

TN
1
AS
Vol. 185
N/C

TRANSACTIONS OF THE AMERICAN INSTITUTE OF MINING AND METALLURGICAL ENGINEERS

(INCORPORATED)

Volume 185

*American Institute of Mining, Metallurgical, and
Petroleum Engineers*

INSTITUTE OF METALS DIVISION, IRON
AND STEEL DIVISION, AND EXTRACTIVE METALLURGY
DIVISION

1949

PAPERS AND DISCUSSIONS PRESENTED AT MEETINGS HELD AT SAN FRANCISCO, FEB. 13-17, 1949; COLUMBUS, SEPT. 25-29, 1949;* CLEVELAND, OCT. 17-19, 1949;* NEW YORK, FEB. 12-16, 1950.* DISCUSSION OF PAPERS PRESENTED AT PHILADELPHIA MEETING, OCT. 25-27, 1948.

* Discussion of papers presented at these meetings will be published in Volume 188 (1950).

PUBLISHED BY THE INSTITUTE
AT THE OFFICE OF THE SECRETARY
29 WEST 39TH STREET
NEW YORK 18, N. Y.

COPYRIGHT, 1950, BY THE
AMERICAN INSTITUTE OF MINING AND METALLURGICAL ENGINEERS
(INCORPORATED)
PRINTED IN THE UNITED STATES OF AMERICA

FOREWORD

This, the 185th volume of the Transactions of the American Institute of Mining and Metallurgical Engineers, contains publications, in new format, of the Metals Branch, and represents another milestone in the science and technology of metals. For the first time the technical papers of the three metals divisions (Institute of Metals, Iron and Steel, and Extractive Metallurgy) are presented in a unit.

The majority of members will appreciate the fact that the vast number of technical papers necessitates the most economical form of publication. Moreover, by this method members obtain at approximately the cost of one volume what was previously published in three. In this period of rapid technologic developments, having available the papers in related fields is of inestimable value.

The discussions are grouped in two sections of the volume. The location of the discussion of a particular paper is listed immediately following the title of that paper in the table of contents. It was not possible to publish the discussions of the papers presented at the 1948 IMD Fall Meeting in Volume 180 (1949 I.M.D. Volume) due to the mechanics inherent in the change of page size. These discussions may be found on pages 297 to 346 of this volume. The discussion of 1949 Annual Meeting papers of all three divisions are on pages 826 to 897. Discussion of papers presented at the 1949 Fall Meetings and 1950 Annual Meeting will appear in the 1950 Transactions Volume 188.

The breadth of scope of the papers from the three metals divisions, which ranges from the highly theoretical to the very practical, is unsurpassed by any other publication in the metallurgical field. It is gratifying to note the high quality of research and development being carried out in the laboratories and plants of the country. The knowledge made available and the stimulation provided by publication are definite assurances of continued progress.

I would like to express my sincerest thanks to the officers of the divisions, members of the publication and program committees, and the headquarters staff, who have worked so unstintingly to produce this outstanding metallurgical volume. Special words of appreciation should be given to the newly formed Extractive Metallurgy Division which in a single year has become a lusty member of the Metals Branch.

FEBRUARY 9, 1950
BARBER, N. J.

A. A. SMITH, JR., *Chairman*
Metals Branch A.I.M.E.

TECHNICAL PAPERS

Institute of Metals Division

| | PAGE |
|---|------|
| Plastic Deformation Waves in Aluminum. By A. W. McREYNOLDS | 32 |
| Discussion | 876 |
| On the Structure of Gold-silver-copper Alloys. By J. G. McMULLIN and J. T. NORTON | 46 |
| Discussion | 857 |
| Stress and Strain States in Elliptical Bulges. By C. C. CHOW, A. W. DANA, and G. SACHS | 49 |
| A Study of Textures and Earing Behavior of Cold-rolled (87-89 pct) and Annealed Copper Strips. By MING-KAO YEN | 59 |
| Discussion | 887 |
| Use of Electrical Resistance Measurements to Determine the Solidus of the Lead-tin System. By R. HULTGREN and S. A. LEVER | 67 |
| Discussion | 859 |
| The Effect of Strain-temperature History on the Flow and Fracture Characteristics of an Annealed Steel. By E. J. RIPLING and G. SACHS | 78 |
| The Densification of Copper Powder Compacts in Hydrogen and in Vacuum. By C. B. JORDAN and P. DUWEZ | 96 |
| Discussion | 893 |
| Influence of Composition on the Stress-corrosion Cracking of Some Copper-base Alloys. By D. H. THOMPSON and A. W. TRACY | 100 |
| Discussion | 862 |
| The Effect of Orientation Difference on Grain Boundary Energies. By C. G. DUNN and F. LIONETTI | 125 |
| Discussion | 860 |
| Solubility Relationships of the Refractory Monocarbides. By J. T. NORTON and A. L. MOWRY | 133 |
| Discussion | 891 |
| Pressure Distribution in Compacting Metal Powders. By P. DUWEZ and L. ZWELL | 137 |
| Discussion | 888 |
| Preferred Orientation in Rolled and Recrystallized Beryllium. By A. SMIGELSKAS and C. S. BARRETT | 145 |
| Discussion | 886 |
| Magnesium-lithium Base Alloys—Preparation, Fabrication, and General Characteristics. By J. H. JACKSON, P. D. FROST, A. C. LOONAM, L. W. EASTWOOD, and C. H. LORIG | 149 |
| Discussion | 867 |
| Self-diffusion in Sintering of Metallic Particles. By G. C. KUCZYNSKI | 169 |
| Discussion | 896 |
| Homogeneous Yielding of Carburized and Nitrided Single Iron Crystals. By A. N. HOLDEN and J. H. HOLLOMON | 179 |
| Discussion | 877 |
| The Surface Tension of Solid Copper. By H. UDIN, A. J. SHALER, and J. WULFF | 186 |
| Discussion | 894 |
| Properties of Chromium Boride and Sintered Chromium Boride. By S. J. SINDEBAND | 198 |
| Discussion | 889 |
| The Hardenability Effect of Molybdenum. By J. M. HODGE, J. L. GROVE, and R. G. STORM | 218 |
| A Method of Examination of Sections of Fine Metal Powder Particles with the Electron Microscope. By LAURENCE DELISLE | 228 |
| The Effect of Ferrite Grain Size on Notch Toughness. By J. M. HODGE, R. D. MANNING, and H. M. REICHHOLD | 233 |
| Recrystallization and Microstructure of Aluminum-Killed Deep Drawing Steel. By R. L. RICKETT, S. H. KALIN, and J. T. MACKENZIE, JR. | 242 |
| Precipitation Phenomena in the Solid Solutions of Nitrogen and Carbon in Alpha Iron below the Eutectoid Temperature. By L. J. DIJKSTRA | 252 |
| The Crystal Structure of Ni ₃ W. By E. EPREMIAN and D. HARKER | 267 |
| The Beryllium-iron System. By R. J. TEITEL and M. COHEN | 285 |
| Discussion, Institute of Metals Division, Fall Meeting, 1948 | 297 |
| Investigation of Temper Brittleness in Low-alloy Steels. By S. A. HERRES and A. R. ELSEA | 366 |

| | PAGE |
|--|------|
| Oriented Arrangements of Thin Aluminum Films on Ionic Substrates. By T. N. RHODIN, JR. | 371 |
| P-type and N-type Silicon and the Formation of the Photovoltaic Barrier in Silicon Ingots. By J. H. SCAFF, H. C. THEURER, and E. E. SCHUMACHER | 383 |
| Microstructures of Silicon Ingots. By W. G. PFANN and J. H. SCAFF | 389 |
| The Study of Grain Boundaries with the Electron Microscope. By J. F. RADAVICH | 395 |
| Transformation of Gamma to Alpha Manganese. By E. V. POTTER, H. C. LUKENS, and R. W. HUBER | 399 |
| Liquid Solubility of Manganese in a Magnesium-aluminum-tin Alloy. By B. J. NELSON and G. F. SAGER | 405 |
| The Comparative Creep Properties of Several Types of Commercial Coppers. By A. D. SCHWOPE, K. F. SMITH, and L. R. JACKSON | 409 |
| The Rapid Determination of Orientations of Cubic Crystals. By C. G. DUNN and W. W. MARTIN | 417 |
| The Vapor Pressures of Zinc and Cadmium over Some of Their Silver Alloys. By C. E. BIRCHENALL and C. H. CHENG | 428 |
| Electrical Resistivity Measurements on Iron-silicon Compacts Prepared by the Powder Metallurgy Procedure. By F. W. GLASER | 475 |
| A Metallographic Description of Fracture in Impact Specimens of a Structural Steel. By M. BAEYERTZ, W. F. CRAIG, JR., and E. S. BUMPS | 481 |
| Recovery and Recrystallization in Brass. By B. L. AVERBACH | 491 |
| Ferromagnetic Alloys in the Systems Cu-Mn-In and Cu-Mn-Ga. By F. A. HAMES and D. S. EPPELSHEIMER | 495 |
| Secondary Recrystallization in Copper. By M. L. KRONBERG and F. H. WILSON | 501 |
| Kinetics of the Reactions of Zirconium with O ₂ , N ₂ , and H ₂ . By E. A. GULBRANSEN and K. F. ANDREW | 515 |
| The Active Slip Systems in the Simple Axial Extension of Single Crystalline Alpha Brass. By R. MADDIN, C. H. MATHEWSON, and W. R. HIBBARD, JR. | 527 |
| The Effects of Molybdenum and Commercial Ranges of Phosphorus upon the Toughness of 0.40 Pct Carbon Chromium Steels. By M. BAEYERTZ, W. F. CRAIG, JR., and J. P. SHEEHAN | 535 |
| The Effect of Quenching on the Age Hardening of Two Aluminum Alloys. By R. D. BARER and M. B. BEVER | 544 |
| Determination of Boundary Stresses during the Compression of Cylindrical Powder Compacts. By M. E. SHANK and J. WULF | 561 |
| A Dilatometric Study of the Sintering of Metal Powder Compacts. By P. DUWEZ and H. MARTENS | 571 |
| The Isolation of Carbides from High Speed Steel. By D. J. BLICKWEDE and M. COHEN | 578 |
| Solubility of Titanium in Liquid Magnesium. By K. T. AUST and L. M. PIDGEON | 585 |
| The Lattice Parameters of High Purity Alpha Titanium; and the Effects of Oxygen and Nitrogen on Them. By H. T. CLARK, JR. | 588 |
| The Mechanism of Martensite Formation. By A. B. GRENINGER and A. R. TROIANO | 590 |
| Structure and Nature of Kink Bands in Zinc. By J. B. HESS and C. S. BARRETT | 599 |
| Analysis of Interstitial Diffusion Using Activity Methods. By A. G. GUY | 607 |
| The Transformation in Beta-CuAl Alloys. By E. P. KLIER and S. M. GRYMKO | 611 |
| Surface Orientation and Rolling of Magnesium Sheet. By R. L. DIETRICH | 621 |
| Recrystallization Texture and Coarsening Texture in High Purity Aluminum. By P. A. BECK and HSUN HU | 627 |
| Annealing Twins in Copper and 70-30 Alpha Brass. By W. R. HIBBARD, JR., YOU-CHAO LIU, and S. F. REITER | 635 |
| The Yielding and Strain-aging of Carburized and Nitrided Single Crystals of Iron. By H. SCHWARTZBART and J. R. LOW, JR. | 637 |
| The Effect of Oxygen, Nitrogen, and Hydrogen on Iodide Refined Titanium. By R. I. JAFFE and I. E. CAMPBELL | 646 |
| The Origin of Annealing Twins in Brass. By R. MADDIN, C. H. MATHEWSON, and W. R. HIBBARD, JR. | 655 |
| Size Effects in Quenching High-purity, Precipitation-hardenable Alloys. By W. L. FINLAY | 668 |
| The Ternary System, Copper-manganese-zinc. By T. R. GRAHAM, J. R. LONG, C. E. ARMANTROUT, and A. H. ROBERSON | 675 |
| Discontinuous Crack Propagation—Further Studies. By L. D. JAFFE, E. L. REED, and H. C. MANN | 683 |
| The Free Energy Change Accompanying the Martensite Transformation in Steels. By J. C. FISHER | 688 |
| Kinetics of the Austenite→Martensite Transformation. By J. C. FISHER, J. H. HOLLOMON, and D. TURNBULL | 691 |
| Simultaneous Aging and Deformation in Metals. By J. D. LUBAHN | 702 |
| The Transverse Bending of Single Crystals of Aluminum. By M. K. YEN and W. R. HIBBARD, JR. | 710 |
| Stages in the Deformation of Monel Metal as Shown by Polarized Light. By D. H. WOODARD | 722 |
| Influence of Temperature on the Stress-strain-energy Relationship for Copper and Nickel-copper Alloy. By D. J. MCADAM, JR. | 727 |
| Kinetics of the Reactions of Titanium with O ₂ , N ₂ , and H ₂ . By E. A. GULBRANSEN and K. F. ANDREW | 741 |
| Structure of Diborides of Titanium, Zirconium, Columbium, Tantalum, and Vanadium. By J. T. NORTON, H. BLUMENTHAL, and S. J. SINDEBAND | 749 |
| The Diffusion and Solubility of Carbon in Alpha Iron. By J. K. STANLEY | 752 |
| Studies of Interface Energies in Some Aluminum and Copper Alloys. By K. K. IKEYE and C. S. SMITH | 762 |
| Preparation and Casting of Beryllium Melts. By J. G. KURA, J. H. JACKSON, M. C. UDY, and L. W. EASTWOOD | 769 |
| Metallographic Examination of Beryllium Alloys. By M. C. UDY, G. K. MANNING, and L. W. EASTWOOD | 779 |
| Seminar on the Kinetics of Sintering. (With discussion). By A. J. SHALER | 796 |
| Discussion, Institute of Metals Division, San Francisco Meeting, February 1949 | 857 |
| Effect of Prestraining Temperatures on the Recovery of Cold Worked Aluminum. By T. E. TIETZ, R. A. ANDERSON, and J. E. DORN | 921 |
| Flow and Fracture Characteristics of a Die Steel at High Hardness Levels. By L. J. KLINGLER, C. C. CHOW, and G. SACHS | 927 |
| Some Observations on the Recovery of Cold Worked Aluminum. By T. V. CHERIAN, P. PIETROKOWSKY, and J. E. DORN | 948 |
| Carbides in Isothermally Transformed Chromium Steels. By W. CRAFTS and J. L. LAMONT | 957 |
| The Properties of Sand Cast Magnesium—Rare Earth Alloys. By T. E. LEONTIS | 968 |
| Cemented Titanium Carbide. By J. C. REDMOND and E. N. SMITH | 987 |
| Intergranular Parting of Brass during Anneals. By F. H. WILSON and E. W. PALMER | 995 |
| The Low Temperature Properties of Tin-antimony and Tin-cadmium Alloys. By F. J. DUNKERLEY, H. B. HUNTER, and F. G. STONE | 1005 |

Iron and Steel Division

| | |
|--|-----|
| The Interaction of Liquid Steel with Ladle Refractories. By C. B. POST and G. V. LUERSSEN | 15 |
| Discussion | 840 |
| The Influence of Temperature on the Affinity of Sulphur for Copper, Manganese, and Iron. By E. M. COX, M. C. BACHELDER, N. H. NACHTRIEB, and A. S. SKAPSKI | 27 |
| Discussion | 837 |
| Relation between Chromium and Carbon in Chromium Steel Refining. By D. C. HILTY | 91 |
| Discussion | 832 |
| The Ionic Nature of Metallurgical Slags. Simple Oxide Systems. By J. CHIPMAN and LO-CHING CHANG | 191 |
| Discussion | 841 |

| | |
|---|-----|
| Sulphur Equilibria between Iron Blast Furnace Slags and Metal. By G. G. HATCH and J. CHIPMAN..... | 274 |
| Discussion..... | 831 |
| What is Metallurgy? By J. CHIPMAN..... | 349 |
| Sintering Characteristics of Minus Sixty-five and Twenty Mesh Magnetite. By A. STANLEY and J. C. MEAD..... | 435 |
| Discussion..... | 834 |
| Equilibrium in the Reaction of Hydrogen with Oxygen in Liquid Iron. By M. N. DASTUR and J. CHIPMAN..... | 441 |
| Optical Temperature Scale and Emissivity of Liquid Iron. By M. N. DASTUR and N. A. GOKCEN..... | 665 |
| Relative Deoxidizing Powers of Some Deoxidizers for Steel. (With discussion). By C. E. SIMS, H. A. SALLER, and F. W. BOULGER..... | 814 |
| Discussion, Iron and Steel Division, San Francisco Meeting, February 1949..... | 826 |
| Evaluation of pH Measurements with Regard to the Basicity of Metallurgical Slag. By C. W. SHERMAN and N. J. GRANT..... | 898 |

Extractive Metallurgy Division

| | |
|--|-----|
| The Morenci Smelter of Phelps Dodge Corporation at Morenci, Arizona. By L. L. McDANIEL..... | 1 |
| Discussion..... | 855 |
| Development of the Modern Zinc Retort in the United States. By H. R. PAGE and A. E. LEE, JR..... | 73 |
| Discussion..... | 850 |
| Cadmium Recovery Practice in Lead Smelting. By P. C. FEDDERSEN and H. E. LEE..... | 110 |
| Discussion..... | 846 |
| Development of Muffle Furnaces for the Production of Zinc Oxide and Zinc at East Chicago, Indiana. By G. E. JOHNSON..... | 118 |
| Discussion..... | 853 |
| The Recovery of Cadmium from Cadmium-copper Precipitate, Electrolytic Zinc Co. of Australasia, Risdon, Tasmania. By G. H. ANDERSON..... | 205 |
| Discussion..... | 844 |
| Electrolytic Zinc at Risdon, Tasmania. Major Changes Since 1936. By S. W. ROSS..... | 211 |
| Discussion..... | 842 |
| Concentration of the SO ₂ Content of Dwight-Lloyd Sintering Machine Gas by Recirculation. By W. S. REID..... | 261 |
| Discussion..... | 848 |
| The Effect of High Copper Content on the Operation of a Lead Blast Furnace, and Treatment of the Copper and Lead Produced. By A. A. COLLINS..... | 347 |
| Discussion..... | 847 |
| Distillation of Zinc from Copper Base Alloys and Galvanizers Drosses. By F. F. POLAND..... | 355 |
| Discussion..... | 855 |
| Cadmium Recovery Practice at the Donora Zinc Works. By G. T. SMITH and R. C. MOYER..... | 360 |
| Discussion..... | 843 |
| Controlled Drying of Retorts. By R. R. FURLONG and D. H. WERTZ..... | 393 |
| Discussion..... | 852 |
| The Use of Oxygen Enriched Air in the Metallurgical Operations of Cominco at Trail, B. C. By R. R. McNAUGHTON, T. H. WELDON, J. H. HARGRAVE, and L. V. WHITON..... | 446 |
| Discussion..... | 848 |
| A Thermodynamic Investigation of the System Silver-Silver Sulphide. By T. ROSENQVIST..... | 451 |
| Autogenous Roasting of Low Grade Zinc Concentrate in Multiple Hearth Furnaces at Risdon, Tasmania. By J. A. B. FORSTER..... | 461 |
| Discussion..... | 849 |
| El Paso Slag Treatment Plant. By T. J. WOODSIDE..... | 472 |
| Discussion..... | 854 |
| Low Pressure Distillation of Zinc from Al-Zn Alloy. By M. J. SPENDLOVE and H. W. ST. CLAIR..... | 553 |
| Titanium Investigations: Research and Development Work on the Preparation of Titanium Chloride and Oxide from Titanium Mattes. By R. G. KNICKERBOCKER, C. H. GORSKI, H. KENWORTHY, and A. G. STAR-LIPER..... | 785 |
| Recovery of Zinc by the Dithionate Sulphur-dioxide Leaching Process. By S. F. RAVITZ and A. E. BACK..... | 792 |
| Discussion, Extractive Metallurgy Division, San Francisco Meeting, February 1949..... | 842 |
| Melting Points in the System TiO ₂ -CaO-MgO-Al ₂ O ₃ . By H. SIGURDSON and S. S. COLE..... | 905 |
| Laboratory Smelting of Titaniferous Ores. By D. L. ARMANT and S. S. COLE..... | 909 |
| Petrology of High Titanium Slags. By C. H. MOORE, JR. and H. SIGURDSON..... | 914 |
| The Fume and Dust Problem in Industry. By H. V. WELCH..... | 934 |
| The Relationship Between Electrical Conductivity and Composition of Molten Lead Silicate Slags. By A. K. SCHELLINGER and R. P. OLSEN..... | 984 |

TECHNICAL NOTES

| | |
|--|------|
| Controlled Grain Growth Applied to the Problem of Grain Boundary Energy Measurements. By C. G. DUNN..... | 72 |
| A Simple Constant Stress Creep Test. By J. C. FISHER and R. P. CARREKER..... | 178 |
| Grain Coarsening in Copper. By P. A. BECK, J. TOWERS, JR., and P. R. SPERRY..... | 203 |
| Solid Nuclei in Liquid Metals. By C. S. SMITH..... | 204 |
| Effect of Recrystallization Texture on Grain Growth. By P. A. BECK and P. R. SPERRY..... | 240 |
| The Sigma Phase in Ternary Cr-Co-Fe and Cr-Co-Ni Alloys. By P. A. BECK and W. D. MANLY..... | 354 |
| The Statistical Nature of the Endurance Limit. By J. T. RANSOM and R. F. MEHL..... | 364 |
| Effect of Carbon and Nitrogen on Temper Brittleness. By D. C. BUFFUM, L. D. JAFFE, and W. P. CLANCY..... | 499 |
| Discontinuous Crack Propagation. By L. D. JAFFE, E. L. REED, and H. C. MANN..... | 526 |
| Rectangular Hysteresis Loops of Co-Ni-Fe Alloys. By R. A. CHEGWIDDEN..... | 570 |
| Effect of Composition on the Wire Textures of Copper and Its Solid Solution Alloys. By W. R. HIBBARD, JR..... | 598 |
| Compression Textures of Copper and Its Binary Alpha Solid Solution Alloys. By W. R. HIBBARD, JR. and D. E. TROUT II..... | 620 |
| Some Observations on the Rate of Secondary Recrystallization in High Purity Copper. By A. M. TURKALO and D. TURNBULL..... | 663 |
| Some Observations in the Structure of Alpha Brass Single Crystals after Cutting and Polishing. By R. MADDIN and W. R. HIBBARD, JR..... | 700 |
| On the Problem of Grain Boundary Movement. By C. G. DUNN, F. W. DANIELS, and M. J. BOLTON..... | 708 |
| High Temperature Scaling of Cobalt. By C. R. JOHNS and W. M. BALDWIN, JR..... | 720 |
| The Thermodynamical Treatment of Very Small Solid Solubilities. By L. GUTTMAN..... | 740 |
| The Relation Between Indentation Hardness and Strain for Metals. By J. H. PALM..... | 904 |
| Notes on the Electrolytic Isolation of Carbides in Steel. By G. WRANGLER..... | 919 |
| The Effect of Working and Heating Eutectic Structures. By J. S. BROWN and A. G. GUY..... | 933 |
| Binary Chart for Interconversions of Mol. Weight, and Volume Per Cent. By J. B. SEABROOK..... | 993 |
| A Proposed Microbending Mechanism of Plastic Deformation. By M. K. YEN..... | 1003 |

The Morenci Smelter of Phelps Dodge Corporation at Morenci, Arizona

L. L. McDANIEL,* Member AIME

COPPER smelters of various kinds have operated in the Morenci district since 1872, but all have been abandoned with the exception of the present Morenci Smelter of Phelps Dodge Corporation, which was completed in 1942.

During the five-year period starting in 1937, the Morenci ore body was prepared for open pit mining, pilot mill test work was carried out, and a complete reduction works, of which the Smelter is a part, was designed and erected. Actual construction work on the Morenci Smelter was started in the fall of 1940, and warming up of the units began on April 1, 1942. Charging of the reverberatory furnaces commenced on April 18, 1942, and the first anode copper was produced on April 26, 1942.

The smelter was originally designed to handle the production of the Morenci Concentrator on a 25,000 ton per day program, but by the time the smelter was in operation, plans were already underway to increase the smelter capacity to handle the production of the concentrator which was being enlarged to 45,000 tons a day capacity as a war-time necessity. This extension to the smelter was completed and the new units were put in operation toward the beginning of 1944.

The original smelter consisted of a smelter crushing plant, bedding plant, two direct-smelting reverberatory furnaces with two waste-heat boilers on each furnace, three converters, an anode department, a stack, and all of the usual accessory smelting equipment. The extension consisted of increasing the bedding plant from three to five beds, the reverberatory department from two to four furnaces, and from four to eight waste-heat boilers, and the converter department from three to six converters. A third converter aisle crane was added and additions were made to the flue systems and conveyor systems throughout the

smelter; but no change was made in the smelter crushing plant or the anode department, and the same stack was used for all additional Smelter units. A blister casting machine was installed at that time in the south end of the converter aisle to handle excess and emergency production above the capacity of the anode department and in 1947 a converter aisle skull breaker and a lime burning plant were added as the final units for a complete plant.

The choice of direct smelting over calcine smelting for the Morenci Smelter was made after careful study by members of the Western organization of Phelps Dodge Corporation and after test runs on direct smelting of Morenci concentrate had been made at the Douglas Smelter of Phelps Dodge Corporation. The Morenci furnace charge is made up of comparatively high grade concentrate with no ores of smelting grade available and with only flux, a small amount of copper precipitate and the usual amount of smelter secondaries to be smelted with the concentrate. The simplicity of direct smelting for this charge and the large amount of waste-heat steam available from direct smelting operations were factors influencing the decision to adopt direct smelting for Morenci. The design of the Morenci Smelter and the type of units selected followed best experience at the Douglas Smelter of Phelps Dodge Corporation.

A description of the original smelter before operations started was given in an article in the May 1942 issue of *Mining and Metallurgy*. The purpose of the present article is to describe the enlarged Morenci Smelter, with a discussion of metallurgy and operating

practice and to show tabulations of operating and metallurgical results obtained. Because of beginning operations during the early years of World War II, many problems caused by labor shortage were encountered, but no major difficulties developed in starting the new plant. However, because of labor shortage, full scale Smelter production was not reached until the fall of 1946.

Fig 1 shows a general plan of the Morenci Reduction Works. The arrangement of the smelter equipment is shown in Fig 2, a sectional view of the smelter is shown in Fig 3, and the smelter flow sheet is shown in Fig 4.

Metallurgy

The metallurgy of direct smelting, being more or less fixed by the character of the charge, is not subject to the control available in calcine smelting. Slags may be modified by the addition of suitable fluxes, but the grade of the matte is determined almost entirely by the iron:copper ratio of the concentrate.

The direct smelting operation involves distributing the wet concentrate along the sidewalls and in the bath of a reverberatory furnace by means of some suitable feeding device and raising the temperature of the charge so that first the moisture is driven off, then the first-atom sulphur is eliminated, and finally the sulphide portion of the charge melts and runs into the bath, carrying with it the non-sulphide portion which has been partially fluxed to form a suitable slag. The fusion of the non-sulphide portion is completed by contact with the iron converter slag which is regularly being poured into the reverberatory furnace. The smelting rate of the charge is influenced by the mineralogical composition of the sulphide portion of the concentrate and by the composition and amount of the non-sulphide portion including the fluxes added.

The copper in Morenci concentrate is chiefly in the form of chalcocite, intimately associated with pyrite, and non-sulphide content is very low so that

San Francisco Meeting, February, 1949.

TP 2488 D. Discussion of this paper (2 copies) may be sent to *Transactions AIME* before April 1, 1949. Manuscript received at the office of the Institute June 1, 1948.

*Smelter Superintendent, Phelps Dodge Corporation, Morenci Branch, Morenci Arizona.

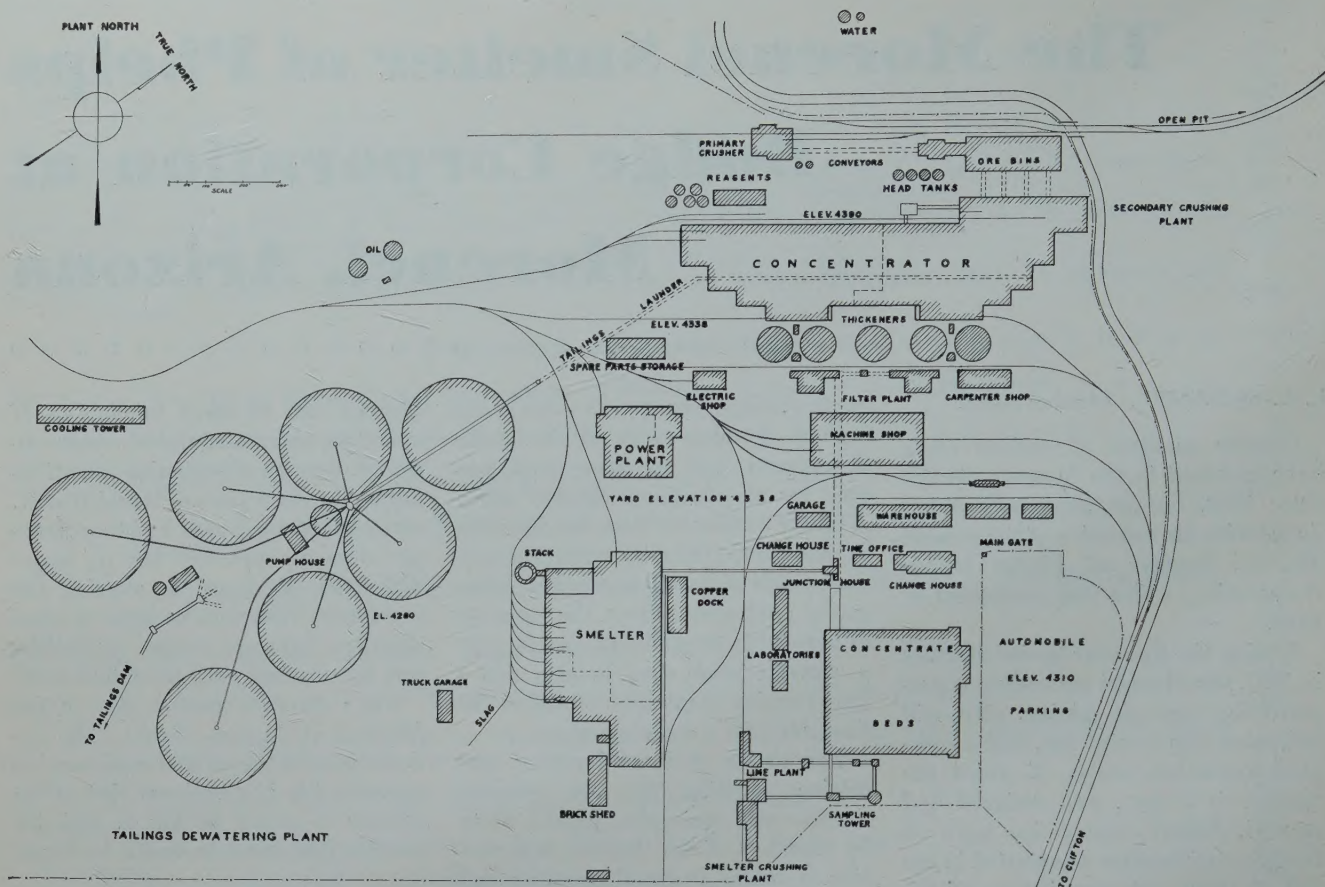


FIG 1—General plan of Morenci reduction works.

the main problem of the smelter is in fluxing and eliminating iron. The copper content of the Morenci concentrate increased appreciably, and the iron content decreased during the first few years of operation. Smelter metallurgy improved correspondingly as the iron burden was lessened and the converters were relieved of part of their work. The concentrate is graded upward 7.0 to 8.0 units of copper in forming matte, the amount being influenced somewhat by the quantity of precipitate on the charge.

There is no metal bearing siliceous flux readily available in the Morenci district and ore from the Open Pit mining operation is too high in alumina to be used alone. It has been necessary therefore, to mine a barren quartzite for use in modifying furnace slags. This is also used in adjusting the silica: alumina ratio of the Pit ore used for converter flux to prevent the formation of excessive amounts of magnetite in converter slags. Limerock is used to flux the non-sulphide content of the concentrate, and at times, additional limerock and quartzite are added to the bedded concentrate to reduce the moisture content of the furnace feed.

The make-up of the furnace charge

is usually quite uniform although at times other material has been smelted. In 1943 and 1944 a large amount of clean-up material from an old smelter in the district was crushed and smelted in the reverberatory furnaces, and during early operations at the smelter a large quantity of reverts accumulated in the converter aisle which eventually were crushed and smelted with the reverberatory furnace charge. At the present time most of the converter reverts are smelted directly in the converters and any excess is crushed and added to the converter flux to modify the high silica content resulting from the use of barren quartzite. Foul slag from the reverberatory furnaces is also crushed and added to the converter flux

for this purpose. Crushing of reverts and foul slag is done simultaneously with the barren quartzite to insure a good mixture.

The dry weight of concentrate received at the smelter is calculated by the concentrator from actual weightometer weights of feed to the ball mills and assays of automatic samples of feed, tailings and concentrate. This method has been very reliable over a considerable period of time. The moisture content of the concentrate is determined by sampling as the concentrate leaves the filter plant.

Smelter slag, stack and mechanical losses are shown in Table 1. Stack loss tests are made regularly and reverberatory slags are sampled at the furnace

Table 1 . . . Losses Expressed as Percent of Input

| | Copper | | | Silver | | | Gold | | |
|------|--------|----------------------|-------|--------|----------------------|-------|------|----------------------|-------|
| | Slag | Stack and Mechanical | Total | Slag | Stack and Mechanical | Total | Slag | Stack and Mechanical | Total |
| 1942 | 1.41 | 0.52 | 1.93 | 1.74 | 0.51 | 2.25 | 2.12 | 0.01 | 2.13 |
| 1943 | 1.50 | 0.69 | 2.19 | 1.65 | 2.71 | 4.36 | 2.87 | 0.55 | 3.42 |
| 1944 | 1.42 | 0.81 | 2.23 | 1.28 | 0.73 | 2.01 | 1.38 | 0.45* | 0.93 |
| 1945 | 1.22 | 0.62 | 1.84 | 1.09 | 1.38 | 2.47 | 1.40 | 0.74* | 0.66 |
| 1946 | 1.12 | 0.94 | 2.06 | 0.99 | 0.89 | 1.88 | 1.03 | 0.30* | 0.73 |
| 1947 | 1.20 | 0.83 | 2.03 | 1.02 | 1.01 | 2.03 | 1.25 | 0.70* | 0.55 |

* Gain

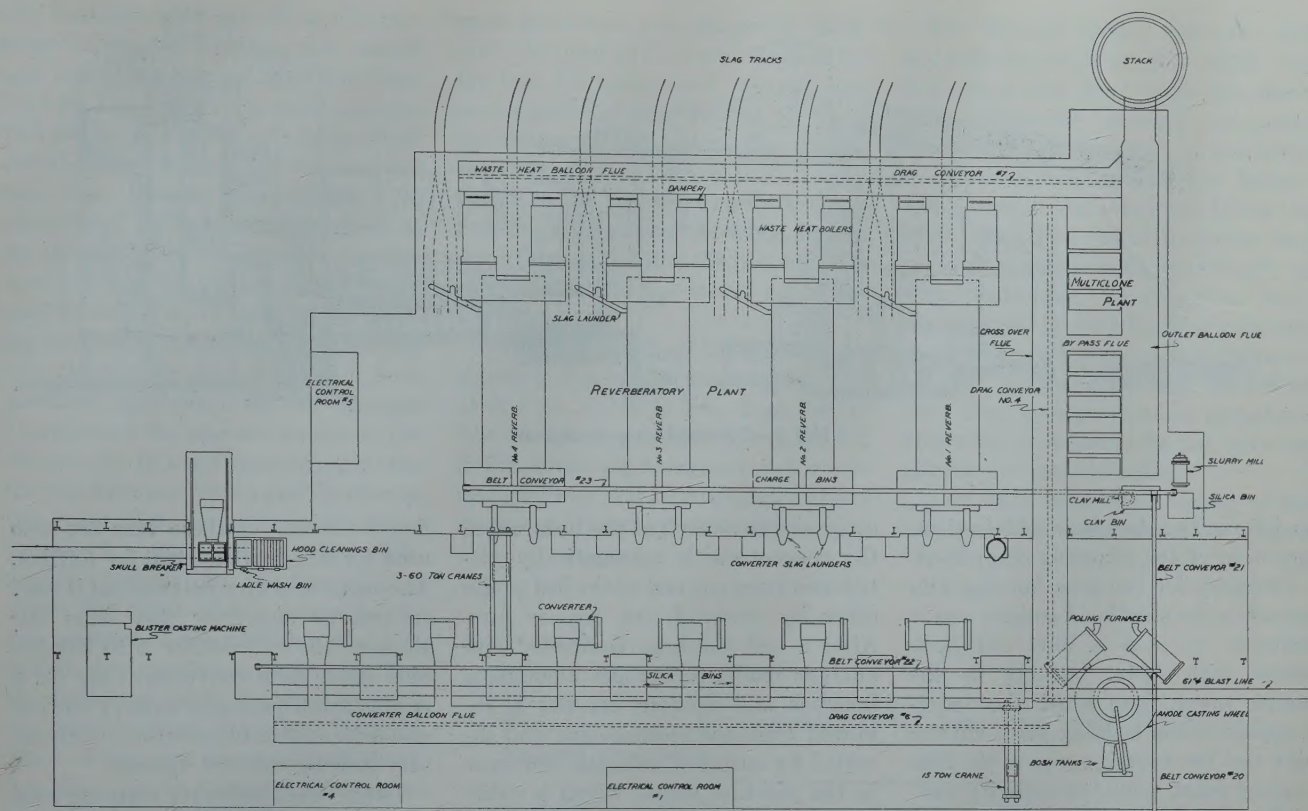


FIG 2—Arrangement of smelter equipment.

and on the dump. Anode copper is weighed and sampled at the refinery for final settlement.

Results have shown that direct smelting of Morenci concentrate has proved successful with a concentrate grade above 25.0 pct copper and an iron:copper ratio of about 1.00, and that smelter equipment and arrangement have been satisfactory. Production figures for the total plant are shown in Table 2. In all tabulations in this paper figures for 1946 are based on 8.4839 months operating time because of a general strike in the industry which caused a shut-down that year.

Smelter Crushing Plant and Lime Burning Plant

The smelter crushing plant was designed to crush Pit ore and siliceous ore for converter flux and limerock and siliceous ore for reverberatory flux, as well as smelter reverts and miscellaneous material required in smelter operations. The crushing plant was also designed to crush limerock for a lime burning plant which is operated by the smelter organization to produce burned lime for the Concentrator.

In order to eliminate crushing of large sized material from open pit shovel mining operations, Pit ore

crushed to $\frac{3}{4}$ in. is drawn from the fine ore bins at the concentrator into 40 yd side dump railroad cars and hauled to the smelter crushing plant and then conveyed to converter flux bins in the bedding plant without further crushings. Barren quartzite is mined in a quarry near the Reduction Works and trucked to the smelter crushing plant. Truck haulage is to be replaced by rail haulage at a later date. Limerock is mined in a quarry near the Open Pit Mine, trucked for a short distance, and loaded into side dump railroad cars for haulage to the smelter crushing plant.

The 100-ton receiving bin in the smelter crushing plant is served by railroad cars or trucks and the material is fed by a 48-in. pan feeder directly into a 36- \times -48-in. jaw crusher. The 4-in. product of the jaw crusher passes over a 5- \times -10-ft mechanically vibrated rod deck screen with $1\frac{1}{2}$ -in. opening, the oversize feeding directly

into a 7-ft standard cone crusher with $1\frac{1}{4}$ -in. setting. This loose setting is required because of crushing smelter reverts containing metallic copper. The combined product of the 7-ft standard crusher and screen passes over another 5- \times -10-ft rod deck screen with $\frac{1}{4}$ -in. opening, the oversize falling into a 4-ft shorthead cone crusher which is in closed circuit with the screen.

In the case of Pit ore and siliceous ore used for converter flux the material by-passes the 4-ft shorthead crusher and goes directly to the 5,000 ton storage bins at the end of the bedding plant. Limerock for flux and other material which is crushed to $\frac{1}{4}$ in. in the shorthead crusher may be delivered either to sections of the storage bins or directly to the beds. The material leaving the crushing plant is sampled by an automatic sampler in a sample tower, which takes a 10 pct cut. The material so far sampled has been barren flux and

Table 2 . . . Operating Data Total Plant

| | Average per Month Tons N.M.B.M. Treated | Pct Copper Input N.M.B.M. | Actual Production Average Month Salable Copper | Power Used Kw Hr Per Ton N.M.B.M. |
|------|---|------------------------------|--|--------------------------------------|
| 1942 | 29,981 | 18.02 | 10,439,844 | 57.90 |
| 1943 | 36,948 | 18.58 | 13,276,948 | 62.26 |
| 1944 | 35,194 | 21.31 | 14,702,658 | 82.68 |
| 1945 | 32,579 | 24.00 | 15,335,529 | 75.22 |
| 1946 | 41,559 | 24.90 | 20,204,926 | 68.41 |
| 1947 | 51,906 | 24.29 | 24,708,705 | 64.77 |

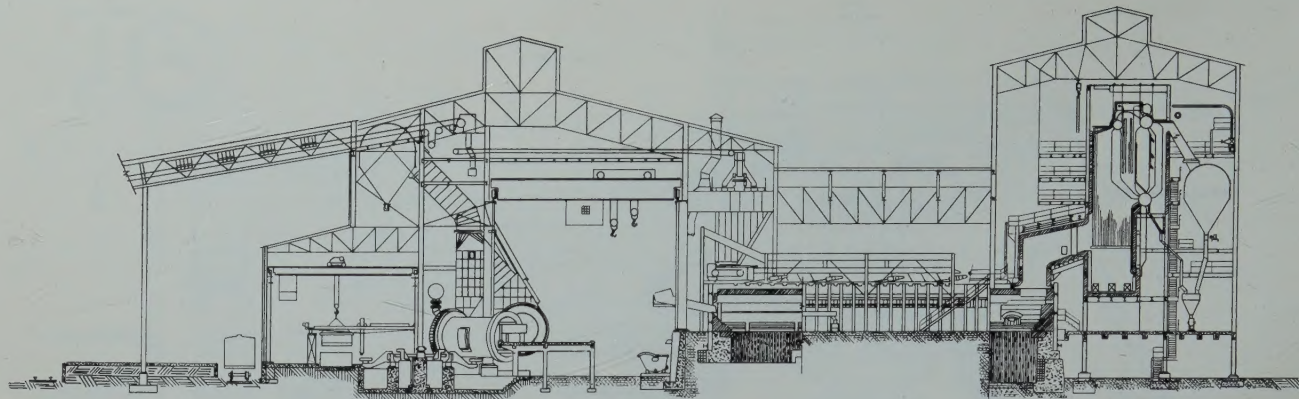


FIG 3—Sectional view of smelter.

no information has been obtained on operation of the sampling equipment.

Limerock for the lime burning kiln by-passes the shorthed crusher and is delivered to a 5- \times 10-ft rod deck screen with $\frac{1}{4}$ -in. opening in the sample tower, from which the under-size goes to the bedding plant storage bins and the oversize goes to the lime burning plant 1,000-ton capacity storage bin. Limerock from this storage bin is delivered by belt conveyor to the 275-ft rotary lime burning kiln which is fired with natural gas and produces 100 tons of burned lime per day.

A lime hydrating plant using a ball mill and classifier for preparation of milk of lime for the Concentrator ad-joins the smelter crushing plant and receives burned lime from the 900 ton storage bin at the discharge end of the lime kiln. Milk of lime is pumped to the Concentrator through a 10-in. pipe.

The smelter crushing plant, sample tower, lime plant and storage bins are provided with dust control systems using wet collectors for the exhaust from the fans.

Bedding and Reclaiming Plant

The bedding plant serves a two-fold purpose: (1) It smooths out daily variations in concentrate composition so that furnace metallurgy and matte grade will be more uniform and, (2) it provides storage capacity to take care of interruptions to operations in either the Smelter or the Concentrator.

There are five beds, completely enclosed to prevent wind losses. The beds are 66 ft wide and 300 ft long with an effective bedding area of 50 \times 250 ft which gives a capacity of 5,000 tons of concentrate each. Concentrate from the filter plant is delivered by two conveyor belts in parallel onto cross-

conveyors over each of the beds where the concentrate is automatically distributed from one end of the bed to the other by motor driven tripper cars. After a bed has been completed and analysis made, the proper amount of limerock and siliceous ore flux is removed from the storage bins and diverted by means of a shuttle conveyor in the junction house, which is a distribution point, to one of the conveyors from the filter plant. The flux is delivered from this conveyor to the overhead conveyor above the bed and distributed over the concentrate on the bed. Flux may also be diverted directly from the smelter crushing plant to the cross conveyors over the beds. A bin in the junction house is provided with a belt feeder to handle copper precipitate and cleanup material from the smelter and feed it onto the concentrate conveyor delivering to the beds. Flue dust from a pug mill is also added to this conveyor in the junction house.

The final bedded mixture of concentrate and flux is removed by a reclaiming machine working into one end of a bed and plowing across the face and delivering the mixture onto a belt conveyor in a trench along the side of the bed. The reclaiming rate is about 150 tons per hr. There are two reclaiming machines which can be moved to any bed by means of a transfer car. This method of bedding and reclaiming furnace charge provides great flexibility in fluxing the charge and results in a very nearly perfect mixture of the charge for the furnaces.

The furnace charge, which is dropped on the trench belt by the reclaiming machine, is delivered through the junction house onto an inclined belt conveyor which transports the material across the converter aisle to a cross conveyor and then to two 265-ton bins above each reverberatory furnace.

Small sections of these bins are also used for siliceous material for fettling. The same conveyor belt system is used to remove converter flux from the storage bins and deliver it to 250-ton bins above each converter. Clay for a mud mill and quartz for a slurry mill are also delivered to bins on the reverberatory floor by this belt system.

Twenty-inch conveyor belts are used on all overhead receiving conveyors and 24-in. conveyor belts are used on the reclaiming system delivering material from the beds to the smelter. All belt conveyors are provided with dust collecting systems at transfer points in the junction house and at the top of the smelter building. In addition, the conveyor gallery above the converter flux bins is kept under slight pressure by a ventilating system delivering 75,000 cfm of fresh air, which keeps the gallery free from smoke and reduces temperature for the comfort of workmen and protection of the conveyor belting. A similar installation in the conveyor gallery over the reverberatory furnace bins discharges 100,000 cfm of fresh air.

Reverberatory Furnaces

The four direct-smelting reverberatory furnaces are located on a block of unexcavated ground 15 ft above the surrounding yard level. Furnace foundations are formed of heavy, re-inforced concrete in a monolithic band around the furnace. Concrete beams were placed between the furnaces, which are on 70-ft centers, and the outer walls of the foundations on No. 1 and No. 4 furnaces were carried downward an additional 8 ft to prevent bending of the longitudinal sections by expansion pressures.

After the concrete foundations for the furnaces were poured and the rods for the end steel bindings were in place

slag bottoms were poured in the furnaces to seal the conglomerate subsoil and to anchor the end steel bindings. Slag for the first two furnace bottoms was melted in a small natural-gas fired reverberatory furnace located between the two furnace foundations. An abandoned reverberatory furnace at an old smelter in the district was dismantled and the brick and steel were used to build the 14 × 50 ft slag melting furnace. Crushed blast furnace slag was obtained from a slag dump from previous operations in the Morenci District and the slag was hauled to the furnace site in trucks and charged into the small furnace with a grab bucket on the boom of a motor crane. Slag was tapped in about 30-ton lots into launders leading into the furnace bottoms. The depth of slag poured in the end sections of the bottoms was 8 ft and in the middle sections 4 ft. The slag remained partly liquid underneath the crust between pours and the final block of slag was dense and relatively free from cracks. About 1200 tons of slag was poured in each bottom. Slag for the bottoms of the last two reverberatory furnaces constructed, No. 3 and No. 4, was run directly from No. 2 reverberatory furnace through launders to the new furnace bottoms.

An attempt was made to fuse in the final furnace bottoms for the first two furnaces with 24 in. of crushed silica at the time the furnaces were started up. However, as soon as charging of the furnaces began, the silica bottoms in both furnaces came up and were lost. The bottoms floated shortly after charging was started and as soon as sufficient matte had accumulated to penetrate beneath the bottom and force it up.

The loss of the silica bottoms occasioned no serious delay to operation, and it developed that the furnaces operated very satisfactorily without the silica bottoms and with a deep bath of matte resting directly upon the original slag bottom that was poured into the furnace at the time the furnaces were constructed. There was no noticeable effect on the furnace foundations from the deep bath of matte, and the bath of matte actually aided in smelting the charge. It was therefore decided to build the two new furnaces, No. 3 and No. 4, without silica bottoms and with the poured slag bottoms at approximately the same elevation as in the first furnaces, that is, about 24 in. below the matte tap holes. This was done and these slag bottoms in all fur-

naces have been very successful. However, the deep bath of matte below the tap hole has not proved advantageous over a period of time because of lack of circulation of the matte. The bottom soon fills up with magnetite to the elevation of the tap holes and it is therefore the present practice when digging out a furnace to leave the bottom at an elevation only a few inches below the tap hole.

Structural details of the furnaces are shown in Fig 5. The furnaces measure 31 ft 3 in. × 110 ft 0 in. from face to face of buckstays and 25 ft 6 in. × 102 ft 6 in. inside the brickwork at the normal slag line. All steel bindings are of exceptionally heavy construction.

The furnace arches, sidewalls and endwalls are made of silica brick. The bridgwall and front walls are faced with chemically bonded magnesite brick and there is a band of magnesite brick completely around the furnace walls, constituting a crucible below the metal line. The furnace uptakes and cross-overs to the boilers are largely of suspended brick construction, with high alumina fire brick in the walls and magnesite brick in the arches. Dampers of light weight insulating brick and alloy steel construction are suspended above the cross-overs for use between the furnace and the boiler.

The 20 in. silica brick arches of the reverberatory furnaces have shown

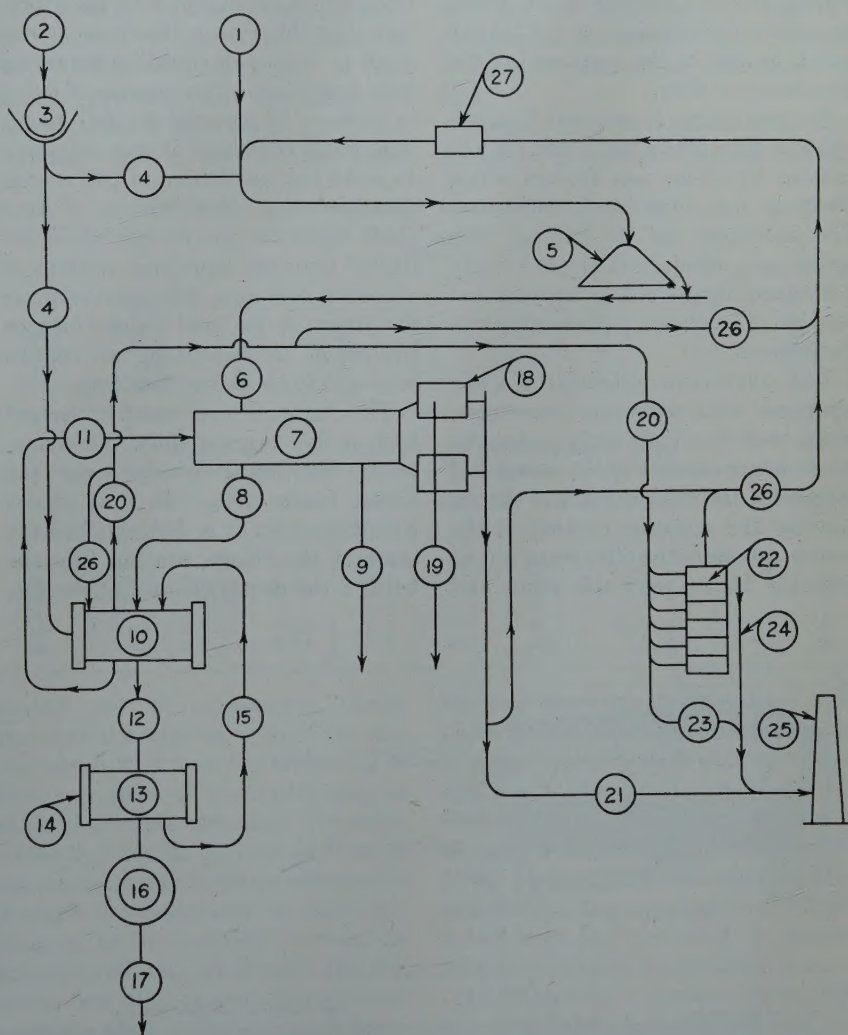


FIG 4—Smelter flowsheet.

- | | |
|---|--|
| 1 Concentrate from filter plant | 15 Slag to converters |
| 2 Flux from smelter crushing plant | 16 Casting wheel (40 ft diam) |
| 3 Flux storage bins | 17 Anodes to refinery |
| 4 Flux to converters and bedding plant | 18 Waste heat boilers (8 boilers, 1143 hp each) |
| 5 Bedding plant (5 beds, 5000 tons each) | 19 Waste heat steam to power house |
| 6 Mixed charge to reverberatories | 20 Converter balloon flue (18 ft diam) |
| 7 Reverberatory furnaces (4 furnaces, 25 ft 6 in. by 102 ft. 6 in.) | 21 Reverberatory balloon flue (15 ft diam) |
| 8 Matte to converters | 22 Multiclone dust collectors (10 sections on converter gases) |
| 9 Slag to dump | 23 Multiclone by-pass flue |
| 10 Converters (6 converters, 13 by 30 ft) | 24 Multiclone outlet flue |
| 11 Converter slag to reverberatories | 25 Stack (reinforced concrete 603 ft 2 in. 39 id bottom, 24 ft id top) |
| 12 Molten blister to anode furnaces | 26 Dust handling system |
| 13 Anode furnaces (2 furnaces, 13 by 25 ft) | 27 Pug mill dust conditioning plant |
| 14 Poles | |

good life under direct smelting conditions, and all of the original arches were still in place at the end of the first 4½ yr of operation, with No. 2 and No. 3 furnaces each having smelted around 400,000 tons of charge and No. 1 furnace, 600,000 tons of charge at that point. Furnace campaigns average 2 to 2½ yr and major repairs consist of digging out the bottom by blasting and slushing and making repairs to brickwork in the bridgewall, sidewalls, front wall and uptakes and cross-over arches. In the future, greater repairs to the main arches are anticipated because of greater length of service. All silica arches and sidewalls are maintained by the slurry gun patching method developed at United Verde Branch of the Phelps Dodge Corporation. A slurry preparation plant using a 6 × 12 ft ball mill is located at the north end of the reverberatory floor.

Furnace charge is removed from the 265-ton bins above each side of the furnace by 54-in. pan feeders which discharge into drag chain conveyors. The conveyors are 80 ft long with spring gate openings in the box every 4 ft which discharge into hoppers and then into 8-in. charge pipes leading into the furnace.

The furnaces originally were equipped with vibrating conveyors, which worked satisfactorily as long as the moisture content of the charge did not exceed the critical point of the vibrators. The moisture content of the concentrate from the filter plant is considerably higher than this point and

Table 3 . . . Reverberatory Furnace Data (Dry Tons Basis)

| | 1942 | 1943 | 1944 | 1945 | 1946 | 1947 |
|-------------------------------|---------|---------|---------|---------|---------|---------|
| Concentrate..... | 214,497 | 355,365 | 365,923 | 346,183 | 316,302 | 550,979 |
| Precipitate..... | 3,431 | 6,391 | 2,231 | 1,014 | 738 | 644 |
| Limerock..... | 9,385 | 19,149 | 15,407 | 18,013 | 24,832 | 38,900 |
| Pit Ore..... | 4,705 | 4,851 | | | | |
| Quartzite..... | 2,088 | 14,974 | 7,742 | 17,823 | 14,823 | 38,667 |
| Reverts and Cleanup..... | 5,643 | 13,079 | 30,642 | 10,642 | 8,232 | 5,007 |
| Total Solid Charge..... | 239,749 | 413,809 | 421,945 | 393,675 | 364,927 | 634,197 |
| Furnace Days..... | 500 | 706 | 829 | 722 | 596 | 1,095 |
| Solid Chg. Fee. Day..... | 479 | 586 | 509 | 545 | 612 | 579 |
| Mil Btu per ton Chg..... | 5,968 | 6,539 | 6,828 | 6,505 | 6,270 | 6,143 |
| Mil Btu per Ton Net..... | 2,670 | 2,851 | 3,039 | 2,958 | 2,960 | 2,844 |
| Converter Slag..... | 174,274 | 269,138 | 248,076 | 213,306 | 211,721 | 353,431 |
| Reverberatory Slag..... | 174,108 | 292,309 | 279,450 | 248,769 | 228,565 | 409,994 |
| Reverberatory Matte..... | 195,755 | 317,579 | 319,101 | 289,524 | 272,061 | 450,680 |
| Lb Steam per Ton Concent..... | 3,408 | 3,980 | 3,932 | 3,668 | 3,387 | 3,394 |
| Pct Waste-heat Recovery..... | 55.6 | 56.4 | 55.5 | 54.5 | 52.8 | 53.7 |
| Pct Boiler Rating..... | 81.4 | 119.4 | 101.9 | 102.8 | 107.1 | 101.6 |

even after it is lowered by flux additions and by some drying on the beds, the moisture is still close to the critical limit; and when this limit is exceeded trouble is encountered with the vibrators. For this reason the decision was made to replace all vibrating conveyors with drag chains, but because of delay in delivery of material for full length drag chain conveyors it was necessary to make the installation in two stages, the first being short sections of drag chain under the pan feeders which delivered onto the remaining sections of vibrating conveyor. Electrical controls for drag chains and other furnace equipment are housed in two control rooms 15 ft above the floor level.

The furnaces are usually charged four or five times a shift, the charge being distributed evenly over the charge banks from both drag chains simultaneously. It is desirable to have some of the charge run out into the bath in the center channel of the fur-

nace, thus exposing greater area to the combustion flame and to the hot bath in the furnace and providing better contact with liquid converter slag for the reduction of magnetite. If the wet charge in the bath becomes too heavy, it is forced down through the slag and comes in contact with the matte and an explosion occurs. Mild explosions are normal and are desirable because they tend to bring more of the charge in contact with the hot bath, which increases the smelting rate; but at times the explosions may be rather violent and may be hazardous to men working around openings in the furnace or boilers and may cause damage to furnace arches. It is the practice at Morenci to attempt to minimize the force of the explosions by keeping the charge banks well filled so that too much charge does not run out into the bath in one place. It is also the practice to keep tie rods tight and to use steel props on the arch to prevent movement.

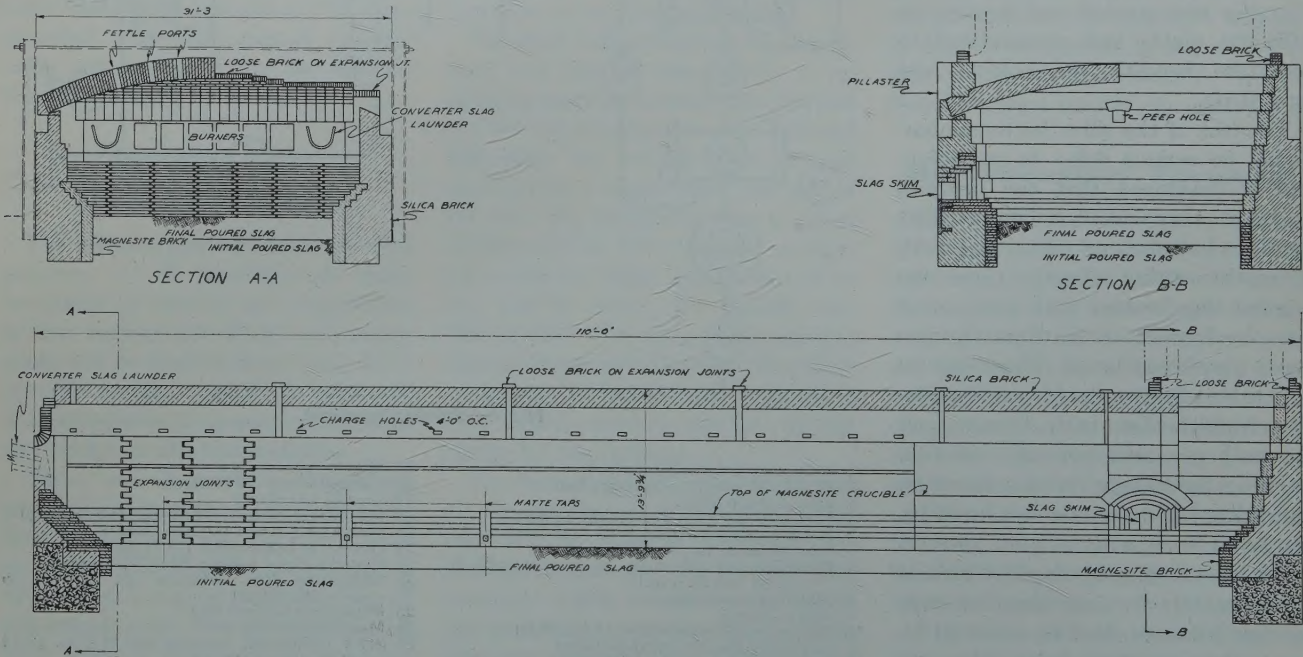


FIG 5—Longitudinal and cross-sectional views of reverberatory furnace brickwork.

The reverberatory furnaces are fired with natural gas and originally were equipped with eight panels of multiple jet burners on each furnace, spaced across the bridgewall with suspended arch construction above the burners. These burners gave satisfactory results, provided the capacity of the burner was not exceeded, but the burners were very difficult to keep clean because of the explosions in the furnace which plugged the burner ports with charge and slag and made control difficult. For this reason and also in order to improve combustion efficiency at higher rates of gas burning a change was made to high pressure burners which enter the bridgewall through large pipes. With large pipes there is less tendency for the burners to become fouled during explosions and combustion control and efficiency are better. The high pressure burners cause somewhat greater arch corrosion as a result of greater turbulence in the combustion zone, but this is not serious and simply requires greater attention to arch maintenance with the slurry gun.

Natural gas from the New Mexico fields is delivered to the plant by pipe line under 300-lb pressure and is then reduced to suitable pressure for use as fuel in the reverberatory furnaces and boilers. Stand-by fuel oil equipment including heaters, pumps and steam atomizing burners has been provided for emergency use and has been used a few times during interruptions to natural gas deliveries.

The natural gas contains about 1100 Btu per cu ft and gas pressure at the burners averages 37 psi, controlled by very sensitive pilot loaded regulators. About 140,000 cfhr of gas is burned in each furnace. Furnace combustion is controlled by frequent analysis of combustion gases with an Orsat apparatus on day shift at a sampling point 75 ft from the bridgewall. Close control of furnace draft is essential to proper combustion and the draft is regulated by automatic dampers back of each waste-heat boiler. Secondary air is largely excluded from the furnace, although some secondary air infiltration is unavoidable and is used to complete the combustion of the natural gas and to burn a small amount of elemental sulphur. No attempt is made to provide excess air for the complete combustion of volatilized first-atom sulphur, as calculations indicate this to be uneconomical. Some sulphur vapor is burned in the furnace, furnace uptakes and boilers, however.

Table 4 . . . Analysis of Reverberatory Solid Charge

| | Au | Ag | Cu | SiO ₂ | Al ₂ O ₃ | Fe | CaO | S | H ₂ O |
|------|-------|------|-------|------------------|--------------------------------|------|-----|------|------------------|
| 1942 | 0.015 | 0.58 | 20.98 | 6.2 | 1.8 | 28.1 | 2.4 | 37.2 | 8.33 |
| 1943 | 0.014 | 0.73 | 20.49 | 8.4 | 1.9 | 26.8 | 2.7 | 35.5 | 8.25 |
| 1944 | 0.017 | 0.86 | 22.49 | 7.2 | 1.7 | 27.8 | 2.0 | 34.8 | 8.09 |
| 1945 | 0.018 | 1.01 | 24.35 | 7.8 | 1.5 | 25.1 | 2.6 | 34.4 | 8.55 |
| 1946 | 0.017 | 0.99 | 24.55 | 8.5 | 1.7 | 23.7 | 3.4 | 33.4 | 8.43 |
| 1947 | 0.015 | 1.00 | 24.10 | 10.4 | 1.8 | 23.1 | 3.2 | 32.8 | 9.04 |

Some trouble has been encountered with magnetite building up in the reverberatory furnace bottoms. The only source of magnetite is through converter slag additions to the reverberatory furnace, but control of magnetite at the converters is difficult because of the high alumina content of the converter flux. Magnetite in the bath of the reverberatory furnace is partly reduced by contact with sulphides and if free silica is available to combine with the resulting ferrous oxide, magnetite can be fairly well controlled. If free silica is introduced with the charge the smelting rate of the charge is affected adversely and a practice has been

each bed and amounts to 70 to 75 pct of the solid charge, or 80 to 85 pct of the concentrate smelted. Matte is tapped through either of three tap holes on each side of the furnace at the bridgewall end, opposite tap holes being used on alternate shifts to allow time for cleaning launders. The matte runs through brick and clay lined launders into 200-cu ft cast steel ladles in the Converter aisle. Two wet pan mills for the preparation of clay for stoppers and launder lining are located at the north end of the reverberatory floor.

Furnace slag is removed from the side of the furnace near the uptake end,

Table 5 . . . Analysis of Concentrate Smelted

| | Au | Ag | Cu | SiO ₂ | Al ₂ O ₃ | Fe | CaO | S |
|------|--------|-------|-------|------------------|--------------------------------|------|-----|------|
| 1942 | 0.0157 | 0.618 | 21.20 | 2.8 | 1.4 | 30.8 | 0.3 | 41.2 |
| 1943 | 0.0156 | 0.806 | 21.35 | 4.3 | 1.3 | 30.3 | 0.3 | 40.9 |
| 1944 | 0.0175 | 0.932 | 23.86 | 4.6 | 1.4 | 29.5 | 0.1 | 38.8 |
| 1945 | 0.0200 | 1.180 | 26.79 | 3.8 | 1.3 | 28.1 | 0.2 | 38.8 |
| 1946 | 0.0190 | 1.126 | 27.49 | 4.7 | 1.5 | 26.6 | 0.1 | 38.3 |
| 1947 | 0.0172 | 1.132 | 27.24 | 5.4 | 1.6 | 26.2 | 0.1 | 37.6 |

Table 6 . . . Analysis of Reverberatory Slag

| | Au | Ag | Cu | SiO ₂ | Al ₂ O ₃ | FeO | CaO | S | Oxygen Ratio |
|------|---------|--------|------|------------------|--------------------------------|------|-----|-----|--------------|
| 1942 | 0.00041 | 0.0140 | 0.39 | 33.6 | 8.2 | 50.7 | 3.3 | 1.7 | 1.78 |
| 1943 | 0.00057 | 0.0165 | 0.42 | 34.1 | 8.5 | 49.1 | 3.7 | 1.5 | 1.85 |
| 1944 | 0.00034 | 0.0160 | 0.46 | 33.5 | 7.3 | 51.3 | 2.9 | 1.5 | 1.73 |
| 1945 | 0.00040 | 0.0170 | 0.46 | 34.2 | 6.7 | 51.4 | 3.3 | 1.4 | 1.72 |
| 1946 | 0.00027 | 0.0155 | 0.43 | 35.2 | 6.6 | 47.7 | 4.6 | 1.3 | 1.83 |
| 1947 | 0.00029 | 0.0156 | 0.44 | 37.3 | 6.9 | 46.0 | 4.7 | 1.1 | 1.99 |

worked out of introducing barren quartzite through the arch of the furnace about 20 ft from the bridgewall so that two piles of quartzite, one on either side of the centerline, are maintained floating on the bath in front of the converter slag launders which enter through the bridgewall on each side adjacent to the junction between the sidewall and the bridgewall. By this means free silica is made immediately available when converter slag is introduced and the smelting rate of the charge is not interfered with. This practice has resulted in marked improvement in the control of magnetite and in the protection of furnace bottoms.

A deep bath of matte is carried in the furnace at all times unless prevented by high furnace bottoms. Matte-fall is quite uniform throughout the life of

the slag skim hole being located just back of the verb arch. The slag is skimmed into 225-cu ft cast steel pots and hauled to the dump by 18-ton electric trolley locomotives. Slag-fall amounts to 65 pct of the solid charge or 75 pct of the concentrate smelted. The slag dump is trimmed and leveled with a bulldozer and the track is thrown with a mechanical track-shifter.

Reverberatory furnace data are shown in Tables 3, 4, 5, 6 and 7.

Table 7 . . . Analysis of Reverberatory Matte

| | Au | Ag | Cu | Fe | S | Fe ₂ O ₄ |
|------|-------|-------|-------|------|------|--------------------------------|
| 1942 | 0.019 | 0.734 | 27.62 | 40.6 | 26.3 | 11.3 |
| 1943 | 0.019 | 0.959 | 28.65 | 39.8 | 25.6 | 8.4 |
| 1944 | 0.022 | 1.131 | 31.10 | 38.3 | 25.9 | 7.7 |
| 1945 | 0.024 | 1.362 | 34.34 | 36.0 | 26.1 | 9.0 |
| 1946 | 0.022 | 1.356 | 34.55 | 35.2 | 26.2 | 6.7 |
| 1947 | 0.021 | 1.393 | 35.72 | 33.9 | 26.3 | 4.3 |

Waste-Heat Boilers

Waste-heat boiler practice with the large water wall area and high steam pressure and temperature has been satisfactory. There are two waste-heat boilers on each reverberatory furnace and each boiler has 11,430 sq ft of total heating surface. Steam is produced at 700 lb ga. pressure and 700°F temperature. The boilers operate at over 100 pct of rating and waste-heat steam produced amounts to 40,000 lb per boiler per hr, which represents a recovery of 53.0 pct of the fuel fired in the reverberatory furnaces.

Combustion gases from the reverberatory furnaces pass through the waste-heat boilers as shown in Fig 2 and 3. The three-drum boilers have internal pendant type superheaters and are equipped with soot blowers using superheated steam on all banks of tubes. The soot blowers are used every 4 hr and are effective in cleaning areas where no sintering or slagging of the dust occurs, but all boilers require complete hand lancing with high pressure air pipes through small ports to remove sintered and caked dust not touched by the soot blowers and to remove slag which forms on the tubes in the area of the boiler inlet from the furnace. Automatic soot blowers on water wall tubes are being considered as a means of lessening hand lancing.

The boiler settings are of fire brick construction with special shapes to fit the water wall tubes. The boiler baffling is shown in Fig 3 and the boilers operate with a draft loss of 0.80 in. of water through the boiler. The cross-over connecting flues between the reverberatory furnaces and the waste-heat boiler were made as short as possible to reduce radiation losses. The boiler structures are quite high and this resulted in a stack effect for incoming gases and a back pressure which made an unsatisfactory smoke condition around the boilers. This condition has been overcome by restricting the outlet of the reverberatory furnaces with dampers so that the back pressure in the boilers can be neutralized without upsetting the furnace draft.

Converters

The arrangement of the converter aisle is shown in Fig 2. The aisle is 63 ft wide and 574 ft 6 in. long, with crane rails 57 ft 6 in. above the ground and a span of 60 ft between crane rails. The three cranes each have two 60-ton hoists driven by 100 hp direct-current

Table 8 . . . Converter Data (Dry Ton Basis)

| | 1942 | 1943 | 1944 | 1945 | 1946 | 1947 |
|-----------------------------------|---------|---------|---------|---------|---------|---------|
| Matte..... | 195,755 | 317,579 | 319,101 | 289,524 | 272,061 | 450,680 |
| Pit Ore..... | 46,854 | 70,420 | 45,801 | 41,956 | 35,530 | 71,244 |
| Other Material..... | 175 | 1,703 | 4,569 | 1,796 | 9 | |
| Quartzite..... | 19,193 | 25,615 | 43,639 | 29,594 | 28,625 | 42,292 |
| Reverts..... | 30,994 | 40,916 | 32,608 | 46,927 | 50,420 | 84,567 |
| Copper..... | 47,027 | 79,740 | 88,315 | 92,110 | 85,794 | 148,402 |
| M Cu Ft air per Ton Cu..... | 244.0 | 233.7 | 210.1 | 172.9 | 165.1 | 171.4 |
| Percent Blowing Time..... | 66.4 | 64.8 | 64.0 | 51.8 | 59.6 | 58.2 |
| Average Converters Operating..... | 2.70 | 2.97 | 3.26 | 2.84 | 3.31 | 4.00 |

motors with magnetic brakes on the motor shaft and gear train. Two 5-ton repair hoists and one 50-ton repair hoist are located above the crane runway.

There are six 13- × 30-ft Pierce-Smith converters located on 60-ft centers. The converter shells are 1½ in. steel plate, welded construction with heavy reinforcing plates along the tuyere section and around the mouth. The welded steel riding rings are riveted to the shell at the outer ends of the shell. The converter ends are made of 1 in. welded plate with 4 beam stiffeners on each end and the ends are held in place by bolts and springs to allow for expansion. The springs have been of value in relieving expansion after repairs, but a point is reached where the springs cannot be used without digging out the entire end sections of the converter and re-setting the end plates in their original position.

The converters are driven by 75 hp dc motors with magnetic brakes, through a speed reducer, intermediate gears and pinion and large gear which is bolted to one of the riding rings. Direct-current for operation of converters, cranes, anode furnaces, and slag locomotives is generated by two 600 kw fly-wheel motor-generator sets and one 300 kw stand-by motor-generator set located in control rooms behind the converters. If the direct current generators and the turbo-blowers in the power house are put out of service by a power failure, the fly wheels can furnish sufficient power to turn down the converters and to allow the cranes to be moved. A signal on the converter air main sounds an alarm when the air pressure drops below a pre-determined point.

The converters have 52 ball valve tuyeres with threaded connections arranged so that 10 tuyeres on each end have 2-in. tuyere pipes and the 32 tuyeres in the center have 1½-in. tuyere pipes. There are two Garr guns, one on each end, for flux which is drawn from overhead bins of 250 tons capacity for each converter into 5-ton

measuring hoppers at each Garr gun. The Garr guns are used alternately to even the wear on the brick lining.

In normal operation, the converters are charged with 5 ladles of matte, amounting to about 70 tons, and additional matte is added after fluxing, blowing and skimming. Air pressure of 13 lb at the converter tuyeres has been found best for converter operation. Air volume averages 23,000 cfm at the tuyere with periods of 25,000 cfm. Air consumption is measured by indicating and recording meters on the 24-in. air line leading to the blast gate and wind box on each converter. An electrical signal system between the converter aisle, the power house, and the smelter office indicates and records the blowing time of each converter and shows which converters and which blowers are in operation at any time.

In making copper charges, matte is blown to white metal in two converters and the white metal from one converter is then transferred to the other and the copper charge finished in that converter. Copper charges average 90 tons and the copper is blown to "worm" copper for the anode plant. Oxide slag is formed in the converter at this stage of the blow and this slag is very corrosive on the brick lining and must be handled with care to prevent explosions when it is skimmed and transferred to another converter. After each transfer or charge of copper is completed the tuyeres are reamed with a cutter bar clamped in a light rotating drill which is supported by hand. This method of reaming tuyeres is much easier on the brick work than the use of a sledge hammer and cutter bar.

Converter campaigns between tuyere line repairs average 9000 tons of copper. No magnetizing of converter linings has yet been practiced. Hard burned chrome-magnesite brick is used in converter linings and repairs are made with the 18-in. four-piece tuyere block shown in Fig 6. The normal repair includes a number of courses in 18-in. wedge brick above and below the tuyere blocks and it is usually necessary

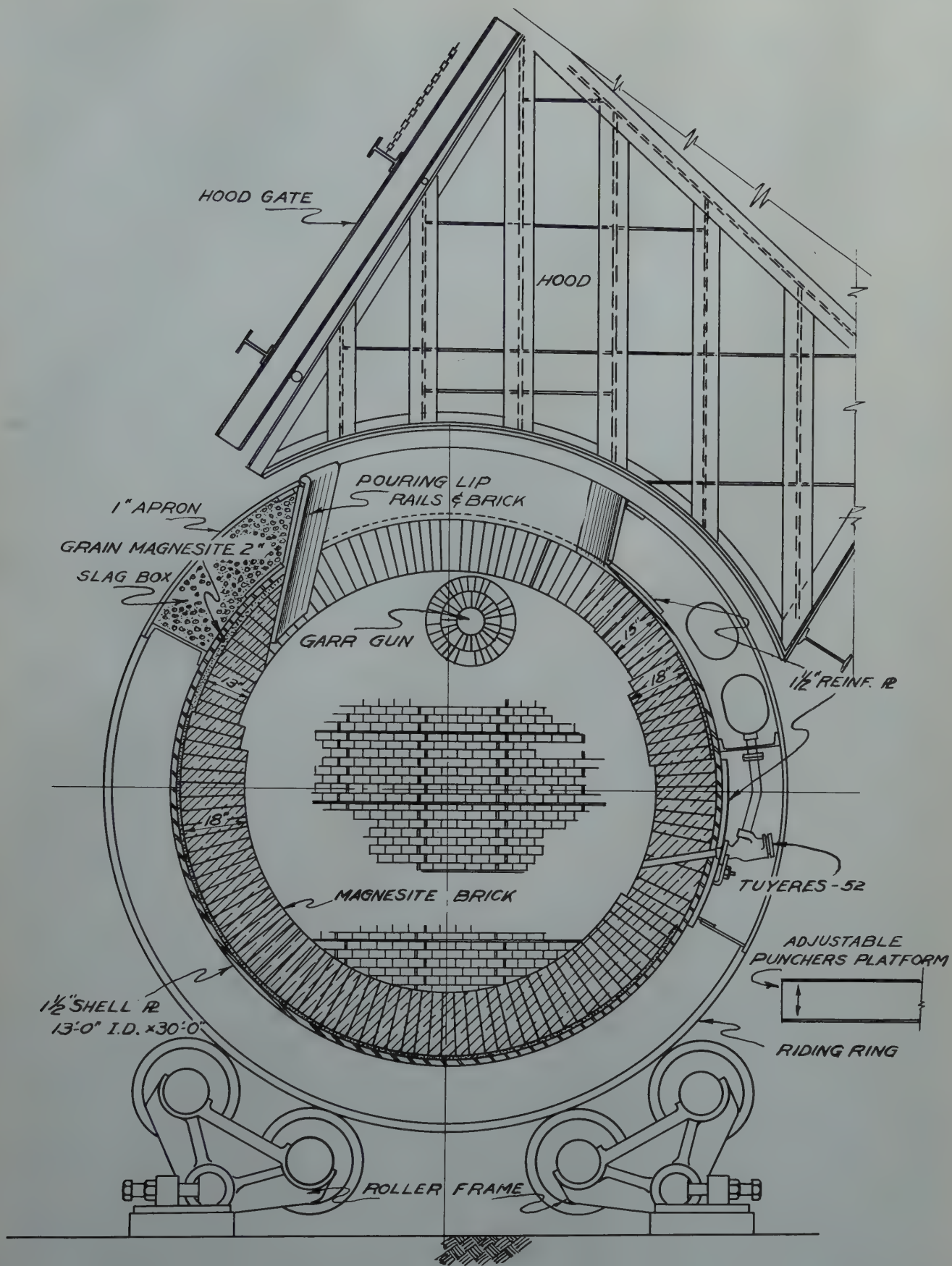


FIG 6—Converter brickwork.

Table 9 . . . Analysis of Converter Slag

| | Au | Ag | Cu | SiO ₂ | Al ₂ O ₃ | Fe | CaO | S | Fe ₃ O ₄ |
|------|--------|--------|------|------------------|--------------------------------|------|-----|-----|--------------------------------|
| 1942 | 0.0038 | 0.0886 | 2.85 | 24.9 | 5.0 | 48.0 | 0.4 | 2.1 | 14.6 |
| 1943 | 0.0020 | 0.0829 | 2.91 | 23.5 | 5.4 | 47.9 | 0.4 | 1.7 | 13.7 |
| 1944 | 0.0016 | 0.0699 | 2.48 | 23.8 | 4.5 | 49.7 | 0.4 | 1.6 | 16.0 |
| 1945 | 0.0018 | 0.0780 | 2.52 | 23.1 | 4.5 | 50.5 | 0.3 | 1.7 | 20.4 |
| 1946 | 0.0014 | 0.0905 | 2.87 | 24.6 | 4.4 | 47.4 | 0.3 | 1.6 | 20.3 |
| 1947 | 0.0013 | 0.0834 | 2.93 | 26.2 | 4.9 | 45.5 | 0.7 | 1.5 | 18.0 |

Table 10 . . . Analysis of Pit Ore for Converter Flux

| | Au | Ag | Cu | SiO ₂ | Al ₂ O ₃ | Fe | CaO | S |
|------|--------|-------|------|------------------|--------------------------------|-----|-----|-----|
| 1942 | 0.0014 | 0.029 | 0.83 | 65.3 | 15.7 | 3.7 | 0.6 | 3.6 |
| 1943 | 0.0012 | 0.041 | 0.96 | 65.3 | 17.5 | 3.4 | 0.5 | 2.9 |
| 1944 | 0.0012 | 0.050 | 1.01 | 65.5 | 18.2 | 3.2 | 0.4 | 2.6 |
| 1945 | 0.0052 | 0.049 | 1.05 | 65.4 | 17.9 | 3.3 | 0.4 | 2.6 |
| 1946 | 0.0012 | 0.050 | 1.09 | 65.1 | 18.1 | 3.4 | 0.2 | 2.7 |
| 1947 | 0.0011 | 0.052 | 1.19 | 65.6 | 17.9 | 3.3 | 0.6 | 2.8 |

to extend the repair to include the arches at the back of the collar, and occasionally necessary to dig out and brick a section in the bottom or front of a converter. Spalling after repairs is avoided entirely by allowing proper expansion joints and by heating the converter very slowly with gas burners for about 48 hr until the entire brickwork is practically at operating temperature and then washing the converter with slag to seal the joints, and charging with matte while the converter is still near maximum temperature. The pouring lips on the converters are made with magnesite brick held in place by rails and grouted with magnesite ganister. The space between the 1-in. apron plate and the shell below the pouring lip is boxed in and filled with magnesite ganister to prevent metal leaks around the brick pouring lip.

Converter hoods are of welded steel construction with cast iron liners in the lower portion. The hood gate rolls on rails and is raised and lowered by motor driven sprockets and chains. A butterfly damper in the circular section of the

converter uptake flue is operated by high pressure air with control valves on the skimmer's platform.

Converter puncher's platforms are raised and lowered for adjustment by hydraulic lifts using oil pressure, and each platform has an air cooling system of overhead ducts with slots for blowing low pressure air from individual motor driven blowers. Stationary platforms behind the converters connect all punchers platforms and also connect with the skimmers platforms.

Converter cleanings, hood cleanings and dust from the hoppers back of the converters are collected in boats on wide gauge cars which are pulled backward behind the converters onto a transfer car running parallel to the converters and reaching the converter aisle under the cranes at the south end of the aisle. The transfer car track is directly underneath the dust hoppers behind each converter and dust is easily drawn into the cars as they are pulled from under the converters. The cleanup in front of the converters is done with a weighted drag handled by the converter crane, and a Traxcavator is used for loading the cold material into boats. Matte and slag ladles are shelled into a skull breaker with an elevated bumping block in the south end of the converter aisle; and cold material from the skull breaker is hauled to the smelter crushing plant in railroad cars.

Converter data are shown in Tables 8, 9, 10, 11 and 12.

Table 11 . . . Analysis of Barren Quartzite for Converter Flux

| | Cu | SiO ₂ | Al ₂ O ₃ | Fe | CaO | S |
|------|------|------------------|--------------------------------|-----|-----|---|
| 1942 | 85.4 | 5.3 | 2.8 | 0.9 | 0.3 | |
| 1943 | 79.4 | 9.5 | 2.8 | 0.8 | 0.3 | |
| 1944 | 80.9 | 8.5 | 2.6 | 0.3 | 0.2 | |
| 1945 | 84.0 | 6.0 | 3.0 | 0.5 | 0.2 | |
| 1946 | 84.8 | 6.3 | 2.5 | 0.6 | 0.2 | |
| 1947 | 85.6 | 5.3 | 2.1 | 0.9 | 0.2 | |

Table 12 . . . Analysis of Mixed Converter Flux

| | Au | Ag | Cu | SiO ₂ | Al ₂ O ₃ | Fe | CaO | S |
|------|--------|-------|------|------------------|--------------------------------|------|-----|-----|
| 1942 | 0.0015 | 0.033 | 0.69 | 71.3 | 12.1 | 3.5 | 0.8 | 2.3 |
| 1943 | 0.0013 | 0.048 | 0.76 | 70.3 | 14.9 | 3.2 | 0.5 | 1.8 |
| 1944 | 0.0015 | 0.074 | 0.89 | 72.6 | 13.0 | 3.2 | 0.4 | 1.5 |
| 1945 | 0.0023 | 0.211 | 2.68 | 66.4 | 10.6 | 8.3 | 0.5 | 2.4 |
| 1946 | 0.0017 | 0.082 | 1.98 | 64.5 | 9.4 | 11.6 | 0.8 | 2.0 |
| 1947 | 0.0013 | 0.063 | 1.43 | 65.0 | 10.6 | 10.2 | 1.5 | 2.0 |

All Morenci copper is produced as anode copper for economy at the refinery. The anode plant is located at the north end of the converter aisle as shown in Fig 2 and contains two refining furnaces of the same type as the converters, but with shells 13 × 25 ft instead of 13 × 30 ft, and one casting wheel. Anode plant practice with rotating furnaces is entirely satisfactory and the arrangement of two refining furnaces and one casting wheel provides flexibility and storage capacity for uniform converter operations.

The anode furnace shells are made of 1½-in. plate, welded construction, with riding rings at the ends and with openings for the poling and skimming door and casting spout. The ends of the vessels are made of 1-in. welded plate with reinforcing beams which are fastened rigidly to the shell. The ends have openings for the receiving spout, burner port and stack outlet. The direct current motors and gear drives are duplicates of those used on the converters.

The anode furnaces are heated with natural gas in burners using high-pressure air for short flame combustion. The burner enters through one end wall well above the metal line. Anode charges average 175 tons of copper and two converter charges usually fill an anode furnace. The anode charges are blown with high-pressure air using two ¾-in. pipes to eliminate the sulphur, the slag is skimmed off and the copper is poled with oak or pine poles which are manipulated with an air operated hoist. The anode furnaces are surrounded by a large concrete platform at an elevation 2 ft below the centerline of the furnaces which provides working space for the blowing, skimming and poling operations.

Copper is poured from the anode furnaces into hydraulically operated pouring spoons and then into copper molds on a circular casting wheel 40 ft in diam with 26 molds. The wheel is electrically driven through gears by duplicate motors which turn the wheel in either direction. All operating controls for the anode vessels, pouring spoons, and casting wheel are located in cabs at each side of the casting wheel. The wheel is moved by an automatic timing device which controls the rate of casting; and the wheel stops automatically with one mold in proper position under the pouring spoon and another mold in proper position for lifting the anode

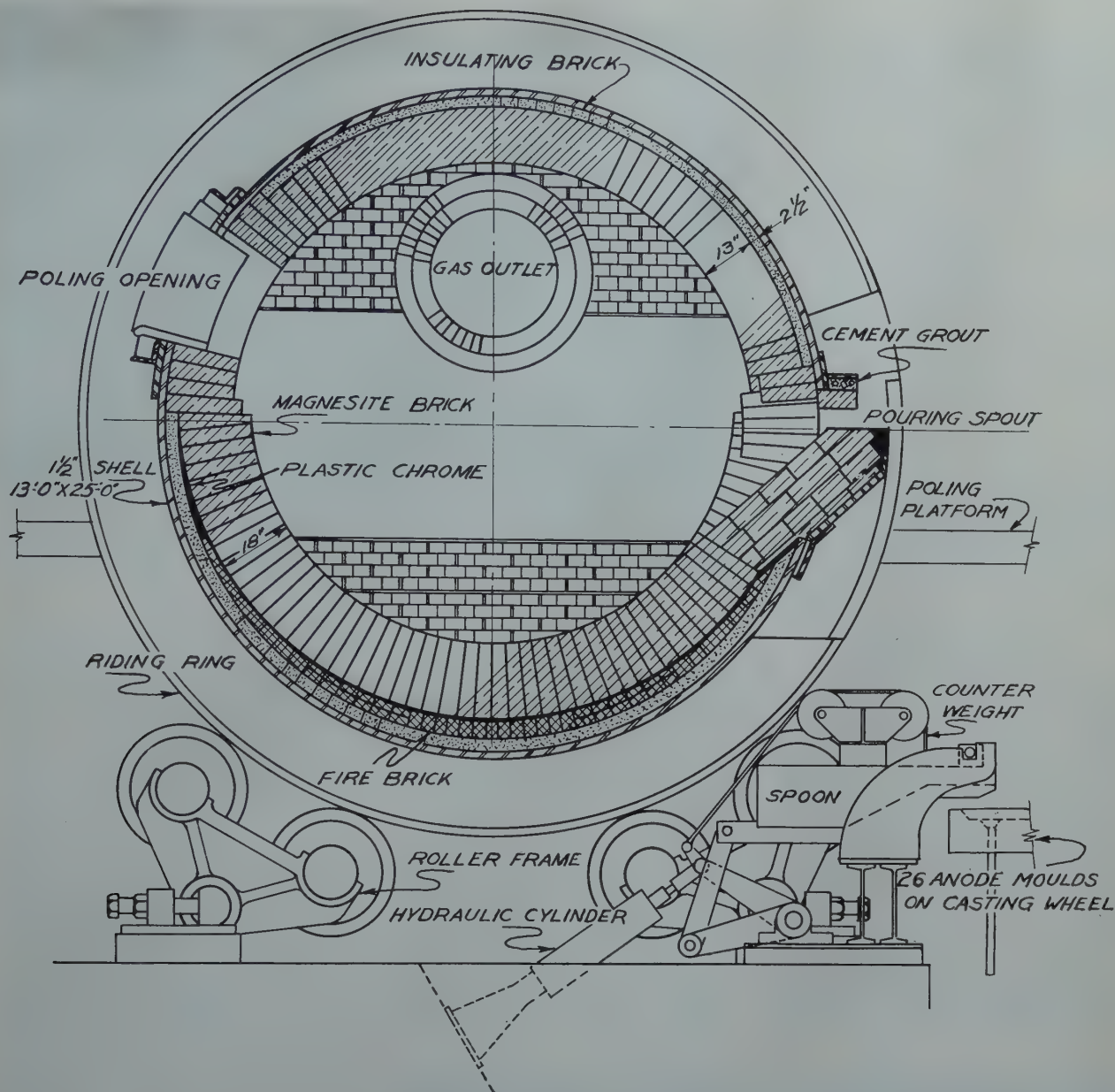


FIG 7—Anode furnace brickwork.

from the mold by tongs. Pouring speed averages 30 tons per hr.

The liquid copper poured into the mold from the spoon must chill on the surface before the casting wheel is moved to prevent rolled edges and fins on the anodes; and a blast of converter air automatically controlled by a solenoid valve, is used to speed up the cooling of the surface of the anode. Water cooling of the molds and anodes is accomplished by spray pipes at definite locations on the wheel. The empty molds on the casting wheel are sprayed inside while hot with an alumina sand wash to keep the anodes from adhering to the mold.

The anodes, which weigh 700 lb, are raised from the molds by pins with sliding contact on an inclined track,

and are lifted from the pins and placed in bosh tanks by manually operated air tongs with control valves at the side of the bosh tanks. Anodes are removed from the bosh tank by a 15-ton crane, inspected and trimmed on the floor adjacent to the anode plant and are then loaded into railroad cars by 2-ton storage battery trucks with vertical lift arms. A large concrete floor across the track from the anode floor is used as a copper dock for storage of anodes during periods of interrupted shipments. This floor and the trimming floor is armored with cast iron grids cast in the concrete.

Pouring spoons are lined with a cement-sand mixture. The spoons and cast iron master molds are heated to the proper temperature for use by indi-

vidual gas burners. Copper molds for the casting wheel and copper tapping plates for the reverberatory furnaces are made on day shift. The copper molds last for about 300 tons of anodes each before cracking too badly to use. One or two new molds are put on the wheel daily and the discarded molds are returned to the converters for smelting with the copper charges.

Anode furnace lining is shown in Fig 7. The chemically bonded magnesite brick has given excellent service and no major repairs to the brick lining have been made in the first six years of operation. Brickwork over the poling doors and around the openings in the ends of the furnaces is maintained by slurry gun patching with magnesite cement when required. The complete

insulation of the shells is desirable for fuel economy and for better working conditions and to prevent filling up of the bottoms with refractory slag.

Anode Plant data are shown in Table 13.

Table 13 . . . Analysis of Anode Copper

| | Au | Ag | Cu | S | O ₂ | Anode Plant Data Per Ton Anode Copper | |
|------|-------|------|-------|--------|----------------|---------------------------------------|--------------|
| | | | | | | Lb Poles | Fuel Mil Btu |
| 1942 | 0.071 | 2.75 | 99.72 | 0.0036 | 0.140 | 80.30 | 1.26 |
| 1943 | 0.071 | 3.50 | 99.72 | 0.0017 | 0.123 | 81.64 | 1.35 |
| 1944 | 0.077 | 3.93 | 99.70 | 0.0021 | 0.128 | 81.73 | 1.36 |
| 1945 | 0.076 | 4.13 | 99.69 | 0.0019 | 0.124 | 98.78 | 1.50 |
| 1946 | 0.070 | 4.03 | 99.74 | 0.0017 | 0.100 | 67.34 | 1.24 |
| 1947 | 0.064 | 4.13 | 99.76 | 0.0018 | 0.098 | 62.08 | 0.89 |

Flues and Stack

The entire flue system in the Morenci Smelter is of steel construction well insulated to prevent heat loss, and of large cross-sectional area to reduce gas velocities. Arrangement of the flue system and stack is shown in Fig 2. The steel balloon flue located back of the converters turns at right angle and rises in a vertical box connection to cross the converter aisle above the crane runway. Gases pass from this flue through mechanical dust collectors consisting of 10 sections of 16-in. Multiclone tubes, and then to the stack. The converter

flue is 18 ft in diam and is covered with 2 in. of fiber glass insulation from a point near the first converter to the dust collectors. The flue immediately back of the converters is not insulated. The mechanical dust collecting system is insulated and also the 18-ft balloon flue leading from the dust collectors to the stack.

A 15-ft steel balloon flue for reverberatory furnace gases, also insulated, leads from the waste-heat boiler outlets and joins the converter flue just in front of the portal of the stack. There is an automatic damper in the reverberatory flue which is operated by a motor

driven worm gear actuated by an electric eye connected to a draft gauge. The necessity for a dust collecting system on the reverberatory gases has not yet been determined.

The stack was built of reinforced concrete with a lining of acid proof brick laid in acid proof mortar and with insulation between the concrete shell and the lining. The stack is 603 ft 2 in. high, with a foundation 9-ft thick and 71 ft in diam standing on a consolidated conglomerate earth foundation with a loading strength of 5 tons per sq ft. The stack was designed to withstand a wind pressure of 100 mph. It is protected by lightning rods with copper cables to the ground. The inside diameter of the stack is 39 ft at the bottom and 24 ft at the top. The concrete shell is 36 in. thick at the bottom and tapers to 7 in. at the top. The total weight of the stack and foundation is about 10,000 tons.

The stack was designed for a draft of 3 in. of water with gases at 500°F and an outside temperature of 60°F and has a total capacity of 1,000,000 cfm at stack conditions. The high stack draft is necessitated by the use of mechanical dust collectors on the converter gases which operate with a pressure drop of 2 in. water. The remaining draft is lost in friction and at the converter hood openings.

The stack was built with two portals, one main portal and a smaller one directly opposite. The smaller portal has been bricked up and will be used only in case it is desired to divert part of the gases through a dust collecting system on the opposite side of the



FIG 8—General view of reduction works.



FIG 9—View of reclaiming machine.

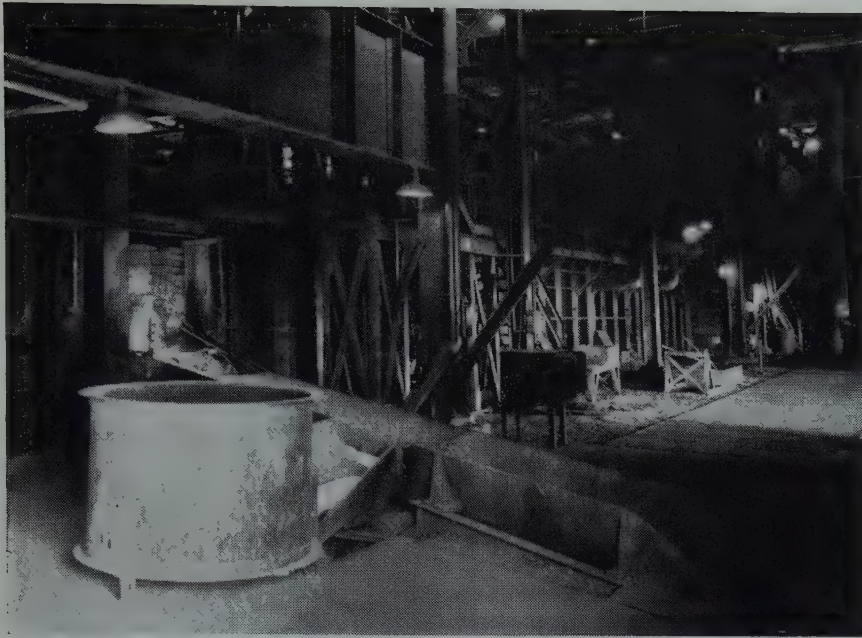


FIG 10—View of reverberatory furnace skimming end.

stack. A test station is located 274 ft above the ground for testing stack gases.

Flue dust handling is accomplished mechanically by means of drag chain conveyors in the bottom of the balloon flues and screw conveyors under the multiclones. The granular abrasive dust from the balloon flue immediately back of the converters however is returned to the converter dust hoppers by gravity through 10-in. pipes at each hopper. The combined dust from the balloon flues and multiclones is collected in a surge bin and is then removed by a short screw feeder, mixed with air and pumped pneumatically to a pug mill located near the junction house through which pass the conveyor belts carrying concentrate from the filter plant to the bedding plant. The flue dust in the pug mill is sprayed with water until properly conditioned and is then discharged onto the layer of concentrate on the belt conveyor and delivered along with the concentrate to the bedding plant.

Power Plant

The Power Plant, which is under separate supervision, is situated about 500 ft from the waste-heat boilers. Steam from the waste-heat boilers at 700 lb pressure and 700°F temperature is delivered to two direct-fired superheaters in the power house, emerging from the superheaters at the proper condition for utilization at the turbine throttle, namely 650 lb ga. pressure and

825°F temperature. Three direct-fired water-wall boilers of 1430 hp each, using natural gas fuel with automatic burner control and air pre-heaters, and with stand-by fuel oil for emergency use, furnish additional steam which is combined with the waste-heat steam in the direct-fired superheaters. About 60 pct of the total steam is produced in the waste-heat boilers and 40 pct in the direct-fired boilers.

Steam is utilized in four 15,000 kva maximum capacity turbo-generators with surface condensers. Power is generated at 13,200 volts and is trans-

mitted to the Concentrator, Smelter, Open Pit mine and pumping stations at this voltage and is there stepped down to 2,300 volts and 440 volts for plant use. A very good power factor results from the use of a large number of synchronous motors in the Concentrator.

Condenser cooling water is pumped through concrete pipes to a cooling tower 1300 ft away. Evaporators are used for boiler feed water make-up and boiler feed water is deaerated, heated to 300°F and pumped to the waste-heat and direct-fired boilers by 8 stage electrically driven centrifugal pumps with steam pumps as stand-by. Waste-heat boiler feed water is delivered through 5-in. welded steel insulated lines with automatic control at the pumps and at the boilers. Steam is returned to the power house from the waste-heat boilers through two 10-in. welded steel insulated lines.

During periods of curtailed power requirement at the Open Pit Mine and Concentrator on scheduled week-end shut-downs, excess waste-heat steam is diverted to a separate condenser plant outside the power house. Cooling water for this condenser plant is circulated through the same system used for the condensers on the turbo-generators and condensate from the condenser plant is returned to the boiler feed water system.

Compressed air at 100 lb pressure is produced in two 3,730 cfm electrically driven compressors located on the ground floor of the power house. Con-

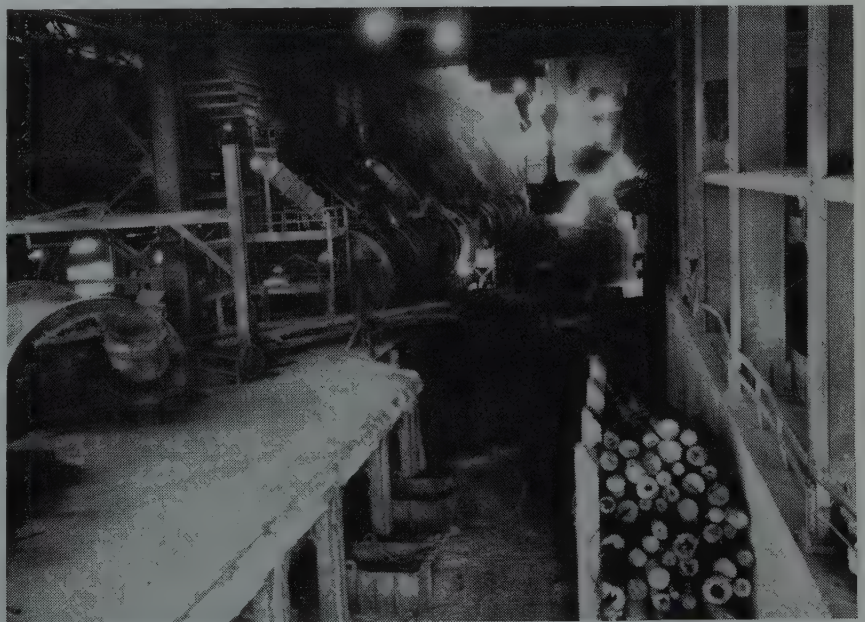


FIG 11—View of converter aisle.

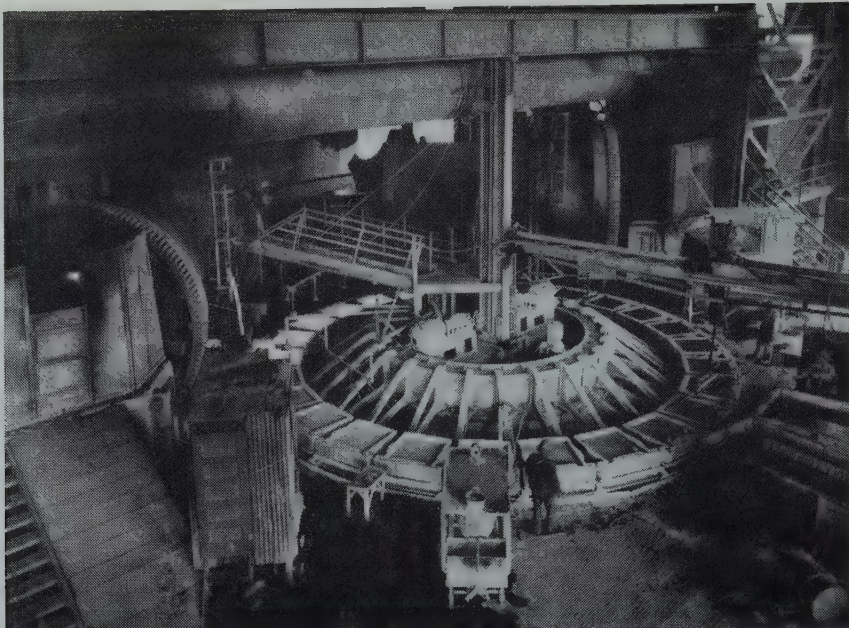


FIG 12—View of anode plant.

verter air is produced by six electrically driven turbo-blowers of 27,500 cfm capacity each at 12.5 lb barometer and 100°F. The blowers are direct-connected to 1500 hp induction motors and operate at constant speed and pressure with automatic regulators controlling impedance vanes on the inlet air ports to adjust air volume to requirements. Converter air is produced at 14 lb pressure and 275°F at the blowers and the blowers discharge into a header pipe connected to a 60-in. air main leading to the converters. Air volume is

metered for each blower between the blower and the header pipe. (Fig 8-12)

Smelter Organization

Smelter operations are under the supervision of the smelter metallurgist, with a general foreman over the reverberatory department and another over the converter department. Shift operations in the reverberatory, converter and anode departments are under the supervision of shift foremen,

and the crushing, bedding and reclaiming plant, lime burning plant, brickmason crew, repair crew and labor crew are each under the supervision of a day shift foreman.

The Smelter maintains a technical staff for plant testing and investigation and a safety department which is a part of the Branch safety organization.

Smelter maintenance work is carried out by the smelter repair crew and brickmason crew, while heavier work is done by the well equipped shops at the Reduction Works.



The Interaction of Liquid Steel with Ladle Refractories

CARL B. POST* AND GEORGE V. LUERSSEN,* Members AIME

It is generally recognized that non-metallic inclusions in steel come from two principal sources. First are the chemical reactions in the furnace, or in subsequent deoxidation, resulting in slag which does not free itself from the metal. Much information has been published concerning these chemical reactions and their control through proper attention to slag viscosity, composition of deoxidizers, and other qualities. The studies of this subject by C. H. Herty, Jr. and others through the medium of physical chemistry have yielded much information for the steel-maker. The second source is erosion of ladle refractories, such as lining brick, stoppers, nozzles and runners, causing entrapped particles of globules of fluxed silicate material. In contrast with the large amount of information available on the first source, relatively little has been published on the subject of erosion which, in the case of basic electric melted steel, is the principal source of nonmetallics. This is probably due to the fact that the problem was assumed to be one of simple mechanical erosion, which could be solved primarily by modification of ladle practices. Good improvements have been made by elimination of slurries in the ladle, better ladle and runner refractories, and more attention to pouring temperatures. It is doubtful, however, that this problem has been recognized in its true light since it is not one of simple mechanical erosion but rather one of chemical reaction between the metal and the refractories; and in this sense is as much a problem of physical chemistry as the reactions involved in the actual steelmaking process.

The influence of ladle refractories on the resulting cleanness of steels was early recognized by A. McCance¹ who examined large inclusions in steels made by both acid and basic practices. His chemical analyses showed the large

influence exerted by the manganese content of the steel on erosion of the ladle and nozzles used in those days. The presence of MnO in such inclusions led McCance to the hypothesis that both basic and acid steels react chemically with the ladle refractories so that small globules of fluxed refractories are carried in the stream into the molds.

This early work of McCance was checked by one of the present authors on basic electric bearing-steel, and it was found that on steels containing as low as 0.40 pct manganese the fluxed surface of the ladle lining after delivering such a heat showed as high as 25 pct MnO by actual analysis. Furthermore, by lowering the manganese content of the steel to 0.20 pct, ladle erosion was decreased with a corresponding decrease in silicate inclusions in the steel. Limitations placed on the manganese content for the required inherent properties made it impossible to pursue this line further, and subsequent attention was concentrated on improved ladle refractories, care in keeping the ladle clean and free from loose refractories up to the time of tapping, and pouring the steel at optimum temperature.

Our study of the chemical reactions at the metal-brick interface between steel and ladle refractories was revived in 1939 as a result of an experimental observation made on the cleanness of alloy steels of the SAE types. This observation showed that the relative cleanness of such steels made in basic

electric arc furnaces of 12 ton capacity and poured in ingots ranging from 1100 to 2200 lb weight was determined to a large extent by the ratio of the manganese and silicon contents, provided other steelmaking variables such as tapping temperature, pouring temperature, pouring time, amount of aluminum added for grain size control, and degree of deoxidation in the furnace were kept reasonably constant. Detailed studies made on the deoxidation and slag practice during the refining period of basic electric furnace practice showed that these two variables exerted some influence on the resulting cleanness of steel in the form of bars and forgings. The important variable, the manganese-silicon balance, was not apparent until heats were made in succession by the best furnace practice kept under fairly rigid metallurgical control.

Another observation pertinent to this work concerned the similarity in the microscope of slag particles causing magnaflux or step-down indications in subsequent rolled bars, and the patches of slag frequently seen on the surface of ingots. These patches are generally believed to come from the glassy metal-brick interface in the ladle and represent an entrapment of such glass (both from the ladle brick and nozzle) in the metal as it flows over the refractories in the neighborhood of the nozzle. These glassy particles are carried down into the mold with the liquid steel, and gradually coalesce into a slag "button" which floats on the surface of the steel as it rises in the molds. Periodically the button is washed to the side of the ingot where it is trapped between the surface of the ingot and the mold, later appearing as a slag patch on the surface of the ingot after stripping.

Even though most of the small glassy particles coalesce into a slag button while the ingot is being poured, it is logical to suspect this step in the steel-making process as being a source of slag lines large enough to cause trouble

San Francisco Meeting, February 1949.

TP 2496 C. Discussion of this paper (2 copies) may be sent to *Transactions AIME* before April, 1949. Manuscript received July 6, 1948.

* Metallurgist and Chief Metallurgist, respectively, The Carpenter Steel Co., Reading, Pa.

¹ References are at the end of the paper.

on subsequent magnaflux inspection in rolled bars. This is especially true when the furnace practice is known to produce clean steel as shown by samples taken from the furnace just before tapping, and also spooned from the ladle before starting to pour. During the pouring of an ingot, the stream from the nozzle is playing in the center of the mold, and the turbulence created by the stream is such that any particles trapped in the stream will be carried for quite a distance down into the molten metal in the mold, and will then be carried over to sides of the molds before finally reaching the upper surface of the metal. It is to be remembered that the metal is freezing rapidly at the wall of the mold, and that a zone of mushy metal extends inward from the wall. Thus the small slag particles stand a good chance of being trapped in this mushy metal and their chance of doing so should increase as the temperature of the metal is colder or as the rate of pouring the ingot becomes slower.

Now, knowing that a relationship exists between the chemical composition of the steel and the resulting magnaflux inspection of bars and forgings, and further, that a large percentage of the slag particles large enough to cause these magnaflux indications appear to have the same silicate characteristics as the so called "ladle-wash" or metal-brick interface, it seemed reasonable that a detailed study of acid slags formed by the interaction of the ladle brick and the liquid steel would lead to an explanation and correlation of these effects. Before proceeding to examine the actual data resulting from this study, we would like to state the problem of this interaction of ladle refractories and liquid steel in qualitative detail.

In the first place, molten steel will be tapped from a basic electric arc furnace into a ladle lined with brick analyzing 65 pct silica, 30 pct alumina, and 5 pct Fe_2O_3 .* At the metal-brick interface there will form as a result of temperature effects a layer of fused glassy slag which will initially be the composition of the brick. The molten steel, however, contains certain elements and constituents such as man-

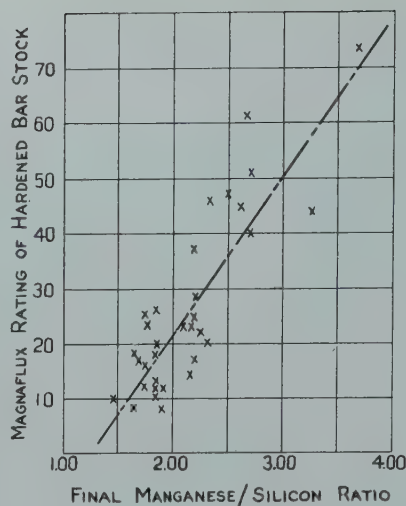


FIG 1—Cleanness of SAE 6150 aircraft quality as a function of the final Mn/Si ratio.

ganese, silicon, and ferrous oxide, which will lead to a change in the chemical composition of the fused glass. The composition of the fused glass interface will be modified therefore so that MnO and FeO make their appearance according to the balanced relationships known to exist between slags containing SiO_2 -MnO-FeO- Al_2O_3 and liquid steel containing Fe-Mn-Si-FeO. Thus, depending upon the manganese and silicon contents of the metal and its temperature, the so-called equilibrium slag will be high or low in manganous oxide and high or low in silica, and consequently of high or low fluidity. The appearance of MnO and FeO in the glassy interface as a result of this reaction will cause a decrease in the weight percentage of SiO_2 and Al_2O_3 due to dilution. Depending upon the final composition of this glassy interface, it will slough off easily or with difficulty, as measured by its fluidity or viscosity at the temperature of the interface. Thus the number and composition of the inverse rain of particles trapped in the flow of the metal near the nozzle and carried through the nozzle with the steel, will depend to a large extent upon the chemical composition of the interface and its fluidity or viscosity. The saturation solubility of SiO_2 in slags of this sort is approximately 50 pct by weight and does not vary greatly with temperature. Furthermore, viscosity studies of acid slags containing MnO, FeO, and SiO_2 show that as the acid slag approaches saturation of SiO_2 the viscosity increases greatly.

In view of the above remarks, it appeared worthwhile to review Körber

and Oelsen's² work on equilibrium in the system Fe-Mn-FeO- SiO_2 - Al_2O_3 and to set up a system of calculation so that their results could be extrapolated to cover the equilibrium between molten steel and the glassy interface at the ladle brick. Such a system allows the composition of the equilibrium acid slag to be calculated if the analysis of the metal is known, and this calculated acid slag can be compared with the experimental values obtained for slag "buttons" or slag patches on the side of ingots. If some agreement is obtained by these methods and the experimental data, then it is reasonable to conclude that the occurrence of these slag patches, and also the greater part of the slag-lines in the finished bars, are influenced largely by the interaction of the molten steel with the ladle brick. Conversely, and this is most important, if the composition of the steel can be shown to influence the final cleanliness of the steel, then the problem can be studied with a view to finding general rules for adjusting the composition of the steel to obtain as clean steel as possible.

This report is accordingly divided into three parts. Part 1 will show the step-down data and operating conditions in the furnace, ladle and pit for two grades of SAE steels, SAE 6150* and SAE 3312†. This part will show that if the furnace practice, ladle and pit practices are kept reasonably constant, then there is a relationship between the manganese and silicon ratio in these two grades of steel and the resulting cleanliness. This conclusion will be based both upon the results of our own inspection department and upon magnaflux inspection data of a leading aircraft engine manufacturer. In addition, performance records of a new deep-hardening roller-bearing steel in which the silicon content is adjusted to balance the high manganese content is compared with a similar grade containing high manganese and low silicon contents.

Part 2 will show the chemical analysis of many heats of steel and of the corresponding slag-buttons and slag-patches taken from the sides of ingots. These data will be correlated to show that the manganese-silicon balance of

* Throughout this paper repeated reference will be made to the metal-brick interface in the ladle as the principal example of metal-refractory interaction. However, in the case of ladles using bonded graphite nozzles, the clay bonding material will react in the same manner we ascribe to the ladle brick. Similar remarks will apply to clay or sand mixtures used in the well of the ladle to seal the nozzle in place, and to the bonded graphite heads and sleeves used on the stopper-rod.

* SAE 6150: 0.48/0.55 C, 0.65/0.90 Mn, 0.20/0.35 Si, 0.040 max. P, 0.040 max. S, 0.80/1.10 Cr, 0.15 V Min.

† SAE 3312: 0.08/0.13 C, 0.45/0.60 Mn, 0.20/0.35 Si, 0.025 Max. P, 0.025 Max. S, 1.40/1.75 Cr, 3.25/3.75 Ni.

Table 1 . . . Typical Melting Log of SAE 6150

| Time | Log | Addition Pounds | Metal Tests | | | | | | | | | Slag Tests | | | | | | | | |
|--|---|--------------------|-------------|------|------|------|-------|-------|------|------|---------------|------------------|------|------------------|-------------|------------------|------|------|------|------|
| | | | C | Mn | Si | P | S | Cr | Ni | V | FeO | SiO ₂ | CaO | CaF ₂ | C (Free) | CaC ₂ | FeO | MgO | CaS | |
| 11:20 AM | Power on | | | | | | | | | | | | | | | | | | | |
| 11:20 to 11:55 | 190 V | | | | | | | | | | | | | | | | | | | |
| 11:55 to 12:15 | 160 V | | | | | | | | | | | | | | | | | | | |
| 12:15 to 12:30 | 130 V | | | | | | | | | | | | | | | | | | | |
| 12:30 | Charged reducing slag— Lime Spar Coke | 300 80 40 | | | | | | | | | | | | | | | | | | |
| 12:55 | No. 1 Carbon test | | 0.42 | 0.45 | | | | 0.55 | | | | | | | | | | | | |
| 12:57 | Spec. test on Metal and Slag (No. 1 and 2) Slag rolling and Car- bide at this point | (No. 1) | 0.42 | 0.43 | 0.02 | | 0.032 | 0.60 | | 0.07 | 0.064 (No. 2) | 17.7 | 51.5 | 11.7 | 0.118 | 0.085 | 0.67 | 10.4 | 0.69 | |
| 1:30 | Spec. test on Metal and Slag (No. 3 and 4) Slag slightly thick and carbide—made addi- tion of spar. | 30 | 0.44 | 0.46 | 0.02 | | 0.022 | 0.62 | | 0.09 | 0.020 (No. 4) | 18.9 | 51.9 | 10.7 | 0.06 | 0.07 | 0.26 | 9.9 | 0.93 | |
| 1:30 | No. 2 Carbon test | (No. 3) | 0.42 | | | | | | | | | | | | | | | | | |
| 1:35 | V ₂ O ₅ charged on reducing slag | 35 | | | | | | | | | | | | | | | | | | |
| 2:00 | Electrodes in bath ½ min. | | | | | | | | | | | | | | | | | | | |
| 2:05 | Charged Wash Metal | 200 | | | | | | | | | | | | | | | | | | |
| | ferro chrome (5 pct C) | 86 | | | | | | | | | | | | | | | | | | |
| 2:10 | Charged ferro-silicon (50 pct Si) | 130 | | | | | | | | | | | | | | | | | | |
| 2:20 | Charged ferro-manganese (7 pct C) | 67 | | | | | | | | | | | | | | | | | | |
| 2:30 | Spec. test on metal and slag. (No. 5 and 6) Slag was slightly thick, non-rolling, carbide. Poured easily. | | (No. 5) | 0.51 | 0.78 | 0.31 | | 0.010 | 0.90 | | 0.15 | 0.015 (No. 6) | 18.7 | 46.7 | 16.4 | 0.06 | 0.1 | 0.21 | 8.3 | 1.14 |
| 2:32 | Aluminum to bath. 5 lb | 4 | | | | | | | | | | | | | | | | | | |
| 2:40 | Tap temperature = 1582°C | | | | | | | | | | | | | | | | | | | |
| Total time heat—4 hr 10 min. Final | | | (No. 1) | 0.52 | 0.70 | 0.32 | 0.019 | 0.009 | 0.92 | 0.05 | 0.17 | | | | | | | | | |
| 19–10 in. ingots, 22 × 10 in. Analysis | | | (No. 2) | 0.53 | 0.71 | 0.31 | | 0.92 | | | 0.17 | | | | | | | | | |
| butt. 1050 lb each | | | | | | | | | | | | | | | | | | | | |
| McQuaid-Ehn Grain Size—7. | | | | | | | | | | | | | | | | | | | | |

the steel determines to a large extent the amount of silica in the slag button or slag patch, and that silica contents of 45 to 50 pct are obtained with manganese to silicon ratios of about unity; and furthermore as the manganese to silicon ratio increases, the amount of silica in the slag button or slag patch decreases, and consequently the viscosity of the slag wash becomes less and will elongate on rolling without shattering.

Part 3 will consider in detail the data of Körber and Oelsen² and J. White³ on equilibrium between silicate slags containing FeO and MnO and molten steel containing Mn, Si, and FeO in solution. The dissociation constants of FeO.SiO₂, MnO.SiO₂, and Al₂O₃.SiO₂ in liquid acid slags will be evaluated through a range of temperatures so that equilibrium can be calculated between acid slags containing SiO₂, FeO, MnO and 25 pct Al₂O₃ and molten steel containing Mn, and Si. The calculated acid slag compositions in equilibrium with steels of various composition will then be compared with the actual slag and metal compositions determined by chemical analyses shown in Part 2.

Part I—Effect of Manganese Silicon Balance on the Cleanness of SAE 6150 and SAE 3312 and a 1.00 pct Carbon Deep-hardening Roller-bearing Steel

The effects of furnace, ladle, and pit practices on the resulting cleanness of steel were studied in considerable detail through a number of years before the manganese-silicon balance was tied down as a source of nonmetallics in the steel. These studies on furnace and pit practice showed that a relatively small effect on cleanness could be definitely tied up with furnace practice. For instance, cleaner steel can be obtained in the SAE grades using slags which deoxidize the metal to a greater degree before metallic deoxidizers (silicon and manganese) are added to the bath. These slags are of low carbide content and are worked on the "wet" side by the use of spar, so that the melter can pour a spoonful of slag and not have to dump it out. High aluminum additions for grain-size control were found to lead to nonmetallic stringers, and the furnace practice was adjusted so that the

minimum of aluminum was added to give grain size test rating of about 7 in SAE 6150. High tapping temperatures were known to give cleaner steel, but there is a limit to the height temperatures can be carried because of obvious effects on furnaces, nozzles, stopper rods, and mold life. Heats of the SAE 6150 type are generally tapped at 1580 to 1600°C, and heats of the SAE 3312 type are tapped at 1600 to 1615°C.

Fast pouring times were found to help the cleanness of the resulting ingot. The heats to be discussed here in detail for the SAE 6150 and 3312 types were cast in 1000-lb ingots measuring approximately 10 in. sq at the top, 8¾ in. sq at the bottom, and about 46 in. high. The pouring time for this size ingot was finally set at 55 to 60 sec from start of pouring the ingot to the shut-off at the bottom of the hot-top.

Table 1 shows a typical log of one of these heats of SAE 6150, showing complete steel and slag analyses throughout the melting process.

After several heats of SAE 6150 were made according to the furnace, ladle, and pit practice summarized in Table 1, the effect of the manganese-silicon

ratio upon cleanness became apparent on steel rated by step-down tests rolled from pilot bars. The pilot bars represented two tops, one middle, and two bottom billets from each heat. The billet stock in all cases was disc inspected before pieces were cut for rolling to 1½ in. rd. bars. Step-down tests representing steps of ⅛ in. off the diam, and ¼ in. off the diam were turned on these rolled bars. The length of each step was approximately 4 to 5 in. in all cases.

In order to rate numerically a heat of steel in terms of its step-down inspection it is convenient to give some numerical weight to the different classes of slag-lines. The routine practice on inspection is to designate the length of slag lines by five classes, and to assign a numerical weight to each of the various classes to penalize the longer slag lines. This system is as follows.

| Class | Length of Lines | Numerical Weight |
|-------|--------------------|------------------|
| 1 | Up to ⅛ in. | 1 |
| 2 | ⅛ to ¼ in. | 2 |
| 3 | ¼ to ⅜ in. | 4 |
| 4 | ⅜ to ½ in. | 8 |
| 5 | Greater than ½ in. | 16 |

This classification for frequency and length of slag lines is extended a step further to penalize slag lines which occur in the tops and middles as compared to the bottoms. The first step in using this system of numerically rating a heat for cleanness is to obtain the sum of the number of lines in each class multiplied by their weight factor, and then to further multiply the top and middle sums by 2. The total summation is then divided by the number of steps inspected to obtain the numerical rating of the heat.

This system is illustrated by the following example:

Pilot Bar Inspection . . . 5 in
Length 1½ rd. Bars

| | ⅜ In. Off Diam | | | | | ¼ In. Off Diam | | | | |
|-------------|----------------|---|---|---|---|----------------|---|---|---|---|
| | Class 1 | 2 | 3 | 4 | 5 | 1 | 2 | 3 | 4 | 5 |
| Top..... | 5 | 2 | 1 | 0 | 0 | 7 | 3 | 1 | 0 | 2 |
| Top..... | 6 | 3 | 0 | 0 | 0 | 5 | 4 | 0 | 0 | 0 |
| Middle..... | 3 | 2 | 0 | 0 | 0 | 2 | 0 | 1 | 0 | 0 |
| Bottom..... | 5 | 0 | 0 | 0 | 0 | 4 | 0 | 0 | 0 | 0 |
| Bottom..... | 6 | 0 | 1 | 0 | 0 | 5 | 0 | 0 | 0 | 0 |

(Average Class) × (Numerical Weight) for Top, Middle and Bottom pilot bars:

Table 2 . . . Magnaflux Rating of SAE 6150, Aircraft Quality
Pilot Bar Inspection, Hardened and Polished

| Heat | 1st Step $\frac{1}{4}$ In. Off Diam CLASS | | | | | 2nd Step $\frac{3}{8}$ In. Off Diam. | | | | | Numerical Rating per 6 In. Length | Mn | Si | Mn/Si |
|--------------------|---|-----------------------------|----------------------------|----------------------------|----------------------------|--------------------------------------|----------------------------|----------------------------|----------------------------|----------------------------|-----------------------------------|------|------|-------|
| | 1 | 2 | 3 | 4 | 5 | 1 | 2 | 3 | 4 | 5 | | | | |
| A | T T M B B | 3 2 0 3 4 | 0 1 0 0 0 | 1 0 0 0 0 | 0 0 0 0 0 | 2 2 1 1 | 1 1 1 0 | 1 0 1 0 | 1 0 0 0 | 0 0 0 0 | 8 | 0.72 | 0.45 | 1.65 |
| B | T T M B B | 0 2 4 1 0 | 2 0 0 0 0 | 0 0 0 0 0 | 0 0 0 0 0 | 0 0 3 0 0 | 0 1 0 0 0 | 0 0 0 0 0 | 0 0 1 0 0 | 0 1 0 0 0 | 12 | 0.73 | 0.40 | 1.82 |
| C | T T M B B | 3 4 3 2 0 | 0 1 2 0 0 | 1 0 0 0 0 | 0 0 0 0 0 | 2 2 2 0 0 | 1 2 1 0 0 | 0 2 1 0 0 | 0 0 1 0 0 | 0 0 0 0 0 | 10 | 0.65 | 0.45 | 1.45 |
| D | T T M B B | 3 3 4 2 5 | 0 0 4 0 1 | 1 0 0 0 0 | 0 0 0 0 0 | 6 1 5 2 5 | 0 0 3 0 0 | 0 0 0 0 0 | 0 0 0 0 0 | 0 0 0 0 0 | 12 | 0.72 | 0.39 | 1.85 |
| E | T T M B B | 4 5 7 1 3 | 3 0 1 0 0 | 0 2 0 0 0 | 1 0 0 0 0 | 4 10 2 2 0 | 3 1 1 0 0 | 0 1 0 0 0 | 2 0 0 0 0 | 0 0 0 0 0 | 20 | 0.68 | 0.37 | 1.83 |
| F | T T M B B | 2 1 1 1 2 | 0 3 2 0 0 | 0 0 0 0 0 | 1 0 0 0 0 | 1 2 4 0 0 | 2 3 2 0 0 | 0 2 0 0 0 | 0 0 0 0 0 | 0 1 0 0 0 | 18 | 0.75 | 0.46 | 1.65 |
| G | T T M B B | 5 7 8 3 11 | 3 3 1 0 0 | 0 0 0 0 0 | 0 0 0 0 0 | 3 2 3 6 5 | 1 0 1 1 0 | 0 1 0 0 0 | 0 0 0 0 0 | 0 0 0 0 0 | 13 | 0.70 | 0.37 | 1.85 |
| H | T T M B B | 5 4 2 5 0 | 1 1 1 0 0 | 0 0 0 0 0 | 0 0 0 0 0 | 4 6 5 9 1 | 0 1 0 0 0 | 0 0 0 0 0 | 0 0 0 0 0 | 0 0 0 0 0 | 8+ | 0.71 | 0.38 | 1.90 |
| I | T T M B B | 2 0 6 2 2 | 0 0 0 0 0 | 0 0 0 0 0 | 0 1 0 0 0 | 1 1 2 0 1 | 1 0 0 0 0 | 0 0 0 0 0 | 1 0 0 0 0 | 0 0 0 0 0 | 12 | 0.79 | 0.45 | 1.75 |
| J | T T M B B | 3 3 3 0 1 | 2 0 0 0 0 | 0 0 1 0 0 | 0 0 0 0 0 | 4 5 0 0 0 | 1 1 0 0 0 | 2 1 0 0 0 | 1 0 0 0 0 | 0 0 0 0 0 | 11 | 0.74 | 0.40 | 1.85 |
| K | T T M B B | 4 5 5 1 | 2 3 0 0 | 2 0 0 0 | 0 0 0 0 | 1 5 5 2 | 2 5 1 0 | 0 0 0 0 | 0 0 0 0 | 0 0 0 0 | 17 | 0.74 | 0.43 | 1.72 |
| L | T T M B B | 1 4 6 0 1 | 2 0 1 0 0 | 1 0 0 0 0 | 0 0 0 1 0 | 4 5 5 0 0 | 8 1 1 0 0 | 1 2 0 0 0 | 0 0 0 0 0 | 1 0 0 0 0 | 16 | 0.72 | 0.41 | 1.75 |
| M | T T M B B | 6 8 13 5 10 | 7 3 1 0 0 | 3 1 0 0 0 | 0 1 0 0 0 | 16 5 10 3 2 | 6 9 3 0 0 | 1 1 1 0 0 | 0 0 1 0 0 | 0 0 0 0 0 | 26 | 0.72 | 0.41 | 1.75 |
| N | T T M B B | 3 4 5 3 0 | 0 3 1 0 0 | 0 0 0 0 0 | 0 1 0 0 0 | 14 4 4 1 2 | 4 4 1 0 0 | 2 1 0 0 0 | 2 0 0 0 0 | 1 0 0 0 0 | 24 | 0.71 | 0.34 | 2.10 |
| O | T T T M B B | 6 1 2 9 12 1 | 0 0 0 0 2 0 | 0 0 1 0 0 0 | 0 0 0 0 0 0 | 4 2 4 7 8 0 | 0 2 3 3 2 0 | 0 1 0 1 0 0 | 0 0 0 0 0 0 | 0 0 0 0 0 0 | 20.0 | 0.74 | 0.32 | 2.30 |
| (4 in. long steps) | | | | | | | | | | | | | | |
| P | T T T M B B | 5 5 3 7 8 6 | 0 2 2 6 1 0 | 0 0 1 0 0 0 | 0 0 0 0 0 0 | 2 5 2 8 1 1 | 0 3 2 2 0 1 | 0 4 1 0 0 0 | 0 1 0 0 0 0 | 0 0 0 0 0 0 | 29.0 | 0.75 | 0.34 | 2.20 |

Table 2 . . . (Continued)

| Heat | 1st Step $\frac{1}{4}$ In. Off Diam CLASS | | | | | 2nd Step $\frac{3}{8}$ In. Off Diam. | | | | | Numerical Rating per 6 In. Length | Mn | Si | Mn/Si | |
|--------------------|--|----|---|---|---|---|----|---|---|---|--|----------|--------------|--------------|--------------|
| | 1 | 2 | 3 | 4 | 5 | 1 | 2 | 3 | 4 | 5 | | | | | |
| (4 in. long steps) | | | | | | | | | | | | | | | |
| Q | T | 2 | 1 | 0 | 0 | 0 | 0 | 1 | 0 | 1 | 0 | 14.5 | 0.71 | 0.34 | 2.10 |
| | T | 2 | 1 | 0 | 0 | 0 | 2 | 1 | 0 | 0 | 0 | | | | |
| | T | 1 | 1 | 0 | 0 | 0 | 5 | 2 | 0 | 0 | 0 | | | | |
| | M | 4 | 3 | 0 | 0 | 0 | 6 | 2 | 0 | 0 | 0 | | | | |
| | B | 8 | 0 | 0 | 0 | 0 | 3 | 0 | 0 | 0 | 0 | | | | |
| B | 3 | 0 | 0 | 0 | 0 | 2 | 0 | 0 | 0 | 0 | | | | | |
| (4 in. long steps) | | | | | | | | | | | | | | | |
| R | T | 5 | 3 | 3 | 0 | 0 | 5 | 3 | 0 | 0 | 0 | 19.0 | 0.74 | 0.40 | 1.85 |
| | T | 1 | 1 | 0 | 0 | 0 | 0 | 0 | 0 | 0 | 0 | | | | |
| | T | 2 | 0 | 0 | 0 | 0 | 3 | 1 | 0 | 0 | 0 | | | | |
| | M | 8 | 2 | 0 | 0 | 0 | 3 | 0 | 0 | 0 | 0 | | | | |
| | B | 8 | 1 | 0 | 0 | 0 | 4 | 1 | 0 | 0 | 0 | | | | |
| B | 10 | 1 | 0 | 0 | 0 | 10 | 0 | 0 | 0 | 0 | | | | | |
| S | T | 11 | 6 | 1 | 3 | 1 | 3 | 1 | 0 | 1 | 1 | 36 | 0.73 | 0.34 | 2.2 |
| | T | 0 | 0 | 0 | 0 | 0 | 1 | 0 | 0 | 0 | 0 | | | | |
| | T | 2 | 0 | 0 | 0 | 1 | 7 | 2 | 1 | 2 | 0 | | | | |
| | B | 20 | 0 | 0 | 0 | 0 | 11 | 1 | 0 | 0 | 0 | | | | |
| | B | 0 | 0 | 0 | 0 | 0 | 0 | 0 | 0 | 0 | 0 | | | | |
| M | 4 | 1 | 0 | 0 | 1 | 12 | 2 | 3 | 0 | 0 | | | | | |
| (4 in. long steps) | | | | | | | | | | | | | | | |
| T | T | 18 | 1 | 2 | 1 | 0 | 12 | 4 | 2 | 0 | 0 | 61 | 0.78 | 0.29 | 2.70 |
| | T | 12 | 1 | 2 | 0 | 0 | 0 | 3 | 2 | 1 | 2 | | | | |
| | T | 2 | 2 | 1 | 1 | 0 | 4 | 7 | 4 | 0 | 0 | | | | |
| | B | 0 | 0 | 0 | 0 | 0 | 0 | 0 | 0 | 0 | 0 | | | | |
| | B | 18 | 0 | 0 | 0 | 0 | 3 | 0 | 0 | 0 | 0 | | | | |
| M | 6 | 1 | 0 | 0 | 0 | 13 | 2 | 1 | 2 | 0 | | | | | |
| (4 in. long steps) | | | | | | | | | | | | | | | |
| U | T | 6 | 1 | 1 | 0 | 0 | 6 | 1 | 1 | 0 | 1 | 47 | 0.70 | 0.30 | 2.33 |
| | T | 1 | 2 | 0 | 0 | 0 | 2 | 1 | 4 | 1 | 1 | | | | |
| | T | 11 | 7 | 2 | 2 | 0 | 0 | 3 | 0 | 0 | 0 | | | | |
| | B | 4 | 0 | 0 | 0 | 0 | 1 | 0 | 0 | 0 | 0 | | | | |
| | B | 1 | 0 | 0 | 0 | 0 | 0 | 0 | 0 | 0 | 0 | | | | |
| M | 11 | 7 | 0 | 0 | 0 | 4 | 1 | 1 | 1 | 0 | | | | | |
| (4 in. long steps) | | | | | | | | | | | | | | | |
| V | T | 5 | 1 | 0 | 0 | 0 | 3 | 1 | 0 | 0 | 0 | 21 | 0.73 | 0.32 | 2.25 |
| | T | 4 | 2 | 1 | 0 | 0 | 2 | 2 | 1 | 0 | 1 | | | | |
| | T | 3 | 2 | 0 | 0 | 0 | 0 | 0 | 1 | 0 | 0 | | | | |
| | B | 2 | 0 | 0 | 0 | 0 | 3 | 0 | 0 | 0 | 0 | | | | |
| | B | 4 | 0 | 0 | 0 | 0 | 3 | 0 | 0 | 0 | 0 | | | | |
| M | 3 | 2 | 0 | 0 | 0 | 1 | 2 | 0 | 0 | 0 | | | | | |
| (4 in. long steps) | | | | | | | | | | | | | | | |
| W | T | 0 | 0 | 0 | 0 | 0 | 2 | 3 | 0 | 0 | 0 | 24 24 | 0.70 0.70 | 0.33 0.33 | 2.12 2.12 |
| | T | 2 | 0 | 0 | 0 | 0 | 1 | 1 | 0 | 0 | 1 | | | | |
| | T | 1 | 1 | 0 | 0 | 1 | 4 | 3 | 1 | 1 | 0 | | | | |
| | B | 5 | 0 | 0 | 0 | 0 | 2 | 0 | 0 | 0 | 0 | | | | |
| | B | 2 | 0 | 0 | 0 | 0 | 1 | 0 | 0 | 0 | 0 | | | | |
| M | 3 | 1 | 0 | 0 | 0 | 6 | 2 | 0 | 0 | 0 | | | | | |
| (4 in. long steps) | | | | | | | | | | | | | | | |
| X | T | 4 | 0 | 0 | 0 | 0 | 0 | 0 | 1 | 1 | 0 | 45 | 0.73 | 0.28 | 2.60 |
| | T | 1 | 0 | 0 | 0 | 0 | 2 | 1 | 3 | 0 | 2 | | | | |
| | T | 2 | 4 | 0 | 1 | 2 | 4 | 2 | 2 | 2 | 1 | | | | |
| | B | 1 | 0 | 0 | 0 | 0 | 0 | 0 | 0 | 0 | 0 | | | | |
| | B | 0 | 0 | 0 | 0 | 0 | 0 | 0 | 0 | 0 | 0 | | | | |
| M | 1 | 0 | 0 | 0 | 0 | 0 | 2 | 1 | 0 | 0 | | | | | |
| (4 in. long steps) | | | | | | | | | | | | | | | |
| Y | T | 3 | 0 | 0 | 1 | 1 | 1 | 2 | 0 | 1 | 1 | 48 | 0.78 | 0.31 | 2.50 |
| | T | 2 | 0 | 0 | 1 | 1 | 8 | 0 | 0 | 0 | 0 | | | | |
| | T | 4 | 0 | 1 | 1 | 2 | 4 | 0 | 0 | 0 | 0 | | | | |
| | M | 2 | 0 | 0 | 1 | 1 | 4 | 0 | 0 | 0 | 0 | | | | |
| | B | 2 | 0 | 0 | 0 | 0 | 1 | 0 | 0 | 0 | 0 | | | | |
| B | 4 | 0 | 0 | 0 | 0 | 0 | 0 | 0 | 0 | 0 | | | | | |
| (4 in. long steps) | | | | | | | | | | | | | | | |
| Z | T | 3 | 1 | 0 | 0 | 0 | 6 | 2 | 0 | 0 | 0 | 25 | 0.83 | 0.46 | 1.80 |
| | T | 2 | 0 | 0 | 0 | 0 | 1 | 0 | 0 | 1 | 0 | | | | |
| | T | 4 | 2 | 1 | 1 | 0 | 2 | 0 | 0 | 1 | 0 | | | | |
| | M | 5 | 4 | 0 | 1 | 0 | 7 | 1 | 2 | 1 | 0 | | | | |
| | B | 1 | 0 | 0 | 0 | 0 | 3 | 0 | 0 | 0 | 0 | | | | |
| B | 1 | 0 | 0 | 0 | 0 | 0 | 0 | 0 | 0 | 0 | | | | | |
| (4 in. long steps) | | | | | | | | | | | | | | | |
| AA | T | 4 | 1 | 0 | 0 | 0 | 3 | 1 | 0 | 0 | 0 | 25.0 | 0.71 | 0.33 | 2.20 |
| | T | 4 | 4 | 1 | 0 | 1 | 6 | 2 | 1 | 0 | 0 | | | | |
| | T | 4 | 2 | 0 | 0 | 0 | 4 | 1 | 0 | 0 | 0 | | | | |
| | M | 7 | 0 | 1 | 0 | 0 | 8 | 0 | 1 | 0 | 0 | | | | |
| | B | 7 | 0 | 0 | 0 | 0 | 2 | 0 | 0 | 0 | 0 | | | | |
| B | 2 | 0 | 1 | 0 | 0 | 2 | 0 | 0 | 0 | 0 | | | | | |

| | $\frac{1}{8}$ In. Off Diam | $\frac{1}{4}$ In. Off Diam |
|------------|----------------------------|----------------------------|
| Tops..... | 12 | 29 |
| Middles... | 7 | 6 |
| Bottoms... | 7 | 5 |

Rating of heat on basis of a weight of 2 for tops and middles equals 20.

The cleanness ratings of successive heats of SAE 6150 made for the aircraft engine industry in 1939 and inspected on the basis of counting visually the slag lines and rating them according to length are shown in Table 2. Fig 1 shows these step-down ratings of the heats as a function of the manganese-silicon ratio for the heats. Here it is seen that as the manganese-silicon ratio decreases the step-down rating becomes less, that is, the heats become progressively cleaner on the step-down inspection.

The dates of melting and inspection of these early heats of SAE 6150 were about 1939 and 1940, and this practice of working to as high a silicon content as possible was adhered to throughout the war. The manganese was kept on the low side of the chemical limit for this specification, and several heats were inadvertently made using a silicon content of 0.60 pct and a manganese content of 0.70 pct. These heats ran true to form, and were cleaner on step-down inspection in $1\frac{1}{2}$ -in. rolled bars.

Recently we have had another confirmation of the effect of the manganese-silicon ratio on the cleanness of rigidly inspected steels made to AMS 6260* which is a modification of SAE 3312. For many years before the war our custom was to melt a proprietary alloy grade similar to SAE 3312 steel to manganese limits of 0.30 to 0.50 pct and silicon limits of 0.25 to 0.40 pct. The SAE limits for 3312 allowed the manganese to be made substantially equal to the silicon content so that the manganese-silicon ratio was approximately unity. When the AMS specifications were set up however, we worked to the upper part of the manganese limits of 0.40 to 0.70 pct because of hardenability requirements and the silicon limits of 0.20 to 0.35 pct, so that a manganese-silicon ratio of at least 1.7 was inevitable, and generally this ratio on actual heats of steel was at least 2.00. From the beginning of manufacture of AMS 6260 it was noticed that the heats were considerably dirtier than our proprietary grade of alloy

* AMS 6260: C 0.07/0.13 pct, Mn 0.40/0.70 pct, Si 0.20/0.35 pct, P 0.040 pct max., Cr 1.00/1.40 pct, Ni 3.00/3.50 pct, Mo 0.08/0.15 pct.

Table 2 . . . (Continued)

| Heat | 1st-Step $\frac{1}{4}$ In. Off Diam CLASS | | | | | 2nd Step $\frac{3}{8}$ In. Off Diam. | | | | | Numerical Rating per 6 In. Length | Mn | Si | Mn/Si | |
|--------------------|--|----|---|---|---|---|----|---|---|---|--|------|------|-------|------|
| | 1 | 2 | 3 | 4 | 5 | 1 | 2 | 3 | 4 | 5 | | | | | |
| (3 in. long steps) | | | | | | | | | | | | | | | |
| AB | T | 8 | 4 | 0 | 0 | 0 | 5 | 0 | 1 | 0 | 0 | 44.0 | 0.73 | 0.22 | 3.30 |
| | T | 6 | 1 | 1 | 0 | 0 | 5 | 4 | 0 | 0 | 0 | | | | |
| | T | 4 | 6 | 2 | 0 | 0 | 7 | 3 | 1 | 0 | 0 | | | | |
| | M | 3 | 1 | 0 | 0 | 0 | 4 | 1 | 0 | 1 | 0 | | | | |
| | B | 8 | 1 | 0 | 0 | 0 | 13 | 1 | 0 | 0 | 0 | | | | |
| | B | 13 | 0 | 1 | 0 | 0 | 12 | 1 | 0 | 0 | 0 | | | | |
| (3 in. long steps) | | | | | | | | | | | | | | | |
| AC | T | 14 | 0 | 1 | 0 | 0 | 6 | 1 | 1 | 0 | 0 | 52 | 0.70 | 0.26 | 2.70 |
| | T | 3 | 0 | 0 | 0 | 0 | 6 | 2 | 1 | 0 | 2 | | | | |
| | T | 4 | 0 | 0 | 0 | 0 | 5 | 2 | 0 | 0 | 0 | | | | |
| | M | 4 | 1 | 0 | 0 | 0 | 8 | 0 | 1 | 0 | 0 | | | | |
| | B | 25 | 0 | 0 | 0 | 0 | 11 | 0 | 0 | 0 | 0 | | | | |
| | B | 9 | 2 | 1 | 0 | 0 | 10 | 0 | 0 | 0 | 0 | | | | |
| (3 in. long steps) | | | | | | | | | | | | | | | |
| AD | T | 5 | 1 | 0 | 0 | 0 | 1 | 2 | 0 | 0 | 0 | 0.70 | 0.32 | 2.20 | |
| | T | 5 | 1 | 0 | 0 | 0 | 3 | 4 | 0 | 0 | 0 | | | | |
| | T | 5 | 0 | 0 | 0 | 0 | 3 | 0 | 0 | 0 | 0 | | | | |
| | M | 2 | 0 | 0 | 0 | 0 | 3 | 2 | 0 | 0 | 0 | | | | |
| | B | 2 | 0 | 0 | 0 | 0 | 1 | 0 | 0 | 0 | 0 | | | | |
| | B | 1 | 0 | 0 | 0 | 0 | 1 | 0 | 0 | 0 | 0 | | | | |
| (3 in. long steps) | | | | | | | | | | | | | | | |
| AE | T | 4 | 3 | 2 | 0 | 2 | 1 | 1 | 1 | 0 | 0 | 74 | 0.92 | 0.25 | 3.7 |
| | T | 3 | 2 | 0 | 1 | 0 | 5 | 2 | 0 | 0 | 1 | | | | |
| | T | 4 | 6 | 6 | 0 | 3 | 2 | 0 | 0 | 0 | 0 | | | | |
| | M | 9 | 1 | 0 | 0 | 0 | 7 | 2 | 0 | 0 | 0 | | | | |
| | B | 5 | 0 | 0 | 0 | 0 | 0 | 0 | 0 | 0 | 0 | | | | |
| | B | 2 | 0 | 0 | 0 | 0 | 2 | 0 | 0 | 0 | 0 | | | | |

similar to SAE 3312 in which the silicon was made about equal to the manganese content.

A cooperative program was arranged with an aircraft engine manufacturer to make two heats of AMS 6260 to limits 0.30 to 0.60 pct for both the manganese and silicon. The performance of these two heats was compared with the performance of previous heats of AMS 6260 made to the high manganese and low silicon limits. All of these heats were of our own manufacture so that complete records were available both in our own inspection department and from the aircraft engine manufacturer's magnaflux reports.

Table 3 shows a typical melting log of AMS 6260, the practice shown being a carryover from the practice used in making SAE 3312 to high standards for cleanliness. Tapping temperatures were held to the range 1600/1615°C, and 1000-lb ingots were poured in 55 to 60 sec.

Table 4 shows the Carpenter inspection data on step-down tests on pilot bars where available, and miscellaneous step-down reports taken from random bars on production orders, and also the percentage rejection on magnaflux inspection of knuckle pins in an aircraft engine manufacturer's plant. The same method of rating the heats on step-down tests was used as that described

above, except that in the case of production lots no weight could be given top and middle as in the pilot bar inspection. (Here it is to be remarked that previously SAE 3312 was supplied for this part for some length of time, and the losses were consistently in the neighborhood of 5 pct or less on final rejection of this difficult knuckle pin and piston pin inspection. On these heats the manganese was held to about

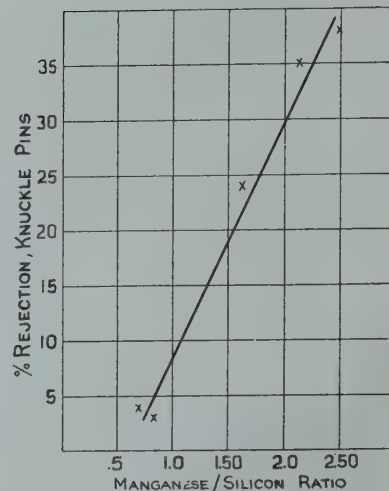


FIG 2—Relationship between Mn/Si ratio heats of AMS 6260 and per cent reduction of aircraft knuckle pins, magnaflux inspection.

0.40 pct and the silicon content was in the neighborhood of 0.35 pct.)

Table 4 shows clearly the relation of manganese to silicon ratio on five heats, to both step-down inspection data in our own plant and magnaflux inspection of finished aircraft parts. Fig 2, plotted from some of the data in Table 4, shows the relationship between the manganese to silicon ratio and the percentage rejection of knuckle pins on magnaflux inspection. Here again the conclusion is obvious that the manganese and silicon contents of the heat of steel can exert a large influence on the resulting cleanliness of the steel when other operating variables are controlled closely.

An additional example can be quoted

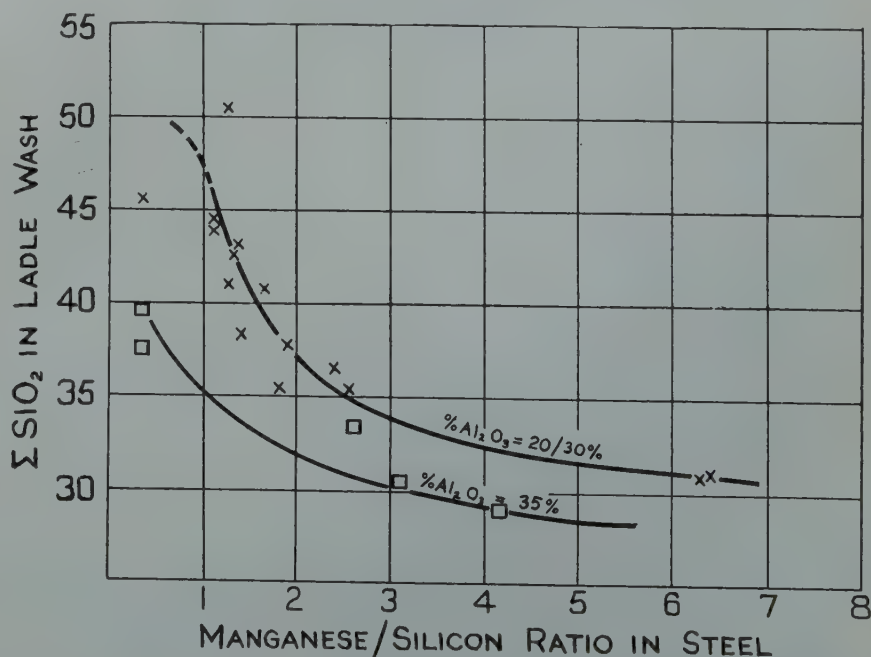


FIG 3—Effect of Mn/Si ratio on the Si content of slag buttons from surfaces of ingots.

to show that the manganese to silicon balance has a large effect on the resulting cleanness of steel when made in the basic electric arc furnace and teemed into ingots from a ladle lined with acid brick. This example has to do with a steel analyzing approximately 1.00 pct C, 1.50 pct Si, 1.50 pct Mn, and 2.50 pct Cr. This steel was developed for the manufacture of large rollers and races which must pass magnaflux testing. The steel previously used analyzed approximately 1.00 pct C, 0.60 pct Si, 1.75 pct Mn and 1.50 pct Cr. When using the latter oil hardening steel the results of hair-line inspection on rollers were very erratic. Some heats were good, but when hair lines occurred they were bad and resulted in rejections of 15 to 50 pct. With the steel containing

Table 3 . . . Typical Melting Log, AMS 6260

Charge 22,000 lb low alloy nickel scrap and plate. Melted down at 0.25 pct carbon and ored down to 0.036 pct carbon.

9:00 AM, . . . No. 2 Preliminary test, C 0.036, P 0.020, S 0.028.

9:10/9:25 Slag-off

9:25 Slag-on. 400 lb lime, 150 lb spar, 20 lb coke breeze. After slag partly fused added 40 lb 50 pct FeSi (lump) and 100 lb crushed 50 pct FeSi.

9:45 Back charge 1000 lb high chromium nickel scrap.

10:00 No. 3 Preliminary test. C 0.048, Mn 0.15, Si 0.12, Cr 1.00 Ni 3.78, S 0.017.

10:35 No. 4 Preliminary test. C 0.054, S 0.017

11:05 96 lb FeCr, 33 lb nickel, 20 lb FeMo.

11:15 115 lb 50 pct FeSi (lump)

11:30 Preliminary test. S 0.010.

11:45 5 lb aluminum in bath

11:50 Tap, tap temperature 1605°C. 3 lb aluminum to ladle.

McQuaid-Ehn Grain Size, 5+

Table 4 . . . Stepdown and Magnaflux Inspection Data on AMS 6260, Aircraft Quality

| Heat | Mn/Si Ratio | Weighted Average per 6 In. Length | | Pct Rejection on Knuckle-Pin Inspection |
|------|-------------|-----------------------------------|------------|---|
| | | Production Orders | Pilot Bars | |
| A | 1.62 | 15.6 | | 24 |
| B | 2.48 | 21.6 | | 38 |
| C | 2.12 | 24.0 | | 35 |
| D | 0.69 | 7.0 | 14.4 | 3.9 |
| E | 0.83 | 8.4 | 5.3 | 3.0 |

1.00 pct C, 1.50 pct Si, 1.50 pct Mn and 2.50 pct Cr, the rejections are uniformly less than 2 pct.

Having established the effect of the manganese-silicon balance on the cleanness of steels when made by carefully

controlled melting and pit practice, the problem was now to find a logical explanation for this effect.

Part 2—The Effect of the Manganese Silicon Ratio on the Silica Content of Slag Patches on Ingot Surfaces

In the introductory remarks we pointed out the possible effect of manganese and silicon contents of molten steel on the chemical composition of ladle wash, as evidenced by the slag patches commonly found on the surface of the metal as it is rising in the molds. It was suggested that the principal effect of the manganese and silicon content of the steel on the ladle brick and metal interface would be to form a slag whose viscosity, or fluidity, would be determined by this balance of manganese and silicon.

Slag buttons were collected from the surface of ingots, and in some cases from the upper surface of the steel as it was poured in the molds. This investigation was not concerned with any particular grade of steel because the general chemical composition of such slag buttons was desired. Consequently a variety of SAE grades of steel were sampled, in addition to several grades of tool steels.

Table 5 shows analysis of the metal and of the corresponding slag buttons collected from these heats. For the purpose of this discussion it is sufficient to show the total silica, total alumina,

total iron as FeO, MnO and Cr₂O₃ composition of these slags.

These slag analyses fall into two groups, first, those having up to about 25 pct Al₂O₃ and second, a few showing approximately 35 pct Al₂O₃. Fig 3 shows the total silica content of these slag buttons as a function of the manganese-silicon ratio of the steel from which they were collected. Two groupings are shown in Fig 3 corresponding to the two Al₂O₃ contents of the slag buttons. Considering first the 25 pct Al₂O₃ group, it is seen that the saturation value for this type of slag approaches 45 to 50 pct by weight, and that the saturation value is rapidly approached as the manganese-silicon ratio approaches unity. At a manganese-silicon balance of 1.5 the silica concentration of these slags drops to 40 pct, and at a ratio of 2.50 the concentration drops steadily to 35 pct. After this the silica concentration drops gradually with increasing manganese to silicon ratios, until in the region of manganese contents of 1.25 to 1.75 pct, with silicon values of about 0.25 pct, the silica concentration is about 30 pct.

The same general conclusions are obtained on the few samples containing approximately 35 pct Al₂O₃. Here the saturation silica concentration seems to be approximately 40 pct, and this saturation value for silica is reached at a manganese-silicon ratio of somewhat less than unity. At a manganese-silicon ratio of unity the silica concentration in the slag buttons is approximately 35 pct, while at a manganese-silicon

Table 5 . . . Composition of Slag Buttons from Surfaces of Ingots

| Heat | Grade | Metal Analysis Per Cent | | | | | | | | Slag Analysis—Per Cent by Weight | | | | | |
|------|--------------|-------------------------|------|------|------|------|------|---|------|----------------------------------|------------------|--------------------------------|------|------|--------------------------------|
| | | C | Mn | Si | Cr | Ni | Mo | V | | Mn/Si | SiO ₂ | Al ₂ O ₃ | FeO | MnO | Cr ₂ O ₃ |
| 1 | SAE 4340 | 0.39 | 0.61 | 0.20 | 0.70 | 1.74 | 0.22 | | | 3.05 | 30.8 | 31.8 | 6.6 | 32.9 | 1.31 |
| 2 | 4340 | 0.41 | 0.70 | 0.29 | 0.68 | 1.83 | 0.28 | | | 2.4 | 36.5 | 27.1 | 3.8 | 33.7 | 0.79 |
| 3 | 3140 | 0.35 | 0.55 | 0.21 | 0.70 | 1.31 | | | | 2.6 | 33.9 | 32.9 | 3.9 | 31.2 | 0.80 |
| 4 | TS* | 0.89 | 1.72 | 0.27 | 0.11 | 0.05 | | | | 6.4 | 30.8 | 25.6 | 6.0 | 40.5 | |
| 5 | TS | 0.92 | 0.26 | 0.16 | 0.15 | | | | | 1.63 | 40.6 | 27.7 | 8.2 | 28.1 | |
| 6 | Band Saw | 0.94 | 0.23 | 0.09 | 0.36 | 0.04 | | | | 2.7 | 35.5 | 31.0 | 6.9 | 25.8 | 1.20 |
| 7 | Band Saw | 0.96 | 0.22 | 0.16 | 0.37 | 0.06 | | | | 1.38 | 38.3 | 29.1 | 5.7 | 25.1 | 1.02 |
| 8 | SAE 6150 | 0.50 | 0.68 | 0.50 | 0.93 | 0.06 | | | | 1.35 | 43.2 | 23.9 | 4.2 | 25.5 | 2.88 |
| 9 | Thread Gauge | 0.20 | 1.38 | 0.22 | 0.09 | | | | 0.21 | 6.3 | 31.0 | 25.3 | 4.8 | 39.5 | |
| 10 | SAE 4340 | 0.38 | 0.70 | 0.17 | 0.75 | 1.87 | | | | 4.7 | 29.0 | 34.5 | 5.1 | 32.9 | 0.74 |
| 11 | 3220 | 0.15 | 0.36 | 0.33 | 1.08 | 1.70 | | | | 1.09 | 44.6 | 18.0 | 5.36 | 26.8 | 4.0 |
| 12 | 4620 | 0.17 | 0.46 | 0.24 | 0.12 | 1.85 | | | | 1.91 | 37.8 | 28.6 | 4.4 | 28.9 | |
| 13 | 52100 | 1.03 | 0.32 | 0.29 | 1.44 | 0.05 | | | | 1.10 | 44.1 | 16.2 | 8.04 | 23.2 | 7.9 |
| 14 | 52100 | 1.07 | 0.40 | 0.32 | 0.45 | 0.04 | | | | 1.25 | 50.5 | 20.7 | 5.1 | 24.3 | 1.5 |
| 15 | 52100 | 1.01 | 0.35 | 0.26 | 1.42 | | | | | 1.35 | 42.9 | 22.2 | 6.2 | 24.6 | 5.4 |
| 16 | 3312 | 0.095 | 0.37 | 0.30 | 1.56 | 3.54 | | | | 1.25 | 42.6 | 19.4 | 5.2 | 25.7 | 4.7 |
| 17 | TS | 0.50 | 0.34 | 0.99 | 0.11 | 0.10 | 0.40 | | | 0.34 | 45.2 | 8.5 | 31.9 | 12.2 | 1.23 |
| 18 | TS | 0.52 | 0.34 | 1.08 | 0.10 | 0.09 | 0.45 | | | 0.32 | 45.2 | 20.0 | 17.7 | 16.5 | 0.70 |
| 19 | TS | 0.50 | 0.65 | 1.92 | 0.22 | 0.04 | | | | 0.34 | 41.7 | 22.9 | 13.9 | 23.5 | |
| 20 | TS | 0.47 | 0.35 | 1.05 | 0.13 | 0.14 | 0.43 | | | 0.33 | 38.6 | 34.8 | 8.2 | 19.4 | |
| 21 | TS | 0.50 | 0.34 | 1.03 | 0.15 | 0.05 | 0.43 | | | 0.33 | 37.4 | 33.4 | 9.9 | 19.3 | |
| 22 | SAE 2515 | 0.11 | 0.46 | 0.26 | 0.09 | 4.96 | | | | 1.75 | 35.3 | 34.8 | 5.4 | 26.4 | |

*TS = Tool Steel.

ratio of 3 the silica concentration is approximately 30 pct by weight.

Fig 3 confirms the results of Körber and Oelsen² on the saturation solubility of silica in acid slags containing about 25 pct alumina, and other quantities of FeO and MnO. Due to the nature of the sampling in our experiments on these slag buttons, some spread in values is to be expected for the total silica content, but the data do indicate that a saturation value of 45 to 50 pct by weight silica is found in these acid slags containing about 25 pct alumina.

From the behavior of the slags containing approximately 35 pct alumina, it is clear that the saturation solubility of silica is evidently lower in these slags than in the 25 pct alumina series. Only 5 heats were found which showed 35 pct alumina in their slag buttons, and the reason for these heats deviating from the 25 pct alumina type is not known.

For the time being it is well to remember that Herty, Conley and Roger⁴ measured the viscosities of slags in the acid slag system FeO-MnO-SiO₂ at about 1550°C. They found that as the silica concentration of the slag approached saturation at this temperature, then the viscosity of the slag increased greatly. Körber and Oelsen² found the saturation solubility of silica in slags composed of FeO, MnO, and SiO₂ to be approximately 50 pct by weight at 1600, 1550 and 1500°C. Körber and Oelsen² also found the saturation solubility of silica to be 50 pct in slags composed of 25 pct alumina, ferrous oxide and manganous oxide.

Part 3—Calculation of Equilibrium between Liquid Metal and Acid Ladle Brick

The foregoing data relating to the effect of the manganese silicon balance on the resulting cleanness of basic electric arc melted steels, and on the silica content of slag buttons and slag patches on the sides of ingots, have been interpreted qualitatively on the basis that the manganese and silicon contents of the steels have a large effect on the chemical composition of the interface between the molten metal and the ladle brick. As the manganese-silicon ratio in steel becomes unity or less, the steels become cleaner on any test which measures the macroscopic cleanness of the steel, such as the magnaflux or step-down methods. Furthermore, we have shown that as the manganese-

silicon ratio becomes unity or less, then the composition of the slag buttons on the sides of ingots becomes such that the silica content is rapidly approaching saturation. From experimental studies on acid slags, we know that the viscosity of such slags increases rapidly as the silica content approaches saturation.

There is another method of attack which can be used to test the hypothesis that the genesis of these slag buttons, and hence the slag lines, is at the metal-brick interface in the ladle, and that is to set up a system to calculate the composition of these slag buttons from the chemical composition of the heat. Such a method can make use of the available laboratory studies which have been made on the equilibrium of molten steel under acid slags. Admittedly the molten steel-brick inter-

Table 6 . . . Silicon-FeO Balanced Reaction in Liquid Steel

| Temperature, °C | [Si] × [FeO] ² |
|-----------------|---------------------------|
| 1600 | 7 × 10 ⁻⁴ |
| 1550 | 2.72 × 10 ⁻⁴ |
| 1500 | 0.78 × 10 ⁻⁴ |

Table 7 . . . Distribution of Free Ferrous Oxide between Slag and Liquid Iron

| Temperature, °C | Mol Per Cent FeO in Slag Pct by Wt. FeO in Metal |
|-----------------|---|
| 1550 | 85 |
| 1575 | 77 |
| 1600 | 69 |

face is not at equilibrium in a strict sense of the word, since the interface is continually breaking up into small globules, and a new interface is being formed by reaction of the steel with the brick which contains approximately 65 pct silica, 30 pct alumina, and 5 pct ferric oxide. However, at the temperatures of molten steel in the ladle there is a good chance that the reaction rates are fast enough so that the composition of the interface approximates the equilibrium composition.

The experiments of Körber and Oelsen² on the equilibrium of molten steel containing manganese and silicon under acid slags containing FeO, MnO and silica, when the slag is saturated with silica, can be used to calculate* the dissociation constants of ferrous and manganous silicates in acid slags. To do this, it is necessary that a value be known for the solubility product of [Si] × [FeO]². The value determined by Körber and Oelsen's² data probably

* The calculations which follow are similar to those made by H. Schenck, *Physikalische Chemie der Eisenhüttenprozesse*, 2, J. Springer, Berlin,

represents the best value available at the present time. Their values for this product, expressed in terms of per cent by weight silicon and FeO in solution in liquid steel are given in Table 6.

The distribution ratio of Herty and Gaines⁵ showing the free mol pct of FeO in liquid slags divided by the pct by weight of FeO in liquid steel may be expressed as in Table 7.

The relationships of Tables 6 and 7 may be combined to give the product of (Si) × (Free mol pct FeO in the slag)² as shown in Table 8.

The experiments of Körber and Oelsen² used liquid steel in sand crucibles in which melts of iron, manganese and silicon were allowed to come to equilibrium with acid slags containing FeO, MnO and silica. Since the crucibles were of sand, the slags were saturated with silica. Considering the constitution of the slag phase, we would like to emphasize that the following remarks on the probable molecular constitution of these slags are made in the light of setting up a set of molecular dissociation constants which may or may not have the correct physical meaning. What we plan to do is to obtain a set of molecular dissociation constants for these acid slags which will reproduce Körber and Oelsen's² data, and then these constants will be used to calculate the probable equilibrium between acid slags and liquid steel under conditions different from those of the laboratory experiments.

Table 8 . . . Balanced Reaction between Pct Si in the Metal and Free Mol-pct FeO in Slags, and by Pct Weight FeO in Slag if the Number of Mol per 100 G, M, is Known

| Temperature, °C | [Si] × (FeO) ² | [Si] × {FeO} ² |
|-----------------|---------------------------|---------------------------|
| 1550 | 1.98 | 1.06 M ² |
| 1575 | 2.72 | 1.43 M ² |
| 1600 | 3.32 | 1.73 M ² |

The constitution of the slags will be FeO, MnO and SiO₂, and the molecular constituents present will be taken to be free FeO, free MnO, free SiO₂, and FeO.SiO₂ and MnO.SiO₂. The ordinary chemical analysis will yield only the

1934. However, different values for the dissociation constants of FeO.SiO₂ and MnO.SiO₂ are used by Schenck in his work than those which we will presently derive. For this reason, we will show briefly our method of calculating and checking those dissociation constants.

total amounts of FeO, MnO and SiO₂. The amount of free FeO, as distinct from the amount of FeO combined with silica can be obtained by use of the silicon-ferrous oxide solubility product. If the silicon content is known, then Table 8 will give the amount of ferrous oxide present in solution, but uncombined with silica, in the slag. Assuming that the mol percent of free FeO can be converted to percent by weight of FeO (this can be done if the molecular weight of the slag is known), then a subtraction of this value from the total per cent by weight of FeO present will yield the amount of FeO combined with silica.

The equilibrium between manganese in liquid steel and free FeO and free MnO in slags is known from the experiments of Krings and Schackmann⁶ and Körber and Oelsen.² This relationship is of the form:

$$K_{Mn} = \frac{\{MnO\}}{\{FeO\}[Mn]} \tag{1}$$

and values for K_{Mn} are shown in Table 9. In Table 9 the FeO and MnO quantities refer to weight percent of uncombined FeO and MnO in the slags.

Table 9 . . . Balanced Reaction between Free FeO and MnO in Slags and Mn by Weight in Liquid Steel

| Temperature, °C | $K_{Mn} = \frac{\{MnO\}}{\{FeO\}[Mn]}$ |
|-----------------|--|
| 1575 | 2.2 |
| 1600 | 2.0 |
| 1625 | 1.8 |

Thus, knowing the manganese content of the liquid metal and the free FeO as determined from the silicon content as outlined above, the free MnO content of the slag can be calculated. A subtraction from the total MnO content as determined by chemical analysis will determine the amount of MnO combined with silica.

J. White³ has published experimental data on the dissociation of FeO.SiO₂ in liquid acid slags at temperatures ranging from 1550 to 1625°C. White's data can be represented by the following relationship:

$$\text{Log} \frac{(\text{FeO}.\text{SiO}_2)}{(\text{FeO})(\text{SiO}_2)} = \frac{7170}{T} - 5.211 \tag{2}$$

where the concentrations are in mol percents, and T is the absolute temperature.

When the dissociation constant for FeO.SiO₂ is determined from Körber

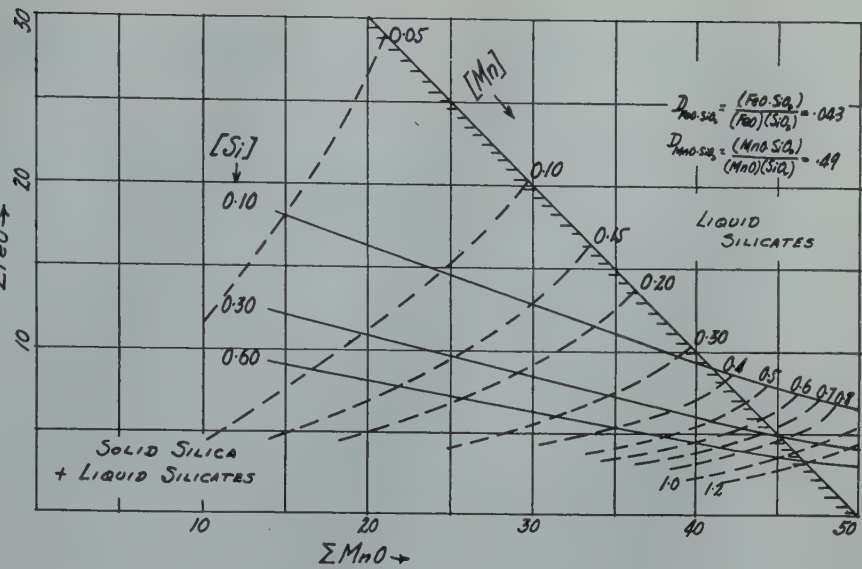


FIG 4—FeO-MnO-SiO₂ slags, 1600°C.

and Oelsen's² data as outlined above, it is found that the value is virtually in agreement with White's value in Eq 2. This indicates that White's dissociation constant is consistent with the data of Körber and Oelsen.² The dissociation constant for MnO.SiO₂ determined from Körber and Oelsen's² data as outlined above is

$$\text{Log} \frac{(\text{MnO}.\text{SiO}_2)}{(\text{MnO})(\text{SiO}_2)} = \frac{6030}{T} - 3.52 \tag{3}$$

where the concentrations are in mol percents, and T indicates the absolute temperature.

Equilibrium at 1600°C in the system Fe-Mn-Si-FeO-MnO-SiO₂ may be computed by means of these two dissociation constants, and Tables 6, 7, and 8. These calculations are summarized in Fig 4, where the MnO and FeO contents of an acid slag are shown as a function of the Mn and Si contents of the bath. The shaded line in Fig 4 indicates the saturation value of 50 pct for silica as found by Körber and Oelsen.² The balanced manganese and silicon content under an acid slag containing 50 pct silica may be determined by reading the intersection of the Mn and Si lines with this 50 pct silica line. Thus, for 0.30 pct Mn, the corresponding silicon content for 50 pct SiO₂ is 0.09 pct; for 0.50 pct Mn the silicon is 0.15 pct; and for 0.70 pct Mn the silicon is about 0.28 pct. Fig 5, curve A shows the experimental Mn and Si contents in liquid steel at 1600°C under acid slags containing 50 pct silica, after Körber and Oelsen.² The calculated values determined from Fig 4 are

shown as squares, and the conclusion is drawn that these dissociation constants for MnO.SiO₂ and FeO.SiO₂ reproduce Körber and Oelsen's² data over a considerable range of Mn and Si contents.

Körber and Oelsen² also determined the Mn and Si contents of liquid steel under acid slags containing 25 pct Al₂O₃ and 50 pct SiO₂ at 1600°C. These data are reproduced in Fig 5, curve B. The dissociation constant for Al₂O₃·SiO₂ = 0.49 (this is the same value as the dissociation constant for MnO.SiO₂ at this temperature) yields the curve shown in Fig 5, labeled curve C. Larger dissociation constants for Al₂O₃·SiO₂ do not make significant changes in this curve, therefore this is as far as this type of analysis can be carried at the present time to determine the dissociation constant for Al₂O₃·SiO₂.

The temperature variation of the dissociation constant for Al₂O₃·SiO₂ is taken to be the same as MnO.SiO₂.

The equations used at temperatures of 1550 and 1500°C to calculate the composition of acid slags containing about 25 pct alumina as a function of the manganese and silicon content of liquid steel are shown below:

25 pct Al₂O₃-FeO-MnO-SiO₂-Slags at 1550°C*

$$\Sigma \text{FeO} = \{ \text{FeO} \} \left[1 + \frac{0.086}{M} \{ \text{SiO}_2 \} \right]$$

* In Eq 4, 5 and 6, [] refers to weight percentage in liquid steel, Σ indicates the total percent by weight of SiO₂, or MnO, etc. in the slag phase, { } indicates the percent by weight of a molecular constituent, such as free SiO₂, free MnO, etc. in the slag phase, and M is the number of mols per 100g when the slag constituents are computed as free FeO, FeO.SiO₂, free MnO, etc.

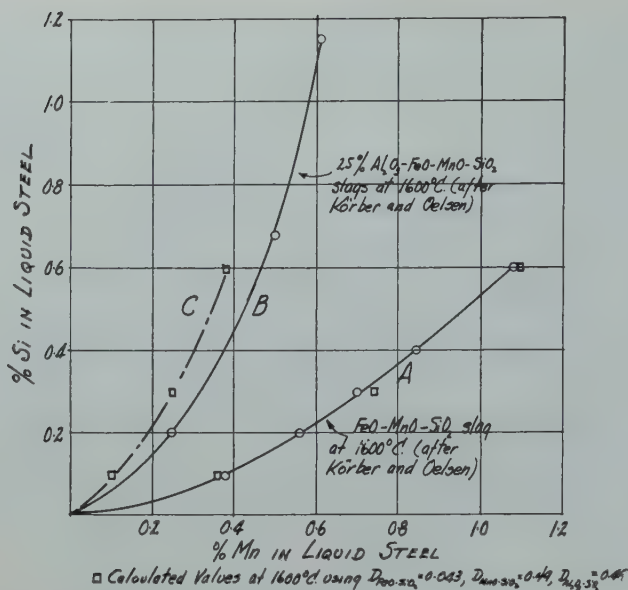


FIG 5—Mn-Si balance at 1600°C in liquid steel under acid slags saturated with silica ($\Sigma\text{SiO}_2 = 50$ pct).

$$\Sigma\text{MnO} = \{\text{MnO}\} \left[1 + \frac{1.00}{M} \{\text{SiO}_2\} \right]$$

$$\Sigma\text{SiO}_2 = \{\text{SiO}_2\} \left[1 + \frac{0.072}{M} \{\text{FeO}\} + \frac{0.84}{M} \{\text{MnO}\} + \frac{0.60}{M} \{\text{Al}_2\text{O}_3\} \right]$$

$$\Sigma\text{Al}_2\text{O}_3 = \{\text{Al}_2\text{O}_3\} \left[1 + \frac{0.97}{M} \{\text{SiO}_2\} \right] = 25 \text{ pct}$$

$$[\text{Si}]\{\text{FeO}\}^2 = 1.06M^2$$

$$[\text{Mn}] = 0.418 \frac{\{\text{MnO}\}}{\{\text{FeO}\}} \quad [4]$$

25 pct Al_2O_3 -FeO-MnO-SiO₂ Slags at 1500°C*

$$\Sigma\text{FeO} = \{\text{FeO}\} \left[1 + \frac{0.11}{M} \{\text{SiO}_2\} \right]$$

$$\Sigma\text{MnO} = \{\text{MnO}\} \left[1 + \frac{1.26}{M} \{\text{SiO}_2\} \right]$$

$$\Sigma\text{SiO}_2 = \{\text{SiO}_2\} \left[1 + \frac{0.11}{M} \{\text{FeO}\} + \frac{1.06}{M} \{\text{MnO}\} + \frac{0.76}{M} \{\text{Al}_2\text{O}_3\} \right]$$

$$\Sigma\text{Al}_2\text{O}_3 = \{\text{Al}_2\text{O}_3\} \left[1 + \frac{1.22}{M} \{\text{SiO}_2\} \right] = 25 \text{ pct}$$

$$[\text{Si}]\{\text{FeO}\}^2 = 0.86M^2$$

$$[\text{Mn}] = 0.32 \frac{\{\text{MnO}\}}{\{\text{FeO}\}} \quad [5]$$

Further, the calculated free, or uncombined, alumina in these slags will be about 2.5 pct by weight when calcu-

lated according to the above sets of formulas, and the mols per 100 g in the slag will be about 0.93 (M). The free silica can be obtained approximately by

$$\{\text{SiO}_2\} = \frac{75 - \{\text{FeO}\} - \{\text{MnO}\}}{1 + \frac{0.158}{M} \{\text{FeO}\} + \frac{1.84}{M} \{\text{MnO}\} + \frac{1.5}{M}} \quad [6]$$

As a sample calculation, let the manganese content of liquid steel in the ladle be 0.70 pct and the silicon content 0.17 pct, and we desire to calculate the total FeO, MnO and SiO₂ contents of the equilibrium slag containing 25 pct Al_2O_3 . Take the temperature as 1550°C. Let $M = 0.93$, then

$$\{\text{FeO}\} = \sqrt{\frac{0.91}{0.17}} = 2.32$$

$$\{\text{MnO}\} = \frac{0.70 \times 2.32}{0.418} = 3.88$$

$$\{\text{SiO}_2\} = \frac{75 - 6.20}{1 + 0.39 + 7.70 + 2.06} = \frac{68.80}{11.15} = 6.2$$

$$\{\text{Al}_2\text{O}_3\} = \frac{25}{1 + 6.48} = 3.34$$

$$\Sigma\text{FeO} = \text{Total FeO} = 2.32$$

$$[1 + 0.572] = 3.64$$

$$\Sigma\text{MnO} = \text{Total MnO} = 3.88$$

$$[1 + 6.68] = 29.80$$

In terms of mol per 100 g, these are $\text{FeO} = 0.0505$, $\text{MnO} = 0.4380$, $\text{Al}_2\text{O}_3 = 0.3470$, and free $\text{SiO}_2 = 0.103$, to give $M = 0.938$. These calculated total FeO and MnO contents of the slag are to be compared with $\text{FeO} = 5.4$ and $\text{MnO} = 32.9$ found experimentally for heat (10) shown in Table 5.

In a similar manner, a broad range of FeO and MnO contents of acid slags containing 25 pct Al_2O_3 and the remainder silica can be calculated as a function of the manganese and silicon content of the liquid steel. These calculations are summarized in Fig 6 and 7 for temperatures of 1550 and 1500°C.

Table 10 shows the predicted MnO and FeO contents in the equilibrium acid slag containing 25 pct Al_2O_3 , balance silica slags for the manganese and silicon contents of the heats shown in Table 5. In general the trend is evident that Fig 6 and 7 predict with reasonable accuracy the composition of the slag buttons found on ingots. Considering the fact that equilibrium is

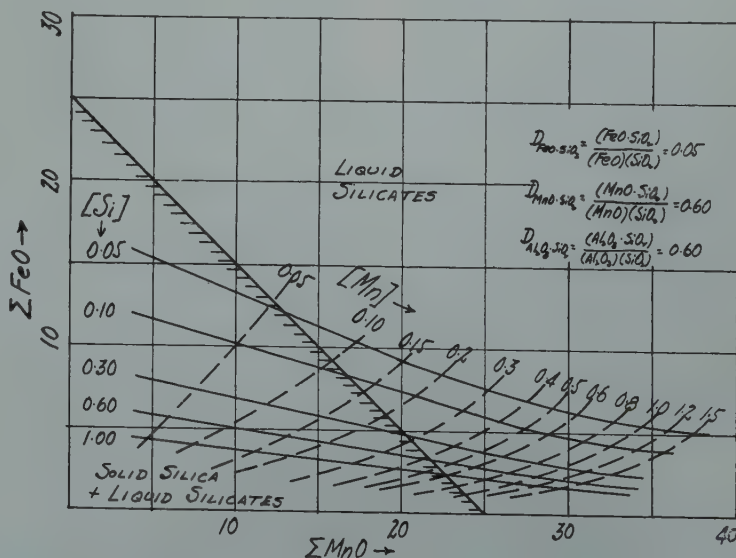


FIG 6—25 pct Al_2O_3 -FeO-MnO-SiO₂ slags 1550°C.

* See footnote on p. 23.

Table 10 . . . Composition of Slag Buttons from Surfaces of Ingots

| Heat | Analysis | | | | | | | Slag Analysis | | | | |
|------|-------------------------|------|------|------|------|------|------|------------------|--------------------------------|------|-------|--------------------------------|
| | C | Mn | Si | Cr | Ni | Mo | V | SiO ₂ | Al ₂ O ₃ | FeO | MnO | Cr ₂ O ₃ |
| 1 | 0.41 | 0.70 | 0.29 | 0.68 | 1.83 | 0.28 | | 36.5 | 27.1 | 3.8 | 33.7 | 0.79 |
| | Predicted slag (1550°C) | | | | | | | | | 3.5 | 27.5 | |
| | Predicted slag (1500°C) | | | | | | | | | 2.5 | 29.0 | |
| 2 | 0.35 | 0.55 | 0.21 | 0.70 | 1.31 | | | 33.9 | 32.9 | 3.9 | 31.2 | 0.80 |
| | Predicted slag (1550°C) | | | | | | | | | 4.0 | 27.0 | |
| | Predicted slag (1500°C) | | | | | | | | | 3.5 | 29.0 | |
| 3 | 0.89 | 1.72 | 0.27 | 0.11 | 0.05 | | | 30.8 | 25.6 | 6.01 | 40.51 | |
| | Predicted slag (1550°C) | | | | | | | | | 2.50 | 35.5 | |
| | Predicted slag (1500°C) | | | | | | | | | 2.0 | 37.5 | |
| 4 | 0.92 | 0.26 | 0.16 | 0.15 | | | | 40.6 | 27.7 | 8.2 | 28.1 | |
| | Predicted slag (1550°C) | | | | | | | | | 6.0 | 22.0 | |
| | Predicted slag (1500°C) | | | | | | | | | 4.5 | 23.5 | |
| 5 | 0.94 | 0.23 | 0.09 | 0.36 | 0.04 | | | 35.52 | 31.0 | 6.9 | 25.8 | 1.20 |
| | Predicted slag (1550°C) | | | | | | | | | 7.0 | 22.5 | |
| | Predicted slag (1500°C) | | | | | | | | | 5.5 | 24.0 | |
| 6 | 0.96 | 0.22 | 0.16 | 0.37 | 0.06 | | | 38.3 | 29.4 | 5.7 | 25.9 | 1.02 |
| | Predicted slag (1550°C) | | | | | | | | | 6.5 | 21.0 | |
| | Predicted slag (1500°C) | | | | | | | | | 5.0 | 23.0 | |
| 7 | 0.50 | 0.68 | 0.50 | 0.93 | 0.06 | | 0.21 | 43.2 | 23.9 | 4.2 | 25.5 | 2.88 |
| | Predicted slag (1550°C) | | | | | | | | | 3.0 | 26.5 | |
| | Predicted slag (1500°C) | | | | | | | | | 2.5 | 28.0 | |
| 8 | 0.20 | 1.38 | 0.22 | 0.09 | | | | 31.0 | 25.3 | 4.8 | 39.5 | |
| | Predicted slag (1550°C) | | | | | | | | | 3.5 | 34.0 | |
| | Predicted slag (1500°C) | | | | | | | | | 2.5 | 34.5 | |
| 9 | 0.38 | 0.70 | 0.17 | 0.75 | 1.87 | | | 29.0 | 34.5 | 5.4 | 32.9 | 0.74 |
| | Predicted slag (1550°C) | | | | | | | | | 4.5 | 29.0 | |
| | Predicted slag (1500°C) | | | | | | | | | 3.0 | 30.5 | |
| 10 | 0.15 | 0.36 | 0.33 | 1.08 | 1.70 | | | 44.6 | 18.0 | 5.36 | 26.8 | 4.0 |
| | Predicted slag (1550°C) | | | | | | | | | 4.00 | 22.0 | |
| | Predicted slag (1500°C) | | | | | | | | | 3.5 | 24.0 | |
| 11 | 0.17 | 0.46 | 0.24 | 0.12 | 1.85 | | | 37.8 | 28.6 | 4.4 | 28.9 | |
| | Predicted slag (1550°C) | | | | | | | | | 4.5 | 25.5 | |
| | Predicted slag (1500°C) | | | | | | | | | 3.5 | 27.5 | |
| 12 | 1.03 | 0.32 | 0.29 | 1.44 | 0.05 | | | 44.1 | 16.2 | 8.04 | 23.2 | 7.92 |
| | Predicted slag (1550°C) | | | | | | | | | 4.5 | 22.0 | |
| | Predicted slag (1500°C) | | | | | | | | | 3.5 | 24.0 | |
| 13 | 1.07 | 0.40 | 0.32 | 0.45 | 0.04 | | | 50.5 | 20.7 | 5.08 | 24.3 | 1.53 |
| | Predicted slag (1550°C) | | | | | | | | | 4.0 | 23.0 | |
| | Predicted slag (1500°C) | | | | | | | | | 3.0 | 25.0 | |
| 14 | 1.01 | 0.35 | 0.26 | 1.42 | | | | 42.9 | 22.2 | 6.2 | 24.6 | 5.36 |
| | Predicted slag (1550°C) | | | | | | | | | 5.0 | 23.5 | |
| | Predicted slag (1500°C) | | | | | | | | | 3.5 | 25.0 | |
| 15 | 0.095 | 0.37 | 0.30 | 1.56 | 3.54 | | | 42.6 | 19.4 | 5.2 | 25.70 | 4.67 |
| | Predicted slag (1550°C) | | | | | | | | | 4.0 | 22.5 | |
| | Predicted slag (1500°C) | | | | | | | | | 3.5 | 24.5 | |

manganese and silicon contents of the liquid steel in the ladle determine to a large measure the chemical nature of the interface between ladle brick and metal.

Summary and Conclusions

1. Data have been presented to show the effect of manganese and silicon contents of basic electric arc melted steel on the resulting cleanliness as measured by the magnaflux test or step down-rating for heats representative of SAE 6150, AMS 6260 and a 1 pct carbon, high manganese, high silicon roller bearing grade of steel. These data show that a high manganese content together with a low silicon content of the steel leads to more nonmetallic indications on step-down tests than are present when the manganese and silicon contents are substantially equal. This effect is quite clear on the three grades discussed here, and the effect was apparent when heats were made in succession by fairly rigid control procedures governing the deoxidation practice, refining slag practice, tapping temperatures and pouring times, and using the minimum of aluminum for grain size control. The data apply particularly to basic electric steels melted in 12-ton furnaces and ingot sizes of 10 to 15 in. square (1000 to 2000 lb ingot weight).

2. Experimental data have also been shown which indicate that the manga-

probably not reached in the glassy brick-metal interface but is approached to some degree before the glassy globules slough off and either rise to the surface of metal in the ladle or are trapped in the stream near the nozzle and carried into the ingot, the calculations are as good as can be expected.

The degree with which the composition of the slag buttons on the surface of ingots melted in the basic electric arc furnace can be calculated, leads to the conclusion that this slag is coming from the ladle and represents globules of the glassy interface between ladle brick and the liquid metal. These compositions were computed on the basis of equilibrium data obtained by allowing liquid steel to come to equilibrium with acid slags in silica crucibles. Thus, the reasonable agreement found between these calculated slags and the composition of the slag button shows that the

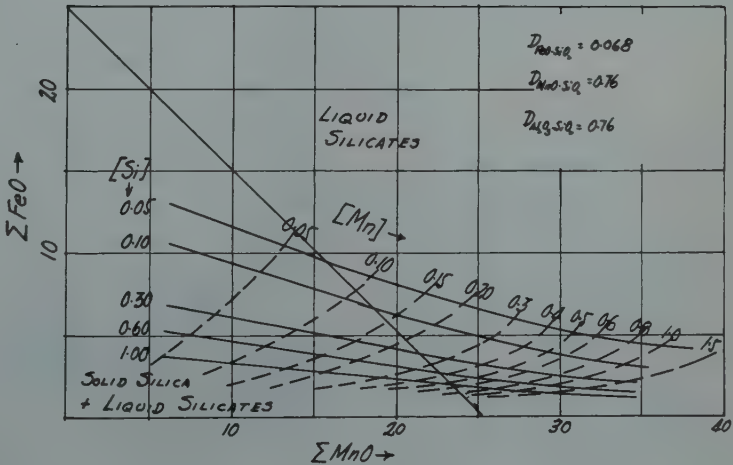


FIG 7—25 pct Al₂O₃-FeO-MnO-SiO₂ slags 1500°C.

nese and silicon contents of the liquid steel, as expressed by the manganese to silicon ratio, do in fact affect markedly the silica content of slag buttons collected from the sides of ingots. Qualitative microscopic data indicate that a large percentage of nonmetallics which cause magnaflux and step-down rejections have the same characteristics as these slag buttons and ladle wash.

3. Detailed calculations are summarized to show that an extension of equilibrium data obtained by Körber and Oelsen² in iron melts containing manganese and silicon under $\text{SiO}_2\text{-FeO-MnO-Al}_2\text{O}_3$ slags accounts reasonably well for the observed slag patch analyses obtained experimentally.

4. A detailed picture of the chemical influence of liquid steel on the physical characteristics of the metal-brick interface is presented in view of the above experimental data. We adopt the outlook that the majority of nonmetallics which are detected by means of macroscopic tests such as the magnaflux test or step-down ratings have their genesis at the interface between liquid steel and ladle brick, and the nozzle. When liquid steel is tapped from a basic electric arc furnace into a ladle lined with brick containing about 65 pct SiO_2 -30 pct Al_2O_3 -5 pct Fe_2O_3 , the brick is first softened or melted at the metal-brick interface. Chemical reactions then take place between the liquid steel and this interface so that its chemical composition approaches that of an equilibrium acid slag containing $\text{SiO}_2\text{-MnO-FeO}$ and Al_2O_3 . The chemical composition of this slag will have a marked influence on its viscosity and hence its ability to resist erosion. For silica contents near the saturation value for such slags, that is about 50 pct SiO_2 , coupled with low

MnO values, the slag will show a somewhat higher viscosity than would result if the silica content were lower than its saturation value. The data we have shown above in fact represent a study of the influence of the manganese and silicon content of liquid steel on the resulting silica content of this metal-brick interface, as reported by the slag buttons and slag patches from the sides of ingots.

As the steel flows through the nozzle of the ladle the inverse rain of acid slag globules coming from the metal-brick interface in the neighborhood of the nozzle are trapped in the steel and carried down into the ingot mold as the metal is being teemed. These nonmetallics are carried for a considerable distance below the surface of the metal as it rises in the molds, and are swept to the sides and upward as a result of the velocity gradients created in the liquid steel by the force of the stream. The metal is freezing from the sides of the mold inward, and a mushy zone of metal extends for a considerable distance into the body of the liquid steel because of the high rate of heat conduction at the mold wall. Thus these nonmetallics stand a good chance of being trapped in this zone of mushy metal as the ingot is being teemed. Cold metal and slow teeming together or separately will lead to more entrapment of these nonmetallic globules, other conditions remaining constant.

Thus, starting with attention focused on tapping temperatures, pouring times and several operating variables in the furnace, the electric furnace operator can take a large step in cleaning up nonmetallics in such steels by focusing attention on the manganese and silicon balance of the steel. The effect is considerable and can be accomplished easily provided chemical specifications will permit.

5. In view of the above effect of manganese and silicon on the cleanness of basic electric arc melted steel, and the importance of such cleanness in aircraft and specialized alloy steel uses, it is suggested that the engineering societies concerned with steel specifications review the silicon contents of these specifications. Such reviews should be directed toward enabling the steelmaker to balance the silicon content against the manganese content where possible, to take advantage of the effect of these two elements on the resulting cleanness of steel.

Acknowledgment

The authors gratefully acknowledge the cooperation of Mr. C. C. Wilson, Superintendent of Melting, the active assistance of Mr. D. G. Schoffstall in the chemical phases of this work, and the encouragement of Mr. J. H. Parker, Chairman of the Board, and Mr. B. H. DeLong, Vice President, The Carpenter Steel Co., without which this work would not have been possible.

References

1. A. McCance: *Jnl. Brit. Iron and Steel Inst.* (1918) 47, 1, 239-286.
2. F. Körber and W. Oelsen: *Mitt. Kaiser-wilhelm Inst. f. Eisenforschung*, 15, 271-309, Dusseldorf (1933); *Stahl u. Eisen*, (1934) 54, 297-298. F. Körber: *Ztsch. Elektrochemie* (1937) 43, 450-460.
3. J. White: Carnegie Scholarship Memoirs, *Brit. Iron and Steel Inst.* (1938) 27, 1-75.
4. C. H. Herty, Jr., J. E. Conley, and M. B. Roger: *Stahl u. Eisen*, (1931) 51, 1174.
5. C. H. Herty, Jr. and J. M. Gaines: *AIME TP 88*, (1928).
6. Krings and Schackmann: *Ztsch. f. Anorg. Chem.* (1932). 206, 337.

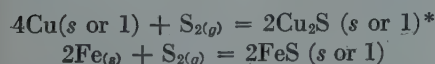
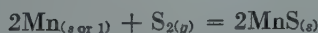


The Influence of Temperature on the Affinity of Sulphur for Copper, Manganese, and Iron

E. M. COX,* M. C. BACHELDER,* N. H. NACHTRIEB* and A. S. SKAPSKI*

As a result of using copper-containing scrap in the steelmaking process, the copper content of steels has been steadily increasing for years. Consequently the possible role copper may play in the steelmaking process and in the finished product begins to attract the metallurgists' attention. Some time ago one of the present authors forwarded the idea—based on the results of the analysis of nonmetallic inclusions extracted electrolytically from steels—that sulphur in plain carbon steels is distributed mainly between copper and manganese, the amount of iron sulphide being very small; and that, consequently, the problem of copper and that of sulphur in steel cannot be treated separately.¹

At the time of the publication of the quoted paper little was known about the relative affinities of copper and manganese for sulphur at high temperatures except that at moderate temperatures (below 1000°C) the affinity of manganese for sulphur is much greater. To gather more experimental data on this subject, the present authors undertook the investigation of the equilibrium constants of the reactions:



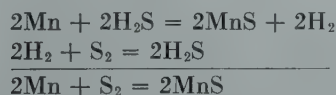
over a range of temperatures wide enough to establish the dependence of these equilibrium constants on temperature. From the equilibrium constants ($K = 1/P_{\text{S}_2}$) the free energy of formation (affinity) can be calculated

from

$$\Delta F^\circ = -RT \ln 1/P_{\text{S}_2} \quad [1]$$

where the standard conditions chosen are: 1 atm of sulphur pressure and the activities of condensed components equal one.

The decomposition pressure, P_{S_2} , of sulphur over the respective sulphides is too small to be measured directly, but there is a way of eliminating this difficulty by measuring the equilibrium constant of the reaction between the sulphide and hydrogen. From the latter and from the equilibrium constant of the thermal dissociation of H_2S we then calculate P_{S_2} for the respective sulphide.



The numerical values of the equilibrium constant of the thermal dissociation of H_2S at different temperatures were taken from Kelley's paper, "The Thermodynamic Properties of Sulfur and its Inorganic Compounds."²

In previous experimental work published by Jellinek and Zakowski³ and by Britzke and Kapustinsky⁴ the equilibrium constants of the reactions *Metal sulphide* + $\text{H}_2 = \text{H}_2\text{S}$ + *metal* were determined by passing hydrogen, at different rates of flow, over the sulphide, analyzing the resulting H_2S + H_2 mixture and then extrapolating the $\text{H}_2\text{S}/\text{H}_2$ ratio (which is a function of the rate of flow) to the zero speed of

flow, a method necessarily involving considerable uncertainty. In the present work the equilibrium ratio was actually measured instead of being extrapolated. The apparatus is shown in Fig 1.

Experimental Procedure

The sulphides were prepared by the following methods:

FeS

Powdered iron which had been reduced with hydrogen (ferrum reductum) was mixed in stoichiometric ratio with sublimed sulphur and carefully ground. The mixture was put into an alundum crucible, covered with pure sulphur, and the reaction started by touching the mixture with a glowing iron rod. After the reaction was completed the product (still containing some metallic iron) was again ground with sulphur, put into a Rose crucible, covered with sulphur, and heated in a strong current of pure hydrogen. Analysis of the final product showed 62.46 pct Fe and 36.59 pct S. Theoretical for FeS: 63.53 pct Fe and 36.47 pct S.

MnS

Manganese sulphide (precipitated and carefully washed with distilled water containing H_2S) was dried in a Rose crucible in an atmosphere of H_2S and heated in a current of hydrogen for 2 hr at red heat. The product was then ground and ignited for several hours at 1000°C in a current of hydrogen sulphide. Analysis showed 64.53 pct Mn and 36.63 pct S. Theoretical: 63.15 pct Mn and 36.85 pct S.

Some MnS samples were prepared from metallic manganese and sublimed sulphur by mixing and grinding them and then heating in a current of hydrogen sulphide in an alundum tube.

San Francisco Meeting, February, 1949.

TP 2505 C. Discussion of this paper (2 copies) may be sent to *Transactions* AIME before April 1, 1949. Manuscript received April 20, 1948; revision received Oct. 13, 1948.

* Institute for the Study of Metals, University of Chicago.

¹ References are at the end of the paper.

* Regardless of the form in which copper sulphide may be found in steel at low temperatures (be it Cu_2S or CuS), the high temperature reactions are concerned only with Cu_2S , CuS being unstable above the temperature of red heat.

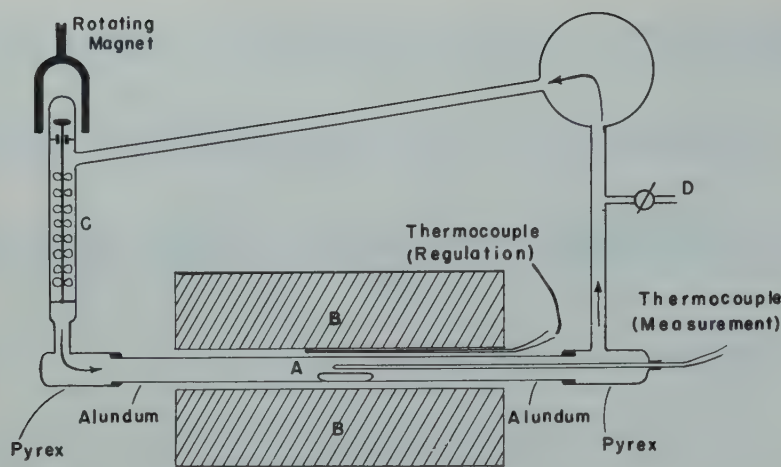


FIG 1—Diagram of apparatus.

No difference was noticed between the MnS samples obtained by the two methods, as far as the value of the equilibrium constants was concerned.

Cu₂S

Reagent grade CuCl₂ was dissolved in hydrochloric acid solution and treated with hydrogen sulphide. The precipitate of cupric sulphide was washed with glacial acetic acid and dried at 110°C. It was then placed in a Rose crucible and heated in a stream of hydrogen at 600°C for 30 min. Analysis showed 79.78 pct Cu and 19.68 pct S. Theoretical for Cu₂S: 79.86 pct Cu and 20.14 pct S.

The alundum boat A containing a few grams of powdered sulphide (or a mixture of sulphide and the respective metal) was placed in a vacuum-tight tube (quartz, mullite, or Norton Co. RA1164 alundum) about 36 in. long and about 1 in. id, which was mounted inside the furnace B; the region of uniform temperature inside the tube was found to exceed the length of the boat by a few inches on each side. The rest of the system was of pyrex glass and was connected to the ends of the furnace tube by means of Apiezon, in the case of the alundum tube. When the quartz furnace tube was employed the connections were by means of graded quartz-to-pyrex seals. When the mullite tube was used, uranium glass was the intermediate in the mullite-to-pyrex seal. The Apiezon connections used for the alundum tube were always kept cool,

if necessary by blowing a current of air on them. After the system had been evacuated and checked for tightness, carefully purified hydrogen (tank hydrogen passed through 1:1 KOH, concentrated KMnO₄, Pd-asbestos at 500°C, and P₂O₅) was admitted up to atmospheric pressure and the system evacuated again, the operation being repeated three times to insure the removal of any traces of oxygen which might have remained in the system after evacuation. The temperature was then set at the desired level and kept constant by means of a Micromax controller. The thermocouple connected with the Micromax was placed *outside* of the reaction tube while the thermocouple measuring the temperature of the reaction was placed *inside* the tube directly over the boat containing the sample. This arrangement assured a considerable constancy of the temperature inside of the tube, where the variations did not exceed $\pm 1^\circ\text{C}$. The hydrogen was circulated over the sample and through the system (the total volume of which was about two liters) by means of a magnetically operated glass propeller C.

Samples of the gas were taken from time to time through the stopcock D with an evacuated 20 ml or 50 ml burette, and the H₂S present absorbed in 2 pct zinc acetate solution. The volume of the remaining hydrogen was measured, temperature and barometric pressure noted and the volume reduced to standard conditions.

The hydrogen sulphide was determined iodimetrically. Either micro-

burettes or 50 ml burettes were used. In the case of the microburettes, the samples were made up to 100 ml with 2 pct zinc acetate solution. An aliquot was acidified with 1.0 ml of glacial acetic acid, titrated with an excess of 0.002 N iodine and back-titrated with 0.002 N thiosulphate. The 50 ml burettes were used when the hydrogen sulphide content of the sample had to be determined as a whole in one analysis. The procedure was the same with the exception of making up to the volume. In either case, the 0.002 N solutions were prepared daily from stock solutions of 0.1N iodine and 0.1 N sodium thiosulphate, and the sodium thiosulphate was standardized with the 0.002 N iodine. The range of hydrogen sulphide content in samples was from 0.015 mg per 100 ml to 1.255 mg per 100 ml. The mean precision was ± 3 pct.

The equilibrium was approached from both sides (excess of H₂ and excess of H₂S). The excess of H₂S was obtained in the following way. The equilibrium ratio H₂S/H₂ increases with temperature; therefore, to raise the concentration of H₂S the sulphide was heated in H₂ up to a temperature higher by a hundred or more degrees than the temperature of the intended measurement and, after the equilibrium had been reached, the temperature was lowered as quickly as possible to the intended level.

Fig 2 gives an example of approaching the equilibrium at 900°C from both sides.

The equilibrium with FeS and Cu₂S was usually reached in less than 24 hr. With MnS, however, four to six days were required to obtain equilibrium and, contrary to the behavior of the other two sulphides, high temperature did not reduce the time needed for the equilibrium to be established. In some runs at temperatures over the melting point of Mn, the sulphide sample was examined after the reaction; its grains were covered with a compact layer of metallic manganese. This layer probably contributed to the difficulty of free diffusion of H₂ and H₂S and to the slowness of the reaction at high temperatures.

The reliability of the results would be expected to depend greatly on the suppression of side reactions, especially between the gas mixture and the refractory furnace tube. This was checked by using different tubes (quartz, mullite, and alundum) at temperatures below 1200°C. No notice-

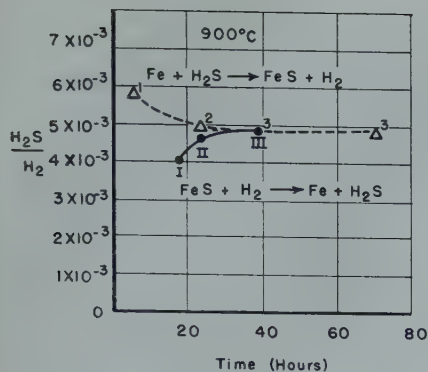


FIG 2—Approach to equilibrium H_2S/H_2 ratio for FeS at $900^\circ C$.

able influence of the kind of refractory material used (or of the presence or absence of Apiezon) on the values of the equilibrium ratio H_2S/H_2 was observed. Quartz tubes, however, crystallized and developed leaks. Even the high quality alundum tubes lost their impermeability to gases, especially at temperatures above $1200^\circ C$, and many runs had to be discarded because of the diffusion of air into the reaction tube. It is known that the presence of H_2S facilitates the reduction of SiO_2 .⁵ The siliceous binding material of the alundum or the silica itself, in the case of quartz, is apparently attacked by this means. Mullite tubes, although they contain silica, withstood the severe conditions to a much better extent than either quartz or alundum, and were used for most of the runs.

Experimental Runs

Table 1 gives a comparison of the $\log H_2S/H_2$ equilibrium values for the reaction $FeS + H_2 = Fe + H_2S$ found by Jellinek and Zakowski, Britzke and Kapustinsky, and in the present investigation. The column "Calc. Kelley" contains Kelley's data, computed from the thermodynamic properties and regarded as quite reliable. It may be seen from Table I that our figures are much closer to those calculated by Kelley than are those of the other authors; the latter, in addition, are in considerable disagreement with one another.

Tables 2, 3 and 4 contain all experimental data for FeS, MnS, and Cu_2S , needed for the calculation of the equilibrium pressure of sulphur over the respective sulphides and of the free energy of formation of these sulphides.

In Fig 3, the values of the logarithm of the equilibrium S_2 — pressure over the sulphides is plotted against $1/T$. The points, though scattered a little, can be represented by straight lines, the slopes of which give the heats of formation of the respective sulphides if we regard this heat of formation (in the first approximation) as independent of the temperature:

$$\log_{10} P_{S_2} = \frac{\Delta H}{2.30RT} + C \quad [2]$$

To avoid any arbitrariness (due to the scattering of the points) in drawing the lines, the most probable straight lines representing the respective sets of points have been calculated, assuming that the error in $1/T$ was much smaller than the error in $\log P_{S_2}$.

For FeS the measurements were taken up to the melting point of the sulphide. Above this point the activity of the condensed components should be taken into account; this requires the knowledge of the actual composition of the liquid phase at the temperature of the measurement. However, as the study of the reaction with FeS was taken up mainly for the sake of comparison of our data with those of other investigators and for the sake of checking the precision which could be obtained, we did not attempt, for the present, to undertake these measurements.

With MnS the case is different. There is no appreciable solubility of

Table 1 . . . Comparison of the $\log H_2S/H_2$ Equilibrium Values

| T (°K) | $\log k$ (exper.) | Source | $\log K$ (our data) | $\log K$ "Calc. Kelley" |
|-------------|----------------------|--------|------------------------|-------------------------------|
| 996 | -2.10 | * | -2.97 | -3.08 |
| 1003 | -2.50 | † | -2.93 | -3.05 |
| 1073 | -1.92 | * | -2.70 | -2.85 |
| 1170 | -1.73 | * | -2.38 | -2.61 |
| 1183 | -2.15 | † | -2.35 | -2.58 |
| 1267 | -1.43 | * | -2.11 | -2.40 |

* Britzke and Kapustinsky,⁴
† Jellinek and Zakowski.³

MnS in liquid manganese and therefore the activity of both MnS and Mn remains equal to unity above, as well as below, the melting point of manganese. The scattering of our points is too great to reveal, in a definite way, the effect of phase transitions on the slope of the $\log P_{S_2}$ vs. $1/T$ line. Therefore all points (up to $1583^\circ K$) were used in the calculation of the most probable straight line representing them.

The case of Cu_2S is, fortunately, simplified by the fact that, although we have two phases (Cu_2S —rich, and Cu—rich phase) in the liquid state, the mutual solubilities of the components are not very different, and change with the temperature in a roughly similar way. Thus the lowering of the activity of Cu is approximately compensated by the lowering of the activity of Cu_2S and consequently all the points within the whole range of temperatures in question lie on the same straight line.

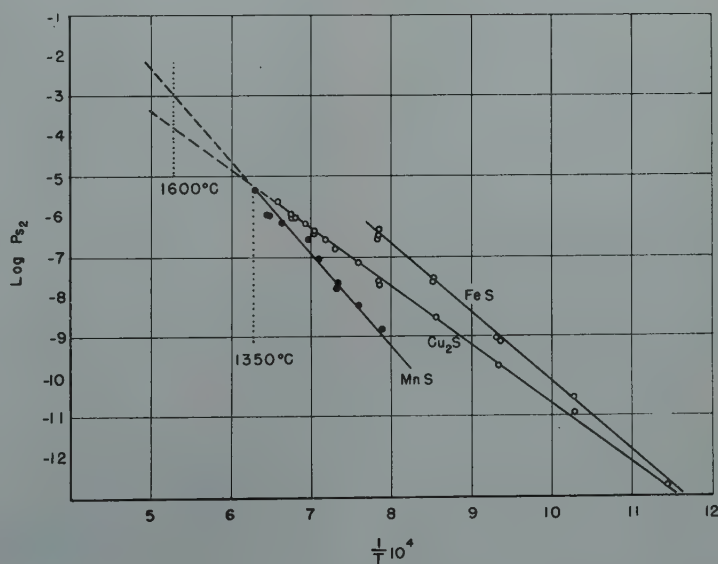


FIG 3—Variation of $\log P_{S_2}$ with $1/T$ for MnS, FeS, and Cu_2S .

Table 2 . . . Free Energy of Formation of FeS

| T (°K) | $\frac{1}{T} \times 10^4$ | FeS + H ₂ = Fe + H ₂ S | | 2H ₂ + S ₂ = 2H ₂ S | 2Fe + S ₂ = 2FeS | |
|-----------|---------------------------|--|----------------------------|---|--------------------------------|---|
| | | $\frac{[H_2S]}{[H_2]}$ | Log $\frac{[H_2S]}{[H_2]}$ | Log $\frac{[H_2S]^2}{[H_2]^2[S_2]}$ | Log P _{S₂} | Free Energy of Formation of FeS (cal per mol S ₂). |
| 770 | 12.986 | 4.60×10^{-6} | -4.337 | 7.127 | -15.801 | -55,670 |
| 873 | 11.455 | 2.98×10^{-4} | -3.526 | 5.690 | -12.742 | -50,890 |
| 973 | 10.277 | 1.02×10^{-3} | -2.992 | 4.582 | -10.566 | -47,040 |
| 1068 | 9.363 | 1.97×10^{-3} | -2.706 | 3.720 | -9.132 | -44,620 |
| 1073 | 9.320 | 2.08×10^{-3} | -2.682 | 3.675 | -9.039 | -44,370 |
| 1173 | 8.525 | 4.80×10^{-3} | -2.319 | 2.920 | -7.558 | -40,560 |
| 1174 | 8.518 | 4.15×10^{-3} | -2.382 | 2.910 | -7.674 | -41,220 |
| 1273 | 7.855 | 9.20×10^{-3} | -2.036 | 2.285 | -6.357 | -37,030 |
| 1275 | 7.843 | 7.02×10^{-3} | -2.154 | 2.270 | -6.578 | -38,370 |
| 1275 | 7.843 | 7.25×10^{-3} | -2.140 | 2.270 | -6.550 | -38,210 |

* All values for log $\frac{[H_2S]^2}{[H_2]^2[S_2]}$ are taken (interpolated) from Kelley's "The Thermodynamic Properties of Sulfur and its Inorganic Compounds."

Discussion of Results

From Fig 3 we see that the intersection of the Cu₂S-line with the MnS-line occurs at 1350°C. At this temperature both MnS and Cu₂S show the same decomposition pressure of sulphur or—what amounts to the same—both Mn and Cu have the same affinity for sulphur (their free energies of formation, $\Delta F^\circ = -RT \ln 1/P_{S_2}$, are the same), provided the activities of the condensed phases are the same. Above 1350°C the decomposition pressure of sulphur over MnS is greater, that is, the affinity of Mn for sulphur is smaller (*ceteris paribus*) than the affinity of copper for sulphur.

The log P_{S₂} vs. 1/T lines in Fig 3 can be expressed by the following equations:

for FeS

$$\text{Log } P_{S_2} = -\frac{17,810}{T} + 7.540 \quad [3]$$

for Cu₂S

$$\text{Log } P_{S_2} = -\frac{14,360}{T} + 3.721 \quad [4]$$

for MnS

$$\text{Log } P_{S_2} = -\frac{21,350}{T} + 8.029 \quad [5]$$

Because these equations refer to the reaction between gaseous sulphur and the condensed metal, the heats of reaction between gaseous sulphur and metal (referred to 1 mol S₂-gas) can be directly calculated from them. We then obtain:

for FeS $\Delta H = -81,990$ cal

for Cu₂S $\Delta H = -65,700$ cal

for MnS $\Delta H = -97,860$ cal

Regarding, in first approximation, these heats as independent of temperature we can subtract the heat of evaporation of rhombic sulphur and calculate the heats of reaction between

the respective metal and rhombic sulphur, referred to 1 mol of the sulphide. Taking for the heat of sublimation of rhombic sulphur 31,360 cal (from Kelley's paper quoted above) we obtain the following values:

for FeS $\Delta H = -25,060$ cal

for Cu₂S $\Delta H = -17,170$ cal

for MnS $\Delta H = -33,160$ cal

The figures thus found for FeS and Cu₂S are in reasonable agreement with the heats of formation experimentally

measured which range from -18,000 cal per mol to -24,000 cal per mol for FeS, and from -18,260 cal per mol to -18,970 cal per mol for Cu₂S. The experimentally found heat of formation of MnS is much more uncertain, the values ranging from -44,390 cal per mol to -62,900 cal per mol. From the aqueous solubility data of MnS⁶ a value of ca. -50,000 cal per mol may be calculated. One single point measured for the equilibrium of the reaction MnS + H₂ = Mn + H₂S by Jellinek and Zakowski⁵ allowed Kelley to calculate the ΔH of formation for MnS as ca. -35,000 cal per mol. The latter value is the nearest to that obtained by us. On the other hand, the error in the experimentally determined heat would work in the direction of higher values because even a slight oxidation would cause a relatively high heat effect. Therefore lower values seem to be more probable. On the whole, one has to remember that the thermodynamical data for the formation of MnS are still far from being settled.²

In Fig 4 the free energies of dissociation of the sulphides per mol of S₂

Table 3 . . . Free Energy of Formation of Cu₂S

| T (°K) | $\frac{1}{T} \times 10^4$ | 2Cu ₂ S + 2H ₂ = 4Cu + 2H ₂ S | | 2H ₂ + S ₂ = 2H ₂ S | 4Cu + S ₂ = 2Cu ₂ S | |
|-----------|---------------------------|---|----------------------------|---|---|--|
| | | $\frac{[H_2S]}{[H_2]}$ | Log $\frac{[H_2S]}{[H_2]}$ | Log $\frac{[H_2S]^2}{[H_2]^2[S_2]}$ | Log P _{S₂} | Free Energy of Formation of Cu ₂ S (cal per mol S ₂) |
| 972 | 10.288 | 6.93×10^{-4} | -3.159 | 4.600 | -10.918 | -48,500 |
| 1069 | 9.354 | 9.55×10^{-4} | -3.020 | 3.700 | -9.740 | -47,600 |
| 1071 | 9.337 | 9.25×10^{-4} | -3.034 | 3.690 | -9.758 | -47,780 |
| 1168 | 8.562 | 1.58×10^{-3} | -2.800 | 2.940 | -8.540 | -45,580 |
| 1273 | 7.855 | 1.92×10^{-3} | -2.717 | 2.285 | -7.719 | -44,920 |
| 1317 | 7.593 | 2.07×10^{-3} | -2.684 | 2.285 | -7.653 | -44,420 |
| 1369 | 7.305 | 2.76×10^{-3} | -2.559 | 2.048 | -7.166 | -43,140 |
| 1393 | 7.179 | 3.03×10^{-3} | -2.519 | 1.780 | -6.818 | -42,660 |
| 1418 | 7.052 | 3.43×10^{-3} | -2.465 | 1.658 | -6.588 | -41,940 |
| 1421 | 7.037 | 3.90×10^{-3} | -2.409 | 1.535 | -6.353 | -41,180 |
| 1440 | 6.945 | 4.24×10^{-3} | -2.441 | 1.524 | -6.406 | -41,670 |
| 1469 | 6.807 | 4.18×10^{-3} | -2.379 | 1.432 | -6.178 | -40,660 |
| 1477 | 6.771 | 4.53×10^{-3} | -2.344 | 1.290 | -6.048 | -40,600 |
| 1477 | 6.771 | 4.09×10^{-3} | -2.388 | 1.260 | -5.948 | -40,140 |
| 1519 | 6.583 | 5.15×10^{-3} | -2.288 | 1.070 | -6.037 | -40,760 |
| | | | | | -5.646 | -39,220 |

Table 4 . . . Free Energy of Formation of MnS

| T (°K) | $\frac{1}{T} \times 10^4$ | 2MnS + 2H ₂ = 2Mn + 2H ₂ S | | 2H ₂ + S ₂ = 2H ₂ S | 2Mn + S ₂ = 2MnS | |
|-----------|---------------------------|---|----------------------------|---|--------------------------------|--|
| | | $\frac{[H_2S]}{[H_2]}$ | Log $\frac{[H_2S]}{[H_2]}$ | Log $\frac{[H_2S]^2}{[H_2]^2[S_2]}$ | Log P _{S₂} | Free Energy of Formation of MnS (cal per mol S ₂) |
| 1267 | 7.893 | 5.68×10^{-4} | -3.246 | 2.320 | -8.812 | -51,050 |
| 1317 | 7.593 | 8.17×10^{-4} | -3.088 | 2.048 | -8.225 | -49,520 |
| 1361 | 7.348 | 1.19×10^{-3} | -2.923 | 1.820 | -7.666 | -47,710 |
| 1364 | 7.351 | 9.95×10^{-4} | -3.002 | 1.803 | -7.808 | -48,690 |
| 1407 | 7.107 | 1.81×10^{-3} | -2.742 | 1.590 | -7.073 | -45,500 |
| 1460 | 6.993 | 2.80×10^{-3} | -2.553 | 1.480 | -6.586 | -43,960 |
| 1500 | 6.662 | 3.08×10^{-3} | -2.511 | 1.145 | -6.167 | -42,300 |
| 1539 | 6.498 | 3.17×10^{-3} | -2.499 | 0.980 | -5.978 | -42,060 |
| 1547 | 6.464 | 3.06×10^{-3} | -2.514 | 0.946 | -5.973 | -41,860 |
| 1583 | 6.317 | 5.40×10^{-3} | -2.268 | 0.788 | -5.324 | -38,530 |

Some runs were repeated at the same temperature and from the tables above the precision of the measurements may be figured out.

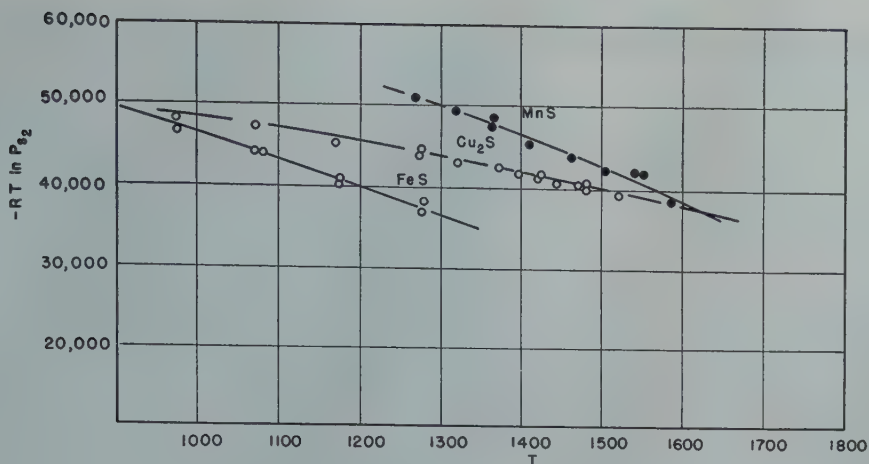


FIG 4—Variation of $-RT \ln P_{S_2}$ with T for MnS, FeS, and Cu_2S .

($\Delta F^\circ = -RT \ln P_{S_2}$) have been plotted against T . The slope of the curves

$$\frac{-\partial \Delta F}{\partial T} = \Delta S$$

represents the entropy

value, which is negative for the formation of the sulphides. The scattering of the points is too great, however, to make its calculation worth while. At any rate, it is evident from these curves and from the fundamental relationship

$$\Delta F = \Delta H - T\Delta S$$

that the entropy term ΔS for the decomposition reaction $2MnS = 2Mn + S_2$ has a larger positive value than for the reaction $2Cu_2S = 4Cu + S_2$, and is responsible for the relatively lower value of the free energy of the first reaction at high temperatures.

The results of the present investigation lead to the following practical conclusions concerning the connection between the amount of copper in the open-hearth furnace scrap and the sulphur content of the bath. Because of the relatively high affinity of copper for sulphur at high temperatures, metallic copper present in the scrap may be expected to pick up sulphur from the heating gases by binding it

into Cu_2S ; thus the sulphur content of the bath would increase with the copper content of the scrap and consequently the desulphurization process would be hampered.

The question remains whether the copper sulphide thus formed is preserved as such in the bath and furthermore, whether it still exists in the ingot after solidification. Though the authors are inclined—on the basis of other experiments—to believe that a comparatively large percent of total sulphur exists in finished steel as copper sulphide, they do not think that the present experimental results can be regarded as supporting directly this point of view. Until the equilibrium diagram Cu-Mn-Fe-S and the influence of other components on its shape have been investigated, no further conclusions can be drawn save that the free energy relations of FeS, MnS and Cu_2S in pure systems give a necessary (though not sufficient) support to the possibility of existence of large amounts of copper sulphide in finished steel.

Summary

The equilibrium constants of the reactions of FeS, MnS, and Cu_2S with H_2 were measured within a range of

temperature wide enough to establish the dependence of these equilibrium constants on temperature. The equilibrium pressures of S_2 over the respective sulphides and the free energy of formation of the sulphides were calculated therefrom.

The affinity of sulphur for copper (as measured by the free energy of formation of the sulphide) is considerably greater than that for iron and begins to exceed that for manganese at temperatures above $1350^\circ C$. It is concluded therefrom that metallic copper which is present in the scrap is to be expected to pick up sulphur from the open hearth furnace gases and thus raise the sulphur content of the bath.

References

1. A. Skapski, A. Kotlinski, W. Goslawski: *Ann. Acad. Sci. Techn., Varsovie*, VI, 23, (1939).
2. K. K. Kelley: *The Thermodynamic Properties of Sulfur and its Inorganic Compounds*. U. S. Bur. of Mines, *Bull.* 406, (1937).
3. K. Jellinek and J. Zakowski: *Ztsch. anorgan. Chem.*, 142, 1, (1925).
4. E. V. Britzke, A. F. Kapustinsky: *Ztsch. anorgan. Chem.* 194, 323, (1930).
5. J. White, H. Skelly: *Jnl. Iron and Steel Inst.*, CLV, No. 2, (1947).
6. I. M. Kolthoff: *Jnl. Phys. Chem.*, 35, 2711, (1931).



Plastic Deformation Waves in Aluminum*

ANDREW W. McREYNOLDS†

Introduction

ONE characteristic of plastic deformation which distinguishes it from elastic strain is the essential inhomogeneity of plastic strains. Elastic strain varies continuously through a material, and average relative displacements of initially adjacent atoms are only small fractions of their initial spacing, (strains of the order of 0.01 or less). On the other hand, plastic flow corresponds to the appearance of discontinuities in strain of the lattice, such as dislocations or slip bands, where local strain, on an atomic scale, is several orders of magnitude higher. These discontinuities are visible on a microscopic scale as the familiar slip lines (Fig 1). In spite of this obvious microscopic inhomogeneity, however, macroscopic measurements almost invariably show a smooth curve of stress vs. strain (Fig 2b) even if measurements of linear strains be made to an accuracy of one part in 10^7 .

This macroscopic homogeneity of strain indicates that the discontinuities in strain on slip planes occur in increments too small or too slow to be recorded individually, and further that they occur sufficiently independent of one another so that the small increments add at random to a smooth stress-strain curve. The present paper describes observations of plastic strain in aluminum of commercial purity and in high purity Al-Cu alloys, where there exists a strong coupling between slip in various regions of the specimen such that once initiated it spreads rapidly through a large volume. The total effect is that of relatively large, rapid, and regularly spaced steps of strain followed by periods of only elastic strain. Fig 2a illustrates the type of "stair-step" stress-strain curve which results. The properties of this cooperative slip phenomenon will be described further in the section on results; in par-

ticular it will be shown that each step corresponds to the propagation of a wave of plastic deformation through the specimen. Some interpretations of the mechanism by which it occurs will be made in the following section.

Although the type of plastic wave phenomena to be described has not previously been reported, there are numerous cases of related effects in the plastic yielding of metals:

YIELD POINT PHENOMENA

The most familiar of such effects is the "yield point" observed in low carbon steels, brass, duraluminum, and the like. It consists in the sudden termination of the elastic portion of the stress-strain curve by a large plastic strain. Since the usual tensile machine is such that yielding of the specimen relieves the load, the resulting curve is as shown in Fig 3. As the strain continues, deformation occurs at a lower stress for some time, then follows a rising curve, but with no further sudden yielding. This effect has been observed in brass by Sachs and Shoji¹ and later by many others. Edwards, Phillips and Jones² made extensive studies of the effect in steel, and of the role of various alloying elements.

Although there seems to be fairly clear evidence that the yield point is caused by a hardening of the material by precipitation of impurities, no satisfactory explanation for the sudden yielding has been given. Winlock and Leiter³ have shown that the stress level of the upper yield point depends strongly on the rate of loading, the yield point increasing by almost a fac-

tor of two as the strain rate goes from 0.002 in. per in. per min. to 4.4 in. per in. per min. This effect would seem to imply an incubation period before yielding is initiated at a certain stress. On the other hand, by going to very slow loading rates, Edwards, Phillips and Jones² showed that the yield point does not become lower and eventually disappear as might be expected, but, on the contrary, begins to rise at loading rates below about 25 lb per in. per min. becoming much higher than at rapid loading rates.

STRAIN AGING

If, instead of continuing straining of a specimen after occurrence of a yield point, the load is removed and the specimen aged, resumption of the test results in occurrence of another yield point as shown by the dotted curve of Fig 3. The new yield stress is generally higher than the previous maximum applied stress. This hardening of the material by straining and subsequent aging is undoubtedly related to quench age-hardening resulting from the aging of a specimen quenched from high temperature. Since neither effect is observed in pure metals, it is generally accepted that quench-aging in all cases is the result of hardening by precipitation of a supersaturated alloying element, and that strain-aging is probably a similar precipitation, accelerated by disruptions of the lattice by previous strain. Pfeil⁴ has shown that strain-aging does not occur in iron from which all of the carbon has been removed, but that only a very small carbon content, around 0.003 pct, is necessary to cause strain-aging. In accord with this observation is recent work by Dijkstra⁵ in this laboratory showing that the solubility limit of carbon in iron is extremely low, less than 0.001 pct at 400°C. Edwards, Phillips and Jones² have shown that the strain-aging effect is also removed by the addition of small quantities of elements such as Mo, Mn, Ti, and the like, which readily form carbides. Their results demonstrate the

San Francisco Meeting, February, 1949.

TP 2499 E. Discussion of this paper (2 copies) may be sent to *Transactions AIME* before April 1, 1949. Manuscript received Sept. 7, 1948.

* This research has been supported by ONR (Contract No. N-6ori-20-IV)

† Research Associate in Physics, Institute for the Study of Metals, University of Chicago.

¹ References are at the end of the paper.

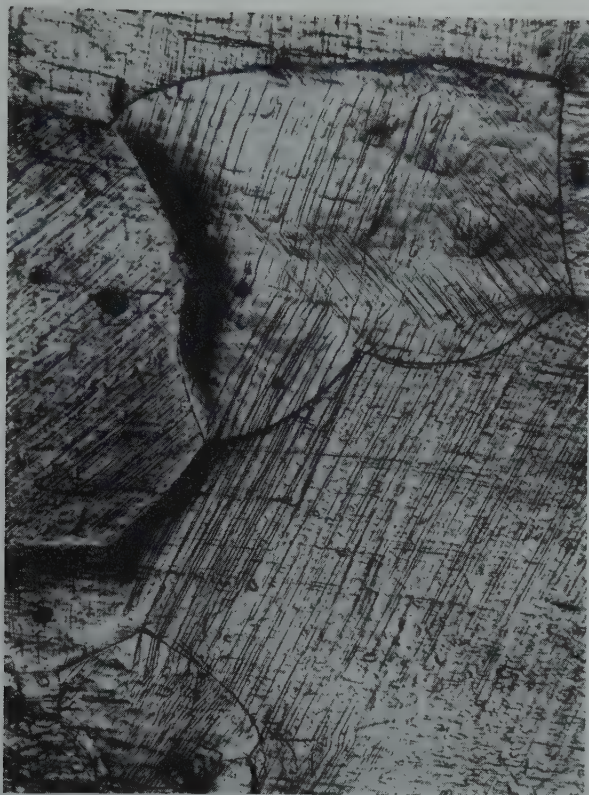


FIG 1—Slip lines in Al-0.5 pct Cu alloy after occurrence of several steps in stress strain curve. Surface electrolytically polished with 2:1 nitric acid methyl alcohol solution prior to straining. Reduced approx. one half in reproduction.

close relation between the yield point phenomena and strain-aging, since both of these effects are destroyed in the same way by addition of carbide forming elements. Their conclusion is that all of the carbon is bound in insoluble carbides and therefore not available for precipitation hardening. Kuroda⁶ has suggested that the yield point is caused by concentration of the carbon around the grain boundaries, forming a hard cementite sheath around each grain. When, at the yield point, this sheath breaks down, the stress during further yielding depends only on the ferrite interiors of the grains and is consequently lower (the lower yield point). It appears at present, however, that the yield point and strain-aging effects can be attributed to precipitation of carbon, but that the detailed mechanism of the precipitation hardening is still uncertain.

SERRATED STRESS-STRAIN CURVES

It has been observed that under some conditions the initial plastic portion of the stress-strain curve exhibits no yield point effect, but that after a small

plastic strain, a series of sudden yields occurs in rapid succession, resulting in a curve as indicated in Fig 4. This type of behavior has been reported in mild steel from 80–250°C by A. Le Chatelier,⁷ in mild steel at 250° by Körber and Pomp,⁸ and in duraluminum (Al-4.8 pct Cu) at room temperatures by Portevin and Le Chatelier.⁹ More recently Sutoki¹⁰ reported similar observations of serrated curves for steels up to 0.9 pct carbon at temperatures of 150°C and higher, duralumin at 20–100°C, 70/30 brass at 450°, and nickel at 300°. In all of these cases, however, strain was either at a relatively rapid rate, so that the observations were complicated by inertial effects and oscillations of the testing machine, or in a machine such that sudden yielding necessarily decreased the stress.

It is to be noted that the serrated curves occur in the same materials which exhibit yield point and strain-aging effects, but that the temperature ranges for the phenomena may differ. In iron, for example, the serrations occur only in an elevated temperature range, around 200°, whereas the yield point occurs at least as low as 20°. Edwards, Phillips, and Liu¹⁰ therefore

expected a yield point in duraluminum at subatmospheric temperatures, since serrations are exhibited at temperatures around 20°. Their tests showed no such yield point, although Sutoki's¹⁰ results show one case of a yield point at room temperature in a quenched and tempered duralumin sample.

LÜDERS' LINES

Lüders¹² reported in 1860 the appearance of large scale markings on the surface of strained mild steel sheet. These markings were later studied systematically by Hartmann¹³ and are well known as "Lüders' lines," stretcher strains, or Hartmann or Piobert lines, but are still only incompletely understood. In cylindrical or strip tensile specimens the "lines" appear as broad bands extending completely across the specimen, at angles of around 50° to the axis of tension, and are visible because the greater plastic deformation within the band causes a depression or change in orientation of the surface. The direction of the bands is determined by the geometry of the specimen and the applied stress, and a band may extend across a number of grains, independent of their orientation.

In mild steel specimens, as the yield point is reached, Lüders lines (or bands) appear on the surface and spread throughout the specimen as the yield point elongation takes place. As described by Fell,¹⁴ the spreading takes place at nearly constant stress, corresponding to the horizontal portion of Fig 3, following the yield point, and further strain within the band begins only after the surface markings have spread over the entire surface, at which time the stress-strain curve resumes an upward trend by strain hardening. The surface markings persist, however, presumably because of differences in the amount of yield point elongation in different bands.

Similar effects have been observed in duraluminum by Hartmann¹³ and more recently by Fell.¹⁵ Fell shows no photographs of markings in aluminum but describes them as a number of parallel bands (more regular than Lüders' lines in steel) inclined at about 60° to the specimen and tension axis and extending across the strip specimen. A photograph of such bands in 24 ST sheet is given by Stang, Greenspan, and Newman¹⁶ (their Fig 1). Fell also observed that a number of successive yields occurred with increasing stress and in each case an inclined

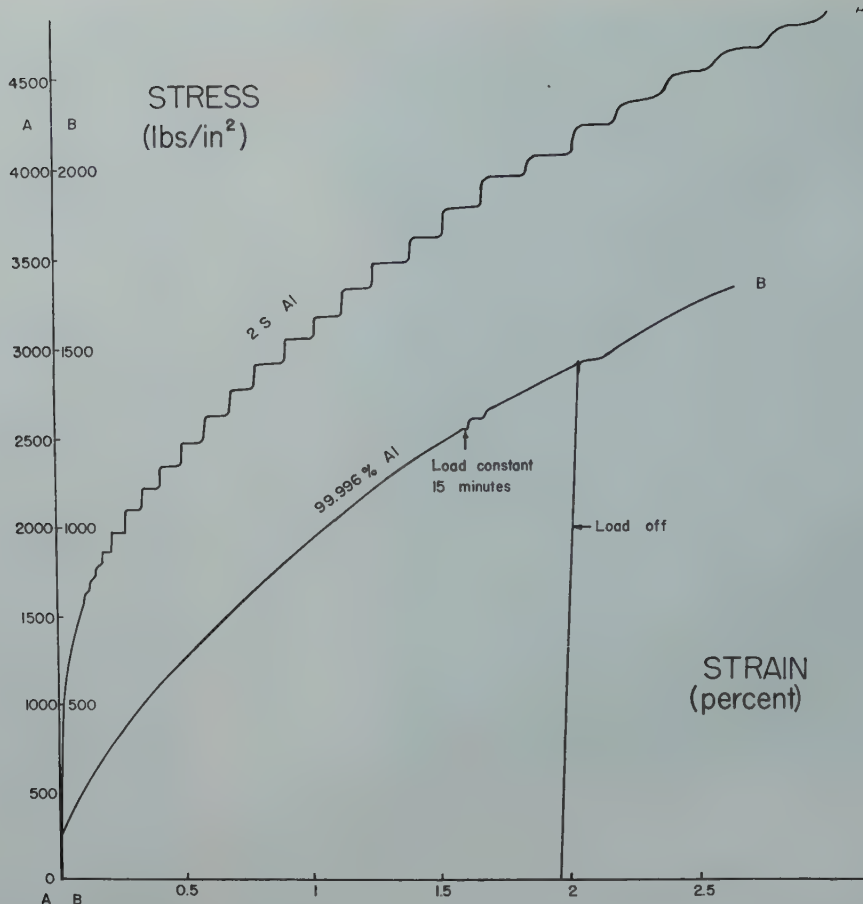


FIG 2—Curves for 0.500-in. diam cylindrical specimens loaded continuously at constant rate of 120 psi per min.

- (A) Typical step curve for 2S-Aluminum—measured over $\frac{3}{4}$ in. of gauge length.
 (B) Smooth curve for pure aluminum under same test conditions. Both removal of load and holding load constant cause slight yield point elongation.

straight line on the surface propagated from one end of the specimen to the other at velocity around 20 cm per sec. Each such yield represented only 0.5–1 pct strain, whereas in steel the yield point elongation is of the order of 5 pct. Portevin and Le Chatelier⁹ also reported that the serrated stress strain curves described above were characterized by the appearance of Lüders' lines on the surface and that each oscillation of stress was accompanied by propagation of the markings along the specimen with an audible "little dry noise."

REPEATED YIELDING

A number of cases of repeated yielding have been observed both at constant load and with increasing load.

Becker and Orowan¹⁷ found that zinc single crystals held at approximately constant stress in a Polanyi machine exhibited sharp steps of from 10^{-5} to 10^{-3} strain at irregular intervals, and

that a temperature increase of 10–20°C resulted in a great increase of frequency. Schmid and Valouch¹⁸ made similar observations. Measurements of creep rate at constant stress in high purity zinc by Tyndall and Wert¹⁹ showed alternate periods of very rapid and slow creep. Andrade²⁰ reported sudden yields at regular intervals in "approximately pure" copper under constant stress.

Classen-Nekludowa²¹ applied increasing shear loads to specimens of NaCl, brass, and aluminum, and found that yielding occurred in very regularly spaced and sharp steps, resulting in a stair-step type stress strain curve. It was found, however, that these steps occurred only in an elevated and limited temperature range, 230–500°C for NaCl, 410–550°C for brass, and 450–550°C for aluminum. Davidenkow²² later presented an interpretation of these results in terms of recrystallization.

The relation of the above repeated

yield phenomena, at nearly constant stress and at elevated temperatures, to the stair-step stress strain curves observed by the author is not readily apparent. An effect which is obviously closely related, however, is Fell's¹⁵ observation of a number of successive yields of duraluminum strip specimens. The resultant stress strain curve is of stair-step form, similar to those observed by the author. It seems likely also that the serrated stress strain curves shown in Fig 4 would also be in the form of rectangular steps if the loading were accomplished by a machine in which oscillations of stress are precluded.

The effects briefly discussed above: yield point elongation, serrated stress-strain curves, Lüders' lines, and stepped stress-strain curves (repeated yielding), have been arbitrarily divided in the discussion for purposes of clarity. It is desired, however, not to differentiate between them, but rather to point out that all appear to be manifes-

tations of the same effect, propagation of plastic deformation waves through the stressed medium. They have in common that:

1. All involve propagation of plastic deformation
2. The presence of certain impurity atoms in appropriate state of solution or precipitation is necessary
3. The required impurity atoms are those which result in quench or strain age-hardening (C in Fe, Cu in Al, Be in Cu)
4. Appropriate test conditions of temperature and loading rate must prevail, although these conditions may differ for the different effects.

The most plausible general hypothesis seems to be that the effect of the impurity atoms is to precipitate in such a manner as to harden the lattice against plastic deformation, and that such precipitation hardening facilitates propagation of the plastic waves. The present studies on the propagation of successive plastic waves in aluminum were made with the objective of further elucidating both the connection between these related phenomena, and the detailed mechanism by which they occur.

Apparatus and Procedure

STRAIN MEASUREMENT

The elongation of specimens was measured in all cases electrically by use of bonded resistance wire gauges similar to the commercial SR-4 gauge. Because of such factors as softness of specimens, diversity of gauge sizes and shapes, and necessity of rapid application, gauges were assembled directly on the specimen instead of gluing on commercial SR-4 gauges. The technique used was to glue on a layer of lens tissue with thinned Duco cement and lay on the paper 6 or 8 strands of 0.001-in. diam hard drawn advance wire, of total resistance 100 ohms, held by several coats of the same cement. The ends were then soldered to heavier wires, also glued to the specimen. Gauges of this type usually lasted to about 3 pct strain before the wire broke, and were sufficiently linear over this range. Calibration could be made by measuring specimen length before and after test. Because of softening of the Duco cement, however, these gauges were reliable only up to about 60°C. For higher temperatures the wires were mounted with DC-804 silicone resin supplied by the Dow-

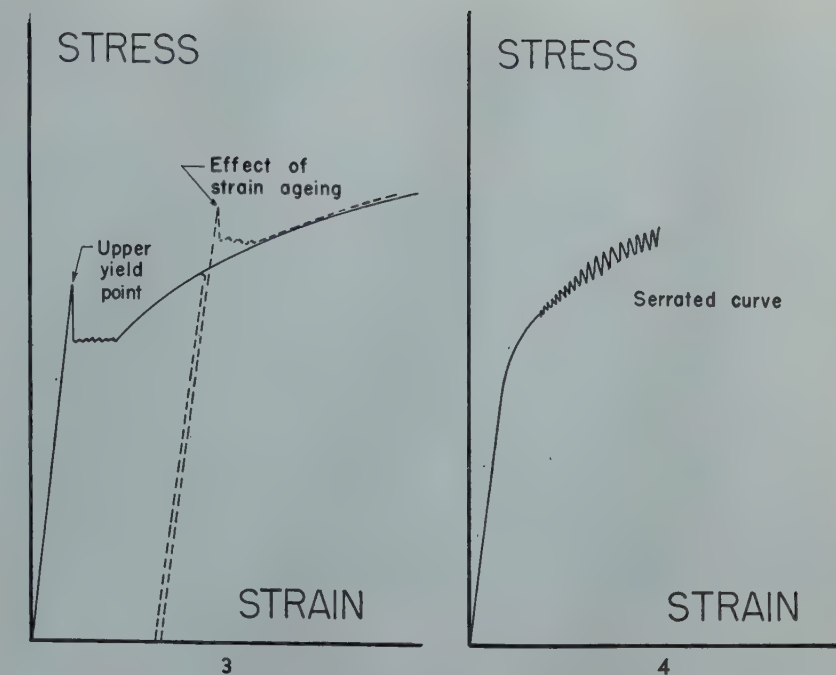


FIG 3—Illustration of yield point phenomena as found in mild steel. Dotted curve shows effect of aging sample after initial strain.

FIG 4—Illustration of serrated stress-strain curve as found in mild steel at 250° or in duralumin at 20°C.

Corning Chemical Co. A thin coat of cement was baked on for $\frac{1}{2}$ hr at 200°C; the wires were then laid on and held by a special jig, covered by a second coat of resin and baked another $\frac{1}{2}$ hr. After removal of the jig a third coat was baked on. These gauges were found usable up to temperatures of 170°C, although some relaxing of the resin sometimes occurred, but the useful strain range was only of the order 1 to 1.5 pct.

The gauge constituted one arm of a Wheatstone bridge, with a second arm consisting of a dummy gauge on an aluminum rod in good thermal contact with the specimen, for temperature compensation. The other arms were dial resistance boxes. Current of the order of 25 ma from a storage battery was passed through each arm of the bridge. Instead of the usual null method of using a galvanometer as detector and repeatedly adjusting the resistors for balance, the resistors were left constant and the bridge unbalance recorded continuously on a Brown "Elektronik" strip chart self-balancing potentiometer with full scale range of 10 mv. Bridge current was usually adjusted so that full scale on the chart was about 1 pct strain, the smallest detectable strain being about 0.1 pct of the full scale, or 10^{-5} strain, although this sensitivity could be increased about five fold if desired. The

chart (see Fig 5) then represented a direct continuous plot of strain vs. time, or, as long as loading rate was constant, strain vs. stress. A chart speed of 30 in. per hr was convenient for most tests, but for rapid strains was increased to 1200 in. per hr, or 0.33 in. per sec.

For measurement of the time relation of strains in different parts of the specimen, four or five gauges were mounted at intervals along its length, each in a separate bridge circuit, and recording each on a separate potentiometer. For these measurements the recorder chart drives were speeded up to 0.33 in. per sec and the four charts were synchronized by periodic electrical pulses.

Since the steps encountered and time intervals between them were in many cases too rapid to be followed by the recording potentiometer, some tests were also made with a 12-channel photographic recording oscillograph with multi-channel amplifier for recording simultaneously the response of several gauges. In this case the bridge current was 5000 cycle ac from an oscillator contained in the amplifier unit, and response time was limited only by the natural frequency (1500 cycle) of the galvanometers. This equipment was kindly made available and operated by Mr. Petersen and Mr. Tahl of the General Motors Electromotive Div.

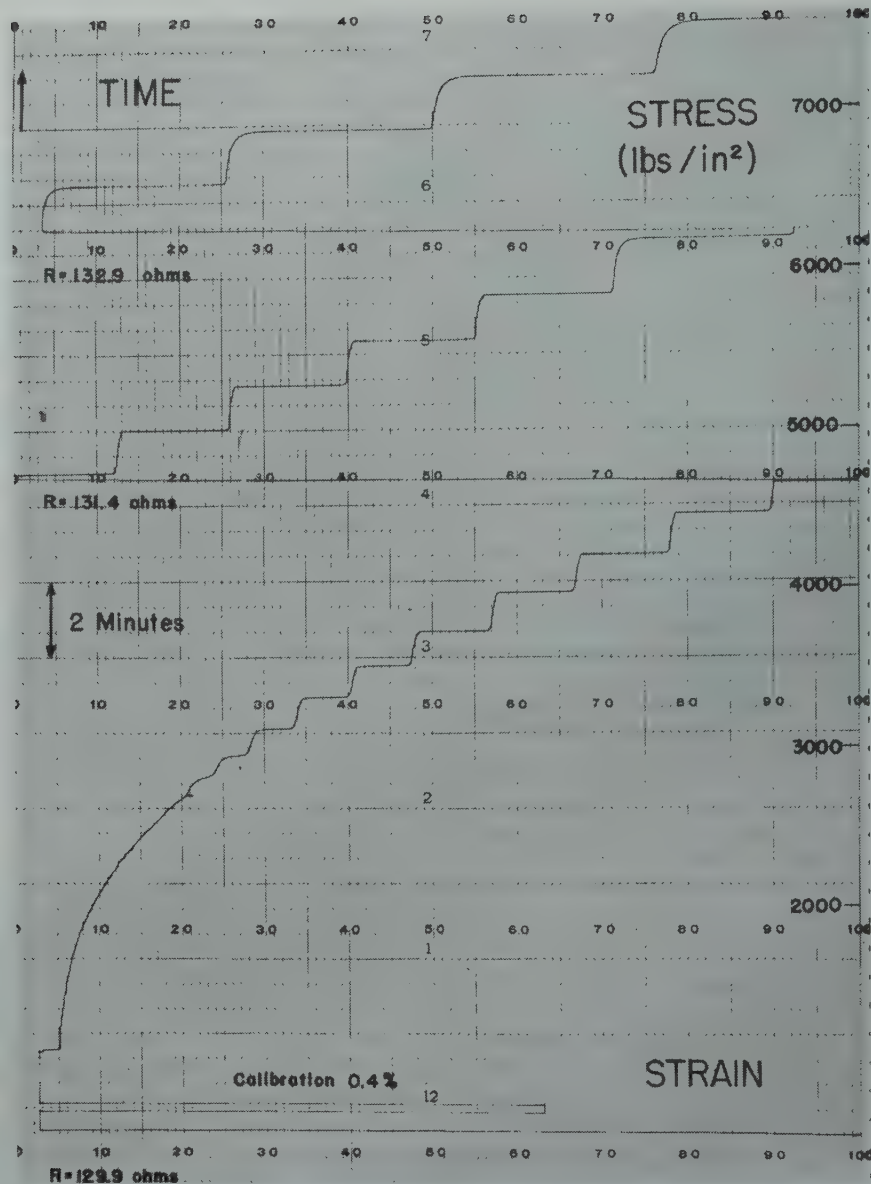


FIG 5—Typical chart record of strain vs. time curve for 2S aluminum at 25°C and continuous loading rate of 240 psi per min. Calibration represents 1 ohm change in one arm of bridge.

Photographic records are shown in Fig. 12.

LOADING APPARATUS

Instead of the standard type of "hard" tensile machine which increases strain at a constant rate, it was desired to have a constant rate of loading (approximately constant stress rate, since strains were small) and to maintain the load during yielding. A simple lever system as shown in Fig 6 was therefore set up. The entire apparatus was on a shock mounted table set on a spring supported concrete block, and the load was communicated to the lever through a soft spring which served the dual purpose of cushioning against external vibration or oscillation of stress during

yielding and of measuring the load by its extension. Load could be read to 0.1 mm on the spring scale, corresponding to 0.5 lb on the specimen. It was applied by draining water through a needle valve into a bucket hanging on the spring scale.

The specimens were turned from $\frac{3}{4}$ -in. diam rod to $\frac{1}{2}$ -in. diam, leaving a shoulder on each end, and were held in end blocks by a split collar arrangement on which the shoulders rested. Tension rods of $\frac{1}{4}$ -in. steel connected to the end block by a hardened ball and cone socket which allowed self-adjustment to axial stress.

Temperature was controlled by circulating alcohol for low temperature, or prestone for high temperature, through $\frac{3}{8}$ -in. copper tubing wound around and

soldered directly to the end blocks, the liquid being driven by a small centrifugal pump and cooled by passing through coils immersed in liquid nitrogen or a dry ice bath or heated similarly. Temperature differential between end blocks and specimen was always less than 2°C and much less except during rapid cooling or heating.

It is to be noted that the tensile testing procedure used differs from conventional engineering practices in several respects.

1. Load is applied by a dead-weight (soft) type of mechanism rather than by the usual (hard) tensile machine in which elongation is at a constant rate. In such a soft machine stress can be increased at a uniform rate since it is unaffected by yielding of the specimen.

2. The strain-sensitive element measures only a localized area of the specimen rather than averaging over most of the length of the specimen. Also the sensitivity, 0.001 pct, is considerably higher than most mechanical strain gauges.

3. A continuous recording of strain is obtained, as is essential for observing the type of small irregularities which were found in stress-strain curves.

ALLOYS USED

The 2S samples were ordinary commercial 3/4-in. rod. Pure aluminum copper alloys were made by melting in vacuum aluminum ingots of 99.996 pct purity, donated by the Aluminum Co. of America, with additions of electrolytic copper shot. The alloys were cast in molds 1 1/4 x 1 1/4 x 6 in. and cold rolled to 3/4 x 3/4-in. square bar, from which specimens were machined. Before testing, each specimen was annealed for 1/2 hr at 500°C in air and cooled to room temperature in a stream of air. Grain diameter of the resulting structure was about 0.1 mm. Chemical analyses of the samples used are given in Table I.

Results

GENERAL DESCRIPTION OF EFFECT

The general plastic properties have been observed from records of strain by single gauges of 3/4-in. length on specimens of 2S and Al-Cu alloys. In an annealed specimen of 2S at 25°C loaded at constant rate of the order of 200 psi per min. the initial portion of the stress-strain curve up to about 0.3 pct plastic strain is smooth. Waves then become perceptible on the record of strain and rapidly become sharper until the curve of strain vs. time assumes a stair-step form with rapid steps of strain (around 0.05 pct) occurring in times of a few seconds and sometimes of 0.1 sec, followed by periods of several minutes during which only elastic extension occurs (see Fig 5). The steps are not random but occur at regular stress intervals of about 250 psi, and adjacent steps represent approximately equal amounts of strain. Actually the spacing and size do not remain constant but become progressively larger with increasing stress, being about proportional to the total stress. Also with increasing stress (or strain) the corners of the

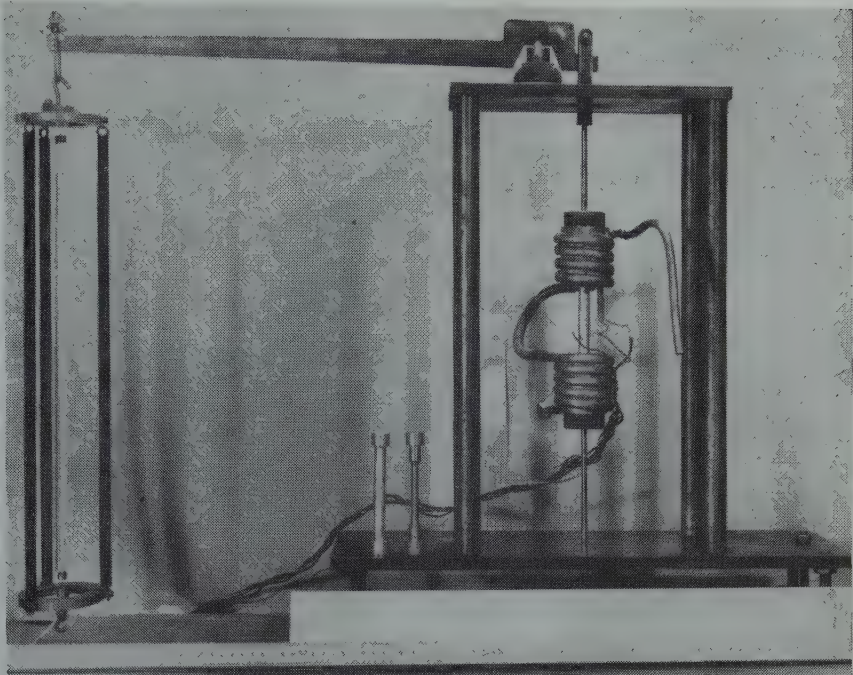


FIG 6—Tensile test machine—constant rate of loading by water flowed into bucket hanging on spring; temperature control by liquid circulating through coils.

Table 1 . . . Chemical Analyses of Samples

| Alloying Elements | Alloy | | | | |
|-------------------|----------------------------|-----------------------|-----------------------|-------------------------|-------------------|
| | A 2S Aluminum Pct | B Al-0.5 Cu Pct | C Al-0.1 Cu Pct | D Al-0.025 Cu Pct | E Brass Pct |
| Copper..... | 0.14 | 0.5 | 0.1 | 0.025 | 69.11 |
| Iron..... | 0.48 | <0.01 | <0.01 | <0.005 | <0.01 |
| Silicon..... | 0.11 | <0.01 | <0.01 | <0.005 | |
| Zinc..... | | | | | 30.80 |
| Lead..... | | | | | 0.01-0.1 |
| Cd, As, Bi..... | | | | | <0.01 |

steps (in 2S Al) become progressively less sharp (see Fig 10, 14). In Fig 7 the height and length of steps is plotted against total stress.

In view of the differences in technique from conventional tensile testing procedure one test was conducted using an ordinary “hard” tensile machine, which operates at approximately constant strain rate, and which allows relief of stress when the specimen yields. Results (Fig 8) verified that the same phenomena occur, although the sharpness of steps is much decreased.

EFFECT OF STRUCTURE AND CHEMICAL COMPOSITION

Tests under similar conditions, and also over a range of temperatures and strain rates, were also performed on 99.996 pct pure aluminum, which was prepared by the Aluminum Co. of

America. Since the pure aluminum in all cases exhibited smooth curves rather than the anomalous curves of the type observed for 2S, anomalies of 2S could be attributed to an effect of the impurity content of the 2S (Cu, Fe, and Si, principally). On that basis copper was chosen as a suitable alloying element and alloys of the 99.996 aluminum with 0.025, 0.1, and 0.5 pct Cu were made up. The observed plastic properties were similar to those of 2S, except that: 1. Steps began at much smaller strains and the first ones are of much smaller size (see Fig 11). 2. Steps are much sharper in 0.1 and 0.5 pct Cu alloys than in 2S. In 0.025 pct alloys the steps are not sharp and appear only under some conditions of previous strain, loading rate, and others. 3. Temperature limits, as discussed below, are different.

The fact that copper content of 0.1 pct is much more effective than

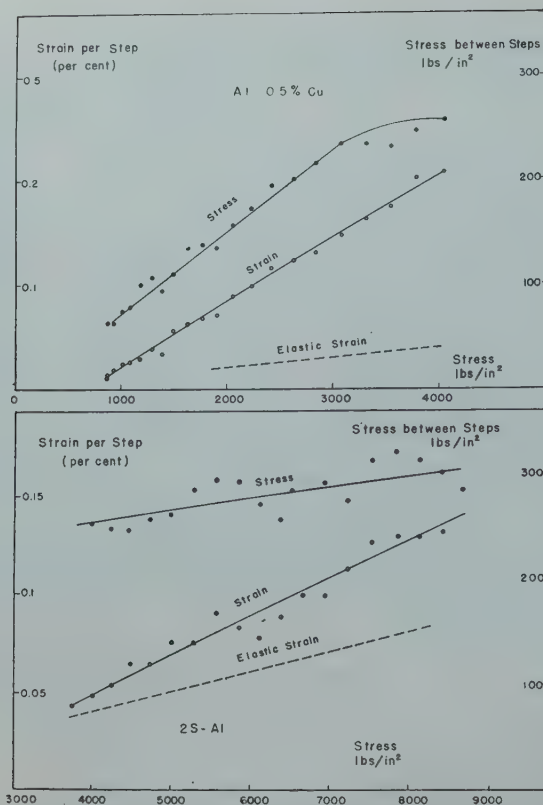


FIG 7—Variation in size of steps with stress. Each curve applies to a single stress-strain curve and each point on curve corresponds to a single step. Horizontal axis is stress at which step occurred.

0.025 pct suggests that the phenomena may depend on precipitation from supersaturated solid solution. Extrapolation of 200–400° data on the aluminum-copper phase-diagram indicates a solubility at 25°C somewhat higher than 0.1 pct, but the solubility limit at this low temperature is rather uncertain. At first it appears surprising that 2S aluminum has less sharp steps than a pure Al-Cu alloy with less Cu content (0.1 pct). It has been shown, however, by Fink, Smith, and Willey²³ that the presence of Fe in Al-Cu alloys greatly decreases their capacity to age-harden, probably by removal of the copper from solid solution. Since Fe is the principal impurity in 2S aluminum, the effective Cu content is thus probably considerably decreased.

Grain size was found to have no profound effect on the qualitative features of the phenomenon although Fig 9 shows that the strength of the alloy is highly dependent on grain size. Note that the step size is greater in the smaller grained structure (where the stress is correspondingly higher) and that the smooth initial portion of the curve continues to greater strains the smaller the grain size.

PROPAGATION

Since continuous plastic flow is observed only until the beginning of the step phenomenon but then ceases, it must be concluded either that the entire region under the gauge remains

elastic except for periodic localized slip, or that each step corresponds to a plastic deformation of the entire region, but leaves it in a hard, elastic condition immediately afterward. Simultaneous measurements of several gauges on different parts of the specimen confirmed the truth of the latter supposition.

A large number of tests was made with multiple gauges along the length of the specimen, to investigate the nature and velocity of the propagating plastic deformation wave. The usual arrangement of gauges was four $\frac{5}{8}$ in. long gauges in a line parallel to the axis, with $\frac{1}{8}$ in. spacing between their ends. Fig 10 shows a typical combined record of four gauges. Although the time differences are barely perceptible on the time scale of Fig 10, steps did not occur simultaneously in all gauges but in rapid succession, and in sequential order. For example, steps would be recorded at intervals of around 1 sec successively on gauges 1, 2, 3, and 4, indicating that strain is initiated at one point and spreads throughout the entire specimen. Thus each step in the stress-strain curve may be considered as the propagation of a plastic deformation wave front along the specimen. It was to be expected that the point of initiation would sometimes lie between gauges and the wave front spread in both directions. It was actually observed that the order of appearance of steps was sometimes, for example, 2, 1, 3, 4, indicating initiation of strain between

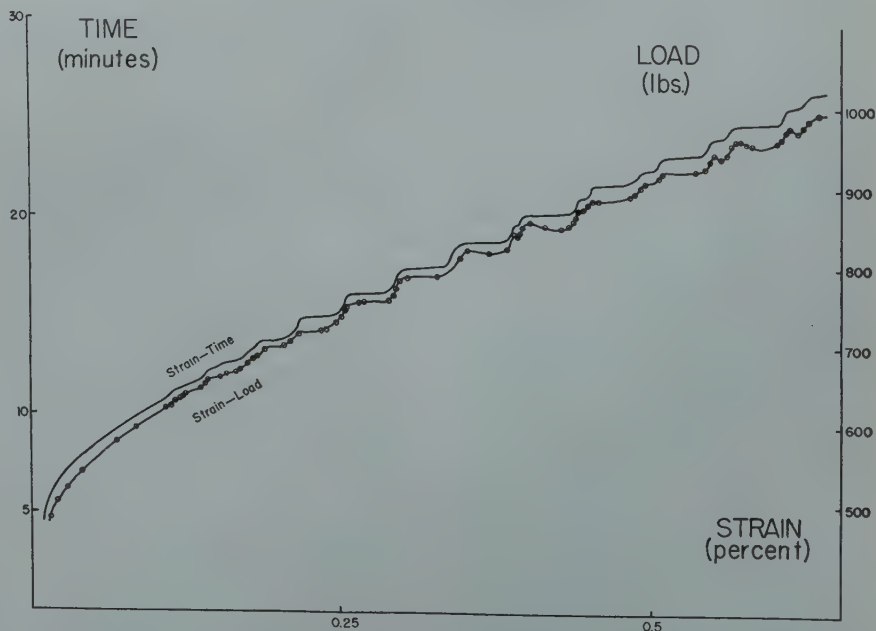


FIG 8—Curve for 2S-Aluminum specimen in standard "hard" tensile test machine. (A) Strain vs. time curve from chart of automatic recorder (B) strain vs. stress curve plotted by combining curve (A) with data read from load dial of machine.

gauges 1 and 2. As strain increased, the steps became more rounded and had no well defined beginning or end (see last steps in Fig 10). Under these conditions it was difficult to distinguish any time difference between strains at different points, and the records showed about the same strain at all four gauges at any instant.

In other cases, however, particularly in Al-Cu alloys, deformation waves propagated only through a limited region of the specimen, then stopped. Strain in the adjoining regions also occurred by the periodic propagation of a wave, but at independent times. This behavior is illustrated in Fig 11. The sharp steps shown occurred at intervals of the order of two minutes, but in every case two or more gauges recorded steps either simultaneously or only a few seconds apart. In Fig. 11 the small numbers beside the four curves indicate relative time in seconds between strain steps which occurred at approximately the same stress. It will be seen that there is a repeated sequential order of occurrence 1-34 . . . 23-4 . . . 1-34 . . . and so on. (See particularly Fig 11 at stresses

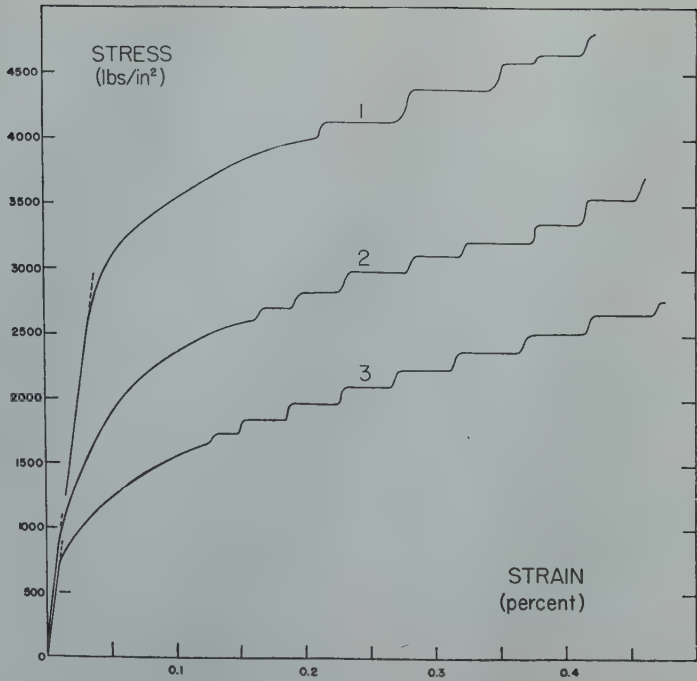


FIG 9—Curves for 2S specimens of different grain size.
Size (1) Grain diam 0.1 mm
(2) Grain diam 1 mm
(3) Grain diam 5 mm (much longer parallel to axis).
Steps begin later but are larger for small grain size.

2300–3300 psi.) This behavior indicates that each strain propagates through a limited region, that some gauges cover parts of separate regions, as designated by A, B, C, and D, and that the sequence of steps in these regions is A–C . . . B–D . . . A–C . . . B–D, and so on.

It can also be seen that appearances of deformation waves in regions A and C are always within a few seconds of each other, and likewise the times of waves in regions B and D are very close. The interaction between such separated regions evidently is not by passage of a plastic wave, however, since no strain is registered by the intervening gauge. The nature of the boundaries of the regions is not known, but as seen from the later steps of Fig 11, and as indicated by the dotted brackets, these boundaries are not entirely fixed but shift with increasing strain.

RATE OF PROPAGATION

The propagation velocity of the deformation wave can be measured roughly from its time of arrival at successive gauges. It was found that:

1. The velocity is relatively slow as compared to sound velocities for propagation of elastic waves, being of the order of a few cm. per second.
2. There

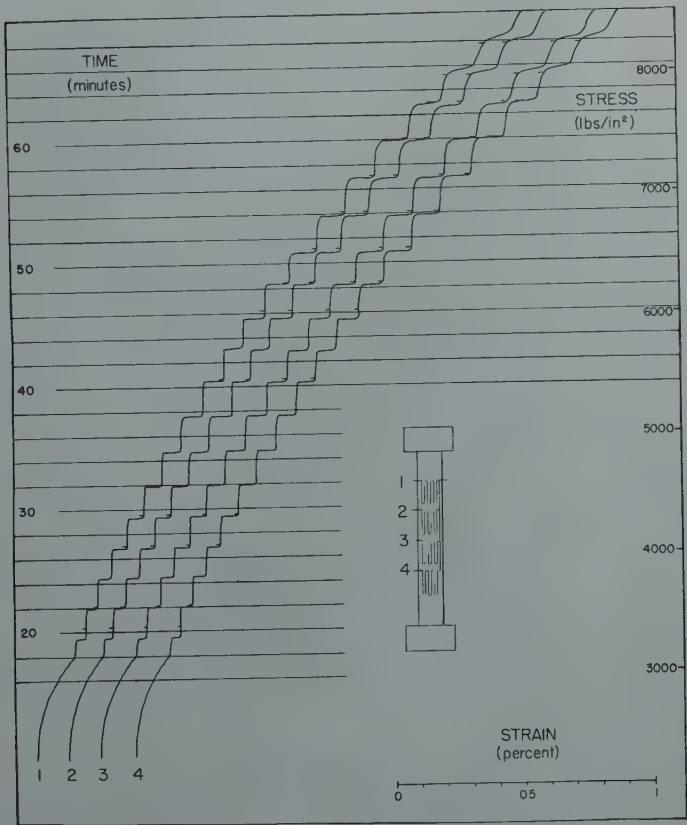


FIG 10—2S Aluminum specimen. Simultaneous records of four gauges arranged as shown along specimen. Sequential order of steps in gauges indicates plastic strain wave starts at one point and propagates through entire specimen.

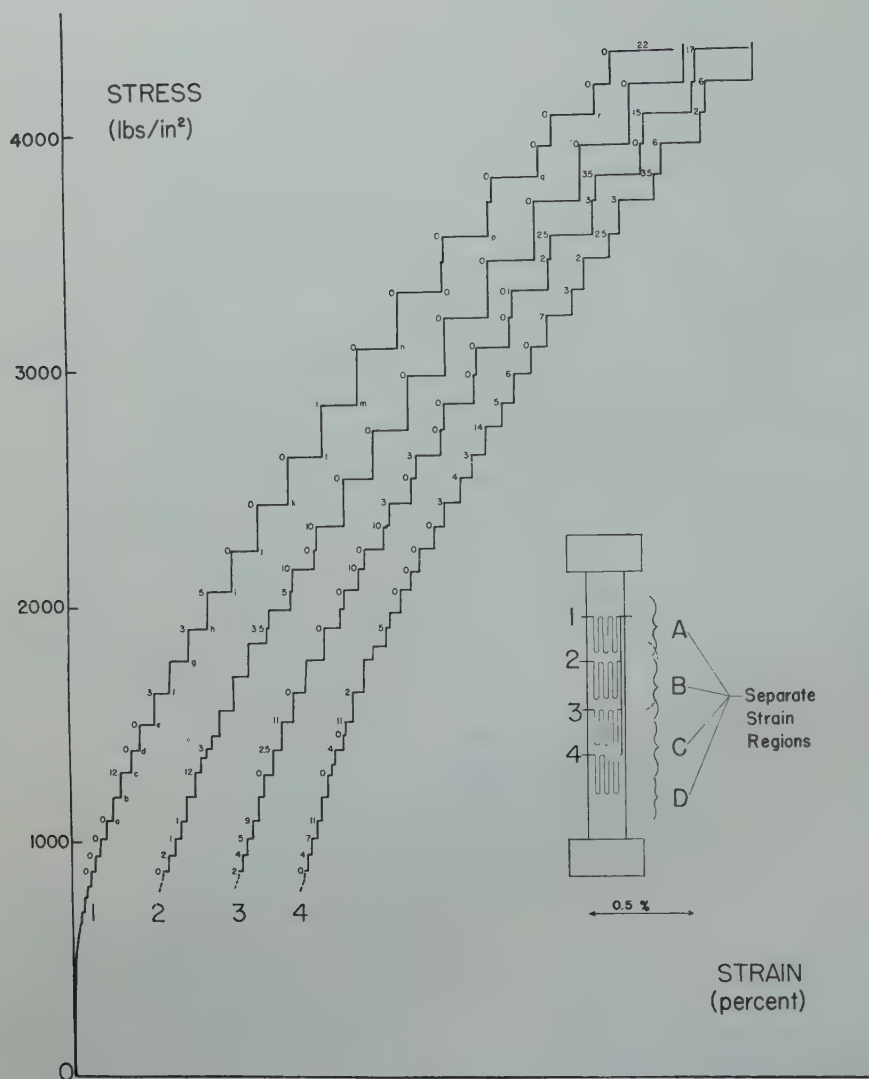


FIG 11—Al-0.5 pct Cu specimen. Simultaneous records of four gauges $\frac{1}{2}$ in. long, $\frac{5}{8}$ in. center to center along specimen. Small numbers beside each step give time in seconds relative to other gauges. Analysis of times of steps in various gauges indicates each step corresponds to deformation throughout one of the regions A, B, C, or D.

is no unique velocity for aluminum or even for a particular composition of aluminum, such as 2S, the velocity depending strongly on the state of strain, and varying over a wide range during a single test.

The wide variation in propagation rate is illustrated by Fig 12. In 12a, all five gauges, ($\frac{1}{8}$ in. long and $\frac{5}{16}$ in. center to center) show steps in rapid succession at average intervals of about 0.01 sec, corresponding to 80 cm per sec velocity; but in 12d the time interval between gauges is of the order of 1 to 1.5 sec, or 0.5 cm per sec velocity. In general it was observed that the rate of propagation was very rapid for the sharp steps observed in pure Al-Cu alloys, all gauges showing steps within a 0.1 sec interval; the rate associated with the less sharp steps characteristic of 2S Al was much less, with intervals up to several

seconds between gauges. Under some conditions, however, 2S also exhibited sharp steps, in which cases propagation was rapid. It thus appears qualitatively that the velocity of propagation increases with sharpness, to a maximum of at least 80 cm per sec. This interdependence of sharpness and propagation velocity is partly but not entirely explained by the consideration that a slower wave front takes longer to traverse the gauge and thus results in a less sharp step. Reference again to the last few steps of Fig 10 shows that the steps have degenerated to rounded waves, but, since the waves are almost in phase, the propagation time must be short compared to the duration of a single wave. A sharp but slowly propagating wave would produce a record on which step 1 is completed before 2 starts, and so on.

Considering the plastic deformation

of the specimen as a plastic wave progressing through it, it is of particular interest to determine the shape of the wave front, that is:

1. Does the wave front advance continuously, with a smooth transition from zero to maximum strain or in discrete steps by the sudden appearance of strained slabs such as the Lüders' bands in mild steel indicate?

2. Is the wave front a plane surface inclined to the axis and along the direction of maximum shear stress?

3. Is the advancing wave front sharp, and does all of the strain occur immediately as it passes, or persist for some distance and time behind?

Some conclusions on point (3) may be drawn from interpretations of Fig 10-12. It will be noted that in the rapid steps of Fig 12 a, b, c, strain at each gauge continues for about 0.1 sec during which time the wave has propagated to all other gauges and thus a distance of several centimeters. Also the initial part of the step seems more rounded than accountable by time for the wave to traverse the $\frac{1}{8}$ -in. gauge. Likewise in the slower steps of Fig 10 and 12d strain continues at a given point long after the wave front has passed. In Fig 10 the length of the region undergoing strain and the time for which strain continues at a given point are both longer than for more rapid steps as in 12a, b, c. The results then lead to the concept of a continuously moving but not necessarily sharp wave of the type indicated in Fig 13.

Investigation of the plane shape, orientation, or continuity of motion of the wave front cannot readily be accomplished by multiple gauge techniques, first, because a large number of gauges of small area would be required and second, because lack of sharpness of the wave front makes precise time of arrival at a point difficult to determine. For this reason a visual or photographic method seems much more appropriate. Preliminary observations on strip specimens, 0.50×0.065 -in. cross-section, of 52 S-O aluminum (nominal composition 2.5 pct Mg, 0.25 pct Cr) show plainly visible bands appearing and spreading along the surface. In this case a narrow straight band, inclined 45-50° to the axis, suddenly appears and rapidly spreads in both directions, the advancing boundaries remaining quite straight and at the original orientation. The bands usually do not spread through the entire specimen. In 2S strip,

strain waves are accompanied by passage along the surface of a disturbance which is perceptible but not distinct enough to determine its shape, and in Al-0.5 pct Cu no surface markings are seen. These latter results are to be expected since the amount of strain per step is smaller than in 52 S-O, where it is 0.5–1 pct. Even in 52 S-O many steps are recorded by the strain gauge before they increase in size enough to be visible on the surface.

It thus can be considered probable that even in cylindrical specimens the wave front is a plane oriented approximately along the direction of maximum shearing stress. Further work is in progress on visual and photographic observations by improved techniques.

EFFECTS OF TEMPERATURE

By use of a liquid circulating system as described above, temperatures could be controlled within 1°C in the range

–60 to 170°C and could be altered within a few minutes without interruption of the test. It was found that the anomalous stepped stress strain curve appears only within a certain temperature range, becoming smooth again above or below that range.

For determination of the upper and lower temperature limits, a series of tests, each on a separate sample and at constant temperature, were made. The results for such a series on 2S aluminum are shown in Fig 14. It will be seen that as the temperature is decreased the step phenomenon begins at greater strains, until at about –20°C the entire curve is smooth except for occasional gentle ripples. On the other hand, increase of the temperature causes the steps to appear at small strains but to fade into a smooth curve, and at sufficiently high temperatures the entire curve is again smooth. Several tests were also conducted in which the temperature was alternately raised or lowered during

the course of the test, either while the load was constant, or without interruption of loading. One of these is shown in Fig 14 and is in agreement with the temperature limits indicated by the other curves. Because of the systematic change in the steps with increasing strain, however, this method was not used for determining temperature limits.

A similar series of tests on pure Al-0.1 pct Cu alloy gave a somewhat wider temperature range, but showed that the onset and termination of the steps is much more abrupt in this purer material. Instead of degenerating to rounded waves the steps give way abruptly to a smooth curve. Although the temperature ranges within which the steps occur are not well defined, they can be specified approximately:

| Material | Temperature Limits | |
|----------------------------|--------------------|----------|
| | Upper °C | Lower °C |
| 2S Aluminum..... | +60 | –10 |
| 99.99 Al + 0.1 pct Cu..... | 120 | +10 |
| 99.99 Al + 0.5 pct Cu..... | 150 | +10 |

EFFECT OF RATE OF STRESS

Several tests have been conducted with 2S specimens, where, without

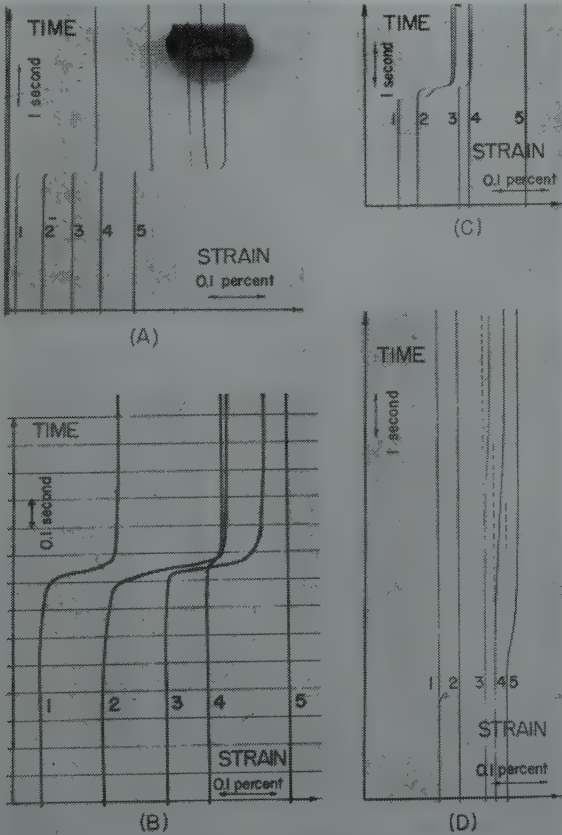


FIG 12—Al-0.5 pct Cu specimen. Oscillograph records of strain at five gauge positions as shown in Fig 13.

- (A) Strains in rapid 1, 2, 3, 4, 5 sequence as plastic wave traverses specimen in about 0.05 sec.
- (B) Plastic wave apparently starts near gauge 2 and propagates both ways. Note that strain continues in gauge 2 after wave has advanced to gauge 4, and that wave stops abruptly before reaching gauge 5.
- (C) Plastic wave in region under gauge 1, then after 0.1 sec delay wave through region under 1, 2, 3.
- (D) Slowly propagating wave takes about 1 sec to traverse distance between gauges. Note that rate of strain is correspondingly slow.

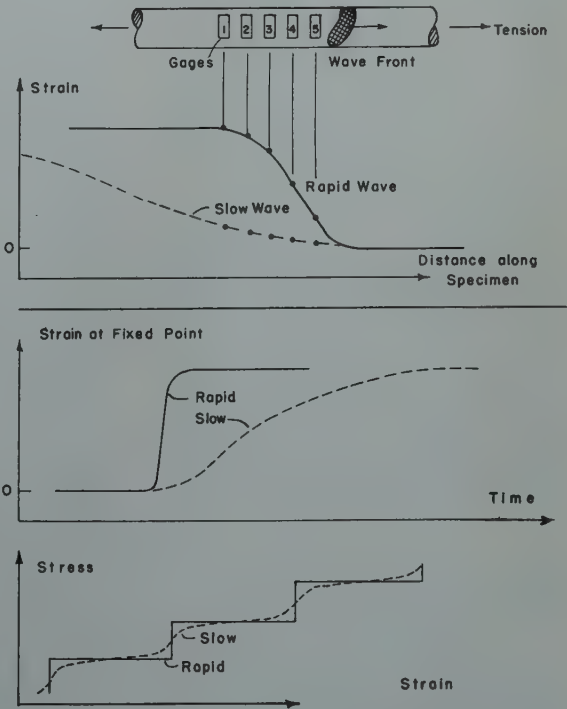


FIG 13—Probable distribution of strain in plastic wave. As shown, slowly propagating wave has longer duration at a fixed point as a result of both low velocity and greater length. Bottom graph shows stress-strain curve which would result from repeated occurrence of such waves.

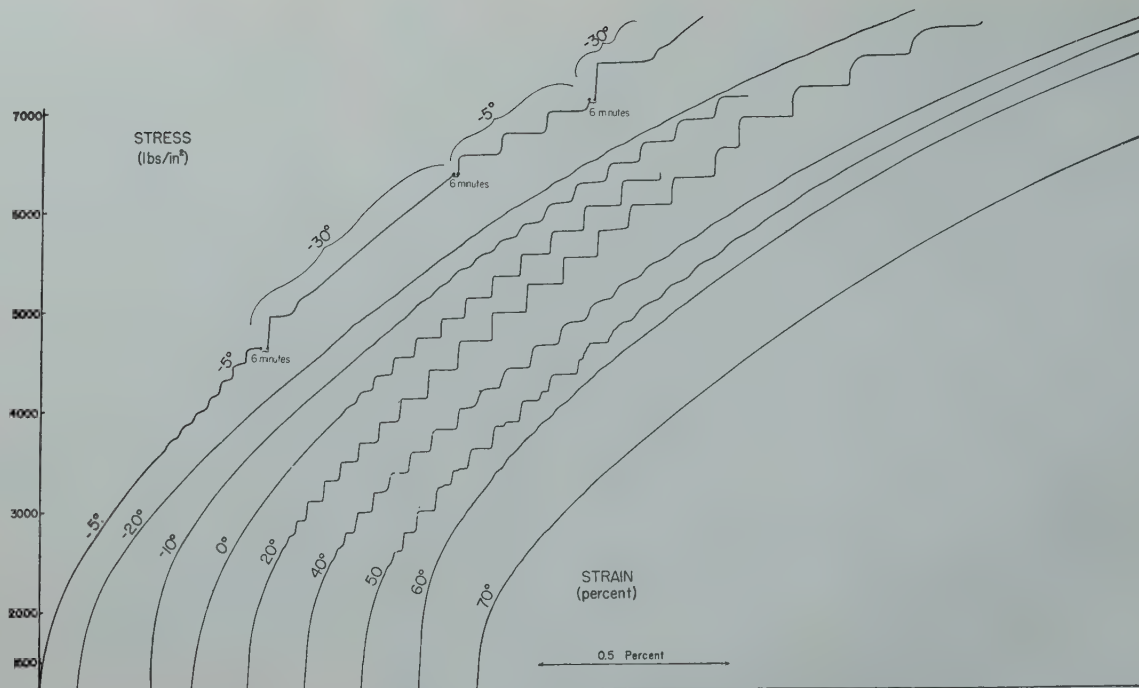


FIG 14—Stress strain curves at various temperatures in 2S Aluminum.

Temperature and loading rate, 120 psi per min, constant in each run, except first curve, where load was held constant for 6 min. during each temperature change.

otherwise interrupting the test, the loading rate has been suddenly changed from slow to rapid rates and vice versa. One of the resulting stress strain curves is shown in Fig 15. It is seen that the size of the steps is affected somewhat, but that variation in loading rate by a factor of 50 causes relatively small changes, less than a factor of 2, in step size and spacing. It is to be expected that the effect of rate may well be much greater near the upper or lower temperature limits, but as yet, the effect of loading rate has been investigated systematically only at room temperature.

In 0.025 pct Cu alloys it is found that steps in the curve appear only under certain conditions. In particular, the rate of loading must be sufficiently slow. This would indicate, in terms of the mechanism postulated in the following section, that with such low copper content, more rapid loading rates do not allow sustained steps because of insufficient time for precipitation hardening between strains.

EFFECT OF AGING AND HEAT TREATMENT

Since the effects observed are shown to depend on the presence of an alloying element in the aluminum and are probably the result of a supersaturated solid solution, appropriate aging or heat treatment might be expected to

affect the plastic properties by changing distribution of the solute atoms in solution, or in precipitation aggregates. The stress-strain curves were found to be unaffected, however, by the difference between a water quench from the annealing temperature of 500°C (which should result in maximum supersaturation) and relatively slow cooling from 500°C, followed by 20 hr annealing at 100°C (which should precipitate out the supersaturated solute atoms). Fig 16 shows the result of a test in which straining was interrupted at intervals for heat treatment. Effects of heat treatment were minor.

It has been observed, however, that specimens of 2S aged around 100 days at 25°C subsequent to annealing deform in sharper steps than those freshly quenched.

STEP PHENOMENON IN BRASS

Several other metals have been tested under conditions similar to the tests of aluminum. Cadmium and high purity copper exhibited only smooth curves, but annealed 70/30 alpha brass had a stepped stress-strain curve similar to those described above, with regular steps of around 0.5 pct occurring at stress intervals of around 150 psi. It was observed that the step phenomenon does not set in until strain of a few percent has occurred.

If the specimen is given a somewhat smaller strain and aged one or two days at room temperature, however, steps begin immediately when plastic straining is resumed. Otherwise no systematic study of the effect in brass has been made.

Discussion and Interpretation

Before attempting to make interpretations of the physical mechanism of the plastic effects observed, the qualitative general results may be summarized. These results apply to fully annealed cylindrical tensile specimens of 2S aluminum and of aluminum-copper alloys with 0.1–0.5 pct copper, strained at a constant rate of loading.

1. The elastic portion of the stress strain-curve is followed by a gradual and smooth plastic region up to 0.1 to 0.3 pct, followed by a short transition region in which the curve changes to the form of square steps of regular height and width. Subsequent deformation occurs almost entirely by steps, the size of which increase proportionally with the total stress. Some homogeneous creep may occur between steps, accelerating just before appearance of a step.

2. The steps are found to be the result of the initiation of plastic strain

at some region in the specimen and its propagation as a wave of plastic deformation along the length.

3. The plastic waves move at velocities up to a maximum of at least 80 cm per sec, the velocity being greater for sharper steps. They do not necessarily traverse the entire sample but may be stopped by structural barriers of undetermined nature. Plastic flow at a given point continues after the wave front has passed several centimeters beyond.

4. If aluminum free of impurities (99.996 pct pure) is used or if the temperature of test lies either above or below a certain range, -30 to $+60^{\circ}\text{C}$ for 2S, $+10$ to 120 – 150°C for Al-Cu alloys, deformation occurs not by the above step process but according to a smooth stress-strain curve.

5. Appearance of the steps is not greatly influenced by heat treatment of either strained or unstrained specimens, although prolonged aging of annealed 2S specimens results in somewhat sharper steps and aging of previously strained specimens decreases the sharpness.

On the basis of experimental results summarized above several postulates can be considered with regard to the physical mechanism by which plastic deformation occurs under these conditions. In this section they will be enumerated and the degree to which they provide an adequate interpretation of observed qualitative features of the phenomena discussed in each case:

1. The presence of alloying elements in aluminum is necessary to harden the lattice against continuous plastic flow between steps. The most probable mechanism by which such hardening is effected is by precipitation of the solute atoms on slip planes.

a. This postulate is based on the observation that pure aluminum (99.996 pct) exhibits a smooth stress-strain curve under conditions where Al-Cu alloys have anomalous curves.

b. Precipitation can occur in relatively short times even at room temperature as evidenced by the well known age-hardening effects of Al-Cu alloys. It should be men-

tioned, however, that extrapolation of higher temperature diffusion rate data would give diffusion rate at room temperature much too low to allow precipitation. It appears therefore that such extrapolation is not valid. In the present case it must be assumed that precipitation is greatly accelerated in the vicinity of slip bands where many lattice vacancies and imperfections exist.

c. Preferential precipitation on slip bands has been shown metallographically in Al-Cu alloys by Fink, Smith, and Willey.²³

d. If hardening is effected by precipitation, the steps would be expected to disappear as the temperature is decreased into a range where precipitation rate becomes too slow. This is in accord with observations that the steps do gradually fade and disappear over a temperature range from 0 to -20°C . (See Fig 14.)

2. Macroscopic steps in the stress-strain curve represent a cooperative effect between grains, by which relaxation on slip bands in one grain initiates slip bands in adjacent grains.

a. Thus plastic deformation occurs as a wave propagating from grain to grain.

b. On a larger scale the wave spreads through large regions of the metal, as a front usually extending entirely across the specimen, as observed both visually and by simultaneous recording of strain at several points on the tensile specimens.

3. Initiation of new slip bands in adjacent grains depends on building up of stress concentrations at the edges of slip planes or, viewed on a larger scale, ahead of an advancing deformation wave front. Consequently, under conditions where continuous relaxation is occurring (on previously formed slip bands or at the grain boundaries), the resultant relief of local stresses may prevent high concentrations, thus preventing propagation of a deformation wave.

a. Disappearance of stress-strain curve steps at higher temperatures (around 60°C for 2S aluminum, 120 – 150°C for Al-Cu alloys of 0.1–0.5 pct Cu) may be explained as a result of the increased creep rate in that range, since creep at constant stress becomes appreciable in roughly the same temperature ranges. The upper temperature limit for appearance of steps has been found to depend not only on temperature but on the amount

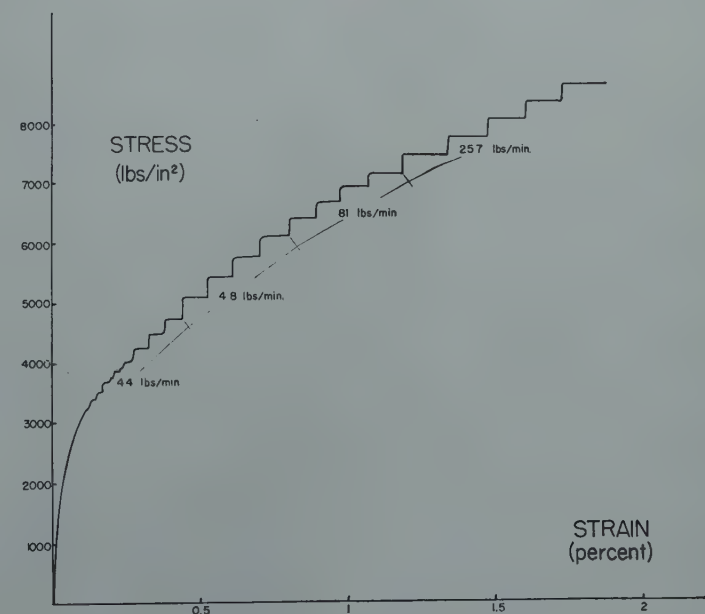


FIG 15—Effect of variation of load rate in 2S Aluminum.

Load applied continuously but with abrupt changes of rate as indicated.

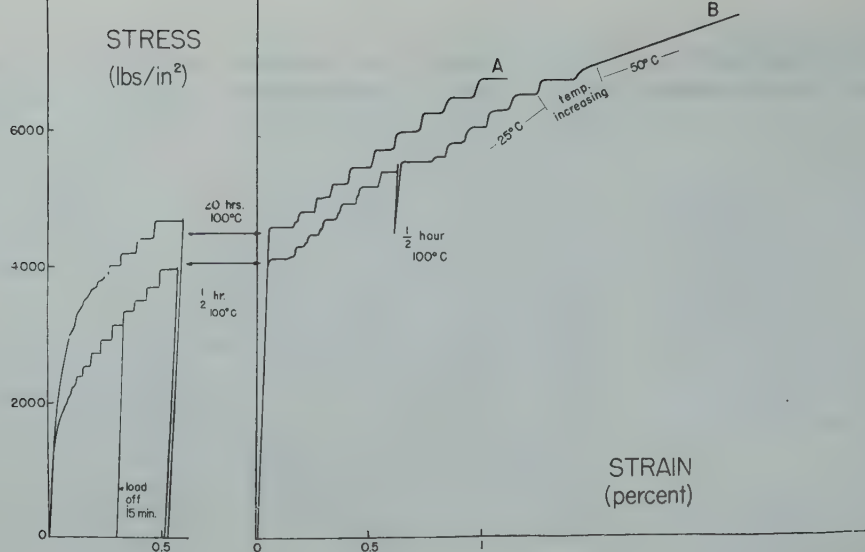


FIG 16—Effect of aging at elevated temperature—2S Aluminum.

(A) Entire tensile test conducted at 25°C but interrupted for 20 hr aging at 100°C. (B) All strain at 25°C except as indicated near end of curve.

and rate of previous plastic strain. That is, at higher temperatures, steps fade at smaller strains. (See Fig 14).

- b. An alternate explanation of the high temperature disappearance of the step phenomenon would be that as solubility increases with temperature a point is reached where the solid solution is no longer supersaturated and therefore does not precipitate. On this basis, however, one would expect widely different upper temperature limits for 0.1 pct Cu and 0.5 pct Cu and also an appreciable effect of heat treatment such as 20 hr aging at 100°C. Since neither of these predictions is found true, it seems unlikely that solubility determines the temperature range for steps.

- c. In all cases where loading was stopped and stress held constant for several minutes, further loading produced a period of elastic strain followed by a sharp and unusually large step of plastic deformation. The same effect was observed under conditions where no steps would otherwise occur (that is, in 99.99 pct pure aluminum or in Al-Cu alloys or 2S aluminum above or below the temperature range for step deformation). In the latter cases, however, step deformation did not persist but rapidly faded. These observations may be explained by the fact that holding stress constant for several minutes allows

cessation of transient creep and thus makes possible enough stress concentration for strain to be propagated from grain to grain as a deformation wave.

- d. It was frequently observed that, in a specimen being loaded at constant rate but at a temperature high enough to give a smooth stress-strain curve, a sudden decrease of temperature of only a few degrees produces a step in the curve. In this case also deformation soon reverts to a smooth stress-strain curve. As demonstrated by Carreker, Leschen, and Lubahn²¹ recently, such a sudden drop in temperature in a stressed material creeping at constant rate momentarily stops all creep, but creep resumes after a short incubation time. Thus immediately after a decrease in temperature the rate of stress relief by creep is low enough to permit propagation of a plastic wave but resumption of creep prevents successive waves.

4. Only a small amount of relaxation in a grain just at the advancing deformation wave front is necessary to initiate plastic slip in adjacent grains ahead of it.

- a. Waves have been observed to propagate with velocity varying over rather wide limits but with maximum around 80 cm per sec. This relatively slow velocity (as compared with the sound velocities for propagation of elastic waves) indicates that there is a

slight delay in transmission of slip from grain to grain, and such a delay would be expected while relaxation on slip bands in one grain proceeds far enough to build up stress sufficient to initiate new bands in the adjacent grain (or to reactivate slip on old bands).

- b. It would be expected that where continuous creep is occurring simultaneously with step deformation, a greater amount of relaxation would be necessary to initiate plastic strain in the next grain and consequently the rate of propagation would be slower. Comparison of different samples indicates that the less sharp the steps (that is, the more continuous creep) the lower the propagation velocity.
- c. It is found in Al-Cu alloys that deformation at one point of a specimen (or more accurately in a region under a 3-mm long gauge) continues after the wave front has travelled 5–10 cm beyond. The strain occurring as the wave front passes is only a small part of the total, and further strain at the point continues at a decreasing rate.

Although the above four postulates represent a fairly consistent outline of the mechanism of transmission of the plastic deformation waves, some observed properties which are not completely explained by the postulates should be discussed. In general, their explanation requires more detailed knowledge of the mechanism, and of

the dynamics of slip bands. Some aspects of the latter subject are to be discussed by C. Zener in the October 1948 ASM symposium on plastic deformation.

1. The steps are not of random size but occur at uniformly increasing stress intervals, approximately proportional to the total stress, and result in uniformly increasing amounts of strain. Further, both beginning and termination of the steps are in many cases sharp. A complete theory of the phenomena must therefore include both an explanation for the uniformity of stress increments between steps and a mechanism by which the deformation in single grains, once started, is terminated sharply at a definite strain value. A balance between these two factors then determines average slope of the stress-strain curve.

2. The exact mechanism by which the alloying elements effect hardening of the lattice to prevent plastic flow is not definitely known. Although it probably results from precipitation of aggregates of copper on the slip planes, it is difficult to picture a precipitation effect which occurs within the 0.1 second duration of the strain in such a way that precipitation hardening terminates the strain at a fixed value. It seems more plausible that each step results in complete relaxation across some slip planes, further strain being prevented by constraints of surrounding regions. Precipitation hardening on that plane then has time to occur before arrival of another deformation wave results in yielding elsewhere, again bringing stress across the same plane.

Summary

1. Plastic deformation of 2S aluminum and Al-Cu alloys is found to proceed according to a stair-step stress strain curve rather than at a continuous strain rate. The same effect is observed in 70/30 alpha brass.

2. The discontinuities are found to result from propagation of waves of plastic deformation along all or part of the specimen length; between occurrence of such waves practically no plastic strain occurs. Under varying conditions waves may be either very sharp or extended and velocities range

from a few millimeters to around 100 cm per sec. Duration of the corresponding strain steps may vary from 0.1 sec to around 1 min.

3. The effect is found to depend on presence of an alloying element such as Cu or Mg in aluminum, and does not occur in 99.99 pct aluminum.

4. Dependence of the phenomenon on such parameters as temperature, amount and rate of strain, and heat treatment or aging has been studied, with results as summarized in the section on discussion. Of particular significance is the fact that the effect does not occur except in a limited temperature range (-10 to 60°C for 2S).

5. The type of deformation observed takes place by appearance of slip bands, but differs from the more usual type in that slip on individual bands is not independent; strain, once initiated, spreads to adjacent grains.

6. It is pointed out that yield point elongation, serrated stress-strain curves and Lüders' or Hartmann lines are examples of a similar propagation of plastic waves. Furthermore, all of these effects have in common that they appear to depend on precipitation hardening.

7. The proposed mechanism for the observed phenomenon of repeated plastic waves may be summarized as follows: Motion on slip bands during strain results in lattice vacancies and imperfections which greatly accelerate general diffusion and precipitation of copper aggregates in the immediate vicinity. Consequent precipitation hardening stops all relaxation on the bands. When stress eventually increases enough to initiate further slip at some point, the hardened condition of the lattice causes high stress concentrations in the vicinity, which facilitate spread of the strain into adjacent grains. As successive grains break down under the stress concentrations, a wave of strain spreads through the metal and is followed by further precipitation hardening, thus starting a new cycle.

Acknowledgments

The author wishes to acknowledge indebtedness to many of the staff of

the Institute for the Study of Metals, particularly Professor C. Zener for stimulating discussions, Mr. David Houghton for carrying out many of the measurements, and Mr. John Gault for technical assistance; and also to Mr. Petersen and Mr. Tahl of the General Motors Electromotive Division for equipment and cooperation in making oscillograph measurements.

References

1. G. Sachs and H. Shoji: *Ztsch. f. Phys.* **45**, 776-796 (1921).
2. C. A. Edwards, D. L. Phillips, and H. N. Jones: *Jnl. Iron and Steel Inst.* **142**, No. 11, 199-222 (1940).
3. J. Winlock and W. E. Leiter: *Trans. ASM* **25**, 163-185 (1937).
4. Pfeil: *Jnl. Iron and Steel Inst.* No. II, 167, (1928).
5. L. J. Dijkstra: Communicated to AIME (1948).
6. Kuroda: *Sci. Papers of Inst. of Phys. and Chem. Res.* **34**, 1528 (1934).
7. A. Le Chatelier: *Rev. de Met.* **6**, 914 (1909).
8. Körber and Pomp: *Mitt. d. Kais. Wilh. Inst. f. Eisenf.* **9**, 346, (1927).
9. A. Portevin and F. Le Chatelier: *Trans. A.S.S.T.*, **5**, 457-478 (1924). (See Fig 13, 14).
10. Sutoki: *Sci. Rep. Tohoku Imp. Univ.* **29**, 673-696 (1941).
11. C. A. Edwards, D. L. Phillips, and Y. H. Liu: *Jnl. Iron and Steel Inst.* **147**, 145-167 (1943).
12. Lüders: *Dinglers Polytechnisches Jnl.* **156**, 18 (1860).
13. Hartmann: *Distribution des Deformations dans les Metaux soumis a des Efforts* (1896) Berger-Levie.
14. E. W. Fell: *Jnl. Iron and Steel Inst.*, **132**, No. 11, 75-91 (1935).
15. E. W. Fell: *Iron and Steel Inst. Carnegie Scholarship Memoirs* **26**, 123-163 (1936).
16. A. H. Stang, M. Greenspan, and S. B. Newman: *Bur. of Stds. Jnl. of Res.*, **37**, 211-221 (1946).
17. R. Becker and E. Orowan: *Ztsch. f. Phys.* **79**, 566-573 (1932).
18. Schmid and Valouch: *Ztsch. f. Phys.* **75**, 531 (1932).
19. E. P. Tyndall and C. Wert: Private Communication.
20. E. N. da C. Andrade: *Proc. Roy. Soc.* **84**, 1-12 (1916).
21. M. Classen-Nekludowa: *Ztsch. f. Phys.* **55**, 555-568 (1929).
22. N. Davidenkow: *Ztsch. f. Phys.* **61**, 46-53 (1930).
23. Fink, Smith, and Willey: *Age Hardening of Metals*, 31-53, ASM Symposium (1939).
24. Carreker, Leschen, and Lubahn: *TP 2477, Metals Tech. AIME*, Sept. 1948.

On the Structure of Gold-silver-copper Alloys

JOHN G. McMULLIN* and JOHN T. NORTON*

Introduction

THE ternary system of gold-silver-copper is characterized by a solid solubility gap and a two phase region in which copper-poor and silver-poor phases coexist. At about 30 pct gold, the two phases become mutually soluble at temperatures below the melting temperature. As the gold content is increased, the solubility temperature of the alloys decreases until at about 80 pct gold, the two phases are soluble down to the lowest temperature at which the alloys will recrystallize.

Although the general form of the two phase region is known, its boundaries do not seem to have been investigated extensively. In an X ray diffraction study, Masing and Kloiber¹ have outlined the boundaries of this two phase field at 400 and 750°C. Using only microscopic techniques, Pickus and Pickus² determined a vertical section of the ternary diagram showing the 14 kt alloys (58.3 pct gold). These two reports are not in complete agreement.

It has been shown³ that some of the ternary alloys are susceptible to age hardening and that the hardening is caused by the separation of a homogeneous alloy into two phases at the aging temperature. While the gold-copper binary system is an outstanding example of super lattice formation, Hultgren⁴ has shown that a few per cent of silver added to gold-copper destroys the tendency for ordering. Because of the age hardening possibilities of these alloys, it seemed advisable to investigate the boundaries of the two phase field more in detail using an X ray diffraction method, so as to permit a better understanding of the aging phenomena and enable predictions as to the behavior of other alloys to be made. This is especially true for the 18 kt alloys (75.0 pct Au) at the lower temperatures since they are known to exhibit age hardening.

Experimental Procedure

Twelve ternary alloys were prepared having the compositions shown in Table 1 and graphically in Fig 1. The gold used was fine gold bars supplied by Handy and Harmon. The silver was a bar of high purity silver from the U. S. Bureau of Standards. The copper was a bar of vacuum-treated, high conductivity copper from the National Research Corporation.

Table 1 . . . Composition of Alloys

| Alloy No. | Composition by Weight Per Cent | | | Solution Temperature °C | Lattice Constant of Solid Solution Angstrom Units |
|-----------|--------------------------------|--------|--------|-------------------------|---|
| | Gold | Copper | Silver | | |
| 1 | 58.33 | 3.00 | 38.67 | 350 | 4.054 |
| 2 | 58.33 | 5.00 | 36.67 | 475 | 4.037 |
| 3 | 58.33 | 10.00 | 31.67 | 570 | 3.999 |
| 4 | 58.33 | 20.83 | 20.84 | 640 | 3.918 |
| 5 | 58.33 | 30.00 | 11.67 | 590 | 3.859 |
| 6 | 58.33 | 36.67 | 5.00 | 390 | 3.810 |
| 7 | 58.33 | 38.67 | 3.00 | 350 | 3.807 |
| 8 | 75.00 | 20.00 | 5.00 | | 3.914 |
| 9 | 75.00 | 12.50 | 12.50 | 380 | 3.966 |
| 10 | 75.00 | 5.00 | 20.00 | | 4.033 |
| 11 | 65.00 | 17.50 | 17.50 | 550 | 3.938 |
| 12 | 70.00 | 15.00 | 15.00 | 475 | 3.954 |

The pure metals in the form of powder were weighed out in proper proportions and melted in graphite in a

high frequency induction vacuum furnace. They were heated to 1100°C and slowly cooled. The ingots were then removed from the crucible, inverted, returned to the crucible and remelted. This remelting procedure was intended to reduce segregation in the ingots. After remelting, the ingots were checked for weight loss. The weight loss in each ten gram ingot was held to less than 25 mg. The remelted ingots were cold rolled and then given a homogenizing heat treatment of 16 hr at 760°C to remove any remaining segregation.

Powder specimens were prepared by cutting the ingots with a fine file, one half the required amount of powder being taken from each end of the ingots. When the X ray diffraction pattern showed any difference in lattice constant between the ends of the ingot, the ingot was remelted and given an additional homogenization treatment.

All powder samples were sealed in evacuated pyrex tubes for heat treatment. Ordinary pyrex proved satisfactory for temperatures up to 650°C but above that temperature it was necessary to use a special high temperature pyrex glass. Annealing at temperatures below 500°C was done in a salt bath whereas for temperatures of 500°C and above an electric muffle furnace was used. In both furnaces the temperature control was $\pm 5^\circ\text{C}$. In all annealing treatments samples of cold worked powder were placed in a furnace which was already at temperature. In this manner the specimens recrystallized directly to the equilibrium structure for that temperature. Time at temperature was selected so as to allow complete recrystallization, but very little grain growth. Specimens were quenched from the annealing temperatures by breaking the pyrex tubes in cold water.

X ray diffraction photograms were made of all the heat treated powders using copper radiation and a Phragmen

San Francisco Meeting, February 1949.
TP 2486 E. Discussion of this paper (2 copies) may be sent to *Transactions AIME* before April 15, 1949. Manuscript received July 1, 1948.
Most of the material presented in this paper has been abstracted from a paper submitted by J. G. McMullin in partial fulfillment of the requirements for the degree of Master of Science from the Massachusetts Institute of Technology. Manuscript received at the office of the Institute July 1, 1948.
* Instructor, Department of Metallurgy and Professor of Metallurgy, respectively, Massachusetts Institute of Technology.
¹ References are at the end of the paper.

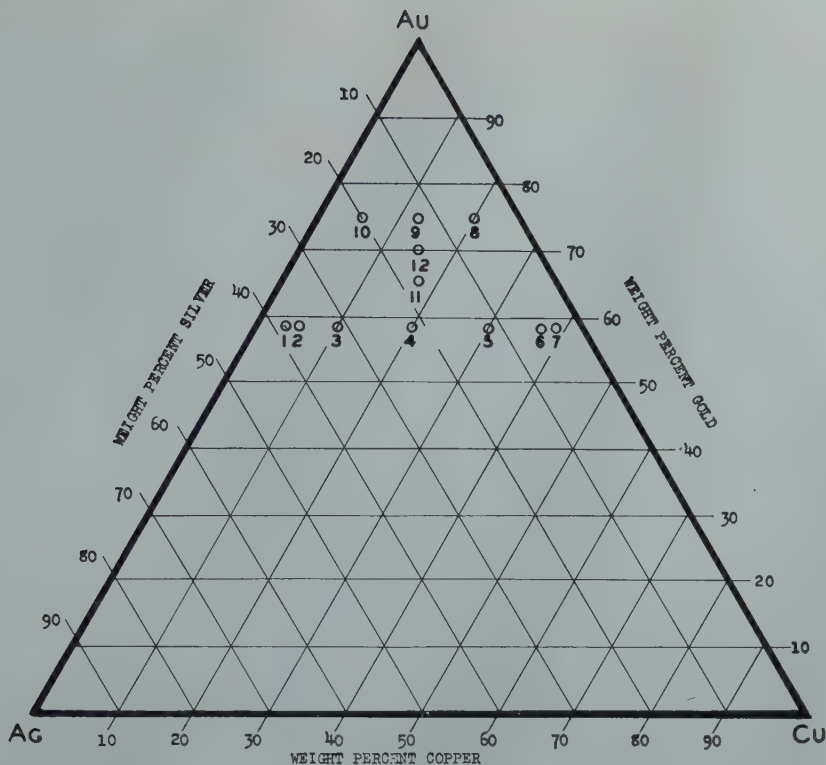


FIG 1—Compositions of the twelve alloys investigated.

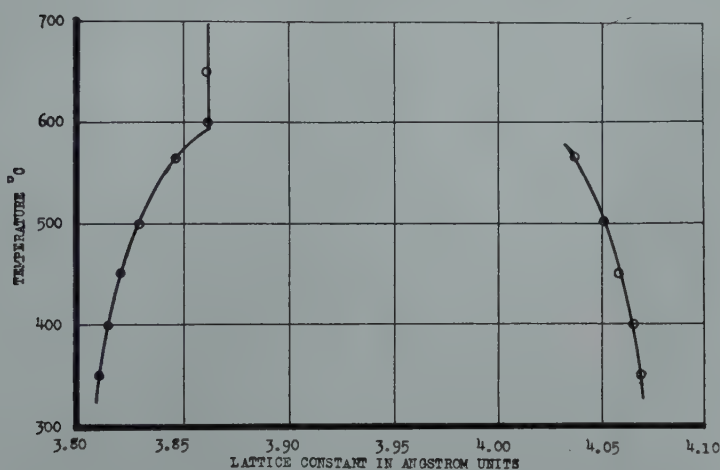


FIG 2—Lattice constants of alloy No. 5 quenched from the annealing temperatures indicated.

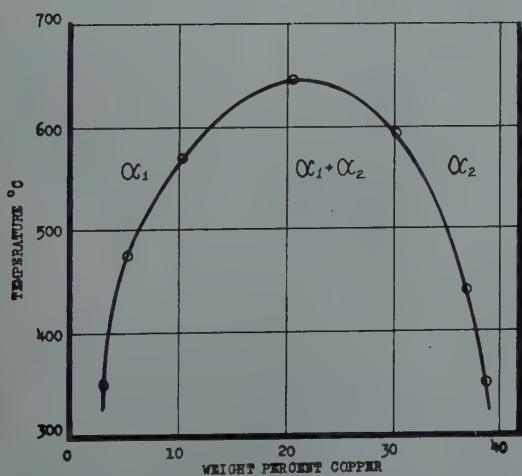


FIG 3—Vertical section through the ternary diagram showing the 14-karat alloys (58.3 pct Au).

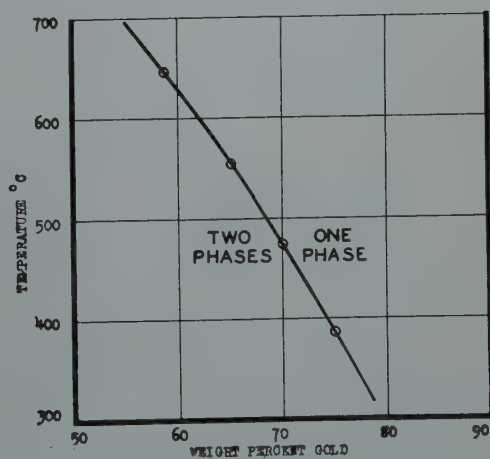


FIG 4—Vertical section through the ternary diagram showing alloys containing equal amounts by weight of silver and copper.

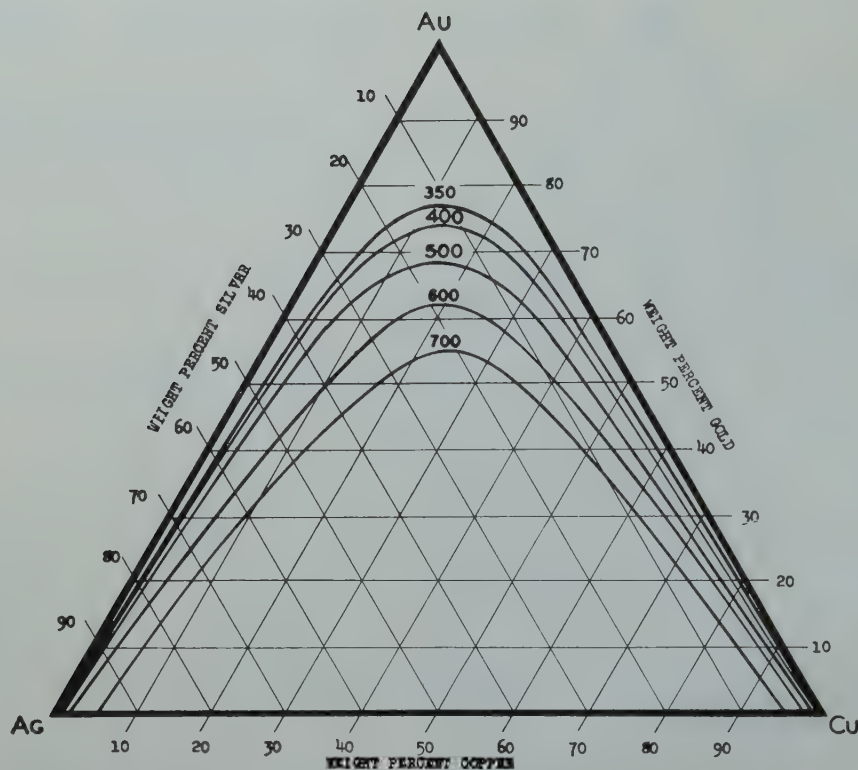


FIG 5—Isothermal sections defining the two-phased region in the gold-silver-copper ternary system.

focusing X ray camera. All the structures observed were face-centered cubic with no indication of ordering or tetragonality. The lattice constants of the phases were determined to ± 0.002 Å based on a copper K alpha one wavelength of 1.54050 Å. In alloys where the pattern of the solute phase was weak this accuracy was not maintained. Also alloy No. 9 did not recrystallize completely when annealed below its solution temperature and its lattice constants were not accurately determined. Since each alloy was annealed at several temperatures above its solution temperature the lattice constants of the solid solutions listed on Table 1 are the average of several determinations and are probably accurate to ± 0.001 Å.

Determination of Phase Boundaries

In order to determine the limits of the two phase field, the twelve alloys listed in Table 1 and plotted in Fig 1 were employed. Cold worked powder specimens of each alloy were annealed at several temperatures and quenched to room temperature. The lattice constants of each specimen were determined by X ray diffraction methods. For each alloy a plot was made of the lattice constant vs. annealing tempera-

ture. Fig 2 is typical of the twelve plots made in this manner. This plot shows the lattice constant of the gold-copper rich matrix phase as well as the larger lattice of the gold-silver rich solute phase. The diffraction pattern of the solute phase is very faint in some alloys, especially at temperatures just under the solution temperature. In alloys No. 1 and 7 the solute phase is present in such a small amount that it gives no visible diffraction pattern. In all alloys the variation in the lattice constant of the solvent phase is so large that the solution temperature can easily be determined. In Fig 2 the lattice constant of the alloy is constant for all temperatures above the solution temperature and decreases as the gold-silver rich phase is precipitated at temperatures below the solution temperature. The exact solution temperature is determined graphically by drawing a vertical line through the points above the solution temperature and the best smooth curve through the points below the solution temperature. The intersection of the vertical line and the curved line determines the solution temperature for the alloy in question. The solution temperatures of ten of the twelve alloys were determined in this manner. The solution temperatures of alloys No. 8 and 10 were below the lowest temperature at which these alloys would recrystallize.

Alloys No. 1, 2, 3, 4, 5, 6 and 7 all lie on one vertical section through the ternary system while alloys No. 9, 12, 11 and 4 lie on another perpendicular to it. These two sections are shown on Fig 3 and 4 where the solution temperatures of the alloys are plotted against their compositions. Using these two vertical sections and the silver-copper binary diagram, it was possible to sketch in the limits of the two phase region at several temperatures in the ternary system as shown in Fig 5.

Results

Fig 5 shows horizontal sections of the ternary diagram outlining the two phase field at five different temperatures. Each section is drawn from three points in the ternary field and two points taken from the binary copper-silver diagram. It is estimated that the error in the position of these boundaries is of the order of ± 2 pct in composition. Fig 4 shows a vertical section for equal parts of copper and silver in the range from 50 to 100 pct of gold.

The horizontal section at 400°C is in good agreement with the results obtained by Masing and Kloiber.¹ The vertical section corresponding to the 14 kt alloys is only in fair accord with the results of Pickus and Pickus² but these investigators presented their results only as approximations.

The horizontal section at 350°C extends into the region of the 18 kt alloys and thus shows how these alloys are susceptible to age hardening by transformation from a single homogeneous phase into two separate phases of different composition.

Acknowledgments

The authors wish to express their indebtedness to Messrs. Leach and Christie of Handy and Harmon for providing the pure gold used in the present investigation, and to Mr. Albert Mahfuz for performing much of the experimental work.

References

1. G. Masing and K. K. Kloiber: *Ztsch. f. Metallkunde*, (1940) **32**, 125.
2. M. R. Pickus and I. W. Pickus: *Trans. AIME* (1943) **152**, 94.
3. J. G. McMullin: *The Age Hardening of Gold-Silver-Copper Alloys*, unpublished.
4. R. Hultgren and L. Tarnopol: *Trans. AIME* (1939) **133**, 228.

Stress and Strain States in Elliptical Bulges

C. C. CHOW,* A. W. DANA,* AND G. SACHS†

Introduction

A GREAT number of the investigations on the plastic flow of metals have been concerned with the establishment of a "universal" stress-strain relation. In such a relation some stress function when plotted against a strain function should yield identical curves for the various stress states.

In the first investigation of this type, Ludwik and Scheu¹ plotted the maximum shearing stress as a function of the maximum principal strain. Later Ros and Eichinger² introduced two universal stress-strain relations, the one relating the maximum shearing stress to the maximum shearing strain, and the other relating a stress invariant, suggested by von Mises and Haigh, to the corresponding strain invariant. (In more recent investigations the stress and strain invariants are frequently supplemented with some factor to render their meaning more lucid.) A further suggestion which has not attracted appreciable attention is that by Baranski³ who used stress and strain deviators.

The most common means of experimentation to determine the relation between stress and strain consists in subjecting thin walled tubes to combined internal pressure and axial tension.^{4a,4b,4c} This method allows the study of plastic flow under stresses which are variable in two directions. However, the plastic flow which can be obtained in this manner is comparatively small, being limited by either tension failure or instability.

For copper,^{4a} only the relation between maximum shearing stress and maximum shearing strain yielded good agreement. On the other hand, tests on a steel^{4b} and on an aluminum alloy^{4c} resulted in systematic deviations if any of the discussed universal stress-strain relations were used. It would seem, therefore, that the agreement mentioned above for copper is only incidental and explained by its high rate of

strain hardening compared to that of other metals.

Much larger strains than experienced in the tube tests can be obtained by subjecting a thin membrane of a ductile metal, which is restrained at its periphery, to a uniform hydraulic pressure. The thin sheet forms a deep bulge before it fails. The stresses and strains in such a bulge increase with increasing distance from the edge of the clamping "die," the maximum stresses and strains occurring at the pole (crown) of the bulge. While the stress and strain states are determined by the contour of the bulge, the absolute magnitude of the stresses and strains depends upon the hydraulic pressure. The bulge contour is in turn correlated with the geometry of the die opening.

The deformation and fracture characteristics of circular bulges, that is, bulges formed with circular clamping dies, have been the subject of numerous experimental and analytical investigations.^{5,6,7} It has been shown that plastically deformed circular bulges develop large and comparatively uniform strains before failure by instability^{6b,6c,6d} and closely assume a spherical shape.^{6d} Also the distribution of strains across the contour of the bulge is dependent on the metal being investigated and is correlated with, but cannot be predicted from, the metal's stress-strain characteristics.

On the other hand, oblong or elliptical bulges, that is, bulges formed with elliptical clamping dies, are not as susceptible to analytical analysis and have not been investigated to the extent that circular bulges have. The few available data^{6a,7c} indicate that stress states are obtained at the poles of the bulges, varying between plane strain and balanced biaxial tension, depending upon the geometry of the die opening.

In this paper, the strain state and curvatures exhibited by three bulge shapes, a circular and two elliptical bulges, Fig 1, are analyzed experimentally using methods described in previous publications.^{6a,6c} An attempt is made to derive the stress-strain relations for these bulges, which represent strain states in which the ratio of the two positive principal strains varied between 1.0 and 0.35. In addition, tension tests yielded data for a value of -0.5 for this strain ratio.

Such an analysis should indicate the applicability of the various laws correlating stress with strain to the stress and strain states occurring in bulged shapes.

Definitions and Nomenclature

The definitions of the major stress and strain quantities used in this paper are as follows:

s_1, s_2, s_3 = principal normal stresses

$$s_1 > s_2 > s_3$$

t = shear stress

e = conventional (unit) strain

$$\epsilon = \ln(1 + e)$$

$\epsilon_1, \epsilon_2, \epsilon_3$ = principal natural strains

γ = shear strain

The maximum shear stress:

$$t_{max} = \frac{s_1 - s_3}{2}$$

Frequently, the flow stress, $s_1 - s_3 = 2t_{max}$, rather than the maximum shear stress is used.

San Francisco Meeting, February, 1949.

TP 2485 E. Discussion of this paper (2 copies) may be sent to *Transactions AIME* before April 15, 1949. Manuscript received at the office of the Institute June 10, 1948.

The work reported in this paper was made possible by the Frederick Cottrell grant received from the Research Corporation, New York.

* Research Laboratory for Mechanical Metallurgy, Case Institute of Technology, Cleveland, Ohio.

† Professor of Physical Metallurgy and Director of Research Laboratory for Mechanical Metallurgy, Case Institute of Technology.

¹ References are at the end of the paper.

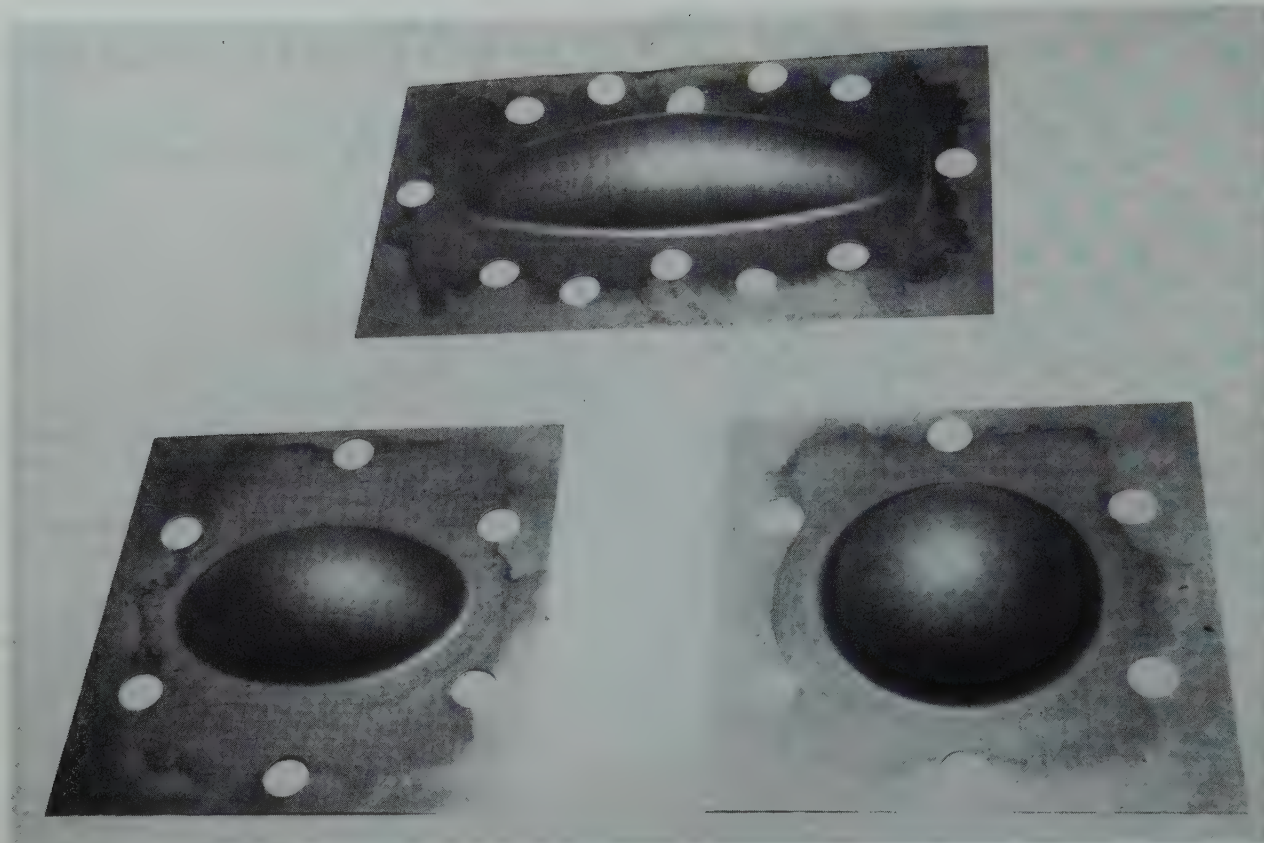


FIG 1—Typical shapes formed on hydraulic bulging of thin sheets.

The largest principal natural strain, ϵ_{max} , is the value of the principal strain having the largest absolute value.

The maximum shear strain:

$$\gamma_{max} = \gamma_2 = \epsilon_1 - \epsilon_3$$

The effective stress:

$$\bar{s} = \frac{1}{\sqrt{2}} \sqrt{(s_1 - s_2)^2 + (s_2 - s_3)^2 + (s_3 - s_1)^2}$$

The octahedral shearing stress, t_{oct}

$$= \frac{\sqrt{2}}{3} \bar{s}$$

The effective strain:

$$\bar{\epsilon} = \frac{\sqrt{2}}{3} \sqrt{(\epsilon_1 - \epsilon_2)^2 + (\epsilon_2 - \epsilon_3)^2 + (\epsilon_3 - \epsilon_1)^2}$$

The octahedral shearing strain, γ_{oct}

$$= \sqrt{2} \bar{\epsilon}$$

The factors in the equations for the effective stress and effective strain serve to render $\bar{s} = s_1$ and $\bar{\epsilon} = \epsilon_1$ for uniaxial tension ($s_2 = s_3 = 0$ and $\epsilon_2 = \epsilon_3 = -\epsilon_1/2$).

Material and Procedure

Cartridge brass (70 pct copper, 30 pct zinc) sheet of 0.040 inch thickness was chosen for the experimental investigation. The rolling and annealing schedule for the sheet was designed to produce isotropic material. To further insure uniformity, the sheet was annealed at 850°F for one-half hour and then air cooled.

In order to determine the degree of isotropy in the sheet, tension tests (specimens $\frac{3}{4}$ in. in width with a 5-in. gauge length) were made parallel to, transverse to, and 45° to the rolling direction. The three stress-strain curves were found to be identical, Fig 2. In Fig 3, the natural strains, ϵ_2 and ϵ_3 , from two series of tests are plotted as a function of ϵ_1 . It is seen that the sheet conforms reasonably to isotropic conditions.

Before bulging, the blanks were photogrided⁸ with a 20 line-to-the-inch net, the grid being parallel and perpendicular to the rolling direction of the sheet.

In all, six bulge shapes were made by using appropriate clamping dies. There were two circular bulges, two ellipses* with a ratio of minor to major axis of 0.60 and two ellipses* with this ratio 0.32. (See Fig 1.)

The equipment and procedure for testing bulges and measuring the pertinent quantities have been described in previous publications on circular bulges.^{6c, 6d} Each bulge was loaded in steps and unloaded after each step. The pressure was recorded and the principal strains and the height

* These contours were not exactly true ellipses but were bulged using clamping dies whose openings were constructed by using arcs of circles. See Ref. 6e for die geometry.

of the bulge surface at various distances from the pole determined.

The strains were measured along the two lines of the photogrid, which were initially located parallel to the short and long axis of the die. Over a considerable area in the center of the bulge, the strain values represent, with sufficient accuracy, the two principal strains in the bulge surface along its intersections with planes containing the pole and the major and minor axis of the die, respectively. Examples of the distribution of these strains are given in Fig 4 and 5. These graphs illustrate that the elliptical bulges exhibited a rather narrow region in the vicinity of the pole in which the strains were nearly constant. As to be expected, the strains decreased rapidly with increasing distance from the pole in the direction of the small axis, but only slowly in the direction of the large axis of the die.

The strain values at the pole obtained from the trend curves in Fig 4 and 5 are taken as the two principal strains, ϵ_1 (perpendicular to major axis) and ϵ_2 (perpendicular to the minor axis), for the respective load value.

Fig 6 and 7 illustrate distributions of the strain state, defined by the ratio of

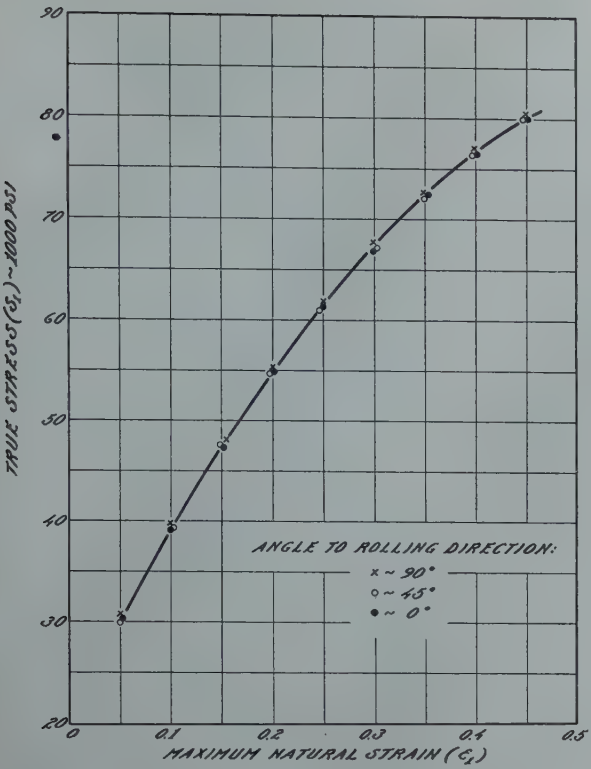


FIG 2—Stress-strain curve for annealed 70-30 brass in tension.

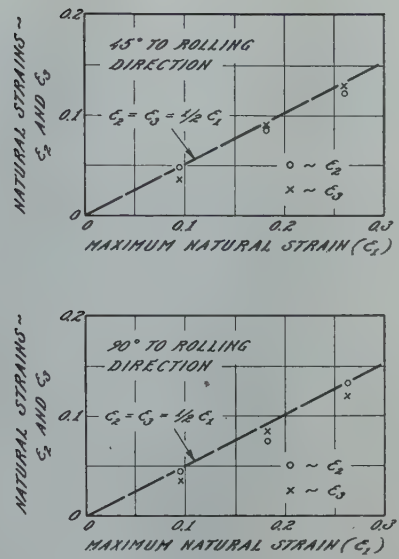


FIG 3—Natural strains ϵ_2 (width) and ϵ_3 (thickness) as a function of ϵ_1 (longitudinal) for tension tests on annealed 70-30 brass sheet (0.040 in. thick).

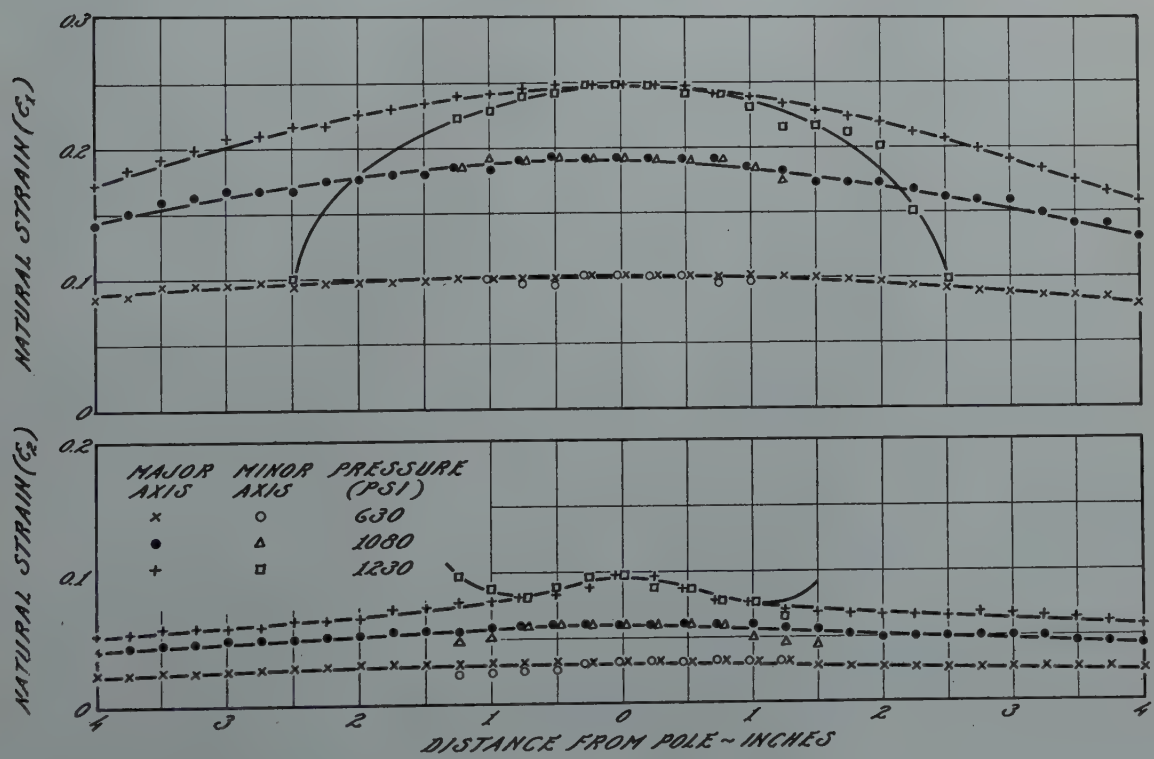


FIG 4—Distribution of strains (ϵ_1 and ϵ_2) at various pressures for annealed 70-30 brass bulged to elliptical contour (ratio of minor to major axis = 0.32).

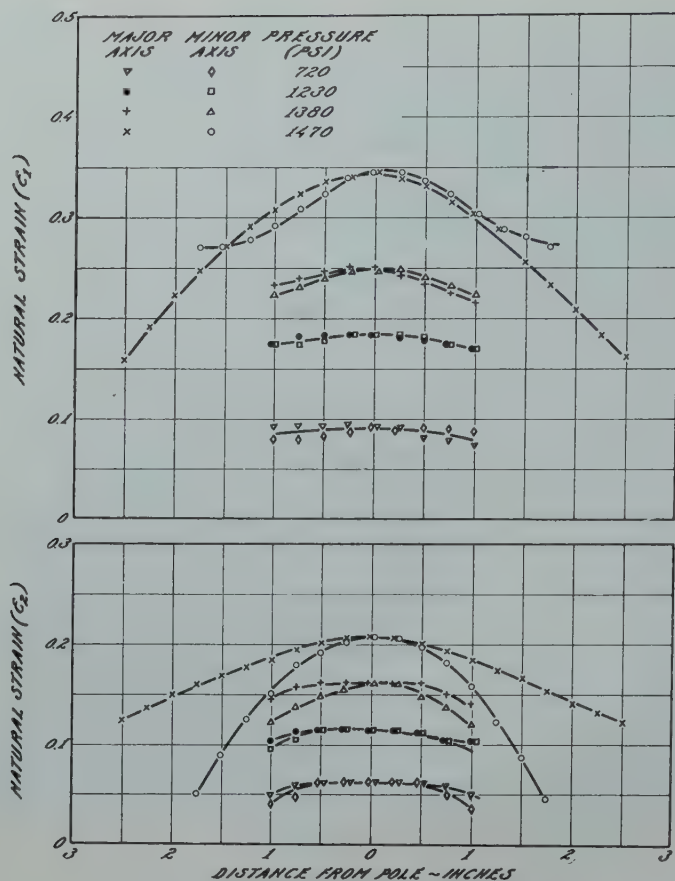


FIG 5—Distribution of strains (ϵ_1 and ϵ_2) at various pressures for annealed 70-30 brass bulged to an elliptical contour (ratio of minor to major axis = 0.60).

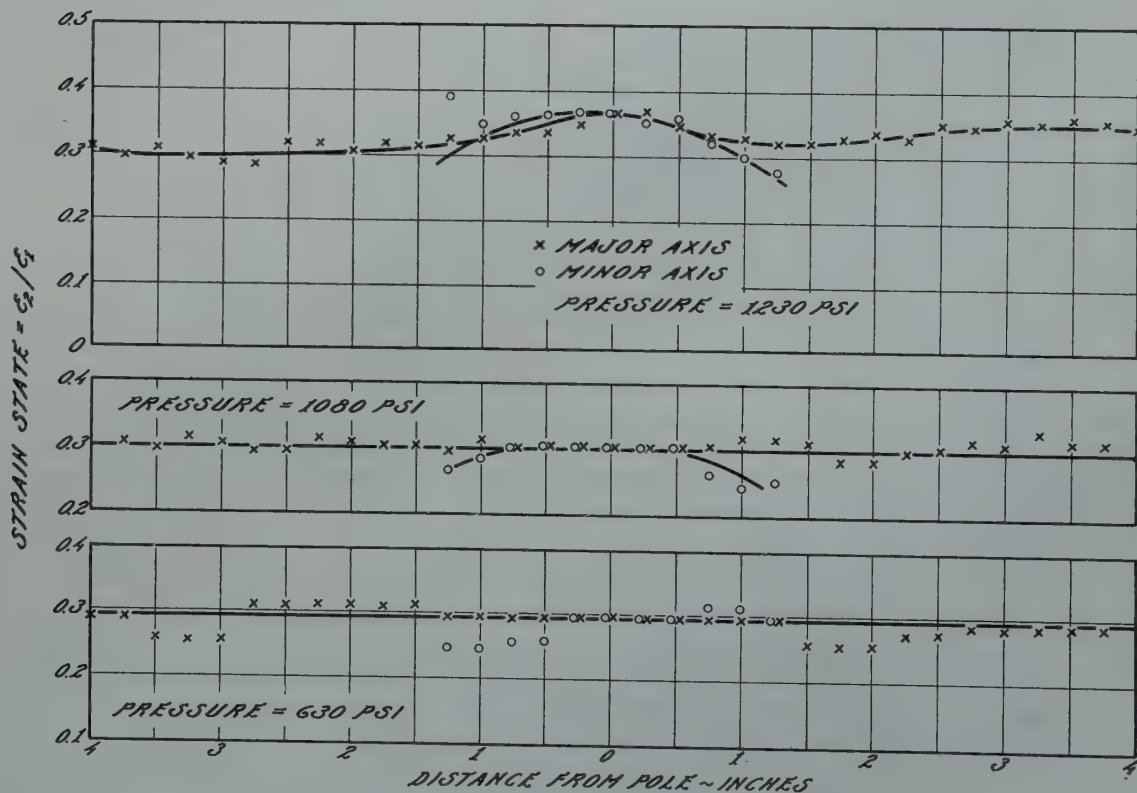


FIG 6—Distribution of strain state (ratio: ϵ_2/ϵ_1) in annealed 70-30 brass bulge (ratio of minor to major axis = 0.32). Derived from Fig 4.

the two principal strains in Fig 4 and 5. According to these graphs, the strain state differed only slightly over the crown of the bulge surface while large variations were noted in areas in the vicinity of the clamped edge.

The radii in the two principal directions of a bulge were determined from the height for various chord lengths, as described in a previous publication.^{5d} An example of the results of this procedure, for a few selected load readings, is shown in Fig 8. The values of the radii extrapolated to zero chord length are considered to be the radii of curvature at the pole, R_1 and R_2 in the two principal directions.

Since the bulge shapes were not fractured (only the one bulge having a ratio of minor to major axis of 0.32 was taken to fracture) it was possible to section the bulges for tension tests. These tension specimens were cut from the center portion of the bulges along the minor axis so that the pole was included. The additional strain resulting from the tension test was measured by using a radial strain gauge. In all cases no appreciable load was carried by the specimen until the specimen had straightened.

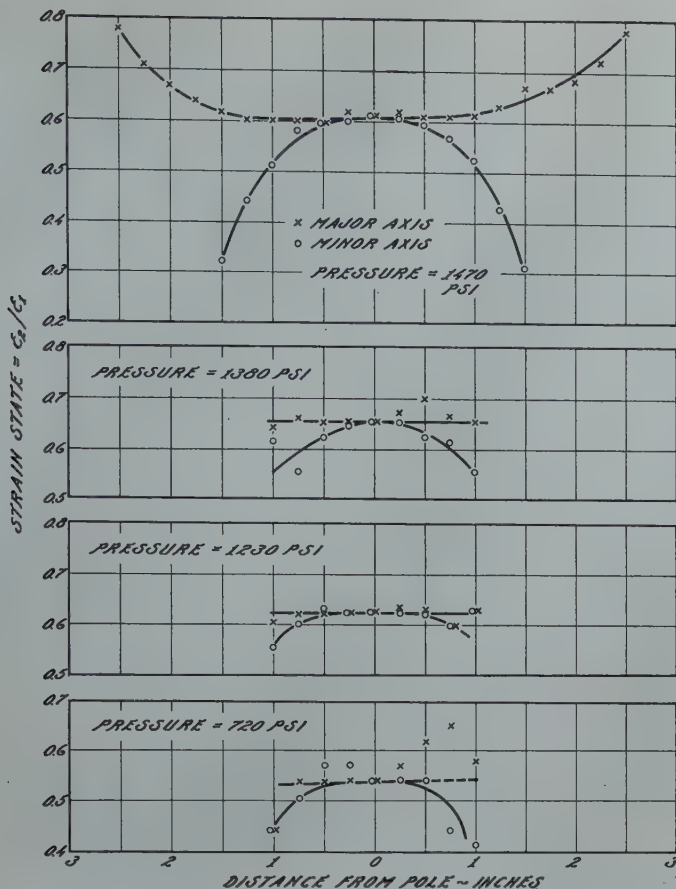


FIG 7—Distribution of strain state (ϵ_2/ϵ_1) in annealed 70-30 brass. Bulge (ratio of minor to major axis = 0.60). Derived from Fig 5.

Results

The bulging data are illustrated in Fig 9 to 12. The pressure, p , is plotted against each of the three principal strains ϵ_1 , ϵ_2 , and $-\epsilon_3$ in Fig 9 to 11, and the radii against the largest principal strain, $-\epsilon_3$, in Fig 12.

The values of ϵ_2 and ϵ_1 are replotted in Fig 13 as functions of $-\epsilon_3$. This graph reveals that during the forming of each bulge the strain state remains practically constant.

For the further analysis, average values of the various quantities obtained from the trendline through the experimental points for the two parallel tests are used. In general, for identical conditions two tests yielded results in close agreement.*

Analysis

The equilibrium of a shell element, Fig 14, yields the following relation:

$$\frac{p}{h} = \frac{s_1}{R_1} + \frac{s_2}{R_2} \text{ or } s_1 = \frac{R_1 p}{h} - \frac{R_1 s_2}{R_2} \quad [1]$$

* In the case of the elliptical bulges having a ratio of minor to major axis of 0.32 some deviation in the values was noted. This probably was due to the considerable slippage during one of the tests. However, this difference was found to be of little influence on the results of the analysis.

The experimental data yield the quantities p , h , R_1 , and R_2 . This leaves two unknowns for which only one equation is available. The other equation must be obtained from some established law of plasticity.

In this analysis the following assumptions will be made concerning conditions at the pole of the bulges:

1. Volume changes can be neglected during plastic flow, or:

$$\epsilon_1 + \epsilon_2 + \epsilon_3 = 0 \quad [2]$$

2. Stress states encountered during bulging are practically biaxial, or:

$$s_3 \approx 0 \quad [3]$$

3. Edge effects are negligible as are any bending or flexural stresses.

EFFECTIVE STRESS AND EFFECTIVE STRAIN

A relation, which is widely accepted, states that the second stress invariant is a function only of the second strain invariant and is independent of the stress state. Thus, for a given value of $\bar{\epsilon}$, the value of \bar{s} is given by the curve for balanced biaxial tension, in Fig 15. The definition of $\bar{\epsilon}$, Eq 4, and the constant volume condition, Eq 2,

$$\bar{\epsilon} = \frac{\sqrt{2}}{3} \sqrt{(\epsilon_1 - \epsilon_2)^2 + (\epsilon_2 - \epsilon_3)^2 + (\epsilon_3 - \epsilon_1)^2} \quad [4]$$

yield values of $\bar{\epsilon}$ for the various bulged shapes, corresponding values of ϵ_1 and

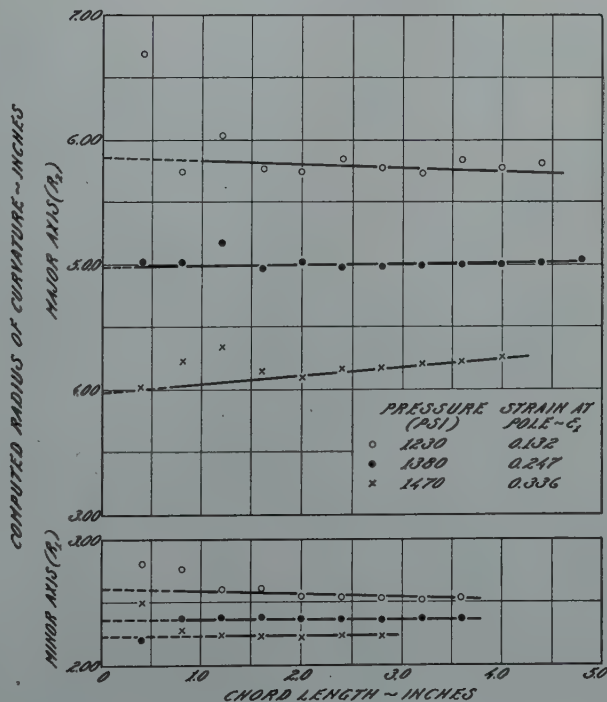


FIG 8—Example of determination of radii of curvature at pole for elliptical bulge (ratio of minor to major axis = 0.60).

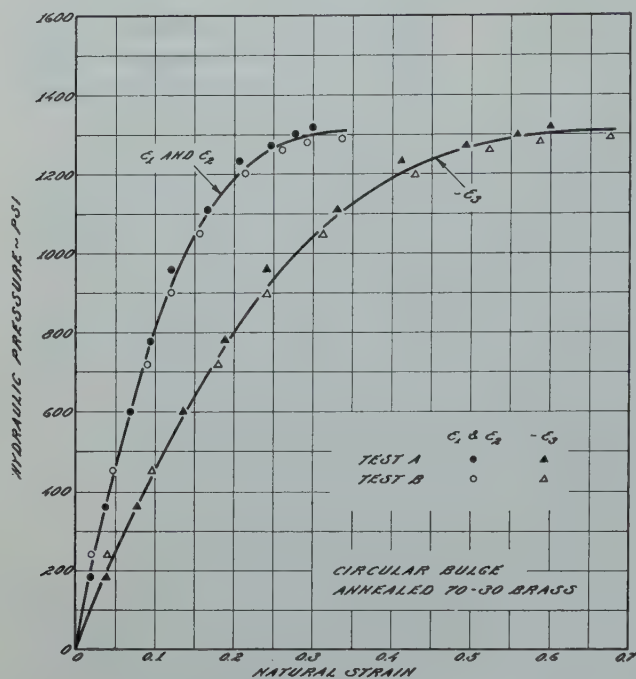


FIG 9—Hydraulic pressure as a function of the three principal natural strains at pole for circular bulging of annealed brass sheet.

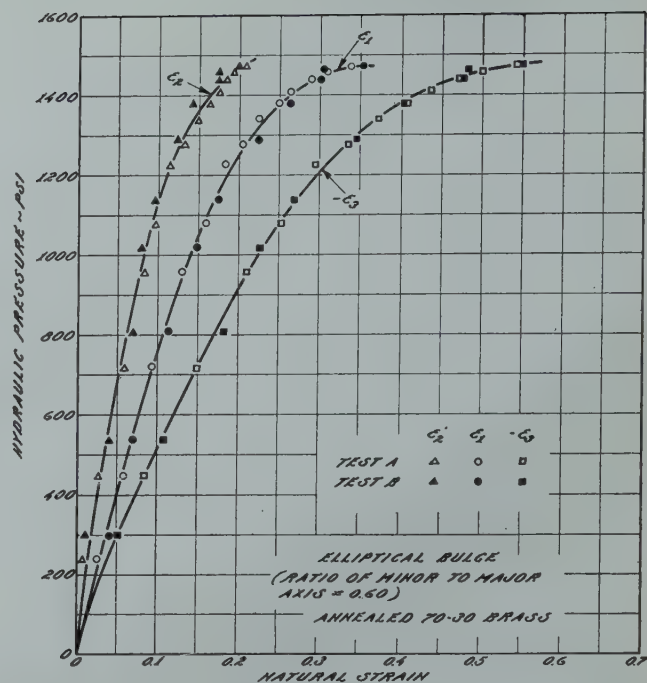


FIG 10—Hydraulic pressure as a function of the three principal natural strains at pole for elliptical bulging of annealed brass sheet.

ϵ_2 being determined experimentally. For these data Fig 9 to 12 then give the pressure, p , and the radii of curvature, R_1 and R_2 , and the value of \bar{s} which is defined as follows:

$$2\bar{s}^2 = (s_1 - s_2)^2 + (s_2 - s_3)^2 + (s_3 - s_1)^2 \quad [5]$$

Simplifying Eq 5 for bulges, where $s_3 \approx 0$:

$$\bar{s}^2 = s_1^2 - s_1 s_2 + s_2^2 \quad [5a]$$

Now by letting $c_1 = \bar{s}$, $c_2 = \frac{R_1 p}{h}$ and $c_3 = \frac{R_2}{R_1}$ and substituting Eq 1 in Eq 5a, a quadratic equation for s_2 is obtained:

$$s_2^2 - s_2 \left[\frac{2c_2 c_3 + c_2}{c_3^2 + c_3 + 1} \right] + \left[\frac{c_2^2 - c_1^2}{c_3^2 + c_3 + 1} \right] = 0 \quad [6]$$

from which:

$$s_2 = \frac{2c_2 c_3 + c_2}{c_3^2 + c_3 + 1} \pm \sqrt{\left[\frac{2c_2 c_3 + c_2}{c_3^2 + c_3 + 1} \right]^2 - 4 \left[\frac{c_2^2 - c_1^2}{c_3^2 + c_3 + 1} \right]} \quad [6a]$$

The corresponding value of s_1 may be obtained by substituting the value of s_2 in Eq 1.

The above calculations were carried out for the two elliptical bulges. However, the value of the ratio of s_2/s_1 were found to be approximately 0.55 in the case of the ellipse with a ratio of minor to major axis of 0.60 and 0.40 in the case of the ellipse with a ratio of 0.32. These values of the ratio s_2/s_1 are not consistent with the experimentally determined strain state. Apparently

the effective stress-effective strain relation is not sensitive to small changes in stress states.

ST. VENANT'S RELATION

An alternative method to determine the stresses present in elliptical bulges, from Eq 5, is to use as the second equation some relation between the known strains ϵ_1 , ϵ_2 , $\epsilon_3 = \epsilon_1 - \epsilon_2$ and the stresses s_1 , s_2 , $s_3 \approx 0$. Such a relation has been suggested by St. Venant. Previous investigations have shown that St. Venant's relation can be used to determine accurately the strains resulting from a varying stress state, such as occurs in deep drawing.⁹ Because of the consistent strain state, $\epsilon_2/\epsilon_1 = \text{constant}$, found to exist in

bulges according to Fig 13, St. Venant's relation also applies to finite strains, rather than to strain rates, as follows*:

* The validity of St. Venant's relation has been investigated repeatedly.^{4,9,10} It can be derived from this data that in the range of strain states occurring in bulging, namely, $\epsilon_1 > \epsilon_2 > 0$, the stress ratio s_2/s_1 may be actually as much as 5 pct larger than that given by St. Venant's relation. However, a correction of this magnitude would change the stress, s_1 , calculated from Eq 8 by not more than one to two percent. A correction of this magnitude does not affect the conclusions derived from the present investigation.

$$\frac{s_1 - s_2}{s_2 - s_3} = \frac{\epsilon_1 - \epsilon_2}{\epsilon_2 - \epsilon_3} \quad [7]$$

yielding for bulging, $s_3 = 0$:

$$\frac{s_2}{s_1} = \frac{\epsilon_2 - \epsilon_3}{\epsilon_1 - \epsilon_3} \quad [8]$$

For the two elliptical bulges investigated, where $\epsilon_2/\epsilon_1 = 0.60$ and 0.36 , respectively (Fig 13), this yields $s_2/s_1 = 0.85$ and 0.70 , respectively. Introducing these values into Eq 1 then permits calculating s_1 for these two bulges from the known quantities represented in Fig 9 to 12, according to the following respective relations:

$$s_1 = \frac{p}{h} \left(\frac{R_1 R_2}{R_2 + 0.85 R_1} \right) \quad (9a)$$

and

$$s_1 = \frac{p}{h} \left(\frac{R_1 R_2}{R_2 + 0.70 R_1} \right) \quad (9b)$$

The results of these calculations are shown in Fig 15, \bar{s}_1 being plotted against the largest principal strain, $-\epsilon_3$. In Fig 16, $s_1 = s_1 - s_3 = 2t_{\max}$ and \bar{s} are replotted as a function of the maximum shearing strain, $\gamma_{\max} = \gamma_2 = \epsilon_1 - \epsilon_3$, and Fig 17 illustrates the relation between s_1 and \bar{s} for the bulges investigated. The corresponding curves for the circular bulges (and also for uniaxial tension) are added to Fig 15 to 17.

The final results of the bulging tests on brass, represented in Fig 15 to 17, agree closely to those of the tests on

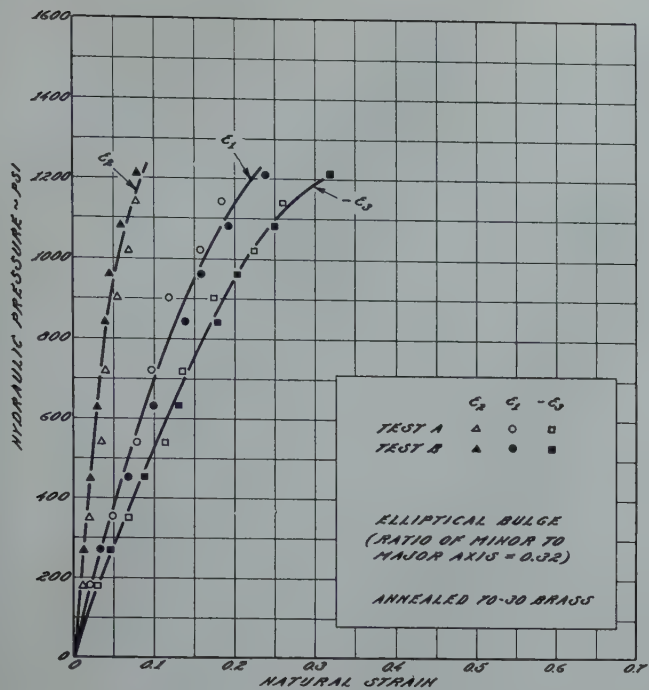


FIG 11—Hydraulic pressure as a function of the three principal natural strains at pole for elliptical bulging of annealed brass sheet.

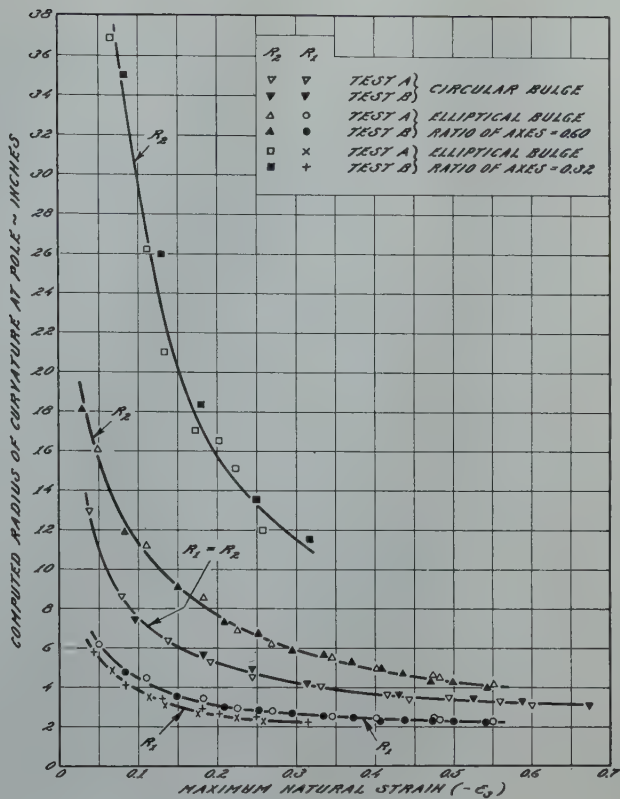


FIG 12—Radii of curvature (R_1 and R_2) as a function of the maximum strain at the pole for the three bulge shapes.

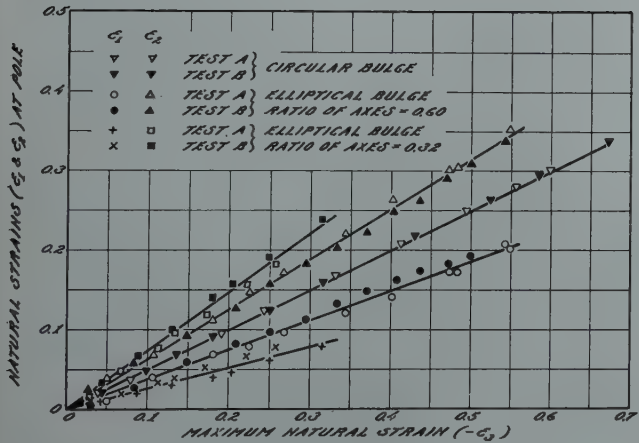


FIG 13—Principal strains (ϵ_1 and ϵ_2) as a function of the maximum principal strain (ϵ_3) for the various bulges made in annealed 70-30 brass.

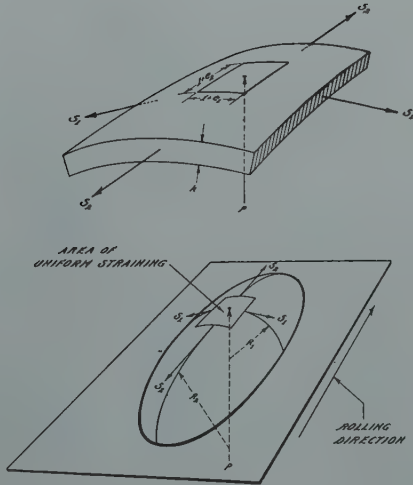


FIG 14—Stress, strain, and geometrical conditions in an elliptical bulge.

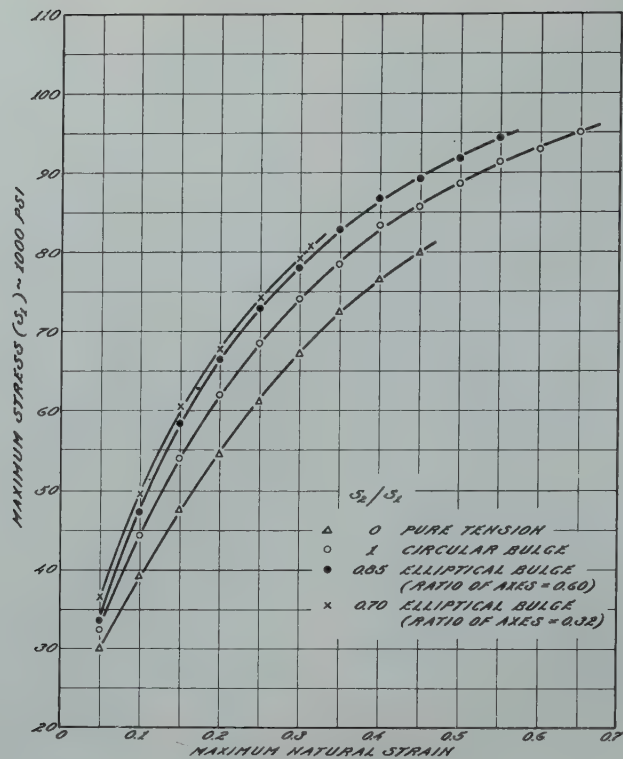


FIG 15—Maximum stress (s_1) as a function of the maximum natural strain ($-\epsilon_3$ at pole for bulges and ϵ_1 for tension test) for annealed 70-30 brass tested under various stress states.

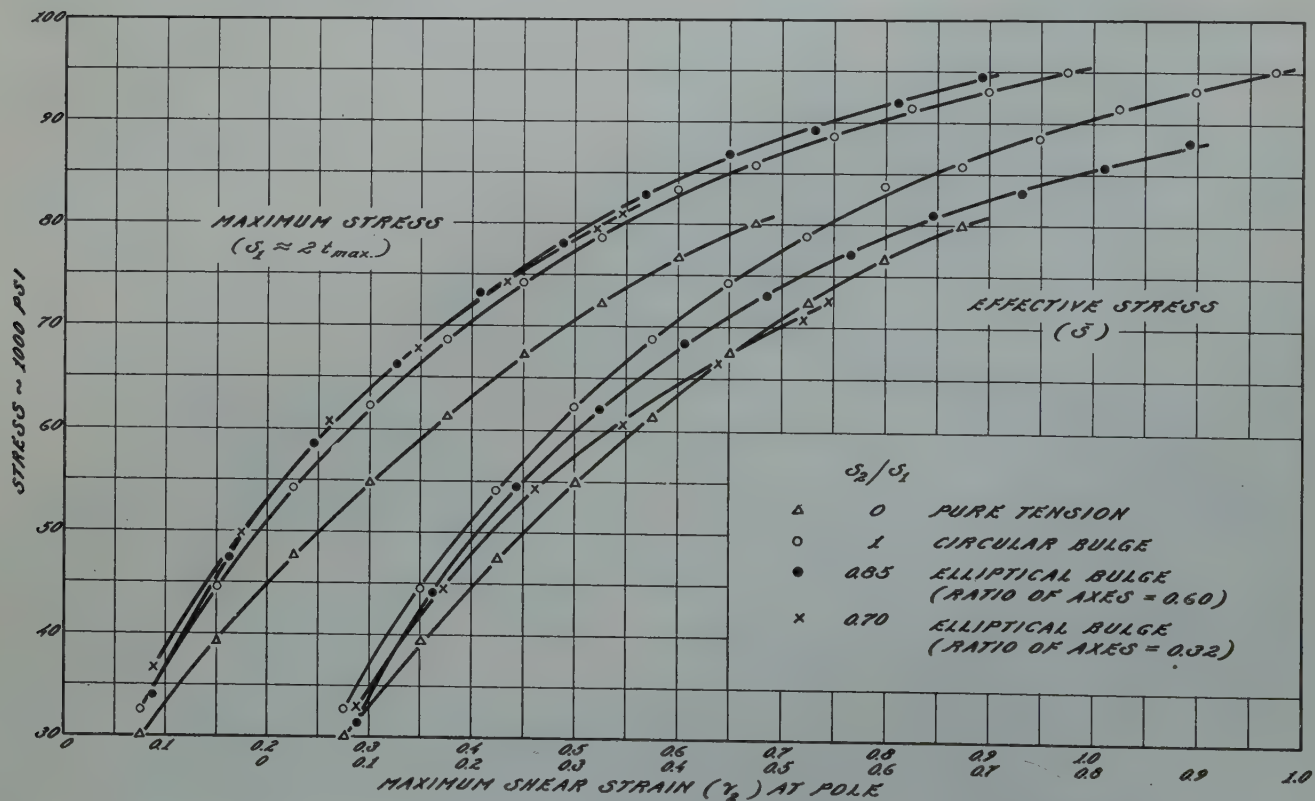


FIG 16—Maximum stress (s_1) and effective stress (s) as a function of maximum shear strain (γ_2) for bulge series and tension test on annealed 70-30 brass (values for bulges at pole).

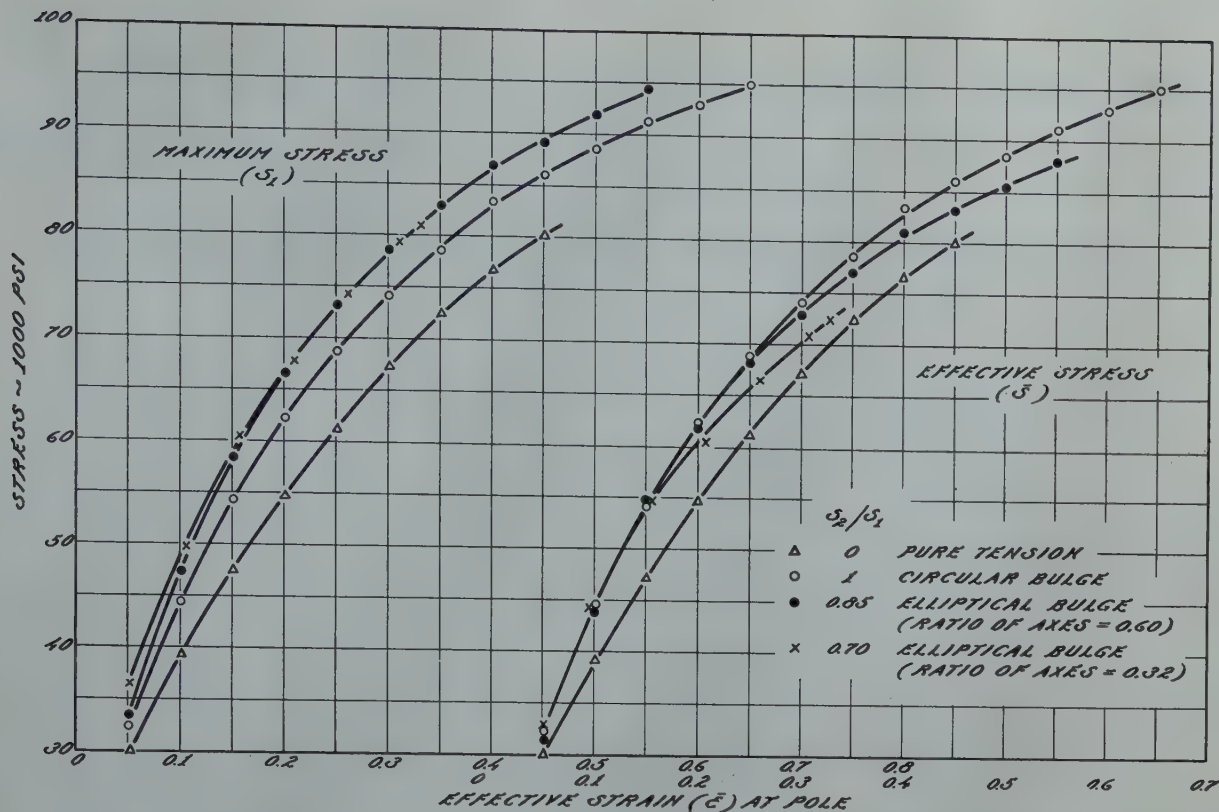


FIG 17—Maximum stress (s_1) and effective stress (s) as a function of effective strain (ϵ) for bulge series and tension test on annealed 70-30 brass (values for bulges at pole).

copper tubes. Of the various types of stress-strain curves, only the relation between the largest principal stress (or more generally between the maximum shearing stress) and the maximum shearing strain yields identical curves for the three bulges investigated, within the limits of experimental accuracy. As discussed in the introduction, this agreement is not universal but appears to apply only to metals with a high rate of strain hardening. The simplest representation of the largest principal stress as a function of the (absolutely) largest principal strain yields, for stress states approaching plane strain, stress values as much as 10 percent higher than for balanced biaxial tension. On the contrary, the effective stress-effective strain ($\bar{s} - \bar{\epsilon}$) relation yields for conditions near plane strain, lower values of the stress invariant than for balanced biaxial tension.

Thus, none of the universal stress-strain relations proposed to date applies accurately, in the range of biaxial tension.

UNIAXIAL AND BIAXIAL TENSION

In order to establish any law of plasticity, some simple stress state must be selected as a basis. In the present investigation, two such stress states were investigated, uniaxial tension, $s_2 = s_3 = 0$ and balanced biaxial tension, $s_2 = s_1$, $s_3 \approx 0^*$ (present in circular bulging).

While any of the recognized theories of plasticity requires identical stress-strain curves for these two stress states, the present tests yielded according to Fig. 15 to 17 considerably higher stresses for balanced biaxial tension than for uniaxial tension.

As mentioned in the procedure the various bulges were sectioned and the strips tested in tension. The results of these tests are shown in Fig 18. The flow stress shown by these specimens closely approximated values expected if the metal had been prestrained in tension. It would seem, therefore, that

* In these tests the pressure did not exceed 1500 psi while s_1 was then almost 100,000 psi. Therefore, s_3 did not exceed one percent of s_1 .

some effect or effects other than anisotropy or stress state, must be operating to cause higher stress values in bulging. One of these effects might well be the nonuniformity of strain values over the bulge contour induced by the lateral restriction of the sheet. In other terms, non-homogeneity of strain in a structure results in higher values for plastic flow than would be called for by the common laws of plasticity. If this effect is sufficient to cause the noted difference between bulging and tension, it would be expected that the amount of this discrepancy would vary with the degree of nonuniformity of the strain.

The main objective of the present tests was to compare the stress-strain relations for bulges of various shapes. Therefore, for the foregoing analysis the stress-strain curve for balanced biaxial tension, where s_1 is given as a function of $-\epsilon_3$, was used as a basis. Between the various investigated bulges the degree of lateral restriction should be approximately the same and since the metal can be considered identical, the observed differences in the stress-

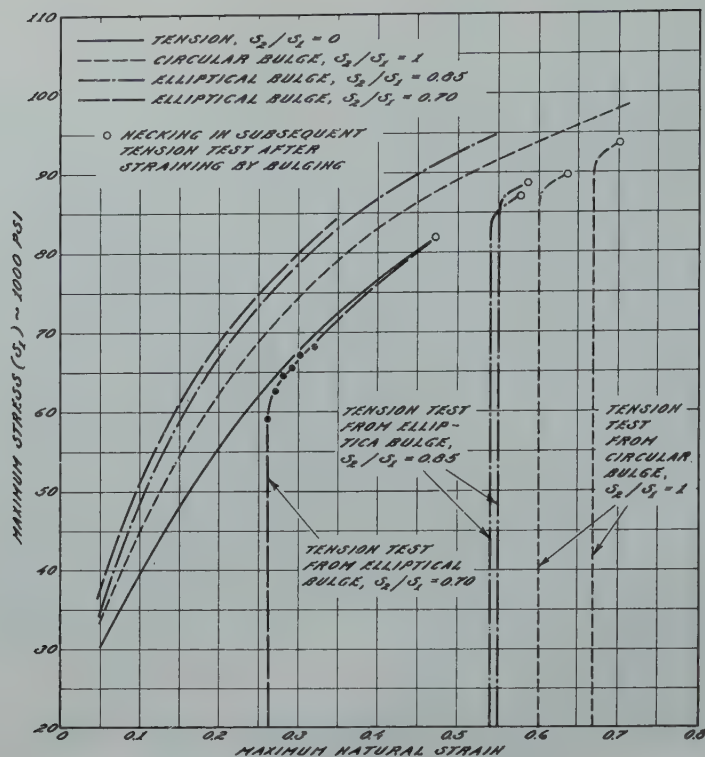


FIG 18—Results of tension tests on pieces sectioned from the various bulges. (The maximum strain in bulging is $-\epsilon_2$, while in tension ϵ_1 is used).

strain curves must be a result of the applied laws of plasticity.

Conclusions

Summarizing the results of this investigation, the following conclusions may be drawn regarding stress and strain states in elliptical bulging:

1. Stress values in elliptical bulges may be analyzed by using St. Venant's law of plasticity and the equation for equilibrium of a shell.

2. Stress states varying between balanced biaxial tension and close to plane strain can be obtained by bulging thin sheet using the proper die geometry.

3. None of the universal stress-strain relations proposed to date applies accurately in the range of biaxial tension.

4. The discrepancy between bulging and tension values of the stress required for plastic flow may be due to the non-homogeneity of strain across the contour of the bulge.

Acknowledgments

The authors are indebted to Mr. W. F. Brown, Jr. and Mr. F. C. Thompson for their help in formulating the program and to Mr. M. F. Jones for his aid in the experimentation.

References

1. P. Ludwik and R. Scheu: Comparison of Tensile, Compression, Torsion, and Rolling Tests. *Stahl u. Eisen*, (1925), 45, 373-381.
2. M. Ros and A. Eichinger: Experimentation on the Problem of Failure. Zurich, 1926, 1928 and 1929.
3. G. Baranski: Tensile Tests Under Plane Plastic Strain, *Ztsch. Metallkunde*, (1934) 26, 173-180.
- 4a. E. A. Davis: Increase of Stress with Permanent Strain and Stress-Strain Relations in the Plastic State for Copper Under Combined Stresses. *Trans. Am. Soc. Mech. Engrs.*, (1943) 65, A187-196.
- b. E. A. Davis: Yielding and Fracture of Medium Carbon Steel Under Combined Stresses. *Jnl. Appl. Mech.*, (1945) 12, A13-24.
- c. W. R. Osgood: Combined Stress Tests on 24ST Aluminum Alloy Tubes. *Jnl. Appl. Mech.* (1947) 14, 147-153.
- 5a. A. N. Gleyzal: Progress Report on Underwater Explosion Research. Bur. of Ships Symbol E139, Part 14, U.S. Navy Dept. TMB Report R-248, (1944), May.
- b. M. A. Greenfield: Progress Report on Underwater Explosion Research, Bur. of Ships Symbol E139, Part 10. U.S. Navy Dept. TMB Report R-248, (1944), May.
- c. W. Mostow: Plastic Deformation of Thin Plates Under Hydrostatic Pressure. U.S. Navy Dept. Bur. of Ships Report No. 1946-1 (NAVSHIPS-250-424-1) (1946).
- 6a. G. Sachs, G. Espey and G. B. Kasik: Circular Bulging of Aluminum Alloy Sheet at Room and Elevated Temperatures. *Trans. Am. Soc. Mech. Engrs.*, (1946) 68, 161-173.
- b. G. Sachs and J. D. Lubahn: Failure of Ductile Metals in Tension. *Trans. Am. Soc. Mech. Engrs.*, (1946) 68, 271-276.
- c. W. F. Brown, Jr. and G. Sachs: Strength and Failure Characteristics of Thin Circular Membranes. *Trans. Am. Soc. Mech. Engrs.*, (1948) 70 (in print).
- d. W. F. Brown, Jr. and F. C. Thompson: Strength and Failure Characteristics of Metal Membranes in Circular Bulging. *Trans. Am. Soc. Mech. Engrs.*, (1948) 70, (in print).
- e. G. Sachs, et al.: War Metallurgy Comm. Reports, Serial Nos. W-105 (1944) and W-125 (1945); and Office of Production Research and Development (WPB) Reports Nos. W-167, W-169, W-195, and W-199 (1945).
- 7a. W. T. Lankford and M. Gensamer: The Plastic Flow of Aluminum Alloy Sheet under Combined Loads. *AIME Met. Tech.*, (1947), TP 2237.
- b. W. T. Lankford and E. Saibel: Some Problems in Unstable Plastic Flow Under Biaxial Tension. *AIME Met. Tech.* (1947) TP 2238.
- c. M. Gensamer, et al.: Reports on the Plastic Flow of Aluminum Aircraft Sheet Under Combined Loads. War Metallurgy Division (NDRC) Reports, Serial Nos. M86, M141, M191, M270, M468, M527, M529, M530.
8. W. F. Brown, Jr. and M. H. Jones: Strain Analysis by Photogrid Method. *Iron Age*, (1946) 158, Sept. 12, 50-55.
9. G. Sachs: Investigations on Deep Drawing. "Spanlose Formung" (1930), 11-38.
10. W. Lode: Tests on the Effect of the Intermediate Principal Stress on the Flow of the Metals Iron, Copper, and Nickel. *Ztsch. Phys.* (1926) 36, 913-939.
11. G. I. Taylor and H. Quinney: The Plastic Distortion of Metals. *Phil. Trans. Roy. Soc., London*, (1931), 230, 329-362.

A Study of Textures and Earing Behavior of Cold-rolled (87-89 pct) and Annealed Copper Strips

MING-KAO YEN*
Junior Member AIME

A CONSIDERABLE amount of work has been reported in the literature in regard to the texture and earing behavior of copper strip. The rolling texture of copper has been confirmed as (110) $\bar{1}\bar{1}2$ and (112) $11\bar{1}$, which yields ears of a drawn cup at the position 45° from the rolling direction.¹⁻³ The recrystallization texture has been established as the cubic or (100) [001] texture, where the earing positions are at 0° and 90° to the rolling direction.⁴⁻⁸ It has also been reported that in the development of cubically aligned grains of copper strips, the percentage of this cubic texture increased with an increase of final reduction and final annealing temperature.^{8,9} A comprehensive study on H.C. copper (British commercial copper of high-conductivity quality = Cu 99.95 pct, O₂ 0.03 pct, Ag 0.003 pct, Fe 0.005 pct and Pb < 0.001 pct) was made by Cook and Richards.⁶ They concluded that the recrystallization textures could be described as one or more of the following textures: (1) a single texture (100) [001], (2) a twin texture (110) $\bar{1}\bar{1}2$ and (3) a random orientation, depending upon the previous history of the specimen concerned.

The effect of various alloying additions in copper was reported by Dahl and Pawlek.¹⁰ They found that certain alloying additions, such as 5 pct Zn, 1 pct Sn, 4 pct Al, 0.5 pct Be, 0.5 pct Cd, or 0.05 pct P suppressed the formation of cubic texture. Brick, Martin and Angier¹¹ reported that the cold rolled textures due to various additions fitted a rather simple pattern. However, the recrystallization textures were subject to very considerable variations. In the discussion of this paper, Baldwin stated that deoxidized copper containing 0.02 pct P gave a complicated recrystallization texture at lower temperature. When this copper was annealed at high temperature, a single texture appeared which was described as (110) $\bar{1}\bar{1}1$ but, according to a pri-

vate communication from Baldwin, this orientation reported was in error and should have been reported as (110) $\bar{1}\bar{1}2$. He also reported that the earing positions of drawn cups were at 60° to the rolling direction.¹²

Recently, Howald, in his discussion on the paper by Hibbard and Yen,¹³ reported that the rolling texture of phosphorus deoxidized copper, containing from 0.006 to 0.020 pct phosphorus, was of the pure copper type. When these coppers were annealed at lower temperatures, they exhibited a random orientation, and when they were annealed at higher temperatures they had a mixed (111) $\bar{1}\bar{1}0$ and (100) [001] texture, depending on the severity of the final reduction and annealing temperature.

However, the specific influence of phosphorus and other impurities on the recrystallization textures and the deep drawing properties of copper strip has not been thoroughly reported. Therefore, an attempt has been made in the present work to determine the rolling and recrystallization textures and also the earing behavior of five types of commercial copper and thereby to evaluate the effect of phosphorus and some other significant impurities on the development of texture for cold reductions of about 87 to 89 pct.

Materials Used

The five types of copper employed in the present investigation were two phosphorus deoxidized coppers of different phosphorus content (0.007 and 0.013 pct P), an oxygen-free copper (OFHC), an electrolytic tough-pitch copper, and a fire-refined tough-pitch copper. These materials were subjected to a thorough spectroscopic and

chemical analysis. The designations and the chemical compositions were as shown in Table 1.

The coppers, FA1, FA2 and FA3, were hot-forged from 3-in. billets into a $\frac{1}{2} \times 6$ -in. plate and cold rolled to the ready-to-finish gauge indicated below. FA4 and FA5 were hot rolled and scalped to ready-to-finish gauge. The grain size of all the materials in the ready-to-finish condition was about 0.030 to 0.045 mm. Table 2 shows the last stage of the production schedule for each copper strip used.

Experimental Procedure

ANNEALING, GRAIN SIZE AND HARDNESS DETERMINATIONS

Specimens of each type of copper were finally annealed in air for periods of one hour at temperatures ranging from 300 to 1600°F and were subsequently cooled in air. The average grain diameter of the annealed specimen was estimated by comparing with a standard grain size chart. Hardness was determined on the Rockwell 15 T scale.

CUPPING TESTS

Cups were made in a blanking and drawing set, in which blanks of 2-in. diam were drawn to a cup of 1.25-in. diam with an average depth of about 0.75 in. The clearance between the punch and die was about 0.032 in. The ears of the cup were measured with a special fixture which read the height of ears to one-thousandth of an inch on every ten-degree interval along the circumference of the cup.

POLE FIGURES

The usual transmission diffraction method with unfiltered copper radiation was employed to determine the pole-figures of the specimens cold-rolled or annealed at 900°F. All the pole-figures were derived from the positions of intensity maxima on 111 diffraction rings of the X ray photographs taken at 10° rotation of a

San Francisco Meeting, February 1949.

TP 2506 E. Discussion of this paper (2 copies) may be sent to *Transactions AIME* before April 25, 1949. Manuscript received September 14, 1948.

* Chase Brass and Copper Co., Waterbury, Conn.

¹ References are at the end of the paper.

Table 1 . . . The Designation and Chemical Compositions of Copper Strips Used

| Designation | Chemical Composition (pct) | | | | | | | | | |
|-------------------------|----------------------------|---------|--------|-------|---------|--------|--------|---------|----------------|---------|
| | Cu | Pb | Fe | Ni | Sn | Si | Zn | P | O ₂ | Misc. |
| FA1 (Phosphorized)..... | 99.97 | <0.0005 | 0.0015 | 0.001 | 0.0002 | <0.001 | <0.005 | 0.013 | Not detected | |
| FA2 (Phosphorized)..... | 99.97 | <0.0005 | 0.0015 | 0.001 | <0.0001 | <0.001 | <0.005 | 0.007 | Not detected | |
| FA3 (Oxygen-free)..... | 99.98 | <0.0005 | 0.001 | 0.001 | <0.0001 | <0.001 | <0.005 | <0.0003 | Not detected | |
| FA4 (Electrolytic)..... | 99.95 | 0.0007 | 0.0015 | 0.001 | 0.0002 | <0.001 | <0.005 | <0.0001 | 0.013 | Te + Se |
| FA5 (Fire Refined)..... | 99.92 | 0.002 | 0.0017 | 0.022 | 0.002 | <0.001 | <0.005 | <0.0001 | 0.025 | 0.029 |

Table 2 . . . The Production Schedule of Copper Strips Used

| Specimen | Ready to Finish Condition | | Final Condition | |
|----------|---------------------------|---------------|-----------------|-----------------|
| | Gauge (in.) | Anneal. (°F) | Gauge (in.) | Reduction (pct) |
| FA1 | 0.291 | 900 | 0.032 | 89.0 |
| FA2 | 0.287 | 900 | 0.033 | 88.5 |
| FA3 | 0.269 | 900 | 0.033 | 88.6 |
| FA4 | 0.291 | As Hot-rolled | 0.033 | 88.7 |
| FA5 | 0.253 | As Hot-rolled | 0.032 | 87.0 |

specimen about its rolling and transverse directions. For specimens annealed at the higher temperatures, a structure integrating camera constructed by Wilson and Brick¹⁴ was used. The camera was designed to cover a specimen area of about 1.5 × 3 cm. The specimens were etched with 50 pct HNO₃ to a thickness of about 0.004 in.

GLANCING PHOTOGRAMS

Photograms obtained with a glancing X ray beam were used to detect the presence of cubically aligned grains and to evaluate the change in recrystallization textures. The X ray beam was directed at an angle θ to the rolling plane and in the transverse plane, where θ is Bragg's angle for the radiation used. By applying Bragg's law, $n\lambda = 2d \sin \theta$, the wavelength of Cu-K α radiation, λ is 1.537 Å, the interplanar distance of the (100) plane of copper, d , is 3.608 Å and for the second order of reflection, $n = 2$, the Bragg angle for 200 diffraction will be about 25°.

Fig 1a and b shows the ideal orientations superimposed upon the outline of the (111) and (100) pole figure of cold-rolled copper.^{3,15} The shaded arc at the vertical position represents the portion of 111 and 200 Debye-Scherrer rings produced in the glancing photograms. It will be seen that both 111 and 200 rings pass nearly through the center of the projection. Therefore, any grains with (111) or (100) planes present in the rolling plane will reflect to the center of the arc of the 111 or 200 diffraction rings, respectively. In addition, these

111 and 200 rings also cross the first order intensity regions of the deformation texture so that any grains in the deformation texture would most probably be detected.

The specimens were etched with 50 pct HNO₃ to a thickness of about 0.015 in., so that any defects or inhomogeneities on the surface could be eliminated. The specimen was then mounted on the goniometer with the rolling direction normal to the X ray beam and the rolling plane inclined at an angle of 25° to the beam. The optimum expo-

sure time was found to be a total of 10 min. with a potential difference of 35 PKV and a current of 10 ma. Similar photograms were also taken by using the structure integrating camera on the samples annealed at 1400 and 1600°F, where the grain size was found to be too large for the setup used for the lower temperature specimens.

Discussion of Results

Fig 2 shows the Rockwell hardness and the average grain size of the five types of copper strips as annealed one hour at various final annealing temperatures. The presence of phosphorus appears to contribute to the grain growth at higher temperatures. The higher softening temperature of specimen FA1, which contained 0.013 pct P, is also quite evident. These results are in good agreement with the work reported by Webster, Christie and Pratt on drawn wires.¹⁶ For the fire-refined copper, FA5, grain growth was suppressed to some extent and a slight effect on the softening temperature was noticed.

The results of the cupping tests and the glancing photograms of each specimen as cold-rolled or annealed at various temperatures are shown in Fig 3 and 4. Specimen FA1 showed no change of earing position at lower temperatures, while at higher temperatures the ears shifted from 45° to an angle of 40° from the rolling direction. Specimens FA3, FA4 and FA5 showed a typical behavior of copper, in that the ears occurred at the 0°-90° position and the earing height increased with the increase in annealing temperature. The earing position of specimen FA2 was somewhat complicated. It appeared that there were two transition zones, at 450° and 1400°F, where the earing position changed from 45° to 0-90° and returned to the 45° position when annealed at 1600°F. Referring to the glancing photogram, Fig 4, some correlation between the earing position and the grain orientation is noticeable. In the series of glancing photograms of

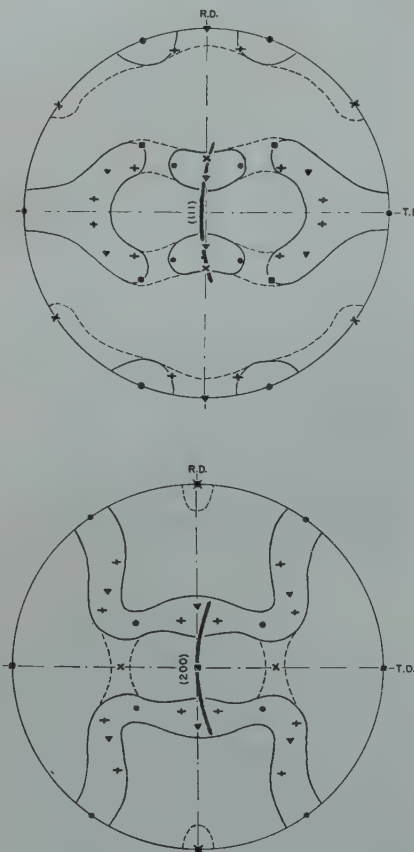


FIG 1—Ideal orientations superimposed upon the outline of the (111) and (100) pole-figures of cold-rolled copper.

The shaded arc at vertical position represents the portion of 111 and 200 Debye-Scherrer Rings produced in glancing photograms. Orientations indicated as follows: ● (110)[$\bar{1}12$], ▼ (112)[11 $\bar{1}$] + (124)[53 $\bar{3}$], ■ (100)[001], × (110)[001]. a. (above). b. (below)

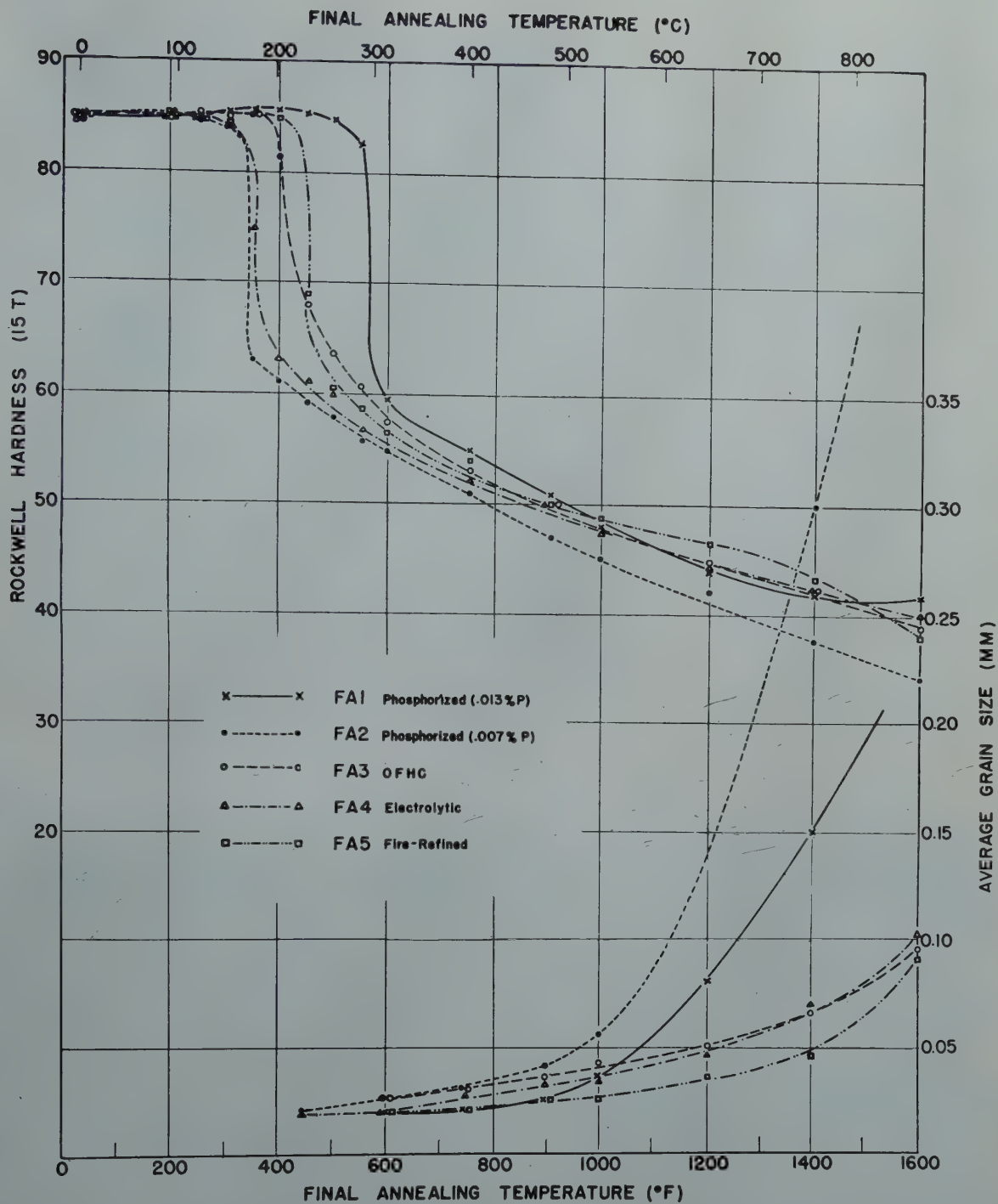


FIG 2—The effect of final annealing temperatures on hardness and grain size of five different types of copper strips.

FA1, the grain exhibited a rather random pattern at 600°F, at which temperature the height of ears was a minimum. A small amount of cubically aligned grains was observed, however. As the preferredness gradually developed the cubically aligned grains diminished and a corresponding increase in the height of the ears was noticed. In specimens FA3, FA4 and FA5 the concentration of cubically aligned grains was found to be considerable even at lower temperatures, while the degree of preferredness of cubic

texture increased with increasing annealing temperature. Similar results were also observed in specimen FA2, annealed at lower temperature.

However, for specimens annealed at 1400 and 1600°F some uncertainties were aroused due to the larger grain size with accompanying lack of definition of these Debye-Scherrer rings. Thus, two series of photograms were taken by the integrating camera as shown in Fig 5. It was noted that, for specimen FA2 annealed at 1400°F, the pattern showed that the grains

possessed certain definite preferred orientations in spite of the fact that practically no ears were observed in the drawn cups. This leads to the assumption that the effect of the presence of the cubic texture which yielded ears at 0° and 90° and that of the other textures yielding ears at 45° were just balanced, so that the resultant effect on ears was neutralized. This assumption was also proposed by Howald¹⁷ in regard to 95-5 Cu-Zn alloy. He found that this alloy with 20 pct cubic texture and 80 pct of (113)[211] plus

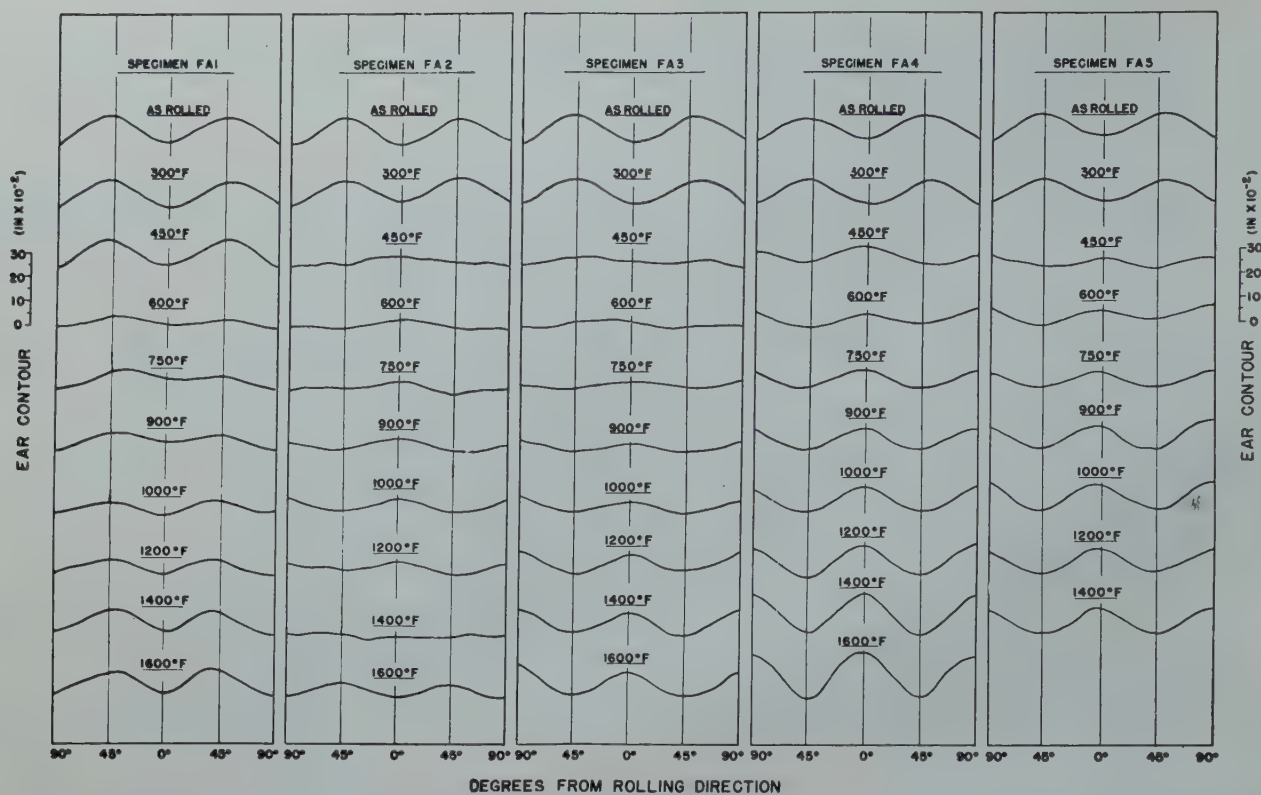


FIG 3—Ear contour on cups drawn from five types of copper strips annealed one hour at the temperatures indicated.

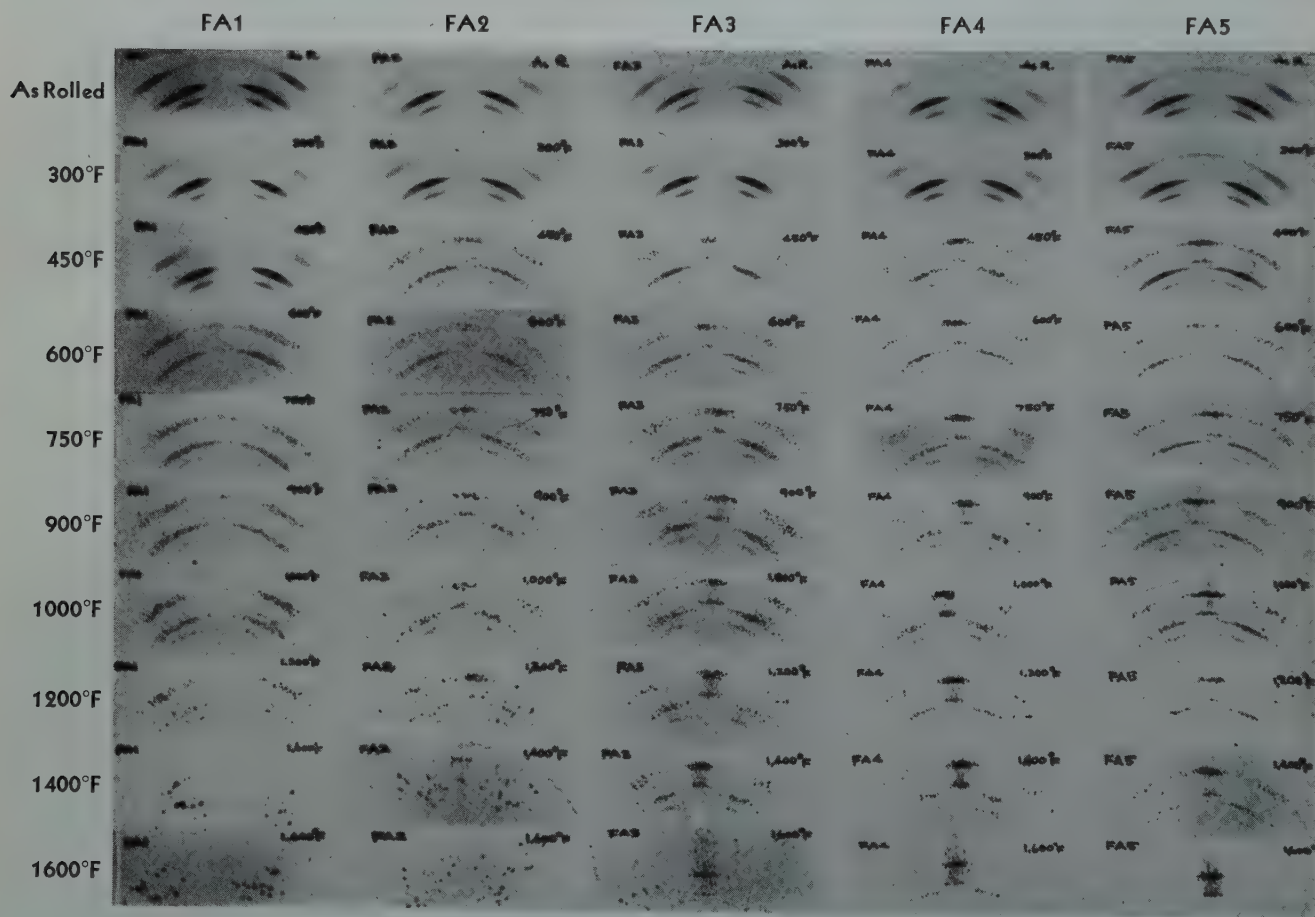


FIG 4—Glancing photographs for five types of copper strips annealed one hour at the temperature indicated. Photographs reduced to one-half the original size.

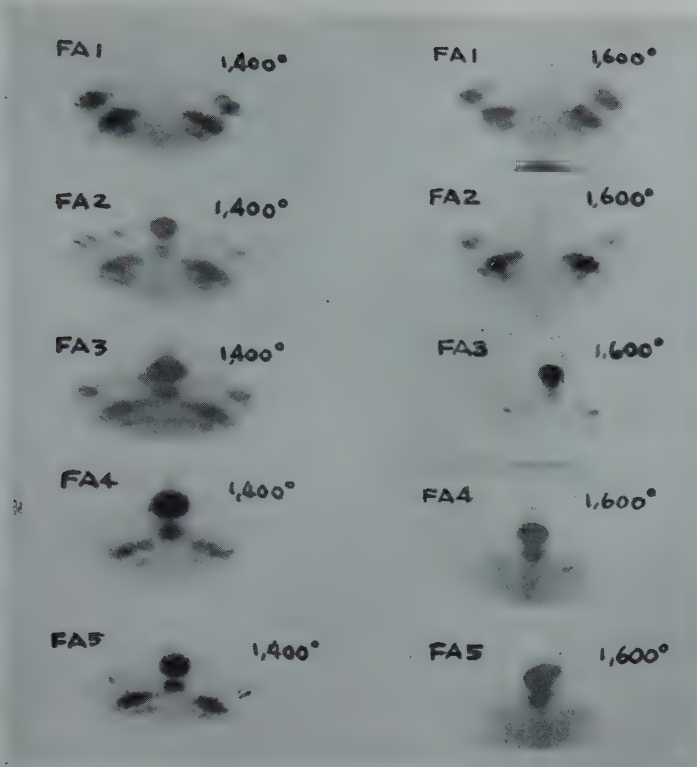


FIG 5—Glancing photograms taken by structure integrating camera for specimens annealed one hour at 1400 and 1600°F.

(11 $\bar{5}$)[321] produced a cup of no ears. Furthermore, for the same specimen annealed at 1600°F, the decrease in the amount of cubic texture resulted in a change in the position of the ears to 45° from the rolling direction.

The pole figures of specimens in the cold-rolled condition were substantially the same as reported by previous investigators.^{3,7,11} The major orientations can be described as (110)[$\bar{1}12$] + (112)[11 $\bar{1}$]. Fig 6 *a*, *b* and *c* shows the rolling texture of specimens FA1, FA3 and FA5. Greater spread of the distribution of (111) planes on the pole-figure of specimen FA1 was noticeable.

Pole figures of all specimens annealed at 900°F were made (Fig 7). No appreciable difference was found between specimens FA2, FA3, FA4 and FA5. The annealing textures were composed of a strong (001)[100] texture superimposed on the retained rolling textures with a mixture of minor orientations (124)[53 $\bar{3}$], (110)[$\bar{1}12$] and (112)[11 $\bar{1}$]. These orientations have been reported as the three important ones in cold-rolled copper.³ In phosphorus deoxidized copper (0.013 pct P), FA1, a somewhat random recrystallization texture was obtained which may be described as a texture composed of (112)[11 $\bar{1}$], (110)[$\bar{1}12$] and (100)[001].

For specimens annealed at higher temperatures, the pole figures were de-

rived from photograms taken by the integrating camera. Fig 8*a* shows the texture of FA1 annealed at 1600°F which can best be described as (112)[11 $\bar{1}$] + (110)[100]. However, no texture of the type (111)[$\bar{1}10$] or cubic orientation¹³ is noticeable. Referring to the photograms of specimen FA1 at 1400 and 1600°F in Fig 5, the absence of (100) or (111) pole in the rolling plane is quite evident. For specimen FA2, annealed at the same temperature, a mixture of textures (113)[$\bar{2}11$], (110)[$\bar{1}12$], and (100)[001], was found. The pole figure of specimen FA3 annealed at 1600°F was similar to that obtained at the lower temperature, except that the intensity of the residual deformation texture decreased to a certain extent. The annealing texture may be stated as a strong (001)[100] texture with a weak (124)[53 $\bar{3}$] texture. For specimens FA4 and FA5, the secondary intensity of the deformation textures was further diminished, and a single texture of (001)[100] was approached. The pole figures were practically the same as reported by the previous investigators.^{7,11}

Several micrographs have been prepared along the rolling plane of specimens FA3, FA4 and FA5 (Fig 9). The specimens were polished and deeply etched with a potassium bichromate solution. The white matrix with two

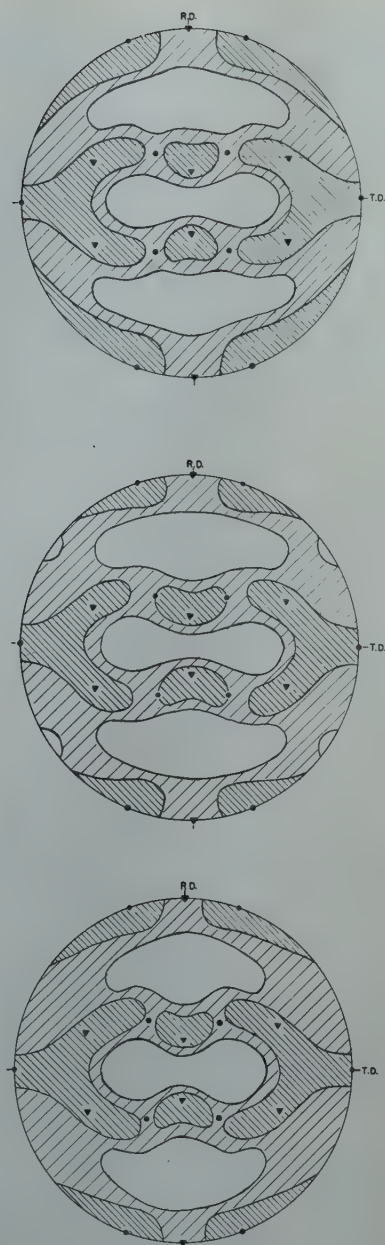


FIG 6—(111) pole figures of cold rolled copper strips.

a. FA1—Phosphorized (0.013 pct P) 89.0 pct Red. *b.* FA3—OFHC 88.6 pct Red. *c.* FA5—fire-refined 87.0 pct Red. Ideal orientations indicated as follows: ● (110)[$\bar{1}12$], ▼ (112)[11 $\bar{1}$]. *a.* (top) *b.* (center) *c.* (bottom).

sets of twin bands at 45° to the rolling direction indicates the grains to be in cubical alignment. It can be seen that there is a certain amount of dark grains other than cubic ones still existing in specimen FA3, whereas for specimens FA4 and FA5, the cubic texture is practically 100 pct.

The effect of phosphorus on the electrical conductivity and softening temperature of copper is well known. The work of Hanson, Archbutt and Ford¹⁸ is typical. They found that the

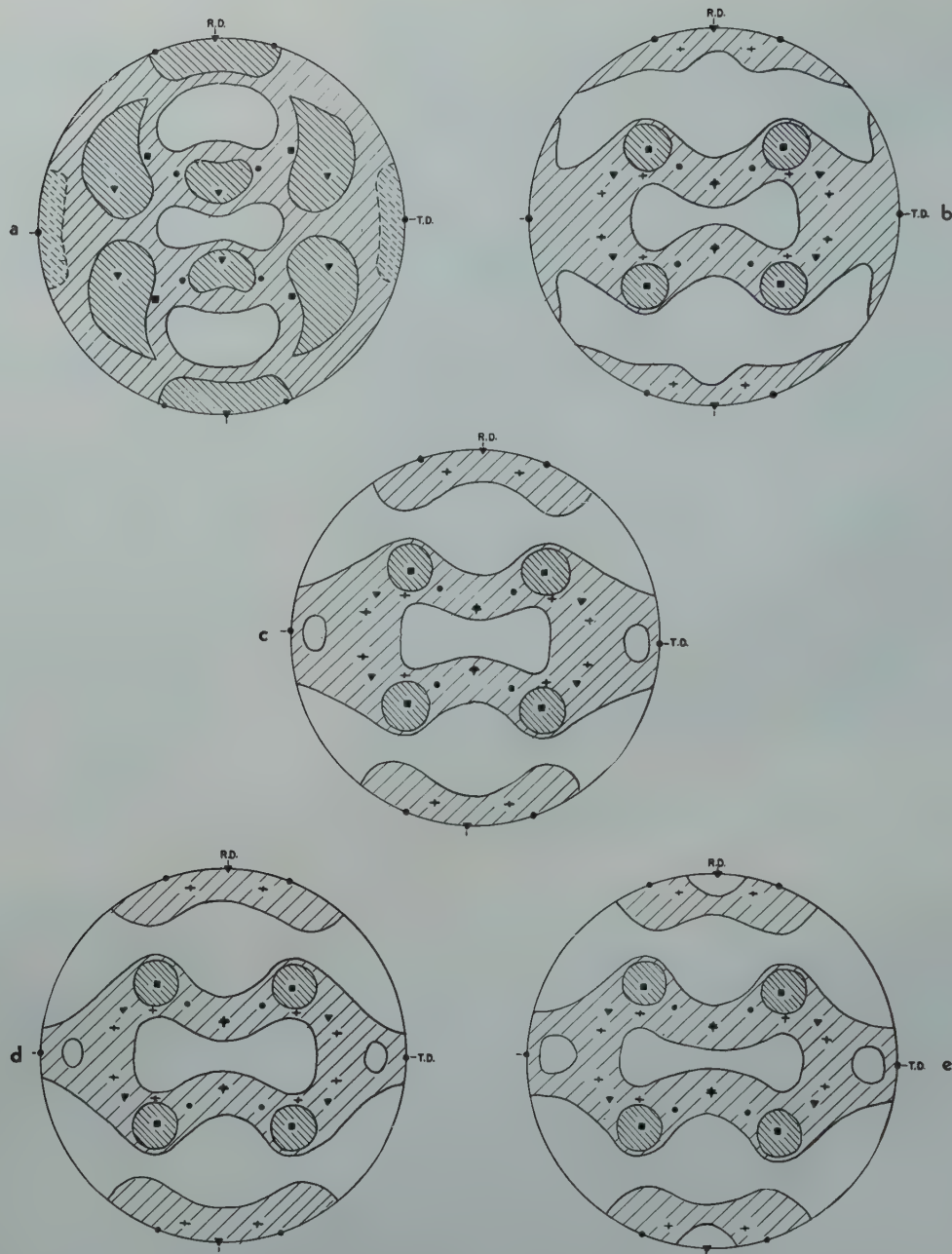


FIG 7—(111) pole figures for cold-rolled copper strips annealed at 900°F for one hour.
a. FA1—phosphorized (0.013 pct P), b. FA2—phosphorized (0.007 pct P), c. FA3—OFHC, d. FA4—electrolytic,
e. FA5—fire-refined. Ideal orientations indicated as follows: ■ (100)[001], ● (110)[$\bar{1}12$] ▼ (112)[11 $\bar{1}$], + (124)[53 $\bar{3}$].

addition of phosphorus yielded a marked increase of softening temperature and a marked decrease of electrical conductivity. Recently, Smart and Smith,¹⁹ stated that phosphorus when present in copper may be either in solid solution or in the oxidized condition. However, only the presence of phosphorus in solution has an important effect on the softening temperature and electrical conductivity. Thus, by comparing the conductivity measurement of specimens FA1, FA2 and FA3 with the results obtained by interpolating from the curves given by Smart and Smith,¹⁹ the following table is obtained.

Table 3 . . . The Effect of Phosphorus on Electrical Conductivity and Softening Temperature of Copper

| | Phosphorus Content pct | Electrical Conductivity pct IACS | Softening Temp. °C |
|-----------------------|------------------------|----------------------------------|--------------------|
| Oxygen-free Alloys | 0.013 | 93.0 | 305 |
| | 0.007 | 97.2 | 292 |
| | 0.0002 | 102.3 | 182 |
| Oxygen-bearing Alloys | 0.013 | 102.1 | 140 |
| | 0.007 | 102.2 | 140 |
| | 0.0002 | 102.3 | 140 |
| FA1 (Phosphorized) | 0.013 | 94.6 | 295 |
| FA2 (Phosphorized) | 0.007 | 101.4 | 170 |
| FA3 (OFHC) | <0.0003 | 101.3 | 200 |

The electrical conductivity of specimens FA1, FA2 and FA3 was measured on samples in a condition comparable to that used by Smart and Smith.¹⁹ However, the softening temperatures of the present specimens were determined from the hardness curves in Fig 2, where the greatest change of slope of these curves occurred. Therefore, the value listed in Table 3 could only be used for a qualitative comparison among each group.

From Table 3, it may be stated that the largest part of the phosphorus in specimen FA2 existed in the oxidized form, whereas that in specimen FA1

was most likely in solid solution with copper. The higher recrystallization temperature of FA1 and the lower value of FA2 also bear out this fact. It has been pointed out that recrystallization textures are subject to considerable variation because of alloying elements in solution. Furthermore, elements which conferred the greatest solution and strain-hardening on copper have shown the most complicated annealing texture.¹¹ It appears, therefore, certain complications will be introduced, in that the amount of phosphorus obtained by chemical analysis may not be used as a guide to specify the influence on the textures. The development of annealed texture for specimen FA1 may therefore be considered as following a different mechanism than that of specimen FA2 because of the different condition of phosphorus in each. In the case of H.C. copper, it was found that a well developed deformation texture—up to 80 to 95 pct reduction—was required before recrystallization would produce the cubic texture. For reductions of 50 to 80 pct, the texture existing in the annealed condition resembled that in the rolling condition.⁶ Referring to the rolling texture of specimen FA1, the greater spread of the major intensity of (111) distribution can be best ascribed to the presence of the minor texture (110)[001], which was found to be one of the intermediate orientations in cold-rolled copper.^{3,20} Thus it may be suggested that the absence of cubic texture in specimen FA1, probably due to the strain-hardening effect of the phosphorus in solid-solution, is analogous to that of H.C. copper deformed below 80 pct reduction. The random orientation at lower temperature and the development of a mixed (112)[111] and (110)[001] texture at 1600°F may also be attributed to the interference of phosphorus with the recrystallization mechanism.

The recrystallization texture of specimen FA2 annealed at lower temperature exhibited the same characteristics as specimens FA3, FA4 and FA5, that is, a strong cubic texture superimposed on a mixed deformation texture. However, when the annealing temperature was sufficiently high, above 1400°F, the cubic texture diminished in intensity and there was a great increase in grain size. The development of the large grains has been reported by Dahl and Pawlek¹⁰ for electrolytic copper of 100 pct cubic

texture annealed at high temperatures. They stated that the texture could be described as (120)[100]. The large grains have also been observed in annealed copper by Cook and Richards²¹ and Baldwin⁸ to possess a texture of (110)[112]. It was also found by Baldwin⁸ that the orientation of the huge grains growing out of a 100 pct cubic texture for lake and electrolytic copper can be best described as: (113) in the rolling plane and between [110],

[301] and $[2\bar{1}1]$ in the rolling direction. It might be suggested that the cubic orientation would be unfavorable under the process of grain growth, or in other words, it is less stable in large grains than other orientations described above. It appears, therefore, that the change of annealing texture as well as earing position in specimen FA2 at 1600°F could be considered to be a result of the absorption of grains of the cubic orientation during the grain growth leaving the other orientations predominant.

Summary

1. The cold-rolled texture of different types of copper strip was found to be less sensitive to the presence of phosphorus or other impurities than the recrystallization one. The ideal orientations of rolling texture may be described as the usual type, (110)[112] + (112)[111], but greater spread of the first intensity of (111) poles in phosphorized copper FA1, (0.013 pct P), may be considered as due to the presence of the minor texture (110)[001].

2. The recrystallization textures of phosphorized copper containing 0.013 pct P exhibited a rather random pattern for annealing at lower temperature, while at high temperature there was produced a texture of mixed orientations (112)[111] and (110)[001]. There was no appreciable change of earing position throughout the whole range of anneal.

3. The texture of phosphorized copper FA2 (0.007 pct P), oxygen-free high-conductivity copper FA3, electrolytic copper FA4 and fire-refined copper FA5, annealed at 900°F was found to be a strong (001)[100] texture superimposed on the retained deformation textures (124)[533], (110)[112] and (112)[111]. These minor orientations usually diminished in their intensities with an increase of final annealing temperature, while, in turn, a single cubic texture was approached in specimens of oxygen-free high-conductivity copper FA3, electrolytic copper FA4 and fire-refined copper FA5. For phosphorized copper containing 0.007 pct P, FA2, annealed at 1600°F, a texture of a mixture of orientations (113)[211], (110)[112] and (100)[001] was found, while the earing position in drawn cups changed from a pure copper type at 0° and 90° to 45° to the rolling direction.

4. In studying the data of electrical conductivity and softening tempera-

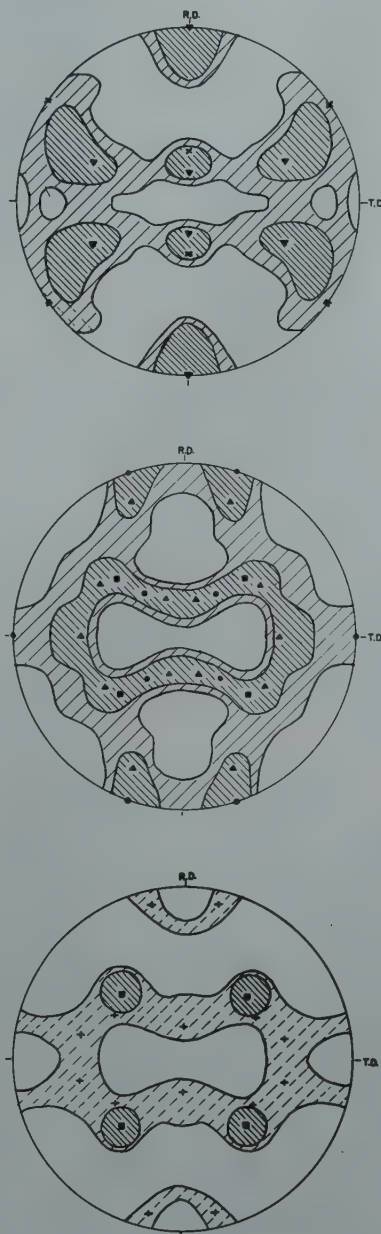


FIG 8—(111) Pole figures for cold-rolled copper strips annealed at 1600°F, for one hour.

a. FA1—Phosphorized (0.013 pct P), b. FA2—Phosphorized (0.007 pct P), c. FA3—OFHC. Ideal orientations indicated as follows: ● (110)[112], ▼ (112)[111], × (110)[001], ■ (100)[001], ▲ (113)[211], + (124)[533]. a (top) b (center) c (bottom)

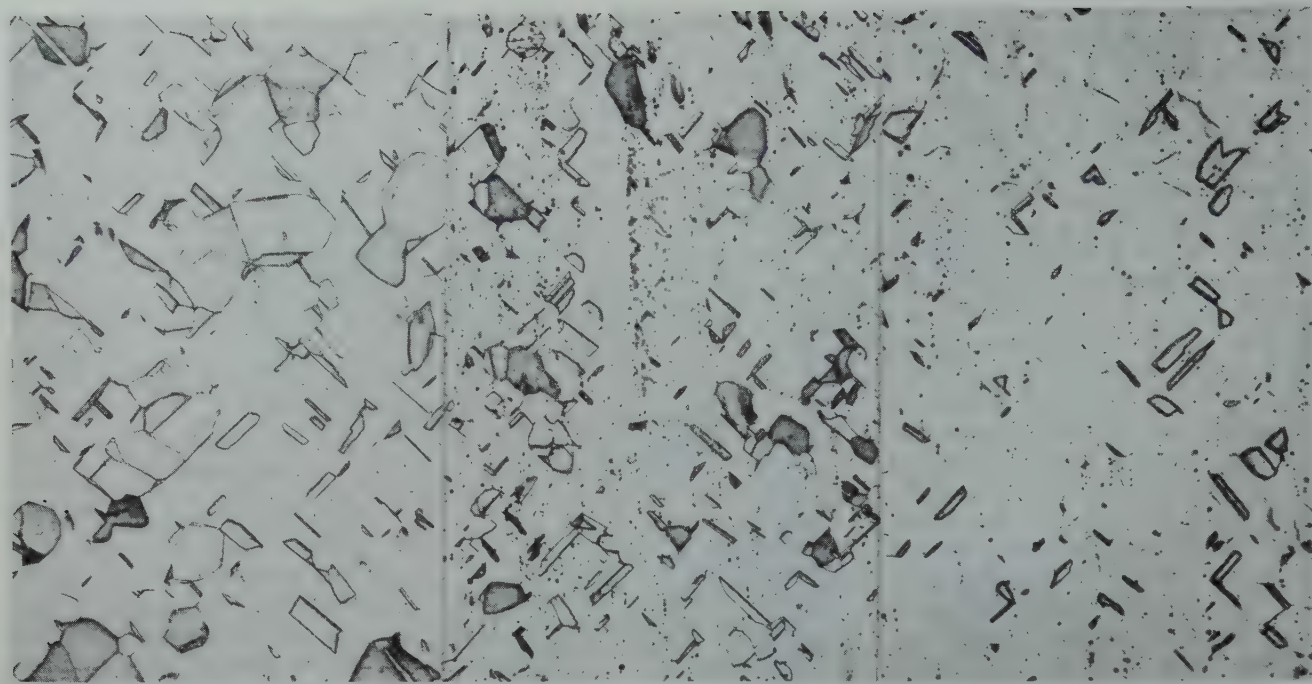


FIG 9—Microstructures of three types of copper strips annealed one hour at 1600°F.
a. FA3—OFHC, b. FA4—Electrolytic, c. FA5—fire-refined. Potassium Bichromate solution etch. $\times 75$. a (left) b (center) c (right)

tures of two types of phosphorized copper, it was suggested that the presence of phosphorus in coppers FA1 (0.013 pct P) and FA2 (0.007 pct P) would be in different conditions. Most of the phosphorus in FA1 may be considered as existing in solid solution with copper; thus the great influences on electrical conductivity, recrystallization temperature as well as textures and earing behavior would result. In specimen FA2, it appeared that most of the phosphorus probably existed in the oxidized form, which had less effect on the texture and earing behavior. However, the change of texture and position of ears at high temperature may be rationalized as the same function of development of various textures in the huge grains where the cubically aligned grains may be less stable than the others.

5. In regard to the earing behavior of these copper strips, it may be stated that the type and degree of preferred orientation are the most significant factors controlling the height and position of ears. An increase in grain size will usually have a tendency toward a preferred orientation, which in turn produces higher ears. The absence of ears in drawn cups may or may not

indicate the absence of preferred orientation, but may be due to the presence of orientations which counteract one another with respect to the earing behavior.

Acknowledgment

The author wishes to acknowledge the advice and suggestions of Dr. D. K. Crampton and Dr. H. L. Burghoff, and the assistance of Mr. J. Cooper, Jr. and other members of the Research Department of the Chase Brass and Copper Co. in the work reported here. Thanks are also due to Professor W. R. Hibbard, Jr., of Yale University for helpful criticism.

References

1. G. Masing and W. Polanyi: *Naturwiss.* (1923) **12**, 177.
2. G. Tamman: *Jnl. Inst. Metals* (1930) **44**, 29.
3. W. Iweronowa and G. Schdanow: *Tech. Phys. USSR Trans.* (1934) **1**, 64.
4. K. Kaiser: *Ztsch. Metallkunde* (1927) **19**, 435.
5. A. Phillips and G. Edmunds: *Proc. ASTM* (1929) **29**, 438.
6. M. Cook and T. Ll. Richards: *Jnl. Inst. Metals* (1940) **66**, 1; (1941) **67**, 203.

7. R. M. Brick and M. A. Williamson: *Trans. AIME* (1941) **143**, 84.
8. W. M. Baldwin Jr.: *Trans. AIME* (1946) **166**, 591. TP 1455, *Met. Tech.* Apr. 1942.
9. M. Cook and T. Ll. Richards: *Jnl. Inst. Metals* (1946) **73**, 1.
10. D. Dahl and F. Pawlek: *Ztsch. Metallkunde* (1936) **29**, 266.
11. R. M. Brick, D. L. Martin and R. P. Angier: *Trans. ASM* (1943) **31**, 675.
12. W. M. Baldwin Jr.: Discussions of Ref 11: *Trans. ASM* (1943) **31**, 696.
13. T. S. Howald: Written discussion on the paper by W. R. Hibbard Jr. and M. K. Yen: *AIME Met. Tech.* Feb. 1948, TP 2334.
14. F. H. Wilson and R. M. Brick: *Trans. AIME* (1945) **161**, 173.
15. C. S. Barrett: *Structure of Metals*, p. 400 (1942) N. Y., McGraw-Hill.
16. W. R. Webster, J. L. Christie and R. S. Pratt: *Proc., Inst. of Metals Div., AIME* (1927) 233.
17. T. S. Howald: Thesis, Case School (1947).
18. D. Hanson, S. L. Archbutt and G. W. Ford: *Jnl. Inst. Metals* (1930) **34**, 41.
19. J. S. Smart Jr. and A. A. Smith Jr.: *Trans. AIME* (1946) **166**, 144. TP 1807, *Met. Tech.* Sept. 1945.
20. H. C. Vacher: *Jnl. Res. Nat. Bur. Std.* (1941) **26**, 385.
21. M. Cook and T. Ll. Richards: *Jnl. Inst. Metals* (1940) **66**, 1.

Use of Electrical Resistance Measurements to Determine the Solidus of the Lead-tin System

RALPH HULTGREN,* Member AIME, and STANLEY A. LEVER†

THE solidus is usually the least satisfactorily determined portion of a phase diagram. Cooling curves, which succeed well with the liquidus, show the solidus inaccurately or not at all because of segregation which occurs during freezing. Heating curves of carefully homogenized alloys might be expected to indicate accurately the solidus, but they are seldom used.

Dynamic methods involving heating or cooling are never completely satisfactory because of uncertainty as to whether equilibrium is attained. A static method in which the specimen may be allowed hours, days, or even weeks to attain equilibrium is to be preferred. In a static method a solid solution, for example, is first made thoroughly homogeneous, then heated to successively higher temperatures. After sufficient time at each temperature to assure equilibrium, some property is measured which should alter strikingly when melting begins. Microscopic examination can be used to detect the beginning of melting, but the method is tedious since the specimen must be quenched, sectioned, polished, and etched before each examination.

Of all the physical properties which change on melting, electrical resistance is probably the most satisfactory to measure. The measurement may be made while the specimen is at temperature without damage to the specimen. It may be repeated indefinitely to ascertain when equilibrium has been achieved. Measurements may be made on a single specimen over the whole range of temperature. Most metals approximately double their resistance on melting. Since an accuracy of a few tenths of a percent is easy to achieve, the method is highly sensitive to the beginning of melting.

In spite of these advantages, which have been perceived for a long time,^{1,2} a reasonable search of the literature

has failed to reveal a single case in which the method has been satisfactorily applied in practice to the determination of solidus temperatures. The use of electrical resistance measurements appears to have been confined in practice to changes in the solid state.

In the work described in the following pages we have applied the electrical resistance method to the solidus of the lead-tin system. We have found the method to be convenient, reproducible, and highly sensitive. We chose the lead-tin system because it leads to few technical difficulties. Furthermore, a number of determinations of solidus have been made in this system by various methods and results could be checked against them. However, all published results are not in good agreement with one another, so this work should help in determining the solidus more precisely.

The Lead-tin Diagram

Because of its commercial importance, there have been numerous investigations of the lead-tin diagram. The results of the most recent work on the solidus are indicated in Fig 7, as well as the results of the present work. The works of Honda and Abe³ and of Stockdale⁴ agree fairly well with each other and with the present work.

San Francisco Meeting, February 1949.

TP 2500 E, January 1949. Discussion of this paper (2 copies) may be sent to *Transactions AIME* before April 15, 1949. Manuscript received September 10, 1948.

Most of the material presented in this paper was abstracted from a thesis submitted by Stanley A. Lever in partial fulfillment of the requirements for the degree Master of Science in Engineering, University of California.

* Professor of Metallurgy, Univ. of California, Berkeley.

† Univ. of California, Berkeley.

¹ References are at the end of the paper.

Jeffery's⁵ data indicate the solidus to be about 50°C lower.

Honda and Abe³ used differential thermal analysis on both heating and cooling cycles. Stockdale⁴ used the microscopic method and also differential heating curves. Stockdale's results were about 4° higher than those of Honda and Abe at low tin contents and lower at higher tin contents. These results also agree with those of Rosenhain and Tucker.⁶

Jeffery⁵ used electrical resistance measurements of the alloy as it was being heated or cooled. Apparently he did not attain equilibrium as his results are about 40°C lower than those of Stockdale⁴ or Honda and Abe.³

MATERIALS AND METHODS

The lead and tin used were of high purity. They were supplied by the American Smelting and Refining Co., who gave the following analyses:

Lead: silver, 0.0016 oz per ton; copper, 0.0008 pct; cadmium, 0.0007 pct; zinc, 0.0002 pct; arsenic, 0.0003 pct; antimony, 0.0002 pct; bismuth, 0.0005 pct; tin, 0.0001 pct; iron, 0.0020 pct; lead (by difference), 99.995 pct.

Tin: antimony, 0.037 pct; arsenic, 0.020 pct; bismuth, 0.004 pct; cadmium, trace; copper, 0.025 pct; iron, 0.004 pct; lead, 0.020 pct; nickel and cobalt, 0.005 pct; silver, 0.0005 pct; sulphur, 0.005 pct; tin (by difference), 99.88 pct.

One hundred grams of metal with the desired proportions of lead and tin was weighed out to the nearest one-tenth of a milligram. The mixture was placed in a silica crucible, covered with charcoal, and melted in a reducing atmosphere in a gas-fired furnace. The alloy was well stirred. Chemical analysis of two of the alloys checked closely with the weighed portions. The compositions of the remainder of the alloys were taken directly from the weighings, without chemical analysis.

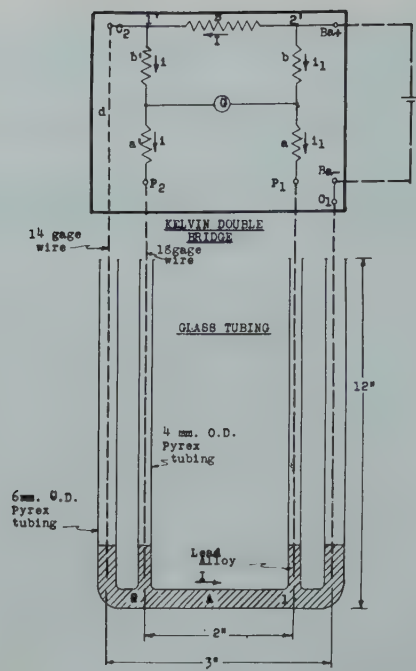


FIG 1—Pyrex U-tube and electrical connections to Kelvin double bridge.

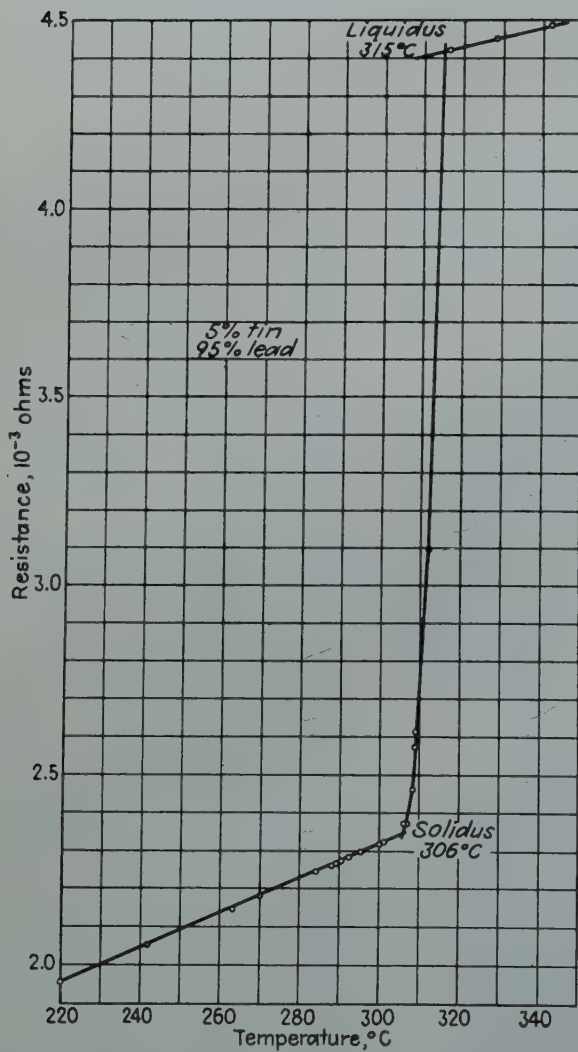


FIG 2—Electrical resistance vs. temperature, 5 pct tin alloy.

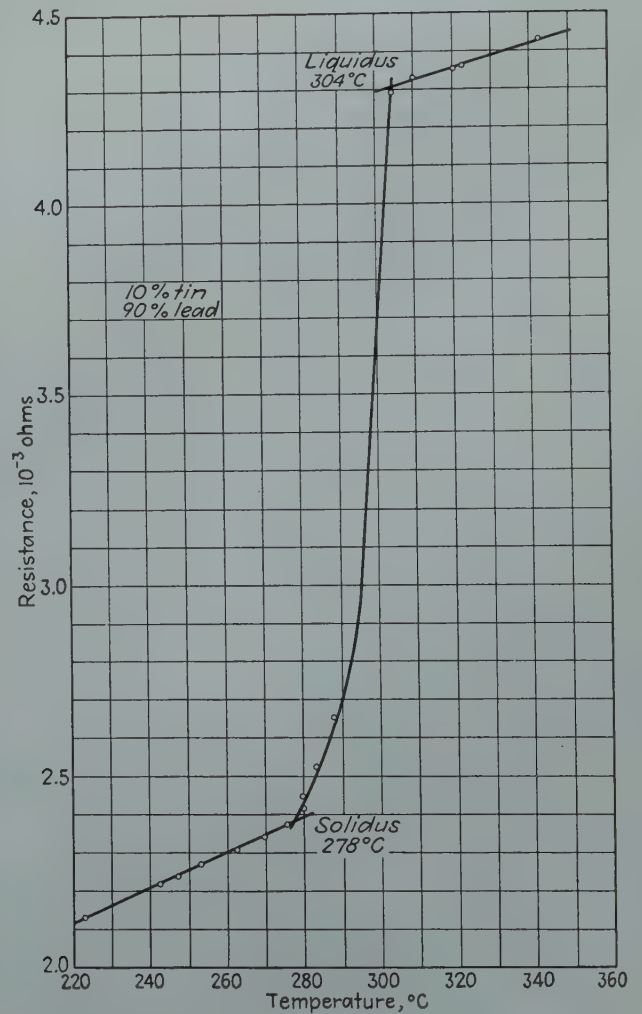


FIG 3—Electrical resistance vs. temperature, 10 pct tin alloy.

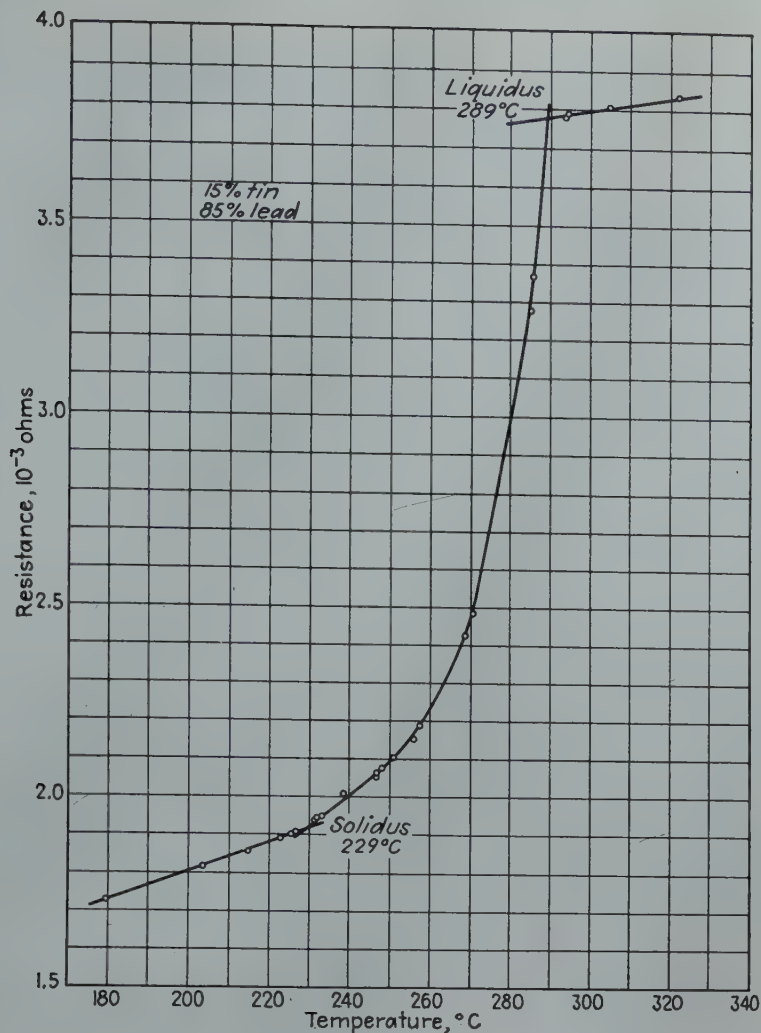


FIG 4—Electrical resistance vs. temperature, 15 pct tin alloy.

The pyrex glass tubing shown in Fig 1 was heated in a Lindberg cyclone furnace and held at a temperature of 400°C. A gas mixture consisting of 98 pct nitrogen and 2 pct hydrogen was passed through it for about one-half hour. The well stirred molten alloy was then poured into the tubing and allowed to remain for about one-half hour while electrical connections were being inserted.

The electric lead wires had been stripped of insulation, cleaned with nitric acid and finally washed with alcohol and dried. Stranded 14-ga copper wires were introduced into the outer arms of the tube, and stranded 18-ga copper wire into the inner arms. Fine (30 ga) iron-constantan thermocouple wires insulated with braided glass were introduced so that the hot junction was at point 1. The tube was then removed from the furnace and cooled rapidly in a stream of cool air in order to minimize segregation on

freezing. Before measurements were taken, the alloy in the tube was given a homogenizing anneal of about two days at a temperature about 50°C below Stockdale's value of the solidus.

For the measurements of electrical resistance the tube was heated in a metal bath composed of lead, tin, and bismuth and having a melting point of about 170°C. The temperature of the bath was held constant to $\pm 1^\circ\text{C}$.

Resistance measurements were made with a Leeds and Northrup Kelvin Double Bridge Ohmmeter. This bridge is more suitable than a Wheatstone bridge for low values of resistance, since the effect of contact resistance is very small. A diagram of electrical connections is shown in Fig 1. External leads are shown as dotted lines. The external electrical leads were approximately 2 ft long. The leads to the connections C_1 and C_2 each consisted of two 14-ga stranded copper wires in parallel, those to P_1 and P_2 of two

18-ga stranded copper wires in parallel. The readings of resistance were estimated to be accurate to about 0.000005 ohms, which is of the order of 0.2 pct.

In making the measurements it was necessary to pass a current of about 7 amp through the metal for a period of less than 15 sec. It can be shown that this is capable of raising the temperature of the alloy less than 2°C . Measurements with the thermocouple imbedded in the alloy indicated the actual temperature rise during a measurement was less than 0.2°C .

Temperature measurements of the alloy were made on a precision potentiometer using the very fine (30 ga) iron-constantan thermocouple mentioned above. Readings are estimated to be accurate to about 0.5°C .

During the homogenizing anneal, electrical resistance measurements were taken from time to time. It was usually observed that the values obtained changed slowly for about two days,

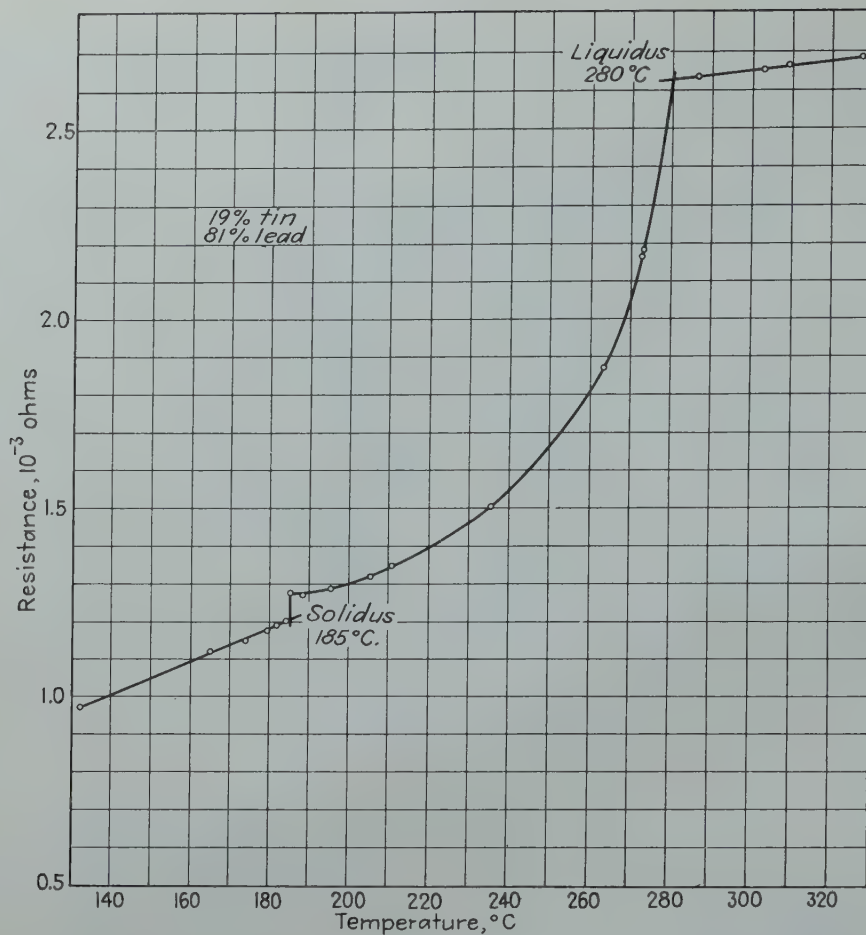


FIG 5—Electrical resistance vs. temperature, 19 pct tin alloy.

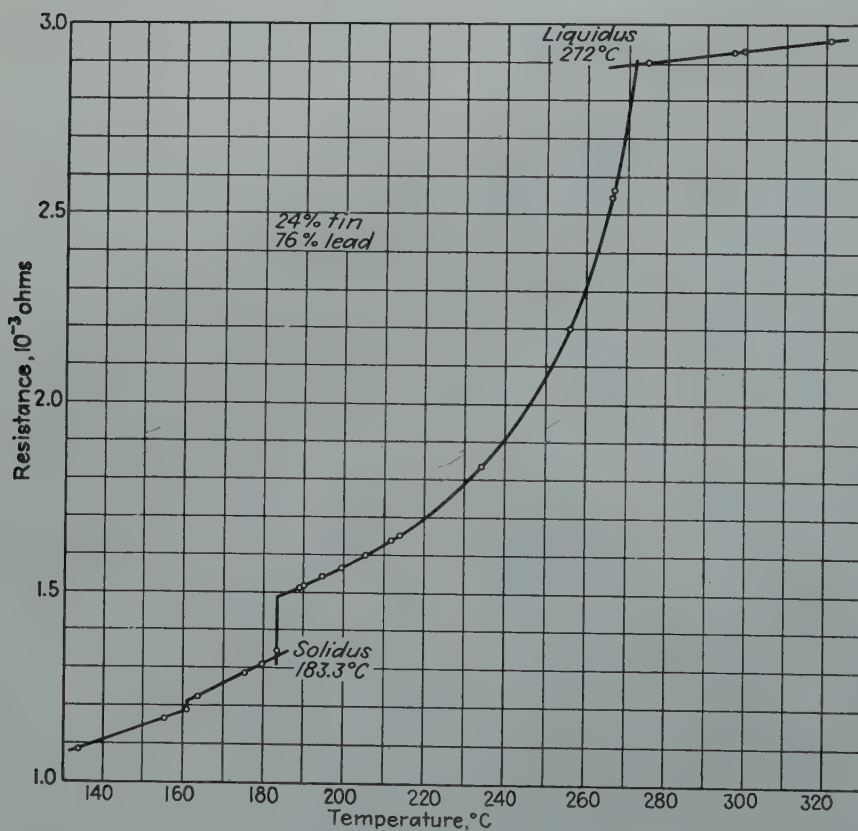


FIG 6—Electrical resistance vs. temperature, 24 pct tin alloy.

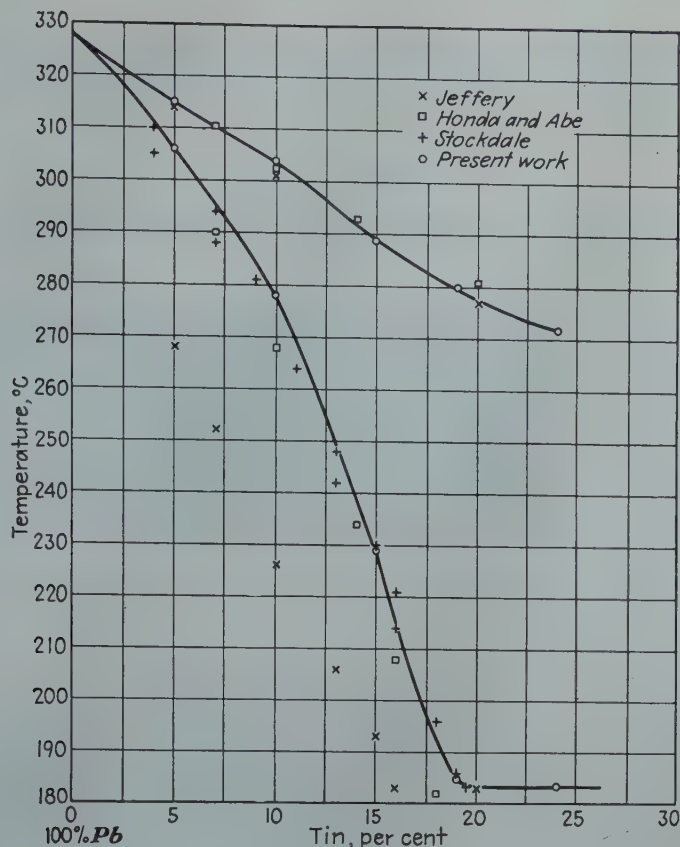


FIG 7—Solidus and liquidus of lead-tin system.

then settled to a constant value. This was taken to indicate that the alloy was homogeneous and the resistance was recorded.

The temperature of the bath was then raised a few degrees and held there until the resistance readings again became constant. Usually five to six hours was allowed for this, although in many cases the alloy remained at temperature overnight. When the resistance did not change for one hour, it was assumed that equilibrium was attained. This process was continued through the solidus and liquidus of the alloy. Temperature intervals in critical regions amounted to only two or three degrees.

Results and Conclusions

The resistance vs. temperature curves obtained are shown in Fig 2-6. As can be seen, these curves are accurate straight lines for the alloy in the solid state. As the alloy begins to melt at the solidus, however, there is a sharp increase in slope of the curve. The experimental points follow the curves accurately, so that the solidus

is determined precisely in each case. There is a similar sharp change in slope at the liquidus.

In the alloys containing 19 and 24 pct tin (Fig 5 and 6), melting begins at 183°C with a small discontinuity in the curve. This is due to the melting of a small amount of the eutectic.

In the alloy containing 24 pct tin, there is also a small but sharp discontinuity at 161°C. We attribute this to a change in the tin-rich phase, which is present in appreciable amount only in this alloy. Other observers⁷ have noted discontinuities in volume and electrical resistance in tin at this temperature although this result is disputed by some. Mason and Pellissier⁷ report that the high temperature X ray camera shows there is no change in phase of tin at elevated temperatures. To add to the confusion, observers have reported discontinuities at a number of other temperatures. We are unable to account for our result.

The solidus and liquidus points determined in this investigation are plotted in Fig 7, along with the results

of other investigators. The liquidus determinations of all workers agree excellently. Except for the work of Jeffery,⁵ the solidus points fall rather closely together. However, our results are somewhat higher than those of Honda and Abe³ at all compositions, and higher than those of Stockdale⁴ at low tin contents. The fact that residual segregation would cause results to be too low rather than too high indicates that our results are to be preferred.

We believe this work has shown that electrical resistance measurement is a convenient method of determining the solidus (and the liquidus) curve with high precision.

References

1. W. M. Guertler: *Jnl. Inst. Metals* **6**, 135 (1911).
2. W. L. Fink: *Metal Prog.* **53**, 530 April (1948).
3. K. Honda and H. Abe: *Sci. Rep. Tohoku Imp. Univ.* **19**, 315 (1930).
4. D. Stockdale: *Jnl. Inst. Metals* **49**, 267 (1932).
5. F. H. Jeffery: *Trans. Faraday Soc.* **24**, 209 (1928).
6. W. Rosenhain and P. A. Tucker: *Phil. Trans. Royal Soc.* **209**, 89 (1908).
7. C. W. Mason and G. E. Pellissier, Jr.: *Trans. AIME* **133**, 280 (1939).

Controlled Grain Growth Applied to the Problem of Grain Boundary Energy Measurements

C. G. DUNN,* Member AIME

THE measurement of interfacial tensions or grain boundary energies in metals is an important metallurgical problem, especially since it bears on growth and nucleation processes. Statistical methods of measuring equilibrium grain boundary angles, which relate interfacial tensions, have been used by some investigators^{1,2} but more direct methods would be preferred.

A direct way, based on a simple extension of a successful method of growing single crystals of silicon ferrite to predetermined orientations in flat specimens,³ is to produce three-grain specimens in such a way that the equilibrium common grain boundary will be perpendicular to the surface of the specimen. The angles to be measured then appear as the grain boundary angles in the surface of the specimen.

The method of producing a single crystal specimen with a predetermined orientation is basically the same as that employed by Yoshida and Fujiwara⁴ in their work on aluminum wires. The specimen, prior to any single crystal transformation, must have a matrix which will support the growth of a crystal of the desired orientation. Growth may occur through exaggerated grain growth or, if the matrix is strained a critical amount, by normal recrystallization. In either case the matrix must have stability at the temperature used to effect the transformation, this stability appearing as a long induction period for exaggerated grain growth or for the formation of recrystallization nuclei. Additional control is gained by using a high temperature gradient through which the specimen is moved at a suitable rate. To obtain the desired orientation, the specimen is fed a short way into the furnace producing one or more crystals in the hot end. After the specimen is removed from the furnace, the orientation of a crystal is determined, so that this crystal may be reoriented by properly deforming a narrow piece of the matrix between the end crystal and the rest of the specimen. This part of the specimen in the case of silicon ferrite is preferably

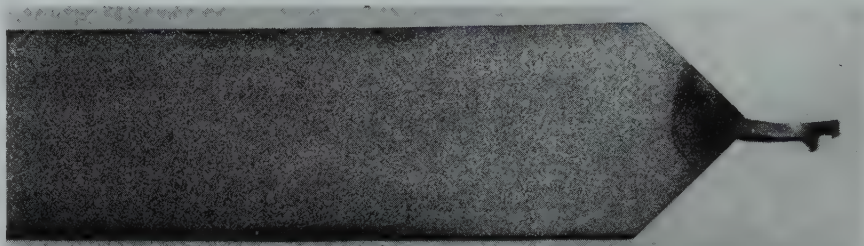


FIG 1—Photograph showing fine grained specimen with reoriented seed crystal in the form of small flag on end of the narrow twisted part of the specimen. Natural size.

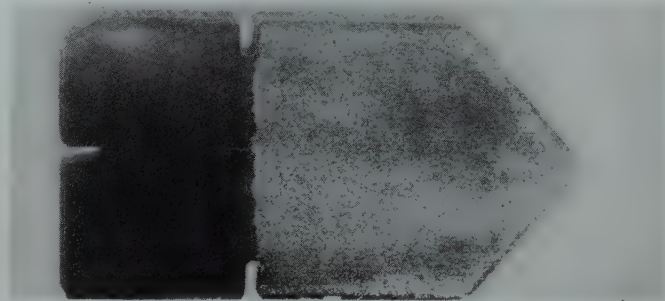


FIG 2—Photograph showing specimen composed of three grains each having a {110} plane in the plane of the specimen. Sample ready to be annealed. $\times 2$.

held at red heat during the reorienting process. Fig 1 shows a specimen which is ready to be transformed into a single crystal through growth of a reoriented "seed" crystal.

When the method just described is applied to the production of a three-grain specimen two crystals are grown first side by side in one end, the specimen is then reversed and the third grain grown from the opposite end. A suitable group of grains each of different orientation is one where all three grains have the same crystallographic plane in the plane of the specimen.[†]

Fig 2 shows a photograph of a three-grain group prepared as described. The notches are introduced in the open

ends of the grain boundaries to anchor them during the final annealing operations which ultimately should bring the grain boundaries to the lowest energy configuration.

Two-grain groups with different crystallographic planes in the plane of the specimen can be similarly prepared and treated. If the two grains have different surface (gas to metal) energies per unit area, the equilibrium condition leads to a curved grain boundary.*

* This feature of the problem was pointed out by J. C. Fisher.

References

1. Cyril Stanley Smith: Grains, Phases and Interfaces: An Interpretation of Microstructure. *Trans. AIME* 175, 15. *Mel. Tech.* TP 2387, June 1948.
2. D. Harker and E. Parker: Grain Shape and Grain Growth. *Trans. A.S.M.* (1945) 34, 156-195.
3. C. G. Dunn, A. Seddon, and R. Wylie: Unpublished Work, 1946-1947.
4. Takeo Fujiwara: A Method of Producing A Long Single-Crystal Wire of Aluminum with any Desired Crystallographic Axis. *Jnl. of Sci. Horoshima Univ. A*, (1939) 9, No. 3, 227.

[†] F. Lionetti and the writer are investigating a series of groups all crystals of which have a {110} plane in the plane of the specimen. Results of this investigation, when complete, will be published.

Technical Note No. 9. Manuscript received September 27, 1948.

* Research Physicist, General Electric Co., Pittsfield, Mass.

¹ References are at the end of the paper.

Development of the Modern Zinc Retort in the United States

H. R. PAGE,* and A. E. LEE, JR.*

From the inception of zinc retorting on a commercial scale in the United States in 1890,¹ the retort employed has undergone wide variations in its composition and manufacture, facilitating in part equally remarkable improvements in furnace capacities. The early day hand made clay retort was charged with carbonates or silicates or with coarse dead roasted concentrates mixed with a large proportion of charge fuel resulting in a relatively low zinc burden and fired 24 hr in direct coal fired furnaces. Its modern counterpart is fabricated in hydraulic presses from clay mixtures containing sizeable amounts of either silicon carbide or silica flour, charged with sintered flotation concentrates to more than three times the early day zinc burden and fired 24 to 48 hr in gas fired furnaces.

This paper does not attempt to describe in detail the early day clay retort practice as it is well outlined in treatises by Ingalls,² Lodin,³ Liebig,⁴ Hofman⁵ and others. A brief review of clay retort practice is presented together with a description of the major developments since 1912.

Clay Retorts

The Belgian type retort, both in the circular and elliptical forms, has been used almost exclusively. Typical dimensions of press made clay retorts around 1910 are shown in Table 1. Variations in these dimensions were used at different plants according to local conditions to a maximum inside diameter of 9 in. and inside length of 54 in. However, the effective heat penetration in a 24 hr firing cycle and the tendency of the retort to bend limited the retort size. Use of the elliptical vessel was an attempt to present a stronger cross-section resisting the tendency to bend and to increase the burden without increasing the depth of heat penetration.

Table 1 . . . Typical Dimensions of Press Made Clay Retorts around 1910

| | Circular, In. | Elliptical, In. |
|----------------------|------------------|--------------------|
| Inside diameter..... | 8 | 7.5 × 10.5 |
| Inside length..... | 50 | 50 |
| Wall thickness..... | 1½ | 1½ |
| Butt thickness..... | 2½ | 2½ |

One exception to the 48-54 in. length was the 60 in. retort used as early as 1905 at Palmerton by means of supporting the last 12 in. at the butt end with a specially designed furnace back-wall. This backwall construction with the 60 in. retort had been developed and used at Bethlehem by G. G. Conners and A. B. DeSaules. An attempt was made at Blende, Colo. to use even larger retorts of the Rhenish type based on European practice and requiring much higher furnace temperatures. Satisfactory plastic clays capable of withstanding these temperatures were not available, and the plant never operated successfully.

PREPARATION OF BATCH

Composition of the clay retort by weight was 40 to 50 pct raw clay and the balance "grog." Generally speaking the mix consisted of 7 parts plastic clay to 9 parts grog by volume. Principal source of the clay used was the Cheltenham vein—sometimes referred to as "St. Louis city clay." A typical analysis was Al₂O₃-31.0 pct, SiO₂-50.0 pct, Fe₂O₃-2.5 pct, MgO-0.3 pct, CaO-1.5 pct and loss on ignition 14.0 pct.

At the smelter the clay was weathered whenever possible and then crushed to 0.08 in. or finer. Grog consisted of calcined adobies, cleaned retort scrap and cleaned refuse fire brick such as old furnace brick, blast furnace linings, and others. Saggars from ceramic plants and calcined flint clay were later used. The grog materials were ground to 0.12 in. or finer. Occasionally coke dust up to 10 pct of the mix was substituted for a part of the grog following European practice.²

Particle size of the grog has a major influence on the retort properties—the larger the grain, the better can the retort withstand thermal shocks, resist bending at furnace temperatures and resist corrosion from slag; the smaller the grain, the lower the loss of zinc vapor through the retort walls. Grog forms the skeleton of the retort, and the clay shrinks around its grains to act as a binder. In the drying process, the grog has a stabilizing effect on the drying rate, decreasing shrinkage and giving up previously absorbed water to the surrounding clay to minimize the danger of cracking or checking.²

Grog and clay were mixed through a horizontal pug mill with 10 to 20 pct water added, depending on whether the retort was to be formed by hand or mechanically, more water being required for the hand process. The batch or "mud" extruded from the pug mill was cut in convenient lengths for handling, stacked in piles or in special rooms, covered with wet burlap and allowed to "rot" or age from 1 to 8 weeks to increase plasticity.

HAND MOLDING

If the retort was to be molded by hand, the mud was repugged after the rotting period and given to the molders. Their molds consisted of 3 sheet iron or wood cylinders, each one third the retort length and defining the outer shape of the retort. Beginning with the bottom section, mud was placed in the form and tamped with a rammer

San Francisco Meeting, February 1949.
TP 2523 D. Discussion of this paper (2 copies) may be sent to *Transactions AIME* before May 15, 1949. Manuscript received September 29, 1948.
* Assistant Superintendent and Metallurgist, respectively, Blackwell Zinc Co., Blackwell, Okla.
¹ References are at the end of the paper.

shaped to correspond with the retort interior. This formed a cup from which the retort walls were built up by winding a sort of rope of mud around the interior periphery of the mold. Each addition was tamped into place and the desired interior contour maintained by smoothing with a semicircular tool. Adjoining edges of the mud were roughened to secure a good bond. This process was continued, adding the remaining mold cylinders as required, until the retort was completed. After standing 48 hr the mold was removed and the retort air dried 1 to 3 weeks before being placed in the hot dry rooms.⁵

AUGUR MACHINE

Hand molding was superseded by use of the augur machine in forming retorts. The method of treating the mud between the rotting rooms and the machine varied at different plants. A few plants fed the mud directly to the machine; others repugged it first either in the mixing pug mill or in a larger more powerful mill extruding a 12 to 14 in. mud cylinder. The augur machine consisted essentially of a circular hopper to receive the mud, a series of blades on a central shaft to force the mud downward and a reduced section die and core representing the cross-section of the retort. The machine was arranged to discharge the retort downward in the form of a pipe which was received on a counterbalanced table passing through a temporary wooden mold. When the proper length cylinder had issued from the machine, the augur was stopped and the cylinder cut off, leaving it encased in the wooden mold. A ball of mud was thrown into the cylinder and tamped into place to form the retort butt. As in the case of the hand made vessel, the mold was left on for 48 hr, and the retort dried in the same manner.⁵

HYDRAULIC PRESS

Following the augur machine, a hydraulic press invented by a Belgian, E. Dor, and manufactured by C. Mehler, Aix-la-Chapelle, came into general use. Retorts made in the press, while more expensive than augur units, were denser and stronger. As a result, losses of zinc by absorption and penetration were reduced, a longer life and greater resistance to bending and corrosion were gained, and the charge could be forced longer at high temperatures to effect better zinc recoveries.² A further refinement in the Mehler

press was effected in the unit made by C. A. Wettengel which formed retorts at higher pressures, was more durably constructed and incorporated a number of labor saving devices.⁵

For use in the press the mud had to be formed into ballots about 16 in. long, 14 in. in diam and weighing 200 lb. Initially this was accomplished by feeding mud from the rotting rooms to a hammering or "Schlag" machine. In time the Schlag machine was replaced by a powerful pug mill extruding a 14 in. diam ballot to be cut off in the proper lengths.

The ballot is placed in the receiver of the press and the die block and cover plate of the press closed and locked. Two rams, one a center punch corresponding to the retort interior and the other an annular ring between the receiver walls and the center punch, rise to compress the ballot. The center ram continues upward to a predetermined distance from the cover plate to form the retort butt while the ring retreats downward in corresponding displacement. After the desired pressure has been reached, the cover plate is swung open and the retort extruded upward between the die block and center ram by pressure from the ring ram. As the retort moves upward, it is guided by a sliding pipe framework with a plate fitting over the retort butt. After trimming to the desired length, the retort is placed in the drying room, no molds being required.

DRYING AND ANNEALING

Freshly made retorts were placed in rooms at atmospheric temperatures for 1 to 3 weeks. Then they were moved to hot rooms at 100 to 140°F for a period of 4 weeks to 6 months to be withdrawn as required by the furnaces. Some plants used a series of 2 or 3 hot rooms each at progressively higher temperatures. Prior to being used in the furnace, the dried retorts were sealed in small kilns and over a period of 15 to 20 hr gradually heated to 1500–1800°F. They were removed at this temperature and placed immediately in the furnace.

PERFORMANCE

The life and performance of clay retorts were materially improved by use of the hydraulic press. Life of a press made clay retort in a 24 hr furnace often averaged as high as 30 days with low iron ores such as coarse Joplin or Willemite. The M & H plant at La

Salle is said to have had an outstanding record in this respect, achieving an average of 90 days with small diameter retorts and low burden of Joplin ore in the early 1900's. With western ores of higher iron content, however, the life was as low as 12 to 14 days in some cases. There was a sizeable loss of zinc vapor by absorption in the walls of the retort (7–9 pct of the retort weight) and by penetration through the walls into the laboratory of the furnace (estimated as high as 2 pct of the zinc in the charge by some operators). Retort failures were caused by excessive bending, build up of loam outside and "rock oxide" inside the retort mouth, cracking from thermal and physical shock, slag boring and corrosion. Among various attempted solutions to these difficulties were glazing² the exterior and/or interior of the retort to reduce vapor absorption and penetration, coating the interior with a noncorrosive basic lining² to resist slag corrosion from iron ores, making the retort bottom thicker than the other walls to give added strength and reduce boring losses, and making the retort in layers⁵ of different materials—the interior to resist corrosion and the exterior to form the body of the retort.

Silicon Carbide Retorts

About 1912 the New Jersey Zinc Co. began experimenting with the use of silicon carbide in the retort mix in an effort to improve the life of the clay vessel. Although the higher cost of the retort was recognized at the outset, there were in addition to longer life and other potential advantages several attractive features at the Palmerton plant. These were the possibility of reducing the amount of St. Louis clay on which the freight charge was high, the nearby commercial electric furnace production of silicon carbide together with the producer's desire to find new uses, and the smelter's large scale use of Willemite ore.

The first retorts were cast units of very high silicon carbide content and failed as a result of thermal shock after a short time. Then followed a period of experimentation using carbide crushed and sized to the recommendation of the Carborundum Co., mixed with plastic clay, and processed in the conventional manner. About 1913 a batch consisting of 88 pct silicon carbide and 12 pct plastic clay by weight was prepared by hand mixing and working over a period of several weeks by Jake

Miller, a skillful potteryman. Ballots were prepared in a Schlag machine and passed through a Mehler press making 2 retorts. After drying and burning in the conventional manner, they were placed together in the middle of the second row of a 4 high Siemens regenerative furnace fired with producer gas made from anthracite coal. One of these retorts lasted 10 months and the other 355 days. A mix of 70 pct silicon carbide and 30 pct plastic clay was finally adopted as the composition which could best be worked with the then existing pottery equipment. Some years later this was changed to 65-35 pct. Under the conditions at Palmer-ton, the method of crushing the silicon carbide was found to be most important, and pan mill ground grain to produce a size distribution approximat-ing Fuller's curve of minimum voids gave the best results.

The advantages realized at Palmer-ton in replacing clay retorts with car-bide have combined to effect savings beyond the additional retort cost. These are: longer life—an average well over 100 days over the years—a more rigid piece of refractory permitting the use of a 5 ft retort without extra butt support, improved zinc recovery, smelt-ing time saved in changing fewer retorts, better heat transfer with conse-quent fuel saving and better control of furnace.

There is a definite reaction between the silicon carbide and basic con-stituents of the charge, including zinc oxide, tending to decompose the car-bide. The practice of salt additions in sintering is prohibited, and its use mixed with the charge is limited to a maximum of 0.25 pct because of the alkali reaction. Basic and alkali bearing dust carried in the producer gas used in firing attacks the exterior of the retort similarly. The highly acidic nature of the residue from the Wil-lemite ore-anthracite coal charge un-doubtedly contributes to the successful results at Palmerton.

Manufacture of silicon carbide re-torts for use with sintered zinc sulphide charges has been described by E. J. Bruderlin⁶ at the Amarillo plant of the American Smelting and Refining Co. Current retort size is 9¼ in. inside diameter, 62 in. inside length, 1½ in. wall, 2½ in. butt, weight burned 224 lb. Amarillo uses 2 classes of retorts—the No. 1 class made with clean, freshly produced silicon carbide and the No. 2 class made with about half new mate-rial and half reclaimed carbide. The

average life in calendar days of these retorts for the period 1940 to 1947 in-clusive was 228.6 days for the No. 1 retort and 123.1 for the No. 2. During this period 24, 28, 32, 36 and 48 hr cycles were used.

Silica Retorts

After the silicon carbide retort had been established successfully at Pal-merton, several smelters experimented with the use of carbide in their retort mixes. However, the high cost, close process control required and relatively difficult furnace working conditions were prohibitive in most instances, and other methods of improving the clay vessel were sought.

During a visit to the Hillsboro plant of the American Zinc, Lead and Smelt-ing Co. about 1915, a German engineer named Salzberg mentioned that Ger-man retort clays contained relatively high silica. In 1919 while experimenting with a wide variety of refractory materials mixed with the regular clay-grog mix in an effort to produce a longer retort which would resist bend-ing, the Rose Lake smelter of the same company tested silica additions from 5 pct through 35 pct by volume of the mix. As a result of this work, the high silica retort mix became regular prac-tice at Rose Lake in 1920, although the volume of silica was not standardized at 25 pct until 1929.

W. F. Rossman⁷ of the American Zinc, Lead and Smelting Co. patented the high silica retort in 1922, specifying proportions by volume of 50 pct plastic clay, 25 pct grog and 25 pct silica flour of minus 140 mesh. Manufacture and performance of this retort at Rose Lake were described by G. L. Spencer, Jr.,⁸ in 1931. The first license under the patent was granted May 1, 1928 to the Hegeler Zinc Co., and within a few years the silica vessel was adopted universally by the other smelters not using silicon carbide.

From the information available, the 25 pct proportion of silica has been followed by the industry, although variations in the volumes of clay and grog have been made. For example, Dumas uses a mix of 45 pct plastic clay, 30 pct grog and 25 pct silica flour. The 5 pct additional grog is intended to further stiffen the retort, but no data are available to prove or disprove the benefits.

A further improvement in the prac-tice of manufacturing both carbide and silica retorts was the use of the de-

airing pug mill. This equipment was developed at the Donora Zinc Works in 1940 and has been described by M. M. Neale.⁹ Greater density and strength of the retort wall are the principal advantages. Another recent innovation is controlled humidity or "quick" dry-ing of retorts, introduced at Donora¹⁰ on a commercial scale in 1947. Un-doubtedly this process removes me-chanical moisture much more rapidly and uniformly than is done during the first 15-45 days in the conventional drying room. However, the value of long aging in addition to drying is considered by some smelters to be of great importance to long retort life, and some believe that aging of quick dried retorts will materially improve them.

As an example of current manufac-ture of silica retorts, the practice of the Blackwell Zinc Co. is described. The retort is of circular cross-section and has the following dimensions burned: inside diameter 9¼ in., in-side length 62 in., wall 1½ in., butt 2¼ in., weight 171 lb.

MATERIALS

Materials used in fabricating the retort and their proportions by volume are 50 pct plastic clay, 25 pct grog and 25 pct silica flour. Wet weights per cu ft and average moisture content of the crushed materials as used are: clay, 78 lb per cu ft, 7.0 pct moisture; grog, 80 and 1.0 pct; silica flour, 68 and 0.5 pct. Missouri clay from the area about 100 miles northwest of St. Louis is used and has approximately the composition shown in Table 2. After weathering 6 to 12 months whenever possible, the clay is sized to minus 0.095 in. Grog is purchased de-aired setter slab mate-rial which has been used in making and burning fire brick. A typical analysis is given in Table 2. Grog is sized to minus 0.120 in. Silica flour is of high quality, assaying approximately 99.5 pct SiO₂, and is in the form of a fine flour, 95 pct through a 150 mesh sieve and 50 pct through 200 mesh.

Table 2 . . . Analysis of Clay and Grog Used in Blackwell Retorts

| | Clay, Pct | Grog, Pct |
|--------------------------------|-----------|-----------|
| Al ₂ O ₃ | 30.5 | 38.9 |
| SiO ₂ | 58.0 | 56.0 |
| Fe ₂ O ₃ | 1.0 | 4.2 |
| MgO | 0.1 | 0.14 |
| CaO | 0.2 | 0.35 |
| S | 0.2 | 0.12 |
| Loss on ignition | 9.8 | 0.0 |

FORMING RETORTS

Desired quantities of clay, grog and silica are bucketed into a horizontal pug mill from adjacent storage bins. Sufficient water, usually 12.5 to 13.0 pct in the mix, is added to produce the desired stiffness. The mud is extruded through a round cornered $7\frac{3}{4} \times 10\frac{3}{4}$ in. opening from the mill, cut and stacked nearby. When approximately 23 tons (enough for 235 retorts) has been made, the feed of raw materials is stopped and the entire batch immediately repugged. It is recut and stacked in rotting rooms for 5 to 6 days. After the rotting period, the mud is fed into a Bonnot de-airing pug mill where it is repugged, shredded, de-aired under a vacuum of 25–27 in. of mercury, and compressed into an ejecting cylinder 15 in. in diam. The ballots are cut off in 17 in. lengths and made into retorts in a Mehler press. The butt is formed with a pressure on the mud of 1050–1100 psi and the walls extruded at 300–350 psi. After trimming to proper length, the retorts are wheeled individually on rubber tired trucks to the drying rooms.

DRYING

Drying rooms have brick walls and a gently sloping frame roof. The floor is made of wood 2×4 's laid flat and spaced $\frac{1}{4}$ in. apart over the floor joists. To a height of 6 ft from the floor, a rough wood wainscoting separates the retorts from the brick walls by a 4 in. airspace. In the roof are constructed 2 ventilators with the outside openings shielded from possible entry of rain and containing dampers for varying the openings. Steam pipes are laid 6 in. below the floor and at the ceiling to effect drying. The average room holds about 1500 retorts.

Prior to using a room for drying, all steam is shut off, the ventilators are closed, and the walls and floor wet down. The retorts are carefully placed in rows beginning against the farthest wall from the door. Each retort is put as close as possible to its neighbors with each row interlocking the preceding row. At the end of each production shift, the exposed row is covered with damp burlap and the door closed. When the room is filled, boards are placed across the doorway to a height of 6 ft, the retorts in the doorway covered with burlap and the door closed.

Depending on outside conditions, the

temperature in the room will average 80°F when filling is completed. Daily checking of the room is required, and its temperature at a regular time each day is recorded on a chart on the door. On the fifteenth day after closing, the ventilators are opened and steam is cracked on the floor coils. Steam additions are carefully controlled so that the temperature rises only 1 or 2° each day. When possible, all drying is effected with the floor coils only. However, after 30 days from start of heating, steam may be turned in the ceiling coils if necessary to maintain the temperature increase until 135°F is reached. Occasionally in cold weather it is necessary to use the top coils to prevent condensation drips from the ceiling.

The room is held at 130–135°F until opened for furnace use. Retorts are in the rooms 90 to 120 days. Loss in drying based on retorts used in the furnaces is quite low as evidenced by the following: 1945—0.12 pct, 1946—0.16 pct, 1947—0.11 pct.

PREHEATING

On the day preceding the prescribed furnace maneuver, the required number of retorts is taken from the oldest drying room and placed in conventional down draft gas-fired kilns. Doors are sealed and the kilns fired at 3 in the afternoon in anticipation of use the following morning between 6 and 9. Heating is gradual to a maximum of 1600–1800°F during the latter part of the period. When retorts are to be withdrawn, the gas is shut off and the doors opened. The retort must be placed immediately in the furnace when taken from the kiln as it is very sensitive to temperature change. During any pause in the removal of retorts over a few minutes duration, the kiln door is closed and the gas reapplied.

Retort loss at the kilns is 4 pct based on retorts used in the furnaces. 1 pct of this is due to errors in firing—primarily spalling from too rapid heating. 3 pct represents breakage from faulty handling on removal from the kiln. All retorts lost at the kilns are collected and returned to the pottery for use as grog. Retorts lost in drying are hard burned in a kiln and used in the same way.

PERFORMANCE

Performance of the silica retort at Blackwell for the period 1943 through

August, 1948, is shown in Table 3. Ores used during this time were about one third low iron sulphide flotation concentrates of about 2.5 pct Fe in the green ore and two thirds containing about 7.0 pct Fe.

Table 3 . . . Performance of Silica Retort at Blackwell

| | LIFE IN FURNACE CYCLES* |
|------|-------------------------|
| 1943 | 22.69 |
| 1944 | 28.54 |
| 1945 | 29.83 |
| 1946 | 31.59 |
| 1947 | 26.20 |
| 1948 | 29.34 |

* Furnace cycle 24 hr before June 1944 and 93 pct at 48 hr since.

Conclusion

The history of the horizontal zinc retort in the United States records a continual effort to enlarge the retort. The two most significant developments in this respect were the use of the hydraulic press in forming retorts and the use of silicon carbide and silica flour mixes. The 62–64 in. inside length employed today is not the limit at which the modern retort can effectively resist bending but is, rather, the supposed practical limit of effective manual charging. Extending the furnace cycle beyond 24 hr has permitted on a practical scale increasing diameter. However, even with the 48 hr cycle the maximum distance for heat penetration appears to be limited depending on the slagging characteristics of the ores charged. Longer life and improved wall density of modern retorts have made possible better zinc recoveries.

While the advantages of both the silicon carbide and silica retorts are easily discernible over the clay vessel, it is difficult to make any such distinction between the former. In the United States only the two primary zinc smelters previously mentioned use carbide retorts, and the balance use silica. In cost the carbide retort is 4 to 6 times as expensive, but correspondingly, its life is 3 to 4 times as long in terms of charge cycles dependent on the composition of ores used and character of the firing fuel.

Heat transfer within the furnace is much more effectively accomplished with the carbide than the silica. Carbide retorts can be and are fired to higher temperatures than silica retorts, resulting in lower zinc in the residue but greater demands on furnace linings. Special refractories are sometimes resorted to where carbide retorts are used. Because of the longer life, more attention must be given to

chiseling out loam build up and "rock oxide." For the same reason, use of carbide retorts in Hegeler furnaces is impractical because of build up of fusible fly ash fastening retorts to the shelves. The use of salt in sintering and in preparing the charge is restricted. Residual sinter sulphur must be held to a low figure, preferably 0.2 pct or lower. The silica retort is subject to boring and corrosion by fusible iron slags but is considerably easier to cut out and replace in the furnace. Thermal shock below furnace temperatures is much more damaging to the silica, even the old clay retort being superior in this respect. Because of the better heat transfer, heavier retort weight and greater difficulty in cutting out retorts, the working conditions are said to be less satisfactory on a silicon carbide retort furnace. On the other hand, changing less retorts per cycle at least partially offsets this. Practical burdens per retort are about the same for both vessels. Other things being equal, the

longer life of carbide retorts should make possible higher recoveries of zinc. Choice of the retort is a matter depending on local conditions at the individual smelter.

Acknowledgment

The assistance of Mr. Francis P. Sinn of the American Metal Co. and Mr. Chester Skinner and the staff at Blackwell in preparing this paper is gratefully acknowledged. Thanks are extended to Mr. Henry Hardenbergh and Mr. L. S. Holstein of the New Jersey Zinc Co. for data on the early history of the silicon carbide retort and its use at Palmerton; to Mr. E. J. Bruderlin of the American Smelting and Refining Co. for data on the use of silicon carbide retorts at Amarillo; and to Mr. Robert Ammon and Mr. G. L. Spencer, Jr. of the American Zinc, Lead and Smelting Co. for the history of the silica flour retort.

References

1. W. R. Ingalls: Lead and Zinc in the United States. 313-315. 1908, New York. Hill Publishing Co.
2. W. R. Ingalls: Metallurgy of Zinc and Cadmium. 216-256. 1903. New York. McGraw-Hill Book Co., Inc.
3. A. Lodin: Metallurgie du Zinc. 594-648. 1905. Paris.
4. R. G. Max Liebig: Zink und Cadmium. 324-373. 1913. Leipzig.
5. H. O. Hofman: Metallurgy of Zinc and Cadmium. New York. 131-154. 1922. McGraw-Hill Book Co., Inc.
6. E. J. Bruderlin: Manufacture of Silicon Carbide Retorts. *Trans. AIME* (1936) **121**, 441-444.
7. W. F. Rossman: U. S. Patent 1424120, July 25, 1922.
8. G. L. Spencer, Jr.: High-silica Retorts at the Rose Lake Smelter. *Trans. AIME* (1931) **96**, 119-124.
9. M. M. Neale: Deaeration in Manufacture of Zinc Retorts. *Trans. AIME* (1944) **159**, 127-129.
10. F. P. Sinn: Annual Review of Zinc Smelting. *Mining and Metallurgy*, (Feb. 1948) 97-98.



A view in an assaying laboratory (Ercker, 1574).

In the background are (left to right), a cementing furnace, a pot for reacting saltpeter and argol to make flux, a double wind furnace, and a muffle furnace for cupellation. The cylindrical tower furnace in the foreground is an Athanor and is making nitric acid for parting. The ring of fire heats silver granules in the pot with sulphur, forming silver sulphide which is subsequently melted to separate the contained gold. The man in the right foreground is smelting copper ore for assay directly in a little blast furnace, the air for which is provided by aeolipile acting as an injector. This is probably the earliest use of steam power for serious purposes.

(Courtesy Cyril S. Smith.)

The Effect of Strain-temperature History on the Flow and Fracture Characteristics of an Annealed Steel*

E. J. RIPLING† and G. SACHS,† Member AIME

Introduction

ALL ferrous alloys can be made brittle by straining at sufficiently low temperatures. However, the changes in mechanical properties for different ferrous materials with decreasing testing temperature do not appear to follow any universal law.

In particular, complex effects of testing temperature have been observed if cold worked steels were subjected to tensile tests at low temperatures.

EFFECTS OF PRETRAINING AT A TEMPERATURE ABOVE THE TESTING TEMPERATURE ON THE FRACTURE CHARACTERISTICS†

A considerable amount of data has been presented by a number of investigators on the fracture characteristics of various cold worked steels.¹ These data usually relate to a two-step procedure first used by Davidenkov,² consisting of stretching by tension to a certain strain or "prestraining" at room temperature and then completing the tensile test, or "testing" at the temperature of liquid air.

On the basis of data of this type made available to date, ferrous alloys can be classified into two groups with respect to their fracture characteristics observed on testing at a low temperature after prestraining at room temperature. Very complex phenomena have been observed for all annealed steels. On the other hand, some observations indicate that steels in certain other conditions represent a fundamentally simpler relation.

In considering the effect of prestraining at one temperature on the properties obtained at some lower temperature, it should be expected that any cold work reduces the ductility

retained in proportion to the magnitude of the cold work. However, the test data presented to date indicate that only heat treated (quenched and tempered) steels appear to conform to this expectation, according to the very limited test data in Fig 1, presented by McAdam, Geil and Mebs. This series of tests, Fig 1, shows that the retained ductility became smaller the larger the prestrain. However, this decrease is less than the amount of prestrain or, in other words, less than the decrease in ductility at the prestraining temperature.

These effects of prestraining are fundamentally identical with those observed by Bridgman³ when a steel was prestrained (in tension) under hydrostatic pressure and then subjected to a regular tension test. It appears, therefore, that the basic effect of prestraining under conditions which yield a higher ductility than the (subsequent)

testing procedure, consists of gradually increasing the total ductility of the metal from the initial low value of testing to the higher value of prestraining.

On the other hand, all annealed steels, if cold worked by tension at room temperature and then tested at a lower temperature, provided that some ductility is retained, showed a far more complex behavior than that discussed above. This relationship is exemplified by Fig 2, for three pearlitic steels.^{4,5} These particular steels were selected because of the various shapes of their ductility-prestrain curves. All three steels, and any other investigated so far, suffered a rapid decrease in retained (and consequently also in total) ductility when subjected to small prestrains. Then, after exceeding a certain prestrain it was generally observed that the ductility recovered.*

This rather complex behavior of annealed steels may be tentatively correlated with the presence of stretcher strains at small prestrains. Heat treated steels do not exhibit stretcher strains. This fact might possibly explain their simpler prestrain-retained ductility relationship.

The destructive effect of these stretcher strains may possibly be associated with the presence of triaxiality, which may occur in any highly non-uniform stress and strain state (and which is retained as residual stress after unloading). Even a small degree of triaxiality may then cause a reduction in ductility, or even embrittlement at a sufficiently low testing temperature.

The discussion presented above deals with the effects of cold working at a high temperature on the fracturing

San Francisco Meeting, February 1949.

TP 2514 E. Discussion of this paper (2 copies) may be sent to *Transactions AIME* before May 15, 1949. Manuscript received June 17, 1948; revision received Sept. 27, 1948.

* This paper is one of a series of reports in a research program conducted at the Research Laboratory for Mechanical Metallurgy, Case Institute of Technology, Cleveland, Ohio, in cooperation with the Office of Naval Research, U. S. Navy.

† Research Laboratory for Mechanical Metallurgy, Case Institute of Technology, Cleveland, Ohio.

‡ In most investigations in which the effect of some variable or variables on the fracturing characteristics is to be determined, it has been found that the ductility generally responds to the variables more simply and accurately than the fracture stress. Consequently, in this paper the main emphasis will be placed on ductility changes.

1 References are at the end of the paper.

* This damaging effect of small tensile strains on the low temperature properties of annealed steels is further revealed by some tests made by Davidenkov and Sakharov² on a 0.20 to 0.25 pct carbon steel. The transition temperature of this steel was found to go through a maximum at small prestrains, as shown in Fig 3.

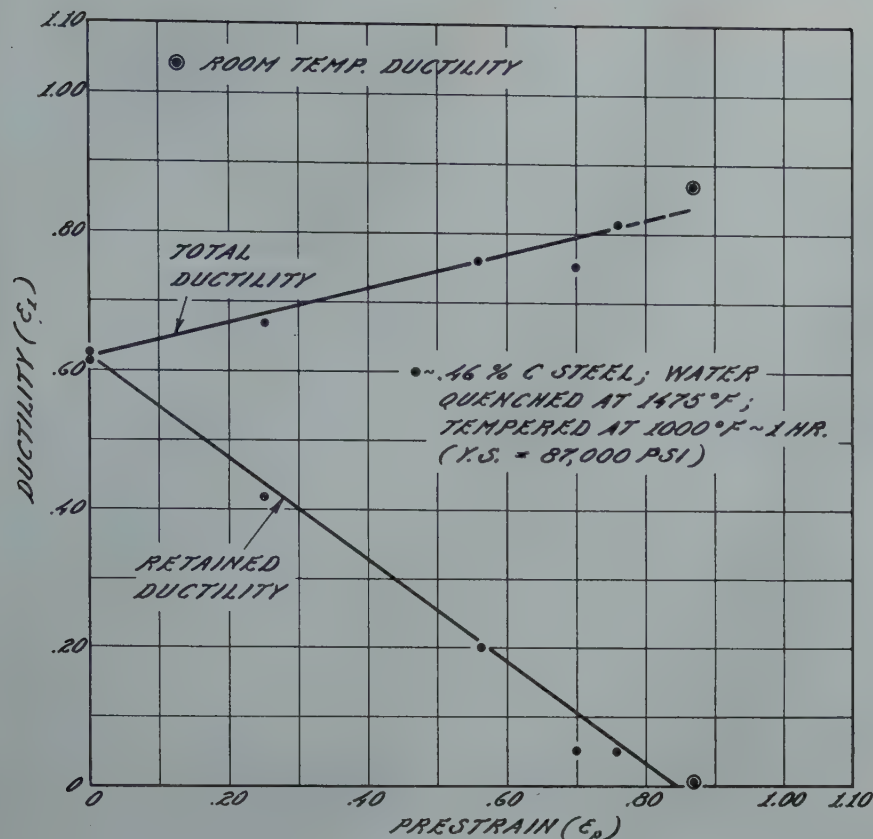


FIG 1—Effect of prestraining in tension at room temperature on the ductility at a low temperature (-190°C) obtained on a heat treated steel (McAdam, Geil, and Mebs).

characteristics at a lower temperature. Apparently, the reverse case, that is, prestraining at a low temperature and testing at a higher temperature to failure, has not yet attracted any attention.

EFFECT OF PRESTRAINING AT ONE TEMPERATURE ON THE FLOW CHARACTERISTICS AT A HIGHER AND A LOWER TESTING TEMPERATURE

The effect of two-step, cold work treatments has also been investigated on another metal characteristic, that is, strain hardening, as represented by the general shape of the stress-strain curve. The very limited data presented by Hollomon⁶ obtained on a 1020 steel have been evaluated by him to prove that the temperature of prestraining has no effect on the strain hardening observed at a given temperature, Fig 4. In other words, the state of strain hardening is independent of the straining temperature, as long as the temperature is sufficiently low to prevent diffusion.

According to some data by Orowan,⁷ however, obtained on copper which was strained in steps at room temperature and at the temperature of liquid

nitrogen, Fig 5, the stress at any particular strain is very greatly affected by the temperature at which the strain was made. Furthermore, in some more recent tests, Dorn, Goldberg and Tietz⁸ prestrained 2SO aluminum at various temperatures and then tested it at both a higher and a lower temperature than the prestraining temperature. Their results were in agreement with those of Orowan in that the flow stress at any particular strain depended greatly on the strain history. Furthermore, they found that prestraining at a high temperature had a greater effect on the flow stress at the low temperature than the reverse process of prestraining at a low temperature and testing at the high temperature. In addition to the work done on 2SO they also prestrained pure aluminum, copper, 65/35 brass, and 18/8 stainless steel at room temperature before testing at a low temperature. The flow stress of each of these materials also showed a great dependence on strain history.

PURPOSE OF PRESENT INVESTIGATION

This investigation was conducted in order to clarify some of the problems discussed above. A low carbon $2\frac{3}{4}$ pct silicon steel was selected for the investigation. Test series were conducted to determine the following:

1. Effect of testing temperature on the properties of the $2\frac{3}{4}$ pct silicon

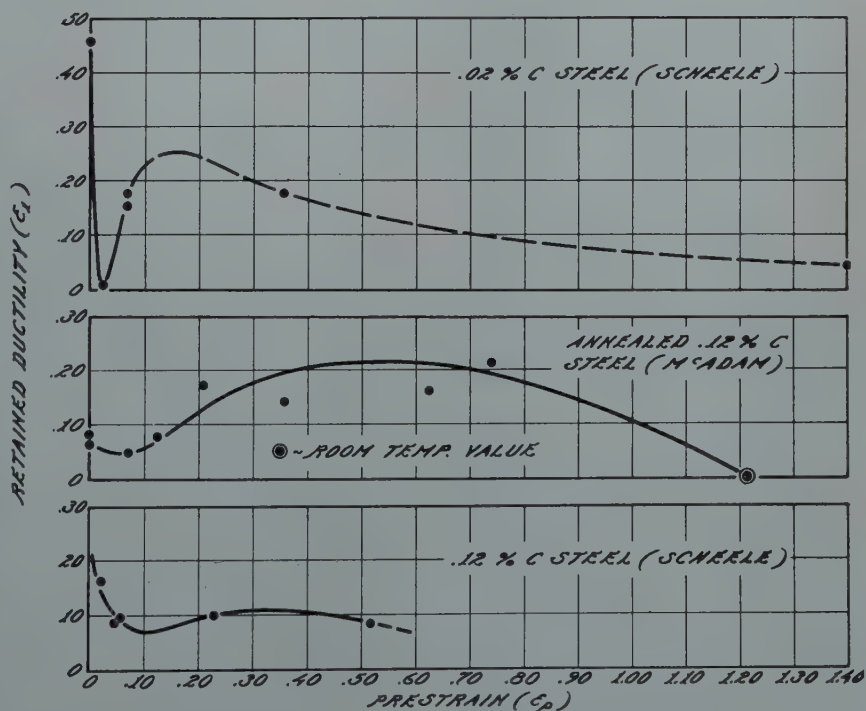


FIG 2—Effect of prestraining in tension at room temperature on the retained ductility at a low temperature (-190°C) obtained on annealed steels.

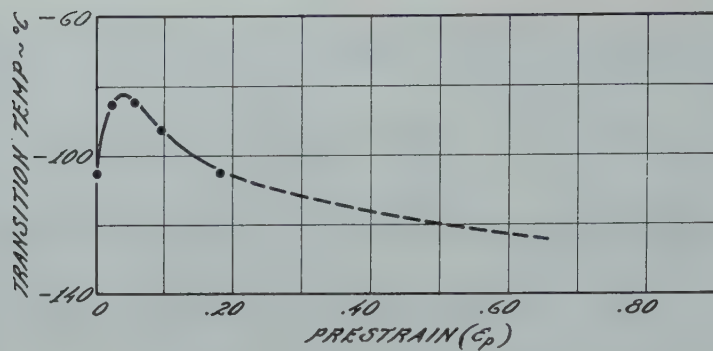


FIG 3—Effect of prestraining in tension at room temperature on the transition temperature of an annealed (coarse grained) 0.20 to 0.25 pct carbon steel (Davidenkov and Sakharov).

steel, to determine the basic effects of testing temperature on the mechanical properties of this metal.

2. Effect of prestraining at room temperature on the properties at various low temperatures.

3. Effect of prestraining at various temperatures on the properties at a constant low temperature.

4. Effect of prestraining at various low temperatures on the properties at room temperature.

Material and Equipment

MATERIAL

The mechanical properties of ordinary low and medium carbon steels behave in general quite peculiarly with varying temperature. As discussed in a later section, most steels, when the temperature of testing is reduced, become considerably stronger while their ductility is only slightly affected over wide limits. However, at some low temperature the ductility drops to very small values over a narrow temperature range. In an investigation of the type proposed here, a steel whose fracturing characteristics behaved in this complex manner would impose a considerable limitation on the results that could be obtained. Consequently, a 2¾ pct silicon steel was selected for this work. The steel, which approached a solid solution type alloy, had the following analysis: C, 0.031; Mn, 0.12; P, 0.011; S, 0.015; Si, 2.73; Ni, 0.098; Al, 0.23; Cu, 0.116; Sn, 0.008. This steel also possessed the advantages that its ductility at room temperature was quite high, while it decreased to a very low value at the lowest temperature obtainable. A high silicon steel of this type also possesses very uniform flow and fracture characteristics.

form of ¾ in. rods had been annealed at 1450–1500°F for 8 hr, so that it possessed quite a large grain size. The steel was used in this “as-received” condition.

EQUIPMENT

The prestraining and testing was done on a 10,000 lb Riehle tensile test machine. All room temperature strains were accomplished with the use of a specially designed loading fixture that yielded an eccentricity of loading of less than 0.001 in. and a radial strain gauge reading in 0.0001 in.⁹ These same loading fixtures were adapted for the low temperature work under which

condition the eccentricity was slightly higher. A remote reading mechanical gauge reading in 0.0001 in. was also developed to be used with this apparatus. A detailed description of this equipment is given in another report.¹⁰

Procedure and Method of Evaluation

PRESTRAINING AND TESTING PROCEDURE

All specimens used in this investigation were initially machined to a 2-in. contour radius at the reduced section, to enforce fracturing at a predetermined location and to facilitate measuring the strains at the neck. The other specimen dimensions are shown in Fig 6.

Specimens that were tested at temperatures less than -78°C (that is, -80 , -100 , -120 , -150 , and -196°C) were finished by polishing in such a manner that the scratches on these specimens were in the direction of the axis of the specimen. Specimens that were prestrained and then tested at temperatures less than -78°C were polished after prestraining. In this series of tests, specimens that were prestrained to less than approximately 30 pct were polished to a 2-in. radius. If the specimens were prestrained to

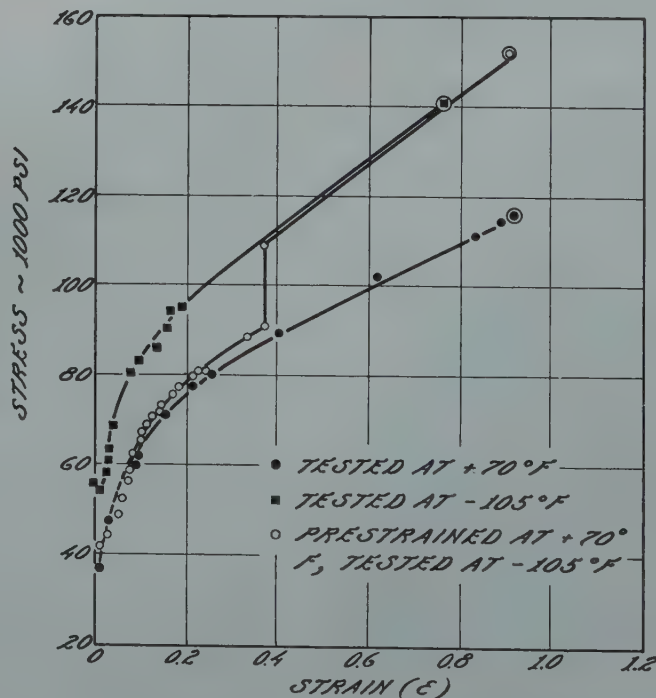


FIG 4—Stress-strain curves for 1020 steel at a high and a low temperature and for prestraining at a high temperature and testing at a low temperature (Hollomon).

more than 30 pct, the contour radius of the strained specimen was determined, and the specimen was polished to this radius. This procedure removed approximately 0.005 in. from the diameter.

All tests were made with the speed of the movable head of the tensile machine approximately 0.04 ipm so that for each specimen strained, a large number of gauge readings could be taken at different loads in order to enable point by point recording of the stress-strain curves. (This, of course, was not possible at temperatures at which the coolant was frozen.) These readings yielded values of the average or "true" stress,* and of the average decrease in diameter of the minimum section. The diameter reduction was converted into the natural maximum strain, ϵ_1 , according to the equation:

$$\epsilon_1 = \frac{\text{Original area}}{\text{Instantaneous area}} - 1 = 2 \ln \frac{\text{Original diameter}}{\text{Instantaneous diameter}}$$

From these data a stress-strain curve was obtained for each specimen strained, showing the true stress as a function of the natural strain. In all instances these natural strains, therefore, relate to the dimensions of the specimen at the beginning of a particular straining operation. However, the use of natural strains made possible the addition of the prestrains and testing strains by the simple graphical operation of plotting the respective stress-strain curves side by side.

In the testing operation, particular care was exercised to observe the load at the moment of fracture so that the fracture stress† could be evaluated. The corresponding fracture strain or "retained ductility" was determined by diameter measurements made with a micro-comparator before and after straining.

METHOD OF EVALUATION

The evaluation of the test data was based primarily on the following two types of graphical representations:

1. A comparison of stress-strain curves obtained at a given temperature for various amounts of prestrains at several different temperatures, see Fig 16 to 21.

2. The dependence of the retained ductility at a given temperature upon the magnitude of prestrain, with the

* The true stress was defined as the ratio of the load to the minimum area of the specimen at the instant at which the load was obtained.

† True stress at fracture.

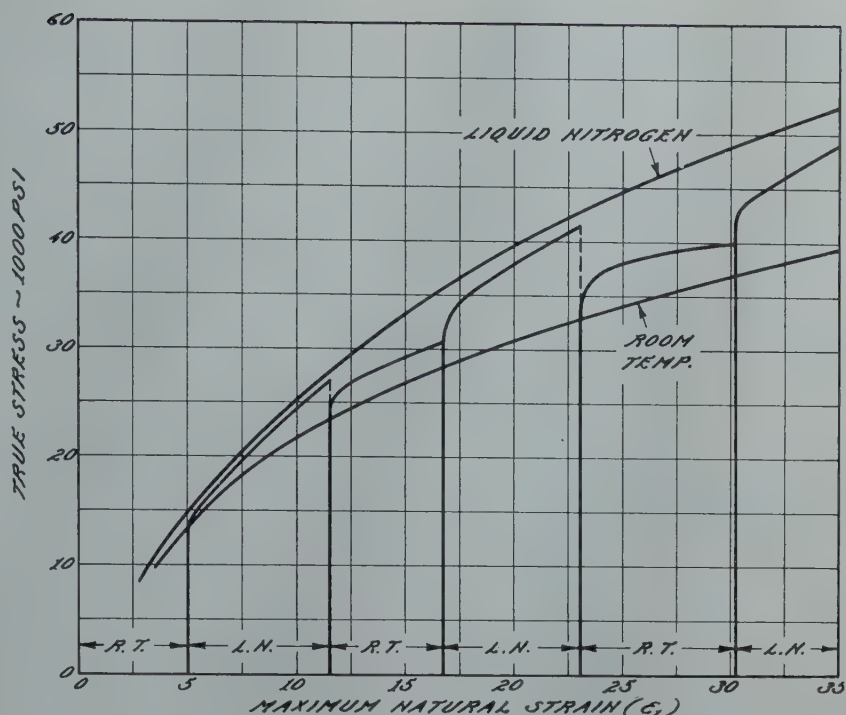


FIG 5—Effect of alternately straining at room temperature and at -196°C on the flow stress of a high conductivity copper (Orowan).

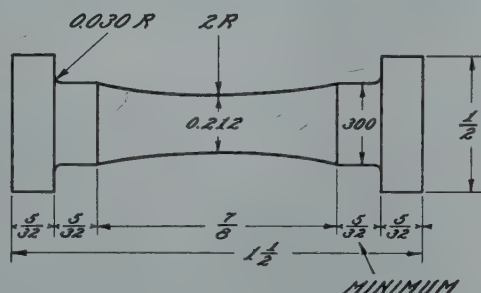


FIG 6—Tensile test specimen.

temperature of prestrain as parameter, see Fig 11 and 15.

These data were obtained, as mentioned before, on tensile test specimens having an initial longitudinal contour radius of two inches. This initial contour and the fact that the specimens developed necks on straining undoubtedly influenced the measured values of stress and ductility. However these effects of specimen shape are superimposed on the phenomena being discussed in this paper, and the measured average stresses and strains appear satisfactory. Furthermore, the principal conclusions derived relate to comparatively small strains and should, therefore, be only slightly influenced by the process of necking.

Discussion of Results

EFFECTS OF TESTING TEMPERATURE ON THE PROPERTIES OF THE UNSTRAINED MATERIAL

For the purpose of this investigation, it was first necessary to investigate the direct effect of testing temperature on the flow and fracture characteristics of the selected steel. Wherever possible, stress-strain curves were determined, which are plotted in Fig 7 and 8. The dependence of the yield strength (1 pct),* the tensile strength, and the

* The yield strength was defined as the stress at 1 pct permanent set instead of the conventional value of 0.2 pct, since the strain gauge used at low temperatures yielded more reliable values at this higher strain.

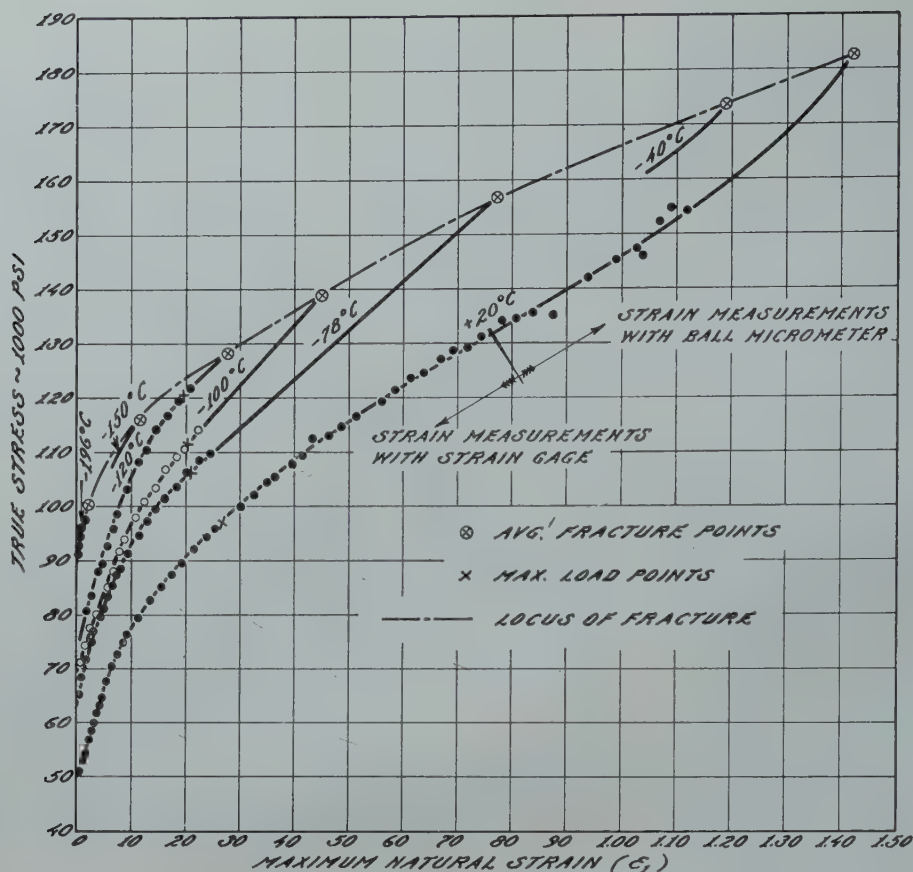


FIG 7—Effect of testing temperature on the stress-strain characteristics of a 2 $\frac{3}{4}$ pct Si steel.

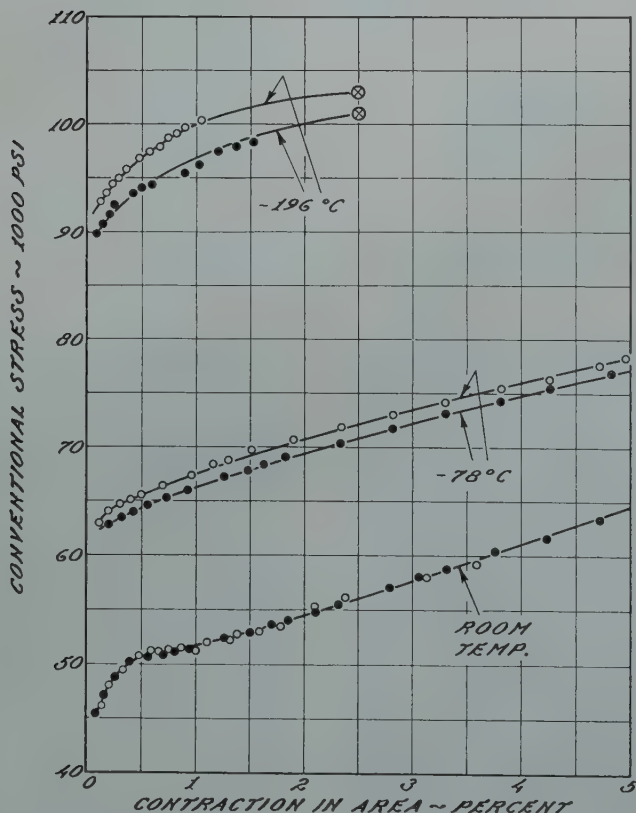


FIG 8—Effect of testing temperature on the stress-strain characteristics of a 2 $\frac{3}{4}$ pct Si steel.

fracture stress upon temperature is shown in Fig 9 and that of the ductility in Fig 10. In both Fig 7 and 10 approximate values of the maximum load strains are also indicated. It can be seen from the stress-strain curves in Fig 7 and from Fig 9 that the value of yield strength changed with temperature at an approximately constant rate over the entire range investigated. The general shapes of the various stress-strain curves in Fig 7 are rather similar. With decreasing temperature, the stress-strain curve moved to higher stresses, increasing its slope, $ds/d\epsilon_1$,* only very slightly. The maximum load strain (which depends upon the relative slope, $ds/sd\epsilon_1$) consequently decreased slightly with decreasing temperature. (See Fig 10.)

The tensile strength, like the yield strength, also changed with temperature at an approximately constant rate down to a temperature of -130°C . The tensile strength values then went through a maximum at about -150°C .

At room temperature the silicon steel curves exhibited a slight but dis-

* Where s = average tensile stress, and ϵ_1 = maximum natural strain.

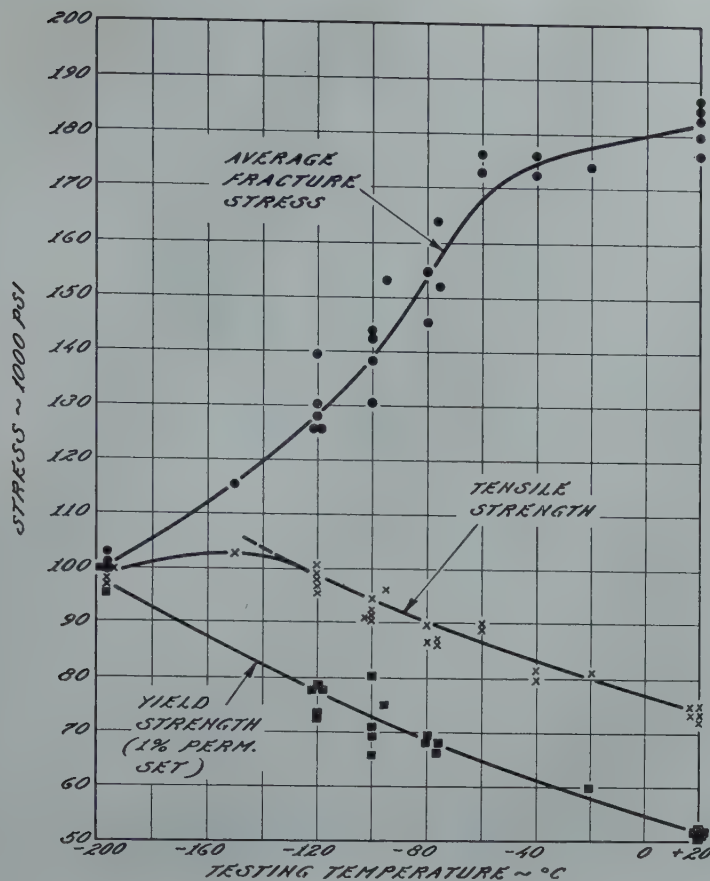


FIG 9—Effect of testing temperature on the strength properties of a 2 $\frac{3}{4}$ pct Si steel.

tinct yield point jog, or reversal in curvature at small strains, as apparent from the conventional stress-strain curves in Fig 8, which are plotted on an enlarged scale.* Fig 8 also includes several stress-strain curves taken at temperatures of -78 and -196°C . (These were the only low temperatures at which reliable small strain measurements were obtained.) The stress-strain curves for -196 and -78°C showed no indication of a yield point jog. It may be concluded, therefore, that the reversal in curvature of the stress-strain curves of the silicon steel decreases with decreasing temperature until it disappears somewhere before -80°C .

The ductility (contraction in area converted to natural strain) of the silicon steel decreased according to Fig 10 with decreasing temperature. At approximately -130°C the ductility became equal to the maximum load strain and at still lower temperatures it rather gradually approached very small values. At the lowest temperature used, -196°C , the steel was still distinctly ductile. (See Fig 8 and 10.)

*The pairs of stress-strain curves in Fig 8 represent tests obtained on pairs of randomly selected specimens at each temperature.

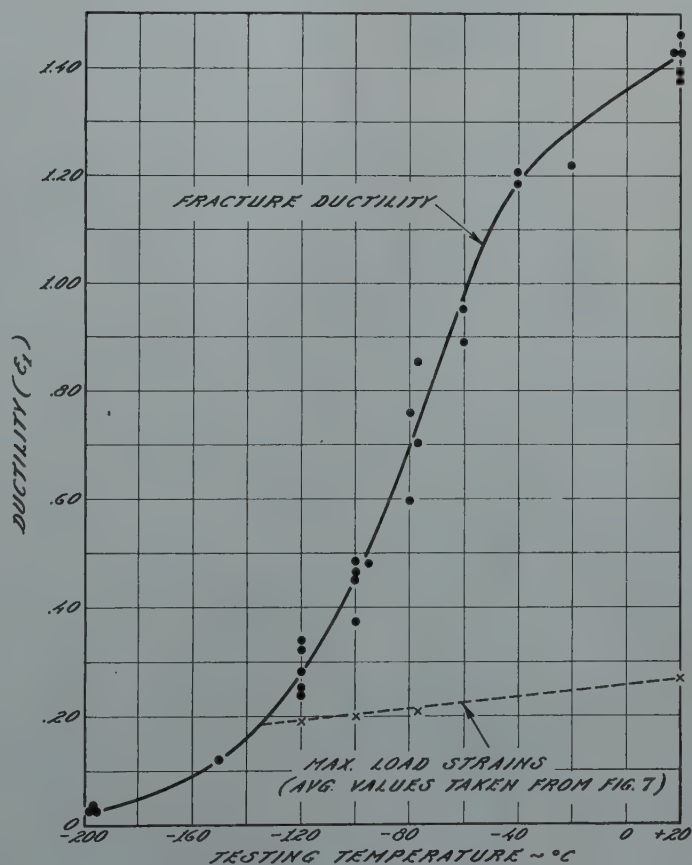


FIG 10—Effect of testing temperature on the ductility of a 2 $\frac{3}{4}$ pct Si steel.

The fracture stress changed with temperature in a manner which showed this property's dependence on both the flow stress (yield strength) and ductility. (See Fig 9 and 10.) This explains the rather slow decrease in fracture stress in the range below room temperature, where the relative change in ductility was also comparatively small. At lower temperatures the (average) fracture stress decreased at nearly a steady rate, to become slightly more than one half of the room temperature value at -196°C .

EFFECT OF PRETRAINING AT ROOM TEMPERATURE ON THE FRACTURING CHARACTERISTICS AT VARIOUS LOW TEMPERATURES

Fig 11 shows the ductility values retained after specimens were prestrained various amounts in tension at room temperature and then tested to failure at various low temperatures.

The retained ductility values went through a minimum, the magnitude of which was proportionally larger the lower the testing temperature. Thus, for example, at -196°C the ductility dropped from $2\frac{1}{2}$ pct with no prestrain to approximately 0.01 pct at

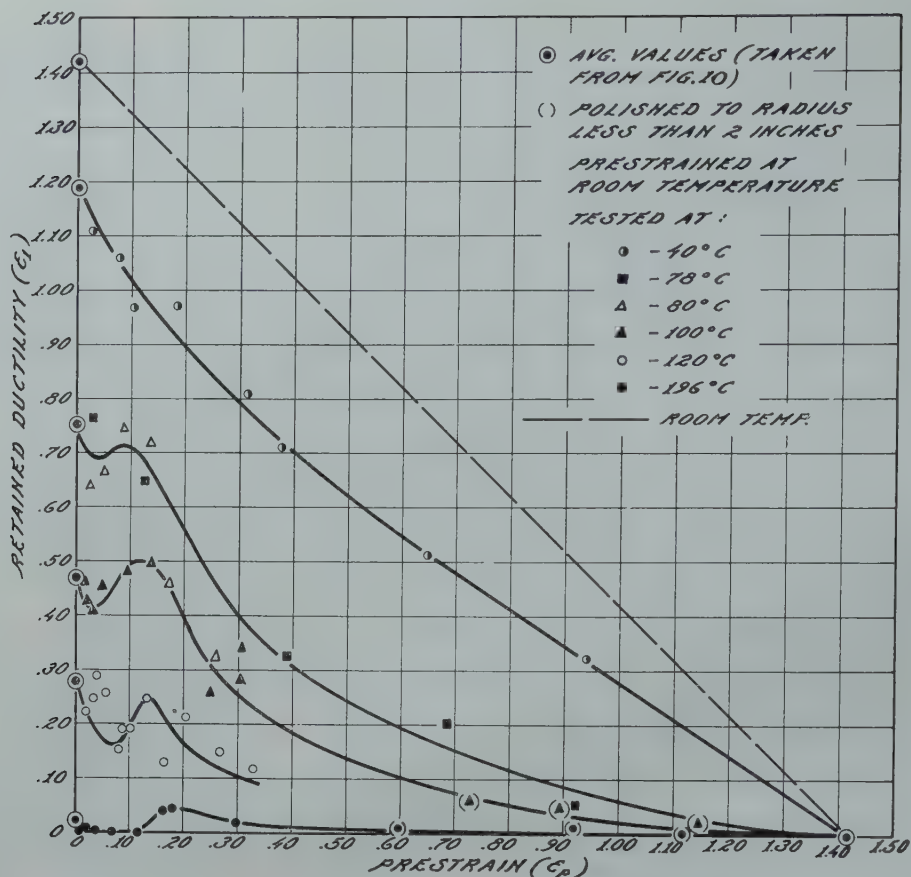


FIG 11—Effect of prestraining in tension at room temperature on the retained ductility at various low temperatures.

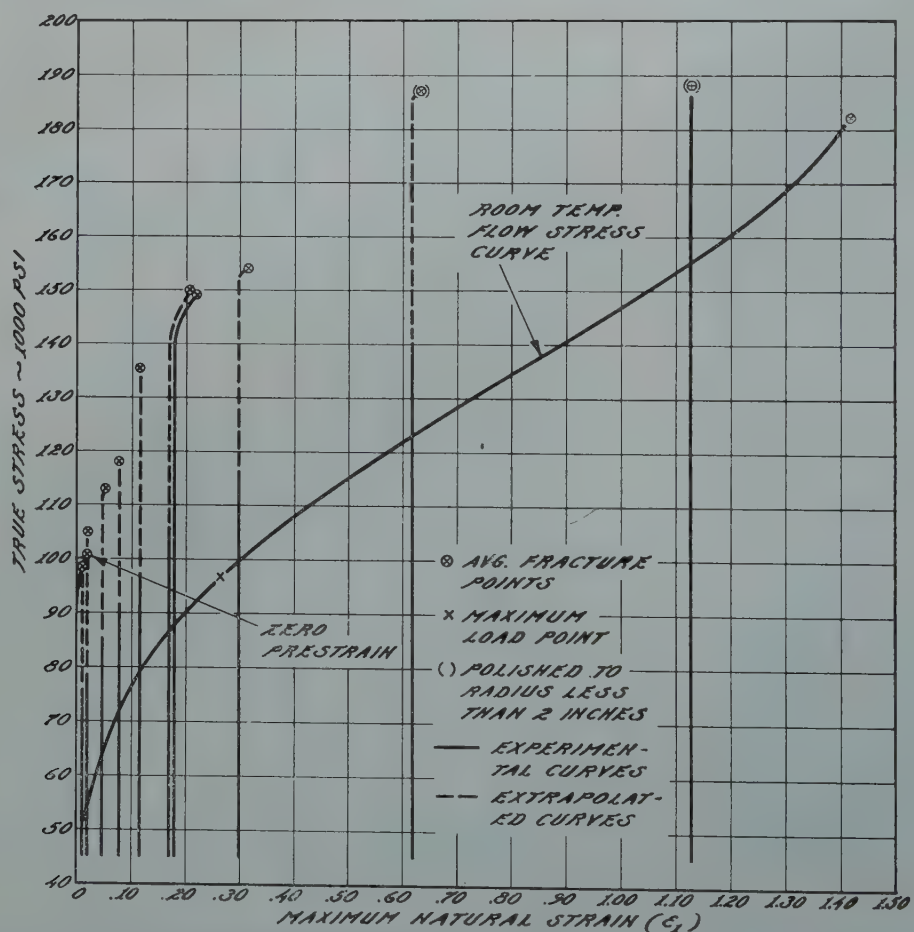


FIG 12—Effect of prestraining in tension at room temperature on the properties obtained at -196°C.

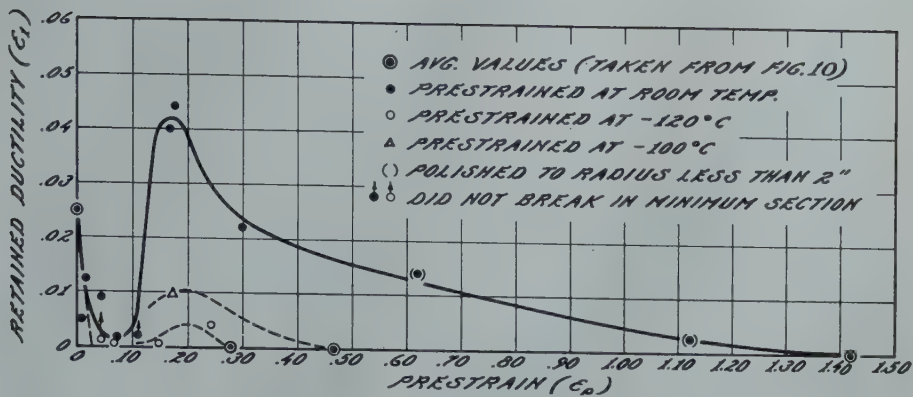


FIG 13—Effect of prestraining at various temperatures on the retained ductility at -196°C .

4 pct prestrain. At -100°C the ductility decreased from about 47 pct at zero prestrain to about 41 pct at a prestrain of 4 pct. At the highest temperature used in testing (-40°C), the minimum disappeared.

These curves also showed a maximum at the lower temperatures which gradually disappeared as the testing temperature was increased. At the lowest temperature used, -196°C , the maximum value of retained ductility (at 18 pct prestrain) was approximately 4 pct. This value was distinctly larger than the ductility of the unstrained metal which averaged only $2\frac{1}{2}$ pct. It also appears that the prestrain value at which this maximum occurred moved to lower prestrains as the testing temperature was increased.

The data presented here confirmed previous test results in that a considerable ductility was generally retained at low testing temperatures even though the magnitude of the prestrains at the high temperature exceeded the total ductility of the steel at the (low) temperature of testing. Only when the prestrain approached its limiting value, that is, the ductility at room temperature, did the ductility retained at the testing temperature also approach zero. Thus, in the range of large prestrains the retained ductility decreased gradually from its maximum value to the value of zero at a prestrain equal to the room temperature ductility.

Fig 12 represents stress-strain curves obtained after prestraining at room temperature and testing at -196°C . These curves are plotted so that their position on the strain axis indicates the magnitude of prestrain. From these curves it can be seen that the points of fracture defined a smooth continuous function of the total strain. The considerable variations in retained ductility, therefore, affected the fracture stress only slightly. The decrease in

fracture stress after small prestrains, frequently observed in previous investigations at -196°C , was therefore either absent or very small for the silicon steel. After prestrains larger than a few the percent, fracture stress increased rapidly with increasing prestrain up to a strain of $\epsilon_1 = 0.30$. After this value of prestrain, the increase in fracture stress became much slower. This can be explained by the increasing depth and sharpness of the neck beyond strains of $\epsilon_1 = 0.30$. Since the ductility retained at this temperature is quite small, the fracture stress should not only be a function of the strain, but also of contour (depth and sharpness) of the neck. Consequently, at high values of prestrain the specimen shape

may account for the low fracture stress values.

EFFECT OF PRESTRAINING AT VARIOUS TEMPERATURES ON THE FRACTURE CHARACTERISTICS AT A CONSTANT LOWER TEMPERATURE

In Fig 13 the ductility retained at -196°C after prestraining at $+20$, -100 , and -120°C , respectively, is plotted as a function of the prestrain. Small prestrains at any of these temperatures reduced the retained ductility to very small values which do not permit definite conclusions regarding any effect of the prestraining temperature. At larger prestrains, however, the ductility was found to be larger the

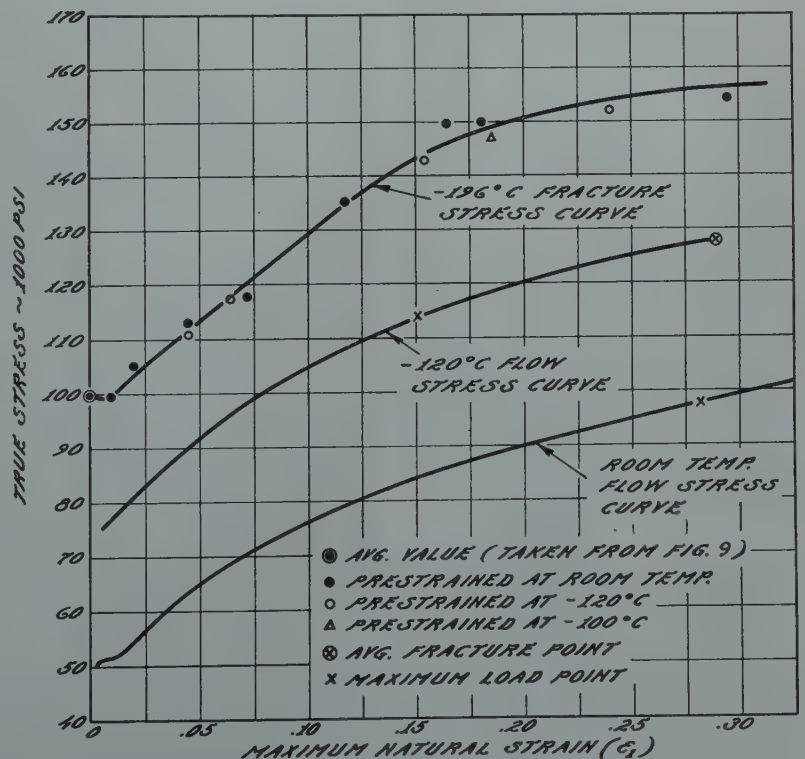


FIG 14—Effect of prestraining at various temperatures on the fracture stress at -196°C .

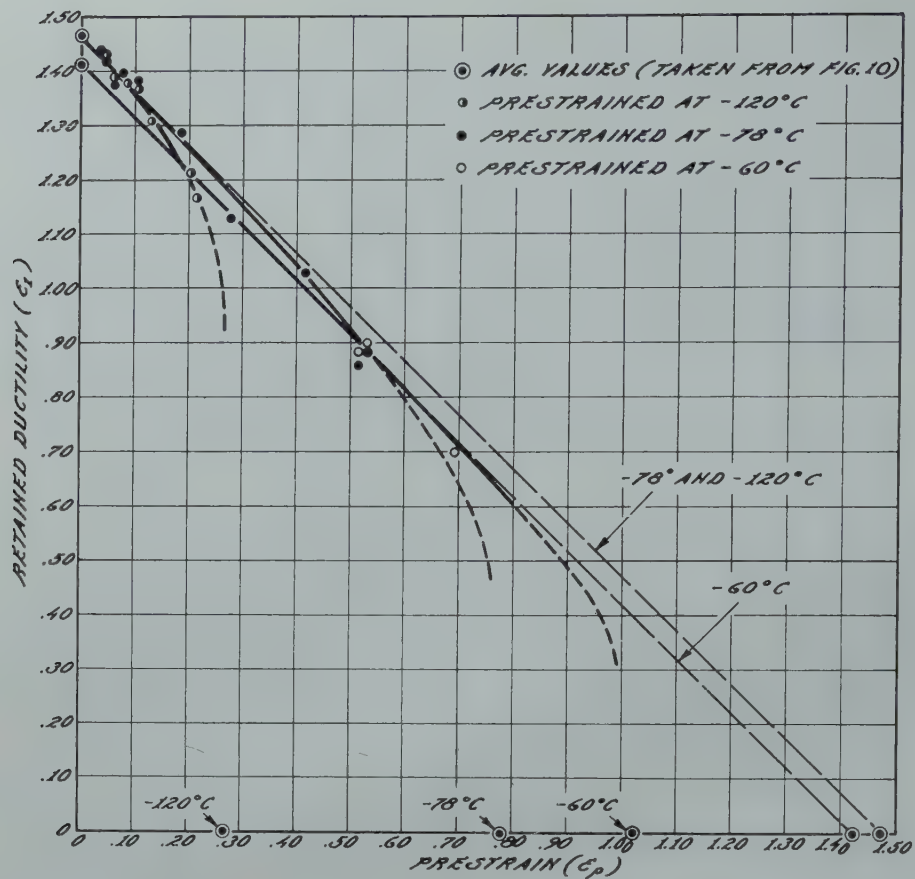


FIG 15—Effect of prestraining at various low temperatures on the retained ductility at room temperature.

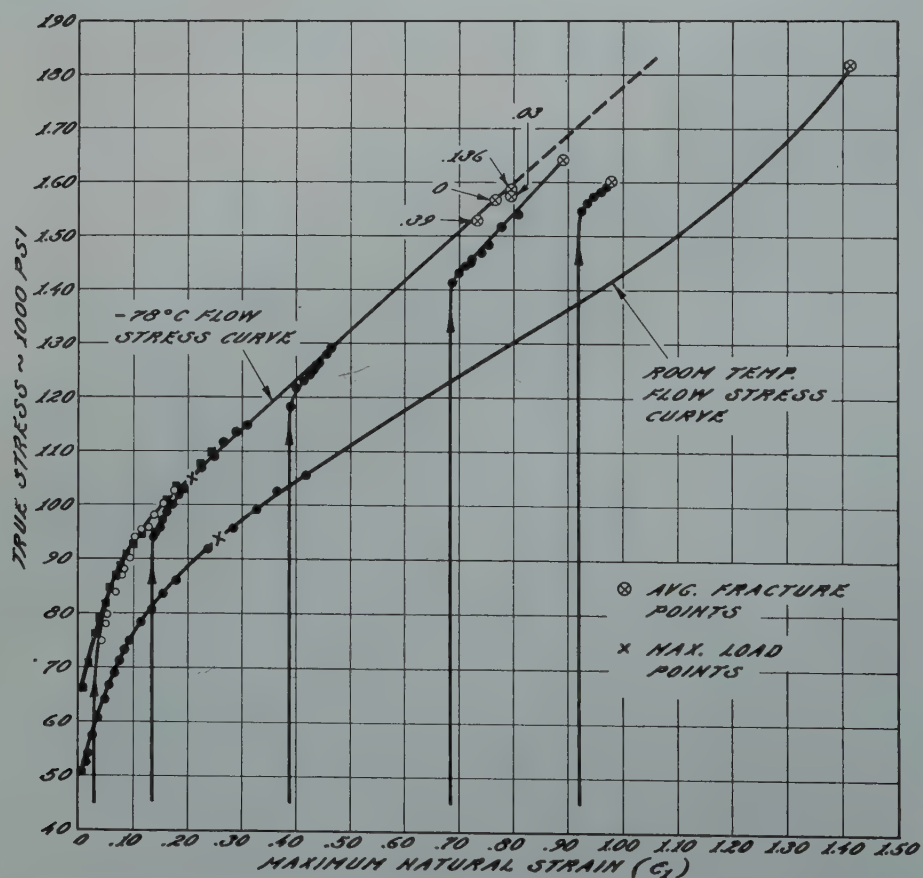


FIG 16—Effect of prestraining in tension at room temperature on the flow characteristics at -78°C .

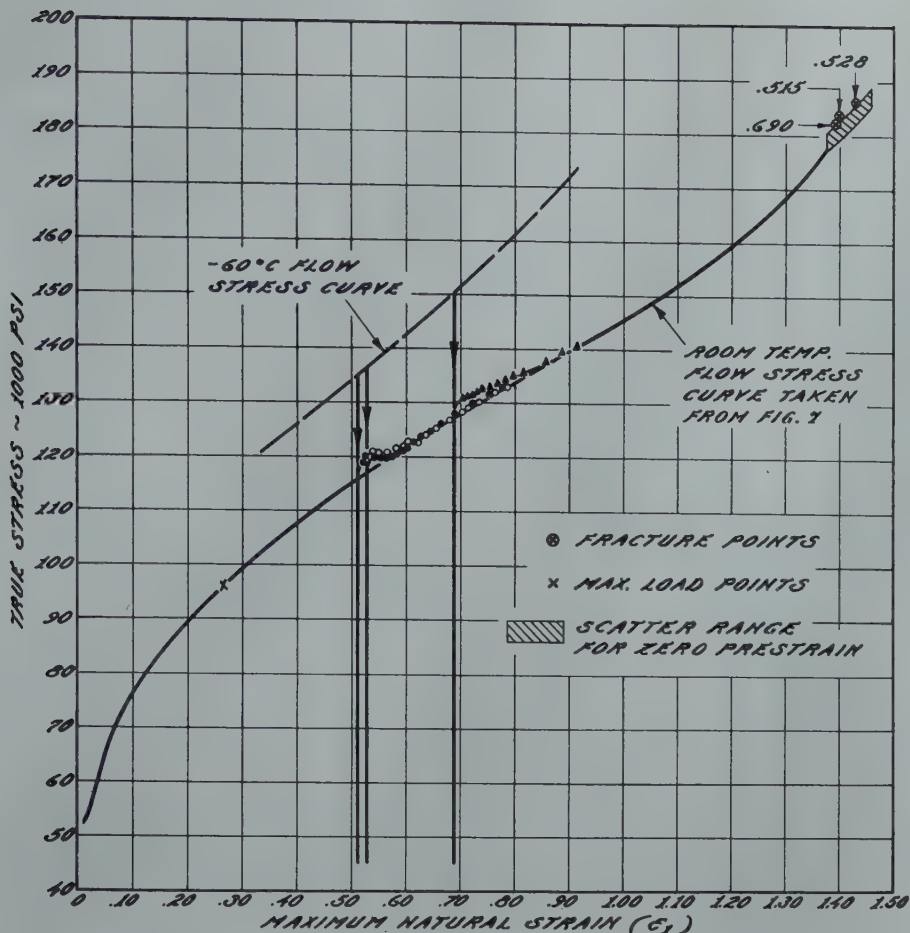


FIG 17—Effect of prestraining at -60°C on the flow characteristics at room temperature.

higher the prestraining temperature, as was to be expected from the results of the first group of tests discussed above.

Fig 14 shows the fracture stress values obtained in these three test series, at the temperature of -196°C . According to this graph, the fracture stress appears to be independent of the prestraining temperature, and only a function of the magnitude of strain. This would be in agreement with some data by Hollomon¹¹ in which a pearlitic steel was prestrained at various temperatures between -110 and $+20^{\circ}\text{C}$ and then tested at -190°C . However, from the fact that the ductility values appeared definitely dependent upon the temperature of prestraining, the conclusion must be drawn that this also applies to the fracture stress. On the other hand, these resulting differences in fracture stress would be very small for the small ductility values observed, assuming that the stress-strain curve is determined only by the magnitude of prestrain. As shown later, this assumption probably does not apply, and this may also cause differences in the fracture stress. Apparently, both these effects are of sufficiently small magnitude to be hidden in the general

scattering of the test results.

EFFECT OF PRESTRAINING AT VARIOUS LOW TEMPERATURES ON THE FRACTURING CHARACTERISTICS AT A HIGH TEMPERATURE

The effects of prestraining at various low temperatures on the ductility retained at the high (room) temperature are shown in Fig 15. It appears that prestraining at any low temperature up to strains close to failure is no more damaging to the metal than if the same strain is accomplished at room temperature. The retained ductility values at room temperature decreased so that they were always equal to the total ductility in testing minus the prestrain. Only at high values of prestrain very close to the ductility of the steel at the temperature of prestraining did the straining appear slightly more harmful at the low temperature than the same strain would have been if the entire test had been conducted at room temperature. This applies to all three temperatures of prestraining.

Since the material used for the -60°C prestrains had slightly different properties than that used for the -78

and -120°C prestrains, two different 45° lines are given in Fig 15.

EFFECTS OF PRESTRAINING ON THE FLOW CHARACTERISTICS

The plastic flow characteristics of a metal are represented by the general shape of its stress-strain curve or, more specifically, by the initial value of the yield strength and the slope of the curve or strain-hardening rate. Consequently, an evaluation of the effect of prestraining on the flow characteristics was based on a determination of the effect of prestraining on these two characteristics. Furthermore, this analysis is based on the fact that straining at any single temperature simply uses up a portion of the initial stress-strain curve equivalent to the magnitude of the prestrain.

A number of stress-strain curves obtained on the silicon steel after prestraining at a temperature higher than the testing temperature are given in Fig 16, and curves after prestraining at different temperatures lower than the testing temperature are presented in Fig 17 to 19. For reasons of clarity the fundamental changes in the stress-

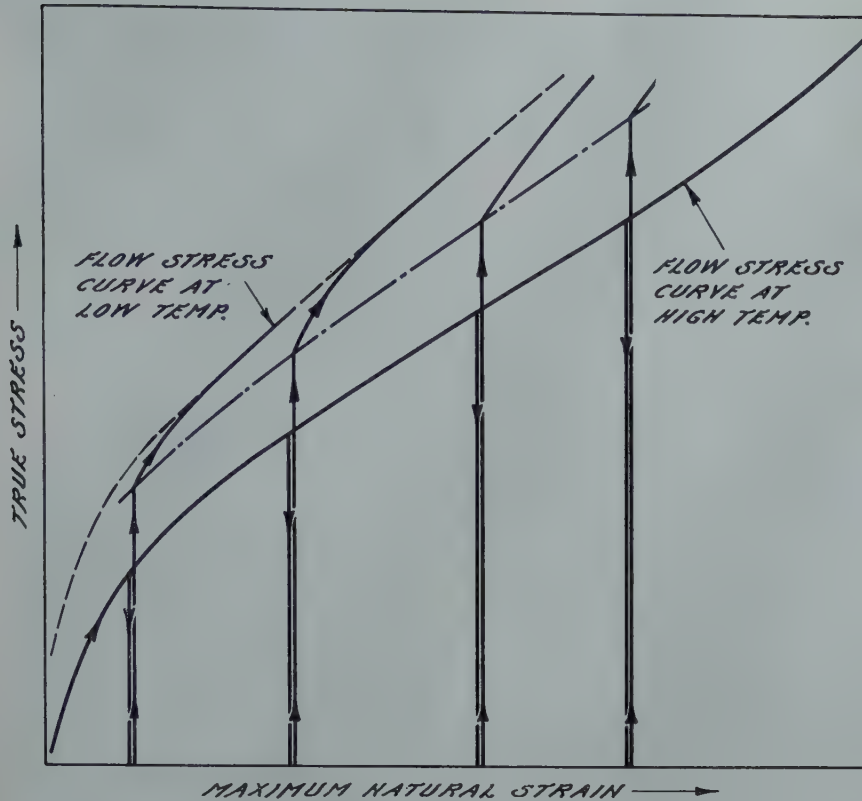


FIG 20—Schematic representation of the effect of prestraining at a high temperature on the flow characteristics at a lower temperature.

strain curves are also schematically shown in Fig 20 and 21. According to these graphs, prestraining at a temperature different from that of testing results in a stress-strain curve distinctly different from that obtained on straining at a constant temperature. These effects are in close qualitative agreement but possibly considerably smaller than those found in other metals.

It can be seen from Fig 16 and 20 that after prestraining at a relatively high temperature the yield strength at the low temperature is considerably reduced from the value that would have been obtained on straining at the low temperature. The subsequent rate of strain hardening, however, is larger after prestraining at the high temperature. Consequently, further straining in testing progressively reduces these deviations both in flow stress and in strain hardening. Both effects increase with increasing prestrain. Consequently, the deviations of the flow characteristics after high temperature prestraining from those after straining at the testing temperature disappear at comparatively small testing strains, if the prestrains are small.

According to Fig 17 to 19 and Fig 21, prestraining at a relatively low temperature causes effects diametrically opposite to those discussed above for

prestraining at a relatively high temperature. The yield strength is raised and the rate of strain hardening is reduced.* Generally, however, these deviations disappear rather rapidly on further straining. It should be expected, furthermore, that the discussed effects increase with increasing difference between prestraining and testing temperature. The test results are not quite conclusive but, in general, in agreement with this expectation.

Conclusions

Based on the test data obtained on this silicon steel, certain conclusions can be drawn on the effect of straining a ferritic material at one temperature on the fracture and flow characteristics at some other temperature.

As far as the *fracturing characteristics* after prestraining at a higher temperature than the testing temperature are concerned, the phenomena observed in these tests are similar to those previously reported for annealed steels. Prestraining small amounts at room temperature caused the retained ductility values at a low testing temperature to pass through a minimum when

*This particular effect may result in a yield point jog which is illustrated more clearly in the conventional stress-strain diagrams in Fig 22, for the same tests illustrated by Fig 18.

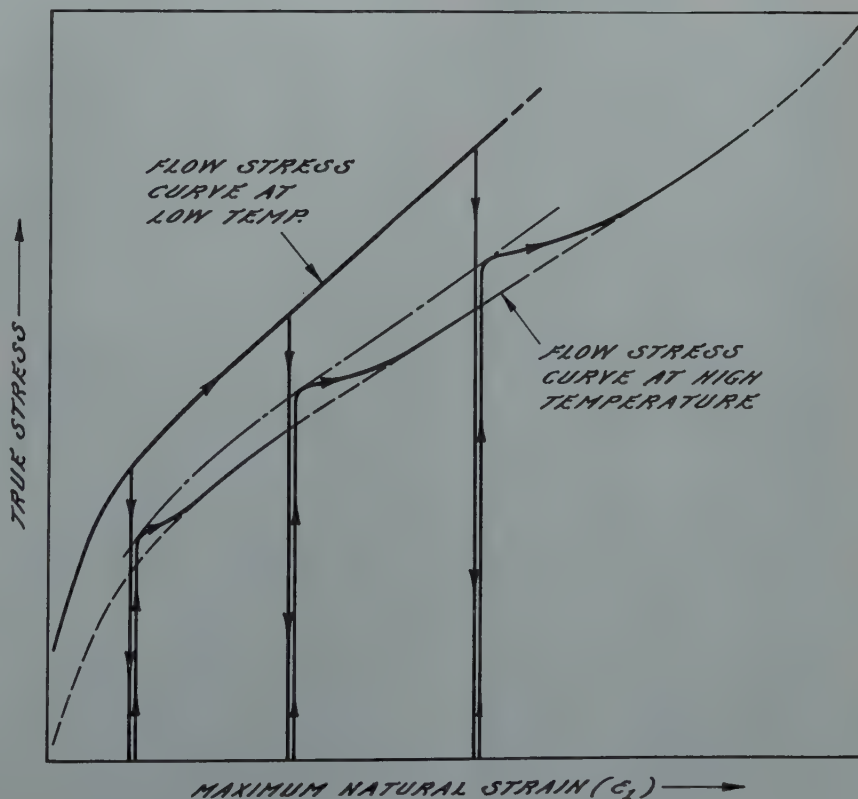


FIG 21—Schematic representation of the effect of prestraining at a low temperature on the flow characteristics at a high temperature.

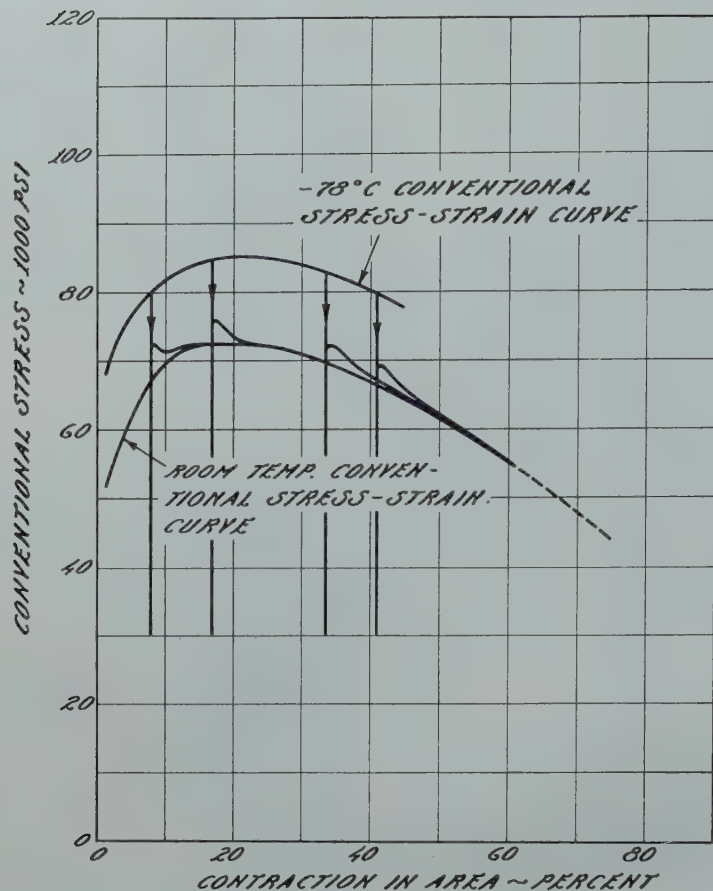


FIG 22—Effect of prestraining at -78°C on the conventional stress-strain characteristics at room temperature.

determined as a function of prestrain. The test data presented here further indicated that the magnitude of this minimum decreased as the temperature difference between the prestraining temperature and the testing temperature was decreased. This behavior of cold worked annealed steels was tentatively correlated with the phenomenon of an uneven yielding illustrated by the yield jog in a tensile test. The correlation was based on the assumption that plastic flow apparently becomes increasingly uniform (at small strains) with decreasing testing temperature.

At sufficiently large prestrains the retained ductility went through a maximum, after which it again decreased at a rate such that the retained ductility did not become zero until the ductility was completely exhausted in prestraining.

A few additional test data indicated that if cold worked material was tested at a low temperature at which the material was still ductile, the retained ductility at this temperature was found to be greater the greater the ductility under the conditions of prestraining.

The fracturing characteristics after prestraining at a low temperature and testing at room temperature appeared to obey a simpler law than that discussed above. It appeared that prestraining at any low temperature was no more harmful than the same magnitude of strain conducted at room temperature until the prestrain values were very close to failure, (Fig 15).

The effects of prestraining at one temperature and testing at another temperature on the flow characteristics for this annealed steel appeared to conform to the behavior of various other metals and alloys, which behavior was discussed in the Introduction. However, the magnitude of the effects was distinctly smaller for this ferritic material (body-centered cubic) than for other metals which crystallize in the face-centered cubic lattice. This can be tentatively correlated with the stress-strain curves, the general appearance of which is less changed with temperature for ferritic materials than for face-centered cubic metals.

The above investigation only reveals a small portion of the laws which

govern the mechanical properties of a ferrous metal subjected to straining, under conditions where the temperature is not kept constant. So far, such practically important conditions have attracted little attention in the laboratory. The present investigation has shown clearly that no predictions can be made from any tests carried out at a constant temperature on the performance of the same metal when the strain-temperature history varies in a more general manner.

Acknowledgments

This work was conducted in cooperation with the Office of Naval Research to which the authors are indebted for permission to publish the report. The authors further wish to express their gratitude to Mr. L. J. Ebert for his suggestions, and to Mr. G. L. Tuer for his aid in the experimental work.

References

1. G. Sachs, et al: Mechanical Relations in Fracturing of Metals. In Cooperation with Office of Naval Research, U. S. Navy, N6ori-273, Task Order 1, Rep. No. 1, May 1947.
2. N. Davidenkov and P. Sakharov: On the Influence of Cold Working Upon the Brittleness of Steel. *Tech. Phys.*, USSR, (1938) 5, 743-757.
3. P. W. Bridgman: Effects of High Hydrostatic Pressure on the Plastic Properties of Metals. *Rev. Mod. Phys.*, (1945) 7, 3-14.
4. H. Scheele: Tensile Tests with Strain Restraint. *Arch. Eisenhuettenw.*, (1941) 14, 513-519.
5. D. J. McAdam, Jr., G. W. Geil and R. W. Mebs: Influence of Plastic Deformation, Combined Stresses, and Low Temperatures on the Breaking Stress of Ferritic Steels. *Metals Tech.*, (Aug. 1947). TP 2220; *Trans. AIME* (1947) 172.
6. J. H. Hollomon: The Mechanical Equation of State. *Metals Tech.*, (Sept. 1946). TP 2034; *Trans. AIME* (1947) 171, 535.
7. E. Orowan: The Creep of Metals. West of Scotland Iron and Steel Inst. (Feb. 1947).
8. J. E. Dorn, A. Goldberg, T. E. Tietz: The Effect of Thermal-Mechanical History on the Strain Hardening of Metals. Univ. of Calif. In Cooperation with Office of Naval Research, U. S. Navy, Contract N7-onr-295, Task II, First Technical Rep.
9. G. Sachs, J. D. Lubahn and L. J. Ebert: Notched Bar Tensile Test Characteristics of Heat Treated Low Alloy Steels. *Trans. Am. Soc. Metals*, (1944) 33, 340-395.
10. E. J. Ripling and G. Tuer: An Apparatus for Low Temperature Tensile Testing. *Products Eng.*, in print.
11. J. H. Hollomon: The Problem of Fracture. *Jnl. Am. Welding Soc.*, Res. Suppl., (1946) 11, 534-583.

Relation between Chromium and Carbon in Chromium Steel Refining

D. C. HILTY,* Member AIME

Introduction

It has long been known that in melting high-chromium steels, some of the carbon might be oxidized out of the melt without excessive simultaneous oxidation of chromium, and that higher temperatures favor retention of chromium. The advent of oxygen injection as a tool for rapid decarburization of a steel bath permits significantly higher bath temperatures, and it was quickly recognized that the use of oxygen injection facilitated the oxidation of carbon to low levels in the presence of relatively high residual chromium contents.

Up to the present time, however, specific data pertaining to the chromium-carbon-temperature relations in chromium steel refining have not been available. Individual steelmakers have evolved practices more or less empirically, but there has been very little real basis for predicting how effective any given practice can be in permitting maximum oxidation of carbon with minimum loss of chromium.

The current investigation, therefore, was undertaken in an effort to establish the fundamental carbon-chromium relationship in molten iron under oxidizing conditions. As reported below, the equilibrium constant and the influence of temperature on that constant have been derived for the iron-chromium-carbon-oxygen reaction in the range of chromium steel compositions with what appears to be a fair degree of precision. The practical application of the result will be obvious.

Experimental Procedure

The laboratory investigation was carried out on chromium steel heats melted in a magnesia crucible in a 100-lb capacity induction furnace at the Union Carbide and Carbon Re-

search Laboratories. The charges for the heats consisted of Armco iron, low-carbon chromium metal, and high-carbon chromium metal, the relative proportions of which were calculated so that the various heats would contain from approximately 0.06 pct carbon and 8 pct chromium to 0.40 pct carbon and 30 pct chromium at melt-down. When the charges were melted, the bath temperatures were raised to the desired level, and the heats were then decarburized by successive injections of oxygen at the slag-metal interface through a 1/2-in. diam silica tube at a pressure of 30 psi. The duration of the oxygen injections was from 30 sec to 2 min. at intervals of approximately 5 to 30 min. It did not appear that length or frequency of the injection periods had any significant effect on the results; consequently, no effort was made to hold them constant and they were controlled only as was expedient to the general working of the heats. Between successive injections, the heats were sampled by means of a copper suction-tube sampler that yields a sound, rapidly-solidified sample representative of the composition of the molten metal at the temperature of sampling. This sampling device is a modification of the one described by Taylor and Chipman.¹

An attempt was made to vary bath temperatures between samples, but it quickly became evident that, unless the variations were small or unless the new temperature was maintained for a minimum of 15 min. during which an injection of oxygen was made in order to accelerate the reactions, a

very wide departure from equilibrium resulted. For most of the runs, therefore, temperature was maintained relatively constant at approximately 1750 or 1820°C. A few reliable observations at other temperatures, however, were obtained.

Temperature Measurement

The high temperatures involved in this investigation were measured by the radiation method, utilizing a Ray-O-Tube focused on the closed end of a refractory tube immersed in the metal bath. The immersion tubes employed were high-purity alumina tubes specially prepared by the Tonawanda Laboratory of The Linde Air Products Co. These tubes were quite sturdy under reasonable mechanical stress at high temperature. They were unusually resistant to thermal shock, and chemical attack on them by the melts was slow. With care, it was found possible to keep these tubes continuously immersed in a heat for as long as 5 hr at temperatures up to 1850°C, before failure by fluxing occurred.

The Ray-O-Tube—alumina tube assemblage was similar to those supplied commercially for lower temperature applications. In operation, the alumina tube was slowly immersed in the molten metal to a depth of approximately 5 in., and the device was then clamped solidly to a supporting jig where it remained for the duration of the run. A photograph of the equipment, in operation with Ray-O-Tube in place and oxygen injection in progress, is shown in Fig 1.

When in position in a heat, the instrument was calibrated by means of an immersion thermocouple and an optical pyrometer. For calibration through the range of temperatures from 1500 to 1650°C, a platinum—platinum + 10 pct rhodium thermocouple in a silica tube was immersed alongside the alumina tube. Output of the Ray-O-Tube in millivolts and the

San Francisco Meeting, February 1949.

TP 2507 C. Discussion of this paper (2 copies) may be sent to *Transactions AIME* before April 1, 1949. Manuscript received September 15, 1948.

* Research Metallurgist, Union Carbide and Carbon Research Laboratories, Inc., Niagara Falls, N. Y.

¹ References are at the end of the paper.

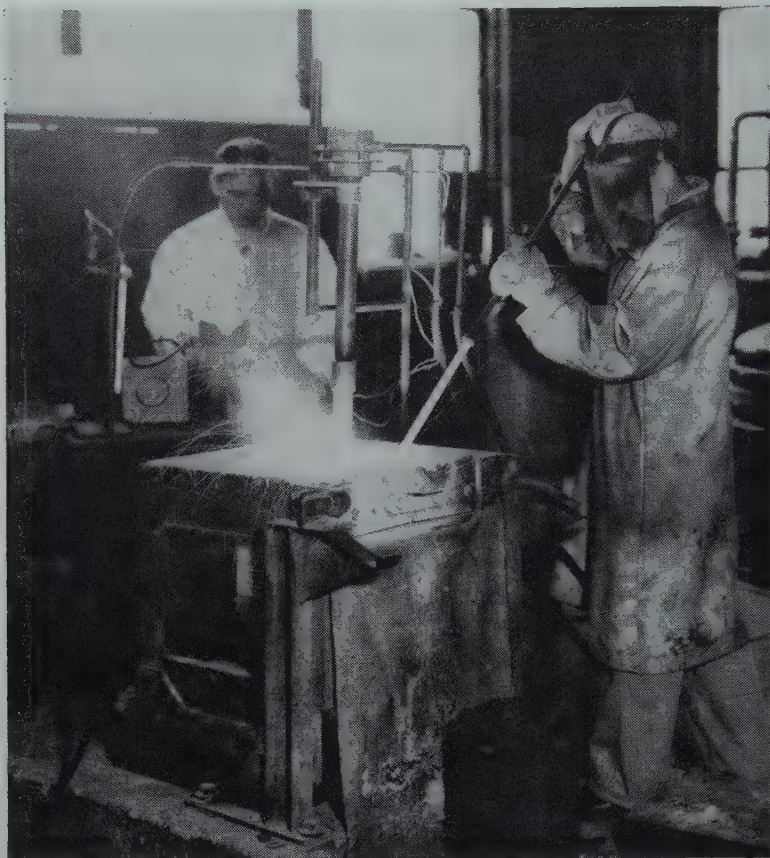


FIG 1—Experimental setup employed.

temperature indicated by the thermocouple were plotted logarithmically. At the same time, the optical pyrometer was standardized against the thermocouple by removing the Ray-O-Tube from its holder and sighting the optical pyrometer on the end of the alumina tube. The calibration was then extended to temperatures above 1650°C with the optical pyrometer.

It was observed that the depth of immersion of the alumina tube had a definite effect on the calibration of the Ray-O-Tube. This was probably at least partially due to the fact that the Ray-O-Tube was equipped with a lens that covered too large a field for the diameter of the alumina tube; but since the Ray-O-Tube was calibrated for each individual run, and the calibration was checked during the course of the runs, possible error due to the depth of immersion effect is considered to have been minimized.

A typical calibration curve is illustrated in Fig 2. It is evident that a fairly accurate calibration was obtained. From this and the calibration curves for the other heats, it appeared that most of the temperature measurements were within $\pm 10^\circ\text{C}$ of the actual temperature.

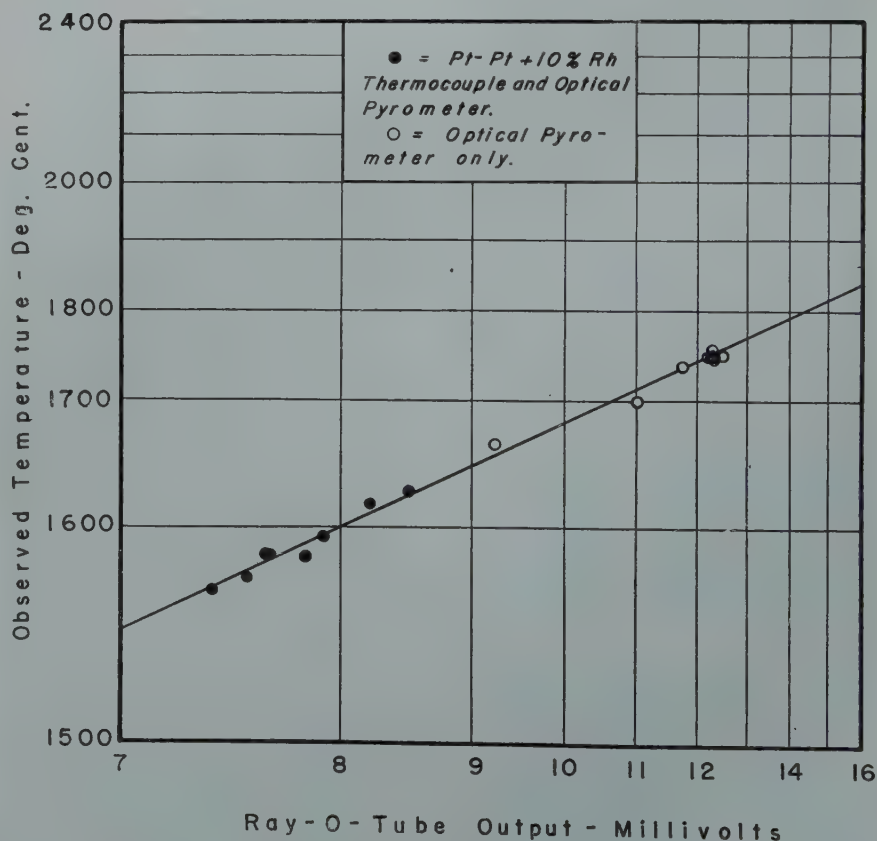
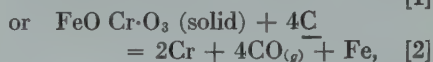
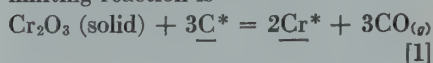


FIG 2—Typical Ray-O-Tube calibration curve.

Observations and Determination of Equilibrium Constant

The carbon and chromium contents and the temperatures of the samples obtained are listed in Table 1 and were plotted to give the equilibrium curves shown in Fig 3.

The oxidation of carbon from a steel bath containing chromium is limited by the simultaneous oxidation of the chromium. Whether decarburization is carried out by ore additions or by injection of gaseous oxygen, the oxygen content of the bath is limited by the formation of an oxide of chromium. Up to the present time, it has been assumed that this oxide is either Cr_2O_3 or $\text{FeO} \cdot \text{Cr}_2\text{O}_3$, and that at one atmosphere pressure of carbon monoxide the limiting reaction is



so that the equilibrium constant would be approximately defined as

$$K_1 = \frac{\text{pct Cr}^2}{\text{pct C}^3} \quad [1a]$$

* Conventionally, underlining of the symbols in a steelmaking reaction indicates that those substances are dissolved in the iron.

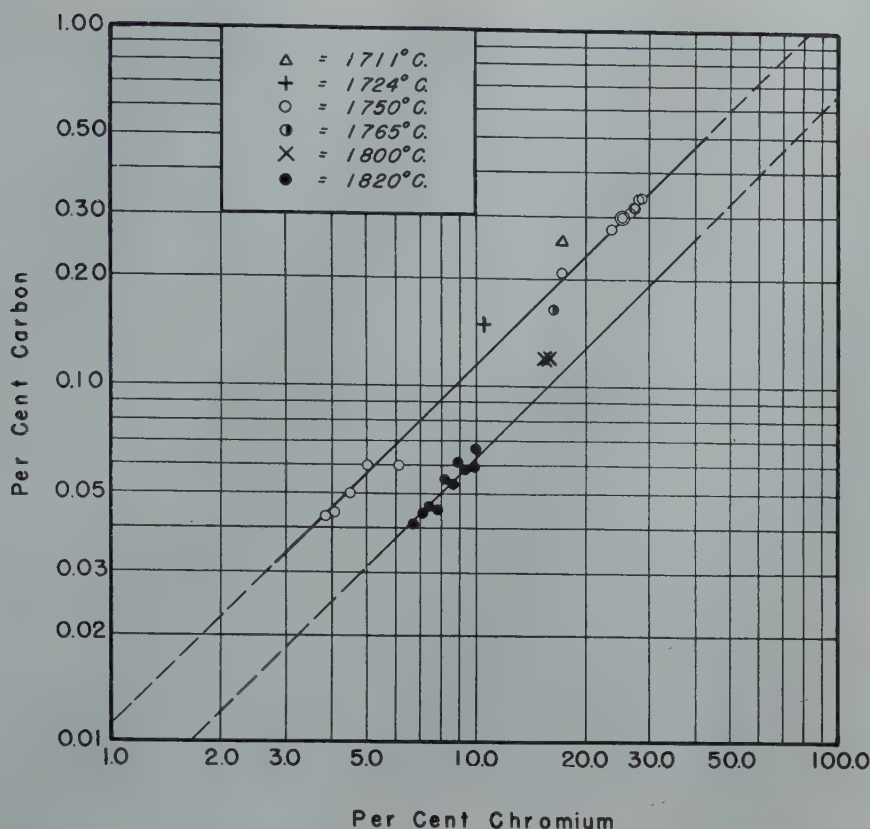


FIG 3—Relation of chromium to carbon in molten chromium steel at constant temperature.

Table 1 . . . Carbon and Chromium Contents and Temperature

| Heat No. | Sam-ple No. | Tem-perature °C | Car-bon Per Cent | Chro-mium Per Cent | $K = \frac{\text{pct Cr}}{\text{pct C}}$ |
|----------|-------------|-----------------|------------------|--------------------|--|
| C-1 | 1 | 1711 | 0.26 | 17.19 | 6.62×10^1 |
| | 2 | 1750 | 0.21 | 17.19 | 8.19×10^1 |
| | 3 | 1765 | 0.17 | 16.37 | 9.63×10^1 |
| | 4 | 1802 | 0.12 | 15.79 | 1.31×10^2 |
| | 5 | 1800 | 0.12 | 15.40 | 1.28×10^2 |
| C-2 | 1 | 1724 | 0.15 | 10.42 | 6.96×10^1 |
| | 2 | 1820 | 0.067 | 9.94 | 1.48×10^2 |
| | 3 | 1822 | 0.059 | 9.86 | 1.67×10^2 |
| | 4 | 1826 | 0.058 | 9.28 | 1.60×10^2 |
| | 5 | 1822 | 0.061 | 8.90 | 1.46×10^2 |
| | 6 | 1822 | 0.053 | 8.61 | 1.62×10^2 |
| | 7 | 1822 | 0.055 | 8.19 | 1.49×10^2 |
| | 8 | 1822 | 0.045 | 7.83 | 1.74×10^2 |
| | 9 | 1822 | 0.046 | 7.40 | 1.61×10^2 |
| | 10 | 1822 | 0.044 | 7.13 | 1.62×10^2 |
| | 11 | 1822 | 0.041 | 6.72 | 1.64×10^2 |
| C-3 | 1 | 1746 | 0.060 | 6.12 | 1.02×10^2 |
| | 2 | 1748 | 0.060 | 5.00 | 8.34×10^1 |
| | 3 | 1750 | 0.050 | 4.50 | 9.00×10^1 |
| | 4 | 1749 | 0.044 | 4.09 | 9.28×10^1 |
| | 5 | 1749 | 0.043 | 3.85 | 8.96×10^1 |
| C-4 | 1 | 1744 | 0.34 | 28.12 | 8.26×10^1 |
| | 2 | 1747 | 0.34 | 27.74 | 8.16×10^1 |
| | 3 | 1751 | 0.32 | 27.33 | 8.54×10^1 |
| | 4 | 1748 | 0.32 | 27.17 | 8.48×10^1 |
| | 5 | 1748 | 0.31 | 26.45 | 8.52×10^1 |
| | 6 | 1748 | 0.30 | 25.37 | 8.46×10^1 |
| | 7 | 1748 | 0.30 | 25.31 | 8.45×10^1 |
| | 8 | 1752 | 0.29 | 24.60 | 8.48×10^1 |
| | 9 | 1752 | 0.28 | 23.61 | 8.45×10^1 |

or
$$K_2 = \frac{\text{pct Cr}^2}{\text{pct C}^4} \quad [2a]$$

These assumptions, however, are not supported by the present experimental evidence. The slope of the curves in Fig 3 is approximately unity, a fact

which strongly indicates that the actual constant is expressed by the equation,

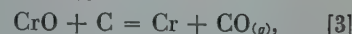
$$K = \frac{\text{pct Cr}}{\text{pct C}} \quad [3a]$$

Equilibrium constants calculated according to Eq 3a are given in the last column of Table 1. It is evident that at constant temperature these K 's are truly constant well within the limits of experimental error.

Two explanations for this departure from the previously accepted hypothesis described by reactions 1 or 2 are suggested. The first is that reactions 1 or 2 do actually represent the equilibrium involved, but that the activity of carbon dissolved in the melt is greatly reduced by the presence of chromium so that it is not proportional to the concentration. This, of course, is possible and is in accordance with the principles of classical thermodynamics; but it seems somewhat improbable in a system that is in reality very far from being saturated with chromium carbides, in view of the magnitude of the effect at moderate chromium concentrations.

The second explanation presumes that the oxide of chromium directly involved is not Cr_2O_3 but CrO , so that

the reaction is



the nonmetallic phase being saturated with CrO and the CO pressure being approximately one atmosphere. At the temperatures of the experiments, the postulation of chromium monoxide does not appear to be unreasonable; it has previously been employed by Chen and Chipman² to account for some of the discrepancies observed in a study of the iron-chromium-oxygen system; CrO was suggested by Clark³ as the oxide of chromium formed during the decarburization of chromium steel heats by magnetite ore; and according to Körber and Oelsen,⁴ chromous oxide is the chief oxide of chromium occurring in acid slags in contact with molten iron-chromium alloys. Moreover, reaction 3 fits the observations without any complications regarding the activities of carbon or chromium. It is, therefore, considered that reaction 3 and Eq 3a are the most probable representations of the limiting equilibrium in the refining of chromium steels.

Effect of Temperature

The equilibrium constants calculated by Eq 3a were plotted logarith-

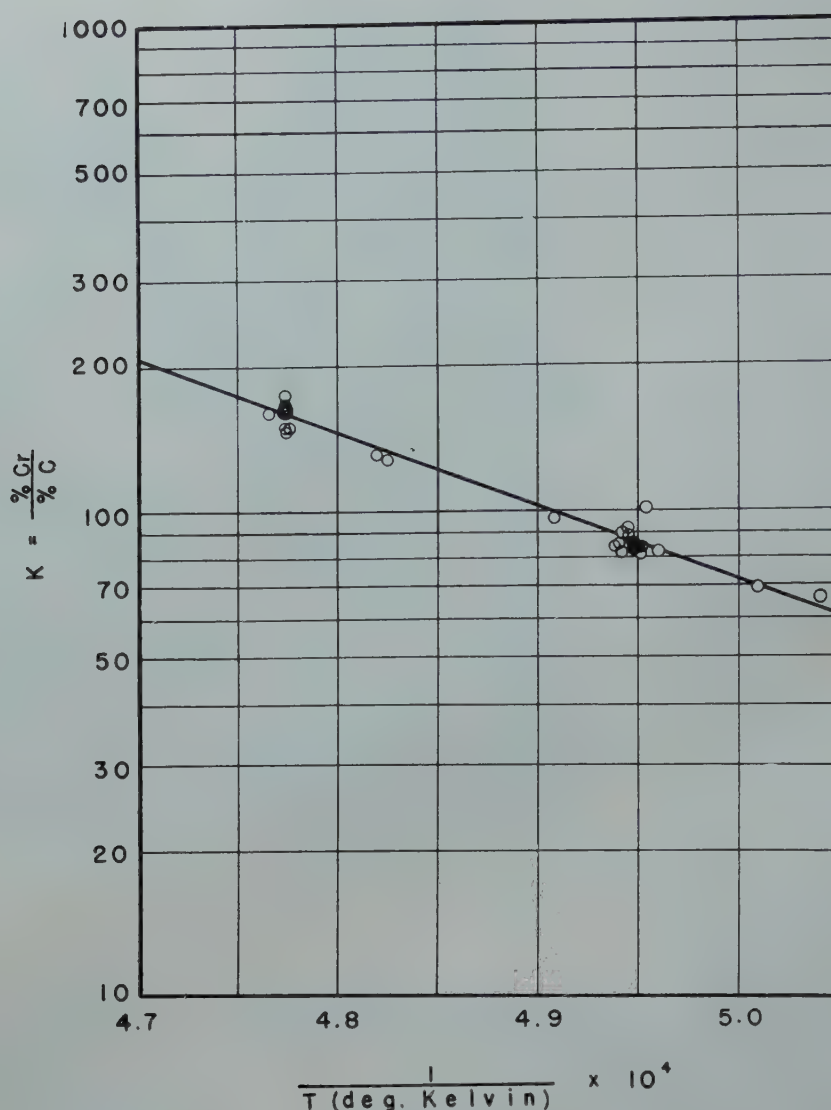


FIG 4—Effect of temperature on the equilibrium constant, $K = \frac{\text{Pct Cr}}{\text{Pct C}}$

mically against the reciprocal of the absolute temperature as illustrated in Fig 4.

The equation of the resulting curve is calculated to be

$$\text{Log } K = -\frac{15,200}{T} + 9.46, \quad [4]$$

in which T is the absolute temperature in degrees Kelvin.

If published⁵ thermal data for the carbon-oxygen reaction and the solution of chromium in molten iron be combined with the heat of reaction 3 calculated from Eq 4, a value of $-106,750$ cal per g mol is obtained for the heat of formation of CrO from the elements. This heat of formation, of course, is subject to considerable uncertainty, but it appears to be quite reasonable; it is of the same order of

magnitude as the heat of formation of manganous oxide, MnO , as, presumably, it should be. Therefore, it seems to be additional evidence in support of the hypothesis stated by reaction 3.

With Eq 4, the carbon-chromium relationship in liquid chromium steel under oxidizing conditions can be calculated for any temperature. This was done for what was believed to be the probable range of steelmaking temperatures as shown in Fig 5. For convenience, the temperatures appearing in Fig 5, and subsequently in this paper, have been converted to Fahrenheit scale in accordance with accepted commercial usage.

Several random observations of chromium and carbon contents at the end of the oxidizing period in commer-

cial arc-furnace heats were available and these were superimposed on the curves of Fig 5 in order to estimate the temperatures attained in commercial practice. Fig 6 illustrates the result.

From Fig 6, it is evident that the heats refined by conventional oreing methods attained temperatures averaging approximately 3025°F . As would be expected, heats made by oxygen practice were considerably hotter—large heats averaging 3275°F and small heats (less than 12 tons) about 3375°F . The maximum temperature appears to be on the order of 3400°F . In this connection, it is notable that in two of the heats, shown in Fig 6 as attaining temperatures close to 3400°F , serious damage to the furnace refractories occurred.

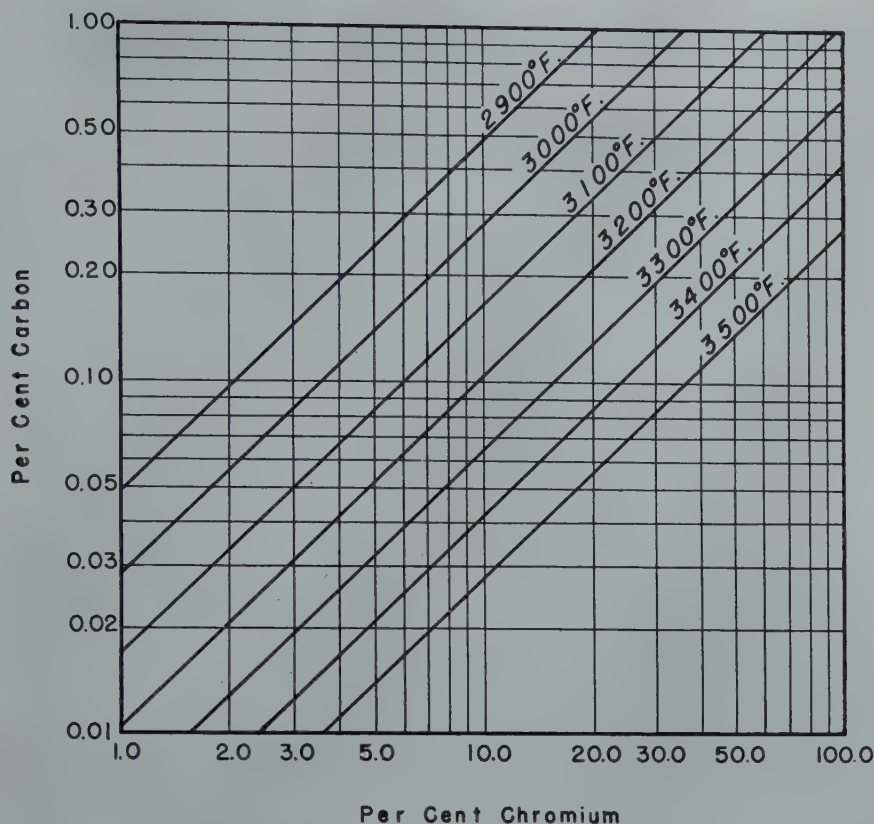


FIG 5—Chromium-carbon relation in chromium steel refining.

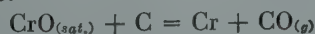
Conclusions

The conclusions drawn from this investigation are as follows:

1. It has been found that at constant temperature the relation between carbon and chromium in chromium steel refining can be expressed by the equilibrium constant,

$$K = \frac{\text{pct Cr}}{\text{pct C}}$$

2. The probable reaction is believed to be:



3. The effect of temperature on the relation has been derived and may be defined by the equation:

$$\log K = -\frac{15,200}{T} + 9.46$$

Acknowledgments

The author is indebted to Walter Crafts, Chief Metallurgist of the Union Carbide and Carbon Research Laboratories, Inc., and to John Chipman, Professor of Metallurgy, Massachusetts Institute of Technology, who contributed many helpful suggestions and reviewed the data and manuscript.

Appreciation is also extended to J. J. Darby and J. J. Mikula who assisted in securing the data from the experimental melts.

References

1. C. R. Taylor and John Chipman: Equilibria of Liquid Iron and Simple Basic and Acid Slags in a Rotating Induction Furnace. *Trans. AIME* (1943), 154, 228-245.
2. Hsin-Min Chen and John Chipman: The Chromium-oxygen Equilibrium in Liquid Iron. *Trans. A.S.M.* (1947), 38, 70-112.
3. Donald Clark: Reduction of Carbon in Presence of Chromium. *Proc. Elect. Furnace Steel Conf.* (1946), 4, 134-135.
4. F. Körber and W. Oelsen: Reactions of Chromium with Acid Slags. *Mit. k. w. Inst. f. Eisenforschung.* (1935) 17, 231-245. Düsseldorf.
5. Basic Open Hearth Steelmaking. Chap. 13 and 16. (1944) AIME.

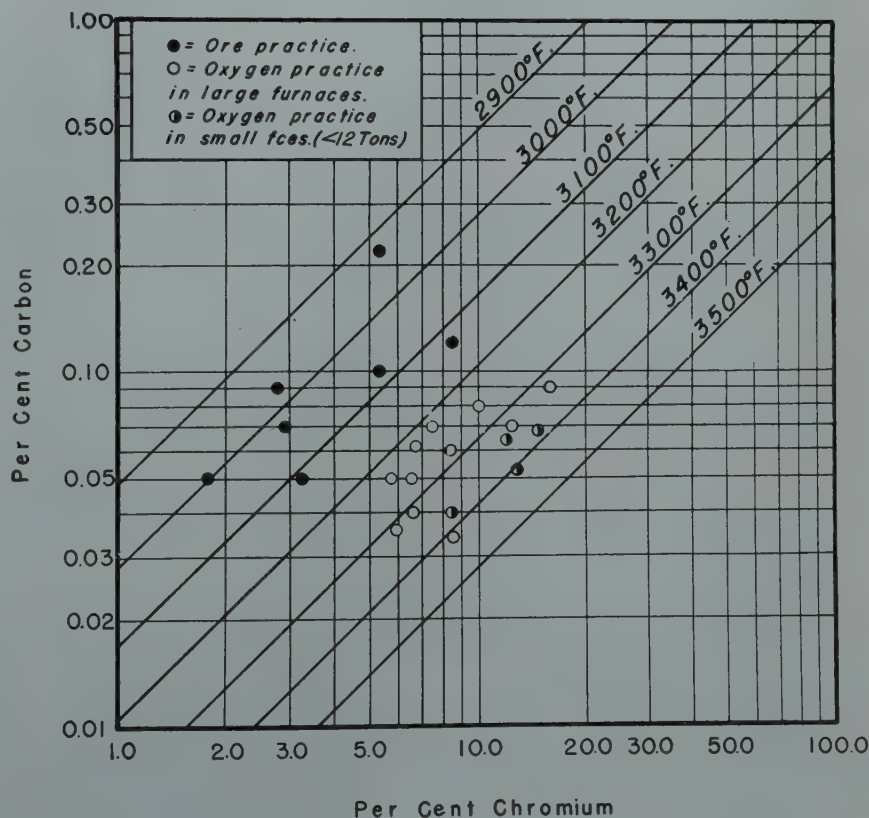


FIG 6—Indicated temperatures at end of oxidizing period in commercial heats made by ore and by oxygen practices.

The Densification of Copper Powder Compacts in Hydrogen and in Vacuum

CHARLES B. JORDAN* and POL DUWEZ*

Introduction

THE phenomenon of the change of volume of pressed powder compacts upon sintering is well known in the field of powder metallurgy. Depending upon the metal or metals involved and the pressure used in forming, a compact may, in the course of time of sintering at a given temperature, expand monotonically, contract monotonically, or first show a volume change of one sign followed by a change of the opposite sign. It is clearly desirable to have accurate knowledge of the magnitude and sign of the change in dimensions to be expected in any given case, both from the point of view of direct usefulness in the fabrication of parts by powder metallurgy, and from the longer range viewpoint of elucidating the fundamental mechanism of metallic sintering.

The present study was therefore undertaken as a first step in acquiring systematic and reasonably quantitative knowledge of the change in density of metal powder compacts during sintering. For practical reasons, copper was selected as the material to be studied first, and its densification followed as a function of temperature and time of sintering in hydrogen and in vacuum.

Experimental Procedure

The copper powder used was that designated by the manufacturer (Metals Disintegrating Co., Elizabeth, N. J.) as MD-151. This powder was sifted through Tyler standard screens to separate the fraction having particle size range between 200 mesh and 325 mesh, and this fraction was used in all the subsequent work. Compacts weighing about 10 g were then pressed in a 1 in. diam round die, using a pressure of 20,000 psi throughout.

Sintering was carried out in commercially built electric furnaces in which the resistance windings are so disposed as to produce a nearly uniform temperature along the axis of the furnace for a length of about 18 in. centrally located. In order to be able to sinter in a controlled atmosphere, a 2 in. stainless steel tubing was inserted in the furnace. Each end of the tube was cooled by a water jacket about 7 in. long, and closed with a rubber stopper. The hydrogen used for one series of specimens was purified as described in Ref. 1. For the other set, a pressure of about 0.5 mm Hg was maintained during sintering by a Welch Duo-Seal pump.

The specimens were heated on square trays made of stainless steel. In placing specimens in the trays, a thin even layer of powdered aluminum oxide was first sprinkled on the bottom of the tray. A copper guard disk about half the thickness of the specimen was then placed in the tray and covered with a second layer of alumina. The actual specimen was then set on the guard disk, and a final coat of alumina sprinkled over the specimen.

This technique was evolved for sintering the specimens in such a way as to reduce the influence of unknown extraneous factors to a minimum. If the specimen is placed directly on the tray and sintered, it is found that the

resulting shape is that of a frustum of a cone, rather than a section of a right circular cylinder, since friction with the tray prevents the bottom of the specimen from contracting at the same rate as the top. In the arrangement used in these experiments, the guard disk provided a support which shrank at the same rate as the specimen, and the alumina powder reduced to a minimum friction between guard disk and tray, and between specimen and guard disk.

The procedure followed in sintering consisted of bringing the furnace to the required temperature, and then inserting the specimen into the central heated portion of the furnace tube in one of the two atmospheres used. At the end of the heating period, the specimen was cooled by bringing it into a portion of the furnace surrounded by a water jacket. These manipulations were carried out without opening the furnace, by means of rods which were attached to the trays and operated through a sliding seal in the rubber stopper.

The progress of densification of the copper compacts was studied at 1300, 1400, 1500, 1600, 1700, and 1800°F. At each of these temperatures, a specimen was allowed to sinter for each of the following time intervals: ½, 1, 2, 4, 8, 16, 32, and 64 hr. The thickness and diameter of each specimen were measured with micrometers before and after sintering, and each was weighed on an analytical balance after sintering.

Results

The techniques described in the preceding section were found to give satisfactory results. The specimens were not detectibly warped after sintering, and were usually of uniform diameter (that is, truly round) to within ± 0.001 in., a very few showing a variation in diameter of ± 0.002 in. All specimens were found to have the same diameter

San Francisco Meeting, February 1949.

TP 2516 E. Discussion of this paper (2 copies) may be sent to *Transactions AIME* before May 15, 1949. Manuscript received November 3, 1948.

* Research Engineer and Associate Professor of Mechanical Engineering and Chief of the Materials Section, respectively, Jet Propulsion Laboratory, California Institute of Technology, Pasadena, Calif.

References are at the end of the paper.

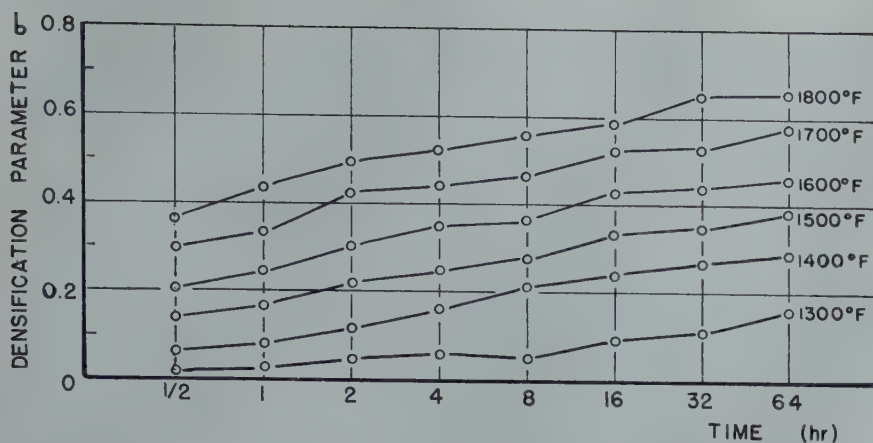


FIG 1—Densification parameter vs. sintering time in hydrogen.

before sintering (namely, 1.039 in.) as was to be expected, since all were pressed in the same die. It was not possible to maintain the same uniformity in thickness, because of slight variations in the amount of powder weighed out, and because of friction in the die during pressing. However, the variation in thickness at various points on a given specimen did not exceed ± 0.004 in., and variations from one specimen to another were of no importance, since the change in dimensions of each was followed separately.

From the measured values of mass, thickness, and diameter of each specimen before and after sintering, the value of the "densification parameter" (defined and explained in the next section of this paper) was calculated. The values of this parameter are plotted as a function of time for the various temperatures used in Fig 1 and 2.

Discussion of Technique

The method of cooling used may appear inadequate in view of the precautions commonly taken in metallurgical work to obtain a very rapid quench. It must be remembered, however, that there is no question of retaining a high temperature structure in the experiments described in this report, and that the only reason for quenching is to define the time of sintering. The water-jacket cooling used certainly accomplishes this end with no greater error than that necessarily introduced at the start of sintering by the time required for the specimen to heat to the required temperature, and possesses the great advantage of keeping the specimen flat and round.

The error introduced by filing the edges of the specimen also requires some consideration. In computing the density, the volume of each specimen was calculated from the measured thickness and diameter, assuming the specimen to be a right circular cylinder. Because of the chamfered edges, the calculated volume will obviously be larger than the true volume, and when used in conjunction with the true mass will give too low a value for the density. In order to estimate this error, several specimens were weighed before and after chamfering. It was found that the specimens which were filed lightly (duplicating conditions of the actual test specimens on which densification measurements were made) lost about 0.5 pct of their mass, while a specimen which was deliberately filed much more heavily than any of those used in the actual tests lost about 1 pct of its mass. This error was therefore considered negligible.

Interpretation of Results

Although the work described in this report was primarily undertaken as an investigation of the sintering of metals, it is important to note that the process actually observed is not one of pure sintering. When a powdered metal compact is heated, not only do the particles gradually bond together, but also the overall volume changes. In the case of the present work on copper, a monotonic shrinkage is observed, the porosity progressively decreasing and the voids becoming smaller and fewer. Evidently this process involves mechanisms other than those of sintering; for example, the overcoming of pressure in the voids due either to gas trapped during pressing, or to volatile impurities present. For this reason, it is more accurate to refer to the progressive shrinkage of copper compacts studied in this work as "densification" rather than as "sintering," since sintering is not the only process taking place. Nevertheless, it is possible to obtain information about sintering by this type of experiment, and it is moreover of practical importance to study sintering under the conditions which exist in the case of powdered metals.

The maximum density which a powder compact can attain is obviously that of the solid metal. This circumstance provides a natural scale on which the progress of densification can be measured. By comparing the observed change in density with the maximum possible change, a convenient dimensionless parameter is obtained, the value of which is initially zero and which becomes unity if the compact attains its maximum possible density.

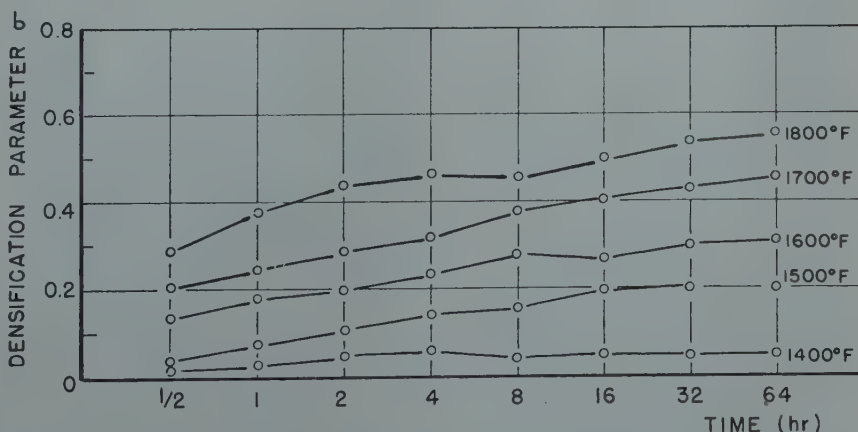


FIG 2—Densification parameter vs. sintering time in vacuum.

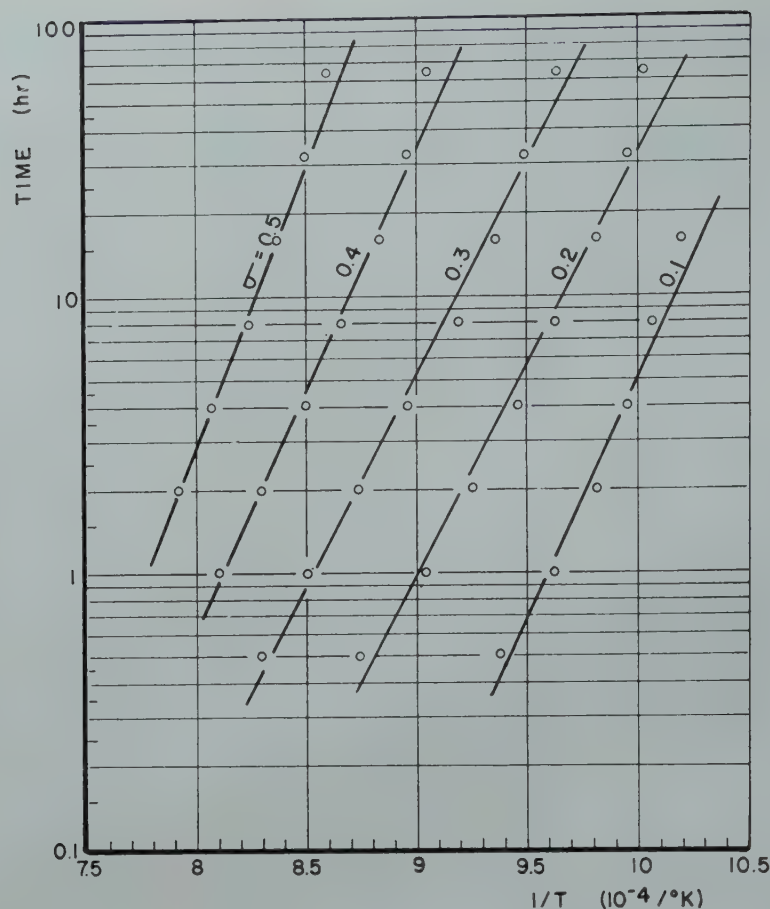


FIG 3—Relation between time and reciprocal of temperature for various values of densification parameter; hydrogen sintering.

Specifically, the “densification parameter” σ is defined as follows:

$$\sigma = \frac{\rho - \rho_0}{\rho_\infty - \rho_0} \quad [1]$$

where ρ = density after partial sintering

ρ_0 = initial density (before sintering)

ρ_∞ = maximum possible density, that is, density of the solid metal.

It is in terms of this parameter that the experimental results are plotted in Fig 3 and 4.

The ultimate goal of the investigation, of which the experiments described in this paper are the first step, is to elucidate the mechanism by which metals bond or sinter together as a result of the application of pressure and heat at temperatures below the melting point. Several hypotheses as to the nature of this mechanism have been advanced (see, for example, Ref. 2, 3, and 4). While no such fundamental theory is developed in this paper, it will be shown that the results of the experiments described may be given a simple interpretation which may serve as a useful guide to future theoretical and experimental investigations.

Briefly stated, it appears possible that densification can be interpreted as a rate process such as that involved, for example, in chemical reactions. Such processes are characterized (see, for example, Ref. 5) by the fact that if a given state is attained in a time t_1 at absolute temperature T_1 , and in time t_2 at some different absolute temperature T_2 , then these four quantities are connected by the relation

$$\log_e \left(\frac{t_1}{t_2} \right) = \frac{Q}{R} \left(\frac{1}{T_1} - \frac{1}{T_2} \right) \quad [2]$$

where R is the gas constant (1.99 cal per mol-°C), and the constant Q is the molal “heat of activation” or “activation energy.” As applied to chemical reactions, for example, Q is proportional to the minimum energy which a molecule must have in order to take part in the reaction (see Ref. 5 for details). In the present case, the progress of the densification “reaction” is measured by the value of the parameter σ . Consequently, to see whether densification may be regarded as a rate process, it is necessary to plot curves of constant σ on a graph of $\log t$ vs. $1/T$, when, if the above relation is to be satisfied, straight lines must

result. Fig 3 and 4 show curves of constant σ plotted in this fashion with the best-fitting straight line drawn through each set of points for comparison. These lines form an approximately parallel set for each of the two sintering atmospheres used, the set representing sintering in vacuum having a larger slope than the set for sintering in hydrogen. The two slopes correspond to values of Q of about 128,000 cal per mol for vacuum sintering, and 80,000 cal per mol for hydrogen sintering, corresponding to the fact (see Fig 1 and 2) that a given time and temperature produce a lower value of σ in vacuum than in hydrogen. A possible explanation of this result is that the hydrogen atmosphere cleans the oxide film from the surface of the particles by reduction, thus making it easier for the clean surfaces to bond together.

It should be noted that there appears to be a systematic deviation of the points from the straight lines drawn in Fig 3 and 4, and that therefore the present results are certainly not conclusive proof that densification is a rate process. It seems plausible, in fact, that densification is the result of superposition of several more fundamental proc-

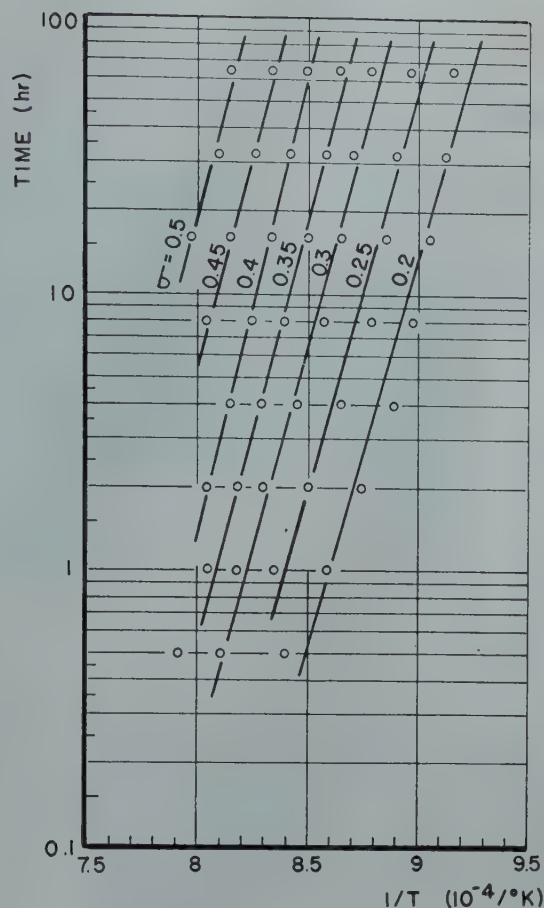


FIG 4—Relation between time and reciprocal of temperature for various values of densification parameter, vacuum sintering.

esses, each of which may be a rate process governed by a different energy of activation. The fact that the overall result may be approximately described as a single rate process would then seem to indicate that one of the fundamental processes predominates over the others.

Summary and Conclusions

From the results of the experimental work described in this paper, it appears that the densification of copper powder compacts in hydrogen and in vacuum may be approximately described as a rate process governed by a heat of activation. The agreement of such a description with the data, however, is not sufficiently good to permit a definite assertion of its validity, and it is suggested only as an hypothesis which may be a useful guide to further work.

The fact that copper powder compacts densify more slowly in vacuum than in hydrogen indicates that the oxide film on the surface of the particles influences the rate of densification. Accordingly, the next step in the experimental investigation will be to study the densification of compacts pressed from powder which has been cleaned of oxide by reduction in hydrogen. It would also be very desirable to investigate the densification of compacts made from powder of more closely controlled particle size, and it is hoped that the practical difficulties involved in obtaining such powder may be overcome sufficiently to permit some work along this line.

Acknowledgment

This work was done at the Jet Propulsion Laboratory, California Institute of Technology, under contract

with the Army Ordnance Department, Washington, D. C. The authors wish to thank this agency for the permission to publish the results of this investigation.

References

1. P. Duwez and H. E. Martens: *The Powder Metallurgy of Porous Metals and Alloys Having a Controlled Porosity*. AIME *Metals Tech.* Apr. 1948, TP 2343.
2. W. D. Jones: *Principles of Powder Metallurgy*. Edward Arnold and Co., London (1937).
3. F. N. Rhines: *Metals Tech.* Aug. 1946, TP 2043; *Trans. AIME* (1946) 166, 474.
4. A. J. Shaler and J. Wulff: *Ind. Eng. Chem.* (May 1948) 40, 838.
5. A. A. Noyes and M. S. Sherrill: *A Course of Study in Chemical Principles*. 1938. New York. The Macmillan Co.

Influence of Composition on the Stress-corrosion Cracking of Some Copper-base Alloys

D. H. THOMPSON* and A. W. TRACY,* Members AIME

SEASON-CRACKING is a type of failure of brass that results from the simultaneous effect of stress and certain corrodants. The object of this paper is to present data that will aid in a more complete understanding of the mechanism of season-cracking and related phenomena. Results presented show that certain high copper alloys are susceptible to season-cracking or stress-corrosion cracking, and possible explanations are discussed. Starting at least as far back as 1906, many papers have been devoted to this subject but the symposium¹ held in Philadelphia in 1944 is the richest source of information.

In order to study season-cracking, several of the many variables were held constant so as to learn the effects of others. Season-cracking is generally understood to refer to the corrosion cracking of brass having internal stresses;^{2,3} it is a special case of the general stress-corrosion cracking. Inasmuch as applied stresses are more readily produced and controlled, they were used exclusively in this research and the resulting phenomenon must be called stress-corrosion cracking.^{2,3} Only constant tensile stresses were used. The agents believed to be most frequently responsible for season-cracking are ammonia, amines and compounds containing them. Both moisture and oxygen also appear to be necessary. Therefore, an atmosphere containing ammonia, water-vapor and air was selected for these tests.

Briefly, the work consisted of exposing sheet metal specimens, having a reduced section $\frac{1}{4}$ by 0.050 in., of copper-base alloys to the effect of static tensile stresses between 5,000 and 20,000 psi and simultaneous contact with a continuously renewed atmosphere containing 80 pct air, 16 pct ammonia and 4 pct water vapor at 35°C. The gas mixture and the speci-

mens were maintained above the dew-point. The time-to-failure in minutes was the primary measure of results. In order to limit the experiment to finite time, it was considered that a specimen which had neither failed nor undergone microscopically detectable cracking in 40,000 min. (4 weeks) while under a stress of 10,000 psi or more could be considered immune to cracking. This is merely a convenient limit and is not to be considered proof of immunity. Supplementary tests in the absence of stress using weight loss or microscopical appearance as measures of attack were made.

Apparatus

The apparatus used in this research is shown in Fig 1. To facilitate the description it may conveniently be divided into six parts: stress-producing units, test chamber, gas train, electrical controls, timers and gas analysis device.

A stress-producing unit is shown in an exploded view at the left in Fig 2. At the right is an assembled unit with a specimen in place in the lower portion; it is this part that remains in the ammonia atmosphere during a test. The upper part contains a spring, a central threaded rod, a large nut and necessary washers, pins, and so forth. Stress is produced in the specimen by

screwing down the top nut against the spring, thus putting a tensile load on the central rod and so on the specimen. The wrench that turns the nut by extending through the upper cap, is seen at the upper right of the figure. The magnitude of the load is gauged by measuring from the pin that extends through the side of the tube, to a fixed point on the large flange. Measurement is made with a vernier beam caliper, shown at the right of the figure. The necessary spring compression to give a desired stress is calculated from the calibration curve of the spring and the dimensions of the specimen.

The test chamber, center Fig 1, consists of a thermally insulated steel box 32 in. long by 10 in. high by 7 in. wide. A horizontal baffle reaching nearly to each end divides the chamber equally. Below this baffle are inlets for air and ammonia, a heating coil and a fan. Thus the gases are warmed and mixed in the lower level and flow past the specimens in the upper level. A thermostat and thermometer project into the upper space. The top is pierced by 12 ports flanked by $\frac{3}{8}$ in. threaded studs. A test starts when a port is opened and a unit containing a stressed specimen is thrust through it and bolted down against a neoprene gasket. The test chamber is held at 35°C.

The gas train, right rear Fig 1, carries ammonia and air continuously to the test chamber. Tank ammonia passes through two reducing valves, a needle valve, a flow meter and into the test chamber. The air from either the plant compressor or a small laboratory compressor passes through wool towers and flow controls to the flow-meter. It then bubbles through water at 34°C and through a heated line to the test chamber.

Electrical controls, left rear, Fig 1, provide rectifiers and mercury relays for the test-chamber and humidifier-heating-control circuits and outlets for

San Francisco Meeting, February 1949.

TP 2518 E. Discussion of this paper (2 copies) may be sent to *Transactions AIME* before May 15, 1949. Manuscript received October 25, 1948.

* Research Assistant and Assistant Metallurgist respectively, The American Brass Co., Waterbury, Connecticut.

¹ Reference are at the end of the paper.

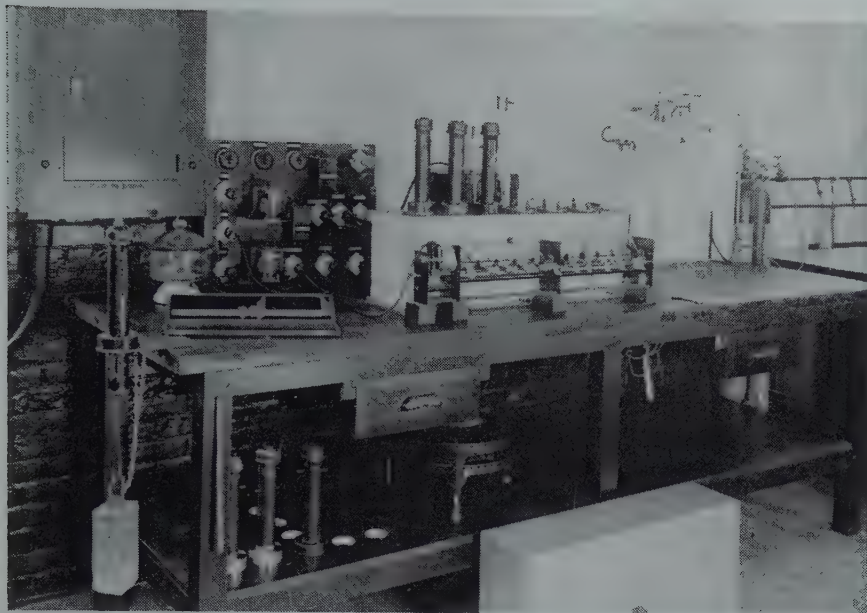


FIG 1—Apparatus for stress-corrosion cracking in moist ammoniacal atmosphere.

gas-line heaters, cover heater, fan and timers.

Timers occupy the space in front of the test chamber. They comprise 12 Veeder-Root counters operated by cams on a shaft driven by a 1 rpm Telechron motor. When a specimen breaks it releases a string which drops a weight stopping a counter. The life of that specimen in minutes is then directly available.

Analysis of the gases contained in the test chamber is performed at the outlet at the right-hand end. The mixed gases are drawn through an absorption train. In the first absorber a known amount of sulphuric acid neutralizes and removes ammonia from the mixture. The moisture is then absorbed in the second tube, which contains silica gel. The volume of air remaining is measured with an aspirator. The gain in weight of both absorption tubes less the known weight of ammonia gives the weight of water. Both ammonia and water are recorded as ml per 500 ml of air, which is the volume per minute delivered to the chamber.

Preparation of Specimens

The following metals and alloys were tested:

- Oxygen-free high-conductivity copper
- Tough-pitch copper
- Copper-zinc alloys containing 0–40 pct zinc
- Copper-phosphorus alloys containing 0–0.9 pct phosphorus
- Copper-arsenic alloys containing 0–1.2 pct arsenic

- Copper-antimony alloys containing 0–1.0 pct antimony
- Copper-silicon alloys containing 0–4 pct silicon
- Copper-nickel alloys containing 0–30 pct nickel
- Copper-aluminum alloys containing 0–8 pct aluminum

Analyses of these alloys are given in Table 1.

The alloys were cast and rolled in the laboratory or obtained from mill production. When possible they were finished with a 50 pct reduction by cold rolling to 0.050 in. gauge. They were sheared to $\frac{3}{8}$ in. by 5 in. and the reduced section filed by the use of a hardened-steel jig to $\frac{1}{4}$ in. by 0.050 in. Holes were drilled near the ends. The specimens were then annealed, usually at 500°C for one hour. Annealing scale was removed by suitable pickles, usually dilute nitric acid, but in every case

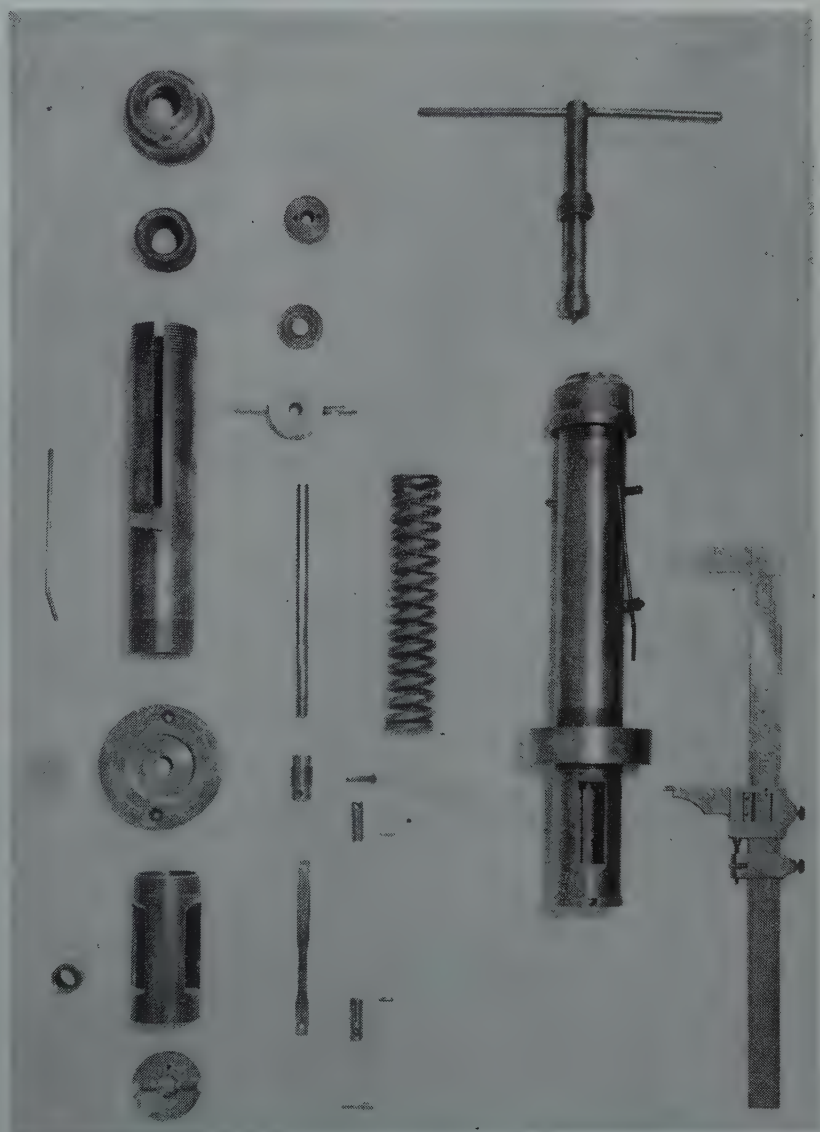


FIG 2—Stress-producing unit.

Table 1 . . . Analyses of Metals Tested

| Alloy No. | Copper + Silver Pct | Oxygen Pct | Sulphur Pct | |
|-----------|---------------------|------------|-------------|------------|
| 1M | 99.962 | 0.0344 | 0.0016 | |
| 2M | 99.950 | 0.038 | 0.003 | |
| 3M | 99.982 | 0.000 | | |
| 4* | 100.000 | 0.000 | Iron | |
| 5* | | Zinc | 0.006 | |
| 6 | 99.861 | 0.12 | 0.006 | |
| 7 | 99.52 | 0.50 | 0.005 | |
| 8 | 99.02 | 0.98 | 0.004 | |
| 9 | 94.81 | 5.18† | 0.005 | |
| 10 | 89.99 | 10.00† | 0.005 | |
| 11 | 79.89 | 20.01† | 0.005 | |
| 12 | 70.16 | 29.82† | 0.010 | |
| 13M | 69.50 | 30.46† | 0.021 | Lead 0.016 |
| 14 | 60.12 | 29.88 | 0.004 | |
| | | Phosphorus | | |
| 15 | 99.996 | 0.001 | 0.006 | |
| 16 | 99.998 | 0.002 | 0.006 | |
| 17 | 99.998 | 0.004 | 0.006 | |
| 18 | 99.998 | 0.007 | 0.006 | |
| 19 | 99.992 | 0.014 | 0.006 | |
| 20 | 99.940 | 0.028 | 0.004 | |
| 21 | 99.942 | 0.056 | 0.004 | |
| 22 | 99.88 | 0.10 | 0.02 | |
| 23 | 99.78 | 0.24 | 0.01 | |
| 24 | 99.54 | 0.46 | 0.01 | |
| 25 | 99.07 | 0.93 | 0.01 | |
| | | Arsenic | | |
| 26 | 99.935 | 0.052 | 0.001 | |
| 27 | 99.858 | 0.126 | 0.002 | |
| 28 | 99.792 | 0.19 | 0.02 | |
| 29 | 99.670 | 0.305 | 0.002 | |
| 30 | 99.592 | 0.36 | 0.004 | |
| 31 | 99.360 | 0.607 | 0.003 | |
| 32 | 98.743 | 1.22 | 0.004 | |

Table 1 . . . (Continued)

| Alloy No. | Copper + Silver Pct | Antimony Pct | Iron Pct | |
|-----------|---------------------|--------------|----------|-------------|
| 33 | 99.968 | 0.010 | 0.014 | |
| 34 | 99.889 | 0.109 | 0.004 | |
| 35 | 99.74 | 0.25 | 0.02 | |
| 36 | 99.52 | 0.47 | 0.01 | |
| 37 | 98.94 | 0.95 | 0.02 | |
| | | Silicon | | |
| 38 | 99.86 | 0.11 | 0.03 | |
| 39 | 99.70 | 0.27 | 0.03 | |
| 40 | 99.48 | 0.46 | 0.02 | |
| 41 | 98.93 | 0.98 | 0.03 | |
| 42 | 97.97 | 1.97 | 0.02 | |
| 43 | 97.00 | 2.96 | 0.04 | |
| 44 | 96.07 | 3.92 | 0.04 | |
| | | Nickel | | |
| 45 | 97.93 | 1.98 | 0.005 | Manganese |
| 46 | 95.17 | 4.78 | 0.005 | 0.08 |
| 47 | 90.00 | 9.84 | 0.005 | 0.077 |
| 48 | 79.69 | 20.16 | 0.004 | 0.21 |
| 49 | 69.28 | 30.06 | 0.005 | 0.28 |
| | | Aluminum | | 0.64 |
| 50 | 99.897 | 0.09 | 0.007 | |
| 51 | 99.74 | 0.24 | 0.009 | |
| 52 | 99.53 | 0.51 | 0.010 | |
| 53 | 98.97 | 1.03 | 0.012 | |
| 54 | 98.00 | 1.98 | 0.012 | |
| 55M | 94.94 | 4.85 | 0.06 | Zinc Nickel |
| 56M | 92.00 | 7.96 | 0.04 | 0.10 0.05 |
| | | Phosphorus | | 0.0 0.00 |
| 57 | 99.966 | 0.024 | 0.002 | |
| 58 | 99.961 | 0.024 | 0.006 | |
| | | Zinc | | |
| 59M | 71.39 | 27.46† | 0.01 | Tin Lead |
| 60M | 70.78 | 29.20† | 0.01 | 1.10 0.006 |
| | | Silicon | | 0.006 |
| 61 | 97.48 | 1.44 | 0.04 | Manganese |
| | | Zinc | | 1.06 |
| 62M | 63.78 | 36.22† | | Arsenic |
| | | | | 0.034 |

M Mill stock. All others cast and rolled in laboratory.

* Chile cathode melted under charcoal. Spectrum shows lead, manganese and iron as traces. Microscope shows no cuprous oxide.

† By difference.

the final dip was cold 20 pct sulphuric acid. After a thorough water rinse the specimens were dipped in alcohol and dried in a blast of hot air. After being measured, they were inserted in units and loaded to the desired stresses. The upper end of each specimen passed out of the test chamber and the opening around it was sealed with wax; the

lower end was held with a pin, which was also imbedded in wax to prevent attack of the specimen at this highly stressed point. Before exposure the whole unit, including the specimen, was warmed to prevent thermal condensation. As each unit was lowered into the test chamber, the appropriate counter was started.

Results

COPPER

Three types of substantially pure copper were subjected to stress-corrosion in the moist ammoniacal atmosphere without the occurrence of cracks. These were tough pitch, OFHC and copper prepared in the laboratory by melting Chile cathode copper under charcoal and pouring through city gas. The magnitude of applied stresses and the length of the exposures are given in Table 2. The column headed "Penetration" describes the result of microscopical examination of a longitudinal section up to an exposed surface. In only one case had any localized corrosion taken place, and in no case was there any evidence of cracking or intergranular penetration.

Table 2 . . . Copper in Moist Ammoniacal Atmosphere Did Not Break Under Stress Within Time Indicated

| | Alloy No. | Stress PSI | Time Min. | Penetration |
|--------------------------------|-----------|------------|-----------|-------------|
| Tough Pitch Copper | 1 | 5,000 | 50,000 | None |
| Touch Pitch Copper | 1 | 10,000 | 50,000 | One Pit |
| Tough Pitch Copper | 2 | 10,000 | 40,000 | None |
| OFHC Copper | 3 | 10,000 | 40,000 | None |
| Copper | 4 | 10,000 | 40,000 | None |
| Copper (4 specimens) | 5 | 15,000 | 50,000 | None |

COPPER-ZINC ALLOYS

Results obtained from copper-zinc alloys are presented graphically in Fig 3. The breaking times of specimens stressed at 5,000, 10,000 and 15,000 psi are plotted against the zinc content in per cent. The corrosion rate in inch per year (ipy) is also plotted against zinc content. Corrosion rate figures were computed from weight loss data on specimens exposed without stress to the same moist ammoniacal atmosphere. It is obvious that the resistance to cracking decreases rapidly as the zinc content increases. The corrosion rate, while relatively stable, does drop slightly with the cracking time, suggesting that the alloys which crack more rapidly are those that corrode less rapidly. Table 3 includes these data and also gives the microscopically observed intergranular penetration that occurred in the unstressed specimens.

Two things should be noted especially: the lack of correlation between cracking rate and corrosion rate, with the suggestion of negative correlation,

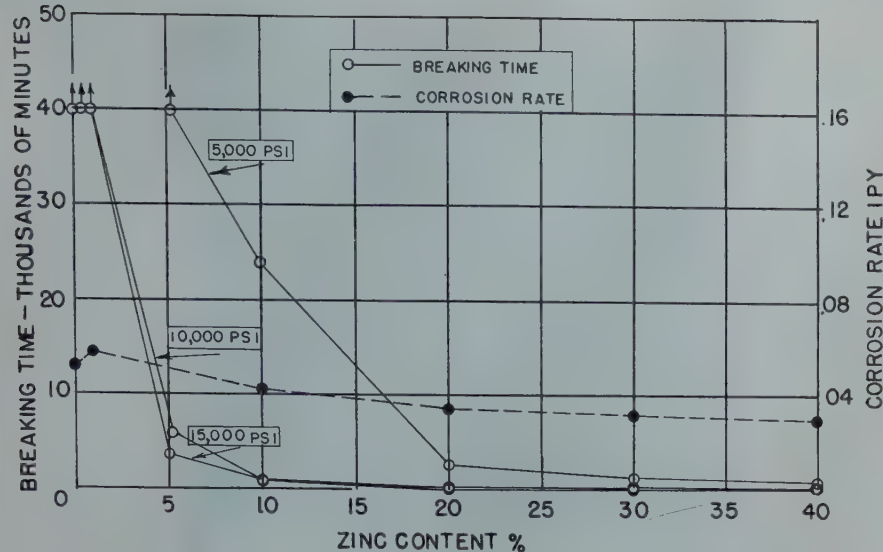


FIG 3—Copper-zinc alloys in moist ammoniacal atmosphere. Breaking time under various stresses vs. zinc content; corrosion rate, no stress, vs. zinc content.

Table 3 . . . Copper-zinc Alloys in Moist Ammoniacal Atmosphere

| Alloy No. | Zinc Pct | Breaking Time—minutes—at | | | Corrosion Rate—IPY | Penetration Grains in 1 Week |
|-----------|----------|--------------------------|------------|------------|--------------------|------------------------------|
| | | 5,000 PSI | 10,000 PSI | 15,000 PSI | | |
| 4 | 00 | 40,000† | 40,000† | 40,000† | 0.052 | None |
| 6 | 0.12 | 40,000† | 40,000† | 40,000† | | |
| 7 | 0.50 | 40,000† | 40,000† | 40,000† | | |
| 8 | 0.98 | 40,000† | 40,000† | 40,000† | 0.058 | None |
| 9 | 5.18 | 40,000† | 5,914 | 3,522 | | |
| 10 | 10.03 | 24,070 | 973 | 757 | 0.042 | 3-4 |
| 11 | 20.01 | 2,689 | 258 | 161 | 0.036 | 1-2 |
| 12 | 29.82 | | 254 | 102 | 0.032 | * |
| 13 | 30.45 | 1,379 | | | | |
| 14 | 39.88 | 943 | 232 | 106 | 0.030 | 1 |

* Several grains at only one region.

† Did not break.

All samples annealed at 500°C for one hour. All metal cast and processed in the laboratory except 13, which was cast and processed to 0.400 in. ga in the mill and finished in the laboratory.

and the occurrence of intergranula penetration in the absence of stress.

COPPER-PHOSPHORUS ALLOYS

Similar results are shown in Fig 4 for copper-phosphorus alloys, although at only one applied stress, 10,000 psi. Comparison of Fig 4 with Fig 3 shows that the curves are similar in shape; the breaking time decreases sharply when either phosphorus or zinc is added to copper. An impressive difference is the extreme rapidity with which the breaking time drops as phosphorus is added. For instance, Table 4 gives 274 min. as the breaking time for the 0.1 pct phosphorus alloy (Alloy No. 22) under 10,000 psi stress in the moist ammoniacal atmosphere, while copper with no phosphorus does not break in 50,000 min. even at higher stresses. Comparison with Table 3 shows that this 0.1 pct phosphorus alloy breaks nearly as rapidly as 80-20 brass under the same conditions.

Table 4 also reveals the rapid attack of the moist ammoniacal atmosphere on annealed copper-phosphorus alloys without stress. A sample containing 0.24 pct phosphorus (Alloy No. 23) was annealed at 800°C for one hour and exposed to the moist ammoniacal atmosphere without stress. After 40,000 min. (1 month) it was found that the intergranular penetration had completely penetrated the 0.050 in. gauge sheet. The specimen could be broken apart into individual grains with the fingers. Some of the grains are shown in Fig 5, a micrograph taken at 30X. Fig 6 is a micrograph taken at 75X of a piece of 0.1 pct phosphorus alloy (Alloy No. 22) that was annealed at 800°C and exposed without stress to the

Table 4 . . . Copper-phosphorus Alloys in Moist Ammoniacal Atmosphere

Breaking Time under Stress
Corrosion Rate and Intergranular Penetration in the Absence of Stress

| Alloy No. | Phosphorus Pct | Breaking Time at 10,000 PSI Min. | Corrosion Rate IPY | Penetration Grains in 1 Week |
|-----------|----------------|----------------------------------|--------------------|------------------------------|
| 4 | 00 | 40,000* | 0.033 | None |
| 15 | 0.001 | 40,000* | | None |
| 16 | 0.002 | 40,000* | | None |
| 17 | 0.004 | 39,459 | | 1-2 |
| 18 | 0.006 | 18,417 | | 4-5 |
| 19 | 0.014 | 6,298 | 0.038 | 4-5 |
| 20 | 0.028 | 642 | 0.027 | 4-8 |
| 21 | 0.056 | 428 | 0.016 | 4-5 |
| 22 | 0.10 | 274 | | 6 |
| 23 | 0.24 | 262 | 0.013 | 6 |
| 24 | 0.46 | 314 | 0.030 | 3-4 |
| 25 | 0.92 | 14,740 | 0.022 | Slight |

* Did not break.

All alloys cast and processed in the laboratory. All samples annealed finally at 500°C for 1 hour.

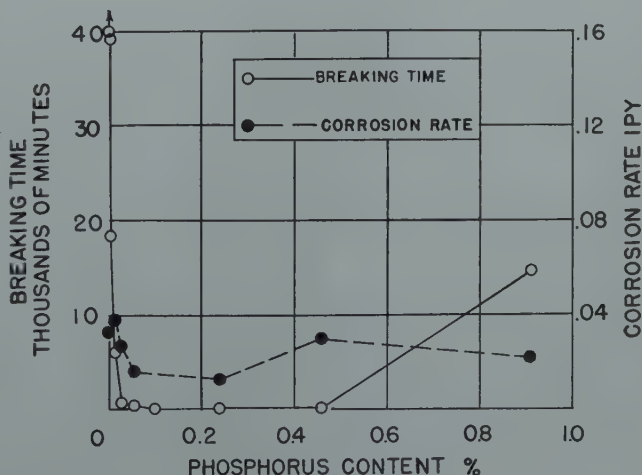


FIG 4—Copper-phosphorus alloys in moist ammoniacal atmosphere. Breaking time under 10,000 psi stress vs. phosphorus content; corrosion rate, no stress, vs. phosphorus content.

moist ammoniacal atmosphere for one week. The depth of penetration is obvious.

The results on the phosphorus alloys are extremely interesting. The addition of phosphorus to copper has a profound effect on the rapidity of stress-corrosion cracking and also on the rate of intergranular penetration in moist ammoniacal atmosphere in the absence of stress. The effect cannot be explained by the removal of oxygen from the copper since OFHC and copper deoxidized with some other elements do not crack. The changes in mechanical and physical properties are negligible except in the case of conductivity and the overall corrosion rate is but slightly affected.

Alloy No. 25 (0.92 pct phosphorus) broke less rapidly than alloys with intermediate phosphorus contents; it is beyond the solid solubility limit of phosphorus in copper. This upswing will be observed in other alloy systems, to be described.

In Fig 3 and 4, points are very close to the axes, but Tables 3 and 4 give the actual values that the points represent. No change in scale was adopted because of the advantage of having all the graphs use the same vertical scale.

COPPER-ARSENIC ALLOYS

Stress-corrosion cracking and corrosion rate curves from data on copper-arsenic alloys in moist ammoniacal atmosphere are shown in Fig 7. These curves are quite different from those presented for copper-phosphorus and copper-zinc in that there is a pronounced minimum in the cracking

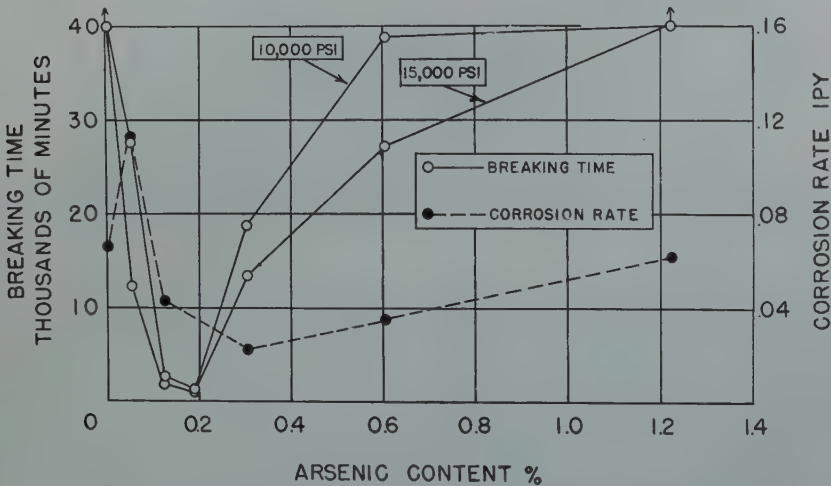


FIG 7—Copper-arsenic alloys in moist ammoniacal atmosphere. Breaking time under various stresses vs. arsenic content; corrosion rate, no stress, vs. arsenic content.

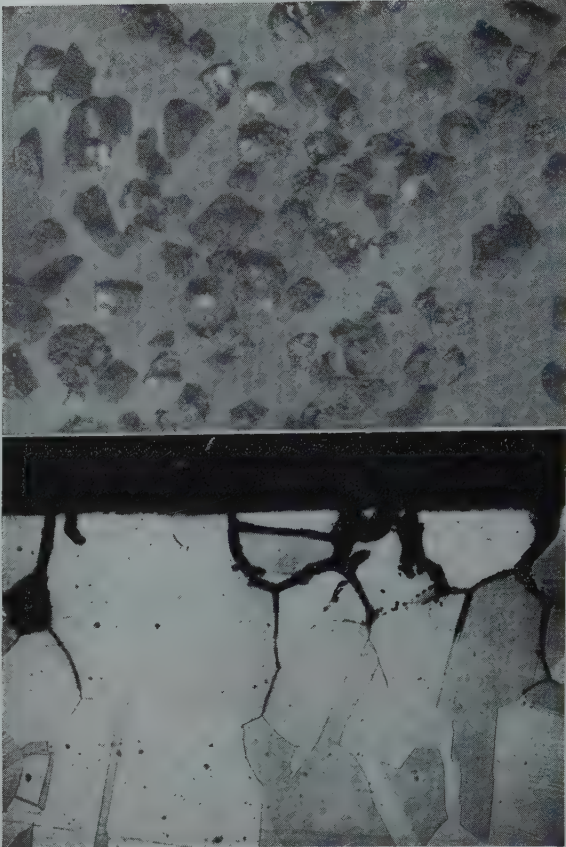


FIG 5 and 6—Copper-phosphorus alloys after exposure to moist ammoniacal atmosphere. FIG 5 (Above)—Alloy No. 23, 0.24 pct phosphorus, 40,000 min., 30 X. FIG 6 (Below)—Alloy No. 22 0.1 pct phosphorus, 10,000 min., 75 X. Potassium bichromate-sulphuric acid etch.

curves at 0.2 pct arsenic and a maximum in the corrosion-rate curve at 0.05 pct arsenic. The 1.2 pct arsenic alloy is immune to cracking within the prescribed limits. Table 5 shows that intergranular penetration is appreciable after four weeks in the lower arsenic alloys. The effect of arsenic content on

Table 5 . . . Copper-arsenic Alloys in Moist Ammoniacal Atmosphere Breaking Time under Stress Corrosion Rate and Intergranular Penetration in the Absence of Stress

| Alloy No. | Arse-nic Pct | Breaking Time at | | Corro-sion Rate IPY | Pene-tration Grains in 4 Weeks |
|-----------|--------------|---------------------|---------------------|---------------------|--------------------------------|
| | | 10,000 PSI Min-utes | 15,000 PSI Min-utes | | |
| 4 | 00 | 40,000† | 40,000† | 0.066 | 0 |
| 26 | 0.052 | 27,609 | 12,342 | 0.113 | Several |
| 27 | 0.126 | 2,674 | 1,899 | 0.043 | Several |
| 28 | 0.19 | 1,417 | 1,093 | | |
| 29 | 0.305 | 18,720 | 13,434 | 0.022 | 1 |
| 30* | 0.365 | 16,905 | 16,484 | | |
| 31 | 0.606 | 38,842 | 27,339 | 0.035 | None |
| 32 | 1.225 | 40,000† | 40,000† | 0.062 | None |

* Cuprous oxide present. † Did not break. All alloys cast and processed in the laboratory. All specimens annealed finally at 500°C for 1 hour.

Table 6 . . . Copper-antimony Alloys in Moist Ammoniacal Atmosphere

Breaking Time under Stress
Corrosion Rate and Intergranular Penetration in the Absence of Stress

| Alloy No. | Antimony Pct | Breaking Time, Min. at | | | Corrosion Rate IPY | Penetration Grains in 1 Week |
|-----------|--------------|------------------------|------------|------------|--------------------|------------------------------|
| | | 5,000 PSI | 10,000 PSI | 15,000 PSI | | |
| 4 | 00 | 40,000* | 40,000* | 40,000* | 0.058 | 0 |
| 33 | 0.01 | | 40,000* | 36,665 | 0.080 | 1-3 |
| 34 | 0.109 | 15,012 | 6,882 | 2,894 | 0.160 | 5-7 |
| 35 | 0.25 | 6,412 | 4,602 | 2,232 | 0.137 | 10-12 |
| 36 | 0.47 | 15,565 | 2,197 | 2,635 | 0.139 | 3-4 |
| 37 | 0.95 | 21,997 | 3,373 | 2,217 | 0.055 | 2-3 |

* Did not break.
All alloys cast and processed in the laboratory.
All specimens annealed finally at 500°C for 1 hour.

Table 7 . . . Copper-silicon Alloy in Moist Ammoniacal Atmosphere

Breaking Time under Stress
Corrosion Rate and Intergranular Penetration in the Absence of Stress

| Alloy No. | Silicon Pct | Breaking Time, Min., at | | Corrosion Rate IPY | Penetration Grains in 4 Weeks |
|-----------|-------------|-------------------------|------------|--------------------|-------------------------------|
| | | 10,000 PSI | 15,000 PSI | | |
| 4 | 0 | 40,000* | 40,000* | 0.052 | None |
| 38 | 0.11 | 23,340 | 13,201 | 0.072 | 2-3 |
| 39 | 0.27 | | 5,178 | 0.034 | 2-3 |
| 40 | 0.46 | 5,250 | 2,881 | 0.024 | 3-4 |
| 41 | 0.97 | 2,537 | 1,972 | 0.034 | Doubtful |
| 42 | 1.96 | 15,735 | 6,280 | 0.047 | |
| 43 | 2.97 | 49,000 | 28,005 | 0.053 | |
| 44 | 3.91 | | 50,000* | 0.082 | None |

* Did not break.
All alloys cast and processed in the laboratory.
All specimens annealed finally at 500°C for 1 hour.

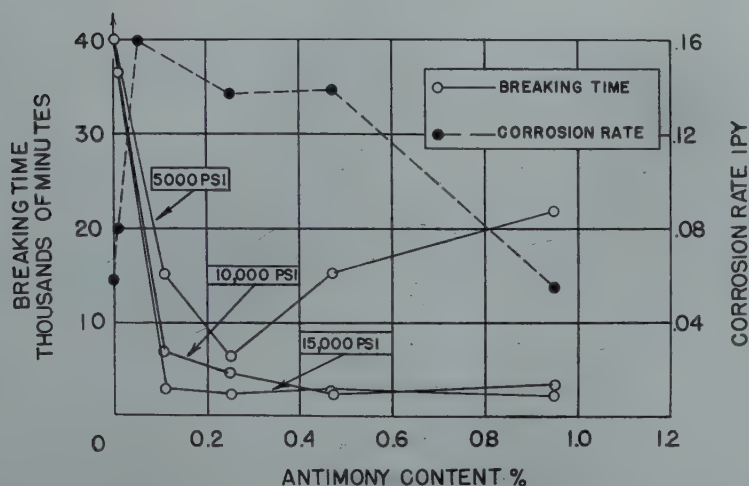


FIG 8—Copper-antimony alloys in moist ammoniacal atmosphere. Breaking time under various stresses vs. antimony content; corrosion rate, no stress, vs. antimony content.

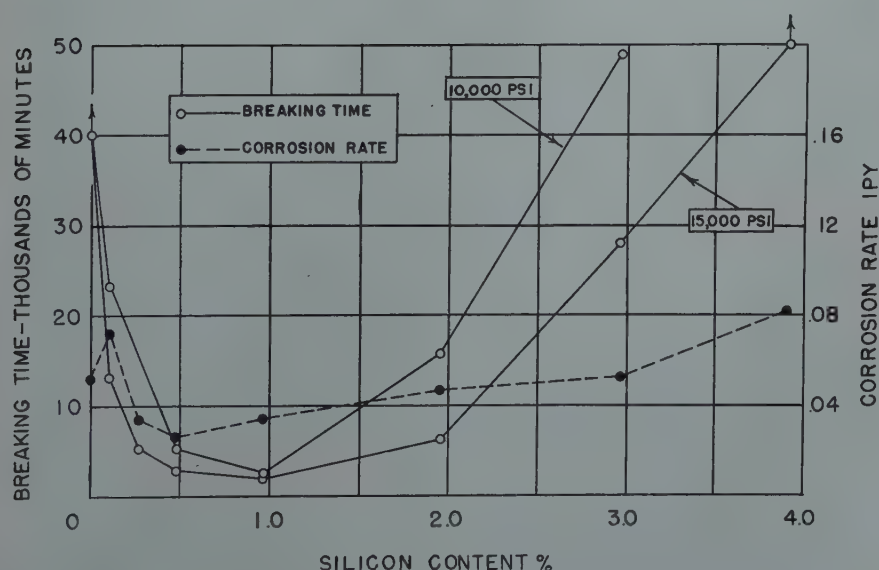


FIG 9—Copper-silicon alloys in moist ammoniacal atmosphere. Breaking time under various stresses vs. silicon content; corrosion rate, no stress, vs. silicon content.

cracking time is not nearly as pronounced as in the case of phosphorus and zinc and it extends over only a very narrow range.

COPPER-ANTIMONY ALLOYS

Fig 8 gives the results for copper-antimony alloys. The minimum cracking time is greater than with the alloy systems previously considered. There is some evidence of a minimum in the antimony per cent versus cracking-time curve. There is a maximum in the corrosion-rate curve. Intergranular penetration is shown by Table 6 to be appreciable in one week.

COPPER-SILICON ALLOYS

Results are given in Fig 9. There is a distinct minimum cracking time at 1 pct silicon, which is a higher percentage than in the case of arsenic. Immunity appears at 4 pct silicon. The corrosion rate is fairly constant. Intergranular penetration given in Table 7 is definite but only after four weeks.

COPPER-NICKEL ALLOYS

Fig 10 gives test results. The minimum in the cracking time is pronounced but the required exposure is long. With this system, as with others, a maximum appears in the corrosion rate curve at a more dilute composition than the minimum in the breaking curve. At 30 pct nickel, the corrosion rate is very small; the samples were hardly tarnished at the end of a week. Table 8 shows that intergranular penetration is almost absent, but it does occur.

Table 8 . . . Copper-nickel Alloys in Moist Ammoniacal Atmosphere

Breaking Time under Stress
Corrosion Rate and Intergranular Penetration in the Absence of Stress

| Alloy No. | Nickel Pct | Breaking Time, Min., at 10,000 PSI | Corrosion Rate IPY | Penetration Grains in 1 Week | Final Anneal °C |
|-----------|------------|------------------------------------|--------------------|------------------------------|-----------------|
| 4 | 00 | 40,000* | 0.043 | None | 500 |
| 45 | 1.98 | 9,426 | 0.070 | 1/8 | 500 |
| 46 | 4.78 | 4,730 | 0.055 | 1/8 | 500 |
| 47 | 9.84 | 9,552 | 0.046 | None | 700 |
| 48 | 20.16 | 13,527 | 0.029 | None | 700 |
| 49 | 30.06 | 40,000* | 0.0006 | None | 750 |

* Did not break.
All samples cast and processed in the laboratory.

COPPER-ALUMINUM ALLOYS

Fig 11 shows a minimum breaking time at 1 pct aluminum. The corrosion-rate curve is relatively constant with only a slight maximum. Intergranular penetration is small in one week as given in Table 9.

OTHER TESTS

In line with Dix's⁴ theories on the role of grain-boundary precipitates in rendering an alloy subject to stress-corrosion cracking, some tests were made to try to show whether the effect is important in copper-phosphorus alloys. About 0.5 pct phosphorus is soluble in copper, but iron phosphide is believed to be only slightly soluble in copper. Therefore, the attempt was made to precipitate iron phosphide and study its effect on cracking. Two alloys were cast; each contained 0.024 pct phosphorus. One contained 0.002 pct iron and the

other contained 0.006 pct iron (alloy Nos. 57 and 58). Thermal treatments were designed to produce precipitation in the grain bodies, in the grain boundaries and to maintain solution. Microscopical examination of these specimens at 1000 diam revealed scattered spheres of some precipitate in all of them in about equal amount. The results of stress-corrosion cracking tests in moist ammonia vapor are given in Table 10. While there is apparently a trend indicating that metal treated to produce precipitation in the grain bodies is most resistant to cracking, followed by material with maximum solution and then that treated to produce grain-boundary pre-

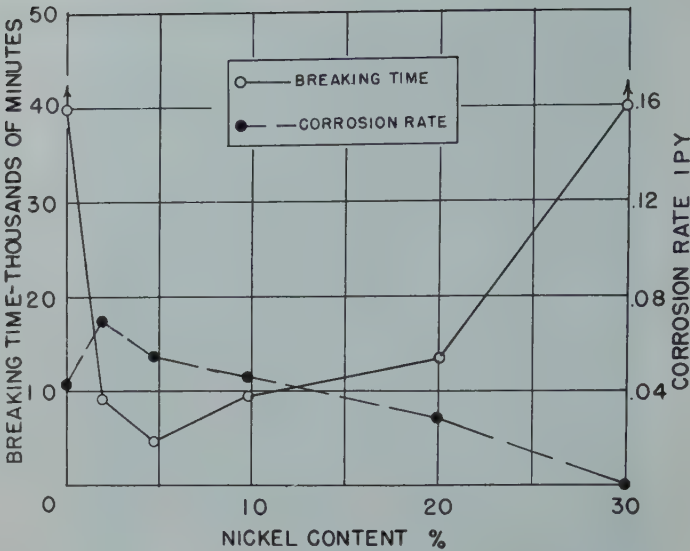


FIG 10—Copper-nickel alloys in moist ammoniacal atmosphere. Breaking time under 10,000 psi stress vs. nickel content; corrosion rate, no stress, vs. nickel content.

Table 9 . . . Copper-aluminum Alloys in Moist Ammoniacal Atmosphere

Breaking Time under Stress
Corrosion Rate and Intergranular Penetration in the Absence of Stress

| Alloy No. | Aluminum Pct | Breaking Time at 10,000 PSI Min. | Corrosion Rate IPY | Penetration Grains in 1 Week |
|-----------|--------------|----------------------------------|--------------------|------------------------------|
| 4 | 00 | 40,000† | 0.042 | None |
| 50 | 0.09 | 40,000† | 0.042 | None |
| 51 | 0.24 | 40,000† | 0.051 | None |
| 52 | 0.51 | 25,583 | 0.043 | 1 |
| 53 | 1.03 | 10,838 | 0.030 | 1 |
| 54 | 1.98 | 13,323 | 0.040 | None |
| 55* | 4.85 | 50,000† | 0.043 | |
| 56* | 7.96 | | 0.046 | |

All alloys cast and processed in the laboratory except
* which were cut from annealed mill stock.
All specimens annealed finally at 500°C for 1 hour.
† Did not break.

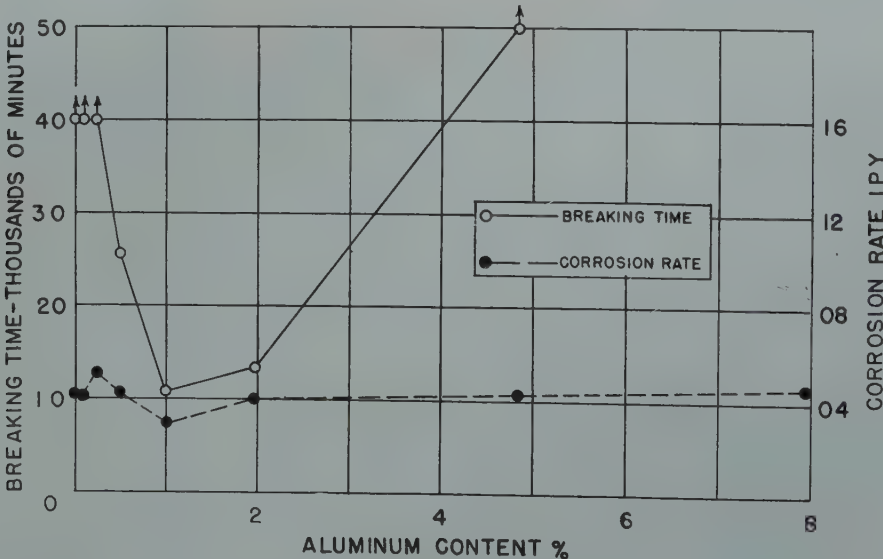


FIG 11—Copper-aluminum alloys in moist ammoniacal atmosphere. Breaking time under 10,000 psi stress vs. aluminum content; corrosion rate, no stress, vs. aluminum content.

Table 10 . . . Stress-corrosion Cracking of Copper Containing 0.024 Pct Phosphorus in Moist Ammoniacal Atmosphere

| Alloy No. | Iron Pct | Ready-to-finish Anneal °C | Cooling | Rolled Pct | Final Anneal °C | Cooling | Breaking Time Min. |
|------------------------|----------|---------------------------|----------|------------|-----------------|----------|--------------------|
| Stressed at 5,000 PSI | | | | | | | |
| 57 | 0.002 | 500 | Air | 50 | 400 | Air | 5,980 |
| | | 800 | Quenched | 50 | 400 | Air | 2,380 |
| | | 800 | Quenched | 50 | 800 | Quenched | 3,136 |
| 58 | 0.006 | 500 | Air | 50 | 400 | Air | 5,049 |
| | | 800 | Quenched | 50 | 400 | Air | 2,244 |
| | | 800 | Quenched | 50 | 800 | Quenched | 4,080 |
| Stressed at 10,000 PSI | | | | | | | |
| 57 | 0.002 | 500 | Air | 50 | 400 | Air | 1,576 |
| | | 800 | Quenched | 50 | 400 | Air | 1,011 |
| | | 800 | Quenched | 50 | 800 | Quenched | 1,453 |
| 58 | 0.006 | 500 | Air | 50 | 400 | Air | 1,649 |
| | | 800 | Quenched | 50 | 400 | Air | 821 |
| | | 800 | Quenched | 50 | 800 | Quenched | 1,610 |

cipitation, there is no difference between the alloy having 0.002 pct iron and the one containing 0.006 pct iron. The statistical procedure, analysis of variance, has been applied to these data and the conclusion is reached that no significant difference exists among them. Either the thermal treatment produced no precipitation, or the sub-microscopic precipitate had no large effect on the breaking time.

Another experiment was performed to show the effect of long-time anneals on the stress-corrosion cracking rate. The results are given in Table 11. The alloy contained 0.1 pct phosphorus, balance copper (alloy No. 22). Four samples were annealed at 500°C for one hour and in addition two of them were held for 64 hr at 350°C. While the long anneal produced a somewhat shorter cracking time, the difference is not significant in the face of the variation among supposedly identical specimens. At 1000 diam these samples also showed tiny, randomly distributed spheres of precipitate, the number of which was not greatly affected by the low temperature anneal. It is believed that such material has not been absorbed from segregation occurring in the casting, because of the relatively small amount of working and annealing of small laboratory castings. More work should be done in connection with the effect of heat treatment on the stress-corrosion cracking of this type of alloy.

PATH OF CRACKS

Although ammonia cracking in brass is usually largely intergranular, there are exceptions in alpha brass as well as in other alloys. Fig 12 at 500 diam

shows typical intergranular cracking in ½ in. diam 70-30 brass rod (alloy No. 60) that failed under 5,000 psi in moist ammoniacal atmosphere. Radically different is Fig 13 at 500 diam, which shows cracking in arsenical admiralty (alloy No. 59) after the same preparation and exposure as the brass. It is difficult to find cracks that are intergranular in this micrograph. The 70-30 brass was annealed at 500°C and the admiralty brass at 550°C for one hour. Similar transcrystalline cracking has been observed in arsenical and non-arsenical admiralty and aluminum brass. Fig 14 is a micrograph at 250 diam of a 65-35 brass gear (alloy No. 62) that was sheared from ¼ in. wrought stock and then exposed to moist ammoniacal atmosphere for 48 hr. The cracks have a strong tendency to pass through the grains.

Fig 15 taken at 500 diam shows cracks in an alloy containing 1.5 pct silicon, 1 pct manganese (alloy No. 61) which failed under 20,000 psi stress in moist ammoniacal atmosphere. Cracks, besides being intergranular, have a tendency to follow twin boundaries, or slip planes.

Discussion of Results

In 1930, Bassett⁵ stated that he had seen copper season-crack, while in 1944 Edmunds⁶ reported that copper is immune to mercury and ammonia stress-cracking. These statements are not necessarily contradictory. Bassett referred to service failures of copper tubes, which are usually deoxidized with phosphorus. Such failures are not frequent but the authors have observed a number of them. One such tube is

Table 11 . . . Effect of Heat-treatment on the Season-cracking of Copper Containing 0.1 Pct Phosphorus in Moist Ammoniacal Atmosphere
Alloy No. 22

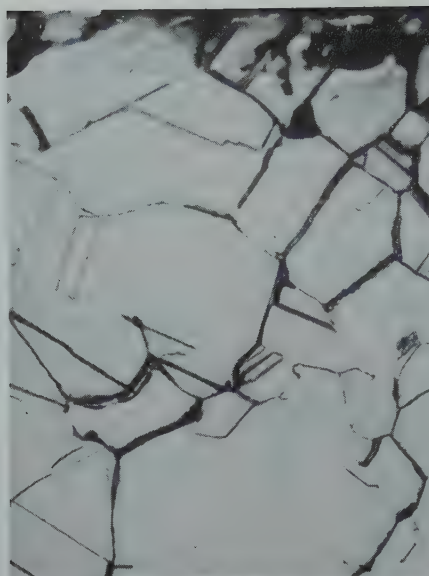
| | 500°C Anneal | 500°C Anneal Followed by 64 Hr at 350°C |
|-----------------------|--------------|---|
| Breaking time..... | 491 | 316 |
| Under 10,000 psi..... | 299 | 286 |
| Average..... | 395 | 301 |

shown in Fig 16. It is a 1½ in. od by 0.082 in. ga wall, hard copper tube containing 0.019 pct phosphorus. In service, presumably a refrigeration plant, it was wrapped in tar paper, twine and two layers of hair felt. The line of the edge of the tar paper is shown as a helical row of pits, and the cracks are obvious. The present paper indicates that phosphorus-deoxidized copper cracks readily under the test conditions. Presumably the paucity of service failures of phosphorus-deoxidized copper is due to the low yield point of copper, which makes the occurrence of high internal stresses impossible. The authors have found no evidence that tough pitch or OFHC copper is subject to season-cracking or to stress-corrosion cracking in moist ammoniacal atmosphere and they therefore agree with Edmunds's statement.

As mentioned above, Dix⁴ suggested that season-cracking is due to corrosion that is accelerated by the potential between grain boundaries and grain bodies and that this difference is caused by the precipitation of an insoluble phase at the grain boundaries and the depletion of the solute atoms surrounding the grain boundary. There seems to be no evidence to support the existence of a precipitated phase in brass. Nor is there evidence of a change in the breaking time curve when the solid solubility of zinc in copper is exceeded. Read, Reed and Rosenthal⁷ attribute this potential difference rather to the high free energy of regions of lattice imperfection such as grain boundaries.

The behavior of phosphorus-deoxidized copper described in the present paper suggested that these theories be reconsidered. It will be recalled that 0.1 pct phosphorus is sufficient to allow rapid cracking of copper with which it is alloyed. Further, this alloy is subject to quite rapid intergranular corrosion in moist ammonia vapor in the ab-

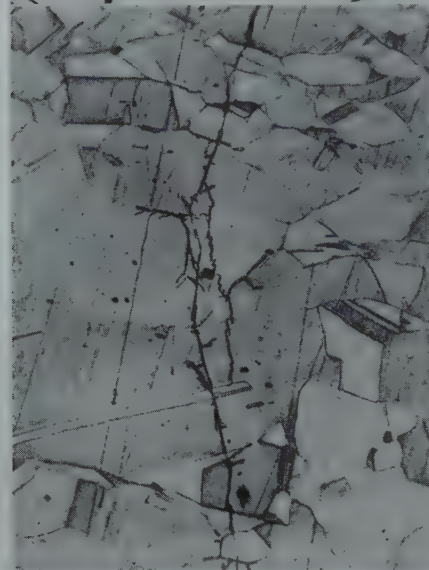
12



13



14



15

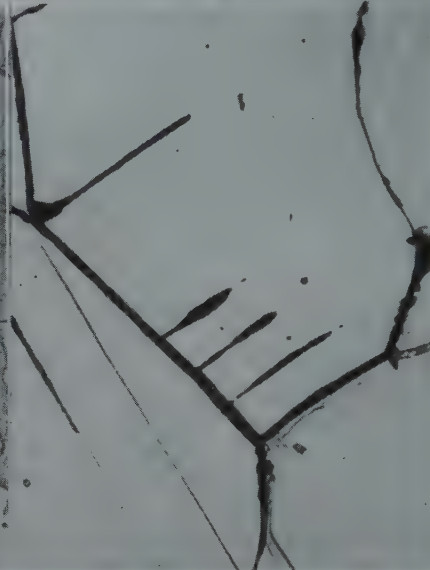


FIG 12 to 15—Types of ammonia cracking.

Fig 12—70-30 brass, alloy No. 60, 5,000 psi stress, 500 X.

Fig 13—Arsenical admiralty, alloy 59, 5,000 psi stress, 500 X.

Fig 14—65-35 brass gear, alloy 62, internal stress, 250 X.

Fig 15—Copper-silicon-manganese, alloy No. 61, 20,000 psi stress, 500 X.

Etchants: Fig 12 and 14—Ammonium hydroxide and hydrogen peroxide.

Fig 13 and 15—Potassium bichromate and sulphuric acid.

sence of stress either internal or external. Thus grain boundaries are open avenues for corrosion by moist ammonia vapor when a little phosphorus is present, but they are closed to traffic when only copper is present. This behavior suggests to the authors that phosphorus is concentrated at the grain boundaries and whether within or beyond the solid solubility limit, the alloy in this region is anodic to the higher-copper grain-bodies. This potential may be the result of lattice dislocation; not that caused by the abutting of adjacent differently-oriented grains at the boundaries but

rather distortion around solute atoms of phosphorus. Such distortion is one of the causes for the large effect phosphorus has on the conductivity of copper.

The behavior of this alloy, if it be typical of season-cracking in general, allows some other conclusions to be drawn. Since intergranular penetration occurs in the absence of stress, it appears that stress merely accelerates the corrosive action of the ammonia, keeping the crack open and a fresh notch available for its action. Another possibility is the formation of protective films. It is conceivable that such

films would form first on the exposed surfaces of the grain bodies, leaving the boundaries highly anodic. In more concentrated alloys the film might cover the *whole* surface and stifle boundary attack. In all the systems studied, except copper-zinc, up to 40 pct zinc, there is at least an indication that the cracking rate decreases as the per cent of alloying element is increased.

The presence of 0.1 pct phosphorus in copper changes the mechanical properties only negligibly and it is impossible to correlate the cracking tendency with yield strength, propor-

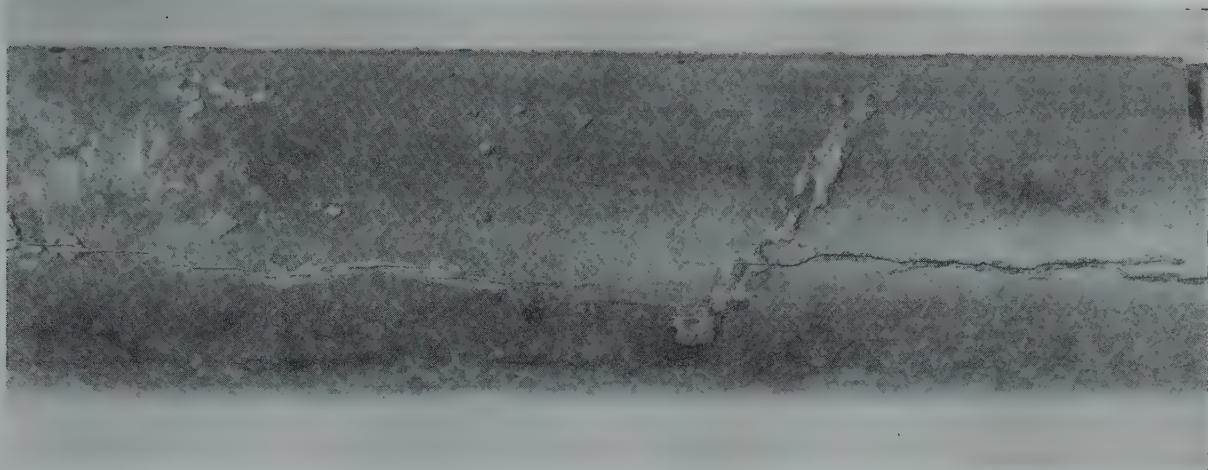


FIG 16—1½ in. od by 0.082 in. gauge hard copper tube containing 0.019 pct phosphorus.
Cracked in service.

tional limit or the like.

It should be emphasized that these tests cannot be used as a basis for predicting service failures by season-cracking. The failures were produced under artificial laboratory conditions and should not arouse fears that phosphorized or arsenical copper tubes will crack in service except in rare instances.

Summary

These tests show that the addition of zinc, phosphorus, arsenic, antimony, silicon, nickel or aluminum to copper forms alloys that are subject to stress-corrosion cracking in moist ammoniacal atmosphere in some composition ranges.

The product of the cracking time and the per cent of the added element is an inverse measure of the cracking tendency per one per cent. From these figures the alloying elements may be formed into a rank of decreasing unit cracking tendency. This order follows: phosphorus, arsenic, antimony, silicon, zinc, aluminum, nickel. Brass cracks more rapidly than any of the other systems mentioned; but zinc is low on the list because so much of it must be added to give a rapid cracking rate.

Another observation is the appearance of a minimum in the per cent of alloying element versus breaking-time curve. This minimum breaking time is distinct in copper-nickel, copper-silicon, copper-arsenic, and cop-

per-aluminum systems; is indicated in copper-antimony and copper-phosphorus and is absent in copper-zinc.

The curves relating per cent of added element to corrosion rate in the absence of stress have a maximum in all systems for one of the more dilute alloys. This maximum is distinct in the copper-arsenic and copper-antimony systems and fairly distinct in copper-nickel, but only slight in the others. The same three, copper-arsenic, copper-antimony and copper-nickel, may be said to exhibit positive correlation between cracking tendency and corrosion rate.

Intergranular penetration in the absence of stress in moist ammoniacal atmosphere places the elements in the following rank in order of decreasing penetration: phosphorus, antimony, zinc, arsenic, silicon, aluminum, nickel. The extent of this phenomenon is very greatly dependent on grain size and the rank is subject to so many variables, that it may be assumed to be nearly enough like the breaking-time rank to support the belief of a common cause.

Conclusion

The data presented are insufficient for a concrete conclusion, but the following are offered for consideration:

The addition of a soluble element to copper produces a concentration of the solute at grain boundaries. This concen-

tration either forms a submicroscopic precipitate, a richer solid solution, or lattice disturbances. Any of these conditions makes the grain boundary region anodic to the grain bodies. Localized corrosion is accelerated and grain boundary penetration ensues. The presence of a tensile stress still further accelerates penetration by opening cracks and forming highly stressed notches.

Work is being continued on this research.

Acknowledgments

The authors are grateful to Mr. John R. Freeman, Jr., Technical Manager of The American Brass Co. for his encouragement during the experimental work and for permission to publish the results. They also wish to acknowledge the advice of Mr. E. W. Palmer and the assistance of many members of the technical staff of The American Brass Co.

References

1. Symposium on Stress-corrosion Cracking of Metals. ASTM-AIME (1944).
2. H. H. Uhlig (Editor): *Corrosion Handbook*. 30. 1948. New York. John Wiley and Sons.
3. ASTM Standards (1946), pt. IB, 134.
4. E. H. Dix, Jr.: *Trans. AIME* (1940). 137, 2.
5. W. H. Bassett: In discussion of Alan Morris, *Trans. AIME* (1930) 273.
6. G. Edmunds: Ref. 1, 87.
7. T. A. Read, J. B. Reed and H. Rosenthal: Ref 1, 108.

Cadmium Recovery Practice in Lead Smelting

P. C. FEDDERSEN,* Member AIME, and HAROLD E. LEE*

Introductory Review

GREENOCKITE is the only known cadmium mineral of importance. It occurs rather universally, in minor concentrations, as a secondary mineral in sphalerite deposits. The world's cadmium output is obtained through the processing of metallurgical by-products, largely from the treatment of residues from electrolytic zinc, retort zinc and lithopone plants. These sources are supplemented by the processing of fumes from lead and copper smelting operations. The development of modern selective flotation practice in the decade 1920-1930, which permitted the economical mining of complex lead-zinc ores, resulted in significant increases in the quantities of cadmium entering lead smelting systems.

Being closely related to zinc as to occurrence, properties and production, most detailed description of cadmium recovery methods are to be found recorded in connection with zinc metallurgy. Other than occasional articles pertaining to particular operational procedures, literature offers but little in the nature of a balanced survey of lead smelter cadmium recovery practices. While many of the basic operations described for the recovery of cadmium from zinc by-products are applicable to the treatment of lead plant products, the inherent problems involved differ widely. In general the cadmium content of related by-products from routine lead smelting operations is present in lower concentrations, exists in a less soluble state and is associated with both a greater quantity and a greater variety of detrimental impurities. To cope with these problems, lead smelter practices are found

to follow the general outline:

Preparatory Processing

1. Concentration operations
2. Sulphation operations

Cadmium Plant Processing

1. Leaching operations
2. Purification operations
3. Sponge precipitation operations
4. Metal recovery operations
5. Refining and casting operations

As in the case of related zinc plant operations, cadmium recovery practices at lead smelters are not standardized. They not only vary as to type, but also extent. Depending upon prevailing conditions, lead smelter cadmium operations range from simple concentration campaigns, for the purpose of sufficiently "up-grading" products for shipment elsewhere, to complete processing steps for the production of refined metal.

Preparatory Processing

The cadmium content of lead smelter receipts is low and, as a rule, proportionate to the zinc content; the usual range of cadmium contained being of the order of 0.01-0.05 pct. Were it not for the low boiling point of cadmium, such small concentrations would, no doubt, be lost in the large tonnages of

slag, metal and other smelter end products. However, the ready volatility of cadmium and its compounds at prevailing lead smelting temperatures results in its concentration in fractional portions of fume collected. This collected fume comprises a circulating load within the smelter system.

Thus, the cadmium content of blast furnace fume* increases with each successive circulation until an equilibrium value is reached when the sum of the cadmium losses, due to handling and in slag, waste gases and other end products, becomes equal to the intake as ore. With ore receipts averaging, say 0.03 pct cadmium, the concentration value obtainable, through fume circulation in a routine manner, approaches 10-12 pct. In such operations, cadmium concentrations in blast furnace fume of from 3-5 pct are readily attainable. However, the concentration gain beyond this range, with each additional circulation, is progressively decreased as a result of mounting losses occurring through handling and in end products. Therefore, to avoid excessive cadmium loss and to enhance the ultimate concentration attainable, it is customary practice to isolate blast furnace fume at some intermediate cadmium content for special concentration procedure.

The most common type cadmium concentration "campaign" involves special smelting operations wherein a relatively high portion of blast furnace fume at 3-6 pct cadmium is incorporated into the sinter charge. This type practice is roughly illustrated by the diagram on p. 111.

Cadmium fume collected from lead blast furnace operations is not amen-

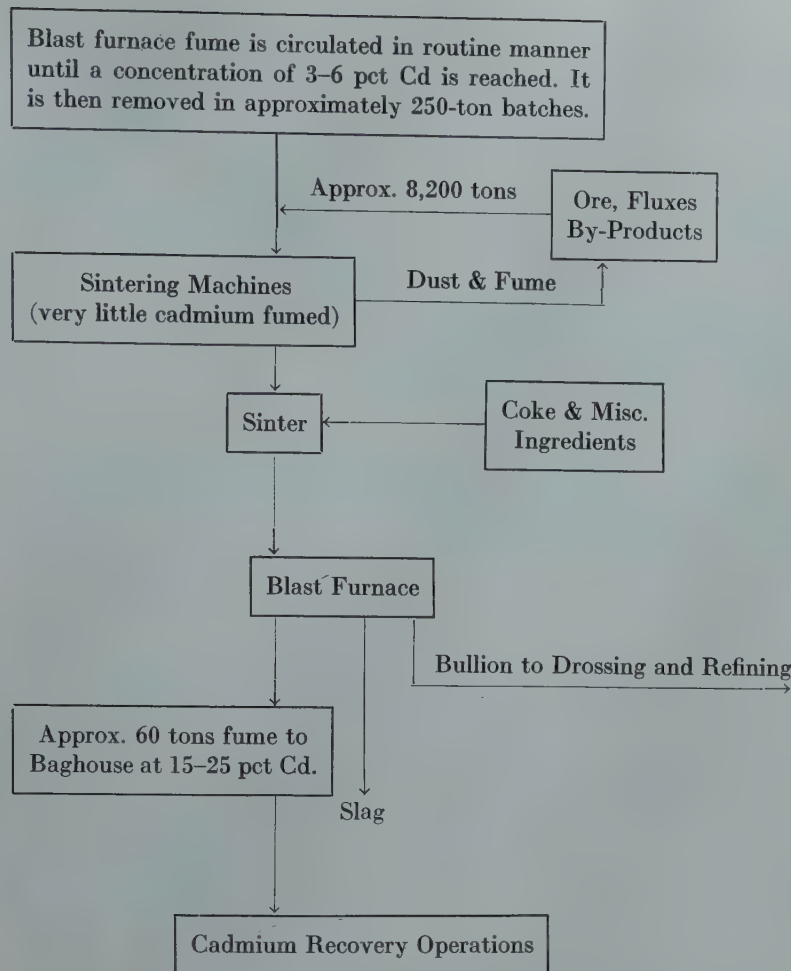
San Francisco Meeting, February 1949.

TP 25091D. Discussion of this paper (2 copies) may be sent to *Transactions AIME* before April 1, 1949. Manuscript received Sept. 20, 1948.

* General Superintendent and Metallurgist, respectively, Bunker Hill Smelter, Kellogg, Idaho.

† References are at the end of the paper.

* The relatively low temperature and contact time which prevails during sintering operations is not conducive to cadmium volatilization. Practically all cadmium elimination occurs during blast furnace smelting operations.



able to direct acid leaching. The cadmium contained is only partially soluble and the fume possesses a sort of "buffer" action which often limits the concentration of dissolved cadmium attainable. It is general practice in the processing of blast furnace fume to "precondition" by pugging with large portions of concentrated sulphuric acid, followed by heat treatment for elongated periods. While this sulphation step effects a high degree of solubility and greatly aids in impurity control, the attendant acid requirement is high and the physical aspects of the operation are not too desirable. At Kellogg, where acid is expensive, the Bunker Hill Smelter developed an alternative concentration procedure whereby a product of high cadmium concentration, amenable to direct acid leaching, is obtained by the fusion of blast furnace fume with silica.

In the fusion process, as in the more common method described above, blast furnace fume is circulated in the regular lead smelting system until a cadmium concentration of 4-6 pct is reached. It is then removed, mixed

with a siliceous flux and fused in a special reverberatory operation. During the fusion, the bulk of the cadmium is distilled and the bulk of the lead retained as a silicate slag. Lead silicate slag is tapped and returned to the blast furnace; the cadmium fume is bag filtered, then sacked for delivery to a cadmium leach plant. In reverberatory melting, the grade of cadmium fume produced is limited by the necessity of excessive temperature in the upper bath layer. However, by limiting the proportion of silica used, and with reasonable care to avoid over-firing, blast furnace fume of 4-6 pct cadmium content may be raised to a product of 30 pct grade.*

At this point in our presentation of cadmium recovery procedures, it should be stated that descriptive terms such as "common," "customary," and so forth, are only used in their most limited sense; departures from the

* In experimental tests under closely controlled temperature conditions such as are readily attainable in an electric furnace, cadmium fume of 60 pct grade has been produced from blast furnace fume containing 6-8 pct cadmium.

practices featured are many. Some of these diversions are itemized below:

TRAIL SMELTER—CONSOLIDATED MINING AND SMELTING CO. OF CANADA, LTD., TRAIL, B. C.

Cadmium-bearing fume from routine lead smelting operations, of 3-5 pct Cd. grade, is periodically forwarded to the zinc oxide leach plant and processed in conjunction with zinc fume from slag treatment operations. The insoluble lead-rich residue is subsequently returned to the lead smelting circuit.

FEDERAL PLANT—AMERICAN SMELTING AND REFINING CO. ALTON, ILL.

Up until 1941, at least, no special concentration campaigns were utilized. Blast furnace fume at about 5 pct cadmium was sulphated directly with concentrated sulphuric acid in preparation for subsequent leaching.

Some of the American Smelting and Refining Co. plants no doubt, practice cadmium concentration in accordance with an assigned patent² granted to R. Teats in 1930. This patent specifies the treating of a finely divided mixture of lead fluedust, carbonaceous material and limestone at 825-850°C to boil off cadmium which is oxidized and collected. The limestone, it is claimed, hinders the volatilization of lead and zinc.

PORT PIRIE WORKS—BROKEN HILL ASSOCIATED PTY., LTD., PORT PIRIE, AUSTRALIA¹

Blast furnace fume from routine lead smelting operations is continuously advanced to a central sump and agitated with water for the solution of fractional portions of the cadmium present. The pulp is then subjected to vacuum filtration, giving two products: (1) Residue, which is returned to the blast furnace and (2) Filtrate, which is treated with sodium carbonate for the precipitation of dissolved cadmium. The cadmium carbonate precipitate is filtered, dried and shipped to the Electrolytic Zinc Co. of Australasia, Ltd., at Risdon.

Survey of Cadmium Production Methods at Lead Smelters

As already indicated, lead smelter METALS TRANSACTIONS . . . 111

Table 1 . . . Outline of Representative Processes for the Production of Cadmium from Lead Smelter Fume

| Plant and Location | U. S. Smelting, Refining and Mining Co. Midvale, Utah | St. Joseph Lead Co. Herculaneum, Mo. | Bunker Hill and Sullivan Mining and Conct. Co., Kellogg, Idaho |
|---|---|---|---|
| Preparatory processing Concentration | Blast furnace fume is circulated in routine manner until reaching cadmium content of 3-6 pct. It is then removed and incorporated in relatively high proportions in sinter charge. Blast furnace smelting of resultant sinter gives a fume product containing 15-25 pct cadmium | Similar to Midvale practice | Blast furnace fume is removed from regular circuit at 4-6 pct Cd., then mixed with siliceous flux and fused in a reverberatory furnace. Furnace products consist of lead silicate slag (returned to blast furnace) and cadmium fume at 25-30 pct Cd. |
| Sulphation | Above fume is pugged with 60° Be H ₂ SO ₄ in batches (400 lb acid per 800 lb fume). After digestion period mixture is charged to furnace and baked 24 hr at low red heat, discharged, cooled and dry ground to 20-mesh in a 3 ft ball mill. | Fume at about 20 pct Cd. Pugged in batches with about 210 lb. 60° Be H ₂ SO ₄ per 500 lb fume. Mixture is charged in 2,000 lb batches to a pan mounted on wheels. Charged pan is rolled on tracks into furnace and baked (no rabbling) for 8 hr at 850°F, then discharged, cooled and broken, and pulverized to -100 mesh. | None |
| Cadmium plant processing Leach Purification | Joint leach and purification practiced. Minus 20-mesh sulphated product is leached with spent electrolyte for 2 hr in a 4 × 8 ft Pachuca tank. Na ₂ S is added to ppt. Cu and final slurry is neutralized with hydrated lime, then filtered and washed in a 2-ft sq. Shriver press. Washed cake is returned to lead smelting circuit. | Pulverized sulphated product is leached in a mechanical agitated, 2,000 gal capacity steel tank with wash water from previous filter operations, then filtered and washed in 3-ft sq. Shriver press. Washed cake returned to lead circuit. Filtrate is treated with a limited quantity of zinc dust for ppt. of Cu and then passed through a clarifier. | Joint leach and purification practiced. Concentrated fume is subjected to a direct dilute H ₂ SO ₄ leach, 800 lb H ₂ SO ₄ being consumed per 6,000 lb of 27 pct cadmium fume. Fe, Sb, As, etc., purification effected by the addition of copperas and oxidizer in conjunction with pH control. Slurry is filtered and washed in a 65 cf capacity Shriver press. Washed cake is returned to lead smelting circuit. |
| Sponge precipitation | None | Pregnant Cd filtrate is drawn from storage tanks through two 4 ft × 2½ ft × 30 ft deposition tanks—each tank containing 96 - 21 × 12 × 2 in. plates. Cadmium ppt. as metallic sponge on zinc plate surfaces. Sponge is removed from tank, dewatered by a rough initial press, then briquetted at high pressure into 8 in. diam × 1 in. thick cakes which are stored under kerosene. | Pregnant solution is drawn from storage tanks in 800 gal batches to a conical-bottomed, high-speed agitation tank. The solution is acidified and treated with zinc dust for Cd sponge precipitation. Initial sponge washing is carried out by decantation and the final dewatering and wash in a Shriver press. Cd sponge is briquetted directly with a Stokes machine. |
| Metal recovery | Pregnant cadmium solution at 120 gpl electrolyzed down to 35 gpl in a cascade, side circulation, cell circuit. Five aluminum cathodes and six durion anodes used in each of 10-30 in. sq. × 40 in. deep California redwood cells. Cathode trees removed each shift, cathodes stripped each 24 hr 78-80 pct Cd at 12 amp per sq ft. Plant capacity = 450 lb cathode cadmium per day. | Cadmium briquettes retorted. Graphite bottles and cast iron condensers used. 3 retorts utilized per 2,000 lb Cd per day. 12 hr retorting time consumed per 500 lb charge. | Cadmium briquettes are retorted, using similar bottles and condensers as employed at Herculaneum plant. Four retorts are used per 1,500 lb of cadmium per day. Retorting time per 600 lb charge variable, depending upon life of bottle and grade of briquettes. Retort residue returned to leach. |
| Refining and casting | No additional refining practiced. Cathodes are rolled and rough melted under cylinder oil and cast into bars. These bars are then melted under a light caustic cover for casting into shapes for market. | Crude retort metal is subjected to two treatments; the first with ZNCl ₂ for the removal of thallium. The TI-bearing ZnCl ₂ is marketed and the metal then treated with NaOH prior to casting into shapes for market. | Crude retort metal is melted under a caustic cover residual from a previous melt. This cover is then drossed and the bath agitated with NH ₄ Cl for thallium removal. The chloride dross is skimmed and stored. New caustic is then added and melted, followed by a brief period of agitation prior to casting into shapes for market. |
| Grade metal produced | | | |
| Copper | 0.0128 | Nil | 0.0002 |
| Lead | 0.0595 | 0.02 | 0.0130 |
| Iron | 0.0048 | | 0.0012 |
| Zinc | 0.0028 | 0.10 | 0.0150 |
| Thallium | | 0.02 | 0.0060 |
| Antimony, arsenic | | | Tr |
| Cadmium | | | 99.9646 |

cadmium operations vary, both as to type and extent. The tonnage intake is low and few smelters pursue operations beyond the concentration stage. Markets for resultant cadmium products of reasonable grade may be found in zinc and chemical industries, and the American Smelting and Refining Co. operate a custom cadmium plant at Denver, Colo. Cadmium bearing products from the various A. S. and R. smelting operations are shipped for treatment at the Globe Plant. Prominent among other lead smelters equipped for cadmium production are the U. S. Smelting, Refining and Mining Co. at Midvale, Utah,* the St.

Joseph Lead Co. at Herculaneum, Mo., and the Bunker Hill and Sullivan Mining and Concentrating Co. at Kellogg, Idaho. To a limited extent, in the past few years, the Bunker Hill plant has been operated on a custom basis.

Table 1 presents an outline of the essential processing steps employed in the three latter plants recorded above. This summary depicts a more or less representative composite of lead smelter practices. Among the component operations outlined may be found most processing steps employed for the recovery of cadmium from lead smelter fume. Though little information regarding recent practices at the Globe plant are available, earlier descriptions of H. R. Hanley³ and T. P. Campbell⁴ indicate no marked departures from the

practices summarized in Table 1. Since an intelligent discussion of a process requires intimate plant knowledge and an appreciation of prevailing plant conditions, any detailed considerations of the practices outlined must be limited to Bunker Hill operations. It is interesting to note, however, that the Midvale process, developed by R. H. Stevens,⁵ was placed in operation in 1915. This plant can probably be credited with the first production of electrolytic cadmium on a commercial scale.

Flow-sheet, Fig 1, was drawn from information supplied by the Bunker Hill Smelter and appeared in an article by John B. Huttie, "Bunker Hill Plant Recovers Metallic Cadmium from Fume," *Eng. and Min. Jnl.*, Apr. 1946, 174 No. 4, 82-85. It is reproduced by permission of *Eng. and Min. Jnl.*

* The Midvale Plant has not been operated since 1944.

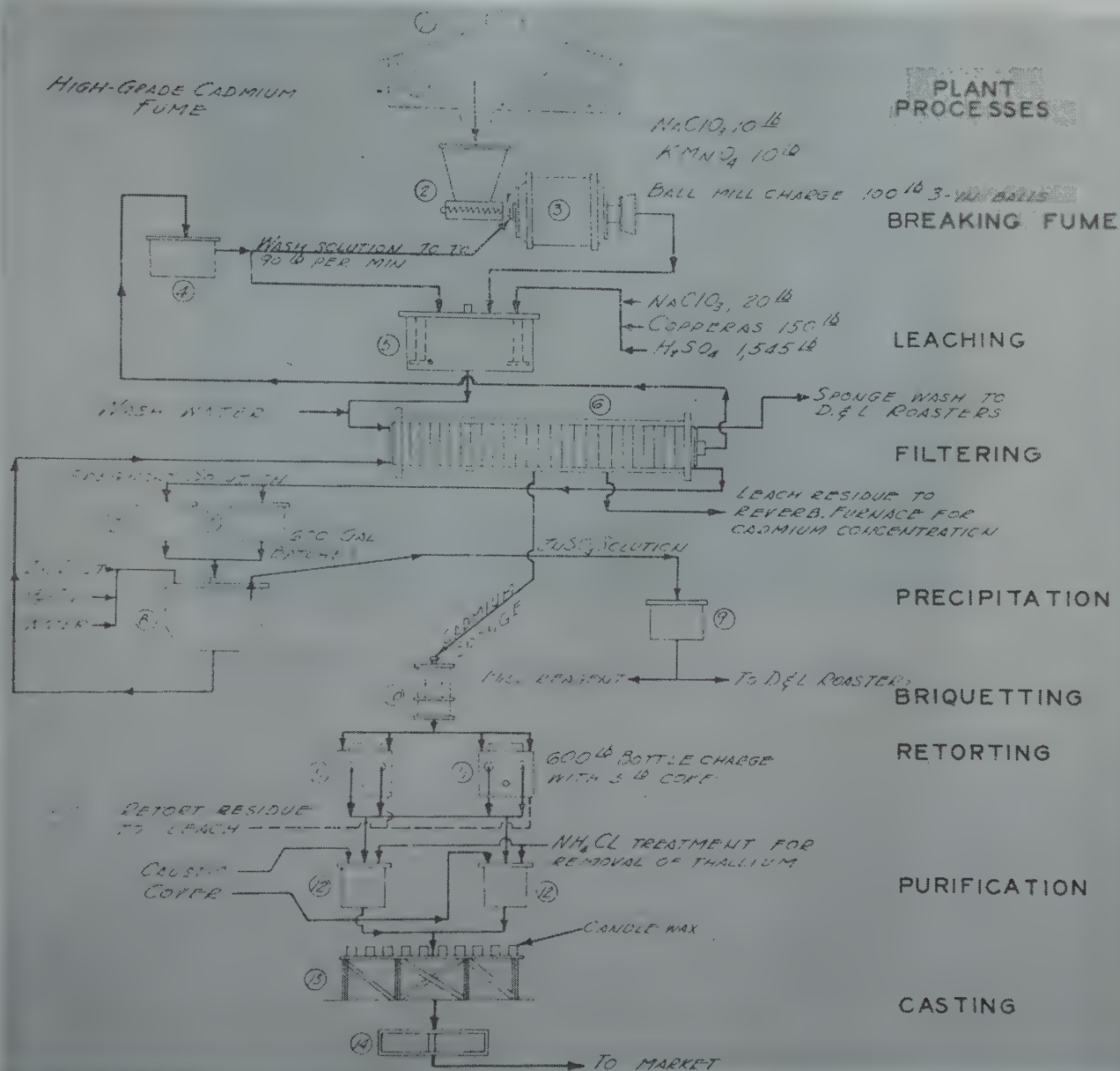


FIG 1—Flow sheet of Bunker Hill cadmium recovery plant.

1. Storage shed.
2. 6000 lb batch leach with screw feeder.
3. 3 × 3 ft ball mill.
4. Wash solution storage tank.
5. 8 × 8 ft lead-lined leach tank.
6. Shriver press, 42 2-in. × 3-ft × 3-ft frames.
7. 5000 gal pregnant solution storage tank.
8. 8 × 8 ft lead-lined precipitation tanks.
9. Zinc sulphate storage tank.
10. Briquette machine.
11. Two-bottle oil-fired retorts.
12. Holding pots, 3000-lb capacity.
13. Ten 4 × 16 × 3/4-in. molds.
14. Cleaning & boxing section.

Bunker Hill Cadmium Recovery Operations

GENERAL DISCUSSION

As already described under "Preparatory Processing" Bunker Hill Cadmium Plant feed consists of fume concentrated by a special reverberatory fusion of a mixture of blast furnace fume and siliceous flux. This product, produced under more favorable oxidiz-

ing conditions than practically attainable in a blast furnace, contains very little sulphide and is amenable to direct leaching in dilute sulphuric acid. As is illustrated by the accompanying flow-sheet, Fig 1, the process employed utilizes a combined leaching and purification operation, followed by sponge precipitation with zinc dust and final metal recovery by retorting. The particular type and sequence of methods depicted were selected after a long

experimental period during which many alternative practices were investigated.

Cadmium recovery obviously involves low tonnage operations wherein efficient processing is most essential to economic production. Processing efficiency is particularly important in the treatment of lead smelter fumes which generally contain high and variable percentages of troublesome impurities. In certain instances primary extraction becomes secondary to flow simplicity

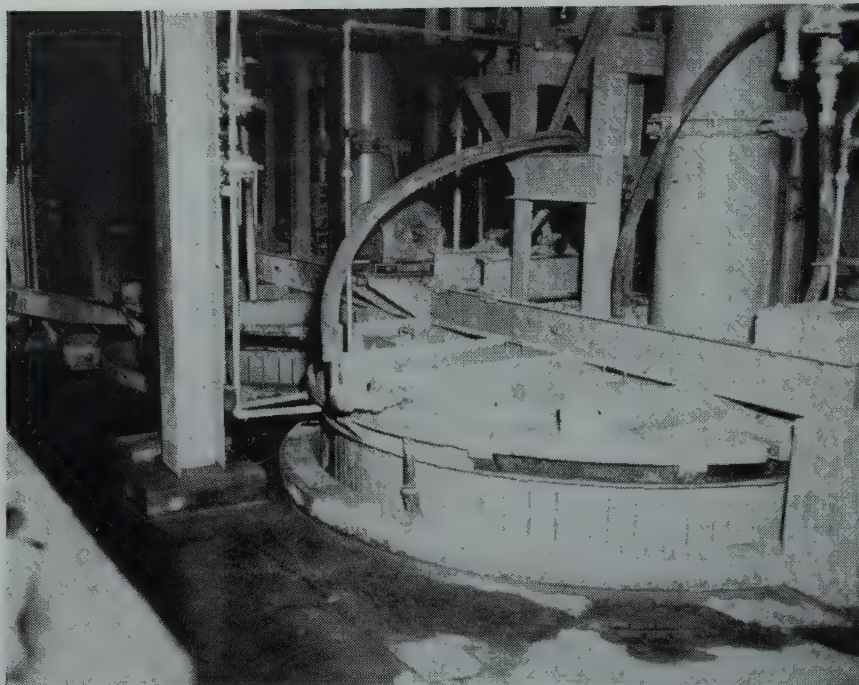


FIG 2—Cadmium leach and precipitation tanks—showing hodding and ventilation system.

and flexibility. In the development of Bunker Hill practice for example, experimental experience indicated that the increased primary extraction attainable by means of separate leaching and purification steps, would not justify the attendant complications of plant flow and the associated increased treatment and capital costs. Similar evaluations resulted in the choice of distillation procedure over electrolysis and sponge precipitation with zinc dust rather than on slab zinc as practiced at Herculanum. For the processing of Bunker Hill fume, the degree of impurity control necessary for successful electrolytic operations would require re-solution of a thoroughly washed sponge in a separate electrolyte circuit. Retorting procedure not only avoided this extra treatment, but also provided operations more readily adjustable to variable capacity conditions. Although the Herculanum type precipitation practice produces sponge of superior retorting grade, such a system would be very cumbersome in the processing of arsenic-bearing products where venting is necessary and every precaution to avoid arsine poisoning must be taken.

GENERAL PLANT DESIGN

The Bunker Hill Cadmium Plant represents a modern installation for the

processing of lead fume, having been placed in operation in June, 1945. It is a compact steel and concrete structure, constructed for the production of 1000 lb of cadmium per day when treating fume of 25 pct grade. Into its design were incorporated all practical facilities to provide both operational ease and favorable working conditions. Equipment units are conveniently located and served by an excellent ventilation system. Solution levels in tanks are observable from strategic points by means of electronic level indicators. Retort temperatures are automatically indicated and recorded, and semiautomatic temperature control with a fuel-air ratio controller, is provided. Both the upper floor, utilized for the receipt and storage of fume and reagents, and the lower floor from which end products emerge, are readily served by truck. Material passes by gravity flow through the leaching, precipitation and metal recovery operations conducted on intermediate levels.

LEACHING AND PURIFICATION PRACTICE

Referring to the accompanying flow-sheet (Fig 1), sacked cadmium fume is weighed and dumped into a steel bin which is screw-discharged into a 3 × 3 ft pulping ball mill located on the leach floor. Circulating wash solution meets

and carries the screw-discharged fume into the scoop box of the pulping mill from which it flows by gravity into a vented, lead-lined, 8 × 8 ft agitator tank. (Fig 2.)

Prior to the flow of ball mill slurry, a predetermined weight of concentrated H_2SO_4 is drawn into the leach-tank along with a small volume of wash water and the agitator started. To this strong acid mixture is then added copperas and sufficient sodium chlorate to oxidize the iron to the ferric state. About mid-run, to offset the reducing effects of fume ingredients, additional chlorate is added at the ball mill and at the close of the run, some potassium permanganate.

While reagent consumption varies widely with changes in fume character, the consumption when treating 6000 lb of 26 pct cadmium grade fume* may be roughly recorded in the range of:

| REAGENT | POUNDS |
|------------------------|--------|
| 60° Be H_2SO_4 | 800 |
| Copperas..... | 200 |
| Sodium Chlorate..... | 30 |
| $KMnO_4$ | 10 |

About two hours is required to pulp 6000 lb of fume. Then, after a short period of additional agitation, the slurry is sampled for acidity. If its pH value runs much lower than 5.3, as shown by a Coleman pH tester, addi-

* Reagent proportions shown on the flow-sheet are for the treatment of high-grade cadmium fume (approx. 45 pct Cd).

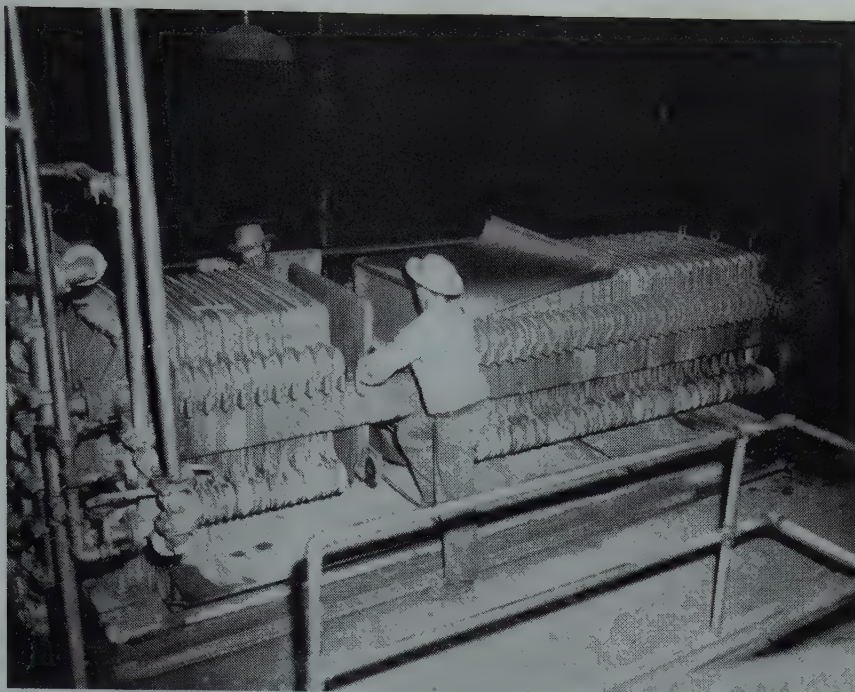


FIG 3—Sixty-five cubic foot capacity Shriver press—utilized for both cadmium leaching and precipitation operations.

tional fume is added. Upon reaching the required acidity range, a filtrate sample is assayed for arsenic. When the arsenic assay shows the presence of less than 10 mg per liter, the slurry is diluted to about 1700 gal and pumped through a 65 cf capacity, closed delivery Shriver press, (forty-two 2 in. \times 3 ft square frames used), to one of two 5000 gal lead-lined, pregnant solution storage tanks. Seventeen hundred gallons of slurry results in about 1500 gal of pregnant solution. One leach cycle is completed per 2-man shift and about 10,000 gal of pregnant solution is obtained in six shifts' operation.

Purification is accomplished through the use of oxidizers and by pH control. Though copperas aids in arsenic removal; considerable arsenic precipitates as a cadmium compound, and the primary extraction attainable varies as the cadmium arsenic ratio; this ranges from a low of about 75 pct for products containing about 6-7 pct As to around 90 pct for products down to 3 pct As. Neutralization to a pH of 5.3 permits practically complete arsenic precipitation. While operations in a higher acidity range allow higher primary extraction, the arsenic purification problem is greatly complicated.

The leach residue is washed in the filter press with about 1500 gal of water which is pumped to an 8 \times 8 ft lead-

lined storage tank for use as make-up solution in a succeeding leach. Upon breaking the filter-press, the washed and blown residue is dropped through a chute to a concrete storage bin on the lowest plant level. From this bin it is conveyed back to the lead smelting circuit, wherein lead is recovered and the cadmium returned to the circulating fume load. (Fig 3.)

SPONGE PRECIPITATION PRACTICE

After two leach days, during which the solution of 8000 to 10,000 lb of cadmium is effected, the crew turns to precipitation operations. Stored pregnant solution, now of known cadmium content, is drawn in 600-800 gal batches into a lead-lined, conical-bottomed precipitation tank served by a high-speed agitator. As in the leach system, this tank is hooded and positively vented by means of a 6400 cfm fan. The vented tank atmosphere is conveyed and discharged into the blast furnace flue system. In this manner, possible hazardous concentrations of arsine are speedily removed and diluted to harmless proportions with 150,000 cfm of blast furnace gas.

Each batch of solution for precipitation is acidified by the addition of H_2SO_4 , to about 4.5 grams acid per

liter. Then, zinc dust is charged in the proportion of about 0.62 lb zinc per lb of cadmium contained. Electro-positive zinc displaces cadmium from solution with the production of cadmium sponge. The action, induced by high-speed agitation, breaks and rolls the sponge masses into dense pellets favorable to washing by decantation. To prevent the precipitation of basic sulphate salts, the solution acidity is not allowed to fall below 2.0 grams per liter and zinc additions are terminated when the solution assay shows a cadmium content below 0.5 grams per liter. At this point, the agitator is shut off, the pellets allowed to settle, and the clarified $ZnSO_4$ solution decanted and pumped to a strong zinc solution storage tank for marketing to the flotation mills of the district. The settled cadmium is then washed by dilution with water and agitation before being pumped to the Shriver press; the filtrate going to a weak $ZnSO_4$ storage tank for delivery to D and L sintering operations.

About 9 similarly treated precipitation batches are accumulated in the filter press prior to a final wash with water. The press is then blown with air until warm, broken, and the contents discharged to a steel storage bin on the retort floor below. To avoid excessive cadmium oxidation, briquetting op-

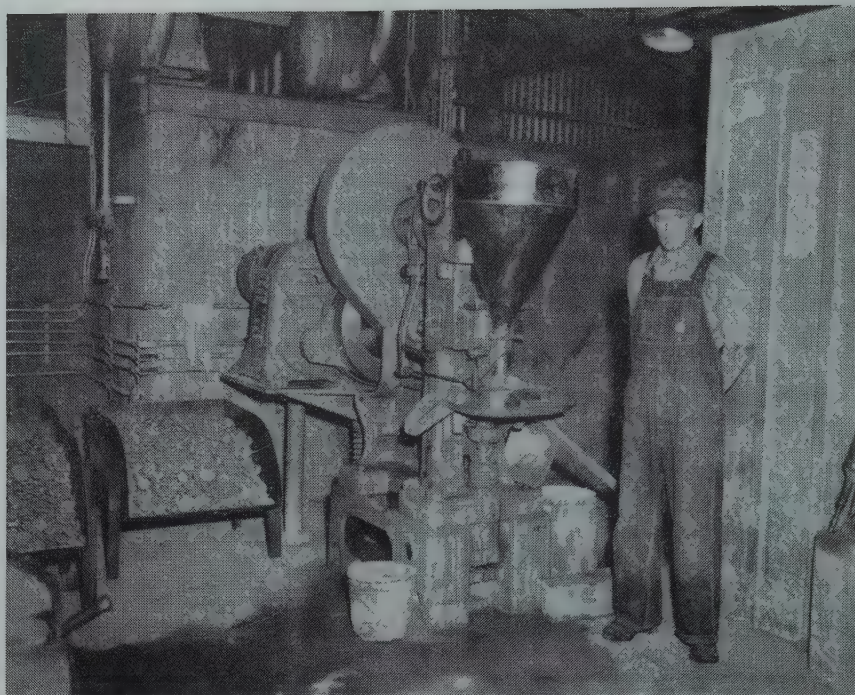


FIG 4—Stokes briquetting machine showing cadmium briquette storage pans.

erations are started soon after a press discharge.

METAL RECOVERY OPERATIONS

Sponge briquetting, with no additive agents and no prior treatment other than granulation through an 8-mesh screen, is practiced. The screened sponge is charged to the hopper of a Model R Stokes machine. The sponge is dewatered and its density increased about three times, by compression under 17 tons pressure, into 2 in. diam by $\frac{1}{2}$ in. thick briquettes. The compressed discs discharge into steel storage pans at the rate of about 1000 lb per hr. Each storage pan has a capacity equivalent to that of a retort bottle. They stand off the floor on legs to permit ready transfer to the retorts by lift truck. (Fig 4.)

Two oil fired retort units are employed for cadmium distillation from briquetted sponge. Each retort unit is of firebrick construction and contains two No. 11 American Crucible Co. graphite bottles set on piers above a brick checker-work arch, which distributes the heat from the firebox below. The retort bottles are manually charged, 600 lb per bottle, 1200 lb per retort unit.

After being charged, portable, partially insulated, cast iron condensers, which fit about the extended neck of the retort bottles, are rolled into place and the bottle-condenser junction sealed with fireclay. The closed, outer

ends of the cylindrical condensers have two $\frac{1}{2}$ -in. holes. The bottom hole is immediately sealed with clay and only opened when tapping metal. The upper hole is kept open for an hour or so after the start of a run to permit the escape of moisture and other gases noncondensable at elevated temperatures. When cadmium vapor is evidenced, the upper hole is sealed.

While the retorting cycle is a variable depending upon the bottle life and briquette character, the average time consumed approaches 20 hr. A description of Bunker Hill retorting practice is as follows:

With the condensers pulled aside, the briquette storage pans are moved to the retorts and the contents shovelled into the bottles. The condensers are then rolled into place and the junctions sealed with clay. Next, the firing is stepped up and the firebox temperature brought to, and maintained at, 2100°F. After about $1\frac{1}{2}$ hr heating, cadmium starts to distill and the upper vent holes are sealed. From then on, at three-hour intervals, the condensers are tapped and the condensed, molten cadmium drawn into steel pans. When the charge is "cooked" as evidenced from the quantity of metal drawn, the condensers are pulled away and the bottles raked clean for the receipt of the succeeding charge.

Retort residue is returned to the leach circuit and the crude metal is charged to one of two pots utilized for refining and casting. Depending upon

bottle life and the grade of briquettes, the operation of two retort units (four bottles) allows a crude metal production of from 1400 to 2000 lb of cadmium per day. (Fig 5.)

REFINING AND CASTING PRACTICE

Two 3000-lb capacity, electrically heated kettles are used for both refining and casting. One pot is being either held or used for casting while the other is being charged for refining. Refining operations are chiefly concerned with thallium removal. The crude retort metal produced meets all impurity specifications except for lead and thallium. All metal is treated for thallium removal; occasional lots destined for sale to bearing manufacturers must be redistilled to meet lead specifications.

Crude retort metal is charged to one of the two kettles and melted under a thin caustic cover. When the kettle is full, the caustic cover is skimmed and 30 lb of ammonium chloride is agitated into the bath over a $\frac{3}{4}$ -hr period. The chloride dross is then removed and 20 lb of new caustic added. About 15 min. additional agitation is given as a precaution against zinc contamination. At this point the agitator is removed and the metal ready for casting.

Refined metal is drawn, by means of a screw-operated valve, through an outlet in the kettle bottom into a casting ladle that is heated by means of a kerosene torch. It is cast into shapes

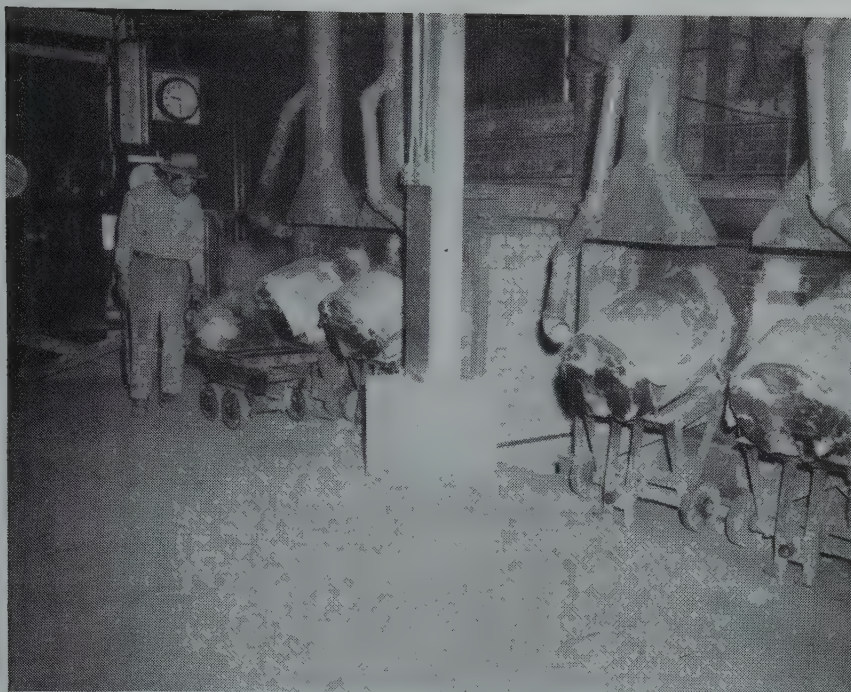


FIG 5—Bunker Hill cadmium retort installation—showing condenser in place and tapping operations.

for marketing in vertical, air-operated molds. The solidified shapes (slabs, balls, sticks) are given a dilute hydrochloric acid dip and wiped dry before weighing and boxing for shipment.

Cadmium Metal Marketing

There are no A. S. T. M. Cadmium specifications. Although attempts have been made in recent years to establish market requirements of more restricted and uniform nature, standardization has not yet been realized. In general, platers are rather lenient with regard to lead (0.05 pct max.) but are insistent on limiting the thallium content to 0.005 pct. The bearing manufacturers, on the other hand, are willing to accept up to 0.05 pct thallium but limit the lead content to 0.02 pct. Some of the diversified marketing specifications are illustrated in Table 2.

As pointed out by John L. Bray,⁶ cadmium is technically one of the younger metals. Although known since 1818, until comparatively recent times there have been but few uses for cadmium. Prior to 1925, the bulk of the world's cadmium was produced in Germany. Production in the United States, at that time, ranged between 25 and 100 tons per year. Concurrent with the use of cadmium as a plating medium, principally in the automotive industry, a marked growth occurred in U. S. production. By 1939, the United States became the world's largest producer.

While up-to-date statistics are unavailable at this writing, evidence points to a 1948 U. S. production approaching the 1947 total of 4,000 tons metallic cadmium. This production is somewhat under the war-time high of 4,300 tons, a decline that parallels a 10 pct decrease in zinc production from its war-time peak. At 4,000 tons per year, metallic cadmium production appears to be somewhat in excess of current domestic requirements. The pattern of current domestic consumption is of the following order:

| | Pct |
|----------------------|-----|
| Electro-plating..... | 75 |
| Bearing alloys..... | 15 |
| Solder alloys..... | 5 |
| Pigments..... | 2 |
| Chemical..... | 2 |
| Miscellaneous..... | 1 |

It is interesting to note that the foregoing pattern is not typical of

Table 2 . . . Marketing Specifications

| BUREAU OF FEDERAL SUPPLY | | Pct |
|------------------------------------|------------|-----|
| Cadmium..... | 99.90 min. | |
| Copper..... | 0.10 max. | |
| Iron..... | 0.01 max. | |
| Lead + silver + tin..... | 0.01 max. | |
| Zinc..... | 0.05 max. | |
| Antimony + Arsenic + Thallium..... | 0.005 max. | |
| PLATING INDUSTRY | | |
| Cadmium..... | 99.90 min. | |
| Lead + Silver + Tin..... | 0.05 max. | |
| Antimony + Arsenic + Thallium..... | 0.005 max. | |
| BEARING MANUFACTURER | | |
| (A) | | |
| Cadmium + Zinc..... | 99.90 min. | |
| Zinc..... | 0.10 max. | |
| Copper..... | 0.02 max. | |
| Lead..... | 0.02 max. | |
| Bismuth..... | 0.01 max. | |
| Antimony..... | 0.01 max. | |
| Tin..... | 0.005 max. | |
| (B) | | |
| Cadmium..... | Remainder | |
| Copper..... | 0.40-0.60 | |
| Silver..... | 0.60-0.80 | |
| Nickel..... | 0.25 max. | |
| Lead..... | 0.05 max. | |
| Zinc..... | 0.05 max. | |
| Tin..... | 0.02 max. | |

foreign consumption. Abroad there is a more extensive use of cadmium in alloys and less in plating. About 10 pct of foreign consumption is also utilized in the manufacture of cadmium-nickel batteries for industrial and railroad units. This type battery has not been extensively used in this country, although within the past few years a small company in New England is reported to have started production.

Acknowledgments

The writers are indebted to Mr. Robert Wallace, Manager, Mr. W. M. Whitecotton, Asst. Smelter Supt., U. S. Smelting, Refining and Mining Co., Salt Lake City, Utah, and to Mr. W. T. Isbell, Supt., St. Joseph Lead Co., Herculaneum, Mo., for information used in references to their respective operations. Credit is also due Mr. C. R. Ince, Manager, Metal Sales Department, St. Joseph Lead Co., New York City, for the provision of cadmium production and marketing details.

References

1. *Proc. Australasian Inst. of Mining and Metallurgy*, (1932) 126.
2. U. S. Patent 1,727,492, Sept. 10, 1930.
3. H. R. Hanley: *Mining and Sci. Press* (1920) 121, 795.
4. T. P. Campbell: *Colo. School of Mines Mag.* Oct. 1930, 26-27.
5. U. S. Patent 1,194,438, Aug. 15, 1916.
6. John L. Bray: *Non-Ferrous Production Metallurgy*. (1941), 64, New York, N. Y.—John Wiley and Sons, Inc.

Development of Muffle Furnaces for the Production of Zinc Oxide and Zinc at East Chicago, Indiana

GUNNARD E. JOHNSON*

Introduction

THE problem of efficient reclamation of zinc base die cast scrap became interesting early in 1930. Die Cast Metal, as referred to in this paper, is a zinc base alloy with various proportions of aluminum, copper, magnesium, antimony and tin.

Many attempts were made to work out some means of reclaiming the discarded die cast metal for re-use as new die cast metal. Difficulties in such reclamation were attributable to contamination by lead and tin from solder, chromium and nickel from electroplated coatings, and iron from iron inserts.

This paper relates the experiments that led to the development of a specialized muffle furnace for the treatment of zinc base die cast scrap for the production of zinc oxide and zinc, and describes the development of the muffle furnace and the equipment now used commercially for these purposes. The Eagle-Picher Co. acquired all patent rights¹ for these developments from the International Smelting and Refining Co. in connection with their purchase of the East Chicago Plant.

Zinc Base Scrap Situation

About 1935, the die cast scrap situation became increasingly acute for scrap dealers. This scrap was accumulating from dismantling automobiles and household appliances which contained die cast parts. Efforts to find an outlet for this type of scrap were intensified.

The International Smelting and Refining Co. began to study the possibilities of a commercial process for the recovery of values from die cast scrap. At that time most of the die cast metal

Table 1 . . . Distribution of Products Produced by Melting Die Cast Scrap

| | Weight in Lb | Per Cent of Weight Charged | Per Cent Zinc | Lb Zinc | Per Cent of Zinc Charged |
|---------------------------|-----------------|----------------------------------|------------------|---------|--------------------------------|
| Charged | | | | | |
| Scrap as received..... | 320,073 | 100.0 | 76.6 | 245,176 | 100.0 |
| Products | | | | | |
| Die Cast Slabs..... | 246,790 | 77.1 | 90.1 | 222,358 | 90.7 |
| Melting Dross..... | 35,620 | 11.1 | 55.1 | 19,627 | 8.0 |
| Iron Rejects..... | 36,491 | 11.4 | 10.0 | 3,649 | 1.5 |
| Ignition Loss..... | 1,172 | 0.4 | 0.0 | | |
| Unaccounted for Gain..... | | | | -458 | -0.2 |
| | 320,073 | 100.0 | | 245,176 | 100.0 |

reclaimed was melted down in small kettles of from one to five tons capacity, the iron inserts being removed by skimming. The dross was skimmed off and disposed of as a zinc dross. The drossed metal was cast into slabs and was given the trade name "die cast slabs." Distribution of the products produced by melting die cast scrap in kettles is shown in Table 1.

American Process Experiments

A method considered for the production of zinc oxide from die cast scrap was an adaption of the standard American Process of zinc oxide manufacture. Thus some die cast scrap was mixed with oxidized zinc materials and charged to Wetherill grates. The zinc oxidized to zinc oxide but, while the aluminum and copper largely remained in the residue, the color of the zinc oxide produced was impaired by copper contamination. As the proportion of

die cast scrap was increased, liquation took place; that is, the metal trickled through the charge then solidified in the openings of the grates.

French Process Experiments

Several hundred tons of die cast scrap were purchased for test purposes and converted into die cast slabs. These slabs were charged into a French Process (horizontal retort) zinc oxide furnace with some electrolytic zinc. A satisfactory grade of zinc oxide was not produced.

Distillation in Belgian Retorts

It was then decided that, rather than attempt to use scrap die cast metal or scrap zinc for the production of zinc oxide, it would be advisable to redistill the die cast slab metal in a Belgian retort furnace.

The opportunity to do so was provided by the closing of the zinc smelter of the Illinois Zinc Co. at Peru, Ill. Arrangements were made for the operation of a Belgian retort furnace for such redistillation purposes. The results of this experiment are summarized in Table 2.

San Francisco Meeting, February 1949.

TP 2526 D. Discussion of this paper (2 copies) may be sent to *Transactions AIME* before May 15, 1949. Manuscript received October 4, 1948.

* General Manager—East Chicago, Indiana, Plant of the Eagle-Picher Co.

¹ References are at the end of the paper.

Table 2 . . . Results of Experiment

| | Weight in Lb | Per Cent Charged |
|-----------------------------|-----------------|---------------------|
| Metal Charged..... | 2,778,541 | 100.0 |
| Production | | |
| Redistilled Metal..... | 1,684,913 | 60.7 |
| Metal from Blue Powder..... | 518,711 | 18.6 |
| Residue Metal..... | 218,287 | 7.9 |
| Loss..... | 356,630 | 12.8 |

All of the zinc produced contained varying amounts of copper, tin and aluminum in sufficient quantities to make it unmarketable. The metals produced, however, were found satisfactory for use in making zinc oxide provided the quantities used were limited to a small fraction of the total metal charged.

Distillation in Graphite Retort Bottles

Some attempts were made to treat die cast scrap in graphite bottles to produce zinc. Very little success resulted from these attempts because graphite bottles had a short life. Also the relative position of the condenser with reference to the retort permitted the condensing metal to contact, and become contaminated with, aluminum and copper.

The next experiment was to produce zinc oxide from the die cast scrap charged to graphite retorts. The zinc oxide produced was conveyed directly to a baghouse by means of a fan and duct system. This zinc oxide was unsatisfactory because of the high copper content and very poor color. Further, contamination with lead and aluminum took place; these elements being mechanically carried into the baghouse when the mouth of the retort bottle was cleaned or when the charge of residue left in the bottle was poured into molds.

It was finally concluded that recognized processes for production of zinc or zinc oxide were not satisfactory for the treatment of die cast metal. Some new approach to the problem was needed.

Experimental Muffle Furnaces

Initial investigation began with the use of a laboratory muffle furnace. This was a rectangular muffle constructed of carborundum tile cemented at the joints. Attempts were made to hold the

level of liquid metal at not over 2 in. in depth. Even with this small depth of metal, serious leakage occurred.

At about the same time, a pilot unit was constructed which provided means for heating the metal bath from above and below. Heat was introduced below the bath by means of a gas flame within a refractory tunnel. This furnace leaked badly after every effort had been made to make it tight enough to contain molten die cast metal.

Shortly afterward a larger experimental unit 5 ft long with a carborundum arch 3 ft wide was built and tested. This unit is illustrated in Fig 1 which shows cross-sectional and longitudinal-sectional views of the furnace.

This pilot unit established the fact that zinc could be vaporized, practically, by means of a large shallow bath and that such vaporizing is less violent and more easily controlled than in the more restricted areas of small retorts.

This furnace provided a monolithic hearth construction arranged within a steel shell to confine the molten metal against escape and loss. Also, operation of the furnace confirmed calculations that it was practical to apply heat to the bath, from above, through a carborundum arch. The zinc vapor did not seep through the carborundum arch.

The metal was charged into the furnace through two small openings in the vaporizing chamber just below the arch. Zinc vapors were conveyed by a short horizontal brick flue to a chamber. Oxidation of the metal vapor to zinc oxide took place at the brick chamber from which the zinc oxide was conducted to a baghouse through a steel flue. This furnace established operating characteristics of the larger furnaces later constructed and pointed out the need for a substantial arch anchorage and related construction problems.

Our experience with these furnaces indicated that satisfactory commercial operations would not be achieved until an integrated unit was produced, having a tight hearth, a tight arch, and

adequate provisions for keeping the zinc or scrap metal heated to the desired temperature, in conjunction with a vaporizing unit from which zinc vapors would be discharged rapidly and at uniform rate. Analysis of experimental operations also led us to believe that commercial operations could proceed upon development of effective means for excluding air from the vaporizing chamber within which the molten bath was being heated. Any air entering this area would react with the vapors to form an oxide film or layer, which inhibits heat transfer to the bath of molten zinc, thus gradually impeding the liberation of zinc vapors from it. This factor was a principal cause of the decline in rate of oxide production soon after the start of operations in the experimental muffle units. It was recognized at the time that the results obtained in small scale equipment would not necessarily be predictive of those obtainable with a larger furnace. However, contemplation of a large scale unit introduced additional questions in respect to confinement of a large bath of molten zinc against escape. A further problem was the accommodation of expansion, under air-seal conditions, of a commensurately large arch capable of sustaining the relatively high temperatures involved.

To meet these requirements, the later design of our commercial furnaces at East Chicago was predicated upon the provision of a monolithic hearth construction arranged within a steel shell to confine the molten zinc against escape and loss. Above the hearth, the arch was sprung from skewbacks along the side walls longitudinally of the furnace whereby widthwise expansion of the arch could bow it without impairing the air-tight seals provided at the skewbacks. At the ends of the furnace, the arch extended into pockets or recesses of the end walls which in turn were filled with an elastic or yieldable cement capable of maintaining an air seal while allowing the expansion movements of the arch. Continued operations over a number of years have

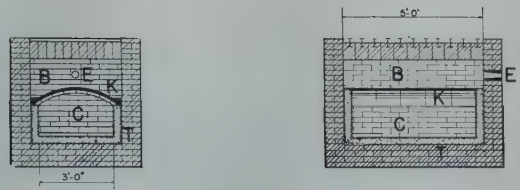


FIG 1—Experimental muffle furnace.

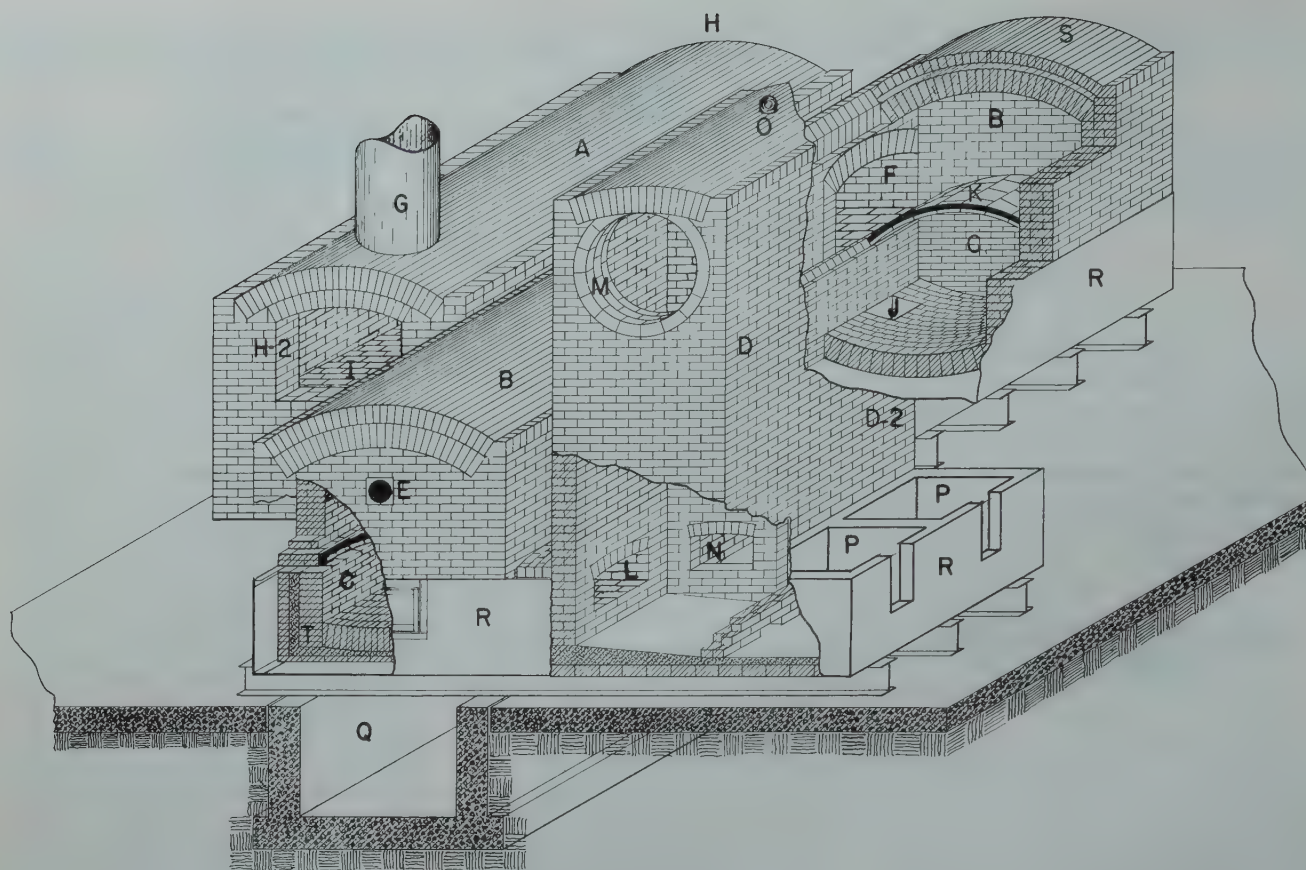


FIG 2—Improved muffle furnace.

Table 3 . . . Results Obtained with Melting Unit

| | Weight in Lb | Per Cent of Weight Charged | Per Cent Zinc | Lb Zinc | Per Cent of Zinc Charged |
|---------------------------------|-----------------|----------------------------------|------------------|---------|--------------------------------|
| Charged | | | | | |
| Die Cast Scrap as received..... | 502,821 | 100.0 | 78.2 | 393,206 | 100.0 |
| Produced | | | | | |
| Metal to Vaporizing Unit | 398,235 | 79.2 | 88.2 | 351,243 | 89.3 |
| Melting Dross..... | 53,299 | 10.6 | 62.0 | 33,045 | 8.4 |
| Iron Rejects..... | 44,751 | 8.9 | 15.0 | 6,713 | 1.7 |
| Unaccounted Loss..... | 6,536 | 1.3 | | 2,205 | 0.6 |
| | 502,821 | 100.0 | | 393,206 | 100.0 |

proven these principles to be effective and reliable.

Commercial Muffle Furnace

The first commercial unit, producing 5 to 7 tons of zinc oxide per day, was equipped with a vertical riser. This brick riser received zinc vapors from the vaporizing chamber and provided for contact of zinc vapor and air to produce zinc oxide. The zinc oxide was conveyed through a steel duct into a baghouse.

In the operation of the first commercial furnace, the die cast scrap was first

melted in kettles (heated by waste heat) to facilitate removal of unmeltables. These kettles were located in a manner that permitted the molten metal from the kettles to overflow into a sealed opening leading into the vaporizing unit. This practice was not satisfactory because of short kettle life.

Later furnaces embodied melting units consisting of a welded steel shell lined with fire brick to enable melting of the scrap continuously on a molten bath. The die cast scrap was charged onto this molten bath. This proved to be more efficient than kettle melting providing the temperature was adequately controlled.

The melting unit now in use consists

of a sloping hearth inclined toward a central point, which discharges into a trough to the vaporizing unit. With controlled melting unit temperatures, the oxidation of zinc is maintained at a minimum. The results obtained with this melting unit are shown in Table 3.

Muffle Furnace

Assembly drawing Fig 2 and sectional views (Fig 4, 5 and 6) along planes as indicated in the plan as shown in Fig 3 may be helpful in a more detailed study of the furnace design. The letters apply to Fig 1 to 6 inclusive.

- A—Melting Unit
- B—Combustion Chamber
- C—Vaporizing Chamber
- D—Riser
- D2—Condenser

The furnace is fired by oil burners at *E* into the combustion chamber *B* which connects through duct *F* with melting unit *A* and combustion gases are vented through stack *G*. The flow of metal through the furnace is counter-current to the flow of gases. The zinc-bearing material is charged through door *H* (not shown) onto the melting

unit hearth *I* which is considerably above and to one side of the bottom of vaporizing chamber *C*. The molten charge drains from the hearth *I* of the melting unit which is pitched toward the center, through a duct entering the vaporizing chamber at point marked *J*. Means for drossing are provided between hearth *I* and outlet *J*. Unmeltables, such as iron inserts, and the like, are raked from the hearth of the melting unit through door *H2*. It will be noted that the combustion chamber *B* is separated from the vaporizing chamber *C* by a comparatively thin arch *K* to expedite the flow of heat from the combustion chamber into the vaporizing chamber. This arch is made up of standard commercial sizes of carborundum blocks. The arch extends into recesses of the end walls which are filled with an elastic material, forming a seal, and providing for expansion.

Under the proper conditions of temperature and pressure, zinc vapors are produced in chamber *C* which flow through opening *L* in the vaporizing chamber into the riser *D*. These vapors may be burned to zinc oxide as they escape from riser *D* through opening *M* to a zinc oxide collector. This assumes that opening *N* is closed. If it is desired to condense the vapors as metallic zinc, *N* is opened permitting the vapors to enter the condenser *D2*. The condenser may be laid up of carborundum brick which aids in condensing the zinc vapors to metallic zinc due to its high heat conductivity. Pressure, if it becomes excessive, is relieved by ball *O* resting on an opening into the condenser. Zinc wells marked *P* are used for tapping condensed metal.

Vaporizing chamber, condensers and zinc wells are all encased in a steel shell marked *R* which rests on supporting I-beams. The arch and side walls of combustion chamber *B* are constructed of a special high grade refractory. An insulating arch *S* covers the combustion chamber. Referring to the front of the vaporizing chamber *C* beneath the oil burner *E* it will be noted that the pan is first lined with a layer of fire brick, upon which is placed refractory concrete, designed to tighten the furnace against the flow of metallic zinc through brickwork *T*. The inverted arch and side walls of the vaporizing chamber *C* are constructed of high quality fire brick. The bottom arch of vaporizing chamber *C* pitches slightly to one end to assist in tapping metal from this chamber. Opening *Q* allows for atmospheric cooling of the furnace bottom

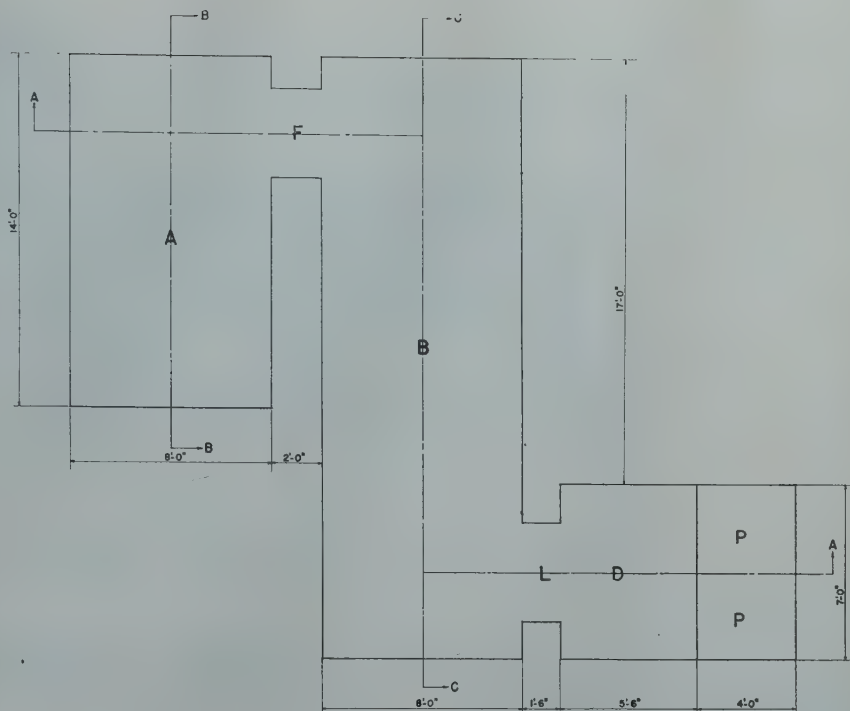


FIG 3—Plan of muffle furnace showing sections.

and provides for inspection of the bottom of the furnace pan.

Metallic Zinc is produced in the Muffle furnace by closing the opening *M*, used in producing oxide and open-communicating door *N* connecting condensers *D* and *D2*. Drains to zinc wells *P-P* are also opened.

This type of furnace construction provided for: Prevention of leakage of molten zinc by means of a monolithic hearth within a steel shell. Escape of vapors and infiltration of air by a tight arch fully sealed throughout its length and breadth and at the points where the arch joined the furnace. Pressure build up within the vaporizing chamber to permit the desired flow of zinc vapor to the riser and condenser. (Fig 7.)

Operating Procedure

The furnace is preheated with a gas flame, gradually raising the temperature to 1600°F. The oil burners are then started and the temperature of the combustion chamber elevated to 2400°F. Preheating requires about ten days.

Charging of metal is started at 2400°F and the production of zinc vapor begins almost at once. Charging is continued at as rapid a rate as possible until a depth of 5½ in. of metal has accumulated in the vaporizing unit.

This accumulation of metal in the bath is exclusive of the metal vaporized during this period. Charging of die cast metal continues at a rate that will increase the depth of the metal in the vaporizing chamber about one inch for each 24 hr of operation until a total depth of 10 in. of metal is reached. This generally requires from six to ten days, depending on the zinc content of the metal charged. Where a high purity zinc is charged exclusively, the cycle may be extended to as much as 60 days without removal of residue metal.

Conditions which determine the end of the cycle are: The rate of zinc vapor production for economical operation of the furnace, a low zinc content in the residue metal, as tapped from the furnace, and a lead content low enough to meet the requirements of the particular zinc oxide being produced.

The cycle is ended by tapping residue metal from the vaporizing chamber, emptying it as far as possible. This metal is drained through a tap, not shown, into cast iron molds. The temperature of the furnace is held constant while it is being drained.

Furnaces have been operated for 72 cycles such as described above. This represents a continuous operation of approximately two years. The economical life of the furnace is determined by the heat transfer efficiency of the carborundum arch.

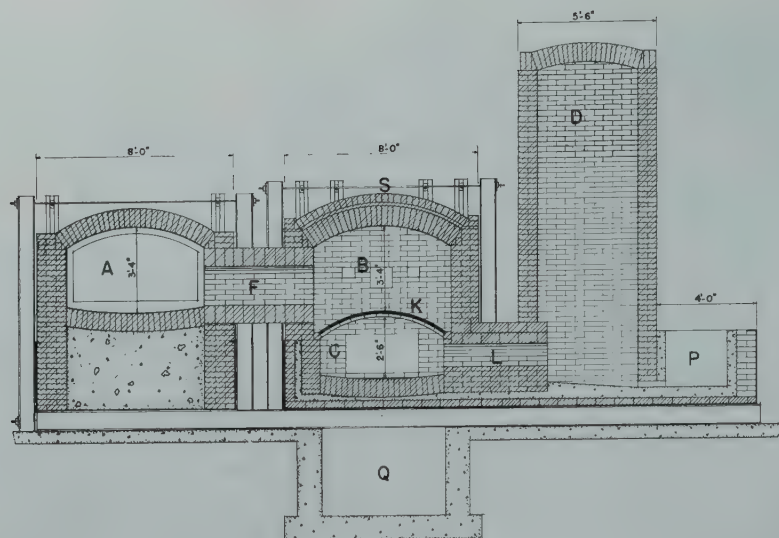


FIG 4—Muffle furnace section on line A-A.

The rate of heat transfer is reduced by: Accretions of zinc oxide which accumulate beneath the carborundum arch, an accumulation of slag on top of the arch and a gradual change in the composition of the arch.

Major furnace repairs are required every two years.

Table 4 . . . Typical Muffle Furnace Zinc Oxide

| | Lead Free | Red Seal | Green Seal | White Seal | U.S.P. |
|---------------------------|-----------|----------|------------|------------|--------|
| Zinc Oxide—ZnO (Pct)..... | 99.1 | 99.2 | 99.3 | 99.3 | 99.3 |
| Lead—Pb (Pct)..... | 0.25 | 0.10 | 0.07 | 0.07 | 0.02 |
| Sulphur—S (Pct)..... | 0.08 | 0.07 | 0.04 | 0.04 | 0.02 |
| Insoluble—(Pct)..... | 0.05 | 0.04 | 0.04 | 0.04 | 0.04 |
| Ignition Loss—(Pct)..... | 0.40 | 0.40 | 0.40 | 0.40 | 0.45 |
| Cadmium—(Pct)..... | 0.10 | 0.06 | 0.04 | 0.04 | |
| Brightness*..... | 83.5 | 86.0 | 90.0 | 91.0 | 92.0 |

* G. E. Recording Spectrophotometer.

Quality of Zinc Oxide

After the initial 20 ft muffle furnace was constructed and placed in operation a gradual improvement became apparent in the color and uniformity of the zinc oxide produced. Many changes in the furnace design improved the quality. The furnace, as now developed, can produce a wide range of zinc oxides including all grades of French Process zinc oxide and with minor modifications has produced acicular zinc oxides. Representative specifications for the French Process zinc oxides that are produced are shown in Table 4.

Production of Zinc

Of the various types of risers tried at East Chicago, several of them indicated the possibility that zinc metal could readily be produced from the muffle furnace. The relative position of the riser with respect to the molten bath of metal in the vaporizing unit seemed ideal to exclude or at least reduce contamination of the zinc metal by copper, aluminum and tin.

A simple design of riser was developed to permit zinc vapors condensed in the risers to be removed through a

trapped opening into a zinc well from which the zinc metal could be removed at convenient intervals. A further development of this idea led to the design of a suitable condenser made of carborundum brick that would permit complete production of zinc metal from all of the vapors leaving the vaporizing units. For the purpose of controlling the rate of zinc condensation, by varying the heat loss, hinged steel frame doors lined with insulation brick were attached to the exterior of the condenser.

Zinc Produced from Secondary Metal

With this type of riser on the furnace, the distillation of zinc from secondary metals became a commercial possibility because the zinc produced in test runs was Prime Western, Brass Special or Intermediate grade. The results of such an experimental run are given in Table 5. In this run die cast slabs and die cast scrap were used as the source of zinc.

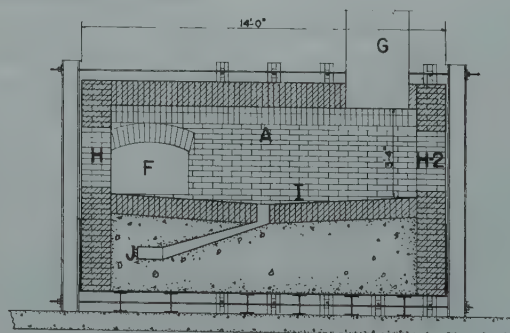


FIG 5—Melting unit section on line B-B.

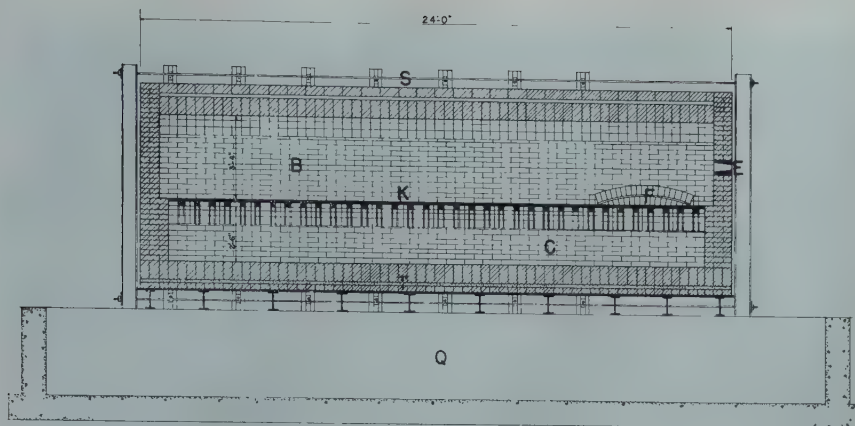


FIG 6—Vaporizing unit section on line C-C.

Table 5 . . . Zinc from Secondary Metals

| | Lb | Per Cent of Metal Charged |
|---------------------------|---------|---------------------------|
| Charged | | |
| Die Cast Slabs..... | 72,685 | 35 |
| Die Cast Scrap..... | 134,180 | 65 |
| | 206,865 | 100 |
| Metal Production | | |
| Condensed Metal..... | 133,165 | 64.4 |
| Residue Metal..... | 11,515 | 5.6 |
| By-products | | |
| Muffle Dross..... | 51,310 | 24.8* |
| Unmeltables..... | 4,915 | 2.4 |
| Unaccounted for Loss..... | 5,960 | 2.8 |

* Dross production should approximate 14.0 pct.

Distillation of Prime Western Zinc

It was recognized that these furnaces could be used for redistillation of impure zinc into higher purity zinc. Results of a test made to determine the efficiency of the redistillation of Prime Western Zinc into higher purity zinc are shown in Table 6.

Table 6 . . . Redistillation of Prime Western Zinc into Higher Purity Zinc

| | Lb | Grade Zinc | Pct of Metal Charged |
|-----------------------|---------|---------------|----------------------|
| Charged..... | 300,095 | Prime Western | 100.0 |
| Metal Production..... | 269,554 | Intermediate | 89.8 |
| | 3,280 | Brass Special | 1.1 |
| | 10,246 | Prime Western | 3.4 |
| By-products.. | 9,238 | Muffle Dross | 3.1 |
| | 1,786 | Blue Powder | 0.6 |
| | 1,316 | Residue Metal | 0.4 |
| | 4,693 | Loss | 1.6 |

Distillation of High Grade Zinc

An experiment was conducted to determine the extent and economics of reducing the lead content of electrolytic high grade zinc in a muffle furnace.

Table 7 summarizes the information obtained.

Table 7 . . . Reduction of Lead Content of Electrolytic High Grade Zinc in Muffle Furnace

| | Pct Lead | Lb | Pct of Metal Charged |
|-------------------------------|----------|---------|----------------------|
| High Grade Zinc Charged..... | 0.0081 | 366,085 | |
| Condensed Metal Produced..... | 0.0032 | 302,225 | |
| Residue Metal..... | | 17,070 | |
| Metal in Process..... | | 44,800 | |
| Recovery..... | | | 99.46 |

In this test the average production of metal per 24 hr was 29,257 lb. The oil consumption averaged 800 gal per 24 hr.

By-products

Several important by-products are produced in the conversion of die cast and zinc scrap into zinc or zinc oxide.

UNMELTABLES

The first by-product obtained is in the form of iron inserts or foreign material that is frequently associated with many forms of zinc scrap. The general term "unmeltables" is used to describe this form of by-product.

The following analysis as shown in Table 8 indicates the metals present in the unmeltables in addition to iron and zinc.

Table 8 . . . Metals in Unmeltables in Addition to Iron and Zinc

| Pb | Cu | Sn | Ni | Cr | Al |
|------|------|------|------|------|------|
| 4.39 | 3.61 | 0.80 | 0.36 | 0.11 | 10.0 |

MUFFLE DROSS

As the scrap is melted in the melting unit or in a kettle some of the zinc is oxidized. The partially oxidized zinc (muffle dross) is screened from the unmeltables and set aside for treatment or sale to zinc smelters. A representative analysis of muffle dross is shown in Table 9.

Table 9 . . . Analysis of Muffle Dross

| Zn | Pb | Cu | Sn | Fe | Al | Insol. |
|------|-----|-----|-----|-----|------|--------|
| 69.7 | 5.1 | 4.0 | 2.3 | 8.5 | 10.0 | 0.4 |

RESIDUE METAL

The distillation of zinc from die cast metal concentrates the other metals (principally aluminum and copper) present in the original alloy. A representative analysis of residue metal is shown in Table 10.

Table 10 . . . Analysis of Residue Metal

| Al | Cu | Zn | Sn | Fe | Pb |
|------|------|-----|-----|-----|-----|
| 33.3 | 51.9 | 8.0 | 2.9 | 3.1 | 0.4 |

RECOVERY OF TIN-LEAD ALLOY FROM RESIDUE METAL

The residue metal is tapped from the furnace at between 5 and 10 per cent zinc content. This metal is remelted in a special liquation furnace in such a manner as to form a two-layer system. The lower layer which consists of a molten lead-tin alloy containing a small



FIG 7—No. 4 muffle furnace.

amount of zinc is tapped from beneath the solid upper layer. This crude lead-tin alloy is refined by removal of the zinc with chlorine and the final refining with caustic soda. It is used as a lead-tin alloy.

RECOVERY OF ALUMINUM FROM RESIDUE METAL

A number of studies were made of the best means of utilizing the aluminum and copper alloy which was left after the zinc, lead and tin had been removed from the residue metal. It was recognized that if the aluminum-copper alloy was freed of undesirable impurities it should be attractive to the die cast producer who could use it by adding electrolytic zinc to produce a high grade die casting alloy.

Extensive experiments were made to electrolyze residue metal in a fused salt cell. The cathode deposits were a high grade aluminum. As the aluminum was removed from the molten electrolyte the copper content of the residue metal increased and reached the point where the operating difficulties of such elec-

trolysis became more and more complex and unattractive. The conclusion was reached that this sort of treatment to recover aluminum from residue metal might prove attractive if low cost power were available.

RECOVERY OF COPPER FROM RESIDUE METAL

The copper content of the residue metal is high enough to interest the copper smelters in its utilization. It has been treated in copper reverberatories along with the melting of scrap copper to produce electrolytic copper. In this treatment the aluminum values are lost in the reverberatory slag.

The residue metal can also be treated in copper converters where the aluminum is oxidized to Al_2O_3 and discarded in the converter slag. Great care, however, is necessary in this type of operation because the reaction between the copper sulphides and metallic aluminum is vigorously exothermic under certain conditions. Large quantities of this residue metal have been sold to manufacturers who find this alloy

useful for their needs. It is obviously a secondary aluminum alloy that contains attractive values for many alloy specifications.

Acknowledgment

Acknowledgment is given to Messrs. George Anderson and R. S. Olsen for their early experimental contributions in the development of the muffle furnace. Appreciation is expressed for the valuable cooperation and assistance of Messrs. P. S. Toney, W. P. Ruemmler and E. F. Weaver of the East Chicago staff in the preparation of the manuscript.

References

1. U. S. Patent No. 2,156,420: Metal Vaporizing Furnace. George Anderson and R. S. Olsen.
U. S. Patent No. 2,174,559: Vaporizing Furnace for Zinc and Other Metals. George Anderson and R. S. Olsen.

The Effect of Orientation Difference on Grain Boundary Energies

C. G. DUNN,* Member AIME, and F. LIONETTI†

THE energy associated with grain boundaries in polycrystalline aggregates is believed to play a major role in grain growth processes and, when growth ceases, to determine the final equilibrium grain boundary angles. Further, the energy of grain boundaries of recrystallization nuclei is a factor in nucleation processes. It is important to know, therefore, how the energy per unit area of a grain boundary, that is, the grain boundary surface tension γ , depends on the difference in orientation of the two lattices of the grains producing the boundary. Although the problem is important, surprisingly little has been done toward a quantitative evaluation of the effect of orientation difference on grain boundary energies.

C. S. Smith¹ recently has discussed this problem and in addition to showing effects of orientation difference on equilibrium angles has shown a variety of interesting effects of surface tension on the appearance of microstructures. Fig 1 and the following relations expressed in Eq 1, which connect equilibrium grain boundary angles and surface tensions, illustrate equilibrium conditions which are believed to hold true in metals.

$$\frac{\gamma_{12}}{\sin \theta_3} = \frac{\gamma_{23}}{\sin \theta_1} = \frac{\gamma_{13}}{\sin \theta_2} \quad [1]$$

Clearly any two of these surface tensions can be expressed in terms of the third when the equilibrium angles θ_1 , θ_2 , and θ_3 are known.

Applied to the present problem for solid state equilibrium of three grains, the angles θ_1 , θ_2 and θ_3 must be measured in a plane perpendicular to the line of junction of the three grains. Normally a direct determination of these angles

from random microsections is impossible. Consequently Harker and Parker² and Smith¹ (except for some measurements on flat specimens) resorted to a statistical method to determine equilibrium grain boundary angles. Smith reported that grain boundaries meet the surface of a piece of metal nearly perpendicularly. He reported also, in connection with direct angle measurements on flat specimens with grains extending through the thickness, that angles varied appreciably from 120° and concluded that there was a measurable effect of orientation difference on surface tension.

Another direct way of determining equilibrium angles and a method adaptable to studying particular configurations, recently suggested by Dunn,³ is to use a three-grain flat specimen with orientations of grains so chosen that the junction line of the three grains will be straight throughout the thickness and perpendicular to the surface of the specimen. Choice of orientations is possible when individual grains of each group can be grown to predetermined orientations through the reorienting and growth of "seed crystals" as described.³ Not only is it possible,

for example, to have grains with the same crystallographic plane in the plane of the specimen, but a given orientation difference between two grains can be made a common factor to an unlimited number of three-grain groups while a series of orientation differences is investigated. Any effect of anisotropy of gas-solid surface tension due to grain orientation should be minimized by having all grains oriented the same with regard to crystallographic plane in the plane of the specimen.

Another feature of the three-grain group is the notched grain boundaries as shown in Fig 2 for one specimen (S4). The notches serve to anchor the end positions of the grain boundaries (especially at high temperatures) while the central and junction point of the grains moves toward an equilibrium position. Final equilibrium should produce straight grain boundaries if the notches are very narrow and if changes in orientation* of the grain boundary do not alter the surface tension.† If one assumes the straight line condition and no change of surface tension with small changes in grain boundary orientation and finds the equilibrium configuration by a minimization of the grain boundary energy, one obtains the relations given in Eq 1.

The approach to straight line boundaries or to minimum energy configurations in specimens containing large grains, such as those used in the present investigation, may be very slow compared with the approach to equilibrium conditions for the grain boundary angles. It may be desirable, as proved to be the case in the present investiga-

San Francisco Meeting, February 1949.

TP 2517 E. Discussion of this paper (2 copies) may be sent to *Transactions AIME* before May 15, 1949. Manuscript received Nov. 3, 1948.

* Research Physicist, General Electric Co., Pittsfield, Mass.

† Formerly Chemist, General Electric Co., Pittsfield, Mass. Now Assistant Professor of Chemistry at Union University, Albany, N. Y.

¹ References are at the end of the paper.

* Change in orientation of a grain boundary is not to be confused with difference in orientation between two grains.

† An effect of grain boundary orientation must exist for crystal orientations near the twinned position. A measurable effect may also exist for other crystal orientations. (See Ref. 1.)

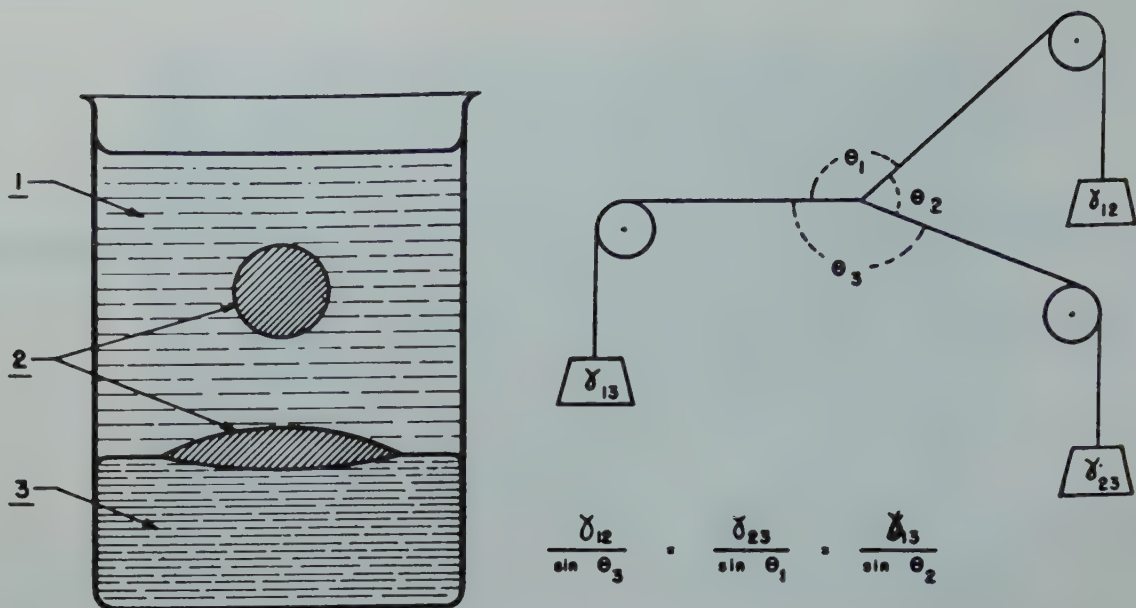


FIG 1—Interface equilibrium between three immiscible liquids and mechanical analogy with triangle of forces. (After Smith.)

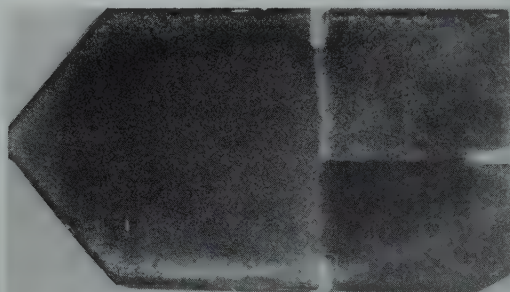


FIG 2—Photograph of S4 showing sample composed of three grains each having a {110} plane in the plane of the specimen. Approx. $\times 2$. (After Dunn.)

tion, to observe relatively small changes in the boundaries near the junction point of the three grains rather than wait for large changes to occur in the grain boundaries prior to making accurate angle measurements.

In the present report a series of groups, each of three grains with the (110) plane in the plane of the specimen, are investigated. The difference in orientation between two grains i and j , with grain boundary surface tension γ_{ij} , is given in terms of an angle Δ_{ij} , which is the angle separating the [001] directions of the two grains. Each three-grain specimen, therefore, has three values of surface tension (γ_{12} , γ_{13} , γ_{23}) corresponding to the three grain boundaries where the differences in orientation of the grains are Δ_{12} , Δ_{13} and Δ_{23} respectively. Each three-grain group has one boundary where the difference in orientation of the grains is 15° , a value chosen somewhat arbi-

trarily. The purpose of the common value of Δ is to permit the calculation of surface tensions in terms of one surface tension (γ_c) which is assumed not to vary much with grain boundary orientation. Values of Δ_{ij} cover the range 5° to 90° .

If orientation of the grain boundary has little effect on the surface tension γ , then γ can be expressed as a simple function of Δ , the difference in orientation. However, even if the orientation of the grain boundary should prove to have little effect in general, the existence of twins with definite composition planes alone indicates an effect of grain boundary orientation when two lattices are near a twinned relation. McKeehan⁴ and Preston⁵ from considerations of the distances between atoms in a lattice and the distance between atoms at a twin boundary, showed that certain composition planes resulted in lower stress or lower

boundary energy. On the basis of measured grain boundary angles, Smith¹ reported that the surface tension for a twin boundary in face-centered cubic metals must be relatively small.

In the present investigation no attempt was made to control the orientation of grain boundaries during the preparation of three-grain groups.

PREPARATION OF SPECIMENS

Silicon ferrite with about 3.5 pct silicon was selected for the investigation because the technique of growing three-grain specimens with each grain in a definite orientation had been previously developed. Furthermore, silicon ferrite remains a single phase even at high temperatures; so temperatures of 1300 – 1400°C , or near the melting point if desired, could be used to effect a more rapid approach to equilibrium.

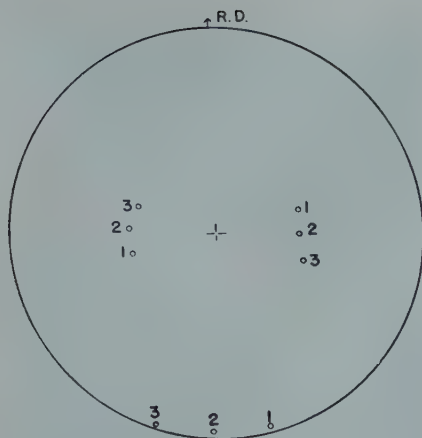


FIG 3—Stereographic projection of the {100} poles of the three grains in S2.

In the laboratory cold rolled strips of silicon steel of commercial grade were made in the form of sheets 0.025 in. thick. These had the property of supporting exaggerated grain growth. Upon lowering pieces of this material into a furnace with a high temperature gradient, large grains formed in the hot end. Two of these grains about one inch apart in each sample were then X rayed and analyzed for orientations. From the stereographic projection of the orientation of each grain, the two angle rotations necessary to bring a (110) plane into the plane of the specimen and a [001] direction into a pre-determined azimuthal position could be read easily from a Wulff net. A small machine with angular scales was used to reorient each crystal, the neck part of the specimen (see Ref. 3 for illustration) being held at red heat during this operation to permit easy plastic flow of the metal.

Each specimen with its two re-oriented seed crystals was then fed into a furnace with a high temperature gradient in order to grow two grains in one end. The speed of a specimen generally was about $\frac{1}{2}$ cm per hr. In a similar manner, a third crystal was seeded, analyzed, reoriented, and grown from the opposite end. Eleven specimens were made, all but S8 by the exaggerated grain growth method. In the case of S8 where one Δ value reached 90°, a strain-anneal type of transformation was used. To facilitate identification, each sample was shaped differently. Also it will be noted that the three initial grain boundary angles obtained in specimens made in the manner previously described, if measured very roughly, will be near 90, 90, and 180° respectively (see Fig 2).

After preparation, the orientations of all grains were determined. Fig 3, which is illustrative of all specimens, shows a stereographic projection of the {100} poles of the three grains 1, 2, and 3 of S2. Tilt of the (110) plane did not exceed 2°. In general since the (110) planes were quite close to the plane of the specimen (within 3°), determining the [001] direction of each grain sufficed for a simple calculation of each orientation difference Δ . The plotting of stereographic projections, as shown in Fig 3, was not necessary since a direct reading analyzer could be used to find the direction of the zone axis of the [001] zone of Laue spots which were present in each Laue photograph. The tilt of the (110) plane could also be read directly from the film.

ANNEALING

On the assumption that well defined equilibrium angles with grain boundaries lacking or nearly lacking in curvature over appreciable distances could be obtained, it was decided to anneal each sample a number of times and observe the approach toward equilibrium. Temperatures near 1300 or 1400°C were considered necessary, and higher temperatures were avoided during long anneals since a failure of the furnace controls while the furnace was unattended could have been disastrous with samples too near the melting point. Furthermore, the higher temperatures favored the sticking of the specimens to supporting plates or surrounding material and this was undesirable. To prevent sticking at high temperatures, samples were separated from supporting and surrounding pieces of silicon iron by a thin layer of alumina powder.

A preliminary anneal of 48 hr at 1350°C with an atmosphere of pure

dry hydrogen disclosed a serious de-siliconization effect for some thin sheets of silicon iron and S3, S4, S5, and S7. Sufficient silicon was removed from the thin sheets of silicon iron to allow them to transform completely by a phase change. S7 and S4 had transformed sufficiently to require replacements. S9, S10 and S11, therefore, were immediately made. S3 and S5 showed some transformation along the edges but this was much less than the transformation in S4, a photograph of which is shown in Fig 4. The photographs of S4, shown before and after the 1350°C hydrogen anneal in Fig 2 and 4 respectively, clearly indicate a change in the grain boundaries near the common grain boundary point.

All samples were then annealed for about 70 hr at 1150°C in pure dry hydrogen. Although grain boundary changes were observable, it appeared expedient to anneal next in dry argon for 48 hr at 1300°C and then obtain some measure of the grain boundary angles. Measurements after the anneal were made at a magnification of 30 diam. Accuracy in the measurements proved difficult to obtain. Additional straightening of the boundaries, however, was anticipated; so the samples were given another anneal of 48 hr, this time at 1350°C in dry argon. Measurements on a number of specimens, especially S5, indicated a stabilizing condition of the angles. A comparison of photographs taken at different times also indicated a marked dropping off of grain boundary movement. A final anneal of 48 hr at 1400°C in an atmosphere of argon was then given the samples. Only minor further changes in grain boundaries occurred in this anneal. Long annealing, therefore, at these high temperatures had not produced the macrochanges sought for as an aid to the quantitative measure of the approach toward equilibrium

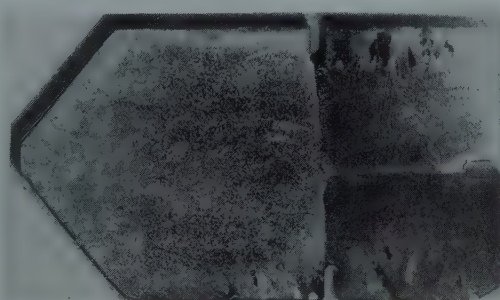


FIG 4—Photograph of S4 after a 48 hr anneal in pure dry hydrogen at 1350°C. Approx. $\times 2$.

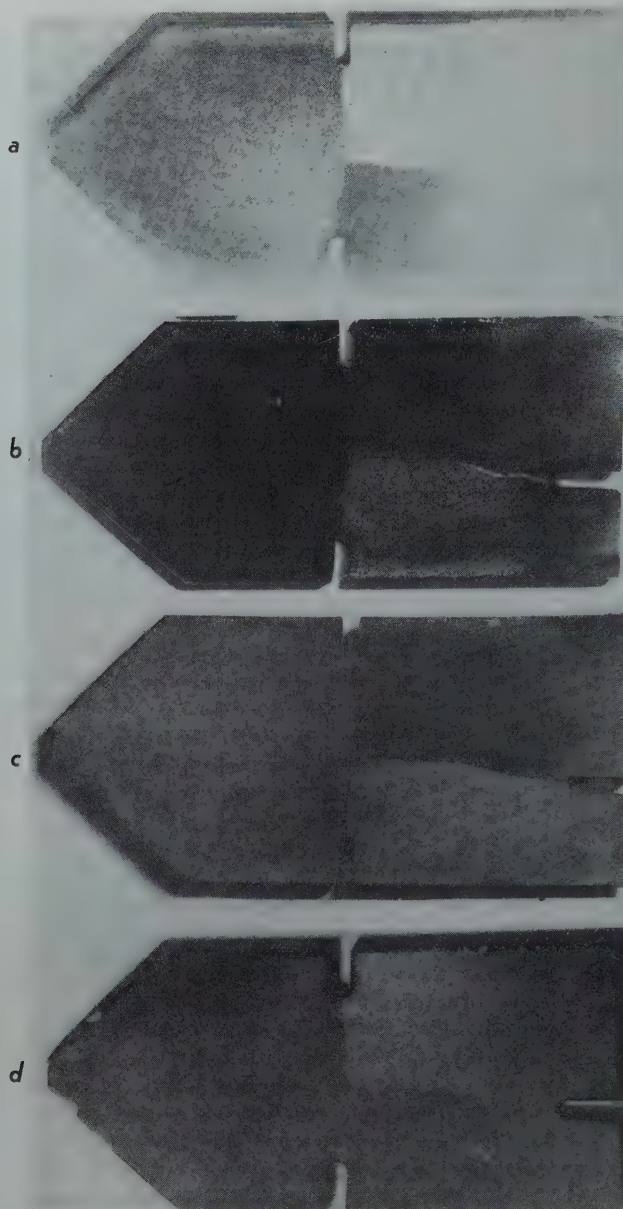


FIG 5—Photographs of S5. Approx. $\times 2$.

- a. Specimen as prepared
b. After 48 hr at 1350°C in pure dry hydrogen
c. After additional 70 hr at 1150°C in pure dry hydrogen and 48 hr at 1300°C in dry argon
d. After final 48 hr at 1400°C in dry argon

Table 1 . . . Orientation Differences, Initial (Gross) Angles, Final Angles after Annealing, Relative Surface Tensions, and Corrected Relative Surface Tensions for Eleven Specimens

| Specimen, No. | Orientation Difference | | | Initial Angles | | | Final Angles | | | Calculated Surface Tensions | | | Corrected Surface Tensions | | |
|---------------|------------------------|---------------|---------------|----------------|------------|------------|---------------|------------|------------|--------------------------------|--------------------------------|--------------------------------|--------------------------------|--------------------------------|--------------------------------|
| | Δ_{12} | Δ_{23} | Δ_{13} | θ_1 | θ_2 | θ_3 | θ_1 | θ_2 | θ_3 | $\frac{\gamma_{12}}{\gamma_0}$ | $\frac{\gamma_{23}}{\gamma_0}$ | $\frac{\gamma_{13}}{\gamma_0}$ | $\frac{\gamma_{12}}{\gamma_0}$ | $\frac{\gamma_{23}}{\gamma_0}$ | $\frac{\gamma_{13}}{\gamma_0}$ |
| 1 | 15. | 7 | 8 | 90 | 90 | 180 | 140 | 143 | 77 | 1 | 0.66 | 0.62 | 1 | 0.66 | 0.62 |
| 2 | 16.5 | 17 | 33.5 | 160 | 90 | 110 | 121.5 | 118.5 | 120 | 1 | 0.98 | 1.01 | 1.04 | 1.02 | 1.05 |
| 3 | 15.5 | 23 | 38.5 | 180 | 80 | 100 | 116.5 | 121 | 122.5 | 1 | 1.06 | 1.01 | 1.01 | 1.07 | 1.02 |
| 4 | 13.5 | 24 | 37.5 | 180 | 90 | 90 | Sample ruined | | | | | | | | |
| 5 | 14 | 25 | 39 | 90 | 180 | 90 | 112 | 129 | 120 | 1 | 1.07 | 0.90 | 0.97 | 1.04 | 0.87 |
| 6 | 15.5 | 29.5 | 45 | 90 | 180 | 90 | 112 | 127.5 | 120.5 | 1 | 1.08 | 0.92 | 1.01 | 1.09 | 0.93 |
| 7 | 16.5 | 53 | 69.5 | 90 | 180 | 90 | Sample ruined | | | | | | | | |
| 8 | 15.5 | 76.5 | 92 | 90 | 180 | 90 | 127.5 | 120 | 113.5 | 1 | 0.86 | 0.94 | 1.01 | .87 | 0.95 |
| 9 | 14 | 26 | 40 | 180 | 90 | 90 | 115.5 | 117.5 | 127 | 1 | 1.13 | 1.12 | 0.97 | 1.10 | 1.09 |
| 10 | 14.5 | 56 | 70.5 | 90 | 180 | 90 | 120 | 133 | 107 | 1 | 0.91 | 0.76 | 0.98 | 0.89 | 0.74 |
| 11 | 14.5 | 57 | 71.5 | 90 | 180 | 90 | 105 | 134 | 121 | 1 | 1.13 | 0.84 | 0.98 | 1.11 | 0.82 |

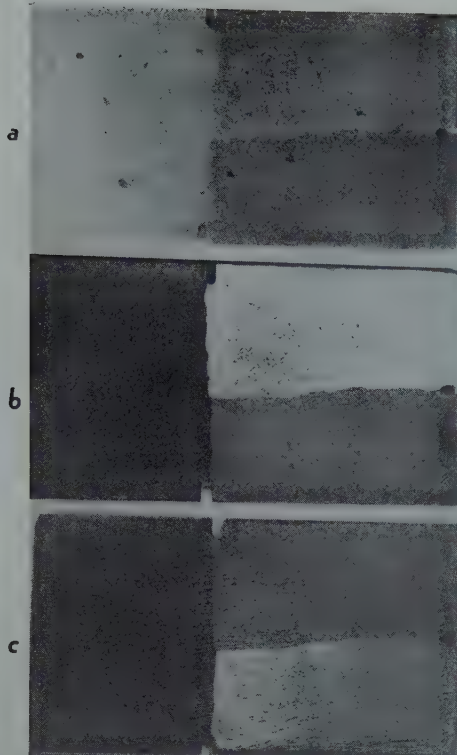


FIG 6—Photographs of S11. Approx. $\times 2$.

- a. Specimen as prepared
- b. After 70 hr at 1150°C in pure dry hydrogen and 48 hr at 1300°C in dry argon.
- c. After additional 48 hr at 1350°C and 48 hr at 1400°C in dry argon

conditions. The angle measurements in some cases agreed well with previous ones; in three cases it was clear that the specimens would first have to be mounted and polished metallographically so that a higher magnification could be used. Angles could be measured fairly accurately on some of the samples in the "as annealed" condition because the grain boundaries were clearly visible.

Experimental Results

STRUCTURE

Photographs of S4 shown in Fig 2 and 4 have already been discussed in connection with the changes produced by the removal of silicon.

Fig 5, showing a series of photographs at slightly less than double magnification of S5, illustrates well the early visible changes and the later stabilization of the boundary positions.

Photographs in Fig 6 likewise show the changes that occurred in S11. From the standpoint of macrochanges which were visible at no magnification, this specimen was the poorest of the

nine used in the determination of grain boundary angles. Only slightly better in this respect was S9. Photographs of S9 are shown in Fig 7, one at about 2 diam magnifications, the other two at 5 diam. These photographs clearly show that grain boundary movement occurred in the 1150°C hydrogen anneal and also in subsequent anneals.

As mentioned previously three of the

samples showed poor macroboundaries. These samples (S1, S9, and S3) were polished and the boundaries observed at 400 diam magnification. Fig 8 shows a photograph of the boundaries of S1, the specimen with the smallest differences in orientation. It is interesting to note that the boundary associated with largest difference in orientation, which stands out sharply in the photograph, is opposite an acute angle. S9,



Fig 7—Photographs of S9.

- a. Specimen as prepared. Approx. $\times 2$.
- b. After 70 hr at 1150°C in pure dry hydrogen $\times 5$
- c. After additional anneals in dry argon gas of 48 hr at 1300°C, 48 hr at 1350°C, and 48 hr at 1400°C. $\times 5$



FIG 8 (above)—Micrograph of S1 after annealing. Nital etch. $\times 400$
 FIG 9 (below)—Micrograph of S9 after annealing. Nital etch. $\times 400$

which has already been discussed in connection with Fig 7, had one grain boundary that continuously curved near the common grain boundary point. This feature is apparent in the photograph shown in Fig 9. Angle measurements were made at 30 diam and then again from the photographic plate taken at 400 diam. One angle, defined by the straight grain boundaries, checked well in these two measurements. Readings from the plate were sufficiently accurate to permit checking the angles to within one degree. The angle measurements of S3 made at a magnification of 400 diam checked quite well with those taken at 30 diam.

Sections were made through a number of grain boundaries to determine how the boundaries passed through the specimen. Although the boundaries in general were close to the perpendicular position, there were some cases of departure from perpendicularity by as much as 5 to 10 degrees.

EQUILIBRIUM ANGLES AND CALCULATED RELATIVE SURFACE TENSIONS

Data for the nine specimens measured are given in Table 1. Following

the columns of orientation differences under Δ_{12} , Δ_{23} , Δ_{13} are the gross initial grain boundary angles listed under initial angles. Referring to Fig 1 it will be noted that θ_3 is the angle opposite the grain boundary formed by grains 1 and 2 where the surface tension is γ_{12} . This is also the boundary where the orientation difference is Δ_{12} . The columns giving the second set of θ values are the final measured angles—the equilibrium angles. Using these angles and Eq 1, relative values of γ were calculated. Results appear in the table under the column headed "calculated surface tensions." A plot of γ against Δ indicated that γ was changing at an

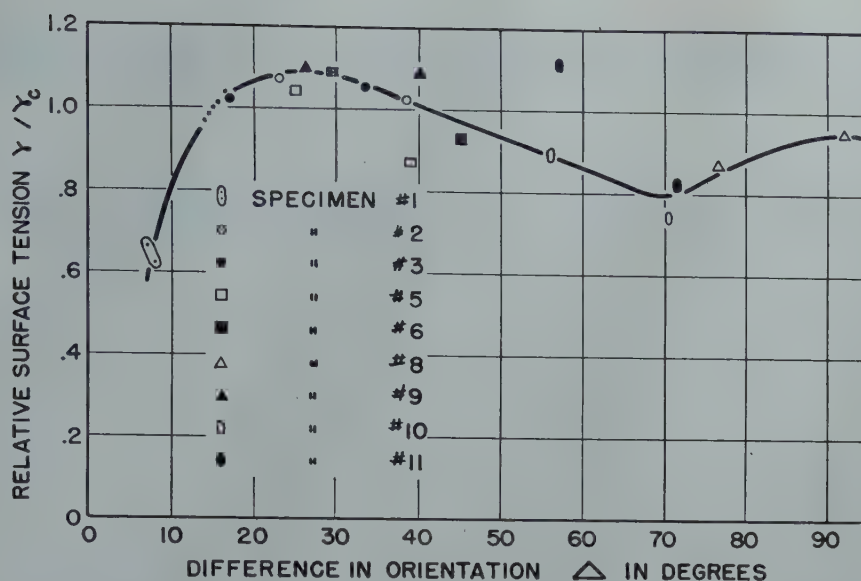


FIG 10—Plot showing variation of relative surface tension γ/γ_c (corrected) with difference in orientation Δ .

appreciable rate with Δ for values of Δ near 15° . Consequently γ for Δ equal to 16.5° , for example, should be slightly larger than γ for Δ equal to 15° , the approximate common value. From the shape of the curve a small correction could be made so that γ_c would apply only to Δ equal to 15° . This correction proved to be less than 4 pct in general. The same percentage change as that made in γ near 15° was also made for the remaining two γ values of each specimen. Results are listed under "corrected surface tensions." A plot of γ/γ_c versus Δ , using the corrected values given in the table, is shown in Fig 10.

Discussion of Results

The relationship between surface tension γ and orientation difference Δ shown by the curve in Fig 10 has three rather striking features: 1. A rapid decrease of surface tension with decreasing Δ for values of Δ less than 15° ; 2. A maximum surface tension for orientation differences in the range of 20 to 30° ; 3. A dip in the curve for orientation differences near 70° .

In regard to the first feature, one would expect some type of approach toward zero surface tension with decreasing Δ since the boundary must vanish at Δ equal to zero. The second point will be discussed later. In the case of the third point, however, one can speculate somewhat on the twin relation. If the boundary between

grains 1 and 3 had been grown near a (112) plane, then approximate artificial (112) twins (grains 1 and 3) might have developed on annealing and a marked dip in the curve expected from the lower energy of a (112) twin boundary. Actually the 1-3 boundary in S10 and in S11 was grown much nearer a (111) plane, but the final configuration not only departed appreciably from the (111) plane but was different in the two specimens. The observed dip in the curve as well as the disagreement for S10 and S11 may reasonably be connected with an effect associated with the twin orientation even though the boundary is removed from a {112} plane. In the particular configuration involving two grains 1 and 3 with (110) planes in the plane of the specimen but differing in orientation by $70^\circ 32'$, the more complete nature of this effect could be investigated by varying the orientation of the 1-3 boundary during the formation of each three-grain group.

S5 and S9, with orientations far removed from any twin position, actually illustrate the variation of grain boundary orientation in the initial samples for a constant set of Δ values. Referring to Table 1, the Δ values for both these specimens are seen to be roughly 15° , 25° , and 40° . The initial gross angles, however, are different except for angle θ_3 which was 90° for both specimens. (Other grain boundary directions and initial gross angles could have been formed by varying the direction of grain growth in each specimen.)

The purpose of making two angles θ_1 different in S5 and S9 was to have θ_1 increase from 90° in S5 and decrease in S9 (if the equilibrium angle was between these two values) until the two reached a common value, or the equilibrium angle. A converse relation would, of course, hold for θ_2 . Lack of the anticipated large grain boundary movements prevented the measuring of the approach toward equilibrium in these samples. As far as angles measured on a small scale are concerned, which finally had to be done, in general the initial gross angles probably have little significance.

Lack of agreement for the final angles for S5 and S9, although possibly due in part to an effect of grain boundary orientation, may be due to failure to reach equilibrium. This view may seem unreasonable at first since long anneals at high temperatures were used in an attempt to reach equilibrium. There is one factor, however, which tends to prevent the reaching of equilibrium conditions as required in the application of Eq 1. Inclusions in a metal exert a constraining force to grain boundary movement, as Smith¹ (see Ref. 24) pointed out in connection with the work of Zener. It was further indicated that, under certain conditions, inclusions should completely stop boundary movement.

With regard to a maximum point on the surface tension curve, it can only be said that one should occur between zero and 70° if there is a marked dropping off of surface tension near 70° .

Considering all nine specimens, and the possibility of some effect of grain boundary orientation, the general consistency of the trend of variation of γ with Δ (especially in the range 15 to 45° where more points have been obtained) indicates that the effect of inclusions in general probably was not too serious. Nevertheless, it would be very desirable to use material of the highest possible purity to insure the attainment of better equilibrium conditions.

Although inclusions may stop a strongly curved grain boundary from moving further, the grain boundary orientation effect may also lead to a curved surface in order to produce a minimum energy configuration (this was also discussed by Smith¹). With reference to the application of the present technique, consider a two-grain specimen with the grain boundary ends anchored and having grains with the same crystallographic plane in the plane of the sheet. If the grain boundary surface tension γ is high for the straight grain boundary compared to other directions, then a curved boundary could correspond to lower energy. We have here the case of minimizing the total energy obtained from the product of boundary area and surface tension, which may be expressed as follows:

$$\text{Total grain boundary energy} = \int \sigma \gamma d\sigma$$

where $d\sigma$ is an element of surface area and the integration is carried out over the entire boundary surface σ . The surface tension γ , of course, is considered to vary from point to point on the surface with orientation of the surface element $d\sigma$. A minimization of grain boundary energy would be valid only when relative sizes of the two grains produce no additional effect on total (internal plus surface) energy.

In any case, the nature of variation of surface tension with grain boundary orientation should be determined in order to obtain a clearer picture of the effect of orientation difference on surface tension. In the case of three-grain groups with common (110) planes, the curve for small values of Δ should be investigated more completely. Finally, three-grain groups with other crystallographic planes in the plane of the specimen should also be investigated and the results of surface tension measurements put on a common relative basis with those of the (110) series.

If relative surface tensions vary with particular orientation differences, as Fig 10 would indicate is actually the case, then some fundamental relationships may be found between surface tension data and recrystallization data involving orientation relationships. In this connection it is interesting to point out some possible correlations, using the shape of the curve in Fig 10 and published facts on recrystallization in silicon ferrite. Dunn⁶ reported a rapid rise in the number of recrystallization nuclei with orientation difference for Δ in the range 10 to 20° and no nuclei with small Δ values. Referring to Fig 10 we note a similar rapid rise in the surface tension starting with small values of Δ . Secondly, the data on recrystallization nuclei show a maximum number of nuclei for Δ equal to approximately 25° with nuclei also having a {110} plane common with the original deformed grain (see Fig 8 of Ref. 6 for curve). The curve of surface tension versus Δ (Fig 10) has a maximum in this same region of orientation difference. However, until other crystallographic relationships are investigated and all values of surface tension are compared, the coincidence of maximum points probably should not be considered too significant. On the other hand some relationships involving either the ease of forming a nucleus or the ability of a nucleus to grow more rapidly in a deformed single crystal because of special orientation relationships is expected.

Experimental data on surface tensions are needed, of course, for application to the problem of grain growth following recrystallization, especially under conditions where recrystallization textures depart from random textures. Further, a strong texture material should have lower total grain boundary energy per unit volume than a random texture material provided both materials have the same grain size and provided the initial part of the curve of relative surface tension does not rise too rapidly to some approximate constant value. A curve of relative surface tension having the form shown in Fig 10 would indicate an appreciable dependence of energy on texture.

Summary

1. Eleven flat specimens of silicon ferrite each composed of three grains were prepared having (110) planes in

the plane of the samples. The common grain boundary point of the three grains was centrally located.

2. Each sample was annealed for long periods of time in the temperature range 1300–1400°C until further change in grain boundaries seemed unlikely and equilibrium angles apparently had been obtained.

3. After annealing, the grain boundary angles were measured and the relative surface tensions calculated. Since each group of grains contained a similar type of boundary (one where the grains had a 15° difference in orientation) it was possible to calculate all surface tensions on a common basis.

4. A curve was obtained showing the variation of relative surface tension (relative energy in the grain boundary per unit area) with difference in crystal orientation.

Acknowledgments

The authors wish to express their appreciation to Drs. J. H. Hollomon and J. C. Fisher for valuable discussions on the problem of measuring surface tensions. Thanks are also extended to Mr. E. F. Welter for aid in the preparation of specimens and the making of X-ray photograms and to Miss Mary Burdette for the micrographs appearing in the manuscript.

References

1. Cyril Stanley Smith: Grains, Phases and Interfaces: An Interpretation of Microstructures. AIME *Metals Tech.* TP 2387 (June 1948).
2. D. Harker and E. Parker: Grain Shape and Grain Growth. *Trans. A.S.M.* (1945) 34, 156–195.
3. C. G. Dunn: Controlled Grain Growth Applied to the Problem of Grain Boundary Energy Measurements. *Trans. AIME Trans.* Jan. 1949, T.N. No. 9.
4. L. W. McKeehan: The Formation of Twin Metallic Crystals. *Nature* (1927) 119, 120, 392.
5. G. D. Preston: The Formation of Twin Metallic Crystals. *Nature* (1927), 119, 600.
6. C. G. Dunn: Effect of Original Orientation on Orientation Changes during Recrystallization in Silicon Ferrite. *Metals Tech.*, TP 1990 (Aug. 1946); *Trans. AIME* (1946). 167, 357.

Solubility Relationships of the Refractory Monocarbides

JOHN T. NORTON* Member AIME and A. L. MOWRY*

THE monocarbides of the A subgroup elements in the fourth and fifth group of the periodic table in addition to being hard and refractory are of special interest in that they are isomorphous in crystalline structure. They are cubic with a sodium chloride type structure in which the metal atoms are essentially close packed in a face-centered cubic arrangement with the carbon atoms placed in the interstices between.

Interstitial structures of this close packed type were first investigated systematically by Hägg¹ and he gave the rule for their formation, stating that the radius ratio of the nonmetal to the metal atom should not exceed the value of 0.59. The carbides of interest are those of titanium and zirconium of the fourth group and vanadium, columbium and tantalum of the fifth group. Table I shows the radius ratio using the Goldschmidt radii for 12 coordination for the metal atoms and the diamond radius for the carbon atom.

It will be noted that while there is considerable variation in the size of the metal atom, in all cases the ratio is smaller than the limit of 0.59 placed by Hägg.

It has been known for some time that these cubic carbides are soluble in one another, at least to some extent or, in other words, the metal atoms can be replaced, one by another without destroying the stability of the structure. Since the stability of these close packed interstitial substances appears to depend more upon geometry than upon the exact chemical nature of the atoms involved, it is of interest to examine the possibilities of replacement in these carbides in some detail.

Hume-Rothery² has pointed out the importance of the difference in size of solute and solvent atom as a factor in limiting the solubility in simple binary

Table 1 . . . Radius Ratio for Metal Atoms and Diamond Radius for Carbon Atom

| Metal | Radius, Metal, A.U. | Radius, Carbon, A.U. | Radius Ratio |
|-------|---------------------|----------------------|--------------|
| V | 1.35 | 0.76 | 0.56 |
| Ti | 1.46 | 0.76 | 0.52 |
| Cb | 1.47 | 0.76 | 0.52 |
| Ta | 1.47 | 0.76 | 0.52 |
| Zr | 1.60 | 0.76 | 0.48 |

solid solutions. Largely on an empirical basis, he states that if the difference in size between solvent and solute atom is more than 14-15 pct of the solvent atom, the range of solubility is very restricted. The atom size was based on the distance of closest approach in the elements involved. While there is some question as to how one should calculate the size of the metal atom in the carbide structures, reference to Table 1 will show that zirconium is the largest and vanadium the smallest of the group and that the difference is about 15 pct. The Ti-Zr difference is about 9 pct and the others are smaller. Thus one would predict that if the size factor controls the solubility, all of the pairs except VC-ZrC would have wide or complete solubility whereas this latter pair is on the border line and might have restricted solubility.

The purpose of the present investi-

gation was to examine the solubility of the several pairs of carbides by heating them together until equilibrium was established and then examining the product by X rays.

Previous Work

Agte³ and his associates prepared various transition metal carbides and determined the melting points of binary mixtures. He concluded from the shapes of the melting point curves that there was extensive solubility in the case of the cubic carbides.

Umanskii⁴ and his colleagues made an investigation of a number of pairs of the cubic carbides, using X rays and plotted lattice parameter vs. composition curves for the systems TaC-TiC, CbC-TiC, TaC-ZrC and CbC-ZrC. All pairs showed a continuous series of solid solutions. The first two pairs gave a linear relation while the latter two showed a negative deviation from Vegard's law.

Kiefer and Nowotny,⁵ in a paper which became available after the present work was well advanced, investigated the binary pairs of the five cubic carbides by means of X rays. Relatively few points were obtained and results indicated that in some cases, at least, equilibrium was not reached at the temperatures used. The results indicated that solubility in the VC-ZrC system was not complete. All of the results of previous investigations indicated the desirability of a more detailed study.

Materials

The raw materials used were monocarbides of titanium, zirconium, vanadium, columbium and tantalum and were the purest which could readily be obtained commercially. Spectrographic qualitative analysis showed that the CbC and TaC contained less than 1 pct

San Francisco Meeting, February 1949.

TP 2527 E. Discussion of this paper (2 copies) may be sent to *Transactions AIME* before May 15, 1949. Manuscript received November 1, 1948.

This investigation was sponsored by the Office of Naval Research, Contract No. N5ori-7817.

* Professor and Research Assistant, respectively, Department of Metallurgy, Massachusetts Institute of Technology.

¹ References are at the end of the paper.

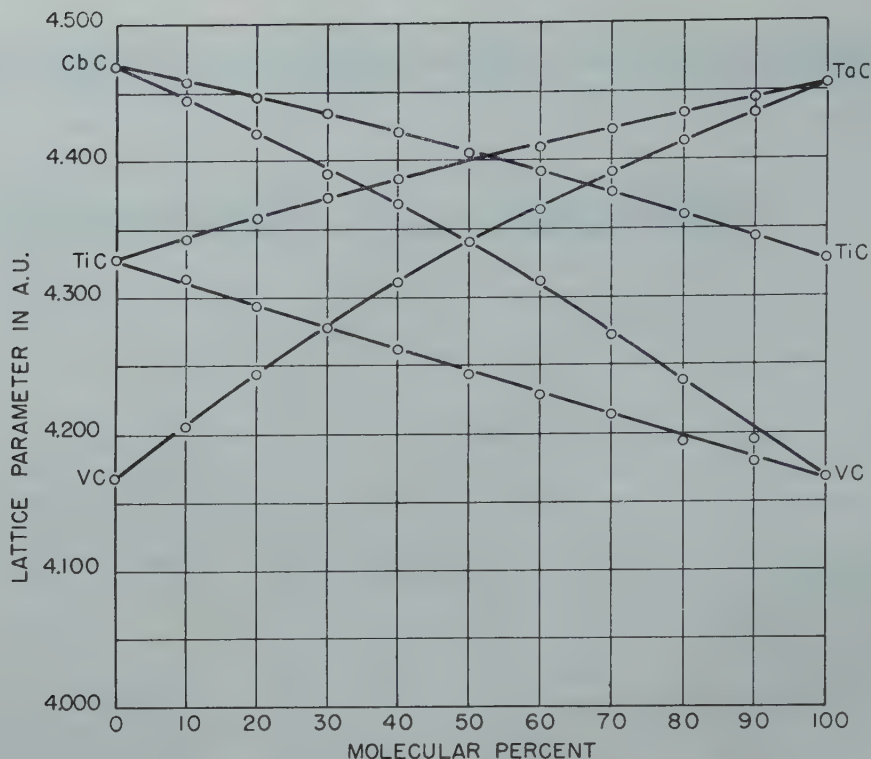


FIG 1—Lattice parameter vs. composition curve for the carbide pairs, CbC-TiC, Cb-VC, TiC-TaC, and VC-TaC.

of other metals. The TiC showed the presence of appreciable amounts of Cr, Fe, Si, V and Zr; the VC contained B, Cr, Fe, M and Si while the ZrC contained appreciable amounts of B, Fe and Ti. All were somewhat deficient in combined carbon content. The results of the investigation were such that the presence of these impurities does not influence the validity of the conclusions.

Experimental Procedure

Heating of the carbide mixtures was carried out in a high frequency vacuum furnace of conventional design, using a graphite crucible. Temperature was measured with a calibrated optical pyrometer sighting through a small tube in the crucible cover directly on the central specimen of the charge. Temperature was maintained by manual control during the heating runs within a limit of $\pm 20^\circ\text{C}$.

The individual carbides were mixed with additional carbon to correct the deficiency and heated in vacuum at 2100°C for 3 hr to recarburize and to volatilize some of the impurities. These carbides were then carefully weighed out and mixed in pairs at 10 molecular pct intervals. The mixing was done in a small stainless steel ball mill using benzene as a dispersing agent. Excess carbon powder was added as well as 1

pct of powdered cobalt to act as a diffusion aid during sintering. After mixing, the powders were pressed into small slugs and sintered.

The sintering was carried out at 2100°C in the vacuum furnace for a period of 3 hr in order to obtain an equilibrium state and then cooled in the furnace. During this treatment practically all of the cobalt was evaporated from the specimens. Equilibrium was judged from the appearance of the X ray diffraction lines which were sharp with well resolved alpha doublets after this treatment. A one hour treatment at temperature appeared to be sufficient in most cases but the longer treatment was used to make certain.

It was not possible to analyze all specimens after sintering but certain specimens selected at random and analyzed chemically for the metal content showed that the compositions as mixed and after sintering, did not differ by more than an amount corresponding to ± 2 molecular pct.

The X ray examination was carried out using radiation from a copper target and a Phragmen type focusing camera which covered the angular range from 45 to 83° . The powder specimens were prepared by crushing the sintered slugs, grinding in a mortar and mounting the fine powder on paper strips with adhesive. Some observa-

tions of relative line intensities were also made with the Norelco recording X ray spectrometer.

The X ray wavelength values used in calibrating the cameras and calculating the lattice constants were as follows:

Copper K beta —1.39217 A. U.

K alpha 1—1.54050 A. U.

K alpha 2—1.54434 A. U.

Thus the lattice constant values are in true Angstrom units. It must be remembered when comparing results with previous work that slightly different values of the wavelengths may have been used in the past.

X ray Results

The structures of the individual carbides were all of the NaCl type with metal atoms at coordinates 0, 0, 0; 0, $\frac{1}{2}$, $\frac{1}{2}$; $\frac{1}{2}$, 0, $\frac{1}{2}$; $\frac{1}{2}$, $\frac{1}{2}$, 0. The carbon atoms undoubtedly are at coordinates 0, 0, $\frac{1}{2}$; 0, $\frac{1}{2}$, 0; $\frac{1}{2}$, 0, 0; $\frac{1}{2}$, $\frac{1}{2}$, $\frac{1}{2}$; although no attempt was made to verify this conclusion in the present research.

The lattice parameters of the individual carbides are given in Table 2.

Table 2 . . . Lattice Parameters of Individual Carbides

| CARBIDE PARAMETER IN A.U. | |
|---------------------------|-------------------|
| ZrC | 4.689 ± 0.001 |
| CbC | 4.470 0.001 |
| TaC | 4.457 0.001 |
| TiC | 4.329 0.001 |
| VC | 4.169 0.001 |

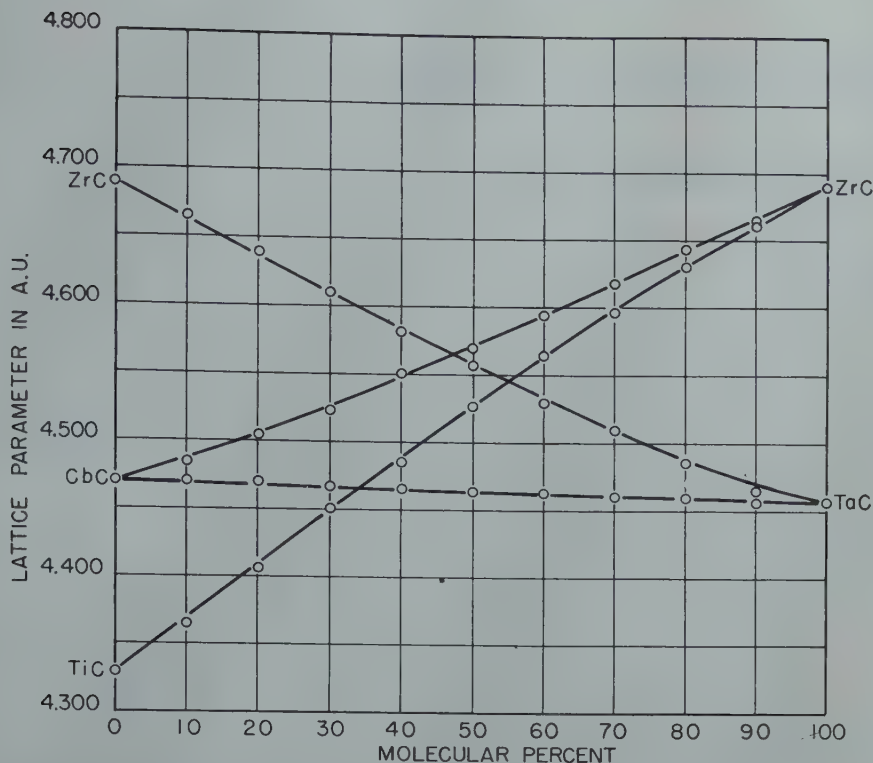


FIG 2—Lattice parameter composition curves for the carbide pairs, ZrC-TaC, CbC-ZrC, CbC-TaC, and TiC-ZrC.

A higher precision in the determination of the parameters of the individual carbides is not warranted in view of the small amounts of impurities present.

With the exception of the VC-ZrC series the X ray photographs of all of the other sintered binary pairs showed the presence of only a single phase having the same NaCl structure as the individual carbides but with varying lattice parameters. Fig 1 and 2 show graphically the variation of lattice parameter with composition of the carbides taken in pairs. It will be observed that the values lie on smooth continuous curves which depart only slightly from straight lines indicating uninterrupted series of solid solutions in each case.

The exception is the VC-ZrC system, the results of which are shown in Fig 3. Here all of the intermediate compositions between 10 and 90 molecular pct show two cubic phases of constant parameter having values close to the individual carbides. This indicates very limited solubility.

At the VC end of series, the lattice constants of the smaller cubic phase in the two-phase field is the same as that of VC, within experimental error. A specimen containing 4 molecular pct ZrC is definitely two-phase. Thus the solubility of ZrC in VC is certainly less than 4 pct and probably less than 1 pct.

At the ZrC end of the series, a defi-

nite but small solubility is indicated since in the two-phase region, the larger cubic phase has a parameter of 4.674 A. U. while that of ZrC is 4.689 A. U. An alloy containing 6 pct VC is two phase. If Vegard's law applies, the solubility would be 4 pct VC. One may conclude that the actual value of solubility of VC in ZrC at 2100°C is approximately 5 molecular pct. Carbides of higher purity would be necessary to obtain a more precise value.

Discussion of Results

The experimental results on the several pairs of carbides show clearly the limit placed on solubility by the size factor. A quantitative expression of the size factor depends upon the method of defining the atom size. One method is to employ the Goldschmidt atomic diameters, obtained from the distance of closest approach in the elements and corrected to a coordination number of 12. Another method is to assume that the metal and carbon atoms are in contact along the cube edge and that the carbon atom has a diameter which is constant for all of the carbides at a value equal to that in the diamond. The metal atom diameter is then calculated from the measured lattice parameter. Still a third method is to calculate the metal-to-metal atom distance in the carbide

based on the measured lattice parameter. Table 3 shows a comparison of these methods of calculation.

Table 3 . . . Atomic Diameters of Metal Atoms in A.U.

| Metal | D ₁ | D ₂ | D ₃ |
|-------|----------------|----------------|----------------|
| V | 2.69 | 2.66 | 2.95 |
| Ti | 2.93 | 2.82 | 3.06 |
| Ta | 2.94 | 2.95 | 3.15 |
| Cb | 2.94 | 2.96 | 3.16 |
| Zr | 3.19 | 3.18 | 3.31 |

D₁ = Diameter from element corrected to coordination number of 12.

D₂ = Diameter from carbide assuming carbon diameter of 1.511 A. U.

D₃ = Distance of closest approach of metal atoms in carbide.

A comparison of these values shows that in the carbides, the metal atoms have closely the same size as in the metals themselves and that in the carbides they are not quite closely packed but are pushed apart slightly by the carbon atoms. The exception is TiC where the diameter of the Ti atom in the carbide is definitely smaller than in the metal. No explanation suggests itself for this fact.

Using the value of D₂ in Table 3 one can calculate the percentage size differences for the several carbide pairs. The results are shown in Table 4.

Thus it can be seen that in this series of solid solutions in which the chemical properties of the elements are very similar but the size factor varies, extended solubility is possible if the

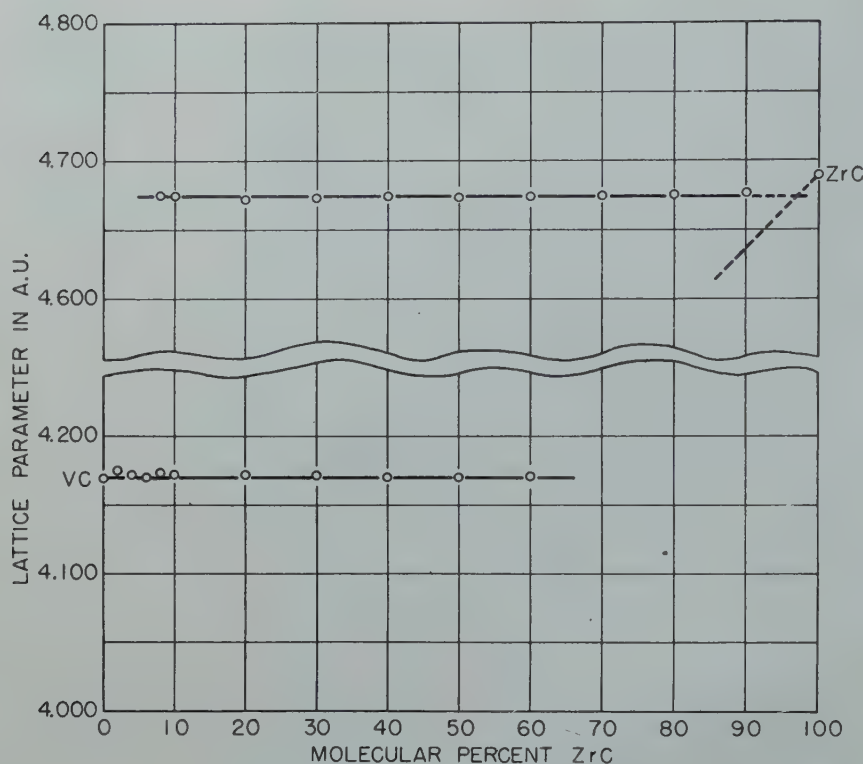


FIG 3—Lattice parameter composition curves for the carbide pair VC-ZrC.

Table 4 . . . Size Difference in Carbide Pairs

| Carbide Pair | Difference in Pct Smaller as Solvent | Difference in Pct Larger as Solvent |
|--------------|--------------------------------------|-------------------------------------|
| VC-ZrC | 21.1 | 16.3 |
| TiC-ZrC | 12.8 | 11.7 |
| VC-CbC | 11.3 | 10.0 |
| VC-TaC | 10.9 | 9.8 |
| TaC-ZrC | 7.8 | 7.2 |
| CbC-ZrC | 7.4 | 6.9 |
| VC-TiC | 6.0 | 5.7 |
| TiC-CbC | 5.0 | 4.7 |
| TiC-TaC | 4.6 | 4.4 |
| TaC-CbC | 0.34 | 0.34 |

difference in size of solute and solvent is 13 pct of the size of the solvent. If this figure increases to 16 pct the solubility is very restricted as in the zirconium-rich end of the VC-ZrC system and is practically zero at 21 pct which is the vanadium-rich end of this same system. This is in good agreement with the rule found for simple binary solid solution alloys.

The lattice parameter composition curves for the binary carbide pairs which form continuous series of solid solutions show slight variations from the linear relation required by Vegard's law. In the systems TiC-VC and CbC-TaC, the line is practically straight. Systems CbC-TiC, CbC-VC, TaC-TiC, TaC-VC and TiC-ZrC show a positive deviation. Systems CbC-ZrC and TaC-ZrC show a negative deviation. The maximum deviation occurs at a composition of about 50 molecular

pct, the maximum positive value being 0.72 pct in the TaC-VC system and the maximum negative value being 0.40 pct in the TaC-ZrC system. At the present, no particular significance can be assigned to these small deviations.

There is no evidence in the sintered solid solution alloys that the distribution of the two kinds of metal atoms on the face-centered cubic lattice is other than random. Calculated and observed X ray line intensities are in good agreement on this basis and no superstructure lines have been observed. It is possible, however, that ordering might be induced by heating for long periods in the temperature range around 1500–1800°C. The system most likely to show ordering would be the TiC-ZrC system since this is the largest size difference for complete solubility. The composition ratios 3–1 and 1–3 should be examined since these compositions are favorable for the face-centered cubic lattice. The difference in atomic number should make it possible to recognize the existence of order in the structure by means of X rays.

The possibility other than ordering is that a solubility gap may exist at temperatures lower than 2100°C. Here again the TiC-ZrC system would be the most likely one. These two points are now under investigation.

Since the solubility of one carbide in another is limited by the change in

lattice energy resulting from the strain produced by the misfit of the atoms, it is interesting to speculate about what would happen in the case of a ternary solid solution. For instance, suppose a mixture of equal parts of VC and ZrC, which are quite insoluble in one another were mixed with increasing amounts of TaC which has a metal atom size about halfway between the two and is capable of completely dissolving both. How much TaC would be required before a single homogeneous phase could be formed? Experiments to investigate this situation are in progress.

Conclusions

1. The monocarbides of the elements titanium, zirconium, vanadium, columbium and tantalum are isomorphous and have a sodium chloride type structure.

2. The binary carbide systems, TiC-ZrC, TiC-VC, TiC-CbC, TiC-TaC, ZrC-CbC, ZrC-TaC, VC-CbC, VC-TaC, CbC-TaC form continuous series of solid solutions.

3. The binary carbide system ZrC-VC shows very small solubility, the limits at 2100°C being 5 pct at the zirconium-rich end and less than 1 pct at the vanadium-rich end.

4. The parameter-composition curves show only slight deviations from Vegard's law but both positive and negative deviations are found.

5. The maximum size difference between atom diameters expressed in percent of the solvent atom diameter for extended solubility is 13 pct. The minimum value for very restricted solubility is 16 pct.

6. In the solid solution, the metal atoms are distributed at random on the points of the metal lattice.

Acknowledgment

The authors wish to acknowledge the services of Mr. Albert Mahfuz and Mr. Robert Bennett who assisted in carrying out these experiments.

References

1. G. Hagg: *Ztsch. Physik. Chem.*, (1929); 6(B), 221 (1930); 7(B), 339 (1930) 8(B), 445.
2. Hume-Rothery: *The Structure of Metals and Alloys*. Inst. of Metals Monograph, p. 52. 1936. London.
3. Agte and Alterthum: *Ztsch. Tech. Physik.* (1930) 11, 182.
4. Kovalskii and Unanskii: *Zhurnal Fizicheskoi Khimii.* (1946) 20, 769.
5. Nowotny and Kieffer: *Metallforschung.* (1947) 2, No. 9, 257.

Pressure Distribution in Compacting Metal Powders

POL DUWEZ* and LEO ZWELL*

Introduction

IN recent years, the problem of pressing metal powder in a die has received much attention. The question has been the object of a Symposium held in New York in March 1947 under the sponsorship of the AIME; an excellent review of the subject may be found in Ref. 1. Various experimental techniques have been used to study the behavior of the powder in a die cavity. Two methods have been particularly successful; one consists of measuring the density distribution^{2,3} and the other makes use of a lead grid in the powder during pressing.⁴ In the present study, the pressure at various points on the bottom and the sides of a die 1.50 in. in diam was measured by means of small piston dynamometers and resistance sensitive strain gauges. In order to correlate the results with previous investigations, the pressure distribution inside the compact has also been determined by an indirect method based on density measurements.

Strain Gauge Measurements of Pressure on Side and Bottom of Die

A schematic drawing of the die used for measuring side pressures is shown in Fig 1. The pressure gauge consists of a 0.25-in. diam piston A which transmits the pressure to a dynamometer B, on which two Baldwin Southwark type A-14 strain gauges are fastened 180° apart. Because the installation of several dynamometer assemblies along the side of the die would have been difficult, the pressure distribution was obtained in successive tests in which the distance from the gauge to the bottom of the compact was adjusted

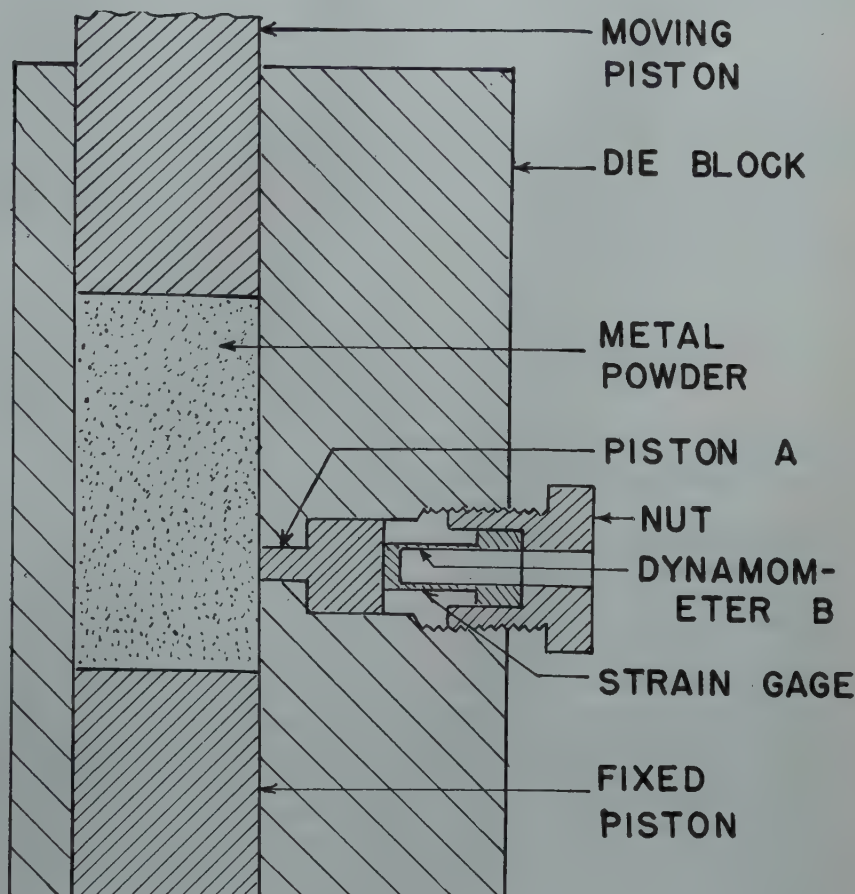


FIG 1—Experimental die for measuring side pressure.

to different values by changing the length of the bottom piston. The dynamometer, disassembled from the die, was calibrated under compressive loads and showed a 1.00 ohm change of

resistance for every 15,300 psi change of pressure (750 lb load change).

All the strain gauge measurements were made with a null type Leeds and Northrup Wheatstone bridge. The sensitivity of the method was better than 1 pct and the accuracy was within 2 pct. These values were considered satisfactory in view of the rather large scatter in the measurements introduced by the random variation in packing the powder in the die. The stable ambient conditions and short time involved in the taking of observations made temperature compensation unnecessary.

The pressure distribution on the bot-

METALS TRANSACTIONS . . . 137

San Francisco Meeting, February 1949.

TP 2515 E. Discussion of this paper (2 copies) may be sent to *Transactions AIME* before May 15, 1949. Manuscript received Nov. 3, 1948.

* Associate Professor of Mechanical Engineering and Chief of the Materials Section, and Research Engineer, respectively, Jet Propulsion Laboratory, California Institute of Technology, Pasadena, Calif.

¹ References are at the end of the paper.

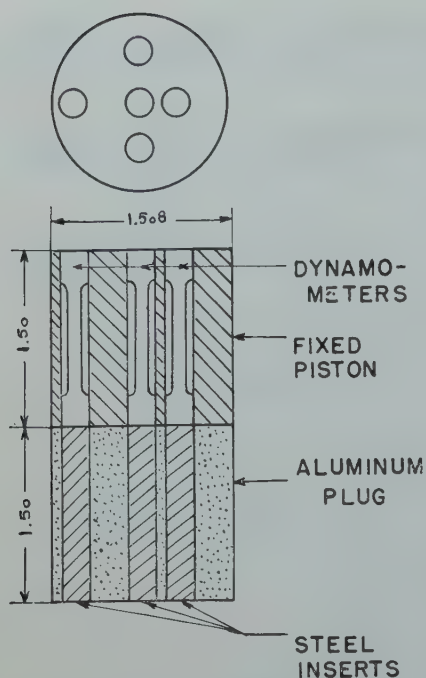


FIG 2—Pressure gauges on fixed piston.

tom of the die was determined with five dynamometers, as shown in Fig 2. The dynamometers were 0.25 in. in diam, 1.5 in. long, and had a 1 in. center length ground to 0.125 in. in diam. One Baldwin Southwark type C-7 strain gauge was pasted on each dynamometer. Under maximum loading, the elastic deformation of the dynamometers caused a relative displacement of about 0.0045 in. between the surface of the gauges and that of the bottom piston. In order to eliminate this source of error, an aluminum plug, 1.5 in. long, was placed under the piston with five steel inserts on which the dynamometers rested. Since the displacement of the aluminum plug with respect to the steel inserts compensated for the displacement of the dynamometers with respect to the bottom piston, the relative motion of the dynamometers to the bottom piston was negligible.

The average pressure acting on the fixed piston was measured by means of a strain gauge arrangement, shown in Fig 3. Four strain gauges, Baldwin Southwark type A-7, were attached around the dynamometer member of the piston. A calibration curve of gauge resistance with pressure was made by applying increasing loads with the moving piston acting directly on the fixed one.

PRESSURE ON THE SIDE OF A DIE

The copper powder used in the experiments was type MD-51 from

Metals Disintegrating Co., Elizabeth, N. J. The stainless steel powder was the 18-8 standard grade made by Unexcelled Chemical Co., New York City. The particle size distribution of the powders is given in Table 1.

Table 1 . . . Particle Size Distributions of Metal Powders

| Screen Size (mesh) Between and | | Weight of Particles in Each Size Fraction (per cent) | |
|--------------------------------------|-----|--|-------------------------|
| | | Copper | 18-8 Stainless Steel |
| 35 | 60 | 0.8 | |
| 60 | 100 | 88.2 | 1.2 |
| 100 | 150 | 5.8 | 5.2 |
| 150 | 200 | 1.2 | 7.0 |
| 200 | 325 | 1.0 | 24.4 |
| through | 325 | 3.0 | 62.0 |

The pressure on the side of the die was measured for both powders. For each location of the gauge with respect to the fixed piston, the applied pressure was increased in steps of 10,000 psi up to a pressure of 60,000 psi and in steps of 5000 psi up to a pressure of 100,000 psi. A family of curves of side pressure vs. applied pressure was then obtained, each curve corresponding to a point at a certain distance from the fixed piston. Typical curves (only two of each family) are shown in Fig 4 for copper and in Fig 5 for stainless steel. Each point on the curve represents the average of at least three measurements.

The results of pressure measurements are more conveniently analyzed by tracing curves of side pressure vs. distance of the gauge from the fixed piston for a given compacting pressure. Such pressure distribution curves are shown in Fig 6 for copper powder and in Fig 7 for stainless steel powder. Although the experimental points are rather scattered, they seem to fall more or less on straight lines. Hence, it may be concluded that the pressure on the side of the die increases almost linearly from the bottom to the top of the compact.

It is significant to note that the side pressure measured for copper powder is about twice as large as for stainless steel. It is probable that the most important factor influencing the side pressure in a die is the plasticity of the powder. A soft powder is likely to flow sidewise and produce a higher lateral pressure than a hard powder. In order to substantiate this statement, side pressure measurements were made by replacing the powder with a cylinder of solid copper. With a fully annealed cylinder (Rockwell F30) the side

pressure was about 50 pct greater than that measured with the powder. With a hard copper cylinder (Rockwell B47) the side pressure was 50 pct less than that observed with the powder. These results suggest that a systematic investigation of the effect of hardness of the powder on the side pressure would be very worthwhile.

PRESSURE DISTRIBUTION ON THE FIXED PISTON

A series of measurements was made with the five small gauges previously described in an attempt to determine the variation in pressure along two perpendicular diameters of the fixed piston. Numerous measurements were made with different thicknesses* of compact and at various compacting pressures. Only a typical set of curves is shown in Fig 8 for compacts of various thicknesses and a compacting pressure of 50,000 psi. The abscissa of the graph of Fig 8 is the distance from the center of the fixed piston expressed as a fraction of the radius of the piston. The results indicate clearly that the

* The word "thickness" refers to the dimension measured after the compact was ejected from the die.

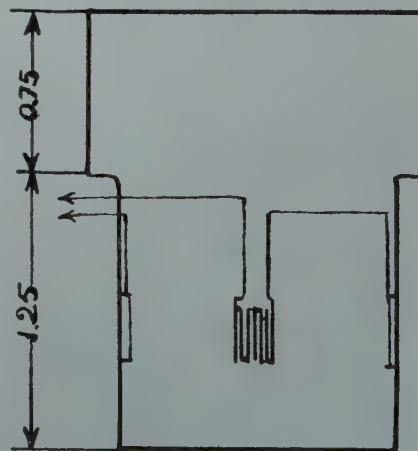
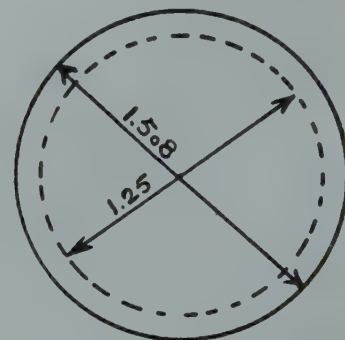


FIG 3—Fixed piston gauge for measuring average pressure.

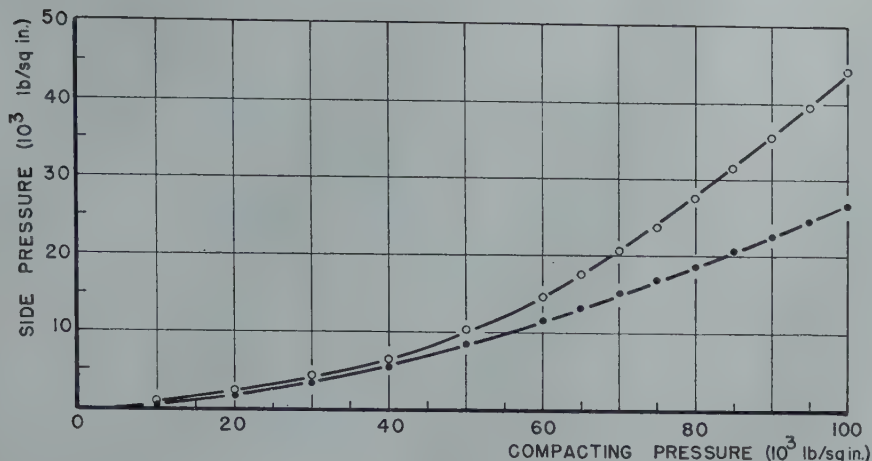


FIG 4—Variation of side pressure with compacting pressure for copper powder, compact thickness 1.15 in., compact diameter 1.51 in.
 (○) 1.0 in. from fixed piston.
 (●) 0.15 in. from fixed piston.

pressure on the fixed piston decreases steadily from the center to the periphery of the piston. Moreover, as the thickness of the compact increases, the average pressure on the fixed piston decreases, but the shape of the pressure distribution curve does not change appreciably, at least within the limits of thickness to diameter ratios considered in these measurements. It is also interesting to note that for a thin compact (ratio of thickness to diameter equal to 0.11 on Fig 8), the pressure at the center of the fixed piston is greater than the compacting pressure.

The results of this series of experiments were substantiated by the measurements of the density distribution within a compact (See "Pressure Distribution within a Compact").

AVERAGE PRESSURE ON THE FIXED PISTON

In spite of the fact that the pressure is not uniform on the fixed piston, the consideration of an average pressure is of interest because it introduces simplifications in both experimental technique and interpretation of the results. Experiments were therefore made with the purpose of relating the average pressure on the fixed piston with the thickness of the compact. The results of measurements are presented in Fig 9. In this diagram, the two variables are dimensionless, the ordinate being the ratio of base pressure to applied pressure and the abscissa the ratio of thickness of compact to diameter. These results were obtained with copper powder at compacting pressures of 40,000 and 100,000 psi. The scatter of the results is relatively large and may

be attributed to the difficulty in obtaining a uniform packing of the powder during loading. In spite of the scatter, it seems reasonable to conclude that, in a first approximation at least, the ratio of bottom pressure to compacting pressure is a function of the ratio of thickness to diameter of compact and in the range of pressures from 40,000 to 100,000 psi does not depend upon the compacting pressure.

The variation of fixed piston pressure with the thickness of a compact is of great practical interest, since it shows what fraction of the compacting pressure is actually transmitted to the bottom of the compact. It is significant to note the rather rapid decrease in bottom pressure with increasing thickness of compact. For the copper powder

used in the present experiments, and with a ratio of thickness to diameter equal to 1.0, only about 30 pct of the compacting pressure is acting on the bottom part of the compact.

The rather simple technique of measuring the average pressure on the fixed piston seems to be best suited to characterize the behavior of a powder during compacting. Its use should prove of great interest for studying quantitatively the effect of lubricants added to the powder or sprayed on the die walls.

Several investigators have proposed theoretical explanations for the decrease in fixed piston pressure with increasing compact thickness. The parabolic expression given by Unckel⁵ does not give a satisfactory agreement with the results found in the present investigation. The exponential relation derived by Taylor⁶ agrees with the results only for compacts having a thickness to diameter ratio less than one.

Pressure Distribution within a Compact

The pressure distribution within a compact was determined by an indirect method, based on the relation between the local density within the compact and the compacting pressure that would be required to obtain such a density. A calibration curve of density vs. compacting pressure was first obtained by pressing $\frac{1}{8}$ -in. thick compacts at various pressures and measuring their densities. In spite of the relatively small ratio of thickness to

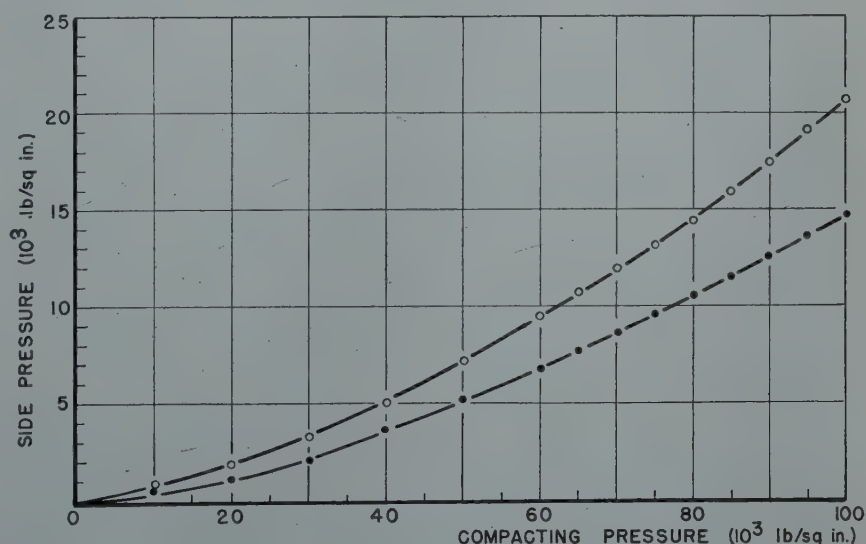


FIG 5—Variation of side pressure with compacting pressure for stainless steel powder, compact thickness 1.27 in., compact diameter 1.51 in.
 (○) 1.0 in. from fixed piston.
 (●) 0.15 in. from fixed piston.

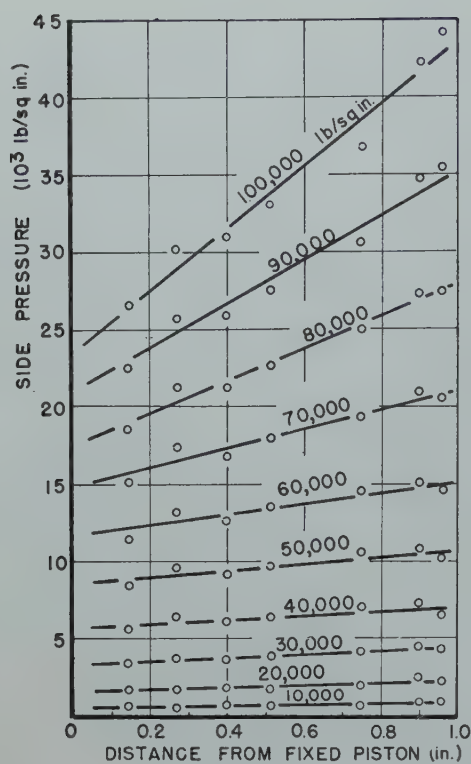


FIG 6—Pressure distribution on the side of a die for copper powder under various compacting pressures; compact thickness 1.15 in.

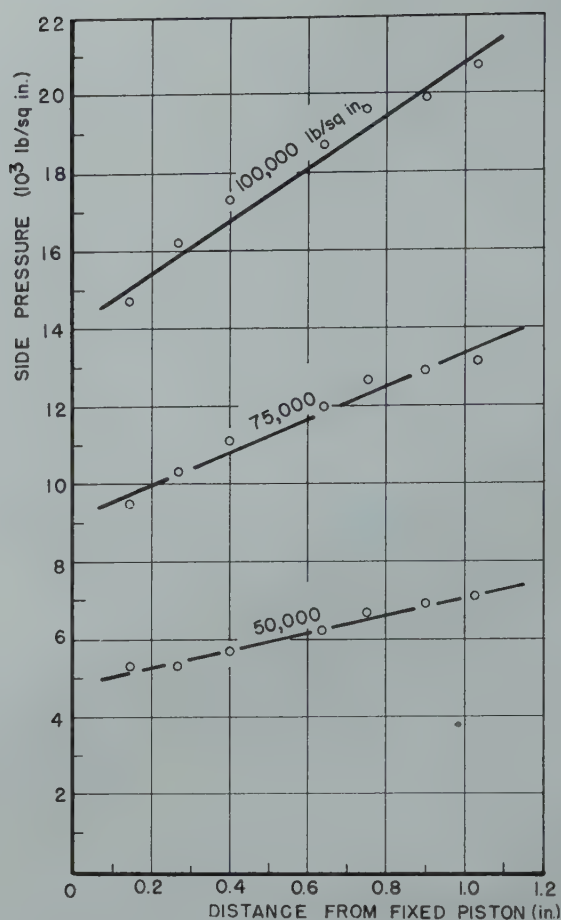


FIG 7—Pressure distribution on the side of a die for stainless steel powder under various compacting pressures; compact thickness 1.27 in.

diameter of these compacts (0.083), the strain gauge pressure measurements showed a base pressure about 6 pct smaller than the compacting pressure. An average pressure was then taken for tracing the calibration curve. Such a curve is shown in Fig 10 for copper powder. The densities of successive layers in a thick compact were obtained by facing off cross-sections of the compact and computing their densities from the dimensions and weights of the compacts before and after machining. In order to eliminate errors due to machining, some compacts were faced from top to bottom, others from bottom to top, and still others from both ends to the center.

The radial distribution of density was determined by turning down the diameter of compacts in steps of 0.20, 0.25, 0.35, and 0.70 in. for thicknesses varying from $\frac{1}{4}$ to $\frac{1}{2}$ in. and computing the densities of these machined cylindrical sections. The densities of the compacts and sections were computed with an uncertainty of about 1 pct and the uncertainty in the pressure values was estimated to be about 6 pct.

The pressure distribution in the vertical direction is shown in Fig 11 for a series of compacts pressed at 100,000 psi. The different symbols used on this

graph refer to specimens having various thicknesses after compacting. The ordinate of the diagram is the ratio of the average effective pressure in a given section of the compact to the applied compacting pressure. The abscissa is also a ratio, obtained by dividing the distance between a section of the compact and the moving piston by the diameter of the compact. This method of presenting the data has the advantage of dealing with dimensionless parameters. The rather large scatter in experimental results (See Fig 11) is probably due mostly to the nonuniform distribution of the powder in the die before pressing. In spite of the scatter, the results indicate that the pressure distribution is about the same for all compacts, regardless of thickness.

As expected, the average pressure decreases steadily from the top to the bottom of the compact. It is interesting to note, however, that for a ratio of thickness of compact to diameter greater than approximately 1.0, the pressure tends to decrease slowly, and approaches a value equal to about 20 pct of the applied pressure on the moving piston.

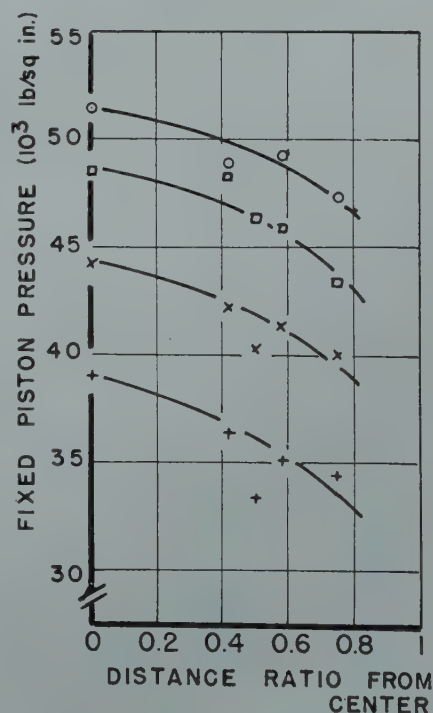


FIG 8—Pressure distribution on fixed piston for copper compacts of various thickness to diameter ratios. (○) 0.11, (□) 0.35, (×) 0.61, (+) 0.88.

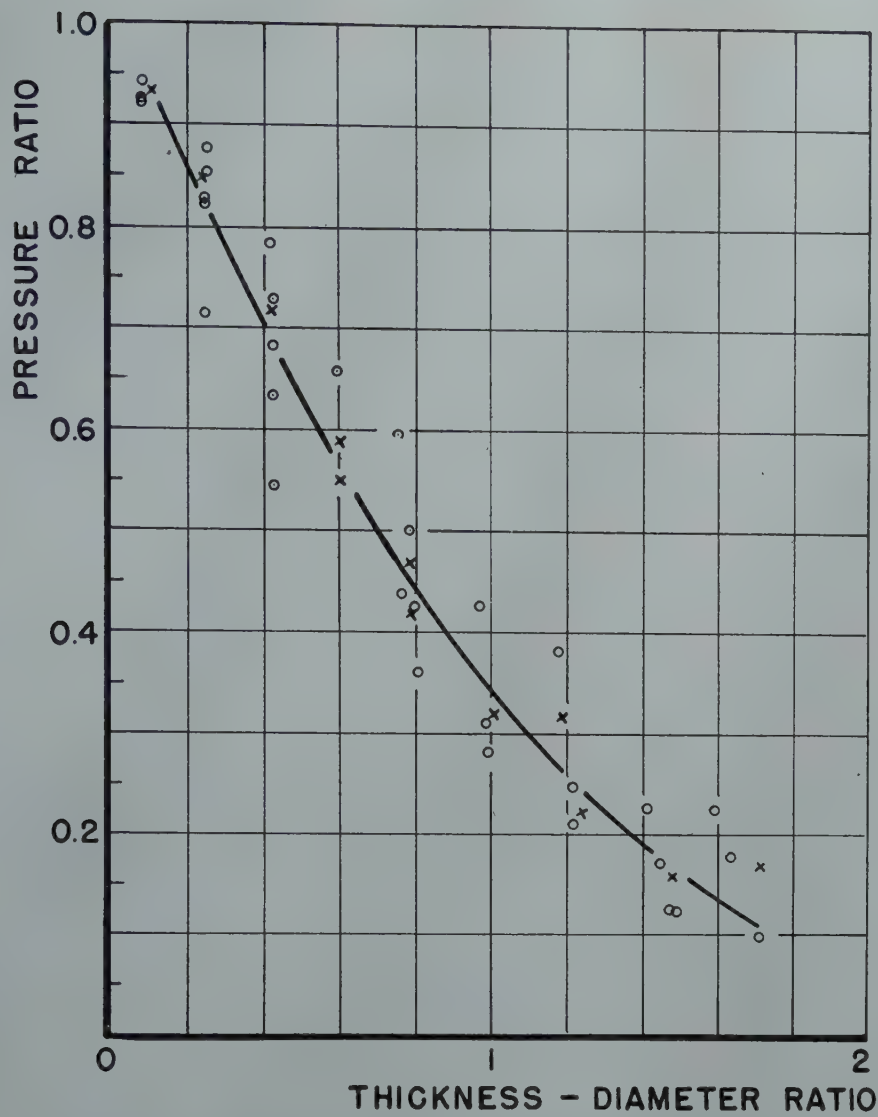


FIG 9—Ratio of average pressure on fixed piston to compacting pressure vs. ratio of thickness to diameter of copper compacts; compacting pressure 100,000 (○) and 40,000 (×) psi.

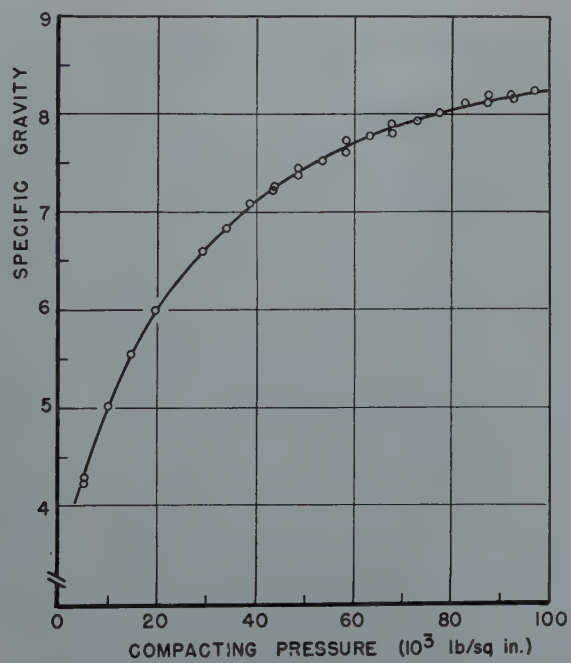


FIG 10—Calibration curve relating density and compacting pressure of copper powder.

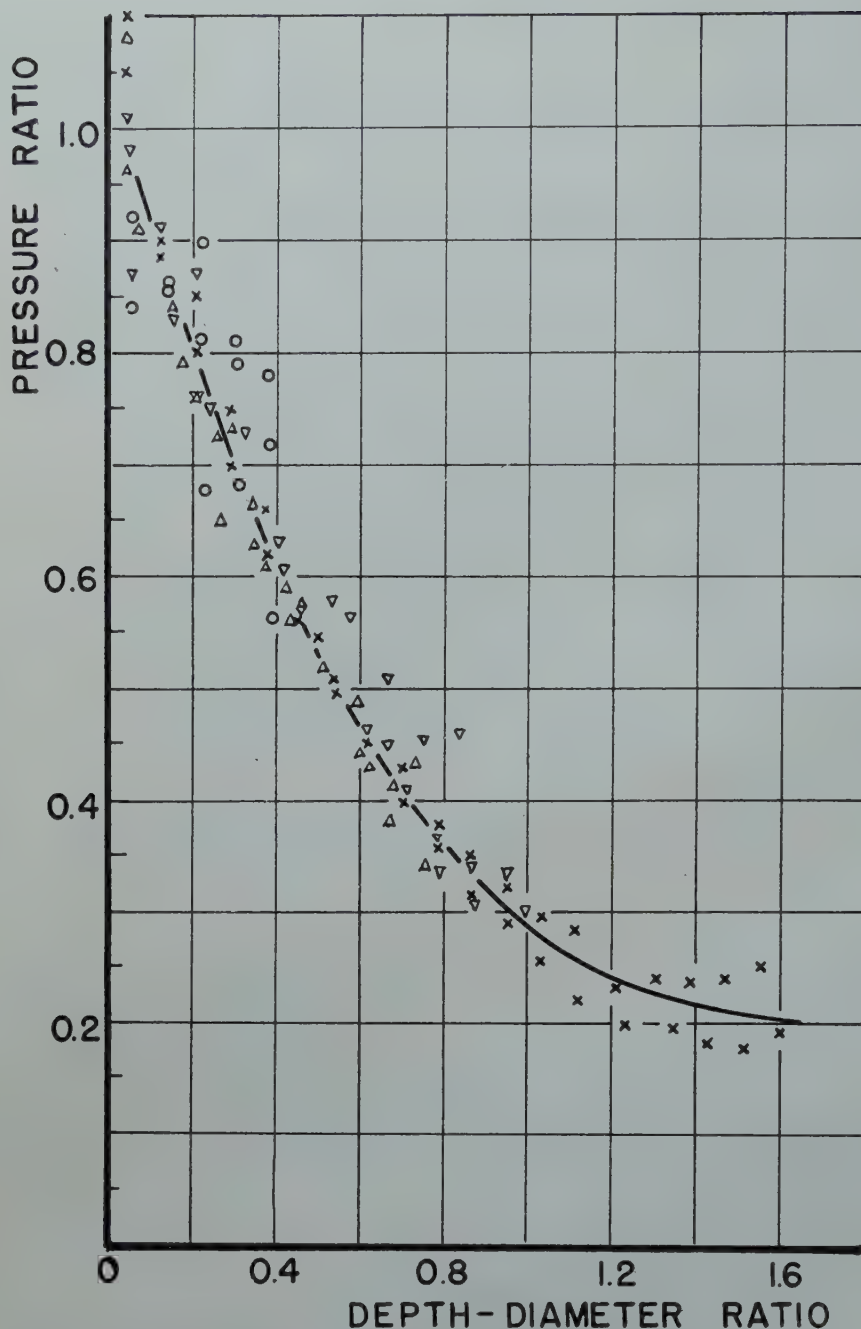


FIG 11—Pressure distribution in copper compacts of various thicknesses, compacting pressure 100,000 psi.
(○) 0.65 in., (△) 1.2 in., (▽) 1.5 in., (×) 2.4 in.

A comparison of the results in Fig 9 and 11 shows that there is satisfactory agreement between the values of the pressures on the fixed piston measured by strain gauges and the values of the pressures at equivalent depths of compacts determined from density measurements. The small difference observed in the two figures (the fixed piston measurements being slightly higher) may be due to the different radial pressure distributions in the two cases and to the different character of the contact layer; that is, at the fixed piston the powder is pressed against a solid support, while within the compact

the powder is pressed against a soft support.

Additional results were obtained at pressures of 80,000 and 40,000 psi. In this case, it was possible to use longer compacts, for which the ratio of thickness to diameter was about 3.4. The results presented in Fig 12 indicate that the pressure distribution curves are reasonably close to the average curve obtained for 100,000 psi. The tendency for the pressure to level off in the bottom portion of long compacts, already mentioned in connection with the measurements made at 100,000 psi, is still more apparent from the graph of

Fig 12. It seems reasonable to conclude that in the range of pressures of 40,000 to 100,000 psi, the pressure distributions in the die are similar. This result cannot be extrapolated to lower pressures. It was found, for example, that for a compacting pressure of 15,000 psi (See Fig 13), the pressure distribution curve does not fall as rapidly as for higher compacting pressures. This observation agrees with a generally recognized fact, that at low compacting pressures the uniformity of pressure (or density) in the longitudinal direction of a cylindrical compact, is relatively better than at high compacting pressures.

The pressure distribution in the radial direction and at various depths within a compact was also investigated by the density method. The results are rather complex, because the three dimensional pattern of pressure distribution depends on the thickness of the compact, and changes continuously as the compacting pressure increases. The results obtained with three compacts of different thicknesses and a compacting pressure of 100,000 psi are presented in Fig 14, 15, and 16. For all three specimens, the effective pressure near the moving piston is much higher at the outer circumference of the compact than at the center. This non-uniformity in pressure distribution decreases with the thickness of the compact and disappears at some distance from the top. In approaching the fixed piston, the situation is reversed, and the pressure decreases from center to periphery. This last observation is in agreement with the pressure measurements made with the five gauges on the fixed piston previously described. By comparing the graphs of Fig 14, 15, and 16, it is evident that the uniformity of pressure on the fixed piston is better for thicker compacts. This uniformity is obtained at the expense of the average pressure, which is, of course, very low on the bottom of a thick compact.

Additional measurements made with a compacting pressure of 50,000 psi did not alter essentially the shape of the pressure distribution curves obtained for 100,000 psi. It is probable that for low pressures of the order of 10,000 or 20,000 psi the distribution of pressure is more uniform. At low pressures, however, density measurements were difficult because of the lack of strength of the compacts.

An attempt was made to represent the distribution of pressure within a compact by tracing lines of equal pres-

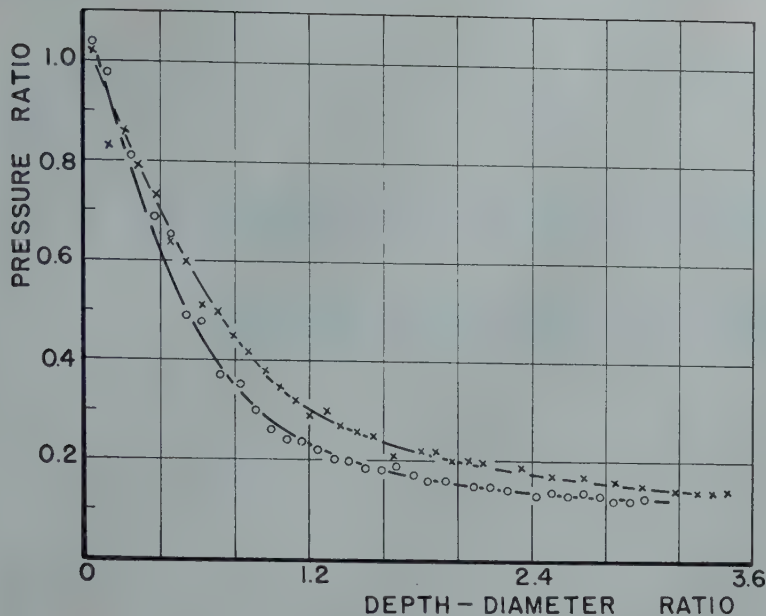


FIG 12—Pressure distribution in copper compacts pressed at 80,000 (○) and 40,000 (×) psi.

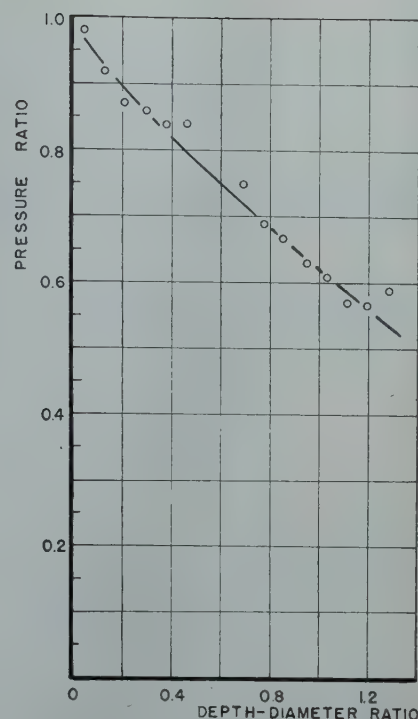


FIG 13—Pressure distribution in a copper compact pressed at 15,000 psi.

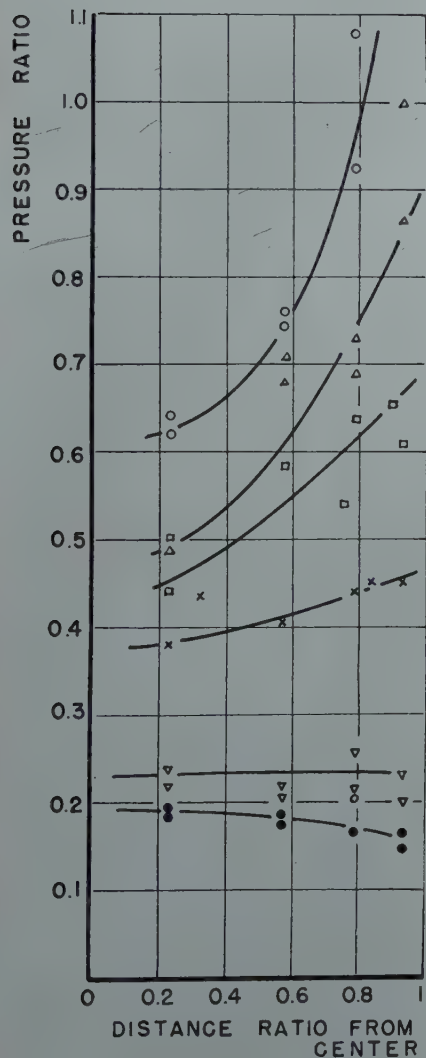


FIG 14—Radial pressure distribution in a copper compact 2.5 in. thick for a compacting pressure of 100,000 psi.

Distance from moving piston:

(○) 0.12 in. (□) 0.63 in. (▽) 1.72 in.
(△) 0.37 in. (×) 0.94 in. (●) 2.2 in.

sure in a longitudinal section. Three cases corresponding to compacts having a thickness to diameter ratio of 0.42, 0.79, and 1.66 are shown in Fig 17. Although these tracings should not be considered as very accurate, they provide a useful illustration of the results previously discussed.

The results of the present investigation of radial and longitudinal distributions of pressure agree in general with those obtained by Kamm, Steinberg and Wulff with the use of a lead grid in the powder during pressing.⁴

Summary and Conclusions

The experiments described in this paper have established the possibility of using resistance type strain gauges for measuring the pressure distribution on the walls and on the fixed piston of a die. The pressure on the walls in a cylindrical die varies almost linearly from the bottom to the top of the compact. On the fixed piston, the pressure decreases from the center to the periphery. The average pressure acting on the fixed piston or the die was also measured by a very simple strain gauge technique.

An interesting curve characterizing the behavior of the powder was obtained by plotting the ratio of the pressure on the fixed piston to the compacting pressure vs. the ratio of thickness to diameter of the compact.

The distance from the moving piston appears to be the basic factor determin-

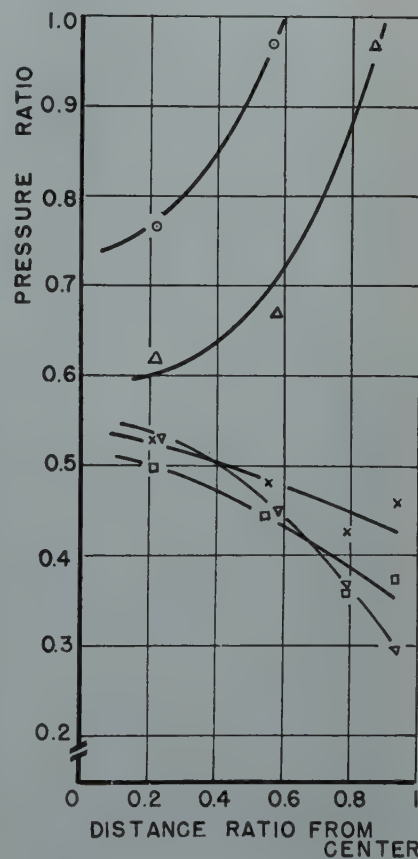


FIG 15—Radial pressure distribution in a copper compact 1.2 in. thick for a compacting pressure of 100,000 psi.

Distance from moving piston:

(○) 0.06 in. (△) 0.19 in. (×) 0.89 in.
(□) 1.01 in. (▽) 1.14 in.

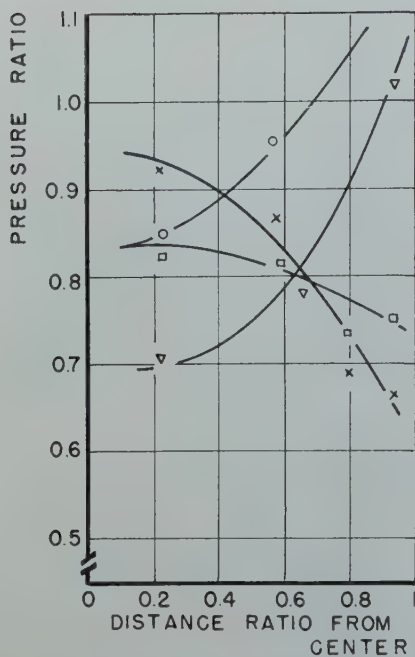


FIG 16—Radial pressure distribution in a copper compact 0.64 in. thick for a compacting pressure of 100,000 psi.

Distance from moving piston:

- (○) 0.06 in. (▽) 0.16 in.
(□) 0.45 in. (×) 0.58 in.

ing the magnitude of effective pressure at any section of a compact; that is, variation of base pressure measurement with thickness of compact (distance from moving piston) agrees reasonably well with the variation of effective compacting pressure with depth of compact (distance from moving piston).

There is a radial distribution of pressure at the top and bottom of the compacts. Near the moving piston, the pressure is high at the outer edge and decreases towards the center. At the fixed piston, the pressure is higher at the center of the compact and decreases towards the outer edge. While the radial distribution at the top is always present, the radial distribution at the base of the compact decreases with increasing thickness of compact until it vanishes, in the case of copper, at a thickness to diameter ratio of about 1.5.

Acknowledgment

This work was done at the Jet Propulsion Laboratory, California Institute of Technology, under contract

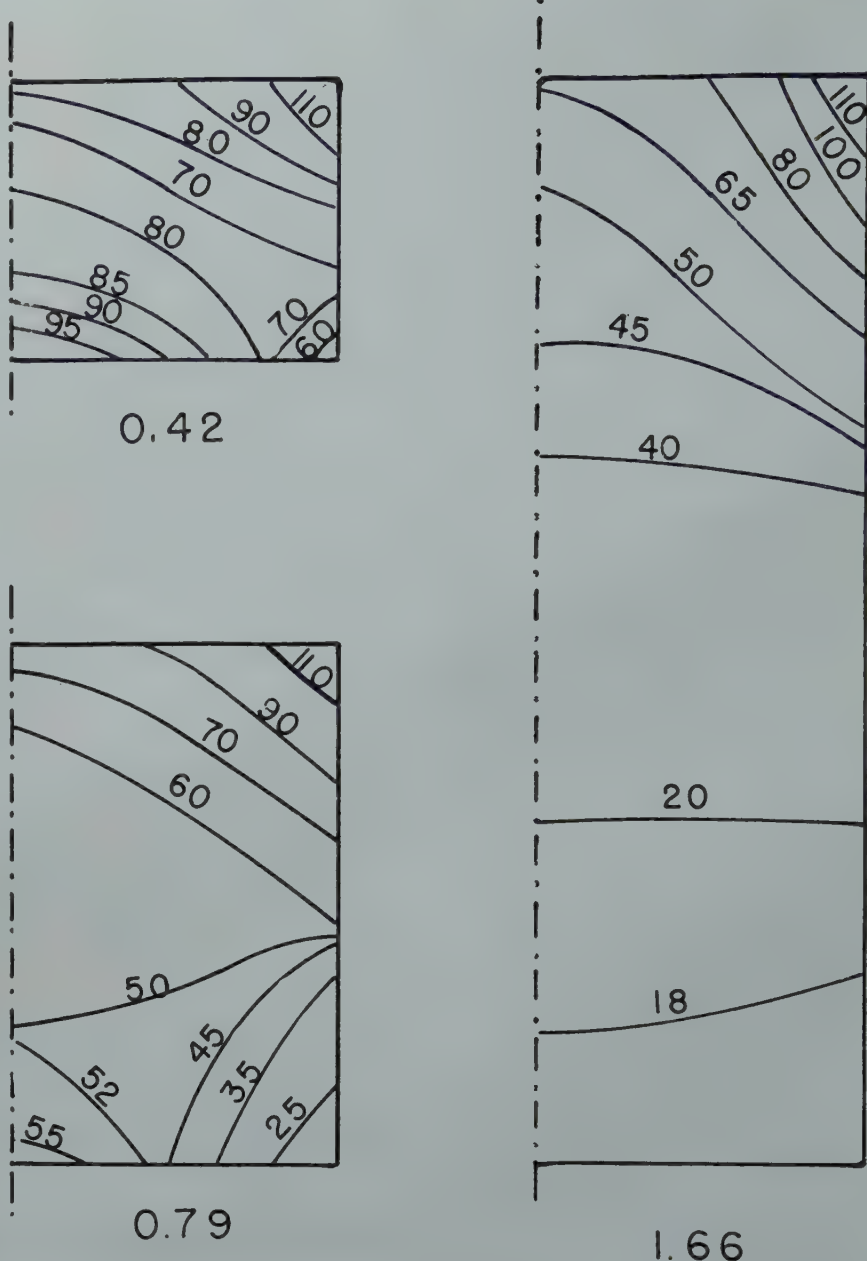


FIG 17—Approximate location of lines of equal pressure in copper compacts of 0.42, 0.79, and 1.66 thickness to diameter ratios, compacting pressure 100,000 psi.

with the Army Ordnance Department, Washington, D. C. The authors wish to thank this agency for the permission to publish the results of this investigation.

References

1. R. P. Seelig: Review of Literature on Pressing of Metal Powders. *Metals Tech.* TP 2236, Aug. 1947; *Trans. AIME* (1947) 171, 506.
2. R. P. Seelig, and J. Wulff: The Pressing Operation in the Fabrication of Articles by Powder Metallurgy. *Metals Tech.*, TP 2044, Aug. 1946; *Trans. AIME* (1946) 166, 492.
3. A. Squire: Density Relationships of Iron Powder Compacts. *Metals Tech.* TP 2165 (April 1947); *Trans. AIME* (1947) 171, 485.
4. R. Kamm, M. Steinberg, and J. Wulff: Plastic Deformation in Metal Powder Compacts. *Metals Tech.* TP 2133 (Feb. 1947); *Trans. AIME* (1947) 171, 439.
5. H. Unckel: *Archiv. Eisenhüttenwesen*, 18, 161, (1945).
6. D. W. Taylor: Research on Consolidation of Clays. Prob. from Dept. of Civil and Sanitary Eng., Mass. Inst. of Tech., Ser. 82 (1942).

Preferred Orientation in Rolled and Recrystallized Beryllium

A. SMIGELSKAS* and C. S. BARRETT,† Member AIME

THERE have been no publications of the deformation and recrystallization orientations of the metal beryllium, yet pronounced textures would certainly be anticipated since it is close-packed hexagonal in structure. Having an axial ratio approximately that of magnesium, beryllium probably deforms by nearly the same slip and twinning mechanisms that operate in magnesium, and the textures are likely to be similar or but slightly different from the magnesium textures. In the tests reported below this is found to be the case; the textures are found to differ from those of magnesium only in the details of the scatter from the average orientation.

This report covers not only samples rolled at room temperature, but some rolled at elevated temperatures. Since magnesium has been suspected by some investigators of altering its crystallographic deformation mechanism at elevated temperatures, it was considered possible that beryllium might do so and alter its textures accordingly. No pronounced alterations were found, however. Unfortunately, the theory of deformation textures is not in a state of development that permits one to deduce the deformation mechanism from a knowledge of the textures, which means that the similarity of textures at different rolling temperatures, reported here, cannot be taken as definite evidence that the deformation mechanism is actually the same at all temperatures. The general similarity of the deformation textures of magnesium and beryllium also extend to the recrystallization textures of the two metals, judging by the pole figures for recrystallized sheet presented in this report.

Methods

Samples were prepared in the form of composite sheets made up of small pieces stacked in a pile. Each piece was trimmed with scissors so that an edge was parallel to the rolling direction, dipped in paraffin, and assembled into the pack by aligning it under the cross hair of a microscope. As the desired orientation was obtained on each piece it was secured in place by touching with a hot wire to melt the paraffin. A stack of ten or fifteen pieces was built up in this way, then trimmed to the shape of a T; the portion to be X rayed was then etched to the shape of a wire about 0.045 in. diam with 6N HCl. This method of shaping the sample is a modification of that used by Bakarian on magnesium.¹ The absorption of the rays in the sample was so slight that it caused no difficulty in interpreting the films.

Exposures were made with a 0.030 in. diam pinhole, using molybdenum radiation (40 kv, 25 ma, Type A film at 5 cm, 2 to 3 hr exposures). With the recrystallized specimens it was found necessary to oscillate the specimen so as to reduce the spottiness of the lines. A range of oscillation of 5° was suffi-

cient to produce reasonably satisfactory patterns, though the quality was somewhat inferior to that of the deformation texture patterns, and only two degrees of intensity were read from the arcs on the films. Typical photographs for each of the deformation textures and the recrystallization texture are assembled in Fig 1.

The pole figures were plotted in the usual way with the intensity of the various portions of the diffraction rings estimated by eye. Seven to nine films were made of each sample and each was carefully read in plotting the pole figures.

Typical series included exposures with the beam normal to the rolling direction and at 11, 26, 41, 56 and 71° to the cross direction, plus two exposures with the beam normal to the cross direction, and at 11 and 79° respectively to the rolling direction.

The rolling was in each case considered sufficient to develop the final texture: the reduction by cold rolling was 84 pct (from 0.0045 to 0.0007 in. thickness), following prior hot rolling in longitudinal and transverse directions and recrystallization; the reduction by hot rolling at 800°C was 90 pct (0.010 to 0.001 in.), following similar prior treatment; the reduction by rolling at 350°C was 88 pct (from 0.005 to 0.0006 in.) after similar prior treatment. The recrystallization texture was determined on a sample rolled at 350° to a reduction of 88 pct (0.0165 to 0.002 in.) after similar prior treatment, then mounted between steel strips to keep it flat and annealed at 700° in an atmosphere of argon.

Discussion of Results

The results of the X ray determinations are assembled in the pole figures of Fig 2, 3, 4 and 5 for rolling at

San Francisco Meeting, February 1949.

TP 2522 E. Discussion of this paper (2 copies) may be sent to *Transactions* AIME before May 15, 1949. Manuscript received November 1, 1948.

* Argonne National Laboratory, Chicago, Illinois.

† Institute for the Study of Metals, University of Chicago; Consultant at Argonne National Laboratory.

¹References are at the end of the paper.

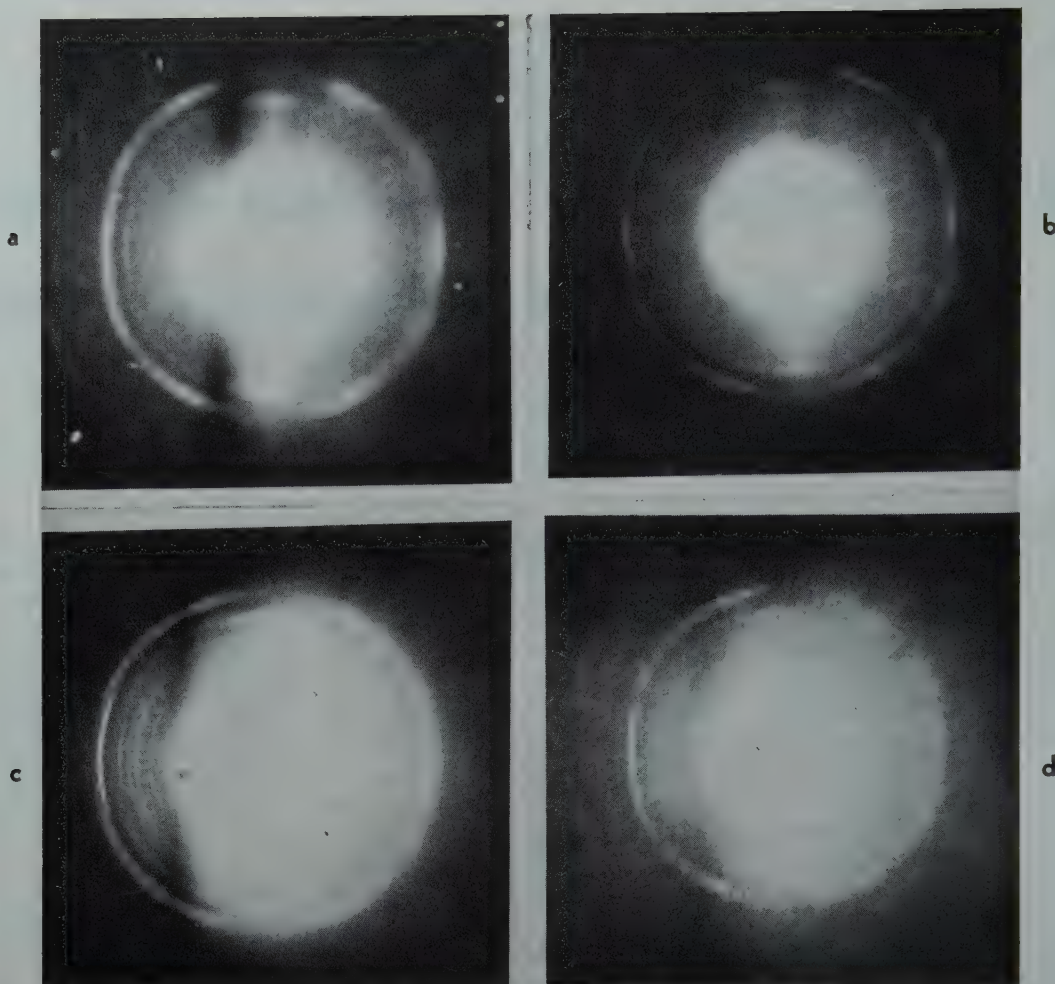


FIG 1—X ray photographs (a) room temperature rolled sheet (b) 350°C rolled sheet (c) 800°C rolled sheet (d) 350°C rolled sheet and recrystallized at 700°C.

Beam 11° to cross direction and 90° to rolling direction vertical. Outmost ring (101) pyramidal planes show eight maxima; next ring (001) basal plane shows two maxima in 3 o'clock and 9 o'clock positions; the inner ring (100) planes show maxima at 6 o'clock and 12 o'clock positions.

25, 350 and 800°C and for 350°C rolled sheet after recrystallization, respectively. The plane of the sheet is parallel to the plane of the stereographic projection in all the figures, with the rolling direction vertical and the transverse direction horizontal. The densities of the arcs on the films are indicated by the closeness of the cross-hatching on the pole figures. The orientations of three different sets of planes are shown, the three with most marked evidence of orientation in the films, (0001), (10 $\bar{1}$ 0), and (10 $\bar{1}$ 1), that is, (001), (100), (101). The conclusions that are drawn from these data are consistent with the pole figures from all three sets of planes.

The texture is of the same type in all specimens. It may be described in terms of an ideal, or mean, orientation plus a scatter, the ideal orientation being (001) parallel to the plane of rolling and (100) perpendicular to the direction of rolling. This orientation is

shown on each of the pole figures by small circles. Thus the basal plane is parallel to the plane of the sheet; two close-packed rows of atoms in this plane make an angle of 30° with the rolling direction, and the third close packed row is parallel to the transverse direction in the sheet.

The scatter from this mean position is such that the hexagonal axis tilts more toward the cross direction than toward the rolling direction. To state it differently, treating the rolling direction as an axis of rotation, the scatter around this axis extends as much as 50° each way from the mean orientation, while the scatter around the cross direction is only about 20° each way from the mean.

From the pole figures it appears that the scatter is greatest with room temperature rolling, is less with 350°C rolling, and still less with 800°C rolling and with recrystallization, the corresponding ranges of scatter around the

rolling direction as an axis being about 65, 50, 40, and 40° from the mean orientation, respectively. Whether these different ranges are significant is problematical, however, for it must be noted that the grain size progressively increases throughout this sequence, hence the films are progressively less able to locate with certainty the exact limits of a pole figure area.

There is no evidence of an abrupt change in texture at an elevated temperature that would necessitate assuming that a different mechanism of deformation sets in above room temperature. But as mentioned earlier, it is not possible at the present time to definitely exclude this on the basis of the pole figure evidence, since a complete understanding of textures and their implications has not yet been reached.

The mean position of the basal plane in rolled beryllium (axial ratio $c/a = 1.568$) is the same as in magnesium, zirconium, and close-packed hexagonal

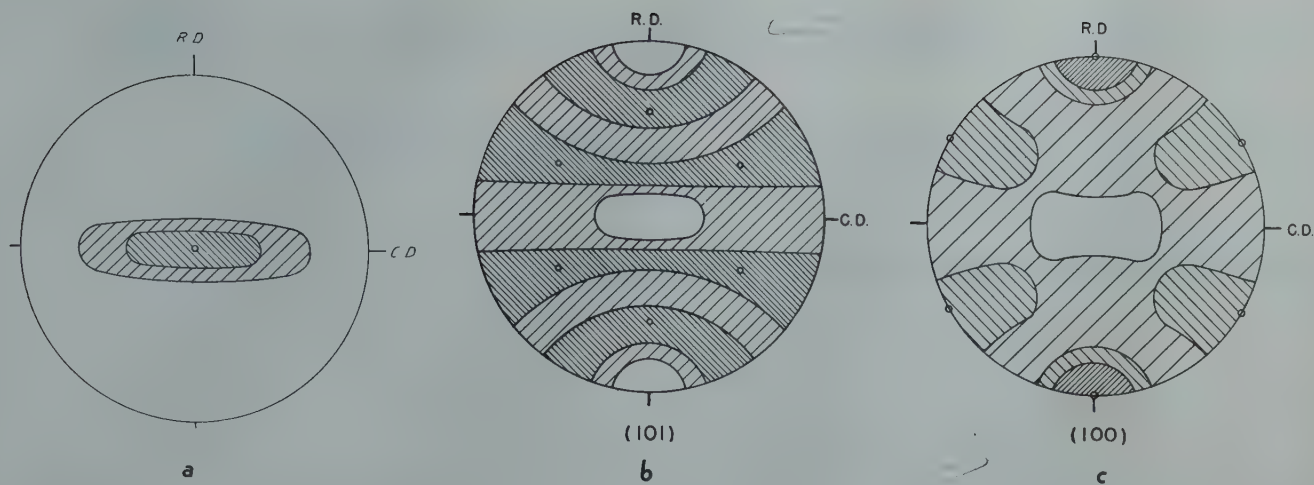


FIG 2—Pole Figures for Beryllium Rolled at Room Temperature (a) (001) Planes, (b) (100) Planes, (c) (101) Planes. Ideal texture indicated by small circles.

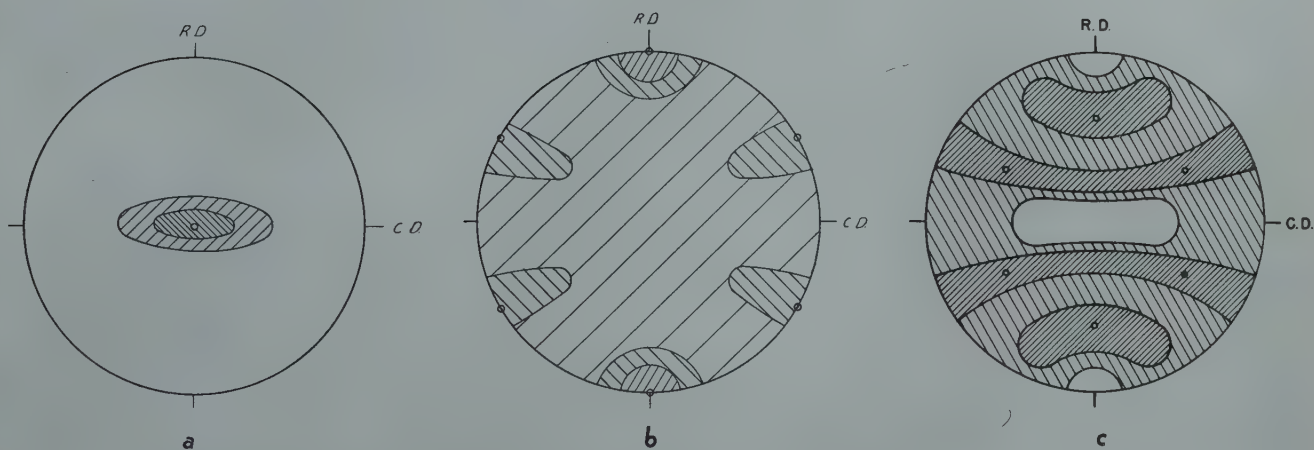


FIG 3—Pole Figures for Beryllium Rolled at 350°C. (a) (001) Planes, (b) (100) Planes, (c) (101) Planes.

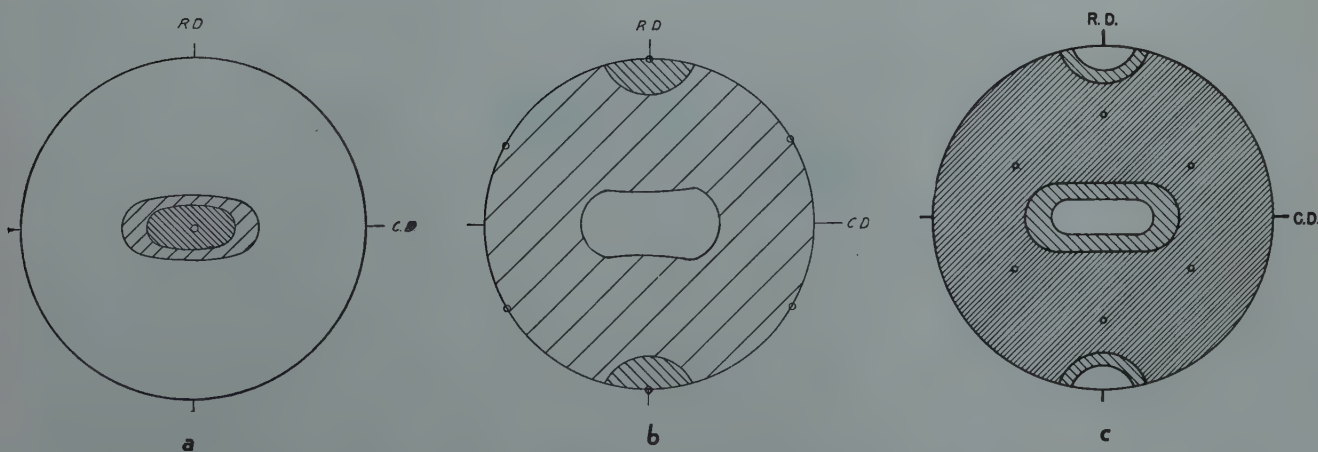


FIG 4—Pole Figures for Beryllium Rolled at 800°C. (a) (001) Planes, (b) (100) Planes, (c) (101) Planes.

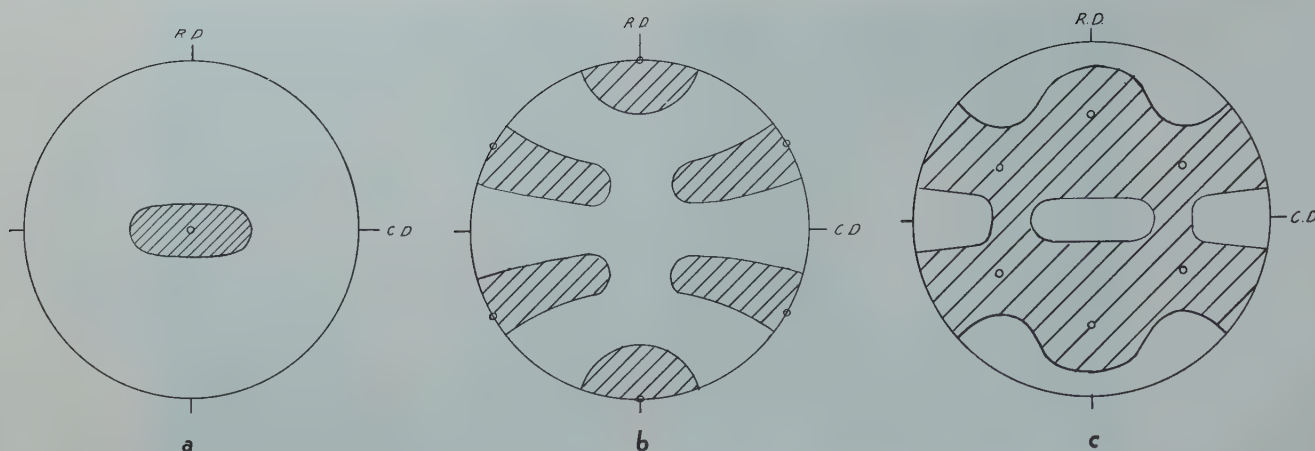


FIG 5—Pole Figures for Beryllium Rolled at 350°C and Recrystallized at 700°C. (a) (001) Planes; (b) (100) Planes; (c) (101) Planes.

cobalt, ($c/a = 1.624, 1.589$ and 1.624 respectively), but differs from that in zinc and cadmium, which have much greater axial ratios (1.85 and 1.88 respectively). Twinning is an important feature of the rolling process for zinc and cadmium and not for the metals of lower c/a ratio, and we now see that beryllium is no exception to this rule, for there is nothing in the texture of beryllium that suggests an appreciable amount of twinning in the final stages of deformation. There may be twinning, of course, in the early stages of deformation before the stable texture is reached.

It is not surprising that the recrystallization texture is the same as the rolling texture, for this is a common behavior in close-packed hexagonal metals.

There is no evidence for the double texture that is observed in certain alloys of magnesium,¹ in which the central spot of the (001) pole figure is

double. The major axis of spread in beryllium is around the rolling direction of the sheet, which is similar to zirconium, rather than around the transverse direction as in magnesium.² Another interesting feature of the beryllium texture is the alignment of the [210] direction parallel to the rolling direction (that is, the alignment of the (100) plane normal to the rolling direction). In the usual textures reported for hexagonal metals there is no marked preference for any direction in the basal plane to be parallel to the rolling direction.

Summary

The rolling texture of beryllium is one in which the preferred position of the basal plane is parallel to the plane of the rolled sheet and close-packed rows of atoms in this plane lie 30° from the rolling direction. There is a scatter of from 40 to 65° in both directions

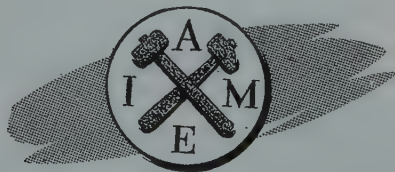
from this orientation around the rolling direction as an axis, and a smaller scatter around the transverse direction in the sheet. The texture is approximately the same for rolling at room temperature, 350 and 800°C , and after recrystallization. There is no evidence of a change of slip mechanism with temperature.

Acknowledgments

We are indebted to Mr. James F. Schumar and Mr. S. Hugh Paine, Jr., for assistance in this work, and particularly to Mr. Robert E. Macherey for the difficult rolling of the samples. The work described in this article was performed under the auspices of the Atomic Energy Project.

References

1. P. W. Bakarian: *Trans. AIME* (1942) **147**, 266.
2. W. G. Burgers and F. M. Jacobs: *Metallwirtschaft*, (1935) **14**, 285.



Magnesium-lithium Base Alloys— Preparation, Fabrication, and General Characteristics

J. H. JACKSON,* P. D. FROST,* A. C. LOONAM,* L. W. EASTWOOD,* and C. H. LORIG,* Members AIME

Introduction

It is well known that for equal weights of material, thin sections of the lighter structural alloys are more resistant to buckling under a compressive stress than thin sections of more dense material. Therefore, structural parts having the same resistance to buckling stresses are generally lightest when they are made of magnesium alloys. Consequently, there is considerable interest in the development of strong alloys having densities equal to or lower than that of magnesium and strength-weight ratios equivalent to those of the strongest aluminum alloys.

The development of commercial magnesium-base alloys has been very successful, and their importance among materials in the structural field has been amply demonstrated. However, an even wider structural application of magnesium alloys might be effected if improvements could be made in the cold rollability and cold-forming characteristics. Such improvements, along with production of less directionality in properties, could be effected if the hexagonal close-packed lattice of present alloys could be replaced with a cubic lattice.

In 1942, a project, having as its objective the improvement of some of the characteristics of commercial magnesium-base alloys, was initiated at Battelle Memorial Institute under the sponsorship of the Mathieson Chemical Corporation. At that time, one of the authors,* then Chief Metallurgist for the Mathieson Chemical Corporation, postulated that the addition of lithium to magnesium in sufficient quantities to change the crystal structure of the resultant alloy from a hexagonal to a

body-centered cubic lattice should produce a magnesium-rich alloy which would have the desired improvements in cold-working characteristics with less directionality in properties. To test this view, a series of alloys was made and was found to have many of the attributes that were predicted.

The view that magnesium-lithium alloys were of structural interest was also held by others. In 1943 and 1945, Dean and Anderson^{1,2} obtained patents on magnesium-base alloys containing from about 1 to 10 pct lithium, from about 2 to about 10 pct manganese, and the balance substantially all magnesium; and on magnesium-base alloys containing from about 1 pct to about 10 pct lithium, from about 2 to about 10 pct manganese, from about 0.5 to 2 pct silver, and the balance substantially all magnesium. They noted that an alloy containing 83 pct magnesium, 10 pct manganese, 5 pct lithium, and 2 pct silver could be cold rolled by any of the usual methods and that this alloy was considerably harder and stronger than most other magnesium-base alloys heretofore available.

In 1945, Hume-Rothery, et al.,³ predicted that magnesium-lithium base alloys should be soft and ductile and that such compositions, to which was added a third element for the purpose of producing a precipitation-hardening type of alloy, should be ductile, strong, and lighter than magnesium itself. Hume-Rothery investigated the

binary magnesium-lithium and ternary magnesium-lithium-silver equilibrium relations and criticized the existing equilibrium diagrams. The binary magnesium-lithium equilibrium diagram has also been investigated by Grube, Von Zeppelin, and Bumm,⁴ Henry and Cordiano,⁵ Sal'dau and Shamrai,⁶ Hofmann,⁷ and Shamrai.⁸ The work of most investigators agreed with that of Grube, whose constitution diagram is shown in Fig 1.

From the standpoint of development of structural alloys, the room-temperature equilibrium relations are of great interest. An examination of Fig 1 reveals that, from 0 to 5.7 pct lithium, the existing phase is alpha, which is a solution of lithium in hexagonal magnesium. The boundary between the alpha, and alpha plus beta regions, occurs at a Mg/Li of 16.5, corresponding to 5.7 pct lithium by weight. Between 5.7 pct and 10.3 pct lithium, there exists a mixture of the alpha phase (lithium dissolved in hexagonal magnesium) and the beta phase (magnesium dissolved in body-centered-cubic lithium). The boundary of the alpha plus beta and beta regions occurs at a Mg/Li of 8.7, corresponding to a lithium composition of 10.3 pct. Much of the work described here was directed toward obtaining an alloy made up of a large proportion, or entirely, of the body-centered-cubic beta structure.

In his early work, Loonam found that specimens of lithium-bearing alloys were very malleable. Ingots of alloys prepared at that time were extruded to $\frac{3}{8}$ -in. diam bars, and the mechanical properties and the effects of heat treatment were then determined. These data are given in Table 1. The outstanding ductility of the alloys, combined with their moderately high strength, evoked considerable interest.

San Francisco Meeting, February 1949.

TP 2534 E. Discussion of this paper (2 copies) may be sent to *Transactions AIME* before May 15, 1949. Manuscript received November 1, 1948; revision received November 26, 1948.

* Battelle Memorial Institute.

¹ References are at the end of the paper.

* A. C. Loonam

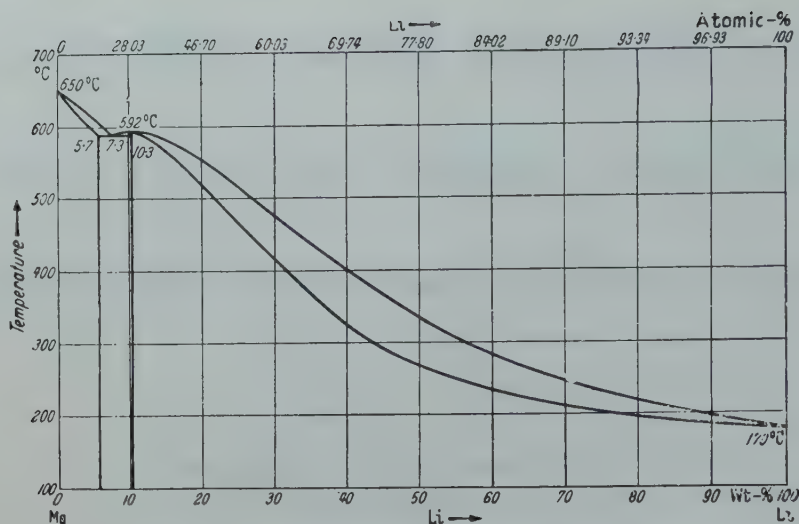


FIG 1—Magnesium-lithium equilibrium diagram (Grube).

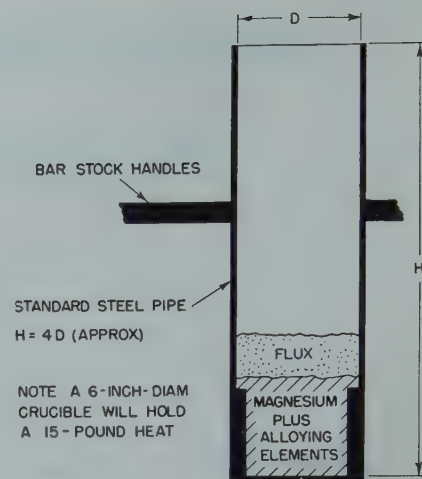


FIG 2—Melting crucible, showing relative positions of flux and metal before lithium addition.

Table 1 . . . Properties of Magnesium-lithium Alloys Prepared at Mathieson Chemical Corporation¹

| Heat No. | Mg/Li | Intended Composition, Pct | | | | | Chemical Analysis, Pct | | | | As Extruded at 450°F ² | | | Brinell Hardness | | |
|----------|-------|---------------------------|------|-----|--------|-----|------------------------|------|---------|------|-----------------------------------|--------------------------|------------------------|------------------|---|---|
| | | Mg | Li | Mn | Al | Zn | Li | Mn | Al | Zn | Tensile Strength, psi | Elongation, Pct in 1 In. | Reduction of Area, Pct | Extruded | Extruded and Air Cooled after 14 Hr at 500°F ³ | Extruded and Water Quenched after 18 Hr at 950°F ³ |
| 2 | 7.6 | 86.9 | 11.5 | 1.6 | | | 12.1 | 0.74 | | | 19,000 | 40 | 42 | 39 | 36 | 40 |
| 4 | 11.3 | 90.4 | 8.0 | 1.6 | | | 9.2 | 1.24 | | | 21,200 | 32 | 43 | 43 | 42 | 44 |
| 5 | 11.2 | 90.0 | 8.0 | | 2.0 | | 8.5 | | 2.05 | | 31,600 | 21 | 27 | 65 | 55 | 77 |
| 6 | 11.0 | 88.0 | 8.0 | | 4.0 | | 8.3 | | 4.15 | | 34,400 | 9 | 11 | 67 | 57 | 78 |
| 7 | 10.7 | 86.0 | 8.0 | | 6.0 | | 8.4 | | 6.20 | | 37,100 | 11 | 13 | 72 | 61 | 85 |
| 8 | 11.4 | 91.0 | 8.0 | | | 1.0 | 8.8 | | | 1.12 | 23,900 | 25 | 50 | 47 | 44 | 44 |
| 9 | 11.2 | 90.0 | 8.0 | | | 2.0 | 9.6 | | | 2.27 | 26,000 | 32 | 42 | 51 | 46 | 50 |
| 10 | 11.0 | 88.0 | 8.0 | | | 4.0 | 8.8 | | | 4.03 | 28,000 | 46 | 58 | 58 | 57 | 53 |
| 12 | 9.0 | 88.2 | 9.8 | | 2.0 Be | | 8.4 | | 0.11 Be | | 20,800 | 29 | 36 | 43 | 39 | 40 |
| 13 | | 98.0 | | 2.0 | | | | 1.53 | | | 45,600 | 2 | 6 | 48 | 47 | 36 |
| Mg | | | | | | | | | | | 31,200 | 4 | 7 | 36 | 34 | 27 |

¹ Alloys were prepared at Mathieson and tested at Battelle.

² Extruded to 3/8-in.-diam rod. Reduction of 10 to 1.

³ Protected from oxidation with argon atmosphere.

The fact that aluminum-bearing alloys, Nos. 5, 6, and 7, were hardened by water quenching from 950°F indicated that, by suitable heat treatment, higher strengths could be obtained. In order to explore completely the possibilities of magnesium-lithium alloys, an extensive project at Battelle was set up by the Mathieson Chemical Corporation. In 1945, when magnesium-lithium base alloys were found to be of military interest, the Navy Department, Bureau of Aeronautics, entered into a cooperative agreement with Mathieson for the sponsorship of further investigational work.

This paper summarizes the results obtained during the several years of investigation of the magnesium-lithium base alloys. These results are described under seven main topics covering melting technique, fabricating practice, density measurements, mechanical properties, work-hardening and stability characteristics, corrosion resistance, and metallographic structure.

Melting Techniques

Magnesium-lithium base alloys can be melted satisfactorily under a flux or under an inert atmosphere. The flux, when it is used, is comprised of lithium chloride and lithium fluoride in the proportions from 75/25 to 82/18, the choice of the composition depending to a great extent upon the alloy composition to be melted. In general, better separation of the metal from the flux is obtained when the salts are in the ratio of 75 to 25; hence, a flux of this composition is selected when a new type of alloy is melted for the first time. However, when this flux is used on certain alloys, especially those containing high percentages of cadmium, it tends to become very viscous. A change to the 82/18 composition will, in most instances, improve the fluidity, although the flux of higher lithium chloride content does not separate from the metal as well as does the flux of lower lithium chloride content.

In most of the experimental work, the quantity of flux used was equivalent to about 35 pct of the weight of the metallic charge. When "large" heats were made, that is, heats weighing 10 lb or more, it was possible to reduce the percentage of flux. The flux can be re-used, and if it becomes too thick for easy handling, the addition of unused material will increase its fluidity. To make certain, however, that the flux would be satisfactory on heats prepared for the experimental studies, fresh materials were used for each melt.

A crucible having a diameter about one-third its height is used in preparing the melts. The flux is melted first to eliminate all traces of water from the hygroscopic flux ingredients. The magnesium and alloying elements other than lithium are then added. In order to insure that the alloying elements dissolve, they are placed in a steel wire basket suspended in the molten magnesium. Before the lithium is added,

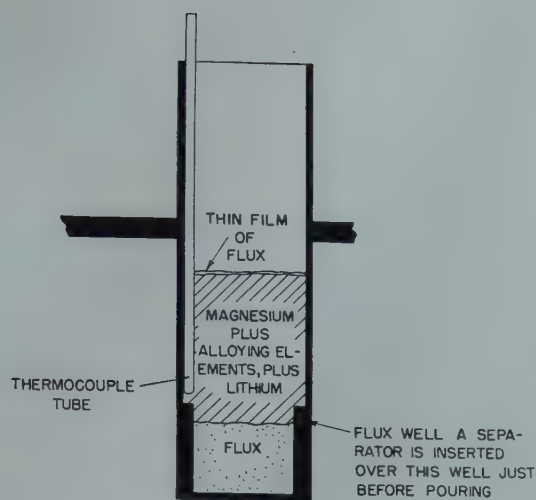


FIG 3—Melting crucible, showing relative positions of flux and metal after lithium addition.

the molten flux is lighter than the metal and provides an effective protective layer on the melt, as illustrated in Fig 2. Lithium, added by means of an inverted cup, is plunged below the surface of the metal bath. After the lithium dissolves, the cup is removed and the melt is thoroughly stirred.

The addition of lithium to the magnesium reduces the density of the alloy to a value lower than that of the flux, and the metal then floats on top of the flux, as shown in Fig 3. If the desired alloy contains elements which can be introduced into the metal more easily by the reduction of the salt of the element, such salt additions are made at this time. This addition can readily be introduced by melting the correct proportion of salt in a separate pot containing lithium chloride-lithium fluoride flux and then pouring the molten salt and flux mixture onto the metal bath. Should the element added in the form of salt not be soluble in molten magnesium alone but soluble in the magnesium-lithium melt, then the above procedure has various obvious advantages.

After all alloying additions are made, the flux is allowed to settle in the crucible. It is often desirable to make additions to the flux in order to increase its density and thus decrease the settling time. An addition of about 10 pct lithium bromide is especially effective.

It is desirable to equip the crucible with a sump in the bottom into which the flux may collect. A convenient method to avoid the mixing of metal and flux during pouring involves the insertion of a cover so that the cover rests on the sump and holds the flux in

the sump while the metal is poured.

Although the flux is heavier than the metal after the lithium addition, a thin film of flux remains on the surface. The protection offered by this film, combined with the stack effect of the deep crucible, reduces the tendency toward burning or excessive oxidation of the metal. Magnesium-lithium base alloys are protected during pouring by a thin film of oxide which envelops the stream. The Durville method of pouring, or a slight modification of it, is necessary if turbulence and attendant inclusion of the oxide skin in the ingot are to be avoided. Therefore, the molds are tilted in such a way that the metal runs down the side with a minimum of turbulence. Ingot molds of either graphite or cast iron are satisfactory. When a cast iron ingot mold is used, a hot top either of graphite or of a refractory baked at high temperature is needed. The surfaces of cast iron molds are coated with acetylene soot. Before pouring, both graphite and cast iron molds are heated to about 250°F to drive off moisture. After pouring, any tendency toward burning on the surface of the ingot hot top is eliminated by the use of G-1 powder (a commercial graphite-base material) or paraffin, or by covering with an air-tight lid. By following the procedure described, the magnesium-lithium base alloys are less likely to burn during melting and pouring than are ordinary magnesium-base alloys.

Magnesium-lithium base alloys may be melted under argon in a capped crucible without the employment of a salt flux. To take full advantage of the inert atmosphere, it is desirable to

place the entire charge, including the lithium, into a cold crucible. After purging the crucible with argon, the heat is melted and poured. Only a slight tendency toward burning during the pour is evident even though no salt flux is used.

A melting procedure combining the use of a flux and an argon atmosphere is also highly satisfactory, and by this technique the amount of flux required can be drastically reduced. The use of an argon atmosphere reduces oxidation and lessens the tendency for the flux to thicken.

Fabrication Practice

For the most part, the magnesium-lithium base alloys were cast into one or more of the various ingots described in Table 2. The ingots were fabricated to produce test material also described in Table 2.

The recrystallization temperature of many magnesium-lithium base alloys of the body-centered-cubic lattice type is about 375°F. The alloys can be hot worked readily by extruding, hammer forging, or hot rolling at temperatures between 400 and 700°F, depending on composition. Finishing temperatures at or just above the recrystallization temperature of 375 to 425°F were used in the experimental work in order to obtain a fine-grained product.

The reduction by hot rolling depended to some extent upon the alloy composition and, in general, was about 30 pct per pass. Hot rolling could be accomplished, however, at reductions as high as 50 pct per pass on most alloys. In order to prevent the magnesium-lithium alloy from adhering to the rolls, the latter were usually coated with kerosene for both hot and cold rolling.

The rolls during cold rolling were usually kept near room temperature. Practically all compositions could be cold rolled to total reductions of at least 15 pct immediately after hot rolling or after solution treating; in some instances, they could be cold rolled to total reductions of over 95 pct. Many of the alloys could be cold reduced as much as 50 to 75 pct per pass, although the general practice was to restrict cold-rolling reductions to 5 to 10 pct per pass.

The magnesium-lithium base alloys could be cold drawn to bar stock only with difficulty because of their tendency to seize on the die and because they

Table 2 . . . Typical Fabrication Procedures Used in Investigation of Magnesium-lithium Base Alloys

| Weight of Heat | Cast Product | Machined Billets | Extruded Product | Disposition |
|----------------|---|--|--|---|
| 1000 g | 2½ ingots, 1½ in. in diam × 8 in. long. | 3 pieces, 1½ in. in diam × 3½ in. long. Balance of ingots saved. | 3 rods, ¾ in. in diam × 30 in. long. | 4 tensile specimens, ¼-in. diam, 1-in. ga length, tested as extruded and as aged 48 hr at 150°F. 4 bend-deflection test specimens, tested as extruded and as aged 48 hr at 150°F. Balance of stock saved. |
| 10 lb | 6 ingots, 2½ in. in diam × 7 in. long. | 6 pieces, 2 in. in diam × 5 in. long. | 5 rods, ⅝ in. in diam × 36 in. long. ¹ 2 strips, ⅞ in. × ¼ in. × 36 in. ² | 10 standard tensile specimens, 10 standard compression specimens, 10 unnotched Charpy impact and 10 notched Charpy impact specimens. These were tested as extruded, and as extruded and aged 48 hr at 150°F. Strips were corrosion test specimens; tested after aging 48 hr at 150°F. |
| 10 lb | 1 forging ingot, 4 × 4 × 12 in. | | | Forged to rolling slab, machined, and rolled to plate or sheet. (Total reduction effected: about 55 to 1.) Used in mechanical testing. |
| 1500 g | 2 ingots, 2½ in. in diam × 7 in. long. | 2 pieces, 2 in. in diam × 5 in. long. Other ingot saved. | 2 strips, 1½ in. × ¼ in. × 36 in. | One strip hot rolled to 0.053 in. and cold rolled 15 pct to 0.045 in. (Total reduction effected: about 55 to 1.) Used in mechanical testing. One strip hot rolled 1-30 pct pass and cold rolled 15 pct. Used in age hardening tests. |

¹ Two billets were homogenized 48 hr at 600°F prior to extrusion.
² One billet was homogenized 48 hr at 600°F prior to extrusion.

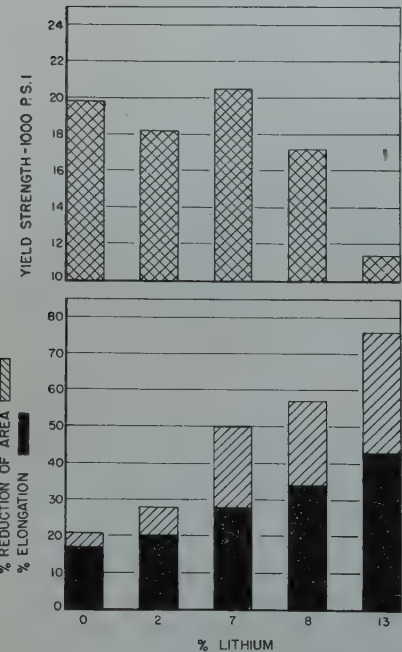


FIG 4—Effect of lithium on ductility and yield strength of extruded magnesium.

work harden only to a limited extent. The latter makes it difficult to strengthen the tip to resist fracture as the bar is started through the die. Various lubricants for cold-drawing operations were tried in an attempt to prevent die seizure. The only lubricating practice that has been successful involved the use of a flash coat of copper applied by dipping the magnesium-lithium bar in a solution of copper sulphate made slightly alkaline by the addition of ammonium hydroxide.

Density of Magnesium-lithium Alloys

One characteristic of great interest is the low density of the magnesium-lithium base alloys. A binary alloy containing 11.5 pct lithium has a density of approximately 1.4 g per cc; however, this binary alloy is so soft and ductile that it has little value from the structural standpoint, except where low strength is permissible and good formability is desired. If sufficient alloying additions of the heavier metals are made to this alloy to improve its strength, the density is often increased to about 1.45 to 1.65 g per cc. It is not difficult to formulate a magnesium-lithium alloy having mechanical properties superior to the commercial magnesium-base alloys and having a density considerably less than 1.8 g per cc, which is approximately the density of most commercial magnesium alloys.

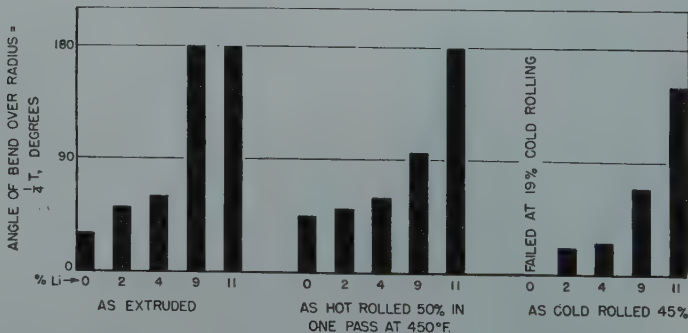


FIG 5—Effect of lithium on bend ductility of magnesium.

Some Mechanical Properties of the Magnesium-lithium Alloys

MAGNESIUM-LITHIUM BINARY ALLOYS

Magnesium-lithium binary alloys have hardnesses of the order of 0 to 10 on the Rockwell E scale, which is equivalent to a Brinell hardness number of about 30 to 35. Magnesium-lithium base alloys having good mechanical properties have hardnesses of the order of 90 Rockwell E, which is equivalent to a Brinell hardness number of about 85.

One of the most important properties which lithium was found to bestow upon magnesium was increased ductility. Although the body-centered-cubic lattice structure does not exist below 5.3 pct lithium, as little as 2 pct lithium markedly enhanced the tensile ductility and formability of pure magnesium. The effect of lithium on tensile ductility is shown in Fig 4. It will be noted that a pronounced increase in reduction of area, accompanied by a marked decrease in yield strength, occurred as lithium was increased from 8 to 13 pct. This is explained by the transition, at 10.3 pct lithium, from the two-phase, hexagonal plus body-centered-cubic structure, to the single-phase, body-centered-cubic structure. Although the single-phase hexagonal and the two-phase alloys were by no means neglected in the experimental work, the greatest attention was paid to alloys with a body-centered-cubic structure.

The influence of lithium on the bend ductility of pure magnesium is shown in Fig 5. The increase in bend ductility of rolled alloys in going from the two-phase region to the region of 100 pct beta was very noticeable. For example, the 9 pct lithium, alpha- plus beta-

phase alloy could not be bent more than 90° while the 11 pct lithium, beta-phase alloy withstood a 180° bend. On the other hand, in the extruded condition, the 9 pct lithium, two-phase alloy, had bend ductility which was equal to that of the 11 pct lithium, beta-phase alloy. The superior bend ductility of the alpha- plus beta-phase alloy in the extruded state can be explained by the mode of occurrence of the alpha phase in the microstructure. The microstructure of the alloy in the extruded and hot-rolled states is shown in Fig 6. The alpha phase occurs in the form of more or less randomly oriented, short patches in the extruded material, whereas in the rolled material it occurs as long platelets, with the plane of the platelets parallel to the plane of the sheet. When the materials are bent, the long, brittle alpha platelets in the sheet are more prone to break and notch the beta material than are the short, brittle alpha patches in the extruded material.

The effect of lithium on the cold rollability of magnesium can be observed from data plotted in Fig 5. Whereas commercially pure magnesium failed in rolling after a cold reduction of 19 pct, the lithium-bearing alloys could be cold-rolled at least 45 pct. In the cold-rolled state, the lithium-bearing alloys retained nearly the same bend ductility they possessed in the hot-rolled state.



FIG 6—Microstructure of extruded and hot-rolled two-phased Mg-Li alloy.

Light areas are alpha and gray matrix is beta. (Etched in 2 pct HF.)

a. Hot-rolled longitudinal section. b. Hot-rolled transverse section.
c. Extruded longitudinal section. d. Extruded transverse section.
Reduced approximately one-third in reproduction.

MAGNESIUM-LITHIUM-BASE TERNARY ALLOYS

Among the original alloys prepared at the Mathieson Chemical Corporation were several which contained aluminum or zinc. The mechanical properties of the alloys with aluminum or zinc gave ample indication that these elements would be of importance in increasing the strength of the ductile magnesium-lithium base. In later work, effects of practically all of the metallic elements on the properties of the magnesium-lithium alloys were investigated by preparing and studying over 1800 individual heats.

The order of solid solubility of the elements in the beta phase at room or slightly elevated temperatures, as determined from the many experimental investigations, is roughly as follows:

| Most Soluble Elements | | |
|-----------------------|----|----|
| Ag | Cd | Al |
| | Hg | In |
| | Zn | Tl |

Slightly Soluble Elements

| | | | | |
|----|----|----|----|----|
| Ni | Cu | Ca | Si | Sb |
| Co | | Sr | Ge | Bi |
| | | Ba | Sn | |
| | | Ce | Pb | |

Relatively Insoluble Elements

| | | | | | |
|---|----|----|----|----|----|
| | Be | Cr | Ti | V | Mn |
| K | B | Mo | Zr | Cb | |
| | | W | Th | | |
| | | U | Fe | | |

The elements which most effectively increased the mechanical strength of the magnesium-lithium base were aluminum, zinc, silver, and cadmium. An example of their effectiveness is shown in Fig 7. In this figure are plotted the maximum and minimum yield strengths obtained from a series of about 50 different ternary alloys of 8.1 Mg/Li base. At the extreme left, the yield strength of the 100 pct beta, 8.1 Mg/Li binary alloy is shown to be 12,000 psi. Antimony added in amounts of 1 to 4 pct and bismuth in amounts of 2 to 4 pct did not increase the yield strength. However, the recovery of

these two elements in magnesium-lithium base alloys has consistently been very low. Copper increased the yield strength somewhat, but 1 pct copper was, for all practical purposes, equally as effective as 8 pct.

Substantial increases in yield strength were brought about by additions of silver, zinc, cadmium, and aluminum. In this series of alloys, 0.5 pct aluminum was as effective as 4 pct zinc, and was much more effective than either 2 pct cadmium or 4 pct silver. The elements which were most effective in alloys with a magnesium-lithium ratio of 8.1 were likewise very effective at other magnesium-lithium ratios.

Some interesting effects of aluminum and zinc on the properties of ternary alloys having various magnesium-lithium ratios are shown in Fig 8 and 9. The alloys with a magnesium-lithium ratio of 24 (24 Mg/Li) are of the hexagonal alpha phase, those with magnesium-lithium ratios of 13.3 and 9.7 consist of alpha plus beta, and those with a magnesium-lithium ratio of 8.1 consist of the body-centered-cubic

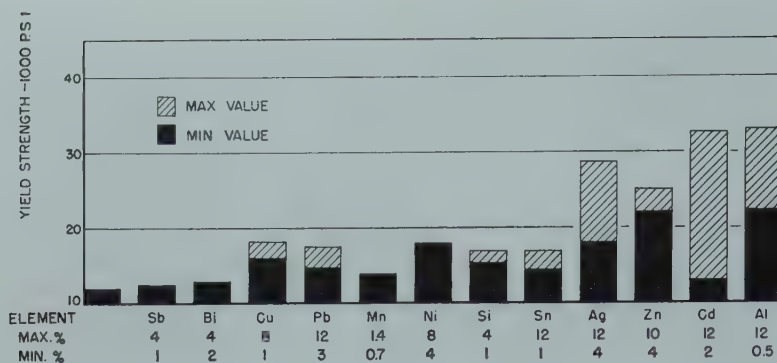


FIG 7—Effect of various elements on the yield strength of the 8.1 Mg/Li beta solid solution. All alloys tested in the as-extruded condition.

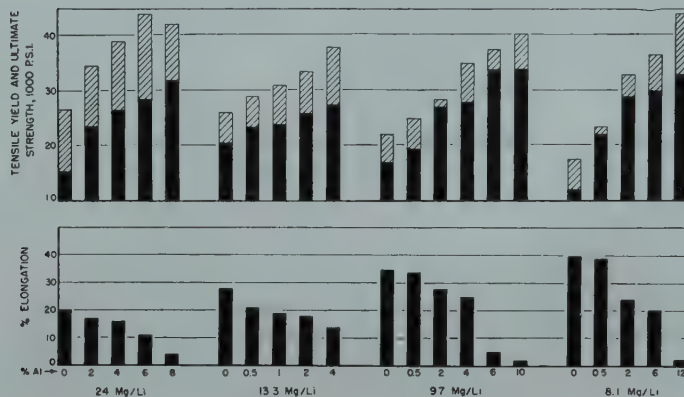


FIG 8—Effect of aluminum at different magnesium-lithium ratios on mechanical properties of extruded ternary alloys.

beta phase. The results plotted in these figures show that (1) several alloys possess rather good properties, a fact which offered an incentive for further investigation; (2) the elongation tends to increase as Mg/Li decreases; and (3) as Mg/Li decreases, there is an increase in the ratio of yield strength to tensile strength. In general, the yield strengths of the high-strength, magnesium-lithium alloys are proportionally high and are the same in tension and compression.

MAGNESIUM-LITHIUM BASE QUATERNARY AND QUINARY LOW-LITHIUM ALLOYS

The favorable properties observed for some of the ternary alloys proved an incentive to investigate quaternary and quinary alloys. The tensile properties of a 24 Mg/Li series of alloys having the hexagonal structure are shown in Fig 10. The average tensile strength of this series of alloys was about 45,000 psi.

MAGNESIUM-LITHIUM BASE QUATERNARY AND QUINARY HIGH-LITHIUM ALLOYS

The above data suggested the possibility of developing interesting alloys having the hexagonal structure or the two-phase, hexagonal plus body-cen-

tered-cubic structure. Of even greater interest have been the beta-phase, cubic lattice alloys, that is, alloys having magnesium-lithium ratios under 8.7. Alloys with magnesium-lithium ratios of 8.1, 7, 6, and 5 have been investigated in detail. A minor amount of work has also been done on 3.5 Mg/Li alloys.

In one series of 12 heats, the effects of variations in aluminum, cadmium, and silver in quinary alloys having a magnesium-lithium ratio of 6, with aluminum varying from 2 to 12 pct, silver varying from 0 to 4 pct, and cadmium varying from 0 to 4 pct were determined. The compositional levels were selected and the experiment performed as a factorial design. By means of this experimental technique, the individual effect of each of the three alloying additions, cadmium, silver, and aluminum, could be determined independent of the effects of the other two additions. The mechanical properties of the alloys are shown in Fig 11. In the as-extruded state, the tensile strength was improved by additions of the alloying elements. Increases in aluminum and cadmium contents caused decreases in mechanical properties in specimens aged at 150°F for 48 hr. The effect of an increase in silver from 0 to 4 pct stabilized the mechanical properties for the same aging treatment. This stabilizing effect of silver on mechanical properties was noteworthy throughout the work on magnesium-lithium base alloys.

The independent effects of variations in magnesium-lithium ratio, zinc, cadmium, and silver, were studied in 36 quinary magnesium-lithium-zinc-cadmium-silver alloys by means of the factorial design technique. In Fig 12

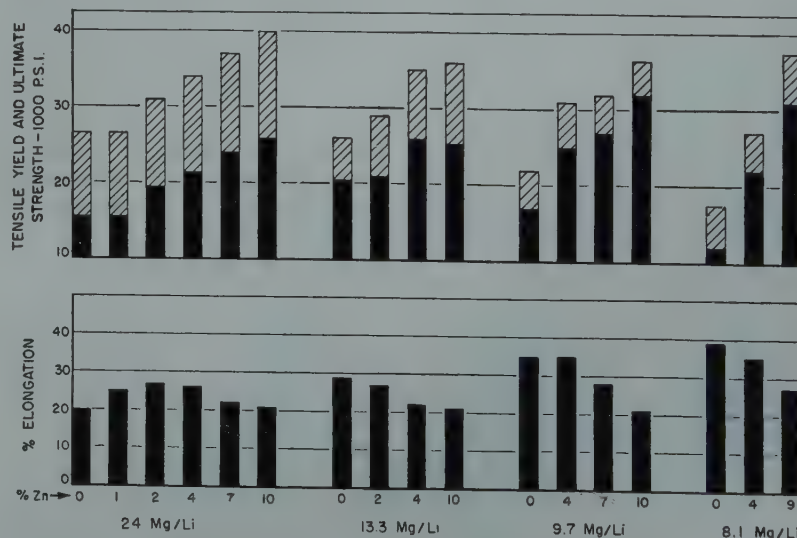


FIG 9—Effect of zinc at different magnesium-lithium ratios on mechanical properties of extruded ternary alloys.

the average yield strengths of the alloys in the as-extruded state and after aging at 150°F for 48 hr are plotted as functions of the composition.

The yield strength of the alloys increased in the as-extruded condition as Mg/Li increased. Aging increased the yield strength of 6 Mg/Li alloys but decreased the yield strength of alloys of higher magnesium-lithium ratio.

Cadmium was similar in its effect in this series of alloys as in the previous series. It increased the yield strength of the alloys in the extruded condition but did not prevent the loss of yield strength upon aging at 150°F. The effects of zinc additions were similar to those produced by cadmium. An increase in silver from 4 to 6 pct had a stabilizing influence as shown by the fact that there was no decrease in yield strength after aging for 48 hr at 150°F.

The effects of aluminum in two series of 6 Mg/Li-aluminum-cadmium-silver alloys are shown in Fig 13. Excellent mechanical properties were obtained with 1 and 2 pct of aluminum in the alloys containing 4 pct silver. The alloys with 4 pct silver were less adversely affected by the 150°F aging treatment than were the alloys with 2 pct silver. As a point of interest, the alloys with 2 pct aluminum were less stable than were the alloys with 0.5 and 1 pct aluminum.

From the results obtained on 36 magnesium-lithium-zinc-cadmium-silver al-

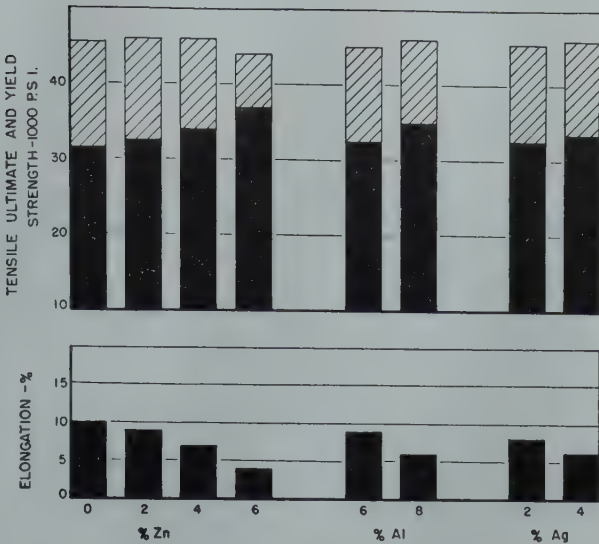


FIG 10—Effect of variations in zinc, aluminum, or silver contents on the tensile properties of extruded 24 Mg/Li-Zn-Al-Ag alloys.

loys prepared according to a factorial design, it was possible to select a number of alloys whose tensile and yield strengths were increased by aging for 48 hr at 150°F. Their mechanical properties after the aging treatment are shown in Table 3. These results are indicative of the excellent mechanical properties which can be obtained in the magnesium-lithium base alloy system. It is noteworthy that these alloys, like

all high-lithium, magnesium-lithium base alloys, have equal compressive and tensile yield strengths and have high elastic limits in both tension and compression. Their notched impact strength, on the other hand, is rather low. The 8.1 Mg/Li alloy is included in this table for comparison purposes. The high-strength alloys of the 8.1 Mg/Li type show a considerably greater loss in strength during the

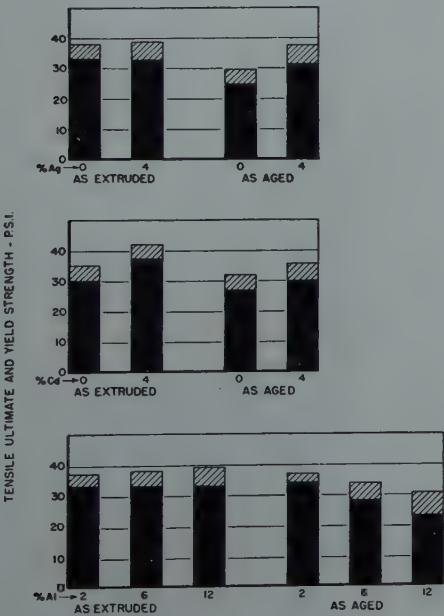


FIG 11—Effect of variation in aluminum, cadmium, or silver contents on the tensile properties of 6 Mg/Li-Al-Cd-Ag alloys as extruded and as aged at 150°F for 48 hours.

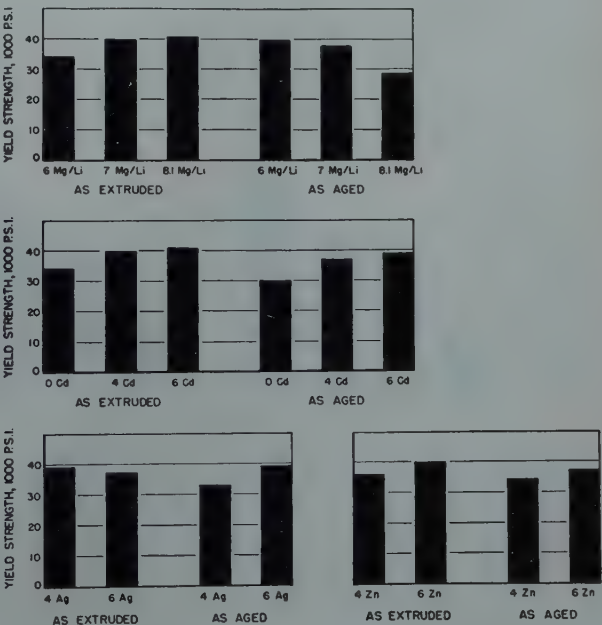


FIG 12—Effect of variation in Mg/Li, Zn, Cd, and Ag on the yield strength of 36 Mg-Li-Zn-Cd-Ag alloys, as extruded and as aged at 150°F for 48 hours.

Table 3 . . . Mechanical Properties of Ten-pound Heats of Selected Mg-Li-Zn-Cd-Ag Alloys after Aging at 150°F for 48 Hr

| Heat No. | Intended Composition, Pct | | | | | | Pre-extrusion Heat Treatment | Tensile Properties ¹ | | | | | | Compressive Properties ¹ | | | |
|----------|---------------------------|------|------|----|----|----|------------------------------|---------------------------------|---------------------|------------------------|--------------------------|------------------------|----------------------|-------------------------------------|---------------------|-------------------------------------|------------|
| | Mg/Li | Mg | Li | Zn | Cd | Ag | | Elastic Limit, psi | Yield Strength, psi | Ultimate Strength, psi | Elongation, Pct in 1 In. | Reduction of Area, Pct | Hardness, Rockwell E | Elastic Limit, psi | Yield Strength, psi | Charpy Impact Strength, Foot-pounds | |
| | | | | | | | | | | | | | | | | Notched | Un-notched |
| | | | | | | | | | | | | | | | | | |
| 1091 | 6 | 75.4 | 12.6 | 6 | 0 | 6 | None | 31,300 | 41,300 | 46,700 | 2 | 4.4 | 94.5 | 36,900 | 47,100 | 0.5 | 2.5 |
| 1095 | 6 | 73.7 | 12.3 | 6 | 4 | 4 | 600°F-16 hr | 30,300 | 43,200 | 48,900 | 3 | 3.7 | 96 | 39,900 | 49,600 | 0 | 2 |
| | | | | | | | None | 34,200 | 48,500 | 53,100 | 1 | 1.9 | 96.5 | 47,700 | 54,900 | 0.5 | 2 |
| 1075 | 6 | 72.0 | 12.0 | 6 | 4 | 6 | 600°F-16 hr | None | | | 0 ² | 0 | 98.5 | 47,800 | 55,300 | 0.5 | 2 |
| | | | | | | | None | 33,200 | 49,100 | 53,200 | 1 | 1.1 | 98.5 | 42,800 | 55,200 | 0.5 | 1 |
| 1076 | 6 | 72.0 | 12.0 | 4 | 6 | 6 | 600°F-16 hr | 40,400 | 50,300 | 48,000 | 0 | 0.4 | 88 | 45,100 | 53,200 | 0.5 | 1 |
| | | | | | | | None | 45,800 | 52,200 | 53,400 | 1 | 2.0 | 84.5 | 46,800 | 54,200 | 0.5 | 1 |
| 1092 | 7 | 76.1 | 10.9 | 4 | 4 | 5 | 600°F-16 hr | 41,800 | 51,500 | 55,200 | 1 | 1.3 | 85 | 45,500 | 53,700 | 0.5 | 1 |
| | | | | | | | None | 32,200 | 39,200 | 43,200 | 20 | 30.1 | 93 | 36,300 | 44,000 | 1 | 5 |
| 1090 | 7 | 75.3 | 10.7 | 4 | 4 | 6 | 600°F-16 hr | 31,000 | 38,400 | 43,100 | 20 | 35.2 | 92.5 | 35,400 | 43,700 | 1 | 5.5 |
| | | | | | | | None | 32,700 | 41,500 | 46,400 | 15 | 26.1 | 95.5 | 42,800 | 49,400 | 0.5 | 3 |
| 1077 | 7 | 75.3 | 10.7 | 4 | 6 | 4 | 600°F-16 hr | 30,000 | 40,200 | 45,700 | 15 | 23.3 | 95 | 37,100 | 47,500 | 0.5 | 3.5 |
| | | | | | | | None | 31,100 | 39,200 | 43,300 | 19 | 34.5 | 88.5 | 36,300 | 43,900 | 1 | 4.5 |
| 1078 | 7 | 73.5 | 10.5 | 4 | 6 | 6 | 600°F-16 hr | 31,500 | 40,800 | 44,400 | 14 | 19.7 | 88 | 36,000 | 44,200 | 0.5 | 4.5 |
| | | | | | | | None | 37,500 | 45,200 | 48,400 | 10 | 13.9 | 90.5 | 42,900 | 54,800 | 0.5 | 3.5 |
| 1093 | 7 | 72.6 | 10.4 | 5 | 6 | 6 | 600°F-16 hr | 32,200 | 46,000 | 51,500 | 8 | 10.5 | 90.5 | 41,400 | 52,300 | 0.5 | 2.5 |
| | | | | | | | None | 31,000 | 41,900 | 49,300 | 9 | 13.5 | 97 | 37,500 | 50,800 | 0.5 | 3 |
| 1094 | 7 | 76.1 | 10.9 | 3 | 7 | 3 | 600°F-16 hr | 30,800 | 40,500 | 49,100 | 6 | 7.4 | 97 | 38,300 | 48,300 | 0.5 | 3 |
| | | | | | | | None | 32,600 | 39,200 | 41,600 | 17 | 27.5 | 91 | 37,300 | 43,200 | 1 | 7 |
| 1079 | 8.1 | 73.0 | 9.0 | 6 | 6 | 6 | 600°F-16 hr | 31,600 | 38,500 | 41,600 | 22 | 38.6 | 90 | 37,400 | 42,900 | 2 | 6.5 |
| | | | | | | | None | 19,700 | 25,600 | 35,000 | 41 | 60.9 | 87.5 | 25,200 | 30,300 | 1 | 4 |
| | | | | | | | 600°F-16 hr | 23,400 | 28,600 | 38,000 | 29 | 46.4 | 89.5 | 25,200 | 30,900 | 2.5 | 4 |

¹ Alloys were extruded from 2-inch-diameter cast billets. Properties are based on average of two specimens.
² Bar too brittle to obtain yield point.

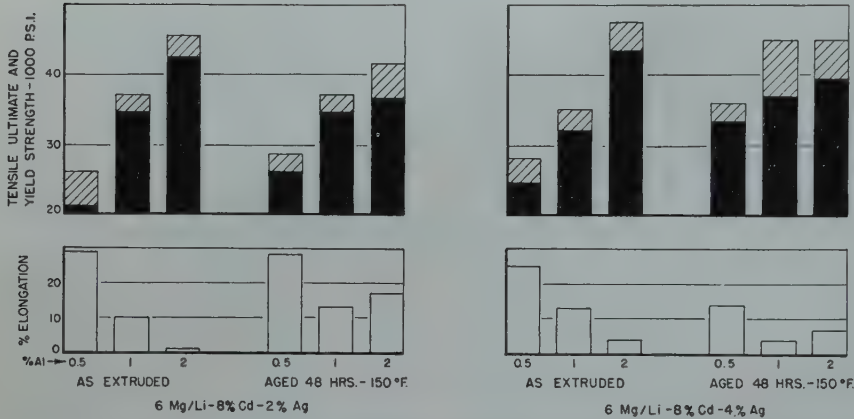


FIG 13—Effect of aluminum at two different silver levels on mechanical properties of a 6 Mg/Li-8 pct Cd base quinary alloy.

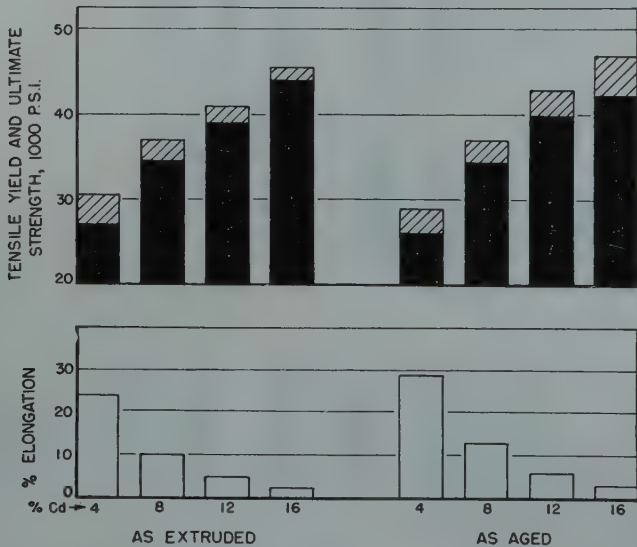


FIG 14—Effect of cadmium on mechanical properties of a 6 Mg/Li-1 pct Al-2 pct Ag alloy. (Aging treatment: 48 hr at 150°F.)

150°F aging treatment than do the alloys, listed in the table, of lower magnesium-lithium ratio.

The high-lithium, magnesium-lithium alloys were capable of dissolving cadmium in much larger amounts than the 6 pct generally added heretofore. Large amounts of cadmium, when substituted for the zinc or aluminum, not only produced high strength but enabled the alloys to retain this strength after aging at 150°F. As shown in Fig 14 and 15, the addition of 12 pct cadmium resulted in high strength which was not reduced by aging 48 hr at 150°F. However, alloys with 16 pct cadmium overaged and lost strength during the 48-hr treatment.

Continued investigation of high-cadmium-bearing alloys showed that, in the absence of zinc and aluminum, 16 pct cadmium could be added without causing overaging during the 48 hr at 150°F treatment. An alloy having the composition, 6 Mg/Li-16 pct cadmium-6 pct silver, was found to retain its high strength for over 1000 hr at 150°F. The mechanical properties of the alloy, after extruding and aging at 150°F for 48 hr, were as follows:

Tensile ultimate strength—48,000 psi
Tensile yield strength —47,000 psi
Elongation in 2 in. —2 pct

Although the ductility of this alloy was low, a slight modification of the composition to 15 pct cadmium and 5 pct silver increased the ductility considerably without seriously affecting the strength or the ability of the alloy

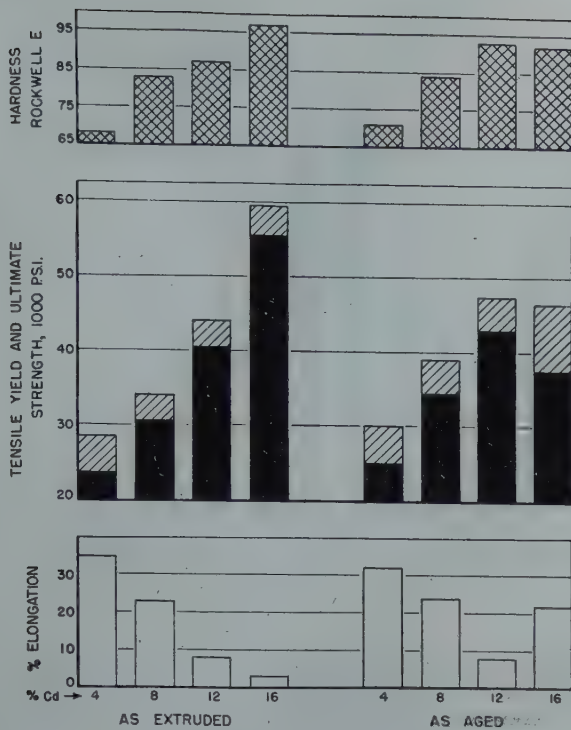


FIG 15—Effect of cadmium on mechanical properties of a 7 Mg/Li-2 pct Zn-4 pct Ag alloy. (Aging treatment: 48 hr at 150°F).

to retain its strength after a prolonged treatment at 150°F.

An extensive study of the fabricating characteristics and strength properties of the 6 Mg/Li-15 pct cadmium-5 pct silver alloy was also conducted. The alloy was easily forged and rolled at 400°F, and after a solution treatment, it could be cold rolled extensively. Its mechanical properties after extruding and aging at 150°F for 24 hr were as follows:

Tensile ultimate strength—46,000 psi
Tensile yield strength —43,000 psi
Elongation in 2 in. —8 pct
Reduction of area —8 pct
Hardness, Rockwell E —92

A stress-strain curve for the 6 Mg/Li-15 pct cadmium-5 pct silver alloy is shown in Fig 16. It is typical for the high-strength, magnesium-lithium base alloys and is characterized by a high elastic limit and a high compressive yield strength. Fig 17 and 18 show respective stress-strain curves for a commercial magnesium alloy and a commercial aluminum alloy. It will be noted that the curve for the magnesium-lithium alloy bears a greater resemblance to the curve for the aluminum alloy than it does to the curve for the magnesium alloy.

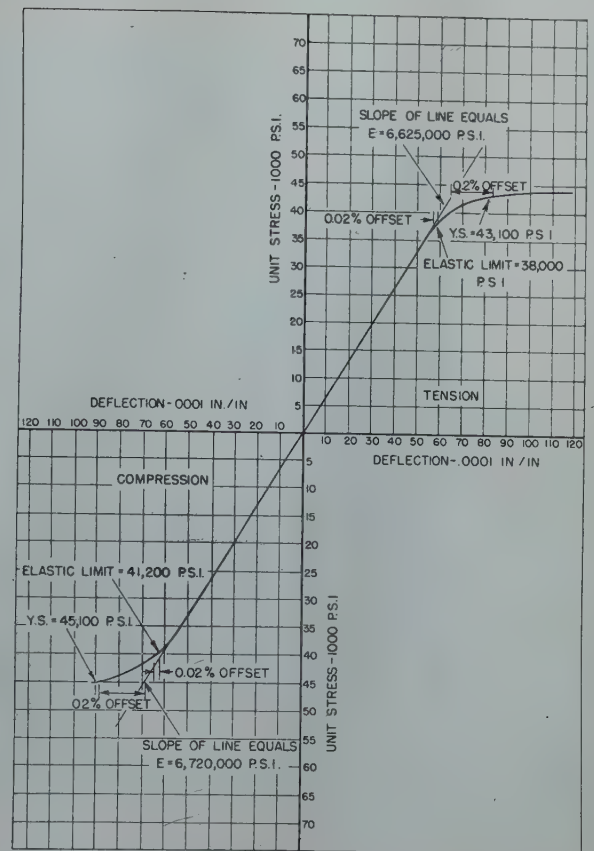


FIG 16—Tension-compression stress-strain curves for the alloy 6 Mg/Li-15 pct Cd-5 pct Ag.

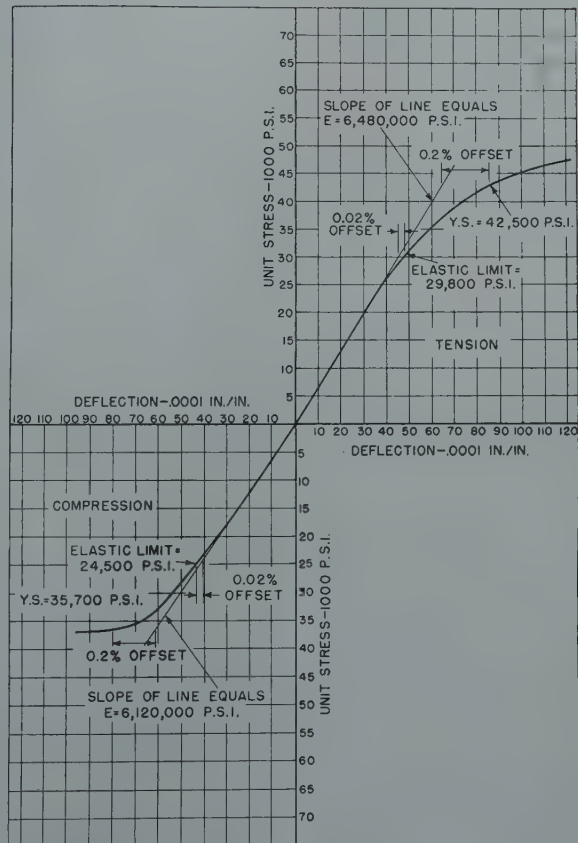


FIG 17—Tension-compression stress-strain curves for commercial magnesium alloy AZ31X.

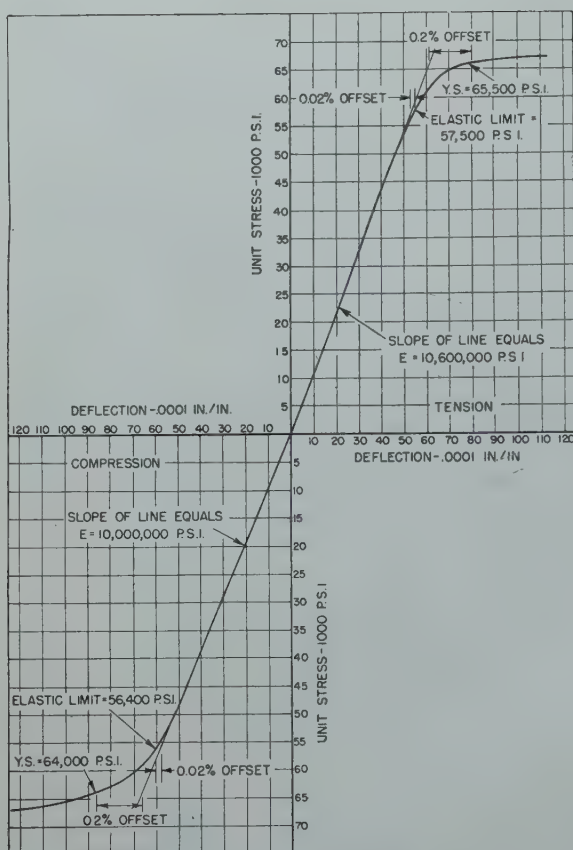


FIG 18—Tension-compression stress-strain curves for commercial aluminum alloy 14S-T.

COMPARISON OF STRUCTURAL CHARACTERISTICS OF MAGNESIUM-LITHIUM BASE ALLOYS WITH OTHER ENGINEERING MATERIALS

The magnesium-lithium base alloys by virtue of their low densities, 1.65 g per cc or less, have considerable advantage when compared to other structural materials on a strength-weight basis.

The strongest available commercial aluminum alloy has a yield strength of the order of 72,000 psi and a density of about 2.8 g per cc. For equivalent strength on a pound-for-pound basis, a magnesium-lithium base alloy, having a density of 1.55 g per cc, should have a yield strength, in compression and tension, of the order of 40,000 psi, while one having a density of 1.65 g per cc should possess a yield strength of about 42,500 psi. As shown in the preceding text, these yield strength values are exceeded in many magnesium-lithium base compositions.

The strength properties of two magnesium-lithium base alloys are compared with other commonly used structural alloys in Fig 19. The strength values representative of the various materials are those obtained

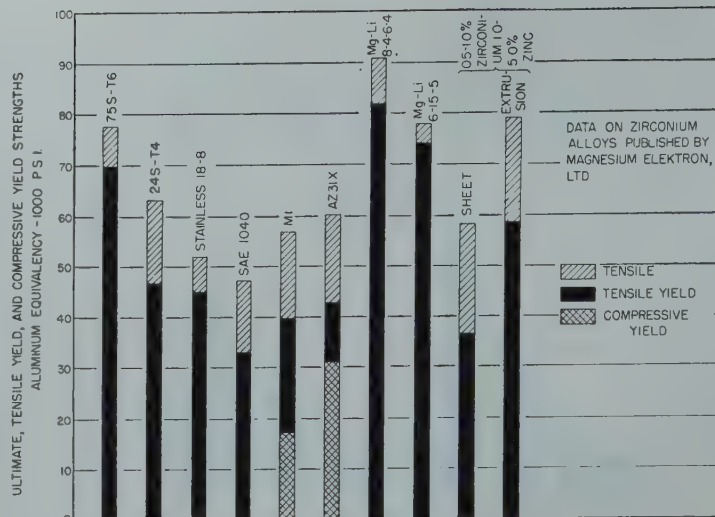


FIG 19—Comparison of strength properties of Mg-Li base alloys with those of other alloys.

fairly high modulus of elasticity (about 6,500,000 psi) of the magnesium-lithium base alloys make these alloys far superior, in this respect, to other structural materials.

Work-hardening Capacity and Stability of Magnesium-lithium Base Alloys

WORK-HARDENING CAPACITY

Early in the study of magnesium-lithium base alloys, it was found that most of the alloys being investigated were incapable of appreciable work hardening. There were a number of indications of the lack of work-hardening capacity, a few of which are enumerated as follows:

1. At rates of tensile loading comparable to those used for testing other materials, such as copper-base, iron-base, aluminum-base, or ordinary magnesium-base alloys, the yield strength of high-lithium, magnesium-lithium base alloys was found to be fictitiously high. The effect of the rate of loading on the yield strength of a few of the early magnesium-lithium base alloys is shown in Table 4. The first three alloys listed therein extended at a rapid rate under a tensile load near their apparent yield strength. The yield strength of the fourth alloy, which was low in lithium content, was not affected by the change in rate of loading.

2. The apparent yield strength of high-lithium, magnesium-lithium base alloys was not appreciably increased by cold stretching. The effect of a prior stretch of 5 and 10 pct on yield strength of four tensile bars is shown in Table 5.

Table 4 . . . Effect of Rate of Loading on the Tensile Yield Strength of a Series of Early Magnesium-lithium Base Alloys

| Mg/Li | Composition, Pct | | | | Yield Strength, psi | |
|-------|------------------|------|----|----|---------------------|---------------------|
| | Mg | Li | Zn | Al | Loaded, 0.02 ipm | Loaded, 0.00004 ipm |
| 9.7 | 87 | 9 | 4 | | 25,200 | 21,500 |
| 9.7 | 87.9 | 9.1 | 2 | 1 | 25,600 | 23,900 |
| 8.1 | 87.2 | 10.8 | 2 | 2 | 24,200 | 21,500 |
| 24 | 94.1 | 3.9 | | 2 | 23,000 | 23,000 |

Table 5 . . . Effect of Cold Stretching on the Tensile Yield Strength of a Series of Early Magnesium-lithium Base Alloys

| Mg/Li | Composition, Pct | | | | Yield Strength, psi | | |
|-------|------------------|------|----|----|---------------------|--------------------|---------------------|
| | Mg | Li | Zn | Al | 0 Pct Cold Stretch | 5 Pct Cold Stretch | 10 Pct Cold Stretch |
| 9.7 | 87 | 9 | 4 | | 25,200 | 25,600 | |
| 9.7 | 87.9 | 9.1 | 2 | 1 | 25,600 | 26,500 | 26,800 |
| 8.1 | 87.2 | 10.8 | 2 | 2 | 24,200 | 26,500 | |
| 24 | 94.1 | 3.9 | | 2 | 23,000 | 34,100 | |

In only the low-lithium alloy was a considerable increase effected in the apparent yield strength by a 5 pct prior stretch.

3. The apparent yield strength of 26,300 psi for an extruded alloy of 87 pct magnesium-9 pct lithium-4 pct zinc was not increased by cold-drawing reductions as high as 55.5 pct.

4. The apparent yield strength of 22,500 psi for a hot-rolled alloy of 87 pct magnesium-9 pct lithium-4 pct zinc could be increased only to 24,000 psi by a 75 pct cold-rolling reduction.

Thus the inability of the first magnesium-lithium base alloys investigated to work harden satisfactorily became readily apparent. The seriousness of this was more fully appreciated when a close relationship was found between the work-hardening characteristics and the stability of the mechanical properties at moderately elevated temperatures. In order to evaluate quickly a large number of compositions and to determine the effect of various addition elements on the work-hardening characteristics of the magnesium-lithium base, a modified test to determine work-hardening capacity was devised. A schematic drawing of the testing equipment is shown in Fig 21.

In this test, the specimens are supported on rails spaced 3 in. apart and loaded in the midpoint as a simple

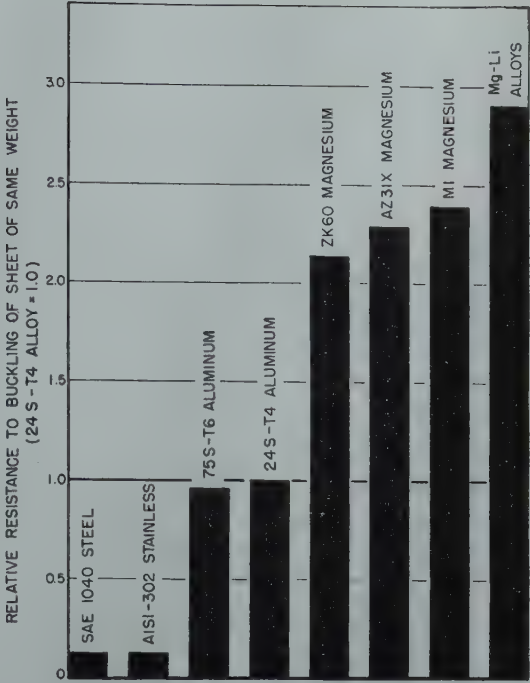


FIG 20—Relative resistance to buckling of various structural alloys compared to that of 24S-T4 aluminum alloy.

beam. The deflections of the bars are measured at the time of loading and then at intervals over a period of a week. The bend-deflection values are plotted against the time elapsed after loading to obtain bend deflection-time curves. Such curves for alloys having good, fair, and poor work-hardening characteristics are shown in Fig 22. The total bend deflection within the 144-hr period of the test and the rate of deflection during the 120- to 144-hr period were used as a measure of the relative merit of the alloys. It will be noted from Fig 22 that deflection readings were taken for 168 hr, in order to obtain an accurate curve in the 120- to 144-hr interval.

Because the bend-deflection test procedure was used primarily to determine alloy additions which would improve work-hardening capacity, the bend tests were made, for the most part, on bars loaded in such a way that the extreme fiber stress exceeded the yield point of the material. The bend-deflection test was of little value for studying age-hardening alloys, because this type of alloy showed marked variations in behavior during the course of the test as a result of aging at room temperature.

Whereas the bend-deflection rate, as measured during the interval between 120 and 144 hr, is of interest and of value in assessing the work-hardening

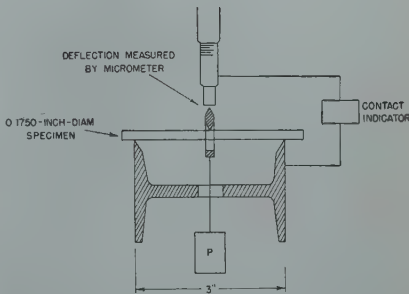


FIG 21—Bend-deflection test apparatus for determining work hardenability.

characteristics of each composition, comparisons between various alloy compositions can be made most easily by examining the total bend deflection during the 0- to 144-hr interval. Results shown in Fig 23 reveal that the ability of a material to withstand bending loads which produce an extreme fiber stress greater than the yield strength apparently depends upon the work-hardening capacity of the material and not upon the yield strength. For example, pure magnesium, with a yield strength nearly twice that of pure aluminum, deflected nearly twice as much as aluminum in 144 hr when tested at an extreme fiber stress of 21,000 psi. It is apparent, from an examination of the 9 bars at the left of the diagram, that the first lithium additions tend to increase the yield strength and to reduce the total bend

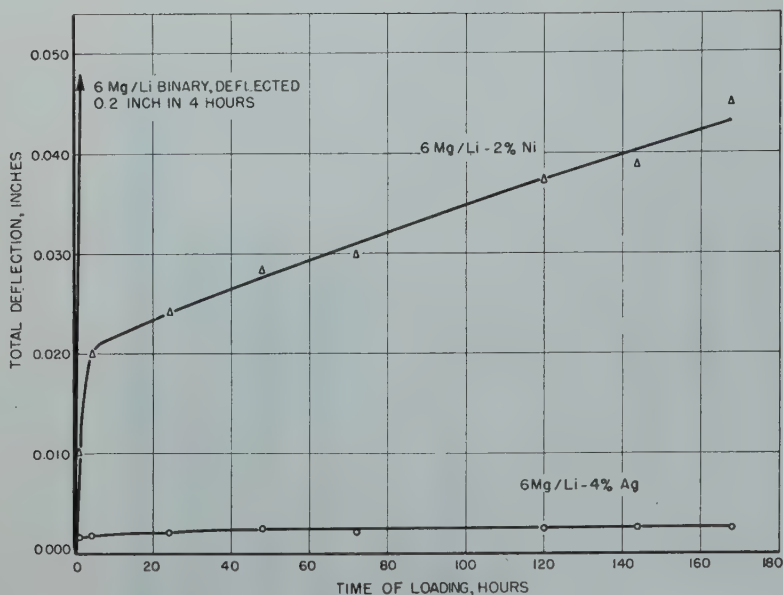


FIG 22—Typical bend-deflection rate curves.

deflection markedly. Larger additions of lithium decreased the yield strength moderately, producing some increase in total bend deflection. This trend continued until a Mg/Li of 8 was reached. At this ratio, and continuing through 6 Mg/Li, the total deflection was high. Thus, with only a slight decrease in yield strength at these high lithium contents, a deflection of 0.2 in. was obtained in 24 hr.

The additions of 4 pct and 9 pct zinc to an alloy of 8 Mg/Li base increased the yield strength to 22,000 and 31,000 psi, respectively, and reduced the total bend deflection to 0.025 in. and 0.010 in., respectively. A 0.5 pct addition of aluminum to the 8 Mg/Li base was equally as effective as a 4 pct zinc addition in raising the yield strength of the material, but was far more effective in reducing the total bend deflection. A 6 pct aluminum addition was responsible for a still more pronounced increase in yield strength. On the other hand, 6 pct aluminum was inferior to 0.5 pct aluminum in reducing the total bend deflection. It is important to note that the zinc- and aluminum-bearing alloys were of the age-hardenable type, and for this reason, strict comparisons of the work-hardening capacities of such alloys, as measured by the bend-deflection test, were not possible.

The most outstanding effect of alloy additions was observed when 4 pct silver was added to an 8 Mg/Li or 6 Mg/Li alloy. The effect of silver is shown in Fig 23.

The mechanism by which an addition such as 4 pct silver or 0.5 pct aluminum improves the work-hardening capacity

of the magnesium-lithium alloy matrix is not entirely clear. It appears, however, that most additions having some solid solubility in the magnesium-lithium base at room temperature will effect some improvement in the work-hardening capacity.

In Table 6 are reported the total bend-deflection values for specimens of the four alloys previously noted in Tables 4 and 5. The total bend-deflection values of the first three alloys shown were high even though an extreme fiber stress of 21,000 psi was appreciably below the apparent yield strength of the alloys. An interesting observation made from results in Table 6 was that the second alloy, which showed some superiority in work-

Table 6 . . . Total Bend Deflection 144 Hr after Loading a Series of Early Magnesium-lithium Base Alloys

| Mg/Li | Composition, Pct | | | | Apparent Yield Strength, psi | Total Bend Deflection, ¹ Inch |
|-------|------------------|------|----|----|------------------------------|--|
| | Mg | Li | Zn | Al | | |
| 9.7 | 87 | 9 | 4 | | 25,200 | 0.0085 |
| 9.7 | 87.9 | 9.1 | 2 | 1 | 25,600 | 0.0069 |
| 8.1 | 87.2 | 10.8 | | 2 | 24,200 | 0.0092 |
| 24 | 94.1 | 3.9 | | 2 | 23,000 | 0.0011 |

¹ Measured 144 hr after loading to an extreme fiber stress of 21,000 psi.

hardening capacity in Tables 4 and 5, also showed a slight superiority to the first and third alloys in resistance to bending. The bend-deflection value for the low-lithium alloy was markedly lower than the values for the three high-lithium alloys.

The bend-deflection test had certain advantages over the other possible methods for determining work-hardening capacity. It could be used to examine a large number of alloys at one time; specimen preparation was a simple matter; and perhaps of greatest importance, temperature was not a variable in the course of the test because it was readily conducted in a room kept at a constant temperature of 85°F.

The increase in hardness obtained by cold rolling a strip of the alloy to a reduction of 15 pct was also used as a measure of the effect of alloy additions on the work-hardening capacity of magnesium-lithium base compositions. It yielded some useful information and generally confirmed the results of the

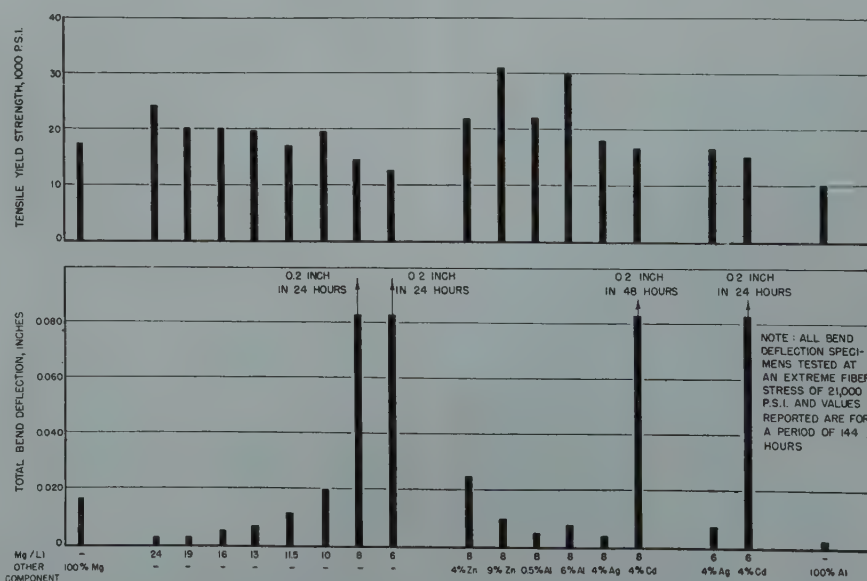


FIG 23—Total bend deflection vs. tensile yield strength for various alloys.

bend-deflection test, but was not so sensitive as the bend-deflection method for revealing the effects of alloying elements. A work-hardening test based on hardness measurements has the objection that the hardness measurement itself depends to some extent on the work-hardening capacity of the material being tested. To determine the stability of work-hardened alloys, the cold-rolled specimens were held at temperatures of 150 and 225°F and their hardness measured at periodic intervals.

The bend-deflection test was also supplemented by the use of a tensile-creep test for the latter is a more sensitive method of determining plastic flow in the region of the yield strength than is the bend creep test. The alloy additions which improved work-hardening capacity, as measured by the bend-deflection test, also improved the tensile-creep characteristics of the alloy.

STABILITY

The properties of high-strength magnesium-lithium base alloys are stable at room temperature. However at 150°F the alloys average slowly, with the magnesium strength being maintained not longer than 1000 hr. The stability is lower at higher temperatures. One of the more important objectives of the present investigation was the improvement of stability of the alloys at 150°F and higher temperatures.

It was found early in the experimental work that alloy additions which improved the bend-deflection characteristics of an alloy also improved the stability of that alloy in the age-hardened state. Silver, which was shown in Fig 22 and 23 to be markedly beneficial, had the following typical effect on stability:

| Composition | As Extruded | | As Aged at 150°F for 48 Hr | |
|---|---------------------|-----------------|----------------------------|-----------------|
| | Yield Strength, psi | Elongation, Pct | Yield Strength, psi | Elongation, Pct |
| 8.1 Mg/Li-6 pct Cd-6 pct Zn..... | 35,800 | 20 | 24,400 | 36 |
| 8.1 Mg/Li-6 pct Cd-6 pct Zn-6 pct Ag..... | 32,700 | 26 | 34,600 | 26.5 |

Other examples of the effect of silver on the stability of mechanical properties were shown in previous figures.

When it was found that silver had an important effect upon the stability characteristics of age-hardened alloys, a considerable portion of the experi-

mental effort was directed to preparing various silver-containing alloy compositions and testing them after extruding, and after extruding and aging at 150°F for 48 hr. The mechanical properties of these alloys were discussed earlier in this paper.

One of the first alloys prepared that showed fairly good stability had the composition 7 Mg/Li-3 pct zinc-7 pct cadmium-3 pct silver. This alloy had the following properties:

| | Yield Strength, psi | Tensile Strength, psi | Elongation, Pct | Reduction of Area, Pct | Hardness, Rockwell E |
|---------------------------------|---------------------|-----------------------|-----------------|------------------------|----------------------|
| As extruded..... | 37,400 | 40,600 | 20 | 44 | 87 |
| As aged at 150°F for 48 hr..... | 35,500 | 39,400 | 28.5 | 43.3 | 88 |

Age-hardening curves for this alloy, at room temperature and at 150°F, are shown in Fig 24. It is apparent from an examination of the curve for 150°F that a reasonably high hardness was maintained for only about 100 hr. Thus, the fact that the mechanical properties after aging for 48 hr at 150°F were not appreciably changed from those obtained in the as-extruded state was no indication that the alloy was stable when held for extended periods at 150°F. It became the practice with subsequent alloys to determine the aging curves, hardness vs. time at temperature, as well as the mechanical properties after various conditions of aging.

Such hardness vs. time at temperature curves showed that an increase in the amount of lithium above that required to make the alloys 100 pct beta was beneficial because it improved the stability. In most alloys investigated, maximum stability was achieved at 6 Mg/Li; therefore, a large number of compositions having a magnesium-

lithium ratio of 6 were studied.

Although many elements were found which could cause precipitation in magnesium-lithium base alloys, it appeared that such precipitate-forming elements as silver, cadmium, aluminum, or zinc would be of major importance.

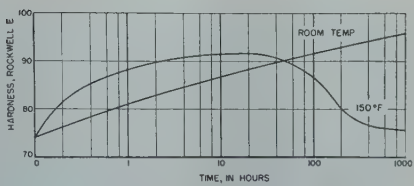


FIG 24—Age-hardening characteristics of the 7 Mg-Li-3 pct Zn-7 pct Cd-3 pct Ag alloy. (Specimens quenched from 475°F.)

Therefore, an investigation of the solubility limits of these elements in the

6 Mg/Li-base alloys was initiated. An indication of the solubility limit for an element was obtained by adding it in small but increasing increments to a magnesium-lithium base, then solution treating the alloys by quenching from 500°F, and finally determining their change in hardness with time at 150°F. The maximum hardness values obtained upon aging are plotted in Fig 25. The apparent effective solubility limits at 150°F for the four elements in the beta-phase alloys of 6 Mg/Li base were roughly 8 pct silver, 12 pct cadmium, 0.5 pct aluminum, and 1.5 pct zinc.

Investigations of this type were also conducted at other ratios of magnesium to lithium. In the beta phase, the solubility at room or at slightly elevated temperatures of almost every element increased as the lithium content increased. For example, at 8.1 Mg/Li, the maximum amount of cadmium that appeared soluble was 6 pct; at 6 Mg/Li, about 12 pct was soluble; and at 5 Mg/Li, over 16 pct was soluble. Silver seemed to be an exception. At 8.1 Mg/Li, over 12 pct silver was soluble; at 6 Mg/Li, only about 8 pct appeared to be soluble; while at 5 Mg/Li, less than 4 pct appeared to be soluble.

In order to determine their effects in age hardening, a large number of elements were added in various concentrations to a 6 Mg/Li-4 pct cadmium-6 pct silver base. The results of this study are shown in Table 7. Although many concentrations of each of the elements shown were studied, only that concentration is reported which had the greatest stabilizing effect on the alloy. It is interesting to note that many additions formed precipitates which were visible under the microscope yet did not cause age hardening.

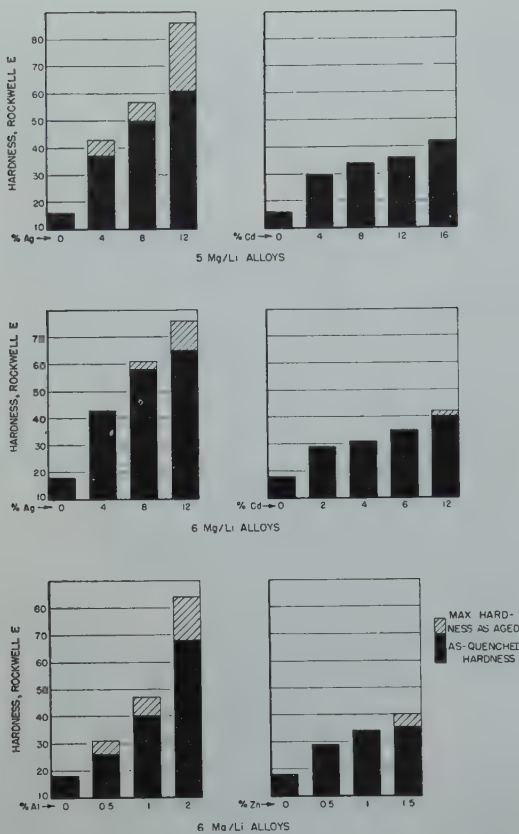


FIG 25—Age-hardening effects of various elements on magnesium-lithium base. Alloys quenched from 500°F and aged at 150°F.

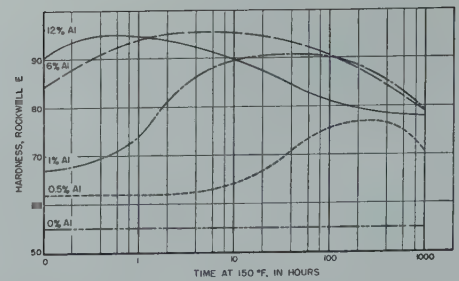


FIG 26—Effect of aluminum on 150°F aging characteristics of a 6 Mg/Li-4 pct Cd-6 pct Ag alloy. (Alloys quenched from 500°F.)

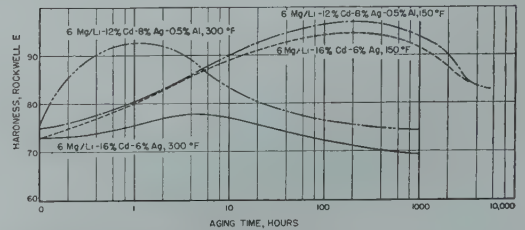


FIG 27—Aging characteristics of two high-strength magnesium-lithium base alloys. (Alloys quenched from 500°F.)

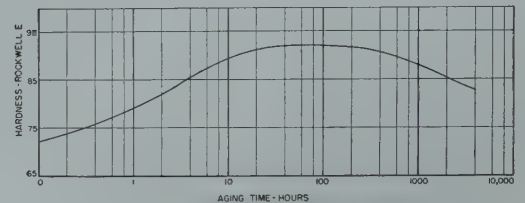


FIG 28—Aging behavior at 150°F of the 6 Mg/Li-15 pct Cd-5 pct Ag alloy following solution treatment at 500°F.

Table 7 . . . Effect of Various Elements¹ on the Age Hardening Capacity of Magnesium-lithium Base Alloys

| Heat No. | Intended Composition, ¹ Pct | | | | Solution Treatment 16 Hr at °F | Aging Temperature, °F | Duration of Aging, Hr | Hardness, Rockwell E | | | Microscopical Examination | |
|----------|--|----|----|--------------------|--------------------------------|-----------------------|-----------------------|----------------------|--------------------|----------------|---|--|
| | Mg/Li | Cd | Ag | Other | | | | As Solution Treated | Maximum As Aged | At End of Test | Solid Solubility, As Quenched from Solution Temperature | Evidence of Precipitation after Aging at 300°F |
| 1414 | 6 | 4 | 6 | | 500 | 70 | | 55 | Did not age harden | | Complete | None |
| | | | | | | 150 | | 55 | Did not age harden | | | |
| | | | | | | 300 | | 55 | Did not age harden | | | |
| 1416 | 6 | 4 | 6 | 8 Ce | 500 | 70 | | 69 | Did not age harden | | Incomplete | Definite |
| | | | | | | 150 | | 67 | Did not age harden | | | |
| | | | | | | 300 | | 66 | Did not age harden | | | |
| 1417 | 6 | 4 | 6 | 4 Ca ² | 500 | 70 | | 63 | Did not age harden | | Incomplete | Definite |
| | | | | | | 150 | | 62 | Did not age harden | | | |
| | | | | | | 300 | | 61 | Did not age harden | | | |
| 1418 | 6 | 4 | 6 | 4 Cu | 500 | 70 | | 68 | Did not age harden | | Incomplete | Definite |
| | | | | | | 150 | | 67 | Did not age harden | | | |
| | | | | | | 300 | | 66 | Did not age harden | | | |
| 1421 | 6 | 4 | 6 | 12 Sr ² | 500 | 70 | 2500 | 61 | Did not age harden | | Incomplete | Definite |
| | | | | | | 150 | | 60 | Did not age harden | | | |
| | | | | | | 300 | | 60 | Did not age harden | | | |
| 1430 | 6 | 4 | 6 | 8 Tl | 600 | 70 | 2000 | 75 | Did not age harden | | Nearly complete | Definite |
| | | | | | | 150 | 3000 | 81 | Did not age harden | | | |
| | | | | | | 300 | | 75 | Did not age harden | | | |
| 1431 | 6 | 4 | 6 | 4 Si | 600 | 70 | 2000 | 70 | Did not age harden | | Incomplete | Definite |
| | | | | | | 150 | | 69 | Did not age harden | | | |
| | | | | | | 300 | | 69 | Did not age harden | | | |
| 1434 | 6 | 4 | 6 | 4 Ba | 600 | 70 | | 58 | Did not age harden | | Incomplete | Definite |
| | | | | | | 150 | | 57 | Did not age harden | | | |
| | | | | | | 300 | | 57 | Did not age harden | | | |
| 1436 | 6 | 4 | 6 | 8 Sn | 600 | 70 | 2000 | 70 | Did not age harden | | Incomplete | Definite |
| | | | | | | 150 | | 88.5 | Did not age harden | | | |
| | | | | | | 300 | | 70 | Did not age harden | | | |
| 1439 | 6 | 4 | 6 | 2 Pb | 600 | 70 | | 59 | Did not age harden | | Incomplete | Definite |
| | | | | | | 150 | | 59 | Did not age harden | | | |
| | | | | | | 300 | | 59 | Did not age harden | | | |
| 1432 | 6 | 4 | 6 | 1.2 In | 600 | 70 | 2000 | 56 | Did not age harden | | Complete | Definite |
| | | | | | | 150 | 3000 | 81 | Did not age harden | | | |
| | | | | | | 300 | | 65 | Did not age harden | | | |
| 1477 | 6 | 4 | 6 | 4 Zn | 600 | 70 | 2500 | 56 | Did not age harden | | Complete | Definite |
| | | | | | | 150 | 2500 | 73 | Did not age harden | | | |
| | | | | | | 300 | | 72 | Did not age harden | | | |

¹ Other elements investigated included Te, Be, P, Bi, Mn, B, and Co, but these were not recovered in the alloys.

² With the exception of these elements, chemical analysis generally showed good recovery of all components.

The effects at 150°F of various quantities of aluminum on the aging characteristics of the 6 Mg/Li-4 pct cadmium-6 pct silver-base alloy, as shown in the age-hardening curves of Fig 26, were particularly interesting. As the aluminum content of the alloy was increased to 6 pct, there was a continuous increase in the maximum hardness obtained by aging. The time at maximum hardness, however, decreased as the aluminum content increased.

A large number of magnesium-lithium, high-cadmium, high-silver alloys were also studied. It was found that the alloys with 6 Mg/Li-12 pct cadmium-8 pct silver-0.5 pct aluminum, and with 6 Mg/Li-16 pct cadmium-6 pct silver, when quenched from 500°F and aged at 150°F, hardened appreciably and maintained their high hardness for a considerable length of time when held at that temperature. The aging characteristics of the two alloys are shown in Fig 27. As noted previously, neither of these alloys had as high ductility as was desired. A slight modification in composition of the alloys from 6 Mg/Li-16 pct cadmium-6 pct silver to 6 Mg/Li-15 pct cadmium-5 pct silver improved the ductility considerably. The aging curve for the latter alloy is shown in Fig 28. The alloy, solution treated to a Rock-

material is about 43,000 psi and the elongation is about 8 pct.

The stability of magnesium-lithium base alloys may be improved by solution treatment. Alloys aged from the hot- or cold-rolled states usually contain residual stresses so that the rate of precipitation is increased and hence stability impaired.

Although the work-hardening capacity and the stability of magnesium-lithium alloys are not yet as desired, nevertheless considerable improvement has been made in these characteristics. It is of interest that the all-alpha phase magnesium-lithium alloys studied were quite capable of work hardening and their mechanical properties at ordinary temperatures were reasonably stable.

Corrosion Resistance

At the inception of the research program, it was expected that the addition of considerable percentages of lithium to magnesium would affect the corrosion resistance adversely. The experimental program was conducted on the premise that, if magnesium-lithium base alloys of satisfactory mechanical properties were developed, a method of protecting them from corrosion by cladding or by the use of paints, lacquers, and varnishes could be effected.

Early in the program, it was found that binary alloys containing about 11 pct lithium were remarkably good in their resistance to corrosion. This was demonstrated by results in Fig 29 which show the corrosive effect of alternate immersion in a 3 pct sodium chloride solution upon a series of magnesium-lithium base alloys. A speci-

men of ASTM No. M-1 magnesium-base alloy, the most corrosion resistant of the commercial alloys, was used for comparison. The immersion cycle was standardized at one-half minute in the solution and two minutes out, the temperature of the solution being maintained at 95°F. The corrosion rates of these alloys are given in Table 8.

It is apparent from the data that the binary magnesium-11 pct lithium alloy (Mg/Li = 8.1) is as resistant to corrosion, at least under the conditions of the test used, as the commercial alloy, ASTM No. M-1.

Results of corrosion tests on a series of magnesium-lithium-zinc-cadmium-silver alloys in a 3 pct sodium chloride solution are shown in Table 9. For comparison purposes, a magnesium-lithium binary alloy, a magnesium-lithium ternary alloy containing 4 pct zinc, and three commercial magnesium-base alloys were also tested. The resistance to corrosion of the magnesium-lithium base complex alloys decreased with an increase in the combined zinc and silver contents, as shown in Fig 30.

Preliminary tests showed that the 6 Mg/Li-15 pct cadmium-5 pct silver alloy also had poor corrosion characteristics. Its resistance to corrosion might be improved by cladding with a more corrosion-resistant material, such as the 8.1 Mg/Li binary alloy or pure aluminum. To give maximum protection, the cladding material should be anodic to the base material. Hence, solution potential measurements were made in a 3 pct sodium chloride solution on the 6 Mg/Li-15 pct cadmium-5 pct silver alloy, on the 8.1 Mg/Li binary alloy, and on 2S aluminum. The results obtained are shown in Fig 31.

Table 8 . . . Corrosion Resistance of Magnesium-lithium and Magnesium-lithium-zinc Alloys Compared with that of Commercial Alloy ASTM No. M-1

| Heat No. | ASTM No. | Composition, Pct | | | | Average Loss of Weight from Corrosion, ¹ Mg per Sq Cm per Day |
|----------|----------|------------------|----|------|------|--|
| | | Zn | Mn | Li | Mg | |
| 251 | M-1 | 1.26 | | | Bal. | 0.62 |
| 871 | | | | 2.0 | Bal. | 4.92 |
| 872 | | | | 4.0 | Bal. | 4.44 |
| 873 | | | | 9.3 | Bal. | 0.77 |
| 874 | | | | 11.0 | Bal. | 0.57 |
| 690 | 4 | 4 | | 9.0 | Bal. | 2.81 |
| 875 | | | | 10.6 | Bal. | 2.83 |

¹ Tested in cyclic immersion in 3 pct NaCl solution for 8 days. Cycle was ½ min. in the solution and 2 min. out. Solutions changed after 4 days' exposure.

well E hardness of about 73, is soft and ductile. Sheet of the material at this hardness can be bent several times through an angle of 180° over a sharp edge (0 radius) and straightened without cracking. The alloy can be aged at 150°F in about 48 hr to a maximum hardness of about 92 Rockwell E. At this hardness the yield strength of the

Table 9 . . . Alternate Immersion, Salt-water Corrosion Resistance of Extruded Mg-Li-Zn-Cd-Ag Alloys Compared with Commercial Magnesium Alloys in Sheet Form

| Heat No. | Mg/Li | Intended Composition, Pct | | | | | | | Average Loss of Weight from Corrosion, ¹ Mg per Sq Cm per Day | Sum of Zn and Ag Contents, Pct |
|----------|-------|---------------------------|------|----|----|----|-----|------|--|--------------------------------|
| | | Mg | Li | Zn | Cd | Ag | Al | Mn | | |
| 1091 | 6.0 | 75.4 | 12.6 | 6 | 0 | 6 | | | 18.7 | 12 |
| 1095 | 6.0 | 73.7 | 12.3 | 6 | 4 | 4 | | | 8.2 | 10 |
| 1075 | 6.0 | 72.0 | 12.0 | 6 | 4 | 6 | | | 12.6 | 12 |
| 1076 | 6.0 | 72.0 | 12.0 | 4 | 6 | 6 | | | 8.8 | 10 |
| 1092 | 7.0 | 76.1 | 10.9 | 4 | 4 | 5 | | | 6.4 | 9 |
| 1090 | 7.0 | 75.3 | 10.7 | 4 | 4 | 6 | | | 10.5 | 10 |
| 1077 | 7.0 | 75.3 | 10.7 | 4 | 6 | 4 | | | 4.7 | 8 |
| 1078 | 7.0 | 73.5 | 10.5 | 4 | 6 | 6 | | | 8.3 | 10 |
| 1093 | 7.0 | 72.6 | 10.4 | 5 | 6 | 6 | | | 10.8 | 11 |
| 1094 | 7.0 | 76.1 | 10.9 | 3 | 7 | 3 | | | 2.2 | 6 |
| 1079 | 8.1 | 73.0 | 9.0 | 6 | 6 | 6 | | | 11.1 | 12 |
| 874 | 8.1 | 89.0 | 11.0 | | | | | | 0.5 | 0 |
| 875 | 8.1 | 85.4 | 10.6 | 4 | | | | | 2.2 | 4 |
| Dow FS-1 | | Bal. | | 1 | | | 2.7 | 0.3 | 0.4 | |
| Dow J-1 | | Bal. | | 1 | | | 6.5 | 0.15 | 0.3 | |
| Dow M-1 | | Bal. | | | | | | 1.20 | 0.5 | |

¹ Average of triplicate specimens.

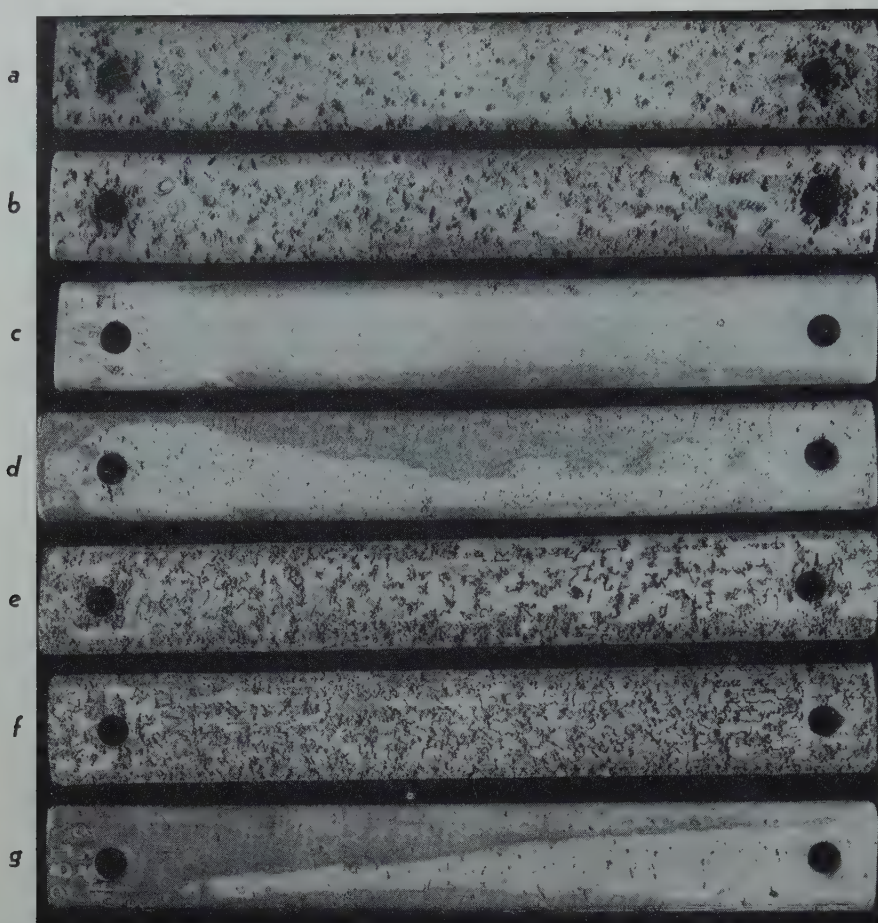


FIG 29—Specimens of magnesium-lithium alloys compared with a 1.26 pct Mn-balance Mg alloy following cyclic immersion corrosion test in 3 pct NaCl.
a. 10.6 pct Li-4 pct Zn-Balance Mg. *b.* 9 pct Li-4 pct Zn-Balance Mg. *c.* 11 pct Li-Balance Mg.
d. 9.3 pct Li-Balance Mg. *e.* 4 pct Li-Balance Mg. *f.* 2 pct Li-Balance Mg. *g.* 1.26 pct Mn-Balance Mg (ASTM No. M-1 alloy). Reduced approximately one-third in reproduction.

It was evident from the data that the 8.1 Mg/Li binary alloy was anodic to the high-strength alloy and, thus, would be expected to offer galvanic protection. On the other hand, 2S aluminum was found to be cathodic to the high-strength alloy and could be expected to afford only mechanical protection.

The 6 Mg/Li-15 pct cadmium-5 pct silver alloy can be clad either with the 8.1 Mg/Li binary alloy or with commercially pure aluminum. To obtain a bond between the materials used in cladding, sheets of the materials assembled in packs were tack welded at the edges and then rolled at temperatures above 600°F. Microscopical examination of the interface between the strong alloy in the core and the 8.1 Mg/Li binary alloy at the surface of the clad structure showed that actual welding had occurred in the process. On the other hand, the interface between the strong alloy in the core and 2S aluminum showed the existence of a thin layer of brittle, intermetallic com-

pounds. For the clad structures in the as-rolled condition, these compounds were not deleterious; but after prolonged heating at 400°F, the intermetallic layer failed, causing the aluminum to separate from the magnesium-lithium base alloy.

The results of a series of corrosion tests made on the clad alloys are shown in Table 10. It appears that the corrosion resistance of the 6 Mg/Li-15 pct cadmium-5 pct silver alloy clad with the 8.1 Mg/Li binary was fairly good, although it did not quite equal that of the commercial magnesium-base alloys, AZ61X or MI. Painting of the cut edges of the clad material was especially effective in reducing corrosion in the simulated marine atmosphere. Cladding with 2S aluminum was advantageous where the edges of the core alloy were protected by paint.

In order to determine the extent of anodic protection offered by the 8.1 Mg/Li cladding on the 6 Mg/Li-15 pct cadmium-5 pct silver alloy, a number of specimens were tested on which a

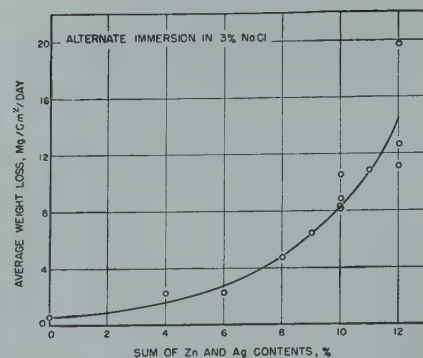


FIG 30—Effect of silver and zinc on corrosion resistance of Mg-Li alloys in salt water.

$\frac{1}{16}$ - to $\frac{1}{4}$ -in. wide strip of the cladding was removed by machining to expose the core material. These specimens were tested in aerated 3 pct sodium chloride and aerated synthetic sea water. As shown in Fig 32, the binary alloy cladding afforded protection to the exposed base alloy when a strip as wide as $\frac{1}{8}$ in. of the base alloy was exposed. These experiments were in agreement with the solution potential measurements reported in Fig 31.

Metallography

A considerable amount of work in connection with microstructural examinations and X ray diffraction studies was conducted on the magnesium-lithium base alloys. In agreement with work of other investigators, it was shown that the beta-phase solid solution had a body-centered-cubic lattice similar to that of lithium. The beta phase was obtained when additions of 10.5 pct of lithium or more were made to magnesium. No attempts were made to establish with any degree of accuracy the exact location of the boundary between the alpha plus beta and the beta-phase regions which, according to the literature, exists at about 10.3 pct lithium.

The ternary Mg-Li-Zn, Mg-Li-Cd, Mg-Li-Al, and Mg-Li-Ag alloys having sufficient lithium to consist of beta solid solution and a sufficient quantity of the third element, may contain a precipitate which has been termed theta. From X ray diffraction studies, theta has been assigned the tentative composition $MgLi \cdot LiX$ where X represents any of the elements zinc, cadmium, aluminum, silver, indium, or thallium. The lattice parameter of the theta phase has a value of about 6.92 Å in the cadmium-bearing alloys, a value of from 6.66 to 6.68 Å in the zinc-bearing alloys, a value of 6.72 Å

in the aluminum-bearing alloys, and a value of 6.78 Å in the silver-bearing alloys. The latter value is in fairly close agreement with the theoretical value of 6.81 Å calculated for MgLi · LiAg.

Partial solution of the theta phase appeared to begin in the neighborhood of 300°F, and complete solution of the theta phase in most of the experimental alloys was evident at temperatures of the order of 450 to 550°F. The experimental alloys for the most part contained relatively small amounts of theta-forming elements, and none of the alloys susceptible to aging contained excessively large amounts of theta. In the Mg-Li-Ag alloys, the lattice parameter of the theta phase was observed to change as aging progressed at 150°F. The highest experimental value obtained was 6.78 Å, but this decreased to 6.70 Å after a long time at 150°F. A similar change in the lattice parameter of the theta phase was also observed in the Mg-Li-Zn and Mg-Li-Cd alloys. Such variations in lattice parameter may indicate that the theoretical structure MgLi · LiX, heretofore assigned to theta, is a transition structure which changes on prolonged aging. Another possible explanation, discussed later in this paper, is that theta only approximates the composition MgLi · LiX and that it may have appreciable quantities of lithium in solution. Attempts to determine the cause of the changes in lattice parameters are planned for later study.

In addition to the theta phase, LiAl has been found in the Mg-Li-Al alloys. Since most of the experimental effort has been devoted to low-aluminum-bearing alloys, and since this phase appears to be more prevalent in the higher aluminum alloys, no specific information about its occurrence has been obtained. It has been observed, however, that LiAl is soluble in the matrix at high temperatures and can be precipitated at low temperatures. Its occurrence has been identified in 8.1 Mg/Li alloys containing as little as 2 pct aluminum after aging at 150°F. Moderate quantities of LiAl occur at 6 pct aluminum and large quantities at 12 pct aluminum, the quantities increasing at both aluminum contents with reduction in lithium content.

In the Mg-Li-Cd alloys, when additions of cadmium were up to 12 pct, an unidentified phase was observed. Although the phase was not identified, it was established that it was neither Mg₃Cd nor LiCd.

The occurrence of the theta phase

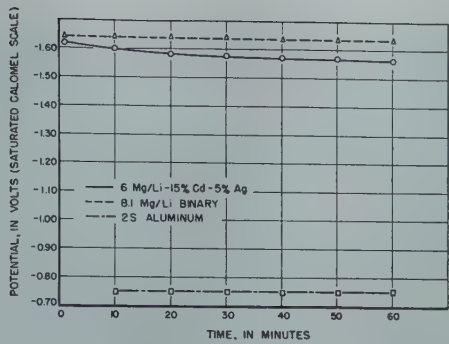


FIG 31—Time-potential values for magnesium-lithium alloys compared with aluminum, 3 pct NaCl solution at 95°F.

and lithium-bearing compounds in ternary alloys is associated with a tendency toward the formation of the alpha phase. Theta and the lithium-bearing compounds appear to remove some lithium from the matrix so that alpha can form in their immediate vicinity. The association of the alpha phase with theta is shown in Fig 33, where a precipitation pattern of theta and alpha occurs in a pearlitic-like structure in the beta background. Fig 34 shows the same type of pearlitic structure after long-time aging, the white material in this case being the alpha phase. This is evidence that theta can absorb sufficient lithium from the magnesium-lithium solid solution to

produce an alloy of predominantly alpha phase, and is probably best explained by considering theta to be a phase in which large quantities of lithium are soluble.

The mode of precipitation of the theta phase in magnesium-lithium base alloys was of interest. A Mg-Zn-Cd-Ag alloy extruded at a temperature sufficiently low to produce some cold working is shown in Fig 35. This alloy was aged 48 hr at 150°F. It is apparent from the micrograph that the precipitated theta phase is concentrated within the cold-worked grains. The same structure at a higher magnification is shown in Fig 36. The strength and ductility of alloys in which precipitation occurs

Table 10 . . . Corrosion Tests on a Clad Magnesium-lithium Base Alloy

| Heat No. or Specimen No. | Specimen Description and Intended Composition, Pct | Type of Corrosion Test and Results ¹ | | |
|--------------------------|--|---|--|--|
| | | 1. Alternate Immersion in 3 pct NaCl at 95°F for 24 Hr. Average Weight Loss, Mg per Cm ² per Day | 2. Partial Immersion in Aerated Sea Water at 95°F. for 24 Hours. Average Weight Loss, Mg per Cm ² per Day | 3. Simulated Marine Atmosphere ² at Room Temperature for 48 Hr. Average Weight Loss, Mg per Cm ² per Day |
| 32 | 6 Mg/Li-15 pct Cd-5 pct Ag alloy, clad on both sides with 8.1 Mg/Li binary | 1.59 | 1.66 | 0.92 |
| 32 | Same, except cut edges of core alloy were protected by paint | 1.55 | 1.52 | 0.290 |
| 33 | 6 Mg/Li-15 pct Cd-5 pct Ag alloy, clad on both sides with 2S aluminum | 50.3 | 48.9 | 1.48 |
| 33 | Same, except cut edges of core alloy were protected by paint | 12.7 | 8.97 | 0.045 |
| 34 | 6 Mg/Li-15 pct Cd-5 pct Ag alloy, clad on one side with 2S aluminum | 41.9 | 47.5 | 5.3 |
| 35 | 6 Mg/Li-15 pct Cd-5 pct Ag alloy, clad on one side with 8.1 Mg/Li binary | 6.12 | 3.94 | 4.14 |
| 36 | Same | 5.51 | 3.54 | 5.27 |
| 2002 | 6 Mg/Li-15 pct Cd-5 pct Ag alloy, unclad | 7.94 | 15.9 | 6.65 |
| 2003 | 8.1 Mg/Li binary | 0.81 | 1.47 | 0.263 |
| 2S | Commercially pure aluminum | 0.00 | 0.07 | 0.00 |
| AZ61X ³ | 6.5 pct Al-1.0 pct Zn-0.2 pct Mn-Balance Mg | 1.21 | | 0.11 |
| M1 ³ | 1.5 pct Mn-Balance Mg | 0.50 | | 0.16 |

¹ The samples were cut from hot-rolled sheet material approximately 0.040 in. thick.
² In this test the cabinet was opened for 8 hr each week day and closed for the remainder of the time.
³ These specimens were exposed for two weeks. Long exposures generally produce lower overall corrosion rates.
The above results are based on averages of two specimens.



FIG 32—Experiment to show the sacrificial protection granted by the 8.1 Mg/Li binary alloy to the 6 Mg/Li-15 pct Cd-5 pct Ag base alloy. Test conditions: 48 hr immersed in aerated sea water at 95°F. (Note: The amount of cladding exposed is the same in all three experiments.)

a. Binary alloy. b. Exposed base alloy, $\frac{1}{8}$ in. c. Binary alloy. d. Binary alloy. e. Exposed base alloy, $\frac{1}{8}$ in. f. Binary alloy. g. Binary alloy. h. Exposed base alloy, $\frac{1}{4}$ in. i. Binary alloy.

in the cold-worked grains are higher than for alloys which are solution treated wherein the grains are equiaxed and where precipitation occurs only at grain boundaries.

Summary and Conclusions

The hexagonal, close-packed crystal lattice of magnesium can be converted to the body-centered-cubic lattice of

lithium by an addition of about 10.3 pct by weight or more of lithium. Additions of lithium of between 5.7 and 10.3 pct produce a structure which is a mixture of lithium dissolved in alpha, hexagonal magnesium, and magnesium dissolved in beta, body-centered-cubic lithium.

The conversion of the crystal lattice from hexagonal to body-centered cubic improves many of the properties of magnesium. Some of these improvements are:

1. Increased ratio of compressive to tensile yield strength; the compressive yield strengths of beta-phase magnesium-lithium base alloys equal or surpass the tensile yield strengths.
2. Increased modulus of elasticity in compression so that the compressive modulus equals the tensile modulus.
3. Improved formability at room temperature.
4. Improved hot- and cold-rolling and extrusion characteristics.

Because of these improvements, a major portion of the experimental work was devoted to the study of the single-phase beta alloys. Considerable attention was also given to the single-phase, lithium-bearing alpha magnesium alloys and the two-phase alloys, since these alloys have certain advantages over magnesium, such as improved working characteristics, but have lower cost than the higher lithium alloys.

The melting of magnesium-lithium alloys is no more difficult than the melting of ordinary magnesium, provided certain precautions are followed. The alloys are generally melted in a steel crucible under an argon atmosphere or lithium chloride-lithium fluoride flux, or a combination of both. They can be poured in air without protection. Cast iron, or graphite ingot molds are quite satisfactory, but they should be dried before they are used.

The magnesium-lithium alloys can be hot worked with ease at temperatures of the order of 450°F. They can be cold rolled without difficulty and total reductions of 50 pct are common for most compositions. Many of the magnesium-lithium base alloys can be cold drawn. However, some difficulty is encountered when starting the cold-drawing operation because the alloys do not work harden well and tips formed on the ends of bars are not sufficiently strengthened to withstand the stresses necessary to start the bar through the die.

Magnesium-lithium base alloys hav-

ing good mechanical properties invariably possess hardnesses of the order of 85 Brinell. High-strength magnesium-lithium base alloys have been developed which have densities of the order of 1.45 to 1.65 g per cc, compared with a density of 1.8 g per cc for present magnesium-base alloys and about 2.8 for aluminum-base alloys. Since yield strengths of approximately 40,000 to 45,000 psi can be obtained with these alloys, they compare favorably on a strength-weight basis with the strongest available commercial aluminum-base alloy, 75ST.

The modulus of elasticity of magnesium-lithium base alloys varies slightly with composition; however, the alloys possess an average value of about 6,500,000 psi, which is the same in tension and compression. This value compares favorably with that for the commercial magnesium-base alloys. Because of the low density of the magnesium-lithium alloys, it can be shown that their resistance to buckling during compressive loading is better than for equivalent weights of commercial magnesium-base alloys or other available commercial structural alloys.

Two characteristics of the magnesium-lithium base alloys containing the body-centered-cubic phase which have been found to be closely interrelated are poor work-hardening capacities and lack of stability of mechanical properties in the age-hardened state. A simple bend-deflection test, in which alloy specimens were loaded above the yield stress, was developed to determine which alloy addition improved the work-hardening characteristics. This test is described in detail. Those alloy additions which were most effective in improving work-hardening characteristics were also very beneficial in improving stability of mechanical properties. The degree of stability was determined by comparing curves showing the relationship of hardness to aging time at 150°F.

By means of these tests, it was found that the addition of silver to the alloys was most effective both in improving the work-hardening capacity of the alloys and in stabilizing the mechanical properties of age-hardened alloys. However, although great progress has been made in improving these characteristics, they are not yet entirely satisfactory.

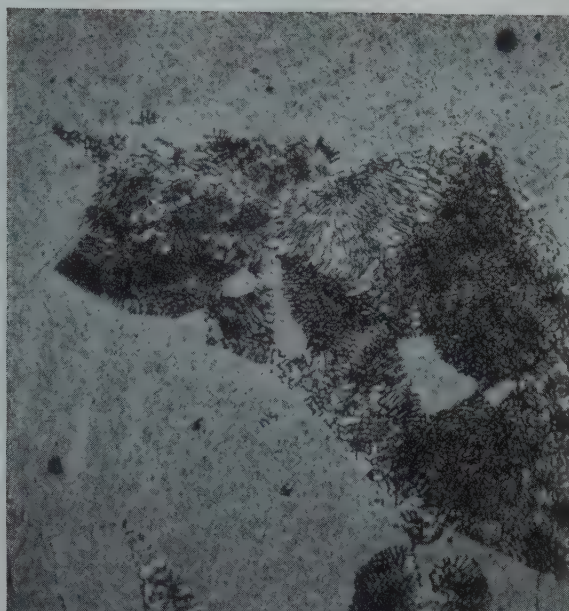
One of the best alloys developed thus far, from the standpoint of stability, has a composition of 68.5 pct magnesium, 11.5 pct lithium, 15 pct

cadmium, and 5 pct silver. Its yield strength of 43,000 psi and its elongation of about 8 pct can be maintained at a temperature of 150°F for an extended period.

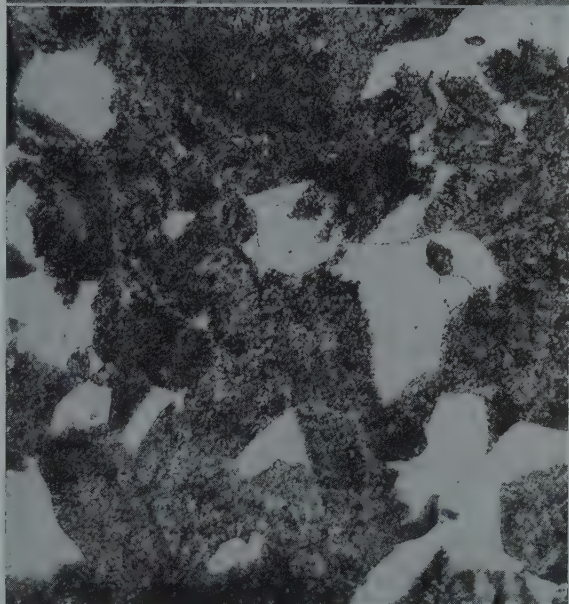
The corrosion resistance of most magnesium-lithium base alloys, especially those containing large quantities of zinc, silver, and/or cadmium is poor; however, it was observed that the magnesium-lithium binary alloy containing about 11 pct lithium had good corrosion resistance. This material can

be used to clad and to protect anodically many of the higher strength alloys.

The magnesium-lithium base alloys containing zinc, aluminum, cadmium, and/or silver can be hardened by the precipitation of a phase, called theta, which was assigned the tentative formula $MgLi \cdot LiX$ where X may be any one of the elements zinc, aluminum, cadmium, or silver. The lattice parameter of theta phase varies slightly with composition and aging time. It was



33



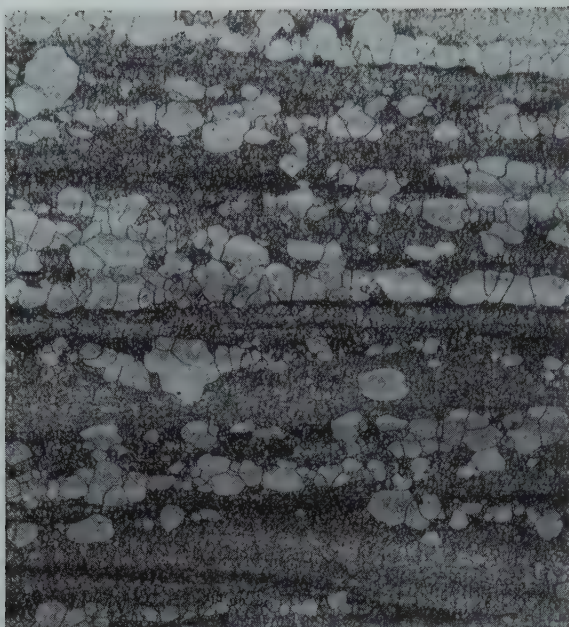
34

FIG 33—(Above) Pearlitic structure with beta background found in Mg-Li-Zn-Cd-Ag alloys after extruding and aging at 150°F. (Etched in 2 pct HF.) $\times 500$.

FIG 34—(Below) Same as Fig 33 but after a prolonged aging at 150°F.

This shows a pearlitic structure with massive alpha phase. Massive alpha phase is found only when large quantities of pearlite are present. (Etched in 2 pct. HF.) $\times 1200$.

35



36

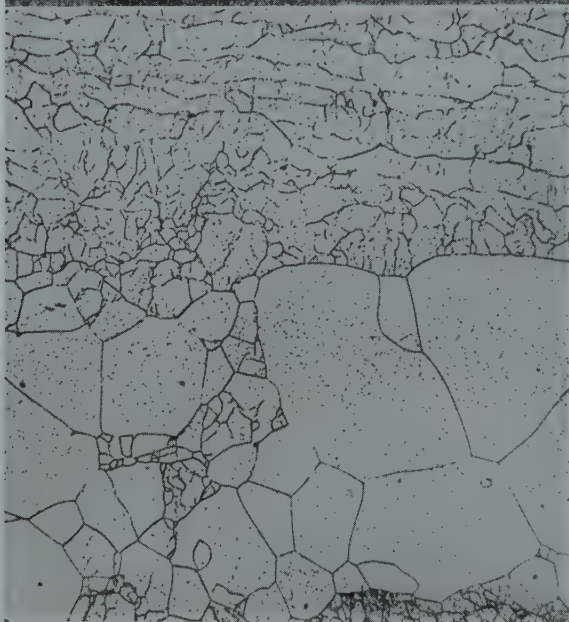


FIG 35 (Above)—Banded structure found in extruded Mg-Li-Zn-Cd-Ag alloys. (Etched in 2 pct HF.) $\times 100$.

FIG 36 (Below)—Same as Fig 35 except at $\times 500$. Note distorted unrecrystallized material. (Etched in 2 pct HF.)

concluded tentatively that the theta phase is a transition structure in which large quantities of lithium are soluble.

Future research on magnesium-lithium alloys will undoubtedly be concerned with improvements in stability, work-hardening capacity, and corrosion characteristics, and with efforts to employ alloying elements which are relatively inexpensive and plentiful.

Acknowledgments

The experimental work discussed herein was conducted under the sponsorship of the Mathieson Chemical Corporation and the Navy Department, Bureau of Aeronautics. Considerable assistance in planning the work was received from individuals representing the sponsors. These men

included Messrs. R. E. Gage, and M. C. Taylor, from Mathieson Chemical Corporation; and Capt. J. E. Sullivan, Messrs. N. E. Promisel, and H. J. Boertzel, of the Navy.

Considerable assistance was received at Battelle from the following: Messrs. E. C. Kron and A. H. Hesse, who supervised and conducted much of the early work and made valuable discoveries and contributions; Dr. C. M. Schwartz and Mr. J. R. Doig, who conducted X ray diffraction studies; and Messrs. A. R. Elsea, and J. L. Stevens, who did the microscopical work. The assistance of Messrs. R. S. Springer, H. S. Sanders, C. R. Owens, R. V. Whittenberg, and T. C. Kronfoth, in the preparation and testing of the various melts is gratefully appreciated. Many others have made valuable contributions to the work, and while no specific acknowledgment is made to them herein, their part in this work is recognized.

References

1. R. S. Dean and C. T. Anderson: Magnesium-Base Alloy, U.S.P. No. 2,317,980 (May 4, 1943).
2. R. S. Dean and C. T. Anderson: Magnesium Alloy, U.S.P. No. 2,376,868 (May 29, 1945).
3. W. Hume-Rothery, G. V. Raynor, and E. Butchers: Equilibrium Relations and Some Properties of Magnesium-Lithium and Magnesium-Silver-Lithium Alloys. *Jnl. Inst. Metals* (1945) **71**, 589-601.
4. G. Grube, H. von Zeppelin, and H. Bumm: Das System Lithium-Magnesium, *Ztsch. Elektrochemie* (1934) **40**, 160-164.
5. O. H. Henry and H. V. Cordiano: The Lithium-Magnesium Equilibrium Diagram. *Trans. AIME* (1934), **111**, 319-332.
6. P. Sal'dau and F. Shamrai: Equilibrium Diagram of the System, Magnesium-Lithium. *Ztsch. anorg. allgem. Chem.* (1935), **224**, 388-398.
7. W. Hofmann: Solubility of Lithium in Magnesium. *Ztsch. Metallkunde* (1936) **23**, 160-163.
8. F. I. Shamrai: The Ternary System Aluminum-Magnesium-Lithium. *Bull. Acad. Sci., U.S.S.R., Sect. of Chem. Sci.* (1947), 605-616, (1948), 83-94.
9. F. R. Shanley: Private Communication.

Self-diffusion in Sintering of Metallic Particles

G. C. KUCZYNSKI,* Member AIME

Two particles in mutual contact form a system which is not in thermodynamical equilibrium, because its total surface free energy is not a minimum. If such a system is left for a certain period of time, the bonding of the two particles will take place in order to decrease the total surface area, even though the temperature is lower than the melting point. This phenomenon of bonding of two or more particles with the application of heat only and at temperatures below melting point of any component of the system will be called sintering, although the powder metallurgists use this term in a broader sense, including the presence of molten phase and pressure. It is the objective of this paper to study this process and the mechanisms involved in it.

This problem is of utmost importance to powder metallurgy and powder ceramics, and its technological aspects have been studied for a good many years. However, the powder metallurgical operations are too complex and include too many superimposing mechanisms, and too many variables for a direct study. It was therefore advisable for the purposes of this study to reduce the variables to a minimum. In this work the radius of the interface formed during bonding in a simple system composed of a spherical particle and a large block of the same metal was studied as a function of time and temperature. It is believed that the mechanism involved in this simple process is fundamental to any sintering operations.

Previous Work

J. Frenkel¹ was the first to make a serious attempt to develop a theory of sintering. He assumed that the process

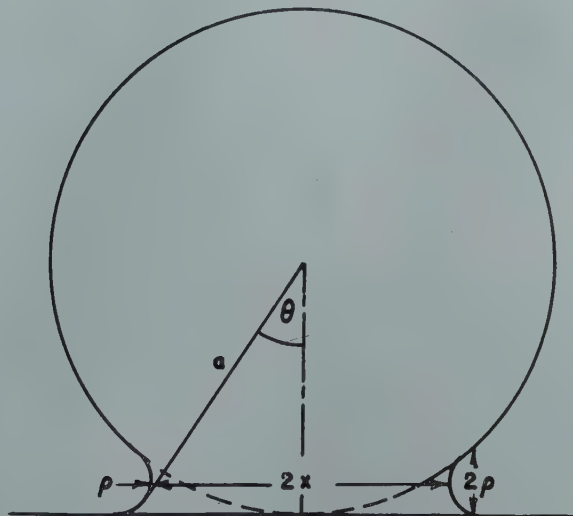


FIG 1—Schematic representation of the cross-section of a spherical particle sintered to a metallic block.

consists of a slow deformation of crystalline particles under the influence of surface tension which reduces to a viscous flow where the coefficient of viscosity η is related to the self-diffusion coefficient D by the following equation

$$\frac{1}{\eta} = \frac{D\delta}{kT} \quad [1]$$

where δ is interatomic distance, k the Boltzman constant, and T the absolute temperature. This type of viscous flow of a crystalline substance is essentially different from the ordinary plastic flow. The latter is a specific property of crystals and cannot take place in amorphous bodies. According to Frenkel this viscous type of flow is due

to the diffusion of the holes or vacancies arising in the lattice. He was able to derive an equation relating the growth of the interface between two spherical crystalline particles or between a particle and a semi-infinite crystal (Fig 1) to time t at constant temperature. This relationship can be written as follows:

$$x^2 = \frac{3}{2} \frac{a\sigma}{\eta} t \quad [2]$$

where x is the radius of the interface assumed to be circular, a the original radius of the sphere and σ surface tension of the material. The other assumptions are that $\frac{x}{a}$ is less than 0.3 and that during the period t the original radius, a , of the metallic particle did not change appreciably.

A. J. Shaler and J. Wulff² followed closely the ideas of Frenkel in their theory of sintering of a mass of metallic powder. Neither Frenkel nor Shaler has validated his theoretical speculations with conclusive experimental data. Two measurements reported by

San Francisco Meeting, February 1949.

TP 2528 E. Discussion of this paper (2 copies) may be sent to *Transactions AIME* before May 15, 1949. Manuscript received November 1, 1948; revision received November 24, 1948.

* Sylvania Electric Products Inc. Bayside, N. Y.

References are at the end of the paper.

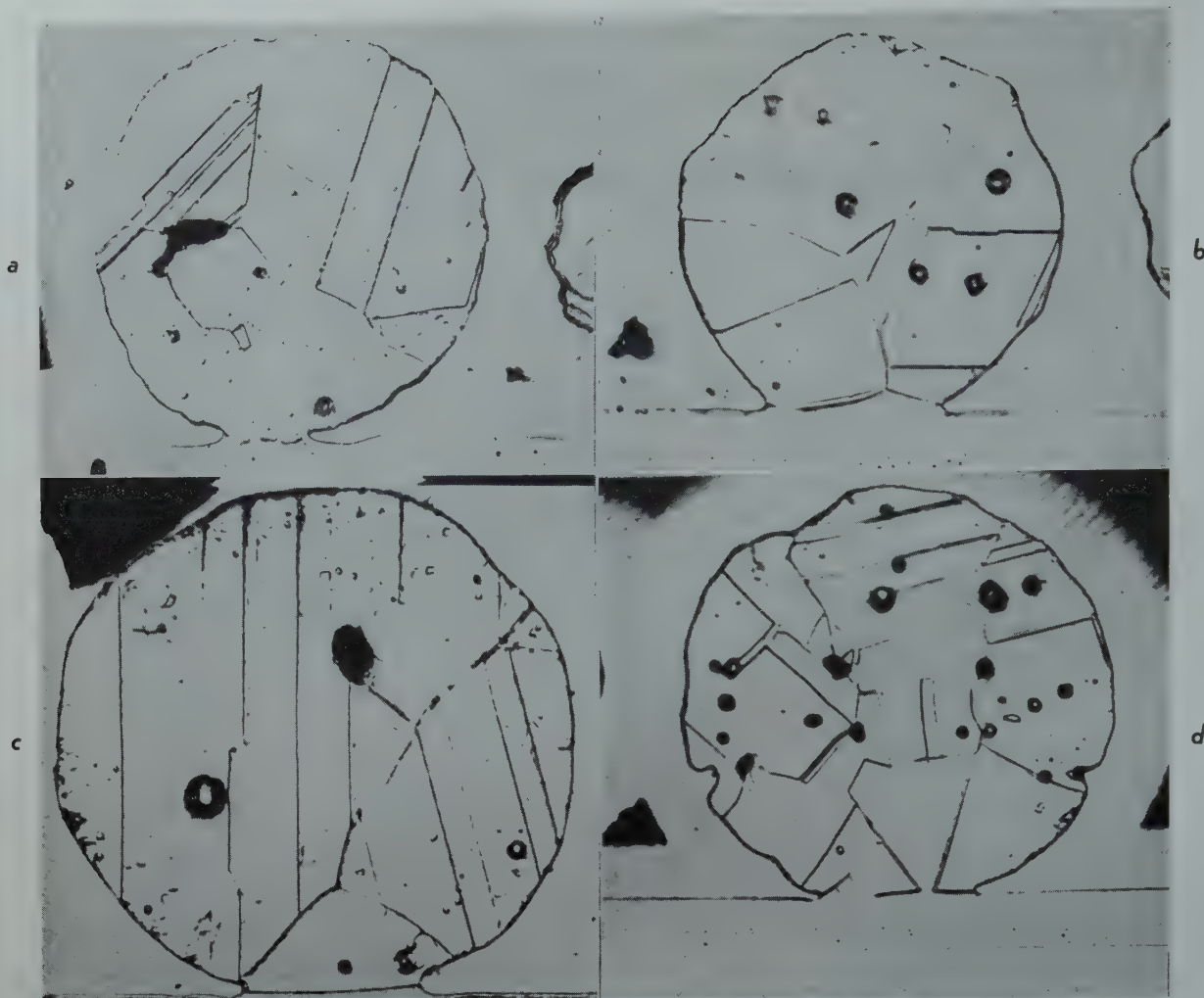


FIG 2—Copper particles sintered to copper blocks. *a.* At 700°C for 4 hr, 800 X. *b.* At 800°C for 2 hr, 900 X. *c.* At 900°C for 1 hr, 1000 X. *d.* At 1000°C for 0.5 hr, 600 X.

Shaler for copper powder sintered at 850 and 900°C yielded a value for the heat of activation of self-diffusion in copper which was 10 pct higher than those obtained by other methods. This is by no means an adequate test of the theory. In the first place two such measurements are not sufficient for evaluating the coefficient of self-diffusion D . More important, however, is the fact that the temperature dependence is of secondary importance only. The final check of this theory will come from the experimental investigations of the time relationships such as [2] above as will be shown later.

B. Ya. Pines³ developed a theory of sintering of the powder compacts based upon different assumptions. According to him the atoms from the surface of the compact migrate by diffusion to the internal voids filling them gradually, or, as Pines puts it, by moving the voids out from the body. This mechanism is essentially different from that postulated by Frenkel. The difference is that

while Pines visualizes sintering as filling of the voids atom by atom, Frenkel envisions them filled by slow viscous creep of the crystal. The conclusions arrived at by Pines are only of qualitative nature and do not render themselves for experimental verification.

Theoretical Considerations

Formation of the common interface between two particles or a particle and a crystal block can be achieved by one, or a combination of, the following mechanisms: viscous or plastic flow, evaporation and condensation, volume diffusion and surface diffusion.

As the objective of this paper is to determine experimentally which of these mechanisms are involved in sintering of the particles it is important to discuss briefly each of these in order to find out what kind of relationships characteristic for each mecha-

nism could be established and tested experimentally.

VISCOUS OR PLASTIC FLOW

This mechanism has already been discussed in connection with Frenkel's paper.¹ If only mechanism of viscous flow were responsible for sintering, the relationship between the radius of the interface and the time of heating at a given temperature would be expressed by Eq 2. A similar expression could be derived for plastic flow with only a different temperature dependent coefficient at variable t .

EVAPORATION AND CONDENSATION

According to the kinetic theory the rate G of evaporation of a gas from a surface above which the equilibrium pressure is p_1 , and the rate of condensation on a neighboring surface of pressure p_2 is

$G = K(p_1 - p_2)$ [3]
 where K is a function of temperature only. The equilibrium pressures are related to the respective radii of curvature. In our case ρ is the radius of the area of condensation and a the radius of the area of evaporation by the well known Kelvin equation:

$$\ln \frac{p_2}{p_1} = \frac{-2\sigma\delta^3}{kT} \left(\frac{1}{\rho} + \frac{1}{a} \right) \quad [4]$$

where σ is the surface tension of the body.

As $\rho \ll a$, $p_2 = p_1 - \Delta p$ and $\frac{\Delta p}{p_1}$ is small, Eq 3 can be written as follows:

$$G = \frac{K'}{\rho} \quad [5]$$

where K' is a function of temperature and p_1 only. In our problem (Fig 1) p_1 can be regarded constant because the radius of the sphere does not change appreciably. The radius of curvature ρ can be approximated as a function of x as follows: From Fig 1, it is obvious that

$$\rho = a(1 - \cos \theta) \text{ or } \rho = 2a \sin^2 \frac{\theta}{2}$$

as θ is very small and equal to $\frac{x}{a}$,

$$\rho = \frac{x^2}{2a}$$

Introducing this value for ρ in [5] we obtain

$$G = \frac{K''}{x^2}$$

The rate of condensation G on the area A of the junction between the particle and the crystalline block should be equal to the rate of mass transport which in turn is proportional to the rate of change of volume of the junction. We can write then

$$AG = \beta \frac{dv}{dt}$$

where β is independent of time.

But $A \cong \pi \frac{x^2}{a}$ and $V \cong \pi \frac{x^3}{2a}$ so

$$\frac{K''}{2\beta} = x^2 \frac{dx}{dt}$$

and after integration

$$x^3 = \frac{3}{2} \frac{K''}{\beta} t \quad [6]$$

In other words if the mechanism of evaporation and condensation were responsible for the formation of interface between particles, the radius of the junction should grow with such a rate that its cube would be proportional to time.

VOLUME DIFFUSION

If we assume the vacancy theory of diffusion, then the area near the

interface should have higher hole concentration than the remaining body of the particle. This is due to the fact that near the interface, where the radius of curvature is small the surface energy is very high and it can be lowered by decreasing the surface area. The decrease in surface area is produced by an increase in the interface volume which is accomplished by a larger concentration of vacancies present in that region. If the interstitial

atom mechanism is assumed, the junction area should be deprived of the interstitial atoms in order to decrease the total surface. This causes the flow of atoms from the other parts of our system to the junction. The third possible mechanism of diffusion known as atom exchange mechanism and sometimes considered possible^{4,13} is automatically eliminated if the actual sintering is caused by diffusion because in this case no concentration gradient

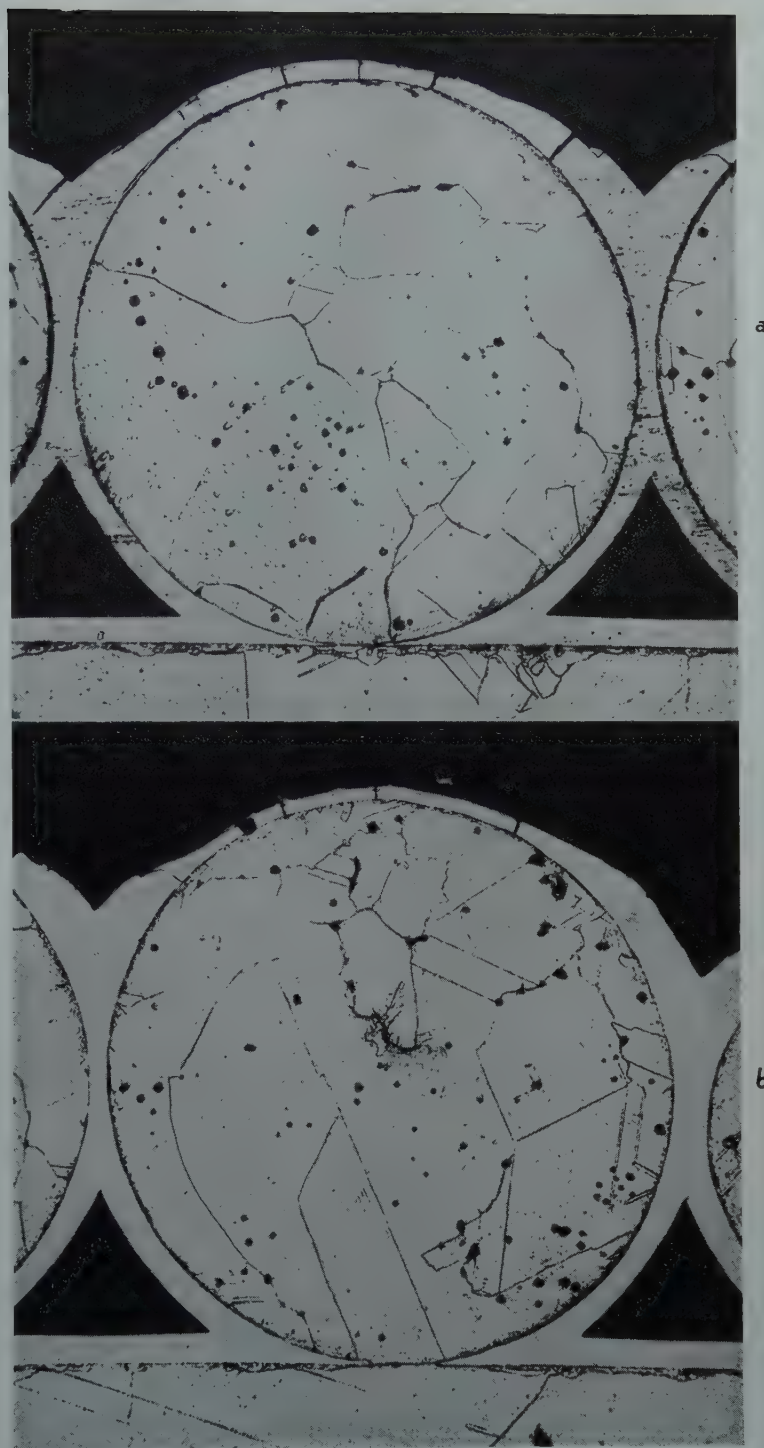


FIG 3—Silver particles sintered to silver blocks. 200 \times . *a.* (above) At 800°C for 24 hr. *b.* (below) At 900°C for 2 hr.

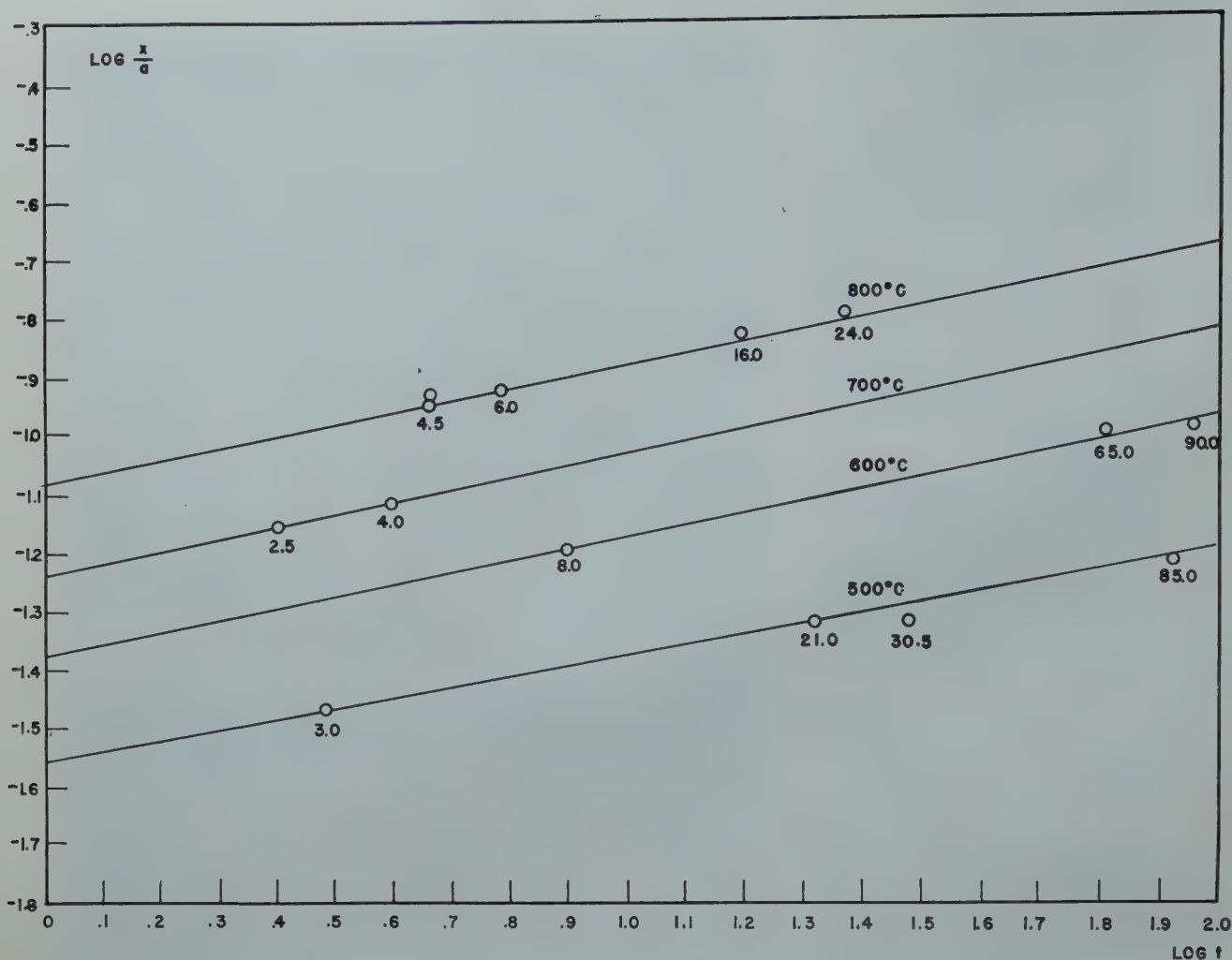


FIG 4—Logarithm of the ratio of the interface radius x to the radius of a copper particle sintered at indicated temperatures, plotted against the logarithm of sintering period t . The numbers at the points express time of heating in hours.

would be present. It is convenient to assume that the hole mechanism is the actual mechanism prevailing in self-diffusion of metals. In such a case, the surface forces tending to decrease the total surface area will build a high concentration of holes³ underneath the surface of the junction between the particle and the crystal block. This increment of concentration ΔC can be calculated from Kelvin's Eq 4

$$\Delta C = \frac{2\sigma\delta^3}{kT} \left(\frac{1}{\rho} - \frac{1}{x} \right) C$$

where C is the equilibrium concentration of the holes equal to $e^{-\frac{E}{RT}}$, E being the energy required to produce such a hole in the lattice. As $x \gg \rho$ the last equation can be written in the following form

$$\Delta C = \frac{2\sigma\delta^3}{\rho kT} e^{-\frac{E}{RT}}$$

As the concentration gradient is approximately equal to $\frac{\Delta C}{\rho}$, we can write the Fick's equation for our case

$$A \frac{\Delta C}{\rho} D' = \frac{dV}{dt} \quad [7]$$

where $\rho \cong \frac{x^2}{2a}$, $A \cong \pi \frac{x^3}{a}$ and $V \cong \pi \frac{x^4}{2a}$ as before and D' the coefficient of holes diffusion which obviously fulfills

the following equation $D' e^{-\frac{E}{RT}} = D_v$, where D_v is the coefficient of volume self-diffusion for a given metal. Introducing all these values into Eq 7 and integrating, we obtain

$$\frac{x^5}{a^2} = \frac{40\sigma\delta^3}{kT} D_v t \quad [8]$$

or in other words if the mechanism of diffusion was responsible for sintering, the fifth power of the interface radius is proportional to time.

SURFACE DIFFUSION

Very similarly we shall obtain the relation between radius x and time t in case the prevailing mechanism is surface diffusion. We have to put only $A \cong 2\pi\delta$ with concentration gradient

and volume rate the same as in the case of volume diffusion.

Integrating the differential equation resulting from Fick's equation we obtain

$$\frac{x^7}{a^3} = \frac{56\sigma\delta^4}{kT} D_s t \quad [9]$$

where D_s is the coefficient of surface diffusion.

Summing up we can tabulate the relationships between radius x of the interface formed during sintering between two particles and time t . These relations are as follows:

| | |
|------------------------------|--------------|
| Viscous or plastic flow | $x^2 \sim t$ |
| Evaporation and condensation | $x^3 \sim t$ |
| Volume diffusion | $x^5 \sim t$ |
| Surface diffusion | $x^7 \sim t$ |

The experiments described in the next paragraph were carried out in order to decide which mechanism or mechanisms actually prevail during sintering.

Experimental Method

In order to study experimentally the

Table 1 . . . Copper Powder

| T°C | t hr | $x \cdot 10^{-4}$ cm | $a \cdot 10^{-4}$ cm | $\frac{x}{a}$ | n |
|-----|------|----------------------|----------------------|---------------|-----|
| 700 | 2.0 | 4.0 | 40.2 | 0.100 | 4.5 |
| | 4.0 | 5.1 | 41.0 | 0.134 | |
| | 8.0 | 7.2 | 41.0 | 0.176 | |
| | 41.0 | 14.0 | 39.0 | 0.250 | |
| 800 | 0.5 | 7.0 | 47.0 | 0.145 | 5.0 |
| | 2.0 | 10.0 | 53.0 | 0.188 | |
| | 3.0 | 7.2 | 36.0 | 0.200 | |
| | 4.0 | 9.0 | 40.1 | 0.222 | |
| | 16.5 | 13.6 | 44.5 | 0.303 | |
| 900 | 0.5 | 12.1 | 41.0 | 0.290 | 5.0 |
| | 1.0 | 14.0 | 43.2 | 0.330 | |

Table 2 . . . Silver Powder

| T°C | t hr | $x \cdot 10^{-4}$ cm | $a \cdot 10^{-2}$ cm | $\frac{x}{a}$ | n |
|-----|------|----------------------|----------------------|---------------|-----|
| 500 | 3.0 | 6.5 | 1.95 | 0.033 | 5.4 |
| | 21.0 | 7.9 | 1.68 | 0.047 | |
| | 30.5 | 9.1 | 1.93 | 0.048 | |
| | 85.0 | 10.2 | 1.79 | 0.060 | |
| | | | | | |
| 600 | 8.0 | 11.6 | 1.88 | 0.062 | 5.0 |
| | 65.0 | 18.8 | 1.87 | 0.100 | |
| | 90.0 | 17.5 | 1.65 | 0.106 | |
| 700 | 2.5 | 12.0 | 1.74 | 0.070 | 4.8 |
| | 4.0 | 14.2 | 1.88 | 0.076 | |
| 800 | 1.0 | 15.9 | 1.90 | 0.084 | 4.9 |
| | 4.5 | 20.2 | 1.83 | 0.111 | |
| | 6.0 | 21.5 | 1.81 | 0.119 | |
| | 16.0 | 25.5 | 1.77 | 0.144 | |
| | 24.0 | 25.0 | 1.55 | 0.162 | |

relationship between the radius of the interface as a function of time and temperature it is necessary to measure this radius directly if possible. This was achieved by a very simple although somewhat laborious method. The metallic particles of spherical shape were dispersed on a flat block of the same metal, heated in a controlled atmosphere (hydrogen in the case of copper, hydrogen or air in the case of silver) at different temperatures and for various periods of time. After heating, the blocks with the particles sintered to them were mounted in bakelite and cut, in order to obtain a diametral cross-section of the particle in contact with the block. This cross-section was then examined under the microscope. The diameters of the particles and their interfaces with the blocks were readily measured with the microscope eyepiece micrometer. In order to assure the greatest accuracy of these measurements, the specimens were successfully polished down and after each of such operations readings of the radius of the interface for each particle were taken until a maximum radius was obtained.

The metals used in these experiments were copper and silver. The copper was round, atomized powder obtained from Greenback Industries, Inc. The shape of the powder particles was nearly

Table 3 . . . The Volume Diffusion Coefficient D_v of Copper

| T°C | t hr | $a \cdot 10^{-4}$ cm | $x \cdot 10^{-4}$ cm | $D_v \frac{\text{cm}^2}{\text{sec}}$ |
|------|------|----------------------|----------------------|--------------------------------------|
| 400 | 6.0 | 20.0 | 0.5 | 4.2×10^{-18} |
| | | 13.0 | 1.0 | 3.2×10^{-14} |
| | | 3.2 | 0.8 | 3.0×10^{-13} |
| 500 | 1.0 | 10.0 | 1.0 | 3.8×10^{-13} |
| | | 4.0 | 1.0 | 2.3×10^{-12} |
| | | 47.5 | 2.0 | 8.2×10^{-15} |
| 65.0 | | 41.5 | 1.9 | 8.3×10^{-15} |
| | | 30.0 | 2.0 | 2.1×10^{-14} |
| 600 | 0.5 | 4.5 | 1.8 | 8.0×10^{-11} |
| | | 15.5 | 1.7 | 3.5×10^{-12} |
| | | 3.8 | 1.7 | 4.5×10^{-11} |
| 3.0 | | 10.0 | 1.7 | 2.0×10^{-12} |
| | | 4.2 | 2.3 | 5.1×10^{-11} |
| | | 40.5 | 4.1 | 1.9×10^{-12} |
| 16.0 | | 28.0 | 3.4 | 1.6×10^{-12} |
| 700 | 0.5 | 4.5 | 2.0 | 1.5×10^{-10} |
| | | 3.5 | 1.7 | 5.5×10^{-11} |
| | | 40.2 | 4.0 | 1.5×10^{-11} |
| 4.0 | | 47.7 | 6.0 | 4.1×10^{-11} |
| | | 41.0 | 5.1 | 2.5×10^{-11} |
| | | 33.0 | 4.8 | 2.8×10^{-11} |
| 26.2 | | 16.0 | 3.1 | 5.0×10^{-11} |
| | | 43.0 | 3.2 | 1.6×10^{-11} |
| | | 39.0 | 7.2 | 6.3×10^{-11} |
| 800 | 0.5 | 47.0 | 8.0 | 1.6×10^{-9} |
| | | 39.8 | 7.0 | 1.1×10^{-9} |
| | | 35.3 | 6.0 | 6.6×10^{-10} |
| 2.0 | | 11.0 | 3.6 | 5.3×10^{-10} |
| | | 53.0 | 10.0 | 9.4×10^{-10} |
| | | 40.1 | 9.0 | 4.9×10^{-10} |
| 16.5 | | 45.0 | 13.6 | 7.3×10^{-10} |
| 900 | 0.5 | 41.0 | 12.1 | 1.8×10^{-8} |
| | | 43.2 | 14.0 | 1.6×10^{-8} |
| | | 30.5 | 11.0 | 9.8×10^{-9} |
| 1000 | 0.5 | 47.0 | 15.0 | 4.3×10^{-8} |
| | | 40.0 | 14.0 | 4.2×10^{-8} |
| | | 37.8 | 14.0 | 4.7×10^{-8} |

spherical as can be seen from Fig 2, *a*, *b*, *c*, and *d*. The diameters of these particles ranged from 4 to 100 μ . The powder was fractionated by the elutriation method into three lots. The first lot contained particles greater than 35 μ in diameter. The second particles between 15–35 μ and the third, particles less than 15 μ . The silver used was coarse atomized powder of about 350 μ in diameter furnished by Stevens Institute of Technology. This powder consisted of almost perfectly spherical particles as can be ascertained from Fig 3, *a* and *b*. The copper powder contained some oxygen so it was reduced by packing it in carbon and heating in a hydrogen atmosphere at 900°C for 18–24 hr. The resulting powder developed some blow holes. The copper blocks were cast of oxygen free high conductivity copper, the silver was spectroscopically pure. Their surfaces were thoroughly polished and cleaned by etching before the powders were dispersed on them. The copper was etched with ammonium hydroxide plus hydrogen peroxide and the silver specimens with potassium dichromate. After heating, the specimens were plated with nickel in order to avoid loosening or deforming the interfaces during the subsequent metallographic operations.

Table 4 . . . The Volume Diffusion Coefficient D_v of Silver

| T°C | t hr | $a \cdot 10^{-4}$ cm | $x \cdot 10^{-4}$ cm | $D_v \frac{\text{cm}^2}{\text{sec}}$ |
|-----|------|----------------------|----------------------|--------------------------------------|
| 500 | 3.0 | 195.0 | 6.5 | 3.4×10^{-12} |
| | 21.0 | 168.0 | 7.9 | 1.3×10^{-12} |
| | 30.5 | 193.0 | 9.1 | 1.8×10^{-12} |
| | 85.0 | 178.0 | 10.2 | 1.2×10^{-12} |
| 600 | 8.0 | 188.0 | 11.6 | 2.7×10^{-11} |
| | 65.0 | 187.0 | 18.8 | 3.7×10^{-11} |
| | 90.0 | 165.0 | 17.5 | 2.5×10^{-11} |
| 700 | 2.5 | 174.0 | 12.0 | 1.4×10^{-10} |
| | 4.0 | 188.0 | 14.2 | 1.6×10^{-10} |
| 800 | 1.0 | 190.0 | 15.9 | 1.3×10^{-9} |
| | 4.5 | 183.0 | 20.2 | 1.0×10^{-9} |
| | 6.0 | 181.0 | 21.5 | 1.1×10^{-9} |
| | 16.0 | 177.0 | 22.5 | 1.0×10^{-9} |
| | 24.0 | 155.0 | 25.0 | 8.1×10^{-10} |
| 900 | 3.5 | 165.0 | 29.5 | 1.2×10^{-8} |

Table 5 . . . The Surface Diffusion Coefficient D_s of Copper

| T°C | t hr | $a \cdot 10^{-4}$ cm | $x \cdot 10^{-4}$ cm | $D_s \frac{\text{cm}^2}{\text{sec}}$ |
|-----|------|----------------------|----------------------|--------------------------------------|
| 400 | 6.0 | 13.0 | 1.0 | 7.0×10^{-12} |
| | | 3.2 | 0.8 | 1.2×10^{-11} |
| 500 | 1.0 | 10.0 | 1.0 | 1.1×10^{-9} |
| | | 4.0 | 1.0 | 1.6×10^{-9} |
| 600 | 0.5 | 4.5 | 1.0 | 2.3×10^{-7} |
| | 1.0 | 3.8 | 1.7 | 8.8×10^{-8} |
| | 3.0 | 4.2 | 2.3 | 1.8×10^{-7} |

Table 6 . . . The Heat of Activation Q_v of self Diffusion and Frequency Factor D_v^0 for Copper as Determined by Various Investigators

| Authors | Q_v cal per mol | $D_v^0 \frac{\text{cm}^2}{\text{sec}}$ |
|---|-------------------|--|
| F. N. Rhines and B. F. Mehl ⁶ | 44,000 | 47.0 |
| B. V. Rollin ⁷ | 61,000 | |
| J. Steigman, W. Shockley, F. C. Nix ⁸ | 57,200 | 0.9–11.0 |
| C. I. Raynor, L. Thomasen, and L. J. Rouse ⁹ | 46,800 | 0.3 |
| M. S. Maier and H. R. Nelson ¹⁰ | 54–61,000 | 0.1–0.6 |
| This Investigation..... | 56,000 | 70.0 |
| Silver | | |
| W. A. Johnson ¹¹ | 45,900 | 0.89 |
| This Investigation..... | 42,000 | 0.60 |

At least ten particles were measured for each temperature or time period. Some micrographs of the observed particles sintered to the metallic blocks are shown in Fig 2, *a*, *b*, *c*, and *d* and Fig 3, *a* and *b*.

Very fine copper particles (less than 10 μ) in diameter were not as round as the coarse ones and consequently yielded more scattered results. Also, it was impossible to polish down these particles, in order to obtain the maximum radius of their interface. Consequently a large number of them were

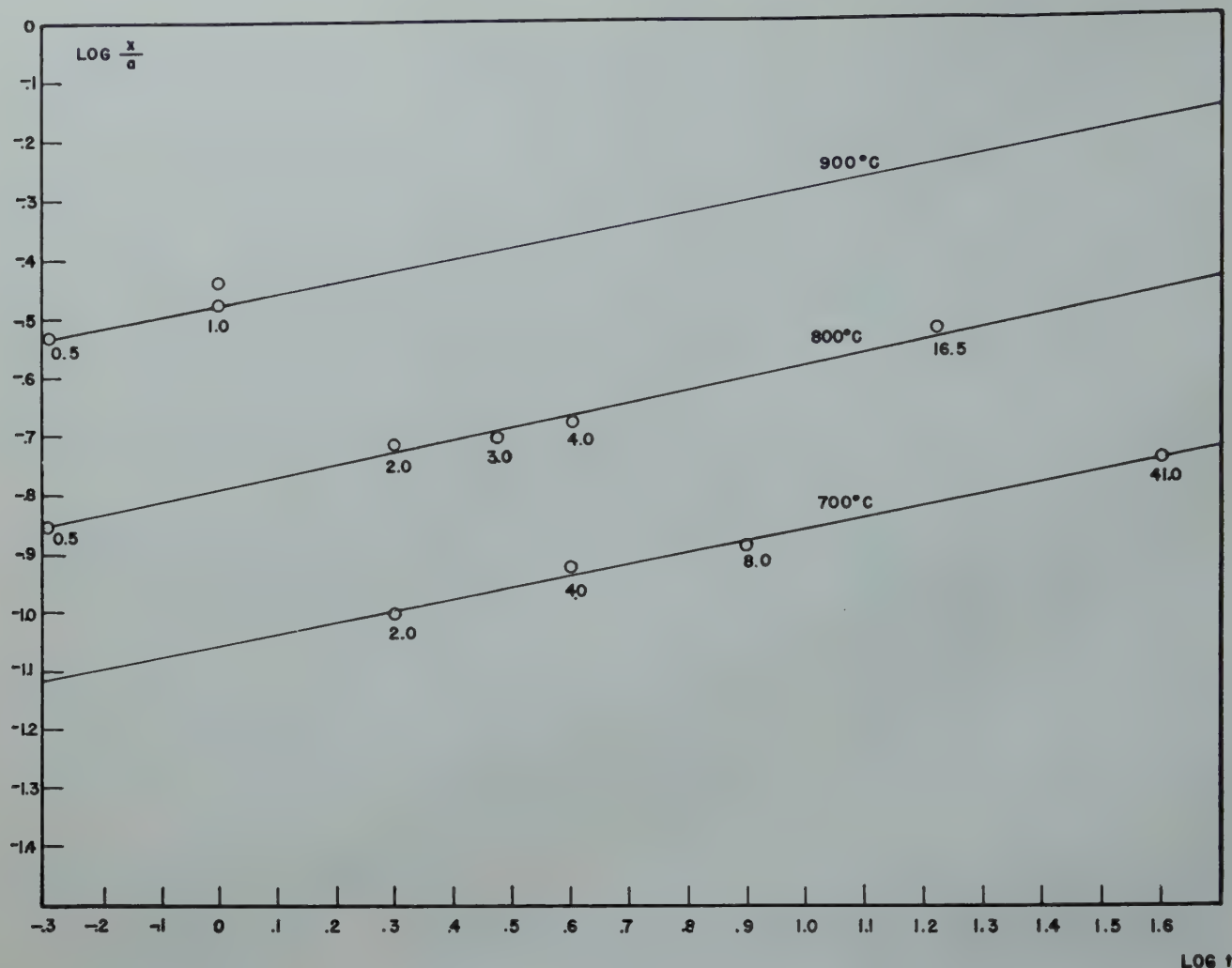


FIG 5—Logarithm of the ratio of the interface radius x to the radius a of silver particles sintered at indicated temperatures, plotted against the logarithm of sintering period t . The numbers at the points express time of heating in hours.

measured and only the largest values of radii were used for future calculations.

Results

Tables 1 and 2 contain the results obtained from measurements of the interface radii of copper and silver particles heated to different temperatures for various periods of time.

In the first and second columns of these tables, the temperature in degrees centigrade and time in hours are listed. The third and fourth column contain the observed radii of the interface and of the particle respectively (in centimeters). In the fifth column the ratios of these radii are given. The $\log \frac{x}{a}$ versus $\log t$ plots are given in Fig 4 and 5. The points fall on the straight lines whose inverse slope n is approximately equal to 5, as can be seen from the sixth volume of tables where the n values are listed.

The numbers at each point express the length of time in hours, for which a given specimen was heated.

The value 5 of the inverse slope n of the $\log \frac{x}{a} / \log t$ plot indicates that

within the range of temperatures, periods of time and particle size, used in this work and listed in Tables 1 and 2, the predominant mechanism of sintering is volume diffusion in agreement with Eq 8. This last equation permits us to evaluate the coefficient of volume diffusion D_v for each temperature provided that the interface radius is known. There is uncertainty in the value of the surface tension of copper and silver as they have not been determined experimentally for solid metals. In this work the values of surface tension as measured for molten metals were adopted, based on the assumption that they should be close to those for solids. The error introduced by this choice would not change the order of

magnitude of the coefficient of diffusion, calculated from Eq 8. Thus, for copper $\sigma = 1200$ ergs per cm^2 and for silver $\sigma = 1000$ ergs per cm^2 was used.⁵ The values of D_v for copper and silver are listed in Tables 3 and 4 respectively, along with temperatures and periods of heating time, radii of the particles and interfaces.

D_v was plotted on the semi-logarithmic scale against $\frac{1000}{T}$. T being absolute temperature. For large particles of 40μ or more in diameter straight lines were obtained as shown in Fig 6 and 7.

The heats of activation of volume diffusion, Q_v , and frequency factors, D_v^0 , were determined from these graphs. Thus for copper Q_v is 56000 cal per mol and $D_v^0 = 70 \frac{\text{cm}^2}{\text{sec}}$ and for silver $Q_v = 42000$ cal per mol and $D_v^0 = 0.6 \frac{\text{cm}^2}{\text{sec}}$. These values are in good

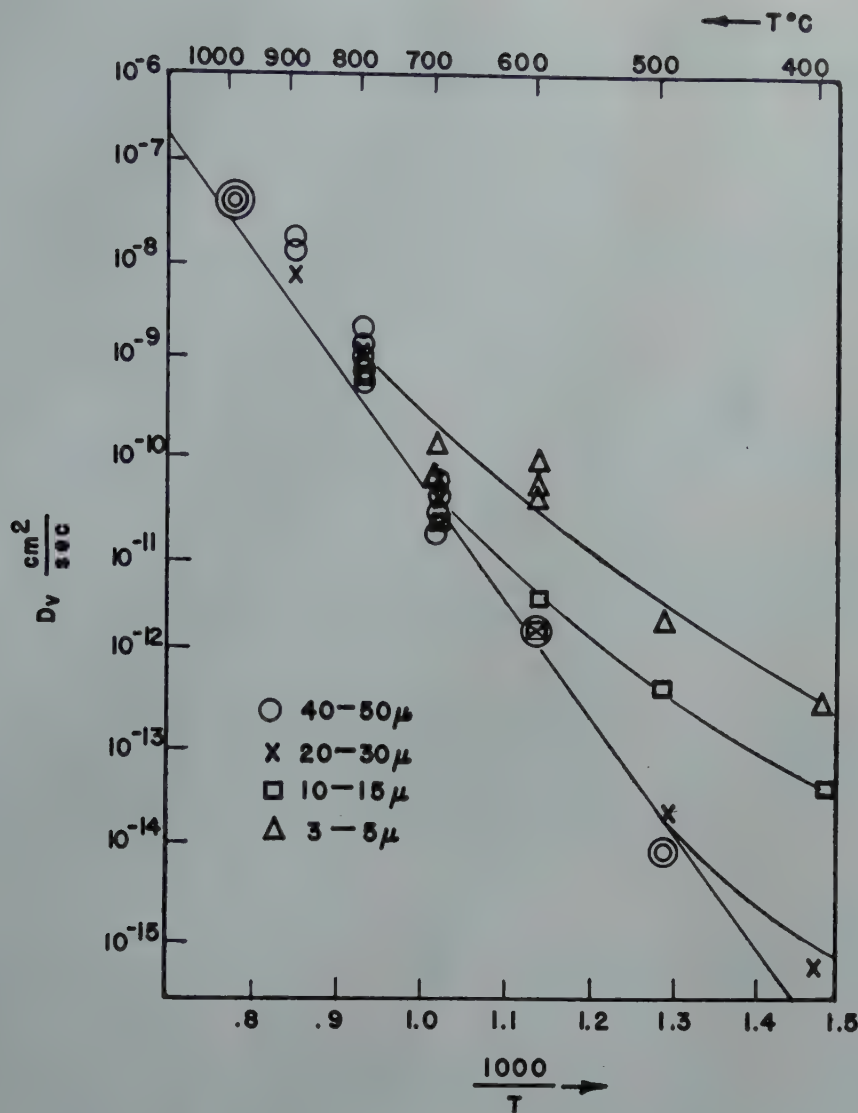


FIG 6—Variation of volume self-diffusion coefficient of copper with temperature as determined from sintering experiments. Logarithm of D_v vs. reciprocal of absolute temperatures.

agreement with those obtained by various workers who used the radioactive tracer method as is shown in Table 6. This suggests that the above described method may successfully be used for determination of the coefficient of self-diffusion of metals without using radioactive tracers. As it is difficult to get a perfectly round metallic particle it is more convenient to use wires and measure their rate of sintering to metallic blocks.*

Fig 6 shows that the coefficients of volume diffusion calculated from the rates of interface growth for small particles, (less than 30μ in diameter) when plotted on the semi-logarithmic

scale versus $\frac{1}{T}$ at lower temperatures

show deviations from the straight line although they fall on this line at higher temperatures; the smaller the particles the greater the deviations. These deviations are due to the surface diffusion mechanism predominant at lower temperatures and for smaller particles as will be proven later. In cases where both mechanisms, volume and surface diffusion, take place, the flow equation will be as follows:

$$\frac{dV}{dt} = n f_v + m f_s \quad [10]$$

n and m are fractions of the overall contributing flow, functions of x and a and obviously fulfill the relationship $n + m = 1$. From Eq 8 and 9 f_v and

f_s are easily calculated their values being as follows:

$$f_v = \frac{16\pi a \sigma \delta^3}{k T x} D_v$$

$$f_s = \frac{16\pi a^2 \sigma \delta^4}{k T x^3} D_s$$

Substituting these values as f_v and f_s into Eq 10, we obtain

$$\frac{dx}{dt} = \frac{8a^2 \sigma \delta^3}{k T x^4} \left(n D_v + m \frac{a}{x^2} D_s \right),$$

since $V \cong \frac{x^4}{2a}$ [11]

When the contact area, or the radius x , is very small one should expect that the contribution of flow due to surface diffusion will be overwhelmingly greater than that due to volume diffusion especially as $D_s > D_v$. In such cases also $m \cong 1$ and Eq 11 reduces to

* The work leading toward experimental testing of this latter method is now in progress in the Sylvania Metallurgical Laboratories.

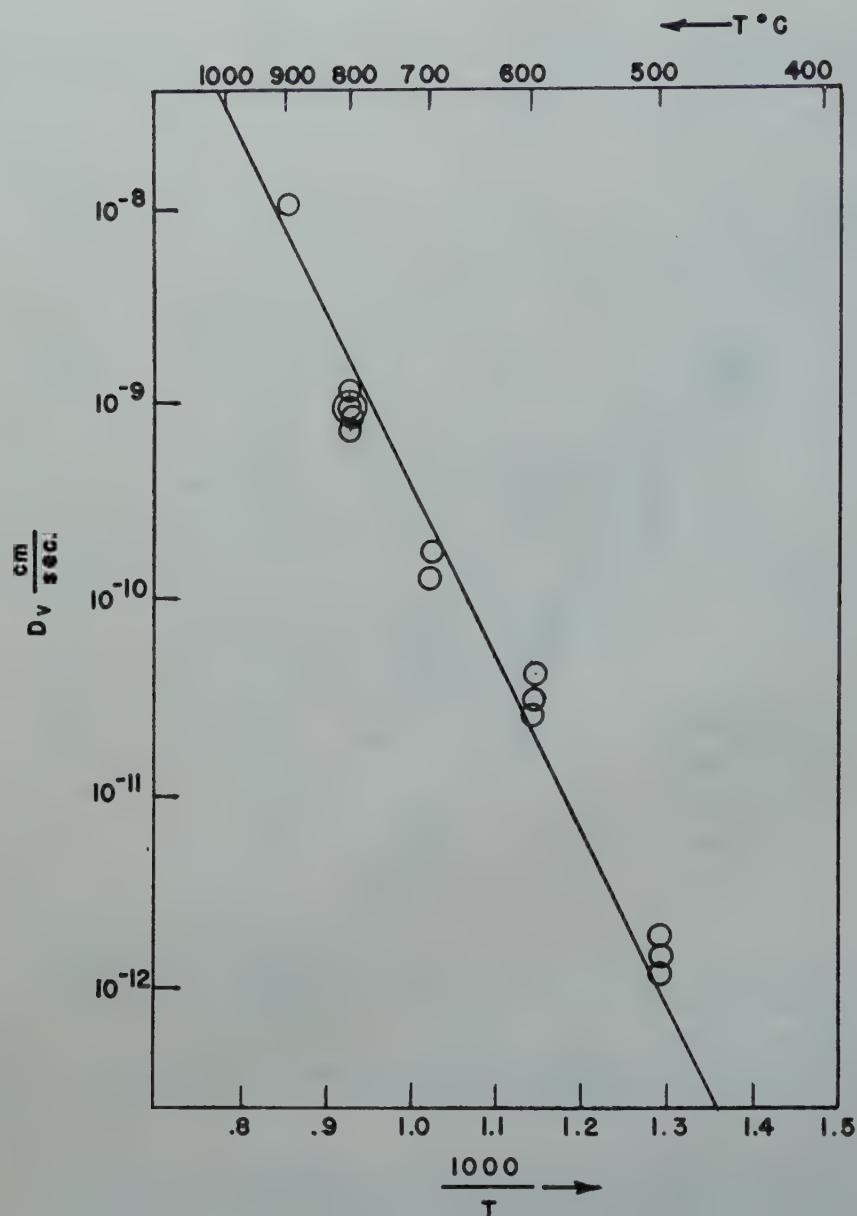


FIG 7—Variation of volume self-diffusion coefficient of silver with temperature as determined from sintering experiments. Logarithm of D_v vs. reciprocal of absolute temperature.

$$\frac{dx}{dt} = \frac{8a^3\sigma\delta^4}{kTx^6} D_s$$

which after integration gives Eq 9. The effect of surface diffusion upon sintering should be noticeable at low temperatures when D_s and x are very small, especially for small particles which have larger surface atom to volume atom ratios, and will sinter by the mechanism of surface diffusion to the longer interface radii x than the large particles. This reasoning seems to be fully substantiated by experiments as seen in Fig 6, where deviations are the larger the smaller are the particles and the lower is the sintering temperature up to about 600°C for the particles

of 10 μ diam or less, the volume diffusion contribution can be neglected and the problem can be treated as surface diffusion only.

In order to prove that the above discussed deviations are really due to surface diffusion, the fine (about 10 μ in diam) copper powder was sintered to the copper block at 600°C for 0.5, 1, and 3 hr. The logarithm of the ratios of the radius of the interface x to the radius of the particle was plotted against $\log t$ (Fig 8) and a straight line was obtained. The inverse slope of this curve $n = 6.5$ is sufficiently close to the theoretical value 7 to indicate that the sintering mechanism in this case is predominantly surface diffusion.

Finally the experimental values of x measured at 400, 500 and 600°C allow us to estimate the surface diffusion coefficients of copper at these temperatures, from Eq 9. The calculated values of D_s are listed in Table 5 along with the values x and a . The semi-logarithmic plot of D_s vs. $\frac{1000}{T}$ is given in Fig 9. The results obtained from two sizes of particles (20 and 8 μ diam) are in excellent agreement with each other. The energy of activation of surface diffusion as determined from the slope of the straight line represented in Fig 9 is $Q_s = 56,000$ cal per mol, the same as for volume diffusion evaluated before. The frequency factor $D_s^0 = 10^7 \frac{\text{cm}^2}{\text{sec}}$ is 10^6 higher than that for volume diffusion which means that although the same energy is required to change the position of an atom on the surface as inside the crystal lattice, the number of atoms possessing this activation energy is much larger on the surface than inside the crystal.

As nobody has ever before measured the coefficient of surface self-diffusion, data obtained in this work cannot be checked but the order of magnitude appears to be reasonable. The fact that energies of activation of volume and surface diffusions are nearly equal may very well be explained by Schottky's¹² mechanism of diffusion. According to him all vacancies are generated on the surface, consequently the energy of the formation of vacancy should be the same in both cases. The only difference should be expected in energies required to move an atom to the adjacent vacancy which in the case of surface migration should be lower than in the case of volume diffusion. It is believed that the greatest part of heat of diffusion is the energy required to make a vacancy on the surface. If this is true the differences in the remaining part of the energy of activation could be small enough to bar detection.

It has therefore been proven that at least for metals of low vapor pressure the rate of interface formation among sintered particles is a process controlled in the early stage by surface diffusion and in the later stage by volume diffusion. No other mechanism such as viscous flow which has been considered by Frenkel¹ and Shaler and Wulff² seems to be involved. The process of sintering by volume diffusion excludes the possibility of an atom exchange mechanism of diffusion^{4,13,14} because in such a case no gradient

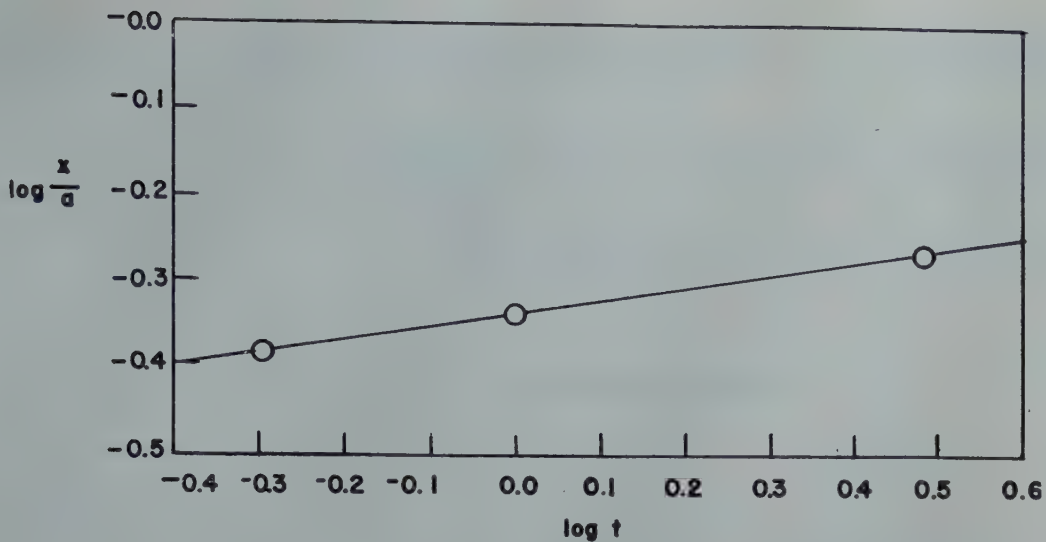


FIG 8—Logarithm of the ratio of the interface radius x to the radius a of the small copper particles (about 4μ) sintered at 600°C , plotted against the logarithm of sintering period t .

driving the atoms towards the interface, is possible. It seems to appear then that diffusion in solids proceeds through the mechanism of imperfections in the lattice such as vacancies or interstitial atoms.

Conclusions

1. It has been proven experimentally that the mechanism of sintering of two metallic particles or of a metallic particle and a flat metallic block at atmospheric pressure is predominantly that of volume diffusion for large particles and higher temperatures.

2. It is possible to measure the coefficient of self-diffusion without radioactive tracers, measuring only the rate of growth of the interface between round particles and a metallic block. The method has been checked successfully in the case of copper and silver.

3. Strong experimental evidence has been presented that at the beginning of sintering surface diffusion is operative.

4. The surface diffusion coefficient of copper has been determined.

Acknowledgment

The author wishes to express his gratitude to Mr. W. E. Kingston, Manager of Sylvania Metallurgical Laboratories, for his support of this project. Greatest indebtedness and gratitude are due to Dr. I. Zavarine of Sylvania Electric Products Inc. for his priceless suggestions and help in the experi-

mental part of this work, and to Dr. C. Herring of Bell Telephone Research Laboratories for frequent helpful discussions of the theoretical part of this

paper. The author wants to thank Mrs. L. Roth of Sylvania Electric Products Inc. for her skillful metallographic work.

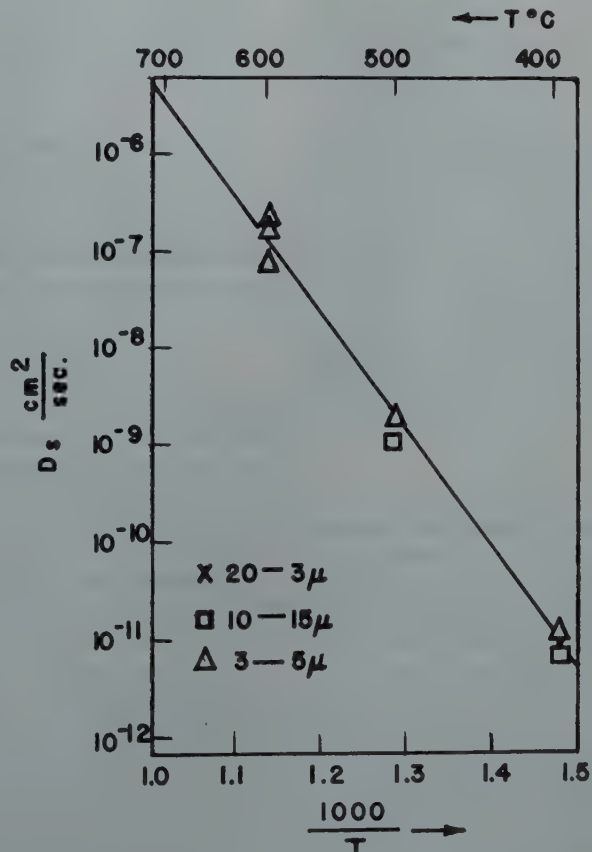


FIG 9—Variation of surface self-diffusion coefficient of copper with temperature as determined from sintering experiments of small particles. Logarithms of D_s vs. reciprocal of absolute temperature.

References

1. J. Frenkel: *Jnl. Phys. U.S.S.R.* (1945) 9, No. 5, 385.
2. A. J. Shaler and J. Wulff: *Ind. Eng. Chem.* (1948) 40, 838.
3. B. Ya. Pines: *Jnl. Tech. Phys.*, (1946) 16, No. 6, 737.
4. R. F. Mehl: *Trans. AIME* (1936) 122, 11.
5. A. Samoilovich: *Acta Physicochimica U.S.S.R.*, (1946) 21, 13.
6. F. N. Rhines and R. F. Mehl: *Trans. AIME* (1938) 128, 285.
7. B. V. Rollin: *Phys. Rev.* (1931) 55, 231.
8. J. Steigman, W. Shockley and F. C. Nix: *Phys. Rev.* (1939) 56, 13.
9. C. L. Raynor, L. Thomassen and L. J. Rouse: *Trans. Am. Soc. Met.* (1942) 30, 313.
10. M. S. Maier and H. R. Nelson: *Trans. AIME* (1942) 147, 39.
11. W. A. Johnson: *Trans. AIME* (1941) 143, 107.
12. W. Schottky: *Ztsch. Phys. Chem. B.* (1935) 29, 335.
13. J. Cichocki: *Jnl. de Phys.* (VII) (1938) 9, 129.
14. F. Seitz: *The Modern Theory of Solids*. (1940) McGraw-Hill.

A Simple Constant Stress Creep Test

J. C. FISHER* and R. P. CARREKER*

CREEP tests are normally constant load tests. Such tests approximate some types of service conditions and therefore are justified from the engineering point of view. Coupled with this consideration is the advantage of simplicity inherent in constant load tests, as contrasted with the comparatively complex requirements of a constant stress test. It is not surprising that the vast majority of creep tests reported are of the constant load type.

Despite the enormous amount of accumulated creep test data, plastic flow is by no means completely understood. The widespread use of constant load tests is at least partly responsible for this lack of understanding. Any attempt to analyze deformation must involve the more fundamental quantity stress, rather than load. It is possible to predict constant load behavior from known constant stress data, but the reverse is much more difficult.

When a metal specimen elongates, as in a creep test, the cross section decreases, maintaining constant volume. Thus

$$\frac{A}{A_0} = \frac{l_0}{l} \quad [1]$$

For a constant stress test the force on the specimen must be decreased as the cross section decreases, that is, this force must be inversely proportional to the elongation of the specimen. Andrade has described three methods of obtaining the constant stress condition,¹⁻³ each of which is relatively complex. The most recent proposal,³ suggests a major simplification which maintains the simplicity of the constant load test while approximating quite closely the desirable condition of constant stress. Andrade's device is admittedly more accurate but the method described below has definite advantages.

Consider a specimen in the form of a

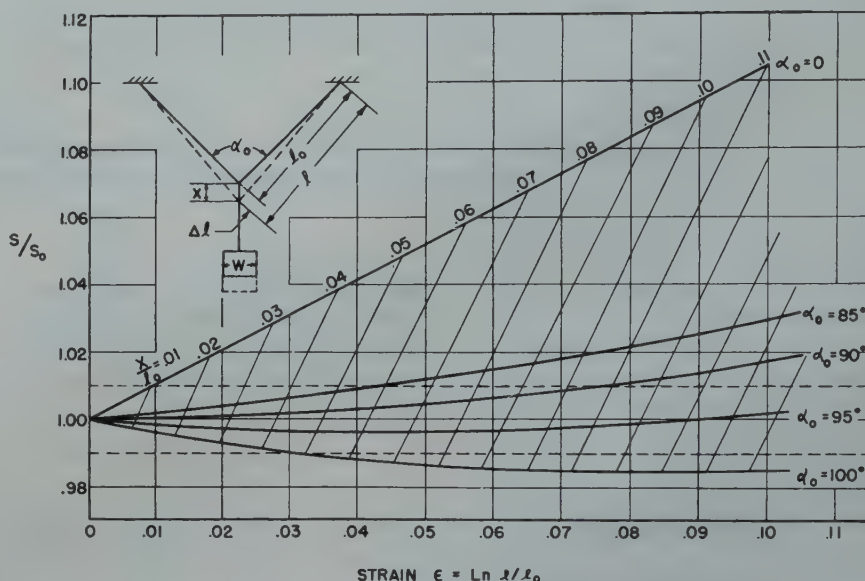


FIG 1—Variation of stress with initial angle.

“V” supported at its ends. If a weight be applied at the vertex of the angle, the stress in each leg of the “V” is

$$S = \frac{w}{z} \cdot \sec \frac{\alpha}{z} \cdot \frac{1}{A} \quad [2]$$

If this stress causes an elongation Δl in each leg of the “V,” the angle decreases from α_0 to a smaller angle α_1 . The quantity $\sec \frac{\alpha}{z}$ thus decreases with specimen elongation while the quantity $1/A$ increases. By selecting proper initial conditions it should be possible to hold S/S_0 very nearly constant at unity.

The proper initial conditions are realized when α_0 is made equal to approximately 90°. Fig 1 compares the ratios of S/S_0 for $\alpha_0 = 85, 90, 95, 100^\circ$, with $\alpha_0 = 0$, that is, a straight speci-

men, for true strains up to $\epsilon = 0.10$. It may prove convenient to measure X , the movement of the vertex, rather than the true elongation Δl . Contour lines of X/l_0 are also plotted in Fig 1.

The method for obtaining constant stress described above is especially suited to the testing of small wires, but may easily be extended to rods of any diameter through the use of a suitable grip which serves as the vertex joining two identical rods forming the legs of the “V.”

References

1. E. N. da C. Andrade: On the Viscous Flow in Metals, and Allied Phenomena. *Proc. Roy. Soc., A*, 84, 1, (1910-11).
2. E. N. da C. Andrade and B. Chalmers: The Resistivity of Polycrystalline Wires in Relation to Plastic Deformation, and the Mechanism of Plastic Flow. *Proc. Roy. Soc., A*, 138, 348, (1932).
3. E. N. da C. Andrade: A New Device for Maintaining Constant Stress in a Rod Undergoing Plastic Extension. *Proc. Phys. Soc.*, 60, (3), 304, (March, 1948).

Technical Note No. 10 E. Manuscript received October 13, 1948.

* General Electric Co., Schenectady, N. Y.

¹References are at the end of the paper.

Homogeneous Yielding of Carburized and Nitrided Single Iron Crystals

A. N. HOLDEN* and J. H. HOLLOMON,* Junior Member AIME

Introduction

INHOMOGENEOUS yielding during the early stages of plastic flow has been observed in many metals and has long been a subject of controversy.

Low carbon steel, when strained at room temperature, exhibits a distinct yield point at which the metal ceases to behave elastically and begins to flow plastically without further increase in stress,[†] often with an actual decrease in stress from that existing at the yield point. One manifestation of this behavior is the familiar Lüders lines. The extent of the yield point elongation (the plastic strain which results without raising the stress above that at the initial yield point) may be several percent.

Several explanations of this type of yielding in steels have appeared in the literature:^{1-3†}

1. The segregation of carbides or other constituents at the grain boundaries of ferrite forms cell-like blocks which break down at a higher stress than that at which the ferrite alone will flow.

2. The precipitation of various constituents within the ferrite itself in some way blocks initial flow until a higher stress is reached, after which a great deal of flow occurs without further increase in stress.

3. The restraining influence of neighboring, less favorably oriented grains in a polycrystal results in a storing up of energy, which on yielding is sufficient to cause the continued propagation of slip bands on the multiplicity of slip systems available in adjacent iron

[†] Other types of inhomogeneous or discontinuous yielding have been observed in aluminum and other aging alloys as well as in some fairly pure metals. The terms inhomogeneous, heterogeneous, or discontinuous yielding used in this paper refer to the particular initial yielding of steel tested at room temperature.

[†] An excellent bibliography of the subject appears in Ref. 2.

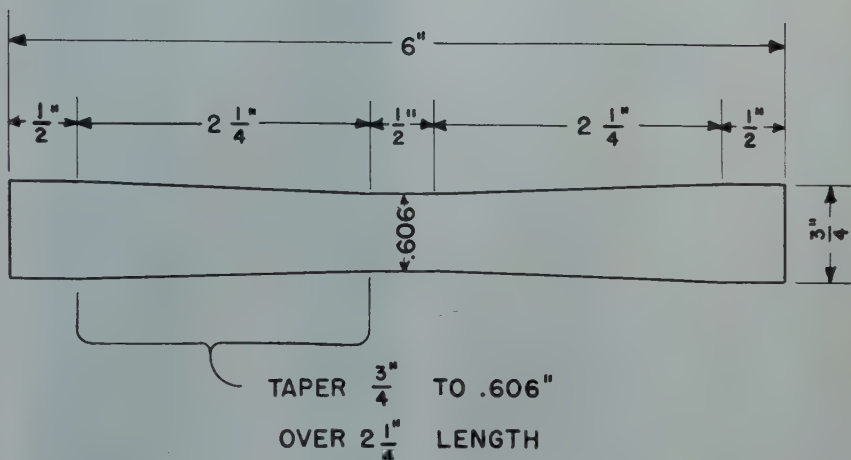


FIG 1—Shape of iron specimens.

crystals without increase in stress.

4. Local segregation of carbon atoms increases the stress required for the initial propagation of dislocations. The stress required for further deformation is lower.³ Such an explanation would require the presence of upper and lower yield points in single crystals.

Low and Gensamer² have shown that heterogeneous yielding can be eliminated by removal of carbon and nitrogen from polycrystalline steels by wet-hydrogen treatment. They also demonstrated that the re-introduction of minute amounts of carbon or nitrogen caused a return of the yield point.

Observations of the initial flow of single crystals containing small amounts of carbon and nitrogen should provide a clue to the explanation of

inhomogeneous yielding. Previous tests of iron crystals⁴⁻⁶ can not be considered conclusive because it is uncertain whether the carbon and nitrogen were satisfactorily removed by the decarburization technique employed.

The purpose of the experiments described herein was to determine whether single iron crystals containing either carbon or nitrogen would exhibit inhomogeneous yielding.

Experimental Procedures

THE PREPARATION OF SINGLE CRYSTALS

All crystals were formed in the following way. Aluminum killed sheet material 80 mils thick was machined into specimens of the outer contour shown in Fig 1. These mildly tapered specimens were decarburized at 730°C for 16 hr in hydrogen that had been bubbled rapidly through water maintained at 70°. The resultant grain size after decarburizing was approximately ASTM 5. Several stress-strain curves were made of the decarburized mate-

San Francisco Meeting, February 1949.

TP 2521E. Discussion of this paper (2 copies) may be sent to *Transactions AIME* before May 15, 1949. Manuscript received June 2, 1948; revision received November 12, 1948.

* General Electric Research Laboratory, Schenectady, N. Y.

¹ References are at the end of the paper.

rial, two of which are shown in Fig 5. The material as-wet-hydrogen treated yielded homogeneously. Nothing is known of the production history of the sheet prior to the decarburization treatment.

The material used for these specimens was analyzed before and after decarburization (carbon was determined by low pressure combustion and nitrogen by a Kjeldahl determination). The analyses were:

| As-received | Pct | Wet-Hydrogen Treated | Pct |
|------------------|---------|----------------------|---------|
| C | 0.090 | C | 0.004 |
| N | 0.0045 | N | 0.003 |
| *Al | 0.09 | *Al | 0.09 |
| †Si | 0.05 | †Si | 0.05 |
| †Mn | 0.25 | †Mn | 0.25 |
| Fe | balance | Fe | balance |
| * Total aluminum | | | |
| † Spectrographic | | | |

After the wet-hydrogen treatment, the tapered specimens were strained until the change in area of the reduced section as measured with a micrometer was 2.7 to 3 pct. Subsequent annealing in pure dry hydrogen at 885°C for 72 hr converted the tapered specimens into large crystals.* Several crystals were as wide as the specimens and 4 in. in length. However, the surface of the specimens contained fine grains which had to be removed by grinding before the large crystals could be revealed by etching. It was found necessary to grind 10 mils off each flat surface with a special wheel. A photograph of a typical specimen after grinding and etching appears in Fig 2, showing the size of recrystallized grains resulting from the treatment described.

The important features of the strain-anneal method used in these experiments are the following: First, the specimens were so shaped that recrystallization was limited to a small volume of critically strained material in the narrowest region. Second, a grain formed in the critically strained region readily grew to the lesser strained regions and larger grains resulted. The lesser strained regions were not deformed sufficiently to recrystallize. Third, the specimens were placed in a hot furnace for the annealing treatments.

Tapered specimens have been employed previously,⁷⁻¹⁰ but tapers used have been more extreme than that used in these experiments.

After forming the large grains, crystal tensile specimens were cut out with a jeweler's saw. All of the tapered specimens did not yield large enough grains from which to cut single crystal

* Similar attempts have been made to obtain large single crystals of a "rimming" steel but as yet none has been successful.



FIG 2—Typical crystal size after strain annealing.

tensile specimens. Data are included for all crystals tested. The single crystal specimens had reduced sections of from 3/4 in. to 2 in. in length and from 3/16 in. to 5/16 in. in width.

HEAT-TREATING AND TESTING OF IRON CRYSTALS

The single crystal tensile specimens were annealed in wet-hydrogen at 850°C for 16 hr. All specimens remained single crystals and it was assumed that all machining strains and any remaining carbon were removed during this treatment. Low and Gensamer² have found the carbon to be less than 0.003 pct after wet-hydrogen treatments. Some of the crystals were carburized by the method used by Low and Gensamer. They were annealed at 675°C

for 4 hr in a mixture of butane and hydrogen. Just enough butane was bled into the furnace to color faintly the flame at the furnace door. Several polycrystals were carburized along with the single crystals to make certain that the process was effective. All of these carburized specimens were then homogenized for 5 hr at 650°C in a nitrogen atmosphere obtained by passing tank nitrogen over copper chips at 500°C and activated alumina. After this treatment, the crystals contained 0.005 pct N₂ and 0.019 pct C.

Nitriding of some of the crystals was carried out by treatments of 4 hr at 525°C in an ammonia atmosphere. The hard nitrided case was ground off to a depth where no nitrides were observable metallographically. The crystals were then stress relieved and homogenized for 5 hr at 650°C in a nitrogen atmosphere. Several polycrystalline specimens were nitrided along with the single crystals to make certain the nitriding was adequate. After treatment, the crystals contained 0.004 pct C, and 0.073 pct N₂. This nitrogen certainly exceeds the limit of solubility and probably the crystals contained a precipitated second phase even though it was not observed metallographically.

All the crystals thus far described were tested in a hydraulic tensile machine with Templin sheet grips mounted on spherical seats. Reasonable care was used in alignment. Strain was measured with a single resistance type strain gauge with a sensitivity of 2 × 10⁻⁶. The rate of testing was the

Table 1 . . . Heat-treating and Testing of Iron Crystals

| Spec. No. | Heat Treatment | Testing |
|-----------|--|-------------------------|
| 12 | Wet hydrogen—850°C | Templin grips—ball seat |
| 13 | Wet hydrogen—850°C | Templin grips—ball seat |
| 23 | Wet hydrogen—850°C | Templin grips—ball seat |
| 34-2 | Wet hydrogen 850°C, carburize at 675°C, homogenize at 650°C in nitrogen | Templin grips—ball seat |
| 35 | Wet hydrogen 850°C, carburize at 675°C, homogenize at 650°C in nitrogen | Templin grips—ball seat |
| 37 | Wet hydrogen 850°C, carburize at 675°C, homogenize at 650°C in nitrogen | Templin grips—ball seat |
| 33 | Wet hydrogen 850°, nitride 525°C, case ground off, homogenized at 650°C. | Templin grips—ball seat |
| 38 | Wet hydrogen 850°, nitride 525°C, case ground off, homogenized at 650°C. | Templin grips—ball seat |
| 39 | Wet hydrogen 850°, nitride 525°C, case ground off, homogenized at 650°C. | Templin grips—ball seat |

same for all crystals and was such as to give 1 pct strain in 45 min. The methods of heat treating and testing are summarized in Table 1 for crystals thus far described.

It later became evident that more accurate methods of evaluating the effect of carbon and nitrogen on the strength of single crystals would be valuable. Therefore, several experiments were performed on pairs of single crystal tensile specimens cut from the same crystal.

An alternative nitriding procedure to that previously employed was used to nitride the crystal pairs. It consisted of passing hydrogen through a catalytic deoxidizer, activated alumina drier, activated charcoal tube, liquid nitrogen trap, ammonia absorber and into the nitriding furnace at 500°C. The ammonia absorber was kept at -78°C to avoid the formation of any hard nitride case which would have to be removed.

In these experiments the carburization of each of the crystals of the pairs was the same as that employed previously.

One nitrided and one carburized crystal together with their identically oriented wet-hydrogen treated counterparts were annealed in vacuum. It was intended that the temperature of the vacuum anneal would not exceed 750°C but inadvertently it exceeded 910°C. These specimens did not remain single crystals, but became very coarsely polycrystalline.

Orientations were determined for all pairs of crystals except the specimens which became polycrystalline. These orientations are shown in Fig 3.

The testing of crystal pairs was done in a hydraulic machine. Eight of these crystals were pulled with long flexible rods so designed that only axial loads were transmitted (see Fig 4), while the others were tested in Templin grips as previously described.

The eccentricity of the strain in the eight accurately aligned specimens was measured by the following means. Two rigid glass fibers about 6 in. in length were cemented to one side of each specimen perpendicular to the tensile axis and about 3/4 to 1 in. apart. The distance between the ends of the fibers was measured with an accurate micrometer-type cathetometer sensitive to 0.001 mm. The 6-in. lever of the fibers gave a multiplication of the eccentricity of about 64. The relation between the change in readings of the cathetometer and eccentricity can be found provided the strain at the center

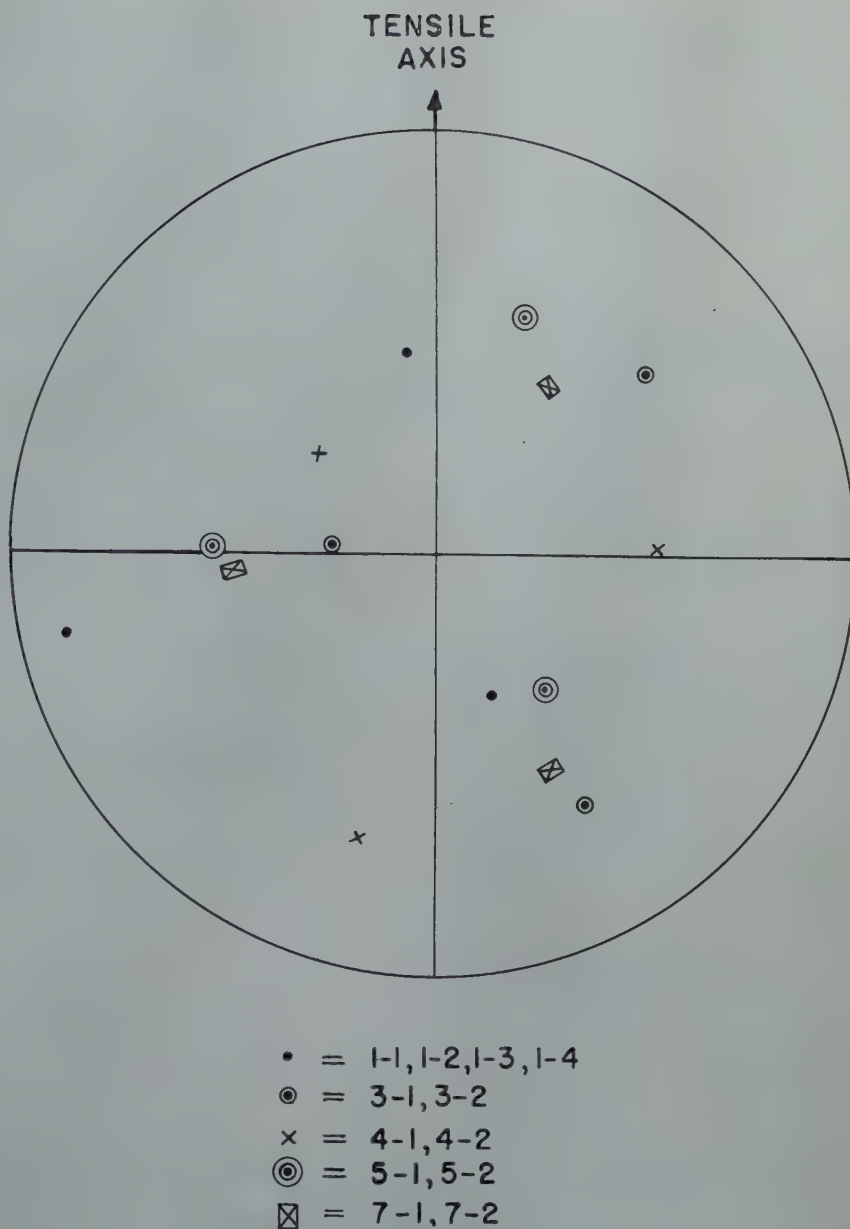


FIG 3—Orientation of crystal pairs (cube poles determined with optical goniometer).

line of the specimen is measured.* The average center line strain was measured with two resistance strain gauges cemented to the opposite flats of the specimen.

The edge strain was within 4 pct of the center line strain without any adjustment of the fixtures other than that automatically applied by the flexible tension members.

The heat treating and testing methods for the crystal pairs is summarized in Table 2.

$$* M = \text{eccentricity} = \frac{e - e'}{e} = \left(\frac{w/2}{l} \right) (e - \Delta)$$

e' = strain at edge of specimen
 e = strain at center line of specimen
 w = width of specimen
 l = length of glass fibers
 Δ = change in distance between fiber ends upon application of strain e .

Results

All the data are presented in the form of stress-strain curves.

Fig 5 compares the flow of polycrystalline specimens in the wet-hydrogen treated, carburized and nitrided states. These tests indicate that either carbon or nitrogen causes the return of the discontinuous yield in material which showed no discontinuity in its flow curve as wet-hydrogen treated. The nitrided polycrystals in Fig 5 contained considerable nitrogen (about 0.07 pct) which accounts for their high yield strength. The carburizing treatment on the other hand was quite mild, and the carburized polycrystals showed less increase in yield strength over the wet-hydrogen treated specimens.

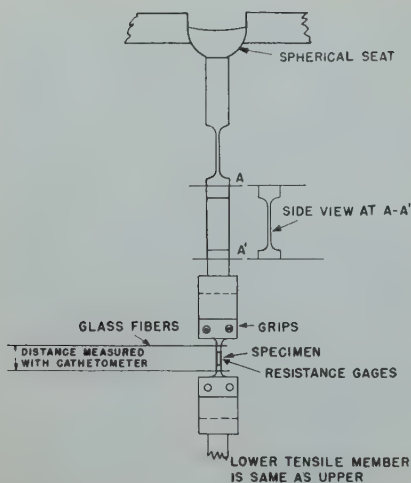


FIG 4—Flexible tensile member for axial loading of iron crystals.

Fig 6, 7, and 8 show the flow curves for nine iron crystals. The crystals whose tensile properties are those of Fig 6 were thoroughly treated in wet-hydrogen. The crystals of Fig 7 were carburized and those of Fig 8 were nitrided. None of these crystals yielded inhomogeneously. The high strength of the nitrided crystals is due to the considerable amount of nitrogen these contained.

Fig 9 and 10 show the effect of the described carburizing treatment on the flow of single iron crystals. In these two figures the flow of carburized crystals is compared with that of decarburized crystals of the same orientation. Fig 9 was obtained by testing four crystals cut from the same grain, two of which were carburized and two of which were decarburized. A scattering of the data for two identical crystals is thus obtained as well as the difference in flow strengths of the two materials. Fig 10 is the result of a test of two different pairs of crystals, one of each pair being carburized while the other was decarburized.

While the tests in Fig 9 and 10 were made in Templin grips with only moderate care in alignment, the results are significant. All crystals yielded homogeneously, and allowing for the scatter of the data, the carburized crystals were 5 to 10 pct stronger up to 0.6 to 0.7 pct strain.

Fig 11 shows the yielding of crystals 5-1 and 5-2 of identical orientation. Crystal 5-1 was nitrided under conditions which did not form a hard case. Crystal 5-2 was completely decarburized in wet hydrogen. The nitrided crystal was slightly higher in flow strength than the decarburized crystal. Both crystals yielded homogeneously.

Table 2 . . . Heat-treating and Testing Procedure for Crystal Pairs

| Spec. No. | Heat Treatment | Testing |
|-----------|--|-------------------------------------|
| 1-1 | Carburized | Templin and ball seat |
| 1-2 | Carburized | Templin and ball seat |
| 1-3 | As wet hydrogen treated | Templin and ball seat |
| 1-4 | As wet hydrogen treated | Templin and ball seat |
| 3-1 | Carburized | Templin and ball seat |
| 3-2 | As wet hydrogen treated | Templin and ball seat |
| 4-1 | Carburized | Templin and ball seat |
| 4-2 | As wet hydrogen treated | Templin and ball seat |
| 5-1 | Nitrided (saturator at -78°C) | Special grips $\dagger M = 2.4$ pct |
| 5-2 | As wet hydrogen treated | Special grips $M = 3.7$ pct |
| *6-1 | Nitrided (-78°C)—vacuum annealed | Special grips $M = 1.81$ pct |
| *6-2 | As wet hydrogen treated—vacuum annealed | Special grips $M = 2.04$ pct |
| 7-1 | Carburized | Special grips $M = 2.3$ pct |
| 7-2 | As wet hydrogen treated | Special grips $M = 3.1$ pct |
| *8-1 | Carburized—vacuum annealed | Special grips $M = 1.92$ pct |
| *8-2 | As wet hydrogen treated—vacuum annealed | Special grips $M = 2.65$ pct |

* Became polycrystalline on vacuum annealing.

\dagger Eccentricity as defined in footnote on p. 181 expressed as a percentage.

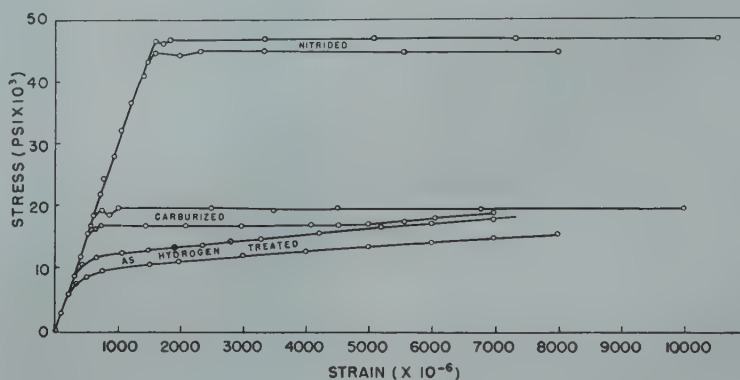


FIG 5—Yielding of polycrystalline iron.

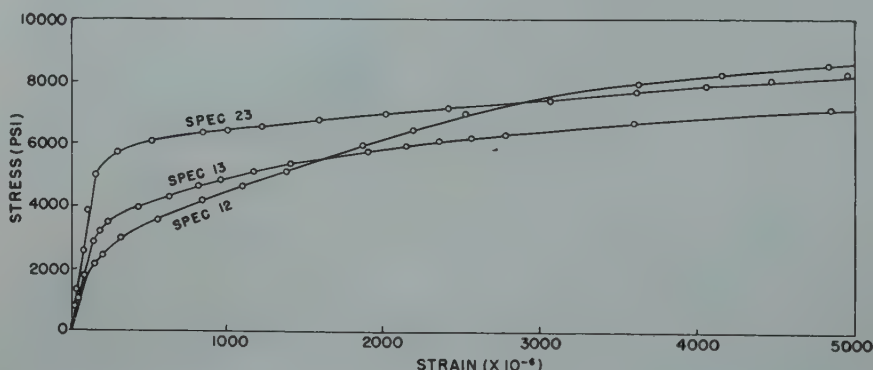


FIG 6—Wet hydrogen treated crystals of iron, random orientation, tested with single gauge in Templin grips.

Fig 12 is a plot of the flow of two identically oriented specimens. 7-1 was carburized, and 7-2 was decarburized in wet-hydrogen. The carburized crystal was considerably stronger than the decarburized crystal. Both crystals yielded homogeneously.

Fig 13 and 14 are plots of the flow characteristics of specimens which became coarsely polycrystalline during a vacuum anneal in which the temperature was inadvertently raised too high.

Fig 13 shows the flow of a nitrided polycrystalline specimen compared to a decarburized polycrystalline specimen in which the grain size was $\frac{1}{4}$ in. or larger in diam. Fig 14 shows the deformation behavior of a carburized polycrystalline specimen in which the grain size is approximately $\frac{1}{4}$ in. in diam. The decarburized polycrystals in both instances did not yield discontinuously. The flow curve of the carburized polycrystal, however, contains a

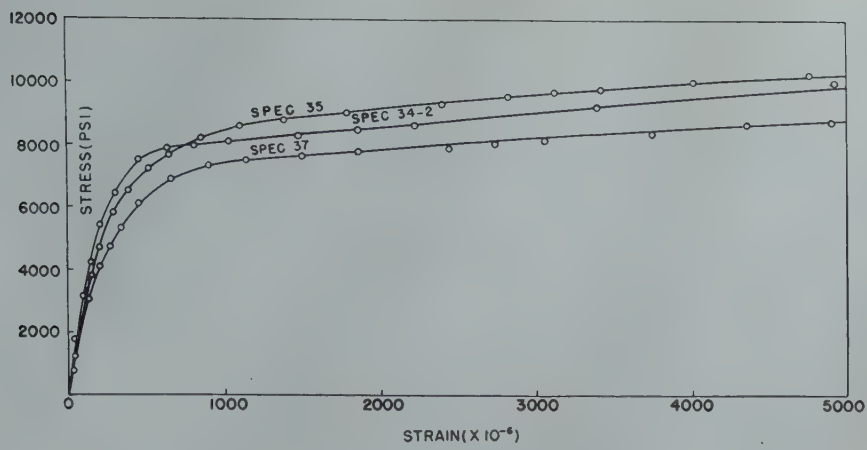


FIG 7—Carburized crystals of iron, random orientation, tested with single gauge in Templin grips.

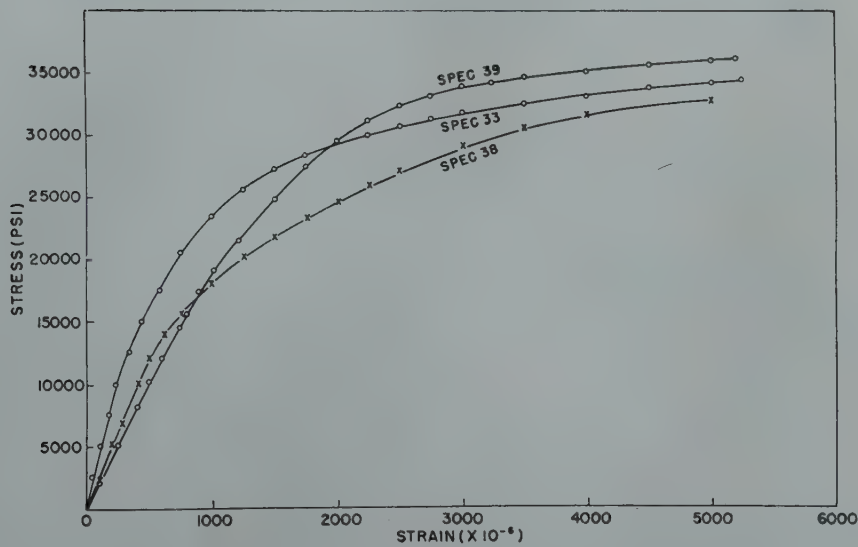


FIG 8—Nitrided crystals of iron, random orientation, tested with single gauge in Templin grips.

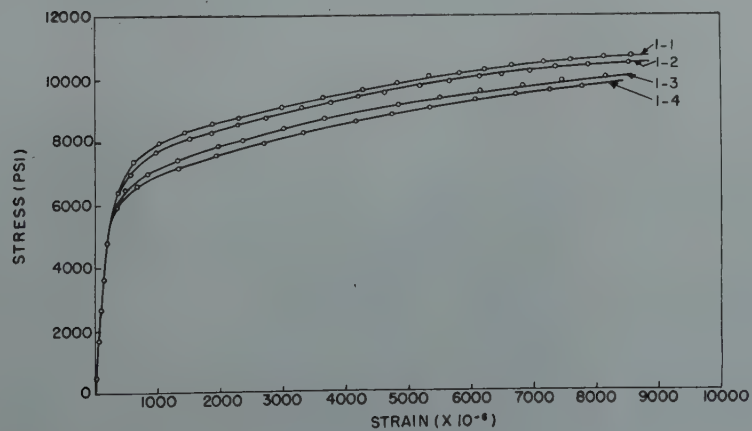


FIG 9—Yielding of four identically oriented iron crystals. 1-1 and 1-2 were carburized. 1-3 and 1-4 were decarburized. Tested with 2 averaging gauges in Templin grips.

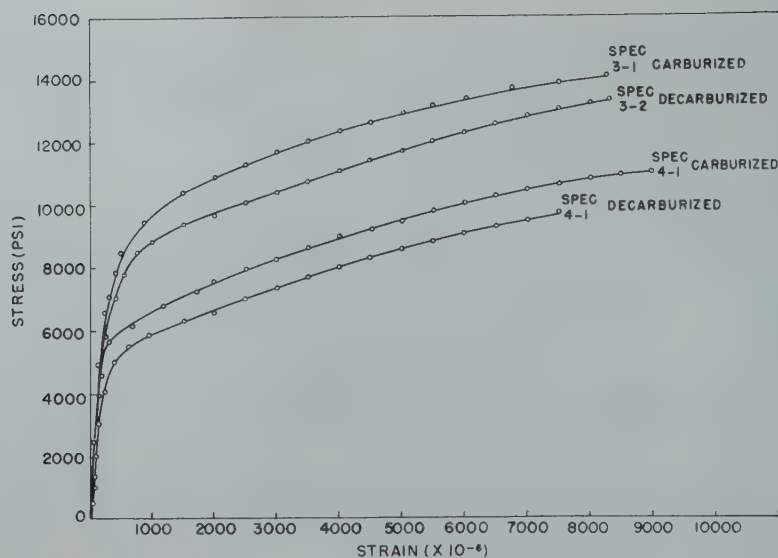


FIG 10—Yielding of iron crystal pairs showing effect of carbon on flow strength. Tested with 2 averaging gauges in Templin grips. Orientation of 4-1 and 4-2 is the same and orientation of 3-1 and 3-2 is the same.

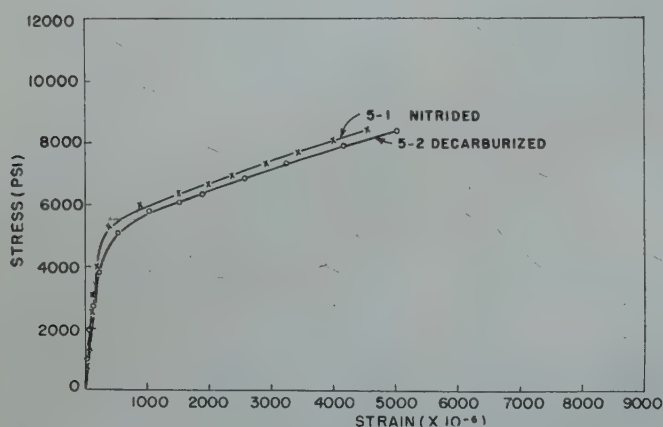


FIG 11—Yielding of identically oriented crystals showing effect of small amounts of nitrogen. Tested with less than 4 pct eccentricity.

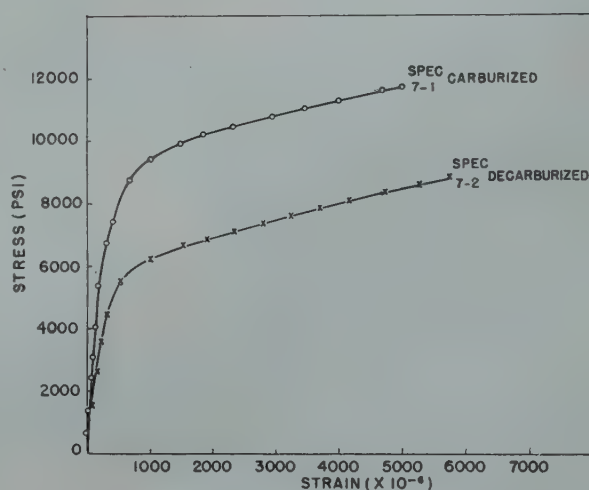


FIG 12—Yielding of identically oriented crystals showing effect of small amounts of carbon. Tested with less than 4 pct eccentricity.

slight upward concavity during initial yielding. The flow curve of the nitrided polycrystal contains no upward concavity, but it does flow at a higher stress initially and then drops to approximately the same flow stress as the decarburized polycrystal as flow progresses. Because of the large grain size it is not expected that the flow of these specimens would be greatly different from single crystals.

The original purpose of vacuum annealing was to ascertain whether the hydrogen presumably occluded in the

specimens eliminated the inhomogeneous yielding. Since the vacuum annealed specimens can be considered essentially hydrogen free, the effect of the hydrogen occluded in the specimens is considered to be negligible.

In general, the data on crystal pairs show that where carbon or nitrogen has increased the flow strength, the higher strength curve remains approximately parallel to the decarburized curve, indicating that the rate of strain hardening was not affected.

The results from the tensile tests in

which the specimens were more accurately aligned fail to indicate inhomogeneous yielding in single crystals of iron.

Conclusions

1. Carbon or nitrogen causes discontinuous yielding in iron polycrystals in substantiation of the findings of Low and Gensamer.

2. Carbon or nitrogen do not appear to cause discontinuous yielding in iron

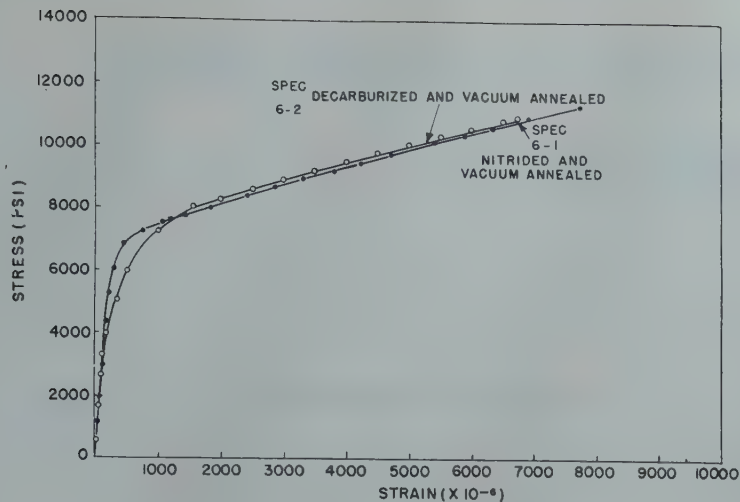


FIG 13—Yielding of extremely coarse polycrystals of iron. Tested with less than 4 pct eccentricity.

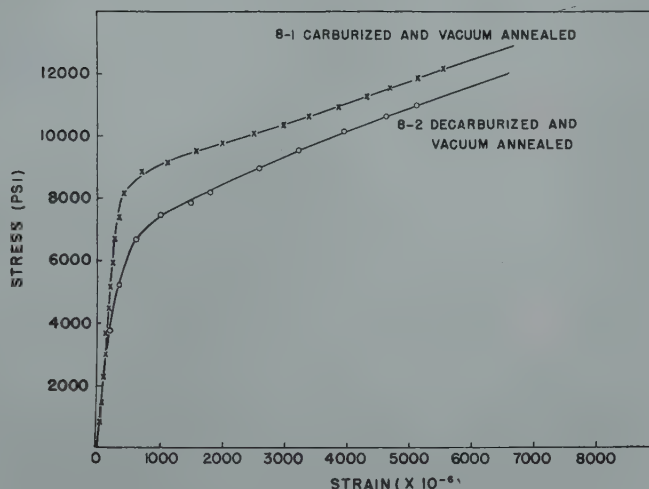


FIG 14—Yielding of extremely coarse polycrystals of iron. Tested with less than 4 pct eccentricity.

single crystals made from aluminum-killed steels. Both elements in small amounts cause an increase in the flow strengths of single crystals, but do not affect the rate of strain hardening.

References

1. A. Nadai: Plasticity. McGraw-Hill, N. Y. (1931) 86-96.
2. J. R. Low and M. Gensamer: Aging and the Yield Point in Steel. *Trans. AIME* (1944) 158, 207.
3. A. H. Cottrell: Effect of Solute Atoms on the Behavior of Dislocations. Report of a conference on Strength of Solids. Phys. Soc., London (1948) 30.
4. C. A. Edwards and L. B. Pfeil: The Tensile Properties of Single Iron Crystals and the Influence of Crystal Size Upon the Tensile Properties of Iron. *Jnl. Iron and Steel Inst.* (1925) 112, 79.
5. C. F. Elam and G. I. Taylor: The Distortion of Iron Crystals. *Proc. Roy. Soc.* (1926) 112, 337.
6. L. B. Pfeil: The Deformation of Iron With Particular Reference to Single Crystals. Carnegie Scholarship Memoirs, Iron and Steel Inst. (1926) 15, 319.
7. H. C. Carpenter and C. F. Elam: Crystal Growth and Recrystallization in Metals. *Jnl. Inst. of Metals.* (1920) 24, 83.
8. C. Chappell: The Recrystallization of Deformed Iron. *Jnl. Iron and Steel Inst.* (1914) 89, 460.
9. D. Hanson: Rapid Recrystallization in Deformed Non-Ferrous Metals. *Jnl. Inst. of Metals.* (1918) 20, 141.
10. H. C. Carpenter and Tamura: Experiments on the Production of Large Copper Crystals. *Proc. Roy. Soc.* (1926) 113, 38.

The Surface Tension of Solid Copper

H. UDIN,* A. J. SHALER,* Member, and JOHN WULFF* Member AIME

Introduction

IN the study of the sintering of metal powders, we have come to the conclusion in this laboratory that further progress requires a more basic understanding of the operating mechanisms. This is emphasized in detail by Shaler.¹ He has shown that a knowledge of the exact value of the surface tension is imperative for a solution of the kinetics of sintering. This force plays a principal role in causing the density of compacts to increase.² Furthermore, a knowledge of the surface tension of solids is also applicable to other aspects of physical metallurgy. C. S. Smith³ points out the relation between surface and interfacial tension and their function in determining the microstructure and resulting properties of polycrystalline and polyphase alloys.

This paper describes one group of results of an experimental program designed for the study of the surface tension in solid metals. As a by-product of this work, considerable information has been obtained on the rate and nature of the flow of a metal at temperatures approaching the melting point and under extremely low stresses, a field of mechanical behavior heretofore scarcely touched by metallurgists. The importance of this additional information to students of powder metalurgy need not be stressed.

Theoretical Considerations

Interfacial tension arises from the condition that an excess of energy exists at the interface between two phases. Gibbs⁴ proves that this energy is a partial function of the interfacial area; thus:

$$\partial F / \partial s = \gamma$$

where $\partial F / \partial s$ is the rate of change of free energy of the system with changing

surface area, at constant temperature, pressure and composition, and γ is the interfacial tension, or interfacial free energy per unit area.

If one of the phases is the pure liquid or solid, and the other the vapor of the substance, γ may properly be termed "surface tension," and is a characteristic of the solid or liquid.

The attempt of a body to lower its free energy by decreasing its surface gives rise to a force in the surface which is numerically equal in terms of unit length to the free energy per unit area of the surface. Thus γ may be expressed either in erg-cm⁻² or in dyne-cm⁻¹. Similarly, surface tension may be determined either by a thermodynamic measurement of the surface energy or by a mechanical measurement of the surface force. We have chosen the latter approach.

Tammann and Boehme⁴ determined the surface tension of gold by measuring the amount of shrinkage or extension of thin weighted foil at various temperatures and interpolating to zero strain. The method is of questionable accuracy because of the tendency of foil to form minute tears when heated under tension. Their assumption of $F = 2W\gamma$, where W is the width of the foil, is unsound, as the foil can decrease its surface area by transverse as well as by longitudinal shrinkage. Although their experimentation was meticulous, the paper does not include details of the

sample configuration required for recalculating γ on a correct basis, even if such a calculation were possible.

In the experimental procedure chosen here, a series of small weights of increasing magnitude are suspended from a series of fine copper wires of uniform cross-section. This array is brought to a temperature at which creep is appreciable under extremely small stress. If the weight overbalances the contracting force of surface tension, the wire stretches; otherwise, it shrinks. The magnitude of the strain is determined by the amount of unbalance, so a plot of strain vs. load should cross the zero strain axis at $w = F\gamma$. If balance is visualized as a thermodynamic equilibrium, the critical load is readily calculated. At constant temperature, an infinitesimal change in surface energy should be equal to the work done on or by the weight:

$$ds = wdl \quad [1]$$

$$\text{For a cylinder, } s = 2\pi r^2 + 2\pi rl \quad [2]$$

If the volume remains constant,

$$r = \sqrt{V/\pi l} \quad [3]$$

$$s = 2\sqrt{\pi V/l} + 2V/l \quad [4]$$

$$ds = (\sqrt{\pi V/l} - 2V/l^2) dl \quad [5]$$

Substituting [5] into [1] gives for the equilibrium load,

$$w = \gamma(\sqrt{\pi V/l} - 2V/l^2) \quad [6]$$

and, again expressing V in terms of r and l ,

$$w = \pi r \gamma (l - 2r/l) \quad [7]$$

Here the end-effect term, $2r/l$, is neglected for thin wires in subsequent work.

Eq 7 can be confirmed by means of a stress analysis. If the x -axis is chosen along the wire, then the stress σ_x is

$$\sigma_x = \frac{2\pi r \gamma - w}{\pi r^2} \quad [8]$$

A cylinder of diameter d is equivalent to a sphere of radius r , insofar as radial surface tension effects are concerned.³ Thus

$$\sigma_y = 2\gamma/d = \gamma/r = \sigma_x \quad [9]$$

For the case of zero strain in the x direction, the strain will also be zero in the y and z directions. Since the wire is under hydrostatic stress, Eq 8 and 9 are

San Francisco Meeting, February 1949.

TP 2530 E. Discussion of this paper (2 copies) may be sent to *Transactions AIME* before May 15, 1949. Manuscript received November 3, 1948.

* Graduate Student, Assistant Professor of Metallurgy and Professor of Metallurgy, respectively, Massachusetts Institute of Technology.

References are at the end of the paper.

equal. Thus

$$2\pi r\gamma - w = \pi r\gamma \quad [10]$$

$$w = \pi r\gamma \quad [11]$$

The end-correction term was again dropped, this time implicitly in Eq 9, which applies to an infinite cylinder.

With certain assumptions it is possible to calculate the strain rate under conditions of unbalance. If pure viscous flow is assumed, there should be no change in lattice energy, and all the strain energy should appear as heat. If the kinetic energy of the moving weight is neglected, the time rate of heat generation must be equal to the rate of change of potential energy and free energy of the system. The system changes its energy by changing both the position of the weight and the area of the copper surface. Thus, under isothermal conditions,

$$dQ/dt = wdl/dt - \gamma ds/dt \quad [12]$$

where Q is the heat of viscous flow.

Frenkel⁶ shows that for a viscous rod under longitudinal strain, the energy dissipated in flow is given by

$$dQ/dt = (6\eta V/l^2)(dl/dt)^2 \quad [13]$$

where η is the coefficient of viscosity. From Eq 5:

$$ds/dt = (\sqrt{\pi V/l} - 2V/l^2) dl/dt \quad [14]$$

Dropping the end-effect term and combining gives:

$$dl/dt = w l^2 / 6\eta V - (\gamma / 6\eta) \sqrt{\pi / V} (l)^{3/2} \quad [15]$$

The equation can be integrated between $t = 0$ at $l = l_0$ and $t = t$, $l = l$;

$$t = 12\eta / \gamma \left\{ -\Delta r + \frac{w}{\pi \gamma} \right.$$

$$\left. \ln \left[\sqrt{\frac{l_0}{l}} \left(\frac{w \sqrt{l} - \sigma \sqrt{\pi V}}{w \sqrt{l_0} - \sigma \sqrt{\pi V}} \right) \right] \right\} \quad [16]$$

Since $dl/dt = l d\epsilon/dt$, $w = \pi r^2 \sigma$, and $V = \pi r^2 l$, ϵ and σ being strain and stress respectively, Eq 15 and 16 reduce to

$$\frac{d\epsilon}{dt} = \frac{1}{6\eta} (\sigma - \gamma/r) \quad [15a]$$

$$t = \frac{12\eta r_0}{\gamma} \left[\frac{\epsilon}{2} + \frac{\sigma r_0}{\gamma} \ln \frac{\sigma r_0^2 - \gamma r}{\sigma r_0^2 - \gamma r_0} \right] \quad [16a]$$

where $r = \frac{r_0}{\sqrt{\epsilon + 1}}$

So long as cylindrical shape is conserved, Eq 16a is an exact expression, despite the presence therein of ordinary stress and strain. This is so because the equation was obtained merely by making the appropriate substitutions in Eq 16. In the actual experiments the strains measured were small enough so that the differential form, Eq 15a, could be employed throughout. It may be written as:

$$\epsilon = \frac{t}{6\eta} \left(\sigma - \frac{\gamma}{r} \right) \quad [15b]$$

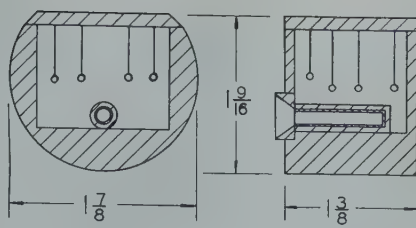


FIG 1—Copper cell with thermocouple well.

Experimental

Two series of experiments were completed, one on five mil and one on three mil copper wire. Eight specimens were used in each test, with copper weights, ranging up to about 60 dynes in the first series and 35 dynes in the second series, welded to the wires. (1 dyne is equivalent to 1.02 mg.) The wires were suspended from the lid of the copper cell, Fig 1.

The ensemble was heated in a nichrome-wound Inconel tube furnace, (Fig 2), which was maintained at a Hg pressure of 3×10^{-5} mm. The cell effectively isolated the specimens, both against contamination from furnace vapors and against loss of wire diameter by evaporation. As the experiments were conducted in a temperature range where the vapor pressure of copper was between 10^{-5} and 5×10^{-4} mm,⁷ a good approximation to the isolated system " $\text{Cu}_s - \text{Cu}_g$ " was attained, at least at the higher temperatures.

The furnace was constructed with three independent windings, tapered in accordance with preliminary heat-loss calculations. At any temperature within its operating limits a 6-in. zone can be held uniform to $\pm 2^\circ\text{C}$. A Tagliabue throttling pyrometer with manual droop control was used as a constant-temperature control device. The shell of the furnace was maintained at a low vacuum with a water-aspirator to protect the highly evacuated tube against collapse.

The marking of reference points on the wire presented a difficult problem. Painting or plating the wires outside a given gauge length was considered but was abandoned as it is evident that anything which adheres to the surface lowers the surface energy. Knotting the wire at two points about 2 cm apart was found to be the simplest expedient. The gauge point is taken as the intersection of the lower loop of the knot with the straight portion of the wire, as viewed from a fixed direction with a measuring microscope. (Fig 3.)

The knotted and weighted wires were mounted and carefully straightened. They were annealed in vacuo for 2 hr at or above test temperature before measuring. A test may last from 24 to 150 hr, depending on the temperature. Initial and final lengths were measured to ± 0.001 cm with a horizontal measuring microscope. Finally, the weights were detached at the lower knot and weighed, and the weight corrected by

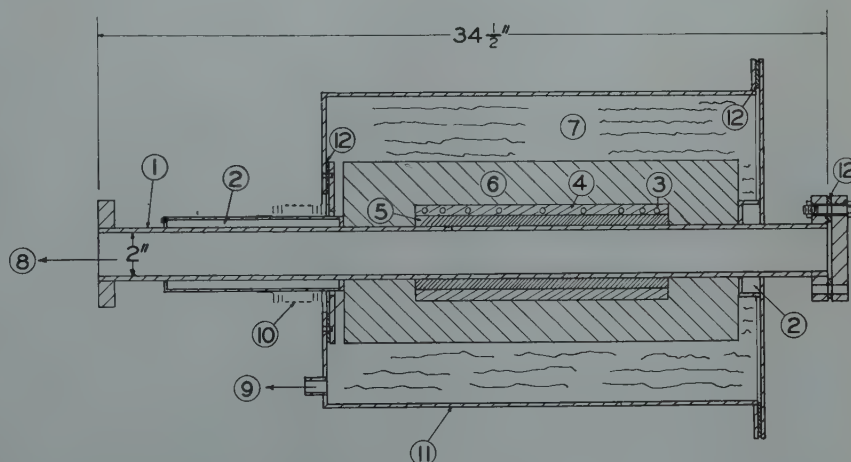


FIG 2—Vacuum furnace.

1. Inconel tube
2. Water jackets
3. Tapered nichrome resistance heater
4. Alumina cement
5. Alumina tube
6. Insulating refractory
7. Crumpled aluminum foil
8. To diffusion pump
9. To water aspirator
10. Syphon expansion joint
11. Steel outer shell
12. Neoprene gaskets



FIG 3—Typical specimen. Arrows show gauge points.

Table 1 . . . Summary of Results

| | | | | | | | |
|----------------------------|--------|--------|--------|--------|--------|--------|--------|
| Test No. | 9 | 10 | 11 | 13 | 14 | 15 | 16 |
| Temperature, °C | 1024 | 999 | 950 | 1049 | 1050 | 1000 | 950 |
| Time, sec $\times 10^{-3}$ | 1.08 | 1.80 | 5.15 | 0.874 | 1.69 | 2.60 | 5.35 |
| Wire radius cm | 0.0064 | 0.0064 | 0.0064 | 0.0064 | 0.0036 | 0.0036 | 0.0036 |

| Spec. No. | Stress Dyne/ Cm ² $\times 10^{-5}$ | Strain $\times 10^3$ | σ | ϵ | σ | ϵ | σ | ϵ | σ | ϵ | σ | ϵ | σ | ϵ |
|-----------|--|-------------------------|----------|------------|----------|------------|----------|------------|----------|------------|----------|------------|----------|------------|
| 1 | 0.091 | -6.1 | 0.069 | -4.4 | 0.076 | -3.9 | 0.091 | -4.5 | 0.096 | -8.9 | 0.072 | -10.7 | * | † |
| 2 | 0.738 | -4.5 | 0.076 | -4.2 | 0.777 | -2.1 | 0.861 | -3.3 | * | * | 1.179 | -5.7 | 1.706 | -3.10 |
| 3 | 1.461 | -3.1 | 1.742 | -1.8 | 1.774 | -1.3 | 1.319 | -2.5 | 2.428 | -5.0 | 2.455 | -2.1 | 3.508 | -0.67 |
| 4 | 2.368 | -.6 | 2.350 | -0.5 | 2.755 | +1.3 | 2.315 | -0.5 | 3.655 | -0.8 | 3.393 | -0.9 | 4.107 | -0.32 |
| 5 | 2.535 | -0.0 | 2.807 | +0.6 | 2.313 | -0.6 | 2.865 | +1.3 | 4.545 | +3.1 | 3.635 | -0.6 | 5.459 | +2.00 |
| 6 | 3.145 | +3.7 | 3.180 | +3.0 | 3.140 | +1.9 | 2.842 | 2.4 | 5.047 | 4.1 | 4.235 | +0.2 | 5.724 | 3.22 |
| 7 | 3.472 | 4.2 | 3.810 | 2.3 | 3.465 | 2.1 | 3.520 | 3.8 | * | * | 5.540 | 4.6 | 6.682 | 4.89 |
| 8 | 4.644 | 3.8 | 4.603 | 5.9 | 4.547 | 4.1 | 4.545 | 5.4 | 7.530 | 9.3 | 8.135 | 9.1 | 8.345 | 6.30 |

* Specimen damaged during measurement.

† Measuring microscope accurate to ± 0.0002 cm used in Test No. 16.

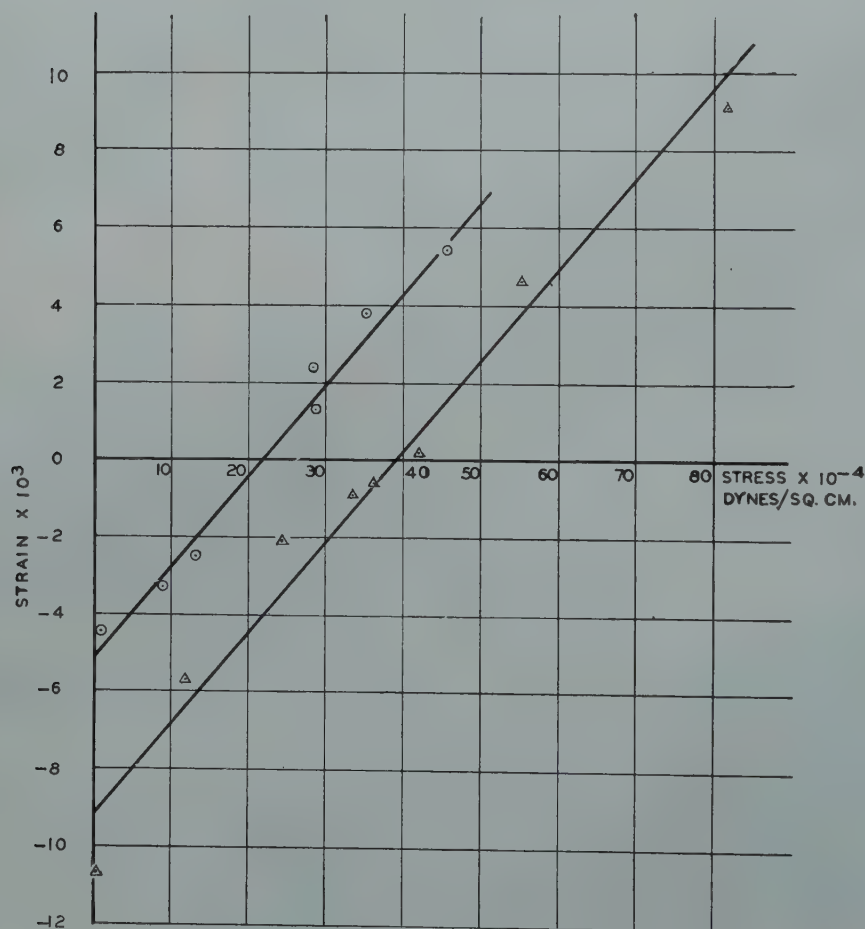


FIG 4—Stress-strain curves for test No. 15 (triangles) and test no. 13 (circles). See Table 1.

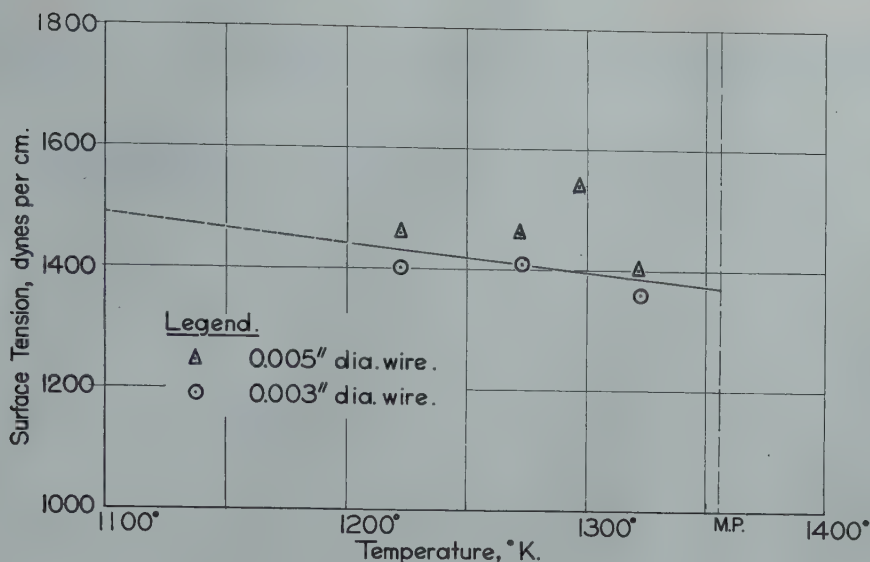


FIG 5—The temperature dependence of surface tension of solid copper.

adding one-half the weight of the gauged length of wire. Table 1 summarizes the results.

Eq 15b is assumed to hold over the range of strains in these tests, and linear least square solutions are plotted. Two such plots are shown in Fig 4. The scatter of the points is within the accuracy of the strain measurements.

Discussion of Results

SURFACE TENSION

It can be seen from Eq 15b that at zero strain the applied stress equals the stress due to surface tension, that is,

$$\gamma = \sigma_{\gamma} r$$

In Fig 5 the surface tensions determined from this relationship are plotted against temperature. If the anomalous point at 1298°K is ignored, a value of 1370 dynes per cm at the melting point is obtained. The temperature coefficient is $-0.46 \text{ dynes cm}^{-1} \text{ }^{\circ}\text{K}^{-1}$, which is consistent, as is to be expected on theoretical grounds,⁸ with an extrapolation to zero in the neighborhood of the critical temperature.

VISCOSITY

As indicated in the introduction, the purpose of this work was to develop an experimental method for the measurement of the surface tension of solid metals. The results on viscosity are a by-product and though interesting should be considered incomplete.

Viscous flow is defined phenomenologically as a process in which strain

rate is proportional to applied shear stress. Recent theory of condensed systems includes the further criterion that the flow must be atomic as well. Steady-state creep is often termed "quasi-viscous" in that the true strain rate, while not proportional to the applied stress, is constant for a constant true stress. Kauzmann⁸ points out that another mode of flow may exist in metals, which involves the motion of blocks rather than single atoms, but which is otherwise proportional to the applied shear stress, at least at low stresses.

Kauzmann's analysis of viscous flow leads to the expression

$$\eta = \frac{\lambda L k T}{2 q A l D} \quad [17]$$

where L = spacing between flow lamellae, normal to flow direction

λ = relative motion of adjacent lamellae, per unit process of flow

q = stress concentration factor, = 1 if no part of the fluid can support shear

A = area of a unit lamella of flow

l = distance between normal and activated state of the flow unit.

D is the coefficient of self-diffusion of the material, if the mechanisms of self-diffusion and of viscous flow are identical. It is only required that the mechanisms correlate. It is not necessary that every unit involved in diffusion be also involved in viscous flow.

For an atom-wise process of self-diffusion, $\lambda = L = (A)^{1/2} = 2l$. For an

atom-wise process of viscous flow under very slight shear, where the probability of a forward jump of an atom exceeds only slightly that of a reverse jump, the relationship $\lambda = 2l$ remains valid. Thus Eq 17 reduces to:

$$\eta = \frac{kT}{\lambda D} = \frac{kT}{\lambda D_0} e^{\frac{Q_D}{RT}} \quad [17a]$$

where λ is now the interatomic spacing. If the Dushman-Langmuir value for D_0 is inserted, the expression becomes:

$$\eta = \frac{h}{\lambda^3} \frac{RT}{Q} \cdot e^{\frac{Q}{RT}} \quad [18]$$

In our experiments the flow is viscous, at least to the extent that the data in Table 1 can be approximated by straight lines. The viscosity is given by

$$\eta = \frac{t}{6\epsilon} \left(\sigma - \frac{\gamma}{\tau} \right) \quad [15c]$$

In Fig 6, the logarithms of the viscosities derived from Eq 15c are plotted against the reciprocal of absolute temperature. The equation of the straight line as drawn is

$$\eta = 130 e^{\frac{95000}{RT}}$$

The activation energy of 59,000 cal per mol is within the range of values reported for self-diffusion of copper.⁹ The action constant, however, is 10^7 times larger than that predicted by Eq 18. The coincidence of activation energies suggests that the atom or atomic vacancy is the unit of flow, but evidently only a very small fraction of vacancies can participate in the flow.

The divergence in viscosity between the two wire sizes, (see dotted lines, Fig 6) indicates that the surface-to-

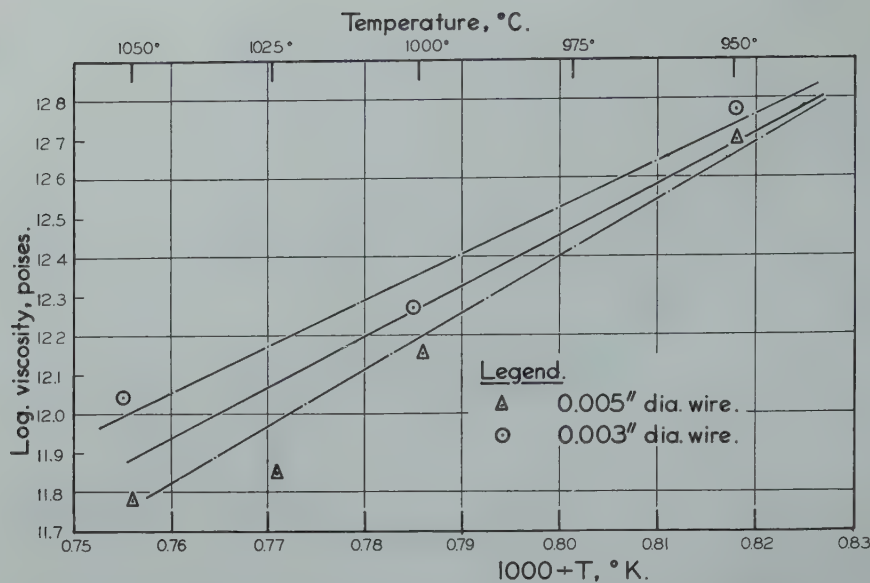


FIG 6—The temperature dependence of viscosity of solid copper.

volume ratio of the specimens may be a factor in determining the flow rate. Apparently the viscosity of the surface phase greatly exceeds that of the interior of the copper.

The mathematics of this condition has not yet been formulated, nor are the data as yet extensive enough to warrant such formulation. Nevertheless some speculation may be justified.

Surface energy owes its existence to the presence of unsatisfied atomic bonds at the surface. However, if surface tension is calculated by merely summing the energy of these broken bonds, the result is too high by roughly 10 pct¹⁰ because the unsevered bonds in the surface layers of atoms distort in such a way as to take up some of the excess energy. These high-energy bonds might account for the strengthening of the surface layer, according to Benedicks.¹¹

In fatigue testing, and in tension test-

ing of brittle materials, failure is initiated at the surface, and the strength of the surface skin plays an important role, even in large section sizes. Benedicks and Ruben¹² investigated a quenched (untempered) carbon steel immersed in various media, and found the strength to be dependent on the surface tension of the medium.

Further experiments are planned with the purpose of determining the thickness of this surface layer, estimating the ratio of its strength to that of the interior metal, and calculating the effect such a layer will have on sintering rates.

Acknowledgment

The writers wish to acknowledge their indebtedness to the Revere Copper and Brass Co., who made the work possible through a Research Grant.

References

1. A. J. Shaler: Seminar on Kinetics of Sintering. AIME *Met. Tech.*, Dec. 1948.
2. F. N. Rhines: *Trans. AIME* (1946) **166**, 474.
3. C. S. Smith: AIME *Met. Tech.*, June 1948, TP 2387.
4. Tammann and Boehme: *Ann. Physik* (1932) **12**, 820.
5. J. W. Gibbs: *Collected Works*, **1**, (1931) N. Y.; Longmans, Green and Co..
6. J. Frenkel: *USSR Jnl. Phys.* (1945) **9**, 385.
7. K. K. Kelley: Contributions to the Data on Theoretical Metallurgy. (1935) USBM Bull. 383.
8. W. Kauzmann: *Trans. AIME*, (1941) **143**, 57.
9. J. Steigman, W. Shockley, and F. C. Nix: *Phys. Rev.* (1939) **56**, 13.
10. W. D. Harkins: *Jnl. Chem. Phys.* (1942) **10**, 268.
11. C. Benedicks: Pittsburgh Internat'l. Conf. on Surface Reactions, (1948) 196. Corrosion Publishing Co. Pittsburgh.
12. C. Benedicks and G. Ruben: *Jernk. Ann.* (1945) **129**, 37. (As quoted by Benedicks in Ref. 11.)



The Ionic Nature of Metallurgical Slags. Simple Oxide Systems

JOHN CHIPMAN,* Member and LO-CHING CHANG,† Junior Member AIME

Introduction

THE perennial and increasing interest in the chemical behavior of steelmaking slags has led to numerous attempts to formulate the thermodynamic properties of these solutions. The classical view is that of a solution of the component oxides in which certain acidic oxides are more or less completely held in combination with basic or metallic oxides, the nature of the interoxide compounds being derivable from the chemical behavior of the slag or from the mineralogy of a solidified specimen. The known electrical conductivity of slags has pointed to the existence of ions in the solution and a number of attempts have been made to account for the observed facts of slag behavior on the basis of a theory of complete ionization of the solution. It is the purpose of this paper to examine, in the light of ionic theory, a number of recently published series of data on slag-metal and slag-gas equilibria, with the purpose of obtaining a more complete or more satisfactory generalization than has been possible on either of the single bases of simple compound formation or complete ionization.

The attempt to formulate the ionic constitution of a complex solution is fraught with many uncertainties. An ion is not something that can be plucked from the solution and examined in detail, nor can its true formula be determined with certainty by any single experimental method. In attempting to express the composition of a slag by various ionic formulas it can be expected that alternative hypotheses of essentially equal merit will present themselves. In the present state of early development of the ionic theory of slags, it may be necessary to make some rather arbitrary choices of ionic formulas in the absence of suffi-

cient information to yield complete certainty.

Acids and Bases

The classification of slag-forming oxides as acidic or basic apparently dates back into the days of Berzelius. It is difficult to see how the concept could have originated in the early twentieth century when it was fashionable to define an acid or a base as an aqueous solution containing hydrogen or hydroxyl ions. It is, however, entirely consistent with the modern and more general theory of acids and bases. In this theory, as originally formulated by G. N. Lewis,¹ a basic molecule is one that has an electron pair which may enter the valence shell of another atom thus binding the two together by the electron-pair bond. An acid molecule is one which is capable of receiving such an electron pair into the shell of one of its atoms. The acid, the base, and the product of neutralization may be either ions or neutral molecules. The product of such a reaction may itself be a base or an acid if it is further capable of giving or accepting an electron pair. Thus a base is a donor of electrons; an acid, an acceptor. In oxide slags the typical and ever-present base is oxide ion, O^{--} . In behavior and in importance it is analogous to hydroxyl ion, OH^- , which is the typical base of aqueous

solutions. There is nothing in the chemistry of slags which is quite analogous to the acid H_3O^+ in aqueous solutions. This is not surprising in slag systems there is nothing which can be designated as a solvent and no ubiquitous positive ion. The chemistry of slags is in fact more complex than the chemistry of aqueous solutions and the concepts which must be evoked in its study are correspondingly broader.

In seeking a basis for a classification of slag-forming oxides as basic or acidic it must be remembered that these terms are not absolute but relative. A substance which acts as a base toward a second substance may act as an acid toward a third. This is less likely to happen among strong bases or acids than among the weak ones; there are numerous examples of weak acids, which under the influence of a stronger acid behave as weak bases. Such substances are called amphoteric. A classification of the glass-forming oxides has been proposed by Sun and Silverman² and further developed by Sun³ in which the oxides are arranged in order of decreasing acidity or increasing basicity, each substance being potentially capable of acting as an acid toward substances below it in the list and as a base toward those above it. It is based upon the relative strengths of the metal-to-oxygen bond as determined by the energy required to dissociate the oxide into its component atoms.⁴ Data are available for computation of this energy, at least approximately, for the oxides of slags and glasses. In general those oxides from which it is most difficult to remove the positive atom are the strong acids while those in which it is most loosely held are the strong bases. It is in the latter, of course, that formation of oxide ion occurs most readily as, for example, in CaO which in solution ionizes to form the weak acid Ca^{++} and the strong base O^{--} . The order of arrangement found by Sun is shown in the first column of Table I, to which have been added the data for

San Francisco Meeting, February 1949.

TP 2529 C. Discussion of this paper (2 copies) may be sent to *Transactions AIME* before May 15, 1949. Manuscript received November 1, 1948; revision received November 26, 1948.

* Professor of Metallurgy, Massachusetts Institute of Technology.

† Crucible Steel Co. of America, New York City.

References are at the end of the paper.

| From Relative Bond Strength ³ | From Carbonate Decomposition ⁵ | From Sulphate Decomposition ⁵ |
|--|---|--|
| B ₂ O ₃ | P ₂ O ₅ | |
| SiO ₂ | B ₂ O ₃ | |
| P ₂ O ₅ | SiO ₂ | |
| Al ₂ O ₃ | TiO ₂ | |
| Sb ₂ O ₃ | | |
| ZrO ₂ | | |
| TiO ₂ | | BeO |
| BeO | | Fe ₂ O ₃ |
| SnO ₂ | | CuO |
| FeO | FeO | CoO |
| PbO | ZnO | NiO |
| MgO | CoO | ZnO |
| MnO | MnO | CdO |
| Li ₂ O | PbO | MnO |
| PbO | CdO | PbO |
| CaO | MgO | MgO |
| SrO | CaO | CaO |
| BaO | Li ₂ O | Li ₂ O |
| Na ₂ O | BaO | BaO |

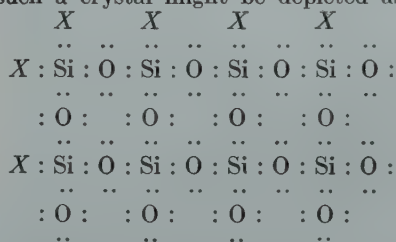
Another method of comparing basic strength of oxides is through studies of the decomposition of such compounds as carbonates and sulphates. The stronger the basic properties of an oxide, the more strongly does it hold fast to CO_2 or SO_3 and accordingly the lower is the decomposition pressure at a given temperature. Acidic oxides may be compared by their relative ability to displace CO_2 from a given carbonate. The information on relative basic strengths derived from experiments of this sort has been summarized by Flood and Förland² and is quoted in the second and third columns of Table 1. It is to be observed that the three columns are in very good agreement although minor discrepancies are present.

On the basis of the Lewis theory of acids and bases the formula for oxide

being used to represent pairs of electrons, not statically placed as in the formula but possessing points of maximum probability which for chemical purposes are sufficiently well represented by the dots. The process of neutralization of the base O^{--} by an acid

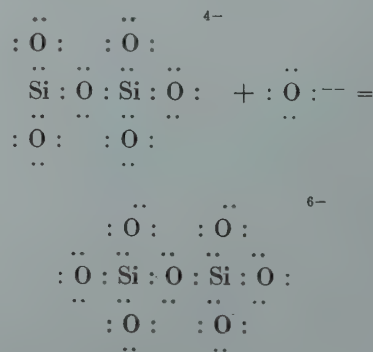
$$\begin{array}{c}
 \text{:}\ddot{\text{O}}\text{:} \\
 \text{:}\ddot{\text{O}}\text{:Si (acid)} + \text{:}\ddot{\text{O}}\text{:}^- \text{ (base)} = \text{:}\ddot{\text{O}}\text{:Si}\ddot{\text{O}}\text{:} \\
 \text{:}\ddot{\text{O}}\text{:} \qquad \qquad \qquad \text{:}\ddot{\text{O}}\text{:} \\
 \text{(metasilicate ion)} + \text{(oxide ion)} = \text{(orthosilicate ion)}
 \end{array}$$
$$\begin{array}{cccccc}
 \text{..} & \text{..} & \text{..} & \text{..} & \text{..} & 2n- \\
 : \text{O} : & : \text{O} : & : \text{O} : & : \text{O} : & : \text{O} : & \\
 \text{Si} : \text{O} : & \text{Si} : \text{O} : & \text{Si} : \text{O} : & \text{Si} : \text{O} : & \text{Si} : \text{O} : & \text{or } (\text{SiO}_3)_n \\
 \text{..} & \text{..} & \text{..} & \text{..} & \text{..} & 2n- \\
 : \text{O} : & : \text{O} : & : \text{O} : & : \text{O} : & : \text{O} : &
 \end{array}$$

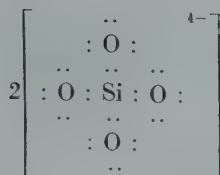
The oxide SiO_2 has a crystal structure consisting of a multiplicity of SiO_4 groups, each silicon being surrounded by four oxygens, arranged tetrahedrally, and each oxygen being shared by two silicons. The surface layers of such a crystal might be depicted as:


$$X: \begin{array}{c} X \\ \vdots \\ \text{Si} \\ \vdots \\ \text{O} \end{array} : \begin{array}{c} \vdots \\ \text{O} \\ \vdots \end{array} + : \begin{array}{c} \vdots \\ \text{O} \\ \vdots \end{array} \rightarrow \begin{array}{c} \vdots \\ \text{Si} \\ \vdots \\ \text{O} \end{array} : \begin{array}{c} \vdots \\ \text{O} \\ \vdots \end{array}$$

metasilicate minerals and which may be depicted by the formula:

Further addition of oxide ion to a silicate melt carries the neutralization a step farther, forming pyrosilicates $[\text{SiO}_{3n+1}]^{(2n+2)-}$. To take the simplest case (and the one which is most probably significant in slags) of a pyrosilicate containing two silicon atoms, its formation is represented by:


$$\begin{array}{ccccccc}
 & \ddot{\text{O}} & & \ddot{\text{O}} & & & 6- \\
 & : & \text{O} : & & : & \text{O} : & \\
 & \ddot{\text{O}} & & \ddot{\text{O}} & & \ddot{\text{O}} & \\
 : & \text{O} : & \text{Si} : & \text{O} : & \text{Si} : & \text{O} : & + : \text{O} : \text{---} = \\
 & \ddot{\text{O}} & & \ddot{\text{O}} & & \ddot{\text{O}} & \\
 & : & \text{O} : & & : & \text{O} : & \\
 & \ddot{\text{O}} & & \ddot{\text{O}} & & &
 \end{array}$$

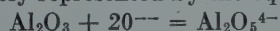


It is evident in these illustrations that the product of neutralization in one reaction may act as an acid in another. The successive steps and the relative acidity of silicon in the several forms may be represented by the following series adapted from the work of Huggins and Sun⁴:

| | Acid | Decreasing Acidity | | | Basic |
|-----------------------------------|------------------|--------------------------------|--------------------------------|--------------------------------|--------------------------------|
| Ion..... | SiO ₂ | SiO ₃ ²⁻ | SiO ₄ ³⁻ | SiO ₅ ⁴⁻ | SiO ₆ ⁴⁻ |
| Atoms of Si per atom of O..... | 0.50 | 0.40 | 0.333 | 0.286 | 0.250 |
| Energy per tetrahedron K cal..... | 3110 | 3123 | 3131 | 3137 | 3141 |

OTHER ACIDIC OXIDES

Phosphorus likewise has a coordination number of four and forms meta-, pyro- and orthophosphate ions whose formulas in order of neutralization are: P₂O₅, PO₃⁻, P₂O₇⁴⁻, PO₄³⁻. Similarly the other acidic oxides react with oxide ion to produce anions which become progressively less acidic as the oxygen content increases. In general the nature of these ions is less thoroughly understood than in the examples cited above, especially with respect to ionic constitution in liquid slags at steelmaking temperatures. It is sometimes possible to deduce the nature of the ion from its known chemical behavior in the slag. For example, in basic open-hearth slags the acidifying effect of one mole of Al₂O₃ is neutralized by addition of two moles of CaO. The neutralization in slags of this kind is therefore very probably represented by the equation:



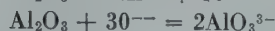
Other oxides of similar formula may form ions of quite different type. Thus the strong acid B₂O₃ if completely neutralized gives



BASIC OXIDES

Any oxide which when added to the slag increases its oxide ion activity is a basic oxide. The most strongly basic oxides are those of the alkali and alkaline earth metals. In addition to oxides, the fluorides, chlorides and sulphides should be considered. Their behavior is altogether analogous to that of oxides, the negative ions F⁻, Cl⁻ and S²⁻ acting as bases.

An amphoteric oxide may function either as an acid or a base depending upon the oxide-ion activity of the solution to which it is added. As a typical example, alumina may ionize in accordance with either of the following reactions:



It may thus increase or decrease the oxide ion activity depending upon whether the basicity of the slag to which it is added is small or great.

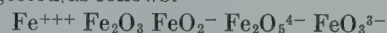
Ionic Solutions

Fused salts are excellent conductors of electricity and, especially in the case of the halides, have long been regarded as highly ionized. Many fused oxides, including the mixtures which we call slags, are also strong electrolytes⁷ and therefore are in considerable measure dissociated into ions. Herasymenko⁸ proposed that open hearth slags are completely dissociated into positive metallic ions and several kinds of negative ions including many of those mentioned in the foregoing section. He showed excellent agreement between theory and observations in many cases of slag-metal equilibrium with acid slags. The success of the theory with respect to basic slags was less noteworthy. Temkin⁹ defined an ideal ionic solution and applied the concept to steelmaking slags. He defined the ion fraction of a positive or negative ion N_i⁺ or N_i⁻ as the ratio of the amount of this ion to the total of all ions of like sign present in the solution. He treated ionic solutions as being "ideal" in the sense that the activity of each ion is equal to its ion fraction. Samarin, Temkin and Shvarzman¹⁰ showed excellent agreement between theory and observations in the distribution of sulphur but unfortunately not for the case of oxygen distribution between slag and metal. We shall refer to the assumed equality of activity and ion fraction as "Temkin's rule."

Liquid Iron Oxide Slags

From the ionic viewpoint, the behavior of liquid iron oxide indicates

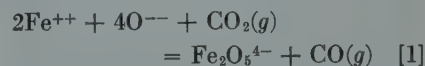
clearly the presence of Fe⁺⁺, O²⁻ and at least one other negative ion containing trivalent iron. That trivalent iron is present as an anion rather than as tripositive ferric ion is shown by the marked increase in ferric iron which attends an increase in slag basicity, other factors remaining constant. Which of a number of possible "ferrite ions" is present in basic slags cannot be decided on the basis of any evidence now available. A series of possible ions formed from ferric ion by successive neutralization with oxide ion is suggested as follows:



Since the composition of the liquid may be expressed in terms of Fe⁺⁺, O²⁻ and any one of the anions suggested, the choice of one of these becomes a matter of convenience. It will be convenient to select the formula which leads to values of activity coefficient nearest to unity, or least variable with composition. A simple calculation from the recent data of Darken and Gurry¹¹ showed that Fe₂O₅⁴⁻ is the most satisfactory of the four ionic formulas suggested, from the standpoint of simplicity of calculation. The occurrence of dicalcium ferrite in solidified basic slags¹² indicates that this choice is not an unreasonable one.

Darken and Gurry¹¹ have established the equilibrium relationship between molten iron oxides and a gas phase containing CO and CO₂. Their data cover a temperature range from 1400 to 1600°C and compositions represented by ratios of oxygen to iron between 1.01 and 1.37. They provide as complete a set of experimental data as could be desired for thermodynamic study of these molten oxides. The data for 1600° are reproduced in Table 2 in which the first three columns are taken directly from Darken and Gurry's Table 6. The figures in the other columns will be discussed later.

In view of what has been said above with regard to the principal ions present in the solution, the principal reaction and its equilibrium constant may be written:



$$K_1 = \frac{p_{\text{CO}}}{p_{\text{CO}_2}} \cdot \frac{a_{\text{Fe}_2\text{O}_5^{4-}}}{(a_{\text{Fe}^{++}})^2 \cdot (a_{\text{O}^{2-}})^4}$$

In this expression the *a*'s represent activities of the ions and it will be well at the outset to state clearly the meaning of this term. Ion activity may be defined like any other activity as

$$a = e^{\frac{\mu - \mu^\circ}{RT}}$$

where μ and μ° are the chemical potentials (free energies) of the ionic component at two concentrations, one of which, μ° , is selected as a standard for reference. The activity has no absolute value since it depends only on the difference in chemical potential; for this reason it is sometimes called the relative activity. Darken and Gurry chose as their standard state a solution in which $N_{\text{O}}/N_{\text{Fe}} = 1.07$ and it was on this basis that the third column of Table 2 was obtained. For our purposes it will be more convenient to adopt $N_{\text{O}}/N_{\text{Fe}} = 1.00$ as the standard state, corresponding to the hypothetical pure liquid FeO. Referred to this standard, the value of $\log a_{\text{FeO}}$ will differ by a constant amount from that of the third column, the new values being given in the fourth. The constant difference of 0.040 was found for each of the experimental temperatures by extrapolation to unit ion fraction of oxide ion. Corresponding values for the activity of FeO are given in the last column.

In the pure liquid FeO the activities of the ions Fe^{++} and O^{--} as well as of the component FeO will be taken as unity. These choices require that

$$a_{\text{FeO}} = a_{\text{Fe}^{++}} \cdot a_{\text{O}^{--}} \quad [2]$$

an equation which we shall use as the definition of the activity of FeO in any slag. It should be noted specifically that nothing has been said about the degree of ionization of FeO. The definition of activity here employed* is equally useful whether the melt is completely or only infinitesimally ionized. The activity coefficient, γ , of an ion will be defined as the ratio of its activity to its ion fraction. For other ions in the solution, such as $\text{Fe}_2\text{O}_5^{4-}$ or Fe^{3+} the reference state will be the infinitely dilute solution in FeO in which the activity is equal to the ion fraction or $\gamma = 1$.

The equilibrium constant of Eq 1 may be obtained from the data of Darken and Gurry.¹¹ For slags in which the ratio of $N_{\text{O}}/N_{\text{Fe}}$ is 1.15 or less and the concentration of Fe^{3+} ion is probably quite small, the calculations are shown in Table 3. The first two columns are the experimental data of Darken and Gurry's Table 6. Columns 3 and 4 are ion fractions computed from column 1 on the assumption that the liquid contains only Fe^{++} , O^{--} and $\text{Fe}_2\text{O}_5^{4-}$. Since the ion fraction of Fe^{++} is unity, the activity of O^{--} is equal to that of FeO by Eq 2. Values of a_{FeO} were shown in Table 2 for 1600° and at

Table 2 . . . Equilibrium Gas Composition and Activity of Ferrous Oxide in Liquid Iron Oxides at 1600°C from Data of Darken and Gurry¹¹

| $N_{\text{O}}/N_{\text{Fe}}$ | $\log \frac{p_{\text{CO}_2}/p_{\text{CO}}}{p_{\text{CO}_2}/p_{\text{CO}}}$ | $-\log a_{\text{FeO}}$ | $-\log a_{\text{FeO}}$ | a_{FeO} |
|------------------------------|--|------------------------|------------------------|------------------|
| (1.00) | | | (0.000) | (1.000) |
| 1.012 | -0.728 | -0.0291 | 0.011 | 0.975 |
| 1.04 | -0.371 | -0.0191 | 0.021 | 0.951 |
| 1.07 | -0.021 | 0. | 0.040 | 0.912 |
| 1.10 | +0.295 | +0.0268 | 0.067 | 0.857 |
| 1.15 | 0.812 | 0.0914 | 0.131 | 0.740 |
| 1.20 | 1.30 | 0.177 | 0.271 | 0.607 |
| 1.25 | 1.80 | 0.290 | 0.330 | 0.468 |
| 1.30 | 2.35 | 0.439 | 0.479 | 0.332 |
| 1.333 | 2.74 | 0.565 | 0.605 | 0.248 |
| 1.34 | 2.82 | 0.593 | 0.633 | 0.233 |
| 1.37 | 3.22 | 0.733 | 0.773 | 0.169 |

Table 3 . . . Equilibrium Constant of Eq 1 at 1600, 1500 and 1400°C

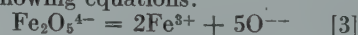
| $N_{\text{O}}/N_{\text{Fe}}$ | $p_{\text{CO}_2}/p_{\text{CO}}$ | $N_{\text{O}^{--}}$ | $N_{\text{Fe}_2\text{O}_5^{4-}}$ | $a_{\text{O}^{--}}$ | K_1 |
|------------------------------|---------------------------------|---------------------|----------------------------------|---------------------|-------|
| Temperature 1600° | | | | | |
| 1.04 | 0.425 | 0.954 | 0.046 | 0.951 | 0.131 |
| 1.07 | 0.952 | 0.912 | 0.088 | 0.912 | 0.134 |
| 1.10 | 1.97 | 0.857 | 0.143 | 0.857 | 0.135 |
| 1.15 | 6.48 | 0.728 | 0.272 | 0.740 | 0.149 |
| Temperature 1500° | | | | | |
| 1.04 | 0.384 | 0.954 | 0.046 | 0.954 | 0.145 |
| 1.07 | 0.886 | 0.912 | 0.088 | 0.912 | 0.144 |
| 1.10 | 1.893 | 0.857 | 0.143 | 0.855 | 0.140 |
| 1.15 | 6.60 | 0.728 | 0.272 | 0.731 | 0.147 |
| Temperature 1400° | | | | | |
| 1.034 | 0.263 | 0.963 | 0.037 | 0.966 | 0.164 |
| 1.04 | 0.338 | 0.954 | 0.046 | 0.956 | 0.164 |
| 1.07 | 0.836 | 0.912 | 0.088 | 0.912 | 0.152 |
| 1.10 | 1.805 | 0.857 | 0.143 | 0.855 | 0.147 |
| 1.117 | 2.82 | 0.819 | 0.181 | 0.815 | 0.143 |
| 1.15 | 6.65 | 0.728 | 0.272 | 0.726 | 0.146 |

other temperatures may be obtained in the same manner from the experimental data. They are listed in the fifth column as $a_{\text{O}^{--}}$. It is to be noted that these experimental values of $a_{\text{O}^{--}}$ agree closely with $N_{\text{O}^{--}}$ thus making $\gamma_{\text{O}^{--}} = 1$ for these solutions.

The activity of this ion thus conforms to Temkin's rule. Now in binary solutions if one component obeys Raoult's law over a given range of composition it follows that the second component obeys Henry's law in the same range. By analogy then, since there are two negative ions, if one obeys Temkin's rule the activity of the other is proportional to concentration in the same range. It follows that in these solutions $\gamma_{\text{Fe}_2\text{O}_5^{4-}}$ (referred to the infinitely dilute solution) is unity. The values of the equilibrium constant computed from the ion fractions are given in the last column, the constancy being surprisingly good. Since deviations occur at higher ratios of oxygen to iron, the values at the lower concentrations are used to obtain the average values of K_1 .

The deviations in K_1 which occur at ratios of $N_{\text{O}}/N_{\text{Fe}}$ greater than 1.15 could readily be treated by imposing an activity coefficient upon any of the ion

fractions involved, for example $\text{Fe}_2\text{O}_5^{4-}$. We prefer to accomplish the same purpose by the hypothesis that at higher ferric contents the concentration of the ferric ion, Fe^{3+} , becomes significant. It is likely that as the concentration of $\text{Fe}_2\text{O}_5^{4-}$ ion increases and that of O^{--} ion decreases, a significant amount of $\text{Fe}_2\text{O}_5^{4-}$ ion dissociates into Fe^{3+} and O^{--} according to some internal equilibrium which we express by the following equations:



$$K_3 = \frac{(a_{\text{Fe}^{3+}})^2 (a_{\text{O}^{--}})^5}{(a_{\text{Fe}_2\text{O}_5^{4-}})}$$

When Fe^{3+} ion is present in significant amount, it becomes no longer possible to calculate the concentration of each constituent directly from the $N_{\text{O}}/N_{\text{Fe}}$ ratios without knowing the constant K_3 and the corresponding activity coefficients. However, we shall proceed to solve the problem from the Darken and Gurry data as follows:

From Eq 1 and our definition of a_{FeO} , and continuing the assumption of unit activity coefficient for oxide and ferrite ions, we may write:

$$K_1 = \frac{p_{\text{CO}}(1 - N_{\text{O}^{--}})}{p_{\text{CO}_2} \cdot (a_{\text{FeO}})^2 \cdot (N_{\text{O}^{--}})^2} \quad [1a]$$

This expression is solved for each of the data to yield $N_{\text{O}^{--}}$ and $N_{\text{Fe}_2\text{O}_5^{4-}}$ (which

* This follows the standard treatment of ion activities by Lewis and Randall; see Ref. 17, p. 326.

Table 4 . . . Calculation of Ferric-ion Activity and of K_3 in Iron Oxide Slags
Temperature 1600°, $K_1 = 0.133$

| $N_{\text{O}}/N_{\text{Fe}}$ | $p_{\text{CO}_2}/p_{\text{CO}}$ | a_{FeO} | $N_{\text{O}^{--}}$ | $N_{\text{Fe}_2\text{O}_5^{4-}}$ | $N_{\text{Fe}^{++}}$ | $a_{\text{Fe}^{++}}$ | $\gamma_{\text{Fe}^{++}}$ | $\gamma_{\text{Fe}^{3+}}$ | $a_{\text{Fe}^{3+}}$ | $K_3 \times 10^4$ |
|------------------------------|---------------------------------|------------------|---------------------|----------------------------------|----------------------|----------------------|---------------------------|---------------------------|----------------------|-------------------|
| 1.20 | 20.0 | 0.607 | 0.622 | 0.378 | 0.939 | 0.976 | 1.04 | 0.48 | 0.029 | 2.09 |
| 1.25 | 63.1 | 0.468 | 0.514 | 0.486 | 0.851 | 0.911 | 1.07 | 0.35 | 0.052 | 2.03 |
| 1.30 | 223.9 | 0.332 | 0.421 | 0.579 | 0.733 | 0.788 | 1.07 | 0.34 | 0.091 | 1.89 |
| 1.333 | 549.5 | 0.248 | 0.374 | 0.626 | 0.638 | 0.664 | 1.04 | 0.36 | 0.130 | 2.00 |
| 1.34 | 668.3 | 0.233 | 0.363 | 0.637 | 0.617 | 0.642 | 1.04 | 0.37 | 0.142 | 1.98 |
| 1.37 | 1660. | 0.169 | 0.327 | 0.673 | 0.520 | 0.517 | 0.99 | 0.39 | 0.187 | 1.95 |

is $1 - N_{\text{O}^{--}}$). The solution is shown in the first five columns of Table 4 of which the first three represent the experimental data. The fourth and fifth columns are obtained by solution of the above equation using values of K_1 from Table 3. The ion fraction of Fe^{++} is found from the stoichiometric requirements (a) that the ratio of the total number of atoms of the two kinds must be that of column one and (b) that the total positive and negative charges must be equal. From these considerations we have:

$$\begin{aligned} (N_{\text{O}^{--}} + 5N_{\text{Fe}_2\text{O}_5^{4-}}) / (2N_{\text{Fe}_2\text{O}_5^{4-}} + n_{\text{Fe}^{++}} + n_{\text{Fe}^{3+}}) &= N_{\text{O}}/N_{\text{Fe}} \quad [a] \\ 2n_{\text{Fe}^{++}} + 3n_{\text{Fe}^{3+}} &= 2N_{\text{O}^{--}} + 4N_{\text{Fe}_2\text{O}_5^{4-}} \quad [b] \end{aligned}$$

Here N represents ion or atom fractions while n is the number of moles of ferrous and ferric ion respectively per mole of total negative ion. Simultaneous solution of Eq a and b leads to the value of $N_{\text{Fe}^{++}}$ shown in column six which in these solutions is equal to $n_{\text{Fe}^{++}}/(n_{\text{Fe}^{++}} + n_{\text{Fe}^{3+}})$.

The activity of ferrous ion in column seven is obtained by Eq 2 from the activity of FeO and the ion fraction of oxide ion which is here assumed equal to its activity. The activity coefficient shown in column eight is remarkably close to unity but the deviations are not negligible.

In order to obtain activity coefficients of Fe^{3+} , we shall assume that the activities of the two positive ions follow the same relationship as that governing the behavior of two components in a binary system. By analogy with the Gibbs-Duhem equation¹⁷ we write:

$$\log \gamma_{\text{Fe}^{3+}} = - \int_0^N \frac{N_{\text{Fe}^{++}}}{N_{\text{Fe}^{3+}}} d \log \gamma_{\text{Fe}^{++}}$$

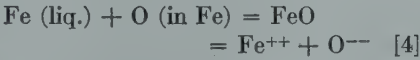
The integration covers the composition range extending to "pure" FeO and consequently involves a rather gross extrapolation. The uncertainty thus introduced corresponds to a constant factor in the activity and hence does not affect the relative accuracy. The resultant values of the activity coefficient and the activity of Fe^{3+} are given in Table 4. Finally the values of K_3 based upon these data are shown in the last column. The surprisingly good

constancy may be due as much to the method of obtaining $\gamma_{\text{Fe}^{3+}}$ as to any other factor, but it should be noted that these values themselves do not vary greatly and a fairly constant K_3 could have been obtained using ion fractions for activities.

The Distribution of FeO between Molten Iron and Oxide Slags

PURE IRON OXIDE SLAGS

From the ionic viewpoint the distribution of FeO between molten iron and liquid iron oxide may be expressed by the following equation:



$$K_4 = \frac{a_{\text{FeO}}}{\% \text{ O}} = \frac{a_{\text{Fe}^{++}} \cdot a_{\text{O}^{--}}}{\% \text{ O}}$$

The experimental data^{13,14} on the distribution of FeO between molten iron and liquid iron oxide containing small amounts of CaO, MgO and SiO₂ are used to determine the distribution constant K_4 . The most probable ion species in these slags are: Ca^{++} , Mg^{++} , Fe^{++} , O^{--} , SiO_4^{4-} and $\text{Fe}_2\text{O}_5^{4-}$. Since the con-

centration of ions other than Fe^{++} and O^{--} is very low, the activity coefficient of Fe^{++} and O^{--} will be close to unity and as an approximation ion fractions may be used for activities.

A plot of $\log K_4$ vs. $1/T$ is shown in Fig 1. The straight line is represented by the equation

$$\log K_4 = +6000/T - 2.57 \quad [4a]$$

This is essentially equivalent to the equation used by Taylor and Chipman¹⁴ to represent the same series of data. It differs slightly because of the different standard state used here and the different method of correcting for impurities.

When the slag is in equilibrium with molten iron, it contains a small concentration of trivalent iron in the form of ferrite ion as shown by the equation



$$K_5 = \frac{a_{\text{Fe}_2\text{O}_5^{4-}}}{(a_{\text{Fe}^{++}})^3 \cdot (a_{\text{O}^{--}})^5}$$

Values of K_5 are readily obtained from the data of Darken and Gurry. Using their limiting gas and oxide compositions, with a small correction to correspond with liquid iron, and our average values of K_1 , we find at temperatures of 1600, 1500 and 1400°C that $K_5 = 0.0255, 0.0316$ and 0.0395 respectively.

IRON OXIDE SLAGS CONTAINING LIME OR MAGNESIA

When liquid iron oxide slags containing varying amounts of lime or magnesia in solution are at equilibrium with molten iron, the concentration of

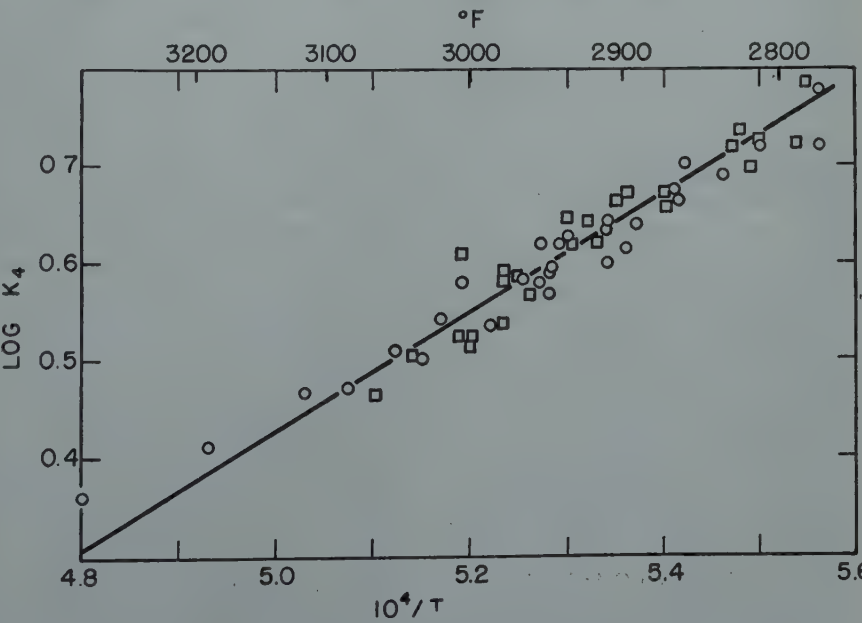


FIG 1—Temperature dependence of the ionic distribution constant for oxygen between iron and iron oxide slags. $K_4 = a_{\text{Fe}^{++}} \cdot a_{\text{O}^{--}}/\% \text{ O}$. Circles, Chipman and Fettes;¹³ squares, Taylor and Chipman.¹⁴

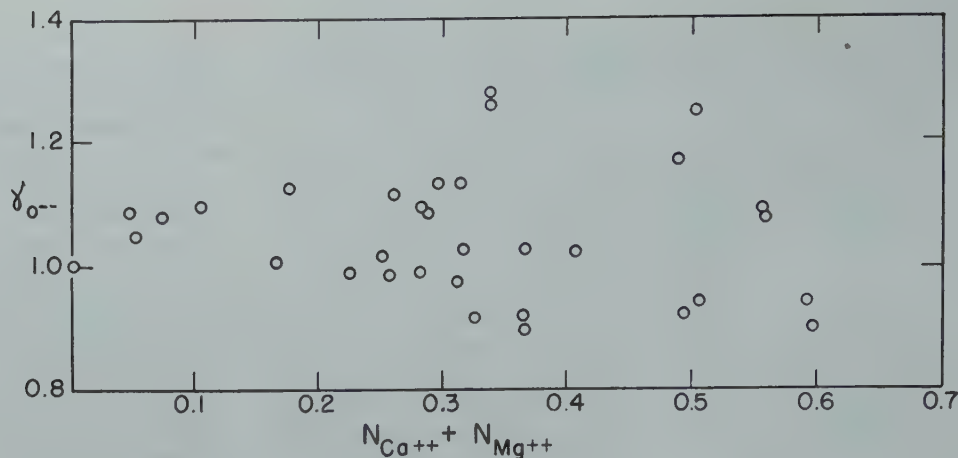


FIG 2—Activity coefficient of oxide ion in slags containing the oxides of iron, calcium and magnesium.

oxygen in the metal phase serves as a convenient measure of the activity of FeO in the slag. The concentration of ferrite ion in the slag at equilibrium with molten iron is relatively low but increases with increasing percentages of CaO or MgO. That of Fe³⁺ is entirely negligible.

Activities of Fe⁺⁺, Ca⁺⁺ and Mg⁺⁺ may be assumed equal to their ion fractions. The activity of O⁻⁻ is obtained from that of Fe⁺⁺, the oxygen content of the molten iron in equilibrium with the slag, and the value of K_4 given in Eq 4a. The data of Taylor¹⁴ and of Fетters and Chipman¹⁵ are used in making the calculations, the results of which are shown in Fig 2. Here the value of the activity coefficient of oxide ion is plotted against the sum of the ion fractions of Ca⁺⁺ and Mg⁺⁺. With a few exceptions the values of γ_{O--} fall in the range 0.9 to 1.15 and appear to be almost independent of the ratio of Ca⁺⁺ to Fe⁺⁺, perhaps increasing slightly with decreasing Fe⁺⁺. The method of computation imposes all of the errors of experiment and of assumptions regarding activities upon the value of γ_{O--} . The fact that the result lies within 10 to 15 pct of unity at all compositions indicates the usefulness of Temkin's rule in these solutions. It shows further that FeO and CaO are almost equal with respect to the amount of oxide ion that each contributes to slags of this type. This finding might reasonably be construed as evidence that both oxides are either completely ionized or not at all.

The activity of Fe₂O₅⁴⁻ ion in these slags may be obtained from the slag compositions and values of K_5 given in the preceding section. The accuracy will be improved somewhat by combin-

ing K_5 with K_4 to obtain the following:

$$K_6 = \frac{a_{Fe_2O_5^{4-}}}{a_{Fe^{++}} \cdot (a_{O--})^3 [\% O]^2} \quad [6]$$

Values of K_6 are given by the following equation which is based upon data previously cited for the other K 's:

$$\log K_6 = +15000/T - 8.32 \quad [6a]$$

Values of the activity coefficient of Fe₂O₅⁴⁻ ion found from these equations and data on lime-iron oxide slags are presented in Fig 3. Here is an entirely different behavior by an activity coefficient than we have found for that of any other ion, the variation being about 100-fold within the observable concentration range. It is true that the method of calculation has piled all the errors of data and assumptions onto this coefficient; but the same data gave activity coefficients for oxide ion approximating unity. Moreover the low coefficient for Fe₂O₅⁴⁻ ion is not related to a high concentration of this ion but is dependent upon a high concentration of the cations Ca⁺⁺ and Mg⁺⁺. It is evident that these two ions exert a very different effect upon Fe₂O₅⁴⁻ than does Fe⁺⁺, the effect being of the nature of an attraction between positive and negative ions. What this means in terms of the structure of the melt cannot be learned from thermodynamics alone. It may be regarded as evidence of a tendency to form complex ions or neutral compounds, or of a more pronounced close-range ordering of positive and negative ions. Flood and Förland⁵ have pointed out other instances in which the stability of similar anions is markedly affected by the nature of the cation. Kheinman¹⁶ called attention to the striking differences between melts of the compositions 2FeO · SiO₂ and 2CaO · SiO₂. The

former is an excellent conductor of electricity and the conductivity is progressively diminished as the latter is added. He regards this as evidence of a change in the coordination numbers of the ions, the Ca⁺⁺ ion being prevented from taking part in the transfer of electricity by a coating of silicate ions. The result is equivalent to the formation of "nondissociated" Ca₂SiO₄. This seems quite analogous to the case of the ferrites.

We now return to the question of what constitutes a basic oxide in slag. How can we, on the basis of ionic theory, account for the differences in behavior between the common basic oxides? That these differences are not due to different degrees of ionization of the oxides themselves has been demonstrated in the case of CaO-FeO slags where the oxide-ion activity is essentially independent of the cation. The evidence thus far presented indicates that differences in the basic strength of oxides becomes apparent only in the presence of anions other than O⁻⁻. And it is the ability of the cation to bind these larger anions into inactive complexes which determines the behavior of the oxide as a base. We shall not attempt a detailed discussion of the nature of these inactive complexes. They may be thought of as neutral ion-groups behaving as molecules or as regions of marked close-range order, or as parts of a network of anions in which the cations of the more strongly basic oxide become more firmly entangled. In representing them by chemical formulas we must for the present disclaim any implication as to structure.

With this understanding we may say that the stronger basic properties of CaO as compared to FeO are due

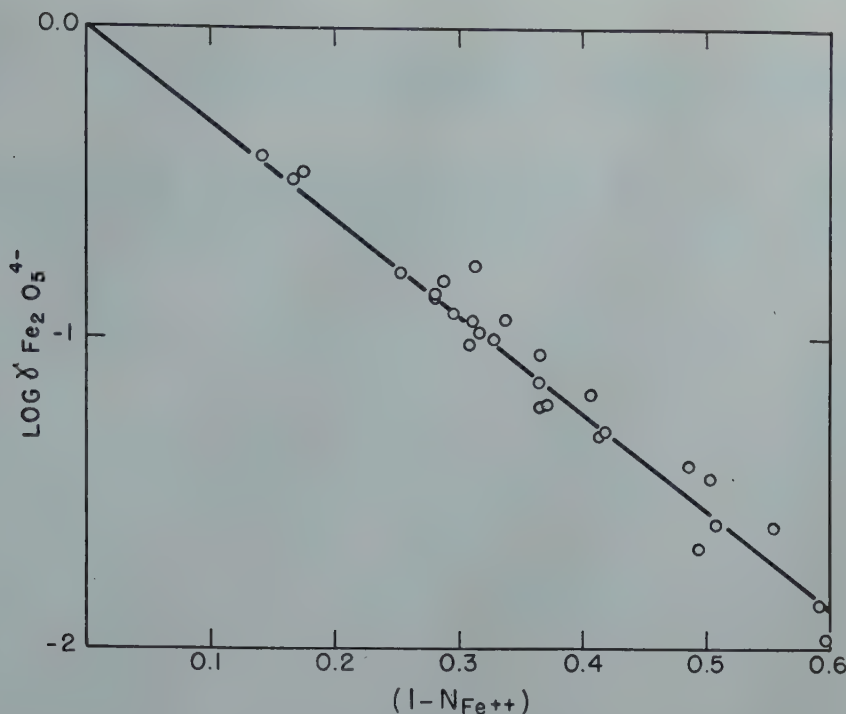


FIG 3—Activity coefficient of ferrite ion in slags containing the oxides of iron, calcium and magnesium.

to the nearer approach to completion of such reactions as: $2\text{Ca}^{++} + \text{Fe}_2\text{O}_5^{4-} = \text{Ca}_2\text{Fe}_2\text{O}_5$ than in the corresponding reaction of Fe^{++} . There is no conflict between this concept and the statement that a basic oxide is one which increases the oxide-ion activity of the slag. Addition of either CaO or FeO to a slag increases the oxide-ion concentration about equally. But the addition of CaO , by inactivating larger ions such as ferrite, increases the effective fraction of O^{--} and thereby causes a further increase in the oxide-ion activity. Kheinman¹⁶ has shown that this concept is capable of quantitative application to silicate slags and leads to satisfactory results for oxygen and sulphur distribution in slags containing up to 30 pct silica. It is our intention to discuss such applications in more detail in a later paper.

Summary

This paper is a step toward a thermodynamic treatment of slag-metal and slag-gas reactions based upon the assumption of ionization in the slag. The Lewis theory of acids and bases is applied to slags. Basic slags contain oxide ion O^{--} which is itself a strong base. The activity of oxide ion in the slag determines its basicity and a basic oxide is one which will increase the oxide-ion activity of the slag. The

step-wise neutralization of acid oxides by oxide ion is illustrated.

The theory of complete ionization of open hearth slags is discussed and it is shown that ion activities may be useful even without knowledge of the degree of ionization. Temkin's use of ion fraction as a measure of ion activity is a useful approximation; ionic solutions which are ideal in this respect may be achieved by judicious selection of ion formulas.

The data of Darken and Gurry on equilibrium of gases with liquid iron oxides are consistent with the ion formulas Fe^{++} , O^{--} , $\text{Fe}_2\text{O}_5^{4-}$ and Fe^{3+} , the last being significant only in highly oxidized slags. Thermodynamic relationships among these ions are deduced from the data.

Data on the distribution of iron oxide between metal and simple oxide slags is shown to be consistent with the same ion formulas and thermodynamic constants. In iron oxide slags the ion activity coefficients are unity. Addition of CaO or MgO has little effect on the activity of oxide ion but causes a sharp decrease in activity coefficient of $\text{Fe}_2\text{O}_5^{4-}$ ion.

The differences in basic strength of oxides in slags are ascribed to differences in the abilities of the cations to form inactive complexes with the larger anions such as $\text{Fe}_2\text{O}_5^{4-}$ and SiO_4^{4-} .

This paper is based upon part of a study of the behavior of metallurgical slags sponsored by the American Iron and Steel Institute.

References

1. G. N. Lewis: *Jnl. Franklin Inst.* (1938) **226**, 293.
2. K. H. Sun and A. Silverman: *Jnl. Amer. Ceram. Soc.* (1945) **28**, 8.
3. K. H. Sun: *The Glass Industry*. (1948) **29**, 73.
4. M. L. Huggins and K. H. Sun: *Jnl. Phys. Chem.* (1946) **50**, 319; (1947) **51**, 438.
5. H. Flood and T. Förland: *Acta Chem. Scand.* (1947) **1**, 592.
6. W. Stegmaier and A. Dietzel: *Glastech. Ber.* (1940) **18**, 297 and 353; *Ceram. Abstr.* (1941) **20**, 235.
7. J. O'M. Bockris, J. A. Kitchener, S. Ignatowicz and J. Tomlinson: *The Faraday Soc. Symp. on the Phys. Chem. of Process Metallurgy* (1948).
8. P. Herasymenko: *Trans. Faraday Soc.* (1938) **34**, 1234; *Archiv für das Eisenh.* (1940) **14**, 109.
9. M. Temkin: *Acta Physicochimica U.R.S.S.* (1945) **20**, 411.
10. A. Samarin, M. Temkin and L. Shvarzman: *Acta Physicochimica U.R.S.S.* (1945) **20**, 421.
11. L. S. Darken and R. W. Gurry: *Jnl. Amer. Chem. Soc.* (1947) **69**, 798.
12. E. C. Smith: *Trans. AIME* (1935) **116**, 13.
13. J. Chipman and K. L. Fethers: *Trans. A. S. M.* (1941) **29**, 953.
14. C. R. Taylor and J. Chipman: *Trans. AIME* (1943) **154**, 228.
15. K. L. Fethers and J. Chipman: *Trans. AIME* (1941) **145**, 95.
16. A. S. Kheinman: *Bull. Acad. Sciences U.R.S.S.* (1946) **10**, 1439.
17. Lewis and Randall: *Thermodynamics* (1923), p. 269 (McGraw-Hill).

Properties of Chromium Boride and Sintered Chromium Boride*

S. J. SINDEBAND,† Member AIME

Introduction

PRIOR to discussing the metallurgy of sintered chromium borides, it is pertinent to outline some of the reasoning behind this investigation and the purposes underlying the work.

This study was initiated as an approach to the ubiquitous problem of a material for service at high temperatures under oxidizing atmospheres, and it was undertaken with a view to raising the 1500°F (816°C) ceiling to 2000°F (1093°C) or better. For the reason that no small, but rather a major, lifting of the high temperature working limit was being attempted, it was felt appropriate that a completely new approach be taken to this problem.

A summary of the thinking behind this approach was published recently by Schwarzkopf.¹ In briefest terms, it was postulated that the following requirements could be set up for a material which would have high strength at high temperatures.

1. The individual crystals of the material must exhibit high strength interatomic bonds. This automatically leads to consideration of highly refractory materials, since their high energy requirements for melting are related to the strength of their atom-to-atom bonds.

2. On the polycrystalline basis, high boundary strength, superimposed on the above consideration, would also be a necessity. Since this implies control of boundary conditions, the powder metallurgy approach would hold considerable promise.

Such materials actually had been fabricated for a number of years, and the cemented carbide is the best example of these. Here a highly refractory crystal was carefully bonded and resulted in a material of extremely high strength. That this strength was maintained at high temperature is exhibited

by the ability of the cemented carbide tool to hold an edge for extended periods of heavy service.

Nowick and Machlin^{2,3} have analytically approached the problem of creep and stress-rupture properties at high temperature and developed procedures whereby these properties can be approximately predicted from the room temperature physical constants of a material. The most important single constant in the provision of high temperature strength and creep resistance is shown to be the Modulus of Rigidity. On this basis, they proposed that a fertile field for investigation would be that of materials similar to cemented carbides, which have Moduli of Rigidity that are among the highest recorded.

The cemented carbide, however, does not have good corrosion resistance in oxidizing atmospheres and without protection could not be used in gas turbines and similar pieces of equipment. It would be necessary then to attempt the fabrication of an allied material based upon a hard crystal which had good corrosion resistance as well.

It was upon these premises that the subject study was undertaken and at an early stage it was sponsored by the U.S. Navy, Office of Naval Research. Since then, it has been carried on under contract with this agency.

Chromium boride provided a logical starting point for such research, since it was relatively hard, exhibited good

corrosion resistance, and, in addition, was commercially available, since it had found application in hard-surfacing alloys with iron and nickel. That chromium boride did not provide a material that met the ultimate aim of the study results from factors which are subsequently discussed. This, however, does not detract from the basis on which the study was conceived, nor from the value of reporting the results which follow.

Chromium Boride

While work on chromium boride proper dates back to Moissan,⁴ there has been a dearth of literature on borides since 1906. Subsequent to Moissan, principal investigators of chromium boride were Tucker and Moody,⁵ Wedekind and Fetzer,⁶ du Jassoneix,^{7,8,9} and Andrieux.¹⁰

These investigators were generally limited to studies of methods of producing chromium boride and determining its properties. Some study, however, was devoted to the chromium-boron system by du Jassoneix,⁷ who did this chemically and metallographically. This system is not amenable to normal methods of analysis by virtue of the refractory nature of the alloys involved, and the difficulties of measurement and control of temperature conditions in their range. Dilatometric apparatus is nonexistent for operation at these temperatures. Du Jassoneix made use of apparent chemical differences between two phases observed under the microscope and reported the existence of two definite compounds, namely: Cr₃B₂ and CrB. These two compounds, he reported, had quite similar chemical characteristics, but were sufficiently different to enable him to separate them.

The easiest method for producing chromium boride is apparently the thermite process, first applied by Wede-

San Francisco Meeting, February 1949.

TP 2519 E. Discussion of this paper (2 copies) may be sent to *Transactions* AIME before May 15, 1949. Manuscript received October 18, 1948; revision received November 26, 1948.

* This paper was also presented, in part, at The International Powder Metallurgy Congress, 1948, Graz, Austria.

† Technical Director, American Electro Metal Corporation, Yonkers, N. Y.

References are at the end of the paper.

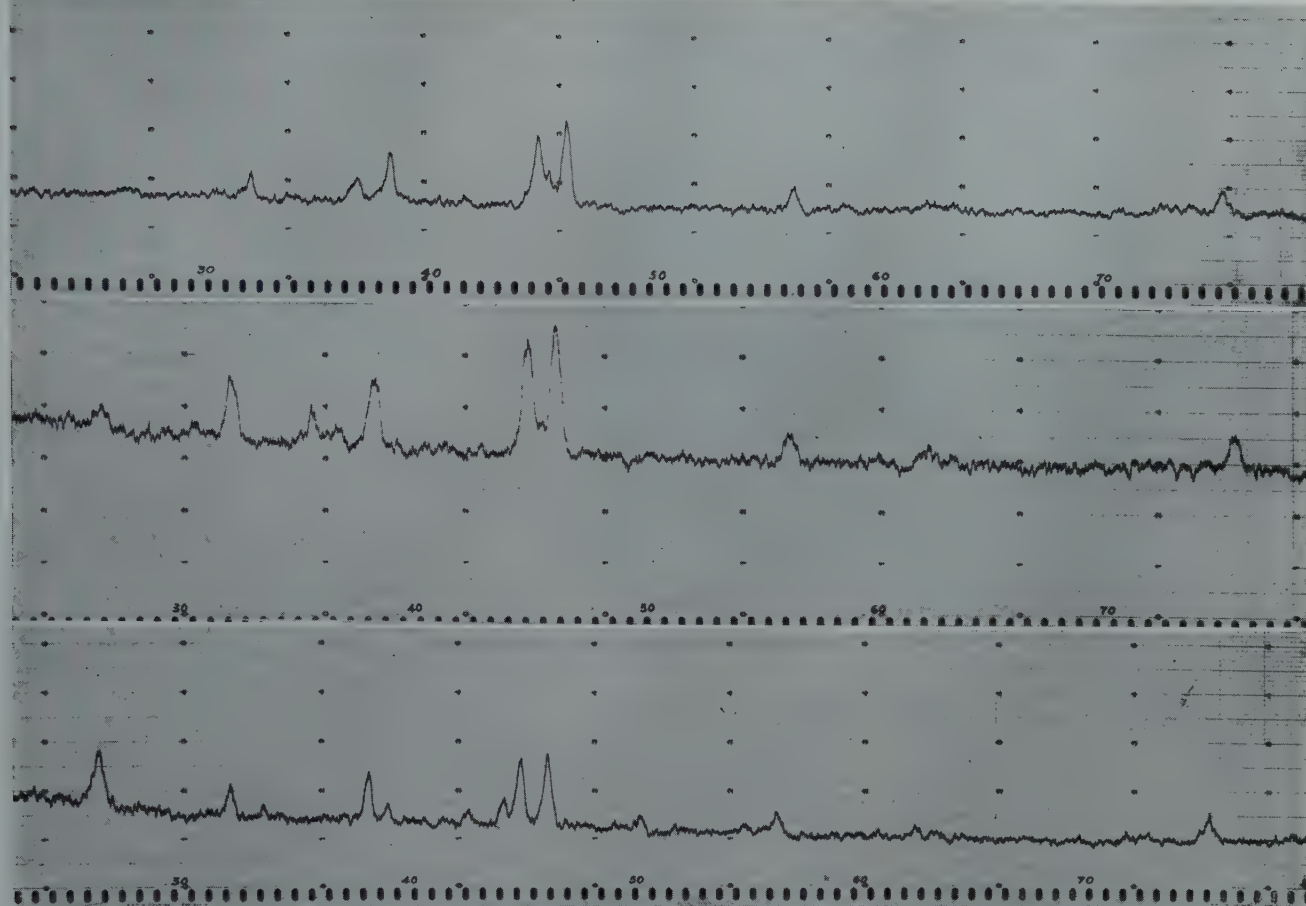


FIG 1 (top)—Chromium boride crystals. (Aluminum thermite.) Pct Boron = 18.0.

FIG 2 (center)—Chromium boride crystals. (Carbon and silicon reduction.) Pct Boron = 14.1.

FIG 3 (bottom)—Chromium boride crystals. (Electrolysis.) Pct Boron = 13.2.

kind and Fetzer.⁶ The commercial product, manufactured in the United States, is also made by thermite processes,¹¹ involving a simultaneous reduction of boric anhydride and chromium oxide Cr_2O_3 . A purer product is obtainable by the electrolysis of fused borate baths described by Andrieux.¹⁰

X ray diffraction studies have been made in the present investigation of chromium borides produced by:

1. Aluminum thermite reduction of B_2O_3 and Cr_2O_3 .
2. Carbon and silicon reduction of B_2O_3 and Cr_2O_3 .
3. Electrolysis of fused borate baths.

Samples having widely different compositions were checked in the boron content range of 12 to 20 pct. This range would include both the compositions Cr_3B_2 and CrB . The X ray diffraction patterns, taken on a Philips Norelco Recorder and using Cu ($K\alpha_1$) radiation, were substantially identical over the entire range. Typical patterns are given in Fig 1, 2, and 3, and the analyses of the samples are given in the next column.

| | Chromium Boride Produced by Aluminum Thermite, Pct | Chromium Boride Produced by Carbon and Silicon Reduction, Pct | Chromium Boride Produced by Electrolysis, Pct |
|----------------|--|---|---|
| Chromium..... | 76.12 | 70.35 | 82.0 |
| Boron..... | 18.0 | 14.1 | 13.2 |
| Iron..... | 0.52 | 2.21 | |
| Aluminum..... | 2.14 | | |
| Carbon..... | 0.03 | 1.86 | 1.7 |
| Silicon..... | 0.44 | 4.23 | |
| Calcium..... | | 2.36 | 0.4 |
| Magnesium..... | | 0.06 | |
| | 97.25 | 95.17 | 97.3 |

In Fig 3 it will be noted that a strong peak appears at 26.6° which is found relatively weaker in Fig 2. This line reflects the presence of graphite impurities.

The conclusion has been drawn that a single phase exists over this entire range, and that this is true regardless of method of fabrication. A single compound exists in this range, and its structure is maintained in adjacent nonstoichiometric compositions. This compound has, apparently, a so-called "subtractive" lattice, that is, it can

lose some boron without affecting its crystal structure. This is a consequence of the small size of the boron atom relative to the chromium atom. This has led to the conclusion that there is only one compound of chromium boride, within the compositions indicated, and that it corresponds to the formula CrB .

An investigation is presently being made of the actual crystal structure of the compound CrB . This is being carried out by Mr. A. J. Frueh, Jr., at the Massachusetts Institute of Technology, and while this is not yet complete, the author, through the kindness of Mr. Frueh, is privileged to be able to present some data on this structure. The structure of CrB is orthorhombic, and its unit cell has the following dimensions:

$$\begin{aligned} a &= 2.95 \text{ A.U.} \\ b &= 7.80 \text{ A.U.} \\ c &= 2.93 \text{ A.U.} \end{aligned}$$

This cell contains four molecules of chromium boride, which is in accord with its measured density, as reported

in a subsequent paragraph. The four chromium atoms have the following coordinates:

| x | y | z |
|-----|-------|------|
| 0 | 0.145 | 0.25 |
| 0 | 0.855 | 0.75 |
| 0.5 | 0.645 | 0.25 |
| 0.5 | 0.355 | 0.75 |

The positions of the boron atoms have not yet been determined exactly, but this problem is presently under study and will be published by Mr. Frueh when his investigation is completed.

It is of interest at this point to recall that Hägg¹² in his study of phases of transition elements in binary systems with boron, carbon and nitrogen, drew certain general conclusions regarding the structure of such phases. He predicted that the structure could only be a relatively close-packed one if the ratio of the diameter of the transition element atom to that of the interstitial atom was in excess of 1.7. In the case of chromium boride, this ratio is between 1.6 and 1.4 in consideration of the indefinite knowledge of the diameter of the boron atom. Since the structure of chromium boride determined by Mr. Frueh is not a close-packed one, this compound apparently behaves in accordance with Hägg's rule.

Various investigators have reported that chromium boride is relatively slowly attacked by acids. Their results vary to some degree, but this is believed to be the consequence of varying impurity contents. In this investigation it was noted that hydrochloric, sulphuric, hydrofluoric and perchloric acids attack it only slowly. The only one of these capable of dissolving it completely is perchloric acid. Nitric acid attacks it almost negligibly and when dilute can be considered, effectively, to fail to attack it at all. Fused sodium peroxide dissolves it completely, as do nitrate-carbonate mixtures.

Densities varying from 5.4 to 6.7 g per cc have been reported for chromium boride. None of these investigators reported the conditions, other than temperature, under which the determination was made. Depending upon composition, the densities noted in the present study were in the range 6.15 to 6.20 g per cc at 18°C, taken in ethyl benzene by the standard pycnometric method.

The hardness of chromium boride has previously been reported to be about 8.5 on Moh's scale.¹⁰

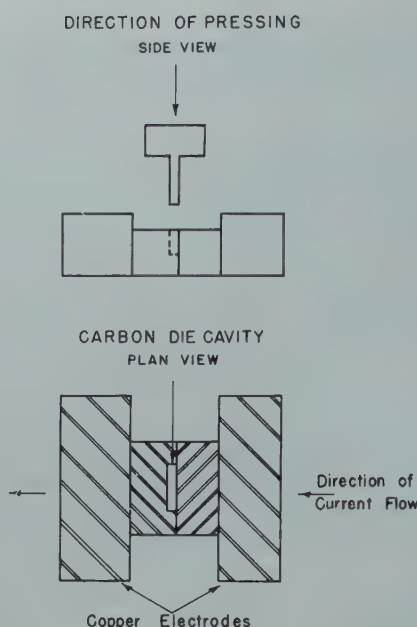


FIG 4—Schematic diagram of hot pressing.

PRESSING AND SINTERING

Attempts to cold press compacts of chromium boride and a binder when the boride content exceeded 75 pct were effectively unsuccessful. Compacts could be obtained but the resultant body, after sintering up to 1500°C in H₂, showed densities which were low and the attendant physical properties suffered. This is considered to be a direct result of the high hardness and negligible room temperature plasticity of the chromium boride. At an early stage in the work, cold pressing and sintering were abandoned in favor of hot pressing. When hot pressing was carried out at temperatures sufficiently high to melt the binder employed, highly dense bodies resulted having interesting properties.

The hot pressing method used is illustrated diagrammatically in Fig 4. A high current was passed through the graphite die proper, and the heat so generated plus heating occurring as a consequence of current passing through the work itself made it possible to raise the temperature to 1500°C in approximately 1–2 min. When the temperature was reached at which pressing was to occur, the current was stopped and pressing accomplished by hydraulic means. No provision for atmosphere was made, and the carbonaceous atmosphere within the die and the short times involved made it possible to avoid any indication of oxidation. The pressure was uniformly held at 1 tsi.

The most effective binder employed proved to be nickel, and the writer will limit himself to mixtures of 85 pct chro-

mium boride, 15 pct nickel, for the purpose of showing the effects of certain parameters. A comparison with other binders will be made in a latter part of this paper.

The chromium boride powder used throughout the following experiments was that produced by aluminum thermite reduction, the analysis of which has already been given. The nickel powder was spectrographically analyzed to be 99.6+ pct nickel, with small impurities, as follows:

| | Pct |
|--------------|-------|
| Iron..... | 0.22 |
| Zinc..... | 0.03 |
| Copper..... | 0.065 |
| Lead..... | 0.025 |
| Sulphur..... | 0.021 |

The chromium boride powder was first ball milled to a given particle size in either a stainless steel or tungsten carbide-lined mill. The latter type was employed only where the particle size desired required milling times which resulted in excessive pick-up of material from the stainless steel mill. The ball milling medium was distilled water. The balls, in each case, were of the same material as the liner. The fine powder was then ball milled again, to mix it with the binder. Water again was the medium employed. After drying the powder with alcohol, the powder mix was ready for hot pressing.

The powders were pressed into a flat bar shape 1 in. × 0.375 in. × approximately 0.200 in. thick. This shape specimen lent itself readily to transverse rupture testing where the span was $\frac{3}{16}$ in. and the load was applied at the center of the bar and span by means of a 10 mm Brinell ball. This test was the main evaluation method for room temperature properties.

The effect of particle size and temperature of pressing proved to be interrelated and interesting. For any given particle size, an optimum temperature of pressing was noted.

The optimum pressing temperature was lower with each reduction in particle size, although this effect became almost negligible once the particle size was down to 3 to 5 microns.

Optimum conditions applied when the particle size was reduced to 3 to 5 microns, and the temperature of pressing, as measured optically on the exterior of the graphite die, was 1300°C. It is estimated that this corresponded to 1550°C inside the die. Under these conditions the Modulus of Rupture was found to be circa 120,000 psi, and the hardness averaged 89 on the Rockwell A scale. Fig 5 shows the effect of temperature of pressing, under the condi-

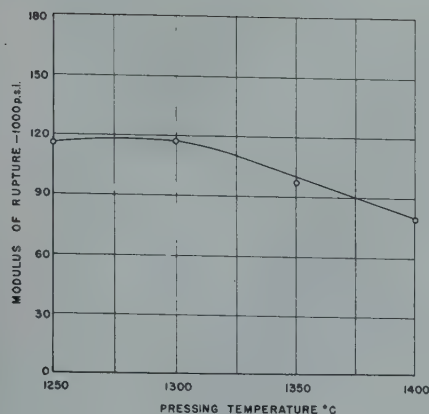


FIG 5—Effect of pressing temperature on Modulus of Rupture. 15 pct nickel binder.

tions indicated above, on the Modulus of Rupture.

Decreasing the particle size further, to a point where it fell between 1 and 2 microns resulted in increased hardness values, that is, 90–91 Rockwell A, but resulted in a decreased Modulus of Rupture optimum. This value fell to 85,000 psi.

Increasing the particle size, or the use of particle size distribution having higher average particle size, resulted in decreasing the Modulus of Rupture as well as the hardness.

The density of a cast 85/15 chromium boride/nickel alloy was measured as 6.17 g per cc and the densities obtained by hot pressing the 3–5 micron powder and 1–2 micron powder, as described above, proved to be circa 5.90 g per cc, so that densities of the order of 96 pct were achieved.

The effect of the use of binders other than nickel is best indicated by the following table, in which the optimum Modulus of Rupture obtained is indicated as well as hardness. The particle size employed was 3–5 microns in all cases, and the composition was 85 pct chromium boride, balance binder.

A typical micrograph of a nickel bound specimen is shown in Fig 6.

HIGH TEMPERATURE TESTING

The following tests have been made to indicate the behavior of this material at high temperatures:

1. Hot hardness (70 pct CrB, 30 pct Ni).
2. Stress rupture.
3. Corrosion in air.

The hot hardness tests were made in an atmosphere of N_2 in a furnace specially designed by E. C. Bishop and M. Cohen.¹³ While the tests were made on a slightly different composition than is presently believed to be an optimum,

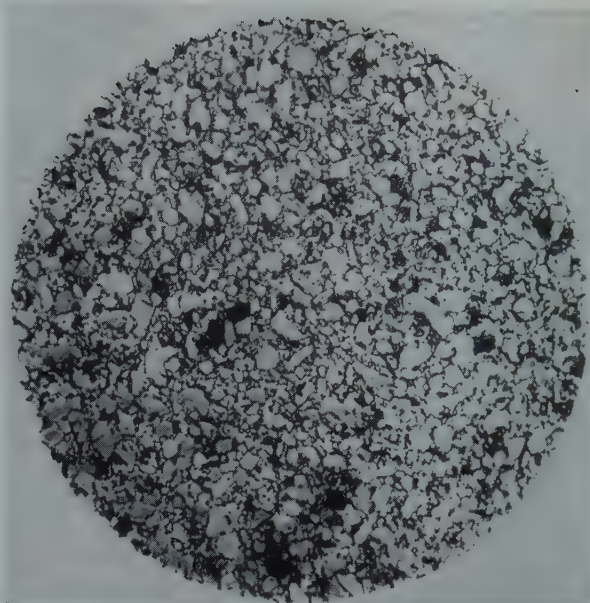


FIG 6—Chromium boride/nickel, 85/15. Etchant: 4 pct Picral. X500

Table 1 . . . Optimum Results of Chromium Boride Sintered with Different Binders (85/15)

| Binder | Modulus of Rupture (psi) | Hardness R _A |
|-------------------------|--------------------------|-------------------------|
| Nickel | 123,000 | 87.4 |
| Nickel-copper (70-30) | 120,000 | 86.7 |
| Nickel-chromium (60-40) | 113,000 | 88.1 |
| Cobalt | 80,000 | 90.5 |

the effect of the use of the 85/15 would have merely translated the curve given in Fig 7 upwards about one point on the hardness scale.

Stress-rupture tests on the 85/15 composition were carried out at the Battelle Memorial Institute, and the results of the tests are given graphically in Fig 8. The hot strength, if taken at the 1000 hr point, is of the order of one

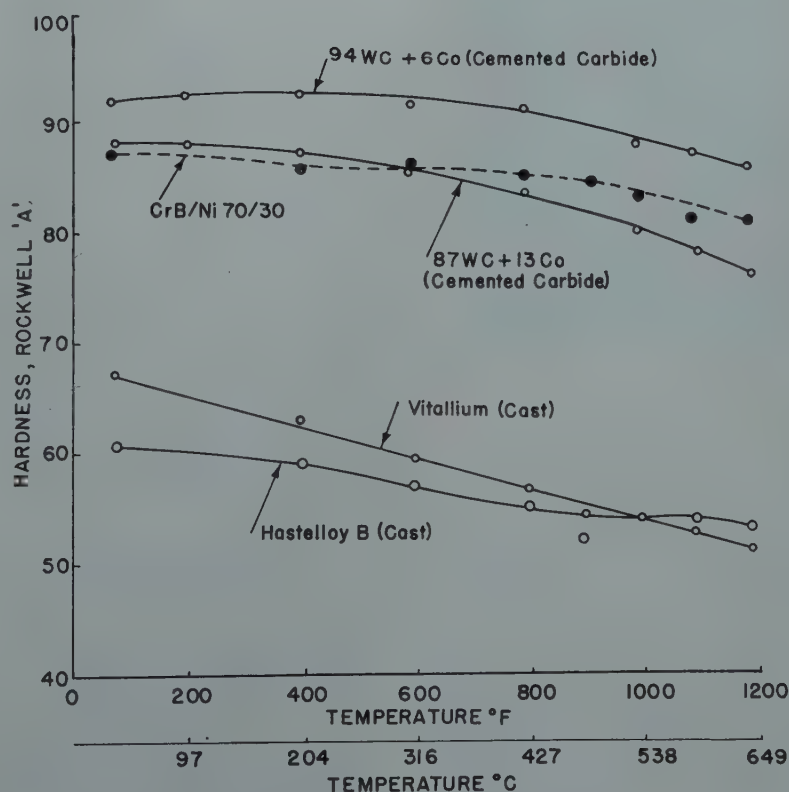


FIG 7—Hardness variation with temperature.

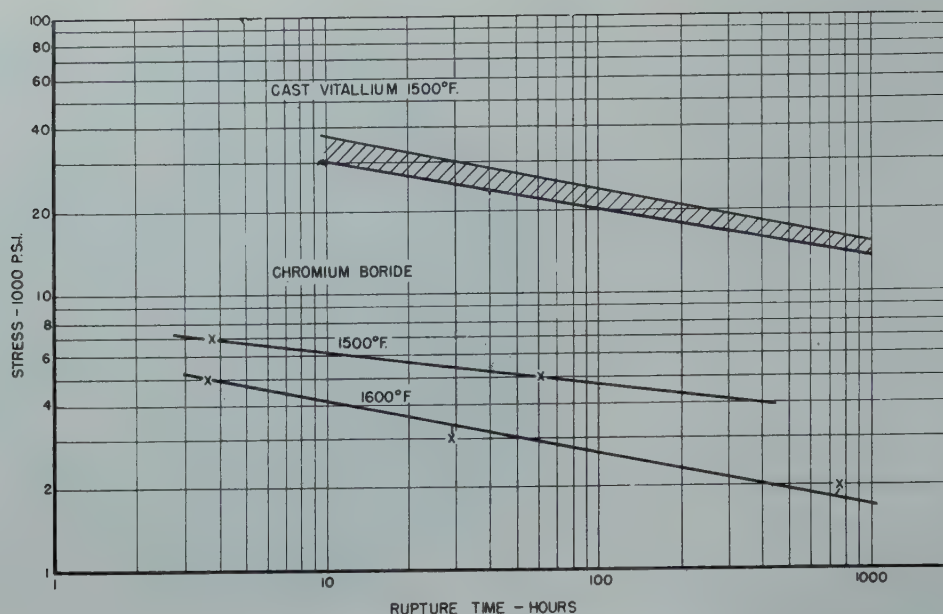


FIG 8—Stress vs. rupture time curves for nickel-bonded chromium boride.

quarter that of cast Vitallium. (Vitallium composition: 0.2 C, 28 Cr, 2.5 Ni, 62 Co, 5.5 Mo, 1 Fe.)

Table 2 gives typical results obtained when the 85/15 CrB/Ni material was tested in air for corrosion.

It was in the above corrosion tests that a serious limitation of this particular material was noted. It can be seen that there are indications of a liquid phase forming at about 1900°F (1038°C). This liquid phase is caused by the development of less refractory nickel borides and systems of these. Their formation limits the use of this material to a maximum temperature of about 1750°F (954°C). There can be no question that the formation of these lower melting point constituents also influenced the observed strength at 1500° and 1600°F (816° and 871°C). Their formation, however, indicated that further work needs to be done to fabricate a material on similar principles in which such a phenomenon will be absent. This work is in progress.

Summary

It has been determined that only one chromium boride compound exists in the range 12 pct to 20 pct boron content, instead of two, as had previously been reported.

The composition of the above compound is postulated to be CrB, and its structure is reported to be orthorhombic. The dimensions of the unit cell are given as well as the coordinates of the chromium atom.

Table 2 . . . Air Corrosion Tests on Chromium Boride/Nickel 85/15

| Material and Sample No. | Temperature | | Atmosphere | Time hr | Remarks |
|-------------------------|-------------|------|------------|---------|---|
| | °F | °C | | | |
| 85/15 CrB-Ni | | | | | |
| 1 | 1525 | 830 | air | 48 | No reportable change |
| 2 | 1600 | 871 | air | 48 | No reportable change |
| 3 | 1725 | 940 | air | 48 | Slight green oxide coat |
| 4 | 1850 | 1010 | air | 48 | Slight green oxide coat |
| 5 | 1900 | 1038 | air | 48 | Initial indication of liquid phase at surface. Hardness drop from RA 88.5 to 80. No grain size change |
| 6 | 2050 | 1121 | air | 48 | Dark coating formed; distortion. |

New data regarding the properties of this boride are presented.

Experimental results are given of an investigation of the pressing and sintering of chromium boride with nickel as a binder. A Modulus of Rupture of 120,000 psi is reported for such material when hot pressed.

Data are given regarding the high temperature strength and corrosion resistance of the above material. The hot strength at 1500°F (816°C) is of the order of one quarter that of cast Vitallium. The formation of a liquid phase at about 1900°F (1038°C) is noted, and a limitation of use temperature is set at 1750°F (954°C).

Acknowledgment

The writer wishes to extend his sincere thanks and appreciation to Dr. Paul Schwarzkopf for his guidance and help, to Dr. J. T. Norton for his assistance in many matters, particularly in the X ray diffraction studies, to Mr. A. J. Frueh, Jr., to Dr. Morris Cohen for the use of his Hot Hardness

Testing equipment, and to Dr. H. Blumenthal and Mr. Alvin Cohan for their overall assistance throughout the above study.

References

1. P. Schwarzkopf: Powder Metallurgy Bull. I, No. 6 (Nov. 1946) p. 86.
2. A. S. Nowick and E. S. Machlin: Nat'l. Advisory Comm. for Aeronautics, Tech. Note No. 1039, April 1946.
3. E. S. Machlin and A. S. Nowick: *Met. Tech.*, Feb. 1947, TP 2137. *Trans. AIME* (1947) 172, 386.
4. H. Moissan: C. R. Acad. Sci. Paris, 119, 185, (1894).
5. S. A. Tucker and H. R. Moody: *Jnl. Chem. Soc.* (1902) 81, 14-17.
6. E. Wedekind and K. Fetzer: *Ber. dtsh. chem. Ges.* (1907) 40, 297-301.
7. Binet du Jassoneix: *Thèse*. Paris, 1909.
8. Binet du Jassoneix: C. R. Acad. Sci. Paris, (1906) 143, 897-899.
9. Binet du Jassoneix: C. R. Acad. Sci. Paris, (1906) 143, 1149-1151.
10. L. Andrieux: *Thèse*, Paris, 1929.
11. N. W. Cole and W. H. Edmonds: U.S. Pat. 2,088,838 (1937).
12. Gunnar Hägg: *Ztsch. Phys. Chem. Abt. B6* (1930) 221-232.
13. E. C. Bishop and M. Cohen: *Metal Progress* 43, Mar. 1943.

PAUL A. BECK,* Member AIME, JOHN TOWERS, JR.,* and PHILIP R. SPERRY*

DAHL and Pawlek¹ found that electrolytic copper develops extremely coarse grains at 1000°C after about 90 pct reduction by rolling. This coarsening occurs only under conditions of penultimate grain size, deformation, and alloying which lead to the "cube" recrystallization texture.^{1,2,3,5} The peculiar angular shapes and straight grain boundaries of the coarse grains were noted by several investigators.^{1,4,6}

On the other hand, coarsening in Fe-containing aluminum or in Al-Mn alloys⁸ does not depend on a "cube" (or any well developed) recrystallization texture. It is true that increasing deformation by rolling, and, therefore, an increasingly well developed recrystallization texture, are associated with decreasing incubation periods of coarsening.^{6,7,8} Nevertheless, coarsening readily develops in aluminum even after only 30 pct reduction by rolling, where the recrystallization texture is very weak.^{6,8} Also, coarsening was observed by Jeffries⁹ many years ago in sintered thoriated tungsten, which presumably has no preferred orientation. In all these cases coarsening is associated with grain growth inhibition by a dispersed second phase.^{8,9} The annealing temperature has to be sufficiently high to overcome the inhibition at a few locations. But if it is too high, growth starts at many points, and the resulting grain size becomes much smaller.⁹ Normally, the coarse grains are more or less equiaxed, and the boundaries have a typical ragged appearance.^{5,8}

Cook and Macquarie⁴ demonstrated that, in addition to the texture-dependent coarsening previously found at 1000°C,¹ electrolytic tough pitch copper may also coarsen at 800°C after 50 pct reduction by cross rolling. The coarse grains formed under such conditions have rounded shapes and ragged boundaries, like those in aluminum. When the annealing temperature is higher, the tendency for their formation decreases. All these observations suggest that the coarsening at 800°C is associated with inhibition by a second phase. Actually, coarsening at 800°C after 50 pct reduction by cross rolling was observed only in tough pitch copper,⁴ which contains Cu₂O particles.

On the other hand, the texture-dependent 1000°C coarsening occurs in both tough pitch and oxygen-free copper;⁴ it does not appear to depend on the presence of a dispersed second phase. However, the interpretation of the 800°C coarsening in Cu after 50 pct rolling as an inhibition-dependent process, similar to the coarsening in Al-Mn alloys, is somewhat weakened by the fact that this coarsening was reported⁴ to occur only after cross rolling, and not after straight rolling. It was, therefore, decided to re-examine this question.

A 1 in. diam electrolytic tough pitch copper rod, No. 2 hard drawn, was annealed for 20 min at 700°C, rolled to 0.5 in., annealed 10 min at 700°C, and straight rolled to 0.064 in. It was then given a penultimate anneal of 20 min at 500°C and it was cut into four sections, which were given final reductions by straight rolling as follows:

- A 30 pct reduction of area
- B 50 pct reduction of area
- C 70 pct reduction of area
- D 90 pct reduction of area

Specimens cut from the four sections were finally annealed at 800°C in an oxidizing atmosphere. Strip A remained fine grained up to 10 hr, but the specimen annealed 12 hr consisted of only 2 large grains. Strip B had a few scattered large ($\frac{1}{2}$ to $\frac{3}{4}$ mm) grains after 1 min, although the balance of the specimen consisted of fine grains of about 0.02 mm. After 5 min there were several 10 to 15 mm grains present, and after 1 hr strip B was completely coarsened. The coarse grains had the same characteristics (see Fig 1) as those obtained by Cook and Macquarie at 800°C after cross rolling. Strip C had several grains of 0.05 to 1 mm after 1 min, but it was still largely fine grained after 12 hr. After 48 hr it consisted entirely of grains of about 0.5 to 4 mm, with an extraordinarily large number of twin bands. Strip D remained com-

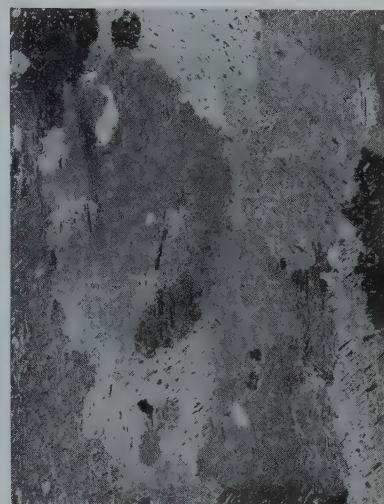


FIG 1—Tough pitch copper after final rolling of 50 pct (strip B) and final anneal of 1 hr at 800°C. The coarse grains have rounded shapes and ragged boundaries. Numerous small twins are entirely surrounded by coarse grains. Magnification 5 X. (Reduced approximately one-half.)



FIG 2—Same copper as in Fig 1, after final rolling of 90 pct (strip D) and final anneal of 25 min at 1000°C. The appearance of this structure is dominated by the characteristically long, straight (twin) boundaries. Magnification 5 X. (Reduced approximately one-half.)

pletely fine grained after 4 hr at 800°C. These results indicate that, in the deformation range of 30 to 70 pct reduction, the incubation period for coarsening as well as the rate of growth and the final size of the coarse grains decreases with increasing deformation. Similar

Technical Note 12. Manuscript received Oct. 18, 1948.

* Assistant Professor, Graduate Student, and Metallographer, respectively, Department of Metallurgy, University of Notre Dame.

¹ References are at the end of the paper.

relations were observed in the "inhibition-dependent coarsening" of Al alloys containing a dispersed phase. However, the behavior of the 90 pct rolled copper strip, which has a cube recrystallization texture, is different. Up to 4 hr it does not coarsen at all at 800°C. It coarsens at 1000°C in 3 to 6 min, in a manner typical of "texture-dependent coarsening" (Fig 2).

It may be concluded that coarsening at 800°C, after 30 to 70 pct reduction by rolling, may develop in straight rolled as well as in cross rolled tough pitch copper. This confirms the view that coarsening in Cu₂O-containing copper after 30 to 70 pct rolling is analogous to the coarsening in alumi-

num containing dispersed particles of a second phase.

Acknowledgment

This work was supported by the office of Naval Research, United States Navy, Contract No. N6 ori-165, T.O. No. 1.

References

1. O. Dahl and F. Pawlek: Kornordnung und Kornwachstum bei Walzblechen. *Zsch. f. Metallkunde* (1936) 28, 266.
2. G. Wassermann: Untersuchungen an Eisen-Nickellegierungen mit Wurfeltextrur. *Zsch. f. Metallkunde* (1936) 28, 262.
3. M. Cook and T. L. Richards: The Structural Changes in Copper Effected by Cold Rolling and An-

- nealing. *Jnl. Inst. Met.* (1940) 66, 1.
4. Maurice Cook and C. Macquarie: Development of Abnormally Large Grain Sizes in Rolled and Annealed Copper Sheet. *Trans. AIME* (1939) 133, 142.
5. Bowles and Boas: The Effect of Crystal Arrangement on "Secondary Recrystallization" in Metals. *Jnl. Inst. Met.* (1948) 74, 501.
6. W. Feitknecht: Crystal Growth in Recrystallized Cold Worked Metals. *Jnl. Inst. Metals* (1926) 35, 131.
7. R. Karnop and G. Sachs: Die Grobkristallisation von Aluminium. *Metallwirtschaft* (1929) 8, 1115.
8. P. A. Beck, M. L. Holzworth and P. R. Sperry: Effect of a Dispersed Phase on Grain Growth in Aluminum-manganese Alloys. AIME TP 2475, *Metals Technology* (Sept. 1948).
9. Z. Jeffries: Grain Growth Phenomena in Metals. *Trans. AIME* (1916) 56, 571.

Solid Nuclei in Liquid Metals

CYRIL STANLEY SMITH, Member AIME

THE partial persistence of grain size and grain shape on melting and resolidifying crystalline substances, as well as the general effects of pre-solidification and of superheating on nucleation rate, have been attributed to the presence in the liquid of crystalline impurities bearing some structural relation to the principal solid and hence capable of serving as nuclei for its crystallization. That such lattice matching does sometimes occur is well established, but it is surely improbable that a compound possessing both high-temperature stability and the requisite structural similarity should be naturally available in almost every system.

It is now suggested that a mechanism for producing appropriate nuclei exists in the crystallization of all but absolutely pure substances. Impurities can be of many kinds. Some will give rise to compounds that are less soluble in the solid crystal than in the liquid. A crystal forming from a melt or solution containing these will be supersaturated in some degree, and the foreign atoms will commence to segregate during or after solidification. They do not necessarily form pure, unstrained, crystals of the precipitating compound with its normal composition and structure. Generally—at least in the metallurgical examples that have been most studied—the first recognizable nuclei have lattice coherency with the surrounding matrix and have practically the same crystal structure and lattice spacing as the material in which they form, differ-

ing only in composition.

An extremely thin oxide layer formed under appropriate conditions on or in a solid metal will tend to be coherent with the metal lattice, and the first few atom layers of the oxide in contact with the metal will differ in both composition and structure from massive crystalline oxide. It will resemble the metal more closely than the oxide. If it did not subsequently change on melting, such an oxide film would constitute an almost perfect "template" or two-dimensional matrix to hold a few atoms of the primary metal in the exact array needed to form a nucleus for solidification.

Any precipitating material will adopt the correct spacing over a few atom diameters, and with appropriate substitution of other atoms of the correct sizes a precipitate can match the parent lattice over large areas of coherence without excessive strain. In metals, the components of a host of oxides, silicides, borides, nitrides, carbides, sulphides, and other compounds are always present in minute amounts. Some of these will be eliminated because of extreme insolubility in the liquid, while others will remain soluble in the solid; occasionally, however, particles will be formed in the solid by coherent precipitation—not of pure substances, but of whatever assortment of atoms best

satisfies the joint requirements of availability, affinity, and appropriate average atom size. Of these, many will disappear on melting, but a few will persist unmelted as little rafts of complex composition, maintaining in the liquid a surface of the exact geometry needed to nucleate the solid on subsequent cooling. Their number and size distribution will determine the resulting grain size; the dimensions of the largest will determine the degree of undercooling that can occur before solidification commences.

A similar process may operate in the case of phase transformations in solids. The coherent precipitation of supersaturated minor constituents in a low-temperature phase should facilitate the nucleation of this phase on subsequent cooling after transforming into another phase at higher temperatures.

At first sight this hypothesis may seem little different from the older ones. It should therefore be emphasized that it does not depend on chance to provide the right compound to form a nucleus, but postulates that every crystal, containing minute amounts of any of a wide range of impurities, automatically engenders particles having the correct surface structure to serve as nuclei for subsequent solidification. It could operate in any system, metallic, organic, or inorganic. The suggested mechanism is closely analogous to the production of antibodies from antigens in living organisms—indeed, it was a description of the matrix theory of this process that suggested to the writer its crystalline analogue.

Technical Note No. 11. Manuscript received November 26, 1948.

* Institute for the Study of Metals, University of Chicago.

The Recovery of Cadmium from Cadmium-copper Precipitate, Electrolytic Zinc Co. of Australasia, Risdon, Tasmania

G. H. ANDERSON*

CADMIUM-COPPER precipitate, a by-product of the purification stage of the zinc plant, is composed mainly of zinc, cadmium and copper in varying amounts depending on the efficiency of precipitation and the cadmium and copper contents of the impure solution treated.

The composition range is approximately: cadmium 10–12 pct, copper 6–8 pct, and zinc 30–35 pct. As received at the cadmium plant, the precipitate is a dark gray to black press cake produced by filter pressing the flocculent cadmium-copper precipitate formed when impure zinc solution is agitated with zinc dust.

The details of the cadmium-copper precipitation are to be found in the paper "Electrolytic Zinc at Risdon, Tasmania," by W. C. Snow. *Transactions AIME*, 121, 501.

The treatment, in addition to recovering cadmium as metal, yields a copper product as a residue for realization and recovers in solution for return to the zinc plant, the excess of zinc dust used during purification.

The recovery of cadmium metal is approximately 200 tons† per year, but, with the amount of copper residue

recovered, varies with the zinc production tonnage, composition of the original concentrates, degree of roasting and other operational factors.

The operations involved in the recovery of the foregoing materials are carried out in a building adjacent to the purification section of the zinc plant and can best be described by dividing the process into the following stages:

1. Oxidation and Grinding of the cadmium-copper precipitate.
2. Leaching and Filtering.
3. Precipitation of cadmium.
4. Oxidation and Grinding of the precipitated cadmium.
5. Leaching oxidized cadmium precipitate and Purification of leach solution.
6. Electrolysis.
7. Melting, Casting and Packing.

A feature of the process is the use of two distinct solution circuits. Spent electrolyte from the zinc plant circuit containing about 10 pct sulphuric acid is used as the primary solvent of the

cadmium and zinc present in the oxidized precipitate. When the cadmium is later separated by precipitation and filtering, the filtrate, originally zinc plant spent electrolyte and now fortified in zinc, is returned to the zinc plant.

The precipitated cadmium, after oxidation, is redissolved in spent electrolyte from cadmium electrolysis which solution is in closed circuit within the cadmium plant except for discards to the zinc plant circuit as mentioned in Section 5 hereinafter. (Fig 1.)

Details of the various operations follow.

1. Oxidation and Grinding of the Cadmium-copper Precipitate

The precipitate having had a preliminary drying by compressed air in Dehne filter presses in the zinc plant is trucked to a storage platform of sufficient length to store 3 to 4 days' production separately.

After 48 hr exposure to atmosphere, oxidation is sufficient to enable all cadmium and zinc but only a portion of the copper to be dissolved in dilute sulphuric acid.

The oxidized precipitate is shovelled into trucks and, after weighing and sampling, is broken in size by means of

San Francisco Meeting, February 1949.

TP 2525 D. Discussion of this paper (2 copies) may be sent to *Transactions AIME* before June 15, 1949. Manuscript received October 1, 1948.

* Assistant Operating Superintendent, Electrolytic Zinc Co. of Australasia Ltd., Hobart, Tasmania.

† Throughout this paper the long ton of 2240 lb and the Imperial gallon are used.

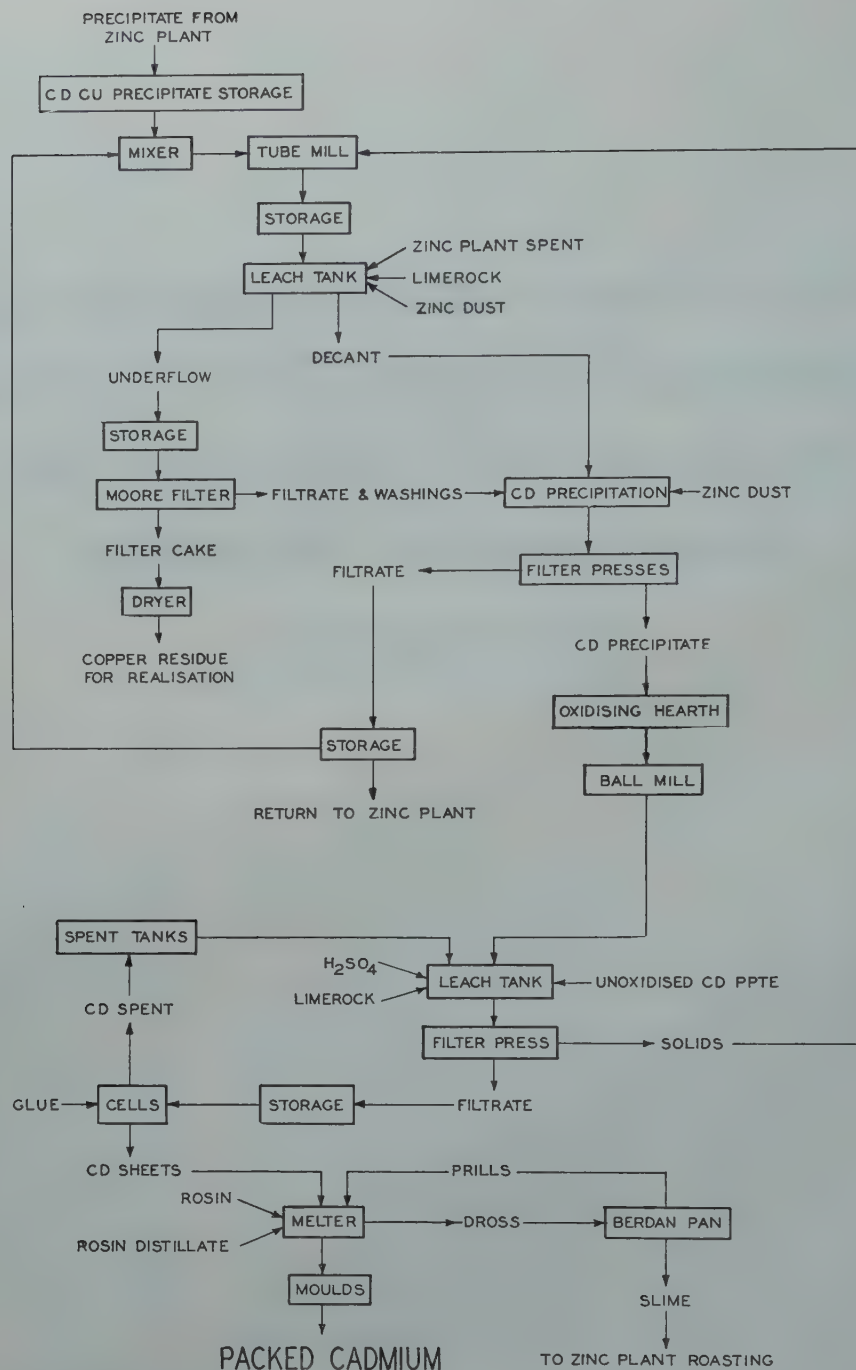


FIG 1—Flowsheet.

right and left handed blades rotating in a shallow mild steel trough.

Return solution (see Stage 3) is added to form a pulp which passes to a tube mill 5 ft long and 3 ft diam having cast steel liners and loaded with flint pebbles.

The use of return solution is restricted to produce a thick pulp which is elevated to a wooden storage tank of 3200 gal capacity and provided with air agitation.

2. Leaching and Filtering

Leaching is carried out in a wooden tank of approximately 14,000 gal capacity, having a conical bottom and provided with both mechanical and air agitation.

Discharge is through a plug cock but, in addition, the tank has a side discharge to which is fitted, inside the

tank, an armored rubber hose for decanting clear solution after settlement of the solids.

The tank is covered and ventilated to atmosphere. Approximately 7000–8000 gal of zinc plant spent electrolyte containing 90–95 g sulphuric acid and 45–50 g zinc per liter are run into the leaching tank and after agitation is started the ground cadmium-copper precipitate is charged until the acidity of the solution falls to 5–6 g sulphuric

acid per liter. Agitation is continued for another 5-6 hr by which time the acidity is reduced to 1-2 g sulphuric acid per liter, then ground limestone is added slowly until a pH 3-4 is reached.

Approximately 30 min. later a sample is taken, tested for copper and the calculated quantity of zinc dust required to remove copper in excess of 0.5 g per liter, is added. (See Appendix 1.)

The zinc dust containing 45-50 pct of minus 250 mesh material, used in this and other stages of the recovery of cadmium, is produced at Risdon by atomizing molten high grade zinc with compressed air at 200 psi pressure.

Control of the copper content of the solution is important, and is considered to have three distinct advantages.

First, its subsequent precipitation with the cadmium in Stage 3 prevents coagulation of the cadmium into metallic balls and facilitates filtering; second, during the cadmium circuit leach (Section 5) arsenic is precipitated or otherwise eliminated, and third, its presence insures a minimum of zinc and cadmium in the copper residue.

If no copper is in the leach solution, sufficient sulphated copper residue is added to give the desired content. Sulphated copper residue is made by mixing copper residue and sulphuric acid and storing in heaps for one or two days.

Approximately 30 min. after the addition of the calculated amount of zinc dust, a further test is taken to determine copper in solution, and if necessary further additions of zinc dust are made.

Agitation is continued for another hour after which solids are allowed to settle for 3 to 4 hr when clear solution is decanted and pumped to the cadmium precipitating tank. (See Section 3.)

The remaining pulp is agitated, air lifted to a wooden storage tank and filtered in a small Moore filter unit.

A cake of about 1/2 in. thickness is formed in 20 min. and washed with water until relatively free of zinc and cadmium.

The filtrate and washings are pumped by wet vacuum pumps to the cadmium precipitation tank containing the decanted leach solution. The filter cake is discharged to a hopper and fed to an oil fired rotary drier 15 ft long and 3 ft 9 in. diam consisting of a mild steel shell lined with 10 ga stainless steel sheet and fitted with suitable angle lifters.

The dried copper residue is bagged

for shipment to a copper refinery at Port Kembla in New South Wales.

Metallurgical and Operating Data

Average figures for year ending June 30, 1948.

CADMIUM-COPPER PRECIPITATE

6.85 tons treated per day.

ASSAY

| | | |
|---|-------|-------------|
| Cd..... | 10.85 | per cent |
| Cu..... | 6.7 | per cent |
| Zn..... | 33.6 | per cent |
| Pb..... | 0.6 | per cent |
| Ag..... | 2.30 | oz per ton. |
| Cadmium extracted by leaching..... | 98.7 | per cent |
| Copper solubility..... | 68.5 | per cent |
| Zinc dust used per ton ppte. leached..... | 269 | lb |
| Limestone used per ton ppte. leached..... | 25 | lb |
| Copper residue factor..... | 12.8 | per cent |
| Copper residue made per filter cake..... | 921 | lb |
| Wash displacement..... | 1.83 | |

COPPER RESIDUE ASSAY

| | | |
|---------|------|-------------|
| Cu..... | 46.5 | per cent |
| Cd..... | 1.07 | per cent |
| Zn..... | 5.85 | per cent |
| Pb..... | 6.0 | per cent |
| Ag..... | 18 | oz per ton. |

3. Precipitation of Cadmium

The precipitation tank is identical in construction to the leach tank previously described except that no decantation hose is fitted and air agitation is not provided.

To the decanted solution, filtrate, and washings derived from the 8000 gal leaching operation described in Section 2 about 600 lb of zinc dust is added after agitation has commenced. Filtered samples of the solution are tested with hydrogen sulphide from time to time and further smaller additions of zinc dust are made until only a trace of cadmium remains.

Approximately 45-60 min. later, if a similar test indicates a satisfactory cadmium content, the pulp is filtered in two 27 in. Dehne filter presses and the filtrate, known as "Return Solution," after by-passing for a few minutes, passes to a storage tank prior to its return to the zinc plant circuit for the recovery of its zinc and cadmium contents.

When the filter presses are full of precipitate, pumping is stopped and a water wash given until a specific gravity of 1.025 shows that the precipitate is almost free of zinc sulphate.

After drying with compressed air the washed precipitate is discharged to hoppers over a drying and oxidizing hearth.

Metallurgical and Operating Data

Average figures for year ending June 30, 1948.

| | | |
|---------------------------------|------|-----|
| Zinc dust efficiency..... | 58.1 | pct |
| Cadmium in return solution..... | 1.08 | gpl |

4. Oxidation and Grinding of the Precipitated Cadmium

The oxidizing hearth is of brick construction with a hearth of cast iron plates, approximately 11 by 9 ft mounted so that gases from an oil burner first pass under the hearth and then over the precipitate which, when dropped from the hoppers above, is raked evenly over the hearth to a depth of 4 to 6 in.

As the precipitate oxidizes readily, a maximum gas temperature of 300°C is set at the rising flue from under the hearth to above the charge but rarely is this limit necessary. Hand rabbling proceeds at intervals until the color of the precipitate indicates that oxidation is complete, at which stage the material is discharged by hand rakes to a ventilated hopper from which the precipitate is screw fed to a mild steel ball mill 4 ft long and 2 ft 6 in. diam loaded with 1 1/2 and 3/4 in. steel balls. Cadmium cell feed solution is added to produce a reasonably thick mill discharge which is stored in a wooden tank ready for air lifting to the leach tank (Stage 5) when required.

For ventilation purposes, a fan handling 10,000-15,000 cfm is connected to the hood over the oxidized precipitate hopper and to a hood over the mill feed screw discharge point. The dust laden air is delivered to the base of a water irrigated wooden scrubbing tower mounted over a concrete sump from which the water is recirculated by means of a pump while the settled pulp is withdrawn at intervals and pumped to the leach tank (Stage 5).

Metallurgical and Operating Data

Average figures for year ending June 30, 1948.

CADMIUM PRECIPITATE

| | |
|-----------------------------------|------|
| | Pct |
| Total cadmium..... | 69.3 |
| Acid sol. cadmium..... | 68.5 |
| Zinc..... | 5.5 |
| Oxidation of cadmium in ppte..... | 97.7 |

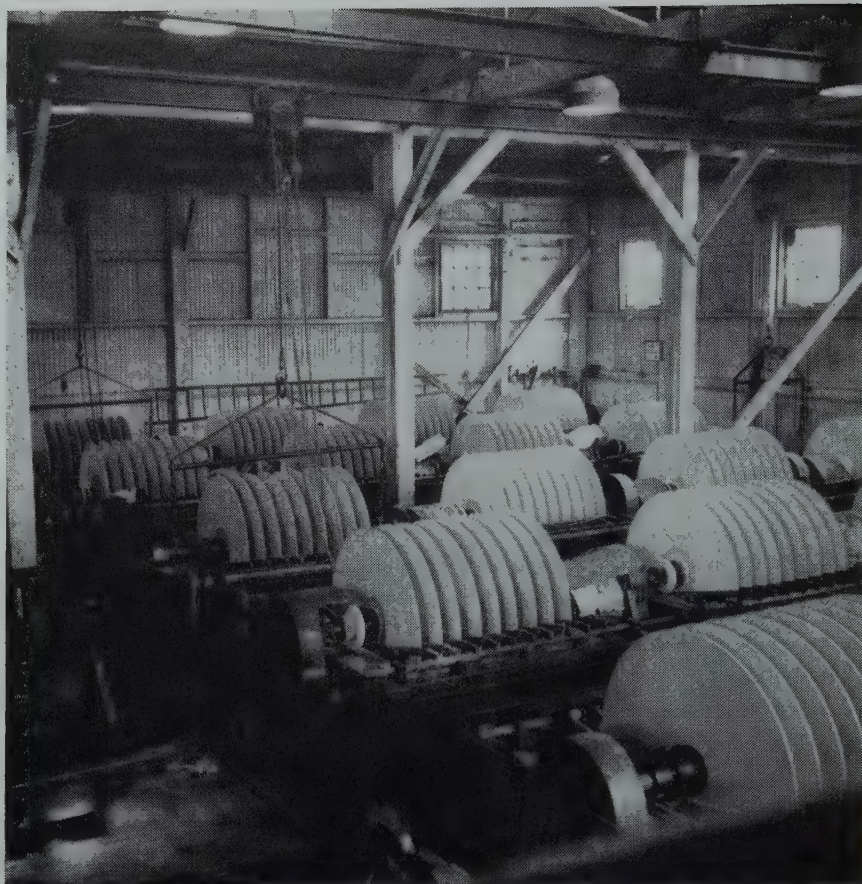


FIG 2—Cell room.

5. Leaching and Purification

Variations in the sulphuric acid content of the leach solution are made from time to time in order to hold both the cadmium content and the volume of the cell feed circuit reasonably constant.

If both are about normal, leaching is done with normal cadmium cell spent electrolyte but if the cadmium content is low, the cell spent electrolyte is fortified 10 to 20 g sulphuric acid per liter. If the volume needs increasing, approximately 600 gal of spent electrolyte are supplemented with 800 gal of water and the whole acidified to 150 g sulphuric acid per liter.

In all cases the volume is 1400 to 1500 gal, and the subsequent leaching operation is the same.

Leaching of the ground cadmium precipitate pulp is carried out in a mechanically agitated lead lined tank, having a working capacity of 2400 gal and ventilated by the suction fan mentioned in Stage 4.

The desired volume of leaching solu-

tion having been run to the leach tank, pulp from the storage tank is charged until the acidity of the solution is approximately, but not less than 10 g sulphuric acid per liter.

A sample of the pulp is filtered and tested for copper by the sodium-sulphide method (see Appendix 2) and if an excessive amount of copper is present, it is reduced by the addition of unoxidized cadmium precipitate.

Leaching is continued until the acidity is reduced to 1-2 g sulphuric acid per liter when tests are made for copper and arsenic (Gutzeit's Test) and if present, more unoxidized precipitate is added. Agitation is continued for 1 hr after copper and arsenic have been reduced to 0.5 and 0.1 mg per liter respectively and if, after neutralizing with hydrated lime, a further test for arsenic is found satisfactory, the pulp is pumped to a Kroog filter press fitted with 36 by 36 by 1½ in. thick frames and plates.

The filtrate is bypassed to the leach tank until free from solid particles as indicated by filtering 500 cc through filter paper and when clarity is satis-

factory the filtrate is diverted to one of two lead lined wooden storage tanks each of 3200 gal capacity, where, if necessary, water is added to reduce cadmium to the desired content of 150 g per liter.

By discarding spent electrolyte to the original cadmium-copper precipitate leach and rebuilding the circuit with fortified spent electrolyte and water leaches the impurities are controlled to 30-40 g zinc, 0.7-0.8 g iron and 30-35 mgm chlorine per liter.

The residue collected in the Kroog press during filtering of the cadmium leach pulp, is returned to the cadmium-copper precipitate mixer (Stage 1).

Metallurgical and Operating Data

Average figures for the year ending June 30, 1948.

| | Pct |
|--|----------|
| Cadmium extraction from acid soluble cadmium in ppte. by leaching..... | 92.5 |
| Cadmium extraction from total cadmium in ppte. by leaching..... | 89.2 |
| Cadmium leach residue factor..... | 25.8 |
| Cadmium leach residue | |
| Assay—Cd..... | 28.7 pct |
| Cu..... | 31.9 pct |

| | |
|--|------------|
| Sulphuric acid used per ton cadmium dissolved..... | 0.287 tons |
| Zinc dust used per ton cadmium dissolved..... | 2470 lb |
| Hydrated lime used per ton cadmium dissolved..... | 56.3 lb |

FEED SOLUTION ASSAY

| | |
|---------|-----------|
| Cd..... | 150.7 gpl |
| Zn..... | 37.55 gpl |
| Fe..... | 0.79 gpl |
| Mn..... | 2.35 gpl |
| Cl..... | 30 mgpl |
| Cu..... | 0.82 mgpl |
| As..... | <0.1 mgpl |

6. Electrolysis

The cell room contains 20 cells arranged in five rows of four cells, each of which is of 3 in. timber, lined first with 8 lb lead and then with 2 in. of a 40 pct sulphur—60 pct sand mixture which has given good service as only 2 linings have failed in 25 yr. Internal dimensions of the cells, which have a volume of 208 gal, are 5 ft square and 2 ft 6 in. deep while the cross-section is semi-rectangular.

The lead of the 10 half-round, 23 in. radius anodes contains 0.01 pct silver to give added rigidity and extend the 4 yr life to 5 yr.

Mounted on a 3 in. diam mild steel shaft and separated at 5½ in. spacing by rubber covered aluminum sleeves are 9 aluminum cathodes, 4 ft diam and ¼ in. thick, each of which has a submerged surface area of 8 sq ft and lasts 7 to 8 yr. To enable the stripped cadmium sheet to be readily broken into four conveniently sized quadrants, each side of the cathode is radially grooved at 90° spacing to a depth of ⅜ in. Before assembly, each cathode is given a matte surface by scrubbing with a steel wire brush and sandstone.

Once each year the cathode assembly is dismantled, inspected, cleaned and, if necessary, faulty parts replaced.

Cathodes are rotated at 10 rpm by suitably driven link chains through gearing from which the cathode assembly may be disengaged without stopping the driving mechanism. Electrically the cells are arranged in series and current is supplied by two motor driven parallel connected generators rotating at 960 rpm and each capable of supplying 650 amp over a range of 25 to 70 volts.

Anode bus bars of 1¼ in. square copper are arranged to give the anode head bars an edge contact and between adjacent cells is a hinged section for short circuiting a cell when cathode assemblies are removed for stripping.

The series circuit is made complete by means of a 9 in. diam brass collector keyed to the cathode shaft and con-

tacting brushes connected by copper cable to the following anode bus bar.

Cell voltage is approximately 3.5 volts per cell.

Feed solution containing 150 g cadmium per liter gravitates from the feed storage tanks through iron pipes of uniform length flanged together for ease of cleaning.

Each cell has a separate feed pipe through which the rate of feed is controlled to hold the acidity of the cell solution at 85–90 g sulphuric acid per liter. Titrations with caustic soda using Congo Red indicator are made every four hours.

Spent overflows from each cell to a launder common to each row and gravitates to a storage tank.

Glue solution containing 0.14 lb glue per gal is added every four hours at a rate equivalent to 2½ to 3 lb per ton cadmium deposited. During deposition, the cadmium surface tends to roughen by the formation of "trees" which are wiped off at intervals with a slotted wooden tool to which rubber strips are attached to make contact with each face of the cathode simultaneously. Trees are cleaned from the cells monthly and returned to the tube mill grinding the original cadmium-copper precipitate.

Stripping periods are either 48 or 96 hr depending on the current density demanded by production. When the current density on the immersed cathode surface is between 10 and 12 amp per sq ft quite a reasonable current efficiency is obtained and the deposit adheres to the cathode, but, when the current density is higher, the stripping period is reduced to 48 hr as beyond this time the current efficiency is found to decrease and the deposited cadmium sheets tend to become detached.

The production of cadmium is not regular owing to variation in the amount of incoming cadmium, consequently both the number of cells used and the current density are varied, but it is aimed to operate at 10 to 12 amp per sq ft; however, at times a higher density is necessary. When the deposit is about to be stripped, the cell concerned is short circuited by means of the hinged section of the anode bus bar, hooks suspended from a bridge of convenient length are attached to fittings on the cathode shaft and the whole cathode assembly is lifted by means of a travelling chain block and lowered on to trestles at the end of the cell row.

The deposit is removed by means of stripping knives, broken into quadrants, stacked almost vertically in

portable racks, weighed and transferred to the melting section.

Before returning the assembly to the cell, each aluminum cathode is hosed, scrubbed with a stiff bristle brush and, if necessary, given a light rubbing with sandstone. (Fig 2.)

Metallurgical and Operating Data

Average figures for year ending June 30, 1948.

| | | |
|-----------------------------|------|--------------------------|
| Average current..... | 800 | amp |
| Current efficiency..... | 88.7 | pct |
| Current density..... | 11.0 | amp per sq ft |
| Cadmium "trees" produced | 6.11 | pct of cathode deposited |
| Number of cells in use..... | 17.6 | |

DISCARD SOL. ASSAY

| | G PER LITER |
|--------------------------------------|-------------|
| Cd..... | 68.2 |
| Zn..... | 37.2 |
| H ₂ SO ₄ | 84.5 |

7. Melting, Casting and Packing

The cadmium sheets are melted, under a cover of molten rosin, in an oil fired cast iron pot, having a capacity of approximately 2500 lb cadmium.

The molten cadmium is handled from the pot to the molds in a mild steel ladle, the pouring spout of which is in the form of a pipe reaching almost to the bottom to prevent dross or flux entering the mold.

Cadmium is cast in various shapes for commercial purposes. (See Appendix 3 and Fig 3.)

Molds are either lubricated with stearin or No. 3 shell grease or sprayed with a fine mist of dilute sulphuric acid in order to give a clean bright surface to the castings which after inspection are packed in Tasmanian oak cases in which are inserted sheets of waxed paper and cardboard to keep the castings from contact with the wood.

Each case is banded with ¾ in. wide banding iron and stamped with particulars of type of casting, gross and net weights, lot and case numbers.

Periodically dross is ladled from the surface of the molten cadmium in the melting pot into mild steel trays and after cooling and weighing is ground in a Berdan grinding pan from which a stream of water carries off the slime to a settling pond, the overflow from which passes into the cadmium-copper precipitate pulp circuit.

The dross slime, collected in a settler,

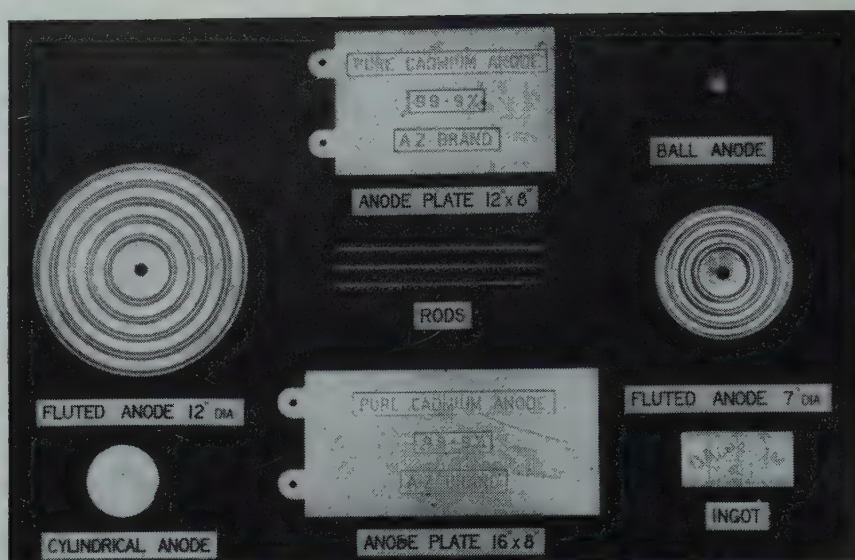


FIG 3—Cadmium castings.

is fed to one of the zinc plant roasting furnaces and eventually returns, via the zinc circuit, to the cadmium plant.

Clean cadmium prills are removed from the pan, dried, weighed and remelted.

It is planned to replace the rosin flux with one of three parts ammonium chloride and eight parts zinc oxide which, in addition to enabling all cell trees to be remelted direct, will dispense with grinding and the return of the dross slime through the zinc circuit and as a result cadmium losses will be reduced.

The melting furnace is enclosed in a mild steel hood from which rosin vapor is exhausted, but before being discharged to atmosphere, passes in series through three vertical, wire packed mild steel cylinders in which approximately 60-70 pct of the rosin is condensed for further use.

Metallurgical and Operating Data

Average figures for year ending June 30, 1948.

| | Pct |
|---|-------|
| Melting efficiency (including returned prills)..... | 95.91 |
| Cadmium prill recovered from dross..... | 7.56 |
| Cadmium in dross slime to roasting plant..... | 1.35 |
| Unaccounted melting loss..... | 2.74 |
| Rosin used (pct cathodes melted)..... | 3.02 |
| Rosin distillate recovered (pct tot. rosin used)..... | 68.3 |

CADMIUM ASSAY

| | Pct |
|---------|---------|
| Cd..... | 99.9590 |
| Cu..... | 0.0009 |
| Zn..... | 0.0263 |
| Pb..... | 0.0136 |
| Fe..... | 0.0002 |

METAL DISTRIBUTION

| | |
|----------------------------|--------------|
| Cd as metal..... | Pct 79.68 |
| Cd in return solution..... | 11.13 |
| Cd in copper residue..... | 1.27 |
| Unaccounted loss..... | 7.92 |
| | 100.00 |

Acknowledgment

The author desires to express his appreciation to the Directors and Management of the Electrolytic Zinc Co. of Australasia Ltd. for permission to publish this paper.

Appendix 1

COPPER TEST—CADMIUM-COPPER PRECIPITATE LEACH

Reagent

Standard comparison solution containing 0.5 gpl copper.

Test

Place 100 cc of standard solution in one comparison tube and 100 cc of filtered leach solution in a similar tube. Compare the blue color against a white background.

1. If leach solution is less blue than the standard but is still perceptibly blue, the leach can be finished.
2. If no blue is perceptible add sulphated copper residue in 100 lb lots until the standard blue is obtained.

3. If the leach solution blue is more intense than that of the standard solution the excess copper must be removed by zinc dust and the quantity

required is estimated as follows:

Determine the quantity of filtered solution which, when diluted to 100 cc with water will match the blue of the standard solution. The quantity of zinc dust required per 1000 gal of leach can be determined from the following formula:

$$\text{Zinc dust per 1000 gal} = \frac{V}{100} \left(\frac{100}{2T} - 0.5 \right)$$

T = Vol. solution (cc) used in test.

V = Vol. leach solution in the leach tank.

Appendix 2

COPPER TEST—CADMIUM PRECIPITATE LEACH

Reagent

Sodium sulphide solution (saturated).

Test

Take 100 cc of filtered leach solution in a stoppered bottle, add 5 drops of sodium sulphide solution, shake vigorously and filter.

The color of the precipitate on the paper is compared with a standard and must be inspected by the shift boss before filtering is permitted.

Appendix 3

CADMIUM SHAPES

| | WEIGHT |
|---|---------------------|
| Rods—12 in. long, $\frac{5}{16}$ in. diam..... | 4 $\frac{1}{2}$ oz |
| Ingots—6 by 3 by $\frac{3}{8}$ in..... | 2 lb |
| Ball anodes—2 in. diam..... | 1 $\frac{1}{4}$ lb |
| Anode plates—12 by 8 by $\frac{1}{4}$ in..... | 9 lb |
| Anode plates—16 by 8 by $\frac{1}{4}$ in..... | 11 lb |
| Fluted anodes—12 in. diam..... | 16 $\frac{1}{4}$ lb |
| Fluted anodes—7 in. diam..... | 7 $\frac{3}{4}$ lb |
| Cylindrical anode—4 in. diam by 1 $\frac{1}{4}$ in..... | 5 $\frac{3}{4}$ lb |

Electrolytic Zinc at Risdon, Tasmania. Major Changes Since 1936

S. W. ROSS*

Introduction

IN 1936 a description of the plant (Fig 1) and process employed by the Electrolytic Zinc Co. of Australasia Ltd. for the recovery of zinc from zinc concentrate by the electrolytic process was prepared.†

During the twelve years which have elapsed since the preparation of the earlier paper, several major changes in the metallurgy of the process have been introduced. It is the purpose of the present paper to give a general description of these changes and thus to bring up to date the description of the plant and process.

Summary

The major changes in Risdon practice since 1936 have been:

1. Replacement of two stage roasting by a preliminary roast followed by the flotation of all the leach residue and the roasting of the flotation concentrate.

2. Screening of all calcine fed to the pachucas.

3. Continuous leaching of calcine and improved classification of pachuca discharge.

4. Close control of hydrogen ion concentration during purification for iron removal.

5. Recovery of cobalt as a good grade oxide.

6. Production of part of the zinc output in the form of "four nines" metal (99.99 pct purity).

7. Closer spacing of electrodes thus increasing the potential output of cathode zinc per cell by 50 pct.

Changes which are in prospect and for which construction work is proceeding at the present time involve the starting up of:

1. Two suspension roasters.

2. A contact acid plant to produce

150 tons† of acid per day and replacing the existing Mills Packard chamber plant.

3. Extra power station capacity to permit greater current flow to existing cell room units. This will increase the output of cathode zinc from about 245 to 290 tons per day.

Plans for the future envisage the building of an ammonium sulphate plant, the first unit of which will produce about 50,000 tons per year, and improved treatment of zinc plant residue for the recovery of zinc, lead and other metals.

At the end of this paper tables of metallurgical data are presented relating to the year ending June 30, 1948.

Details of Changed Practice Output

In 1936 the production of cathode zinc amounted to about 200 tons per day. This has since been increased to about 245 tons per day while plant extensions are practically complete which will permit of an output of about 290 tons per day in the near future.

Roasting Division

ROASTING POLICY

A major change has occurred in the roasting policy. Twelve years ago the method in use was to carry out a two

stage roast in the first stage of which sulphide sulphur was reduced to about 6 pct. The pre-roast calcine was re-roasted in modified Leggo furnaces using coal as fuel, sulphide sulphur being reduced to about 0.8 pct. The whole procedure was described on pp. 482-491 of the earlier paper.

Although this roasting procedure had certain advantages it possessed some distinct disadvantages. For instance, it appeared uneconomical to heat up the entire input of pre-roast calcine to roasting temperature by the expenditure of fuel in order to oxidise a few per cent of sulphide sulphur. It was argued that if the pre-roast calcine were leached and a process could be developed for the recovery of a zinc sulphide concentrate from the leach residue, this concentrate, small in weight compared with the pre-roast calcine, would probably roast autogenously, thus virtually eliminating the expenditure of fuel as well as greatly increasing the weight of sulphur oxidised per square foot of furnace hearth area.

The obvious method of producing a suitable concentrate from leach residue was by flotation. It will be recalled (see p. 495 of the earlier paper) that when two-stage roasting was practised the leach residue was classified, the granular fraction was ground and floated while the slime fraction was thickened, filtered and dried ready for shipment to a lead smelter. This process worked quite successfully. However, when trials were made of leaching a calcine carrying several per cent of sulphide sulphur the granular fraction still floated well, but the slime fraction carrying 8-10 pct sulphide sulphur yielded very poor results when subjected to flotation. This fact held up the application of "pre-roast" leaching for many years. However, successful flotation of the slime fraction of leach residue was finally achieved and in August 1940 the slime flotation plant began operation, while the leach-

† Throughout this paper the long ton of 2240 lb and the Imperial Gallon are used.

San Francisco Meeting, February 1949.

TP 2524 D. Discussion of this paper (2 copies) may be sent to *Transactions AIME* before May 15, 1949. Manuscript received October 1, 1948.

* Technical Assistant to the General Superintendent, Risdon Works of Electrolytic Zinc Co. of Australasia Ltd.

† W. C. Snow: *Electrolytic Zinc at Risdon, Tasmania, AIME Trans.* 121, 482.



FIG 1—General view of works.

ing of pre-roast calcine became an accomplished fact. A description of the flotation section will be given later in the present paper. Calcine leached at the present time carries from 5–6 pct sulphide sulphur while the mixture of concentrates from the granular and slime flotation sections carries about 22–24 pct sulphide sulphur. This mixed concentrate is roasted for the most part in modified Skinner furnaces.* The flotation tailing, carrying 1.5–2.5 pct sulphide sulphur, is filtered and dried and becomes the final zinc plant residue. The loss of sulphide sulphur in residue is little higher than it was when two stage roasting was practised.

It is not proposed to set out the arguments of single stage roasting to low sulphide sulphur versus the present method of roasting with intermediate flotation. However, it should be stated that the present method permits of high roasting rates and in some of the newer furnaces an oxidation rate of 12–13 lb sulphur per square foot of hearth area per day has been achieved without the use of any fuel. With a very small fuel addition (less than 0.5 pct of oil) the figure has risen to 14–16 lb.

* See contemporary paper, J. A. B. Forster: Autogenous Roasting of Low Grade Zinc Concentrate in Multiple Hearth Furnaces at Risdon, Tasmania.

CALCINE SCREENING SECTION

The introduction of continuous leaching, described later in this paper, made it imperative to screen the calcine on its way to the Leaching Division. Preliminary trials of continuous leaching when using unscreened calcine were unsatisfactory because many of the larger lumps would not move from pachuca to pachuca and accumulated in the first and second units of the series. A plant for the screening of all calcine entering the Leaching Division was, therefore, built and this has removed the trouble.

The screening station consists of two vibrating screens each 8×3 ft and fitted with $\frac{1}{4}$ in. wire mesh. The oversize falls to a bin and is fed intermittently to a swinging arm breaker. A bucket elevator returns the crushed oversize to the screens.

Leaching and Purification Division

LEACHING

The leaching of calcine and the purification of the resulting solution were described fully in the earlier paper (see pp. 491–510). No modifica-

tion of the fundamental principles of this division has occurred but many important changes have taken place in details.

The batch leaching of calcine was described in the earlier paper. Although quite successful in operation, batch leaching employs a relatively big labor force, it uses the pachucas inefficiently in that much lost time occurs in filling and emptying while the discharge of pulp at a low level loses head and under Risdon conditions makes improved classification of pachuca discharge difficult. These considerations coupled with the somewhat restricted space available for building new pachucas for increased production led to the introduction of continuous leaching in 1945.

Ten pachucas, each 12 ft diam and 34 ft stave and arranged in two rows of five, were previously employed in batch work (nine in 1936). These have been so connected that all ten may be used together if so desired, but any one or more can be cut out for repairs. In normal practice the ten units are divided into two groups of five each and one set only is in use at a time. It has been found that five pachucas, used in continuous flow, leach as well as ten employed on batch work.

Screened calcine enters a small bin of

80 tons capacity which feeds an 18-in. belt running centrally above and between the two rows of pachucas. From this belt calcine is fed continuously by means of a tripper to the head pachuca while spent solution from the electrolytic division is fed to the same pachuca.

At the top of each column and placed to one side is a swinging launder so arranged that it picks up part of the discharge from the top of the column and transfers it to a short launder feeding the next pachuca. This equipment permits the coarser particles rising in the column to be transferred to the next pachuca at the same time maintaining the same pulp level in all pachucas of the series. The discharged pulp flows to a launder placed beneath the operating floor and running between the two rows. From time to time scuttling of one or more pachucas becomes necessary and a low level launder—used previously for batch leaching—takes the discharge.

The flow of solution through the pachucas for the present output of about 245 tons of cathode zinc per day amounts to about 800,000 to 1,000,000 gal per day while 600–700 tons of calcine is leached. The spent electrolyte carries up to 100 g acid per liter and this is reduced to 1.5–2.0 g per liter before discharge.

Continuous leaching has proved advantageous in that it is simpler, saves labor, uses 35 psi air in place of 90 lb air, the equipment is utilised more efficiently while improved classification and flotation results have been made possible.

CLASSIFICATION AND THICKENING OF PACHUCA DISCHARGE

The classification of pachuca discharge has been improved by the addition of a V shaped box 42 ft 9 in. long, 10 ft wide at the top and 10 ft deep. The pachuca discharge enters at one end at the top and flows the length of the box. The fine fraction of the solids passes over the lip and enters five 50 ft diam by 15 ft stave Dorr thickeners. The granular fraction, discharged from the bottom of the V shaped box through six spigots, is dewatered in six duplex Dorr classifiers (see item 2 p. 494 of the earlier paper). The underflow from the classifiers is delivered to the granular flotation section while the overflow from the classifiers joins that from the V box on its way to the thickeners, where the pulp is thickened to a specific gravity of about 1.8. The

thickener underflow is elevated to pulp holding tanks whence it is delivered to the slime flotation plant.

FLOTATION OF LEACH RESIDUE

The granular flotation section described on p. 495 of the earlier paper remains unchanged in principle but has been enlarged, while improved classification has been achieved by the addition of a 12 ft diam cone dealing with the tailing. The underflow from the cone is dewatered in a small simplex Dorr classifier and returns to the tube mills for regrinding. The overflow from the cone goes to the five primary thickeners and so granular tailing normally joins the feed to the slime flotation section.

The slime flotation section consists essentially of three main parts, pulp preparation, flotation, and thickening of concentrate and tailing.

Pulp preparation consists of two main steps:

1. A 12 ft diam \times 12 ft stave tank mechanically agitated receives the slime pulp from the leaching division. This tank is normally kept full. Spent electrolyte is added to maintain an acidity of about 1.75 g per liter. Finely ground manganese cell mud is added. The supply of pulp, acid and manganese dioxide is more or less continuous to this tank. An air lift elevates the pulp to a bucket feeder which consists of eight stainless steel buckets attached to a 3 ft 6 in. diam wheel. The discharge from the buckets is divided by a movable cutter, one part going forward for flotation and the other part returning to the pulp tank. In this way a continuous and constant feed rate is maintained.

2. The discharge from the bucket feeder enters the first of five air agitated processing boxes each 4 ft square. Finely divided limestone pulp is fed to the first box for neutralising excess acid. Then cresylic acid and eucalyptus oil are added and finally the pulp is diluted with circuit solution to a pulp density of about 3–3.5 lb solids per gallon. A pulp density recorder controller maintains the pulp at the required specific gravity.

The processed pulp then goes forward to the flotation boxes. There are sixteen boxes arranged in two rows of eight. Each box is 3 ft 6 in. \times 3 ft 6 in. \times 5 ft 2 in. deep. The impellers, 18 in. in diam, are made of stainless steel and revolve at 370 rpm. Each pair of impellers is driven by a single vertical

12 hp motor, while air from a Connorsville blower is supplied through an adjusting valve to each box. Each row of eight boxes has a common pulp level since each partition between boxes has an aperture 2 ft wide \times 6 in. deep cut 8 in. from the bottom. The froth level is controlled by inserting riffles in slots. No mechanical scraping is necessary since the froth flows very freely.

The sixteen boxes are divided into three groups, namely, five rougher concentrate, three cleaner concentrate and eight scavenger. Potassium xanthate is added to the pulp leaving the rougher boxes and entering the scavenger boxes.

The tailing flows to two 50 ft diam \times 15 ft stave Dorr thickeners. The overflow is returned to the flotation circuit while the thickened pulp is filtered and dried as described on pp. 496 and 497 of the earlier paper. Oil has replaced coal for firing the driers.

The combined concentrate from the two flotation sections is thickened in two 50 ft diam \times 15 ft stave Dorr thickeners. The overflow is returned to the main zinc plant circuit while the underflow is filtered in two six-leaf 8 ft 6 in. diam disc filters. The discharge from these filters is not washed and is forwarded by belt conveyor for roasting.

It has been found that the zinc content of the circuit solution in the slime flotation section is of importance and an endeavor is made to keep zinc in the range 80–90 g per liter. This is done by bringing washings and other low zinc tenor liquors into the flotation section and using them for pulp dilution.

IRON PURIFICATION

The overflows from the five primary thickeners dealing with pachuca discharge combine and the solution goes forward for the removal of iron, silica, arsenic and antimony, by the addition of finely divided limestone. This procedure was described on pp. 497 and 498 of the earlier paper and the basic principles remain unchanged. Considerable refinement in detail has taken place however, and this has effected a marked improvement in the filtering properties of the precipitate while the effectiveness of purification has been increased considerably.

In 1936 there were four 28 ft diam \times 12 ft stave agitators in series. An extra agitator has been added and each of the first three in the series has been divided into two by building a partition across

a diameter in order to reduce the effect of short circuiting. The first agitator receives thickener overflow at about 1.5 to 2.0 g acid per liter. Here ground manganese mud is added for the oxidation of iron. During the leaching of preroast calcine up to 1.0 g iron per liter is dissolved and part of this is reduced by sulphides to the ferrous state and up to 300–400 mg of ferrous iron per liter may be present. The bulk of this is oxidized in the first agitator.

The conditions in the second agitator of the series are critical and it is here that considerable improvement has occurred. It was discovered that both the physical state and the chemical composition of the precipitate resulting from the addition of limestone are profoundly altered according to the hydrogen ion concentration at which precipitation occurs. It has been determined that if the pH of the pulp in the precipitating tank is maintained at a figure greater than about 4.0 the physical state of the resulting precipitate is such that it filters rapidly while the iron is present almost wholly as ferric hydroxide with but small formation of basic ferric sulphate.

The effect of this procedure on the filtering rate of the ensuing pulp is remarkable. If limestone is added to the acid solution so that the pH slowly rises to the critical figure the time of filtering the pulp under otherwise similar conditions will be about five times as long as it is if the pH is maintained at about 4.0 during precipitation. Similar results are obtained if the neutralising agent is finely ground calcine instead of limestone.

The control of pH is achieved by the continuous addition of finely ground limestone and the intermittent return to the purifying tank of every second primary filter cake. A pH indicator and also a recorder have been installed and it is proposed to add a controller to the recorder.

No material change has occurred in the amount of silica removed during iron purification but the recognition of the part played by silica during purification has been of importance. In the course of leaching traces of germanium are dissolved, and, if this element is not removed almost completely, it increases the reversion of cadmium during the filtration of copper cadmium precipitate and reduces current efficiency during subsequent electrolysis. It is believed that the presence of at least 1.0 g per liter and preferably about 1.3 g per liter of silica in the solution

entering the iron purification tanks is effective in controlling germanium.

The filtration of iron precipitate was described in detail on pp. 498–501 of the earlier paper. The number of leaves per filter basket has been increased in the ratio of five to four while a rest period in hot water has been introduced to remove incrustations of gypsum from the canvas. These factors coupled with the greatly improved filtering properties of the precipitate have enabled the section to handle with ease the solution flow equivalent to 245 tons of cathode zinc per day, whereas previously, difficulty was often encountered when the output was only 200 tons. It is anticipated that existing equipment will handle without difficulty the solution flow when output increases to 290 tons of cathode zinc per day.

COPPER CADMIUM PURIFICATION

The removal of copper and cadmium was described on p. 501 of the earlier paper. The section has been enlarged somewhat and the general results improved. Eight purifiers are now employed and filtration takes place in 3 × 3 ft Dehne presses as previously. The solution for purification now contains about 90–120 mg copper and 150–180 mg cadmium per liter. The zinc dust charge is normally 250–300 pct of theoretical requirements.

The filtration of the discharge from the purifiers has been improved by feeding both ends of the presses which are now fitted with 68 frames 1½ in. thick built up from mild steel. The improved feeding arrangement coupled with the 1½ in. frames permits the filling of a press in approximately 12 hr. Control of germanium during iron purification, quicker filling of presses and a greater excess of zinc dust coupled with a constant watch by shift chemists on the cadmium content of press filtrate, have combined to produce a purified solution carrying 1.5–2.5 mg cadmium per liter.

The filter cake is treated for the recovery of metallic cadmium and of copper in the form of a copper rich residue in a separate plant.*

COBALT PURIFICATION

The method of removing cobalt from solution was described in detail on pp.

501 and 502 of the earlier paper. No change, except in minor detail, has occurred in the method of purification during the ensuing twelve years.

COBALT OXIDE PLANT

A major change has taken place in the method of disposing of the cobalt precipitate which was previously wasted. Many attempts were made to find uses for this precipitate and to recover economically valuable by-products from it, but all such early attempts ended in failure.

The precipitate after filtration is a mixture of cobalt nitroso beta-naphtholate, gypsum, basic zinc sulphate and unconsumed slaked lime, mixed with zinc sulphate solution. It was discovered that the cobalt nitroso beta-naphtholate would float and if conditions were right, a relatively high grade concentrate could be produced. A plant was, therefore, built and has operated successfully since 1936. One of the features of this process is that the concentrate froth is produced quite readily in the absence of any addition agent.

The cobalt precipitate pulp is transferred from the purification section by pulping it with water and pumping it to the cobalt oxide plant. Two mechanically agitated tanks 9 ft diam × 11 ft stave receive the pulp. These tanks are used alternately, one receiving the pulp one day and the other receiving it the next day. When the day's output of precipitate is transferred, sulphuric acid is added until the acidity reaches about 3 g per liter. Basic zinc sulphate and calcium hydroxide are consumed during a short period of agitation. The pulp contains about 2½ lb of solids per gal and is pumped to the first of a row of ten flotation boxes each 3 ft × 2 ft 9¼ in. × 5 ft deep. The ten boxes all have a common pulp level since the partitions between boxes do not extend to the bottom and leave a gap of 3 in. On the floor of each box is a canvas aerator stretched over a rectangular frame of 1¼ in. copper pipe. Air is supplied to the aerator at a pressure of 1½–2½ psi while the froth level is controlled by riffles fitted into slots. The first box of the series is used as a digester and returned circuit solution is added to bring the pulp density to about one pound per gallon. The next six or seven boxes are used for concentrate production while the last two or three make a middling which is returned to the feed.

* See contemporary paper, G. H. Anderson: The Recovery of Cadmium from Cadmium Copper Precipitate—Electrolytic Zinc Co. of Australasia Ltd.

The tailing is normally a milky white suspension of fine gypsum crystals in zinc sulphate solution.

The process is very sensitive to the volume of air supplied to the aerators and the flow of concentrate froth must be extremely gentle otherwise gypsum is entrained in it. A normal calcium content of the concentrate is about 0.02 pct but it is very easy to multiply this many times by the use of too much air. Another impurity of importance is iron. If iron escapes precipitation in the iron purification section some of it is later precipitated along with cobalt. The flotation of cobalt precipitate does not differentiate between iron and cobalt so that virtually all the iron present in the precipitate appears in the concentrate.

The concentrate flows to a 9 ft diam \times 9 ft stave holding tank whence it is pumped to a Moore filter. The basket consists of six leaves each 4 ft \times 3 ft 6 in. After filtration the basket is transferred to a washing tank where thorough washing removes most of the water soluble zinc. The cake is blown off to a hopper from which it is fed to an oil fired hand rabbled reverberatory furnace 20 ft long \times 4 ft wide where the organic material is burned off, and a final product of reasonably pure cobalt oxide is discharged from the furnace. This is placed into steel drums ready for the market. During the war years some cobalt sulphate and metallic cobalt were produced for special purposes.

SOLUTION COOLING

The plant for the cooling of purified solution prior to its being pumped to the electrolytic division which was described on p. 504 of the earlier paper, has been extended by the building of a second cooling tower similar to the one described previously. The two towers are used alternately so that during the cleaning of one tower the other is in use.

Electrolytic Division

The electrolytic division was described in detail on pp. 511-519 of the earlier paper. Basically, the same procedure is still employed but some quite important modifications have been introduced.

FOUR NINES ZINC

The specification of the Standards Association of Australia for zinc base

die casting alloy sets an upper limit for lead of 0.007 pct. Attempts at Risdon over many years failed to produce zinc conforming to this specification. The best results had been obtained with 1 pct silver lead anodes but the zinc still contained 0.01 pct lead or even more. During the war a considerable demand for high quality die castings developed and renewed efforts were made to meet the specification. Following a suggestion made by Mr. W. H. Hannay of The Consolidated Mining and Smelting Co. of Canada success was achieved by the simple expedient of cooling the electrolyte in cells fitted with 1 pct silver lead anodes to about 28°C. Many thousands of tons of zinc containing about 0.005 pct lead have now been produced by this method and have been used for the production of die casting alloy. There is no production of ingot zinc of this very high grade since all cathodes not used for the manufacture of die casting alloy are melted with the ordinary make of plant zinc. The anodes used are not perforated and conditions of electrolysis are standard except in regard to temperature. Experiments in which the temperature was reduced to 20°C showed no further improvement in the lead content of zinc.

CLOSER SPACING OF ELECTRODES

In 1936 the cells in the four big units contained 34 anodes and 33 cathodes while the current flow was nominally 12,000 amp. The spacing of anodes center to center varied between 4 in. and 3½ in. in the various units. The urge for increased power efficiency and later

for increased output focussed attention on the closer spacing of electrodes. A suitable double cone porcelain spacing insulator was developed and two of these were fitted to each anode. (See Fig 2). In this way it was found possible to insert 45 anodes and 44 cathodes into each cell at 3 in. spacing. The current flow can be increased to 18,000 amp and the output from a single unit increased from about 46 to about 69 tons per day.

At the present time the four big units have all been fitted with rolled copper bus-bars capable of carrying the increased current. However, only two units are as yet supplied with the full power input. The other two units will be supplied as soon as a new converter station, now under construction, is completed.

ELECTRODES

The size and shape of electrodes are virtually the same as they were in 1936 except that now plain ¼ in. aluminum sheets are used as cathodes.

Twelve years ago the life of a cathode was extended by attaching protective strips of aluminum above solution level. This was effective because maximum corrosion occurred about 1½ in. above solution level. In recent years solution line corrosion has increased markedly possibly related to an increase of fluorine in the electrolyte from about 15-20 mg per liter up to 30-35 mg per liter. Protective strips which give no benefit at the solution line have therefore been discarded but cathode cost per ton of zinc has increased considerably.

Trials of re-rolled used cathodes have

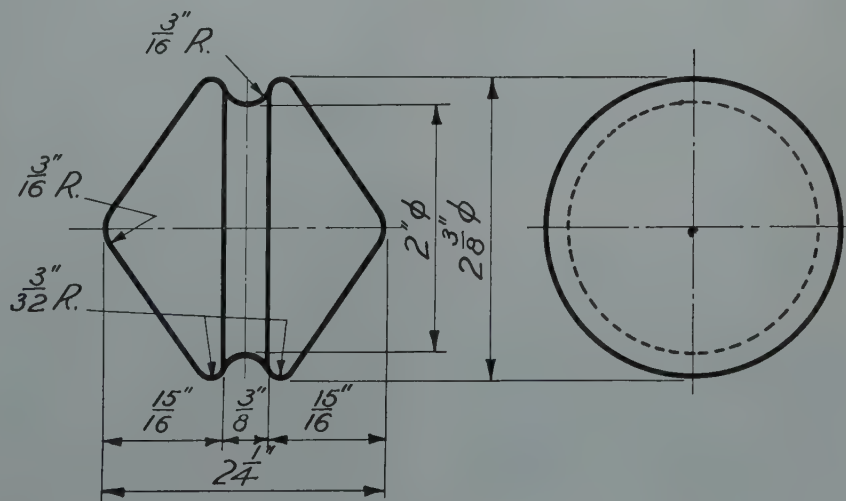


FIG 2—Anode spacing insulator. Glazed porcelain.

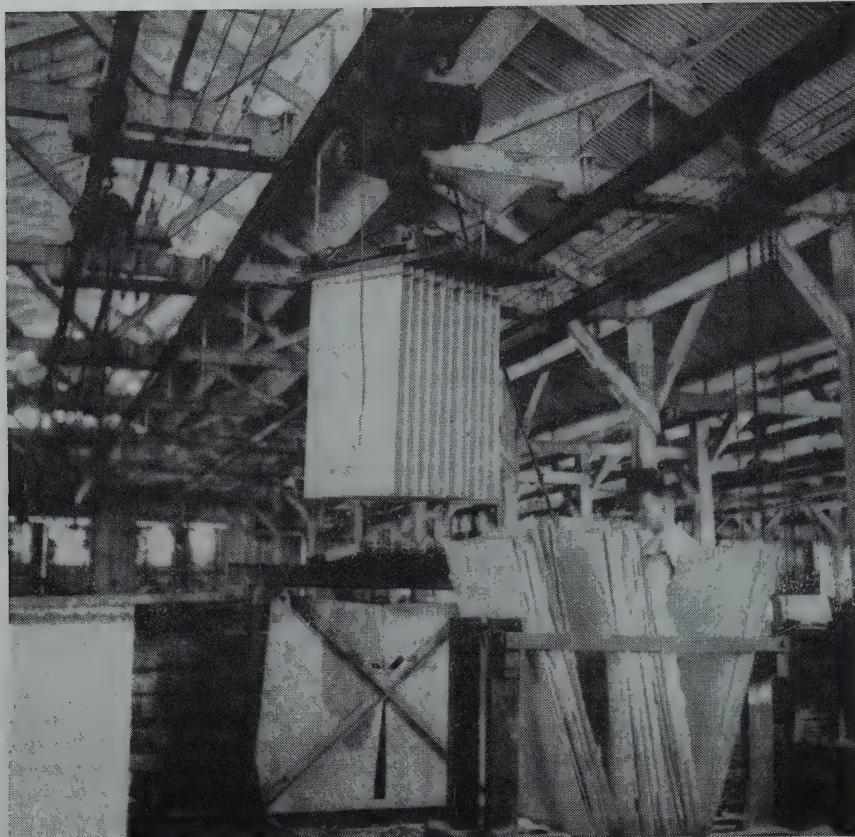


FIG 3—Hoist in action.

been made with only moderate success.

Anodes now contain 0.012 pct silver. This addition has been made to increase the stiffness and to reduce the need for anode straightening. This small addition probably is responsible for a reduction in the lead content of normal cathode zinc to a figure of about 0.012 pct. An interesting minor modification has been made in the treatment of new anodes prior to placing them in the cells. It was discovered that if the anodes were painted with a slurry of cell mud while they were still hot after casting, the conditions of electrolysis were much improved during the first two or three stripping periods. Prior to the introduction of this practice current efficiency was low during the first few stripping periods.

COOLING OF ELECTROLYTE

The adoption of closer spacing and greater current flow has called for more cell cooling. There is not room for more than about four cooling coils per cell and in these circumstances the temperature of the electrolyte during the hotter months of the year tended to be unduly high. Experimental work has indicated that the greatest yield of

cathode zinc per unit of power occurs when the temperature of the electrolyte is about 32–33°C. In practice an endeavor is made to keep the temperature below 35°C.

The demand for a greater extraction of heat from the cells stimulated an investigation into the design and cleaning of the cooling coils described on p. 514 of the earlier paper. The outstanding result of this investigation was the recognition that even when cleaned thoroughly by hand scraping and brushing, a coil quickly lost up to one half of its effectiveness due to the formation of a thin hard scale on the outer surface.

A system of electrolytic cleaning has been developed in which the coils are made cathodic in a dilute solution of sulphuric acid. An input of about 75–100 amp per coil is effective in removing adherent scale during overnight treatment. The efficiency of the coil as a heat remover has been restored to about 90 pct of that of a new clean coil and temperature control of the electrolyte is now not difficult even in the hotter months of the year.

LIFTING OF CATHODES

The hand operated chain blocks for

lifting groups of cathodes for stripping and described on pp. 514–515 of the earlier paper are still in use but at the time of writing this paper a change-over is being made to electrically operated hoists. One of these has been on trial for a long period and has proved very satisfactory. Another twelve are being installed and it is hoped to equip the whole cell room with these hoists—one hoist for every three cascades. (Fig 3.)

ADDITION AGENTS

The use of about 24 mg glue per liter and 10 mg beta naphthol per liter, referred to on pp. 514, 516 and 517 of the earlier paper is still maintained.

It is no longer necessary to add antimony since improved technique in solution purification appears to have overcome many of the difficulties previously experienced during electrolysis. Current efficiency averaging about 92 pct is maintained with a 72 hr stripping period.

Melting and Casting Division

This operation was described in detail on pp. 519–526 of the earlier paper. The major change introduced during the intervening years has been the abandonment of coal firing and the use of oil in its place. No leaded zinc has been produced for some years.

Metallurgical Data

The following tables refer to average figures for a four weekly period during the year ended June 30, 1948.

Feed solution was taken for analysis in June, 1947. During the year ended June 30, 1948 average cathode zinc output was 211.2 tons per day although it had risen to about 245 tons at the close of the year.

Roasting Division

The data relevant to this division will be found in contemporary paper by J. A. B. Forster.

Acknowledgment

The author wishes to express his appreciation to the Directors and Management of the Electrolytic Zinc Co. of Australasia Limited for permission to publish this paper. Also, his thanks are due to those who have helped in various ways in its preparation.

Leaching Division

Table 1 . . . Pachuca Section

| | |
|--|-------|
| New calcine leached—tons..... | 11660 |
| Circulating load calcine and dross leached—tons..... | 3909 |
| Total calcine leached—tons..... | 15569 |
| Assay calcine leached | |
| Sulphate S Pct..... | 1.38 |
| Sulphide S Pct..... | 5.79 |
| Total Zn Pct..... | 56.6 |
| Sol. Zn Pct..... | 42.1 |
| Pb Pct..... | 1.0 |
| Fe Pct..... | 9.2 |
| Cu Pct..... | 0.18 |
| Cd Pct..... | 0.31 |
| Ag oz..... | 4.3 |
| Au oz..... | 0.017 |
| Spent electrolyte—acid grams per liter.. | 90.5 |
| Acid added to circuit—tons..... | 283 |
| Granular residue to flotation, pct of total calcine leached..... | 24.2 |
| Slime residue to flotation, pct of total calcine leached..... | 26.8 |

Table 4 . . . Copper Cadmium Cobalt and Chlorine Purification Sections

| | |
|---|------|
| Zinc dust used—tons..... | 71 |
| —lb per ton cathode zinc.. | 26.7 |
| —pct of chemical equivalent of copper plus cadmium..... | 298 |

| | Solution Composition | |
|--------------------------------------|----------------------|-----------------|
| | Before Treatment | After Treatment |
| Copper—mg per liter..... | 112 | 0.1 |
| Cadmium—mg per liter..... | 176 | 1.8 |
| Copper cadmium precipitate—tons..... | | 192 |

| | Zn Pct | Pb Pct | Cu Pct | Cd Pct | Ag Oz. |
|---|--------|--------|--------|--------|--------|
| Assay copper cadmium ppt..... | 33.6 | 0.6 | 6.7 | 10.85 | 2.3 |
| Cobalt removed—lb..... | | | | | 1801 |
| Beta naphthol used—lb per lb cobalt..... | | | | | 10.0 |
| Sodium nitrite—lb per lb cobalt..... | | | | | 6.9 |
| Caustic Soda—lb per lb cobalt..... | | | | | 3.17 |
| Lime—lb per lb cobalt..... | | | | | 14.2 |
| Chlorine removed—lb..... | | | | | 1090 |
| Silver loss—oz per lb chlorine removed..... | | | | | 0.99 |

Table 2 . . . Flotation Section

| | |
|---|-------|
| Granular residue treated—tons..... | 3696 |
| Assay sulphide sulphur—pct..... | 17.52 |
| Slime residue treated—tons..... | 4095 |
| Assay sulphide sulphur—pct..... | 8.02 |
| Combined concentrate—tons..... | 4041 |
| Slime tailing (or final residue)—tons..... | 3028 |
| Slime tailing pct of new calcine leached—pct..... | 26.0 |

| | Combined Concentrate | Slime Tailing |
|--------------------------|----------------------|---------------|
| Sulphur sulphur pct..... | 22.5 | 1.99 |
| Total Zn pct..... | 49.4 | 22.3 |
| Pb pct..... | 0.8 | 4.0 |
| Cu pct..... | 0.21 | 0.14 |
| Cd pct..... | 0.70 | 0.13 |
| Ag oz..... | 10.2 | 6.5 |
| Au oz..... | 0.03 | 0.026 |

| Addition Agents | Pot. Xanthate | Eucalyptus | Cresylic Acid |
|----------------------------------|---------------|------------|---------------|
| Granular circuit—lb per ton..... | nil | 0.35 | nil |
| Slime circuit—lb per ton.. | 0.04 | 0.04 | 0.03* |

* Cresylic acid was not added throughout the year. This figure represents the normal addition when it was used.

Table 5 . . . Cobalt Oxide Section

| | |
|---|------|
| Cobalt precipitate treated—tons..... | 42.5 |
| Cobalt content of crude precipitate—pct.. | 1.93 |
| Acid used—tons..... | 2.47 |

| | Ca Pct | SiO ₂ Pct |
|---|--------|----------------------|
| Cobalt concentrate assay..... | 0.023 | 0.151 |
| Oil used in roasting—tons..... | | 11 |
| Finishing temperature °C (approximate)..... | | 750 |
| Output of oxide—tons..... | | 1.0 |

| | Co Pct | Fe Pct | Zn Pct | Ca Pct | SiO ₂ Pct |
|-----------------------|--------|--------|--------|--------|----------------------|
| Cobalt oxide assay... | 64.3 | 2.5 | 1.6 | 0.50 | 6.77* |

* This figure is abnormally high. It is usually about 2 pct.

Table 3 . . . Iron Purification Section

| Solution treated—gal per day..... | Solution Composition | |
|-----------------------------------|----------------------|-----------------|
| | Before Treatment | After Treatment |
| Sulphuric acid—g per liter... | 1.95 | neutral |
| Total iron—mg per liter..... | 470 | 0.3 |
| Ferrous iron—mg per liter..... | 290 | |
| Silica—gms per liter..... | 1.65 | 0.112 |
| Arsenic—mg per liter..... | 2.65* | 0.2 |
| Antimony—mg per liter..... | 0.44* | 0.1* |
| Limestone used—tons†..... | | 600 |
| Iron precipitate—tons†..... | | 1200 |
| —Total zinc pct..... | | 7.0 |
| Water soluble zinc pct..... | | 3.5 |

* These figures are representative but are not necessarily yearly averages.

† The figures for limestone used and weight and composition of iron precipitate are typical but due to minor changes in procedure during the year do not depict the year's average work.

Melting and Casting Division

Table 8 . . . Data on Melting

| | |
|---|-------|
| Cathode zinc melted—tons..... | 5877 |
| Proportion of scrap therein—pct..... | 2.02 |
| Zinc slabs cast—tons..... | 5658 |
| Dross produced—tons..... | 272 |
| Flue and baghouse dust (estimated) tons | 37 |
| Zinc content of dross—pct..... | 79.4 |
| Zinc recovery as slab zinc—pct..... | 96.27 |
| Oil consumed—pct of zinc fed..... | 2.29 |
| Ammonium chloride—lb per ton feed... | 1.32 |

Table 9 . . . Analyses of Products

| | High Grade Slab Zinc, Pct | Four Nines Cathode Zinc, Pct |
|--------------|---------------------------|------------------------------|
| Zinc..... | 99.9838 | 99.9918 |
| Lead..... | 0.0116 | 0.0048 |
| Copper..... | 0.0012 | 0.0011 |
| Cadmium..... | 0.0025 | 0.0023 |
| Iron..... | 0.0009 | <0.00001 |
| Arsenic..... | <0.00001 | <0.00001 |

Electrolytic Division

Table 6 . . . Analysis of Feed Solution (June 1947)

| | Grams Per Liter |
|---------------------------|-----------------|
| Zinc..... | 111.9 |
| Manganese..... | 20.8 |
| Calcium..... | 0.44 |
| Magnesium..... | 1.7 |
| Sodium..... | 3.7 |
| Potassium..... | 1.36 |
| Sulphate..... | 219.4 |
| | Mg Per Liter |
| Cobalt..... | 9.4 |
| Copper..... | 0.11 |
| Cadmium..... | 1.6 |
| Silica..... | 102 |
| Total Chlorine..... | 139 |
| Chloride chlorine..... | 99 |
| Chlorate chlorine..... | Nil |
| Perchlorate chlorine..... | 40 |
| Fluorine..... | 32 |
| Arsenic..... | <0.1 |
| Antimony..... | 0.09 |

| | Mg Per Liter |
|-------------------------------|----------------|
| Total Nitrogen..... | 142 |
| NH ₄ nitrogen..... | 138 |
| Nitrite nitrogen..... | 3 |
| Nitrate nitrogen..... | Possible trace |
| Phosphate..... | Trace |
| Aluminum..... | 0.44 |
| Lead..... | 0.07 |
| Bismuth..... | 0.001 |
| Nickel..... | 0.2 |
| Selenium..... | Nil |
| Tellurium..... | Nil |
| Tin..... | 0.065 |
| Silver..... | 0.35 |
| Iron (total)..... | 1.2 |
| Iron (after filtration)..... | <0.1 |
| Solids in suspension..... | 74 |
| Specific Gravity..... | 1.344 |

Table 7 . . . Data on Electrolysis

| | |
|---------------------------------------|-------|
| Output of cathode zinc—tons..... | 5917 |
| Anode current density—amp per sq ft | |
| At 12000 amp..... | 28.3 |
| At 18000 amp..... | 32.1 |
| Cathode current density—amp per sq ft | |
| At 12000 amp..... | 26.2 |
| At 18000 amp..... | 29.4 |
| Voltage per unit at 12000 amp..... | 502 |
| Voltage per unit at 18000 amp..... | 507 |
| Current efficiency—pct..... | 92.0 |
| Zinc deposited—lb per dc hp day..... | 12.59 |
| Zinc deposited—lb per ac hp day..... | 11.47 |
| Glue—lb per ton cathode zinc..... | 0.84 |
| Beta naphthol—lb per ton cathode zinc | 0.33 |

The Hardenability Effect of Molybdenum

J. M. HODGE,* J. L. GIOVE,* Members AIME, and R. G. STORM*

Introduction

THE hardenability effect of molybdenum has been evaluated by a number of investigators, including one of the present authors.^{1,2,3,4,6} Considerable discrepancy exists, however, among the results of these various investigators, and two of them, Brophy³ and Kramer,⁴ have indicated that the apparent hardenability effect of molybdenum would vary, depending upon the other alloying elements in the steels being considered. The results of previous, unpublished work conducted at the Duquesne Works Laboratory of the Carnegie-Illinois Steel Corporation also have indicated significant differences in the hardenability effect of molybdenum in nickel and in chromium steels.

The present investigation was undertaken in an effort to establish the mechanism governing this difference in the hardenability effect of molybdenum. This work involved both end-quench hardenability and isothermal transformation tests on two series of steels of varying molybdenum content. One steel contained 3 pct nickel and the other 1 pct chromium. It was hoped that such studies would shed further light on the mechanism of this behavior.

Materials and Experimental Work

MATERIALS

The chemical compositions of the steels used in this investigation are shown in Table 1. These steels were furnished by Battelle Memorial Institute in the form of 100-lb induction furnace ingots. The top half of each ingot was forged to 1 $\frac{3}{8}$ -in. square billets and then rolled to 1-in. round bar stock for isothermal transformation studies.

Table 1 . . . Results of Ladle Chemical Analyses—Per Cent
3 Pct Nickel Steels

| C | Mn | P | S | Si | Cr | Ni | Mo | Al |
|------|------|-------|-------|------|----|------|------|-------|
| 0.41 | 0.70 | 0.019 | 0.030 | 0.28 | | 3.02 | 0.0 | 0.020 |
| 0.39 | 0.68 | 0.021 | 0.028 | 0.27 | | 3.01 | 0.08 | 0.025 |
| 0.40 | 0.69 | 0.018 | 0.028 | 0.32 | | 2.99 | 0.18 | 0.025 |
| 0.40 | 0.71 | 0.019 | 0.028 | 0.26 | | 3.00 | 0.32 | 0.025 |

| 0.95 Pct Chromium Steels | | | | | | | | |
|--------------------------|------|-------|-------|------|------|------|------|-------|
| 0.41 | 0.68 | 0.018 | 0.027 | 0.27 | 0.95 | 0.05 | 0.0 | 0.025 |
| 0.41 | 0.69 | 0.018 | 0.028 | 0.21 | 0.95 | 0.05 | 0.08 | 0.025 |
| 0.42 | 0.69 | 0.018 | 0.028 | 0.23 | 0.94 | 0.05 | 0.18 | 0.025 |
| 0.42 | 0.65 | 0.018 | 0.028 | 0.20 | 0.94 | 0.05 | 0.32 | 0.025 |

* Note: For calculating ideal diameters, these analyses were corrected to 0.40 pct C, 0.70 pct Mn, and 0.25 pct Si.

tion studies. The bottom half of each ingot was forged into approximately 1 $\frac{1}{4}$ -in. rounds for end quench tests. All of the steels were normalized from 1650°F and tempered at 1100°F before machining to end quench or isothermal samples.

END-QUENCH TESTS

Standard 1-in. diam end-quench tests were made on each of the steels. The test bars were austenitized at 1600°F for 30 min., quenched in a standard Jominy jig, and hardness surveys were made in all tests. The 95 pct martensite point was determined from hardness values⁵ and checked by metallographic examination. The Jominy distance values for 95 pct martensite were converted to hardenability values in terms of ideal

diameter (D_1), using a revised curve for the relationship between Jominy distance and ideal diameter. This curve was based on the cooling time from the A_1 to the bainite nose temperatures rather than on the usual criterion of half-temperature time. The cooling rates as determined by Russell and Williamson⁹ were used as a basis for this relationship. The derivation of this curve is described in detail in the appendix.

ISOTHERMAL TRANSFORMATION STUDIES

Samples for the isothermal transformation studies were quarter sectors of $\frac{1}{16}$ -in. thick slices from the 1-in. round bars. All samples were austenitized for a total time of 15 min., transferred rapidly to a lead bath for isothermal transformation, and brine quenched from the lead bath. A time of 3 sec was allowed for the sample to come to the temperature of the lead bath, and this time was not included in the isothermal transformation times.

Each sample was examined metallographically at a magnification of 100 diam. The per cent transformation was estimated by comparison with standard micrographs, and the values were plotted against time on log/log coordinate paper. At least 4 and as many as 10 points were plotted for each steel. A line was drawn through the points for each steel, and the times for 5 pct transformation were obtained from the plot for each steel.

Isothermal transformation diagrams in terms of 5 pct total transformation, covering the temperature range of 800 to 1200°F, were determined in this manner for an austenitizing temperature of 1600°F. The times for 5 pct transformation at the bainite nose for austenitizing temperatures of 1800 and 2000°F were also determined in the same manner.

These times for 5 pct total transformation

Cleveland Meeting, October 1949
TP 2520 E. Discussion of this paper (2 copies) may be sent to *Transactions AIME* before Dec. 15, 1949. Manuscript received November 1, 1948.
* Carnegie-Illinois Steel Corporation, Pittsburgh, Pa.
References are at the end of the paper.

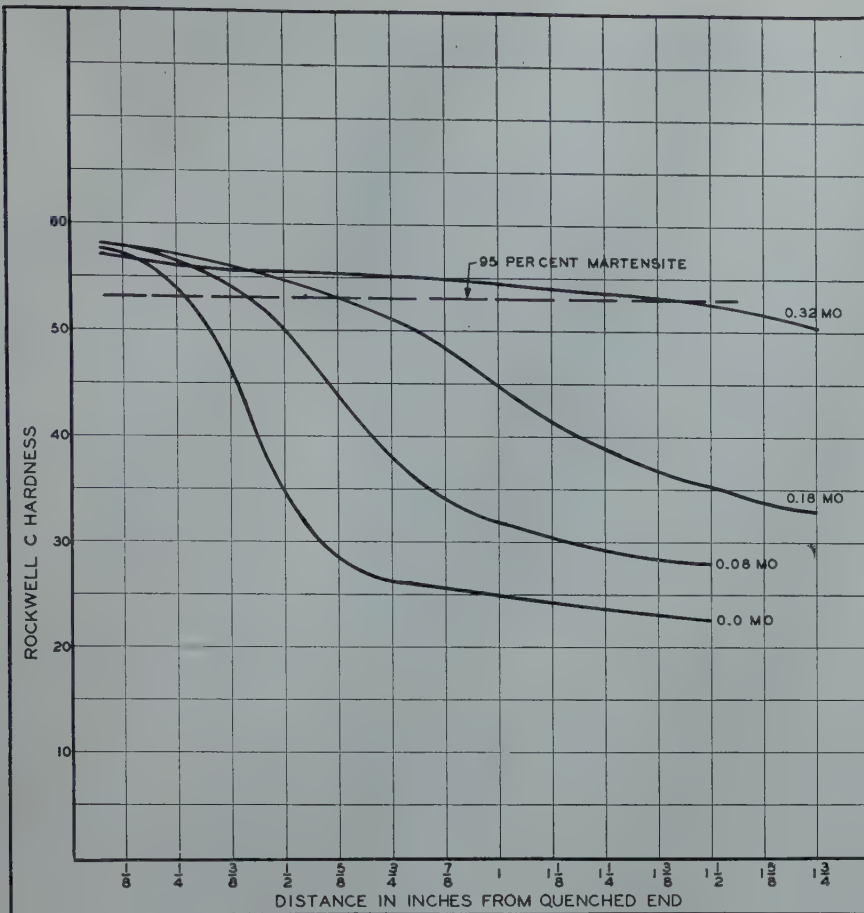


FIG 1—End quench hardenability curves for a series of 3 pct nickel steels.

mation at the bainite nose were converted to hardenability values in terms of ideal diameter by multiplying them by a factor of 1.5 and correlating the results with the cooling times from the A_1 to the bainite nose temperature in an ideal quench. This method is described in detail in the appendix.

Results and Discussion

The results of the hardness surveys on the end-quenched samples, austenitized at 1600°F, are shown in Fig 1 and 2. The 95 pct martensite points, determined microscopically, are also indicated on these curves. The location of this microstructure corresponds in general with the hardness value for 95 pct martensite as reported in Ref. 5. The hardenability factors for molybdenum, determined by dividing the ideal diameters of the steels containing molybdenum by the ideal diameters of those containing no molybdenum, are shown in Fig 3. It is evident that the hardenability effect of molybdenum is much more pronounced in the nickel than in the chromium steels. It is, perhaps, significant that the hardenability factors for molybdenum in the

chromium steel correspond approximately to those originally determined by Grossmann,¹ which are also shown.

The microstructures at the 95 pct martensite point on the end-quench test samples of each series containing 0.18 pct molybdenum are shown in Fig 4 and 5. The nonmartensitic products are predominantly bainitic in both steels. Some acicular ferrite is to be noted, however, and the nickel steel shows somewhat more of this apparently ferritic constituent.

The isothermal transformation studies were undertaken principally to determine if the hardenability differences noted in the results of end-quench tests reflected actual differences in the rate of transformation to bainite, or if they were associated with incubation effects or differences in nucleation which occurred during continuous cooling. The results of the isothermal transformation studies from samples austenitized at 1600°F are summarized by isothermal transformation diagrams in Fig 6 and 7. It is apparent from the diagrams that the transformation rates in both the pearlitic and bainitic regions have been decreased in both types of steel by the addition of molybdenum. There are also large differences in the

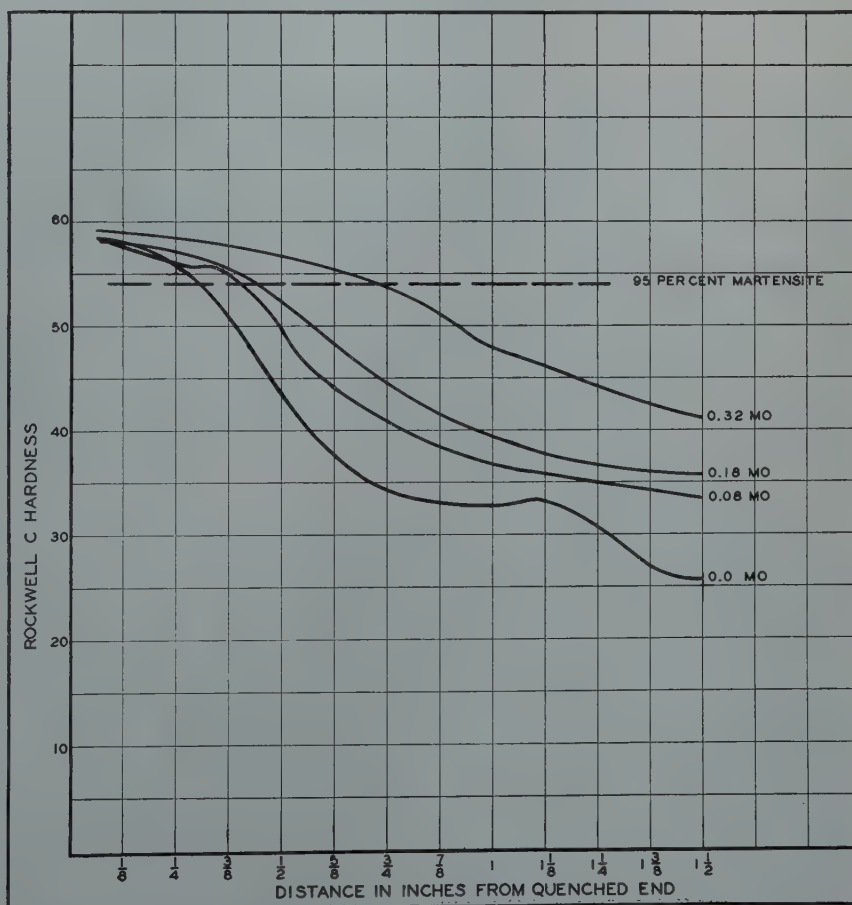


FIG 2—End quench hardenability curves for a series of 0.95 pct chromium steels.

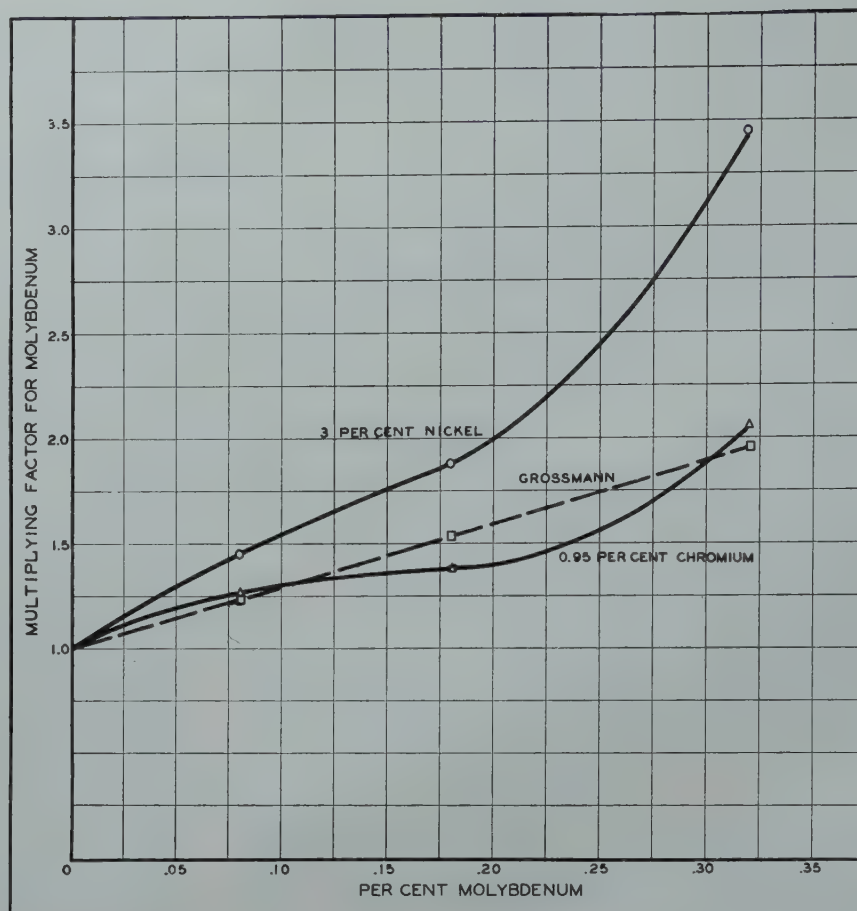


FIG 3—The hardenability effect of molybdenum in 3 pct nickel and 0.95 pct chromium steels. End quench tests.

magnitudes of these effects in the two types of steel. The molybdenum was much more effective in decreasing the transformation rates, in the temperature range 1000 to 1200°F, in the nickel than in the chromium steels.

As will be evident, this effect on the rates of transformation at the higher temperatures is not particularly pertinent to the present investigation, which is concerned with 95 pct martensite hardenability, the nonmartensitic products being predominantly bainitic. However, the large differences in the rates of transformation in the pearlitic range in the two types of steel would be very important if one were concerned with transformation to pearlitic microstructures.

There are also evident differences in the effect of molybdenum on the transformation rates at the bainite nose in the two types of steel. On converting these transformation time values to hardenability values, by the methods mentioned above and described in detail in the appendix, it is evident that these differences in the hardenability effects, as expressed by the multiplying

Table 2 . . . End Quench Test Results and Corresponding Hardenability Values

| 3 Pct Nickel Steels | | | | 0.95 Pct Chromium Steels | | | |
|---------------------|-------------------|-------------------|-------|--------------------------|-------------------|-------------------|-------|
| Pct Mo | J_D (Inches) | D_I (Inches) | M_F | Pct Mo | J_D (Inches) | D_I (Inches) | M_F |
| 0.0 | 0.27 | 2.05 | 1.00 | 0.0 | 0.31 | 2.19 | 1.00 |
| 0.08 | 0.40 | 2.97 | 1.45 | 0.08 | 0.388 | 2.76 | 1.26 |
| 0.18 | 0.625 | 3.87 | 1.88 | 0.18 | 0.45 | 3.03 | 1.38 |
| 0.32 | 1.41 | 7.06 | 3.44 | 0.32 | 0.733 | 4.51 | 2.06 |

Note: J_D = Jominy bar distance to 95 pct martensite
 D_I = Ideal diameter
 M_F = Multiplying factor

factors, are identical with those observed in the end-quench tests. The hardenability values for the end-quench and the isothermal transformation tests are given in Tables 2 and 3, respectively. It is apparent that, although the ideal diameters determined from the results of the end-quench tests are larger than those determined from the isothermal studies from an austenitizing temperature of 1600°F, the multiplying factors for molybdenum, calculated from the results of both tests, are substantially the same. These multiplying factors expressing

the hardenability effect of molybdenum in both the end-quench and isothermal transformation tests are plotted as a function of molybdenum content in Fig 8. Thus the hardenability effect of molybdenum and the differences in its effect in the two types of steel, as shown by the results of end-quench tests, are seen to be fully accounted for by the effect of molybdenum on the isothermal transformation rate to bainite.

Micrographs illustrating the appearance of the transformation products which formed at the nose temperature

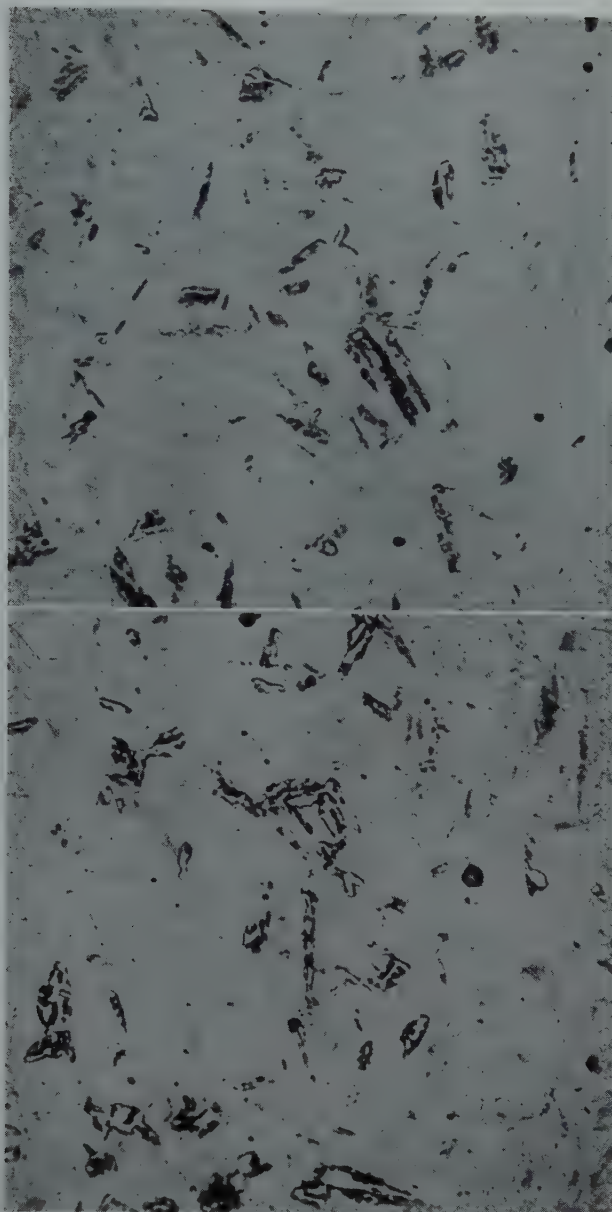


FIG 4—(Above) Microstructure of the end-quench bar at approximately 95 pct martensite in the 3 pct nickel, 0.18 pct molybdenum steel. Picral-zephiran chloride etch. $\times 1000$.

FIG 5—(Below) Microstructure of the end-quench bar at approximately 95 pct martensite in the 0.95 pct chromium, 0.18 pct molybdenum steel. Picral-zephiran chloride etch. $\times 1000$.

after about 5 pct transformation are shown in Fig 9 and 10. These products are similar in appearance to those observed at the 95 pct martensite point in the end-quench test samples. As would be expected, however, the transformation during the continuous cooling of the end-quench test samples evidently occurred at a somewhat lower average temperature than the isothermal nose temperature.

One plausible explanation for this difference in the hardenability effect of molybdenum in nickel and in chromium steels might be that it reflects differ-

ences in the rate of carbide solution in the two steels, at a given austenitizing temperature. In order to check this hypothesis, isothermal transformation studies were made at the bainite nose temperature, using austenitizing temperatures of 1800 and 2000°F. The results of these studies are superimposed on the isothermal transformation diagrams of Fig 6 and 7, and the corresponding hardenability values as a function of austenitizing temperature are shown in Fig 11 and in Table 3. The multiplying factors expressing the hardenability effects of molybdenum

in samples austenitized at these higher temperatures are superimposed on Fig 8 along with corresponding factors for 1600°F austenitization. It can be seen that, although the transformation rates to bainite are markedly decreased by increasing the austenitizing temperature, the hardenability effect of molybdenum and the differences in its effect on the two series of steels, remains unchanged with changes in the austenitizing conditions within the temperature range 1600 to 2000°F.

The probability appears remote that the rate of carbide solution with in-

Table 3 . . . Isothermal Test Results and Corresponding Hardenability Values

| Isothermal Tests | | | | | | | |
|------------------|------------------------------|----------------|-------|--------|------------------------------|----------------|-------|
| Pct Mo | Bainite Nose Times (Seconds) | D_I (Inches) | M_F | Pct Mo | Bainite Nose Times (Seconds) | D_I (Inches) | M_F |
| 1600°F | | | | | | | |
| 0.0 | 2.33 | 1.73 | 1.00 | 0.0 | 3.42 | 1.68 | 1.00 |
| 0.08 | 4.06 | 2.38 | 1.38 | 0.08 | 4.60 | 2.04 | 1.21 |
| 0.18 | 8.84 | 3.25 | 1.88 | 0.18 | 7.60 | 2.43 | 1.45 |
| 0.32 | 26.8 | 5.97 | 3.45 | 0.32 | 11.8 | 3.43 | 2.04 |
| 1800°F | | | | | | | |
| 0.0 | 5.17 | 2.48 | 1.00 | 0.0 | 7.0 | 2.47 | 1.00 |
| 0.08 | 9.8 | 3.54 | 1.43 | 0.08 | 10.0 | 3.07 | 1.24 |
| 0.18 | 18.6 | 4.56 | 1.84 | 0.18 | 16.0 | 3.76 | 1.52 |
| 0.32 | 55 | 8.30 | 3.35 | 0.32 | 24 | 4.83 | 1.96 |
| 2000°F | | | | | | | |
| 0.0 | 13.7 | 4.19 | 1.00 | 0.0 | 13.4 | 3.36 | 1.00 |
| 0.08 | 23.6 | 5.78 | 1.38 | 0.08 | 21.4 | 4.41 | 1.31 |
| 0.18 | 48 | 7.60 | 1.81 | 0.18 | 29.6 | 5.02 | 1.49 |
| 0.32 | 132 | 13.3 | 3.17 | 0.32 | 52 | 7.00 | 2.08 |

Note: D_I = Ideal diameter
 M_F = Multiplying factor

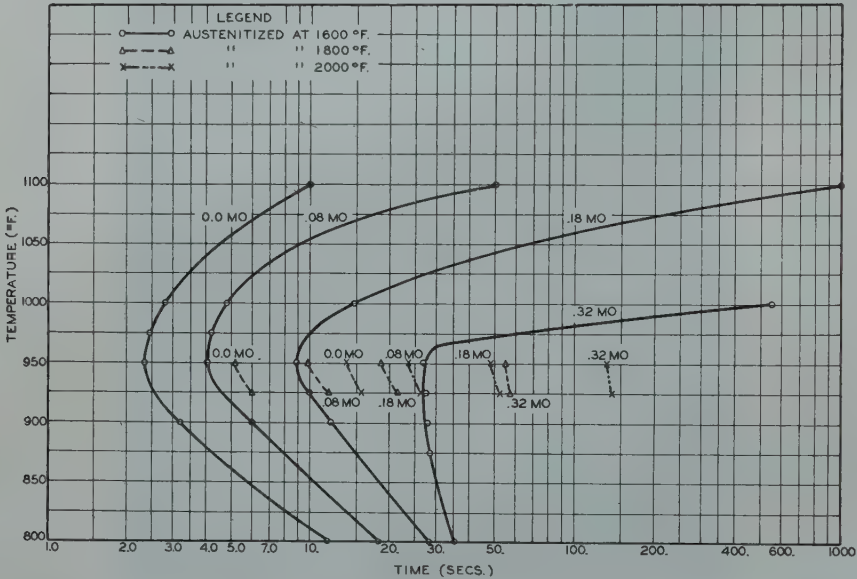


FIG 6—Isothermal transformation diagram for 5 pct total transformation in 3 pct nickel-molybdenum steels.

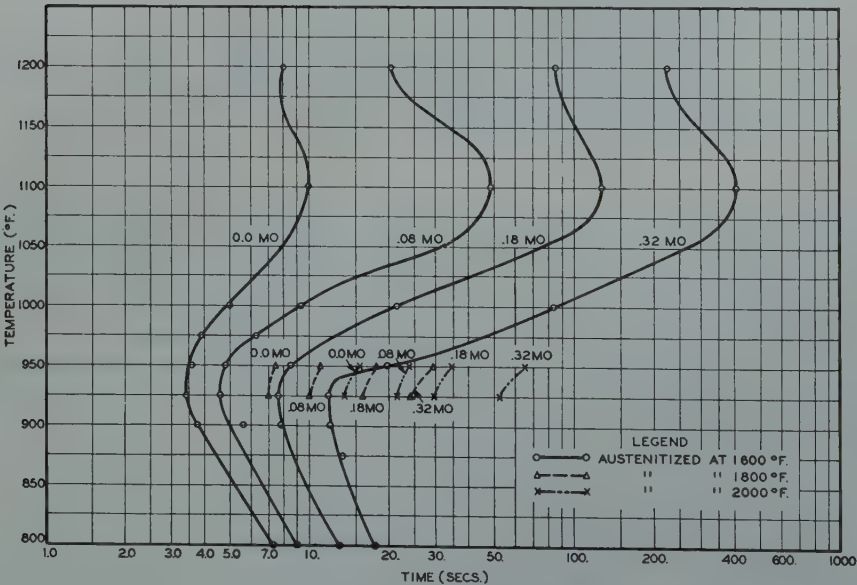


FIG 7—Isothermal transformation diagram for 5 pct total transformation in 0.95 pct chromium-molybdenum steels.

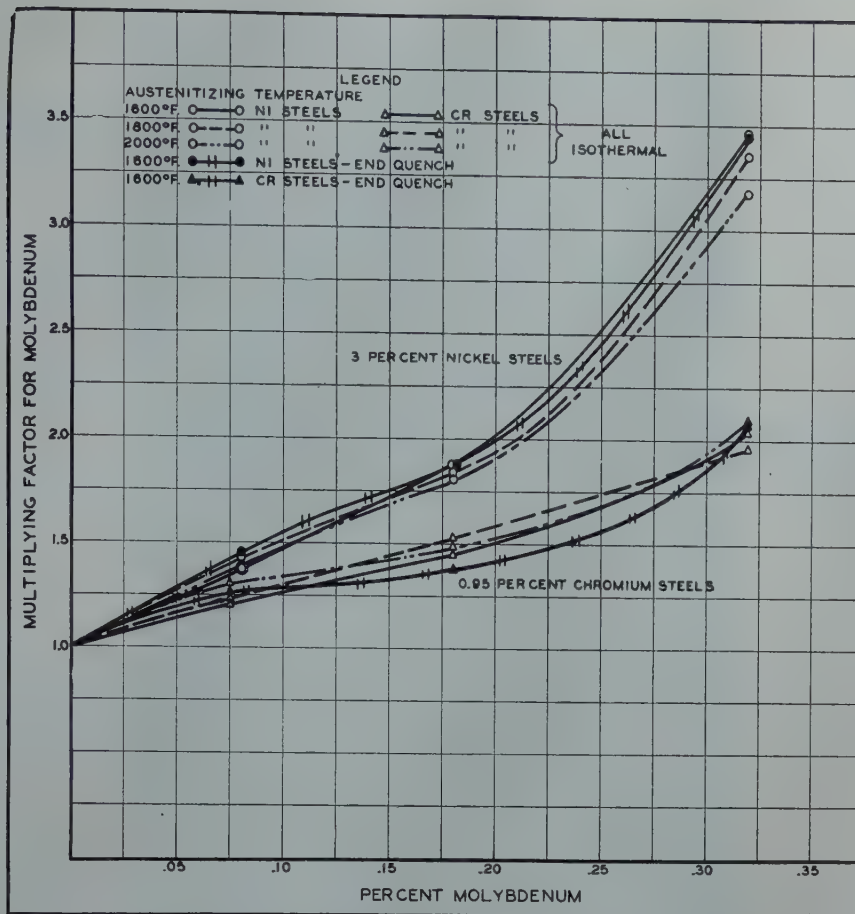


FIG 8—The hardenability effect of molybdenum as determined by end quench and isothermal transformation tests.

creasing austenitizing temperatures has caused these large increases in hardenability, because no undissolved carbides were observed in any of the steels after austenitizing at 1600°F. Furthermore, the increase is as marked in the nickel steel without molybdenum as it is in the chromium steel with 0.32 pct molybdenum. The increase in hardenability correlates roughly with the increase in grain size which accompanied the increased austenitizing temperature. This increase in hardenability, however, seems rather large to be ascribed altogether to the increased grain size, particularly as it is based on transformation rates in the bainite region.

Conclusions

1. The hardenability effect of molyb-

denum, based on end-quench tests of two series of steels, one with a base composition of 0.40 pct carbon and 3 pct nickel and the other with a base composition of 0.40 pct carbon and 1 pct chromium was more pronounced in the nickel steels; 0.32 pct molybdenum was about twice as effective in the presence of 3 pct nickel as in the presence of 1 pct chromium.

2. The hardenability effect of molybdenum in both steels, and the difference in its effect in the presence of nickel and chromium are quantitative reflections of its effect on the rate of transformation at the bainite nose temperature.

3. The hardenability effect of molybdenum in the presence of either nickel or chromium is unaffected by changes in austenitizing temperature over the temperature range of 1600 to 2000°F.

4. The explanation of the difference

in the effect of molybdenum on transformation rates to bainite in the presence of nickel or chromium was not apparent, but it did not seem to reflect differences in the rate of carbide solution in the two types of steels.

Appendix

CALCULATION OF HARDENABILITY VALUES FROM END-QUENCH AND ISOTHERMAL DATA

As mentioned in the body of this report, the hardenability values, as derived from the results of either the end-quench or isothermal transformation studies, are based on the cooling time from the A_1 to the bainite nose temperatures. This criterion was chosen because it permitted the isothermal transformation times at the bainite

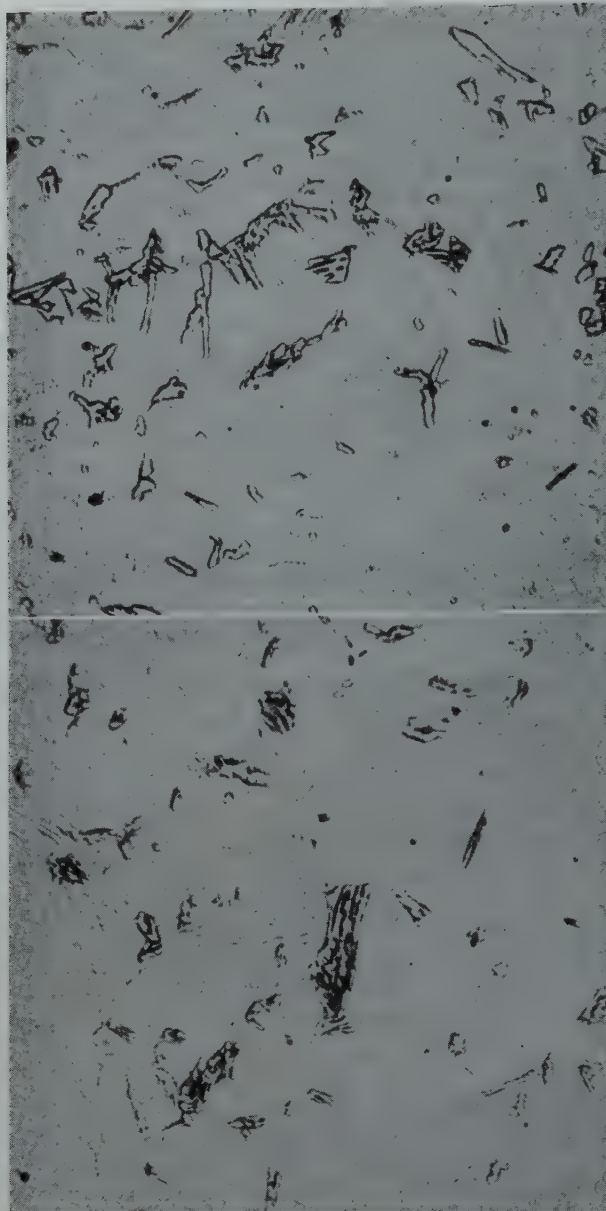


FIG 9—(Above) Microstructure of isothermal sample at the bainite nose temperature after about 5 pct transformation in the 3 pct nickel, 0.18 pct molybdenum steel. Picral-zephiran chloride etch. $\times 1000$.

FIG 10—(Below) Microstructure of isothermal sample at the bainite nose temperature after about 5 pct transformation in the 0.95 pct chromium, 0.18 pct molybdenum steel. Picral-zephiran chloride etch. $\times 1000$.

nose to be converted to hardenability values by the method developed by Grange and Kiefer.⁷ For consistency, therefore, the same criterion was used in evaluating the end-quench test results.

The correlation curves between Jominy distance and ideal diameter for the two series of steels, based on this criterion, are shown in Fig 12. The cooling time from A_1 to the bainite nose

temperatures, on which the ideal diameter values of these curves are based, were determined from the cooling rates along the end-quench bar which were recently published by Russell and Williamson.⁹ These cooling rates, plotted in terms of fractional temperature as a function of time, are reproduced in Fig 13.

In order to convert the cooling times from the A_1 to the bainite nose tem-

peratures to ideal diameter values, such cooling times for a series of cylinder sizes, assuming an infinite quench and diffusivity of 0.0099 sq. in. per sec were calculated from Russell's tables.⁸ From these times, plots correlating cooling time and ideal diameter were prepared for austenitizing temperatures of 1600, 1800, and 2000°F. These plots are shown in Fig 14, 15, and 16.

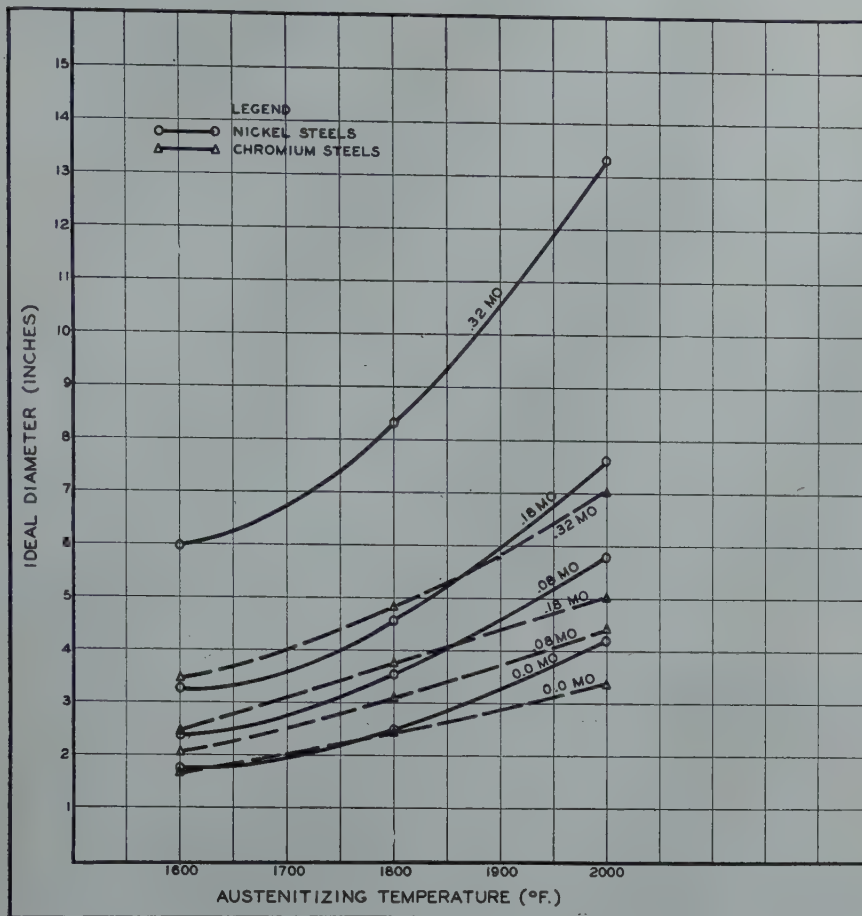
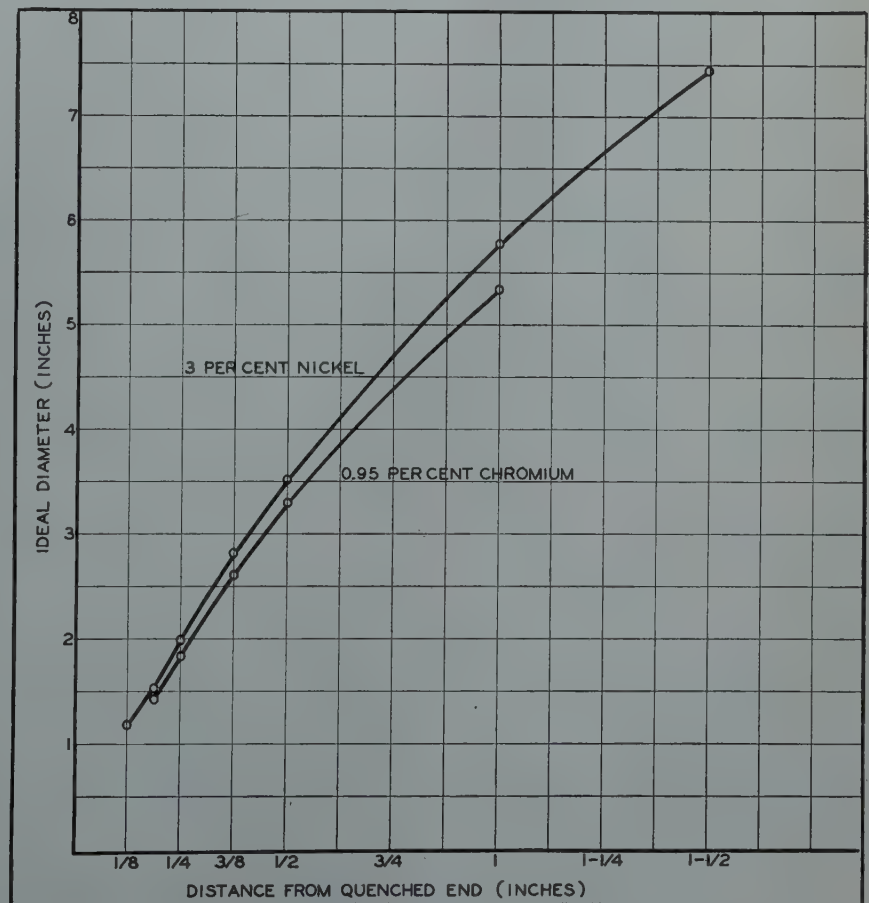


FIG 11—Hardenability as a function of austenitizing temperature in nickel-molybdenum and chromium-molybdenum steels.

FIG 12—Relationship between Jominy distance and hardenability based on cooling time from A_1 to the bainite nose temperature.



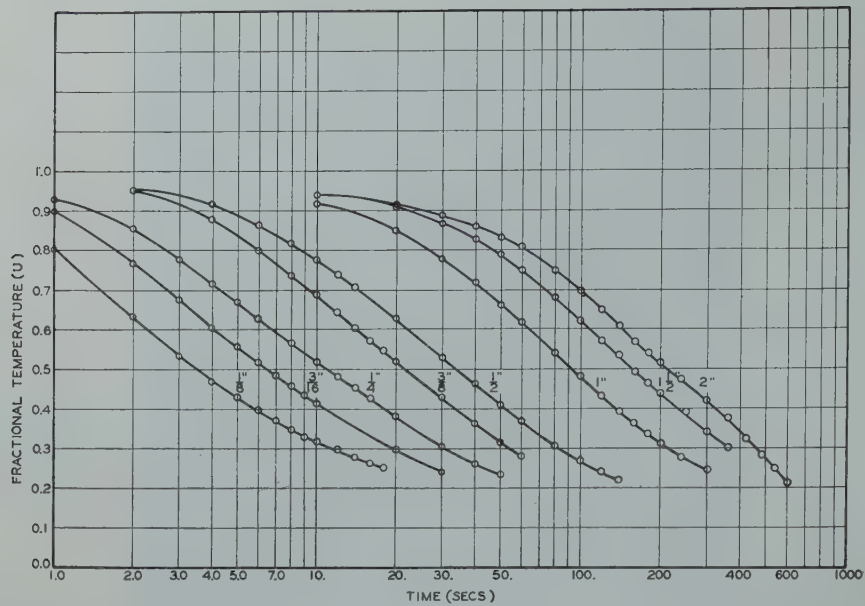


FIG 13—Cooling rates at different locations along an end quench bar quenched from approximately 1600°F. (Russell and Williamson.)

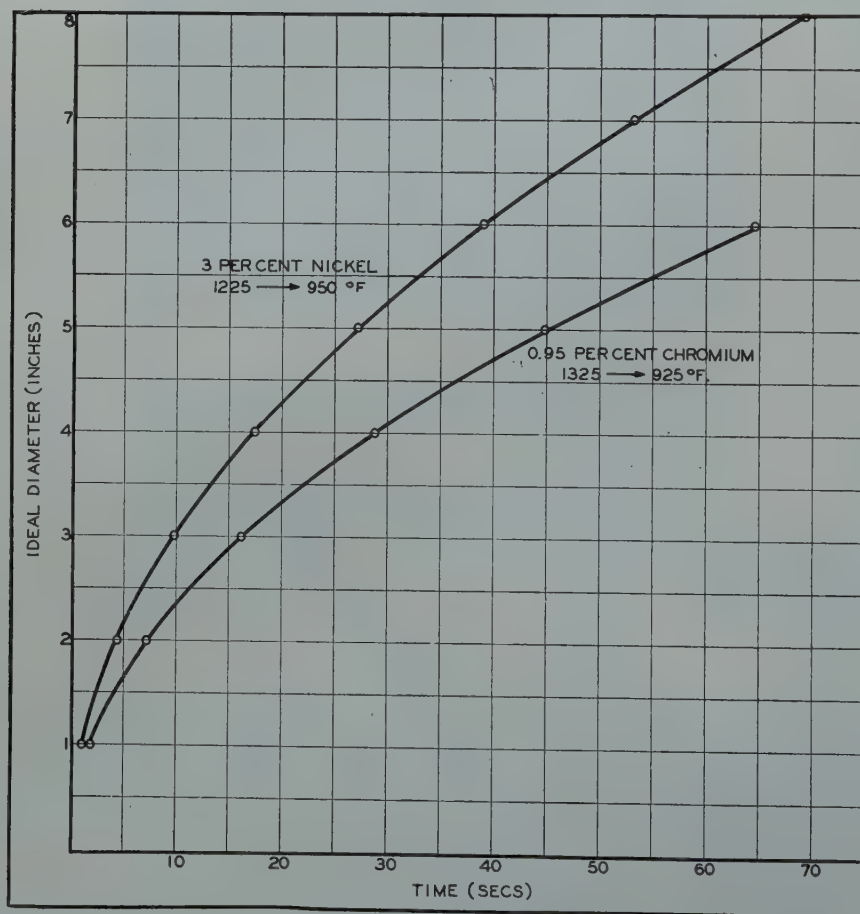


FIG 14—Relationship between ideal diameter and time to cool from the A_1 to the bainite nose temperatures. Austenitized at 1600°F.

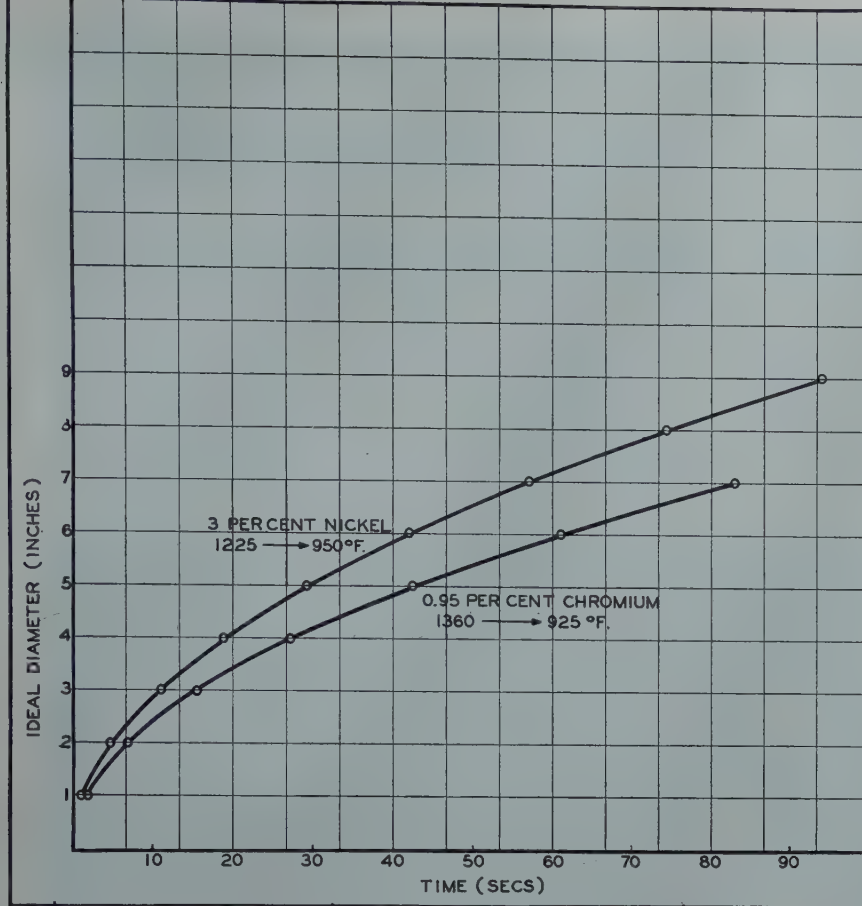


FIG 15—Relationship between ideal diameter and time to cool from the A_1 to the bainite nose temperatures. Austenitized at 1800°F.

The relationships between the distance from the quenched end of the Jominy bar and the ideal diameter, as shown in Fig 12, are therefore based on the cooling times as determined from Fig 13, and the relationship between cooling time and ideal diameter as shown in Fig 14. The hardenability values corresponding to the isothermal transformation times at the bainite nose were likewise determined from Fig 14, 15, and 16. These isothermal transformation times were multiplied by a factor of 1.5 before making this conversion. This factor of 1.5 represents the average relationship between the continuous cooling time from the A_1 to the nose temperatures and isothermal transformation time at the nose temperature, as determined by Grange and Kiefer.⁷

References

1. M. A. Grossmann: Hardenability Calculated from Chemical Composition. *Trans. AIME* (1942) 150, 227.
2. Walter Crofts and J. L. Lamont: The Effects of Some Elements on Hardenability. *Trans. AIME* (1944), 158, 157.

3. G. R. Brophy and A. J. Miller: An Appraisal of the Factor Method for Calculating the Hardenability of Steel from Chemical Composition. TP 1933, *Metals Tech.*, Oct. 1945; *Trans. AIME* (1946), 167, 654.
4. I. R. Kramer, S. Seigel, and J. G. Brooks: Factors for the Calculation of Hardenability. TP 2029, *Metals Tech.*, June 1946; *Trans. AIME* (1946), 167, 670.
5. J. M. Hodge and M. A. Orehoski: Relationship between Hardenability and Percentage of Martensite in Some Low-alloy Steels. TP 1800, *Metals Tech.*, Sept. 1945; *Trans. AIME* (1946), 167, 627.
6. J. M. Hodge and M. A. Orehoski: Hardenability Effects in Relation to the Percentage of Martensite. TP 1994, *Metals Tech.*, April, 1946; *Trans. AIME* (1946), 167, 502.
7. R. A. Grange and J. M. Kiefer: Transformation of Austenite on Continuous Cooling and Its Relation to Transformation at Constant Temperature. *Trans. Amer. Soc. for Metals*, (1941) 29, 85.
8. T. F. Russell: Some Mathematical Considerations on the Heating and Cooling of Steel. First Report of the Alloy Steels Res. Comm. The Iron and Steel Inst. (British), Spec. Rep. No. 14, (1936), 149.
9. T. F. Russell and J. C. Williamson: Surface Temperature Measurements during the Cooling of a Jominy Test-Piece. Symposium on the Hardenability of Steel, The Iron and Steel Inst. (British), Spec. Rep. No. 36, (1946) 34.

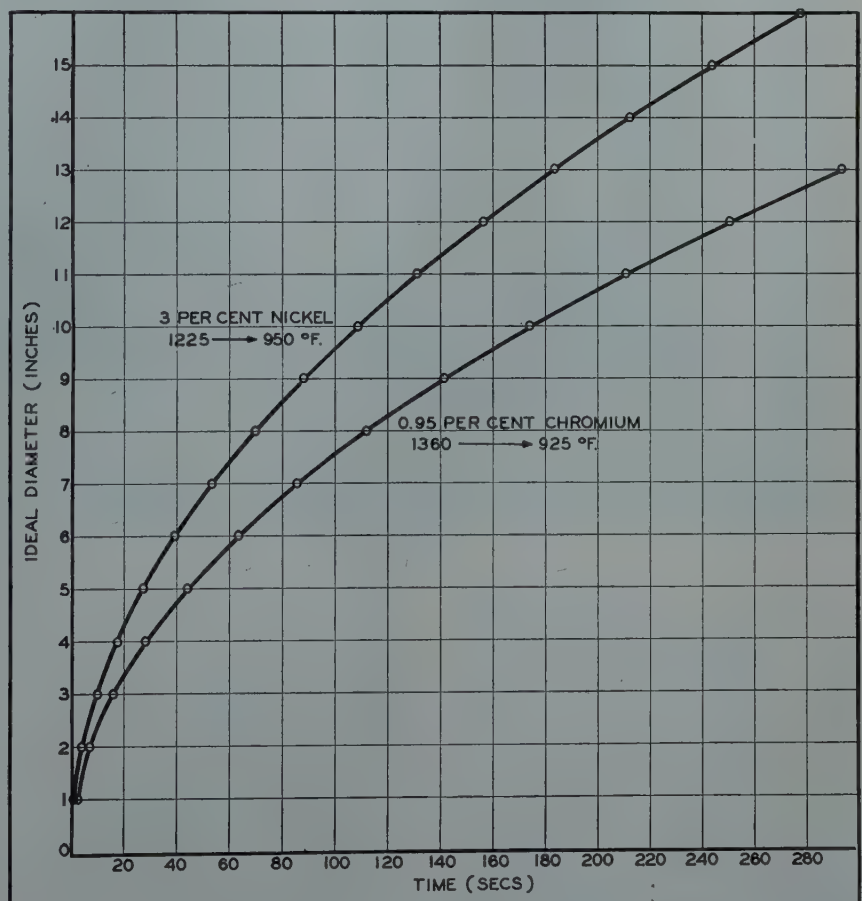
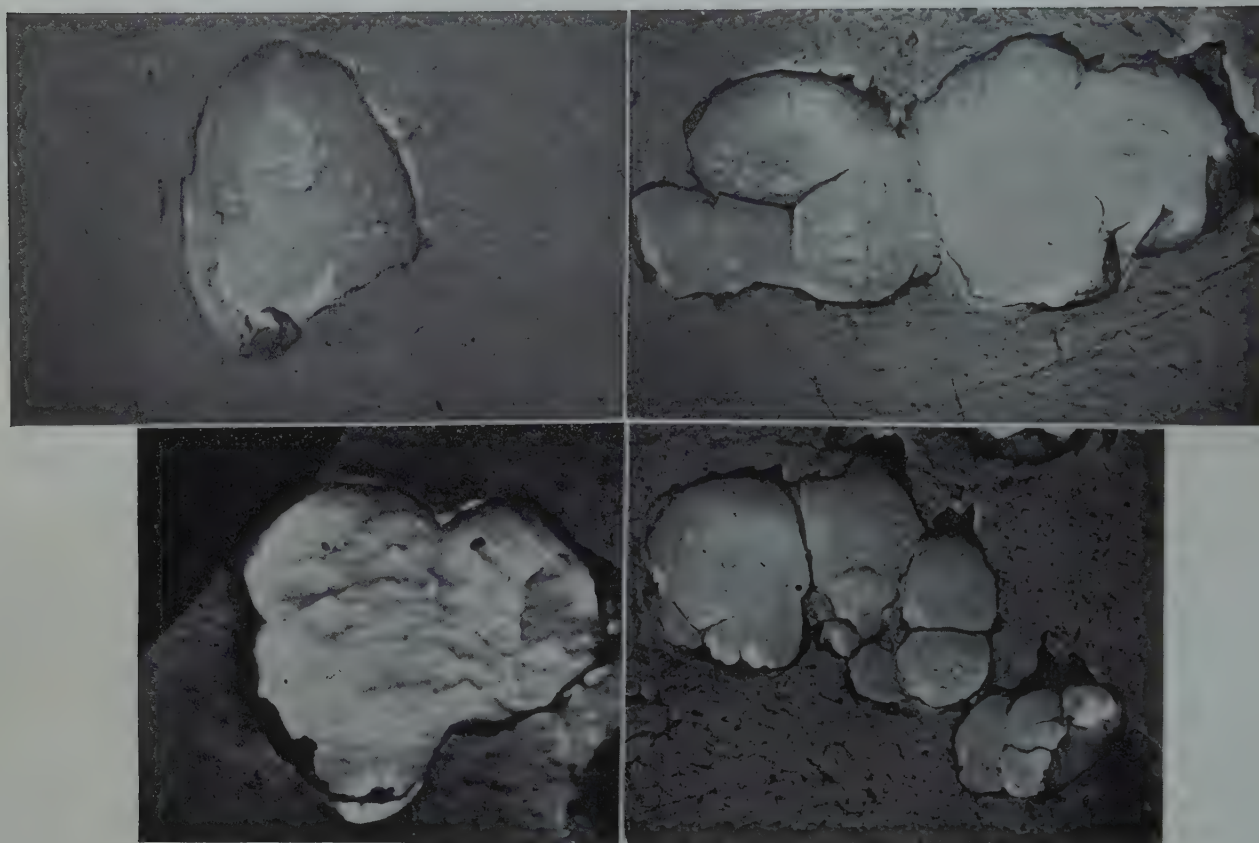


FIG 16—Relationship between ideal diameter and time to cool from the A_1 to the bainite nose temperatures. Austenitized at 2000°F.

A Method of Examination of Sections of Fine Metal Powder Particles with the Electron Microscope

LAURENCE DELISLE*



FIG—1 Tungsten powder particles $\times 10,000$. Reduced approximately one fourth in reproduction.

Introduction

THE aim of this paper is the description of a technique to be applied to the study of sections of metal powder particles, less than 20 microns in diam, with the electron microscope, by the replica method, using for replica a material such as formvar or parlodion.

This work originated with the study of particles of tungsten powders. Such particles were too small to be examined in sufficient detail with the light microscope. On the other hand, examination with the electron microscope of the

powders dispersed in the supporting film was not found satisfactory because: 1. It did not permit differentiating between single particles and aggregates. 2. It did not show the true outlines of the particles but only the projection of a whole surface. 3. No details appeared. For that reason it was

attempted to make replicas of sections of the particles imbedded in a mounting material suitable for polishing and etching. The method proved satisfactory for the examination of tungsten powder and was then extended to carbonyl nickel and carbonyl iron powders.

Procedure

Several mounting materials commonly used in ordinary metallography were investigated. The problem consisted in finding a mounting material

Cleveland Meeting, October 1949.
TP 2538 E. Discussion of this paper
(2 copies) may be sent to *Transactions*
AIME before Dec. 15, 1949. Manuscript received October 14, 1948; revision received December 7, 1948.
*Sylvania Electric Products Inc.,
Bayside, N. Y.

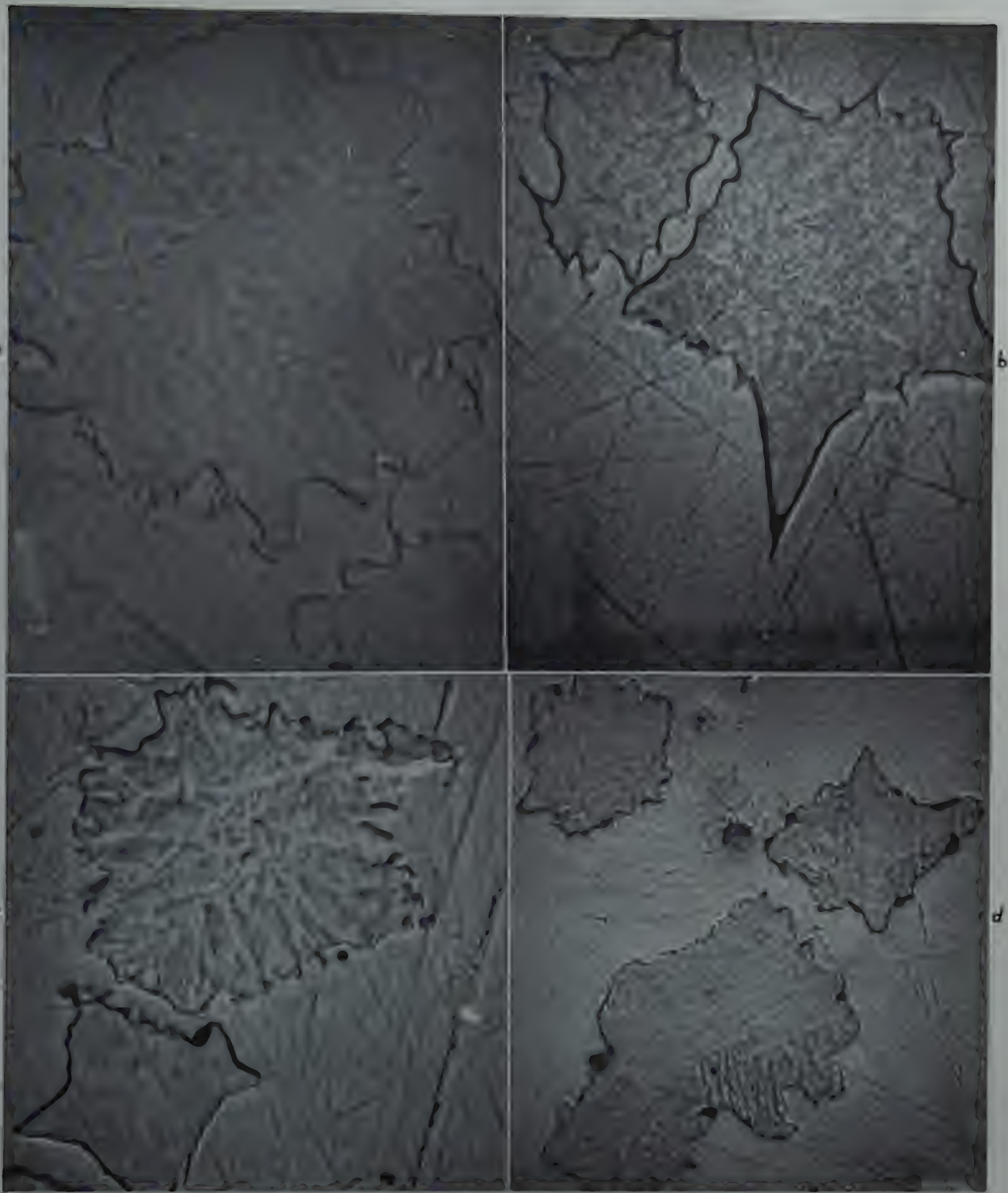


FIG 2—Particles of carbonyl nickel powder, a, b, c, $\times 10,000$, d, $\times 5,000$. Slightly reduced in reproduction.

that would (1) wet the metal particles, (2) be of proper hardness to give, after polishing, a fairly smooth surface from which a replica could be stripped, (3) resist the attack of etchants, (4) be incompatible with the replica material to permit stripping.

Of the mounting materials investigated, aerotex M-3, a water soluble melamine formaldehyde plastic, was found to be the easiest to use. A thick

paste was made by mixing the powder in a little aerotex. A thin layer of this mixture was spread on a square of glass, about $\frac{1}{2}$ in. on the side, thick enough to permit easy holding during polishing. The best final surface was obtained by spreading the mixture of powder in aerotex into a film as thin as possible. Under such a condition, the aerotex polymerizes into a continuous film that seems to gain strength from the glass

backing. A thick layer of aerotex gives a porous rough surface after polymerization. Polymerization was carried out in a drying oven at 140°C for 2 hr. The specimens were then carefully polished and etched* in the ordinary man-

* Standard etchants were used as follows:
 Powder Etchant
 Tungsten 10g NaOH, 10g $\text{FeK}_3(\text{CN})_6$, 100cc water
 Nickel Merica's solution: HNO_3 (70 pct) 50cc; CH_3COOH (50 pct) 50cc
 Iron 2 pct nital
 All etchants were applied by flooding.

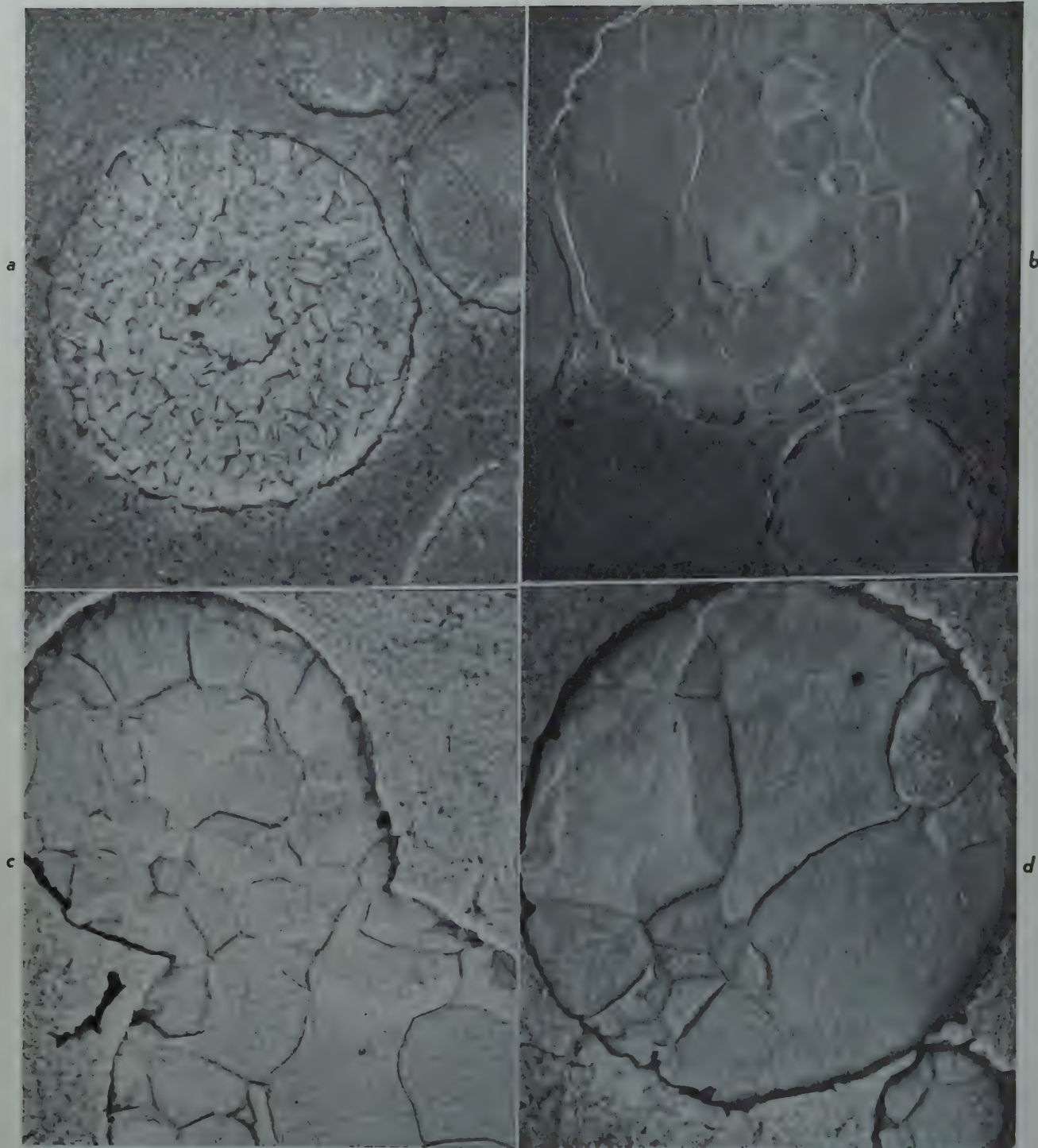


FIG 3—Particles of carbonyl iron powder illustrating differences in grain size. $\times 10,000$. Slightly reduced in reproduction.

ner for metallographic work through emery papers, silk cloth and velvet. The usual precautions to prevent removal of inclusions from metallographic specimens had to be observed; consequently most of the polishing was carried out on the silk wheel with alumina from Linde Air Products Co. as an abrasive. Either formvar or parlodion replicas could be stripped from the surface and shadow-cast as is customary.

Results

Fig 1 shows sections through particles of a sample of tungsten powder. The shape and microstructure of the particles are clearly visible. Evidently many aggregates actually consist of small particles sintered together; the sintering probably took place during reduction of the tungsten oxide in the preparation of the metal powder. The

resolution power of the light microscope is not sufficient to permit such an observation. Examination with the electron microscope of the powder dispersed in the supporting film also fails to indicate whether the aggregates consist of separate particles just touching one another or of particles bonded together into actually much larger particles.

Fig 2 shows sections through particles of a sample of carbonyl nickel

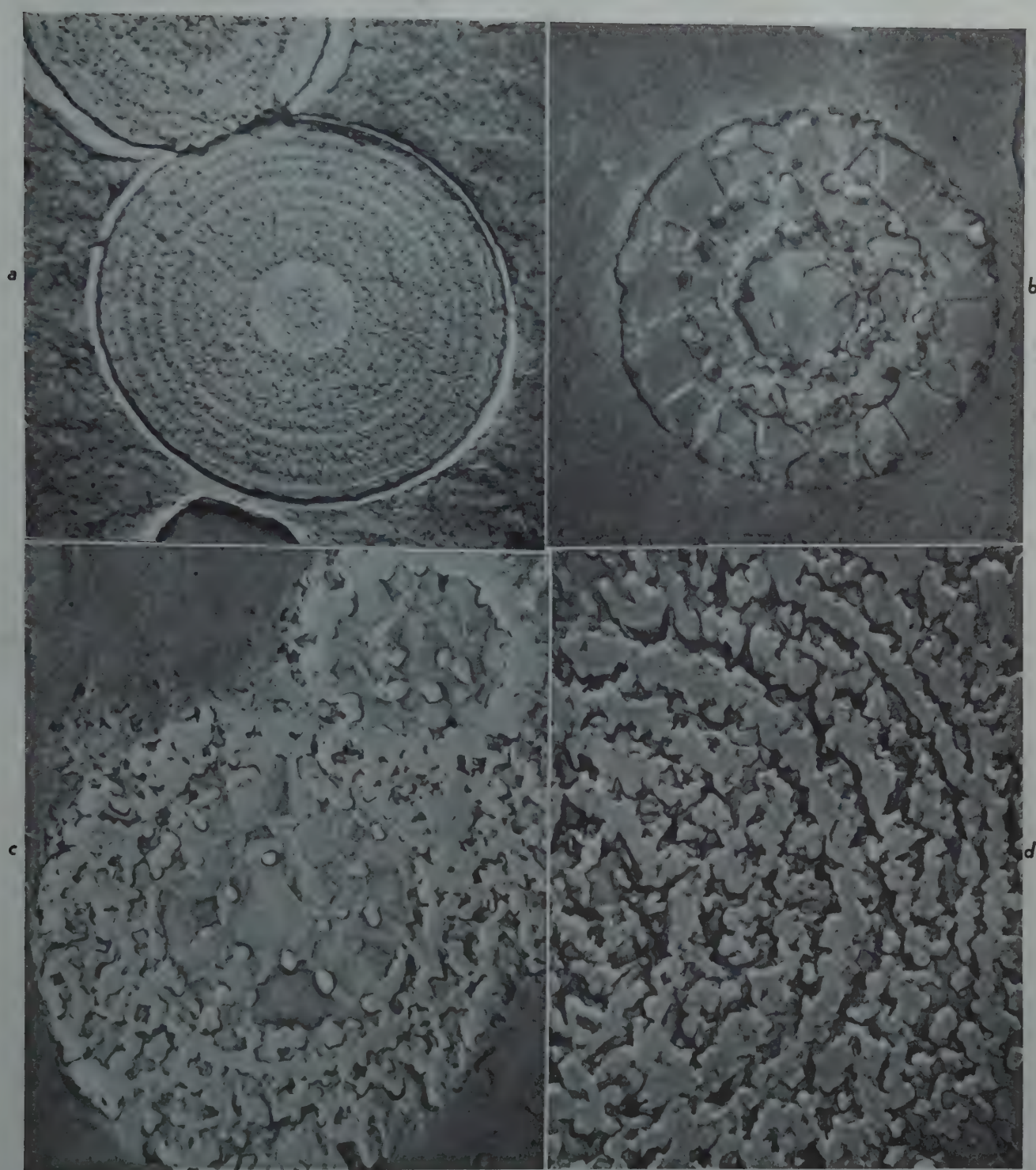


FIG 4—Particles of carbonyl iron powder illustrating differences in the structure. $\times 10,000$. Slightly reduced in reproduction.

powder. In this case, the large specific area of the powder is evidenced by the jagged outline of the particles. Again the resolution power of the light microscope is too low to reveal the surface condition of the particles of such a powder. Examination with the electron microscope of the powder dispersed in the supporting film would also fail to bring out the surface details of the powder or would, at least, show them less clearly than replicas of the sections

do.

Fig 3, 4 and 5 show sections through particles of a sample of carbonyl iron powder. The shape and microstructure of the particles are again clearly visible. The diversity in grain size and structure of the particles of a small sample of a powder is striking. Fig 3 illustrates differences in grain size; Fig 4 brings out differences in the structure of particles with the characteristic "onion skin" appearance; Fig 5 is a micro-

graph of the same particle as Fig 4a at a higher magnification; it emphasizes the presence of two finely dispersed constituents which are alternately in larger proportions forming concentric darker and lighter rings. The number and sharpness of the structural details visible with the electron microscope is greatly increased over those brought out with the ordinary microscope. From observations with the ordinary microscope, for instance, one might be temp

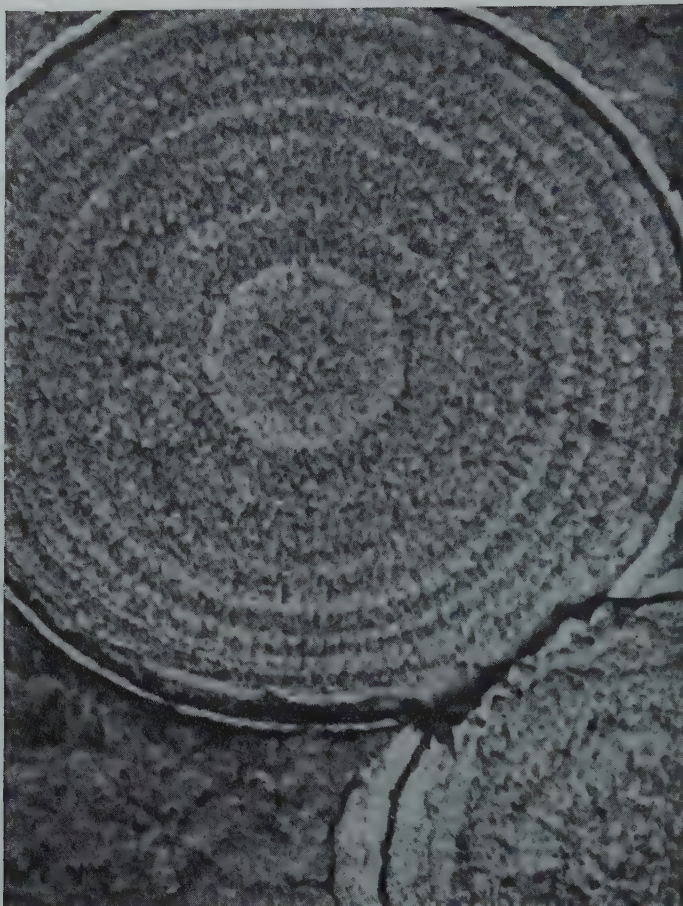


FIG 5—Particles of carbonyl iron powder. Micrograph of Fig 4a at a higher magnification. $\times 15,000$.

ted to exaggerate the occurrence of particles with an "onion skin" structure and to attribute the absence of such a structure in a large number of particles to improper etching. Really many particles consist of polyhedral grains of iron too small to be resolved with the light microscope.

Conclusions

The micrographs in this paper prove that the application of the electron microscope to the study of fine metal powders can be extended to the examination of sections of the particles. The microstructure of such particles can thus be revealed beyond the range of resolution of the light microscope. Added information can also be obtained

on the size, shape and surface condition of metal particles by a study of their cross-sections with the electron microscope over the information obtainable with the same instrument from a study of the powders dispersed in supporting films.

Acknowledgment

The author is grateful to Sylvania Electric Products, Inc. for its generous support of this work. The author also wishes to extend her thanks to Mr. W. E. Kingston, Manager of Metallurgical Research, for his patient guidance, to Mr. G. A. Davis, Section Head of Physical Metallurgy, for his assistance and constructive criticism, and to Dr. B. Kopelman, Section Head of Basic Research, for his advice on plastics.

References

1. V. J. Schaefer and D. Harker: Surface Replicas for Use in the Electron Microscope. *Jnl. of Appl. Phys.*, (1942), 13, 427-433.
2. V. J. Schaefer: New Methods for Preparing Surface Replicas for Microscopic Observation. *Phys. Rev.*, (1942), 62, 495-496.
3. V. J. Schaefer: Dry Stripping Replicas for the Electron Microscope. *Science*, (1943) 97, 188.
4. D. Harker and M. J. Murphy. A Study of Age-hardening Using the Electron Microscope and Formvar Replicas. *AIME Trans.* (1945) 161, 75-89.
5. L. Thomassen, R. C. Williams and R. W. G. Wykoff: Surface Replicas for Electron Microscopy. *Rev. of Scient. Instruments*, (1945) 16, 155.
6. Helmut Thielsch: Shadow Cast Replicas for Use in the Electron Microscope. *Metals Tech.*, Feb. 1946, TP 1977; *Trans. AIME* (1946) 166, 37.

The Effect of Ferrite Grain Size on Notch Toughness

J. M. HODGE,* R. D. MANNING,* Members AIME, and H. M. REICHHOLD*

Introduction

THE work reported in this paper represents the first of a series of investigations of the factors governing notch toughness in ferritic materials. This paper is concerned with two of these factors, namely, the effect of ferrite grain size, and the effect of an alloy content of 3.64 pct nickel. Every effort has been made to hold other variables constant in order to isolate the effects of these two. The compositions chosen for study were 0.02 pct carbon in order to eliminate the variable of carbide distribution, one steel being a plain carbon steel and the other alloyed with 3.64 pct nickel. Both steels were fully killed with silicon, without an aluminum addition, so that the variable of deoxidation practice was held constant. Finally, all samples were water quenched from 1200°F and tempered 24 hr at 300°F in order to hold the quench aging variable constant and to decrease the tendency for grain boundary carbide precipitation.

The ferrite grain size was varied by heat treatment over the range of A.S.T.M. grain size numbers of about 2 to 6 in each steel so that the effect could be evaluated individually and the notch toughness of each steel could be compared at comparable ferrite grain sizes.

Table 1 . . . Composition of Steels—Per Cent

| Heat No. | C | Mn | P | S | Si | Ni | Al (acid sol.) | N* | O* |
|----------|------|------|-------|-------|------|------|-------------------|-------|-------|
| 3539 | 0.02 | 0.52 | 0.009 | 0.018 | 0.17 | 0.03 | 0.009 | 0.002 | 0.019 |
| 3537 | 0.02 | 0.55 | 0.011 | 0.017 | 0.18 | 3.64 | 0.006 | 0.005 | 0.018 |

* By vacuum fusion analysis.

Materials and Experimental Procedure

MATERIALS

The materials for this investigation were obtained from Battelle Memorial Institute as 250 lb induction melts which were forged into 1½ in. square bars and then rolled into 0.6 in. square bars. Both steels were deoxidized with silicon, the aluminum content being held to a minimum. Check analyses of these materials are shown in Table 1.

HEAT TREATMENT FOR GRAIN SIZE

The grain size was varied by varying both the cooling rate and the austenitizing temperatures.

The heat treatments used and the corresponding grain size values are tabulated in Table 2.

A semicontinuous network of grain boundary carbide was observed in the microstructure of both the plain carbon and nickel steels in the as rolled condition and an additional heat treatment was necessary to eliminate this variable. Therefore, all samples were water quenched from 1200°F and tempered 24 hr at 300°F as a final treatment before testing. This heat treatment served to eliminate to a great extent the grain boundary carbide network and to hold the quench aging effect constant.

IMPACT TESTING

Standard keyhole Charpy impact tests were machined after heat treatment. A bath of acetone and dry ice was used for refrigeration of the samples down to temperatures of -94°F (-70°C) and a bath of either methylcyclohexane or isopentane, cooled by

Cleveland Meeting, October 1949.
TP 2553 E. Discussion of this paper (2 copies) may be sent to *Transactions AIME* before Dec. 15, 1949. Manuscript received Nov. 1, 1948; revision received Dec. 18, 1948.

* Carnegie Illinois Steel Corporation.



FIG 1—Microstructure of rapidly cooled plain carbon steel, Heat 3539, Code C, illustrating ferrite grain size of 5. Nital etch. $\times 100$.

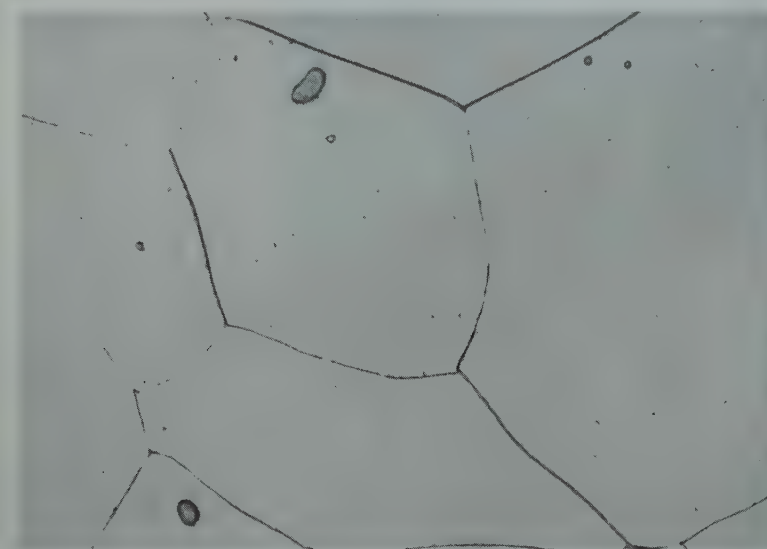


FIG 2—Microstructure of rapidly cooled plain carbon steel, Heat 3539, Code C. Nital etch. $\times 1000$.

Table 2 . . . Summary of Heat Treatments and Corresponding Hardness Ferrite Grain Size, and Transition Temperature

| Heat No. | Code | Austenitizing Temperature, °F | Cooling Method | Hardness RB | Ferrite Grain Size No. | Transition Temperature, °F |
|----------|------|-------------------------------|---|-------------|------------------------|----------------------------|
| 3539 | B | 1800 | Quenched in lead at 1300°F, held 2 hr—air cooled | 61 | 5 (4-6) | - 88 \pm 12 |
| 3539 | C | 1700 | Quenched in lead at 1000°F, held 15 min.—air cooled | -63 | 5 (4-6) | - 82 \pm 12 |
| 3539 | M | 1700 | Quenched in brine | 63 | 5 (4-7) | - 73 \pm 14 |
| 3539 | K | 2000 | Quenched in brine | 62 | 3-4 (2-5) | - 20 \pm 35 |
| 3539 | S | | AS ROLLED | 62 | 3-4 (3-5) | - 39 \pm 16 |
| 3539 | A | 1800 | Furnace cooled at 20°F per hr to 1000°F—air cooled | 48 | 2-3 (2-4) | - 12 \pm 17 |
| 3539 | R | 2000 | Furnace cooled at 20°F per hr to 1000°F—air cooled | 51 | 1-2 (0-3) | \pm 45 \pm 25 |
| 3537 | V | 1650 | Quenched in brine | 77 | 6 (5-7) | -177 \pm 17 |
| 3537 | N | 1650 | Air cooled | 76 | 6 (5-7) | -171 \pm 19 |
| 3537 | E | | AS ROLLED | 77 | 5 (4-6) | -133 \pm 14 |
| 3537 | H | 1950 | Quenched in lead at 1100°F, held 2 hr—air cooled | 76 | 4-5 (4-6) | -112 \pm 16 |
| 3537 | D | 2200 | Furnace cooled at 20°F per hr to 1000°F—air cooled | 72 | 3 (2-4) | - 85 \pm 13 |
| 3537 | T | 2400 | Furnace cooled at 20°F per hr to 1000°F—air cooled | 73 | 2 (0-4) | - 57 \pm 16 |

Notes:
After above treatments all bars were heated at 1200°F for one-half hour and water quenched, and then were heated for 24 hr at 300°F and air cooled.
Numbers in parentheses under Ferrite Grain Size Number refer to the range of grain sizes present.

liquid nitrogen, was used for the lower temperatures. Wherever possible, three tests were broken at a given temperature. In the vicinity of the beginning and ending of the transition temperature range, testing was conducted in such a way as to restrict the testing interval to 10°F. The appearance of the fracture was noted on each test and was recorded in terms of the percent of the area which showed a cleavage type of fracture.

ESTIMATION OF FERRITE GRAIN SIZE

The ferrite grain size was estimated by comparison of the microstructure at a magnification of 100 with standard grain size charts. The grain size reported is the predominant grain size, as a range of grain sizes was present in most samples. The values represent an average of the estimations of three independent observers.

HARDNESS MEASUREMENT

Rockwell B hardness measurements were made on impact samples from each heat treatment.

END-QUENCH TESTS

Standard $\frac{1}{2}$ in. end-quench tests, austenitized at 1700°F, were made on each steel to study the effect of cooling rate on ferrite grain size. Ferrite grain size as a function of the distance from the quenched end of the bar was determined by metallographic examination.

Results and Discussion

MICROSTRUCTURE

Typical microstructures of the two steels after the final treatment are shown in Fig 1-4.

RELATIONSHIPS AMONG FERRITE GRAIN SIZE, NICKEL CONTENT, TRANSITION TEMPERATURE AND IMPACT VALUES

Plots of the impact values as a function of testing temperature for each of the steels at each grain size value are shown in Fig 5-17. The corresponding transition temperature was determined from each of these plots. This was defined as the middle of the temperature range over which an impact value of 40 ft-lb was obtained. These temperatures and the temperature ranges at 40 ft-lb for each of the conditions are

tabulated in Table 2. The value of 40 ft-lb was chosen as a criterion inasmuch as most of the actual test results fell either below or above this value and it therefore represents the point at which the energy is changing most rapidly with changes in transition temperature.

The transition temperature values for the two steels are plotted as a function of ferrite grain size in Fig 18. A straight line relationship between ferrite grain size and transition temperature for each of the steels is indicated by these results. An increase of ferrite grain size of one A.S.T.M. grain size number is thus seen to raise the transition temperature by 30°F in each steel. The transition temperature of the 3.64 pct nickel steel is, however, 60°F lower at a given ferrite grain size than the plain carbon steel, even though the nickel steels are at a somewhat higher hardness level. Inasmuch as the other variables were held constant, this improvement in notch toughness, represented by the lower transition temperatures of the nickel steels, is apparently a specific effect of nickel as an alloying element in ferrite.

The average impact values at room temperature for both steels are plotted as a function of ferrite grain size in Fig 19. A fair correlation also exists between these room temperature values and ferrite grain size, an increase in ferrite grain size of one A.S.T.M. grain size number decreasing the impact value by approximately 8 ft-lb. This relationship, however, appears to be independent of nickel content, as the nickel steel does not show consistently higher impact values than the plain carbon steel at a given grain size level.

FACTORS GOVERNING FERRITE GRAIN SIZE

The range of ferrite grain sizes studied in this investigation was obtained by varying both the austenitizing temperature and the cooling rate. The relationships among austenitizing temperature, cooling rate and ferrite grain size for the steels of this investigation are summarized in Fig 20. It was found that, at a constant cooling rate, the ferrite grain size changed rather slowly with changes in austenitizing temperature, an increase in austenitizing temperature from 1800 to 2000°F corresponding to an increase in ferrite grain size of about one grain size number. Increasing the cooling rate, however,

was much more effective in decreasing the ferrite grain size of the plain carbon steel than that of the nickel steel. Increasing the cooling rate from a furnace cool at 20°F per hr to a brine quench, decreased the ferrite grain size of the plain carbon steels by approximately two grain size numbers, while a similar change in cooling rate resulted in a decrease of only one grain size number for the nickel steel.

The effect of cooling rate on the ferrite grain size in the two steels was further evaluated by end quench tests. One-half inch diameter specimens were used because of the size limitation, and the standard procedure for ½ in. end quench tests was followed. The specimens of both steels were austenitized

at 1700°F, and the results are plotted in Fig 21 in terms of ferrite grain size as a function of distance from the quenched end. Here again, the plain carbon steel shows a much more pronounced effect of cooling rate on ferrite grain size than does the nickel steel.

The above results are explainable on the basis that the ferrite grain size for a given austenite grain size reflects the average temperature at which ferrite precipitates during cooling. The slower transformation rate of the nickel ferrite would thus result in a lower average temperature of ferrite precipitation at a given cooling rate and a correspondingly smaller, final ferrite grain size. Furthermore, the differences in the effect of cooling rate on ferrite grain

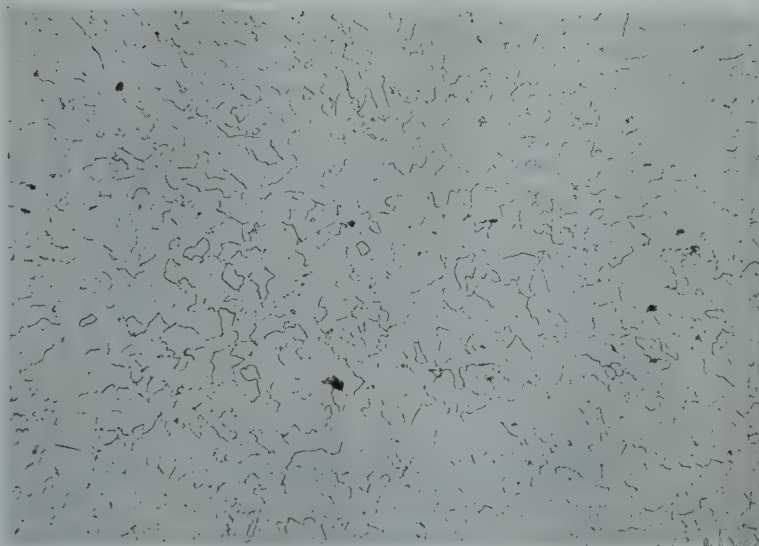


FIG 3—Microstructure of rapidly cooled nickel steel, Heat 3537, Code N, illustrating ferrite grain size of 6. Nital etch. $\times 100$.

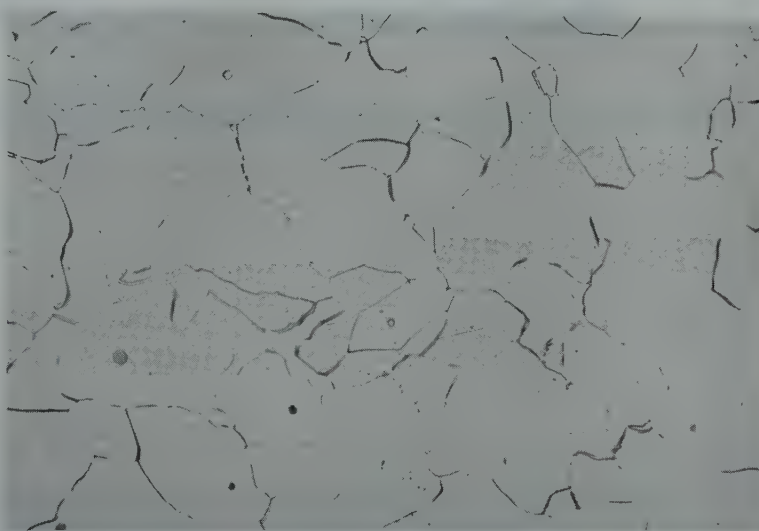


FIG 4—Microstructure of rapidly cooled nickel steel, Heat 3537, Code N. Nital etch. $\times 1000$.

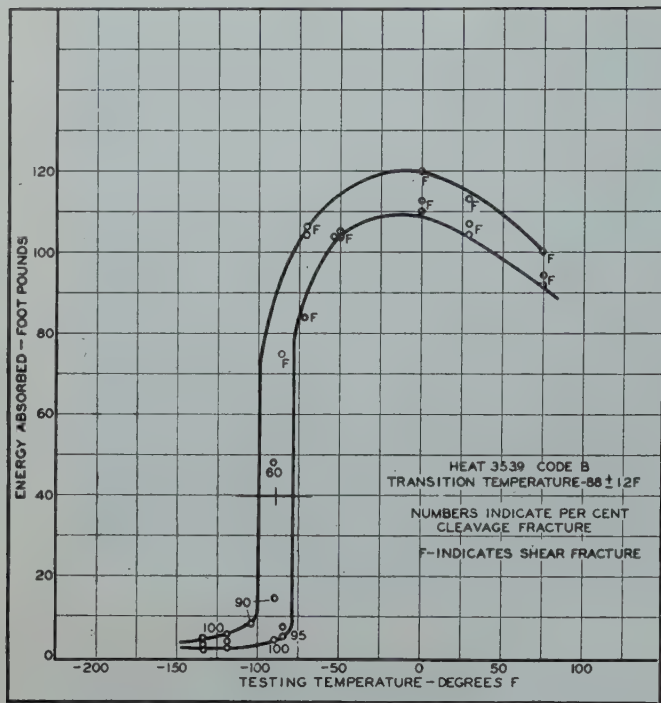


FIG 5—Impact-temperature curve for plain carbon steel at a ferrite grain size of 5.

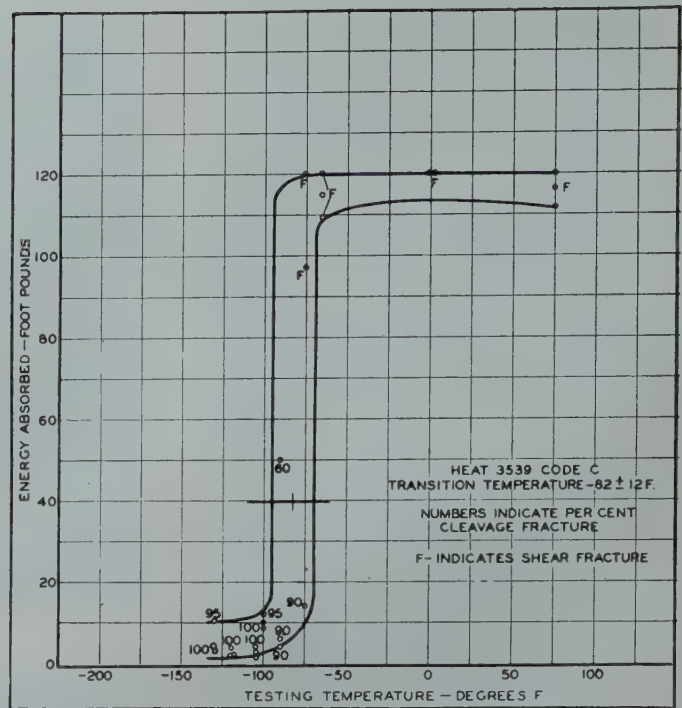


FIG 6—Impact-temperature curve for plain carbon steel at a ferrite grain size of 5.

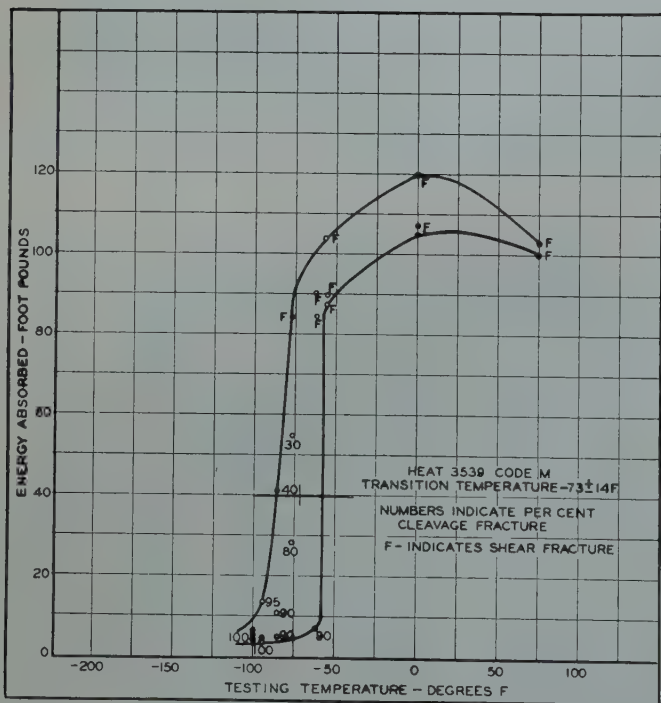


FIG 7—Impact-temperature curve for plain carbon steel at a ferrite grain size of 5.

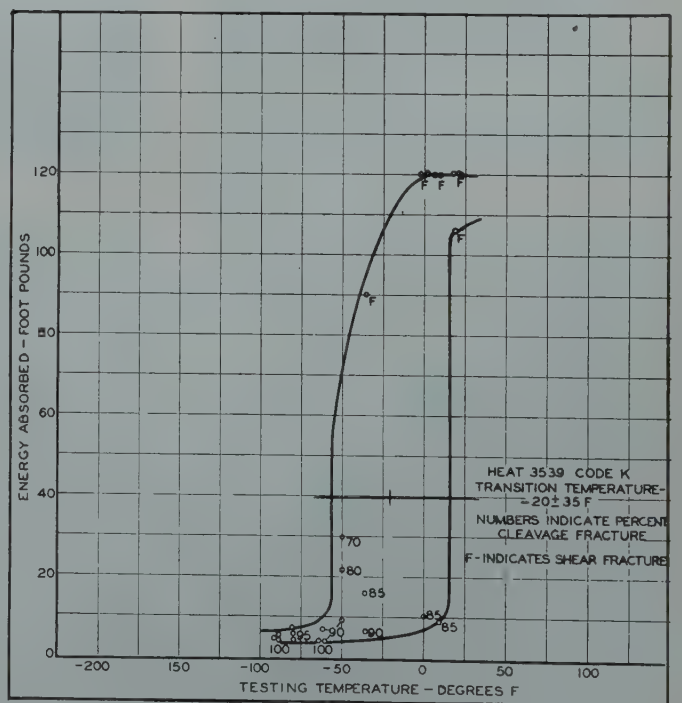


FIG 8—Impact-temperature curve for plain carbon steel at a ferrite grain size of 3-4.

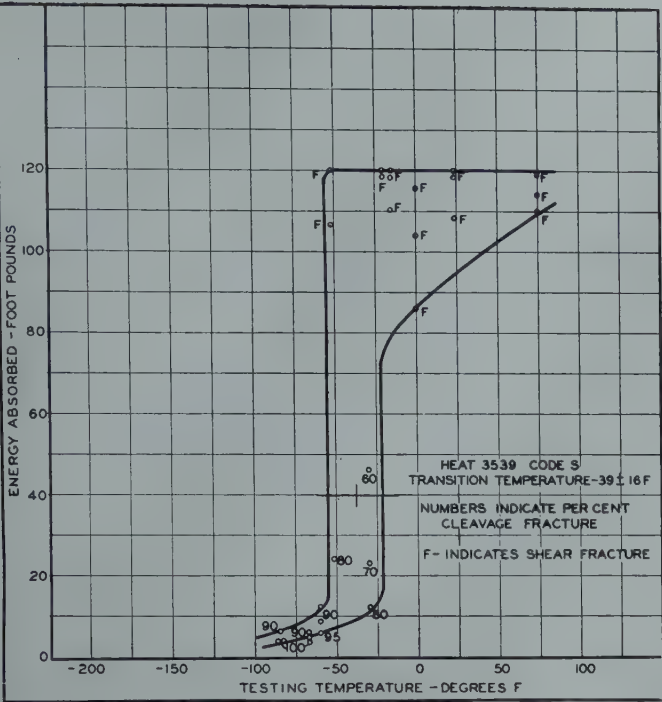


FIG 9—Impact-temperature curve for plain carbon steel at a ferrite grain size of 3-4.

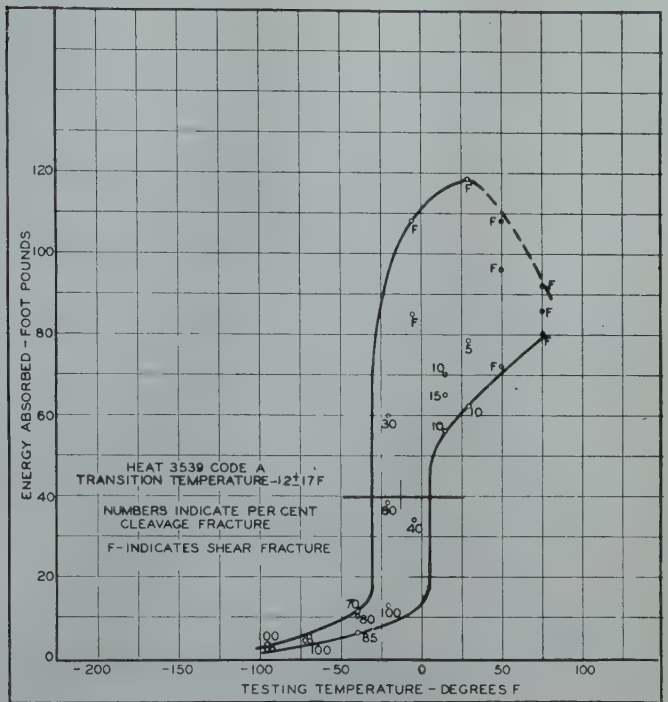


FIG 10—Impact-temperature curve for plain carbon steel at a ferrite grain size of 2-3.

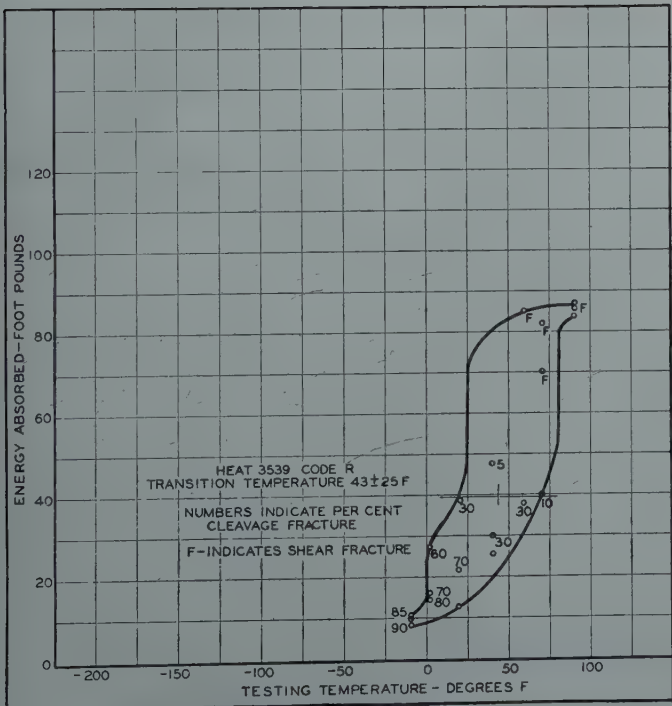


FIG 11—Impact-temperature curve for plain carbon steel at a ferrite grain size of 1-2.

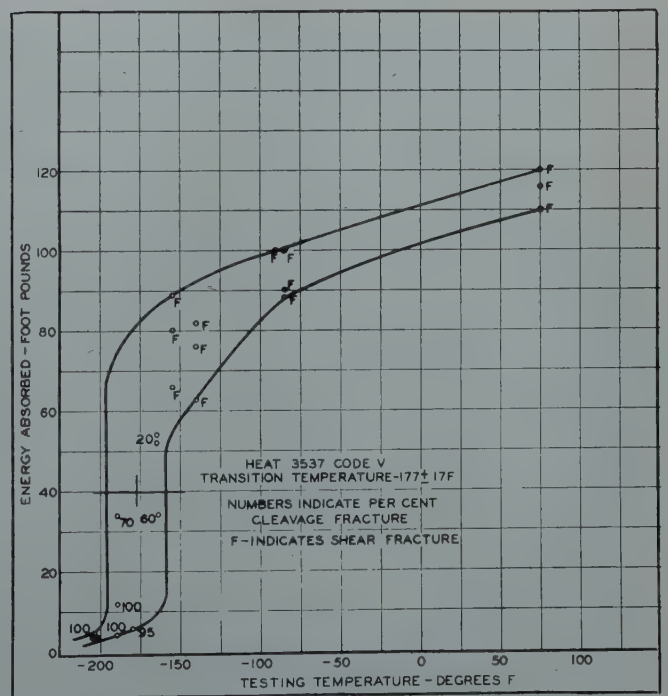


FIG 12—Impact-temperature curve for nickel steel at a ferrite grain size of 6.

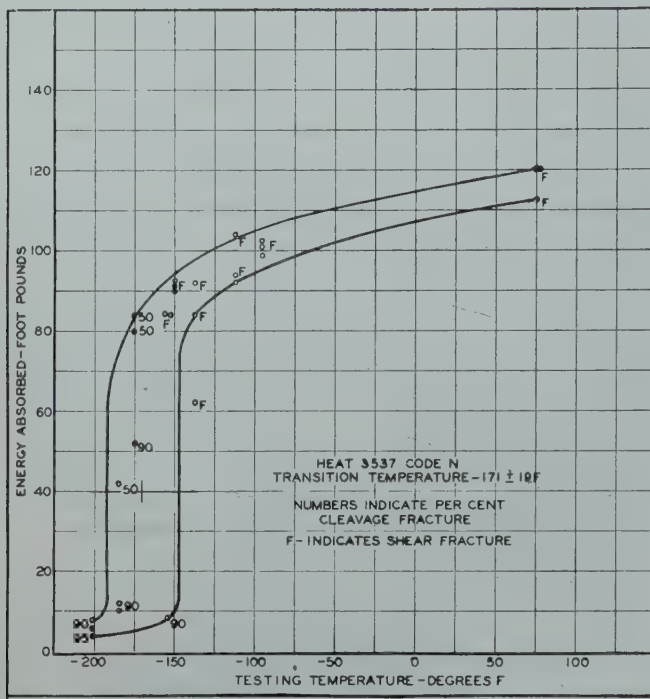


FIG 13—Impact-temperature curve for nickel steel at a ferrite grain size of 6.

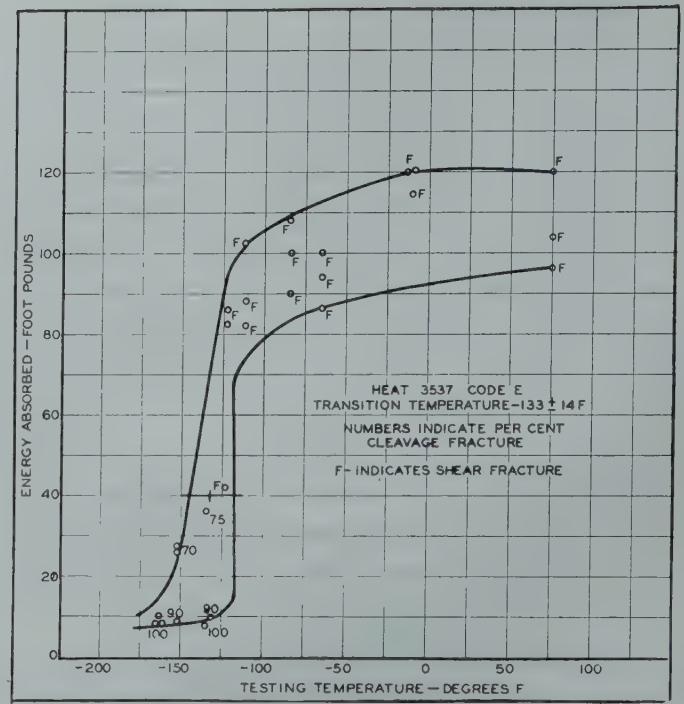


FIG 14—Impact-temperature curve for nickel steel at a ferrite grain size of 5.

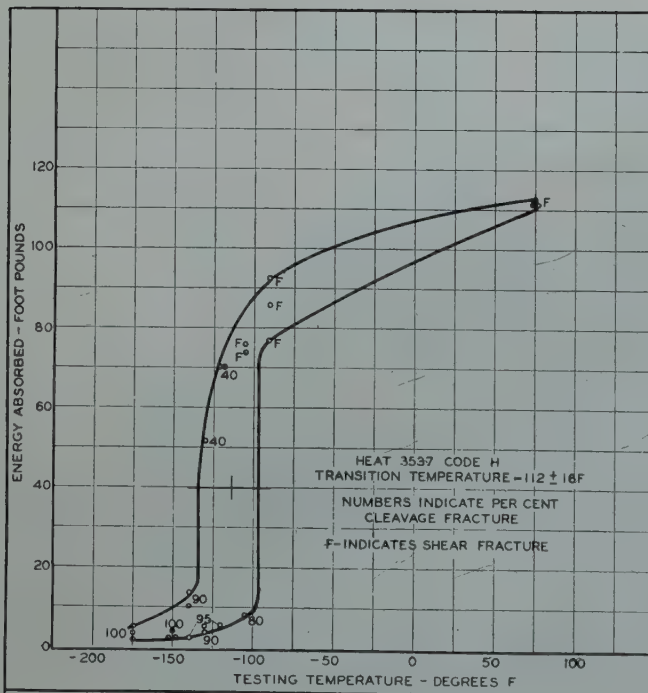


FIG 15—Impact-temperature curve for nickel steel at a ferrite grain size of 4-5.

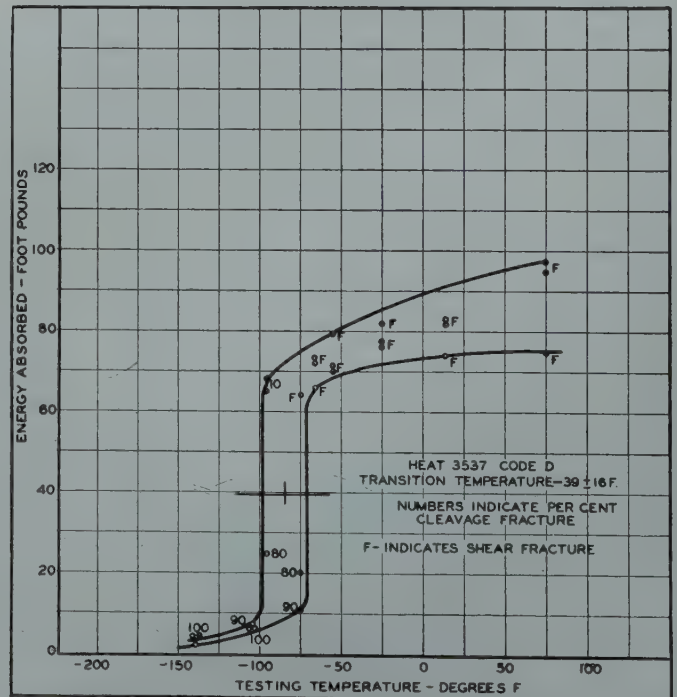


FIG 16—Impact temperature curve for nickel steel at a ferrite grain size of 3.

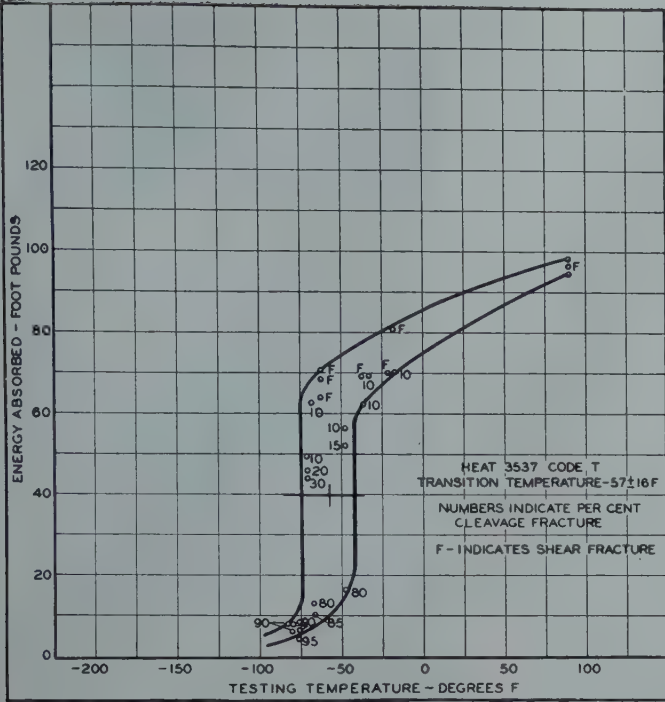


FIG 17—Impact-temperature curve for nickel steel at a ferrite grain size of 2.

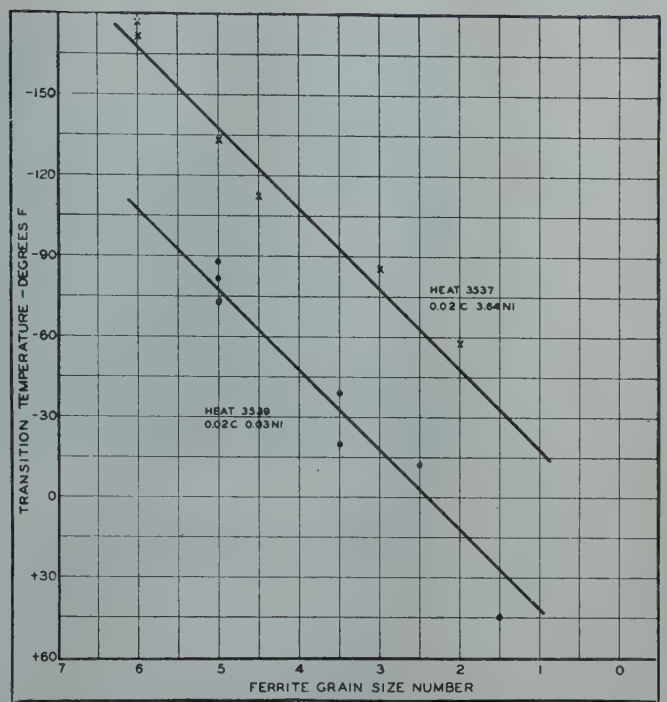


FIG 18—Transition temperature as a function of ferrite grain size of a plain carbon and a nickel steel.

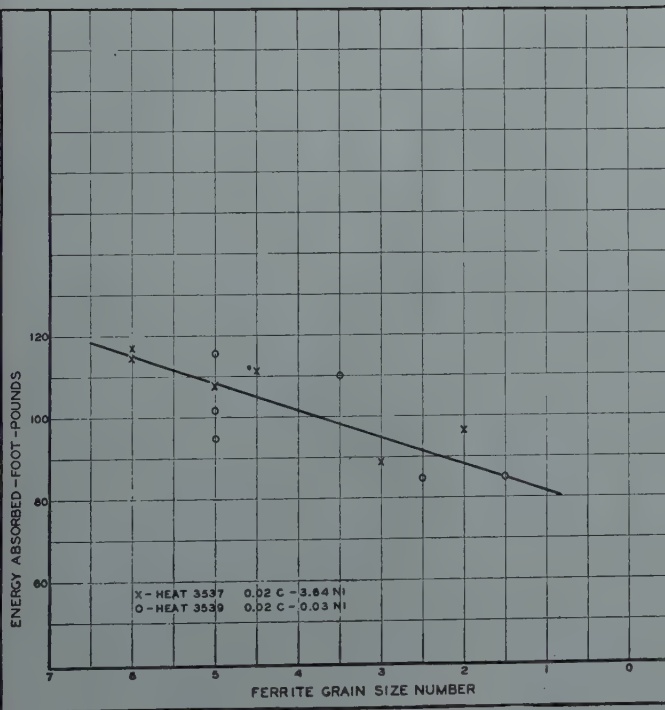


FIG 19—Energy absorption at room temperature as a function of ferrite grain size.

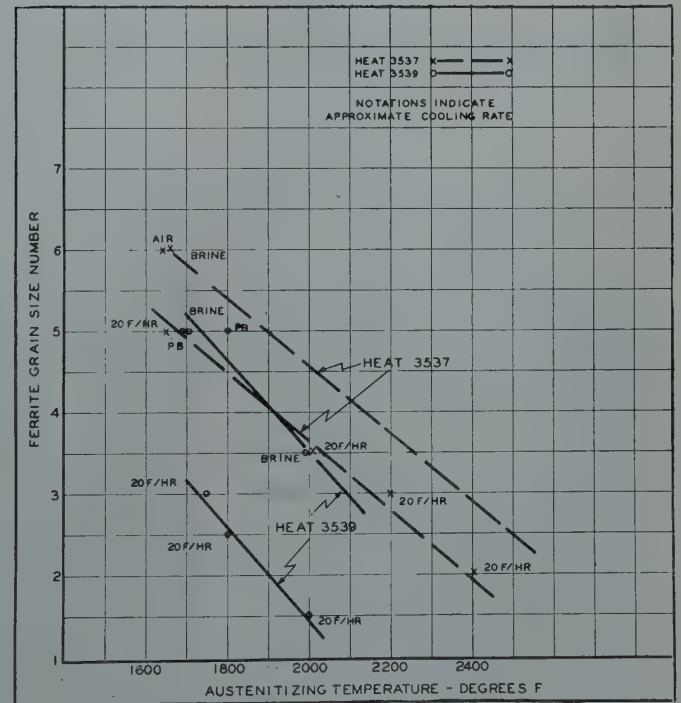


FIG 20—Relationship among austenitizing temperature, ferrite grain size and cooling rate.

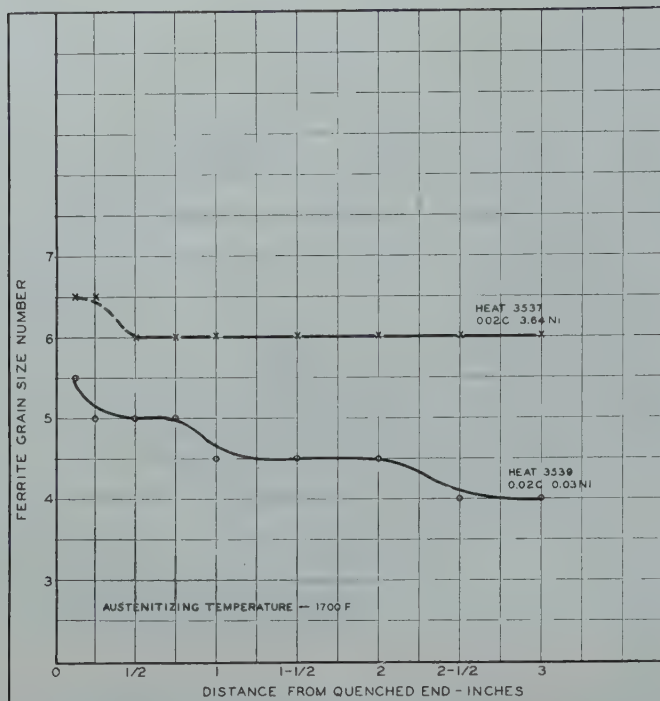


FIG 21—Ferrite grain size as a function of cooling rate in $\frac{1}{2}$ -in. diam end-quench tests.

size would be expected to be larger at the slower cooling rates inasmuch as the differences in transformation rates to ferrite between nickel and plain carbon steels are generally more pronounced at the higher transformation temperatures.

Conclusions

1. The keyhole notch Charpy transition temperature of 0.02 pct carbon steels is a straight line function of the ferrite grain size, the transition temperature being raised 30°F by an increase in ferrite grain size of one A.S.T.M. grain size number.

2. The keyhole notch Charpy transition temperature is lowered 60°F at a constant ferrite grain size in 0.02 pct carbon steels by alloying with 3.64 pct nickel.

3. The room temperature impact value in the keyhole Charpy impact test for each steel is also a function of the ferrite grain size, increasing as the grain size decreases.

4. At a given ferrite grain size, the room temperature impact value in the keyhole Charpy impact test is unaffected by alloying with 3.64 pct nickel.

Effect of Recrystallization Texture on Grain Growth

By PAUL A. BECK,* Member AIME, and PHILIP R. SPERRY*

It has been shown¹ that in polycrystalline strips of high purity aluminum with a fairly random orientation distribution, grain growth progresses gradually until the average grain diameter reaches a value approximately equal to the strip thickness. Recent work at this laboratory led to the realization that grain growth might be impeded to a considerable extent in the presence of a sharply defined texture, where orientation differences between neighboring grains are small.

In order to investigate this effect the following experiment was carried out with the same lot of high purity aluminum previously used for grain growth studies in randomly oriented material.¹ Very large grain size was

developed by grain growth at 650°C in specimens of 0.200 in. thickness. These specimens were then rolled to a thickness of 0.050 in. or 1.25 mm—a reduction of 75 pct. In the rolled strip each large grain corresponded to an elongated area easily identified by etching. After annealing for 1 to 25 min at 600°C and re-etching, these elongated areas were again recognizable. Within each area, corresponding to a single

large grain before annealing, there formed by recrystallization a multitude of new grains with a fairly well developed preferred orientation. The orientation and the size of the new grains formed in areas corresponding to different large grains, varied widely depending on the orientation of the parent grains with respect to the rolling direction and the plane of rolling. Many areas were found where the average grain size was considerably smaller than the specimen thickness. Such an area occurred in a specimen cut in half before annealing. One half, containing a portion of the area in question, was annealed 1 min at 600°C, the other half, with the remaining portion of this area, for 25 min at the same tempera-

Technical Note 13. Manuscript received Nov. 22, 1948.

* Associate Professor and Metallographer, respectively, Department of Metallurgy, University of Notre Dame.

¹ References are at the end of the paper.

ture. It was apparent that the annealing time had very little effect on the size of the small grains produced by recrystallization from a single large grain of the original rolled specimen. They possessed a very well developed preferred orientation, which made it somewhat difficult to detect the grain boundaries for accurate grain size determination. However, after some experimentation, it was found possible to make fairly accurate determinations. These are presented in the Table 1, which also includes for comparison the grain sizes obtained by similar anneals in specimens from the same bar of aluminum, rolled to the same final thickness, but exhibiting little preferred orientation (penultimate condition: fine grained, polycrystalline; last reduction: 33 pct).

Table 1 . . . Effect of Annealing Time and Orientation on Grain Size

| Annealing Conditions | Average Grain Size, mm | |
|----------------------|------------------------------|--------------------|
| | Strong Preferred Orientation | Random Orientation |
| 1 min at 600°C..... | 0.33 | 0.61 |
| 25 min at 600°C.... | 0.36 | 1.0 |

The fact that with a strong texture the grain size remained practically constant from 1 to 25 min at 600°C, at a value much smaller than the specimen thickness, proves that in a highly oriented aggregate of crystals, grain growth is greatly reduced, if not entirely impeded. It is quite possible that this reluctance of grains to grow, even though they are small, when their orientations are very nearly the same, is a result of the low surface tension values associated with grain boundaries under such conditions.²

The close connection between a certain type of coarsening and the inhibition of gradual grain growth by a dispersed second phase has been known for a long time.³ These relationships were recently explored in a quantitative and rather detailed manner.⁴ However, from the results of Dahl and Pawlek⁵ and of Cook and Macquarie⁶ it may be concluded^{4,7} that in certain metals coarsening may also occur *without* a dispersed second phase, provided that the conditions of penultimate grain

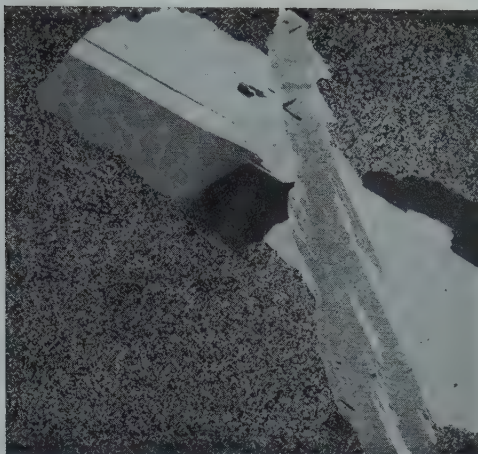


FIG 1—Partially coarsened tough pitch copper specimen, cold rolled 90 pct, annealed 3 min. at 1000°C. Magnification 5 ×. (Reduction approximately one-half.)

size, of amount of reduction by rolling, and of composition are such that a strongly developed cube texture results upon recrystallization. This texture, in which the fine recrystallized grains have very closely identical orientation, appears to resist gradual grain growth up to relatively high temperatures. In copper with the cube recrystallization texture, extremely coarse grains abruptly develop when the temperature is raised to approximately 1000°C (see Fig 1). These very large grains have a fairly well developed preferred orientation of their own,^{5,8} different from that of the fine grained recrystallized matrix in which they grow. This fact may be interpreted as an indication that in a highly oriented fine grained matrix, the rate of growth of a grain strongly depends on its orientation with respect to the preferred orientation of the matrix. The alternative interpretation, namely, that the preferred orientation of the coarse grains is a result of the presence in the matrix of "nuclei" of a certain orientation only⁸ appears less convincing. It seems justified to assume that "texture-dependent coarsening" is intimately connected with the above described restraint of gradual grain growth by virtue of a strongly developed texture, just as "inhibition-dependent coarsening" is connected with grain growth inhibition by a dispersed second phase.

This work was supported by the Office of Naval Research, Contract No. N6 ori-165, T.O. no. 1.

References

1. P. A. Beck, J. C. Kremer, L. J. Demer, and M. L. Holzworth: Grain Growth in High Purity Aluminum and in an Aluminum-magnesium Alloy. AIME TP 2280, *Metals Technology* (Sept. 1947).
2. C. G. Dunn and F. Lionetti: The Effect of Orientation Difference on Grain Boundary Energies. *Trans. AIME (Jnl. of Metals)*, Feb. 1949) 125.
3. Z. Jeffries: Grain Growth Phenomena in Metals, *Trans. AIME* (1916) 56, 571.
4. Paul A. Beck, M. L. Holzworth, and Philip R. Sperry: Effect of a Dispersed Phase on Grain Growth in Al-Mn Alloys, AIME TP 2475, *Metals Technology* (Sept. 1948).
5. O. Dahl and F. Pawlek: Kornordnung und Kornwachstum bei Walzblechen. *Ztsch. f. Metallkunde* (1936) 28, 266.
6. M. Cook and C. Macquarie: Development of Abnormally Large Grain Sizes in Rolled and Annealed Copper Sheet. *Trans. AIME* (1939) 133, 142.
7. Paul A. Beck, John Towers, Jr., and Philip R. Sperry: Grain Coarsening in Copper. *Trans. AIME (Jnl. of Metals)*, T.N. 12, Feb. 1949).
8. J. S. Bowles and W. Boas: Effect of Crystal Arrangement on "Secondary Recrystallization" in Metals. *Jnl. Inst. Met.* (1948) 74, 501. and W. G. Burgers and J. Sandee: *Physica* (1942) 9, 996.

Recrystallization and Microstructure of Aluminum Killed Deep Drawing Steel

R. L. RICKETT,* Member, S. H. KALIN,† and J. T. MACKENZIE, JR.,‡ Junior Member AIME

ALUMINUM killed low carbon steel,§ which is now used extensively for severe deep drawing or other difficult forming operations, is unusual in that its grain structure, after cold reduction and box annealing in accordance with conventional continuous sheet or strip mill practice, often is elongated, although at times it is equiaxed. Since this unusual structure has been found superior for many, but not all, severe forming operations, recrystallization of the steel, both at constant temperature and on continuous heating, was investigated and compared with that of rimmed steel in the hope that something might be learned about the mechanism of, and the factors controlling, the formation of such elongated grains.

In this structure, the grains are elongated both in the lengthwise direction of the strip and transverse to this direction, even though nearly all of the extension in both hot and cold rolling is in the lengthwise direction. The grains are thus roughly pancake-shaped, being longer and wider than they are thick, as observed also by Burns and McCabe,¹ and as illustrated by the typical structures shown in Fig 1. Fig 1a, representing a conventional longitudinal section, shows the length and thickness of the grains, whereas Fig 1b shows their length and width as seen by examining a section parallel to the sheet surface. Both illustrate the very irregular grain boundaries usually associated with the elongated grain shape. A finer equiaxed grain structure in this same grade is shown in Fig 1c. Either the elongated or the equiaxed structure may be present in the annealed product, and in rare instances the two types may coexist in a single specimen, as shown in Fig 1d.

Table 1 . . . Composition of Steels Investigated

| Steel | Type | | Composition—Pct* | | | | | | |
|-------|------------|---|------------------|------|-------|-------|-------|-------|--------------------------------|
| | | | C | Mn | P | S | Si | Al | Al ₂ O ₃ |
| A | Rimmed | Hot rolled strip 0.095 in. thick | 0.07 | 0.36 | 0.008 | 0.024 | 0.008 | 0.008 | 0.005 |
| B | Al. Killed | Hot rolled strip 0.075 in. thick | 0.05 | 0.32 | 0.010 | 0.025 | 0.010 | 0.09 | 0.008 |
| C | Al. Killed | Hot rolled strip 0.075 in. thick | 0.04 | 0.34 | 0.010 | 0.023 | 0.008 | † | † |
| D | Al. Killed | Hot rolled strip 0.085 in. thick | 0.05 | 0.30 | 0.012 | 0.028 | 0.008 | 0.08 | 0.008 |
| E | Al. Killed | Hot rolled strip 0.085 in. thick | 0.05 | 0.32 | 0.010 | 0.022 | 0.010 | 0.08 | 0.007 |
| F | Al. Killed | Cold rolled strip 0.053 in. thick (40 pct red.) | 0.05 | 0.33 | 0.008 | 0.023 | 0.010 | † | † |
| G | Al. Killed | Cold rolled strip 0.053 in. thick (45 pct red.) | 0.05 | 0.33 | 0.006 | 0.023 | 0.008 | 0.05 | 0.012 |
| H | Al. Killed | Cold rolled strip 0.053 in. thick (45 pct red.) | 0.06 | 0.39 | 0.007 | 0.021 | 0.006 | 0.06 | 0.014 |

* Values underlined are check analyses, others are heat analyses.
† Al and Al₂O₃ in these steels not determined but the heats were made by the same practice as the other aluminum killed steels.

Isothermal Recrystallization of Rimmed and Aluminum Killed Steel

An aluminum killed steel known to have an elongated grain structure after conventional processing (Steel B, Table 1), was selected for the initial recrystallization studies; for comparison, a rimmed steel, A in Table 1, was used. Samples of each in the form of hot rolled strip 0.075 and 0.095 in. thick, respectively, were cold rolled on a small laboratory mill in steps of about 0.010 in. per pass to obtain total reductions

of 40 and 60 pct. Small pieces of the cold reduced strip were heated in lead at selected constant temperatures for one of several periods of time, then cooled in air. Rate of heating in the lead was, of course, very fast. Hardness of the cooled specimen was measured and a longitudinal section examined metallographically.

Isothermal recrystallization curves for these two steels at 1050°F, based on hardness of the air cooled specimens, are shown in Fig 2 in which the amount of recrystallization corresponding to each plotted point is indicated. The marked difference in the behavior of these two types of steel is evident. After a corresponding amount of cold reduction, the rimmed steel recrystallizes in a much shorter time than the killed steel and the shape of its recrystallization curve, (plotted on a logarithmic time scale), is very different. The curve for rimmed steel indicates that recrystallization is analogous to isothermal transformation of austenite in that it proceeds at a progressively faster rate up to some 50 pct recrystallization, then at an increasingly slower rate. For the aluminum killed steel, however, the start of

Cleveland Meeting, October 1949.
TP 2552 E. Discussion of this paper (2 copies) may be sent to *Transactions AIME* before Dec. 15, 1949. Manuscript received October 26, 1948.
1 References are at the end of the paper.
* Research Laboratory, United States Steel Corporation, Kearny, N. J.
† Carnegie-Illinois Steel Corporation, Gary Sheet and Tin Mill, Gary, Ind.
‡ United States Steel Export Co.
§ This type of steel comes within the special killed steel category of the American Iron and Steel Institute; cf. AISI Steel Products Manual, Sections 11, 12, and 13.

recrystallization is followed by a period during which little further change occurs, after which recrystallization of the remaining cold worked metal proceeds at a relatively fast rate. The hardness curve thus exhibits an initial gradual drop, then a nearly horizontal portion or "shelf" and finally a rather sharp drop. The "shelf" is lowered by increased cold reduction and, as discussed later, by increased temperature.

These two types of steel also differ considerably in microstructure both during and after recrystallization, as shown in Fig 3 and 4. In rimmed steel, Fig 3, the first recrystallized grains are nearly equiaxed, and remain so as they grow and new grains continue to form. In the aluminum killed steel however, Fig 4, the small new grains, which may be equiaxed as first formed, become elongated as they grow, apparently because resistance to growth in the thickness direction of the sheet is greater than in the lengthwise or crosswise direction. Both rate of growth and rate of formation of new grains (nucleation) are much less in the aluminum killed than in the rimmed steel.

Grain growth restraint in the aluminum killed steel appears to be greatest at boundaries of the cold worked grains, as illustrated in Fig 5. Even in the rimmed steel, Fig 5a and 5b, there is some tendency for grain growth to stop at former grain boundaries but this tendency is much more marked in the killed steel, Fig 5c and 5d. This grain boundary restraint, together with the relatively slow rate of nucleation in this type of killed steel, apparently is responsible for its relatively coarse elongated grain structure after recrystallization. The presence of thorium oxide particles, similarly, has been shown to restrain grain growth and result in an elongated grain structure in recrystallized tungsten wire.^{2,3} It still is not clear, however, why grain growth of aluminum killed steel is restrained more effectively in the thickness direction than it is in the lengthwise or crosswise direction of the sheet, as it must be if such restraint is responsible for the plate-like shape of the recrystallized grains. This effect suggests the possible presence in the steel of fine particles distributed more or less in layers parallel to the sheet surface.

As expected, increased cold reduction reduces the time required for complete recrystallization of either of the steels represented in Fig 2 and increases their hardness as fully recrystallized. This

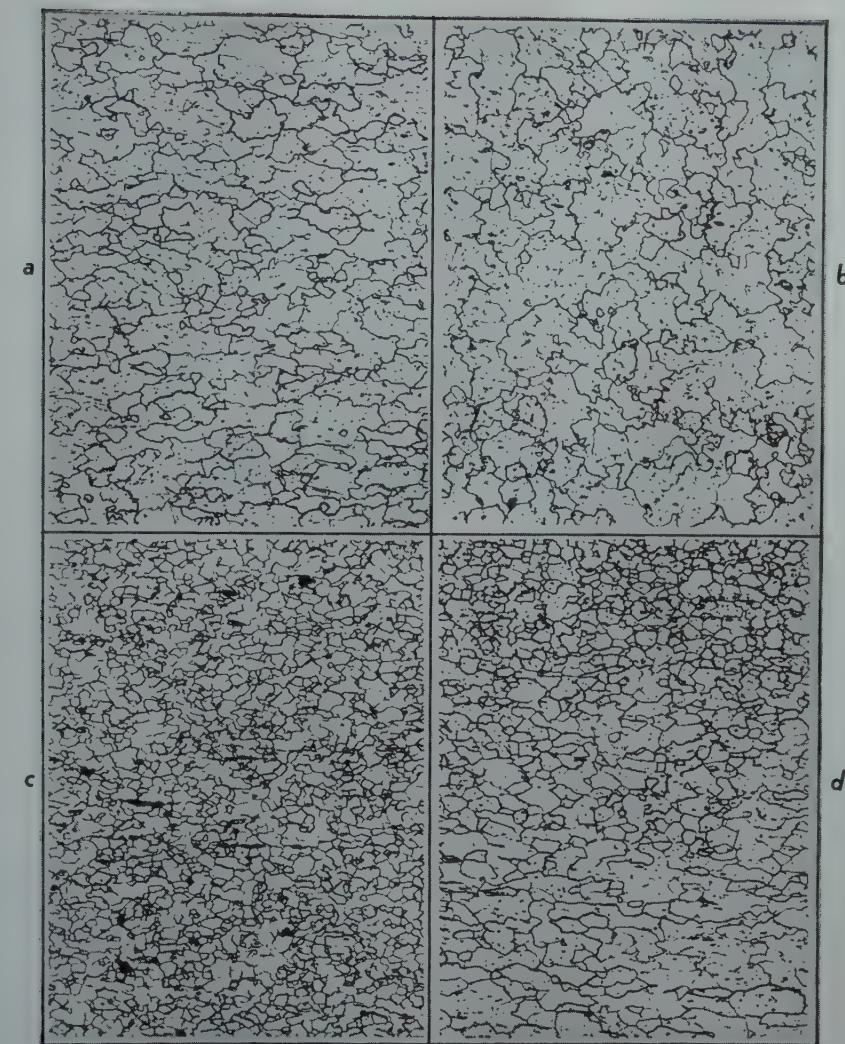


FIG 1—Types of microstructure observed in aluminum killed steel after cold reduction and box annealing. 100 \times . Nital etch.

a. Typical elongated grains, conventional longitudinal section. b. Same specimen as a but section parallel to sheet surface. c. Equiaxed ferrite grains, longitudinal section. d. Equiaxed grains (top) and elongated grains in a single specimen.

increased hardness is due to a finer grain size, as illustrated in Fig 6. For the same amount of prior cold reduction the killed steel, with its elongated grain structure, is softer, and its grain size coarser, than the equiaxed rimmed steel.

Effect of Temperature of Isothermal Recrystallization

The effect of temperature on rate of isothermal recrystallization was investigated, again using rimmed steel A and killed steel B of Table 1, each cold reduced 40 pct. For rimmed steel, Fig 7a, the shape of the recrystallization curve is not altered appreciably by change in temperature, although as would be expected the time required for a comparable amount of recrystalli-

zation is less the higher the temperature. Fig 7a shows that over the range 1000 to 1100°F, hardness of this steel after complete recrystallization is nearly independent of recrystallization temperature; final grain size, likewise, was found to be about the same for all.

The effect of temperature, in the range 1050 to 1200°F, on isothermal recrystallization of the aluminum killed steel is shown in Fig 7b. At each temperature investigated, the amount of recrystallization remains nearly constant over an appreciable period of time, resulting in a "shelf" in the recrystallization curve. The amount of recrystallization corresponding to this shelf increases, and the time to attain it decreases, with increased temperature. Duration of the shelf period also is shorter the higher the temperature. Hardness of this steel as fully recrystallized increases as the recrystalliza-

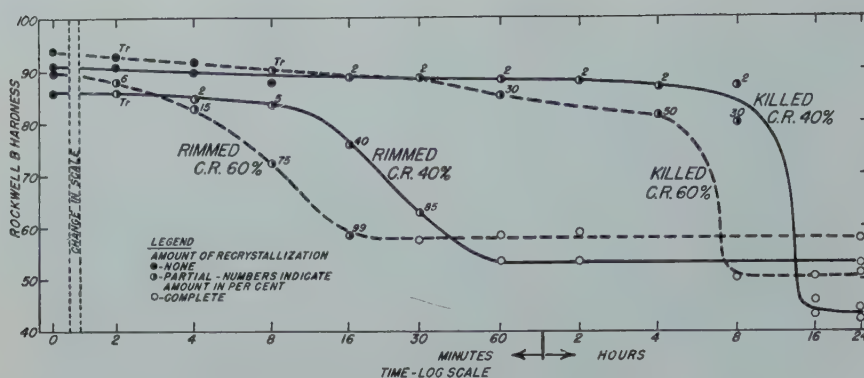


FIG 2—Rate of isothermal recrystallization of rimmed steel A and aluminum killed steel B at 1050°F after 40 pct and after 60 pct cold reduction.

tion temperature is raised, Fig 7b, the higher hardness resulting from a finer, more equiaxed grain structure, as shown in Fig 8.

The aluminum killed grade thus differs from rimmed steel in requiring a longer time for complete recrystallization at comparable temperature, in having a “shelf” in its isothermal recrystallization curve, and in becoming finer grained as the recrystallization temperature is raised.

Effect of Treatment Prior to Cold Reduction

Early in this investigation, it was discovered that normalizing the aluminum killed steel at about 1700°F after hot rolling, but before cold reduction, resulted in an equiaxed rather than an elongated grain structure after subsequent cold reduction and box annealing. This observation led to a more extensive study of the influence of such heating prior to cold reduction on final grain structure.

Specimens of steel B of Table 1, in the form of hot rolled strip 0.075 in. thick, were heated at each of a series of temperatures for 20 min. then air cooled. Another set was prepared in which the heating time was 2 hr. The specimens of both sets were then cold reduced 40 pct in thickness, using a small laboratory rolling mill, after which they were annealed 16 hr at 1275°F in a protective atmosphere. The laboratory annealing cycle simulated commercial box annealing practice, both heating and cooling rates being in the range of 20–50°F per hour. Microstructure, after cold reduction and annealing, of the specimens heated

for 20 min. or 2 hr prior to cold reduction is shown in Fig 9. Holding 2 hr at 1000°F had little effect on the final structure, but 2 hr at 1100°F resulted in a mixed elongated and equiaxed structure, whereas holding

2 hr at 1200°F or above resulted in a final structure that is almost entirely equiaxed.

The change in grain structure, as box annealed, from elongated to equiaxed is accompanied by an appreciable increase in hardness of the annealed material. Fig 10 shows the relationship between temperature of heating, prior to cold reduction, and hardness of the subsequently cold reduced and box annealed product. The two curves in Fig 10 are for 20 min. and 2 hr at temperature in the initial treatment, and show that the longer time lowers the temperature range over which the change in final structure and hardness takes place. Fig 11 shows that prior heating for as long as 24 hr at 800 or 1000°F had no appreciable effect on final hardness whereas 2 hr at 1200°F or 5–10 min. at 1300°F increased hardness of the cold-rolled, annealed material to a maximum; this maximum hardness corresponds to a substantially equiaxed grain structure. Fig 10 and 11 thus demonstrate that the change in

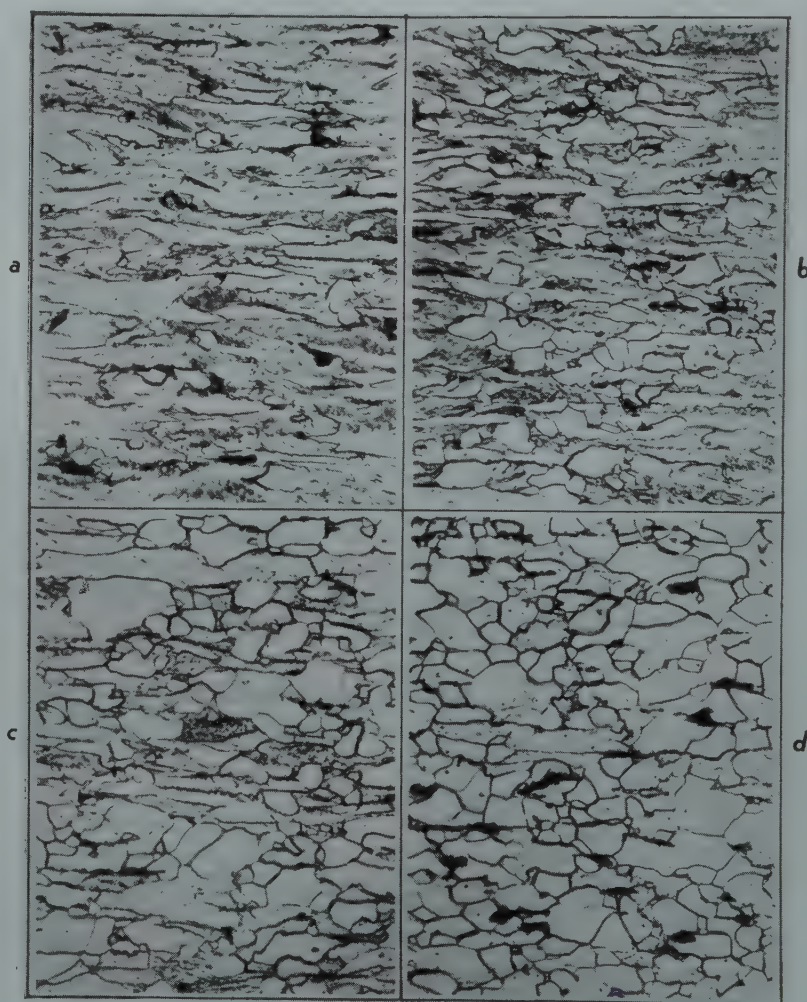


FIG 3—Progress of isothermal recrystallization of rimmed steel A at 1050°F after 60 pct cold reduction. 500 ×. Nital etch.
a. 2 min. b. 4 min. c. 8 min. d. 12 min.

structure and hardness as annealed is dependent upon both time and temperature of the treatment prior to cold reduction, the time required being shorter the higher the temperature, within the range investigated.

The foregoing observations indicate that slow rather than rapid cooling of this aluminum killed steel directly following hot rolling should yield an equiaxed grain structure after subsequent cold reduction and annealing. This was confirmed by cooling samples at three rates after heating to 2150°F and hot rolling from 0.15 to 0.085 in. (43 pct reduction) in a single pass through a small laboratory rolling mill. The three rates of cooling were obtained by: (1) quenching in oil, (2) cooling in air, and (3) placing in a furnace at 1500°F immediately after hot rolling and cooling with the furnace (1 hr to cool from 1500 to 1350°F). After cold rolling 40 pct and box annealing 16 hr at 1275°F, grain structure of the previously oil quenched or air

cooled samples was elongated, whereas that of the slow-cooled sample was equiaxed, as shown in Fig 12.

The foregoing experiments demonstrate that the thermal history between hot rolling and cold reduction is an important factor in determining whether the grain structure of this aluminum killed steel, when recrystallized after cold reduction, will be elongated or equiaxed. Either slow cooling from the temperature at which hot rolling is finished, or suitably reheating more rapidly-cooled strip leads to the formation of equiaxed grains in the final annealed product similar to those commonly found in box annealed rimmed steel. This raised the question whether the recrystallization of "equiaxed" aluminum killed steel may not also resemble that of rimmed steel, rather than being much more sluggish as is characteristic of the elongated-grain type (Fig 2 and 7). To answer this question, suitable samples cold rolled 40 pct were recrystallized isothermally

at 1050°F, with results shown in Fig 13 and 14.

To determine the effect of cooling rate on isothermal recrystallization at 1050°F, Fig 13, specimens of steel D, Table 1, were hot rolled in regular production, and cooled rapidly to about 1330°F; a portion was then cooled slowly below this temperature, whereas another portion was cooled much more rapidly. The rapidly cooled portion, subsequently cold rolled and completely recrystallized at 1050°F, had an elongated grain structure, and, as shown in Fig 13, its recrystallization curve exhibits the "shelf" characteristic of such material. The more slowly cooled strip when cold reduced and recrystallized had an equiaxed grain structure like that of rimmed steel; the recrystallization curves for this and for the rimmed steel in Fig 13 likewise are similar in shape, although the killed steel recrystallized somewhat more slowly. Fig 14 shows the effect of reheating to 1300°F after hot rolling on isothermal recrystallization after cold reduction, the steel being the same aluminum killed steel as in Fig 2. The effect of this treatment on recrystallization is the same as that of slowly cooling the strip directly after hot rolling; recrystallization proceeds more rapidly, and in more continuous fashion than when the strip is cooled rapidly after hot rolling and is not reheated. Final recrystallized grain structure of this steel previously heated at 1300°F before cold reduction was equiaxed, whereas without such treatment it was elongated.

Fig 13 and 14 thus demonstrate that when the treatment of aluminum killed steel prior to cold reduction is such that the final recrystallized grain structure is equiaxed rather than elongated it recrystallizes more readily and its recrystallization curve exhibits no "shelf," thus resembling rimmed steel in these respects.

Recrystallization on Continuous Heating

In regular commercial practice cold rolled strip or sheet is box annealed in the approximate temperature range 1200–1350°F after cold reduction. Rate of heating is necessarily rather slow, because a large amount of metal is annealed in each batch, and partial or complete recrystallization occurs during the heating period. Since the structure of aluminum killed deep drawing

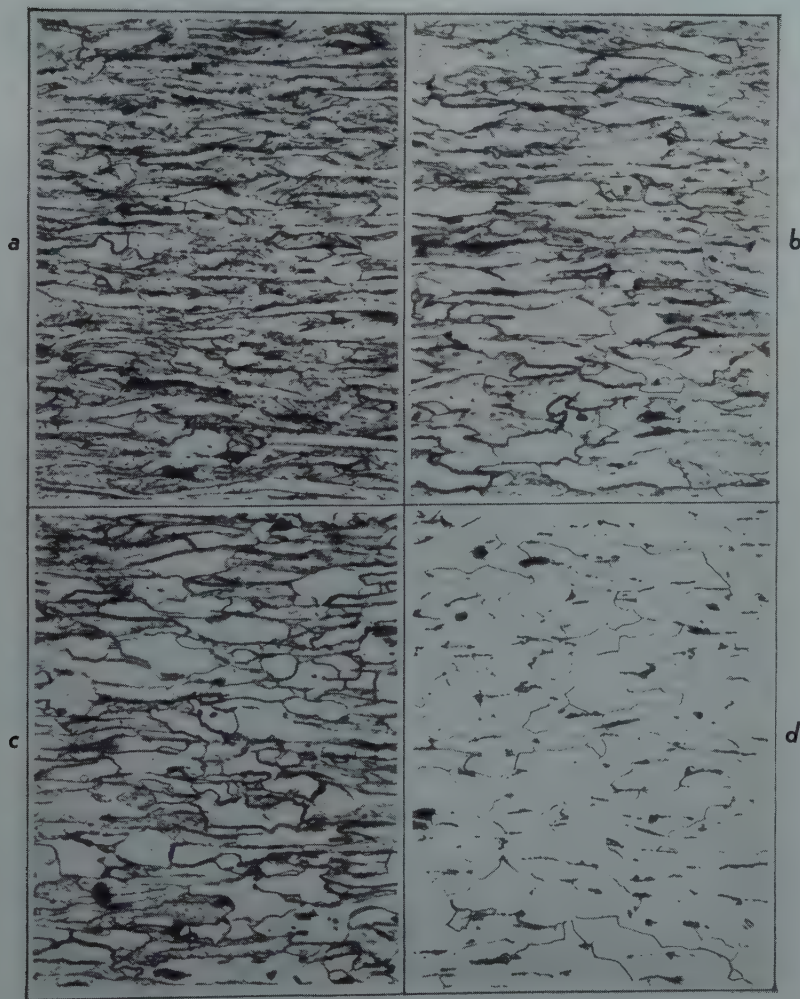


FIG 4—Progress of isothermal recrystallization of aluminum killed steel B at 1050°F after 60 pct cold reduction. 500 X. Nital etch.
a. 8 min. b. 1 hr. c. 4 hr. d. 5 hr.

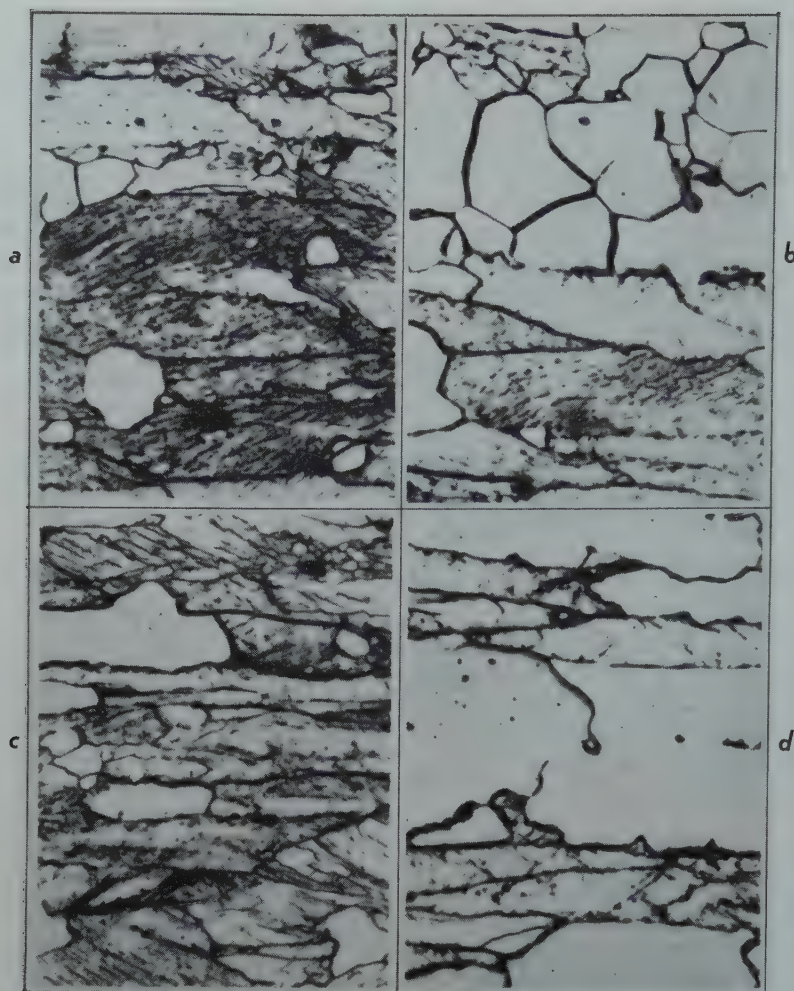


FIG 5—Comparison of microstructure of rimmed and aluminum killed steels partially recrystallized isothermally at 1050°F after 60 pct cold reduction. 2000 \times . Nital etch.

a. Rimmed steel, 2 min. b. Rimmed steel, 8 min. c. Killed steel, 8 min. d. Killed steel, 4 hr.

sheet varies with the temperature at which it is recrystallized (Fig 8) it was decided to investigate the recrystallization of this steel on continuous heating at several rates, and the effect of such variation in heating rate on the final grain structure.

For this purpose, Steels *E*, *F*, *G*, and *H* of Table 1 were used; *E* was cold reduced 40 pct in the laboratory, the others were cold rolled in regular production. Several specimens of each were heated at a controlled constant rate of 20, 50, or 300°F per hr in lead, starting at 700°F. As each selected temperature was reached, a specimen was removed from the lead and air cooled.

Results of these tests for Steels *F*, *G* and *H* are shown in Fig 15. When heated continuously at 20°F per hr, Fig 15a, steel *F* started to recrystallize at about 1050°F but had not recrystallized completely on reaching 1150°F, the highest temperature investigated. The hardness curve for Steel *G* follows closely that for Steel *F*; however, *G* was completely recrystallized on reaching 1100°F. Steel *H* differs from the others in that it recrystallized over a considerably lower temperature range. Structure of all three steels after recrystallization was elongated.

As would be expected, the effect of increasing the heating rate, Fig 15b and 15c, is to raise the recrystallization temperature range. The curve for Steel *G* heated at 300°F per hr exhibits a "shelf" not apparent at slower heating rates; the curve for Steel *H* also has a

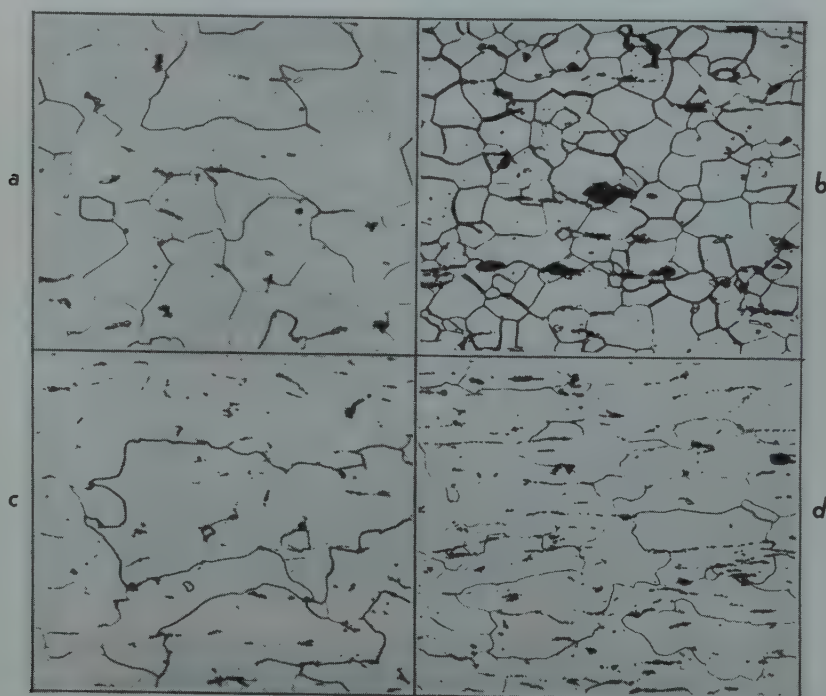


FIG 6—Effect of amount of prior cold reduction on structure of rimmed and aluminum killed steels after complete recrystallization at 1050°F. 500 \times . Nital etch.

a. Rimmed steel cold red. 40 pct. b. Rimmed steel cold red. 60 pct. c. Aluminum killed steel cold red. 40 pct. d. Aluminum killed steel cold red. 60 pct. Slightly reduced in reproduction.

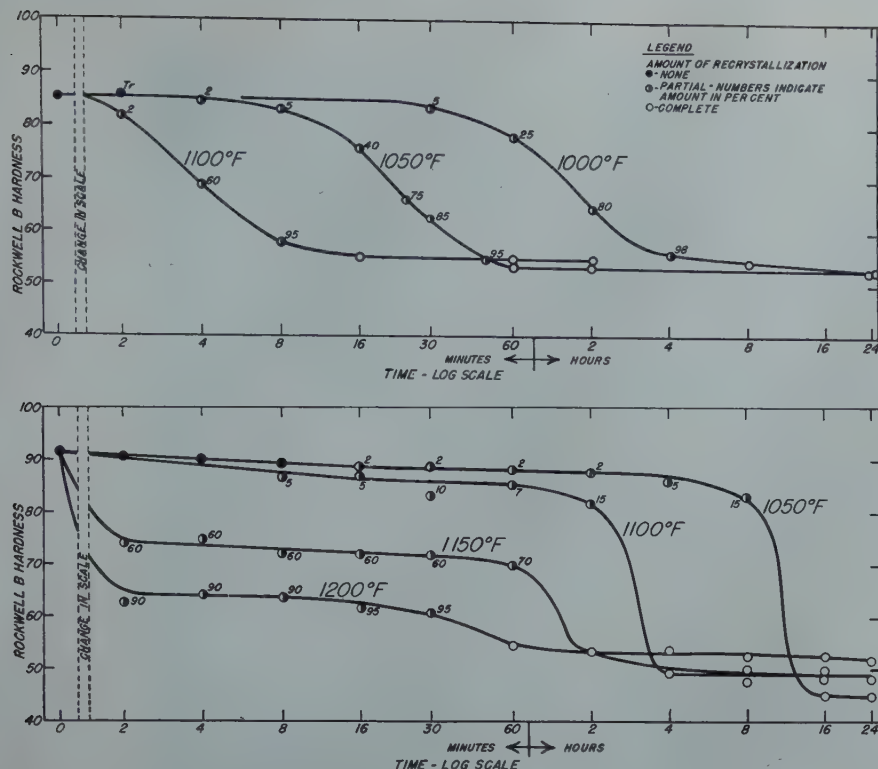


FIG 7—(a. Above). Effect of temperature on rate of isothermal recrystallization of rimmed steel A and aluminum killed steel B (b. Below). Cold reduced 40 pct.

“shelf” at somewhat lower hardness. This latter steel is unusual in that its recrystallized grain structure becomes much finer and more nearly equiaxed when the rate of heating is raised from 50 to 300°F per hr. No such effect was found in the other steels over the range of heating rate investigated.

Differences among these steels do not seem to be related to their composition, as given in Table 1, but are believed to be due to differences in prior processing, as discussed below, although this is not known with certainty.

Recrystallization on continuous heating, like isothermal recrystallization, is influenced by treatment of the steel prior to cold reduction. Fig 16 shows the effect of heating Steel E, Table 1, 20 min. at 1300°F before cold rolling as compared to the same steel hot rolled only before cold reduction. The 1300°F treatment prior to cold reduction lowers the recrystallization temperature range for each of the three heating rates and results in an equiaxed rather than an elongated recrystallized grain structure. From this, it appears likely that Steel H, Fig 15, was cooled after hot rolling in such a man-

ner that its tendency toward an elongated grain structure, on recrystallization, was only partly destroyed rather than completely destroyed as was that of Steel E when heated to 1300°F after hot rolling.

Summary

The results of this investigation show that the recrystallization of rimmed steel at constant temperature proceeds in a regular and continuous manner, once it starts, as is already well known. On the other hand, the recrystallization of aluminum killed steel of the elongated-grain type takes place in three rather distinct stages: (1) an initial period resembling the start of recrystallization in rimmed steel; (2) a second period during which recrystallization proceeds very slowly; and (3), comparatively rapid recrystallization of the remaining unrecrystallized portion. The length of time required for complete recrystallization is ordinarily much greater for the aluminum killed steel than for rimmed steel at a comparable temperature. Except at the very start, the recrystallized grains in this type of killed steel are definitely elongated



FIG 8—Effect of recrystallization temperature on structure of isothermally recrystallized aluminum killed steel cold reduced 40 pct. 100 X. Nital etch.
a. 1050°F. b. 1100°F. c. 1150°F. d. 1200°F.

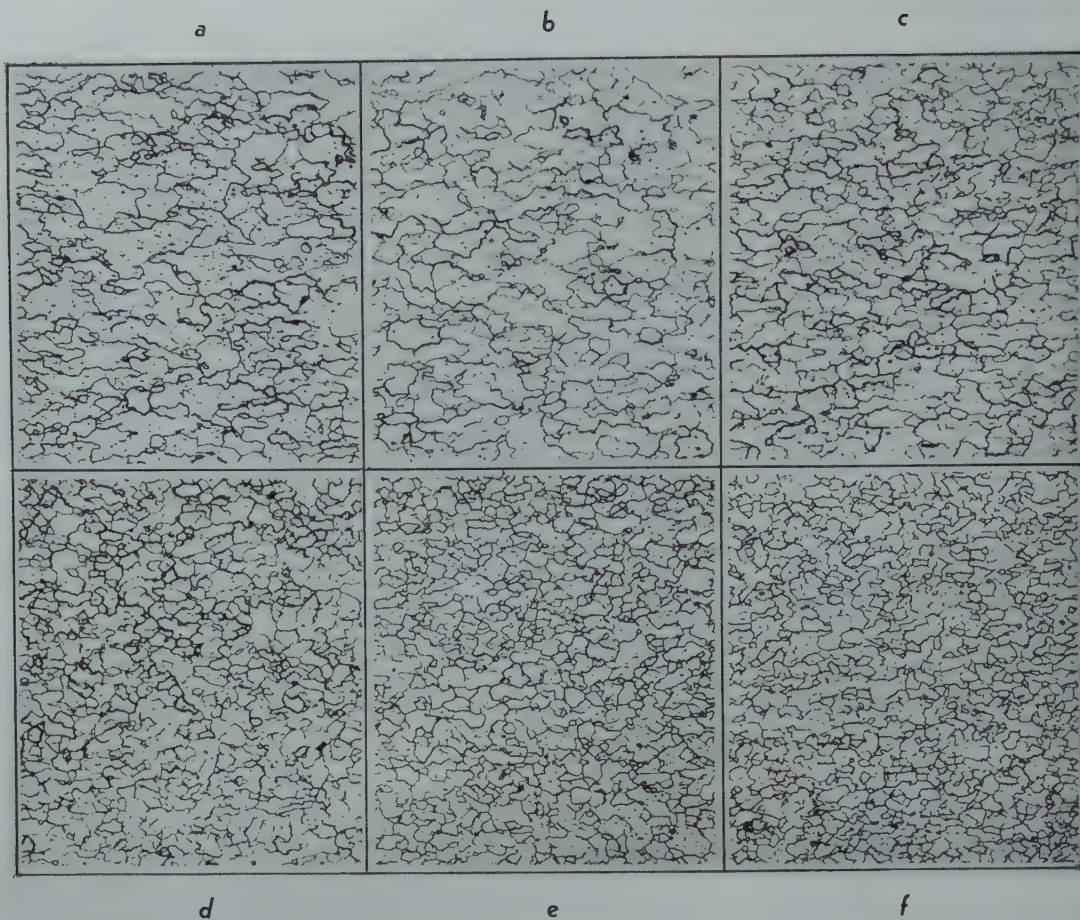


FIG 9—Effect of prior heating on grain structure of aluminum killed steel B annealed 16 hr at 1275°F after 40 pct cold reduction. 100 X. Nital etch.

Treatment before cold reduction: *a.* None, hot rolled only. *b.* 2 hr at 1000°F. *c.* 2 hr at 1100°F. *d.* 2 hr at 1200°F. *e.* 20 min. at 1300°F. *f.* 20 min. at 1650°F.

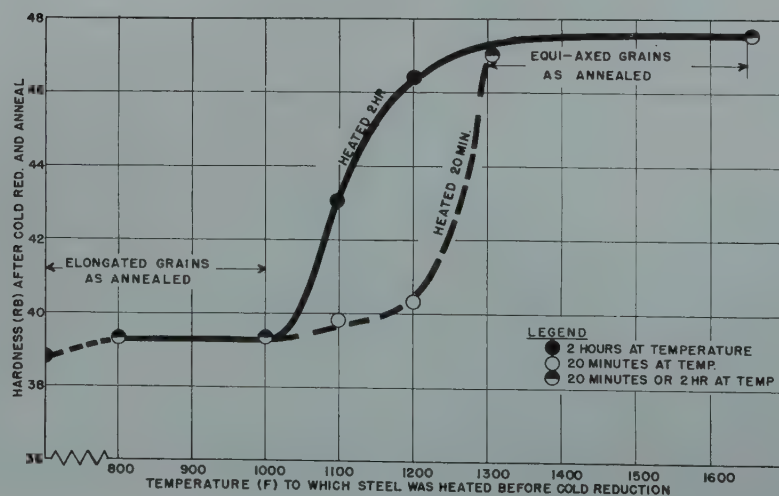


FIG 10—Effect of heating aluminum killed steel B for 20 min. or 2 hr at indicated temperature on hardness after subsequent cold reduction (40 pct) and box anneal (16 hr at 1275°F).

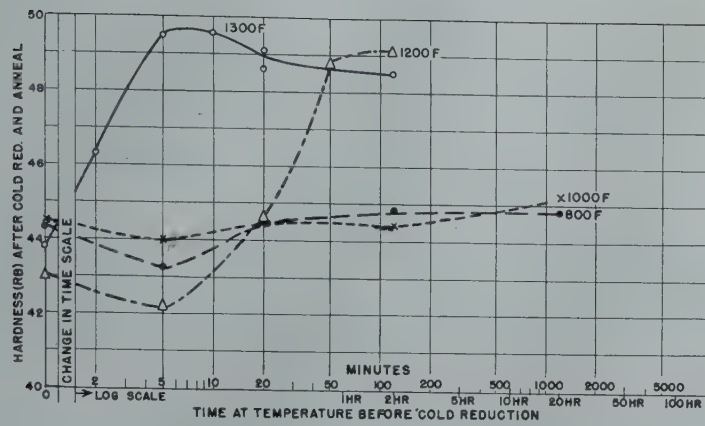


FIG 11—Effect of time at indicated temperatures on hardness of aluminum killed steel subsequently cold reduced 40 pct and box annealed (16 hr at 1275°F).

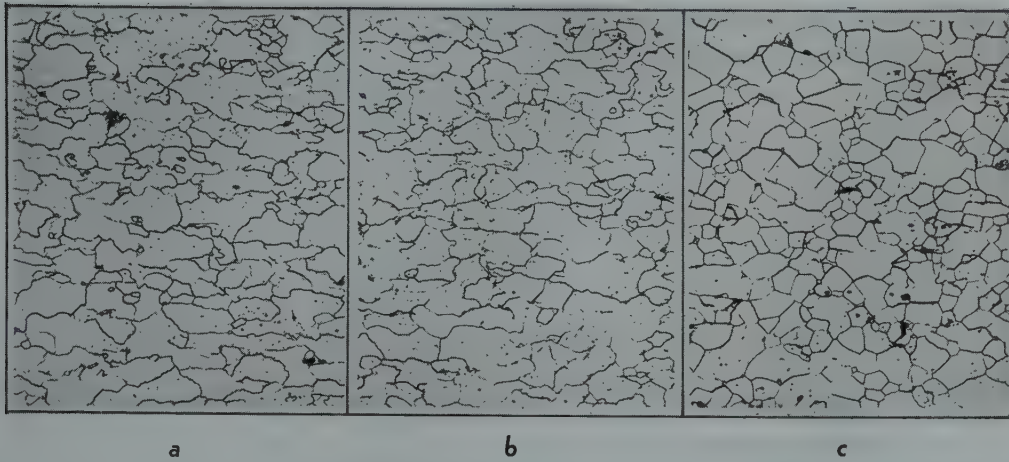


FIG 12—Effect of method of cooling, following hot rolling, on grain structure of aluminum killed steel after subsequent reduction (40 pct) and box annealing. 100 X. Nital etch.
a. 0.085 in. thick hot rolled strip oil quenched. b. 0.085 in. thick hot rolled strip air cooled. c. 0.085 in. thick hot rolled strip placed in furnace at 1500° F and furnace cooled.

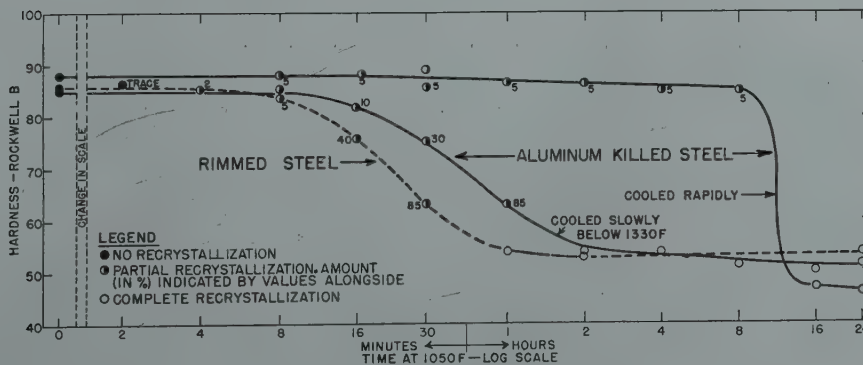


FIG 13—Effect of cooling rate after hot rolling on isothermal recrystallization of aluminum killed steel D at 1050°F, following 40 pct cold reduction. Curve for rimmed steel cold reduced 40 pct reproduced from Fig 2 for comparison.

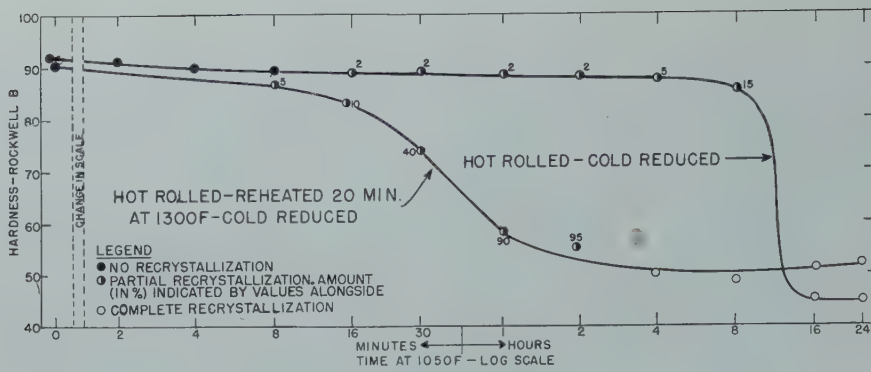


FIG 14—Effect of heating aluminum killed steel B at 1300°F on subsequent recrystallization at 1050°F following 40 pct cold reduction.

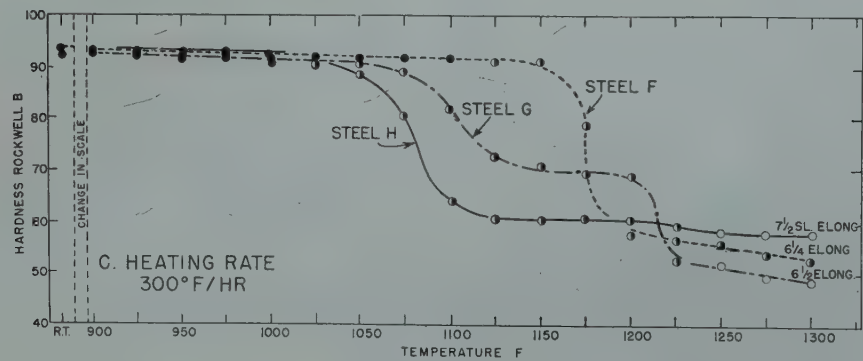
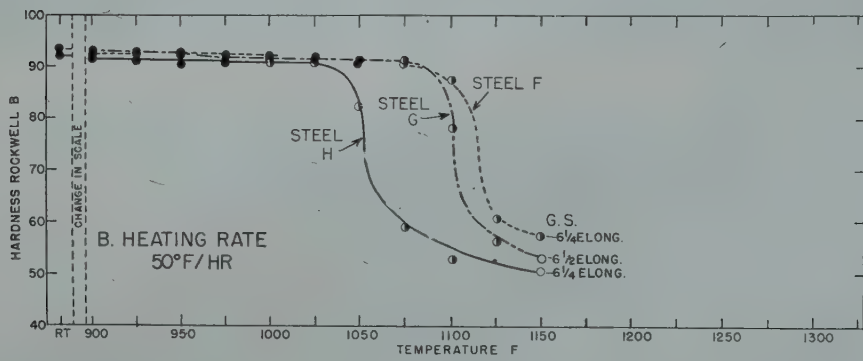
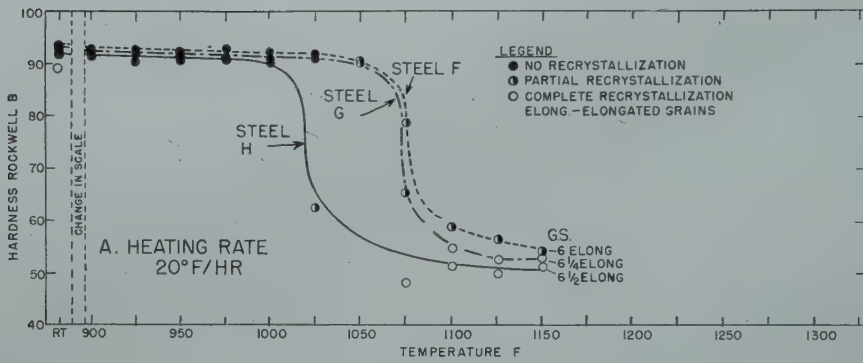


FIG 15—Effect of heating rate on recrystallization of aluminum killed steel during continuous heating after 40 pct cold reduction.

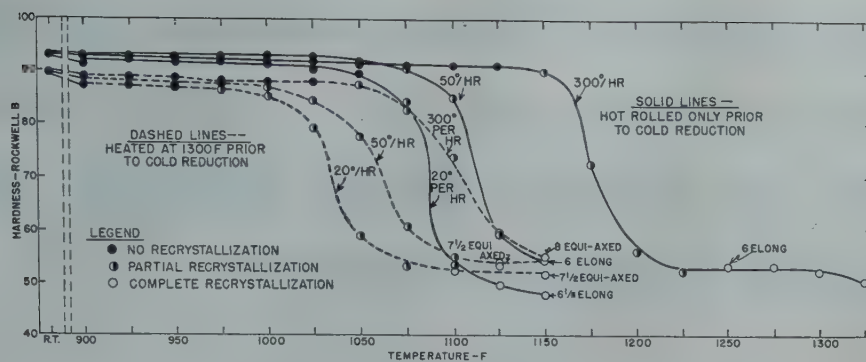


FIG 16—Effect of prior treatment at 1300°F on recrystallization of aluminum killed steel E when heated continuously at 20, 50 or 300°F per hr after 40 pct cold reduction.

whereas the grains in rimmed steel are predominantly equiaxed.

An increase in temperature accelerates the recrystallization of rimmed steel but does not essentially change the *shape* of the isothermal recrystallization curve; final grain size and hardness are changed to a minor extent, if at all. In the isothermal recrystallization of aluminum killed steel, increase in temperature increases the amount of recrystallization which takes place in the initial stage, shortens the second and third stages but does not eliminate them, and makes the grain size finer and more nearly equiaxed.

The isothermal recrystallization pattern of subsequently cold reduced aluminum killed sheet steel may be made to approach that of rimmed steel by slowly cooling the hot rolled strip or by reheating it for a sufficient length of time to a temperature of approximately 1200°F or above, then cooling at any convenient rate; the recrystallized grain size is then comparatively fine and the grains tend to be equiaxed.

The recrystallization temperature range on continuous heating of aluminum killed steel is raised by increasing the rate of heating and in some instances the grain structure becomes finer and more equiaxed. Treatments prior to cold reduction that result in an equiaxed structure on subsequent recrystallization lower the recrystallization temperature range on continu-

ous heating.

It was observed that when killed steel recrystallizes to an elongated-grain structure the first new grains to form are widely scattered and initially may be more or less equiaxed; as they grow they have considerable difficulty in crossing the cold-worked grain boundaries and consequently become elongated in shape like the original deformed grains. Recrystallization gradually progresses to adjacent cold-worked grains so that the final recrystallized grains are, to some extent, built up of elongated units which correspond to the original deformed grains. When recrystallization takes place at a comparatively low temperature, the number of locations or nuclei where new grains start is limited and the final grain size is coarse; but as the recrystallization temperature is increased, more nuclei form, the final grain size becomes finer, and the grains tend to be less elongated. In rimmed steel, or in killed steel which recrystallizes to give an equiaxed structure, the number of nuclei increases rapidly as recrystallization progresses and becomes much greater than in killed steel of the elongated-grain type at the same temperature; resistance to growth across the old grain boundaries is also less; the result is an equiaxed grain structure and, generally, a finer grain size. The formation of coarse, elongated, recrystallized grains appears, therefore, to

be due to some factor which reduces the number of effective recrystallization nuclei and also restrains grain growth. The precise nature of this restraining influence has not been established.

Acknowledgments

This investigation was suggested by Dr. John Johnston, then Director of Research, United States Steel Corporation. The assistance of various operating personnel, particularly at Gary Sheet and Tin Mill and Irwin Works of Carnegie Illinois Steel Corporation, in supplying materials and that of Gary Works Laboratory in making the hot rolling tests is greatly appreciated, as are the suggestions of associates in both the Research Laboratory and operating companies. Messrs. H. M. Evers and L. B. Haberman helped with portions of the experimental work.

References

1. Burns and McCabe: U. S. Pat. No. 2,381,435 (Aug. 7, 1945).
2. S. J. Smithells: *Tungsten*. (1926), 79-87, Chapman and Hall, London.
3. S. J. Smithells: *Impurities in Metals*. (1931), 83-85, John Wiley & Sons, New York.

Precipitation Phenomena in the Solid Solutions of Nitrogen and Carbon in Alpha Iron below the Eutectoid Temperature*

L. J. DIJKSTRA†

Introduction

DURING the past several years an extensive study has been made of the internal friction of iron containing carbon or nitrogen in solid solution.^{1, 2, 3, 4, 5} It has been found that a sharp peak is observed in a plot of the internal friction vs. temperature of measurement. With a frequency of about one cycle per second, this peak occurs at 20°C for N and 36°C for C. The physical origin of this anomalous internal friction was traced by Snoek¹ to the local tetragonal symmetry of the interstitial positions in body centered cubic (bcc) iron. A change in stress induces a change in the equilibrium distribution of the interstitial atoms among the three types of interstitial positions, the three types corresponding to the three directions along which the tetragonal axis may lie. It is the continual striving of the interstitial atoms to maintain an equilibrium distribution that gives rise to a phase lag between strain and stress during oscillation, and hence, to internal friction. A similar type of internal friction has been observed in the bcc lattice of tantalum containing in interstitial solid solution C, N or O⁶.

The theory of this anomalous internal friction leads to the prediction that its magnitude is strictly proportional to the concentration of either the carbon or the nitrogen in solid solution, provided the concentrations are small. This prediction has been verified³ for the range of solubilities obtainable in alpha iron. This proportionality provides us with a new tool for the study of nitrogen and carbon in alpha iron. It thus enables one directly to follow the precipitation of either of these solute atoms from solid solution and also directly to measure their solubility as a function of temperature. A

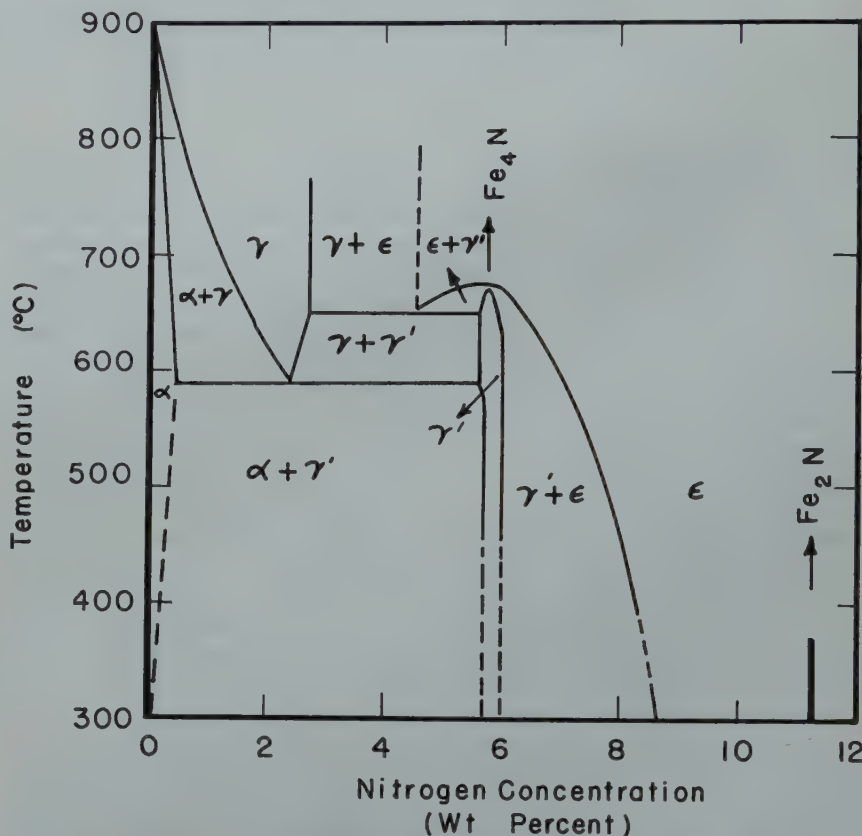


FIG 1—(Above) Fe-N equilibrium diagram (after Lehrer-Eisenhut and Kaupp²).

preliminary study of precipitation using this method has already been presented by the author.³ The purpose of this paper is to present more extensive observations upon the precipitation of N and C in alpha iron, as well as to present observations upon the solubility of N and C in alpha iron which, at least in the lower tempera-

ture range, are believed more accurate than those previously obtained by other methods.

The interpretation of the observations upon precipitation involves the use of the appropriate equilibrium diagrams. For ease of future reference in this paper the equilibrium diagrams for the Fe-N and Fe-C systems are accordingly reproduced as Fig 1 and 2, respectively.

Experimental Procedure

The specimens were made of Westinghouse Puron iron and consisted of wires 0.025 in. in diam and about 1 ft long. By a wet hydrogen treatment the specimens were purified of C and N. In

Cleveland Meeting, October 1949.
TP 2540 E. Discussion of this paper (2 copies) may be sent to *Transactions AIME* before Dec. 15, 1949. Manuscript received November 19, 1948; revision received December 20, 1949.

* This research has been supported by ONR Contract No. N-6ori-20-IV, NR 019 302.

† Institute for the Study of Metals, University of Chicago.

References are at the end of the paper.

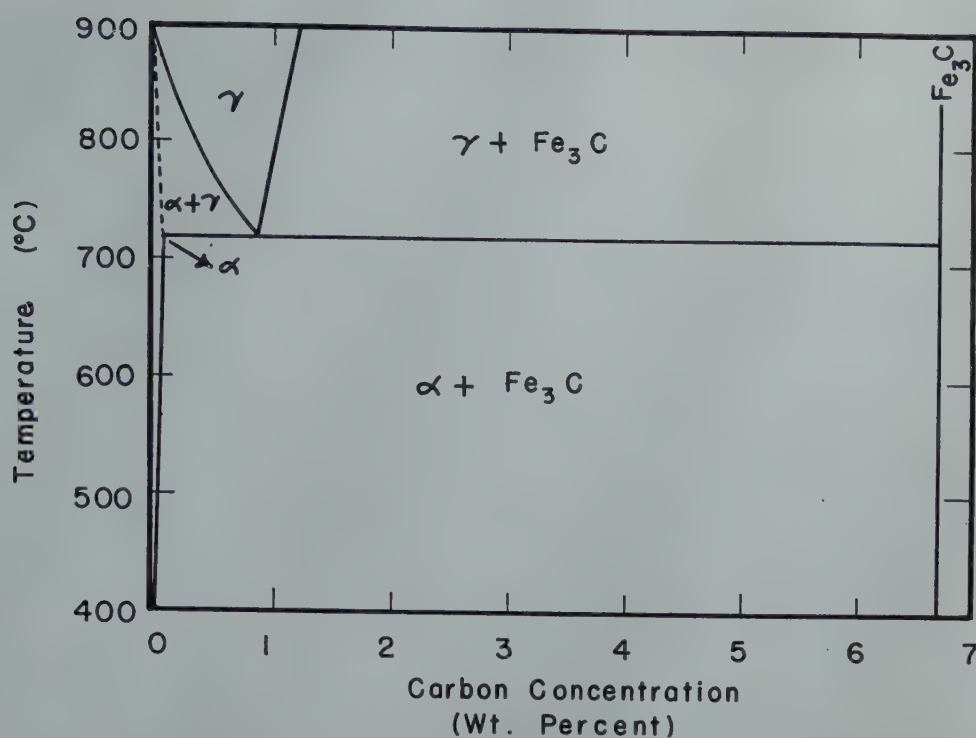


FIG 2—(Below) Fe-C equilibrium diagram.

order to make internal friction measurements the wires were used as the suspension element in a torsional pendulum system with a period of vibration of about 1 sec. The damping is determined by measuring the logarithmic decrement of the free torsional vibration using a very small vibrational amplitude. The apparatus is very similar to that previously described by T. S. Kê.⁴ The wire was surrounded by a furnace to enable us to vary the temperature, which variation is necessary in locating the maximum in the internal friction. All data have been corrected for a relatively small background damping of $Q^{-1} = 0.001$. Here, as in the following, we shall take as the quantitative measure of internal friction the quantity Q^{-1} , which is $\frac{1}{2}\pi$ times the logarithmic decrement, $(\frac{1}{2}\pi)$ times the specific damping capacity. A calibration of the value of Q^{-1} at the maximum of the internal friction peak, Q_{max}^{-1} , vs. resistivity, and a comparison of Köster's⁷ resistivity vs. concentration curves, has shown that Q_{max}^{-1} is equal, within the 10 pct accuracy of the measurements, to the wt pct concentration in the case of both carbon and nitrogen in solid solution.

The N was introduced in the standard way by annealing the specimen in a mixture of H₂ and 3-5 pct (by volume) of NH₃ at 580° for some hours, until the wire was homogeneously

loaded with N. The homogeneous distribution throughout the specimens could be checked microscopically after precipitation. By varying the partial pressure of the NH₃ in the mixture the amount of N introduced could be controlled. After quenching from 580°C by immersion into cold water or by exposure to a compressed air stream all the N was retained in supersaturated solid solution, as was verified by varying the quenching rate.

The C was introduced in a similar way by annealing the sample at 700°C in a mixture of H₂ and benzene, followed by quenching in cold water.

The introduction of N and C by this method has the disadvantage that atomic H is generated which will readily enter into the Fe-lattice. It is well known that the absorption of H affects the mechanical properties of Fe. Most of the H will diffuse out again by heating in a neutral atmosphere. Iron which was pickled in acid, and which had thereby taken up a large amount of H, did not show any contribution by H to the internal friction in the temperature region between -40 and 100°C. How far the specimen may have been damaged by the H, for example, by causing small rifts and thus affecting the precipitation phenomena, we do not know, but assume it is not serious.

The general procedure was as follows. After being quenched from the

nitriding or carburizing temperature to room temperature, the specimens were tempered at a definite temperature. In order to determine the C or N content still present in solid solution after increasing periods of tempering, the specimens had to be quenched to room temperature to measure Q_{max}^{-1} , which took about 5 min. The drop in Q_{max}^{-1} due to aging during this short interval was generally negligible. Sometimes the time intervals of tempering were rather short (15 sec), necessitating rapid heating to the tempering temperature. For this purpose hydrogen was used as the tempering atmosphere at moderate temperatures (heating time was 3 sec in H₂, 30 sec in air). At temperatures above 400°C we used He since the N and C content of the wire decreased noticeably at these temperatures in a hydrogen atmosphere.

It was found possible to use a single specimen in a whole series of measurements. After aging or tempering, during which the N or C had been rejected partially or completely from solid solution, the original state of complete solid solution was reestablished by what we shall call a re-solution heat treatment. This re-solution heat treatment consisted of a 580°C (or 720°C for C) anneal for about 1 sec and subsequent quenching. This was repeated more than 50 times without any change being noticed in the initial value of

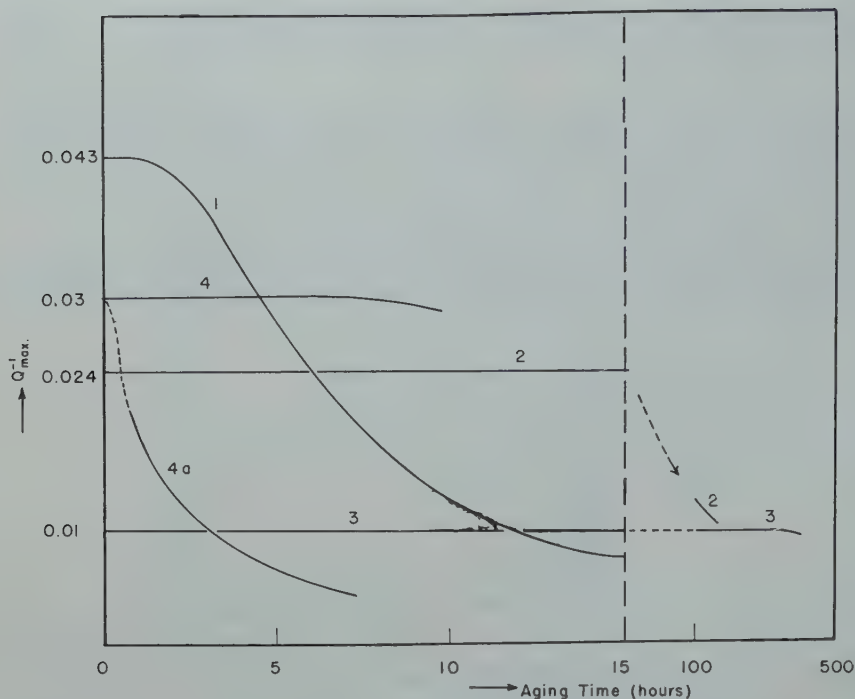


FIG 3—Typical room temperature aging curves; 1,2,3,4 as quenched; 4a same as 4, except for cold work following quench.

Q_{max}^{-1} . Even after extended tempering times at higher temperatures no more than 5 sec were required to eliminate the tempering effects. After this re-solution heat treatment one could start again and find the measurements reproduced quite satisfactorily.

Internal Friction Measurements

We first confine ourselves to the case of nitrogen in solid solution. A brief discussion of carbon in solid solution will be given at the end of this section.

Fig 3 shows typical aging curves for four specimens. They were all slowly cooled from 950°C and afterwards loaded with different amounts of N as indicated by the initial Q_{max}^{-1} . After a re-solution heat treatment specimen 4 has been cold worked to 48 pct reduction in area. The corresponding aging-curve is denoted as 4a. These curves show clearly the large influence of the initial concentration of N and of the state of cold work upon the rate at which N is rejected from solid solution. To investigate the effect of temperature these two factors should be kept constant; this was assured by the re-solution heat treatment.

In Fig 4a and 4b are reproduced a typical set of tempering curves for a series of temperatures ranging from 0 to

500°C. The curves for the temperatures 250, 275, and 300°C are only partially drawn in Fig 4a; the complete tempering curves are given in Fig 4b. All the measurements were made on the same specimen, which, before nitriding, had been slowly cooled from 950°C. The various measured initial values of Q_{max}^{-1} , of about 0.042, corresponding to a total N content of about 0.04 pct, show how nicely they are reproduced by the re-solution treatment. The time scale is a logarithmic one. We wish to point out the following:

1. If a linear time scale is used instead of a logarithmic one, a number of curves, especially those for the lower temperatures, still show the very small initial slope which rapidly increases. This may mean that some nucleation stage is involved, usually called incubation or induction period.

2. After the initial drop (*dash*) the curves approach a horizontal section. This indicates that a stationary state, which can be temporary, is approached in which the N concentration in solid solution has decreased to a certain constant value. This residual value is zero within the limits of measurements, at temperatures below 100°C, but increases rapidly for higher temperatures.

3. For more extended tempering times at intermediate temperatures a second drop (*solid line*) starts and continues until a final equilibrium state is

reached, which final state proved to be permanent even for very extended tempering times. The tempering times for temperatures below 250°C have been too short to observe the second drop, though there can hardly be any doubt that it must also be present below this temperature.

At temperatures above 250°C there seems to be no opportunity for the intermediate, "stationary" state to develop completely, due to the interference with the second drop. Above 300°C the first drop has completely disappeared and only the second process remains. The final residual solubility rapidly increases with temperature and at 500°C no decrease of Q_{max}^{-1} on tempering could be observed for this N content.

4. If we further compare the dashed tempering curves for different temperatures in Fig 4a, then we see there is a shift to the left with increasing temperature. This shift is almost parallel as long as the curves drop to a low value. Above 250°C this shift to the left reverses into a shift to the right, towards longer tempering times. The solid curves show about the same behavior.

Considering the dashed curves, we shall define a half time value $t_{1/2}$ as being the time necessary to reach the Q_{max}^{-1} midway between the initial and residual value. In Fig 5 $\log t_{1/2}$ has been plotted against $1/T$ in the region 0 to 200°C. The dots and circles refer to two different successive runs through the whole temperature region. The curves seem rather straight, but show a somewhat sudden bend at 100 and just below 20°C. This bend was reproducible and seems to indicate that the phenomenon is rather complicated.

5. The specimen was then annealed for $\frac{1}{2}$ hr in wet H_2 at 700°C and afterwards for some hours in dry H_2 at 500°C to assure a homogeneous distribution of the N. After this treatment the Q_{max}^{-1} was 0.023, corresponding to a total N content of about 0.02 pct. The tempering curves for this concentration in Fig 6 show the same general behavior as those in Fig 4. The dashed curves, as well as the solid one, seem to approach the same equilibrium values of Q_{max}^{-1} as the curves in Fig 4. (The Q_{max}^{-1} scale is different in Fig 4 and 6.) The only obvious effects of the concentration difference are, first, a large increase in $t_{1/2}$ below 100°C so that the sudden bend in the curve at 100°C in Fig 5 has disappeared, and secondly, a lowering of the temperature at which

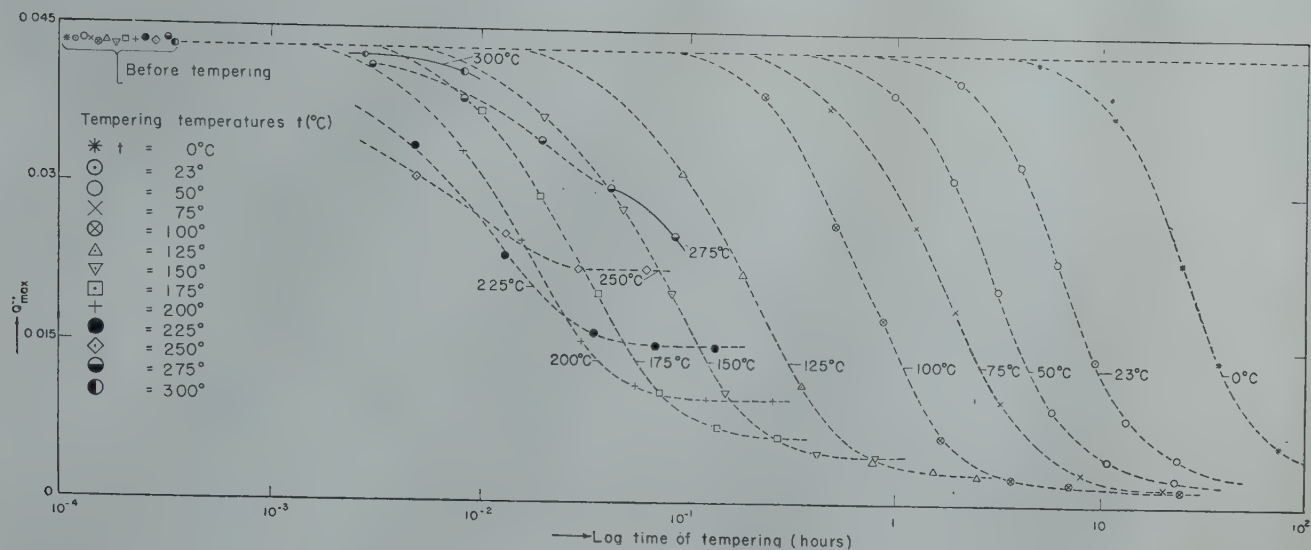


FIG 4a—Effect of aging at low temperatures ($R.T.$ — 300°C). All measurements are at room temperatures following indicated aging. Initial concentration of nitrogen is 0.043 wt. pct.

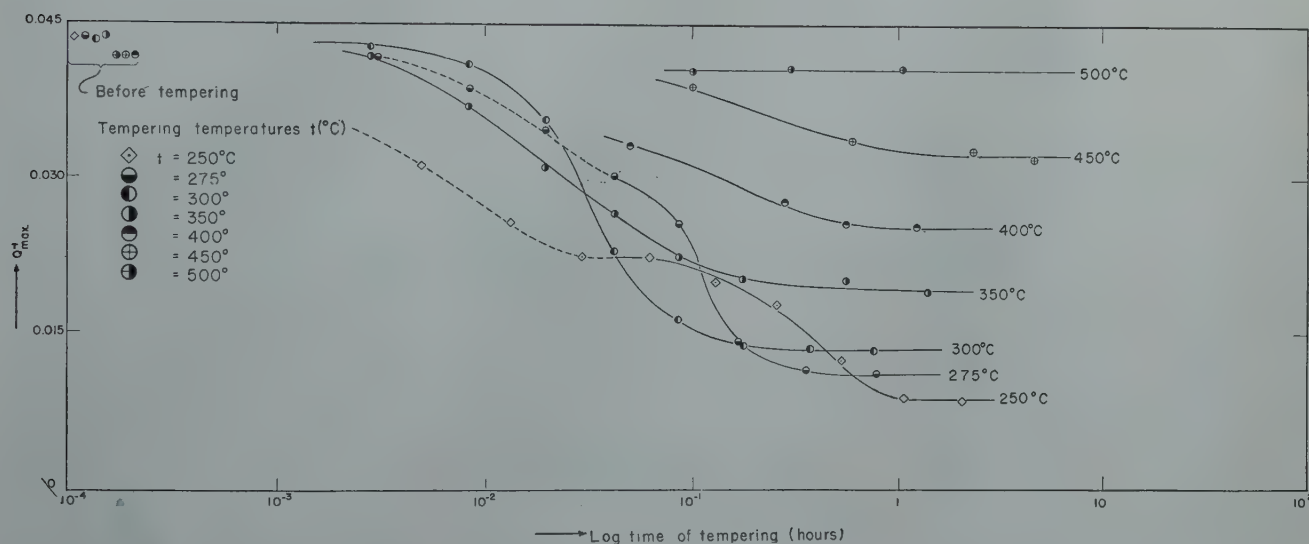


FIG 4b—Effect of aging at high temperatures (250 – 500°C). Dashed lines: intermediate precipitation. Full lines: precipitation of Fe_4N .

the first drop disappears. The solid curves for 250°C in Fig 4b and 6 are almost identical, although in Fig 4b a large first drop has preceded it.

We may briefly summarize the above observations as follows: At intermediate temperatures the rejection of N from the supersaturated solid solution takes place according to two different successive processes. By lowering the temperature the earlier reaction will predominate; by raising the temperature, the later one. The fact that the completion of the earlier rejection process does not seem a necessary condition for the beginning of the second one (in a certain temperature region we even observe that the temperature dependence of the rate of both

processes has a different sign), suggests that the two processes occur independently of each other with rates having a different temperature dependence.

It seems most natural to relate each quasi-stationary or stationary state in the tempering curves to the existence of some Fe-N phase, whatever it may be. The height of a horizontal part represents the solubility of N in α -iron in equilibrium with the corresponding Fe-N phase. According to the preceding paragraph, it appears, then, that the observed Fe-N phases are independent of one another, that the earlier phase is not an intermediate or transitional state of the final phase.

In the case of a perfect solid solution

the solubility $[c]_{\text{sat}}$ must satisfy a relation of the type

$$\left(\frac{\partial \ln [c]_{\text{sat}}}{\partial T}\right)_p = \frac{\Delta H}{RT^2}$$

or

$$\ln [c]_{\text{sat}} = -\frac{\Delta H}{RT} + \text{const.}$$

ΔH is the heat of solution per gram mol. of the precipitated phase. In Fig 9 the values of $[c]_{\text{sat}}$ as given by the horizontal parts in Fig 4, and in a number of curves which we did not reproduce, have been plotted on a logarithmic scale versus $\frac{1}{T}$ both for the intermediate phase (curve 1) and for the final phase (curve 2), which we assume to be Fe_4N . The values

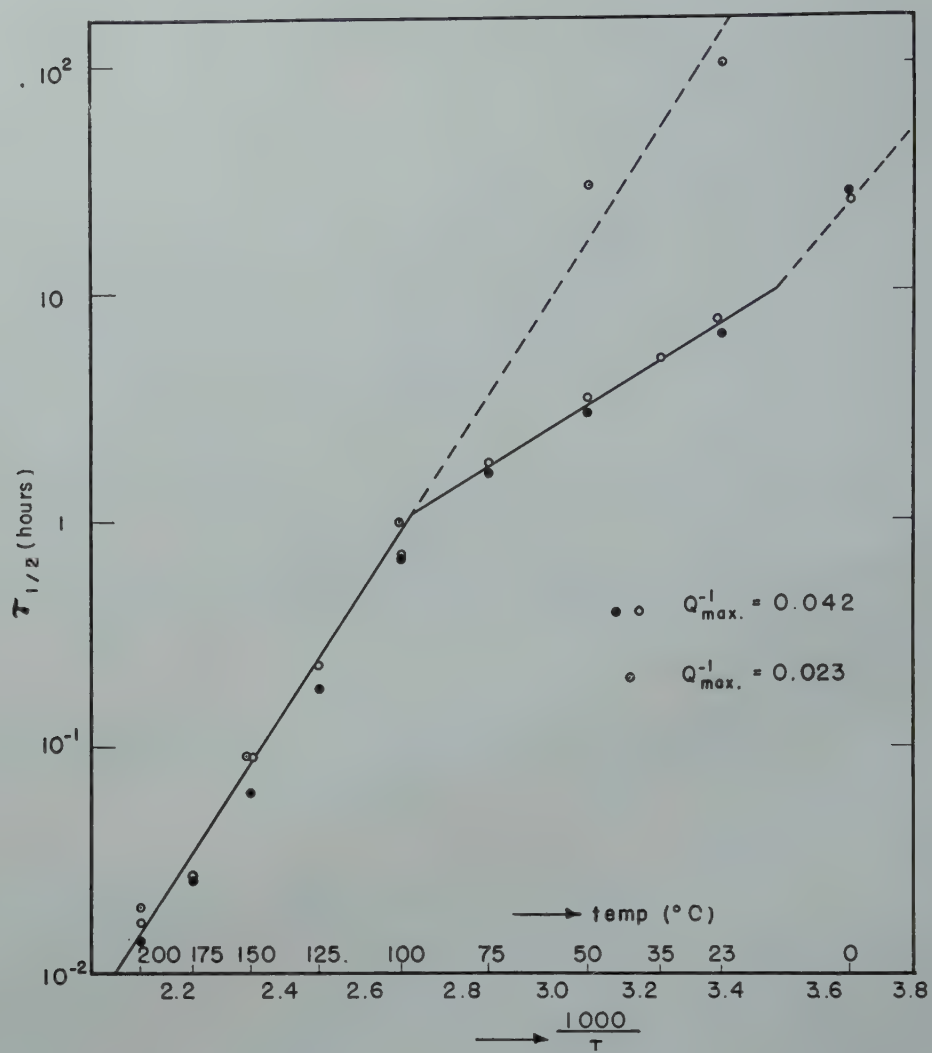


FIG 5—Temperature dependence of time required for precipitation to be one-half complete for two initial concentrations.

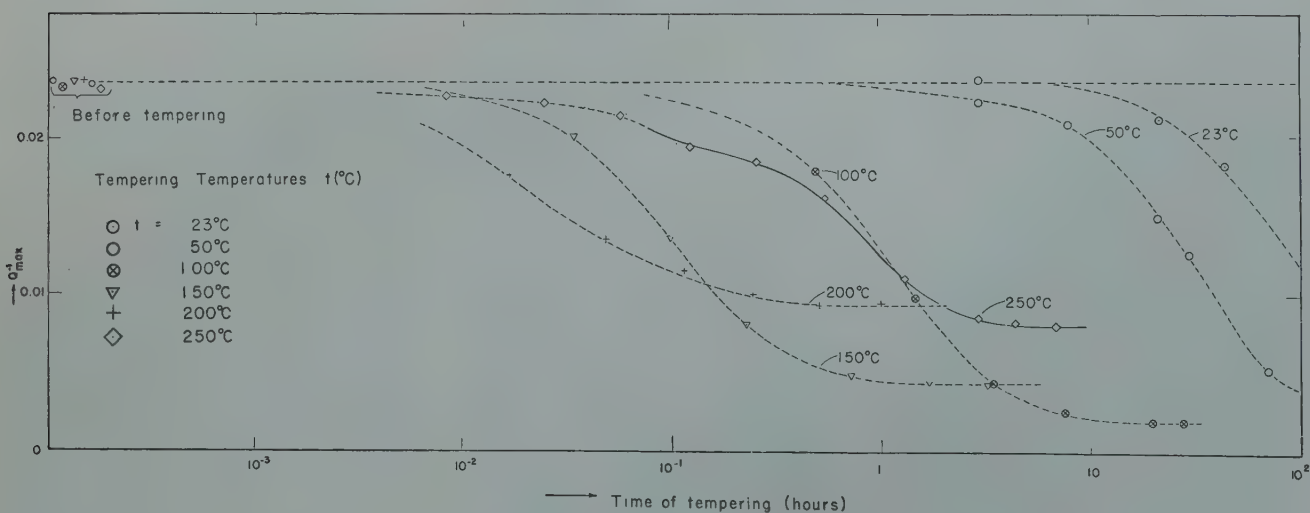


FIG 6—Effect of aging at low temperatures (*R.T.*—300°C). All measurements are at room temperatures following indicated aging. Comparison with Fig 4*a* illustrates effect of initial concentration upon rate of precipitation.

for Fe_4N from Fig 4a for the lower temperature are probably too high because the tempering times have been too short to reach real equilibrium. At the highest temperatures we met with the difficulty that the N content seemed to decrease during tempering, even using He as a gas atmosphere. Therefore we followed another way and nitrided the specimen at 575°C for a sufficiently long time in $\text{H}_2 + \text{NH}_3$ mixtures of increasing NH_3 content until no further increase in Q_{max}^{-1} was observed. This final value of Q_{max}^{-1} gives us the solubility for Fe_4N at 575°C . It would take us too long to do the same for all the lower temperatures. Therefore we simply annealed this loaded specimen at the desired lower temperatures in adequately rich $\text{H}_2 + \text{NH}_3$ mixtures, during which Q_{max}^{-1} dropped until the equilibrium value was reached. These values are given by the black dots in Fig 9 and seem to us to be the best ones. From the slope of the curve we calculate that ΔH for both precipitates is of the order of 8,000 cal per mol. An extrapolation of our data to 590°C , the eutectoid temperature for the Fe-N system, gives for the maximum solubility about 0.10 pct.

It is possible to get higher concentrations of N into solid solution in the following way: by annealing in $\text{H}_2 + \text{NH}_3$ mixtures above the eutectoid temperature some f.c.c. γ -phase is formed (see Fig 1) which by rapid quenching down to room temperatures apparently transforms into the bcc α -phase. During this quenching no precipitation takes place, though there must have been some diffusion of N between adjacent interstices in order to obtain the cubic phase and not a martensitic structure. In this way we have observed values for Q_{max}^{-1} of 0.12. These highly supersaturate solutions are extremely unstable and precipitate at room temperature in about 5 min.

The precipitation of C from a supersaturated solid solution has been investigated along lines similar to that for N. The value of Q_{max}^{-1} in the freshly quenched state was 0.02, which corresponds roughly to a carbon content of 0.02 pct by weight. The tempering curves did not show any observable sign of a double stage character at any temperature. The half time value for well annealed material was about 2-3 hr at 100°C , about 2 min. at 200°C , and about 10 sec at 300°C . For higher temperatures precipitation was so rapid that we were able to observe only the final equilibrium values.

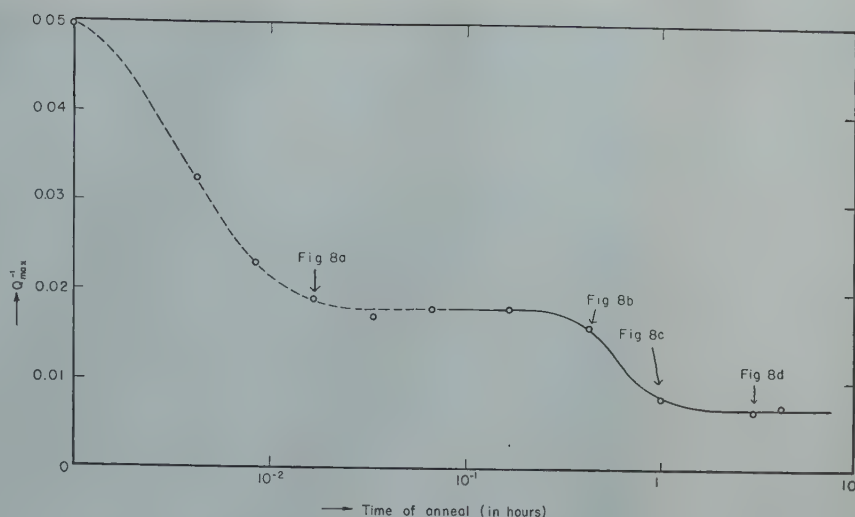


FIG 7—Aging history of specimens whose micrographs are given in Fig 8.

Table 1 . . . Solubility of Carbon in Alpha Iron in Equilibrium with Fe_3C .

| t ($^\circ\text{C}$) | 250° | 400° | 450° | 500° | 550° | 600° | 650° | 700° | 710° |
|--|-------|-------|-------|-------|-------|------|-------|-------|-------|
| $Q_{\text{max}}^{-1} \simeq [\text{c}]_{\text{sat}}$ | 0.001 | 0.002 | 0.003 | 0.004 | 0.007 | 0.01 | 0.012 | 0.016 | 0.020 |

These data are plotted in Fig 9 and from the slope of Curve 3 we calculate for the heat of solution of Fe_3C in α -iron about 10,000 cal per mol.

The above determined values of the solubility of C in α -iron with respect to Fe_3C are only about one-half the values reported by Köster.⁷ The extrapolated value at the eutectoid temperature of 723°C obtained from the above data is, however, in excellent agreement with the value of 0.025 wt pct given by Smith⁹ from an extrapolation of his higher temperature data on the equilibrium of C in α -iron with C in γ -iron.

Results of Microscopic Investigation

A specimen purified of C by wet H_2 treatment was loaded with N. The initial value of Q_{max}^{-1} was 0.049. The tempering curve for 250°C is shown in Fig 7. After a re-solution heat treatment the tempering treatment at 250°C was repeated. Micrographs of the various stages during tempering were made on small samples cut from the quenched specimen after increasing tempering periods. Some of them with tempering times indicated by arrows in Fig 7, and which were most characteristic, have been reproduced in Fig 8 (a-d). No micrographs were taken for other tempering temperatures. The magnification was $500\times$; the etchant was

pical. The big dark spots are oxide impurities. After some seconds the micrographs reveal the very early stages of some visible precipitation process. After 1 min., when the first equilibrium state in Fig 7 is reached, these early stages have developed into a highly dispersed but well-defined structure shown in Fig 8a. The measured distance between the dark etched N-rich regions is about 10^{-4} cm. This value is consistent with the calculated diffusion distance X according to $X = \sqrt{Dt}$, in which t is tempering time in seconds and the atomic diffusion coefficient² D is $5.2 \times 10^{-4} e^{-20,000/RT}$ $\text{cm}^2\text{sec}^{-1}$. From the initial concentration of about 0.05 pct N we now calculate easily that the thickness of the platelets precipitated must be of the order of 10\AA , assuming that each observed platelet is not a series of smaller parallel platelets. That they nevertheless show up so markedly in the micrograph must be an etching effect which is probably due to the fact that a large region around the precipitate is in a state of high internal strain caused by the precipitate itself.

Though Fig 7 shows that no further precipitation from the α -Fe phase takes place for tempering times between 1 and 30 min., successive micrographs during this period demonstrate that the structure has not reached a steady state. The distance between the platelets gradually increases, presumably due to a coagulation process. After 30 min. the regular geometrical pattern

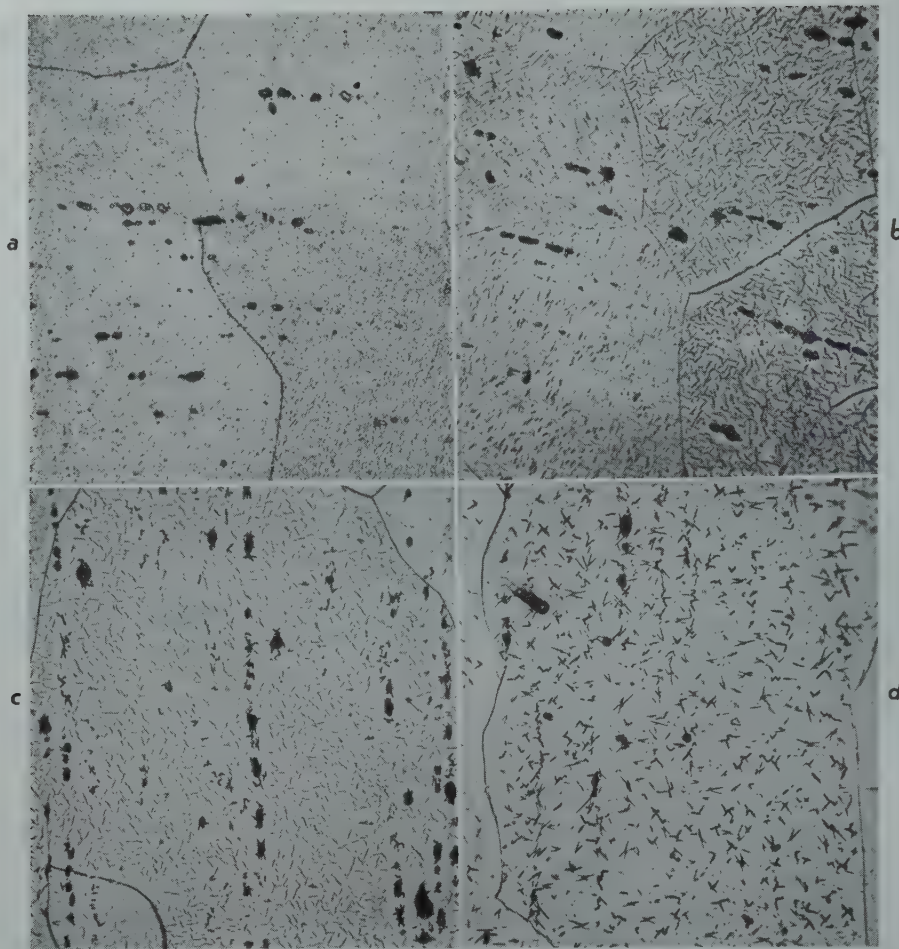


FIG 8—Illustration of two types of precipitates: *a* and *b*, intermediate phase; *c*, intermediate and Fe_4N phase; *d*, Fe_4N phase. Aging history given in Fig 7. $\times 500$. Reduced approximately one third in reproduction.

of Fig 8*b* is obtained. Similar platelike structures arranged along definite crystal planes (the so-called Widmanstätten structures) are quite common in precipitation phenomena¹⁰ though their explanation is still unsatisfactory. Very often the dark etched regions consist of a series of mostly parallel, close, rather short plates, which cause the wavering character of the etching marks.

The pattern in Fig 8*b* generally shows no more than 3 different orientations of the plates, and from simple geometrical considerations it is clear that these plates of a precipitated Fe-N phase must be arranged parallel to the (100) planes of the bcc iron matrix. Very often the polishing plane itself is parallel to a (100) plane and then the Widmanstätten pattern shows only 2 orientations at right angles, as in some of the crystal grains in Fig 8*b*. Moreover, in this case the polishing plane sometimes cuts just across a plate in its own plane and we see round etched areas which are vaguely visible in the rectangular spaces between the dark

lines; they do not show up well in the micrographs. They prove that the precipitate is indeed plate-shaped and not needlelike. The thickness of these plates must be of the order of 50 Å. Micrographs made of these tempered specimens after a second anneal at 600°C followed by quenching (re-solution heat treatment) did not show any trace of precipitate in accordance with the internal friction measurements.

At this time and even earlier a new precipitate (indicated by II to distinguish it from the former precipitate I) suddenly develops here and there. It is easily observed because it etches much darker with picral than I. Precipitate II almost directly shows the well known plate structure of the iron nitride Fe_4N . Fig 8*c* corresponds to a tempering time of 40 min. During the second drop of the curve in Fig 7 the micrographs show that the number and size of the Fe_4N plates increase, while phase I is fading away, especially in the vicinity of the Fe_4N plates.

After 1 hr phase I is still visible, al-

though only faintly; after 3 hr of tempering we distinguish only the Fe_4N plates (Fig 8*d*). The Widmanstätten patterns of phase I and Fe_4N are quite different. The large number of different orientations of the "nitride needles" in Fig 8*d* indicates that the lattice planes of the matrix along which the plates of the phase Fe_4N are arranged must be of a higher order. According to the literature¹¹ Fe_4N precipitates in plates along the (210) plane of the bcc matrix lattice, which generally causes 12 different orientations of the needles in the micrograph.

We were not able to detect any clearly pronounced relationship between the two precipitates. The Fe_4N plates seem to originate from nuclei inside or very close to the plates of phase I as well as somewhere else. The fact that the phases I and II precipitate on quite different lattice planes of the matrix is reason to suppose that there exists no definite relationship and that phase I is not an intermediate transition state of phase II, as for in-

stance is observed in the precipitation of Cu and Ag in Al.¹² We thus see that this microscopic work confirms the conclusions in section 3 regarding the independence of the nucleation of phase II from the presence of phase I.

As mentioned in the preceding section, the curves of internal friction vs. time of tempering did not suggest the presence of an intermediate precipitate in the Fe-C system. Micrographs showing successive stages during tempering at 250°C revealed only small round dots of precipitate which coagulated somewhat during extended tempering times.

Kinetics of Precipitation

Certain observations reported above which, at least on the surface, appear anomalous may be readily understood when cognizance is taken of the standard nucleation theory. This theory has been discussed in great detail by Volmer,¹³ so only the results of the theory need be herein reproduced.

According to the standard nucleation theory the rate of formation of new nuclei, N , is given by the product of two factors each of which depends upon temperature in a characteristic manner. Thus

$$N = DS. \quad [1]$$

The first factor D , known as the diffusion factor, decreases rapidly with a decrease in temperature according to the well known equation

$$D \sim e^{-H/RT}, \quad [2]$$

where H is the heat of activation for the diffusion of the solute atoms. The second factor, S , known as the statistical factor, varies with temperature in a quite different manner, namely as

$$S \sim e^{-T_0^3/T(T_0-T)^2}, \quad [3]$$

where T_0 is the equilibrium temperature corresponding to the concentration of the atoms in solid solution. The temperature T_0 is a function of the geometry of the nucleus, its interface surface tension with respect to the surrounding matrix, and its heat of solution. The precise manner in which T_0 depends upon these parameters need not concern us here. The characteristic manner in which S varies with temperature is determined by the factor $(T_0 - T)^2$ in the denominator of the exponent. This exponent insures that the nucleation factor rapidly approaches zero as the temperature T increases towards the equilibrium temperature.

Reference to Fig 4a, 4b and 6 shows that as the temperature of tempering is gradually increased above room temperature, the time required for precipi-

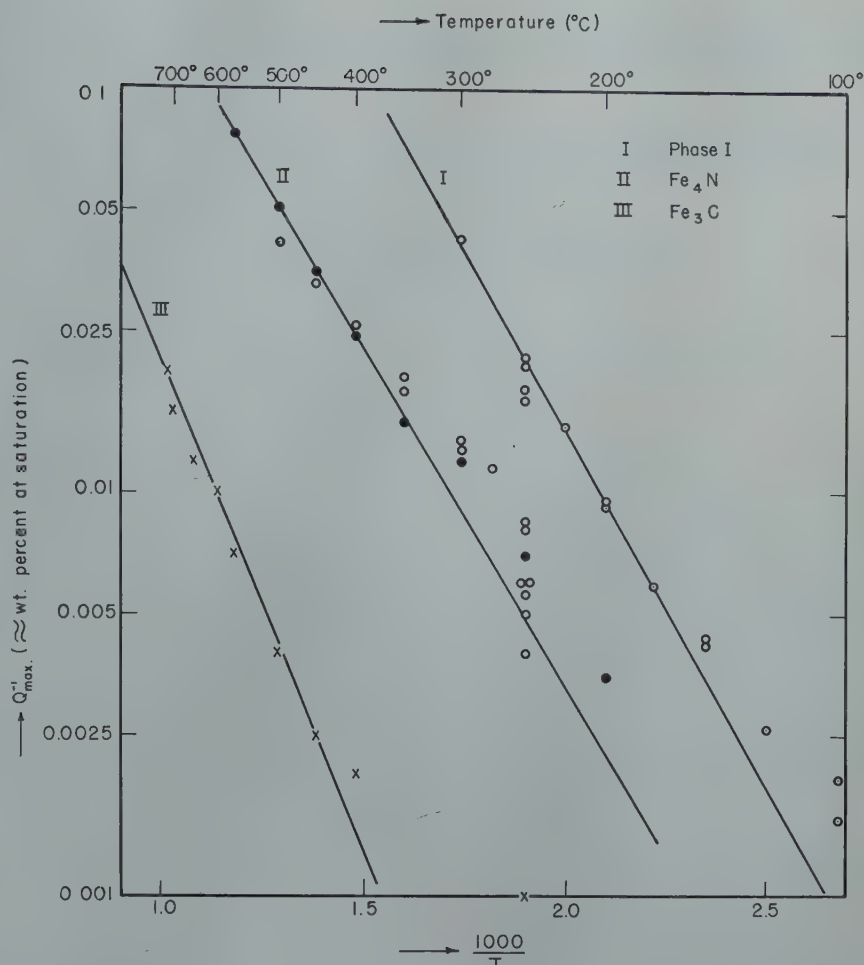


FIG 9—Concentration of N in equilibrium with intermediate phase (Curve I), with Fe_4N (Curve II), and concentration of carbon in equilibrium with Fe_3C (Curve III).

tation to be half complete, $t_{1/2}$, at first decreases and then finally rapidly increases at the highest temperatures. According to the above discussion, we are to interpret the lower temperature range, in which $t_{1/2}$ decreases with a rise in temperature, as that range in which the temperature dependence of D dominates. Thus in this temperature range precipitation is limited primarily by the rate of diffusion. On the other hand, the upper temperature range, in which $t_{1/2}$ increases with a rise in temperature, is that range in which the temperature dependence of S dominates. Thus in this temperature range precipitation is limited primarily by the statistical probability of the presence of nuclei of a critical size for spontaneous growth.

Reference to Fig 3 shows that the time for precipitation to be half complete, $t_{1/2}$, is a marked function of the concentration of the solute atoms, rapidly increasing as the concentration is lowered. The same conclusion is reached upon comparing Fig 6 with Fig 4a. This marked dependence of $t_{1/2}$ upon initial concentration may be

interpreted simply as an increase in T_0 with an increase in concentration at a fixed temperature of tempering. Such an increase in T_0 may be seen, from Eq 3, to result in an increase in the statistical factor S . Thus an increase in initial concentration is seen to affect S in precisely the same manner as a decrease in temperature, namely through an increase in the temperature of undercooling, $(T_0 - T)$.

Specimens in which the N precipitates at 23°C in some hours can be stabilized by a preceding tempering treatment at, for example, 250°C. By this we mean that the rate of precipitation at 23°C, after a preceding tempering treatment at 250°C which took out let us say 60 pct of N from solid solution, is much smaller than if the same amount had been rejected from solid solution during preceding aging at 23°C. The explanation must be the different degree of dispersion of the nuclei. It is to be noted that the rate of nucleation is very slow at 23°C after 60 pct of N has been rejected from α -iron.

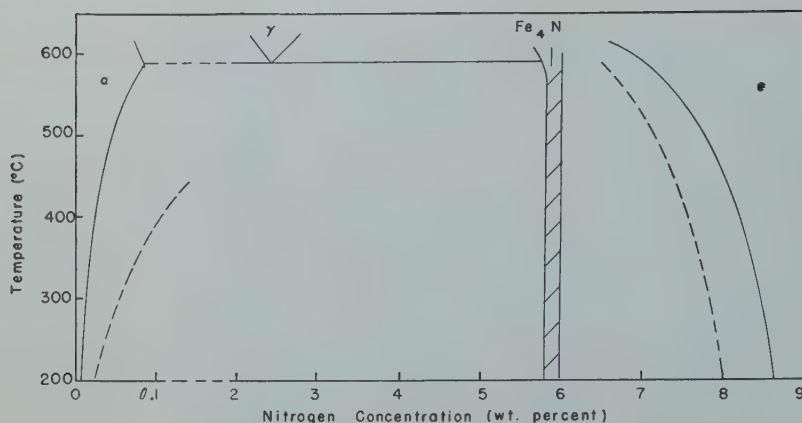


FIG 10—Equilibrium diagram of Fe-N system including metastable intermediate phase.

We have yet to interpret the formation of the intermediate phase in the Fe-N system. A tentative interpretation may be arrived at as follows. From our observations it appears that the Fe_4N phase is very difficult to nucleate. The origin of this difficulty is at present unknown. It may possibly reside in an unusually large interface energy between Fe_4N and the surrounding α -iron matrix. Reference to Fig 1 shows that if the solid solution of N in α -iron is sufficiently undercooled the solution will become supersaturated with respect to the ϵ -phase. This possibility is clarified by the tentative equilibrium diagram of Fig 10. According to this diagram the dashed boundaries of the α and ϵ phases represent the actual boundaries in the absence of the Fe_4N phase. The dashed boundary of the α phase has been drawn from the data in Fig 9. The dashed boundary of the ϵ phase has been drawn merely schematically.

The above interpretation of the intermediate phase in the Fe-N system automatically interprets likewise the nonoccurrence of an intermediate phase in the Fe-C system. In the latter system the only stable phase lying to the right of Fe_3C is graphite. This phase actually has a lower solution pressure than does Fe_3C . It could not, therefore, form an intermediate phase.

Effect of Cold Work

It is a well known experimental fact that distorted regions are favorable places for precipitation. The reason was pointed out above. An amount of cold work of 1 to 5 pct reduction in area did not have very much effect on the rate of precipitation of N from supersaturated α -iron. Certainly the

distances between the distorted regions for this small amount of cold work are too large to affect the precipitation in the specimen as a whole. The effect of 46 pct reduction in area was previously shown in Fig 3. Micrographs of these cold worked specimens being tempered in the region 250–300°C did not show any trace of precipitate. This means that it must be and stay submicroscopically dispersed even at 300°C and that this precipitate modification must be more stable than the usual microscopic Fe_4N plates. A determination of the solubility of N for this precipitate, by the internal friction measurements, indeed proved this to be the case. The solubility at 300°C was about 0.0025 pct, at 400°C about 0.006 pct, while the corresponding values for the Fe_4N plates were respectively 0.012 and 0.025 pct. At higher temperatures the solubility very rapidly increased, partly in an irreversible way due to the fact that the state of cold work is gradually annealed out.

The observed lowering of the solubility of N by plastic deformation is in agreement with the idea advanced by Cottrell that carbon and nitrogen are trapped by dislocations.¹⁴

Summary

Precipitation of carbon and of nitrogen from solid solution in alpha-iron has been studied at different tempering temperatures by internal friction measurements.

In the case of nitrogen these measurements suggested the presence of two successive stages in precipitation. This suggestion was then verified by metallographic examinations. In the first stage plates of an unknown precipitate are formed on the (100) planes of the

matrix. During the second stage the well known Fe_4N plates are formed. The former unknown phase appears to be less stable than Fe_4N , but cannot be considered as a transition state of Fe_4N .

The observed rate of precipitation follows the general behavior to be anticipated from the standard theory of diffusion and nucleation, namely low rates at low temperatures (diffusion limitation), low rates at high temperatures near the critical temperature (nucleation limitation) and a maximum rate in an optimum temperature range. The half time for precipitation is found to increase rapidly with a decrease in the initial concentration, again in accord with nucleation theory.

Plastic deformation (studied only in the case of N) was found not only to increase the rate of precipitation, but also to lower the final solution concentration presumably in equilibrium with the precipitate. It appeared, therefore, as if the precipitate induced by plastic deformation was not identical to that which forms in annealed material. This viewpoint was confirmed by metallographic examination which failed to reveal visible precipitates even after the final equilibrium solute concentration had been attained.

References

1. J. L. Snoek: *Physica's Grav.* (1941) 8, 711.
2. D. Polder: *Philips Res. Rep.*, (1945) 1, 5.
3. L. J. Dijkstra: *Philips Res. Rep.* (1947) 2, 357.
4. T. S. Kê: *AIME Metals Tech.*, June 1948, TP 2370. T. S. Kê: *Phys. Rev.* (1947) 71, 533.
5. C. Zener: *Anelasticity of Metals*. (1948) University of Chicago Press, 115–126.
6. T. S. Kê: *Phys. Rev.* (1948) 74, 9, 16, 914.
7. W. Köster: *Arch. des eisenh. Wesen*, (1928–29) 2, 503, (1929–30) 3, 637.
8. M. Hansen: *Aufbau der Zweistofflegierungen*.
9. R. P. Smith: *Jnl. A.C.S.* (1946) 68, 1163.
10. C. S. Barrett: *Structure of Metals*. (1943) McGraw-Hill Book Co., 466.
11. R. F. Mehl, C. S. Barrett, H. S. Jerabek: *Trans. AIME* (1934) 113, 211.
12. J. L. Burns: *Trans. AIME* (1934) 113, 239.
13. M. Volmer: *Kinetik der Phasenbildung*. (1939) Dresden.
14. A. H. Cottrell: *Strength of Solids*. Report of 1947 Bristol Conf., The Phys. Soc., London (1948), 30.

Concentration of the SO₂ Content of Dwight-Lloyd Sintering Machine Gas by Recirculation

W. S. REID,* Member AIME

IN March, 1938, E. P. Fleming, metallurgist for the American Smelting and Refining Co. inaugurated an investigation into the possibilities of recirculating the gases from Dwight-Lloyd sintering machines operating on lead charge, with the twofold object of concentration of the SO₂ content and reduction in volume of total gas produced.

The possibility of recovering a commercial grade of SO₂ gas from D & L machines operating on lead charge had previously been considered by several investigators.

Early History of Recirculation

The Selby Smelter Commission Report, published by the Bureau of Mines in 1914, contains a chapter by A. E. Wells regarding results obtained at Selby, wherein some of the richer gas was recirculated through a hood over the pallets.

Oldright and Miller of the U. S. Bureau of Mines had also made tests at Trail, B.C., and at Kellogg, Idaho.

R. C. Rutherford, while at the Chihuahua, Mexico, Smelter of the American Smelting and Refining Co., in May, 1937, proposed recirculation of D & L gases to decrease the volume of gas handled by the baghouse.

At none of these plants, however, was the operation commercialized.

In July, 1938, Mr. Fleming, in correspondence with the Selby Plant, inquired regarding the possibility of obtaining 6 pct SO₂ gas from the Selby D & L machines.

At that time, the writer advised that there was slight possibility of obtaining 6 pct SO₂ gas without re-

circulation, but believed that it was possible with recirculation, and that experimental work toward that end should be tried at some plant where spare D & L machines were available.

The foregoing statement was based on the following information then available—

1. Tests on Selby first-over machines showed 2.28 pct SO₂ from first windbox and 1.03 pct SO₂ from second windbox, and corresponding figures for second-over charge of 0.81 pct SO₂ for first windbox and 0.08 pct SO₂ for second windbox.

2. Oldright and Miller (U.S. Bureau of Mines) in 1932 at Bunker Hill, on 42 in. × 22 ft machines found:

a. First-over charge—Maximum SO₂ concentration (leaving cake) of 9.5 pct.

b. First-over charge—SO₂ concentration of over 8 pct from the 4 ft to the 12 ft points beyond the front deadplate and that the concentration then dropped rapidly.

c. That approximately 80 pct of the total sulphur eliminated on the second-over machines occurred during the travel of the pallets from the 1 ft to the 6 ft distances from the deadplate.

d. That approximately 94 pct of the total sulphur eliminated on the second-over machines occurred over the first windbox.

3. Oldright and Miller (U.S. Bureau of Mines) in 1932, at Trail, on 42 in. × 50 ft machines found:

a. First-over charge—SO₂ varied

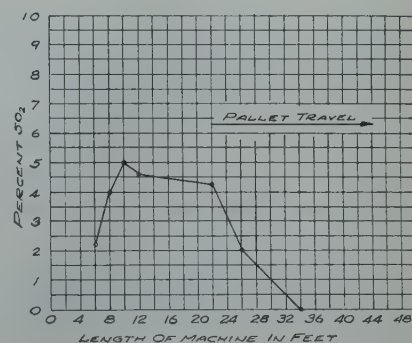


FIG 1—Sulphur elimination curve.

from 2.0 pct to 5.5 pct (leaving cake) from the 12 ft to 28 ft points from the deadplate.

b. That the average SO₂ increased from 1.0 pct at 7 ft from deadplate to maximum of 3.3 pct at 20 ft, then dropped to 1.5 pct at 40 ft.

c. That on a 22 ft, second-over machine with an 11 in. bed the SO₂ varied from 4.5 pct to 6.5 pct from the 2 ft to the 8 ft points from the deadplate.

d. That on the final roast, the SO₂ concentration also varied across the pallets; that is, 2½ pct at the side, increasing to 6.0 pct, 5 in. in, and to 7.0 pct at 10 in. to 20 in. in, then decreased vice versa at the opposite side.

e. Concluded that most of the sulphur on a 22 ft machine was removed over the first 7 ft of the first windbox; therefore, they partitioned the first windbox so that the exit gas from the second 4 ft section was returned to the surface of the pallets over the first 7 ft section, and during a seven-day trial the gas from the 4 ft section averaged 2.4 pct SO₂, while the recirculated gas from the first 7 ft section only increased to 3.8 pct SO₂. (Excess suction over the 7 ft section to prevent escape of SO₂ laden gas from the 4 ft section caused dilution by air.)

San Francisco Meeting, February 1949.

TP 2554 D. Discussion of this paper (2 copies) may be sent to *Transactions AIME* before July 15, 1949. Manuscript received Nov. 14, 1948; revision received January 11, 1949.

* Selby Smelting Works, American Smelting and Refining Co., Selby, California.

f. That recirculation had the advantage of filtering out the dust contained in the recirculated gas.

g. That second-over charge on a 50 ft machine gave SO₂ concentrations ranging from 2.4 pct at 6 ft to 4.0 pct at 8 ft; to 5.0 pct at 10 ft, to 4.6 pct at 12 ft; to 4.3 pct at 22 ft; to 2.0 pct at 26 ft; to 1.0 pct at 30 ft; to trace at 34 ft from deadplate.

If the figures under g are plotted, we have what is now known as a sulphur elimination curve, which is shown in Fig 1.

Preliminary Work at Selby

At the Selby, Calif., Plant of the American Smelting and Refining Co., the company, since 1937, had been operating a 40-ton per day Contact Acid Plant on gases from the roasting of pyritic gold concentrates on a seven hearth Wedge Roaster. This conversion of SO₂ to H₂SO₄ was beneficial in reducing the output of SO₂ from the smoke stack.

At that time (1938) some consideration was also being given to the construction of a liquid sulphur dioxide plant to utilize still more of the SO₂, normally exhausted through the stack.

During Sept., 1938, the first investigation was made at Selby in connection with the feasibility of obtaining a good grade of SO₂ gas from the D & L machines.

Holes were drilled in the sides of various pallets in such a manner that a sample pipe could be inserted to the center of the bed, just under the grate bars. Gas samples taken through the pipe, as the pallets passed over the windboxes, were then analyzed for SO₂.

These first tests on a 42 in. x 22 ft D & L machine, operating with a 4-in. bed at a pallet speed of about 29 ipm, 25 to 30 pct return sinter on a very fine charge, with windbox suction at 12 in. to 12½ in. H₂O, fan volume at 17,500 cfm, and sulphur in charge reduced from 13.0 pct to 5.3 pct, showed as follows for the first windbox: Pct SO₂ under grates—4.6 pct to 9.2 pct—Average—7.4 pct Pct SO₂ leaving windbox—1.1 pct to 1.35 pct—Average—1.25 pct

It was obvious that the principal source of air leakage was between the pallets and the windbox and over the deadplates, with smaller amounts through the shrinkage fissures at the junction of the sinter cake with the side of the pallet, between the pallet

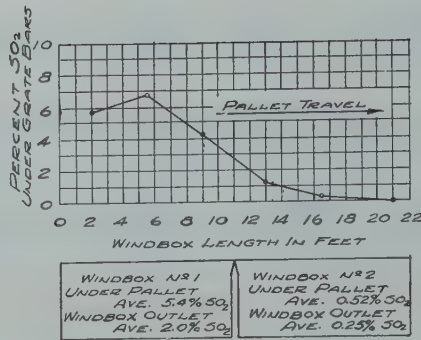


FIG 2—First-over charge—12 pct sulphur.

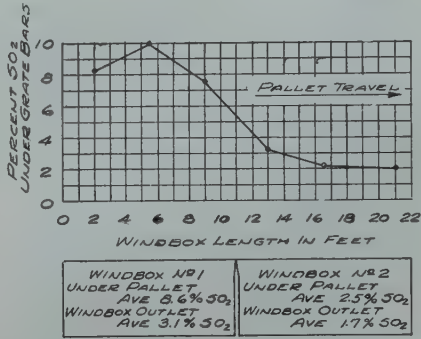


FIG 3—Second-over charge—4.5 pct sulphur.

ends, and around windbox cleanout doors, and the like.

The second windbox on the same charge showed SO₂ concentrations under the grates varying from 6.5 pct to 10.0 pct, and averaging 7.8 pct.

These tests indicated that on this very tight charge, the sulphur elimination continued high throughout the length of machine.

Tests were then made on a second-over machine, operating with a 5¼ in. bed at 19 ipm speed, with windbox suction at 6½ in. H₂O, and fan at 15,000 cfm. These tests showed peak sulphur elimination about midway of the first windbox, after which it dropped rapidly as the pallets passed to and across the second windbox.

A typical set of SO₂ readings showed 2.3 pct SO₂ at the 2 ft mark, a peak of 5.5 pct midway of the first windbox, then decreasing amounts to the second

windbox, which averaged only 0.15 pct for its entire length. It was evident that the first windbox was doing about 90 pct of the work as far as actual sulphur elimination was concerned. The second windbox was serving, principally, as a cooler for the hot sinter cake.

These preliminary tests clearly indicated that, in order to secure a good grade of SO₂ gas, it would be necessary to recirculate the intermediate grade gas through hoods covering the entire pallet including ends and the sealing strip, and collect the concentrated gas from a relative short section of the machine where the SO₂ concentration was highest.

Preliminary Work at Murray

Further experimental work along the lines of Mr. Fleming's suggestion was performed under the supervision of Mr. A. L. Labbe at the Murray, Utah, Plant of the American Smelting and Refining Co. This work was started in Nov., 1938, on standard 42 in. x 22 ft D & L machines on both first-over and second-over charge. By taking gas samples from 2 in. below the grate bars as the pallets passed over the windboxes, the SO₂ concentrations at various points along the machine were determined.

Fig 2 shows, in graphic form, the resultant data for a "first-over" charge and Fig 3, the same for a "second-over" charge.

These graphs illustrate how the SO₂ concentration increases to a peak about midway of the first windbox and then rapidly decreases as the pallets proceed to and over the second windbox.

The comparison of strength of gas under the pallets vs. strength of gas in the outlet from the windbox brings out the often overlooked fact that an unbelievably high leakage of air occurs under and around the pallet ends and over the deadplates. The following tabulation, based on the foregoing data, might demonstrate more clearly this high leakage factor of the ordinary D & L machine:

| | First Windbox | | | Second Windbox | | |
|-------------------------|----------------------------------|-------------------------------------|-----------------|----------------------------------|-------------------------------------|-----------------|
| | Pct SO ₂ Under Grates | Pct SO ₂ Leaving Windbox | Pct Air Leakage | Pct SO ₂ Under Grates | Pct SO ₂ Leaving Windbox | Pct Air Leakage |
| First-over Charge..... | 8.6 | 3.1 | 277 | 2.5 | 1.7 | 147 |
| Second-over Charge..... | 5.4 | 2.0 | 270 | 0.52 | 0.25 | 208 |

Or, for the machines as a whole:

First-over Charge—231 pct air leakage

Second-over Charge—263 pct air leakage.

Later tests on varying charges, depths of bed, and others, indicated air leakages varying up to 400 pct.

Recirculation at Murray

In March, 1939, the first actual recirculation of gases at Murray, Utah, was tried out on a standard 42 in. \times 22 ft D & L machine. This initial installation consisted of a recirculation fan, which delivered the gases from the second windbox through a duct to a hood over the pallets on the first windbox. On a firstover charge, carrying 11.0 pct S, it effected an SO_2 concentration averaging 5.1 pct SO_2 in the reduced volume of gas delivered to the Cottrell flue. However, this final gas varied from 4.0 pct SO_2 to 6.5 pct SO_2 , depending on variations in the moisture content and uneven porosity of the bed. The uneven porosity was due principally to segregation of coarse and fines in the charge hopper above the machine.

This first trial installation also demonstrated the importance of a baffle plate over the windbox partition to minimize the interchange of the weak and strong gases, and, likewise, the partitioning of the conventional windboxes, or construction of different sized windboxes to obtain the maximum concentration of the SO_2 .

To summarize, this first trial installation effected the following on first-over charge:

Gas volume reduced from 19,000 cfm to 6,850 cfm.

SO_2 concentration in final gas increased from 1.7 pct to 5.1 pct.

At this time, it was realized that the same proportional decrease in volume would not be possible from a wider machine because the volume resulting from side leakage is approximately the same regardless of the width of the machine.

This initial installation at Murray is still in service, but utilized solely to decrease the volume of gas going to the Cottrell treaters.

Patent

Based upon data obtained on this preliminary work, Mr. Labbe applied

for, and was subsequently granted, U. S. Patent No. 2,235,261, entitled, "Method and Apparatus for Sintering."

Prior commercial applications of utilizing the oxygen content of weak gas for additional roasting, or in effect further concentration of the SO_2 content of these gases, had accomplished their purpose by returning the weak gases from the last windbox to a closed hood over a limited central section. Attempts on a two-windbox machine to return the gases to a hood confined over the sinter bed of the first windbox had failed, due to the SO_2 in the circulated gases smothering the combustion in the sinter bed proper.

The main features of the sintering machine of Mr. Labbe's patent may be summarized as follows:

Although it is applicable to multiple windbox machines, its application to a two-windbox machine is described merely for simplification.

A hood is provided over most or all of the bed, including pallet ends and wheels, over the second windbox and a large proportion of the first windbox. It cannot be extended any farther over the first box on account of the ignition muffle. The hood also extends over the discharge end of the machine.

There are no cross-sectional baffles in the hood to confine the direction of the smoke to any one portion of the sinter bed. The smoke is free to establish its own course or equilibrium over the entire surface of the sinter bed. Part of the circulated smoke may be drawn back through the same bed of the second windbox.

An inner hood with an opening adjacent to the ignition muffle extends back under the recirculation hood proper, for a distance, over the sinter bed of the first windbox. This allows some outside air to enter and freely support combustion, yet diverts the

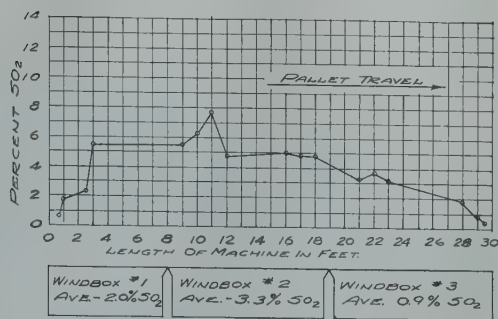


FIG 4—Data obtained over 5-day period on a first-over charge averaging 10.5 pct S.

recirculated gas around the ends of the pallets and thus substitutes this SO_2 laden gas for the air that is ordinarily drawn in as leakage on an unhooded machine.

Trial Recirculation at Selby

By Sept. 1939, the D & L machines at Selby had been enlarged, the sintering practice improved and serious consideration was being given to the utilization of D & L gases for the production of liquid SO_2 .

As a result, a new series of tests were made on the gases by taking samples from under the grate bars by inserting a sample pipe through holes near the top of the various windboxes. A sulphur elimination curve depicting the average data obtained over a 5-day period on a first-over charge averaging 10.5 pct is shown in Fig 4.

While this sulphur elimination curve showed a 15-ft section of the machine producing better than a 5 pct concentration of SO_2 , the actual SO_2 concentration leaving the windboxes averaged only 2.1 pct. This indicated a high infiltration of air around windbox seals, between the pallets at the side of the machine, over the deadplates, and through the shrinkage space between the bed and sides of the pallets.

This machine was reducing 200 tons of charge from 10.5 pct S to 4.5 pct S per day with the fan handling a volume of 25,000 cfm at 440°F.

Gas concentration from the windboxes varied widely, depending on the nature of the charge. A tight charge increased the air leakage, thereby decreasing the SO_2 content of the gases leaving the windboxes. Variations in the depth of the bed on various machines resulted in SO_2 concentrations varying from 0.6 pct to 2.32 pct.

The first trial recirculation unit at

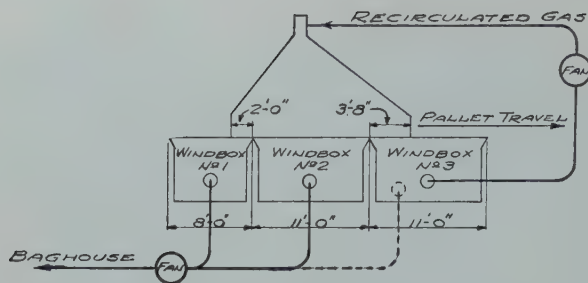


FIG 5—Recirculated gas.

Selby was completed and put into service on May 10, 1940, and consisted of a No. 9 Type P. B. American Blower Co. Exhauster Fan for concentration of the SO_2 content of the gas from a three-windbox D & L machine, 42 in. wide \times 30 ft long, operating on "first-over" charge.

The design for this recirculation unit, including the location of the hoods, was based upon the sulphur elimination curve for the average charge handled by the machine. The so-called sulphur elimination curve, or a knowledge of the data from which it might be drawn, is fundamental in designing a recirculation unit. The pattern varies with different sized machines and with variations in the charge on the same sized machines.

The sulphur elimination curve of a machine on "first-over" charge is quite different from the same sized machine or "second-over" or final charge.

The procedure which has been developed for making a sulphur elimination curve is as follows: 1. Have D & L machine operating normally, with uniform feed.

2. Determine SO_2 content of gases directly under the grate bars at intervals throughout the passage over the windboxes.

Under (1) it is important that the charge be uniform as to analyses, size and moisture content, as well as being uniformly laid down on the pallets. Uniformity of material on the pallets is of major importance because it is impracticable to take and determine gas samples from numerous points throughout the length of the machine simultaneously. As the gas samples must be taken progressively, it is obvious that conditions must be comparable during the entire sampling period. Particular care should be exercised to prevent major segregation of coarse and fines in the feed hoppers

over the machine, yet at the same time obtain a uniform segregation of coarse and fines as the charge is laid down on the pallets. This last mentioned condition is secured by proper design of the feeding mechanism and close control of the talus pile. A high talus pile usually causes "sloughing" which results in a spotty bed, while a "low" talus pile tends to "break" the segregation, which is so desirable at this point.

Under (2) the actual data for plotting the sulphur elimination curve is obtained by sampling the gas directly under the grate bars. In actual practice, these samples are now taken by inserting a curved pipe through openings near the top of the windboxes, allowing same to follow the travel of the pallet a sufficient length of time to draw a measured volume of gas sample through an iodine solution for analysis. In this manner, a sample is obtained which is undiluted by the enormous air leakage normally occurring under and around the ends of the pallets. By taking several of the samples at each location, the average SO_2 concentration at this particular point may be determined and from this a sulphur elimination curve may be plotted.

This first recirculation unit at Selby was entirely for experimental purposes as no utilization of the concentrated gas was made.

The first-over machines at that time were delivering up to 28,000 cfm of approximately 1.5 pct SO_2 gas to the baghouse. This grade of gas was entirely too low in sulphur dioxide to maintain the conversion temperatures at the Contact Acid Plant.

The 42 in. machine equipped for this experimental work had three windboxes, the first box being 8 ft long and the second and third boxes, 11 ft each. The gas from the No. 3 box was returned by the recirculation

fan to a hood over part of No. 1 box and all of No. 2 box, as indicated in Fig 5.

It was soon learned that maintaining proper balance of draft in the recirculation hood was essential. Actual pressure in the recirculation hood caused a smoke nuisance in the building. Excess draft permitted infiltration of air and resultant dilution of the concentrated gas. A definite drop in the concentration was noted whenever the draft in the recirculation hood exceeded 0.02 to 0.03 in. water. This precise regulation was later accomplished by the installation of a damper controlled by a Bristol free-vane controller. Recording draft gauges were also installed in the various windboxes and an SO_2 recorder installed to indicate and continuously record the SO_2 concentration in the concentrated gas.

On the first-over charge, averaging about 13.0 pct S, the recirculation fan handled a volume of 5,000 to 9,000 cfm at temperatures ranging from 700 to 800°F.

By close attention to all operating details, it was demonstrated that with the high sulphur charge being handled at that time gas concentrations of 6 to 8 pct SO_2 could be obtained, but that with this degree of concentration the speed of the machine was reduced about 10 pct in order to effect the same overall sulphur elimination. Overall gas volume to the baghouse with recirculation was approximately 11,800 cfm at 385°F, as compared to approximately 23,100 cfm at 330°F without recirculation. Subsequent improvements in the windbox, duct, and hoop designs corrected this loss in tonnage feature. The first step was to by-pass part of the gas from Windbox No. 3 to the main fan, as indicated by the dotted lines in Fig 5. This practically doubled the suction in Windbox No. 3 and equalized it with No. 1 and No. 2 Windboxes.

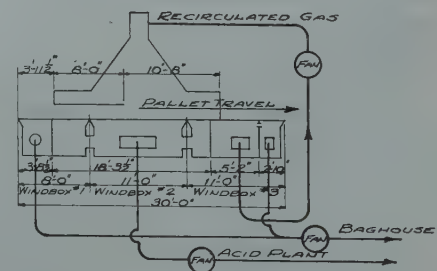


FIG 6—Schematic diagram of first-over recirculation.

These preliminary tests, along with the sulphur elimination curve of the machine indicated that the installation of partitions in the first and third windboxes, whereby the weak gas from the end sections could be segregated and by-passed direct to the baghouse, would be advisable. These tests also showed that when recirculating approximately 3,000 cfm the total fan power consumed was about 69 hp, as compared to 60 hp with the machine operating normally, that is, without recirculation.

During April, 1942, an improved recirculation system for the first-over machine at Selby was completed and further tests proceeded. This new installation consisted of a recirculation fan which drew the recirculated gases through a series of vertical pipe coolers before returning them to the hoods over the pallets. This cooler was later abandoned. The windboxes were also subdivided.

Fig 6 shows a diagrammatic flow sheet of the gases and sizes of various windboxes.

This layout demonstrated that when handling a raw feed mix, averaging 12 pct S, the machine would produce an average of 5,900 cfm at 310°F, of 7.0 pct SO₂ gas for possible utilization at an acid or SO₂ plant.

The concentration of SO₂ varied with the charge, depending largely on the physical characteristics and also on the proportion of sulphide sulphur in the raw feed. Sulphur present as pyrite, for example, was much more desirable than a charge in which part of the sulphur was present as sulphate. Low SO₂ in the concentrated gas invariably accompanied high volume and vice versa. For example:

7.0 pct SO₂ (20 tons S per day)—

Volume, 6,400 cfm at 250°F

8.75 pct SO₂ (16 tons S per day)—

Volume, 5,200 cfm at 330°F

Volume of the recirculated gas varied with the charge between limits as follows:

4.0 pct SO₂—3,500 cfm at 400°F

7.0 pct SO₂—1,500 cfm at 300°F

The distribution of volumes was roughly as follows:

| | |
|--|---|
| First Windbox (4 ft long)..... | Cfm |
| Middle Windbox (concentrated gas)..... | 3,000 |
| Recirculation Windbox (net)... | 5,900 |
| Last Windbox..... | 1,500 |
| Main Bistle Pipe and Fan Leakage..... | 3,500 |
| | 1,100 |
| Total Volume at Main Fan.... | 15,000 at 375°F and 4.5 pct SO ₂ |

Leakage between the deadplate and the pallets was largely accountable for

the high volumes from the end windboxes.

Test runs over a period of months on this machine indicated that, with a charge averaging about 11.0 pct S, it was possible to produce approximately 6,300 cfm of 7.0 pct SO₂ gas, leaving the middle windbox. This amounted to about 18.8 tons of S per day, or sufficient to produce around 50 tons of H₂SO₄ per day.

Commercial Recirculation at Selby

By the middle of 1942, the War Production Board's famed Order L-208 had seriously curtailed the production of pyritic gold concentrates from the California gold mines. High sulphur concentrates, formerly received in excess of the capacity of the one Wedge roaster at Selby dwindled to the point where lower sulphur concentrates containing lead and zinc had to be substituted in order to keep the 40-ton per day Contact Sulphuric Acid Plant supplied with SO₂ gas. However, the gradually decreasing receipt of pyritic concentrates was acutely curtailing the production of sulphuric acid, which was a critically needed war supply. Barren pyrite was even being used at a loss to enrich the Wedge charge.

As a result of the urgent need for sulphuric acid and based upon the favorable results obtained on the experimental recirculation unit on the D & L machine, an appropriation request was filed in Aug. 1942, to equip a second machine with a recirculation unit and to collect and convey the concentrated gases from both machines to the sulphuric acid plant.

This application was made during the height of difficulties in obtaining priority ratings from the War Production Board. However, after much red tape, preparation of minutely detailed lists of materials, substitutions of used motors, and other procedures, an A-1-A Rating was finally obtained and the work got under way, late in 1942.

Wartime delays in delivery of materials and equipment postponed completion of this unit until March 8, 1943.

The D & L gas was at first mixed with the Wedge gases, but after 26 hr operation it was apparent that special conditioning of the D & L gases would be required in order to recover any

appreciable amount of the solids in the Cottrell treater through which the Wedge gases had previously been treated.

Conditioning equipment, consisting of water sprays, and SO₃ gas, direct from the Acid Plant, was installed in the distribution chamber ahead of the Cottrell (Plate) Treater and considerable work done in closing up leaks in the Cottrell unit and the flue system.

For the next three months, the Acid Plant alternated periodically from D & L to Wedge gases as various operating "bugs" were discovered and corrected.

Starting on July 26, 1943, the Acid Plant operated regularly on D & L gas from first-over machines with the Wedge utilized merely as a standby unit to keep the Acid Plant going during occasional periods when the Sinter Plant was shut down.

Since that time, the 40-ton per day Contact Acid Plant has continued to operate on D & L gases concentrated by recirculation.

Sulphuric acid made from SO₂ gases originating from a straight pyritic concentrate roasted in a multiple hearth roaster is normally water-white in color. However, when the supply of pyritic gold concentrates began to dry up and complex flotation concentrates were substituted, it was noted that the resultant sulphuric acid was, at times, discolored, and with greater percentages of the complex concentrates on the charge the acid was close to a coffee-brown in color.

It is believed that this color imparted to the sulphuric acid is caused by hydrocarbons originating from flotation reagents which carry through the scrubbing towers, mist precipitators and coke filters to the drying tower, where they are picked up by the drying acid and act as a dye to all acid produced.

The colloidal carbon imparting the color is so finely divided that no settling as a sediment ever takes place. It is more in the nature of a dye, and in no way lowers the purity of the acid or decreases its usefulness in the normal commercial uses to which it is put. However, as this discoloration is objectionable to certain customers, particularly the food processing plants, it was deemed desirable to clarify the product and a method for so doing has been devised by Mr. Walter F. Johnson, Research Dept. metallurgist.

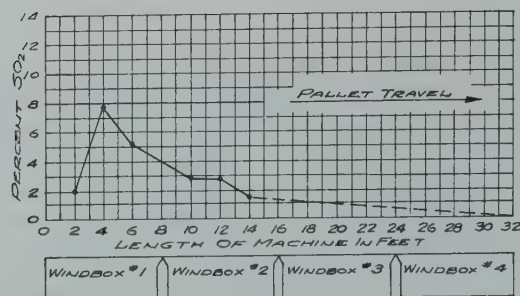


FIG 7—Sulphur elimination curve showing typical graph of data obtained.

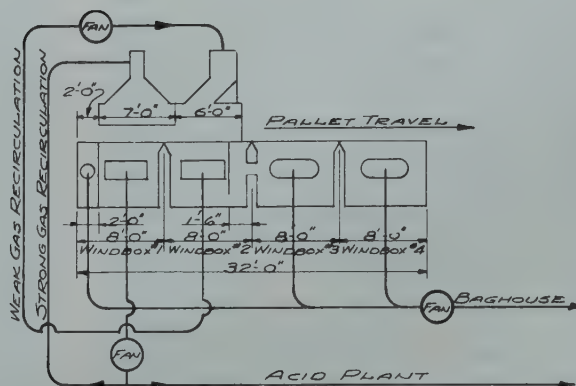


FIG 8—Schematic diagram of second-over recirculation.

In May, 1945, a new recirculation system on a 63 in. \times 32 ft, "second-over" D & L machine was completed. This unit consists of two 10,000 cfm fans, hoods, ducts, control instruments, and other items.

This installation was made for the threefold purpose of (1) obtaining practical operating data on second-over charge; (2) supplemental SO_2 supply for the acid plant; and (3) SO_2 supply for a liquid sulphur dioxide plant to be constructed at some future date.

Prior to designing the recirculation unit for this 63 in. second-over or Final Product Machine, numerous tests were made to determine the sulphur elimination characteristics.

The sulphur elimination curve in Fig 7 shows a typical graph of the data obtained.

It will be noted that this sulphur elimination curve is quite different from the curve for a machine handling first-over charge.

Here, after the charge is ignited, the bed roasts rapidly, coming to a peak about midway of the first windbox

and then tapering off rapidly over the second windbox. Very little sulphur is eliminated over the third windbox and practically none over the fourth or last windbox.

Fig 8 shows the windbox and hood design for this machine and a diagrammatic outline of the flow of gases.

Following a preliminary test period, the concentrated gases from this machine were diverted to the Acid Plant on June 18, 1945, and have been utilized periodically since that time to supplement the concentrated gases from the first-over machines.

At the present time, the concentrated gases from the second-over machine are actually higher in SO_2 content than those from the higher sulphur first-over charge.

In Sept. 1947, a 15-ton per day liquid sulphur dioxide plant was completed at Selby and, since that time, both the sulphur dioxide plant and the sulphuric acid plant have been operated entirely on D & L lead charge gases, concentrated by recirculation.

The sulphur dioxide plant is not dependent on a certain grade gas, as is

the contact acid plant. It will function on any strength gas from the roasters and operates smoothly and efficiently on the 5 to 6 pct SO_2 in the gases normally produced by the recirculation units on the Dwight-Lloyd machines.

The SO_2 plan is a patented process,* developed by the American Smelting and Refining Co. Research Dept., under the able direction of Mr. E. P. Fleming. It functions by the absorption of SO_2 in dimethylaniline flowing counter current to the gas stream in a tower consisting of a series of bubble-cap trays. The pregnant D.M.A. solution then goes to a stripping tower where the SO_2 is expelled by boiling with steam heated calandrias. The wet SO_2 gas is dried by passing through sulphuric acid in a third bubble-cap tower, then compressed to liquid and transferred to storage tanks from which the entire production is shipped in railroad tank cars.

* U.S. Patents Nos. 2,295,587 and 2,399,013.

The Crystal Structure of Ni₄W

E. EPREMIAN* and D. HARKER†

THE constitution of the nickel-tungsten system has been studied by a number of investigators, the most recent of which are Ellinger and Sykes.¹ On the basis of metallography, electrical resistivity and hardness measurements and some X ray diffraction work, they constructed a constitution diagram (Fig 1). Ellinger and Sykes report a_0 for the alpha face-centered cubic phase (nickel saturated with tungsten) as 3.66\AA .[‡] The gamma phase (tungsten saturated with nickel) is given as body-centered cubic, but no value of a_0 is recorded. At 43 pct tungsten by weight (approximately 20 at. pct) a beta phase is reported, but structure and lattice parameter are not known. Primarily on the basis of metallographic evidence, they conclude that beta is a new phase and rule out the possibility of formation of a superlattice since they observe a new phase in the microstructure.

Grube and Schlecht² report an ordering reaction in a system similar to the Ni-W (Ni-Mo) and Harker³ has shown that Ni₄Mo forms a superlattice upon the pre-existing face-centered cubic lattice of the alpha phase. Ellinger and Sykes observed a change in the diffraction pattern of a 43 pct W alloy upon aging and attributed it to the formation of a new phase.

Thus, there appears to be some question as to the character of the beta phase reported by Ellinger and Sykes. The purpose of the present work is to determine precisely the structure and nature of the beta phase in the Ni-W system of X ray diffraction methods.

Experimental Procedure

One inch diameter ingots of 43.66

[‡] Distances are reported in true angstrom units throughout this work. Distances in kX must be multiplied by 1.00202 to give distances in angstroms.

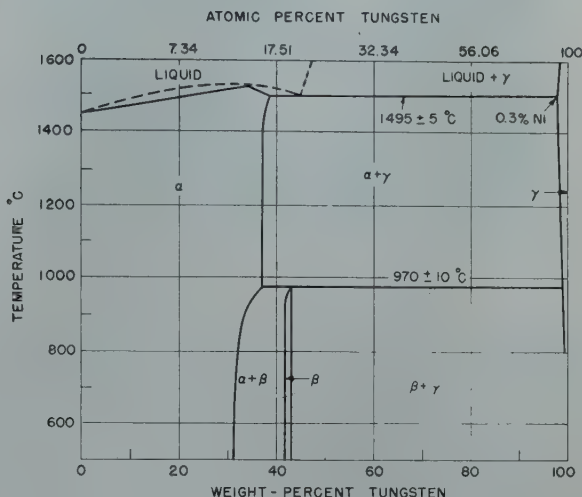


FIG 1—Constitution diagram of the nickel-tungsten system after Ellinger and Sykes.

pct, 40.15 pct and 34.06 pct tungsten by weight (19.8, 17.6 and 14.1 at. pct respectively) were melted and cast under vacuum from electrolytic nickel and pure wire filament grade tungsten. The ingots were soaked for 16 hr at 1300°C in a hydrogen atmosphere furnace, then swaged at this temperature and finally drawn to 0.020 in. diam wire. Some of the bar stock was retained in ½ in. diam rod for hardness and metallographic studies. Wire samples for diffraction work were sealed in evacuated quartz tubes and subjected to the various solution and aging heat treatments in a hydrogen

furnace. X ray photographs were taken in a Debye-Scherrer camera using copper K radiation filtered by nickel foil.

Results

X RAY DIFFRACTION

The lattice parameters of the alpha and gamma phases at saturation were determined by an X ray photograph of the 19.8 at. pct W alloy after solution heat treatment at a temperature well within the alpha-gamma range above the peritectoid temperature (17 hr at 1150°C—oil quenched). The alpha phase was found to be face-centered cubic with a_0 of $3.594 \pm 0.001\text{\AA}$, while the gamma phase was determined as body-centered cubic with a_0 of $3.153 \pm 0.001\text{\AA}$. Exactly the same phases and parameters were obtained with the 17.6 at. pct W alloy for the same solution heat treatment.

Thorough analysis was made of an X ray photograph of a 19.8 at. pct alloy sample in the quenched and aged condition (solution treated 17 hr at

Cleveland Meeting, October 1949.
TP 2551 E. Discussion of this paper may be sent to *Transactions AIME* before December 15, 1949. Manuscript received October 13, 1948.

* Formerly associated with the Research Laboratory of the General Electric Co.; now a graduate student in the Dept. of Metallurgical Engineering, Carnegie Institute of Technology.

† Research Associate, Research Laboratory of the General Electric Co.

References are at the end of the paper.

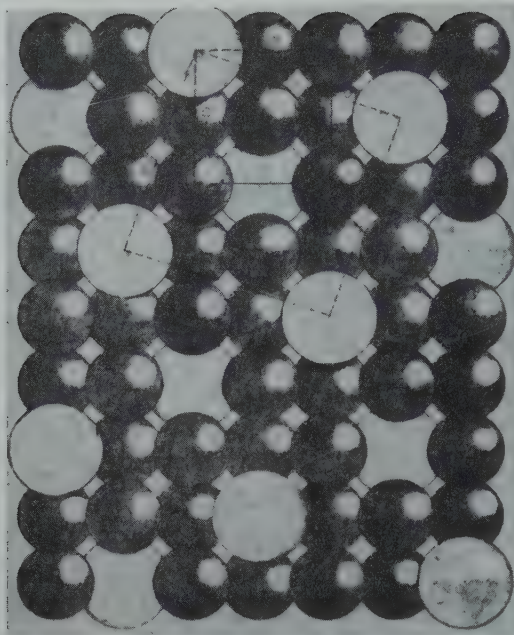


FIG 2—View of the structure of Ni_4W along $[001]$.

1150°C—oil quenched; aged 65 hr at 950°C—oil quenched). An attempt was made to index the lines of the pattern on the basis of a tetragonally distorted face-centered cubic unit cell, but it was found that all of the new lines could not be accounted for. The lattice parameters of the small tetragonal unit cell were determined to be $a_0 = 3.6248 \pm 0.001$ and $c_0 = 3.553 \pm 0.001 \text{ \AA}$ with $c/a = 0.980$.

It was necessary to choose a large tetragonal unit cell in order to assign indices to all of the lines appearing in the pattern. The dimensions of this unit cell are $a'_0 = 5.730 \pm 0.001$ and $c'_0 = 3.553 \pm 0.001 \text{ \AA}$ with $c/a = 0.620$.

The structural relationship between the two cells is shown in Fig 2. The following equations relate the indices of the small cell to those of the true large cell. (Primed indices refer to the new large cell):

$$\begin{aligned} h' &= \frac{3h - k}{2} \\ k' &= \frac{h + 3k}{2} \\ l' &= l' \end{aligned}$$

The volume of the large cell is 2.5 times the volume of the small tetragonal cell, $a'_0 = \left(\frac{5}{2}\right)^{1/2} a_0$ and $c'_0 = c_0$.

Those lines which could be indexed on the basis of the small unit cell have indices for which $2h' + k'$ or $h' + 2k'$ is a multiple of 5. These lines, which are quite sharp and strong, make their appearance by splitting from the lines of the alpha face-centered cubic phase.

The lines were indexed by making use of the relation $\text{Sin}^2 \theta = A(h^2 + k^2) + B(l^2)$ where A and B are constants involving the lattice parameters and

$$\text{wave length (from } \text{Sin}^2 \theta = \frac{\lambda^2}{4} \left[\frac{h^2 + k^2}{a^2} + \frac{l^2}{c^2} \right]).$$

This relation was applied to the $\text{Sin}^2 \theta$ values for several low order planes whose hkl indices were known with certainty to predict the $\text{Sin}^2 \theta$ values for planes with higher indices. The A and B values were fitted with the observed data and the lines indexed. These lines which were newly assigned indices were in turn used to assigned planes of still higher order, the process being repeated until all of the lines were identified. This method gives a self-consistent solution to the data, and automatically provides accurate values of the lattice parameters at values of θ (the Bragg angle) near 90°. It was found that $h + k + l$ for all planes was even, which indicates that the structure is body centered. Table 1 summarizes the results obtained for the ordered structure.

Since the unit cell of Ni_4W is body-centered, and since there are 2 W atoms and 8 Ni atoms in a unit cell, there are three possibilities for the space group of the ordered structure, which are as follows (in the notation of ⁵):

1. $S^2_4 - I\bar{4}$: 2W in 2 (a)
8Ni in 8 (g)
parameters x, y, z
2. $C^5_4 - I\bar{4}$: 2W in 2 (a)
8Ni in 8 (c)
parameters x, y, z

3. $C^5_4h - I\bar{4}/m$: 2W in 2 (a)
8Ni in 8 (h)

parameters x, y

All of these structures have the same projection on the x, y plane, but differ in the projection on the z -axis.

Intensity calculations were made to determine which of the three possible space groups correspond to the structure of Ni_4W . The relative intensities of lines were calculated by means of the following formula:

$$I = \text{Constant } x \frac{1 + \text{Cos}^2 2\theta}{\text{Sin}^2 \theta \text{ Cos } \theta} P_{hkl} F^2_{hkl} A_\theta$$

$\frac{1 + \text{Cos}^2 2\theta}{\text{Sin}^2 \theta \text{ Cos } \theta}$ is the Lorenz and Polarization Factor

P_{hkl} is the multiplicity factor

F^2_{hkl} is the structure factor

A_θ is the absorption factor

θ is the Bragg angle

Since the ordered structure is formed primarily from the alpha face-centered phase, it appeared likely that the atoms would be in an arrangement which is nearly that of cubic close packing. In this case, the approximate positions of the 10 atoms in the unit cell are as follows:

W at $xyz = 000$ and $\frac{1}{2}\frac{1}{2}\frac{1}{2}$
Ni at $xyz = \frac{1}{10} \frac{3}{10} \frac{1}{2}; \frac{3}{10} \frac{1}{10} \frac{1}{2}; \frac{1}{10} \frac{1}{10} 0; \frac{3}{10} \frac{3}{10} 0;$
 $\frac{3}{10} \frac{1}{10} \frac{1}{2}; \frac{1}{10} \frac{3}{10} \frac{1}{2}; \frac{1}{10} \frac{1}{10} 0; \frac{3}{10} \frac{3}{10} \frac{1}{2};$
 $\frac{3}{10} \frac{1}{10} 0; \frac{1}{10} \frac{3}{10} \frac{1}{2}.$

and the space-group is $C^5_4h - I\bar{4}/m$. It is seen that half of these atomic positions are merely lattice translations of the others. Thus, the approximate positions are:

W at 000

Ni at $\frac{2}{5} \frac{1}{5} 0; \frac{1}{5} \frac{2}{5} 0; \frac{3}{5} \frac{1}{5} 0; \frac{1}{5} \frac{3}{5} 0$, that is, at $\frac{2}{5} \frac{1}{5} 0$ and positions derived from this by operation of the four-fold axis.

The structure factor formula for $I\bar{4}/m$ is:

$$F_{hkl} = 2\{f_W + 2f_{Ni}[\text{Cos } 2\pi(hx + ky) + \text{Cos } 2\pi(kx - hy)]\}$$

where f_W is the atomic scattering factor for tungsten

f_{Ni} is the atomic scattering factor for nickel

hkl are the indices of the plane
 xy are the coordinates of one of the Ni atoms.

Using the above structure factor formula in the equation for intensity, and properly taking into account the change in atomic scattering factor, Lorenz factor, and absorption factor with change in the Bragg angle, the intensities of all the lines were calculated. Table 1 includes a comparison between the observed and calculated intensities of the lines for $x = 0.400$,

$y = 0.200$. Complete intensity calculations were made in which x and y were varied in steps of 0.005 between 0.390 – 0.410 and 0.190 – 0.210 respectively. The best agreement was obtained for $x = 0.400$ and $y = 0.200$, which, as is seen, was excellent. Attempts to improve the agreement using the two other possible space-groups were fruitless. Hence, in the absence of any evidence to the contrary, the structure of Ni_4W is that based on $\text{C}_{4h}^5 - \text{I } 4/m$ with $x = 0.400$ and $y = 0.200$.

The structure is such that each atom has twelve nearest neighbors; W has twelve nearest Ni neighbors, and Ni has three nearest W neighbors and nine nearest Ni neighbors. A Ni atom has one W and three Ni neighbors at a distance of 2.5626 Å in the same basal plane, and two W and six Ni neighbors at 2.5377 Å in parallel planes above and below the basal plane.

The mechanism by which Ni_4W forms was studied by determining the sequence of changes in the intensities and positions of the lines in X ray diffraction patterns. Samples were aged for various times at temperatures between 750 and 950°C, after an initial solution treatment and quench from 1150°C.

The X ray photographs of the 19.8 at. pct W alloy in the ordered state for shorter aging times also included lines corresponding to the gamma body-centered cubic phase. In all cases, the intensities of the gamma lines were less in the photograph of the ordered state than in the solution treated state, and decreased further upon longer aging. Thus, the gamma phase, as well as the alpha phase, is involved in the reaction which produces the beta phase.

There are two possible mechanisms by which Ni_4W might form, each having a characteristic sequence of diffraction patterns. In an ordering reaction, "the crystal structure of the alloy changes gradually as time proceeds; the lines of the initial pattern change intensity, become diffuse, split into other lines, and, finally, the new lines move into constant positions and become sharp."⁴ A phase change on the other hand is indicated by a sequence in which "the lines on the initial pattern remain almost unaltered in position and sharpness, but decrease in intensity during the reaction, while new lines appear and increase in intensity without much change in sharpness or position."

Table 1 . . . 19.8 Atom Percent W Alloy: Solution Treated 17 Hours at 1150°C—Oil Quenched. Then Aged 65 Hours at 950°C—Oil Quenched. Copper K_α Radiation.

| hkl | θ | Observed Intensity | Ratio of Intensities $x = 0.400$ $y = 0.200$ $z = 0$ | | |
|----------------|----------|--------------------|--|------|------------|
| | | | Observed | | Calculated |
| 110 | 11.081 | 8 | | | |
| 101 | 14.897 | 10 | | | |
| 200 | 15.651 | 5½ | 101/110 | 1.25 | 1.30 |
| 211 | 21.840 | 40 | 200/101 | 0.55 | 0.56 |
| 220 | 22.414 | 5 | 211/200 | 7.27 | 15.0 |
| 310 | 25.221 | 25 | 220/211 | 0.13 | 0.04 |
| 002 | 25.785 | 10 | 310/220 | 5.0 | 10.2 |
| 301 | 27.306 | 6 | | | |
| 112 | 28.287 | 6 | 301/310 | 0.46 | 0.14 |
| 202 | 30.767 | 5 | 112/301 | 1.00 | 0.97 |
| 321 | 32.164 | 8 | 202/112 | 0.83 | 0.89 |
| 400 | 32.586 | 2 | 321/202 | 1.60 | 1.91 |
| 330 | 34.867 | 3 | 400/321 | 0.25 | 0.24 |
| 222 | 35.331 | 4 | 330/400 | 1.50 | 1.25 |
| 411 | 36.622 | 5 | 222/330 | 1.33 | 1.44 |
| 420 | 37.039 | 13 | 411/222 | 1.25 | 1.97 |
| 312 | 37.467 | 25 | 420/411 | 2.60 | 3.14 |
| 103 | 41.651 | 4 | 312/420 | 1.92 | 1.91 |
| 510 | 43.351 | 4 | 103/312 | 0.16 | 0.08 |
| 402 | 43.742 | 4 | 510/103 | 1.00 | 1.01 |
| 501 | 45.038 | 20 | 402/510 | 1.00 | 1.01 |
| 431 | | | 501 | 5.00 | 23.4 |
| 213 | 45.859 | 13 | 431/402 | | |
| 332 | | | 213/501 | 0.65 | 0.54 |
| 422 | 47.928 | 13 | 332/431 | | |
| | | | 422/213 | 1.00 | 0.97 |
| 521 | 49.198 | 8 | 332 | | |
| 440 | | | 521 | 0.62 | 0.22 |
| 303 | 49.891 | 4 | 440/422 | | |
| | | | 303/521 | 0.50 | 0.41 |
| 530 | 51.681 | 5 | | | |
| 600 | 53.748 | 2 | 530/303 | 1.25 | 1.03 |
| 512 α_1 | 54.278 | 9 | 600/530 | 0.40 | 0.55 |
| 323 α_1 | | | 323 | 6.75 | 8.02 |
| 512 α_2 | 54.440 | 4½ | 512/600 | | |
| 323 α_2 | | | | | |
| 611 | 57.822 | 5½ | | | |
| 620 α_1 | 58.284 | 8 | 611/323 | 0.41 | 0.56 |
| 620 α_2 | 58.481 | 4 | 512 | | |
| 413 α_1 | 58.758 | 5 | 620/611 | 2.18 | 3.00 |
| 413 α_2 | 58.976 | 2½ | 413/620 | 0.63 | 0.35 |
| 004 α_1 | 60.223 | 5 | | | |
| 004 α_2 | 60.477 | 2½ | * | | |
| 442 α_1 | 61.134 | 5 | | | |
| 442 α_2 | 61.399 | 2½ | 442/413 | 1.00 | 0.56 |
| 114 α_1 | 62.622 | 10 | | | |
| 541 α_1 | | | 114/442 | 2.00 | 3.35 |
| 114 α_2 | | | | | |
| 541 α_2 | 62.910 | 5 | | | |
| 532 α_1 | 63.683 | 8 | 532/114 | 0.80 | 0.72 |
| | | | 541 | | |
| 532 α_2 | 63.937 | 4 | | | |
| 204 α_1 | 65.274 | 5 | 204/532 | 0.63 | 0.57 |
| 204 α_2 | 65.563 | 2½ | | | |
| 602 α_1 | 66.300 | 5 | 602/204 | 1.00 | 1.00 |
| 602 α_2 | 66.647 | 2½ | | | |
| 631 α_1 | 68.035 | 20 | 631/602 | 4.00 | 13.4 |
| 631 α_2 | 68.421 | 10 | | | |
| 433 α_1 | 69.332 | 30 | 433/631 | 1.50 | 2.04 |
| 503 α_1 | | | | | |
| 433 α_2 | 69.620 | 15 | | | |
| 503 α_2 | | | | | |
| 224 α_1 | 71.188 | 5 | 224 | 0.64 | 0.70 |
| 550 α_1 | 71.867 | 16 | 550/433 | | |
| 224 α_2 | | | 710/503 | | |
| 710 α_1 | | | | | |
| 550 α_2 | | | | | |
| 710 α_2 | 72.329 | 8 | | | |
| 622 α_1 | 72.639 | 16 | 622/224 | 0.83 | 0.93 |
| 622 α_2 | 72.112 | 8 | 550 | | |
| 314 α_1 | 74.956 | 20 | 710 | 1.25 | 1.34 |
| | | | 314/622 | | |
| 314 α_2 | 75.543 | 10 | | | |
| 523 α_1 | 76.649 | 10 | 523/314 | 0.50 | 0.21 |
| 523 α_2 | 77.214 | 5 | | | |

* I_{001} does not vary with change in x, y .

At 750°C, for aging times up to 17 hr, the alpha and gamma lines retain their position and intensity, indicating that there is no change in structure. Perhaps longer times at this temperature would have produced appreciable X ray diffraction effects. At 775°C and higher temperatures (800, 850, 900 and 925°C) new lines appear in the diffraction patterns. For shorter aging times, the change in structure is indicated by a blurring of the lines,

and, on further aging, the lines sharpen and move into position and new weak lines appear. This behavior is evidence of a mechanism similar to an ordering reaction as opposed to an ordinary phase change.

At 950°C, however, the initial lines retain their position and sharpness, but decrease in intensity while new lines appear in the pattern in the manner characteristic of a phase change. The final structure obtained at this



Fig 3

Fig 4

Fig 5

Fig 6

Fig 7

FIG 3—Solution treated for 17 hr at 1150°C—oil quenched. Strong lines of face-centered cubic alpha and weak lines of body-centered cubic gamma.

FIG 4—Solution treated, then aged for 4 hr at 925°C—oil quenched. Beta lines split from alpha lines.

FIG 5—Solution treated, then aged from 17 hr at 925°C—oil quenched. Beta lines shift toward their final positions.

FIG 6—Solution treated, then aged for 17 hr at 950°C—oil quenched. Alpha lines are sharp and strong. Beta lines make their appearance in their final positions.

FIG 7—Solution treated then aged for 65 hr at 950°C—oil quenched. Structure is entirely beta. All lines are in their final positions.

temperature by a phase change is the same as that obtained by a different reaction at the lower temperatures. Thus, the mechanism, but not the product, of the reaction appears to depend upon the temperature. Diffraction patterns illustrating the two sequences of changes in the 19.8 at. pct W alloy are given in Fig 3-7.

The X ray diffraction pattern of a quenched and aged sample of the 17.6 at. pct W alloy (17 hr at 1150°C—oil

quenched, and aged 65 hr at 950°C—oil quenched) showed the alpha face-centered cubic phase as well as somewhat diffuse lines of the ordered, body-centered tetragonal structure. Several gamma lines were present in the patterns for shorter aging times, but they decreased in intensity with increased time of aging, indicating that gamma is unstable in the 17.6 at. pct W alloy at 950°C. The beta phase obtained with this sample was not as

perfectly crystalline as that shown by the 19.8 at. pct W alloy for the same heat treatment, confirming the fact that the latter is closer to the stoichiometric ratio of the ordered compound.

Samples of the 17.6 at. pct W alloy were aged at various temperatures below 950°C and examined by X ray diffraction. It was found that samples aged below 850°C consist of only the beta phase, while those aged above this temperature are composed of the



FIG 8a-d—17.6 atom percent W alloy. Slightly reduced in reproduction.

- a. Solution treated for 17 hr at 1150°C—oil quenched. Alpha matrix with spheroids of gamma. 500 X.
- b. Solution treated then aged for 17 hr at 950°C—oil quenched. Alpha matrix with spheroids of gamma and newly formed regions of beta.
- c. Solution treated, then aged for 65 hr at 950°C—oil quenched. Alpha and beta matrix with residual spheroids of gamma.
- d. Same sample as Fig 8b, but with oblique light at 1000 X. Beta phase with striations.

alpha phase as well. These results are evidence that the range of solid solubility of the beta phase is wider than reported by Ellinger and Sykes. It appears that the beta region in the constitution diagram should be extended to the left below 850°C to at least 17.6 at. pct W. No data are available to establish the boundary on the right, that is, at W concentrations above 20 at. pct.

The diffraction pattern of a solution treated (17 hr at 1150°C—oil quenched) sample of the 14.1 at. pct W alloy (34.06 pct by weight), showed lines of only the alpha phase with $a_0 = 3.584 \pm 0.001 \text{ \AA}$. This result is in agreement with the boundary drawn by Ellinger and Sykes between the alpha and alpha plus gamma fields.

Aging this alloy for 17 hr at 850°C and at 900°C produced no change in the diffraction pattern, although Ellinger and Sykes found a marked increase in hardness for these heat treatments.

METALLOGRAPHY

The microstructure of the alloys in both the quenched and aged conditions were examined. The 19.8 and 17.6 at. pct W alloys in the quenched state showed an alpha solid solution matrix with spheroids of gamma. The alloy with lower tungsten content had less gamma phase. For the aged condition, the microstructures of these two alloys display a decrease in the amount of gamma and the formation of new areas

in the matrix. There is no difference in the type of microstructure obtained with samples aged at 850 and 950°C. These new areas are no doubt the regions of ordered Ni_4W , since they form where gamma is present. Micrographs of the various structures are shown in Fig 8 and 9.

Ellinger and Sykes report that the microstructure of the 14.1 at. pct W alloy in the quenched condition shows a homogeneous solid solution of alpha. After long aging, there is a thickening of grain boundaries and a general darkening of the alpha grains. These authors conclude from this observation that the alloy has decomposed into two phases. This need not be the case, since the same changes in appearance can occur on ordering.



FIG 9a-c—19.8 atom percent W alloy. Slightly reduced in reproduction.

a. Same heat treatment and phases as Fig 8a.
b. Same heat treatment and phases as Fig 8b.
c. Same heat treatment and phases as Fig 8c.

ELECTRICAL RESISTIVITY

Electrical resistivity measurements were made on the 19.8 and 17.6 at. pct alloys in the solution treated and aged conditions. The results obtained are tabulated below:

Table 2 . . . Results of Electrical Resistivity Measurements

Electrical resistivity at room temperature in microhms per cm

| Atom percent W | Solution Treated* | Aged† |
|----------------|-------------------|-------|
| 19.8 | 110.2 | 54.4 |
| 17.6 | 125.4 | 81.2 |

* 17 hr at 1150°C—oil quenched

† 17 hr at 1150°C—oil quenched

65 hr at 950°C—oil quenched

The sharp drop in electrical resistivity upon aging indicates the migration of atoms to periodically arranged sites in the structure, that is, increasing order. The fact that the resistivity of the 17.6 at. pct W alloy does not drop to as low a value as does the 19.8 at. pct W alloy upon aging at 950°C is

explained either by the fact that the former consists of alpha and beta whereas the latter is entirely beta, or that the 19.8 at. pct W alloy is better ordered, being nearer the stoichiometric ratio Ni_4W .

HARDNESS

The hardness of the 19.8 at. pct alloy as a function of the time and temperature of aging was determined. These results are shown in Fig 10, and it is seen that the hardness of the alloy increases in the usual manner as the time and temperature are increased. There is a definite indication of over-aging at all temperatures, and the time of overaging increases with decreasing temperature. The hardening curves at 850 and 950°C appear to be similar in form, but differ from that obtained at 750°C.

Hardness data obtained by Ellinger and Sykes for an alloy similar to the

17.6 at. pct alloy show much the same behavior except that the maximum hardnesses attained are less than those developed in the 19.8 at. pct W alloy.

It is apparent that Ni_4W may be classified as an intermetallic compound since it has a narrow range of homogeneity, a simple stoichiometric formula, and an ordered structure.⁶ Beta, as formed in these experiments, is characterized by extreme brittleness, high hardness, and relatively high electrical resistivity.

Summary and Conclusions

At approximately 20 at. pct tungsten in the Ni-W system there exists an ordered beta phase which is an intermetallic compound Ni_4W . Its structure is body-centered tetragonal with $a'_0 = 5.730 \pm 0.001\text{\AA}$, $c'_0 = 3.553$

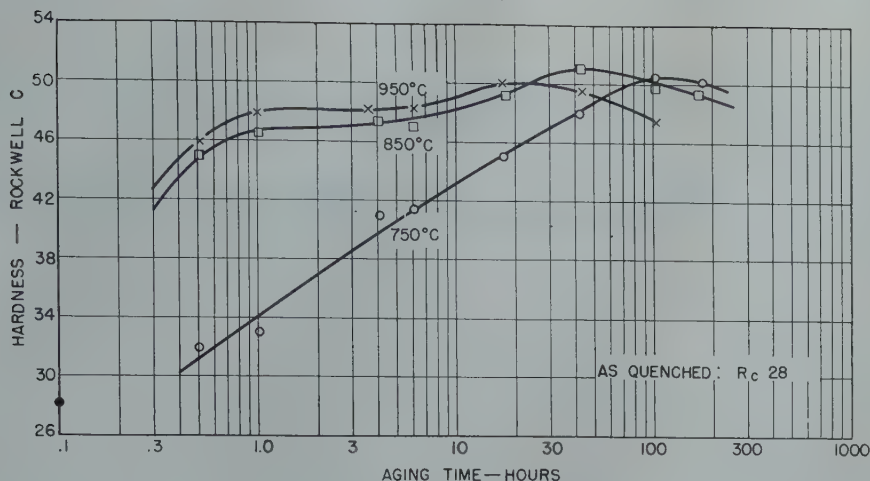


FIG 10—Hardness of 19.8 atom percent W alloy as a function of time and temperature of aging after quenching from 1150°C.

$\pm 0.001\text{\AA}$ and $c/a = 0.620$. The unit cell contains two W atoms at 000 and $\frac{1}{2} \frac{1}{2} \frac{1}{2}$ and eight Ni atoms at 0.100 0.300 0.500; 0.200 0.600 0; 0.300 0.900 0.500; 0.400 0.200 0; 0.600 0.800 0; 0.700 0.100 0.500; 0.800 0.800 0; 0.900 0.700 0.500 (space group C_{4h}^{24} — $I4/m$.)

Beta forms upon prolonged heating below $970 \pm 10^\circ\text{C}$ from an alpha face-centered cubic phase and a gamma body-centered cubic phase. The structure of Ni_4W is based primarily on the alpha face-centered cubic lattice which undergoes a slight tetragonal distortion. The true unit cell, however, has a volume which is 2.5 times the volume of the small tetragonal cell.

The mechanism of formation of Ni_4W appears to be temperature dependent. On the basis of the sequence

of changes in the diffraction patterns, it is concluded that up to quite high temperatures the reaction proceeds by a mechanism similar to ordering but at still higher temperatures occurs by a phase change.

Evidence is presented which shows that the range of solid solubility of the beta phase is wider than reported previously.

The hardness, electrical resistivity, and microstructures of the alloys are discussed.

Acknowledgment

The authors of this paper are indebted to Dr. Roman Smoluchowski for several useful and provocative discussions. It is also a pleasure to

acknowledge the aid given by H. W. Becker, E. T. Asp, and C. Cherry.

References

1. F. H. Ellinger and W. P. Sykes: The Nickel-Tungsten System. *Trans. Amer. Soc. for Metals* (1940) **28**, 619.
2. G. Grube and H. Schlecht: *Ztsch. f. Electrochemie* (1938) **44**, 413.
3. D. Harker: The Crystal Structure of Ni_4Mo . *Jnl. Chem. Phys.* (July 1944) **12** (8), 317.
4. D. Harker: Ordering Hardening: Its Mechanism and Recognition. *Trans. Amer. Soc. for Metals* (1944) **32**, 21.
5. Internationals Tabellen zur Bestimmung von Krystallstrukturen. (1935) Gebruder Borntraeger, Berlin.
6. C. S. Barrett: Structure of Metals. (1943) McGraw-Hill Book Co., New York.



Sulphur Equilibria between Iron Blast Furnace Slags and Metal

GERALD G. HATCH* and JOHN CHIPMAN,* Member AIME

ONE of the important functions of the iron blast furnace is the desulphurization of pig iron before it enters the steelmaking furnaces. However, the increasing concentrations of sulphur in the metallurgical coke, source of approximately 90 pct of the sulphur present in the blast furnace charge, and demands for higher rates of production within recent years have increased the need for greater desulphurization within the iron blast furnace. Furnace operators are beginning to look for desulphurizing agents other than blast furnace slag to accomplish the desired degree of desulphurization. A considerable amount of work has been done on desulphurization outside the furnace with soda ash, calcium carbide and various synthetic slags. Whether the desulphurization of pig iron is accomplished wholly inside the furnace or partly inside and the remainder outside, will be determined by the economics involved. Regardless of which is the case, it is believed that it is necessary to have a better understanding of the physical chemistry of desulphurization by blast furnace slags. To this end, it is the object of the present investigation to attempt what is believed to be the first equilibrium study of the distribution of sulphur between liquid pig iron and a wide range of blast furnace slag compositions.

Review of Literature

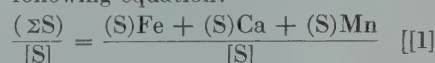
There is a considerable amount of information in the literature concerning the desulphurizing power of iron blast furnace slags, the solubility of various sulphides in the slags, and the effect on desulphurization of temperature, of elements dissolved in the liquid iron, and of viscosity. However, there is nothing to indicate that the equilibrium distribution of sulphur between liquid iron saturated with carbon and iron blast furnace slags has been studied

experimentally.

Wentrup¹ has made probably the most detailed study of the desulphurization of pig iron to date. He considered that there are three distinct aspects involved, namely: 1. Desulphurization within the blast furnace (by lime and manganese). 2. Subsequent desulphurization by manganese. 3. The effect of subsidiary reactions on the desulphurization by manganese.

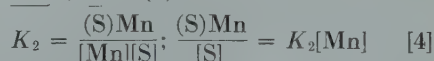
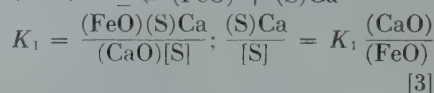
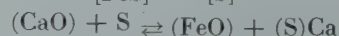
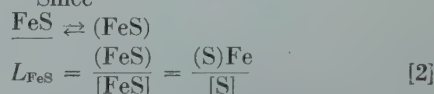
The experimental work carried out by Wentrup was devoted mainly to obtaining a better understanding of how desulphurization by manganese was accomplished in the mixer and the ladle. Particular attention was given to the part played by carbon, silicon, and phosphorus associated with manganese in the iron, and the effect of temperature on desulphurization. The experimental results indicated that desulphurization by manganese is purely a process of crystallization of manganese sulphide. The addition of silicon to iron melts containing 3.5 pct carbon and less than 0.5 pct manganese had no noticeable effect on desulphurization, but with 1-2 pct manganese the silicon additions improved the desulphurization. Additions of phosphorus also resulted in improved desulphurization by manganese, but the effect was not as marked as in the case of silicon. It was also found that desulphurization by manganese was further improved by lowering the temperature.

In order to explain desulphurization inside the blast furnace, Wentrup considered the system iron, sulphur, calcium, oxygen, manganese, (silicon). The distribution of sulphur between the metal and slag was represented by the following equation:

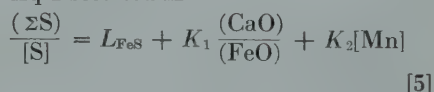


The parentheses and the brackets represent the equilibrium concentrations in weight per cent of the slag and metal constituents, respectively.

Since



Substitution of Eq 2, 3, and 4 into Eq 1 resulted in



Eq 5 was used to calculate $\frac{(S)}{[S]}$ and $[S]$ at 1480°C for slags containing 30-50 pct lime, 0.1-2.5 pct iron oxide, 0-26 pct silica, 2 pct sulphur and iron analyzing 1.5 pct manganese. The value for L_{FeS} at 1480°C was found to be equal to 4.5, based on the experimental work of Bardenheuer and Geller.² The results of the calculations are shown in Table I. Although the slags are hypothetical and do not represent the range of compositions found in ordinary blast furnace practice, the calculations indicate that lime is effective in controlling desulphurization only if the iron oxide and silica contents of the slag are kept low. Schenck³ did not claim K_1 to be a true equilibrium constant, but an empirical value which varied with the silica content of the slag.

San Francisco Meeting, February 1949.

TP 2556 C. Discussion of this paper (2 copies) may be sent to *Transactions AIME* before July 15, 1949. Manuscript received November 4, 1948.

This paper is based upon a thesis submitted by Gerald G. Hatch in partial fulfillment of the requirements for the degree of Doctor of Science at the Massachusetts Institute of Technology.

* Massachusetts Institute of Technology.

References are at the end of the paper.

Table 1 . . . Calculations for the Fe-S-Ca-Mn-O-(Si) System
(By Wentrup)

| | Pct CaO | Pct FeO | Pct SiO ₂ | Pct [Mn] | (S)Fe [S] | (S)Ca [S] | (S)Mn [S] | (ΣS) [S] | Pct (S) | Pct [S] |
|----|------------|------------|-------------------------|-------------|--------------|--------------|--------------|-------------|------------|------------|
| 1 | 30 | 0.1 | | 1.5 | 4.5 | 857 | 15 | 876.5 | 2 | 0.0023 |
| 2 | 30 | 1.0 | | 1.5 | 4.5 | 85.7 | 15 | 145.2 | 2 | 0.0138 |
| 3 | 30 | 2.5 | | 1.5 | 4.5 | 34.3 | 15 | 53.8 | 2 | 0.0380 |
| 4 | 50 | 0.1 | | 1.5 | 4.5 | 1430 | 15 | 1449.5 | 2 | 0.0014 |
| 5 | 50 | 1.0 | | 1.5 | 4.5 | 143 | 15 | 162.5 | 2 | 0.0135 |
| 6 | 50 | 2.5 | | 1.5 | 4.5 | 57.3 | 15 | 66.8 | 2 | 0.030 |
| 7 | 30 | 0.1 | 26 | 1.5 | 4.5 | 40 | 15 | 59.5 | 2 | 0.034 |
| 8 | 30 | 1.0 | 26 | 1.5 | 4.5 | 4 | 15 | 23.5 | 2 | 0.085 |
| 9 | 30 | 2.5 | 26 | 1.5 | 4.5 | 1.6 | 15 | 21.1 | 2 | 0.095 |
| 10 | 40 | 0.1 | 26 | 1.5 | 4.5 | 53.4 | 15 | 72.9 | 2 | 0.027 |
| 11 | 40 | 1.0 | 26 | 1.5 | 4.5 | 5.34 | 15 | 24.84 | 2 | 0.081 |
| 12 | 40 | 2.5 | 26 | 1.5 | 4.5 | 2.13 | 15 | 21.63 | 2 | 0.093 |
| 13 | 50 | 0.1 | 26 | 1.5 | 4.5 | 66.8 | 15 | 86.3 | 2 | 0.023 |
| 14 | 50 | 1.0 | 26 | 1.5 | 4.5 | 6.7 | 15 | 26.2 | 2 | 0.075 |
| 15 | 50 | 2.5 | 26 | 1.5 | 4.5 | 2.6 | 15 | 22.1 | 2 | 0.090 |

Holbrook^{5,6} and Joseph studied the desulphurizing power of blast furnace slags. From their experiments carried out under standardized laboratory conditions, desulphurizing power was defined as being equal to the ratio:

$$\frac{\% \text{ sulphur in slag}}{\% \text{ sulphur in metal}} = \frac{(\% \text{ S})}{[\% \text{ S}]}$$

No mechanical method of mixing the slag and metal was employed in this work, as the investigation was not concerned with attainment of equilibrium but with the determination of the relative desulphurizing powers of slags under controlled laboratory conditions. It was found that in magnesia-free slags the desulphurizing power increases rapidly as lime replaces silica; less rapidly as lime replaces alumina and slowly as alumina replaces silica. The desulphurizing power decreases slightly with the addition of magnesia to the acidic slags and increases markedly when magnesia is added to the very basic slags. Magnesia decreases the viscosity of the slags, and thereby allows the very basic slags to exhibit their inherently strong desulphurizing qualities. Holbrook and Joseph also suggested that the evolution of carbon monoxide accompanying desulphurization retards the descent of falling metal drops and carries calcium sulphide and globules of metal away from the bath interface and into the slag, contributing to the effectiveness of the reaction.

McCaffrey and Oesterle⁷ have carried out comprehensive experiments on the solubility of calcium sulphide and manganese sulphide in slags of the ternary system, silica, lime, and alumina. Their results indicate that the solubility limit of sulphur as calcium sulphide and manganese sulphide is considerably higher than the sulphur content of ordinary blast furnace slags, and that the actual chemical composition of the slag is of less importance than the temperature of the slag in affecting sulphur solubility.

Imhoff⁹ has claimed that sulphur occurs in three forms in blast furnace slags: (1) combined as calcium sulphide; (2) free sulphur held in solution in the slag and (3) sublimed sulphur, the result of excess sulphur in the burden.

Martin, Glockler, and Wood¹⁰ examined in the laboratory the forms in which ferrous sulphide, manganese sulphide, and calcium sulphide occur in a blast furnace slag. The glasses obtained by quenching a molten slag to which the sulphides were added separately, were shown to contain a colloidal phase. The data indicated that the sulphides are present also in solution in the slag. The authors believed that the colloidal particles were sulphides and that the colloidal condition was present in the molten slag, as heat treatment below the softening point did not affect the intensity of the colloid. In order to explain the stability of the colloidal phase in molten slags Martin and Glockler proposed an ionic constitution for blast furnace slags.

The work by Martin and Derge¹⁶ on the electrical conductivity of molten blast furnace slags has provided further evidence of high degrees of ionization. Herasymenko¹⁷ has proposed that molten slags are completely ionized.

In contrast to the ionization concept has been the older molecular theory of blast furnace constitution. The researches of McCaffrey,¹¹ Field and Royster,⁸ Hay¹² and others on the viscosity of mixtures of lime, silica, alumina, and magnesia at temperatures well above their melting points, show that the slags behave in a manner similar to simple solutions, the changes in viscosity with change of composition being relatively small. However, McCaffrey,¹³ and Colclough¹⁴ have stated that in the temperature range 50–100°C above the melting range blast furnace slags are composed of minerals of definite composition and properties.

Abell¹⁵ also was convinced that molten blast furnace slags are composed of molecular compounds. However, he proposed that the slags are composed of spinels and silicates and maintained that the silicates act as comparatively inert solvents for the spinels which alone are capable of reacting with the sulphur in the iron.

Experimental Method

FURNACE

In order to study the equilibrium distribution of sulphur between iron blast furnace slags and liquid iron saturated with carbon, a small induction furnace was built, which held a graphite crucible containing 200 g of metal and 400 g of slag. The amount of metal was determined by the maximum number of samples that would be required in any run. The comparatively large amount of slag was believed to be sufficient to maintain the slag at constant composition over the narrow temperature range employed.

Carbon monoxide gas is evolved in the desulphurization reaction. If an equilibrium state was to be maintained, the partial pressure of this gas had to be held constant. Thus carbon monoxide was used as the furnace atmosphere. Since the crucible was to be made of graphite, little or no stirring of the metal could be expected from electro-magnetic forces. Thus it was proposed to attain the equilibrium state by stirring the slag and metal with a graphite stirring rod.

The induction furnace is shown in Fig 1. The graphite crucible, *M*, is 7 in. long and 2¼ in. id with a wall thickness of ⅜ in., and it contains a well, 1 in. in diam and ¼ in. in depth, which provides an additional depth of metal for sampling. The crucible is insulated on all sides by a porous carbon tube, *K*, and by porous carbon blocks, *L* and *P*. Lampblack is packed between the porous carbon tube and the silica tube, *I*, to further insulate the furnace. The silica tube is placed in an annular slot, fitted with a silicone gasket, on the soapstone base.

A water-cooled brass plate, *C*, closes off the top end of the silica tube. The brass plate is fitted with a rubber gasket. Three holes were drilled in the plate to serve as inlets for taking samples and temperature measurements, for inserting the graphite stirring rod and the graphite tube containing the carbon monoxide gas.

The graphite stirring thimble is threaded into the stirring rod, which is attached to the chuck of a $\frac{1}{6}$ hp variable speed electric motor. Carbon monoxide gas contained in a high pressure cylinder is passed first through a precision bore rotameter tube, before entering the furnace by means of a graphite tube. This graphite tube is $\frac{1}{8}$ in. id and 21 in. long with a $\frac{3}{16}$ in. wall thickness. The tube rests on the furnace bottom, thus causing the gas to flow through both the metal and slag layers. Both the stirring rod and graphite tube are fitted with brass bushings which rest on the brass plate. The furnace is thus closed to the atmosphere at all points except for the sampling-temperature measuring hole. This insures that all the carbon monoxide is withdrawn from the furnace and burned at one point.

METAL AND SLAG CHARGES

High-carbon wash metal was used as the source of iron. When it was desired to approach equilibrium from the side of high sulphur in the metal, ferrous sulphide was added to the metal. In order to approach equilibrium from the slag side a low sulphur melting stock was prepared, which consisted of electrolytic iron melted in contact with a graphite rod, and calcium sulphide was used as the source of sulphur in the slag. In those runs in which the silica content of the slag was high, silicon metal was added to the metal charges to decrease the amount of transfer of silicon from slag to metal. In order to homogenize the slags as much as possible before using them in the experimental furnace, a series of eight master slags were melted in graphite crucibles. These master slags were made up from mixtures of chemically pure lime, purified silica sand, alumina, and magnesia. They were crushed, sampled, and analyzed. Slag charges for the experimental runs were readily prepared from the master slags, with small additions of the pure constituents as required to produce slags of the desired analyses.

TEMPERATURE MEASUREMENT

In the first run, the temperature was measured with both an optical pyrometer and a platinum-platinum, 10 pct rhodium thermocouple. The optical pyrometer was sighted down a $\frac{1}{2}$ in. id graphite tube, which had its lower end closed off. The readings taken with the thermocouple inside

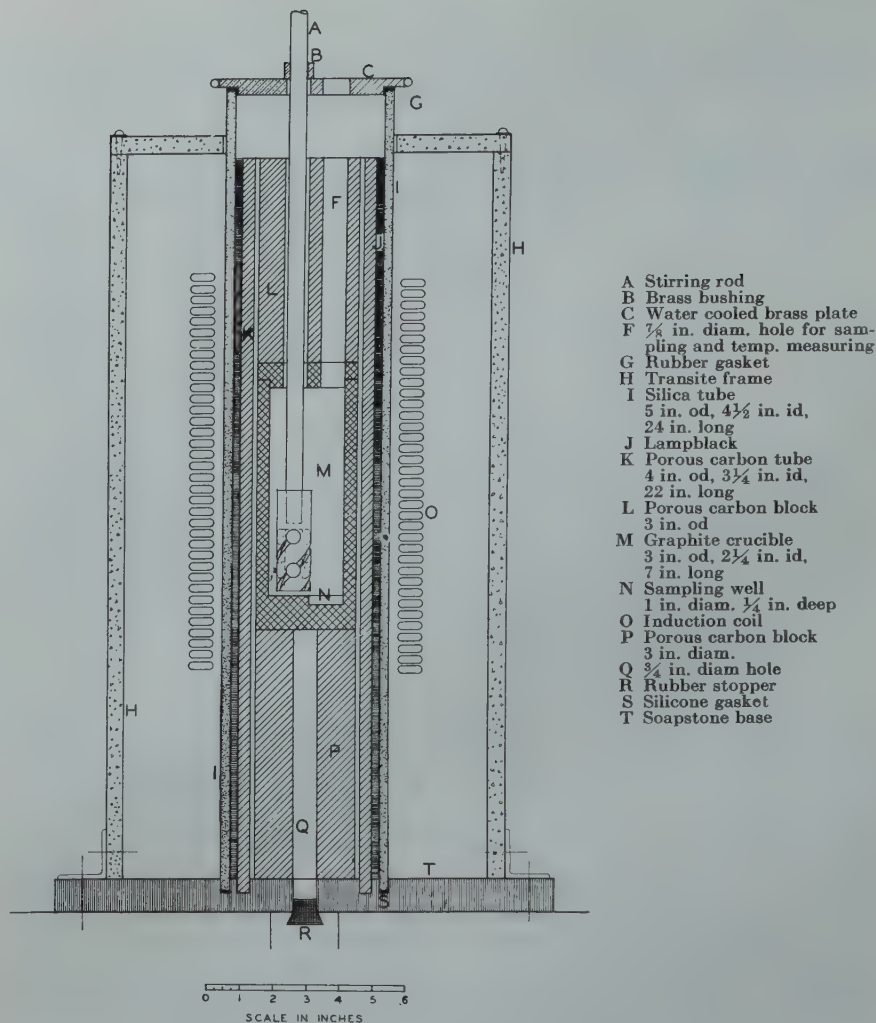


FIG 1—Details of furnace.

the graphite tube checked within $\pm 2^\circ\text{C}$ at 1500°C with those taken simultaneously with the optical pyrometer. Thus, since the true black body temperature was obtained with the optical pyrometer, and as the temperature was so readily measured this way, the optical pyrometer was used exclusively in all subsequent runs. The platinum-platinum, rhodium thermocouple served to check the optical pyrometer periodically. The main source of error with respect to temperature was not in the measurement but in the difficulty of maintaining the temperature constant by means of the manually operated power supply. It was found that the temperature could be held only within $\pm 10^\circ\text{C}$ of the desired value for the duration of each run.

FURNACE OPERATION

From the experience gained in the early runs the following procedure was

found to be satisfactory in establishing equilibrium:

Two hundred grams of wash metal were charged into the crucible. With the stirring rod resting on the metal charge, the graphite cover, the porous carbon insulating block and the brass plate were placed in position. Four hundred grams of slag of the desired composition and having 1.5 pct sulphur as calcium sulphide were then introduced into the crucible by means of a funneled pyrex tube. The water and power were turned on and the furnace was purged out with nitrogen. After the charge was melted, the stirring mechanism was clamped so that the bottom of the stirring thimble was $\frac{1}{8}$ of an inch from the bottom of the crucible. The stirrer was started and operated at 500 rpm. The nitrogen gas was turned off and carbon monoxide was introduced, at approximately 900 ml per min., down into the melt by means of the graphite tube which rested on the furnace bottom. A pilot

flame was maintained at the mouth of the sampling hole to insure that the carbon monoxide burned as it was discharged from the furnace. In case any carbon monoxide escaped unburned, an exhaust hood was placed close to the furnace.

The temperature was adjusted to the desired value and maintained at that value for the duration of each run by adjusting the power input. Experience with various slags indicated that the sulphur equilibrium was attained in 4 to 6 hr time, depending on the viscosity, temperature, and composition of the slag. As a result, the duration of the runs was established at 7 hr. Metal samples were taken at end of 5, 6, and 7 hr. The metal sampler consisted of thin-walled silica tube, $\frac{3}{16}$ in. id, attached to a rubber aspirator bulb. No real difficulty was experienced in obtaining sound 10 to 15 g samples provided the slag was not too viscous. The slag was sampled at the end of the run by dipping a $\frac{5}{8}$ in. diam brass rod into the slag layer. The last metal sample was analyzed for sulphur, carbon, and silicon, while the first and second samples were analyzed for sulphur only. A complete analysis was made on the slag sample. Both the metal and slag samples were analyzed for sulphur by the combustion method. This method consists of igniting the sample at 1300 to 1400°C in a stream of oxygen. The gas given off from the sample is bubbled into a 3 pct solution of hydrochloric acid and titrated as it is evolved with potassium iodate solution. The combustion method takes less sample, 1 g of metal or 0.2 g of slag, than either the volumetric or gravimetric method. It is more accurate than the volumetric and is much less tedious to perform than the gravimetric. The sulphur determinations on the metal samples by this method are accurate within ± 0.001 pct sulphur. An analysis is completed in less than 10 min. time.

SLAG VISCOSITY AND SLAG-TO-METAL TRANSFER OF SILICON

At temperatures above 1500°C, a few preliminary runs demonstrated that in a graphite crucible liquid iron could absorb as much as 10 pct silicon from a slag containing more than 40 pct silica. Since the effect of such high percentages of silicon on the equilibrium con-

centration of sulphur has not been determined experimentally, it was planned to maintain the silicon content in the metal at less than 2 pct. In order to do this, the maximum allowable concentration of silica in the slag was estimated to be 35 pct, with a maximum temperature of 1500°C. On the other hand, since the viscosity of slags increases with decrease in temperature, for any given slag there is a temperature below which it is not feasible to carry out any equilibrium studies. The work by McCaffrey on viscosity measurements of blast furnace slags proved invaluable in determining this lower temperature limit. From McCaffrey's data and from the experience gained in the first seven runs it was found that 1400°C was about the lowest temperature at which an appreciable range of slag compositions could be investigated.

On the basis of the above considerations, a series of runs was made at 1425°C in order to determine the relationship between slag composition and desulphurization. Runs were also made at 1500°C to study the effect of temperature on desulphurization.

In runs H-31 and H-37 the silicon concentrations in the metal were 3.23 and 4.80 pct, respectively. These higher silicon concentrations did not appear to affect the sulphur equilibrium. In addition, calculations by Chipman on the activities of liquid iron in the iron-silicon-carbon system indicated that the activity of iron is only slightly affected by additions of up to 10 pct silicon to liquid iron saturated with carbon. Also, the work of Wentrup on the desulphurization of pig iron by manganese showed that silicon did not affect desulphurization provided that the manganese concentration was less than 0.5 pct. On the basis of these facts it was assumed that silicon does not greatly affect the sulphur equilibrium concentration in liquid iron saturated with carbon.

Although the present investigation was concerned primarily with the equilibrium distribution of sulphur between slag and metal it was interesting to determine whether an equilibrium was established with respect to silicon. It was found that the silicon equilibrium was much more slowly attained than was the sulphur equilibrium between slag and metal. This fact was demonstrated when runs H-19, H-24, H-25, and H-36 were remelted and more sulphur was added in order to study the effect of an increase in the sulphur content of the slags on the sulphur

equilibrium. In these remelted runs, it was observed that the silicon concentrations in the metal were higher than they had been in the original runs, showing that equilibrium with respect to silicon had not been originally attained. It was interesting to note that in the original runs, even though the silicon equilibrium was not attained, lowering the temperature from 1550 to 1425°C caused the silicon slag-to-metal transfer to reverse, and hence resulted in a decrease in the silicon content of the metal. This indicated that the temperature coefficient for the silicon equilibrium is very high.

In run H-33, the silicon equilibrium was approached from both sides by first holding the temperature at 1500°C for 6 hr, followed by 1 hr at 1600°C and then $3\frac{1}{2}$ hr at 1500°C. The equilibrium state was found to lie between 1.71 and 2.29 pct silicon in the metal. This run was remelted and maintained at 1500°C for another 7 hr. At the end of this period the metal analyzed 2.08 pct silicon. On the basis of these results, the remelted runs H-34, and H-44 to H-48, are considered to have approximated equilibrium with respect to silicon.

ATTAINMENT OF THE SULPHUR EQUILIBRIUM

Ferrous sulphide was the only source of sulphur available in the early runs. Consequently at the beginning of each run the slag-metal system was far removed from equilibrium and the initial sulphur transfer to the slag was extremely rapid as was evidenced by the strong bubbling of the slag and the evolution of carbon monoxide gas. However, the bubbling action soon stopped and the rate of sulphur transfer proceeded extremely slowly thereafter, so slowly that the sulphur content of the metal had not reached a constant value after 5 hr with a stirrer speed of 100 rpm. In order to improve the possibility of attaining equilibrium within a reasonable length of time, the speed of the stirring rod was increased to 500 rpm in run H-8. However, the increased stirring speed did not greatly improve the rate of attaining equilibrium.

Since the equilibrium concentrations of sulphur in the metal for the various slags studied appeared to be quite low it was believed that the equilibrium state might be more readily approached from the side of high sulphur in the slag. In runs H-9 and H-14, sulphur, as calcium sulphide, was added to the slag charge. The sulphur reached a con-

stant value after 4 and 2 hr in runs H-9 and H-14, respectively. This difference in the time required to reach equilibrium was occasioned by (1) temperature, run H-9 being at 1425°C and H-14 at 1500°C, and (2) slag composition, the slag used in run H-14 being much more basic than in run H-9.

In an effort to further decrease the time to equilibrium carbon monoxide was bubbled into the metal and slag at approximately 600 ml per min. in run H-17. Thus with calcium sulphide as the source of sulphur, with the stirrer operating at 500 rpm and with carbon monoxide bubbling through the bath, it appeared that 4 or 5 hr was sufficient time for any slag to come to equilibrium with the metal. Consequently, in run H-19 the temperature was held constant at 1500°C for 5 hr and then it was decreased to 1425°C where it was maintained for 4 hr. This procedure was adhered to from run H-19 to H-30, except where viscosity and silicon-transfer considerations did not permit the slag to be studied at both 1500 and 1425°C.

The results of the analyses on these runs showed that the sulphur content of the metal increased when the temperature was lowered from 1500 to 1425°C. However, the analyses also revealed that equilibrium had not been attained in all these runs. Thus, beginning with run H-31, the furnace was held at one temperature for 7 hr and the rate of flow of carbon monoxide was increased from 600 to 900 ml per min. This practice insured the attainment of equilibrium, and was followed in all the succeeding runs.

It must be pointed out that in every run in which calcium sulphide was used as the source of sulphur, the successive metal samples did not increase in sulphur, but rather decreased, until the equilibrium concentration was obtained. A typical example of this fact is shown in Fig 2. This was true even when electrolytic iron which contained less than the equilibrium concentration of sulphur was used. The high sulphur content of the first metal samples was probably due to the calcium sulphate present in the calcium sulphide charged into the crucible.

The plot of per cent sulphur in the metal against the time sampled, shown in Fig 3, demonstrates that the sulphur equilibrium can be approached from the slag side. Calcium sulphide was the source of sulphur in this run. The temperature was maintained at 1425°C for 6 hr so as to allow the transfer of

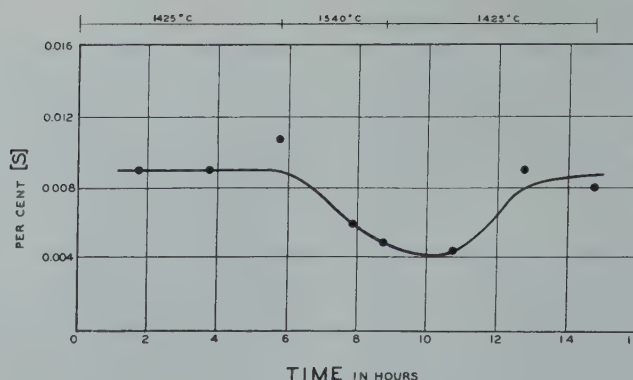


FIG 2—Typical determination of equilibrium at 1500°C.

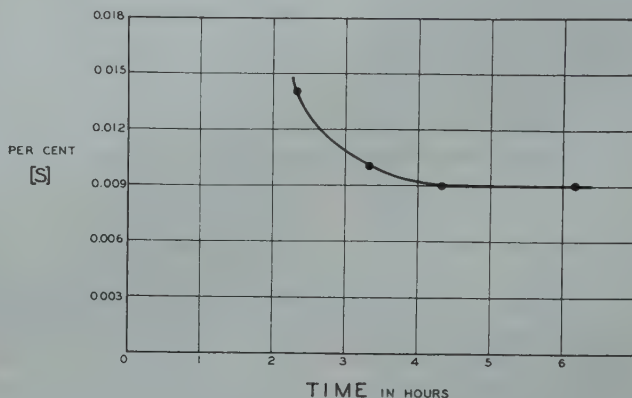


FIG 3—Equilibrium approached from slag and metal sides.

sulphur from the metal to the slag until equilibrium was attained. The temperature then was increased to 1550°C and held constant for 3 hr, in order to decrease further the sulphur concentration of the metal. Nitrogen gas was bubbled through the melt during this period to aid in the metal-to-slag transfer of sulphur. At the end of the 3 hr period, the temperature was lowered again to 1425°C and maintained for 6 more hours. The sulphur content returned to its former value corresponding to equilibrium at this temperature.

SULPHUR CONTENT OF THE SLAGS

The slags in most of the first 38 runs analyzed 1.5 pct sulphur. This percentage of sulphur in the slag resulted in very low sulphur concentrations in the metal, especially with the more basic slags. Thus it was believed desirable to increase the sulphur concentration in the slags in order to increase the sulphur content of the

metal, and thereby improve the accuracy of the sulphur determinations on the metal samples. Nine of the original runs were remelted and iron sulphide was added in quantities to give approximately 2.5 pct sulphur in the slags. Examination of the analytical results for these runs indicated that the sulphur concentration in the metal did not increase proportionally to the increase of sulphur in the slag. As a result, three runs were made with slags containing approximately 5 pct sulphur. Although the percentages of sulphur found in the metal samples for these runs were higher than would occur with similar slags containing 1.5 pct sulphur, they were much lower than would be the case if the sulphur in the metal was proportional to the sulphur in the slag.

IRON CONTENT OF THE SLAGS

Iron is probably present in blast furnace slags as iron oxide, iron sulphide and as metallic iron. Although it is known that the concentration of

Table 2 . . . Iron Content of Slags at 1500°C

| Run No. | Pct FeO | Run No. | Pct FeO |
|---------|---------|---------|---------|
| H-19 | 0.027 | H-44 | 0.034 |
| H-24 | 0.033 | H-47 | 0.044 |
| H-31 | 0.046 | H-48 | 0.030 |
| H-34 | 0.030 | H-49 | 0.026 |
| H-37 | 0.026 | H-51 | 0.039 |
| H-39 | 0.031 | H-54 | 0.100 |
| H-40 | 0.029 | H-55 | 0.065 |
| H-41 | 0.020 | H-56 | 0.050 |

iron is low in blast furnace slags, it was believed to be advantageous to determine the quantity of combined iron present in the slags studied in the present investigation. The mixing of the slag and metal by the graphite stirring rod caused iron to be dispersed throughout the slag. As a result, even though the slag was allowed to stand for at least one minute before being sampled, tiny droplets of iron were present in the slag samples. This magnetic iron was separated roughly by means of a magnet. The concentration of iron remaining after this separation was found to be 0.2 to 0.5 pct, reported as iron oxide (Table 3). In order to determine the degree to which the simple magnet had removed the metallic iron, several slag samples were passed over a Franz iso-dynamic separator. These slag samples included slags containing 1.5, 2.5, and 5.0 pct sulphur. The samples were passed over the separator until their iron contents became as nearly constant as could be detected by the colorimetric method used for chemical analysis. The results of these analyses are shown in Table 2 where the iron is reported as iron oxide. These figures do not give a true value for iron oxide as they include any iron sulphide present in the slag, but they provide a good indication of the amounts of chemically combined iron in blast furnace slags at equilibrium with liquid iron saturated with carbon. The iron content did not appear to be related to the sulphur concentration in the slag.

Results

The results of chemical analyses of the slag and metal samples for the equilibrium runs are shown in Table 3. The only significant sources of error from chemical analysis occurred in the analytical results obtained for sulphur in the metal. Eight metal samples that had been analyzed for sulphur were re-labeled and submitted for analysis

Table 3 . . . Chemical Analyses of Slag-metal Samples

| Run No. | Temp. °C | Iron Analysis, Pct | | | Slag Analysis, Pct | | | | | |
|-----------------|-------------|--------------------|------|--------|--------------------|------------------|-------|--------------------------------|------|------|
| | | C | Si | S | CaO | SiO ₂ | MgO | Al ₂ O ₃ | FeO* | S |
| H-9 | 1425 | 4.67 | 0.53 | 0.013 | 42.70 | 35.14 | 7.75 | 13.72 | 0.20 | 2.07 |
| H-14 | 1500 | 4.83 | 0.55 | 0.005 | 48.30 | 29.69 | 10.58 | 10.14 | 0.46 | 1.58 |
| H-15 | 1425 | 4.18 | 2.41 | 0.058 | 35.20 | 42.88 | 5.70 | 14.68 | 0.20 | 1.48 |
| H-16 | 1425 | 4.27 | 1.37 | 0.038 | 39.95 | 38.65 | 5.97 | 14.86 | 0.20 | 1.51 |
| H-17 | 1500 | 4.76 | 0.65 | 0.006 | 49.52 | 30.06 | 5.71 | 14.92 | 0.35 | 1.56 |
| H-18 | 1425 | 4.25 | 1.62 | 0.028 | 35.79 | 33.67 | 5.36 | 26.26 | 0.41 | 1.54 |
| H-19 | 1500 | 4.54 | 1.40 | 0.006 | 50.01 | 34.20 | 5.65 | 10.48 | 0.23 | 1.59 |
| | 1425 | 4.41 | 1.05 | 0.007 | | | | | | 1.58 |
| H-21 | 1500 | 4.78 | 0.91 | 0.009 | 35.04 | 29.70 | 14.84 | 19.86 | 0.25 | 1.51 |
| | 1425 | 4.62 | 0.74 | 0.011 | | | | | | 1.49 |
| H-24 | 1500 | 4.53 | 1.41 | 0.009 | 48.60 | 33.42 | 0.08 | 16.82 | 0.28 | 1.47 |
| H-25 | 1500 | 4.86 | 0.79 | 0.006 | 34.90 | 31.10 | 18.65 | 13.54 | 0.25 | 1.50 |
| | 1425 | 4.65 | 0.45 | 0.007 | | | | | | 1.51 |
| H-28 | 1500 | 4.48 | 1.76 | 0.013 | 45.58 | 32.10 | 1.47 | 19.98 | 0.22 | 1.45 |
| H-31 | 1500 | 4.12 | 3.23 | 0.017 | 35.79 | 30.48 | 6.68 | 25.98 | 0.27 | 1.53 |
| H-32 | 1500 | 4.28 | 2.53 | 0.012 | 40.00 | 34.24 | 8.34 | 17.28 | 0.19 | 1.62 |
| | 1425 | 4.29 | 1.83 | 0.013 | 39.79 | 34.44 | 8.45 | 17.14 | 0.30 | 1.61 |
| H-33 | 1500 | 4.51 | 2.28 | 0.0075 | 40.14 | 33.63 | 13.53 | 12.20 | 0.30 | 1.59 |
| | 1425 | 4.56 | 0.91 | 0.008 | | | | | | 1.56 |
| H-34 | 1500 | 4.42 | 2.05 | 0.010 | 48.60 | 33.42 | 0.08 | 16.82 | 0.20 | 2.24 |
| (H-24 remelted) | | | | | | | | | | |
| H-35 | 1500 | 4.71 | 1.23 | 0.007 | 38.03 | 35.45 | 18.19 | 7.79 | 0.19 | 1.48 |
| | 1425 | 4.71 | 0.69 | 0.010 | | | | | | 1.48 |
| H-36 | 1500 | 4.00 | 0.84 | 0.007 | 39.81 | 31.64 | 16.19 | 11.40 | 0.19 | 1.54 |
| H-37 | 1500 | 3.70 | 4.80 | 0.011 | 41.80 | 37.86 | 5.33 | 14.30 | 0.19 | 1.57 |
| | 1425 | 3.76 | 3.79 | 0.015 | | | | | | 1.56 |
| H-38 | 1500 | 4.33 | 2.18 | 0.011 | 35.40 | 28.96 | 9.80 | 25.70 | 0.20 | 1.56 |
| H-39 | 1500 | 3.95 | 2.53 | 0.011 | 37.27 | 34.00 | 15.03 | 12.40 | | 2.47 |
| (H-8 remelted) | | | | | | | | | | |
| H-40 | 1500 | 3.27 | 6.04 | 0.011 | 47.86 | 40.00 | 5.41 | 5.80 | | 2.56 |
| (H-6 remelted) | | | | | | | | | | |
| H-41 | 1500 | 3.82 | 4.14 | 0.014 | 37.20 | 31.54 | 10.70 | 18.84 | 0.23 | 2.61 |
| (H-13 remelted) | | | | | | | | | | |
| H-42 | 1425 | 4.24 | 2.46 | 0.019 | 35.79 | 30.48 | 6.68 | 25.98 | | 1.61 |
| H-44 | 1500 | 4.47 | 1.85 | 0.006 | 49.66 | 33.80 | 5.94 | 10.92 | | 2.25 |
| (H-19 remelted) | | | | | | | | | | |
| H-45 | 1500 | 4.68 | 1.24 | 0.009 | 34.90 | 31.10 | 18.65 | 13.54 | | 2.35 |
| (H-25 remelted) | | | | | | | | | | |
| H-46 | 1500 | 4.44 | 2.08 | 0.009 | 40.14 | 33.63 | 13.53 | 12.20 | 0.30 | 2.34 |
| (H-33 remelted) | | | | | | | | | | |
| H-47 | 1500 | 4.04 | 3.37 | 0.010 | 46.25 | 30.84 | 1.21 | 21.10 | | 2.18 |
| (H-28 remelted) | | | | | | | | | | |
| H-48 | 1500 | 4.76 | 1.19 | 0.006 | 39.46 | 31.18 | 16.55 | 12.00 | | 2.48 |
| (H-36 remelted) | | | | | | | | | | |
| H-49 | 1500 | 3.52 | 5.28 | 0.016 | 31.00 | 32.20 | 9.35 | 25.92 | 0.30 | 1.54 |
| H-51 | 1500 | 4.45 | 1.93 | 0.007 | 51.70 | 36.08 | 1.45 | 10.32 | 0.30 | 1.61 |
| H-54 | 1500 | 3.01 | 7.25 | 0.024 | 35.40 | 35.50 | 9.49 | 16.40 | | 4.66 |
| H-55 | 1500 | 3.63 | 5.04 | 0.017 | 38.41 | 33.36 | 9.44 | 15.66 | | 4.59 |
| H-56 | 1500 | 3.99 | 3.80 | 0.012 | 46.80 | 35.56 | 7.50 | 7.12 | | 4.83 |
| H-57 | 1425 | 4.29 | 1.69 | 0.009 | 42.50 | 34.86 | 7.51 | 12.96 | | 1.35 |

*FeO after incomplete magnetic separation. Compare Table 2 showing results after repeated magnetic treatment.

again. The two sets of results differed in all but one case, by not more than 0.001 pct sulphur. (Table 4.) However, the desulphurization ratio, $\frac{(S)}{[S]}$, weight per cent of sulphur in the slag divided by weight per cent of sulphur in the metal, can be considerably affected by even this small change in the sulphur content of the metal. A comparison of run H-19 with H-44 illustrates this point. Run H-44 was a remelt of run H-19 to which more sulphur as iron sulphide had been added.

| | (S) | 1st Analysis | | 2nd Analysis | |
|---------|------|--------------|-------------------|--------------|-------------------|
| | | [S] | $\frac{(S)}{[S]}$ | [S] | $\frac{(S)}{[S]}$ |
| H M 19d | 1.59 | 0.006 | 265 | 0.005 | 318 |
| H M 44c | 2.25 | 0.006 | 375 | 0.007 | 322 |

These figures demonstrate the difficulties involved not only in correlating the desulphurization ratio with slag composition, with the more basic slags, at a constant sulphur concentration in the slag, but also in determining whether or not the sulphur in the metal is directly related to the sulphur in the slag.

Table 4 . . . Rechecked Sulphur Determinations on Metal Samples

| Run No. | Pct Sulphur | |
|---------|--------------|--------------|
| | 1st Analysis | 2nd Analysis |
| H-19 | 0.006 | 0.005 |
| H-24 | 0.009 | 0.009 |
| H-34 | 0.010 | 0.012 |
| H-39 | 0.011 | 0.012 |
| H-40 | 0.011 | 0.012 |
| H-41 | 0.014 | 0.013 |
| H-44 | 0.006 | 0.007 |
| H-46 | 0.009 | 0.009 |

EFFECT OF SLAG COMPOSITION ON DESULPHURIZATION

Since the majority of the runs were made at 1500°C with slags containing 1.5 pct sulphur, it was believed that a relationship between desulphurization and slag composition could best be established from the data collected in these runs. Desulphurization of pig iron is known to depend on the basicity of the slag; thus there was the possibility that the desulphurization ratio, $\frac{(S)}{[S]}$, might be simply related to an index of basicity.

All slag analyses were converted to mols per 100 g of slag. In the chemical analysis of the slags all the calcium present was reported as lime. Any calcium present in the form of calcium sulphide was included in the total molar concentration of lime and was, therefore, considered to act as a base.

Plots were made of the desulphurization ratio versus the molar ratios

$\frac{\text{CaO}}{\text{SiO}_2}$, $\frac{\text{CaO}}{\text{SiO}_2 + \text{Al}_2\text{O}_3}$, $\frac{\text{CaO} + \text{MgO}}{\text{SiO}_2}$, and $\frac{\text{CaO} + \text{MgO}}{\text{SiO}_2 + \text{Al}_2\text{O}_3}$, respectively. Of these plots the one of $\frac{(\text{S})}{[\text{S}]}$ versus $\frac{\text{CaO} + \text{MgO}}{\text{Al}_2\text{O}_3 + \text{SiO}_2}$

(Fig 4) gave by far the best correlation in relating the desulphurization ratio to basicity. In this plot it was noted that all but one of the points below the line represent slags containing more than 6 pct magnesia, while all but one of the points above the line represent slags containing less than 6 pct magnesia. This fact indicated that magnesia is not as effective a desulphurizing agent as lime. The substitution of various factors for K in the basicity ratio $\frac{\text{CaO} + K \cdot \text{MgO}}{\text{SiO}_2 + \text{Al}_2\text{O}_3}$ showed that the factor of $\frac{2}{3}$ resulted in the closest correlation of the points representing slags with high and low magnesia concentrations. (Fig 5)

It can be said that the relating $\frac{(\text{S})}{[\text{S}]}$

to a basicity ratio, a good correlation of the data might be obtained by the use of factors for any or all of the four constituents lime, magnesia, silica, and alumina. Thus it was believed that a more quantitative relationship might be developed if the desulphurization ratio could be expressed as some function of excess base, in a manner analogous to that employed by Grant and Chipman⁴ in their study of sulphur equilibrium between liquid iron and basic open hearth slags. Since blast furnace slags are considered to consist mainly of bisilicates, it was first assumed that 1 mol of acid neutralized 1 mol of base, that 1 mol of magnesia was equivalent to 1 mol of lime, and that 1 mol of alumina was as effective as 1 mol of silica. Excess base thus became equal to BASES $(\text{CaO} + \text{MgO}) - \text{ACIDS } (\text{SiO}_2 + \text{Al}_2\text{O}_3)$. A graph of the desulphurization ratio versus this expression for excess base (Fig 6) produced a scattering of the points comparable to that obtained when the

ratio $\frac{\text{CaO} + \text{MgO}}{\text{SiO}_2 + \text{Al}_2\text{O}_3}$ was employed as

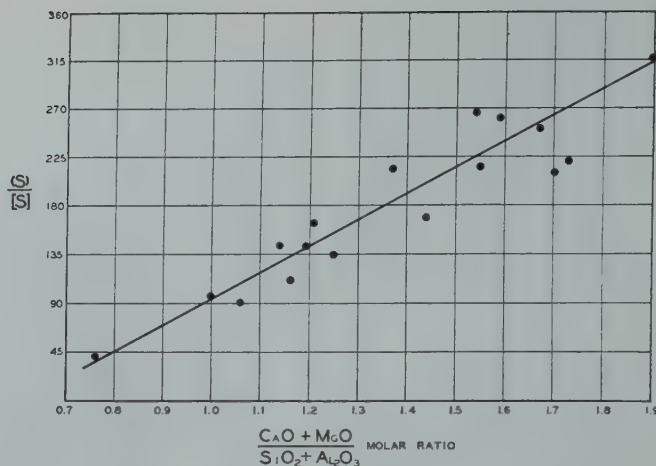


FIG 4—Effect of $\frac{\text{CaO} + \text{MgO}}{\text{SiO}_2 + \text{Al}_2\text{O}_3}$ on desulphurization at 1500°C.

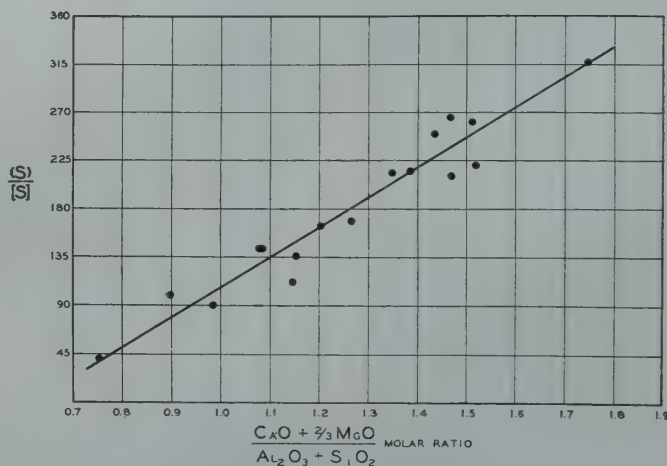


FIG 5—Effect of basicity on desulphurization at 1500°C.

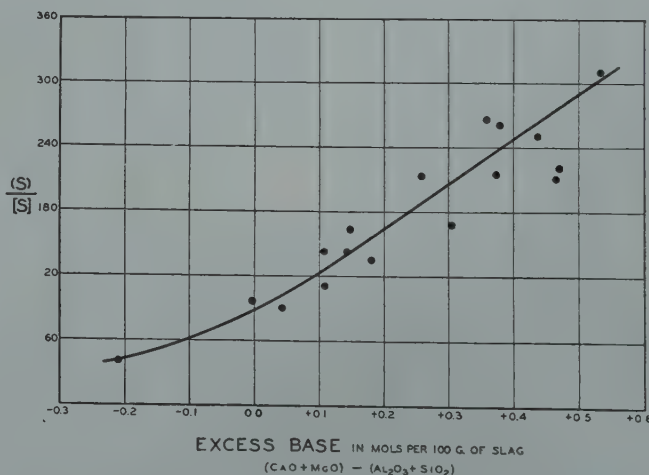


FIG 6—Effect of $(\text{CaO} + \text{MgO}) - (\text{SiO}_2 + \text{Al}_2\text{O}_3)$ on desulphurization at 1500°C.

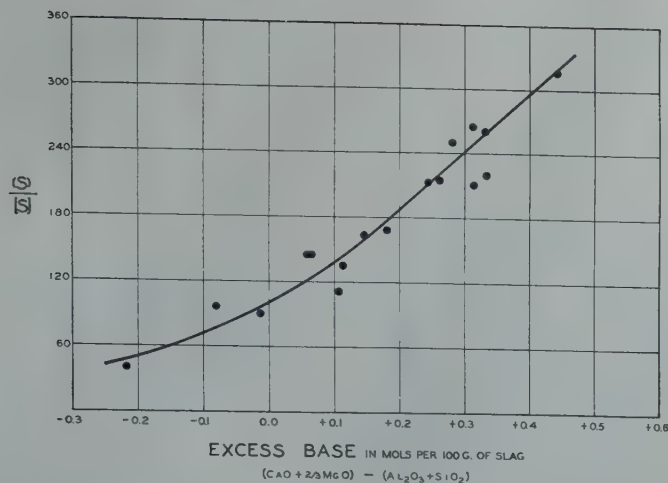


FIG 7—Effect of excess base on desulphurization at 1500°C.

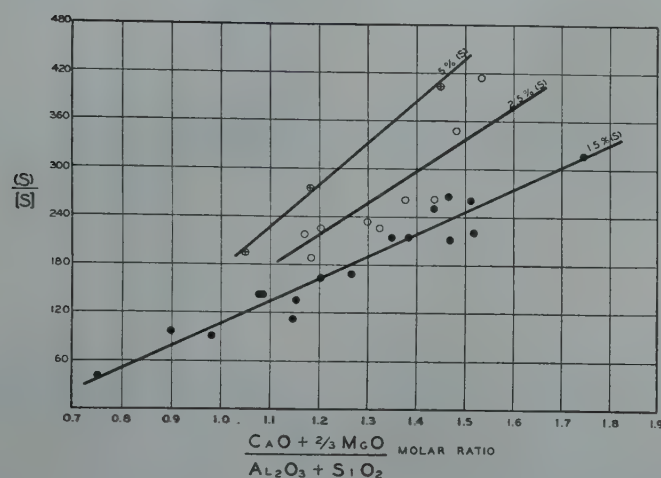


FIG 8—Relationship between basicity and desulphurization at 1500°C for 1.5 to 5 pct sulphur slags.

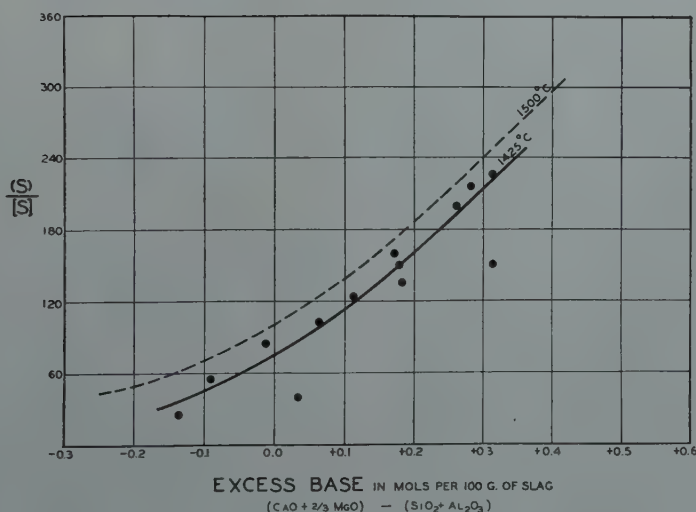


FIG 9—Effect of temperature on desulphurization.

the abscissa (Fig 4).

In order to improve the correlation between the desulphurization ratio and excess base, it was assumed that 1 mol of magnesia was equivalent to only $\frac{2}{3}$ of a mol of lime, that is, $1\frac{1}{2}$ mols of magnesia were equal to 1 mol of base, and the other assumptions were considered to remain the same as before. Excess base was then defined as being equal to $(\text{CaO} + \frac{2}{3}\text{MgO}) - (\text{SiO}_2 + \text{Al}_2\text{O}_3)$. The variation of the sulphur distribution ratio with this expression for excess base is shown in Fig 7. Considering the accuracy of the data this graph represents a very good correlation.

It was expected that the relationships developed for the 1.5 pct sulphur slags would correlate the data for all the slags at 1500°C irrespective of their sulphur content. However, in the plot of $\frac{(S)}{[S]}$ versus $\frac{\text{CaO} + \frac{2}{3}\text{MgO}}{\text{SiO}_2 + \text{Al}_2\text{O}_3}$ for slags containing 1.5, 2.5, and 5.0 pct sulphur three curves were obtained as shown in Fig 8. This was also true for the plot of $\frac{(S)}{[S]}$ versus excess base,

Fig 7. These curves indicate that an increase in the sulphur concentration of the slag does not result in a proportional increase in the sulphur content of the metal, within the range of slag compositions studied. This phenomenon cannot be readily explained with the present data.

EFFECT OF TEMPERATURE ON DESULPHURIZATION

Fig 9 shows the effect on the desulphurization ratio of decreasing the temperature from 1500 to 1425°C. Because magnesia was shown to be two-thirds the equivalent of lime on a molar basis, it is approximately equivalent to lime on a weight per cent basis. Thus from the two curves in Fig 9 it was possible to plot on a ternary diagram iso-sulphur lines at 1500°C and 1425°C, the coordinates being weight per cent $\text{MgO} + \text{CaO}$, SiO_2 , and Al_2O_3 , as shown in Fig 10. This diagram summarizes the effect of slag composition and temperature on the equilibrium sulphur concentrations in liquid pig iron. Although the sulphur concentrations plotted in Fig 10 were obtained for slags containing 1.5 pct sulphur, on the basis of the observations made with slags of higher sulphur content, these concentrations can be regarded as apply-

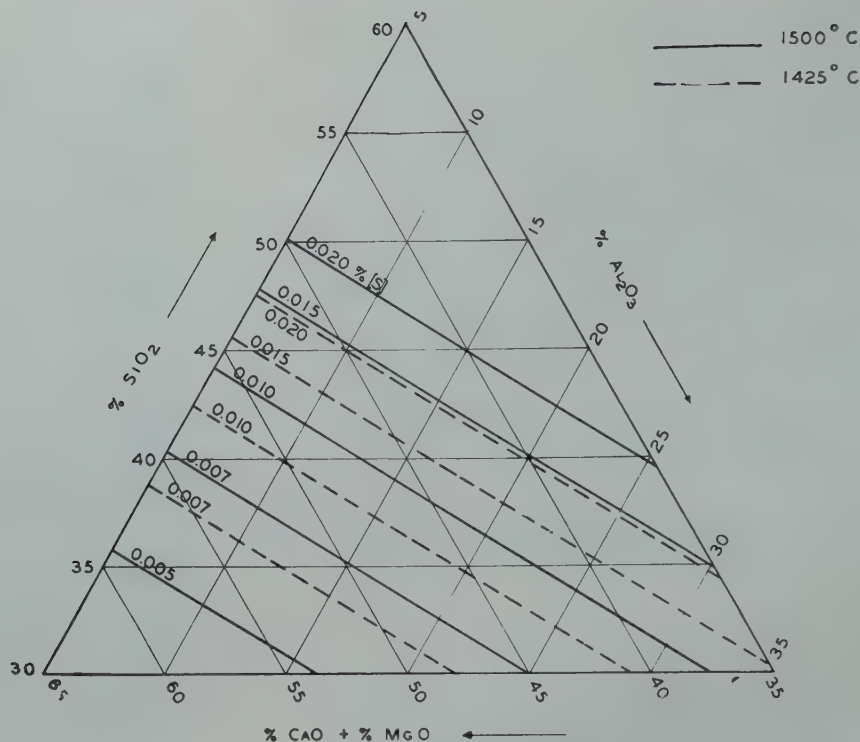


FIG 10—Metal iso-sulphur lines for 1.5 pct sulphur slags at 1500°C and 1425°C. (Slag composition in weight per cent.)

ing to slags analyzing 1.25–2.00 pct sulphur.

Discussion of Results

Although the basicity ratio

$$\frac{\text{CaO} + \frac{2}{3}\text{MgO}}{\text{SiO}_2 + \text{Al}_2\text{O}_3}$$

correlated the data for the 1.5 pct slags, the expression developed for excess base, $(\text{CaO} + \frac{2}{3}\text{MgO}) - (\text{SiO}_2 + \text{Al}_2\text{O}_3)$ in mols per 100 g of slag, is considered to offer a better means of interpreting the results, as it provides a more direct measure of the effective concentrations of the basic constituents present in the slags. Some of the acid slags contained excess acid according to this expression, but this does not necessarily mean that there is “free” acid present, but rather that alumina, because of its amphoteric nature probably acts partly as a base and only partly as an acid. The tendency of alumina to behave as a base is well demonstrated in Fig 7 by the marked decrease in the slope of the curve in the region representing the more acid slags. With alumina considered as acting partly as a base, a

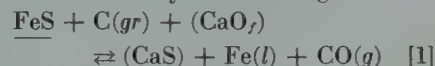
recalculated value for excess base would increase the slope of the curve in this region. From these observations it can be concluded that alumina acts like silica, on a molar basis, in reducing the desulphurizing power of a basic slag; in the more acid slags it is less harmful than silica.

It was observed that three of the very basic slags (47 to 50 pct lime) disintegrated into a fine powder on solidification. This behavior is a well known characteristic of calcium orthosilicate. Thus it appears that these basic slags contain appreciable quantities of calcium orthosilicate, and therefore, that more than 1 mol of lime has been used to neutralize 1 mol of silica. If this is true, the basic slags contain smaller quantities of excess base than described by the expression $(\text{CaO} + \frac{2}{3}\text{MgO}) - (\text{SiO}_2 + \text{Al}_2\text{O}_3)$.

Thus with alumina acting partly as a base in the more acid slags and with the basic slags containing appreciable quantities of calcium orthosilicate a true graph of the desulphurization ratio versus excess base would have a much steeper slope than occurs with the present expression for excess base.

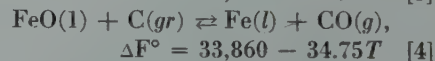
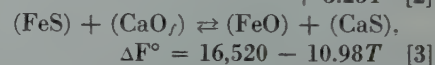
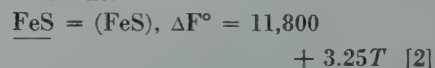
If sulphur is present in blast furnace

slags mainly in the form of calcium sulphide, then desulphurization can be described by the following reaction:



$$K_1 = \frac{a_{\text{CaS}} \cdot a_{\text{Fe}} \cdot p_{\text{CO}}}{a_{\text{FeS}} \cdot a_{\text{C}} \cdot a_{\text{CaO}_f}}$$

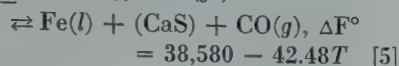
(CaO_f) represents the free or uncombined lime in the slag. An approximate value for the equilibrium constant K_1 at 1500°F can be calculated from the reactions:



Eq 2 was derived from the work of Bardenheuer and Geller² on the distribution of sulphur between liquid iron and iron oxide slag. The expression for the standard free energy of reaction [3] as a function of temperature was developed from the calculations made by Darken and Larsen¹⁹ on Bardenheuer and Geller's data for sulphur equilibria between lime-iron oxide slags and liquid iron. Eq 4 was obtained from Chipman's²¹ tabulations of the

free energy of formation of liquid iron oxide and carbon monoxide at steel-making temperatures.

Addition of Eq 2, 3, and 4 results in $\text{FeS} + (\text{CaO}_f) + \text{C}(gr)$



therefore,

$$K_1 = 3.39 \times 10^4 \text{ at } 1500^\circ\text{C}$$

Since the reaction is endothermic, the equilibrium transfer of sulphur to the slag increases with an increase in temperature, as observed in the experiments.

Under the conditions set up for the experimental work the activity of both the carbon dissolved in the iron and the carbon monoxide gas was equal to unity, the standard states for these two substances being graphite and 1 atm pressure, respectively. The activity of liquid iron was also constant at approximately 0.55 at 1500°C , as determined from Chipman's¹⁸ thermodynamic calculations on the iron-silicon-carbon system. Assuming that activity is proportional to mol fraction for calcium sulphide, iron sulphide and lime, as was done in the determination of the constant K_1 and where N_s and N_m are the number of mols per 100 g of slag and metal, respectively, Eq 1 is transformed to

$$K_1 = 3.39 \times 10^4 = 0.55$$

$$\times \frac{(\text{mols CaS}) \times N_s \times N_m}{N_s \times \text{mols} [\text{FeS}] \times (\text{mols CaO}_f)} = 0.55 \times \frac{(\% \text{ S}) \times N_m}{[\% \text{ S}] \times (\text{CaO}_f)}$$

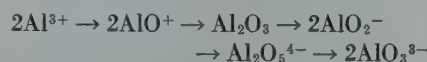
but since N_m is essentially constant and equal to 2.1, then at 1500°C

$$2.94 \times 10^4 = \frac{(\% \text{ S})}{[\% \text{ S}]} \times \frac{1}{(\text{CaO}_f)} \quad [6]$$

According to Eq 6 the desulphurization ratio $\frac{(\text{S})}{[\text{S}]}$ is proportional to the number of mols of free lime per 100 g of slag. This is in agreement with what was observed when $\frac{(\text{S})}{[\text{S}]}$ was plotted against mols of excess base for a given sulphur concentration in the slags. However, the slope of the curve $\frac{(\text{S})}{[\text{S}]}$ versus excess base for the 1.5 pct sulphur slags at 1500°C was only equal to 560, compared with 2.9×10^4 for the slope of the curve $\frac{(\text{S})}{[\text{S}]}$ versus free lime, as given by Eq 6. Thus the large value calculated for K_1 provides further evidence that the expression $(\text{CaO} + \frac{2}{3}\text{MgO}) - (\text{Al}_2\text{O}_3 + \text{SiO}_2)$ does not give a true value for the excess base, the actual excess being somewhat smaller.

Previously, in discussing the relationship between desulphurization and slag composition, it has been assumed that molten slags are composed of molecular compounds and their constituent oxides. However, the expression of slag composition in terms of excess base can be used equally well whether slags are composed of ions or of molecules. In the ionization theory the basic oxides produce oxygen ions which are absorbed by silica and alumina to form complex ions of the form $(\text{Si}_2\text{O}_7)^{-6}$, $(\text{SiO}_4)^{-4}$, $(\text{Al}_2\text{O}_5)^{-4}$. As the basic oxides replace the acid oxides the oxygen ion concentration increases.

The conclusions previously reached regarding the amphoteric properties of alumina in blast furnace slags can be stated in terms of the ionization theory by the following series of steps representing the transition from acidic to basic solutions, each step requiring the addition of oxide ions:



The presence of calcium orthosilicate in the basic slags is shown by the formation of the stable orthosilicate ion SiO_4^{4-} from the metasilicate ion in a similar series.



The concept of ionization also explains the fact that 1 mol of magnesia was not found to be equivalent to 1 mol of lime. The binding forces between magnesium and oxygen ions are greater than those between calcium and oxygen ions.²⁰ Hence the substitution of 1 mol of magnesia for 1 mol of lime in a slag would result in a decrease in the oxygen ion concentration of the slag. This means that magnesia is not as active a base as lime, and therefore, not equivalent to lime on a molar basis.

Thus, either the molecular or the ionic theories can be employed in explaining the behavior of the various slag constituents. However, blast furnace slags involve such complicated chemical systems that fundamental knowledge is as yet inadequate for the quantitative determination of their properties in the molten state, and therefore it is impossible at present to determine the true value for excess base. This does not mean that the expression $(\text{CaO} + \frac{2}{3}\text{MgO}) - (\text{SiO}_2 + \text{Al}_2\text{O}_3)$ has no real significance. The equilibrium desulphurization ratios for slags containing about 1.5 pct sulphur have been well correlated with this expression for excess base. The result

is shown in the ternary diagram (Fig 10), which allows the equilibrium values of sulphur in the metal to be determined for blast furnace slags at 1500°C and 1425°C .

Since none of the slags studied contained any manganese oxide, it would be of considerable interest to study under equilibrium conditions the effect on desulphurization of manganese oxide in the slag. Also, in order to better understand the constitution of molten slags, activity measurements should be made of simple binary slag systems. These studies can be made by means of either reversible electromotive force measurements, as described by Chang and Derge²² or by slag-metal equilibrium investigations.

PRACTICAL CONSIDERATIONS

The present investigation has shown that the equilibrium sulphur concentrations in the metal are considerably lower than those found in practice. Hence, the problem of attaining better desulphurization with blast furnace slags is controlled by the kinetics and not by the thermodynamics of the metal-to-slag transfer of sulphur. It is important that investigations be carried out to determine the mechanism by which desulphurization takes place, in the manner initiated by Chang and Goldman.²³ Of more immediate significance to blast furnace operators would be a study of the desulphurization attained by various methods of mixing slag and metal. It should not be concluded that such an investigation is not warranted because the time required to reach equilibrium was so great in the present study. A simple process of pouring the metal through the slag might well show that considerable quantities of sulphur can be removed by taking advantage of the inherently strong desulphurizing powers of commercial slags without resorting to other desulphurizing agents.

Summary

From the 57 runs made in the experimental furnace covering a range of slag compositions, consisting of 30 to 50 pct lime, 29 to 40 pct silica, 1 to 19 pct magnesia and 6 to 27 pct alumina at 1500°C and 1425°C , the following conclusions have been reached:

1. The sulphur concentrations in pig iron at equilibrium with blast furnace slags are considerably lower than those found in practice.

2. The desulphurization ratio, $\frac{(S)}{[S]}$,

for slags containing approximately 1.5 pct sulphur is controlled by excess base, where excess base is equal to $(CaO + \frac{2}{3}MgO) - (SiO_2 + Al_2O_3)$ in mols per 100 g of slag.

3. The effect of lowering the temperature from 1500°C to 1425°C is to increase the equilibrium sulphur concentration in the metal. This increase amounted to 0.001 to 0.004 pct in metal containing 0.005 to 0.020 pct sulphur.

4. Magnesia is only two-thirds the equivalent of lime as a desulphurizing agent on a molar basis, or approximately equal on a weight basis.

5. Alumina acts like silica in reducing the desulphurizing power of a basic slag; in the more acid slags it is less harmful than silica.

6. The sulphur concentration in the metal is not directly proportional to the sulphur in the slag.

Acknowledgments

The authors wish to express their thanks to Mr. Donald L. Guernsey and his associates for making the large number of chemical analyses involved. They also wish to thank the Republic Steel Corporation for its generous support of this investigation.

References

1. Wentrup: The Desulfurization of Pig Iron and the General Laws Governing the Desulfurization of Iron. Iron and Steel Inst. Carnegie Scholarship Memoirs (1935) 24, 103.
2. Bardenheuer and Geller: Ueber die Grundlagen der Entschwefelung von Roheisen und Stall. Mitt. Kaiser Wilhelm Inst. für Eisenforschung, (1934) 16, 77.
3. Schenck: Introduction to the Physical Chemistry of Steelmaking. Translation by H. J. Goldschmidt, Part III, 472.
4. Grant and Chipman: Sulphur Equilibria between Liquid Iron and Slags. *Metals Tech.* TP 1988 (April 1946); *Trans. AIME* (1946) 167, 134.
5. Holbrook and Joseph: Relative Desulphurizing Powers of Blast-furnace Slags. *Trans. AIME* (1936) 120, 99.
6. Holbrook: Relative Desulphurizing Powers of Blast-furnace Slags, II. *Trans. AIME* (1938) 131, 127.
7. McCaffrey and Oesterle: Desulphurizing Power of Iron Blast-furnace Slags. *Trans. AIME* (1923) 69, 606.
8. Field and Royster: Viscosity Measurements of Blast Furnace Slags. U. S. Bur. of Mines. T. P. Nos. 157, 187, and 189.
9. Imhoff: Sulfur as a Component of Furnace Slags. *Blast Furnace and Steel Plant*, 308, July, 1917.
10. Martin, Glockler, and Wood: Form of Sulfur Occurrence in Blast Furnace Slag. U. S. Bur. of Mines, R. I. 3552.
11. McCaffrey:
 - a. Research on Blast-furnace Slags. *Trans. AIME* (1932) 100, 65.
 - b. Determination of Viscosity of Iron Blast-furnace Slags. *Trans. AIME* (1932) 100, 86.
12. Hay: The Viscosity Determination of Blast Furnace Slags. *Jnl. of the West of Scotland Iron and Steel Inst.* (1941) 49, 89.
13. McCaffrey and Oesterle: The Constitution of Iron Blast Furnace Slags. *Amer. Iron and Steel Inst.* (1924) 285.
14. Colclough: The Constitution of Blast Furnace Slags in Relation to the Manufacture of Pig Iron. *The Jnl. of the Iron and Steel Inst.*, (1936) 134 No. 2, 547.
15. Abell: The Theory of the Silicate Residues of Blast Furnace Slags. *The Industrial Chemist* (1932) 8, 110-113, 128-130, 191-194.
16. Martin and Derge: The Electrical Conductivity of Molten Blast-furnace Slags. *Trans. AIME* (1943) 154, 104.
17. Herasymenko: *Ztsch. Elektrochemie*, (1941) 47, 588.
18. Chipman: *Trans. Faraday Soc.* (In press).
19. Darken and Larsen: Distribution of Manganese and of Sulphur between Slag and Metal in the Open-hearth Furnace. *Trans. AIME* (1942) 150, 87.
20. Slater: Introduction to Chemical Physics, chap. 21, 22, 23, and 26.
21. Chipman: Basic Open-Hearth Steel-making, chap. 16. Seeley W. Mudd Series. *AIME* (1944).
22. Chang and Derge: Electrochemical Study of Properties of Molten Slags of the Systems $CaO-SiO_2$ and $CaO-Al_2O_3-SiO_2$. *Metals Tech.* TP 2101 (Oct. 1946); *Trans. AIME* (1947) 172, 90.
23. Chang and Goldman: Kinetics of the Transfer of Sulphur Across a Slag-metal Interface. *AIME Metals Tech.* TP 2367 (June 1948). *Trans. AIME* (1948) 176.



Determining density by Archimedes method
(Ercker, 1574).

The man in the foreground is weighing a sample in water against an adjustable mixture of gold and silver granules. In the background are the cupelling furnace and accessories and the large matrass for parting gold and silver with nitric acid. (Courtesy Cyril S. Smith.)

The Beryllium-iron System*

R. J. TEITEL† and MORRIS COHEN,‡ Member AIME

Introduction

THERE is considerable interest in beryllium because of its low density (1.84 g per cu cm), high modulus of elasticity (40×10^6 psi), high melting point (1280°C), and special nuclear characteristics. Moreover, it has fair resistance to corrosion and oxidation. However, the purest beryllium known to the authors is relatively brittle at room temperature, and cannot be fabricated readily. The search for improved properties leads naturally to investigations of beryllium alloys and the phase relationships upon which they are based.

The present paper is concerned with the alloys of beryllium and iron, primarily from the standpoint of the equilibrium diagram. Iron was selected (1) because of its all-round importance in metallurgy, and (2) because the beryllium-iron system is known to be quite complex.

The most recent diagram in the literature is that of Gaev and Sokolov,¹ and covers only the iron-rich end up to 16 wt pct beryllium. Beryllium markedly restricts the austenitic field, closing the gamma loop at about 0.4 wt pct (3 at. pct). On the other hand, beryllium is soluble in α -ferrite up to a maximum of 7.5 wt pct (34 at. pct) at the eutectic temperature of 1160°C. The eutectic composition lies at 10 wt pct beryllium (42 at. pct) and corresponds to a mixture of α and FeBe₂ (called β in the present paper). The solid solubility of beryllium in the α phase decreases with decreasing temperature, and makes precipitation-hardening possible. These findings substantiate the earlier work of Oesterheld,² Wever and Mueller³ and Laissus.⁴

In addition to the FeBe₂ (β) mentioned above, Misch⁵ has reported on

Table 1 . . . Analyses of Raw Materials

| Element | Beryllium | | Iron | | |
|---------------------------|-------------------|---------|-----------------------------|-----------------------------------|----------------------------------|
| | Chemical Analysis | | Chemical Analysis Wt Pct | Spectrographic Analysis Wt Pct | Vacuum Fusion Analysis Wt Pct |
| | Wt Pct | At. Pct | | | |
| Silicon | 0.034 | 0.011 | | 0.010 | |
| Aluminum | 0.12 | 0.040 | | Slight trace | |
| Molybdenum | | | | 0.0007 | |
| Iron | 0.10 | 0.016 | | | |
| Copper | | | | 0.0006 | |
| Magnesium | 0.005 | 0.002 | | | |
| Tin | | | | 0.0001 | |
| Nickel | | | | Trace | |
| Titanium | | | | 0.00005 | |
| Vanadium | | | | Trace | |
| Chromium | | | | Trace | |
| Manganese | | | | Trace | |
| Tantalum | | | | Not found | |
| Columbium | | | | Not found | |
| Tungsten | | | | Not found | |
| Carbon | 0.02 | 0.02 | 0.006 | | |
| Nitrogen | 0.015 | 0.010 | 0.0007 | | 0.0005 |
| Oxygen | | | | | 0.0267-0.0359 |
| Hydrogen | | | | | 0.00005 |
| Beryllium Assay | 99.4 | | | | |

FeBe₅, and indicated evidence for another compound containing still more beryllium.

A preliminary diagram by Gordon,⁶ not hitherto published, is given in Fig 1. Besides the phases previously named, there are shown a solid solution of extended range (ϵ), a compound of limited solubility (ζ), and a high temperature phase (η). Beryllium is designated as θ . The ϵ field contains the

compound composition FeBe₅, and the ζ phase undoubtedly corresponds to the beryllium-rich compound found by Misch.⁵ The region around the ζ phase was proposed by R. J. Teitel based on Gordon's data. The details of the diagram are self-explanatory. It was the unusual complexity of this system that prompted the authors to undertake the present studies. By the same token, more emphasis was placed on the beryllium-rich than the iron-rich end of the diagram.

Experimental Details

RAW MATERIALS

The beryllium employed in this investigation was one of the purest grades available. Its chemical analysis after vacuum melting is given in Table 1. The metal assayed 99.4 wt pct beryllium.

Vacuum melted electrolytic iron of purity shown in Table 1 was the source of iron.

Cleveland Meeting, October, 1949.
TP 2550 E. Discussion of this paper (2 copies) may be sent to *Transactions AIME* before December 15, 1949. Manuscript received November 1, 1948.

* This paper is based on a thesis submitted by R. J. Teitel at the Massachusetts Institute of Technology in partial fulfillment of the requirements for the degree of Doctor of Science in Metallurgy, June 1948.

† Associate Metallurgist, Brookhaven National Laboratories, Upton, N. Y.

‡ Department of Metallurgy, Massachusetts Institute of Technology, Cambridge, Mass.

References are at the end of the paper.

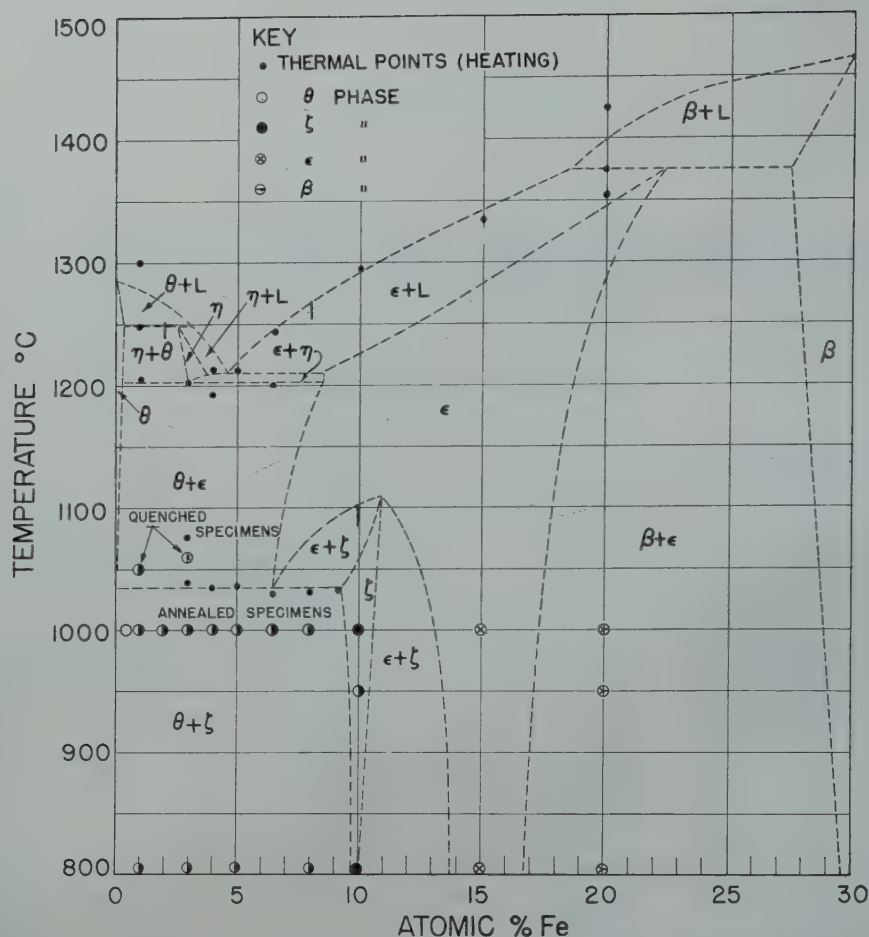


FIG 1—Beryllium-iron system developed by Gordon,⁶ based on preliminary studies leading up to the present investigation.

APPARATUS AND PROCEDURE

The alloys were prepared in a vacuum induction furnace, using beryllia crucibles. The resulting ingots were approximately 2 in. high \times 1½ in. diam, and weighed 60–150 g depending on composition. The ingots were analyzed top and bottom, and accepted only if the determinations checked within ± 0.1 wt pct.

Thermal analysis and solution-quenching experiments were performed in the vacuum furnace shown in Fig 2. It consisted of a molybdenum-wound alundum core, mounted in a water-jacketed steel shell with electrical and vacuum fittings introduced through the sides, thus leaving the top and bottom completely accessible for various interior designs.

The interior arrangement for the thermal analysis runs is shown in Fig 3. The thermocouple was located with respect to the melt by means of a re-entrant tube integral with the bottom of the beryllia crucible. The rate of temperature rise or fall was controlled by varying the furnace volt-

age through an induction regulator driven by a telechron motor. The rates were usually adjusted to 1–2°C per min. Temperatures were recorded automatically for the survey runs, and measured with a K-2 precision potentiometer for the critical determinations. Calibrated platinum-platinum rhodium thermocouples were used for all the critical determinations. It is believed that the accuracy of measurement was within $\pm 10^\circ\text{C}$ above 1350°C, and $\pm 5^\circ\text{C}$ below.

In the solution-quenching experiments, the temperatures were probably accurate to $\pm 2^\circ\text{C}$. Fig 4 illustrates how this operation was carried out in the vacuum furnace of Fig 2. Small pieces of the alloys to be treated were placed in thin-walled iron capsules for identification and guidance through the furnace. When the solution temperature was believed to approach or exceed the solidus, the iron capsules were lined with beryllia to avoid sticking or iron contamination. The beryllia linings were also employed when powder specimens were treated for X ray measurements. After the furnace

had been evacuated and stabilized at the predetermined temperature, the capsules were pushed into the furnace, one by one, via the charging tube shown at the top right of Fig 4. Each specimen was detained in the heating chamber for the desired time by a molybdenum vane operated from the outside, and then allowed to drop into an externally-cooled silicone oil bath. After all the capsules in the charging tube had been solution-treated and quenched, the bath was disassembled from below, and the samples recovered. Further details on the design and operation of the above equipment are being published elsewhere.

The metallographic techniques used were fairly standard, except for the alloys in the range of 8 to 45 at. pct iron (36 to 84 wt pct). The latter were extremely brittle, and were polished on a Graton semiautomatic unit.* No suitable etchant was found for these compositions. However, they could be examined successfully with polarized

* This polishing was done by Mr. Charles Fletcher at Harvard University.

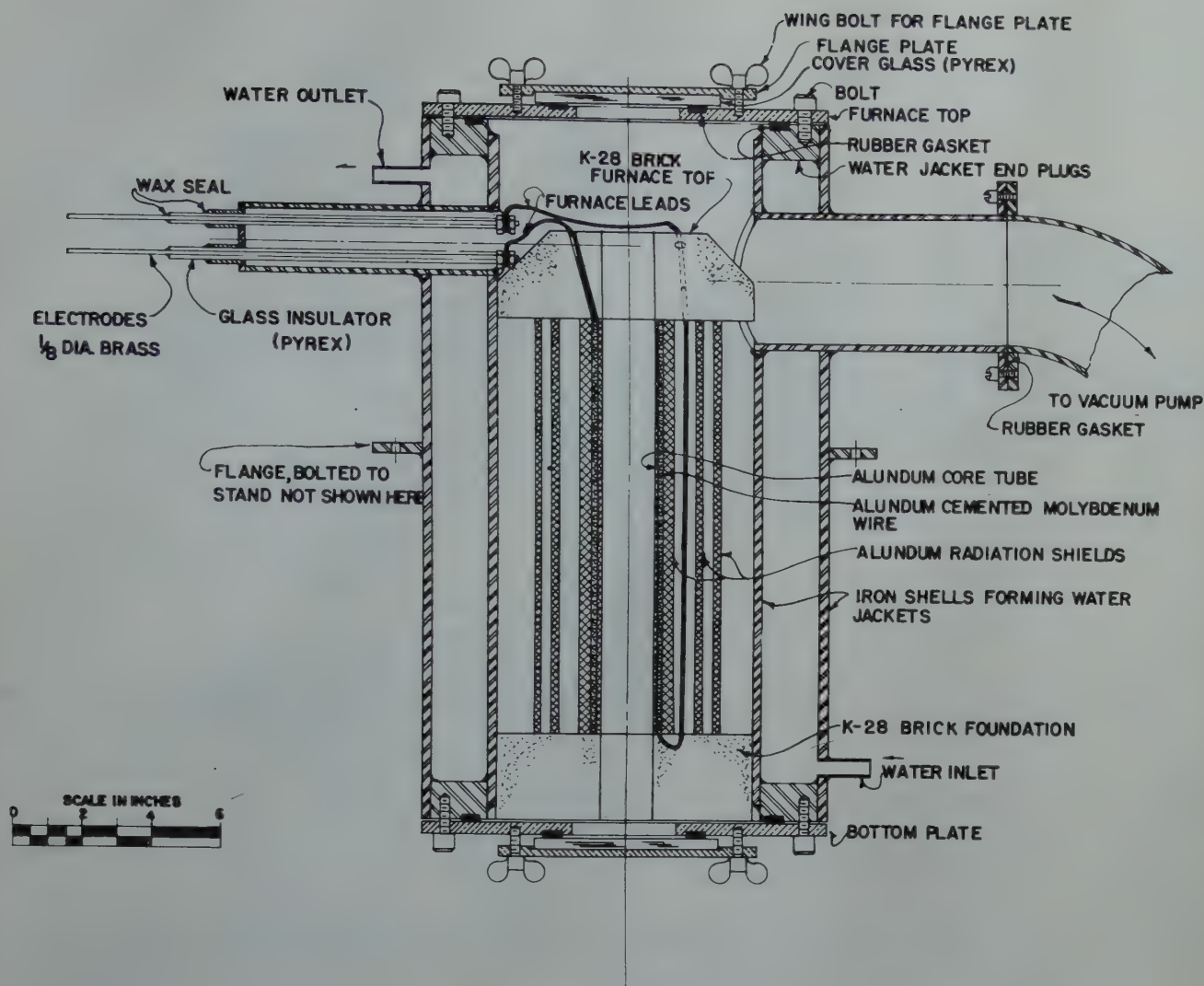


FIG 2—Vacuum furnace used for thermal analysis and solution-quenching experiments. (See Fig 3 and 4.)

light. Alloys containing 0 to 8 at. pct iron were etched with 1 pct HF, while those containing 45–100 at. pct iron were etched with 1 pct nital.

The structures of the phases were studied by standard X ray diffraction procedures using Debye-Scherrer and Phragmen cameras with CoK_α radiation. Most of the solid solubility limits were determined by the lattice-parameter and disappearing-phase methods.

Experimental Results

The individual solid phases are first discussed, starting with beryllium and proceeding in the direction of iron. Following this, the thermal, X ray and metallographic data leading up to the diagram itself are presented in two sections: (1) 0–8 at. pct iron and (2) 8–100 at. pct iron. All compositions are henceforth expressed as atomic percent iron, until at the very end, the

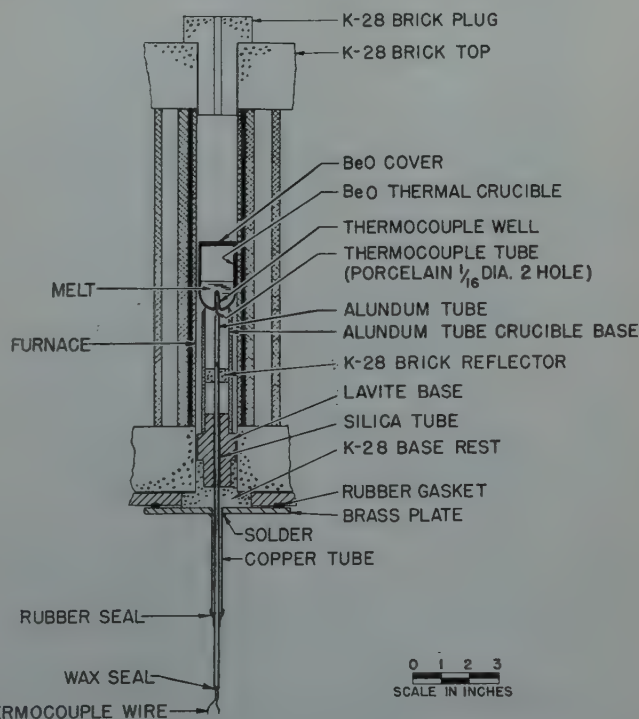


FIG 3—Interior arrangement of vacuum furnace for thermal analysis. (See Fig 2.)

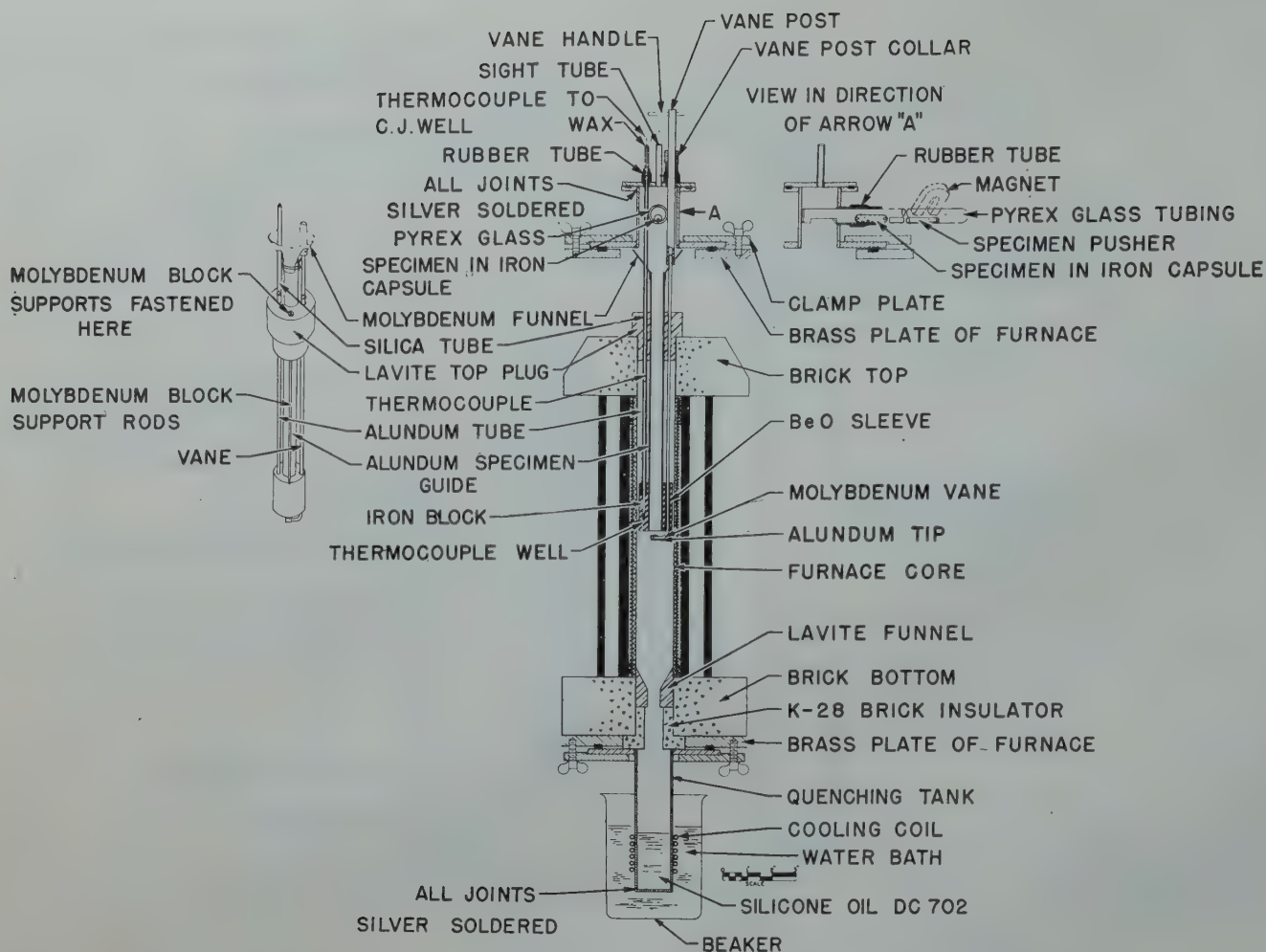


FIG 4—Interior arrangement of vacuum furnace for solution-quenching experiments. (See Fig 2.)

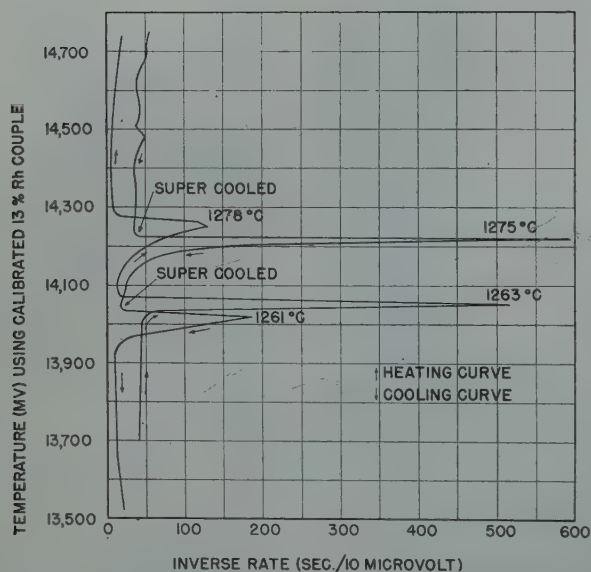


FIG 5—Inverse-rate thermal curves for vacuum melted beryllium stock.

proposed diagram is redrawn with iron at the left and compositions expressed as weight percent beryllium to comply with the convention adopted by the 1948 Metals Handbook. With this arrangement, the phase designations fall into proper sequence.

θ PHASE (Be)

Thermal analysis of the vacuum-melted beryllium stock revealed a double arrest near the melting point, both on cooling and heating (Fig 5). Other sources of beryllium, having different amounts of impurities, also displayed these two heat effects. The upper arrest varied from sample to sample, but the lower one remained quite constant, except when iron was present in excess of 0.1 at. pct. Furthermore, the ratio of the heat liberated (or absorbed) at the two arrests varied from sample to sample. Both Sloman⁷ and Losano⁸ have likewise observed a double break in the thermal curves for beryllium. Losano⁸ reported that the upper arrest is raised to 1284°C with

Table 2 . . . Summary of Phase Structures*

| Phase Symbol | Formula | Lattice | Number of Atoms Per Cell | Lattice Dimensions (A.U.) | | | Density G Per cc (calc) |
|--------------|--------------------|---------|--------------------------|---------------------------|-------|-------|-------------------------|
| | | | | a | c | c/a | |
| θ | Be | H.C.P. | 2 | 2.281 | 3.577 | 1.568 | 1.845 |
| ζ | FeBe ₁₁ | Hex. | 18 | 4.13 | 10.71 | 2.59 | 2.43 |
| ϵ | FeBe ₃ | F.C.C. | 24 | 5.884 | | | 3.272 |
| β | FeBe ₂ | H.C.P. | 12 | 4.212 | 6.853 | 1.626 | 4.629 |
| α | Fe | B.C.C. | 2 | 2.861 | | | 7.870 |

* Typical X ray diffraction patterns are shown in Fig 12 and 20.

increasing purity and the lower arrest completely disappears at extremely high purity (99.962 wt pct beryllium). Sloman⁷ also attributed the double arrest to impurities, oxygen in particular.

The same conclusion was reached in this work, but the possibility of an allotropic transformation occurring near the melting point was also considered. This alternative was finally judged to be improbable on the following grounds:

1. The heat involved in the lower arrest was too large relative to that of the upper arrest for these phenomena to be regarded as allotropic and melting transformations respectively.

2. Careful study of the temperature-time cooling curves (rather than the inverse-rate curves in Fig 5) indicated that the upper transformation actually took place over a temperature range, while the lower break constituted an isothermal hold. This suggested a binary liquidus and eutectic reaction, and not complete freezing followed by a solid-solid transformation.

3. In addition, when the resulting beryllium-iron diagram was drawn to include the hypothetical allotropic change, it called for completely solid phases in alloys of 0.5 and 1.5 at. pct iron at temperatures of 1190 to 1225°C (refer to Fig 10). However, when these alloys were quenched from this region, they displayed definite evidence of melting.

If the double arrest is caused by an impurity, other than iron, the beryllium-iron alloys under investigation should be considered as ternary rather than binary compositions. It was established that iron was not the active impurity because beryllium samples with as little 0.001 at. pct iron showed a marked double heat effect, very similar to that exhibited by the stock beryllium containing 0.016 at. pct iron. Moreover, all of the experimental findings on the beryllium-iron alloys were consistent with concept that (1) they belonged on a section through a ternary system, and (2) that the "pure" beryllium behaved as if the presence of an

impurity caused primary beryllium to crystallize over a range of temperatures down to a binary eutectic temperature where the rest of the beryllium and the impurity-constituent crystallized simultaneously and isothermally.

This is in line with the observations of Sloman⁷ who ascribed the eutectic to Be + BeO. However, in the present work, no eutectic configuration could be seen in the microstructure of the beryllium; nor could the BeO phase be identified as such, although there were many inclusions visible (Fig 6). Inasmuch as oxygen analyses were not available for correlation purposes, it appeared preferable to designate the impurity-constituent as *X*. These relationships will be discussed more fully in the section dealing with 0-8 at. pct iron.

The solid solubility of iron in beryllium⁸ was found to be quite limited (less than 0.4 at. pct iron) and no

change in lattice parameter could be detected. The lattice constants of beryllium are listed in Table 2, along with data for the other solid phases to be discussed.

§ PHASE (FeBe₁₁)

Misch⁵ found diffraction lines from a complex beryllium-rich phase judged to be FeBe₉. In the current investigation, a compound was located between 7.8 and 8.2 at. pct iron, which corresponds to the formula FeBe₁₁ (or possibly FeBe₁₂), rather than FeBe₉. All the diffraction lines from this phase can be indexed on the basis of a hexagonal cell of dimensions shown in Table 2. According to the measured density (2.50 g per cc), the number of atoms per unit cell is 18. This is a peculiar result because it implies that there are 1½ formula weights per unit cell. Until a complete solution of the structure by single-crystal analysis is available, the present findings cannot be rationalized.

The range of solubility in the ζ phase is too limited to show a variation of lattice parameter with composition. It transforms on heating via a congruent reaction at 1075°C into the ϵ phase. It is extremely difficult to polish because of brittleness, but when this is properly done, it can be easily identified in the microstructure under polar-



FIG 6—Inclusions in beryllium stock. Larger particles are beryllium carbide; smaller ones are probably a silicon-rich phase. Unetched. Mag. 500 X.

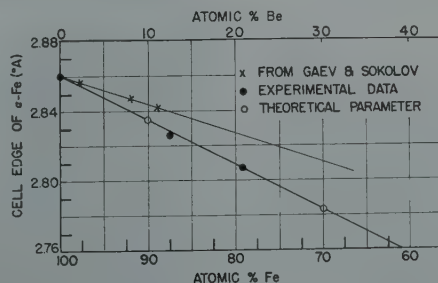


FIG 7—Lattice parameter of F.C.C. ϵ phase as a function of iron content.

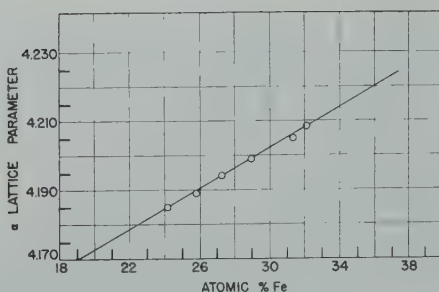


FIG 8—Basal plane parameter of H.C.P. β phase as a function of iron content. c/a ratio does not change measurably over this range.

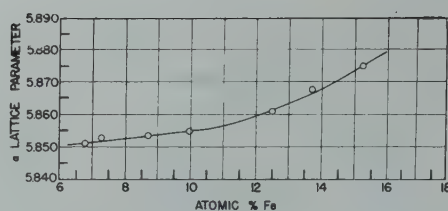


FIG 9—Lattice parameter of B.C.C. iron as a function of beryllium content.

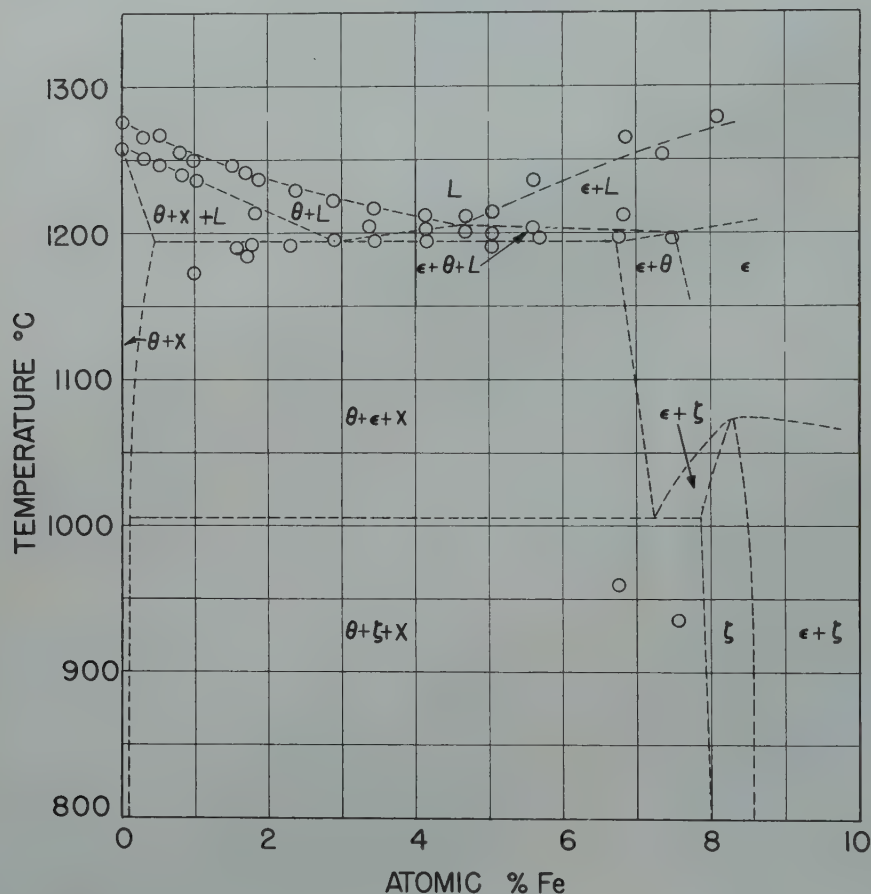


FIG 10—Results of thermal analyses on cooling of 0–8 at. pct iron alloys. Phase fields are drawn to be consistent with X ray results of Fig. 11.

ized light by the feathery appearance illustrated in Fig 21.

ϵ PHASE (FeBe_5)

Misch⁵ determined the structure of this phase to be face-centered cubic and assigned the formula FeBe_5 . This was confirmed in the present work (Table 2) except that the phase was found to enjoy a wide range of homogeneity at elevated temperatures (7 to 18 at. pct iron). At lower temperatures,

however, the range becomes narrow (15–17 at. pct iron), but still includes the composition FeBe_5 (16.7 at. pct iron). The variation of lattice parameter with composition, obtained by solution quenching, is given in Fig 7.

Because of its cubic symmetry, ϵ does not exhibit extinction effects upon rotation under polarized light (Fig 21) and is thereby readily distinguished from ζ on the one hand and β on the other, both of which are optically anisotropic.

β PHASE (FeBe_2)

This compound was first observed by Oesterheld.² Later, Misch⁵ reported the structure to be hexagonal close-packed of the MgZn_2 type, and this was substantiated here (Table 2).

The β phase was found to extend from 21 to 37.5 at. pct iron, and Fig 8 shows the variation of the basal parameter with iron content. The c/a ratio does not change measurably over this range of composition.

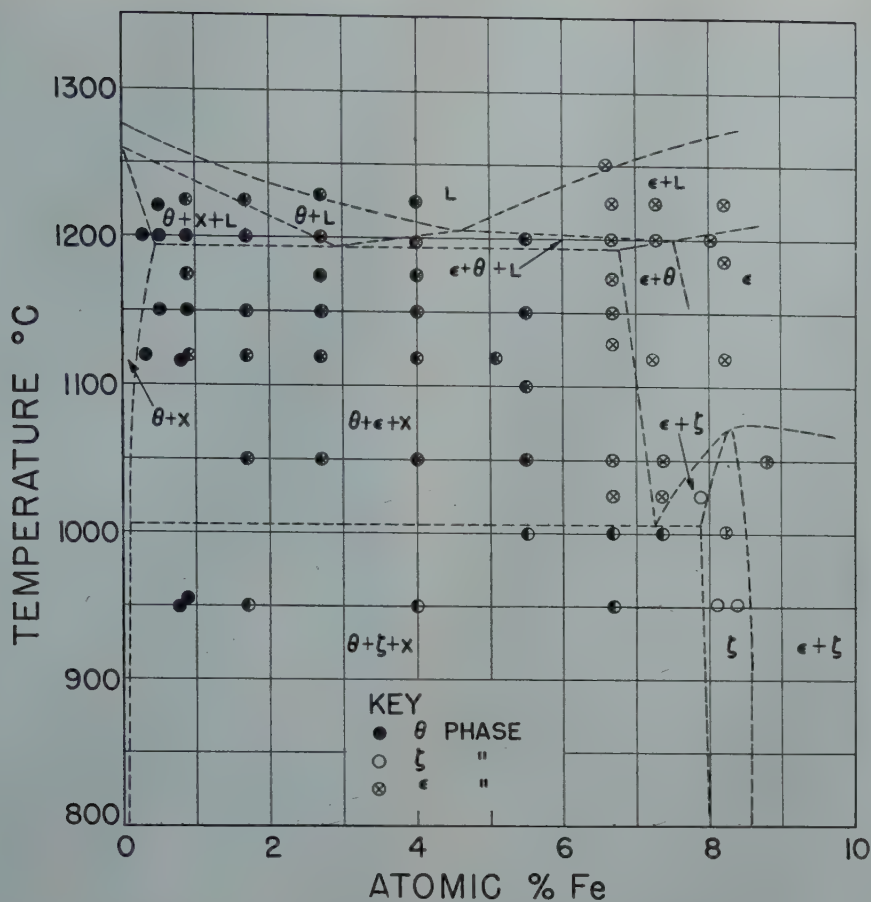


FIG 11—Summary of X ray results on solution-quenched alloys containing 0–8 at. pct iron. Phase fields are drawn to be consistent with thermal data of Fig. 10.

| TREATMENT | ANGLE θ FOR Co K_{α} RADIATION | | | ATOMIC % Fe | PHASES | WEIGHT % Fe |
|------------------------------|--|----|----|----------------|---|----------------|
| | 0 | 45 | 90 | | | |
| ABOVE 1010°C BELOW 1010°C | | | | 0. | θ | 0. |
| BELOW 1010°C | | | | 1.0 | $\theta + \zeta$ | 6.0 |
| BELOW 1010°C | | | | 3.0 | $\theta + \zeta$ | 15.9 |
| ABOVE 1010°C BELOW 1010°C | | | | 4.1 | $\theta + \epsilon$ $\theta + \zeta$ | 20.9 |
| ABOVE 1010°C | | | | 6.8 | $\theta + \epsilon$ | 31.0 |
| ABOVE 1010°C BELOW 1010°C | | | | 8.0 | ϵ ζ | 35.4 |

FIG 12—X ray diffraction patterns of alloys containing 0–8 at. pct iron, quenched from above and below 1010°C.



FIG 13 (Above)—1.0 at. pct Fe, as solidified. Large primary grains of θ with ϵ at grain boundaries (degenerate eutectic). Precipitate within the primary grains is also ϵ . Etched with HF. Mag. 100 \times .

FIG 14 (Below)—2.3 at. pct Fe, as solidified. Primary grains of θ surrounded by eutectic. Etched with HF. Mag. 100 \times .

β melts congruently at approximately 1480°C, corresponding to the composition 33 at. pct iron or FeBe_2 .

Metallographically, β is easily identified because of its polarizing effects. On the beryllium-rich side of the above range, the grains of β are uniformly clear (Fig 22), but at the iron-rich side, a fine lacy structure appears within the grains (Fig 23).

α PHASE (Fe)

Beryllium is appreciably soluble in ferrite, and its effect on the lattice parameter of body-centered cubic iron is given in Fig 9. The present results depart somewhat from those of Gaev and Sokolov,¹ and are in better agreement with the calculated parameter based on atomic radii.

The critical points of pure iron used in the final diagram were taken from the 1948 Metals Handbook as A_3 at

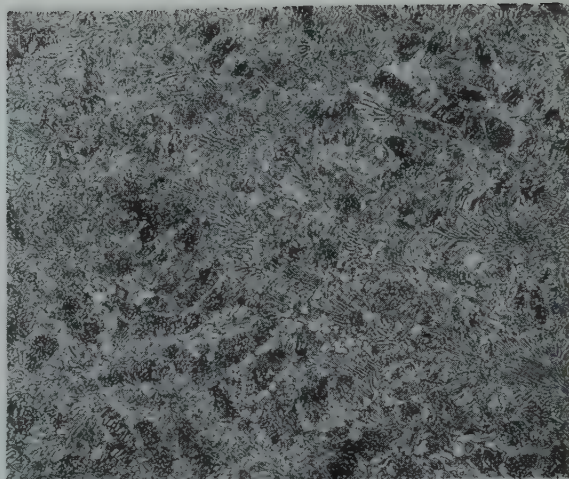
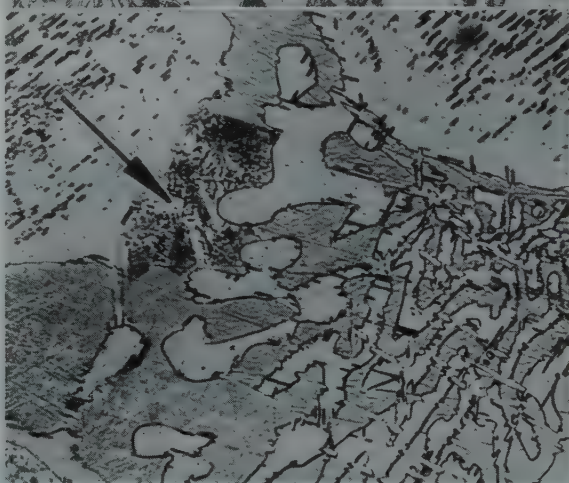


FIG 15 (Above)—4.1 at. pct Fe, as solidified. Mixture of coarse and fine "eutectics." Etched with HF. Mag. 100 \times .

FIG 16 (Center)—5.2 at. pct Fe, as solidified. Primary grains of ϵ with coarse and fine "eutectics." Etched with HF. Mag. 100 \times .

FIG 17 (Below)—1.7 at. pct Fe, as solidified. Primary grains of θ separated by ternary eutectic. Precipitate of ϵ in θ grains. Matrix of eutectic is ϵ , one region of which has undergone eutectoid decomposition to $\theta + \zeta$ (arrow). Other constituents of eutectic are particles of θ and needles of unknown phase polished in relief. Etched with HF. Mag. 1000 \times .



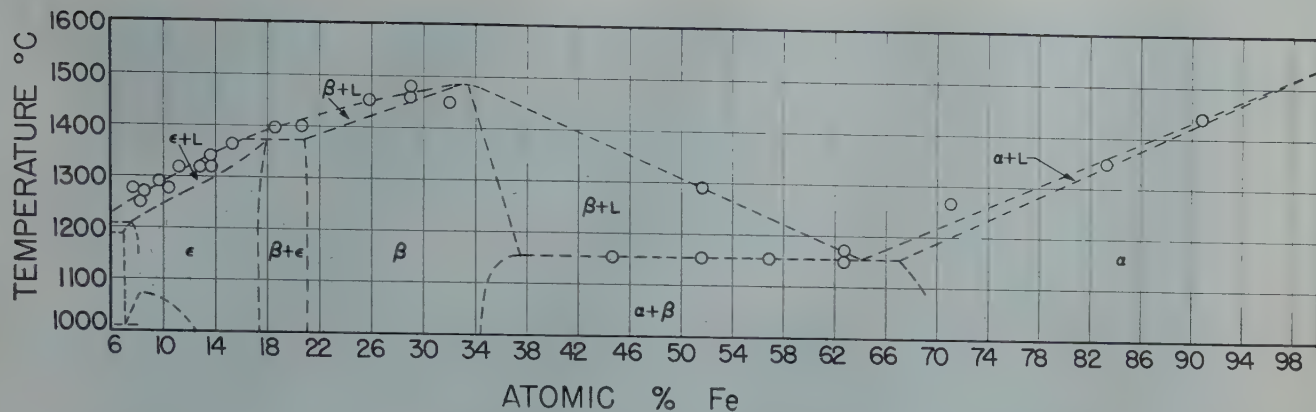


FIG 18—Results of thermal analysis on cooling 8–100 at. pct iron alloys.

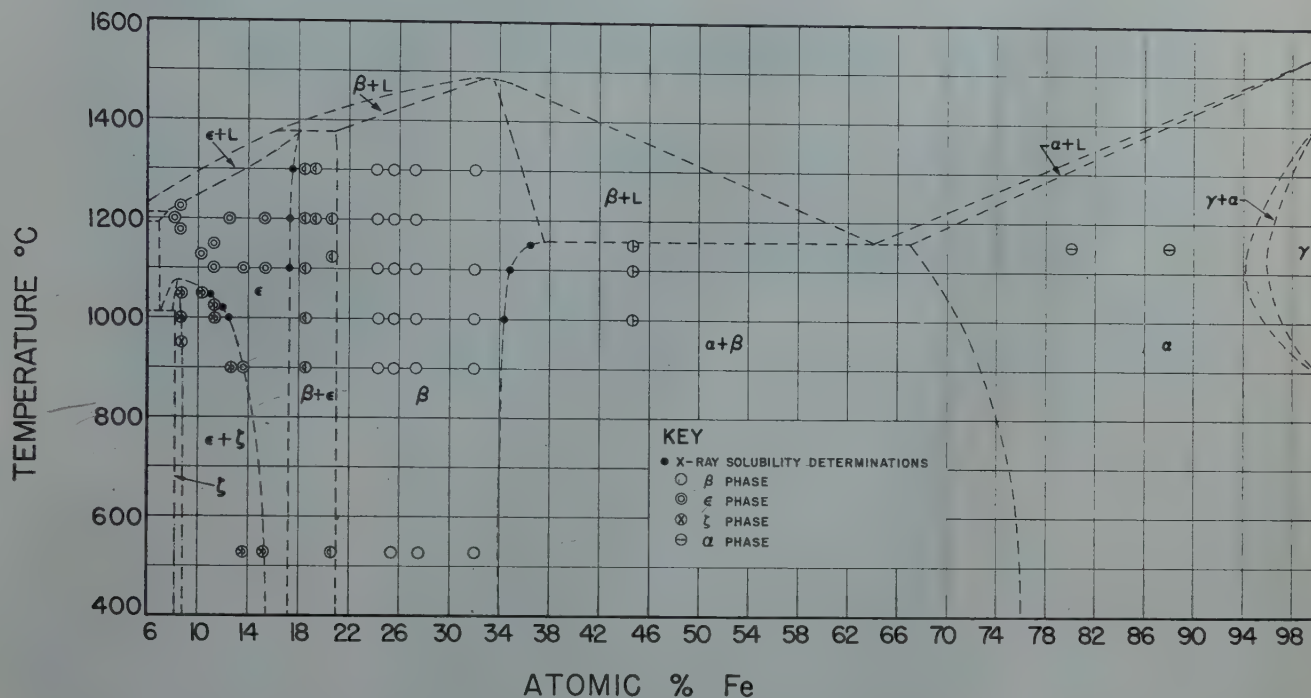


FIG 19—Summary of X ray results on solution-quenched alloys containing 8–100 at. pct iron.

910°, A_4 at 1400° and $m.p.$ at 1539°C. No studies were made of the austenitic and ferritic phase boundaries. The gamma loop and alpha solubility limits of Gaev and Sokolov¹ were adopted.

0–3 AT. PCT IRON (0–35 WT. PCT)

The results of thermal analyses on cooling of alloys lying in this range are summarized in Fig 10. The liquidus line descends from “pure” beryllium, and reaches a minimum at 4.7 at. pct iron. This occurs at 1210°C, and corresponds to the maximum heat effect in the series. The lower arrest of beryllium descends with increasing iron, and meets the 1190°C isothermal line at about 3.0 at. pct iron, where it yields

the maximum heat effect in this series.

The phase fields outlined in Fig 10 were drawn to be consistent, not only with the thermal points shown, but also with the X ray (Fig 11) and metallographic results of the solution-quenching experiments.*

The latter observations were given more weight in cases where supercooling was suspected to have influenced the thermal arrests. For example, the two points at 950°C in Fig 10 were found to be in error because of supercooling. Hence, the isothermal reaction indicated at 1010°C was ascertained on the basis of the quenching experiments.

* Due regard was also given to the phase rule as applied to ternary systems.

Fig 12 offers a comparison of the diffraction patterns of several alloys after quenching from above and below 1010°C.

The transformations corresponding to the various lines in Fig 10 and 11 are deducible from the microstructures. Up to 2.9 at. pct iron, the as-solidified alloys exhibit increasing amounts of an eutectic-like structure, (Fig 13 and 14) which is evidently connected with the 1190° isothermal line. At the same time, the amount of primary θ diminishes. Beyond 3.0 at. pct, a coarse duplex structure appears and reaches a maximum at 4.7 at. pct iron, corresponding to the 1210° intersection. A comparison of the two “eutectics” is found in Fig 15.

| TREATMENT | ANGLE θ FOR Co K α RADIATION | | | ATOMIC % Fe | PHASES | WEIGHT % Fe |
|------------------|--|----|----|----------------|--------------------|----------------|
| | 0 | 45 | 90 | | | |
| ALL BELOW 1000°C | | | | 8.0 | ζ | 35.4 |
| | | | | 13.6 | $\zeta + \epsilon$ | 49.2 |
| | | | | 15.3 | $\zeta + \epsilon$ | 52.8 |
| | | | | 20.5 | $\beta + \epsilon$ | 61.5 |
| | | | | 25.5 | β | 67.9 |
| | | | | 32.0 | β | 74.2 |
| | | | | 44.7 | $\alpha + \beta$ | 83.5 |
| | | | | 100. | α | 100. |

FIG 20—X ray diffraction patterns of alloys containing 8–100 pct iron. Annealed below 1000°C.

When the iron is increased above 4.7 at. pct, primary grains of ϵ begin to appear in conjunction with the two “eutectics” (Fig 16). The mottling in the primary ϵ is due to partial decomposition into $\theta + \zeta$ via the eutectoid reaction at 1010°C. In some instances, even the ϵ associated with the “eutectic” structures undergoes such decomposition (Fig 17). However, if the alloys are quenched from above 1010°C, the phase is retained intact. As shown in Fig 13 and 17, some precipitation from the θ phase occurs during slow cooling, in accordance with the sloping solubility limit.

It is believed that the coarser of the two “eutectics” results from the univariant reaction $L \rightarrow \theta + \epsilon$ in the vicinity of 1210°C, and the finer one from the nonvariant reaction $L \rightarrow \theta + \epsilon + X$ at 1190°C (Fig 10). Unfortunately, no evidence was obtained as to the identity of the X constituent. Fig 17 shows primary grains of θ separated by a network of the ternary eutectic. The θ particles and ϵ matrix of the eutectic are clearly distinguishable, but there is also a third phase (polished in relief) in the form of needles that run through the eutectic, causing jagged interfaces between the θ and ϵ . No diffraction lines attrib-

utable to this phase were observed.

8–100 AT. PCT IRON (35–100 WT. PCT)

Since the assumed impurity was introduced in proportion to the beryllium content, it was reasonable to expect the ternary behavior of the system to vanish gradually with increasing percentages of iron. Thus, the higher iron range could be treated as a regular binary diagram without undue violation of the phase rule.

The results of thermal analysis for the above composition range are plotted in Fig 18. The liquidus rises to approximately 1480°C at the melting point of the compound FeBe_2 (β), then falls to 1165°C (the eutectic of β and α), and finally rises to 1539° at the melting point of pure iron.

The solution-quenching experiments are summarized in Fig 19. Fig 20 illustrates the diffraction patterns of typical alloys in this range.

From the shape of the liquidus lines and extension of the solid phase boundaries, a peritectic reaction was deduced at approximately 1375°C: $L + \beta \rightleftharpoons \epsilon$. No thermal evidence for this reaction was found but the microstructure of an alloy in this range did show signs of β surrounded by ϵ . Furthermore, the

peritectic temperature agrees with that of Gordon's diagram in Fig 1.

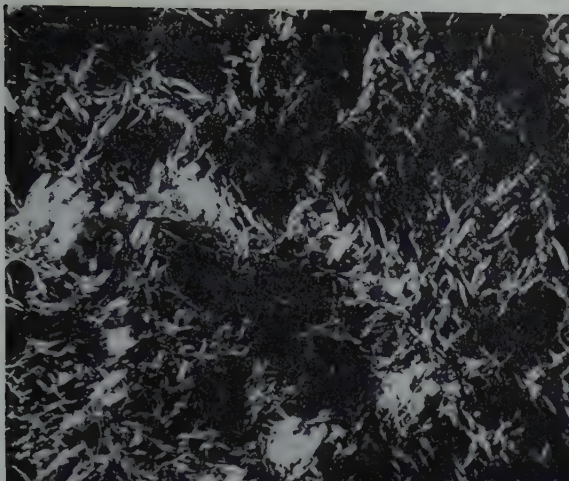
The micrographs in Fig 21 to 25 illustrate the types of structures observed. Fig 21 shows a mixture of ζ (light and feathery) and ϵ (dark masses). Fig 22 and 23 are examples of β . Fig 24 typifies the primary β plus eutectic ($\alpha + \beta$) structure, and Fig 25 shows an iron-rich alloy with β precipitated from the α solution matrix.

Final Diagram

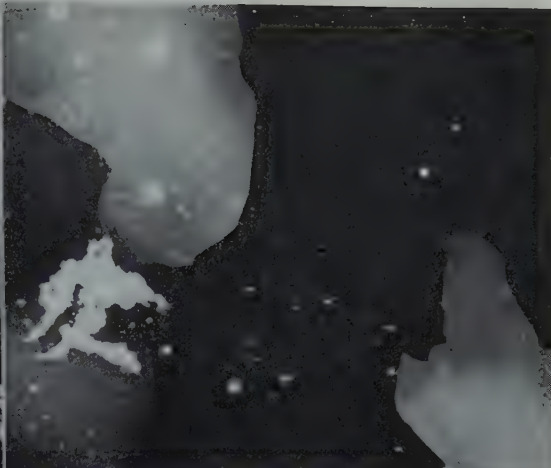
The entire diagram is assembled in Fig 26. At the beryllium-end, the ternary behavior is eliminated by collapsing the three-phase regions in an attempt to estimate the nature of the true beryllium-iron binary system. This practice is somewhat arbitrary because there is no information as to the critical temperatures and compositions in the absence of the interfering impurity. However, it is likely that the observed liquidus and solidus temperatures would rise slightly with increasing purity, as found by Losano⁸ for beryllium itself.

Fig 26 embodies all these considerations, and is redrawn to conform to the method of presentation adopted by the 1948 Metals Handbook.

21



22



23



24



25

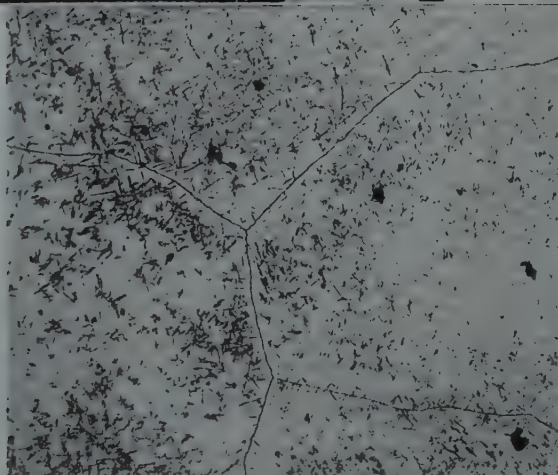


FIG 21—12.5 at. pct Fe, as solidified. ϵ phase is black and massive. ζ phase is light and feathery. Unetched. Illuminated by polarized light. Mag. 100 \times .

FIG 22—27.3 at. pct Fe, as solidified. All β phase. Unetched. Illuminated with polarized light. Mag. 100 \times .

FIG 23—32.0 at. pct Fe, as solidified. All β phase. Note fine pattern within grains. Unetched. Illuminated with polarized light. Mag. 100 \times .

FIG 24—51.2 at. pct Fe, as solidified. Primary grains of β and eutectic of $\alpha + \beta$. Etched with nital. Mag. 100 \times .

FIG 25—70.5 at. pct Fe, as solidified. Primary grains of α with precipitate of β . Etched with nital. Mag. 100 \times .

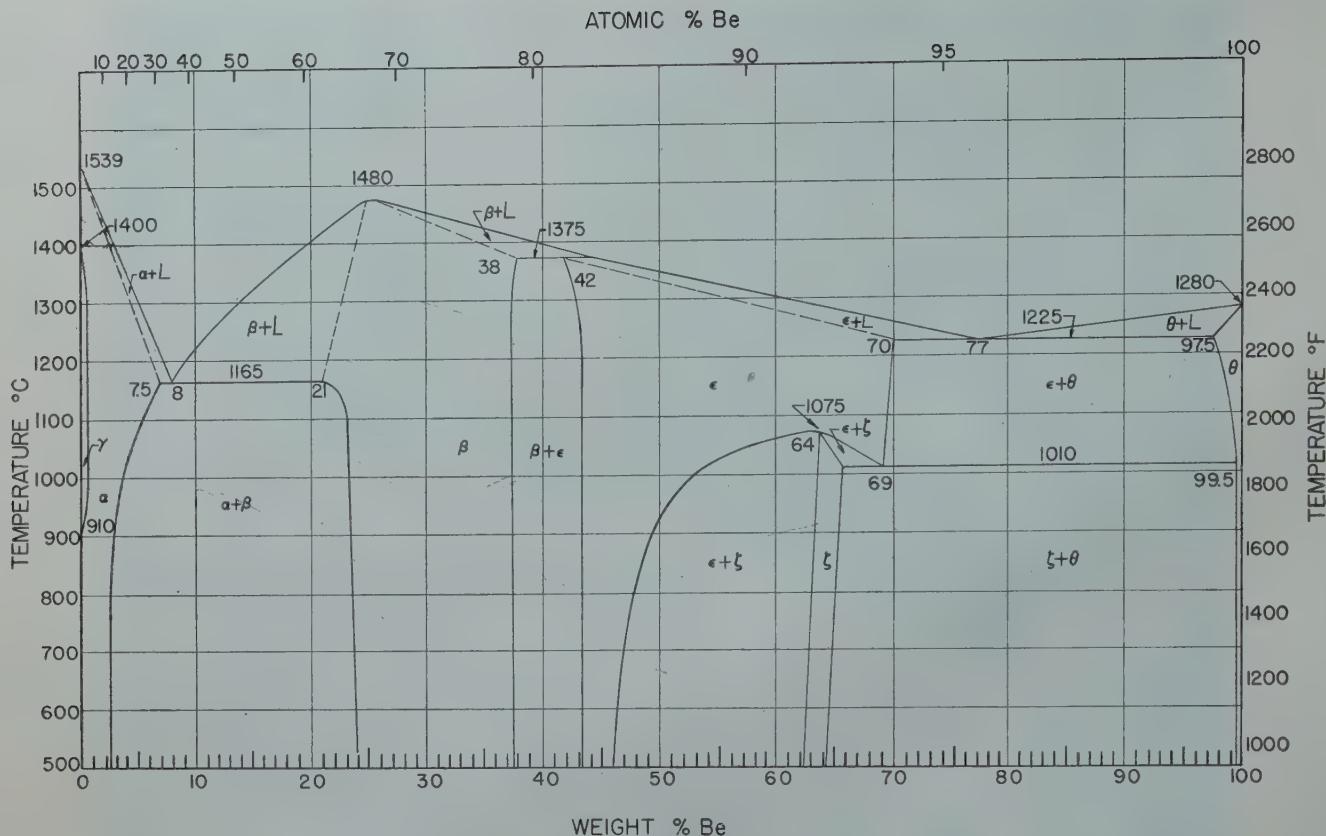


FIG 26—The beryllium-iron system.

Conclusions

1. The available beryllium (99.4 wt pct) was sufficiently impure to exhibit a double arrest at the melting point.

2. Because of the binary nature of this beryllium, the beryllium-iron diagram investigated turned out to be a section through a ternary system. The experimental data were analyzed on this basis, and then the beryllium-iron binary was deduced by allowing the three-component relationships to degenerate into a two-component diagram, thus eliminating one degree of freedom. This approximation was only necessary at the beryllium-end of the system.

3. The solid phases in the system have been identified as listed in Table 2.

4. The beryllium-iron diagram contains two eutectics: one at 1225°C, $L_{7.5} \rightleftharpoons \theta_{0.4} + \epsilon_7$; and the other at 1165°C, $L_{64} \rightleftharpoons \beta_{37} + \alpha_{67}$. There is also a peritectic at 1375°C, $L_{16} + \beta_{21} \rightleftharpoons \epsilon_{18}$; and an eutectoid at 1010°C, $\epsilon_7 \rightleftharpoons \theta_{0.1} + \zeta_8$. The subscripts indicate atomic percent

iron. The corresponding weight percentages are given in Fig 26.

5. The ζ phase decomposes congruently on heating into ϵ at 1075°C, and the β melts congruently at about 1480°C.

6. There are appreciable ranges of solubility in the α , β and ϵ phases, but very limited solubility in the ζ and θ phases.

Acknowledgment

The authors wish to express their appreciation to Mr. Paul Gordon for permission to publish Fig 1 which summarizes his preliminary work leading up to the present investigation; to Dr. A. R. Kaufmann for his criticisms and aid; to Mr. A. B. Bompane who assisted in the thermal analyses; to Miss H. P. Roth for the general metallographic work; to Mr. Charles Fletcher for the special polishing of the brittle alloys; and to Mr. V. M. Mahady for making the beryllia crucibles.

The research was carried out in the Department of Metallurgy at Massachusetts Institute of Technology under the auspices of the Manhattan Project, Contract No. W7405-eng-175.

References

1. J. S. Gaev and R. S. Sokolov: The System Iron-Beryllium. *Metallurg* (1937) 4, 42-48.
2. G. Oesterheld: Concerning the Alloys of Beryllium with Aluminum, Copper, Silver and Iron. *Ztsch. Anorg. Chem.* (1916) 97, 6.
3. F. Wever and A. Müller: Structures of Mixed Crystals of Iron with Beryllium and Aluminum. *Ztsch. Anorg. Allgem. Chem.* (1930), 193, 337-345.
4. M. J. Laissus: Cementation of Iron and Iron Alloys by Ferroberyllium. *Rev. de Met.* (1935) 32, 293, 351, 401.
5. L. Misch: On Two Intermetallic Compounds of Beryllium with Iron. *Naturwissenschaft* (1935) 23, 287-288.
6. P. Gordon: Unpublished research, Manhattan Project at M.I.T. under Contract No. W7405-eng-175.
7. H. A. Sloman: Researches on Beryllium. *Jnl. Inst. Metals* (1932) 50, 365.
8. L. Losano: Investigation on Beryllium. I. Properties of Beryllium of a High Degree of Purity. *Alluminio* (1939) 8 (2) 67-75.

CORRECTION FEBRUARY ISSUE

"Development of the Modern Zinc Retort in The United States." By H. R. Page and A. E. Lee, Jr.
On page 73, column 1, line 3, of February 1949 *Journal of Metals Transactions* the date 1890 should read 1860.

Discussion, Institute of Metals Division

Contents

| | PAGE |
|---|------|
| The Cobalt-chromium Binary System (paper by A. R. Elsea, A. B. Westerman, and G. K. Manning, <i>Met. Tech.</i> June, 1948, TP 2393)..... | 298 |
| Mechanism of Precipitation in a Permanent Magnet Alloy (paper by A. H. Geisler and J. B. Newkirk, <i>Met. Tech.</i> Aug. 1948, TP 2444)..... | 300 |
| Some Effects of Applied Stresses on Precipitation Phenomena (paper by W. L. Finlay and W. R. Hibbard, Jr., <i>Met. Tech.</i> Sept. 1948, TP 2470)..... | 301 |
| Diffusion of Carbon in Austenite with a Discontinuity in Composition (paper by L. S. Darken, <i>Met. Tech.</i> Sept. 1948, TP 2443)..... | 304 |
| An Electron Diffraction Study of Oxide Films Formed on Nickel-chromium Alloys (paper by J. W. Hickman and E. A. Gulbransen, <i>Met. Tech.</i> June 1948, TP 2372)..... | 305 |
| An Electron Diffraction Study of Oxide Films Formed on Copper-nickel Alloys at Elevated Temperatures (paper by J. W. Hickman and E. A. Gulbransen, <i>Met. Tech.</i> June 1948, TP 2391)..... | 307 |
| Decarburization of Chrome Nickel Alloys by Their Surface Oxides in High Vacua and at Elevated Temperatures (paper by E. A. Gulbransen, W. S. Wysong, and K. Andrew, <i>Met. Tech.</i> Sept. 1948, TP 2438)..... | 307 |
| Fractographic Study of Cast Molybdenum (paper by C. A. Zapffe, F. K. Landgraf and C. O. Worden, <i>Met. Tech.</i> Aug. 1948, TP 2421)..... | 308 |
| Effect of Composition on Grain Growth in Aluminum-magnesium Solid Solutions (paper by L. J. Demer and P. A. Beck, <i>Met. Tech.</i> June 1948, TP 2374)..... | 309 |
| Effect of a Dispersed Phase on Grain Growth in Al-Mn Alloys (paper by P. A. Beck, M. L. Holzworth and P. Sperry, <i>Met. Tech.</i> Sept. 1948, TP 2475)..... | 310 |
| Statistical Rate Theory of Metals—Mechanism of Flow and Application to Tensile Properties (paper by J. W. Fredrickson and H. Eyring, <i>Met. Tech.</i> Aug. 1948, TP 2423)..... | 315 |
| Nucleation of Slip Bands (paper by J. G. Leschen, R. P. Carreker, and J. H. Hollomon, <i>Met. Tech.</i> Sept. 1948, TP 2476) and.. | 318 |
| Transient Plastic Deformation (paper by R. P. Carreker, J. G. Leschen, and J. D. Lubahn, <i>Met. Tech.</i> Sept. 1948, TP 2477)... | 318 |
| Plastic Deformation of Large Grained Copper Specimens (paper by W. R. Hibbard, Jr., <i>Met. Tech.</i> Sept. 1948, TP 2469).... | 323 |
| Plastic Flow in Anisotropic Sheet Steel (paper by L. R. Jackson, K. F. Smith, and W. T. Lankford, <i>Met. Tech.</i> Aug. 1948, TP 2440)..... | 323 |
| The Effect of Thermal-mechanical History on the Strain Hardening of Metals (paper by J. E. Dorn, A. Goldberg, and T. E. Tietz, <i>Met. Tech.</i> Sept. 1948, TP 2445)..... | 325 |
| The Room and Elevated Temperature Properties of Some Sand Cast Magnesium-base Alloys Containing Zinc (paper by T. E. Leontis, <i>Met. Tech.</i> June 1948, TP 2371)..... | 327 |
| The Low Temperature Properties of Tin and Tin-lead Alloys (paper by H. S. Kalish and F. J. Dunkerley, <i>Met. Tech.</i> Sept. 1948, TP 2442)..... | 335 |
| Thermal and Electrical Properties of Ductile Titanium (paper by E. S. Greiner and W. C. Ellis, <i>Met. Tech.</i> Sept. 1948, TP 2466)..... | 335 |
| Property Changes during Aging (paper by A. H. Geisler, <i>Met. Tech.</i> Aug. 1948, TP 2436)..... | 337 |
| Factors Affecting the Tensile Notch Sensitivity of Magnesium Alloy Extrusions (paper by I. Cornet, <i>Met. Tech.</i> Aug. 1948, TP 2419)..... | 338 |
| Effect of Grain Size on Tensile Strength, Elongation and Endurance Limit of Deep Drawing Brass (paper by H. L. Walker and W. J. Craig, <i>Met. Tech.</i> Sept. 1948, TP 2478)..... | 339 |
| A Copper-base Alloy Containing Iron as a High-strength, High-conductivity Wire Material (paper by W. Hodge, R. I. Jaffee, J. G. Dunleavy, and H. R. Ogden, <i>Met. Tech.</i> Aug. 1948, TP 2422)..... | 340 |
| A High Strength-High Conductivity Copper-silver Alloy Wire (paper by W. Hodge, R. I. Jaffee, J. G. Dunleavy, and H. R. Ogden, <i>Met. Tech.</i> June 1948, TP 2366)..... | 340 |
| The Effect of Chromium on the M _s Point (paper by J. B. Bassett and E. S. Rowland, <i>Met. Tech.</i> Aug. 1948, TP 2417).... | 341 |
| The Kappa Eutectoid Transformation in the Copper-silicon System (paper by W. R. Hibbard, Jr., G. H. Eichelman, Jr., and W. P. Saunders, <i>Met. Tech.</i> Sept. 1948, TP 2441)..... | 343 |
| Stabilization of the Austenite-martensite Transformation (paper by W. R. Harris, Jr. and M. Cohen, <i>Met. Tech.</i> Sept. 1948, TP 2446)..... | 344 |
| Secondary Hardening of Tempered Martensitic Alloy Steel (paper by W. Crafts and J. L. Lamont, <i>Met. Tech.</i> Sept. 1948, TP 2439)..... | 345 |

This discussion is TP 2533 E.

The Cobalt-chromium Binary System

By A. R. ELSEA, A. B. WESTERMAN, Junior Members, and G. K. MANNING, Member AIME

DISCUSSION

(G. E. Doan and W. L. Fink presiding)

A. H. SULLY*—There are two points relating to this paper which I would like to discuss.

The first relates to the purity of the alloys. I note that, whereas all the alloys examined were analyzed for nitrogen, no estimations of the oxygen content appear to have been made and, in discussing the purity of the materials, although the authors refer to the oxygen content of the electrolytic cobalt (0.034 pct), they appear to have ignored the oxygen present in the electrolytic chromium. It was first shown by Adcock⁸ that the oxygen content of electrolytic chromium may be, and usually is, considerable, the content of chromium oxide Cr_2O_3 being commonly of the order of 1–2 pct. Brenner, Burkhead and Jennings⁹ have recently confirmed this fact and have made a comprehensive investigation of the variation of the oxygen content with conditions of electro-deposition. Work in progress at the Fulmer Research Institute on the preparation of high purity chromium-rich alloys has illustrated the difficulty of removing the oxygen content; and we have found that chromium-rich alloys can continue to oxidize when melted under moderate vacuum conditions (5–20 microns). For this reason, chromium-cobalt alloys with up to 20 pct cobalt, made from electrolytic chromium containing initially about 1.6 pct Cr_2O_3 may contain, after vacuum melting, up to 2.5 pct Cr_2O_3 . The oxygen content may be determined readily by dissolving the alloy in dilute acid and weighing the insoluble residue of Cr_2O_3 . The same method may be used for the determination of the oxygen content of electrolytic chromium, if the chromium is first heated for a period of a few hours at a temperature of about 800°C.

While the oxide content is unlikely to have any serious effect on the phase transformations, it must be remembered that the chromium content of the oxide will be withheld from solid solution and this will have a minor effect on the location of the boundaries in the chromium-rich alloys. A statement by the authors of the oxygen content of their alloys would enable an assessment to be made of the probable precision in the location of the $\epsilon/\gamma + \epsilon$ phase boundary.

The second point which I wish to make concerns the identity of the γ phase. During a preliminary survey of the cobalt-chromium system, my colleague, Mr. T. J. Heal, and I¹⁰ found that this phase was isomorphous with the sigma phase, of the iron-chromium. Andrews,¹¹ in commenting on our result, has since stated that there appears to be a third isomorphous phase in the system Fe-V. The present investigation places the composition of this phase at the CO_2Cr_3 composition, confirming the earlier work of Wever and Haschimoto.¹² In the iron-chromium system the isomorphous sigma phase forms at the ratio Fe-Cr. In both systems, however, solution seems to be confined to the low chromium side of the relevant stoichiometric composition. The reason for the variation of the stoichiometric ratio for the isomorphous phase between the Co-Cr and the Fe-Cr system is an interesting subject for speculation, and further study of this phase in the two systems may throw further light on the difficult subject of atomic bonding in alloys of the transition metals.

N. J. GRANT* and L. W. KATES*—Several points in this paper that are not quite clear or in complete agreement with our work at Massachusetts Institute of Technology include the following:

The structure of an all-alpha specimen (Fig 4) could be interpreted as a two-phase structure rather than a single phase one. Specimens of chromium contents 10.6, 16.8, 23.0, and 28.8 pct when heated at temperatures of from 1800 to 2200°F (980 to 1205°C) for periods of time ranging from 1 to 48 hr followed by water quenching, invariably showed both F. C. C. and H. C. P. lines on X ray diffraction examination. In addition, these same specimens, when examined metallographically, using such etchants as chrome regia and Marble's Reagent, showed a rather poorly defined but unmistakable two-phase structure. We wondered, in those treatments where the initial structure was "all alpha," if this were checked by X ray diffraction patterns. It was not made clear, but we presumed that the alpha structure was retained at room temperature by water quenching. Our work has indicated that there is a metastable martensitic form of beta which is formed on quenching from within the alpha range which accounts for the H. C. P. lines and the microstructure observed in quenched alpha specimens. If that is the case, the so-called

"all alpha" structures are not truly equilibrium structures. It would seem that a true equilibrium alpha structure does not exist at room temperature and that a study of the α to β transformation would best be done by transferring the hot all alpha specimen directly to the aging temperature without the intermediate quenching step.

Although no attempt was made at Massachusetts Institute of Technology to establish the boundaries of the gamma phase field, the presence of gamma phase in alloys as low in chromium as 15 pct seems questionable. It is interesting to note that alloys V-20, V-26, and V-31 were cold worked initially to form beta and all these showed a gamma precipitate when aged for 65 hr at from 600 to 850°C. Alloy V-14, however, which had a homogenized structure initially, did not. It seems possible, therefore, that the so-called gamma precipitate is, in fact, some residue of the initial cold-worked structure. This is further suggested by the fact that Alloy V-36 which also had a homogenized initial structure showed no gamma precipitate at 600°C, although at 650°C and above, presumably, massive gamma, as exemplified in Fig 8, was found.

We took note of the treatments for developing gamma shown in Table 4 and repeated one of the experiments using our 28.8 pct chromium alloy. The specimen was heated at 1000°C for 1 hr and water quenched and metallographic examination showed the usual two-phase structure. The specimen was then held for 50 hr at temperatures of 875, 850, 830, and 890°C with metallographic and X ray examination being made between each different treatment. The structure in every case was the same, namely a single phase H. C. P. structure. There was no evidence of gamma precipitate similar to Fig 7 resulting from any of the treatments. Several attempts were made to use the etchant described in the paper for identifying the gamma phase; all were unsuccessful. The etchant finally adopted was Marble's Reagent which showed the beta grain boundaries quite well.

Regarding etchants 1, 2, and 3, used by the authors, we never, at any time, were successful in using them as described in the paper on our own alloys. We are not surprised that prior alpha structure did not transform to beta in 50 hr in alloys of less than 20 pct chromium. We did note, however, that a 28.8 pct chromium alloy transformed from alpha to beta com-

*Fulmer Research Institute, Stoke Poges, Buckinghamshire, England.

⁸ References are at the end of discussion.

*Massachusetts Institute of Technology.

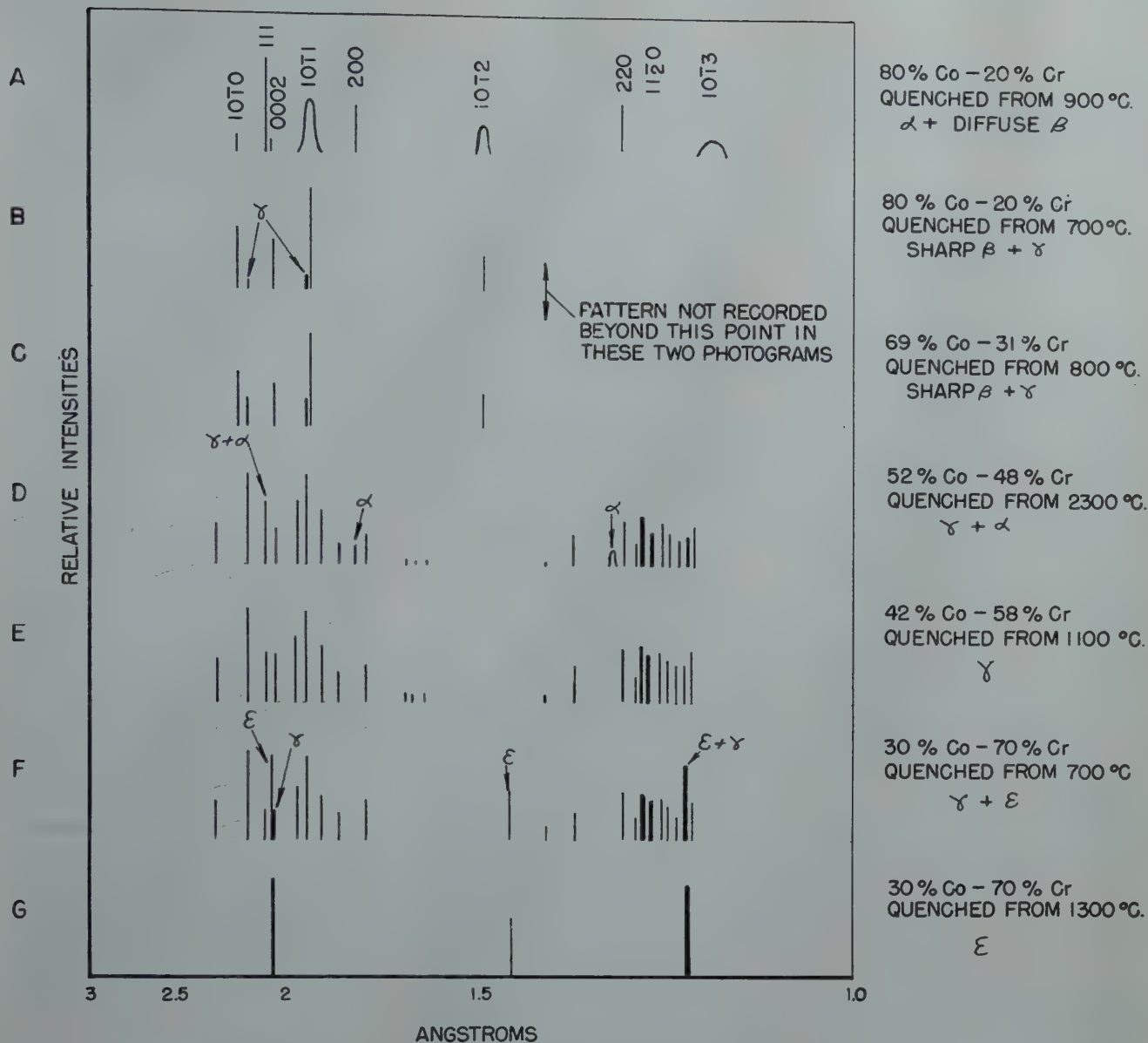


FIG 17—Plots of patterns of various alloy compositions of cobalt and chromium.

paratively easily when cooling in a dilatometer at a rate of about 5°C per min. We found that the 23 and 28.8 pct chromium alloys transformed readily from alpha to beta and vice versa, simply by heating and cooling in a well insulated furnace, but that the 10.6 and 16.8 pct alloys did not transform on cooling (alpha to beta) even at very slow cooling rates.

H. S. AVERY*—Rockwell hardnesses are mentioned in the paper, but I did not see any values. I should like to suggest that the authors will make this more valuable as a reference if in their written reply to the discussions they would include microhardness readings for the various constituents, and also give enough of their X ray crystallographic data to enable other workers to check their data against

those described in this paper.

W. O. SWEENEY*—The authors should be complimented on their very thorough investigation. We feel it is very timely now because of the necessity to know more about the high temperature alloys, as well as to obtain fundamental data which will enable the development of newer and better alloys for even higher temperatures.

The results of the work which were reported are in substantial agreement with the previous work that has been published and the work done at Union Carbide and Carbon Research Laboratories in Niagara Falls. It is also in line with the work we have done at the Haynes Stellite Co. Of course, the latter has been devoted primarily to more complex alloys.

However, we think it is noteworthy

* Haynes Stellite Co.

that the results the authors have obtained are not inconsistent with what we found in more complex alloys of this type.

A. R. ELSEA (authors' reply)—Mr. Sully has raised a very interesting question regarding the oxygen content of the cobalt-chromium alloys studied in this investigation. The electrolytic chromium used as melting stock in preparing these alloys contained 0.28 to 0.50 pct oxygen. Alloys V-7, V-20, V-26, and V-31, listed in Table 1 of the paper, contained 0.015, 0.14, 0.09, and 0.18 pct Cr₂O₃, respectively, as determined by a wet analysis method similar to the one described by Mr. Sully, but in which a correction was made for the amount of chromium nitride present in the residue. Microstructures of the vacuum-melted alloys, such as those described above, contained numerous oxide inclusions, while the

structures of the alloys melted in an alundum crucible under purified argon were almost free from oxide inclusions. After considerable study, it was concluded that chromium oxide in the melt went into solution in the alundum crucible, thus lowering the oxygen content of the melt.

The observation made by Mr. Sully that the cobalt-chromium gamma phase is isomorphous with the sigma phase of the iron-chromium system substantiates similar observations made at Battelle.

Dr. Grant and Mr. Kates have raised a number of questions regarding phase identification, experimental techniques, and interpretation of the data. In our opinion, the specimen shown in Fig 4 of the paper was alpha phase at the heat-treating temperature used; but upon cooling to room temperature partial transformation to beta phase occurred by a martensite type reaction similar to the reaction observed in pure cobalt by Troiano. This explains the acicular structure observed in Fig 4 and also partially accounts for the diffuse pattern of beta phase observed in the X ray diffraction patterns shown in Fig 17 of this discussion. It was because of this partial transformation during the quench that the aged specimens with alpha prior structures were transferred directly from the preheating furnace to the aging furnace, as described in the paper.

There is no question in our minds regarding the presence of gamma phase in cobalt-chromium alloys containing as little as 20 pct chromium. All of the binary alloys containing 20 pct or more chromium when aged at temperatures 20 to 50°C below the lower limit of the alpha-beta transformation range were found to contain gamma phase. The presence of gamma phase in these specimens was established by both metallographic and by X ray diffraction studies.

Dr. Grant's unsuccessful attempts to use the metallographic etchants described in the paper are difficult to explain. We have used these etchants throughout the study of the binary system and in our studies of the cobalt-chromium-iron, cobalt-chromium-nickel, and cobalt-chromium-nitrogen systems with success. The higher chromium alloys require a much longer etching time, but if the proper etching technique is used, metallographic

identification of the phases in this system is not difficult.

The Rockwell hardness impressions referred to by Mr. Avery were made on metallographic specimens to determine the nature of the slip lines or the type of fracture that was produced in the various phases by slight cold work. The microhardness values requested by Mr. Avery are as follows:

| Phase | Knoop Hardness (500-g load) |
|-------------------------|--------------------------------|
| Gamma..... | 940 to 960 |
| Epsilon (84 pct Cr).... | 630 to 686 |
| Beta (31 pct Cr)..... | 330 to 360 |
| Alpha* (31 pct Cr).... | 250 to 340 |

* The hardness of alpha was determined at room temperature and, therefore, it was not pure alpha but was alpha plus beta which formed while cooling to room temperature.

The following discussion of the X ray diffraction data was prepared by Dr. C. M. Schwartz of the Battelle staff, who conducted the X ray diffraction studies:

Plots of representative X ray patterns of alloys of various compositions and heat treatments are shown in Fig 17. Filings were used in Debye cameras with Co, Ni, or CrK radiation; or where greater resolving power was required, block samples were used with CrK radiation in a 20-cm-diam unsymmetrical focussing camera. Since the techniques varied, the photograms could not be compared directly, and it was necessary to resort to the graphical plot in Fig 17.

Pattern A, obtained from a 20 pct chromium sample quenched from 900°C, not far above the transformation zone, illustrates the existence of the "diffuse" hexagonal beta phase in samples quenched from the high-temperature F.C.C. alpha region. The corresponding indices of the reflections are indicated above the pattern. The appearance of beta is in agreement with that reported in pure cobalt by Edwards and Lipson.[†] Some lines are sharp, others diffuse, owing to stacking faults as explained by these authors. The existence of this faulted hexagonal phase is well correlated with the Widmanstätten-like appearance of the microstructure of alpha phase in Fig 4 of the paper. The question whether this structure results in part from quenching strains has not yet been settled from X ray data. Small amounts of "diffuse" hexagonal remain in samples of filings examined in a high-temperature camera

[†] *Proc. Roy. Soc.*, (1942) 180A, 268.

at temperatures just above the transformation zone, after moderate holding times. The amount does not increase on rapid cooling to room temperature; however, the strain introduced in this way is not comparable to that in a quenched block sample. Experiments are contemplated in which samples will be held and examined at temperatures far above the transition to see whether the hexagonal structure will tend to disappear.

It is to be noted that the (111) cubic and (0002) hexagonal reflections are resolved; complete resolution is attained in the focussing camera, using chromium radiation. This makes it possible to compare the relative intensities of the lines of the hexagonal phase. In spite of the diffuse nature of some of the lines, there is no marked discrepancy among the intensities, as has sometimes been claimed for cobalt itself.

Patterns B and C were obtained from 20 pct and 31 pct Cr block samples hot forged in the beta region, and subsequently heat treated and quenched from 700 and 800°C, respectively. Under these conditions sharp hexagonal beta-phase patterns are obtained free from alpha. The two strongest lines of gamma phase also appear faintly, in agreement with the phase diagram in Fig 3. Note again that the relative intensities of the first three lines of beta agree in Patterns A, B, and C.

Patterns D, E, and F contain gamma phase. Pattern E is single-phase gamma, with lattice spacings corresponding almost to the limit of chromium solubility. The solubility range is small, and the shift in spacing is readily detected only in the back-reflection lines. Pattern G, that of the chromium-rich solid-solution phase epsilon, is given so that its presence in Pattern F may be easily identified.

References

8. F. Adcock: *Jnl. Iron and Steel Inst.*, (1927) 115, 369.
9. A. Brenner, P. Burkhead and C. Jennings: *Jnl. Res. Nat'l. Bur. Standards* (1948) 40, 131.
10. A. H. Sully and T. J. Heal: *Research*, (1948) 1, 238.
11. K. W. Andrews: *Research*, (1948) 1, 478.
12. F. Wever and V. Haschimoto: *Mett. K. W. Inst. Eisenforschung*, (1929) 11, 293-330.

Mechanism of Precipitation in a Permanent Magnet Alloy

By A. H. GEISLER, Junior Member AIME, and J. B. NEWKIRK

DISCUSSION

(G. E. Doan and W. L. Fink presiding)
W. L. FINK*—For some years many

* Aluminum Co. of America.

of us have believed that the age hardening mechanism consisted simply of precipitation by nucleation and growth in which the precipitation occurred by the usual Widmanstätten mechanism, and

during the early stages of which the precipitate is coherent with the matrix.

Dr. Geisler has been working on this problem—one system after another—and he has succeeded in proving that mechanism for several alloys. He is doing a very excellent job. I feel that today

he skipped rather lightly over one of the important parts of this work—the streaks that are obtained on the Laue patterns from single crystals. I wonder if he would like to say a little more about the streaks.

A. H. GEISLER (authors' reply)—The interpretation of streaks in Laue photographs represents a specialized but important part of the precipitation problem. It has been demonstrated elsewhere⁸ that the streaks can be interpreted generally as the result of small dimensions of the precipitate particles that have a new structure related to the matrix by coherency. As such, the small particles should warrant no special consideration as a step in the precipitation process discrete from the larger, coherent particles that produce normal sharp diffraction. This was suggested by the discussor 8 or 10 years ago and has since been confirmed for several alloys. Indeed, the present study illustrates that age-hardening need not be contingent upon the structure that is responsible for streaks since the major part of the hardening of Cunico occurs after the particles have grown to a size large enough to produce sharp diffraction.

R. M. BRICK*—This aging is a little different from the normal precipitation process. Constitutionally it is almost a eutectoid reaction. You use the word "recrystallization" in discussing the lamellar stage of precipitation. I assume that you imply that if reheated after complete softening, when again in the single phase structure, there would be a completely different matrix grain structure than there was originally. Is that true?

A. H. GEISLER—The difference between the precipitation process in this

type alloy and the usual is that here the precipitate has the same structure as the matrix whereas usually the precipitate has a structure different from the matrix. In this respect the reaction here is more remote from the eutectoid reaction where both decomposition products usually have structures different from each other and different from the parent phase. Furthermore, the basic constitutional difference exists: that of the absence of a specific reaction temperature and composition as in the eutectoid reaction. Grain refinement in some alloys can be induced by the nodular reaction. The best evidence for this has been obtained on single crystals using the Laue X ray diffraction technique. Single crystals of some alloys, notably Cu-Be, Ag-Cu and Ni-Au are replaced by a polycrystalline aggregate when heat-treated crystals are aged and re-solution heat treated.

A. E. FLANIGAN*—I should like to comment on Dr. Geisler's remarks concerning a novel method for obtaining grain refinement.

It is implied that in the case of certain precipitation-hardening alloys it has been found possible to obtain grain refinement of the solid solution by means of a process involving precipitation followed by resolution. Presumably, precipitation of the discontinuous "lamellar" type in the region of the grain boundaries of the solid solution is attended by recrystallization of the matrix. Upon re-solution, it is implied, the new orientations of the previously lamellar patches are preserved thus effecting grain refinement of the solid solution.

This mechanism and its possible practical importance interested me several years ago and at that time an attempt

* University of California.

was made to induce grain refinement in this manner. A magnesium base casting alloy containing 9 pct aluminum and 2 pct zinc was employed. (ASTM B80-45T grade AZ92.) About ten cycles of the above-described treatment were employed and measurements of the grain size of the solid solution were made after each cycle. No changes in grain size were detected, however, even after this large number of cycles.

A. H. GEISLER—The application of the nodular reaction as a grain refinement method depends both upon alloy and thermal treatment. Since this is a recrystallization of the matrix it can be suppressed by the relief of strain through prior recovery in much the same manner as the suppression of recrystallization of cold worked metal. Thus, by slow heating to the solution temperature, it has been possible to recover single crystals by reabsorbing the recrystallized nodules. For grain refinement, such a reversion would have to be prevented; the nodular reaction would have to be carried to a sufficient degree of conclusion by aging and the heating rate to the solution temperature would have to be sufficiently fast to avoid reversion to the original grain structure. Naturally, if the rate of grain growth to a stable structure is very rapid at the solution heat treating temperature, as it may well be in some alloys, this method would be of little avail as a possible method of grain refinement.

References

8. A. H. Geisler and J. K. Hill: Analyses and Interpretations of X ray Diffraction Effects in Patterns of Aged Alloys. *Acta Crystallographica*, Nov. 1948, 1, (5), 238-252.

Some Effects of Applied Stresses on Precipitation Phenomena

By WALTER L. FINLAY and WALTER R. HIBBARD, JR., Members AIME

DISCUSSION

(G. E. Doan and W. L. Fink, presiding)

V. G. PARANJPE*—Have the authors investigated, or theoretically looked into, the effect of these large hydrostatic pressures on the equilibrium diagram itself? Of course, the change in the equilibrium relationships would depend on the amount of heat evolved, and the change of volume associated with the reaction. The effect may be computed by straightforward thermodynamics. It may be that the effect of hydrostatic pressures

which the authors describe in their paper might arise appreciably from the change in the equilibrium relationships only.

W. L. FINLAY (authors' reply)—Mr. Paranjpe has raised a very interesting point. We have no information on the effect of pressure on this system and have had no opportunity to investigate it.

I might point out that intermittently through the aging sequence specimens were removed for periods up to two hours in order to make the hardness measurements. Occasionally specimens were examined microscopically and nothing unusual compared to atmosphere-pressure-aged specimens was noticeable

under the microscope.

Also, the hydrostatic-aged specimens had hardness properties, which, although they were significantly different from atmosphere-pressure-aged specimens, nevertheless were not of a different order such as no hardening at all. This would make me wonder if the solubility relationship had been markedly changed, but I have no information on that.

C. S. BARRETT*—If you had examined the microstructures, would you say whether there is a tendency for orientation of the precipitates as a result

* Massachusetts Institute of Technology.

* University of Chicago.

of the applied stresses?

W. L. FINLAY—I am afraid that again we have no data to offer on that point. Optical microscopy gave no pertinent evidence and no X ray work was done in the investigation.

C. S. BARRETT—Did you happen to notice whether the precipitate tended to be aligned on slip planes, or was it distributed generally, and with equal numbers of precipitated particles on the different crystallographic planes that are equivalent in the matrix?

W. L. FINLAY—At the aging temperature involved (100°C), Widmanstatten figures are not developed in these alloys and precipitation particles were aligned on slip planes.

R. M. BRICK*—Do you have any data regarding the volume changes involved in the systems?

W. L. FINLAY—In so far as 100°C aging is concerned, there is a volume contraction in Al-Zn and Al-Cu; data are not available for 75S.

R. M. BRICK—If there is volume contraction, then you would expect pressure to accelerate precipitation just from a volume standpoint?

W. L. FINLAY—Yes, you would expect more precipitate to come out from that standpoint. You are placing the matrix under compression, and, in the Al-Zn case, the zinc is in tension and you are relieving the elastic strain. Therefore, you would tend to extend the amount of coherency. Both Drs. Barrett and Brick have touched on the interesting possibility that the application of external stresses during aging might affect the mode of precipitation, that is, by changing the relative amounts of precipitation on different matrix planes which, although crystallographically equivalent, are differently oriented to an applied uniaxial tensile stress; or by changing the plane of precipitation by altering the relative spacings of matrix and precipitate. An investigation of these possibilities using single crystals would appear to be worthwhile.

G. CHAUDRON,† J. HERENGUEL‡ and P. LACOMBE§ (*Translation*)—The paper by Messrs. Finlay and Hibbard draws attention to the importance of stresses on the kinetics of structural hardening, particularly at a temperature of 100°C where abundant precipitation of a second phase can be observed in most solid solutions of aluminum.

We should like to call attention to some observations which we made with regard to these alloys. We have shown¹² that structural hardening is very rapid at room temperature for an alloy containing 12 pct zinc. Moreover, in the

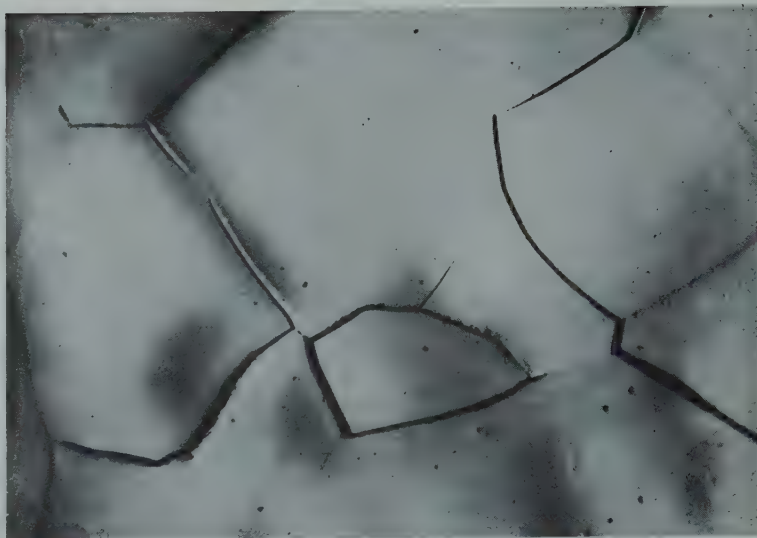


FIG 17—Intergranular decohesion observed spontaneously on aluminum alloy containing 12 pct zinc, electrolytically polished then aged at 20°C after quenching from 400°C. $\times 300$.

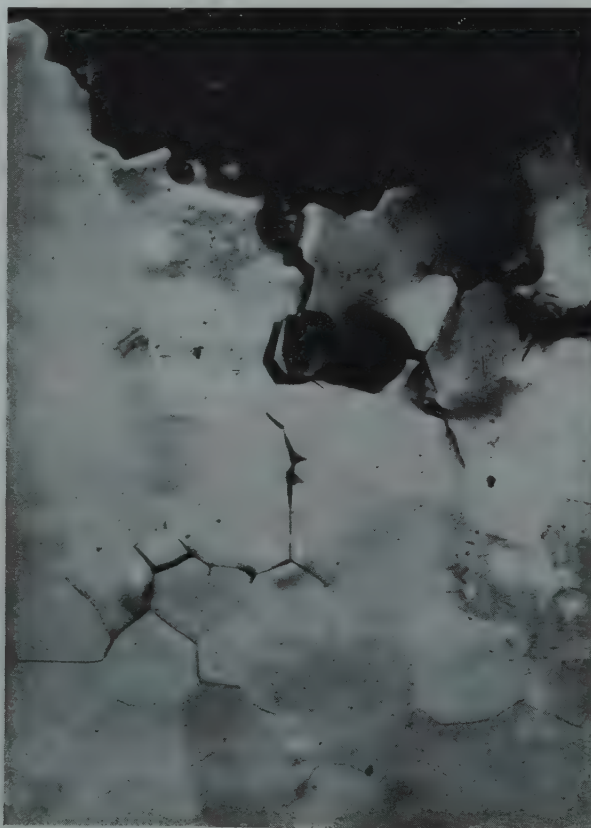


FIG 18—Aluminum-zinc-magnesium alloy hardened at room temperature and then stressed after electrolytic polishing. $\times 150$.

course of a more or less prolonged aging this group of alloys starting with a zinc content greater than 3 pct presents, depending on composition, a very important phenomenon which we have called "intercrystalline decohesion."¹³ This phenomenon is characterized by intergranular separation, producing a very great brittleness of the alloy (Fig 17).

This brittleness can be observed both in hardening under vacuum and in the presence of more or less humid air. In addition, an external mechanical stress applied to the metal accelerates this cohesion¹⁴ whether the tested specimens are exposed to air or are protected by plating, varnish or anodic oxidation. The resulting fracture is definitely inter-

* University of Pennsylvania.

† Director, Laboratory of Vitry-sur Seine

(France). National Center of Scientific Research.

‡ Director, Wire Drawing Plants and Rolling

Mills Research Center, LeHavre, France.

§ Research Director of Vitry Laboratory, France.

¹² References are at the end of the discussion.

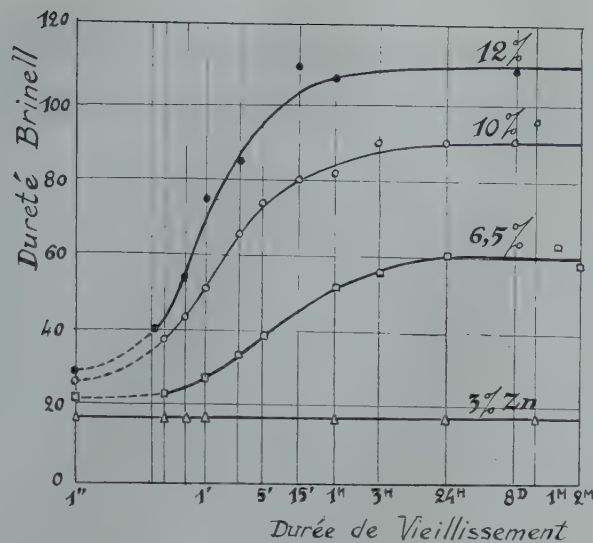


FIG 19—Dureté Brinell = Brinell hardness. Durée de Vieillessement = Aging time.

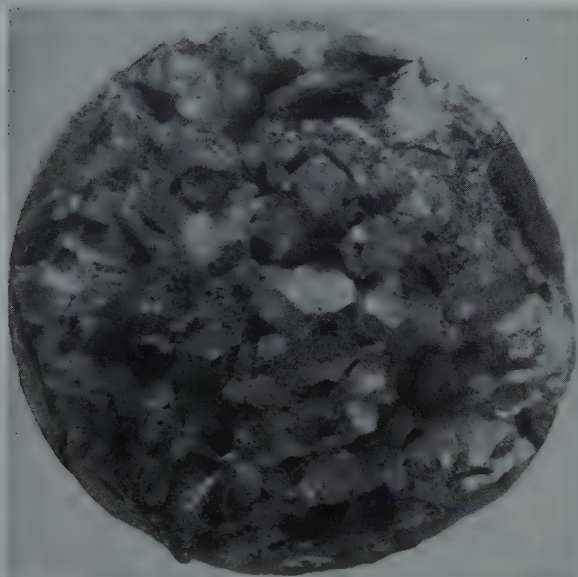


FIG 20—Macrograph of Intercrystalline Fracture of 12 pct Al-Zn after 5 hr at 100°C under 20,500 psi Tensile Stress. Tensile specimen was $\frac{1}{2}$ in. diam. Original magnification 13 \times . Reduced approximately one-half in reproduction.

granular (Fig 18) as found by Finlay and Hibbard at a temperature of 100°C.

As regards the hardness tests made by the authors, we are happy to notice complete agreement with our own tests carried out in 1943 on the same alloys, prepared likewise by starting with pure metals. (Fig 19). With regard to an alloy richer in zinc, 20 pct for example, it becomes impossible to perceive an increase in hardness after quenching, the latter taking place in a few seconds. In the course of the same study, we determined the specific effect of certain impurities, particularly iron and magnesium, on the kinetics of hardening. Additions of iron restrain the intensity

of hardening without slowing it up. Magnesium, on the contrary, even in extremely small quantities (0.02 pct) reduces the hardening speed. Thus one realizes that preceding studies made on impure alloys were not able to reveal this structural hardening.

Finally, it seems that after tests made on Al alloys containing 12 pct Zn, Messrs. Finlay and Hibbard intended to associate the phenomenon of retrogression with the particular way of aging under stress. Although the authors confirmed that 200°C was the optimum retrogression temperature for Al-Cu alloys, they adopted for their creep aging tests on this alloy the temperature of 100°C. It

seems to us that the choice of this temperature no longer allows comparison of these two alloys from the point of view of the mechanism of redissolving the mass of atoms in the course of retrogression.

W. L. FINLAY (authors' reply)—The interesting discussion contributed by Messrs. Chaudron, Herenguel, and Lacombe is very welcome. The authors were familiar with the publications of these investigators and, in common with a great many others, accord them the greatest respect. The following remarks are offered regarding the various points raised by these discussers:

1. The spontaneous "intercrystalline

decohesion" discussed by Messrs. Chaudron, Herenguel, and Lacombe was never observed by us in an experience comprising perhaps a dozen ingots with compositions from 8 to 25 pct zinc from which several hundred specimens were heat treated and observed on occasion over a two-year period. The discussers' micrographs establish very clearly, however, that their specimens did suffer intergranular fracture, and we have no explanation for the apparent discrepancy. The brittle, intercrystalline fracture we reported is illustrated in the accompanying macrophotograph (Fig 20). Unlike

the spontaneous failures reported by the discussers, all of ours occurred after a period of stress at an elevated temperature.

2. The very rapid age hardening at room temperature of quenched high purity aluminum-zinc alloys, shown in our paper and in the discussers' Fig 19, was first reported by Fink and Van Horn* based on both hardness and electrical resistance. Since this feature was only of incidental interest to our main

* W. L. Fink and K. R. VanHorn: Equilibrium Relations in Aluminum-zinc Alloys of High Purity. *Trans. AIME*, (1932) 99, 132-140

purpose, space did not permit mentioning the gratifying agreement with the work of the French investigators.

References

12. J. Herenguel and G. Chaudron: *Comptes Rendus Acad. Sci. Paris*, (1943) 216, 687. *Rev. de Métallurgie* (1943) 41, 33.
13. J. Herenguel and P. Lacombe: *Métaux et Corrosion* (1944) 19, 39. G. Chaudron, J. Herenguel and P. Lacombe: *Comptes Rendus Acad. Sci. Paris*, (1944) 218, 404.
14. J. Herenguel: *Rev. de Métallurgie* (March-April 1947) 44, 77.

Diffusion of Carbon in Austenite with a Discontinuity in Composition

By L. S. DARKEN, Member AIME

DISCUSSION

(R. Smoluchowski and M. L. Fuller, presiding)

R. SMOLUCHOWSKI*—Thank you for the very interesting paper. It seems to me that these experiments provide a classical example of the role of activity in diffusion. You mentioned that in your experiment you had a rather wide two-phase region. This is possible in a ternary system only if there is migration of the third component and I do not think that under the conditions of your experiment this was possible.

L. S. DARKEN (author's reply)—The two phase region in the first experiment (Fig 1) does indeed arise by virtue of the migration of the third component (carbon). In a binary system there can be no gradient of activity in a two phase region and hence such a region cannot be obtained by isothermal diffusion. In a ternary system, however, a two phase region is not incompatible with an activity gradient. In fact the data of R. P. Smith demonstrate that in the two phase region (austenite + ferrite), at constant ratio of iron to silicon the activity of carbon rises, though slightly, with increasing carbon content.

V. G. PARANJPE†—I would like to ask Dr. Darken if this technique would not be a godsend in estimating the influence of alloying elements on the activity of carbon. For example, the steel contain-

ing various alloying elements might be welded on to an alloy in which the activity of carbon is known. The diffusion experiment would thus give an approximate idea about the change in the activity of carbon due to the presence of alloying elements in the former steel.

L. S. DARKEN—Mr. Paranjpe's suggestion seems good in principle. As to whether this method would be easier than others would depend upon the particular circumstances. This diffusion method is inherently longer than the gas equilibration method used by Smith and requires a multiplicity of analyses for each sample. However, the diffusion method does not require such precise control of the gas atmosphere and might be adaptable to a relatively uncontrolled atmosphere—for example, by plating the "sandwich" with an element relatively impermeable to carbon.

J. T. MILEK*—I wonder if the diffusion could also be explained as an ionic mechanism—that is, a movement of the carbon ions, if we could say they exist. I do not know if there is such a thing as a carbon ion in steel.

It was brought out recently that carbon can migrate under the influence of an electric current—a dc current electrolysis. I wonder if you would see this reaction by performing an electrolysis test, instead of waiting 14 days, that is, to impress a high d-c current through the weld and also note that diffusion or transportation of carbon, whether it is ionic or atomic.

L. S. DARKEN—I agree with Mr. Milek's implication that the carbon in

austenite is ionic in nature. It migrates under the influence of a potential gradient (direct current); I have observed this effect myself. However, I do not believe anything can be gained in the present type of experiment by the passage of an electric current. In fact, I would expect that the potential gradient would give rise to approximately equal force on the carbon atoms no matter which side of the weld, and that the resulting motion of the carbon would tend to mask the effect considered in this paper. The superimposed effect of the electric current would certainly complicate the interpretation at any rate.

Since the publication of this paper, I have been informed of the prior work of Seith and Bartschat¹² on this subject. They welded an iron-carbon alloy (0.965 pct C) to each of several low carbon alloys (Ni-Fe, Co-Fe, Cr-Fe, Cu-Fe) and held each welded specimen at 940°C for one day. Although "uphill" diffusion was not encountered under these circumstances, a discontinuity in carbon content at the weld was found in several cases. This discontinuity was most pronounced at the weld involving a 19.2 pct nickel alloy—the carbon being 0.39 pct on the high nickel side and 0.66 pct on the iron-carbon side of the weld. A slight discontinuity (about 0.07 pct C) was found at the weld involving a 10 pct cobalt alloy. No discontinuity was found with the copper (2.7 pct Cu) or chromium (10.2 pct Cr) alloy.

Reference

12. W. Seith and F. Bartschat: *Ztsch. für Metallkunde* (1942) 34, 125.

* Carnegie Institute of Technology.

† Massachusetts Institute of Technology.

* Babcock and Wilcox Co.

An Electron Diffraction Study of Oxide Films Formed on Nickel-chromium Alloys

By J. W. HICKMAN, Member AIME, and E. A. GULBRANSEN

DISCUSSION

(R. Smoluchowski and M. L. Fuller, presiding)

F. R. MORRAL*—This paper presents some very interesting data on two types of Ni-Cr alloys. The authors give, it is believed, too much importance to the oxide films formed as being the controllers of the useful life of the alloys at high temperatures. The data, summarized here-with in Table 6 by types of life (more than 100 hr, 50 hr) seem to indicate that alloying elements, such as Si and Mn, are of special significance. The effect of the small amounts of Zr, Ca and Al cannot be properly evaluated. The study of another set of alloys with these elements present and 1.7 pct Mn would be necessary.

The presence of the 1.7 pct Mn is definitely detrimental to the useful life, although the oxide film is the same as that on the alloy showing the longest life (245 hr). Heating and cooling cycles may have an effect on the oxide films, although Fig 7 and 8 show that the high temperature oxides are retained on cooling down to room temperature for all six alloys.

The somewhat larger amount of Cr (3.5 pct) is beneficial even at higher temperatures. This effect was not so pronounced on the alloy containing 1.3 pct Si.

It may be of interest to mention that a salt bath has been found which at 1850°F (1010°C) in less than 10 min. removed the difficulty of eliminating film present on nichrome rods and wire.

The authors are to be thanked for making available this type of valuable data.

E. A. GULBRANSEN (authors' reply) We are indebted to Dr. Morral for his interesting comments. The original choice of heater alloys was made on a historical basis. It would be of scientific interest now to study the effect of one alloying element at a time on both the lifetime and structural factors of the oxide film. This would require a long and intensive study.

We have not made in our conclusions comparisons between alloys of the 80 Ni-20 Cr and the 61 Ni-16 Cr-23 Fe series because the useful life data are made at different temperatures. We agree that the individual effects of Mn and the small amounts of Zr, Ca and Al cannot be separated from the data in the alloys studied. The effect of Si on the useful life and on the structure of the oxide film is very marked in the case of the 80 Ni-20 Cr alloy. The beneficial effect of Cr is also noted.

We would like to restate our inter-

Table 6 . . . Indicating Special Significance of Alloying Elements

| Group | Useful Life at | | Alloy Analysis | | | | | Oxide Films at 950°C | | |
|-------|----------------|-----|----------------|------|-----|-----|--------|----------------------|---|------------|
| | °C | Hr | -46 | Cr | Si | Mn | Others | Fig | Electron Diffraction Pattern | Lines |
| I | 1125 | 245 | 133 | 16.6 | 1.2 | | Yes | 4 | NiO.Cr ₂ O ₃ | Sharp |
| | 1175 | 157 | 120 | 20 | 1.3 | | Yes | 1 | Cr ₂ O ₃ | S |
| II | 1175 | 86 | 122 | 20 | | | Yes | 2 | NiO.Cr ₂ O ₃ , Cr ₂ O ₃ | Medium |
| | 1125 | 66 | 126 | 16.6 | | | Yes | 5 | Cr ₂ O ₃ | S |
| III | 1175 | 25 | 132 | 20 | | 1.7 | No | 3 | NiO.Cr ₂ O ₃ | S-Oriented |
| | 1125 | 21 | 134 | 16.2 | | 1.7 | No | 6 | NiO.Cr ₂ O ₃ | S |

pretation of the oxidation resistance of heater alloys. We feel that the oxide film cannot be considered as a separate entity but rather in combination with the interface and the alloy itself. The processes by which oxidation occurs involve the transport of metal ions from the alloy through the interface and oxide to the surface. The rates of these processes are determined by the structure factors in the alloy, interface and oxide. We also feel that the stability of the oxide to decomposition and solid phase reactions on heating and cooling are of great importance and are not shown by a single cooling experiment.

F. E. BASH*—The work reported by the authors of this paper is very timely in view of the great demand for information leading to the development of better alloys for high temperature service. It is hoped that this work and other work now being undertaken will lead us to a better understanding of the mechanism of oxidation resistance of alloys when subjected to high temperature.

The alloys which were studied in this investigation were prepared in a laboratory high-frequency induction furnace, casting ingots weighing approximately 14 lb. These were forged and a portion rolled to 1/4 in. rod and drawn to 0.025 in. wire for life test. The other portion was rolled to strip for this electron diffraction study. Heat 13246 represents the old Nichrome LV (80Ni-20Cr). Heats 12246 and 12046 represent improvements in

Attention should be called to the life test figures given. It will be noted, for example, that Heat 12046 of Nichrome V (80Ni-20Cr) has a useful life of 157 hr at a temperature of 1175°C (2150°F). This compares with a life of 245 hr at 1125°C (2050°F) for Heat 13346 of Nichrome (60Ni-16Cr-Bal. Fe). It might be thought, in considering these figures, that the Nichrome wire had a useful life approaching that of Nichrome V. It must be understood, however, that the life of a nickel-chromium alloy wire varies as a power of the temperature. For example, 157 hr life for Nichrome V at 1175°C (2150°F) is equivalent to 450 hr at 1125°C (2050°F) for the same wire. We have found, also, that the durability of the nickel-chromium and nickel-chromium-iron alloys is affected by the size of the heat cast. The life on standard production heats of the same alloy composition is considerably higher than on that of the same alloy made in the laboratory furnace. The authors refer to a paper by H. D. Holler,* in which he noted the loss of chromium at high temperatures and the higher temperature coefficient of resistivity of the remaining wire. Due to the increased temperature coefficient, he concluded that the wattage density (and temperature) would be increased in sections of the wire where the chromium was more depleted. I should like to call attention to the effect of varying chromium content on specific resistance and temperature coefficient:

| Alloy | Spec. Resis. at 25°C | Spec. Resis. at 1177°C (2150°F) | Av. TC 27-1177°C |
|-------------|----------------------|---------------------------------|------------------|
| 80-20 Ni-Cr | 650 ohms per cmf | 700 ohms per cmf | 0.000067 |
| 85-15 Ni-Cr | 566 ohms per cmf | 612 ohms per cmf | 0.000072 |
| 90-10 Ni-Cr | 545 ohms per cmf | 585 ohms per cmf | 0.000081 |
| A Nickel | 60 ohms per cmf | 300 ohms per cmf | 0.0035 |

composition leading to the present Nichrome V (80Ni-20Cr). In the same way, Heats 13446 and 12646 represent the progress of development of Nichrome (60Ni-16Cr-Bal. Fe).

It will be noted from the above that the cold resistance of the nickel-chromium alloys is reduced considerably with re-

* Preprint 9207, Oct. 1947, of the Electro-Chem. Soc., "Observations on the Failure of 80 Nickel-20 Chromium Alloy at Excessive Temperatures."

* American Cyanamid Co.

* Driver-Harris Co.

duction of chromium content. It should be noted that the hot resistance also is reduced. The temperature coefficient increases rather slowly with decrease of chromium from 20 to 10 pct. The temperature coefficient of the pure nickel is, of course, very much higher. In view of this information, it is obvious that any areas which may have lost more chromium than the *average* for the wire would not have a greater wattage density (I^2R), since the specific resistance at this point would be lower than the average. Eventually the sectional area reduces more at one point than at others for reasons unknown, and the wattage density increases at this point causing failure of the wire.

I should also like to call attention to an article by A. H. Sully, entitled "A Simple Method for the Study of Metallic Diffusion in Certain Binary Alloys Systems."^{*} Sully determined the concentration gradient of chromium in an 80Ni-20Cr wire 0.021 in. diam after having been at high temperature for a period of time. He combined electrolytic etching techniques with X ray diffraction and thus obtained the chromium content at the surface of the wire and at various depths. He showed the center of the wire to have the original composition, or thereabouts, while the chromium at the surface had decreased to approximately 8 pct. The work of Holler confirms the loss of chromium in prolonged heating of nickel-chromium alloys.

C. L. GUETTEL†—I wish to ask a question concerning the nature of the reaction $2Cr + 3NiO \rightleftharpoons Cr_2O_3 + 3Ni$, involving sample 12046, the new Nichrome V. The paper states that this reaction is probable "since Cr_2O_3 is observed both by reflection and transmission above 600°C." However, what becomes of the reaction product, 3Ni? Even if this resulting nickel were immediately oxidized, why would not the NiO be found either in the outer film or next lower oxide layer? Your previous paper states that a spectrochemical analysis failed to detect nickel in the electrolytically removed film.¹² Thus, considering the latter, would not the reaction, $2Cr + \frac{3}{2}O_2 \rightleftharpoons Cr_2O_3$ be more probable?

E. A. GULBRANSEN—I think that both the direct oxidation reaction $2Cr + \frac{3}{2}O_2 \rightleftharpoons Cr_2O_3$ and the solid phase reaction $2Cr + 3NiO \rightleftharpoons Cr_2O_3 + 3Ni$ contribute to the formation of Cr_2O_3 in the film. The Ni ion in the latter reaction diffuses back to the metal. Eventually as the Cr is depleted in the surface of the metal NiO may form at the metal oxide interface. We have confirmed, by X ray diffraction studies of the same alloys, the fact that Ni is not observed in the films at least during the early periods of the reaction.

C. L. GUETTEL—During the discussion period following the presentation of your papers at the AIME meeting of Nov. 1946, I suggested the possibility that a difference in results may occur if the sample were heated electrically instead of by radiation. (My remarks incorrectly were attributed to Dr. C. G. Goetzel). Sully's work on an 0.021 in. 80 pct Ni, 20 pct Cr wire, to which Mr. Bash has already referred, shows that after prolonged heating at high temperature, the remaining metal core nearest to the oxide layer is the most depleted in chromium. The rate and direction of further atom diffusion may be affected in a different manner when an electric current passes through such a core than when the core is heated by radiation. Also, radiation heating places the source of heat on the atmosphere side of the oxide. And electrical heating, in effect, places the heat source on the metal side of the oxide. In view of these comments and the fact that, in actual use, furnace and appliance elements are heated electrically in air, I would like to suggest the following investigation based on the work of Sully and the authors of this paper: Mount and start 16 samples of the same spool of Nichrome V (of known analysis and physical properties) according to the ASTM "Standard Method of Accelerated Life Test for Metallic Materials for Electrical Heating."¹³ After one hour, subject two of the samples to the following tests:

1. A temperature determination.
2. A hot resistance determination.
3. A cold resistance determination.
4. Electron diffraction, reflection technique, to determine the identity of the surface oxide.
5. Electron diffraction, transmission technique as applied to the electrolytically removed oxide layer to identify the oxides occurring on the outer surface and in the body of the oxides.

6. X ray diffraction, applied to the remaining metal conductor in conjunction with the electrolytic etching of successive metal layers from the core according to the method of Sully, to determine the transverse chromium distribution at this specific time period.

7. Metallographic examination, transverse and longitudinal sections, to determine the degree and direction of the oxidation.

Repeat the above for other pairs of samples at suitable intervals during the life test. Apply 4, 5, 6, and 7 to the last pair after total life near the point of burnout. It does not appear necessary that 4, 5 or 6 would have to be applied to any sample when heated, as it is unlikely that different oxides would exist at an elevated temperature than when cool, after subjecting each sample to hundreds of two minute heating and cooling cycles prior to the diffraction tests (the one hour samples excepted).

Such a series of tests could relate the formation of the specific oxides with the chromium distribution in the remaining metal core at various time intervals under the standard conditions of the A.S.T.M. life test, and would be supplemented by metallographic information, and thermal and resistance measurements. The same series of tests could be applied to the older types of Nichrome V (80Ni-20Cr) and to experimental modifications of the same alloy. The application of the tests to Nichrome (60Ni-16 Cr-Bal. Fe) would depend on the adaptability of the Sully technique to tertiary alloys.

E. A. GULBRANSEN—Mr. Guettel has outlined a very ambitious program and I think a very good one. We have been doing some thinking along this line but we are not in the position to carry out such a program. We are arranging to make an X ray diffraction study of a number of heater alloys in the following manner: The specimen will be alternately heated and cooled following the ASTM life test procedures. X ray diffraction patterns will be taken of the sample only while the sample is hot. This will be done several times during the life of the specimen. This can be carried out by opening and closing suitable shutters on the X ray tube. A series of patterns also could be taken during the cold cycle of the test. A comparison of the hot and cold pictures as a function of the oxidation may add much useful information to structural changes in the metal and oxide film.

The Sully technique also appears to be a very useful method for studying the change in composition of the metal surface as a result of oxidation.

J. H. SCAFF*—I would like to ask the author if it is safe to assume that the composition of the oxide films produced at pressures of 0.1 mm of oxygen would be the same as those oxidized at pressures corresponding to the oxygen pressure of the atmosphere.

E. A. GULBRANSEN—The pressure of 1.0 mm of oxygen is chosen as a matter of convenience in evacuating the camera. In the case of nickel we do not anticipate any change in the structure of the oxide films due to the low pressure. This follows from the fact that NiO is the only oxide ever observed over the temperature range in any work known to us. One point should be carefully noted and that concerns the decomposition of NiO to the metal. If high enough temperatures are reached NiO may not form at 1 mm of O_2 while it would form in higher oxygen pressure atmospheres.

J. T. MILEK†—I wish to give my compliments to the authors for their valuable contribution.

I recall some years ago reading Professor Winchell's work on spinels. It seems

* *Jnl. of Scient. Instr.*, p. 244, Dec. 1945.

† Driver-Harris Co.

¹² References are at end of discussion.

* Bell Telephone Laboratories, Inc.

† Babcock and Wilcox Co.

to me that nickel oxide and chromium oxide form a continuous series of solid solutions in which one would have variable nickel oxide and chromium oxide contents and this should show up in the X ray data. I have not read the paper, and I apologize for that, but I wish the authors would comment on the continuous series of solid solutions and also the replacement of the bivalent end of the spinel.

For example, $\text{NiO} \cdot \text{Cr}_2\text{O}_3$ —the NiO can be replaced by MnO or MgO , and likewise the trivalent oxide can be replaced by some other oxide as B_2O_3 .

Have the authors tried an atmosphere of hydrogen sulphide and what kind of pattern is obtained in a sulphur dioxide

atmosphere?

E. A. GULBRANSEN—I failed to mention the problems one encounters in determining the crystal structure of the oxides on the surface. Some of these problems we have mentioned in previous publications. One has the problem of solid solutions of one oxide in another as well as the formation of the spinel structure. The spinel system as Mr. Milek mentioned is a very flexible one in which various oxides can fit. This represents the main difficulty in completely specifying the composition of the oxide. Both X ray and electron diffractions indicate only the lattice spacings and give no direct information about what atoms are in the crystal. The spinels represent a wide

variety of oxides which give similar parameters for the common metals used in heater alloys.

To answer your other question, we have not tried atmospheres containing hydrogen sulphide or sulphur dioxide. We have not made such experiments and I would prefer not to comment until we have done so.

References

12. Gulbransen, Phelps and Hickman: *Ind. Eng. Chem., Anal. Ed.* 18, (1946) 640.
13. A.S.T.M. Test B76-39: Prepared by Committee B-4.

An Electron Diffraction Study of Oxide Films Formed on Copper-nickel Alloys at Elevated Temperatures

By J. W. HICKMAN, Member AIME, and E. A. GULBRANSEN

DISCUSSION

(R. Smoluchowski and M. L. Fuller presiding)

J. T. MILEK*—I wonder if Dr. Gulbransen is justified in using the equilibrium constant as a criterion for evaluating which oxide will form. I think, thermodynamically, it is better to use the free energy of formation in his calculations rather than the equilibrium

constant and to determine how the free energy of formation varies with the temperature. These thermodynamic relationships might explain in a more logical way why a certain oxide will form in preference to some other oxide than can be explained by the equilibrium constant relationship.

E. A. GULBRANSEN (authors' reply)—The free energy ΔF and the equilibrium constant K are related by the equation

$$\frac{-\Delta F}{2.3 RT} = \log K$$

It does not make any difference which you use in discussing equilibria.

G. V. PORTER*—At what composition of copper and nickel are there enough electrons contributed by copper to fill the d band of the alloy? You have not mentioned in your talk at what combination this occurs.

E. A. GULBRANSEN—The composition is 40 at. pct nickel.

* Babcock and Wilcox Co.

* Leeds and Northrup Co.

Decarburization of Chrome Nickel Alloys by Their Surface Oxides in High Vacua and at Elevated Temperatures

By E. A. GULBRANSEN, W. S. WYSONG, and K. ANDREW

DISCUSSION

(R. Smoluchowski and M. L. Fuller, presiding)

E. N. SKINNER*—In this paper, Dr. Gulbransen and his associates have employed their usual beautiful experimental techniques to offer a fundamental contribution to our meager knowledge of high temperature gas-metal equilibria.

* The International Nickel Co., Inc.

Although the procedures adopted in this work are above reproach, there are several questions which might be raised concerning the interpretation of the data.

It has been considered that all carbon in the three heater-type alloys studied has been entirely in solid solution within 700–910°C, the range of temperatures investigated. This assumption is not consistent with observed micro-structural

changes occurring in carbon-containing Ni-Cr and Ni-Cr-Fe alloys. The solid solubility of carbon in alloys of this type is not definitely known but is conceded to be extremely low. For example, carbide inclusions have been noted after appropriate heat treatment at 450°C in an alloy of 15 Cr, 6 Fe, balance Ni which contained the uncommonly low carbon content of 0.02 pct. A similar base com-

position containing 0.04 pct will exhibit an unmistakable precipitate of carbide after heating the solution-treated alloy for two hours at 875°C. It is therefore highly probable that the 80/20 and 62/16 samples, containing carbon levels of 0.08, 0.12, and 0.06 respectively, consisted of a carbide-studded matrix at the temperature of testing.

If the ribbon upon which the present work was conducted was in the soft condition, this strand-annealing operation probably consisted of rapid cooling from temperatures at or above 1100°C. Subsequent heating to temperatures in the range of 700–910°C after this solution-anneal would be expected to promote the precipitation of carbides preferentially in the grain boundaries. Assuming that this condition existed, the two rates of decarburization noted by the authors might conceivably be explained by a rapid rate of outward migration to the oxide interface by the carbon atoms located in the grain boundaries and along slip and twinning planes and a slower

rate of migration through the lattice.

In comparing the decarburization by high vacua vs. hydrogen, we are interested in learning whether the loss in weight of the specimen was appreciably affected by the dissociation of NiO in the Ni-Cr spinel or by loss of residual constituents such as Ca, Zr, Al, Mg, or Si.

E. A. GULBRANSEN and K. ANDREW (authors' reply)—We are in complete agreement with Dr. Skinner about the presence of carbides in the chrome-nickel alloys. This should have been made clearer in our paper. In order to calculate the equilibria of carbon and the oxides in the film it is necessary to assume that the carbon is in solid solution since the thermodynamics of the carbides at the temperatures under discussion is not known. The equilibria calculated with this assumption is an estimate of the actual equilibria which must involve the carbides.

Dr. Skinner has suggested an alternative explanation of the two rates of decarburization noted in the experiments.

There is one fact which is in opposition to the mechanism proposed, namely, the second rate is observed after the surface oxide film has been removed. We feel that we are dealing with a reaction between carbon, which is in a large excess in most of the experiments, and two different sources of oxide, the surface oxide reaction with carbon being the more rapid reaction. Such an explanation overcomes the objection noted above.

We have not studied the loss in weight due to dissociation of NiO or loss of residual constituents such as Ca, Zr, Mg, Al or Si.

M. LACHANCE*—Has any conclusion been drawn regarding varied silicon content in an alloy as it affects the decarburized weight losses observed?

E. A. GULBRANSEN and K. ANDREW—We have not studied the decarburization rates as a function of the silicon content in the chrome-nickel series of alloys.

* Battelle Memorial Institute.

Fractographic Study of Cast Molybdenum

By C. A. ZAPFFE, Member AIME, F. K. LANDGRAF and C. O. WORDEN

DISCUSSION

(D. L. Martin and J. E. Burke, presiding)

H. S. AVERY*—Would you comment on the type of illumination that you use to give the depth of focus in your high magnification photographs?

C. A. ZAPFFE (authors' reply)—In fractography, depth of focus or at least an illusion of depth of focus, is attained by oblique lighting, which serves much as the etch does on polished samples to improve the pattern by varying the reflection from grain to grain. Cleavage facets may be studied visually without oblique illumination, but for photography it is essential.

H. S. AVERY—With your oblique lighting do you use a conventional vertical illumination or dark field illumination?

C. A. ZAPFFE—We have tried both, and by far prefer the conventional vertical illumination. Polarized and other types of illumination, such as "sensitive tint," can also be used. There is no special restriction.

J. H. BOSS*—What kind of microscope do you use?

C. A. ZAPFFE—We used a Bausch and Lomb MILS for this work but have used Zeiss, Leitz, and others. There is no special restriction in type of microscope, except that obliquing has an exaggerated importance.

C. W. HORSTING†—Do you use anything else besides the carbide to deoxidize the molybdenum?

C. A. ZAPFFE—Other deoxidizers

could undoubtedly be used, but carbon has the feature of forming a gaseous deoxidation product which can be removed from the system under the conditions of the vacuum.

F. R. MORRAL*—I read this paper with interest. The authors should be congratulated for the interesting and clear fractographs. I note that on p. 3 of their paper only one molybdenum carbide is discussed although there is a possibility that two are present in the MoC diagram as shown by Sykes in the 1948 ASM handbook, p. 1183. I wonder if the MoC would be one of the two discussed in item 4 under the conclusions on p. 21 of the paper.

C. A. ZAPFFE—Professor Morral raises a good point with regard to MoC, which we are glad to accept as he suggests.

* Philadelphia Naval Base.

† Caryl, Radio Corporation of America.

* Syracuse University.

Effect of Composition on Grain Growth in Aluminum-magnesium Solid Solutions

By LOUIS J. DEMER, Junior Member, and PAUL A. BECK, Member AIME

DISCUSSION

(D. L. Martin and J. E. Burke, presiding)

C. G. DUNN*—May we have more detail on the time required for recrystallization? How did you determine when recrystallization was complete?

L. S. DEMER (authors' reply)—In order to determine the point of complete recrystallization, the specimens of material were annealed for various periods of time and their hardness values were determined. Then hardness was plotted vs. the time, both to logarithm scales, and it was found that when the recrystallization was not complete, the points fell on a line which had a slope. When recrystallization was complete, specimens annealed for longer periods of time fell on the horizontal line. We took the point of complete recrystallization to be the juncture of these two lines.

C. G. DUNN—The break in the hardness-time curve probably does mean something. On the other hand, it is possible to have recovery of physical properties prior to recrystallization. In other words, the metal may soften without any appreciable recrystallization actually occurring. Furthermore, as grain size increases, there may also be a softening from this source. I am not too familiar with the application of hardness tests to the determination of the course of recrystallization and therefore want the authors' views on the reliability of this method.

L. J. DEMER—This was the method of determining the point of complete recrystallization. Then it was checked by examining the specimens microscopically and those points were taken as points of complete recrystallization.

C. G. DUNN—To make a contrast on the reliability of the hardness test, I would say it does not apply to large grains or single grains of silicon ferrite. For example, we have observed on the basis of a Knoop Hardness test complete softening prior to recrystallization. Therefore, the hardness test may, in my opinion, introduce undesirable complexities into the study of the extent of recrystallization.

P. A. BECK (authors' reply)—We made some X ray diffraction patterns for the aluminum-magnesium alloys, as well as for pure aluminum, and the X ray method confirmed the hardness method

as to the time necessary for complete recrystallization.

C. G. DUNN—Concerning another point brought out by the authors I would like more information on the effect of the second phase on the recrystallization process. Your data show a smaller grain size as well as longer time for complete recrystallization with the 2 pct Mg alloy. Unless the induction period is considerably lengthened by the second phase, these two facts would indicate a slower grain boundary movement in the presence of a second phase. As I understand it, the main driving force for recrystallization is internal strain energy. We have here then a grain boundary moving in the presence of a second phase but under the action of strain energy. Could the action of the second phase be discussed further?

P. A. BECK—To my knowledge, no complete analysis has as yet been made of the effect of a dispersed second phase on the two rates pertinent to recrystallization, namely the rate of nucleation and the rate of growth. However, it seems very likely that the main effect of a dispersed second phase in decreasing the rate of recrystallization is exerted through decreasing the rate of growth of the new grains, rather than through an effect on the rate of nucleation.⁷

J. E. BURKE—Would it not develop that all of the observations could be explained by saying that the rate of nucleation was constant but that the rate of nucleus growth had been decreased?

P. A. BECK—Yes, at least qualitatively.

C. G. DUNN—I would like to make one more comment on growth in a strained matrix because the following paper by Professor Beck and coworkers will have more on growth presumably in the absence of strain. If true nucleation occurs, new surfaces are developed and energy is required for this. As long as the matrix is in a strained condition the energy needed for nucleation and growth may be obtained from the matrix. If deformed grains instead of nuclei grow in the strained matrix, the picture is different.

J. E. BURKE—Anderson and Mehl⁸ made an observation that is possibly pertinent to this paper. They found that the rate of nucleus growth during recrystallization increased with decreasing

grain size of the deformed material. That is, the rate of nucleus growth is greater in an originally fine grained specimen than in a coarse grained specimen, even though the two specimens were deformed by identical amounts. This could indicate that interfacial energy as well as deformational energy, is important in controlling the rate of growth of recrystallization nuclei.

P. A. BECK—I think that there is a more likely explanation of that phenomenon. The fine grained material, when cold worked to the same reduction of area, develops considerably higher hardness than coarse grained material. Thus, in spite of the same geometry, the effective cold work is greater. This accounts for the higher rate of recrystallization.

D. C. JILLSON*—I believe that only one set of fabricating conditions was studied, ending with a final cold reduction of 33 pct. Since changes in fabricating conditions might be expected to affect recrystallization phenomena, and hence might alter some of the conclusions, it might be well to state this limitation in the conclusions.

P. A. BECK—The conclusions are meant to apply under the conditions of the experiments, as fully described under "Experimental Procedure." It appears somewhat impracticable to repeat all those conditions in the "Conclusions."

J. E. BURKE—I have two questions I should like to have the authors comment upon. First, what is the influence of magnesium content upon the average rate of grain growth? The second question concerns the activation energy for recrystallization. Anderson and Mehl reported values ranging from 64,500 cal per mol to 52,100 cal per mol for elongations of from 5 to 15 pct. The present authors report a value of 44,000 cal per mol for a deformation of 33 pct. The range of values encountered serves to emphasize the uncertainty of the physical meaning of the computed "heats of activation." It would seem probable that the change in temperature dependence indicates a change in the atomic mechanism occurring during recrystallization.

The differences in the amount of deformation can account for only a few calories per mole in residual energy left

* General Electric Co., Pittsfield, Mass.

⁷ References are at the end of the discussion.

* New Jersey Zinc Co.

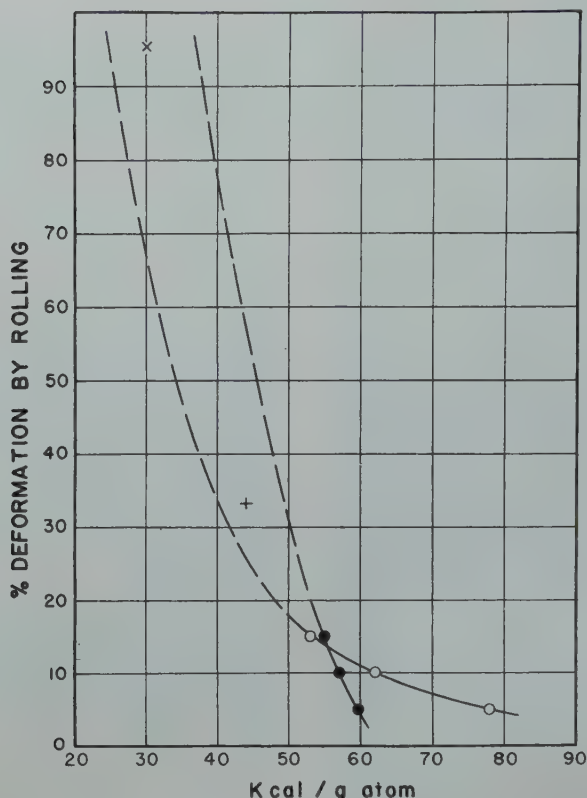


FIG 16—Energy of activation for recrystallization in high purity aluminum.

- Activation energy for nucleation. (Anderson and Mehl)⁸
- Activation energy for growth. (Anderson and Mehl)⁸
- + Overall activation energy for complete recrystallization. (Present paper)
- x Overall activation energy for complete recrystallization. (Calvet, Trillat and Paic)⁹

in the metal, and thus cannot account for the difference of several thousand calories per mole in the apparent heat of activation.

P. A. BECK—Concerning Dr. Burke's first question, I should like to refer to Fig 14 and 16 of Ref 1. It is shown there that at small grain sizes the in-

stantaneous rate of growth $\frac{dD}{dt}$ is higher for pure aluminum than for the 2 pct Mg alloy. However, in pure aluminum the rate decreases faster than in the alloy, so that eventually the relative rates are reversed. After about 4300 min. at 400°C, the grain size in the Al + 2 pct Mg alloy

was larger, in spite of a smaller grain size, as recrystallized.

Dr. Burke observed the difference between the heat of activation values reported by us on the one hand and by Anderson and Mehl on the other for the recrystallization of pure aluminum. He concluded that this difference emphasizes the uncertainty of the physical meaning of the computed heats of activation. He has, however, neglected to consider the fact clearly shown by Anderson and Mehl, that the Q values for both the rate of nucleation and the rate of growth decrease with increasing prior deformation. Fig 16 shows the data from Fig 23 of Anderson and Mehl's paper,⁸ and dotted lines indicate the extrapolation of their curves for higher deformation values. Since in our work the two factors, nucleation and growth, were not separated, the heat of activation for the overall process of recrystallization may be expected to lie in between the two extrapolated curves. As seen in Fig 16, this condition is well satisfied, regardless of the uncertainty of extrapolation. The Q value estimated from older data of Calvet, Trillat and Paic⁹ for 95 pct deformation also falls between the reasonably extrapolated lines. Far from agreeing with Dr. Burke, we feel justified in concluding that, as far as comparisons can be made at all, the data shown in Fig 16 are indeed quite consistent with each other.

References

7. See also Discussion, *Trans. AIME* (1943) 152, 117.
8. W. A. Anderson and R. F. Mehl: Recrystallization of Aluminum in Terms of the Rate of Nucleation and the Rate of Growth. *Trans. AIME* (1945) 161, 140, 160.
9. Calvet, Trillat and Paic: Sur la recristallisation de l'aluminium pur. *Comptes Rendus de l'Acad. Sc.* (1935) 201, 426.

Effect of a Dispersed Phase on Grain Growth in Al-Mn Alloys

By P. A. BECK, Member AIME, M. L. HOLZWORTH and P. SPERRY

DISCUSSION

(D. L. Martin and J. E. Burke, presiding)

J. S. SMART, JR.*—From the data presented by the authors, it appears plausible to speculate on the possibility of the existence of a size factor which governs the effectiveness of the precipitated particles in inhibiting grain growth. For instance, the 650° curve of Fig 4 indicates that sufficient precipitate was dissolved in one minute at temperature to remove the inhibiting effect completely.

However, the authors noted that the precipitate did not completely dissolve in such short time, but in fact, required something under 125 min. to reach a sub-microscopic stage. This behavior seems to indicate that the inhibiting effect is due primarily to particles of very small size which would dissolve rapidly at sufficiently high temperature. If so, it can be readily understood why this curve approximates the behavior of a solid solution alloy despite the presence of the remaining precipitated particles of large size during the whole of the straight

section of the curve. Furthermore, this mechanism would explain why the inhibiting effect is strong even though very little visible precipitate is present, as the authors have found elsewhere.

If this reasoning is extended further, the "incubation period" at low annealing temperatures would appear to be the time required for sufficient coalescence to take place to allow the small and effective particles to grow to an innocuous size. At higher annealing temperatures, the incubation period might then depend on a combination of the rates of solution and coalescence of the particles. The apparent anomaly that specimens containing large amounts of manganese

* American Smelting and Refining Co.

compound should have shorter incubation periods, as noted by the authors on p. 14 of the paper, would thus be explainable on the basis that they were in a more advanced stage of coalescence to begin with, and therefore required a shorter period for the coalescence to continue beyond the critical size range.

The interpretation placed by the authors on the experiments to investigate the effect of various degrees of deformation ascribes a very considerable effect to various degrees of prior reduction. However, from Table 7, it is evident that the process annealing procedure varied from 5 min. at 530°C for the samples reduced 90 pct to 65 min. at 530°C for those rolled 20 pct. This treatment would therefore have resulted in increasing amounts of precipitated compound in the specimens of descending order of reduction. Since the final anneal was at 625°C, which is very close to the solvus point for the alloy used, it does not appear strange to find that the specimens which have the greatest reductions, and the least precipitated compound, lose their restricted status the earliest, as the precipitate dissolves. Is it therefore not unlikely that the differences in process annealing are significant and should be included with differences in reduction in any explanation of the behavior shown in Fig 13 and 14?

P. A. BECK (authors' reply)—Mr. Smart noted the initial slope of the 650°C line for the 1.1 pct Mn alloy in Fig 4 of the paper is approximately equal to the slope for high purity aluminum, as extrapolated to the same temperature from Fig 6 of Ref. 36. From this fact he concluded that in the Mn alloy "sufficient precipitate was dissolved in one minute at temperature to remove the inhibiting effect completely," even though compound particles were found microscopically after much longer periods of annealing. This conclusion is based on the idea that the slope of the $\log D$ vs. $\log t$ line represents the rate of growth. However, as described on p. 10 of Ref. 36, this is not the case. For any value of D , the instantaneous rate of growth $\frac{dD}{dt}$ depends on the parameter K as well as on the slope n . If a grain growth line is obtained for high purity aluminum at 650°C by extrapolation from Fig 5 of Ref. 36, it is easily seen, by comparison with the 650°C line of Fig 4 of the present paper, that actually the instantaneous rate of growth for high purity aluminum is about 200 times larger than that for the alloy, compared at the same grain size. This suggests that the manganese compound particles seen under the microscope are in fact very effective in reducing the rate of growth. There appears to be at present little basis for the suggestion that the inhibiting effect is due primarily to particles of very small size. Actually, it is expected that any difference in inhibiting effectiveness that may be ultimately

traced back to a particle size effect, would turn out to be rather small. Every indication points to the fact that it is the total number of dispersed second phase particles that primarily determines the effectiveness of inhibition. It is, of course, obvious that if the same total amount of precipitate is present in the form of smaller particles, the effect is larger, simply because the number of particles is then larger.

Mr. Smart is correct in observing that the series of specimens in Table 7, prepared for the study of the effect of increasing prior deformation, did not receive identical processing. The situation was, however, not nearly as unfavorable as it appears from consulting Table 7 only. As shown in Table 3, the treatment previous to the varying 530°C anneals of Table 7 was a series of anneals at 550 and 530°C common to all specimens. As a result, the differences in processing the specimens of series C, D, E, F and G, had no significant effect on their coarsening characteristics. This was also shown in a later experiment, not included in the present paper, where the attempt to finish with the same specimen thickness was given up, and instead the processing treatment was kept constant. In this experiment the decrease of the incubation period with increasing reduction by rolling was confirmed.

C. G. DUNN*—I want to congratulate the authors on their excellent results. They certainly are adding fundamental knowledge to grain growth processes, and this we need. The effect of dispersed phases is particularly important, I think. Using the authors' term "coarsening," it perhaps should be mentioned that phenomena other than the effect of a dispersed phase can be associated with coarsening, particularly in fine grained materials where textures play an important role. Would the authors care to say something on this aspect of coarsening?

P. A. BECK—Dr. Dunn, knowing about our latest results, is offering us here a welcome opportunity for presenting them in this discussion.

Cook and Macquairie⁴⁴ showed that in tough pitch copper two different types of coarsening may occur. The one type, which they produced by annealing at 750 to 850°C, after about 50 pct reduction by cross rolling, did not occur in oxygen-free varieties of copper. It was recently found⁴⁶ that this type of coarsening, which is characterized by fairly round coarse grains with irregular, "ragged" boundaries and small, completely enclosed twins (Fig 31), may be obtained in tough pitch copper after straight rolling, as well as cross rolling. It appears very likely that this type of coarsening depends on the presence of finely dispersed Cu₂O particles in the copper, and that it is, therefore, closely related to the

coarsening phenomena in Al-Mn alloys, described in the paper. The term "random coarsening" used in the introduction of the paper, is descriptive only in the sense that these coarse grains may lack any preferred orientation, and that this type of coarsening does not depend on the presence of a texture in the fine grained recrystallized matrix. However, as shown by Bowles and Boas⁴⁶ in a paper published after the present paper was submitted for publication, it is possible for the coarse grains growing in commercial aluminum (which contains dispersed phases) to possess a preferred orientation. For this reason it now seems preferable to describe this coarsening as "inhibition-dependent" rather than "random."

The other type of coarsening in copper found by Cook and Macquairie, and before them by Dahl and Pawlek,²⁹ does not require Cu₂O particles. It may occur in oxygen-free copper as well as in tough pitch copper. What it does require, is a well-developed "cube texture" in the matrix, as recrystallized. In the presence of such a sharply defined texture the small recrystallized grains, most of which have fairly closely the same orientation, show great reluctance to undergo gradual grain growth. Copper with the "cube texture" remains quite fine grained up to high temperatures. Finally at about 1000°C (or at a lower temperature after a longer period of annealing) it abruptly develops very large grains. Fig 32 shows such grains embedded in the fine grained matrix in which they grew. Typical of the coarse grains of this type is the presence of very long, straight twin boundaries, inclined at about 45° to the direction of rolling (Fig 33). These coarse grains have a well-developed preferred orientation, different from that of the fine grained matrix. The orientation relationships were recently studied by Bowles and Boas.⁴⁶ It was recently found at this laboratory that, even in high purity aluminum, gradual grain growth was practically prevented in the presence of a very sharply defined texture,⁴⁷ regardless of the orientation with respect to the rolling direction. Apparently, the determining factor here is the similarity of the orientation of neighboring grains of the fine grained recrystallized matrix. When high purity aluminum with such a structure is annealed long enough at 500–600°C, abrupt coarsening sets in. Grains many times larger than the specimen thickness may be obtained by this mechanism.

The views expressed in the introduction of the present paper are thus confirmed: there are at least two different types of coarsening, the one depending on a dispersed second phase, the other on the presence of a very well developed texture. The common feature of both types of coarsening is the suppression of the continuous or gradual type of grain growth and the abrupt development of extremely large grains which grow by feeding

* General Electric Co.

⁴⁴ References are at the end of the discussion.

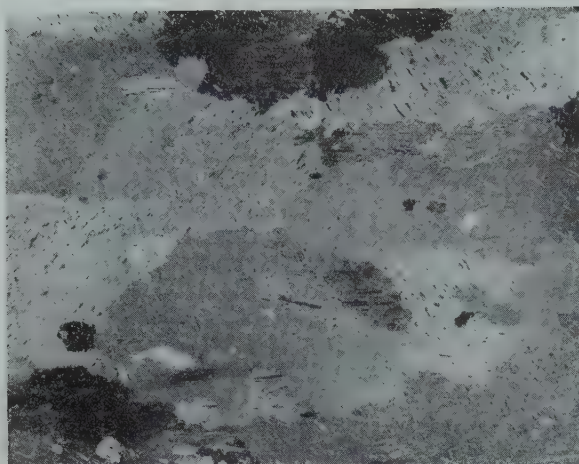


FIG 31—Tough pitch copper after final rolling of 50 pct and final anneal of 1 hr at 800°C.

The coarse grains have rounded shapes and ragged boundaries. Numerous small twins are entirely surrounded by coarse grains. Magnification $\times 5$. Reduced one half in reproduction.



FIG 32—Same copper as in Fig 31, cold rolled 90 pct, annealed 3 min. at 1000°C.

Coarse grains in fine grained matrix. Magnification $\times 5$. Reduced one half in reproduction.

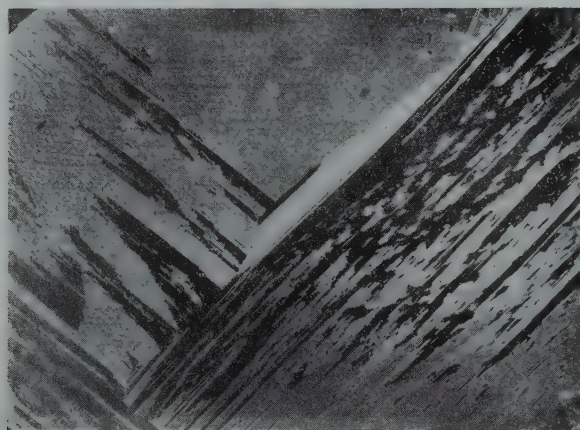


FIG 33—Same copper as in Fig 31, after final rolling of 90 pct and final anneal of 25 min. at 1000°C.

The appearance of this structure is dominated by the characteristically long, straight (twin) boundaries. Magnification $\times 5$. Reduced one half in reproduction.

directly on the fine grained matrix.

C. S. SMITH*—It is, perhaps, somewhat undesirable to use the term "attraction," as do the authors on p. 25 of their paper, for the interaction between the grain boundary and a particle of the second phase. Surely, though a boundary will cling to an inclusion once it has met it, and can be retained in positions that involve considerable curvature, it will not be influenced by an inclusion at a distance.

The effectiveness of such an anchor is relatively little dependent on the surface energy of the inclusion. It is essentially a question of geometry, for the numerical value of the interfacial tension of the boundary cancels out, being both the force for driving and for restraint. If the second phase is not rigid, it will become lenticulate in shape under the influence

of the triangle of surface forces around its edge, but such departures from a spherical shape will increase the length of the line of contact, and hence the restraining force, by factors of not more than two or three except when the dihedral angle approximates zero and the second phase spreads as a film separating the grains.

I have come to believe strongly in the simple geometric theory of grain growth, first clearly enunciated by Harker and Parker. The initial contact between grains will produce a random network of surfaces and points of contact. Each internal intersection must involve three grain boundary surfaces meeting along a line and six grain boundaries (and four edges shared with four grains) meeting at each point. If all surfaces exert the same surface tension they will tend to establish angles of 120° with each other and the edges will tend toward the stable "tetrahedral" angle of $109^\circ 20'$ with each other.

Except with ideal stacking of minimum-area tetrakaidecahedra (the three-dimensional equivalent of hexagons), curvatures are inevitably introduced to reconcile the required angles with the random points of contact and this introduces instability. The surfaces will then tend to move toward their centers of curvature, allowing further continual readjustment of the edges. This will proceed smoothly (at a rate dependent on the temperature and the local curvature) until more than three surfaces meet together at an edge or more than four edges meet at a point. The moment this happens the system becomes locally highly unstable and the surfaces will rapidly assume new positions of local equilibrium. Occasionally there will be formed tetrahedral grains, all of whose sides are convex and therefore bound to move inwards, bringing the points of contact with the four neighboring grains together in a stable balance as the grain disappears. Only as this happens will the number of grains decrease or the average grain size increase. This is illustrated two-dimensionally by the accompanying figures. The boundaries of the five-sided and four-sided grains shown in Fig 34A will move progressively toward their centers of curvature through the positions shown by the dotted line, to reach eventually approximately the configuration shown in the solid lines of Fig 34B. If the surfaces are all of equal energy, the moment four of them meet they become highly unstable, for, in place of the original six equilibrium angles of 120° , there are now two angles of 120° and two of 60° . The slightest disturbance will cause the films to seek new equilibrium with a new interface forming at approximately 90° to the one that has disappeared, and there will be accompanying readjustments throughout, as shown by the dotted lines in Fig 34B. The net result is that the five- and four-

* University of Chicago.

sided grains have become respectively four- and three-sided, with the addition of one side to each of two neighboring grains. The three-sided grain can now disappear completely by its sides moving toward their centers of curvature without any further instability occurring.

If something should happen to render the intersection of four surfaces or five edges stable, further grain growth could not take place. The situation that normally is followed by the most rapid motion now constitutes a complete block. Such an obstacle can be caused either by inclusions (where the requirement is only that all boundaries meet its surface at 90°) or by the grain boundary energy differing from boundary to boundary. In a single-phase alloy, although the energy is clearly not highly sensitive to orientation over most of the range of mismatch, it is likely—in fact, the recent experiments of Dr. C. G. Dunn make it certain—that in the range of slight mismatch there is a high dependence on orientation. Consider the grains shown in Fig 34B with the four interfaces momentarily meeting at a point. This is unstable if the four interfaces and the new interface that must be produced all have equal energies. If, on the other hand, the new interface (the horizontal one in the figure) should have a higher interfacial tension than the resultant of the other four tensions in its direction (that is, if it has a value greater than the diagonal of the polygon of forces they produce) the four films will be quite stable in contact with each other, unless and until movement of other parts of the boundary allows changes of the local angles to such an extent that the above criterion is no longer true. Such four-grain corners are frequently seen in two-phase structures (for example in the case of alpha-beta brass, where the grain boundary between two alpha grains has about 1.3 times the energy of the other possible interfaces) and it can occasionally be found in normal single-phase polycrystalline metals, particularly if the metal possesses a high degree of preferred orientation. The formation of these stable points can completely stop grain growth unless the grain size is extremely small and the curvatures high. Such a blocked network of grain boundaries will be quite stable on indefinite annealing unless some other action sets in to release it, whereupon—if it occurs locally—one grain may become much larger than its neighbors and continue to grow, for a former block will no longer be effective against the new, high, local curvatures. This sudden removal of a block could occur if it were possible for grains to change their orientation under the influence of surface forces (or if orientation changes as a result of local plastic deformation or new nucleus formation), with resultant change of interface energy and upsetting of the local force-polygon. If blocking is due to inclusions, the solution of the finest par-

ticles would have a similar effect. In either case, some grains would become considerably larger than their neighbors, the effective negative curvature of their boundaries larger, and thereafter their boundaries would progress continually and at a more or less constant rate into the network of smaller grains in which motion remains blocked. This will continue until the growing grain encounters another one of the same type. The frequency of nucleation will determine whether the grains are only a little larger, as in the case of abnormal grain growth in steels, or enormously larger, as in the general case of "secondary recrystallization."

In addition to blocking at a point by inclusions or by the necessity for the formation of a high-energy interface, it is also possible for a grain boundary to be blocked away from an intersection by inclusions, or by surface forces alone if the boundary, moving toward its equilibrium position, has to change its angle and pass through a minimum energy direction in relation to the two lattices that it divides. Unless the curvature is great enough to overcome this, the boundary will have a definite tendency to "hang" along certain preferred directions between the two crystals. In practice it is probable that the stopping of grain growth is due to a combination of all these factors. It does seem to be a fact that "secondary recrystallization" occurs only in material that has substantially ceased growing in the normal fashion. It is an interesting speculation as to whether primary recrystallization is also a result of a somewhat similar reaction taking place in a much finer network of interfaces.

Although a phenomenon as complex as grain growth clearly cannot be the result of a simple system of causes, it is nevertheless possible to account for many of the observations on the simple basis of the geometry that would result from various interfaces interacting in accordance with the principles enunciated by Plateau, Gibbs, and others in the nineteenth century.

P. A. BECK—Dr. Smith's interesting contribution to the discussion is much appreciated. In the absence of plastic deformation, grain boundary migration in pure metals, resulting in a gradual increase in the average grain size, is undoubtedly motivated by the interfacial tension connected with the grain boundaries. This view was clearly expressed by H. Althertum⁴⁸ about 25 years ago. The detailed theory of the geometry of grain boundary migration, as stated by Dr. Smith, was developed more recently by Harker and Parker.⁴⁹ Although the latter authors used an atomistic terminology, it has been certainly quite clear that they investigated the behavior of grain boundaries in single phase metals under the influence of what is phenomenologi-

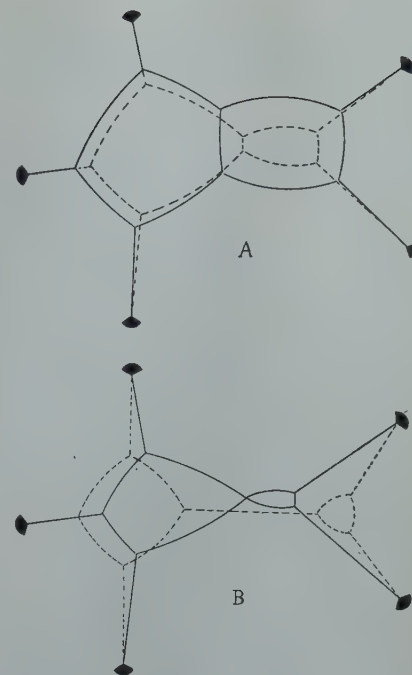


FIG 34—Tracings of soap bubbles illustrating idealized shapes and adjustment of grain boundaries moving under the influence of surface tension.

cally described as surface tension forces. Their considerations are, in the main, doubtless correct, but require two corrections. First, the relative lattice orientation of neighboring grains affects the value of the interfacial tension.⁵⁰ This brings about large deviations of the equilibrium dihedral angles from 120°, depending on the orientation. Also, it is becoming increasingly clear that the simple surface-tension theory of grain growth needs to be completed by consideration of the effects of orientation, probably even beyond those just mentioned. Secondly, although the grain boundary movements serve the tendency to approximate equilibrium angles and straight boundary surfaces, the deviations and irregularities are nevertheless self-perpetuating. Stable grain boundary geometry is thus not actually reached through grain growth, as was originally postulated by Harker and Parker. It was clearly shown by recent isothermal grain growth studies with high purity aluminum³⁶ that grain growth continues until stopped by the outside surfaces of the specimen.

It is gratifying that Dr. Smith agrees with the view set forth in the present paper, that coarsening is motivated by essentially the same forces that produce gradual grain growth. Whether the coarsening results in the formation of grains only ten to a hundred times larger than the fine grains of the matrix, as in steels, or 10³ to 10⁴ times larger, as it does under certain conditions in copper, the process is always actuated by surface tension, modified by the requirements of orientation. Terms like "abnormal grain

growth" and "secondary recrystallization," which were somewhat discredited by ambiguous usage, tend to confuse this picture.

As described in the paper, *inhibition-dependent coarsening* is a type of grain growth that starts at isolated points in a fine grained structure, after general gradual grain growth had been halted by the inhibitive effect of a dispersed second phase. In the examples described, the inhibition was locally overcome by the re-solution and coalescence of particles of the dispersed phase. Once a certain grain, through favorable local conditions, succeeded in growing considerably larger than its fellows, it will continue to grow with relative ease at the expense of neighboring small grains. This effect of "grain size contrast" was found long ago by Z. Jeffries.^{1,2}

It should be emphasized here that the above outlined mechanism for coarsening does not require any preferred orientation of the small grains of the matrix. Neither could it conceivably lead to a preferred orientation of the coarse grains formed from a random matrix. However, the mechanism considered may be still operative if the fine grains of the recrystallized matrix did possess a certain amount of preferred orientation. In such a case, it would be expected that all grains which happened to have local conditions of inhibition favorable for growth would not be, in general, equally likely to grow. Those having a particularly favorable orientation relative to their neighbors will be preferred. Thus the presence of a preferred orientation in the fine grained recrystallized matrix leads to a preferred orientation of the coarse grains. This condition is simply a result of the dependence of the rate of growth of a grain upon its orientation with respect to the preferred orientation of its neighbors. There is no need to assume the formation of "nuclei" of a certain orientation, or to postulate that residual portions of the deformed structure remain to serve as nuclei after surviving recrystallization, general grain growth and long periods of recovery at high temperatures.

Although preferred orientation of the coarse grains may occur in inhibition-dependent coarsening, it is by no means a necessary condition. On the other hand, in the case of *texture-dependent coarsening*, as explained above in the answer to Dr. Dunn, the fine grained recrystallized matrix *must* have a sharply defined texture in order to restrain gradual grain growth; therefore, the coarse grains growing in this highly oriented matrix have, of necessity, a preferred orientation of their own. The specific mechanism proposed by Dr. Smith for the restraint of gradual grain growth in a fine grained metal with a strong texture, is interesting. Whether or not it actually accounts for the observed facts remains to be estab-

lished by further research.

J. P. NIELSEN*—Referring to Dr. Smith's discussion on interfacial energies between grains not identically oriented, I wonder if, in the case of close-packed hexagonal metals, a new and perhaps important factor does not also enter into the picture: the difference in thermal expansion coefficients between two adjacent grains at the surface contact. Such a factor would depend of course on the increase in temperature above that at which the metal is completely relaxed.

C. G. DUNN—In the low range of orientation differences, I believe we actually need more data. This work on grain boundary surface tensions, which I hope to report at the next meeting of the Institute, actually was somewhat exploratory in nature. The groups of crystals investigated—each a three-grain group as was described in a technical note⁵¹—had crystals with a (110) plane in the plane of the sheet. The only variable, therefore, was the direction of the cube edge in the plane of the specimen.

Since the orientations were controlled, it was possible to have two grains in each three-grain group with the same difference in orientation. An arbitrary value of 15 was used. With this common orientation difference providing communication between groups, an entire range of orientation differences could be investigated.

Omitting a description of the entire curve, the shape of the curve indicated values of surface tension at orientation differences of 6 to 8° that were about one half the maximum value. The shape of the curve in this range of orientation differences is important to the understanding of strong texture materials such as copper and nickel-iron with the "cube texture." Strong texture materials should have less grain boundary energy than weak texture materials with the same average grain size.

So much for the surface tension measurements. I would like to say something about orientation relations as a factor in growth processes. First, there is the well known principle that a difference in orientation is required for growth. Secondly, certain orientation relationships, as for example twins, appear to be less favorable than other orientation relationships for growth.

With orientation relationships in mind let us consider the behavior of fine grained copper or nickel-iron with a strong cube texture. What grows in these materials by coarsening or secondary recrystallization always has an orientation which is different from that of the cube texture. Pawlek in 1935 reported that the orientation of the large grains in nickel-iron were as follows: a (120) plane in the plane of the sheet and a [001] direction parallel with the rolling direction. Similar results have been reported for

copper but there are also other textures. Omitting twin orientations (actually appreciable material is present as twins in the large grains) there are still many definite preferred orientations remaining. From symmetry they can be reduced in number and classified in relation to the cube texture. All fall 20 to 30° away from the cube texture. One orientation relationship reported recently by Bowles and Boas in Australia has a (111) plane common with the cube texture.

If we call coarsening of the grain structure, starting with a strong texture fine grain matrix, as "strong-texture dependent coarsening" in contrast to "dispersed phase inhibited coarsening," we still need another type designation to describe the case of development of the strong (110) [001] texture in silicon iron.* Unlike copper and nickel-iron, the final large grained silicon iron sheet, to which I have reference, has a strong single texture. Furthermore, the large grains do not have any unusual characteristic shapes or shapes with straight boundaries as Professor Beck pointed out is the case for oriented coarsening in copper and nickel-iron. The prior fine grained material in the as-recrystallized condition does not have a strong single texture as does the copper or nickel-iron examples but has a rather weak texture composed probably of two or more weak preferred crystal orientations. The development of large grains in silicon iron, therefore, is quite different from the development of large grains in materials having the cube texture. Nevertheless, I think it could be classified also as "texture-dependent" but certainly not as "strong-texture dependent."

P. A. BECK—Dr. Dunn's results, and his method for determining interfacial energy as a function of the relative orientation of the adjoining grains are indeed very interesting and pertinent to the questions discussed. We have also noted the fact, referred to by him, that the preferred orientation of the coarse grains usually deviates about 20 to 30° from the preferred orientation of the fine grained matrix. It would be interesting to speculate on the possible causes of preferential growth with an orientation difference of this particular range.

On the basis of information now available to us concerning the coarsening in silicon-iron, it appears that this is not of the "texture-dependent" type. It may be suspected, however, that it depends on inhibition by at least one dispersed second phase. With a complex material of commercial purity, which probably contains several dispersed phases, the exact role of each is difficult to ascertain. But it seems that the dispersed manganese sulphide, which is removed during annealing, may have an important role

*The (110) [001] texture was discussed at the 1948 ASM Symposium on "Cold Working of Metals," under the subject "Recrystallization Textures."

* College of Engineering, New York University

in the process. It was shown recently⁵² that under certain conditions nitrogen (perhaps in the form of dispersed aluminum nitride particles) may provide so much additional inhibition that coarsening is prevented altogether. The role of the much smaller amount of nitrogen normally present in silicon ferrite has not yet been clarified. Possibly, the coarsening reaction depends on the combination of two or more inhibitors, in analogy to the double inhibitor used with tungsten, as described in the Introduction of the present paper. In this connection it should be mentioned that, in the method most generally used for the manufacture of coarse grained tungsten filaments, the inhibitor used is potassium silicate. Most of this inhibitor evaporates during the first heating of the filament, while the coarse grains are formed. However, a portion of it remains in the filament. Here, too, the situation is quite similar to that described in the paper for the coarsening of Al-Mn alloys. As explained above in the answer to Dr. Smith's discussion, preferred orientation of the coarse grains may occur under conditions of inhibition-dependent coarsening, so that the phenomena in silicon-iron do not appear to necessitate a separate class of coarsening.

J. E. BURKE*—The authors have presented an excellent paper and have demonstrated very clearly the importance of growth inhibiting dispersed phase in promoting the appearance of very coarse grains. I should like to present a partial explanation of the role of the inhibiting phase. As Zener has shown, and as the authors demonstrate in this paper, there is a definite relationship between the concentration of the inhibiting constituent, and the limiting grain size, or limiting boundary curvature. Grain growth will cease when the driving force for grain growth, the curvature of the grain boundaries, is just balanced by the inhibiting effect of second phase inclusions.

Now, considering the situation in two dimensions, all grains are composed of sides and corners, and at the corners three boundaries usually meet at angles of about 120°. If all the grains have six

sides, the sides also can be flat, and as Harker and Parker⁴⁹ showed, there will be no tendency for grain growth. If the boundaries always meet at corners at angles of 120°, the curvature of the faces will increase as the number of sides on a grain increases, being concave outwards for more sides than six and concave inwards for less sides than six. In a reasonably uniform aggregate of grains, the number of sides on grains will vary from three to about eight or nine. In these cases, no very large curvatures are encountered. If now, due to some fluctuation, a much larger grain is produced, it will have many sides, being bounded by small grains. These sides will have more pronounced curvatures than those of more or less uniform grains. Thus, the amount of second phase impurity that inhibits the migration of grain boundaries in the uniform matrix will be insufficient to prevent the migration of the boundary between the larger grain and its smaller neighbors, and the large grain will consume its smaller neighbors. The rate of migration of this boundary is presumably proportional to the curvature of the individual curved sections. Since this is controlled almost entirely by the size of the small grains, the boundary should migrate at a uniform rate. Furthermore, the large grain will continue to grow until the small grains are entirely consumed, and it contacts another large grain. Growth will then stop. The ultimate grain size will thus be controlled solely by the number of large grains that appear.

This argument does not explain the nature of the fluctuation that leads to the appearance of the initial large grains. It could result from the local disappearance of a few inclusions, as the authors suggest, which would permit the local appearance of a very coarse grain. Any other cause for producing a large grain should lead to the same final sequence of events.

P. A. BECK—Dr. Burke gave a clearly formulated picture of the conditions of preferential growth of a large grain in a fine grained matrix (Jeffries' grain size contrast effect) in terms of the Harker-Parker mechanism. This picture is entirely in accord with our own thoughts on the subject, provided the fine grained matrix has no preferred orientation. When this preferred orientation is not

negligible, however, the picture needs to be supplemented by a mechanism which provides the strong dependence of the rate of growth of the large grain on its relative orientation with respect to its neighbors, as stated above. The exact nature of that mechanism is not yet completely clear.

References

1. Z. Jeffries: Grain Growth Phenomena in Metals. *Trans. AIME* (1916) 56, 571.
2. Z. Jeffries and R. S. Archer: The Science of Metals. McGraw-Hill (1924).
29. O. Dahl and F. Pawlek: Kornordnung und Kornwachstum bei Walzblechen. *Ztsch. f. Metallkunde* (1936) 28, 266.
36. P. A. Beck, J. C. Kremer, L. J. Demer and M. L. Holzworth: Grain Growth in High Purity Aluminum and in an Aluminum-magnesium Alloy, AIME TP 2280. *Met. Tech.* Sept. 1947.
42. C. S. Smith: Grains, Phases and Interface. AIME TP 2387. *Met. Tech.* June 1948.
44. M. Cook and C. Macquarie: Development of Abnormally Large Grain Sizes in Rolled and Annealed Copper Sheet. *Trans. AIME* (1939) 133, 142.
45. P. A. Beck, J. Towers, Jr. and P. R. Sperry: Grain Coarsening in Copper. *Trans. AIME*, 185, 203: *Jnl. of Met.*, Feb. 1949.
46. J. S. Bowles and W. Boas: Effect of Crystal Arrangement on "Secondary Recrystallization" in Metals. *Jnl. Inst. of Metals* (1948) 74, 501.
47. P. A. Beck and P. R. Sperry: Effect of Recrystallization Texture on Grain Growth. *Trans. AIME*, 185, 240: *Jnl. of Met.*, March 1949.
48. H. Althertum: Zur Theorie der Rekristallisation. *Ztsch. fur Metallkunde* (1922) 14, 417.
49. D. Harker and E. R. Parker: Grain Shape and Grain Growth, *Trans. A.S.M.* (1945) 34, 156.
50. C. G. Dunn and F. Lionetti: The Effect of Orientation Difference on Grain Boundary Energies. *Trans. AIME*, 185, 125: *Jnl. of Met.*, Feb. 1949.
51. C. G. Dunn: Controlled Grain Growth Applied to the Problem of Grain Boundary Energy Measurements. *Trans. AIME*, 185, 72: *Jnl. of Met.*, Jan. 1949.
52. Weston Morrill: Improved Silicon-Irons for Electrical Equipment, *Metal Progress*, (1948) 54, 675.

* University of Chicago

Statistical Rate Theory of Metals—I. Mechanism of Flow and Application to Tensile Properties

By JAY W. FREDRICKSON and HENRY EYRING

DISCUSSION

(G. Gensamer and W. R. Hibbard Jr., presiding)

G. WENSCH*—The authors have

further advanced the basic fundamentals in the science of rheology. Upon the teachings of Bingham, Scott Blair, Houwink, and others we are approaching the solution of the inelastic behavior of metals.

In consideration of Fig 10, as the authors point out, the stress-strain curve follows line *MF* even after interruptions provided that relaxation effects do not occur. However if relaxation effects do occur, such that the behavior of the metal is inconsistent with the concept of an

* International Nickel Co. Graduate Fellow in Metallurgical Engineering, University of Illinois.

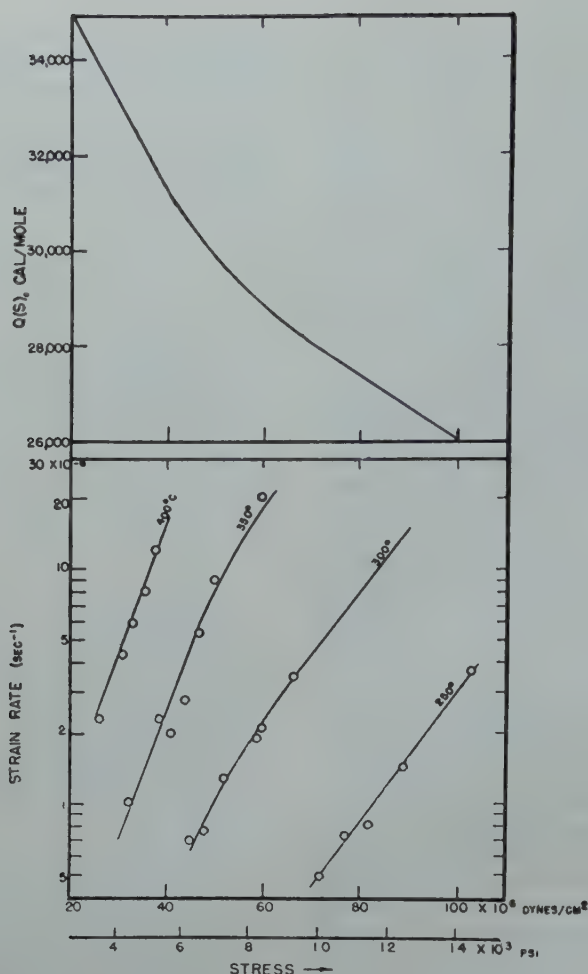


FIG 24—Analysis of Dushman's data after Ref. 43.

equation of state, transient phenomena will appear as clearly shown by the work of Carreker, Leschen and Lubahn.⁴²

W. C. ELLIS*—The authors in this paper have advanced a theory for plastic flow in metals which involves the translation of relatively small flow units or domains into existing holes made up of a number of adjacent unoccupied lattice sites. From the mathematical analysis of the stress-strain curves for a number of steels they have calculated an average value for the hole involved in flow. A range of values was found which group around about 200\AA^3 at room temperature. This volume corresponds to about 8 unit lattice cells which is a large hole in an atomic universe but a small one in relation to available measuring tools such as the electron microscope.

The mathematical analysis, by itself, seems to be merely suggestive and constitutes no proof of the physical existence of such holes, and it should be added that the authors do not contend that it does. Explicit evidence for the existence of such holes, if they be a reality, would be welcome for it would provide a firm foundation for a mechanism of plastic

flow, a foundation which does not exist, in my opinion, for any of the present theories. I would therefore like to ask if there is a method, or prospect of developing methods, of arriving explicitly at the physical reality of such holes in metallic structure. This paper is a valuable one in that it presents a new concept and it is hoped that investigation along this line will be continued.

C. ZENER* and T. S. KË*—The authors conclude that the heat of activation ΔH^* for the elementary act of plastic flow is essentially zero, and hence, that the free energy of activation ΔF^* is entirely an entropy effect. This conclusion, if correct, must form the starting point for any further development of the theory of plastic deformation. It is of utmost importance that their underlying assumptions be carefully scrutinized to see if this conclusion of a zero ΔH^* could possibly arise simply as a consequence of an artificial assumption.

The authors assume that the rate of an elementary flow process depends upon the applied stress S in the manner:

rate $\sim e^{-(\Delta F^*/kT)} \{e^{(VS/kT)} - e^{-(VS/kT)}\}$, [42] where the free energy of activation ΔF^*

and the volume V may depend upon the temperature but not upon the applied stress. Now one of the most characteristic features of crystalline plasticity, as opposed to amorphous plasticity, is the relative insensitivity of the flow stress S to changes in temperature. Thus by passing from room temperature to 1°K the flow stress corresponding to a given strain rate is increased by, at most, a factor of five. The assumption (Eq 42) is compatible with this characteristic fracture of crystalline plasticity only if both the ratios V/T and $\Delta F^*/T$ are relatively insensitive to changes in temperature. A zero heat of activation ΔH^* then follows from the constancy of the ratio $\Delta F^*/T$. The conclusion of the authors that the free energy of activation is essentially an entropy effect is, therefore, a direct consequence of the assumption (Eq 42).

In writing Eq 42 one implicitly assumes that the heat of activation Q of an elementary flow process is a linear function of the applied stress S . One of the writers (C. Z.)⁴³ has, in collaboration with J. H. Hollomon, shown that the extensive creep data of Dushman, Dunbar and Huthstein¹⁸ may most readily be interpreted through a relaxation of this assumption, that is, by regarding the heat of activation as a function $Q(S)$, the precise form of which is to be determined by experiment. Thus, in place of Eq 42 one has

$$\text{rate} \sim (e^{-Q(S)/kT} - e^{-Q-(S)/kT}). \quad [43]$$

The example of $Q(S)$ for pure aluminum is presented as Fig 24. Fisher and MacGregor,²⁸ whose data have been analyzed by Fredrickson and Eyring according to Eq 42, showed that their own data were consistent with Eq 43.

The present writers wish to ask Messrs. Fredrickson and Eyring if their physical picture of plastic flow necessarily demands a rate dependence containing the applied stress to the first power in the exponent, as in Eq 42, and whether a relaxation of this condition of an exponent linear in stress would not drastically modify their conclusions. They further wish to point out to Messrs. Fredrickson and Eyring that creep data at very low stress levels is not in agreement with the conclusion of a zero heat of activation. Such data have been analyzed by Kanter⁴⁴ who found that at those low stress levels where the creep rate is proportional to the stress itself, the creep rates for iron and for brass have heats of activation comparable to those for self diffusion.

J. W. FREDRICKSON and H. EYRING (authors' reply)—The authors wish to extend their appreciation for the interest shown in this paper.

The transient phenomena mentioned by Mr. Wensch has been observed⁴⁵ by the senior author in a subsequent investigation. A continuation of these transient investigations promises to enlighten us further on the flow mechanism.

* Bell Telephone Laboratories.

⁴² References are at end of discussion.

* University of Chicago.

The question proposed by Mr. Ellis regarding the physical reality of "flow holes" in a metallic structure is a very intriguing problem and deserves serious consideration. As is emphasized by Mr. Ellis, the authors have not established the physical existence of such holes. It does seem to be a reasonable assumption however, that in order for flow to occur by the movement of domains these domains must be provided with a space to occupy in their new positions. A mechanism for flow has been explained by some theories through the operation of dislocations. It is not our wish to enter into a discussion at present as to the difference between a "dislocation," "imperfection" or "hole." It suffices to say that some medium is apparently required to explain flow and the medium of holes has been used in this paper to provide the mechanism for flow. If one assumes that the size of the domain that moves is an inverse function of the applied stress, as appears to be the case, then the mechanism of flow could also occur by the creation of holes or new "home sites" by the domain itself as it moves.

At present there is apparently no method of determining explicitly the physical existence of holes in metallic structures. As Mr. Ellis suggests, the development of such a method would contribute greatly to the knowledge of flow in metals. It is the authors' belief that such a determination can be secured by the methods of statistical mechanics and further work is being directed toward this end.

Messrs. Zener and Kê have presented a very interesting and thoughtful discussion. The points introduced in this discussion are well taken and merit consideration not only by the authors but by others interested in flow mechanisms.

The rate equation for the elementary flow process shown as Eq 42 in the discussion was developed after careful consideration of various flow processes occurring in solid materials including that of viscous flow. The fact that the apparent heat of activation ΔH^* for flow was essentially zero, and thus the free energy of activation ΔF^* was entirely an apparent entropy effect, was a direct consequence of the application of the elementary rate equations to metallic deformation. That this result might possibly have occurred by the use of some other assumption can not be categorically denied. But first, let us examine the equation a little more closely.

If in Eq 42 $VS \gg kT$ we have

$$\text{rate} \sim e^{-\frac{\Delta F^*}{RT}} e^{\frac{VS}{kT}} \quad [44]$$

and the equation gives the same type of exponential dependence of rate on stress that is found empirically. On the other hand if $VS \ll kT$, one has approximate proportionality of the rate to the stress as in viscous liquids and as shown by Maxwell.³³

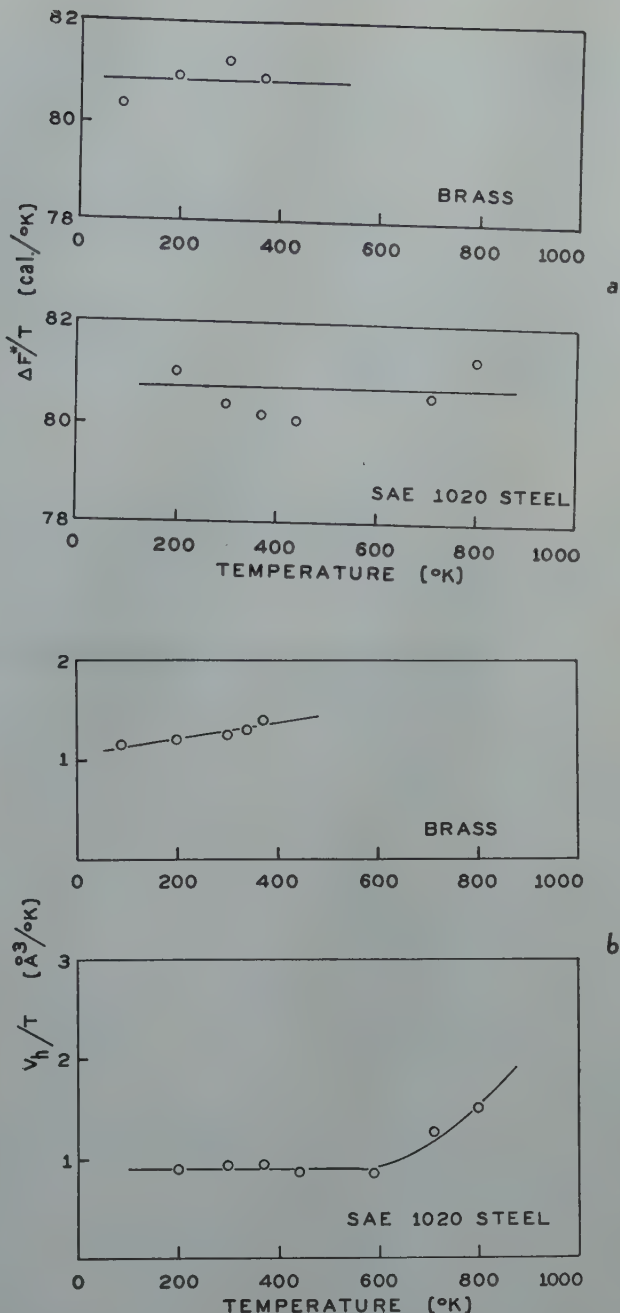


FIG 25—(a) (above) Curves showing $\Delta F^*/T$ vs. temperature relationship. (b) (below) Curves showing V_h/T vs. temperature relationship.

If one rewrites Eq 44 in the form

$$\ln \text{rate} \sim -\frac{\Delta F^*}{RT} + S \frac{V}{kT} \quad [45]$$

the stress is shown as a function of the logarithm of the rate. Eq 45 is clearly seen to fit the curves of Fig 24.⁴³

A further analysis of the data in the paper shows that $\Delta F^*/T$ and V_h/T are relatively insensitive to changes in temperature, as was deduced by Messrs. Zener and Kê. Fig 25, representing Fig 2 and 3 from this analysis, shows the relationship of $\Delta F^*/T$ and V_h/T as a function of T .⁴⁶

It has been determined by the senior author in a separate subsequent investigation of creep⁴⁶ that both the free energy

of activation ΔF^* and the hole volume V_h are inversely dependent upon the applied stress. Because of this stress dependency, one must be careful in making an analysis that the underlying mechanism does not change within the stress range.

One may well consider that the mechanism of flow occurs by the process of self-diffusion in that at equilibrium the energy barriers that must be crossed are sufficiently high to prevent flow, or conversely, the probability for flow in any one direction is as likely as in any other and therefore flow will not occur without a directed driving force. The action of the applied stress is to provide the driving force for flow by raising and lowering the

equilibrium positions on each side of the energy barrier as depicted by Fig 2. Thus, if the barriers are lowered in a preferred direction by some means, flow can occur by self-diffusion of domains across the barrier.

Messrs. Zener and K₂ have proposed a rate equation as shown by Eq 43. It appears that in order for this equation to fit the curves shown in Fig 24 the parameter Q must be some linear function of stress. If Q is some linear function of the stress, then Eq 42 and 43 differ only in the definitions of the exponents. Deter-

mining which equation is the more correct will require further investigation. It is the belief of the authors that the amount of data so far analyzed has been too meager to be used as a definite criterion to determine the nature of the parameters in the equation. In any event it is gratifying that separate investigations do produce such qualitative agreement.

References

42. R. P. Carreker, J. G. Leschen and

J. D. Lubahn: Transient Plastic Deformation, AIME *Metals Tech.* Sept. 1948, TP 2477.

43. C. Zener and J. H. Hollomon: *Jnl. Appl. Physics* (1946) 17, 69.

44. J. J. Kanter: *Trans. AIME* (1938) 131, 385.

45. Unpublished report.

46. H. Eyring, J. W. Fredrickson and D. McLachlan, Jr.: The Mechanism of Flow for Solid Metals, *Proc. Nat. Acad. of Sci.* (1948) 34, No. 6, 295-304.

Nucleation of Slip Bands

By J. G. LESCHEN, Junior Member, R. P. CARREKER, and J. H. HOLLOWOMON, Junior Member AIME

and

Transient Plastic Deformation

By R. P. CARREKER, J. G. LESCHEN, Junior Member AIME, and J. D. LUBAHN

JOINT DISCUSSION

(G. Gensamer and W. R. Hibbard, Jr., presiding)

G. WENSCH*—Messrs. Carreker, Leschen and Lubahn are to be congratulated on their excellent paper "Transient Plastic Deformation." As the authors correctly point out little thought has been given to transient phenomena in metallurgical experimentation; however, considerable effort has been made to analyze the rheological behavior of solids by mathematical treatment.

By the proper combination of visco-elastic models such as the Maxwell and Kelvin bodies one can imitate many of the observed behaviors in metals, such as the elastic after-effect, yield point and the transient behavior.^{7,8}

With a slight modification of the visco-elastic model system given by Burgers⁹ one can obtain a generalized strain-time curve similar to that of Fig 2 in the above-mentioned paper. By the proper evaluation of the constants of viscosity and elasticity the two curves would probably be unique. The writer submits a sketch of a visco-elastic model which would exhibit generalized transient behavior, see Fig 9.

The solution of the differential equation of the model is:

$$1. x = \phi_1 \int_0^t P dt + \phi_2 \int_0^t P(t_1) e^{-(t-t_1)\phi_2/\alpha_2} dt$$

$$2. \text{ when } P = P_1, 0 < t < t_1$$

$$x = \phi_1 t P_1 + \alpha_2 P_1 (1 - e^{-t/\alpha_2})$$

$$\mu = \frac{\alpha_2}{\phi_2}, P_1 > P_2$$

$$3. \text{ when } P = P_2, t_1 < t < t_2$$

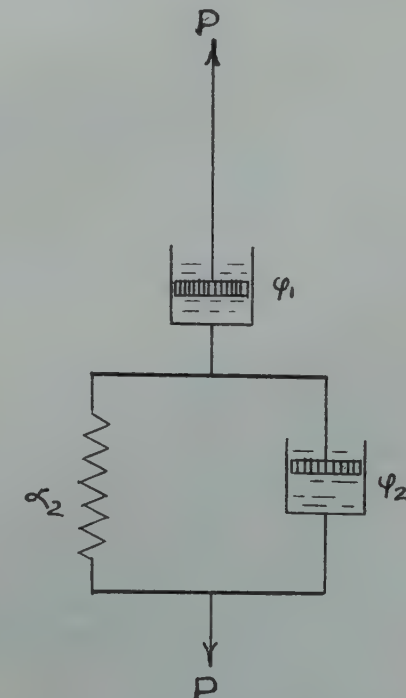


FIG 9—Rheological model which demonstrates transient behavior.

$$x = \phi_1 P_2 (t - t_1) + \alpha_2 P_2 (1 - e^{-\frac{t-t_1}{\alpha_2}}) + \phi_1 P_1 t_1 + \alpha_2 P_1 (1 - e^{-\frac{t_1}{\alpha_2}})$$

By proper evaluation of the constants ϕ_1 , ϕ_2 and α_2 , the strain x may be plotted versus the time t to give a curve similar to the upper curve of Fig 2 in paper discussed. (Fig 10).

Perhaps the authors can be induced to comment on visco-elastic model analysis as a means of interpreting transient behavior.

It appears that the authors did not

account for the change in the cross-sectional area of the wire which occurred during their investigation. Did the authors find this area reduction to be negligible?

J. G. LESCHEN (authors' reply)—With a suitable combination of springs and dash-pots one can undoubtedly reproduce many experimental results. The authors prefer not to depend too much on this sort of model since they feel that in many cases it does not represent adequately any real mechanism in the metal. However, this type of model is frequently of considerable value.

In the initial experiments no account was taken of the change in cross-sectional areas of the wires, since the reduction was negligible. In the experiments with which the sigmoidal curve was determined, the stress was automatically maintained constant by the device described by Fisher and Carreker.¹⁰

R. MADDIN* and W. R. HIBBARD, JR.*—The very interesting study of the dynamics of slip bands is a welcome addition towards the general solution of the problem of plastic deformation of metallic single crystals. There are two points which should be considered in light of recent experiments conducted at Hammond Laboratory.

In conjunction with Professor Henry A Lepper, Jr. (Department of Civil Engineering, Yale University), a single crystal of alpha brass 37 mm in diam was slit into 6 square crystals 180 mm long by 3.6, 4, 5.2, 7, 7.9 and 13 mm on the edge, respectively. Each crystal was etched to remove cold-work, homogenized for 20 hr at 800°C, polished electrolytically and X rayed via the back reflection method to insure that the machining operation left

* Yale University.

* International Nickel Co. Graduate Fellow in Metallurgical Engineering, University of Illinois.
7,8 References are at the end of discussion.

the orientation unchanged. An SR-4 strain gauge, type A-1, was glued on each specimen and the crystals were stressed to just beyond the yield point. The slip lines were counted on four of the specimens (too much glue on the remaining two specimens obscured the lines). The largest specimen showed a total of 70 lines observable at a magnification of 600 diam along a 150 mm gauge length whereas the smallest crystal showed over 8000 lines observable at $600\times$ for a 25 mm (only $\frac{1}{8}$ of gauge length). The number of lines on the other crystals was intermediate between those for the two extreme sizes and decreased with increasing size of the specimen. These preliminary results of this investigation, which is still in progress, have thus far produced experimental evidence which is not in accord with the statements made by the authors on p. 3 of their paper, "Nucleation of Slip Bands."

In the investigation of Ono quoted by the authors, two variables existed, namely, specimen diameter and orientation. Recent work being conducted at Hammond indicates that alpha brass single crystals of the same diameter pulled in tension under similar conditions but with differing orientations, when referred in the usual manner to the principal [111] plane in the principal $\langle 110 \rangle$ direction, give values for critical resolved shear stress too widely separated to be accounted for by experimental inaccuracies. Thus, variations in crystal orientations might account for Ono's differing critical resolved shear stress values. Furthermore, the curves redrawn from Ono in Fig 3 represent resolved shear stresses at shear equal to 4×10^{-5} and shear equal to 100×10^{-5} rather than a true critical resolved shear stress. The curve representing the resolved shear stress at shear equal to 0 (that is, the critical resolved shear stress) does not show so marked a downward trend and the data points deviate from the drawn curve making them difficult to generalize. It is also possible that the downward trend in Ono's curves and those redrawn in Fig 3 of the current paper might conceivably be rationalized on the basis of a variation of rate of strain hardening as a function of specimen diameter.

J. G. LESCHEN—We now realize our error in including in the present paper the curves from Ono and admit that they should be interpreted with caution.

However, a size effect is still to be expected. It should be a more complicated one than the present paper indicates, since the displacement per slip band δ and the number of slip bands N per unit length of specimen should also be considered. For example, if one assumes that the formation of a slip band in a specimen of diameter D relieves all the elastic energy stored in an approximate volume D^3 , δ should vary as the product τD where τ is the stress at which

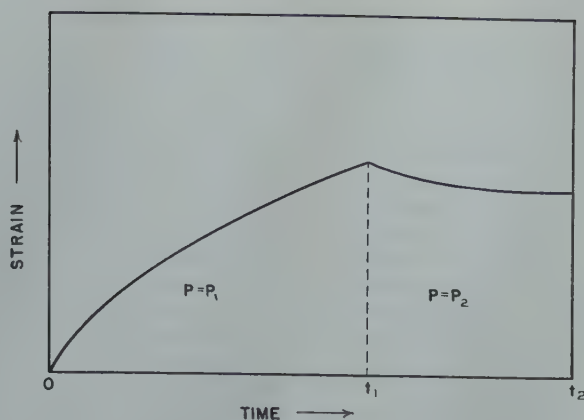


FIG 10—Schematic strain-time curve.

the slip band started. The observed strain would then vary as $N\tau D$.

Now as I understand these experiments with brass crystals, the specimens were pulled to a constant strain and then the number of slip bands counted. Is that correct?

R. MADDIN—Relatively.

J. G. LESCHEN—Constant strain requires the product $N\tau D$ to be approximately constant. This requirement is consistent with the observations of Messrs. Maddin and Hibbard that N decreases with increasing D . It is difficult to say how τ should vary under these circumstances, and a report of any such variation in these experiments would be very interesting. The situation is further complicated by the likelihood that all the slip bands did not start at the same stress.

L. D. JAFFE*—The theory outlined by the authors is obviously worthy of most careful consideration, especially in view of its successful prediction of certain transient effects. I should like, however, to confine my remarks to Fig 4 of the paper, "Nucleation of Slip Bands," and the text pertaining to this figure.

The authors explain the portion of the observed yield strength vs. $T^{-1/4}$ curve that represents a straight line through the origin (Fig 4) on the basis of the first exponential in Eq 3. They attribute the deviation at higher temperatures to the influence of the second exponential and to decrease in the modulus G . However, the second exponent differs from the first simply by a factor of 2. A brief calculation shows that even if the whole variation in yield strength with temperature were attributed to the second exponential, the slope would be increased by a factor of $2^{1/4}$, or only 19 pct. The observed increase, according to Fig 4, is obviously very much greater than this. Thus, the second exponential of Eq 3 is of little help in accounting for the change in slope. Do the authors, therefore, believe that the deviation observed is primarily due to decrease in the modulus?

* Watertown Arsenal Laboratory.

W. C. ELLIS*—Jay Fredrickson in our Laboratories has conducted creep tests similar to those for which Carreker, Leschen and Lubahn report the results in Fig 2 of their paper, "Transient Plastic Deformation." These tests were made on high purity lead with tensile specimens of rectangular cross-section, approximately 0.500×0.100 in. The strain rate curves as a function of time were similar to that shown in Fig 2 including the high rate of strain on initial application of stress decreasing slowly with time to a nearly constant rate. When the stress level was decreased the strain rate became zero for some time and then increased gradually to a nearly constant rate smaller than that for the initially higher stress. These are qualitatively the same transient effect as reported by the authors and would follow from the relationships developed in the companion paper, "Nucleation in Slip Bands."

The energy relationships which the experimental evidence qualitatively confirms were developed from the concept of nucleation in slip bands and the experimental findings are therefore qualitatively consistent with the nucleation concepts, as the authors have stated. There is a tendency when such an agreement is found between experimental data and a postulated mechanism to go further and to consider that the consistency observed points to a high probability for the physical reality of the mechanism.

There is a question, however, of whether a postulated mechanism, such as this, can be said to be unique from confirmation by property relationships alone, when such relationships might conceivably arise from other physical mechanisms. I would like, therefore, to ask Mr. Leschen to discuss this in more detail. How strongly do the experimental findings point to nucleation in slip bands as a part of the physical mechanism of flow in metals?

J. G. LESCHEN—Thank you, Dr. Ellis. I am glad to learn that someone else has performed this sort of experi-

* Bell Telephone Laboratories.

ment and obtained similar results.

I should like to emphasize that the present papers are not primarily concerned with the physical mechanism of slip. They simply seek to determine whether or not the nucleation concepts are applicable to the slip process. The results of the experiments indicate that slip bands do behave like anything else that is nucleated. Nucleation concepts should therefore be applicable to any mechanism of slip, whether that mechanism be described by dislocation theory or by the theory of Fredrickson and Eyring or by any other theory.

D. W. WHITE*—As I understand it, one corollary of this theory is that the small surface imperfections in the crystal would tend to facilitate the nucleation of the slip. On the other hand, Dr. McAdam showed us this morning that the low stress of a specimen on a larger scale is raised as you introduce the triaxial by means of a notch.

This seems on first appearance a little inconsistent with this matter of the function of surface imperfections by the nucleation theory. I was wondering if this is really a contradiction or just something imaginary on my part.

J. G. LESCHEN—The stress field in the vicinity of a notch is not as simple as that assumed in the present papers. It is difficult to say what the effect would be on the nucleation and growth of a slip band.

G. H. BOSS†—The authors of these two papers have outlined a very provocative theory and have presented the results of some very beautiful experiments. Their theory is certainly as tenable as are some of the others which attempt to explain slip. However, it is not necessary to postulate nuclei as the generators of slip in order to explain the curves which they have derived from the results of these excellent experiments.

While a metal is in the steady stage of creep it is being subjected to two opposing phenomena. One of these is the work hardening which occurs as the result of the deformation to which it is being subjected; the other is the recovery anneal, which occurs at a rate determined by the temperature to which the metal is heated.

In the following discussion it is assumed that the temperature is held constant, thereby fixing the rate of recovery annealing: If a metal is creeping at a steady rate caused by a load L , it will be work hardened to the extent determined by the balance between the rate of extension and the speed of recovery anneal. Now, if the load is increased by an amount ΔL , the balance is upset because the metal has only the work hardening of the lower load to resist the newer, greater load. Consequently the metal is deformed at a very great rate, which gradually diminishes as the work

hardening of the metal is increased. It finally reaches a steady rate which is somewhat higher than the original. Then if we reduce the load back to its original value of L the balance is again upset, because the metal is work hardened to the extent demanded by the higher load. Consequently the rate of extension is greatly reduced, and remains so until recovery has restored the balance by reducing the work hardening of the metal.

A. H. COTTRELL*—The idea that slip may be nucleated by the formation on a slip plane of a disc-like patch of slipped material which subsequently grows by the outward advancement of its boundary across the slip plane is much older than the authors suggest. It was proposed and discussed by Orowan¹⁴ in 1934. In reintroducing the idea, the authors suggest that it is in some way different from the dislocation theory; this is strange in view of the fact that Orowan and many others have emphasized that the boundary (which divides the slipped and unslipped parts of the slip plane) of the disc-like patch constituting the nucleus of slip is rigorously definable as a dislocation. This model of slip nucleation has been discussed, explicitly and implicitly, many times^{1,15,16,17,18,19,20} since 1934 and the general conclusion has now been reached that an extremely high energy of formation precludes the existence of slip nuclei as equilibrium features of a crystal under external stress, unless this stress approaches $G/10$ in order of magnitude, where G is the shear modulus. Accordingly, modern opinion holds that such nuclei exist only as metastable features in crystals, the dislocations which form their boundaries being trapped in potential energy troughs caused by the stress fields of impurities, crystal boundaries, and other dislocations. In the absence of these troughs, or of a very high shear stress on the glide planes, the nuclei must disappear.

The concept of a slip nucleus which the authors propose on p. 2 of "Nucleation of Slip Bands," as a basis for their theory is perplexing. It is founded on the assumption "that a growing semicircular interface, *across which no shear stress is supported*, advances slowly into the crystal." The clause in italics must mean that the material in the slip nucleus is incapable of supporting a shear stress, or that it happens to be free from stress at the time considered. From the work of Bragg,¹⁸ who has studied the second possibility in detail, one can conclude:

1. That it arises when the applied shear stress τ bears a certain relation to the amount of slip (which is fixed by the crystal structure) in the slip nucleus, a relation which also involves the size of the nucleus and the elastic properties of the medium,

2. That, when its consequences are

fully analyzed, it reduces the above model of slip to a particular case of the dislocation theory model, in which the stress fields from the applied load and the dislocation constituting the boundary of a slip nucleus approximately cancel each other inside that nucleus.

The authors evidently have in mind the first possibility (that is, that the slipped region cannot support a shear stress), since:

1. No suggestion is made of any critical relation between the applied stress and the amount of slip; in fact the amount of slip is not mentioned at all.

2. The energy of nucleation is taken to be made up of a term representing relief of shear stress in the vicinity of the nucleus and a surface energy term proportional to the area of the slipped region.

To suppose that the slipped region cannot support a shear stress must mean either that the material in the disc-like patch has become a fluid (see below) or that the two atomic planes which have slipped over each other in this region have parted company, thus forming a crack. The authors presumably favor the latter since they compare the disc-like patch to a slit.

What is now very difficult to understand is how this model can describe the process of plastic gliding since the picture it gives is of the spreading of a crack across a slip plane, which is something quite different. If the material within the slipped region cannot support a shear stress, then, when the "slip" has propagated across the entire slip plane, the two halves of the crystal divided by the slip plane must become separated. Brittle failure along a slip plane, and not plastic flow, should result.

The conclusion seems unavoidable that no other model of a slip nucleus is conceivable except the strict dislocation model in which the atoms in the slipped region have slipped past each other to congruent positions where they are as firmly bound and are as capable of supporting a shear stress as those in the unslipped region. Only the dislocation itself, where a special atomic configuration exists, is incapable of supporting a shear stress, and this only in the sense that the dislocation will move in that direction which causes the crystal as a whole to give way to the stress.

The fact that a crystal as a whole cannot support a shear stress without undergoing plastic flow, if it contains dislocations, raises the possibility that the authors may regard their slip nucleus as a macroscopic, disc-like piece of crystal containing many slip nuclei of the strict dislocation type. This is an alternative to the crack interpretation and could be regarded as a refinement of the concept of the slipped region as a "fluid." In such a case the energy required to form the macroscopic slip nucleus would be the sum of the self energies and interaction

* General Electric Co.

† U. S. Naval Base, Naval Air Material Center.

* University of Birmingham, England.

energies of all the nuclei (of the dislocation type) from which it is made up. We shall now show that the energy of formation is impossibly high for even a single slip nucleus of the dislocation type. Consider the formation of a circular patch of slip in the interior of a crystal, constituting a single slip nucleus of the dislocation type. (The slightly more complicated case of slip starting from the surface can also be treated by making use of Koehler's¹⁷ surface image force.) The critical radius determining whether the nucleus will grow or disappear under a given stress is found by equating the forces acting on the dislocation forming the boundary of the nucleus. Three forces act:

1. An outward force, causing the dislocation to spread, which is due to the applied stress. This force increases as the nucleus grows.
2. An inward force due to the attraction towards each other of the parts of the dislocation on opposite sides of the nucleus. This force decreases as the nucleus grows.
3. An inward force due to the fact that, as the nucleus grows, the length of the dislocation round its boundary increases and so the amount of highly strained material in the core of the dislocation increases. It can be shown^{17,18} that the strain energy of the material in the core of a dislocation is generally smaller than the interaction energy of the strain fields which causes force (2), so that, in a rough calculation, force (3) can be neglected in comparison with force (2).

A balance between forces (1) and (2) is obtained approximately when the stress fields acting on any part of the dislocation due to the applied stress and the dislocation on the other side of the nucleus are equal. This defines the critical radius of the nucleus roughly as $\gamma = G\lambda/2\pi\tau$ where G and τ have their previous meanings and λ is the slip distance ($\sim 3\text{\AA}$). The energy of such a nucleus could be computed accurately, but for a rough estimate we can note that the energy of a dislocation is, at least, $1eV$ per atom along its length.²⁰ Hence under a stress τ , the energy of nucleus formation is about $2\pi\tau/\lambda = G/\tau$ eV. Strictly, one should subtract from this the work done by the external forces, but, unless these are such that $\tau > G/100$, the inclusion of this work does not affect the order of magnitude of the result.¹⁹ For soft metals G is of the order of 1000τ , so that an energy of about 1000 eV is required for slip nucleation. With a Boltzmann factor of $e^{-40,000}$ operating, there can be no possibility of stable slip nuclei at the elastic limits of soft metals. Only under exceedingly high stresses ($\sim G/10$) could the possibility be admitted. While the above estimate is undoubtedly rough, it ought to be correct in order of magnitude. More exact treatments have been developed^{17,18,19} for nuclei bounded by straight

dislocations, which give essentially the same results.

The experiments on transient plastic deformation⁷ cannot be regarded as providing evidence uniquely supporting the slip nucleation theory since Orowan²¹ has shown that the same effects are to be expected on the recovery theory of creep. Indeed, the times of the induction periods noted (~ 10 min. for lead and > 5 hr for copper) seem more in accord with a recovery theory than the theory of slip nucleation.

A. H. SULLY*—Although the paper, "Transient Plastic Deformation," makes no reference to the fact, it may be presumed that the wires on which these tests were carried out were polycrystalline aggregates and not single crystals. In this case, it seems more than probable that the results obtained in the tests, involving a reduction of stress during creep, are complicated by normal creep recovery effects. Creep recovery always accompanies stress reduction in polycrystalline aggregates, due to the redistribution of elastic stress between differently orientated crystals, which have different values of the resolved shear stress along the slip plane, and, consequently, have varying degrees of elastic and plastic distortion. In the case shown in Fig 2, where a small reduction of stress results in an apparently constant strain for a short period before creep recommences, it seems possible that this could be due to a balance between recovery processes in some crystals and continuing creep in others. If this were true, an actual diminution of strain would be expected to occur if the stress reduction was larger, and it is unfortunate that the authors do not give the results of experiments with larger reductions of stress, since this would be a more critical test of their theory. The statement in the introductory paragraphs that transient effects have not previously been recognized in experimental work is incorrect. Tapsell²² has published data illustrating creep recovery and in particular has shown for a 3 pct nickel steel at 400°C the effect on the creep of reducing the stress from 16 tsi to 14 tsi. This shows, after allowing for the elastic strain, strain first diminishing, due to recovery effects, and then increasing and gradually approaching a new steady state creep rate.

The shape of the curve shown in Fig 3 from one minute onwards, relating the length of the period of zero strain rate to the time of prior application of the higher stress, can similarly be accounted for on existing theory if Andrade's division of creep into transient and quasi-viscous components is accepted and it is taken that only transient creep is recoverable in polycrystalline aggregates. There is adequate evidence that this is the case, for example, Chalmers²³ on the creep of

tin. After the time of exhaustion of primary creep, the recovery accompanying a constant stress reduction therefore remains the same, irrespective of the period for which the higher stress is applied, in accordance with the authors' observed approach to constancy of their "incubation" period. The rapid increase in creep rate and subsequent decrease to a constant rate observed on increasing the stress can similarly be explained on the basis of existing theory by Orowan's²¹ concept of an activation energy for glide increasing with the creep deformation along a curve similar to the normal stress-strain curve. An increment in the stress therefore results in a sudden lowering of the activation energy for further slip and consequently a further stage of transient creep, the exhaustion of which corresponds with the achievement of a constant creep rate, observed by the authors. It may be suggested, therefore, that the authors' results can be satisfactorily explained on the basis of existing knowledge of transient creep, and of the deformation of polycrystalline aggregates, and the evidence in favor of the theory of Leschen, Carreker, and Holloman would only be convincing if they observed identical effects, especially those accompanying stress reduction, in single metallic crystals.

J. G. LESCHEN—The authors regret that a misunderstanding has arisen with Professor Cottrell through their apparent failure to make sufficiently clear certain points in their introduction. They did not mean to imply that the idea of an advancing boundary of slip was at all new or that the dislocation and nucleation concepts are incompatible with one another. The authors merely wished to suggest that since nucleation theory can be successfully applied to the growth of cracks and of particles of a second phase, it might likewise be applicable to the growth of slip bands. In order to determine if it were so applicable, they selected a simple model—undoubtedly an oversimplified one—and then qualitatively investigated the characteristics of that model. Since these characteristics proved to be in reasonably good agreement with experiment, as reported both in the present papers and in a later development by Hollomon,²⁴ a nucleation theory of slip seems to merit further attention and a more quantitative development.

The present rudimentary treatment did not seem to warrant any undue concern with the atomistic mechanism by which slip takes place. In future developments of the theory the mechanism will have to be taken into account, and there can be little doubt that dislocations will here play a large part. In this regard the comments of Professor Cottrell should be of great help. The authors take issue with several of his remarks but feel that a discussion of most of them belongs more properly in a future note or paper

* Fulmer Research Institute, England.

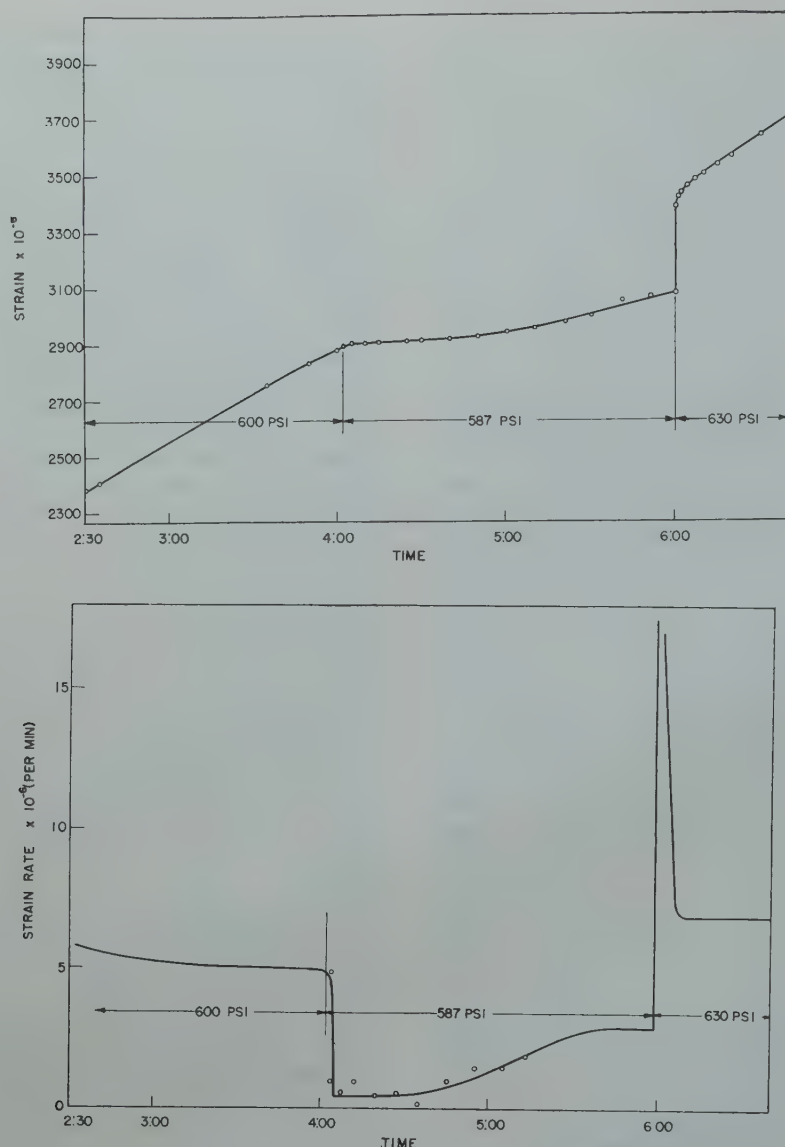


FIG 11—Transient effects in creep test on single crystal of lead.

than in the present discussion. However, several points can be made. For example, in calculating the Boltzmann factor for nucleating a dislocation, Professor Cottrell neglects the fact that yielding may begin at places where the local stress is significantly higher than the average applied stress. At such places, as Cottrell points out, the work done by the external forces cannot be neglected. Furthermore, we wonder whether the value of 1 eV , taken from the calculations of Nabarro, is a total energy or is it the free energy that must be used in computing the Boltzmann probability.

Mr. Sully is quite correct in presuming that the wires used in the original experiments were polycrystalline. However, tests have since been carried out with single crystals, and the results of the few experiments thus far completed indicate that the behavior of single crystals is essentially the same as that of polycrys-

talline specimens. Fig 11* illustrates, for instance, the response of a lead specimen to changes of stress at room temperature. Etching and visual examination of this particular specimen before the creep test indicated that it was a single crystal. X ray diffraction photographs made several days after the test showed the specimen to possess some lineage structure and a few small grains (possibly from local recrystallization). The suggestion that experiments be made with larger reductions of stress is a very valuable one and the authors have undertaken such tests.

Although the paper by Tapsell is not at present available to the authors, the

*The strain rate-time curve was obtained by graphically determining the slope of the strain-time curve, except in the region following the decrease of stress. Here the strain-time curve was so flat that accurate measurements of the slope could not easily be made, and the method of differences was therefore used. This method yielded points with appreciable scatter, and it accordingly seemed appropriate to show them in Fig 11.

type of results which he observes, as reported by Mr. Sully, is familiar.²⁵ However, this sort of transient does not appear to be the same as that discussed in the present papers, since the authors observed no contraction other than an immediate elastic one upon reduction of the stress. The transients of Tapsell probably require more complicated explanations of the kinds summarized by Leschen²⁶ and Zener.²⁷

In reply to Dr. Jaffe, it does indeed appear that the decrease of modulus with increase of temperature is primarily responsible for the deviation of the yield strength versus $T^{-1/2}$ curve from a straight line. The work of Kê²⁸ indicates that the decrease in modulus of single crystals is appreciable; and there is reason to believe²⁹ that as the melting point is approached the modulus, of polycrystals at least, falls toward zero.

Messrs. Cottrell, Sully, and Boss point out that the observed transient effects can be explained equally well by the creep recovery theory of Orowan. An experiment which would differentiate between this and the nucleation theory is difficult to conceive. A choice between the two will perhaps depend upon which can be the more adequately developed.

The nucleation theory of slip will no doubt require considerable modification. Meanwhile, it should serve to direct attention to the type of experiment involving sudden changes of stress, strain rate, or temperature. Then, if the theory should ultimately prove to be untenable, it will at least have been of heuristic value.

References

(Transient Plastic Deformation)

7. R. Houwink and W. G. Burgers: Elasticity, Plasticity and Structure of Matter, Cambridge (1937), 64.
8. A. M. Freudenthal: Notes on The Inelastic Behavior of Materials and Structures, Department of Theoretical and Applied Mechanics, University of Illinois, Urbana (1947) Parts I and II.
9. J. M. Burgers: First Report on Viscosity and Plasticity. Amsterdam (1935), Chap. II.
10. J. C. Fisher and R. P. Carreker: A Simple Constant Stress Creep Test. *Trans. AIME*, **185**, 178; *Jnl. of Met.*, Feb. 1949.

References

(Nucleation of Slip Bands)

1. F. Seitz and T. A. Read: *Jnl. Applied Phys.* (1941), **12**, 100, 170, 470, 538.
7. R. P. Carreker, J. G. Leschen and J. D. Lubahn: *AIME, Metals Tech.*, Sept. 1948, TP 2477.
14. E. Orowan: *Ztsch. f. Phys.* (1934), **89**, 634.

15. J. M. Burgers: *Proc. Roy. Acad. Sci. Amsterdam* (1939), **42**, 293; *Proc. Phys. Soc.* (1940), **52**, 23.
16. E. Orowan: *Proc. Phys. Soc.* (1940), **52**, 8; *Inst. Met. Symp. on Internal Stresses* (1947), 47.
17. J. S. Koehler: *Phys. Rev.* (1941), **60**, 397.
18. W. L. Bragg: *Nature* (1942), **149**, 511; *Trans. N.E. Coast Inst. Eng. Shipbuilders* (1945), **62**, 25; *Inst. Met. Symp. on Internal Stresses* (1947), 221; *Report of Bristol Conf., Phys. Soc.* (1948), 26.
19. F. R. N. Nabarro: *Proc. Phys. Soc.* (1947), **59**, 256.
20. N. F. Mott and F. R. N. Nabarro: *Report of Bristol Conf., Phys. Soc.* (1948), 1.
21. E. Orowan: *Jnl. West Scotland Iron and Steel Inst.*, 1947.
22. H. J. Tapsell: *De Ingenieur*, 1946, **30**, (2), 57.
23. B. Chalmers: *Jnl. Inst. Metals*, 1937, **61**, 103.
24. J. H. Hollomon: *Nucleation of Deformation. ASM Symposium on Cold Working of Metals* (1948).
25. J. D. Lubahn: *Creep of Metals. Ibid.*
26. J. G. Leschen: *Plastic After-effects. Ibid.*
27. C. Zener: *Anelasticity of Metals. TP 1992, Metals Tech.* (Aug. 1946): *Trans. AIME* (1946) **167**, 155.
28. T. S. Kê: *Experimental Evidence of the Viscous Behavior of Grain Boundaries in Metals. Phys. Rev.* (1947) **71**, 533.
29. L. Brillouin: *On Thermal Dependence of Elasticity in Solids. Phys. Rev.*, (1938) **54**, 916.

Plastic Deformation of Large Grained Copper Specimens

By W. R. HIBBARD, JR., Junior Member AIME

DISCUSSION

(R. F. Mehl and J. C. McDonald
presiding)

R. F. MEHL*—It is certainly pleasant to have a paper in the field of the plasticity of metal crystals that modestly undertakes to study some of the complexities from a phenomenological point of view, advancing new and good information and employing theory with judgment and restraint. In the long view, progress ought to come from a nicely calculated mixture of theory and experiment; and the proportions of each in that mixture should be chosen with some regard for the stage of development and the degree of complexity involved. Despite the great attention that has recently been given to physical theory in the field of metal behavior generally—the many symposia, the innumerable papers, the approval that is accorded semi-religiously to any effort so long as dislocations or lattice vacancies are intoned—it seems clear to this observer that progress in understanding plasticity has been shockingly slight. A proper sense of responsi-

bility should be shown in a field of research; theory should not far outrun experiment, for even though there is good sport in this, the purpose is not one of entertainment. Nor should undirected experiment be the rule; but at the present the error is not in this. There is a need of systematic experimentation in this field, and from this a formulation of general modes of behavior, for which then we might hope to have theories of behavior, and not before. The metallurgical profession ought to remember this, as Dr. Hibbard evidently does, and as some physicists do not.

As to the problem at hand, the plasticity of aggregates, it is possible that some of the difficulties arise in a lack of knowledge of the conditions of flow under various circumstances of restraint. We have based our thinking on the Polanyi-Schmid principle of a critical resolved shear stress for slip, providing slip on that lattice plane and in that direction for which the resolved shear stress is a maximum; it is possible that if this principle is not general, we could profitably restudy aggregates. Dr. R. Smoluchowski

in the Carnegie Metals Laboratories has recently demonstrated that slip in single crystals of aluminum in the form of thin plates does not conform to the Polanyi-Schmid principle, but that the length of the slip direction through the piece itself is a determinant—that slip is the reader the shorter this direction, that slip may occur in a given plane in a given direction when the length of the slip direction is short even though this slip system does not exhibit the maximum resolved shear stress. This effect of external geometry is in the category of restraint; it would be very interesting to see whether the change in basic thinking which this experiment implies might alter our conceptions of how aggregates should behave.

W. R. HIBBARD, JR. (author's reply)—I should like to thank Dr. Mehl for his kind remarks. His philosophy of scientific progress is a very important guide to investigations and, unlike the chicken or egg story, gives us a lead to the answer of which should come first, theory or experimental fact.

Dr. Smoluchowski's findings are extremely interesting and important. We now have another variable to consider in deformation studies.

* Carnegie Institute of Technology.

Plastic Flow in Anisotropic Sheet Steel

By L. R. JACKSON, Member AIME, K. F. SMITH and W. T. LANKFORD

DISCUSSION

(R. F. Mehl and J. C. McDonald
presiding)

R. HILL*—Apart from notation, the anisotropic stress-strain relations used by the authors are equivalent, in the special case when the directions of principal

stress and orthotropy coincide, to those which I have derived by other methods in an earlier paper.⁷ The criterion of yielding which I proposed is also similar in form to the authors' expression $\bar{\sigma}$, although I cannot make out whether they

⁷ A Theory of the Yielding and Plastic Flow of Anisotropic Metals. *Proc. Roy. Soc.*, (1948) 193-A, 281.

actually identify $\bar{\sigma}$ with the function governing yielding. It seems that they do not, since in the second paragraph of their summary and conclusions they state that their method is consistent with the idea that "the flow is governed primarily by considerations of shear-strain energy."

The value of the paper would have been greatly enhanced if detailed data had been given concerning the observed strain-ratios in the bulge tests. These can

* Cavendish Laboratory, Cambridge, England.

be predicted theoretically from the stress-strain relations in terms of the measured strain-ratios in the tension tests at right-angles. An immediate test of the validity of the stress-strain relations is then possible. Would the authors be good enough to give these data? I should also be very interested to check the relations given in my paper between the yield stresses in the orthotropic directions and the parameters occurring in the stress-strain relations.

I have found it very difficult to make out what fundamental postulates the authors are making with regard to the influence of cold work on the values of the anisotropic parameters. They appear to assume tacitly that these parameters increase in strict proportion. This seems rather unlikely on general grounds, but if it is true it certainly makes the problem of plastic anisotropy considerably easier. (In my own paper I left open the question of the dependence of the anisotropic parameter on the strain-history.) The second postulate made by the authors appears to be that the effective stress $\bar{\sigma}$ is a function only of the total plastic work. This is the natural assumption to make by analogy with the isotropic theory. However, could it not have been tested more directly by comparing the results of the two tension tests at right-angles? Would the authors please give the relevant data for this comparison?

The agreement between the bulge and tensile tests is, on the face of it, very satisfactory, but here again the authors have withheld the data that would enable a reader to assess whether the agreement is significant.

R. F. MEHL*—I would like to ask Mr. Jackson what are his ideas concerning the departure of Cor-Ten in behavior from his calculations.

L. R. JACKSON (authors' reply)—We have no concrete ideas as to just why Cor-Ten behaved as it did; however, throughout the analysis we made assumptions which may not have been justified in the case of Cor-Ten. Three such assumptions are: 1. That the flow curves in tension and compression are identical. 2. That the materials being investigated were orthotropic and that the orthotropic axes could be identified with the length, width, and thickness directions in the sheet. 3. That differences in the rate of straining in the bulge and tension tests had a negligible effect on the shape of the flow curves. 4. That the bulge test applies stresses only along the orthotropic axes. This last assumption is not correct and is particularly evident for circular bulges where there is no real choice of axes. 5. We also believe that the methods of measuring the parameters K_{xx} and K_{yy} are crude and not particularly precise.

R. F. MEHL—Do you think it possible that your results might be affected by

variations in the ductility properties in the thickness direction?

L. R. JACKSON—We attempted to minimize the effect of nonuniform thickness by measuring the thickness of test pieces at numerous locations and selecting only those which were uniform within narrow limits.

R. F. MEHL—It is disturbing that we have hitherto been forced to consider plastic properties, even when the behavior in the transverse direction is important, on the assumption that the ductility in the transverse direction (the thickness direction in plate or sheet) shows no special characteristics. Recent studies at Carnegie on the transverse mechanical properties of heat-treated forging steels show that the transverse ductility properties vary greatly from the longitudinal; and though this doubtless originates in the structural anisotropy caused by alloy segregation and its consequences in heat-treatment, it is possible that a similar mechanical anisotropy, perhaps less in degree, may occur in simpler alloys; there is no information on this point, and it should be developed. The effect might well be present in Cor-Ten, which the author studies, for this is an alloy steel, and should show a degree—not necessarily a harmful one—of alloy segregation and resultant mechanical anisotropy.

M. F. SAYRE*—Was any measure-

* Union College.

ment made on stresses in the 45° direction? From the theoretical point of view, evidence of anisotropy should be much more evident with measurements at 45° than with measurements taken 90° apart.

L. F. JACKSON—We did not measure the tensile properties in directions other than the rolling direction and the width direction; however, we are making these tests now.

MEMBER—How did you calculate the stresses in the elliptical bulge?

L. F. JACKSON—We had some difficulty in this measurement. We did not believe that the conventional method of computing stresses by assuming that the ellipse is a figure of revolution was precise enough, so the method had the following steps: 1. A bulge was blown to some selected height and the pressure released. 2. Either Tuckerman or wire strain gauges were mounted at the top of the bulge along the rolling direction and width direction. 3. The oil pressure under the bulge was then gradually increased to the value it had when the pressure was released. Simultaneous strain and pressure readings were taken during this period and a relation between the two strains and the pressure was obtained. The stresses existing at the maximum pressure were then computed from the strains by conventional methods.

MEMBER—How constant did that ratio remain during your test?

L. F. JACKSON—Do you mean the ratio between the stresses in the longi-

Table 3 . . . Bulge Stress-strain Data

| Test and Material | Stress in K psi | | | | R_z Inches | R_y |
|--|-----------------|--------------|------------|--------------|-----------------|-------|
| | σ_x | ϵ_x | σ_y | ϵ_y | | |
| Rimmed, annealed, long. elliptical (Fig 4) | 52.8 | 0.0640 | 67.0 | 0.0956 | 16.0 | 7.7 |
| | 55.6 | 0.0777 | 69.4 | 0.1196 | 14.1 | 7.1 |
| | 60.0 | 0.0934 | 71.4 | 0.1556 | 12.5 | 6.7 |
| Rimmed, annealed, trans. elliptical (Fig 5) | 56.2 | 0.0745 | 47.2 | 0.0409 | 8.8 | 18.4 |
| | 61.0 | 0.1024 | 52.8 | 0.0546 | 7.8 | 16.1 |
| | 65.1 | 0.1239 | 56.6 | 0.0654 | 7.3 | 14.2 |
| Rimmed, annealed, circular, (Fig 6) | 51.5 | 0.0506 | 50.9 | 0.0494 | 12.9 | 12.5 |
| | 56.6 | 0.0697 | 55.3 | 0.0690 | 11.0 | 10.9 |
| | | | | | 9.1 | 9.1 |
| Al. killed, annealed long. elliptical (Fig 7) | 64.2 | 0.1096 | 62.7 | 0.1105 | | |
| | 44.4 | 0.0321 | 58.8 | 0.0505 | 22.5 | 10.6 |
| | 48.3 | 0.0393 | 63.0 | 0.0638 | 19.9 | 9.3 |
| Al. killed, annealed transverse elliptical (Fig 8) | 49.6 | 0.0458 | 66.2 | 0.0768 | 18.2 | 8.7 |
| | 52.7 | 0.0540 | 68.9 | 0.0944 | 16.5 | 8.0 |
| | 56.1 | 0.0519 | 53.8 | 0.0334 | 10.5 | 20.0 |
| Al. killed, annealed circular (Fig 9) | 61.0 | 0.0701 | 54.8 | 0.0440 | 8.5 | 17.5 |
| | 64.1 | 0.0850 | 57.1 | 0.0522 | 7.9 | 16.5 |
| | 67.6 | 0.1028 | 61.2 | 0.0620 | 7.3 | 14.8 |
| Al. killed, T.R. long., elliptical (Fig 10) | 48.5 | 0.0420 | 48.5 | 0.0344 | 13.3 | 13.5 |
| | 53.8 | 0.0524 | 55.8 | 0.0442 | 12.0 | 12.1 |
| | 55.0 | 0.0623 | 57.4 | 0.0538 | 11.1 | 11.2 |
| Al. killed, T.R. trans. elliptical (Fig 11) | 57.5 | 0.0722 | 61.0 | 0.0637 | 10.3 | 10.3 |
| | 58.9 | 0.0853 | 62.3 | 0.0766 | 9.7 | 9.7 |
| | 45.5 | 0.0327 | 56.0 | 0.0521 | 20.5 | 9.9 |
| Al. killed, T.R. circular (Fig 12) | 49.1 | 0.0449 | 60.6 | 0.0736 | 17.6 | 8.6 |
| | 53.3 | 0.0574 | 63.9 | 0.0983 | 15.5 | 7.7 |
| | 56.6 | 0.0699 | 67.3 | 0.1193 | 13.1 | 7.1 |
| Cor-Ten long, elliptical (Fig 13) | 55.8 | 0.0529 | 44.7 | 0.0315 | 9.9 | 20.6 |
| | 60.8 | 0.0732 | 50.0 | 0.0422 | 8.6 | 17.8 |
| | 64.6 | 0.0994 | 54.2 | 0.0564 | 7.6 | 15.6 |
| Cor-Ten trans. elliptical (Fig 14) | 67.0 | 0.1174 | 55.7 | 0.0659 | 7.2 | 14.3 |
| | 54.3 | 0.0499 | 52.9 | 0.0484 | 12.8 | 12.8 |
| | 58.0 | 0.0663 | 56.5 | 0.0638 | 11.1 | 11.0 |
| Cor-Ten circular (Fig 15) | 60.6 | 0.0810 | 59.3 | 0.0782 | 10.2 | 10.3 |
| | 64.8 | 0.0991 | 62.5 | 0.0955 | 9.5 | 9.6 |
| | 76.0 | 0.0282 | 95.3 | 0.0404 | 22.5 | 11.3 |
| Cor-Ten long, elliptical (Fig 13) | 80.8 | 0.0367 | 101.6 | 0.0528 | 20.2 | 9.9 |
| | 86.0 | 0.0504 | 113.1 | 0.0748 | 16.9 | 8.6 |
| | 84.2 | 0.0249 | 70.1 | 0.0158 | 13.2 | 27.3 |
| Cor-Ten trans. elliptical (Fig 14) | 92.5 | 0.0366 | 71.6 | 0.0230 | 11.2 | 22.9 |
| | 100.5 | 0.0479 | 76.7 | 0.0302 | 9.9 | 20.4 |
| | 104.3 | 0.0678 | 86.1 | 0.0420 | 8.7 | 17.6 |
| Cor-Ten circular (Fig 15) | 93.9 | 0.0576 | 104.0 | 0.0536 | 12.4 | 12.4 |
| | 97.3 | 0.0674 | 100.5 | 0.0636 | 11.6 | 11.6 |

* Carnegie Institute of Technology.

tudinal and transverse directions?

MEMBER—Yes.

L. F. JACKSON—The ratio remained quite constant for any one test; however, the ratio obtained depended on the kind of steel.

The authors regret that Dr. Hill's excellent paper was not available at the time theirs was submitted and are glad to have the opportunity afforded by his discussion to acknowledge it.

With regard to his suggestions we have the following comments.

Within the precision of our measure-

ments which was not high, the anisotropy parameters do not vary with cold work within the range covered. We wish to point out, however, that we did not explore the region in the vicinity of the yield point in detail because the assumption of incompressibility is not valid there. The parameters appeared to be essentially constant even after necking started when measured at the minimum section of the neck.

We are inserting Table 3 giving the data on the bulge tests requested by Dr. Hill. In the table we are also giving the

radii of curvature at the top of the bulge, since this data would be required in order to take into account the fact that the bulge tests do not apply stresses only along the orthotropic axes. This should be taken into account in attempting to compute the strain ratios as Dr. Hill suggests. As noted in the paper, we did not take this factor into account in computing $\bar{\sigma}$.

The tension data for the two directions can be computed from the tension curves given in the figures through the use of Eq 21 and 22.

The Effect of Thermal-mechanical History on the Strain Hardening of Metals

By J. E. DORN, Member AIME, A. GOLDBERG and T. E. TIETZ

DISCUSSION

(R. F. Mehl and J. C. McDonald
presiding)

G. W. GEIL* and N. L. CARWILE*—Tests of a type similar to those reported in this paper were carried out recently by the writers at the National Bureau of Standards with ingot iron. Complete true stress-true strain curves, up to the point representing fracture, were obtained for specimens prestrained at one temperature and extended to fracture at a different temperature. The curves were derived from simultaneous load and diameter measurements made during the tension tests. The results are in agreement with those reported in this paper in that they do not conform to the assumptions proposed for a mechanical equation of state. Tension tests made previously with an ingot iron, an 0.12 pct carbon steel and an 0.46 pct carbon steel, in which the specimens were prestrained various amounts at room temperature and then extended to fracture at 85°K gave similar results. These results were discussed in a paper on the "Influence of Plastic Deformation, Combined Stresses and Low Temperature on the Breaking Stress of Ferritic Steels" by D. J. McAdam, Jr., G. W. Geil and R. W. Mebs, published in *Metals Technology*, Aug. 1947.

The results of tension tests made at room and at low temperatures on commercially pure aluminum (99.4 pct) and high purity aluminum (99.97 pct) were discussed in a paper on the "Effect of Combined Stresses and Low Temperatures on the Mechanical Properties of Some Non-ferrous Metals" by D. J. McAdam, Jr., G. W. Geil, and R. W. Mebs published in the *Transactions of the American Society for Metals*, (1946)

37. The true stress-strain curve for aluminum extended at 85°K, warmed to room temperature, and subsequently extended further at 85°K, was not a continuous curve. The warming of the metal to room temperature resulted in some softening or crystal recovery. On subsequent retesting at 85°K, the stress-strain curve was lower than that which would have been obtained if the specimen had not been warmed to room temperature. The softening of aluminum prestrained at 85°K, warmed to 194°K, and retested at 85°K should be less than the softening resulting from warming to room temperature. This softening effect also is indicated by the curves in Fig 12 and 13 for aluminum as presented by Dorn, Goldberg and Tietz. Fig 12 shows the effects of prestraining at 78°K on the true stress-true strain curves at 292°K. The slope of these curves is due to the combined influence of the ordinary strain hardening at room temperature and the room temperature softening following the previous strain hardening at the lower temperature.

The slope of these curves decreases as the amount of prestrain at 78°K increases. With extension to maximum load or necking these curves approach the curve obtained in the single stage test at 292°K. Fig 13 presents the effects of prestraining at 78°K on the true stress-true strain curves at 194°K. With extension to necking, however, these curves still remain considerably above the curve obtained in the single stage test at 194°K, indicating less softening than in the test results shown in Fig 12.

J. H. HOLLOMON*—Inherent to the problem of plastic deformation is the relationship between the effects of strain

introduced under differing conditions. In treating the engineering problem of materials, the simplest assumption that can be made with respect to prior strain history is that its effect is negligible if no phase transformations take place during the deformation. This assumption was made in the early part of this century by Ludwik and was justified by a few experiments. Other investigators have utilized the qualitative conclusions derived from this assumption in discussing and describing the effects of temperature and strain rate on the resistance to plastic flow. Certainly the notion permits a rationalization of such gross features of deformation as the relations between necking in tension and in creep tests.

On the basis of a few experiments on steels, I showed that the effects of prior strain history were exceedingly small. More recently, experiments have been performed by G. Sachs and E. J. Ripling* that are in almost complete agreement with my earlier experiments. It appears that particularly at low temperatures, and for ferritic steels, there is only a small effect of prior strain history even at large strains. On the other hand, the results of the authors show a pronounced effect of prior strain history. Orowan† has shown that the effect of prior strain history becomes progressively greater with increasing strain. The authors of the present paper have carried out a thoroughly competent investigation of the effect of strain history for their materials.

In Fig 18 of their paper, the authors show a difference in the equivalent strain depending on whether or not the specimen was first deformed at a high or a low temperature. Another equivalent strain may be definable that is independent of

*The Effect of Strain-temperature History on the Flow and Fracture Characteristics of an Annealed Steel. *Trans. AIME Vol. 185, 78, Journal of Metals*, Feb. 1949, 78.

†West of Scotland Iron and Steel Inst. (1947).

* National Bureau of Standards.

* General Electric Co.

the sequence of the deformation temperatures. It seems reasonable that the shift in the stress strain curves should have been such as to make them asymptotic at large strains rather than identical at smaller strains. If the coincidence was assured at large strains, then the equivalent strains for the two sequences of temperature changes would have been nearly identical. There is some basis for defining an equivalent strain in this fashion. One would expect transient effects immediately upon reapplication of the load at the new temperature which would disappear with deformation at the second temperature.

Aside from such transient effects, the authors' experiments by themselves in no way invalidate the concept of the mechanical equation of state. The authors have simply shown either that there is no mechanical equation of state or that plastic strain is not an adequate measure of deformation. The self consistency of their results and an intuitive feeling with regard to the behavior of matter seem to require the latter conclusion. In order to demonstrate definitely that there is in fact little or no effect of prior deformation history when deformation is properly defined the following kind of experiment is necessary. Two specimens that are deformed the same amount (to the same equivalent strain in the authors terminology) must be deformed at some third temperature and their flow curves determined. If then these flow curves are identical, then the existence of a mechanical equation of state would have been demonstrated. Such a critical experiment is important to the further rationalization of the mechanism of deformation. It is conceivable that the equivalent strain if it does exist measures some fundamental properties of the material. Dr. D. J. McAdam,* and Dr. J. C. Fisher and I† have suggested that perhaps a proper measure of deformation fulfilling this condition is the stored internal energy. At a single temperature stored energy is probably a monotonic function of strain. However, this functional relationship may be different at different temperatures. Under such conditions, the work done during deformation may be a better measure of the stored energy. When the stress data of these investigators and of Orowan are plotted versus work, much less effect of prior strain history is noticeable.

Certainly the concept of equivalent strains is a good approximation to the way the authors' specimens behaved. If such equivalent strains are determined properly as can be done by investigations similar to the authors, and the significance of these equivalent strains is rationalized, a long step forward in un-

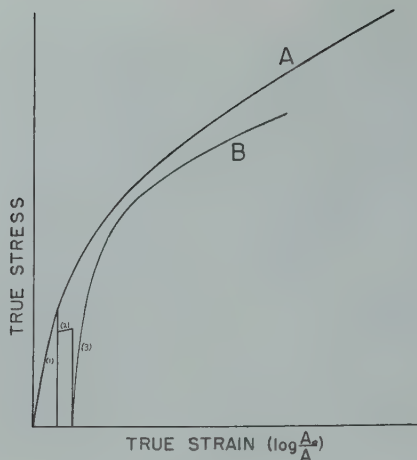


FIG 20—Effect of thermal prior strain history.

derstanding plastic deformation and predicting creep behavior would have been made. I fully agree with the authors that their data imply that at least for large strains all previous relations between the strength of metals and temperature are utterly confused by including both a variation in strength itself and a variation of the degree of deformation.

D. H. WOODWARD*—I would like to mention some results obtained at the National Bureau of Standards on the effect of thermal prior strain history. Curve A in Fig 20 was the type obtained at room temperature with the annealed material and curve B was the type obtained with the prior strained material. The schedule of prior straining was as follows: 1. The annealed material was extended 32 pct at room temperature. 2. The load was removed, the temperature raised, and the specimen deformed a small amount at a creep rate. 3. The load was removed, the temperature lowered to room temperature, and the flow curve obtained at that temperature. In such a case, not only is the shape of the latter flow curve different, that is, it is impossible to transpose it, but the resultant ductility is reduced.

J. H. HOLLOMON—That is 35 pct at room temperature, then heat it to what?

D. H. WOODWARD—Heat it to 350°F, that is, room temperature deformation followed by heating to 350°F. Deform a small amount in creep. Then complete the test at room temperature. The material was Monel.

E. J. RIPLING†—I should like to add here that there is no reason to suppose that results obtained on the fracturing characteristics after straining at two different temperatures are necessarily related to the flow characteristics under these conditions.

For example, work has been done at Case in which steel specimens were first

prestrained at room temperature and then tested at some lower temperature. These results, which should be published shortly, indicate the very complex behavior of the fracturing characteristics in a two-step test. When the retained ductility at the low temperature was plotted as a function of the prestrain conducted at room temperature, the curve possessed a very sharp minimum and maximum. However, the flow stress for these same specimens could be represented by a smooth curve always possessing a positive shape.

D. J. McADAM, JR.*—A few years ago, in my discussion of Dr. Hollomon's paper, "A Mechanical Equation of State," I referred to some experiments with aluminum, described in an earlier paper.²² These experiments showed that after aluminum has been plastically deformed at liquid air temperature, there is considerable relaxation when the metal is returned to room temperature. The results thus implied that an equation of mechanical state is not applicable to aluminum between room temperature and -188°C. At that time, I thought it possible that an equation of mechanical state might apply, throughout this temperature range, to metals with higher melting point, such as steel and nickel. However, in a paper published in August, 1947²³ we presented evidence that the flow stress for steels in liquid air is higher when the plastic deformation has been entirely at that temperature, than it is when part of the same total plastic deformation has been at room temperature. This evidence is found in Fig 6, 8 and 11 of that paper. Moreover, in Fig 2 of a paper published in Jan., 1948, we presented similar evidence concerning the flow stress of ingot iron.²⁴

During the last four months, I have studied the evidence in a series of our papers. The results have been assembled

* Presented as discussion at the Seminar on Cold Working, ASM, Philadelphia, 1948.
† Ibid.

* National Bureau of Standards.
† Case Institute of Technology.

* National Bureau of Standards.
²² References are at end of discussion.

in 23 full page illustrations, and are discussed in a paper to be offered for publication by AIME. The results, like those presented in the paper by Dorn, Goldberg, and Tietz, show clearly that the rate of real work hardening increases with decrease in the temperature of flow. The results indicated that the conception of an equation of mechanical state is invalid.

J. E. DORN, A. GOLDBERG and T. E. TIETZ (authors' reply)—The authors wish to take this opportunity to thank Mr. I. Kramer of the Office of Naval Research for his competent oral presentation of this paper at the AIME meeting at Philadelphia, Oct. 26, 1948. They also express their appreciation to those contributing discussions to this paper, and are gratified to hear that the results of other workers are in substantial agreement with those given here.

The results reported in the text of this paper prove that the concept of equivalent strains is fundamentally untenable. The authors agree with Dr. Hollomon, however, that properly determined equivalent strains may possibly be of considerable practical usefulness for correlations of stress strain data obtained under various strain-rate and temperature histories. On the other hand it must be recognized that such correlations become acceptable only for small strains and that the concept of equivalent strains will not assist in arriving at a better understanding of work hardening.

The comments of G. W. Geil, N. L. Carwile and also Dr. D. J. McAdam on recovery of aluminum at room temperature after straining at liquid nitrogen temperature are appreciated by the authors. Recent tests on pure aluminum (99.987 pct) have shown that the rate of recovery at 90°F is approximately twice as great after straining at liquid nitrogen temperature as after straining at room temperature when the amounts of prestrain at liquid nitrogen and room temperature are so selected as to result in the same value of initial flow stress were the tests immediately continued at liquid nitrogen temperature.

In the present paper the authors reported a test in which a specimen of high purity aluminum was prestrained at room temperature and then tested at liquid nitrogen temperature. From the data given in Fig 14, it is evident that the flow stress for pure aluminum tested at liquid nitrogen temperature after 0.15 prestrain at room temperature falls about 9,000 psi below that obtained when the specimen is strained the same amount at liquid nitrogen temperature. The amount of recovery which occurred after prestraining at room temperature before continuing the test at liquid nitrogen has been determined from a series of recovery tests to be not more than 400 psi, accounting for only a small part of the difference noted. Although recovery of high purity aluminum does occur at atmospheric temperature, such recovery

cannot account for the observed failure of the so-called "mechanical equation of state."

Any possible recovery of 2S-0 at atmospheric temperature after prestraining at liquid nitrogen temperature would have decreased the observed difference between the flow stresses of Fig 12 at room temperature. In the absence of recovery, therefore, somewhat greater effects of the past strain history would have been obtained than those recorded in Fig 12. The observed effects of past strain history on the flow stress described in this paper therefore are only slightly affected by recovery. The conclusion that the postulated "mechanical equation of state" is incorrect appears to be inescapable.

References

22. D. J. McAdam Jr., G. W. Geil, and R. W. Mebs: Effects of Combined Stresses and Low Temperatures on the Mechanical Properties of some Nonferrous Metals. *Trans. Am. Soc. Metals*, (1946) 37, 497-537.
23. D. J. McAdam Jr., G. W. Geil, and R. W. Mebs: Influence of Plastic Deformation, Combined Stresses, and Low Temperatures on the Breaking Stress of Ferritic Steels. *Trans. AIME* (1947) 172, 323; *Metals Tech.* TP 2220, Aug. 1947.
24. D. J. McAdam Jr., G. W. Geil, D. H. Woodard, and W. D. Jenkins: Influence of Strain Aging on the Fracture Stress of Low-carbon Steel. *AIME Metals Tech.* TP 2318, Jan. 1948.

The Room and Elevated Temperature Properties of Some Sand Cast Magnesium-base Alloys Containing Zinc

By T. E. LEONTIS, Junior Member AIME

DISCUSSION

(P. R. Kosting and W. A. Johnson
presiding)

JAY R. BURNS*—The presentation of this paper represents another significant advance in the field of magnesium metallurgy. The higher creep strength of the magnesium-zinc base alloys should place these materials in many applications which stand waiting.

Dr. Leontis has shown a comprehensive picture of the relative merits of many conceivable magnesium-zinc base alloy compositions. Work in the Materials Laboratory has substantiated the good properties obtained from such alloys at

room temperature although no elevated temperature testing has been done. One factor which has been evident in the work, however, is the tendency of these alloys to produce a dirty casting. Apart from the microporosity, small oxide skins appear prevalent in cast test bars. The proper use of screens and steel wool obviated the difficulty in the bars but some difficulties might be expected in larger castings. The presence of zirconium was found to emphasize the difficulties of obtaining sound and clean bars whereas Mischmetal reduced the trouble.

Certain other investigators have reported yield strengths of about 28,000 psi and corresponding elongations of 6-8 pct for magnesium-zinc-zirconium alloys. The Materials Laboratory has also obtained such figures from these alloys but the number of tests has not been very large. I should like to ask the author if he

believes the figures 24,000 psi and 3 pct for yield strength and elongation are more in line with the typical figures for the alloy.

T. E. LEONTIS (author's reply)—The comments of Mr. Burns are most welcome.

In regard to the tendency of magnesium-zinc alloys to produce dirty castings, I cannot say that we have had the same experience. The binary alloys and all the ternary alloys with which we have worked, except those containing zirconium, do not require any more special treatment than either of the two commercial magnesium sand-casting alloys, AZ63 and AZ92, to produce clean castings. It is true that zirconium does introduce more flux, oxide skins, and nonmetallic inclusions, but here again, either by careful flux treatment and settling or by proper chlorination, clean

* Materials Laboratory, Air Materiel Command.

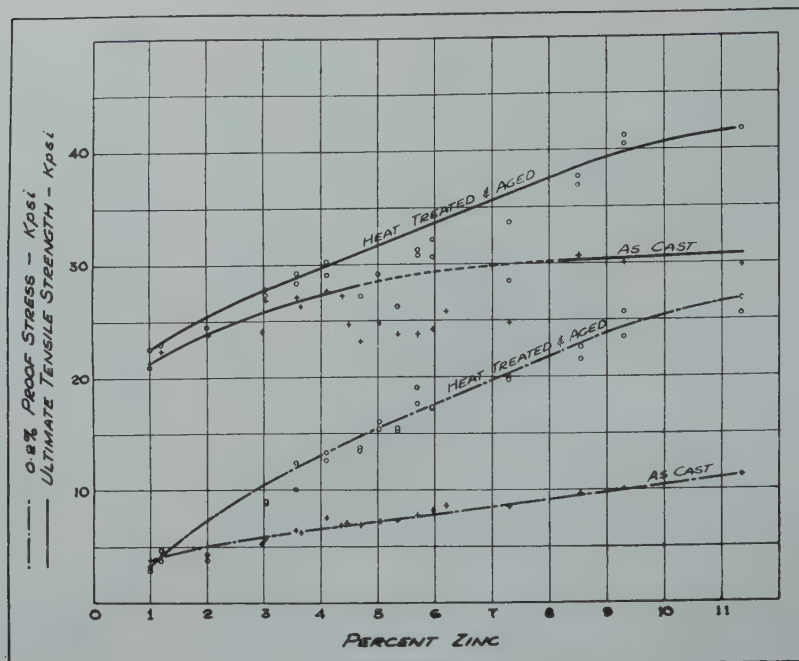


FIG 26—Tensile properties at room temperature for binary Mg-Zn alloys.

castings can be made. We have not experienced any more difficulty in making clean castings of production size than in making clean test bars.

Certain differences also exist between our observations on the microporosity of Mg-Zn alloys and those of Mr. Burns. Binary magnesium-zinc alloys have a high porosity tendency. This tendency is most markedly reduced by the addition of Mischmetal as Mr. Burns states, but we have observed that the addition of zirconium or any of the other elements investigated, with the exception of manganese, also reduces the microporosity to the point where relatively sound castings can be produced. The soundness of these castings compares favorably with that of AZ63 alloy. Alloys containing 0.7 to 2.0 pct manganese, on the other hand, produce very porous castings.

In reply to Mr. Burns' question about the mechanical properties, I do not believe we are in a position as yet to say what the typical properties of Mg-Zn-Zr alloys are. I am assuming that the properties which Mr. Burns has cited refer to an alloy containing 5 to 6 pct zinc and 0.7 pct zirconium. We have also seen 28,000 to 30,000 psi yield strengths and 6 to 8 pct elongations in certain batches of this composition. I used the somewhat lower figures in this paper because those were the room temperature properties of the batch on which I also had elevated temperature data. I consider that these properties are related directly to the grain size. Whether one obtains 28,000 psi, and even higher, or 24,000 psi, and

somewhat lower, depends on whether the grain size is 0.002 to 0.004 in. or 0.007 to 0.014 in., respectively. The control of the grain size of these alloys, particularly in production size castings having sections of varying thickness, is a problem that requires considerable further investigation.

J. W. MEIER*—The paper by Dr. Leontis covers a very wide field and represents a considerable amount of experimental work. The author is to be congratulated for his effort and the presentation of the results.

Experimental work on higher strength magnesium alloys at the Canadian Bureau of Mines included also many alloys based on the Mg-Zn system. Since most of our work is still not published, I would like to mention only some of the results which differ from the data presented by Dr. Leontis.

Our results of tensile properties at room temperature for the binary Mg-Zn alloys, both in the "as cast" and the "HTA" conditions, show (Fig 26) an increase of UTS for the zinc range of 8–11 pct to over 30,000 psi and over 40,000 psi respectively, with elongations of 7–8 pct.

These results are based on alloys prepared from high-purity magnesium and electrolytic zinc, without any manganese additions.

The mechanical properties at room temperature for Mg-Zn-Zr alloys, reported by the author, would seem to be somewhat lower than average results

achieved in our investigations. As already reported* "as cast" ZK61 alloy test bars showed average UTS of 38–40,000 psi, 0.2 pct PS of 20–22,000 psi and elongations over 10 pct. Grain sizes of the Mg-Zn-Zr alloys, shown in Table 2, reveal that the "effective" zirconium content in alloys 18–24 was rather low. Our investigation showed that the best mechanical properties in these alloys can be achieved only if the zirconium content is well above 0.7 pct and the average grain size is in the range of 0.001–0.002 in., in any case below 0.003 in.

Special heat treatment cycles were established for these alloys which increased considerably the mechanical properties without any effect on the grain size. Maximum results on fully heat treated ZK61 alloy castings of 48,000 psi UTS, of 35,000 psi 0.2 pct PS, and of 7–12 pct elongation were achieved. Considering the strength-to-weight ratio, these alloys have tensile properties superior to any aluminum casting alloys.

Another interesting characteristic of the Mg-Zn-Zr alloys is room temperature aging. "As cast" test bars, stored for some time at room temperature, show considerable increase of proof stress and hardness, as well as some increase of the UTS. Although a more systematic study of this problem is still under way, it may be said that increases of UTS up to 3,000

*J. W. Meier and H. Livingstone: A Study of Magnesium-Zirconium Sand Casting Alloys. Paper presented at the General Meeting, Canadian Inst. of Min. and Met., Vancouver, B.C., Apr. 7, 1948.

* Canadian Bureau of Mines, Ottawa, Canada.



FIG 27—Risers cut from test bar castings—Binary Mg-Zn alloys. Each melt treated with equal amounts of hydrogen compound.



FIG 28—Same as Fig 27, risers sectioned to reveal internal porosity.

psi, and of 0.2 pct PS up to 6,000 psi, have been found.

The effect of calcium additions to Mg-Zn-Zr in the range of 4-6 pct Zn was found to be detrimental to the tensile properties causing a considerable decrease of both the UTS and the elongation.

H. S. SPENCE*—This paper is a valuable contribution to the growing literature of magnesium and its alloys and the author is to be congratulated on both the work accomplished and its presentation.

There is one point which has been mentioned very briefly but which has important practical significance. This concerns the sensitivity to porosity of the binary magnesium-zinc alloys. Mr. Leontis states, in part, "Binary alloys containing more than 2 to 3 pct zinc . . . have a high porosity tendency. . . . All other binary and polynary alloys investigated were essentially free of porosity." Is it correct to infer that the binary magnesium-zinc alloys below 2-3 pct zinc were found to be essentially free of porosity?

It is stated that all alloy melts were prepared according to the 'crucible method' described by Nelson. Was any degassing attempted in the high zinc binary alloys using chlorine or any other agent?

Personal experience in alloying experiments confirms the findings of greater susceptibility to porosity in the higher zinc content binary alloys. This is certainly true with reference to hydrogen and the sensitivity in the range 2 to 6 pct zinc appears to be a function of zinc content. Fig 27 and 28 show this effect quite clearly; these illustrate risers cut from test bar castings from three melts containing respectively 1.89, 3.98 and 6.02 pct zinc. To each melt was added an identical quantity of hydrogen in the form of a metal hydride. The effect of zinc content in repressing the solid solubility of hydrogen is evident. Flushing similarly prepared melts with chlorine did not prove satisfactory in eliminating the hydrogen, even when using a quantity and treatment time in excess of that consistent with practical considerations.

Returning to Dr. Leontis' paper, it is interesting to note that his work does not

confirm earlier published data (J. A. Gann,⁶ National Physics Laboratory,⁶ P. Spitaler⁷) which indicate a fairly sharp maximum UTS of as-cast binary Mg-Zn alloys somewhere in the range between 4 and 6 pct zinc. While the earlier workers were not in agreement as to maximum UTS or its corresponding per cent zinc, all three curves indicated a definite maximum as opposed to the findings now reported which show a constant UTS over the range from 2 to 7 pct zinc. Does the answer to this difference lie in the number of determinations made in the present work with the consequent elimination of erratics, or is it in variations in the foundry techniques used by the different investigators? I suggest it may be the latter since, as these alloys respond to heat-treatment, varying cooling rates after casting may produce effects equivalent to different degrees of partial heat-treatment.

M. W. MARTINSON*—This paper has been a valuable contribution to the magnesium industry, particularly to

⁶ References are at end of discussion.

* Dominion Magnesium Limited, c/o Bureau of Mines, Ottawa, Canada.

* Dominion Magnesium Limited, Haley, Ont., Canada.

those associated directly with the development of new and better alloys and should serve as a basis for the further study of magnesium base alloys containing zinc, zirconium and rare earths.

Mr. Leontis states that, "The addition of 3 pct cerium added to Mg-3Zn improves the strength properties at 300 and 400°F, but is detrimental to room temperature strength. The addition of 3 pct zinc to Mg-3Zn to make Mg-6Zn alloy, however, results in still higher properties at elevated temperatures than those of the alloy containing cerium, and at the same time, is beneficial to the strength at room temperature."

Reviewing the creep data presented for these alloys we find that Mg-3Zn-3Ce is considerably superior to Mg-6Zn at both 300 and 400°F at all loads tested.

Early in our investigations carried out at the Canadian Bureau of Mines in Ottawa, we concluded that zinc had the advantage of raising the mechanical properties of magnesium base alloys intended for elevated temperature use up to 300°F, but above this temperature its presence was detrimental, particularly increasing the creep rate of these alloys.

This raises a question. From the engineering point of view, at what point does the author consider tensile properties to be overshadowed by creep properties in the final evaluation of a magnesium base alloy for elevated temperature use?

In the making of the various magnesium base alloys containing cerium and zirconium: 1. Was it necessary to degas the melt in any manner before or after the zirconium chloride fused salt addition, or was the refining effect from the fused salt mixture sufficient? 2. To what degree did a varying iron content in the Mischmetal added affect the final zirconium analysis? 3. Could the author give an idea of the initial alloying efficiency to be expected for both the rare earths and zirconium additions? 4. What recovery of rare earths and zirconium can be expected on remelt, and what methods are used to revivify the rare earths and zirconium losses to restore the initial properties of the alloy?

C. J. P. BALL*—My metallurgical staff and I were greatly interested in the paper by Mr. Leontis and I attach some detailed comments by my staff upon certain points in which they are particularly interested. Since Mr. Leontis touches upon the development and usage of magnesium-zirconium alloys, I think you would be interested to learn the present position in the United Kingdom as regards the magnesium-base casting alloys containing zinc and zirconium with and without Mischmetal.

At our Clifton Junction works we have carried out, over a number of years, a considerable volume of research and develop-

ment work on these zirconium-containing alloys. Two major problems presented themselves, and both had to be solved at a reasonable cost. The first was the introduction of sufficient zirconium in effective form without serious chloride contamination, the second, the suppression of microporosity, which has always presented a danger with all forms of magnesium alloys, and which can also ruin castings in high strength zinc-zirconium containing alloys unless the correct technique is used.

I am glad to say that special alloying compounds and fluxes have been evolved by my company, which enable the alloying to be carried out simply and at a reasonable cost, with no danger of flux contamination, and which yield a zinc-containing alloy virtually free from microporosity even in the thickest sections. As a result this alloy, Z5Z, (4.5 pct zinc, 0.7 pct zirconium) is being called for in rapidly increasing quantities for many structural castings, particularly in the aircraft industry. The properties of the casting are remarkably uniform, and frequently exceed those of separately cast test bars. Because of the ease with which this alloy can be handled in the foundry and the superior mechanical properties at room temperature, it is expected that this alloy will replace the greater part of the magnesium-aluminum-zinc alloys at present used for structural purposes.

The advances made recently in the magnesium-base alloys containing Mischmetal in addition to zirconium and zinc have been most striking. Because of their resistance to creep at temperatures around 200°C, their main applications so far have been elevated temperature work. The ZRE1 alloy (2.7 pct zinc, 2.7 pct Mischmetal and 0.7 pct zirconium) has made particular progress. Its properties at room temperature are—

| | |
|------------------|-------------|
| Yield | —14,000 psi |
| Tensile strength | —23,000 psi |
| Elongation | —5 pct |

Around 200°C its resistance to creep is practically identical with that of RR.50, the well-known general-purpose aluminum-base alloy widely used in the United Kingdom for service at elevated temperatures. Incidentally, the tensile strength of 15,000 psi given in the recent American Specification AMS.4428 would seem to compare most unfavorably with the corresponding figure for ZRE1, particularly since the small margin of 2,000 lb only between tensile and yield indicates the inherently brittle nature of this alloy at room temperature in the cast state.

Practical experience in the fabrication of the largest and most complicated castings, even as high as 900 lb net weight, has proved conclusively that the ZRE1 alloy containing not less than 2 pct Mischmetal is inherently free from any tendency to microporosity.

This concludes my short resume of the development and present position of the

magnesium-zirconium-zinc and magnesium-zirconium-zinc-Mischmetal alloys in this country.

Writing as a member of the AIME, it is my hope that this survey will be found of interest to Mr. Leontis and to those who have taken part in the discussion.

As we understand that considerable work on magnesium-zirconium-zinc and magnesium-zirconium-zinc-Mischmetal alloys is also being carried on in the U.S., perhaps some of the members taking part in the discussion would be able to answer the following questions: 1. Are magnesium-zirconium containing castings now being produced readily free from flux inclusions? 2. Can large castings be made readily in magnesium-zinc-zirconium free from microporosity? 3. Are alloys of magnesium-zirconium-zinc-Mischmetal readily available to the trade?

A. C. JESSUP* and J. B. WILSON*—Mr. Leontis has presented extensive data on magnesium alloys, and since his paper summarizes the properties for many alloys for which published values are not otherwise available, it provides most interesting reading for all workers in the magnesium industry. The article is, however, a little difficult to follow, and the comments and figures occasionally appear somewhat contradictory, nor do we in all cases agree with the inferences which have been drawn.

For instance, Fig 29 shows the effect of adding calcium in amounts up to 1 pct to a Mg-Zn-Zr alloy; in our opinion this shows calcium to be positively injurious. We would agree that the addition of cerium produces a similar reduction in room temperature properties, but for high temperature service the advantage of enhanced creep resistance more than outweighs the disadvantage of lower room temperature properties.

On p. 19 of his paper, the author claims that the Mg-6Zn-0.5Mn alloy is comparable for strength and ductility at all temperatures with the Mg-6Zn-1Zr alloy, and quotes Fig 10. We are not able to substantiate this sweeping statement. While we do not recommend the use of Mg-Zn-Zr alloys at temperatures above 300°F, and favor a lower Zn content, our experience based upon hundreds of tests and many tons of production, has satisfied us that the room temperature properties of a Mg-4.5Zn-0.7Zr alloy when prepared with the proper alloying reagents are certainly higher than the author quoted for Mg-6Zn-0.5Mn at room temperature. In Fig 10, the room temperature properties of the manganese containing alloy are given as:

| | |
|------------------|-------------|
| Yield | —24,000 psi |
| Tensile strength | —38,000 psi |
| Elongation | —5 pct |

* Magnesium Elektron Limited, London, England.

* Magnesium Elektron Limited, Clifton Junction, Manchester, England.

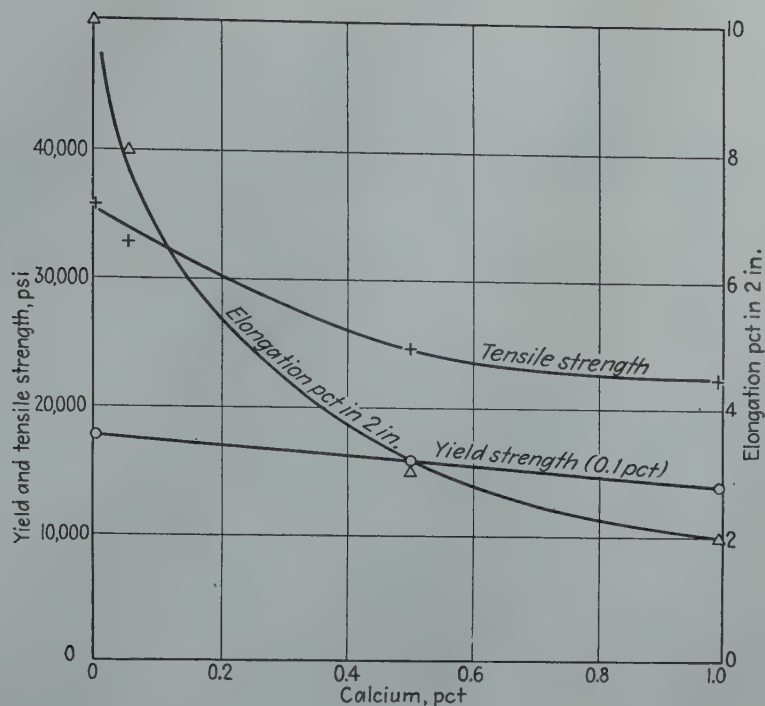


FIG 29—Effect of adding calcium in amounts up to one per cent to Mg-Zn-Zr alloy.

Comparable properties for a Mg-4.5Zn-0.7Zr alloy when tested as an unmachined "American" type test bar, after an annealing treatment of 10 hr at 350°F, are:

Yield —27,000 psi
Tensile strength—40,000 psi
Elongation —5 pct

Moreover, pronounced freedom from microporosity and grain coarsening on heat treatment, and small variation in mechanical properties between test bars and specimens cut from the casting, make this alloy particularly attractive to the foundryman. We have not had much experience with the 6 pct zinc-0.5 pct manganese alloy, but such as we have had has shown it to be even more microporous than AZ92, which in turn suffers much more from microporosity than the 4.5 pct zinc-0.7 pct zirconium alloy.

The improvements offered by the Mg-Zn and similar alloys over the AZ92 and AZ63 alloys are noted with interest. We feel, however, that the all-round properties of these alloys do not offer to magnesium founders the great advances and improvements in properties and casting techniques which they can obtain from the Mg-Zr-Ce alloys developed by Murphy and Payne or from the alloys of Mg-Zn-Zr-Ce, designated ZRE1 and ZRE2, recently developed in the United Kingdom by Magnesium Elektron

Ltd. These latter contain nominally Mg-2.7Zn-0.7Zr-2.7Ce and Mg-4.5Zn-0.7Zr-2.0Ce, respectively. Mr. Leontis has tested two closely similar compositions (his alloys 28 and 30) and finds them among his most promising alloys at 300°F. It was surprising to find therefore, that he did not investigate this type of alloy in more detail at 400°F, particularly in view of their extremely attractive combination of properties over the 60–400°F range. In Fig 30, we have plotted several of the author's results from Tables 6 and 7 at 300 and 400°F and have added a few of our own obtained at 400°F. In this diagram we consider *creep rates* only, since, in our opinion, the use of an arbitrary "creep limit" is likely to prove misleading.

Our results include the ZRE1 and ZRE2 alloys and also the Mg-3Ce-0.7Zr composition (MCZ) as developed by Murphy and Payne. We find that there is little to choose between the MCZ and ZRE1 alloys over the 60–400°F range of temperatures. The zinc containing alloys are, however, distinctly easier to handle in the foundry. The superiority of the cerium bearing alloys at 400°F requires no comment.

The author states on p. 29 and 31 of the paper that zinc lowers the creep resistance of Mg-Ce alloys. This may well be true in the particular case of zinc

additions to the binary Mg-Ce alloy. However, all our experience has shown both in tests and in practical foundry production that if the full amount of effective zirconium is present, considerable amounts of zinc may be tolerated without adverse effect upon creep resistance. This is demonstrated by Mr. Leontis' own experience with compositions 28 and 30 and our experience with the alloys ZRE1 and ZRE2. This may be due to the suppression of the formation of zinc phase when zirconium is present, which would in turn prevent the "dilution" of the cerium compound by zinc compounds at the grain boundary, and would enable it to act as if the zinc were absent. If Mr. Leontis did not find the Mg-Ce-Zn-Zr alloy quite as satisfactory as the Mg-Ce binary for creep, then judging from the results he quotes for other zirconium containing alloys, it would seem to be probable that his results are unsatisfactory because he has not been able to introduce into his alloy the necessary amount of effective zirconium to counteract the zinc.

In conclusion, we should like to record that these differences of experience and interpretation apply only to a small part of the paper, the majority of which is entirely in accord with our own work and experience.

T. E. LEONTIS (author's reply)—It is

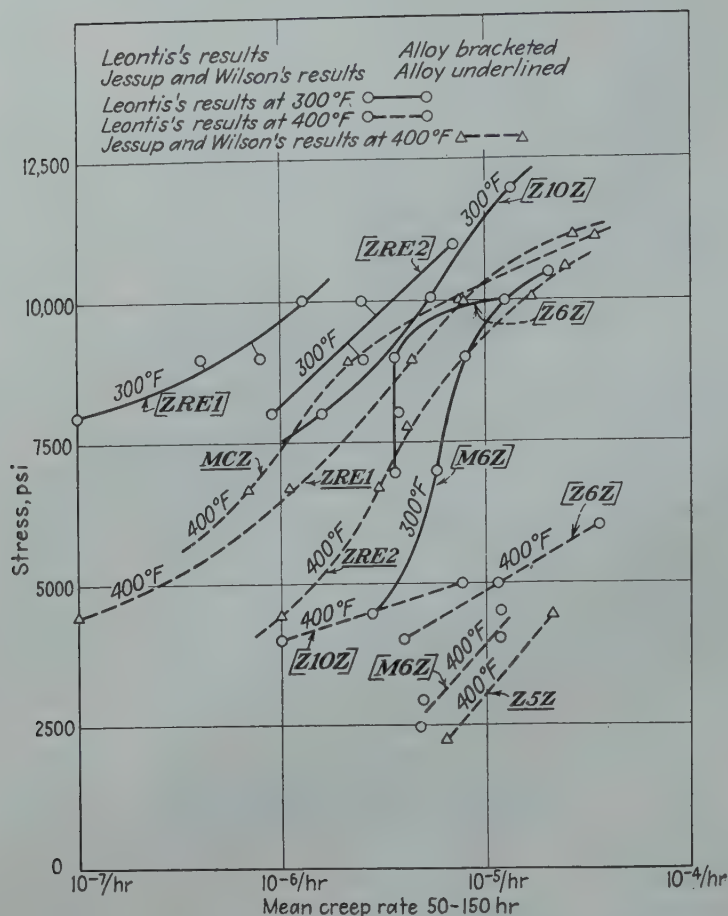


FIG 30—Plot of results from Tables 6 and 7 at 300° and 400°F, and others at 400°F.

gratifying to see that this paper has aroused so many interesting discussions from our friends in Canada and Great Britain. In the following, I shall attempt to present briefly my views on the many questions raised by the various contributors.

Mr. Meier and Mr. Spence have mentioned the properties of binary Mg-Zn alloys. It is interesting to note that the tensile yield strength of their alloys both in the as-cast and in the heat treated and aged condition, as shown in Fig 26 of Mr. Meier's discussion, are in reasonably good agreement with the values given in Fig 6, particularly if the curve for the heat treated and aged condition is drawn through all the points as is done in Fig 6. In regard to the tensile strength, if one looks at the experimental points rather than the curves drawn in Fig 26, again the agreement is good between the two sets of data up to 7.5 pct zinc. The absence of a sharp maximum in this property between 4 and 6 pct zinc that was observed by earlier investigators, as mentioned by Mr. Spence, is noted also in Fig 26. The markedly higher values de-

picted by Mr. Meier's results in alloys containing 8 to 11 pct zinc must be associated with differences in foundry practice. Perhaps the conditions of preparing the alloys were such as to result in a finer grain size and, what is more important in alloys containing a large amount of zinc, in a finer distribution of the intermetallic compound. Other factors that also may affect the tensile strength of Mg-Zn alloys have been cited by Mr. Spence. In reply to the question about the porosity of binary Mg-Zn alloys, my observations of freedom from porosity in alloys containing up to 2-3 pct zinc were made on cast test bars. The evidence that Mr. Spence has presented indicates that difficulty can be expected in larger casting even in the lower zinc contents. Attempts made to minimize porosity in Mg-6Zn alloy by chlorination have not been very successful.

In line with the observations of Mr. Burns, Mr. Meier has reported some still more spectacular properties for cast ZK60 alloy. Their high strength and ductility values are associated undoubtedly with the very fine grain size that Mr.

Meier was able to achieve in his alloys. As he has noted, in many of the alloys in the paper the zirconium content mentioned is below 0.7 pct, an amount which he feels must be exceeded in order to attain the finest possible grain size. However, alloys prepared recently in which the zirconium content exceeded his minimum have not confirmed his findings either with respect to grain size or properties.

Turning to the comments of Major Ball concerning Mg-Zn-Zr alloys, I was very interested to hear of his successful application of these alloys in the foundry. We have been successful in producing certain castings in ZK60 alloy free from flux, porosity, and cracking. The flux problem can be eliminated by proper treatment as discussed above. However, difficulties are sometimes encountered with porosity and cracking when more intricate castings are made from this alloy. The ingredients for making up these alloys are freely available in the United States on the open market.

The question of room temperature strength vs. elevated temperature strength and creep resistance raised by

Table 10 . . . Comparison of Alloys

| Temp. °F | Mg + 6Ce | | | Mg + 3Ce | | | Mg + 3.1Zn + 2.7Ce + 0.45Zr | | |
|----------|----------|----------|------|----------|----------|------|-----------------------------|----------|------|
| | Pct E | TYS | TS | Pct E | TYS | TS | Pct E | TYS | TS |
| | | 1000 psi | | | 1000 psi | | | 1000 psi | |
| Room | 1.0 | 17.0 | 20.4 | 1.5 | 12.4 | 20.5 | 3.8 | 13.4 | 22.3 |
| 300 | 2.0 | 14.9 | 19.3 | 7.0 | 12.9 | 17.9 | 14.4 | 11.9 | 21.7 |
| 400 | 2.0 | 14.7 | 18.6 | 4.7 | 11.9 | 16.8 | 19.8 | 11.6 | 18.4 |
| 500 | 4.0 | 13.4 | 17.9 | 11.7 | 11.3 | 17.9 | 44.0 | 9.7 | 14.4 |
| 600 | 12.5 | 9.8 | 14.3 | 24.2 | 8.8 | 13.5 | 66.5 | 6.7 | 9.1 |

The data are self-explanatory.

Mr. Martinson is one which is frequently asked but it is not answered very often, at least not to the satisfaction of designers and engineers. Certainly, if a part is to be exposed to sustained loads of predetermined value at elevated temperatures, the resistance to creep at those temperatures would necessarily be the controlling factor in design. However, it is always necessary to make provision for overloading which may occur during operation or during assembling of the part. For this reason, it will be found that the highest possible static properties are desired both at room temperature and at elevated temperatures in order to reduce failures to a minimum. Thus, in the selection of an alloy for elevated temperature service, a compromise may have to be made between static properties and creep resistance. The answers to questions of Mr. Martinson concerning foundry practice are as follows: 1. This has been answered adequately in reply to Mr. Burns' discussion. 2. We have no data from a systematic investigation of this effect. There unquestionably is a lowering of zirconium content resulting from the introduction of iron when Mischmetal is added to the melt and it certainly would be expected that the degree of lowering will be dependent on the amount of iron added. 3. The initial alloying efficiencies of rare earths and zirconium are:

Pct
Rare earths..... 80-90
Zirconium..... 20-40
4. The losses of rare earths and zirconium in absolute amount upon remelting are approximately:

Pct
Rare earths..... 0.5
Zirconium..... 0.1-0.2
The revivification of rare earths and zirconium is accomplished by adding the amount lost after remelting. The additions are made on the basis of the alloying efficiencies given above.

The discussion of Messrs. Jessup and Wilson contains many interesting points, some of rather controversial nature. I was interested to see their results on the effect of calcium on the properties of Mg-4.5Zn-0.7Zr alloy. It will be noted in the paper that the claim for an enhancement of the properties by the addition of 0.3 pct calcium was made only for the

composition Mg-1Zn-0.7Zr. Fig 9 of the paper shows that the same addition of calcium to Mg-3.5Zn-0.7Zr results, if anything, in a slight decrease in room temperature tensile strength. It is apparent from these data and those of Messrs. Jessup and Wilson that the effect of a small addition of calcium to these alloys depends upon the zinc content; at low zinc contents there is an increase in strength which appears to go through a maximum between 0 and 3 pct zinc, and at zinc contents above 3-3.5 pct zinc there is a definite decrease in strength resulting from the calcium addition.

The properties of Mg-6Zn-0.7Zr (ZK60) and Mg-6Zn-0.5Mn (ZM60) are more readily compared in Table 9. With the data available at the time of the writing of the paper, I cannot see any great differences between the properties of the two alloys with the exception of the somewhat lower ductility of ZM60 at 300 and 400°F. It is true that higher strengths can be attained in ZK60; in fact, considerably higher properties than those cited by Messrs. Jessup and Wilson have been shown by Mr. Meier. As for the foundry characteristics of the two alloys, the statements made in the paper were based on observations from the casting of test bars and a few relatively simple castings. Since the writing of the paper, more extensive tests on the foundry characteristics both of ZK60 and ZM60 have shown that the latter alloy has a much greater porosity tendency in larger castings than the zirconium-containing alloy.

Both Major Ball and Messrs. Jessup and Wilson have indicated that for elevated temperature service they would favor an alloy of the Mg-Zn-Ce-Zr type. It has been the thesis of this paper that Mg-Zn-Zr alloys offer a combination of room temperature properties equivalent to those of the present Mg-Al-Zn commercial alloys and significantly higher creep resistance at elevated temperatures than the commercial alloys. Mg-Al-Zn alloys have been used widely in parts exposed to temperatures up to 300°F. With the higher resistance to creep of the Mg-Zn-Zr alloys, there is every reason to believe that these alloys would be satisfactory in many parts operating at temperatures as high as 400°F.

For applications at temperatures above 400°F, we in the United States have been recommending Mg-Ce alloys. Major Ball's comparison of the laboratory properties of ZRE1 alloy with those of E6 (Mg + 6 pct Ce) alloy as specified in AMS4428 is not proper. Specified minimum properties are always set lower than typical values. A more realistic comparison can be made by using laboratory data for both alloys. This is done in Table 10 where the properties of an alloy having an analysis similar to that of Major Ball's alloy and those of two Mg-Ce alloys are presented over a wide temperature range. All these alloys are in the heat treated and aged condition.

It is the contention of Messrs. Jessup and Wilson that the elevated temperature creep resistance of Mg-Zn-Zr-Ce alloys is equivalent to that of the Mg-Ce alloys. Since the writing of the paper a few alloys of the former type have been tested in creep at 400°F. The results of these tests together with the corresponding properties of two Mg-Ce alloys are tabulated below. All the alloys were tested in the heat treated and aged condition. In order to present a complete picture, the creep limits based on three levels of extension are given in Table 11: (1) 0.1 pct creep extension, (2) 0.2 pct total extension, and (3) 0.5 pct total extension. I prefer the use of a creep limit based on a specified amount of extension to the use of an actual creep rate for several reasons. In the first place, a creep limit can be used directly in design calculations. Secondly, during creep tests of short duration, the creep rate very often does not attain a constant value. Thus, such creep rates are unreliable for predicting behavior in practice. It can be seen from the above summary that the best creep resistance is offered by Mg + 6 pct Ce alloy. This fact, coupled with the superior strength of this alloy at elevated temperatures, renders the material more attractive than the Mg-Zn-Ce-Zr alloys for applications up to 600°F. On the basis of the above data, particularly the stress values for 0.2 and 0.5 pct total extension, it appears that the alloy ZRE1 approaches the creep resistance of Mg + 3Ce. Inasmuch as Messrs. Jessup and Wilson have presented only creep rates in

their discussion, it would be interesting to compare their figures with those obtained in the present tests. The values for the Jessup and Wilson alloys given in Table 12 were taken from their Fig 30. There are apparently wide discrepancies between the two sets of data. If creep rate were used exclusively for evaluating the creep characteristics of the alloys, the present author's results indicate a very significant superiority of the Mg + 3Ce alloy over the zirconium-containing alloys.

There is one factor that has not been considered as yet. Whereas all the results that I have presented were obtained on alloys in the heat treated and aged condition, there is no mention of any heat treatment made by Messrs. Jessup and Wilson. Presumably, all their tests were performed on material in the as-cast or in the as-cast plus aged condition. At the present time, I have creep data available on Mg + 4.4Zn + 3.7Ce + 0.55Zr at 300°F in both conditions. These are presented in Table 13 together with the corresponding information for Mg + 3.23Ce. On the basis of creep limits there is little to choose between the two conditions of heat treatment, but the creep rates show the ACA condition to render the alloys somewhat more resistant to creep. The Mg-Ce alloy is again superior to the zinc-containing alloy both on the basis of creep limits and of creep rates in spite of the somewhat lower cerium content. This information indicates that the lower creep rates reported by Messrs. Jessup and Wilson may be attributed to their testing the alloys in the ACA condition. However, this emphasizes the hazards of using only the creep rate in evaluating alloys for elevated temperature service. Inasmuch as the total extension obtained is the same in both cases, the lower creep rate of the alloys in the ACA condition means that more of the extension is obtained during loading and less during the creep test.

It has been proposed that perhaps the lower resistance to creep of the Mg-Zn-Ce-Zr alloys used in the present paper may be due to our inability to introduce a sufficient amount of zirconium in our alloys. The zirconium content of most of my alloys is admittedly lower than that claimed by Messrs. Jessup and Wilson as being necessary for attaining the highest possible creep resistance. However, reference to Table 1 in the paper shows that alloy No. 28 has the lowest zirconium content of the cerium-containing alloys and at the same time has been shown to have the highest creep resistance. In fact, the creep rates of the alloy with no zirconium given above are lower than those of either of the two zirconium-containing alloys. The data show that high creep resistance is associated with a high Ce/Zn ratio emphasizing again the predominant position of cerium in magnesium alloys for elevated temperature

Table 11 . . . Creep Limits Based on Three Levels of Extension

| Alloy | Creep Limit — 1000 psi (400°F) | | |
|------------------------------------|--------------------------------|-----------------------------------|-----------------------------------|
| | 0.1 Pct Creep in 100 hr | 0.2 Pct Total Extension in 100 hr | 0.5 Pct Total Extension in 100 hr |
| Mg + 6.33Ce | 10.7 | 9.6 | 11.8 |
| Mg + 3.23Ce | 10.0 | 8.3 | 9.9 |
| Mg + 3Zn + 2.8Ce | 7.8 | 5.7 | 8.4 |
| Mg + 3.1Zn + 2.7Ce + 0.45Zr (ZRE1) | 7.7 | 7.0 | 9.1 |
| Mg + 4.4Zn + 1.7Ce + 0.66Zr (ZRE2) | 5.8 | 5.8 | 7.4 |
| Mg + 4.4Zn + 2.8Ce + 0.57Zr | 6.4 | 6.2 | 8.0 |

Table 12 . . . Values of Alloys

| Creep Rate per hr (400°F) | | | | | |
|---|------------------------|-----------------------|---|-----------------------|----------------------|
| Mg + 3.1Zn + 2.7Ce + 0.45Zr ZRE1 Alloy | | | Mg + 4.4Zn + 1.7Ce + 0.66Zr ZRE2 Alloy | | |
| Stress psi | Present Data | Jessup and Wilson | Stress psi | Present Data | Jessup and Wilson |
| 7000 | 3.9×10^{-6} | 1.4×10^{-6} | 6000 | 6.8×10^{-6} | 2.4×10^{-6} |
| 9000 | 16.9×10^{-6} | 4.6×10^{-6} | 7000 | 18.8×10^{-6} | 3.3×10^{-6} |
| 11000 | 302.0×10^{-6} | 20.0×10^{-6} | 9000 | ∞ | 4.7×10^{-6} |

| Mg + 3.23Ce Alloy | | | Mg + 3.1Zn + 2.7Ce Alloy | | |
|-------------------|-----------------------|-------------------|--------------------------|-----------------------|-------------------|
| Stress psi | Present Data | Jessup and Wilson | Stress psi | Present Data | Jessup and Wilson |
| 8000 | 1.0×10^{-6} | | 5000 | 0.42×10^{-6} | |
| 9000 | 8.7×10^{-6} | | 6000 | 1.2×10^{-6} | |
| 10000 | 9.0×10^{-6} | | 8000 | 4.4×10^{-6} | |
| 11000 | 68.0×10^{-6} | | | | |

creep resistance. As for the necessity of the presence of zirconium to suppress the formation of the zinc intermetallic compound, it has been my observation that even small amounts of cerium alone added to alloys containing up to 6 pct zinc will produce this effect.

In conclusion, only time and further experience can settle current differences of opinion on the preferred magnesium alloys for either room or elevated temperature service. Relative costs based on the alloying elements used, and the foundry efficiencies attained, will certainly be a factor. At elevated temperatures, the actual temperature concerned, and the appropriate creep strengths in the best condition of heat treatment, will affect the decision. An urge for simplicity in foundry operations may result in a compromise of a few alloys of good average properties, rather than more alloys each with its specialized field of use.

I would like to thank all the contributors to the discussion of this paper for their stimulating comments and criticism. I shall be looking forward to seeing the results of their investigations in formal papers.

References

6. J. L. Houghton and W. F. Prytherch: Magnesium and Its Alloys. H. M. Stationery Office, London (1937)

p. 35, Fig 10. (Original from *Ind. and Eng. Chem.* (1927) 19, 1193.) National Physical Lab. Ibid, p. 38, Fig 15.

7. A. Beck: The Technology of Magnesium and Its Alloys. F. A. Hughes and Co., Ltd., London (1940), p. 133, Fig 168.

Table 13 . . . Creep Data on Mg + 4.4Zn + 3.7Ce + 0.55Zr at 300°F

| | Creep Limit—1000 psi (300°F) | | |
|--------------------------------------|------------------------------|-----------------------------------|-----------------------------------|
| | 0.1 Pct Creep in 100 hr | 0.2 Pct Total Extension in 100 hr | 0.5 Pct Total Extension in 100 hr |
| Heat Treated + Aged (HTA) | | | |
| As-cast + Aged (24 hr at 350°F (ACA) | 11.2 | 8.1 | 11.3 |
| Mg + 3.23Ce (HTA) | 11.5 | 7.8 | 11.8 |
| | 13.0 | 10.0 | 12.5 |

| Stress psi | Creep Rate per hr (300°F) | | |
|------------|-----------------------------|----------------------|----------------------|
| | Mg + 4.4Zn + 3.7Ce + 0.55Zr | | Mg + 3.23Ce |
| | HTA | ACA | HTA |
| 8000 | 0.6×10^{-6} | 0.2×10^{-6} | |
| 10000 | 0.8×10^{-6} | 0.4×10^{-6} | |
| 11000 | | 0.4×10^{-6} | |
| 12000 | 7.3×10^{-6} | 0.6×10^{-6} | 0.2×10^{-6} |

The Low Temperature Properties of Tin and Tin-lead Alloys

By H. S. KALISH and F. J. DUNKERLEY, Junior Members AIME

DISCUSSION

(P. R. Kostling and W. A. Johnson
presiding)

R. I. JAFFEE*—I should like to amplify the work of Kalish and Dunkerley on the basis of some work we did in conjunction with the National Lead Co. about three years ago, which is to be published in *Metal Progress* early in 1949.

In general, we confirmed the statement that 50-50 lead-tin is brittle at low temperatures. However, we investigated the lead-rich range, and found, as might be expected, that the lead plus $2\frac{1}{2}$ pct silver alloy and lead-rich lead-tin alloys had rather good low temperature properties, both in ductility, strength, and in Charpy impact values.

One observation made on alloys between the high tin range investigated by Kalish and Dunkerley and the high-lead range was that alloys with about 15 pct tin did not decrease materially in impact strength or in ductility, as temperature went down to -295°F . This point, it seems to us, should be emphasized, since the presence of tin, at least up to 15 pct, in a lead-tin solder is rather important for commercial applications because of the improvement tin makes in solderability and wetting power.

J. R. LOW, JR.†—The authors have presented a very interesting paper and one of the few describing a systematic investigation of the relationship between microstructure, composition and low-temperature brittleness in a series of alloys.

The only comment I should like to make is that I believe the use of the term "ultimate tensile strength" over the full range of the curve so labelled in Fig 3 of

the paper is misleading. As far as engineering design is concerned, this is a valid use of the term; however, in thinking about the mechanical properties of the metal, a distinction should be made between the quantity measured above and below the transition temperature. Above the transition temperature the ultimate tensile strength is a measure of the stress at which necking begins and is therefore related to the rate of strain hardening. Below the transition temperature, the fracture strength of the metal is being measured. For this reason the maximum ultimate tensile strengths referred to throughout the paper are in a sense fictitious maximums.

H. S. KALISH and F. J. DUNKERLEY (authors' reply)—The authors wish to thank Drs. Jaffee and Low for their comments on this paper. From the results reported here, we would predict a lead-silver alloy containing $2\frac{1}{2}$ pct silver would remain ductile at low temperatures and we are glad that Jaffee's work confirms this as well as our other work on the tin-lead alloys. It might further be speculated in agreement with Brick and Seigle¹⁶ that any alloy formed by the combining of any two or more face-centered cubic metals, such as silver and lead, should remain ductile to absolute zero.

The superior ductility of the 85-15 lead-tin alloy is indeed important as emphasized by Dr. Jaffee. Again this would be predicted if the T_B curve of Fig 11 were extrapolated to higher lead contents. Kostenets¹⁷ found that a tin-lead alloy containing 25 pct tin still remained ductile at -253°C , only 20°C above absolute zero.

We agree with Dr. Low that it would have been desirable to separate the so-called ultimate tensile strength above T_B

from that measured quantity below T_B . However, since we did not have true stress-strain, yield strength, work hardening moduli and other fundamental data available, we were not able to separate all the variables quantitatively and preferred to present the engineering tensile data in the form most useful to engineers. These necessary fundamental data, however, are being obtained in this laboratory so that a more rigorous analysis of these low temperature properties can ultimately be made.

Dr. Low is quite right that the rate of strain hardening is the most important factor in determining the tensile strength above T_B , while below T_B the fracture strength is the main component. In neither case, however, is the strain hardening or the fracture stress, respectively, the only component. For example, the ultimate tensile strength, Fig 3, could not be labelled fracture strength below T_B because considerable ductility remained to make an appreciable work hardening contribution to the tensile strength feasible. The necessary qualitative rationalizations of the tensile data of this survey report should be clarified and amplified by the forthcoming fundamental data currently being obtained in this laboratory.

References

16. L. Seigle and R. M. Brick: Mechanical Properties of Metals at Low Temperatures; A Survey. *Trans. Amer. Soc. for Met.* (1948), 40, 813.
17. V. I. Kostenets: Mechanical Properties of Metals under Static Load at Low Temperatures. *Jnl. Tech. Phy.* (U.S.S.R.) (1946), 16, I, IV, 515.

Thermal and Electrical Properties of Ductile Titanium

By E. S. GREINER and W. C. ELLIS, Members AIME

DISCUSSION

(P. R. Kostling and W. A. Johnson
presiding)

P. DUWEZ*—We would like first to

congratulate the authors for a very interesting piece of work on a difficult subject. We have been studying the thermal expansion of pure titanium for some time and have found the coefficient of expansion between room temperature and

800°C to agree closely with the value given by the authors. We are particularly interested, however, in the thermal expansion anomalies accompanying the $\alpha \rightleftharpoons \beta$ allotropic transformation.

On specimens machined out of a bar

* Jet Propulsion Laboratory, California Institute of Technology.

manufactured by the vapor deposition process (obtained from Foote Minerals) we have observed a contraction on heating and an expansion on cooling, both around 880°C. The change in length varied somewhat from sample to sample, but was about 0.05 pct. This anomaly in the expansion curve was almost negligible on heating and completely absent on cooling when the bar was cold worked (reduction of area about 30 pct) before the test. The same experiments made on sintered titanium (from Bureau of Mines powder) did not reveal any thermal expansion anomalies.

We would like to ask the authors if they have made any measurements of thermal expansion across the α , β critical temperature and we would appreciate very much their comments on the subject.

W. C. ELLIS and E. S. GREINER (authors' reply)—The discussion by Professor Duwez of the volume changes in the 885°C transformation as evidenced by linear expansion measurements is particularly interesting and the additional data are welcomed. The authors made similar measurements on Bureau of Mines titanium (magnesium-reduced) but did not report the results in the paper because of uncertainty as to their significance. In these experiments there was always a volume decrease on heating through the transformation but no detectable discontinuity on cooling. The result was a shortening of the specimen as it was cycled through the transformation. The cause of the shortening was tentatively assigned to a further sintering of the expansion specimen in traversing the transformation. This was possible since the expansion specimen was only approximately 75 pct reduced in area from the sintered compact and could reasonably be expected to contain a distribution of fine voids.

Sintering of the expansion specimens during test in the temperature range below 800°C, for which data were given in the paper, was insignificant, since the slopes of expansivity on heating and cooling in this temperature range were nearly identical. At the transformation temperature, however, because of the spontaneous rearrangement of atoms the facility for sintering appears to be greatly increased.

B. W. GONSER*—The authors did a very fine job, and everything is very much in order for the work that was covered.

My discussion is a little broader than the subject covered by the paper, but it is activated by noting the purity or type of titanium used. This whole subject of titanium purity is becoming very involved because of the difficulty of defining the metal which is used as the base for many fundamental investigations.

The Bureau of Mines powder, of course,

is not nearly as pure as that produced by iodide refining. Likewise, even iodide titanium varies quite widely in analysis. As measured by hardness, for example, it may go all the way from a Vickers hardness of 60 to 115. Therefore one should define very closely the base material used to give an indication of what the properties are going to be. This is involved because of the difficulty of determining many constituents. Particularly the non-metallics, as oxygen, nitrogen, or carbon, are difficult to determine, and yet are very profound in their effects.

I think if more fundamental work is done on titanium it should be done with very well defined iodide titanium, or even purer metal if there is a better method of making it, to get consistent results on a reasonably sound base.

This choice of base material is important because so much is being done with titanium on different bases and results can be confusing. A lot of work is probably going to have to be done over again from time to time with titanium of improved purity.

J. T. MILEK*—Did the authors observe the phenomenon which J. D. Fast and DeBoer, I believe, observed in their experiments with zirconium wire, that is, by impressing a dc current voltage on a zirconium wire one can change the wire from an embrittled wire to a ductile wire? The explanation given by the authors is that the oxide and/or nitride which cause the embrittlement in the wire are transported to one pole—I believe it was the cathode. While the above work was carried out on zirconium, did the authors observe the same phenomenon with the titanium wire?

Communicated: This phenomenon was observed by J. H. DeBoer and J. D. Fast and reported in *Rec. Trav. Chim.*, Vol. 2, pp. 161–167, (1940). DeBoer and Fast reported that as a piece of brittle zirconium containing oxide is placed under a high vacuum and a dc potential of such a magnitude that the wire attains a temperature of approximately 900°C, the oxygen will migrate through the bar and collect at the anode. This migration can be reversed any number of times by changing the polarity of the current. Ductility can be restored through the cathode by such treatment.

While the above phenomenon has been observed in zirconium metal it is not unreasonable to assume that it can occur in titanium metal, or perhaps by a stretch of the imagination, even in titanium alloys. This latter process may find commercial applications.

W. A. JOHNSON†—I find the results given in Fig 3 for the variation of the resistance with temperature rather interest-

ing, since above the transformation temperature the resistivity seems to decrease with rising temperature.

This is a rather uncommon behavior, and I wonder whether possibly the transformation does not occur quite as rapidly as is indicated, and this decrease in resistivity perhaps is simply a gradual transformation with an increasing amount of a lower resistance phase.

W. C. ELLIS—Dr. Gonser brought up the matter of the purity of the metal which was investigated. It was not high purity in the sense of some of our more usual metals, as shown by the analyses in the paper. I agree with Dr. Gonser that it is desirable to carry out fundamental investigations on metals of high purity. However, in view of the increasing commercial importance of titanium and the fact that the methods which produce the high purity titanium are expensive and have produced only small quantities in a lot, we think there is good reason to have data on the properties of magnesium-reduced titanium.

Mr. Milek brought up a very interesting fact. Ionic transport is not only found in impure zirconium, but is of general interest in other alloy systems. We ordinarily think of electrical conduction as electronic in metals, but in some metal systems there is good evidence that there is a transport by one of the ions. Data have been reported on transport of carbon in steels by applying dc voltage.

In answer to Mr. Milek's question, no experiments of this character were made in our work on titanium.

Mr. Johnson discussed the unusual occurrence of a decrease in electrical resistivity with temperature in the high temperature phase of titanium. The authors are also mystified by this, but believe that it is a real effect, and not the result of a slow transformation. On cycling the specimens through the transformation a number of times, the temperature of the transformation as shown by the electrical resistivity data occurred always at the same level.

J. L. WYATT*—In line with this discussion which has been completed, would you mind telling us how long you held your specimens at temperature before taking your measurements above 885°C.

E. S. GREINER—The sample used for the electrical resistance measurements at temperatures above 885°C was maintained at the respective temperatures for 15 to 30 min. Stabilized conditions for the measurement at the respective temperatures were established by the obtaining of essentially constant values of the resistance in two successive determinations.

* Battelle Memorial Institute.

* Babcock and Wilcox Co.
† Westinghouse Research Laboratories.

* National Lead Company.

Property Changes during Aging

By A. H. GEISLER Junior Member AIME

DISCUSSION

(P. R. Kosting and W. A. Johnson
presiding)

P. MELARA*—Dr. Geisler, would you say that the physical properties of tensile, yield, and ductility for an aluminum alloy aged at room temperature are comparable to the physical properties obtained by the aging at elevated temperature of the same alloy? I would consider the aging at room temperature to be for an indefinite period of time, for example, ten, twenty, or even fifty years.

A. H. GEISLER (author's reply)—I think that the properties which could ultimately be obtained by aging at room temperature can be predicted from those developed by aging at elevated temperatures. Although 50 years is probably not long enough for the strength of an alloy like 24S to attain that provided by aging at elevated temperature, eventually the strength on aging at room temperature should be greater. If a finite rate of precipitation obtains, I see no reason why room temperature should be any exception from the conventional behavior that the maximum strength or hardness and the time to attain it both increase with decreasing temperature of isothermal aging. Care must be exercised, however, to compare analogous portions of the aging curves; changes during the first few days of aging at room temperature may correspond to the initial hardness peak (as in the case of 24S alloy) whereas the main portion of the curve for elevated temperature aging corresponds to the second hardness peak.

J. B. HESS†—My comment involves a minor, and probably obvious point in connection with Dr. Geisler's description of the mechanism of "discontinuous precipitation," which he calls the "grain boundary reaction." According to the present viewpoint, this reaction is fundamentally recrystallization, with complete decomposition of the matrix accompanying the recrystallization. The author suggests that this recrystallization results from plastic strains produced by prior precipitation at the grain boundary areas.

A characteristic feature of the aging of magnesium base alloys is the onset of the grain boundary reaction at a very early stage of the process. In fact, metallographic and electron microscopic studies tempt one to believe that grain boundary precipitation in these alloys is of the pearlitic form, and therefore typically of the recrystallization type, from the very

start. Based upon the hypothesis of prior precipitation, it is also difficult to rationalize the fact that the recrystallization reaction frequently proceeds from the grain boundary into only one of the adjoining grains.

Fortunately another source of the strains to initiate recrystallization suggests itself. Thermal contraction is anisotropic in magnesium, so that in polycrystalline samples this property should produce strains during cooling from the solution heat treatment, identical in character to those reported to produce fatigue by thermal cycles in tin, cadmium, and zinc. While no evidence of thermal fatigue in magnesium has been reported, so that the severity of such strains in magnesium are probably less, still I have been able to demonstrate their existence by use of Barrett's X ray microscopy technique.

The grain boundary reaction has also been reported to be almost the exclusive type of precipitation in tin alloys containing bismuth (J. E. Burke and C. W. Mason: *Trans. AIME* (1942) 147, 300) where thermal contraction strains should be more severe.

Accordingly, the mechanism of "discontinuous precipitation" should probably be generalized to include recrystallization resulting from strains other than those of prior precipitation.

A. H. GEISLER—Perhaps the precipitation strains are not always responsible for the recrystallization reaction but quenching strains in anisotropic metals may sometimes contribute. On the other hand, these could hardly account for the reaction frequently observed with alloys of the isotropic metals Al, Cu, and Fe. In addition, I do not think that the existing data are sufficient to conclude that the recrystallization reaction can progress in the absence of general precipitation in any alloy system.

I appreciate the usefulness of the electron microscope in extending the resolution of precipitates but some of the existing replica techniques do not permit full utilization of this increased resolution. I would not conclude that general precipitation was absent without consulting X ray patterns of single crystals. While a minimum quantity in excess of a few percent by volume must be present in order to detect the precipitate by X ray diffraction, the restricting particle size may be well below that for electron microscopy as currently applied to metals.

A slight misstatement of my conclusions regarding the recrystallization reaction should probably be clarified. This process is presumed to result from plastic strains produced by precipitation throughout the grains, not at the grain

boundaries alone. It is nucleated at grain boundaries not because of preferential precipitation here but because the activation energy is lower much as in the cases of localized precipitation and the decomposition of austenite into pearlite. I see no difficulty in rationalizing the morphology of the recrystallized nodules; it is identical with that of pearlite. Growth into only one of two adjoining grains suggests a favored orientation relationship between the distorted matrix and the recrystallized matrix analogous to a recrystallization texture.

F. C. HULL*—One of the previous discussers asked whether long time aging at room temperature would be comparable to a shorter period at an elevated temperature. I believe the results as judged from physical property tests might be very similar, but that if one could count the number and size of "coherent" regions and precipitated particles, a difference would be found. In the case of the isothermal transformation of austenite to pearlite at subcritical temperatures, it has been found that the rate of nucleation increases more rapidly with undercooling than the rate of growth.† At low transformation temperatures, therefore, the austenite reacts to form a larger number of smaller pearlite nodules. Nucleation and growth in age hardening systems might behave in a similar manner.

A. H. GEISLER—It is generally agreed that the rate of growth of the precipitate as controlled by rate of diffusion decreases with aging temperature whereas the rate of nucleation as controlled by both the rate of diffusion and degree of undercool goes through a maximum with decreasing temperature of isothermal precipitation. Thus, complete precipitation results in more numerous but smaller particles at the lower aging temperature, a condition which has been assumed to be responsible for the greater ultimate hardness and strength.

W. A. MUDGE‡—I do not think we should allow the chairman to close this meeting without an expression of gratitude for the excellent work which has been done in this case by Dr. Geisler. It is only through such careful work as this that we may hope to understand eventually what happens in the complicated commercial age-hardening alloys, particularly those of high melting point, such as the nickel-base material, where age hardening is accomplished by two or

* Grumman Aircraft Engineering Corporation.
† University of Chicago.

* Westinghouse Research Laboratories.
† F. C. Hull, R. A. Colton, R. F. Mehl: Rates of Nucleation and Growth of Pearlite. *Trans. AIME*, (1942) 150, 185.
‡ International Nickel Co.

three elements. I hope that Dr. Geisler and his associates will at some future time have an opportunity to study these more complicated systems.

A. H. GEISLER—While studies of the mechanism of precipitation have been confined in the past to binary alloys for simplicity, they are now being extended to multi-component alloys. The first step has been considered alloys in which only one phase precipitates but eventually it will be desirable to study alloys in which two or more phases can precipitate simultaneously.

R. A. RANDEBAUGH*—It has been suggested by Bain that quench hardening might be considered a special case of age hardening, the properties as quenched being compared to the maximum properties in age hardening alloys, quenched and subsequently aged to develop optimum precipitated particle size.

I wonder if the author has given any consideration to the application of his theories to quench hardenable alloys?

A. H. GEISLER—Yes, the concept of coherency and the characteristics associated with this state have been considered for other reactions in solid solutions. The work in progress is concerned with superlattice formation but the eutectoid reaction will be investigated also. Current consideration of the martensite reaction as a nucleation and growth process and recognition of the product as a coherent transition lattice will facilitate the analogy.

A. GUINIER†—It is obvious that in

the regions where the concentration of foreign atoms becomes abnormally high, the matrix lattice is more or less disturbed.

On the other hand, the evidence indicates in many cases that it is not possible to describe the structure of these zones as the structure of the precipitate with slight changes due to the size of the nucleus and the coherency with the matrix lattice.

For instance, in Al-Cu alloys,³⁹ the streaks, visible on the X ray patterns (with monochromatic rays) in the early stages of aging, split, in a further stage, into diffuse spots definitely different from the spots of the θ' precipitate. That means that the structure of the "G.P. zones" cannot be considered as an imperfect θ' structure.

In Al-Ag or Al-Zn⁴⁰ alloys, the beginning of the aging is characterized by the fact that each node and also the center of the reciprocal lattice is surrounded by the same scattering zone which has the shape of a spherical shell. Such a diffraction effect is quite different from the one- or two-dimensional diffraction effects quoted by Dr. Geisler. This effect cannot be explained on the basis of the structure of the precipitate (Zn or Al-Ag₂); but it is very easily accounted for by the hypothesis of nuclei enriched in solute atoms and keeping without great change the structure of the matrix lattice.

Recent reports show that the zones of gathering of the solute atoms are by no means always plate-like, but that they also can be nearly spherical.⁴¹

A. H. GEISLER—The discussion so kindly submitted by Dr. Guinier is concerned with the interpretation of diffuse X ray diffraction effects, a subject that

was not discussed in the present paper but was considered in detail in Ref 77. Unfortunately, the latter was not yet in print when the present paper appeared. I entirely agree that the diffraction effects do not always suggest plate-like particles but change gradually as one, then two and finally three dimensions of the particle become adequate for sharp diffraction through normal growth at anisotropic rates. On the other hand, the evidence mentioned for Al-Cu alloys is no criterion for concluding that the structure causing the diffuse diffraction effects is different from the θ' structure. Results for an Al-Mg-Si alloy described in Ref 7 show that while spots in patterns for thin platelets do not coincide with those for large particles of precipitate, the configurations in reciprocal space determined by the analysis of not one but of many patterns are intimately related. In this case there is no question that the diffuse diffraction effects originate in a structure similar to that of the thick precipitate particles rather than the matrix. A possible explanation of the spherical zone of diffraction about matrix nodes of Al-Ag and Al-Zn alloys based upon structure of the precipitate is discussed in the cited reference.

References

7. *Acta Crystallographica*, Nov. 1948, 1 (5), 233-252.
39. *Jnl. de Phys.* VIII (1942) 124.
40. *Metaux et Corrosion* (1943) 18, 209.
41. F. R. N. Nabarro: Symposium on Internal Stresses—Inst. of Metals—London (1947) p. 237.

Factors Affecting the Tensile Notch Sensitivity of Magnesium Alloy Extrusions

By I. CORNET, Member AIME

DISCUSSION

(P. R. Kostling and W. A. Johnson
presiding)

J. C. McDONALD*—The type of work presented here by Professor Cornet had its origin in field observations which

seemed to indicate that magnesium was more notch sensitive than aluminum. As it was shown in our previous ASTM paper¹¹ and as confirmed by Professor Cornet's results, the static notch sensi-

tivity of wrought magnesium is similar to that of wrought aluminum. As shown in our ASTM paper, the field observations noted above were actually a consequence of the greater toughness of the high strength wrought aluminum alloys compared to the wrought magnesium alloys.

* Dow Chemical Co., Midland, Mich.

¹¹ Amer. Soc. for Test. Materials: *Proc.* (1946) 46.

Effect of Grain Size on Tensile Strength, Elongation, and Endurance Limit of Deep Drawing Brass

By H. L. WALKER, Member AIME, and W. J. CRAIG

DISCUSSION

(A. I. Blank and E. W. Palmer presiding)

A. I. BLANK*—This paper is a valuable addition to the published data on the effect of grain size on endurance properties of deep drawing brass sheet. Previous investigators^{7,8} of annealed wrought copper alloys have dealt mainly with the commercial ranges of grain size, and it is interesting to note that the data presented in this paper for commercial grain sizes closely confirm the earlier findings. This is probably the first time, however, that endurance properties for deep drawing brass of less than 0.010 mm grain size have been reported. Full advantage should be taken of the high endurance strength which is associated with these very small grain sizes.

As the authors have pointed out briefly, however, such grain sizes provide less ductility for forming purposes and, in addition, it will be appreciated that very small grain sizes are not too readily obtained in ordinary commercial practice. Special processing schedules and precise control of even nominal impurity content would normally be required to produce such grain sizes consistently and without the danger of incomplete recrystallization. These limitations are not intended, however, to detract from the merit of the authors' contribution.

H. L. WALKER (authors' reply)—The specimens upon which this work was conducted are from normal commercial production. The mill does not find it to be such a difficult task to control the grain size rather closely and the specifications call for a rather small variation in grain size. I should say the smaller grain sizes can be controlled within ± 0.002 mm diam. It is important to know the effects of ready-to-finish grain size and the amount of final cold reduction, and especially the latter. We have not encountered difficulties in securing complete recrystallization during the final anneal. The times and temperature of annealing are such that coalescence does not readily take place, which gives considerable flexibility in the annealing schedule. I should again like to point out that brass with the grain sizes reported here is being produced commercially.

L. W. GLEEKMAN†—I trust Professor Walker will not find me overbearing when I bring up a topic he said was not

going to be developed in this paper. That was with regard to the effect of grain size on tensile strength and grain size.

I notice your Fig 3 does not go beyond the value of grain size of 0.024 mm diam. I was curious as to whether the curve of elongation vs. grain size would show a maximum elongation at an intermediate grain size. My reason for this is that work I did on a 14-carat gold alloy showed that the elongation rose to a maximum at a grain size of 0.025 mm and then fell off rather appreciably at higher grain sizes. I recall that Jeffries and Archer⁹ and also D. K. Crampton,¹⁰ showed similar results for elongation versus grain size.

I wonder if elongations for the two larger grain sizes were reported, would you get that maximum and subsequent decrease?

H. L. WALKER—Professor Gleekman is not overbearing in asking the question. We felt that the larger grain sizes with respect to tensile strength and elongation had already been reported in the literature a number of times. I should expect the elongation to reach a maximum value and then decrease with very large grain size. The tensile strength would not however reach a minimum value and then increase with increased grain size.

E. W. PALMER*—I have a couple of points that I would like to bring up. One of them is concerned with the fact that starting with an initially small grain size and giving fairly heavy reductions is a very fine way to develop directionality in a material. I am wondering if Professor Walker cares to comment on what influence directionality might have had on his work, especially with respect to the direction of test of a fatigue specimen.

There is another point. In explanation of some of the annealing curves, there is some discussion of a recovery period. If this starting material were stress relief annealed to start with, I am puzzled as to what you mean by "recovery period," in Fig 1.

H. L. WALKER—With respect to the production of directionality I wish to comment that we believe the rolling schedule affects the production of directionality. In the paper as originally written the rolling schedule was specified, but the reviewers declared it to be unimportant and it was deleted from the manuscript. The rolling schedule does affect directionality and stresses. We have found that some alloys prone to fire

cracking during annealing may have the tendency to fire crack mitigated with proper adjustment of the rolling schedule. The diffraction patterns after recrystallization, and the tensile strength at 45 and 90° to the direction of rolling did not indicate any marked degree towards directional properties.

As to recovery, I consider recrystallization phenomena cover three distinct processes, the first called recovery, the second called recrystallization, and the third called coalescence.

Recovery I take to mean when in the X ray diffraction pattern there is a sharpening of the lines without appearance of any other visual changes. In other words, I believe there is a bringing together of the atoms into positions which give much sharper lines. Some may call this the incubation period for recrystallization. There may be the establishment of nuclei, but if so, they are not apparent from a diffraction pattern nor are they visible under the microscope.

The second process, recrystallization itself, I would define as the production of strain free grains through nucleation and growth, and strain free grains growing at the expense of strained grains for the establishment of an essentially strain free structure.

The third process, coalescence, is the growth of strain free grains at the expense of other strain free grains, and probably the driving force, or the energy exchange, is surface energy.

E. W. PALMER—With regard to recovery, would not that process of relief of strain on an atomic scale have occurred already in the strain relief anneal given to the material with which you started?

H. L. WALKER—Certainly some would have taken place. There is no question about that. But it does not necessarily indicate that it was complete, because I believe that recovery did take place in the series of anneals shown in Fig 1.

References

7. C. H. Greenall and G. R. Gohn: Fatigue Properties of Non-Ferrous Sheet Metals. *Proc. Am. Soc. Testing Mats.*, (1937) 37, Part II, 160.
8. H. L. Burghoff and A. I. Blank: Fatigue Properties of Some Coppers and Copper Alloys in Strip Form. Annual Meeting, June 1948, of Am. Soc. Testing Mats.
9. Jeffries and Archer: The Science of Metals. 1924, p. 161, McGraw-Hill, N. Y.
10. D. K. Crampton: *Metals Progress*, (1936) 29, 39-42.

* Chase Brass and Copper Co.

† University of Delaware.

^{7,8} References are at the end of the discussion.

* American Brass Co.

A Copper-base Alloy Containing Iron as a High-strength High-conductivity Wire Material

By W. HODGE, R. I. JAFFEE, Junior Member AIME, J. G. DUNLEAVY and H. R. OGDEN

DISCUSSION

(A. I. Blank and E. W. Palmer presiding)

P. G. MAGANUS*—The type of work we do is in the resistance welding field, and we are wondering if this particular alloy might not be satisfactory in the making of these particular machines we have in mind. We would like to know what the magnetic properties of this par-

* Progressive Welder Co.

ticular alloy are. In other words, if put in the field on current, we would like to know whether or not it would heat up.

W. HODGE (authors' reply)—I cannot give a definite answer to your question. The alloy we know is ferromagnetic. As to applying it to the application about which you have asked, we have done no experimental work along that line.

L. PESSEL*—What are the fatigue

* Radio Corporation of America.

properties of the alloy?

W. HODGE—We have actually made no fatigue tests on the alloy.

P. G. MAGANUS—I thought about melting and casting. I also happen to be a foundryman. I was wondering what this "Riser-X" was. The authors have it in quotes. Is that an iron base? I would imagine so, since it is exothermic.

H. R. OGDEN (authors' reply)—Yes, it is.

A High Strength-High Conductivity Copper-silver Alloy Wire

By W. HODGE, R. I. JAFFEE, Junior Member, J. G. DUNLEAVY and H. R. OGDEN, Junior Member AIME

DISCUSSION

(A. I. Blank and E. W. Palmer presiding)

W. HODGE—Since this paper was written the Signal Corps has sponsored the commercial development of this alloy. Work was carried out by the American Brass Co. under the able direction of R. D. Hull, and we are quite certain now that it is possible to produce an alloy of 6½ pct silver which will have high strength and high conductivity.

M. G. CORSON*—I am not in the habit of congratulating authors and I am quite sure they are in no need of congratulations, but I am glad that due to their efforts silver might become far more useful technically than it is today.

The characteristics of Cu-Ag alloys intrigued me long ago and it is now more than ten years since I broached the subject to the late W. H. Bassett of the American Brass Co. I did not experiment to such a great extent as the present authors did, nor did I get highly precise and uniform results. I saw, however, that with as little as 3 pct silver one might have copper conductor wire with over 100,000 psi strength and a conductivity of 90 pct. Besides, such wire is immune to permanent softening when exposed to a temperature up to 450°C.

Mr. Bassett could not see my suggestion from the commercial viewpoint, for obviously a wire with 3 pct silver would cost at least double the price of ordinary

copper. It is a fact that OFHC copper in spite of all its advantages has hard sledding because its price is about one cent higher per pound. This cost question will form an enormous stumbling block in the way of Cu-Ag alloys, but I hope the future belongs to it.

By the way, I also suggested such uses of copper to the Mexican government, for that country could produce far more silver if there were a demand for it. My suggestion was not even honored with a reply. It is ridiculous that silver cannot have a definite price because it is obtained mostly as a byproduct, and the price of silver depends upon the arbitrarily fixed value of residues from copper, lead and zinc production. If we were not still under the spell of the idea that silver is a precious metal of an inherently high price, the latter might (and should) drop enormously and silver would become just a technical metal; that is where it belongs.

Regarding the degassing of Cu-Ag alloys I should suggest to the authors that they try blowing into the molten alloy first a stream of carbon monoxide in order to eliminate oxides and oxygen, then a stream of dry, oxygen-free nitrogen to remove whatever CO is retained. I found the method to work well in a number of cases.

P. J. MAGANUS*—I am in full agreement with Mr. Corson on the fact that these alloys are rather expensive, because

we have worked with these alloys, too, in an experimental foundry that we have. If it were not for the fact that the stuff costs around 80 cents a pound, we probably could use it also in the resistance welding field.

One of the questions that I have is the fact that, in our foundry, when we used magnesium as a deoxidizer it also acted as a hardener all right, but it has the effect of absorbing gases or at least we get a lot of porosity when we have magnesium. When we forget to add magnesium and add other deoxidizers such as lithium or calcium borate or some of the other deoxidizers that work pretty well, we do not have that trouble. Can the author give us an idea?

In Fig 1 he gives the conductivity of these various elements and how much they depress the copper. I was wondering what magnesium does. In other words, I know that in the work we have done magnesium can knock down our conductivity to around 80 to 85 pct of copper, and with this conductivity we feel that we should not use it. Has the author some information on that?

W. HODGE (authors' reply)—The point you brought up, of porosity caused by magnesium, is very pertinent. In the laboratory we did not have trouble from porosity caused by magnesium, presumably because of the small melt.

When we attempted to cast larger ingots for cold rolling, the porosity caused by magnesium ruined our entire first

* Consulting Engineer, New York City.

* Progressive Welder Co.

attempt, and Mr. Hull, of the American Brass Co., finally decided to throw some borax on top of the melt, and by so doing he was able to get rid of most of the porosity caused by magnesium. Otherwise we could not have cast the alloy in the air at all. It would have had to be cast quite in a protected atmosphere.

On the other point on conductivity, I could only refer you to a rather old article by M. G. Corson, in which he de-

scribed the effect of magnesium copper alloys. I think it was written in about 1930 and occurs in the *AIME Transactions*.

E. W. PALMER*—I should like to congratulate the authors on the very fine development work that has resulted in these two new high-strength high-conductivity alloys.

The situation in copper-silver and copper-iron was gone over carefully years

* American Brass Co.

ago, looking for precipitation hardening effects. When no hardening was discovered, the systems were dropped.

The discovery by Mr. Hodge and his co-workers, that these precipitation hardened matrices have enormously high rates of work hardening that permit them to be drawn to very high strength is of fundamental importance, and the authors deserve a great deal of credit for this development.

The Effect of Chromium on the M_s Point

By J. B. BASSETT and E. S. ROWLAND, Junior Member AIME

DISCUSSION

(C. S. Smith and A. R. Troiano presiding)

A. E. NEHRENBURG*—From the practical viewpoint it is not particularly important whether 1 pct chromium lowers the M_s temperature of steels containing 1 pct carbon 65°F as indicated by the data just presented, or about 40°F as shown by Klier and Troiano.² This is because such high carbon steels are not austenitized commercially at a high enough temperature to dissolve all of the carbides present. In such cases the actual M_s temperature is considerably higher than one would predict on the basis of the known effects of the alloying elements present. However, it is somewhat disturbing that there should be this disagreement among these investigators. Perhaps a few comments on this discrepancy would be in order.

It seems to this discussor, in spite of the arguments of the authors to the contrary, that the possibility exists that the time allowed for the hot oil quench used for temperatures below 350°F may not have been long enough to permit the specimens to reach the bath temperature before they were tempered. It may be significant that in the authors' Fig 6 which shows the relation between the M_s point and chromium content for the two carbon levels studied, the five points which do not agree with published data all were obtained using hot oil for the initial quench. For the compositions which have M_s temperatures high enough so that molten salt could be used for their determination, there is good agreement with published data, even at the 1 pct carbon level. It is recognized, however, that there is one point based on a hot oil quench which does not deviate from the expected value.

In their paper Klier and Troiano² indicated that steps were taken to establish that the temperatures of the quenching baths used were attained. There is no indication that this was done in the investigation just described. Therefore this discussor is inclined to agree with Klier and Troiano that 1 pct chromium lowers the M_s temperature of steels no more than about 40°F irrespective of variations in carbon from about 0.40 to 1.3 pct.

It is of interest to compare the M_s points reported in the present paper with calculated values. Formulas which have been proposed for calculating M_s temperatures contain factors for carbon which vary from 540 to 650.^{1,8,9} The significance of this variation in the carbon factor can be established if common factors are assigned for each of the alloying elements in these formulas other than carbon.

The M_s temperatures shown in Table 6 were calculated by using the Grange-Stewart and the modified Payson-Savage formulas with common factors of 70 and 40 for Mn and Cr, respectively. The effect of the residual Si and Ni was neglected.

It will be noted that when the carbon content is about 0.50 pct the difference in the carbon factor used in these formulas has no effect on the accuracy of the calculated M_s temperature, and that there is good agreement with the measured values. The maximum deviation is only 20°F. When the formula containing the higher carbon factor is used 9 of the 12 steels have calculated M_s points which differ by only 10°F or less from the measured values. When the formula containing the lower carbon factor is used the calculated M_s temperatures of 10 of the 12 steels differ by no more than 10°F from the measured values.

At the 1.0 pct carbon level, however, calculations based on the formula having the higher carbon factor tend to be con-

siderably lower than those based on the one with the lower carbon factor, as the table indicates, and do not agree as well with the measured values.

Earlier in this discussion it was suggested that the M_s temperatures shown for the five higher chromium steels might be low. If that is so, there would be even better agreement between calculated and measured M_s points for the modified Payson-Savage formula than the table indicates and a greater deviation for the Grange-Stewart formula. Be that as it may, the results as they stand indicate that the modified Payson-Savage which contains the lower carbon factor appears to be more satisfactory at this high carbon level. Additional data which confirm this fact were presented in my discussion of the Grange-Stewart paper.

The carbon factor used in the Grange-Stewart formula is based on data published by Greninger¹⁰ and by Digges¹¹ which showed that 1 pct carbon in pure iron-carbon alloys lowers the M_s temperature 650°F. The carbon factor in the modified Payson-Savage formula was also based on data published by Greninger¹⁰ which showed that 1 pct carbon in commercial iron-carbon alloys corrected to 0 pct Mn lowers the M_s temperature 540°F. Since these differences in the carbon factor were reported by a single investigator it seems reasonable to conclude that the impurities present in carbon steels have an effect on the rate of lowering of the M_s temperature with increasing carbon.

Grange and Stewart in the closure to their paper¹ also presented data to show the effect of variations in carbon on the M_s temperature of carbon steels. These data and those of Greninger, corrected to 0 pct Mn, are plotted in Fig 7. There is good agreement among these investigators. Grange and Stewart not only confirm that 1 pct carbon lowers the M_s temperature of commercial steel 540°F, but

* Crucible Steel Co. of America.

² References are at the end of the discussion.

also show that the effect of carbon is not linear above about 1 pct. The rate of lowering of the *Ms* temperature with increasing carbon above 1 pct gradually decreases so that a correction based on Fig 7 must be made if the *Ms* temperature for a steel containing more than this amount of carbon is to be calculated.

It cannot be emphasized too strongly that *Ms* temperatures can be calculated only when the austenitizing temperature is sufficiently high so that there are no residual carbides present. Since this generally occurs commercially in only the medium carbon steels where either of the formulas discussed above is equally accurate, it usually makes little difference whether one or the other is used for the calculation of the *Ms* temperature. However, it should be remembered that the effect of carbon in commercial steels is somewhat less than the Grange-Stewart formula implies.

If it is desired to calculate the *Ms* temperatures of steels containing 1 pct carbon only the modified Payson-Savage formula can be used to obtain values which will be reasonably accurate.

The authors conclude that "as far as steels containing chromium are concerned, no simple formula is adequate for the accurate calculation of *Ms* points." This is contradicted by the fact that there is reasonable agreement with the authors' own data when the *Ms* temperatures are calculated using the modified Payson-Savage formula. Furthermore, data presented in my discussion of the Grange-Stewart paper showed that the agreement between calculated and measured *Ms* temperatures was remarkably good for the chromium steels 5140 and 52100 and for the 1 pct carbon steels containing from 1 to 9 pct chromium studied by Klier and Troiano.

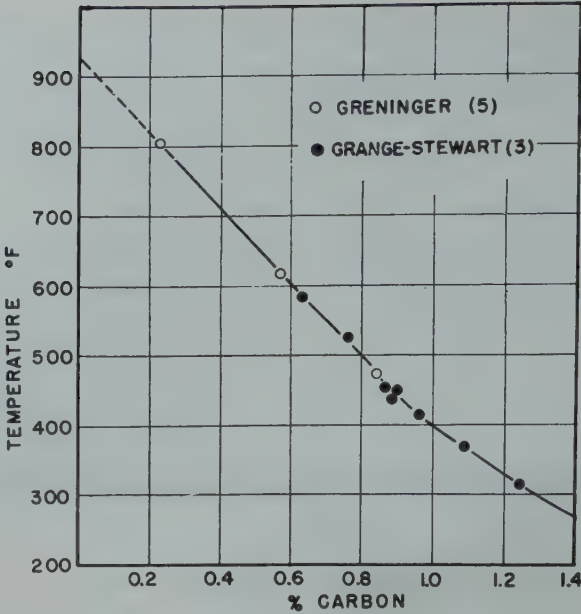


FIG 7—Effect of carbon on *Ms* temperature of carbon steels. Variations of carbon in plain carbon steels between about 0.2 and 1 pct lower the *Ms* temperature at the rate of 540°F per 1 pct carbon.

A. R. TROIANO*—There seems to be some question about the disagreement in the rate of lowering of *Ms* with chromium in the high carbon steels. Did the authors make any grain size determinations, or could they tell us approximately what the grain size was? In the work that Dr. Klier and I did, we had exceptionally large grains, and since we now know that the grain size may change *Ms* by as much as 35°C, it is possible that the disagreement may be caused by this phenomenon.

* University of Notre Dame.

If the authors had a smaller grain size, the deviation would be in the right direction.

E. S. ROWLAND (authors' reply)—The authors are indebted to the discussers of this paper for their comments and criticisms.

First, in answer to Mr. Nehrenberg, we fear that he missed the implication contained in the opening paragraph of the paper in regard to the effect of small variations in chromium content on the *Ms* temperature. The curve of Fig 11 of the Grange and Stewart¹ paper indicates that the effect of chromium on *Ms* might be very much greater than previously anticipated in the range of chromium contents normally expected to be in solution in the austenite of SAE 52100 at its commercial austenitizing temperature (about 1550°F). It was conceived possible that small variations in austenitizing conditions might produce a significant shift in the martensite temperature range if the above curve expressed the true relationship. Mr. Nehrenberg is right in stating that the difference between 40 and 65°F per 1 pct chromium is unimportant but an effect two or three times either of these values at low chromium contents would have been important. As it turned out, the relationship between chromium and *Ms* temperature is undoubtedly linear and this effectively disposes of any such arguments.

Mr. Nehrenberg's second criticism is much more serious since it throws doubt upon the validity of all the data obtained by questioning the fact that the specimens actually reached the quenching bath temperature. In the first place, the

Table 6 . . . Effect of Carbon Factor on Calculated *Ms* Temperatures

| Steel | C | Mn | Si | Ni | Cr | Measured <i>Ms</i> , °F | Calculated <i>Ms</i> | | Deviation | |
|--------|-------|------|-------|------|------|-------------------------|------------------------------------|------------------------------------|-------------------------|-------------------------|
| | | | | | | | 540 (a) Carbon Factor, °F | 650 (b) Carbon Factor, °F | 540 Carbon Factor | 650 Carbon Factor |
| 1 | 0.53 | 0.79 | 0.30 | 0.12 | 0.01 | 590 | 590 | 600 | 0 | +10 |
| 2 | 0.505 | 0.79 | 0.29 | 0.12 | 0.24 | 586 | 590 | 605 | +4 | +19 |
| 3 (1) | 0.51 | 0.79 | 0.30 | 0.11 | 0.51 | 575 | 580 | 595 | +5 | +20 |
| 4 (2) | 0.46 | 0.80 | 0.355 | 0.14 | 0.56 | 610 | 605 | 625 | -5 | +15 |
| 5 | 0.51 | 0.80 | 0.28 | 0.12 | 0.74 | 575 | 570 | 585 | -5 | +10 |
| 6 | 0.505 | 0.79 | 0.29 | 0.12 | 1.03 | 570 | 560 | 575 | -10 | +5 |
| 7 | 0.495 | 0.77 | 0.29 | 0.12 | 1.27 | 565 | 555 | 570 | -10 | +5 |
| 8 | 0.50 | 0.80 | 0.28 | 0.12 | 1.54 | 555 | 545 | 560 | -10 | +5 |
| | 0.47 | 0.80 | 0.355 | 0.21 | 2.09 | 555 | 535 | 555 | -20 | 0 |
| 17 | 0.485 | 0.34 | 0.24 | 0.11 | 1.05 | 620 | 600 | 620 | -20 | 0 |
| 18 | 0.48 | 0.35 | 0.25 | 0.11 | 1.32 | 600 | 595 | 610 | -5 | +10 |
| 19 | 0.48 | 0.34 | 0.26 | 0.13 | 1.45 | 595 | 590 | 605 | -5 | +10 |
| 9 | 1.075 | 0.33 | 0.30 | 0.12 | 0.01 | 330 | 325 | 275 | -5 | -55 |
| 10 | 0.95 | 0.35 | 0.24 | 0.11 | 0.27 | 400 | 380 | 350 | -20 | -50 |
| 11 (1) | 0.965 | 0.35 | 0.255 | 0.10 | 0.53 | 380 | 365 | 330 | -15 | -50 |
| 12 (2) | 0.965 | 0.35 | 0.34 | 0.12 | 0.55 | 365 | 365 | 330 | 0 | -35 |
| 13 | 0.97 | 0.35 | 0.26 | 0.11 | 0.78 | 335 | 350 | 315 | +15 | -20 |
| 14 | 0.97 | 0.35 | 0.24 | 0.12 | 1.04 | 330 | 340 | 305 | +10 | -25 |
| 15 | 0.965 | 0.35 | 0.28 | 0.12 | 1.28 | 313 | 335 | 300 | +22 | -13 |
| 16 | 0.96 | 0.36 | 0.265 | 0.12 | 1.54 | 300 | 325 | 290 | +25 | -10 |
| | 0.97 | 0.37 | 0.35 | 0.13 | 2.05 | 275 | 300 | 265 | +25 | -10 |

(a) *Ms* (°F) = 930 - 540 C - 70 Mn - 40 Cr (Based on Payson-Savage Formula)

(b) *Ms* (°F) = 1000 - 650 C - 70 Mn - 40 Cr (Based on Grange-Stewart Formula)

specimens used were rough cut to the sizes indicated in the text but by the time they were cleaned up by hand grinding, the actual sizes were about $\frac{3}{32}$ in. square and $\frac{5}{32}$ in. square, respectively. Nevertheless, actual cooling times were obtained on $\frac{1}{8} \times \frac{1}{8} \times \frac{1}{2}$ in. long specimens, after austenitizing at 1800°F, during a salt quench at 350°F. This work was done by welding 24 ga thermocouples to each of two specimens and connecting them to two channels of a Hathaway 12 channel recording oscillograph. The strings had a dc sensitivity of 55 mm per mil amp at 1 meter distance and a natural frequency of 400 cycles per sec. The results showed that both specimens were within 10°F (about the experimental error of the determination) of the bath temperature in 4 sec.

At several times during the investigation, the smaller specimens were checked against the larger, using the austenitizing conditions and quenching times in both salt and oil described for the high carbon steels. In all cases the results were identical. Furthermore, both oil and salt were used interchangeably in the range of 300 to 350°F with the same results on many check runs. Finally, duplicate specimens quenched together using the oscillograph produced differences in temperature of 25°F when only 50°F above the bath temperature and separate runs showed even greater deviations. It is believed that these data support the contention that reproducibility of results is a satis-

factory indication that the specimens have actually reached the quenching bath temperature. So many variables enter into the actual quenching operation that reproducibility is out of the question if the specimen is removed from the bath while still above the bath temperature.

Mr. Nehrenberg also criticizes our statement that no simple formula will suffice to express the relationship between the effects of carbon and chromium on the *Ms* temperature and in defense of his objection shows that the modified Payson-Savage formula will predict the *Ms* points within 25°F. Our statement was based on the fact that the effects of carbon and chromium on the *Ms* points of these steels are interdependent and not independent as formulas of the Payson-Savage and Grange-Stewart type assume. Either or both may arrive at a reasonable prediction by a series of compensating errors, but a more complex formula would obviously be required to express accurately the true relationship between carbon and chromium in this regard.

In answer to Dr. Troiano's question regarding the grain size of the specimens after the austenitizing treatment, samples of 1.5 pct chromium steel were heated for 20 min. at 2100°F and isothermally transformed at 1300°F for 3 min. to delineate the grain size. The resulting ASTM grain size was No. 2. We are unable to assess this result in terms of Dr. Troiano's statement of "exceptionally large grains" obtained in his work.

Since the manuscript for this paper was submitted, both Dr. Troiano and Dr. Cohen have shown an effect of grain size on *Ms*. Since high austenitizing temperatures are necessary for the complete solution of high carbon chromium steels, coarse grain size is unavoidable and its effect on *Ms* difficult to separate from carbide solution since both are changing simultaneously. Our only pertinent observation in this regard was that with increasing austenitizing temperature, the *Ms* became constant shortly after the complete disappearance of carbide in the quenched microstructure and did not change upon a further increase of austenitizing temperature of 100°F.

References

1. R. A. Grange and H. M. Stewart: The Temperature Range of Martensite Formation. *Trans. AIME* (1946) **167**, 467-501.
2. E. P. Klier and A. R. Troiano: Ar'' in Chromium Steels. *Trans. AIME* (1945) **162**, 175-185.
3. E. S. Rowland and S. R. Lyle: The Application of *Ms* Points to Case Depth Measurement. *ASM Trans.* (1946) **37**, 27-47.
4. A. E. Nehrenberg: Discussion of Ref. 3.
5. A. B. Greninger: The Martensite Thermal Arrest in Iron-Carbon Alloys and Plain Carbon Steels. *ASM Trans.* (1942) **30**, 1-26.
6. T. G. Digges: Transformation of Austenite on Quenching High Purity Iron-Carbon Alloys. *ASM Trans.* (1940) **28**, 575-607.

The Kappa Eutectoid Transformation in the Copper-silicon System

By W. R. HIBBARD, JR., Junior Member, G. H. EICHELMAN, JR., Student Associate AIME, and W. P. SAUNDERS

DISCUSSION

(C. S. Smith and A. R. Troiano presiding)

C. S. SMITH*—The authors refer to some earlier work of mine containing reference to the pearlitic structure of these alloys. It should, perhaps, be pointed out that the two-phase structure most reminiscent of pearlite is formed when gamma precipitates from super-saturated alpha phase or from an alpha-kappa mixture rich in alpha. This is not a eutectoid decomposition involving three different phases, but is a case of discontinuous precipitation involving two phases (one, however, possibly of two different compositions). It seems not unlikely that a typical nearly-parallel-plate form of pearlite occurs only when there

are three interfaces of approximately equal energy meeting at the advancing boundary of the transformed alloy. When alpha forms from kappa in an oriented manner, the resulting interface is of extremely low energy and the gamma phase can co-precipitate with alpha without the constraint of the third interface.

C. S. BARRETT*—Dr. Smith recently gave me a set of samples of copper-silicon alloys that I have been X raying after different heat treatments. The investigation is not yet completed, but it is already clear that the decomposition of a sample of homogeneous kappa into alpha plus gamma on cooling below the eutectoid temperature is crystallographically very different from the precipitation of

alpha from kappa on heating above 600°C. The diffraction patterns in the two cases are as strikingly different as the appearance of the microstructures, and in the way one might expect from the microstructures: there are normal reciprocal lattice points for all phases after the eutectoid transformation, but after the precipitation, which produces the remarkable striations in the microstructure that Dr. Smith has reported,⁵ reciprocal lattice points are often seen that are greatly elongated. Elongated points are found after only one minute at a precipitation temperature of 750°C but none is found after times up to 45 hr at 500°C.

A. R. TROIANO*—Dr. Barrett has

* University of Chicago.

* University of Chicago.

* University of Notre Dame.

raised an interesting point. Care must be taken in generalizing the term "pearlite" if one is going to draw the analogy with steel. One may have very pearlitic-looking microstructures that do not originate from the eutectoid decomposition of the parent phase.

W. R. HIBBARD, JR. (authors' reply)
—Dr. Smith has emphasized a point which

the authors failed to realize, perhaps because it is somewhat difficult to understand how kappa, even in an alpha-kappa structure, can decompose to plate-like alpha and gamma without involving the eutectoid transformation (see Fig 20 of Ref. 5).

Dr. Troiano's caution regarding the use of the term "pearlite" is most timely.

The striated structure of alpha and kappa formed above 600°C from kappa described by Dr. Barrett obviously is not a eutectoid structure, since gamma is not involved, and it probably looks more "twin"-like than "pearlite"-like, anyway.

Stabilization of the Austenite-martensite Transformation

By W. J. HARRIS, JR., Junior Member, and M. COHEN, Member AIME

DISCUSSION

(C. S. Smith and A. R. Troiano presiding)

A. R. TROIANO*—This paper is full of new observations.

It is very interesting to me to see that now we can rationalize why in some cases one may observe stabilization without any decomposition at all. I distinctly remember how in the laboratories at Notre Dame we found this phenomenon and then tried to check it in other steels and it did not seem to be there. We were beginning to wonder if the original determinations were valid. Now we can see good reasons why it was not observed in all steels.

I wonder if the authors would care to state just how general the relationship between σ_s and M_s might be.

C. S. BARRETT†—Our investigation of the transformation in lithium and lithium-magnesium alloys, which is somewhat like the martensite transformation in steels,¹⁴ is continuing. We are using an improved X ray diffraction unit that has been built by D. F. Clifton to see whether there is stabilization of the high temperature phase on cooling, and to investigate further a behavior that looked like stabilization of the low temperature form during reversion to the high temperature form on heating. Detailed information of this kind for the lithium transformation should be quite helpful in arriving at sound theories of stabilization.

B. S. LEMENT‡—I just want to point out that even though stabilization of austenite can result from quenching to and holding at some temperature below σ_s , the extra austenite at room temperature is not stabilized against room temperature transformation. The reason for the apparent contradiction has been pointed out by Dr. Morris Cohen in his Campbell Memorial Lecture. There are

two different mechanisms involved in the transformation of austenite to martensite. On cooling the transformation probably occurs by a process of nucleation and shear; whereas the isothermal transformation at room temperature probably occurs by growth of the existing martensite plates. Any extra austenite that results from stabilization on cooling to room temperature behaves quite similarly to the other retained austenite with regard to isothermal transformation at room temperature. If more austenite is retained, more transformation occurs on aging at room temperature. This phenomenon is of great importance from the standpoint of dimensional stability of tool steels.

L. D. JAFFE*—The authors have certainly done a fine job in clarifying and establishing many points only suggested by previous work. On one matter, however, there seems to be some disagreement. The authors' Eq 1 indicates that for constant percent martensite (P), M_s-T is a constant. In other words, all curves of percent martensite vs. temperature are the same, except for a uniform shift along the temperature axis. This is not in accord with the data of Grange and Stewart,²⁵ obtained by technique similar to that of authors. As the writer has pointed out,²⁶ these data indicate that M_s-T increases as M_s decreases. Can the authors throw any light upon these apparently contradictory findings?

It may be noted that the discrepancy just mentioned does not affect the authors' conclusion that all the (unstabilized) martensite transformation curves conform to a single function, in which M_s is the only metallurgical variable. This same conclusion was, indeed, drawn by the writer in the discussion cited.²⁶

M. COHEN (authors' reply)—The σ_s

relationships that Dr. Troiano has inquired about seem to hold for the following ranges of composition: 0.75 to 1.35 pct carbon, 0–5½ pct nickel, and 0–3 pct chromium. These limits are not definitely fixed and may be extended when future work is done on additional steels. However, considerable deviation may be expected when the composition is changed radically, as in the case of high speed steel.

We agree with Dr. Barrett that his contemplated studies on lithium and lithium-magnesium alloys will have a significant bearing on the theory of stabilization. For example, in working with steels, we are inclined to wonder about the role of carbon in the stabilization process, whereas if true stabilization occurs in a high-purity metal, one may well question the importance of solute elements in the phenomenon.

Mr. Lement is entirely correct in emphasizing that the term stabilization used in this paper refers only to the inhibition of the cooling austenite-martensite transformation. The increment of retained austenite resulting from stabilization is subject to isothermal transformation in the same sense as normal quantity of austenite retained in the absence of stabilization. In fact, this is one of the main reasons for suspecting that the isothermal transformation of austenite to martensite²⁷ may occur, at least in part, by the growth of existing plates, rather than by the formation of new ones as in the cooling transformation.

It is worth repeating here that the σ_s temperatures determined in this paper are all based on holding times of ½ hr. At the moment, the relation between σ_s and holding time is not known. However, regardless of this possible variation, the main trends should persist, with stabilization becoming more pronounced, the larger the amount of martensite present.

Dr. Jaffe rightly points out that discrepancies exist between the martensite transformation curves presented here and those of Grange and Stewart. No positive explanation is available at the

* University of Notre Dame.

† University of Chicago.

‡ Massachusetts Institute of Technology.

* Watertown Arsenal Laboratory.

¹⁴ References are at the end of discussion.

moment, although it should be pointed out that the method used by the latter investigators was only semi-quantitative. The form of the transformation curves as given by Eq 1 is identical with the one found by Howard² for carbon contents ranging from 0.75 to 1.35 pct. On the other hand, Grange and Stewart covered a wider range of carbon contents, and their data may indicate trends that are not detectable in a more limited series of compositions. However, according to

our experience, quantitative measurements are quite difficult in the lower carbon steels and may lead to questionable results even when lineal analysis is employed.

References

R. T. Howard and M. Cohen: Austenite Transformation Above and Within the Martensite Range. *Met. Tech.* Sept. 1947, TP 2283.

14. C. S. Barrett: Low Temperature Transformations in Lithium and Lithium-magnesium Alloys. *Met. Tech.* (April 1948) TP 2346.
25. R. A. Grange and H. M. Stewart: The Temperature Range of Martensite Formation. *AIME Trans.* 167 (1946) 467-490.
26. L. D. Jaffe: Discussion of Ref. 25. *AIME Trans.* 167 (1946) 493-494.
27. B. L. Averbach and M. Cohen: The Isothermal Transformation of Martensite and Retained Austenite. A.S.M. Preprint No. 1 (1948).

Secondary Hardening of Tempered Martensitic Alloy Steel

By W. CRAFTS, Member AIME, and J. L. LAMONT

DISCUSSION

(C. S. Smith and A. R. Troiano presiding)

R. BALLUFFI* and M. COHEN*—

In the tempering research conducted at M.I.T., carbide precipitation from martensite or retained austenite has never been found to produce an expansion. Consequently, the expansion effects of Fig 11 and 12, attributed by the authors to alloy carbide precipitation, are of some concern to us. We have observed such expansions, but have accounted for them on the basis of retained austenite decomposition. The authors have not used this explanation because they assumed that the retained austenite in their samples had been reduced to negligible amounts by previous refrigeration in liquid oxygen.

With the cooperation of the authors, we undertook a critical experiment to settle this issue. The authors kindly sent us four of the alloy steels under consideration, of which we selected the following two for test:

| Designation | Heat | Pct C | Pct Mn | Pct Si | Pct Cr | Pct V |
|-------------|-------|-------|--------|--------|--------|-------|
| Cr | 4-24 | 0.52 | 0.37 | 0.19 | 11.73 | |
| V | 4-257 | 0.48 | 0.54 | 0.12 | | 2.02 |

Two dilatometric specimens of each composition were austenitized at 2300°F (1260°C) for 12 min.† and quenched in oil. One of each was immediately refrigerated in liquid nitrogen. All four specimens were then subjected to dilatometric runs, covering the significant range of 600–1300°F in 2 hr. The results are plotted in Fig 22 in a manner analogous to that of Fig 11.

The expansion effect is definitely smaller for the refrigerated steels than for the as-hardened steels. This clearly suggests

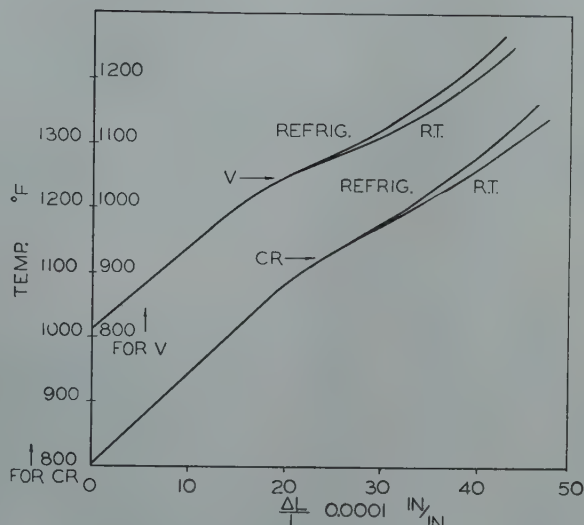


FIG 22—Dilation on heating 0.5 pct carbon, chromium and vanadium steels, after oil quenching from 2300°F and after refrigeration in liquid nitrogen.

that the expansion phenomenon is the result of retained austenite decomposition inasmuch as the refrigerated specimens undoubtedly contain less retained austenite than the as-hardened ones. If the expansion during tempering were caused by carbide precipitation from the martensite, the refrigerated specimens should exhibit at least as much expansion as the as-hardened ones, and probably slightly more because of the martensite increment produced by the cold treatment. It is also worthy of note that the tempering expansion of the refrigerated specimens represents a sizable fraction of the expansion of the as-hardened specimens. This means that the cold treatment does not convert anything like all of the retained austenite.

These findings should not reflect upon the authors' conclusions as to the cause of secondary hardening in the 0.50 pct carbon steels under study here. While the retained austenite decomposition should not be ignored, we quite agree that alloy carbide precipitation plays an important role in the secondary hardening observed.

D. J. BLICKWEDE*—I would like to point out to the authors two phenomena which occur during the isolation of carbides from steels that might affect their electron micrographs.

One is that carbon in the matrix does not ionize during electrolysis. Instead it

* Massachusetts Institute of Technology.

† Time at temperature.

* Naval Research Laboratory, Washington, D.C.

either comes down as free amorphous carbon or reacts with hydrogen to form hydrocarbon gases. The presence of free amorphous carbon might affect the electron micrographs.

The second phenomenon occurs in the case of alloy steels, in which particles of the matrix material—that is, the steel itself—remain undissolved and will come down with the carbide precipitate. Thus it is quite likely that pieces of matrix material itself could be the carbide residue and show up in the electron micrographs.

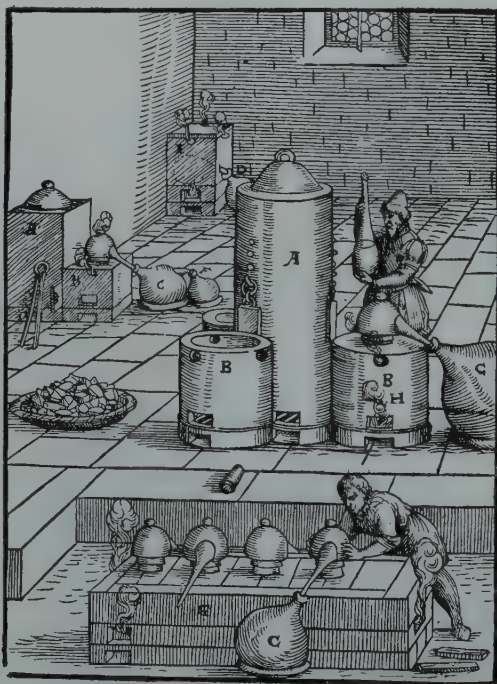
W. CRAFTS (authors' reply)—The examination of isothermally transformed bainite should be very informative. A preliminary survey of bainite specimens has indicated that the carbide structures are exceedingly fine and probably quite complex, so that a good deal of difficulty in experimental technique and interpretation may be anticipated. It is expected however, that electrolytic extraction of the carbides may provide a useful tool for furthering our understanding of the nature of bainite. The carbide of a 3 pct chromium steel in the bainitic condition was found to change on tempering from Fe_3C to Cr_7C_3 in about the same temperature range as steel in the martensitic condition, but the specimens were not examined to determine the appearance of the carbides during the transition. In

view of the apparently complex nature of the carbides in bainite, it might be expected that the transition might not be as simple and straightforward as in tempered martensitic steels.

In reference to the discussion by Robert Balluffi and Morris Cohen it should be noted that the analyses given in their discussion represent the same steels that are shown in Fig 11. By an oversight these specimens were indicated in the text to have come from the same heats as those used for the metallographic investigation. The dilation tests indicate that the larger amount of residual austenite in the unrefrigerated specimens increased the amount of dilation on heating in the 1000–1300°F range. It is also quite probable that the refrigerated specimens contained an amount of residual austenite that was too small to be detected in our tests. However, it is felt that a more positive test should be made before eliminating the possibility that the expansion is in part due to transition of the carbide phase. As is pointed out, the actual amount of retained austenite is too small to affect significantly the conclusions regarding the effect of transition to alloy carbide on the rehardening phenomenon.

In electrolytic extraction, as stated by D. J. Blickweide, a certain amount of car-

bide is decomposed to hydrocarbons and amorphous carbon. The attack occurs largely during electrolytic solution of the metal and, although subsequent solution by the electrolyte has been substantially eliminated, the recovery of carbide is never complete and in slightly tempered specimens may be quite low. Thus, the carbide residue is only a partial representation of the total amount and individual carbide particles may be altered from their original condition. The X ray indications, therefore, may be incomplete, but positive results may be accepted, and the appearance of the carbides parallels the collateral properties sufficiently well to give a credible confirmation that the observed structures are significant. Relatively little difficulty due to undissolved particles of matrix material has been encountered in steels that are free from large amounts of residual austenite and the presence of metallic iron in the residue has been found to be a useful criterion of retained austenite. Undissolved carbides and matrix material are too coarse to present any difficulty in the electron microscope examination. Although electrolytic extraction requires careful experimental technique, it offers a means of examining carbide structures that is much more revealing than methods of examination suitable for solid specimens.



Furnaces for the distillation of nitric acid. (Ercker, 1574.)

The tall tower was filled with charcoal which burned only at the bottom and the hot gases passed through the side chambers to heat the alembics containing vitriol, saltpeter and other materials. Fresh charcoal descended to replace that burned, and the furnace would maintain constant heat for as long as a day without refueling or other attention.

(Courtesy C. S. Smith)

The Effect of High Copper Content on the Operation of a Lead Blast Furnace, and Treatment of the Copper and Lead Produced

A. A. COLLINS,* Member AIME

When we speak of high copper on a lead blast furnace we think in terms of 4 to 5 pct, or any lead charge carrying over 1 pct. Any copper on charge will produce its corresponding troubles such as lead well, extra slag losses, drossing problems, and the working up of the dross.

This is indeed a very interesting subject and one that used to give the old-time lead metallurgists such as Eiler, Hahn and Iles many worries, not so much in the actual operation of the blast furnace but in the working up of the copper. When the American metallurgists commenced with the American rectangular-shaped lead blast furnace in the 1870's and got away from the reverberatories such as were in use in Germany and other parts of the world, they went to greater tonnages, as 80 to 100 tons per day in comparison to the 20 to 30 tons per day in the other processes.

With the greater tonnages along with insufficient settling capacity, the silver losses in some cases were increased. Hence the lead-fall was low, for there were no leady concentrates in those days to assist the metallurgist to gain lead or an absorber for the *precious* metals; and in some cases copper sulphides were added intentionally to the charge to produce a copper matte to lessen the silver losses through the dump slag. The operators in those days thought that where some copper was always present in the lead ores the copper should not enter into the reduced lead and alloy with it. This, by the way, is just the reverse of our present-day practice, when we try to put all of the copper into the blast furnace lead and to remove the same through the drossing kettles. Therefore the furnace was operated to produce a certain amount of matte or artificial sulphides, since, due to the great

affinity of copper for sulphur, any copper present would enter the matte almost completely. Thus, the lead bullion produced was practically free from copper.

The products of the furnace were metallic lead or lead bullion, containing 85 to 95 pct of the lead and about 96 pct of the silver which were in the ore—a lead-copper-iron matte which contained nearly all the copper in the ore and the slag, the waste product.

In the United States, up through the year 1892, we find the small furnace $100 \times 32\frac{1}{2}$ in. with 12 tuyeres, some 6 on each side, plagued with a small amount of poorly roasted sulphides—either from heap or hand roasters that produced matte.

This matte was roasted and if poor in copper was returned for the ore smelting. Otherwise it was smelted either alone or with additions of rich slags or argentiferous copper ores, the products being lead and a highly cupriferous matte, the latter being subsequently worked up for its copper.

The lead metallurgists kept trying and improving on furnace and roasting equipment designs until we find Malvin W. Iles constructing at the old Globe Plant at Denver what came to be the modern furnace. That is, in 1900 he built a furnace of 42 in. width by 140 in. at the tuyeres with a 10 in. bosh and a 16-ft ore column. This type has been more or less standard to the present time, though modified in width and length to meet the demand for large tonnages and improvements in structural details. In 1905 at Cananea, Mexico, Dwight and Lloyd developed

the present down-draft sinter machine that has meant so much in producing a well-processed material for the lead blast furnace.

In 1912 Guy C. Riddell came forth with double roasting at the East Helena Plant of the American Smelting and Refining Co., which removed the "zinc mush plague." Incidentally, with the introduction of double roasting, which most lead plants were forced into after 1924, when lead flotation came into its own, less matte or no matte was produced.

When this stage arrived, the copper was forced into the dross and the casting of lead at the blast furnace lead-wells was stopped. In plants with a fair copper carry 1 pct or better on the blast furnace charge, the lead wells became inoperative once the production of matte stopped. The copper drosses clogged the lead wells and even with bombing, either water or dynamite, the operators could not keep them open. Thus, the lead wells were abandoned in some plants, such as at the El Paso and Chihuahua smelters of the American Smelting and Refining Co., and all lead taken out through the first settlers.

The elimination of sulphur, especially sulphide sulphur, from the blast furnace charge and the nonproduction of matte resulted in a great saving of time, energy and equipment in the recirculation of the copper.

With the copper content in the dross and dross-fall ranging in quantities from a few percent up to 60 pct, such as at El Paso, a drossing problem was created.

As the old-time operators hated dross and buried the same in the shipping bullion, the modern metallurgists from 1925 on decided that with increasing dross-falls they would have to adopt the lead refiner's ideas of drossing kettles with subsequent treatment of the lead with a sulphur addition to have the shipping lead of 0.01

San Francisco Meeting, February 1949.

TP 2576 D. Discussion of this paper (2 copies) may be sent to *Transactions AIME* before July 1, 1949. Manuscript received Nov. 1, 1948.

* Manager, Chihuahua Smelter, Chihuahua, Chih., Mexico.

pct copper content or less.

With the cleaning up of the bullion and thus the copper remaining in the lead smelters, the dross reverberatory was developed at the Selby Plant of the American Smelting and Refining Co. and brought to its present stage of development by Mr. O. P. Chisholm, the former superintendent of the East Helena Smelter.

Since 1925, when the real flotation of lead sulphide commenced, the concentrators have gone in some cases from a 10 to a 64 pct lead in the lead concentrates, and the copper has also increased in the same concentrates, in some cases up to 14 pct. Consequently, the lead smelters have received a considerable amount of copper in these lead concentrates.

These higher copper-lead concentrates along with complex copper, zinc, lead ores after roasting give a high copper charge to the lead blast furnaces, say up to 5 pct, and have in no way retarded the furnace speeds. On the contrary, the furnace tonnages have increased. The copper minerals contained in the original ores and concentrates have been mainly chalcopyrite and chalcocite and have assisted in producing a good, fast-smelting sinter at the blast furnaces. The copper sulphides have retarded the lead fusion and permitted a greater degree of zinc sulphide roasting. Thus, the copper sulphides have aided in sintering.

Therefore, high copper on a lead blast furnace, if in the form of a well roasted sinter, will not cause any trouble in the working of the furnace.

Copper in the form of dross, when added to a lead furnace and necessitating a sulphur addition for matte making, will foul a furnace and cause it to work inefficiently. Any sulphides added raw to matte out the copper in combination with zinc will produce a zinc mush, along with accretions and an irregular working of the blast furnace.

Any copper on the furnace charge with the present-day double roasting will go either to the speiss, lead or slag, the amount depending upon the arsenic on charge, as the speiss and the slag losses will depend upon the quality of the sinter.

The blast furnace speiss production will vary from plant to plant, depending upon local conditions and the amounts of copper and arsenic on the charge. I well remember at the El Paso smelter for the years 1939 through 1944, with an average of about 0.6 pct arsenic on the furnace charge, that no

speiss was produced with over 1.5 pct copper on charge. However, with under 1.5 pct copper we always showed some speiss.

The copper in the blast furnace speiss can be reclaimed through the dross reverberatory, using the iron arsenide in the speiss as a collector for more copper or else the iron speiss can be ball-milled and roasted for arsenic and the resultant calcine worked up in a copper reverberatory or blast furnace.

The copper slag losses were in no way affected by the speiss-fall.

For our present-day roasting program, the degree of roasting can be ascertained by the amount of copper in the slag. I have a rule of thumb that the copper on charge multiplied by 0.16 should give the percent of copper in the furnace slag. Any amounts below this figure indicate excellent roasting.

The furnace lead with a heavy dross-fall will be hotter and cause extra troubles from the dross separating in transfer pots, along with a greater strain in the lead receiving kettles due to heavy accretions formed on sides of the kettles and necessitating more frequent barring down of the same. Frequently at El Paso, with its heavy dross-fall, I have seen a full 65-ton kettle show about 20 tons of lead after the drossing operations. The reduction in no way will affect the quantity of dross produced.

Blast furnace lead containing its copper in the form of dross and varying from a few percent up to, say, 60 pct will be deposited on the surface of the lead in the drossing kettles and will be worked up in either one of three ways, viz: 1. Fluxing with soda ash in the dross reverberatory. 2. Using the arsenic in the blast furnace speiss as the collector of copper in the dross reverberatory. 3. Fluxing with silica and using a sulphide as a collector for the copper.

The copper products from the reverberatory, such as the matte and speiss, can be sent direct to a copper department; or the speisses, especially of soda, can be roasted with an iron diluent for arsenic elimination and the resultant calcine sent to the copper department.

The benefits from copper in a lead smelter are as follows:

1. Better sinter and a good furnace tonnage, especially if chalcopyrite.
2. If a baghouse is used to collect the sinter fume, the bag life will be aided by copper as a more alkaline dust will be produced at the sinter machines

with slightly more fume.

3. Copper has a great affinity for arsenic and will prevent the arsenic from entering the lead bullion. I have seen the reduction badly off on a lead furnace, even up to 2.5 pct lead in the slag, with 4 pct copper and 2 pct arsenic on the furnace charge, yet the bullion was below 0.1 pct As.

The problems from copper are as follows:

1. Lead wells are apt to be useless and on high copper charges, with the lead removed through the first settlers, the copper will cause a hotter lead and probably result in more frequent tap-hole changes.
2. More dross-fall and creating problems at the drossing kettles.
3. More cost at dross reverberatory to work up the dross.
4. Higher metal losses in dump slags.

Conclusions

1. Copper will not affect the operation of a lead blast furnace, if in the form of a well roasted sinter; but if contained as a dross, definitely it will.
2. Copper will not affect the fume or flue dust production on the blast furnace.
3. Copper will not affect the reduction on a lead blast furnace.
4. Copper will affect the secondaries produced—thus more dross-fall.
5. Copper will affect the slag losses.
6. Copper will affect and produce a hotter lead.
7. Copper will affect and cause lead-well trouble.

Thus, it is preferable to remove copper at the lead concentrators and make a copper concentrate which can be shipped to a copper smelter. In this way, the copper losses will be considerably lessened, for a lead plant will show possibly a 10 pct copper loss depending upon conditions, against a copper smelter's loss of, say, 2 pct. In addition to the extra losses in the lead plant, one must consider the higher as well as additional processing costs which are incurred when any copper is routed into a lead works, since any copper into a lead smelter must eventually be sent to a copper plant to be worked up into blister copper.

Therefore, to conclude this paper, the writer believes that with the present high metal prices the benefits, such as are obtained in the sinter and the baghouse aids, are apt to be outbalanced by the increased costs for processing and the metal losses.

What Is Metallurgy?

JOHN CHIPMAN,* Member AIME

There is no better way of paying tribute to the memory of a scientist than by developing and carrying forward those ideas which he has contributed to science and which are for us the very essence of his immortality. For a lecturer who has not had the great privilege of studying under Professor Howe or even of knowing him in person, these ideas must be transmitted through the printed word. It is our great good fortune that Professor Howe left to us a rich heritage of publication, not only in his classic monograph on the "Metallography of Steel and Cast Iron" but in a wealth of earlier books and papers in the transactions of this Institute and of other scientific and engineering bodies. An outstanding characteristic of this published record is the great breadth of interest and of vision which it portrays. His was not a narrow specialization in only the scientific aspects of ferrous metallography. On the contrary many of his important contributions had to do with a far broader field of metallurgical endeavor. He insisted that his students be well grounded in the fundamentals underlying the whole field and not led into the narrow groove of specific applications. Among his first major publications we find papers on copper smelting, extraction of nickel, the efficiency of fans and blowers, thermic curves of blast furnaces, the cost of coke, and the manufacture of steel. These are the papers of a metallurgical engineer and it was among engineers that Henry Marion Howe made his early and well-merited reputation.

These early engineering contributions display very clearly the strongly scientific inclination of their author.

The classic work on "The Metallurgy of Steel" published in 1890 contains a thorough and critical discussion of all that was known at the time concerning the alloys of iron and of what we would now call the physical metallurgy of steel. In addition it describes steel-making processes in use and some that had become obsolete, and points out in critical fashion the reasons for success and failure. Steel mill design and layout were included as well as some pertinent discussion of refractories. The book is indeed an embodiment of one of Howe's outstanding characteristics—breadth. It is both the science and the engineering of steel production as known in that day.

One of Howe's earliest technical papers was entitled "What is Steel?" That was nearly seventy-five years ago when many new processes and new kinds of steel were being developed. The time was ripe for such a question and the answers which Howe was able to give were helpful in understanding the phenomena of heat treatment. Twenty-five years ago Professor Sauveur repeated the question as the title of the first Henry Marion Howe Memorial Lecture. It seemed to him that this question, "What is Steel?," had served as Howe's motto throughout the remainder of his life.

Today I shall present for your consideration a question of another sort: "What is Metallurgy?" Perhaps it is not too much to hope that in the answer we may obtain a clearer and possibly broader view of the nature of our

science and our profession. The time is ripe for giving careful consideration to what we mean by metallurgy. If our Metals Branch is to become in fact an American Institute of Metallurgical Engineers, it is essential that we understand what is meant by metallurgical engineering. I am convinced that the best interests of the profession have not been served by a narrow interpretation of these terms. We must now place emphasis on the breadth of metallurgy as a science and as an engineering profession.

With its usual brevity and wit, Webster's dictionary defines metallurgy as "the science and art of extracting metals from their ores, refining them and preparing them for use." I shall not assume that the words "science" and "art" and "metal" are so well understood as to require no defining but others among our contemporaries are better qualified than either your lecturer or the dictionary to present the broad meanings of these terms. When we say that metallurgy is among the oldest of the arts we are not classifying it with painting or sculpture or music but rather with the making of tools or weapons or the building of bridges or chariots or cathedrals. In short we are saying that metallurgy is among the oldest of the engineering professions.

The question "What is metallurgy?" has been one of rather more than ordinary concern to those of us who have the task of developing a curriculum for the education of students in this field. This development has been going on in a number of universities over a period of some years, but there seems to be as yet no unanimity as to what such a curriculum should contain. I believe there is fairly complete agreement that it must be founded upon sound

San Francisco Meeting, February 1949.

Howe Memorial Lecture.

TP 2614 C. Manuscript received March 7, 1949.

*†Department of Metallurgy, Massachusetts Institute of Technology.

basic training in the sciences and that it should contain the elements of an engineering education. The recognition of metallurgy as both science and engineering is fairly widespread among metallurgists. It is not so well understood in other circles.

The terms "metallurgy" and "metallurgical engineering," if each is used in the broadest sense, mean exactly the same thing. I know of two metallurgical departments that have similar curricula, one of which graduates metallurgists, the other metallurgical engineers. For purposes of this discussion, however, I shall use the term "metallurgy" as the broader one to include on the one hand metallurgical engineering and on the other the science of metals.

In connection with our efforts to establish a rational curriculum for students of metallurgy we thought it would be extremely helpful to have before us a concise outline of the entire field. Now it is no small task to prepare such an outline. Metallurgy is a large subject and it overlaps many others so that a clear-cut line of demarcation between it and its neighbors cannot be drawn. The various parts of metallurgy are closely interrelated and cannot be divorced. Nevertheless it is possible to set down in some sort of logical sequence the names of the principal parts of the science and art of extracting metals from their ores, refining them, and preparing them for use.

In presenting the outline I must emphasize that, while the chief impetus for its preparation was pedagogic, it is in no sense an outline of a curriculum. It is not my intention to discuss the pros and cons of the several items which compose the academic bill-of-fare. But this outline which evolved in the course of such discussions may have other than academic uses, and moreover the purpose for which it was developed can best be served by offering wide opportunity for criticism.

There is no universally accepted terminology corresponding to that used in the outline. Other schemes of classification have been employed, for example, "extractive metallurgy" may cover not only the first two engineering divisions and "adaptive metallurgy" the other two, but each term may include also the appropriate parts of metallurgical science. Similarly the term "production metallurgy" could be used to cover some eighty percent of what I have called "metallurgical engineering." Two terms which are conspicuously absent from the outline

A. Metallurgical Engineering

Extractive Metallurgy

1. Mineral Dressing

- Comminution of ores
- Separation of minerals
- Leaching

2. Process Metallurgy

- Roasting and sintering
- Reduction and smelting
- Fuels and combustion
- Refractories and furnaces
- Heat and fluid flow
- Electrometallurgy
- Melting, refining and alloying
- Casting and solidification

Adaptive Metallurgy

3. Metal Processing

- Hot and cold forming
- Foundry practice
- Joining
- Surface treatment
- Powder metallurgy
- Heat treatment

4. Application Metallurgy

- Quality control
- Selection and specification
- Alloy design
- Service behavior

B. Metallurgical Science

1. Chemical Metallurgy

- Crystal chemistry and mineralogy
- Thermodynamics
- Reaction kinetics
- Surface chemistry
- Electrochemistry
- Corrosion

2. Physical Metallurgy

Metallography

- Constitution and phase diagrams
- Macro, micro and lattice structure
- Grain size and texture
- Grain growth and recrystallization
- Phase transformations

Physics of Metals

- Electrical and thermal properties
- Atomic bonding and cohesion
- Magnetism
- Diffusion
- Theory of the solid state

Mechanical Metallurgy

- Elasticity
- Anelastic behavior
- Plastic flow and work hardening
- Rupture and fatigue
- Creep
- Correlation of structure and mechanical properties

are "ferrous" and "nonferrous." These terms may be useful industrially but the division of science or engineering along such lines would not be profitable. I have no quarrel with those who would select a different set of words nor indeed with those who would interchange the terms "metallurgy" and "metallurgical engineering."

There is of necessity much overlapping in the outline, just as there must be in any attempt to set forth the content of any science. There are interrelationships throughout the outline so numerous that any attempt to show them by subheadings and tie-lines would simply cross-hatch the entire page. The purpose of the outline is not to divide metallurgists into classifications but rather only to simplify the task of examining our metallurgical profession to find out what it contains. To continue this study of the anatomy of metallurgy, let us consider briefly each of the major divisions of the outline.

Metallurgical Engineering

Metallurgical engineering is the direct descendant of that ancient art first brought to man by the titan demigod Prometheus. He it was who dared oppose the will of newly-crowned Zeus when that cruel monarch planned to sweep mankind off from the world and plant a newer race there. He stole fire from heaven and brought it down to earth for men to use. He taught men the motions of the stars and devised for them numbers and letters. He originated ships and was first to yoke horse to chariot. And, in the words of this first metallurgical engineer:

"For the other helps of man hid underground

The iron and the bronze, silver and gold
Can any dare affirm he found them out
Before me? None, I know! unless he
choose

To lie in his vault. In one word learn the
whole—

That all arts came to mortals from
Prometheus."

MINERAL DRESSING

Metallurgical engineering begins with what is "hid underground," the ore, thus illustrating a constantly recurring phenomenon, that the metallurgist is intimately concerned with nonmetals. Metallurgy must in practice begin with the ore and its first operations are those of mineral dressing. Here it is very closely allied to such fields as solid fuels, ceramics and nonmetallic minerals and like them it is here intimately associated with economic geology and mining. In brief this first segment of metallurgy constitutes also a portion of a broad field which is quite properly termed mineral engineering. Much of the scientific background lies in the fields of crystal chemistry, surface chemistry, mineralogy, hydrodynamics and other branches of knowledge not too familiar to most metallurgists but indicative of the breadth of the field.

The importance of the field is obvious in that almost every ore that comes from the ground requires some processing before smelting or reduction can be undertaken with profit, and it will not be many years before the word "almost" can be omitted. The very question of whether or not a given deposit can be considered an "ore" is conditioned upon the state of the mineral dressing art. The ores from which

the bulk of our copper is now produced were of no value fifty years ago. The development of flotation converted worthless rock into a natural resource. Much of our iron ore of the future must come from rock which today cannot profitably be smelted. We face here one of the great tasks of metallurgical engineering.

PROCESS METALLURGY

Process metallurgy has a long and honorable history too familiar to most metallurgists to require discussion. This is the very stuff on which the Iron and Steel Division is made. It is the succession of steps or processes by which impure mineral is reduced to metal, refined, alloyed and delivered according to a specification. It is an old art, but with the aid of chemical science it has become a chief part of modern metallurgical engineering. It is closely akin to chemical engineering with which it has many ideas and problems in common. The study of the field in terms of processes rather than by metals here follows the lead of chemical engineering education with its emphasis on the "unit processes."

It is worth noting that process metallurgy is not narrowly concerned only with the metal it produces. It has much to do with nonmetals. Operations begin with minerals and fuels and refractories, and the use of these materials is an essential part of the whole. In nearly every melting process a non-metallic by-product, a slag, is formed and in many cases this slag is itself a necessary reagent for carrying on the chemical reactions of the process. The chemistry of slags and of slag-metal reactions is extremely important in the control of such processes.

Process metallurgy is concerned also with certain principles which are common to many processes. Among them may be mentioned the flow of gases, combustion, heat flow, material balances and yields, heat balances and thermal efficiency, rates of reactions and the laws of chemical equilibrium. It is the quantitative application of such principles in the smelting and refining of iron and steel which has been the guide to efficient utilization of pressure and of oxygen and which will continue in the future to point the way to new efficiency and economy.

METAL PROCESSING

The more physical aspects of production metallurgy, the methods of

forming into useful shapes, are grouped in the outline under *Metal Processing*. Among these we note the overlapping of metallurgy with recognized trades or professions such as welding, founding, forging, electroplating. These fields are as much parts of metallurgical engineering as are steelmaking or heat treatment, and they deserve as much interest and recognition on the part of the metallurgical profession. For too long a time they have been relegated by metallurgists to rule-of-thumb control. Much can be accomplished here by the application of science and of sound engineering as witness recent advances in welding and the current renaissance in the foundry industry. Here we have seen in recent years the doubling of the strength of gray iron by persuading the graphite to form nodules rather than flakes. We have seen more than the doubling of the dependability of steel castings through control of soundness.

APPLICATION METALLURGY

The task of putting the right metal in the right spot with full regard for cost and service is an important part of metallurgical engineering. The selection and specification of metals and of their heat treatment is often a task of large proportions involving all the skill and understanding of an experienced metallurgist. The more complex the structure, the more kinds of metals must be taken into consideration; the greater the quantity of production, the more urgent it becomes to select for each part the right alloy, the right quality, for economic manufacture and service. It is in this field particularly that the science of physical metallurgy finds its practical engineering applications, and that metallurgy becomes the servant of all engineering. The metallurgist is constantly working with and for engineers of different backgrounds. He must know their language. He must understand the rudiments of design, of stresses and vibration, of fabrication and inspection and assembly. His success is gauged by his ability to serve his fellowman in adapting the right metal for each use.

Then comes the time when there is no satisfactory metal known for the given task; a new alloy must be designed to fit the job; a research and development program is required. As alloys are obtained which fill the need the requirements go up, still better alloys are required and the process

must continue. We are constantly in the midst of such developments, rapid progress being made at present in the development of high-temperature metals. The design of a new alloy for a given purpose may be a very simple or an extremely difficult task, depending upon the availability of basic scientific data needed. The development of our N. E. steels during the war was an example of alloy design on a grand scale, the success of which was assured by adequate knowledge of such controlling factors as steelmaking practice, strength, ductility and hardenability.

Metallurgical Science

A celebrated nuclear physicist when asked "What is the difference between science and engineering?" replied, "About fifteen years." He implied that it takes engineering about fifteen years to utilize the new things of science.

No one believes that the full engineering use of nuclear fission can be developed in any such short time, but it is true that the nuclear engineering tasks which have already been accomplished (the bomb, and commercial production of radio-isotopes) required much less. In metallurgy the difference in time is likely to vary from plus fifty to minus fifty years. Many a scientific result is left to molder on the shelf for years while others which appear to offer the prospect of economic reward may be converted into engineering application with breath-taking speed. On the other hand engineering developments frequently must be pushed forward without benefit of science. In Professor Howe's view engineering is essentially application, while the function of science is correlation with or without discovery. In 1917 he said: "Pure science in its relation to engineering seems today to be in an intermediate stage of its asymptotic evolution from the state of a follower to that of an absolute dictator." As one who has spent some years in study of the science underlying the art of steelmaking, I feel privileged to say that it is a blessing to humanity that the development of steelmaking practice did not have to await the full understanding of the scientific principles upon which it rests. At the same time I must express the conviction that the science will become more useful to the art as its growth progresses—indeed that it will approach asymptotically,

as Professor Howe has said, although it can never quite reach the state of "an absolute dictator."

CHEMICAL METALLURGY

The great dependence of process metallurgy upon the basic science of chemistry has been illustrated many times in such activities as the operation of blast furnaces and open hearths and the smelting and refining of all sorts of metals.

Production processes require time; hence, the rates of reactions, the rates of transfer of impurities such as sulphur from metal to slag, the rates of reduction of oxides and other phenomena of chemical kinetics are important to nearly every process. Of perhaps even more basic importance is the question whether or not a proposed reaction will occur at all. We do not make aluminum or zinc in a blast furnace, much as we should like to do so if it were possible. There is also the question of how far a process will go before it reaches equilibrium and finds itself run down like a clock. We do not get all the carbon or sulphur or phosphorus out of a heat of steel for just this reason. Consider the slags which are so important in the conduct of smelting and refining processes. We used to think of them as being made up of various mineral species. Some of us liked to regard them as molecular solutions. Nowadays it seems more probable that they are made up chiefly of ions, electrically charged atoms or groups of atoms, some of the groupings being fairly complex. There is much that is not yet known about slags but a knowledge of their actual structure would undoubtedly aid in understanding their proper control. These are chemical questions and illustrate the dependence of all of our processes upon chemical metallurgy, particularly upon kinetics and thermodynamics.

Certain metals which have only recently come into use and others which, like titanium, are still in the chemical stage give added emphasis to the close relationship between chemistry, process metallurgy and chemical engineering. Every new metal that is brought into use will bring its own problems and its own chemical processes. Many of the metals which are now shrouded in obscurity will inevitably be brought into practical use in the years to come. By the time our metal-hungry civilization has become sufficiently discriminating to demand

the highly individualistic properties of some of our rarer metals we will witness the introduction of new and strange methods of production. The metallurgy of gadolinium or dysprosium, for instance, may well involve such processes as solvent extraction, ion exchange, fractional distillation, fluorination, and electrolysis. These are the things which chemistry has in store for metallurgists and they will become as much a part of process metallurgy as the blast furnace or the converter.

Our interest in chemistry must not end with the production of the metal. Reactions occur within the solid and it is these reactions which provide the basis for heat treatment. Reactions occur also on the surfaces of metals and these provide troubles aplenty for all who are concerned with their service behavior. The control of metal corrosion has become an important engineering activity, but in spite of the great advances that have been made, the world's corrosion bill amounts to several billion dollars every year. The scientific study of corrosion is an important part of chemical metallurgy. To the metallurgist it is obviously dependent upon many factors which we think of as physical metallurgy, since the corrosion behavior of a metal depends not alone upon its chemical nature but upon its structure. But it is highly dependent upon its chemical environment, its electrical contact with other metals and upon that physico-chemical super-mystery, passivity.

PHYSICAL METALLURGY

Physical metallurgy is the science of the metallic state. Offspring of physics and physical chemistry, it is intimately concerned with the structure of metals and alloys and with the phenomena which occur within this structure. The study of metal structures and of the processes which determine them is called *metallography*. It is regrettable that this term has become widely used to connote only the microscopic observation of structure. Its real significance is far wider. In its broad sense it signifies the whole science of metal structure. This includes all knowledge of equilibrium in metallic systems as shown in the many phase diagrams that have been published and the nearly infinite number which remain to be studied. It includes recrystallization and grain growth and precipitation within metallic phases. The whole complex series of changes, by which soft

austenite is converted into tough bainite or hard martensite and the latter is tempered to produce structures of desired properties, is a part of this science of metallography. It was in this broad sense that Professor Howe used the word in his "Metallography of Steel and Cast Iron," and I urge that we return to this usage.

Progress in the development of new alloys as well as in understanding and improving the old ones, would be materially accelerated by a more thorough understanding of the nature of the solid state. The forces by which the atoms are bound together in a crystal are far greater than the overall strength of even our best metals. Why cannot we utilize all of this force to produce a steel ten times as strong as our present strongest? Atoms are bound together by electronic forces. Do the electrons spread throughout the structure as a sort of cloud, or do they resonate between several alternative interatomic positions? The answer lies in electrical, magnetic and thermal properties of alloys, and although we do not yet know how to read this answer, we may be confident that it will ultimately play its part in attaining such practical ends as the making of stronger or more ductile steels. The search for a better understanding of the solid state is not something that the metallurgist can leave entirely to the physicist. The two must work together as both kinds of background are needed. The *physics of metals* is an essential part of metallurgy.

Metals are useful primarily because of their mechanical properties, their strength, ductility, elasticity. The study of such phenomena is *mechanical metallurgy*. The metallurgist's approach to studies of elastic and plastic deformation is basically different from that of the mathematical stress analyst. A metal is not a mere three-dimensional continuum possessed of properties expressible in differential equations. It is a complex aggregate of crystals which may differ greatly among themselves and whose properties may change with strain and with time. Why does such an aggregate fail under load, and how? What is the mechanism of the characteristically metallic phenomenon called slip? Why and how are blocks of metal atoms able to glide for great distances over slip planes? Do they really behave like a panful of soap bubbles? By blocking slip planes we can raise the tensile strength. When are we going to learn to do this so effectively as to double the useful strengths of steels?



The Province of Metallurgy and Neighboring Areas.

Metallurgical Education

One of the principal reasons for asking the question, "What is metallurgy?" has been the need for a system of guide-posts along the road to metallurgical education. With the outline acting as a small-scale map of the province let us have a brief look at the path which a student may follow. One fact stands out clearly—the area is large and the terrain in some parts is rugged. The neophyte, planning to spend four years in becoming acquainted with the area, cannot hope to have time to dig deeply into each interesting vein nor to pick all of the daisies that he passes in the field. In planning his tour we must assure that he has an opportunity to see at least a part of each principal area. We must reserve enough time on his itinerary for him to examine in some detail the areas in which he is most interested and we must see that he is equipped with tools for digging in these areas. In addition we must recognize that he is going to spend a part of his time in daisy-picking and other nontechnical activities and we should teach him the difference between wild grape and poison ivy and how to avoid the pitfalls and the rattlesnakes. In introducing him to the province of metallurgy we must see

that he learns to mingle not only with his fellow explorers but with the great variety of people whom he will encounter within the field and in adjacent areas.

It is neither feasible nor desirable that all students who spend four years in metallurgical study be subjected to the same instruction. The world has need for many kinds of technically trained people and indeed many kinds of metallurgists. Happily there are enough individualists among metallurgical educators to provide a variety of curricula at the several institutions that offer the subject. In general, departments of metallurgy or of metallurgical engineering have given heed to Professor Howe's warning against Procrusteanism. "You remember Procrustes," he said, "who made his bed fit every traveler by lopping off the tall one's legs and stretching the short ones on a rack. Beware the narrow and cocksure Procrustean of every walk of life who would have all institutions shaped to fit their own pet ideals regardless of the need of the world of widely different products."

Perhaps it is not generally recognized outside of academic circles that a student of metallurgy devotes only about one-third of his effort during a four-year course to studies of metal-

lurgy. One half of his time is spent on basic science and engineering. This provides a minimum of preparation for entering and exploring the province of metallurgy. Nearly one-fifth is spent on the arts and humanities (daisy-picking and mingling) and this leaves less than one-third for metallurgy. Now it is obviously impossible to cover all that is included or implied in our outline of metallurgy in one-third of a four-year course. A large amount must be omitted and in fact should be. It is quite feasible, however, to teach the fundamental principles underlying most of the subjects listed, provided the student is not overburdened with mere description or with a plethora of specific applications. These rather bare fundamentals plus one or two advanced or specialized studies and a thesis requiring independent laboratory work on a subject, preferably of the student's own choosing, complete the metallurgical part of his schooling.

It is far more important that the student have a real grasp of physical chemistry than that he know the dimensions of the biggest blast furnace or the latest wrinkle in instrumentation. It is far more important that he understand what goes on inside a piece of steel during heat treatment than that he be able to distinguish between

bainite and fine pearlite under the microscope. It is far more important that he be able to *think* than that he know the characteristics of a wide variety of alloys. And it is in the teaching of the fundamentals that the instructor has his best opportunity to help the student learn to think. It seems perfectly clear to me that no part of the fundamentals of metallurgy should be omitted in order to substitute a college professor's idea of how an open hearth furnace ought to operate!

I have been talking of undergraduate instruction; what about postgraduate study? For the great majority of metallurgists this is directly related to a job and is therefore specialized. In many industries definite and well-planned training programs have been set up; these are of very great value to the young metallurgist and to the industry as well. The modern scheme of engineering education is becoming more and more dependent upon such training, and both the universities and the industries are according greater recognition to the responsibilities of the latter in the training of engineers.

Graduate training in the universities generally has one or the other of two objectives: further preparation for a professional career by extension of

undergraduate training both in breadth and in depth along some one or two lines of specialization; or preparation for a research career or for leadership in some field in which research plays a dominant part. In a field that is as young and vigorous as metallurgical science, graduate work has much to recommend it. It is, however, by no means to be regarded as a necessary part of a metallurgical education for those whose undergraduate training has been sufficiently basic and sufficiently broad.

Summary

In summary permit me to repeat that metallurgy is a field of great breadth. Since it is inhabited by metallurgists these must be people of wide vision. I have heard important persons who ought to know better speak of metallurgy as a narrow field of specialization. Nothing could be farther from the truth. It does, of course, contain within its boundaries many fields in which a metallurgist may specialize to his heart's content. But no other branch of engineering can compare with it in breadth if that breadth be gauged by the number of other fields

with which it has a common frontier. No other field of applied science draws so heavily upon both of the two basic sciences of physics and chemistry. No field of endeavor exhibits a greater wealth and diversity of achievement. Nowhere can scientists of such a wide variety of interests find a more fruitful or more stimulating field for research.

And now we must attempt to answer the question "What is a metallurgist?" Surely there must be thousands of answers to this question for it is obvious to any observer that no two metallurgists are alike. If we state that "a metallurgist is one whose scientific or professional work is directed toward the production or use or understanding of metals," what more need be said? We have here a definition broad enough to include all of us. However, it is too broad; it needs to be made specific; it requires illustration. Let us add then—"like Henry Marion Howe." And we have no longer a mere definition but an aspiration. For here was a man whose memory still inspires us. Here was a metallurgist whose interests reached into every corner of the province of metallurgy, whose work has influenced every segment of metallurgical science and engineering.

The Sigma Phase in Ternary Cr-Co-Fe and Cr-Co-Ni Alloys

PAUL A. BECK,* Member and W. D. MANLY,† Junior Member, AIME

In a recent note Sully and Heal¹ showed that the Cr-Fe sigma phase is isomorphous with the Cr-Co gamma phase, and that the lattice constants are also nearly identical. In a preliminary investigation of the ternary Cr-Co-Fe system at 800°C at this laboratory the above findings were confirmed, and it was found by microscopic techniques, using various etching reagents, that the two binary phases form an uninterrupted series of solid solutions with each other. These solid solutions occupy a straight narrow band which cuts across the 800°C isothermal section of the ternary system, connecting the two binary phases.

A detailed investigation of the Cr-Co-Ni ternary system at 1200°C

disclosed that here, too, the Cr-Co gamma phase extends deep into the ternary system in the form of a long narrow lip. The fact that this sigma type lattice is sustained even when well over half of the Co atoms in it are replaced by Ni atoms, with relatively little change in the Cr content, clearly indicates that Ni itself has a certain

tendency to form the sigma phase with chromium. This tendency is hidden in the binary Cr-Ni alloys, where the sigma phase is not known to occur, but it becomes operative in the presence of a sufficient amount of Co. The interpretation of these facts in terms of electron concentrations is rendered difficult by the uncertainty of our present knowledge of the valency electron structure of the transition elements in their alloys. However, Sully and Heal's results and the present work suggest that intermetallic phases with sigma type lattice may occur more frequently in these little investigated alloys than heretofore suspected. In particular, it is expected that a similar phase may exist in the V-Co and perhaps in the V-Ni system, in analogy to the known sigma type phase in the V-Fe system, and that all these sigma type phases may form extensive solid solutions with one another.

Technical Note 14 E. Manuscript received March 28, 1949.

This work was supported by the National Advisory Committee for Aeronautics, Contract No. NAW-5438.

* Associate Professor, University of Notre Dame.

† Research Engineer, Metallurgical Division, Oak Ridge National Laboratory.

¹ A. H. Sully and T. J. Heal: *Research*, March 1948, 1, 288.

Distillation of Zinc from Copper Base Alloys and Galvanizers Drosses

FRANK F. POLAND*

The purpose of this paper is to describe the recent applications and improvements made in the process and equipment for the recovery of metallic zinc from secondary metals by means of high temperature electric resistor furnace distillation.

The process and high temperature furnace, as developed by Revere Copper and Brass Incorporated, Research and Development Department, was described in a previous paper.†

Since the publication of that paper the process and equipment have been licensed to others. Consequently its field of application has been expanded, particularly for the treatment of scrap brass, galvanizers dross and scrap zinc. Other applications are being considered, particularly the melting of metallic titanium and special alloys requiring a controlled atmosphere. Consideration is also being given to modification in design that would allow the melting of copper cathodes for the production of oxygen-free and electrolytic tough pitch copper shapes without the necessity of blowing and poling.

In the design of a furnace for melting copper cathodes it is intended that the fundamental principle of charging the solid material into a large pool of molten metal through a double door charging vestibule as shown in Fig 3 of the previous paper,† would be adhered to and, in addition, either dehydrated and desulphurized producer gas or commercial nitrogen, that is, approximately 96 pct nitrogen, 2 pct hydrogen 2 pct CO, also dehydrated, would be

used to provide a protective atmosphere for the resistors and to flush out more soluble gases from the molten copper.

The operation of a small unit producing approximately 1000 lb of copper per hr has shown that the commercial nitrogen will allow the production of tough pitch electrolytic copper when the metal is transferred from the melt-down unit contemplated to a special type induction unit where the oxygen absorption and temperature can be controlled.

Standard practice in treating low grade scrap brass has been to oxidize the zinc by blowing air through the molten metal. This operation results in the recovery of approximately two-thirds or less of the zinc content of the brass in the form of an impure zinc oxide having only a fraction of the value of the zinc in metallic form. The balance of the zinc is lost to slag, fume and drosses. Fig 1 shows the revised flow sheet of the process for the treatment of scrap brass. For this application and as shown on the flow sheet a low frequency induction furnace has

been substituted for the Wilkins-Poland type as a melting unit. This type of furnace has been found the most suitable for the purpose as will be shown by the following discussion.

Scrap Brass

The melting of refinery scrap brass preparatory to distillation presents a melting problem quite different from the usual melting of brass mill scrap for recasting because refinery scrap is a heterogeneous mixture of alloys each having different melting and boiling points, and coated with a variety of corrosion products and foreign materials. In addition, brass and copper plated pieces of sheet iron, stainless steel, ceramic materials, and others are present that do not melt except at temperatures above the boiling point of the liquid bath.

In the previous paper it is noted that difficulty was encountered in the melting of refinery grade scrap brass without excessive loss of zinc by volatilization and that 5 to 10 pct razorite flux was used to alleviate this condition. While this flux was successful in preventing the excessive loss of zinc by volatilization it interposed a low heat conductivity layer between the source of heat and liquid charge and resulted in lowering the melting rate of the furnace. This same problem presents itself in all types of furnaces in which the metal is heated by radiation and conduction from above the charge.

It has been found in melting this type material that the melting rate per hour or per square foot of hearth area

San Francisco Meeting, February 1949.

TP 2577 D. Discussion of this paper (2 copies) may be sent to *Transactions AIME* before July 15, 1949. Manuscript received December 7, 1948; revision received February 4, 1949.

* Administrative Assistant to Vice President in Charge of Research and Development, Revere Copper and Brass Inc., Rome, N. Y.

† F. F. Poland: Distillation of Zinc and Refining of Residual Metals from Copper-base Alloys. TP 2065, *Metals Tech.* (Sept. 1946): *Trans. AIME* (1949) 182 (to be published).

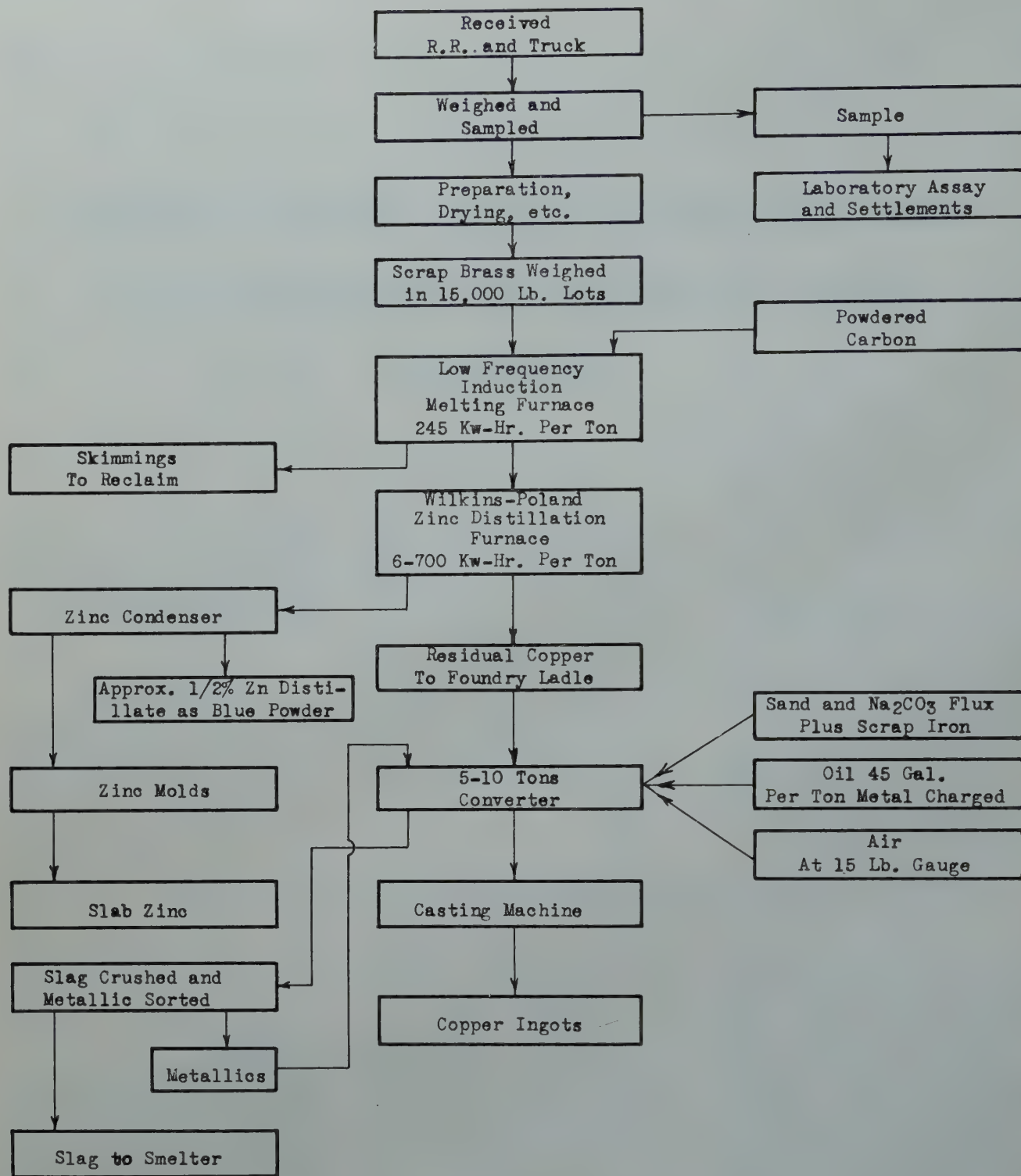


FIG 1—Flowsheet of process for treatment of scrap brass.

for all types of furnaces is considerably less (of the order of 50 pct) than when the same furnace is used for melting scrap alloys or metal of a uniform composition. Allowance for this difference in melting capacity for any given size furnace must be made when designing the melting equipment.

The induction type furnace, because

of its generating heat in the charge below the surface, allows the use of a flux or carbon cover so that the benefits of such a cover may be obtained without interference with the heat input to the charge. This type furnace is constructed without any cover or roof which is an advantage in charging bulky material and allows the use of

mechanical means for pushing the cold charge into the liquid bath.

The usual secondary winding, that is, heating ducts, in induction furnaces designed for general brass mill casting are not satisfactory for the melting of low grade scrap because this type material does not ordinarily contact the liquid metal enough to absorb the

full rated energy of the furnace, consequently the metal in the secondary boils, pinching off and thereby reducing the power input. A low frequency furnace designed for this particular purpose has larger ducts and more circulation than normally supplied and, in addition, is provided with hydraulic rams to push the cold charge into the liquid bath.

The amount of dross formed when melting this type scrap is ordinarily much greater than that produced when melting scrap brass of uniform composition or even when melting turnings. However, it has been found that a layer of two or more inches of finely divided carbon, or preferably lamp-black, on top of the liquid metal, used in conjunction with a hydraulic ram increases the rate of melting to a maximum and reduces the loss of copper and zinc to skims and fume to a minimum.

The finely divided carbon cover on top of the liquid metal produces a very strong reducing atmosphere at the melting zone and experiments have shown that this atmosphere, high in carbon monoxide, will reduce zinc oxide to metal.

Consequently this is an ideal condition and one that is difficult if not impossible to reproduce commercially in any other type of melting furnace.

In melting clean scrap brass, such as mill scrap that contains no ceramic material or other contaminants, there is practically no loss of zinc when melting under the finely divided carbon cover. From these considerations it is believed that the loss of zinc to skims and fume in melting under the conditions described has been reduced to an absolute minimum. The effects on the economics of the operation are shown by the following metallurgical results.

METALLURGICAL RESULTS

The following are the results obtained from the treatment of a mixture of approximately 1,000 tons of light and heavy miscellaneous yellow brass scrap melted in a low frequency induction furnace equipped with mechanical pushers and using a carbon cover on top of the liquid metal.

The approximate analysis as charged to the induction melting furnace was copper 64.2 pct, zinc 25.5 pct, lead 2.0 pct, tin 1.0 pct, nickel 0.7 pct, aluminum, silicon, manganese 0.3 pct, iron (varies widely) 3.3 pct, infusible material, oil, other combustibles, H₂O, etc., 3.0 pct.

There was produced the following, as indicated in Table 1:

| Table 1 . . . Production | | |
|---|---------------------|--|
| | Pct Gross Scrap | |
| Melting furnace skims..... | 7.7 | |
| Zinc slabs..... | 21.4 | |
| Blue powder..... | .5 | |
| Residue copper..... | 67.9 | |
| Volatile and combustible loss..... | 2.5 | |
| | 100.0 | |
| Approximate Zinc Distribution | Pct Gross Scrap | |
| Zinc slabs..... | 21.4 | |
| Blue powder..... | .5 | |
| Melting furnace skims at 15 pct zinc..... | 1.2 | |
| 2.7 pct of residue copper..... | 2.0 | |
| Fume..... | .4 | |
| | 25.5 | |
| Zinc Recovery | Pct Zinc Contents | |
| Zinc slabs..... | 83.9 | |
| Blue powder..... | 2.3 | |
| | 86.2 | |
| Sub Total Recovery..... | | |
| Distribution of Zinc Losses | | |
| to melting furnace skims..... | 4.5 | |
| to copper shot..... | 7.8 | |
| volatile..... | 1.5 | |
| | 13.8 | |
| Sub Total Losses..... | | |
| Total..... | 100.0 | |
| | Pct Copper Contents | |
| Copper produced in residue metal..... | 96.5 | |
| to melting furnace skims..... | 3.5 | |
| | 100.0 | |
| Total..... | | |

Melting in the reverberatory or converter type furnace results in a zinc loss to slag and fume of between 18 to 30 pct, a fair average being about 23 pct of the total zinc contents. The copper loss to skims is also proportionately greater than in the induction furnace.

The increased amount of zinc lost and the additional amount of by-products to be treated for the recovery of copper results in an estimated difference in returns of approximately \$20.00 per ton of scrap brass treated, in favor of the induction furnace.

The amount of zinc left in the residual copper from the distillation is under the control of the operators and it has been commercially varied from less than 1.5 to 3.5 pct depending upon the planned disposal of the residual metal. The results enumerated above were predicated upon a use where it was desirable to obtain the maximum production and anything under 3 pct zinc in the residual copper was adequate. The temperature of the residual copper as tapped from the distillation furnace was approximately 3200°F. However, these furnaces have been run for considerable periods at much higher temperatures, and in one plant the operating temperature is sufficiently high to reduce the zinc content of the residual metal to less than 1.5 pct. This corresponds to a metal temperature of approximately 3500°F.

There have been no changes made in the condenser or furnace operating temperature from that described in the previous paper. Therefore the copper content of the zinc slabs produced is approximately the same, that is, 0.75

pct. The lead content of the zinc produced was 3+ pct which is normally liquated to Prime Western quality.

In general, it has been found that from 35 to 45 pct of the lead content of the scrap metal is distilled with the zinc. All of the other contaminants have very low vapor pressures at the operating temperatures and consequently copper and lead are the only metals in significant quantity carried to the condenser by the zinc vapor.

CONVERTING RESIDUAL METALS

Since the publication of the previous paper the plants that have installed this equipment have desired the residual metal for purposes different from those described in that publication. In one plant the residual metal was intended to be made into shot for the manufacture of copper sulphate. In another the residual metal was intended for electrolytic copper refining and in others the residual metal was to be converted for use in the manufacture of copper base ingot alloys. The revised flow sheet (Fig 1) shows the use of a 5 to 10 ton converter instead of the 50 ton previously described. In operating this small converter the residual metal is transferred directly from the distillation furnace and copper oxide added in definite amounts or air blown through the metal to some definite control point, for instance, iron to -0.02 pct, depending upon the end uses as enumerated above. There is nothing particularly new in this general operation. However, it is believed of interest to note that the iron can be reduced to the third decimal point in percentage while 0.75 to 1 pct zinc is still present and that in so doing only about 10 pct of the lead and tin present is removed. After the iron is removed the zinc, tin, lead and nickel are eliminated concurrently but in the order given.

It is common practice in recovering zinc from galvanizers dross to use the retort process. It is well-known by those operating such equipment that it is becoming more and more difficult to obtain labor that is willing to perform the hot, smoky and dirty task connected with this process.

One of the Wilkins-Poland units designed for handling scrap brass was modified to permit a pilot plant operation on the distillation of galvanizers dross, scrap die castings and other scrap zinc and subsequently the engineering company licensed to build these furnaces has designed a unit especially

Table 2 . . . Comparison of Wilkins-Poland Unit vs. Retort Plant

| | | |
|---|--|-----------------------|
| | Recovery Retort Plant | |
| Zinc content of galvanizers dross | average | 93.5 |
| Zinc slabs produced—pct of gross weight | | 86. |
| Losses of Gross Weight | | 5. |
| to melting skims | | 5-6 |
| to retort residues—28 pct Zinc | | 1-2 |
| to blue powder | | 1-2 |
| to fume and other volatile | | 86 |
| Pct recovery Zinc Slabs | 93.5 | 92 |
| Initial cost estimated | | \$30,000.00 |
| | Recovery Wilkins-Poland Unit with Ajax-Tama Melting Furnace Attached | |
| Zinc content of galvanizers dross | average | 93.5 |
| Losses | | 3 |
| to melting skims | | 5 |
| to retort residue—8 pct zinc | | 2 |
| to blue powder and volatile | | 90 |
| Zinc slabs recovered | | 90 |
| Pct recovery | 93.5 | 96 |
| Initial cost estimated | | \$100,000.00 |
| | Estimated Operating Cost per Ton in Retort Plant Producing 15 Tons per Day | |
| Labor—5 hr per ton at \$1.50 per hr | | \$ 7.50 |
| Retorts at \$200. each | | 4.00 |
| 100 gal fuel oil | | 10.00 |
| Repairs and replacements retorts | | 2.00 |
| | | \$23.50 |
| 50 pct overhead | | 11.75 |
| | | \$35.25 |
| Amortization of equipment, 10 pct of \$30,000. operating 325 days per yr and producing 4875 tons per yr | | 0.62 |
| | | \$35.87 |
| | Estimated Operating Cost per Ton in Wilkins-Poland Furnace Producing 15 Tons per Day, 750 KVA Capacity | |
| Labor—2 men each shift—48 labor hr—3.2 at \$1.50 | | \$ 4.80 |
| Power—1150 kw hr per ton at 0.9 cents | | 10.35 |
| 150 kw hr per ton melting—1150 | | |
| 1000 kw hr per ton distilling— | | |
| Repairs at \$2.00 per ton | | 2.00 |
| | | \$17.15 |
| 50 pct overhead | | 8.57 |
| | | \$25.72 |
| Amortization of equipment, 10 pct of \$100,000 operating 325 days per yr and producing 4875 tons per yr | | 2.05 |
| | | \$27.77 |
| This comparison shows that the savings in operating costs per ton in Wilkins-Poland furnace are | | \$ 8.10 |
| In addition there is an estimated 4 pct additional recovery which amounts to 2000 lb × 4 pct × 18 cents | | 14.40 |
| Total savings to be expected from the use of the Wilkins-Poland furnace | | \$22.50 per ton dross |
| Inasmuch as a production of 4875 tons per yr is involved, a total savings would amount to about \$109,000 per yr. | | |

adapted for this purpose. This unit consists of a special type low frequency furnace connected directly to the Wilkins-Poland distillation furnace of standard type.

Table 2 summarizes the results of the pilot plant operation, the estimated cost and the savings to be made. The comparison has been based on the operation of one Wilkins-Poland unit of 750 KVA capacity which is capable of processing 15 tons of dross per day vs. a retort plant equipped with 10 retorts of 4,000 lb capacity each. There will probably be plants in which this size unit would be too large and it is therefore planned to also build these units in sizes about one-half this capacity. This smaller size unit may result in a slightly higher labor cost as compared to the larger unit. However, the savings as compared with the operation of an equivalent retort plant would be in proportion.

It should be noted that the above savings are a comparison in the operating cost between the two types of equipment and that there would be additional savings in freight and treat-

ment charges where the equipment was installed at a galvanizing plant.

In presenting the foregoing figures I am aware that cost figures will vary from plant to plant and from month to month in a given plant. The figures given represent a pilot operation on full scale equipment insofar as the treatment of drosses in the resistor furnace is concerned. They do not, however, comprehend the over-all operation of a large plant.

The cost projected for a retort plant operation represents the best average that could be established on information supplied by operators of plants of this type.

A typical analysis on galvanizers dross is copper 0.01-0.04 pct, lead 0.2-1.0 pct, iron 2.9-3.5 pct, aluminum nil, zinc balance. The slab zinc produced from this type of material will run less than 0.02 pct iron and under Prime Western requirements in lead. The balance is zinc.

The furnace as designed for the distillation of galvanizers dross and other scrap zinc products has a relatively deep hearth so that the iron residue

may be accumulated for several days at which time it becomes necessary to stop charging and increase the temperature of the furnace to the melting point of the iron, that is, approximately 2750°F. This allows the residue to be tapped as a liquid containing approximately 8 pct zinc and the balance iron and lead. This residue can be sold to plants operating lead blast furnaces. However, there has been no credit given to the Wilkins-Poland furnace cost estimate for this item.

In the pilot plant operation galvanizers dross, scrap die castings and other scrap zinc, and the like, were re-distilled, producing slab zinc running between intermediate and high grade quality. This was accomplished by placing a small condenser in series with a regular condenser and returning an approximately 10 pct fraction condensed in the first condenser to the furnace. The principal reason for doing this was to obtain zinc extremely low in aluminum. The bulk of the material under these conditions was spectroscopically free from this element.

In distilling zinc from galvanizers

dross and other scrap zinc, the furnace can be operated so as to deliver a quite uniform amount of vapor to the condenser. This should prove very desirable in the production of zinc dust which is usually made from this source of zinc.

FURNACE IMPROVEMENTS

Improvements in construction have been made to the resistor furnace to reduce the heat losses, particularly at the top and side walls above the metal line. This was accomplished by more liberal use of lampblack insulation between the carbon and refractory lining on the side walls and by raising the insulators to a more remote location from the roof plates over the resistors. In consequence of this the weight of the roof and therefore the crane capacity to remove it when necessary was reduced from approximately 15 tons to approximately 5 tons. The power consumption on this later designed furnace is approximately 100 kw hr per ton less than on the original design.

Nonmagnetic steel has been inserted in the area influenced by the magnetic field of the lead-in terminals and the use of noninductive busses combined with the noninductive arrangement of the resistors results in a power factor of between 93 and 96 pct. This high power factor and steady load are of distinct advantage in that the lowest power rates are granted and the initial cost for electrical equipment is at a minimum.

Electric arc furnaces have been and are being used successfully for the melting of electrolytic copper cathodes and a further extension of this application is being made. The difference in the characteristics between the arc furnace and the Wilkins-Poland resistor furnace are such that a considera-

ble reduction in the installed KVA for any given capacity would result in a substantial saving. Increased efficiency due to the reduced radiation losses and extremely low replacement cost of the resistors as compared with arc electrodes makes the resistor furnace more economical than the arc furnace.

Special applications of the Wilkins-Poland furnace are being given consideration where the use of helium, argon, chlorine and nitrogen are to be used as atmospheres. Past experience with nitrogen as an atmosphere has shown that this type furnace can be made practically gas-tight and therefore it is practical to use these expensive gases where necessary.

There have been no changes in the dimensions or design of the condenser. However, one installation is being built in which a small primary condenser will be inserted between the furnace and the regular condenser. The purpose of this is to condense a 10 to 15 pct fraction of the zinc at this point in order to reduce the copper and lead in the approximate 85 pct remainder.

ECONOMICS

As stated in the previous publication the initial investment for building a plant to recover metallic zinc from scrap brass is appreciably less for this process and equipment than for any previous processes. The operating labor hours and other items as given in the previous publication are still applicable. However, the power required has been reduced approximately 100 kw hr per ton.

Summary

It has been shown that the high temperature electric resistor furnace distillation of zinc from secondary metals has proven, with further de-

velopment and use, to be superior in economic and metallurgical results to the older equipment and process.

The economics of melting miscellaneous scrap brass for the recovery of metallic zinc has been discussed and it has been shown that induction electric melting is more economical for this purpose than fuel fired furnaces.

The electric melting of electrolytic copper cathodes has been suggested as an application for the resistor furnace because it is believed to be more economical than the present 250 ton fuel fired reverberatory furnace practice for the production of tough pitch or oxygen free shapes. For this purpose the Wilkins-Poland resistor type furnace would be competitive in installation and operating costs.

Several new installations are in the engineering stage. These plants will be located both in this country and in Europe.

Although it is rather difficult to obtain prompt delivery of the transformers and other electrical equipment necessary for these furnaces at this time, the expansion in their use to date and the degree of interest as shown by inquiries for its application to other fields give every reason to believe that this new metallurgical furnace will find a wide and diversified use in the metallurgical field in the future.

Acknowledgments

Acknowledgment is made for data obtained from Mr. Fred Rehns, Brooklyn Chemical Co., Baltimore, Md.; Mr. Daniel Ogden, The American Metal Co., New York, N. Y.; Mr. Mario Tama, Ajax Engineering Corporation, Trenton, N. J., and to Mr. R. A. Wilkins for permission to publish the information contained.



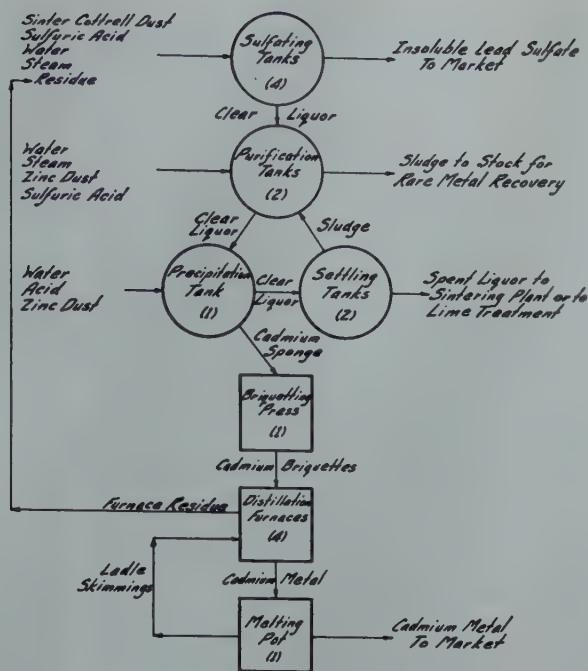


FIG 1—Flow sheet. Fire metallurgy of cadmium.

stacks. The bottoms of the tanks slope, 1 in. per ft, to 4 in. Everdur bronze gate valves. There are air, steam, water, acid and weak liquor connections to each tank.

In the treatment of dust, 3 to 4 ft of water, or weak cadmium wash liquor from a previous batch, is added to the sulphating tank. While this solution is being agitated a bucket of dust is placed on the dumping ring on the tank and the dust added slowly over a period of 15 to 30 min. An average bucket of Cottrell dust weighs 5 or 6 tons.

Acid sludge, when available, is added at this point to supply the necessary sulphuric acid for treatment. Care must be taken that too much sludge, and consequently too much sulphuric acid, is not added. All excess acid must later be neutralized with zinc dust. When no acid sludge is available 60° Baume sulphuric acid, from the Cadmium Plant storage tank, is used. The sulphating tank is then brought to a boil with steam to dissolve soluble material. Usually 4 to 6 hr of boiling and agitation are needed. The acidity is so adjusted that, upon final dilution with water, the solution will show approximately 1 pct acid. After dilution the steam is shut off and the lead sulphate allowed to settle. This settling period may be 6 to 8 hr.

To determine the acidity of the solution, a 10 ml sample of the liquor is titrated with sodium hydroxide using methyl orange as the indicator. It may be necessary to filter the sample before titration.

The purpose of the sulphating treatment is to put cadmium and zinc into solution and to convert lead to lead sulphate. The lead sulphate is practically insoluble and settles to the tank bottom leaving 7 or 8 ft of clear liquor above it. When the sample cup shows that the lead sulphate has settled sufficiently, a suction hose, from a lead LaBour pump, is dropped to within 6 in. of the mud level of the tank and the clear liquor decanted to one of the purification tanks. When the batch of clear liquor has been pumped out, the tank is ready for treatment of more dust. Usually two buckets of Cottrell dust and two tanks of acid sludge may be treated before it is necessary to remove accumulated lead sulphate. If no sludge is available, and sulphuric acid is being used in treatment, three buckets of dust may sometimes be treated before lead sulphate removal.

The above treatment and settling time will vary somewhat with the density, moisture content, chemical characteristics, and physical properties of the dust and sludge.

After the second or third batch of

clear liquor has been pumped to the purification tanks, the remaining lead sulphate is given a 1 pct sulphuric acid wash and several water washes. The acid wash is decanted to the purification tanks and treated as regular pregnant cadmium solution. The final washes of 2° Be' or less are decanted to storage for subsequent use as make-up water in the sulphating tanks. The accumulated lead sulphate is then pumped, as a slurry, to 25 × 50 ft concrete storage bins where it can again settle, and the water can be decanted off as necessary.

The lead sulphate is allowed to accumulate during the winter and in summer weather it is air-dried for shipment to lead smelters. This finished lead sulphate assays approximately 63 pct lead, 1 pct zinc, 0.2 pct cadmium, and may contain small amounts of silver. The use of acid sludge increases the lead content of the lead sulphate.

Purification

The two purification tanks are 8½ ft in diam and 15 ft deep. They are equipped with agitators, and individually ventilated. Each tank has a hinged cleanout door at the bottom which closes with a wheel clamp. These tanks

are agitated while the clear acid liquor from the sulphating tanks is being pumped into them. Zinc dust, or fine zinc skimmings, is added during agitation in sufficient amount to neutralize the solution. This addition of zinc precipitates part of the cadmium and nearly all impurities such as lead, tin, copper, silver, gallium, indium and germanium. It is very important that these purification tanks be well ventilated because of evolution of nascent hydrogen from the reaction of zinc and sulphuric acid.

The zinc dust or skimmings used as a precipitant is a mixture of metallic zinc and 5–10 pct zinc oxide. Normally 100 to 200 lb of zinc dust are needed to raise the hydrogen ion concentration of the batch to 5.5. The neutral point is checked with methyl red or preferably with Hydrion pH test paper. The tank is then agitated for several hours and allowed to settle. When the solution has settled a suction hose is dropped to within 6 in. of mud level and the clear liquor decanted to the precipitation tank by a LaBour pump. The purification tank is then ready for another batch of liquor from the sulphating tanks.

The liquor pumped to the purification tanks will have a Baume of 20 to 25° and, as stated before, will run about 1 pct acid. Higher acidity may cause a violent evolution of hydrogen and excessive foaming. The Baume must also be kept within reason, since usually the higher Baume solutions settle very slowly. When sufficient sludge has accumulated to prevent the tank from settling properly it is removed as discussed later under "Rare Metal Recovery."

Precipitation

The precipitation tank is identical with the two that are used for purification. The clear liquor from the purification tanks is pumped into this tank and enough sulphuric acid added to raise the acidity to 0.5 pct. Screened zinc dust or zinc skimmings is then added slowly to the agitated solution to precipitate cadmium sponge. Hydrogen is evolved by the reaction of zinc and sulphuric acid, therefore good ventilation is also necessary here. The solution must be kept acid, since a basic solution will precipitate a sponge which is not suitable for briquetting. A polished strip of metallic zinc is used to determine when all the cadmium has been precipitated. The zinc strip

will show no black stain when dipped in liquor from which all cadmium has been removed. The experienced operator can usually determine the end point visually as there is considerable gas evolved. At this point care must be taken to prevent excessive foaming or the tank may overflow.

When the end point is reached, the agitator is turned off and the grey metallic sponge settles quickly to the bottom of the tank. The clear liquor is then decanted to a settling tank. The sponge is not removed after each precipitation but is allowed to accumulate until 2000 to 3000 lb are in the tank. When ready for removal, the sponge is given a 1 pct cold acid wash followed by about six cold water washes. After pumping off the final water wash, the bottom door of the tank is opened and the sponge shoveled into barrels. The barrels of sponge are immediately covered with water to prevent oxidation. If allowed to stand in the air, the sponge becomes very hot and changes to the oxide. The sponge contains 90 to 95 pct cadmium, 1 to 2 pct zinc, 1 to 2 pct lead plus other impurities in small amounts. Most of these impurities are carried from the purification tank to the precipitation tank mechanically since the liquor does not always settle water clear. Also, pockets of gas in the mud on the tank bottom are released as the liquor above is removed and this disturbance in the tank causes some impurities to be carried over.

Following the precipitation tank are two settling tanks 10 ft in diam and 10 ft deep with agitators. The liquor pumped from the precipitation tank usually contains small amounts of cadmium which either are not precipitated or have gone back into solution. A small amount of zinc dust is added to the liquor pumped to the settling tank for removal of this last trace of cadmium and to neutralize any remaining acid. The tank is agitated until a test with tri-methyl-phenyl-ammonium iodide shows no cadmium in solution. The tank is allowed to settle clear.

This clear liquor is then pumped to a storage tank. The sponge which collects in these tanks is removed periodically and returned to the purification tanks, as it is not suitable for briquetting.

Part of this liquor is pumped to the sintering plant and serves as a wetting agent in the charge going to the sintering machines. Any excess wash liquor is treated with lime at the Cadmium Department and the precipitated zinc oxide and calcium sulphate, after being

filtered and dried, is sent to the sintering plant.

Briquetting

The cadmium sponge from the precipitating tank is briquetted in a Watson-Stillman press operated by an Oilgear hydraulic pump. This hydraulic press has a mold 6 in. in diam and 4 in. deep. The sponge is removed from the stock barrels and placed on the press table. To make a briquette, the mold is filled with sponge and pressure is applied. The upper plunger moves down and forces the pressure plate into the mold. Pressure is applied until the water and gas are squeezed out of the sponge and plunger stops moving—a matter of 5 to 10 sec. The upper plunger is then withdrawn and a lower plunger comes up, forcing the briquette from the mold. The briquettes are removed, as made, to a weighing scale, until 500 lb have been made. These 500 lb batches of briquettes are then returned to a barrel and again covered with water.

The finished briquette is 6 in. in diam and from $\frac{1}{2}$ to 1 in. thick. The total pressure applied is approximately 3500 psi. The water and fine particles of sponge, draining away from the press, are returned to the purification tank. This press will make from 1500 to 2000 lb of briquettes per 8 hr shift. The finished briquettes contain about 10 pct water. The briquettes apparently are not affected by being stocked under water, although when held for a considerable time hydrogen gas is slowly evolved.

Smelting

There are four tilting type furnaces for the distillation of the cadmium briquettes, each of which contains a Lava No. 40 graphite type retort and a cast iron condenser. They are fired by natural gas using a zero gas governor which gives a constant gas and air ratio. The distillation furnace is mounted with short axles on cast iron trunions and may be tilted by a hand wheel gear and pinion from a 30° distillation angle to a horizontal position for cleaning. The furnace is a cylindrical steel shell lined with firebrick and has two tangential burner ports diametrically opposite at the base of the shell to give the gas a swirling motion for uniform heating of the retort. The cast iron condenser is mounted on a four

wheeled iron carriage for convenient removal.

About an hour before charging a retort, 500 lb of briquettes are removed from under water and allowed to drain. The 500 lb charge is then placed in the hot retort. The cast iron condenser is placed in position over the retort and sealed with clay. In approximately one hour, steam from the charge is driven off and the metal begins to distill. The distilled cadmium is tapped, as often as necessary, into iron molds. Ordinarily it takes from 16 to 20 hr for a charge to work off. When the cadmium has distilled, the condenser is removed and the residue and slag scraped from the retort. The retort is then ready for recharging as before. An average 500 lb charge of briquettes will produce about 375 lb of metal and 35 lb of residue plus some condenser cleanings.

Cadmium residue, from the retorts, is crushed and accumulated for retreatment in the sulphating tanks with acid. The acid insoluble material is sent to the Waelz Oxide Plant for removal of residual cadmium. Any slag formed during smelting is also collected and sent to the Waelz Oxide Plant. Condenser cleanings are usually high in metallic cadmium and are recharged into a retort in separate batches. Fumes and dust from the furnaces are collected by hoods and recovered by a cyclone and Dracco dust catcher. This dust and fume are accumulated and acid treated along with residues.

The cadmium metal recovered from briquettes is ordinarily too high in lead for commercial use and must be redistilled. A 1000 lb charge of metal is placed in a relatively new retort and distilled as above, tapping metal from the condenser as often as necessary. A 1000 lb charge will normally produce

975 lb of metal ready for casting into commercial shapes.

Remelting

Redistilled cadmium is accumulated until a sufficient amount is on hand to fill an order or until it is convenient to recast it into commercial shapes. The cast iron melting pot is gas fired. It is hemispherical in shape, being approximately 4 ft in diam. A considerable amount of skimmings, consisting of a mixture of cadmium oxide and metal, collects on the pot of molten metal and must be skimmed off occasionally. These skimmings are accumulated for recharging into the cadmium furnaces. If the pot of molten metal is held at a high temperature too long, small amounts of zinc present will burn off and the cadmium metal will oxidize excessively. The temperature is kept slightly above the melting point of 320.9°C. The molten cadmium is ladled from the melting pot and cast into commercial shapes. The finished metal will run less than 0.1 pct zinc and less than 0.02 pct lead, plus spectrographic traces of several other elements.

Rare Metal Recovery

As stated under the heading of "Purification," the impurities removed from the cadmium liquor collect on the tank bottom until this bulk becomes so great that the solution in the tank will not settle properly. At this point, the accumulated sludge must be removed. This sludge contains cadmium, zinc, lead, tin, chromium, copper, germanium, indium, gallium and traces of

other elements below zinc in the Electromotive Series. Besides the cadmium and zinc, the only other elements being recovered from this sludge at present are the gallium, indium and germanium.

Previous to its removal, the sludge is given several acid washes to dissolve as much cadmium as possible. Before these washes are allowed to settle, they are made basic with a small amount of zinc dust to reprecipitate any rare metals which may have gone into solution. These decanted washes are treated in the precipitating tank to recover cadmium. The sludge remaining in the purification tank is then given a strong acid treatment to put as much material in solution as possible. After settling, the clear portion of this solution is decanted to the precipitating tank and treated with zinc dust. The precipitated sponge, containing rare metals, is removed, briquetted, and charged as usual into the cadmium furnace. The residue is saved for rare metal recovery. This sponge is occasionally too slimy to briquette and, in this case, is dried on a hot plate prior to treatment for rare metals. Such material may contain 4-7 pct germanium, 5-10 pct indium and less than 1 pct gallium.

The insoluble material remaining in the purification tank, after the strong acid treatment, is mainly lead sulphate and contains approximately 5 pct cadmium, 0.7 pct germanium, and 0.1 pct indium. This residue is pumped as a slurry to a storage bin for future treatment.

A separate set of tanks is used for rare metal recovery. Gallium, indium and germanium are currently being recovered and purified but it is beyond the scope of this paper to go into the methods of concentration and purification.



Technical Notes

On Feb. 16, 1948, the Board of Directors of AIME authorized the publishing of "Technical Notes" in METALS TECHNOLOGY (as of Jan. 1, 1949, *Transactions Section, JOURNAL OF METALS · TECHNOLOGY · PRACTICE*). The purpose is to provide *prompt* publication of *very short* items of the following general types:

1. Results of short investigations which do not warrant a paper.

2. The conclusions of extensive investigations of insufficient general

interest to justify a regular paper.

3. Conclusions arising in the course of an investigation, which, because of interest to others in the field, the author wishes to present prior to completion of the investigation.

4. Pertinent factual comment (not mere argument) on the subject matter of previous "Notes."

Such Notes will be subject to the approval of the Auxiliary and AIME Publications Committees, but can be handled more promptly than regular

papers because they need not be referred to readers. The recommended maximum length is 500 words; notes in excess of 1,000 words will not be considered for this type of publication. A graph or photograph may be included as part of the note when particularly illustrative. As with regular papers, contributions to the new section should be submitted to the Secretary of the AIME. Please furnish two copies each complete with illustrations.

The Statistical Nature of the Endurance Limit

[illegible]

J. T. RANSOM,* Junior Member, and R. F. MEHL,† Member, AIME

For many years the Metals Research Laboratory of Carnegie Institute of Technology has been concerned with the statistical nature of the engineering properties of steel from an experimental viewpoint, particularly those properties representing ductility.¹ In the past three years new work has been directed toward evaluating the statistical nature of the endurance properties. It has been shown that both the fracture curve and the endurance limit in fatigue are markedly statistical in nature.

The *S-N* curve (and the endurance limit) of ferrous materials is often determined with specimens which number as few as ten. The common procedure is to test the first specimen at a stress well above the expected endurance limit. Each succeeding specimen

is then tested at a progressively lower stress, until, after five or six tests, a specimen runs ten million or so cycles without failing. Two or three more specimens are then used to find the

Technical Note 15 E. Discussion of this note (2 copies) may be sent to *Transactions AIME* before August 1, 1949. Manuscript received February 14, 1949; revision received April 8, 1949.

* Formerly graduate student, Department of Metallurgical Engineering, Carnegie Institute of Technology, Pittsburgh, Pa.; now Research Metallurgist, Engineering Research Laboratory, E. I. duPont deNemours & Co., Inc., Wilmington, Delaware.

† Head, Department of Metallurgical Engineering, and Director, Metals Research Laboratory, Carnegie Institute of Technology, Pittsburgh, Pa.

¹References are at the end of the note.

highest stress at which failure will not occur; the limiting stress determined in this way is called the endurance limit. It has now been found, however, that the variability in the fracture curve and in the endurance limit in heat-treated alloy forging steels is so great that $S-N$ curves must be drawn on the basis of distribution curves which can be appraised only by statistical methods.

Two methods have been adopted in this study: (1) straightforward statistical studies of cycles to fracture of a number of specimens at each of a series of stress levels, and (2) a new abbreviated statistical method, known as "staircase testing."² The latter consists in testing a series of specimens, one by one, with the test stress for any given specimen automatically

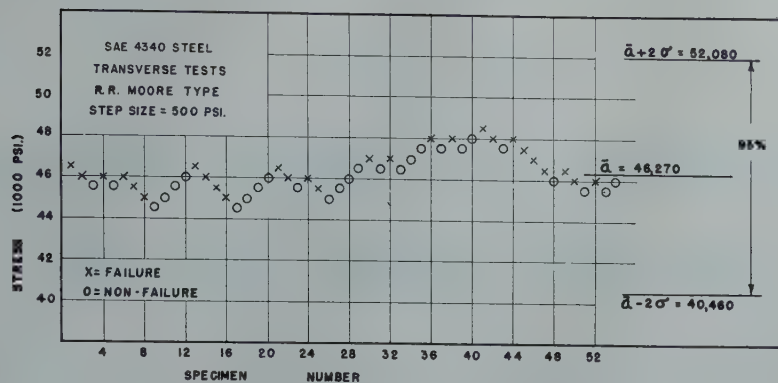


FIG 1—Results on a SAE 4340 steel.

determined by whether the preceding specimen failed or ran out unbroken through ten million cycles. The stress for the first specimen is chosen at a level where 50 pct failures would be expected if a large number of specimens were so tested, that is, at about one-half the tensile strength for steels. If the first specimen fails, the stress for the second specimen is decreased by one step, say 500 psi. If the first specimen "runs out" unbroken, the stress for the second specimen is raised by one step, and so on. The results on a SAE 4340 steel are plotted chronologically as X's (failures) or O's (non-failures), as in Fig 1. The X's and O's are then used to compute \bar{a} , the average endurance limit (the stress at which 50 pct of the specimens would fail and 50 pct run out), and σ , the standard deviation (if each of a very large number of specimens reveals its own exact endurance limit, the range $\bar{a} \pm 2\sigma$ would include 95 pct of these values). Calculation of the data in Fig 1 results in the prediction that the true scatter range in terms of $\pm 2\sigma$ extends from 40,460 to 52,080 psi.

This result is in conformity with findings of the usual statistical approach; 146 specimens were tested at

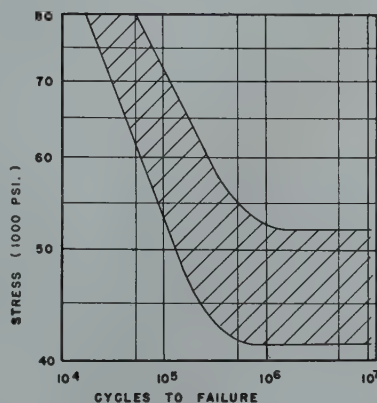


FIG 2—Value of $\pm 2\sigma$ for endurance limit.

stress levels distributed evenly over the 12,000 psi range indicated, and to this were added 64 specimens tested at stresses above the indicated average endurance limit. The value of $\pm 2\sigma$ for the endurance limit as calculated from these data gave 11,250 psi, Fig 2. Similar results were found for other forging steels in both the transverse and the longitudinal directions. It is interesting to note that groups of ten specimens chosen from the 210 samples in a manner to simulate the conventional testing procedure, but otherwise at random, provided eight *S-N* curves with points for each agreeing

with the drawn curve as well as on most published curves, but each curve showing wide divergence from one another, giving endurance limits ranging from 50,000 psi to 41,000 psi; such is the way that chance may operate, to the deception of the observer, in a statistical universe.

It is evident that estimates of the true endurance limit and of the fracture curve may be substantially in error when based on the small number of tests commonly employed. It appears that the fatigue properties of such steels can be appraised only on statistical grounds. Moreover, it appears that the endurance limit must be used in design in full recognition of its statistical nature; if design is based upon a stated stress level for the endurance limit, then, on principle, a fixed number of fatigue failures must be expected.

References

1. C. Wells and R. F. Mehl: Transverse Mechanical Properties in Heat Treated Wrought Steel Products. (1948) ASM Preprint No. 23.
2. Statistical Analysis for a New Procedure in Sensitivity Experiments. (1944). AMP Report No. 101.1R, Statistical Research Group; Princeton No. 40.



[illegible]

S. A. HERRES* and A. R. ELSEA,* Junior Member AIME

Temper brittleness refers to the loss in the notched-bar impact resistance encountered in most medium- or low-alloy steels when they are tempered within the temperature range of 700 to 1100°F or slowly cooled from a higher tempering temperature. Temper brittleness is important because it impairs the service properties of otherwise suitable steels over the range of hardnesses obtained at medium tempering temperatures and because it is impractical to cool pieces of large section rapidly enough from higher tempering temperatures to prevent temper brittleness.

The problem of temper brittleness has always been closely associated with ordnance manufacture because armor plate and gun steels require good shock resistance and are often heat treated in heavy section. However, it is now realized that many brittle failures in structural alloy steel parts are attributable to temper brittleness, and there is little question that it contributes to the low impact resistance of alloy steels used in the hot-rolled or normalized condition which are slowly cooled from the hot-rolling or normalizing temperature.

Recently Hollomon¹ has presented a comprehensive summary of the literature on the subject and an excellent description of the manner in which temper brittleness affects the notched-bar impact resistance and other mechanical properties of steel.

Carpenter and Robertson² have given a good analysis of the probable mechanism of temper brittleness, which is similar in many respects to the precipitation-hardening phenomenon. Fig 1 is their diagram illustrating the response to tempering of a susceptible steel. Three changes are recognized as the temperature of tempering a previously quenched steel is raised: (1) pre-

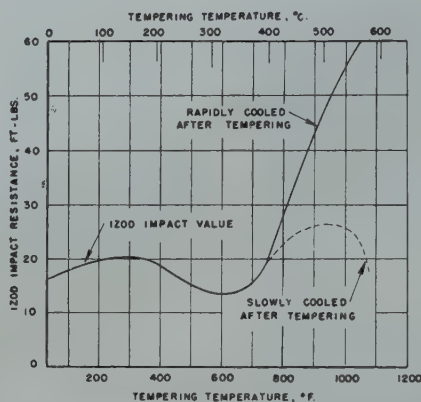


FIG 1—Effect of tempering on impact toughness.²

cipitation occurs more rapidly and to a greater extent and the notched-bar impact value falls to a minimum; (2) coalescence of the precipitated particles begins to be effective and the impact values for both rapidly cooled and slowly cooled specimens increase; (3) the precipitate goes back into solution at higher tempering temperatures and the impact values of specimens cooled rapidly enough to retain the solution increase, while reprecipitation occurs in slowly cooled specimens and their impact values decrease again. No change must proceed to completion before the following one begins and there is overlapping in temperature ranges.

Although there have been a large number of experimental investigations

of temper brittleness, insufficient evidence has been accumulated to permit definite identification of the precipitate which causes temper brittleness nor have the specific effects on it of various alloy elements and impurities in steel been definitely established. This lack of evidence is largely a result of the lack of a suitable measure for temper brittleness.

Temper brittleness is evidenced by an increase in the temperature of brittle failure of notched-bar impact specimens, but most of the data are in the form of an arbitrary susceptibility ratio of the room-temperature impact value for specimens quenched from a high tempering temper to that of similar specimens furnace cooled from the temper. It is obvious that this numerical ratio is dependent upon the type of specimen used and the specific conditions of testing rather than the characteristics of the steel.

In general, manganese, chromium, and nickel alloy steels are most susceptible to temper brittleness and molybdenum has been used to decrease

Cleveland Meeting, October 1949.
TP 2574 E. Discussion of this paper
(2 copies) may be sent to *Transactions*
AIME before December 15, 1949.
Manuscript received December 6,
1948.

¹ References are at the end of the paper.

* Metallurgist, Battelle Memorial Institute.

Table 1 . . . Chemical Analyses of Experimental Steels

| Type Steel,* Pct | Per Cent | | | | | | |
|--------------------------|----------|------|------|-------|-------|----------------|------------------|
| | C | Mn | Si | P | S | Al Addition | Others |
| 1.0 Mn | 0.23 | 0.92 | 0.19 | 0.020 | 0.018 | 0.10 | |
| 1.5 Mn | 0.25 | 1.58 | 0.17 | 0.022 | 0.019 | 0.10 | |
| 0.5 C, 1.0 Mn | 0.47 | 1.03 | 0.20 | 0.020 | 0.017 | 0.10 | |
| 3.0 Ni | 0.27 | 0.19 | 0.27 | 0.018 | 0.017 | 0.10 | 2.9 Ni |
| 5.0 Ni | 0.23 | 0.20 | 0.16 | 0.022 | 0.017 | 0.10 | 4.95 Ni |
| 0.75 Cr | 0.26 | 0.21 | 0.26 | 0.018 | 0.016 | 0.10 | 0.72 Cr |
| 1.5 Cr | 0.24 | 0.20 | 0.18 | 0.020 | 0.015 | 0.10 | 1.44 Cr |
| 0.5 Mo | 0.25 | 0.20 | 0.18 | 0.019 | 0.017 | 0.10 | 0.63 Mo |
| 1.0 Mo | | | | | | | 1.0 Mo |
| 2.0 Ni, 0.1 Ti | 0.26 | 0.20 | 0.20 | 0.018 | 0.017 | 0.10 | 2.0 Ni, 0.09 Ti |
| 2.0 Ni, 0.1 V | 0.27 | 0.23 | 0.26 | 0.014 | 0.016 | 0.10 | 2.0 Ni, 0.12 V |
| 3.0 Ni, 0.1 P | 0.25 | 0.20 | 0.16 | 0.110 | 0.016 | 0.10 | 3.0 Ni |
| 1.0 Mn, 0.75 Cr | 0.24 | 1.08 | 0.27 | 0.016 | 0.019 | 0.10 | 0.77 Cr |
| 1.0 Mn, 0.75 Cr, No Al | 0.25 | 1.11 | 0.24 | 0.018 | 0.020 | None | 0.76 Cr |
| 1.0 Mn, 0.75 Cr, 0.20 Mo | 0.23 | 0.99 | 0.20 | 0.016 | 0.019 | 0.10 | 0.78 Cr, 0.20 Mo |
| 1.0 Mn, 0.75 Cr, 0.50 Mo | 0.23 | 1.06 | 0.22 | 0.017 | 0.016 | 0.10 | 0.76 Cr, 0.50 Mo |
| 1.0 Mn, 0.75 Cr, 0.75 Mo | 0.24 | 1.03 | 0.26 | 0.018 | 0.017 | 0.10 | 0.77 Cr, 0.75 Mo |
| 1.0 Mn, 0.75 Cr, 0.06 P | 0.24 | 1.05 | 0.26 | 0.057 | 0.018 | 0.10 | 0.78 Cr |
| 1.0 Mn, 0.75 Cr, 0.005 P | 0.26 | 1.08 | 0.24 | 0.006 | 0.020 | 0.10 | 0.75 Cr |
| 1.5 Mn, 0.005 P | 0.27 | 1.51 | 0.22 | 0.005 | 0.021 | 0.10 | |

* The intended base analysis was 0.25 pct carbon, 0.20 pct manganese, 0.20 pct silicon, 0.02 pct phosphorus, 0.02 pct sulphur (0.1 pct aluminum added).

temper brittleness. The apparent effect of phosphorus in increasing temper brittleness has been attributed by Hollomon¹ to an increase in the temperature of brittle failure of nonembrittled steels of high phosphorus content which in many instances brings the divergence in the impact curves between embrittled and nonembrittled specimens closer to room temperature.

Various investigators have suggested that the temper-brittleness precipitate is a carbide, a nitride, a phosphide, or an oxide. Hollomon¹ states that the rate of diffusion of the responsible element is such that either nitrogen or carbon appears to be involved.

A recent study³ indicated that neither variations in the nitrogen content of susceptible steels, nor the addition of nitride stabilizing elements such as boron, aluminum, titanium, or zirconium have any appreciable influence on temper brittleness. It is possible to develop a form of temper brittleness in low-carbon Armco ingot iron which appears to be a result of iron carbide precipitate at the grain boundaries. However, when the carbon content is increased to about 0.15 pct and there are a large number of carbide particles throughout the grain, the grain boundary precipitate does not appear and unalloyed carbon steels do not seem to be noticeably temper brittle.

Copper and tin have lower solubility in ferrite at normal temperatures than in ferrite at higher temperatures and when present in sufficient amounts (much larger than normal) may produce a form of temper brittleness. Phosphorus has a solubility of about 1 pct in iron, and would, therefore, not

be expected to be a direct cause. Neither oxygen nor sulphur is believed to have the solubility characteristics in ferrite which would lead to temper brittleness, nor do the effects of other elements on temper brittleness fit in with their probable behavior.

This brief discussion indicates the need for further data on the specific influence of various elements on temper brittleness. The remainder of this paper discusses an investigation of the susceptibility to temper brittleness of a series of experimental low-alloy steels.

Materials and Test Procedures

Twenty experimental steels of the compositions indicated in Table 1 were melted by a standard induction furnace practice in a magnesium oxide crucible. Armco ingot iron was used as a base for all except the last two steels, for which electrolytic iron was used. One-tenth pct each of manganese and silicon was added as ferroalloys with the charge. Carbon and alloy elements were added after melt down. Final deoxidation was made 2 min. before pouring, using ferromanganese and ferrosilicon in all melts and aluminum in all but one. All melts were cast into 50-lb cast-iron ingot molds at a pouring temperature of 2950–3000°F as measured by an optical pyrometer.

The 50-lb ingots were forged to 1¼- × 4-in. billets and then rolled in the longitudinal direction to ½-in. plate at a finish rolling temperature of 1950°F. Impact bars were cut parallel to the rolling direction and ground to

½ in. square before heat treatment. After heat treatment, the bars were finish ground to 0.394 in. square, and a standard Charpy "V" notch was machined on a side perpendicular to the original plate surface. This notch orientation on rolled plate avoids split fractures and meaningless high impact values frequently encountered on specimens from forged bar or plate notched parallel to the rolled surface.

Heat treatments were as indicated in Table 2. The cooling rate on bars furnace cooled from the tempering temperature averaged 30°F per hr over the temperature range of 1100 to 700°F. Impact bars were broken in a standard Amsler impact testing machine with 103 ft lb initial energy in the hammer. Bars tested at subatmospheric temperatures were immersed in a dry ice-acetone bath for at least 15 min. before testing and broken within a few seconds of removal from the bath. Notched-bar impact values are given in Table 2. Rockwell A hardnesses taken on a ground surface of bars representing each heat treatment and Brinell equivalents obtained from the conversion tables supplied by the Wilson Instrument Co. are also given in Table 2.

Discussion of Results

The impact results given in Table 2 are limited to +75°F and –40°F. A steel which retains a relatively high impact value for the standard Charpy V-notch test at the latter temperature is generally regarded as sufficiently tough for most applications. However, it is not certain that a steel which had

Table 2 . . . Results of Notched-bar Impact and Hardness Tests

| Type Steel,* Pct | Quench | | Tempering Temperature, † °F | Hardness | | V-Notch Charpy Impact Ft Lb | | | |
|--------------------------|-------------|-------|-----------------------------|------------|-------------|-----------------------------|----------|--------------|----------|
| | Temp., † °F | Media | | Rockwell A | Approx. Bhn | Water Quench | | Furnace Cool | |
| | | | | | | +75°F | -40°F | +75°F | -40°F |
| 1.0 Mn | 1625 | Brine | 1200 | 54-55 | 181 | 103, 103 | 87, 103 | 103, 103 | 93, 97 |
| | 1900 | Brine | 1200 | 54-55 | 181 | | 103, 103 | | 103, 103 |
| 1.5 Mn | 1625 | Brine | 1200 | 56-57 | 197 | 92, 92 | 85, 101 | 82, 82 | 11, 5 |
| 0.5 C, 1.0 Mn | 1625 | Brine | 1200 | 58½-59½ | 217 | 62, 67 | 34, 38 | 62, 65 | 23, 23 |
| | | | 1250 | 57-58½ | 209 | 77, 72 | 33, 36 | 65, 70 | 25, 25 |
| 3.0 Ni | 1625 | Brine | 1200 | 54-55 | 181 | 103, 103 | 103, 103 | 103, 103 | 96, 100 |
| | 1900 | Brine | 1200 | 54-55 | 181 | | 103, 103 | | 103, 102 |
| 5.0 Ni | 1625 | Brine | 1200 | 55-57 | 192 | 86, 90 | 58, 57 | 100, 101 | 88, 103 |
| | | | 1150 | 56½-57 | 199 | | 103, 103 | | 102, 98 |
| 0.75 Cr | 1625 | Brine | 1200 | 58-59 | 214 | 103, 103 | 103, 103 | 103, 103 | 103, 103 |
| | 1900 | Brine | 1200 | 58½-59½ | 217 | | 103, 103 | | 103, 103 |
| 1.5 Cr | 1625 | Brine | 1200 | 59-60 | 223 | 103, 103 | 103, 103 | 103, 103 | 90, 100 |
| | 1750 | Brine | | 58½-59 | 215 | | | | 103, 92 |
| | 1900 | Brine | | 59-60½ | 226 | | 103, 103 | | 49, 15 |
| 0.5 Mo | 1625 | Brine | 1200 | 61-61½ | 236 | 102, 101 | 65, 38 | 103, 103 | 83, 58 |
| | 1900 | Brine | 1200 | 61½-62½ | 241 | | 64, 42 | | 66, 46 |
| 1.0 Mo | 1625 | Brine | 1200 | 62-63 | 248 | 91, 92 | 37, 30 | 81, 81 | 33, 27 |
| | | | 1250 | 61-62 | 238 | | 38, 36 | | 41, 41 |
| 2.0 Ni, 0.1 Ti | 1625 | Brine | 1200 | 55-56 | 181 | 103, 103 | 59, 79 | 103, 103 | 92, 40 |
| | | | 1250 | 53-54½ | 178 | 103, 103 | 94, 91 | 103, 103 | 74, 77 |
| | 1900 | Brine | 1200 | 58-59 | 214 | 97 | 27 | 78 | 18 |
| 2.0 Ni, 0.1 V | 1625 | Brine | 1200 | 62-62½ | 243 | 103, 97 | 49, 44 | 101, 101 | 31, 15 |
| | | | 1250 | 60-61 | 232 | 103, 103 | 71, 54 | 103, 101 | 36, 41 |
| | 1900 | Brine | 1200 | 62-63 | 248 | 100 | 28 | 87 | 23 |
| 3.0 Ni, 0.1 P | 1625 | Brine | 1200 | 56-57 | 197 | 103, 103 | 84, 58 | 57, 60 | 5, 4 |
| | 1900 | Brine | 1200 | 56-56½ | 194 | 103, 103 | 93, 82 | 69 | 30, 27 |
| 1.0 Mn, 0.75 Cr | 1625 | Water | 1200 | 59-60 | 223 | 103, 103 | 97, 96 | 62, 60 | 7, 6 |
| 1.0 Mn, 0.75 Cr, No Al | 1900 | Water | 1200 | 59-60 | 223 | 103 | 100 | 86 | 9 |
| | 1550 | Water | 1200 | 59-60½ | 226 | 93, 93 | 79, 58 | 33, 30 | 3, 4 |
| | 1625 | Water | 1200 | 59½-60 | 226 | 93, 102 | 57, 98 | 7, 8 | 2, 3 |
| | 1900 | Water | 1200 | 59-60½ | 226 | | 41, 52 | | 2, 2 |
| 1.0 Mn, 0.75 Cr, 0.20 Mo | 1625 | Water | 1200 | 60½-61½ | 235 | 103, 103 | 98, 93 | 103, 86 | 86, 81 |
| | 1900 | Water | 1200 | 60-61½ | 233 | | 102, 103 | | 103, 103 |
| 1.0 Mn, 0.75 Cr, 0.50 Mo | 1625 | Water | 1200 | 62-63 | 248 | 87, 88 | 82, 85 | 86, 79 | 88, 87 |
| | 1900 | Water | 1200 | 62½-63 | 251 | 95 | 93 | 95 | 81 |
| 1.0 Mn, 0.75 Cr, 0.75 Mo | 1625 | Water | 1200 | 63-63½ | 256 | 103, 96 | 82, 92 | 72, 69 | 48, 52 |
| 1.0 Mn, 0.75 Cr, 0.06 P | 1625 | Water | 1200 | 60-61 | 232 | 82, 85 | 38, 49 | 2, 2 | 1, 1 |
| 1.0 Mn, 0.75 Cr, 0.005 P | 1625 | Brine | 1200 | 54½-56½ | | 80, 82 | 78, 77 | 80, 80 | 73, 77 |
| 1.5 Mn, 0.005 P | 1625 | Brine | 1200 | 58-60 | | 90, 91 | 94, 95 | 96, 99 | 82, 71 |

* The intended base analysis was 0.25 pct C, 0.20 pct Mn, 0.20 pct Si, 0.02 pct P, and 0.02 pct S.

† Time at temperature = 1 hr.

‡ Time at temperature = 2 hr.

equivalent values for furnace-cooled and water-quenched specimens at -40°F testing temperature would not show temper brittleness at lower testing temperatures.

Some measure of the temper brittleness of the various steels as tested at -40°F may be obtained by subtracting the average value for the furnace-cooled specimens from the average value for the water-quenched specimens. This is believed to give a better picture than the susceptibility ratio which is affected greatly by small differences in the value used for the denominator. The relative temper brittleness of the steels as indicated by this measure is shown in Table 3.

Tables 2 and 3 indicate trends for the influence of various addition elements on temper embrittlement of the base analysis (0.25 pct carbon, 0.20 pct manganese, 0.20 pct silicon, 0.02 pct sulphur, and 0.02 pct phosphorus) as described in the following paragraphs.

Approximately the same increase in hardenability, as calculated by the Grossmann method, should be obtained in the 1.0 pct manganese, 3.0 pct nickel, 0.75 pct chromium, and 0.5 pct molybdenum steels. Microscopic examination indicated that these steels transformed

Table 3 . . . Relative Temper Embrittlement of Experimental Steels at -40°F Testing Temperature

| Type Steel, Pct | Quenching Temperature (1) | |
|--------------------------|---------------------------|--------|
| | 1625°F | 1900°F |
| 1.0 Mn | 0 | 0 |
| 1.5 Mn | 85 | |
| 0.5 C, 1.0 Mn | 13 9(2) | |
| 3.0 Ni | 5 | 0 |
| 5.0 Ni | | 0(3) |
| 0.75 Cr | 0 | 0 |
| 1.5 Cr | 8 | 71 |
| 0.5 Mo | 0 | 0 |
| 1.0 Mo | 3 0(2) | |
| 2.0 Ni, 0.1 Ti | 0 17(2) | 9 |
| 2.0 Ni, 0.1 V | 23 24(2) | 5 |
| 3.0 Ni, 0.1 P | 67 | 59 |
| 1.0 Mn, 0.75 Cr | 90 | 91 |
| 1.0 Mn, 0.75 Cr, No Al | 75 | 44 |
| 1.0 Mn, 0.75 Cr, 0.20 Mo | 12 | 0 |
| 1.0 Mn, 0.75 Cr, 0.50 Mo | 0 | 12 |
| 1.0 Mn, 0.75 Cr, 0.75 Mo | 37 | |
| 1.0 Mn, 0.75 Cr, 0.06 P | 42 | |
| 1.0 Mn, 0.75 Cr, 0.005 P | 2 | |
| 1.5 Mn, 0.005 P | 18 | |

(1) Tempering temperature 1200°F unless otherwise designated.(2) 1250°F tempering temperature.(3) 1150°F tempering temperature.

almost completely to martensite during quenching as $\frac{1}{2}$ -in.-square bars. All of the steels but the 0.5 pct molybdenum one maintained high impact values at -40°F , and none of them showed temper brittleness on slow cooling from the temper.

A further increase in nickel content

to 5 pct lowered the critical temperature sufficiently that an intercritical structure with resultant low impact values was obtained for a 1200°F temper, but no temper brittleness was apparent when this steel was properly tempered at 1150°F . An increase of chromium content to 1.5 pct produced slight embrittlement, as did 0.5 pct carbon with 1 pct manganese, and 0.1 pct vanadium or titanium with 2 pct nickel.

Extreme temper embrittlement was produced by increasing the manganese content of the base analysis to 1.5 pct, by the combination of 1 pct manganese and 0.75 pct chromium, or by the addition of phosphorus to a 3 pct nickel steel.

Further experiments with the 1.0 pct manganese, 0.75 pct chromium-type steel were made to investigate the influence of deoxidation practice and molybdenum additions. Comparison of the steels, with and without aluminum addition austenitized at different temperatures to produce marked variation in austenitic grain size, showed no direct influences of these factors on temper embrittlement. Impact values for both water-quenched and furnace-cooled specimens were higher for the

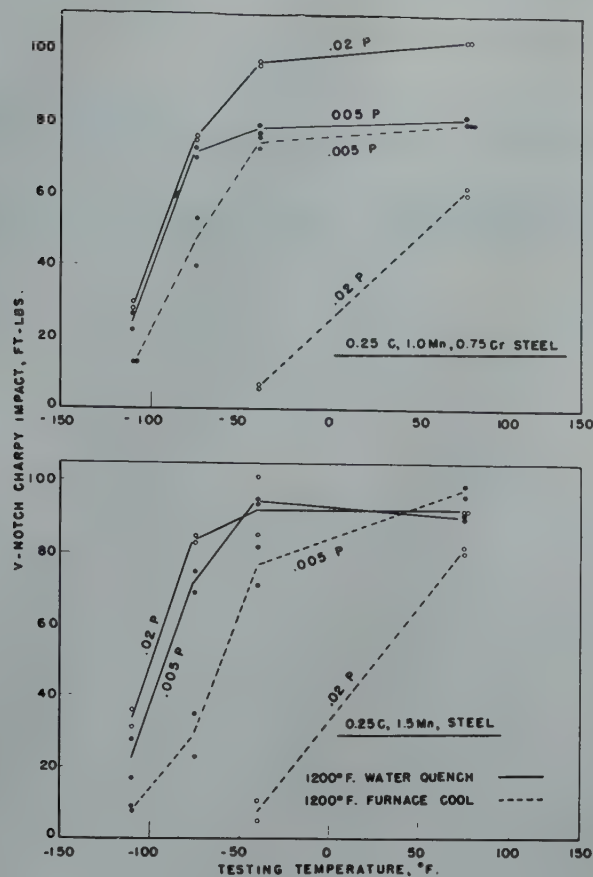


FIG. 2—Comparative impact values for 0.02 pct P and 0.005 pct P steels quenched from 1625°F and tempered as indicated.

aluminum-killed steel than for the silicon-killed steel and higher for the silicon-killed steel austenitized at low temperature to give fine grain size.

The influence of molybdenum on temper brittleness is quite complex. An addition of about 0.20 pct molybdenum has a well-known beneficial effect in decreasing the apparent temper embrittlement of susceptible steels. Kishkin⁴ reported that additions of molybdenum or columbium, which were effective in preventing temper brittleness of susceptible steels quenched from 1690°F, were ineffective or even increased embrittlement if the steels were quenched from 2280–2370°F. This difference was attributed to solution of the molybdenum or columbium carbides in austenite at the higher, but not at the lower, quenching temperature. Pellini and Queneau⁵ reported that temper embrittlement developed in steels with high molybdenum content during extended holding at tempering temperatures as high as 1200°F.

The data of Maurer, Wilms, and Kiessler⁶ indicate that, if the molyb-

denum content is increased beyond a critical amount, the susceptibility to temper brittleness increases again. The results given in Tables 2 and 3 for molybdenum additions to the manganese-chromium steel indicate an optimum molybdenum addition which is less for a higher austenitizing temperature. However, these data on molybdenum additions, as well as the results obtained for 0.5 pct molybdenum, 1.0 pct molybdenum, 2.0 pct nickel-0.1 pct titanium, and 2.0 pct nickel-0.1 pct vanadium steels heat treated at 1625 and 1900°F austenitizing temperatures, and 1200 and 1250°F tempering temperatures, are quite inconclusive as far as establishing any clear picture of the role of these carbide-forming elements on temper embrittlement.

In view of the pronounced effect of an increase in phosphorus content on temper brittleness of the 3 pct nickel steel, two additional melts of the most susceptible steels (1.0 pct manganese, 0.75 pct chromium, and 1.5 pct man-

ganese) were made with an effort to obtain a minimum phosphorus content (0.005 pct phosphorus). A very marked decrease in the temper brittleness of these two steels as indicated by tests at -40°F (Tables 2 and 3) accompanied the decrease in phosphorus from 0.02 to 0.005 pct. In order to determine whether this could be an indirect effect of lowering the transition temperature for brittle failure of both water-quenched and furnace-cooled specimens, additional impact tests were made at -75 and -110°F testing temperatures.

The complete notched-bar impact data for normal and 0.005 pct phosphorus steels are given in Table 4 and plotted in Fig 2. Since lowering the phosphorus content has not improved the impact resistance of the specimens water quenched from the temper, the great improvement in the impact values for furnace-cooled specimens of the 0.005 pct phosphorus steel over those of the 0.02 pct phosphorus steel is attributed to a decrease in the susceptibility to temper embrittlement. As mentioned previously, these steels

Table 4 . . . Notched-bar Impact Values for Normal and Low-phosphorus Steels

| Type Steel, Pct | Temper, °F | V-Notch Charpy Impact, Ft Lb | | | |
|--------------------------|------------|------------------------------|---------|--------|---------|
| | | + 75°F | - 40°F | - 75°F | - 110°F |
| 1.0 Mn, 0.75 Cr, 0.02 P | 1200 WQ(1) | 103, 103 | 97, 96 | 75, 76 | 27, 22 |
| | 1200 FC(2) | 62, 60 | 7, 6 | | |
| 1.0 Mn, 0.75 Cr, 0.005 P | 1200 WQ | 80, 82 | 79, 77 | 73, 70 | 23, 30 |
| | 1200 FC | 80, 80 | 73, 76 | 53, 40 | 13, 13 |
| 1.5 Mn, 0.02 P | 1200 WQ | 92, 92 | 85, 101 | 83, 85 | 31, 36 |
| | 1200 FC | 82, 82 | 11, 5 | | |
| 1.5 Mn, 0.005 P | 1200 WQ | 90, 91 | 94, 95 | 75, 69 | 23, 17 |
| | 1200 FC | 99, 96 | 82, 71 | 35, 23 | 8, 9 |

(1) Water quenched
(2) Furnace cooled

were made by similar melting procedures and the only known difference, other than phosphorus content, is that electrolytic iron was used for melting stock of the low-phosphorus steel and ingot iron for the normal phosphorus steel.

These results indicate that phosphorus must have a much more important part in temper embrittlement than has been generally supposed. Several explanations are possible, but in view of the lack of fundamental data on the solubility of phosphorus in iron-carbon alloys, its influence on the solubility of carbon, and its reactions with other alloy elements in steel, no theory is advanced at this time.

Summary

Twenty experimental low-alloy steels were tested for temper embrittlement by comparing notched-bar impact values at +75 and -40°F testing temperature of specimens water quenched and furnace cooled from the tempering temperature.

For these conditions of testing, no embrittlement was apparent for nickel additions up to 5 pct to the base analy-

sis of 0.25 pct carbon, 0.20 pct manganese, 0.20 pct silicon, 0.02 pct phosphorus, and 0.02 pct sulphur. Chromium of 1.5 pct or either 0.1 pct vanadium or 0.1 pct titanium with 2 pct nickel gave slight embrittlement. Manganese of 1.5 pct or 1 pct manganese with 0.75 pct chromium produced extreme embrittlement. Deoxidation practice or grain size did not appear to have any direct influence on embrittlement. A moderate amount of molybdenum decreased embrittlement of the manganese-chromium steel. Increasing the phosphorus content of a 3 pct nickel steel produced temper brittleness, and decreasing the phosphorus content from 0.02 to 0.005 pct greatly decreased the embrittlement of the susceptible 1.5 pct manganese and 1.0 pct manganese-0.75 pct chromium steels.

Impact-resistance, transition-temperature curves for the latter steels indicate a real influence of small differences in phosphorus content on temper brittleness, but in the absence of fundamental data on the behavior of phosphorus in relation to carbon and alloy elements in steel, no theory of the mechanism of this influence is apparent.

Acknowledgments

This work was carried out as a part of the fundamental research program of Battelle Memorial Institute. Appreciation for encouragement of the work is expressed to Dr. B. D. Thomas, Dr. C. H. Lorig, and Mr. C. T. Greenidge.

References

1. J. H. Hollomon: Temper Brittleness. *Trans. Amer. Soc. for Metals*, (1945), 36, 473-542.
2. H. Carpenter and J. M. Robertson: *Metals*. London, 1939, Oxford Press.
3. S. A. Herres and C. H. Lorig: Influence of Metallurgical Factors on the Mechanical Properties of Steel. *Trans. Amer. Soc. for Metals*. (1948), 40, 775-805.
4. S. T. Kishkin: The Mechanism of the Effect of Molybdenum and Columbium on the Temper Brittleness of Steel. *Bul. Acad. Science URSS*, No. 4, 91-4, (1941) (*Chem. Abstr.*, (1942) 36, 1578).
5. W. S. Pellini and B. R. Queneau: Development of Temper Brittleness in Alloy Steels. *Trans. Amer. Soc. for Metals*, (1947) 39, 139-161.
6. E. Maurer, O. H. Wilms, and H. Kiessler: Effect of Phosphorus and of Various Alloying Elements on the Temper Brittleness and Hot Brittleness of Structural Steel. *Stahl and Eisen*, Jan. 29, (1942), 81-89, Feb. 5, (1942), 115-121.



Oriented Arrangements of Thin Aluminum Films on Ionic Substrates

T. N. RHODIN, JR.*

Introduction

There can be two types of films on solids, those which are stable in monolayers and those which tend to aggregate into three dimensional structures. A great number of metal films formed by condensation onto a solid base are unstable in the sense that they will aggregate into crystals providing the atoms possess sufficient surface mobility. The crystalline structure of the film is strongly influenced by the base in many systems and, in some cases, a single orientation prevails when the force fields around the atoms in the supporting crystal are sufficiently strong.¹ Relatively little is available in the literature about the nature of these forces and the role they play in promoting a preferred orientation of the atoms arriving at the substrate surface. An understanding of their periodicity and magnitude relative to the surface forces characteristic of the film itself should provide insight into the critical dependence of film orientation on the nature and temperature of the substrate.

In addition, this effect may be very useful in preparing samples for surface studies. The study of the physical and chemical characteristics of pure metal surfaces has been severely handicapped by the presence of strongly adherent foreign films. Furthermore, the randomness of the surface orientation has obscured interpretation of experimental results. Evaporation of metals in high vacuum onto carefully selected substrates under ideal conditions for preferred orientation appears suited to the preparation of flat, oxide-free, oriented films for surface reaction studies. Many factors influence their structure and some understanding of the mechanism of their formation is a necessary prerequisite for obtaining satisfactory surfaces for study. The dominant factors

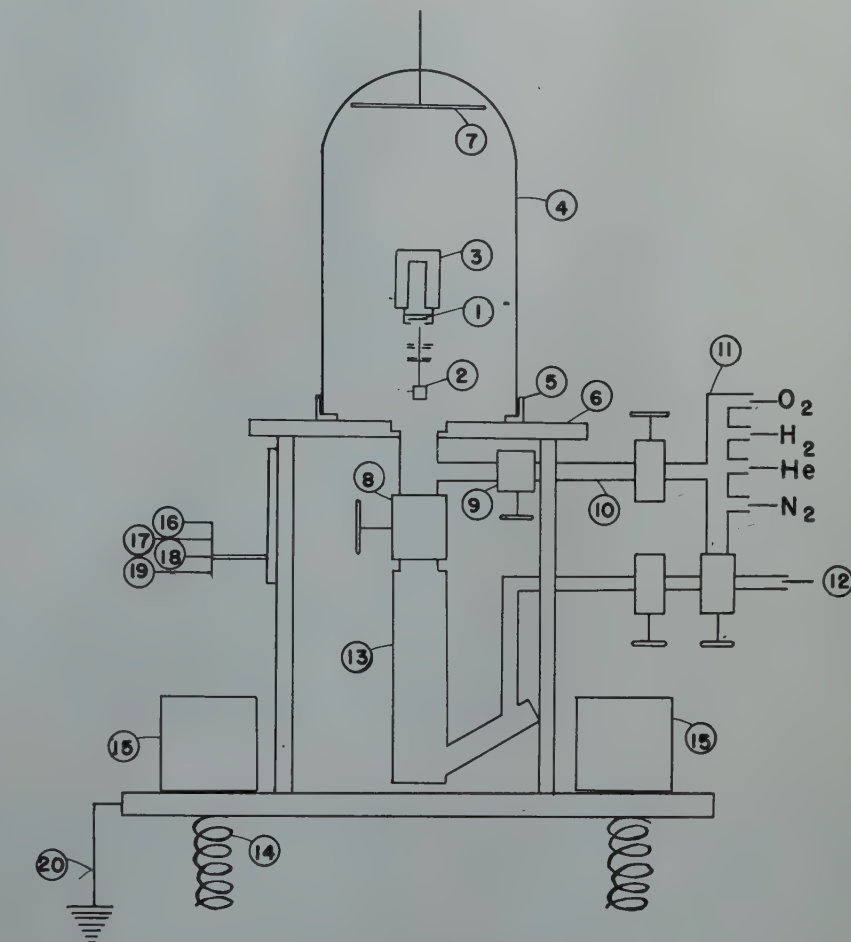


FIG 1—Vacuum evaporator.

- | | |
|---------------------------------|----------------------------------|
| 1. Substrate | 11. Purified Gases |
| 2. Molecular Beam Source | 12. Holding Pumps |
| 3. Furnace | 13. High Capacity Diffusion Pump |
| 4. 18 in. Glass Bell Jar | 14. Shock Mount |
| 5. Right Angle Neoprene Gasket | 15. 200 lb Weights |
| 6. Polished Steel Plate | 16. Thermocouple Pressure Gauge |
| 7. High Voltage Cathode—5000 V. | 17. Ionization Gauge |
| 8. 4 in. Packless Valve | 18. Temperature Controller |
| 9. 2 in. Packless Valve | 19. Electronic Heater |
| 10. Manifold | 20. Electrical Ground |

in defining film structure are film thickness and growth rate and the nature, condition, and temperature of the substrate.

Procedure

GENERAL ASSEMBLY

The system was enclosed in an 18 in. bell jar which rested on an L-shaped neoprene gasket on a ground steel plate as indicated in Fig 1. Rapid evacuation of the system to 10^{-6} mm mercury was facilitated by a 4 in. manifold, 2 in. packless valve, and an extra large diffusion pump. Suitable arrangement of valves on a secondary manifold readily permitted introduction of purified gases

Cleveland Meeting, October 1949.
TP 2575 E. Discussion of this paper (2 copies) may be sent to *Transactions AIME* before December 1, 1949. Manuscript received November 19, 1948.

* Research Associate, Institute for the Study of Metals, University of Chicago.

¹ References are at the end of the paper.

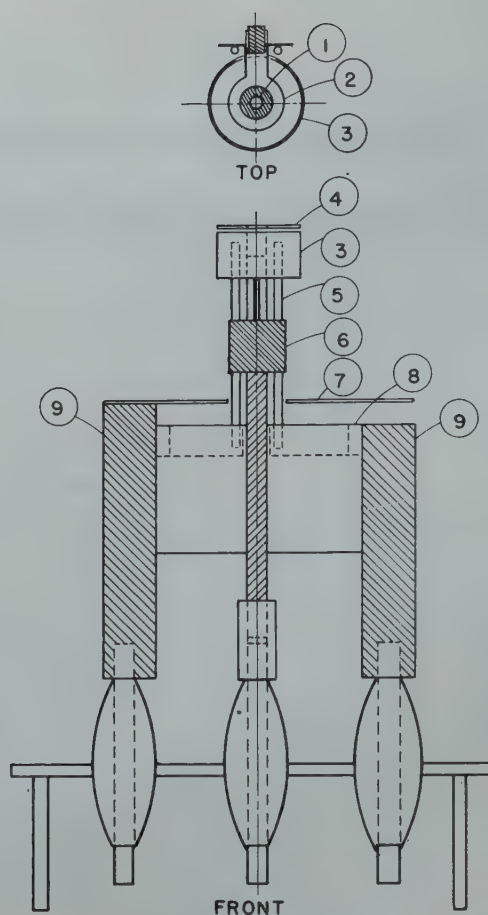


FIG 2—Electronic heater.

1. Tantalum Crucible
2. Tungsten Filament
3. Tantalum Shield
4. Tantalum Lid
5. Nickel Leads
6. Crucible Electrode
7. Stainless Steel
8. Mykroy Spacer
9. Filament Electrodes

into the chamber. Outgassing of the entire internal surface in a glow discharge was greatly expedited by a 5000 V copper cathode mounted at the top of the bell jar. The entire frame was carefully shock-mounted to isolate the microbalance from building vibration. The lead-ins for control and power were situated in the steel base. Pressures from 10 to 10^{-6} mm mercury could be measured and temperatures of the substrate and crucible could be independently controlled and measured. Atmosphere pressure seated the bell jar hard on the gasket when the latter was evacuated. When it was filled with dry nitrogen at one atmosphere it could be readily elevated out of reach.

FORMATION OF THE FILM

The film was produced by evaporating high purity (99.99 pct) aluminum from a microcrucible in a good vacuum (10^{-6} mm) and condensing it on an independently heated substrate. With

a suitable slit system a uniform, concentrated, direct molecular beam resulted. The arrangement of the source, slits, and substrate is indicated by items 2 and 1 in Fig 1.

The substrate (item 1) was mounted 25 mm above the source in a copper frame which held it in place against an externally heated copper block. In this manner the lower face was exposed to the beam and maintained at the desired temperature by heating from the upper face. The temperature was regulated to one percent by a proportionating potentiometer controller. The substrate consisted of a square plate of an ionic salt approximately 5 mm on the side and 1 mm thick. A freshly cleaved face was exposed just prior to a run. A thermocouple probe in contact with the lower face of the substrate indicated the film temperatures. Two additional platinum probes 2.0 mm apart were in contact with the surface. The appearance of the first few layers of the film was indicated by the sudden

decrease in resistance measured between the probes.

The source (item 2) of the beam was a small tantalum crucible located directly below the substrate. The microcrucible held a charge of 100 mgms. The inside diameter of the crucible was 3 mm but the beam was actually emitted through a 0.1 mm orifice in a tantalum cap placed over the top of the microcrucible. The cap prevented splattering and also promoted thermal equilibrium of the atoms before they were emitted. The charge was outgassed by prefusing *in situ* before evaporating during which time the substrate was protected by an externally manipulated shield.

The heating of the crucible was very satisfactorily effected by an arrangement for direct electron heating indicated in Fig 2. The crucible is shown with the lid off as item 1. Electrons emitted from an incandescent 30 mil tungsten filament (item 2) around the crucible are accelerated by a positive

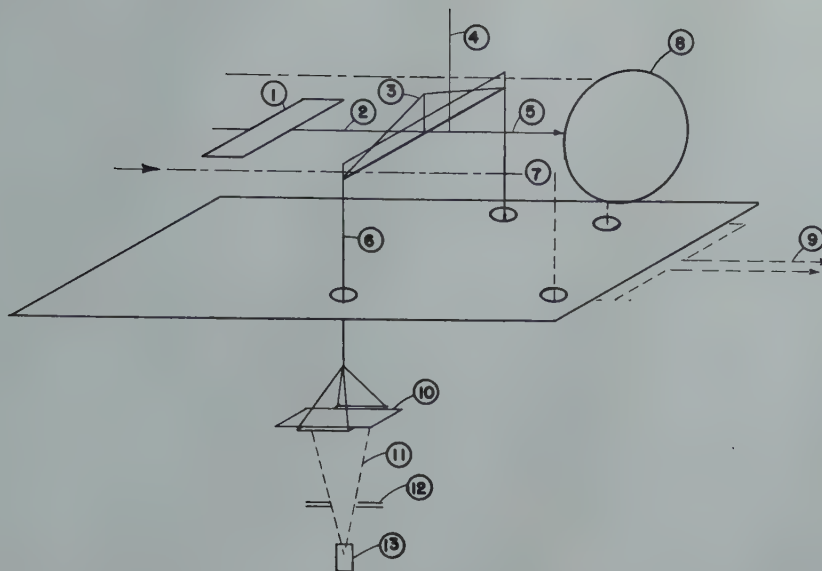


FIG 3—Quartz torsion microbalance.

- | | |
|-------------------|-----------------------|
| 1. Bow Fibre | 8. Graduated Wheel |
| 2. Static | 9. Single Field Image |
| 3. Beam | 10. Substrate |
| 4. Hang-up | 11. Molecular Beam |
| 5. Torsion Fibre | 12. Collimating Slit |
| 6. Hang-down | 13. Source |
| 7. Image of Index | |

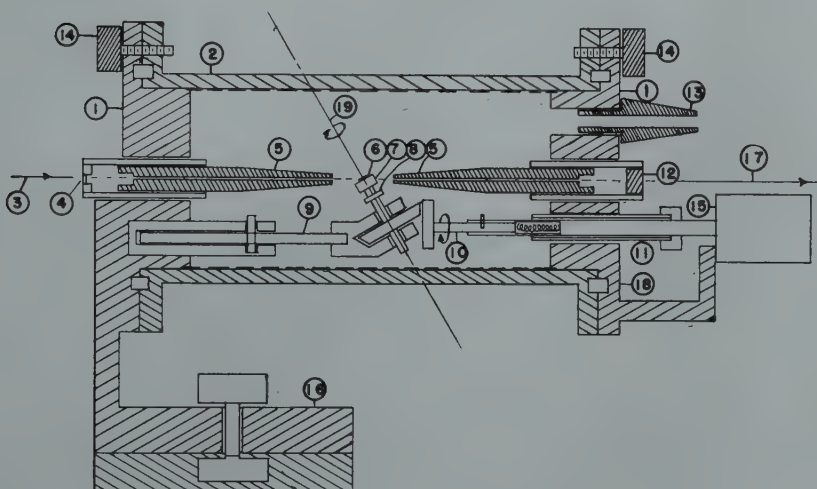


FIG 4—X ray vacuum camera.

- | | |
|-----------------------|-------------------------------|
| 1. End Plates | 11. Rotor Vacuum Seal |
| 2. Film Case | 12. Lead Glass Window |
| 3. Entrance Beam | 13. Vacuum Outlet |
| 4. Beryllium Window | 14. Plate Nuts |
| 5. Pin Holes | 15. Motor |
| 6. Specimen | 16. Track Clamp |
| 7. Lucite Spacer | 17. Exit Beam |
| 8. Lock-nut | 18. Neoprene Gaskets |
| 9. Rotor Assembly | 19. Axle of Specimen Rotation |
| 10. Drive Wheel Shaft | |

potential towards it. A tantalum shield (item 3) around the assembly reduced heat losses and another tantalum lid (item 4) shielded the substrate from direct exposure to the filament. The temperature of the microcrucible could be accurately adjusted and maintained at any temperature up to 1500°C within 2–3 pct by regulating the filament emission and the accelerating potential. This high fidelity temperature control is necessary in the determina-

tion of the substrate temperature condensation-pressure relationship for various substrates. The substrate was tied in at the same potential as the crucible to eliminate the possibility that metal ions formed in or around the crucible may be spuriously accelerated towards the substrate.

The critical vapor pressure for condensation on a given substrate at a given temperature could be determined as follows: In this measurement

the crucible temperature was slowly increased until the rate of evaporation of the aluminum was just enough to cause condensation on the substrate for a given base temperature. The rapid decrease in the film resistance between the probes was used to indicate the formation of the initial layer. The process was reversible, that is, a small increase in base temperature for a critical pressure caused the film to evaporate. The microcrucible could be readily removed

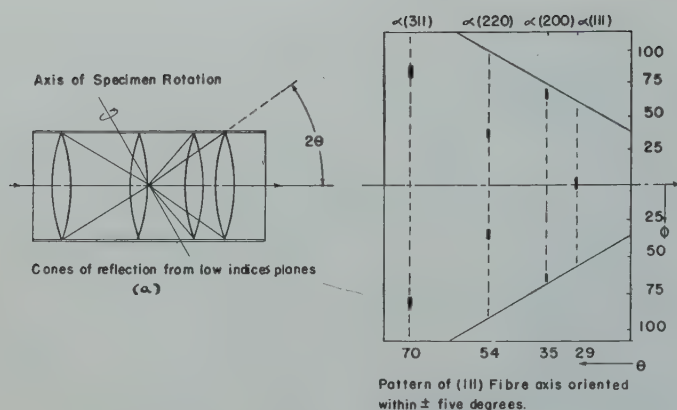


FIG 5—X ray pattern.

from the crucible electrode (item 6) for replacement and the position could be lined up easily by adjusting the eccentric at the base. The crucible temperature was measured by a chromel-alumel thermocouple mounted in the bottom.

DETERMINATION OF FILM THICKNESS

The condensation rate for a given crucible and substrate temperature was determined by weighing *in situ* a thin glass slide hanging on a quartz fibre over the molecular beam as indicated in Fig 3. A sensitive quartz torsion microbalance facilitated accurate and quick measurements in vacuum. The torsion fibre was rotated by magnetic coupling through the glass wall. The sensitivity of the weighing was 10^{-6} gm with a 23 mu. quartz torsion fibre (item 5). The thickness corresponding to weight increments was calculated for a constant area assuming the film to be flat and continuous and the film density to be comparable to the mass density. A microgram corresponded to a hundred angstroms thick layer of aluminum for the film area used. The condensation rates for various substrate and crucible temperatures were calibrated in this manner.

EXAMINATION OF THE FILM

Metallography

Upon completion of the run the substrate was cooled *in situ* and removed for examination. Reflectivity of the surface varied from very mirror-like to cloudy as the film thickness and substrate temperature increased. Metallographic examination of the samples was considerably hampered by their fragility. In the cases where it was possible to observe grains without destroying the film the average grain size was 2000 to

5000 Å for a film of the same thickness.

X ray Diffraction

The structure was determined with X ray diffraction using a surface reflection pin-hole technique in a vacuum camera as indicated in Fig 4. A Picker-Waite diffraction unit was used with a water-cooled chromium target. The exposure time varied from 2 to 15 hr for film thicknesses from 5000 to 500 Å with an accelerating potential of 50 kv and a space current of 10 milliamp. The sample (item 6) was anchored flat on the turntable (item 7) and rotated around an axis (item 19) normal to the surface of the sample. The axis of rotation was inclined away from the incident beam an amount corresponding to the Bragg angle for reflection from the plane of preferred orientation. The camera was particularly designed to suit the geometry and orientation unique to the samples studied. The simplicity of the film patterns indicated in Fig 5a and 5b clearly shows the advantage obtained. Preferred orientation is characterized by segmentation of the lines into local marks as shown by the heavy marks of 5° length on the dashed reflection lines in Fig 5b. The vertical distance from the center line measures the orientation azimuths characteristic of a preferred orientation. The value of the orientation azimuth (ϕ) can be calculated for any preferred orientation,^{1a}

$$\cos \rho = \cos \beta \sin \theta + \sin \beta \cos \theta \cos \phi \quad [1]$$

ρ = angle between oriented plane and reflecting plane.
 β = angle between normal to oriented plane and incident beam.
 θ = Bragg angle for reflection from reflecting plane.
 ϕ = orientation azimuth for oriented plane.

The values of ϕ calculated for reflection of K_α and K_β chromium radiation from the (111), (200), (220) and (311) planes of aluminum for (111), (100) or (110) orientation are listed in Table 1. The kind of orientation can be readily determined from the pattern defined by the characteristic values of ϕ . A semi-quantitative value for the degree of orientation with a maximum error of 10 pct in this determination can be obtained by measuring the opaqueness of the spot relative to the integrated opaqueness of the whole line with a Leeds and Northrup recording microphotometer. The error is introduced by the assumption that the intensity at any one spot on the film is linearly proportional to the amount of radiation reflected to that point and the dependence is the same for all azimuth angles.

Table 1 . . . Bragg Angles and Orientation Azimuths Chromium Radiation on Aluminum

| Radiation Crg. | Re-reflecting Plane | Bragg Angles | Orientation Azimuths | | |
|----------------|---------------------|--------------|----------------------|---------|--------|
| | | | (111) | (110) | (100) |
| α | (111) | 29.5 | 0.83 | 41, 109 | 64 |
| β | (111) | 26.8 | 0.80 | 39, 105 | 62 |
| α | (200) | 34.7 | 68 | 55, 119 | 0, 119 |
| β | (200) | 31.0 | 65 | 53, 111 | 0, 111 |
| α | (220) | 54.4 | 63 | 0, 118 | 82 |
| β | (220) | 47.0 | 52 | 0, 94 | 68 |
| α | (311) | 70.0 | 95, - | 104 | 89 |
| β | (311) | 59.2 | 58, 142 | 63 | 50 |

Orientation Results

GENERAL

A quantitative dependence of degree of preferred orientation on film thickness and substrate temperatures was found over a considerable range of thickness and temperature for eleven aluminum-substrate pairs. It was necessary, however, to make a preliminary evaluation of four other factors sufficiently well so as to minimize their influence. The pertinent results of the preliminary survey are herewith presented in condensed form as a background against which the significance of the quantitative aspects can be considered more intelligently.

Film Growth Rate

Foremost is the important influence of film growth rate on structure. Since the experimental system was not propitiously suited for studying this aspect it was maintained at a constant value in all experiments. The evaporation

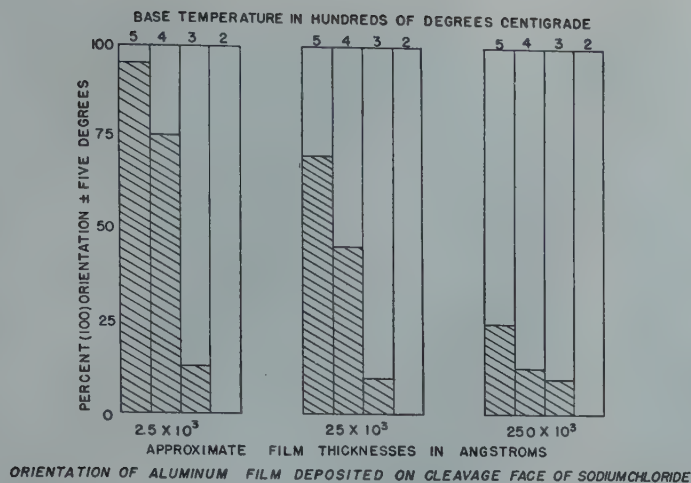


FIG 6—Orientation and base temperature (1).

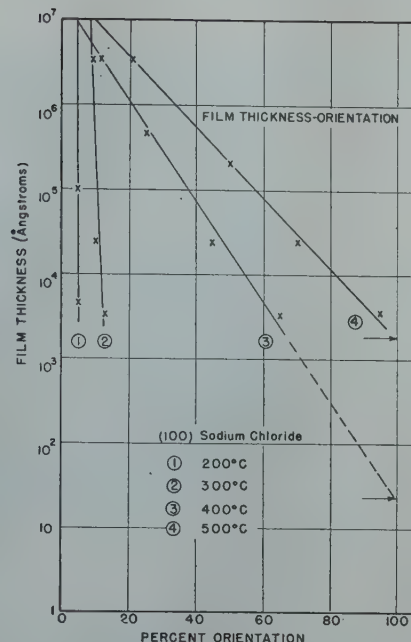


FIG 7—Orientation and film thickness.

rate was adjusted for each substrate temperature corresponding to an effective film growth rate of ten to thirty monolayers of aluminum per second. In the case of the binding energy determinations, however, the film growth rate was not controlled since it was desired only to determine the condition for minimum condensation.

Heat Treatment

Heat treating of the substrates with or without adherent metal film caused no striking change in the resulting orientation. The films were therefore usually kept at constant temperature during formation and then permitted to cool by radiation in a vacuum. Annealing a randomly oriented film at elevated temperatures (up to 600°C) in helium resulted only in grain growth. Likewise oriented structures were not markedly altered by annealing under similar conditions. This temperature stability of the structures is in contrast to the temperature sensitive orientations of thinner aluminum films (ca. 400 Å) previously reported.²

Atmosphere Effects

The influence of gases present even at 10^{-6} mm pressure was also considered. The pressure of purified quantities of helium, oxygen, nitrogen and hydrogen at low pressures (10^{-4} mm) decreased the orientation to a relatively small extent. The effect was not unique to any one gas or substrate and appeared solely to hamper the steady evolution of aluminum vapor. In no case was a gas such as helium observed to improve the film orienta-

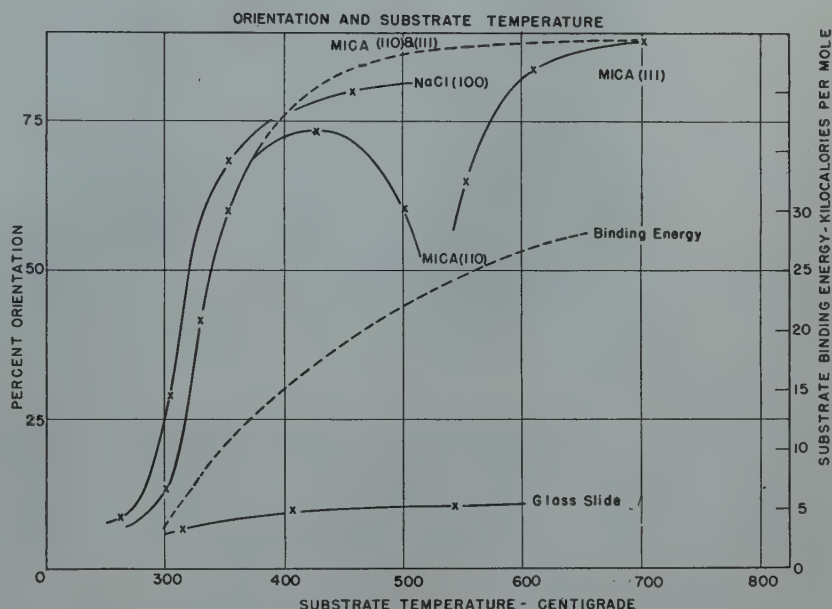


FIG 8—Orientation and base temperature (2).

tion as reported by others for thinner films.³

Substrate Condition

The contamination of the substrate surface itself by the gases previously listed was not considered to be critical. Oriented films could be formed on freshly cleaved rock salt which had been preheated in oxygen and hydrogen atmospheres. In all cases, however, the cleanliness of the substrate was a critical requirement and best results were

always obtained with freshly cleaved ionic surfaces whose lattices had an arrangement of ions, the geometry and dimensions of which showed a certain correlation to that of aluminum. The limited number of such salts emphasized the preparation of oriented substrates by other means. Even after repeated polishing, etching, and annealing, use of NaCl and LiF surfaces obtained in this manner was only moderately successful. Successful techniques for exposing any desired sub-

strate orientation in a suitably clean and flat condition would be most useful for future studies.

SPECIFIC FACTORS

Film Thickness

Initial studies made it evident that degree of orientation was very thickness dependent for all film-substrate pairs. This characteristic will be described first since it depended only on temperature and film thickness and was general to all substrates. The percent orientation for films on the (100) face of rock salt for various thicknesses and base temperatures are plotted in Fig 6 as an illustration. An exponential dependence of orientation on film thickness was observed, and the data plotted in Fig 7 indicate a typical case. It is interesting to note that a critical film thickness for perfect orientation at each temperature is suggested by extrapolation of the straight line to small film thicknesses. A striking temperature dependence is also indicated by the distinctly small slope of curve 2 compared to curve 3 in Fig 7. The validity of a strong base temperature-dependence for maximum orientation is also indicated in Fig 8 for a variety of film-substrate pairs. Discussion of the temperature dependence is, however, temporarily postponed until right after the discussion of the thickness effect.

The thickness dependence may mean that the oriented arrangement is constant at all points in the film and merely decreases as the film thickens. It seems more reasonable to assume that the orientation is strongly dependent on the substrate and produces an orientation large at the inner film surface and decreasing towards the outer film surface. The latter possibility is in agreement with the surface reflection characteristics of X rays. In this case a disproportionately large fraction of the radiation producing the pin-hole pattern is reflected from the outer planes of the film. A quantitative illustration of this can be presented by calculating the intensity of radiation reflected from successive layers of metal atoms as follows.⁴ The intensity (I_t) reflected from a thickness (t) relative to the intensity (I_d) reflected from an infinitely thick film can be expressed:

$$\frac{I_t}{I_d} = \frac{\int_0^t I_2 dt}{\int_0^\infty I_2 dt} \quad [2]$$

$$\text{where, } I_2 = kI_0 e^{-4\left(\frac{\mu}{\rho}\right)\rho\left(\frac{td}{\lambda}\right)} \quad [3]$$

Neglecting the scattering of the ray after it has emerged from the sample, I_2 is the final intensity, I_1 the intensity, upon reflection from a diffraction volume element at a depth, (t), below the surface, and I_0 is the incident intensity before entering the sample. The term $\left(\frac{4td}{\lambda}\right)$ is a linear expression of the total distance traveled in the sample when the ray penetrates a depth, (t), and undergoes a Bragg angle reflection. The other symbols are,

k = efficiency constant \leq unity

I_0 = initial intensity of incident beam

$\left(\frac{\mu}{\rho}\right)$ = mass absorption coefficient

ρ = film density

d = interplanar distance of oriented planes

t = film thickness penetrated

λ = wavelength of X ray radiation.

Values of $\frac{I_t}{I_d}$ for a limiting thickness of $5 \times 10^5 \text{ \AA}$ have been calculated from Eq 2 for successive depths of penetration into the sample. The amount of radiation from each layer characterizes the degree of orientation in that layer and the over-all variation of apparent orientation with film thickness indicates the decrease of average orientation with increasing film thickness. The calculations were made for the K_α radiation from a chromium target diffracted by the (100) oriented planes of aluminum. The results in Table 4 are presented: Column 1, depth of penetration (\AA); Column 2, thickness penetrated relative to limiting thickness, and Column 3, the corresponding percent intensity for that thickness penetrated over the total radiation recorded on the film.

Although the pin-hole pattern is an integrated effect of orientation through the entire layer, it is obvious that the pattern is a weighted average heavily in favor of the extreme surface. For example, with a chromium target twice as much radiation is reflected from the outer half thickness than from the inner half thickness of an aluminum film 5000 \AA thick. Hence, in the film thickness study the orientation of the outer surface was essentially observed. The orientation is greatest in the region nearest to the substrate-film interface.

Substrate Temperature

A base temperature dependence in which orientation of the film increased rapidly at some characteristic tem-

perature for each substrate illustrated in Fig 8 was typical of all substrates. The less the maximum orientation, however, the smaller the dependence on the characteristic temperature. This is illustrated by the contrast in the curves for (100) orientation on rock salt and glass. The temperature dependence may mean that the metal atoms must possess a minimum kinetic energy corresponding to the observed temperature for maximum orientation for them to take up the preferred positions suggested by the substrate. The transition of a (110) orientation of the film on mica at low temperatures to a (111) orientation at higher temperatures indicates that a higher minimum mobility is required for formation of the second configuration. In all cases the rate at which orientation increased with base temperature as well as the maximum value it approached was typical of the substrate. It indicates that production of ordered arrangements is governed not only by the interaction of the substrate and metal but by a relatively slow temperature dependent surface diffusion process as well. Calculation of activation energies for orientation seems premature until the mechanism of arrangement is better defined. The characteristic values of base temperature and maximum observed orientation are plotted in Fig 8 for rock salt, mica, and glass, and listed for eleven substrates in columns 2 and 4 of Table 2.

Experimental data for mica in the temperature region intermediate between the (110) and (111) orientations were inconclusive. It is noteworthy that the most oriented configurations corresponded to the higher temperatures. This characteristic is a general one for all the substrates studied. It is illustrated by the dashed curve in Fig 8 in which the orientation temperature as abscissa is plotted against the substrate binding energy as ordinate on the right. The substrate binding energy, heretofore undefined, is described in a subsequent section and shown to be proportional to the percent of the observed film orientation.

Nature of Substrate

From the facts presented so far it seems clear that the nature and degree of the observed orientation was critically dependent on the substrate. This dependence held in general for all the substrates studied. In every case there was a correlation of some kind between

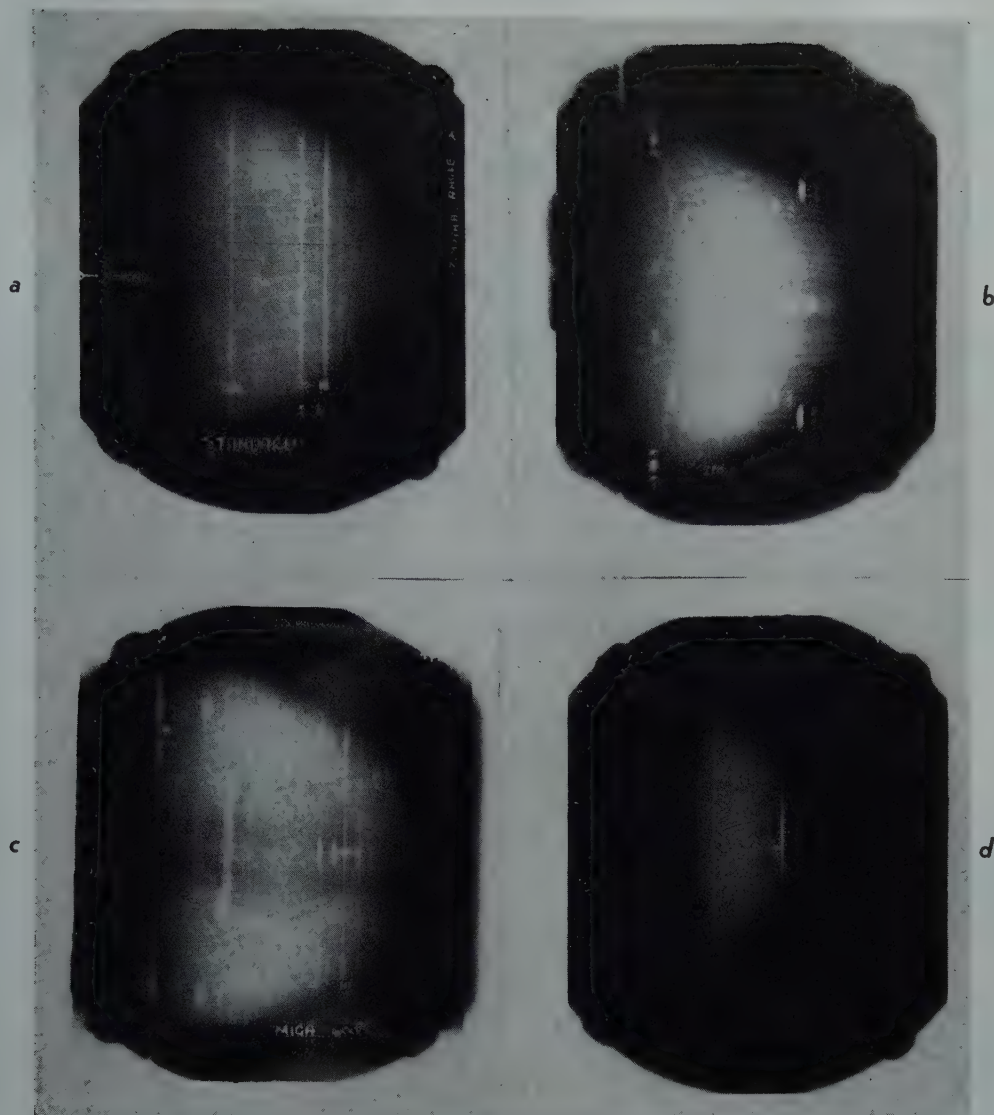


FIG 9a—Aluminum-glass random orientation (10,000 Å).
 FIG 9b—Aluminum—(100) sodium chloride 80 pct (100) orientation (1200 Å).
 FIG 9c—Aluminum—(111) mica 87 pct (111) orientation (1300 Å).
 FIG 9d—Aluminum-glass 10 pct (100) orientation (1000 Å).

the geometry and dimensions of the underlying lattice and that plane of aluminum preferentially oriented parallel to it. For example, the (100) face of aluminum was the only orientation observed on the (100) face of the alkali halide substrates. Similarly the (111) planes of aluminum tended to be preferentially oriented parallel to substrates with hexagonal cleavage or hexagonal-polished faces, providing the base temperature and film thickness were favorable. In other cases (110) orientation was observed to occur on (110) oriented substrates. This is not a general effect, however, since cases occur where substrates stabilize preferred film orientations other than their

own, but in most cases that orientation of aluminum occurred for which the geometry and spacing of the metal atoms yielded the best fit on the substrate. The data are summarized in

columns 1, 2, 3, 4 of Table 2 in order of decreasing orientation. The direction of orientation in the film listed in the third column is the same as that of the substrate for the first seven items. A small

Table 2 . . . Structure Characteristics of Thin Aluminum Films

| Substrate | Temp. Orient. °C | Direct. Orient. | Pct Orient. | Pressure × 10 ⁴ cm Hg | A kc per m | Δ kc per m | A - Δ kc per m | E _c kc per m |
|-------------------|------------------|-----------------|-------------|----------------------------------|------------|------------|----------------|-------------------------|
| mica | 600 | [111] | 87 | 0.007 | 42 | 20 | 22 | 22 |
| mica | 450 | [110] | 75 | 1.52 | 28 | 10 | 18 | 20 |
| NaCl | 350 | [100] | 80 | 0.003 | 31 | 15 | 16 | 18 |
| NaCl | 350 | [110] | 50 | 0.024 | 21 | 10 | 11 | 12 |
| LiF | 400 | [111] | 55 | 0.022 | 33 | 20 | 13 | 10 |
| LiF | 300 | [100] | 50 | 0.012 | 25 | 15 | 10 | 10 |
| CaCO ₃ | 300 | [111] | 15 | 0.012 | 25 | 20 | 5 | 5 |
| Glass | 400 | [100] | 10 | 6000 | 15 | 15 | 0 | |
| CaF ₂ | 300 | [111] | 10 | 700 | 20 | 20 | 0 | 2 |
| ZnS | 300 | [111] | 10 | 700 | 21 | 20 | 1 | 4 |
| Sodalite | 300 | [111] | 10 | 700 | 21 | 20 | 1 | 2 |

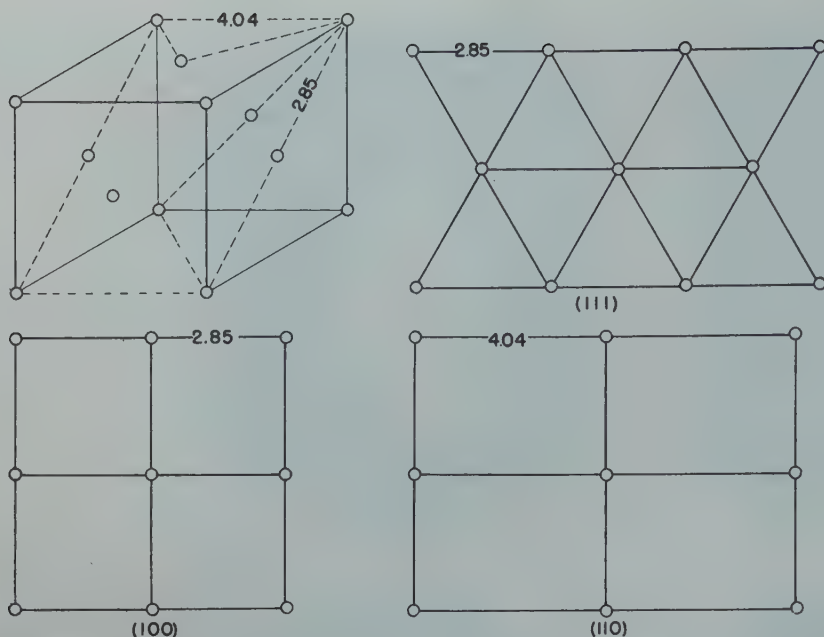


FIG 10—Aluminum unit cell.

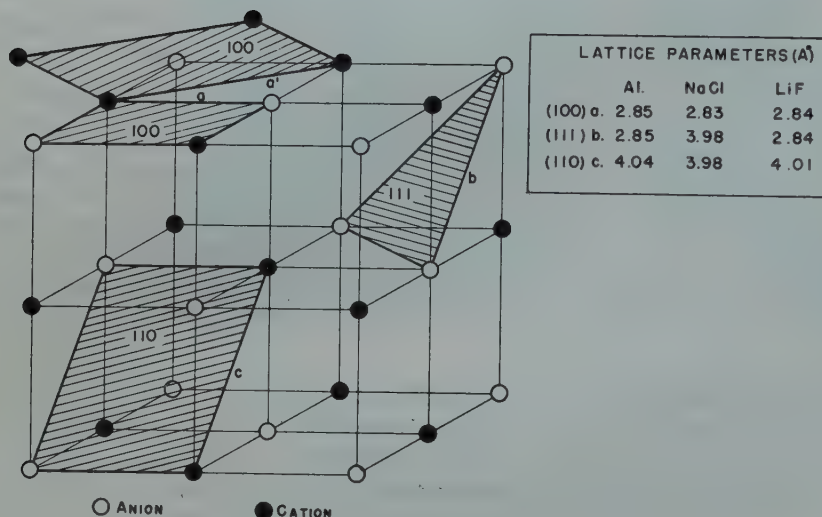


FIG 11—Alkali halide unit cell.

orientation was observed on glass which, of course, possesses no definable surface arrangement. The small degree of orientation on fluorite was barely measurable. The (111) orientation on zinc blende and sodalite was also very small. The last two substrates possess cubic lattices with good (110) cleavage faces and are examples of film orientation differing from that of the substrate. Some typical surface reflection X ray film patterns are illustrated in Fig 4. The interpretation is handicapped by the poor contrast of the aluminum lines,

the strong and complex pattern caused by reflection from the substrate, and the poor reproduction, but the over-all pattern analysis is quantitatively unique for each orientation. Continuous reflection from all the low indices reflection planes indicate complete randomness in Fig 9a. The sharply defined orientation of a (100) aluminum film on rock salt is illustrated in Fig 9b. Fig 9c is greatly complicated by the mica pattern but arrows indicate the discrete aluminum reflections corresponding to (111) orienta-

tion. A poorly oriented film on glass tending towards (100) orientation is included for comparison (Fig 9d).

Discussion of Results

GEOMETRIC CONSIDERATIONS

The good correlation between substrate and film orientation is in accord with the excellent matching between the oriented aluminum plane and the geometry and dimensions of the surface lattice upon which it forms. Similar results have been reported for thinner films.⁵ The striking geometric kinship between the three low indices planar arrangements: (100), (110), (111), of aluminum in Fig 10 and the geometry of the corresponding planes in sodium chloride and lithium fluoride in Fig 11 suggests that such correspondence between film and substrate promotes a related orientation in the former. This hypothesis is suggested by the table of lattice distances summarized in Fig 11. They agree within a few percent in each case except for the (111) sodium chloride face, for which the lattice spacing is 40 pct greater than the corresponding spacing in the (111) aluminum plane. It is doubtful whether this correlation is generally essential for substrate-metal interaction but it is significant that no (111) orientation of aluminum was ever observed on a (111) sodium chloride surface. Corresponding orientations were observed in every other case.

Substrates with hexagonal cleavage faces of atomic dimensions corresponding to the (111) face of aluminum yielded (111) oriented aluminum films. The fairly complicated surface structure of mica accommodated (110) arrangement of aluminum as well. The arrangement of the atoms in the hexagonal cleavage faces of mica, calcite and fluorite are drawn to scale in Fig 12. The matching of lattice distances was poorer than for the cubic face cleavage substrates and the observed degree of orientation was also correspondingly poorer with the exception of mica. The (110) cleavage faces of cubic zinc blende and sodalite are not indicated but the matching was relatively poor for both substrates and they were unsatisfactory as (110) directing surfaces.

In all cases studied the nature and degree of the observed film orientation bore a close relationship to the geometry and dimensions of the underlying substrate. It appears that directing forces are geometrically distributed on

the substrate surfaces in close correspondence to the atomic distribution in the substrate plane. An interpretation based on this approach will be discussed in the next section.

CHARACTERIZATION OF SUBSTRATE

In an effort to characterize the substrates an effect, discovered by Wood⁶ and studied by Estermann,⁷ was used in a modified form. When a beam of metal vapor is directed at a heated substrate, condensation will occur if the pressure is sufficiently high or the substrate temperature sufficiently low. Whether most of the atoms bounce off the surface losing none or relatively little of their kinetic energy or whether they are accommodated on the surface depends on the relative values of the aforementioned variables plus a third, the attraction of the substrate for the metal atoms. Since the relationship between these factors can be quantitatively expressed, the attraction of the substrate may be determined providing the corresponding pressures and base temperatures can be measured. This pressure-temperature dependence was determined as follows for all the substrate-metal pairs at those substrate temperatures at which maximum orientation was known to occur in each case. The substrate temperature was measured with a thermocouple probe on the surface. The metal pressure was not measured directly but calculated from the crucible temperature using the free energy of vaporization values for aluminum.⁸ The minimum vapor pressure was accurately determined for each base temperature at which condensation of the first layers took place. The formation of the first layer was indicated by measuring the sudden drop in film resistance between two probes on the surface. The corresponding values of pressure and base temperature for a group of typical runs are plotted in Fig 13. The pressure-temperature relationship can be expressed,

$$p = a_1 e^{-A/RT} \tag{4}$$

- where,
- p = pressure of metal vapor
- a_1 = constant, insensitive to temperature
- T = absolute temperature of the substrate
- A = an energy term, characteristic of the film and the substrate.
- The values of a_1 could be evaluated from the intercept on the pressure axis of the curves plotted in Fig 13. It is

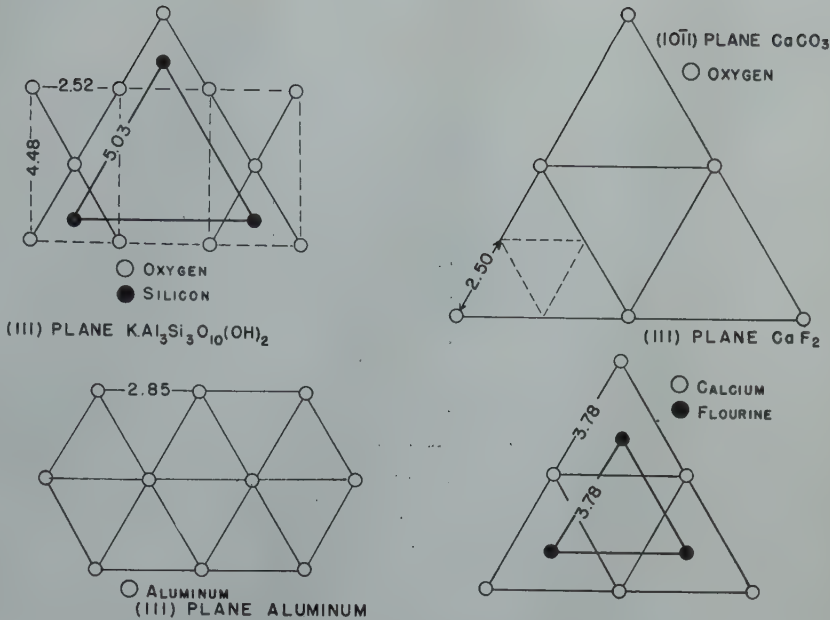


FIG 12—Hexagonal substrates.

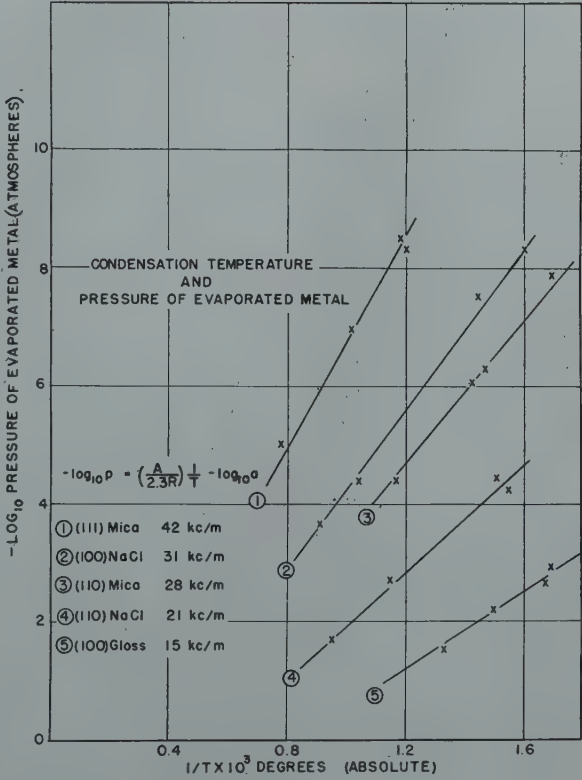


FIG 13—Condensation temperature and pressure.

insensitive to the nature of the substrate and to the base temperature for the conditions observed. Hence, it was of little use for characterizing the substrates on a relative basis. It, however, includes at least three significant terms describing: (1) geometry of the system; (2) size of the condensing particles; (3) a linear temperature correction. Hence,

an interpretation of the mechanism of condensation would eventually require an analysis of a_1 into its component terms. The values of A could be readily interpolated from the slopes of the straight lines plotted in Fig 13. Some typical values are listed there in order of decreasing magnitude. Correspond-

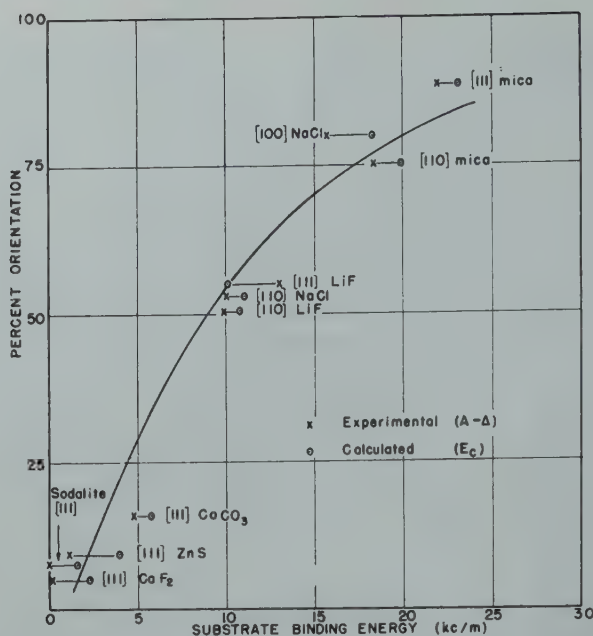


FIG 14—Orientation and substrate.

ing values of temperature, pressure, and A are more completely listed in columns 2, 5 and 6 of Table 2.

A definite trend of A in Table 2 from 42 kc per m to 20 kc per m is evident. This trend corresponds to decreasing observed orientation. It is significant that the values of A are smallest for the ionic substrates at the end of the table for which the orientation was poorer. The smaller surface free energy of the (111) arrangement corresponds to the observation that the A values for (111) substrate-film orientations are somewhat greater than those for (110) and (100) orientations for each substrate-metal pair.

An interpretation of A as describing the heat of condensation of the first layer of metal atoms on the substrate is indicated by the temperature dependence relationship established by the straight lines in Fig 13, and by the empirical findings of Wood and Estermann. A theoretical analysis of their work by Semenoff⁹ applied to these results indicates that

$$A = E + \Delta \quad [5]$$

where,

E = the adhesive energy of binding of the metal and substrate

Δ = the energy of binding of the aluminum atoms in the first layer, that is, the surface energy characteristic of the metal film itself.

If the first term is large the substrate is likely to influence strongly the formation and arrangement of the atoms in the first layer providing the atoms pos-

sess sufficient mobility to assume those positions on the surface of lowest potential energy. If it is small, relative to the second term, that is the adhesive forces between metal and substrate are negligible compared to the cohesive binding between metal atoms, the film formation will be relatively independent of the substrate and, should any orientation occur, it will be that arrangement for which the surface free energy is smallest. Formation of an oriented first layer under the first condition would facilitate the occurrence of the same orientation for subsequent layers. The degree of observed orientation should increase with the value of E providing other factors are also favorable, that is, mobile atoms and relatively thin films. Formation of an oriented layer under the second condition may also occur but the degree of orientation will likely be considerably less. It is noteworthy that the values of A varied from 42 kc per m for aluminum on mica to 15 kc per m for aluminum on glass (column 6, Table 2). In the latter case one might consider the interaction between the glass and the metal to exert a relatively small influence on the film structure and the measured heat of condensation to correspond mainly to the cohesive forces in the (100) plane of aluminum. Since there are about one-third the number of bonds in this configuration compared to that of massive aluminum, the surface energy can be roughly approximated to be one-third of the molar heat of vaporization or 22 kc per m. For this

crude approximation the order of magnitude agrees with the experimentally determined value measured on an amorphous substance like glass. Neglecting the entropy correction, the substrate binding energy for the other substrate-metal pairs may be similarly approximated by subtracting an energy, Δ , corresponding to the cohesive binding energy of the film, from A , the total energy of condensation. In view of the assumptions involved the values obtained are speculative but the resulting values (E) listed in column 8 of Table 2 are of the right order of magnitude. These approximations compare favorably with values calculated on the same basis as Van der Waals interaction. The trend of the experimental values of E is in qualitative accord with the trend of observed orientations for each metal-substrate pair. This is indicated by the data on the maximum orientation and the substrate binding energies listed in columns 4 and 8 in Table 2. The correlation is also evident in Fig 14 in which the maximum observed orientation is plotted as ordinate against the substrate binding energy as abscissa. The calculated values, included for comparison, are now discussed.

VAN DER WAALS INTERACTION

Understanding of the binding between a metal and an ionic surface would provide considerable insight as to the nature of the metal-substrate interaction. A rigorous attempt to define the binding is well beyond the scope

of this paper, but some speculation in this direction seems justified. The characteristics of the binding, namely its relative magnitude and non-specificity, suggest the validity of an approach based on Van der Waals interaction between the first layer of metal and the substrate. An analysis similar to a certain extent to the calculation of heats of adsorption of gases physically adsorbed on ionic surfaces near the boiling point of the gas seems justified. It is obvious that the chief distinguishing characteristic between metal and physically adsorbed gas films, other than the different temperature range in which they form is the marked importance of the cohesive forces in the former case. It is conceivable nevertheless that a strong periodicity in the potential energy surface of the substrate towards the metal atom may be sufficient to start the condensation in a favored direction. The energy of Van der Waals binding of aluminum on each of the substrates was calculated on this basis.

The Van der Waals interaction between non-polar molecules has three important constituent parts: (1) the attraction between fluctuating dipole and induced dipole (dispersion effect), varying inversely as the sixth power of the distance; (2) the attraction between fluctuating quadruple and induced dipole varying inversely as the eighth power of the distance; and (3) the repulsion energy decreasing exponentially with the distance. A fourth constituent part is unique to ionic surfaces: the so-called influence effect. The latter is due to the fact that the charged ions of the substrate induce a dipole moment in the metal atom, which results in an attraction between the ions and the induced dipole. At the equilibrium distances characteristic of the metal films, the first of the four terms is by far the most important. The calculations were made on an approach similar to Orr¹⁰ in which he calculated heats of physical adsorption of argon on potassium chloride.

The dispersion effect was introduced by London¹¹ in the calculation of heats of adsorption. The dispersion potential ϕ , between an atom of metal and an ion of the substrate can be written

$$\phi = -\frac{C}{r^6} \quad [6]$$

where r is the equilibrium distance and C , the dispersion constant, is given by

$$C = \frac{3}{2} \alpha \alpha' \frac{JJ'}{J + J'} \quad [7]$$

where

α = polarizability of the metal

α' = polarizability of the ion

J = characteristic energy of the metal

J' = characteristic energy of the ion

The interaction between an atom and the entire surface of the substrate can be very simply calculated if one assumes that the distance between atom and ion is not smaller than the distance between ions. In this case the summation over the ions of the substrate can be replaced by an integration. In the case of alkali halide substrates this approximation will yield values that are too low by 25 to 30 pct. For the mutual dispersion energy of an infinitely large surface and an isolated atom,

$$\phi = -\int \frac{C}{r^6} N dv = -\frac{N\pi C}{6r^3} \quad [8]$$

where N = number of ions per cc, and

dv is the volume element. Substituting Eq 6 for the dispersion constant

$$\phi = -\frac{N\pi \alpha \alpha'}{4 r^3} \frac{JJ'}{J + J'} \quad [9]$$

An exact evaluation from Eq 8 is not possible because some of the experimental data are missing, particularly the value of J for aluminum. Nevertheless, to show the order of magnitude calculations were made using the first ionization potential. The value of N for the substrates other than the alkali halides was calculated from the density. The distance, r , between an ion and an aluminum atom was assumed to be made up of two parts after London.¹²

$$r = \frac{d_1}{2} + \frac{d_2}{2} \quad [10]$$

For $d_1/2$, half the distance between ions in the substrate was used and for $d_2/2$, half the interplanar distance for that plane of aluminum observed to be

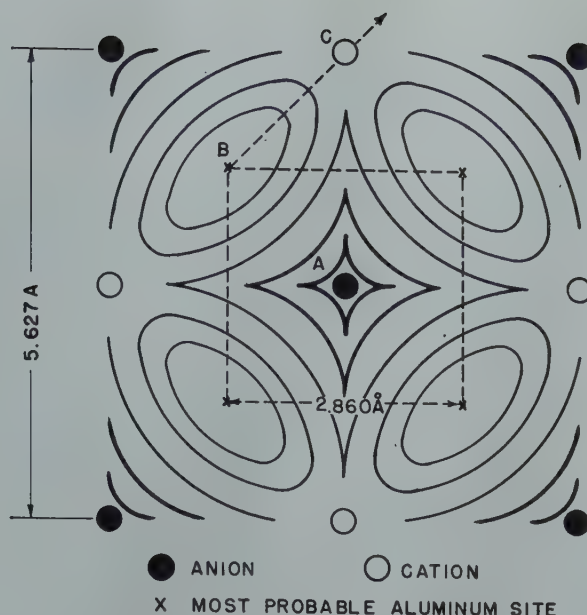


FIG 15—Potential energy surface aluminum on (100) sodium chloride.

Table 3 . . . Dispersion Effect. Aluminum on Ionic Substrates

| Substrate | Plane | Position Center of Face | Ionic Polarizability $\alpha \times 10^{24} \text{ cm}^3$ | Characteristic Energy $\epsilon \times 10^{12} \text{ ergs per mol}$ | Dispersion Constant $C \times 10^{60} \text{ ergs cm}^6$ | Binding Energy $E \times 10^{-3} \text{ cal per mol}$ |
|---|-------|-------------------------|---|--|--|---|
| Sodium Chloride (NaCl) | (100) | two ions | 3.27 | 16.4 | 251 | 18 |
| | (110) | two ions | 3.27 | 16.4 | 251 | 12 |
| | (111) | two ions | 3.27 | 16.4 | 251 | 6 |
| Lithium Fluoride (LiF) | (100) | two ions | 0.93 | 24.3 | 80.8 | 10 |
| | (110) | two ions | 0.93 | 24.3 | 80.8 | 10 |
| | (111) | two ions | 0.93 | 24.3 | 80.8 | 10 |
| Mica (KAl ₃ Si ₃ O ₁₀ (OH) ₂) | (110) | oxygen ion | 3.88 | 20.5 | 321 | 20 |
| | (111) | oxygen ion | 3.88 | 20.5 | 321 | 22.0 |
| | (111) | silicon ion | 0.17 | 2.0 | 3.6 | 2 |
| Calcite (CaCO ₃) | (101) | oxygen ion | 3.88 | 20.5 | 321 | 5 |
| Fluorite (CaF ₂) | (111) | fluorine ion | 1.04 | 19.4 | 84.4 | 2 |
| Zinc Blende (ZnS) | (110) | sulphur ion | 10.2 | 17.5 | 544 | 4 |
| Sodalite (Na ₄ Al ₃ Si ₃ O ₁₂ Cl) | (110) | oxygen ion | 3.88 | 20.5 | 321 | 2 |

preferentially oriented. The identity and geometry of the important ions in the substrate were not always definitely established and a choice had to be made in some cases. The ion was chosen whose arrangement on the surface best fitted the observed aluminum orientation. For example, the oxygen ions were chosen, instead of the silicon ions, in mica. The calculated binding energy for both is listed in Table 3 for comparison. The atomic polarizabilities were taken from Van Vleck¹³ if possible, or calculated,

$$\alpha = \frac{e^2}{4\pi^2 m \omega^2} \quad [11]$$

where ω is the characteristic frequency of the atom and the other symbols have the customary significance. The polarizability and characteristic energies for the ions of the alkali halides were taken from Mayer's¹⁴ analytical treatment of the lattice energy characteristics of alkali halides. The validity of the physical constants in this case warranted more extended consideration. A potential energy surface for the system (100) aluminum-sodium chloride was constructed after Orr.¹⁵ It is schematically represented in Fig 15. The potential hole in the center represents a position of the aluminum in which the potential energy is 7 kc per m lower than a position over the cation. The position over the anion corresponds to the highest potential energy on the surface. For this system it is evident that the central site is relatively large but is deeper by 7 kc per m than the next most favorable site and corresponds to a binding energy of approximately 18 kc per m. It is noteworthy that the atoms of the (100) aluminum plane could be laid over the grid formed by the potential energy holes with negligible distortion. The calculations are summarized in Table 3, in which the atom positions, the ionic polarizabilities, the characteristic energies, the dispersion constants and the calculated substrate binding energies are tabulated for thirteen substrate-metal pairs in columns 1 to 7.

Considering the approximations involved in the theory and the uncertainties in the assumed values of J and r

Table 4 . . . Disproportionate Variation of Intensity of Diffracted X ray Radiation with Depth of Penetration

| (1) | (2) | (3) |
|-----------------|---------------------|-----------------------|
| t (Å) | Pct $\frac{I}{I_d}$ | Pct $\frac{I_t}{I_d}$ |
| 5×10^2 | 1 | 9 |
| 5×10^3 | 6 | 24 |
| 5×10^4 | 25 | 53 |
| 1×10^5 | 50 | 76 |
| 5×10^5 | 100 | 100 |

one cannot expect, in general, more than an agreement in the order of magnitude between calculated and experimental values. The calculated values (E_c) in column 9, Table 2, should be evaluated on that basis. It is considered fortuitous that the calculated values other than for the alkali halides agree as well as they do with the experimental values (column 8). It is significant, however, that the highest values correspond to the substrates upon which the best oriented aluminum films were formed and that the trend definitely agrees with that characteristic of the percent orientation for all eleven substrates and with the indirectly determined substrate binding energies.

It is evident that the periodicity of the potential energy surface of the substrate-atom pair is a very important factor in defining the arrangement of the metal atoms.

Conclusion

The structure of thin aluminum films condensed in vacuum on clean ionic substrates is strongly influenced by the nature, geometry and temperature of the ions in the base. The degree of orientation of the film with respect to the base can be semiquantitatively correlated with a binding energy characteristic of the substrate. The values of the substrate binding energy are of the same order of magnitude as Van der Waals binding between a single atom and an infinite ionic surface. The characteristics of the film structures show this method to be effective for the preparation of oxide-free oriented alu-

minum surfaces for studying surface reactions.

Acknowledgments

The writer is indebted to many of the research faculty for opportunities to discuss the subject and particularly to Professors Charles Barrett, Clarence Zener and Cyril Smith of the Institute for the Study of Metals and to Professor Joseph Mayer of the Institute for Nuclear Studies. In addition, all the structure determinations were made in Professor Barrett's X ray Diffraction Laboratory with the assistance of Messrs. Donald Clifton and James Hess, whose cooperation is gratefully acknowledged.

References

1. C. S. Barrett: Structure of Metals. Crystallographic Methods, Principles and Data. McGraw-Hill (1943), p. 441. New York.
- 1a. Ibid. p. 156.
2. R. Dixit: *Phil. Mag.* (1933) 16, 1049.
3. O. Beeck, A. Smith, and A. Wheeler: *Proc. Royal Soc.*, (1940) 62A.
4. James B. Hess: (Institute for the Study of Metals). Private communication to the author.
5. L. Bruck: *Ann. Physik* (1936) 26, 233.
O. Rudiger: *Ann. Physik* (1937) 30, 505.
- G. Finch, A. Quarrell, and H. Wilman: *Trans. Faraday Soc.* (1935), 31, 1051.
6. R. Wood: *Phil. Mag.* (6), (1916) 32, 365.
7. I. Estermann: *Ztsch. Elektrochem.* (1925) 31, 411.
8. K. Kelley: The Free Energies of Vaporization and Vapor Pressures of Inorganic Substances. Bull. 383, Bur. of Mines (1935).
9. N. Semenov: *Ztsch. Phys. Chem.* (1930) B7, 471.
10. W. Orr: *Trans. Faraday Soc.* (1939) 35, 1247.
11. F. London: *Ztsch. Phys. Chem.* (1930) B11, 222.
12. Ibid.
13. Van Vleck: Electric and Magnetic Susceptibilities, p. 225. Oxford, 1932.
14. J. Mayer: *Jnl. Chem. Physics* (1933) 1, 270.
15. *Loc. cit.*

P-type and N-type Silicon and the Formation of the Photovoltaic Barrier in Silicon Ingots

J. H. SCAFF,* Member, H. C. THEUERER* and E. E. SCHUMACHER,* Member AIME

The microwave region of the radio spectrum was effectively utilized in radar designs during the recent war and it has become of increasing interest in the field of communications. Work in this field has led to an important use for silicon—that of the point contact rectifiers† in the frequency converter of microwave (radar or radio) receivers—and has stimulated considerable interest in the electrical properties and preparation of silicon and its alloys.

Silicon is an electronic semiconductor. Its conductivity at room temperature results principally from the presence of certain impurities. While for metals an increase in impurity content increases the resistivity, for semiconductors such as silicon the opposite occurs and, in general, the addition of impurities lowers the resistivity. Silicon materials may be classified into one of two groups depending upon the manner in which the impurities contribute to electrical properties. These have been termed for convenience p-type or n-type. P-type silicon develops a very large positive thermal emf against metals, has a Hall coefficient of positive sign and a low resistance direction in point contact rectification with the silicon positive with respect to the point. N-type silicon, on the other hand, develops a negative thermal emf against metals, has a Hall coefficient of negative sign and a low resistance direction in rectification with the silicon negative with respect to the point. Impurities which produce n-type silicon are called donors inasmuch as these elements contribute to electrical conductivity by donating electrons to an unfilled energy band in the silicon. On the other hand, elements which produce p-type silicon are known as acceptors as these impurities contribute to the electrical conductivity

by accepting electrons from a filled energy band permitting what is known as conductivity by “holes” in which the sign of the carriers appears to be positive. A general treatment of the mechanism of conduction in semiconductors from the viewpoint of modern band theory has been given recently by Pearson,² by Becker, Green and Pearson,³ and by Torrey and Whitmer.⁴

In this investigation boron and aluminum have been found to be acceptors, and phosphorus, arsenic, and antimony to be donors in silicon. Data on the effect of boron and phosphorus on the electrical properties, when present singly and in combination, have been acquired. These data are discussed in the present paper.

Raw Materials Used and Methods for Adding Second Constituents

Silicon from two sources was used in this work and these will be referred to as A and B respectively. Silicon A is a material of high purity supplied by the Electro Metallurgical Co. It is prepared by chemical purification of “commercial” silicon obtained from the arc furnace reduction of SiO_2 . It contains 99.8 pct silicon, minimum, with small amounts of calcium, iron, aluminum,

boron, and phosphorus as the principal impurities. This material was extensively employed in these studies as well as in the commercial preparation of rectifier materials. Silicon B is a material of high purity from the du Pont Co. It is prepared by a pyrolytic reduction of SiCl_4 and is free of analytically detectable amounts of boron and phosphorus. Its use permitted study of the effect of boron and phosphorus individually on the properties. This material contains, however, spectroscopic traces of a number of metals, some of which affect electrical and rectification properties.

Typical analyses for the two grades of silicon are given in Table 1.

Table 1 . . . Analyses of Silicon Used in Point Contact Rectifier Investigations

| | Silicon A† | Silicon B |
|----|------------|--------------|
| Si | 99.84 | |
| Ca | 0.003 | 0.005* |
| Na | | 0.005* |
| Cu | | 0.001* |
| Mg | 0.007 | 0.001* |
| Mn | 0.002 | 0.001* |
| Al | 0.020 | Not detected |
| Fe | 0.031 | 0.03* |
| C | 0.019 | |
| O | 0.061 | |
| H | 0.001 | |
| N | 0.008 | |
| P | 0.011 | Not detected |
| B | 0.005 | Not detected |

* These are estimated upper limits as determined by spectrographic methods.

† Analysis furnished through the courtesy of Mr. E. F. Doom, Union Carbide and Carbon Research Laboratories, Inc.

To make controlled additions of boron to the charge it was necessary to employ a low boron content master alloy since the quantity of boron to be added was usually only a few thousandths of one percent. The alloy containing nominally one percent boron was prepared by melting chemically pure boron with silicon A using the melting techniques for 320 g silicon

Cleveland Meeting, October, 1949.
TP 2586 E. Discussion of this paper (2 copies) may be sent to *Transactions AIME* before November 15, 1949. Manuscript received January 24, 1949.

* Metallurgists, Bell Telephone Laboratories, Inc., Murray Hill, N. J.

† These are, essentially, the modern version of the “crystal detector” in which rectification is obtained by applying a point contact to the surface of a semiconductor.

‡ References are at the end of the paper.

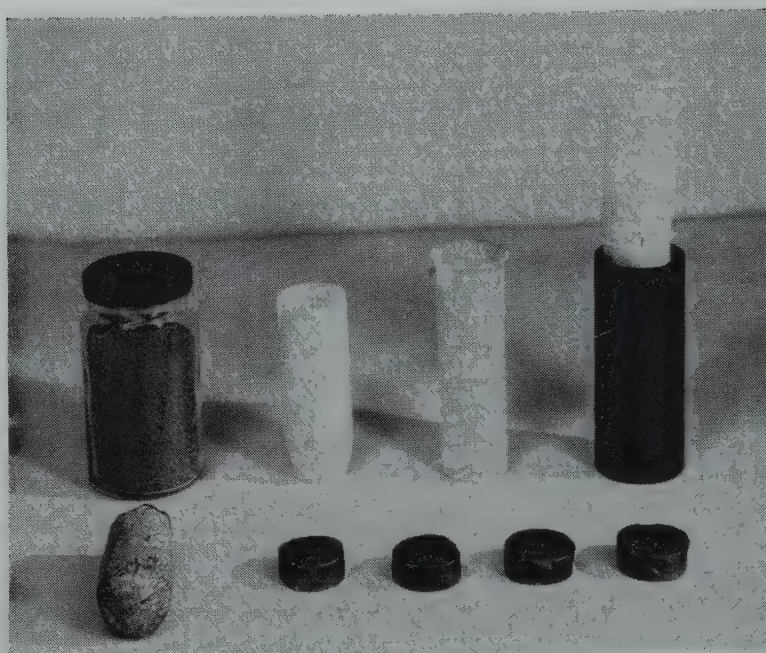
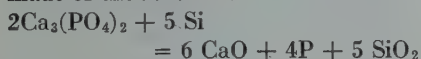


FIG 1a—Silicon ingot preparation.

Silicon granules and crucible arrangement in background. Ingot and ingot sections in foreground.

ingots to be described in the next section. This alloy was crushed in a hardened steel die, ground to a fine powder in an agate mortar, thoroughly mixed and analyzed for boron. Portions of this master alloy were then used in preparing the experimental ingots.

Direct additions of phosphorus were not feasible because of its low melting point and volatility. Instead use was made of the reaction:



When this method was used, spectrochemical analysis revealed that no calcium was retained by the silicon. Apparently also, calcium oxide formed by the reaction does not affect the properties, for the direct addition of calcium oxide to silicon ingots caused no changes in either rectifying characteristics or resistivity.

Additions of aluminum, arsenic and antimony for the qualitative tests described were made by adding these elements directly to the furnace charge.

PREPARATION OF SILICON INGOTS

The ingots of silicon were prepared in silica crucibles in an atmosphere of helium in a high frequency induction furnace. Since silicon cannot be heated by direct induction, a graphite heater which fitted around the melting crucible was used. Most of the early work was done with 45 g ingots. In preparing the ingot the charge was fused and then

slowly cooled by reducing the power applied to the induction coil. Freezing occurred largely from the top surface downward and to a lesser extent inward from the sides and upward from the bottom. During freezing, normal impurity segregation occurred. That is, the silicon at the top of the ingot was highest and that at the core of the melt was lowest in purity.

It was difficult to produce crack-free ingots by this method because of the expansion of silicon during solidification. If a mass of silicon is allowed to freeze in the normal manner, in the final stages of freezing a liquid core will be surrounded by a solid shell which may be easily ruptured by the expansion of the freezing liquid. By changes in solidification technique, however, means were found for preparing 320 g ingots free of cracks throughout the major part of the ingot. Such ingots were prepared in cylindrical silica crucibles of $1\frac{3}{4}$ in. diam and 5 in. tall. Melting was accomplished in the same manner as for the smaller charges, using graphite heaters, but freezing was controlled by gradually removing the furnace tube from the induction coil while power was still applied to the coil. Thus the top of the melt froze first, and solidification progressed slowly downward, the total time for solidification being about 20 min. This not only avoided cracking



FIG 1b—Longitudinal section of 320 gram silicon ingot.

but gave precise control over impurity distribution in the ingot. Due to segregation of impurities, the silicon at the top of the ingot had the highest purity, while the last material to freeze, at the bottom portion of the ingot, had the lowest purity. Fig 1a shows the crucible assembly, a typical 320 g silicon ingot and several sections cut from an ingot. The macrostructure of the ingot is shown in the longitudinal section, Fig 1b.

ELECTRICAL CHARACTERISTICS AND STRUCTURAL FEATURES OF THE EARLY SILICON INGOTS

The early ingots (45 g) prepared from selected lots of silicon A were found to consist of zones of p-type and n-type separated by a photovoltaic barrier.⁵ The p-type zone was located in the region of the ingot which solidified first while the n-type zone was located in the region of the ingot which solidified last. The macrostructure of the ingots is illustrated in the diagram, Fig 2. Relatively large columnar crystals extend downward from the top surface of the ingot to a depth of about one-half inch. Columnar grains are also found extending inward from the sides and upward from the bottom for about one-eighth inch. Beyond the columnar grains irregular grains are found with a network of a second phase in the grain

boundaries. The central portion of the ingot is porous presumably as a result of gas evolution in the last stages of solidification. The outer part of the columnar zone is p-type, the inner part n-type. The central portion of the ingot, containing the irregular grains is also n-type. The boundary between the p- and n-zones is approximately 1 mm in width and extends across the columnar grains, following in general the contour of the ingot surface. Since solidification occurred not only from the top surface downward but also to some extent inward from the bottom and sides of the crucible, the boundary is elliptical in cross-section and encloses the n-zone. It is evident that the boundary follows the contour of the freezing surface as it advanced during solidification. In the 320 g ingots similar effects are observed. However, in this case the solidification of the melt is substantially unidirectional, progressing from the top surface downward. The boundary then extends across the ingot and the portion of the ingot above it is p-type and below it is n-type.

If ingots are rapidly cooled by shutting off the power in the induction coil when the charge has melted, the resulting macrostructure is quite different. The crystallites are no longer columnar but are quite irregular in shape. In each grain an island of p-type is found within a matrix of n-type. The p- and n-zones are again separated by a barrier layer, but the photovoltages developed are lower than those for the barriers of the slowly cooled ingots. The structures of both the rapidly and slowly cooled ingots may be resolved microscopically and are discussed in a companion paper.⁶

Photovoltaic cells may be prepared from the slowly cooled ingots by cutting samples so that one part is p-type, the other n-type separated by the barrier. Such cells are sensitive both to visual and infra-red radiation. They are quite stable and have shown no change in characteristics over a period of several years. Moreover, the effect persists even after annealing at 1000°C for a number of hours.

Associated with the internal photovoltaic boundary are two related effects of interest. Specimens containing these boundaries show both a rectification effect and a pronounced thermoelectric effect. The rectification effect is similar to that obtained in copper oxide or selenium cells. In specimens containing these internal boundaries rectification

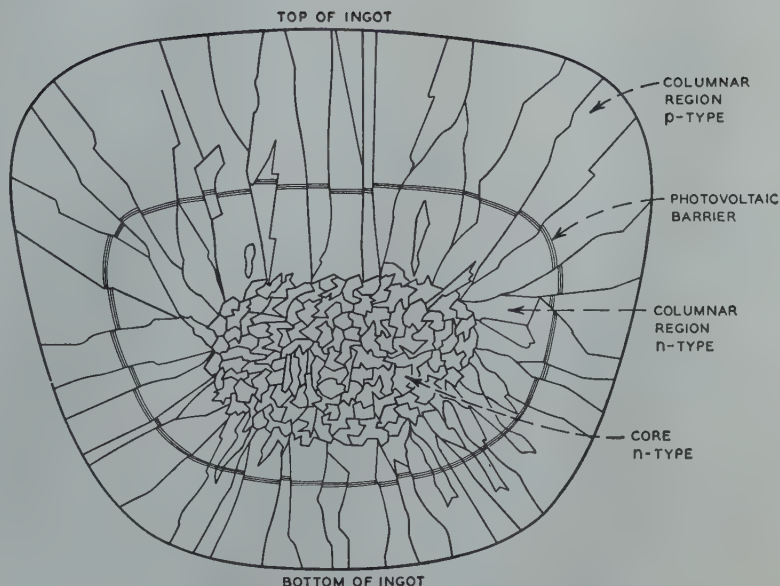


FIG 2—Schematic representation of 45 gram silicon ingot showing barrier.

ratios above 500 at 1 volt have been obtained. Similar rectification and photovoltaic effects in germanium have been reported by Benzer.⁷

Measurement of the resistivity of the silicon at different positions in the ingots containing p-n boundaries revealed an interesting relationship. Since increasing the concentration of impurities in semiconductors decreases the resistivity and since chemical analysis had shown the segregation of impurities in the ingots to be normal it was expected that the resistivity would decrease steadily from a high value for the material which solidified first to a lower value for the material which solidified last. Instead it was observed that in the p-region the resistivity was least for the first frozen material and that it increased with depth to a high value at the barrier. In the n-region the resistivity was highest near the barrier and then decreased with distance from the barrier reaching its lowest value in the region of the ingot which solidified last. The variation in resistivity in the p- and n-zones of a 320 g ingot is shown in Curve 1, Fig 3, which will be discussed at a later point in the paper.

Several other significant facts were observed in the early studies. For a given lot of silicon A the location of the barrier and the relative amounts of p- and n-silicon were precisely reproduced from ingot to ingot but differences were obtained between lots. The mean resistivity in the p-silicon was also related to the location of the barrier and in general it decreased as the amount of p-silicon in the ingot

increased. This clearly indicated the important role of impurities in determining properties and led to a detailed study of the electrical properties of silicon containing different alloying constituents in trace amounts.

EFFECT OF BORON ON THE RESISTIVITY AND RECTIFICATION CHARACTERISTICS OF SILICON

To obtain quantitative data on the effect of boron on resistivity and the rectification properties ingots were made with boron additions ranging from 0 to 0.01 pct. These ingots were prepared using 320 g charges of silicon A mixed with appropriate quantities of the silicon-boron master alloy. The resistivity measurements were made on rectangular specimens, approximately $1 \times \frac{1}{8} \times \frac{1}{8}$ in. in size. These were cut from the ingots so that the long axis was parallel to the top surface of the ingot. Current leads were affixed to the ends of the specimen by electroplating with nickel and soldering. The potential drop across probes on the surface of the specimen was then determined for small known currents by a potentiometric method. From these data, the dimensions of the sample and the distance between probes, the resistivity may be calculated. The sign of rectification, that is, whether the silicon was p- or n-type, was determined by applying a point contact to the surface of the specimen and observing the polarity for the easy direction of current flow.

The resistivities of the central sections of the specimens were determined for a number of vertical positions in

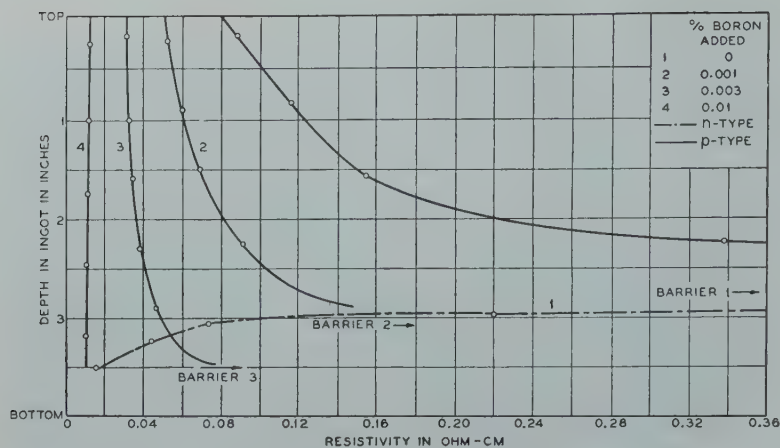


FIG 3—Effect of boron additions on the electrical properties of silicon A.

each ingot. Resistivity measurements in the n-region were possible, however, only for the initial sample in the series to which no boron was added. In the other ingots the n-region was too restricted in size to permit several points to be obtained.

These data are plotted in Fig 3. It will be seen that within this composition range increasing the concentration of boron in silicon A has three significant effects: 1. It increases the amount of p-silicon and lowers the position of the barrier (Curves 1, 2 and 3); if sufficient boron is added only p-type is formed (Curve 4). 2. It lowers the mean resistivity of the silicon. 3. It increases the uniformity of resistivity for a considerable part of the material in the ingot and for the 0.01 pct boron addition substantially no variation is observed throughout the ingot (Curve 4).

In the preparation of silicon point contact rectifiers the uniformity of the finished rectifiers is determined to a considerable extent by the uniformity of resistivity of the silicon used. It was desirable for this reason to attain the uniformity of the 0.01 pct boron composition at higher levels of resistivity also. To determine whether this could be achieved in silicon of higher purity, several ingots were prepared from silicon B. After fusion without alloying additions this material is p-type and its specific resistance is of the order of one ohm-cm. Addition of 0.001 pct boron, however, markedly lowers its resistivity as shown in Curve 1, Fig 4. The resistivities for this alloy ranged from 0.07 ohm-cm at the top of the ingot to about 0.03 ohm-cm at the bottom. Thus no improvement in uniformity of resistivity was obtained by

the use of silicon of extreme purity as the base material. It will be noted, however, that the resistivity *decreased* with depth in the ingot. Hence, in silicon containing only boron as the principal alloying constituent the variation of resistivity in the ingot is in the manner to be expected from a normal segregation. This is in contrast to the increase in resistivity with depth observed in ingots of silicon A containing comparable amounts of boron.

EFFECT OF BORON AND PHOSPHORUS ON THE PROPERTIES OF ULTRA-HIGH PURITY SILICON

To explain the anomalous resistivity gradient observed in ingots of silicon A the presence of a second active impurity which also affected conductivity was assumed. Further investigations revealed that traces of phosphorus were responsible for the anomalous resistivity variations and the formation of n-silicon and the photovoltaic

boundary in the ingots of this material.

To study the effects in silicon of phosphorus and boron in combination, a number of alloys were prepared from silicon B. Specimens were cut from these ingots through the central vertical axis and the resistivity and direction of rectification then determined at $\frac{1}{8}$ in. intervals. The data for typical alloys are given in Table 2 and Fig 5.

Table 2 . . . Resistivity of Silicon-boron and Silicon-Phosphorus Alloys

| Composition | Resistivity at Room Temperature of Samples from Different Locations in the Ingot | | | |
|-------------|--|------------|---------------|---------------|
| | Pct | Top ohm-cm | Middle ohm-cm | Bottom ohm-cm |
| Silicon B | +0.001 B | 0.067 | 0.050 | 0.040 |
| Silicon B | +0.01 B | 0.015 | 0.011 | 0.006 |
| Silicon B | +0.0029 P* | 0.041 | 0.034 | 0.017 |
| Silicon B | +0.0058 P* | 0.031 | 0.023 | 0.008 |

* Added as $\text{Ca}_2(\text{PO}_4)_2$.

These data show that:

1. The addition of boron to pure silicon produces p-silicon while the addition of phosphorus produces n-silicon. The resistivity of such alloys decreases with increasing concentration of the added element (Table 2 and Curves 1 and 2).

2. If ingots of silicon containing either boron or phosphorus are prepared by freezing from the top surface downward, normal segregation occurs and as a result the resistivity decreases with depth in the ingot. The rate of segregation of phosphorus is somewhat greater than that of boron as shown by a more steeply sloping resistivity curve (Curves 1 and 2).

3. If in silicon containing both boron

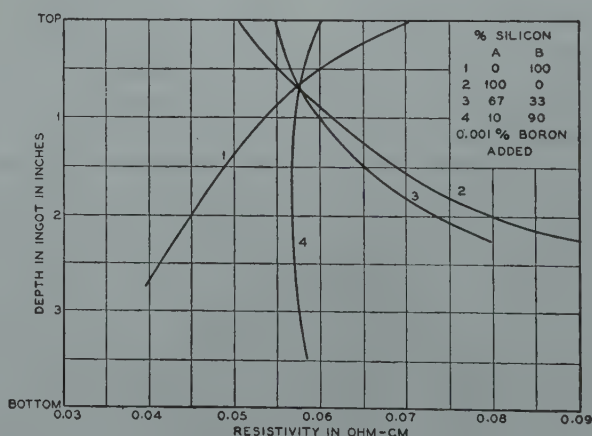


FIG 4—Resistivities of various alloys of silicon A and B.

and phosphorus, the boron exceeds the phosphorus by a small molar amount, of the order of 0.0002 pct, and the ingot is prepared by solidifying slowly from the top downward, then zones of p- and n-silicon will be formed, separated by the photovoltaic boundary (Curve 3). It is therefore possible to reproduce completely the resistivity, rectification and other properties observed for silicon A by adding the correct relative amounts of boron and phosphorus to silicon B. Since boron and phosphorus are both present in silicon A it is a reasonable conclusion therefore that they are the principal impurities responsible for the electrical effects observed in this material.

The mechanism of formation of the p- and n-zones and the barrier may now be interpreted in terms of an electrical interaction or compensating effect of equivalent amounts of donor and acceptor impurities. Referring to Fig 6, Curves 1 and 2 are hypothetical segregation curves for boron and phosphorus with phosphorus segregating more rapidly than the boron. At a depth of 3 in. in the ingot the curves cross and at this point the molar concentrations of boron and phosphorus are equal. Since it is believed that these impurities neutralize one another electrically, no residual impurities are available at this point to contribute to the conductivity of the silicon.* As a result high resistivity and poor point contact rectification are to be expected. This is actually the case in the region of the barrier. Above this region boron is in excess by an amount which is indicated by the difference between the two segregation curves at each location in the ingot. This amount is given by Curve 3, Fig 6 which shows that the free (excess) boron decreases with depth in the ingot from a value of 0.001 pct at the top to 0 pct at the barrier. Since boron is in excess the silicon is p-type, and since the concentration of free boron diminishes with depth, the resistivity increases correspondingly. Below the barrier phosphorus is in excess of boron by an amount equal to the difference between their concentrations at each location. The concentration of free phosphorus below the barrier, given by Curve 4, Fig 6, increases from 0 at the barrier to 0.0015 pct at the bottom of the ingot. Since phosphorus is in excess in this region the silicon is n-type and its resistivity decreases with

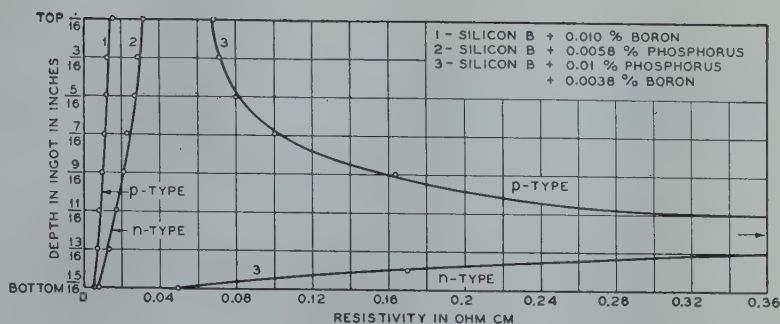


FIG 5—Effect of boron and phosphorus on the electrical properties of silicon B.

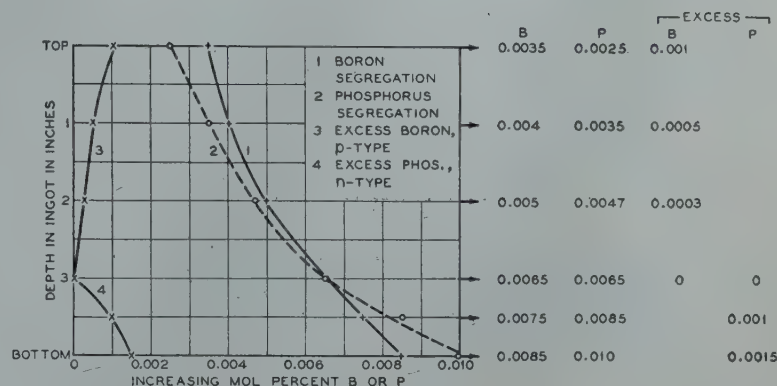


FIG 6—Mechanism of formation of barrier in silicon ingots.

depth in the ingot.

If silicon having the characteristics of Fig 6 were remelted and 0.001 pct more boron were added, the boron segregation Curve No. 1, would shift to the right and would intersect the phosphorus curve at a lower point. Thus, the photovoltaic barrier would appear at a lower point, the amount of p-silicon would be increased, and, since the excess of boron at the top of the ingot would also increase, the mean resistivity of the p-silicon would be lower. If instead, the boron concentration were held constant and the concentration of phosphorus reduced, Curve 2 would shift to the left, and again, the barrier would have occurred lower in the melt, the free boron concentration above the barrier would have increased and the mean resistivity would have been lowered.

It may be seen, therefore, that the electrical characteristics of the silicon ingots may be explained in terms of the differential segregation of boron and phosphorus. The hypothesis has not been checked by direct analysis, however, because of difficulties in determining accurately the small concentrations of boron, and phosphorus at the different locations in the ingot. It

is believed, however, that the hypothetical values given in Fig 6 are correct as to order of magnitude.

While these studies have been concerned principally with boron and phosphorus in silicon it has also been shown that aluminum additions produce p-type silicon, while arsenic and antimony produce n-type silicon. Moreover, photovoltaic barriers have been produced by the addition of arsenic to silicon B. It seems to be generally true therefore that the addition to silicon of elements of group 3, with 3 valence electrons produces p-silicon while elements of group 5, with 5 valence electrons, produces n-silicon.

DEPENDENCE OF UNIFORMITY OF RESISTIVITY ON THE BORON PHOSPHORUS RATIO

It has been shown that in silicon ingots containing only one principal impurity, the resistivity varies with location in the ingot. On the other hand, if 0.01 pct boron is added to silicon A practically no variation in resistivity is observed throughout the ingot. This suggested that uniformity of resistivity throughout the ingot might be related to the relative

* Similar phenomena have been reported in lead sulphide photoconductive cells by Starkiewicz, Sosnowski, and Simpson⁸ and by Sosnowski, Soole, and Starkiewicz.⁹

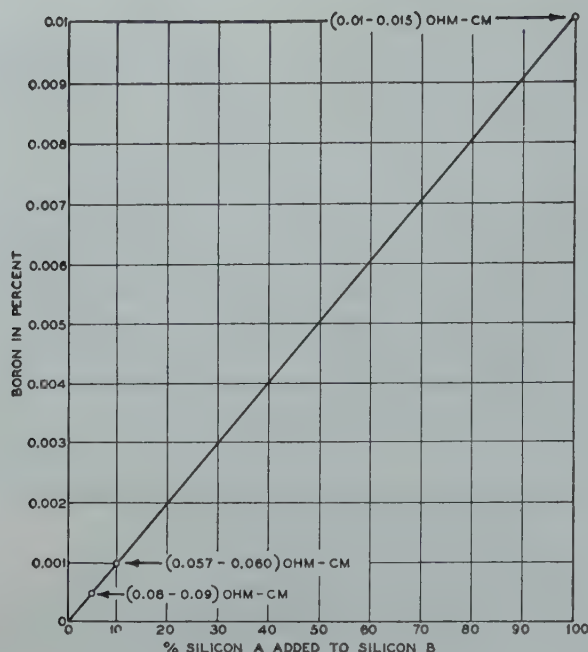


FIG 7—Boron additions to various mixtures of silicon A and B to obtain uniform resistivity in silicon ingots.

The values in parenthesis are the resistivity ranges observed for each composition.

amounts of boron and phosphorus in the charge and that under the correct conditions the uniformity of the 0.01 boron composition might also be attained in materials of high resistivity. To check this experimentally several melts were prepared using as raw materials different proportions of the silicon A and B, adding 0.001 pct boron to each charge. Since the A silicon contained both boron and phosphorus while the B silicon is free of analytically detectable quantities of these elements this series provided samples with a range of boron and phosphorus concentrations in which the relative proportions were systematically varied in the direction of increasing the boron to phosphorus ratio.

Resistivity as a function of location in the ingot for this series is plotted in Fig 4. As the concentration of phosphorus is decreased by increasing the proportion of silicon B in the charge, the variation in resistivity with depth decreases. The least variation is obtained with the 90-10 composition.

Thus, uniform ingots of silicon of desired resistivity may be prepared by making the proper boron additions and maintaining a critical boron to phosphorus ratio. This ratio is about 5

boron atoms for each phosphorus atom. Fig 7 shows the amounts of boron which must be added to various mixtures of silicon A and B to maintain the required 5 to 1 ratio and gives the resistivity range obtained in each ingot. It will be seen that sensibly uniform ingots with any resistivity desired in the range from 0.01 to 0.1 ohm-cm may be obtained in this way. These proportions would vary slightly if the composition of silicon A changed significantly from lot to lot.

Summary

Boron and aluminum are acceptors in silicon, and phosphorus, antimony, and arsenic are donors forming respectively p-type or n-type silicon. The presence of boron or phosphorus alone markedly reduces the specific resistance of silicon. If ingots of silicon containing small amounts of either boron or phosphorus are solidified from the top downward, normal segregation occurs and the resistivity decreases with depth in the ingot. If boron and phosphorus are present together in certain amounts, ingots may be prepared in which the top section is p-type and the bottom

is n-type silicon, in which a barrier region with interesting rectification and photovoltaic properties separates the p-type and n-type regions. In the p-zone the resistivity increases rapidly as the barrier is approached, reaches a maximum at the barrier and then decreases in the n-zone. The formation of the barrier and the variation of resistivity with depth in the ingot are interpreted as being due to interaction between donors and acceptors, in this case boron and phosphorus, in which one mol of boron compensates one mol of phosphorus. Boron and phosphorus segregate at different rates under the solidification conditions used so that in the region of the ingot which solidifies first boron is in molar excess and the silicon is p-type. In the region which solidifies last phosphorus is in molar excess and the silicon is n-type. At the location in the ingot where the molar concentrations of boron and phosphorus are equivalent, the barrier is found.

Addition of phosphorus to boron silicon compositions improves the uniformity of the resistivity in the ingot. In spite of the extreme sensitivity of the resistivity to impurities means were found to obtain sensibly uniform resistivities by maintaining the correct boron to phosphorus ratio.

References

1. J. H. Scaff and R. S. Ohl: Development of Silicon Crystal Rectifiers for Microwave Radar Receivers. *Bell System Tech. Jnl.*, (Jan. 1947) 26, No. 1, 1-30.
2. G. L. Pearson: The Physics of Electronic Semi-conductors. *Trans. Amer. Inst. Elec. Eng.*, (1947) 66, 209-214.
3. J. A. Becker, C. B. Green and G. L. Pearson: Properties and Uses of Thermistors. Thermally Sensitive Resistors. *Elec. Eng. Trans.* 65, 711-725, Nov. 1946.
4. Henry C. Torrey and Charles A. Whitmer: *Crystal Rectifiers*. McGraw-Hill Book Co., Inc., N. Y. 1948.
5. R. S. Ohl: U. S. Pat. 2,402,661, 2,402,662, 2,402,663 and 2,407,678; J. H. Scaff: U. S. Pat. 2,402,582.
6. W. G. Pfann and J. H. Scaff: Microstructures of Silicon Ingots. *Metals Trans.*, this volume, p. 389.
7. S. Benzer: Excess Defect Germanium Contacts. *Phys. Rev.* 72, No. 12, p. 1267.
8. Starkiewicz, Sosnowski, and Simpson: Photovoltaic Effects in High Resistance Semi-conducting Films. *Nature*, 158, 28, July 6, 1946.
9. Sosnowski, Soole and Starkiewicz: Occurrence of Random Photovoltaic Barriers in Photoconductive Layers. *Nature*, 160, 471, Oct. 4, 1947.

Microstructures of Silicon Ingots

W. G. PFANN,* Junior Member, and J. H. SCAFF,* Member AIME

Introduction

The effects of impurities on the electrical properties of silicon are discussed in a companion paper by Messrs. Scaff, Theuerer, and Schumacher.¹ It was shown that an ingot of silicon which contained boron and phosphorus in certain concentrations consisted partly of p-silicon and partly of n-silicon² and that the common boundary between these regions was the source of a photovoltage. These features were ascribed to the segregation of boron and phosphorus during solidification of the ingot. Because of different rates of segregation the first portion of the ingot to freeze contained a molar excess of boron over phosphorus and hence was p-silicon. The last-solidified region contained a molar excess of phosphorus and was n-silicon.

This paper is concerned with the microscopic examination of such ingots. The microstructures are rather unusual in certain respects and their study has helped to show how the segregation of minor elements modifies the electrical properties of silicon. The microstructures of ingots prepared from two lots of silicon, designated 1 and 2, will be described. These lots were obtained from the Electro Metallurgical Co. Both contain 99.8+ pct silicon, but they differ in impurity analysis. For each lot will be shown the microstructure of a slowly cooled ingot, for which the time of solidification is 6 min., and that of a rapidly cooled ingot, for which the time of solidification is 2 min. The ingots were prepared from 45 g charges of silicon.

When an alloy freezes a cored structure is generally produced because of insufficient diffusion to remove concentration differences established during freezing. As a result of coring the first portion of a crystal to freeze is usually poorer in solute than equilibrium requires, while the last material to solidify is richer. In a columnar grain, growth is principally unidirectional and coring can produce a concentration gradient along the entire grain. By carrying the picture of the coring

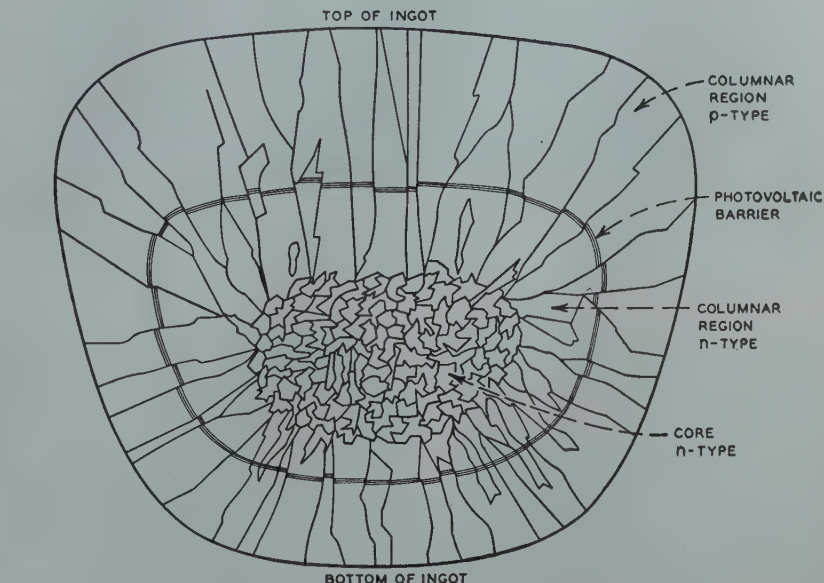


FIG 1—Sketch showing features of slowly-cooled ingot of silicon. Vertical section through center of ingot.

process from a single grain to an entire ingot in which columnar grains are aligned more or less radially, one can easily see that a composition gradient could be established between the outside and center of the ingot. This, to a considerable extent, occurs during the solidification of a slowly cooled ingot of silicon.

Slowly Cooled Ingot

In slowly cooled ingots of both lots of silicon, columnar grains which are approximately radial in direction and longest at the top of the ingot enclose a region in which the shapes and align-

ment of the grains are considerably less regular. The central region is last to solidify and contains cavities and inclusions. The sketch of Fig 1 illustrates some of these features, as well as others which will be described below.

If a polished section of an ingot is etched in a mixture of 20 pct HF and 98 parts of HNO₃ the p-n barrier becomes visible. The overall shape of the barrier in a slowly-cooled ingot is roughly oval, as may be seen in Fig 1. The proportion of n-silicon, that is, the region enclosed by the barrier, is considerably greater in ingots of lot 1 than in those of lot 2.

A sample about $\frac{1}{2} \times \frac{1}{8} \times \frac{1}{8}$ in. was cut from a slowly cooled ingot of lot 1 with its long direction extending from the top of the ingot to the porous region. Thus its upper half was p-silicon, its lower half n-silicon. A longitudinal face was polished and etched in the acid mixture. The areas of interest are identified in Fig 2. A band of parallel markings extends across the sample in the columnar region. These striae are roughly parallel to the upper surface of the ingot and cross grain boundaries with only slight deviations. They are quite distinct in the n-silicon,

Cleveland Meeting, October 1949.
TP 2587 E. Discussion of this paper (2 copies) may be sent to *Transactions AIME* before November 15, 1949. Manuscript received Jan. 24, 1949.

* Metallurgists, Bell Telephone Laboratories, Inc., Murray Hill, N. J.

¹ J. H. Scaff, H. C. Theuerer, E. E. Schumacher: "P-type and N-type Silicon and Formation of the Photovoltage Barrier in Silicon Ingots," *Metals Transactions*, this volume, p. 383.

² The reader is referred to Ref. 1 for definitions of p- and n-type semiconductors and of donor and acceptor impurities.

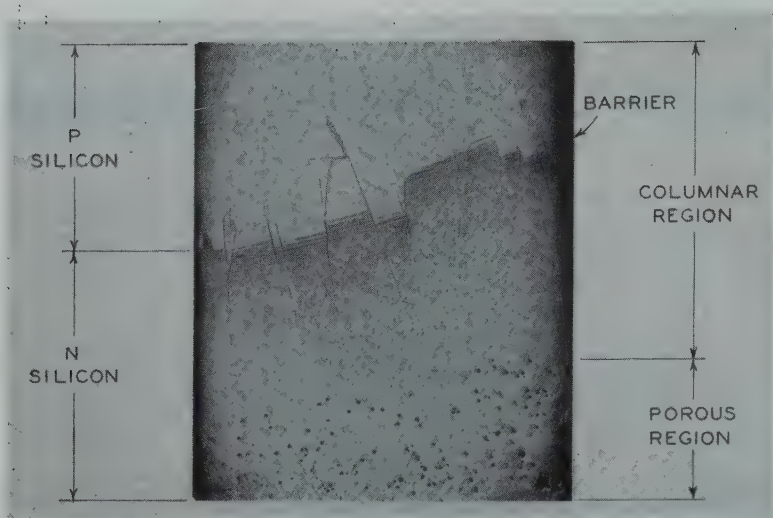


FIG 2—Longitudinal section of slowly-cooled ingot of lot 1. Etched in acid mixture. $\times 14$.
Reduced one-third in reproduction.

especially near the p-type area. Striae are present in the p-silicon but are not visible in Fig 2.

Photovoltaic activity is confined to points on the sample which are common to both p- and n-silicon. It was possible to determine the locations of such points very accurately by connecting a suitable recording instrument to the ends of the sample and then exploring the specimen surface at high magnification, using the illuminating beam of the microscope as a source of light.

A portion of the p-n region of Fig 2 is shown at higher magnification in Fig 3.

Examination of Fig 2, 3 and 5 will show that although a few n-striae are completely isolated, most of the n- and p-striae are connected to the main bodies of n- and p-silicon respectively. The striae may be said to be interlocking rather than alternating. Hence the boundary which is common to the main bodies of n- and p-silicon is quite long. A result of this feature is an enhancement of the photo-current obtained on illumination.

The difference in the behavior of the two etchants which have been used in this study is interesting. A warm, aqueous, 5 pct solution of sodium hydroxide forms etch-pits whose shapes depend on crystal orientation. At moderate and low magnifications this effect is seen as a uniform darkening of entire grains which varies in degree in individual grains. Hence this reagent is helpful in showing grain size and shape. It is entirely insensitive, however, to the presence of the p-n boundary or the effect which produces the striae.

On the other hand the mixed acid etchant reveals the striae and the p-n boundary. It produces an overall brightening and delineates the grain boundaries.

The following explanation is advanced for the microstructures of a slowly cooled ingot:

When freezing begins columnar grains form at the outside of the melt and grow inward, those originating at the upper surface growing most rapidly. At any time during solidification the shape of the liquid-solid interface roughly parallels the outer surface of the ingot. This advancing front is more or less unbroken except for small differences in growth of individual grains and irregularities at the grain bound-

aries. The striae in the columnar region are believed to be the result of minor undulations in the composition gradient which are caused by disturbances in the liquid adjacent to the advancing solid. They record the positions of the liquid-solid interface throughout the solidification of the columnar region. Since an overall concentration gradient of impurities is established during the freezing of the columnar grains the striae may also be regarded as contours of constant composition.

An explanation of the alternating strips of p-silicon and n-silicon at the boundary is given by the hypothetical curve of Fig 4, which shows the concentrations of excess boron or phosphorus as a function of distance from the top of the ingot for a single columnar grain. The reversals represent the local variations in composition which are associated with the striae, while the major trend of the curve depicts the general effect of coring on the difference between the concentrations of phosphorus and boron. Since silicon changes from p-type to n-type at zero difference, it is possible to have a number of alternate bands of p-silicon and n-silicon in a polished section if the fluctuations are of sufficient amplitude. This situation is shown in Fig 4, where two narrow strips of p-silicon and two of n-silicon appear, and is a characteristic feature of slowly cooled ingots, as may be seen from Fig 5 and from Fig 2 and 3. The dark edges between the p- and n-areas in Fig 5 do not necessarily indicate the presence of a substance at the boundary but are an

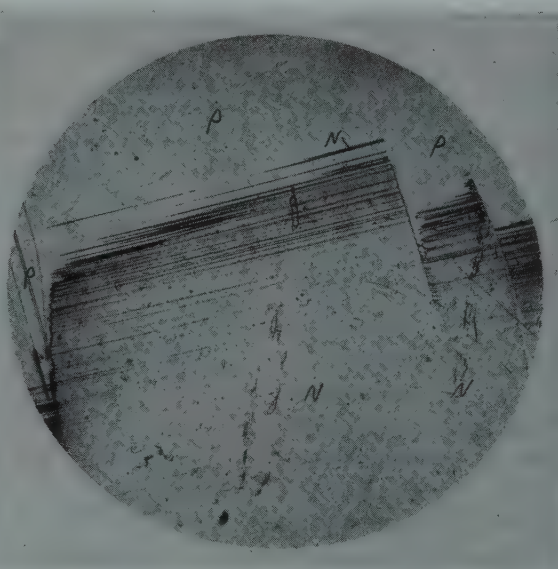


FIG 3—Area from Fig 2. $\times 50$.
Reduced approximately one-third in reproduction.

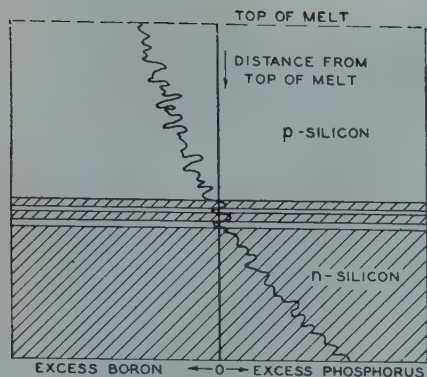


FIG 4—Relation between excess impurity concentration and distance from top of ingot.

etching effect. The p-silicon is attacked more rapidly by the acid etchant, leaving raised peninsulae of n-silicon whose sides are oblique, and hence are dark in vertical illumination.

Rapidly Cooled Ingot

If the molten silicon is cooled rapidly, nucleation occurs throughout the melt rather than only at the surface and instead of columnar crystals an equiaxed grain structure results. Such an ingot differs from a slowly cooled ingot electrically and microstructurally. During solidification coring produces at the center of each grain a region which is poor in impurities and which is surrounded by layers of increasingly higher concentration. In contrast, the region weak in impurities in a slowly cooled ingot is at the outside of the ingot and is continuous. In a rapidly cooled ingot inclusions are found in the last-solidified

parts of each grain and are distributed throughout the ingot instead of being concentrated in the center, as in a slowly cooled ingot. In short, in a slowly cooled ingot segregation may be regarded as a feature of the ingot as a whole, while in a rapidly cooled ingot it is in general localized to individual grains.

If the relative concentrations of boron and phosphorus vary in a single grain as they do in a slowly cooled ingot, one would expect to find a p-n boundary having the shape of a closed figure in that grain. Examination of rapidly cooled ingots has shown this to be so. The microstructures may be described as islands of p-silicon in a background of n-silicon. Measurements of the direction of point contact rectification, made by using a sharply pointed probe to touch individual grains, showed that invariably the islands were p-silicon while the surrounding areas were n-type.

Fig 6 shows an area in a rapidly cooled ingot of lot 1 in which several islands of p-silicon are visible. These islands were concentrated at the top of the ingot where, despite the non-columnar grain growth, freezing did take place first. The remainder of the ingot was entirely n-type. Thus, in addition to local coring in each grain, some segregation had occurred in the ingot as a whole.

An area from a rapidly cooled ingot of lot 2 is shown in Fig 7 and 8. Here the p-n boundaries are near the grain boundaries. The major part of each grain is p-silicon surrounded by a thin

strip of n-silicon. Again some segregation occurred over the ingot as a whole, as some grains at the top of the ingot contained only p-silicon and the grains containing the greatest proportion of n-silicon were at the center of the ingot.

It was stated in the discussion of slowly cooled ingots that those of lot 2 contained more p-silicon than those of lot 1. As Fig 6 and 7 show, this relationship is also true for the individual grains in rapidly cooled ingots.

Although the p-n boundaries in the two types of ingot are unlike in many respects, they are basically similar. Their shapes and locations differ because the ingots solidify in dissimilar ways. The appearance of the boundary in a slowly cooled ingot is further modified by the effect responsible for the striae. Apparently this effect is seldom present in rapidly cooled ingots.

The irregular shapes of the p-n boundaries, especially in rapidly cooled ingots, make it unlikely that they are localized to certain crystallographic planes. Their locations and appearance at high magnification distinguish them from grain boundaries. Illustration of these points is offered in Fig 9 and 10.

Summary

The microstructures of ingots of two lots of silicon have been described, both as prepared by slow cooling and by rapid cooling. The dependence of the distribution of the p- and n-regions on segregation has been indicated. When the ingot freezes slowly the grains are columnar, the regions of p-silicon form

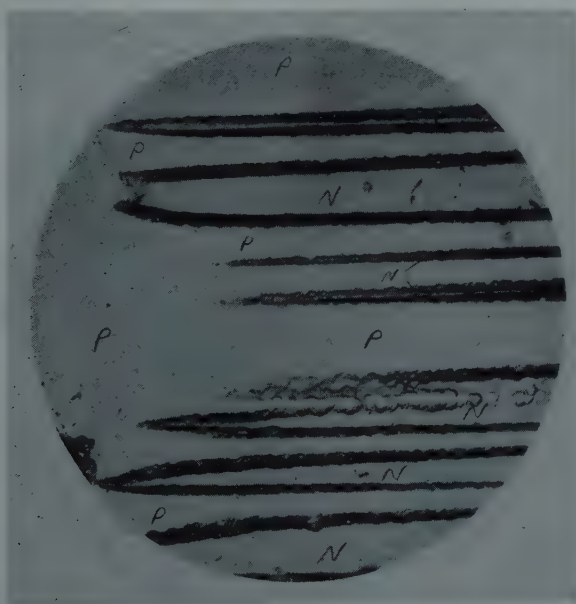


FIG 5—Interlocking strips of n- and p-silicon in slowly cooled ingot of lot 1. $\times 1000$.
Reduced approximately one-third in reproduction.

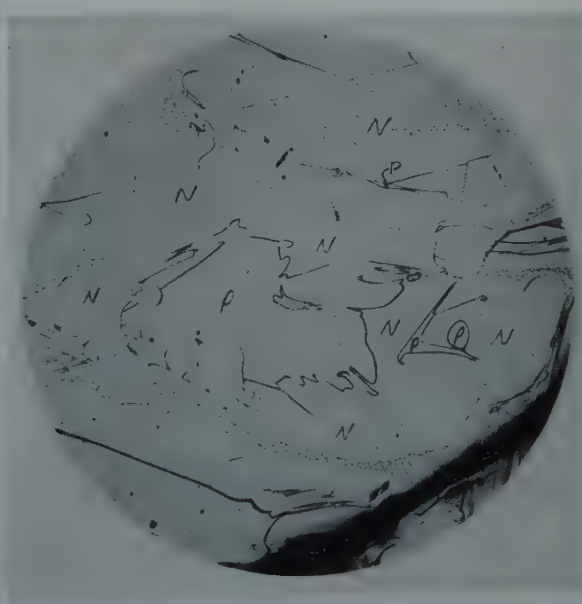


FIG 6—Rapidly-cooled ingot of lot 1. Etched in acid mixture. $\times 50$.
Reduced approximately one-third in reproduction.

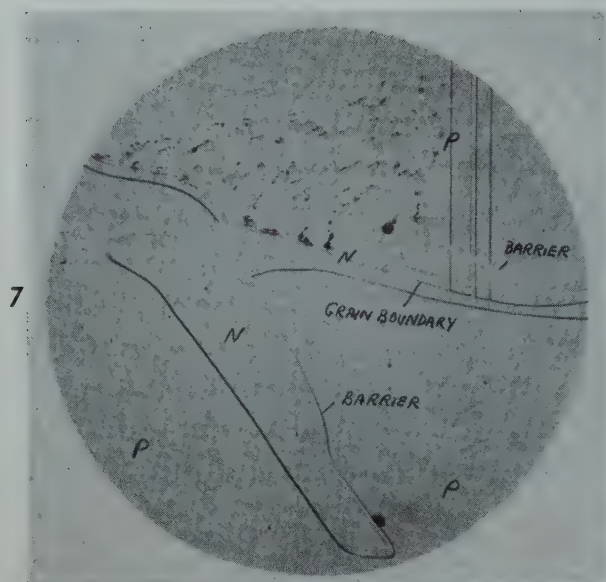


FIG 7—Rapidly-cooled ingot of lot 2. Etched in acid mixture. $\times 100$.

Reduced approximately one-third in reproduction.

FIG 8—Area from Fig 7 showing two p-n barriers separated by a grain boundary. Oblique illumination. $\times 250$.

Reduced approximately one-third in reproduction.

FIG 9—P-N barrier in rapidly-cooled ingot of lot 1.

Note irregular shape and variation in thickness. Etched in acid mixture. $\times 500$. Reduced approximately one third in reproduction.

a continuous zone which encompasses the n-silicon, and the p-n boundaries are relatively continuous. When cooling is more rapid, nucleation occurs throughout the melt and grain growth is disorderly, with the result that the p-silicon and the p-n boundary in each grain are separated from the corresponding regions in adjacent grains by layers of n-silicon.

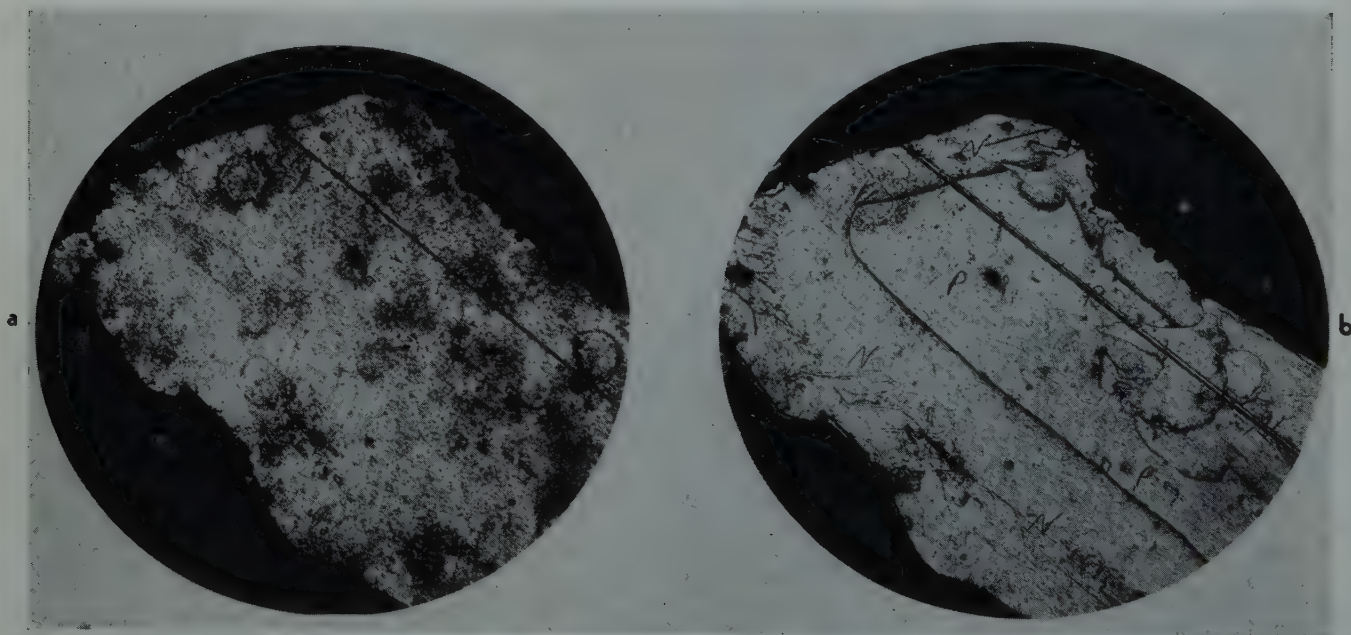
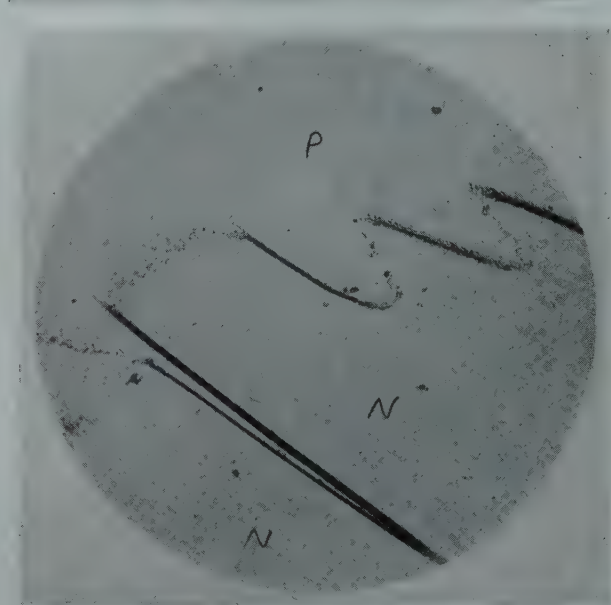
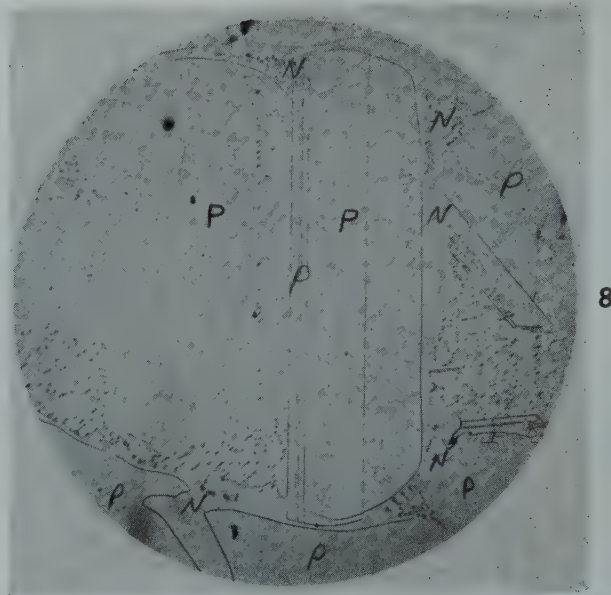


FIG 10—(a) Grain in rapidly-cooled ingot of lot 1. Etched in warm 5 pct KOH. (b) Same grain, after etching in acid mixture followed by re-etching in KOH. P-N barrier is now visible. $\times 50$.

Reduced approximately one-third in reproduction.

Controlled Drying of Retorts

R. R. FURLONG* and D. H. WERTZ*

Dry room equipment at Donora Zinc Works is of the design which prevailed at the time the plant was built in 1915. It consists of 11 adjoining rooms, each being 99 ft long, 11 ft wide, and 7 ft high and having a capacity for 1040 retorts. Heat is supplied by steam coils beneath the slatted wood floor and by warm air ducts at the ceiling. Drying practice is about the same as that generally followed in the industry except that, under normal zinc furnace operations, the maximum drying time is 45 days.

During certain seasons of the year the drying process was seriously affected by varying weather conditions which frequently resulted in a scrap loss of 5 to 7 pct. Because of these unfavorable conditions, which caused uneven drying and strains in the retorts, increased retort failures in the zinc furnaces were recorded. Regulation of temperature and humidity under all conditions appeared to be the logical solution of this problem.

Controlled drying had been developed for a number of ceramic products and investigation of several such drying processes in this area revealed favorable results. Along with control of drying conditions and the attendant decrease in scrap losses, plant operators also reported a material reduction in drying time.

Another factor affecting the decision to proceed with this development was

the drastic change in market conditions for retort clay. Curtailment of shipments from the chief source of supply made it necessary to proceed with blending of other available clays, but quality of these clays was questionable for adequate retort life in the 24 hr furnace cycle. Rapid furnace testing of new mixtures was desirable but impossible with the prolonged drying schedule. Therefore development of a controlled drying process for zinc re-

torts offered the solution to the problem of rapid testing of retort mixtures.

Description of Process and Equipment

The freshly extruded retort is cylindrical in shape, 58 in. long, 9 in. id and has $1\frac{1}{8}$ in. side walls. One end is closed and approximately 2 in. thick. The moisture content of this "green" retort is about 17 pct which means a necessary removal of 30 lb of water per retort. Retorts are set on the slatted floor of the dry room with the closed end down.

The controlled drying process depends upon the circulation of a large volume of conditioned air at low velocity. To provide for uniform distribu-

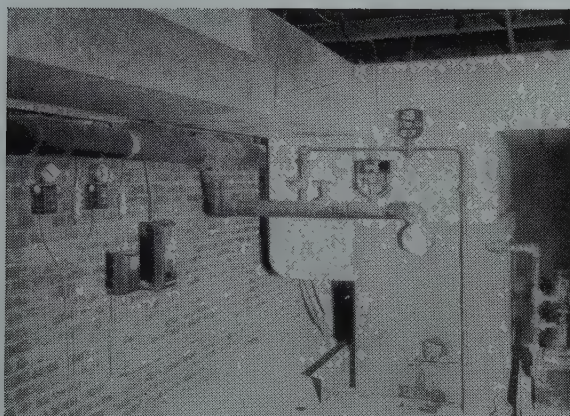


FIG 1—Front view of Carrier Heater unit.

San Francisco Meeting, February 1949.

TP 2555 D. Discussion of this paper (2 copies) may be sent to *Transactions AIME* before Aug. 15, 1949. Manuscript received October 28, 1948.

* Foreman, Pottery Department, and Ceramic Engineer, respectively, American Steel and Wire Co., Donora Zinc Works, Donora, Pennsylvania.

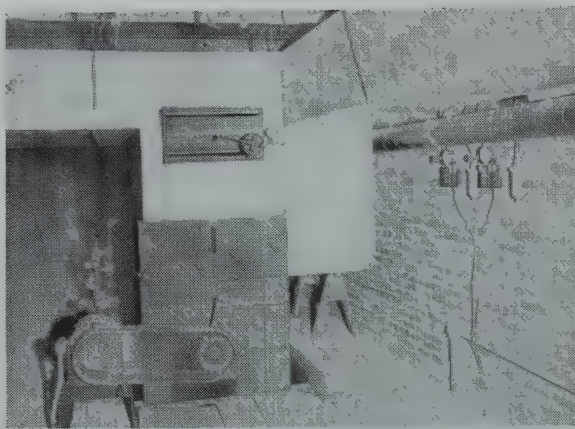


FIG 2—Rear view of Carrier Heater unit.

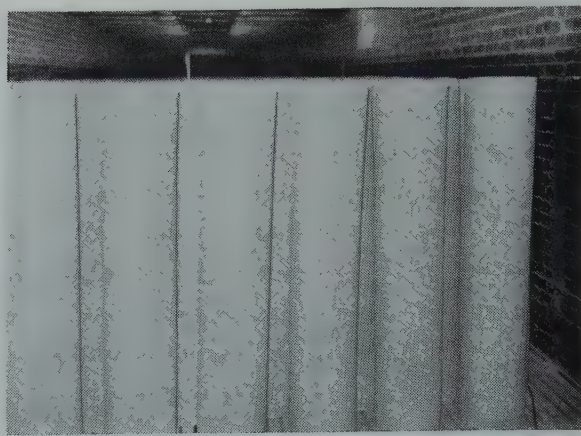


FIG 3—View of retorts in drying room.

tion of the air stream, the heater units should discharge into a large chamber. The only available space for this, in the existing dry rooms, was under the slatted floor. Two inverted type Carrier Heater units, each with a fan capacity of 17000 cfm, were installed in the middle one of three dry rooms, and connected to each adjacent room with short ducts leading into wall openings above and below floor level. Manually operated interlocked dampers within the unit regulate the flow of air to either room.

To control conditioning of the air stream, each heater unit is provided with wet and dry bulb temperature instruments located beneath the floor of each room opposite the duct opening. These control instruments actuate air operated valves on the steam lines to the heater coils and to the steam spray (Fig 1). These supply heat and moisture as required. During the drying cycle a slight pressure is maintained in the dry room and make-up air is introduced through a fresh air damper (Fig 2). This damper, located in the rear wall of the heater unit above the steam coils, is operated by an air valve which in turn is controlled by the dry bulb instrument.

After considerable experimental work a standard practice for quick controlled drying of zinc retorts has been developed to suit conditions at this plant.

Loading of the room requires about two days production from the retort press. Retorts are placed in staggered

rows 3 in. apart and this widespacing provides free movement of the rising warm air around the retorts (Fig 3). Incidentally, this spacing has reduced the capacity of each room from 1040 to 760 retorts.

After loading, the stack damper and doors of the room are closed and retorts are allowed to stand at existing conditions until the following morning. Air circulation is then started and continued for 48 hr at a dry bulb temperature of 120°F and 72 pct relative humidity. The wet bulb temperature for this humidity is 110°F which temperature remains constant throughout the drying cycle. On the third day the dry bulb temperature is held at 130°F for 8 hr with a relative humidity of 53 pct. For the next 16 hr the dry bulb temperature is fixed at 140°F with a corresponding decline in relative humidity to 38 pct. During the first 6 hr of the fourth day the dry bulb temperature is increased in 10° intervals until 170°F is reached, with a final relative humidity of 17 pct. At this point the fresh air and stack dampers are opened. Fresh air heated to 170°F is allowed to sweep through the room for the next 16 hr to complete the drying cycle. Steam is then shut off and the fan is used to cool the room.

Summary

1. It is evident from the above description of drying practice that the

principles of controlled drying can be beneficially applied to the manufacture and quick testing of zinc retorts.

2. The drying cycle has been reduced from 45 days to 4 days with assurance that drying conditions can be duplicated. This feature is extremely valuable in the rapid testing of new retort mixtures.

3. Retort losses in drying have been reduced to less than one percent. This is about half the normal loss expected with the slow drying practice.

4. Close regulation of temperature and humidity has eliminated their fluctuation caused by variations in the weather.

5. Numerous zinc furnace tests have not shown any failure of retorts which could be associated with the quick drying process. At the same time no improvement in service in the furnaces has been detected.

6. The capacity of the present installation is not large enough to supply total retort requirements for current furnace operations. Therefore the equipment is used to quick-test the quality of retort mixtures to be dried by the slow process, and as additional capacity for emergency production. In these respects the installation has been satisfactory.

7. Quick drying equipment of sufficient capacity for the entire smelting furnace requirements would reduce the number of drying rooms by one-half with a corresponding decrease in retort inventory.

The Study of Grain Boundaries with the Electron Microscope*

J. F. RADAVIDH†

Introduction

Many heats of steel of low carbon value have been known to produce brittle pieces of steel. The brittleness is believed to be due to the impurities located within the grain boundaries. Such brittle steels have been examined with an optical microscope to ascertain the nature and the amount of the impurities present at the grain boundaries. Due to the relatively low resolving power of the optical microscope, the impurities are not visible in fine detail.

The writer obtained some sheet steel and proceeded to determine the location of the impurities and to show the application of the electron microscope to the study of grain boundaries. One sample was known to be capable of becoming embrittled, whereas another sample was believed to be much less susceptible to embrittlement.

Treatment of Specimens

The specimens were embrittled by annealing above the A_3 point under mildly oxidizing conditions. One piece of ingot iron could not withstand a 90° bend, whereas another piece of ingot iron was not affected and could withstand a 90° bend. The brittle piece was then annealed at a high temperature in a hydrogen atmosphere.

The annealed ingot iron was termed *cured* and could withstand a 90° bend very easily. The three specimens examined will be designated as *brittle*, *good*, and *cured* in the discussion that follows.

Procedure

The sizes of the specimens were as follows: one piece of brittle ingot iron— $\frac{3}{8}$ by $\frac{1}{8}$ in.; one piece of good ingot iron— $\frac{3}{8}$ by $\frac{1}{8}$ in.; one piece of cured ingot iron— $\frac{3}{8}$ by $\frac{1}{8}$ in.

The specimens were too small to be

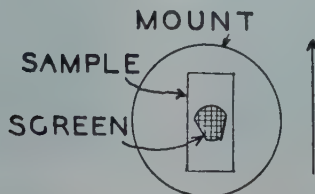


FIG 1—Cut-down screen for narrow specimens.

polished by hand and therefore were mounted in bakelite. The polishing procedure was carried out in the conventional manner with the use of 1/0 through 3/0 papers, and the final polish was done with alumina on a billiard cloth. The specimens were then etched in a 4 pct solution of picral in alcohol, and then they were examined through an optical microscope. An area was chosen that showed distinct grain boundaries, and an effort was made to keep near this area when pulling the replicas

REPLICA TECHNIQUE

The replica technique used in the preparation of the replicas for examination under the electron microscope is described in *Electron Metallography*.¹ It consists essentially of the following steps:

1. Obtaining a suitably etched specimen.
2. Applying a swab of ethylene dichloride on the surface.
3. Applying a formvar solution on the surface.
4. Placing a screen on any desired spot.
5. Breathing on the formvar layer.
6. Applying scotch tape on the screen and film.

7. Pulling the film and the screen up with the Scotch tape.

8. Separating the screen from the Scotch tape.

This replica technique is very similar to the one described by Harker and Shaefer.² However, with the added step, the percentage of replicas removed is very much higher regardless of the length of the time from the etching of the specimen to the actual pulling of the replica.

The replicas were then shadow cast with manganese at a filament height to replica distance ratio of $1\frac{1}{2}:7$. This produced a very high contrast replica for use in the electron microscope.

One of the difficulties encountered with this study was the restricted area of the specimen. The width of the specimens was the same as that of the 200 mesh nickel supporting screen. In order to increase the effective area, the screens were cut down as shown in Fig 1. The arrow indicates the direction in which the replica was pulled. This operation made it possible to obtain a large percentage of good replicas.

Fig 3 shows an electron micrograph of a brittle piece of ingot iron and a grain boundary that was polished mechanically. The surface is very rough probably due to the incomplete removal of the flowed layer by the picral etchant. The grain boundary does show evidence of impurities. It was decided to electropolish the specimens to obtain a much smoother surface than the one obtained by mechanical polishing.

ELECTROPOLISHING

The specimens were cut in half to expose the metal on the back side. The exposed metal had sufficient area to make good electrical contact and electropolishing was carried out easily.

The conditions for electropolishing were 0.9 amp, 35 volts, and 25 sec. in an electrolyte composed of 850 cc of ethyl alcohol, 100 cc distilled water, and 50 cc of perchloric acid.

The polished specimens were then etched in the 4 pct picral solution for a shorter time than was necessary for

Cleveland Meeting, October 1949.
TP 2623 E. Discussion of this paper (2 copies) may be sent to *Transactions AIME* before November 15, 1949. Manuscript received January 25, 1949.

*Graduate Student Prize Paper, Seventh National Student Prize Paper Contest, AIME, 1949.

†Dept. of Physics, Purdue University.

¹References are at the end of the paper.

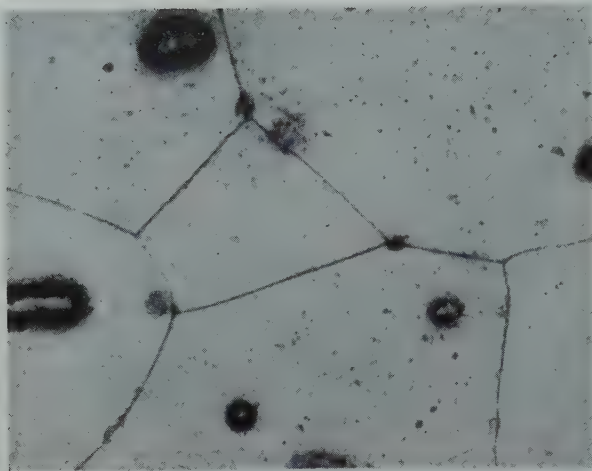


FIG 2—Ingot iron brittle. Mag. 1000 X.
Reduced approximately one-fourth in reproduction.

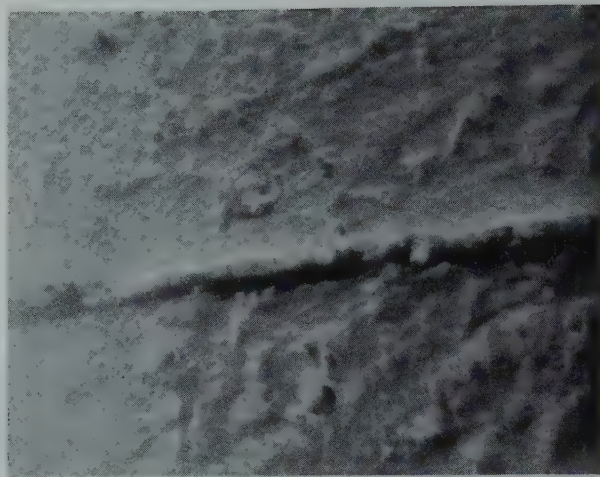


FIG 3—Ingot iron brittle. Mag. 18,500 X.
Reduced approximately one-fourth in reproduction.



FIG 4—Ingot iron brittle. Mag. 18,500 X.
Reduced approximately one-fourth in reproduction.

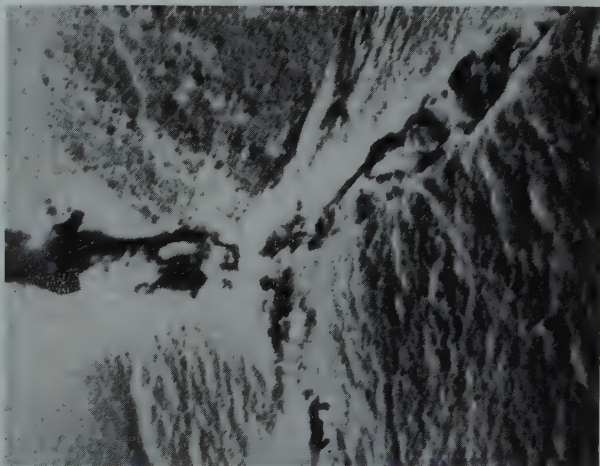


FIG 5—Ingot iron brittle. Mag. 18,500 X.
Reduced approximately one-fourth in reproduction.

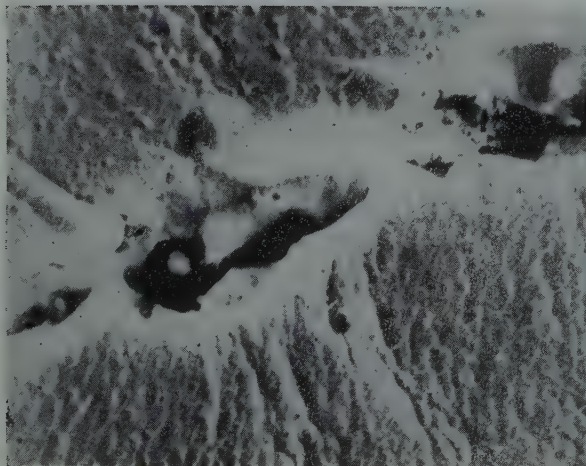


FIG 6—Ingot iron brittle. Mag. 18,500 X.
Reduced approximately one-fourth in reproduction.

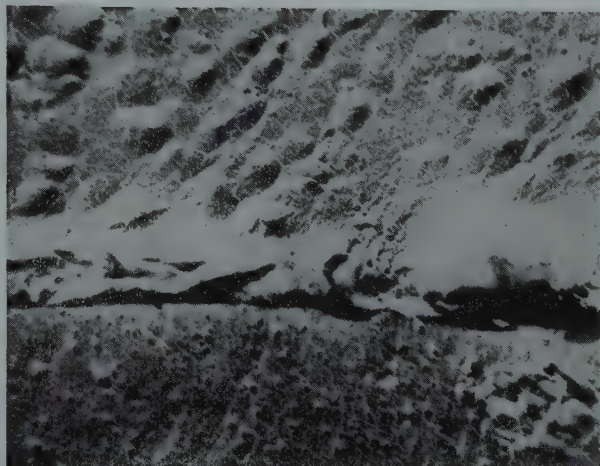


FIG 7—Ingot iron brittle. Mag. 18,500 X.
Reduced approximately one-fourth in reproduction.



FIG 8—Ingot iron brittle. Mag. 18,500 \times .
Reduced approximately one-fourth in reproduction.

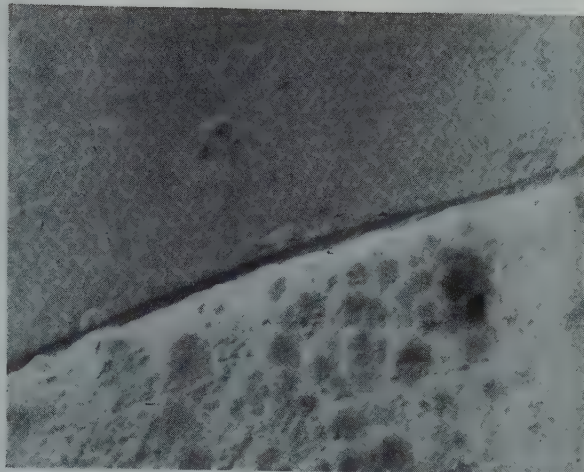


FIG 9—Ingot iron good. Mag. 18,500 \times .
Reduced approximately one-fourth in reproduction.

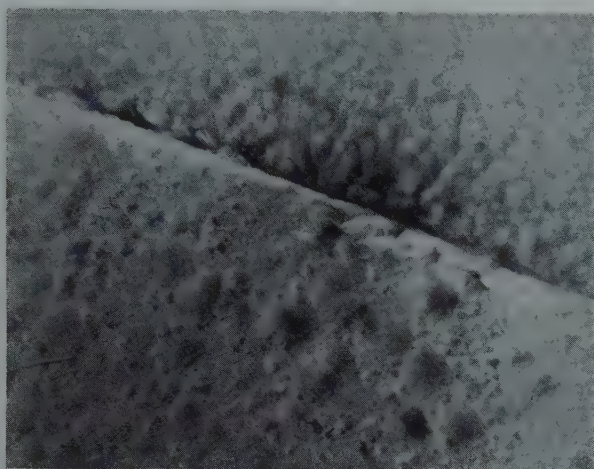


FIG 10—Ingot iron good. Mag. 18,500 \times .
Reduced approximately one-fourth in reproduction.

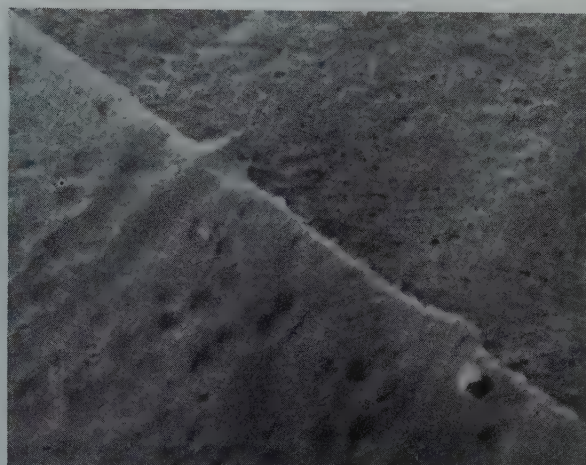


FIG 11—Ingot iron good. Mag. 18,500 \times .
Reduced approximately one-fourth in reproduction.

specimens polished mechanically. The grain boundaries were clearly defined and the number of scratches was small, Fig 2.

EXAMINATION OF THE GRAIN BOUNDARIES

In order to gain the maximum contrast, the objective aperture was installed in the electron microscope. The background electrons were eliminated, and the electron micrographs showed good contrast. The rough surface background caused by the flowed layer as seen in Fig 3 was eliminated.

The brittle piece of ingot iron was carefully examined to locate the grain boundaries and whatever impurities the grain boundaries might contain. It was noticed that a large quantity of impurities existed at the grain boundaries. These findings were recorded on photographic plates and are represented by Fig 4-8.

The good piece of ingot iron was then similarly examined to observe the amount of impurities present. Fig 9-12

show the typical structures that were observed in the electron microscope.

The cured piece of ingot iron was then similarly examined to see the effects at the grain boundaries produced by the hydrogen anneal. Fig 13 and 14 show two representative pictures of the cured metal.

Discussion of Micrographs

The optical micrograph is included to show the grain boundaries at 1000 \times . The electron micrographs will be divided into three groups showing the grain boundary structure of each group. The electron micrographs were taken at 7500 \times and then enlarged to 18,500 \times .

The electron micrographs illustrated are lacking in detail especially at the grain boundaries. This loss of detail is due to the enlargements and printing from the original plates.

BRITTLE IRON

Fig 3 is an electron micrograph show-

ing the lack of contrast due to the rays of scattered electrons which build up a general hazy background. The impurities are shown at the grain boundaries. The white areas are shadows cast by the oblique rays of evaporated manganese. The stringers shown in the ferrite areas are probably due to the incomplete removal of the flowed layer by the etching solution.

Fig 4 was taken with the objective aperture in the electron microscope. The grain boundary is very regular and is about 0.5 microns wide.

Fig 5 shows the intersection of the three grains of ferrite. In each case the boundary is large and the impurities are clearly shown. The width of the grain boundaries is about 0.4 to 0.6 microns. The same size boundary exists in Fig 7, but the shadow cast was parallel to the grain boundary. This produced a loss of details within the shadows.

Fig 7 shows the structure of the ferrite (top) which is rough and projecting. The lower grain which is

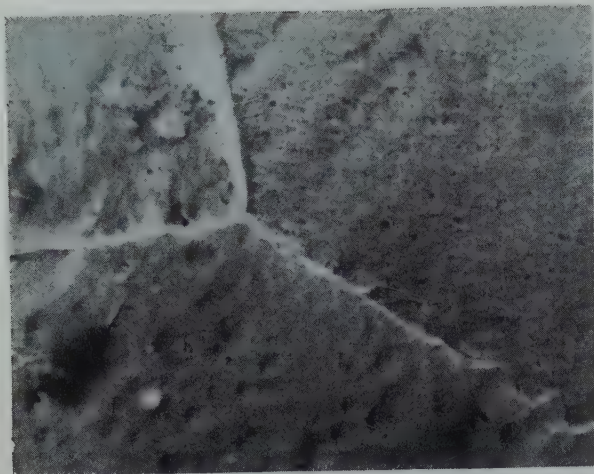


FIG 12—Ingot iron good. Mag. 18,500 \times .
Reduced approximately one-fourth in reproduction.

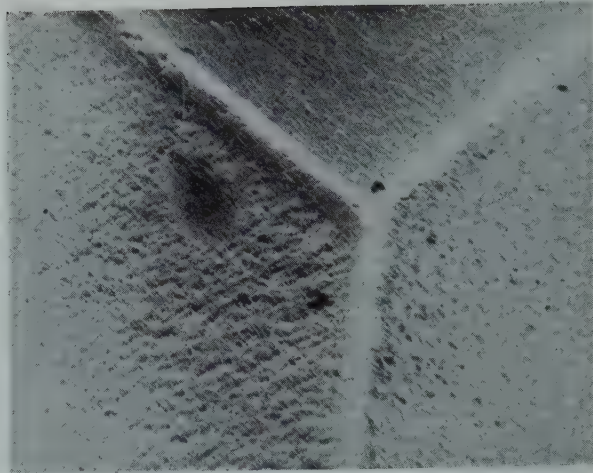


FIG 13—Ingot iron cured. Mag. 18,500 \times .
Reduced approximately one-fourth in reproduction.

oriented differently is smooth, with particles of manganese producing shadows. The grain boundaries of Fig 7 and 8 show the impurities, and the average width of the grain boundaries is about 0.5 microns.

GOOD IRON

Fig 9, 10, and 11 show the grain boundaries as narrow areas in comparison to the brittle ingot iron. The width of the grain boundaries is about 0.08 microns. However, in Fig 12 the grain boundary is wide and contains some impurities. Due to the printing process, the details within the grain boundary are missing.

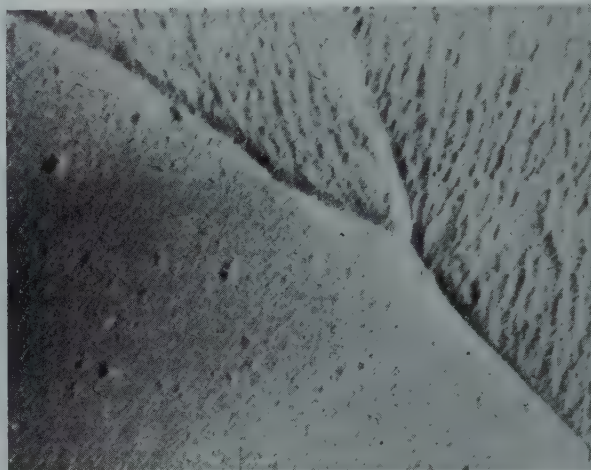


FIG 14—Ingot iron cured. Mag. 18,500 \times .
Reduced approximately one-fourth in reproduction.

CURED IRON

Fig 13 and 14 show the condition of the grain boundaries after the hydrogen anneal. The most noticeable fact is that the impurities have been completely removed. The grain boundaries show the grains meeting each other very tightly. The white grain boundary effect seen in Fig 13 and 14 is due also to the printing process which prohibits the fine details from being reproduced.

Fig 5 and 13 show the striking comparison of the grain boundary conditions of the brittle and the annealed ingot iron specimens.

Conclusions

From the electron microscope examination of the various pieces of ingot iron which were brittle, good, and cured, it is evident that the cause of the embrittlement may be due to the segregation of impurities at the grain boundaries. This embrittling material

is probably in the form of various oxides.

In the brittle state, the grain boundaries have been broadened by the impurities which have segregated at the grain boundaries. From observation of all the plates, it has been concluded that the metal as a whole becomes brittle if the width of the grain boundaries is 0.4 microns or greater. The grain boundaries of the brittle ingot iron fall in such a range.

The good piece of ingot iron has an appreciable amount of impurities at its boundaries, but the distribution is such that the grain boundaries are not excessively large. The grain boundaries average from about 0.08 microns to 0.2 microns. It is believed that with an additional oxidizing period the good ingot iron would have gathered more impurities at the boundaries and become brittle.

The hydrogen anneal has caused the grain boundaries to give up the im-

purities and the bond between grains reestablished itself. There were no evidences of impurities within the grain boundaries of the cured iron. The ferrite grains were a great deal smoother and contained less inclusions than were found in the brittle and good ingot iron.

The electron microscope has proven that an actual study of the grain boundary size in various metals can shed light on many problems against which metallurgists have come. In the study of this problem, the electron microscope has shown that the grain boundaries may hold the answers to many properties of polycrystalline metal.

References

1. John F. Radavich: Electron Metallography. Thesis Submitted For The Degree of Master of Science in Metallurgical Engineering. (1948).
2. V. J. Shaefer and D. Harker: Surface Replicas for Use in the Electron Microscope. *Jnl. Appl. Phys.* (1942) 13, 427-433.

Transformation of Gamma to Alpha Manganese

E. V. POTTER,* H. C. LUKENS,* and R. W. HUBER,† Junior Member AIME

For a number of years, it has been known that manganese made by electro-deposition under certain conditions is ductile while under other conditions it is very brittle. The ductile metal is gamma manganese normally stable only between 1100 and 1138°C¹; the brittle metal is alpha manganese, stable up to 727°C. The ductile metal is not stable, but gradually changes to the brittle form; the time required to complete the transformation is about 20 days at room temperature. Other observations have indicated that the transformation is completed in 10 to 15 min. at about 125°C, while at -10°C, no appreciable change occurs in 9 months.

The properties of gamma and alpha manganese in the pure state are ordinarily difficult to determine because the gamma structure cannot be retained by normal quenching procedures and alpha manganese is so brittle, it is difficult to obtain specimens free from flaws. In a recent investigation² some properties of gamma and alpha manganese were determined by studying the ductile electrolytic metal and determining the changes in its properties as it transformed to the brittle alpha form. These investigations provided an excellent opportunity for following the progress of the transition and studying its mechanism. The results of a series of such investigations are reported in this paper.

Procedure

Various properties of manganese were determined starting with the metal in the original ductile gamma form and following the subsequent changes in its properties as the metal transformed to the brittle alpha form. These observations were made at various temperatures, the data providing information regarding the mechanism of the transformation as well as

the effect of temperature on the transition rate. Structure and resistivity values gave the most significant results, so this paper is concerned primarily with them.

The structure was studied microscopically as well as by X ray diffraction. The resistivity was determined on strips of the metal by measuring the potential drop across a given length of the specimen. Current was passed through the specimen by wires soldered to its ends, and the potential connections were made by wires looped around the specimen near its center. The current was determined by the potential drop across a standard resistor connected in series with the specimen, the potential drop being measured on a potentiometer.

In the temperature range from room temperature to 100°C an ordinary drying oven was used to heat the specimen. This was entirely satisfactory except at 100°C, where the time required to heat the specimen was long compared to the transition time, making the initial section of the resistivity curve unsatisfactory. To overcome this limitation, at 100°C and higher a thermostatically controlled oil bath was used to heat the specimens. The block on which the specimen was mounted was plunged into the hot oil at the start of each test. The

heating time was thereby reduced from 5 min. to about 6 sec, and dependable resistivity values could be obtained through 160°C. At this point the whole transition, including the warm-up time for the specimen, required only about 20 sec and it was not considered worth while trying to extend the temperature range further.

Aside from the heating problem, the problem of making a sufficient number of accurate resistivity determinations became more and more difficult as the temperature was raised. Using the manually operated potentiometer, 100°C was about as far as it was possible to go. At this temperature and above, a self-balancing photoelectric recording potentiometer was used. Its response was quite rapid, and it proved to be entirely satisfactory all the way through 160°C, where the tests were stopped because of the specimen heating problem rather than any limitation of the potentiometer recorder.

The metal used in these tests was prepared at the Salt Lake City laboratory of the Bureau of Mines. The method of preparation is discussed in a paper by Schlain and Prater.³ The sheets were about 2 $\frac{3}{8}$ by 5 $\frac{3}{16}$ in. and varied from 10 to 16 mils in thickness. They could be cut readily into pieces suitable for the various tests. X ray and microstructure determinations were made on pieces about $\frac{1}{8}$ to $\frac{1}{4}$ in. wide and about 1 in. long, while resistivity measurements were made on strips as long as possible and about $\frac{1}{2}$ in. wide. The thickness of each sheet was not uniform over all its surface. This had no bearing on the X ray and microstructure determinations, but sections as nearly uniform and free from flaws as possible were chosen for the resistivity determinations.

The gamma manganese was electro-deposited at 30°C, the time of deposition ranging from 5 to 12 hr for each sheet. Whenever possible, the tests were started directly after the metal was stripped from the cathode; otherwise the sheet was placed immediately

Cleveland Meeting, October 1949.
TP 2583 E. Discussion of this paper (2 copies) may be sent to *Transactions AIME* before December 1, 1949. Manuscript received February 17, 1949; revision received February 28, 1949.

Papers by authors on the U.S. Bureau of Mines Staff are not subject to copyright.

* Physicists, Salt Lake City Branch, Metallurgical Division, Bureau of Mines, Salt Lake City, Utah.

† Metallurgist (Physical), Salt Lake City Branch, Metallurgical Division, Bureau of Mines, Salt Lake City, Utah.

¹ References are at the end of the paper.

in an electric refrigerator and stored at about -10°C until needed. In no case was there any appreciable difference in the behavior of the fresh and stored metal.

Results

X RAY AND MICROSTRUCTURES

Microscopic examinations of the specimens were unsatisfactory. In no case could the individual grains be identified or the different phases be distinguished. The grains are apparently too small to be studied by this method. The X ray diffraction patterns gave good results, however. In each case the pattern changed from that for gamma manganese to that for alpha manganese, the relative intensities of the two patterns changing as the transition progressed. No attempt was made to determine quantitatively the relative amounts of the two phases. It is significant, however, that no beta manganese was found at any time. Since this is the intermediate phase between alpha and gamma manganese, it might be expected that the beta phase would be an intermediate step in the transformation. Either this is not the case and gamma manganese transforms directly to alpha manganese, or any beta manganese formed transforms so rapidly to alpha manganese that the amount of beta manganese present at any time is very small.

Resistivity

Resistivity measurements were made during the progress of the transformation from gamma to alpha manganese at temperatures ranging from 20 to 160°C . The results are given in Tables 1 to 11. Examination of these data shows the change in resistivity to be slow at first, increasing as the transition progresses and again slowing as the transition nears completion. This is shown clearly in Fig 1, which shows the variation of resistivity with time at 25°C . This S-shaped curve is typical of all the resistivity data as well as the hardness and density data and is apparently characteristic of this type of transition. The effect of temperature on the transition rate is shown in Table 12, where the time required for the transition to be about half completed is given for various temperatures. The time ranges from 455 hr at 20°C to about 8 sec at 160°C , decreasing

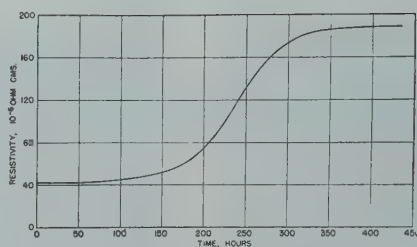


FIG 1—Variation of resistivity with time at 25°C .

ing by a factor of about 2 for each 10°C rise in temperature.

Transformation Theory

Data such as those given in Tables 1 to 11 provide an excellent means for studying the transition of gamma manganese and determining the transition-rate constants, but before this can be done it is necessary to develop a theory for the mechanism of the transformation which will satisfactorily explain the observed behavior. Let us assume that the resistivity at any time is given by the expression

$$R = \alpha R_{\alpha} + \gamma R_{\gamma} \quad [1]$$

where R is the measured resistivity, R_{α} and R_{γ} are the resistivities of alpha and gamma manganese, respectively, and α and γ are the fractions of alpha and gamma manganese present at any time. It is assumed, based on X ray observations, that no beta manganese is present. Then, since $\alpha + \gamma = 1$, the amount of alpha and gamma present at any time is given by the relations:

$$\alpha = \frac{R - R_{\gamma}}{R_{\alpha} - R_{\gamma}} \quad [2]$$

and

$$\gamma = \frac{R_{\alpha} - R}{R_{\alpha} - R_{\gamma}} \quad [3]$$

From Eq 2 and 3 we see that

$$\frac{d\alpha}{dt} = \frac{1}{R_{\alpha} - R_{\gamma}} \frac{dR}{dt} \quad [4]$$

and

$$\frac{d\gamma}{dt} = \frac{-1}{R_{\alpha} - R_{\gamma}} \frac{dR}{dt} \quad [5]$$

or that the rate of change of the amounts of alpha and gamma manganese with respect to time is directly proportional to the rate of change of resistivity. Thus, with only a change in vertical scale, resistivity curves such as Fig 1 also represent the variation of the amount of alpha and gamma manganese with respect to time.

From Fig 1, based on the above discussion, we see that the rate of

Table 1 . . . Variation of Resistivity with Time at 20°C

| Time, Hr | Resistivity, 10^{-6} ohm-cm | Time, Hr | Resistivity, 10^{-6} ohm-cm |
|----------|-------------------------------|----------|-------------------------------|
| 0 | 44.9 | 474.3 | 144.3 |
| 26 | 45.0 | 505 | 159.7 |
| 44.5 | 45.4 | 522.8 | 166.6 |
| 75.8 | 46.0 | 545.8 | 174.1 |
| 138.5 | 47.0 | 569.8 | 181.9 |
| 163 | 48.2 | 597 | 188.0 |
| 209.5 | 51.5 | 618 | 192.6 |
| 239 | 54.8 | 642 | 198.2 |
| 260 | 58.3 | 666.8 | 202.1 |
| 282 | 63.6 | 690.3 | 204.6 |
| 306 | 71.8 | 713.8 | 206.2 |
| 330 | 79.2 | 739.5 | 207.7 |
| 355.8 | 87.3 | 767.8 | 209.6 |
| 379.3 | 93.5 | 786.5 | 210.5 |
| 403.5 | 103.5 | 815.5 | 211.9 |
| 427.8 | 114.4 | 858 | 212.5 |
| 451.3 | 126.09 | 979.5 | 213.8 |

Table 2 . . . Variation of Resistivity with Time at 25°C

| Time, Hr | Resistivity, 10^{-6} ohm-cm | Time, Hr | Resistivity, 10^{-6} ohm-cm |
|----------|-------------------------------|----------|-------------------------------|
| 0 | 42.8 | 240 | 119.3 |
| 16.8 | 43.1 | 256.5 | 137.4 |
| 23.8 | 42.4 | 263.3 | 144.1 |
| 40.5 | 42.5 | 304.5 | 176.5 |
| 47.5 | 43.0 | 312.3 | 179.4 |
| 64.3 | 43.1 | 332 | 183.9 |
| 71.5 | 42.5 | 336 | 184.2 |
| 88.3 | 42.8 | 353 | 186.3 |
| 95.5 | 44.6 | 357.7 | 186.8 |
| 136.3 | 49.1 | 376.3 | 187.5 |
| 144.0 | 50.3 | 400 | 189.0 |
| 160.5 | 53.9 | 408.3 | 188.6 |
| 167.3 | 56.2 | 424 | 187.8 |
| 184 | 63.7 | 431.8 | 188.8 |
| 192 | 68.7 | 472.3 | 189.5 |
| 208.3 | 83.4 | 480 | 189.2 |
| 216 | 92.0 | 496.3 | 189.8 |
| 232 | 109.3 | | |

Table 3 . . . Variation of Resistivity with Time at 40°C

| Time, Hr | Resistivity, 10^{-6} ohm-cm | Time, Hr | Resistivity, 10^{-6} ohm-cm |
|----------|-------------------------------|----------|-------------------------------|
| 0 | 44.4 | 46.67 | 106.5 |
| 0.17 | 44.6 | 48.0 | 112.6 |
| 0.67 | 45 | 49.5 | 118.8 |
| 1.67 | 44.1 | 51 | 126.1 |
| 3.0 | 45.5 | 52.5 | 132.7 |
| 5.0 | 45.5 | 54 | 140.3 |
| 7.0 | 45.8 | 55 | 145.6 |
| 9.0 | 46.1 | 56 | 151.0 |
| 11.0 | 45.8 | 59.16 | 166.5 |
| 13.0 | 46.6 | 65 | 192.6 |
| 15.0 | 47.7 | 66.5 | 198.2 |
| 16.0 | 47.7 | 69 | 206.0 |
| 19.0 | 49.0 | 71 | 211.1 |
| 23.0 | 52.3 | 73 | 214.8 |
| 25.0 | 54.2 | 75 | 217.8 |
| 27.0 | 55.9 | 78 | 220.5 |
| 30.0 | 60.4 | 80 | 221.8 |
| 34.0 | 67.1 | 91 | 224.3 |
| 36.0 | 72.4 | 94.5 | 224.7 |
| 38.0 | 76.9 | 99.0 | 224.9 |
| 43.0 | 92.3 | 115 | 225.4 |
| 44.75 | 98.9 | | |

formation of alpha manganese is slow at first, gradually increasing to a maximum near the point where half of the gamma manganese has transformed and again decreasing as the amount of untransformed gamma manganese decreases toward zero. The slow rate of formation of alpha manganese at the start, accelerating as the transition progresses, can be explained as follows: In its initial state the metal consists of atoms arranged in the form of a face-centered tetragonal structure characteristic of gamma manganese, each

unit cell consisting of 4 atoms. Alpha manganese, however, has a body-centered cubic structure consisting of 58 atoms to the unit cell. Before the transition can start, it is necessary that enough atoms arrange themselves in the form characteristic of alpha manganese, so that a particle of alpha manganese can form. This will occur as a result of the random motion of the atoms in the metal, the probability of enough atoms becoming arranged in the proper grouping being less for alpha manganese, however, than it would be for a more simple structure. Alpha manganese has a higher density than gamma manganese, so once a particle of alpha manganese has formed, it will try to occupy a smaller volume than the original gamma manganese, and owing to interatomic forces, the alpha manganese particle and the surrounding gamma manganese will be under stress. Alpha manganese is the lower energy form, but particles of alpha manganese below a critical size will be unstable and reconvert to gamma manganese. Particles large enough for the decrease in volume energy to exceed the increase in surface and strain energy will be stable however, and form nuclei about which more alpha manganese can form. The rate of formation of alpha manganese about any nucleus will depend on the size of the nucleus and will increase as the particle grows, new alpha manganese being formed at an accelerating rate around each nucleus. New particles of alpha manganese will also be forming throughout the body of the metal, and each of these will grow, the rate of formation of alpha manganese accelerating as the transformation progresses.

The acceleration in growth of an individual particle will continue only so long as the alpha manganese particle is completely surrounded by gamma manganese. Ultimately a point will be reached where two or more alpha manganese particles will touch each other. Their active surface is then decreased and the acceleration in growth is less. This will occur at more and more points in the specimen as the transition progresses, until a point is reached where the rate of formation of alpha manganese is a maximum and must then decrease, necessarily becoming zero when there is no more gamma manganese. Thus, curves of the general shape shown in Fig 1 can be explained on the basis of the variation with time of the interface between two

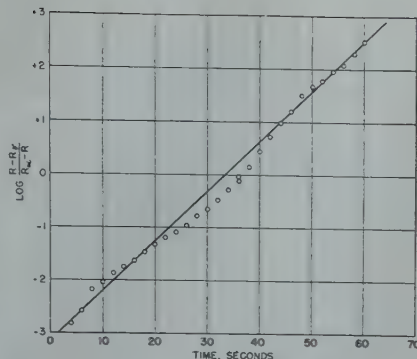


FIG 2—Log $(R - R_\gamma)/(R_\alpha - R)$ vs. time at 140°C.

phases, the interface necessarily being zero at the beginning and end of the transition and a maximum somewhere in between.

When the particles of alpha manganese are completely surrounded by gamma manganese, the rate of formation of the alpha manganese will be proportional to the volume of the gamma manganese under stress. This volume will be the product of the interface area times an effective depth of penetration of the stress into the surrounding gamma manganese. It is reasonable to suppose that this depth of penetration will be proportional to the size of the alpha-manganese particle. Then, the effective volume of the gamma manganese under stress will be proportional to the volume of the alpha-manganese particle, or

$\frac{d\alpha}{dt} = K_1\alpha$. This expression is incomplete, however, as it does not provide

for a decrease in $\frac{d\alpha}{dt}$ as the alpha-manganese particles grow together and the interface area decreases. This factor cannot be accounted for in an exact manner, but the desired effect can be obtained by multiplying by gamma, as in the following equation:

$$\frac{d\alpha}{dt} = K_1\alpha\gamma \quad [6]$$

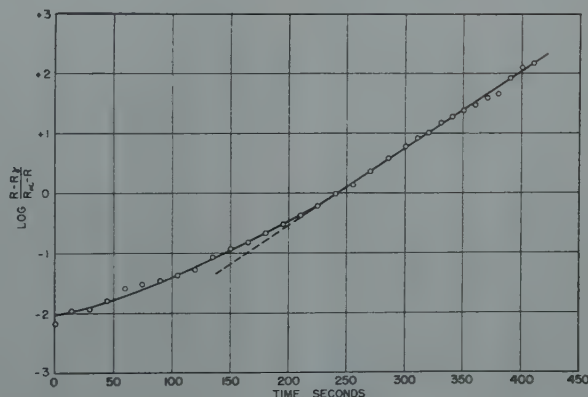


FIG 3—Log $(R - R_\gamma)/(R_\alpha - R)$ vs. time at 115°C.

Table 4 . . . Variation of Resistivity with Time at 58°C

| Time, Min. | Resistivity, 10^{-6} ohm-cm | Time, Min. | Resistivity, 10^{-6} ohm-cm |
|------------|-------------------------------|------------|-------------------------------|
| 10 | 44.1 | 502 | 93.9 |
| 25 | 45.5 | 517 | 99.1 |
| 40 | 46.3 | 532 | 103.0 |
| 55 | 46.5 | 562 | 116.2 |
| 77 | 46.2 | 592 | 129.2 |
| 100 | 47.0 | 624 | 144.9 |
| 115 | 47.0 | 657 | 159.5 |
| 130 | 46.7 | 725 | 189.5 |
| 170 | 48.0 | 779 | 202.7 |
| 240 | 50.3 | 804 | 205.8 |
| 290 | 53.9 | 826 | 207.7 |
| 325 | 57.0 | 854 | 209.8 |
| 345 | 59.4 | 889 | 210.6 |
| 374 | 62.7 | 914 | 211.1 |
| 423 | 71.2 | 950 | 211.6 |
| 445 | 76.9 | 1002 | 212.0 |
| 475 | 84.5 | 1198 | 212.6 |
| 487 | 88.1 | 1306 | 212.9 |

Table 5 . . . Variation of Resistivity with Time at 80°C

| Time, Min. | Resistivity, 10^{-6} ohm-cm | Time, Min. | Resistivity, 10^{-6} ohm-cm |
|------------|-------------------------------|------------|-------------------------------|
| 0 | 37.3 | 78 | 93.2 |
| 2 | 40.0 | 80 | 99.2 |
| 4 | 40.9 | 82 | 106.2 |
| 6 | 41.6 | 84 | 113.2 |
| 10 | 42.8 | 86 | 121.2 |
| 15 | 43.5 | 88 | 131.0 |
| 19 | 43.9 | 89 | 135.5 |
| 27 | 44.8 | 91 | 145.4 |
| 33 | 45.7 | 92 | 151.4 |
| 39 | 47.5 | 93 | 154.9 |
| 43 | 49.1 | 94 | 157.9 |
| 48 | 52.1 | 96 | 161.7 |
| 52 | 55.3 | 98 | 165.9 |
| 55 | 58.1 | 100 | 169.7 |
| 59 | 61.8 | 102 | 173.5 |
| 65 | 69.7 | 105 | 178.6 |
| 67 | 73.3 | 107 | 180.4 |
| 70 | 77.3 | 109 | 182.1 |
| 72 | 80.8 | 112 | 183.2 |
| 74 | 84.5 | 117 | 184.5 |
| 76 | 88.9 | 123 | 185.2 |

Table 6 . . . Variation of Resistivity with Time at 100°C

| Time, Min. | Resistivity, 10^{-6} ohm-cm | Time, Min. | Resistivity, 10^{-6} ohm-cm |
|------------|-------------------------------|------------|-------------------------------|
| 0 | 56.6 | 13 | 91.4 |
| 1 | 56.7 | 14 | 105.5 |
| 2 | 56.8 | 15 | 119.2 |
| 3 | 57.5 | 16 | 134.1 |
| 4 | 57.8 | 17 | 146.8 |
| 5 | 58.5 | 18 | 158.6 |
| 6 | 59.5 | 19 | 167.3 |
| 7 | 61.1 | 20 | 173.3 |
| 8 | 63.7 | 21 | 176.9 |
| 9 | 65.3 | 22 | 178.8 |
| 10 | 69.3 | 23 | 180.2 |
| 11 | 75.3 | 23.5 | 180.6 |
| 12 | 82.9 | | |

Table 7 . . . Variation of Resistivity with Time at 115°C

| Time, Sec. | Resistivity, 10 ⁻⁶ ohm-cm | Time, Sec. | Resistivity, 10 ⁻⁶ ohm-cm |
|------------|--------------------------------------|------------|--------------------------------------|
| 0 | 64.3 | 240 | 125.2 |
| 15 | 64.9 | 255 | 135.9 |
| 30 | 65.0 | 270 | 152.0 |
| 45 | 65.5 | 285 | 162.8 |
| 60 | 66.6 | 300 | 171.2 |
| 75 | 67.1 | 310 | 175.3 |
| 90 | 67.7 | 320 | 178.9 |
| 105 | 68.8 | 330 | 181.4 |
| 120 | 69.9 | 340 | 183.5 |
| 135 | 73.6 | 350 | 184.9 |
| 150 | 76.3 | 360 | 185.9 |
| 165 | 80.1 | 370 | 186.7 |
| 180 | 85.5 | 380 | 187.3 |
| 195 | 92.0 | 390 | 188.5 |
| 210 | 100.5 | 400 | 189.0 |
| 225 | 110.7 | 410 | 189.2 |

Table 8 . . . Variation of Resistivity with Time at 130°C

| Time, Sec. | Resistivity, 10 ⁻⁶ ohm-cm | Time, Sec. | Resistivity, 10 ⁻⁶ ohm-cm |
|------------|--------------------------------------|------------|--------------------------------------|
| 0 | 67.6 | 75 | 120.4 |
| 6 | 68.3 | 78 | 128.5 |
| 12 | 68.6 | 81 | 136.9 |
| 18 | 69.1 | 84 | 147.3 |
| 24 | 69.7 | 87 | 155.9 |
| 30 | 70.7 | 90 | 162.6 |
| 33 | 71.5 | 93 | 167.8 |
| 36 | 72.7 | 96 | 172.1 |
| 39 | 73.9 | 99 | 174.8 |
| 42 | 75.2 | 102 | 177.5 |
| 45 | 76.0 | 105 | 179.0 |
| 48 | 77.6 | 108 | 180.5 |
| 51 | 79.7 | 111 | 181.4 |
| 54 | 82.0 | 114 | 182.1 |
| 57 | 84.7 | 117 | 182.7 |
| 60 | 89.2 | 120 | 183.0 |
| 63 | 93.9 | 123 | 183.4 |
| 66 | 98.6 | 126 | 184.0 |
| 69 | 105.4 | 129 | 184.1 |
| 72 | 112.3 | | |

Table 9 . . . Variation of Resistivity with Time at 140°C

| Time, Sec. | Resistivity, 10 ⁻⁶ ohm-cm | Time, Sec. | Resistivity, 10 ⁻⁶ ohm-cm |
|------------|--------------------------------------|------------|--------------------------------------|
| 0 | 74.8 | 32 | 103.7 |
| 2 | 75.4 | 34 | 113.9 |
| 4 | 75.7 | 36 | 127.3 |
| 6 | 75.8 | 38 | 143.2 |
| 8 | 76.3 | 40 | 158.7 |
| 10 | 76.5 | 42 | 170.4 |
| 12 | 77.0 | 44 | 177.7 |
| 14 | 77.5 | 46 | 181.4 |
| 16 | 78.1 | 48 | 184.7 |
| 18 | 79.3 | 50 | 185.8 |
| 20 | 80.6 | 52 | 186.2 |
| 22 | 82.3 | 54 | 186.8 |
| 24 | 83.9 | 56 | 187.1 |
| 26 | 86.5 | 58 | 187.5 |
| 28 | 91.1 | 60 | 187.7 |
| 30 | 96.0 | 62 | 187.9 |

Thus, in the early stages of the transition, when gamma is nearly 1, Eq 6 says that $\frac{d\alpha}{dt} = K_1\alpha$ as was reasoned above. However, as alpha increases, gamma decreases, and $\frac{d\alpha}{dt}$ increases until alpha equals gamma or the transition is half complete. After this the decrease in gamma causes $\frac{d\alpha}{dt}$ to decrease, approaching zero as the transition nears completion. Introducing gamma into the equation may not be strictly correct, but it does have the

desired effects of reducing the rate of formation of alpha manganese as the particles grow and their surfaces meet and of reducing the rate to zero at the end of the transformation.

From Eq 6 by integration we get

$$\ln \frac{\alpha}{1-\alpha} = \ln \frac{\alpha}{\gamma} = K_1 t + C$$

and from Eq 2 and 3

$$\ln \frac{R - R_\gamma}{R_\alpha - R} = K_1 t + C_1 \quad [7]$$

This equation indicates that, if the above theory is correct, values of

$\ln \frac{R - R_\gamma}{R_\alpha - R}$ when plotted against t

should follow a straight line. Using values of R from Tables 1 to 11,

values of $\log \frac{R - R_\gamma}{R_\alpha - R}$ were calculated

and plotted against time. Logarithms to the base 10 were used instead of natural logarithms for convenience. Typical curves are shown in Fig 2 and 3. In every case, by proper choice of R_α and R_γ , curves such as Fig 2 can be obtained and represented by a straight line if the deviations shown are not considered serious or significant. On the other hand, curves such as shown in Fig 3 can also be obtained in which the upper portion of the curve fits a straight line very well, whereas the lower portion deviates more and more toward zero time. Considering the accuracy with which the resistivities can be determined and the closeness to which the points fit a smooth curve, curves such as Fig 2 were not considered satisfactory fits and an attempt was made to modify Eq 6 so as to obtain a fit throughout the whole transition comparable in that shown in Fig 3 for the upper part of the curve.

From Fig 3, it can be seen that the slope of the actual curve, $\log \frac{R - R_\gamma}{R_\alpha - R}$ versus time, is less during the first half of the transformation than that of the straight line determined by the upper half of the curve. The deviation of the actual values of $\log \frac{R - R_\gamma}{R_\alpha - R}$ from a projected straight line fitting the upper half of the curve is very nearly proportional to $\frac{1}{\alpha}$. Therefore, by subtracting a term $\frac{K_2}{\alpha}$ from

Table 10 . . . Variation of Resistivity with Time at 150°C

| Time, Sec. | Resistivity, 10 ⁻⁶ ohm-cm | Time, Sec. | Resistivity, 10 ⁻⁶ ohm-cm |
|------------|--------------------------------------|------------|--------------------------------------|
| 0 | 77.7 | 19 | 127.6 |
| 4 | 78.3 | 20 | 141.6 |
| 7 | 79.0 | 21 | 153.1 |
| 9 | 80.4 | 22 | 161.1 |
| 10 | 81.2 | 23 | 167.2 |
| 11 | 82.5 | 24 | 172.5 |
| 12 | 83.8 | 25 | 176.1 |
| 13 | 85.8 | 26 | 178.2 |
| 14 | 88.5 | 27 | 179.4 |
| 15 | 91.9 | 28 | 180.1 |
| 16 | 96.0 | 29 | 180.8 |
| 17 | 103.4 | 32 | 181.0 |
| 18 | 114.1 | 34 | 181.6 |

Table 11 . . . Variation of Resistivity with Time at 160°C

| Time, Sec. | Resistivity, 10 ⁻⁶ ohm-cm | Time, Sec. | Resistivity, 10 ⁻⁶ ohm-cm |
|------------|--------------------------------------|------------|--------------------------------------|
| 0 | 83.2 | 7 | 111.9 |
| 1 | 84.5 | 8 | 144.3 |
| 2 | 85.1 | 9 | 176.8 |
| 3 | 86.9 | 10 | 187.4 |
| 4 | 88.2 | 11 | 188.3 |
| 5 | 91.9 | 12 | 188.9 |
| 6 | 97.0 | 13 | 189.6 |

$\log \frac{R - R_\gamma}{R_\alpha - R}$, it should be possible to obtain points following a straight line throughout the whole transition. Eq 7 thus becomes

$$\ln \frac{\alpha}{\gamma} - \frac{K_2}{\alpha} = K_1 t + C$$

or

$$\ln \frac{R - R_\gamma}{R_\alpha - R} - K_2 \frac{R_\alpha - R_\gamma}{R - R_\gamma} = K_1 t + C \quad [8]$$

The data shown in Fig 2 were recalculated on this basis and are shown in Fig 4. It can be seen that, by proper choice of R_α , R_γ , and K_2 , the data fit a straight line very well from practically zero time to completion of the transition. The deviation at zero time cannot be considered serious, as it is uncertain just when the specimen has become uniformly heated, and readings before this are unreliable.

Eq 8 seems to be a satisfactory representation of the experimental data, and from it, by differentiation, we get the relation,

$$\frac{d\alpha}{dt} = K_1 \alpha \gamma \frac{\alpha}{\alpha + K_2 \gamma} \quad [9]$$

Comparing this equation with Eq 6, we see that a new factor, $\frac{\alpha}{\alpha + K_2 \gamma}$ has been introduced. When alpha is small compared to $K_2 \gamma$ this factor equals $\frac{\alpha}{K_2}$ and approaches zero as alpha ap-

Table 12 . . . Time Required for the Transition to be Half Completed

| Temperature, °C | Time | Temperature, °C | Time |
|-----------------|------|-----------------|------|
| 20 | Hr | 115 | Sec |
| 25 | 455 | 130 | 240 |
| 40 | 238 | 77 | 77 |
| | 53 | 140 | 36.5 |
| | Min. | 150 | 19.3 |
| 58 | 590 | 160 | 7.7 |
| 80 | 83 | | |
| 100 | 15 | | |

Table 13 . . . Values of Constants in Eq 8 for Various Temperatures

| Temp. °C | R _α micro-ohm-cm | R _γ micro-ohm-cm | K ₂ | K ₁ (based on time in min.) |
|----------|-----------------------------|-----------------------------|----------------|--|
| 20 | 241.1 | 43.8 | 0 | 0.0001962 |
| 25 | 189.8 | 42.6 | 0 | 0.0005475 |
| 40 | | | 0.34 | 0.002843 |
| 58 | 212.6 | 37.5 | 0.123 | 0.01543 |
| 80 | 185.8 | 33.3 | 0.220 | 0.1481 |
| 100 | 182.3 | 52.4 | 0.0501 | 0.5305 |
| 115 | 190 | 62 | 0.0279 | 1.832 |
| 130 | 184.2 | 66 | 0.0317 | 6.368 |
| 140 | 187.6 | 73.1 | 0.0582 | 17.77 |
| 150 | 181.6 | 76.37 | 0.0252 | 28.55 |
| 160 | 190 | 83 | 0.0767 | 101.8 |

proaches zero, making $\frac{d\alpha}{dt}$ smaller during this part of the transition. The factor $\frac{\alpha}{\alpha + K_2\gamma}$ increases as alpha increases, becoming $\frac{1}{2}$ when alpha equals $K_2\gamma$, and is equal to 1 when alpha is large compared to $K_2\gamma$. In the latter case Eq 9 is equivalent to Eq 6, and represents the upper part of the curve in Fig 3. This equation was obtained empirically and has no obvious physical interpretation. Its exact form cannot be considered too significant. A number of equations could be obtained which might represent the experimental data as well. One of these is

$$\frac{d\alpha}{dt} = K_1\alpha\gamma(1 - e^{-\frac{\alpha}{K_2\gamma}}) \quad [10]$$

In this case, the factor $(1 - e^{-\frac{\alpha}{K_2\gamma}})$ is equal to $\frac{\alpha}{K_2}$ as alpha approaches zero, increases to 0.632 when $\alpha = K_2\gamma$, and becomes 1 when alpha is large compared to $K_2\gamma$. This is almost exactly the way the factor $\frac{\alpha}{\alpha + K_2\gamma}$ in Eq 9 varies with alpha. Again, however, this factor has no obvious physical significance, and in addition Eq 10 cannot readily be integrated and the constants cannot readily be evaluated from the experimental data. The important thing to be noted is not the exact form of the modifying factor but rather the manner

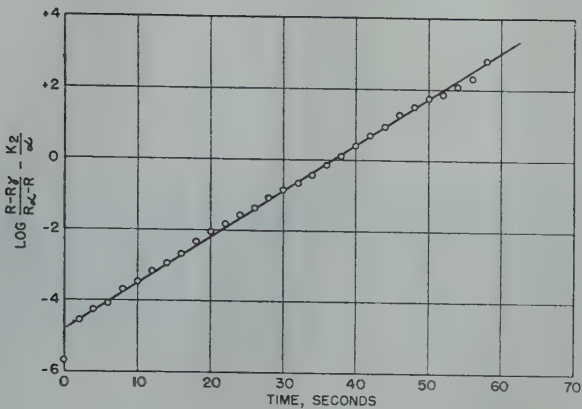


FIG 4—Log (R - R_γ)/(R_α - R) - K₂ $\frac{R_{\alpha} - R_{\gamma}}{R - R_{\gamma}}$ vs. time at 140°C.

in which it affects the value of $\frac{d\alpha}{dt}$ as alpha varies.

The physical nature of the factors retarding the transformation in the initial stages is not known. It is probably due to the greater tendency for small alpha-manganese particles to revert to gamma manganese than for the larger ones. This would slow the net formation rate of alpha manganese at first. Formation of beta manganese might also be a factor, but it is hard to see how this could have a great effect, since more than a few percent of beta manganese could hardly be present without being detected and such small amounts could hardly affect the transition appreciably.

The transformation theory presented above is necessarily greatly simplified in order to facilitate mathematical treatment, and a number of factors influencing transformations in metals have not been considered. It is to be noted, however, that this simple theory fits the observed experimental data very well for the latter half of the transition and with a relatively simple modification can be made to fit throughout the whole transition. The data in Tables 1 through 11 are included for the benefit of those who might wish to reinterpret the data.

Transition Rates

Based on Eq 8, values of $\log \frac{R - R_{\gamma}}{R_{\alpha} - R} - \frac{K_2(R_{\alpha} - R_{\gamma})}{(R - R_{\gamma})}$ were plotted against t as in Fig 4 for all the data in Tables 1 to 11, inclusive, values of R_{α} , R_{γ} , and K_2 being chosen to give the best straight line. This is not difficult, since the best values of R_{α} and R_{γ} can be obtained very closely

from the original data and R_{γ} is not influenced at all by K_2 . R_{α} and K_2 are somewhat interdependent but not seriously so, since R_{α} can be approximated very closely from the original resistivity data. The values R_{α} , R_{γ} , K_1 , and K_2 thus obtained are given in Table 13.

The values of R_{α} and R_{γ} are quite interesting. With only two exceptions, the values of R_{α} fall between 180 and 190 micro-ohm-cm. R_{γ} varies considerably but the values up to 58°C indicate an average value of 44 micro-ohm-cm. The variation of R_{α} with temperature is small, indicating a low temperature coefficient, while the variation of R_{γ} with temperature indicates a high temperature coefficient in the order of $60 \text{ to } 80 \times 10^{-4}$. Obviously these values are not accurate but they compare very well with observations reported in another paper.²

To see how the transition rate constants (K_1 in Table 13) vary with temperature, these data were treated according to the equation

$$K_1 = \frac{kT}{h} e^{-\frac{\Delta F^{\ddagger}}{RT}} \quad [11]$$

given by Glasstone, Laidler, and Eyring⁴, where K_2 is the specific reaction-rate constant, T is the absolute temperature, ΔF^{\ddagger} is the free energy of activation, and R , K , and h are constants. From this relation,

$$\text{Log } \frac{K_1}{T} = \text{Log } \frac{k}{h} - \frac{1}{2.3026} \frac{\Delta F^{\ddagger}}{R} \frac{1}{T}$$

Values of $\text{Log } \left(\frac{K_1}{T} \right)$ were calculated and plotted against $\frac{1}{T}$. These values are shown in Fig 5. The points follow rather closely to a straight line, the greatest deviation being shown by the 160°C point. Considering the rapidity of the transition at this temperature

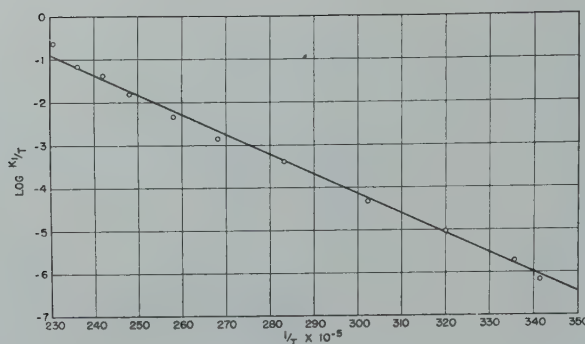


FIG 5—Log (R_1/T) vs. $1/T$.

and the time required to heat the specimen, this value may be considerably in error and its deviation is not necessarily significant. As a whole, the points fit a straight line satisfactorily, and from the slope of this line the free energy of activation was calculated to be 21,200 cal per mol.

Summary and Conclusions

The change in structure and resistivity of electrolytic manganese as it transformed from ductile gamma to brittle alpha manganese was determined. The values were found to follow a typical S curve when plotted against time. The rate of change was small at first, increased to a maximum as the transition was about one-half complete, and then decreased as the transition neared completion.

Resistivity determinations proved to be the most satisfactory way to follow the transition, and studies were made at temperatures from 20 to 160°C. It was found that the transformation curve during the latter half of the transformation could be represented by

an equation based on the theory that the rate of formation of alpha manganese was determined by the amount of interface between the alpha and gamma manganese or

$$\frac{d\alpha}{dt} = K_1\alpha\gamma$$

The observed rate of formation of alpha manganese at the beginning of the transition was smaller than this theory predicted, however, and a modification of this equation

$$\frac{d\alpha}{dt} = K_1\alpha\gamma \frac{\alpha}{\alpha + K_2\gamma}$$

was found to represent the data quite well throughout the whole transition. The physical significance of this additional factor is not obvious. Apparently there are some factors operating in the initial stages of the transformation which retard the formation of alpha manganese but become less active as the amount of alpha manganese increases and are negligible during the latter half of the transition. This effect probably arises from a tendency on the part of the alpha manganese to revert to gamma manganese when the alpha-

manganese particles are small, this tendency becoming less and less as the alpha-manganese particles grow in size.

References

1. E. V. Potter and H. C. Lukens: Hydrogen Content of Electrolytic Manganese and Transition Points in Electrolytic Manganese. AIME *Metals Tech.*, Sept. 1946.
2. E. V. Potter, H. C. Lukens, and R. W. Huber: Some Properties of Gamma and Alpha Manganese and the Effect of Hydrogen and Lattice Expansion on Them. To be Published.
3. David Schlain and John D. Prater: Electrodeposition of Gamma Manganese. *Jnl. Electrochem. Soc.*, Aug. 1948, **94**, 58.
4. Glasstone, Laidler, and Eyring: The Theory of Rate Processes. McGraw-Hill Book Co., (1941) 195.
5. H. Eyring: *Jnl. Chem. Phys.* (1935) **3**, 107.
6. K. K. Kelley, B. F. Naylor, and C. H. Shomate: The Thermodynamic Properties of Manganese. Bur. of Mines (1946) Tech. Paper 686.
7. E. V. Potter and R. W. Huber: The Effect of Hydrogen on X-ray Parameters and Structure of Electrolytic Manganese. *Phys. Rev.*, **68**, 1 and 2, July 1945, p. 24.

CORRECTION MAY ISSUE

Discussion of "The Room and Elevated Temperature Properties of Some Sand Cast Magnesium-base Alloys Containing Zinc." On page 329, column 1, line 8, of May 1949 *Journal of Metals Transactions*, discussor should be N. S. SPENCE.

Liquid Solubility of Manganese in a Magnesium-aluminum-tin Alloy[†]

B. J. NELSON,* Junior Member, and G. F. SAGER,* Associate Member AIME

Magnesium alloy forgings offer higher and more uniform mechanical properties than heat treated magnesium alloy castings and are used principally for light weight parts that may be stressed in fatigue or subject to impact loads, or where space limitations do not permit the use of the necessarily bulkier magnesium alloy castings.

Compositions and Properties of Magnesium Forging Alloys

The nominal compositions and properties of the principal commercial magnesium forging alloys are given in Table 1.

The two that are most commonly used are AMC58S and AM65S. The former has the highest strength and is, therefore, employed for heavy duty applications. However, the forging of this alloy and of AMC57S ordinarily requires the use of slow speed hydraulic presses.

The forging alloy AM65S combines good, although somewhat lower, mechanical properties with excellent forging characteristics. This alloy can be forged on hammers, upsetters, rolls, and mechanical presses, as well as on hydraulic presses. These characteristics make it particularly useful for many applications.

Manganese Segregation in AM65S

The alloy AM65S contains 5 pct tin, 3½ pct aluminum, and a small amount of manganese, the manganese being added to insure satisfactory resistance to corrosion. Some manganese segregation was occasionally encountered in this alloy. In many applications, such

Table 1 . . . Magnesium Forging Alloys

| A. M. C. Alloy | A. S. T. M. Alloy | Nominal Composition (Pct) | | | | Typical Properties | | |
|----------------|-------------------|---------------------------|-----|----|------|--------------------|-----------|---------------------|
| | | Al | Zn | Sn | Mn | T.S. psi | Y.S.* psi | Elong. Pct in 2 in. |
| AMC57S† | AZ61X | 6.5 | 1 | | 0.2 | 42000 | 26000 | 10 |
| AMC58S† | AZ80X | 8.5 | 0.5 | | 0.2 | 45000 | 30000 | 7 |
| AMC58S-T5† | AZ80X | 8.5 | 0.5 | | 0.2 | 50000 | 34000 | 6 |
| AM65S | TA54 | 3.5 | | 5 | 0.2‡ | 40000 | 28000 | 12 |

* Yield strength is the stress at which the material exhibits a permanent set of 0.2 pct.

† Wrought alloys with the letter "C" in their designation are of controlled high purity, iron and nickel being held to less than 0.005 pct each. The same nominal compositions without guaranteed iron and nickel limits but with identical mechanical properties are available as AM57S, AM58S and AM58S-T5. The "-T5" temper is obtained by artificial aging after forging.

‡ When this investigation was started, the nominal manganese content of AM65S was 0.5 pct.

segregation is of no particular consequence, but when forgings are acid dipped prior to the application of various chemical coatings, the segregated particles of manganese constituent may stand in relief. The resultant surface roughening may impair appearance and is undesirable in forgings employed in the textile industry, where very smooth surfaces are essential to avoid the catching and breaking of fine threads. An effort was therefore made to determine the cause of manganese segregation in this alloy and find a method for its elimination.

Radiographic examination of a series of cast ingot sections and extruded samples of the AM65S type having manganese contents ranging from zero to about 0.7 pct revealed no appreciable manganese segregation when the manganese was less than about 0.4 pct. A

small amount was observed with a manganese content of 0.46 pct and considerable with manganese contents of 0.6 pct or higher.

Attempts to eliminate the manganese segregation by variations in the melting and casting conditions were unsuccessful and it soon became apparent that the trouble was attributable to the fact that the manganese contents that caused segregation were in excess of the amounts that would remain in solution at temperatures encountered in the melting and/or casting operations prior to the complete solidification of the ingots.

A knowledge of the amounts of manganese that would be soluble in molten alloys of the AM65S type at various temperatures was obviously desirable. The liquid solubilities of manganese in binary Mg-Mn alloys and in Mg-Al-Mn and Mg-Zn-Mn alloys have been determined by Tiner and others,* but no data on the solubility of manganese in molten magnesium alloys containing tin and aluminum are given in the literature. For this reason, an investigation to determine the solubility of manganese in a magnesium alloy containing 5 pct tin and 3.5 pct aluminum (AM65S type) was undertaken.

* Tiner: *Trans. AIME* (1945) 161, 351.

Cleveland Meeting, October 1949.

TP 2602 E. Discussion of this paper (2 copies) may be sent to *Transactions AIME* before December 1, 1949. Manuscript received October 29, 1948.

* Aluminum Research Laboratories, Aluminum Co. of America, New Kensington, Pa.

† Except for the variations in manganese content, this alloy corresponds to the American Magnesium Corporation Alloy AM65S or A.S.T.M. alloy TA54.

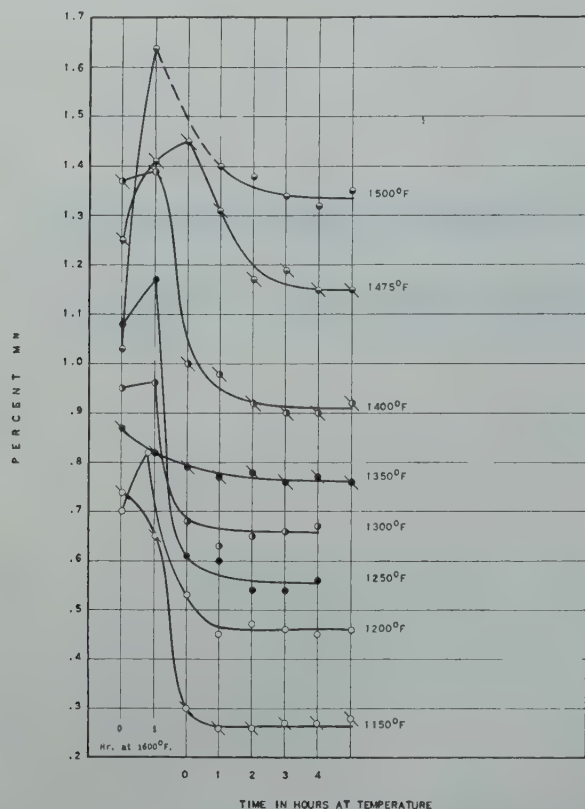


FIG 1—Manganese contents of molten AM65S as a function of holding time.

Liquid Solubility Determinations

The settling procedure was selected as the most suitable method for determining the solubility of manganese in alloys of the type under consideration. Briefly, this method involved saturating the alloy with manganese at a temperature substantially above that at which the solubility was to be determined, then cooling the melt to the latter temperature and holding it at that temperature for a substantial period of time. Samples for analysis were carefully ladled from the upper portion of the melt at hourly intervals during the aforementioned holding period. After the ladling of each sample, the melt was stirred to redistribute some of the manganese that had already settled, because it appeared that when the latter particles of manganese again settled, they aided in carrying down more of the manganese and thus hastened the attainment of equilibrium.

The melts were prepared and held in a No. 8 Tercod crucible holding approximately 4 lb of metal. The manganese was added either in the form of a prealloyed ingot (Dow M) containing about 1.5 pct manganese or by the use of a flux (Dow 250) containing man-

ganese chloride. In calculating the flux additions, it was assumed that the manganese introduced would be equal to 22 pct of the total weight of the flux. Temperatures were measured with an iron-constantan thermocouple enclosed in a seamless steel tube, the lower end of which was welded shut. This protection tube also served as a stirring rod. The samples ladled from the upper portions of the melts at the various intervals were analyzed for tin, aluminum, manganese, and iron. Table 3 shows the complete analyses for manganese, tin, aluminum and iron, together with the limiting solubilities of manganese used in drawing the solubility curve.

These manganese contents are plotted as a function of the holding time in Fig 1. It will be noted that the curves become nearly horizontal when the longer holding periods are reached, indicating that the manganese contents are approaching the equilibrium values for the various holding temperatures.

The solubility of manganese so determined at various temperatures is plotted in Fig 2. In general, the points fall on a fairly smooth curve and indicate that the solubility of manganese increases from about 0.45 pct at 1200°F to approximately 1.32 pct at 1500°F.

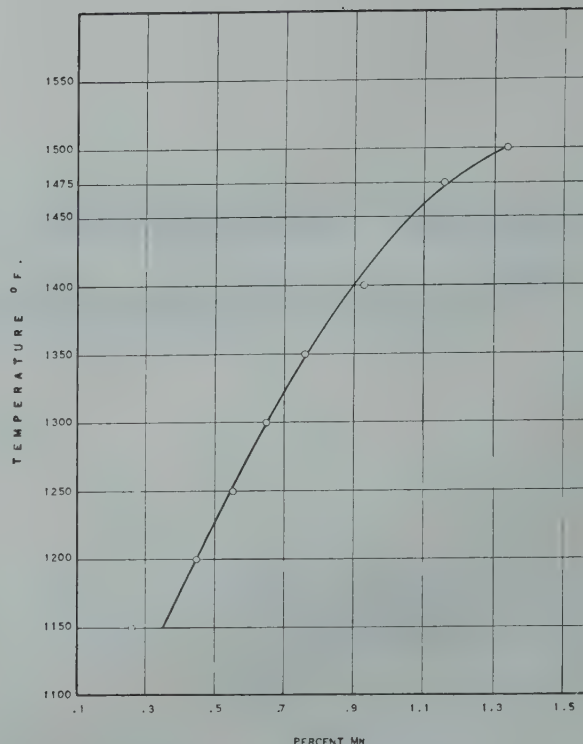


FIG 2—Solubility of manganese in molten AM65S.

The value for the lowest temperature (1150°F) is somewhat lower than that which would be predicted from an extrapolation of the main portion of the curve to this temperature. One possible explanation of this deviation would be the existence of a "quaternary peritectic" at a temperature between 1150 and 1200°F.

Considerable difficulty was encountered in obtaining consistent equilibrium values for the manganese solubility at temperatures near 1400°F. It was suspected that the trouble might be attributable to small variations in the aluminum contents of the alloys. In order to check this hypothesis, settling tests were conducted on alloys containing several slightly different amounts of aluminum. The results of these tests are shown in Fig 3. These results indicate that the solubility of manganese in alloys of the type under discussion decreases markedly and almost linearly with increasing aluminum contents.

While the above effect of aluminum on the solubility of manganese might be due merely to the decrease in the solubility of one element with increasing concentrations of a second solute, it was suspected that a compound containing both aluminum and manganese might be precipitating. This would, of course, result in a concentration of aluminum as well as man-

Table 2 . . . Effect of Manganese Content on the Tensile Properties of AM65S Type Extruded and Forged Samples*

| S No. | Pct Mn | Extruded† | | | Press Forged‡ | | | Hammer Forged‡ | | |
|-------|--------|-----------|------------|------------------|---------------|------------|------------------|----------------|------------|------------------|
| | | T.S. psi | Y.S. § psi | El. Pct In 2 in. | T.S. psi | Y.S. § psi | El. Pct In 2 in. | T.S. psi | Y.S. § psi | El. Pct In 2 in. |
| 88434 | 0.00 | 36700 | 26700 | 15.0 | 48200 | 37100 | 7.0 | 34800 | 16900 | 15.7 |
| 88435 | 0.17 | 43500 | 33500 | 15.2 | 49400 | 42400 | 11.8 | 39400 | 26300 | 19.5 |
| 88436 | 0.26 | 45100 | 36900 | 14.7 | 49100 | 42800 | 11.8 | 40300 | 27100 | 18.7 |
| 88437 | 0.37 | 44900 | 33900 | 14.0 | 48900 | 43300 | 8.8 | 40900 | 28200 | 17.8 |
| 88438 | 0.46 | 45300 | 32800 | 14.0 | 49500 | 43500 | 11.5 | 39600 | 26600 | 16.8 |
| 88439 | 0.66 | 45200 | 31600 | 14.0 | 47800 | 37500 | 10.7 | 38700 | 25600 | 15.8 |

* All values are averages for 3 specimens.
† Tests made on standard 1/2 in. diam A.S.T.M. tensile specimens machined from 3/4 in. diam rod.
‡ Specimens of the 3/4 in. diam rod were forged down to strips 3/16 in. thick. Standard A.S.T.M. sheet-type tensile specimens were machined from these strips. Both surfaces of the specimens were machined to eliminate surface imperfections.
§ 0.2 pct set.

ganese at the bottom of the melts. In order to check this point, an AM65S melt containing 1.2 pct manganese was prepared in a tapered graphite crucible. After heating to a temperature of 1550°F, the melt was cooled and held for 3 hr at a temperature of 1350°F. In order to avoid complications that might be introduced if iron dissolved from the thermocouple protection tube, temperatures were measured by a thermocouple wired to the outside of the crucible. At the end of the three-hour holding period, the crucible was removed from the furnace and cooled by a fine spray of water directed on the bottom until freezing was complete. Fig 4 shows the macrostructure of a section of the solidified melt adjoining the bottom of the crucible. The concentration of manganese constituent at the bottom is plainly evident. Analyses of the bottom zone and the main portion of the melt gave the following results:

| Location | Per Cent | | | |
|--------------------|----------|------|------|-------|
| | Al | Sn | Mn | Fe |
| Main portion . . . | 3.17 | 4.82 | 0.50 | 0.001 |
| Bottom | 5.83 | 4.99 | 4.62 | 0.10 |

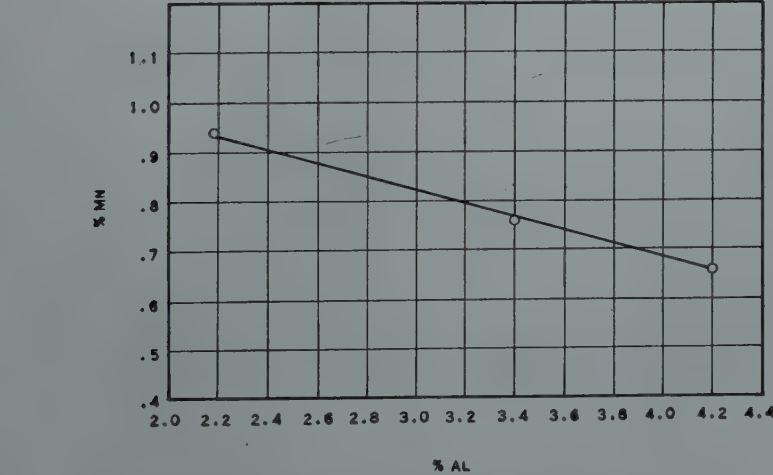


FIG 3—Effect of aluminum content on solubility of manganese in alloys of the AM65S type at 1350°C.

It will be noted that the amounts of aluminum, manganese, and iron in the bottom zone are substantially greater than those in the main portion of the melt.

Effect of Manganese on Tensile Properties and Resistance to Corrosion

It is obvious that manganese is likely to precipitate and segregate in AM65S melts if the manganese contents of these melts exceed the values indicated in Fig 3 for temperatures corresponding to those involved in the melting and casting of such melts. This naturally raises a question regarding the possible effect on mechanical properties and resistance to corrosion of decreasing the manganese to a value at which precipitation and segregation of that element are not encountered.

Tensile tests conducted on as-extruded, press forged and hammer forged samples of AM65S type alloys having various manganese contents ranging from zero to 0.66 pct gave the results shown in Table 2. The manganese content of the alloy can be

Table 3 . . . Summary of Analytical Data Used in Obtaining the Limiting Solubility of Manganese in Molten AM65S

| Setting Temp. <i>T</i> S ₂ No. Analytical No. Time, Etc. | 1150°F 93531 1-84745 | | | | 1200°F 93509 1-84745 | | | | 1250°F 94065 1-85983 | | | | 1300°F 94384 1-86581 | | | | 1350°F 93507 1-84745 | | | | 1400°F 95542 1-89009 | | | | 1475°F 94841 1-87612 | | | | 1500°F 94470 1-86817 | | | | |
|--|----------------------------|-------|------|------|----------------------------|-------|------|------|----------------------------|-------|------|------|----------------------------|-------|------|------|----------------------------|-------|------|------|----------------------------|-------|------|------|----------------------------|-------|------|------|----------------------------|-------|------|------|--|
| | % Mn | % Fe | % Al | % Sn | % Mn | % Fe | % Al | % Sn | % Mn | % Fe | % Al | % Sn | % Mn | % Fe | % Al | % Sn | % Mn | % Fe | % Al | % Sn | % Mn | % Fe | % Al | % Sn | % Mn | % Fe | % Al | % Sn | % Mn | % Fe | % Al | % Sn | |
| 0 hr./1600°F | 0.74 | 0.011 | 3.65 | 5.22 | 0.70 | 0.005 | 2.30 | 3.35 | 1.08 | 0.025 | 3.64 | 5.15 | 0.95 | 0.017 | 3.58 | 4.98 | 0.87 | 0.004 | 1.75 | 2.57 | 1.37 | 0.04 | 3.51 | 5.14 | 1.39 | 0.016 | 3.44 | 5.14 | 1.25 | 0.005 | 3.65 | 5.18 | |
| 1 hr./1600°F | 0.65 | 0.018 | 3.57 | 5.27 | 0.82 | 0.015 | 3.57 | 4.96 | 1.17 | 0.006 | 3.56 | 5.25 | 0.79 | 0.020 | 3.54 | 5.13 | 0.82 | 0.019 | 3.68 | 2.12 | 1.39 | 0.06 | 3.44 | 5.14 | 1.41 | 0.01 | 3.72 | 5.14 | 1.41 | 0.01 | 3.72 | 5.25 | |
| 0 hr./T | 0.30 | 0.001 | 3.26 | 5.20 | 0.53 | 0.001 | 3.31 | 5.07 | 0.67 | 0.001 | 3.20 | 5.26 | 0.69 | 0.002 | 3.53 | 5.13 | 0.79 | 0.008 | 3.58 | 2.16 | 1.00 | 0.02 | 3.33 | 5.16 | 1.00 | 0.02 | 3.33 | 5.16 | 1.00 | 0.02 | 3.33 | 5.23 | |
| 1 hr./T | 0.26 | 0.001 | 3.25 | 5.24 | 0.45 | 0.001 | 3.35 | 5.11 | 0.60 | 0.001 | 3.24 | 5.25 | 0.68 | 0.002 | 3.48 | 5.20 | 0.77 | 0.008 | 3.56 | 2.16 | 0.98 | 0.002 | 3.23 | 5.22 | 0.98 | 0.002 | 3.23 | 5.22 | 0.98 | 0.002 | 3.23 | 5.33 | |
| 2 hr./T | 0.26 | 0.001 | 3.18 | 5.20 | 0.47 | 0.001 | 3.46 | 5.11 | 0.54 | 0.002 | 3.20 | 5.26 | 0.68 | 0.003 | 3.49 | 5.28 | 0.78 | 0.008 | 3.49 | 2.52 | 0.92 | 0.002 | 3.20 | 5.18 | 0.92 | 0.002 | 3.20 | 5.18 | 0.92 | 0.002 | 3.20 | 5.33 | |
| 3 hr./T | 0.27 | 0.001 | 3.12 | 5.24 | 0.40 | 0.001 | 3.43 | 5.11 | 0.54 | 0.001 | 3.18 | 5.26 | 0.68 | 0.003 | 3.52 | 5.28 | 0.78 | 0.007 | 3.46 | 2.52 | 0.90 | 0.002 | 3.20 | 5.24 | 0.90 | 0.002 | 3.20 | 5.24 | 0.90 | 0.002 | 3.20 | 5.41 | |
| 4 hr./T | 0.27 | 0.002 | 3.17 | 5.29 | 0.45 | 0.001 | 3.36 | 5.03 | 0.56 | 0.002 | 3.19 | 5.30 | 0.67 | 0.006 | 3.48 | 5.25 | 0.77 | 0.006 | 3.46 | 2.50 | 0.90 | 0.004 | 3.14 | 5.29 | 0.90 | 0.004 | 3.14 | 5.29 | 0.90 | 0.004 | 3.14 | 5.37 | |
| 5 hr./T | 0.28 | 0.001 | 3.15 | 5.22 | 0.46 | 0.001 | 3.32 | 5.07 | 0.46(3) | 0.001 | 3.15 | 5.32 | — | — | — | — | 0.76 | 0.006 | 3.49 | 2.50 | 0.92 | 0.003 | 3.10 | 5.24 | 0.92 | 0.003 | 3.10 | 5.24 | 0.92 | 0.003 | 3.10 | 5.37 | |
| Limiting Solubility at <i>T</i> . | 0.27 | | | | 0.45 | | | 0.55 | | | | | 0.65 | | | | 0.76 | | | | 0.92 | | | 1.16 | | | | | | | 1.33 | | |



FIG 4—Macrostructure of section of solidified melt adjoining bottom of crucible.
Original mag. 10 \times . Etch 2 pct nital.

reduced to approximately 0.2 pct without impairing tensile properties. However, complete elimination of the manganese causes substantial reductions in the tensile and yield strengths.

Accelerated and atmospheric corrosion tests conducted on extruded samples of AM65S type alloys having various manganese contents showed that the manganese content could be lowered to about 0.2 pct without impairing resistance to corrosion. However, the complete elimination of the manganese impaired this characteristic to a significant extent.

Conclusions

1. The solubility of manganese in

molten AM65S alloy increases with temperature from a value of about 0.45 pct at 1200°F to 1.32 pct at 1500°F.

2. The manganese solubility at a given temperature decreases markedly with increasing aluminum content.

3. Manganese segregation in the alloy can be controlled by maintaining the manganese content below the amount soluble at the lowest temperatures encountered in the melting and casting of the alloys.

4. The manganese content can be lowered to a sufficient extent to avoid appreciable segregation without impairing tensile properties or resistance to corrosion, but the complete elimina-

tion of the manganese would adversely affect both the strength and the resistance to corrosion.

Acknowledgment

The authors express their appreciation to the Aluminum Company of America for permission to publish this work. They also express their appreciation of the constructive guidance and advice of Dr. Wm. L. Fink, under whose supervision the investigation was carried out and to Mr. Richard Patz, who assisted in the preparation and sampling of a number of the melts.

The Comparative Creep Properties of Several Types of Commercial Coppers

A. D. SCHWOPE,* Junior Member, K. F. SMITH,* and L. R. JACKSON,† Member AIME

Burghoff and Blank¹ have pointed out that the creep properties of hard-drawn coppers are closely associated with their individual softening characteristics and have further shown that the creep resistance of various types of copper is improved, under certain circumstances, by cold stretching.

In the design of certain types of electrical machinery, it is important to have the creep resistance as high as possible; furthermore, short-time creep strength is important since in many cases stresses are large only during warming-up and cooling-down periods.

In this paper, data are presented showing the effect of cold work on the short time creep strengths of various types of commercial copper under several conditions. It is shown that trends from short-time creep tests are evident at longer times.

Materials Used in the Investigation

The coppers used in this investigation were commercial grade and of two basic types, oxygen free high conductivity (OFHC) and tough pitch. Additions of silver in amounts of 15 and 25 oz per ton were added to each of the two coppers. The analyses of these six coppers are given in Table 1. Originally, they started as wire bars 4 × 4 × 54 in.

A square rod was made by hot rolling the wire bars to 1/16-in. rod in 8 passes. This rod was then cold drawn to 0.445-in.-diam rod and annealed for 3 1/2 hr at 1000°F. It was then cold drawn to 0.325-in. rod and again annealed at 1000°F for 3 1/2 hr. Hard square rods were then made by cold rolling to 0.257 × 0.257-in. rod. Soft wire was made from the hard-

Table 1 . . . Analyses of Types of Copper Used in Investigation
(Per Cent by Weight)

| Material | Tough Pitch | Tough Pitch + 15 oz Silver per Ton | Tough Pitch + 25 oz Silver per Ton | OFHC | OFHC + 15 oz Silver per Ton | OFHC + 25 oz Silver per Ton |
|---------------|-------------|------------------------------------|------------------------------------|---------|-----------------------------|-----------------------------|
| Sb | 0.0004 | 0.0015 | 0.0018 | 0.0010 | 0.0008 | 0.0012 |
| As | 0.0004 | 0.0007 | 0.0006 | 0.0004 | 0.0002 | 0.0004 |
| Bi | None | <0.0001 | None | None | 0.0001 | 0.0001 |
| Fe | 0.0005 | 0.0021 | 0.0005 | 0.0007 | 0.0010 | 0.0007 |
| Pb | 0.0006 | 0.0005 | 0.0008 | 0.0002 | 0.0005 | 0.0003 |
| Ni | 0.0018 | <0.0011 | | 0.0011 | 0.0008 | <0.0008 |
| O | 0.031 | 0.03 | 0.060 | None | None | None |
| Se | 0.0004 | <0.0002 | 0.0002 | 0.0001 | 0.0003 | <0.0004 |
| Ag | 0.0019 | 0.063 | 0.072 | 0.0011 | 0.0537 | 0.0755 |
| S | 0.0013 | 0.0020 | 0.0015 | 0.0011 | 0.0014 | 0.0017 |
| Te | None | <0.0002 | 0.0004 | None | None | <0.0006 |
| Sn | 0.0002 | <0.0005 | | None | 0.0001 | <0.0001 |
| Cu (by diff.) | 99.9615 | >99.8981 | 99.8622 | 99.9943 | 99.9411 | >99.9182 |

drawn material by annealing at 650°F for 3 hr.

The final rolling was performed using a set of 9-in. grooved rolls revolving at 30 rpm, which produced square wires. Reductions of approximately 5, 20, 30, and 40 pct were obtained using several passes in the same direction for the large reductions.

The 5 pct reduction by drawing was accomplished using a steel die having 2 parallel bearing surfaces. The die angle was 7 1/2 degrees and the wires were lubricated with a paste of ceresin wax dissolved in carbon tetrachloride. The speed of drawing was 13 fpm. Since work was done on only two sides of the wire simultaneously, it was necessary to rotate it 90 degrees each pass to insure uniform deformation.

The room-temperature tensile properties of the various tempers are given in Table 2. The grain size of the an-

nealed 0.257-in. wires was uniform and averaged about 0.035–0.045 mm.

Experimental Procedures for Short-time Creep Tests

Standard creep-test frames (Fig 1) were used for the testing. Special fixtures were designed to apply axial compressive and tensile loads to the copper wires. The compression specimens were 1 in. long and the ends were ground flat and parallel. The creep in compression was indicated by the movement of reference marks scratched on intersliding platinum strips attached to the moving heads of the fixture. The movement was measured with an optical micrometer fitted with a filar eyepiece on which the smallest division was 0.00005 in.

The tensile creep specimens were 4 in. long which provided ample gripping surface for the jaw-type grips. The platinum strips were attached to a one-inch gauge length of the wire and the creep measured as previously described.

The single-specimen furnaces were connected to individual power and control sources. The controlling equipment consisted of Foxboro controllers

Cleveland Meeting, October 1949
TP 2605 E Discussion of this paper (2 copies) may be sent to *Transactions AIME* before December 1, 1949. Manuscript received January 3, 1949.
* Research Engineers, Battelle Memorial Institute.
† Supervisor, Battelle Memorial Institute.
1 References are at the end of the paper.

specially fitted with anticipating thermocouples which controlled the temperature to less than 3°F of the control setting which was 572°F (300°C). Two thermocouples were mounted on each specimen, one to the controller and the other to the recorder and potentiometer for measuring the temperature.

The specimen was mounted in its fixture and placed inside the furnace and assembled in the test frame. The furnace was brought up to temperature, with a zero load on the specimens, in approximately 30 min. A no-load reading was taken and the load applied by means of dead weights on the lever arm. Readings were taken thereafter at suitable intervals and the test continued until a secondary or minimum creep rate was well established. The tests averaged twenty-four hours in duration.

Discussion of Results

The results of these tests are summarized in Table 3, which lists the creep stress, initial deformation, total creep, minimum creep rate and the total time of test. The initial deformation is seen to vary only slightly among the various coppers for similar degrees of cold work. Total creep is defined as the total strain minus the initial strain. The initiation of the third or rapid stage of creep is indicated in the table, with its approximate time.

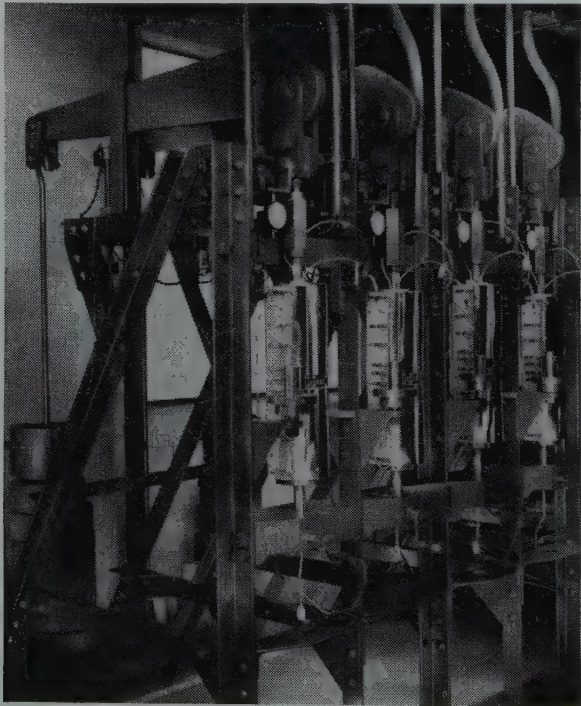


FIG 1—Creep-test Frames.

Table 2 . . . Room-temperature Tensile Properties of Wires

| Material | Temper, Pct Cold Reduction | Yield Strength, psi* | Tensile Strength, psi | Elongation, Pct in 10 in. |
|--------------------------------|----------------------------|----------------------|-----------------------|---------------------------|
| Tough pitch | Drawn 5 | 17,500 | 33,400 | 34 |
| | Rolled 5 | 17,500 | 33,500 | 33 |
| | Rolled 20 | 43,400 | 45,700 | 3.5 |
| | Rolled 30 | 46,500 | 47,200 | 3.0 |
| Tough pitch + 15 oz Ag per ton | Rolled 40 | 49,000 | 50,200 | 2.5 |
| | Rolled 5 | 24,000 | 36,300 | 33 |
| | Rolled 20 | 44,000 | 45,300 | 3.5 |
| | Rolled 30 | 47,500 | 48,800 | 3.0 |
| Tough pitch + 25 oz Ag per ton | Rolled 40 | 49,500 | 50,700 | 2.5 |
| | Drawn 5 | 18,600 | 35,700 | 34 |
| | Rolled 5 | 19,300 | 35,900 | 34 |
| | Rolled 20 | 43,400 | 45,600 | 3.5 |
| OFHC | Rolled 30 | 47,600 | 48,800 | 3.0 |
| | Rolled 40 | 51,000 | 52,000 | 2.5 |
| | Drawn 5 | 14,700 | 32,800 | 36 |
| | Rolled 5 | 15,000 | 33,000 | 35 |
| OFHC + 15 oz Ag per ton | 20 | 43,000 | 44,600 | 5.0 |
| | 30 | 45,800 | 46,900 | 4.0 |
| | 40 | 48,500 | 49,500 | 3.0 |
| | Rolled 5 | 15,500 | 33,100 | 36 |
| OFHC + 25 oz Ag per ton | Rolled 20 | 44,500 | 45,400 | 2.0 |
| | Rolled 30 | 45,500 | 46,700 | 3.0 |
| | Rolled 40 | 49,500 | 50,600 | 2.5 |
| | Drawn 5 | 14,600 | 33,000 | 35 |
| | Rolled 5 | 14,700 | 33,000 | 35 |
| | Rolled 20 | 43,000 | 45,300 | 5.5 |
| | Rolled 30 | 46,500 | 47,700 | 4.0 |
| | Rolled 40 | 49,300 | 50,600 | 3.0 |

* Stress at 0.2 pct offset from initial slope of stress-strain curve.

Typical of the types of curves obtained are those shown in Fig 2 comparing various degrees of cold work. Although the hardness and the strength properties of the wires increased as the per cent reduction by cold work increased, the creep rates are not so simply affected. It is normally supposed that as the strength properties increase, the creep properties, such as rate and total deformation, are benefited. This can be considered true only as long as some competing process does not set in. As was pointed out by Burghoff and Blank, recrystallization,

as manifested by softening, takes place when the strained metal is heated within a critical temperature range and the creep rate thereby increased. In a previous paper,² the relation between degree of cold work and the course of recrystallization for most of the coppers used in this investigation was described. It was pointed out that as the cold work increased, the temperature for softening decreased, or in isothermal annealing, the softening time decreased.

It is important, then, in analyzing creep data to keep in mind that recrystallization and creep are taking place simultaneously. Thus, in Fig 2 the curves for 5 pct cold-rolled OFHC copper appear to be normal, having progressed into the constant creep-rate stage. However, the wires rolled 20, 30, and 40 pct show decidedly different characteristics. It is evident that the beginning of the stage of rapid or acceleration creep occurs sooner as the creep stress and the degree of cold work increase.

Since softening is occurring simultaneously with creep, it is reasonable to expect the yield strength to decrease from the cold-worked value to that of soft material during testing. The majority of these creep tests were made using stresses higher than the yield strengths of the soft material so that at some time during the tests the yield stress must equal the applied creep stress. When this occurs, it is postulated that the third or final stage of creep should be initiated.

Utilizing the relations set forth in a previous paper,² the time for the yield strength to drop to the applied creep

Table 3 . . . Results of Short-time Creep Tests at 572°F (300°C)

| Material | Temper, Pct Cold Reduction | Stress, psi | Type of Test | Initial Exten- sion, Pct | Total Creep, Pct | Creep Rate, Pct per Hr | Total Time of Test, Min. |
|-----------------------------------|----------------------------------|----------------|-----------------|-----------------------------------|------------------------|---------------------------------|--------------------------------|
| OFHC | Rolled 5 | 8,000 | Comp. | 0.145 | 0.105 | 0.0032 | 1790 |
| OFHC | Rolled 5 | 10,800 | Comp. | 0.17 | 0.23 | 0.0074 | 1310 |
| OFHC | Rolled 5 | 15,000 | Comp. | 0.24 | 1.12 | 0.025 | 1460 |
| OFHC | Drawn 5 | 8,000 | Comp. | 0.145 | 0.120 | 0.0035 | 1580 |
| OFHC | Drawn 5 | 10,700 | Comp. | 0.155 | 0.19 | 0.0075 | 1150 |
| OFHC | Drawn 5 | 15,000 | Comp. | 0.170 | 1.10 | 0.034 | 1540 |
| OFHC | Rolled 5 | 7,500 | Tension | 0.16 | 0.06 | 0.0018 | 1500 |
| OFHC | Rolled 5 | 10,750 | Tension | 0.18 | 0.17 | 0.0040 | 1460 |
| OFHC | Rolled 5 | 12,500 | Tension | 0.20 | 0.26 | 0.0062 | 1490 |
| OFHC | Drawn 5 | 7,500 | Tension | 0.16 | 0.11 | 0.0026 | 1330 |
| OFHC | Drawn 5 | 10,000 | Tension | 0.18 | 0.15 | 0.0046 | 1390 |
| OFHC | Rolled 20 | 7,500 | Tension | 0.10 | 2.52 | | 1445 3rd stage, 440 min. |
| OFHC | Rolled 40 | 7,500 | Tension | 0.15 | 2.59 | | 195 3rd stage, 10 min. |
| OFHC | Rolled 30 | 12,500 | Tension | 0.23 | 8.71 | | 725 3rd stage, 50 min. |
| OFHC | Rolled 20 | 12,500 | Tension | 0.12 | 2.61 | | 1200 3rd stage, 390 min. |
| Tough pitch | Rolled 5 | 7,500 | Comp. | 0.19 | 0.54 | 0.0170 | 1590 |
| Tough pitch | Rolled 5 | 10,000 | Comp. | 0.205 | 1.26 | 0.0366 | 1465 3rd stage, 1200 min. |
| OFHC + 15 oz Ag per ton | Rolled 5 | 7,500 | Tension | 0.155 | 0.060 | 0.0014 | 1440 |
| | Rolled 5 | 12,500 | Tension | 0.180 | 0.16 | 0.0045 | 1440 |
| | Rolled 20 | 7,500 | Tension | 0.07 | 0.18 | 0.0052 | 1360 |
| | Rolled 20 | 12,500 | Tension | 0.16 | 0.29 | 0.010 | 1440 |
| | Rolled 30 | 7,500 | Tension | 0.06 | 0.14 | 0.0049 | 1375 |
| | Rolled 30 | 12,500 | Tension | 0.16 | 0.32 | 0.011 | 1355 |
| | Rolled 40 | 7,500 | Tension | 0.04 | 0.16 | 0.0052 | 1440 |
| | Rolled 40 | 12,500 | Tension | 0.17 | 0.31 | 0.0074 | 1440 |
| OFHC + 15 oz Ag per ton | Rolled 20 | 17,500 | Tension | 0.265 | 0.680 | 0.023 | 1430 |
| Tough pitch + 15 oz Ag per ton | Rolled 5 | 7,500 | Tension | 0.160 | 0.185 | 0.0063 | 1440 |
| | Rolled 5 | 12,500 | Tension | 0.175 | 0.580 | 0.0192 | 1440 |
| | Rolled 20 | 7,500 | Tension | 0.100 | 0.320 | 0.010 | 1395 |
| | Rolled 20 | 12,500 | Tension | 0.170 | 0.700 | 0.0246 | 1415 |
| | Rolled 20 | 17,500 | Tension | 0.295 | 0.765 | | 315 |
| | Rolled 30 | 7,500 | Tension | 0.105 | 0.265 | 0.0094 | 1370 |
| | Rolled 30 | 12,500 | Tension | 0.185 | 0.755 | 0.022 | 1380 |
| | Rolled 40 | 7,500 | Tension | 0.085 | 0.320 | 0.0125 | 1400 |
| | Rolled 40 | 12,500 | Tension | 0.175 | 0.795 | 0.0272 | 1400 |
| OFHC + 25 oz Ag per ton | Rolled 5 | 7,870 | Comp. | 0.15 | 0.16 | 0.0021 | 1505 |
| | Rolled 5 | 10,600 | Comp. | 0.18 | 0.18 | 0.0051 | 1455 |
| | Rolled 5 | 12,500 | Comp. | 0.20 | 0.36 | 0.0089 | 1540 |
| | Drawn 5 | 7,960 | Comp. | 0.16 | 0.18 | 0.0032 | 1430 |
| | Drawn 5 | 10,700 | Comp. | 0.19 | 0.23 | 0.0070 | 1490 |
| | Drawn 5 | 12,500 | Comp. | 0.20 | 0.47 | 0.0113 | 1550 |
| | Rolled 5 | 7,500 | Tension | 0.18 | 0.04 | 0.0010 | 1400 |
| | Rolled 5 | 10,000 | Tension | 0.20 | 0.05 | 0.0016 | 1415 |
| | Drawn 5 | 7,000 | Tension | 0.19 | 0.07 | 0.0012 | 1235 |
| | Drawn 5 | 10,000 | Tension | 0.20 | 0.09 | 0.0018 | 1425 |
| | Rolled 5 | 12,500 | Tension | 0.12 | 0.24 | 0.0079 | 1205 |
| Tough pitch + 25 oz Ag per ton | Rolled 5 | 7,500 | Comp. | 0.19 | 0.24 | 0.0054 | 1410 |
| | Rolled 5 | 10,000 | Comp. | 0.20 | 0.25 | 0.0078 | 1340 |
| | Drawn 5 | 7,500 | Comp. | 0.19 | 0.20 | 0.0060 | 1200 |
| | Drawn 5 | 10,000 | Comp. | 0.205 | 0.42 | 0.0102 | 1340 |
| Tough pitch + 25 oz Ag per ton | Rolled 5 | 7,500 | Tension | 0.19 | 0.16 | 0.0047 | 1240 |
| | Rolled 5 | 10,000 | Tension | 0.20 | 0.28 | 0.0078 | 1275 |
| | Drawn 5 | 7,500 | Tension | 0.19 | 0.21 | 0.0057 | 1400 |
| | Drawn 5 | 10,000 | Tension | 0.205 | 0.26 | 0.0096 | 1250 |
| | Rolled 20 | 12,500 | Tension | 0.19 | 0.885 | 0.030 | 1440 |
| | Rolled 40 | 12,500 | Tension | 0.170 | 0.880 | 0.031 | 1340 |

stress can be approximated. The detailed calculations are given in Appendix A. The arrows on the creep curves indicate these computed times. Fair agreement between calculated and actual points of inflection is observed. It is to be emphasized that this relation is an empirical approximation which enables the engineer to choose a suitable degree of cold work for a particular temperature application. This relation is most effective at low amounts of cold work where the yield strength has not been appreciably changed or at temperatures where it is little affected.

Tension vs. Compression Creep

The majority of the compression creep tests covered only small ranges of strain and only in the cases where

the third stage of creep set in, did local instability occur. Typical of the curves obtained are those shown in Fig 3. Tension and compression creep are compared in Fig 4 and 5.

It will be noted that the creep rate in compression is markedly higher than that for tension. In cold-drawn or cold-rolled materials, as were used here, this difference may be connected with the Bauschinger effect.

CREEP IN COLD-DRAWN VS. COLD-ROLLED MATERIALS

From Fig 4 and 5, it will be noted that in general, the cold-drawn material has a higher creep rate under comparable conditions than the cold-rolled material. This effect is probably connected with the manner in which the two methods of cold deformation distribute the cold deformation

throughout the cross-section of the material. Fig 6 shows the results of a Knoop hardness transverse through drawn, rolled, and annealed tough-pitch copper. It will be noted that while the drawn material is harder at the outside, the rolled material is harder at the center. The area under the hardness curve is about 5 pct greater for the cold-rolled material than for the cold-drawn. It will also be noted from Table 2 that the yield and tensile strengths are, in general, slightly higher for the rolled than for the drawn material. These two factors probably account for the differences in creep rate observed. The nonuniformity in strain hardening evident in Fig 6 for the 5 pct cold-worked wires persists in the wires rolled 40 pct.

EFFECT OF SILVER ON CREEP PROPERTIES

It is well known that silver added to copper increases the resistance to recrystallization. Likewise, it might be expected that it should have a similar effect on the creep properties of cold-worked material. Qualitatively, this is true, but quantitatively, the relation is not simple. Fig 7 shows the recrystallization curves of the various coppers. These results are based on the fractional change in yield strength of hard drawn (84.4 pct reduction in area) 0.081-in. wire, annealed for 1 hr at various temperatures. There is little difference among the silver-bearing coppers, as far as the recrystallization curves are concerned.

The effect of silver on the secondary creep rate is illustrated in Fig 8. It is evident that silver, while effective in reducing the creep rate of both tough-pitch and OFHC coppers, does not equalize the two types as it did in the softening properties. Although the effect of silver is comparatively small at low amounts of cold working, it is very active at greater cold reductions. Its effectiveness is manifested in the delaying of the third stage of creep.

Long-time Creep Tests

During the course of this investigation, long-time tensile creep tests (>1000 hr) were performed on commercially drawn (0.081 in.) wires of tough-pitch, OFHC, and OFHC plus 15 oz of silver per ton, coppers. Three commercial tempers were included in these tests; annealed, half hard (37.1 pct red. in area), and hard drawn

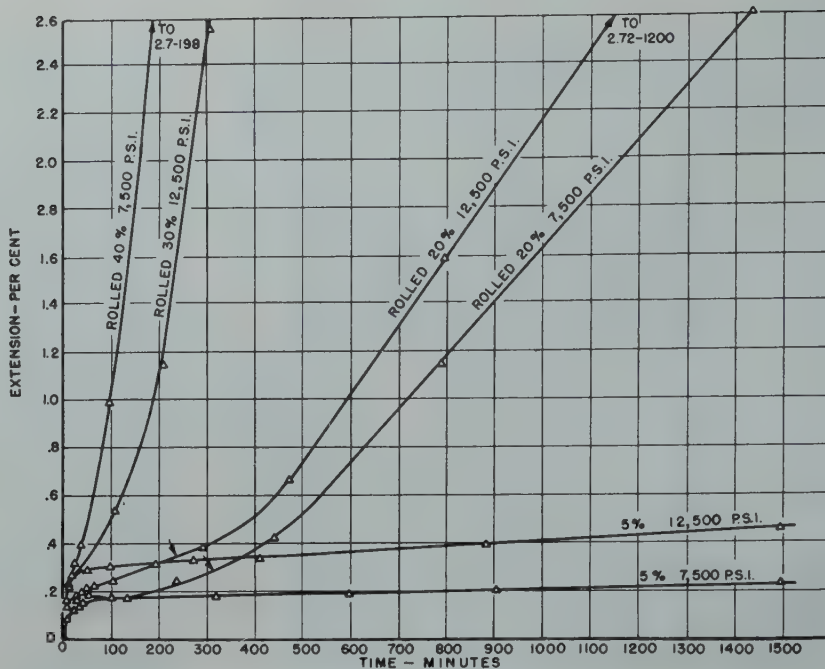


FIG 2—Time-extension curves for OFHC copper, rolled to reductions of 5, 20, 30 and 40 pct. Tested at 572°F.

Arrows indicate recrystallization has reached critical stress level.

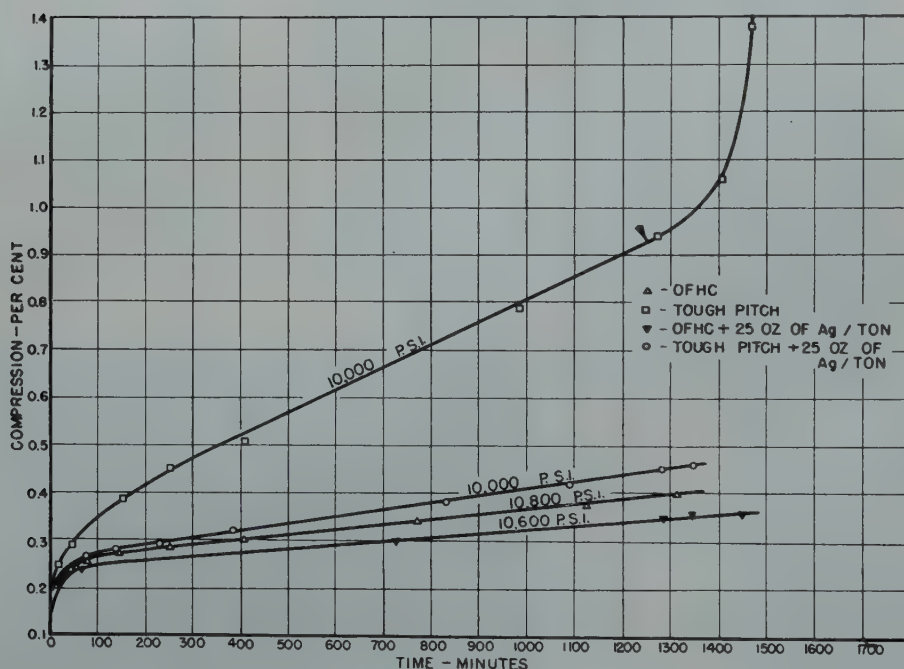


FIG 3—Time-compression curves at 572°F for various coppers cold rolled 5 pct.

(84.4 pct red. in area). An additional temper, 10 pct cold worked, was produced by pulling annealed wire in tension until the desired deformation was produced. The room-temperature tensile properties are given in Table 4.

These tests were carried out at lower temperatures and higher stresses than the short-time tests. The details of the creep tests are given in Table 5. Typical creep curves for the three coppers are

shown in Fig 9, 10, and 11. The results of these tests are consistent with the short-time tests, although in some instances the effects of cold work and silver are greater than in the short-time tests.

The long-time tests serve to establish more firmly an optimum degree of cold work for each temperature and the beneficial influence of silver on the creep properties of copper. It will

be observed that the long-time tests rate the various coppers in the same order as the short-time tests.

The comparative data on creep rates of OFHC and tough-pitch copper in Table 4 appear to be at variance with the results of Burghoff and Blank, who found little difference between the creep rates of some OFHC and ETP copper both in the annealed and cold-drawn condition. It should be pointed

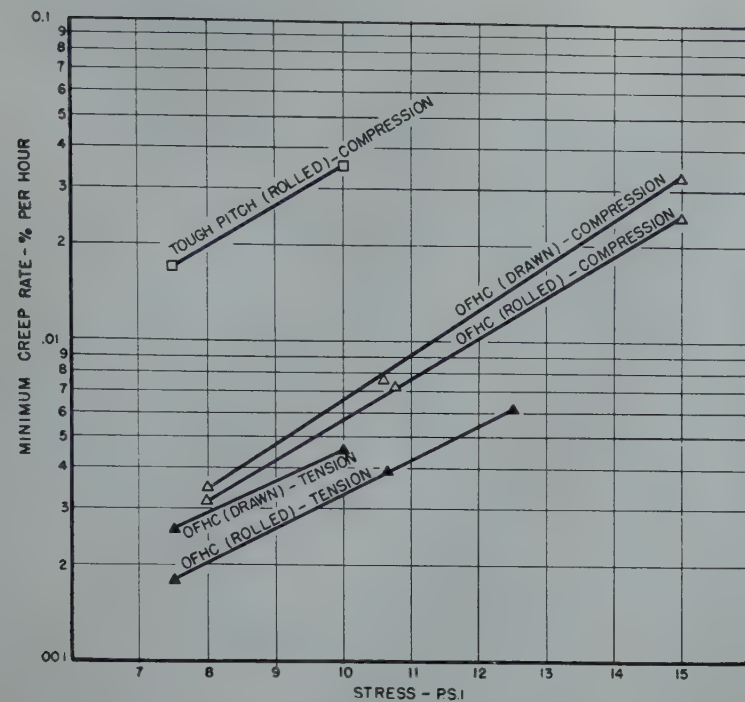


FIG 4—Stress-creep rate relationship at 572°F for coppers rolled and drawn 5 pct. Tested in tension and compression.

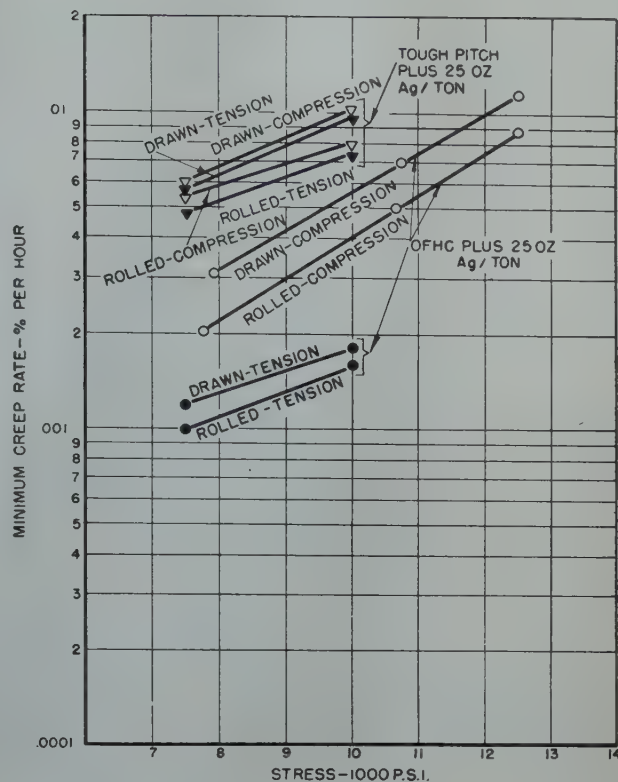


FIG 5—Stress-creep rate relationship at 572°F for coppers rolled and drawn 5 pct. Tested in tension and compression.

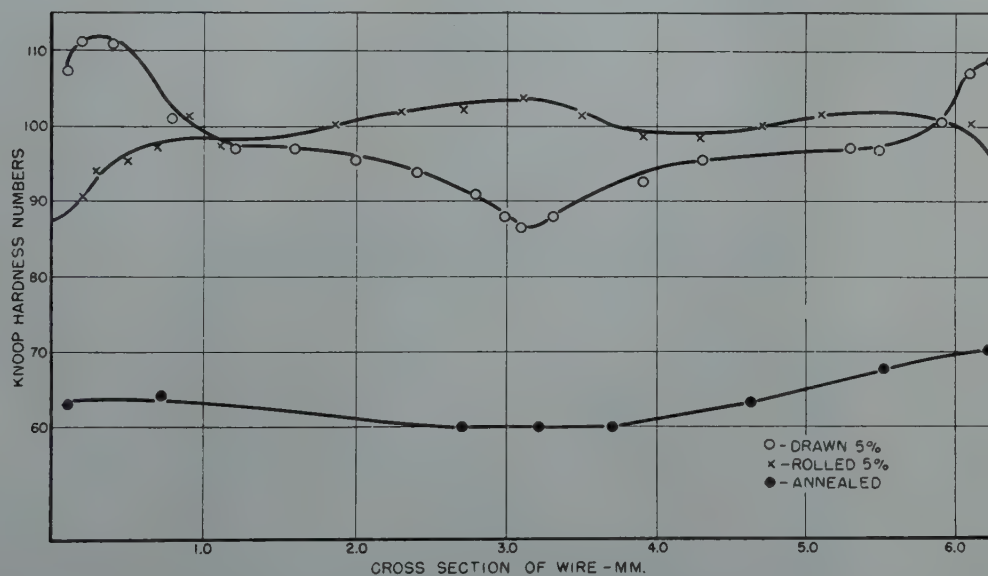


FIG 6—Knoop hardness numbers vs. location. Tough-pitch copper.

out, however, that these authors also found little difference between the softening characteristics of the two lots of copper they used in this investigation.

Summary

The effect of cold work on the creep characteristics of tough-pitch

and OFHC coppers, unalloyed and silver bearing, has been determined for temperatures from 200 to 572°F. The most important results are:

1. Cold work increases the creep strength of copper; however, the benefit from cold work is lost at temperatures where recrystallization is rapid. This temperature varies with the

amount of cold work and the type of copper.

2. The addition of silver to either tough-pitch or OFHC copper raises the temperature at which rapid recrystallization occurs; the effect is approximately the same on both types of copper.

3. While additions of silver effec-

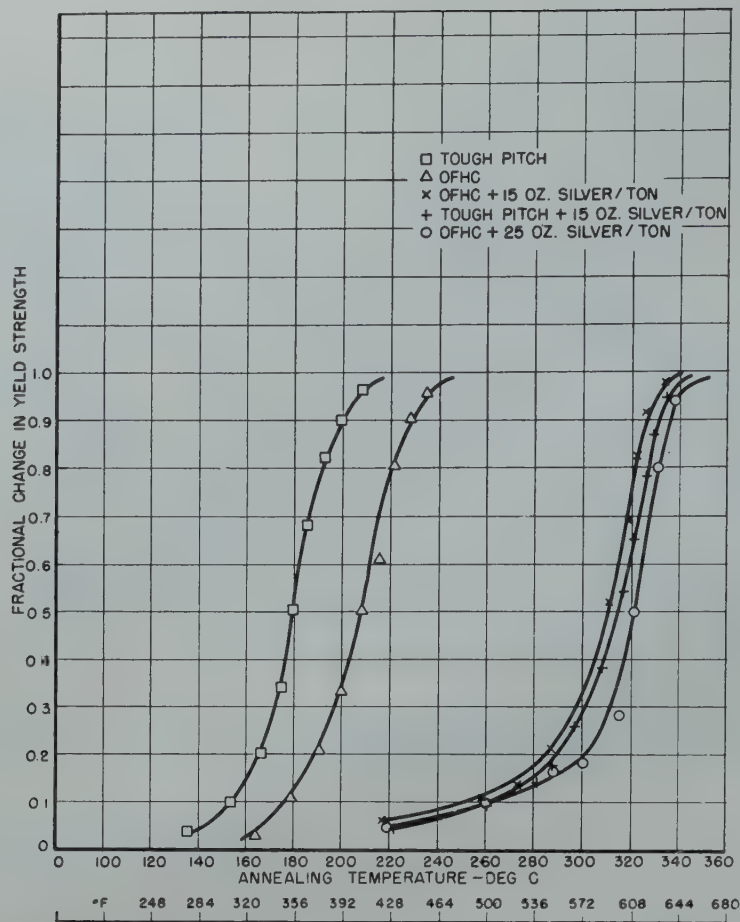


FIG 7—Softening curves for hard-drawn (84.4 pct R. A.) copper wires held one hour at temperature.

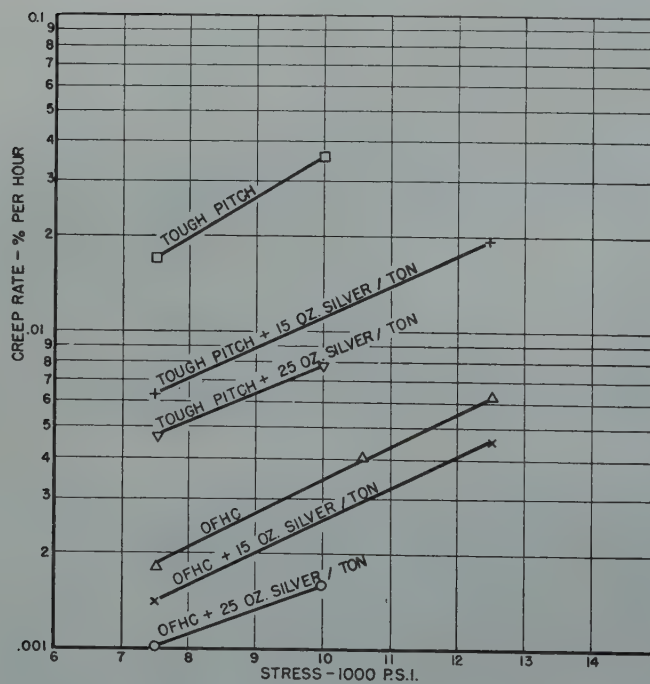


FIG 8—Effect of silver on the secondary creep rate of various coppers cold rolled 5 pct. Tested in tension. Short-time tests at 572°F.

tively lower the creep rate of both tough-pitch and OFHC copper as cold worked, the silver-bearing OFHC copper has a markedly lower creep rate than comparable tough-pitch copper.

Appendix

In a previous paper, an equation was presented by which the process of recrystallization, as evidence by softening, could be charted at low temperatures—long-time from short-time high-temperature tests. The validity of this relationship has been shown and useful curves derived by its application. The equation

ln t = ln ln (1 / (1 - x)) - A + Q / RT

in which the terms for tough pitch copper, cold worked 5 pct, and under creep test at 300°C and 10,000 psi (Fig 3) are

t = time in hours for the yield strength to drop to 10,000 psi.

x = fraction recrystallized corresponding to a drop in yield strength to 10,000 psi.

A = a constant = 22.5 for tough pitch, taken from Fig 6 of the reference paper. (Table 6).

Q = energy of activation = 30,000 cal per mol.

R = gas constant = 1.99 cal per degree per mol.

T = temperature, degrees Kelvin = 573°K.

This equation solved for t yields a value of 21 hr at which time the yield

Table 4 . . . Tensile Tests on Copper Wires

| Material | Cold Reduction After Last Anneal, Pct | Yield* Strength, psi | Tensile Strength, psi | Elongation, Pct in 10 In. |
|-----------------------------------|---------------------------------------|----------------------|-----------------------|---------------------------|
| Tough pitch | 84.4 (hard) | 65,000 | 65,200 | 1.5 |
| Tough pitch | 37.1 (half hard) | 55,000 | 57,000 | 2.0 |
| Tough pitch | 10.0 | 32,000 | 37,200 | 25.0 |
| Tough pitch | Annealed | 6,500 | 34,200 | 39.0 |
| OFHC | 84.4 (hard) | 66,000 | 66,300 | 1.5 |
| OFHC | 37.1 (half hard) | 57,000 | 57,500 | 2.0 |
| OFHC | 10.0 | 33,500 | 39,300 | 27.0 |
| OFHC | Annealed | 6,500 | 37,000 | 40.0 |
| OFHC plus 15 oz per ton of silver | 84.4 (hard) | 65,700 | 65,900 | 1.5 |
| | 37.1 (half hard) | 57,400 | 57,600 | 2.0 |
| | 10.0 | 33,000 | 38,100 | 27.0 |
| | Annealed | 9,000 | 36,100 | 40.0 |

* Stress at 0.2 pct offset from initial slope of stress-strain curve.

Table 5 . . . Results of Long-time Creep Tests

| Material | Temper | Test Temperature, °F | Stress, psi | Total Creep, † Pct | Minimum Creep Rate, Pct per Hr | Duration of Secondary Stage, Hr | Total Time of Test, Hr | |
|-----------------------------|-----------|----------------------|-------------|--------------------|--------------------------------|---------------------------------|------------------------|-------------------------|
| Tough pitch | Hard | 200 | 15,000 | 0.051 | 0.0000066 | 4500 | 5000 | |
| Tough pitch | Hard | 200 | 20,000 | 0.10 | 0.000010 | 3300 | 5000 | |
| Tough pitch | Hard | 200 | 25,000 | 0.136 | 0.000017 | 3000 | 5000 | |
| Tough pitch | Hard | 230 | 20,000 | 0.200 | | | 1260 | Accelerating creep rate |
| Tough pitch | Hard | 230 | 25,000 | 0.210 | | | 1000 | Accelerating creep rate |
| Tough pitch | Soft | 250 | 25,000 | 1.75 | | | 1440 | Decreasing creep rate |
| Tough pitch | 10 pct | 250 | 25,000 | 1.85 | | | 2200 | Decreasing creep rate |
| Tough pitch | Half hard | 250 | 25,000 | 0.400 | 0.000056 | | 4800 | |
| Tough pitch | Hard | 250 | 25,000 | 1.75 | | | 1180 | Accelerating creep rate |
| Tough pitch | Hard | 300 | 5,000 | 1.5 | | | 1100 | Decreasing creep rate |
| Tough pitch | Hard | 300 | 10,000 | 2.5 | | | 190 | Accelerating creep rate |
| OFHC | Hard | 200 | 25,000 | 0.033 | 0.0000049 | | 5000 | |
| OFHC | Soft | 230 | 20,000 | 1.08 | 0.000042 | | 5000 | |
| OFHC | Soft | 230 | 25,000 | 1.33 | 0.000067 | | 5000 | Decreasing creep rate |
| OFHC | Hard | 230 | 20,000 | 0.046 | 0.0000065 | | 5000 | |
| OFHC | Hard | 230 | 25,000 | 0.072 | 0.0000090 | | 5000 | |
| OFHC | 10 pct | 250 | 25,000 | 0.48 | 0.000060 | | 5000 | |
| OFHC | Half hard | 250 | 25,000 | 0.240 | 0.000026 | | 4800 | |
| OFHC | Hard | 250 | 25,000 | 0.167 | 0.000027 | | 4800 | |
| OFHC | Soft | 300 | 20,000 | 0.800 | 0.00028 | | 1000 | |
| OFHC | Soft | 300 | 25,000 | 1.4 | 0.00048 | | 1000 | Decreasing creep rate |
| OFHC | Hard | 300 | 15,000 | 0.4 | 0.00029* | 260 | 1000 | Increasing creep rate |
| OFHC | Hard | 300 | 20,000 | 1.67 | 0.00058* | 200 | 1000 | Increasing creep rate |
| OFHC | Hard | 300 | 25,000 | 1.67 | 0.00068* | 150 | 680 | Increasing creep rate |
| OFHC + 15 oz silver per ton | Soft | 230 | 25,000 | 0.38 | 0.000025 | | 5000 | |
| | Soft | 250 | 25,000 | 1.00 | 0.000090 | | 4200 | Decreasing creep rate |
| | 10 pct | 250 | 25,000 | 0.170 | 0.000013 | | 5000 | |
| | Hard | 240 | 25,000 | 0.033 | 0.0000032 | | 4800 | |
| | Half hard | 250 | 25,000 | 0.10 | 0.0000040 | | 4800 | |
| | Soft | 300 | 20,000 | 0.750 | 0.00021 | | 1100 | |
| | Soft | 300 | 25,000 | 0.880 | 0.00025 | | 1100 | |
| | Hard | 300 | 25,000 | 0.066 | 0.000045 | | 1000 | |

* Only approximate, due to extremely short second stage.
† The total creep does not include the initial elastic elongation. This quantity was not measured in these tests.

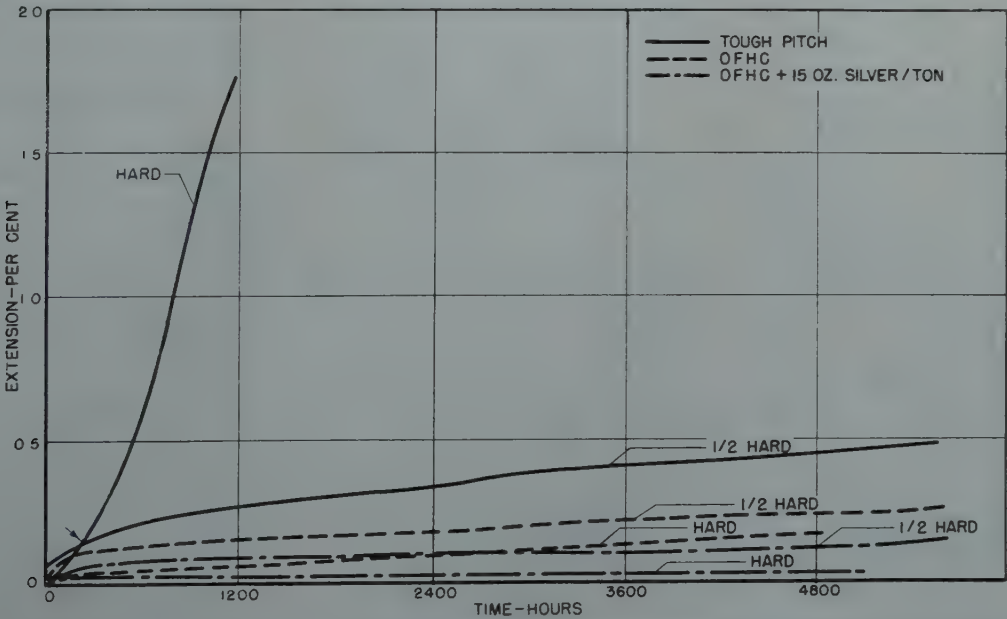


FIG 9—Time-extension curves at 250°F and 25,000 psi. Wires half hard and full hard (37.1 pct and 84.4 pct cold worked).

Arrows indicate recrystallization has reached critical stress level.

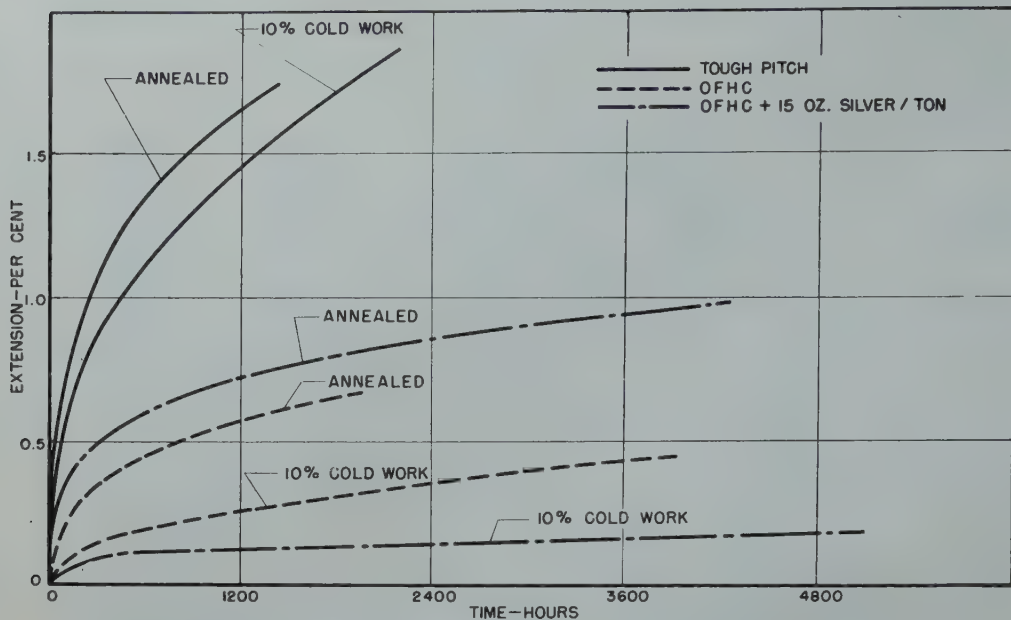


FIG 10—Time-extension curves at 250°F and 25,000 psi. Wires annealed and prestrained in tension 10 pct.

strength has dropped to 10,000 psi. At this time conditions are favorable for the initiation of the third stage of creep. When this value is placed on the curve of Fig 3 it is found to correspond closely to the inflection point. Values of *A* for the other types of

copper and degrees of cold work are listed in Table 6.

Considering a creep test at 25,000 psi and 300°F and neglecting the effect of strain hardening, recrystallization might be expected to reduce the yield strength to 25,000 psi for the various

Table 6 . . . Value of *A* for Various Types of Copper and Degrees of Cold Work

| Pct Cold Reduction in Area | Tough-Pitch Copper | OFHC Copper | OFHC + 15 Oz of Silver per Ton of Copper |
|----------------------------|--------------------|-------------|--|
| 5.0 | 22.5 | 20.2 | 19.5 |
| 20.0 | 26.6 | 25.3 | 23.1 |
| 30.0 | 27.9 | 26.0 | 23.7 |
| 37.1 | 29.4 | 26.9 | 23.85 |
| 40.0 | 29.1 | 27.1 | 24.0 |
| 84.4 | 32.9 | 30.9 | 25.3 |

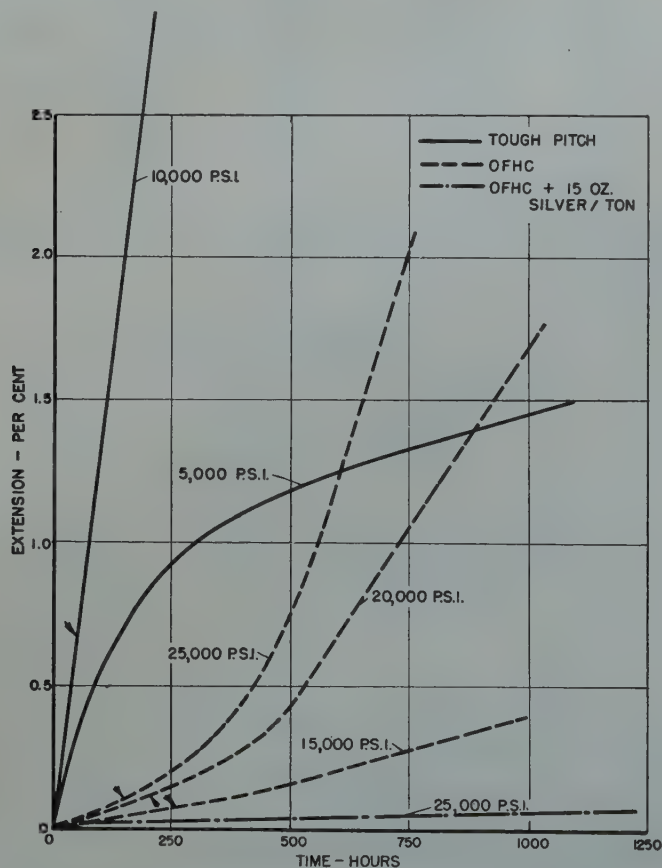


FIG 11—Time-extension curves at 300°F. Wires full hard (84.4 pct cold worked).

Arrows indicate recrystallization has reached critical stress level.

hard-drawn coppers in the following times: tough pitch—20 hr, OFHC—150 hr, OFHC + 15 oz silver per ton—10,000 hr. The times for the yield strengths to drop to the stress imposed during the creep tests are indicated by arrows on the time-extension curves.

Acknowledgments

The authors are grateful to the American Metal Co. for initiating and supporting the experimental work leading to this paper. They particularly wish to thank Mr. D. L. Ogden, Mr. H. M. Burkey, and Mr. H. M. Schleicher of that company for their cooperation.

References

1. H. L. Burghoff and A. I. Blank: The Creep Characteristics of Copper and Some Copper alloys at 300, 400, 500°F. *Proc., Am. Soc. Test. Mat.*, (1947) 47.
2. L. R. Jackson, A. M. Hall, and A. D. Schwobe: The Comparative Properties of Several Types of Commercial Coppers, as Cold Worked and as Recrystallized, *Metals. Tech.*, Sept. 1947, TP 2274. *Trans. AIME* (1948) 175, 296.

The Rapid Determination of Orientations of Cubic Crystals

C. G. DUNN,* Member AIME and W. W. MARTIN†

Introduction

Various X ray diffraction techniques have been developed for determining orientations of crystals. Transmission and back-reflection Laue methods^{1,2,3} in particular have been found to be very useful. In many applications, however, a need still exists for a simplification of the details of analysis so that orientations can be determined more rapidly, and operators with little or no training in crystallography can be easily instructed in the necessary procedures.

Filling this need in part is a system of analysis that has been in use for several years in the Metals Section of the Laboratory, General Electric Co., Pittsfield, Mass. This method is an extension of the one of Majima and Togino,⁴ which uses fifty-five indexed standard transmission Lauegrams to cover the entire range of crystal orientations. Greater rapidity in determining the orientation of a crystal is achieved by using a slightly larger set of standard Lauegrams and by systematizing the steps followed. This system of analysis in its present form constitutes the subject matter of the present paper. Although the method uses transmission X ray Laue patterns, many of the operations are applicable to the analysis of back-reflection Lauegrams.

Very briefly the method is based on the fact that Bragg and azimuthal angles for two or more identified Laue diffraction spots completely determine the orientation of a crystal, and standard Laue photographs of the Majima and Togino type provide a ready means for identifying Laue spots. After a preliminary analysis, which consists of identifying the pattern in terms of one of the standard patterns, a correctly marked Lauegram is selected to carry out the final analysis. From measured Bragg and azimuthal angles, the normals (poles) of the reflecting planes for the selected Laue spots are located on a stereographic projection and the orientation of the crystal determined (in terms of the positions of cube poles for

example) by a few additional operations on a Wulff net.

The actual procedure followed will be illustrated in detail after a brief treatment of X ray problems connected with orientation determinations and a discussion of useful principles and techniques.

X Ray and Plotting Problems

RELATIVE ADVANTAGES OF BACK-REFLECTION AND TRANSMISSION LAUE DIFFRACTION METHODS

In the back-reflection Laue method

it is easy to make a direct measurement of the tilt of a zone of Laue spots. Specimen thickness also is generally no problem. In the case of thin specimens, however, the time of exposure is less for the transmission Laue method. For example, with silicon ferrite this advantage holds up to a thickness of 0.6 mm if tungsten radiation at 40 kv peak voltage is used. Furthermore, the transmission photograph represents the entire thickness of the crystal whereas the back-reflection picture represents only a surface layer (a thickness of less than 0.05 mm for silicon ferrite), the deeper layers supplying a negligible amount to the diffraction pattern. If a crystal is distorted, the transmission Laue pattern gives more information particularly with regard to the orientation of the crystal and the overall amount of spread in orientation. Finally a $3\frac{1}{4} \times 4$ in. film suffices for transmission photograms; a 4×5 in. or 5×7 in. film with a central hole is needed for back-reflection patterns. Not only is the manipulation of film easier because of the size of film, but

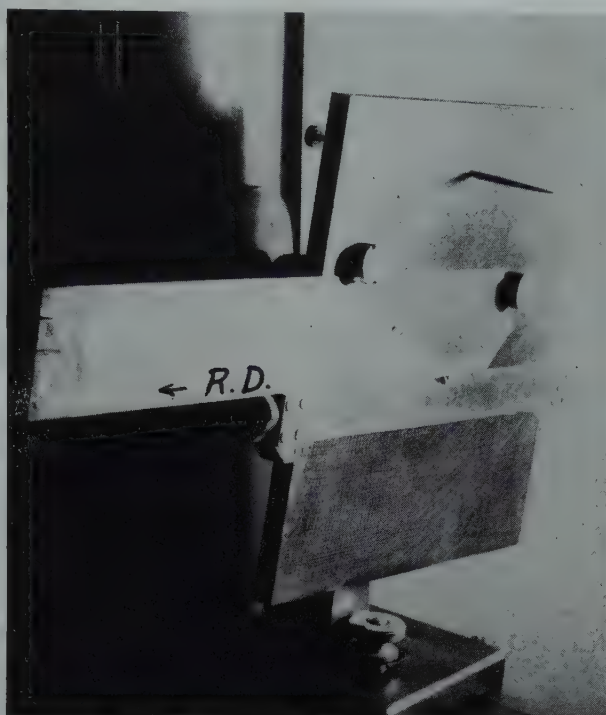


FIG 1—Photograph of a Laue transmission X ray camera with specimen in position.
Film holder not shown.

Cleveland Meeting, October 1949.

TP 2637 E. Discussion of this paper (2 copies) may be sent to *Transactions AIME* before December 1, 1949. Manuscript received January 21, 1949.

* Research Physicist, General Electric Co., Pittsfield, Massachusetts.

† Formerly Metallurgist, General Electric Co., Pittsfield, Massachusetts; now Metallurgist, University of California, Sandia Base, New Mexico.

¹ References are at the end of the paper.

there is also less work involved in camera loading with film requiring no central hole.

AIDS FOR THE LAUE METHOD

A convenient method for mounting flat specimens is shown in Fig 1. A collimating tube is joined centrally to a 5 in. square steel plate with the rear pinhole flush with the surface. An adjustable clamp to provide vertical and horizontal movement of the sample without rotation rests on the square plate in such a way that its upper edge is always 90° to a line passing from the rear pinhole to the long pin located near the top of the large plate (see Fig 1). The purpose of this pin is to transfer a reference direction directly to the film in the form of a pin-prick and thereby solve the alignment problem for measuring azimuthal angles. The specimen shown in Fig 1 is held in position by one clamp and two Alnico magnets. Larger specimens can be held with auxiliary clamps or with scotch tape. Further, the camera shown in Fig 1 can also be used as a specimen holder for a back-reflection camera.

RELATIONS FOR PLOTTING THE POLE OF A PLANE

The positions of poles of planes that appear in stereographic projection depend on which surface of a flat specimen is used for reference. Our procedure is to use the surface which is visible when the sample is mounted for X ray-ing, either for transmission or back-reflection photography (as shown in Fig 1). Fig 2 diagrammatically shows the position of the normal *N* to a plane which diffracts X rays to a point *L* on the film. The normal *N* makes an angle δ with the surface of the sample, and the diffraction spot *L* makes an azimuthal angle ϕ with the reference direction, *R.D.* The distance *r* from the central image *O* to the spot *L* is given by Eq 1:

$$r = D \tan 2 \delta^* \tag{1}$$

where *D* is the distance between specimen and film.

The incident beam, the diffracted beam, and the normal to the reflecting plane, lie in a plane which intersects the film along the line *OL* at an angle ϕ to the reference direction of the sample. This relationship also determines ϕ for plotting the pole of the plane in stereographic projection. The distance *r* determines the value of δ according to

* A similar equation holds for back-reflection, the angle δ being replaced by $90^\circ - \delta$.

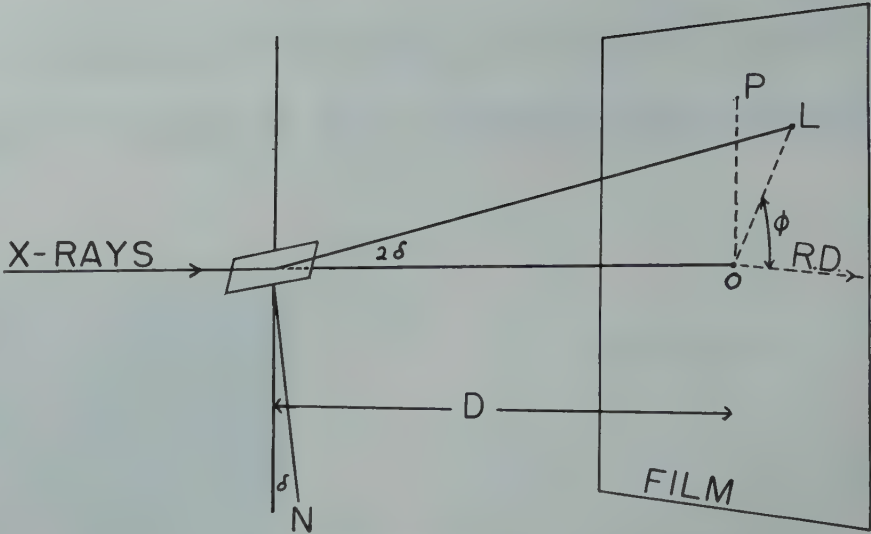


FIG 2—Schematic diagram showing angular relations for the Laue method.

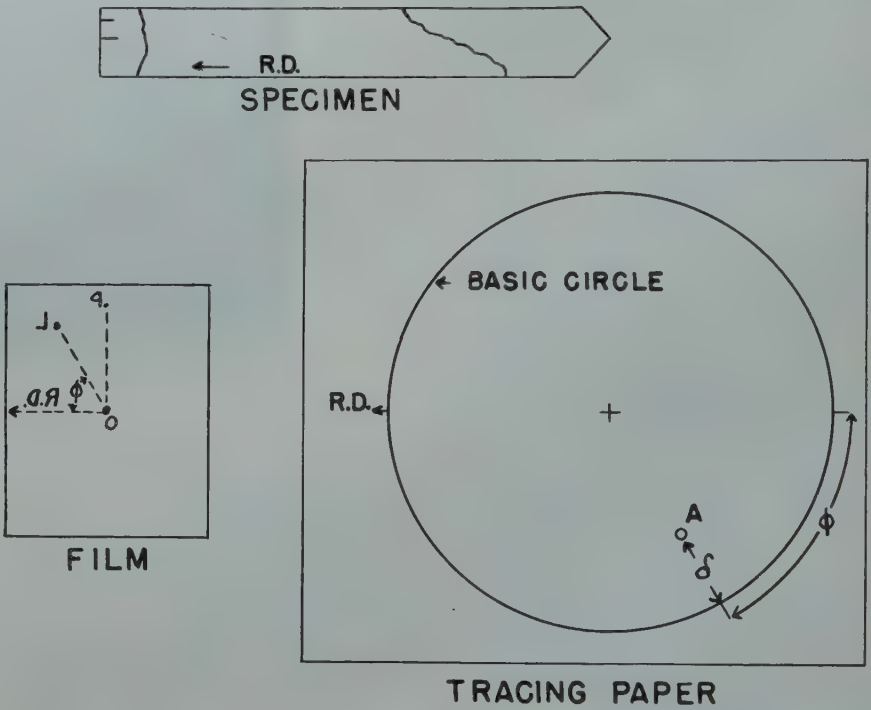


FIG 3—Schematic diagram showing correct relation for film, specimen, and stereographic projection.

The point *A* locates the direction of the pole of the plane which reflects X rays to the point *L* on the film.

Eq 1; therefore, a direct reading net can be easily made for measuring δ . Later a photograph will be shown of an arrangement for holding the film and measuring δ and ϕ directly (it is called a δ, ϕ analyzer).

To keep relationships correct during analysis the film is held so the observer looks through the film onto the surface of the sample. This applies to both transmission and back-reflection work. Fig 3 showing specimen, film, and the plot of one pole in stereographic projection illustrates this for transmission. As in Fig 2, the pole of the reflecting

plane is diametrically opposite the Laue spot.* Its distance from the basic circle, which coincides with the plane of the sample, is δ degrees measured along a diameter. The basic circle and two diameters of a Wulff net are properly graduated for making this plot. The meridian and latitude lines of the Wulff net are also indispensable for plotting crystallographic directions from the known angular relationships between planes. Therefore, the plot is

* In back-reflection work the pole of the reflecting plane and the Laue spot fall on the same side of the incident beam.

most conveniently carried out on tracing paper superimposed on a Wulff net.^{5*}

In a Laue photograph certain groups of diffraction spots lie on conic sections (ellipses, parabolas, and hyperbolas). Such groups are called zones. In stereographic projection poles of planes for a zone fall on a meridian line when the plot is correctly rotated about the center of the Wulff net (in space they lie in a common plane). The direction 90° away (and this will fall on an equator when the poles of the zone are superimposed on a meridian line) is the zone axis of the zone. When a zone axis is within 45° of the center of projection, the zone of Laue spots on the film is an ellipse; when a zone axis is at 45°, the zone is a parabola; and when a zone axis is beyond 45°, the zone is a hyperbola. In back-reflection Laue photographs all zones are hyperbolas.

Crystallographic Relationships in Cubic Crystals

ANGLE BETWEEN PLANES

The angle θ between two planes $(h_1k_1l_1)$ and $(h_2k_2l_2)$ or two directions $[h_1k_1l_1]$ and $[h_2k_2l_2]$ can be calculated from Eq 2 when the Miller indices are known.

$$\begin{aligned} \cos \theta = & \frac{h_1h_2 + k_1k_2 + l_1l_2}{\sqrt{(h_1^2 + k_1^2 + l_1^2)(h_2^2 + k_2^2 + l_2^2)}} \quad [2] \\ \text{when } h_1h_2 + k_1k_2 + l_1l_2 = 0, \theta = 90^\circ. \end{aligned}$$

ZONE AXIS

$$\begin{aligned} \text{Since } h_1u + k_1v + l_1w = 0 \\ \text{and } h_2u + k_2v + l_2w = 0 \\ \text{when } \begin{cases} u = a(k_1l_2 - k_2l_1) \\ v = a(l_1h_2 - l_2h_1) \\ w = a(h_1k_2 - h_2k_1) \end{cases} \quad [3] \end{aligned}$$

(where a is a suitable constant to make u, v , and w small integers) the direction $[uvw]$ is 90° from the directions $[h_1k_1l_1]$ and $[h_2k_2l_2]$, which are the poles of planes $(h_1k_1l_1)$ and $(h_2k_2l_2)$ respectively since the system is cubic. The line of intersection of the planes $(h_1k_1l_1)$ and $(h_2k_2l_2)$ is the direction $[uvw]$.

$$\begin{aligned} \text{Also } h_iu + k_iv + l_iw = 0 \quad [4] \\ \text{when } \begin{cases} h_i = mh_1 + nh_2 \\ k_i = mk_1 + nk_2 \\ l_i = ml_1 + nl_2 \end{cases} \text{ for any integral values of } m \text{ and } n. \end{aligned}$$

Consequently, the direction $[uvw]$ makes an angle of 90° with all direc-

tions of the form $[h_ik_il_i]$ and, therefore, is the zone axis of all planes $(h_ik_il_i)$. Example: starting with Miller indices $\bar{1}, 0, 1, 1, \bar{1}$, and 0 for h_1, k_1, l_1, h_2, k_2 , and l_2 respectively and using values of 3 and 2 for m and n respectively, we obtain $[111]$ for the zone axis of the $(\bar{1}01)$, $(1\bar{1}0)$, and $(1\bar{2}3)$ planes.*

The Relationship between Film Nets and Stereographic Projection Nets

When poles of planes for a zone are plotted in stereographic projection, points are obtained which fall on a meridian line. Also, if the direction of plotting is reversed, a meridian line of a Wulff net becomes a conic section on a film net. Let us call the conic section thus obtained, however, a zone or meridian line on a film net. Similarly a latitude line of a Wulff net can be plotted to obtain a latitude line of a film net. The reverse plotting must be carried out according to whether the net is to be used for transmission Lauegrams or back-reflection Lauegrams. Using an arrow to indicate the operation of plotting, the following relations can be indicated for well known nets.

| Film Net | Projection Net | Use of Film Net | Lit. Ref. |
|--|---|----------------------------|-----------|
| Greninger \rightleftharpoons | Wulff net | Back-reflection Laue | 3b |
| Leonhardt zero-tilt \rightleftharpoons | Wulff net | Transmission Laue | 6 |
| Leonhardt 90°-tilt \rightleftharpoons | Polar net | Either B.R. or Trans. Laue | 6 |
| Leonhardt w -tilt \rightleftharpoons | Intermediate net between Wulff and Polar net. | Transmission Laue | 6 |

Fig 4 shows one-half of a Leonhardt zero-tilt net;⁶ the dotted curves spaced at 10° intervals are meridians and the solid line curves spaced at 5° intervals are latitude lines. The distance D satisfies Eq 1, r becoming equal to D when δ equals 22½°. An illustration will be given later showing how angles between planes can be obtained with this net upon placing a zone of Laue spots on a meridian (by interpolation) and reading differences in latitude between Laue spots.

Fig 5 shows a new diagram that we have developed and which we shall call an isogonal net because each curve represents a constant angle from a point on the base line—the straight line graduated in 5° intervals. The net is a combination of tilted Leonhardt curves (w equal to 5, 15, and 25°) with no meridian lines and with two

sets of latitude lines. One set gives the 45, 90, and 135° differences in latitude, the other set the 30, 60, 90, and 120° differences in latitude measured from correct points on the base line. The base line must be used for all measurements of angle between planes except those of a zone. In this particular case, as will be illustrated later, the angles between planes for a zone can be read directly when one Laue spot of a zone is placed on the base line.

The Greninger net has been adequately described elsewhere. An illustration, however, using such a net will be given later.

The film net shown in Fig 6 is very useful for plotting poles of planes and directions of zone axes in stereographic projection. When used for these purposes, however, the net must be coupled with a scale for measuring the azimuthal angle ϕ . The angle δ for any Laue spot can be read from the polar scale which is drawn in half circles. The tilt of a zone measured from the center of projection can be read directly from the net when the zone of Laue spots is correctly located by interpolation among the zones of the net. Unlike the zones of the Greninger net, however, the accuracy of measure-

ment of tilt falls off rapidly near 90° and the position of Laue spots in the direction of the zone axis must be used for an accurate determination of the tilt of the zone.

Standard Laue Photographs

For several years Majima and Togino standards, which were re-indexed for simplicity of analysis as will be described later, were used for identifying Laue spots and zones of Laue spots. Experience thus gained indicated a need for a larger set to cover all possible orientations more uniformly; so 75 patterns were made and these were prepared in two sets—one for *preliminary analysis* and the other for *final analysis*.

In all 300 patterns were made for the body-centered cubic lattice and the face-centered cubic lattice. However, it is not the purpose of this paper

* This article, incidentally, gives an excellent treatment of the properties and uses of a Wulff net.

* Standard projections (see Ref. 1) can also be used to determine members of a zone and the zone axis.

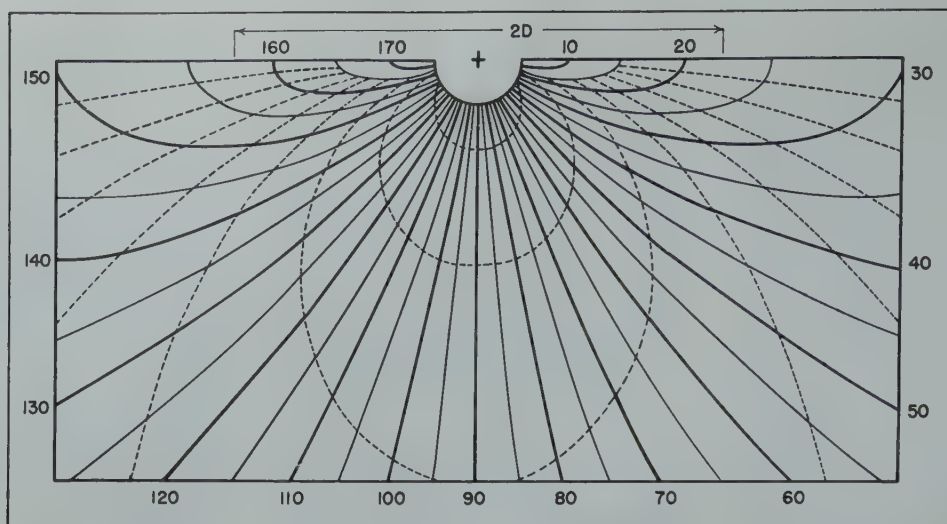


FIG 4—A Leonhardt zero-tilt net showing meridians (dotted-lines spaced at 10° intervals) and latitude lines (solid-lines spaced at 5° intervals).
Net to be used on films where film to sample distance is D .

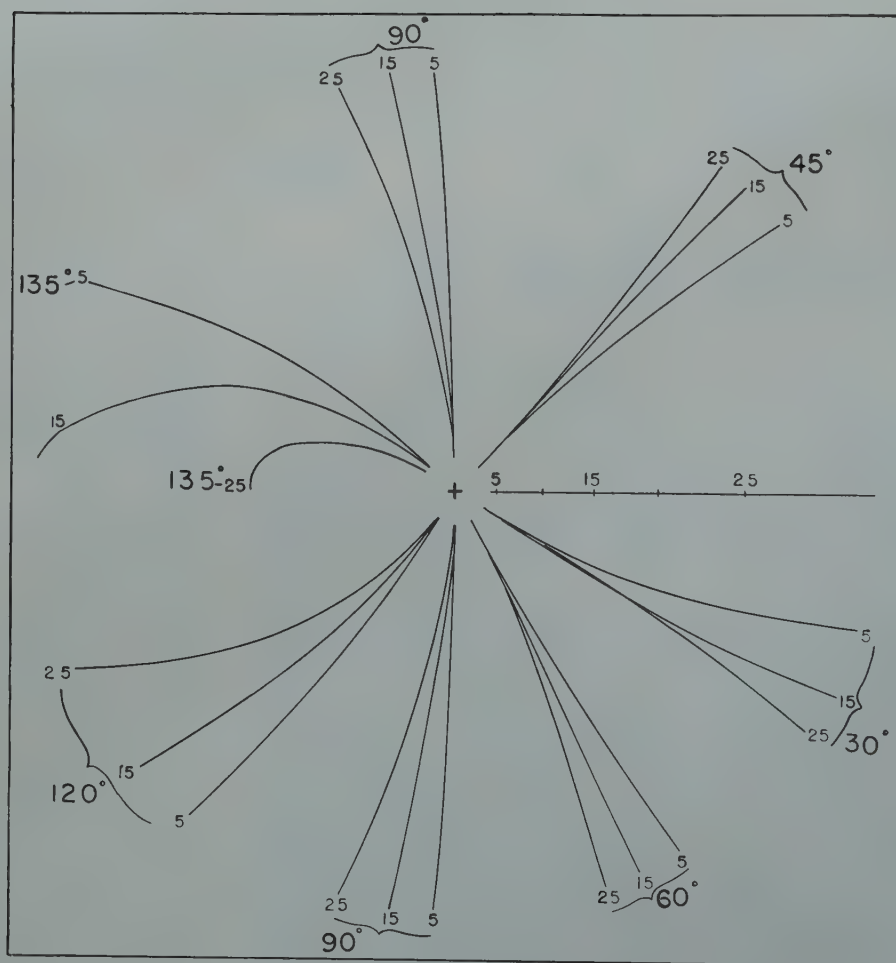


FIG 5—An isogonal film net for determining special angle relations as an aid to the identification of a Laue pattern.

To same scale as the Leonhardt net of Fig 4.

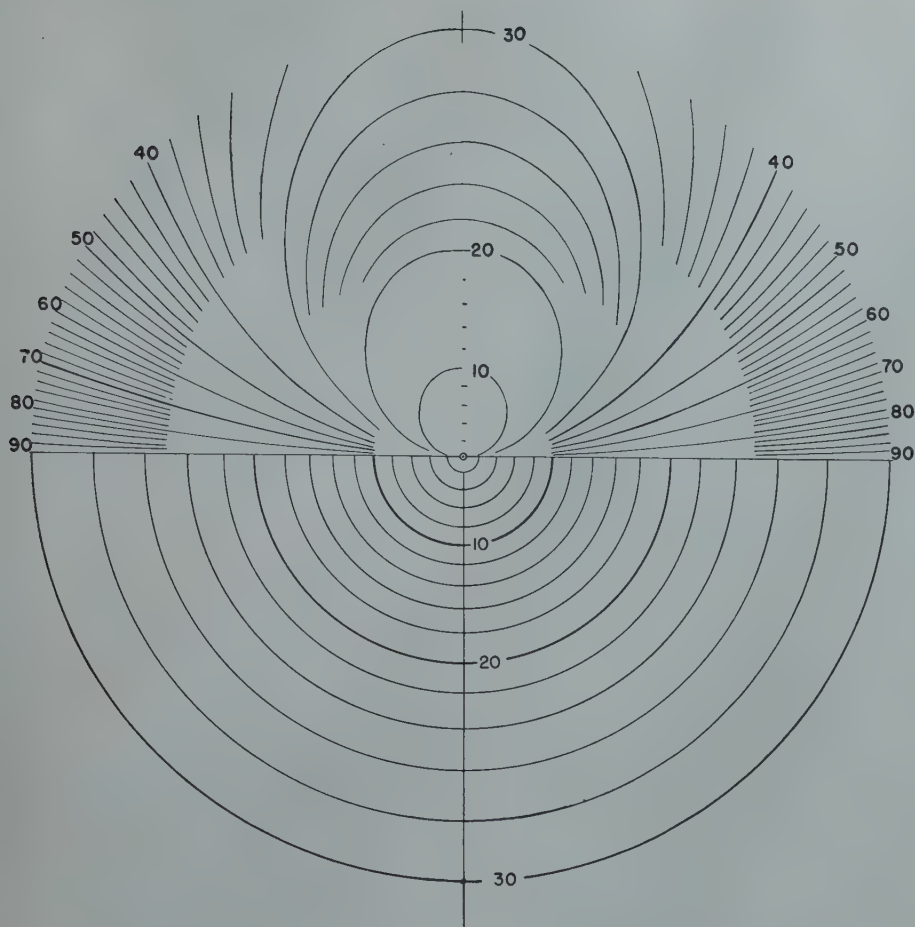


FIG 6—A film net for transmission Laue patterns when used as part of a δ , ϕ analyzer.

One half consists of latitude lines of a polar net graduated in 2° intervals; the other half consists of zones spaced at 2° intervals. To same scale as the Leonhardt net of Fig 4.

to present all 300 patterns in full size reproduction; rather the aim is to illustrate how such patterns may be used for rapid analysis.

COORDINATES OF STANDARD LAUE PATTERNS

The two angular coordinates to be considered now and discussed in relation to Fig 7a and 7b locate only the crystallographic direction that is parallel to the incident X ray beam. They are not sufficient to determine the orientation of a crystal because rotation about the X ray beam as an axis is still indeterminate.

Fig 7a shows diagrammatically the angles α and β used by Majima and Togino with their standard Laue patterns and the angles α and β' used by the present authors with a new set of standards. The relationship between β and β' is

$$\tan \beta' = \cos \alpha \tan \beta \quad [5]$$

When α and β are zero, β' is also zero and the X ray beam is then normal to a cube plane.

The stereographic projection can be treated in two ways to show the angles

α and β' . One way makes use of the unit stereographic projection triangle (see Fig 7b) formed by the [100], [110], and [111] directions of orientation A, which is plotted in terms of cube poles. The values of α and β' are zero for orientation A. Now any crystallographic direction P whatsoever may be found in the unit triangle and its position determined by two angles α and β' if we understand that the direction P is actually to be brought to the center of projection. The coordinates of P, which may be given by α and β' , then specify the crystallographic direction which coincides with the incident X ray beam. Suppose P is brought to the center of projection by two angular rotations—one of α degrees about a vertical axis in the plane of the paper, the other of β' degrees about a horizontal axis in the plane of the paper. Expressed in terms of cube poles, the final orientation is C and the intermediate orientation after the α -rotation is B. On the Wulff net, α gives the change in longitude whereas β' gives the change in latitude of point P during this rotation of A to C.

The unit triangle will be used again later.

The second way of determining α and β' for orientation C is given simply as follows: place the outermost cube pole on an equator of a Wulff net and read directly the angles α and β' , which are determined entirely by the cube poles of orientations C and A as indicated in the figure. This relationship, incidentally, provides a quick and convenient check of the analysis made with the aid of a standard Laue pattern.

Similarly α and β may be found in two ways from the stereographic projection. First if the coordinates of P are expressed in terms of meridian intercepts on two diameters at 90° as shown, the angular distances to the center of the projection are α and β . Secondly, they can be found from the cube poles of the orientation C by constructing a diameter through the correct cube pole and locating its point of intersection in the corresponding {100} plane. Actually no diameter need be drawn when the plot is on tracing paper because the equator of a Wulff net becomes the desired diameter upon placing the correct cube poles on a meridian line.

In the unit stereographic projection triangle, a point indicates that crystallographic direction which is parallel to the incident X ray beam. Directions for the Majima and Togino set of standards, which are 0,0; 5,0; 5,5; etc. to 45,45 in α , β units, are shown in the unit triangle form in Fig 8a. Each direction falls at the center of a circle of 2° radius. These circles, forming horizontal and vertical rows, fall on meridian lines. Positions of the new standards (see Fig 8b) were chosen so that horizontal rows would fall on latitude lines and the coverage of the unit triangle would be generally both complete and uniform. Some points, which are marked with central black dots, did not fit into the otherwise regular scheme. Inaccuracies in both Fig 8a and 8b are due largely to the errors in the enlarged Wulff net, which was used to make the plots. Results for the crystallographic directions for the new set of standards in α , β' coordinates are given in Table 1, each position in the table corresponding to a similar position in the triangle in Fig 8b.

PREPARATION AND NATURE OF NEW STANDARDS

A small experimental error occurred

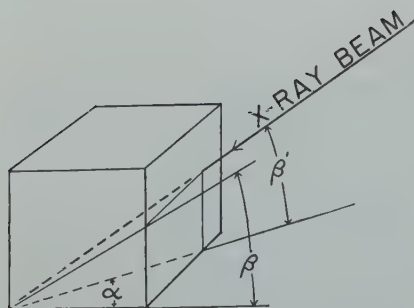
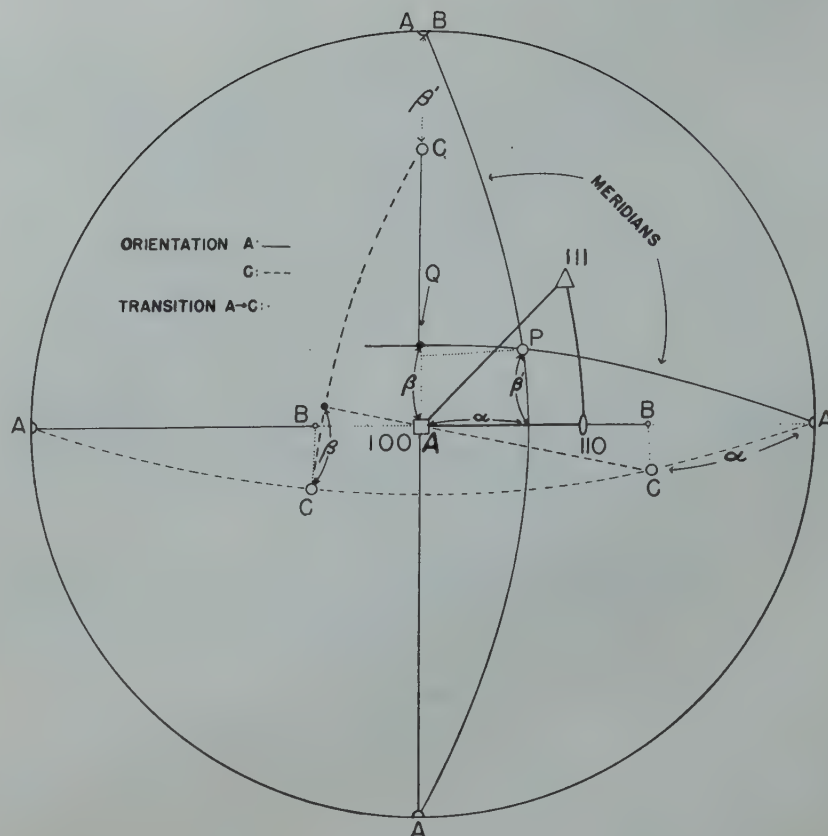


FIG 7—Schematic relationship showing direction of incident X ray beam on a cubic crystal.

(a) Three dimensional drawing showing the angles α , β , and β' .

in obtaining Lauegrams for crystals oriented as outlined in Table 1; so the actual coverage represented by final standards is somewhat poorer than that indicated in Fig 8b. Nevertheless, the error is generally less than one degree, and this has little effect on the usefulness of the standards. The Laue photographs were taken on Kodak type K X ray film without any intensifying screen, using tungsten radiation at 40 kv (higher voltages introduce additional Laue spots—see later note). The distance between film and sample was 3.2 cm. Three crystals of silicon ferrite each 0.2 mm (0.008 in.) thick were used to obtain 75 patterns for the body-centered cubic lattice. No crystal rotation about an axis perpendicular to the X ray beam exceeded 20°. Exposure times were one hour, and the weaker Laue spots were well recorded. One crystal of aluminum 0.4 mm (0.015 in.) thick was used to obtain all 75 Lauegrams for the face-centered cubic lattice. Exposure times were 15 min. for the aluminum crystal.

Lauegrams obtained on $4\frac{1}{2} \times 5$ in. film and with dark Laue spots on a relatively clear background are called the original positives. From them, marked negatives $3\frac{3}{4}$ in. \times $3\frac{3}{4}$ in. in size were made as follows: first a correctly marked piece of tracing celluloid was superimposed on the positive and the composite was then printed on contrast process ortho film; secondly, this procedure was repeated using another type of celluloid tracing but the same original



(b) Stereographic projection for X ray beam in the center of projection and the crystal in orientation C , showing the angles α , β , and β' in relation to orientation A .

positive. In this way 300 negatives, to be used in making final positives on commercial ortho film,* were obtained from the 150 original Lauegrams. Except for the very intense Laue spots, which became enlarged in the reproduction process, final positives made on film were good duplicates of the original Lauegrams.

Sets of standards for preliminary analysis may be mounted between large glass plates in the arrangement partially shown in Fig 9 and 10 for the body-centered (set *B*) and face-centered (set *F*) lattices respectively. Here the positions correspond to those in Fig 8b, and individual patterns have the (010) Laue spots along a vertical line above the central image. The [111] and [001] zones of set *B* and the [101] and [001] zones of set *F* are marked in lightly to show con-

tinuity of the pattern with rotation of the crystal and to aid somewhat in the more rapid scanning of the group while locating the pattern which is similar to the one being analyzed.

Standards of the second set for use in the final analysis are kept individually in an index file and are marked so that steps to be taken in the analysis are nearly self-evident. Illustrative examples of such standards are shown in Fig 11 to 16. Miller indices for a zone of Laue spots (the zone axis) are enclosed in brackets and located near the zone; those for a Laue spot (the reflecting plane) are located adjacent to the Laue spot. During the final analysis when the angles δ and ϕ are to be measured, the correct standard is taken from the file and superimposed on the film being analyzed. The identification of zones and Laue spots to use are determined quickly in this way, and zones or Laue spots on films do not have to be marked.

Table 1 . . . The 75 Standards in α, β' Coordinates

1-1 4-3 5-1 7-4½ 9-1 9-8 11-4½ 13-8 15-4½ 17-1 17-15 19-11½ 21-15 21-8 23-4½ 25-1 27-4½ 29-1 31-4½ 33-1 35-4½ 37-1 41-1 43-4½ 45-1
 12-10½ 13-8 15-11½ 17-8 19-11½ 21-15 23-11½ 25-8 27-11½ 29-8 31-11½ 33-8 35-11½ 37-8 39-11½ 41-8 43-11½ 45-8
 19-18 23-18½ 25-22 27-18½ 29-22 31-25½ 33-22 35-18½ 37-22 39-18½ 41-22 43-18½ 45-22
 28-25 31-25½ 33-22 35-25½ 37-29 39-32 41-29 43-32½ 45-29
 33-28.7 37-29 39-32 41-29 43-32½ 45-29

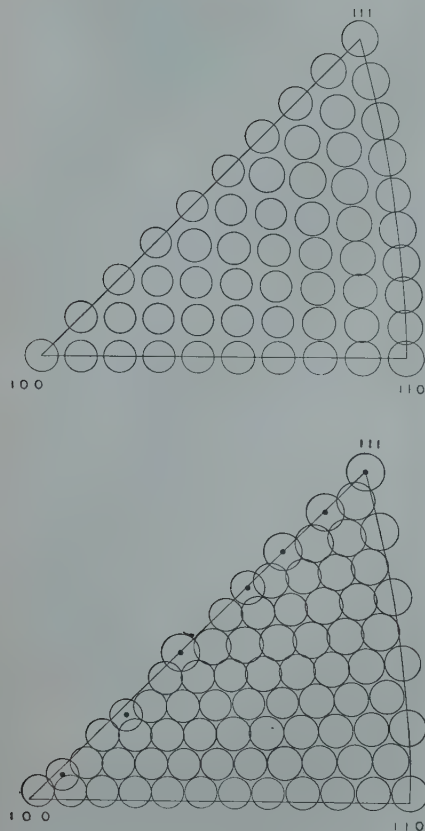


FIG 8—Directions of incident X ray beam in unit triangle form of projection.

(a) (above) The 55 directions used by Majima and Togino in obtaining standard Lauegrams.
(b) (below) The 75 directions used by the authors in a new group of Lauegrams.

In using standard 1-1 of set *B* shown in Fig 11, it is important to know that the poles of the (031) and ($\bar{0}\bar{3}1$) planes fall $143^{\circ}8'$ apart (according to Eq 2). Halfway between them is the pole of the (001) plane. The (010) pole lies on the same meridian 90° from the (001) pole. The [100] direction, the zone axis of the (031) and ($\bar{0}\bar{3}1$) planes, lies 90° away, a point easily located with the aid of a Wulff net. The tilt of the (100) plane obtained this way, however, is not accurate; so the pole of the ($\bar{3}01$) or the pole of the (301) plane should be used to determine the tilt. The [301] direction for example is between the [001] and [100] directions, $18^{\circ}26'$ from the latter. The [111] zone, which is also marked, need not be used except as a check.

The steps of analysis using standard 1-1 of set *F* are the same as those for 1-1 of set *B*. However, the strong $\langle 101 \rangle$ zones, which may be used for checking purposes, can be used very conveniently alone if desired to make the complete analysis.

A very simple procedure for carrying out an analysis, which applies to most standards, can be illustrated

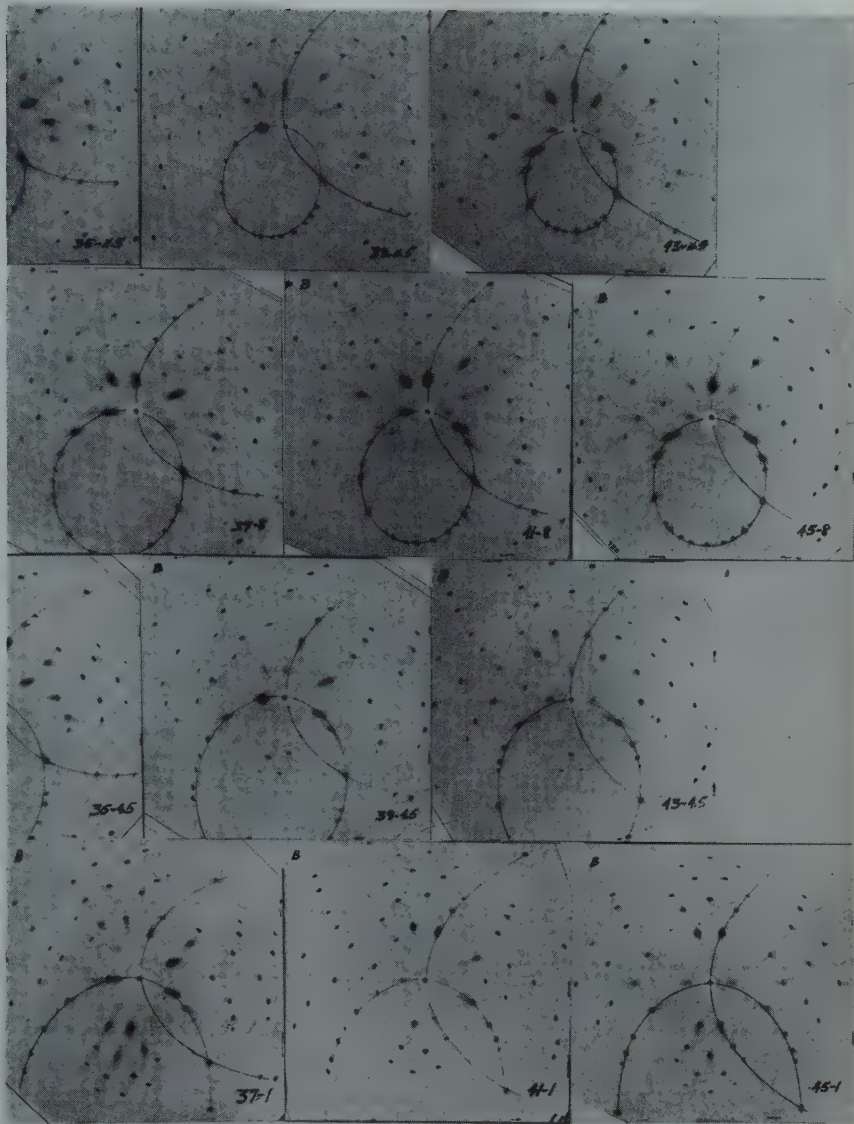


FIG 9—Laue patterns of the body-centered cubic lattice for determining $\alpha\text{-}\beta'$ in a preliminary analysis.

with standards 29-15 shown in Fig 13 and 14. Plot three poles from the [001] zone including the (010) and ($\bar{1}\bar{1}0$) poles if the Laue spots show on the film. Finally, to complete the analysis in terms of cube poles, plot the (001) and (100) poles with the aid of a Wulff net.

In other Laue patterns which do not contain the (010) or the ($\bar{1}\bar{1}0$) Laue spot, the procedure of analysis is only slightly modified. Standards of the type illustrated in Fig 15 and 16 (crystals are in the threefold symmetry position) are examples. The poles of the ($\bar{1}30$) and ($3\bar{1}0$) planes for the [001] zone, referring to Fig 15, are $126^{\circ}52'$ apart (according to Eq 2); halfway between them is a (110) pole, and this serves to locate the (010) and (100) poles which belong to the [001] zone. The [010] zone need not be used except as a check on the analysis. The {111} poles are sometimes useful

in making an analysis; so {111} Laue spots are marked on some standards. Similar in procedure for analysis is the use of the standard shown in Fig 16. The ($\bar{1}20$) and ($2\bar{1}0$) poles, in this case, fall $143^{\circ}8'$ apart.

If crystallographic directions other than those marked in the standards are desired, they can be easily located on the stereographic projection from the positions of the cube poles. Therefore, there is no need to index many of the Laue spots. As a matter of fact, it is our opinion that a minimum of indexing of the standards is an aid to more rapid analysis.

It should be pointed out here that there are a number of errors in the standards of Majima and Togino. The errors of indexing can be easily corrected, however, with the aid of equations for crystallographic relations or with standard projections of the poles of planes. Another point con-

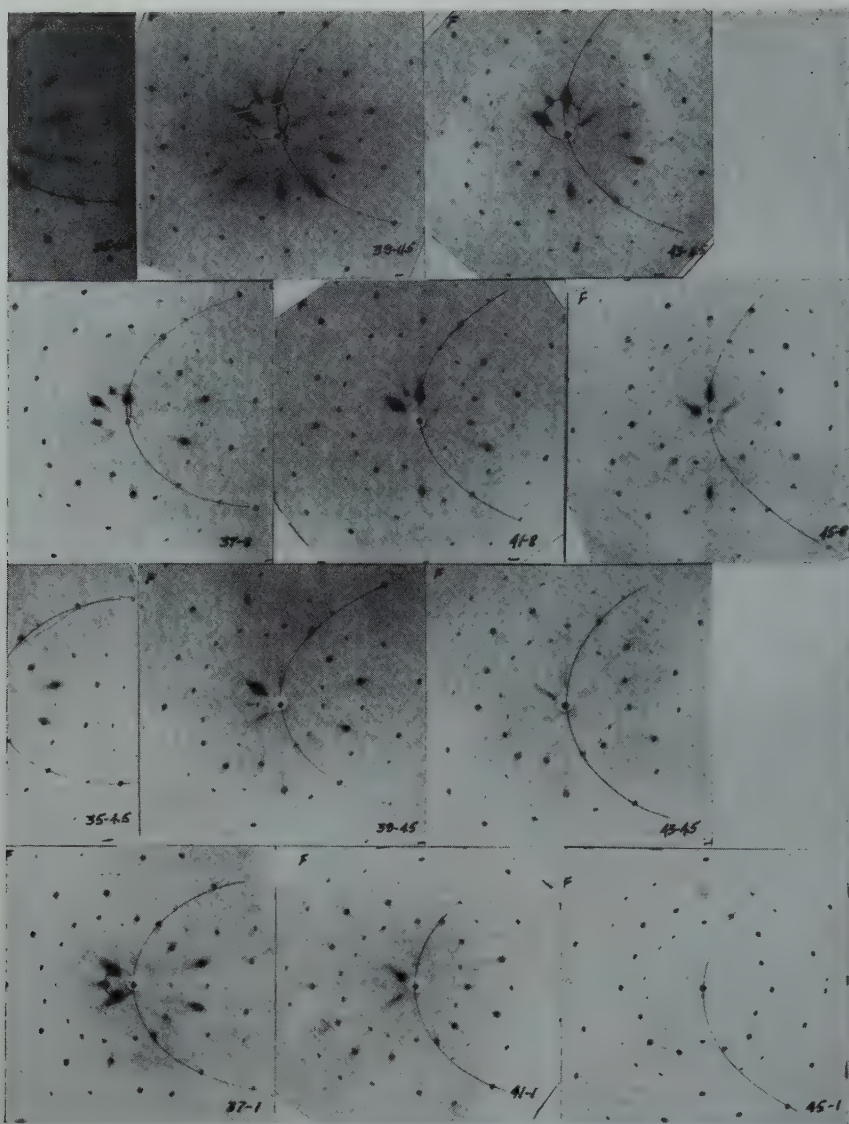


FIG 10—Laue patterns of the face-centered cubic lattice for determining $\alpha-\beta'$ in a preliminary analysis.

cerns the voltage used on the X ray tube. Referring to standard 45-0 of the body-centered cubic lattice as published by Majima and Togino,⁴⁶ it is observed that {321} Laue spots are present. A voltage of 35 kv was used according to their report; but 40-45 kv peak voltage is needed theoretically to bring out these particular Laue spots. On the other hand, the same Laue spots are absent in our 45-1 standards exposed at 40 kv peak voltage and show only on patterns taken at higher voltages.

Analysis

PRELIMINARY ANALYSIS

A preliminary analysis involves determining which standard Lauegram of the 75 mounted between glass plates resembles most closely the unknown pattern. To obtain agreement some

films obviously have to be turned over. They also have to be held in the correct rotational position. When held properly, the [111] zone always falls between 6:00 and 7:30 o'clock except near 45-35.3 where Laue spots of the zone fail to register on the photographic film. The [001] zone lies between 1:30 and 3:00 o'clock except near 0-0 where it fails to register on the film. The [101] zone lies between 9:00 and 12:00 o'clock and fails to show near 45-0.

The [111] and [001] zones for the body-centered cubic lattice often can be correctly recognized at a glance; determining the standard to use for analysis is then an easy matter. When difficulty arises in finding the proper standard, film nets can be used as illustrated in Fig 17 and 18 to help identify the zones. The zone of Laue spots falling on the meridian line of the Leonhardt net in Fig 17 clearly

shows a sequence of angular separations of 30° (spots on 20, 50, 80, 110 and 140 latitude lines) thus indicating that the zone is of the $\langle 111 \rangle$ form. This same relationship as well as a 135° relationship for a $\langle 100 \rangle$ zone is shown even more clearly in Fig 18, the common (110) Laue spot falling on the base line. Having established the [111] and [001] zones of this pattern, the identification of the Lauegram as one very near 29-15 follows quickly upon comparison with the standards.

The [101] and [001] zones of the face-centered cubic lattice generally need to be recognized for a rapid identification of the unknown pattern. When difficulty arises, the film nets again can be used as an aid. Although the isogonal net shown in Fig 5 is not constructed for direct application on a [101] zone, it can be used if a rough interpolation only is needed.

FINAL ANALYSIS

In order to plot the orientation of a crystal in stereographic projection, a method for measuring the angles δ and ϕ (see Fig 2 and 3) is required. The δ , ϕ analyzer shown in Fig 19 with δ ranging from zero to 30° and ϕ from zero to 360° fills this need very well; a complete analysis of a film often can be made with it in a time of five minutes or less. A film net as shown in Fig 6 but photographed on glass is mounted in a frame and located over a good source of light. To provide a carrier for the Lauegram, a circular clear piece of film approximately 8 in. in diam is clamped to a metal ring, which is graduated in degrees and is seated in the base concentrically with the film net in such a way that the assembly is free to rotate with the Lauegram while the clear film remains in contact with the surface of the stationary film net. The Lauegram is held against the surface of the clear film with scotch tape, the central spot of the Lauegram coinciding with the center of the film net and the pinprick falling on the single radial line (a reference line) when the scale reads 270. In this position the reference direction *R.D.* should coincide with the zero direction on the scale.

Continuing with the Lauegram used as an illustration in Fig 17 and 18, standard 29-15 from the index file is now laid over the Lauegram on the analyzer. An identified Laue spot is then brought to the reference line of the net. A final position with the (010)

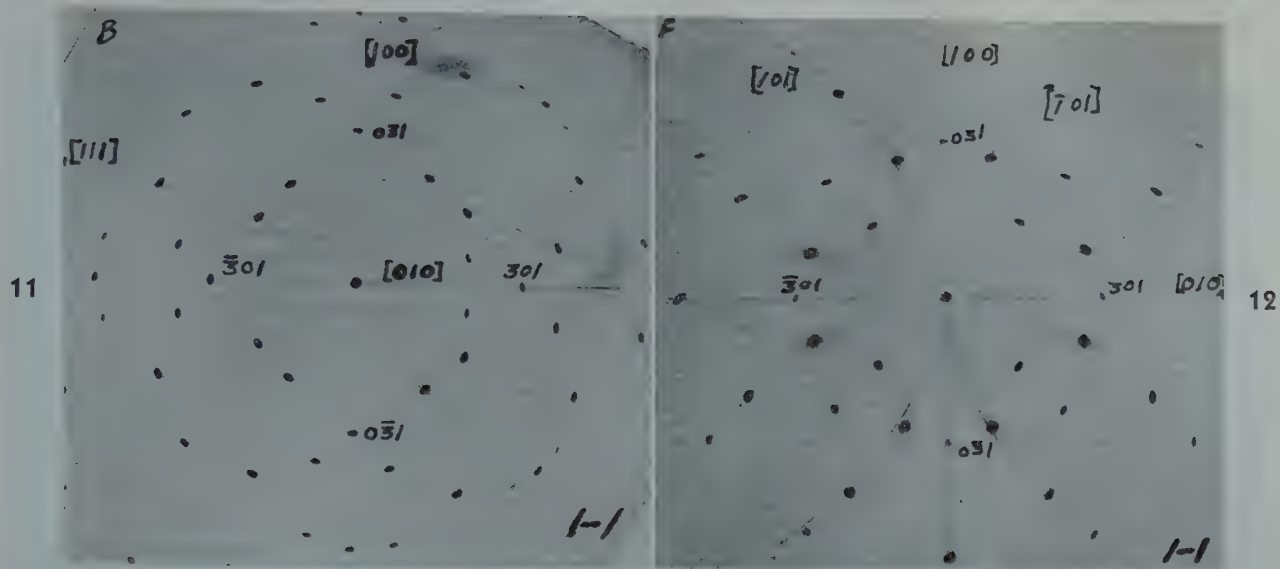


FIG 11—An indexed Lauegram for the body-centered cubic lattice in position 1-1.
 FIG 12—An indexed Lauegram for the face-centered cubic lattice in position 1-1.

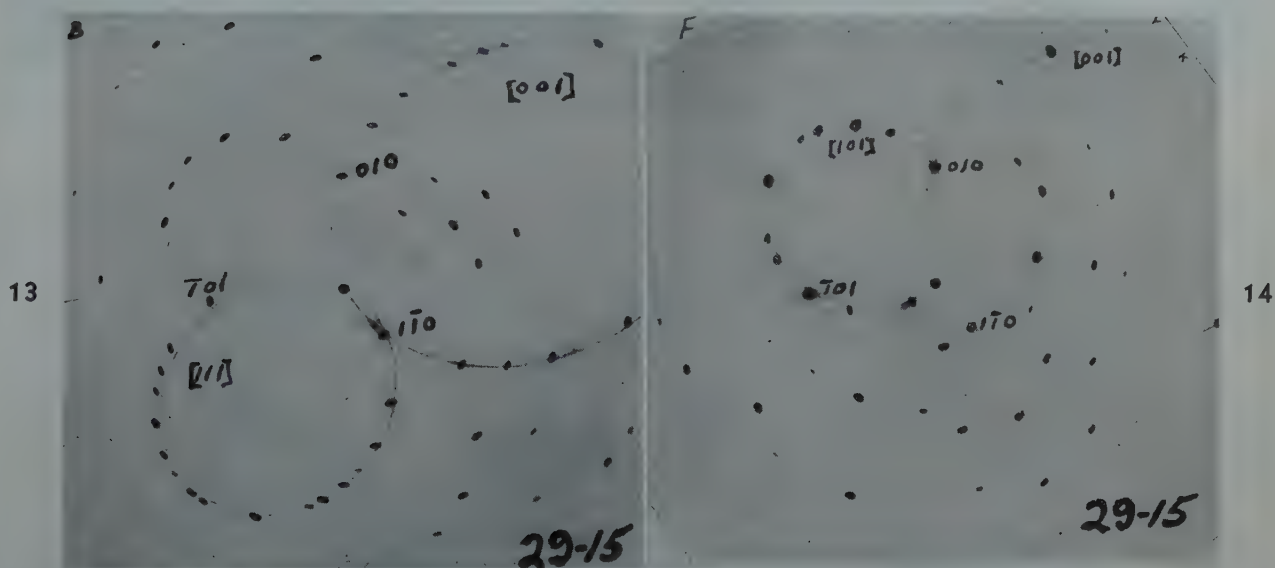


FIG 13—An indexed Lauegram for the body-centered cubic lattice in position 29-15.
 FIG 14—An indexed Lauegram for the face-centered cubic lattice in position 29-15.

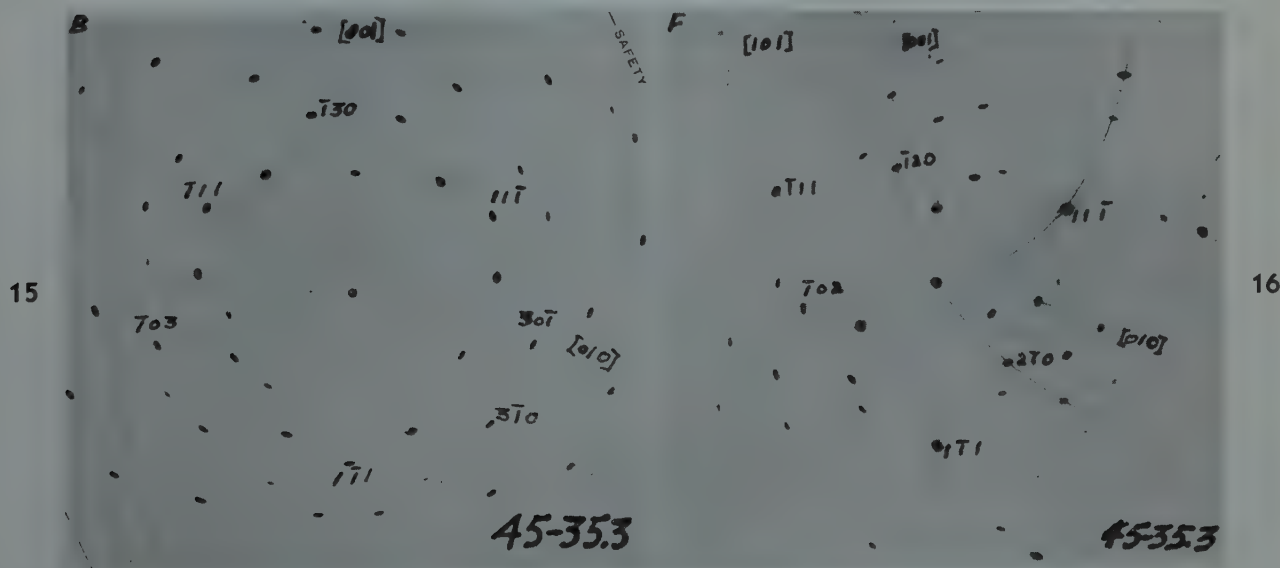


FIG 15—An indexed Lauegram for the body-centered cubic lattice in position 45-35.3.
 FIG 16—An indexed Lauegram for the face-centered cubic lattice in position 45-35.3.

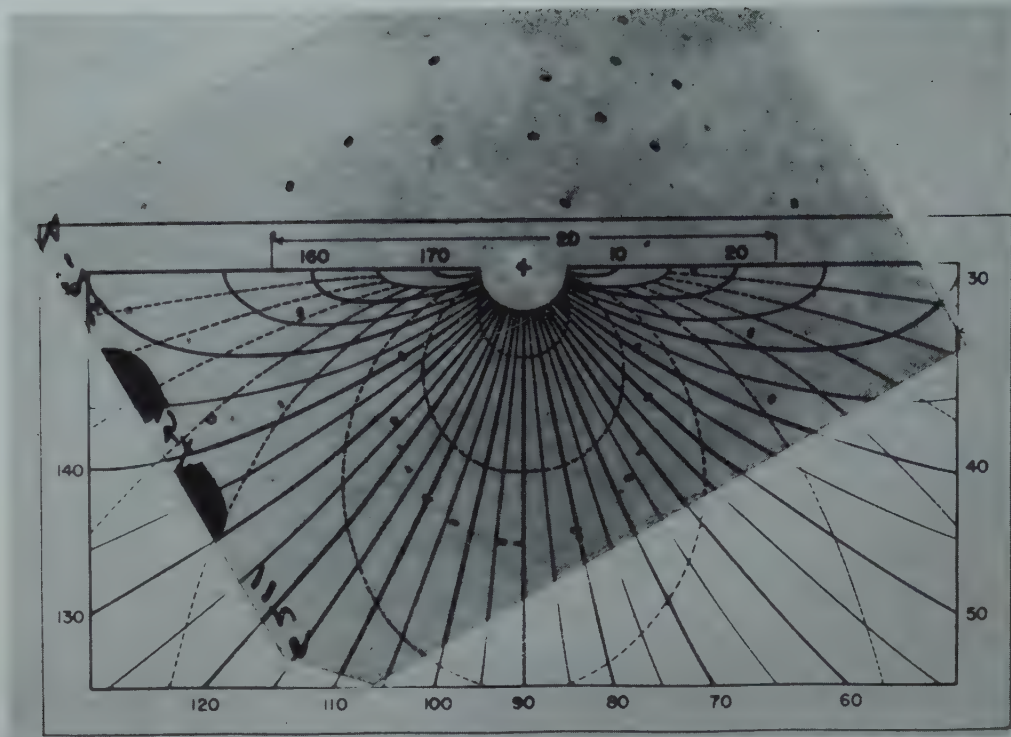


FIG 17—The Leonhardt zero-tilt net superimposed on a zone of Laue spots for measuring angles between planes.

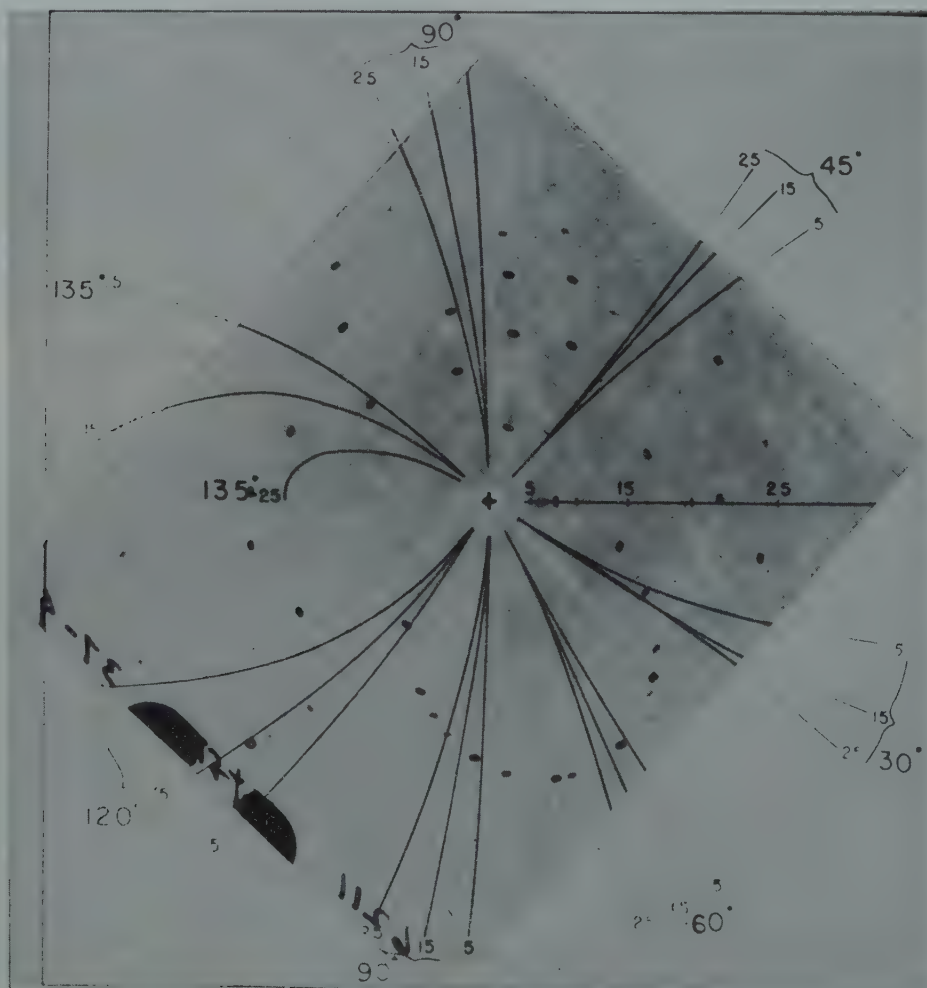


FIG 18—The isogonal net superimposed on a Lauegram for measuring angles between planes.



FIG 19—The δ , ϕ analyzer with transmission Laue pattern in position for determining the angles δ and ϕ .

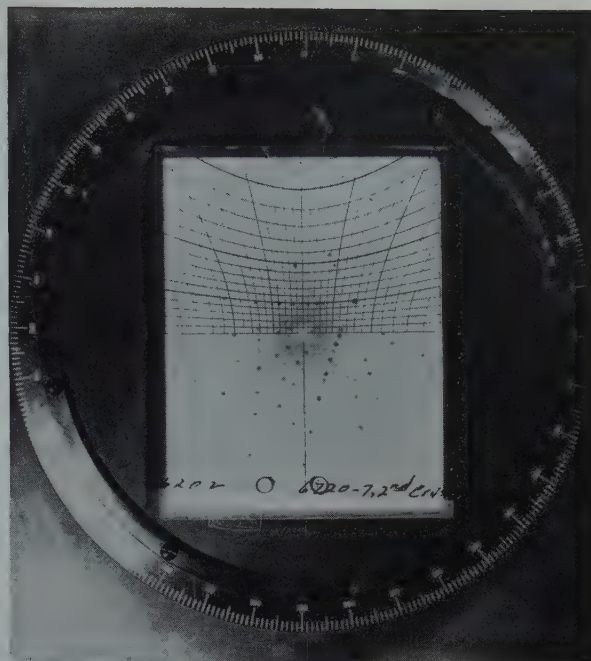


FIG 20—Analyzer employing a Greninger net and showing correct setting for a zone of Laue spots.

Laue spot falling at angles 16° and 187° for δ and ϕ respectively is illustrated in Fig 19. The angles δ and ϕ are essentially polar coordinates and must be so used in plotting the pole of the (010) plane in stereographic projection as was explained in the discussion of Fig 3.* The (110) and another Laue spot (one with larger δ for greater accuracy) are similarly plotted to determine the [001] zone. With the [001] zone on a meridian line of a Wulff net, the pole of the (100) plane and the pole of the (001) plane—the latter coinciding with the [001] zone axis—can be located directly to complete the analysis for the orientation of the crystal involved.

If a zone axis is to be plotted directly, the angles for doing this are obtained upon placing the zone of Laue spots as parallel as possible to the meridian lines of the net and reading tilt and azimuth from the analyzer.

Final analyses by the present method actually are more difficult to make near some of the common symmetry positions than for other positions. For example, in the face-centered lattice the position 45-0 (twofold symmetrical) is more difficult to analyze than is 29-15 shown in Fig 14. Likewise 0-0 (fourfold symmetrical) for iron is one of the more difficult positions to analyze rapidly.

In the usual back-reflection Laue

method, however, symmetry conditions are a great aid to both preliminary and final analyses. Zones are generally more useful than individual Laue spots for plotting the orientation in stereographic projection. A suitable set of marked standards could be made for the more rapid identification of zones in back-reflection Lauegrams.

A convenient method for measuring tilt and azimuth on such patterns is shown in Fig 20. Here a Greninger net comprises part of the analyzer. The Laue pattern is 44-18 in α , β' coordinates. Angle coordinates for a $\langle 111 \rangle$ zone, which has been placed parallel to the meridian lines of the net, are a tilt out of the plane of the sample of almost 10° and an azimuthal angle of 191° . These angles can be used with a Wulff net to plot the zone axis in stereographic projection.

Latitude lines on the Greninger net are useful for determining directly angles between planes in the same manner described previously for the zero-tilt Leonhardt net. For example, a {112} Laue spot is 30° from the {110} spot, the strongest Laue reflection for the $\langle 111 \rangle$ zone shown in Fig 20.

Acknowledgment

The amount of work represented by the final marked standard Laue patterns is considerable. The production of the negatives and positives from

the original Lauegrams alone is quite a task and the authors are indebted to the Photographic Department of the General Electric Co. for completing this work. The authors are also indebted to Dr. Arthur A. Burr, of Rensselaer Polytechnic Institute, for helpful suggestions in the preparation of the manuscript and to Eugene F. Welter of the Metals Section for assistance in the X ray work.

References

1. E. Schiebold and G. Sachs: Graphische Bestimmung der Gitterorientierung von Kristallen mit Hilfe des Laueverfahrens. *Ztsch. Krist.* (1926) **63**, 34.
2. E. Schmid and W. Boas: Kristallplastizität, p. 51, Berlin, 1935. Springer.
3. A. B. Greninger: (a) Determination of Orientations of Metallic Crystals by Means of Back-reflection Laue Photographs. *Trans. AIME* (1935) **117**, 61.
(b) A Back-reflection Laue Method for Determining Crystal Orientation. *Ztsch. Krist.* (1935) **91**, 424.
4. M. Majima and S. Togino: (a) The Radiograph of a Crystal having the Face-centered Cubic Lattice. *Sci Paper I.P.C.R. Tokyo*, (1927) **7**, No. 111, 75.
(b) The Radiograph of a Crystal having the Body-centered Cubic Lattice. *Sci Paper I.P.C.R. Tokyo*, (1927) **7**, No. 126, 259.
5. C. S. Barrett: The Stereographic Projection. *Trans. AIME* (1937) **124**, 29.
6. J. Leonhardt: Die Deutung der Laue diagramme deformierter Kristalle. *Ztsch. Krist.* (1924) **61**, 100.

* The Wulff net may be marked with ϕ ranging from 0° to 360° in a way to permit direct plotting of the data.

The Vapor Pressures of Zinc and Cadmium over Some of Their Silver Alloys

C. E. BIRCHENALL,* Junior Member, and C. H. CHENG,* Student Member AIME

Introduction

The fundamental problem in the thermodynamics of solid solutions is the determination or calculation of the activities of the components as a function of temperature and composition. Since the theory of metals is not sufficiently developed to allow *a priori* calculation of these quantities, they must be obtained from experiment. C. Wagner¹ has reviewed the literature of this subject for the period before 1940. Although several important and extensive studies have been made in the meantime, the number of systems to which any sort of quantitative information can be assigned is vanishingly small. These data have become of great potential importance in studies of the structure of solid solutions² and intermetallic compounds, the nature of the diffusion process,^{3,4} and perhaps even the mechanism of mechanical deformation.⁵ For these reasons, it seems very worthwhile to extend the experimental data in this field.

Although there is little use in duplicating Wagner's review, attention should be directed to the most recently reported investigations. A brief enumeration of the methods of measurement previously employed also should be valuable. The most direct method is the determination of the partial pressure of the components in the vapor phase in equilibrium with the solution. Both equilibrium and kinetic methods have been tried in metal systems, but almost exclusively on liquid phases. Only in the case of carbon in iron alloys and in the copper-zinc system have extensive measure-

ments been made which include solid phases.

When one of the components is an element, such as nitrogen or carbon, which forms compounds which are very volatile and stable at normal temperatures and pressures (CH_4 , CO_2 , CO , NH_3), it is frequently possible to equilibrate mixtures containing these (such as $\text{CH}_4\text{-H}_2$, $\text{CO}_2\text{-CO}$, $\text{NH}_3\text{-H}_2$) independently with the elements (C, N) and with the metal (Fe, Ni, etc.). Such measurements have been made for carbon in iron, iron-silicon, and iron-manganese alloys by Smith⁶ and in iron and iron-nickel alloys by Toensing.⁷ Differences between carbon activity values at the same temperature and carbon content when carbon is introduced from $\text{CH}_4\text{-H}_2$ mixtures or CO-CO_2 mixtures indicate that the effects of hydrogen and oxygen in the system are not negligible, and one can only hope that the true value lies somewhere between these sets of results, probably nearer the $\text{CH}_4\text{-H}_2$ data since hydrogen is less soluble in iron than oxygen. This is essentially an equilibrium method, although flowing gas is employed.

A kinetic method has been employed which consists of sweeping an inert gas (generally hydrogen) over the alloy at

a series of rates, condensing the metal vapor out, and analyzing it. The metal content can be extrapolated to zero flow rate (equilibrium). Wejnarth's⁸ work on Cd-Mg and Zn-Mg is a good example of this frequently used method. A variant of this consists of equilibrating a known volume of inert gas with the alloy, sweeping it out quickly, and analyzing for metal. In common with the above method, it has the disadvantage that the "inert" gas is generally somewhat soluble in the alloy. Moreover, the former continuously displaces the system from equilibrium and may give low values if solid diffusion is involved.

The dew point method applied by Hargreaves⁹ to the alpha and beta brasses and by Schneider and Stoll¹⁰ to Al-Zn avoids the introduction of another component to the system, but is useful only in systems in which one component is much more volatile than the other. The alloy sealed in one end of an evacuated silica tube is heated to the desired temperature. The temperature of the other end is lowered until droplets of the volatile component condense. When the temperature is raised slightly, the droplets will evaporate. By careful adjustment of temperature, the range between evaporation and condensation can be narrowed appreciably. An independent determination of the vapor pressure of the pure volatile component is necessary to give the partial pressure over the alloy. This is the method employed here to determine the vapor pressures of zinc and cadmium over their silver alloys up to 34 pct in cadmium and 76 pct in zinc. The former involves only the α solid solution, but the latter covers the α , β , γ , and ϵ fields.

In recent determinations, Herbenar, Siebert, and Duffenback¹¹ used the

Cleveland Meeting, October 1949.
TP 2601 E. Discussion of this paper
(2 copies) may be sent to *Transactions*
AIME before November 15, 1949.
Manuscript received February 9, 1949.
* Member of Staff and Research
Assistant, respectively, Metals Re-
search Laboratory, Carnegie Institute
of Technology.

¹ References are at the end of the
paper.

absorption of light to determine the concentration of zinc in the vapor phase over copper-zinc alloys. This is probably the method most free from objections arising from disturbance of equilibrium.

To calculate thermodynamic activities with pure metals as the standard states, independent determinations of the vapor pressures of pure components are necessary. For many metals, these have been made by two general types of measurement—the Knudsen method of effusion through an orifice and the method of free vaporization from a surface. The latter usually involves an assumption about the accommodation coefficient of the surface, and insofar as this is in doubt, the data obtained by the method are questionable. Therefore, the Knudsen method is more desirable. A recent experimental triumph is the determination of the vapor pressure of graphite in this manner.¹²

The calculation of thermodynamic activities from vapor pressure data has been described in a recent paper by Birchenall and Mehl³ for similar data on copper-zinc alloys. The methods are the same here. Another method sometimes employed in the determination of activities involves the measurement of the electromotive force of electrolytic cells. This is only feasible when the electrode reactions can be established beyond reasonable doubt and the cells are reversible in nature.¹³

Experimental

APPARATUS

With the exception of a few minor changes, the apparatus was similar to that of Hargreaves.⁹ The alundum furnace tube ($18 \times 1\frac{1}{4}$ in. id) was heated by three main resistance windings, with auxiliary coils to heat the tubes to the observation windows and the end plugs which were inserted to avoid draughts of cold air. The fine adjustment coil was movable in the direction along the tube. A low power cathetometer telescope was used to observe the droplets in the cooler end of the tube. A sketch of the apparatus appears in Fig 1.

TEMPERATURE CONTROL

Since the accuracy and reproducibility of this experiment are dependent chiefly upon the control and measurement of the temperatures at the ends of the fused quartz sample

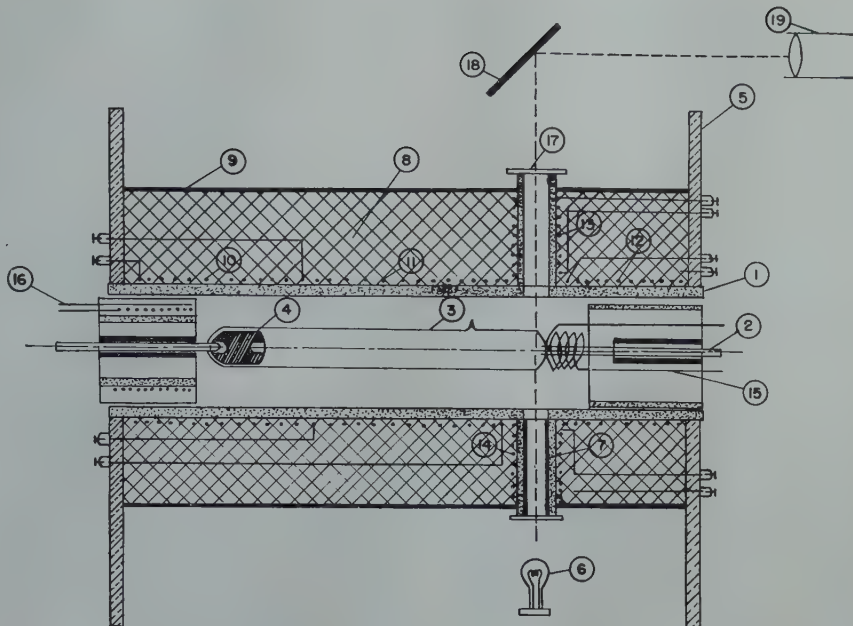


FIG 1—Apparatus for the determination of the vapor pressures of zinc and cadmium over their silver alloys by the dew point method.

- 1—Alundum furnace tube $18 \times 1\frac{1}{4}$ in. id
- 2—Quartz thermocouple protection tube
- 3—Quartz sample chamber
- 4—Specimen
- 5—Transite sheet
- 6—Lamp
- 7—Reflector
- 8—Silocel
- 9—Galvanized steel sheet
- 10—Coil A, No. 13 kanthal wire, 8 turns per in., 2.8 ohms at 20°C
- 11—Coil B, No. 13 kanthal wire, 7 turns per in., 2.2 ohms at 20°C
- 12—Coil C, No. 18 nichrome wire, 4 turns per in., 4.1 ohms at 20°C
- 13 to 16—Auxiliary coils
- 17—Glass plate
- 18—Mirror
- 19—Telescope

tube, considerable attention has been devoted to these factors. The voltage across each resistance winding could be adjusted independently of the others with "Powerstats." For long heating periods, automatic control equipment was employed. Fluctuations in temperature were quite small after the furnace had been stabilized. It was possible to achieve a controlled temperature difference of 400°C between the ends, considerably more than required in these systems.

SAMPLE PREPARATION

Silver powder (99.9 pct, lot no. 4203-D, U. S. Metals Refining Co.) was melted by induction heating in a graphite crucible, the inner walls of which were coated with alundum cement. Metallic zinc (99.99 pct) or cadmium (99.95 pct) was added making allowance for vaporization losses. The melt was stirred gently with a fine quartz tube and allowed to stand for about 2 min. before being permitted to freeze in the crucible. After a thin layer of the surface was machined off, the ingot was sealed in an evacuated pyrex

capsule and homogenized for 24 hr at 650°C . From this a cylinder was machined about $\frac{5}{8}$ in. high by $\frac{7}{16}$ in. diam and a shallow well drilled in one end to receive the thermocouple protection tube. The samples weighed about 10 g.

PROCEDURE

The specimen was sealed in a transparent quartz tube after flushing several times with dry hydrogen and pumping to a few microns pressure. The tube was inserted in the furnace and heated overnight, the high end stabilized by a controller. The run began by lowering the temperature at the other end slowly until droplets condensed in the field of the telescope. These were reevaporated by raising the temperature. Then the cycle was repeated several times, more slowly, to narrow the range between condensation and evaporation. The differences could be reduced to about 2°C at 10 mm pressure, 3°C at 5 mm pressure, and $4\text{--}5^{\circ}\text{C}$ at 1 mm pressure. The times required to establish these were about 15 min. at 10 mm and 2 hr at 1

mm. The true equilibrium temperature was assumed to lie midway between the condensation and evaporation temperatures.

It was customary to begin with a specimen temperature about midway between the extremes then take the upper and lower points. This prevents overlooking changes which might occur progressively in the alloy to produce errors which would appear systematic if the temperature was always changed in the same direction.

SAMPLING

Samples for chemical analysis were taken from chips removed in shaping the samples before the run, others were machined off after the run. In only one case did these disagree by more than duplicate analyses on the final sample. This indicates that the homogeneity of the cylinders was quite satisfactory. Even if heterogeneity existed on a scale too small to be detected by the sampling method, it would have little effect on the results if the surface was representative. Vapor transport would quickly homogenize the surface where the determination was really made.

In a number of alpha Ag-Zn runs, the droplets formed at the low temperature end were collected and analyzed to determine the validity of the assumption that the condensate consisted of nearly pure zinc. Only the lowest zinc sample showed even a trace

of silver, too small to be determined quantitatively. Under the conditions of the analysis, it could not have been as great as 0.1 pct. This was checked by spectrographic analysis which also revealed minute traces of iron, silicon, magnesium, and copper.

Because of its greater volatility, conditions were even more favorable in the cadmium case, and no attempt was made to analyze the droplets.

ERRORS

Although no exact determination of the errors is possible, a reasonable estimate may be given. These are principally of two types—those associated with establishment, measurement, and control of temperatures and those relating to the composition of the sample and droplets. Errors may also be introduced into the calculations due to errors in the vapor pressure data for pure zinc and cadmium, but it is believed that the equations K. K. Kelley¹⁴ employed here are correct to within a few per cent.

Temperatures were measured with chromel-alumel thermocouples standardized against the freezing point of pure aluminum and a Bureau of Standards secondary standard couple. At these low operating temperatures, no contamination or recrystallization of the couples was observed. There was a possibility of error in the failure of the couples to measure the effective temperature of the sample or droplets

due to the steep thermal gradient in the furnace. However, care was always taken to see that the specimen covered one thermocouple well, and the droplets formed on the other. A 1°C error in temperature reading produced a relative error of about 1½ pct in the calculations. It seems probable that the error from this source averages less than 5 pct for individual points and less when several points are correlated as below.

Of the compositional errors, those arising from impurities appear to be negligible. Pure metals were used in melting, and any oxygen introduced would be tied up as ZnO. The latter would make the analyzed Zn content slightly higher than that participating in the process. To minimize this, the surface was cleaned several times before sealing in the quartz tube. The spectrographic analyses indicate that the zinc may have reduced a trace of silicon from the quartz tube.

Heterogeneity of composition may have been present from three sources. Since the specimens were made from castings, some segregation may persist even after fairly long annealing. But the experiment itself is an annealing process, and the samples taken at the end should represent the real composition well. Furthermore, the reproducibility of points was found to be quite good at different stages during the run.

Long heating in a temperature gradient could produce a concentration gradient in the specimen, but the vapor pressure would still approach the true value for the average composition and temperature. It is unlikely that this effect is important here.

Repeated evaporation and condensation might cause considerable differences between the surface and the interior of the sample. In the 20 cm long tube of about 1.3 cm id, it is possible to have 0.01 g of zinc in the vapor phase at 100 mm pressure. This is increased by the necessity of forming droplets of finite size for visual resolution.

There should also be a time dependent hysteresis in the surface layer, as zinc is first evaporated, then condensed. However, by slowing the rate of temperature changes, the gap could be narrowed to the point that the equilibrium value was in little doubt.

Since the analytical deviations average between 1 and 2 pct, the calculated activities may contain errors which aggregate to more than 10 pct for

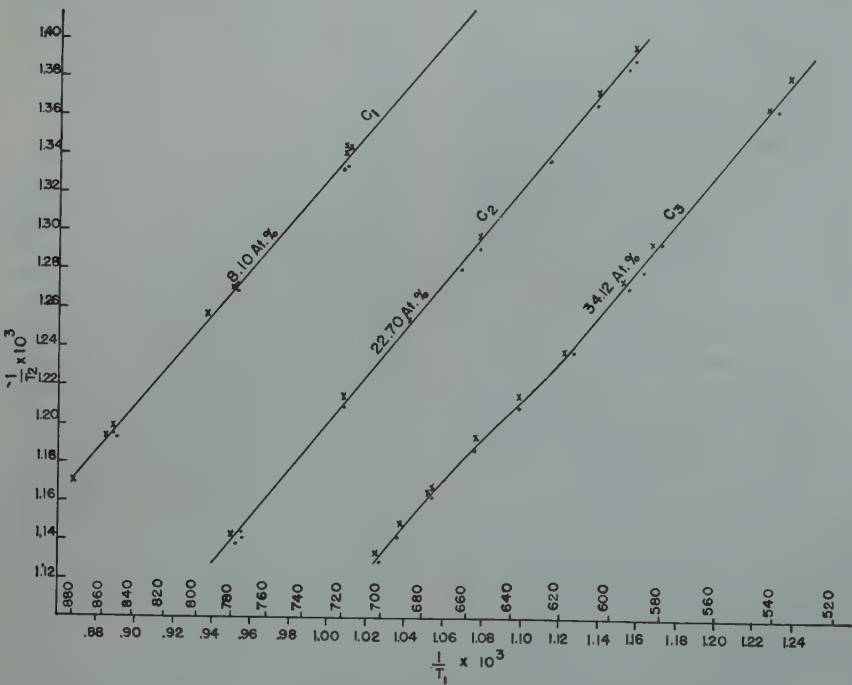


FIG 2—Graph of 1/T₁ vs. 1/T₂ for alpha silver-cadmium alloys. T₁ is the temperature of the alloy in equilibrium with cadmium droplets at temperature T₂.

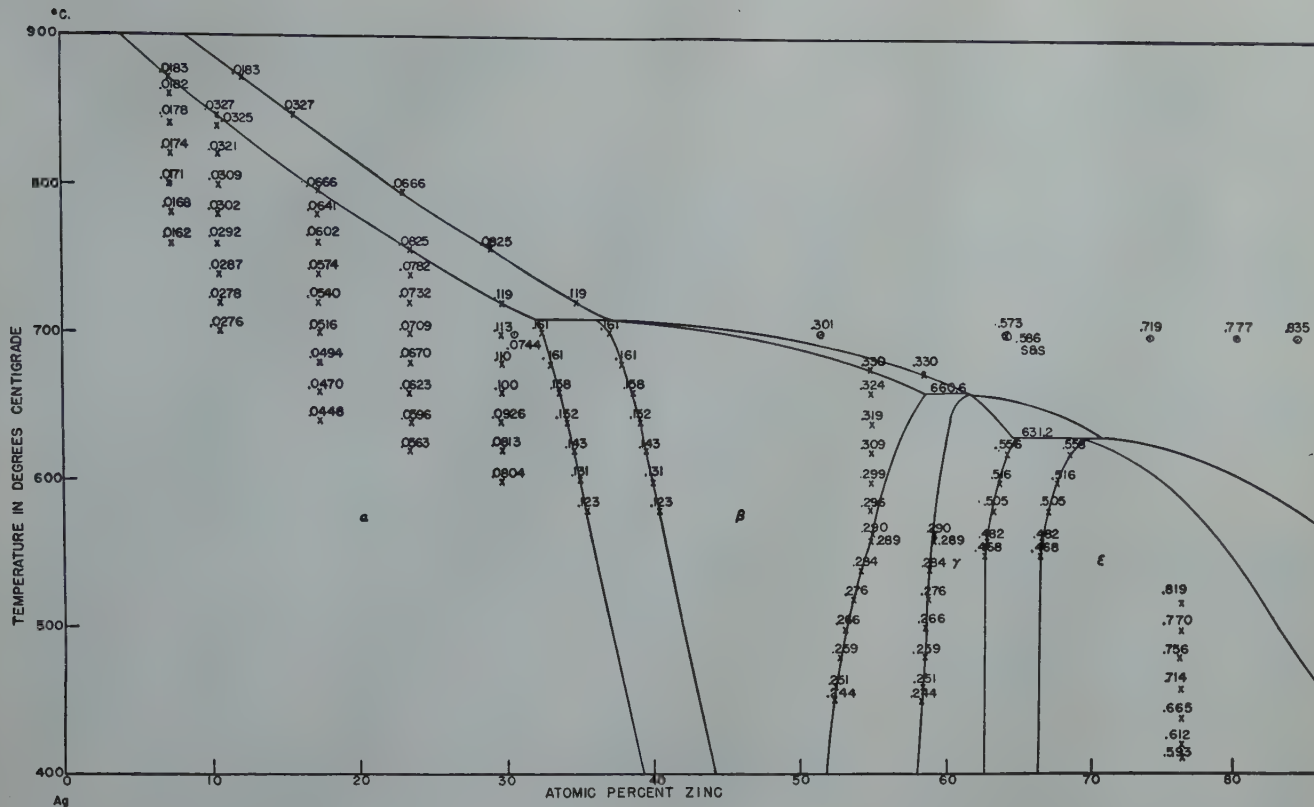


FIG 3—Phase diagram of the silver-zinc system according to Andrews, Davies, Hume-Rothery and Oswin, with the activities of zinc referred to pure liquid zinc as the standard state. The circled points are those of Schneider and Schmid.

single points, but the data taken as a whole should be better than this.

Discussion of Results

The Clapeyron-Clausius equation

$$\frac{\partial \ln p}{\partial T} = \frac{\Delta H}{RT^2} \quad [1]$$

relates the vapor pressure, p , the absolute temperature, T , the gas constant, R , and the heat of vaporization, ΔH . Over a narrow range of temperature, ΔH will be nearly constant. Then

$$\ln p = -\frac{\Delta H}{RT} + C. \quad [2]$$

If p_1 is the partial pressure of zinc or cadmium over the alloy at temperature T_1 , and p_0 is the vapor pressure of zinc or cadmium over the pure liquid metals at T_2 , they will obey

$$\ln p_1 = -\frac{\Delta H_1}{RT} + C_1 \quad [3]$$

$$\ln p_0 = -\frac{\Delta H_0}{RT} + C_0 \quad [4]$$

At equilibrium, $p_1 = p_0$, and

$$\frac{\Delta H_1}{R} \left(\frac{1}{T_1} \right) = \frac{\Delta H_0}{R} \left(\frac{1}{T_2} \right) + C_1 - C_0. \quad [5]$$

Since R , C_1 , C_0 are constants and ΔH_1 and ΔH_0 are nearly so, this is nearly a linear equation in $1/T_1$ and $1/T_2$. This is the form in which the experimental data were plotted for correlation. The

best smooth curve was drawn through the points, and values were read off at intervals of about 20°C. (As an example, the curves for silver-cadmium are given in Fig 2.) Tables 1 and 2 list the vapor pressures, activities, and activity coefficients for zinc and cadmium calculated from points read from these curves. It is possible by standard methods to calculate the other thermodynamic quantities for these systems as exemplified by the free energy of solution which will be discussed below.

Liquid zinc and cadmium have been chosen as the standard states for the calculation of activities using the vapor pressure equations of K. K. Kelley.¹⁴ Other standard states might have been employed. Particularly in the alpha solid solution ranges, the infinitely dilute solutions offer an attractive state independent of other determinations, but this is hardly suitable for extension to the other phases. Of course it is a simple matter to recalculate these points on the basis of any arbitrary reference state.

Since the activity coefficients for the constituents of two phase alloys depend on the location of the phase boundaries, it was necessary to assume that the diagram for silver-zinc given by Andrews, Davies, Hume-Rothery, and Oswin¹⁵ is correct. This diagram is

given in Fig 3 with the activities of zinc marked on it. Any deviations in this diagram will produce errors in the computed values given here. This problem did not arise in silver-cadmium because no two phase alloys were studied.

The few activities reported for solid phases in both systems by Schneider and Schmid¹⁶ are considerably lower than those observed here. This may be a result of allowing too little time for solid diffusion to supply zinc to the vapor. This seems especially likely since their liquid values seem to be quite consistent with the results obtained by extrapolating our data to the solidus line and with our one liquid point on silver-zinc.

It is interesting to examine the alpha solid solutions of the systems Cu-Cd, Ag-Cd, Ag-Zn, and Cu-Zn from the point of view of size factor, electronegativity, and the free energy of solution of liquid zinc or cadmium in silver or copper. According to Weibke and Matthes,¹⁷ the heat of formation is least in the case of Cu-Cd and increases in the order given to Cu-Zn. This is also the order for the free energy decrease given by Biltz.¹⁸ The data of Schneider and Schmid¹⁶ also leave little doubt that in the liquid phase Cu-Cd shows the least decrease

in free energy and Cu-Zn the greatest, but Ag-Zn and Ag-Cd are too close to separate. Using the Gibbs-Duhem equation (see ref. 3), it is possible to obtain activities for silver at 25 at. pct zinc or cadmium for 700°C. The partial molar free energy, $\Delta\bar{F}$, of a substance relative to some arbitrary standard state is given by

$$\Delta\bar{F}_i = RT \ln a_i, \quad [6]$$

and the total free energy change for a binary solution (a measure of its stability) is obtained from this by

$$\Delta F = X_1\Delta\bar{F}_1 + X_2\Delta\bar{F}_2, \quad [7]$$

where the X 's are mole fractions.

Substituting from above this becomes

$$\Delta F = RT(X_1 \ln a_1 + X_2 \ln a_2). \quad [8]$$

This is the equation employed in calculating ΔF in Table 3, corresponding to the reaction

Ag or Cu (solid) + Zn or Cd (liquid) \rightarrow solid solution (25% Zn or Cd)*

From this table, it appears that the stabilities of the Ag-Zn and Ag-Cd solutions are nearly identical with Ag-Cd slightly favored.

The size factors for the four systems are as follows: Cu-Zn, 1.04; Ag-Cd, 1.03; Ag-Zn, 1.08; Cu-Cd, 1.16. Only Cu-Cd exceeds the 1.15 set as the limiting value for extensive solubility. This is confirmed by the observation that Cu-Cd has an alpha solid solution extending to less than 2 at. pct cadmium while the other systems extend to 30 to 40 pct. Thus the repulsion due to large discrepancies in size makes very little free energy available through mixing copper and cadmium. Schneider and Schmid¹⁶ found that liquid solutions of copper and cadmium show positive deviations from ideal behavior while all the other systems above give negative deviations.

The most reasonable measure of electronegativity should be the Fermi energy of the crystalline metals. The differences should give a rough measure of the attraction between the components. Using the values of Slater,¹⁹ the following are obtained (in volts): Cu-Zn, 1.1; Ag-Cd, 0.8; Ag-Zn, 0.4; Cu-Cd, 2.3. Cu-Cd has already been eliminated by the size factor, so the solutions are favored in the decreasing order Cu-Zn, Ag-Cd, Ag-Zn as observed.

* The liquid states of Zn and Cd are used as reference states since they are the stable phases of the pure metals at the temperatures considered. Later in the discussion of short range order one of the assumptions requires the use of a fictitious solid reference state.

Table 1 . . . Vapor Pressure of Silver-Zinc Alloys in the α , β , γ and ϵ Fields

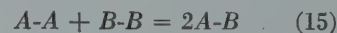
| Phase | T°C | P _{Zn} | P _{°Zn} | α | γ |
|------------------|-----|-----------------|------------------|----------|----------|
| 7.34 At. pct Zn | | | | | |
| α + liq. | 872 | 9.50 | 520 | 0.0183 | 0.249 |
| α | 860 | 8.25 | 453 | 0.0182 | 0.248 |
| α | 840 | 6.55 | 367 | 0.0178 | 0.243 |
| α | 820 | 5.08 | 292 | 0.0174 | 0.237 |
| α | 800 | 3.98 | 233 | 0.0171 | 0.233 |
| α | 780 | 3.05 | 181 | 0.0168 | 0.229 |
| α | 760 | 2.30 | 142 | 0.0162 | 0.221 |
| 10.53 At. pct Zn | | | | | |
| α + liq. | 847 | 13.00 | 398 | 0.0327 | 0.310 |
| α | 840 | 11.93 | 367 | 0.0325 | 0.309 |
| α | 820 | 9.38 | 292 | 0.0321 | 0.305 |
| α | 800 | 7.20 | 233 | 0.0309 | 0.293 |
| α | 780 | 5.46 | 181 | 0.0302 | 0.287 |
| α | 760 | 4.14 | 142 | 0.0292 | 0.277 |
| α | 740 | 3.10 | 108 | 0.0287 | 0.273 |
| α | 720 | 2.28 | 82.0 | 0.0278 | 0.264 |
| α | 700 | 1.67 | 60.5 | 0.0276 | 0.262 |
| 17.33 At. pct Zn | | | | | |
| α + liq. | 796 | 14.70 | 222 | 0.0662 | 0.382 |
| α | 780 | 11.60 | 181 | 0.0641 | 0.370 |
| α | 760 | 8.55 | 142 | 0.0602 | 0.347 |
| α | 740 | 6.20 | 108 | 0.0574 | 0.331 |
| α | 720 | 4.43 | 82.0 | 0.0540 | 0.312 |
| α | 700 | 3.12 | 60.5 | 0.0516 | 0.298 |
| α | 680 | 2.20 | 44.5 | 0.0494 | 0.285 |
| α | 660 | 1.51 | 32.1 | 0.0470 | 0.271 |
| α | 640 | 1.03 | 23.0 | 0.0448 | 0.259 |
| 23.45 At. pct Zn | | | | | |
| α + liq. | 757 | 11.30 | 137 | 0.0825 | 0.352 |
| α | 740 | 8.45 | 108 | 0.0782 | 0.333 |
| α | 720 | 6.00 | 82.0 | 0.0732 | 0.312 |
| α | 700 | 4.29 | 60.5 | 0.0709 | 0.302 |
| α | 680 | 2.98 | 44.5 | 0.0670 | 0.286 |
| α | 660 | 2.00 | 32.1 | 0.0623 | 0.266 |
| α | 640 | 1.37 | 23.0 | 0.0596 | 0.254 |
| α | 620 | 0.90 | 16.0 | 0.0563 | 0.240 |
| 29.65 At. pct Zn | | | | | |
| α | 720 | 9.75 | 82.0 | 0.1189 | 0.401 |
| α | 700 | 6.82 | 60.5 | 0.1127 | 0.380 |
| α | 680 | 4.89 | 44.5 | 0.1099 | 0.371 |
| α | 660 | 3.20 | 32.1 | 0.0997 | 0.336 |
| α | 640 | 2.13 | 23.0 | 0.0926 | 0.312 |
| α | 620 | 1.30 | 16.0 | 0.0813 | 0.274 |
| α | 600 | 0.90 | 11.2 | 0.0804 | 0.271 |

It is apparent that the size factor and electronegativity correlate quite well in a qualitative way with the observed free energies for these metallic solid solutions. However, it should be emphasized that it is unlikely that constants for the pure metals in themselves give an adequate representation of the state of these atoms in solution. This need not detract from their great usefulness which has been demonstrated in many instances.

The similarity in the deviations from ideal solution laws in the systems Ag-Zn and Ag-Cd to those in Cu-Zn suggests that the same considerations regarding the progression of structures applied earlier to the brasses² should also apply here. The progression of structures α , β , γ is, of course, very similar with only moderate shifts of phase boundaries corresponding to the quantitative differences in activities. The great differences in the free energies in the Cu-Cd system are reflected in the very different appearance of its phase diagram.

Short Range Ordering

Our attention has recently been called to an error in ref. 2* where Eq (18) relating the equilibrium constant, K , for the reaction of bonds



to the fraction, x , of bonds which are $B-B$ at 25 at. pct B has been mistakenly rewritten in Eq (19).

$$K = \frac{(1-4x)^2}{2x(1+2x)} = 4e^{-\Delta F^\circ/RT} \quad (\text{correct}) \quad (18)$$

$$K = \frac{(1-4x)^2}{2x(1-x)} = 4e^{-\Delta F^\circ/RT} \quad (\text{incorrect}) \quad (19)$$

ΔF° is the standard free energy for reaction (15).

When the values of x for 25 at. pct zinc in copper are recalculated for 950°C and 700°C, the first approxi-

* The authors wish to thank Professor C. S. Samis of the Univ. of British Columbia for discovering this error. The equation numbers from the earlier paper will be used in this section in parentheses.

Table 1 . . . (Continued)

| Phase | $N(\alpha)$ | $N(\beta)$ | $T^{\circ}C$ | P | P° | a | $\gamma(\alpha)$ | $\gamma(\beta)$ |
|-------------------------|--------------|------------|------------------|-------|-------------|-------|----------------------|-----------------|
| 37.15 At. pct Zn | | | | | | | | |
| $\alpha + \beta$ | 0.3235 | 0.370 | 700 | 9.75 | 60.5 | 0.161 | 0.498 | 0.435 |
| $\alpha + \beta$ | 0.3295 | 0.3795 | 680 | 7.15 | 44.5 | 0.161 | 0.489 | 0.425 |
| $\alpha + \beta$ | 0.3355 | 0.3860 | 660 | 5.08 | 32.1 | 0.158 | 0.471 | 0.410 |
| $\alpha + \beta$ | 0.340 | 0.391 | 640 | 3.50 | 23.0 | 0.152 | 0.447 | 0.388 |
| $\alpha + \beta$ | 0.345 | 0.395 | 620 | 2.28 | 16.0 | 0.143 | 0.415 | 0.362 |
| $\alpha + \beta$ | 0.350 | 0.400 | 600 | 1.47 | 11.2 | 0.131 | 0.374 | 0.327 |
| $\alpha + \beta$ | 0.354 | 0.404 | 580 | 0.94 | 7.63 | 0.123 | 0.348 | 0.304 |
| 54.87 At. pct Zn | | | | | | | | |
| $(\beta + \text{liq.})$ | 0.5487 | | 675 | 13.5 | 41.0 | 0.330 | 0.600 | |
| β | 0.5487 | | 660 | 10.4 | 32.1 | 0.324 | 0.590 | |
| β | 0.5487 | | 640 | 7.33 | 23.0 | 0.319 | 0.581 | |
| β | 0.5487 | | 620 | 4.95 | 16.0 | 0.309 | 0.563 | |
| β | 0.5487 | | 600 | 3.35 | 11.2 | 0.299 | 0.545 | |
| β | 0.5487 | | 580 | 2.26 | 7.63 | 0.296 | 0.539 | |
| $\beta + \gamma$ | 0.5487 | 0.5923 | 564 | 1.58 | 5.45 | 0.290 | 0.529 | 0.489 |
| $\beta + \gamma$ | 0.548 | 0.592 | 560 | 1.47 | 5.08 | 0.289 | 0.527 | 0.488 |
| $\beta + \gamma$ | 0.542 | 0.590 | 540 | 0.930 | 3.28 | 0.284 | 0.524 | 0.481 |
| $\beta + \gamma$ | 0.536 | 0.588 | 520 | 0.580 | 2.10 | 0.276 | 0.515 | 0.470 |
| $\beta + \gamma$ | 0.531 | 0.587 | 500 | 0.349 | 1.31 | 0.266 | 0.501 | 0.453 |
| $\beta + \gamma$ | 0.527 | 0.586 | 480 | 0.207 | 0.810 | 0.256 | 0.485 | 0.437 |
| $\beta + \gamma$ | 0.525 | 0.585 | 460 | 0.119 | 0.480 | 0.248 | 0.472 | 0.424 |
| $\beta + \gamma$ | 0.524 | 0.584 | 450 | 0.089 | 0.365 | 0.244 | 0.465 | 0.418 |
| 64.29 At. pct Zn | | | | | | | | |
| γ | 64.29 | | 620 | 8.90 | 16.0 | 0.556 | 0.865 | |
| $\gamma + \epsilon$ | 63.7 | 67.8 | 600 | 5.78 | 11.2 | 0.516 | 0.810 | 0.761 |
| $\gamma + \epsilon$ | 63.3 | 67.1 | 580 | 3.85 | 7.63 | 0.505 | 0.798 | 0.753 |
| $\gamma + \epsilon$ | 62.8 | 66.7 | 560 | 2.45 | 5.08 | 0.482 | 0.767 | 0.722 |
| $\gamma + \epsilon$ | 62.7 | 66.5 | 550 | 1.91 | 4.08 | 0.468 | 0.746 | 0.703 |
| liquid | | | 700 | 34.70 | 60.5 | 0.573 | $\gamma(l)$ 0.891 | |
| 76.45 At. pct Zn | | | | | | | | |
| Phase | $T^{\circ}C$ | P_{Zn} | P°_{Zn} | a | γ | | | |
| 76.45 At. pct Zn | | | | | | | | |
| ϵ | 500 | 0.940 | 1.31 | 0.718 | 0.940 | | | |
| ϵ | 480 | 0.595 | 0.810 | 0.735 | 0.962 | | | |
| ϵ | 460 | 0.335 | 0.480 | 0.698 | 0.913 | | | |
| ϵ | 440 | 0.181 | 0.273 | 0.662 | 0.867 | | | |
| ϵ | 420 | 0.093 | 0.153 | 0.608 | 0.795 | | | |
| ϵ | 410 | 0.067 | 0.113 | 0.593 | 0.776 | | | |

mations give $\frac{1}{20.4} = (0.0490)$ and

$\frac{1}{23.0} = (0.0435)$ respectively. These

results are in good agreement with those of Guttman²⁰ calculated from the equation of Takagi,²¹

$$\frac{v_{AA} + v_{BB} - 2v_{AB}}{kT} = \ln \frac{(c-x)^2}{x(1-2c+x)} \quad [9]$$

x has the same meaning as above, c is the atomic fraction of component B in the solution, and $\Delta F^\circ = N(2v_{AB} - v_{AA} - v_{BB})$ where N is Avogadro's number. Eq 9 may then be rewritten in exponential form

$$e^{-\Delta F^\circ/RT} = \frac{(c-x)^2}{x(1-2c+x)} \quad [9a]$$

Inserting $c = \frac{1}{4}$, this reduces immediately to Eq (18).

Repeating the procedure used in ref. 2 for $c = \frac{1}{3}$ and $c = \frac{1}{2}$ and substituting these values in Eq 9a, again gave two sets of identical equations.

For

$$c = \frac{1}{3}, e^{-\Delta F^\circ/RT} = \frac{(1-3x)^2}{3x(1+3x)}$$

$$c = \frac{1}{2}, e^{-\Delta F^\circ/RT} = \frac{(1-2x)^2}{4x^2}$$

It therefore appears that the methods of Birchenall and Takagi are equivalent for the treatment of short range order.

For calculations of short range order, the pure solid materials make the most convenient reference states. For zinc and cadmium, this involves an extrapolation of the vapor pressure equations for the solid beyond the melting point. In the case of zinc, the extrapolation is probably fairly good but cadmium is rather uncertain. Nevertheless this has been done here in determining the activity coefficients referred to the solid, approximate bond energies, free energies for reaction (15), and the short range order for the systems Cu-Zn, Ag-Zn, and Ag-Cd for 700°C and 25 at. pct Zn or Cd. In an ideal solution x , the fraction of Zn-Zn or Cd-Cd bonds would be 0.0625 ($\frac{1}{16}$),

Table 2 . . . Vapor Pressure of Alpha Silver-Cadmium Alloys

| $T^\circ C$ | $P_{mm. Hg}$ | P° | a | γ |
|------------------|--------------|-----------|--------|----------|
| 8.10 At. pct Cd | | | | |
| 880 | 63.0 | 2100 | 0.0300 | 0.370 |
| 860 | 50.0 | 1790 | 0.0279 | 0.344 |
| 840 | 40.2 | 1500 | 0.0268 | 0.313 |
| 820 | 31.7 | 1230 | 0.0258 | 0.319 |
| 800 | 24.8 | 1025 | 0.0242 | 0.299 |
| 780 | 19.0 | 850 | 0.0224 | 0.277 |
| 760 | 14.6 | 695 | 0.0211 | 0.260 |
| 740 | 11.1 | 565 | 0.0196 | 0.242 |
| 720 | 8.20 | 445 | 0.0184 | 0.227 |
| 700 | 6.00 | 342 | 0.0175 | 0.216 |
| 680 | 4.36 | 269 | 0.0162 | 0.200 |
| 660 | 3.15 | 203 | 0.0155 | 0.191 |
| 22.70 At. pct Cd | | | | |
| 800 | 117 | 1025 | 0.1141 | 0.503 |
| 780 | 90.5 | 850 | 0.1064 | 0.469 |
| 760 | 70.0 | 695 | 0.1007 | 0.444 |
| 740 | 52.5 | 565 | 0.0929 | 0.409 |
| 720 | 39.1 | 445 | 0.0876 | 0.386 |
| 700 | 29.0 | 342 | 0.0848 | 0.374 |
| 680 | 21.0 | 269 | 0.0781 | 0.344 |
| 660 | 15.0 | 203 | 0.0739 | 0.321 |
| 640 | 10.5 | 155 | 0.0677 | 0.298 |
| 620 | 7.15 | 115 | 0.0622 | 0.274 |
| 600 | 4.82 | 85.0 | 0.0567 | 0.250 |
| 580 | 3.22 | 62.5 | 0.0515 | 0.227 |
| 34.12 At. pct Cd | | | | |
| 720 | 130 | 445 | 0.292 | 0.856 |
| 700 | 96.0 | 342 | 0.281 | 0.823 |
| 680 | 71.5 | 269 | 0.266 | 0.780 |
| 660 | 52.8 | 203 | 0.260 | 0.762 |
| 640 | 40.2 | 155 | 0.259 | 0.759 |
| 620 | 29.8 | 115 | 0.259 | 0.759 |
| 600 | 20.1 | 85.0 | 0.236 | 0.694 |
| 580 | 13.5 | 62.5 | 0.216 | 0.633 |
| 560 | 8.80 | 43.7 | 0.201 | 0.590 |
| 540 | 5.60 | 30.4 | 0.184 | 0.539 |
| 520 | 3.48 | 20.8 | 0.167 | 0.489 |

P = pressure of zinc or cadmium in mm. Hg over alloy.

P° = pressure of zinc or cadmium over pure liquid metal at the same temperature.

$a = P/P^\circ$, the activity of zinc or cadmium.

$\gamma = a/N$, the activity coefficient.

N = mole fraction of zinc or cadmium.

but in all three cases it is less than this. The tabulation follows (Table 4).

Using Darken's²² correlation of the activity coefficients for solid silver-gold solutions and Eq 9, the x 's have been calculated for mol fractions 0.25, 0.50, and 0.75 at 700°C and several temperatures along the solidus line. Even in this completely isomorphous system and so near the melting points the ordering is seen to be appreciable.

The scatter of data did not permit estimating the dependence of ΔF° on temperature for reaction (15) for silver and gold. Consequently, the mol fractions and x 's apply to either component, the deviations showing up most markedly in the value of x for the dilute component (Table 5).

Summary

The vapor pressures of cadmium in equilibrium with three alloys in the alpha solid solution field in silver have been measured over a temperature range of about 200°C. Similar measure-

Table 3 . . . Free Energies of Solution at 25 At. Pct Zinc or Cadmium at 700°C for Ag-Zn, Ag-Cd, and Cu-Zn

| System | a ₁ | a ₂ | log a ₁ | log a ₂ | ΔF |
|--------|----------------|----------------|--------------------|--------------------|-------|
| Ag-Zn | 0.718 | 0.0788 | -0.144 | -1.1035 | -1710 |
| Ag-Cd | 0.642 | 0.1060 | -0.193 | -0.975 | -1730 |
| Cu-Zn | 0.611 | 0.0470 | -0.214 | -1.328 | -2190 |

Note: Subscript (1) refers to Ag and Cu, (2) to Zn and Cd.

Table 4 . . . Short Range Order and Bond Energies for Cu-Zn, Ag-Zn, Ag-Cd at 700°C and 25 At. Pct Zn or Cd

| System | (Stabilization Energy of A - B over B - B) | ΔF° | X _{Zn or Cd} |
|--------|--|-----------------------------|-----------------------|
| Cu-Zn | B = Cu 264 Zn 852 cal per mol of bonds | + 1116 cal per mol of bonds | 0.0435 |
| Ag-Zn | Ag 54.5 Zn 644 | - 699 | 0.0503 |
| Ag-Cd | Ag 202 Cd 536 | - 738 | 0.0492 |

Table 5 . . . Short Range Order in Silver-Gold Alloys

| Atom Fraction | x (ideal) | x (calculated) | | | |
|---------------|-----------|----------------|--------|--------|--------|
| | | 700°C | 990°C | 1015°C | 1040°C |
| 0.25 | 0.0625 | 0.0532 | 0.0553 | | |
| 0.50 | 0.250 | 0.233 | 0.237 | 0.237 | |
| 0.75 | 0.563 | 0.553 | 0.555 | 0.555 | 0.555 |

ments have been made on nine alloys of silver and zinc from 8 to 76 at. pct zinc and over a somewhat narrower temperature range. These alloys include the α, β, γ, and ε fields, as well as yielding activities along several of the liquidus lines.

The thermodynamic activities and activity coefficients have been calculated for the volatile component in each case. In the silver-zinc system, the activity coefficients of two phase alloys are based on the phase diagram of Andrews, Davies, Hume-Rothery, and Oswin.

At 700°C and 25 at. pct, the free energies of solution for liquid zinc and cadmium in solid silver have been computed for comparison with those of copper-zinc. The free energies of these systems have been compared with each other and copper-cadmium with respect to size factor, electronegativities and the progression of stable phases in the phase diagram.

The methods for calculating short range order developed by Birchenall and Takagi have been shown to lead to identical results. Application has been made to the alpha solid solutions of silver-zinc, copper-zinc, and silver-cadmium at 700°C and 25 at. pct zinc or cadmium and to the silver-gold

system. These calculations indicate a greater proportion of A-B bonds than would be present in ideal solution.

Acknowledgments

This work was done on a contract between the Office of Naval Research and the Metals Research Laboratory of Carnegie Institute of Technology. The chemical analyses were performed by Martha M. Helzel. Many of the runs were carried out by Wilbert Walker, and a few of the alloys were melted by William J. Reichenacker. Their assistance is gratefully acknowledged.

References

1. C. Wagner: Handbuch der Metallphysik, Vol. 1, pt. 2, Leipzig, 1940. Contains complete references to previous work.
2. C. E. Birchenall: *Metals Tech.*, June 1947, TP 2169; *Trans. AIME* (1947) 171, 166.
3. C. E. Birchenall and R. F. Mehl: *Metals Tech.*, June 1947, TP 2168; *Trans. AIME* (1947) 171, 143.
4. J. C. Fisher, J. H. Hollomon, and D. Turnbull: *Metals Tech.*, Feb. 1948.
5. A. H. Cottrell: Effect of Solute Atoms on the Behavior of Dislocations. Bristol Conf. 7989. June, 1948.

6. R. P. Smith: *Jnl. Am. Chem. Soc.* (1946) 68, 1163; *ibid.* (1948) 70, 2724.
7. E. Toensing: Doctorate Thesis, Carnegie Inst. of Tech., Dept. of Chem., 1947.
8. A. Wejnarth: *Technisk Tidskrift* (1942) 72, 33.
9. R. Hargreaves: *Jnl. Inst. of Metals* (1939) 64, 115.
10. A. Schneider and E. K. Stoll: *Ztsch. Elektrochem.* (1941) 47, 519, 527.
11. A. W. Herbenar, C. A. Siebert, and O. S. Duffenback: Unpublished paper.
12. L. Brewer, P. W. Gilles, and F. A. Jenkins: *Jnl. Chem. Phys.* (1948) 16, 797.
13. A. Wachter: *Jnl. Am. Chem. Soc.* (1932) 54, 4609.
14. K. K. Kelley: *Bur. of Mines Bull.* 383, (1935).
15. K. W. Andrews, H. E. Davies, W. Hume-Rothery, and C. R. Oswin: *Proc. Roy. Soc. (London)* (1941) 177A, 149.
16. A. Schneider and H. Schmid: *Ztsch. Elektrochem.* (1942) 48, 627.
17. F. Weibke and H. Matthes: *Ztsch. Elektrochem.* (1941) 47, 623.
18. W. Biltz: *Ztsch. Metallkunde* (1937) 29, 73.
19. J. C. Slater: Introduction to Chemical Physics. New York, 1939, McGraw Hill Book Co.
20. L. Guttman: *Metals Tech.*, Feb., 1948, TP 2330; *Trans. AIME* (1948) 175, 178.
21. Y. Takagi: *Proc. Phys. Math. Soc., Japan* (1941) 23, 44.
22. L. S. Darken: *Metals Tech.*, Jan., 1948, TP 2311; *Trans. AIME* (1948) 175, 184.

Sintering Characteristics of Minus Sixty-five and Twenty Mesh Magnetite

ALAN STANLEY,* Junior Member AIME, and JOSEPH C. MEAD

Introduction

The MacIntyre Development of the National Lead Co. is located at Tahawus, N. Y. The operations involve the mining and concentrating of a titaniferous iron ore to produce an ilmenite concentrate and a magnetite concentrate.

Construction of the MacIntyre plant was commenced during the summer of 1941, when world conditions threatened to cut off the supply of Indian ilmenite. An open pit mining operation was developed and the crushing and milling equipment put in operation in July 1942. A general description of the operation was given in the Adirondack Issue of *Mining and Metallurgy* for November 1943. The metallurgy of the mill operation was described by Mr. Frank R. Milliken,* Plant Manager, National Lead Company, MacIntyre Development, and presented at the AIME New York Meeting, February 1948.

The magnetite concentrate produced in the milling operation was too fine (minus 20 mesh) to be used directly in iron blast furnace operation, and most of the magnetite had to be stockpiled in 1942 and 1943.

In 1943, the Defense Plant Corp. built a Greenawalt sintering plant at Tahawus, N. Y., to put the magnetite concentrate in a more suitable form for use in the iron blast furnace.

The Greenawalt sintering plant consists of three 10 by 25 ft sintering pans

designed to produce 1800 gross tons of sinter per 24 hr. The vacuum to each pan is produced by two Greenawalt fans in series, pulling approximately 30,000 cu ft of air per minute at 50 in. water gauge vacuum. The plant started operation in August 1944. The present plant production averages 25 tons per operating pan hour (approximately 224 lb per operating hour per square foot of grate area) of plus 1 in. sinter.

Raw feed to the plant consists of 61 pct magnetite, 4 pct anthracite coal culm, and 35 pct minus 1 in. return fines which are conveyed to a pug mill where the materials are mixed thoroughly and water added to give the mixture 5.5 to 6 pct moisture. The mixed prepared feed is conveyed to two 4 by 10 ft vibrating screens where the minus 1 in. plus $\frac{5}{8}$ in. return fines are screened out and discharged into a surge bin for use as a hearth layer. The minus $\frac{5}{8}$ in. prepared feed is discharged into another surge bin for use as prepared feed.

A charge car, electrically operated, having a capacity of one charge of prepared feed and several charges of hearth layer, lays a thin layer of plus $\frac{5}{8}$ in. return fines and $9\frac{1}{2}$ in. depth of

prepared feed into the pans. A fluffing roll and a vibrator on the car fluffs and spreads the prepared feed into the pans.

An ignition car, electrically operated, ignites the top of the bed with a 30 sec flash burn. The $9\frac{1}{2}$ in. bed sinters in approximately 13 min. Dumping the pan, and recharging and igniting the bed requires 2 min.

To improve the quality of the ilmenite concentrate produced in the mill and to reduce the amount of titanium dioxide lost in the mill tailings and in the magnetite product, extensive research work and pilot plant operations have been done on grinding the crude ore to minus 65 mesh size (rather than to minus 20 mesh) and concentrating it by a combination of magnetic separation (for magnetite recovery) and flotation (for ilmenite recovery). These tests have proved successful in increasing ilmenite recovery and grade.

With the development of the ilmenite flotation process to a stage where a full scale flotation plant was in the design stage, the problem arose of handling the 65 mesh magnetite concentrate that would be produced. In order to study and solve the problems of handling and sintering the 65 mesh magnetite in the sinter plant, a pilot sinter plant was secured from John E. Greenawalt.

The effect of using 65 mesh magnetite in the sintering operations was then studied on the 2.4 sq ft test pan, operating under conditions as similar to the large plant as could be set up in the laboratory.

A series of tests were run in the test pan on present sinter plant feed that had been mixed in the plant pug mill. An average production and an average quality of sinter produced in this series

San Francisco Meeting, February 1949.

TP 2597 BC. Discussion of this paper (2 copies) may be sent to *Transactions AIME* before Aug. 1, 1949. Manuscript received Nov. 27, 1948.

* General Engineer and Sinter Plant Superintendent, respectively, MacIntyre Development, Titanium Division, National Lead Co., Tahawus, N. Y.

* Frank R. Milliken: Metallurgy at National Lead Company. TP 2355, *AIME Mining Tech.* (May 1948).

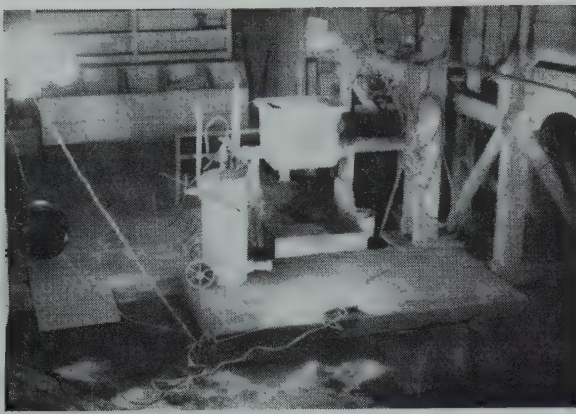


FIG 1—Sinter pan and kerosene burner.

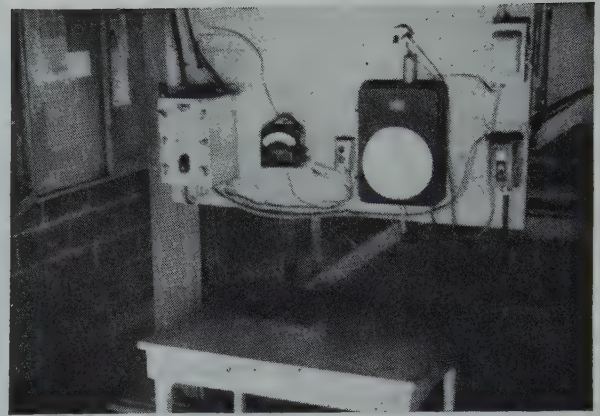


FIG 2—Instrument panel.

of tests was established as a "Standard" (8.8 lb per min) to compare the sintering of minus 20 mesh magnetite with that of minus 65 mesh magnetite.

The high points on each series of tests were repeated twice as a check on the original, to be sure that some unknown variable did not cause the change in the sintering performance. A test run of 10 pans was made on the mixture found to give the best production and quality.

Procedure

The pilot sinter plant included a sintering pan 20¾ by 16¾ in. and 9 in. deep, an ignition hood, a pressure kerosene burner for ignition, a dust collector, and a 400 cfm vacuum fan rated at 54 in. of water (see Fig 1 and 2 for instrument panel, sinter pan and kerosene burner).

Vacuum was recorded on a Bristol meter, and exhaust temperatures were read from an electrical pyrometer.

Magnetite of 65 mesh was prepared by grinding stockpile (20 mesh) magnetite, to the desired size, in a batch ball mill, and filtering in a laboratory pressure filter, Table 1.

The moisture obtained by this method of filtering was too high for pilot plant use (averaging about 9 pct) and it was necessary to dry a portion of the magnetite prior to its use in the sintering operation.

For the final "production run" tests, rod mill screen undersize (20 mesh) was ground to 65 mesh, and the magnetite was concentrated in a laboratory

Crockett.

Coal was obtained from the sinter plant stockpile, and when necessary, ground in a ball mill to the desired size. After several tests had to be discarded because of poor results caused by coal with high ash content, all coal samples were submitted to the laboratory for ash determination. In order to eliminate one variable, only coal with a 10 pct or less ash content was used in the test work.

Sawdust, when needed, was obtained from local mills; limestone and slaked lime were obtained from the Chazy Lime and Stone Co.

The return fines, unless otherwise noted, were obtained by crushing plus 1 in. sinter, produced in the pilot plant, in a jaw crusher and rolls and screening it to the desired size on a laboratory vibrating screen.

Screens for screening the sinter were made locally, as were sample racks and storage bins for the raw materials. A ¼ yard gasoline concrete mixer was connected to an electric drive and used for the mixing of all batches. Balances and a hot plate were provided for moisture determinations, and an electric clock with a sweep second hand was used for timing the tests.

A group of five persons was found to be the most efficient, as continuous test work required constant work by one man grinding magnetite and coal, one man preparing sized return fines, two men preparing batches for burning, and one man completing the necessary calculations and paper work. The last three men were required when the batches were burned.

Each batch mixed contained enough material for two tests. The charge was calculated in advance. A weighted mixture of dry and filtered magnetite was added to the mixer. This material was then mixed for 5 min and a moisture determination made. Using this moisture it was possible to calculate the exact amount of magnetite that had to be removed or added to the mixer to leave the required weight of magnetite at 5 pct moisture.

Then the remaining materials were added dry, and the necessary amount of water to provide the required moisture was sprinkled, with a sprinkling can, into the revolving mixer. When trouble with pellet formation occurred, the procedure was changed so that the necessary water was added to the return fines, and then the wet returns were added to the mixer. The latter method was more satisfactory.

Each batch, unless otherwise noted, was mixed for 5 min again.

A 15 lb bedding charge (minus 1 in. plus ½ in. sinter) was added to the pan for each burn. This gave a bedding depth of 1 in. Then the sinter pan was filled, with a weighed amount of mix, and dumped by hand through a 1 in. screen. The bed then was made level by scraping off the excess material. The weight of the mix in the pan was obtained by difference. The ignition hood was lowered into place over the pan, and the pressure kerosene burner was ignited, as the vacuum was turned on, and ignition took place for 30 sec. The hood was then raised. A record was made of the exhaust temperature as the burning proceeded and vacuum was recorded continuously with the Bristol meter. When the bedding on the grate bars glowed red (viewed by means of a mirror mounted to make the grates visible through a hole covered with glass in the bottom of the pan) the vacuum was turned off and the

Table 1 . . . Screen Analysis of Magnetite Products

| | +28 | +35 | +48 | +65 | +100 | +150 | +200 | −200 |
|--------------|-----|------|------|------|------|------|------|------|
| 20 mesh..... | 8.3 | 16.4 | 19.5 | 14.8 | 12.1 | 9.2 | 5.2 | 14.5 |
| 65 mesh..... | | | | 3.0 | 11.2 | 19.8 | 15.8 | 50.2 |

Note: All references to 65 and 20 mesh magnetite refer to minus 65 and minus 20 mesh material.

sintered charge was dumped by inverting the pan.

The results of the first pan of the mix were usually poor because a cold pan did not approximate actual operating conditions. The second, or hot pan, gave results that could be compared more directly with sinter plant practice.

After each pan was burned, the material was passed over a 1 in. Ty-Rock screen three times. The material remaining as plus 1 in. was "sinter." The minus 1 in. material was passed over a ½ in. Ty-Rock screen twice, and the plus ½ in. material was "bedding." The remainder of the material (minus ½ in.) was "return fines" (note: in all references to return fines in this paper, the bedding is excluded).

In order to have a strength comparison of the sinter formed by various mixes, a "quality" figure was initiated. This figure was determined by screening the cold (the plus 1 in. sinter was allowed to air cool overnight) sinter in the same manner as above. The weights of the plus 1 in. and the plus ½ in. were combined, and this total weight was divided by the weight of the hot 1 in. sinter to obtain relative "quality."

Cycle time was figured by adding 2½ min to the burning time to allow for dumping and recharging the pan. Theoretical production in pounds per minute was determined by dividing the pounds of plus 1 in. sinter by the cycle time. In quite a few tests the amount of bedding and return fines produced was not sufficient for repeat operations. Because of this some of the plus 1 in. sinter had to be taken to provide the amounts of these materials needed. Actual production was then the weight of plus 1 in. sinter remaining after bedding and return fines requirements were met, divided by cycle time.

Discussion of Factors Investigated

The following factors were investigated during the test period:

(1) return fines, (2) coal, (3) moisture, (4) slaked lime and miscellaneous reagents, (5) oxidation, (6) limestone, (7) sawdust, (8) pellets, (9) "dust," (10) mixing time, and (11) production runs.

RETURN FINES

As far as is known, there is no sinter plant in the United States that employs sized return fines as a necessary

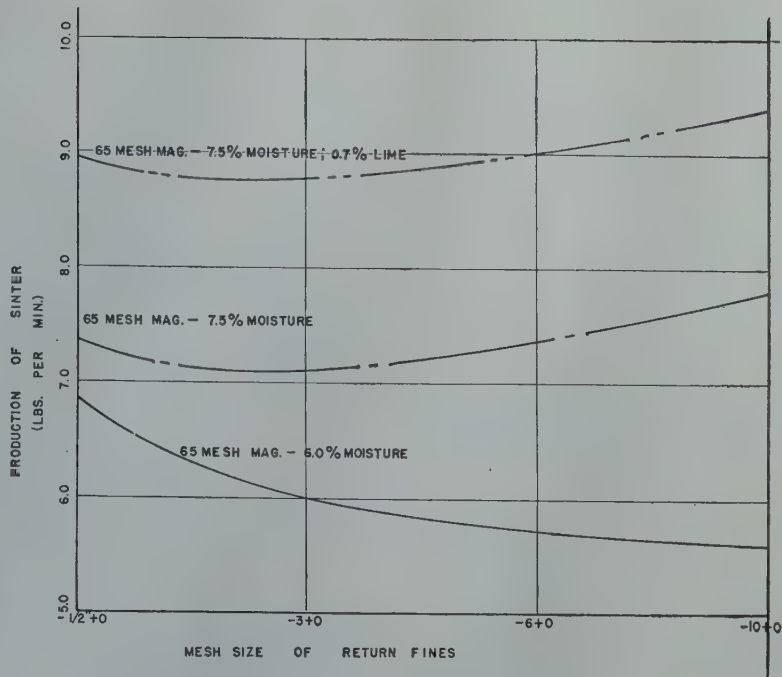


FIG 3—Results of return fines series.

metallurgical requirement for its operation. Mr. Worm Lund, on a visit to MacIntyre from Sweden, suggested the possibility of sized return fines in the sintering of 65 mesh magnetite.

In the test plant at 20 mesh, return fines were not necessary for the production of good sinter. In many cases the return fines were detrimental to test plant production. This is especially true when the returns consisted mainly of raw magnetite, coal, and dust from the dust collectors.

For sintering 65 mesh and finer magnetite, return fines are absolutely necessary for sinter production. If efficient operation and economical sinter are to be had, it is necessary to have these return fines fall within definite size ranges. The secret of sintering fine concentrates is to obtain proper porosity in the "bed" so that air can be uniformly distributed throughout and burning can progress.

A series of tests were run using minus ½ in. plus 3; minus 3 plus 6, minus 6 plus 10, minus 10 plus 20, minus 10 plus 35, and minus 20 plus 35 mesh return fines. The best results were obtained from the minus 10 plus 35 mesh tests. Because of the difficulty that would be incurred by screening to these close sizes, a series was run using minus ½ in. plus 0, minus 3 plus 0, minus 6 plus 0, and minus 10 plus 0. The results of this series can be seen in Fig 3. These tests were run with 4.0 pct coal and 25 pct return fines.

As can be seen (Fig 3) the best re-

sults were obtained using minus 10 mesh plus 0 return fines. The best percentage of this size return fines was determined by a series of tests (Fig 4). The results were satisfactory only as long as the minus 35 mesh portion did not exceed 25 pct of the total return fines weight. (This then would give a calculated minus 10 plus 35 mesh return fines figure of 18.75 pct of the total weight of the charge.)

A study of the results obtained using various amounts and sizes of return fines indicated:

1. Proper porosity is essential in producing sinter economically:

- Too much porosity causes too rapid burning and results in poor sinter.
- Insufficient porosity increases the burning time beyond economic limits.

2. Excess returns weaken the sinter and cause a drop in production.

3. By proper control of the size and amount of returns it should be possible to sinter magnetite finer than 65 mesh.

4. More efficient sinter plant operation could be obtained if the dust from the dust collectors and the finer portion of the returns were returned to the original source of sinter plant feed (for example: to magnetite filter).

A 20 mesh magnetite will sinter without the addition of return fines, providing adequate bedding is supplied, but blast furnace operations object to fines; this requires that the fine material be screened out and recirculated.

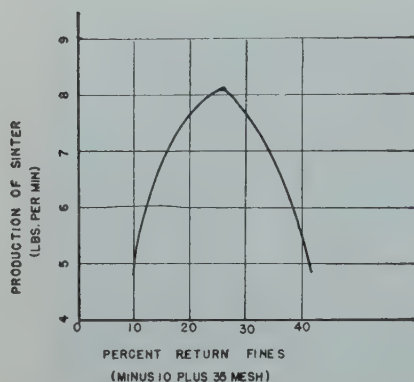


FIG 4—Results of various percentages of minus 10 plus 35 mesh returns.

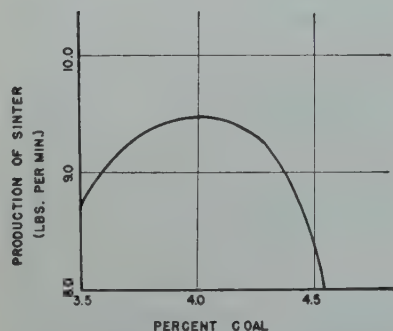


FIG 5—Effect of various percentages of anthracite culm 4 and 5 buckwheat coal on sinter production using 65 mesh magnetite.

COAL

Coal is used in MacIntyre sintering as the most economical local source of carbon.

The amount and size of coal used is an important factor in a sintering operation.

As can be seen in Fig 5, 4.0 pct coal produced the best results in sintering 65 mesh magnetite. Both greater and lesser amounts of coal tended to slow the burning time and reduce the production of sinter. Insufficient coal did not produce enough heat for proper sintering and excess coal caused too high a temperature, resulting in slagging and overoxidation with resultant poor sinter. This overoxidation was caused by an oxidizing atmosphere, and while reduction may have taken place during the initial phases of the burning, the final result was excess oxidation.

On the theory that coal used in sintering should be approximately the same particle size as the magnetite, the coal for the sintering tests was ground to 65 mesh. This fine coal, at first, seemed to help sinter production, but sawdust was being used in conjunction with it. As testing progressed,

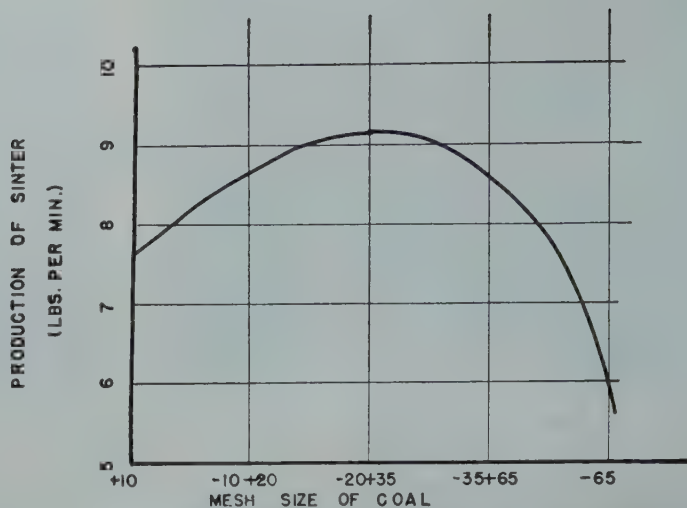


FIG 6—Effect of various mesh sizes of coal on sinter production using 65 mesh magnetite.

satisfactory results were not obtained, and it was decided to test various sizes of coal. These tests (Fig 6) proved that fine coal, rather than help, did much to deter good sinter production. The No. 4 and 5 buckwheat anthracite culm, as received for 20 mesh sintering, gave excellent results and made it possible to eliminate sawdust from the mix.

The fine coal tended to plug most voids, and made proper air flow impossible. The coarser coal left large voids as it burned, causing lower vacuum and faster burning time.

MOISTURE

The amount of water that can be added to a 65 mesh magnetite "mix" is limited. The "mix" will sinter, if all other proportions are correct, at a moisture between 6 and 8 pct, with the best results obtained at 7.5 pct moisture (Fig 7).

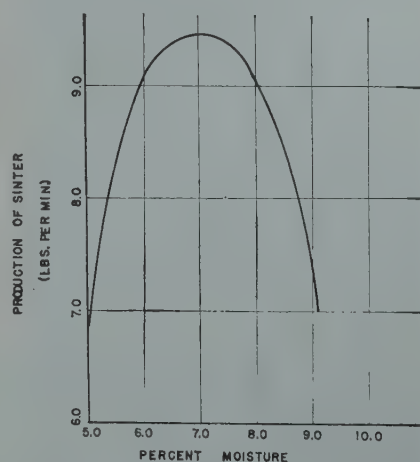


FIG 7—Effect of various percentages of moisture on sinter production with 65 mesh magnetite.

If the moisture is too high, the mix becomes semifluid and it is impossible to draw air through the bed. Thus, ignition is impossible. If the moisture is low, holes tend to form as the material is pulled through the grates. The air, following the path of least resistance, is drawn through the holes and thereby short-circuits the bed. Poor burning results and less sinter is produced.

With 20 mesh magnetite, a wider moisture range is possible. Good sinter was produced with a moisture as low as 3 pct, and as high as 8 pct. However, with 20 mesh magnetite, the percentage of moisture required is closely related to the amount of dust present in the returns. If there were more than 35 pct of minus 35 mesh material in the return fines, it was necessary to use a moisture of 7.5 pct (production with the same mix at 7.5 pct moisture was 10.8 lb per min and at 6.0 pct moisture, production was 9.6 lb per min). If the returns contain less than 35 pct minus 35 mesh material, best results are obtained with a 6 pct moisture.

SLAKED LIME AND MISCELLANEOUS REAGENTS

In an effort to reduce burning time, and thus increase production, slaked lime was added to the charge. A 10 pct increase in production was obtained with the addition of 0.7 pct lime to the 65 mesh mix (Fig 8).

If an excess of lime is added, the charge will burn hot and fast, with little sinter being produced. It is thought that the lime causes an increase in the surface tension of the water. With this higher surface tension, the water would fill less voids in the

Table 2 . . . Effect of Lime on Varying Amounts of Coal

| | Production (Lb per Min) | Cycle Time (Min) | Temperature Exhaust Gas Degree C | Quality | Vacuum In. of Water | | Per Cent Lime |
|--------------------|-------------------------------|------------------------|--|---------|---------------------|-----|------------------|
| | | | | | Start | End | |
| With 3 pct coal... | 5.5 | 9.0 | 520 | 81.5 | 61 | 48 | 0.75 |
| With 4 pct coal... | 11.0 | 10.0 | 325 | 82.2 | 57 | 53 | 0.75 |

Table 3 . . . Effects of Various Reagents on 65 Mesh Magnetite Sinter

| Reagent | Per Cent Reagent | Production, Lb per Min | Per Cent Plus 1 In. Sinter | Quality | Cycle Time, (Min) |
|-----------------------|---------------------|---------------------------|-------------------------------|---------|----------------------|
| Standard..... | | 9.0 | 65.1 | 78.9 | 13.1 |
| Lime..... | 0.7 | 9.9 | 63.6 | 78.0 | 11.5 |
| Detergent..... | 0.005 | 8.1 | 64.2 | 86.0 | 15.0 |
| Oleic acid..... | 0.05 | (would not burn) | | | |
| Calcium chloride..... | 2.0 | 9.7 | 61.4 | 74.8 | 12.0 |
| Pine oil..... | 0.05 | 5.1 | 52.2 | 88.2 | 20.5 |
| Zinc stearate..... | 0.5 | (would not burn) | | | |
| Aluminum dust..... | 0.5 | 5.8 | 54.8 | 78.9 | 18.0 |

mix, thus leaving greater and more numerous voids than possible with un-adjusted water. With more numerous voids, a greater volume of air was drawn through the bed, lowering the vacuum, decreasing the burning time, and causing a higher burning temperature. The addition of excess lime increased the surface tension to such an extent that an excess volume of air was drawn through the charge, causing such rapid and hot burning that little sinter was produced.

If the percentage of lime was held constant and the coal percentage dropped, less sinter was formed because of higher burning temperatures. Higher burning temperatures slag the sinter.

The results of Table 2 show that with 3 pct coal and 0.75 pct slaked lime, the mix burned hotter, and gave poorer results than those obtained using 4 pct coal and 0.75 pct slaked lime. This can be explained by the knowledge that a higher percentage of carbon causes excess slagging. This slagging reduces the amount of voids, and this tends to slow the burning rate. This shows, again, how critical the addition of lime would be in actual plant practice. If lime were added in excess, production would drop. If the amount of lime remained constant and the percentage of carbon dropped, production would again drop. Thus, if lime is used in actual plant practice, efficient metallurgical and quantity controls must be provided.

In order to check the surface tension theory, a series of tests were made using the following reagents (Table 3): (1) detergent ("Dreft"), (2) oleic acid, (3) calcium chloride, (4) pine oil, (5) zinc stearate, and (6) aluminum dust.

It is known that a detergent reduces the surface tension of water. Thus, if a

detergent is added to the mix, a poorer sinter should result, because with a lower surface tension, the water would fill more voids. The results obtained by test work checked with this idea. When 50 g of detergent were added to the mix, the mix became "putty-like" in appearance and semifluid in nature. The sized return fines were completely disintegrated when they were placed in water containing a detergent. When this mix was added to the pan it was impossible to draw air through it, and thus it could not be ignited.

Calcium chloride, which gives a substantial increase in the surface tension of water, was next added to the mix. The calcium chloride decreased the burning time, but produced a weak sinter. The sinter cake actually expanded during burning when calcium chloride was in the mix. Why this expansion took place is unknown. Calcium chloride could not be used in sinter plant operation because of the large amounts of chlorine gas liberated during the burning; however, it was used in the pilot plant because it was known to increase the surface tension of water.

All other reagents tried gave poor results.

OXIDATION

For a short while during the test work, it was thought that the oxidation of the FeO to Fe₂O₃ was an important factor in strong sinter. To check this point many assays were made on magnetite feed, and sinter produced from this magnetite. As a result of a study of these assays it is thought that oxidation to a certain extent does produce stronger sinter by causing the iron molecules to share oxy-

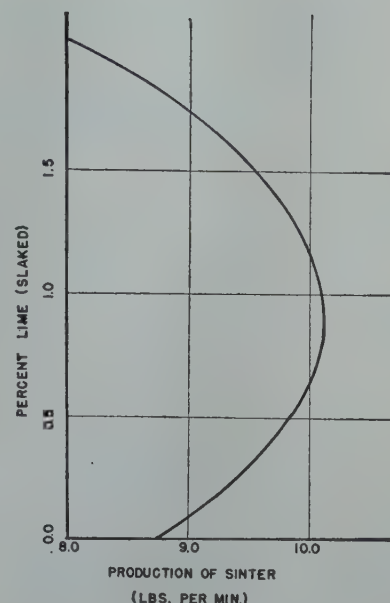


FIG 8—Effect of various percentages of slaked lime on sinter production with 65 mesh magnetite.

gen atoms. When oxidation progresses too far, the iron is oxidized completely and no longer shares oxygen atoms, thus producing weaker sinter. When oxidation is low, there is little sharing of oxygen atoms and again the sinter is weak.

Table 4 . . . Effects of Oxidation upon Quality of Sinter

| Magnetite | | | Sinter | | | Qual- ity |
|-----------|-------|--------------------------------|--------|-------|--------------------------------|--------------|
| Fe | FeO | Fe ₂ O ₃ | Fe | FeO | Fe ₂ O ₃ | |
| 57.0 | 31.04 | 46.99 | 56.8 | 21.78 | 57.06 | 75.8 |
| 56.7 | 31.61 | 45.91 | 56.0 | 16.52 | 61.68 | 87.8 |
| 58.0 | 32.33 | 46.97 | 56.5 | 9.63 | 70.05 | 72.8 |

Table 4 is representative of the average assays completed, and shows weaker sinter on both the high and low oxidation samples.

LIMESTONE

Because of the cheaper costs of limestone compared to slaked lime, it was thought desirable to check the effects of limestone in the "mix." The limestone was sized from minus 6 plus 10, minus 10 plus 20, minus 20 plus 35, and minus 35 plus 65 mesh. In no case did the limestone help. This was probably caused by the fact that the heat necessary to slake the lime evaporated all the moisture before the limestone was slaked, and thus the effect of the slaked lime on the water was lost.

SAWDUST

Sawdust was helpful when 65 mesh coal was used in the mix. The sawdust

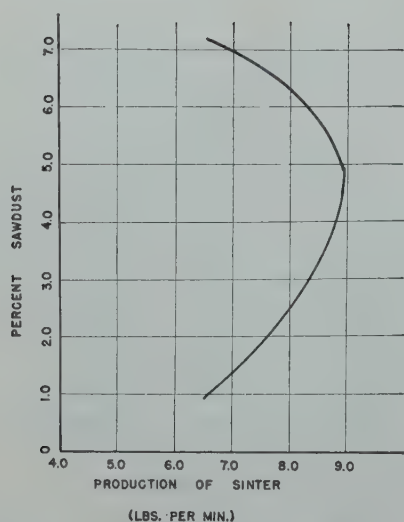


FIG 9—Effect of various percentages of sawdust on sinter production with 65 mesh magnetite.

had a tendency to “fluff” the mix in the pan, and it also made voids for air passage as the mix was burned. Fig 9 shows a high point for sawdust addition. As the percentage of sawdust was increased above 5, the mix burned very hot and fast and sinter production dropped. Sawdust elimination simplified the general problem because of the difficulties that its handling would have entailed if it were needed for 65 mesh magnetite sintering. The use of No. 4 and 5 buckwheat coal eliminated the need for sawdust.

PELLETS

A rotary mixer was used for pilot plant mixing. During the mixing of some batches, pellets were formed by magnetite building up around particles of return fines. The coarser the return fines, the larger the pellets would become. These pellets interfered with sinter production by causing short-circuiting of air around them because they had no porosity. Therefore they were unable to be sintered. The pellets were baked by the heat around them, but crumbled when subjected to the slightest pressure. No figures were obtained and the only method of making these determinations was by visible observation.

In sinter plant operation, pug mills are used for mixing and this problem should not occur. However, if pellets do form, some method to eliminate them must be provided. This does not infer sintering of a completely pelletized charge was undertaken. In all cases the pellets were mixed with unpelletized material, and under such conditions, were detrimental.

DUST

Dust is defined in this test work as material in the return fines, less than 65 mesh for 20 mesh magnetite sinter and minus 200 mesh for 65 mesh magnetite sinter. After it was known that excess fine material would reduce sinter production with 65 mesh material, tests were made to determine what effects “dust” would have on minus 20 mesh material. It was found that if the moisture was increased as the percentage of “dust” increased, the amount of “dust” in the “mix” had little effect on sintering of 20 mesh magnetite.

MIXING

Early in the project, several mixing tests were run using pug mill discharge. When this material was further mixed in the rotary mixer, a sharp production increase was noted. This mixing was checked again at the end of the project, and no increase in production could be attained by further mixing. In some cases production fell off after additional mixing, probably caused by water filling the voids in the return fines. It is thought that the pug mill blades, and other plant conditions were responsible for the poor results obtained during the first testing, but with the pug mills in good shape, as far as blade wear is concerned, a complete mix should be attainable. It was found that a 5 min rotary mix, after the magnetite had been brought to the correct moisture, gave the best results for rotary mixing in the test plant.

PRODUCTION RUNS

When the test work was completed it was necessary to test the best results. For this purpose, several pans were burned in rapid succession to see how the “mix” would react in a hot pan over a period of time. The recommendations made were on the basis of the production run results.

Conclusions

The best quality and quantity of sinter on this test pan were obtained with the following mix:

- 4.0 pct coal
- 25.0 pct return fines¹(minus 10 mesh plus 0)
(at least 18.75 pct minus 10 mesh plus 35 mesh)
- 70.3 pct magnetite (minus 65 mesh size)

0.7 pct slaked lime.

The average production on the test pan with the above “mix” was 9.9 lb per min or 246 lb per hr per sq ft of grate area. This is slightly higher than average production in the sintering plant pans on minus 20 mesh magnetite.

The pilot plant work indicates that minus 65 magnetite can be sintered in the sinter plant if close control can be maintained over the following items:

1. Adequate amount of bedding material (minus 1 in. plus ½ in. return fines for hearth layer.
2. Sized return fines (minus 10 mesh plus 0).
3. Anthracite coal (size and moisture percentage).
4. Moisture percentage in the “mix.”
5. Magnetite (moisture percentage).
6. Percentage of magnetite, coal, lime, and return fines in the prepared feed to the plant.

The results obtained in the sinter testing show that a more accurate metallurgical control on overall operation will be necessary for sintering minus 65 mesh magnetite than is needed in present plant operation for sintering minus 20 mesh magnetite.

Before the present sintering plant can handle minus 65 mesh magnetite, the plant flowsheet will have to be changed to include the conveying, cooling, screening, storing, and weighing of both return fines and bedding material.

Because of the difference between the size of the test pan (2.4 sq ft grate area) further development work will be needed in the sintering plant. A production run of at least two months would be required on minus 65 mesh magnetite to study the effect of the finer mesh size magnetite on the operation and maintenance of the plant.

Acknowledgment

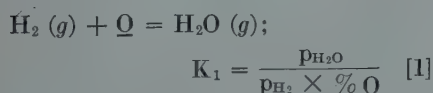
The authors wish to thank the following individuals for their suggestions and help in making the sintering tests and for their help in making it possible for them to write this paper: Messrs. Gloyd M. Wiles, Chairman of the Mining Committee, National Lead Co., Frank R. Milliken, Plant Manager, MacIntyre Development, National Lead Co., A. R. Reiser, former Assistant Plant Manager, M. F. Morgan, Arthur G. McKee & Co., John E. Greenawalt, and the following metallurgical personnel of MacIntyre Development; Messrs. Ernest M. Spokes and Elton Geist.

Equilibrium in the Reaction of Hydrogen with Oxygen in Liquid Iron

MINU N. DASTUR,* Student Associate, and JOHN CHIPMAN,† Member AIME

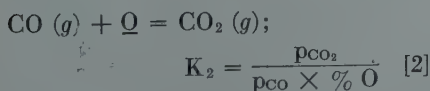
The importance of dissolved oxygen as a principal reagent in the refining of liquid steel and the necessity for its removal in the finishing of many grades have stimulated numerous studies of its chemical behavior in the steel bath. From the thermodynamic viewpoint the essential data are those which determine the free energy of oxygen in solution as a function of temperature and composition of the molten metal. A number of experimental studies have been reported in recent years from which the free energy of oxygen in iron-oxygen melts can be obtained with a fair degree of accuracy for temperatures not too far from the melting point. Certain discrepancies remain, however, which imply considerable uncertainty at higher temperatures; also several sources of error were recognized in the earlier studies. It has been the object of the experimental work reported in this paper to reexamine these sources of uncertainty and to redetermine the equilibrium condition in the reaction of hydrogen with oxygen dissolved in liquid iron.

The reaction and its equilibrium constant are:

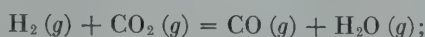


Here the underlined symbol $\underline{\text{O}}$ designates oxygen dissolved in liquid iron. The activity of this dissolved oxygen is known to be directly proportional to its concentration^{1,2} and is taken as equal to its weight percent.

The closely related reaction of dissolved oxygen with carbon monoxide has also been investigated:^{3,4,5}



The two reactions are related through the water-gas equilibrium:



$$K_2 = \frac{p_{\text{CO}} \times p_{\text{H}_2\text{O}}}{p_{\text{H}_2} \times p_{\text{CO}_2}} \quad [3]$$

and with the aid of the accurately known equilibrium constant of this reaction, it has been shown⁵ that the experimental data on reactions [1] and [2] are in fairly good, though not exact, agreement.

Experimental Method

Great care was taken to avoid the principal sources of error of previous studies, namely, gaseous thermal diffusion and temperature measurement. The apparatus was designed to provide controlled preheating of the inlet gases and to permit the addition of an inert gas (argon) in controlled amounts, two measures found to be essential for elimination of thermal diffusion. A known mixture of water vapor and hydrogen was obtained by saturating purified hydrogen with water vapor at controlled temperature. This mixture, with the addition of purified argon, was passed over the surface of a small melt (approximately 70 g) of electrolytic iron in a closed induction furnace. After sufficient time at constant temperature for attainment of equilibrium the melt was cooled and analyzed for oxygen.

GAS SYSTEM

A schematic diagram of the apparatus is shown in Fig 1. Commercial hydrogen is led through the safety trap *T* and the flowmeter *F*. The catalytic chamber *C*, held at 450°C, was used to convert any oxygen into water-vapor. A by-pass *B* with stopcocks was provided so that the hydrogen could be introduced directly from the tank to the furnace when desired. From the catalytic chamber the gas passed through a water bath *W*, kept at the desired temperature by an auxiliary heating unit, so that the gas was burdened with approximately the proper amount of water vapor before it was introduced into the saturator *S*.

All connections beyond the catalytic chamber were of all-glass construction. Those connections beyond the water bath were heated to above 80°C to prevent the condensation of water vapor. After the saturator, purified argon was led into the steam-hydrogen line at *J*, and finally the ternary mixture was introduced into the furnace.

THE SATURATOR

The saturator unit comprised three glass chambers, as shown in Fig 1, the first two chambers packed with glass beads and partially filled with water, and the third empty. Each tower had a glass tube with a stopper attached for the purpose of adjusting the amount of water in it. The unit was immersed in a large oil bath, which was automatically controlled with the help of a thermostat relay to constant temperature, $\pm 0.05^\circ\text{C}$, using thermometers which had been calibrated against a standard platinum resistance thermometer. The performance of the saturator over the range of experimental conditions was checked by weighing the water absorbed from a measured volume of hydrogen; the observed ratio was always within 0.5 pct of theoretical.

New York Meeting, February 1950.
TP 2661 C. Discussion of this paper (2 copies) may be sent to *Transactions AIME* before April 1, 1950. Manuscript received March 31, 1949.

This paper is based on a thesis submitted by M. N. Dastur in partial fulfillment of the requirements for the degree of Doctor of Science at the Massachusetts Institute of Technology.

* Metallurgical Engineer, H. A. Brassett & Co., New York.

† Professor of Metallurgy, Massachusetts Institute of Technology, Cambridge, Mass.

‡ References are at the end of the paper.

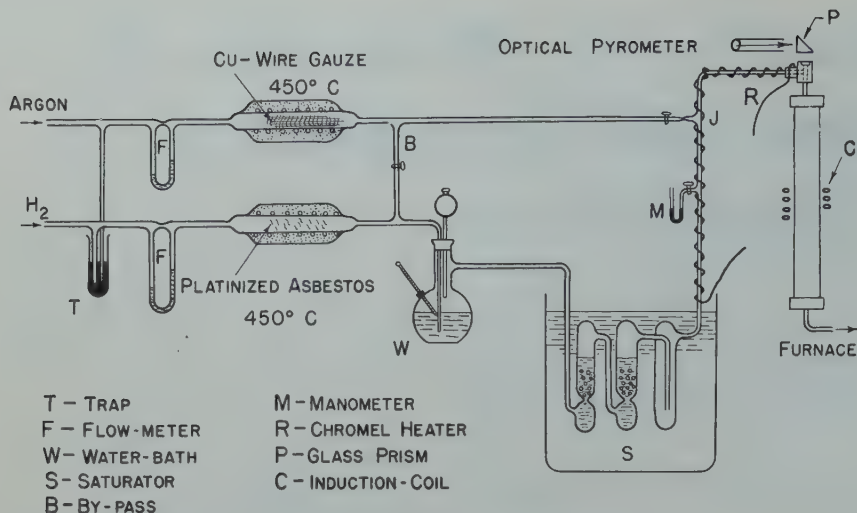


FIG 1—Diagram of apparatus.

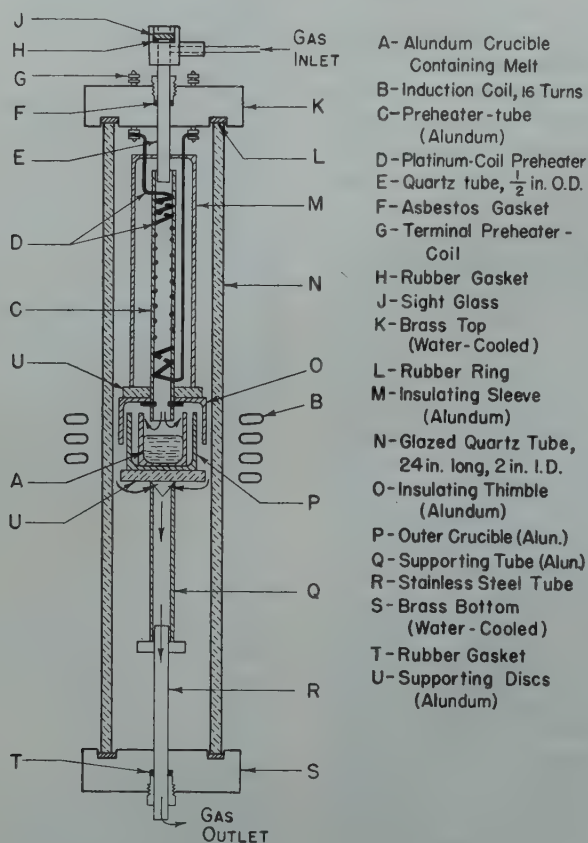


FIG 2—Furnace arrangement.

FURNACE ARRANGEMENT

The furnace arrangement is shown in Fig 2. A glazed-surface silica tube *N*, 24 in. long and 2 in. id, was used throughout. It worked satisfactorily and was impermeable to gases at elevated temperatures. The furnace was equipped with water-cooled brass top *K* and bottom *S* and rubber gaskets *L*. The brass head *K* was fitted with a sight glass *J* made of pyrex glass, 1/2 in. diam and 1/16 in. thick. A gas inlet and outlet were provided at the top and

bottom of the furnace respectively. A small silica tube, 1/2 in. od and 5 in. long, was used to carry the mixture into the furnace. It was fixed to the furnace head by means of an asbestos gasket *F*. The preheater tube *C* was suspended from the small silica tube.

The alumina crucible *A* was placed inside an outer alumnum thimble *P*, resting on an alumnum disc *U* which was in turn supported on top of an alumnum tube *Q*, 1/2 in. id, and steel tube *R* which passed through the bottom by means of a rubber gasket and which

could be slid up or down as desired. This proved to be very effective in positioning the melt inside the induction coil *B* to get the desired electrical coupling. The power needed for melting was from 10 to 14 kw, supplied by a 35 kva high frequency unit, and only 5 to 8 kw were necessary to hold the metal at any temperature between 1535° and 1800°C.

THE PREHEATER

The preheater tube *C* made of alumnum, 1/2 in. id, was tapped with 12 threads to the inch for a length of 6 in.; a coil of platinum wire *D*, 0.025 in. diam, which served as the heating element, was screwed into position in the threads. Later on, a bigger and better preheater was made 9 in. long and with a heavier wire, 0.030 in. diam, using platinum-10 pct rhodium instead of pure platinum. This enabled the entering gaseous mixture to be heated up to the temperature of the melt before coming in contact with it. The leads were taken out through holes drilled in the preheater tube and were fastened to terminal connectors at *G*. The preheater was covered with an alumnum insulating sleeve *M*, 12 in. long and 1 1/2 in. diam, resting on an alumnum disc *U* and another sleeve *O*, 1 1/2 in. long and 1 3/4 in. diam, to prevent excessive radiation. The incoming gases came in direct contact with the heated platinum wire and hence the preheating was very efficient.

OXYGEN ANALYSIS

Oxygen analyses were made by the vacuum fusion method on an apparatus which has been used in this laboratory for over ten years. It had been calibrated previously against measured gas volumes and checked by exchange of samples with the National Bureau of Standards. Results reported are the mean of two or more concordant determinations.

AVOIDANCE OF THERMAL DIFFUSION

In a mixture of gases of unlike molecular weight any temperature gradient tends to produce corresponding composition gradient, the lighter gas diffusing toward the hotter region. This is a well known effect which has given rise to troublesome errors in many studies of gas-metal reactions. When the metal is heated by induction a sharp temperature gradient may be set up near its surface; in some of the early

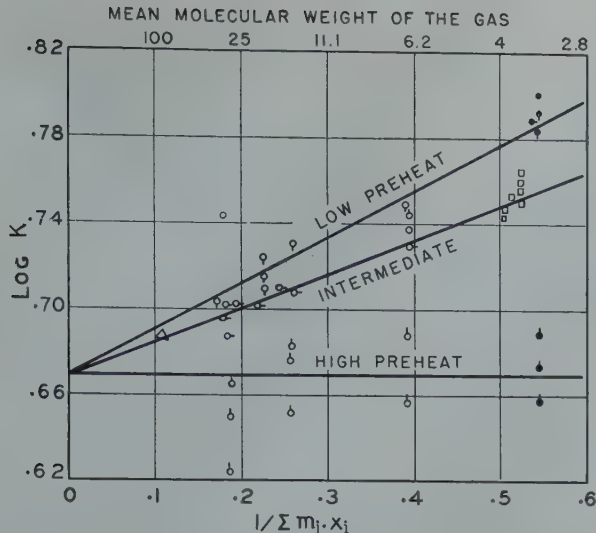


FIG 3—Experimental values of the apparent equilibrium constant at 1563° C. Log K approaches a limiting true value with addition of inert gas of high molecular weight.

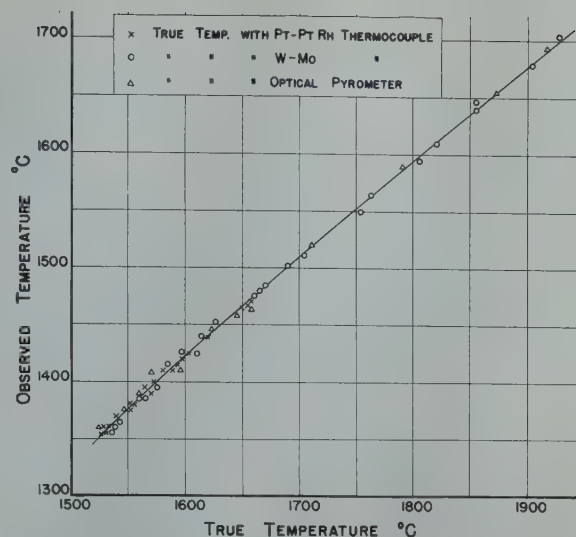


FIG 4—Calibration curve for optical pyrometer sighted on a clean surface of liquid iron.

studies of reaction [1] this resulted in apparent values of K_1 which are now known to have been too high.

A study of the factors affecting thermal diffusion⁶ indicated two practical methods of minimizing errors from this source. The first is the obvious one of preheating the gases entering the system so as to eliminate as far as possible the thermal gradient near the surface of the melt. The second is based upon Gillespie's⁷ simplified treatment of the phenomenon which showed that the thermal separation is diminished by admixture of a gas of high molecular weight. According to this theory the error in log K_1 should be proportional to the reciprocal of the mean square root of the molecular weight of the gas. Fig 3 shows the results of a detailed experimental study⁸ at 1563°C using three degrees of preheat, the apparent value of log K being plotted against the reciprocal of the mean square root of the molecular weight. From the data it was concluded that the error is eliminated by adequate preheating and greatly minimized by addition of a heavy gas. The average value using the highest, and apparently adequate, preheat agreed with results obtained at lower preheat by extrapolation to infinite molecular weight. In later experiments, including all those made above 1563°C, the preheater was operated at the same apparent temperature as the melt, corresponding to the highest preheat of Fig 3, and argon was added in the approximate ratio 4:1.

TEMPERATURE MEASUREMENTS

All temperature measurements were made by means of a disappearing-

filament-type optical pyrometer sighted on the clean surface of the melt. The following is a brief description of the calibration of this method, the details of which are published elsewhere.⁸ Two optical pyrometers were calibrated against a standard instrument using a tungsten strip filament lamp. A special beryllia crucible was constructed having a reentrant tube in the bottom which provided a small "black body" at the temperature of the molten metal contained in the crucible. This crucible filled with liquid iron was held in the furnace under exactly the same conditions as those used in equilibrium determinations. Simultaneous temperature readings were made on the metal surface and on the "black body" using duplicate windows and prisms and occasionally exchanging the positions of the two optical pyrometers.

Similar calibrations were carried out using a thermocouple instead of the lower optical pyrometer, the bead of the couple being inserted into the reentrant tube. For temperatures up to 1650°C a platinum-platinum-rhodium couple was employed; this was checked before and after use at the melting point of palladium. For higher temperatures extending to 1930°C an independently calibrated tungsten-molybdenum couple⁹ was used. The resulting calibration curve which was used throughout this study is shown in Fig 4. The estimated uncertainty in temperature measurement is less than $\pm 5^\circ\text{C}$ at the lowest and slightly greater at the highest temperatures.

Experimental Procedure

The charge consisted of about 70 g of

electrolytic iron which had been previously cleaned, pickled, washed and dried. This was held in a crucible of high-purity alumina. The whole system including the furnace was flushed out with hydrogen for about an hour. The saturator, the water bath and connecting tubing were brought to the desired temperatures.

Since the object of this series of experiments was to determine the effect of temperature upon the Fe-H₂O equilibrium, it was necessary to let the various melts attain equilibrium at different temperatures, the range covered being from 1563° to 1750°C. Frequent temperature measurements were made and in general these did not deviate more than $\pm 3^\circ\text{C}$ from the desired value. The optical pyrometer was occasionally checked against the melting point of iron. The flow rates were adjusted to give an argon-to-hydrogen ratio of approximately 4:1 in all heats.

Preliminary runs had demonstrated that under the experimental conditions equilibrium in the reaction of hydrogen with oxygen dissolved in liquid iron was attained within fifteen minutes. All heats were continued for a minimum of forty-five minutes under steady conditions after which the metal was cooled as rapidly as possible.

To increase the rate of solidification, attempts were made to quench the melt directly into water at the end of the heat. A deep tank was arranged so that the water level was above the bottom of the furnace tube, thus excluding air, and the entire furnace bottom with the crucible and its supports was dropped into the water. The resulting ingots were mostly irregular and unsound and of very high oxygen content. Substitu-

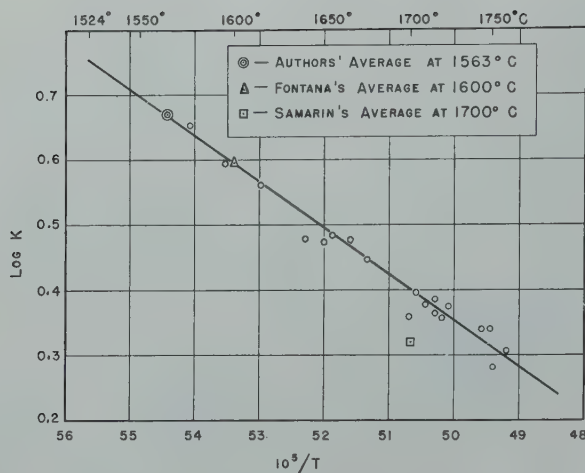


FIG 5—Effect of temperature upon the equilibrium constant

$$K_1 = \frac{p_{H_2O}}{p_{H_2} \times \% O}$$

tion of chlorinated biphenyl for water resulted in a high-carbon ingot. The method finally adopted was to lower the melt into the cold part of the furnace, simultaneously cutting off the preheater and increasing the rate of flow of argon. Solidification occurred in five to fifteen seconds.

Most of the ingots were sound with very little or no porosity. The ingots were cut into pie-sections with a hacksaw. Grinding and pickling were used to clean the samples which were analyzed for oxygen by the vacuum fusion method. This method gives the total oxygen content of the sample and includes all the oxygen which was in solution in the melt and any oxide particles which may be entrapped in the specimen. Microscopic examination showed that the ingots were fairly clean and contained no appreciable amount of foreign oxides.

Experimental Results

The series of experiments at 1563°C which have been discussed in connection with thermal diffusion lead to a value of K_1 at that temperature of 4.68 ± 0.15 . Results at higher temperatures are shown in Table I. It is to be noted that the oxygen content of all samples is far below the saturation value in the liquid and hence there was little chance for loss during cooling. There was no visible evidence of ejection of oxide and no marked segregation in the ingots examined microscopically. Oxygen analyses were usually duplicable within ± 2 pct; in the five cases of larger deviation it is uncertain whether the cause was analytical error or actual segregation.

The results are plotted in Fig 5 in which are also shown the average values at 1600° and 1700°C reported respectively by Fontana¹ and by Samarin.² The best line through the data is represented by the equation:

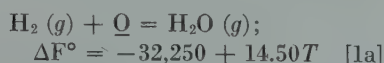
$$\log K_1 = 7050/T - 3.17$$

This agrees very closely with Fontana's average but deviates from that of Samarin by about 18 pct in the value of K at 1700°.

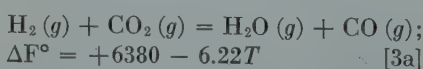
Thermodynamic Calculations

COMPARISON WITH DATA ON FE-C-O SYSTEM

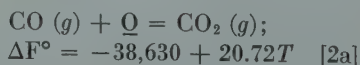
From the equation given above for the temperature dependence of K_1 we obtain the following for the change in free energy:



The free energy change in the similar reaction of carbon monoxide with dissolved oxygen to form carbon dioxide is obtained from this with the aid of the free energies of the four gases involved. The data given in "Basic Open Hearth Steelmaking"¹⁰ are in excellent agreement with the most recent compilation of the National Bureau of Standards.¹¹ From them we find for the water-gas reaction:



When this is subtracted from Eq 1a the result is:



Several investigators have studied this

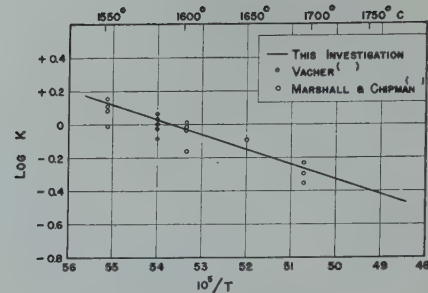


FIG 6—Effect of temperature upon the equilibrium constant

$$K_2 = \frac{p_{CO_2}}{p_{CO} \times \% O}$$

Table 1 . . . Equilibrium Data on Reaction of Steam with Liquid Iron

| Heat No. | $\frac{p_{H_2O}}{p_{H_2}}$ | Metal Temp. °C | Oxygen Percent | K |
|----------|----------------------------|----------------|----------------|------|
| 65 | 0.1051 | 1574 | 0.0234 | 4.49 |
| 66 | 0.1040 | 1595 | 0.0265 | 3.92 |
| 67 | 0.1042 | 1650 | 0.0350 | 2.98 |
| 68 | 0.1039 | 1700 | 0.0456 | 2.28 |
| 87 | 0.1052 | 1615 | 0.0291 | 3.64 |
| 88 | 0.1052 | 1640 | 0.0350 | 3.01 |
| 89 | 0.1053 | 1720 | 0.0464 | 2.27 |
| 90 | 0.1053 | 1752 | 0.0552 | 1.91 |
| 103 | 0.1039 | 1665 | 0.0347* | 3.0 |
| 104 | 0.1040 | 1704 | 0.0419 | 2.49 |
| 105 | 0.1040 | 1724 | 0.0438 | 2.37 |
| 106 | 0.1040 | 1750 | 0.0476 | 2.18 |
| 124 | 0.1042 | 1760 | 0.0516* | 2.02 |
| 128 | 0.1385 | 1745 | 0.0632 | 2.18 |
| 300 | 0.1052 | 1716 | 0.0432* | 2.43 |
| 301 | 0.1060 | 1716 | 0.0457* | 2.31 |
| 140 | 0.0977 | 1710 | 0.0411* | 2.38 |
| 141 | 0.0982 | 1655 | 0.0324 | 3.03 |
| 142 | 0.0984 | 1675 | 0.0352 | 2.79 |

* Average deviation about 0.0020; in all other cases less than 0.0006

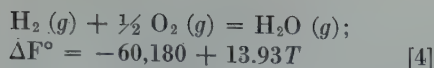
equilibrium but it is only the results at very low carbon content that can be directly compared with the equation. The data of Marshall and Chipman⁵ and of Vacher³ for carbon contents below 0.02 pct are shown in Fig 6. The straight line represents the equilibrium constant calculated from Eq 2a which is given by the expression:

$$K_2 = \frac{p_{CO_2}}{p_{CO} \times \% O}; \log K_2 = +8440/T - 4.53 \quad [2b]$$

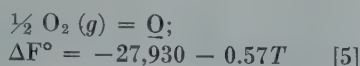
It is noted that the calculated line falls within the limits of experimental uncertainty at all temperatures and in fact represents the experimental data very satisfactorily. The precision of the data for the Fe-C-O system is not as good as that for the steam-hydrogen equilibrium so that the agreement should be recorded only within limits of about ± 0.07 in $\log K_2$. This represents rather good agreement for high temperature data.

FREE ENERGY OF OXYGEN IN IRON

The free energy of formation of water vapor is given by the equation:¹⁰



When this is combined with Eq 1a we have:

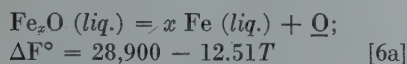


FREE ENERGY OF LIQUID FERROUS OXIDE

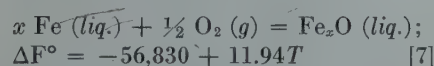
The liquid oxide phase which exists in equilibrium with solid or liquid iron has a composition represented by the formula Fe_xO where the value of x is a function of temperature and, in the range considered here, lies between 0.96 and 0.99. The free energy of this equilibrium phase per gram atom of oxygen is obtained from its solubility in liquid iron and Eq 5. Its solubility^{12,13} is represented by the expression:

$$\log \% \text{O} = -6320/T + 2.734 \quad [6]$$

This may be paraphrased by the equation:



which, with Eq 5, gives:

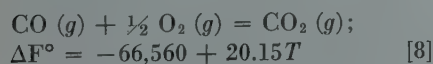


This is equivalent to the partial molal free energy of formation of FeO in the liquid oxide of equilibrium composition. From this the oxygen pressure of oxygen-saturated liquid iron is:

$$\log p_{\text{O}_2} = -24,850/T + 5.22 \quad [7a]$$

COMPARISON WITH DATA OF DARKEN AND GURRY

The oxygen pressure of oxygen-saturated iron may be calculated also from the experimental data of Darken and Gurry.¹⁴ These investigators have found the ratio $p_{\text{CO}_2}/p_{\text{CO}}$ in equilibrium with iron and iron oxide over a wide range of temperatures, the pertinent values being reproduced in Table 2. From the known free energies of the several gases¹¹ we have:



$$K_8 = \frac{p_{\text{CO}_2}}{p_{\text{CO}} \times p_{\text{O}_2}^{1/2}}; \log K_8$$

$$= +14,550/T - 4.405 \quad [8a]$$

Values of K_8 are included in Table 2. From these data the logarithm of the oxygen pressure is found as given in the fifth column. The sixth shows the same quantity computed from Eq 7a.

Table 2 . . . Computation of the Oxygen Pressure of Oxygen-Saturated Iron

| Temp. °C | $\frac{p_{\text{CO}_2}}{p_{\text{CO}}}$ | $\log \frac{p_{\text{CO}_2}}{p_{\text{CO}}}$ | $\log K_8$ | $\log p_{\text{O}_2}$ (D and G) | $\log p_{\text{O}_2}$ (Eq 7a) |
|-------------|---|--|------------|------------------------------------|----------------------------------|
| 1371 | 0.282 | -0.550 | 4.447 | -9.99 | |
| 1524 | 0.208 | -0.682 | 3.690 | -8.74 | -8.61 |
| 1575 | 0.194 | -0.713 | 3.470 | -8.37 | -8.24 |
| 1600 | 0.187 | -0.728 | 3.363 | -8.18 | -8.05 |

The discrepancy between these two series of computed oxygen pressures is very small.* It is, however, a real discrepancy since the difference is greater than the apparent uncertainties in any of the subsidiary data. Perhaps the least certain of these is the solubility of oxygen in liquid iron. The data employed here are about 30 pct lower than those which were generally accepted prior to 1941.¹² However, if the older data are substituted the discrepancy becomes greater; thus the calculation upholds the lower solubility data.

It seems quite possible that in spite of all the careful calorimetric and spectroscopic work that has been done, minor errors may remain in the free energy values of the gases which would be large enough to account in part for the discrepancies found. Inconsistencies in values of the water-gas constant, K_8 , have been pointed out by Darken and Gurry¹⁴ and until these uncertainties have been removed the small discrepancy shown in Table 2 should be no cause for worry. We may conclude then that the present data are in good agreement with the requirements of the oxygen solubility of Taylor and Chipman and the equilibrium data of Darken and Gurry.

Summary

An experimental study has been made of equilibrium in the reaction of hydrogen with oxygen in liquid iron in the temperature range 1563°–1760°C. The primary purpose was to secure more dependable data by elimination of certain errors which were inherent in earlier work.

Errors of thermal diffusion in the gas mixture were eliminated by preheating the entering gas stream to the temperature of the metal. A further safeguard was the admixture of pure

*It is considered that earlier discrepancies below the melting point of iron have been adequately explained by Darken and Gurry.

argon with the gas stream in a ratio of about 4 to 1.

Temperature measurements were made by an optical pyrometer sighted on the clean surface of the melt. This system was calibrated in the range 1530°–1930°C against optical and thermoelectric measurements in a reentrant tube in the bottom of the crucible. This reduced uncertainties in temperature measurement to about $\pm 5^\circ$.

The experimental results are represented by:

$$K_1 = p_{\text{H}_2\text{O}}/p_{\text{H}_2} \times \% \text{O};$$

$$\log K_1 = 7050/T - 3.17$$

Related thermodynamic quantities are derived. The results confirm the oxygen solubility data of Fетters, Taylor and Chipman and are in good agreement with equilibrium data on the system iron-oxygen of Darken and Gurry.

Acknowledgments

The authors wish to express their thanks to Noble E. Hamilton and Nevzat A. Gökcen for assistance in building the apparatus and in conducting some of the experiments; also to Mrs. Catherine Kallal and Mrs. Marion Matheny for the vacuum fusion analyses. This research was begun with the aid of a grant from the Republic Steel Corporation and completed as part of Contract N5ori-07816, Task Order XVI, NR-031-186, Office of Naval Research.

References

1. M. G. Fontana and J. Chipman: *Trans. A. S. M.* (1936) **24**, 313.
2. J. Chipman and A. M. Samarin: *Trans. AIME* (1937) **125**, 331.
3. H. C. Vacher: Nat. Bur. of Standards, *Jnl. Res.* (1933) **11**, 541.
4. G. Phragmen and B. Kalling: *Jernkontorets Annaler* (1939), **123**, 199.
5. S. Marshall and J. Chipman: *Trans. A. S. M.* (1942) **30**, 695.
6. M. N. Dastur and J. Chipman: The Faraday Soc. Symposium on the Physical Chemistry of Process Metallurgy (1948).
7. L. J. Gillespie: *Jnl. Chem. Phys.* (1939) **7**, 530.
8. M. N. Dastur and N. A. Gökcen: To be published: *Trans. AIME* (1949) *Jnl. of Metals* **185**.
9. R. D. Potter: Sc. D. Thesis, Mass. Inst. of Tech. (1948).
10. "Basic Open Hearth Steelmaking."
11. "Selected Values of Chemical Thermodynamic Properties," Nat. Bur. of Standards (1948).
12. J. Chipman and K. L. Fетters: *Trans. A. S. M.* (1941) **29**, 955.
13. C. R. Taylor and J. Chipman: *Trans. AIME* (1943) **154**, 228.
14. L. S. Darken and R. W. Gurry: *Jnl. Am. Chem. Soc.* (1945) **67**, 1398; (1946) **68**, 798.

[illegible]

Oxygen enriched air is being used paper, the use of oxygen enriched air Cottrell precipitator. The discharges

Most of the ore treated in the Trail metallurgical plants comes from Cominco's Sullivan Mine at Kimberley, B.C. At Kimberley the ore is milled to produce lead and zinc concentrates which are shipped to Trail for further treatment to metal.

A second section of the paper describes the use of oxygen enriched air in operations at the lead smelter. There oxygen enriched air is used in the blast to the lead blast furnaces and in the slag fuming furnace which recovers the lead and zinc contained in lead blast furnace slag.

The Use of Oxygen Enriched Air in the Suspension Zinc Roasters

Suspension roasting is carried out at Trail in converted standard 25 ft diam Wedge roasters. The 2nd, 3rd, 4th and 5th roasting hearths have been removed and the drying hearth covered over. Drying of the concentrate is done on the drying hearth and the 1st roasting hearth. The dried concentrate, after any lumps have been broken up in a ball mill, is fed to a single burner located in the upper part of the combustion chamber. Oxygen is introduced at the burner fan along with the gases from drying, returned combustion gases from the waste heat boiler outlet and the required amount of new air. Up to 60 pct of the concentrate settles out on the 6th roasting hearth, the rest passing out of the roaster. The product collected in the waste heat boiler is finished calcine, but the dust collected in the cyclones after the boilers is returned to the base of the combustion chamber where the sulphate is decomposed. Gases from the cyclones go to a

Following small scale tests started in 1933, oxygen enriched air has been used continuously in the suspension roasting of zinc concentrate in Trail, beginning in 1937. A significant factor in promoting its use in this operation was the availability of by-product oxygen from the Company's near-by Chemical and Fertilizer Division. To-day it is standard practice at Trail to use oxygen enriched air for zinc concentrate roasting.

High solubility of zinc requires that the sulphide sulphur and zinc ferrite in the calcine be kept low. These are both functions of temperature and time, with formation of zinc ferrite also dependent on contact between the iron and zinc particles. One of the inherent advantages of suspension roasting is that minimum time and contact are achieved. The limit on temperature is imposed by the fusion point of the concentrate and not by the need to control zinc ferrite formation. Operating temperatures are normally maintained within the limits of 1725° and 1850°F. A relatively low zinc sulphate in the calcine is required at Trail, and this results from discharging the calcine from the high sulphur dioxide atmosphere at a temperature above 1600°F.

* Manager, Metallurgical Division, Superintendent, Zinc Department, Superintendent, Lead Smelting Department, Superintendent of Development, Metallurgical Division, respectively. The Consolidated Mining and Smelting Company of Canada, Limited

The rate of elimination of sulphur from the concentrate and the control of zinc ferrite formation depend in practice principally on the following factors: 1. The composition of the concentrate. 2. The fineness of the concentrate. 3. The temperature in the roaster. 4. The time allowed for roasting. 5. The concentration of oxygen in the roaster.

The limitations that exist to restrict the operation are: 1. The size of the combustion chamber. 2. The capacity for grinding the concentrate. 3. The supply of oxygen.

To control sulphur dioxide concentration in the gas to the Acid Plant and maintain this at a maximum consistent with the production of satisfactory calcine is a secondary objective. For normal operation without the addition of oxygen the furnace outlet gas contains 8.5 pct SO₂, which corresponds to a concentration of 9 pct SO₂ in the combustion chamber. This latter concentration has a calculated theoretical maximum for Trail operations of about 14 pct, with no oxygen enrichment.

The controls used in roasting are: 1. Measurement of temperature in the combustion chamber. 2. Analysis of the calcine for sulphide sulphur. 3. Continuous recording of the sulphur dioxide concentration in the roaster gases.

The calculated and observed advantages of the use of oxygen enriched air in the suspension roasting of zinc concentrate may be summed up as follows: 1. Increased capacity and greater flexibility of operation. 2. Increased concentration of sulphur dioxide. 3. Greater overall heat recovery. 4. Faster starting up and steadier operations.

To calculate the oxygen enrichment of the new air used in suspension roasting is of little value where recirculation of gases to the burner is practised. Therefore, only the volumes of oxygen used are given. These volumes are at 0°C and 760mm Hg. The advantages will now be considered in detail:

INCREASED CAPACITY AND GREATER FLEXIBILITY OF OPERATION

Increasing the concentration of oxygen in the furnace gases has a marked effect on sulphur elimination in the suspension roasting of zinc concentrate. This most important advantage may be made use of in several ways. For a given roaster capacity where the sulphide sulphur in the calcine being produced is not the lowest that it is possible to attain, a calcine lower in sulphide

sulphur can be produced. If lower sulphide sulphur in the calcine is not required then the roaster capacity can be increased, or a coarser concentrate can be roasted. The foregoing indicates the greater flexibility of the roaster operation when oxygen is being used.

Current zinc concentrate treated at Trail is about 95 pct minus 200 mesh, and its analysis, and that of the corresponding calcine, are given in Table 1.

Table 1 . . . Typical Analyses of Normal Zinc Concentrate and Calcine

| | Zinc Concentrate, Pct | Zinc Calcine, Pct |
|-----------------------|-----------------------|-------------------|
| Zinc..... | 48.5 | 53.8 |
| Iron..... | 12.2 | 14.2 |
| Lead..... | 5.0 | 5.2 |
| Moisture..... | 4.5 | |
| Total sulphur..... | 32.3 | 1.5 |
| Sulphate sulphur..... | | 0.8 |
| Sulphide sulphur..... | | 0.7 |

The increased capacities obtained with increased additions of oxygen are shown in Table 2. Oxygen volumes are given in cubic feet per minute at N.T.P. and the supply analyzes 98.5 pct oxygen.

Table 2 . . . Increased Capacities Obtained with Increased Additions of Oxygen

| Rate of Roasting (tons per day) | Percent Sulphide Sulphur in Zinc Calcine with Increasing Oxygen | | | |
|---------------------------------|---|---------|---------|-----------|
| | 0 cfm | 200 cfm | 400 cfm | 1,000 cfm |
| 120 | 0.6 | 0.3 | 0.1 | |
| 140 | 1.3 | 0.7 | 0.4 | |
| 160 | 2.0 | 1.4 | 0.8 | 0.1 |
| 210 | | 3.7 | 2.1 | 0.3 |

From Table 2 it will be seen that an increase of 20 tons per day is realized for each 200 cfm of oxygen. At rates above 150 tons per day it becomes necessary to provide cooling in the combustion chamber to control the temperature there. This is normally accomplished by recirculating cooled gas from the waste heat boiler outlet back into the combustion chamber. At Trail the capacity limitations for recirculation required that additional cooling at very high tonnages be obtained by spraying water into the combustion chamber. This operation was found necessary during the test using 1,000 cfm of oxygen for the rate of 210 tons per day, about 20 lb of water per min. being sprayed into the lower half of the combustion chamber.

At increased roasting rates extra air

is also used with the increased oxygen. Indications are that the total oxygen supplied must be at least 50 pct in excess of the theoretical required. Although there is some increase in the excess oxygen required at the higher tonnages, this alone does not account for the increased rates of sulphur elimination. The full explanation must take into account the fact that the combustion chamber temperature tends generally to be higher at the higher rates.

INCREASED CONCENTRATION OF SULPHUR DIOXIDE

The first requisite of the roasting operation is to maintain a low sulphur in the zinc calcine. Gas strength at Trail is secondary to quality of calcine but is still important. Before installing the permanent oxygen supply for zinc roasting, it was decided to verify the effect of oxygen on gas strength. For this purpose a test was carried out at a normal roasting rate, using 140 cfm of oxygen. The increase in gas strength in the combustion chamber, as determined by the averages of a great many tests, was 0.3 units (9.0 pct SO₂ to 9.3 pct SO₂).

In appraising the long term benefit of oxygen as regards gas strength, many variables must necessarily be taken into account. Relatively large tonnages of acid are required at Trail, and, at times, this has necessitated the roasting of iron concentrate to supplement the gases from zinc roasting. Maximum theoretical gas strength is lower when roasting the pyrrhotite concentrate than when roasting the marmatitic concentrate. However, the use of oxygen in zinc concentrate roasting has assisted in maintaining high overall gas strength. At the same time it has also permitted higher tonnages of zinc concentrate to be roasted.

When allowances are made for all of the variables, there is always an increase in gas strength with increased oxygen, and at least as great as that obtained in the test reported above. Highest gas strengths are obtained when greatest quantities of oxygen are used to replace part of the air required for combustion.

The full range of gas composition in the combustion chamber has not yet been established by test work for comparison with theoretical requirements. In a high tonnage test the concentration of oxygen in the combustion chamber was 10.3 pct for a concentration of sulphur dioxide of 9.1 pct at the

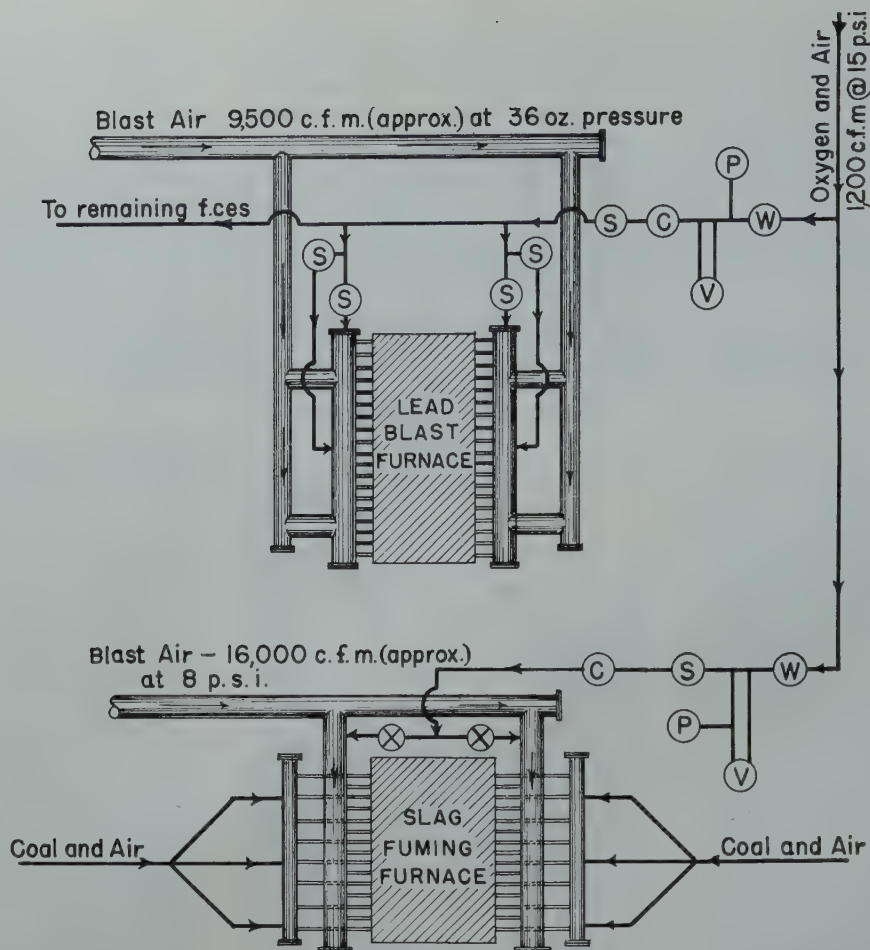


FIG 1—Smelter oxygen system.
 Volumes shown are at 0°C and 760 mm Hg
 X—Gate valve
 C—Check valve
 S—Spur gear valve
 V—Volume gauge
 P—Pressure gauge
 W—Water trap

furnace outlet. Of course this is not the maximum sulphur dioxide concentration reached in the combustion chamber, but it does indicate satisfactory conditions for high tonnages. Any extra oxygen in the roaster gases is an advantage in converting SO_2 to SO_3 in the Acid Plant.

GREATER OVERALL HEAT RECOVERY

The use of oxygen permits greater economy in heat recovery, both through increased capacity for drying the concentrates to be roasted and in increased steam production per pound of concentrate roasted. In a test to show the increased drying rate to be gained by using oxygen at a normal roasting rate it was established that 140 cfm of oxygen increased the drying capacity by about 40 pct. The results of tests carried out to determine the greater heat recovery from the gases are given in Table 3.

Table 3 . . . Results of Tests to Determine Heat Recovery from Gases

| Rate of Roasting (Tons per day) | Increase in Heat Recovery Using 400 cfm of Oxygen Pct |
|------------------------------------|---|
| 120 | 21 |
| 140 | 18 |
| 160 | 11 |

FASTER STARTING UP AND STEADIER OPERATION

Of less importance, but certainly a definite advantage of the use of oxygen in zinc roasting, is the greater speed that is achieved in getting the roaster up to temperature to produce satisfactory calcine. The lower temperature at which ignition of the concentrate occurs and the more rapid rise in temperature mean quicker starting after a shutdown. This results in a saving of fuel oil and minimum dilution of the roaster gases during starting up.

Fluctuations in the chemical and physical properties of the concentrates being fed, which occur particularly in treating a variety of customs concentrates, are more easily taken care of

when oxygen is being used to enrich the air for combustion. The normal procedure is to maintain the oxygen supply constant and make the other necessary adjustments. The result is a much steadier operation.

SUMMARY

Tests have been carried out using up to 1,000 cfm of oxygen on one suspension zinc roaster to obtain satisfactory operation up to 210 tons per day. The suspension zinc roasters at Trail are normally supplied with about 300 cfm of oxygen per roaster. The greatest single advantage has been to increase the individual roaster capacity from 120 tons per day to 150 tons per day. Gas strengths have been increased up to 5 pct. Heat recoveries have been increased up to 15 pct with the use of oxygen.

Advantages are achieved in proportion to the actual oxygen being used. Operation may be varied to obtain the maximum of the advantage desired at

a particular time. A much steadier roaster operation is achieved when oxygen is being used and the operation is more flexible.

Consideration is being given to the use of even greater quantities of oxygen. The object of this is to increase the capacity of present roasting equipment still further, and to obtain increased concentration of sulphur dioxide in the gases going to the Acid Plant for increased acid production.

The Use of Oxygen Enriched Air in the Slag Fuming Furnace and Lead Blast Furnaces

The use of oxygen enriched air has interested both ferrous and nonferrous pyrometallurgists for many years. The Trail Lead Smelter is fortunate in having available a limited supply of by-product oxygen from the Company's Chemical and Fertilizer Division. This fact led to the institution of a test program on the use of oxygen enriched air in both the lead blast furnaces and the slag fuming furnace.

To date most of the test work with oxygen enriched air at the Lead Smelter has been carried out on the slag fuming furnace, where both throughput and zinc recovery have been notably improved. The test work on the lead blast furnaces, although not very far advanced, has indicated a definite coke-saving and much smoother furnace operation.

The compressor delivering oxygen to the Lead Smelter handles a constant volume of 1,200 cfm, which is delivered to the Smelter at 15 psi. When less than 1,200 cfm of oxygen is used, air is introduced into the compressor to make up the difference and the Smelter receives a mixture of air and oxygen. This is fed into the bustle pipes on the slag fuming and blast furnaces with suitable measuring and control devices as shown in Fig 1. All volumes are given at 0°C and 760 mm Hg. 1,000 cfm of oxygen at N.T.P. equal approximately 65 tons per day.

SLAG FUMING FURNACE TESTS

Details of construction and operation of the slag fuming furnace have been published in *Transactions AIME 121*, "Slag Treatment for the Recovery of Lead and Zinc at Trail, B. C." by R. R. McNaughton. Briefly, the furnace is 10 ft wide by 24 ft long and 10 ft high with 36 2-in. tuyeres on each side. Pul-

verized coal and air are blown through the slag bath where the ZnO is reduced to Zn with the temperature of the bath maintained at about 2,200°F. Above the bath the Zn is oxidized again to ZnO. The furnace gases carrying the ZnO pass through a waste heat boiler where they are cooled to 900°F. They then pass through an economizer and finally reach the baghouses at something less than 220°F.

Normally the total volume of air to the furnace is approximately 16,000 cfm at 8 psi ga. Pulverized coal is used at a rate of approximately 200 lb per min. Operation of the fuming furnace is a batch operation and the furnace charge is 55 tons of molten lead blast furnace slag analyzing 16.5 pct zinc, 20 pct silica, 10 pct lime and 28 pct iron. Until recently the standard cycle of operations was 9 blows in 24 hr or 160 min. per blow.

The rate of elimination of the zinc from the molten slag charge depends in practice principally upon the following factors: 1. The composition of the slag. 2. The temperature of the slag. 3. The concentration of CO in the gases agitating the slag.

There are limitations in the existing plant equipment that control the operation, such as: 1. The gas handling capacity of the waste heat boiler and subsequent equipment. 2. The capacity of the blower to supply blast air. 3. The working capacity of the furnace (agitation of the charge must not splash slag into the flue). 4. The cooling capacity of the water jackets (limits furnace temperature).

Altogether about 100 tests, using up to a maximum of 26.5 pct oxygen in the blast, have been carried out on the slag fuming furnace to show the effect of oxygen. Some 30 of these were averaged to give the three sets of figures given in Table 5, which are graphed in Fig 2. In Table 6 the capacity and recovery increases for 23.4 pct oxygen in the blast (500 cfm oxygen added) are shown. In these calculations an empirical figure of 81 pct is used to obtain the tons of slag discharged from the furnace in relation to the tons of slag charged.

Although there is a slight increase in coal consumption the measurement of this has not been accurate enough for comparative purposes. The small increase in steam production is relatively insignificant.

Without the addition of oxygen the slag temperature, as measured by a locally developed continuous optical

temperature recorder, averaged about 2150°F. The use of oxygen has enabled temperatures slightly in excess of 2300° to be maintained. Limitations of the existing equipment prevent operation at higher temperatures.

The points of greatest interest on the curves in Fig 2 fall between blowing times of 100 and 140 min. In this range the rate of zinc elimination commences to fall off. It may be possible that the use of still greater proportions of oxygen to give slightly higher temperatures will permit the development of the operation of a continuous process. Of course, the economics of changing metal prices combined with production costs must be included in any calculations made to establish an operating program.

LEAD BLAST FURNACE TESTS

Details of operation of the lead blast furnaces at Trail have been published in *Transactions AIME Vol. 121*, "Lead Blast Furnace Practice at Trail, B. C." by G. E. Murray. The dimensions of the Trail furnaces have in some cases been altered. Therefore the significant dimensions are given in Table 4 and also the normal blast air volumes.

Table 4 . . . Furnace Dimensions

| Furnace Number | 9 | 10 | 11 | 12 |
|------------------------------------|-------|-------|-------|--------|
| Length (in.)..... | 180 | 270 | 180 | 270 |
| Width at Tuyeres (in.) | 98 | 65 | 65 | 69 |
| Width at Top of Shaft (in.)..... | 120 | 82 | 82 | 76 |
| Normal Blast Air Volume (cfm)..... | 8,500 | 9,500 | 7,500 | 10,000 |

Table 5 . . . Slag Fuming Furnace—Analyses of Slags

| Blowing Time (minutes) | Zinc Remaining in Slag with Oxygen Content in Blast Air of | | |
|------------------------|--|--------|--------|
| | 20.9 % | 23.4 % | 24.8 % |
| 0 | 16.8 % | 16.9 % | 16.4 % |
| 20 | 14.3 | 13.6 | 13.2 |
| 40 | 12.1 | 11.4 | 10.8 |
| 60 | 10.0 | 9.1 | 8.4 |
| 80 | 7.9 | 6.9 | 5.9 |
| 100 | 6.0 | 4.9 | 3.9 |
| 120 | 4.3 | 3.3 | 2.6 |
| 140 | 3.3 | 2.2 | 1.4 |
| 160 | 2.9 | 1.6 | 0.9 |

Table 6 . . . Slag Fuming. Capacity and Recovery Increases for 23.4 Pct Oxygen in Air (500 cfm)

| | | | |
|--------------------------------|------|------|-------|
| Oxygen—Pct in Blast Air..... | 20.9 | 23.4 | 23.4 |
| Length of Blows—min..... | 160 | 160 | 133 |
| Number blows per 24 hr..... | 9 | 9 | 11 |
| Slag Blown—Tons per 24 hr..... | 495 | 495 | 605 |
| Pct Zn. in Slag—In..... | 16.8 | 16.9 | 16.9 |
| Out..... | 2.9 | 1.6 | 2.6 |
| Tons Zn.—In Slag Charged..... | 83.2 | 83.7 | 102.3 |
| Off in Fume..... | 71.6 | 77.3 | 89.5 |
| In Slag Tapped..... | 11.6 | 6.4 | 12.8 |
| Zn Production Increase—Tons.. | | 5.7 | 17.9 |
| Pct..... | | 8 | 25 |

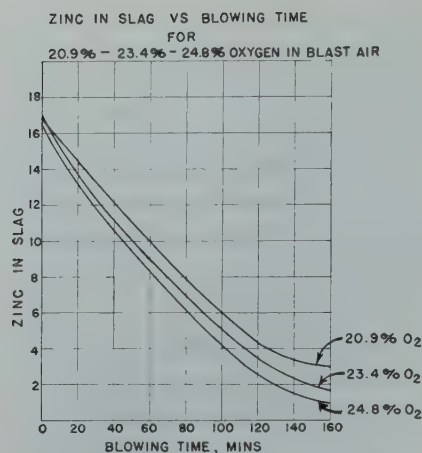


FIG 2—Effect of oxygen on slag fuming operation.

Interruptions in the supply of oxygen have made it impossible to carry through a prolonged continuous test on one blast furnace. Nevertheless the following figures will give some indication of advantages to be expected. A comparison of No. 10 blast furnace using 22.3 pct oxygen in the blast with No. 12 blast furnace using no oxygen showed a coke saving of 3.9 pct. Using 23.0 pct oxygen in the blast on No. 10 furnace and comparing the operation again with No. 12 blast furnace, the coke saving amounted to 12.1 pct. There were corresponding production increases of 20 pct and 30 pct for No. 10 furnace over No. 12. However, comparing the operation of No. 10 furnace using oxygen with its own previous operation for a comparable two months' period without oxygen, the increase in production amounted to only 15 pct for the total period it was using oxygen.

Oxygen has been valuable in blast furnace operation in preventing the formation of, or aiding to smelt out quickly, the crusts which generally form in the lower shaft or crucible. The normal time of smelting out these crusts is about 3 days, whereas the use of up to 27.5 pct oxygen in the blast enables them to be smelted out in one day or less by increasing bottom temperatures.

Although records do not indicate any marked increase in maximum furnace temperatures, slag temperatures are

on the average somewhat higher and better conditions do prevail in the upper shaft to give steadier furnace operation.

To summarize the rather small amount of test work carried out on the lead blast furnaces, it can only be said that indications point to a reduction in coke requirements of about 10 pct with an increase in furnace capacity of 15 to 20 pct for an oxygen enrichment giving 23.4 pct oxygen in the blast air. The regular use of 22.1 to 25.0 pct oxygen enriched blast with occasional applications up to 27.5 pct oxygen enrichment to smelt out crusts should prove to be economic in lead blast furnace operation. For enrichments greater than the above it will probably be necessary to make alterations in furnace design to achieve best results.

CONCLUSIONS

The value of oxygen in the slag fuming operation at Trail is in increased furnace throughput and higher zinc recovery. Further development work will require modifications in furnace design. These are already under consideration. Ultimately a continuous operation may be obtained.

In the lead blast furnaces the indications are that oxygen reduces coke consumption and increases furnace capacity. This work is continuing and will do so until the limits of the present equipment are reached. Alterations in

design will probably then be necessary as in the case of slag fuming.

The Precautions Necessary with the Use of Oxygen Enriched Air in Plant Operations

The use of oxygen enriched air in plant operations requires that certain precautionary measures be taken because of the following characteristics of oxygen:

1. Oil and grease may react violently with oxygen.
2. Spontaneous combustion occurs more readily in the presence of oxygen. The probability of a spark causing ignition during a static discharge is increased.
3. Oxygen accelerates combustion. It has been stated that the rate of acceleration increases rapidly up to a concentration of 40 pct oxygen with little difference noted between 40 and 100 pct oxygen.

The only positive method of preventing oxygen flow beyond a given point in a line is to insert a blind flange. It is strongly recommended that this procedure be adopted where any work is to be carried out in a system beyond a given cut-off point. Also, the system beyond this point should be completely purged of oxygen with large volumes of air.

A Thermodynamic Investigation of the System Silver-silver Sulphide

TERKEL ROSENQVIST*

Introduction

From the chemical, metallurgical, and mineralogical points of view, the importance of thermodynamic data for metal-sulphides and sulphur dissolved in molten metal has long been realized. Such data will give a basis for thermodynamic calculations of processes such as roasting and the distribution of sulphur between molten metal and slags. Furthermore, it will help us understand the chemical forces which tie sulphur to the metal and to the melt.

Thermodynamic studies of solid sulphides and the equilibria between solid sulphides and metals have been carried out in a rather large number of cases by several investigators. An excellent review of this work is given by Kelley.¹ On the other hand, very little is known about the thermodynamic properties of molten sulphides and of sulphur dissolved in molten metal. The only system which previously has been investigated in this respect is the iron/sulphur system.

The purpose of the present investigation was primarily to obtain further data for metal/sulphur melts and the system silver/sulphur was chosen, not because this system was expected to be of special interest in itself, but because the silver/sulphur system is a typical example of a metal/sulphur system. Because of the low melting temperatures, the work could be carried out without appreciable furnace and refractory difficulties. The sulphur in this system possesses a rather high escaping tendency compared to most other metal/sulphur systems. By the method employed (reaction with hydrogen to form hydrogen sulphide) this gives ratios P_{H_2S}/P_{H_2} up to 0.30, which may be determined accurately.

Thermodynamic investigations of the heterogeneous reaction $Ag_2S + H_2 \rightarrow 2Ag + H_2S$ have previously been carried out by Pelabon,² Keyes and Felsing,³ Jellinek and Zakowski,⁴ Watanabe,⁵ and Britzke and Kapustinsky.⁶

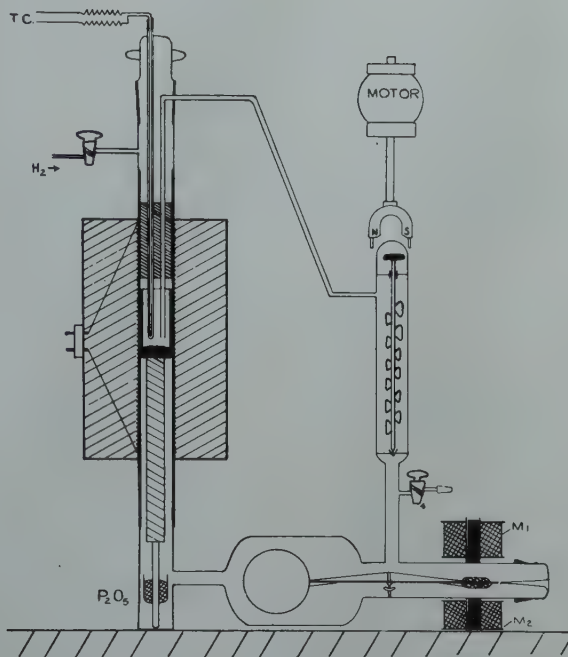


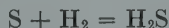
FIG 1—Apparatus for studies of gas-metal equilibria.

Their results are in rather poor agreement.

Experimental Part

PRINCIPLE

In the present investigation the escaping tendency of sulphur from the condensed phase was determined by the reaction:



The ratio P_{H_2S}/P_{H_2} is at constant temperature, directly proportional to the escaping tendency of sulphur and to its chemical activity in the condensed phase. (This ratio will subsequently be denoted by H_2S/H_2 .) From this ratio and its variation with temperature and with change in the com-

position of the condensed phase, thermodynamic quantities such as free energy and heat of reaction can be derived. The apparatus used is shown in Fig 1. The silver/sulphur alloy was placed in a crucible inside the refractory tube and mounted inside the furnace to the left. The tube was a part of a closed, gas-tight system in which the gas mixture could circulate until equilibrium was established. Circulation was maintained by the glass propeller to the right, driven by an external magnet, and promoted by the chimney action of the furnace. The gas passed up through the furnace, down into the crucible where it came in contact with the alloy, passed rapidly up through a narrow tube and out of the hot zone.

After equilibrium was established between the gas and the condensed phase, the composition of the gas mixture was determined from its density. In its circulation, the gas mixture passed through a chamber (lower right on Fig 1) containing a buoyancy-balance, where the density of the gas was determined by magnetic balancing. From the measured density,

Columbus Meeting, September 1949.

TP 2649 D. Discussion of this paper (2 copies) may be sent to *Transactions AIME* before December 1, 1949. Manuscript received December 27, 1948.

* Instructor, Institute for the Study of Metals, University of Chicago.

¹ References are at the end of the paper.

corrected for pressure and temperature, the H_2S content, and consequently the $\text{H}_2\text{S}/\text{H}_2$ ratio were determined. For the gas compositions in question (1–25 pct H_2S) this method is more accurate than the usual chemical analytical methods for H_2S determination. The method further has the advantage compared with chemical analysis, that no gas is removed from the system during the determination. Thus, the progression of the gas-metal reaction could be followed by means of a large number of density determinations, until constant density indicated attainment of equilibrium. This would take from 4 to 5 hr, but the runs were always continued to a total of 12 hr. Prolonged heatings for another 24 hr, which were tried on some samples, produced no further change in the gas composition.

The equilibrium ratios could be determined for any number of temperatures during one heating, without need for withdrawal of gases for analysis or replenishment of the alloy.

After the end of each run, the sulphur content of the alloy was determined by analysis. In order to avoid any back reaction with the gas during cooling, the system was always evacuated to a few mm pressure after the last measurement had been taken (usually at about 1000°C) and cooled in vacuum.

For analysis, the alloy was oxidized by solution in hot concentrated nitric acid and the sulphate thus formed precipitated and weighed as BaSO_4 in the usual way.*

EXPERIMENTAL DETAILS

Materials

The silver/sulphur alloys used were made from electrolytically refined silver, 99.99 pct pure, and sublimed sulphur. Silver sulphide was prepared by heating together stoichiometric amounts of the elements in evacuated and sealed quartz tubes at a temperature of $500\text{--}700^\circ\text{C}$. This reaction was always complete. Silver/sulphur alloys of different compositions were obtained when weighed amounts of silver and silver sulphide were mixed and heated together during the run.

Thermocouple

For all temperature readings, a Pt-13 pct PtRh thermocouple was used. This thermocouple was calibrated by

*Thanks are due to the analytical laboratory of the Institute and particularly to Mr. R. E. Fryxell for the chemical analyses.

means of the melting points of antimony, silver, gold, and palladium—the last two by the wire-bridge method. (A short wire of the calibration metal is inserted in the thermocouple junction and heated until the wire melts, breaking the circuit.)

Furnace

A platinum resistance furnace was used. In order to obtain constant temperature for a period of time, the furnace was fed with current from a constant voltage transformer, and the input was regulated with a variable transformer. In this way, a temperature constancy of $\pm 2.5^\circ\text{C}$ was obtained for days. This is somewhat poorer than by a good temperature controller, but is more dependable in the long run. In the table of experimental results, the temperature is always given to the nearest 5°C .

Refractories

A tube of mullite was used for the main reaction tube. It proved to be absolutely vacuum tight during the entire work (which covered more than 30 runs over a period of about one year). The thermocouple tube and the outlet tube for the gas were of high grade porcelain, approximating mullite in their composition. However, leaks soon developed in the thermocouple tube. Therefore, an inner thermocouple tube of vitreous quartz, sealed gas tight to the porcelain tube, was used. After a couple of runs this quartz tube devitrified and had to be replaced.

A plug of alundum was cemented on to the thermocouple and outlet tubes and acted as a baffle to prevent heat radiation and gas convection to the upper part of the system.

The crucibles were of sintered high purity aluminum-oxide, (Pure-oxide from Norton Co.) free of silica. They stood up well and no chemical reaction seemed to have taken place between the crucible and the gas, or between the crucible and the alloy.

With exception of the crucibles, all other refractories contain some combined silica which gradually would be reduced by the gas at high temperatures. The refractories were therefore reduced with hydrogen at 1300°C before they were used. Nevertheless, some reduction always occurred during the runs. The water-vapor thus formed was absorbed in P_2O_5 placed in a small cup in the cold zone of the system.

Contamination of the alloy with

silicon from the refractories is a usual source of error in work of this kind; therefore a few of the alloys were examined spectroscopically for silicon. The alloys were found to be free of silicon.

The Buoyancy Balance

The buoyancy balance is in principle similar to what is earlier described by Stock,⁷ but certain changes have been made. It was built primarily of Pyrex glass. The beam was built of fine tubes of Pyrex glass with fine porcelain tubes fused on internally for increased rigidity. The bulb was blown of Pyrex glass to about 230 cm^3 and weighed less than 20 g. The counterweight was a Pyrex tube in which some lead was fused together with a small sheet of transformer iron. Eventually this tube was evacuated and closed so that the reaction gas did not come in direct contact with any metal parts. For the same purpose, the knife edge and the support for the balance were made of mullite porcelain, ground to shape and fused in place with uranium glass. The balance was operated by means of the external magnet M_1 (Fig 1) which contained a core of transformer iron. A current was passed through the magnet coil until a fine needle on the counterweight was just level with a corresponding stationary needle. In order to reduce the effect of magnetic hysteresis, the balanced position was always approached from a highly magnetized state, and in such a way that oscillation of the balance in the magnetic field was avoided. In this way, the effect of magnetic hysteresis was reduced to considerably less than 1 pct.

Between the readings, the balance was kept steadily in place by passing current through the lower magnet M_2 . This current, as well as the current for the propeller, was shut off the moment a density reading was taken.

The balance was so made that it was just balanced, without any magnetic influence, for a gas density slightly less than pure hydrogen at atmospheric pressure. This offers the widest operating range and greatest sensitivity for low H_2S contents.

The balance was calibrated by means of gases of known density. As such, dry air, nitrogen, helium and hydrogen were used. By varying the pressure of the calibration gas, a wide range of densities could be covered. The density of the gas was plotted as a function of the current in the magnet. The calibration was tested on known mixtures of

hydrogen and hydrogen sulphide and a satisfactory agreement with the calibration was found.

From the observed density of the gas mixture, the average molar weight M of the gas was derived. This gives the percentage of H_2S in the gas and the H_2S/H_2 ratio:

$$\%H_2S = \frac{M - 2.016}{32.06} 100$$

and

$$\frac{H_2S}{H_2} = \frac{M - 2.016}{34.08 - M}$$

The sensitivity of the balance in itself was about 0.3 mg corresponding to about 0.1 vol. pct of hydrogen sulphide. However, because the balance had a tendency to change position on its support, mainly due to vibration from the gas propeller, the calibration shifted somewhat back and forth. The balance was therefore recalibrated between every run. Nevertheless, the practical accuracy, as far as one could judge from parallel runs, would be about 0.2–0.3 pct H_2S which, for a gas of 20–30 pct H_2S , would represent a relative accuracy of 1 pct.

SOURCES OF ERROR

The value we are interested in is the ratio H_2S/H_2 of the gas when it is in equilibrium with the condensed phase in the hot zone. But the gas was analyzed at room temperature. Thus the question arises whether or not this analysis is representative of the hot gas.

Two different factors may tend to change the composition of the gas on cooling:

1. The gas mixture, in the hot zone, will hold a small amount of sulphur vapor as S_2 gas according to the equilibrium:



In the present work, the sulphur pressure in the hot zone, P_{S_2} , may be as high as 5 mm Hg.

The sulphur vapor will be carried along with the gas flow and on cooling, will react with H_2 to give H_2S . This will increase the ratio H_2S/H_2 in the cooled gas. That this reaction actually occurred is evident from the fact that no condensation of sulphur was observed in the cold part of the system.

In order to obtain the gas ratio H_2S/H_2 in the hot zone, the value observed in the cold zone must therefore be corrected. This correction has been disregarded by most investigators who previously have done work of this kind. But it can be shown that in extreme cases it may attain 10 pct.

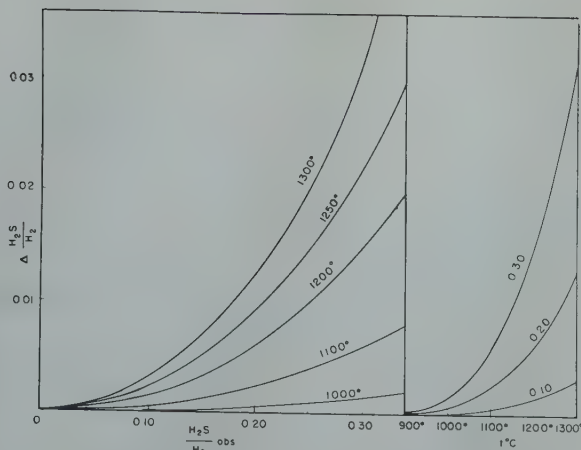


FIG 2—Correction curves for H_2S/H_2 .

The curves to the left give the correction as a function of $H_2S/H_{2(obs)}$ for five different temperatures. The curves to the right give the correction as a function of temperature for three different values of $H_2S/H_{2(obs)}$.

If the correction should be done arithmetically on the basis of the observed gas ratio and the equilibrium constant for the reaction $2H_2S \rightarrow 2H_2 + S_2$, it would involve solving a third order equation. However, it can be done rather easily by a graphical method.

From a series of arbitrarily chosen values for the gas ratio in the hot zone, called $H_2S/H_{2(corr)}$, the equilibrium concentration of S_2 vapor was calculated. On cooling, each S_2 molecule combines with $2H_2$ molecules and gives $2H_2S$ molecules. Consequently, the expected gas ratio at room temperature, $H_2S/H_{2(obs)}$, could be calculated. The difference

$$\Delta H_2S/H_2 = H_2S/H_{2(obs)} - H_2S/H_{2(corr)}$$

was then plotted graphically against $H_2S/H_{2(obs)}$. When this was done for a series of temperatures, (for example, 1000, 1100, 1200, 1250 and 1300°C) a series of smooth curves were obtained (see Fig 2). From these curves, the correction for any experimental $H_2S/H_{2(obs)}$ could be made with sufficient accuracy. It will be seen that for temperatures below 1000°C and also for small H_2S/H_2 ratios, the correction is negligible.

2. The effect of thermal diffusion may cause considerable errors.

It was shown by Soret (1881) that a homogeneous aqueous solution, in response to a thermal gradient, develops differences in concentration in the cold and hot zones. It was later shown by Emmett and Schultz⁸ that the same effect occurred in mixtures of gases having different densities, and that this caused considerable errors in studies of gas-metal equilibria if performed in a *static* system. For the equilibrium of metal-metal oxides

with an H_2O-H_2 atmosphere, the error in the equilibrium constant could be as much as 40 pct. Chipman and Dastur⁹ have shown that the same effect arises in a *dynamic* system if the gas was insufficiently preheated before it reached the condensed phase.

In the present work, special precautions have been taken to avoid this source of error. The gas must be expected to be sufficiently preheated before it reaches the metal as it passes from below, through the resistance heated furnace, up outside the crucible and then down into it.

The fact that the gas circulates at a rather high rate (about 30 to 50 cm³ per min.) prevents inhomogeneity when going from the hot to the cold zone. No appreciable change occurred in the gas composition when the flow rate was varied by a factor of two (by speeding up or slowing down the propeller) indicating that the flow rate was sufficient to eliminate the thermal diffusion. That inhomogeneity would occur if there were no circulation, was shown in one experiment: A "dynamic equilibrium" was established at 1055°C (Run 17) and a gas ratio of 0.218 (corr), 0.220 (obs), was found. Then the circulation was arrested by turning the ground joint top of the apparatus. After the system had been left overnight at the same temperature, a gas ratio of 0.325 (obs) was measured. This is about 50 pct higher than the "dynamic composition." The original value was reproduced when the circulation was started.

EXPERIMENTAL RESULTS

After a number of preliminary runs (which were made to work out the

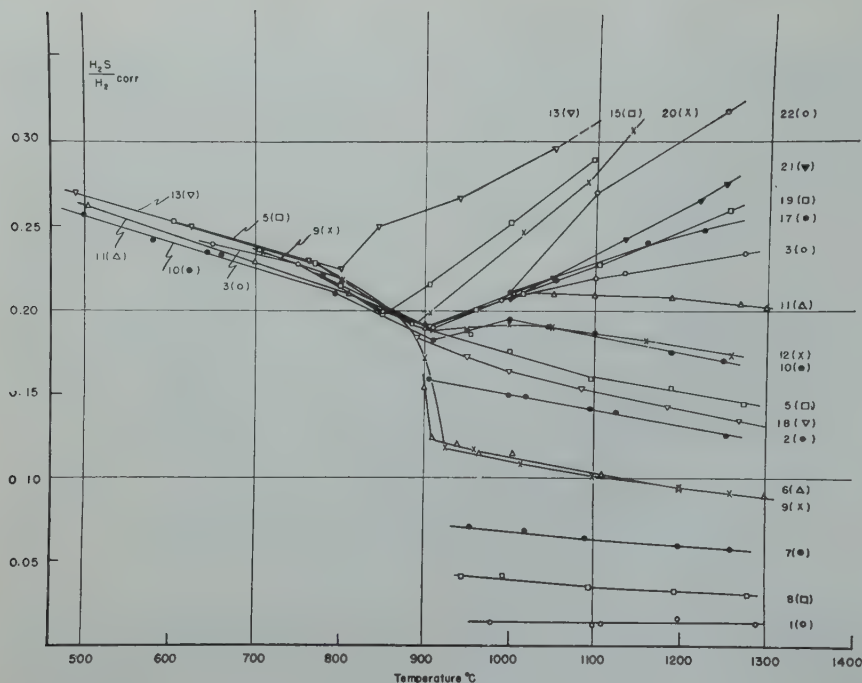


FIG 3—Ratio H_2S/H_2 for runs 1–22.

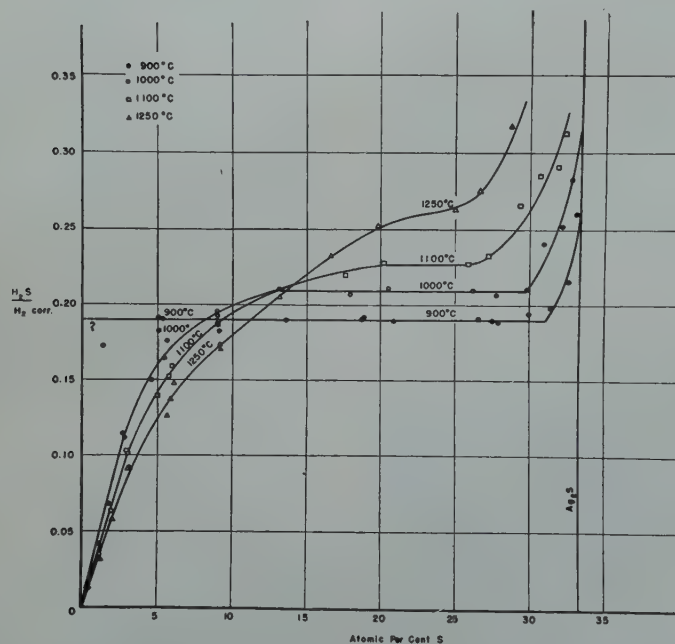


FIG 4—Equilibrium ratios as a function of composition of the alloy.

method) 22 main runs were done with sulphur contents varying from 0.4–33.3 at. pct (0.14–13.9 wt pct). In most of these runs the initial gas was pure hydrogen. However, some runs were started with an initial H_2S/H_2 mixture of a ratio 0.25, thus approaching the equilibrium from the high side. These runs gave values in agreement with the rest of the work.

In Table 1, the runs are tabulated in the order they were made; likewise are the readings at different temperatures listed in the sequence in which they

were carried out. In the first column is given the number of the run, the weight of the alloy, and the volume of the gas. The volume is reduced to 760 mm pressure and 0°C. The composition of the silver/sulphur alloys is given in atomic per cent. The compositions which are *italicized* are the ones obtained by chemical analysis. The compositions at other temperatures of the same run are recalculated from the analytical data, on the basis of the change in gas composition with temperature, the weight of the alloy, and

Table 1 . . . Experimental Runs

| Run No Alloy Weight Gas Volume (in Liter) | t°C | Sulphur Content | Ratio H_2S/H_2 |
|--|--|-----------------------------|---------------------|
| | | At. Pct | Corrected |
| No 1 30.22g 1.40 l | 1100 | 0.47 | 0.013 |
| | 1200 | 0.47 | 0.016 _s |
| | 1290 | 0.45 | 0.014 |
| | 1105 | 0.47 | 0.013 _s |
| | 980 | 0.46 | 0.013 _s |
| | 1200 | 0.47 | No reading made |
| No 2 8.84g 1.36 l | 905 | 4.13 | 0.159 |
| | 1000 | 4.66 | 0.149 _s |
| | 1095 | 5.03 | 0.142 |
| | 1255 | 5.70 | 0.126 |
| | 1115 | 5.10 | 0.140 |
| | 1010 | 4.66 | 0.149 |
| No 3 9.18g 1.35 l | 650 | 17.0 | 0.239 _s |
| | 750 | 17.5 | 0.227 _s |
| | 850 | 18.6 | 0.199 |
| | 910 | 18.9 | 0.190 |
| | 990 | 18.2 | 0.206 |
| | 1135 | 17.5 | 0.222 _s |
| | 1275 | 16.6 | 0.234 |
| | 1100 | 17.6 | 0.219 _s |
| No 4 19.18g 1.33 l | 800 | 5.2 | 0.216 |
| | 900 | 5.2 | 0.192 |
| | Runs at higher temperature failed because crucible broke | | |
| No 5 21.73g 1.38 l | 605 | 4.23 | 0.253 |
| | 705 | 4.52 | 0.236 |
| | 770 | 4.68 | 0.227 _s |
| | 885 | 5.40 | 0.191 _s |
| | 955 | 5.49 | 0.186 |
| | 1095 | 6.02 | 0.160 |
| | 1190 | 6.08 | 0.153 _s |
| | 1270 | 6.24 | 0.144 |
| | 1000 | 5.68 | 0.176 |
| | | | |
| No 6 29.04g 1.38 l | 900 | 2.05 | 0.154 |
| | 910 | 2.57 | 0.124 |
| | 940 | 2.64 | 0.120 |
| | 965 | 2.72 | 0.114 _s |
| | 1110 | 2.96 | 0.102 |
| | 1200 | 3.09 | 0.093 _s |
| | 1300 | 3.15 | 0.089 |
| No 7 30.18g 1.38 l | 1005 | 2.74 | 0.114 _s |
| | 955 | 1.83 | 0.070 _s |
| | 1090 | 1.94 | 0.064 |
| | 1200 | 2.01 | 0.060 |
| | 1260 | 2.05 | 0.057 _s |
| No 8 30.48g 1.38 l | 1020 | 1.85 | 0.068 _s |
| | 945 | 1.19 | 0.041 |
| | 1095 | 1.30 | 0.035 |
| | 1195 | 1.35 | 0.032 _s |
| | 1280 | 1.37 | 0.030 _s |
| No 9 20.36g 1.36 l | 995 | 1.17 | 0.041 _s |
| | 710 | 0.16 | 0.235 _s |
| | 805 | 0.50 | 0.218 _s |
| | 900 | 1.48 | 0.171 _s |
| | 925 | 2.68 | 0.118 _s |
| No 10 29.12g 1.36 l | 960 | 2.71 | 0.117 |
| | 1100 | 3.06 | 0.101 _s |
| | 1200 | 3.22 | 0.093 _s |
| | 1260 | 3.23 | 0.092 |
| | 1015 | 2.90 | 0.108 _s |
| | 660 | 8.53 | 0.232 _s |
| | 580 | 8.39 | 0.241 _s |
| | 430 | equilibrium was not reached | |
| No 11 29.63g 1.36 l | 500 | 8.20 | 0.256 _s |
| | 652 | 8.48 | 0.235 |
| | 795 | 8.83 | 0.210 |
| | 910 | 9.22 | 0.182 |
| | 950 | 9.13 | 0.188 |
| | 1045 | 9.07 | 0.190 _s |
| | 1100 | 9.10 | 0.187 |
| | 1190 | 9.25 | 0.175 |
| | 1250 | 9.25 | 0.170 _s |
| | 1000 | 9.01 | 0.195 |
| | | | |
| No 12 29.12g 1.34 l | 700 | 13.3 | 0.229 _s |
| | 810 | 13.4 | 0.209 _s |
| | 505 | 12.8 | 0.262 |
| | 900 | 13.7 | 0.190 |
| | 1050 | 13.4 | 0.210 _s |
| | 1190 | 13.4 | 0.207 _s |
| | 1270 | 13.4 | 0.204 |
| | 1300 | 13.4 | 0.201 _s |
| No 13 15.42g 1.33 l | 1100 | 13.4 | 0.209 _s |
| | 1005 | 13.4 | 0.210 _s |
| | 910 | 9.16 | 0.188 |
| | 950 | 9.18 | 0.187 |
| | 1050 | 9.13 | 0.190 |
| No 14 15.42g 1.33 l | 1160 | 9.18 | 0.182 _s |
| | 1260 | 9.24 | 0.174 |
| | 1000 | 9.11 | 0.192 |
| | 490 | 33.1 | 0.270 |
| | 625 | 33.4 | 0.249 _s |
| No 15 15.42g 1.33 l | 762 | 33.7 | 0.230 |
| | 800 | 33.7 | 0.225 |
| | 845 | 33.3 | 0.250 |

Table 1 . . . (Continued)

| Run No Alloy Weight Gas Volume (in Liter) | t°C | Sulphur Content | Ratio H ₂ S/H ₂ |
|--|---|--------------------|--|
| | | At. Pct | Corrected |
| No 14 24.63g 1.37 l | 940 | 33.1 | 0.267 |
| | 1050 | 32.6 | 0.295 _s |
| | (1100) (extrapolated) | (32.4) | (0.312 _s) |
| | 780 | 17.4 | 0.221 |
| | 910 | 17.8 | 0.192 |
| No 15 27.89g 1.35 l | 950 | 17.7 | 0.200 |
| | Runs at higher temperature failed because crucible broke | | |
| | 800 | 32.68 | 0.215 |
| | 905 | 32.68 | 0.215 _s |
| No 16 29.15g 1.37 l | 1095 | 31.95 | 0.289 _s |
| | 850 | 32.81 | 0.198 _s |
| | 1000 | 32.32 | 0.252 _s |
| | 905 | 27.6 | 0.190 |
| | Runs at higher temperature failed because crucible broke | | |
| No 17 23.87g 1.38 l | 1055 | 20.96 | 0.189 |
| | 1160 | 20.51 | 0.218 |
| | 1225 | 20.15 | 0.240 _s |
| | 1000 | 20.00 | 0.247 _s |
| | 1000 | 20.59 | 0.211 _s |
| No 18 26.41g 1.38 l | 890 | 5.21 | 0.183 _s |
| | 950 | 5.41 | 0.173 |
| | 1085 | 5.71 | 0.154 |
| | 1185 | 5.90 | 0.142 _s |
| | 1270 | 6.00 | 0.134 |
| | 1000 | 5.56 | 0.164 |
| No 19 14.75g 1.39 l | 905 | 26.7 | 0.191 |
| | 1105 | 25.9 | 0.226 _s |
| | 1180 | 25.4 | 0.246 _s |
| | 1255 | 25.0 | 0.259 |
| | 1015 | 26.3 | 0.209 |
| No 20 28.10g 1.36 l | 900 | 31.5 | 0.198 _s |
| | 1090 | 30.7 | 0.276 _s |
| | 1140 | 30.4 | 0.307 _s |
| | 1015 | 31.0 | 0.247 |
| | 905 | 27.95 | 0.189 |
| No 21 23.31g 1.39 l | 1135 | 27.25 | 0.242 _s |
| | 1220 | 26.95 | 0.265 |
| | 1050 | 27.55 | 0.219 _s |
| | 1250 | 26.70 | 0.275 |
| | 1000 | 27.85 | 0.206 |
| No 22 26.67g 1.33 l | 850 | 30.07 | 0.200 _s |
| | 895 | 30.15 | 0.194 |
| | 1100 | 29.39 | 0.265 _s |
| | 1250 | 28.80 | 0.317 |
| | 965 | 30.02 | 0.206 |
| | 1000 | 29.98 | 0.210 _s |

the volume of the gas. For a few runs in the medium composition range, the alloys were not analyzed but their sulphur contents calculated from their original composition by correcting for the sulphur losses to the atmosphere. These values are given with one decimal place less than the others and are not underlined.

In Fig 3 is plotted the gas ratio, H₂S/H₂(corr), as a function of temperature for all runs.

Fig 4 gives the variation of the gas ratio with composition of the alloy for four different temperatures: 900, 1000, 1100, and 1250°C. When no experimental value existed for the exact temperature, the points were obtained by interpolation from Fig 3.

In Fig 5 is plotted log H₂S/H₂ against 1/T for a number of compositions as they are taken from Fig 4. It is obvious that the data given in Fig 5 do not represent the experimental data directly, but are obtained by

interpolating between them. Therefore they give an idealized picture where experimental scatterings are smoothed out. On the other hand, they are derived from a large number of experimental data, and no appreciable error should be introduced by this procedure.

Discussion of Results

COMPARISON WITH THE RESULTS OF PREVIOUS INVESTIGATORS

The heterogeneous equilibria between phases rich in Ag₂S and Ag have been investigated by Pelabon,² Keyes and Felsing,³ Jellinek and Zakowski,⁴ Watanabe,⁵ and Britzke and Kapustinsky.⁶ Their data are plotted in Fig 6, together with the present data for the same heterogeneous equilibria.

The data of the previous investigators are derived by using different techniques. Pelabon as well as Keyes and Felsing established the equilibrium composition of the gas mixture inside a container kept at constant high temperature. The gas mixture was then quenched to room temperature and analyzed. Pelabon quenched the entire container (a quartz tube); Keyes and Felsing withdrew the gas from the hot zone into an evacuated burette. As seen, there is poor agreement between their values. It should be noted that Pelabon worked with rather small gas volumes and that an inaccuracy in the chemical analysis is possible. Keyes and Felsing's values are the averages of a series of parallel runs which in themselves deviated as much as 10 pct from the mean value.

Watanabe established his gas equilibrium in the hot end of a tube, and withdrew gas for analysis from the cold end. It is obvious that this leads to inhomogeneity of the gas by thermal diffusion, and that his values for the gas-ratio must be too high. In fact the value which in the present investigation was obtained by closing off the circulation, and which in Fig 6 is denoted by an *, agrees with what one should expect by extrapolation from Watanabe's data.

The data of Jellinek and Zakowski run rather parallel to those of the present investigation but are about 25 pct higher. Their method was a dynamic one in which the gas passed only once over the condensed phase. In order to correct for incomplete reaction, they made several runs of different flow rates, and the equilibrium compo-

sitions were obtained by extrapolation to zero flow rate. By this extrapolation they actually introduce to some extent, the effect of thermal diffusion. Their experimental runs were made at flow rates from 6 to 1 cm³ per min., flow rates at which the thermal diffusion already plays an important role.

The data of Britzke and Kapustinsky are in best agreement with those of the present work. They were obtained by a static method of measuring the partial pressure of hydrogen in the hot zone by letting it diffuse through the walls of a platinum bulb. However, some uncertainty must exist in this method too; their data show a minimum for the gas ratio at 957°C, although no break in the curve is to be expected at this temperature from the equilibrium diagram.

THE EQUILIBRIUM DIAGRAM OF THE SYSTEM

The experimental data confirm previous data that a region of liquid immiscibility exists in the system. At the monotectic temperature of about 900°C,* the silver-rich phase has a composition of 5.5 at. pct sulphur (corresponding to run 5) and the sulphur rich phase about 31.0 at. pct. This agrees with the compositions obtained from thermal analysis by Kracek: 5.8 and 31.1 at. pct sulphur.¹⁰ At higher temperatures, the immiscibility gap becomes narrower and disappears at a critical temperature of about 1125°C (±25°C) and a critical composition of 24 at. pct sulphur. This corresponds to a rather unsymmetrical shape of the immiscibility region. The immiscibility region and the neighboring parts of the equilibrium diagram are shown in Fig 7.

The present investigation gives little information as to the solid solubility of sulphur in silver. Run 9 shows that the solid solubility at 800°C is not greater than 0.50 at. pct (0.15 wt pct) sulphur. The actual solid solubility is probably much less.

Thermodynamic Calculations

Thermodynamic calculations will be carried out separately for the different regions of the system.

* Kracek¹⁰ found the monotectic temperature equals 906°C. The present work indicates a temperature of 895–900°C. However, the temperature reading in this work may be a few degrees off, and it is further probable that hydrogen dissolved in the liquid metal will lower the freezing point another couple of degrees. Therefore, the value of Kracek is regarded as most reliable.

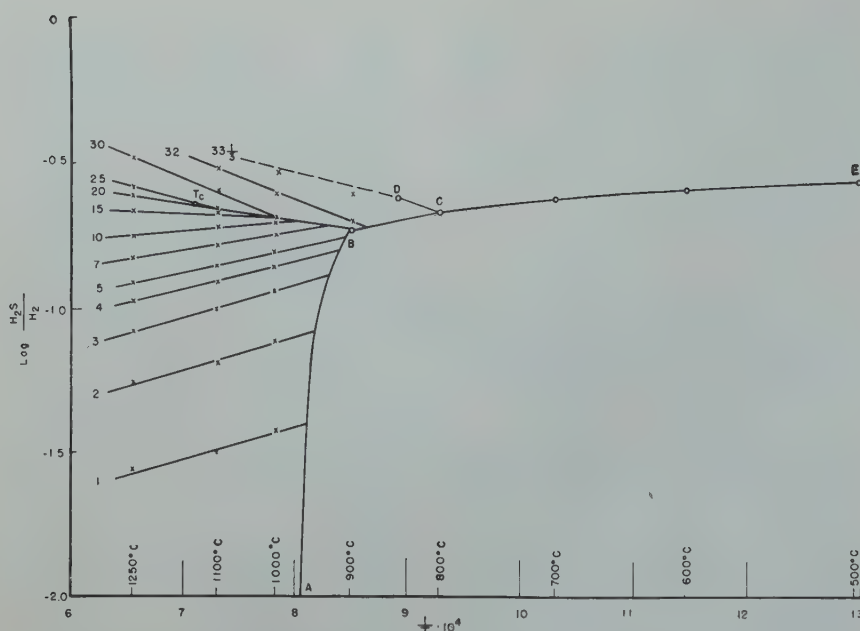
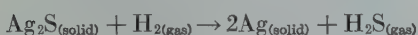


FIG 5—Log H_2S/H_2 as a function of $1/T$.
Figures to the left give sulphur content of the alloy in atomic per cent.

1. Below 800°C , the investigated equilibrium corresponds to the reaction:



The equilibrium gas ratio is independent of the relative amounts of the two solid phases, as long as they are both present.

The mean values of the equilibrium constant, averages of five runs, are listed in Table 2 for four different temperatures.

The standard Gibb's free energy ΔF° for the reaction is derived by the expression $\Delta F^\circ = -RT \ln Kp$

The slope of $\log Kp$ plotted against $1/T$ as done in Fig 5, gives us the heat of the reaction:

$$\Delta H = \frac{-R d \ln Kp}{1/T}$$

Furthermore:

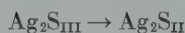
$$\left[\frac{d\Delta H}{dT} \right]_P = \Delta Cp$$

where ΔCp is the increase in specific heat resulting from the reaction.

In the following, a calculation will be carried out to derive expressions for the heat and Gibb's free energy of the reaction, as a function of temperature, on the basis of the experimental data and the specific heats of the components involved. The procedure for these calculations is the same as that used by Watanabe, except that more recent data are applied for the specific heats. For the specific heats Cp , the values listed by Spencer,¹¹ for the gases, and by Kelley,¹² for the solids, are used.

Silver sulphide exists, according to Kracek,¹⁰ in three modifications de-

noted III (below 176°C), II (176 – 586°C), and I (586 – mp). The heat of transformation at $176^\circ\text{C} = 449^\circ\text{K}$ is given by Kelley.



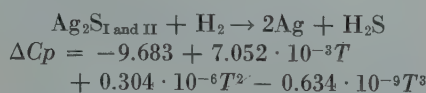
$$\Delta H_{449} = 1000 \text{ cal/mol}$$

The heat of transformation $Ag_2S_{II} \rightarrow Ag_2S_I$ is not known. Kracek finds that the heat effect at 586°C is less than one-tenth of the heat effect at 176°C . This indicates that the heat of the reaction $Ag_2S_{II} \rightarrow Ag_2S_I$ is less than 100 cal which is inside the experimental error of the present work.

Likewise no data exist on the specific heat of Ag_2S_I . It cannot, however, be much different from that of Ag_2S_{II} , and no appreciable error will be introduced by using this value above 586°C also.

Thus, the transformation at 586°C is entirely disregarded in the present calculations.

For the reaction:



and

$$\Delta H = 4720 - 9.683T$$

$$+ 3.526 \cdot 10^{-3}T^2 + 1.01 \cdot 10^{-6}T^3$$

$$- 0.159 \cdot 10^{-9}T^4 \quad [1]$$

$$\Delta F^\circ = 4720 + 22.29T \log T$$

$$- 3.526 \cdot 10^{-3}T^2 - 0.051 \cdot 10^{-6}T^3$$

$$+ 0.053 \cdot 10^{-9}T^4 - 65.11T \quad [2]$$

From the last expression, ΔF° and $\log Kp$ are calculated for comparison with the experimental data. They are listed in the last columns in Table 2. The agreement is satisfactory.

If the expressions 1 and 2 are com-

Table 2 . . . Mean Values of Equilibrium Constant

| $Ag_2S_{(s)} + H_{2(g)} \rightleftharpoons 2Ag_{(s)} + H_2S_{(g)} \quad Kp = \frac{H_2S}{H_2}$ | | | | | |
|--|-------------------|-----------|------------|-----------------------|------------------------|
| $t^\circ\text{C}$ | $T^\circ\text{K}$ | Kp exp. | Kp calc. | ΔF° exp. | ΔF° calc. |
| 500 | 773 | 0.263 | 0.264 | 2050 cal | 2043 cal |
| 600 | 873 | 0.249 | 0.248 | 2414 cal | 2418 cal |
| 700 | 973 | 0.232 | 0.231 | 2830 cal | 2836 cal |
| 800 | 1073 | 0.215 | 0.214 | 3281 cal | 3289 cal |

bined with corresponding expressions for the reaction $H_2S \rightarrow H_2 + \frac{1}{2}S_2$, one obtains the heat and free energy for the reaction $Ag_2S \rightarrow 2Ag + \frac{1}{2}S_{2(gas)}$; and one can also derive the partial pressure of S_2 vapor. These calculations will not be done here.

On the basis of Eq 1 and 2, the values for the heat and free energy at the transformation temperature 449°K are obtained.

For the reaction $Ag_2S_{II} + H_2 \rightarrow 2Ag + H_2S$

$$\Delta H_{449} = 1084 \text{ cal and } \Delta F^\circ_{449} = 1316 \text{ cal}$$

and for the reaction $Ag_2S_{III} + H_2 \rightarrow 2Ag + H_2S$

$$\Delta H_{449} = 1084 + 1000 = 2084 \text{ cal}$$

$$\Delta F^\circ_{449} = 1316 \text{ cal}$$

Below 449°K , one has:

$$Ag_2S_{III} + H_2 \rightarrow 2Ag + H_2S$$

$$\Delta H = 4370 - 6.683T$$

$$+ 3.526 \cdot 10^{-3}T^2 + 0.101 \cdot 10^{-6}T^3$$

$$- 0.159 \cdot 10^{-9}T^4 \quad [3]$$

$$\Delta F^\circ = 4370 + 15.39T \log T$$

$$- 3.526 \cdot 10^{-3}T^2 - 0.051 \cdot 10^{-6}T^3$$

$$+ 0.053 \cdot 10^{-9}T^4 + 46.01T \quad [4]$$

This gives for $298^\circ\text{K} = 25^\circ\text{C}$

$$\Delta H_{298} = 2693 \text{ cal} \quad \Delta F^\circ_{298} = 1692 \text{ cal}$$

The heat and free energy of the reaction $H_2S = H_2 + S_{rh}$ at 298°K are known¹

$$\Delta H_{298} = 4800 \text{ cal} \quad \Delta F^\circ_{298} = 7865 \text{ cal}$$

Combining these two sets of values, one obtains for the formation of 1 mol of silver sulphide from the elements at room temperature:

$$2Ag + S_{rh} = Ag_2S_{III}$$

$$\Delta H_{298} = -7493 \text{ cal}$$

$$\Delta F^\circ_{298} = -9557 \text{ cal}$$

The largest uncertainties in the present calculation are in specific heats of the silver-sulphides which are known with an accuracy of only 5 pct, which causes an uncertainty of 600 cal in the calculation of the heat and free energy at room temperature. The determination of the heat of reaction at high temperature is probably correct to ± 200 cal; hence the total uncertainty in ΔH_{298} and ΔF°_{298} will be 800 cal.

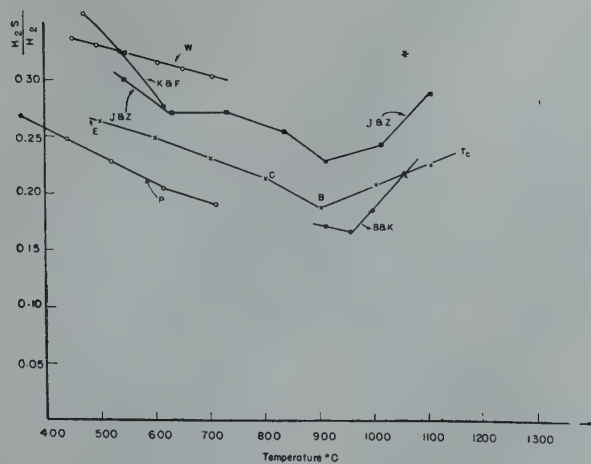


FIG 6—Comparison of present results with results of previous investigators.

P = Pelabon
K & F = Keyes and Felsing
J & Z = Jellinek and Zakowski
ECBTC = Result of the present work
W = Watanabe
B & K = Britzke and Kapustinsky
* = Gas ratio for run without circulation allowing thermal diffusion to take place

The heat of formation of Ag_2S from the elements has been determined experimentally by Zeumer and Roth¹³ to $\Delta H_{293} = -6,660 \pm 200$ cal.

The standard free energy of formation is listed by Latimer¹⁴ as $-9,500$ cal, a value with which the present result is in very good agreement. Latimer's value is the average of independent measurements of equilibrium constants in aqueous solutions.

The standard free energy has also been given by Kelley as $-8,680$ cal, but his value is based on the equilibrium constants at high temperature by Keyes and Felsing, Jellinek and Zakowski, and Watanabe in combination with the heat of reaction adapted from Zeumer and Roth.

THERMODYNAMIC RELATIONS IN THE MOLTEN STATE

Calculations of the heats of reaction and free energies for the heterogeneous reactions above the melting point, for instance Ag_2S -rich melt + $\text{H}_2 \rightarrow \text{Ag}$ -rich melt + H_2S , can be done in the same way as for the solid equilibrium. Such calculations have rather little physical significance as they involve phases in which the composition changes considerably with the temperature.

A clearer description of the thermodynamics in the molten state is obtained by plotting the partial thermodynamic functions for sulphur and silver as a function of the composition. The partial atomic heat content of sulphur dissolved in the melt can be expressed in different ways, depending on what standard state is chosen:

The heat of the reaction $\text{H}_2\text{S} \rightarrow \text{H}_2$

+ $\text{S}_{(\text{dissolved})}$ will be denoted by $\Delta \bar{H}_S$ and is the heat required to transfer one gram atom of sulphur from hydrogen sulphide to the melt—the melt being kept at constant composition.* $\Delta \bar{H}_S$ is given by the expression

$$\Delta \bar{H}_S = R \frac{d \ln \text{H}_2\text{S}/\text{H}_2}{d \ln T}$$

and can be obtained from the slope of the curves in Fig 5.

If, on the other hand, the partial heat content of sulphur is referred to monoatomic sulphur vapor as the standard state, it will be denoted by $\Delta \bar{H}_S'$. In the temperature region 1000 – 1250°C $\Delta \bar{H}_S$ and $\Delta \bar{H}_S'$ will differ by $74,680$ cal which is the heat of the reaction $\text{H}_2\text{S} \rightarrow \text{H}_2 + \text{S}_{(g)}$ in this temperature range, calculated from Kelley's data.¹

The partial heat content of silver, $\Delta \bar{H}_{\text{Ag}}$, is related to the corresponding value for sulphur by the equation

$$N_{\text{Ag}} d\Delta \bar{H}_{\text{Ag}} + N_{\text{S}} d\Delta \bar{H}_S = 0$$

N_{Ag} and N_{S} mean the atomic fractions of silver and sulphur respectively. This equation is independent of what standard state is chosen for sulphur. Integrating this equation graphically, the partial heat content of silver referred to pure molten silver as standard state, can be derived. The partial heats $\Delta \bar{H}_S$, $\Delta \bar{H}_S'$ and $\Delta \bar{H}_{\text{Ag}}$ are plotted in Fig 8, all as a function of composition.

A few points became apparent from Fig 8; the partial atomic heat of sulphur is independent of concentration in the dilute range 0 – 3 at. pct sulphur, that is, Henry's law is followed.

Between 3 and 30 at. pct sulphur, the

* $\Delta \bar{H}_S$ is independent of the partial pressure of H_2S , which behaves as a perfect gas.

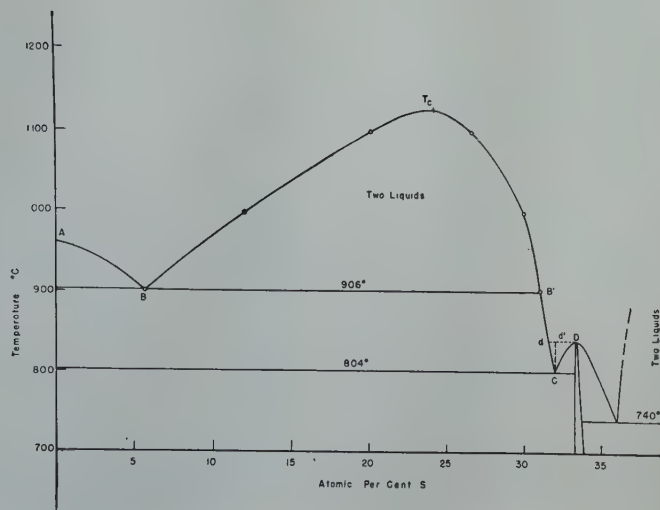


FIG 7—Phase diagram for the melting region of the system silver/silver-sulphide.

partial heat of sulphur $\Delta \bar{H}_S$ decreases linearly with the sulphur content. Between 30 and $33\frac{1}{3}$ at. pct sulphur, the atomic heat seems to increase somewhat. The experimental data are not too good here, however, and a considerable error is possible.

Contrary to what is usually the case for a solute, the partial heat of sulphur decreases with increasing concentration. In a later section this phenomenon will be more thoroughly discussed, as well as its relation to the immiscibility phenomenon in this system.

The chemical potential μ_S and the chemical activity a_S of sulphur in the melt are given by the equations

$$\mu_S = RT \ln \text{H}_2\text{S}/\text{H}_2 + \mu_S^0$$

$$a_S = K_1 \cdot \text{H}_2\text{S}/\text{H}_2$$

The standard potential μ_S^0 and the constant K_1 depend again on what standard state is chosen for sulphur.

Using the Gibbs-Duhem equation, we can derive the chemical activity of silver a_{Ag} :

$$N_{\text{Ag}} d \ln a_{\text{Ag}} + N_{\text{S}} d \ln \text{H}_2\text{S}/\text{H}_2 = 0$$

This equation is integrated graphically and pure molten silver is given the activity one.

The chemical activity of Ag_2S is defined by the expression

$$a_{\text{Ag}_2\text{S}} = K_2 (a_{\text{Ag}})^2 \cdot \text{H}_2\text{S}/\text{H}_2$$

The constant K_2 is so chosen as to make $a_{\text{Ag}_2\text{S}}$ unity at the stoichiometric composition.

In Fig 9, the chemical activity of silver, the $\text{H}_2\text{S}/\text{H}_2$ ratio and the chemical activity of Ag_2S are plotted for the temperature 1125°C (the critical temperature of immiscibility).

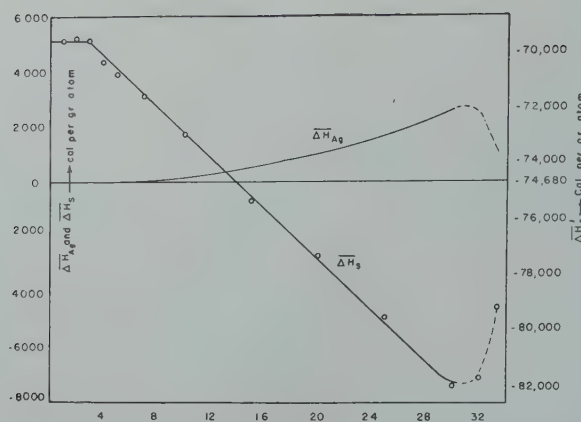


FIG 8—Partial atomic heat content of silver and sulphur.

Figures along the abscissa indicate atomic pct sulphur.
 $\Delta \bar{H}_S$ and $\Delta \bar{H}_{Ag}$ are read on the scale to the left.
 $\Delta \bar{H}_S'$ is read on the scale to the right.

The typical positive deviation from Raoult's law is apparent for all three curves, and they all have a horizontal tangent at 24 at. pct sulphur, corresponding to the critical composition.

One can further see that the activity of silver has a considerable value even for a melt of composition Ag_2S . Thus, the system $Ag-Ag_2S$ cannot be treated thermodynamically as a simple binary system but only as part of the system $Ag-S$.

The activity of silver follows Raoult's law in the silver rich part of the system—the activity of sulphur following Henry's law.

THE HEAT OF FUSION OF Ag_2S

The heat of fusion of Ag_2S may be determined in two different ways:

1. The break in the curve ECB (Fig 5) at the eutectic temperature $804^\circ C$ corresponds to about 900 cal. This would be equal to the heat of fusion if there were no change in the partial heat content and partial free energy of molten Ag_2S between 31 and $33\frac{1}{3}$ at. pct sulphur. Because this assumption is not strictly correct, the actual heat of fusion will be somewhat less than 900 cal.

2. Knowing the variation of the activity of Ag_2S in the melt between 31 and $33\frac{1}{3}$ at. pct sulphur, and the lowering of the freezing point of Ag_2S by addition of silver, the heat of fusion can be determined by the equation

$$\frac{dT_m}{dx} = \frac{RT_m^2}{\Delta H_m} \left(\frac{\partial \ln a_{Ag_2S}}{\partial x} \right)_T$$

x = atomic fraction of silver

T_m = freezing temperatures

ΔH_m = heat of fusion of Ag_2S

The chemical activity of Ag_2S is proportional to the product $(a_{Ag})^2$. H_2S/H_2 ; the freezing point lowering is

obtained from the work of Kracek,¹⁰ and a value for ΔH_m of about 700 cal is obtained.

This method involves a considerable degree of uncertainty and the obtained value must be regarded as preliminary.

It seems likely, however, that the heat of fusion is considerably lower than the 3400 cal per mol listed by Kelley.¹⁵ The disagreement is so large that a redetermination by more accurate methods is desirable.

A value for the heat of fusion of 700–900 cal is amazingly low and would correspond to an entropy of fusion of less than one calorie per degree per mol. Very few substances are known to have an entropy of fusion that low (a value from 2–5 units per mol is usual). On the other hand, a very low entropy of fusion is to be expected from the crystal structure of solid Ag_2S which according to Rahlfs¹⁶ shows a high degree of disorder. In this crystal structure the silver atoms are almost randomly distributed and can be compared with the atoms in a liquid, whereas only the sulphur atoms form a regular lattice. Therefore, the entropy of fusion should correspond to the breaking down of the sulphur lattice only.

A Tentative Theory for the Relation between Thermodynamics and Structure of the Melt

Little is known about the structure of molten metals and alloys and especially meager is our knowledge of the structure and chemical forces in molten metal-sulphur systems. For the following treatment, a few known facts will be summarized:

1. Solid silver crystallizes in a close packed cubic structure with coordination number 12 and distance between nearest neighbors = 2.88\AA .

2. Molten silver has a structure closely related to that of solid silver but lacks the long range regularity of the solid state. The coordination number is 11–12 and nearest neighbor distance slightly more than in the solid. In the following, an average coordination number of 11.5 will be assumed. In both solid and liquid silver, the interatomic bond is metallic.

3. Solid Ag_2S (modification II) crystallizes in a cubic structure, where the silver atoms are almost randomly distributed (per unit cell 4 silver atoms can occupy 42 positions).¹⁶ Each sulphur atom has about seven nearest silver neighbors at a distance of about 2.6\AA . The distance to the nearest eight sulphur atoms is 4.225\AA . Each silver atom has on the average about ten nearest silver neighbors at a distance of about 3.0\AA . The crystal structures of modifications I and III are not known in detail but are regarded as closely related to modification II. Therefore, the number of nearest neighbors and the distance between them should be about the same as in modification II. As the heat of fusion of Ag_2S seems to be very low, the structure of the melt should not be expected to differ very much from the solid state.

The nature of the interatomic bond in Ag_2S can be described as predominantly metallic since the compound exhibits electronic conductivity with a negative temperature coefficient.¹⁷ There is no reason to assume the nature of the interatomic bond to be any different in the liquid than in the solid state.

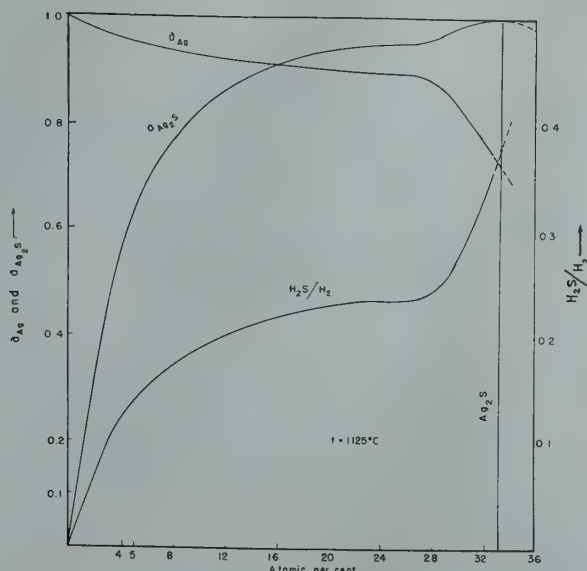


FIG 9—Chemical activities for silver and silver sulphide and the ratio H_2S/H_2 at $t = 1125^\circ C$.

The gas ratio is a measure of the chemical activity of sulphur.

One should, therefore, in this compound apply the atomic radii for metallically bonded atoms rather than the ionic radii. The atomic radii which are in best harmony with the interatomic distances are 1.5\AA for silver and 1.1\AA for sulphur.

The ratio R_s/R_{Ag} is close to 0.73. For a close packing of atoms, this would correspond to a coordination number: 8 (silver neighbors around each sulphur atom) while 7 is actually found in solid Ag_2S . For the discussion of the structure of the melt, the average coordination number is assumed equal 7.5.

We will discuss the energy required to introduce one gram-atom of sulphur from monatomic vapor into molten silver or into a silver-sulphur melt, the melt being kept at constant temperature. This energy equals $\Delta\bar{H}_S'$ from the preceding section. It will be necessary to expand one of the interstitial positions in the silver melt to make room for each sulphur atom. Structural consideration indicates that this requires the breaking an average of 1.5 Ag-Ag bonds, and a slight adjustment of the silver atoms. If more and more sulphur atoms are added to the melt, more interstitial positions are expanded, each requiring the breaking of 1.5 Ag-Ag bond. When one gram atom sulphur has been added to 2 g atoms silver corresponding to a composition Ag_2S , 1.5 N out of 11.5 N Ag-Ag bonds have been broken, leaving 10 N bonds unbroken, corresponding to each silver atom being surrounded by 10 silver neighbors. This agrees with the coordination number 10 which is actually found in solid Ag_2S .

The energy required to introduce one gram atom of sulphur from monatomic vapor into the melt will be the energy required to break $N \cdot 1.5$ Ag-Ag bond minus the energy liberated by the formation of new interatomic bonds. The energies of the interatomic bonds will be denoted by the symbol V .

For a diluted solution of sulphur in molten silver, the individual sulphur atoms will be sufficiently separated not to interact and

$$\Delta\bar{H}_S' = N \cdot (1.5V_{Ag-Ag} - 7.5 V_{Ag-S})$$

As $|\Delta\bar{H}_S'|$ according to Fig 8 equals $-69,500$ cal for a dilute solution, and $N \cdot V_{Ag-Ag}$ is calculated from the heat of vaporization of liquid silver equal $12,000$ cal, one obtains the energy of N silver-sulphur bonds, $N \cdot V_{Ag-S}$, equal $11,650$ cal.

With increasing sulphur concentration, we find that $\Delta\bar{H}_S'$ decreases and reaches a value of about $-82,000$ cal when the composition approaches Ag_2S .

This decrease in heat content is very likely due to the fact that more and more sulphur atoms will occupy neighboring "expanded interstitial" positions, that is, they will be second nearest neighbors in the melt, and that these sulphur neighbors exhibit attractive forces on each other. Thus, bringing two sulphur atoms into neighboring "interstitial" positions will liberate a certain energy V_{S-S} .

The fact that the energy of the sulphur-sulphur bond has a positive value means that each sulphur atom will tend to attract other sulphur atoms to have as large a number of sulphur neighbors as possible. On the other hand, thermal

agitation will tend to distribute the sulphur atoms statistically among the available positions to make the entropy as large as possible. The net effect is a distribution of the atoms which gives the lowest free energy. The number of sulphur neighbors in neighboring "interstitial" positions will be somewhat larger than corresponds to random distribution. We will have a type of short range order in the melt. (See Fig 10.)

The total free energy of mixing can, for a given temperature, be expressed in the following terms:

$$\Delta F(x, n) = \Delta H(x, n) - T\Delta S(x, n)$$

x is the mol fraction of sulphur and n the number of sulphur-sulphur bonds. ΔH will decrease with increasing value of n , and ΔS will decrease with increasing value of n in excess of what corresponds to random distribution.

If the exact dependencies of ΔH and ΔS with respect to n were known, the minimum value of ΔF and the degree of short range order could be obtained by setting

$$\left(\frac{\partial \Delta F}{\partial n}\right)_x = 0$$

Such a statistical derivation, especially of the entropy, cannot at the present be carried out.

The energy of the sulphur-sulphur bond can be derived from the difference in $\Delta\bar{H}_S$ for a stoichiometric and a diluted melt. This difference is $12,500$ cal. On the assumption that each sulphur atom has 8 sulphur neighbors in a melt of stoichiometric composition, as it has in solid Ag_2S , the energy of N sulphur-sulphur bonds will be: $N \cdot V_{S-S} = 1560$ cal.

The energy of the interatomic bonds will not vary much with temperature. By decreasing temperature however, the term $T\Delta S$ in the free energy expression will decrease, allowing an increase in the degree of short range order. But an increase in short range order of this kind cannot go on indefinitely with maintenance of the homogeneity of the melt. The sulphur atoms will more and more accumulate into clusters separated from each other by regions where concentration of sulphur atoms is small. When the cluster formation has reached a certain extent, large enough to overcome the surface tension, the melt will break down into two liquids, one rich in sulphur corresponding to the Ag_2S -rich phase and one low in sulphur corresponding to the Ag-rich phase.

Thus there is a close relationship between the decrease in $\Delta\bar{H}_s$ with increasing sulphur concentration, the degree of short range order in the melt, and the fact that it separates into two layers by cooling.

The author is aware of the fact that this last section has been rather speculative and suffers from errors of oversimplification. Thus, for example, it is not strictly correct to assume the size of the atoms, and consequently the coordination number, to be absolutely constant all through the system. The assumption that the energy of the individual interatomic bonds are independent of the composition is also probably incorrect. But the errors thus introduced will be small compared with the large variation of $\Delta\bar{H}_s$ going from diluted to stoichiometric composition.

The main idea has been to introduce a general concept of the structure of a metal/sulphur melt and show that such a concept is consistent with observed thermodynamic properties. It is unlikely that the atomic arrangement in other metal/sulphur systems is in principle different from that of the system silver/sulphur. Most metal/sulphur systems show either immiscibility between a metal melt and a sulphide melt, or miscibility with a pronounced positive deviation from Raoult's law. Also in these cases, short range order should exist in the melt, although there is no reason to assume the existence of defined sulphide molecules. It follows therefore, that the discussion of which sulphides do exist, for example, in molten steel (a discussion which is common among metallurgists) is somewhat beside the point. One should rather discuss the influence of different

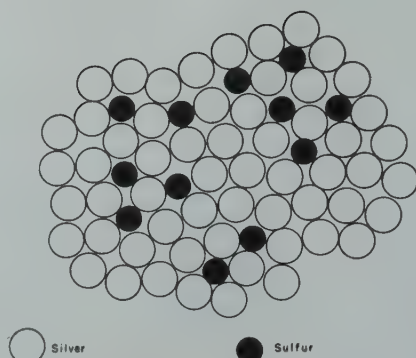


FIG 10—Two dimensional sketch of the suggested atomic arrangement for a silver-sulphur melt containing about 20 at. pct sulphur, indicating short range ordering of the sulphur atoms.

alloying elements on the chemical activity of dissolved sulphur, and on the interatomic arrangement.

The author hopes, in another paper, to return to this last subject.

Summary

A thermodynamic investigation of the system silver-silver sulphide has been undertaken. The principle of this investigation is the reaction of sulphur from the silver sulphur alloys with hydrogen to form hydrogen sulphide, the equilibrium ratio $\text{H}_2\text{S}/\text{H}_2$ being a measure of the escaping tendency of sulphur.

An apparatus was designed in which the equilibrium gas ratio was obtained by circulating the gas mixture over the specimen, and the composition of the gas mixture was subsequently determined from its density by means of a buoyancy-balance (see Fig 1). The possible sources of error were discussed.

Altogether, 22 samples containing up to 33.3 at. pct sulphur have been studied over the temperature range 500–1300°C. The equilibrium ratios $\text{H}_2\text{S}/\text{H}_2$ are plotted as a function of temperature in Fig 3 and 5 and as a function of alloy composition in Fig 4.

It was shown that the immiscibility region in the system has a critical temperature of about 1125°C corresponding to a critical composition of 24 at. pct sulphur (see Fig 7).

The heat and standard free energy of the reaction $\text{Ag}_2\text{S}_{(s)} + \text{H}_{2(g)} \rightarrow 2\text{Ag}_{(s)} + \text{H}_2\text{S}_{(g)}$ were obtained from the experimental data and are expressed as functions of temperature.

The heat and standard free energy of formation of Ag_2S from the elements have been calculated for room temperature,

$$\Delta H_{298} = -7493 \text{ cal and}$$

$$\Delta F^\circ_{298} = -9557 \text{ cal}$$

The heat of fusion of Ag_2S has been estimated to 700–900 cal.

The partial heat content and chemical activity of sulphur in the liquid phase have been computed and the corresponding values for silver have been calculated by means of the Gibbs-Duhem equation (see Fig 8 and 9).

The last section contains a discussion of the relation between thermodynamics and the structure of the silver-silver sulphide melts. A model of the structure is suggested, the model being consistent with observed thermodynamic data and also with the existence of immiscibility in the system. (See Fig 10.)

Acknowledgment

This research has been supported in part by grants from Union Carbide and Carbon Corporation.

It is a pleasure for the author to acknowledge the help of many members of this Institute. Thanks are especially due to Professor A. Skapski (now at University of Nebraska) for interesting discussions, and Professor N. H. Nachtrieb and Professor J. W. Stout for reading the manuscript with valuable criticism.

References

1. K. K. Kelley: U. S. Bur. of Mines Bull. 406.
2. M. H. Pelabon: *Ann. Chem. Phys.*, VII (1902), 25, 365.
3. F. G. Keyes and W. A. Felsing: *Jnl. Am. Chem. Soc.* (1920), 42, 246.
4. K. Jellinek and J. Zakowski: *Ztsch. Anorgan. Chem.* (1925), 142, 1.
5. M. Watanabe: *Sci. Rep. Tohoku Imp. Univ.* (1933), 22, 905.
6. E. V. Britzke and A. F. Kapustinsky: *Ztsch. Anorgan. Chem.* (1932), 205, 95.
7. A. Stock: *Ztsch. Phys. Chem.* (A) (1928), 139, 47.
8. P. H. Emmett and J. F. Schultz: *Jnl. Am. Chem. Soc.* (1933), 55, 1376.
9. J. Chipman and M. N. Dastur: *Discussions Faraday Society* (1948) 4, 100.
10. F. C. Kracek: *Trans. Am. Geophys. Union* (1946), 27, 364.
11. H. M. Spencer: *Jnl. Am. Chem. Soc.* (1945), 67, 1859. See also: *Idem*, (1934), 56, 2311.
12. K. K. Kelley: U. S. Bur. of Mines Bull. 371.
13. H. Zeumer and W. A. Roth: *Ztsch. Phys. Chem.* (A), (1935), 173, 365.
14. W. M. Latimer: *Oxidation, Potentials*. New York 1938.
15. K. K. Kelley: U. S. Bur. of Mines Bull. 393.
16. P. Rahlfs: *Ztsch. Phys. Chem.* (B) (1936), 31, 157.
17. C. Wagner: *Ztsch. Phys. Chem.* (B) (1933), 21, 42. (1933), 23, 469. See also: F. Seitz: *Modern Theory of Solids*, New York (1940) 67.

Autogenous Roasting of Low Grade Zinc Concentrate in Multiple Hearth Furnaces at Risdon, Tasmania

J. A. B. FORSTER*

The operations of the Electrolytic Zinc Co. of Australasia Ltd. involve the preliminary roasting of zinc concentrate from Broken Hill, New South Wales, at a number of acid-making centers on the Australian mainland. The partially roasted material is shipped to the Tasmanian plant where it was formerly re-roasted prior to leaching,¹ but this practice was gradually abandoned in favor of the flotation of leach residue for the recovery of a concentrate containing about 22 pct sulphide sulphur and known as secondary or Risdon concentrate.² This change, together with increased zinc production, called for new furnaces at Risdon for the roasting of 40-50 tons† of secondary concentrate and 90 tons of new concentrate per day.

The war situation made it imperative that construction be commenced without delay and to save time it was decided to base the design on that of Skinner type furnaces which had been built in South Australia twenty years earlier.

This involved some sacrifice of desirable features but did not prevent the incorporation of provisions which had enabled small Herreshoff type furnaces to roast secondary concentrate autogenously. The roasting rate in existing furnaces was 10-12 lb sulphide sulphur per sq ft of hearth area per day, and eleven hearths, 20 ft in diam, were provided in the two new furnaces in anticipation that they would prove capable of the autogenous roasting of 130-140 tons of concentrate per day from 28-29 pct sulphur down to 4.5-5 pct, with an oxidation rate of 11-11.5 lb S/S per sq ft of hearth area per day.

It was soon realized, when the first of the furnaces went into operation, that a much better performance than this might be given, and the purpose

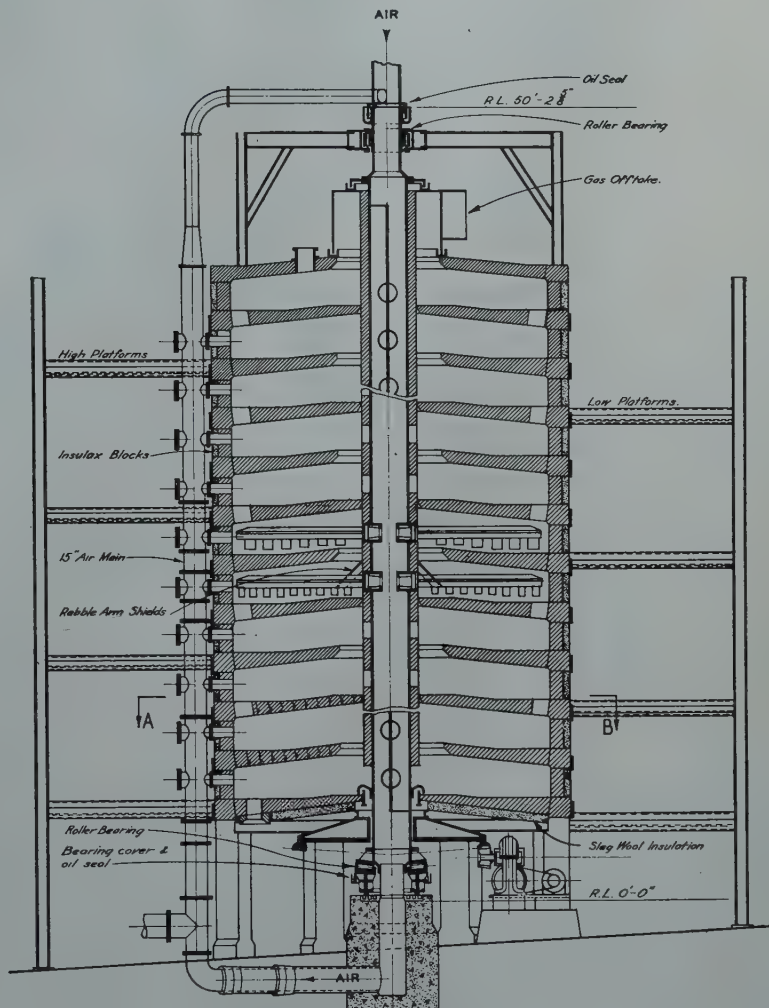


FIG 1—Composite section.

San Francisco Meeting, February 1949.

TP 2624 D. Discussion of this paper (2 copies) may be sent to *Transactions AIME* before October 1, 1949. Manuscript received October 1, 1948; revision received April 8, 1949.

* Superintendent, Roasting and Casting Division, Risdon Works, Electrolytic Zinc Co. of Australasia, Ltd., Tasmania.

† Throughout this paper the ton is 2240 lb.

¹ References are at the end of the paper.

of this paper is to show how a treatment rate of 100 tons per furnace day, and oxidation rates approaching 15 lb S/S per sq ft per day have been reached.

Furnace Design

General specifications for the design were based on the results of experience with several other types of furnace and on the special operating conditions

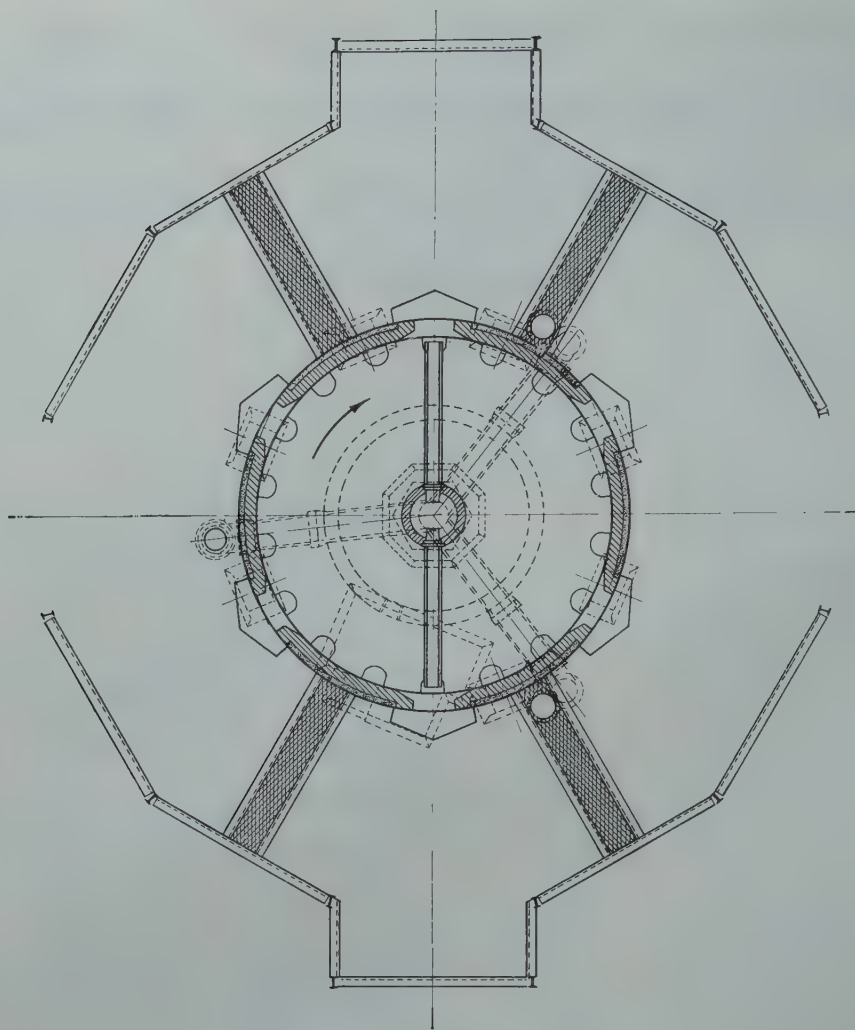


FIG 2—Plan A-B (See Fig 1).

expected. The general arrangement is shown in Fig 1, 2 and 3.

The original hearths had a camber of 8 in. and were very difficult to keep clean. To build flat hearths involved major changes in design, and a compromise was reached by thickening the haunch blocks and five outer rings of hearth blocks as much as minimum door size would allow, but the original camber remains in the central portions of the hearths.

The working doors are covered by outer doors which form chutes right down the face of the furnace to hoppers in the basement where spillage and cake from the hearths are collected. These chutes are ventilated by a fan which exhausts from both top and bottom of each chute so as to be effective when any door is open.

The column and rabble arms are air cooled, and the air leaving the bottom of the column is distributed

to three mains rising alongside the furnace. Air is supplied to the hearths from these mains through ports controlled by disc valves. The tops of the mains are connected through a damper to the fan supplying the rabble-cooling air. This arrangement permits hot air to be supplied to all hearths when necessary, while cold air may be used down to any desired level of the furnace. Hot air may be exhausted to atmosphere when desired.

In the second furnace, Nos. 6, 7, and 8 hearths are each provided with an additional port for the injection of dust recovered from the furnace gases by means of cyclones. An additional port in No. 9 hearth accommodates a small oil burner which is not in continuous use.

Rabble arms are of cast iron and have an indefinite life. The rabble teeth in No. 1 hearth are of special cast iron and last 2-3 years; all other

teeth are 27 pct Cr and the average life is 3½ years.

Design and Arrangement of Rabble Teeth

A large contribution to the present performance of these furnaces has been made by improvement in the design and arrangement of rabble teeth. There are five factors of importance in design: angle of approach, throw, spacing, depth and overlap. These have not always had the attention they deserve, though this may mean the difference between failure and success of a furnace.

Angle of approach is the angle between the blade of the tooth and the tangent to its circle of movement. If this angle is too large the material being rabbled will not slip across the blade but will tend to build up in front

and to be pushed around the furnace; an overloaded condition will quickly develop. If the angle is smaller than need be the blade of the tooth will be too long and heavy in relation to the work required of it. The smaller the angle and the longer the tooth the more difficult it will be to clean the blades when necessary. The angle may be relatively large for material moving down a slope or outward across the hearth, but must be smaller for the same material on upward slopes and for inward rabbling. Free moving material like dry sand can be worked with the most economical angle, 45° , on outward traverses, but angles of less than 30° may be necessary for sluggish or "sticky" material on inward traverses.

The throw is the radial distance between the leading and trailing edges of the teeth; it is rather more than the effective radial distance of the movement of material because of "slip"—that is, the material which, as the trailing edge passes on, slips back from the rill of the tooth into its path. In the first place the throw determines the number of times the roasting material will be turned over during its traverse of the hearth; consequently it has an important bearing on the amount of roasting done on the hearth. Long throw thins the mobile bed and may be a factor in overcoming an overloading tendency. Throw also determines, to some extent, the spacing of the teeth, and hence the convenience with which tooth cleaning is done, and its frequency.

Spacing, the center to center distance of the teeth on the arm, must not be too small or the cleaning of teeth becomes a difficult operation likely to result in mishap. Under heavy loads close spacing also means increased friction in the passage of material between teeth and makes the development of overloading more probable, besides decreasing the exposure of the material to the furnace atmosphere. In determining spacing, allowance must be made for any tendency of the material to crust on the teeth as this of course decreases the effective spacing between successive cleanings. Spacing must not exceed the throw multiplied by the number of arms in the hearth if the whole of the hearth is to be swept by the teeth, but if the material rills easily and a deep mobile bed is desired, it is possible even to double this figure and have considerable bands of unswept hearth, par-

ticularly if the throw is relatively small.

The depth of the teeth determines firstly the depth of immobile bed on the hearth, and secondly, in conjunction with spacing, the maximum cross section of material which can be moved effectively at each pass of the arm. Where the material has to traverse a slope it is the depth of tooth nearest the crest which is the determining or effective depth of all teeth on the hearth. If the effective depth of tooth divided by the spacing is less than the tangent of the angle of rest of the material, the furnace will be unable to attain its possible transport capacity, but it is not of much advantage for this value to be exceeded greatly unless a deep, slow-moving bed is to be maintained by having the spacing exceed the throw multiplied by the number of arms, or unless two teeth of opposite throw are used together to form a "scoop" for gathering material into a drophole.

On a flat hearth "slip" is normally a little less than one-eighth of the mobile load gathered by the tooth; on downward slopes and outward traverses it is less, on upward slopes and inward traverses it is more. On cambered inward rabbling hearths, the greater slip tends to increase slip still further, so that there is a distinct tendency for such hearths to become overloaded and, finally, completely choked. It is important in such cases to keep the upward slope to a minimum by having as little immobile bed as possible near the crest. A further

and effective remedy is the use of some overlap, that is, having the paths of teeth on one arm overlap the paths of those on the preceding and following arms. It is present when spacing is less than throw multiplied by the number of arms; (by 2 in the special case where four arms operate as two effective pairs). This is, of course, a particular case of the general principle that increased throw tends to thin the mobile bed, for the simplest way of getting overlap is to increase the throw of the teeth without altering the spacing.

Where two teeth of opposite throw are used to form a V or scoop for gathering large quantities of material, as in the case of a final hearth where the whole load has to be concentrated to a single drophole, it is essential that the base of the scoop be sufficiently open to leave a considerable trail of material behind it. The ideal opening will permit so much to escape that the scoop will have accumulated its full load only shortly before it reaches the drophole. In the final hearth it is also desirable, if the load is large, that each arm should carry a scoop commanding the drophole, but these scoops should not work over identical paths.

A significant factor in all rabbling is that on outward rabbling hearths the load is being spread over a larger and larger area, as it progresses, while the reverse is the case on inward rabbling hearths. To secure the best possible combination of roasting and transport capacities the throw of teeth

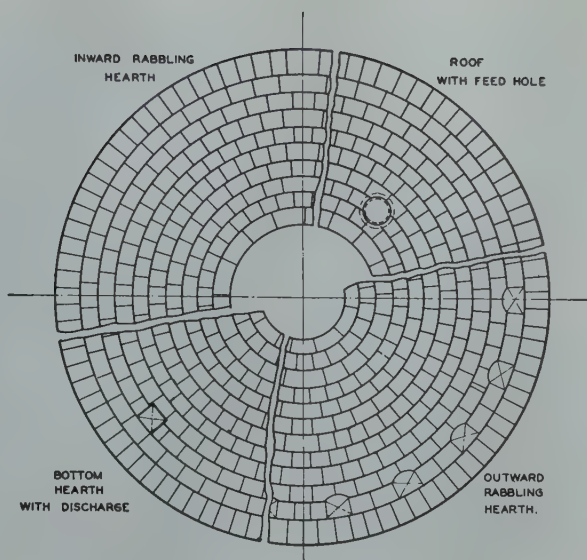


FIG 3—Composite hearth plan.

should be at the practical minimum at the outer ends of the arms and increase progressively inwards. This calls for a great diversity of patterns, and, except for the use of some overlap, has not been adopted in the Risdon furnaces, mainly because roasting capacity has already reached a level which makes gas velocity through the third hearth dropholes as high as is desirable; the use of shorter throw teeth in the outer parts of the lower hearths is contemplated as a means of still further improving the completeness of the roast.

Within a few weeks of starting, the first furnace was being operated to the full capacity of its hearth transport system, which proved, under test, to be about 75 tons per day, nonstop. It was obvious that the furnace had by no means attained its full roasting capacity, and if this were to be realised an increase of transport capacity must be obtained. In fact, a very big increase would be necessary for, in any furnace roasting galena bearing concentrate, the transport capacity must considerably exceed roasting capacity if smooth, efficient operation is to be obtained. The reasons for this are that the best roasting temperature is not far below the softening point of galena, and that hearth temperatures tend to rise with deepening of the mobile bed. If the furnace is being operated at near its full transport capacity a slight increase of feed rate, or delay in the routine of tooth cleaning will deepen the beds slightly, and the consequent rise of temperature may make the galena sticky; mobility decreases, teeth become dirtier, and in consequence of this vicious circle the hearth soon becomes seriously overloaded.

The functioning of the teeth was studied in all parts of the furnace and also in wooden model hearths constructed to scale and using dry sand and pigments. New teeth were designed for special purposes in different parts of the furnace; new combinations were worked out, and within a few months transport capacity was raised to over 100 tons per day. An average rate of 105 tons per 24 hr, nonstop, has been maintained for weeks on end, but the actual maximum transport capacity is uncertain, as there must always be some safety margin to guard against overloading. The above rates refer to operation at the normal column speed of 0.52 rpm; 120 tons per day has been reached at 0.61 rpm.

The first problem was the outward rabbling top hearth. The secondary concentrate carries 14 pct moisture, and having been filtered from a strong zinc sulphate solution, it has a very "sticky" stage during drying. The concentrate tended to reach the dropholes in this condition and grew and baked in the openings to the detriment of draught. As the cover arch is similar to an inward rabbling hearth, and the feed-hole is outside the gas offtake, the inner fifth of the first hearth was not being used. From immediately under the feed-hole inwards, one arm was dressed with narrow angle, short throw teeth, the remainder of this arm and all the other being dressed with narrow angle, long throw teeth in place of the original wide angle, short throw teeth. This arrangement caused feed to be spread over the central portion of the hearth; but as the inward throw is less than the outward throw there is no congestion. The arrangement is shown diagrammatically in Fig 4. The narrow angle permitted the concentrate to be moved more freely in the sticky stage and the long throw thinned the bed. Drying was now completed on the first hearth, and at most of the dropholes roasting had begun, so that a second sticky stage, caused by the presence in secondary concentrate of a small amount of elemental sulphur, had also been passed.

The second major problem was the congestion of the inward rabbling hearths, especially the most active fourth, mainly due to camber. Some alleviation was obtained by lengthening the inner teeth at the expense of making the immobile bed rather too thin to permit easy removal of hearth cake. The later, fully effective solution was the use of teeth with overlap across the whole cambered portion of the inward rabbling hearths. A subsequent modification was to reduce the number of overlap teeth in the eighth hearth and to eliminate them from the tenth to increase the depth of mobile bed and consequently the time of passage of these hearths. The reason for this is that it was observed, when the furnace was stopped for some hours except for a half-turn half-hourly, that the prolonged soaking greatly increased the penetration of the roast into the small aggregates which form very freely during the drying of secondary concentrate, owing to the zinc sulphate content. It is quite practicable to operate these lower

hearth with lower transport capacity because galena is no longer present.

At higher loading rates spill from the inside of outward rabbling hearths increased. The teeth nearest the column on these hearths were elongated so that the leading edges of the blades almost touch the column.

The outward teeth most generally used in the Risdon furnaces have the following characteristics:

| | Outward Teeth | | | Inward Teeth | | |
|-------------------|---------------|-----|-----|--------------|-----|-----|
| Throw—in..... | 6½ | 5 | 4* | 8 | 6½ | 5 |
| Spacing—in..... | 13 | 10 | 8 | 13 | 13 | 10 |
| Angle of approach | 32° | 45° | 30° | 32° | 32° | 28° |

* Designed for lower hearths but not yet installed.

Fig 4 shows, diagrammatically, the arrangements used in various positions.

Operation

Consistent roasting performance depends on regular feeding of an evenly graded concentrate, effective temperature control, clean rabbling and a smoothly running furnace.

Because of the characteristics of the feed components and the necessary arrangements for their delivery to the furnaces, the labor needed to obtain satisfactory feed control is much more than the average for other roasting plants. About half the feed consists of secondary concentrate delivered direct from a continuous disc leaf filter liable to vary from hour to hour in amount and from day to day in grade. The remainder, known as the "high grade" feed, is a mixture of screened dross and flue dust from the zinc melting furnaces with high grade zinc concentrate derived from any of four sources and with distinctly differing characteristics; this mixture carries from 26.5 to 28.5 pct sulphide sulphur whereas the secondary concentrate has from 21 to 24 pct. The general effects of this diversity of feed material are described in connection with furnace performance; as far as feed control is concerned it makes feeding at a constant tonnage rate entirely unsuitable. Effort must be directed at keeping the input of sulphide constant.

Secondary concentrate is weighed on a belt conveyor as it leaves the filter and begins its half-hour journey to the furnaces. The rate of high grade feed is adjusted hourly in accordance with the delivery rate and current grade of secondary concentrate. It is a cumbersome system needing conscientious

operators but the sulphide input is consistently within 2 pct of the set figure, and adjustments of other major controls because of changes in effective input are not frequent.

Temperature control is maintained through the draughting and blast system. The following values are under regular observation and are logged hourly:

1. Gas temperatures in hearths 2, 3, 4, 5, 6, 8, 10, and column exit.
2. Furnace load (ammeter reading also continuously recorded.)
3. Blast pressure at column exit.
4. Draught between main damper and first hearth.
5. Sulphur dioxide in offtake gas (continuous recorder).

Control is exercised through adjustments of one or more of the following:

1. Furnace main damper: normal draught on the furnace side of the damper is 0.04 in., water gauge.
2. Blast fan damper: requisite settings for any given sulphur input are known and any need for departure from normal, as indicated by marked rise or fall of blast pressure at the column exit from the normal 0.5 in. w.g., is an indication of irregularity in rate or grade of feed.

3. Cold air by-pass damper: the fourth and fifth hearths are always fed with cold air in normal circumstances and hearths below the seventh with hot air; operation of the damper mainly determines the extent to which the sixth hearth receives cold air or hot. When regaining temperatures after a stoppage no cold air is fed to begin with but as temperatures rise an increasing amount is used.

4. The disc valves on blast ports: the three ports on any hearth are all opened to the same extent, and the close regulation of the temperature of each hearth is effected by variation of these openings as deemed necessary.

The current feed rate and the settings of all dampers and valves, as made, are recorded on blackboards mounted near the instrument panel.

The temperature objectives in autogenous and "higher sulphate"* roasting are:

| | Autogenous | "Higher Sulphate" |
|---------------------|------------|-------------------|
| Hearths 3 to 6..... | 820°C | 820°C |
| Hearth 8..... | 770-780°C | 800-820°C |
| Hearth 10..... | 700-750°C | 680-700°C |

The condition of hearths and teeth

* See later in this section.

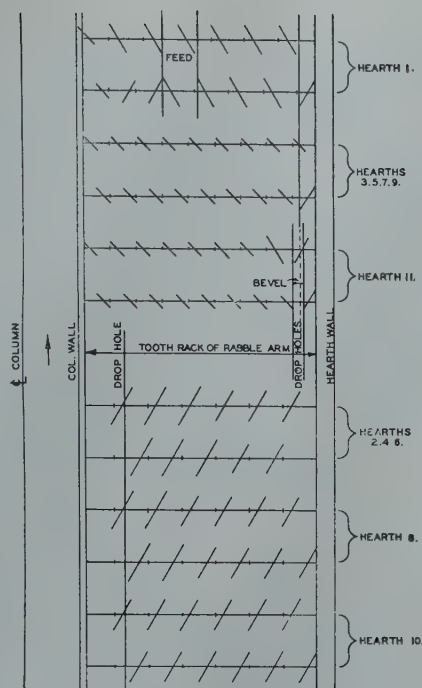


FIG 4—Tooth dressing.

is examined at the beginning and toward the end of each 8 hr shift; where necessary a rough cleaning is carried out. During the main part of the shift the furnacemen start at the top of the furnaces and work down, cleaning all teeth thoroughly and also cleaning such of the arms, shields and portions of the walls and hearths as are allocated to them. The teeth in the lower hearths are changed once in a few months for inspection and for removal of any hard crust, but on hearths 3 to 6 they are changed every two weeks. This is made necessary by the presence of galena which has a significant vapor pressure at 850°C. Some volatilized lead sulphide comes in contact with the teeth, which are at a lower temperature because of the cooling of the arms, and condenses on them in a finely crystalline form, too adherent to be removed by the ordinary process of cleaning. The deposit occurs on the underside of the teeth as well as on the sides and soon causes a "drag" which raises the power input and will ultimately become sufficient to stop the furnace.

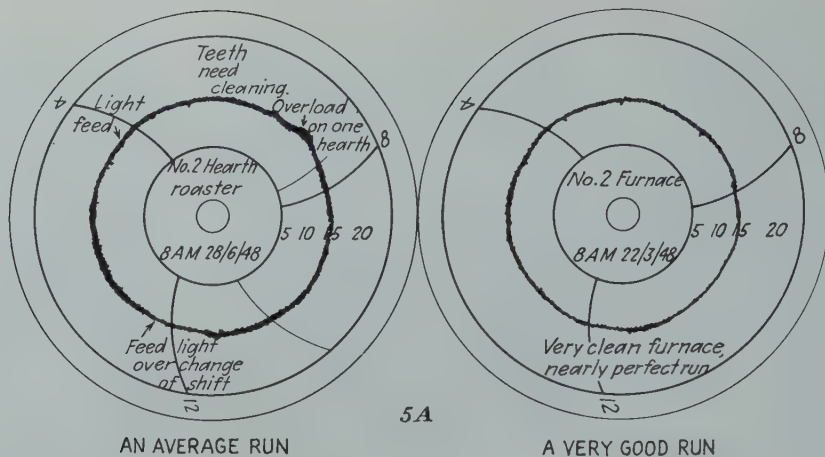
It is characteristic of all zinc concentrate roasting that the immobile bed cakes hard and if not broken up regularly begins to exert an excessive drag which will either break arms or stop the furnace. The treatment of these beds differs in practically all plants, and practice at Risdon has

passed through several phases. Initially the hearths were barred or chiselled at intervals of several days. The work proved to be much less arduous, less material was removed and no more labor was required when the intervals were reduced, but it has been found preferable to fill the hearths to tooth level with coarse sand.

It was found impossible to maintain these beds intact; owing to changes of temperature in hearths, column and rabbles, to the disturbance caused by tooth cleaning and to the growth of galena "shoes" on teeth, the upper part of the sand is displaced and a crust of calcine is formed which behaves to some extent like ordinary hearth cake. These developments take time, however, and it has been found that a furnace can be maintained in free running condition provided the sand beds are renewed periodically. The fourth and fifth hearths are resanded every three months, and the other hearths every six months except the first which is done yearly when its teeth are inspected.

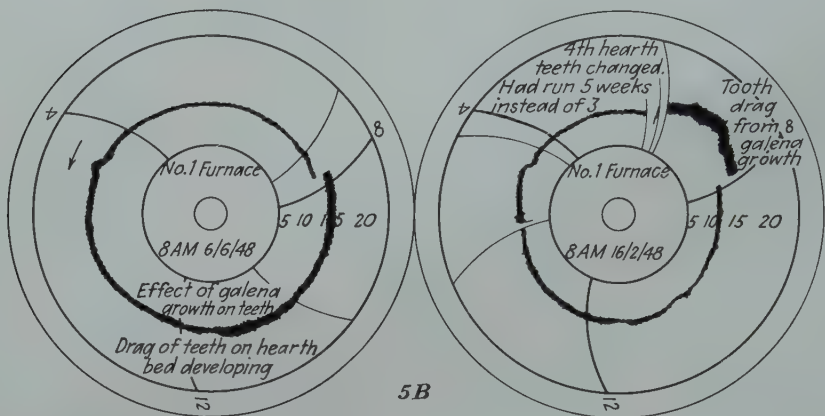
During the week before two hearths are to be resanded, they are chiselled thoroughly, the work being in the opposite direction to the rotation of the arms. The hearths done together (except in the case of the first hearth) are always an inward rabbling hearth and the one below it. The feed is cut off for one and a half hours. When material has practically ceased coming into the first hearth to be sanded, a few teeth are removed from the hearth above it and the furnace is restarted. Furnacemen at each door push material off the inward rabbling hearth at a steady rate until the hearth is clean. They then start to pull off the hearth below while sand is shovelled into the clean hearth—sufficient to form the immobile bed of two hearths—about 7 cu yd. As soon as the surplus sand has worked in from the outer part of the hearth the tynes are replaced in the hearth above. The one and a half hours allowed is ample, and it should be noted that, in the case of lower hearths, the feed will be on again long before the hearth cleaning starts. Temperatures are regained very rapidly and the furnace is usually normal within four hours.

After allowing for the cost of sand and of putting it in place, the wage saving resulting from the almost complete elimination of chiselling is not very great but the ultimate benefit from the reduction of wear and tear on the hearths and mechanism will be

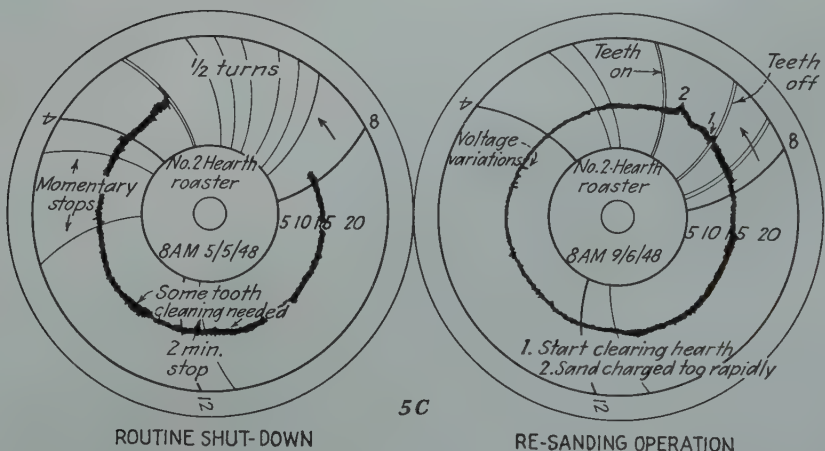


AN AVERAGE RUN

A VERY GOOD RUN



EFFECT OF GROWTH OF GALENA ON BOTTOM FACES OF TEETH



ROUTINE SHUT-DOWN

RE-SANDING OPERATION

FIG 5a—(Left) An average run. (Right) A very good run.
5b—Effect of growth of galena on bottom faces of teeth.
5c—(Left) Routine shut-down. (Right) Re-sanding operation.

quite considerable.

A recording ammeter gives invaluable guidance as to the general condition of the furnace and reveals irregularities or neglect unfailingly. Typical records are shown in Fig 5a, 5b, and 5c.

The furnace section must be closed down for about five hours once a fortnight to permit cleaning of gas fans.

Auxiliary equipment is overhauled and every effort is made to have all maintenance work involving stoppage carried out at the same time; big jobs may extend the stoppage to eight hours, but these are infrequent now. Supplementary equipment is provided for disposing of the gas which is emitted at the feed-hole, and full feed is kept on the furnaces right up till shut-down

time, but all blast valves are shut off earlier; column cooling air is reduced to a minimum and turned to atmosphere. Some air leaks into the furnace through rabble sockets, and the chimney effect of the furnace causes ingress of air to the lower half of the furnace wherever doors are not air-tight. Unless the column drive or bearing is being overhauled, the column is turned for

one minute every half hour. This prevents the crusting of beds and presents new surfaces to the air available; a fair amount of roasting goes on, so that for several hours temperatures do not fall much except in the lower hearths where there is little sulphide available. A typical example of such temperatures is given in Table 1.

If the roasting is strictly autogenous, the recovery of the lower hearth temperatures is rather slow, taking about four hours for each hour of shut down, unless calcine grade is sacrificed to a serious extent. If an oil burner is used at Hearth 9 to assist recovery, the time is reduced by half at an expenditure of about 6 gal of oil per furnace per hr, and calcine grade does not suffer appreciably.

If a stoppage extends beyond eight hours for external reasons the furnaces are then run and fed for five minutes in every thirty or forty. This retards further temperature drop almost completely. If the bottom hearth becomes seriously overloaded, it may be relieved by discharging into the basement.

The addition of the cyclone dust from both furnaces to the middle hearths of one furnace results in about 100°C drop in bed temperature and necessarily affects roasting rate. The lowering of feed grade resulting from the addition of dross also causes a drop in roasting performance. It was decided to abandon strictly autogenous roasting, therefore, and use a small oil-burner on each furnace as required, to help restore temperatures after the furnace stoppages and to make good the effect of cyclone dust addition. Experience shows that the burners are used to best advantage in the ninth hearth, and consumption of fuel oil amounts to about 0.15 pct on the material roasted or about 0.7 pct on the sulphur oxidized.

Additional fuel oil has been used during most of the last year in order to increase the formation of sulphate, which is done by reducing the sulphide much below the level attainable with autogenous roasting at high feed rates. The temperature objectives have been given earlier in this section, and the consumption of fuel oil is shown in Table 6.

Equipment designed for the changing of rabble arms and teeth is very satisfactory and good team work has developed in its use. Where changing is frequent the set of teeth on an arm is removed and replaced in 3-5 min.

Lost time was very heavy initially.

Table 1 . . . Gas Temperature °C during Stoppage

| Time | Hearth 2 | Hearth 4 | Hearth 6 | Hearth 8 | Hearth 10 |
|---------|----------|----------|----------|----------|-----------|
| 9 a.m. | 780 | 830 | 810 | 760 | 650 |
| 11 a.m. | 760 | 820 | 800 | 720 | 580 |
| 1 p.m. | 740 | 810 | 760 | 640 | 510 |
| 3 p.m. | 740 | 810 | 750 | 590 | 450 |

Furnace stopped 8 a.m.

Table 2 . . . Furnace Stoppage Analyses

| Analysis Headings | Percentage Loss of Furnace Time | | | | | |
|--|---------------------------------|--------|--------|--------|--------|-----------|
| | 1943-4 | 1944-5 | 1945-6 | 1946-7 | 1947-8 | Objective |
| Feed and calcine conveyors..... | | 1.06 | 0.60 | 0.72 | 0.48 | Nil |
| Gas disposal, power, etc..... | | 1.03 | 0.55 | 0.60 | 0.55 | Nil |
| Routine shut down..... | | 4.87 | 3.83 | 2.80 | 1.92 | 1.5 |
| Furnace work including changing arms, shields, teeth and renewal of sand beds. | | 2.12 | 1.29 | 1.19 | 1.04 | 0.75 |
| Renewal of column bearing..... | | | | | 1.05 | |
| Total lost time pct..... | 10.8 | 9.08 | 6.27 | 5.31 | 5.04 | 2.25 |

Table 3 . . . Assays of Concentrates

| Assay Pct | B.H.N.* (a) | B.H.S.* (a) | B.H.Z.* (a) | Mixed B.H. | | Rosebery | | Risdon | |
|--------------------|----------------|----------------|----------------|------------|-------|----------|-------|--------|-------|
| | | | | (b) | (c) | (a) | (d) | (e) | (d) |
| Zn | 52.2 | 53.10 | 52.5 | 51.1 | 49.0 | 54.4 | 55.5 | 49.7 | 49.65 |
| Pb | 1.3 | 1.1 | 1.6 | 1.1 | 1.3 | 3.7 | 2.0 | 1.6 | 0.9 |
| Mn | 1.58 | 1.4 | 1.42 | | | 0.14 | | 1.0 | |
| Cu | 0.08 | 0.07 | 0.11 | 0.109 | 0.118 | 0.51 | 0.295 | 0.23 | 0.20 |
| Cd | 0.22 | 0.168 | 0.189 | 0.201 | 0.196 | 0.137 | 0.139 | 0.69 | 0.64 |
| Fe | 9.91 | 8.32 | 8.76 | 9.3 | 8.8 | 5.9 | 6.05 | 8.1 | 9.4 |
| T/S | 31.83 | 32.00 | 31.74 | 30.97 | 29.34 | 32.7 | 32.50 | 23.7 | 24.0 |
| SO ₄ /S | | | | 0.43 | 1.06 | 0.16 | 0.23 | 1.7 | 1.47 |
| S/S | | | | 30.54 | 28.28 | 32.54 | 32.27 | 22.0 | 22.53 |
| H ₂ O | 8 | 8 | 8 | 8 | 8 | 8 | 8 | 14 | 14.5 |

(a) Mill production, year ended June 1942.

(b) Mainly current material delivered to furnaces, year ended June 1948.

(c) Deliveries mainly from storage dumps, year ended June 1948.

(d) Deliveries to furnaces, year ended June 1948.

(e) Deliveries, 4 weeks ended 22nd Sept. 1943.

* Broken Hill North, Broken Hill South, and Zinc Corporation.

Table 4 . . . Laboratory Roasting Tests

| | B.H.N.* (a) | B.H.S.* (a) | B.H.Z.* (a) | Rosebery. (b) | Risdon (b) | Ros.-Ris. (c) |
|--|----------------|----------------|----------------|------------------|---------------|------------------|
| Assays pct | | | | | | |
| Total Sulphur..... | 31.35 | 31.27 | 31.46 | 32.55 | 24.9 | 28.7 |
| Sulphate Sulphur..... | 0.12 | 0.15 | 0.16 | 0.25 | 1.7 | 0.95 |
| Sulphide Sulphur..... | 31.23 | 31.12 | 31.30 | 32.3 | 23.2 | 27.75 |
| Zinc..... | 50.7 | 52.5 | 52.0 | 54.5 | 48.5 | 51.5 |
| Sizings pct (Tyler) | | | | | | |
| +100..... | 4.55 | 20.1 | 24.75 | 2.6 | 0.2 | |
| +150..... | 16.3 | 20.6 | 18.4 | 3.4 | 1.5 | |
| +200..... | 16.2 | 12.7 | 9.9 | 8.9 | 6.7 | |
| +250..... | 9.0 | 5.9 | 4.2 | 7.8 | 7.0 | |
| +250..... | 53.95 | 40.7 | 42.75 | 77.3 | 84.6 | |
| Sulphur oxidation rate, lb per sq ft per day (to 4 pct S/S)..... | 16.9† | 14.8 | 13.4 | 16.9 | 12.65 | 15.75 |
| | 17.4‡ | 17.1 | 16.5 | 18.2 | 15.8 | 17.7 |
| Sulphation Levels | | | | | | |
| Pct SO ₄ /S with S/S at 8 pct..... | 0.37 | 0.48 | 0.46 | 0.62 | 1.57 | 1.11 |
| Pct SO ₄ /S with S/S at 6 pct..... | 0.48 | 0.63 | 0.56 | 0.74 | 1.80 | 1.28 |
| Pct SO ₄ /S with S/S at 4 pct..... | 0.66 | 0.90 | 0.73 | 0.96 | 2.12 | 1.54 |
| Pct SO ₄ /S with S/S at 2 pct..... | 1.08 | 1.35 | 1.04 | 1.65 | 2.60 | 2.15 |

(a) Mill production samples, early 1943.

(b) Deliveries to furnaces, week ended 16th June 1943.

(c) Mixture in equal parts of concentrates marked (b).

* See footnote, Table 3.

† Roasting in muffle without chimney.

‡ Roasting in muffle with chimney.

Table 5 . . . Percentage of +250 Mesh (Tyler) Material in Feed Components

| Four weeks ending | Broken Hill Mixture | | | Rosebery | | | Risdon | | |
|-------------------|---------------------|------|------|----------|------|------|--------|------|------|
| | Av. | Max. | Min. | Av. | Max. | Min. | Av. | Max. | Min. |
| 2/4/47 | 42.9 | 53.6 | 28.2 | 15.8 | 25.2 | 11.9 | 37.6 | 46.5 | 24.9 |
| 30/4/47 | 44.4 | 51.0 | 36.6 | 18.5 | 38.2 | 10.8 | 30.3 | 41.2 | 18.3 |
| 28/5/47 | 48.3 | 56.2 | 40.8 | 18.7 | 27.1 | 15.8 | 32.4 | 46.6 | 19.3 |
| 25/6/47 | 52.4 | 58.3 | 48.5 | 18.8 | 31.8 | 16.2 | 27.6 | 36.9 | 20.0 |
| 23/7/47 | 50.3 | 59.4 | 44.4 | 19.1 | 21.0 | 15.8 | 27.1 | 32.8 | 16.4 |
| 20/8/47 | 43.3 | 49.3 | 37.8 | 17.9 | 25.2 | 14.3 | 31.6 | 45.8 | 19.8 |
| 17/9/47 | 42.3 | 47.7 | 38.0 | 17.9 | 26.7 | 14.0 | 31.0 | 54.6 | 15.7 |
| Av. | 46.3 | | | 18.1 | | | 31.1 | | |

To a large extent this was caused by blockage or breakdown of auxiliary equipment much of which was 20 yr old, but there were many short stoppages in connection with furnace work. Much effort was concentrated on eliminating causes of trouble and the progress made is shown in Table 2.

The final column gives the minimum times in which it is considered possible to carry out essential operations such as fan cleaning, teeth changing and renewal of sand beds.

Roasting Characteristics of Feed Components

The feed to the furnaces is always a mixture of concentrates from any or all of four sources, three Broken Hill mills and the Company's own mill at Rosebery, together with secondary concentrate (called Risdon) recovered from leached calcine residues, and latterly about 5 pct of dross and flue dust from zinc melting furnaces. (See Table 6.) Since feed composition inevitably varies, a knowledge of the roasting characteristics of the different components and mixtures is essential.

The objectives are not constant. The requirements of the zinc plant as a whole, the position in regard to stocks and certain subsidiary operations lead to variations in the stress laid on obtaining maximum oxidation of sulphides which is incompatible with relative completeness of oxidation and production of sulphate.

Table 3 gives analyses of typical samples of the five concentrates. In the Broken Hill concentrates the iron is largely present as the zinc-iron sulphide, marmatite, whereas in Rosebery concentrate there is both zinc-iron sulphide and pyrite; and in Risdon concentrate the iron is present partly as oxide but principally as zinc ferrite. Lead is present as galena in the primary concentrates but as sulphate in Risdon concentrate while the latter also contains a little elemental sulphur.

The gross thermal values of the concentrates on complete oxidation, as calculated from analyses (a), (d) and (e), Table 3, range from 1180 to 1150 C.H.U. per lb for the Broken Hill concentrates and are 1125 and 720 C.H.U. per lb for Rosebery and Risdon concentrate respectively. Particle sizes are more important than minor differences in gross thermal value in influencing roasting rate, and relative roasting rates for the various dried

concentrates have been studied under controlled conditions in the laboratory (by E. Z. Research Department).

An iron roasting dish with a false bottom was used in an electrically heated muffle with and without a small exhaust chimney, and temperature was closely controlled throughout. A half inch bed of material was well rabbled every five minutes and the most difficult concentrate was dead-roasted in 2 hr at 800°C under these conditions. In all cases roasting was faster at a bed temperature of 800°C than at 750 or 850°C, and the rates for the various concentrates always fell in the same order. Sulphate is formed to any extent only when sulphide content is relatively low, and under these conditions is more prevalent in the coarse fraction containing aggregates than in -10 mesh material. Rosebery and Risdon concentrates sulphate much more readily in both coarse and fine fractions than the Broken Hill materials. Table 4 gives assays, sizings, roasting rates and sulphate formation in the tests described and it should be noted that, in general, the progressive or instantaneous isothermal roasting rate for any concentrate is directly proportional to the progressive sulphide concentration and to a proportionality factor which is characteristic of the material and of the conditions of the roast.

The sizing relationships are perhaps more clearly expressed through the specific surfaces as determined by the Fisher sub-sieve sizer; typical concentrate samples gave the following results:

| | Specific surface |
|-----------------------|-----------------------|
| B. H. North | 740- 810 sq cm per g |
| B. H. South | 680- 710 sq cm per g |
| B.H. Zinc Corporation | 545- 600 sq cm per g |
| Rosebery | 1310-1520 sq cm per g |
| Risdon | 1940 sq cm per g |

For the several Broken Hill concentrates, the ratios of specific surface and roasting rates are close enough to indicate some connection, and it can be assumed that the low grade of the Risdon concentrate tends to offset the advantage of its fineness. The rates for Rosebery concentrate are not nearly as high as its fineness would lead one to expect. The explanation is to be found in its high galena content. It ignites much more rapidly than the others and roasts so actively that it is almost impossible to prevent fusion of galena which makes the roast become "sticky" and "ball-up."

The same facts explain why the

Rosebery-Risdon mixture has better rates than the averages of the rates of the components. The ready ignition of the Rosebery concentrate gives the roast a good start, while its high activity which tends to run temperature out of control is moderated by the low grade material.

Experimental roasting times are well borne out in practice. It is impossible to get satisfactory results with mixtures containing much Broken Hill concentrate at above the normal speed of furnace column. With Rosebery-Risdon mixture the speed may be raised from 0.52 rpm to 0.615 rpm, an increase of 18 pct.

While the sizings of the various concentrates are fairly consistent when long term samples are examined, there is a by no means insignificant day to day variation. Table 5 gives a clear indication of the extent to which these variations are experienced.

Performance

The complete performance record of the furnaces has been summarized in Table 6 and shown graphically in Fig 6. In this summary, the results have been arranged for periods of varying length, each period having some common feature which more or less determined or characterized the performance. The reference letters in the table and graph refer to the following explanations of the grouping:

A. The first four-weekly period during which furnace crews were becoming accustomed to the equipment, and initial difficulties were being overcome.

B. A period during which it was apparent that roasting capacity exceeded hearth transport capacity, and the lower hearths were doing very little roasting. Efforts were made to raise the temperatures of the hearths by "split drafting." Gas offtakes were connected to the bottom hearth, and from Hearth 7 the furnace was drafted downward. The temperatures of the lower hearths improved, but drying was slower and the activity of the upper hearths decreased. With a drier and higher grade feed, very active on the upper hearths, the method has definite advantages, but feed grade was tending to fall.

C. The effect of hearth camber was reduced by deepening the inner teeth of inward rabbling hearths, and column speed was increased from 0.52 to 0.61 rpm. More feed was handled and

Table 6 . . . Performance

| Reference | A | B | C | D | E | F | G | H | J | K | L | M |
|---------------------------|-------------|-----------------|-----------------|---------------|-----------------|-----------------|------------------|-----------------|----------------|-----------------|------------------|-----------------|
| Number of weeks ended. | 4 7.4.43 | 20 25.8.1943 | 20 12.1.1944 | 8 8.3.1944 | 44 10.1.1945 | 20 30.5.1945 | 24 14.11.1945 | 40 21.8.1946 | 4 18.9.1946 | 44 23.7.1947 | 20 10.12.1947 | 24 26.5.1948 |
| Furnaces operated. | 1 | 1 | 1 | 1 | 2 | 2 | 2 | 2 | 2 | 2 | 2 | 2 |
| Cyclone dust returned. | No | No | No | No | No | No | No | No | Yes | Yes | Yes | Yes |
| Feed Composition Pct | | | | | | | | | | | | |
| Rosebery Conc. | 49.7 | 51.5 | 38.5 | 25.5 | 29.6 | 7.9 | 22.5 | 9.9 | 22.4 | 12.0 | 23.4 | 22.2 |
| Broken Hill Conc. | | | | | 5.1 | 27.1 | 19.3 | 39.0 | 30.4 | 32.8 | 28.5 | 21.3 |
| Dross, etc. | | | 0.4 | | 0.8 | | 0.8 | 1.0 | 7.4 | 5.0 | 4.9 | 5.4 |
| Risdon Conc. | 50.3 | 48.5 | 61.1 | 75.5 | 64.5 | 65.0 | 57.4 | 50.1 | 39.8 | 50.2 | 43.2 | 51.1 |
| Feed | | | | | | | | | | | | |
| Tons per furnace per day. | 61.3 | 64.7 | 75.0 | 92.7 | 72.8 | 80.0 | 80.3 | 93.8 | 76.1 | 92.7 | 88.0 | 93.8 |
| S/S Pct. | 27.2 | 27.8 | 26.0 | 25.25 | 25.8 | 25.8 | 26.2 | 26.4 | 25.8 | 25.4 | 26.2 | 24.7 |
| Lb S per sq ft per day | | | | | | | | | | | | |
| Input. | 11.6 | 12.44 | 13.5 | 16.2 | 13.0 | 14.6 | 14.6 | 17.2 | 13.6 | 16.3 | 16.0 | 16.1 |
| Oxidized. | 9.4 | 11.1 | 11.9 | 13.2 | 11.3 | 11.25 | 12.6 | 14.4 | 11.4 | 13.2 | 14.0 | 14.6 |
| S oxidation Pct. | 80.6 | 89.2 | 87.9 | 81.5 | 86.7 | 78.6 | 86.4 | 83.6 | 83.3 | 80.8 | 88.0 | 90.8 |
| Calcare Assays | | | | | | | | | | | | |
| SO ₂ /S Pct. | 2.09 | 3.38 | 3.08 | 2.36 | 2.48 | 1.36 | 1.76 | 1.33 | 1.63 | 1.22 | 1.52 | 1.68 |
| S/S pct. | 5.76 | 3.29 | 3.46 | 5.15 | 3.74 | 6.11 | 3.92 | 4.80 | 4.71 | 5.38 | 3.51 | 2.50 |
| SO ₂ /S formed | | | | | | | | | | | | |
| Tons per furnace per day. | 1.16 | 1.98 | 2.11 | 1.98 | 1.64 | 0.98 | 1.28 | 1.12 | 1.13 | 1.02 | 1.22 | 1.44 |
| Fuel Oil used | | | | | | | | | | | | |
| Pct of S oxidized. | | | | | | | | | | | 1.54 | 2.19 |
| Stoppages | | | | | | | | | | | | |
| Lost time Pct. | 10.4 | 9.7 | 11.7 | 10.4 | 10.2 | 8.15 | 5.95 | 5.7 | 6.3 | 5.1 | 4.6 | 3.7 |

temperatures in the lower hearths improved.

D. Teeth with longer throw, giving overlap, were introduced on the inner half of inward rabbling arms. Higher feed rate resulted and the greater roasting capacity of the furnaces, even with a very low grade feed, was clearly demonstrated.

E. The second furnace came into operation, and the gas disposal system which was shared with two other furnaces proved inadequate for the operation of both the new furnaces at the higher roasting rate achieved in the previous period.

F. One of the other furnaces was shut down, and draught improved but appreciable quantities of B.H.S. and B.H.Z. concentrate were introduced for the first time, and considerable difficulty was experienced in producing an acceptable grade of calcine. Column speeds were restored to 0.52 rpm and were even reduced to 0.46 rpm for part of the period, but for no month did calcine average below 5.5 pct S/S.

G. During this period the feed mixture varied several times, the high grade portion being alternately all Rosebery and all Broken Hill concentrate, but the several changes afforded opportunities for close comparison of techniques. Traverse rates were reduced in Hearths 8 and 10, and calcine of under 5 pct S/S was eventually produced from Broken Hill-Risdon mixture, with a roasting rate of 12.5 lb S per sq ft per day which was then regarded as the acceptable minimum.

H. New supplies of Broken Hill concentrate contained no B.H.Z. and were mainly B.H.N. No difficulty was experienced in increasing roasting rates

to 14.5 lb S per sq ft per day, even when there was no Rosebery concentrate present and while maintaining calcine at less than 5 pct S/S.

J. A four-week period during which shortage of concentrate occurred and the furnaces were run, for a time, on the minimum load at which temperatures could be maintained. During this feed shortage the last of the old furnaces was shut down, and it became necessary to include zinc melting furnace dross and flue dust in the roaster feed to the extent of about 5 pct. Dust from the cyclones, formerly roasted in the old furnace, now had to be returned, at first to the feed though soon afterwards provision was made for delivering it to the middle hearths of No. 2 furnace.

K. This period was, in most respects, a continuation of period H, but marked by the dilution of the feed with dross and the effect of returning cyclone dust, which combined to reduce roasting rate from 14.4 to 13.4 lb S per sq ft per day. The admixture of dross with concentrates results in more rapid hardening of hearth beds and quicker fouling of teeth. Fortunately the developmental work on sand beds had been completed and both furnaces were soon bedded throughout. The labor saved from hearth cleaning was more than enough to enable better attention to be given to tooth cleaning.

The dust addition reduced the middle hearth temperatures of No. 2 furnace and therewith the roasting rate. Continuous addition at one point causes a drop of 100°C in bed temperature, but as the addition was spread over two hearths, the effect of the dust was not so sharply evident in

temperatures. The most noticeable effect was in calcine assays, those of No. 2 furnace being consistently about 1 pct S/S higher than those of No. 1 in spite of adjustment of feed distribution to insure equal overall sulphur inputs to the two furnaces.

The higher calcine assays, now tending to be just over the acceptable 5 pct S/S, prevented any attempt to restore sulphide input by increasing feed rate to make up for the dilution. Excluding from period K four weeks during which 40 pct of the feed was B.H.Z. concentrate, and calcine went to 8 pct S/S, the effects of dross and cyclone dust can be fairly assessed over two comparable 40 week periods. The feed rates were nearly equal, 93.8 and 92.6 tons per furnace-day respectively.

Dilution caused sulphur input to fall from 17.2 to 16.4 lb per sq ft per day. Temperature reduction by dust caused oxidation efficiency to fall from 83.6 pct to 81.6 pct so that sulphur oxidized fell from 14.4 to 13.4 lb per sq ft per day. The chief effect is caused by dilution, though it may not be immediately clear why, with a lower sulphide input, the oxidation efficiency should not be expected to increase.

The reason is that, in autogenous roasting, maintenance of temperature and of the limited roasting rate in the lower hearths is dependent on the carriage of sufficient amounts and concentrations of heat and sulphide in the calcine from the middle hearths, and on close control of air input. The addition of cyclone dust to the middle hearths affects the balance; calcine temperature is reduced while more sulphide is carried down. The latter can be corrected, as was done, by feed ad-

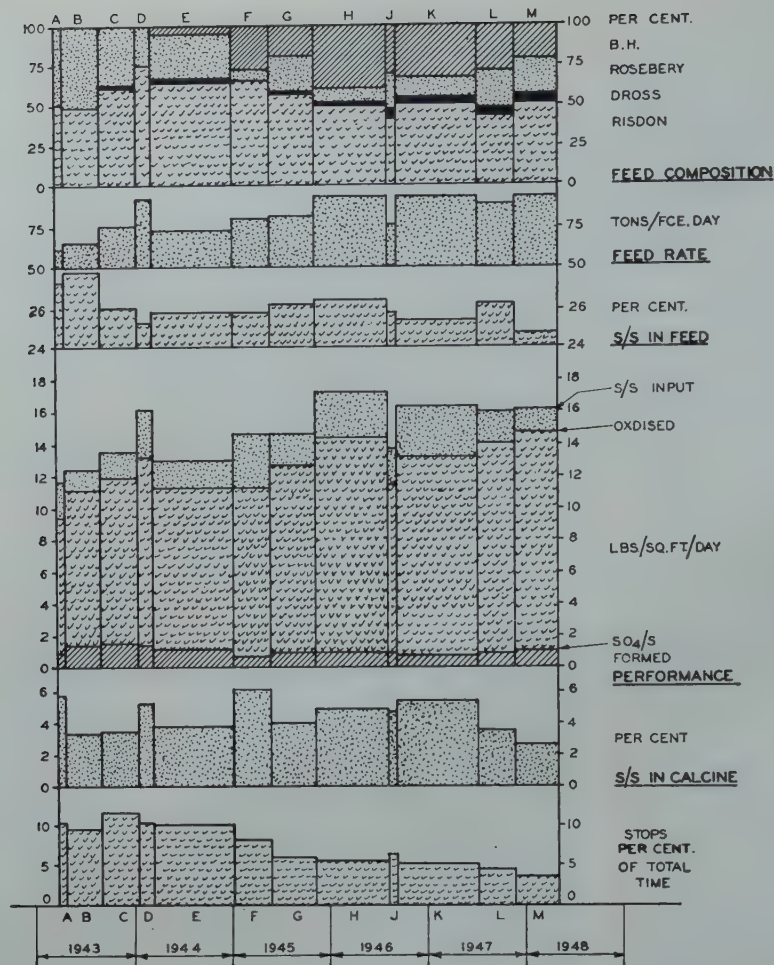


FIG 6—Performance data.

justment, but the temperature effect cannot be remedied without use of extraneous fuel.

On the upper middle hearths, where the roast is most active, it is usually necessary to depress that activity by use of cold air in order to avoid overheating. Even low grade concentrates are more than sufficiently active and by increasing input it is possible, up to a point, to maintain oxidation rate on these hearths. The limit is reached when the amount and concentration of sulphide passing to the lower hearths tend to get out of balance.

By comparing the work of different months in periods *H* and *K*, in which feed grade and sulphide input are nearly the same, it is found that the effect due to cyclone dust addition is only one-third of that due to dilution by dross, that is, about 25 pct of the total decrease of 1 lb per sq ft per day.

It appears, then, that the dust addition is being made too low in the furnace, and that it should be made in

the zone in which depression of activity is required. Gas velocity through the dropholes is so high in this zone however that return of dust to it would cause a large circulating load to build up. The dust is added to the moderately active sixth and seventh hearths.

L. It was decided to make use of small oil-burners to overcome the temperature drop due to cyclone dust in No. 2 furnace and to hasten recovery of both furnaces after long stoppages. At the time the burners became available there was a demand for an increase of sulphate formation and as this increases with decrease of sulphide, it was decided to operate the burners more or less continuously to stimulate roasting in the lower part of the furnace.

A short test was made to determine the consumption of oil for the original purposes; it was 0.17 pct of the tonnage roasted or 0.75 pct of the sulphur oxidized. To stimulate sulphate production, about three times as much is

Table 7 . . . Autogenous vs. Moderately Assisted Roasting

| Duration | Period <i>K</i> , Best 24 Weeks of 44 | Period <i>M</i> , Consecutive 24 Weeks |
|---|--|---|
| Feed rate, tons per furnace per day | 93.2 | 93.8 |
| Feed grade, pct S/S | 25.7 | 24.7 |
| Sulphide input, lb per sq ft per day | 16.6 | 16.1 |
| Sulphide oxidized, lb per sq ft per day | 13.7 | 14.6 |
| Sulphur oxidation pct. | 82.6 | 90.8 |
| Calcine assay, pct SO ₄ /S | 1.30 | 1.68 |
| Calcine assay, pct S/S | 4.94 | 2.50 |
| Fuel oil used pct of S oxidized | | 2.19 |

used. The most effective position for an oil burner was found to be the ninth hearth.

M. The experimental work on the application of fuel oil being completed and good supplies of high grade concentrates being available to give a regular feed mixture, the furnaces settled down to a long run of extraordinarily consistent performance. Both the quick recovery from the fortnightly stoppages due to the use of fuel oil and

a greater stability of furnace crews than existed in wartime and immediately afterwards, contributed to these results. By way of making allowance for the latter factor in comparing periods *K* and *M*, the best 24 weeks' work in the former period has been selected to compare with the 24 consecutive weeks' work of the latter; the results are given in Table 7.

The benefits derived have been calculated on the basis of 90 pct of unroasted sulphide being recovered as secondary concentrate from calcine leach residue and are found to be, for each ton of fuel oil used:

- 2.69 tons sulphur oxidized,
- 2.24 tons sulphuric acid, equivalent of extra sulphate formed,
- 1.34 tons of high grade concentrate (32 pct S/S) saved,
- 18.5 tons of low grade concentrate (22.5 pct S/S) which does not have to be returned for roasting.

The last item in this saving is more important than it may seem at first sight; it means not merely a decrease by one-sixth in the secondary concentrate to be treated by the furnaces, but it effects an increase of 0.6 pct in a feed grade already uncomfortably low for the maintenance of high roasting activity. That this increase was not actually obtained was due to a greater intake by the zinc plant of less well roasted calcine from other sources.

Heat Balances and Gas Tenors

Some heat balances were made in 1944 and showed radiation losses slightly in excess of 20 pct of the heat input. The work was done under great practical difficulties, including irregular operation, and there is some reason to believe that the loss is scarcely so high; but whether the actual loss is 10 pct or 20 pct is immaterial to the discussion of gas tenor in relation to heat balance which follows.

In Table 8 there are shown three balances calculated from recent performance figures, and average gas tenors, and an assumed radiation loss which is proportional to average furnace temperature, using the observed figure of the 1944 balances as basis. To simplify presentation, heat contents have been referred to atmospheric temperature instead of the more usual 0°C.

Table 8 . . . Heat Balances

| Condition (see below) | Per Hour for Two Furnaces | | | | | |
|---|-----------------------------|-------|-----------------------------|-------|-----------------------------|-------|
| | (A) | | (B) | | (C) | |
| | C.H.U. × 10 ³ | Pct | C.H.U. × 10 ³ | Pct | C.H.U. × 10 ³ | Pct |
| Input | | | | | | |
| Oxidation of concentrate..... | 13,371 | 100.0 | 14,449 | 94.1 | 15,353 | 98.1 |
| Combustion of Fuel Oil..... | | | 900 | 5.9 | 300 | 1.9 |
| Totals..... | 13,371 | 100.0 | 15,349 | 100.0 | 15,653 | 100.0 |
| Outgo | | | | | | |
| In calcines..... | 1,403 | 10.5 | 1,205 | 7.8 | 1,580 | 10.1 |
| In water vapor, ex conc..... | 1,700 | 12.7 | 1,559 | 10.2 | 1,759 | 11.2 |
| In water vapor, ex air..... | 99 | 0.7 | 130 | 0.8 | 124 | 0.8 |
| In dry gases..... | 7,181 | 53.7 | 9,474 | 61.7 | 9,167 | 58.5 |
| Loss from dust returned..... | 47 | 0.4 | 56 | 0.4 | 56 | 0.4 |
| Radiation loss..... | 2,941 | 22.0 | 2,925 | 19.1 | 2,967 | 19.0 |
| Totals..... | 13,371 | 100.0 | 15,349 | 100.0 | 15,653 | 100.0 |
| Conditions | | | | | | |
| Fuel oil used, tons per day..... | | | 0.92 | | 0.31 | |
| Feed rate, tons per day..... | 186 | | 176 | | 203 | |
| Feed, pct moisture..... | 10.9 | | 10.5 | | 10.5 | |
| Feed assay, pct S/S..... | 25.7 | | 26.3 | | 26.0 | |
| Calcine assay, pct S/S..... | 5.0 | | 2.54 | | 4.32 | |
| Calcine assay, pct SO ₄ /S..... | 1.3 | | 1.78 | | 1.4 | |
| Calcine discharge, °C..... | 677° | | 617° | | 697° | |
| Gas volume, N.T.P., cfm..... | 13,200 | | 16,500 | | 16,500 | |
| Gas offtake temperature °C..... | 450° | | 470° | | 450° | |
| Offtake gas, SO ₂ , pct..... | 5.0 | | 4.2 | | 4.5 | |
| Sulphur oxidized, lb per sq ft per day..... | 13.7 | | 14.6 | | 15.6 | |
| Sulphur eliminated, lb per sq ft per day..... | 13.5 | | 14.2 | | 15.3 | |

The conditions chosen for these balances are:

A. The best 24 weeks performance for autogenous roasting of mixtures including dross, as shown in Table 7.

B. The comparable performance when using some fuel oil continuously to improve sulphate formation, also as shown in Table 7, except that feed grade is raised to that which would have resulted had other calcine received by the zinc plant remained of the same grade as in the first period.

C. Performance when using fuel oil only intermittently to make good losses of temperature due to stoppages and the introduction of cyclone dust. The furnaces have been operated under this condition for a short time only but actual performance has been slightly better than that assumed for Table 8.

The amount of heat radiated does not vary much and so a larger fraction of the heat must be carried away by the gases when the space rate of roasting is increased. The upper temperature of the gases is limited to that which gives the fastest roasting and consequently an increase in the space rate must be accompanied by a fall in gas strength. It is nevertheless true that the whole of the heat input to the furnace could be carried by better grade gas than is actually being made, and without exceeding the maximum desirable temperature of 820°C. As low gas tenor is the chief disadvantage of hearth roasters in comparison with

flash roasters it is worth examining why the gas from these furnaces is so low.

In the first place an open feed-hole and main damper slot together account for a dilution of at least 10 pct. Secondly, activity is so great on the fourth hearth that 20-25 pct of the roasting is done there and an excess of air must be used to prevent the desired temperature being exceeded. Finally, in the lower hearths hot air is used as blast and this air can never attain the same percentage of sulphur dioxide as the cold air input because of the imposed maximum temperature.

Apart from the sealing of the feed-hole, the grade of gas produced could be increased by moving the material much more quickly over the most active hearths and much more slowly over the lower hearths. Differential rabbling rates are already being used in these furnaces almost to the limit of practical convenience but with furnaces having three or four arms per hearth greater differentiation is possible and it is by no means certain that the hearth roaster will be finally outmoded by the flash roaster.

References

1. W. C. Snow: Electrolytic Zinc at Risdon, Tasmania. *Trans. AIME* (1936) 121, 482 et seq.
2. *Idem*: p. 495, and S. W. Ross: *Trans. AIME* 185, 211: *Jnl. of Metals*, Mar. 1949.

El Paso Slag Treatment Plant

T. J. WOODSIDE*

Prior to 1927 the lead blast furnace charge at El Paso consisted principally of direct-smelting carbonate ores, very low in zinc, and the resulting slag seldom carried more than 4.0 pct. With the exhaustion of the mines in Northern Mexico which supplied these ores, they were supplanted with a much smaller tonnage of sulphide concentrates containing appreciable amounts of zinc, and the zinc content of the slag rose to 10.0 pct.

The Anaconda Company's slag fuming plant at East Helena, Montana, had then been in successful operation for several years, and it was immediately recognized that, while at that time the production of high zinc slag was small, if the grade held, a plant for the recovery of zinc from the accumulated slag might some day be practical. The grade not only held but became increasingly higher so that by 1946 sufficient slag had been accumulated to warrant the construction of a fuming plant regardless of future slag production from the blast furnaces, and with the removal of Government restrictions on construction at the end of the war the project was undertaken.

The general design of the plant follows that at Bunker Hill, with waste heat boiler, unit coal pulverizers and even more extensive instrumentation and automatic control.

The area around the lead blast furnaces is rather congested, being cut off from the nearest feasible site for the fuming plant by the copper plant, so that the most practical route for hot slag transfer is through the converter aisle. For this reason and also to make use of the existing converter cranes to serve the fuming furnace, an unused reverberatory at the north end of the converter building was dismantled and the fuming furnace and boiler located in its place. A flue at right angles to the furnace and boiler runs northward to the U-tube coolers and baghouse (Fig 1). From the baghouse a steel flue runs eastward to an existing and long unused 300 ft con-



FIG 1—U-tube coolers, baghouse, and de-leading kilns.



FIG 2—Fuming furnace.

San Francisco Meeting, February 1949.

TP 2651 D. Discussion of this paper (2 copies) may be sent to *Transactions AIME* before October 1, 1949. Manuscript received Jan. 26, 1949; revision received May 13, 1949.

* Superintendent, El Paso Smelting Works, El Paso, Texas.

crete stack. The coal handling system and de-leading plant lie north of the furnace and east of the cooling tubes and baghouse.

The furnace is conventional, 8 × 21 × 33 ft high inside and completely water jacketed (Fig 2). There are 21



FIG 3—Soot blowers.

double-inlet tuyeres on each side of the furnace, with center line of tuyeres $5\frac{1}{2}$ in. above the furnace bottom, and tuyere pipes extending 7 in. inside the furnace. Tuyere pipes were originally water-jacketed, but since these proved to have very short life they have been replaced with $3\frac{1}{2}$ in. od \times $1\frac{1}{2}$ in. id hydraulic tubing. Slag is tapped through two 5 in. water jacketed tap holes simultaneously into two 300 cf air dumped slag pots.

A water jacketed flue connects the furnace to the water-wall combustion chamber of the B. & W. two drum sterling type boiler which is rated at 72,000 lb of steam per hr at 400 lb pressure and 700° total temperature. Combustion chamber, boiler and economizer are equipped with a total of 35 fully automatic Diamond soot-blowers, Fig 3, operating on compressed air. The soot-blower installation has been very satisfactory, no hand lancing being required to keep tubes free of fume. Two motor driven A B C fans, each rated at 51,000 cfm, and connected in parallel, deliver gases from the economizer outlet to a 7 ft diam balloon flue leading to the U-tube coolers. Furnace draft is automatically controlled by louvre dampers in the fan inlets. The U-tube coolers are in two banks, each bank consisting of forty 30 in. \times 58 ft tubes. Additional cooling is supplied when required by an automatically operated damper which admits air into the gases as they leave the U-tubes. A second pair of fans

with capacity of 75,000 cfm each and automatically dampered like the boiler fans deliver gases to the baghouse.

The baghouse is constructed entirely of concrete, including roof and thimble floor, and is divided into seven chambers each containing 160 18 in. \times 30 ft woolen fume bags. Six chambers are used to collect zinc fume from the furnace gases and the other collects lead oxide fume from the deleading kilns.

The bags are shaken automatically when the pressure differential across the bags reaches a predetermined maximum, the chambers being shaken consecutively until the pressure drops to the desired minimum. In order to keep a slight draft on the inlet side of the baghouse, and thus prevent leakage of fume through screw conveyors, the outlet flue is evacuated by a Sirroco type induced draft fan with a capacity of 180,000 cfm, delivering gas to the stack.

Combustion chamber, boiler, economizer, balloon flue, U-tubes and baghouse chambers are equipped throughout their length with screw conveyors which operate continuously and discharge fume into a system of drag and belt conveyors which carry it to the de-leading plant.

Washed 1 \times 0 in. slack coal from Dawson, New Mexico, is dumped into a track hopper. Coal analysis is approximately as follows:

| Ash | Volatile | Fixed Carbon | Btu |
|------|----------|--------------|--------|
| 12.0 | 38.0 | 49.00 | 13,000 |

From the track hopper, coal is passed through a hammer mill and is pneumatically conveyed to a 300 ton storage tank. A Merrick Feedoweight delivers coal from the tank to a Redler elevator and rotary conveyor which distribute it to the three 30 ton pulverizer bins. The pulverizers are B. &



FIG 4—Coal pulverizers.

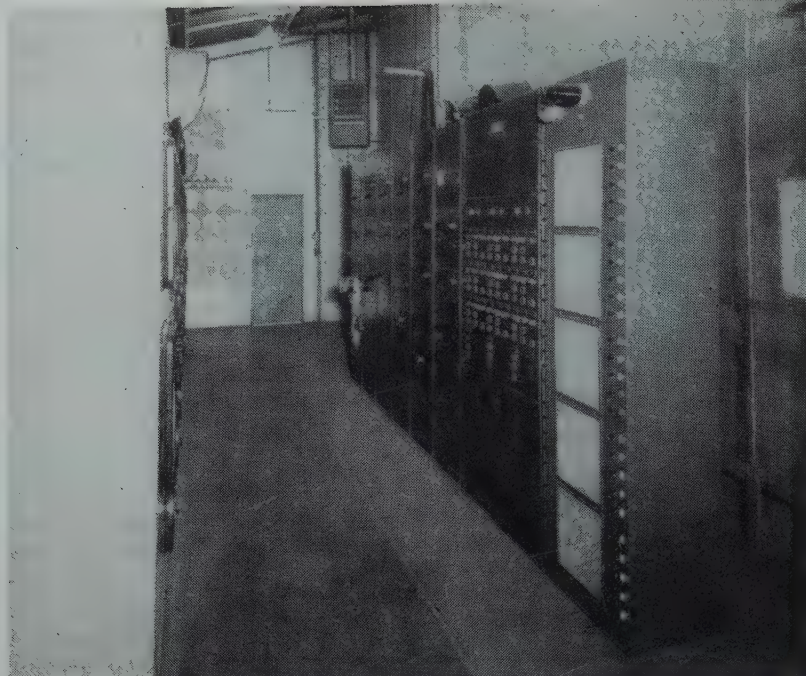


FIG 5—Control panel.

W. type E, size 47, two being operated with the third in reserve (Fig 4). Furnace blast is supplied by an Elliott turbine driven blower with a capacity of 18,000 cfm at 10 lb. The blast is divided by automatically operated butterfly dampers into primary and secondary air. The primary air passes through the pulverizers, picking up the coal and carrying it to the primary inlets of the tuyeres. The secondary air goes directly to the tuyeres. A 15,000 cfm motor driven blower was installed to inject low pressure air through a number of 2½ in. pipes into the upper part of the furnace and the crossover flue to oxidize completely all coal and metallic zinc. This was found to be unnecessary, however, as furnace draft pulls in enough air through the charging hole, and the blower is no longer in use.

A central control room located at the furnace contains a very complete set of Bailey indicating and recording instruments and control devices, with turbo-blower, pulverizers and flue system drafts all being controlled automatically from that point (Fig 5).

The furnace is now treating 20,000 tons of slag per month. Dump slag is mined by a bulldozer and ripper and remelted in the blast furnaces, no cold dump slag being charged direct to the fuming furnace. Molten slag is brought to the converter aisle in 12.5 ton ladles carried on transfer cars. Four ladles, including the shells, constitute a charge. Blowing time varies from 90 to 110 min., depending on rate of slag production at the blast furnaces.

Coal flow to the furnace is controlled by the velocity of primary air passing through the pulverizers. Since back pressure at the tuyeres is 6 lb when the furnace is empty and increases to 11 or 12 lb when it is fully charged, the volume of primary air, measured in terms of free air at sea level, must be constantly increased to maintain the same velocity. When charging starts, coal flow is reduced in order more nearly to complete combustion, the resulting high temperature serving to heat up the slag and smelt the shells. During this period, total air is held at 14,000 cfm and primary air ranges between 5,000 and 6,000 cfm, maintaining a coal flow of 140 lb per min. After the last shell is charged, usually in about 20 min., total air is reduced to 13,000 cfm and primary air increased to 6,500 cfm, raising coal flow to 190 lb per min. Volume of primary air is never allowed to exceed that of the secondary to prevent blow-back of coal into the secondary lines. The best indicator of rate of fuel consumption is the steam flow from the boiler and under charging conditions this is held at 40,000 lb per hr. During the reducing blow it is maintained at 58,000 lb per hr. Gases enter the boiler at a temperature of 2300° and leave the economizer at 590°. Temperature at inlet to U-tubes is 540 and 225° entering the baghouse. Jacket cooling water amounts to 3,700 gpm and absorbs 2 million Btu's per min. or 44 pct of total heat input.

The blast furnace slag now averages 13 pct zinc and de-zincd slag 1.8 pct

zinc, which indicates a recovery of 89.2 pct after allowance for shrinkage. Lead is reduced from 0.80 pct in the heads to 0.03 in the tails. Combined fume from the boiler flues, coolers and baghouse weighs 50 lb per cf and has the following analysis:

| Zn | Pb | Cu | SiO ₂ | Fe | As |
|------|-----|------|------------------|-----|------|
| 68.0 | 6.0 | 0.25 | 0.9 | 0.8 | 0.20 |

This fume is deleaded by the process developed at Tooele, which consists of roasting in rotary kilns with a small amount of coke breeze to volatilize lead oxide. From a 300 ton surge bin, the fume is carried by screw conveyor and bucket elevator to a hopper which feeds either or both kilns. 1.0 pct coke breeze is added by screw feeder. The two kilns are 5 ft 6 in. id by 75 in. long, and are fired with natural gas. Temperature is automatically maintained at 2300°F by radiation pyrometers focused on the clinker at the point of discharge. Lead oxide fume is drawn from the kilns through twenty-four U-tubes, by a 20,000 cfm fan and discharged into the lead section of the baghouse. The collected fume, carrying 38 pct Pb and 30 pct Zn is returned to the lead plant. The de-leaded clinker, weighing 150 lb per cf and carrying 76.0 pct Zn and 2.0 pct Pb drops into a Traylor tube cooler, one of which is provided for each kiln, is crushed to pass a ⅜ in. screen, and is loaded into cars for shipment to a re-tort smelter.

Electrical Resistivity Measurements on Iron-silicon Compacts Prepared by the Powder Metallurgy Procedure

FRANK W. GLASER*

Introduction

Iron-silicon alloys have had a great influence, in many ways, in modern industry. Silicon steels have been used almost exclusively for the construction of electrical machinery, but have also become an important material for structures which benefit by the high tensile and yield strengths of this material. In elaborating on the early history of work done on iron-silicon alloys, Greiner, Marsh and Stoughton¹ went back as far as 1808, and pointed to Berzelius as the first producer of ferrosilicon. During the last twenty years some very important contributions in the form of studies of the iron-silicon system, as well as of the physical properties of these alloys, have been published. In consideration of the brittleness and poor machinability of alloys containing more than 5-6 pct Si, commercial interests have stimulated the research done on iron-silicon alloys, but mainly in the range of 0 to 6 pct Si. Yensen² has shown the influence of im-

purities, such as carbon, sulphur and phosphorus on the magnetic properties of 2, 4, and 6 pct Si alloys. Corson³ extended his investigation of physical properties to approximately 32 pct Si, and attributed the brittleness of the high-silicon material to the particular constitutional features of the alloys. Though mentioned earlier in the literature, the effect of nitrogen on crystal growth and magnetic permeability of iron-silicon alloys has been demonstrated recently by Morrill⁴ and Rostoker,⁵ respectively. In all the above quoted investigations, except that of Rostoker,⁵ sand or chill casting processes were employed for the preparation of samples.

A major advantage of the powder metallurgy process is that it does away with time-consuming machining in many applications. The powder metal industry is always interested in pro-

ducing a finished product employing a material which has presented considerably greater difficulties in manufacture by other methods. Steinitz⁶ described preparation and testing of various Fe-Si alloys which were produced by the powder metallurgy process for the manufacture of armatures for small electric motors or generators. While Steinitz investigated alloys up to 6 pct Si, Rostoker⁵ went as high as 9 pct Si. The author⁷ previously discussed the diffusion of iron-silicon compacts containing 6 and 10 pct silicon.

It is the object of this paper to study the progress of diffusion occurring in iron-silicon alloys by electrical resistivity measurements. All samples were prepared by pressing and sintering of compacts. Iron, silicon, and Fe-Si powders of various mesh size and compositions were employed to obtain test samples. It was assumed that complete diffusion had been obtained when the electrical resistivity reached a constant value characteristic for that particular alloy. To this end, electrical resistance measurements were used to follow the progress of alloying under various conditions.

Cleveland Meeting, October 1949.
TP 2660 E. Discussion of this paper
(2 copies) may be sent to *Transactions*
AIME before December 1, 1949.
Manuscript received March 11, 1949.
* American Electro Metal Corpora-
tion, Yonkers, N. Y.

¹ References are at the end of the
paper.

Table 1 . . . Raw Materials Employed

| Powder No. | Type | Typical Analysis, Pct | | | | | | | | Wt. Loss in H ₂ |
|------------|-------------------|-----------------------|-----|------|-----|-------|-------|-------|------|----------------------------|
| | | Fe | Mn | Ni | Cr | C | Al | Ca | Si | |
| 1 | Electrolytic iron | bal. | | | | 0.004 | | | | 0.65 |
| 2 | Fe-Si (85-15) | 83.1 | 0.6 | 0.3 | 0.2 | 0.70 | 0.3 | trace | 15.4 | |
| 3 | Fe-Si (75-25) | 74.0 | | | | 0.03 | | | 25.2 | |
| 4 | Fe-Si (50-50) | bal. | 0.4 | 0.15 | 0.1 | 0.04 | 1-1.2 | 0.08 | 49.8 | |
| 5 | Silicon | 0.82 | | | | 0.10 | 0.75 | 0.25 | 97.6 | |

The difficulty of microscopic evaluation of the degree of diffusion and of approach to homogenization in Fe-Si alloys was a prime cause for this investigation. Although there have been some important publications during recent years, they have not helped to clarify the rather complex situation occurring in compacts wherein diffusion may be only partial.

Materials, Preparation of Samples and Testing Methods

Table 1 gives data concerning the powders employed for this work. All powders were mixed in appropriate proportions to give the desired overall silicon content, and were subsequently tumbled for one hour.

Samples 2.5 cm × 1 cm × 1 cm were produced by single action hot pressing in graphite dies heated by direct conduction. The hot pressing procedure was chosen in order to avoid compacting difficulties which otherwise occur during cold pressing operations with high silicon-containing powders. Relatively high initial densities were obtained by this method. In certain cases an expansion of samples was observed during the initial subsequent heating period, and was attributed mainly to the evolution of gases, an occurrence

Table 2 . . . Densities of Fe-Si Alloys

| Pct Si | Values obtained by | | |
|--------|--------------------|-------------------|--------------------|
| | Bedel* | ASTM ⁹ | This Investigation |
| 6 | | 7.43 | 7.46 |
| 10 | 7.1 | | 7.13 |
| 25 | 6.15 | | 6.18 |
| 50 | 4.7 | | 4.68 |

* Bedel's results were plotted, and the tabulated values were taken from this curve.

frequently encountered in Fe-Si materials. This effect was never large enough to interfere with subsequent and continued densification, although sintering was slowed down to some extent. Pressures employed during hot pressing ranged from 1 to 2 tsi, and the hot-pressing temperature was selected to be below the melting point of the alloy.

Heating was done in a Globar-heated furnace in an atmosphere of either hydrogen or cracked ammonia. Atmosphere purity was controlled to a high degree by the use of drying towers and gettering.

Electrical testing was done with a Kelvin Bridge in which the potential drop for a current of 10 amp was measured over a length of 1.5 cm at room temperature.

In 1932 Bedel⁸ published data of experimentally determined densities of cast specimens. The data of Table 2

are as reported by Bedel and have been accepted as a theoretical density basis for all specimens prepared during this investigation. These are in good agreement with results obtained in this investigation. The comparison is given in Table 2.

Homogenization Study of Individual Alloy Compositions

50 PCT SILICON

Samples containing 50 pct silicon were prepared from: (1) silicon powder mixed with electrolytic iron powder (*powders 1 and 5*) and (2) prealloyed 50/50 ferrosilicon (*powder 4*).

Only coarse powders, through 100 mesh, could be employed during the processing of this composition, since all compacts of finer powders could not be prevented from oxidizing during heat treatment.

Samples in group (1), above, which were hot pressed at 1080°C, showed an initial increase of electrical resistivity during the first hours of heat treatment at 1180°C. After reaching a maximum, the resistivity dropped to a constant level after about 8 hr at temperature. This is similar to previously reported behavior for hot-pressed samples.⁷ Fig

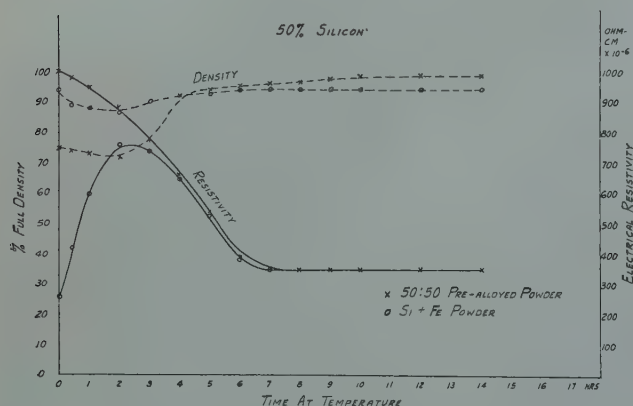


FIG 1—Density and electrical resistivity vs. time at 1180°C after hot pressing. Alloy: 50 pct silicon.

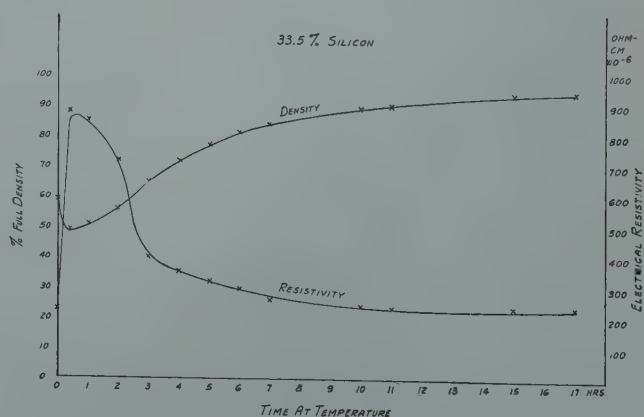


FIG 2—Density and electrical resistivity vs. time at 1180°C after hot pressing. Alloy: 33.5 pct silicon.

1 shows density and electrical resistivity behavior after hot pressing and during the heating cycle. The minimum resistance value in the "as hot pressed" state is far above that of pure iron, and it is therefore believed that some diffusion had already taken place during hot pressing, thereby setting up high silicon grain boundary "barriers" to the current through a "series-resistance" network. The formation of this high resistance skeleton continued with time at temperature and increasing diffusion. After approximately 1 hr and 50 min. at temperature (1180°C), a maximum resistivity was reached for the 50 pct Si material, whereas, as previously reported, only 25 min. were necessary for the 6 and 10 pct Si materials to reach this peak value.⁷

Another possible explanation for this maximum is the formation of an Fe-Si-C phase, since some carbon was introduced during hot pressing through the use of graphite dies, and was still present at this point in the heat treatment. An intergranular phase was visible upon microscopic examination. The microhardness of this phase was much closer to that of an iron-silicon alloy than that of silicon carbide. This seems to favor the first theory. It was found that progressive decarburization of the compacts occurs during heat treatment.

Diffusion seemed to be completed after approximately 8 hr, at which point a resistivity value of 350 microhm-cm was reached. The density was relatively high for this material throughout the heat treatment and seemed to reach a maximum point of densification after only 4 hr of heating.

When prealloyed 50/50 ferrosilicon powder was hot pressed at 1080°C and heat treated at 1180°C, both the density and resistivity showed behavior

Table 3 . . . Density and Resistivity of Homogenized Material After Hot Pressing

| Hot Pressing Temp. °C. | Density Pct | Resistivity Microhm-cm |
|------------------------|-------------|------------------------|
| 1080 | 86.0 | 255 |
| 1150 | 95.5 | 250 |
| 1200 | 96.0 | 250 |

otherwise encountered only after sintering operations (see Fig 1). Contact resistance showed a gradual decrease as continued solid bonding took place between the particles. As soon as pore space was greatly reduced by densification and the measured cross-section became a true measurement (after approximately 6 hr), the same resistivity of 350 microhm-cm was reached. When this prealloyed material was hot pressed at 1200°C, this resistivity value was reached immediately, and the concomitant density was approximately 100 pct. The use of higher hot pressing temperature thus eliminates approximately 6 to 8 hr of heat treatment.

The density of iron-silicon powder mixtures, initially hot pressed at this higher temperature (1200°C), did not differ from that obtained at a lower hot pressing temperature (1080°C). Resistivity, however, was approximately 125 microhm-cm higher at this initial stage, due, presumably, to further progress of diffusion. The curve then followed substantially the aforementioned trend of peak and decrease, reaching complete diffusion at similar time and resistivity values. Samples containing 48.3, 44.1 and 42.2 pct Si, by analysis, were prepared by this same method and showed similar behavior in the relationship between time at temperature and both resistivity and density. Resistivity data for these

compositions are reported in a subsequent portion of the text.

33.5 PCT SILICON

This composition was prepared by mixing silicon powder with electrolytic iron powder and hot pressing at 1080°C. Coarse and fine powders behaved alike, and in general it can be said that resistivity and density followed the same general trend as the 50 pct Si alloys throughout the heating period (Fig 2). Only after 10-12 hr was homogenization accomplished. The final resistivity value reached, at complete diffusion, was 235 microhm-cm. This is in agreement with values obtained by Corson³ for cast materials of similar composition. Some of the completely homogenized material was crushed to powder (through 100 mesh), and re-pressed at various temperatures. Table 3 gives the results for these homogenized materials when hot pressed at various temperatures.

It is obvious from Table 3 that the resistivity is not dependent on the density in this range. Complete diffusion had occurred in all three cases during the prealloying, and the slightly higher resistivity of these samples was attributed to thin grain boundary oxide films which were found to be present during metallographic examinations. The structure of the above three specimens was substantially the same as for samples fully homogenized by heating for 11 hr.

20 TO 27.5 PCT SILICON

A 27.5 pct Si alloy was prepared by mixing a 50/50 Fe/Si master alloy with electrolytic iron powder. The powders (-325 and -100 mesh mixtures) were hot pressed at 1080°C and after a subsequent heat treatment of

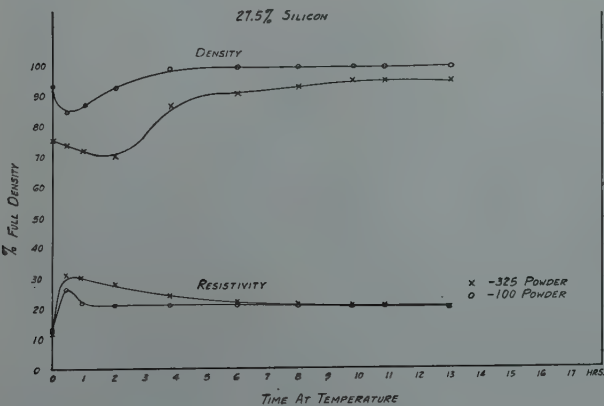


FIG 3—Density and electrical resistivity vs. time at 1180°C after hot pressing. Alloy: 27.5 pct silicon.

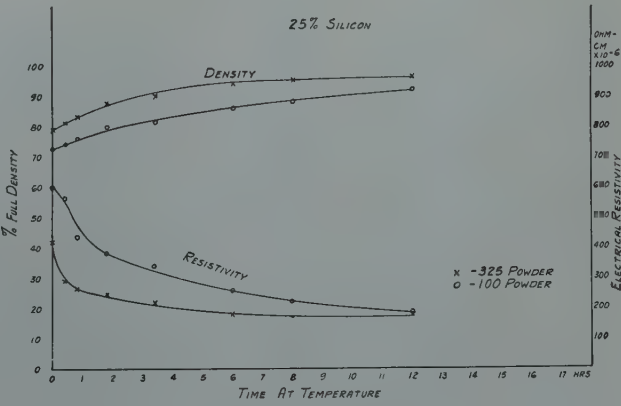


FIG 4—Density and electrical resistivity vs. time at 1180°C after hot pressing. Alloy: 25 pct silicon.

Table 4 . . . Resistivity of Specimens Hot Pressed at 1080°C and Heat Treated at 1180°C

| Composition | | | Resistivity, Microhm-cm | | | |
|--------------|--------------|-------------|-------------------------|---------------------|-----------------------|---------------------|
| Alloy Pct Si | Master Alloy | Iron Powder | This Investigation | Corson ³ | Rostoker ⁵ | Yensen ² |
| 6 | 2 and 3 | 1 | 85 | 80 | 83.5 | 78 |
| 9 | 2 and 3 | 1 | 110 | 103* | 98.6 | 110† |
| 10.1 | 2 and 3 | 1 | 115 | 105* | | |
| 11.5 | 3 | 1 | 116 | 98* | | |
| 12.5 | 3 | 1 | 60 | 85* | | |
| 13.1 | 3 | 1 | 55 | 75* | | |
| 15.2 | 3 | 1 | 55 | 40* | | |
| 16.6 | 3 | 1 | 62 | 60* | | |
| 18.2 | 3 | 1 | 65 | 80* | | |

*Interpolation not too accurate, due to scale of curve.
†Extrapolated.

approximately 6 hr at 1180°C a constant resistivity level was reached.

The 25 pct Si alloy was made up by hot pressing a commercial, pre-alloyed 75/25 alloy at 1080°C with a subsequent heat treatment at 1180°C. A state of constant resistivity was obtained after approximately 8 hr of heat treatment for both fine and coarse powders.

The 20 pct Si sample was produced by mixing a 75/25 master alloy with electrolytic iron powder. Only a -325 mesh powder was employed for this composition.

Fig 3, 4 and 5 show the relationship of both the resistivity and density to time at temperature. Trends substantially similar to those observed in previous experiments are noted. Some difference in behavior is noticeable if one considers the particle sizes employed.

For the 27.5 pct Si alloy, the coarse powder follows a rather normal pattern to complete homogenization. The process was slowed down considerably in the case of finer powder because relatively more surface area is exposed to oxidation. This is contrary to the usual alloying process occurring in powders, where the finer powder mixes usually

Table 6 . . . Fe-Si Alloys Annealed in H₂ and Cracked NH₃ Atmospheres

| Approx. Pct Si | Resistivity, Microhm-cm | |
|----------------|------------------------------------|---|
| | Samples Annealed in H ₂ | Samples Annealed in Cracked NH ₃ |
| 6 | 83.5 | 85 |
| 9 | 104.5 | 110 |
| 10 | 111 | 115 |
| 12.5 | 60 | 60 |
| 20 | 151.5 | 152 |
| 25 | 210 | 205 |
| 32 | 239 | 235 |
| 50 | 355 | 350 |

reach equilibrium faster.

The 25 pct Fe-Si alloy behaved normally; the finer powder was densified in about half the time required for the coarser powder. Apparently the 50/50 Fe/Si master alloy which was employed in producing the 27.5 pct Si sample had a greater tendency to oxidize than did the 75/25 master alloy.

When fully homogenized 20 pct and 27.5 pct Si alloys were crushed to pass through a 100 mesh and hot pressed at 1080°C, their final resistivity values were obtained immediately on hot pressing. For the commercial, pre-alloyed 75/25 Fe/Si alloy, the hot pressing temperature had to be raised to 1200°C, in order to reach the final

Table 5 . . . Percent Carbon in Fe-Si Compacts After Various Heat Treatments

| Pct Si | Pct Carbon | | | | |
|--------|----------------|-------------------|------|-------|-------|
| | As Hot Pressed | 25 Min. at 1180°C | 4 Hr | 10 Hr | 15 Hr |
| 6 | 0.12 | 0.10 | 0.08 | 0.07 | 0.04 |
| 10.1 | 0.13 | 0.04 | 0.04 | 0.04 | |
| 12.5 | 0.13 | 0.03 | 0.03 | | |

resistivity value of this material immediately after hot pressing. When pressed at a lower temperature (1080°C) 8 hr of subsequent heat treatment were needed to attain constant resistivity.

A similar behavior had been noticed with regard to the 50/50 alloy. The precise reason for this difference is not known. Also, the method of manufacture of the commercial material is not known. It is known, however, that the homogenized powders used in this investigation (made by hot pressing and heat treating) were used within a fairly short time after crushing (12 hr max.), and were stored in desiccators even during this interval. Surface oxide film on the commercial powder may account for the increased resistance values found in the hot pressed (1080°C) condition.

6 TO 18 PCT SILICON

All compositions were prepared as shown in Table 4. Testing was done for heat treating times ranging from 25 min. to 17 hr and, with regard to electrical resistivity and density, all materials followed the trends discussed before for other Si alloys. Final resistivity values are also given in Table 4. Some values found in the literature have been entered in the table for comparison.

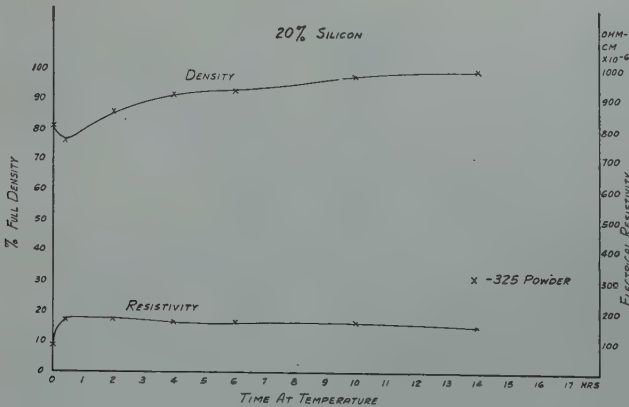


FIG 5—Density and electrical resistivity vs. time at 1180°C after hot pressing. Alloy: 20 pct silicon.

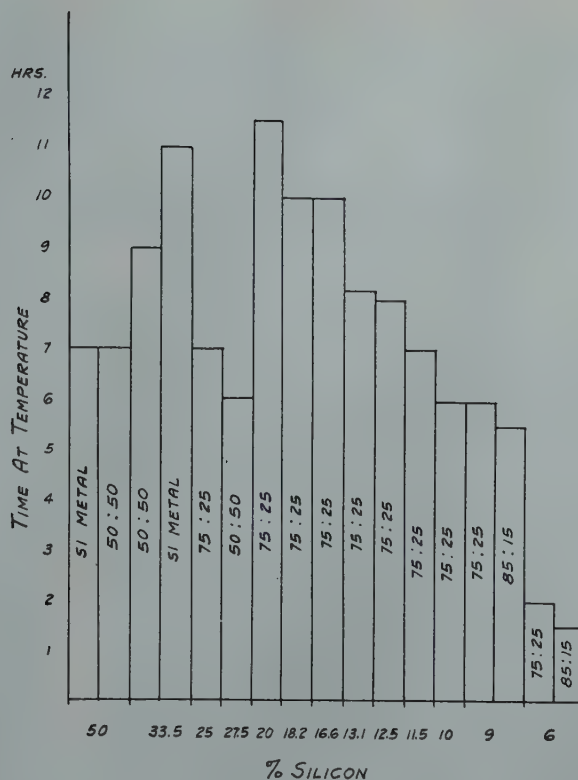


FIG 6—Time needed for complete diffusion for iron-silicon samples prepared from different master alloys. Hot pressing temperature 1080°C. Subsequent heat treatment at 1180°C.

Table 7 . . . Resistivity Values for Fe-Si Alloys After Complete Diffusion

| Pct Si (by analysis) | Resistivity (microhm-cm) | Pct Si (by analysis) | Resistivity (microhm-cm) |
|----------------------|--------------------------|----------------------|--------------------------|
| 6.0 | 85 | 20.1 | 152 |
| 9.0 | 110 | 25.2, 25 | 182, 180.5 |
| 10.1 | 115 | 27.6 | 200 |
| 11.5 | 116 | 33.5 | 240 |
| 12.5 | 60 | 42.2 | 303 |
| 13.1 | 55 | 44.1 | 320 |
| 15.2 | 55 | 48.3 | 340 |
| 16.6 | 62 | 49.8 | 350 |
| 18.2 | 65 | | |

Fig 6 indicates the time needed for different samples to reach complete diffusion. It is interesting to note that when master alloys are sintered by themselves, both the 50/50 and the 75/25 require the same time (7 hr at 1180°C) to reach constant resistivity.

For a given alloy mixture, 85/15 master alloy requires a somewhat shorter time at temperature, as compared with 75/25, to reach constant resistivity. Also, the less iron added to the 75/25 mixtures (approaching the composition of the master alloy), the longer the time required for equilibrium. If not hot pressed, much longer times at temperature than those reported in Fig 6 are necessary to obtain

complete diffusion in iron-silicon materials produced by powder metallurgy processes. Hot pressing temperatures were controlled optically and it is probable that the indicated temperatures were no more precise than plus or minus 20–30°C. Considering the fact that a few degrees C in this temperature range, which is quite critical for these Fe-Si materials, will influence the speed of diffusion considerably, the times reported in Fig 6 represent approximate values.

Carbon analyses have been run for some materials containing 6, 10.1 and 12.5 pct Si, and the results are tabulated in Table 5.

Inasmuch as the original raw material contained less than 0.03 pct C, the C picked up during hot pressing seems to be as high as 0.09 to 0.10 pct.

Metallographic examination disclosed substantial surface carburization of the compacts, and certainly a good portion of both the increased carbon found on hot pressing and the loss of carbon observed after heat treating can be attributed to the carburization and subsequent decarburization going on in the skin of the compact during its cycle.

A comparison has also been made for resistivities obtained with samples annealed in H₂ vs. samples annealed in

cracked ammonia. Table 6 shows that the nitrogen contained in this latter atmosphere does not seem to have much influence on the electrical resistivities of Fe-Si alloys.

A characteristic trend of minimum, maximum and constant resistivity level was established as a function of diffusion time for iron-silicon samples prepared from powder mixes.

At the minimum resistivity (the “as hot pressed” stage), diffusion of the silicon into the iron was far from complete, but a certain amount of bonding between particles had taken place. The current passed through a low resistance network. After a given time interval at temperature, diffusion created a high resistance silicon-iron network, accounting for the maximum resistivity. Diffusion, progressing with time, reduced the resistivity to a constant level. If a given ferrosilicon composition was prealloyed by the hot pressing and heat treating procedure, and subsequently crushed to –100 mesh, final resistivity was obtained immediately on hot pressing at 1080°C.

Hot pressing temperatures, higher by 120°C, were required for commercial prealloyed powders to obtain final resistivity immediately upon hot pressing. Grain boundary oxide films are

believed to be the cause for the necessity of this higher hot pressing temperature. If a commercial, prealloyed, powder was hot pressed at normal hot pressing temperature, 8 hr of subsequent sintering time was needed to arrive at final resistivity values.

General Discussion of Results

Table 7 shows the resistivity values the author measured for various Fe-Si alloys after complete diffusion. Data as given by Corson³ have been plotted together with these values in Fig 7.

Distinct differences between the values obtained in these two investigations, especially in the 20–30 pct Si ranges, can be noticed in Fig 7. The present values are generally higher than those reported by Corson, whose specimens were prepared by casting. A comparison of grain size of the alloys employed during the respective investigations disclosed striking similarities. Since no comparisons with regard to chemical purity can be made it can only be pointed out that all Si percentages employed in this investigation have been carefully checked by chemical analysis, and tests have frequently been repeated to minimize any source of error. It will also be recalled that while the samples for the author's experiments have been produced by several methods, the final test results have never varied more than 3 to 5 pct.

All samples were tested for hardness, and Fig 8 shows the relationship of Rockwell hardness vs. silicon content for the fully homogenized samples. Hardness values in Fig 8 are higher for the higher silicon ranges than the values reported by Corson. There may be some relationship between the higher hardness and the higher resistivities as reported in Fig 7.

Metallographic examination of specimens in the 11–25 pct region suggest no cause for the shape of curves for hardness and resistivity. One explanation, recorded by Hansen,¹⁰ was the presence of an order-disorder transformation. An X ray diffraction study of 12.5 pct and 16.6 pct Si alloys showed the presence of lines which were absent in a 10.1 pct Si alloy. These lines corresponded to the calculated positions of the 111 and 200 reflection, and thus are taken to indicate the existence of an ordered state. In this connection it

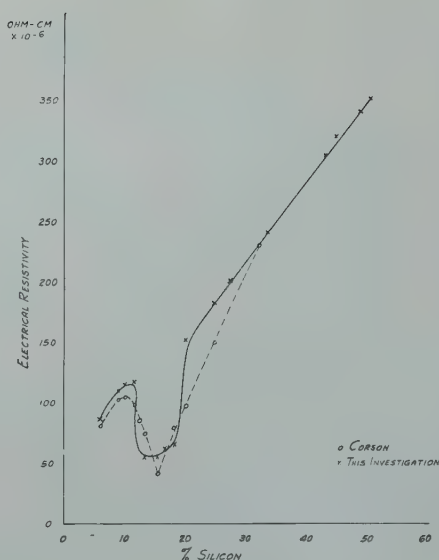


FIG 7—Electrical resistivity vs silicon content for fully homogenized samples.

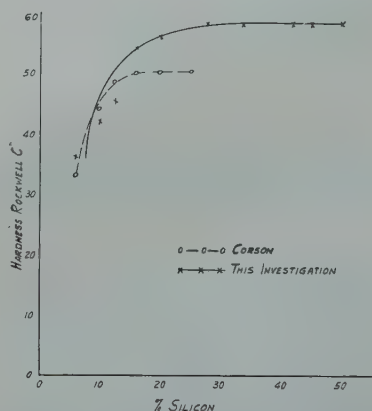


FIG 8—Hardness vs silicon content for fully homogenized samples.

might be of interest to note that some heat treatment experiments have been made with a 15.2 pct Si-containing material. One specimen was kept at 1180°C for 72 hr and cooled to room temperature over a period of approximately 5 hr, while another specimen was quenched in water after this prolonged time at temperature. In both cases the resistivity values as reported for this composition in Fig 7 were still found and no marked difference in structure between these two specimens could be found upon metallographic examination.

Summary

1. It has been shown that the degree of diffusion in iron-silicon alloys prepared by the powder metallurgy process

can be followed by electrical resistivity measurements. In the higher density ranges, the electrical resistivity is a function only of the diffusion process and is very much influenced by changes of the Si concentration in a non-homogeneous Fe-Si alloy.

2. Values for the specific electrical resistivity of iron-silicon alloys containing between 6 and 50 pct silicon have been determined.

3. It has been further shown that the hot pressing and heat treating process can be used to produce iron-silicon materials in suitable forms.

4. No major effects upon the electrical resistivity of an atmosphere containing nitrogen were detected for iron-silicon alloys.

5. The resistivity curve shows a break between approximately 11 and 25 pct Si.

Acknowledgment

A portion of this investigation was carried out under Contract NOa(s)-8959, of the U.S. Navy, Bureau of Aeronautics, and the results are presented with the permission of this agency. The author wishes to express his thanks to this Bureau for permission to publish these data.

The writer also wishes to express his gratitude to Messrs. W. Ivanick, R. Steinitz, S. J. Sindeland and R. Wachtell, for their advice and assistance in the preparation of this paper, as well as to Professor J. T. Norton for his cooperation in carrying out the X ray diffraction study.

References

1. E. J. Greiner, J. S. Marsh and B. Stoughton: *The Alloys of Iron and Silicon*. McGraw-Hill, 1933, pp. 5, 70.
2. T. D. Yensen: *Trans. A.I.E.E.* (1924) 43, 145.
3. M. G. Corson: *Trans. AIME* (1928) 80, 249.
4. W. Morrill: *Metal Progress* (1948) 54, 5, 675.
5. W. Rostoker: *Trans. AIME* (1949) 180, 672. *Metals Tech.* Oct. 1948 TP 2437.
6. R. Steinitz: *Powder Metallurgy Bull.* 2, 135 (1947).
7. F. W. Glaser: *Powder Metallurgy Bull.* 4, 19 (1949).
8. C. Bedel: *Compt. rend.* 195, 329 (1932).
9. A.S.T.M. Standards (1946) p. 648.
10. M. Hansen: *Der Aufbau der Zweistofflegierungen*, Springer Verlag, Berlin, (1936) p. 735.

A Metallographic Description of Fracture in Impact Specimens of a Structural Steel

M. BAEYERTZ,* Member AIME, W. F. CRAIG, JR.* and E. S. BUMPS*

Metallurgists have looked at fractures macroscopically for many years and have evolved a vocabulary in which such words as "cleavage," "brittle," "shear," "ductile," "granular," "fibrous," and "silky" are used to describe the appearance of the fractured surface; but the meaning of these words in terms of metal structure is not well established. Observations of the structural meaning of "brittle" and "ductile" fractures in plate steels have been made, notably, by Kramer and coworkers¹ and by Tipper.² Grossman³ has studied the fracture of tempered martensite and combinations of ferrite and martensite. Notwithstanding these and other less concerted attacks on the problem, present understanding of fracture rests more on assumptions and logic than on experiment. It is the purpose of this paper to add a little to the growing fund of experimental observations of the nature of fractures in steel. The particular fractures to be described were obtained in conventional impact testing of an ordinary structural steel shape.

In impact tests of the Charpy type, the specimens fail in a characteristic manner that depends on the steel and the temperature of testing. With ordinary structural and many other steel products, an appropriate range of testing temperature will cause a considerable change in the energy absorbed before fracture. This change is known as the energy transition and is accompanied, more or less closely, by alteration in the appearance of the fracture. At testing temperatures below the transition, the terms "brittle," "cleavage," or "granular" are used to describe the fracture; above it, "ductile" or "shear" are often used. Within the transition, the fracture changes from "brittle" to "ductile" by a progression in appearance, wherein the "brittle" portion of the fracture becomes restricted to a smaller and smaller central area of the fracture, as the testing temperature is

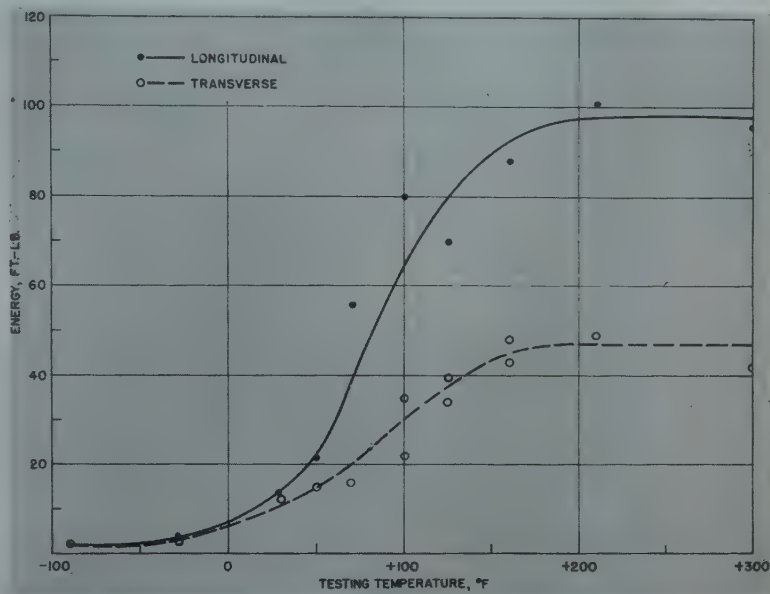


FIG 1—Relation of energy to testing temperature obtained from V-notch Charpy specimens from an ordinary structural steel shape.

raised and the "ductile" type of fracture is approached. All this is well known to metallurgists.

The specimens under consideration are of the conventional V-notch Charpy type. They were taken from a structural steel shape of the following analysis:

| C | Mn | P | S | Si |
|------|------|-------|-------|------|
| 0.17 | 0.46 | 0.009 | 0.029 | 0.03 |

Both longitudinal and transverse specimens were tested and examined. Fig 1 shows the energy values plotted against testing temperatures in the usual way. The curves for both longitudinal and transverse specimens show an energy transition, although the maximum energy absorbed at testing

temperatures above the transition is greater in the case of the longitudinal specimens.

Fig 2 illustrates the changes in the macroscopic appearance of the fractures that are associated with the energy transitions shown in Fig 1. Macrographs of the fractured surfaces of the specimens have been identified with the fracture ratings at intervals on each fracture curve. The numerical fracture rating on the ordinate of Fig 2 indicates the percentage of the area of each fracture that was considered to be "brittle" on macroscopic observation. Such rating of the fracture type in impact tests is now customary in many laboratories. Hereafter the specimens will be identified by reference to Fig 2 as 90 pct "brittle," 80 pct "brittle," and so on, in accordance with this macroscopic evaluation of the appearance of the fractured surface.

The discussion of the fractures is divided into three parts. The first two are concerned with the mode of fracture and its relation to general structural features. As the same metallographic features occur in both longi-

Cleveland Meeting, October 1949.
TP 2635 E. Discussion of this paper (2 copies) may be sent to *Transactions AIME* before December 1, 1949. Manuscript received March 4, 1949.
* Armour Research Foundation of Illinois Institute of Technology.
¹ References are at the end of the paper.

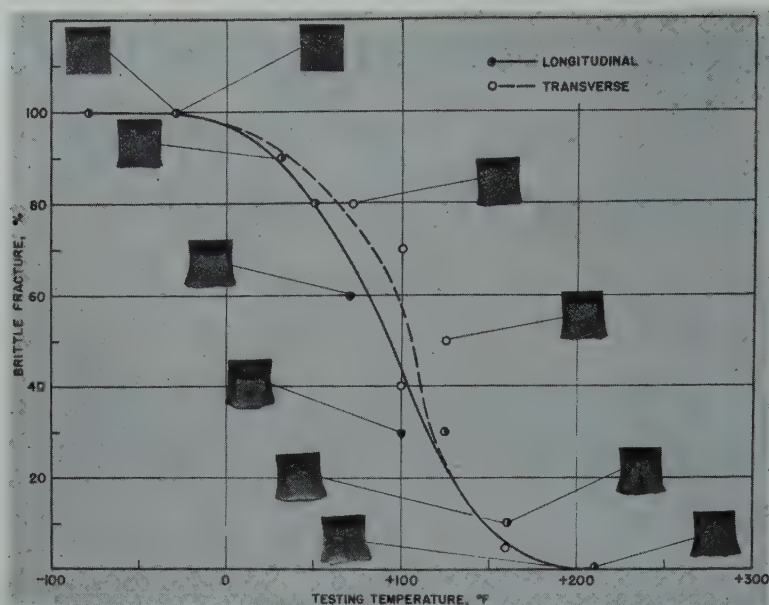


FIG 2—Relation of type of fracture to testing temperature obtained from V-notch Charpy specimens from an ordinary structural steel shape. Corresponding energy curves are shown in Fig 1.

tudinal and transverse fractures, differing in degree and distribution but not in kind, the illustrations and description are drawn from both types of specimens. The third part of the discussion deals with some relations between the structural features of fracture and the energy values obtained in the test. In this part the relation between longitudinal and transverse data will be discussed.

Character of the Fractured Surface

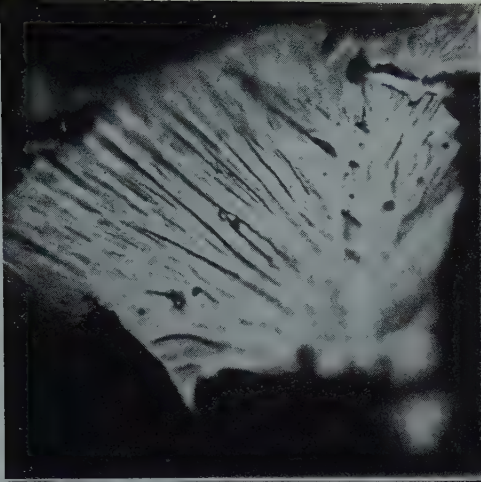
Leaving aside for the moment consideration of "ductile" fracture, the most prominent feature of the fractured surfaces in Fig 2 is the group of shiny facets to be seen on the "brittle" regions. These facets look alike and are of about the same size regardless of testing temperature, as



FIG 3—Microscopic appearance of cleavage facets on fractured surfaces of impact specimens. Series covers transition range from 100 pct "brittle" fracture to 100 pct ductile fracture.

- a—100 pct "brittle" fracture. 750 ×
 - b—90 pct "brittle" fracture. 750 ×
 - c—80 pct "brittle" fracture. 750 ×
 - d—60 pct "brittle" fracture. 750 ×
 - e—60 pct "brittle" fracture. 750 ×
 - f—30 pct "brittle" fracture. 750 ×
 - g—10 pct "brittle" fracture. 750 ×
 - h—10 pct "brittle" fracture. 750 ×
 - i—5 pct "brittle" fracture. 750 ×
 - j—0 pct "brittle" fracture or 100 pct "ductile" fracture. (Same as Fig 3 k but focused at slightly lower plane.) 750 ×
 - k—0 pct "brittle" fracture or 100 pct ductile fracture. (Same as Fig 3 j but focused at slightly higher plane.) 750 ×
- All micrographs slightly reduced in reproduction.

e



f



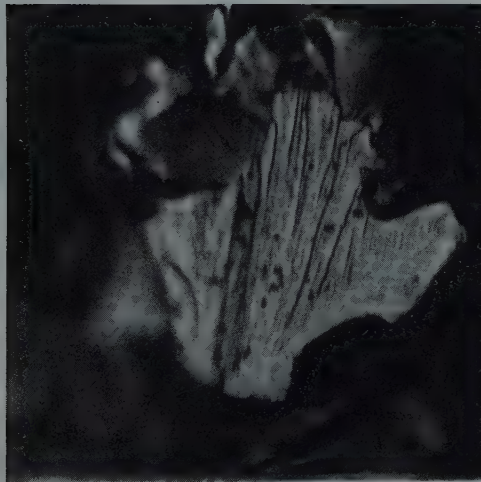
g



h



i



j



k





FIG 4—Section through 90 pct "brittle" fracture. "Brittle" portion of fracture is enclosed by bracket.
50 X. Etchant 2 pct nital. Reduced approximately one fourth in reproduction.

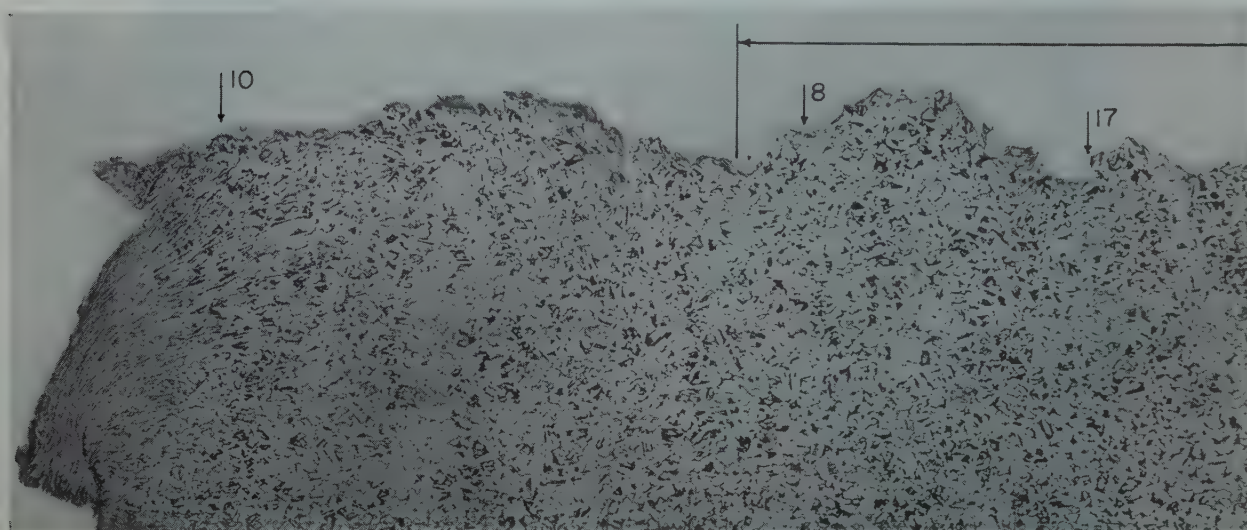


FIG 5—Section through 60 pct "brittle" fracture.
"Brittle" portion of fracture is enclosed with bracket. Arrows indicate figure numbers of micrographs showing detail. 50 X. Etchant 2 pct nital. Reduced approximately one fourth in reproduction.

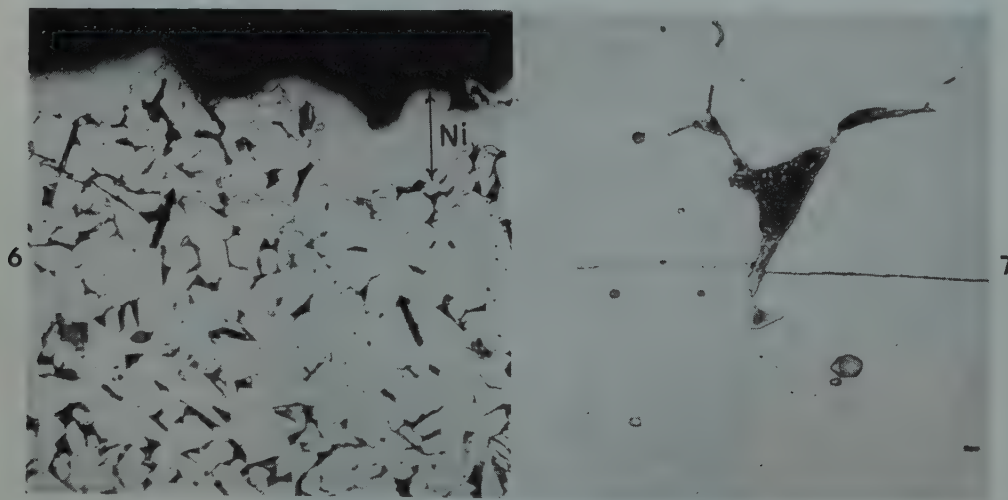


FIG 6 (left)—Portion of "brittle" region of 30 pct "brittle" fracture.
Single arrows indicate ferrite cleavages below the path of main fracture. 150 X. Etchant 2 pct nital.
FIG 7 (right)—Detail of cleavages in the two ferrite grains indicated by the arrow on the right of Fig 6.
Note that the cleavage was apparently interrupted by the pearlite colony. 1000 X. Etchant 2 pct nital. Both micrographs slightly reduced in reproduction.

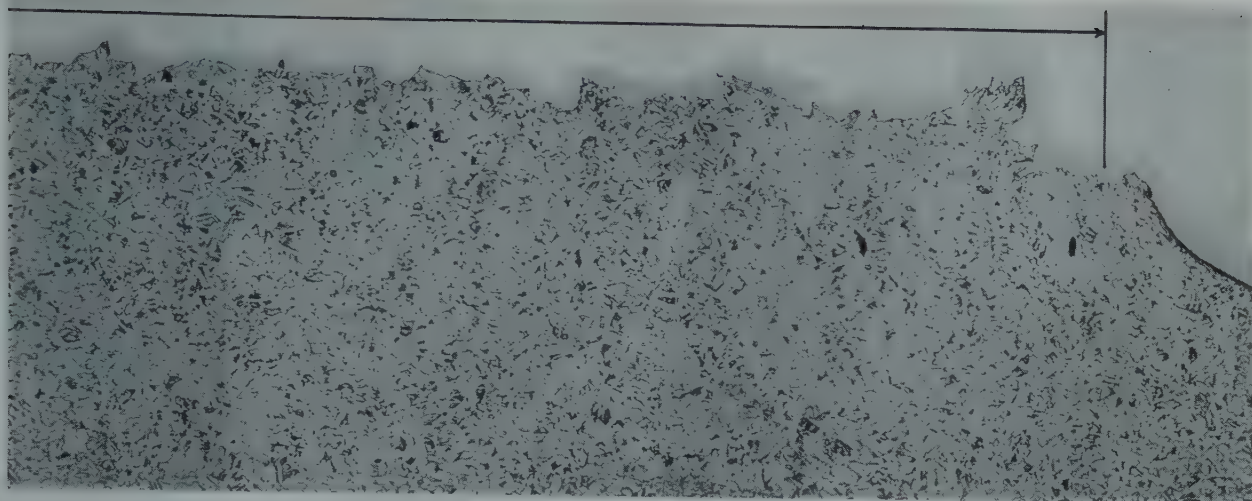


Fig 4—(Continued)

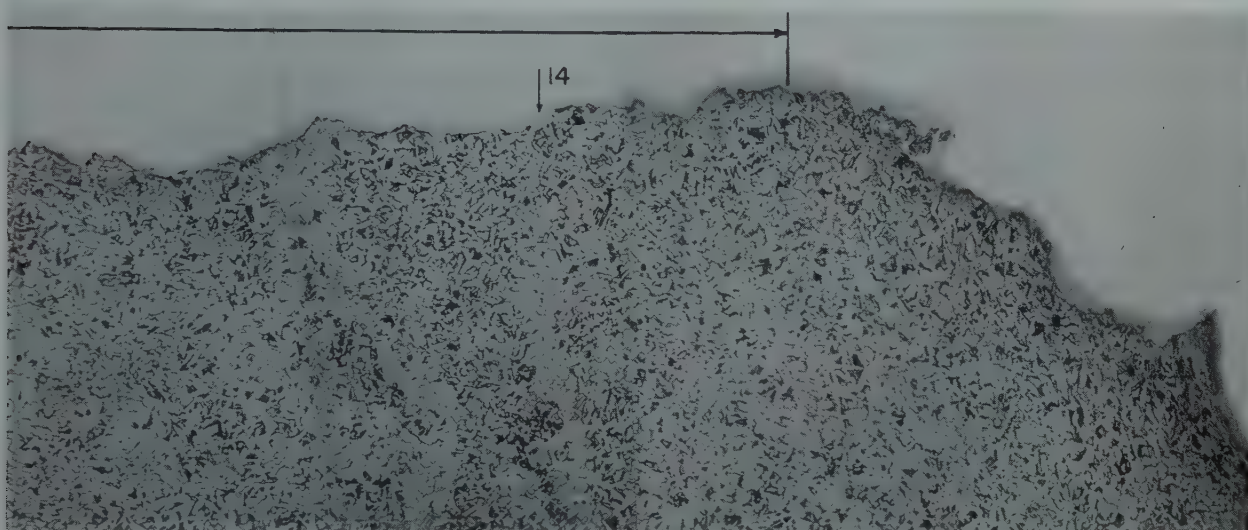


Fig 5—(Continued)

long as they appear at all. This suggests a relation to the structure of the steel.

On raising the magnification, but still looking toward the fractured surface, the facets have the appearance illustrated by Fig 3. It now becomes apparent that the facets are not alike, as they seemed at lower magnification. Instead, straight cleavage planes characterize the low temperature end of the transition range, while definite and then pronounced evidence of deformation is observed on the cleavage facets as the high temperature end of the transition range is approached. "Cleavage" as used here and in the rest of the paper is crystallographic cleavage, not the loose application of the term to describe the macroscopic appearance of the fracture.

At low testing temperatures, represented by the specimens with 100 pct

and 90 pct "brittle" fractures, the cleavage planes are flat and resemble the cleavage facets of ferrite described by Zapffe and Moore⁴ and by Kramer and coworkers.² The cleavage planes make well defined angles with each other that appear to be the 90° angles to be expected from the {100} cleavage observed in ferrite by Barrett, Ansel and Mehl.⁵ Tipper² has found that the {100} cleavage is that shown by the ferrite in ship plate fractures.

As the testing temperature is raised, the tendency for multiple cleavage on several of the {100} family appears to diminish, giving rise to the larger, comparatively smooth facets shown by the 80 pct "brittle" fracture. Also there is another change in the character of the fracture. Small ripples appear on the cleavage surfaces. These ripples are believed to be caused by cold work, either prior to or at the time of

cleavage. It is difficult to distinguish between prior and concurrent cold work, but the complexity of slip directions to be seen as the testing temperature is raised suggests that at least a part of the slip occurs in the ferrite before cleavage takes place. A part of the rippling may be caused by the stress waves set up by the operation of cleavage.

Multiple slip in three directions on single cleavage facets may be seen in the micrographs of the 30 pct and 10 pct "brittle" fractures. The extent of such slip probably is related to the orientation of the ferrite grain with respect to the stress pattern. Two micrographs are included in Fig 3 for the 60 pct and 10 pct "brittle" fractures. Each pair of photographs shows qualitatively the range in the amount of slip observed on the various cleavages of the fracture.

The final micrographs in the series in Fig 3 illustrate the highly distorted cleavage planes observed in the 0 pct "brittle" fracture obtained with a testing temperature of 210°F. Macroscopically this fracture appeared to be 100 pct "ductile," as may be seen in Fig 2. Microscopically the same sort of cleavage facets are to be seen in the central region of this "ductile" fracture as were observed on the "brittle" regions of the other fractures, with the exception that the cleavage facets of the "ductile" fracture are so rumpled by cold work that they do not reflect enough light to be detected macroscopically as cleavage facets. Thus, under the triaxial loading in an impact specimen during testing, "ductile" fracture appears to be initiated by ferrite cleavage in essentially the same way as in the more "brittle" fractures that are obtained at lower testing temperatures.

The Mode of Fractures

Turning from examination of the fractured surface to the metal below the surface, even more light is shed on the mode of impact fracture in ordinary structural steel. For this part of the study, the fractured specimens were plated with nickel, sectioned and prepared for metallographic examination. In each specimen the section studied lay on a plane that was normal to the fractured surface and extended from the notch to the back of the specimen.

Fig 4 and 5 are illustrations of the

structural features observed in the metal below the "brittle" and "ductile" portions of fractures. Fig 4 shows a section normal to a 90 pct "brittle" fracture. The portion on which the ferrite cleavages were observed is included by the bracket. Similarly, Fig 5 shows a section normal to a 60 pct "brittle" fracture. The thickness of the specimen after fracture (distance between the notch and the back of the specimen) indicated the greater reduction before final rupture in the specimen having the 60 pct "brittle" fracture. In Fig 5, the region of ferrite cleavage is restricted and cold work, especially at the notch, has become more apparent than in the 90 pct "brittle" specimen in Fig 4. For the purpose of orienting the reader, the figure numbers of photographs at higher magnification to be described below have been placed in their respective positions along the fracture in Fig 5.

On examination of the metallographic sections at higher magnifications, the mode of development of the fracture becomes evident. With the exception of shock twinning at low testing temperatures, to be discussed later, the essential details of cleavage, deformation and fracture did not vary throughout the transition range, although these features apparently differed in amount with change in testing temperature. Because of this similarity in the mode of cleavage, deformation and fracture, illustrations will be drawn from several of the specimens broken within the transition.

The metallographic evidence sup-

ports the following sequence of events leading to the final rupture of the specimens. As the hammer of the impact testing machine strikes the specimen and bends it, elastic and then plastic deformation occurs. Within the general region of greatest triaxiality of loading located somewhat back of the notch in the specimen, the restraint to deformation and the nature and temperature of the steel are such as to cause cleavage within the ferrite grains when the tensile stress normal to a cleavage plane reaches an appropriate value. The ferrite cleavage may occur either within the elastic or the plastic portion of deformation depending upon the testing temperature. The cleavage occurs only in grains or groups of grains whose cleavage planes are favorably oriented with respect to the stress pattern. Such cleavage involving two ferrite grains is indicated by the arrow on the right side of Fig 6, and is shown at higher magnification in Fig 7. Other similar cleavages are shown in Fig 8. In the fractured specimens, such cleavages were observed only in the immediate vicinity of the fracture.

As described previously and illustrated by Fig 3, cleavage at the low temperature end of the transition apparently occurs before the yield point is reached. At the high temperature end of the transition, there is evidence of cold work preceding cleavage. Intermediate stages between these two extremes occur within the transition range. Evidence of deformation before cleavage at the high temperature end of the transition is to be seen also in the samples prepared for metallographic study. Fig 9 shows cleavage involving three ferrite grains in a 10 pct "brittle" specimen. The bent cleavage on the right side of the micrograph is taken as an indication of cold work before cleavage. Deformation after cleavage would be expected to separate the two surfaces of the cleavage in the manner illustrated by the cleavage at the fracture surface in Fig 8.

To continue with the events preceding final rupture, the greater the extent of cleavage the less will be the effective section of the metal left to withstand subsequent loading during the test. Also the stress pattern will be altered, because each cleavage will now have become an internal notch. In the next stage the metal between the cleavages, and that in the peripheral regions of low triaxiality of

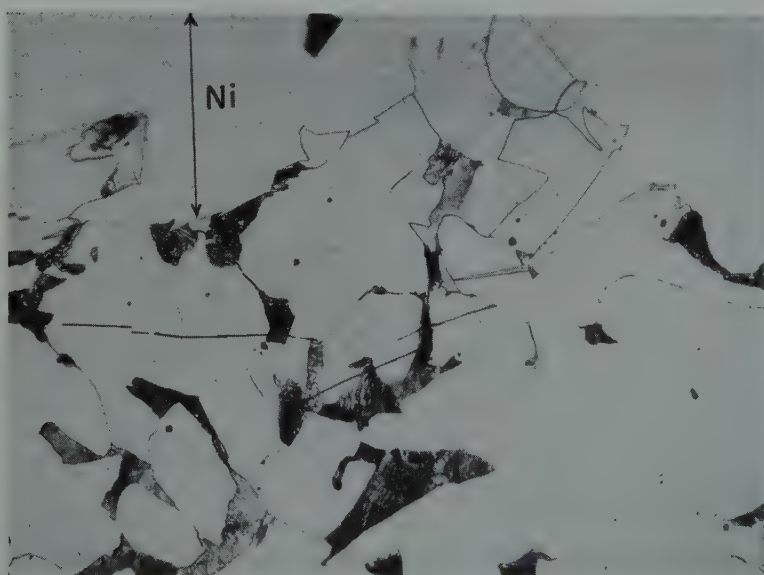


FIG 8—Cleavages observed in the "brittle" portion of the 60 pct "brittle" fracture. 500 X. Etchant 2 pct nital.

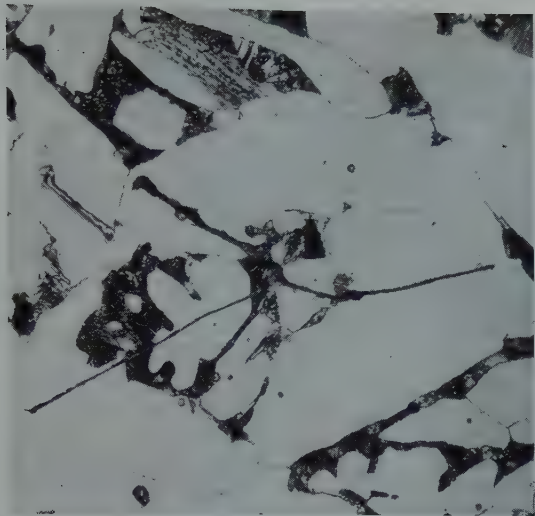


FIG 9—Cleavages in three ferrite grains in a 10 pct "brittle" fracture.

The bent cleavage on the right side of the micrograph indicates plastic deformation before cleavage. 500 X. Etchant 2 pct nital.

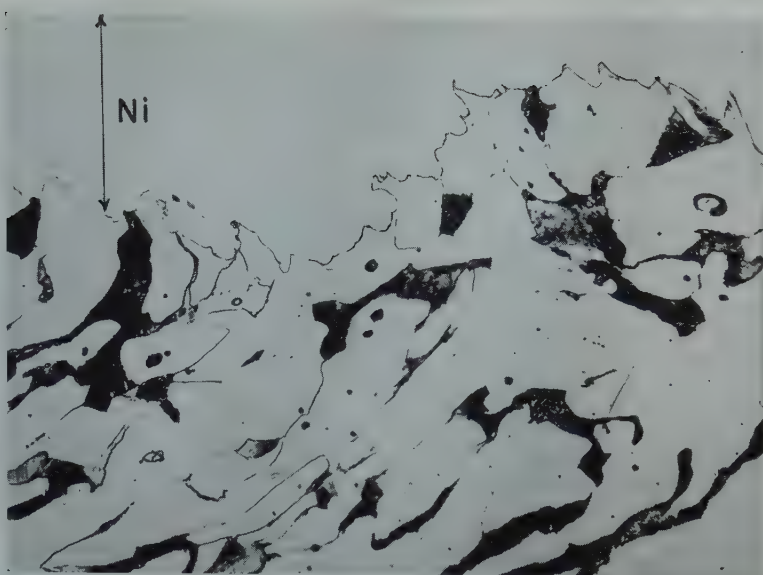


FIG 10—Evidence of deformation in the peripheral "ductile" region of a 60 pct "brittle" fracture.

500 X. Etchant 2 pct nital.

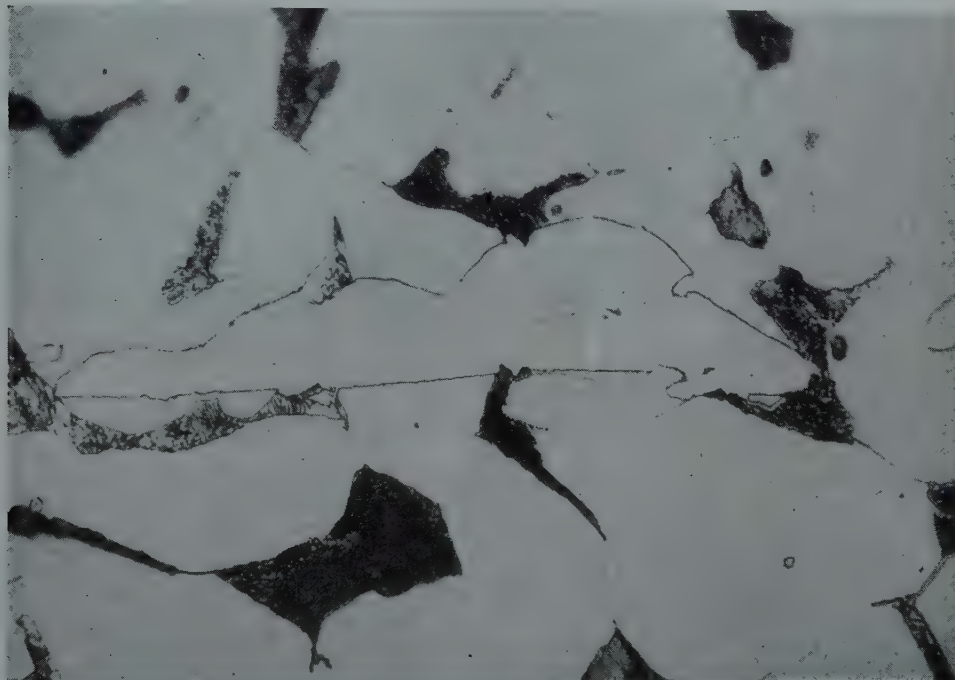


FIG 11—Detail of the nickel filled crack indicated by the arrow on the left of Fig 6.

Two colonies of pearlite were pulled apart. 1000 X. Etchant 2 pct nital.

stressing, deform and fracture. Evidences of deformation in the peripheral "ductile" region have been illustrated already in Fig 2, 4 and 5. Microscopically, the fracture of such regions is illustrated by Fig 10.

In the central "brittle" region, one feature of the deformation after the cleavage is the pulling apart of cleavages formed earlier. Numerous cleavages are formed in the general region of the final rupture, but only a limited number form a part of the path of ultimate rupture. Some of the cleavages remain intact as indicated by the

arrow on the right side of Fig 6 and in Fig 7. Others are pulled apart as indicated by the arrow on the left side of Fig 6. This crack was filled with nickel when the specimen was plated. It may be seen in more detail in Fig 11. The upper surface of the cleavage has pulled away from the lower surface, and in so doing, has broken apart two colonies of pearlite. Similar pulling apart of cleavages may be seen in Fig 8. Fig 12 shows an instance in which stepwise slip occurred on the upper half of the cleavage during deformation subsequent to cleavage but

preceding final rupture. Apparently ferrite grain boundaries constitute a weak region where the cleavage extends through adjacent grains, as illustrated by Fig 13.

When more than one cleavage occurs in a ferrite grain, as on the left of Fig 8, the final path of fracture may include the several cleavages. In such a case the final rupture occurs by tearing between the cleavages, as indicated in Fig 14. The arrows indicate the torn edges.

In the absence of experimental observations, there has been an inclination

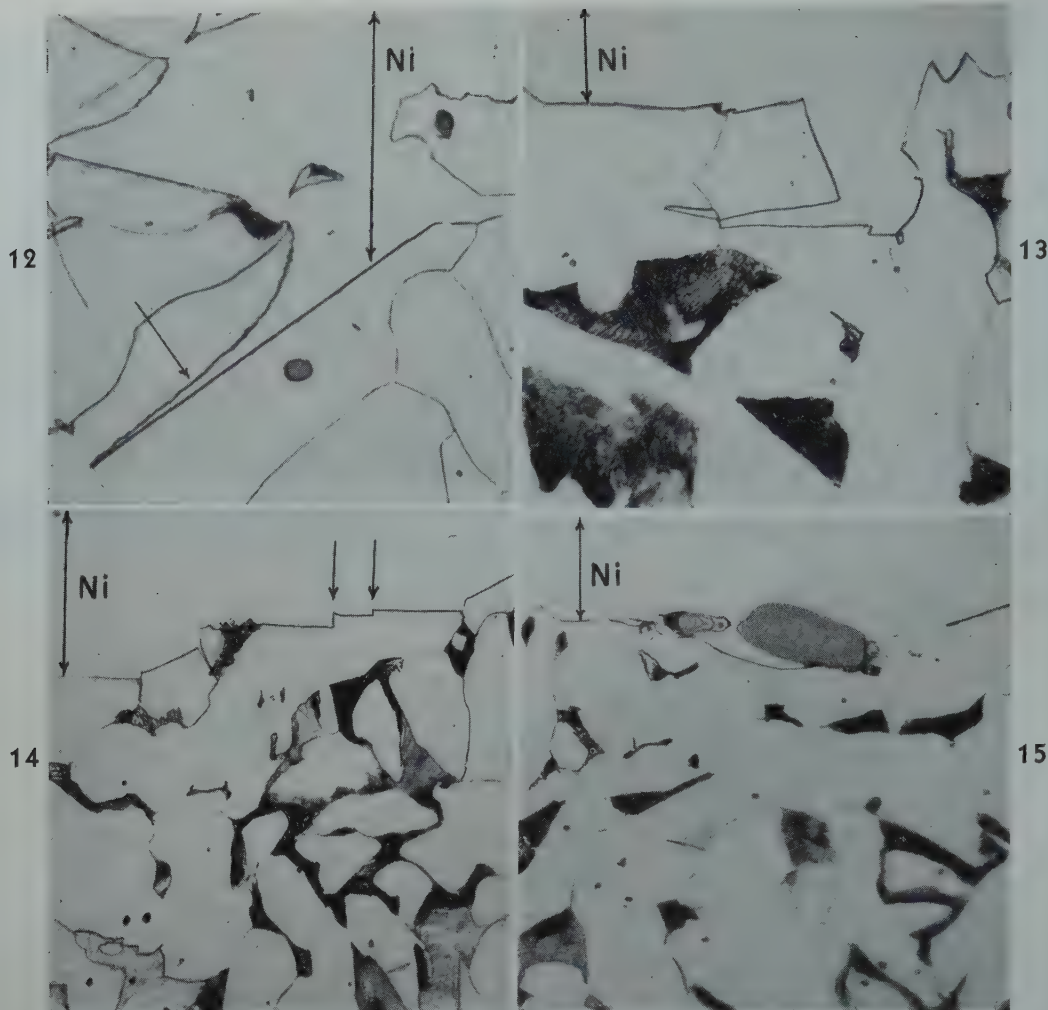


FIG 12—Evidence of stepwise slip that preceded final rupture in a 60 pct "brittle" fracture.
1200 X. Etchant 2 pct nital.

FIG 13—A 90 pct "brittle" fracture.

Cleavage in adjacent ferrite grains is joined by fracture along a grain boundary. 1000 X. Etchant 2 pct nital.

FIG 14—Example of tearing between cleavages as observed in a 30 pct "brittle" fracture.
500 X. Etchant 2 pct nital.

FIG 15—A (Mn, Fe)S inclusion adhering to a torn region of the fracture of an 80 pct "brittle" fracture.
500 X. Etchant 2 pct nital. Micrographs slightly reduced in reproduction.

on the part of some metallurgists to blame the initiation of "brittle" fracture on phases of little ductility such as carbides or nonmetallic inclusions. No evidence of this has been obtained in this study. On the contrary, the evidence suggests that the cleavage of ferrite initiates "brittle" fracture. To support this viewpoint are the observations of intact pearlite colonies, as in Fig 7 where the cleavage has involved ferrite grains on both sides of the pearlite colony.

There were far fewer inclusions than pearlite colonies in the steel, so that the opportunity to observe their role was limited; however, none of the observed ferrite cleavages could be definitely attributed to inclusions. The inclusions were as apt to be present in the torn regions between the cleavages as near the cleavages. Fig 15 shows a (Mn, Fe)S inclusion

still adhering to a torn region of the fracture. While the evidence presented here does not prove conclusively that cementite or inclusions do not initiate the cleavage, yet it seems sufficient to cast doubt on this explanation as the primary cause of the cleaving of ferrite in the impact test. More experimental observations are needed.

Shock twins occurred frequently near the fracture in specimens broken at the low temperature end of the transition, and grew infrequent and then practically disappeared as the testing temperature was raised. Thus a greater proportion of energy went into the formation of twins at the lower than at the higher testing temperatures. Typical shock twins are indicated by the arrows in Fig 16. There was no evidence that the observed ferrite cleavage follows the plane of shock twinning. This was to be antici-

pated from the work of others⁴ who have reported that the twinning and cleavage planes in ferrite are {112} and {100} respectively. The lack of coincidence is illustrated by Fig 16 in which the shock twins and a cleavage facet occur at a slight but definite angle with respect to each other. If the cleavage had resulted from weakness of lattice registry along the interface between the shock twin and the parent ferrite grain, one would not expect the structure shown in Fig 16.

Dependence of Transverse and Longitudinal Energy Values on Structure

This portion of the discussion is based on more limited observations than the foregoing description of the mode of fracture; however, it seems

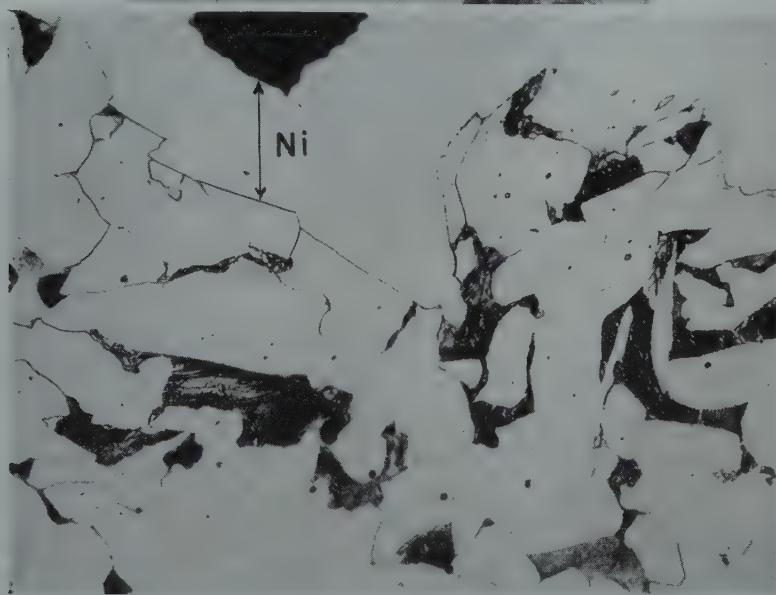
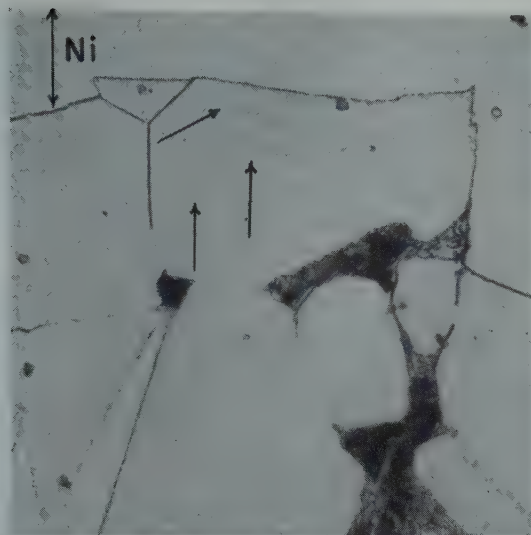


FIG 16—(above) The arrows indicate shock twins near the surface of a 90 pct "brittle" fracture.

Note that the shock twins and the cleavage facets occur at a slightly different angle.
1500 X. Etchant 2 pct nital.

FIG 17—(below) Evidence that cleavage is sometimes arrested by pearlite colonies.

500 X. Etchant 2 pct nital.

worthwhile to present it in an attempt to explain the differences between longitudinal and transverse energy values. It may be noted in Fig 1 that the energy curves for both longitudinal and transverse specimens start to rise at about the same testing temperature. Also, although the maximum energy values differ, both types of specimens reach their maximum energy value at about the same testing temperature. Furthermore, the macroscopic fracture appearance is similar for both longitudinal and transverse specimens at each testing temperature. These observations strongly suggest that the mechanism of the fracture is the same in both longitudinal and transverse specimens, but that the ease of fracture is altered by the well known anisotropy of rolled steel products such

as the structural shape used in this work. We believe that the explanation of the ease of fracture in the transverse specimens is to be found in the ferrite banding in the steel.

In Fig 4, ferrite cleavage occurs quite generally throughout the "brittle" region of the fracture. This is the case for both longitudinal and transverse specimens of 80 pct and 90 pct "brittle" fractures. There is not much divergence of the energy curves in Fig 1 with these fractures.

The situation is quite different with fractures from the middle of the transition. In these fractures ferrite cleavage is more prevalent in the ferrite bands, whereas the bands containing more pearlite show greater deformation before fracture. It may be that pearlite even arrests the

cleavage. There is some evidence for this, as illustrated by Fig 17, where the cleavage that ends in the pearlite colony has not advanced. Instead, the steel to the right of the cleavage has deformed considerably after the formation of the ferrite cleavage. Whether pearlite stops the cleavage may be open to some question, although it seems to be the case.

It has been shown already that ferrite cleavage constitutes the initial stage of the failure. Now, in the transverse specimens the uninterrupted bands of ferrite lie roughly parallel to the surface of final fracture, as illustrated by Fig 18. It seems reasonable to suppose that there would be more ferrite cleavage in these bands in the initial stages of fracture than in the rest of the structure. In this case the

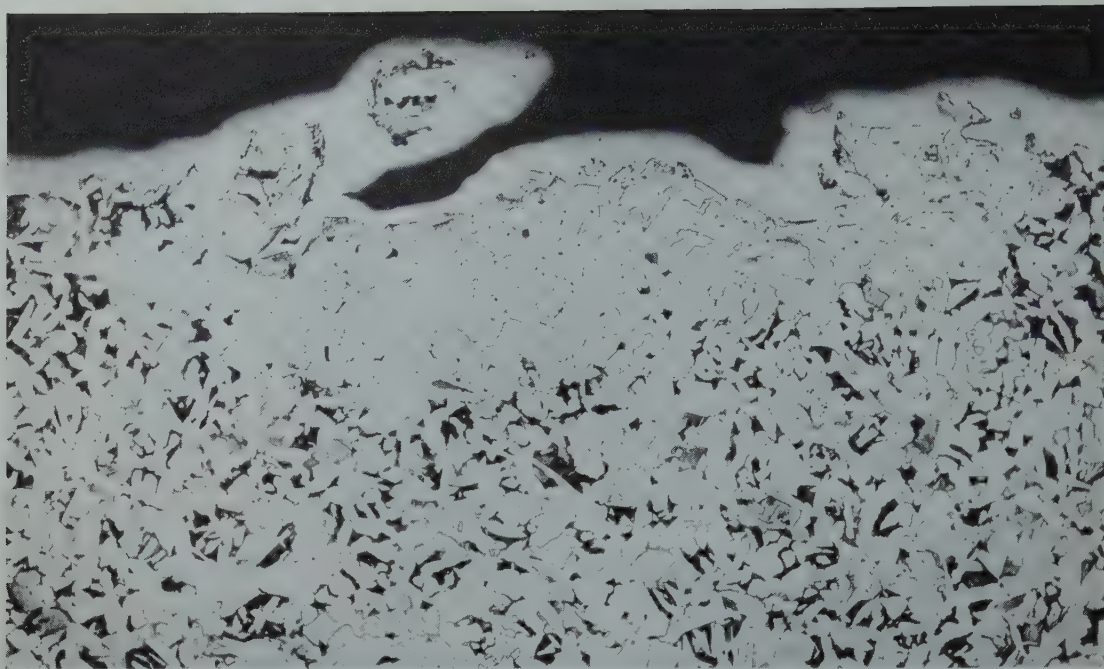


FIG 18—Cleavage in a ferrite band in a 50 pct "brittle" fracture of a transverse specimen.
100 X. Etchant 2 pct nital.

ferrite bands would form a potential path of fracture, only needing to be joined by rupture of the intervening bands that contain pearlite. This explanation assumes a greater amount of ferrite cleavage in the "brittle" part of the fracture of transverse specimens, in order that the absorbed energy of the transverse specimens be less than for the corresponding longitudinal specimen in the middle and upper portions of the transition range. This was not checked quantitatively because of the experimental difficulties involved, so that the above explanation is to be considered only as a reasonable assumption based on the observed mode of fracture.

Summary

It cannot be too strongly emphasized that the fractures that have been described were observed in impact specimens from a single structural steel shape. The essential details of the mode of fracture are thought to be common to mild steel of this type,

but more observations are needed to round out the general picture.

Throughout the transition revealed by the impact test, fracture in this steel was initiated by cleavage of ferrite grains situated in the general region of maximum triaxiality of stressing during the test. At the low temperature end of the transition, ferrite cleavage occurred during or soon after the end of elastic deformation. It was often accompanied or preceded by shock twinning of the ferrite. At higher testing temperatures within the transition, shock twinning gave way to deformation by slip. In the high temperature end of the transition, cold work apparently occurred both before and after the ferrite cleaved.

After the initiation of the fracture by ferrite cleavage, a second stage of the fracture consisted of opening up the ferrite cleavages and deformation and rupture of the metal between the cleavages. Deformation and rupture of the peripheral regions of the specimen also formed a part of the second stage of fracture.

The experimental observations sug-

gest that hard phases such as cementite and inclusions are not to blame for initiating ferrite cleavage in mild steel. In fact, there was some evidence that pearlite could arrest ferrite cleavage and confine it to a ferrite band, at least in the middle and the high temperature end of the transition.

The tendency for the initial ferrite cleavage to extend quite generally throughout the ferrite band and the directional extent of these bands in rolled mild steel products is offered as a possible explanation of the difference in the energy values obtained with longitudinal and transverse specimens.

References

1. I. R. Kramer, A. E. Ruark, W. J. Ferguson, H. L. Smith, G. A. Hornbeck, P. E. Shearin, R. M. Trimble and H. N. Michie: NRL report 0-2796, Nov. 22, 1946.
2. C. F. Tipper: *Jnl. Iron and Steel Inst.* (1948) **158**, Pt. 3, p. 335.
3. M. A. Grossmann: *Trans. AIME*, (1946) **167**, 39-79; *Mel. Tech.* (April 1946) TP 2020.
4. C. A. Zapffe and G. A. Moore: *Trans. AIME* (1943) **154**, 335.
5. C. S. Barrett, G. Ansel and R. F. Mehl: *Trans. ASM* (1937) **25**, 702-733.

Recovery and Recrystallization in Brass

B. L. AVERBACH,* Junior Member AIME

Recovery and primary recrystallization in cold worked metals are usually considered as two competing processes. Some of the effects which usually accompany recovery are: alleviation of stress corrosion tendencies, changes in thermal emf,¹ damping capacity,² electrical resistivity,² and magnetic properties,³ and only minor changes in hardness or the related strength properties. During primary recrystallization new unstrained grains are formed at the expense of the strained matrix. These new grains eventually become visible metallographically, and nucleation and growth kinetics have been indicated for this process.^{4,5}

Frequent attempts have been made to study the cold-working phenomenon by observations on the line broadening by X ray diffraction patterns. Relatively few measurements of line intensities have been made, although Brindley and his collaborators,^{6,7,8} by means of film techniques, compared the intensities of cold worked Cu, Ni, and Rh patterns with those from chemically precipitated powders. These precipitated powders were presumed to be strain free, and it was found that the intensities for the cold-worked materials progressively decreased as the Bragg angle increased except for the first line, where there was an increase due to reduction in extinction. This was interpreted as a randomness in atomic position induced by cold work. Such randomness is similar to that caused by thermal agitation and has been described as "frozen heat" displacement of 0.08–0.10 Å from the mean atomic position.

In a recent study⁹ on the effect of cold work in metals on their powder pattern intensities, the changes in integrated intensity for heavily cold worked alpha brass were observed as a function of the annealing temperature. These measurements were made with a manually operated Geiger-counter spectrometer using $\text{CuK}\alpha$ radiation monochromated with a rock salt crystal. Intensity measurements were made with a scaling meter over small intervals of angle, and the equipment

was so arranged that the diffracted and incident beams made equal angles with the specimen. Intensities could be compared directly by simply interchanging specimens, and comparisons from day to day were made with a standard whose line intensities did not change on aging. It was shown that a cold worked alpha brass standard was stable for at least a year.

Table 1 indicates the results of the integrated intensity measurements on a 70 Cu-30 Zn brass. In the sample preparation, a brass plate was first cold rolled 50 pct and then filed, screened to -325 mesh, compacted into briquettes at a pressure of 60,000 psi and finally annealed for one hour at various temperatures up to 400°C. The briquetting pressure did not seem to influence the integrated intensities, and most of the cold work was introduced by the filing. Although this method of cold work is not quantitative, it was used to obtain random orientation (and thus uniform diffraction lines) in order to make accurate measurements of integrated intensity. Back reflection patterns were taken in each case to check the uniformity of the lines, and from the observed line broadening it was apparent that this type of plastic deformation was quite severe.

Care was taken to traverse the entire background of the pattern and to assign to each peak the total intensity above this background. The bases of the diffraction lines were quite broad and spread out over several degrees, even for the narrow peaks. The theoretical intensities were calculated to include a temperature correction, a dispersion correction, and a Lorenz-

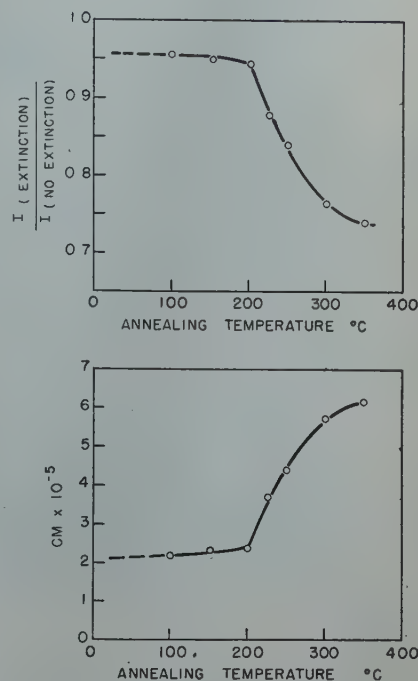


FIG 1—(above) Change of extinction coefficient with annealing temperature for cold worked brass (70 Cu-30 Zn).

FIG 2 (below)—Effective particle sizes calculated from extinction coefficients.

polarization factor corrected for the crystal monochromated beam. In Table 1 it was necessary to match the calculated and observed values at only one point, and the rest of the experimental values were converted directly to this arbitrary scale. The integrated intensities in Table 1 are listed in arbitrary units, and the accuracy was sufficient to reproduce any of the measured line intensities to within ± 1.5 units. It is evident that the percentage error on the strongest line (111) was quite low.

The calculated values and the observed intensities for the cold worked material matched reasonably well. As the annealing temperature was raised, however, the intensity of the strongest reflections, particularly the (111), decreased measurably. Since the background intensities of all of these patterns were identical, such behavior could be interpreted as a primary

Cleveland Meeting, October 1949.
TP 2636 E. Discussion of this paper (2 copies) may be sent to *Transactions AIME* before December 1, 1949. Manuscript received Feb. 28, 1949; revision received April 29, 1949.

* Assistant Professor, Department of Metallurgy, Massachusetts Institute of Technology, Cambridge, Mass.

¹ References are at the end of the paper.

Table 1 . . . Effect of Cold Work and Annealing on Integrated Intensities of X ray Diffraction Lines

| Brass (70 Cu-30 Zn)—Cold Worked at 25°C | | | | | | | | |
|---|------------------------|--------------------------|------|------|------|------|------|------|
| Line | Calculated Intensities | Annealing Temperature °C | | | | | | |
| | | 25 | 100 | 200 | 225 | 250 | 300 | 350 |
| (111) | 193 ↔ | 193 | 184 | 182 | 170 | 162 | 148 | 143 |
| (200) | 93.6 | 89.5 | 87 | 85 | 86 | 84 | 76 | 75 |
| (220) | 50.5 | 48 | 48 | 48 | 46 | 47 | 43.5 | 41 |
| (311) | 57.1 | 57.5 | 55 | 55 | 54 | 55 | 53 | 48 |
| (222) | 16.5 | 18.3 | 19.1 | 17.1 | 15.7 | 16.1 | 15.7 | 13.1 |
| (400) | 10.0 | 9.6 | 8.4 | 8.7 | 10.6 | 8.7 | 9.6 | 8.7 |

↔ Indicates where calculated and measured intensities were matched.

extinction effect, and it is apparent that cold work reduces this extinction considerably. The calculated values take no account of extinction, and the agreement between the cold worked and calculated intensities indicates that the deformation induced by filing was severe enough to practically eliminate extinction. The extinction coefficient, $\frac{I \text{ (with extinction)}}{I \text{ (without extinction)}}$, was calculated from the (111) lines, since the accuracy is greatest here, and these coefficients are plotted in Fig 1.* There is a sharp break at 200°C, and this sudden increase in extinction was subsequently associated with the onset of primary recrystallization.

The data presented in Table 1 are not sufficiently accurate to determine whether the intensities of the back reflection lines in the cold worked material were measurably lower than those of the annealed samples. The observations listed here were made in such a way as to accentuate the accuracy of the low angle high intensity lines. When more accurate intensity determinations were made in the high angle region,⁹ it was shown that both cold worked and annealed materials diffracted the same integrated intensity for the relatively weak (400) line if all of the intensity above the true background was considered. The determinations based on film measurements can suffer inherent difficulties in the comparison of intensities from one film to another, and in the determination of the true background. These discrepancies may be sufficient to account for the diminished intensity originally observed in the high angle lines of cold worked materials.

In order to determine the cause for the sudden change in the extinction curve in Fig 1, observations were made on the hardness, the half-maximum

diffraction line width, and on the metallographic structure. For the hardness test, the surfaces of the compacts were first given a metallographic polish with diamond dust and a large number of Tukon hardness readings were made on the individual filings at a load of 25 g. Although some scatter was obtained because of insufficient support under individual filings it was felt that the hardness readings from one specimen to another were comparable and the results are plotted in Fig 3. Each point in the figure is the average of at least five readings. The sharp dip in the hardness at about 225°C is usually taken as indicating the inception of primary recrystallization. Similarly the half-maximum line widths (plotted in minutes) also fall rapidly at about 225°C and this is indicated in Fig 4. It should also be noted that prior to this sharp dip the lines did not behave in uniform fashion, some lines increasing in width and others decreasing in width as the recovery temperature was raised.

From the microstructures, which are shown in Fig 5 and 6, it is difficult to determine the inception of recrystallization. Because of the heavy cold working the recrystallized grain size is very small and although there seems to be a subtle difference between the structures at 200 and 225°C, the strain-free grains are not observed in the microstructure until considerable growth has occurred. The X ray pattern first became spotty after a 400°C treatment and the microstructure in Fig 5 indicates that visible growth has occurred by then. The combined evidence can be taken, however, to indicate that recrystallization takes place starting at 225°C.

It is difficult to assign directly the cause for the reduction in primary extinction by plastic flow in a crystal. Above 200°C, recrystallization, and therefore grain growth, is involved and the extinction could be assumed to be a particle size effect. If the classical Darwin formula* is applied to these data one obtains an "effective particle size" of $2-6 \times 10^{-5}$ cm. These particle sizes are plotted in Fig 2 as a function of annealing temperature, and if the data are extrapolated below 100°C, one obtains an effective particle size of 2×10^{-5} cm at room temperature. Each of the measured particle sizes

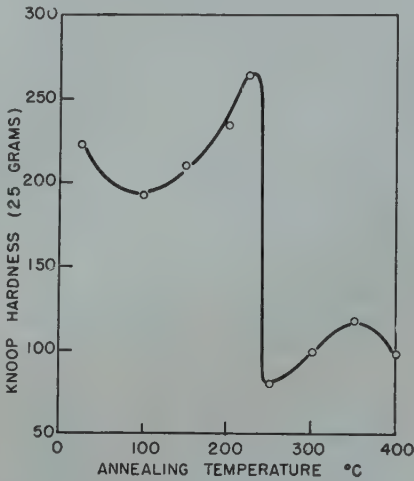


FIG 3—Tukon Hardness (25g load) of brass filings.

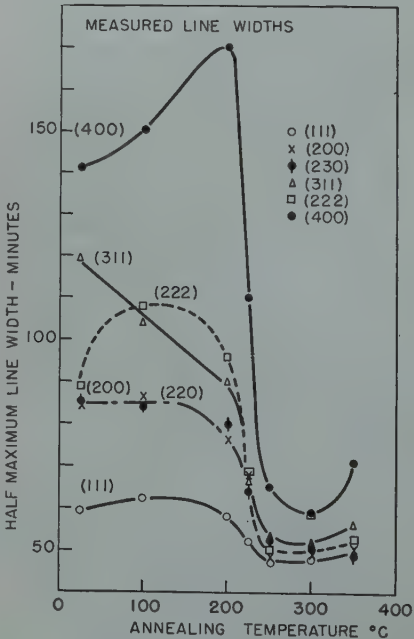


FIG 4—Change in half-maximum line widths with annealing temperature in brass (70 Cu-30Zn).

* The point at 150°C was determined from a measurement of the integrated intensity of the (111) line. The rest of the pattern was not measured and is, therefore, not listed in Table 1.

* $\frac{I \text{ (with extinction)}}{I \text{ (without extinction)}} = \frac{\tanh xq}{xq}$
 x = no. of planes taking part in the reflection
 q = reflected amplitude per lattice plane

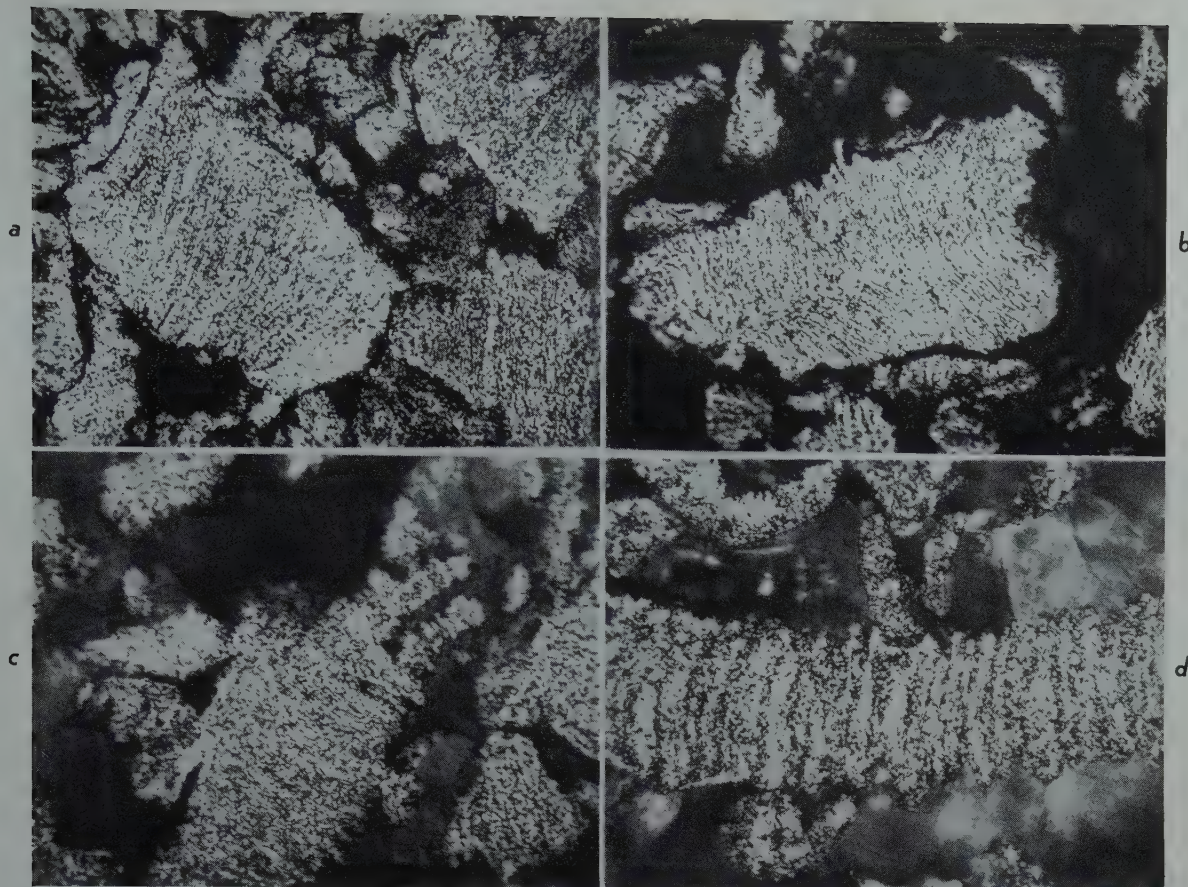


FIG 5—Micrographs of brass filings. 750 \times .

a. Cold worked. b. Annealed 1 hr at 150°C. c. Annealed 1 hr at 200°C. d. Annealed 1 hr at 225°C.

is accurate to at least one significant figure and if the experimental error in the measurement of the cold worked (111) line is computed it can be seen that the cold worked particle size is probably not smaller than 1×10^{-5} cm and is probably closer to the extrapolated value of 2×10^{-5} cm. If the recrystallized grain size is estimated at 400°C from the micrographs in Fig 6 one obtains about 20×10^{-5} cm. The X ray beam averages the extinction of both the cold worked and the annealed regions, so that for the entire specimen one obtains a weighted average value of about 7×10^{-5} cm and this fits the extrapolated X ray-values quite well.

The presence of a nonuniform strain, even if it is an elastic strain, can also reduce extinction in crystals. It would be possible, therefore, to ascribe at least part of the extinction effect to nonuniform strains introduced by the deformation. However, Heidenreich and Shockley,¹⁰ using an electron microscope technique obtained a particle size of about 0.2×10^{-5} cm in cold worked aluminum, and observed in addition a two stage process of

growth. The first stage consisted of a rather slow growth of a few small strain-free areas, and this corresponded to the usual recovery stage. In the second stage a very rapid growth of strain-free areas occurred and this is the phenomenon usually observed during recrystallization. It would be difficult to interpret Heidenreich's results in terms of an overall strain relief, so that it seemed reasonable to assume that the small change in extinction during the recovery stage could have been caused by the slow growth of strain free areas by a method entirely analogous to what is later called recrystallization. Some overall relief would also occur simultaneously. Since recrystallization is a process of nucleation and growth the early stage corresponds to a prolonged incubation period and it seems unnecessary to specify a separate mechanism for recovery. The data presented here, however, are not accurate enough to show definitely whether there is a slow growth of particle size during recovery, and a more extended study on materials with a greater temperature range for recovery is needed.

Table 2 . . . Broadening of X ray Diffraction Lines in Brass (70 Cu-30 Zn) Cold worked at 23°C and annealed for 1 hour at temperatures indicated.

| Line | θ° | Annealing Temperature °C | | | | |
|-------|----------------|--------------------------------|-----|-----|-----|-----|
| | | 25 | 100 | 200 | 225 | 250 |
| | | Reduced Line Widths— (min.) | | | | |
| (111) | 21°10' | 36 | 39 | 33 | 20 | 0 |
| (200) | 24°35' | 68 | 70 | 58 | 30 | 0 |
| (220) | 36°10' | 80 | 68 | 63 | 40 | 14 |
| (311) | 43°47' | 101 | 90 | 74 | 44 | 15 |
| (222) | 46°20' | 72 | 91 | 77 | 36 | |
| (400) | 56°30' | 118 | 138 | 157 | 94 | 30 |

These data do indicate, however, that the most important process during the recovery stage may not be stress relief. If any substantial stress relief had occurred, it would have been reflected in a rather large change in extinction coefficient prior to recrystallization. Since the extinction remained virtually constant during recovery, it is suggested that the mechanism of recovery consists of the slow growth of existing strain free nuclei with a linear dimension of about 2×10^{-5} cm.

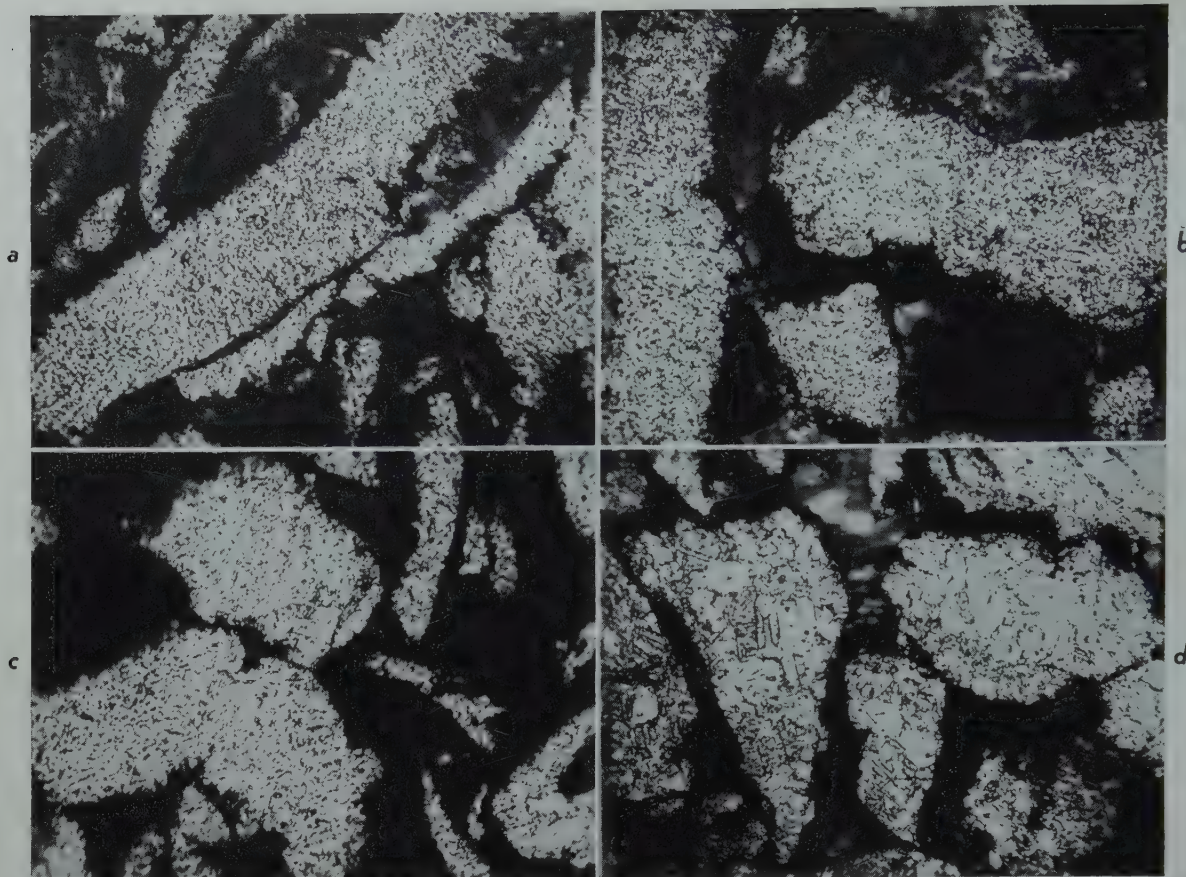


Fig 6—Micrographs of brass filings. 750 X.

a. Annealed 1 hr at 250°C. b. Annealed 1 hr at 300°C. c. Annealed 1 hr at 350°C. d. Annealed 1 hr at 400°C.

The line broadening observed for these cold worked materials is also consistent with such an interpretation. Perfect crystals have a very narrow range of perfect reflection, but if the crystal is cold worked, the intensity distribution can be taken as an indication of the deviation from ideality of the radial distance to successive nearest neighbors. As recrystallization starts, certain small regions become strain-free, they reflect sharply, and the line broadening decreases.

The half-maximum line widths were reduced to include only the broadening due to cold work by assuming that the lines at 300°C and beyond did not contain cold work broadening. Then: B (due to cold work)

$$= \sqrt{B^2 (\text{cold worked}) - B^2(300^\circ\text{C})}$$

and the resulting line widths are shown in Table 2. It has been suggested that the cold-work broadening should be a linear function of $\tan \theta$, and Fig 7 indicates that there is too much scatter in the data to check this concept. Greater precision in line widths is needed to put this phase of the work on a more satisfactory basis.

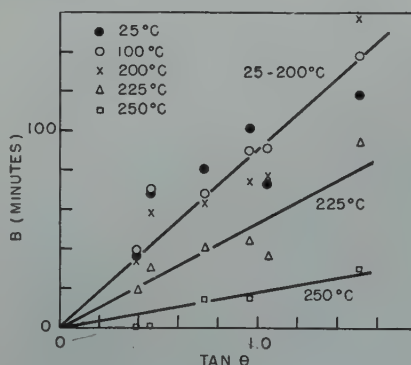


FIG 7—Line broadening due to cold work in brass (70 cu-30 Zn).
Annealed 1 hr at temperatures indicated.

Summary

On the basis of X ray extinction measurements it is concluded that recovery may be a process analogous to recrystallization. It is possible that small strain-free grains are formed during recovery, and that recrystallization is observed to occur when there is a rapid growth in the size of these strain-free regions. Recovery and recrystallization could then be two stages of the same process, and it would seem unnecessary to prescribe a separate mechanism, such as strain relief, for the recovery stage.

Acknowledgments

The author would like to express his appreciation to Professor B. E. Warren for his many helpful suggestions during the course of this investigation, and to Mr. Sergei Lorris and Mr. William Clancy for their assistance in obtaining the data.

References

1. G. W. Brindley: Rep. Conf. Strength Solids. Phys. Soc. (1948).
2. J. T. Norton: *Trans. AIME* (1940) 137, 49.
3. J. K. Stanley: *Trans. AIME* (1945) 162, 106.
4. W. A. Anderson and R. F. Mehl: *Trans. AIME* (1945) 164, 140.
5. M. Cook and T. L. Richards: *Jnl. Inst. Met.* (1946) 73, 1.
6. G. W. Brindley and F. W. Spiers: *Phil. Mag.* (1935) 20, 882, 893.
7. G. W. Brindley and P. Ridley: *Proc. Phys. Soc. (London)* (1938) 50, 501.
8. G. W. Brindley: *Proc. Phys. Soc. (London)* (1940) 52, 117.
9. B. L. Averbach and B. E. Warren: (in the press).
10. R. D. Heidenreich and W. Shockley: Rep. Conf. Strength Solids. Phys. Soc. (1948).

Ferromagnetic Alloys in the Systems Cu-Mn-In and Cu-Mn-Ga*

F. A. HAMES,† Junior Member and D. S. EPPELSHEIMER,‡ Member, AIME

The ferromagnetic copper-manganese-aluminum and copper-manganese-tin alloys (Heusler alloys) owe their ferromagnetism to the beta phases (body-centered cubic structure) in their respective systems.^{1,2,3} The ternary beta phase regions in these systems are extensions of the beta fields of the binary copper-aluminum and copper-tin systems into the ternary models of the copper-manganese-aluminum and copper-manganese-tin systems respectively.

X ray analysis has indicated the presence of long-range order in the more strongly magnetic alloys.^{3,4,5} The ideal ordered structure is obtained in alloys of compositions Cu_2MnAl and Cu_2MnSn ; the copper atoms occupy positions at cube centers while the aluminum (tin) and manganese atoms alternate at cube corners. This atomic arrangement is illustrated in Fig 1. The compositions Cu_2MnAl and Cu_2MnSn are also those that show maximum magnetic saturation moment.^{3,4,6,7} Departures from these compositions result in a decrease in the degree of order attainable and a decrease in magnetic saturation moment.

In view of the chemical similarities of aluminum, tin, indium, and gallium, and the existence of beta phases in the binary systems copper-indium and copper-gallium, it may be suspected that ternary beta phases exist in the systems copper-manganese-indium and copper-manganese-gallium, and that these are ferromagnetic. The purpose

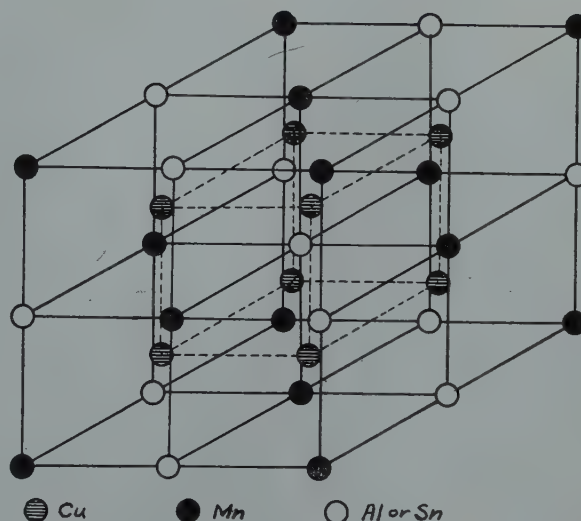


FIG 1—Atomic Arrangement in Ordered Beta Cu_2MnAl and Cu_2MnSn .

Cleveland Meeting, October 1949. TP 2600 E. Discussion of this paper (2 copies) may be sent to *Transactions AIME* before December 1, 1949. Manuscript received December 6, 1948.

* A part of a thesis submitted by F. A. Hames to the Graduate School of the University of Missouri in partial fulfillment of the requirements for the degree of Doctor of Philosophy, July, 1948.

† Assistant Professor of Metallurgy, The University of British Columbia, Vancouver, B.C., Canada. Formerly Research Fellow in Metallurgy, Missouri School of Mines and Metallurgy, Rolla, Mo.

‡ Professor of Metallurgical Engineering, Missouri School of Mines and Metallurgy, Rolla, Mo.

¹ References are at the end of the paper.

of this investigation was to determine whether ferromagnetic beta phases exist in the systems copper-manganese-indium and copper-manganese-gallium analogous to the ferromagnetic beta phases in the systems copper-manganese-aluminum and copper-manganese-tin.

Previous Work

At the time this investigation was started no information could be found regarding the constitution of copper-manganese-indium and copper-manganese-gallium alloys, nor of the binary manganese-indium and man-

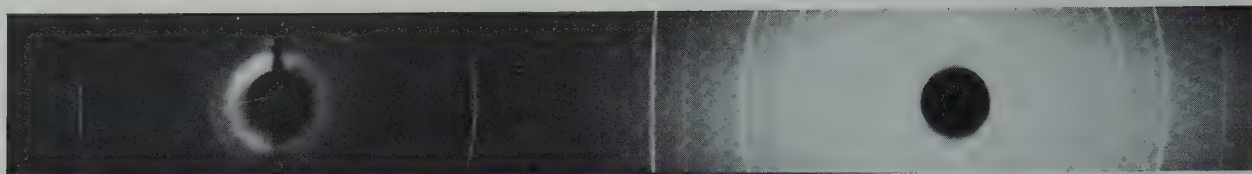


FIG 2—X ray Diffraction Pattern of Copper-Manganese-Indium Alloy I-1, Quenched from 500°C.

ganese-gallium alloys. The general features of the equilibrium diagrams of the systems copper-indium and copper-gallium are known however, and these are next considered with special reference to the beta phase fields.

SYSTEM COPPER-INDIUM

Weibke and Eggers have worked out a constitution diagram for the copper-indium system on the basis of thermal, microscopic, and X ray studies.⁸ These investigators showed by X ray analysis that the beta phase in this system has the body-centered cubic structure. Powder diffraction photographs of quenched beta alloys taken at room temperature showed extra diffraction lines indicative of a superlattice.

Hume-Rothery and coworkers re-investigated the beta phase area in the copper-indium system,⁹ their beta phase field boundaries being in good agreement with those of Weibke and Eggers. High temperature X ray powder photographs taken by Hume-Rothery and coworkers of alloys in the homogeneous beta area showed only the lines to be expected from a simple body-centered cubic structure. They concluded that the extra lines on the films of Weibke and Eggers are characteristic of quenched alloys, rather than of the actual structure at high temperatures.

SYSTEM COPPER-GALLIUM

Weibke has published a constitution diagram for the copper-gallium system based on thermal, microscopic, and X ray studies.¹⁰ Weibke reported a beta phase having a body-centered cubic structure, but that the beta copper-gallium alloys particularly resemble beta copper-aluminum alloys in that the structure of quenched alloys depends on the cooling velocity.

Hume-Rothery and Raynor¹¹ re-examined the constitution of copper-gallium alloys in the region 18–32 at. pct of gallium and published a diagram which shows a high temperature

Table 1 . . . Composition of Alloys Studied

| Alloy Designation | Weight Pct | | | |
|-------------------|------------|------|------|------|
| | Cu | Mn | In | Ga |
| I-1 | 42.5 | 18.0 | 39.5 | |
| G-1 | 49.5 | 21.6 | | 28.9 |
| G-2 | 62.3 | 13.0 | | 24.7 |
| G-3 | 57.8 | 16.0 | | 26.2 |

beta phase having boundaries that agree well with those of Weibke. Hume-Rothery and Raynor reported that the beta structure is retained by quenching from the homogeneous beta area only in alloys containing 22.5–23.8 at. pct of gallium. Beta alloys lying outside these composition limits decomposed on quenching. The same investigators also reported two modifications of the beta phase which they designated as beta' and beta'', and suggested that a third modification exists below 420°C.

In later papers by Hume-Rothery and coworkers,^{9,12} it appears that they have combined the beta' and beta'' fields in a single field, representative of the beta phase (close-packed hexagonal structure). High temperature X ray powder photographs taken by these investigators showed that the beta phase has a simple body-centered cubic structure. They call attention to the fact that experiments with quenched alloys may give quite misleading results and point to the existence of a non-equilibrium phase having a simple close-packed hexagonal structure in alloys quenched from the homogeneous beta area.

Experimental

Alloys were prepared from copper of 99.99 pct purity; indium of 99.97 pct purity; Eagle-Picher gallium (purity not specified); and vacuum-sublimed or electrolytic manganese, both of 99.96 pct purity. The electrolytic manganese was treated for removal of hydrogen by heating at 500°C for

one hour in a silica tube under a vacuum of 20 microns.¹³

One copper-manganese-indium alloy and three copper-manganese-gallium alloys were prepared and studied. The alloys were analyzed for copper and manganese and indium and gallium contents were obtained by difference. Analyses are listed in Table 1.

Alloy I-1 was prepared by melting indium and copper-manganese master alloy (composition Cu₂Mn) in an aluminum thimble under a vacuum of 17 microns, with the use of a high-frequency induction coil. Alloy G-1 was prepared by melting copper, manganese, and gallium together in an aluminum thimble under helium. Alloys G-2 and G-3 were prepared by remelting portions of alloy G-1 with added copper in evacuated Vitreosil tubes.

The compositions of alloys I-1 and G-1 were intended to correspond to atomic proportions Cu₂MnIn and Cu₂MnGa, respectively. Actual compositions as listed in Table 1 correspond to atomic proportions Cu_{2.00}Mn_{0.952}In_{1.00} and Cu_{1.97}Mn_{1.00}Ga_{1.05}.

Alloy specimens for heat treatment were sealed in evacuated pyrex glass or Vitreosil tubes and heated in an electric pot furnace. Temperatures below 200°C were measured with a mercury thermometer, and temperatures above 200°C with a chromel-alumel thermocouple calibrated against the melting points of lead, zinc, and antimony. Temperature was adjusted by a Variac and was held within 10° of the desired temperature.

Powder diffraction photographs were taken with the Straumanis technique in a cylindrical camera of 57.3 mm diam. Unfiltered iron-K radiation from a Baird Associates X Ray Diffraction Unit was used. Powders were prepared from lump-annealed specimens and the powders were annealed as specified. The powder specimen was mounted in the camera on a glass fiber with the aid of vaseline, and rotated during exposure.

Approximate values of specific satu-

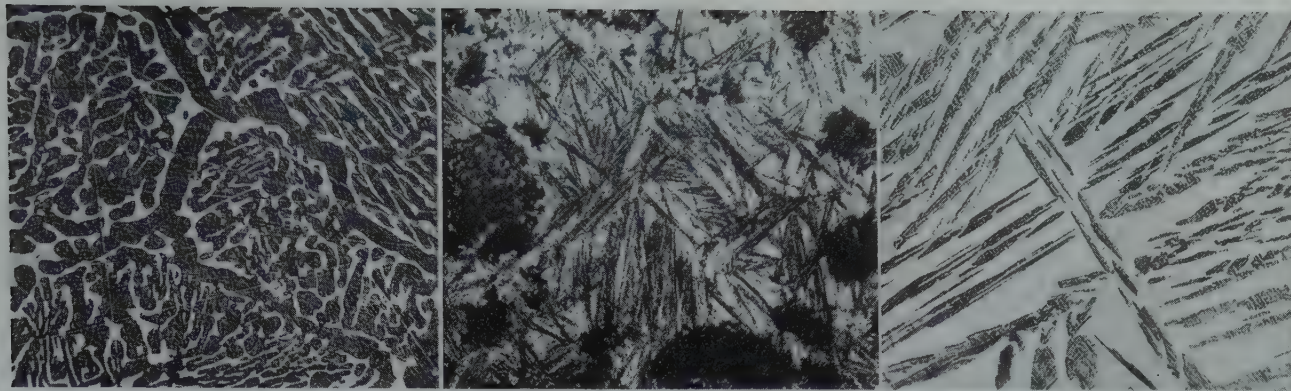


FIG 3—(left) Copper-Manganese-Gallium Alloy G-1, Quenched from 500°C. 100 X
Potassium Dichromate Etch.

FIG 4—(center) Copper-Manganese-Gallium Alloy G-2, Quenched from 750°C. 100 X
(Black Spots are Holes.) Alcoholic FeCl₃-HCl Etch.

FIG 5—(right) Copper-Manganese-Gallium Alloy G-3, Cooled in Furnace from 750°C. 100 X
Potassium Dichromate Etch.

ration intensity of magnetization were measured at room temperatures with a magnetic balance constructed from an old magnetic ore separator. The balance is similar in design to balances used by Fereday,¹⁴ Buehl and Wulff,¹⁵ and Carapella.¹⁶ The force per unit mass exerted on a small specimen placed in an inhomogeneous magnetic field is compared with the force per unit mass exerted on a standard specimen, in this case electrolytic nickel of 99.95 pct purity. The balance was arranged so that the force was exerted vertically and the force was measured with an analytical balance.*

Results and Discussion

SYSTEM COPPER-MANGANESE-INDIUM

The copper-manganese-indium alloy,

* For details concerning the magnetic balance, see thesis.

Table 2 . . . X ray Diffraction Data
for Ferromagnetic Cu-Mn-In
Alloy I-1

| Radiation | hkl | dobs. | dcalc | Intensity | |
|--------------|------------------------|--------|--------|-----------|--------------------|
| | | | | Observed | Relative $F^2_p U$ |
| FeK α | \dagger 111 | 3.592 | 3.583 | w | 9.2 |
| α | \dagger 200 | 3.108 | 3.103 | ww | 2.0 |
| β | *220 | 2.196 | 2.194 | ww | 85.0 |
| α | *220 | 2.190 | | s | |
| β | \dagger 311 | 1.868 | 1.871 | ww | 4.5 |
| α | \dagger 311 | 1.868 | | w | |
| α | *222 | 1.790 | 1.792 | ww | 0.5 |
| α | *400 | 1.548 | 1.552 | m | 26.0 |
| α | \dagger 331 | 1.420 | 1.423 | w | 2.0 |
| α | \dagger 420 | 1.395 | 1.388 | ww | 0.6 |
| α | *422 | 1.266 | 1.267 | m | 33.0 |
| α | \dagger {511 333} | 1.194 | 1.194 | w | 2.0 |
| β | *440 | 1.096 | | ww | 19.0 |
| α | *440 | 1.098 | 1.097 | m | |
| α_1 | \dagger 531 | 1.049 | | w | 4.2 |
| α_2 | \dagger 531 | 1.049 | 1.049 | ww | |
| α_1 | \dagger {600 442} | 1.034 | 1.034 | w | 1.5 |
| α_2 | \dagger {600 442} | 1.037 | 1.034 | ww | |
| α_1 | *620 | 0.9814 | 0.9813 | ss | 100.0 |
| α_2 | *620 | 0.9812 | | w | |

* Fundamental (body-centered cubic) lines.

\dagger Superstructure lines.

I-1, was magnetic as prepared. Homogenized for three days at 500°C and quenched, this alloy was magnetic, and under the microscope appeared to consist of a single phase. The specimen was badly cracked and preparation of a suitable metallographic specimen was difficult.

Fig 2 shows the X ray diffraction pattern obtained from a powder specimen of alloy I-1 quenched from 500°C, and Table 2 summarizes the diffraction data for this alloy. Reflections were found which correspond to those expected for an ordered body-centered cubic structure with $a_0 = 6.206$ Å. This alloy appears to be structurally analogous to the ferromagnetic beta phases in the systems copper-manganese-aluminum and copper-manganese-tin. Following the analogy, an alloy of composition Cu₂MnIn, when fully ordered, would have an atomic arrange-

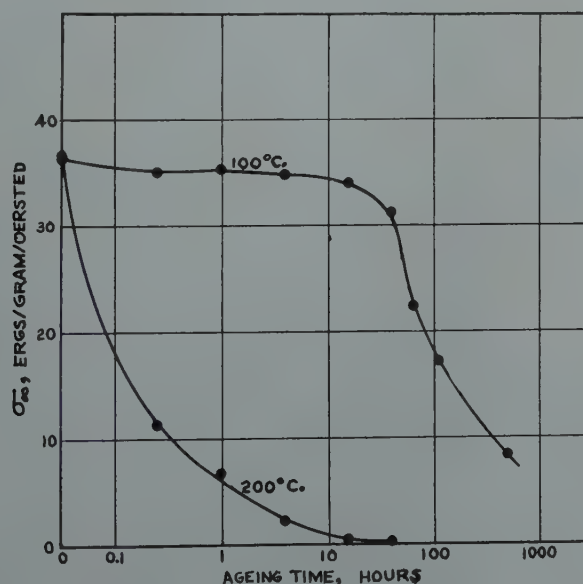


FIG 6—Effect of Aging on Saturation Magnetization of
Copper-Manganese-Gallium Alloy G-3.

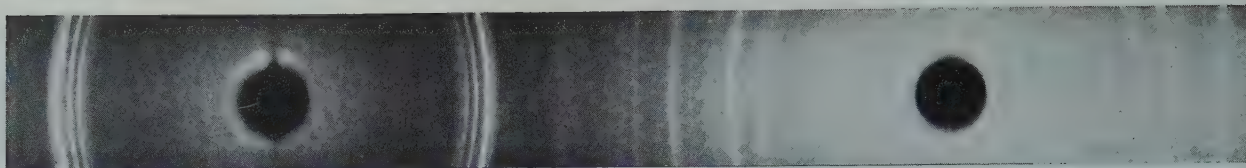


FIG 7—X ray Diffraction Pattern of Copper-Manganese-Gallium Alloy G-3, Quenched from 750°C.

ment like that shown in Fig 1 with indium atoms in place of aluminum (tin) atoms. This structure is based on space group O_h -Fm3m. Relative intensities were calculated as being proportional to $F^2 p U$, where F is the structure factor, p is the multiplicity factor, and U is the Lorentz-polarization factor. These are listed in Table 2 together with visually estimated intensities for comparison. With the data at hand, nothing quantitative can be said about the degree of order in this alloy. It is certainly not fully ordered as it is deficient in manganese (composition $Cu_{2.00}Mn_{0.952}In_{1.00}$.)

After the present work was practically completed, the authors discovered an article by Valentiner and Pusicha¹⁷ concerning the system aluminum-indium, in which mention was made of a ferromagnetic copper-manganese-indium alloy of composition Cu_2MnIn having the same structure as beta Cu_2MnAl and Cu_2MnSn . In a later brief paper,¹⁸ Professor Valentiner has summarized his findings regarding the copper-manganese-indium system. He states that the composition Cu_2MnIn shows the highest intensity of magnetization. The structure is the same as that of Cu_2MnAl and Cu_2MnSn , with $a_0 = 6.2 \text{ \AA}$. This alloy has a very small hysteresis and coercive force (less than 0.4 oersted). The specific electrical resistivity is about three times as great as that of iron. The alloy is very brittle. The Curie temperature is about 270°C. Thermal treatment has but a very slight effect on the magnetic properties of copper-manganese-indium alloys, in contrast to the behavior of the copper-manganese-aluminum and copper-manganese-tin alloys.

SYSTEM COPPER-MANGANESE-GALLIUM

The copper-manganese-gallium alloy G-1 was not magnetic as prepared, and a series of heat treatments was therefore carried out to determine whether it could be rendered magnetic. Specimens were quenched from temperatures between 500°C and 750°C and aged at 100°C and 200°C for times

Table 3 . . . X ray Diffraction Data for Alloy G-3, Quenched from 750°C

| Intensity | Radiation | d |
|-----------|-------------|-------|
| ww | $FeK\alpha$ | 2.446 |
| ww | β | 2.294 |
| m | α | 2.286 |
| ww | β | 2.122 |
| s | α | 2.127 |
| m | β | 2.019 |
| ss | α | 2.018 |
| m | α | 1.968 |
| m | α | 1.556 |
| m | α | 1.532 |
| m | α | 1.371 |
| ww | β | 1.328 |
| m | α | 1.335 |
| ww | β | 1.292 |
| s | α | 1.295 |
| s | α | 1.207 |
| w | α | 1.148 |
| m | α | 1.135 |
| ss | α | 1.108 |
| m | α | 1.076 |
| w | β | 1.062 |
| m | α | 1.067 |
| w | α | 1.011 |

ranging up to 110 hr following quenching. Saturation magnetization was measured after quenching and at intervals during aging.

The specimens were only feebly magnetic, as quenched, and the effect of aging on magnetization was very slight. A notable exception was a specimen quenched from 650°C. This had a saturation magnetization about $2\frac{1}{2}$ pct of that of nickel as quenched. Aging at 100°C for 110 hr doubled this value while aging at 200°C reduced this value ten-fold.

All quenched specimens showed two constituents under the microscope. Fig 3 shows a typical microstructure. In view of the feeble magnetism of alloy G-1 and the complexity of interpretation of the microstructure, this alloy was abandoned. The composition of alloy G-1 corresponds to atomic proportions $Cu_{1.97}Mn_{1.000}Ga_{1.05}$. It will be a matter of interest to determine whether an alloy of exact composition Cu_2MnGa ever exists as a single phase, analogous to the beta phases of compositions Cu_2MnAl , Cu_2MnSn , and Cu_2MnIn .

Alloys G-2 and G-3 were prepared by remelting portions of alloy G-1 with added copper. After homogenizing for 15 hr at 750°C the alloys were quenched in water and examined under the microscope. Both alloys showed an acicular (martensitic) structure and there was

no evidence of the presence of more than one constituent. This is illustrated in Fig 4.

Both alloys G-2 and G-3 were magnetic after quenching. Experiments were carried out on alloy G-3 to determine the effect of certain heat treatments on magnetization. A portion of this alloy, when cooled in the furnace, became nonmagnetic and under the microscope had the appearance of Fig 5. A transformation is indicated. This behavior is similar to that of slowly cooled copper-manganese-aluminum and copper-manganese-tin ferromagnetic beta alloys.

Specimens of the quenched G-3 alloy were aged at 100°C and 200°C, and magnetization measured at intervals. The magnetization of the specimen aged at 200°C decreased with aging time, and after 40 hr was very feebly magnetic. The effect of aging at 100°C was also to cause a decrease in magnetization but at a slower rate. This behavior is shown graphically in Fig 6.

X ray diffraction photographs were taken of powder specimens of alloy G-2 and G-3, quenched from 750°C. Similar patterns were obtained for the two alloys. Fig 7 shows the pattern for alloy G-3 and Table 3 lists interplanar spacings and visually estimated line intensities for this pattern.

The diffraction patterns could not be interpreted satisfactorily. In particular, no combination of lines could be found which is reconcilable with lines to be expected from a body-centered cubic structure, simple or ordered. The occurrence of martensitic structures in quenched alloys (Fig 4) suggests strongly that the high temperature equilibrium structure is not retained by quenching. The acicular structure of quenched beta copper-gallium alloys has been noted by Hume-Rothery and Raynor,¹¹ and it is quite possible that this behavior persists in the ternary beta copper-manganese-gallium alloys. Also, Weibke¹⁰ noted the resemblance of beta copper-gallium alloys to beta copper-aluminum alloys which are known to develop martensitic structures on quenching.¹⁹

It is therefore suggested that the quenched alloys G-2 and G-3 consist of a transition phase derived from the beta phase of the system copper-manganese-gallium, the beta phase being stable at high temperatures but not retained by quenching. This description is based on indirect evidence: by analogy with beta copper-gallium and copper-aluminum alloys. It should be possible to clarify the structure of the ferromagnetic copper-manganese-gallium alloys with the aid of high temperature X ray diffraction data.

Summary

A ferromagnetic copper-manganese-indium alloy has been prepared having an ordered body-centered cubic structure, and it is probably structurally analogous to the ferromagnetic beta copper-manganese-aluminum and copper-manganese-tin alloys (Heusler alloys).

Ferromagnetic copper-manganese-gallium alloys have been prepared. An alloy of composition $\text{Cu}_{1.97}\text{Mn}_{1.000}\text{Ga}_{1.05}$ variously heat treated is feebly magnetic and has a two-phase structure. It is questionable whether an alloy of the exact composition Cu_2MnGa ever exists as a single phase analogous to the beta phases of compositions Cu_2MnAl , Cu_2MnSn , and Cu_2MnIn .

With higher copper contents, quenched copper-manganese-gallium alloys are strongly magnetic. Quenched alloys show martensitic structures and are tentatively described as consisting of a transition phase derived from the beta phase of the system copper-manganese-gallium, the beta phase being stable at high temperature but not

retained by quenching. Quenched alloys lose their magnetism on aging. Slowly cooled alloys also lose their magnetism, and this loss is correlated with a transformation which is observable under the microscope.

Acknowledgments

Grateful acknowledgment is made of metal donations from the following companies: The Indium Corporation of America (indium); The Electro Manganese Corporation (electrolytic manganese); The Eagle-Picher Company (gallium); and The National Research Corporation (copper).

One of the authors (F. A. H.) is grateful to the Board of Curators of the University of Missouri for the award of a Research Fellowship at the Missouri School of Mines and Metallurgy.

References

1. O. Heusler: Zur Kenntnis der Heuslerschen Legierungen: Über das Mangan-Aluminium-Kupfer. *Ztsch. anorg. Chem.* (1928) **171**, 126.
2. H. H. Potter: The X-Ray Structure and Magnetic Properties of Single Crystals of Heusler Alloy. *Proc. Phys. Soc.* (1929) **41**, 135-142.
3. L. A. Carapella and R. Hultgren: The Ferromagnetic Nature of the Beta Phase in the Copper-Manganese-Tin System. *Trans. AIME* (1942) **147**, 232-242.
4. O. Heusler: Kristallstruktur und Ferromagnetismus der Mn-Al-Cu-Legierungen. *Ztsch. Metallkunde* (1934) **25**, 274-277.
5. A. J. Bradley and J. W. Rodgers: The Crystal Structure of the Heusler Alloys. *Proc. Roy. Soc. (A)* (1934) **144**, 340-359.
6. F. Heusler and E. Take: The Nature of the Heusler Alloys. *Trans. Faraday Soc.* (1912) **8**, 169.
7. E. Take and A. Semm: Magnetische

Messungen von den Heuslerschen Zinn-Mangan Bronzen. *Verh. der deut. phys. Gesell.* (1914) **16**, 971.

8. F. Weibke and H. Eggers: Das Zustandsdiagramm des Systems Kupfer-Indium. *Ztsch. anorg. Chem.* (1934) **220**, 273-292.
9. W. Hume-Rothery, G. V. Raynor, P. W. Reynolds, and H. K. Packer: Constitution and Structure of Alloys of Intermediate Composition in the Systems Copper-Indium, Copper-Aluminum, Copper-Germanium, Silver-Aluminum, and Silver-Germanium. *Jnl. Inst. Metals*, (1940) **66**, 209-239.
10. F. Weibke: Das Zustandsdiagramm des Systems Kupfer-Gallium. *Ztsch. anorg. Chem.*, (1934) **220**, 293-311.
11. W. Hume-Rothery and G. V. Raynor: The Constitution of the Copper-Gallium Alloys in the Region 18 to 32 Atomic Per Cent of Gallium. *Jnl. Inst. Metals*. (1937) **61**, 205-222.
12. W. Hume-Rothery, P. W. Reynolds, and G. V. Raynor: Factors Affecting the Formation of 3/2 Electron Compounds in Alloys of Copper, Silver, and Gold. *Jnl. Inst. Metals*, (1940) **66**, 191-207.
13. E. V. Potter, E. T. Hayes, and H. C. Lukens: Hydrogen Content of Electrolytic Manganese and Its Removal. *Trans. AIME* (1945) **161**, 373-381.
14. R. A. Fereday: Measurements of Magnetic Susceptibilities at High Temperatures. *Proc. Phys. Soc.*, (1934) **46**, 214-230.
15. R. Buehl and J. Wulff: A Simple Magnetic Apparatus for Phase Transformation Studies of Ferrous Alloys. *Rev. Sci. Inst. N.S.* (1938) **9**, 224-228.
16. L. A. Carapella: The Ferromagnetic Nature of the Beta Phase in the Copper-Manganese-Tin System. Doctor's Thesis, Harvard Univ., 1941.
17. S. Valentinier and I. Pusicha: Das System Aluminium-Indium. *Metallforschung* (1947) **II-4**, 127.
18. S. Valentinier: Über den Ersatz des Aluminiums und des Zinns durch Indium in den Heuslerschen Legierungen. *Naturwissenschaften* (1947) **4**, 123.
19. A. B. Greninger: The Martensite Transformation in Beta Copper-Aluminum Alloys. *Trans. AIME* (1939) **133**, 204-227.

Effect of Carbon and Nitrogen on Temper Brittleness

D. C. BUFFUM,* L. D. JAFFE,* Junior Member AIME, and W. P. CLANCY*

Many earlier workers have suggested that the temper brittleness of steel is associated with the presence of carbon or nitrogen.† Nevertheless, no investigations on the effect of removal of these elements upon susceptibility to temper brittleness have been published. It was therefore decided to determine whether temper brittleness would develop in an iron alloy contain-

ing very little carbon and nitrogen. The alloy,‡ in the form of a 10-lb ingot, was prepared by melting purified materials under argon. Its composition, in per cent, was:

| C | Mn | Si | S | P | Ni | Cr | Mo | N | O | H |
|-------|------|-------|-------|-------|------|------|-------|--------|-------|---------|
| 0.003 | 0.80 | 0.020 | 0.005 | 0.002 | 1.49 | 0.61 | 0.002 | 0.0004 | 0.017 | 0.00006 |

This analysis, except for carbon content, is within the specified range for SAE 3140, which has been demonstrated by previous work at this laboratory² to be markedly susceptible to

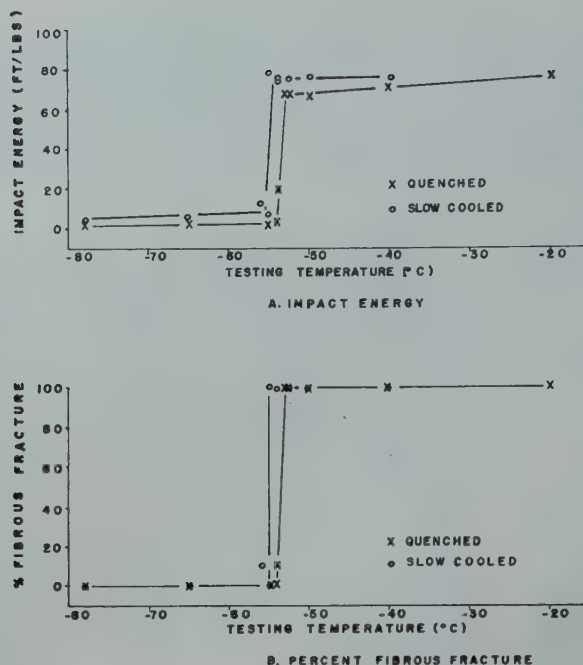


FIG 1—Toughness vs. testing temperature curves for alloy of S.A.E. 3100 composition with 0.003 pct carbon.

temper brittleness.

Charpy blanks machined from the alloy were heat treated as follows:

°F °C

10 min. at 2100 (1150), water quench
10 min. at 1650 (900), water quench
30 min. at 675 (360), air cool
60 min. at 1250 (675)

Half the blanks were water-quenched from the final temper and half were furnace-cooled. The treatment produced an austenitic grain size of ASTM 3-2 and a microstructure which was entirely ferritic.

The blanks were machined to sub-sized V-notched Charpy specimens 7.5 mm square, 55 mm long, with a 45° V-notch 1 mm deep and having a 1/8 mm radius at its base.* The specimens were tested on a standard (217 ft-lb) impact machine, with the results given in Fig 1.

The transition temperatures of the quenched and slow cooled specimens were -53 and -54°C, respectively, as

shown in Fig 1. Since these temperatures are the same within the limits of experimental error, the results are consistent with the view that temper brittleness cannot develop in the absence of carbon and nitrogen. It may be pointed out, however, that two alternative explanations are possible. First, embrittlement may occur so slowly that furnace cooling provides insufficient time for appreciable embrittlement. Second, embrittlement may occur so rapidly that complete embrit-

tlement develops even on the water-quench from the temper.² In an alloy of the composition used, it is considered unlikely that either of these alternative views is valid.

It is interesting to note that the material used apparently does not quench-age, but the amounts of carbon and nitrogen present are sufficient to cause strain-aging.

Further work is planned on the same composition, as well as on alloys with carbon and nitrogen added separately and together, since an alloy to which carbon and nitrogen are added will still differ from commercial steel in phosphorus content.

References

1. H. Jolivet and R. Chouteau: Sur la fragilité de revenu des aciers. *Rev. Metallurgie* (1943) **40**, 14-24.
2. L. D. Jaffe and D. C. Buffum: Temper Brittleness of Plain Carbon Steels. *Trans. AIME* (1949) **180**, 513. *Metals Tech. Dec.* 1948, TP 2482.
3. D. C. Buffum: Investigation of Square V-Notched Charpy Specimens. Accepted for publication, *ASTM Bulletin*.

Technical Note No. 17E. Manuscript received March 23, 1949.

This note has been published by permission of National Military Establishment.

* Watertown Arsenal Laboratory, Watertown, Mass.

The statements or opinions in this note are those of the authors and do not necessarily represent the views of the Ordnance Department.

† These suggestions have been reviewed by Jolivet and Chouteau.¹

‡ Made by National Research Corporation.

¹ References are at the end of the note.

* Behavior of these specimens is compared with that of full-size Charpy bars in a forthcoming paper.³

Secondary Recrystallization in Copper

M. L. KRONBERG* and F. H. WILSON,† Member AIME

The low temperature recrystallization of very heavily rolled copper produces a fine grained structure with a high degree of preferred orientation. Additional heating to within a few hundred degrees of the melting point may induce an abrupt and pronounced increase in the grain size, with the resulting crystals having new orientations. This behavior at high temperatures is commonly termed "secondary recrystallization."

Several investigations have dealt with the phenomenon and have served to bare many features of the behavior.¹⁻⁴ In general, observations have been made on the sizes and shapes of the grains, and data have been presented showing the existence of an induction period in isothermal experiments.

Although it has been well established that the orientation before the change is statistically (100) [001], the so-called "cubically aligned" texture, there is no such agreement on the orientation after the change. For example, Dahl and Pawlek¹ describe it as being equivalent to an approximately 30° rotation about the [100] axis of the ideal cubic texture which is parallel to the rolling direction, the resulting orientation being near (210)[001]; and Cook and Richards² find an orientation of approximately (110)[112].

Since the completion of most of the work to be reported in this paper, Bowles and Boas³ have published their very illuminating paper on "secondary recrystallization," in which they present convincing evidence for a third orientation and show that their experiments give no evidence for either of the other two orientations. The orientation is described as equivalent to an approximately 30° rotation about a [111] pole of the ideal cubic orientation.

The existence of a variety of reported orientations is not unique for copper, for a similar state of affairs exists for other systems that have been studied—

aluminum, nickel, nickel-iron alloys, and others. It seems therefore that the existence of this variety does not necessarily constitute a contradiction, but rather indicates that different experimental conditions yield different results.

The fundamental nature of the phenomenon has not been elucidated. However, it has been generally recognized that the large grains could be the end product of growth of a few select grains already existing in the sample in minor amounts—too small to allow detection—or that entirely new ones could be formed by a process of nucleation and growth. Existing experimental evidence does not distinguish between these two most apparent possibilities. Nevertheless, the former has been more generally favored largely because our current understanding of the state of an annealed metal has not made it seem reasonable to expect a nucleation event to occur at temperatures above those required for the primary recrystallization.

Observations on the Preparation and Heating of Twin-bearing Cubically Aligned Copper

The starting material used throughout the investigation was a bar of OFHC copper, forged and annealed at 950°C. Visual inspection showed the grain size to be around 0.5 mm, and did not disclose any preferred orientation.

A chemical analysis showed the following composition:

| | |
|----------|------------|
| Cu + Ag— | 99.99 pct |
| S — | 0.005 pct |
| O — | <0.005 pct |

For the preparation of cubically aligned copper, ¾ in. thick slabs were cut from the bar, heavily pickled in concentrated HNO₃ and cold rolled to sheets about 0.012 in. thick. The reduction in thickness was approximately 98.5 pct. Standardized annealing techniques were followed. Samples to be heated were lightly dusted with alumina in order to prevent sticking and then sandwiched between ⅛ in. copper plates. The resulting sandwich was heavily wrapped with copper sheet, and then annealed in air. The protection was such that only very thin films of oxide were formed. That the associated light oxidation of the samples had no specific effect on the recrystallization behavior was shown by the similar results that could be obtained on annealing in highly purified and dried hydrogen.

Two methods were used in bringing samples to temperature: (1) by placing the package directly in the furnace at temperature and (2) by placing the package in the furnace at room temperature, and then slowly increasing the temperature. The corresponding heating rates are illustrated in Fig 1, and will be referred to as "rapid" and "slow," respectively. Unless specified otherwise, all anneals will be of the former type.

Metallographic examination was made on samples prepared by electrolytic polishing and etching as described in the Metals Handbook.*

STRUCTURES FOUND BEFORE "SECONDARY RECRYSTALLIZATION" OCCURS

Annealing the rolled material for 1 hr at 400°C produced a heavily twinned, cubically aligned structure, the grain size being of the order of 0.03

Cleveland Meeting, October 1949.
TP 2634 E. Discussion of this paper (2 copies) may be sent to *Transactions AIME* before December 1, 1949. Manuscript received March 10, 1949.

*Formerly Copper Research Lab. The American Brass Co; now Hammond Lab., Yale University.

†Copper Research Laboratory, The American Brass Co., Waterbury, Conn.

¹References are at the end of the paper.

*A.S.M. Metals Handbook, p. 901.

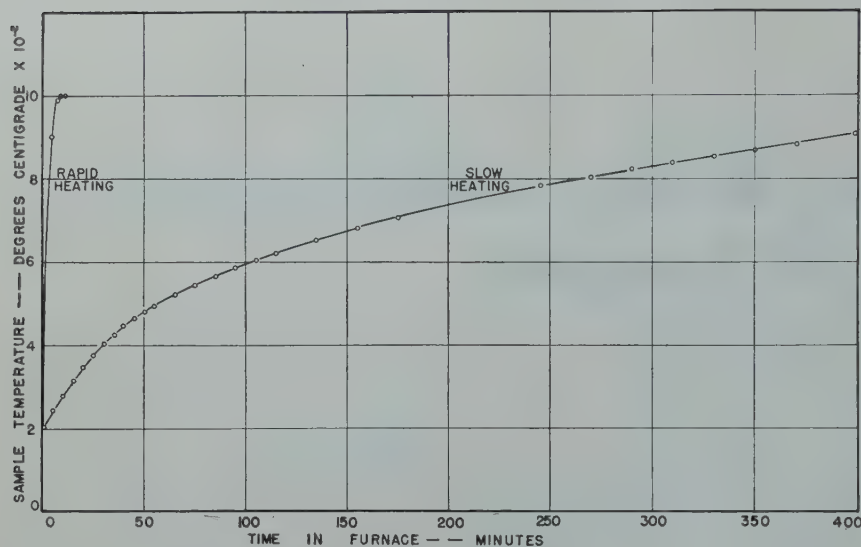


FIG 1—Rates of heating in two annealing techniques used for secondary recrystallization of copper.

mm. The effect of annealing at progressively higher temperatures was to cause an increasing consumption of the twins, and a moderate increase in the size of the grains. With a 1 hr anneal at 850°C the grain size increased to around 0.08 mm. Fig 2 illustrates the microstructure of the resulting material. Only a light etch is needed to reveal the twins, whereas the individual cubic grains as seen in the figure are revealed by a heavier etch. Still heavier etching develops the familiar aligned cubic etch pits characteristic of the material. The effect is illustrated in Fig 3.

Fig 2 also discloses that the grain boundaries are generally curved, and

that there is a wide variation in the angles between the boundaries. These conditions indicate that the equilibrium state of grain growth by boundary migration has not been achieved.

The resolution of the grain boundaries between a grain and its various neighbors varies considerably, some of the boundaries being scarcely visible at all. This observation leads to the conclusion that there is a variation in the extent of mismatch in the relative positioning of the individual crystals—presumably the closer the match, the finer the grain boundary. Apparently the material can be described equally well as a very imperfect single crystal or as a polycrystal having a high de-

gree of preferred orientation.

It has been observed that heavy rolling reductions cause the edges of the strip to tear and thus to form protruding “ears.” When the rolling is completed these “ears” have undergone a different kind of deformation from the bulk of the material, and thus on recrystallization do not have a well developed “cubic” texture. On the other hand, the grain size within such a region after a 400°C anneal is approximately the same as that of the “cubic” grains. Annealing at higher temperatures, however, develops larger grains within the “ears,” and indeed at temperatures of around 800–900°C the size is several fold larger. (Fig 4). Thus it can be concluded that grain growth in cubically aligned copper is very sluggish because of the great similarity in the orientations of the individual grains.

STRUCTURES RESULTING FROM “SECONDARY RECRYSTALLIZATION”

Although a 1 hr anneal at 850°C resulted only in grain growth of the cubic grains, heating samples for longer times, of the order of 2 hr, at 850°C sometimes induced “secondary recrystallization,” thereby verifying the existence of an induction period. In general, in those samples showing the large grains, the treatment had not resulted in a complete absorption of the cubic material. Longer annealing

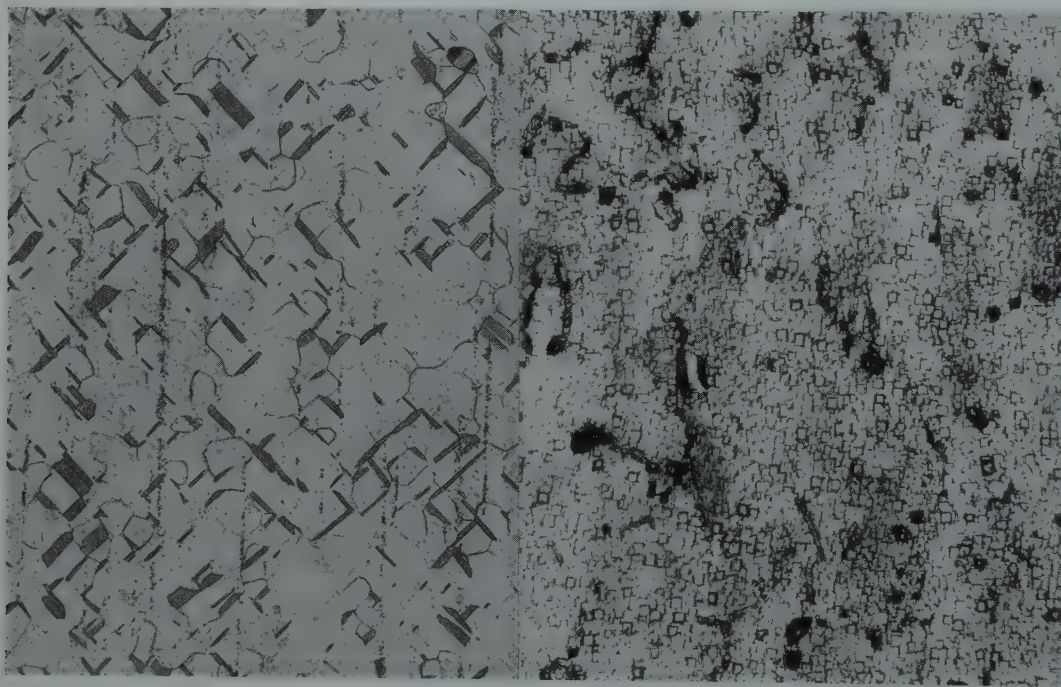


FIG 2 (left)—Structure of twin-bearing cubically aligned OFHC copper. Starting grain size approx. 0.5 mm, rolled 98.5 pct, annealed 1 hr at 850°C. 75 ×
FIG 3 (right)—Cubic etch pits in cubically aligned copper. 250 ×

times, of the order of 4 hr, were needed in order to complete the absorption, but growth always stopped at the "ears." The foreign orientations existing in these edge fragments could not be absorbed even by annealing for 4 hr at 900°C. Higher temperatures were needed for invasion of these areas and in general many of the grains resisted consumption even after annealing for 4 hr at 1000°C. Thus it is seen that the cubically aligned grains are absorbed much more readily than grains of other orientations.

Examination of numerous samples showing partial consumption of the cubic material revealed no specific tendency for growth to initiate at the "ears." Rather, growth almost always started within the body of the sample and then spread toward the edges. Thus there is a pronounced tendency for growth to start within the cubically aligned grains, rather than among the foreign orientations existing at the edges. Fig 4 shows two illustrations of the transition region between residual cubically aligned grains and those existing at an edge of a sample almost entirely converted to large crystals.

The shape of the boundary between a growing large grain and the residual cubic ones has been observed. It is illustrated in Fig 5. One sees that the boundary is scalloped, being pointed toward the boundaries of the cubic grains. Thus growth is proceeding in accord with the principles of boundary migration.^{5,6}

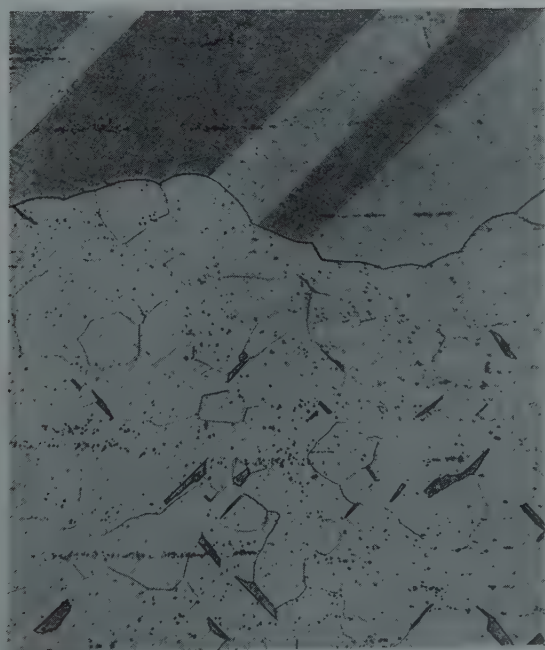


FIG 5—Advancing boundary of a large grain.
150 X.



FIG 4—Structure of the transition region between cubically aligned copper and the more random orientations near torn edges.
75 X. Reduced approximately one-third in reproduction.

Experimentation showed that for ultimate temperatures of 900–1000°C the sizes of the large grains are strongly influenced by the heating rate, the more rapid the heating the smaller the grain size. For example, slow heating often produced grains with from 1–8 sq in. in surface area, whereas the rapid heating produced grains with approximately $\frac{1}{16}$ – $\frac{1}{4}$ sq in. Fig 6 illustrates typical samples formed by the two heating methods.

The illustrations show that the individual grains formed during "sec-

ondary recrystallization" have a highly preferred orientation. Two types are formed: those characterized by, (a) prominent twin traces at approximately 45° to the rolling direction, and (b) elongation parallel to the rolling direction and frequently showing no twins at all. The former are formed almost exclusively if the heating rate is rapid through the region of 800–1000°C and the latter form in minor concentrations if the rate is slow in this temperature region, or if rapidly heated samples are held at temperature in the

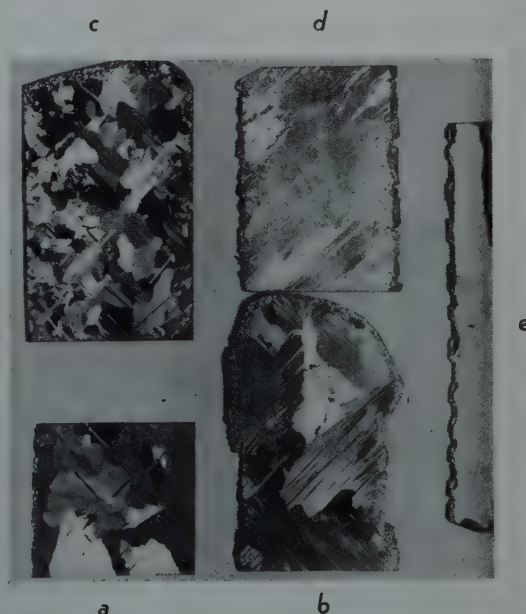


FIG 6—"Secondary recrystallization" of twin-bearing cubically aligned copper.

a. Rapidly heated to 900°C + 1 hr. b. Slowly heated to 900°C. c. Rapidly heated to 1000°C + 1 hr. d. Slowly heated to 1000°C. e. Rapidly heated to 1000°C + 1 hr. b, d, and e are particularly illustrative of stoppage of growth at torn edges. $\frac{3}{8}$ X.

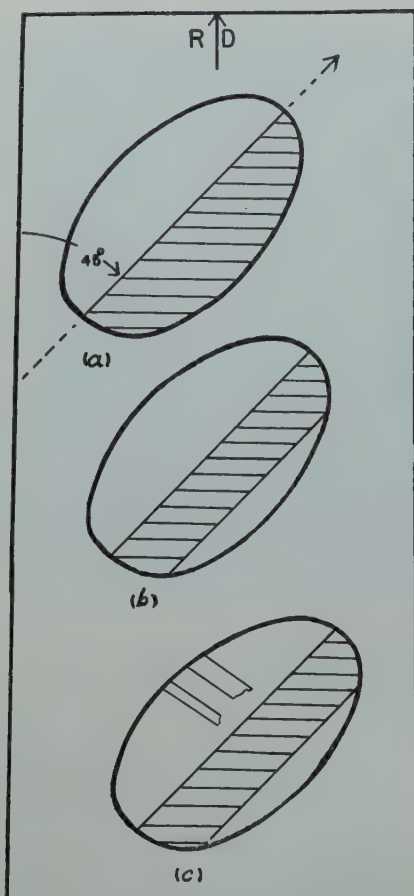


FIG 7—Schematic representation of grain shapes commonly found in rapidly heated samples.

region of 850–900°C. Examples of the latter type are the “white” grains at the upper and lower left of sample (a) and near the upper center of sample (b) in the figure.

A careful examination of the grains formed by rapid heating to 1000°C shows a tendency for the development of a characteristic shape and a characteristic positioning of the twin boundaries. It is convenient to describe the grains in terms of these fundamental characteristics, and Fig 7 illustrates the idealized shapes in a highly schematic way. The simplest shape (a) is an ellipse with the major axis coinciding with the trace of a twin boundary. Indeed, around 70 real crystals approximating such a shape and composed of a single twin pair have been observed. In a more common variety (b) one of the twins appears as a band dividing the grain about equally. Careful examination of grains with relatively thick bands has shown, however, that it is not the band which divides the grain, but rather one of its boundaries. Some of the grains (c) show additional twins within either or both of the components. Fig 8 (a and b) shows some particularly illustrative grains.

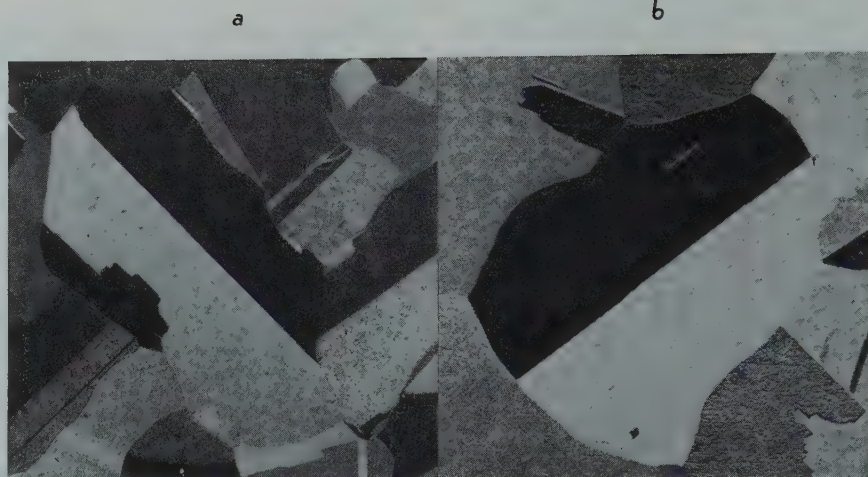


FIG 8—Elongated twinned grains found in samples rapidly heated to 1000°C. Rolling direction vertical. 10 X. Slightly reduced in reproduction.

The repeated appearance of roughly elliptical grains containing a twin boundary near the center and along the major axis suggests that growth develops a twinned crystal as the first unit of growth and continues most rapidly parallel to the twin boundary. If it occurs by the development of a grain already existing in the material, then this starting grain would be a single twin pair. If it occurs by nucleation and growth, then the nucleation would presumably occur at a twin boundary. During the growth, either member of the twin pair could twin on a parallel plane generating another unit of the complementary orientation, and both orientations could give rise to second generation twins on other (111) planes.

There are some observations indicating that growth initiates most readily at the surfaces of the samples and proceeds most rapidly parallel to the surface. Specimens displaying the early stages of growth show some grains extending over $\frac{1}{4}$ in. along the surface, but only a few thousandths of an inch below the surface. Others show grains extending $\frac{1}{2}$ in. along the surface, but meeting other grains growing from the other surface approximately half way.

In brief summary, “secondary recrystallization” occurs after an induction period at temperatures above about 850°C in twin-bearing cubically aligned OFHC copper, the induction period being shorter at higher temperatures. Slow heating through the temperature range of 800–1000°C produces much larger crystals than rapid heating. The latter process produces one kind of orientation, type (a), and the former produces an additional one, type (b), in minor concentrations.

Type (a) always contains a twin boundary at about 45° to the rolling direction, whereas type (b) frequently is twin free. When formed by rapid heating, the type (a) grain is often approximately equally divided by a twin boundary and is elongated in the direction of the boundary.

Growth of the large grains occurs readily in cubically aligned copper but is slowed drastically when grains of other orientation are met at the torn edges. There is no particular tendency for growth to initiate at the torn edges. The contour of the boundary of a growing grain is in accord with the predictions of the principles of grain growth by boundary migration.

CRYSTALLOGRAPHIC ORIENTATIONS RESULTING FROM “SECONDARY RECRYSTALLIZATION”

Orientations of the grains resulting from “secondary recrystallization” were determined using the back-reflection Laue technique of Greninger.⁷ Eleven samples were used. Four were formed by “rapid” anneals for 1 hr at 900°C and seven by “slow” anneals at 950°C. The resulting orientations of both types of grains, (a) and (b), apparently were not affected by the variation in heating rate.

The analysis of the data showed that the position of the octahedral pole common to a twin pair (type (a) grain) is close to the position of one of the octahedral poles of the ideal “cubic” orientation. The location of this pole for 52 grains is plotted in stereographic projection in Fig 9, in which the plane of projection is the plane of the copper strip. The distribution of poles is shown in relation to the 5° radius circles

around the $[111]$ poles of the ideal "cubic" orientation. The plot is to be compared with Fig 10, showing a pole figure of the "cubic" texture plotted from X ray photographs of unconsumed material in one of the samples annealed at 900°C . For comparison, 5° circles are drawn around the $[111]$ poles of the ideal orientation. The great similarity in the two distributions suggests that the orientations of the new grains may be formally related to those of the old by rotations around a $[111]$ pole.

The character of the indicated rotations can be investigated rather simply if one confines the analysis to those poles falling within a densely populated region. For this purpose, the area defined by the 5° circles about the ideal cubic position has been selected. The positions of the corresponding central $[100]$ poles of the selected crystals are plotted in Fig 11 after bringing their $[111]$ poles into the same quadrant, and 5° circles are drawn to cover the most densely populated regions. By plotting the poles of both twins in some cases, a total of 63 orientations on 40 $[111]$ poles is included. It is seen that nearly all the poles are enclosed by the circles, but that there is a spread of a few degrees in the directions of greater and lesser rotation. The corresponding distribution is roughly of the form that would be required for a discrete, or unitary, rotation, that is, one involving an exact angular relationship between each grain and its parent. The poles within the circle would arise from cubic grains whose $[111]$ poles lie within the defined 5° circle, and whose central $[100]$ poles would lie within a 5° circle about the ideal position of those poles. In the pole figure of cubically aligned copper, there is an appreciable concentration extending several degrees outside the 5° circle, and thus with unitary rotation the observed kind of spread would develop. An amount of rotation can be estimated by the angular distance from the center of the plot to the centers of the 5° circles. It is seen that the rotations are opposing ones of approximately 22 and 38° , the individual rotations corresponding to the members of a twin pair.

With one exception, specific directions of rotation are observed. Around the south-east and north-west $[111]$ poles the 22 and 38° rotations are found to be clockwise and counter-clockwise respectively, and for the other two poles the directions are re-

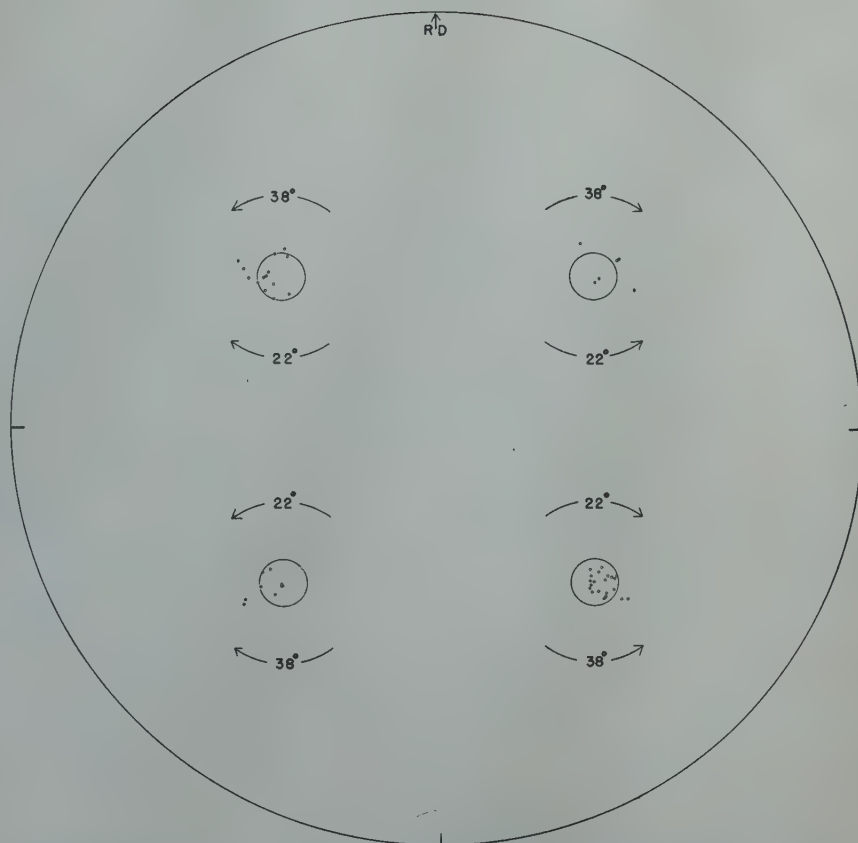


FIG 9—The positions of the $[111]$ poles of 52 large crystals which lie near the $[111]$ poles of $(100)[001]$.
 $\pm 5^{\circ}$ circles are centered on the $[111]$ positions of $(100)[001]$.

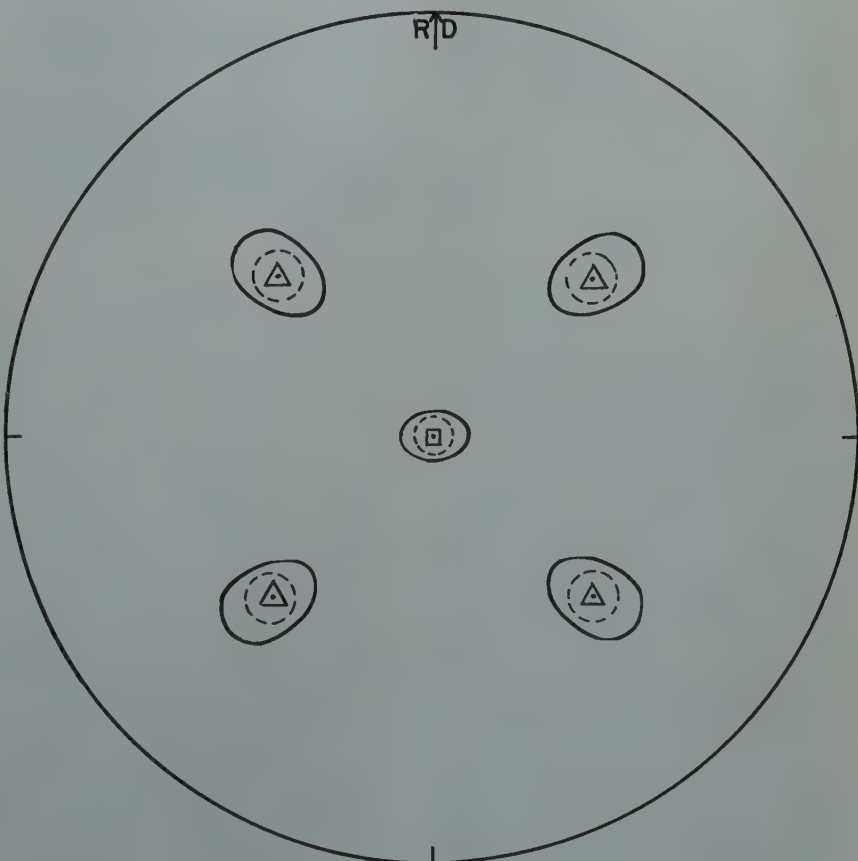


FIG 10—Pole figure of cubically aligned copper.
 Broken $\pm 5^{\circ}$ circles give indication of extent of deviation from $(100)[001]$.

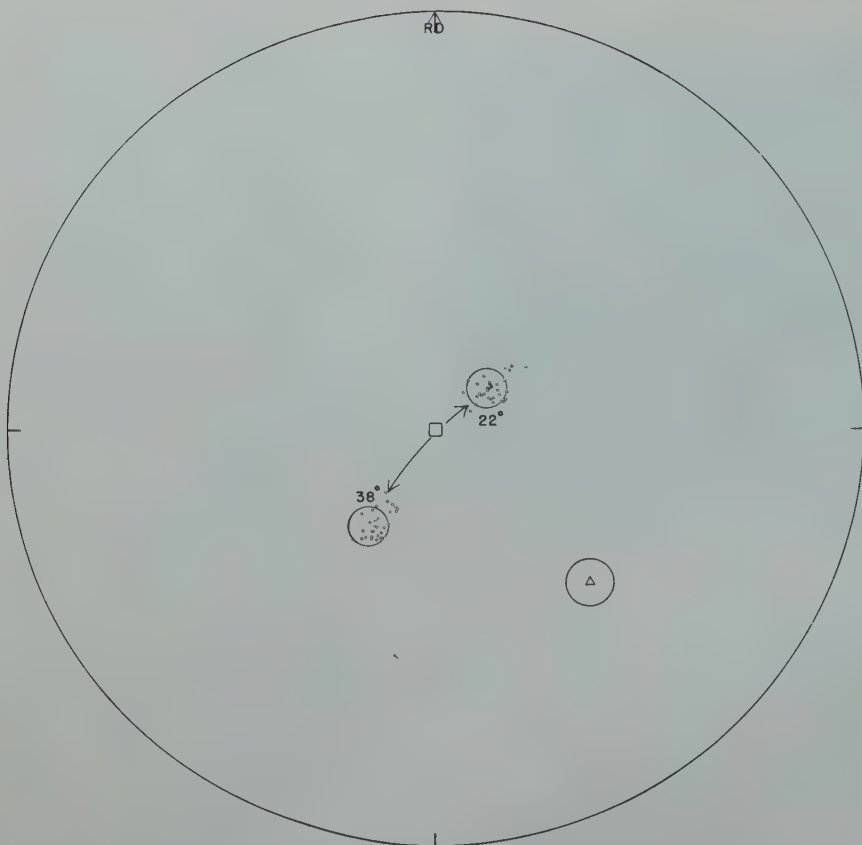


FIG 11—The positions of the central cube poles of 63 large crystals which are derived by rotation about $[111]$.

Centers of $\pm 5^\circ$ circles are at indicated rotations of the center of projection about $[111]$.

versed. The effect is illustrated in Fig 9. Thus in the formal relationship developed, the pole figure shows a loss of the four-fold axis associated with cubic symmetry, but the planes of symmetry are preserved.

Coincidence Plot for a 22° Rotation

The nature of the relationship between the two highly preferred orientations involved suggests that a discrete mechanism operates in the formation of the "secondary" crystals. It has previously been shown that the primary unit of growth is probably a twin and that this unit forms in cubically aligned copper which has been observed to contain twins. This circumstance suggests that the twinned unit might be derived from a twin pair in the starting material by a mechanism which rotates the unit by a 22° or 38° rotation about the twinning pole. In order to attempt to gain an insight into the nature of the mechanism thereby suggested, it is useful to examine the relationship between the crystallographic orientations, before and after "secondary recrystallization." Referring to Fig 12, the small

filled circles of net A represent the positions of the atoms in a (111) plane of the ideal cubic orientation. The large filled circles then represent the positions of the atoms in a neighboring layer. Net B is derived by a 22° rotation of the latter net (or a 38° rotation in the opposite direction) about an arbitrary point of this net. The positions

of the open circles in the resulting net then represent the positions of the atoms of a (111) plane for the orientation after "recrystallization." This formal construction is not intended to imply that the orientation change actually occurs by means of the indicated rotational shear operation. Rather, it serves only to illustrate the relative positions of the atoms in a (111) plane before and after "secondary recrystallization."

However, examination of the figure reveals several striking features. It is seen that $\frac{1}{4}$ of the atoms of the new orientation are in coincidence with atoms of the old orientation, and the positions of these coincidence atoms define a unique equilateral net which is a multiple of the primitive net. Moreover, the remaining atoms can be brought onto the sites of the new net by a very simple movement of the order of $\frac{1}{3}$ of an interatomic distance.

In order to effect a three dimensional change in orientation, formally speaking, it is necessary to consider neighboring layers. The corresponding coincidence sites for such a layer are shown by small annular rings in net A. Fig 13 shows the completed re-orientation in detail for two layers, and in one section for three layers. Coincidence sites in the second layer are defined by triangles in this figure. The remainder of the structure is derived by a repeated stacking of such groups of three.

Although it appears that the formal operations have produced a 22° rotation of the structure, such is not the case. Actually, study of the plots shows

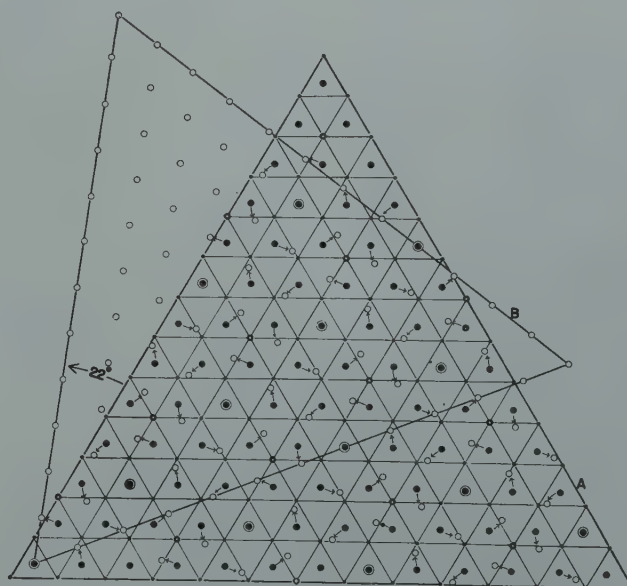


FIG 12—Coincidence plot showing relation between positions of atoms in an octahedral plane before and after a 22° rotation.

the new orientation to be a twin of the starting orientation, rotated by 22° . Thus in the formal conversion of a twinned cubic crystal to the newly oriented twin, each part can be described as being related to its parent as a twin rotated 22° , or as its own orientation rotated 38° in the opposite direction.

Examination of the figure which shows the re-orientation for three layers reveals several interesting geometrical features. One sees that the coincidence positions uniquely define a multiple face-centered cubic lattice. All other original sites can be brought to their new positions by relatively short displacements.

A fundamental characteristic of the cluster of atoms composed of a coincidence atom plus its nearest neighbors is readily discerned. An atom in a cubic closest packed structure is surrounded by twelve nearest neighbors, six "around the waist" in any given $\{111\}$ plane, three in the parallel plane above and three in the plane below—the latter six forming an octahedron about the central atom. For the case of twins, the packing of the three layers involving the composition plane and its contiguous neighbors corresponds to hexagonal closest packing. Thus, for a coincidence atom lying in the composition plane the atoms in the two sets of three nearest neighbors in adjacent planes define a triangular prism. Considering either case, in order to effect the formal orientation change under discussion, the six "waist" atoms all move in one direction, whereas the re-

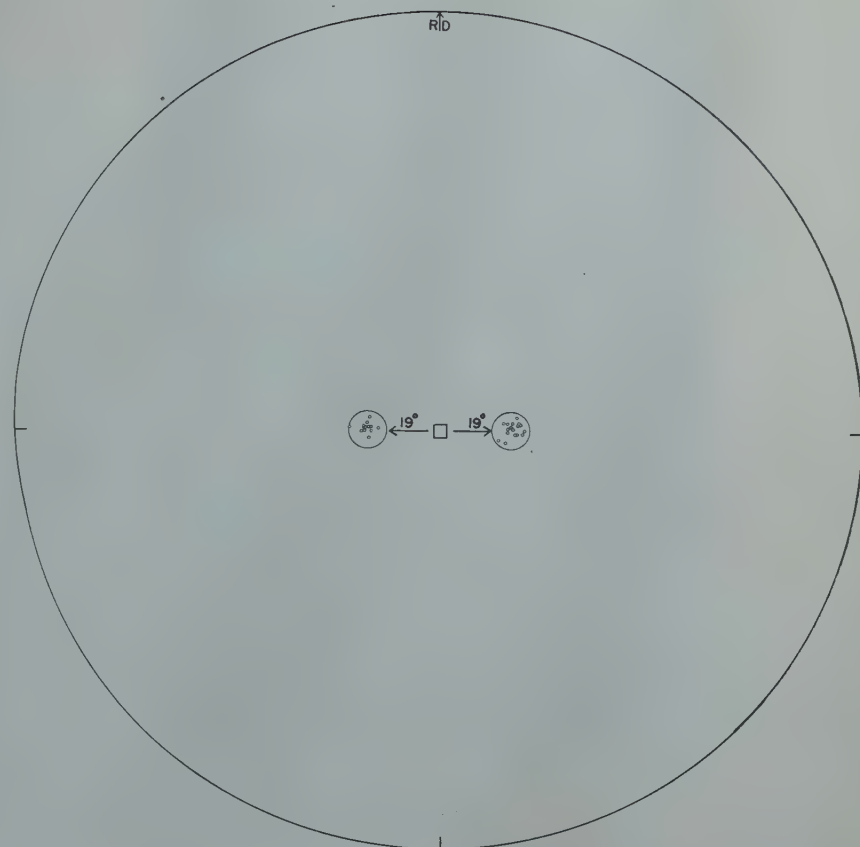


FIG 14—The positions of the central cube poles of 30 large crystals which are derived by rotation about $\{001\}$.

maining two groups of three move in the opposite direction.

There are no obvious clues to a possible origin of the type (b) crystals which form most readily on slow heating. However, they exist with a very high degree of preferred orientation and there is a definite geometrical relationship between the atomic positions

before and after "secondary recrystallizations." Fig 14 is a pole figure showing that the orientation can be related to that of the cubic by a $\pm 19^\circ$ rotation about a $[100]$ axis parallel to the rolling direction. It is significant to note that the degree of preferred orientation is apparently considerably greater than that of the "cubic" material. Fig 15 illustrates the relative positions of the atoms before and after "recrystallization."

Observations on the Preparation and Annealing of Twin-free Cubically Aligned Copper

In order to test whether the occurrence of "secondary recrystallization" is dependent upon the presence of twins in the cubically aligned material, experiments were performed on apparently twin-free samples. It is known that the effect of a progressively diminishing grain size of the material prior to the heavy rolling reduction is the development of cubic material containing correspondingly diminishing amounts of twins.¹⁶ Experiments in the current investigation have shown that, for starting grain sizes of the order of 0.01–0.1 mm, cubic material can be

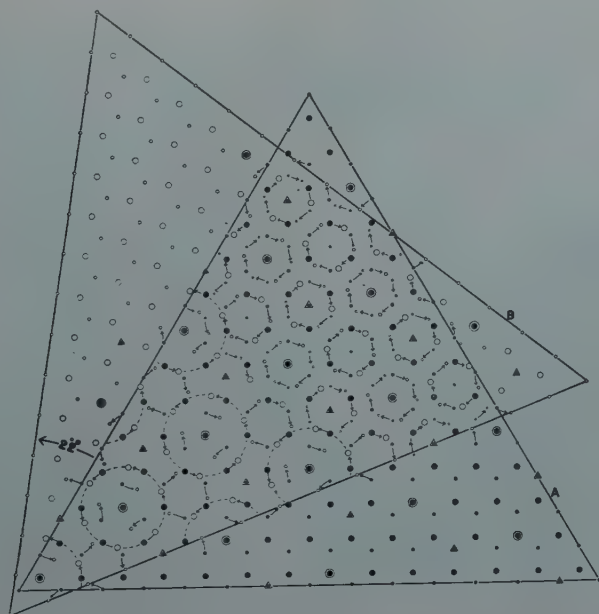


FIG 13—Coincidence plot showing relationship for two and three octahedral planes before and after a 22° rotation.

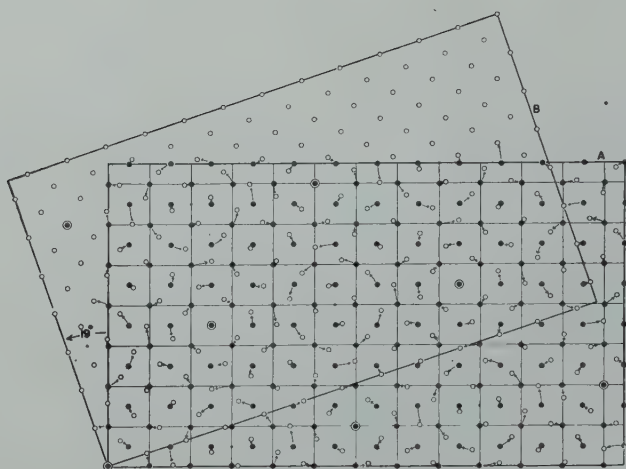


FIG 15—Coincidence plot showing relation between positions of atoms in a cube plane before and after a 19° rotation.

produced in which twins have not been detected by microscopic methods.

Starting with 0.5 mm grain size stock, samples of the finer grain size were produced by repeated cold forging and 300°C annealing treatments. Heavy cold rolling reductions and subsequent anneals were performed as described for the 0.5 mm material.

Fig 16 illustrates the kinds of samples obtained by rapid annealing to 1050°C. It is seen that all grains touch the edges of the sheet suggesting that growth has initiated at these boundaries. Careful examination of around 50 samples of the kind illustrated has shown that all the grains have this characteristic. Study of the microstructures of the sheared and torn edges of sheets annealed 1 hr at 850°C, a treatment which develops the structure existing just prior to "secondary recrystallization," revealed the presence of twinned cubically aligned grains along with other grains of varying orientations. By pickling the sheared edges of cold-rolled samples, regions where such grains might develop were removed and it was possible to obtain material apparently free of twins which did not undergo "secondary recrystallization" even during 6 hr anneals at 1050°C. Thus, twin-free cubically aligned copper does not undergo "secondary recrystallization" under the conditions of experimentation.

Fig 17 illustrates the microstructure of the twin-free material after a 6 hr anneal at 1050°C, and is to be compared with Fig 2, showing the microstructure of twin-bearing material after annealing at 850°C for 1 hr. Comparison shows that the grains persist in shapes characteristic of a nonequilibrium state of growth, displaying highly curved boundaries and

varying angles between boundaries. The deviations from equilibrium shapes appear to be even more pronounced in the twin-free material. In this connection, it has been observed that the processing which develops the formation of twin-free material yields a markedly higher degree of preferred orientation than the processing which forms the twin-bearing material. Thus it would be expected that the former material would be the more sluggish in approaching the equilibrium state.

With regard to the sheets showing edge growth, an extensive study of the orientations of the large grains has not been made because of the lack of knowledge of the orientations existing at the cut and torn edges. However, the same kinds of orientations as were found in the twin-bearing material were also found in such samples, but

with somewhat more spread in orientation. Several generations of twins were sometimes found in these grains. Also the type (b) rotations about a [100] pole are now found to occur about poles parallel to both the rolling and cross-rolling directions, and the relative abundance of these orientations is greater than for the grains arising in cubic material containing twins in the body of the sheet. Some additional orientations are occasionally encountered, but they have not been determined to date.

Fig 18 illustrates the shapes of grains grown by rapid annealing at 1000°C for 1 hr in a sample with edges sheared after the rolling reduction. It shows that growth of several crystals proceeded from the shorter edges at an approximately constant rate, thus meeting in the center of the sample. The large grains are all of the (a) and (b) types, as initially described.

Annealing at lower temperatures of the order of 850–900°C, a region in which the rates of growth are relatively slow, allows the development of characteristic shapes. Fig 19 illustrates the phenomenon, samples (a) and (b) having all edges sheared, and (c) and (d) having sheared edges parallel only to the cross-rolling direction. Again, all grains are of the (a) or (b) type in these samples, but some contain additional generations of twins. Unconsumed cubic material can be seen in the illustration. The existence of the characteristic shapes simply means that some planes are developed more readily than others. Previous investigators have ob-

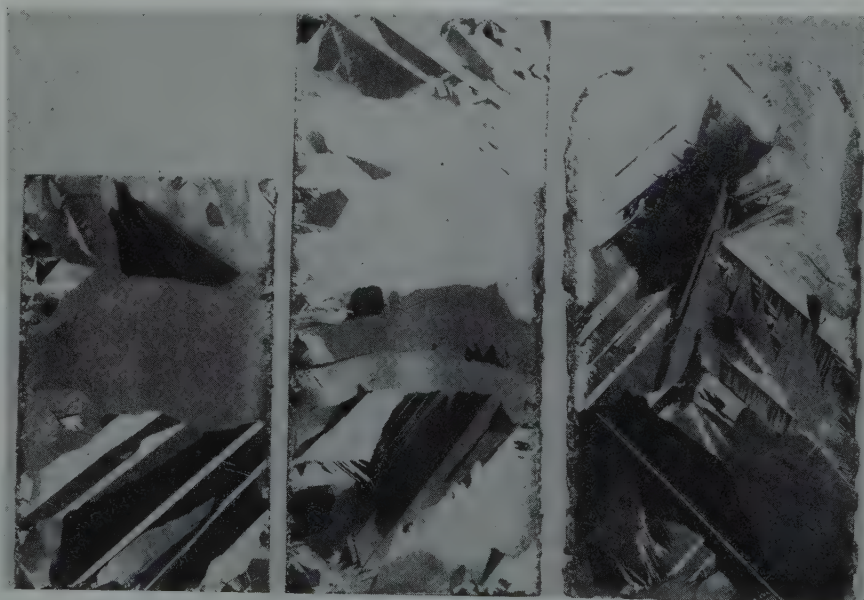


FIG 16—Growth from edges, annealed 1 hr at 1050°C.
Actual size.

served and described such typical shapes.^{1-4,8}

It is important to note that elaborate lineage-like structures have been observed in the large grains. There has been no opportunity to study the nature of these structures, but it seems probable that they will afford additional clues to the dynamics of "secondary recrystallization."

The results of these experiments do not help particularly in determining whether the large grains grow in this kind of material from favorably oriented ones already existing at the edges, or by nucleation and growth of new ones in these regions. Nevertheless, the positive result that "secondary recrystallization" does not occur in twin-free cubically aligned copper, but does in twin-bearing material to form twinned units having orientations so discretely and simply related to the parent cubic orientation is the strongest kind of experimental evidence in favor of the concept of nucleation of new orientations at a twin boundary in the cubically aligned material.

On this basis, therefore, it would seem feasible to try to understand why a reorientation might occur at a twin boundary. The packing of layers in the face-centered cubic lattice follows the sequence: ABCABCABCABC . . . , corresponding to cubic closest packing whereas the sequence for a twinned crystal is: ABCABCACBA . . . , in which there is a region of three layers corresponding to hexagonal closest packing: . . . BCB . . . Since

copper does not crystallize in the hexagonal closest packed structure it can be concluded that the associated mode of packing is higher in energy content than that associated with cubic closest packing. There would, therefore, be an inherent tendency for the atoms to rearrange so as to eliminate the fault.

Annealing Lightly Deformed Twin-free Cubically Aligned Copper

There is much current interest in the question of whether stacking faults are produced in face-centered cubic metals during deformation. For over twenty years, Mathewson has

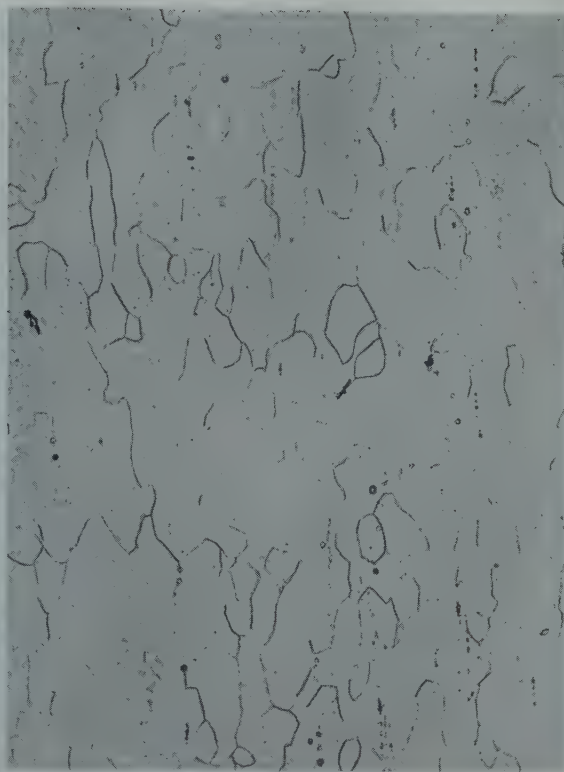


FIG 17—Structure of twin-free cubically aligned OFHC copper.

Starting grain size approx. 0.05 mm, rolled 98.5 pct, annealed 6 hr at 1050°C. Edges sheared and pickled before the anneal. 75 ×



FIG 18—Growth from sheared edges, annealed 1 hr at 1000°C.

Actual size.



FIG 19—Growth from edges, showing characteristic shapes. Annealed 850-900°C.

a and b. All edges sheared. c and d. Edges parallel to cross-rolling direction sheared. Actual size.



FIG 20 (left)—Deformation lines in peened twin-free cubically aligned copper.

FIG 21 (right)—Structure after peening and annealing.

75 \times .
10 \times .

held the view that annealing twins probably originate in copper during primary recrystallization from twins, or twin faults as he has more recently described them, arising within slip bands, during cold work,^{9,10} and has presented experimental evidence showing that twins begin to form within slip bands during the annealing of worked copper. More recently Barrett has pointed out from structural considerations that twin faults might have nearly a 40 pct chance of forming during slip.¹¹ Thus, if twin faults can be induced in twin-free cubically aligned copper by cold work, it might be anticipated that primary recrystallization should produce twinned crystals of the same kind and orientation as are observed to form during "secondary recrystallization" in twin-bearing material. As a corollary, the formation of these kinds of crystals could be taken as evidence for the formation of the faults during deformation. This interesting possibility has been subjected to a preliminary investigation by three techniques: peening, stretching, rolling.

Twin-free cubically aligned material was prepared from starting stock having a grain size of approximately 0.05 mm. Heavy rolling reductions were performed as already described, the edges of the resulting cold worked sheets were all sheared and pickled and

the samples were then annealed for 1 hr at 1050°C. The microstructure of the kind of material thus formed has been illustrated by Fig 17.

A light ball peening produces copious deformation lines emanating from the peened spot and making approximately 45° angles with respect to the rolling direction, as shown by Fig 20. Recrystallization at temperatures as low as 600°C induces growth of twinned crystals in the regions of these markings, having twin directions at approximately 45° to the rolling direction and possessing orientations the same as those described for "secondary recrystallization." Orientations of type (b) are also found. Annealing at higher temperatures causes these grains formed by "primary recrystallization" to consume the remainder of the sample by grain growth. Fig 21 illustrates typical crystals formed during a 900°C anneal.

Annealing of samples containing deformation lines produced by tensile stretchings of the order of 5–10 pct yields the same kinds of results. Thus it is seen that both types of experiments are confirmatory and, in addition, show that the corresponding "primary recrystallization" occurs at temperatures several hundreds of degrees below those required for "secondary recrystallization" of unworked

twin-bearing cubically aligned copper.

Light rolling reductions of the order of 1–5 pct yield similar effects as illustrated by Fig 22, except that in most samples the [111] rotations appear to be shifted from 22° toward a region around 30°, and the [100] rotations are shifted toward a region around 15° and now occur about the [100] pole that is normal to the sheet. The [111] poles of rotation and the central [100] poles of 18 large grains which grew on annealing lightly rolled twin-free cubically aligned copper are plotted in Fig 23. Presumably, the very close correspondence of the [111] poles to their "cubic" positions is simply a reflection of the very high degree of preferred orientation existing in the parent material.

The significance of this apparent change in the amount of rotation has not been evaluated. Perhaps the deformation process has caused the indicated additional rotation at the site of nucleation. On the other hand, coincidence plots very similar to those presented for the 22 and 38° rotations about [111] can be drawn for 28 and 32°, as shown by Fig 24, and a similar kind of plot can be constructed for [100] at 16°. Thus there is an alternative possibility that the reorientation of the rolled material proceeds according to the geometry of these new coincidence plots.

In this connection it is to be noted that in Fig 11 the spread is somewhat asymmetric, being greater in a clockwise direction. Thus, it is possible that a few of the orientations might be better described in terms of the 28 and 32° plots. An analysis based on considerably more data would be needed in order to evaluate properly this possibility.

Exploratory experiments on the recrystallization of more heavily rolled samples have revealed the very interesting finding that there is no pronounced change in the recrystallization orientation for deformations as high as approximately 35 pct, the limit of reduction that has been tried. It is interesting to note, in this connection, that Baldwin¹² has determined the orientation of 45 large grains produced by a 540°C anneal of cubically aligned copper that had been reduced 22 pct in thickness by rolling. He found a very high degree of preferred orientation which was described as:

| Rolling Plane | Rolling Direction |
|---------------|--|
| (113) | Between [110] and [301] 21° from [301] |
| (113) | Between [301] and [211] 10° from [301] |

Examination of the data shows, however, that the orientation can also be described about as well by an approximately 30° rotation about [111].

On the other hand, the grain size de-

creases continuously as a function of increasing deformation, being of the order of $\frac{1}{2}$ in. or more for a 5 pct reduction and approximately $\frac{1}{32}$ in. for a 35 pct reduction. At the same time, the density of twins increases and the components become increasingly thinner, giving rise to a fine lamellar structure. It can be observed that growth in undeformed twin-free material (Fig 16, 18, and 19) produces a minimum

number of twins, and therefore the suggestion arises that perhaps the formation of twins during growth in the deformed material might be associated with twin faults produced during the deformation.

The importance of the observation that the orientations of the grains resulting from the recrystallization of the rolled samples are essentially insensitive to the degree of rolling cannot be overemphasized, for it indicates the action of a fundamental, discrete mechanism of deformation and recrystallization throughout the range of deformation studied. An extensive study of the effects of deformation on the recrystallization orientations and structures is currently being prosecuted, and will be the basis of a separate, detailed publication.

Considerations Concerning A Possible Mechanism

The considerable evidence in favor of a nucleation hypothesis warrants an investigation of a possible mechanism for "secondary recrystallization." Indeed, the final acceptance or rejection of such an idea may well depend on the outcome of a detailed analysis of the energetics of such a process. The experimental data and the geometrical relationships derived therefrom are of a suitable form to allow such an investigation. If it can be proven that nucleation cannot occur, then one is left with the apparent conclusion that reorientation occurs by the highly selective growth of constituents present in amounts too small to be detected. As a beginning, it seems that the following

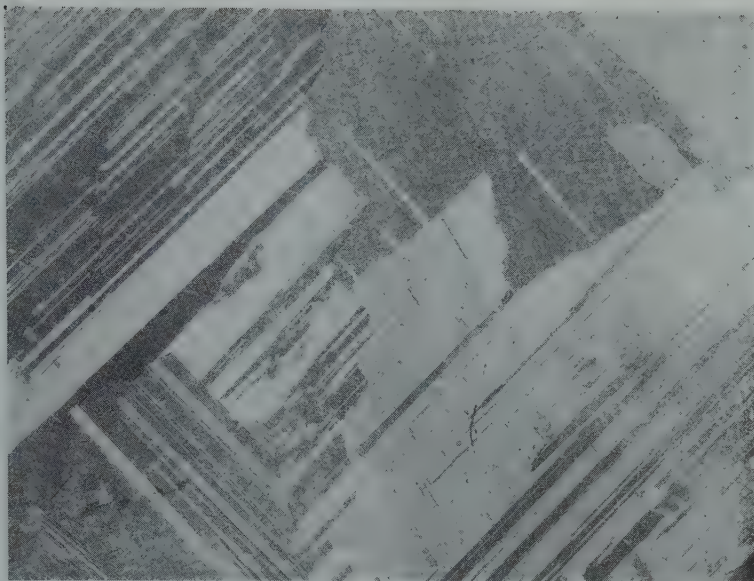


FIG 22—Structure after light rolling and annealing cubically aligned copper. 20 X.

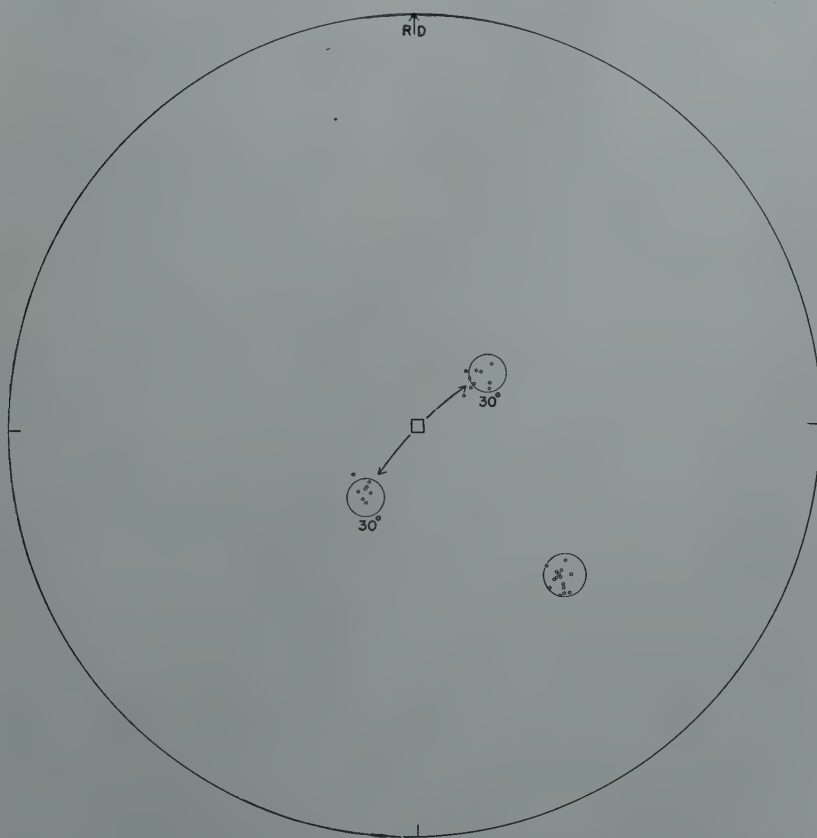


FIG 23—The positions of the octahedral poles of rotation and the central cube poles of 18 large crystals arising during annealing of lightly rolled cubically aligned copper. Centers of the $\pm 5^\circ$ circles correspond to the 30° rotations about [111].

kinds of information should be given attention.

The lowest energy state of an assemblage of atoms in the solid state is a single crystal, and thus the polycrystalline cubically aligned material containing twins is naturally proceeding in the direction of this ideal state when it converts into huge single crystals. Grain boundaries are removed and therefore would be the most probable source of the driving energy required for the change. On the other hand, there is a change in orientation altering the geometrical distribution of atoms exposed at the surface of the specimen and, if this lowers the surface tension, the corresponding decrease in energy would likewise contribute to the driving force. The fact that the conversion occurs only if twin boundaries are present indicates that the energy associated with the stacking fault existing at a twin boundary is probably involved in the activation energy, in part at least. Experiments indicating that growth initiates at a surface, where the atoms have the greatest freedom of movement and are correspondingly more energetic, can be interpreted to mean that the associated surface energy likewise probably contributes to the activation energy. Other likely contributions could come from the localized statistical fluctuations in the distribution of thermal energy among the various atoms, and the distortional energy of imperfections such as vacant sites, foreign atoms, and others.

A reasonable picture, therefore, would have the most favored site of nucleation be the region of intersection between a grain boundary, a twin boundary and the surface. A necessary condition to the atomic reorganization occurring during nucleation would be the disappearance of the grain boundary region involved. A disordered area would therefore vanish and the corresponding imperfections would be discharged at the surface. Experimental observations indicate that the twin boundary would be maintained, but would be reoriented.

It is important to point out that a structurally perfect twinned crystal would not be expected to undergo recrystallization, even though the region of the boundary is a place of higher energy than the remainder of the interior of the crystal, for this energy is locked up for a perfect crystal. Thus it is necessary to evaluate the interaction of structural imperfections, such as vacant sites or the disorganization

associated with a grain boundary, with this faulted region. The balance of forces normally maintaining the atoms in their faulted positions would be upset by the entry of imperfections into the boundary region, and might therefore promote the initiation of an atomic rearrangement in accord with the inherent tendency to de-twin or remove the fault. Indeed, inspection of Fig 12 and 13 shows that the nearest three atoms to a coincidence site in the plane above and in the plane below it actually travel in the directions of de-twinning sites in the formal picture, but achieve the equilibrium positions corresponding to the observed reorientation by moving only somewhat more than one-half the distance to a normal de-twinning site. Thus in this picture the reorientation might be described as the end product of an abortive attempt to de-twin.

It is interesting to note that the r.m.s. value of the amplitude of the thermal vibration of the atoms at the temperatures of the re-arrangement is roughly 0.3\AA , which corresponds to approximately $\frac{1}{3}$ the total distance of formal travel between sites. Statistical fluctuations are considerable and become more pronounced with increasing temperatures. Thus, it would be desirable to evaluate the probability that an atom, or perhaps a few atoms, in cooperation with an imperfection such as a vacant site, might spontaneously execute oscillations favoring the initiation of the rearrangement.

Presumably, a critical number of atoms would have to reorient in accord with the formal cooperative movements indicated by the coincidence plots of Fig 12 and 13 in order to form a stable nucleus. Once this critical size is reached, the remaining atoms in the crystal involved in the nucleation would reorient rapidly by cooperative movements. Further increase in size would be achieved by boundary migration, and presumably would proceed readily because of the favorable orientation relationship.

It seems reasonable that the induction period observed for isothermal recrystallization might, in part at least, be essentially a reflection of the improbability of the nucleation event. Accordingly, few nuclei would form, and huge grains would consequently be developed. The observation that the grain size decreases with increased heating rate might be interpreted as follows. The probability that a nucleus will form at any given temperature de-

pends on the time the sample is held at that temperature. Thus, on slow heating one nucleus might form at a relatively low temperature and consume the entire sample before another nucleation event could occur. On rapid heating, there would not be as great a probability for nucleation to occur at so low a temperature. Rather, initial nucleation would occur more probably at a higher temperature. Since the frequency of nucleation will increase with temperature as a result of the increased amplitude of thermal vibration the overall result would be the formation of many grains.

The significance of the experimental observation of specific directions of rotation about the individual [111] poles has not been evaluated, but is apparently an important clue to an understanding of the structural nature of the reorientation phenomenon.

In the very important case of the recrystallization of the lightly deformed samples of cubic material, there is no difficulty in understanding the nature of the driving force. It is the residual energy of cold work. Although its structural nature is not too well understood, it is quite possible that a deeper insight might result from continued studies of recrystallization utilizing the concepts of atomic rearrangement as revealed in the studies of "secondary recrystallization."

General Application of Coincidence Plots to Secondary Recrystallization

None of the orientations observed during the current investigation has corresponded with those described by either Dahl and Pawlek¹ or Cook and Richards.² However, the orientation study of the latter team was on material prepared by a rolling reduction of 85 pct, and it is known that such a reduction is insufficient to promote the kind of "secondary recrystallization" studied in the current investigation.

Bowles and Boas³ have reported rotations of approximately 30° about [111] on the basis of a study of 11 large grains produced in their experiments. Examination of the method of analysis employed in the evaluation of their data shows that the 30° figure results from an averaging process of all observed rotations. It seems that re-evaluation of the data might show it

to fit the 22 and 38° regions reported in the current study.

One element in common with nearly all the reported observations of new orientations produced by "secondary recrystallization" in cubically aligned metals and alloys is that old and new orientations are related by rotations about [111] and [100] axes. It would seem feasible to attempt to evaluate the significance of the variety of recorded observations utilizing the variety of possible coincidence plots, although it is to be emphasized that very carefully acquired and analyzed data will be needed. For [111], there are plots corresponding to 28, 22, 18, 15, 13, $11\frac{1}{2}$ °, etc., but there are no experiments indicating rotations other than the two discussed. For those values less than about 15°, the density of coincidence sites is relatively low and the corresponding plots can probably be ignored. For [100], there are plots corresponding to 37, 28, $22\frac{1}{2}$, 19, 16, 14, $12\frac{1}{2}$ °, etc. A commonly reported rotation for both copper and 50:50 nickel-iron alloys is approximately 30°,⁴ and there is one report¹³ of 37–38° for a 30:70 nickel-iron alloy, a coincidence plot for which is shown in Fig 25.

Some Implications of the Concept of Coincidence Plots

In applying the concepts of atomic rearrangement suggested by the experiments on "secondary recrystallization" to the experiments on lightly deformed cubically aligned copper, the deformation was considered as a means for inducing faults locally comparable in structure to twin boundaries. Nevertheless, the reorientation on annealing is fundamentally primary recrystallization and suggests that this approach may be a good tool for the study of both deformation and primary recrystallization. If extensive orientational relationships of the nature described by coincidence plots are found between deformed and recrystallized grains, they will provide strong evidence in support of the suggested atomic rearrangements; and detailed studies of recrystallization orientations accordingly should make it possible to learn more about the fine structure of deformed metal. The fruitfulness of this field of investigation is indicated by some observations which appear to be consistent with the present concept. Further research will be necessary to evaluate them.

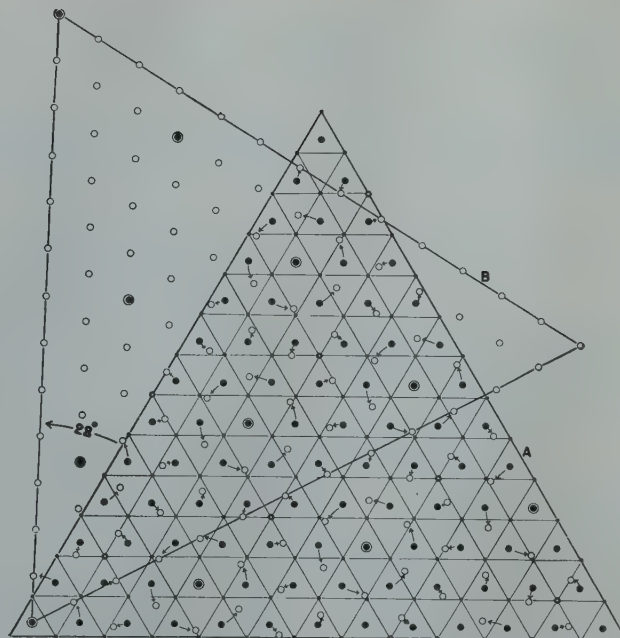


FIG 24—Coincidence plot showing relation between positions of atoms in an octahedral plane before and after a 28° rotation.

Although the structure of aluminum is based on the face centered cubic lattice it is well known that annealing twins are rarely formed by this metal. Thus, it can be predicted that a modified picture of the deformation and recrystallization processes, as developed for copper, should result from similar studies on cubically aligned aluminum. Exploratory experiments have shown that twin-free cubically aligned "high-purity" aluminum does not undergo "secondary recrystallization" on annealing in air at 650°C for 24 hr. On the other hand, recrystallization of lightly rolled samples produces the same kinds of orientations as observed for twin-bearing copper after "secondary recrystallization," with both types of orientations, (a) and (b), being found. Twinned crystals are almost entirely absent, and the rotations about [111] are predominantly of the 38° type.

In this connection, it is interesting to note that Barrett¹⁷ has observed clusters of orientations of new grains produced by the recrystallization of deformed single crystals of aluminum, compressed so as to avoid the formation of deformation bands. The orientations of these clusters can be related with considerable success to the deformation orientations by approximately 38° rotations about the [111] poles.

It was pointed out by Cook and Richards¹⁴ that components of the (100)[112] rolling deformation texture of brass are related to components of the so-called (113)[112] recrystallization texture by a 30° rotation about a

[111] pole near the rolling direction. It is possible to reproduce the pole figure, referred to as (113)[112] quite well by a 22° rotation in one direction and a 38° rotation in the other around the same [111] poles of a single component of the deformation texture. This would, of course, also be true of any of the other metals having the same textures. Rotations may occur also in wires which have a [111] fiber axis and recrystallize to the same fiber texture, as copper and aluminum are reported to do—although the rotation of each crystal would be definite in amount and the random distribution around the axis would arise from the randomness of distribution in the deformation structure. Moreover, triangular coincidence plots of the basal plane of hexagonal close packed metals would be similar to those illustrated for the octahedral planes of the face centered cubic lattice, and similar rotations might be expected. Thus, the retention of the [00.1] axis normal to the plane of the sheet during recrystallization of heavily rolled hexagonal close packed metals is comparable to retention of the [111] fiber axis in wires of face centered cubic metals. Likewise, worked material of random orientation could retain the randomness on recrystallization if each grain undergoes a rotation during the recrystallization. Although the "cubic" texture, having no complements, is considerably simpler than the deformation texture from which it arises, there is a component of deformation texture which is related to "cubic" by a 38° rotation about [111].

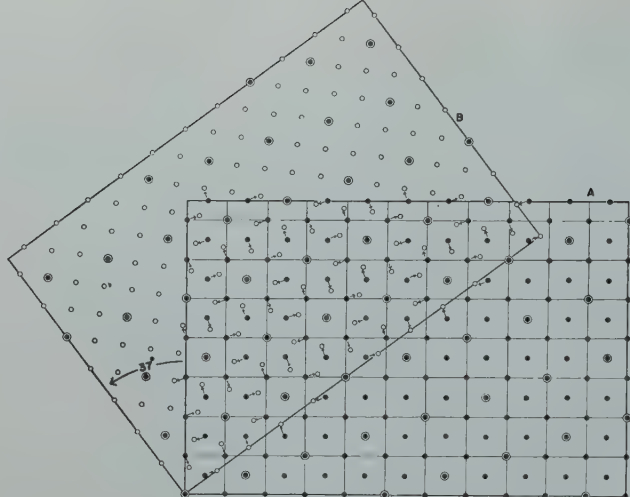


FIG 25—Coincidence plot showing relation between positions of atoms in a cube plane before and after a 37° rotation.

The conversion of the so-called (113)[112] low temperature recrystallization texture of brass to (110)[112] at higher temperatures¹⁵ may be a form of "secondary recrystallization" without the development of very large grains. This reversion to the deformation texture could be accomplished by a reversal of the rotations occurring during primary recrystallization.

Dunn has observed clusters of orientations of recrystallized grains formed on annealing lightly deformed iron-silicon crystals,¹⁸⁻¹⁹ and it would be pertinent to determine whether these new orientations can be related to the deformation orientations by means of coincidence plot relations. One might anticipate coincidence relationships on (110) planes, since they are the most densely packed ones in the body centered cubic lattice.

Summary

A formal relationship between pairs of orientations, which can explain extensive apparent rotations of a structure in terms of short, cooperative atomic movements, has evolved from a study of the orientations of the large grains that can be produced during the "secondary recrystallization" of twin-bearing cubically aligned copper. Experimental evidence indicates that the large grains are formed by a process of nucleation and growth of new orientations, with nucleation apparently initiating at twin boundaries. Two types of orientations are found. Each can be related formally to the ideal cubic orientation by rotations about [111] and [100] poles, respectively. The former always contains twins at approximately 45° to the rolling direction. There are simple relationships between the relative positions of the atoms

before and after "secondary recrystallization," which indicate that the reorientation probably occurs by a cooperative movement of atoms.

Twin-free cubically aligned copper, when lightly deformed by peening or tensile elongation, recrystallizes to form grains of the same kinds and orientations as are produced by "secondary recrystallization" of unworked twin-bearing cubically aligned copper. This result supports the hypothesis that twin faults form during the deformation, and participate in the recrystallization of the worked material to form annealing twins.*

Some speculative comments are made concerning a possible mechanism of "secondary recrystallization," pointing out the need for a theoretical analysis, and emphasizing the apparent necessity of considering imperfections in searching for the driving and activation forces. The driving force is probably mainly the energy associated with the disorganization existing at a grain boundary, but the differential in surface energy between the orientations before and after reorientation must be considered in addition. The activation energy is probably associated with a combination of the energies corresponding to the stacking fault existing at a twin boundary, imperfections such as vacant sites, the localized fluctuations of thermal energy amongst the various atoms, and the relatively loose binding of surface atoms.

A detailed account is given of the observations made on the prepara-

* By private communication, Dr. Robert Maddin of the Hammond Laboratory of Yale University informs us of some particularly timely results of his current work on the tensile elongation and subsequent annealing of single crystals of alpha brass. After recrystallization, twinned crystals are found whose orientations can be related to the parent orientation by opposing rotations of approximately 22 and 38° about a [111] pole.

tion and annealing of cubically aligned copper, and a description is given of the sizes, shapes and orientations of grains formed by "secondary recrystallization."

Some implications of the results of the "secondary recrystallization" studies are discussed as they might be related to recrystallization phenomena in general.

Acknowledgments

Acknowledgment is made to the American Brass Co. for permission to publish; to Mr. John R. Freeman, Jr., Technical Manager, whose interest and support made the work possible; and to Mr. E. W. Palmer, in charge of the Copper Research Laboratory, for sponsoring the work and for his critical advice and encouragement. The staffs of the laboratories of the Company deserve much credit for assistance throughout the project.

Before the paper was written, various aspects of the experimental results were discussed with Professors P. Debye, J. D. H. Donnay, and C. H. Mathewson. We wish to thank these gentlemen for their kindly and stimulating consideration.

References

1. O. Dahl and F. Pawlek: *Ztsch. Metallkunde* (1936) **28**, 266.
2. M. Cook and T. L. Richards: *Jnl. Inst. Metals* (1940) **66**, 1.
3. J. S. Bowles and W. Boas: *Jnl. Inst. Metals* (1948) **75**, 449.
4. W. G. Burgers: *Rekristallisation, Verformter Zustand und Erholung. Handbuch der Metallphysik, Band III, II Teil*, (1941).
5. D. Harker and E. R. Parker: *Trans. A.S.M.* (1945) **34**, 156.
6. C. S. Smith: *Metals Tech.*, (June 1948) TP 2387. *Trans. AIME* (1948) **175**, 15.
7. A. B. Greninger: *Trans. AIME* (1935) **117**, 75.
8. Cook and Macquarie: *Trans. AIME* (1939) **133**, 142.
9. C. H. Mathewson: *Trans. AIME* (1928) **78**, 7.
10. C. H. Mathewson: Campbell Memorial Lecture. *Trans. A.S.M.*, (1944) **32**, 138.
11. C. S. Barrett: A.S.M. Seminar on Cold Working of Metals. Philadelphia, Oct. 1948.
12. W. M. Baldwin: *Metals Tech.* (April 1942) TP 1455; *Trans. AIME* (1946) **166**, 591.
13. G. Wassermann: *Ztsch. Metallkunde* (1936) **28**, 266.
14. M. Cook and T. L. Richards: *Jnl. Inst. Metals* (1943) **69**, 351.
15. F. H. Wilson and R. M. Brick: *Trans. AIME* (1945) **161**, 173.
16. M. Cook and T. L. Richards: *Jnl. Inst. Metals* (1941) **67**, 201.
17. C. S. Barrett: *Trans. AIME* (1940) **137**, 128.
18. C. G. Dunn: *Trans. AIME* (1944) **158**, 372.
19. C. G. Dunn: *Trans. AIME* (1945) **161**, 98.

Kinetics of the Reactions of Zirconium with O_2 , N_2 and H_2

EARL A. GULBRANSEN* and KENNETH F. ANDREW*

Introduction

The gas-metal reactions of zirconium are very interesting. The metal is extremely stable at room temperature to reactions with the several gases present in air and the metal will stay bright indefinitely. However, at temperatures of several hundred degrees higher the metal reacts readily with oxygen, nitrogen and hydrogen. This behavior, in addition to the fact that zirconium is one of the higher melting point metals which might have high temperature applications under the proper conditions, resulted in the work reported in this communication.

There are several factors which indicate that zirconium might have good oxidation resistance at elevated temperatures. These are: (1) the high melting point of approximately 1860°C, (2) the high melting point of the oxide of approximately 2675°C, (3) the high degree of thermodynamic stability of the oxide to chemical reaction and the low decomposition pressure of the oxide and (4) the possible formation of a continuous oxide film since the volume ratio of oxide to metal is greater than unity. The unfavorable factors are: (1) the metal reacts to form nitrides, hydrides and carbides, (2) the oxide is soluble at elevated temperatures in the metal and (3) the oxide ZrO_2 undergoes crystal structure transformations at high temperature.

The oxidation resistance of this metal is not only a question of the rate of film formation but is complicated by the fact that the oxide and other reaction products dissolve in the metal which in turn will affect the physical and mechanical properties of the metal.

The protection of the metal to nitride formation must be considered separately from the oxide problem. One unfavorable factor is that the volume ratio of the nitride to the metal is about unity. This indicates that a discontinuous film might be

formed. This paper will present measurements on the rates of reaction of the metal with O_2 , H_2 and N_2 over a wide temperature and pressure range. The reaction in high vacuum and the stability of the several compounds formed will be presented. The results are correlated with fundamental rate theory and with the physical and chemical structure of the metal and film.

Literature

Although many papers have been published on the chemical reactions of zirconium with various gases, comparatively few are concerned with the protective nature of the metal and its reactions at normal pressures. The studies in the pressure range below 0.01 mm of Hg gas pressure are largely of interest in the nature of the adsorption of gases by hot filaments in high vacuum apparatus. The reactions of zirconium in this pressure range have been reviewed by Fast⁸ and by Raynor.²⁷ In spite of certain differences of opinion as to the maximum adsorption temperatures for various gases, the low pressure range is qualitatively understood. Some of these papers will be mentioned briefly here.

1. LOW PRESSURE

Ehrke and Slack⁷ find that oxygen reacts above 885°C and hydrogen above 760°C. Nitrogen does not react up to a temperature of 1527°C. Fast⁹ on the other hand observes that oxygen is absorbed above 700°C and nitrogen at temperatures exceeding 1000°C.

Hydrogen is absorbed from 300° to 400°C and liberated between 500° and 800°C. It is readsorbed at 862°C and released above 862°C.

Hukagawa and Nambo²² find a rather complicated picture for the absorption of oxygen. A rapid initial absorption is found between 180° to 230°C. Further oxygen is not taken up until a temperature of 450°C is reached. The optimum temperature for complete absorption is 650° to 700°C. Nitrogen is found to be completely adsorbed at 600°C. However some of the gas is evolved at higher temperatures. Their data on the absorption of hydrogen indicate some of the gas is removed at 550°C.

Guldner and Wooten¹⁷ in a study of the low pressure reactions of zirconium with various gases observed that the reaction with oxygen occurs at temperatures above 400°C and that the oxide is formed. The reactions with carbon monoxide and carbon dioxide occur rapidly at temperatures of about 800°C with the oxide and carbide being formed. Zirconium reacts at temperatures of 400°C slowly and at 800°C rapidly to form the nitride and with hydrogen and water at 300°C to form the hydride and a mixture of the oxide and hydride respectively.

2. NORMAL PRESSURE

DeBoer and Fast³ in a study of the electrolysis of oxygen in zirconium find that the metal absorbs up to 40 at. pct of oxygen without forming a new phase. The solubility of nitrogen in the lattice has been studied by de Boer and Fast⁴ and Fast¹⁰ and is found to be considerable. At higher temperatures the oxide dissolves in the lattice at an appreciable rate according to Fast¹⁰ and the zirconium surface becomes active.

De Boer and Fast⁴ and Hägg¹⁸ have studied the solubility of hydrogen and find that at room temperature the solubility corresponds to $ZrH_{1.95}$. Desorption occurs on lowering the pressure. Hydrogen is stated to be more soluble in the β -form and the

Cleveland Meeting, October 1949.
TP 2659 E. Discussion of this paper
(2 copies) may be sent to *Transactions*
AIME before December 1, 1949.
Manuscript received December 15,
1948; revision received April 18, 1949.

* Westinghouse Research Laboratories,
East Pittsburgh, Pa.

⁸ References are at the end of the
paper.

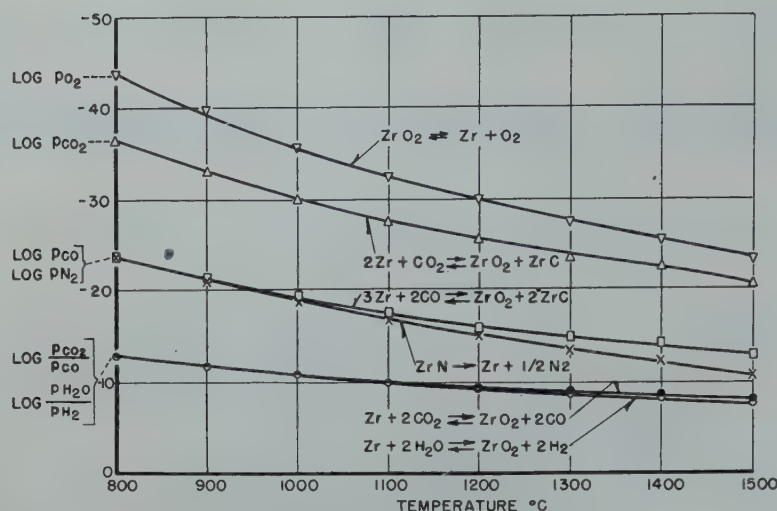


FIG 1—Equilibrium calculations on Zr reactions.

transition between the α and β forms occurs at 865°C.

Hall, Martin and Rees¹⁹ have studied the solubility of hydrogen in zirconium and Zr-O solid solutions at temperatures up to 1000°C and at pressures of 1 to 760 mm of Hg. The hydrogen desorbed on lowering the pressure.

3. CRYSTAL STRUCTURE

The crystal structures of the oxide films formed on zirconium at temperatures from 300° to 600°C using the electron diffraction method have been studied by Hickman and Gulbransen.²¹ The monoclinic form of ZrO_2 was observed over the temperature range. ZrO_2 is reported to exist in at least three crystalline modifications: monoclinic,²⁰ cubic⁵ and tetragonal²⁸ from X ray diffraction studies. Kelley and co-workers²³ from a specific heat study of the oxide ZrO_2 have shown the existence of an (α) and a (β) form with a transition at 1205°C.

Zirconium forms a nitride ZrN having a cubic lattice of the sodium chloride type.² The reaction with hydrogen has been studied by Hägg.¹⁸ Several phases are observed. Hydrogen is adsorbed up to 5 pct in the hexagonal close packed lattice without an appreciable change in lattice parameters. The lattice constants of the solid solutions of oxygen and nitrogen have been given by Fast.⁸

4. STABILITY

The stability of the several oxides of zirconium has been studied by Cohn and Tolksdorf.⁵ They found the monoclinic modification to be stable to 1000°C and the tetragonal modification above 1000°C. The latter may be cooled

to room temperature. After long heating above 1900°C a trigonal modification was found to form. When cooled a transition occurs at 625°C.

5. EQUILIBRIUM CALCULATIONS ON THE REACTION OF ZIRCONIUM WITH SEVERAL GASES

Zirconium reacts with most of the common gases to form stable compounds with the exception of the inert gases. The chemical equilibrium of these reactions may be evaluated for reactions in which the end products are ZrO_2 , ZrN or ZrC . Data are not available on the reaction with hydrogen.

The following reactions of zirconium with O_2 , H_2O , CO_2 , CO and N_2 can be evaluated from thermodynamic data:

1. $Zr(s) + O_2(g) \rightleftharpoons ZrO_2(s)$
2. $2 Zr(s) + CO_2(g) \rightleftharpoons ZrO_2(s) + ZrC(s)$
3. $3 Zr(s) + 2 CO(g) \rightleftharpoons ZrO_2(s) + 2 ZrC(s)$
4. $Zr(s) + \frac{1}{2} N_2(g) \rightleftharpoons ZrN(s)$
5. $Zr(s) + 2 CO_2(g) \rightleftharpoons ZrO_2(s) + 2 CO(g)$
6. $Zr(s) + 2 H_2O(g) \rightleftharpoons ZrO_2(s) + 2 H_2(g)$

The letters (s) and (g) refer to the solid and gaseous states respectively.

The free energy of formation of ZrO_2 (α) and ZrO_2 (β) is calculated from the data given by Thompson³¹ and using the recent data of the Pacific Experiment Station of the Bureau of Mines²³ on the entropy of ZrO_2 (α) and the heat content of ZrO_2 (α) and ZrO_2 (β). The free energy of formation of ZrC is calculated from an equation given by Kelley.²³ This equation is open to some question and may involve a maximum error of ± 2 in the logarithm of the pressures calculated for the reactions

in which ZrC is involved. The results of the calculations are shown in Fig 1. The logarithm of the gas pressure or pressure ratios are plotted against the temperature in °C for the several reactions.

The results show the following: (1) ZrO_2 , ZrN and ZrC are stable at all temperatures shown in the graph and zirconium from a thermodynamic point of view will remove O_2 , N_2 , CO and CO_2 at the lowest pressures used in modern vacuum technology, (2) the reactions of water and carbon dioxide to form the oxide and hydrogen and carbon monoxide respectively are possible below 1100°C in vacua of the order of 10^{-7} mm of Hg.

Apparatus

BALANCE

The microbalance with its auxiliary apparatus is similar to that previously described.^{12,13} The sensitivity of the balance is 0.86 divisions (0.001 cm) per microgram and the weight change can be estimated to 0.3×10^{-6} g. The balance zero point is constant and the instrument is insensitive to pressure and to small changes in the temperature of the surroundings.

VACUUM SYSTEM

The vacuum system has been changed from that previously described.¹² The length of the glass tubing connecting the several parts of the apparatus has been decreased and the diameter increased to a minimum of one inch. In addition, a high speed single jet mercury diffusion pump of the Illinois design has been added to increase the pumping speed at the outlet of the pumps by a factor of ten. The Illinois pump is backed by a two jet Princeton type of mercury diffusion pump and a Cenco Hyvac fore pump. No grease, wax, cement or metal seals are used in the system.

FURNACE TUBES

Previous to this work we have used pyrex, Vycor and quartz tubing for the construction of the furnace vessel. For higher temperatures and better vacuum conditions we have recently found synthetic mullite or zircon to be very valuable materials for the construction of furnace vessels. These materials are vacuum tight when properly made and can be sealed directly to pyrex. This feature allows double walled furnace

vessels to be constructed in which the outer tube serves as a protecting vacuum.

McLeod gauge pressures of 10^{-6} mm or lower can be achieved with these vessels at temperatures of 1175°C and perhaps higher. Leak rate measurements with the McLeod gauge on these furnace tubes show values as low as 1.4×10^{-9} mm liters per sec. after pumping over night at 900°C . We do not infer that such readings represent conditions in the furnace vessel itself since a cold trap is used on the system.

The determination of the pressure in the furnace tube is a difficult problem and any apparatus for such a task must be incorporated in the tube itself. This problem will be discussed in a later communication. For chemical and metallurgical purposes the chemical reactivity of the furnace atmosphere is of more importance than the absolute value of the pressure. This can be measured by observing the reaction rate of an active metal such as zirconium in the furnace tube itself.

GAS PURIFICATION

The purification of the oxygen and hydrogen are the same as previously described.¹² The nitrogen is purified by passing the tank gas over hot copper turnings at 400°C and removing water vapor by passing over $\text{Ba}(\text{ClO}_4)_2$. The gas is next passed over palladium asbestos at 400°C and then through another column of $\text{Ba}(\text{ClO}_4)_2$ and ascarite. It is finally passed over a liquid nitrogen trap at 0.1 atmosphere pressure.

SAMPLES

The specimens of zirconium are cut from a five mil sheet of the metal obtained from the Foote Mineral Co. No accurate analytical data are available on the material. However, the supplier states that it contains approximately 3.0 pct hafnium and about 0.04 pct iron. We are indebted to Mr. W. C. Lilliendahl of our Bloomfield Works for furnishing additional information on the presence of carbon, nitrogen and oxygen in zirconium samples. Several samples of 0.05 in. drawn wire have shown the following analysis: carbon 0.01–0.05 pct; nitrogen 0.01 pct; and oxygen 0.02–0.04 pct.

The specimens weigh 0.6840 g and have a surface area of about 15 cm^2 . Most of the samples were abraded starting with No. 1 grit and finishing with 4/0 paper. The last stage of the

abrading is carried out under purified kerosene.

Results and Discussion

HIGH VACUUM REACTION

A consideration of the high vacuum reactions of the metal under investigation is essential if a film free metal is desired at the start of the experiment. For most metals this can be achieved by heating the metal to the reaction temperature in a vacuum of the order of 10^{-6} mm of Hg and then reducing the film initially present with pure hydrogen.

The problem of preparing and keeping an active metal such as zirconium in a film free condition is practically impossible. Zirconium not only acts as a getter but the oxide ZrO_2 is not reduced by hydrogen or other reducing gases. Since the oxide is soluble in the metal at high temperatures, the oxide film may be removed by heating. However, on cooling, a film will again form in the vacuum. This procedure results also in the addition of oxide and other impurities to the metal.

Since the oxides are not reducible we have adopted the use of abraded specimens. Every effort is made to keep the films formed during abrasion to a minimum. On heating the specimen in vacuum to the reaction temperature an additional film forms. With many metals this film is only several atomic layers thick. However, zirconium forms an unprotective film and the film forms continuously in the best vacuums that we have been able to obtain.

It is of interest to show the extent of the vacuum reaction of zirconium in a furnace tube made from zircon or mullite. The furnace tube consists of two concentric tubes closed at one end and sealed at the other end to pyrex.

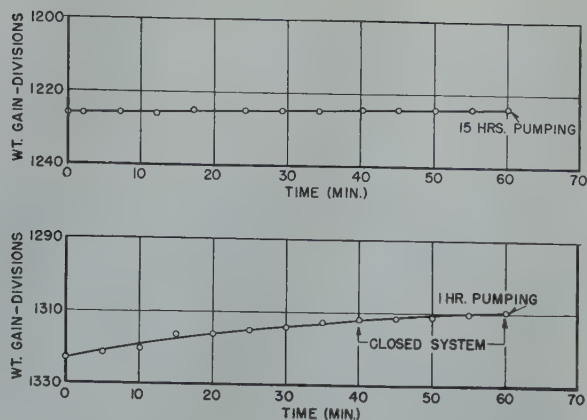


FIG 2—Reaction Zr in vacua-zircon furnace tube 900°C .

The space between the concentric tubes is evacuated. Fig 2 shows the results of heating a zirconium specimen. The weight gain is given in scale divisions (1 division = 1.2 micrograms). Two curves are shown for a temperature of 900°C and for a McLeod gauge pressure of 1×10^{-6} mm of Hg or lower. The weight gain of a sample of zirconium suspended in the furnace tube is plotted against the time in minutes. The first curve shows the reaction rate after one hour of pumping time. A reaction rate of 0.2 divisions per min. is observed. This corresponds to 0.016 micrograms per cm^2 per min. or about 1 Å of ZrO_2 per min. assuming a surface roughness ratio of unity. The second curve shows the reaction rate after 15 hr of pumping. A reaction rate of 0.04 divisions per min. is observed which corresponds to 0.0032 micrograms per cm^2 per min. or 0.2 Å per min. The calculations on thickness are based on the assumption that the film is composed largely of ZrO_2 .

We are interested also in the nature of the reaction at temperatures below 425°C and for practical pumping times of up to one hour. These are the conditions that we use in our rate studies. Experiments indicate that the maximum film formation observed is of the order of 0.70 micrograms per cm^2 for one hour of reaction at 425°C . If this is assumed to be ZrO_2 , a maximum thickness of 43 Å may be formed. In most of our measurements the vacuum formed film will be a fraction of this value.

REACTION WITH OXYGEN

The reaction is studied as a function of the time, temperature, pressure and surface treatment. The results are presented in Fig 3, 4, 5, 6 and 7. The weight gain in micrograms per cm^2 is plotted against the time in minutes.

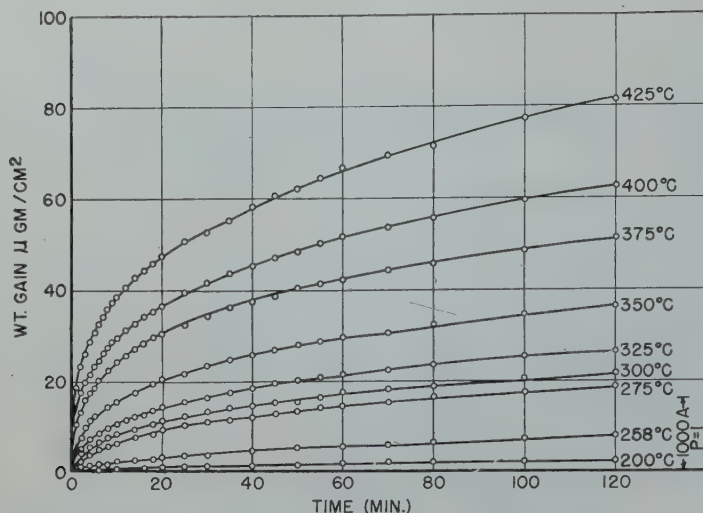


FIG 3—Reaction Zr with O₂ 7.6 cm. Effect of temperature 200–425°.

Assuming the ratio of real area to measured area to be unity ($P = 1$) and the oxide film to be ZrO₂,²¹ the thickness of the oxide film in Angstroms is 61.5 times the weight gain in micrograms per cm². Unless specifically mentioned the samples are abraded.

Time

Several experiments are made at 7.6 cm pressure and at 375°C to check the method and the reproducibility of the surface preparation. The results on the oxygen reaction can be duplicated within several percent. One run is extended for 7 hr but no additional information is obtained over the 2 hr experiments.

The shapes of the oxidation curves are similar to those observed for other metals.¹⁵ A fast reaction rate is observed in the early stages of the reaction which gradually decreases as the film thickens. In this sense the oxide film may be said to have protective properties.

Time and Temperature

Fig 3 shows the effect of temperature on the reaction for the range of 200° to 425°C. At the right of the curves is shown the weight gain corresponding to a thickness of 1000Å. A comparison of the 200°C curve with the 425°C curve after 2 hr of reaction shows a film thickness of 150Å at 200°C and a thickness of 5000Å at 425°C.

Time and Temperature Equations

Three equations have been used to explain the time variation of the oxidation rate. The parabolic rate law was

first derived by Pilling and Bedworth²⁶ on the basis of diffusion of oxygen through the oxide lattice. It has been derived more recently by Wagner and Grünewald³³ and by Mott.²⁴ The equation is

$$W^2 = Kt + C$$

Here W is the weight gain, t is the time and K and C are constants. Mott²⁵ has recently modified the parabolic law to account for the presence of a potential due to oxygen ions on the surface. The field resulting from this potential is greatest for thin films and becomes small for thick films.

The logarithmic rate law has been derived by Tammann and Köster.³⁰ This equation states that

$$t = \beta (e^{W/\alpha} - 1)$$

Here α and β are constants. The physical basis for this rate law has not been well established although Wagner³⁴ has recently derived the law from physical considerations.

The linear rate law is given by the equation

$$W = Kt + C$$

This equation states that the reaction rate is independent of film thickness and the limiting factor in the reaction rate is not a simple diffusion mechanism.

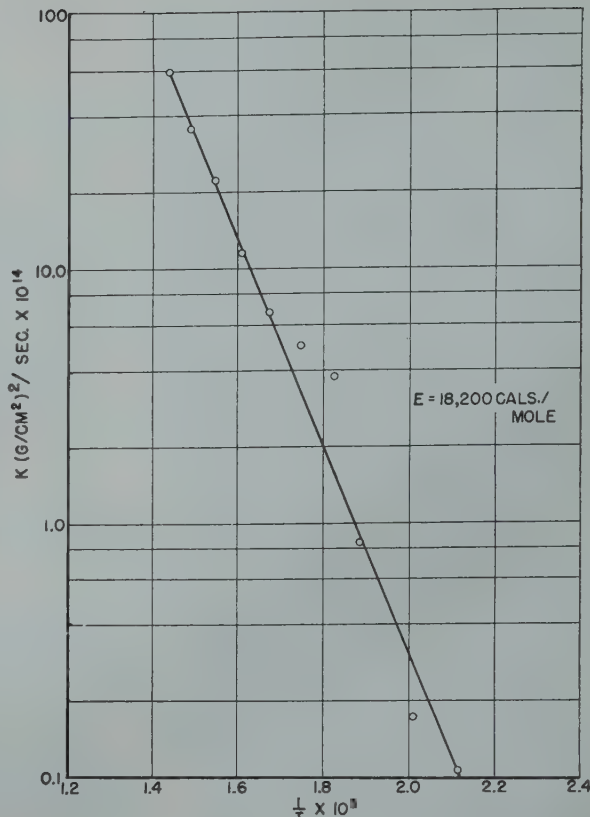


FIG 4—Reaction Zr with O₂ 7.6 cm. Parabolic rate constant vs. $1/T$.

Dunn⁶ first applied the Arrhenius equation to the temperature coefficient of oxidation rate measurements. The Arrhenius equation as applied here states that

$$K = Ae^{Q/RT}$$

Here K is the parabolic reaction rate constant, Q the activation energy and A is a constant.

Mott²⁴ has considered the physical interpretation of Q for the case where ions and electrons are diffusing through the oxide to react with oxygen at the gas interface.

One of the authors¹⁶ has applied the transition state theory of chemical reactions and diffusion processes as developed by Eyring and coworkers¹¹ to the oxidation reaction. The parabolic rate law constant K is given by the following equation:

$$K = \frac{2kT}{h} \lambda^2 e^{\Delta S^*/R} e^{-E/RT}$$

Here ΔS^* is the entropy of activation and E the energy of activation. λ is the interatomic distance between diffusional states, k is Boltzman's constant and h is Planck's constant. This equation is useful since both ΔS^* and E can be calculated. ΔS^* is the probability or steric factor of the particular barrier limiting the reaction.

Time and Temperature Correlation

The applicability of the parabolic and logarithmic rate laws can be tested by plotting the square of the weight gain against time in the former case and the weight gain against the logarithm of the time in the latter case. A straight line would show that the law is obeyed.

Parabolic plots are made of the data. Although some deviations are observed from a straight line during the initial stages of the reaction, there appears a trend to approach a straight line for the longer periods of the reaction.

Plots of the weight gain against the logarithm of the time show smooth curves of increasing slope. The logarithmic rate law does not apply for this reaction over the complete time and temperature range studied.

The linear rate law is not found to fit the data as can be seen by an examination of Fig 3.

It is necessary to conclude that none of the simple rate laws suggested adequately explains the data. The modification of the parabolic rate law as suggested by Mott is useful since it predicts the sign of the deviation as well as the general shape. However, the theory has not been developed in sufficient detail to apply to the data.

Temperature Dependence

The temperature coefficient of the reaction rate is a very useful quantity to evaluate. If the reaction rate can be related to a mechanism an energy of activation may be calculated for the process. If the theory or mechanism is unknown it is possible to show the thickness or time dependence of the temperature coefficient. Assuming that one mechanism has a constant temperature coefficient it may be possible to show whether one or more than one mechanism is responsible for the reaction. We will use both points of view in the discussion that follows.

1. *Energy and Entropy of Activation.* Fig 4 shows the parabolic rate law constant K plotted against $\frac{1}{T}$. The temperature range is from 200°–425°C. The limiting slopes at long times are used where the data deviate in the earlier stages of the reaction from the straight line.

The energy of activation of the rate determining process is calculated from the plot. A value of 18,200 cal per mol is found. The temperature independent factor $e^{\Delta S^*/R}$ is calculated from the

Table 1 . . . Parabolic Rate Constants and Diffusion Constants, Entropies, Energies and Free Energies of Activation, for the Oxidation Process

| $t^\circ\text{C}$ | $K, \text{cm}^2 \text{ per sec}$ | $D_0, \text{cm}^2 \text{ per sec.}$ | ΔS^* Cal per mol per $^\circ\text{C}$ | E Cal per mol | $-T\Delta S^*$ Cal per mol | ΔF^* Cal per mol |
|-------------------|----------------------------------|-------------------------------------|---|-----------------------|----------------------------------|--------------------------------|
| 200 | 0.0391×10^{-14} | 4.92×10^{-8} | -24.6 | 18,200 | 11,650 | 29,850 |
| 225 | 0.0633×10^{-14} | 3.10×10^{-8} | -25.6 | 18,200 | 12,750 | 30,950 |
| 258 | 0.311×10^{-14} | 4.94×10^{-8} | -24.8 | 18,200 | 13,200 | 31,400 |
| 275 | 1.413×10^{-14} | 12.6×10^{-8} | -23.1 | 18,200 | 12,660 | 30,860 |
| 300 | 1.87×10^{-14} | 8.35×10^{-8} | -24.0 | 18,200 | 13,750 | 31,950 |
| 325 | 2.50×10^{-14} | 5.6×10^{-8} | -24.8 | 18,200 | 14,800 | 33,000 |
| 350 | 4.28×10^{-14} | 5.3×10^{-8} | -25.1 | 18,200 | 15,600 | 33,800 |
| 375 | 8.26×10^{-14} | 5.7×10^{-8} | -25.0 | 18,200 | 16,200 | 34,400 |
| 400 | 13.20×10^{-14} | 5.36×10^{-8} | -25.2 | 18,200 | 17,000 | 35,200 |
| 425 | 22.15×10^{-14} | 5.55×10^{-8} | -25.2 | 18,200 | 17,600 | 35,800 |

Table 2 . . . Summary of Data Temperature Effect

| $t^\circ\text{C}$ | $T^\circ\text{K}$ | $\frac{1}{T} \times 10^3$ | $\frac{dW}{dt}$ (micrograms per cm^2 per min) $P = 7.6 \text{ cm O}_2$ | | | | | | |
|-------------------|-------------------|---------------------------|---|-------|-------|-------|-------|--------|--|
| | | | At the Following Thicknesses (micrograms per cm^2) | | | | | | |
| | | | 10 | 20 | 30 | 40 | 50 | 60 | |
| 300 | 573 | 1.7542 | 0.280 | 0.113 | | | | | |
| 325 | 578 | 1.6722 | 0.445 | 0.113 | | | | | |
| 350 | 623 | 1.6051 | 1.46 | 0.345 | | | | | |
| 375 | 648 | 1.5432 | | 1.10 | 0.156 | | | | |
| 400 | 673 | 1.4859 | | 1.79 | 0.459 | 0.173 | 0.125 | 0.0782 | |
| 425 | 698 | 1.4327 | | 5.91 | 1.03 | 0.382 | 0.272 | 0.179 | |
| | | | | | 1.97 | 1.08 | 0.555 | 0.418 | |

parabolic rate law constant as expressed by the transition state theory. The equations for the parabolic rate law constant K and the diffusion constant D_0 are as follows

$$K = \frac{2kT}{h} \lambda^2 e^{\Delta S^*/R} e^{-E/RT}$$

$$D_0 = \frac{K}{2e^{-E/RT}}$$

The significance of the terms has been previously discussed. The parabolic rate law constants vary from $0.0391 \times 10^{-14} \text{ cm}^2 \text{ per sec}$ at 200°C to $22.15 \times 10^{-14} \text{ cm}^2 \text{ per sec}$ at 425°C. In terms of Angstroms of film thickness, the above rates correspond to 2 Å per sec at 200°C to 50 Å per sec at 425°C.

Table 1 shows the values for the parabolic rate law constants and diffusion constants and the entropies, energies and free energies of activation of the rate determining process. The K values are connected to thickness by the use of the density of the oxide and the stoichiometric ratio of oxygen in the oxide. A surface roughness ratio P of 1 is assumed.

The energy of activation 18,200 cal per mol is lower than that observed for several other metals previously studied. The entropies of activation are negative and are close to those observed for the oxidation reactions on iron and aluminum. ΔS^* is a measure of the (frequency factor) or the probability of an ion with a definite energy getting through the lattice. For most metals ΔS^* is negative although tungsten and molybdenum show positive

values. The free energy of activation is made up of the energy of activation E and the term $T\Delta S^*$. The sign and magnitude of the term $T\Delta S^*$ thus determines whether the effective barrier ΔF^* is increased or decreased by the steric factor. The values of ΔF^* for the oxidation of zirconium vary from 29,850 to 35,800 cal per mol. These are somewhat lower than those observed for other metals at 400°C, for example, the ΔF^* for the oxidation of zirconium is 35,200 cal per mol while the following values are obtained for iron, tungsten, molybdenum and aluminum respectively: 39,150, 37,700, 36,260 and 39,900 cal per mol.

2. *Temperature Coefficient as a Function of Film Thickness:* The data shown in Fig 3 are plotted on a large scale and a smooth curve drawn through the points. The slopes of these curves $\frac{dW}{dt}$ are determined for film thicknesses of 10, 20, 30, 40, 50 and 60 micrograms per cm^2 by Lagrange's formula for determining slopes at a given point. These slopes are tabulated in Table 2 at the same film thickness as a function of the temperature. Fig 5 shows the slopes plotted on a logarithmic graph as a function of $\frac{1}{T}$. A series of straight lines of approximately the same slope are observed. This result indicates an approximately constant temperature coefficient over a wide thickness range. This suggests that one mechanism may be responsible for the reaction.

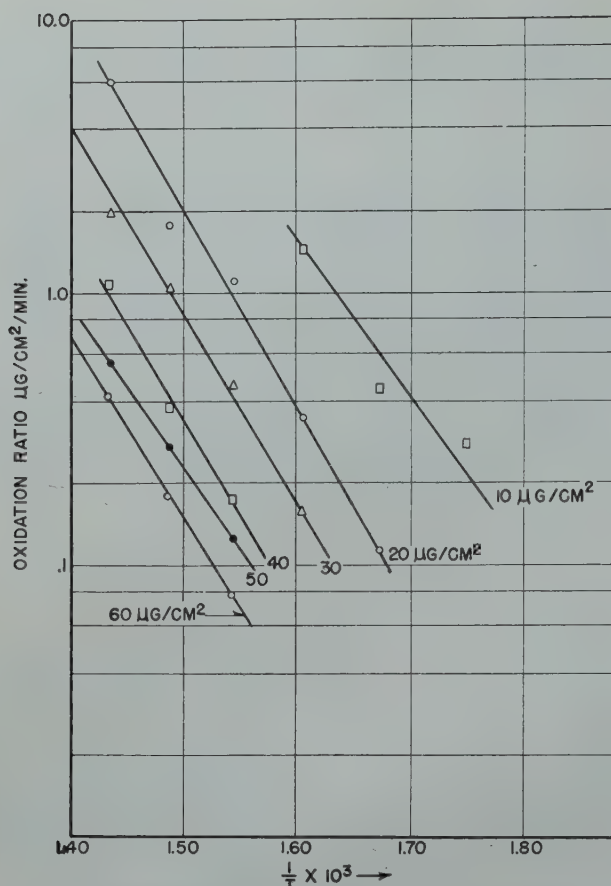


FIG 5—Oxidation rate vs. temperature at film thickness of 10–60-g per cm².

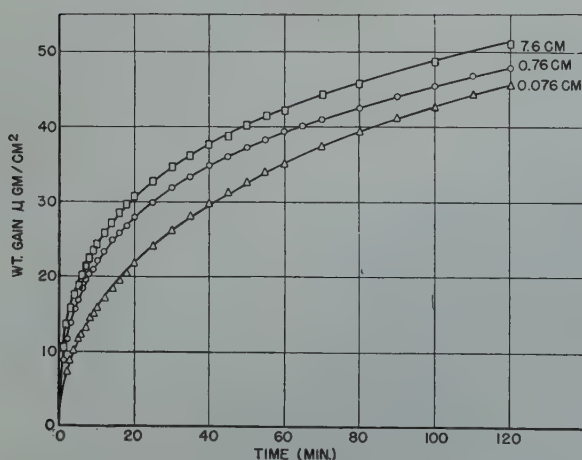


FIG 6—Reaction Zr with O₂ 375°C. Effect of pressure.

Pressure Effect

The effect of pressure on the reaction at 375°C is shown in Table 3 and in Fig 6. The pressure is varied by a factor of 100 from 7.6 cm to 0.076 cm of oxygen. The effect is largest for the thin film range and decreases with increasing film thickness. No simple relationship with the pressure has been determined.

Effect of Abrasion

Fig 7 shows a comparison of the reac-

tion of an abraded sample and an unabraded sample. The abraded sample oxidizes more rapidly than the unabraded sample. The effect may be related to one or more of the following factors: (1) increased surface area, (2) removal of initial oxide film, and (3) change in the size and state of the surface crystals.

REACTION WITH NITROGEN

In this section the reactions of zirconium with purified lamp grade of nitrogen are studied in detail as a

Table 3 . . . Summary of Data Pressure Effect

| Pressure Atmospheres | $\frac{dW}{dt}$ (micrograms per cm ² per min) $T = 375^\circ\text{C}$ | | | | |
|----------------------|---|------|------|------|------|
| | At the Following Thicknesses (Micrograms per cm ²) | | | | |
| | 0 | 10 | 20 | 30 | 40 |
| 0.1 | 15.9 | 5.35 | 1.1 | 0.46 | 0.24 |
| 0.01 | 14.1 | 3.33 | 1.02 | 0.35 | 0.17 |
| 0.001 | 8.6 | 1.36 | 0.82 | 0.31 | 0.20 |

function of time, temperature and pressure and a comparison of two gas sources is used to show the strong effect of impurities. The results are shown in Fig 8–11 and discussed in the following subsections. In all of the figures the weight gain in micrograms per cm² is plotted against the time and where necessary the temperature is given at the top of the graph.

1. *Purity of Nitrogen:* A study of the reaction of nitrogen with zirconium presented the problem of obtaining a sufficiently pure gas to make the reaction with impurities a small part of the nitrogen reaction. To show this effect we can compare the results of the reaction using purified commercial nitrogen and purified lamp grade of nitrogen. The time course of the reaction of the purified commercial nitrogen at 350°C is identical with the reaction using the purified lamp grade of nitrogen at 700°C.

Mass spectrometer analysis of the gases showed the presence of 0.3 pct oxygen in the commercial gas source before purification. The lamp grade of nitrogen shows 0.01 pct. The gas analyses are not complete since hydrogen is not determined at low concentrations by our mass spectrometer.

It is of interest to note that colored films are formed using the purified commercial nitrogen while no films are observed in the experiments at the higher temperatures using the purified lamp grade of nitrogen. Electron diffraction studies show the outer layers of the colored films to be the monoclinic form of ZrO₂ while no diffraction patterns were obtainable with the higher temperature experiments using lamp grade of nitrogen. We do not conclude that no oxide or hydride is formed with the purified lamp grade of nitrogen but rather that the reaction rate is so slow that one has to use a higher temperature to observe an appreciable reaction. The temperatures used in the nitride study are in general above the decomposition temperature of the hydride. At temperatures above 500°C both the

nitride and oxide appear to be soluble in the metal and colored films would not be expected to be observed.

The stability of the nitride to vacua of the order of 10^{-6} mm of Hg has been tested experimentally. The reaction products formed with purified nitrogen at 750°C are stable to temperatures of at least 900°C. However, if the reaction products formed with purified commercial nitrogen at 425°C are heated, part of the product decomposes at 490°C. This may indicate the presence of a nitride of low stability or a hydride. The decomposition of the hydride occurs at about this temperature.

These experiments show: (1) that impurities of oxygen and hydrogen are very important in determining the rate of reaction and (2) that purified lamp grade of nitrogen is a rather pure source of nitrogen.

2. *Time and Temperature:* The time behavior of the nitride reaction for several temperatures from 400° to 825°C is shown in Fig 8. In all of the experiments the reaction rate decreases as the film thickens. The effect of temperature on the reaction rate is quite uniform.

The shape of the weight gain curves indicates that a parabolic rate law may agree empirically with the data. Fig 9 shows a plot of the weight gain squared against the time for the nitriding reaction at 750°C. The agreement is very good even for very small amounts of reaction. The agreement with the parabolic law at other temperatures is tested and except for the 400° and 500°C experiments is found to be good. At the lower temperatures deviations are observed for the initial stages of the reaction.

Although the data may obey the parabolic rate law the mechanism of the reaction may be quite different from the oxidation reaction since the nitride is soluble in the metal at these temperatures.

If we consider that the diffusion of ionic species through the surface film and surface interface reactions is not limiting the reaction it is possible to apply the results of diffusion theory to the reaction.

Van Liempt³² has considered the problem of the degassing of metals and he has by the aid of an approximation method obtained a solution to the problem. His equation is

$$Q/Q_0 = \frac{8}{d} \sqrt{\frac{Dt}{\pi}}$$

Here Q is the quantity of gas evolved

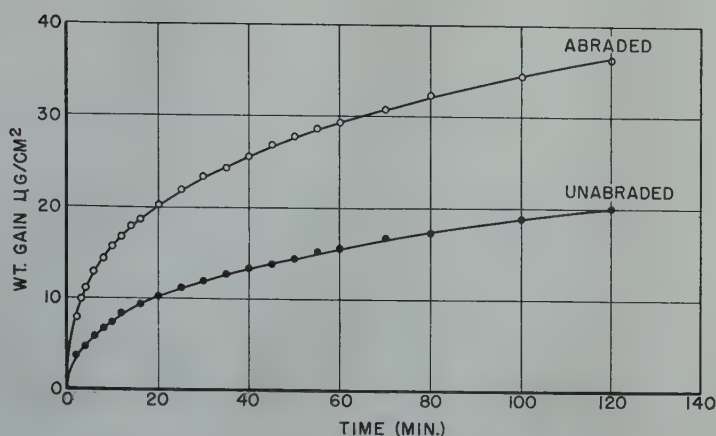


FIG 7—Reaction Zr with O_2 350°C. Effect of abrasion.

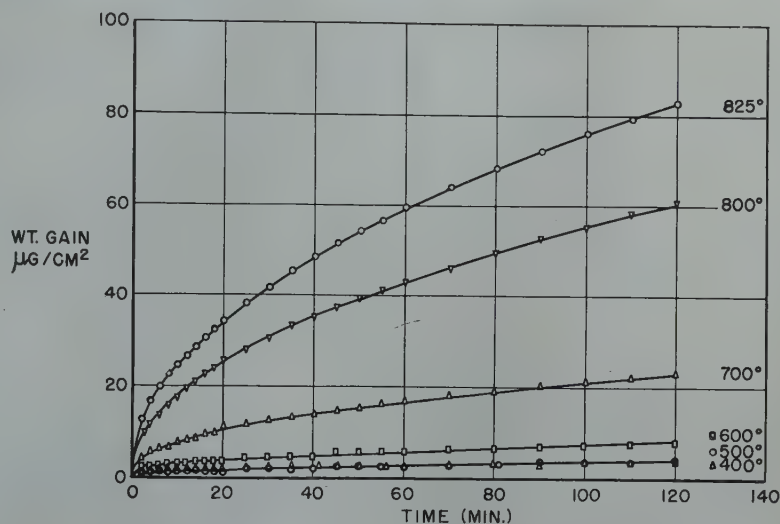


FIG 8—Reaction Zr with pure N_2 —7.6 cm. Effect of temperature.

or taken up at any time t , Q_0 is the original quantity of gas in the metal and D is the diffusion coefficient. This expression can be reduced to the parabolic law,

$$W/W_0 = K\sqrt{t}$$

In the van Liempt expression the only term that depends upon the temperature is D . Since the data fit the parabolic rate law it is of interest to evaluate the temperature dependence and relate this to the energy of activation E for the diffusion process.

Table 4 shows the values of the parabolic rate law constants for the temperature range of 400° to 825°C. Fig 10 shows a logarithmic plot of the parabolic rate law constant against $\frac{1}{T}$. A

straight line is found for the temperature range of 600° to 825°C. Below 600°C the data fall away from a straight line. An energy of activation of 39,200 cal per mol is calculated.

3. *Pressure:* Fig 11 shows the effect of pressure on the time course of reaction with purified lamp grade nitrogen at a temperature of 750°C. The rate of

Table 4 . . . Reaction Zirconium with Nitrogen 7.6 Cm

| Parabolic Rate Law Constants | | | |
|------------------------------|-------------|-------------------|---|
| $t^\circ C$ | $T^\circ K$ | $1/T \times 10^3$ | $K(g \text{ per cm}^2)^2 \text{ per sec}$ |
| 400 | 673 | 1.4859 | 2.082×10^{-16} |
| 500 | 773 | 1.2935 | 1.835×10^{-15} |
| 600 | 873 | 1.1453 | 7.77×10^{-15} |
| 700 | 973 | 1.0276 | 6.85×10^{-14} |
| 750 | 1023 | 0.9774 | 1.90×10^{-13} |
| 800 | 1073 | 0.9319 | 5.13×10^{-13} |
| 825 | 1098 | 0.9107 | 9.60×10^{-12} |

reaction is nearly independent of the pressure in the range of 7.6 cm to 0.15 cm pressure. This evidence indicates that mechanism of reaction is very different from what is observed in the reaction with hydrogen which is presented in Fig 14 and discussed in the section *Reaction with Hydrogen* of this paper. In the case of hydrogen it is shown that the reaction rate is proportional to the square root of the pressure at a given temperature.

Barrer¹ has summarized several systematic studies of the permeation of hydrogen through metals. Two possible

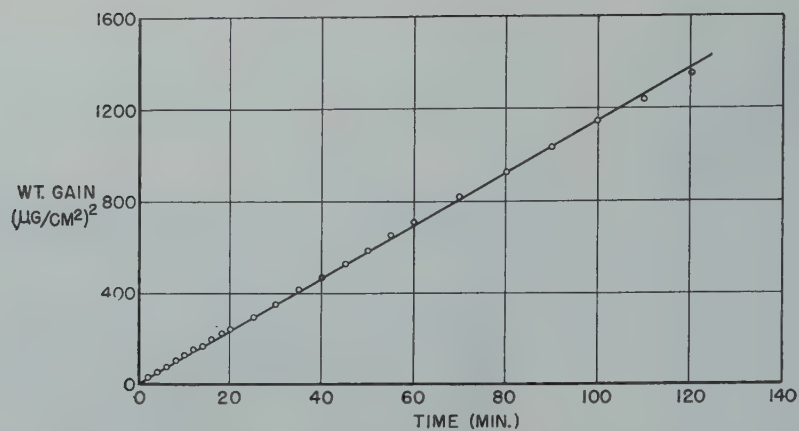


FIG 9—Reaction Zr with pure N_2 —7.6 cm. Parabolic plot.

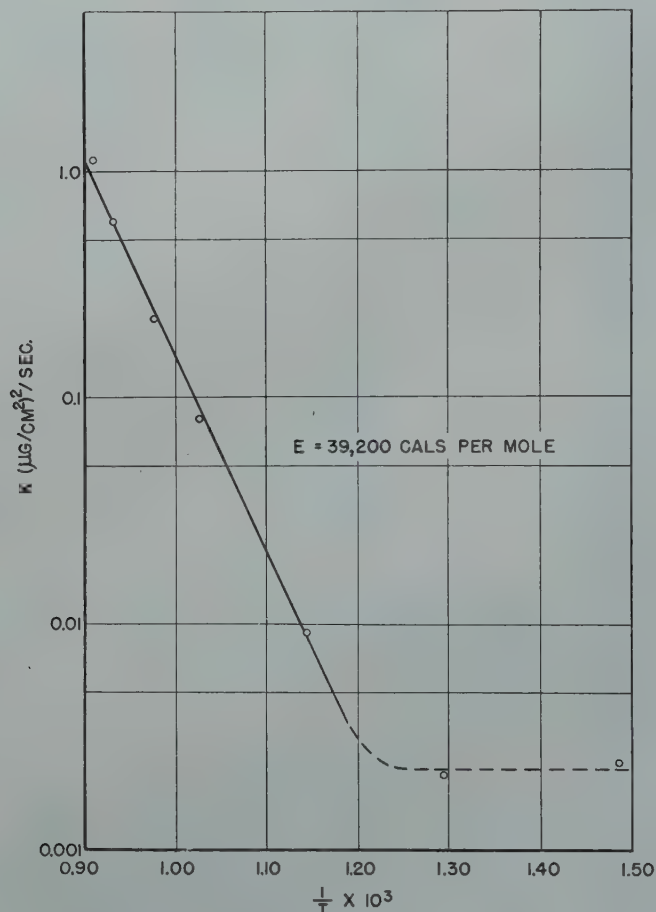


FIG 10—Reaction Zr with pure N_2 — $\log K$ vs. $\frac{1}{T}$.

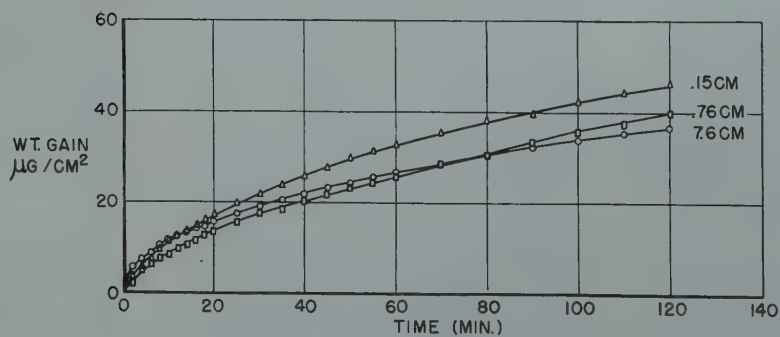


FIG 11—Reaction Zr with pure N_2 —Effect of pressure.

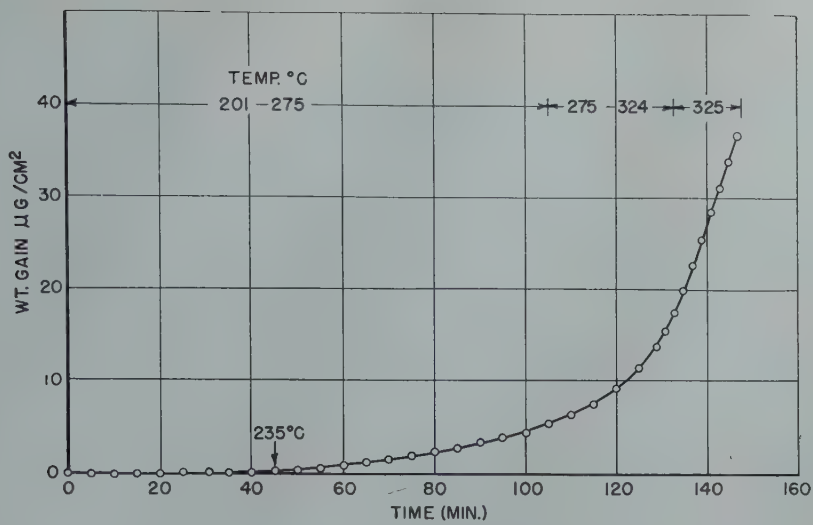


FIG 12—Reaction Zr with H_2 2.2 cm 201°–326°.

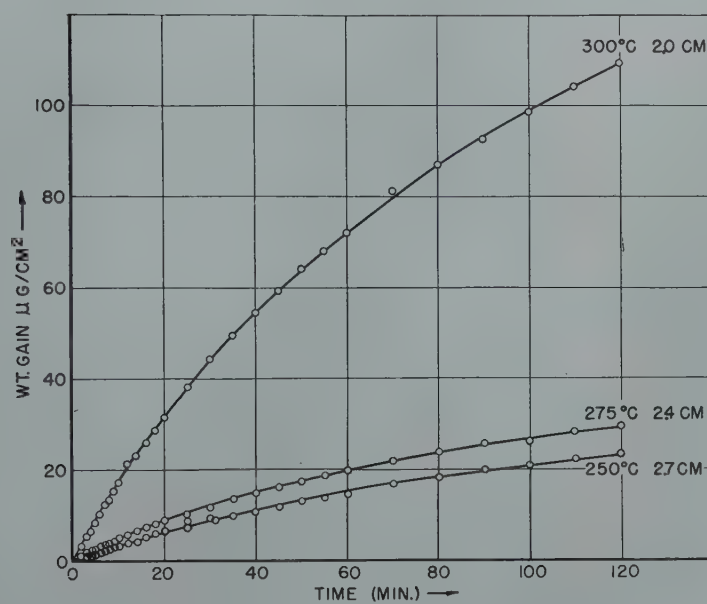


FIG 13—Reaction r with H_2 . Effect of temperature.

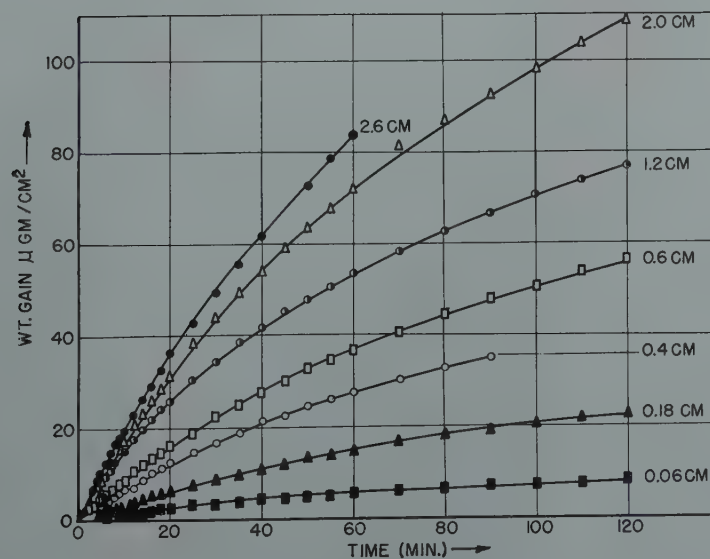


FIG 14—Reaction Zr with H_2 300°C. Effect of pressure.

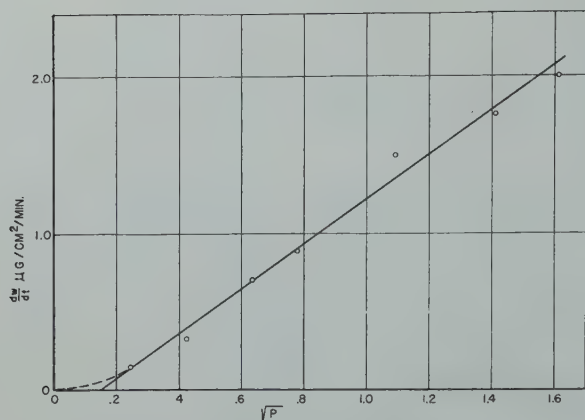


FIG 15—Reaction Zr with H_2 300°C. Initial reaction rate vs. $P^{1/2}$.

rate-pressure relationships have been found:

(1) Activated diffusion without dis-

$$\text{sociation } \frac{dW}{dt} = -kpe^{-b/T}$$

(2) Activated diffusion with dis-

$$\text{sociation } \frac{dW}{dt} = -kp^{1/2}e^{-b/T}$$

Here $\frac{dW}{dt}$ refers to the rate of reaction, p the pressure, t the time, T the temperature and k and b are constants. This expression predicts for the diffusion of atoms in the crystal of zirconium at constant temperature an expression of the type $\frac{dW}{dt} = Ap^{1/2}$.

It is rather surprising that the reaction does not follow one of the rate-pressure relationships. This evidence indicates that the reaction is not occurring on a bare metal surface but rather through a film of the nitride, the nitride in turn dissolving in the metal. Upon evacuation the nitride continues to dissolve but no further film formation is possible. After a certain time bare metal will be exposed and this is the condition in which we find the metal after completion of the experiment. The thickness of the nitride film is governed by the rate of reaction which is a reciprocal function of the thickness and the rate of solution of the nitride. The square root relationship of pressure is not expected to govern a reaction in which a film is present since the nitride is diffusing under a constant concentration gradient.

REACTION WITH HYDROGEN

The reaction is studied as a function of time, temperature and pressure. The stability of the reaction product is studied as a function of the temperature under high vacuum conditions. Fig 12–

16 show the results. The hydrogen is prepared by diffusion through a palladium tube after a preliminary purification. A maximum pressure of 2.6 cm of hydrogen is used in the experiments since greater pressures required rather long preparation times.

Fig 12 shows a preliminary study of the reaction as a function of temperature for a pressure of 2.2 cm of hydrogen. The reaction appears to start at a temperature of 235°C and the rate of reaction increases rapidly with the temperature. A visual examination of the film showed no evidence of a surface film. It is assumed that the hydrogen is dissolving in the metal to form a compound or stable complex. On evacuating the hydrogen from the specimen shown in Fig 12 no decomposition is noticed. This evidence supports the point of view that the hydrogen is forming a compound or complex.

1. *Time and Temperature:* It is of interest to examine the time behavior of the reaction rate. Typical curves are shown in Fig 13 for temperatures of 250° to 300°C. The reaction rate falls off with time. An analysis of the change of slope with time shows that there is no great difference in the way the rate is changing with time for the three curves in spite of the great difference in the amount of hydrogen taken up during the reaction.

The 300°C curve after two hours of reaction shows a hydrogen uptake corresponding to the formula $ZrH_{0.216}$. Hall and co-workers¹⁹ have found a saturation value of $ZrH_{1.95}$ for 20°C. No attempt is made to determine the saturation value.

If the rate determining process in the uptake of hydrogen is the diffusion of hydrogen into the metal, it is possible

to account qualitatively for the decrease in reaction rate as due to a change in the diffusion constant D or to a change in the concentration gradient.

2. *Temperature:* A study of the reaction with hydrogen as a function of temperature is necessary if the details of the reaction mechanism are to be worked out. However, the reaction is very sensitive to the pretreatment and to the presence of surface films. In addition, the reaction is very sensitive to temperature, especially in the temperature range of 275° to 300°C. Very little reaction occurs at 250°C while at 300°C a very rapid reaction rate is observed. The temperature coefficient has not been determined for this reaction.

3. *Pressure:* The effect of pressure on the permeability of metals to hydrogen has been discussed by Barrer¹ and summarized in the section on *Reaction with Nitrogen* of this paper. Two possible rate-pressure relationships were proposed: (1) Activated diffusion without dissociation, and (2) activated diffusion with dissociation. Mechanism (2) is expected to govern the diffusion of hydrogen in metals since the openings in the metal structure are not large enough to allow molecules to diffuse directly.

The reaction rate may then be expressed at a constant temperature as follows:

$$\frac{dW}{dt} = Ap^{1/2}$$

Fig 14 shows the effect of pressure on the time course of the reaction for a temperature of 300°C. The pressure is varied from 2.6 to 0.06 cm. The results show that pressure has a large effect on the reaction.

To test the application of the square root law Fig 15 shows a plot of the initial reaction rate $\frac{dW}{dt}$ as a function of $p^{1/2}$. Good agreement is observed. This correlation shows that the diffusion of hydrogen into the metal is mainly by atoms of hydrogen.

It may be noticed that the curve bends at low pressure and is not linear with $p^{1/2}$ in this range. This effect has been discussed by Smithells and Ransley²⁹ for the permeation of hydrogen through metals. The rate should include a term which is a function of the fraction of surface covered θ .

4. *Stability:* Fig 16 shows the stability of the hydrogen complex with zir-

conium as a function of temperature in a vacuum of 10^{-6} mm of Hg. H_2 is added to zirconium at $250^\circ C$ and 2.5 cm pressure. After evacuation the temperature is gradually raised. The temperature is given at the top of the graph. At a temperature of $436^\circ C$ the hydrogen is given off. All of the hydrogen is removed as is shown in the figure. Above $700^\circ C$ the specimen is reacting with its environment and gaining weight. We are not sure whether the specimen is readsorbing hydrogen and other gases given off by the furnace. The addition of hydrogen to a low pressure appears to increase this reaction.

Conclusion

The kinetics of the reactions of ductile zirconium with oxygen, nitrogen and hydrogen are studied as a function of time, temperature, pressure, surface preparation and stability of the particular film. The vacuum microbalance method is used for all of the measurements.

The oxidation reaction showed an appreciable rate at $200^\circ C$. No simple rate law is found to fit the data over a wide temperature range. However, the modification of the parabolic rate law suggested by Mott predicts the general shape of the time curve. An analysis of the parabolic rate law plots for long periods of reaction time shows straight lines. Using the transition state theory of gas-metal reactions an energy of activation of 18,200 cal per mol and an entropy of activation of -25.6 cal per mol per $^\circ C$ are calculated. These are compared to similar calculations on other metals.

A study of the temperature dependence of the oxidation rate as a function of film thickness shows a constant relationship. This fact suggests that one mechanism is controlling the rate over a wide thickness range. No evidence was found for an unstable oxide.

The nitride reaction is of special interest. The reaction is found to be very sensitive to traces of oxygen and hydrogen in the reacting gas. The rate of reaction of zirconium with nitrogen is much slower than the reactions with oxygen and hydrogen. The data agree well with the predictions of the parabolic rate law although reaction films are not observed on the metal. An energy of activation of 39,200 cal is calculated from the temperature co-efficient of the parabolic rate law constants.

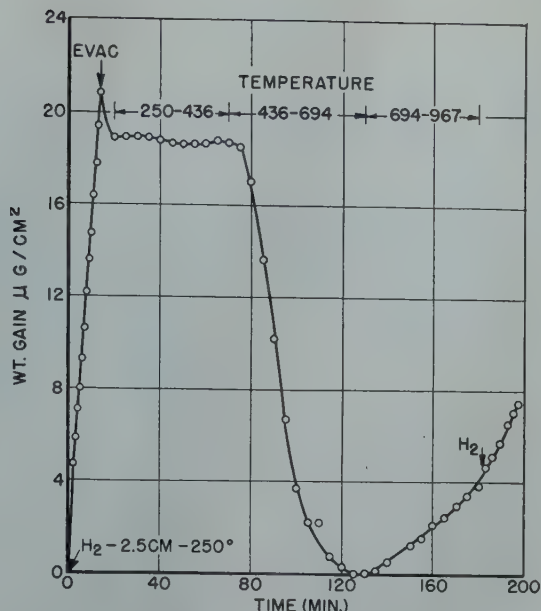


FIG 16—Stability of Zr hydride 250° – $1000^\circ C$.

The nitride reaction is insensitive to pressure and the reaction does not follow any simple pressure function. A theory of the reaction is presented in which the limiting factor is the diffusion of the nitride into the metal under the conditions of a constant concentration at the surface.

The stability of the nitride is tested and the nitride is found to be stable to a temperature of at least $900^\circ C$.

The hydride reaction obeys the square root of pressure law. In this case, a film is not formed and it appears that hydrogen diffuses into the zirconium lattice as atoms. The time behavior of the reaction deviates from a linear law. This deviation may be due to changes in the concentration gradient in the metal or to a change in the diffusion constant. The hydride is stable in vacua up to a temperature of about $440^\circ C$.

References

1. R. M. Barrer: *Diffusion In and Through Solids*. P. 170, Univ. Press, Cambridge (1941).
2. K. Becker and F. Ebert: *Ztsch. f. Phys.* (1925) **31**, 268–272.
3. J. H. de Boer and J. D. Fast: *Rec. trav. chim.* (1940) **59**, 161–167.
4. J. H. de Boer and J. D. Fast: *Rec. trav. chim.* (1936) **55**, 459.
5. W. M. Cohn and S. Tolksdorf: *Ztsch. Phys. Chem.* (1930) **B8**, 331.
6. J. S. Dunn: *Jnl. Chem. Soc.* (1929) 1149–1150.
7. L. F. Ehrke and C. M. Slack: *Jnl. Appl. Phys.* (1940) **11**, 129–137.
8. J. D. Fast: Foote Prints 13, No. 1 (1940).
9. J. D. Fast: Quoted by W. M. Raynor (ref. 27).
10. J. D. Fast: *Metallwirtschaft* (1938) **17**, 641.
11. Glasstone, Laidler and Eyring. *The Theory of Rate Processes*. McGraw-Hill (1941).
12. E. A. Gulbransen: *Trans. Electrochem. Soc.* (1942) **81**, 187–197.
13. E. A. Gulbransen: *Rev. Sci. Instr.* (1944) **15**, 201–204.
14. E. A. Gulbransen and K. Andrew: To be published.
15. E. A. Gulbransen: *Trans. Electrochem. Soc.* (1947) **91**, 431–461.
16. E. A. Gulbransen: *Trans. Electrochem. Soc.* (1943) **83**, 301–313.
17. W. G. Guldner and L. A. Wooten: *Jnl. Electrochem. Soc.* (1948) **93**, 223–235.
18. G. Hägg: *Ztsch. Phys. Chem.* (1931) **B11**, 433.
19. M. N. A. Hall, S. L. H. Martin and A. L. G. Rees: *Trans. Faraday Soc.* (1945) **41**, 306–316.
20. J. D. Hanawalt, H. W. Rinn and L. K. Frevel: *Ind. Eng. Chem., Anal. Ed.* (1938) **10**, 457.
21. J. W. Hickman and E. A. Gulbransen: *Jnl. Anal. Chem.* (1948) **20**, 158–165.
22. S. Hukagawa and J. Nambo: *Electrotech. Jnl.* (Japan) (1941) **5**, 27–30.
23. K. K. Kelley: U. S. Bur. of Mines Bull. (1935) 384, (1937) 407; also Private Communication.
24. N. F. Mott: *Trans. Faraday Soc.* (1940) **36**, 472.
25. N. F. Mott: *Jnl. Inst. Metals* (London) (1946) **72**, 367–380.
26. N. B. Pilling and R. E. Bedworth: *Jnl. Inst. Metals* (1923) **29**, 529–582.
27. W. M. Raynor: Foote Prints (1943) **15**, No. 2, 3–10.
28. O. Ruff and F. Ebert: *Ztsch. anorg. allgem. Chem.* (1929) **180**, 19.
29. C. Smithells and C. E. Ransley: *Proc. Roy. Soc.* (1935) **150A**, 172.
30. G. Tammann and W. Köster: *Ztsch. anorg. allgem. Chem.* (1922) **123**, 196.
31. M. deKay Thompson: *The Total and Free Energies of Formation of the Oxides of Thirty-Two Metals*. The Electrochemical Society, Inc., New York 1942.
32. J. van Liempt: Quoted by Barrer.¹
33. C. Wagner and K. Grünwald: *Ztsch. Phys. Chem.* (1938) **40B**, 455.
34. C. F. Wagner: Private Communication.

Discontinuous Crack Propagation

L. D. JAFFE,* Junior Member, AIME, E. L. REED,* and H. C. MANN*

It has been generally believed that fracture originates at a point and, if the stress is sufficient, propagates across the material from this point. Evidence to the contrary is given in Fig 1. This micrograph shows an area close to the fracture of a steel containing

| C | Mn | Si | Cr | Mo | V |
|------|------|------|------|------|------|
| 0.28 | 0.74 | 0.20 | 1.00 | 0.49 | 0.12 |

The material had been quenched from 1675°F and tempered at 1150°F as a round about 10 in. in diam, and had a static tensile strength of 132,000 psi and a static yield strength of 105,000 psi. The steel was broken in 3000 cycles of reversed bending at a nominal max. fiber stress of 110,000 psi at a speed of 10,000 rpm. It was in the form of a standard R.R. Moore specimen with 45° V-notch, 0.015 in. radius and 0.220 in. diam at base of notch. The fractured edge in Fig 1 is part of the central portion of the specimen which broke during the final sudden fracture.

Attention is directed to the short cracks which appear as dark lines within the specimen. Similar cracks were found in another specimen of the material, broken in 1,798,000 cycles at a nominal stress of 40,000 psi. The cracks were found in several areas close to the path of the final sudden fracture. This final fracture appeared microscopically to be wholly brittle and transcrystalline. Closer to the surface of the specimens, near the path of progressive fracture, which presumably advanced gradually during many cycles, there was microscopic evidence of some local deformation, but no microcracks. Neither were microcracks observed in areas distant from the main fracture path.

The following explanation is offered: In the sudden fracture of the specimen, a crack propagates along a crystallographic plane, with little or no plastic deformation of the adjacent material, until it reaches a grain boundary or a particle of carbide or inclusion which stops its advance. (The particle or boundary may be outside the plane of polish and not visible in the micrograph.) A stress concentration occurs about the end of the stopped crack. One or more new cracks are likely to start in the zone of this stress concentration. They may lie in the same grain as the first crack or in an adjacent

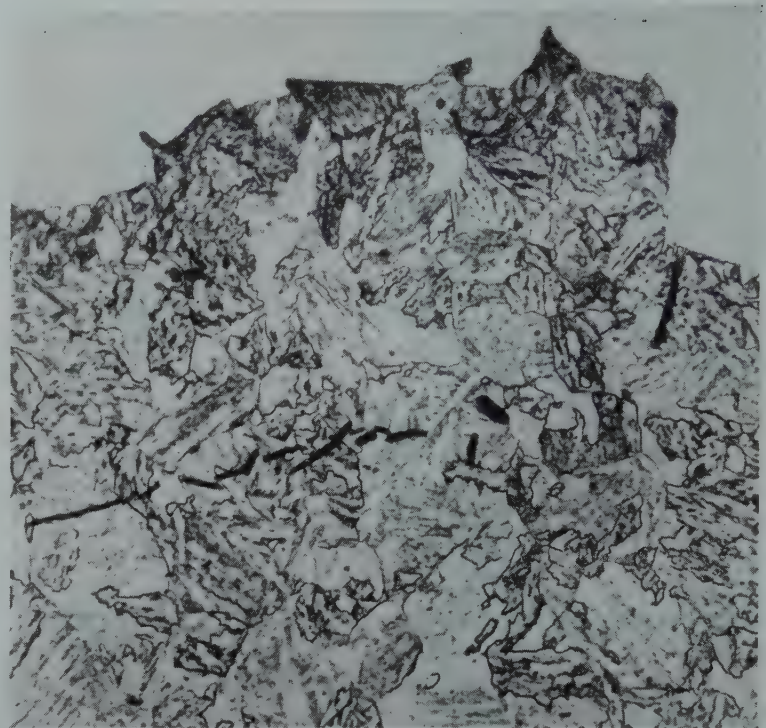


FIG 1—Microcracks near fracture of fatigue test specimen.
× 500. Vilella etch.

grain. New cracks may occasionally start in a nearby but not adjacent grain whose orientation with respect to the stress leads to more ready fracture than does that of the grain between. Once started, these cracks propagate along crystallographic planes in their grains and the process repeats. This leads to discontinuous, branching chains of microcracks.

As the process continues, microcracks probably tend to link up by fracture of intermediate material under the influence of increasing stress concentration. Occasionally, too, there may be a series of nearby grains of similar orientation so that there is a certain continuity of fracture across them. In either case the effective size of a crack is increased, resulting in greater stress concentration at its ends and a greater likelihood of further increase of size of the continuously-fractured region. When one continuous crack crosses the entire specimen, macroscopic fracture has occurred. The fractured edge of the specimen in Fig 1 represents a

series of microcracks which became continuous across the entire specimen. The short, dark-appearing cracks in the figure did not become continuous over a large area. The row of microscopic stress concentrations at their ends may link up with those of the "main crack" outside the plane of polish.

The above explanation does not imply that microcracks develop at the same rate in all portions of the specimen. They will develop most rapidly where the macroscopic tensile stress and macroscopic stress concentration are greatest. Viewed on a scale large compared to the grains, the fracture would appear to progress continuously across the specimen.

Although Fig 1 shows a specimen broken in a fatigue test, it is believed that the microcracks discussed do not depend on the repetitive nature of the stressing used, since they are in the region where "sudden" fracture occurred, presumably in a single stress cycle. The whole process of microcrack propagation outlined above is thought to have occurred during this single cycle.

It is believed that discontinuous crack propagation may be universal in brittle transgranular fracture of crystalline solids. Further experiments are under way.

Technical Note No. 16 E. This note has been published by permission of National Military Establishment. Manuscript received April 4, 1949.

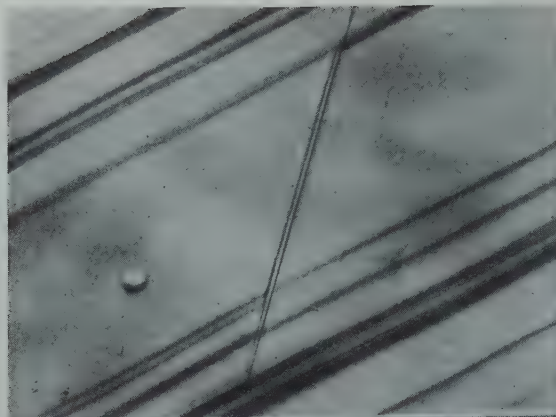
* Watertown Arsenal Laboratory, Watertown, Mass.

[illegible]

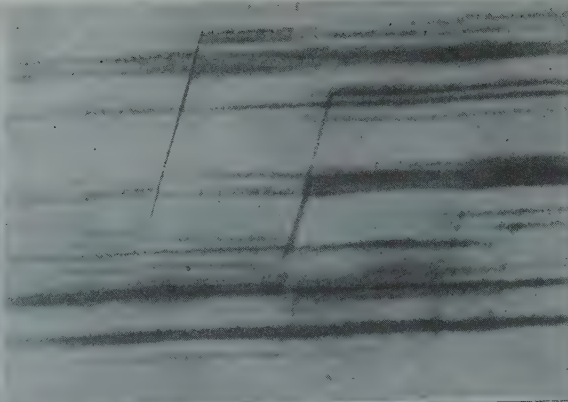
ROBERT MADDIN,[†] Junior Member, C. H. MATHEWSON,[‡] Member, and W. R. HIBBARD, Jr.,[‡] Junior Member AIME

Metals Transactions, Vol. 185 . . . 527

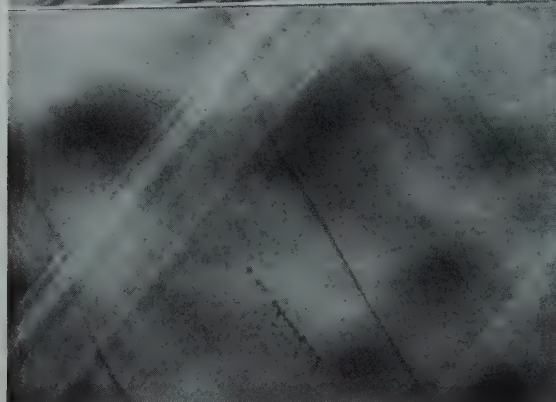
1



2



3



4

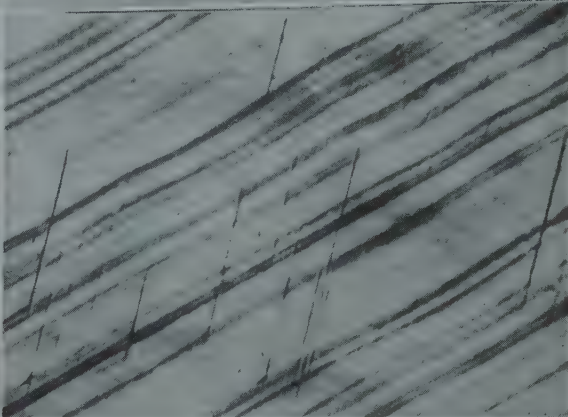


FIG 1—Resolution of cross-slip lines at a position perpendicular to the plane containing the slip direction and the specimen axis. Stress axis is vertical.

Shear is 0.0009. $\times 1000$

FIG 2—Prominent cross-slip at a position perpendicular to the plane containing the pole of the primary glide plane and the specimen axis. Stress axis is vertical.

Shear is 0.053. $\times 1000$

FIG 3—Displacement of a third set of markings by a cluster of primary slip lines at a position perpendicular to the plane containing the pole of the cross-slip plane and the specimen axis. Stress axis is vertical.

(Oblique illumination) Shear is 0.0009. $\times 1000$

FIG 4—Relatively long segmented cross-slip lines at a position perpendicular to the plane containing the slip direction and the specimen axis. Stress axis is vertical.

Shear is 0.102. $\times 1000$

specimen was found in perfect alignment with the classical conjugate slip lines and hence it may be concluded that both effects were caused by the same family of octahedral planes.

In order to observe critically the direction of slip on the cross-slip plane, a crystal was prepared as in the previous manner but without any flat surfaces. It was then extended an amount sufficient to produce a large number of slip lines.

In any metallic single crystal, slip lines are visible because the linear translation of the glide planes displaces the surface. There are, however, two positions (180 degrees apart) on the circumference of a cylindrical crystal at which this displacement is parallel to a surface plane and hence slip lines would not be visible. These positions lie in planes containing the specimen axis and the slip direction.

By observing the presence or absence of cross-slip in planes parallel to the plane containing the specimen axis

and each of the three possible slip directions in turn, the plane of observation in which cross-slip could no longer be observed would identify the direction of slip. The technique becomes critical if the three observation planes are suitably placed about the periphery of the cylindrical specimen. Accordingly, careful microscopic observations were made at all positions on the circumference of the crystal. The position where cross-slip could not be observed coincided with the position where primary slip lines could no longer be seen. Furthermore, since cross-slip could be seen at all other positions, two of the three possible slip directions were eliminated. Hence it may be concluded that both the primary and cross-slip planes possess the same slip direction.

Summarizing this situation, the slip systems involved in the plastic extension of the face-centered cubic alpha brass are: 1. The (primary) system required by the classical Taylor and Elam analysis. 2. A system exhibiting

the octahedral plane which contains the same slip direction as the first octahedral plane, now constituting the active direction as in the other system. 3. The conjugate system required by the classical Taylor and Elam analysis. 4. A system exhibiting the octahedral plane which contains the same slip direction as the plane normally acting in conjugate slip, now constituting the active direction as in the case of the conjugate system.

The slip produced by System 2 was originally termed "cross-slip" because its trace as observed in the first experiments cut across the trace of the primary slip and the early evidence of other cross markings now traceable to the conjugate slip system (acting prematurely) was not conclusive.

It should be noted that the same "cross-slip" plane is associated with both primary slip and conjugate slip but the direction differs in accordance with the associated plane. Therefore, three slip planes and two directions

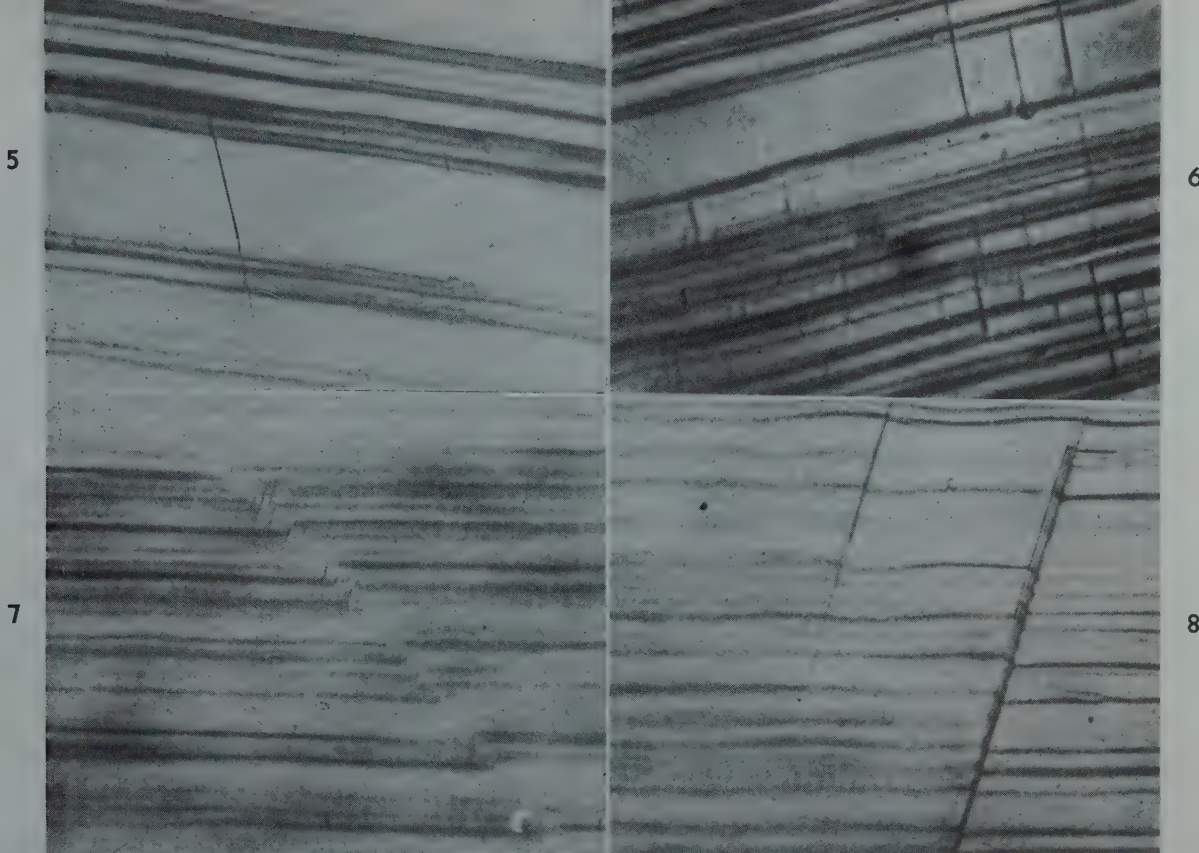


FIG 5—Appearance of primary and cross-slip lines perpendicular to the plane containing the specimen axis and the slip direction. Stress axis is vertical.

Shear is 0.102. $\times 1000$

FIG 6—Clustered cross-slip at a position perpendicular to the plane containing the slip direction and the specimen axis.

Stress axis is vertical.

Shear is 0.174. $\times 1000$

FIG 7—"Twin" appearance of cross-slip at a position perpendicular to the plane containing the pole of the primary glide plane and the specimen axis. Stress axis is vertical.

Shear is 0.174. $\times 1000$

FIG 8—Displacement by cross-slip lines of the primary slip lines at a position perpendicular to the plane containing the pole of the primary glide plane and the specimen axis. Stress axis is vertical.

Shear is 0.257. $\times 1000$

of slip have been observed in these experiments.

X-ray Results

No measurable amount of asterism could be noted in the Laue spots during the deformation corresponding to shears through 0.463. At the beginning of classical conjugate slipping, a large amount of asterism could be observed. In some cases, the streaks encompassed as much as seven degrees.

After the crystal had been elongated 12.8 pct corresponding to a shear of 0.257, Debye rings amounting to at least 20 degrees of arc could be seen in the back-reflection photograms corresponding to areas such as those shown in Fig 8, whereas they could not be observed in photograms representing areas of the type shown in Fig 9. This effect became more pronounced throughout the specimen during the later stages of the deformational

process. At the beginning of classical conjugate slip, the fragmentation rings, sometimes as great as 180 degrees of arc, could be noted wherever there was a dense concentration of cross-slip (Fig 12) but was noticeably absent for areas of the type shown in Fig 13.

The lattice rotations for the various extensions of the specimen are plotted in Fig 15. These rotations follow, generally, the theoretically predicted course. It may be noted, however, that in the initial stages of deformation, the reorientations observed from the X ray data exceeded the calculated; they agreed in the vicinity of the symmetry curve and, in the final stages, the observed reorientations lagged behind the theoretical.

It may be well to point out that for the first five extensions, λ and χ values (λ is the angle between the specimen axis and the slip direction, and χ is the angle between the specimen axis and the primary slip plane) were observed from a series of photo-

grams made only at the center of the specimen, whereas, the λ and χ values for the last seven extensions were averaged from photograms made at the ends and center.

Stress-strain Results

The initial stress-strain curve for the specimen with a constant rate of loading of 100 lb per min. is plotted in Fig 16. Correspondingly, stress-strain curves for several series of consecutive loadings of the crystal to the yield point, generally with the same rate of loading, are plotted in Fig 17, 18, 19 (a larger shear and a ten-fold increase in the rate of loading) and 20. It may be noted that no noticeable rise in proportional limit results from this type of extension. However, by plotting the first loading of each group superimposed upon one another, Fig 21 is obtained, in which it is evident that strain hardening

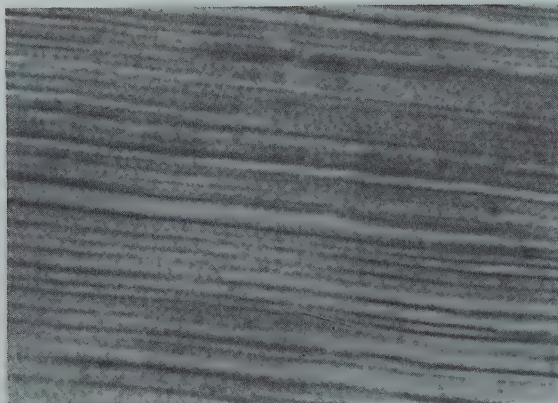


FIG 9—Lack of cross-slip and density of primary slip lines on a surface diametrically opposite to the one shown in Fig 8. Stress axis is vertical. Shear is 0.257. $\times 1000$

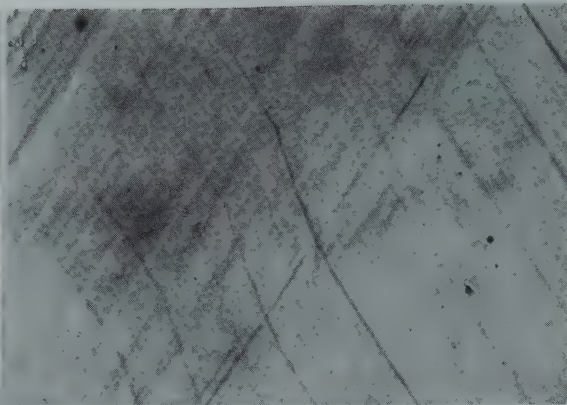


FIG 10—Displacement of the third set of markings by primary slip lines about 30 degrees from a position perpendicular to the plane containing the slip direction and the specimen axis. Stress axis is vertical. Shear is 0.257. $\times 1000$

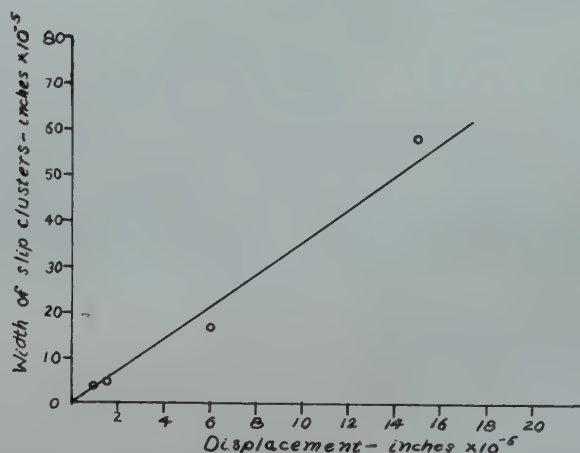


FIG 11—Displacement of the third set of markings by primary slip clusters of different widths. Data obtained from Fig 10.

has occurred. Moreover, the plot of the critical resolved shear stress for each of these curves against the prior shear, Fig 22, is in good agreement with the strain hardening curve for brass of the same composition as reported by von Göler and Sachs.⁶ Whereas the von Göler and Sachs curve, Fig 23, indicates that, shear strengthening begins at a value of shear of about 0.18, the present curve shows that hardening begins at a value located between shears of 0.174 and 0.257. Beyond these points there is apparently a sharper rise in the present curve than in the one reported by von Göler and Sachs.

Discussion of Results

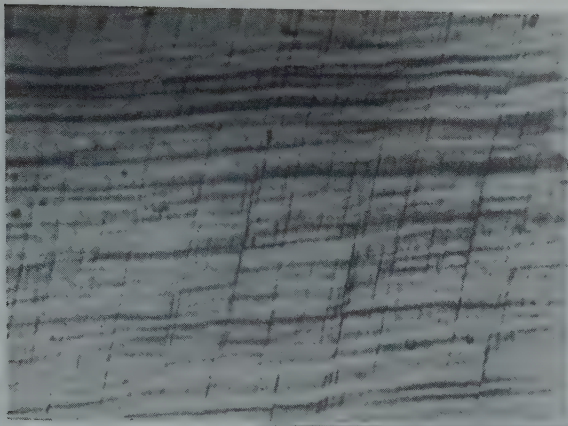
The methods by which the different parts of a metallic single crystal reorient during deformation and at the same time adjust themselves to the constraints of adjacent matrix material and the specimen grip ends have been

the subject of many investigations. These investigations have postulated in the main a bend-gliding mechanism (*Biegeleitung*)⁷ and a crystal fragmentation⁸ followed by the rotation of minute crystallites. Asterism has been cited as evidence of both these mechanisms. However, the absence of asterism and the presence of collateral slip on hitherto unpredicted systems in a strained crystal oriented wholly within the hypothetical single slip region suggest that the above postulated mechanisms can be considerably modified, perhaps in the direction of simplification.

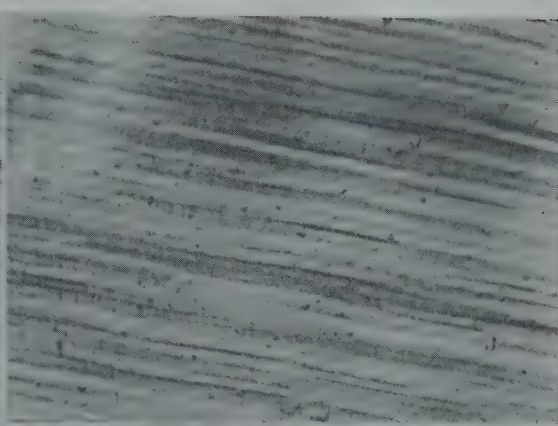
Consider, for example, the constraints imposed by the material adjacent to a latent glide plane. Once slip has occurred along this plane forming a visible slip line at the surface, the crystal has already reoriented. The actual reorientation can be considered as formative during the gliding and completed once the slip line has appeared. Consequently, in order for reorientation to occur, the gliding

plane must be in a state of flexure (of the type reported by Polanyi⁷), caused by the stresses due to the unslipped adjacent material. This bending causes compression of the gliding plane on the concave side and tension on the convex side and is assumed to be directed about an axis in the plane of slip at right angles to the direction of slip ($\langle 112 \rangle$). A set of octahedral planes favorably situated to reduce these stresses would be the conjugate slip planes which cut across the primary planes at a wide angle (70 degrees) and it is not surprising to observe their participation in the process long before the advent of classical conjugate slip. Bending moments arising from the action of these intersecting octahedral planes would be opposite in the rotational sense although not entirely symmetrical since the $\langle 112 \rangle$ axes in question do not lie in the same plane. In order to produce glide plane curvature without plastic action, the potential glide plane would have to be bent elastically in the modified sense of elastic shear and flexure outside the range of perfect elastic behavior, that is, by an anelastic process or an initial elastic stage of flexural gliding. However, instead of full flexural glide, relief could take place by action of the conjugate slip planes just prior to slip on the primary glide plane carrying the highest conventionally resolved shear stress. It might be predicted, therefore, not only that a set of secondary markings would always be associated with the primary slip lines but that this set would also be displaced by the primary lines. This was found to be the case with the present specimens in which the markings in question have been described as the third set, and with other

12



13



14



FIG 12—Dense cross-slip at a position perpendicular to the plane containing the pole of the primary glide plane and the specimen axis. Stress axis is vertical.

Shear is 0.973×1000

FIG 13—Absence of cross-slip at a position diametrically opposite the one shown in Fig 12. Stress axis is vertical.

Shear is 0.973×1000

FIG 14—Conjugate slip cluster showing cross-slip in both the conjugate slip cluster and the primary slip lines at a position perpendicular to the plane containing the pole of the primary glide plane and the specimen axis. Stress axis is vertical.

Shear is 0.973×1000

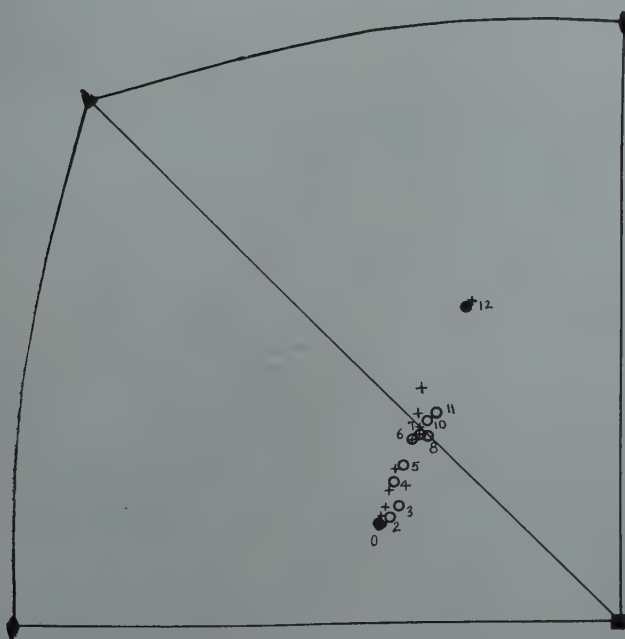


FIG 15—Theoretical and observed lattice rotations for crystal investigated. Numbers refer to specific loading.

+ Theoretical position after successive loading
o Observed positions

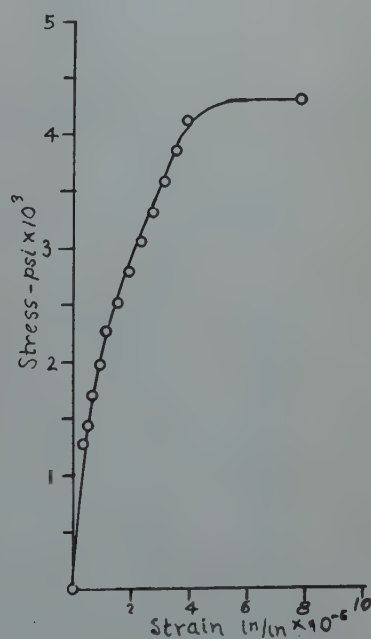


FIG 16—Initial stress-strain curve.

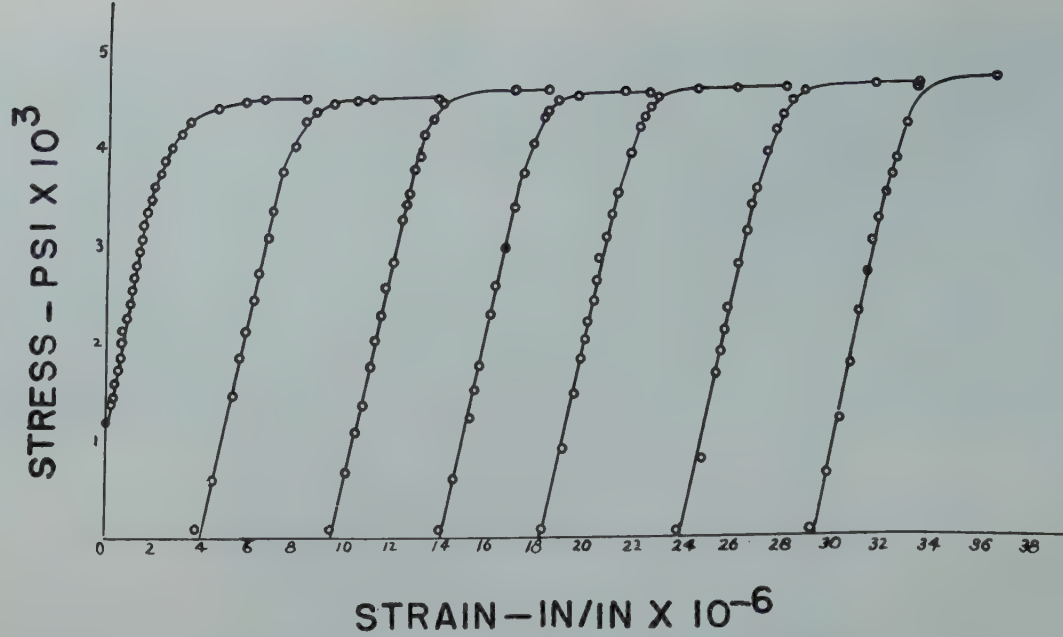


FIG 17—Seven consecutive loadings of the specimen to its yield point.
Prior shear is 0.174.

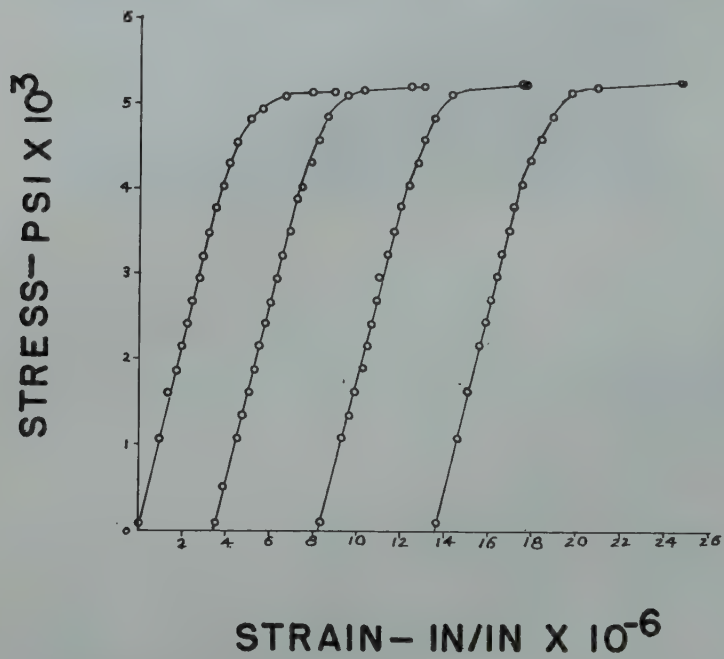


FIG 18—Four consecutive loadings of the specimen to its yield point.
Prior shear is 0.257.

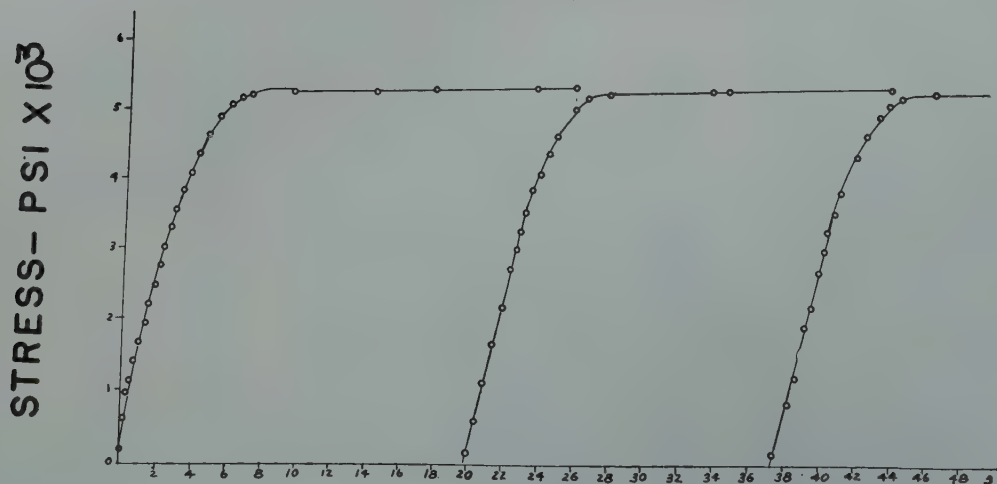


FIG 19 (left half)—Six consecutive loadings of the specimen to its yield point. Rate of loading is 1000 lb per min.
Prior shear is 0.265.

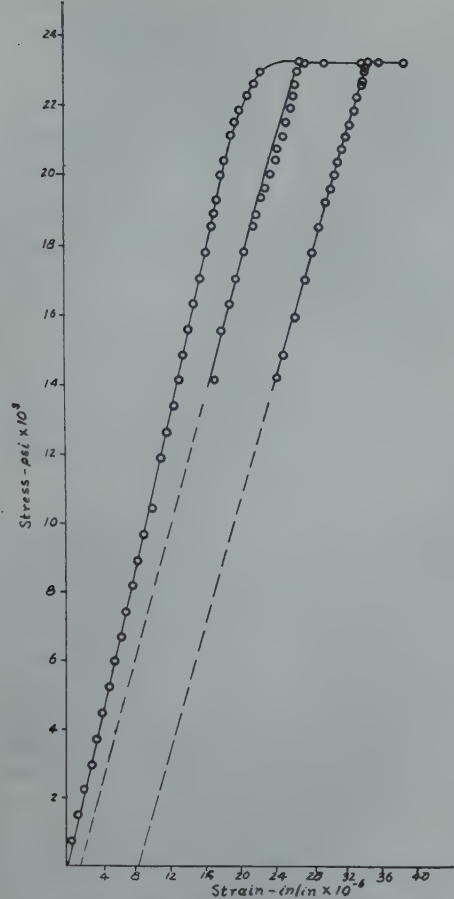


FIG 20—Three consecutive loadings of specimen to its yield point.
Prior shear is 0.973.

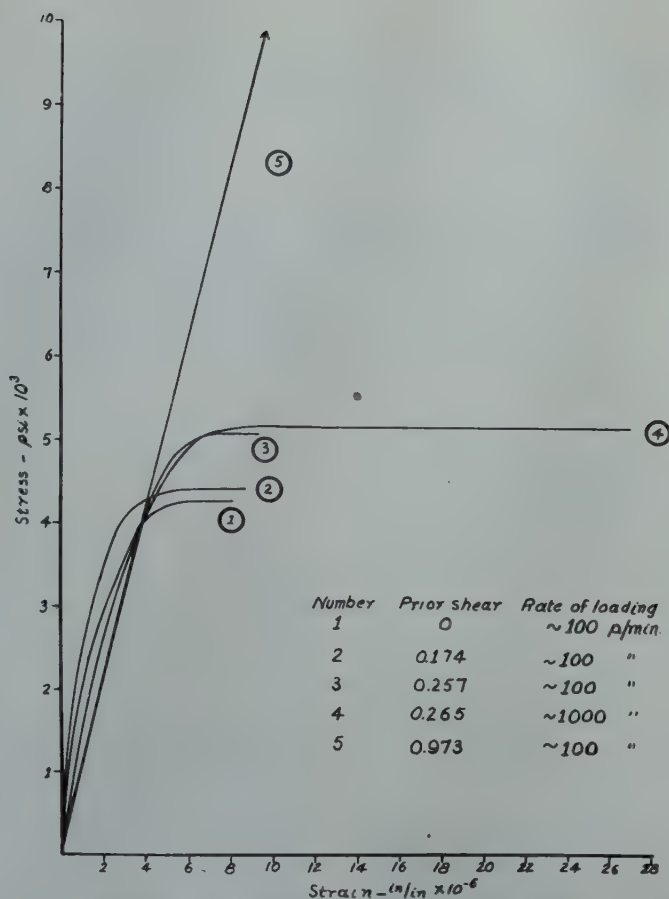


FIG 21—Superimposed stress-strain curves for the first loading of each total extension shown in Fig 16, 17, 18, 19 and 20.

crystals investigated in the Hammond Laboratory.

The cross-slip plane was identified as the one having a common slip direction with the major slip plane. Since it has also been found that the slip direction is the same for both the cross-slip plane and the major slip plane, shear may now be pictured as occurring simultaneously along a pair of planes forming steplike folds, with the cross-slip plane corresponding to the short leg of the fold. Whether this

can be clarified in the mechanics of stress action in a perfect crystal with regard for inhomogeneities at the stepped ends of the lamellae, or must be explained in terms of dislocations or other abnormalities in the crystal must be determined by further study.

In the initial stages of the deformation process, back-reflection Laue photographs were made with the X ray beam incident in the central region of the crystalline rod where the major deformation had occurred as shown

by the much larger number of slip lines in this area. Consequently, the lattice reorientation observed from the X ray data exceeded the reorientation as calculated from the initial and final gauge lengths representing the over-all elongation of the specimen. In the vicinity of the symmetry curve where the theoretical and observed reorientations agreed, slip had taken place throughout the crystal and the X ray data represented an average of exposures made at different points of

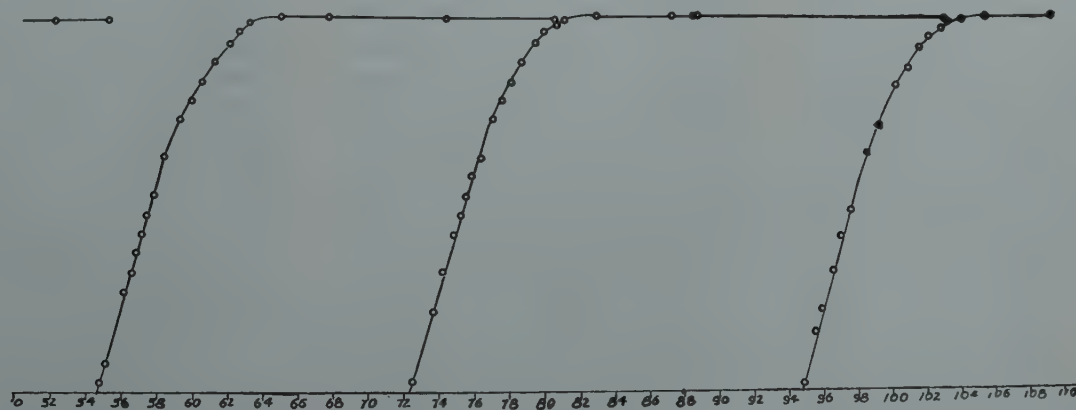


FIG 19 (right half)—Strain—in/in $\times 10^{-6}$.

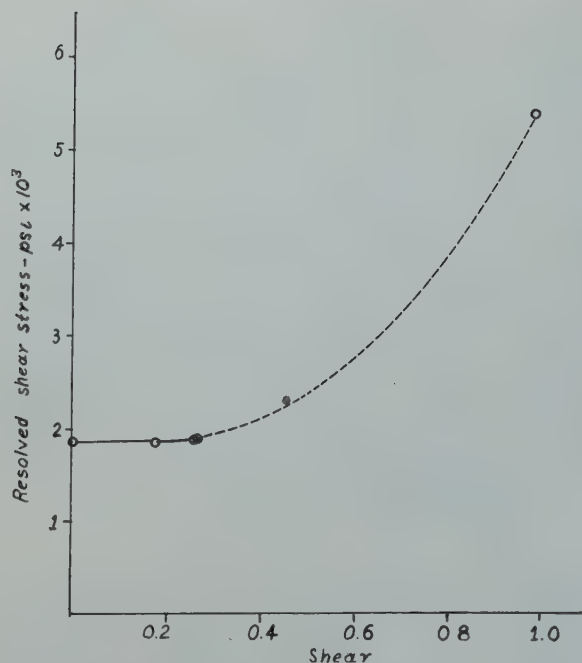


FIG 22—Shear strengthening curve for specimen investigated.

the specimen and thus gave a more truly representative macro-history of the lattice reorientation.

In the later stages, the observed reorientations lagged behind the theoretical ones. This lag has previously been reported by von Göler and Sachs.⁶ An explanation of this latter behavior might stem from a consideration of the additional amount of glide on the cross-slip planes as compared with the small amount during the early stages of deformation. Cross-slip first occurred either simultaneously or in close association with primary slip since neither the primary nor the cross-slip lines were displaced. During the later stages of deformation, however, additional glide occurred on the cross-slip planes as noted by their displacement of primary lines. In this way, the theoretical reorientation did not represent the true reorientation since it gave no account of glide on the cross-slip planes.

Although consecutive loadings to the yield point show no strain hardening, shear strengthening can be observed after the separate extensions. One possible explanation for this behavior might be sought in the hypothesis that recovery rates are greater while deformation is proceeding than after deformation has stopped.

Summary

The observations reported seem to suggest that plastic deformation in single crystals of alpha brass of

approximately 70-30 composition begins by gliding on octahedral planes possessing cross-slip folds. This stage of the deformation process is not accompanied by measurable strain hardening. To cause slip to proceed along planes segmented into folds would conceivably require a greater stress than along other planes and, consequently, slip is diverted to undisturbed areas. Hence there would be no over-all measurable strain-hardening. When all available unslipped areas are eliminated, it would seem that greater stress would be required to cause further glide in previously slipped areas. This stage of the deformation process appears to be the beginning of shear strengthening and would be accompanied by the occurrence of further glide on the cross-slip and primary slip planes. Since shear strengthening begins to occur at about the point where additional glide has also occurred on the cross-slip planes as well as on the primary planes and since this stage of the deformation process is accompanied by notable fragmentation wherever there is a large amount of prominent cross-slip it would seem that shear strengthening may be caused primarily by the necessity of forcing glide along planes segmented into folds. With additional deformation which increases fragmentation, the stress rises sharply until the classical stage of conjugate slip begins. Cross-slip also occurs during conjugate slip and on the same slip plane that operated before true conjugate slip began.

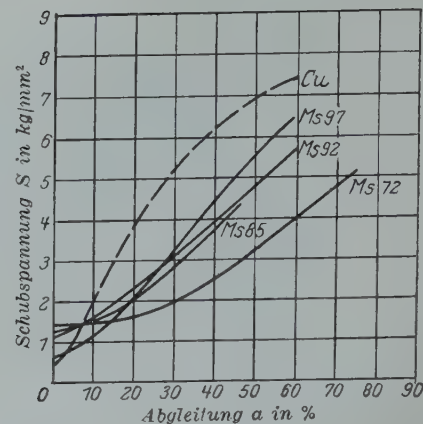


FIG 23—Shear strengthening curves for copper and a series of brasses.
(von Göler and Sachs)

When associated with either the primary or conjugate slip plane it assumed the appropriate common direction.

Acknowledgment

The authors' thanks are due to the Bridgeport Brass Company for having supplied the brass rod from which the crystals were made.

References

1. Maddin, R., Mathewson, C. H. and Hibbard, W. R. Jr.: Unpredicted Cross-slip in Single Crystals of Alpha Brass. *Metals Tech.* Feb. 1948, TP 2331. *Trans. AIME* (1948), 175, 86.
2. Maddin, R.: Anomalies in the Appearance of Glide Ellipses. *Metals Tech.* Feb. 1948, TP 2332. *Trans. AIME* (1948), 175, 355.
3. Taylor, G. I. and Elam, C. F.: Distortion of an Aluminum Crystal. *Proc. Roy. Soc.*, (1923), A102, 645.
4. Greninger, A. B.: A Back-reflection Laue Method for Determining Crystal Orientations. *Trans. AIME*, (1935), 117, 61.
5. Heidenreich, R. D.: Electron Microscope and Electron Diffraction Study of Slip in Metal Crystals. *Jnl. Appl. Physics*, (1947), 18, 11, 1029.
6. von Göler, F. and Sachs, G.: Zugversuche an Kristallen aus Kupfer und Alpha Messing. *Ztsch. Physik*, (1929), 55, 581.
7. Polanyi, M.: Deformation, Rupture and Hardening of Crystals. *Trans. Faraday Soc.*, (1928), 24, 72.
8. Taylor, G. I.: Resistance to Shear in Metal Crystals. *Trans. Faraday Soc.*, (1928), 24, 121. (cf Collins, J. A., and Mathewson, C. H.: Plastic Deformation and Recrystallization of Aluminum Single Crystals. *Trans. AIME*, (1940), 137, 150; Burgers, W. G., and Lource, P. C.: Zusammenhang Zwischen Deformationvorgang und Rekristallizationstextur bei Aluminium. *Ztsch. Physik*, (1931), 67, 605; Andrade, E. N. da C., and Roscoe, R.: Glide in Metal Single Crystals. *Proc. Phys. Soc.*, London (1937), 49, 2, 152; Barrett, C. S., and Levenson, L. H.: Structure of Iron after Drawing, Swaging and Elongation in Tension. *Trans. AIME* (1939), 135, 327.)

The Effects of Molybdenum and Commercial Ranges of Phosphorus upon the Toughness of 0.40 Pct Carbon Chromium Steels

M. BAEYERTZ,* Member AIME, W. F. CRAIG, JR.* and J. P. SHEEHAN*

This paper deals with molybdenum modifications of 5140 steel that have the same hardenability but a better tolerance for phosphorus than the AISI-SAE 5140 grade. Lack of toughness in steels with higher than normal phosphorus contents is well known to metallurgists. This problem is troublesome even within normal phosphorus ranges, if the heat treatment or the design of the part or the service is critical. Under such unfavorable conditions and also in the case of phosphorus contents toward the upper side of the commercial range, the use of molybdenum to replace a part of the chromium in 5140 steel provides a factor of safety.

The toughness of steel is variously exhibited in different mechanical tests; broadly the term is applied to the capacity of the steel to deform prior to fracture. Defined in this way, toughness is considered to be an inherent quality that depends upon the composition and structure of the steel, and also upon its temperature during deformation and fracture in the test. In the present state of our knowledge, the type of mechanical test needs to be included in any discussion of toughness, because the revelation of this quality in steel depends on the stress state and rate of stressing imposed by the test.

In comparing the toughness of one steel with another by laboratory testing, it has long been customary to use notched tests that impose severe constraint to deformation, and then to test over a range of temperatures to obtain the so-called transition. At temperatures above the transition, the steel fails after considerable deformation and absorption of energy. Below the transition, less energy is absorbed as the steel fails largely by cleavage. The transition range itself is characterized by a more or less abrupt change

in energy absorption and type of fracture. The conventional V-notch Charpy impact test has been used exclusively in the work covered by this report. For the steels under study, rather sharp transitions are obtained with this test, at testing temperatures that are easily obtained in the laboratory. The position of the transition on the testing temperature scale provides a rather sensitive index of the toughness of the steel, when the steels under study are similar in character as they are in this work.

Turning to the metallurgical reasons for the greater toughness of one steel as compared to another, the authors propose to limit the discussion to the small field under study. Only one structural state is considered, tempered martensite of a hardness of about 28 Rockwell C or 269 Brinell. The study deals first with the loss of toughness in AISI-SAE 5140 steel caused by increasing the phosphorus content from about 0.020 to 0.040 pct. A second part of the work deals with counteracting this loss in toughness by replacing a part of the chromium by molybdenum. A series of molybdenum modifications was studied, in each of which the chromium was reduced sufficiently to duplicate the hardenability of 5140 steel.

Phosphorus affects the toughness of steel in two ways. An inherent lack of toughness of phosphorus-bearing ferrite as compared to low phosphorus ferrite has often been noted. Jolivet and Vidal¹

have shown that phosphorus has the same effect in tempered martensite in chromium steels. The other well known effect of phosphorus is to make steel susceptible to temper embrittlement. Temper brittleness is a loss in toughness brought about by tempering steel within a limited temperature interval somewhat below the A_1 temperature. In most of the standard AISI-SAE alloy steels, this temperature interval is approximately 850–1100°F. Either of these types of loss in toughness is easily followed by the shift in the transition temperature obtained with the notched-bar impact test. The data to be presented show the beneficial effect of substituting molybdenum for a part of the chromium in 5140 steel with either moderate (0.020 pct) or high (0.040 pct) phosphorus contents. Both the inherent lack of toughness of phosphorus-bearing steel and temper brittleness are counteracted by this use of molybdenum.

The work of Jolivet and Vidal mentioned above shows the detrimental effect of phosphorus on the toughness of tempered martensite in the absence of temper embrittlement, as well as the temper brittleness caused by phosphorus. They used two steels, essentially 0.25 pct C-1.4 pct Cr, with 0.044 and 0.012 pct P, respectively. The nonembrittled state was obtained by quenching in oil from 1610°F, then tempering for one hour at 1200°F and quenching in water. In this state the transition temperature range of the low phosphorus steel in the notched-bar impact test was below that of the steel with 0.044 pct P. An additional treatment of 24 hr at 975°F (that is, in the embrittling range) caused both steels to lose toughness, but the high phosphorus steel showed the greater embrittlement.

Recently Hollomon² has published a comprehensive survey and bibliography of the literature on temper brittleness, to which the reader is re-

Cleveland Meeting, October 1949.
TP 2654 E. Discussion of this paper
(2 copies) may be sent to *Transactions*
AIME before December 1, 1949.
Manuscript received June 22, 1948;
revision received May 2, 1949.

* Armour Research Foundation of
Illinois Institute of Technology.

¹References are at the end of the
paper.

ferred for a general review of the subject. Carbon, nitrogen, phosphorus, oxygen, and various alloying elements as well have been blamed for the embrittlement. Other pertinent papers have appeared subsequently. Cohen, Hurlich, and Jacobsen³ and McLean and Northcott⁴ have studied metallographic etchants for revealing the temper brittle state. Pellini and Quenau⁵ have obtained data which they interpret as indicating carbon to be the cause of temper brittleness. Their conclusion is based on the observation of isothermal development of brittleness at temperatures below the A_1 temperature but above that of the iron-nitrogen eutectoid. In the light of data to be presented later in this paper, it may be noted that their steel that developed brittleness at this high temperature contained 0.029 pct P, an amount which might be suspected as the cause of the embrittlement.

The inception of the case against phosphorus, as a factor in temper brittleness, dates from World War I. However, in this early work and to some extent in later investigations conclusions are based on tests made only at room temperature. Andrew⁶ reported that steels with phosphorus in the lower part of a range of 0.01 to 0.058 pct did not exhibit temper brittleness, while in the upper part of this phosphorus range the difference in impact strength between water quenched and slowly cooled specimens was as much as 50 pct.

Ashdown⁷ stated that temper brittleness was observed in large chromium-nickel steel forgings with phosphorus contents of 0.03 to 0.04 pct while he also observed its absence in aircraft crankshaft forgings of the same steel except with phosphorus below 0.02 pct.

Data presented by Andrew⁶ and also by Green⁸ show the influence of phosphorus in a series of 0.35 pct C-3.5 pct Ni steels alike in composition and treatment but with variable phosphorus content. The 0.018 and 0.039 pct P steels had susceptibility ratios of one; in those with 0.058 pct and higher phosphorus contents the ratio rose consistently with the phosphorus content. The susceptibility ratio is the impact value of the unembrittled steel divided by that of the same steel in the embrittled state. The ratio applies to a single testing temperature, usually room temperature.

Greaves and Jones⁹ obtained similar data using Cr, Ni and Cr-Ni steels with about 0.3 pct C, from which they concluded that phosphorus up to 0.04

pct has little influence on temper embrittlement but that higher phosphorus has a marked effect in raising the susceptibility ratio.

Reporting work on various plain carbon and alloy steels, Mauer, Wilms and Kiessler¹⁰ and also Bischof and Bottger¹¹ have added to the observations of the deleterious effect of phosphorus.

Bennek¹² studied the role of phosphorus in temper brittleness using susceptibility ratios, and in some instances supplemented these with determinations of the impact transition curves. Phosphorus contents ranged from less than 0.01 to 0.11 pct. Manganese, Ni, Cr, Cr-Ni and Cr-Ni-Mo steels were employed. Carbon contents were between 0.25 and 0.30 pct. Prolonged heating either above or below the critical range lessened the intensity of embrittlement developed on subsequent heat treatment; presumably phosphorus diffused from regions of high phosphorus segregation during the anneal. The low phosphorus steels exhibited little or no temper brittleness provided that the alloy content was restricted to 1.5 pct Mn, Ni, or Cr; however, a steel with 3.58 pct Ni, 0.92 pct Cr and only 0.012 pct P showed a marked shift in transition temperature on furnace cooling compared to water quenching after tempering. This apparent influence of hardenability on susceptibility to temper brittleness seems of importance, although, for fully hardened specimens, a reason is not obvious.

The greater tendency to embrittlement in steels containing both chromium and nickel, as compared to either alone, had often been observed by investigators of temper brittleness. Recently Hollomon² has shown a rather consistent relationship between the susceptibility ratio (specimens broken at -40°F) and the combined hardenability contributed by manganese, nickel, and chromium in a series of twenty-one 0.30 pct C, Cr-Ni-Mo steels. Manganese varied from 0.76 to 1.52 pct, nickel from a trace to 3.41 pct and chromium from 0.45 to 2.57 pct. Phosphorus was hardly variable as the entire range for the series was 0.009 to 0.014 pct.

Plan of Investigation

In the present work, a straight chromium grade was chosen to avoid the confusion of a number of alloying elements. Heats of 5140 steel were made

with phosphorus contents varying between 0.020 and 0.036 pct. The lower side of the phosphorus range was selected in an attempt to duplicate a usual residual for open hearth steels. The upper side was chosen to fall within the AISI-SAE specification for the grade. Then, because molybdenum has been the element most widely used for reducing or delaying the onset of temper brittleness, another series of modified 5140 steels was studied in which a part of the chromium was replaced by molybdenum, keeping the hardenability essentially constant. Phosphorus was varied as in the 5140 series.

It might be argued that reduction in chromium content would assist in reducing the susceptibility to temper brittleness but, in adding molybdenum, either the hardenability of the steel or the basic 5140 composition must be altered. In view of the apparent relation between hardenability and temper brittleness noted by many investigators and also from the standpoint of providing a steel with the same hardenability as 5140 but with a good tolerance for phosphorus, the substitution of molybdenum for part of the chromium seemed the best procedure, and the one of greatest commercial significance. If molybdenum were added to the 5140 base analysis without reduction in chromium, the 4140 grade of considerably higher hardenability would be approached.

In both the 5140 steels and the molybdenum modifications aluminum was used to produce fine grained steels, which would be comparable with a large part of the commercial production of 5140. Another reason for adding aluminum was to remove both oxygen and nitrogen from the metal phase and thus materially reduce the possibility of a contribution to temper brittleness by these elements.

The tempering treatments were illustrative of common commercial cycles. In considering the choice of a tempering cycle, it is desirable to have reference specimens in an unembrittled state of the same hardness as the embrittled specimens. In isothermal studies this has been done by tempering all specimens between the A_1 temperature and the embrittling range and then quenching in oil or water. Subsequent isothermal treatment in the embrittling range does not change the hardness materially, and the quenched specimens without subsequent isothermal treatment provide a nonembrittled norm.

While isothermal tempering of small

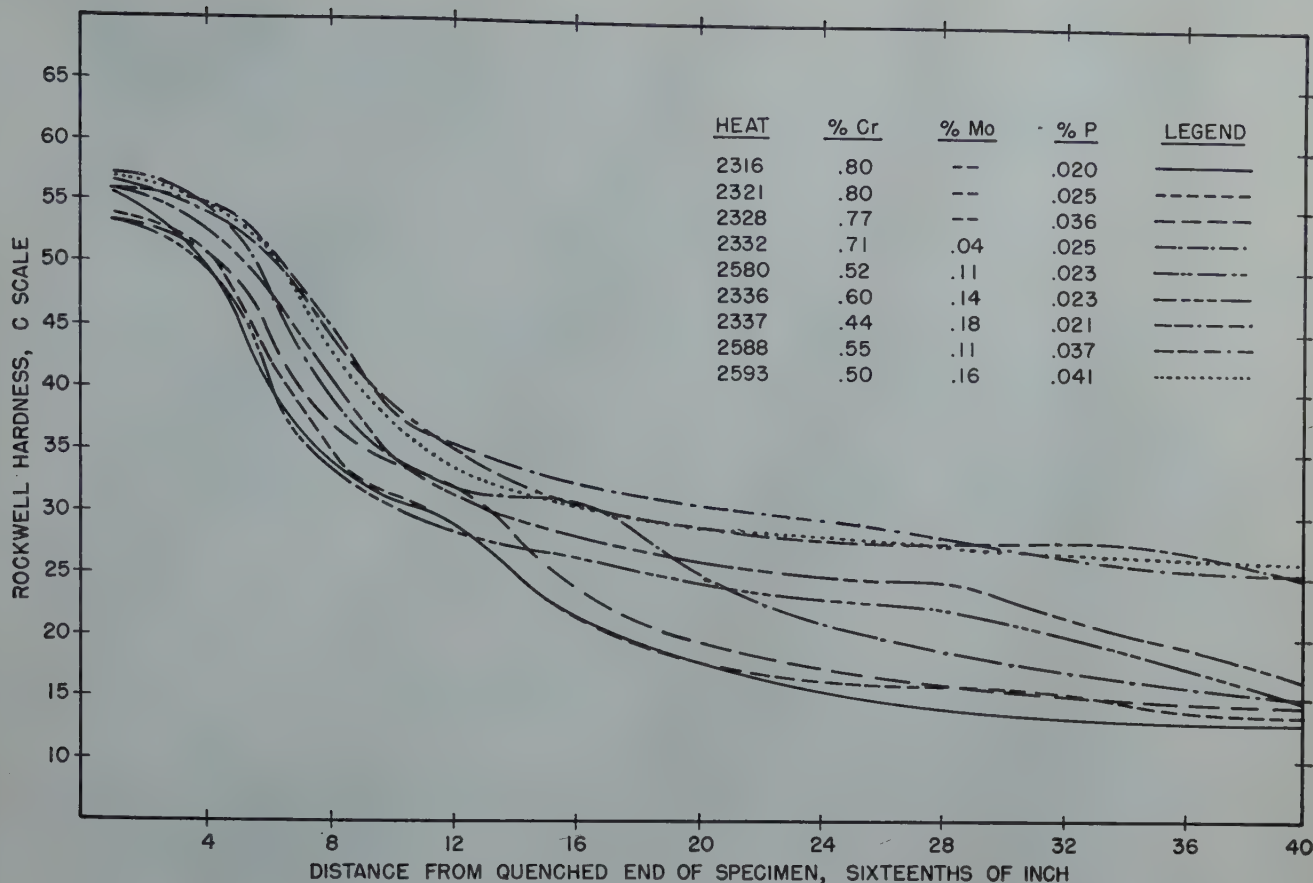


FIG 1—Hardenability band of 5140 and molybdenum-chromium steels with variable phosphorus.
Standard Jominy test, quenching temperature 1550°F.

specimens is attractive for the study of the embrittling reaction, it does not simulate commercial practice in the tempering of machine parts in which loss of toughness would be of practical importance. For the purpose of this work it seemed preferable to temper above the embrittling range and to obtain progressive embrittlement by cooling at various rates through the temper brittle range. A tempering temperature of 1150°F and a range of cooling rates wide enough to simulate those generally encountered in commercial heat treatment were chosen. Specimens quenched in water from the tempering temperature provided a non-embrittled norm for the evaluation of temper brittleness, and also for determination of the effect of the replacement of chromium by molybdenum on toughness in the nonembrittled state.

Another consideration in selecting the tempering treatment was the variable amounts of chromium and molybdenum in the steels, and the influence of these elements on the tempering rate. Their effect on tempered hardness is least at high tempering temperatures such as 1150°F chosen for this study. That the tempering treatments selected were fairly suc-

cessful in obtaining uniform hardness is shown by a maximum range in Rockwell C values of 25 to 31 for both the 5140 and the molybdenum-chromium steels. The molybdenum-chromium steels tended to be slightly higher in hardness than the 5140 steels at each cooling rate, and the hardness of both series decreased slightly with slower rates of cooling from the tempering temperature.

The transition range of the notched-bar test was used as a measure of toughness.

Preparation of the Steels

In order to have comparable steels, 500 lb laboratory induction furnace heats were made, using Armco iron from a single open hearth heat as the charge. Uniform furnace practice was maintained. The steel was deoxidized with 1½ lb of aluminum per ton in the furnace. The analyses of the steels are given in Table 1.

As phosphorus is one of the elements most apt to segregate in steel ingots, it was desired that the experimental data would approach those which might be obtained with the same phosphorus

contents in commercially produced steels. With this in mind, one ingot of 460 lb weight with hot top was poured from each heat and only the top half of each ingot was used in the study of temper brittleness.

The top halves of the ingots were forged to ½ by 2½ in. bars for the impact tests and 1¼ in. round bars for the Jominy tests. All stock was normalized from 1550°F and stress relieved at 1200°F prior to machining the specimens.

Determination of Hardenability

The standard Jominy test was used for the determination of hardenability. The Jominy bars were quenched from 1550°F. The hardenability band for the 5140 steels with variable phosphorus and for the molybdenum modifications is shown in Fig 1. The 5140 steels vary little in hardenability, but the band is unavoidably somewhat wider at the lower hardness levels as a result of the effect of molybdenum.

The austenite grain sizes of the various steels were ASTM No. 8 to 9, as determined by polishing a section from each Jominy test bar.

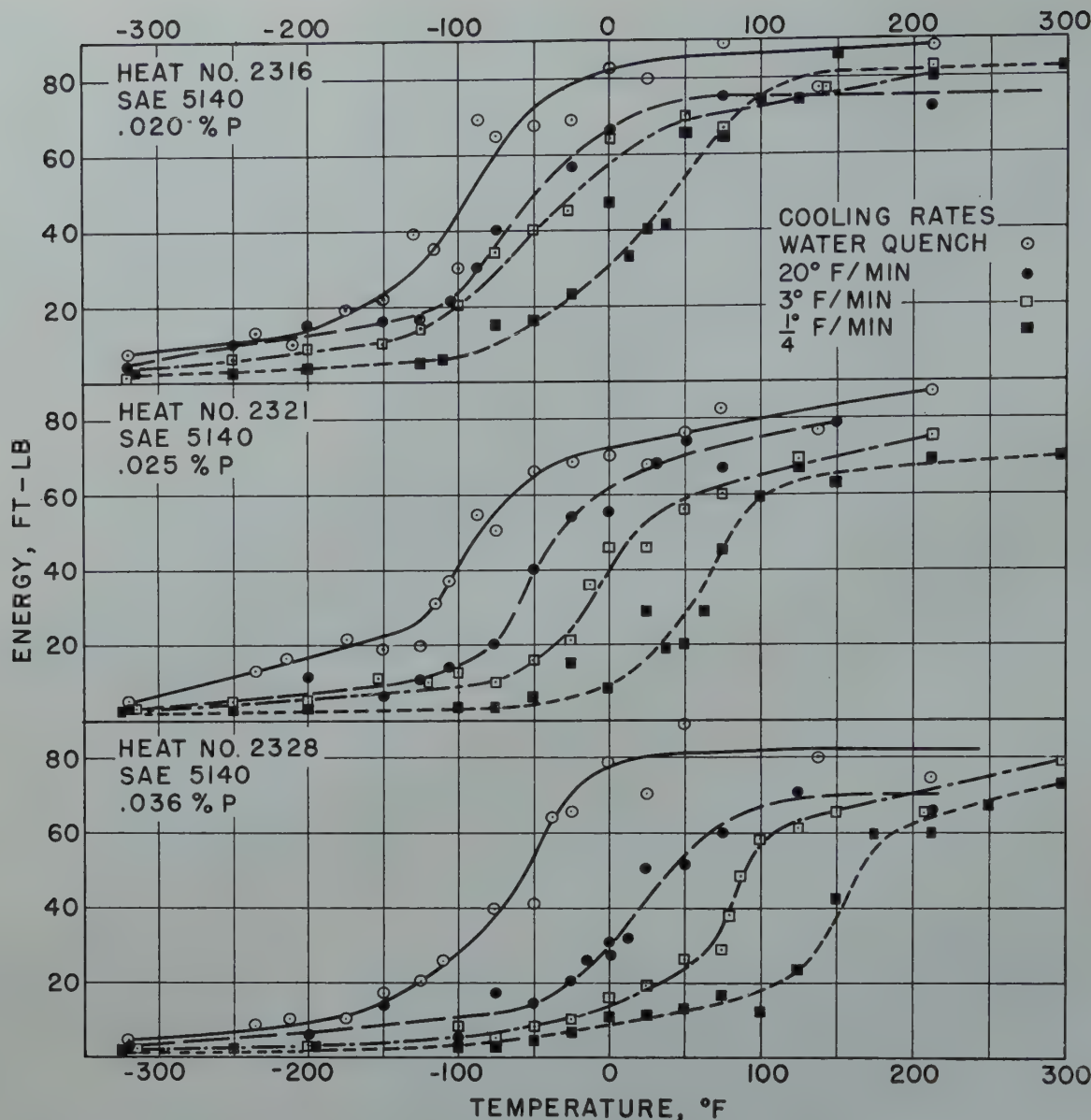


FIG 2—Impact transition curves for 5140 steel with variable phosphorus. Specimens quenched in oil from 1550°F, tempered for one hour at 1150°F and cooled at the rates indicated in the legend.

Determination of the Transition Ranges

Longitudinal Charpy specimens with a 45° V-notch of 0.010 in. root radius¹³ were used. They were machined in groups of four from the central portion of the ½ × 2½ in. bars.

The specimens, 0.016 in. oversize, were heat treated before grinding to size and notching. The base of the notch was perpendicular to the longitudinal direction of the bars, and extended between the specimen surfaces representing the top and bottom, 2½ in. wide surfaces of the bars. The notches were roughed out with a high speed steel milling cutter, and finished with a carefully ground and checked carbide tipped fly cutter. The radii of the notches were 0.010 in. and were held to a tolerance of ±0.001 in. by

Table 1 . . . Chemical Analyses

| Grade | Heat | C | Mn | P | S | Si | Cr | Mo |
|-------|------|------|------|-------|-------|------|------|------|
| 5140 | 2316 | 0.44 | 0.73 | 0.020 | 0.025 | 0.26 | 0.80 | |
| | 2321 | 0.39 | 0.77 | 0.025 | N.D.* | 0.30 | 0.80 | |
| | 2328 | 0.42 | 0.76 | 0.036 | N.D.* | 0.27 | 0.77 | |
| Mo-Cr | 2332 | 0.43 | 0.72 | 0.025 | 0.027 | 0.26 | 0.71 | 0.04 |
| | 2580 | 0.41 | 0.81 | 0.023 | 0.020 | 0.24 | 0.52 | 0.11 |
| | 2336 | 0.43 | 0.73 | 0.023 | 0.024 | 0.20 | 0.60 | 0.14 |
| Mo-Cr | 2337 | 0.40 | 0.79 | 0.021 | 0.021 | 0.26 | 0.44 | 0.18 |
| | 2588 | 0.42 | 0.81 | 0.037 | 0.021 | 0.23 | 0.55 | 0.11 |
| | 2593 | 0.42 | 0.80 | 0.041 | 0.019 | 0.24 | 0.50 | 0.16 |

*Not Determined.

checking every sixth specimen at 50 diam with an optical comparator.

The heat treatment consisted of quenching in oil from 1550°F, tempering for one hour at 1150°F and cooling at different rates from this temperature to 700°F. The cooling rates used were approximately ¼, 3, and 20°F per min., and water quenching. The 3 and 20°F per min. rates were nominal averages of the actual rates between 1150 and 700°F. The ¼°F per min.

rate was maintained with a program controller. All specimens were cooled in air from 700°F.

Specimens of each steel with each treatment were broken over a sufficient range of temperature to determine the transition range. A Sonntag Universal impact testing machine of 120 ft-lb capacity and a striking velocity of 17 ft per sec was used. The capacity was raised to 240 ft-lb when impact values over 90 ft-lb were expected. The data

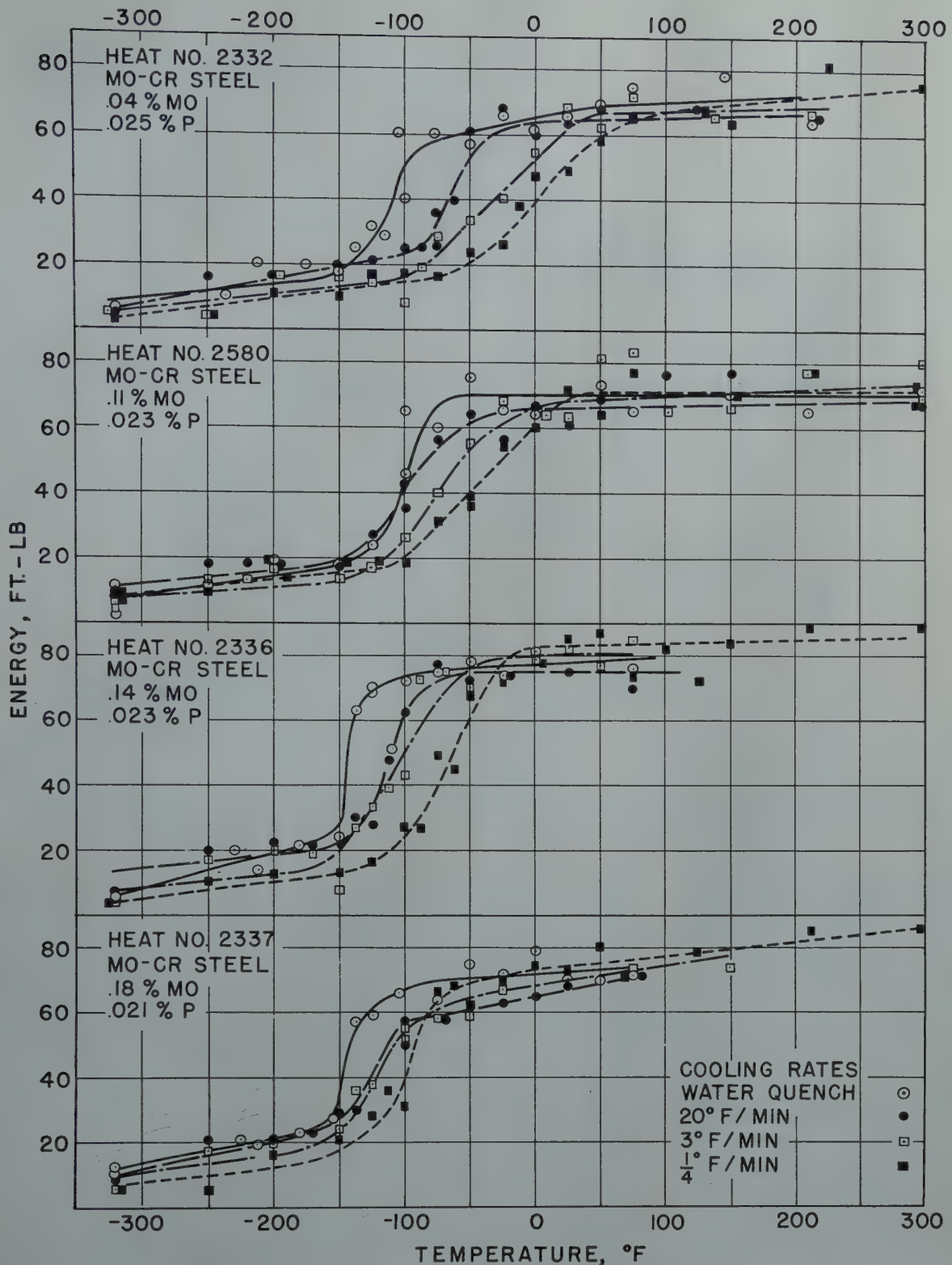


FIG 3—Impact transition curves for molybdenum-chromium steels with 0.021 to 0.025 pct phosphorus. Specimens quenched in oil from 1550°F, tempered for one hour at 1150°F and cooled at the rates indicated in the legend.

are assembled in Fig 2, 3, and 4, in which the impact values have been plotted against testing temperatures in the conventional way. The points shown in the figures signify individual impact values, not averages. All of the data represent completely fractured specimens.

Rockwell C hardness values obtained on the impact specimens of the various

steels with each cooling rate are listed in Table 2.

Effect of Phosphorus in 5140 Steel

Fig 2 illustrates the changes in toughness that attended an increase in phosphorus from 0.020 to 0.036 pct in

5140 steel. Even in the specimens that were quenched in water after tempering, a rise in the transition temperature range with increase in phosphorus content is to be noted. This agrees with the previously noted observations of Jolivet and Vidal. As it seems unlikely that quenching in water allows sufficient time for embrittlement during cooling of an impact specimen, this effect of

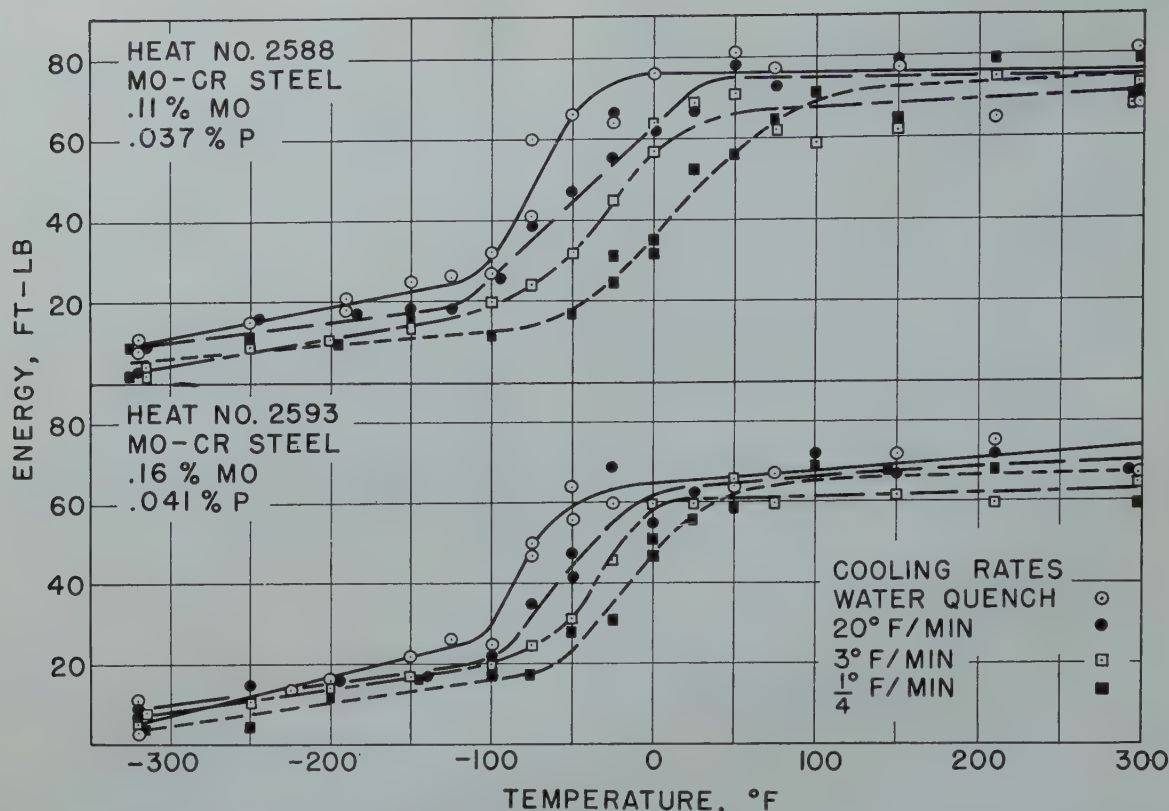


FIG 4—Impact transition curves for molybdenum-chromium steels with 0.037 to 0.041 pct phosphorus. Specimens quenched in oil from 1550°F, tempered for one hour at 1150°F and cooled at the rates indicated in the legend.

phosphorus might be attributed either to inherent brittleness of the phosphorus-bearing ferrite phase in tempered martensite or to embrittlement during the period of tempering at 1150°F. While this question was not answered unequivocally, enough work was done to show that the result is essentially the same in tempering periods of one and three hours at 1150°F. Specimens from the three 5140 steels were heat treated in the same way as the water quenched specimens of Fig 2 except that the tempering period was extended to three hours. The impact transition curves for both the one- and three-hour treatments are shown in Fig 5. Only slight differences in transition were produced in each steel by the additional two hours at 1150°F. These data strongly suggest that the increase of phosphorus from 0.020 to 0.036 pct has raised the transition of 5140 steel, even in the probable absence of temper brittleness.

In Fig 2, temper brittleness becomes apparent with cooling rates less than that of the water quench. To aid in visualizing the influence of phosphorus (and later the combined effects of phosphorus and replacement of chromium by molybdenum), it seems desirable to have a numerical value for the transition temperature. The difficulty is the definition of a transition

Table 2 . . . Average Rockwell C Hardness of Impact Specimens

| Grade | Heat | Cr | Mo | P | Rockwell C Hardness, with Cooling Rate of: | | | |
|-------|------|------|------|-------|--|---------------|--------------|--------------|
| | | | | | Water Quench | 20°F per Min. | 3°F per Min. | ¼°F per Min. |
| 5140 | 2316 | 0.80 | | 0.020 | 29 | 29 | 26 | 26 |
| | 2321 | 0.80 | | 0.025 | 29 | 28 | 27 | 25 |
| | 2328 | 0.77 | | 0.036 | 28 | 27 | 27 | 26 |
| | 2332 | 0.71 | 0.04 | 0.025 | 31 | 30 | 29 | 28 |
| Mo-Cr | 2580 | 0.52 | 0.11 | 0.023 | 28.5 | 28.5 | 27.5 | 26 |
| | 2336 | 0.60 | 0.14 | 0.023 | 30 | 28 | 27 | 26 |
| | 2337 | 0.44 | 0.18 | 0.021 | 31 | 30 | 30 | 27 |
| | 2588 | 0.55 | 0.11 | 0.037 | 29.5 | 29.5 | 28.5 | 26.5 |
| | 2593 | 0.50 | 0.16 | 0.041 | 31 | 31 | 29.5 | 27 |

Table 3 . . . Transition Temperatures Read from Fig 2, 3, and 4 at Impact Value of 45 Ft-Lb

| Grade | Heat | Cr | Mo | P | Transition Temperature, °F, with Cooling Rate of: | | | |
|-------|------|------|------|-------|---|---------------|--------------|--------------|
| | | | | | Water Quench | 20°F per Min. | 3°F per Min. | ¼°F per Min. |
| 5140 | 2316 | 0.80 | | 0.020 | -100 | -55 | -35 | 35 |
| | 2321 | 0.80 | | 0.025 | -95 | -40 | 10 | 75 |
| | 2328 | 0.77 | | 0.036 | -60 | 30 | 85 | 160 |
| | 2332 | 0.71 | 0.04 | 0.025 | -105 | -60 | 20 | 10 |
| Mo-Cr | 2580 | 0.52 | 0.11 | 0.023 | -100 | -95 | -65 | -40 |
| | 2336 | 0.60 | 0.14 | 0.023 | -145 | -115 | -105 | -70 |
| | 2337 | 0.44 | 0.18 | 0.021 | -145 | -120 | -115 | -95 |
| | 2588 | 0.55 | 0.11 | 0.037 | -80 | -50 | -25 | 20 |
| | 2593 | 0.50 | 0.16 | 0.041 | -80 | -50 | -30 | -5 |

temperature as a single temperature in the transition range. Such a definition is still a moot question among metallurgists. The most sensitive values for purposes of comparison would lie on the steepest portion of the energy curve, and, with this in mind, it appears possible to define the transition temperature arbitrarily for the data under consideration.

Inspection of Fig 2, 3, and 4 will indicate that the value of 45 ft-lb falls near the middle of the steepest portion of all the transition curves, and represents the relative placement of the transition ranges with respect to testing temperature. The transition temperatures read from the curves at 45 ft-lb are assembled in Table 3. The authors hold no brief for the value of

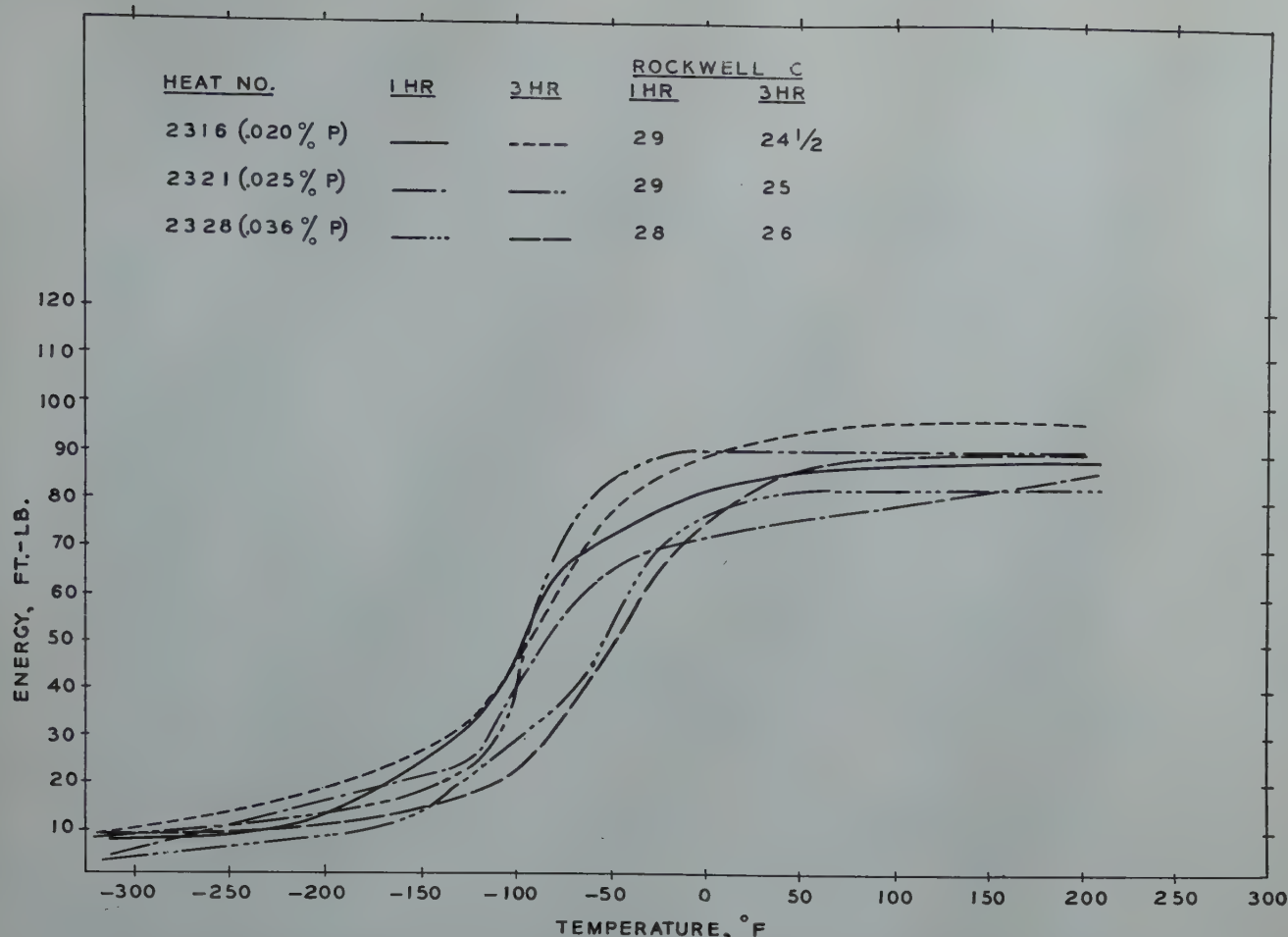


FIG 5—Comparison of transition curves of 5140 steel with variable phosphorus after one and three hours at 1150°F. Specimens quenched in oil from 1550°F, tempered for one and three hours at 1150°F and quenched in water.

45 ft-lb except to represent this particular set of data. All of the experimental points have been shown in Fig 2, 3, and 4, so that the reader may select his own criterion, should he not agree with the authors'.

Using the transition temperatures listed in Table 3, Fig 6 was prepared to illustrate the influence of an increase in phosphorus in 5140 steel. The ordinate is transition temperature, beginning arbitrarily at -150°F . Thus the transition temperatures indicated by the upper ends of the bars are significant, but not their length. It might be thought desirable to reduce this axis to the increase in transition temperature of the embrittled as compared to the nonembrittled state. This was avoided for two reasons. It would not show the relation of transition temperature in the water quenched state to the phosphorus content. Secondly, the rise in transition temperature brought about by an embrittling treatment may be only a qualitative measure of the degree of embrittlement, unless the transition temperatures of two steels being compared are essentially the same in the nonembrittled

state. At present there is no reason to suppose that the same rise in transition temperature, if it occurs in quite different temperature ranges, represents an equal change in toughness.

In Fig 6 the transition temperatures of the 0.020 and 0.025 pct P steels are essentially alike in the nonembrittled state, but show an increasing divergence as the cooling rate through the embrittling range is reduced. The divergence is small at a cooling rate of 20°F per min., but is larger with the slower cooling rates. The rise in transition temperature over the entire series of cooling rates is less for the 0.020 pct P steel than for the steel with 0.025 pct P. In the same figure, the transition temperature of the 0.036 pct P steel in the nonembrittled state is 40°F higher than that of the steels with lower phosphorus contents, but the rise in transition temperatures over the series of cooling rates is 220°F as compared to 135°F for the steel with 0.020 pct P and 170°F for the steel with 0.025 pct P. These observations indicate that phosphorus is a major cause of temper brittleness.

Effect of Phosphorus in Molybdenum-chromium Steels with Hardenability Similar to 5140 Steel

Fig 3 and 4 illustrate the extent to which the replacement of chromium by molybdenum in 5140 steel counteracts the loss in toughness caused by phosphorus.

In Fig 3 the steels have a phosphorus level of 0.021 to 0.025 pct; in Fig 4, 0.037 to 0.041 pct. With each steel the transition temperature rises progressively as the cooling rate is reduced from water quenching to $\frac{1}{4}^{\circ}\text{F}$ per min. Taken together with the data on 5140 steels in Fig 2, the impact transition curves of the molybdenum-chromium steels indicate that the replacement of chromium by molybdenum reduces the embrittlement caused by phosphorus to an extent dependent upon the phosphorus level and the amount of the replacement. To effect a similar reduction in embrittlement, the higher phosphorus steels require a greater addition of molybdenum than the steels with moderate phosphorus contents.

From the transition temperatures

listed in Table 3, Fig 7 has been prepared to show the combined effects of an increase in phosphorus and the replacement by molybdenum of a part of the chromium in 5140 steel. For the purposes of this comparison, average values of the transition temperatures were taken for heats 2316 and 2321, and for heats 2336 and 2337. The trends of transition temperature with both phosphorus and molybdenum are progressive throughout the data; only the transition temperature for the water quenched specimens of the 0.11 pct Mo steel with moderate phosphorus falls out of line. In the water quenched 0.020 to 0.025 pct P series (with the exception of the 0.11 pct Mo steel) replacement of chromium by molybdenum lowers the transition temperature slightly, amounting to about a 40°F shift for 0.16 pct Mo. In the 0.036 to 0.041 pct P series, the decrease in transition temperature for the same molybdenum content is less, amounting to about a 20°F shift in transition temperature. In each steel, the transition temperature in the nonembrittled state is raised by increasing the phosphorus content from the moderate to the higher level.

Turning to the evidence for temper brittleness shown in Fig 7, temper embrittlement is minimized by molybdenum but not entirely eliminated in any of the steels under study. In general, phosphorus increases the manifestation of temper brittleness, and the replacement of chromium by molybdenum lowers the transition temperature for each phosphorus level and cooling rate under consideration. In the range of 0.020 to 0.025 pct P, the beneficial effect of molybdenum is evident at all cooling rates (except the water quenched series of the 0.11 pct Mo steel). In the 0.036 to 0.041 pct P range the difference between no molybdenum and 0.11 pct is considerable, but the difference between 0.11 and 0.16 Mo is evident only in the cooling rates of 3 and of 1/4°F per min.

Discussion of Results

One effect of phosphorus is to cause a brittleness of tempered martensite which appears to be essentially the inherent brittleness of phosphorus-bearing ferrite so often noted by metallurgists. Confirmation of this was obtained in the present study of 5140 steels with 0.020, 0.025, and 0.036 pct P. The structural condition of the steel was martensite tempered for one and

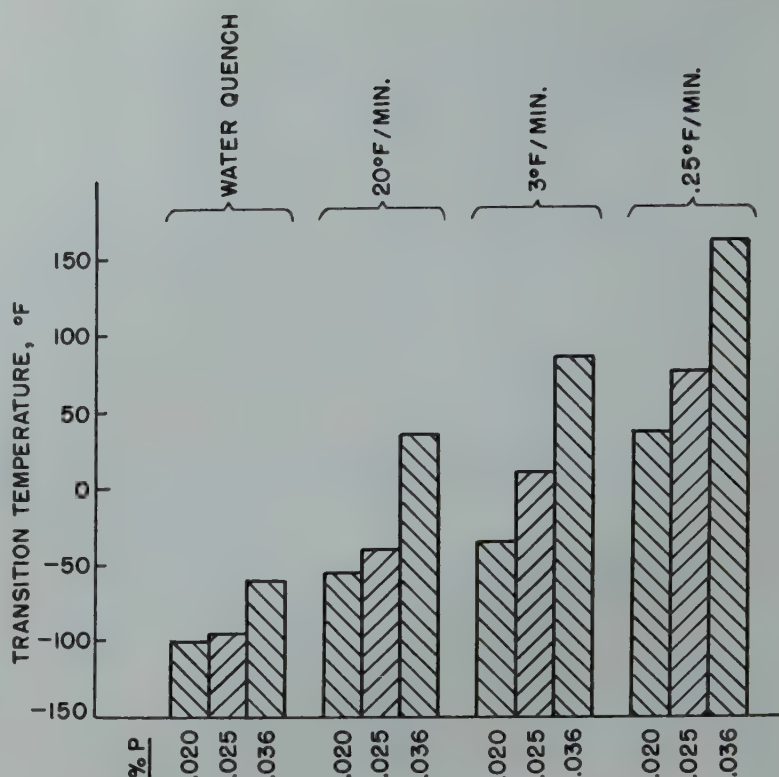


FIG 6—Effect on transition temperature of an increase of phosphorus in 5140 steel. Transition temperatures taken from Table 3.

for three hours at 1150°F, followed by quenching in water. While the difference in tempering period had little effect on the transition temperature at each phosphorus level, a definite loss of toughness accompanied raising of the phosphorus from 0.025 to 0.036 pct. If this is caused by temper brittleness, nearly maximum temper embrittlement must have developed during the one-hour period of 1150°F. Such rapid development of temper brittleness seems improbable in view of the slow isothermal embrittlement in this temperature range shown by Pellini and Queneau for their high phosphorus steel. Thus it seems reasonable to conclude that phosphorus reduced the toughness of the tempered martensite, in the absence of temper brittleness. As deformation in tempered martensite occurs by slip in the ferrite phase, this loss of toughness is assumed to be the already well-known brittleness of phosphorus-bearing ferrite.

The inherent brittleness of phosphorus-bearing martensite described above appears to be counteracted to a slight extent by the replacement of chromium by molybdenum in 5140 steel, as illustrated by Fig 7. With the higher phosphorus level, the use of 0.11 and 0.16 pct Mo in this way lowered the transition temperature about 20°F. With the lower phosphorus level, the steel with 0.11 pct Mo appears to be

out of line as mentioned earlier; however, a recession of the transition to lower temperatures may be noted in the 0, 0.04, and 0.16 pct Mo series. The use of 0.16 pct Mo lowered the transition temperatures about 40°F as compared to 5140 steel.

The data obtained in this study substantiate the evidence presented by numerous investigators that phosphorus can cause temper brittleness in tempered martensite. Temper brittleness was observed to depend on phosphorus content in 5140 steel and also to a degree in the molybdenum modifications of this grade. Using the transition temperature as a measure of the degree of embrittlement, the susceptibility to temper brittleness in the molybdenum-chromium steels decreases as more of the chromium is replaced by molybdenum.

In the 5140 grade chosen for study, it has been demonstrated that a good tolerance for phosphorus can be obtained by the use of molybdenum to replace a portion of the chromium without essential alteration of the hardenability of the steel. The desirable amount of such replacement would depend upon the phosphorus level to be expected and the tempering cycle to which the steel is to be subjected. In commercial alloy steels made by the basic open hearth or electric process, the ladle analyses for phosphorus are

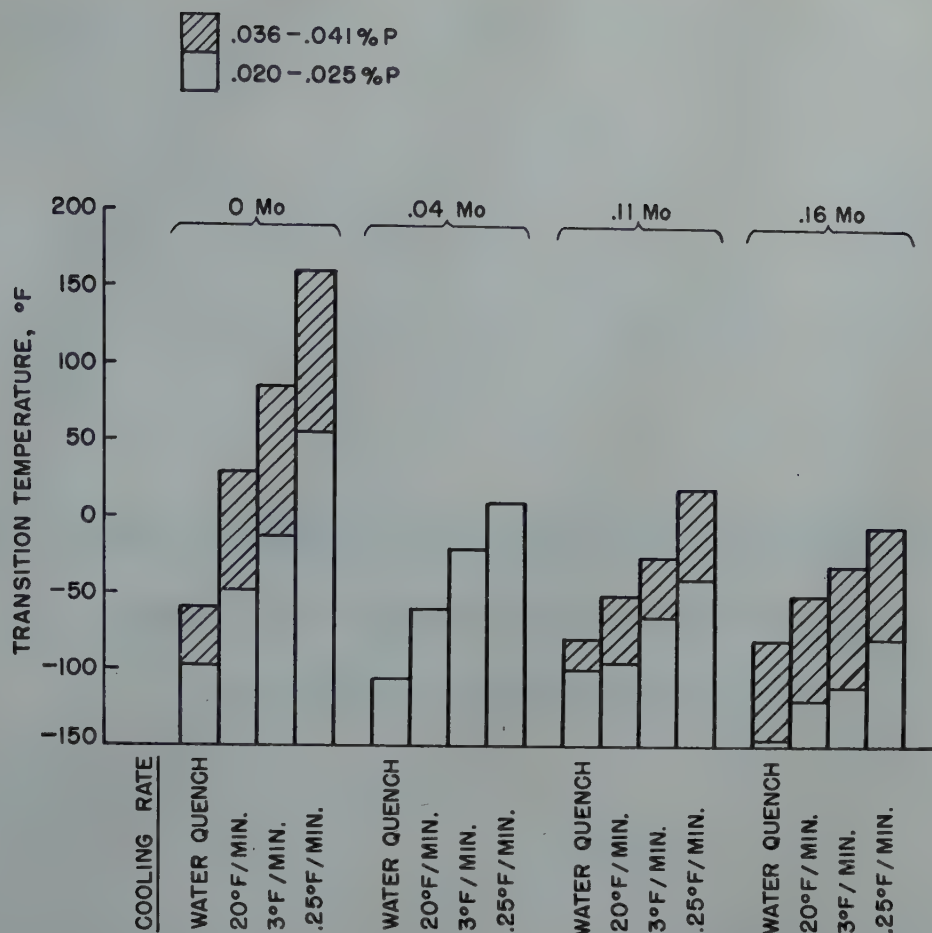


FIG 7—Combined effect on transition temperature of phosphorus and replacement by molybdenum of part of the chromium in 5140 steel. Transition temperatures taken from Table 3.

usually well below the maximum limits permitted by current AISI-SAE specifications. Because of segregation, however, substantially higher levels of phosphorus are frequently encountered, especially in material from the upper central portion of the ingots. It is in such material that the beneficial effect of replacing chromium by molybdenum would be greatest. The extent to which loss of toughness due to phosphorus segregation can be overcome is demonstrated by the 0.16 pct Mo-Cr steel with 0.041 pct P which had a lower transition temperature than the 5140 steel with 0.020 pct P when given an embrittling treatment, namely, cooling at $\frac{1}{4}$ °F per min. after tempering at 1150°F.

The work reported here has dealt entirely with 5140 steel and molybdenum modifications of essentially the same hardenability. Similar work is already under way on the effect of replacing a part of the manganese by molybdenum in 1340 steel, in an effort to evaluate further possibilities in the development of steels with good tolerance for phosphorus.

Conclusions

1. Phosphorus reduces the toughness of tempered martensite even in the absence of temper brittleness. In 5140 steel this loss in toughness can be partially compensated by replacement of part of the chromium by molybdenum with no essential change in the hardenability of the steel.

2. Confirmation has been obtained of the conclusion of a number of earlier investigators that phosphorus accentuates temper embrittlement of martensite. (Structures other than tempered martensite were not included in this work.)

3. The replacement by molybdenum of part of the chromium in 5140 steel materially reduces its susceptibility to loss of toughness by temper embrittlement.

4. A study of 5140 steels and molybdenum modifications of similar hardenability has shown that replacement of part of the chromium by molybdenum can be used to improve the toughness at phosphorus levels encountered in commercial steels.

Acknowledgment

The authors gratefully acknowledge a grant of funds for this work from the Kennecott Copper Corporation.

References

1. H. Jolivet and G. Vidal: *Rev. de Met.* (1944) 41, 378, 403. Read in translation.
2. J. H. Hollomon: *Trans. A.S.M.* (1946) 36, 473.
3. J. P. Cohen, A. Hurlich and M. Jacobsen: *Trans. A.S.M.* (1947) 39, 109.
4. D. McLean and L. Northcott: *Jnl. Iron and Steel Inst.*, Feb. 1948, p. 169.
5. W. S. Pellini and B. R. Queneau: *Trans. A.S.M.* (1947) 39, 139.
6. J. H. Andrew: *Jnl. Iron and Steel Inst.* (1920) No. I, 621.
7. H. H. Ashdown: Discussion of paper by R. H. Greaves and J. A. Jones. *Jnl. Iron and Steel Inst.* (1920) No. II, 219.
8. G. W. Green: Discussion of paper by R. H. Greaves and J. A. Jones. *Jnl. Iron and Steel Inst.* (1920) No. II, 219.
9. R. H. Greaves and J. A. Jones: *Jnl. Iron and Steel Inst.* (1925) No. I, 231.
10. E. Mauer, O. H. Wilms and H. Kiessler: *Stahl und Eisen* (1942) 62, 81 and 115. Read in translation.
11. W. Bischof and L. Bottger: *Arch. Eisenhuttew.* (1948) 19, 29.
12. H. Bennek: *Tech. Mitt. Krupp* (1935) 3, 205; *Stahl und Eisen* (1942) 62, 116.
13. Fig 4, ASM Handbook, 1948 ed. p. 113.

[illegible]

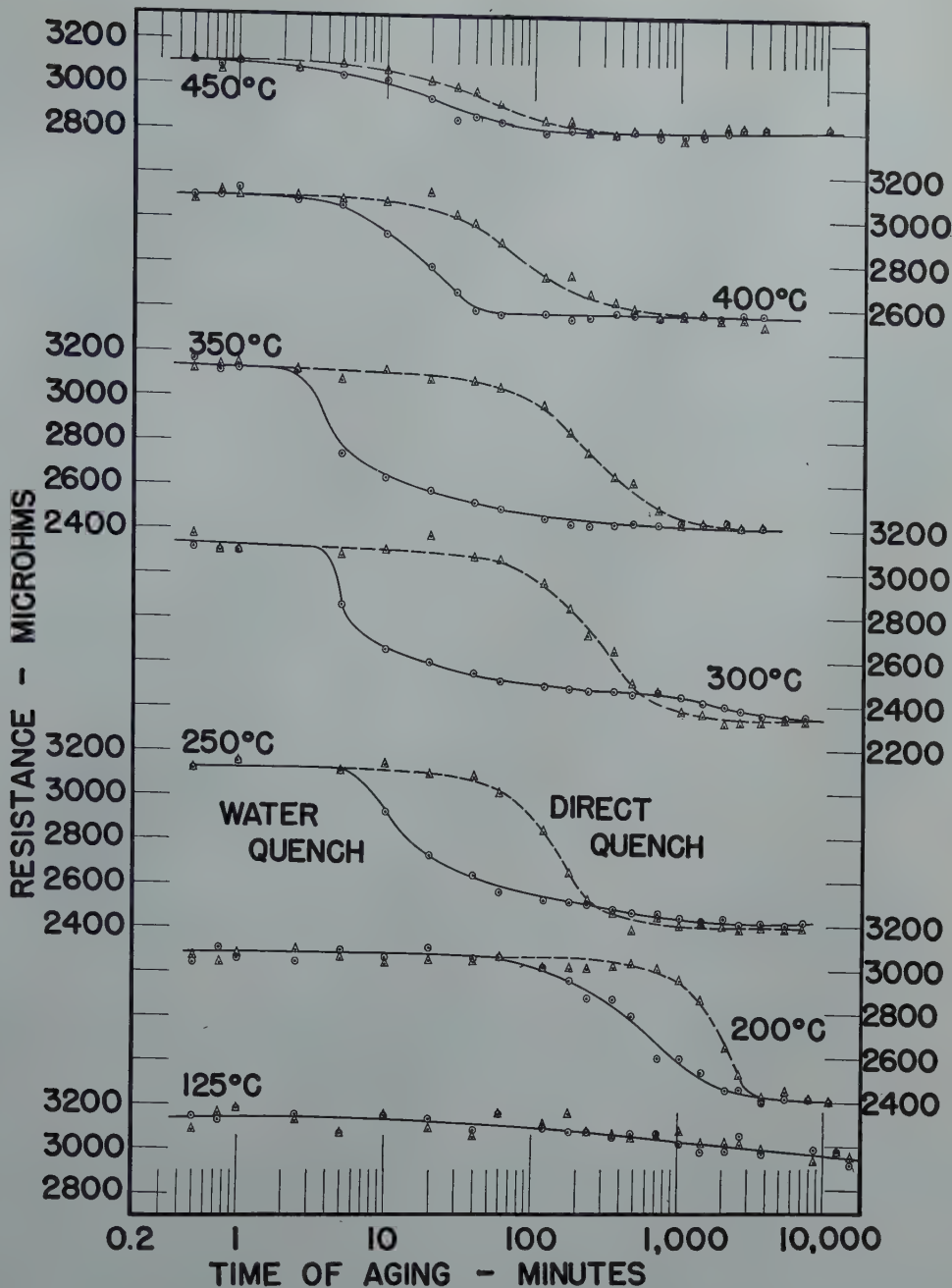


FIG 1—Electrical resistance as a function of aging time at constant aging temperatures in water quenched and directly quenched specimens of an aluminum-copper alloy.

copper alloys quenched into cold water and aged at 200°C while specimens aged after quenching into boiling water or oil at 153°C showed precipitation throughout the grains. They correlated these structural observations with hardness-time curves for various aging temperatures and concluded that the rapid hardening of specimens quenched into water resulted from accelerated precipitation in regions plastically deformed by quenching. Other investigations¹¹⁻¹⁸ have confirmed that severe quenching promotes age hardening compared to cooling at slower rates from the solution treatment.

Experimental Procedure and Results

The alloys were received as hard-rolled sheet 0.066 in. thick. They had the following compositions:

| | Aluminum-copper, pct | Aluminum-silicon, pct |
|---------------|----------------------|-----------------------|
| Cu | 4.13 | 0.004 |
| Si | 0.002 | 0.97 |
| Fe | 0.003 | 0.005 |
| Mg | 0.001 | 0.001 |
| Al (by diff.) | 95.86 | 99.02 |

Specimens for hardness tests were cut from the sheet stock; they measured $\frac{1}{2}$ by $\frac{5}{8}$ in. (aluminum-copper) and $\frac{3}{8}$ by $\frac{5}{8}$ in. (aluminum-silicon). Specimens for electrical resistance measurements were prepared by wire drawing.

The aluminum-copper wire measured 0.0392 ± 0.0002 in. in diam and the aluminum-silicon wire 0.0385 ± 0.0003 in. For heat treating, the wires were cut into equal lengths of about $3\frac{1}{2}$ in.

The solution heat treating and artificial aging operations were carried out in salt or oil baths heated by electrical resistance units. The temperature was automatically controlled to $\pm 2^\circ\text{C}$ for solution treating and to $\pm 1^\circ\text{C}$ for aging. At and above 200°C a special heat treating salt mixture was used; at 125° and 70°C a light mineral oil proved suitable.

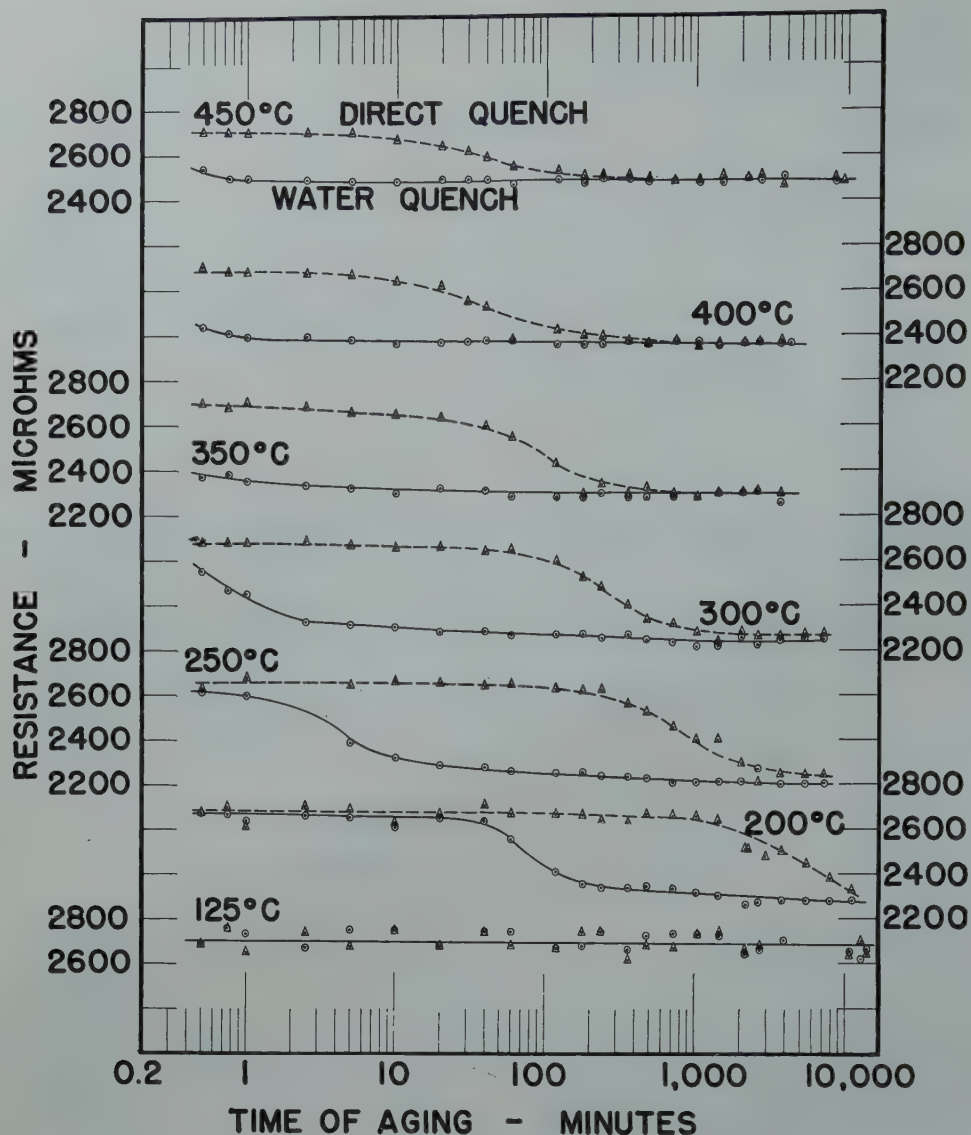


FIG 2—Electrical resistance as a function of aging time at constant aging temperatures in water quenched and directly quenched specimens of an aluminum-silicon alloy.

The solvus temperature is approximately 515°C for aluminum containing 4.13 pct copper¹⁹ and 525°C for aluminum containing 0.97 pct silicon.²⁰ The aluminum-copper alloys were solution treated at 524°C and the aluminum-silicon alloys at 535°C for a period of 6 hr. In preliminary experiments the hardness of water quenched aluminum-copper samples became approximately constant after 3 to 4 hr of solution treatment at 521°C. No undissolved second phase could be found by metallographic examination. Specimens treated for 10–12 hr showed marked grain growth.

After 6 hr of solution treatment one wire and one rectangular specimen were transferred rapidly to the aging bath. These will be referred to as directly quenched specimens. Another wire and rectangular specimen were

quenched in water at $20^{\circ} \pm 1^{\circ}\text{C}$ and were then placed in the aging bath. The directly quenched specimens aged at 70°C were quenched into water at that temperature and transferred to an oil bath for aging. Aging treatments of less than 20 min. were timed to within a few seconds and similar precision was maintained for longer aging times. The specimens were staggered so that only one rectangular and one wire sample were ready for testing at a time.

The specimens were quenched from the aging furnace in water at 20°C. Each wire was removed from the water bath after 10–15 sec and its electrical resistance measured. The hardness was then determined on the rectangular specimen. This small delay did not appreciably affect the hardness. For specimens aged less than 5 min., the

schedule was modified so as to allow almost immediate determination of resistance and hardness.

Electrical resistances were measured on a Kelvin double bridge using an effective specimen length of 2.376 in. The resistances were determined in microhms and are so reported here. Care was exercised not to deform or mar the wires, and any variations in tension applied by the holder were negligibly small.

The Rockwell F scale could be used with good reproducibility on the aluminum-copper samples, but was unsatisfactory for the aluminum-silicon alloys. All hardness values were therefore determined by superficial hardness tester on the Rockwell 15-T scale. Hardness readings on the same specimen of aluminum-copper alloy agreed within two or three points, but the

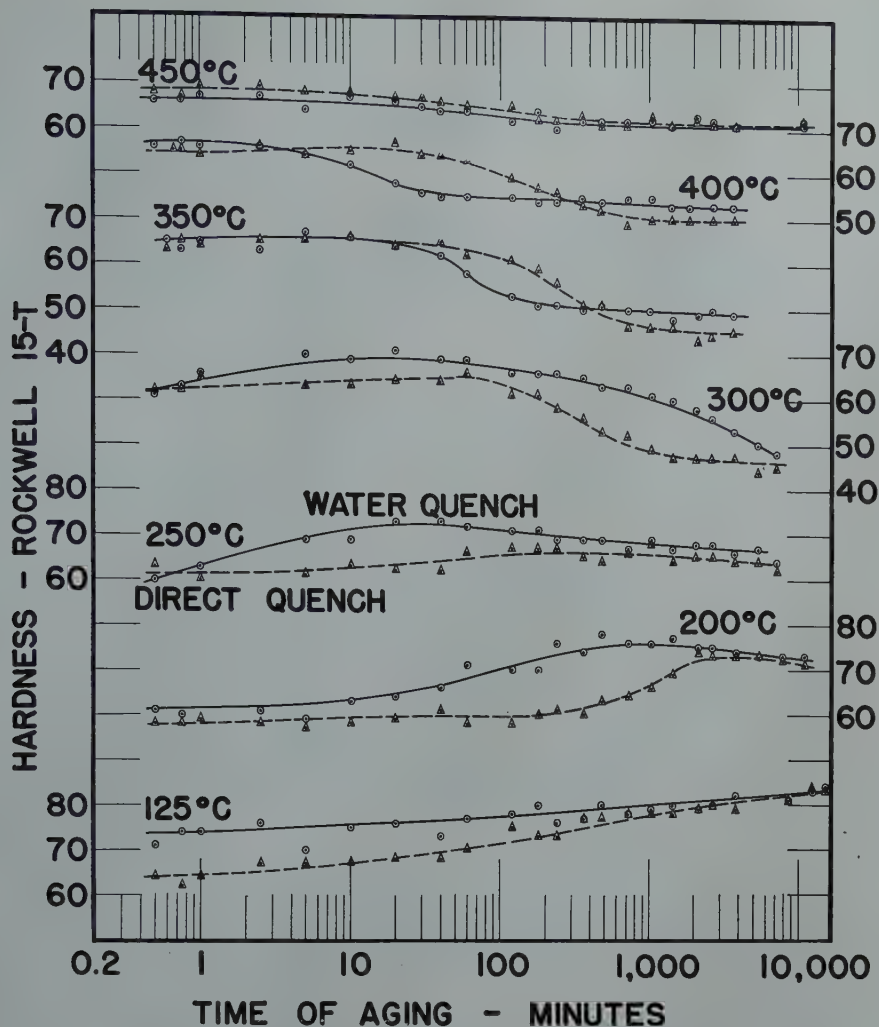


FIG 3—Hardness as a function of aging time at constant aging temperatures in water quenched and directly quenched specimens of an aluminum-copper alloy.

spread obtained with the aluminum-silicon specimens was large. Five, and occasionally six, separate readings were taken on each specimen in a standardized geometrical pattern. Only the averages of these readings are reported.

Both alloys were aged at 70, 125, 200, 250, 300, 350, 400 and 450°C. Fig 1-5 report all observed values graphically.

Discussion of Results

SOURCES OF ERROR

Measurements of hardness and resistance were made at room temperature on separate samples for each aging temperature and time. Aside from experimental advantages, this procedure made it possible to compare all data directly without reducing them to a common temperature. It should be kept in mind that each point plotted in Fig. 1-5 represents a different specimen.

The data obtained for aging temperatures above 300°C fit simple curves well. The observed values become less regular for aging below 300°C and are somewhat erratic at 125° and 70°C.

The resistance and hardness of samples in the water-quenched condition before aging were also determined. While the hardness values showed good agreement, the resistance values were spread over a considerable range, probably owing in large measure to variations in the quenching action. It is known^{18,21} that the quenching rate affects the properties of aluminum alloys in the water quenched condition much more than after aging.

GENERAL FEATURES OF AGING CURVES

The aging curves (Fig 1-5) show the effects of aging temperature, type of quench and alloy composition on the aging process. Before discussing these factors individually, some general features of the curves will be considered.

The first statement is general; the comments under (2) to (5) refer only to aging at 200°C and above, while the curves for 70° and 125°C are discussed under (6) and (7).

1. The changes in hardness and in electrical resistance are not directly comparable even for the same time and temperature of aging. Aside from the different nature of hardness and electrical resistance, in this investigation the two properties were measured on specimens of different size and shape. The resulting different quenching strains complicate any comparison by an additional variable.

2. The electrical resistance reaches steady values after sufficiently long aging. These values vary with the aging temperature, but are nearly equal at any temperature for water quenched and directly quenched samples. This applies to both alloys.

3. The resistance of the aluminum-copper alloy decreases sooner after a water quench than after a direct quench. At 250° and 300°C the de-

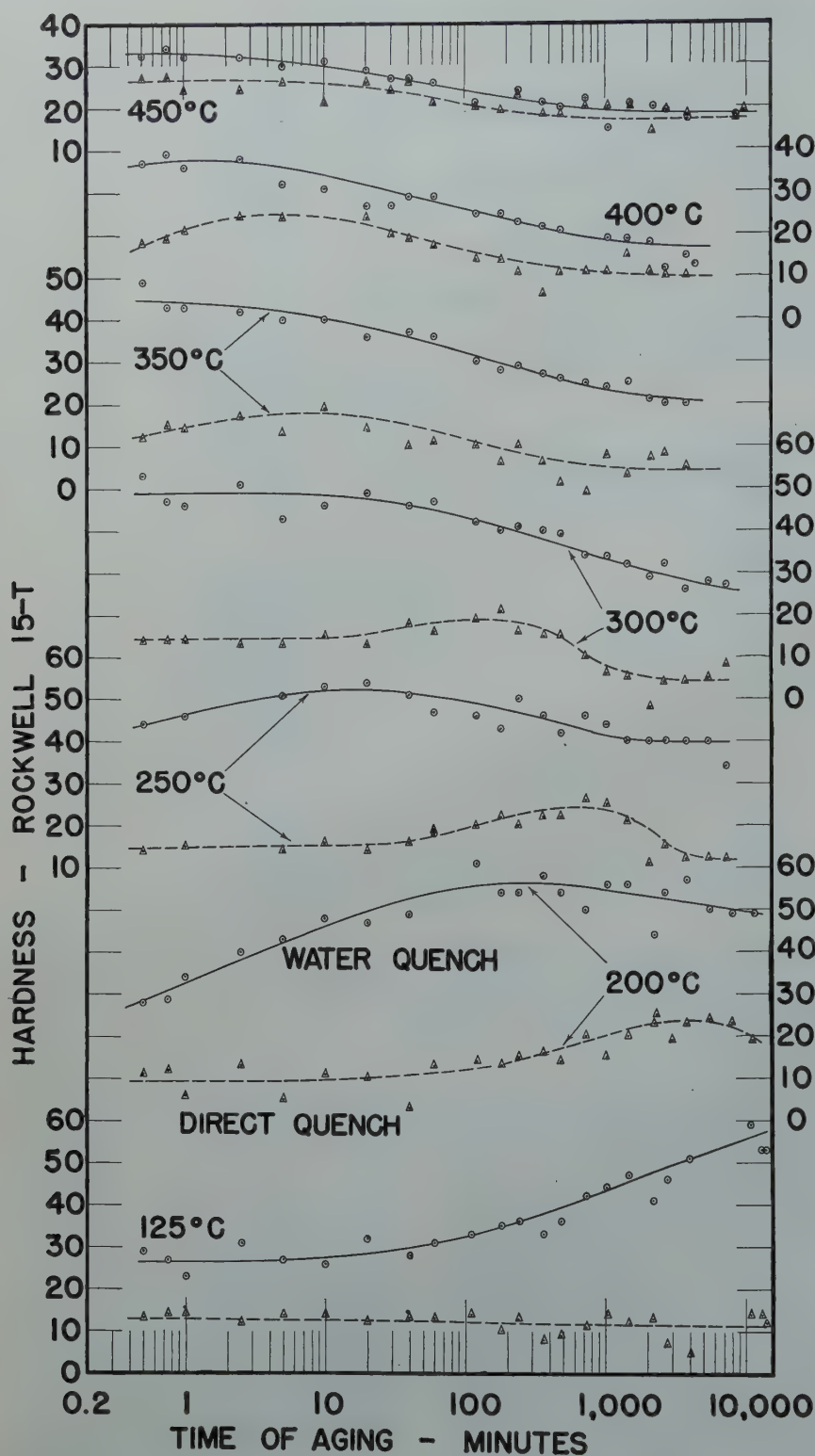


FIG 4—Hardness as a function of aging time at constant aging temperatures in water quenched and directly quenched specimens of an aluminum-silicon alloy.

crease in resistance slows down more in the water quenched than in the directly quenched specimens toward the end of the aging period so that the curves cross.

4. The resistance of water-quenched aluminum-silicon alloys decreases very rapidly at temperatures above about 250°C; a large fraction of the total

decrease occurs in the first minute of aging. The decrease in resistance of directly quenched aluminum-silicon alloys begins slowly and requires considerable time for its completion.

5. The alloys harden more rapidly after a water quench than after a direct quench. The maximum hardness of the water quenched specimens exceeds

that of the directly quenched specimens in most cases. The difference in the rate of hardening and in the maximum hardness reached tends to be larger in the aluminum-silicon than in the aluminum-copper system.

6. The difference in quenching interval between water quenching and direct quenching decreases as the aging temperature is lowered, but even at 70°C the two quenching treatments do not lead to identical results in all respects. Regardless of the type of quench the resistance of aluminum-copper alloys aged at 125° and 70°C decreases slowly, possibly after a small initial rise. During the aging times used the resistance of the aluminum-silicon alloys undergoes no change as the result of aging at 125° and 70°C.

7. The hardness of aluminum-copper alloys increases slowly with aging at 125° and 70°C. At the latter temperature the directly quenched samples lead by a small margin over the water quenched samples. This fact is consistent with the observation of Gayler¹⁶ who found that quenching into boiling water promoted the age hardening at 130°C of an aluminum alloy containing 4 pct copper more effectively than quenching into cold water. The behavior of the hardness of the aluminum-silicon alloys aged at 125° and 70°C is particularly interesting; the directly quenched samples show no change during the longest periods of aging employed while the water quenched samples increase steadily in hardness.

THE EFFECT OF AGING TEMPERATURE

Fig 6 and 7 show the total changes in resistance of the aluminum-silicon alloys against the aging temperature for different times. The plotted points are taken from the curves in Fig 2 and 5. Resistance-temperature curves for aluminum-copper alloys show the same pattern as the aluminum-silicon alloys although in a less pronounced manner. For each aging period the decrease in resistance reaches a maximum at some intermediate temperature. As the aging period is lengthened the maxima become more marked. They also shift to lower temperatures because the depletion of solute from the solid solution causes the reaction to reach a maximum at lower temperatures where a sufficient degree of supersaturation can be expected.

The hardness-temperature curves were simple only for water-quenched aluminum-silicon alloys (Fig 8). The

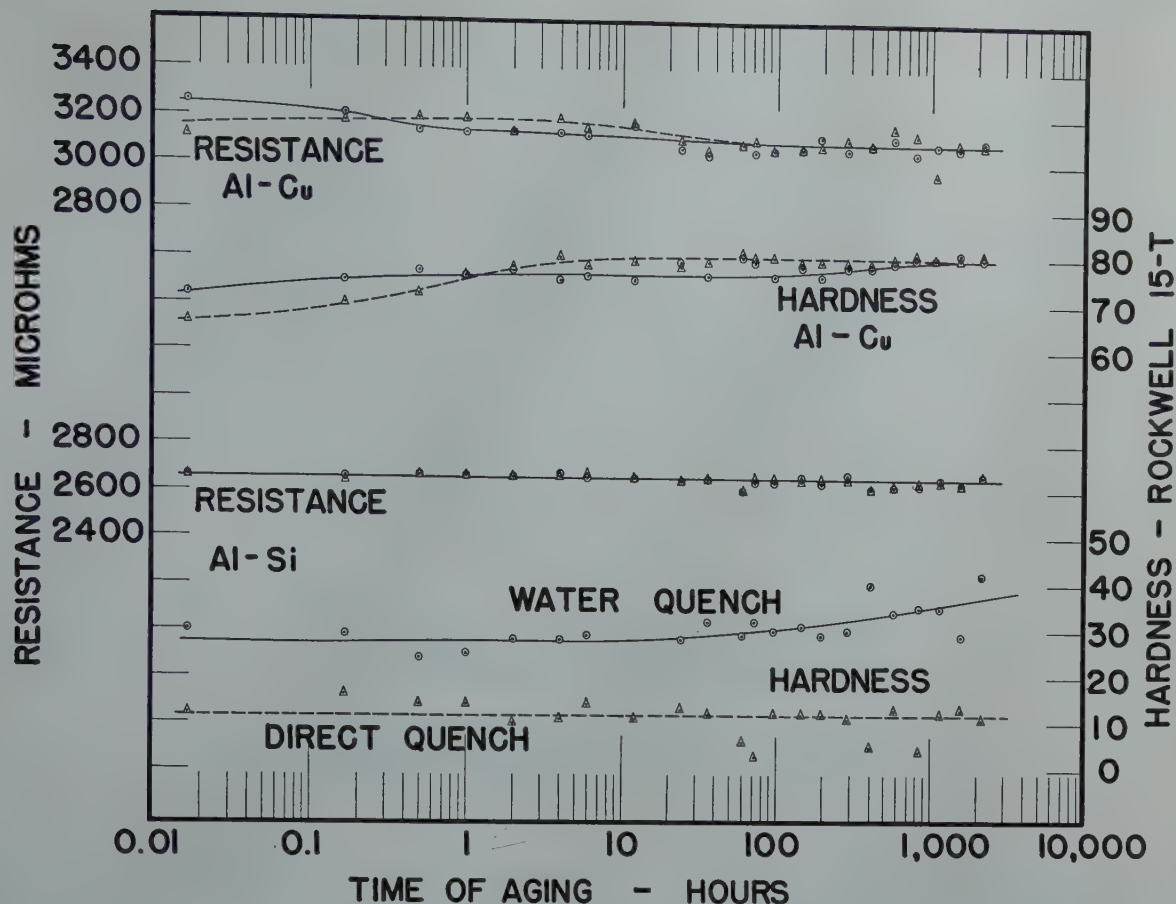


FIG 5—Electrical resistance and hardness as functions of aging time in water quenched and directly quenched specimens of an aluminum-copper alloy and an aluminum-silicon alloy aged at 70°C.

hardness peak was attained at lower temperatures as the aging period was lengthened. Hardness curves for aluminum-copper and directly quenched aluminum-silicon alloys did not show such a simple pattern.

Chevenard, Portevin and Waché⁸ found a maximum hardness value at 200°C for a water-quenched aluminum alloy containing 0.63 pct silicon and 0.13 pct iron aged 8 hr. This value is in good agreement with the corresponding result of the present investigation. In experiments of Jetter and Mehl¹⁴ with aluminum-silicon alloys a maximum of initial dilation against temperature of aging seemed to be approached at 236°C which was the upper temperature limit of their observations.

The temperatures for maximum total change in resistance (Fig 6 and 7) are not necessarily identical with the temperatures for maximum rates of resistance changes. In fact there is no satisfactory method of defining these rates in a manner which would allow an absolute comparison between different aging temperatures. The terminal solubility of copper and silicon in

aluminum increases with temperature and the resulting resistance of the saturated solution increases also. The change in resistance is therefore smaller the higher the aging temperatures.

A comparison on the basis of the completion of a specified fraction of the aging reaction is not a comparison in absolute terms. It implies that the aging curves have or should have similar shapes. For complex reactions in the solid state this assumption is not warranted. Nevertheless such arbitrary measures of the rate as the time required for half the total reaction are of some value and have been used for finding activation energies.

ACTIVATION ENERGIES

The rate of the aging process may be expressed by the equation

$$r = c \exp - \frac{Q}{RT}$$

In this equation the reaction rate r must be measured by some arbitrary standard such as the reciprocal of the time required for one-half of the total change in resistance or the reciprocal of the time required to reach maximum hardness. Q is the activation energy for

the over-all process, T is the temperature and R and c are constants.

The activation energy may be found from a plot of the logarithm of the rate against the reciprocal of the absolute temperature. Such curves were straight in the temperature range of 200–250°C, and in some instances up to 300°C. At higher temperatures some of the curves became erratic, but in most cases they bent back toward the abscissa. This behavior is to be expected from the eventual reversal of the aging rate with increasing temperature.

The activation energies determined from the straight portions of the curves are listed in Table 1. In every instance the activation energy was larger for the water-quenched than the directly quenched alloy. The faster aging rate of the water-quenched samples therefore must have been due to differences in the value of the factor c .

Guy, Barrett and Mehl¹⁷ found that the activation energy for precipitation in the copper-beryllium system is less than the activation energy for diffusion of beryllium in copper. A similar relation had been noted by Jetter and Mehl¹⁴ in their investigation of alu-

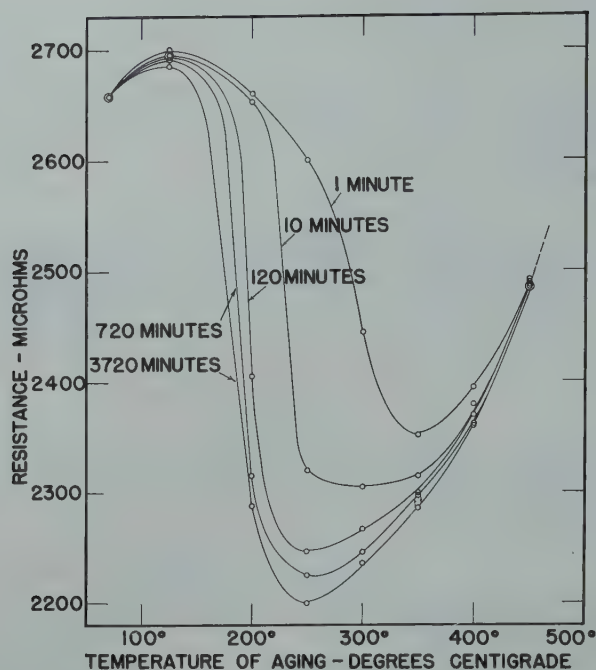


FIG 6—Electrical resistance of water quenched specimens of an aluminum-silicon alloy as a function of temperature at constant aging times.

Table 1 . . . Activation Energies (in Calories)

| Alloy | Based on Resistance | | Based on Hardness | |
|--------------------------|---------------------|---------------|-------------------|---------------|
| | Water Quench | Direct Quench | Water Quench | Direct Quench |
| Aluminum-copper | 30,500 | 24,100 | 34,200 | 25,100 |
| Aluminum-silicon | 24,300 | 15,900 | 24,100 | 22,900 |

minum-silicon alloys. In the investigation reported here this relation between activation energies of diffusion and of aging was confirmed.

THE EFFECT OF QUENCHING

As stated in the description of experimental procedure, the directly quenched samples aged at 70° and 125°C were quenched into media which were different from those used with all other directly quenched specimens. While the latter were transferred from the solution bath into the salt bath and remained there for aging, the specimens aged at 125°C were quenched into a bath of oil in which they were aged and the specimens aged at 70°C were quenched into water at that temperature and aged in oil. This difference in quenching procedure is one reason why the quenching stresses cannot be considered as continuous or simple functions of the aging temperature.

The sequence of molten salt (200°C and over), oil (125°C) and water (70°C), however, parallels the increase in quenching severity resulting from the decrease in temperature. A correlation of all runs on the basis of decreasing temperature is therefore reasonable.

While the final values of the resistance of water quenched and directly quenched samples are alike for any aging temperature, the rates at which these values are approached are generally more rapid after water quenching than after quenching directly to the aging temperature. This accelerating action of water quenching is particularly pronounced in the medium temperature range of aging. The water quench also accelerates the rate of hardening and with some minor exceptions raises the maximum hardness obtainable.

The accelerating effect of the water quench may be owing to one or both of two causes. In the first place, the number of available nuclei is larger at room temperature than at elevated temperatures according to Becker's analysis of nucleation.⁴ This is a simple effect of temperature. Secondly, rapid cooling by quenching into water produces thermal stresses and the resulting strains create favorable regions for the progress of age hardening. This effect results from the rapid change in temperature.

The number of nuclei is larger at

room temperature than at elevated aging temperatures because the critical radius for a stable nucleus decreases as the temperature is decreased. The greater undercooling and the greater degree of supersaturation with a receding solvus cooperate toward this decrease in critical nucleus size. In order to be effective in subsequent aging at elevated temperatures, however, the nuclei must remain in existence. They must, therefore, grow at room temperature or during heating so that they will not be below the critical size characteristic of the higher temperature.

If it is assumed that even a fraction of the nuclei existing at room temperature survives on heating, a difficulty arises from the generally accepted explanation of the phenomenon of retrogression or restoration. According to this explanation the property changes of an alloy aged at room temperature revert partially in the direction of the unaged state because on heating active aggregates go again into solution. Since the nuclei resulting from a short period at room temperature are smaller than the aggregates resulting from long-time aging at this temperature, they can be expected to resist the effects of higher temperature less strongly.

A difference exists between room-temperature age hardening and room-temperature nucleation: the matrix surrounding the hardening aggregates

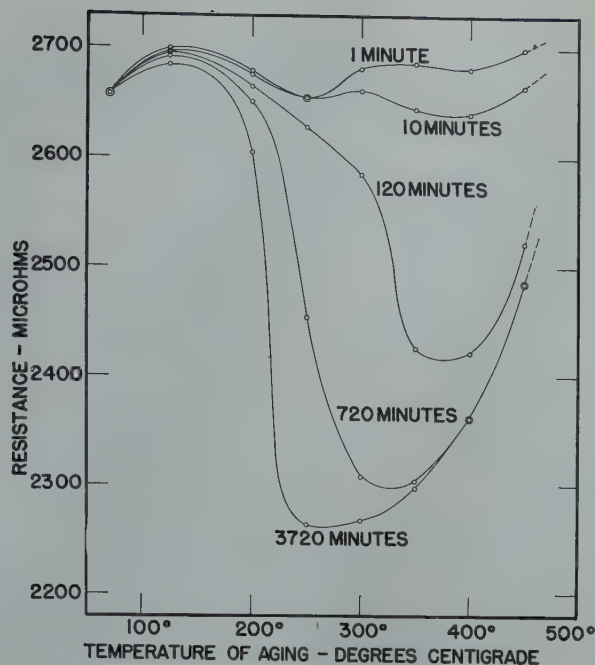


FIG 7—Electrical resistance of directly quenched specimens of an aluminum-silicon alloy as a function of temperature at constant aging times.

approaches closer to the equilibrium state than does the matrix which surrounds the nuclei existing at room-temperature. The supersaturated matrix may have a stabilizing effect on the nuclei which is absent in the matrix after aging. Whether such a stabilizing effect is sufficiently strong to protect small nuclei at a temperature where retrogression would occur is open to question. It can be stated with certainty only that the effect of room temperature on nucleation favors the aging of quenched alloys to whatever extent nuclei survive upon reheating.

An alternative or additional explanation of the acceleration of aging caused by water quenching is based on the effect of strains on the age hardening process. Plastically deformed regions are regions of instability. Their high energy favors any rearrangement which tends toward a more stable condition. In addition to explaining the increase in the rate of aging, strains can also explain the greater total hardness obtained by water quenching than by direct quenching. Following an argument of Fink and Smith,¹⁰ the increase in hardness results from the presence of zones of preferential aging throughout the grains; the spread in time between aging at the grain boundaries and in the bodies of the grains is thus reduced and this causes a more concentrated aging effect and greater

hardness. It should be emphasized, however, that a corresponding argument can be based on the nucleation effect of low temperatures.

It may be argued that the effects of strains are removed on reheating to elevated aging temperatures. Hartnagel¹² concluded from his work that relief of quenching stresses takes place and this is also to be expected from the work of Kempf and Van Horn²² on residual stresses in aluminum alloys. Regardless of the relief of residual stresses during aging, the plastic strains due to the thermal shock of quenching create regions of instability in which the aging process takes place preferentially. In fact, the process by which the effects of plastic deformation are relieved in age hardening is probably closely related to the aging process.

THE EFFECT OF ALLOY COMPOSITION

When the aging curves of the two alloys are compared, several differences become apparent. Except for aging at 125° and 70°C, the electrical resistance of water quenched aluminum-silicon specimens decreases more rapidly than that of the water quenched aluminum-copper specimens. The rates of hardening behave correspondingly, although to a less marked degree. At the two lowest aging temperatures the water

quenched aluminum-silicon alloy aged less rapidly than the aluminum-copper alloy, especially when considered in terms of the first appreciable aging effect.

The directly quenched samples of both alloys changed in resistance and in hardness at comparable rates at most temperatures but the directly quenched aluminum-silicon alloys showed almost no effect of aging at 125° and 70°C.

With minor exceptions the accelerating effect of water quenching is thus more marked for the aluminum-silicon than for the aluminum-copper alloy. This observation must be interpreted in the light of the fact that the age hardening mechanism is simpler in the aluminum-silicon than in the aluminum-copper system.

Summary and Conclusions

Two alloys of aluminum were aged at various temperatures after quenching from the solution treatment directly to the aging temperatures and also after first quenching into water. The progress of the aging reaction was followed by electrical resistance and by hardness measurements.

The absolute amount of change in electrical resistance as a function of the aging temperature went through a maximum. This was true for both

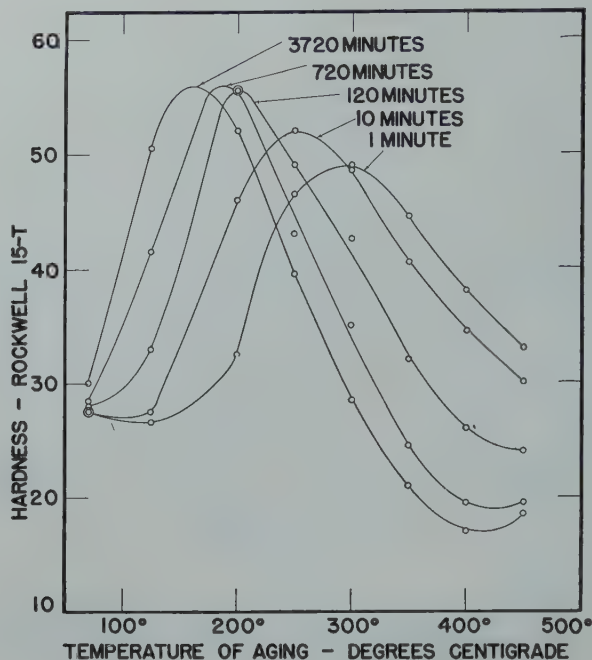


FIG 8—Hardness of water quenched specimens of an aluminum-silicon alloy as a function of temperature at constant aging times.

alloys and regardless of the type of quench, given a certain minimum time of aging. The change of hardness behaved similarly although some of the curves were of complicated shape. It may also be concluded that the age hardening rates went through maxima at intermediate temperatures, although no absolute basis exists for comparing these rates at different temperatures.

At most temperatures water quenching greatly accelerated the rate of aging compared to directly quenched samples. This accelerating effect is the result of strains caused by the thermal shock of quenching assisted to an unknown extent by the effect which exposure to room temperature has on nucleation.

At most temperatures the water-quenched aluminum-silicon alloy aged more rapidly than the aluminum-copper alloy, while the directly quenched alloys aged at comparable rates. At the two lowest aging temperatures, however, the water quenched aluminum-silicon alloy aged less rapidly than the aluminum-copper alloy and the directly quenched aluminum-silicon alloy showed almost no effect of aging. At most temperatures, the accelerating effect of water quenching over direct

quenching is larger for aluminum-silicon than for aluminum-copper alloys.

Acknowledgments

The authors gratefully acknowledge the help received from several staff members of the Department of Metallurgy at the Massachusetts Institute of Technology. They desire especially to record their indebtedness to Professor Morris Cohen. Thanks are also due to the Aluminum Company of America for furnishing the high-purity alloys used in this investigation.

References

1. R. F. Mehl and L. K. Jetter: Symposium on Precipitation Hardening (Age Hardening) A.S.M., Cleveland 1940, p. 342
2. M. L. V. Gayler: Symposium on Internal Stresses, Inst. of Metals, London, 1948, p. 255
3. A. H. Geisler: Property Changes during Aging. *Trans. AIME* 180 (1949) 230. *Metals Tech.* Aug. 1948, TP 2436.
4. R. Becker: *Ann. Phys.* (1938) (5), 32, 128
5. G. Borelius: *Ann. Phys.* (1938) (5) 28, 507
6. C. H. Johansson and O. Hagsten: *Ann. Phys.* (1937) (5), 28, 520

7. C. L. Wilson, H. F. Silliman and E. C. Little: Contribution No. 11, AIME, Feb. 1933 (Abstract: *Trans. AIME* (1933) 104, 131
8. P. A. Chevenard, A. M. Portevin and X. F. Waché: *Jnl. Inst. Metals*, (1929) 42, 337
9. A. Phillips and R. M. Brick: *Trans. AIME* (1934) 111, 94
10. W. L. Fink and D. W. Smith: *Trans. AIME* (1938) 128, 223
11. G. Wassermann: *Ztsch. Metallkunde* (1938) 30, 62
12. W. Hartnagel: *Ztsch. Metallkunde* (1938) 30, 81
13. W. P. Sykes: *Trans. A.S.M.* (1940) 28, 892
14. L. K. Jetter and R. F. Mehl: *Trans. AIME* (1943) 152, 166
15. R. H. Harrington: *Trans. A.S.M.* (1944) 33, 494
16. M. L. V. Gayler: *Jnl. Inst. Metals*, (1946) 72, 243
17. A. G. Guy, C. S. Barrett and R. F. Mehl: *Trans. AIME* (1948) 175, 216. *Metals Tech.* Feb. 1948, TP 2341.
18. B. M. Loring, W. H. Baer and G. M. Carlton: *Trans. AIME* (1948) 175, 401. *Metals Tech.* Feb. 1948, TP 2337.
19. G. Borelius, J. Andersson and K. Gullberg: *Ingeniörsvetenskapsakademins Handl. Nr. 169*, Stockholm, 1943
20. E. H. Dix Jr. and A. C. Heath Jr.: *Trans. AIME* (1928) 78, 164
21. W. L. Fink and L. A. Willey: *Trans. AIME* (1948) 175, 414. *Metals Tech.* Aug. 1947, TP 2225
22. L. W. Kempf and K. R. Van Horn: *Trans. AIME* (1942) 147, 250

Low Pressure Distillation of Zinc from Al-Zn Alloy*

MAX J. SPENDLOVE† and HILLARY W. ST. CLAIR,† Junior Member AIME

Introduction

The problem frequently arises, particularly in refining metals or smelting scrap metals, of separating metals in the metallic state. Many metals may be separated by taking advantage of their difference in vapor pressure. Such separations can be made at atmospheric pressure, but the separations are much more selective and can be carried out at considerably lower temperatures if the distillation is done at pressures of a few millimeters or less in an evacuated enclosure. Until recently, this has not been considered feasible as a metallurgical operation, but the recent improvements that have been made in vacuum technology have broadened the applicability of vacuum processes and have prompted re-examination of low-pressure distillation of metals as a practicable process. The distillation of zinc from lead is one separation that has already been reduced to practice.¹

This paper is the first of a series of studies being made on separation of nonferrous metals by distillation at low pressures. Although these experiments were confined to the separation of zinc from aluminum, the significance of the results is by no means confined to these two metals. The purpose has been to investigate a metallurgical technique rather than merely to devise a means of separating specific metals.

The experimental work on distillation of zinc from zinc-aluminum alloys at reduced pressure grew out of earlier work on distillation at atmospheric pressure.² The earlier work indicated that it would not be practicable to decrease the zinc in the alloy much below 10 pct owing to the high temperature required. Therefore attention was turned to distillation at low pressures, at which lower temperatures are required. After preliminary tests were made in a small, evacuated tube furnace, a larger furnace having a capacity

of 100 to 150 lb of metal per charge was constructed. Distillation tests were first made on pure zinc and then on aluminum-zinc alloys of various composition. Particular attention was given to the limit to which zinc could be reduced in the residual metal. Data were also taken on the rate of evaporation, and heat balances were made for both the crucible and the condenser.

Distillation Furnace

The vacuum-distillation unit is illustrated schematically in Fig 1. The major components are the induction furnace, the condenser, the vacuum system, and the power-conversion unit. Power is supplied to the induction furnace from a 50-kw 3000-cycle motor-driven alternator. The pressure in the furnace is reduced by a vacuum pump having a nominal pumping speed of 10 liters per sec. When in operation, the metal vapors travel upward from the furnace to the water-cooled condenser where they are collected in amounts of 50 to 100 lb. The condenser is removed with aid of an electric hoist. When the system is under vacuum, the condenser is made self-sealing by a rubber gasket between the smooth-faced, water-cooled flanges at the top of the furnace and the bottom of the condenser. The pressure of the atmosphere is more than sufficient to insure sealing. At the conclusion of an experiment, the residual

metal can be removed from the furnace by removing the condenser and tilting the furnace with the electric hoist. The metal was cast into the molds carried on a mold truck. A photograph of the furnace and auxiliary equipment is shown in Fig 2.

The details of the vacuum furnace are illustrated in Fig 3. The furnace proper is made vacuum-tight with rubber gaskets placed at each end of a fused quartz cylinder. A clamping plate at the bottom and a ring at the top are made to squeeze the rubber between the metal and the end of the quartz tube. A large graphite crucible placed inside the quartz cylinder is thermally insulated and physically supported by refractory insulating bricks. A thermocouple in a quartz protection tube is located at the bottom of the crucible; the leads pass through a rubber seal in the bottom plate. The supporting structure for the furnace is an angle iron frame with transite board sides.

The condenser is made in the form of a water jacketed cylinder with an opening to the vacuum line at the top. The bottom has a projecting skirt inside the machined flange to provide additional cooling for the rubber gasket. Condenser sleeves are made in the form of two semicylindrical pieces of sheet metal that fit snugly inside the cooling jacket. The split sleeve facilitates removal of the condensate.

Measurement of Temperature and Pressure

The metal temperature was measured by a platinum-platinum rhodium thermocouple inserted in a well extending up into the bottom of the graphite crucible. During rapid evaporation there is a wide difference in temperature between the surface and the main body of metal in the crucible because of the large amount of heat that must be conducted to the surface to supply the heat of evaporation. The heat of

New York Meeting, February 1950.

TP 2671 D. Discussion of this paper (2 copies) may be sent to *Transactions AIME* before April 1, 1950. Manuscript received March 29, 1949; revision received June 14, 1949.

* Papers by authors of the U. S. Bureau of Mines Staff are not subject to copyright.

† Electrical Engineer and Metallurgist, respectively, College Park Branch, Metallurgical Division, Bureau of Mines, College Park, Md.

¹ References are at the end of the paper.

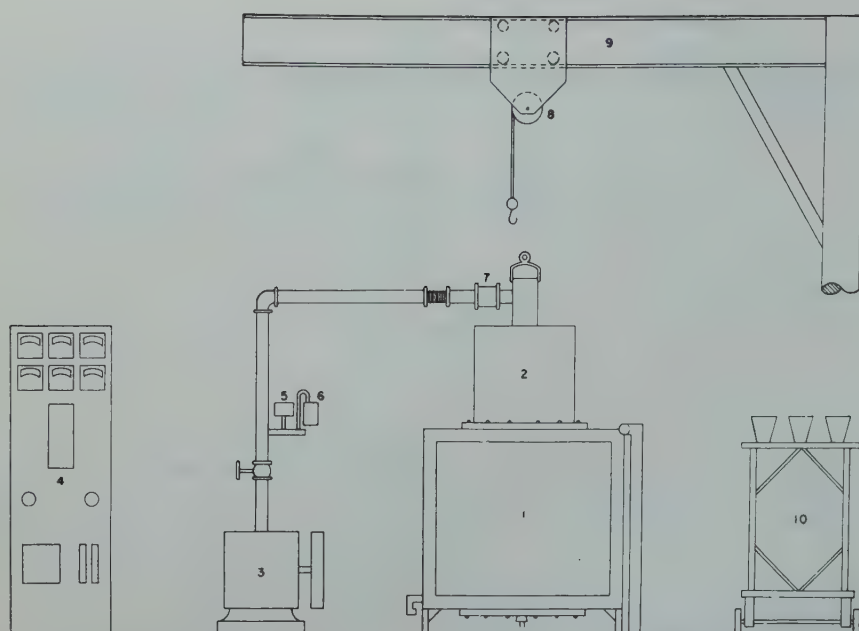


FIG 1—Diagrammatic sketch of equipment for vacuum distillation.

- | | |
|----------------------|------------------------|
| 1. Induction furnace | 6. McLeod gauge |
| 2. Condenser | 7. Dust trap |
| 3. Vacuum pump | 8. Electric hoist |
| 4. Control panel | 9. Mono-rail jib crane |
| 5. Televac | 10. Mold truck |

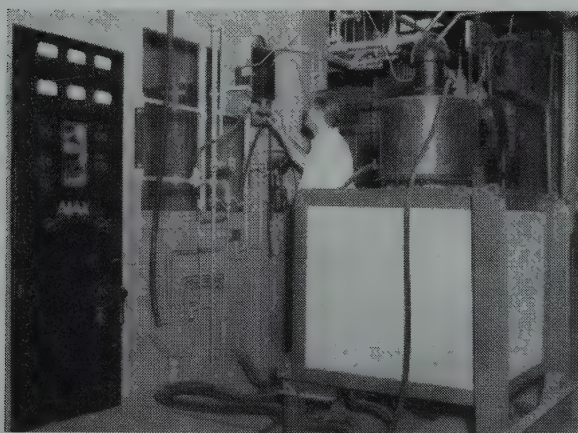


FIG 2—Vacuum distillation furnace.

evaporation amounts to about 200,000 cal per lb of zinc. The temperature gradient required for conducting heat to the surface, neglecting the effect of stirring of the melt due to induced currents in the metal, will be of the order of 10 to 30°C per cm. Therefore, during rapid evaporation, the temperature of the main body of the melt as measured by the thermocouple at the bottom of the crucible may be as much as 100°C higher than the surface temperature. Nevertheless, the temperature of the metal is quite sensitive to changes in the temperature at the surface and gives a fairly accurate representation of relative temperature changes at the surface even though the actual recorded temperatures are considerably higher.

The pressure in the system was measured by a McLeod gauge and by a thermocouple gauge connected to the recording potentiometer. The vacuum indicated by the potential across the thermocouple gauge was checked frequently by the McLeod gauge. Dust filters and cold traps, cooled with dry ice, were placed between the vacuum gauge manifold and the vacuum line. A Pirani gauge was used for leak detection. A small jet of helium was passed over the walls where leaks might occur. When the stream of helium impinged against the leak, the Pirani gauge would indicate a sudden rise in pressure.

The pressure indicated by the vacuum gauge is the partial pressure of the residual gas in the system. There

is no way of directly measuring the partial pressure of the zinc vapor. During evaporation the partial pressure of the residual gas in the region between the metal and the condenser is much lower than is indicated by the vacuum gauge because the zinc vapor tends to sweep the residual gases toward the condenser. In other words, the zinc vapor acts as a diffusion pump, removing gases from the crucible and discharging them at the condenser. Therefore, during rapid evaporation the vapor above the metal is virtually all zinc vapor. The pressure of the residual gases indicated by the vacuum gauges applies only to the condenser and the lines to the vacuum pump.

Experimental Procedure

Weighed amounts of zinc or zinc and aluminum were melted together in the carbon crucible preceding the test. After the metals were thoroughly melted and blended, a sample was taken for chemical analysis. The condenser and baffle were put in place and the metal was allowed to freeze before the system was evacuated. If this precaution was not taken, the rapid evolution of gas from the molten metal during initial stages of evacuation sometimes caused spattering of the alloy into the condenser. After the system was evacuated, the metal was remelted, and the power was increased to the desired level. The flow of cooling water to the condenser was regulated during the test to keep the temperature of the water leaving the condenser less than about 90°C. The flow of water was measured by a rotameter. At the conclusion of a test the condenser was removed from the furnace and allowed to cool. Samples were taken from the condensate and the residual metal for chemical analysis and the condensate and residual metal were weighed.

Experiments 1 to 6 were made with charges of pure zinc. The purpose of these tests was to remedy any operating difficulties before introducing the aluminum and to obtain data on pure zinc for comparison with those to be obtained on zinc-aluminum alloys.

After the preliminary tests, cylindrical sleeves were placed in the condensing chamber to permit easy removal of the condensate. These sleeves were painted before each test with a thin paste of lampblack and water to prevent the condensate from adhering to the sleeve. The paste was allowed

to dry before placing the sleeves in the furnace.

Radiation baffles were placed between the crucible and condenser to prevent direct radiation of heat to the condenser and to equalize the distribution of condensate. Three types of baffles were tried as shown in Fig 4. The baffles were constructed of iron and painted before each experiment with lampblack to protect the iron from the hot zinc vapor.

Experiment 1 was run without the radiation baffle. The deposit was clean and fairly dense but showed evidence of refluxing. The condensate from experiment 3, with a single-deck baffle in place, was cleaner, denser, and showed no evidence of refluxing. Improvements in the condensing sleeve were worked out in experiments 3 and 4. In these experiments the single-deck baffle directed most of the vapors to the lower portion of the condenser, thereby constricting the path of the vapor as the deposit grew out from the walls. In experiment 5 the baffle was inverted to direct the flow of vapor higher into the condenser. This change overcorrected the distribution, resulting in excessive condensation at the top of the condenser and clogging the exit to the vacuum line. In experiment 6, a two-deck baffle was made and placed within the condenser as shown in Fig 4. This baffle gave a fairly uniform deposit. Although baffles were useful in this furnace, it is doubtful that they are absolutely necessary. The same effects doubtless could be reached by properly proportioning the diameters of the upper part of the crucible and the condenser.

The metal temperature provides a good indication of what is happening in the distillation furnace. As the temperature reaches the melting point, an arrest is indicated on the temperature chart. The temperature climbs steeply until it reaches the point at which evaporation begins; then, as the heat supplied is gradually offset by the heat required for evaporation, the temperature levels and remains nearly constant for the remainder of the test. The beginning of distillation is also marked by a sudden rise in the temperature of the cooling water from the condenser as heat is transferred to the condenser by the zinc vapor. A typical temperature curve for the metal temperature is shown in Fig 5, together with a corresponding curve showing the variation of temperature of the cooling water from the condenser. It will be ob-

served that the temperature rises linearly after melting, as shown by section *AB*. The beginning of evaporation is indicated by *C*, the point at which the temperature curve begins to break away from *AB*. It will also be observed that the temperature of the cooling water starts to rise at the melting point and then begins to rise abruptly as the temperature reaches *C*. The rate of evaporation in each experiment was calculated, using point *C* as a starting point.

Distillation Tests on Pure Zinc

Six tests were made on distillation of pure zinc (99.99 pct Zn); the data for these tests are summarized in Table 1.

Evaporation began when the metal temperature reached about 470°C. The maximum metal temperature during evaporation was determined chiefly by the power input; for an input of 10 kw, the temperature leveled at about 500°C and for 30 kw at about 550°C. The metal temperature was also influenced by the distance

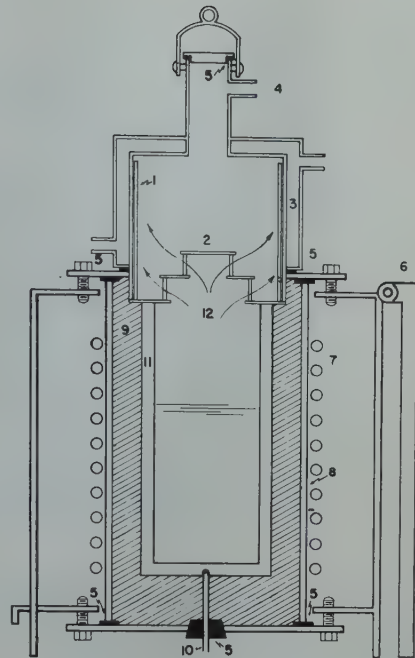


FIG 3—Cross-section of 50 kw distillation furnace.

- | | |
|---------------------------|------------------------------|
| 1. Split condenser sleeve | 7. Induction coil |
| 2. Radiation baffle | 8. Quartz tube |
| 3. Water jacket | 9. Insulation |
| 4. To vacuum pump | 10. Quartz thermocouple well |
| 5. Rubber seal | 11. Graphite crucible |
| 6. Furnace pivot | 12. Vapor path |

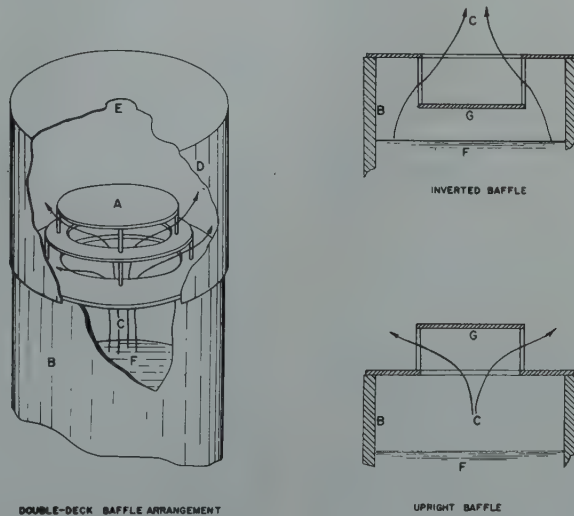


FIG 4—Arrangement of baffles between crucible and condenser.

- | | |
|-----------------------|-----------------------|
| A. Double-deck baffle | E. Vacuum take-off |
| B. Carbon crucible | F. Metal surface |
| C. Zinc vapor | G. Single-deck baffle |
| D. Condenser | |

between the evaporation and condensing surfaces and by an obstruction to the flow of vapor to the condenser. This effect is shown by the temperature curves for tests 3, 4, 5, and 6 shown in Fig 6. Tests 3 and 4 were run with the single-deck baffle. This baffle constricted the flow of the vapor as it left the crucible and directed it toward the walls of the condenser. Most of the zinc condensed as large clusters of

crystals in the lower part of the condenser. In test 5 the baffle was inverted as shown in Fig 4, thereby constricting the flow even more than in tests 3 and 4 and directing the vapor to the top of the condenser. This caused the temperature to rise to 540°. The double-deck baffle used in test 6 offered much less impedance to the vapor flow and caused more uniform distribution of the deposit. This ex-

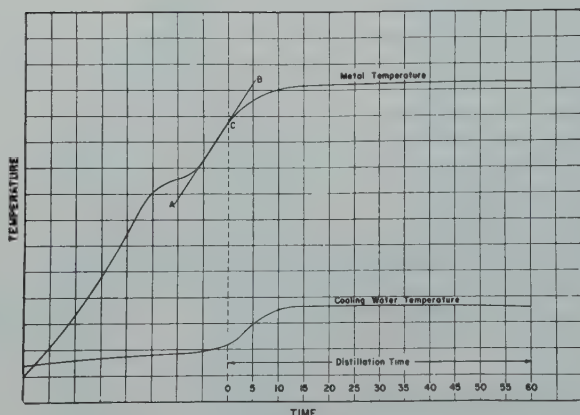


FIG 5—Furnace temperature and cooling water temperature during typical distillation test.

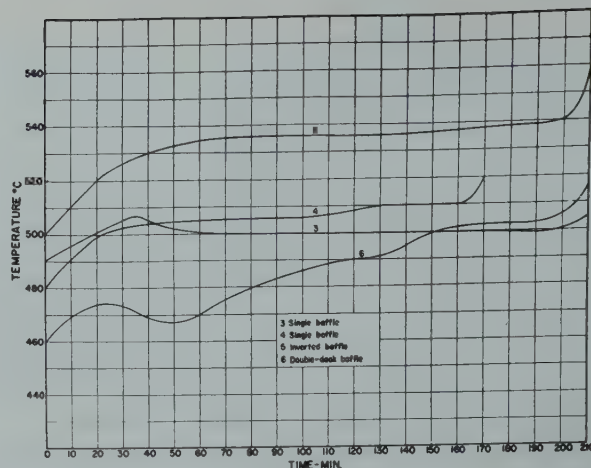


FIG 6—Metal temperatures for tests 3 to 6 showing effect of baffles.

Table 1 . . . Distillation Tests on Molten Zinc

| Number | 1 | 2 | 3 | 4 | 5 | 6 |
|--|-------|-------|-------|-------|-------|-------|
| Power input, kw | 27.5 | 25 | 10 | 10 | 10 | 10 |
| Duration, min | 16.5 | 60 | 220 | 115 | 215 | 230 |
| Zn distilled, lb | 9.8 | 33 | 58 | 41 | 50 | 61 |
| Metal temp., avg. °C at which evap. starts | 545 | 536 | 500 | 507 | 533 | 486 |
| Final pressure, mm Hg | 0.700 | 4.30 | 0.050 | 0.120 | 0.100 | 0.060 |
| Rate of evaporation, lb per min | 0.594 | 0.550 | 0.264 | 0.264 | 0.232 | 0.264 |
| Power consumption kw-hr per lb | 0.772 | 0.758 | 0.622 | 0.630 | 0.716 | 0.629 |

plains the low average metal temperature during test 6. The temperature first leveled slightly above 470°; during the early part of the test the vapor traveled only a very short distance before it was condensed. As the zinc gradually condensed higher on the walls of the condenser where cooling was more effective, the temperature of the metal gradually rose to 500°C, the same as for test 3.

Referring to Table 1, it will be noted that the rate of evaporation is related more directly to the power input than to the metal temperature. This is not surprising since the rate of evaporation is determined by the rate at which heat is conducted to the surface of the metal; the metal temperature automatically adjusts itself to bring the two in balance. The relationship between rate of evaporation and metal temperature will be discussed again later.

Distillation Tests on Zinc-aluminum

Six distillation tests were made on zinc-aluminum alloy containing about 80 pct zinc. The alloy was made up of commercially pure aluminum (99.89 pct Al) and pure zinc. The zinc and the aluminum were melted and heated

until the aluminum was dissolved. The melt was then skimmed thoroughly before the condenser was placed on top of the furnace. In the first series of tests, only 60 to 80 pct of the zinc was distilled. Tests were made with the power input adjusted to 10, 20, 30 kw, respectively. Temperature of the metal, pressure of the system, and temperature of the cooling water of the condenser were all recorded automatically on a strip-chart potentiometer. A photograph of the chart for test 9 is shown in Fig 7. The chart is calibrated to read the furnace temperature directly in hundreds of degrees centigrade. The pressure and water temperature are recorded on the same chart in arbitrary units. Several actual values for the water temperature and pressure are shown on the chart. The horizontal lines indicate ten minute intervals.

In this test it will be observed that the metal temperature, which had been raised to about 700°C to dissolve the aluminum, dropped abruptly as soon as the vacuum pump was started. The rapid cooling of the metal is a result of rapid evaporation. When the power was turned on the metal gave off dissolved gases and the pressure in the system rose from 80 to 130 microns, then gradually decreased to about 90 microns as the metal was degassed.

The water-temperature variations

were a result of manual adjustment of the flow of cooling water. It was intended that the water should remain at 80°C but the valve adjustment was too coarse to permit accurate control during this test.

The undulations in the metal temperature are interesting. They were always observed when the temperature of the metal was in the liquidus-solidus range. They are explained as follows: As evaporation continues, the zinc in the melt is decreased until the metal temperature is equal to or perhaps less than the liquidus temperature. Then the solid phase crystallizes out; and since it is lighter than the melt, it floats on top. This forms a protective layer on the surface and decreases the rate of evaporation, allowing the temperature to rise until the solid phase is redissolved. Then the same sequence starts all over again, producing a series of undulations in the temperature. It will be noted that simultaneous variations occur in the pressure, indicating that gas evolution increases and decreases with the temperature throughout the test.

The temperature of the melt gradually increases as the proportion of zinc decreases. The vapor pressure of zinc in zinc-aluminum alloys shows a positive deviation from Raoult's law; that is, the vapor pressure is greater than that calculated by multiplying the vapor pressure of zinc by the molal fraction of zinc in the melt. The vapor pressure of zinc-aluminum alloys was measured by Schneider and Stoll³ at 650 to 800°C. They found that their data were in good agreement with Hildebrand's⁴ equation for activity of a solute, in which the coefficient β equals 0.50 or

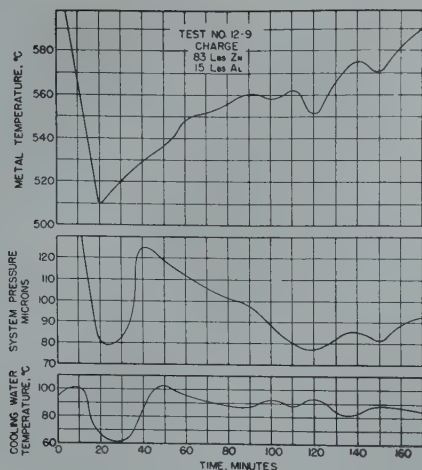


FIG 7—Potentiometer chart for test 9 showing metal temperature, pressure in system, and temperature of water from condenser.

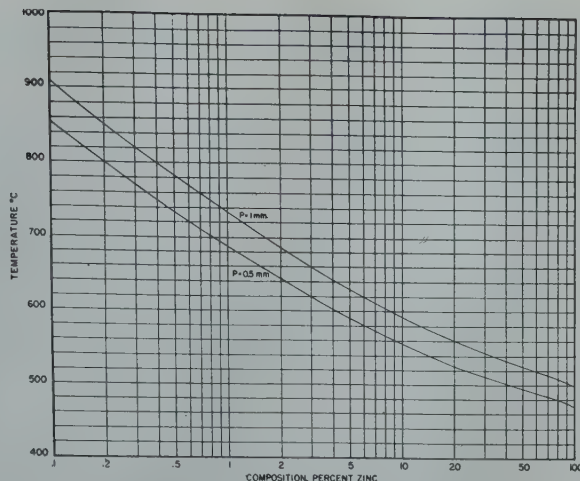


FIG 8—Temperature-composition curves for constant partial pressure of zinc over zinc-aluminum melts.

$$\log \lambda_{Zn} = \log \frac{p}{x_{Zn}p_0} = 0.50 (x_{Al})^2$$

where p_0 is the vapor pressure of zinc; x_{Zn} and x_{Al} are the respective molal fractions. From this equation and the vapor pressure of pure zinc it is possible to calculate the vapor pressure of molten zinc-aluminum alloys at any temperature and composition.

Evaporation of pure zinc begins when the vapor pressure reaches about 0.5 mm as indicated by the metal temperature. This would mean that evaporation begins at about 470°C for pure zinc, 560° for 10 pct Zn, 690° for 1 pct Zn, and 800° for 0.1 pct Zn.

If we carry this assumption farther it might be expected that the temperature of the surface of the metal would vary in such a way as to maintain a constant vapor pressure with changing composition. In that case, the temperature at constant power input would vary as in Fig 8, in which are shown the isobaric temperature curves for zinc-aluminum melts having partial pressures of 0.5 mm and 1.0 mm of mercury. However, it was observed, as shown by the temperature curves in Fig 9, that the temperature actually increased more than would be indicated by the isobaric curves of Fig 8. For example, the temperature of test 8 at a power input of 10 kw should have increased 15 to 20°C, according to the change in composition of the residual metal, but the observed increase in temperature shown in Fig 9 was 70°C. The discrepancy for the other two tests at higher heating rates is even greater. As we have already pointed out, the metal temperature may differ appreciably from the surface temperature

during rapid evaporation; but even after taking this into account, it is apparent that the isobaric temperature curves do not provide an adequate guide for predicting the rise in metal temperature.

Another factor to be considered is the nonuniformity of composition arising from rapid evaporation of the zinc at the surface. Zinc will tend to evaporate faster than aluminum can diffuse away from the surface, thereby causing a surface enrichment in aluminum. Accordingly, the observed temperature rise could be explained if the actual surface concentration of zinc in test 8 were between 10 and 20 pct zinc instead of 70 pct as given by the average composition. Likewise, an even greater concentration of aluminum at the surface would be expected at the higher heating rates in tests 11 and 14. The temperature rise in test 14 would indicate only about 2 pct zinc at the surface at the end of the test.

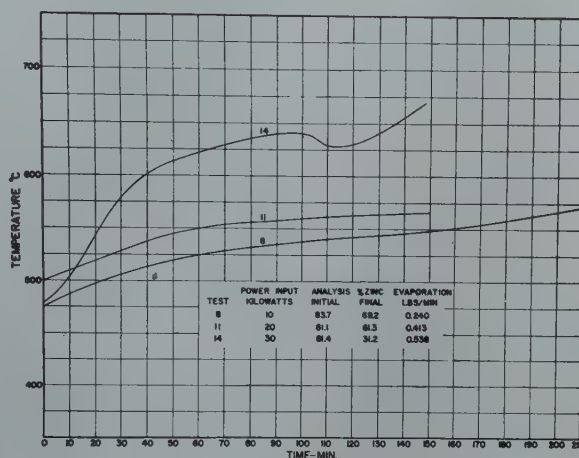


FIG 9—Variation of metal temperature during distillation of zinc from zinc-aluminum melts.

Extent of Removal of Zinc from Aluminum

A series of three tests was run in which the zinc in the alloy was reduced in successive steps. The progressive rise in metal temperature during these tests is shown in Fig 10. The power input to the furnace during the three tests was held at 10 kw. During the first test the metal temperature rose to 512° and remained constant to the end of the test; about 60 pct of the zinc was evaporated, leaving residue containing 34.5 pct zinc. In the second test, about 35 pct more of the zinc was distilled. The metal temperature during this time rose from 512 to 620°. During the final test the temperature rose continuously to more than 900°C and the zinc in the metal was reduced to 0.21 pct.

Comparative tests were made on alloys prepared from aluminum and from aluminum scrap to determine the effect of impurities and other metals

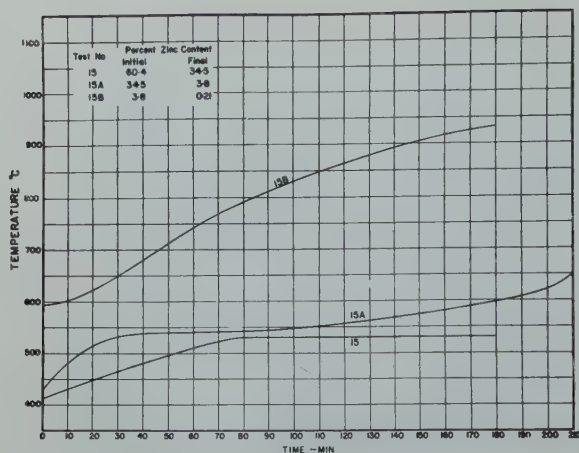


FIG 10—Metal temperature during three successive distillation tests on which zinc was reduced from 60 to 0.2 pct.

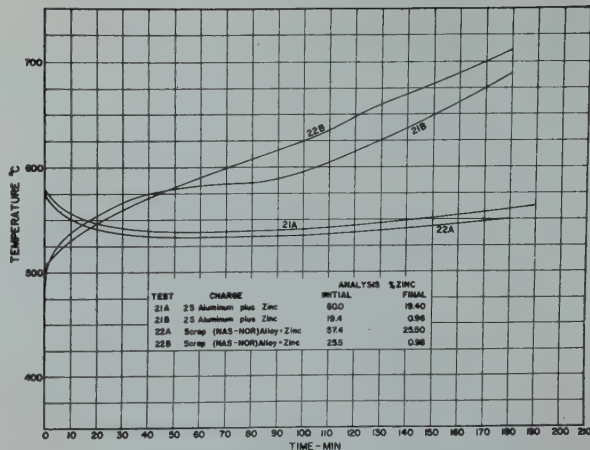


FIG 11—Metal temperature curves for comparative tests with pure aluminum and aluminum scrap.

Table 2 . . . Summary of Distillation Tests on Zinc-Aluminum Alloys

| Test Number | 8 | 9 | 10 | 11 | 12 | 14 | 15 | 15A | 15B | 21A | 21B | 22A | 22B |
|-----------------------------------|-------|-------|------|-------|------|-------|-------|------|------|-------|-------|-------|-------|
| Power input, kw. | 10 | 20 | 20 | 20 | 30 | 30 | 10 | 10 | 10 | 10 | 10 | 10 | 10 |
| Temperature, °C | | | | | | | | | | | | | |
| Final | 575 | 590 | 550 | 570 | 555 | 630 | 532 | 610 | 930 | 565 | 685 | 550 | 710 |
| Average | 546 | 557 | 554 | 553 | 555 | 605 | 504 | 558 | 771 | 549 | 594 | 543 | 613 |
| Zn content, Pct | | | | | | | | | | | | | |
| Initial | 83.7 | 55.8 | 75.2 | 81.1 | 81.4 | 81.4 | 60.4 | 34.5 | 3.8 | 60.0 | 19.4 | 57.4 | 25.5 |
| Final | 69.2 | 23.6 | 66.3 | 61.3 | 77.1 | 31.2 | 34.5 | 3.8 | 0.21 | 19.4 | 0.96 | 25.5 | 0.98 |
| Rate of distillation, lb per min. | 0.240 | 0.441 | | 0.413 | | 0.538 | 0.205 | 100 | | 0.187 | 0.123 | 0.215 | 0.103 |
| Power consumption, kw-hr per lb. | 0.695 | 0.811 | | 0.808 | | 0.930 | 0.814 | 1.67 | | 0.892 | 1.35 | 0.776 | 1.62 |

present in the scrap in minor amounts. The scrap aluminum came from melted aircraft scrap from the Naval Air Station at Norfolk, Virginia. It was designated by the symbol, "NAS-NOR." A representative analysis is given as follows:

| Analysis of NAS-NOR Alloy in Percent | |
|--------------------------------------|-------|
| Aluminum | 93.88 |
| Zinc | 1.09 |
| Iron | 0.91 |
| Silicon | 0.31 |
| Copper | 3.81 |

Tests 21A and 21B (Fig 11) were run with 2S aluminum and tests 22A and 22B, with NAS-NOR alloy. The original alloy for each test was made up to about 60 pct zinc. Each test was interrupted after 3 hr and a sample was taken of the residual metal. Then evaporation was continued for another 3 hr, during which the zinc in the residual metal was decreased to less than 1 pct. There was no appreciable difference in the metal temperatures during the first 3-hr period but during the last 2 hr the metal containing the impurities was about 30° hotter. The over-all rates of evaporation were very nearly the same, although more zinc was distilled in the first half of the test with scrap aluminum. All in all, there was no significant difference in the general behavior of the two alloys during distillation.

The important data for all the tests

on zinc-aluminum alloys are summarized in Table 2.

Nature of Condensate

The lower section of the condensate consists of large, dendritic clusters of crystals projecting outward from the walls and in a direction opposite that of the vapor flow. The deposit in the upper part of the condenser is thinner, more compact, and the crystals are much finer. This is illustrated by the photograph in Fig. 12. The form of the crystals in the crystal aggregates is greatly influenced by the rate of condensation and the partial pressure of the permanent gas in the system. At low evaporation rates and low pressures, the condensate is composed largely of fine, loosely compacted, needle-shaped crystals. At higher rates of condensation, the crystal aggregates become more massive and compact and at very high rates the deposit becomes compact and the surface becomes smooth and rounded as though the zinc were deposited in the molten state. The same effects are observed when the pressure is increased, except that the surface takes on a dull appearance instead of the bright, metallic surface produced at low pressures. The dull appearance may result in part from some surface oxidation at higher pressures.

The principal impurities found in the condensate were aluminum, iron, and cadmium. The iron is usually less than 0.02 pct; it was probably introduced as a result of contact with the condenser walls. The cadmium was introduced as a minor impurity in the zinc. It was present only in trace amounts. Aluminum is the only impurity that is inherently important. The vapor pressure of aluminum is only about 10^{-9} times that of zinc at 500°C, but when an alloy of aluminum and zinc is distilled the temperature increases and the partial pressure of the zinc decreases thereby increasing the proportion of aluminum in the vapor. For example, the aluminum in the vapor from a 10 pct zinc alloy at 600° is less than 10^{-4} pct. At 900° the vapor pressures of zinc and aluminum are 700 mm and 1.3×10^{-3} mm, respectively. The vapor pressure of zinc over a 0.1-pct zinc alloy is calculated as 0.91 mm, so that the condensate from such an alloy would contain aluminum and zinc in the proportions to give a deposit containing 0.14 pct aluminum.

The average analyses of the condensates obtained in these tests range from less than 0.01 to about 0.5 pct aluminum. The analyses of the condensates and residual metal for tests 15, 21, and 22, the three series in which the zinc in the residual metal was

reduced below 1 pct, are listed as shown below. The analyses for tests 21B and 22B show that the aluminum in the condensate increases markedly as the zinc is depleted in the residual metal. Furthermore, the aluminum content

| Test Number | 15 | 15A | 15B | 21A | 21B | 22A | 22B |
|-----------------------------|------|------|------|------|------|------|------|
| Residual metal, pct Zn..... | 34.5 | 3.8 | 0.21 | 19.4 | 0.96 | 25.5 | 0.98 |
| Condensate, pct Al..... | 0.20 | 0.10 | | 0.04 | 0.34 | 0.05 | 0.56 |

of the condensate greatly exceeds that which can be explained on the basis of evaporation of aluminum, indicating that the aluminum in the condensate is largely a result of spattering.

Spattering seems to occur chiefly during degassing of the molten metal. As the dissolved gas is expelled it carries with it a fine spray of metal formed when the bubbles break at the surface. Spattering from this cause can be reduced considerably by heating the metal very slowly during the time gases are being released. By following such a procedure, it was possible to reduce the aluminum in the condensate to less than 0.01 pct. However, when the zinc in the residual metal is reduced to a few tenths percent, some spattering seems to occur even when there is no evidence of gas evolution. This might be explained on the basis of the concentration of aluminum at the surface during a rapid evaporation. Normally vapor is formed only at the surface because the vapor pressure of the zinc is so low that the hydrostatic pressure even slightly below the surface is too great to permit the formation of bubbles. But as the surface layer becomes depleted in zinc, the temperature will rise to a point where the vapor pressure in the metal immediately under the surface layer will suffice to offset the slight hydrostatic pressure thereby allowing bubbles of zinc vapor to form just below surface. The breaking of these very small bubbles will cause a fine spray of metal some of which may be mechanically entrained in the zinc vapor and carried to the condenser. These droplets must be very minute to be carried by the attenuated zinc vapor, so it is likely that they would be extremely difficult to separate from the vapor. Therefore the condensate probably will contain several tenths of 1 pct aluminum when the zinc in the residual metal is reduced below 1 pct, even though elaborate precautions are taken to avoid contamination by spattering.

Heat Requirements

After distillation has reached a constant rate, the heat requirements consist of the heat of vaporization at the distilling temperature and the

heat necessary to supply losses by radiation and conduction. The heat required for vaporization is transferred by the vapor to the condenser and absorbed by the condenser cooling water. The remainder of the heat input is lost by radiation and conduction from the walls of the furnace and is approximately equivalent to the heat required merely to maintain the furnace temperature.

Tables 3 and 4 give the heat balances for the furnace and the condenser, respectively, for the six tests on distillation of pure zinc. Table 3 was determined by balancing the electrical power input to the furnace, after correcting for the losses in the electrical circuit, against heat removed by radiation and evaporation. The heat losses of the furnace by radiation and conduction were measured by a preliminary test in which the power requirements were determined for maintaining the furnace at various

Table 4 . . . Heat Balance for Condenser

| Test No. | Heat of Condensation Kg-Cal per Min. | Heat Abstracted by Cooling Water Kg-Cal per Min. | Heat Not Accounted for Kg-Cal per Min. |
|----------|--------------------------------------|--|--|
| 1 | 128.10 | 181.44 | -106.75 |
| 2 | 118.60 | 164.4 | -45.80 |
| 3 | 65.80 | 86.39 | -20.59 |
| 4 | 58.80 | 61.18 | -2.38 |
| 5 | 51.35 | 69.14 | -17.79 |
| 6 | 57.15 | 60.30 | -3.15 |

Heat of Condensation = ΔH_v for Zn_g → Zn_l at 100°C
= 215.76 kg-cal per lb

temperatures when no distillation was taking place.

Evaporation of Metals at Low Pressure

Evaporation of liquids at low pressure is in many respects quite different from evaporation at atmospheric pressure. At low pressures the atmosphere above the liquid is made up almost entirely of molecules of vapor from the liquid. Vapor forms only at the surface and not in the body of the liquid such as occurs when volatile liquids boil at atmospheric pressure. Evaporation takes place at a rapid rate at low temperatures because the diffusion of vapor molecules away from the surface is not retarded by the presence of other gas molecules. The acceleration of evaporation by reduction in pressure is frequently explained

Table 3 . . . Heat Balance for Distillation Furnace

| Test No. | Power Input Kw | Temp. °C | Rate of Evaporation, Lb per Min. | Heat Input* Kg-Cal per Min. | Heat of Vaporization Kg-Cal per Min. | Heat Loss Rad., Cond. Kg-Cal per Min. | Losses Not Accounted for Kg-Cal per Min. |
|----------|----------------|----------|----------------------------------|-----------------------------|--------------------------------------|---------------------------------------|--|
| 1 | 27.5 | 545 | 0.594 | 362.5 | 117.8 | 87.5 | 157.2 |
| 2 | 25 | 536 | 0.550 | 329.5 | 109.1 | 85.0 | 135.4 |
| 3 | 10 | 500 | 0.305 | 131.8 | 60.8 | 76.2 | -5.2 |
| 4 | 10 | 507 | 0.273 | 131.8 | 54.3 | 77.5 | -0.0 |
| 5 | 10 | 533 | 0.238 | 131.8 | 47.2 | 84.2 | +0.4 |
| 6 | 10 | 486 | 0.265 | 131.8 | 52.9 | 72.8 | 6.1 |

* Calculated on basis of average electrical efficiency of 92 pct applied to furnace input.

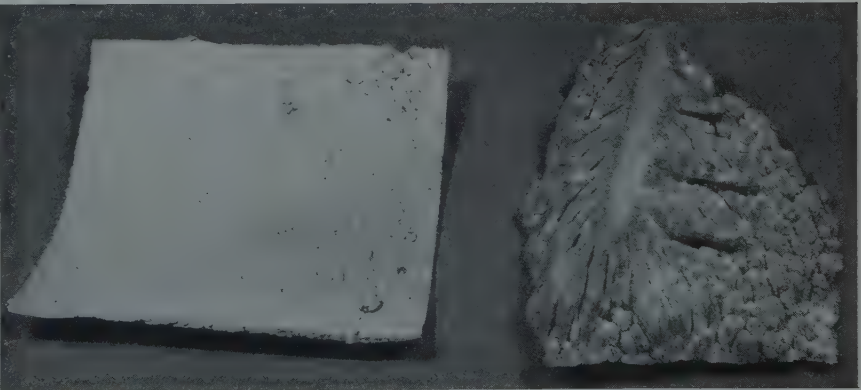


FIG 12—Zinc condensate showing large dendritic clusters found near bottom of deposit and dense fine grained deposit from upper wall.

as a result of the reduction in boiling point. This explanation applies as long as the total pressure remains appreciably greater than the partial pressure of the liquid, the boiling point being defined as the temperature at which the vapor pressure of the liquid is equal to the pressure of the permanent gas in the system. However, at very low pressures the rate of evaporation is limited not by the gas molecules but by the vapor molecules themselves. Under such circumstances the vapor pressure immediately above the liquid exceeds the partial pressure of the permanent gas and the boiling point no longer has any meaning.

The rate at which molecules of vapor leave the surface of the liquid is given by the effusion formula:

$$\omega_0 = p_0 \sqrt{\frac{M}{2\pi RT}} \quad [1]$$

where ω = rate of evaporation in grams per sq cm per sec.;

p_0 = vapor pressure of liquid in dynes per sq cm

M = molecular weight

R = gas constant in ergs per mol per °C

T = temperature °K

Expressing the rate of evaporation in grams per minute, the rate of evaporation of zinc is given by

$$\omega = 28.29 \frac{p_0}{T^{1/2}} \text{ g per sq cm per min.} \quad [2]$$

This equation gives the rate at which zinc would be evaporated into a vacuum or when evaporation is taking place at a comparatively slow rate. However, at high rates of evaporation the molecules of zinc leaving the surface interfere with each other and some of them return to the liquid. The effusion formula [1] may also be used to express the rate at which zinc is being recondensed on the surface:

$$\omega' = p \sqrt{\frac{M}{2\pi RT}} \quad [3]$$

where p now equals the partial pressure of the zinc vapor in contact with the surface. Therefore the net rate of evaporation is given by the difference between ω_0 and ω' or

$$\omega = (p_0 - p) \sqrt{\frac{M}{2\pi RT}} \quad [4]$$

For zinc, this becomes

$$\omega = \frac{28.29}{T^{1/2}} (p_0 - p) \quad [5]$$

When the rate of evaporation reaches a steady state the net rate of evapora-

tion as given by Eq 5 will be equivalent to the rate at which heat is transferred to the surface. The heat required to evaporate 1 g of zinc is 439 cal per g at 500°C. The temperature gradient required to conduct heat to the surface for evaporating at the rate of 1 g per sq cm per min. is equal to 53°C per cm. Therefore, the surface temperature at high rates of evaporation is a good deal lower than the temperature of the main body of metal.

The net rate of evaporation must also be equal to the rate at which vapor is diffused away from the surface. The rate of diffusion is determined by the pressure gradient of the zinc vapor between the evaporating and condensing surfaces. This explains why the temperature of the metal during evaporation is so responsive to obstructions between the crucible and condenser or changes in the distance between the evaporating and condensing surfaces. Any increase in the length of path of the vapor flow or in the pressure of the zinc at the condenser surface produces a corresponding increase in p , the pressure of the zinc at the evaporating surface. This requires a corresponding increase in the vapor pressure, p_0 , and the metal temperature as defined by Eq 5.

Another interesting effect to be considered in connection with the flow of zinc vapor to the condenser is the adiabatic cooling it undergoes. The temperature of the vapor in expanding from pressure p_1 at the crucible to pressure p_2 at the condenser decreases in the ratio

$$\frac{T_1}{T_2} = \left(\frac{p_1}{p_2}\right)^{\gamma} \quad [6]$$

The pressure of the zinc vapor at the evaporating surface is considerably less than the vapor pressure of zinc at the surface temperature or its temperature is above the dew point. However, as it is cooled adiabatically, the vapor becomes saturated so that even before it reaches the condenser, the temperature may be below the saturation temperature so that the condensation takes place from a supercooled vapor. For example, if the pressure of zinc vapor at the surface is 0.20 mm when the surface temperature is 500°C, the vapor at this point is only 20 pct saturated. However, when the vapor has expanded to a pressure of 0.15 mm the temperature will have dropped to the melting point, at which the vapor pressure of zinc is only 0.12 mm, and so the vapor is supersaturated with respect to liquid zinc. If the initial

pressure were a little lower the vapor would become saturated at a temperature below the melting point and would be supersaturated with respect to solid zinc.

This provides an explanation of the marked change in appearance that is found in the condensate at different rates of evaporation. At low rates the condensation takes place from a vapor that is supercooled with respect to the solid phase so the vapor condenses directly as a crystalline solid. At higher rates of evaporation, the vapor condenses from a vapor that is supercooled with respect to the liquid phase, so the vapor condenses momentarily as a liquid, chilling immediately to a solid. This deposit is more dense and compact and explains the rounded surfaces that give the appearance of having been melted.

These interesting aspects of low-pressure distillation of metal are discussed briefly to give a qualitative picture of the interrelation of the various factors that determine the rate of evaporation and the nature of the condensate. A more detailed study is being made of these phenomena which will be given a more extensive discussion in a later paper.

Acknowledgment

This investigation has been made by the Metals Recovery and Refining Section at the Eastern Experiment Station of the Bureau of Mines, College Park, Maryland. Acknowledgment is made to L. H. Banning and H. Bizot, formerly members of this group, who participated in the early experiments. Special acknowledgment is made to George E. Biser for his able assistance in constructing and operating the furnace; to A. M. Sherwood for the chemical analyses; to M. J. Peterson for spectrographic analyses; and to other members of the Eastern Experiment Station who contributed to this work.

References

1. W. T. Isbell: Vacuum Dezincing in Lead Refining. *Metals Tech.* April 1947, TP 2138. *Trans. AIME* (1949) 182.
2. H. W. St. Clair and D. D. Blue: Recovery of Aluminum from Crude Aluminum-silicon Alloy by Extraction with Molten Zinc. *Bur. of Mines Rept. of Investigations.* (In press.)
3. A. Schneider and E. K. Stoll: Vapor Pressure of Zinc Over Aluminum-zinc Alloys. *Ztsch. Electrochem.* (1941) 47, 527-535.
4. Joel H. Hildebrand: Solubility of Non-electrolytes. *Rheinhold Publ. Co., N. Y.*, (1936) p. 44.

Determination of Boundary Stresses during the Compression of Cylindrical Powder Compacts

M. E. SHANK,* Junior Member and JOHN WULFF,* Member AIME

Introduction

At the present time, the designer of dies for metal powder pressing is handicapped by relative ignorance of stress distribution and frictional effects at the interior surface of the die. Unckel¹ was the first to develop a method for the study of wall friction. He used three Brinell balls on which the die rested during pressing. The total frictional wall force was determined by the size of impression these balls left on a soft metal plate. Since the method does not give radial pressures, or distribution of such pressures, coefficients of friction could not be determined. Although Unckel measured density distribution, he was not able to determine radial or shear stresses. Shaler² has proposed theoretical expressions for the stress and density distribution within cylindrical compacts during pressing, in accordance with the experimental results of Kamm, Steinberg, and Wulff.³

By application of Siebel's method,⁴ Kamm et al³ plotted stress trajectories for two compacts. From the stress trajectories they calculated coefficients of friction from point to point along the die wall. As pointed out by Shaler in the discussion of Ref. 3, these values are based on progressive point-to-point calculations on finite size grid squares across the compact. In the region of the die wall such calculated values may therefore have considerable cumulative error.

The purpose of the present paper is to develop an experimental method by which the nonhydrostatic pressures and shears acting on the interior wall of a cylindrical die can be measured. Such measurements can then be correlated with existing data to aid in the explanation of the pressing process.

The method used is based on the elastic properties of the thick-walled

tube used as the die. The principle of super-position of force systems on an elastic body is assumed to hold. Electric strain gauges were mounted in adjacent positions on the exterior die wall in order to get an exact measurement of the variation of tangential strain over the length of the die during pressing. While in this paper, measurements in terms of only tangential strains are considered, it is well to note that similar calculations may be set up for axial strains. The latter are not preferred, since they tend to be smaller than the tangential strains and therefore permit less sensitive measurements. Discussion in this work is restricted to compacts pressed from both ends, since the elastic deformation of the die is then more amenable to analysis.

Before choosing the electric strain gauge method, a more direct line of attack was considered and discarded. The discarded idea was the insertion of a pressure gauge through a hole in the die wall.* The gauge would have been in the form of a small piston. If pressure were exerted against such a gauge, it would move outward along a radius of the die. One disadvantage of the scheme is its inability to measure shears along the die wall. Another

* Since the completion of this paper a manuscript,⁵ now published, was received. This work describes an investigation employing such a piston pressure device. The results, insofar as radial pressures are concerned, are at complete variance with the findings of this author. They are discussed more fully below.

Cleveland Meeting, October 1949.
TP 2678 E. Discussion of this paper (2 copies) may be sent to *Transactions AIME* before December 1, 1949. Manuscript received April 25, 1949; revision received June 28, 1949.

* Instructor and Professor of Metallurgy, respectively, Massachusetts Institute of Technology.

¹ References are at the end of the paper.

more serious disadvantage is the disturbance caused by the device itself. It would serve to change the forces it was designed to measure. No matter how small the movement of the gauge, when pressure is applied a discontinuity would exist in the wall surface at that point. Due to the stress concentration caused by the hole, abnormal deflections of the die wall would occur around the gauge. During pressing, powder would be forced into the resulting depression. The depression would then become larger with increasing compacting pressure. Powder, not being a fluid, is capable of supporting shear. The ease with which it would flow into the die wall depression to further move the piston is an indication, not of the radial pressure at that point, but of the state of shear retarding the movement. Thus the "pressure" gauge is really a criterion of flowability, and of the capability of the powder to support shear. For these reasons, it was decided that the electric strain method, herein employed, was more reliable, if more indirect. The gauges and lead wires, mounted on the external die wall do not in any way affect the behavior of the metal powder or the die during pressing.

Theory of the Method

THE EFFECT OF RADIAL PRESSURE ON THE DIE WALL

Effect of a Single Small Band of Hydrostatic Pressure

Consider a die which is a thick-walled cylinder of outer radius R_o and inner radius R_i . If over a small finite length L there is a normal pressure P , a tangential strain distribution at the outer wall results. This is shown schematically in Fig 1. The exact shape of the curve may be predicted by an extension of the theory of a semi-infinite beam on an elastic foundation.⁶ This

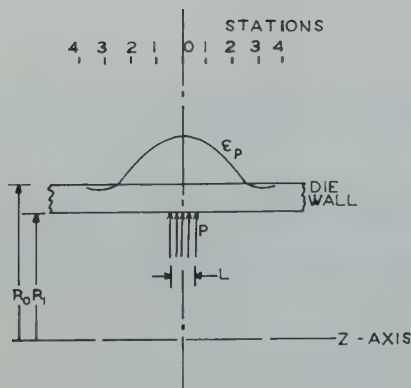


FIG 1—Schematic illustration of strain due to a single increment of pressure.

Note that in all figures, strain abscissa correspond with outer die wall unless otherwise indicated. Z-axis is the axis of the die.

extension has been developed and experimentally verified by MacGregor and Coffin⁷ in their work on symmetrically-loaded thick-walled cylinders. For the calculation of external strains due to increments of pressure the accuracy of their theory is well within 5 pct for very small strains, and within 2 pct for larger strains. Since in our experiments the ends of the tube are not capped, the normal forces in the axial direction are carried by the die plungers, and we thus need not consider the effect of an axial tensile force on the die wall.

Using the above-mentioned theory, values of strain may be calculated along the length of the die at stations a distance L apart (See Fig 1). It is well to note that L should be small enough so that a powder compact of height L will exhibit fairly uniform normal pressure over its length while under compression. The calculations may be verified by filling the die with a hydrostatic fluid in sufficient quantity to occupy a length L in the die, the pressure P being exerted by loading the die plungers in a press. Readings may then be taken on the tangential electric strain gauges.

The calculated tangential strain ϵ_P caused by P is noted at each station.

Values of $F_n = \frac{\epsilon_P}{P}$ may then be calculated, and F_n is called the pressure influence factor. The subscript n indicates the station (distance) from the center of increment L . Since the die is elastic, if the value of P is increased, ϵ_P will increase in proportion. If a measured tangential strain ϵ_{Pn} at station n is caused by an unknown pressure P , then:

$$P = \frac{\epsilon_{Pn}}{F_n} \quad [1]$$

Effect of Several Small Bands of Hydrostatic Pressure

In a compact pressed from both ends, conditions will be symmetrical about the center.⁸ Suppose for the time being that the compact exerts no shear force on the die wall, and that the length of the compact is broken down into five increments, each of length L . Each increment L is assumed to exert uniform radial pressure over its length, as shown in Fig 2. The strain due to each pressure band (increment) is similar in shape to that of a single band. By the principle of elastic superposition the total strain at any point along the die axis is the sum of the five individual strains at that point (see Fig 2). The previously calculated influence factors hold for each of the five individual strain curves. Applying these elastic influence factors to each of the five strain curves, there result five expressions for the total strain due to pressure at stations 0 to 4 inclusive:

$$\begin{aligned} (\epsilon_P)_0 &= F_0 P_0 + 2F_1 P_1 + 2F_2 P_2 \\ (\epsilon_P)_1 &= F_1 P_0 + (F_0 + F_2) P_1 + (F_1 + F_3) P_2 \\ (\epsilon_P)_2 &= F_2 P_0 + (F_1 + F_3) P_1 + (F_0 + F_4) P_2 \\ (\epsilon_P)_3 &= F_3 P_0 + (F_2 + F_4) P_1 + (F_1 + F_5) P_2 \\ (\epsilon_P)_4 &= F_4 P_0 + (F_3 + F_5) P_1 + (F_2 + F_6) P_2 \end{aligned}$$

The above constitute five equations for the three unknowns P_0 , P_1 , and P_2 , any three of which may be used for a solution after measurement of $(\epsilon_P)_0$, $(\epsilon_P)_1$, etc. by the electric strain gauges. A similar equation may be written for the total tangential strain at any point along the die.

EFFECT OF SHEAR ON THE DIE WALL

Effect of a Single Small Band of Uniform Shear

A compact undergoing compression will exert shear force in an axial direction on the inner die wall. Consider a shear stress exerted over an increment of length L in the die. The total resultant force T on the wall is then:

$$T = 2\pi R_i L \tau \quad [3]$$

Fig 3 shows this wall shear force T ; it is statically equivalent to the compressive force B , plus the moment couple $T-C$. From the separate consideration of the couple and the com-



FIG 3—Shear system and equivalent moment-compressive force system.

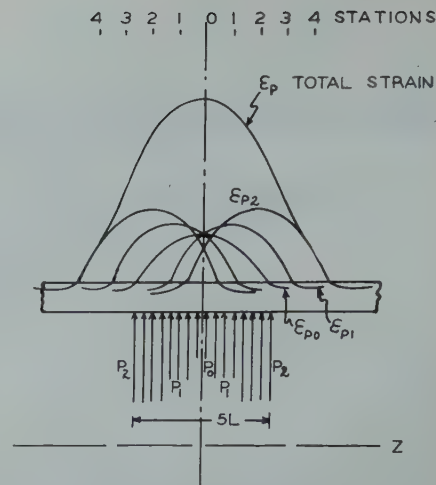


FIG 2—Schematic illustration of strain due to five increments of pressure.

pressive force one may calculate the shape of the strain curve due to the shear stress τ acting over the increment L . The compressive force gives rise to a linearly increasing tangential strain ϵ_r'' throughout the increment L . This strain is then a constant along the remainder of the tube to the end, where an equal and opposite shear force T must be applied to maintain equilibrium. The couple causes the strain ϵ_r' , which is antisymmetrical about the center of L . In effect, to the left of L the tube is constricted. To the right it is bulged. The sum of two curves is ϵ_r , the total tangential strain caused by the shear stress and is shown in Fig 4.

Since the total strain curve due to shear is asymmetrical account must be taken of this in denoting stations. As shown in Fig 4, positive stations will be taken on the side of positive strain; negative stations on the side of negative strain. At each station a shear influence factor $f_n = \frac{\epsilon_r}{\tau}$ is calculated.

On the positive strain side of the shear curve, the strain approaches a constant value (end effect). Correspondingly, for all stations in this region, the shear influence factors will be constant, and will be designated as f_e . The subscript e signifies end effect. Shear influence factors may then be tabulated.

Calculations of shear influence factors may be verified by placing a suitable material, such as metal powder, in the die. It should be of such quantity that a compact of length L will result after compaction to some arbitrary plunger pressure. While maintaining the plunger pressure an axial force T is applied to the circumference at one end of the die (see Fig 5). Such force should not be large enough to cause the

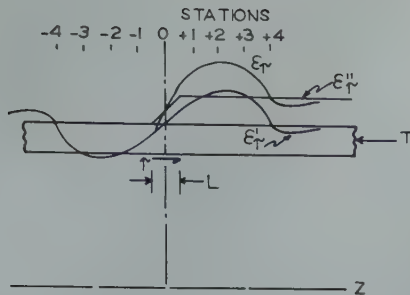


FIG 4—Schematic illustration of strain due to a single increment of shear.

die to slide by the compact. Readings may now be taken on the electric strain gauges. Such readings represent the sum of strain due to radial pressure exerted by the compact, and strain due to the applied shear. The shear force T is then removed. Readings of the strain gauges are again taken. Such readings represent strain due to pressure only. Difference between the two sets of readings yields values of strain due to shear. The shear stress is known from Eq 3, and the shear influence factors may then be checked.

Effect of Several Small Uniform Bands of Shear

Here, use is again made of the fact that in a compact pressed from both ends conditions will be symmetrical about the center. According to Kamm et al,⁸ the powder at the center does not move axially during pressing. The wall shear will therefore vary symmetrically about the center, with a value of zero for the center increment.

Consider in such a compact the strains due to shear caused by two shear increments equally and oppositely placed about the center. Strain distributions are schematically illustrated in Fig 6. Unlike the case of the single increment of shear, the die no longer need be supported at one end by a force T in order to be in equilibrium. Instead the compressive (end) effect of one increment is opposed by the compressive effect of the opposite increment. The compressive effect thus exists only between the increments, and does not persist down to the end of the die, as in the single increment case. In effect, the strain abscissa is moved up to 0-0 (see Fig 6), thus sub-

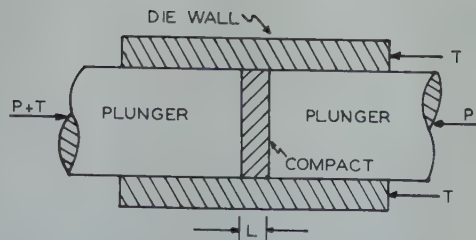


FIG 5—Schematic diagram for the arrangement for a shear check test.

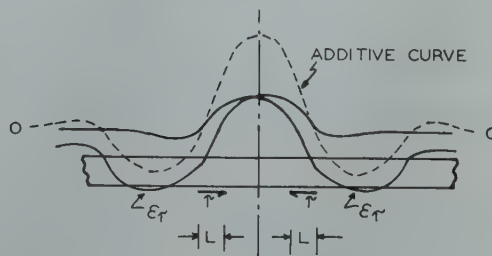


FIG 6—Schematic illustration of the addition of strains due to equal and opposite shear increments. The new strain abscissa is indicated by the line O-O.

tracting the end effect strain beyond the increments (the portion of the die between either end and the edge of the nearest increment). Mathematically, this is accomplished in subsequent equations by subtracting the influence factor for end effect f_e from all terms involving the addition of strains due to opposite shear increments.

Note that the foregoing correction does not invalidate the principle of superposition. It is necessitated only because the boundary conditions of the force system (with several shear increments now present) are different from the boundary conditions for the single increment of shear. In effect, the force T has been moved from the end of the die to the body of the die.

With this correction in mind, and the fact that the wall shear at the compact center is zero, the expressions may be written (analogous to Eq 2) for total strain due to shear at any point. For five increments these are:

Similar equations may be written for the total strain due to shear at any station.

SOLUTION OF BOUNDARY STRESSES ON THE INTERIOR DIE WALL

In pressing of metal powder compacts from both ends, Eq 2 relates tangential strains with radial pressures on the die wall, and Eq 4 relates strains with shear. When both shears and pressures are present, as is usually the case, the expressions of Eq 1 and 2 are additive for each station.

Terms shown in the boxes are the ones of interest for a compact divided in three increments.

In the above, values of F_n and f_n are calculated. Strain values may be determined by experiment. Solution for the unknown shears and pressures may then be carried out.

Eq 5 treats the powder compact as a

$$\begin{aligned} (\epsilon_r)_0 &= 2(f_{+1} - f_e)\tau_1 + 2(f_{+2} - f_e)\tau_2 \\ (\epsilon_r)_1 &= (f_0 + f_{+2} - f_e)\tau_1 + (f_1 + f_{+3} - f_e)\tau_2 \\ (\epsilon_r)_2 &= (f_{-1} + f_{+3} - f_e)\tau_1 + (f_0 + f_{+4} - f_e)\tau_2 \\ (\epsilon_r)_3 &= (f_{-2} + f_{+4} - f_e)\tau_1 + (f_{-1} + f_{+5} - f_e)\tau_2 \\ (\epsilon_r)_4 &= (f_{-3} + f_{+5} - f_e)\tau_1 + (f_{-2} + f_{+6} - f_e)\tau_2 \end{aligned} \quad [4]$$

$$\begin{aligned} \epsilon_0 &= \boxed{F_0 P_0 + 2F_1 P_1} + 2F_2 P_2 + \boxed{2(f_{+1} - f_e)\tau_1} + 2(f_{+2} - f_e)\tau_2 \\ \epsilon_1 &= \boxed{F_1 P_0 + (F_0 + F_2)P_1} + (F_1 + F_3)P_2 + \boxed{(f_0 + f_{+2} - f_e)\tau_1} + (f_{+1} - f_{+3} - f_e)\tau_2 \\ \epsilon_2 &= \boxed{F_2 P_0 + (F_1 + F_3)P_1} + (F_0 + F_4)P_2 + \boxed{(f_{-1} + f_{+3} - f_e)\tau_1} + (f_0 + f_{+4} - f_e)\tau_2 \\ \epsilon_3 &= F_3 P_0 + (F_2 + F_4)P_1 + (F_1 + F_5)P_2 + (f_{-2} + f_{+4} - f_e)\tau_1 + (f_{-1} + f_{+5} - f_e)\tau_2 \\ \epsilon_4 &= F_4 P_0 + (F_3 + F_5)P_1 + (F_2 + F_6)P_2 + (f_{-3} + f_{+5} - f_e)\tau_1 + (f_{-2} + f_{+6} - f_e)\tau_2 \end{aligned} \quad [5]$$

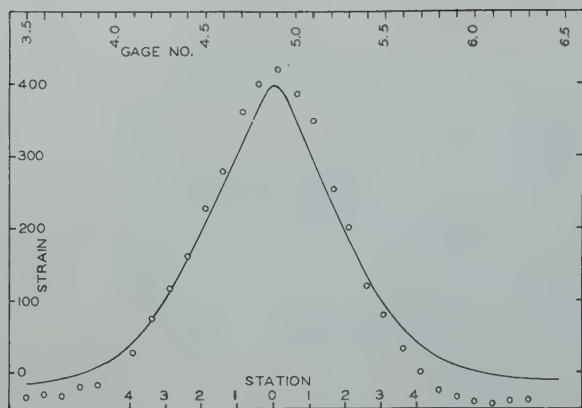


FIG 7—Check tests for 0.20 in. increment of hydrostatic pressure.

Strain in microinches per inch plotted along die length. Solid line indicates theory. Circles indicate experimental values. 55,000 psi pressure.

series of average pressures and shears, varying in steps, over short increments of length L . For a given length of compact the approximation will be bettered by using a greater number (necessarily an odd number) of increments. A practical consideration limits this number. The labor of solving linear simultaneous equations increases roughly as the square of the number of unknowns. A mathematical consideration also enters. Consider, for instance, the array of numbers making up the coefficients on the right hand side of Eq 5. This array constitutes the determinant of the system of equations. If by chance this determinant has a value near zero, small errors (on the order of 0.01 pct) in the coefficients will cause huge errors (on the order of 100 pct or more) in the answers. Should the determinant approach zero, the answers approach infinity, regardless of other considerations. In either case, the error in the calculated answer may far exceed the magnitude of the true answer.

Equations similar in form to Eq 5 may be written for compacts divided into even numbers of increments. As will be pointed out, such equations were considered and discarded in the course of the present investigations.

Experimental Procedure

For investigation of boundary stresses the die must satisfy two conflicting requirements. It must be strong enough not to fail, yet be built lightly so that it will undergo large elastic strains in use. The die was therefore made ten inches long with external diameter of 2.000 ± 0.0005 in., and internal diameter (diamond lapped) of 1.128 ± 0.0005 in. Two plungers

were used, each 6 in. long and lapped to have 0.001 in. clearance with the die.

The material was an air-hardening, high carbon, high chromium steel (Airdi 150, Crucible Steel Co.), heat-treated to final hardness of Rockwell C 64. The die showed no sign of wear at the conclusion of the investigation.

Tangential strain gauges (Baldwin SR-4, type A-12) were mounted on the outer wall every 0.10 in. along the axial distance of the central portion of the die, and every 0.80 in. near the ends. Alternate gauges were 180° apart on the die. A total of 41 gauges was employed. The die was then placed in a loose-fitting frame, baked in a drying oven, and the gauges then wax-coated to seal out moisture. Two devices were available for strain measurement. The first was a manual SR-4 indicator, and the second an automatic scanning recorder which read and recorded all 41 gauges in less than a minute.

Pressing of compacts was performed on a standard type of testing machine. Lubricated spherical seats were mounted on the top and bottom platens of the press to prevent transmission of bending forces to the die.

After all equipment was assembled, the behavior of the gauges was checked by loading the die internally with oil under hydrostatic pressure. This method was also used to find the modulus of elasticity of the die steel which was $E = 31.65 \times 10^6$ psi. Poisson's ratio was determined as 0.273. Both the constants were necessary for calculation of the influence factors for pressure and shear (see Tables 1 and 2).

Check tests for the influence factors were performed in accordance with the principles previously described. As a hydrostatic medium, paraffin sealed in a thin rubber bag (0.002 in. wall) to

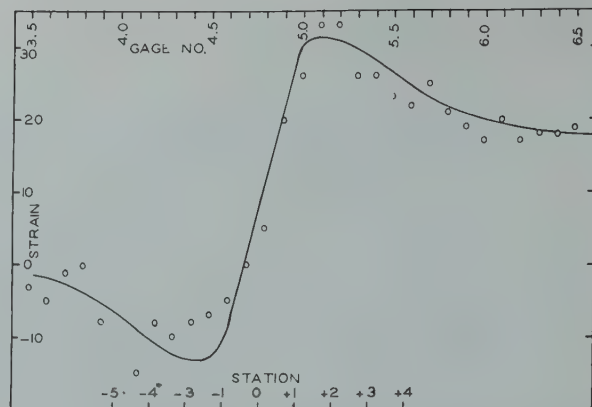


FIG 8—Check test for 0.20 in. increment of shear.

Strain in microinches per inch plotted along die length. Solid line indicates theory. Circles indicate experimental values. 6381 psi shear stress.

Table 1 . . . Influence Factors for 0.20 In. Increment of Pressure

| Station | f_n |
|---|---------------------------|
| 0 | 7.21614×10^{-3} |
| 1 | 5.71976 |
| 2 | 3.56168 |
| 3 | 1.83945 |
| 4 | 0.71276 |
| Influence Factors for 0.20 In. Increment of Shear | |
| $(L = 0.20 \text{ in.})$ | |
| Station | f_s |
| -4 | -1.05417×10^{-3} |
| -3 | -1.60524 |
| -2 | -2.00169 |
| -1 | -1.75064 |
| 0 | 1.46280 |
| 1 | 4.60424 |
| 2 | 4.85529 |
| 3 | 4.45884 |
| 4 | 3.90777 |
| e | 2.85360 |

Table 2 . . . Influence Factors for 0.33 In. Increment of Pressure

| Station | f_n |
|---|---------------------------|
| 0 | 11.58639×10^{-3} |
| 1 | 7.12757 |
| 2 | 2.40515 |
| 3 | 0.20805 |
| 4 | -0.36247 |
| Influence Factors for 0.33 In. Increment of Shear | |
| $(L = 0.33 \text{ in.})$ | |
| Station | f_s |
| -4 | -0.18367×10^{-3} |
| -3 | -0.96538 |
| -2 | -2.37457 |
| -1 | -3.37675 |
| 0 | 2.35422 |
| 1 | 8.08519 |
| 2 | 7.08301 |
| 3 | 5.74978 |
| 4 | 4.89211 |
| e | 4.70844 |

prevent leakage was employed. The amount of paraffin was such that it occupied the proper length in the die while under pressure. The center of the paraffin plug was located by measuring the distance which the plungers extended beyond the die. Results of one pressure check test are plotted in Fig 7. For the shear check test, a copper powder compact, exactly 0.20 in. high under 40,000 psi plunger pressure was used. The die was placed in the press, with the compact inside, and with the plungers loaded. A known force was then applied axially to the die wall, in accordance with the previously described principles. (See Fig 5.) Strain readings were then taken, the load re-

moved, and readings taken again. Results for one test appear in Fig 8. The scattering about the theoretical curve in Fig 8 is due largely to the low strain being measured.

In subsequent pressing tests it is certain that no powder was squeezed up into the space between plungers and die wall (except test C-10-a, copper, at 60,000 psi), since the plungers could be pulled out by hand following the tests.

Wall lubrication was used in several of the pressing tests. Stearic acid was one lubricant employed, and was applied by dissolving in benzene, until a supersaturated slurry was formed. Three coats of this slurry were painted on the die wall. Each was allowed to dry thoroughly before application of the next coat. This procedure resulted in a final heavy coating of stearic acid which completely covered the wall. Molybdenum sulphide, when used as a wall lubricant, was applied in similar fashion. It was not, however, possible to build up a heavy coating of this material on the wall. When colloidal graphite (Aquadag) was employed, a very thin coat was painted onto the die wall and dried for two hours by means of an electric fan. A heavy coating of graphite was found to interfere with insertion of the plungers in the die.

Altogether, thirty successful tests were performed. The weight of powder used in each test was adjusted so that the final height of a compact was either 0.20, 0.60, or 1.00 in. From the recorder chart in each case the strain distribution along the length of the die was plotted and stations noted. For a compact with final height of 0.20 in., the average radial pressure was calculated directly by application of the pressure influence factors of Table 1. A compact of 0.60 in. height was broken into three increments. Shear and pressure influence factors of Table 1 were inserted into the boxed-in expressions of Eq 5, resulting in three simultaneous equations. With strain values at stations 0, 1 and 2 (determined from the

test curve) solution for average pressure and shear at each station was carried out.

It had been originally intended to solve the 1.00 in. compacts by the five increment solutions of Eq 5, using values listed in Table 1. However, the value of the determinant of the system was close to zero and the solutions of the equations were therefore meaningless. Equations were then derived for four increments, but in this case the determinant was even closer to zero. Solutions of the 1.00 in. compacts were finally accomplished by treating them as composed of three increments. Method of solution is exactly as described for a 0.60 in. compact, except that influence factors listed in Table 2 are used. Stations, of course, are then 0.33 in. apart, rather than 0.20 in.

Since there is symmetry to the left and right of station 0, strain values for like-numbered stations either side of station 0 should be alike. In the values of strain used in the equations, small differences at such stations were therefore averaged. With such averaging, reproducibility of strain data at any station was within ± 3.6 pct for the smallest values of strain involved. Large values of strain were completely reproducible. This was demonstrated by repeating two pressing experiments. The range of ± 3.6 pct is due to lack of sensitivity in the scanning recorder at low strain readings. The strain gauges themselves are accurate to ± 1 pct. Two other considerations enter into the final accuracy of solutions to the simultaneous expressions of Eq 5. The first is error in the calculated influence factors (Tables 1 and 2). As pointed out, it may amount to ± 5.0 pct for the numerically smaller factors and much less for the larger. The second consideration is the method employed to solve the simultaneous equations.⁹ With the errors in theory and data enumerated, the method¹⁰ employed in the present investigation was found to propagate a maximum possible error

of ± 23 pct in the final calculated values of pressures and shears.

Selected and typical data are presented in Table 3. A total of fourteen pressing tests were performed on type LB (−100 mesh) electrolytic copper powder (U. S. Metals Refining Co). Eight of these were pressed, without lubrication, to a final height of one inch. Compacting pressures varied from 3900 to 60,000 psi. Of these eight, two (tests C-16-a and C-13-a) were duplicates of other tests. Two compacts, with final heights of 0.20 and 0.60 in., were pressed, without lubrication, at 40,000 psi. Wall lubrication was used in four other compacts, all of 1.00 in. final height. Three of these were pressed at 30,000 psi, and the fourth at 18,600 psi. Stearic acid, molybdenum sulphide, and colloidal graphite (Aquadag) were the lubricants employed.

The second series of three tests was performed on type C (−325 mesh) electrolytic copper powder (U. S. Metals Refining Co.). All of the compacts were pressed to a final height of 1.00 in. without lubrication. Compacting pressures of 7100, 9200 and 18,600 psi were employed.

Carbonyl iron, type L (General Analine and Film Co.) was used for a third series of six compacts. Two each were pressed at 9100, 21,000 and 32,000 psi. Stearic acid was used as a wall lubricant in one of the compacts pressed at each pressure. All final heights were 1.00 in.

For the fourth series, Swedish sponge iron, type MH (−100 mesh Ekstrand and Tholand Co.), was used. Pressures, height, and lubricants were the same as for the six carbonyl iron compacts, so that a direct comparison could be made.

Experimental Results

From data such as are recorded in Table 3, certain conclusions may be drawn immediately. For a constant

Table 3 . . . Tabulation of Typical Data and Results
Copper—Type LB, −100 Mesh

| Test No. | Plunger Pressure Psi | Final Height Inches | Wall Lubrication | Strain-microinches per Inch | | | | | Weight of Powder Grams | Pressure-Psi | | Shear-Psi 1 | $\frac{\tau_1}{P_1}$ Coef. of Friction | Pct of Solid Density |
|----------|----------------------|---------------------|---------------------------------|-----------------------------|------|-------|------|-------|------------------------|--------------|-------|-------------|--|----------------------|
| | | | | 0 | 1 | | 2 | | | P_0 | P_1 | | | |
| | | | | | Left | Right | Left | Right | | | | | | |
| C-2-a | 40000 | 1.00 | None Unloading of Test C-2-a | 525 | 415 | 400 | 160 | 160 | 118.5 | 23129 | 15756 | 4799 | 0.304 | 80.9 |
| C-2-b | | | | 192 | 150 | 158 | 80 | 86 | 118.5 | 9503 | 7213 | -3098 | 0.430 | 80.9 |
| C-3-a | 40000 | 0.20 | | 135 | 105 | 105 | 60 | 64 | 25.6 | 18711 | | 0 | 0 | 87.5 |
| C-4-b | 40000 | 0.60 | None | 390 | 336 | 330 | 200 | 214 | 73.0 | 32584 | 12120 | 4632 | 0.381 | 83.2 |
| C-7-c | 30000 | 1.00 | None | 370 | 280 | 286 | 112 | 100 | 105.3 | 17588 | 10288 | 2898 | 0.282 | 72.0 |
| C-12-b | 30000 | 1.00 | Stearic Acid | 377 | 285 | 290 | 133 | 125 | 109.2 | 19722 | 10837 | -887 | 0.081 | 74.5 |
| C-14-a | 30000 | 1.00 | Molybdenum Sulphide | 375 | 285 | 270 | 115 | 109 | 107.2 | 20636 | 8917 | 1302 | 0.146 | 73.1 |
| C-15-a | 30000 | 1.00 | Aquadag | 370 | 275 | 271 | 112 | 104 | 107.2 | 20515 | 8513 | 1622 | 0.180 | 73.1 |

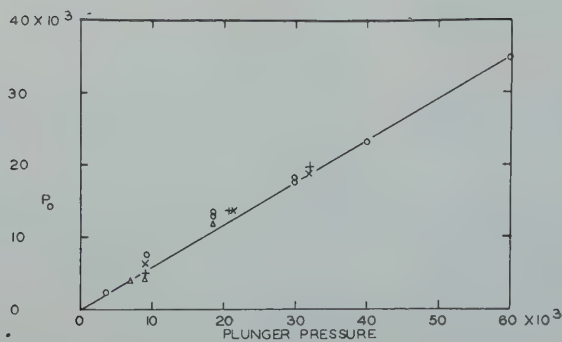


FIG 9—Variation of radial pressure P_0 (center increment) with plunger pressure, both in pounds per square inch.

One inch compacts, no lubrication.
 ○ Copper LB (—100 mesh)
 △ Copper C, (—325 mesh)
 × Swedish Sponge Iron (—100 mesh)
 + Carbonyl Iron L

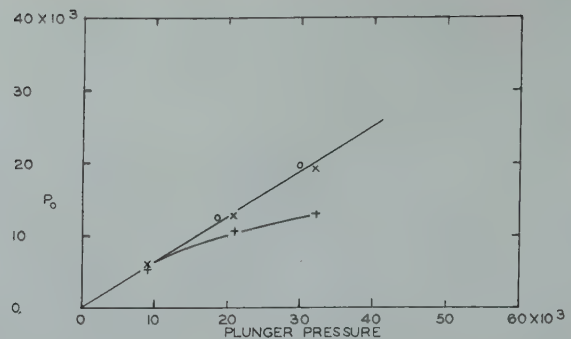


FIG 10—Variation of radial pressure P_0 (center increment) with plunger pressure, both in pounds per square inch.

One inch compacts, stearic acid wall lubrication.
 ○ Copper LB (—100 mesh)
 × Swedish Sponge Iron (—100 mesh)
 + Carbonyl Iron L

final height of compact, average density increases with compacting pressure. Likewise, for constant compacting pressure and die diameter, average density decreases with increasing height of compact. Side wall lubrication is of great importance in securing greater average density of compact. When wall lubrication was employed, the average density of the compact was always greater than that of an unlubricated compact of the same final height and pressed at the same pressure. The foregoing also confirms the work of previous investigators.^{3,8}

In addition, it was found that in all cases but one (Test E-1-3, in which there was evidence of the die acting in bending) the average radial pressure exerted on the die was greater at the center increment of the compact than at the end increments (adjacent to the plungers). In other words, P_0 , the pressure at the center, is greater than P_1 , the pressure at the ends. A possible explanation of this is based on the fact that the most dense part of the compact is at the outer circumference adjacent to each plunger, and the least dense part is at the middle outer circumference.³ Thus the metal powder adjacent to the plungers comes closest to behaving like a solid metal. On the other hand, the central portion of the compact is closer to being an aggregate of metal powder particles. Such an aggregate if placed between two plungers (with no surrounding die wall present) and squeezed, would flow radially, retarded only by the interparticle friction.

A solid plug, if similarly pressed, would offer considerable resistance to any such flow. As a consequence, in a compact undergoing compression from both ends in a die, the central portion, being the least dense, is the most capa-

ble of exerting radial pressure. Of course, the foregoing picture is highly simplified. Strain-hardening of the metal powder particles, change of particle shape, and bonding of the particles during pressing all play a role. The picture is supported, however, by the low radial pressure (18,000 psi for P_0) measured in compact C-3-a (type LB copper powder) which had a final height of 0.20 in. after compaction at 40,000 psi. This compact was pressed to 87.5 pct of solid density. In compact C-2-a, made of the same material and at the same pressure, but with a final height of 1.00 in. the value of the radial pressure P_0 at the central increment was 23,129 psi. Compact C-2-a was only 80.9 pct of final density.

The compact of intermediate length, C-4-b, again of the same material, pressed at the same pressure, but to a final height of 0.60 in., at first examination does not support the above argument. For this compact, the average radial pressure of the center increment is higher than that in either of the two compacts cited above. This is due, it is believed, to compact C-4-b being broken down into 0.20 in. increments for calculation, whereas compact C-2-a was broken into 0.33 in. increments. Since the central portion of a compact has the highest radial pressure, then the shorter the center increment length L over which an average is calculated, the higher such average will be. As a corollary of this statement, it follows that since the end increment has the lowest radial pressure the shorter the length over which it is figured, the lower its average will be. This is the case. The average and radial pressure P_1 for compact C-4-b was 12,120 psi, less than for either of the other two. (In compact C-3-a 0.20 in. high, figured as composed of one increment, P_1 is iden-

tical with P_0 .)

As mentioned previously other investigators,⁵ whose results were received after completion of the present experiments, found a completely different type of radial pressure distribution. Their work was performed on compacts pressed from one end. Their method of measurement employed a piston-type pressure gauge, set in a hole through the die side wall. They state that radial pressure varies from a maximum at the end of a compact adjacent to the moving plunger, to a minimum at the static plunger, in linear fashion. In terms of a compact pressed from both ends, it would mean a V-type distribution of radial pressure, with the point of lowest pressure at the center, and the point of highest pressure next to the plungers. The nature of the results obtained by the above workers may be attributed to the fact that their piston type pressure gauge disturbs the uniform flow of powder and measures the ability of the powder to support shear. Thus as pointed out in the introduction it measures the flow of the powder rather than true radial pressure.

It is unfortunate in the present investigation that the one inch compacts could be treated only as composed of three increments. As a consequence no indication of point to point stress distribution along the length of a compact could be ascertained. Certain general trends are nevertheless evident. Fig 9 shows a plot of average radial pressure P_0 (center increment) versus compacting pressure. It indicates a straight line relationship between radial and compacting pressure for all four metal powders pressed without lubrication.

Fig 10 shows a similar plot, but for tests in which stearic acid wall lubrication was used. Again for copper, type

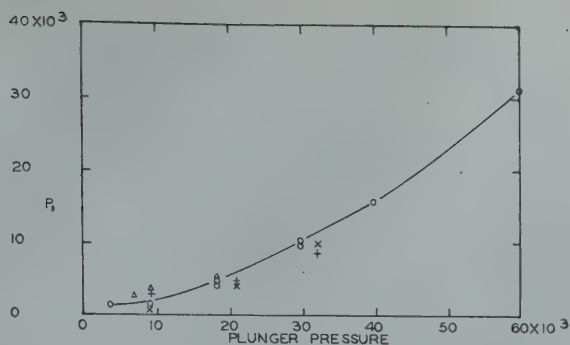


FIG 11—Variation of radial pressure P_1 (end increment) with plunger pressure, both in pounds per square inch.

One inch compacts, no lubrication.
 ○ Copper LB (-100 mesh)
 △ Copper C (-325 mesh)
 × Swedish Sponge Iron (-100 mesh)
 + Carbonyl Iron L

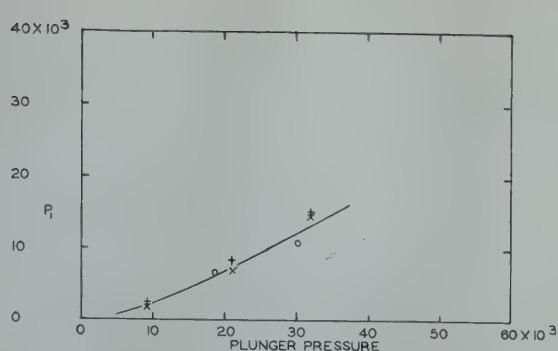


FIG 12—Variation of radial pressure P_1 (end increment) with plunger pressure, both in pounds per square inch.

One inch compacts, stearic acid wall lubrication.
 ○ Copper LB (-100 mesh)
 × Swedish Sponge Iron (-100 mesh)
 + Carbonyl Iron L

C (-100 mesh) and Swedish sponge iron, a straight line relationship exists. The slope of the line is almost identical with that in Fig 9. Within the limits of experimental error, the values of P_0 are equal for like metals (except carbonyl iron) pressed at like pressures in both wall-lubricated and unlubricated compacts. For carbonyl iron, with wall lubrication, the values of P_0 , when plotted as in Fig 10, fall well below the straight line relationship, and well below the P_0 values for unlubricated carbonyl iron powder. If, as has been proposed, radial pressure is in some fashion inversely proportional to densification (as distinguished from density distribution) then one would expect Fig 9 and 10 to have similar plots. It is not clear why carbonyl iron should depart from this. It may be related to the fact that of all the powders here used carbonyl iron compacted with wall lubrication showed the greatest increase in percent of solid density over compaction in the unlubricated state. It thus behaves more like a solid than the other powders used.

Fig 11 and 12 are plots of average radial pressure P_1 (end increment) versus compacting pressure. Fig 11 is for metal powders pressed without lubrication, and Fig 12 for those pressed with stearic acid wall lubrication. Both plots are in the form of shallow curves, slope gradually increasing with plunger pressure. For copper powder, type C, pressed at like pressures, values of P_0 (within the limits of experimental error) are equal for lubricated and unlubricated compacts. For Swedish and carbonyl irons, (especially the latter) pressed with wall lubrication, values of P_0 in Fig 12 appear to be somewhat higher than for the unlubricated state. It cannot be said whether or not the departure is due to error, since it is not a marked deviation. It is possible

that the stearic acid wall lubrication, being in a thick coating, is acting as a semifluid, transmitting pressure to the die wall in a quasihydrostatic fashion.

Some of the most significant results obtained are those concerning average shear stress τ_1 and coefficient of friction on the die wall adjacent to the plungers. These results are for unlubricated pressing to a final height of one inch. (See Fig 13 and 14). For copper, type LB (-100 mesh), the curve of shear stress (Fig 13) rises sharply with steadily increasing slope. The point for 60,000 psi compacting pressure (Test C-10-a) is very low because of extrusion of copper into the space between plunger and die wall. Due to such extrusion a large shear stress was acting on the wall toward the ends of the die (negative shear). This caused the average value of shear stress to be very low. The shear stress curve for copper type C (-325 mesh) follows more or less parallel and below the curve for type LB. There are only three points on this curve, however. The ductility of the copper undoubtedly accounts for the sharp rise of the copper shear curves. At the beginning of pressing, the copper particles have only point contact with the wall. As pressing continues they deform, increasing the area in contact with the die wall, and thus increasing the shear stress acting on that wall. The type C copper, having only fine particles, initially has a smaller total contact area with the die wall and thus a lower shear stress for given plunger pressure. As the fine particles are pressed, they do not pack as well as the type LB copper, which has a wider particle size distribution. Consequently the area of contact with the die wall, while it increases, never reaches (for a given plunger pressure) that of the type LB copper. Thus the curves of shear stress versus plunger

pressure rise sharply, in parallel fashion for the two types of copper powder.

The shear stress plot (Fig 13) for carbonyl iron appears to be a straight line, and that for Swedish iron nearly so. This is because of the lesser ductility of the two metals as compared to copper. While at low compacting pressures the shear stresses for iron are higher than those of copper, this is not true at higher pressures. The wall-particle contact area cannot increase as rapidly. Plots for the two types of iron are nearly parallel, with the carbonyl iron values being higher, even though the Swedish iron is more ductile. This is in part related to the fact that Swedish sponge iron cannot (under like conditions) be compacted to as high an average density as carbonyl iron. The less dense packing of the former contributes to a lower wall-particle contact area. In addition, the wide difference in chemical composition of the two types of irons affects their mechanical behavior.

Fig 14 shows the variation of coefficient of friction with compacting pressure. The plots for all the metal powders (with the exception of copper, type C, for which only three points are known) show an increase, followed by a decrease. The decrease is especially marked for type LB copper due to the low shear stress of test C-10-a before noted. Initial increases, with higher compacting pressure are due to increase in wall-particle contact area by particle deformation. The final decrease is probably caused by the compact reaching a point where strain hardening of the metal slows down the deformation of particles. Thus the wall-particle contact area and shear stress no longer increase rapidly. The coefficient of friction $\frac{\tau_1}{P_1}$ then decreases because the radial pressure P_1 continues to rise

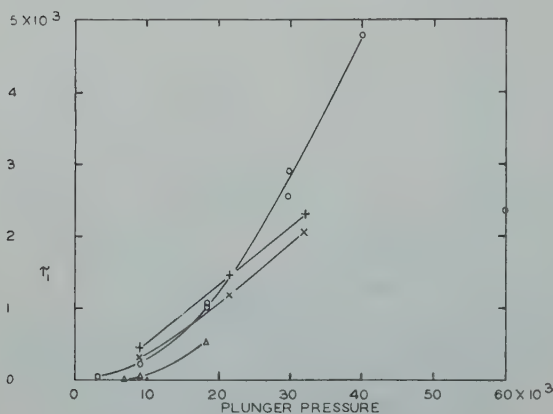


FIG 13—Variation of shear stress τ_1 (end increment) with plunger pressure, both in pounds per square inch.

One inch compacts, no lubrication.
 ○ Copper LB (-100 mesh)
 △ Copper C (-325 mesh)
 × Swedish Sponge Iron (-100 mesh)
 + Carbonyl Iron L

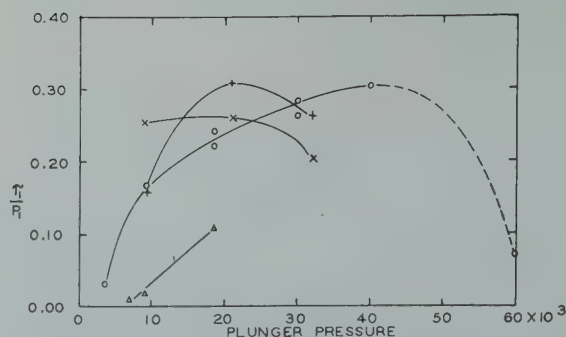


FIG 14—Variation of coefficient of friction $\frac{\tau_1}{P_1}$ (end increment) with plunger pressure, the latter in pounds per square inch.

One inch compacts, no lubrication.
 ○ Copper LB (-100 mesh)
 △ Copper C (-325 mesh)
 × Swedish Sponge Iron (-100 mesh)
 + Carbonyl Iron L

steadily as compacting pressure becomes greater. (See Fig 11 and 12). This explanation is borne out by the curve, in Fig 14, for copper. It strain hardens less rapidly than iron, and therefore the coefficient of friction does not reach a maximum until plunger pressure is quite high. The curves for iron fall off much sooner.

From the curves of shear stress and coefficient of friction versus compacting pressure plotted in Fig 13 and 14, we may draw some conclusions about ejection pressures. For soft ductile metals, the ratio of ejection pressure to compacting pressure should be high. On the other hand, harder, less plastic powders should have a low ratio of ejection pressure to compacting pressure. It is known that tin compacts, for instance, require a greater force for removal from the die; they seem to "drag" on the die wall. Tungsten compacts, pressed under like conditions, are much more easily ejected.

The data for shear and coefficients can be compared to some results obtained by Kamm, Steinberg and Wulff,³ working with lead grids. These authors calculated point-to-point values of the coefficient of friction. One of their compacts, number S-66 (carbonyl iron, type L), was pressed in a die of 0.560 in. diam, at 32,000 psi, from an initial height of 0.55 in. No lubrication was used, and pressing was from one end only. The average coefficient of friction, over the entire final height (obtained by averaging their point-to-point data) was 0.282. The test in the present investigation that compared to their compact was number E-5-d. This was performed on the same material, pressed from both ends at the

same pressure, without lubrication, but to a final height of 1.00 in. The die was 1.128 in. in diam. The average coefficient of friction over the end increment ($L = 0.33$ in.) was 0.261. Even with the entirely different sizes of compact and die and different method of measurement the results are within 8.0 pct of each other. In their point-to-point calculation Kamm et al found the coefficient of friction to be zero adjacent to the static plunger. Therefore in pressing from both ends, the shear stress would be zero at the center of the compact. This was the assumption made in developing the present theory.

The surprising results of the present tests are the relatively small magnitudes of wall shear stresses. The largest is less than 5000 psi. The test results are confirmed, however, by the small magnitude of shear stress that could be supported without slippage between compact and die in the check test, described under *Experimental Procedure*. It was 6381 psi, and its value was ascertained by a direct calibration. Since sliding friction is in general less than static friction, the magnitude of stress encountered in the die must be of that order, or less.

All shear stresses in compacts pressed with stearic acid wall lubrication were in the neighborhood of zero, some in fact being negative. This latter has no physical significance, being due rather to errors of the method. It can only be concluded then that stearic acid, when used as a wall lubricant, reduces wall shear stress to nearly zero. Tests C-12-b, C-14-a, and C-15-a give comparative data for different wall lubricants. All three compacts were type LB copper, pressed at

30,000 psi to a final height of one inch. They show that stearic acid is most effective in reducing shear, while colloidal graphite and molybdenum sulphide are not as good. The last two lubricants are, however, better than none.

A further interesting experiment was performed with compact C-2-a (copper type LB) after the plunger pressure had been released. The compact had been pressed to a final height of one inch, at 40,000 psi. Radial pressure P_0 in the center increment of the compact was 23,129 psi; that in the end increment, P_1 , was 15,756 psi. The average shear τ_1 over the end increment, acting axially on the die wall toward the center of the compact, was 4799 psi. After release of plunger pressure in test C-2-a, another strain record was taken. This showed P_0 had dropped to 9503, P_1 to 7213, and τ_1 to -3098 psi. The negative sign before the shear stress indicates a reversal of direction. The shear stress then acted on the die wall away from the center of the compact. (Or, if looked at the other way around, the shear acting on the compact is toward the center.)

Physically interpreted, the results may explain the cause of lamination cracks in hard powders. When compacting pressure was released, the die (which had been bulged elastically), contracted about the compact. This tended to squeeze it axially from the center of the die towards the ends, thus reversing the direction of shear acting on the die wall. This squeezing action causes the center of the compact to be extruded toward the ends of the die. The circumferential surface of the compact, in contact with the die wall,

cannot move. Thus it is along the axis that such extrusion takes place. The plane of the center of the compact (parallel to the end of the die) is subjected to axial tensile stress. In a hard powder this causes a crack to start, which spreads across the compact resulting in a laminar crack. If such be the case, lamination cracks probably originate while the compact is still in the die, following the release of plunger pressure. They spread to the surface following ejection from the die.

The foregoing explanation of lamination cracks has immediate practical implications. Wall lubrication, by lowering the retarding friction, will permit the circumference of the compact to move with the axial portion, and prevent laminar cracking following the release of plunger pressure. The tendency to crack will thus be reduced. It is well known that hard powders, compacted without lubrication, will almost always form cracks. However, the cracking of compacts made of soft powders, but pressed at extremely high pressures, is also explained. Because of the high pressure, the elastic bulge of the die will be large. After release of plunger pressure, the shear stress acting on the die wall toward the ends of the die is therefore very large. The extruding force, acting to push the axial portion of the compact toward the end of the die, is also large. Consequently, even though the compact is of a comparatively soft, ductile material, a laminar crack will result. The most important implication, however, is of interest to the die designer. Since cracks are caused by the elastic bulge of the die during pressing, the controlling factor in die design is rigidity, not strength. Whereas a die wall ratio (ratio of outer wall diameter to bore diameter) of 3 or 4 might satisfy even the highest requirements for strength, it may very well not result in a die rigid enough to prevent cracking in the compaction of hard powders. With knowledge of radial pressures acting on the interior die wall, it is possible, in the light of existing theory,⁷ to calculate elastic strains and deflections of the die.

Discussion of Results and Conclusions

By analysis of elastic strains of the die during pressing, average shear and radial pressures may be calculated over the length of a compact pressed from

both ends. The results of the analysis aid in forming a picture of the pressing process. During compaction, the powder flows axially through the die, propelled by the plunger. If the die walls are smooth and well-lubricated, the flow will be fairly even across the die and thus a higher average density, and a more even density distribution result. If the die walls are rough, or there is no wall lubrication, frictional effects cause marked retardation of powder movement at the die wall. More flow then takes place in the axial portion than in the circumferential portion. Average density will, as a result, be lower and density distribution will be less even. Die wall friction is therefore one of the most important factors controlling the density distribution of a metal powder compact.

Friction between the compact and the die wall is responsible for shear stresses at the wall of the die. Such stresses are of least magnitude at the middle circumference of the compact (when pressed from both ends) and highest adjacent to the plungers. Radial pressures on the other hand are distributed in a reverse fashion, the maximum stress being at the middle circumference and the minimum at the plungers. The magnitude of the radial pressures are, as to be expected, largely a function of the compacting pressure employed. The one exception found in this work was the extremely fine and hard carbonyl iron powder.

Wall shear stresses during compaction without lubrication are functions of ductility and particle size distribution of the metal powder. Fine particle size (with attendant less dense packing and low wall-particle contact area) in general gives rise to lower shear stresses. Hard metal powders, the particles of which cannot deform to a great degree, will have a relatively low wall-particle contact area for a given compacting pressure. Because of strain hardening, this area does not increase rapidly. For soft, ductile powders, the opposite is true. Consequently, for the latter type, shear stresses rise rapidly as compacting pressure increases.

The same two factors, ductility and particle size distribution, affect the variation with compacting pressure of the coefficient of friction. Radial pressure increases steadily with increasing plunger pressure. Therefore, the coefficient of friction at first increases as wall-particle contact area increases

rapidly and then decreases as strain hardening effects arise. Hard powders usually strain-harden at a faster rate than ductile powders. For the former, therefore, maximum coefficient of friction is reached at a lower compacting pressure.

The results of the present investigation also show that the strength of a die may not necessarily be the controlling factor in the problem of proper die design. A die may adequately withstand, without plastically yielding, the stresses involved in pressing. During pressing, however, the center portion may bulge elastically. Following the release of plunger pressure, the walls try to assume their normal configuration. Die-wall friction then retards movement of the compact surface, yet the center is squeezed in the axial direction. The resulting axial tension starts a laminar crack, which more often spreads to the surface following ejection from the die. While the condition can be partially relieved by wall lubrication, a more satisfactory solution lies in design of the die. The die should be strong enough to not only withstand the stresses, but also to prevent large elastic radial deflections. A thin-walled steel or carbide die is then best mounted in a heavy-walled steel or cast-iron jacket.

The experimental work reported in this paper may be summarized as follows:

1. For a given height of compact, average density increases with compacting pressure. For constant compacting pressure and die diameter, average density decreases with increasing height of compact.
2. Radial pressure on the die wall is greatest at the center of the compact, and least at the ends. Shear stress has the reverse type of distribution.
3. Die-wall friction is the most important single factor controlling density. With no lubrication, frictional shear stresses are a function of particle size distribution and ductility of the metal powder. Wide particle size distribution, with attendant dense packing, causes the shear stresses to be high. Soft metal powders cause shear stresses to increase rapidly with compacting pressure.
4. The coefficient of friction between powder and die wall first increases, then decreases with increasing compacting pressure. Increasing radial pressure, which continues to rise steadily with compacting pressure, is responsible for the decrease in coefficient of friction.

cient of friction. For soft powders (low rate of strain hardening) the coefficient of friction reaches a maximum at a higher compacting pressure than for hard powders.

5. For a die with smooth interior wall, frictional shear stresses may be reduced to practically zero by the use of wall lubricants.

6. Because of elastic deformation of a die during pressing, rigidity rather than strength is a necessary criterion for die design. Elastic bulging of a die results in the formation of laminar cracks.

References

1. H. Unckel: Mechanical Properties

of Sintered Iron for Porous Bearings. *Arch. Eisenhüttenwesen* (1944) 18, 5-6, p. 125.

2. R. P. Seelig: Introduction to Seminar—Review of Literature on the Pressing of Metal Powders (with Discussion). *Trans. AIME* (1947) 171, 506. *Metals Tech.* Aug. 1947. TP 2236.

3. R. Kamm, M. Steinberg and J. Wulff: Plastic Deformation in Metal Powder Compacts. *Trans. AIME* (1947) 171, 439. *Metals Tech.* Feb. 1947. TP 2133.

4. E. von Siebel: Plastic Forming of Metals III. Investigation of Distribution of Deformation and Stress in Drawing, Pressing and Piercing. *Steel* (Apr. 9 and Mar. 10, 1934).

5. P. Duwez and L. Zwell: Pressure Distribution in Compacting Metal Powders. *Trans. AIME* 185, 137.

Jnl. of Met., Feb. 1949.

6. S. Timoshenko: Strength of Materials, Part II. D. Van Nostrand Co. (1941).

7. C. W. MacGregor and L. F. Coffin, Jr.: Approximate Solutions for Symmetrically Loaded Thick-walled Cylinders. *Jnl. Appl. Mech. A.S.M.E.* (1947) 4, A-301.

8. R. Kamm, M. Steinberg and J. Wulff: Lead Grid Study of Metal Powder Compaction. *Trans. AIME* (1949) 180, 694. *Metals Tech.* Dec. 1948, TP 2487.

9. E. R. Holiday: Spectrophotometry of Proteins I. *Biochem. Jnl.* (1936) 30, 1785.

10. P. D. Crout: A Short Method for Evaluating Determinants and Solving Systems of Linear Equations with Real or Complex Coefficients. *Trans. A.I.E.E.* (Mar. 1942) 60.

Rectangular Hysteresis Loops of Co-Ni-Fe Alloys

R. A. CHEGWIDDEN*

In view of the current interest in magnetic materials having rectangular hysteresis loops, as for example those obtained with the grain oriented 50 nickel 50 iron alloys,[†] we wish to call attention again to the results obtainable with the permivar (Co-Ni-Fe) alloys heat treated in a magnetic field.

Data taken from direct current measurements made prior to and during World War II give the typical values shown below for two of the permivar alloys. Fig 1 and 2 show the hysteresis loops for these samples.

The first sample above consisted of small rings punched from 0.014 in. sheet stock. These rings were heat treated at 1000°C for one hour in a hydrogen atmosphere and then cooled with the furnace to 750°C at which point they were subjected to a magnetic field of 15 oersteds maintained during cooling to room temperature. The molybdenum permivar sample consisted of a spirally wound core of 0.001 in. tape. The heat treatment was the same except that box annealing methods were used and no hydrogen atmosphere was employed. Even better properties might be expected using hydrogen. The heat treating temperatures and cooling rates are not critical. Rectangular hysteresis loops produced in other permivar alloys by heat treatment in a magnetic field were described earlier.^{1,2}

Properties similar to those described

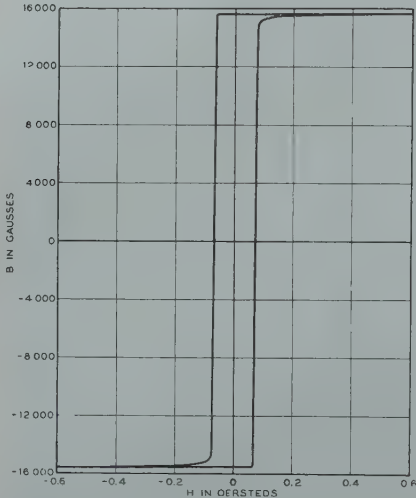


FIG 1—Hysteresis loop for 0.014 in. permivar rings (43 Ni 34 Fe 23 Co) heat treated in a magnetic field.

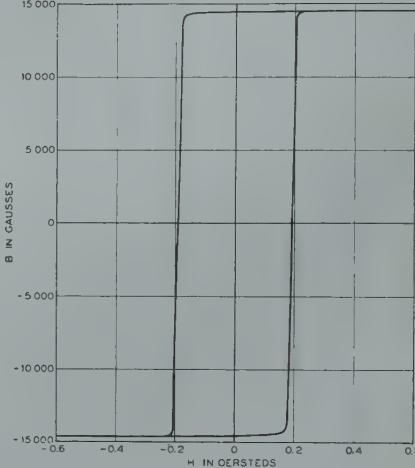


FIG 2—Hysteresis loop for 0.001 in. molybdenum permivar tape core (34 Ni 34 Fe 29 Co 3 Mo) heat treated in a magnetic field.

| Nominal Composition | Thickness | B _{max} | B _r | B _r /B _{max} | H _c | Approx. μ _{max} | ρ |
|------------------------|-----------|------------------|----------------|----------------------------------|----------------|--------------------------|----|
| 43 Ni 34 Fe 23 Co | 0.014 in. | 15650 | 15600 | 0.995 | 0.07 | 150,000 | 20 |
| 34 Ni 34 Fe 29 Co 3 Mo | 0.001 in. | 15200 | 14500 | 0.955 | 0.19 | 72,000 | 52 |

B_{max} = flux density in gauss at H = 20 oersteds
B_r = residual flux density in gauss
H_c = coercive force in oersteds
μ_{max} = maximum permeability
ρ = resistivity in microhm-cm

above are realized in permivars manufactured by conventional methods. Drastic cold working which in practice limits the final thickness and is gen-

erally expensive may thus be avoided. This information may be of interest to those concerned with magnetic alloys and the development of contact rectifiers, magnetic amplifiers and so on.

References

1. G. A. Kelsall: *Physics*. 5, 169-172, June, 1934.

2. R. M. Bozorth, J. F. Dillinger: *Physics* 6, 279-284, Sept., 1935.

Technical Note 21E. Manuscript received May 31, 1949.
* Magnetics Research Dept., Bell Telephone Laboratories.
† Orthonol, Orthonik, Deltamax and similar materials.
¹ References are at the end of the paper.

A Dilatometric Study of the Sintering of Metal Powder Compacts

POL DUWEZ* and HOWARD MARTENS†

Introduction

Dimensional changes generally occur during the sintering of metal powder compacts. These changes may have several causes and their magnitude depends upon the numerous variables involved in the process, such as the nature of the powder, size and shape of the grains, compacting pressure, rate of heating, maximum temperature, length of time at temperature, and furnace atmosphere. Among all the variables, time, temperature, and compacting pressure are probably the most important ones, and the effect of each one of the other variables can be studied separately once the effect of these is well understood.

The most precise method of studying the phenomenon of dimensional changes in a compact consists of heat treating the compacts at various temperatures for different lengths of time. In this method, only very small specimens can be used, in order to achieve rapid rates of heating and cooling. The technique involved in these measurements is very simple, but is time consuming. Another experimental approach to the problem consists of measuring the change in length of a compact as it is being heated at a constant rate. Although the two variables, time and temperature, are combined into a single one (rate of heating), the results obtained by this technique may be of great interest from both practical and theoretical points of view. The purpose of this paper is to describe a systematic investigation of the change in length during sintering of compacts made of one or several metal powders.

Experimental Procedure

The change in length of compacts

during sintering was measured with an automatic recording dilatometer. In this instrument the change in length and the temperature are recorded as

Cleveland Meeting, October 1949.
TP 2673 E. Discussion of this paper (2 copies) may be sent to *Transactions AIME* before December 1, 1949. Manuscript received May 5, 1949.

* Associate Professor of Mechanical Engineering and Chief of the Materials Section of Jet Propulsion Laboratory, California Institute of Technology, Pasadena, Calif.

† Research Engineer, Jet Propulsion Laboratory, California Institute of Technology.

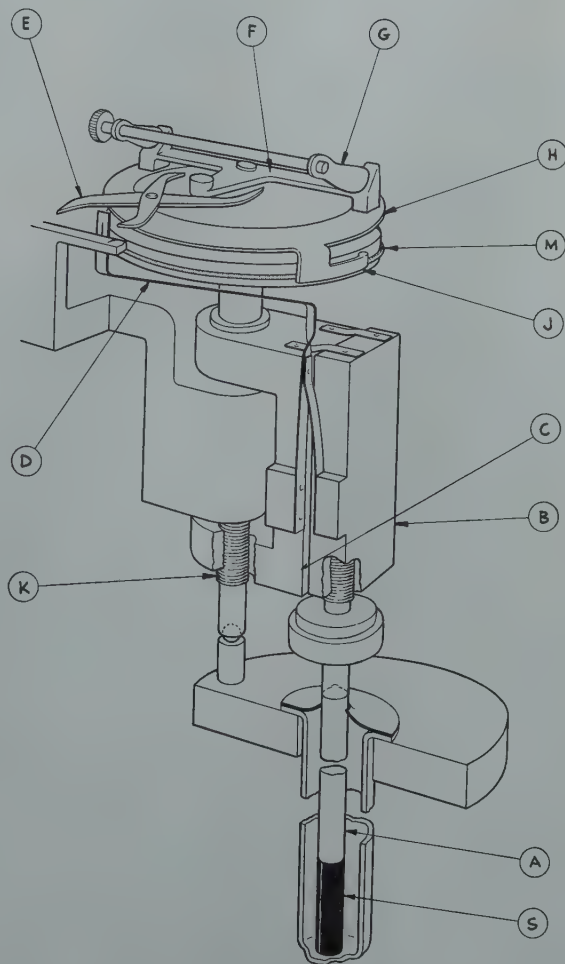


FIG 1—Principle of the dilatometer pick-up mechanism.

functions of time on two separate charts and the rates of heating and cooling may be varied from 1 to 20°F per min. The temperature may be kept constant at any value up to 2200°F during any predetermined length of time and the change in length recorded as a function of time. Provision is made for atmosphere control inside the fused silica tube containing the specimen. Three different magnifications are provided, so that 1 in. on the chart corresponds to 0.002, 0.005, or 0.010 in. change in length.

The mechanism following the change

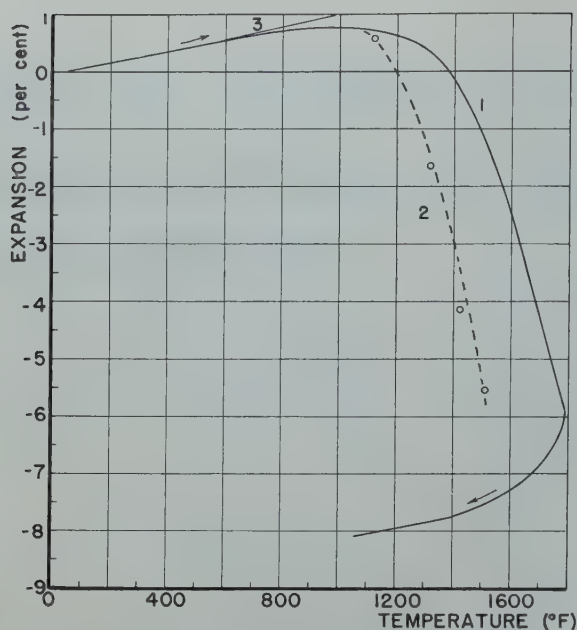


FIG 2—Thermal expansion curve of copper compacted at 20,000 psi.

(1) Rate of heating 7°F per min. (2) Results of isothermal test.
(3) Solid copper.

in length of the specimen consists of a mechanical pickup coupled with an electrical transmission to the recorder. The principle of this method is shown in Fig 1. The motion of the specimen is transmitted by the quartz rod to the movable section *B* of a reed gauge mechanism. When the movable section *B* of the gauge is displaced with respect to the fixed section *C*, the wand *D* is displaced from its equilibrium position. The scissors mechanism *E* transfers the movement of this wand as an angular displacement of the clutch bar *F*. The rotating cams *G* reposition the clutch bar *F* to equilibrium position causing rotational movement of the drive disk *H* and the contactor *J*. This motion also rotates the lead screw *K* which causes the fixed section *C* of the reed mechanism to follow the motion previously imposed on the movable section *B* and thus return this mechanism to equilibrium. The position of the contactor *J* on the slide wire *M* is transmitted electrically to the slide wire in the recorder.

The standard specimen used in this investigation was 1 in. long and $\frac{1}{4}$ in. square in cross-section. These specimens were compacted in a hard steel die in which the pressure was applied in a direction perpendicular to the length of the specimen. All tests were performed in an atmosphere of pure hydrogen.

Compacts Made of a Pure Metal

A thermal expansion curve which

may be considered as typical of a pure metal compact is shown in Fig 2. This curve was obtained with a copper specimen compacted at 20,000 psi and made of a classified powder having particle sizes between 74 and 43 microns. The compact was heated at a rate of 7°F per min. The first portion of the curve, up to a temperature of about 600°F represents the normal thermal expansion of copper. As soon as sintering takes place in the compact, shrinkage counteracts the normal thermal expansion and the curve deviates from that of a solid bar of copper. As the temperature increases, shrinkage proceeds faster, the thermal expansion curve reaches a maximum, and finally drops very rapidly.

The change in length occurring during cooling at a constant rate can be measured, and the shape of the expansion curve is also shown in Fig 2. At the beginning of the cooling stage, the contraction of the specimen is larger than that which would correspond to the normal coefficient of thermal expansion of the metal. It is probable that during this period some sintering is still in progress, but at a lesser rate than during the heating period in the same temperature range. As the temperature is lowered the expansion curve follows closely that of a solid metal, showing that all contraction caused by sintering has ceased.

In interpreting the thermal expansion curves of a compact during sintering, it must be remembered that the two variables, time and temperature, are combined into one. Obviously, such curves do not represent equilibrium

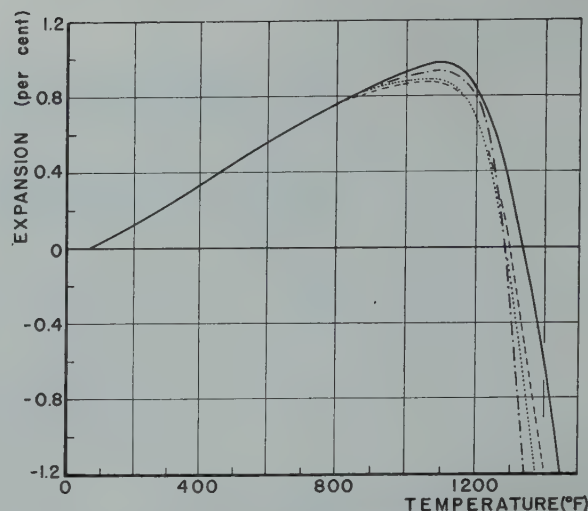


FIG 3—Thermal expansion curves of copper compacted at 80,000 psi.

Recorded at various rates of heating:

— 3°F per min. — 7°F per min. — 11°F per min. — 18°F per min.

conditions, and would be affected by the rate of heating. For rates of heating normally used in practice, however, the effect is relatively small. A series of curves obtained at rates of heating from 3 to 18°F per min is shown in Fig 3. As could be expected, after definite contraction has set in, the expansion curve drops faster for smaller rates of heating. There should be a limit, however, to the shift of the expansion curve toward greater shrinkage as the rate of heating becomes smaller. The limiting curve, which would correspond to an infinitely slow heating can be approximated by making isothermal experiments and measuring the change in length of a compact versus time. Such experiments have been described in a previous paper¹ and the results obtained with a copper powder with particle size ranging from 74 to 43 microns are reproduced in Fig 4, in which the percentage shrinkage is plotted as a function of time. For a given temperature, shrinkage proceeds very fast during the first few hours, and little additional decrease in dimensions is obtained after a long sintering time. From these results it is not possible to decide whether the shrinkage, after the initial period of sintering, tends toward a limiting value or increases at a constant rate. In any case, the shrinkage obtained after a sintering time of the order of 50 hr may be assumed to represent a practical limiting value. Within this approximation, it is possible to trace on the graph of Fig 2 the limiting thermal expansion curve which would correspond to a very small rate of heat-

¹ References are at the end of the paper.

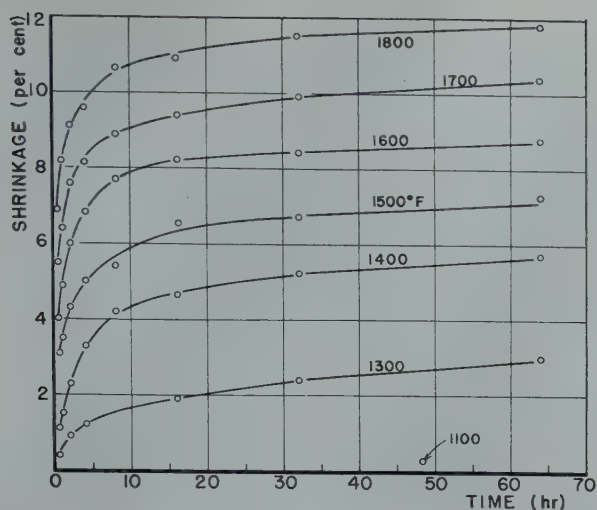


FIG 4—Shrinkage vs. time curves during sintering of copper compacts at various temperature.

ing. Above the temperature at which shrinkage becomes measurable, this curve deviates from that recorded at a rate of 7°F per min but both curves have essentially the same shape. It is particularly interesting to note that both curves separate from the normal thermal expansion curve of solid copper at almost the same temperature. Hence, the thermal expansion curve of a compact recorded at a normal rate of heating can give valuable information on the minimum temperature at which sintering proceeds at a measurable rate.

The influence of the compacting pressure can also be detected by thermal expansion analysis. In general, the expansion curves illustrate clearly the well known fact that the shrinkage of a compact is greater for smaller compacting pressure. As an example, a series of thermal expansion curves recorded for copper, cobalt, and molybdenum compacts prepared at various compacting pressures are shown in Fig 5, 6, and 7, respectively. All the curves are essentially of the type previously described as normal, and for the three metals the effect of increasing the compacting pressure is to increase the temperature at which a given percentage shrinkage is reached.

Most of the pure metal powder compacts studied in this laboratory so far have exhibited the normal type of thermal expansion curves described above. One of the copper powders tested, however, showed an abnormal behavior under compacting pressures above approximately 60,000 psi. At a temperature of about 1600°F, an abnormal expansion or swelling took place. This swelling, almost negligible at 60,000 psi, became greater with

increasing compacting pressure and was about 1.2 pct at 90,000 psi. The thermal expansion curves recorded with this particular copper powder have been published elsewhere.² Thermal expansion curves showing a similar swelling of copper compacts have been obtained by other investigators.³

The first possible explanation for the swelling of a compact is based on the existence of gas pockets enclosed in the compacts by the high compacting pressure. When the temperature is increased, sintering may start before the gas can escape between the particles and the increasing gas pressure may cause plastic flow of the partially sintered metal. In the particular case considered here, the explanation was weakened by the results of experiments made with the same copper powder in which both the pressing of the compact and the recording of the thermal expansion curve were done in vacuum.⁴ The specimens still expanded at high temperature and essentially the same thermal expansion curves were measured. The entrapped gas theory would still remain an explanation, however, if it were supposed that the gas pockets were already inside the particles of powder before pressing and are therefore not affected by vacuum. The existence of such gas inclusions is consistent with the spongy structure of the powder, and the explanation seems at the present time a logical one.

Special Case of Iron Compacts

The dimensional changes taking

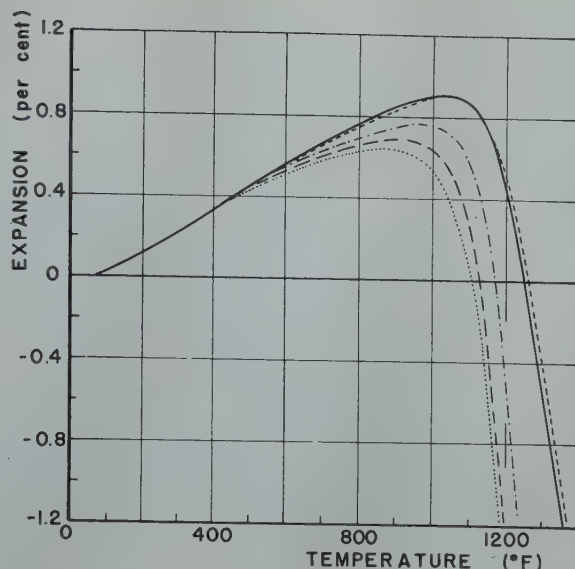


FIG 5—Thermal expansion curves of copper compacted at various pressures and recorded at a rate of heating of 7°F per min.

place during the sintering of iron compacts are greatly influenced by the allotropic change from α to γ iron. The thermal expansion curve (see Fig 8 A) is of the normal type previously described, up to the critical temperature at which an abrupt contraction indicates the transformation from α to γ iron. As soon as this transformation has taken place, the curve starts upward with a slope corresponding approximately to the coefficient of expansion of γ iron. As the temperature increases, shrinkage due to sintering becomes noticeable and the curve deviates from the normal thermal expansion of solid iron, as in the α range.

Before discussing the particular shape of the thermal expansion curve of iron, other features shown in Fig 8 require a short explanation. The influence of compacting pressure, which is quite apparent in the two sets of curves, is in accordance with the previous observation on other pure metal compacts. The influence of the particle size is not very marked, and it would be difficult to base any conclusion from the small difference existing between the two sets of curves, mostly because the two powders are probably different in impurity content. The effect of impurities is clearly shown by the temperature at which the transformation took place. The critical temperature of the fine powder is 1670°F, which is that of pure iron. The coarse powder transformed at about 1570°F, and this low critical temperature is an indication of the presence of impurities, most probably carbon.

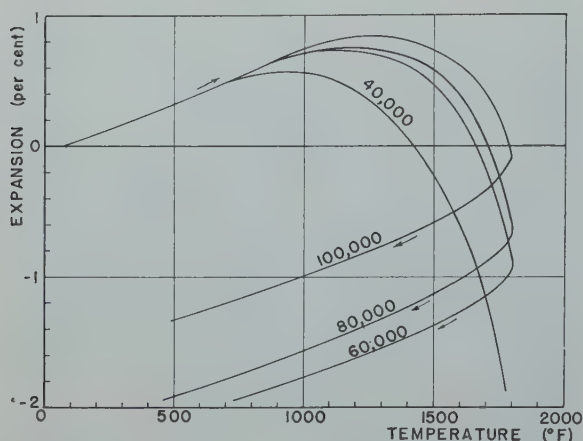


FIG 6—Thermal expansion curves of cobalt compacted at various pressures and recorded at a rate of heating of 7°F per min.

As stated above, the most important feature of the thermal expansion curves of iron compacts is the upward trend of the curve just above the critical temperature. The discontinuity in the rate at which shrinkage proceeds through the critical temperature suggests that near the transformation point the rate of sintering of γ iron is much smaller than that of α iron. In an effort to bring more evidence to this conclusion, the following experiment was performed: An iron compact, prepared with MD-111 powder, was heated in the dilatometer at a rate of 7°F per min. up to a temperature of 1620°F, that is, slightly below the transformation. At this temperature the shrinkage was recorded as a function of time. A second compact was then investigated by the same method, but the isothermal measurements were started at 1690°F, that is, slightly above the $\alpha \rightarrow \gamma$ transformation. The two resulting curves are reproduced in Fig 9, in which the expansion (or shrinkage) is plotted versus time, together with the temperature versus time curves of the two experiments.

Up to 1620°F, the two expansion curves are obviously very close to each other, the slight difference being due to experimental errors and most probably also to the lack of perfect similitude of the two specimens after compacting. During the isothermal part of the test it is quite clear that the sample maintained below the critical temperature contracted at a much faster rate than that maintained above the critical temperature. The net shrinkage one hour after the temperature reached a constant value was 0.85 pct for the specimen heated to 1620°F and only 0.05 pct for the specimen heated to 1690°F. The obvious conclusion is that in the region of the $\alpha \rightarrow \gamma$ transforma-

tion temperature, the rate of sintering is much greater in the α range than in the γ range.

This result may be correlated with observations previously reported by various investigators. For example,⁵ it was shown that both density and tensile strength of sintered iron compacts increase first with sintering temperature, but undergo a marked drop in the vicinity of the critical temperature. Most of the systematic investigations of sintered iron, however, have been made at sintering temperatures above the transformation.⁶ The fact that the rate of shrinkage of a compact heated just below the critical temperature is greater than that above this temperature might be used advantageously in practical application where maximum density and hence maximum tensile strength are desired. In this case, the sintering should be carried on at approximately 1600°F for as long a time as practical, then the temperature should be increased to a higher value, for example 2000°F as was used in Ref. 6. By this technique, advantage could be taken of the rapid rate of shrinkage occurring in the α range, while the final high temperature treatment would achieve a satisfactory sintering.

Case of Alloyed Powders

Apriori, it could be stated that the mechanism of sintering of a compact made of alloyed powder is not essentially different from that of a pure metal compact. As far as the dimensional changes are concerned, this statement has been verified in the cases of a copper-nickel powder (30 pct copper and 70 pct nickel) and a stainless steel powder of the 18-8 type. A

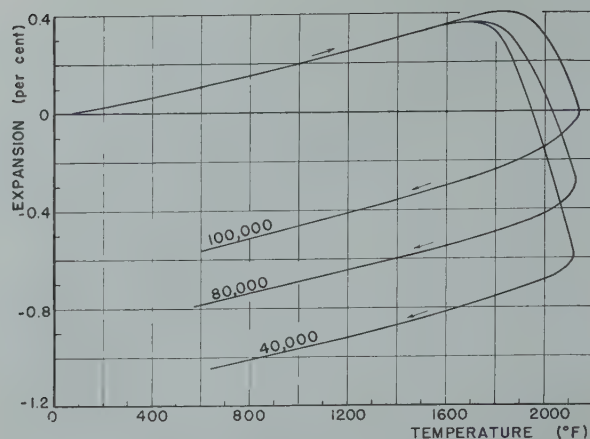


FIG 7—Thermal expansion curves of molybdenum compacted at various pressures and recorded at a rate of heating of 7°F per min.

set of thermal expansion curves of compacts made with the copper-nickel powder is shown in Fig 10, and similar curves for stainless steel powder have previously been published.⁷ All these curves are of the normal type generally encountered with pure metals.

Compacts Containing Two Metal Powders

During sintering of a compact containing two metal powders, relatively large dimensional changes are frequently observed. The swelling of copper-tin and copper-zinc compacts are familiar examples. These dimensional changes may be studied by dilatometric measurements. The interpretation of thermal expansion curves, however, is often more complicated than in the case of a pure metal. To make this interpretation as clear as possible, it is recommended procedure to prepare the mixtures with powders which, tested individually, would have the normal type of thermal expansion curve described in the previous section. If this precaution is taken, any abnormal swelling observed during the sintering of the mixture is most probably due to interaction between the two powders. As a result of numerous experiments performed at this laboratory on the sintering of compacts made of two powders, it was found that the thermal expansion curves during sintering were of two basic types. These two types will first be described and tentative explanations for the dimensional changes will then be discussed.

COPPER-NICKEL COMPACTS

During the sintering of copper-nickel compacts, no abnormal expan-

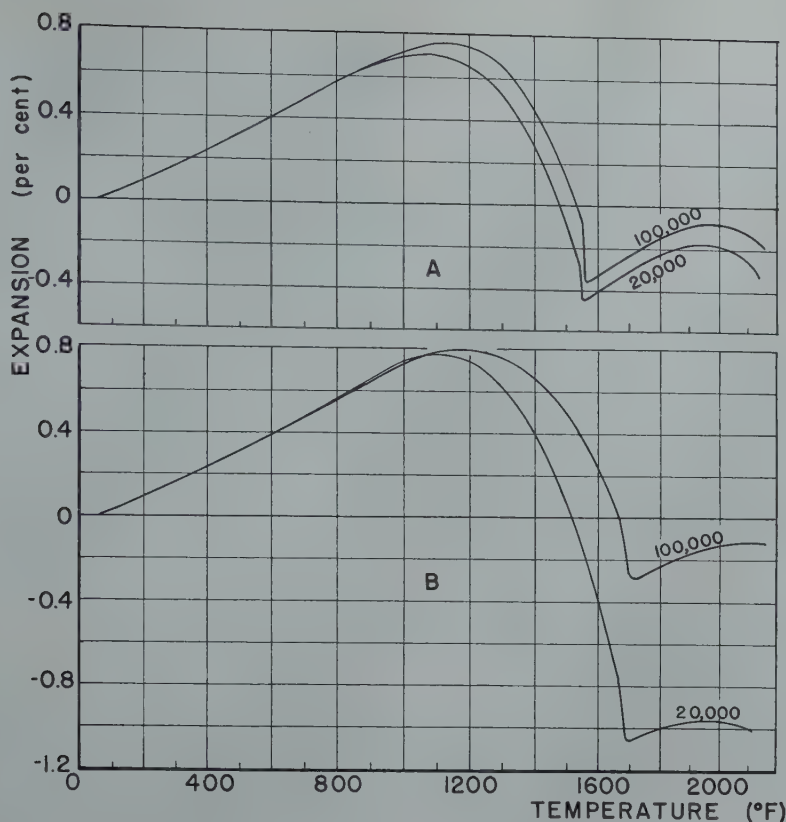


FIG 8—Thermal expansion curves of iron powder compacts recorded at a rate of heating of 7°F per min.
A. Particle sizes between 147 and 104 microns.
B. Particle sizes smaller than 43 microns.

sion has been observed. The thermal expansion curves recorded with powders of various kinds and pressed at compacting pressures varying from 20,000 to 100,000 psi were all of the normal type which is characteristic of each powder taken separately. This study was supplemented by X ray diffraction measurements which showed that simultaneously with the shrinkage of the compact, diffusion takes place and when the compact reaches a temperature of 2200°F at a rate of 6°F per min. its structure is that of the equilibrium solid solution between copper and nickel. The details of this investigation have been published elsewhere.^{2,8}

As far as the present study is concerned, suffice it to say that for copper-nickel compacts the diffusion of the metals into each other does not cause any perturbation in the progression of the normal shrinkage during the process of sintering and the thermal expansion curve is of the type observed for a normal pure powder.

COPPER-ZINC COMPACTS

The salient feature of the thermal expansion curves of copper-zinc compacts during sintering is a large swelling of the compact in a range of temperature from about 300 to 700°F. This has been previously discussed for compacts

containing 70 pct copper and 30 pct zinc.² It was shown that the critical temperature marking the beginning and the end of this abnormal expansion depended upon the fineness of the powders but not upon the compacting pressure. The effect of composition has been recently investigated, and typical thermal expansion curves for compacts containing from 5 to 45 pct zinc are shown in Fig 11. The copper powder

(MD-151) from Metals Disintegrating Co., Elizabeth, N. J.) used for these measurements was 50 pct between 200 and 325 mesh and 50 pct finer than 325 mesh and the zinc (MD-201 from the same source) was all finer than 325 mesh. The curves of Fig 11 indicate clearly that by increasing the percentage of zinc in copper, the magnitude of the swelling of the compact is steadily increased, but the two temperatures between which this swelling occurs do not seem to be affected.

A study of the various phases present during the sintering of 70-30 copper-zinc compacts has been previously made by X ray diffraction.² It was shown that the temperature at which the thermal expansion curve has a sudden increase coincides with a rapid diffusion of zinc into copper and at 300°F the presence of the ϵ phase was already noticed. At all temperatures along the ascending portion of the expansion curve, pure zinc and intermediate phases were present and at the end of the ascending portion (about 550°F) all the zinc had been absorbed into β and α phases. It is therefore apparent that the abnormal thermal expansion between 300 and 550°F coincides with the progressive disappearance of the particles of zinc and their absorption by the particles of copper. A tentative explanation of the increase in volume during the sintering of copper-zinc compacts may be based on the assumption that during the process of diffusion, the zinc particles are absorbed by the copper particles, which, as a result, grow in size leaving cavities in place of the zinc particles. The mass transfer of zinc into copper

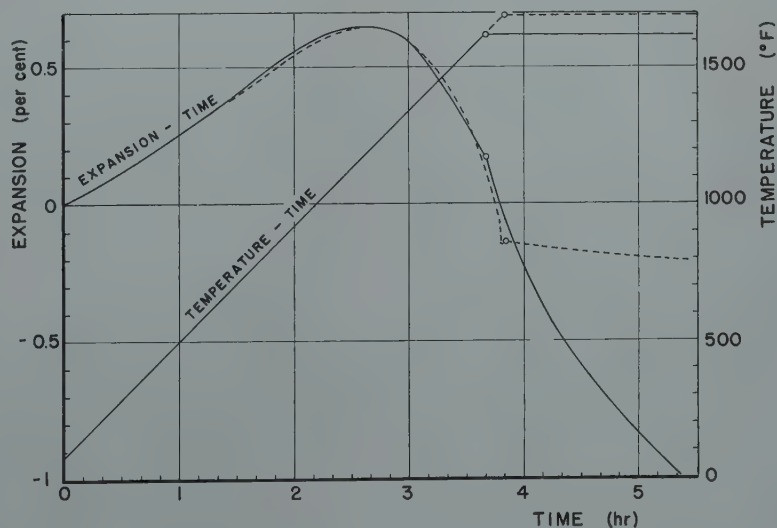


FIG 9—Expansion and temperature vs. time curves for two experiments made with iron powder compacts pressed at 80,000 psi.
— Isothermal test in α range
--- Isothermal test in γ range

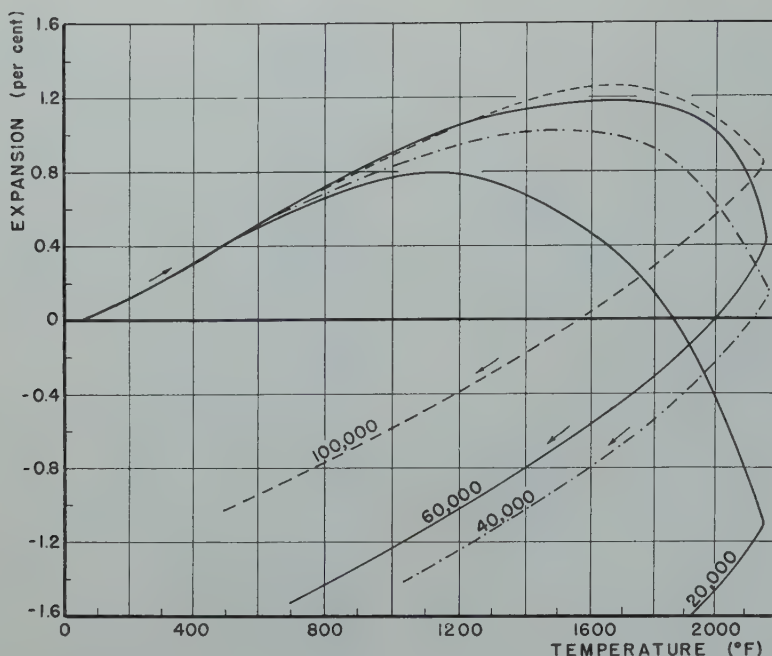


FIG 10—Thermal expansion curves of alloyed copper-nickel powder compacts.

during diffusion is the main hypothesis in this explanation. It may be justified on the basis that zinc is soluble in copper, whereas copper is practically insoluble in zinc. The results of the measurements described above provide a new argument in favor of the absorption of zinc hypothesis. It is indeed quite clear that if zinc moves into the copper particles, cavities are formed and the amount of swelling of the compact should increase steadily with the percentage of zinc. This is exactly what has been found experimentally, as shown by the curves of Fig 11.

FACTORS INFLUENCING THE DIMENSIONAL CHANGES OF COM-PACTS CONTAINING TWO POW-DERS

The nature of the phase diagram between two metals is a determining factor controlling the occurrence of the swelling of the compact. In the case of copper-nickel, in which no abnormal expansion is observed, the two metals form a complete series of solid solutions, so that either one of the two metals is able to dissolve the other. This condition may be necessary to prevent any swelling, but does not seem to be sufficient. Experiments performed on chromium-molybdenum compacts ranging in composition from 10 to 90 pct, by steps of 10 pct, exhibited a maximum increase in dimensions of 16 pct, as shown in the curve of Fig 12, and yet these two metals form a complete series of solid solutions.⁹

There is therefore another condition

which must be fulfilled to prevent swelling of the compact during diffusion, and it is quite logical to believe that this condition is that the rates of diffusion of either one of the two metals into the other should be approximately the same. This condition is satisfied in the copper-nickel system. Unfortunately it is not possible to apply it at present to the chromium-molybdenum system because the diffusion constants for this pair of metals have not been determined.

The explanations suggested for the swelling of the copper-zinc compacts are supported by several experimental results obtained in this laboratory. The system copper-10 pct tin exhibits a swelling which, by means of X ray diffraction, has also been related to the absorption of tin into copper.² Compacts made of 25 pct molybdenum and 75 pct nickel also have an abnormal thermal expansion. The mechanism is, in this case, similar to that described for the copper-zinc system, since molybdenum is soluble in nickel up to about 35 pct at 2500°F while molybdenum does not dissolve any appreciable amount of nickel and in addition, three intermediate phases are present in the phase diagram.

Conclusions

The results of experiments described in this paper have demonstrated the usefulness of the dilatometric method in studying the sintering of metal powder compacts. In the case of a compact made of a pure metal, the thermal expansion curves recorded on a dilatometer at a constant rate of heating give valuable information on the rate at which shrinkage proceeds as the temperature is increased. In addition, a dilatometric test offers a simple means of detecting the abnormal behavior of some metal powder compacts which exhibit a swelling during sintering.

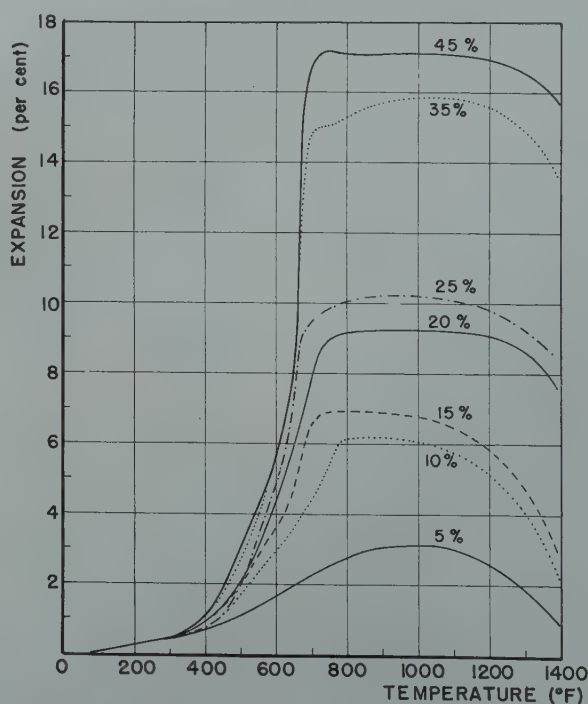


FIG 11—Thermal expansion curves of copper-zinc compacts containing various amounts of zinc and pressed at 40,000 psi.

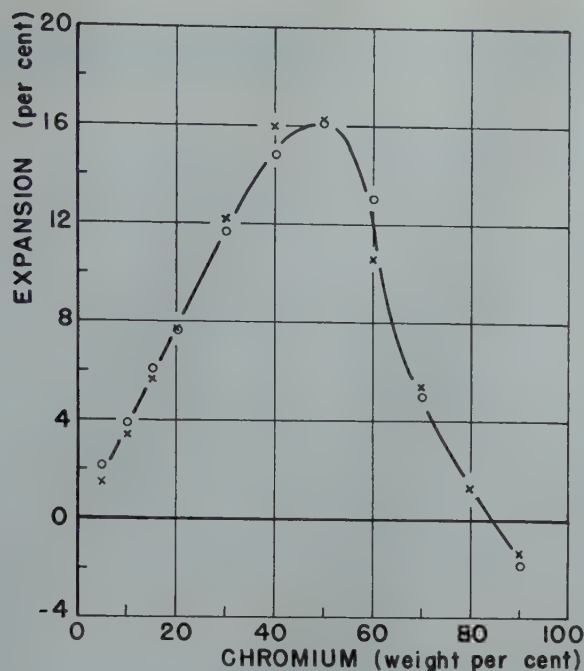


FIG 12—Expansion of chromium-molybdenum compacts measured after sintering for 4 hr at 2500°F.

When a binary alloy is prepared by powder metallurgy by mixing the two powders before pressing, abnormal dimensional changes are likely to take place as the result of diffusion. In most cases, a swelling is observed in the range of temperature in which one of the constituents is absorbed by the other. This critical range of temperature is clearly detected on a thermal expansion curve. Since in the sintering of large compacts the temperature may not be uniform during sintering, the existence of large dimensional changes may result in an objectionable distortion of the compact. There is therefore an advantage in reducing the rate of heating in the critical range of temperatures determined from dilatometric measurements.

As stated before, the thermal expansion curves of a compact during sintering do not provide the kind of data that would contribute most to the search for a theory of sintering, the reason being that the two independent variables, time and temperature, are combined into one, namely the rate of heating. The importance of the dilatometric method should not be mini-

mized, however, in view of the fact that it has already furnished very valuable results, especially in the determination of the critical range of temperatures of compacts containing two metal powders. Considered as a first step, the method is of great help in determining the conditions under which the more reliable, but also more tedious, isothermal experiments should be conducted to bring out the maximum amount of information in the minimum time.

Acknowledgment

This work was done under contract with the Army Ordnance Department, Washington, D. C. The authors wish to thank this agency for the permission to publish the results of this investigation.

References

1. Charles B. Jordan and Pol Duwez: The Densification of Copper Powder Compacts in Hydrogen and in Vacuum. *Jnl. of Metals Trans.* 185, Feb. 1949, p. 96-99.

2. Pol Duwez: The Formation of Alloys by Diffusion in Powder Metallurgy. Presented at the International Congress of Powder Metallurgy, Graz, Austria, July 12-16, 1948.
3. R. Kamm, M. A. Steinberg, and J. Wulff: Lead Grid Study of Metal Powder Compaction. *Trans. AIME* 180, 694. *Metals Tech.* Dec. 1948 TP 2487.
4. W. F. Nash: An Investigation of Certain Phases of the Powder Metallurgy of Copper and of Silver Manganese Alloys. Ph. D. Thesis, Calif. Inst. of Tech., Pasadena, Calif., 1942.
5. J. Libsch, R. Volterra, and J. Wulff: The Sintering of Iron Powder. Chap. 35 in *Powder Metallurgy*, ed. by J. Wulff, Amer. Soc. for Metals, Cleveland, O., 1942.
6. A. Squire: Density Relationships of Iron Powder Compacts. *Trans. AIME* 171, 472. *Metals Tech.*, April 1947 TP 2165.
7. Pol Duwez and H. E. Martens: The Powder Metallurgy of Porous Metals and Alloys Having a Controlled Porosity. *Trans. AIME* 175, 848. *Metals Tech.* April 1948 TP 2343.
8. Pol Duwez and C. B. Jordan: Application of the Theory of Diffusion to the Formation of Alloys in Powder Metallurgy. *Trans. ASM*, 1948.
9. W. Trzebiatowski, H. Ploszek, and J. Lobzowski: X-ray Analysis of Chromium-Molybdenum and Chromium-Tungsten Alloys. *Analytical Chemistry* 19, no. 2 (93-95) 1947.

Introduction

Review of the Literature

Table 1 . . . Analyses of Steels

| Steel Designation | C | W | Mo | Cr | V | Si | Mn | S | P |
|-------------------|------|------|------|------|------|------|------|-------|-------|
| A | 0.83 | 6.09 | 5.06 | 4.07 | 1.85 | 0.16 | 0.33 | 0.008 | 0.013 |
| B | 0.82 | 5.73 | 4.23 | 4.23 | 1.51 | 0.26 | 0.26 | 0.014 | 0.019 |
| C | 1.09 | | | 1.52 | | 0.29 | 0.32 | 0.018 | 0.005 |
| D | 1.08 | | | 2.83 | | 0.29 | 0.27 | 0.010 | 0.006 |

Composition of Steels

Four steels, of the compositions given in Table 1, were used for the experiments to be described. Steel A is the present-day grade of M-2 high speed steel. Steel B is the war-time equivalent of the same grade, with reduced alloying elements. Steels C and D are low-alloy laboratory heats being studied for other purposes at M. I. T.

These materials were received in the form of annealed (spheroidized) centerless-ground bars, $\frac{1}{4}$ in. in diam.

The Citrate Cell

PROCEDURE

A number of double electrolytic cells based on that of Treje and Benedicks¹⁴ were built in an attempt to devise a method which would permit rapid, yet quantitative isolations of the carbides from high speed steel. The apparatus found most satisfactory is illustrated in Fig 1. Its principal features are:

1. The anolyte is an aqueous solution of 15 pct sodium citrate, 1 pct potassium bromide and 0.1 pct potassium iodide, having a pH of 7.0 ± 0.2 . The catholyte is an aqueous solution of 10 pct copper sulphate.

2. The specimens to be dissolved are 5 in. long by $\frac{1}{4}$ in. diam and are supported in pairs from the bottom on the fixture shown in Fig 2. These rods form the anode of the cell, and are rotated at 1 rpm during electrolysis to promote even solution.

3. The anode and cathode compartments are separated by a porous cylinder made by cutting the bottom off a porcelain cup used for Daniel cells.

4. Continuous removal of the iron-rich anolyte and replenishment with fresh solution is necessary to prevent the anolyte from becoming too acidic during the course of electrolysis. The cell in Fig 1 provides for such replenishment automatically. With this arrangement, the pH of the anolyte drops only to about 6.6 after a 24 amp-hr run. Without it, the pH decreases to 3.6 over the same period.

After a normal run of 24 hr at 1 amp,* the two specimens are not completely dissolved, and in the case of the annealed steels, a large proportion of the carbides adheres to the remainder of the specimens. The specimens are removed from the cell, and the attached carbides are scraped into a beaker with a rubber "policeman" and a jet of water. The syphon that

Wt. pct of carbides

$$= \frac{(\text{Wt. of filter crucible} + \text{contents}) - (\text{Wt. of filter crucible})}{(\text{Wt. of specimens before run}) - (\text{Wt. of specimens after run})} \times 100 \quad [1]$$

* Current density = 0.14 amp per sq in.

supplies fresh anolyte from the reservoir is shut off, and the solution in the anode chamber is drawn through the alundum filter crucible (Fig 1) with the aid of an aspirator pump. When the anolyte level drops below the ground-glass joint just above the filter crucible, the joint is broken and the filter assembly is lowered away from the apparatus. The carbides in the aforesaid beaker are transferred to the filter crucible, and the entire residue thus collected is washed with 300 cc of distilled water, followed by 50 cc of 1:20 ammonium hydroxide* and finally 500 cc of distilled water. The filter crucible and its contents are then dried in vacuum at 165°F (60°C) for 12 to 14 hr.

The carbide content of the steel is taken as:

* The ammonium hydroxide wash is used to dissolve any tungsten acid which may possibly form from the tungsten originally in the steel matrix.

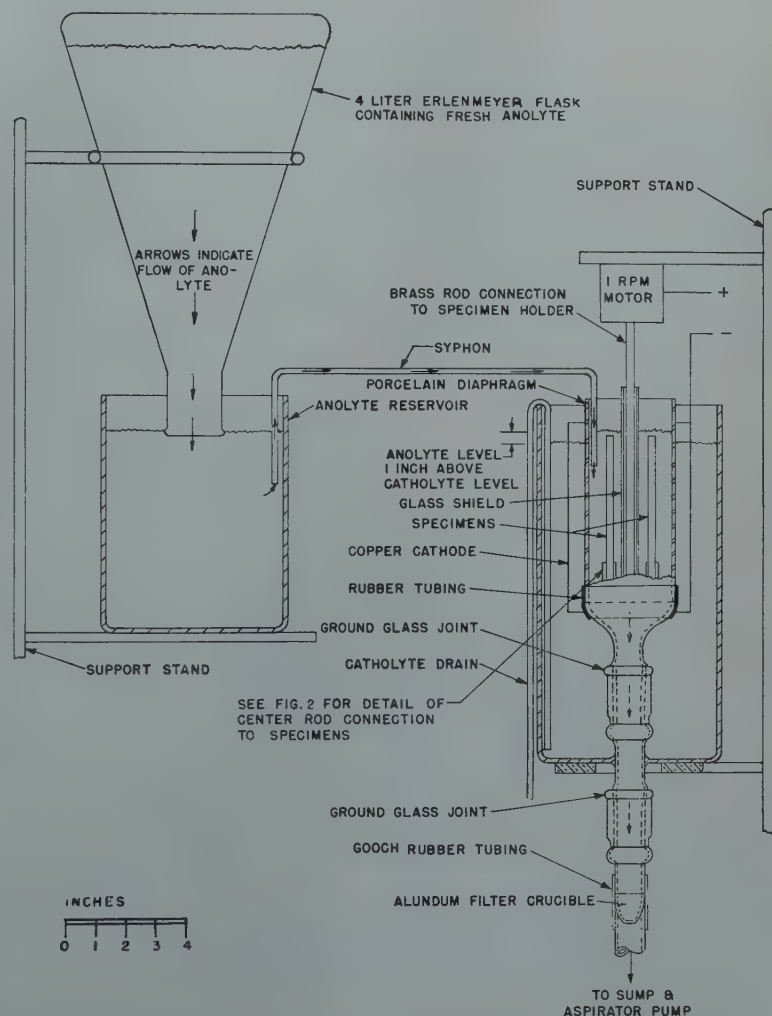


FIG 1—Schematic diagram of sodium citrate cell for electrolytic isolation of carbides. Anolyte: aqueous solution of 15 pct sodium citrate, 1 pct potassium bromide and 0.1 pct potassium iodide. Catholyte: aqueous solution of 10 pct copper sulphate.

RESULTS ON ANNEALED SPECIMENS

The amounts and compositions of the residues obtained by citrate-cell extractions of annealed steels B, C and D in the annealed condition are listed in Table 2.

The fact that the carbon content of the residues isolated from the low alloy steels C and D closely approximates the theoretical composition of cementite (6.67 wt. pct) offers one criterion that the cell is quantitative, even for low alloy carbides. In addition, it is known that virtually all the carbon in the three annealed steels is tied up in the carbides. This circumstance may be employed as a second criterion for the quantitative-ness of the isolation, since the amount of carbon in the residue can be compared with that originally existing in the steel as electrolyzed:

Fraction of carbon of steel found in residue

$$= \frac{(\text{Wt. of residue}) \times (\text{Wt. pct carbon in residue})}{(\text{Wt. of steel dissolved}) \times (\text{Wt. pct carbon in steel})} = \frac{(\text{Wt. pct residue})}{100} \times \frac{(\text{Wt. pct carbon in residue})}{(\text{Wt. pct carbon in steel})} \quad [2]$$

On this basis, the data of Table 2 demonstrate that all of the carbon in each steel is accounted for in the extracted residue.

Steel A did not dissolve like the other three during electrolysis. Rather, a porous skin of partially attacked metal remained around the specimens after the runs. Inasmuch as it was difficult to wash the adhering carbides from beneath this skin, the results ob-

Table 2 . . . Amounts and Compositions of Residues Obtained from Isolations of Annealed Steels in Sodium Citrate Cell*

| Steel Designation | Weight Pct Residue | Composition of Residue—Weight Pct | | | | | | Fraction of Carbon of Steel Found in Residue |
|-------------------|--------------------|-----------------------------------|-------|-------|-------|------|-------|--|
| | | C | W | Mo | Cr | V | Fe | |
| B | 21.0 | 3.84 | 25.76 | 18.98 | 11.44 | 6.56 | 27.75 | 0.98 |
| C | 17.0 | 6.49 | | | 8.36 | | 83.70 | 1.01 |
| D | 16.3 | 6.65 | | | 15.58 | | 77.00 | 1.00 |

* These investigations did not include M-2 high speed steel.

tained for steel A are not considered sufficiently accurate to be included in Table 2. Numerous attempts were made to eliminate the undissolved skin by carefully degreasing the specimens, altering the surface finish, and varying the current density, but no success was achieved. The method devised for coping with this troublesome occurrence will be discussed later in the paper.

RESULTS ON HARDENED STEELS

To test the behavior of hardened

Table 3 . . . Comparison of Amounts of Residue Obtained in Two Types of Electrolytic Cells from Steel B Quenched from Various Temperatures

| Temp. °F | Wt Pct Residue | |
|----------|---------------------|------------------------|
| | Sodium Citrate Cell | Hydrochloric Acid Cell |
| Annealed | 20.9 | 21.4 |
| 1700 | 17.2 | 18.1 |
| 1900 | 16.9* | 16.0 |
| 2100 | 18.3* | 14.7 |
| 2200 | 21.4* | 9.9† |

* Peeling occurred, no magnetic separation applied.
† Peeling occurred, but magnetic separation was applied.

austenitizing temperature is raised to 1900°F (1040°C), and then increases with further increase in temperature. The latter trend is distinctly anomalous, and indicates that the cell operation becomes unreliable when the austenitizing temperature is too high. It was found that somewhat the same phenomenon occurs during the electrolysis of quenched steel B as previously described for annealed steel A; that is, a tenuous layer of metal remains undissolved. However, unlike the case of the annealed steel, the metallic skin tends to split during the run (probably due to the relief of quenching stresses while the electrolysis proceeds), and drops into the filter crucible along with the isolated carbides. This undesirable state of affairs seems to become more pronounced as the alloy content of the steel matrix is increased, and accounts for the erroneous results after austenitizing at the higher temperatures.

The authors are not aware that this "peeling" phenomenon has been observed before in the electrolysis of high speed steel, but Gulyaev¹⁰ has mentioned that it occurs with high-alloy chromium steels, electrolyzed in 1:20 hydrochloric acid. He further states that it may be eliminated by using more concentrated acid. Consequently, experiments were undertaken in the present work with hydrochloric acid cells in an effort to avoid the "peeling" of high speed steel. At the same time,

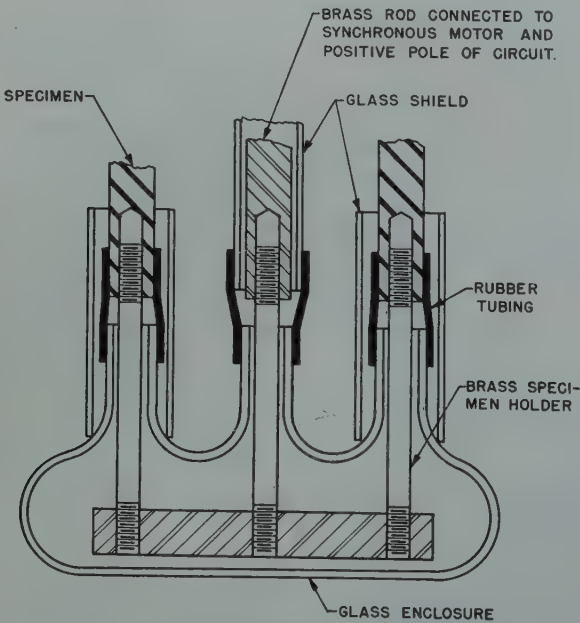


FIG 2—Fixture for holding and rotating specimens in electrolytic cell of Fig 1.

because of the increased danger of carbide attack by the electrolyte in this type of cell, the quantitative aspects of the isolations were cross-checked by lineal analysis¹⁶ and density measurements as well as by chemical analysis.

The Hydrochloric Acid Cell

PROCEDURE

A schematic drawing of the hydrochloric acid cell finally adopted is shown in Fig 3. The anode is a single specimen 5 in. long by ¼ in. diam, the general arrangement being quite similar to that used by Bain and Grossmann.⁷ Satisfactory runs are carried out at 0.5 amp* for 48 hr in an electrolyte of 1 part hydrochloric acid (sp. gr. = 1.19) and 10 parts distilled water. About half the electrolyte is replaced with fresh solution at the end of 24 hr; otherwise iron may deposit loosely on the cathode and fall into the carbide residue when the cathode is disturbed.

When hardened specimens of steel B are electrolyzed in this simple cell, it is found that the peeling phenomenon occurs only with austenitizing temperatures above 2100°F (1150°C). Thus, although the acid cell does not completely eliminate this interfering condition, it does help appreciably.

The particles of the undissolved skin that contaminate the carbide residue are ferromagnetic and are strongly attracted to a permanent magnet. Fortunately the carbides themselves are nonferromagnetic and this circumstance provides the basis for a method of separation in those runs where the peeling occurs. After electrolysis the spent electrolyte is decanted from the residue in the cell-beaker through a fine-porosity fritted-glass filter crucible, while an Alnico-5 horseshoe magnet is held under the spout of the beaker to prevent magnetic particles from going into the filter. The residue retained in the cell-beaker is then transferred to a smaller beaker together with the particles adhering to the specimen. About 50 cc of 1:20 hydrochloric acid is added to form a slurry, and any large agglomerates of the residue are dispersed with a glass rod. Then, the Alnico-5 magnet enclosed in a thin-walled lucite box is immersed in the slurry, withdrawn and the liquid is allowed to drain back into the beaker. The lucite box is next held over a third beaker, the magnet is removed and the particles adhering to

the box are washed into the third beaker with a stream of distilled water. This operation is repeated several times until no magnetic particles can be withdrawn from the original residue.

Then the same procedure is carried out on the magnetic residue thus transferred, and the nonmagnetic particles finally remaining are added to the first batch of nonmagnetic residue. This is filtered, washed (200 cc of 1:20 hydrochloric acid and 100 cc of distilled water in that order) and dried in vacuum at 165°F (60°C). The magnetic residue, consisting of relatively coarse particles of undissolved steel, settles readily and requires no filtering. The supernatant water is merely decanted off and the residue is washed with alcohol and ether, after which it is dried in vacuum.

The carbide content of the steel is calculated as:

$$\text{Wt. pct carbides} = \frac{(\text{Wt. of filter crucible} + \text{nonmagnetic residue}) - (\text{Wt. of filter crucible})}{(\text{Wt. of specimen before run}) - (\text{Wt. of specimen after run}) - (\text{Wt. of magnetic residue})} \times 100 \quad [3]$$

The magnetic separation described above requires due care but is entirely practicable when applied in conjunction with the hydrochloric acid cell. This is not the case with the citrate cell because of the continuous-filtration feature. In other words, the complexity of the citrate cell is hardly worth contending with, if magnetic separation is necessary—provided, of course, that the hydrochloric acid cell can be shown to yield quantitative results.

RESULTS ON ANNEALED AND HARDENED SPECIMENS

Table 3 offers a comparison of extractions performed on steel B with both the citrate and hydrochloric acid cells. These data cast a favorable light on the acid cell, at least for studies on high speed steel, because it not only alleviates the tendency toward peeling but gives good agreement with the citrate cell in those cases where peeling does not interfere. Where peeling does occur, however, it remains to test the quantitateness of the procedure in which the magnetic process is used to correct for it. Steel A was selected for this purpose.

Weight percentages and compositions of the carbides isolated from steel A are given in Table 4. The heat treated specimens were austenitized for 10 min. in a salt bath at the indicated temperatures and quenched in

Table 4 . . . Weight Percentage and Composition of Carbides Obtained from Steel A in Hydrochloric Acid Cell

| Austenitizing Temp. °F | Weight Pct Carbides | Composition of Carbides, Wt Pct | | | | | |
|------------------------|---------------------|---------------------------------|------|------|------|------|-----|
| | | C | W | Mo | Cr | V | Fe |
| Annealed | 21.7 | 3.72 | 27.3 | 21.4 | 9.34 | 8.05 | Bal |
| 1700 | 19.5 | 3.90 | 29.5 | 22.8 | 5.28 | 7.70 | Bal |
| 1900 | 17.3 | 3.97 | 31.9 | 23.7 | 4.26 | 7.38 | Bal |
| 2000 | 16.2 | 3.69 | 31.6 | 22.8 | 2.83 | 6.73 | Bal |
| 2100 | 14.8* | 3.60 | 30.5 | 21.5 | 2.31 | 7.69 | Bal |
| 2150 | 13.3* | 3.60 | 31.6 | 22.6 | 1.72 | 6.93 | Bal |
| 2200 | 11.6* | 3.22 | 32.3 | 23.8 | 2.31 | 6.02 | Bal |
| 2250 | 10.7* | 3.12 | 22.9 | 32.1 | 1.81 | 5.22 | Bal |

* Peeling occurred, but magnetic separation was applied.

oil. It is interesting to note that steel A as annealed does not exhibit an undissolved skin when electrolyzed in the hydrochloric acid cell, unlike the results obtained with the citrate cell. Furthermore, virtually all the carbon of the annealed steel is accounted for

in the extracted carbides (using Eq 2:

$$\frac{21.7}{100} \times \frac{3.72}{0.83} = 0.97).$$

It might be possible to find all the carbon in the residue even if the carbides were partially decomposed by the hydrochloric acid because free carbon could be precipitated. Hence, the results were checked independently by density measurements and lineal analysis. It can be shown that

$$\text{Density of carbides} = (\text{Density of steel}) \times \frac{(\text{Wt. pct of carbides})}{(\text{Vol. pct of carbides})} \quad [4]$$

In addition to the weight percentage of carbides in the steel as determined by extraction, the other three quantities are directly measurable: the density of the carbides by the pycnometer method,¹⁷ density of the steel by the loss-of-weight in water,¹⁸ and volume percentage of the carbides by lineal analysis¹⁶ on the butt ends of the electrolyzed specimens. Table 5 shows a comparison of the density of the carbides from annealed steel A, as measured and as calculated from Eq 4. The close agreement indicates that, as far as the annealed steel is concerned, the hydrochloric acid cell not only isolates the carbides quantitatively, but leaves them intact.

Unfortunately, in the case of the hardened specimens, the extracted carbides are found to be contaminated

* Current density = 0.28 amp per sq in.

with free carbon which materially reduces the measured density of the carbides. This trend is shown by the

Table 5 . . . Comparison of Measured and Calculated Density of Carbides Obtained from Annealed Steel A in Hydrochloric Acid Cell

| Austenitizing Temp. °F | Weight Pct of Carbides* | Volume Pct Carbides | Density of Steel | Density of Carbides Measured | Density of Carbides Calculated |
|------------------------|-------------------------|---------------------|------------------|------------------------------|--------------------------------|
| Annealed | 21.7 | 23.2 | 8.19 | 7.71 | 7.65 |
| 1900 | 17.3 | 16.3 | 8.08 | 6.73 | 8.58 |
| 2000 | 16.2 | 12.0 | 8.06 | 5.54 | 10.90 |

* Average of 2-4 runs.

data in Table 5. The true density of the carbides increases with the austenitizing temperature in accordance with the calculated values, but the measured density changes erroneously in the opposite direction. In view of the excellent correlation obtained with the annealed steel, it is believed that the free carbon in the residues of the quenched specimens comes from the martensite-austenite matrix and not from decomposition of the carbides themselves. Attempts to determine the amount of free carbon in the residues by chemical and differential oxidation techniques were unsuccessful. Accordingly, the carbon contents shown in Table 4 for the hardened specimens are undoubtedly somewhat too high and should be regarded as uncertain.*

CORRELATION WITH FILTRATE ANALYSES

Since the foregoing density determinations shed little light on the quantitiveness of the cell operation with hardened specimens, this approach cannot be used for testing the efficacy of the magnetic separation when peeling occurs. Consequently, an analysis was made of the filtrate remaining from one of the extractions in which abundant peeling took place. The specimen (steel A) was austenitized at 2200°F (1205°C), electrolyzed in the hydrochloric acid cell, and the undissolved particles of steel in the residue were separated magnetically. From the quantity of the filtrate and its composition, the weights of tungsten, molybdenum, chromium and vanadium dissolved from the steel

were calculated. Similarly, the weights of these elements in the nonmagnetic residue were also determined.

The resulting weight balance is given in Table 6. It is evident that there is satisfactory agreement between the weight of each element in the steel electrolyzed and the sum of the respective weights in the filtrate and carbides. Thus the magnetic separation process is suitably quantitative. A weight balance based on carbon is not feasible because part of the matrix carbon is lost from the cell in gaseous form and part reports in the residue as free carbon. The fact that the other four elements check each other so well indicates that there is not enough free carbon to affect the weight percentage of the residue materially. The maximum error in the weight percentage of the residue, and therefore in the alloy analyses, due to the free carbon and the magnetic-separation technique appears to be no greater than 1 part in 20.

However, the error in the carbon analyses of the carbides may be 5 or

Table 6 . . . Comparison of Residue and Filtrate Compositions with Composition of Steel A, Quenched from 2200°F (1205°C) and Electrolyzed in 1:10 Hydrochloric Acid (Residue = 12.6 pct by weight)

| Element | A Gm Element in Filtrate per 100 Gm Steel Electrolyzed | Composition of Residue Wt. Pct | B Gm Element in Residue per 100 Gm Steel Electrolyzed | A + B | Composition of Steel Wt. Pct |
|---------|--|--------------------------------|---|-------|------------------------------|
| W | 1.81 | 32.3 | 4.07 | 5.88 | 6.09 |
| Mo | 2.02 | 23.8 | 3.00 | 5.02 | 5.06 |
| Cr | 3.58 | 2.31 | 0.29 | 3.87 | 4.07 |
| V | 1.05 | 6.02 | 0.76 | 1.81 | 1.85 |

10 times larger because of the uncertainty in the amount of free carbon.

Despite the advantages of the hydrochloric acid cell over the more complicated citrate cell for these studies on high speed steel, it should be emphasized that the latter seems to give more reliable results when cementite is present. It was pointed out under THE CITRATE CELL—Results on Annealed Specimens, that the citrate cell operates quantitatively for the cementite in annealed low alloy steels. This is not the case with the hydrochloric acid cell. For example, an annealed steel with 1.11 pct carbon

and 4.11 pct chromium yielded a residue of 8.2 wt. pct of the steel electrolyzed, and the composition was: 8.13 pct carbon, 28.50 pct chromium and 61.38 pct iron. Thus, less than two-thirds of the carbon in the steel could be accounted for in the residue $\left(\frac{8.2}{100} \times \frac{8.13}{1.11} = 0.60\right)$. Evidently the low alloy cementite was partially decomposed during the acid electrolysis. However, since cementite is not found in the M-2 high speed steel under consideration even when the citrate cell is used, the hydrochloric acid cell can be adopted with reasonable assurance for the work at hand.

The Carbides in M-2 High Speed Steel

NATURE OF THE CARBIDES

X ray diffraction analysis of the residues extracted from steels A and B indicates that three carbide phases exist in M-2 high speed steel. These may be designated here as M_6C , $M_{23}C_6$ and MC , the M representing the sum of the metal atoms.

M_6C is a face-centered cubic carbide with a lattice parameter of 11.04₄ A.U. It is identical with the (Fe, W, Mo, Cr, V)₆C phase commonly found in high speed steels.^{19,20}

$M_{23}C_6$ is a face-centered cubic carbide with a lattice parameter of 10.56₄ A.U. Its diffraction pattern also corresponds to that of $Cr_{23}C_6$ as determined by Westgren.^{21,22} Like the M_6C , this phase is capable of dissolving iron, tungsten, vanadium and molybdenum, along with the chromium.

MC is a face-centered cubic carbide with a lattice parameter of 4.18 A.U. It is essentially a vanadium-rich carbide.^{23,24}

The above carbides are present in M-2 high speed steel in the annealed condition and after austenitizing. Therefore, the observed weight percentages and compositions of the extracted residues are not representative of single carbides, but of carbide mixtures. The lattice parameters of these carbides are not appreciably affected by austenitizing, and hence it may be assumed that no gross variation in composition of the individual carbides occurs as result of hardening. This suggests that the observed changes in composition of the extracted carbides as a function of austenitizing temperature (Table 4) are due primarily to a shift in the relative amounts of the three carbides.

* Gulyaev¹⁰ estimates that the free carbon in extracted residues of 18-4-1 high speed steel, austenitized at 2370°F (1300°C), is 0.25 pct of the steel electrolyzed.

METALLOGRAPHIC IDENTIFICATION OF THE CARBIDES

Once the existence of the three carbides in the residues was established, a systematic study was made of their etching characteristics in the solid steel in an effort to identify them under the microscope. Reliable techniques were developed which not only disclosed these carbides positively but rendered it possible to determine their volume percentages by lineal analysis. Diamond dust polishing was necessary to prevent the carbides from standing in relief or from being partly smeared by the softer matrix.

All three carbides are nicely outlined by 1 pct nital or 4 pct picral. This permits the measurement of the total volume percentage of the carbides. After repolishing, the M_6C phase can be etched selectively in a 4 pct aqueous solution of sodium hydroxide saturated with potassium permanganate. The M_6C particles are outlined and stained brown in 4–5 sec. The $M_{23}C_6$ and MC carbides are not attacked. After repolishing once more, the MC carbide is darkened selectively with an elec-

trolytic etch in 1 pct chromic acid, stainless steel being the cathode. In 3–4 sec at about 3 volts, the MC particles are colored grey or black. The M_6C and $M_{23}C_6$ carbides are not attached. Lineal analysis is applied after each of the above etches, and the volume percentage of $M_{23}C_6$ is taken by difference. Proof of the effectiveness of these procedures is presented elsewhere.²⁵

EFFECT OF AUSTENITIZING TEMPERATURE

The pertinent results obtained by lineal analysis on the carbides as polished and by chemical analysis of the carbides as isolated are summarized in Fig 4. For correlation purposes, the percent of retained austenite is also shown.

It is immediately evident that the $M_{23}C_6$ carbide dissolves more readily than the other two on austenitizing, and is practically absent above 2000°F (1090°C). The M_6C carbide dissolves more gradually, while the MC carbide hardly dissolves at all below 2200°F (1205°C). In the customary austen-

itizing range of 2200–2250°F (1205–1235°C), there remains 5–8 vol. pct M_6C and 0.5–1 vol. pct MC. The progressive solution of the $M_{23}C_6$ and M_6C carbides causes an increase in the carbon and alloy contents of the matrix, as shown by the partition curves in Fig 4. These values are calculated from the alloy content of the steel and that of the isolated carbides (Tables 1 and 4). It is interesting to note that most of the chromium in the steel dissolves in the austenite at relatively low temperatures, and this coincides with the decrease in the amount of $M_{23}C_6$ carbide, the amount of M_6C and MC then remaining essentially unchanged. Clearly, $M_{23}C_6$ is a chromium-rich carbide. While the solution of the other elements proceeds during this early stage, signifying that $M_{23}C_6$ also contains these elements, most of the tungsten, molybdenum and vanadium and part of the chromium go into solution above 2000°F. Here the $M_{23}C_6$ has disappeared, the MC remains constant and the M_6C is decreasing. Therefore, the M_6C phase certainly contains tungsten, molybdenum, chromium and vanadium. Other evidence²⁵ not considered here shows that most of the tungsten and molybdenum in the carbides is associated with the M_6C phase, while MC is a vanadium-rich phase.

The curve in Fig 4 showing the partition of carbon between the matrix and the carbides must be regarded as very approximate. The values plotted are admittedly questionable because the carbon analyses of the carbide residues tend to be high in view of the free carbon that precipitates during electrolysis of the quenched samples. The other partition curves in Fig 4 do not suffer from this uncertainty.

Conclusions

1. Two electrolytic methods have been studied for the quantitative isolation of carbides from M-2 high speed steel. The double citrate cell, with continuous filtration of the anolyte, yields quantitative extractions for annealed low alloy as well as high speed steels. This is established on the basis that (a) the theoretical carbon content of cementite is found in the extracted residues of annealed low alloy steels, and (b) the total carbon of these steels and of annealed M-2 steels is accounted for in the residues.

2. The citrate cell possesses the experimental disadvantage, aside from its complexity, that portions of the

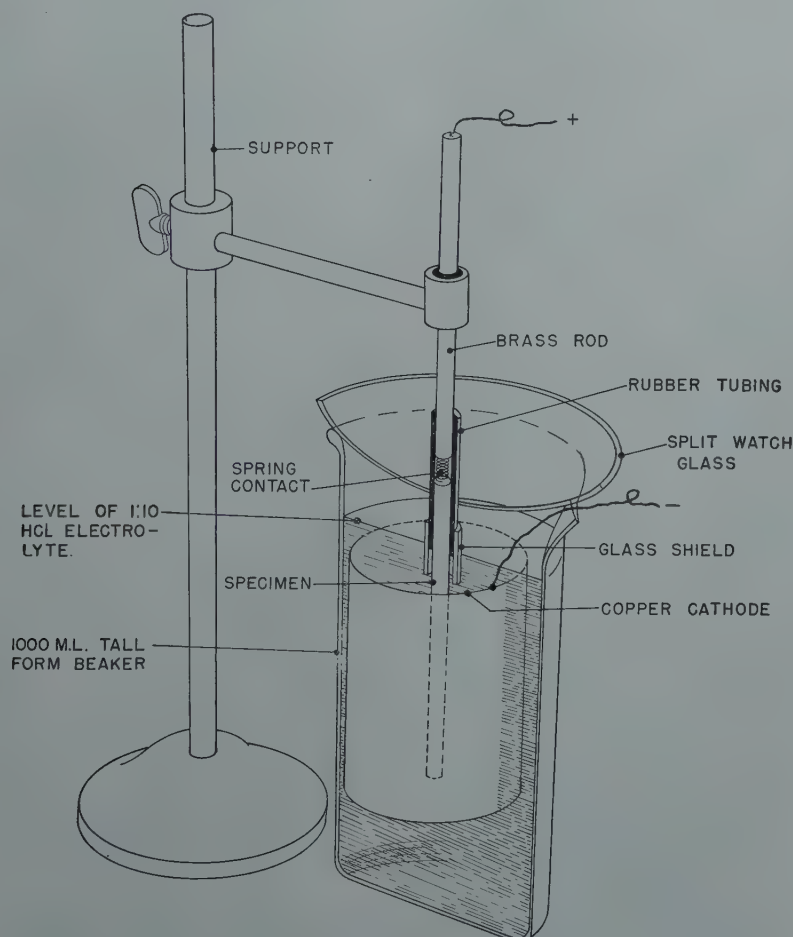


FIG 3—Schematic diagram of hydrochloric acid cell for electrolytic isolation of carbides.
Electrolyte: 1:10 hydrochloric acid.

matrix of high alloy steels may not dissolve during the electrolysis and may thus contaminate the carbide residue. This characteristic becomes more pronounced, the higher the austenitizing temperature. Because the steel particles are ferromagnetic and the carbides are not, it is possible to effect a magnetic separation. However, this procedure is not convenient with the citrate cell.

3. Electrolysis in a simple 1:10 hydrochloric acid cell reduces the extent of the above contamination, and when it does occur, the particles of base metal can be separated reliably with a magnetic method. The hydrochloric acid cell yields quantitative extractions on annealed M-2 steel as shown by the fact that (a) all the carbon in the steel is accounted for in the residue, and (b) the measured densities of the carbide residues are in good agreement with the calculated values based on lineal analysis of the solid steel. The magnetic separation procedure is also quantitative since the total amount of each alloying element in the residue plus electrolyte checks that present originally in the steel.

4. In the electrolysis of hardened M-2 steel, both cells precipitate free carbon from the martensite-austenite matrix. The presence of free carbon lowers the observed density of the carbides extracted from quenched specimens but is not sufficient in weight to have a significant effect on the weight percentage or composition (except for carbon) of the carbides. The carbon values reported for such carbides are undoubtedly high.

5. Three face-centered cubic carbides exist in M-2 steel: M_6C which is based on a complex iron-tungsten-molybdenum carbide, $M_{23}C_6$ which is essentially a chromium-rich carbide, and MC which is a vanadium-rich carbide. $M_{23}C_6$ dissolves completely on austenitizing at temperatures above 2000°F; M_6C dissolves partially, and MC hardly at all. Curves are presented showing the quantitative solution of these carbides and the corresponding partition of the elements between the carbides and the matrix.

Acknowledgments

The authors are grateful to the Vanadium-Alloys Steel Co. for a grant-in-aid to finance this research, for furnishing the steels to be investigated, and for making most of the chemical

analyses. The cooperation of Dr. George A. Roberts, Chief Metallurgist of the above Company, is sincerely appreciated.

References

1. J. P. Gill: High Speed Steel, Carbide Segregate and Grain Size. Campbell Mem. Lecture, *Trans. A.S.M.* (1936) 24, 736.
2. R. F. Mehl: The Decomposition of Austenite by Nucleation and Growth Process. Third Hatfield Mem. Lecture, *Jnl. Iron and Steel Inst.* (1948) 159, No. 2, 113.
3. F. Abel: Final Report on Experiments bearing upon the Question of the Condition in which Carbon Exists in Steel. *Proc. Inst. of Mech. Eng.* (1885) 30.
4. F. C. G. Müller: Grundzüge einer Theorie des Stahls. *Stahl u. Eisen* (1888) 8, 291.
5. J. O. Arnold and A. A. Read: The Chemical Relations of Carbon and Iron. *Jnl. Chem. Soc.* (1894) 65, 788.
6. E. D. Campbell: A Pure Carbide of Iron. *Amer. Chem. Jnl.* (1896) 18, 836.
7. E. C. Bain and M. A. Grossmann: The Nature of High Speed Steel. *Jnl. Iron and Steel Inst.* (1924) 110, 249.
8. W. Crafts and C. M. Offenhauer: Carbides in Low-chromium Steel. *Trans. AIME* (1942) 150, 275.
9. W. Crafts and C. M. Offenhauer: Carbides in Low Chromium-molybdenum Steels. *Trans. AIME* (1943) 154, 361.
10. A. P. Gulyaev: Phase Analysis of Steel. *Zavodskaya Lab.* (1946) 12, 9.
- 10a. A. P. Gulyaev: A Study of the Phase Composition of High Speed Steels. *Stal* (1946) 6, 188.
11. W. Crafts and J. L. Lamont: Secondary Hardening of Tempered Martensitic Alloy Steel. *Trans. AIME*

- (1949) 182, 471. *Met. Tech.* (Sept. 1948) TP 2439.
12. E. D. Campbell: The Constitution of Carbon Steels. *Jnl. Iron and Steel Inst.* (1908) 78, 318.
13. A. Hultgren: The Isothermal Decomposition of Austenite. *Trans. A.S.M.* (1947) 39, 915.
14. R. Treje and C. Benedicks: A Method for the Electrolytic Extraction of Slag from Iron and Carbon Steel. *Jnl. Iron and Steel Inst.* (1933) 128, No. 2, 205.
15. E. Houdremont, P. Klinger and G. Blaschczyk: A New Electrolytic Isolation Method for the Determination of Iron Carbide. *Arch. f. Eisenhütt.* (1941) 15, 257.
16. R. T. Howard, Jr. and M. Cohen: Quantitative Metallography by Point-counting and Lineal Analysis. *Trans. AIME* (1947) 172, 413; *Met. Tech.* (Aug. 1947) TP 2215.
17. V. Reilly and W. E. Reay: Physico-Chemical Methods. Methuen and Co., London (1943) pp. 475-479.
18. S. G. Fletcher and M. Cohen: The Effect of Carbon on the Tempering of Steel. *Trans. A.S.M.* (1944) 32, 333. Cf. reply to discussion of this paper.
19. A. Westgren and G. Phragmen: On the Double Carbide of High Speed Steel. *Trans. A.S.S.T.* (1928) 13, 539.
20. M. Cohen and P. K. Koh: The Tempering of High Speed Steel. *Trans. A.S.M.* (1939) 37, 1015.
21. A. Westgren: Complex Chromium and Iron Carbides. *Nature* (1933) 132, 480.
22. F. Morral, G. Phragmen and A. Westgren: Carbides of Low Tungsten and Molybdenum Steels. *Nature* (1933) 132, 61.
23. E. Mauer, T. Doring and W. Pulewka: One or Two Vanadium Carbides in Steel. *Arch. Eisenhut.* (1940) 13, 336.
24. B. S. Lement and M. Cohen: The Tempering of Two High-Carbon, High-Vanadium High Speed Steels. *Trans. A.S.M.* (1942) 30, 1021.
25. Paper being submitted to A.S.M. (1949).

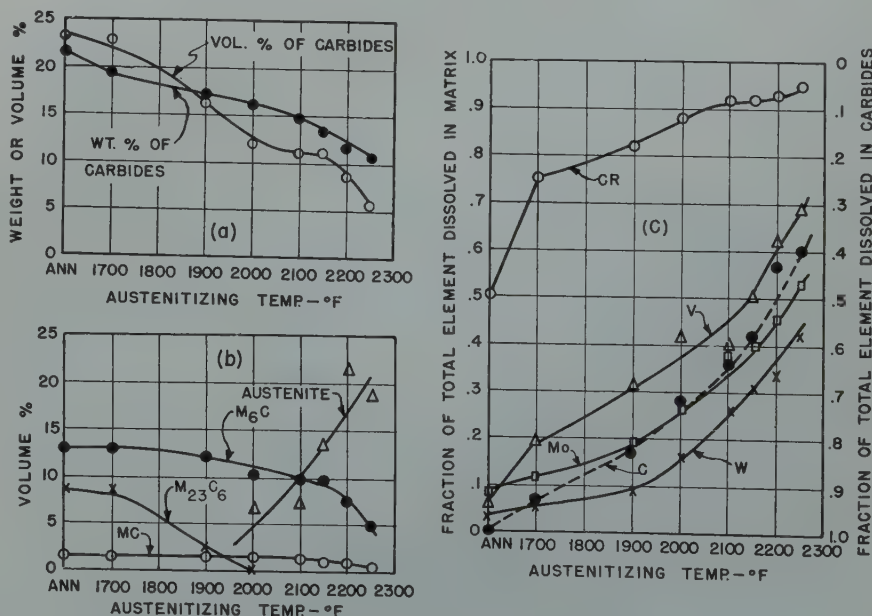


FIG 4—Effect of austenitizing temperature on (a) weight and volume percentages of carbides, (b) amounts of the individual carbides and retained austenite, and (c) partition of elements between carbides and matrix.

M-2 high speed steel (Steel A, Tables 1 and 4).

Solubility of Titanium in Liquid Magnesium

K. T. AUST* and L. M. PIDGEON*

There has been considerable interest in the possible use of titanium in magnesium alloys.¹ Zirconium has shown some promise in this connection² and its general similarity with titanium suggests that the latter might act in a similar manner. A literature survey revealed that quantitative data on the Mg-Ti system was unavailable. Several patents³ have claimed that titanium additions from 0.2 to 4 pct to magnesium alloys were possible, but no mention was made as to the form in which the titanium existed in the alloy. Kroll⁴ succeeded in introducing only traces of titanium into magnesium by bubbling $TiCl_4$ through the metal under argon or by reacting it with sodium titanium fluoride. The application of theoretical data given by Carapella⁵ based on Hume-Rothery's principles, involving atomic size factor, crystal structure, valency and the electro-chemical factor, suggests that a Mg-Ti alloy is a favorable case, and the system appeared to warrant experimental examination.

Experimental Procedure and Results

THERMAL ANALYSIS

If titanium is appreciably soluble in magnesium, a change in the melting point of the magnesium might be detectable using standard cooling curve methods. Magnesium was melted in graphite crucibles under an argon atmosphere, the assembly being enclosed in a silica tube. Graphite thermocouple protection tubes served also to stir the melts. The apparatus was very similar to Fig 1, with the addition of a refractory and baffle system to prevent undue heat losses from the top of the crucible. Chromel-alumel thermocouples were calibrated using Al of 99.97 pct purity.

Dominion Magnesium Limited sup-

plied redistilled high purity magnesium of the analysis given above.

Titanium was added in three different forms:

1. Titanium powder -100 mesh, from the Titanium Alloy Manufacturing Co., Niagara Falls, N. Y.

2. Sheet titanium from the U.S. Bureau of Mines, produced by Mg reduction of $TiCl_4$.

3. Magnesium -50 pct titanium master alloy from Metal Hydrides Inc., Beverly, Mass.

The melting point of the high purity magnesium used was measured experimentally as 651.0°C. More than a dozen tests were conducted using titanium from the three sources referred to above, in calculated additions up to 20 pct titanium, at temperatures between the melting point and 1000°C and holding periods up to 6 hr. In no case was evidence obtained of solubility of titanium in magnesium, using inverse-rate and time-temperature curves. The melting point of the magnesium was unchanged within the accuracy of measurement, namely $\pm 0.5^\circ\text{C}$; and no other thermal arrests were detected.

Metallographic investigation of the thermal analysis billets indicated that the titanium additions were apparently mechanically entrapped in the magnesium in segregated areas. Consequently, these samples were not analyzed for titanium. The master alloy proved to be a mechanical mixture of titanium particles in a magne-

sium matrix.

These results indicated that the titanium solubility, if such existed, could not be obtained by the usual thermal methods.

X RAY DIFFRACTION INVESTIGATION

In an effort to detect solubility of titanium in magnesium, samples were investigated using both the Debye-Scherrer and the Focusing Back-Reflection methods. Filings from samples of the thermal analysis billets and from pure magnesium were annealed in argon one hour at 350°C to relieve mechanical strain. Measurements made of the interplanar spacings showed no difference between the Mg-Ti samples and pure magnesium. The interplanar spacings could be measured to within 0.0002Å, and the greatest variation found was 0.0004Å, in the back-reflection method. The diffraction lines for magnesium were not shifted by the titanium additions indicating that the solid solubility of titanium in magnesium is of a very low order—less than 0.5 pct. From both diffraction methods, a d or interplanar spacing of 0.817Å was obtained for the redistilled high purity magnesium. This latter value is not given in the standard X ray diffraction cards for magnesium metal or vacuum distilled magnesium. Theoretical calculations for a close-packed hexagonal space lattice for magnesium indicate that the planes {2134} should give a line which was found. The relative intensity for this reflection at 0.817Å is slightly less than that at 0.870Å for magnesium.

SOLUBILITY OF TITANIUM IN LIQUID MAGNESIUM

The Mg-Mn system was examined by Grogan and Haughton⁶ who were

| Al | Mn | Fe | Ni | Cu | Si | Pb | Ca | Mg |
|-------|---------|--------|-------|--------|--------|-------|--------|---------------|
| 0.007 | <0.0005 | 0.0013 | 0.001 | 0.0005 | 0.0012 | 0.004 | <0.004 | 99.98 minimum |

Cleveland Meeting, October 1949.
TP 2680 E. Discussion of this paper
(2 copies) may be sent to *Transactions*
AIME before December 1, 1949.
Manuscript received Nov. 18, 1948;
revision received May 20, 1949.

* Department of Metallurgical Engineering,
University of Toronto.

¹ References are at the end of the
paper.

and 0.08 pct. These erratic analytical results suggested that finely divided titanium particles, despite the substantial density difference, do not settle readily in liquid magnesium and may not be employed as a source of titanium in liquid solubility tests. Titanium sheet, obtained from the U.S. Bureau of Mines, was used in the remainder of the tests.

Experimental Procedure

The apparatus used for the solubility tests is shown in Fig 1. Each charge consisted of 135 g of the high-purity magnesium and 15 g of titanium sheet. The titanium sheet was wrapped around the graphite thermocouple protection tube and kept in the molten magnesium during the holding periods at the desired temperature. The graphite protection tube also acted as a stirrer during the early portion of each holding period. It was assumed that titanium and graphite would not react to form titanium carbide in any appreciable quantity at the temperatures used in these solubility tests. Cylinder argon of commercial purity was passed through an oil filled bubbler, absorbent glass wool, anhydrous calcium chloride, and a "getter" furnace which contained magnesium chips at 600°C to remove oxygen and nitrogen. The purified argon passed to the system through the steel tube as shown, and escaped to a water trap and bubbler, maintaining a positive pressure of argon in the melt chamber. A chromel-alumel thermocouple was placed in the top part of the melt and the temperature was maintained within $\pm 5^\circ\text{C}$ by an automatic temperature controller.

Sampling

After each holding period, the Ti sheet was lifted from the melt and a steel sampling tube was quickly lowered into the top half of the melt. A liquid sample was pulled into the tube by a static vacuum sufficient to remove samples ranging from 2 to 5 g. After removal from the melt, the steel was stripped from the magnesium, and the entire sample analyzed for titanium except for a very small portion taken for metallographic purposes. Drillings were taken from the top section of the solidified billet to obtain the solubility at the freezing point. The analysis of titanium in magnesium was done colorimetrically using an adaptation of a well-known color reaction.¹² The method was calibrated with a standard titanium solution prepared from ti-

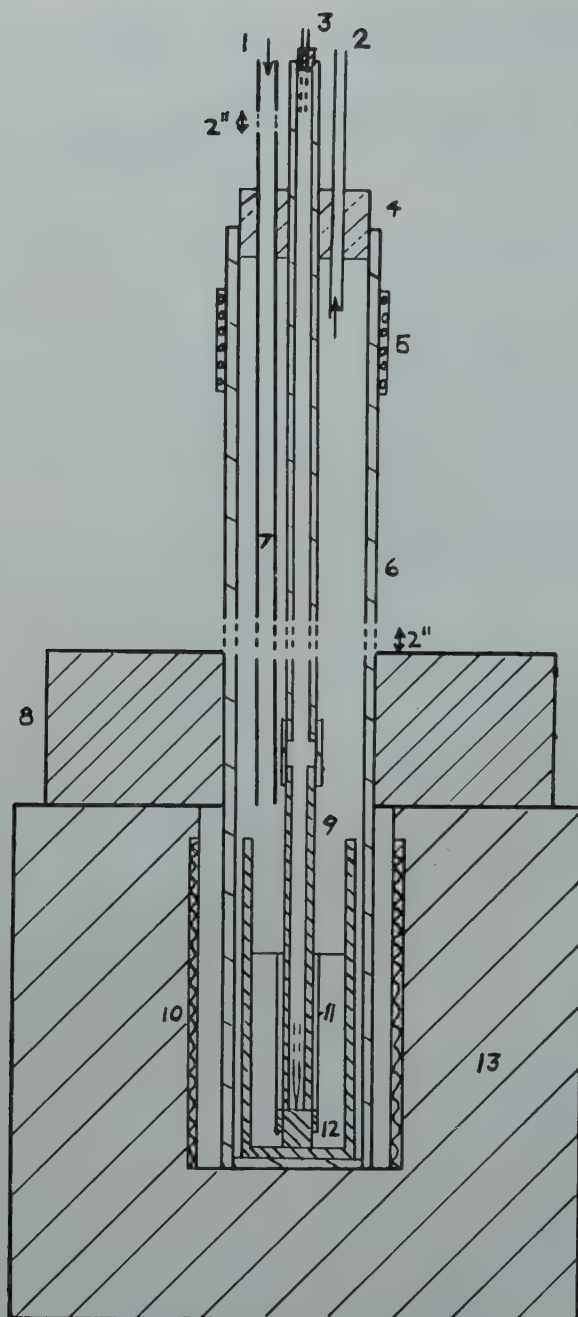


FIG 1—Liquid solubility apparatus.

- | | |
|-------------------------------|--------------------------|
| 1. Argon Inlet | 8. Refractory |
| 2. Argon Outlet | 9. Graphite Thermocouple |
| 3. Thermocouple Tube | Tube and Crucible |
| 4. Rubber Stopper | 10. Furnace Coil |
| 5. Water Cooled Cu Coil in Pb | 11. Ti Sheet |
| 6. Steel Tube | 12. Melt (Mg) |
| 7. Steel Sampling Tube | 13. Furnace Refractory |

unable to determine the liquidus line by thermal analysis, since it was found impossible to obtain any definite evidence of arrest points. The liquidus line, however, was successfully determined by the analysis of dip samples taken from the top of the melt at definite temperatures. This method has proved satisfactory where the primary insoluble crystals separating from the liquid have a different density from the liquid. A similar technique was used by Fink and Van Horn⁷ to determine the liquidus line for the Al-Ti system and

has also been employed by other investigators.^{8,9,10,11} It was decided to apply this method to the Mg-Ti system.

In preliminary tests, titanium powder was added to liquid magnesium under an argon atmosphere. Analytical results on these dip samples showed gross segregation. For example, titanium analyses of triplicate portions from a test that had been held at 850°C for 8 hr gave 0.012, 0.57 and 0.052 pct, while another group which had been held at 700°C for 8 hr showed 0.28, 0.01

tanium dioxide (NBS Std 154). A blank run of the apparatus with no titanium introduced gave no indication of titanium which, under the conditions of the method, means a content of less than 0.001 pct. None of the other elements present in the magnesium in normal amounts interferes with the analysis.

Experimental Results

If incomplete separation of melt and solid had taken place, the liquid samples as withdrawn might contain some of the solute metal as solid particles. If such had occurred, erratic results would again have appeared, the presence of such an error would be obvious, and those samples would be disregarded. The analytical results obtained on different samples from the same test strongly support the belief that the titanium found was in solution when the sample was taken from the melt (Table 1). The average results are plotted in Fig 2. Fig 3 is a typical photograph taken from the cross-section of the liquid solubility samples. Small dark particles of Ti which have come out of solution on cooling from the sampling temperature to the freezing point may be seen. Magnesium samples without titanium additions did not show this second phase. The even size and distribution of these particles support the belief that they were in solution at the sampling temperature.

Table 1. Experimental Results

| Test No. | Temp. °C | Holding Time, Hours | Pct | Titanium |
|----------|----------|---------------------|--------|----------|
| 35 | 651 | | 0.0027 | 0.0027 |
| 46 | 651 | | 0.0028 | 0.0023 |
| 40 | 651 | | 0.0043 | 0.0025 |
| 42 | 651 | | 0.0020 | 0.0013 |
| 42 | 700 | 48 | 0.0062 | 0.0066 |
| 35 | 775 | 24 | 0.011 | 0.010 |
| 40 | 775 | 24 | 0.013 | |
| 41 | 850 | 24 | 0.015 | 0.019 |
| 46 | 850 | 48 | 0.015 | 0.014 |

Conclusions

1. The solubility of titanium in liquid magnesium is extremely small, increasing approximately from 0.0025 pct at the freezing point of magnesium to 0.015 pct at 850°C. This titanium solubility is far less than that reported for zirconium¹³ or for iron in magnesium.¹⁴

2. Solid solubility of titanium in magnesium could not be detected using X ray diffraction methods.

3. The freezing point of redistilled high-purity magnesium is 651.0°C.

4. An interplanar spacing or d value was obtained for magnesium, 0.817Å, a value which has not been reported in the standard X ray diffraction card index system.

Acknowledgments

The financial assistance received from the Ontario Research Council is gratefully acknowledged by the junior author (K. T. Aust). The authors are indebted to Mr. R. G. Ernst, Research Chemist of the United States Metals Refining Co., N. J., for the titanium analyses, and to Dr. E. J. Allin of the Department of Physics, Toronto, for advice in the X ray analysis.

References

1. Exploratory Investigations of Ti Additions to Mg Alloys. Bur. of Mines, Ottawa, July 31, 1947. Unpublished.
2. C. Bull: Outstanding Properties of the Mg-Zr Alloys. *Metallurgia* (1947) 35 (207) 125-129.

3. Burkhardt, Riederer: U.S. Pat. 2,251,266, Aug. 5, 1941. Christen: U.S. Pat. 2,340,795, Feb. 1, 1944.
4. Kroll: Rare Metals as Constituents in Light Alloys. *Light Metal Age* (1945) 3, No. 12, 23-30.
5. L. A. Carapella: Fundamental Alloying Nature of Mg. *Metal Progress* (Aug. 1945) No. 48.
6. Grogan, Haughton: Alloys of Mg. *Jnl. Inst. Metals* (1943) 69, 241.
7. Fink, Van Horn, Budge: Constitution of High-Purity Al-Ti Alloys. *Trans. AIME* (1931) 93, 421.
8. N. Tiner: Solubility of Mn in Liquid Mg. *Trans. AIME* (1945) 161, 351.
9. Fink, Willey: Equilibrium Relations in Al-Zr Alloys of High-Purity. *Trans. AIME* (1939) 133, 69.
10. Kemp, Van Horn: Solubility of Pb and Bi in Liquid Al and Al-Cu Alloys. *Trans. AIME* (1939) 133, 81.
11. G. Edmunds: Liquidus Determinations in Zinc-rich Alloys. *Trans. AIME* (1944) 156, 263.
12. E. B. Sandell: Colorimetric Determination of Traces of Metals. P. 420—Interscience Publ. Inc. (1944).
13. Nowotny, Wormnes and Mohrnhelm: Investigation in the Systems Al-Ca, Mg-Ca, Mg-Zr. *Ztsch. Metal.* (1940) 32 (2), 39-42.
14. D. W. Mitchell: Solubility of Fe in Liquid Mg. *Metals Tech.* Jan. 1948. TP 2309: *Trans. AIME* (1948) 175, 570.

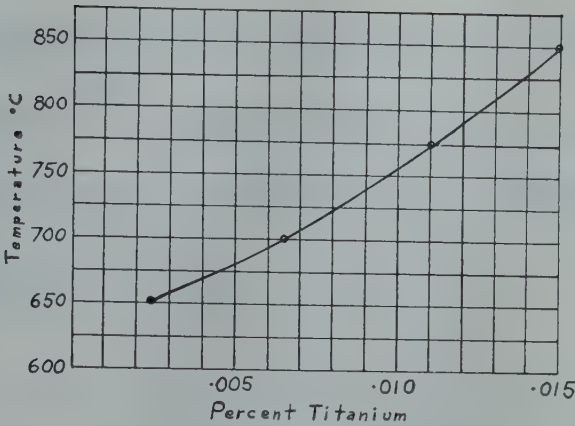


FIG 2—Solubility of Ti in liquid Mg.



FIG 3—Cross-section of typical solubility sample showing precipitated Ti in Mg.

× 150. Etched with 10 pct sodium bicarbonate.

The Lattice Parameters of High Purity Alpha Titanium; and the Effects of Oxygen and Nitrogen on Them*

HOWARD T. CLARK, JR.,† Member AIME

Introduction

Within the last twenty years at least three sets of lattice constants for the room temperature (alpha, hexagonal close packed) phase of titanium have been reported in the literature. These values, summarized in Table 1, differ one from another by amounts far greater than can be explained on the basis of inaccuracies in parameter measurements.

This paper presents new values determined for high purity titanium. It also details the effect of two elements, oxygen and nitrogen, on these parameters and shows that two of the previously reported values are probably in error because of the presence of one or both of these elements in the material used for examination.

Preparation of Samples

The titanium‡ used for this study was prepared by the thermal decomposition of titanium tetraiodide⁷ on a hot titanium filament. This titanium rod was prepared for X ray examination by melting about 10 g in purified argon in an electric arc furnace on a cold hearth. This cast button was cold rolled to 0.040 in. thick sheet, cleaned, annealed in vacuum at 1000°C and cold rolled to 0.020 in. thickness. About 0.003 in. of surface material was then removed by hand grinding on papers to remove any contamination caused by the rolls and the sample was bent to the radius of the focusing camera. The sample was then vacuum annealed at 600°C, a temperature just high enough to cause recrystallization, producing a fine grained structure. Such a structure is essential in sheet

Table 1 . . . Summary of Literature† Values of Alpha Titanium Lattice Parameters

| Worker | a_0 | | c_0 | | c/a |
|--------------------------------|-------|----------|-------|---------|-------|
| | KX | Å | KX | Å | |
| G. Haag ¹ | | 2.953 | | 4.729 | 1.60 |
| J. D. Fast ² | 2.945 | (2.951)* | 4.67 | (4.68)* | 1.59 |
| Greiner and Ellis ³ | 2.945 | (2.951) | 4.684 | (4.694) | 1.591 |

* Figures in parentheses have been calculated from the reported KX units for comparison (KX units $\times 1.00203$ = Angstroms).

† Since the preparation of this paper the following values for the lattice parameters of high purity alpha titanium have been published by Bruce W. Gonser (*Metals Progress* (1949) 55, p. 346):

$a_0 = 2.946$ KX units (2.952 Å), $c_0 = 4.686$ KX units (4.695 Å). A comparison of these values with those presented in this paper and with other literature values shown in Table 1 suggests that the X ray samples used by Gonser were contaminated with oxygen and/or nitrogen. This conclusion is based on the fact that his value of a_0 is approximately correct, but that his value of c_0 is extremely high compared with both Fast's value and the writer's, the writer's explanation for which is detailed in this paper.

specimens prepared for focusing cameras in order to have a sufficient quantity of grains to develop continuous diffraction lines.

The use of sheet specimens rather than powder samples appears to be essential for the X ray examination of titanium. This is because of titanium's exceptionally high gettering power and its rapid absorption of adsorbed gases, water vapor, and the like at annealing temperatures. While the effect of this contamination may be neglected for sheet specimens, its effect on 200–300 mesh powder is appreciable.

Titanium alloys of oxygen and nitrogen were prepared by a technique simi-

lar to that described above except that the required amount of the highest purity titanium oxide or nitride available was added prior to melting in the arc furnace. These materials were added by placing them in holes drilled in the titanium. A small weight loss invariably occurs during the melting of these oxygen and nitrogen alloys. This is believed to be due entirely to the loss of some of the powdered compound in the blast of the electric arc, an assumption which is justified on the basis that there is no weight loss during the melting of titanium metal and that wet analyses for nitrogen on representative samples have checked with the calculated analyses when it was assumed that the entire loss during melting was due to the loss of titanium nitride powder. These alloy buttons were reduced to sheet in the same manner as used for the unalloyed titanium.

Experimental Procedure

A North American Phillips 12 cm diam symmetrical precision focusing vacuum camera and copper radiation

Cleveland Meeting, October 1949.
TP 2656 E. Discussion of this paper (2 copies) may be sent to *Transactions AIME* before December 1, 1949. Manuscript received April 26, 1949.

* This paper is part of a dissertation to be presented by the author to the Faculty of the Graduate Division of the School of Engineering of Yale University in partial fulfillment of the requirements of the degree of Doctor of Engineering.

† Research Metallurgist, Remington Arms Co., Inc., Bridgeport, Conn.

¹ References are at the end of the paper.

‡ This material was prepared by Battelle Memorial Institute under contract for the Remington Arms Co., Inc.

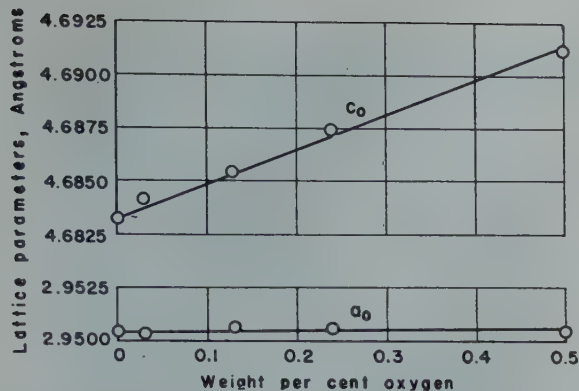


FIG 1—The effect of the addition of small amounts of oxygen on the lattice parameters of alpha titanium.

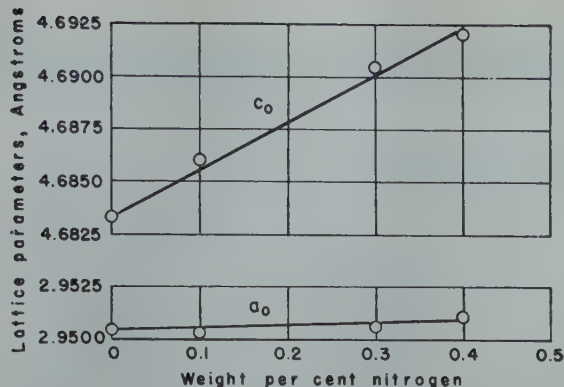


FIG 2—The effect of the addition of small amounts of nitrogen on the lattice parameters of alpha titanium.

were used for all determinations. The films were measured with a conventional measuring unit employing a micrometer screw with a drum graduated in 0.002 mm divisions. Calculations were made using Cohen's⁵ least squares method. The results were analyzed for probable error by the Jette and Foote⁶ method. Table 2 summarizes a typical calculation, the details of which are obvious if reference is made to Cohen's and Jette and Foote's papers.

Table 2 . . . Details of Calculation for Titanium Sample No. 4

Cu $K\alpha_1 = 1.540522 \text{ \AA}$ Cu $K\alpha_2 = 1.544367 \text{ \AA}$
Cu $K\beta_1 = 1.39218 \text{ \AA}$

| Line | Plane | Experimental $\sin^2 \theta$ | Calculated $\sin^2 \theta$ | $\sin^2 \theta \times 10^6$ |
|-----------------------------------|-------------------|------------------------------|----------------------------|-----------------------------|
| 1 | (0006) α_1 | 0.97399 | 0.97400 | - 1 |
| 2 | (0006) α_2 | 0.97400 | 0.97401 | - 1 |
| 3 | (3032) α_1 | 0.92587 | 0.92592 | - 5 |
| 4 | (3032) α_2 | 0.92592 | 0.92592 | 0 |
| 5 | (1233) α_1 | 0.87953 | 0.87939 | +14 |
| 6 | (1233) α_2 | 0.87950 | 0.87939 | +11 |
| 7 | (1234) β_1 | 1.06873* | 1.06877 | - 4 |
| 8 | (2025) β_1 | 1.03963 | 1.03964 | - 1 |
| 9 | (3030) α_1 | 0.81741 | 0.81752 | -11 |
| 10 | (3030) α_2 | 0.81753 | 0.81752 | + 1 |
| $a_0 = 2.9503 \pm 0.0005^\dagger$ | | | | |
| $c_0 = 4.6827 \pm 0.0004$ | | | | |
| $c/a = 1.587$ | | | | |

* Values of $\sin^2 \theta$ greater than 1.0 result from the conversion of measured values of $\sin^2 \theta$ to equivalent Cu $K\alpha_1$ values.

† A probability of 0.05 has been taken for determining limits of accuracy.

Room temperature remained fairly constant at about $25 \pm 2^\circ\text{C}$ during these exposures. The camera is so constructed that the synchronous motor used to oscillate the sample does not appreciably increase the sample temperature.

Experimental Results

Table 3 lists the lattice parameters of several different samples prepared from different titanium tetraiodide decomposition runs and reduced to sheet as discussed above. All values for both a_0 and c_0 agree very well.

Oxygen and nitrogen form interstitial solid solutions with alpha titanium, and, as would be expected for interstitial solutes, increase the titanium parameters. The amount of this change produced by each of these elements is shown in Fig 1 and 2 respectively.

Discussion of Results

It will be noted in examining Fig 1 and 2 that the addition of the common contaminants to alpha titanium expands the lattice in the c direction much more than in the a direction. With this in mind, it is interesting to look again at Table 1 and to compare the values presented there with those of Table 3. Such an examination leads to the following conclusions:

1. Fast's values, which were determined on titanium prepared by the same method used for preparing the titanium employed in this investigation, agree with the writer's values.

2. All reported values of a_0 agree within reasonable limits, a condition which is to be expected.

3. The reported values of c_0 vary greatly, the two values reported by Haag and Greiner and Ellis being appreciably higher than the values re-

ported here and by Fast. Greiner and Ellis worked with titanium⁷ produced by the Kroll⁴ process which is reported to have small amounts of manganese, magnesium, and silicon present. This material was prepared by powder metallurgy, and undoubtedly also contained oxygen and nitrogen picked up during both the reduction and the leaching and grinding operations, and diffused into the metal during sintering.

Conclusions

1. The lattice constants of alpha titanium are:

$$a_0 = 2.9504 \text{ \AA} \pm 0.0003$$

$$c_0 = 4.6833 \text{ \AA} \pm 0.0003$$

2. The lattice constants of alpha titanium, especially the value of c_0 , are increased appreciably by the addition of small amounts of oxygen or nitrogen.

Acknowledgments

Permission from the Remington Arms Co., Inc. to publish the data in this paper is acknowledged. Assistance was received from several members of the Remington Metals Research Unit, particularly J. A. Snyder on sample preparation, and P. F. Darby on the statistical analysis of the data.

References

1. G. Haag: *Ztsch. f. Phys. Chem.*, Sect. B, II (1931), 433.
2. J. D. Fast: *Rec. Trav. Chim.* (1939) 58, 972-983.
3. E. S. Greiner and W. C. Ellis: *Trans. AIME* (1949) 180, 657. *Metals Tech.* Sept. 1948, TP 2466.
4. U. S. Pat. No. 2,205,854, Kroll (1940).
5. M. U. Cohen: *Rev. Sci. Instr.* (1935) 6, 68-74.
6. E. R. Jette and F. Foote: *Jnl. of Chem. Phys.*, (1935) 3, 605-616.
7. U. S. Pat. No. 1,671, 213, Van Arkel et al (1928).

Table 3 . . . Lattice Constants of Several Different Samples* of Titanium

| Sample | a_0 | c_0 | c/a |
|---------|------------------------------------|------------------------------------|-------|
| 1 | 2.9508 \AA | 4.6834 \AA | 1.587 |
| 2 | 2.9498 \AA | 4.6836 \AA | 1.588 |
| 3 | 2.9509 \AA | 4.6837 \AA | 1.587 |
| 4 | 2.9503 \AA | 4.6827 \AA | 1.587 |
| average | 2.9504 \AA (2.9444 KX) | 4.6833 \AA (4.6737 KX) | 1.587 |

* Battelle's best estimate of the chemical composition of these iodide titanium samples is: titanium 99.95 pct, nitrogen 0.002 pct, oxygen undetermined, and carbon, iron, silicon, and aluminum each present in amounts less than 0.03 pct.

[illegible]

SEPTEMBER 1949

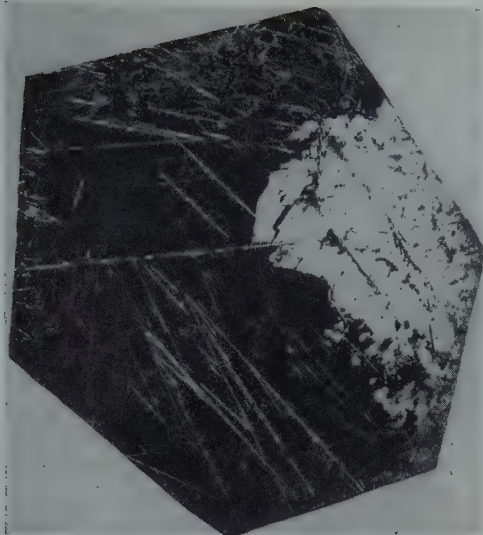


FIG 1—Martensite crystal in nickel steel.
White area is a single crystal of martensite; see text for details of specimen preparation. Etched with Nital. $\times 6$.

Most martensite crystals in steel are far too small for the above method to be practical. Judging from past experience, it was decided that the alloy that offered the best chance of success would be a steel containing about 22 pct nickel and 0.8 pct carbon. This alloy is all austenite at room temperature (even after very slow furnace cooling), and small amounts of martensite may be formed by cooling to -77°C . Accordingly, 35 separate 50-g melts of this alloy were prepared in a high-vacuum molybdenum-wound resistance furnace, using as raw materials a 1.3 pct carbon drill-rod steel and nickel shot.* Many ingots were remelted and all melts were solidified very slowly. Resulting austenite grain size averaged about 1 cm. Suitable ingots were cut and ground to form specimens about 1 cm cube, which were then given a metallographic polish on all six surfaces. Each specimen was carefully cooled by successive stages in mixtures of solid CO_2 and acetone; the cooling was halted after a few martensite crystals had formed. The largest martensite plates were about 2 or 3 mm^2 in area, and about 30 microns thick; most crystals were considerably smaller than this. Suitable specimens were then ground and carefully polished on a surface parallel to a single martensite plate, exposing the crystal for an area of 1 mm^2 or more. Four martensite crystals from 4 different ingots were prepared in this manner; the largest crystal of this group is illustrated in Fig 1. Back-reflection Laue patterns

* Most of the ingots were used to prepare specimens for shear studies, described in the second section of this report.

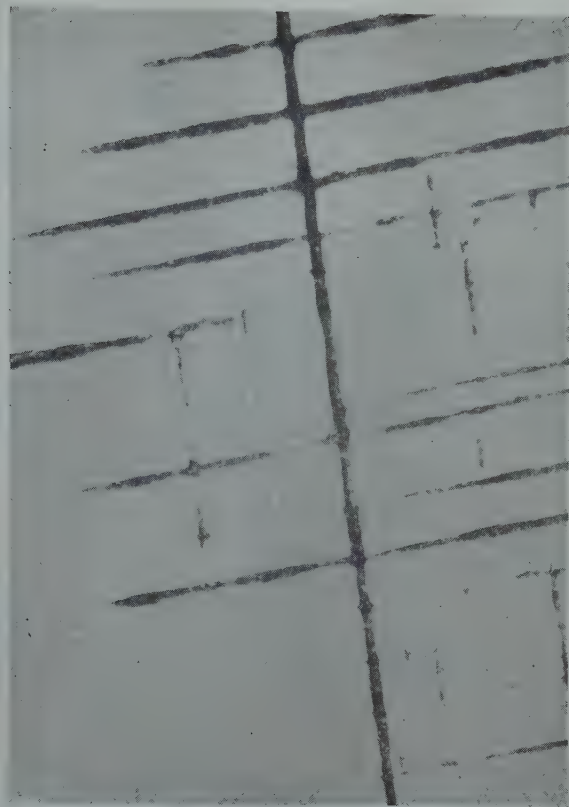


FIG 2—Martensite crystal of Fig 1.
Etched with Nital. $\times 1000$.

were obtained from martensite crystals and the matrix austenite both before and after tempering. The location of the basal plane pole of martensite was checked by means of oscillating crystal X ray patterns.

In addition to the above orientation work, several Debye X ray patterns were prepared from slivers (cut from the ingots utilized) deformed and recrystallized at 1100°C and then cooled to -195°C . Austenite lattice parameter was $3.592 \text{ \AA} \pm 0.005$; martensite parameters were $a_0 = 2.845 \text{ \AA}$, $c/a = 1.045$, both ± 0.005 .

RESULTS

All 4 martensite crystals studied yielded the same solution ($\pm 0.5^{\circ}$); these relationships are expressed in gnomonic projection in Fig 3. It will be noted that the (111) austenite plane is not parallel to the (101) of martensite; the planes are separated by an angle of about 1° . Likewise, no important zones are parallel. Except for the nonparallelism of these two closely packed planes, the evaluated relationship may be described as about midway between the Kurdjumov and Sachs and the Nishiyama relationships. The relationship shown in Fig 3 is for the untempered "tetragonal martensite"; in the process of tempering the relation-

ship changes slightly. The first evidences of tempering are observed in the back-reflection Laue patterns (after only 2 or 3 days at room temperature) by an elongating of the Laue spots on the $[11\bar{1}]$ zone. After a month at room temperature, these spots are considerably elongated, while the spots on both the $[\bar{1}11]$ and $[10\bar{1}]$ zones remain nicely rounded, but shift position slightly. After tempering 2 days at temperatures between 500 and 900°C ,* all spots from the tempered martensite crystal are well rounded, $(111)\gamma$ and $(101)\alpha$ are parallel, and the lattice relationship departs only about 1° from the Nishiyama relationship. Note that the slight change in lattice relationship that occurs during the tempering process (the approximate direction of shift is indicated by the small arrows in Fig 3) is decidedly not in the direction that one would expect from a simple change in axial ratio from 1.045 to 1.

The narrow, dark-etching bands illustrated in Fig 2 were found to be parallel to $\{112\}$; 6 trace normals were located and all of these deviated less than 2° from a $\{112\}$ pole of martensite. The bands are thus probably twin bands, which may have formed during

* After one-half hour at 1000°C , the tempered martensite disappears and the original all-austenite crystal is retained at room temperature; if the austenite is heated to 1100°C , it recrystallizes.

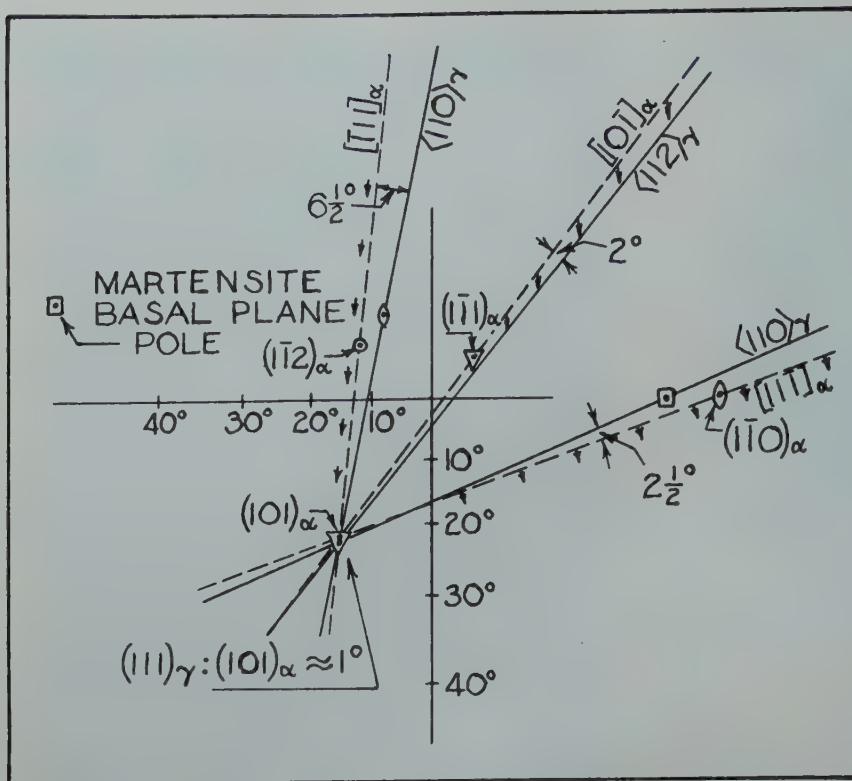


FIG 3—Orientation relationships between austenite and martensite in nickel steel. Relationships are projected gnomonically. Plane of projection is the plane of the martensite plate.

the polishing operation. Individual twin bands seldom are continuous across the midrib of a martensite crystal, and occasionally very small (less than 0.5°) angular differences are observed between bands on opposite sides of the midrib. It is safe to conclude that the midrib plane represents a discontinuity in the lattice of a martensite crystal.

The Martensite Shear*

If a suitable specimen of metastable austenite is polished metallographically and cooled to some subatmospheric temperature to form small amounts of martensite, the martensite may then be seen as a relief effect on the polished surface. This fact has been known for many years, but evidently no one has attempted to measure and analyze this relief.

Fig 4 and 5 illustrate the appearance of the relief formed by martensite in the steel used in the present investigation. A careful inspection of many of these "needles" led us to the conclusion that the relief is caused by a deformation that closely resembles homogeneous shear and that the shear must be in the plane of the martensite plate. Now, it

may readily be proved stereographically that it is impossible to transform a face-centered cubic lattice into a pseudobody-centered tetragonal lattice by a single shear. However, it is possible that two shears are involved in the transformation. If so, and if the first shear can be described by analyzing the martensite relief, then it should be possible to determine the remainder of the transformation mechanism by simple subtraction, inasmuch as the final result of the transformation is known from the lattice relationship and habit information given in Fig 3. Accordingly, attempts were made to analyze the visible martensite shear by methods outlined in Fig 11, Appendix A; the results of this analysis are summarized below.

RESULTS

Twelve martensite crystals in 3 specimens from 3 different ingots were studied. The results obtained for the direction of shear and the shear angle are shown by the small arrows and numbers on the primitive circle of Fig 6; the average γ_0 of the 12 measurements is 10.75° . The accuracy of an individual measurement is about $\pm 10^\circ$ in direction and about $\pm 2^\circ$ in angle. Some measurements were considerably better than this, notably the fifth arrow from the top in Fig 6, which is believed

good to within 5° in direction and 0.5° in angle. If a martensite crystal could be found having a surface like that shown in Fig 4 on two faces of a specimen, the direction could be evaluated to within less than 1° and the angle to within a few minutes. Unfortunately, no near-perfect martensite crystal of this type was found in the dozens of specimens examined, though, of course, only plates that were reasonably well formed were measured. The plates with perfect faces show a definite tendency to be grouped at the centers of the specimen surfaces, instead of at the edges where they must be if they are to be analyzed.

A continuation of the stereographic manipulation yielded the following important result: When the austenite lattice was deformed stereographically in accordance with the average experimentally determined direction and angle of shear, it was found that a second shear could transform this triclinic lattice into a pseudobody-centered tetragonal lattice of the same orientation and almost the same parameters as martensite (having an atomic volume equal to that of austenite). Furthermore, this second shear is on the (112) martensite plane in the $[11\bar{1}]$ direction; these are the elements for twin gliding in the body-centered cubic or tetragonal lattice. This second shear cannot, of course, be homogeneous on a macroscopic scale, though atomically it is; it must be confined to the volume of the triclinic lattice produced by the first shear. In the twinning shear of the body-centered cubic lattice, points on every sixth (112) layer are common to both the twinned and the untwinned lattices.¹⁴ In the second shear of the martensite mechanism, the shear angle (the optimum angle is between 12° and 13°) is about one-third as large as the shear angle for twinning, hence the second shear will take place in layers of about 18 atomic planes. The deformation of the austenite lattice into a martensite lattice by means of these two shears is illustrated stereographically in Fig 6,* and the data and results of calculations are summarized in Tables 1 and 2. An inspection of Tables 1 and 2 and of Fig 6 will reveal that the optimum calculated direction for shear No. 1 has been bracketed by directions A and B of Fig 6.

Another possibility for the second shear is that it be on $(123)_\alpha$ in the direction $[11\bar{1}]_\alpha$. These shear elements give

* Readers will find it advisable to examine Appendix A before continuing with this paper. Symbols, equations, and conventions are defined or derived in Appendix A.

* The stereographic portion of this analysis was carried out with the aid of a 15.75 in. diam stereographic net.

slightly better results than (112) and [111] but not sufficiently better to warrant their selection as the true elements. No better results are obtained with irrational shear planes and directions for the second shear.

The missing parameter that makes it impossible at present exactly to define the mechanism from beginning to end concerns the change in atomic volume. When a volume of austenite transforms to martensite, it increases about 4 pct in size; this volume increase is uninfluenced by carbon content (see Table 3). Shear can produce no change in volume; hence, a small but nonetheless important part of the transformation consists of an expansion. If the expansion occurs either at the beginning or end of the transformation, it would produce no change in orientation, and the spacing changes are readily calculated. If the expansion occurs during the transformation, it could have a maximum effect of about 1° on the resulting orientation of the martensite lattice. The "unexpanded martensite" interplanar spacings listed in Tables 1 and 2 were calculated from the measured martensite parameters of the steel used in this study, assuming that the expansion is merely one of a change in atom radius.

Most of the experimental results described above will be discussed in the following section.

The Mechanism of the Martensite Transformation

In the following is presented a brief exposition of the movement of atoms in a martensite transformation. The general statement is really nothing more than a rewording of the experimental results reported in this paper. Application of the theory in a specific case will provide a solution for both lattice relationship and orientation habit for any martensite transformation in steel occurring near room temperature or below. The probable effect of the temperature variable is predicted and it is pointed out that the most important problem awaiting solution is the complete experimental determination of the effect of temperature change on the mechanism of an individual martensite transformation.

GENERAL STATEMENT

In a martensite transformation, billions of atoms move from their positions on the matrix lattice to positions

Table 1 . . . Orientation and Spacing Changes Resulting from the Martensite Shears

| Before Shearing; Austenite Indices | After Shearing; Martensite Indices | Shear No. | Data | | | Calculated | | d-Values† Unexpanded Mart. | Deviation‡ in Degrees |
|------------------------------------|------------------------------------|-----------|-------------|-------------|------------------|-------------|-----------|----------------------------|-----------------------|
| | | | ρ | ϕ | α^\dagger | γ | α' | | |
| (200) | (002) | 1 | 34. ° | 20. ° | 1.796 | 6° 36' | 1.645 | 1.468 | 1 |
| | | 2 | 48.5 ° | 0. ° | 1.645 | 5° 12' | 1.470 | | |
| (022) | (020) | 1 | 153. ° | 49.5 ° | 1.270 | 6° 00' | 1.331 | 1.405 | 1 |
| | | 2 | 149.5 ° | 52. ° | 1.331 | 6° 22' | 1.410 | | |
| (022) | (200) | 1 | 136. ° | 70. ° | 1.270 | 2° 02' | 1.313 | 1.405 | 1 |
| | | 2 | 147. ° | 52. ° | 1.313 | 6° 06' | 1.396 | | |
| (220) | (112) | 1 | 31. ° | 33.5 ° | 1.270 | 6° 20' | 1.178 | 1.181 | 1 |
| | | 2 | No movement | 0. ° | 1.796 | 4° 08' | 1.972 | 1.987 | 1.3 |
| (002) | (110) | 1 | 125.5 ° | No movement | 2.074 | 1° 11' | 1.990 | 2.030 | 0.5 |
| | | 2 | 63. ° | 57.5 ° | 2.074 | No movement | 2.057 | 2.030 | 0.3 |
| (111) | (101) | 1 | 177.5 ° | 23. ° | 2.074 | 10° 12' | 2.079 | 2.030 | 1 |
| | | 2 | No movement | No movement | 2.074 | 0° 09' | 2.012 | 2.030 | 1 |
| (111) | (011) | 1 | 136. ° | 88.5 ° | 2.074 | 10° 48' | 2.125 | 2.030 | 1 |
| | | 2 | 4.5 ° | 32.5 ° | 2.079 | 7° 11' | 2.072 | 2.030 | 1 |
| (111) | (011) | 1 | 165.6 ° | 48. ° | 2.074 | 11° 00' | 1.781 | 1.987 | 1 |
| | | 2 | 2. ° | 32. ° | 2.125 | 2° 30' | 1.996 | | |
| (020) | (110) | 1 | 10. ° | 76.5 ° | 1.796 | 7° 34' | | | |
| | | 2 | 135.5 ° | 0.5 ° | 1.781 | | | | |

* Refer to Fig 6; shear No. 1 is on the plane of the martensite plate in the direction of Trial Shear "A" with $\gamma = 11^\circ$; shear No. 2 is on (112) α in the direction [111] α with $\gamma = 13^\circ$.
† Calculated from austenite $a_0 = 3.592 \text{ \AA}$.
‡ Calculated from Debye pattern of martensite after changing parameters to make atomic volume equal that of austenite; for unexpanded martensite: $a_0 = 2.810 \text{ \AA}$, $c/a = 1.045$.
§ Angle between the pole resulting from the shear movements and the corresponding martensite pole experimentally located (from the lattice relationship information given in Fig 3).

Table 2 . . . Orientation and Spacing Changes Resulting from the Martensite Shears

| Before Shearing; Austenite Indices | After Shearing; Martensite Indices | Shear No. | Data | | | Calculated | | d-Values† Unexpanded Mart | Deviation‡ in Degrees |
|------------------------------------|------------------------------------|-----------|-------------|-------------|------------------|------------|------------|---------------------------|-----------------------|
| | | | ρ | ϕ | α^\dagger | γ | α_1 | | |
| (200) | (002) | 1 | 31.5° | 9. ° | 1.796 | 7° 02' | 1.649 | 1.468 | 1.3 |
| | | 2 | 50. ° | 0. ° | 1.649 | 4° 51' | 1.475 | | |
| (022) | (020) | 1 | 153. ° | 60. ° | 1.270 | 4° 22' | 1.316 | 1.405 | 2.3 |
| | | 2 | 150.5 ° | 53. ° | 1.316 | 6° 24' | 1.390 | | |
| (022) | (200) | 1 | 134. ° | 61. ° | 1.270 | 2° 36' | 1.328 | 1.405 | 1 |
| | | 2 | 147.5 ° | 51. ° | 1.328 | 6° 20' | 1.413 | | |
| (112) | (220) | 1 | 31.5° | 42. ° | 1.270 | 5° 24' | 1.192 | 1.181 | 0.5 |
| | | 2 | No movement | No movement | | | | | |

* Refer to Fig 6. Shear No. 1 is on the plane of the martensite plate in the direction of Trial Shear "B" with $\gamma = 10.5^\circ$; shear No. 2 is on (112) α in the direction [111] α with $\gamma = 13^\circ$.
†,‡,§ See Table 1.

Table 3 . . . Atomic Volumes of Austenite and Martensite

| Pct Carbon | Temp Range* °C | Atomic Volume Cubic Angstroms per Atom | | $\frac{\text{At. Vol. Mart.}^\dagger}{\text{At. Vol. Aust.}}$ | Reference |
|------------------------------|-------------------|--|------------|---|-----------------------------------|
| | | Austenite | Martensite | | |
| Plain Carbon Steels | | | | | |
| 0.90 | 230° to 20° | 11.526 | 12.058 | 1.046 | Hägg ¹⁶ |
| 1.20 | 160° to 20° | 11.664 | 12.128 | 1.040 | Hägg ¹⁶ |
| 1.58 | 90° to 20° | 11.771 | 12.300 | 1.045 | Hägg ¹⁶ |
| 1.74 | 70° to 20° | 11.900 | 12.450 | 1.046 | Honda and Nishiyama ¹⁷ |
| 1.80 | 65° to 20° | 11.928 | 12.419 | 1.041 | Greninger (unpublished) |
| Nickel Steel (22 pct nickel) | | | | | |
| ~0.80 | −60° to −195° | 11.586 | 12.032 | 1.038 | this publication |

* Approximate temperature range in which martensite formed. See Ref 5.
† In pure iron, the ratio of the atomic volume of ferrite to that of austenite¹⁹ is: at 900°C, 1.007; at 20°C, 1.039. The average temperature coefficient of expansion of gamma iron is almost twice that of alpha iron. See Ref 18.

on the martensite lattice. This change in position can be described almost entirely by two homogeneous shears (if the transformation cannot be accomplished by one shear, as it can be for the transformation: hexagonal close-packed \rightleftharpoons face-centered cubic). The function of the first shear is to create a

lattice containing a unique set of parallel atomic planes whose interplanar spacing and atom positions are the same as those of a set of parallel atomic planes in the martensite lattice; a second shear, on this unique plane, will then be capable of generating the martensite lattice. In the usual case,

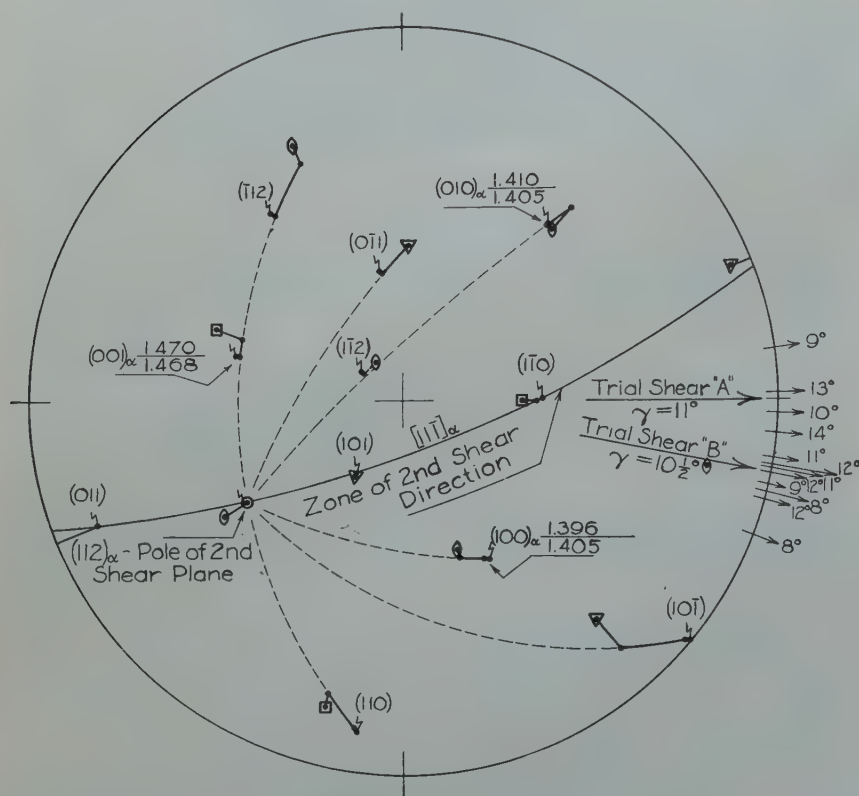
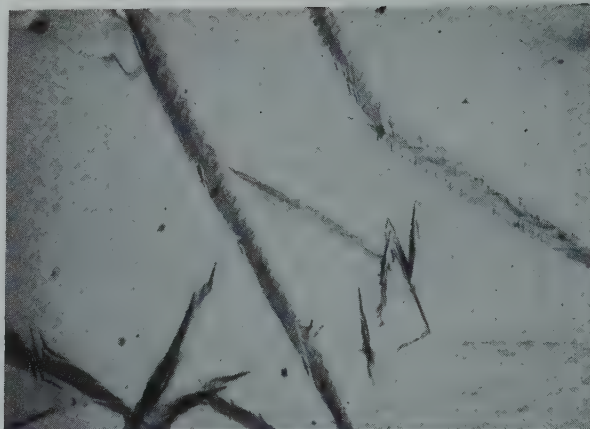
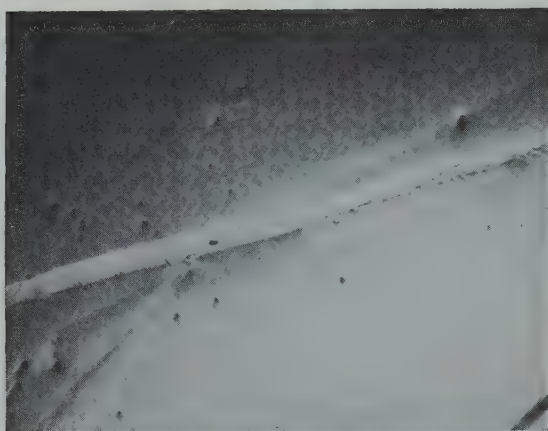


FIG 6—Stereographic projection illustrating the transformation from austenite to martensite by means of two homogeneous shears.

Plane of projection is the plane of the martensite plate (plane of shear No. 1). Small arrows and figures at the right represent the experimentally determined directions and angles of shear for shear No. 1. Trial shears "A" and "B" are directions for shear No. 2 assumed and for purposes of calculating orientation and spacing changes of planes in the austenite lattice. Squares, triangle, and oval designate $\{100\}$, $\{111\}$, and $\{110\}$ austenite poles respectively. Austenite and martensite poles were plotted from experimental data of Fig. 3. The travel of each austenite pole as a result of shear No. 1 is along an equatorial line; the additional shift resulting from shear No. 2 is along a great circle joining the pole of the second shear plane (see Tables 1 and 2). The numbers attached to indices of the axial planes of martensite are (1) numerators—interplanar spacings calculated from shear data—and (2) denominators—actual interplanar spacings of the "unexpanded martensite" lattice.

the complete transformation cannot be accomplished *precisely* by two shears; hence a very small readjustment will be needed, most logically after the first shear. The selection of planes and directions for the two shears will be governed by considerations of minimum shear angle and minimum readjustment. The second shear plane will probably be a low-indices plane of the martensite lattice, the first shear plane

(and direction) will be an irrational plane in the matrix lattice because its selection is governed by requirements that cannot be expressed in terms of the matrix lattice itself. The solution of the above problem begins with the selection of the second shear plane.

THE PLANE OF THE SECOND SHEAR

The designation of the second shear plane is arrived at from a comparison of

interplanar spacings of, and atom positions on, the lattice planes of the matrix and martensite lattices; the object is to designate a martensite plane that most easily may be generated from an austenite plane. This comparison must be made with due regard to the principles of lattice shear illustrated in Fig 10, Appendix A. For the transformation face-centered cubic \rightarrow body-centered cubic, the following combinations* are most probable; other possible combinations will have indices higher than those shown:†

- $$\begin{aligned} (a) \quad & (220)_\gamma \rightarrow (112)_\alpha \\ (b) \quad & (331)_\gamma \rightarrow (123)_\alpha \\ (c) \quad & (442)_\gamma \rightarrow (134)_\alpha \end{aligned}$$

If expression (a) can be fulfilled exactly, then expressions (b) and (c) cannot be. Actually, neither (a) nor (b) nor (c) can be fulfilled exactly; the differences in readjustments required by expressions (a) and (b) are so small that for the extension of this analysis, it makes no difference which of the two is selected, or which one actually operates as the second shear plane.

THE PLANE AND DIRECTION OF THE FIRST SHEAR

If $(220)_\gamma \rightarrow (112)_\alpha$ could be fulfilled exactly, the plane and direction of the first shear for minimum γ could be accurately determined mathematically. Actually, the expression cannot be exactly fulfilled, and the optimum plane and direction of the first shear are more readily located by trial-and-error meth-

* The expression $(220)_\alpha \rightarrow (112)_\gamma$ means: As a result of a single homogeneous shear in the austenite lattice, the orientation, the interplanar spacing, and the atom positions of the $(220)_\gamma$ plane become (very nearly) the same as those of the $(112)_\alpha$ plane.

† These expressions (with the direction of the arrows reversed) must also hold for the reverse transformation body-centered cubic \rightarrow face-centered cubic.

ods of stereographic manipulation; of course, there can be no single solution, but instead the shear plane will be located as a small area and the shear direction as a small oriented angle. The spread or scatter for the plane and for the direction will be a function of the readjustments required for the generation of $(112)_\alpha$. For the case of the martensite transformation illustrated in Fig 6, the permissible scatter for the pole of the shear plane was determined stereographically as about $\pm 4^\circ$ and for the shear direction about $\pm 5^\circ$; both of these agreed with those experimentally determined.

LATTICE RELATIONSHIPS

After the elements of the two shears have been determined, the resulting lattice relationship may be solved stereographically. For the transformation face-centered cubic to body-centered cubic, a pseudo body-centered tetragonal lattice of axial ratio greater than 1 will always form; for the reverse transformation, the tetragonal cell must have an axial ratio slightly less than 1 (see Fig 6). The continuation of the transformation to the final cubic form may be hindered by the presence of certain solute atoms;* notably, carbon is responsible for the retention of the tetragonal lattice of martensite in steel. For the martensite transformation in iron-nickel alloys, the tetragonal stage is not retained; we may confidently predict that for nickel contents above about 29 pct† this transformation will proceed along the same paths as the transformation shown in Fig 3, and that the final lattice relationships will be very close to the Nishiyama relationship.‡

THE EFFECT OF TEMPERATURE

It is quite likely that with an increase in the temperature of the transformation, there will be a tendency for the first shear elements to assume lower indices and higher symmetry. However, a change in the elements of the first shear will be possible only when the temperature of the transformation and thus the atomic mobility is increased sufficiently so that larger readjustments are possible. A stereographic

* It is probable that the temporary retention of the tetragonal transition lattice is always due to the proper ordering of solute atoms. The tetragonal lattice that results from the martensite transformation in β brass¹⁰ is remarkably stable; there is good reason to believe that quenched β brass is ordered.¹⁰

† See the first footnote in the next column.

‡ No explanation is advanced for the small lattice-relationship changes observed to occur during the change from tetragonal to cubic martensite, and illustrated in Fig 3.

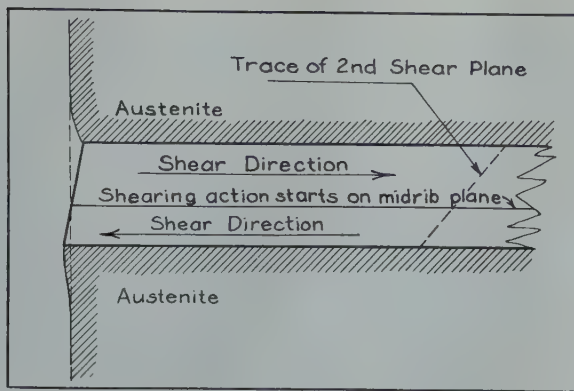


FIG 7—Origin of the martensite midrib.

solution for probable first-shear planes and directions of higher symmetry suggests that the shear plane should become $(422)_\gamma$ and the direction of shear $[\bar{1}\bar{1}\bar{1}]_\gamma$.* The resulting lattice relationship would then be $[110]_\gamma \parallel [11\bar{1}]_\alpha$, and $(111)_\gamma \cdot (101)_\alpha = 0^\circ$ to 3° , depending upon the directions of readjustment; the readjustments necessary are 3 to 5 times as great as those required by the "lowest temperature" mechanism shown in Fig 6. For still higher temperatures, the only probable change in the pole of the first shear plane would be along the $[01\bar{1}]_\gamma$ zone in the direction of $(111)_\gamma$ and for highest temperature, the first shear should be on $(111)_\gamma$ in the direction $[2\bar{1}\bar{1}]_\gamma$ —these are the elements of twinning shear for the face-centered cubic lattice. The above statements are based upon the assumption that the elements of second shear do not change with temperature; there should be no tendency for change, inasmuch as at lowest temperatures, the elements of the second shear are the same as those of the twinning shear in the body-centered cubic lattice. With increasing temperatures, there should be an increasing probability that actual twins will be produced in the body-centered cubic lattice.†

THE MARTENSITE MIDRIB

The plane of the martensite midrib represents a region of discontinuity in

* This predicted shear plane is located only 5° from the experimentally determined plane of martensite plates in plain carbon steel containing 0.9 to 1.4 pct carbon.⁹ Martensite of this habit is also formed in iron-nickel-carbon alloys in certain composition ranges. Martensite in iron-nickel alloys has the "lowest temperature" irrational habit for nickel contents above about 29 pct nickel; for lower nickel contents the habit is octahedral, but poorly developed.

† Abundant twinning results from the $\gamma \rightarrow \alpha$ transformation in iron; see Ref. 15. For the martensite transformation: body-centered cubic \rightarrow hexagonal close-packed, the plane of second shear is $(10\bar{1}\bar{1})$, and polysynthetic twinning on $(10\bar{1}\bar{1})$ results from this transformation at moderately low temperatures; see Ref. 6.

the lattice of a martensite crystal.* The manner in which this plane of discontinuity probably originates is illustrated in Fig 7. Shearing action starts on the plane of the midrib, and is propagated in parallel but opposite directions on both sides of this plane. The final tetragonal crystal could be identical and continuous on both sides of the midrib plane if the transformation could be completed without readjustments. The small readjustment that must occur would permit a difference in orientation of about 0.5° , hence a discontinuity at this plane of contact. An additional and probably more important consideration is that it is very unlikely that the shear can be perfect near its plane of origin when it must be propagated on both sides of this plane.

Summary

An X ray and microscopic study of the martensite transformation in steels containing about 22 pct nickel and 0.8 pct carbon has been made, and a brief exposition of the movement of atoms in this martensite-type transformation has been advanced. The martensite crystal is formed from an austenite crystal almost entirely by means of two homogeneous shears. The function of the first shear is to create a lattice containing a unique set of parallel atomic planes whose interplanar spacings and atom positions are the same as those of a set of planes in the martensite lattice; a second shear on this unique plane will then generate the martensite lattice.

The theory predicts both lattice relationships and orientation habits for martensite transformations. The two

* See p. 592. Another fact supports this statement: The midrib plane is the region where carbon first precipitates when martensite is tempered.

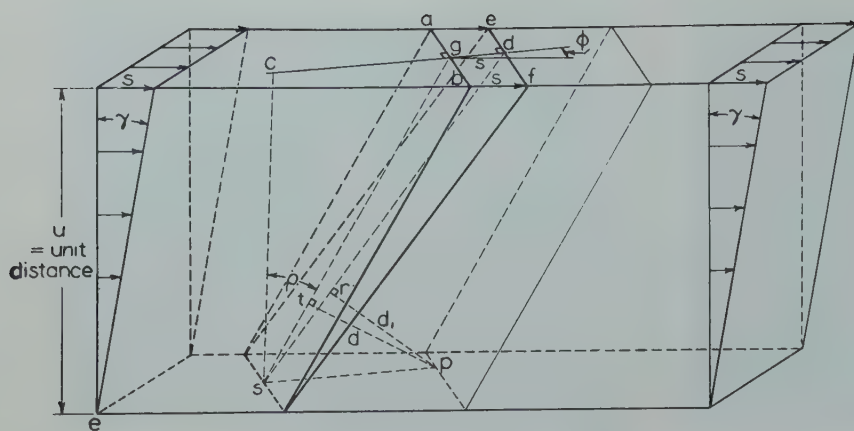


FIG 8—Parallel perspective of homogeneous shear.

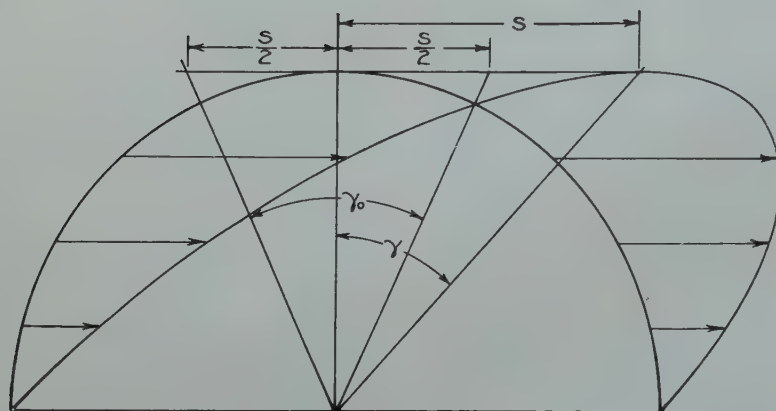


FIG 9—Deformation of a circle into an ellipse.

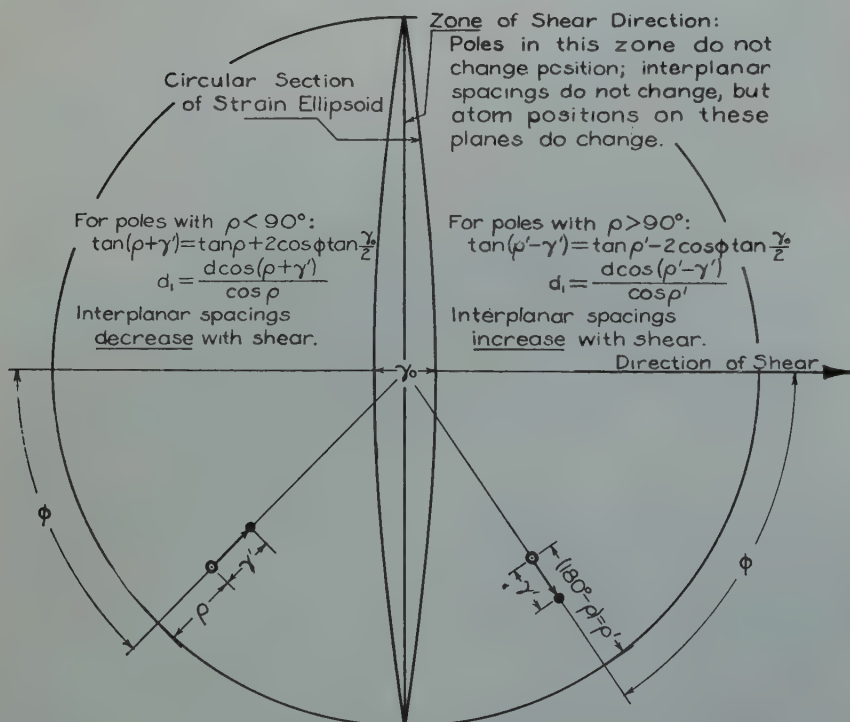


FIG 10—Stereographic summary of shear.
Plane of projection is the plane of shear.

principal experimental determinations were:

1. The evaluation of the lattice relationship between austenite and individual crystals of martensite. (See Fig 3.)
2. The measurement and analysis of the change in position that a volume of austenite undergoes when it transforms into a crystal of martensite (see Fig 6).

Appendix A

The Stereographic Analysis of Shear

In Fig 8 a lattice segment having the shape of a rectangular parallelepiped is deformed by homogeneous shear upon the basal plane in the direction of the long axis. The displacement of any point within the lattice segment is a linear function of its distance from the undistorted base plane. The displacement at unit distance from this base plane is s ; the shear angle is γ . Plane abs is any lattice plane in the undistorted segment; as a result of the deformation, plane abs moves to its new position efs . The position of plane abs is fixed with respect to the plane and direction of shear by the modified spherical polar coordinates ϕ and ρ . ϕ is the angle between the trace normal of plane abs (on the shear plane) and the direction of shear, and ρ is the angle between abs plane normal and the shear plane; ρ is measured in a clockwise direction from the shear plane, and thus may have values between 0° and 180° . The plane $spdgrq$ is perpendicular to planes abs and efs . pt is perpendicular to plane abs , and pr is perpendicular to plane efs . If, then, we designate the angle between planes abs and efs as γ' , the following relations obtain:

$$\tan \gamma = \frac{s}{u}$$

$$\tan \rho = \frac{cg}{u}$$

$$\tan (\rho + \gamma') = \frac{cd}{u}$$

$$qd = s \cos \phi$$

$$\therefore \tan (\rho + \gamma') = \frac{\tan \rho + \tan \gamma}{\cos \phi} \quad [1]$$

In the undistorted lattice, planes parallel to plane *abs* have interplanar spacing *d*; after the deformation, the interplanar spacing of these planes in their new positions is *d*₁. Then,

$$\begin{aligned} \cos \rho &= \frac{pq}{ps}, & \cos (\rho + \gamma') &= \frac{pr}{ps} \\ \therefore d_1 &= \frac{d \cos (\rho + \gamma')}{\cos \rho} \quad [2] \end{aligned}$$

All angular distances contained in Eq 1 and 2 are depicted stereographically in Fig 10, in which the plane of projection is the plane of shear and the direction of shear is as indicated. Note that the shear angle γ has been replaced by the quantity γ_0 . (The reason for doing this is that γ_0 is the quantity that is directly determined in the stereographic solution of a shear problem—see Fig 11.) The relation between the shear angle γ and the angle γ_0 is shown in Fig 9. γ_0 is the angle between the circular section of the strain ellipsoid* and the plane that all points on this section occupied in the undistorted lattice; these two surfaces are represented as great circles in Fig 10.

The relationships expressed in Fig 10 are quite general; they may be applied to any case of a single homogeneous shear.† Note that as a result of shear, all poles travel along equatorial lines; the only poles that do not change position are those lying in the zone of the shear direction. The angular displacement, γ' , as well as the change in interplanar spacing may be calculated precisely for any pole that is plotted, so long as the plane and direction of shear and γ_0 are known.‡ The value of γ' and thus of d_1 , are relatively insensitive to small errors in ϕ and ρ .

In the experimental problem that arises, the conditions are the reverse of those outlined above; namely, we measure γ' , ϕ , and ρ for two poles and we wish to solve for the direction of shear and γ_0 . This problem and its stereographic solution are illustrated in Fig 11. In Fig 11, a small plate-shaped volume of the crystal has undergone a deformation as illustrated. Within the distorted volume, surface I has moved to a new position I_a ; similarly, surface II is now in position II_a . If we assume that the deformation has been a homogeneous shear along the plane of the plate, we may evaluate the direction and angle of shear. The measurements that must be made are: (1) those ordinarily needed to plot the location of a pole from the measurements of

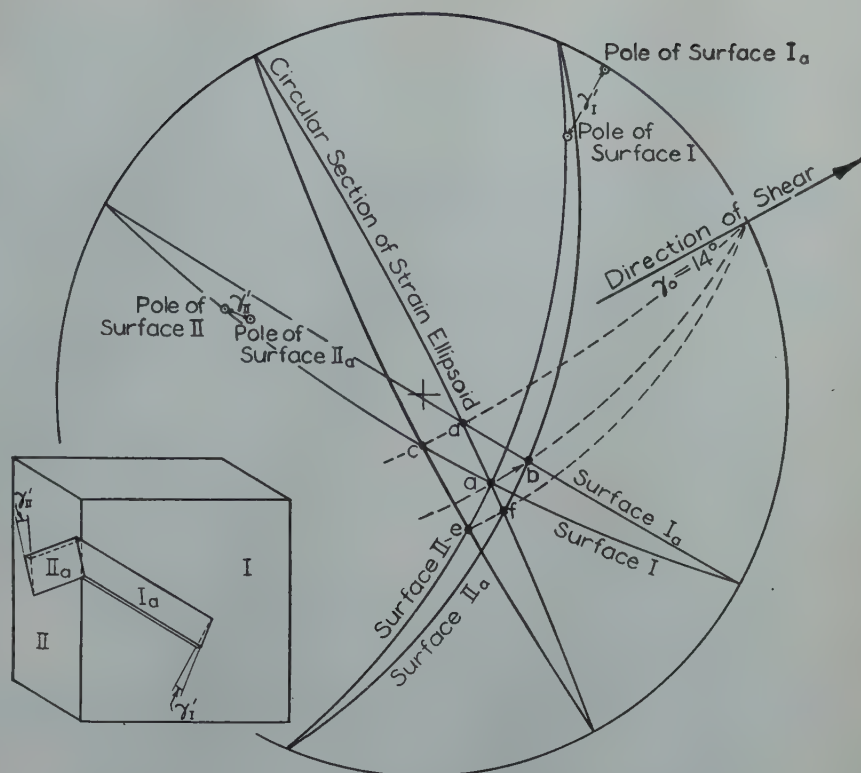


FIG 11—Stereographic determination of the direction and angle of shear. Plane of projection is the plane of shear.

traces of the plane on two surfaces, and (2) angles γ_I' and γ_{II}' ; these latter are measured with an optical goniometer. The steps in the stereographic solution are as follows:

1. With surface I as the plane of projection, plot stereographically the poles of surfaces I, I_a , II, and II_a , and the pole of the shear plane.
2. Rotate the projection to make the shear plane the plane of projection.
3. Replot surfaces I, I_a , II, and II_a as great circles. (This stage is illustrated in Fig 11.)
4. Point a then represents a line in the undistorted crystal (the intersection of surfaces I and II), and as a result of the deformation this line has moved to the position represented by point b (the intersection of surfaces I_a and II_a).

5. The stereographic net is then rotated until a and b lie on the same great circle, and the straight line joining the two diametrically opposite poles of this great circle is parallel to the shear direction. The direction of movement is ascertained from the fact that a moves to b (not b to a), hence the direction of shear indicated by the arrow in Fig 11.

6. To evaluate γ_0 , the stereographic net is rotated until its equator coincides with the direction of shear, and points c and d are located by the requirement

that great circles fad and ec must be at equal distances from the center of the projection and points c and d must lie on the great circle that is shown. Another way of stating the requirement is that the angle between point c and the equator must be equal to the angle between point d and the equator. Angle cd is then equal to γ_0 and angle ef must be equal to cd inasmuch as all points on the great circle ec move to positions on the great circle fad as a result of the deformation.

The stereographic method for solving the above problem represents a graphical solution of two simultaneous equations of form (1). If it is possible to measure γ_I' and γ_{II}' to within a few minutes of arc, and extreme precision is needed, then the shear direction and γ may be solved as follows:

Two equations of form (1), after substituting the known values of γ_I' and ρ for surfaces I and II, reduce to

$$\tan \gamma \cos \phi_I = a \quad [3]$$

$$\tan \gamma \cos \phi_{II} = b \quad [4]$$

divide [3] by [4]

$$\frac{\cos \phi_I}{\cos \phi_{II}} = c \quad [5]$$

then, inasmuch as $(\phi_I + \phi_{II})$ is known, an accurate solution of expression [5] may be obtained by trial and error.

* The other circular section of the strain ellipsoid is, of course, the undistorted base plane. Crystallographers usually designate these two planes as K_2 and K_1 , respectively.

† In the information given by Fig 9, the following space relationships between the hemisphere of projection, the specimen, and the observer are either stated or implied: The hemisphere is located between the specimen and the observer; the shear direction is toward the right of the observer; plane normals proceed from the specimen toward the observer, and intersect the hemisphere of reference in their path; the distortion that is analyzed lies between the undistorted base plane and the hemispherical surface.

‡ The angular displacement may also be determined by stereographic manipulation (see Ref. 13). For most work, however, the stereographic solution of γ' provides insufficient accuracy.

References

1. G. Kurdjumow and G. Sachs: Über den Mechanismus der Stahlhärtung. *Ztsch. Phys.* (1930) **64**, 325-343.
2. G. Wassermann: Über den Mechanismus der $\alpha \rightarrow \gamma$ Umwandlung des Eisens. *Mit. K. W. I. Eisenforsch.* (1935) **17**, 149-155.
3. Z. Nishiyama: X-ray Investigation of the Mechanism of the Transformation from Face-Centered Cubic Lattice to Body-Centered Cubic. *Sci. Repts. Tohoku Imp. Univ.* (1934) **23**, 637-664.
4. R. F. Mehl and G. Derge: Studies Upon the Widmanstätten Structure, VIII, The Gamma \rightarrow Alpha Transformation in Iron-Nickel Alloys. *Trans. AIME* (1937) **125**, 482-496.
5. A. B. Greninger and A. R. Troiano: Kinetics of the Austenite \rightarrow Martensite Transformation in Steel. *Trans. Amer. Soc. for Metals* (1940) **28**, 537-562.
6. A. B. Greninger: The Martensite Transformation in Beta Copper-Aluminum Alloys. *Trans. AIME* (1939) **133**, 204-221.
7. G. Sachs: Allgemeine Gesetzmäßigkeiten der Gefüge- und Eigenschaftsänderungen bei Umwandlungsvorgängen. *Ztsch. f. Metallkunde* (1932) **24**, 241-247.
8. R. Mehl, C. Barrett, and D. Smith: Studies upon the Widmanstätten Structure, IV, The Iron-Carbon Alloys. *Trans. AIME* (1933) **105**, 215-249.
9. A. B. Greninger and A. R. Troiano: Crystallography of Austenite Decomposition. *AIME Metals Tech.*, Aug. 1940.
10. A. B. Greninger and V. G. Mooradian: Strain Transformation in Metastable Beta Copper-Zinc and Beta Copper-Tin Alloys. *Trans. AIME* (1938) **128**, 337-355.
11. G. Phragmén: Austenitsönderfallet och martensitomyvandlingarna ur termodynamisk synpunkt. *Särtryck ur Teknisk Tidskrift* (1938) **23**, 1-12.
12. A. B. Greninger: A Back-Reflection Laue Method for Determining Crystal Orientation. *Trans. AIME* (1935) **117**, 61-74; *Ztsch. f. Kristallog.* (1935) **91-A**, 424-432.
13. W. A. Wooster: A Text-book on Crystal Physics. Cambridge Univ. Press, London, 1938.
14. C. H. Mathewson and G. H. Edmunds: The Neumann Bands in Ferrite. *Trans. AIME* (1928) **80**, 311-333.
15. A. B. Greninger: Transformation Twinning of Alpha Iron. *Trans. AIME* (1936) **120**, 293-303.
16. G. Hägg: X-ray Investigation on the Structure and Decomposition of Martensite. *Jnl. Iron and Steel Inst.* (1934) **130**, 439-451.
17. K. Honda and Z. Nishiyama: On the Nature of the Tetragonal and Cubic Martensites. *Sci. Repts. Tohoku Imp. Univ.* (1932) **21**, 299-331.
18. H. Esser, W. Eilender, and K. Burgardt: Röntgenographische Untersuchungen von Metallen bei hohen Temperaturen. *Archiv Eisenhüttenwesen* (1938) **12**, 157-161.

Effect of Composition on the Wire Textures of Copper and Its Solid Solution Alloys

WALTER R. HIBBARD, Jr.,* Junior Member AIME

It has been proposed¹ on the basis of slip and flow that the ideal deformation texture of drawn wire for face-centered cubic metals is a [111] direction parallel to the wire axis. Under these considerations, an intermediate [100] texture is permissible but should eventually change to the stable [111] orientation. This theory does not explain why copper and its alloys containing up to about 30 pct nickel, 5 pct zinc and 1 pct aluminum were found to have a double [111], [100] texture, while alloys with at least 8 pct zinc and 2 pct aluminum developed essentially a single [111] texture.^{1,2} It does suggest, however, that the [100] component of the former alloys should disappear with additional deformation.³ Some evidence exists to support this suggestion. Howald⁴ reported that annealed copper wire previously drawn 93.8 pct and 98.5 pct developed a single [111] texture. Since, in wire, the drawn and annealed textures are similar, these wires probably had a single [111] deformation texture before annealing. In addition, although cold rolled polycrystalline copper and 80-20 brass were found to form different types of pole figures,^{5,6} single crystals of these metals when rolled from the stable (110) [112] orientation were found to produce essentially the same pole figure.^{7,8} It may be, therefore, that while the addition of solute elements changes the path by which the final

texture is obtained, the final texture is not changed.

Experimental Results

The wires remaining from the previous investigation¹ already drawn about 50 pct reduction in diameter were further drawn to 86 pct and then to 96.4 pct total reduction in diameter. The textures were determined after these stages by transmission X ray photograms taken with a copper K-alpha beam rotated θ degrees toward the wire axis. It was found that the ratio of the [111] and [100] intensities of the double texture in copper and its alloys containing 0.94 pct aluminum, 30.70 pct nickel, 2.61 pct zinc and 4.99 pct zinc increased from about 3:1 for the 50 pct reduction to about 9:1 for the 86 pct reduction. After 96.4 pct reduction, these wires exhibited essentially a single [111] texture.

Summary

Thus, the drawn wire deformation texture of copper and its alpha solid solution alloys containing aluminum,

nickel or zinc is essentially a single [111] texture as predicted by theoretical considerations of slip and flow.¹ For copper and its alloys containing up to about 1 pct aluminum, 5 pct zinc and at least 30 pct nickel, an intermediate [100] component is found after about 50 pct reduction in diameter, but disappears after about 95 pct reduction in diameter. For alpha solid solution alloys containing at least about 2 pct aluminum and 8 pct zinc the single [111] texture is developed considerably more easily and is found after about 50 pct reduction in diameter. No explanation of this compositional effect is apparent. Similar work is contemplated for cold rolled and cold compressed alloys.

References

1. W. R. Hibbard, Jr. and M. K. Yen: *Trans. AIME* **175**, 126. *Metals Tech.*, Feb. 1948, TP 2334.
2. W. R. Hibbard, Jr. and D. E. Trout, II: *Trans. AIME* **185**, 620. *Jnl. of Metals*, Sept. 1949, TN 18.
3. W. R. Hibbard, Jr.: Disc. of R. M. Brick's paper on Deformation Textures, ASM Symp. on Cold Working of Metals, Oct. 1948.
4. T. S. Howald: Disc. of Ref. 1. *Trans. AIME*, **175**, 126. *Metals Tech.* Aug. 1948, TP 2449.
5. R. M. Brick, D. L. Martin and R. P. Angier: *Trans. ASM* (1943) **31**, 675.
6. O. Dahl and F. Pawlek: *Ztsch. Metall.* (1936) **28**, 266.
7. C. S. Barrett and F. W. Steadman: *Trans. AIME* (1942) **147**, 57.
8. J. E. Burke and C. S. Barrett: *Trans. AIME* **175**, 106. *Metals Tech.*, Feb. 1948, TP 2327.

Technical Note No. 19 E. Manuscript received May 12, 1949.

* Assistant Professor of Metallurgy at Yale University, New Haven, Conn.

¹ References are at the end of the note.

Structure and Nature of Kink Bands in Zinc*

J. B. HESS,† Junior Member, and C. S. BARRETT,† Member AIME

Single crystal rods of cadmium collapse under uniaxial compression into peculiar kinks if the (0001) glide plane is nearly parallel to the axis of compression. In his report first describing this behavior, Orowan¹ proposed that these "kink bands" do not develop entirely by ordinary gliding and twinning but by a special mechanism in which glide lamellae of uniform thickness snap abruptly to a tilted position that permits lattice continuity across the glide planes. He concluded that a portion of each boundary of a kink band consists of a plane (non-crystallographic) which bisects the angle between the glide planes on the two sides of it, and along which the bending and the dislocations are concentrated.

The data presented by Orowan seemed to us to be insufficient to conclude that a wholly new mechanism of deformation was responsible for the kinks. Therefore, we have investigated zinc, which is hexagonal close-packed and has an axial ratio near to cadmium, to see whether similar bands are produced, and whether the ordinary mechanisms of glide, bend-gliding, twinning, and the formation of deformation bands can account for its mode of deformation.

We find that kinks form profusely in zinc as shown in Fig 1. The structure of these kinks, reported below, seems to require no new mechanism for their explanation, but indicates that kink bands are a special form of deformation bands and develop gradually, solely from basal glide. A theory covering the formation and structure of the bands is presented in detail because it is seldom possible to study deformation bands under such simple conditions, yet many principles applying to these kinks

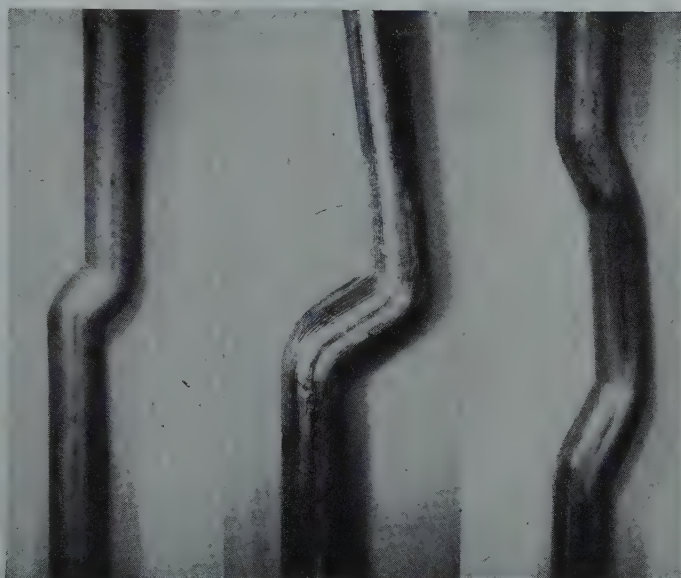


FIG 1—Typical kink bands in compressed single-crystal zinc rod. 3X.

should also apply to deformation bands in general.

Experimental Procedures

Single crystal rods of 2–3 mm diam and 10–15 cm length were grown by the Bridgman technique from swaged wire of Horsehead Special zinc in uncoated pyrex tubes. Orientations of the rods were determined with an optical goniometer after cleaving the rods at

liquid air temperature. Crystals of desired orientations were then selected and used as "seeds" to grow additional crystals approximately 4 ft in length from which all specimens were cut.

The wires were compressed in two ways: in a simple hydraulic handpress—a "soft" machine—and in a Riehle hydraulic testing machine modified to produce very "stiff" action by the simple expedient of inserting lengths of steel bars at the sides of the zinc crystals between the compression plates.

For metallographic examination, the specimens were mounted in sealing wax. Hand polishing was employed, with no grits coarser than No. 1 paper; following the abrasives about 0.025 in. was removed by an etch-polishing reagent.* Final etching to reveal ori-

Cleveland Meeting, October 1949.
TP 2688 E. Discussion of this paper (2 copies) may be sent to *Transactions AIME* before December 1, 1949. Manuscript received May 2, 1949.

* This research was supported in part by the Office of Naval Research, USN (Contract N-6ori-20-IV).

† Institute for the Study of Metals, Univ. of Chicago.

¹ References are at the end of the paper.

* 200 g CrO₃, 15 g Na₂SO₄ (or 34 g Na₂SO₄·10H₂O), 1000 ml water, applied by swabbing.



FIG 2—End-kinked crystals, illustrating the increase in kink length with increasing specimen length.

The unsupported length is indicated. The first kink to form in the shortest specimen is shown by the arrow. Specimens *a* and *b* are shown at higher magnification in Fig 1b and 1c respectively.

entations was with 50 pct HCl,² swabbed for about 5 sec. An optical goniometer was used for orientation determinations.

Experimental Results

CONDITIONS FOR KINK FORMATION

A single crystal zinc rod of suitable orientation deforms by kinking when it is compressed axially provided the rod ends are restrained from rotating. Such restraint is provided by inserting the ends into axially aligned holes in the compression plates, or, with short specimens, merely by permitting the squared-off ends of the crystals to rest directly upon the compression plates.

Axial compression alone is not sufficient to cause kinking, for when the ends of a zinc rod are inserted into hardened steel caps having axially-aligned conical points which rest against the compression plates, kinking does not result. Instead, the crystals buckle into a smooth sine-curve without abrupt bend angles on either the convex or concave surfaces. Continuing compression under these conditions leads to twinning at the convex (tension) surface and ultimately to cleavage on the new basal planes of the twinned region; the fracture is then propagated jerkily across the section by the process of further (10 $\bar{1}2$) twinning at the base of the crack and basal cleavage through these twins, and the final cleavage surface has a striated, stepped appearance in units corresponding to the widths of the succes-

sive twin bands. Crystals subjected to pure bending without simultaneous compression deform and cleave in like manner.

All crystals having their basal (0001) planes nearly parallel to the wire axis could be made to kink. As the inclination of the basal plane to the wire axis increased, kinking became erratic, so the present work was done on crystals having the basal plane within 3° of the wire axis. The appearance of the kink bands in zinc, Fig 1, 2, and 5 are identical to the photographs of kinks in cadmium published by Orowan.

The kinks occur at several reasonably definite locations along the specimen lengths. For example, in one group of 14 specimens of widely differing lengths, the first kink to appear in 5 specimens occurred at the end of the unsupported length, that is, where the rod entered the hole in the compression plate; in 5 others the first kink formed $\frac{1}{3}$ of the way along the unsupported length, and the remaining 4 kinked at $\frac{1}{4}$ -length positions. Invariably the kinks that formed at the ends formed only in those specimens whose surfaces appeared to be completely free of pits, small laps, or other defects. Conversely, the $\frac{1}{3}$ and $\frac{1}{4}$ locations occurred in specimens containing such blemishes, and, with only few exceptions, the kinked regions were observed to terminate at such visible defects.

There was no correlation between specimen length and kink location. However, in the case of end-kinked specimens, there appeared to be a direct relation between the specimen length and the length of the kink that



FIG 3—A kinked crystal subsequently cleaved on the basal plane. 3X.

formed—the longer the specimen the longer the kink, as illustrated in Fig 2, and equal length specimens yielded equal length kinks. Furthermore, whenever a second kink formed in such specimens, the new kink was always shorter than the initial kink and always tilted the opposite way. An example is shown in Fig 1c.

The sudden buckling discussed by Orowan is characteristic only of kinking in a “soft” machine; in a “stiff” machine the kinks form gradually, with progressive reorientation of the crystal within the kink bands. For a typical example, a simple kink such as shown in Fig 1a was found to have the basal planes bent 12.5° at the kink notches when it was first unmistakably recognized, but continued compression in a “stiff” machine increased these angles gradually to 27.5° before the test was halted. Final bend angles as large as 88° have been measured.

REORIENTATION IN SIMPLE KINK BANDS

The reorientation caused by kinking is a rotation around an axis that lies parallel to the glide planes. This fact is demonstrated convincingly by cleaving a kinked crystal at liquid air temperature so that the bends and curvatures of the glide planes are revealed, as shown in Fig 3. During the initial stages of kinking the rotation axis is normal to the [2 $\bar{1}10$] slip direction that lies closest to the compression axis. In the late stages the rotation axes

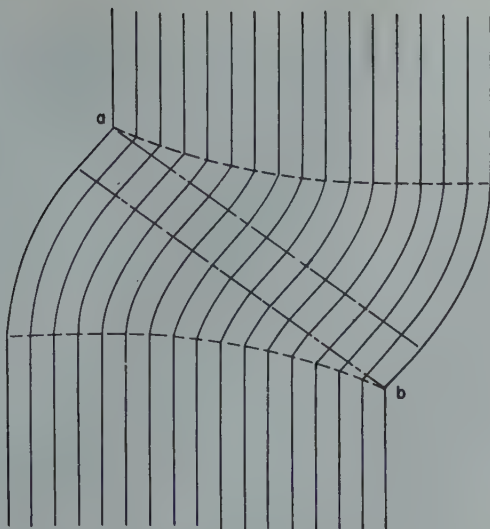


FIG 4—Structure of typical simple kink.

Thin parallel lines indicate glide planes; broken lines, kink boundaries; dash-dotted lines, undistorted parallelogram.

deviate slightly from this crystallographic direction to become non-crystallographic and more nearly normal to the rod axis, though still remaining parallel to the glide planes. For the special case in which a $[2\bar{1}10]$ direction is parallel to the rod axis, the rotation axis does not shift from a position that is normal to both the rod axis and the slip direction.

It is simpler to consider the latter case and to represent the orientations present by a sketch in which the rotation axis is normal to the plane of the drawing. This is done in Fig 4 for a simple kink. It will be noted that on the cross-section of the specimen illustrated in this figure there are two symmetrical areas of oppositely bent glide planes, between which there is a parallelogram of unbent, but rotated, material. The parallelogram has diametrically opposite corners at the kink grooves *a* and *b*. At an earlier stage in the development of a simple kink such as this, the grooves are at the same places and the parallelogram is wider, with sides extending across from grooves *a* and *b* more nearly perpendicular to the wire axis, and with the orientation of material within the parallelogram more nearly like that of the original undeformed crystal. At a later stage in the compression of such a crystal the sides of the parallelogram may meet, leaving no unbent area. When this happens the loci of those parts of the crystal that have been rotated the greatest amount then lie along the line joining the grooves.

In the regions of a simple kink band neighboring the parallelogram of un-

distorted material, the bent glide planes approach the form of arcs of concentric cylinders, with their axes of curvature at the grooves on the surface, as indicated in Fig 4. However, where the arcs approach junction with the undeformed matrix, their radii of curvature decrease progressively, with the centers of curvature for these decreasing radii lying in the two symmetrical boundaries of the kink band. The bending of the glide planes may be considered a special case of the "bend-gliding" studied by the early investigators of crystal plasticity.

KINK BAND BOUNDARIES

The abrupt bends in the glide planes at the boundaries of a kink band, which are the loci of centers of the various radii of curvature mentioned above, mark out a pair of surfaces which are slightly but definitely curved and nearly normal to the axis of the wire at the convex side. The angle of abrupt bending at these boundaries is a maximum at the groove on the surface and decreases gradually across the specimen toward the convex side, corresponding to the changes in radii of curvature.

To study the structure of a kink at the very earliest stage of its formation, a wire was coated with diluted Canada Balsam cement and dried for several days at room temperature. The coated specimen was then compressed in small increments and examined microscopi-



FIG 5—Macrograph of ridges produced in late stage of kinking.

(The striations are due to the method of preparing the single crystals, but in this example correspond to the traces of the (0001) planes as well). 11 X.

cally after each increment until two small cracks were detected in the brittle cement coating. At this stage no macroscopic bend was measurable, but metallographic examination of the cross-section at the cracks revealed a single pair of boundaries, approximately normal to the specimen axis, where abrupt bending through a slight angle occurred. The boundaries extended entirely across the specimen with uniform (though slight) contrast, differing in this respect from the later stage of Fig 4, where contrast increases on approaching the grooves. The material between the boundaries appeared to be unbent, though slightly rotated.

The abrupt boundaries of a simple kink are fixed in the earliest detectible stages of deformation and do not wander through the specimen as deformation proceeds.

SECONDARY BOUNDARIES AND RIDGES

A number of complexities were noted. Additional faint boundaries of abrupt orientation changes were frequently detected. These boundaries occurred either as branches from the primary or other secondary boundaries, or as new and independent boundaries. Their low contrast indicated that their abrupt bend angles were small.

Ridges like those shown in Fig 5 and sketched in Fig 6 often develop in the later stages. Goniometric measure-

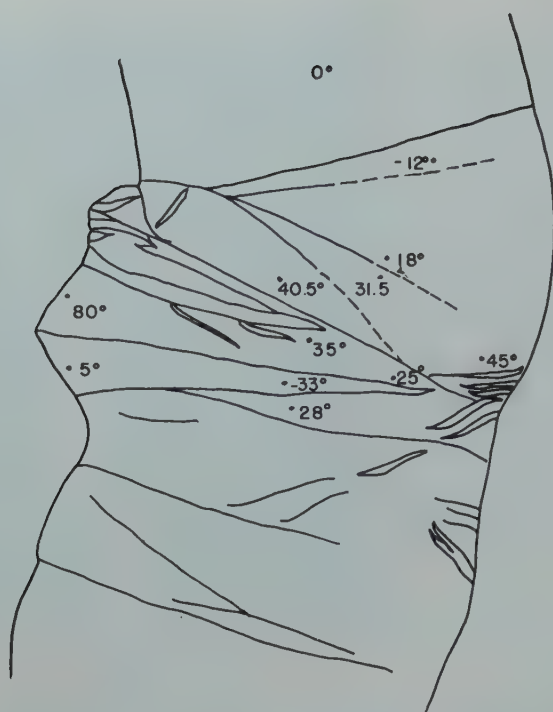


FIG 6—Structure of complex kink of Fig 5.

Numbers at the dots indicate the rotation of the glide planes from their original orientation (0°) parallel to the rod axis. Abrupt bending of the glide planes occurs across the boundaries shown as thin solid lines. Overlapping segments and varying orientations within a segment are seen.

ments such as those recorded in Fig 6 indicate that the ridges are at the boundaries of segments that are rotated in opposite direction, an amount that increases with the amount of deformation. In one example, the bend at a boundary reached 110° . The ridges form on the curved surfaces of prior simple kink bands only after several of these have formed elsewhere along the specimen, and when the local stress conditions must have been greatly altered. They form on the side of the specimen where the compressive strain is the greatest. Branched, intersecting, and overlapping ridges are not uncommon. The ridge and segment boundaries do not, in general, extend across the entire cross-section.

Deformation twinning does not appear to be involved in any manner in the sequence of events of kinking. While there were occasional twins pre-existing in some of the specimens, these did not appear either to initiate or to inhibit kinking. Orientation measurements in the segments at the ridges indicate that these are not twins; the directions of their boundaries are incompatible with twinning, as is also the fact that the ridge angle becomes gradually more acute with continued deformation.

Discussion of Results

The characteristics of kink bands in zinc (and we believe in cadmium also) allow them to be classified as a special form of deformation bands. Deformation bands are lamellar regions in crystals and polycrystalline grains within which there has been reorientation by rotation as a result of slip, the amount of rotation increasing gradually with increasing strain. There are abrupt changes in orientation at the boundaries of deformation bands, and fre-

quently there is also bending (bend-gliding) within the bands. While deformation bands have apparently not been reported previously in zinc, they are a common mechanism of deformation in many cubic metals,³ and no principle is known that would indicate that they should not occur in zinc, cadmium, or other hexagonal crystals provided the applied stress does not first cause twinning. Since compressive stress directed along the basal plane is required for kink bands, they can be expected only in those crystals that are not subject to twinning from this type of stressing, hence only in hexagonal metals or alloys having an axial ratio c/a greater than 1.732.

Actually, nearly analogous structures have been reported by R. F. Miller^{2,4} near the grips in zinc single crystals elongated in tension. Miller identified a "bend-plane"—the locus of abrupt bend angles in the basal plane—and showed that it was non-crystallographic and that its orientation was dependent upon the amount of deformation. However, he described the phenomenon as a new type of twinning, and failed to recognize the structures as deformation bands.

Orowan's suggestion¹ that a new mechanism of deformation is involved in the formation of kink bands seems unnecessary, at least in zinc, since the structure and formation of the bands can be accounted for by the accepted mechanisms of slip and bend-gliding that operate in forming deformation bands. Contrary to Orowan's conclusions regarding kinking in cadmium, the glide planes do not snap over suddenly to the kinked orientation, nor is there a " k plane"¹ extending from the grooves to the center of the wire over which there is a constant bend angle equal to the bend angle at the groove.

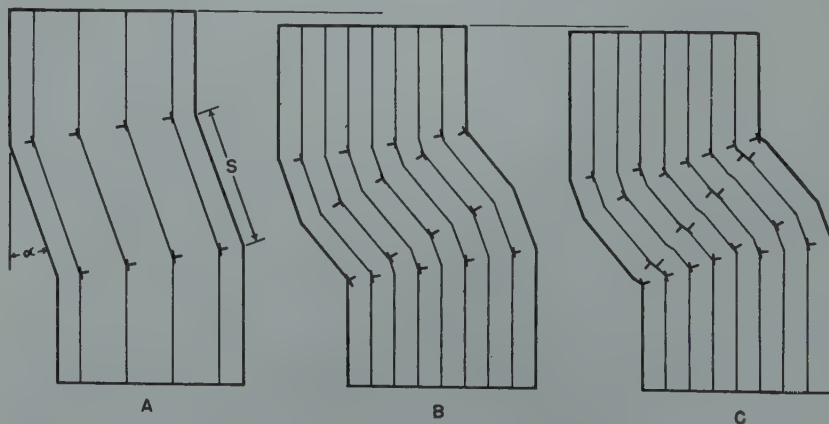


FIG 7—Formation of a kink by dislocations.

Each dislocation is marked by a T with the extra plane of atom indicated by the stem of the T . Successive stages are shown in drawings A, B and C.

However, we are in agreement with Orowan's suggestion that there are dislocations concentrated in the boundaries, and we develop in the following section a detailed qualitative theory of the bands based on the formation and movement of pairs of dislocations.

The fact that there is an axis of rotation lying in the glide plane of zinc and parallel to the boundaries of the band, suggests that rotation axes may be similarly oriented in deformation bands of other metals, but observations on this point seem to be lacking. The rotation axis should be crystallographic and lie in the glide plane normal to the glide direction when a single slip system operates, but could well have irrational indices if two glide systems are active. A single slip system appears to be active in zinc during the initial stage of kinking, because the rotation axis $[01\bar{1}0]$ is exactly that predicted for such behavior.

In a crystal oriented with the glide direction parallel to the axis of compression, the rotation is such as to keep the maximum resolved shear stress in the glide plane continually parallel to the glide direction. Wandering of the maximum resolved shear stress direction occurs, however, in less symmetrically oriented crystals and may ultimately induce glide in a second glide direction, with a corresponding change in the axis of bending of the glide planes. If two glide directions are at equal angles to the axis of compression initially, they would be expected to remain so throughout, and bending would then be around $[1\bar{2}10]$. Such behavior was confirmed experimentally in most specimens of this orientation; however, a few did exhibit less symmetrical rotation and had axes with irrational indices. In these exceptional cases the behavior was not consistent throughout the region of a single kink,

suggesting that defects are possible in a glide plane which do not affect all slip directions equally.

A DISLOCATION THEORY OF KINK BANDS

The development of a kink band can readily be described in terms of dislocations. Initial plastic flow in these specially oriented zinc crystals appears to be confined to the volume of the kink band and does not extend to the ends of the specimen. From this and considerations discussed below we conclude that flow begins by the generation, within the volume that is to become the band, of pairs of dislocations of opposite sign, the positive and negative dislocations collecting, respectively, in two parallel planes that are nearly perpendicular to the glide planes.

The generation of such pairs of dislocations may be expected from consideration of the elastic distortions produced in slender rods by compressive loading. According to the theory of elasticity,⁵ an isotropic slender rod with fixed ends buckles in the shape of one full period of a cosine function, the ends being tangent to the wave at successive crests. If the anisotropic zinc crystals of the present experiments are assumed to buckle elastically in similar cosine shape, then this distortion produces a shear stress along all the basal planes, the magnitude of which is a sine function of position along the rod length and is proportional to the amplitude of the cosine flexure. Shear stress maxima consequently occur at the points of inflection of the cosine flexure, the quarter-length locations. Further decrease of the distance between the compression plates increases the amplitude of the cosine flexure, and hence increases the shear stresses. At

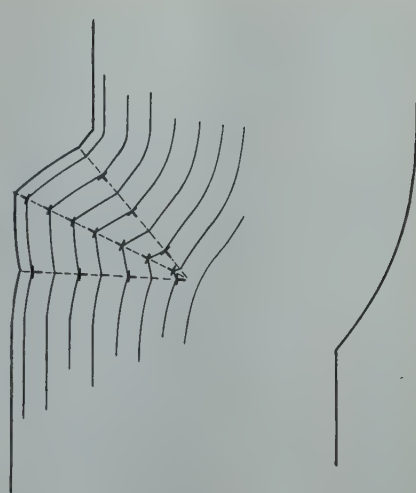


FIG 9—Formation of a ridge by dislocations.

some critical shear stress a pair of dislocations of opposite signs might be generated, either as linear dislocations, or more probably as screw dislocations spreading out from some point, possibly at the surface, and becoming a pair of linear dislocations. Since the critical shear stress is attained on all planes simultaneously but is localized to a short length of area on each, its relief must entail the generation of pairs of dislocations on many separate planes approximately evenly spaced over the cross-section rather than the generation of an equal number of pairs on one, or only a few, planes. We conclude that the positive and negative dislocations must collect, respectively, into planar arrays because, if they did not, there would be additional local stresses set up around them that would increase the strain energy of the structure.

The result of such a pair of planar arrays of dislocations of opposite signs is a slight bend of the glide planes at one of the planes of dislocations and an equal reverse bend at the opposite plane of dislocations. This bend is illustrated in Fig 7a for the simplest case where a slip direction is initially parallel to the rod axis. Each plane of dislocations bisects the angle between the glide planes on the two sides of it because, if it did not, the interplanar spacings of the glide planes could not be equal on both sides of the bend angle, and hence the strain energy of the configuration would be increased. Because the symmetrically oriented planar array is a configuration of minimum strain energy for a given bend angle, individual dislocations that depart from it will be forced back into it. Strain energy considerations also

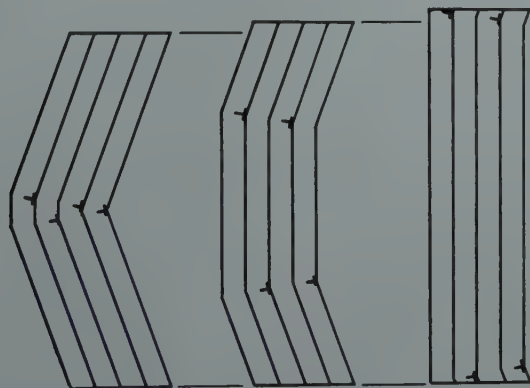


FIG 8—Tensile strain by the separation of like planar arrays of dislocations.

lead to the conclusion that dislocations are approximately evenly spaced over these planes, from one side of the wire across to the other side, because if this were not so some portions of the crystal would be bent more than others and an additional strain energy would be introduced. Local lattice imperfections and stress raisers might distort the regular array of dislocations on a local (atomic) scale, but on the average there should be a remarkably uniform distribution over the planes.

The planes of dislocations are forced apart by the applied stress and thereby shorten the distance between the compression plates. The possibility of deformation by the movement of such arrays of dislocations has previously been proposed by Bragg.⁶ For the case sketched in Fig 7a the shortening is given by the formula $s(1 - \cos \alpha)$ where s is the distance between the planes of dislocations, and α is the bend angle at each. This angle is proportional to the number of dislocations in the arrays.

The planes of dislocations move apart until they are stopped by some agency, discussed below, where they become the permanent boundaries of the kink band. Further compressive strain occurs not by increasing the spacing between the boundaries but by increasing the rotation, that is, by generating new pairs of dislocations. Since the glide planes within the band are now rotated to a position where they have a higher resolved shear stress than the glide planes in the matrix outside of the band, the new pairs will be generated within the band.

The new dislocations array themselves on a new pair of planes, the position of minimum energy for them. These planes begin to separate as the first pair did, and continue until they encounter the first set, as illustrated in Fig 7b. Since each of the second pair of planes bisects the glide planes on each side of it, and since the second pair is generated in glide planes that have already been reoriented by the first pair, it follows that the second pair will be tilted with respect to the first pair in the manner illustrated (in an exaggerated way) in the sketch, and the first contact of the second pair with the first pair will be at the grooves. As successive pairs are generated (Fig 7c), the bend angle at the groove will steadily increase. If each pair has about the same number of dislocations in it, the result of many successive pairs of planes will be a bending of the

glide planes into concentric cylinders with the axis of the cylinders centered at the grooves.

However, if the movement of all successive planes of dislocations were stopped by initial contact with the first planes as sketched in Fig 7b, there would be no visible grooves extending nearly half-way around the rod circumference such as is observed experimentally. Instead it appears that the movement of the second pair of dislocation planes is not stopped immediately by contact with the first pair at the groove locations, but is merged with the first set over part of its area, increasing the uniform bend angle over the coalesced area and producing bending elsewhere as sketched in Fig 7c. Then if succeeding pairs contact the boundary set along progressively decreasing areas following their encounters at the grooves, the final pattern of dislocations will yield the orientations sketched in Fig 4. The boundaries will be slightly curved, as indicated in Fig 4 and 7c, and the minimum strain energy argument would suggest that the boundaries be curved so as to bisect the abrupt bend angle of the glide planes at all points.

Reasoning from the minimum strain energy argument, we would expect complete merging of two arrays of dislocations that have contacted each other at a point, because near the contact region there would be local distortions on an atomic scale from the close approach of the arrays that would not be required for a coalesced array, so that progressive merger should ultimately produce the minimum strain energy configuration. Accordingly, the failure to merge completely indicates an opposing tendency in the convex regions of the kinks, the probable nature of which is indicated in the sketches of Fig 8. From these it is evident that if a volume of crystal containing two arrays of like sign is subjected to tensile stress, then minimum strain energy obtains when the arrays have moved as far apart as possible; hence we conclude that the convex regions are under slight tensile stress. High tensile stress should produce twinning, which was never observed.

The formation of kinks at the $L/4$ point of the rod length has already been shown to be a consequence of the points of inflection of the initial cosine flexure of the rods, for the case of rigidly fixed ends. The $L/3$ location can result from the slightly different case

where one end is rigidly fixed while the other end is merely constrained to axial alignment but remains free to rotate, since in this case the flexure shape⁵ has a point of inflexion at $L/3$. As the single crystal nature of our specimens precluded the possibility of forcing the specimen ends into the aligning holes so as to secure really rigid mounting, it is quite possible that the slight rotations needed to permit the second type of buckling occurred frequently. When both ends of the rod are free to rotate, the flexure shape corresponds to $1/2$ period of a sine function and has no points of inflexion; hence, kinking should not occur, as was confirmed experimentally.

The grip-end kink locations require a different explanation. We shall consider, for the moment, the initial stage of kink generation shown in Fig 7a when a single pair of planar arrays of dislocations of opposite signs have formed at either the $L/4$ or $L/3$ locations and have moved apart the distance s . This movement has displaced the axis in the matrix just above the upper array from the axis just below the lower array, and since the rod ends are still axially aligned, these matrix segments must be resisting bending moments tending to curve them in opposite directions. Minimum strain energy requires that the respective radii of curvature be equal. Let us now assume that the pair of arrays may move as a unit along the rod keeping their separation s unchanged, and inquire whether there exists any more favorable location of lower strain energy. It can be shown that the strain energy is a maximum for the paired array at $L/2$ and that the energy decreases continuously as the paired array moves toward $L = 0$ or 1 ; so that, if such migration be possible, the kinks would always be expected to have migrated to the grip-ends long before they attained even microscopically observable size or shape. We conclude, therefore, that the kinks observed at $L/4$ and $L/3$ positions have been prevented from migrating from their points of origin by the surface defects observed, almost without exception, at both kink boundaries in such specimens, while the end-locations occurred only in specimens so nearly perfect that migration of the arrays through the crystal lattice is unimpeded.

In the defect-containing specimens, the kink lengths are certainly determined when the migration of the first

pair of arrays is stopped at the nearest defects. In the other specimens where the movement of the planes of dislocations is apparently unhindered, the formula $s(1 - \cos \alpha)$ suggests that the first pair of planes should separate without limit, to the full length of the specimen. However, we have already seen that the separation of the first pair of arrays creates a bending moment in the rest of the wire, and examination shows that the curvatures in these elastically bent sections produce strain gradients across the glide planes of such nature that they must oppose the advance of the separating pair of arrays. For example, if the dislocations of the upper array in Fig 7a have their extra plane of atoms on the left side of the glide planes, then in the neighborhood of each dislocation the atoms at the left side of the glide plane are compressed because of the extra plane of atoms, and similarly the atoms at the right are under tensile strain. But the rod section ahead of the advancing array is elastically bent with radius of curvature to the left, so that the atoms to the left of the glide planes are already compressed with respect to those at the right, and hence would resist the introduction of dislocations of similar strain gradient. At sufficiently great curvatures the opposing force may reach such magnitude that it becomes easier to generate a new pair of arrays within the undistorted parallelogram than for the first pair of arrays to separate further. Then the first pair would stop separating and fix the ultimate kink length. Under such conditions the kink length would become a function of the specimen length, as our experiments have suggested, for presumably the critical buckling moment would correspond to a definite radius of curvature.

The above theory accounts for the observed locations of the kink bands and for their lengths. It accounts for the fact that in simple kink bands the arcs formed by the bent glide planes always occur in symmetrical pairs, with the arcs at the two convex sides of a band being equal in length; that the grooves always occur in symmetrical pairs with bend angles equal to each other; that the bend angles at the grooves depend upon the lengths of the arcs; that the glide planes at band boundaries may be bent through progressively greater angles the nearer they lie to the grooves. In simple kink bands in zinc these features are all observed.

The planes of dislocations of each successive pair are parallel. The material between them is rotated from its original orientation but remains unbent (or nearly so). On the longitudinal cross-section, with slight or intermediate amounts of compressive strain, there will be a parallelogram within which there is negligible bending. Two diagonally opposite corners of the parallelogram will be located at the grooves at the surface (Fig 4) and the upper and lower sides of the parallelogram will be parallel because there are equal numbers of positive and negative dislocations on the two sides; hence they will be at equal angles to the glide planes between them. With increasing strain, the parallelogram rotates and narrows, becoming finally a line connecting the two grooves, after which no unbent material remains. At all places where glide has occurred it is possible, of course, that faults in stacking of the glide planes are left.

When a single kink band forms, it creates a bending moment on the rest of the rod. There is a tendency for this bending moment to be relieved by the generation of one or more kinks of reversed tilt elsewhere in the wire. When pairs of reverse kinks form, the axes of bending of the glide planes are initially always the same crystallographic direction and are parallel in the two; this has been observed in a rod with as many as four pairs.

To account for secondary boundaries in kink bands, one assumes that successive planar arrays of dislocations may be forced to contact and coalesce over part of their areas at places other than the grooves. Secondary boundaries would be expected when stress conditions change suddenly during the straining of a specimen, for example, when a new kink band starts to form and introduces a bending moment not previously present. Some secondary boundaries may result, also, from planes of dislocations that are stopped at places other than the grooves. This, too, may be a result of local imperfection or changed stress conditions that give a plane of dislocations power to penetrate otherwise insurmountable barriers, or on the other hand, that stop its migration prematurely. Change in rotation axis due to the onset of duplex slip could also be a factor.

Ridges are understandable as the result of planes of like dislocations being forced together, as sketched in Fig 9. Suppose double pairs of dislocations are generated, approximately

simultaneously, with the positive dislocations collecting in planes that are closer to each other than the negative dislocations. As progressive straining forces the positive planes together they come to rest at a plane boundary that extends out to a ridge on the surface. The negative dislocations, meanwhile, form the opposite boundary of the segment. Thus, a ridge is located on the boundary between two crystal segments within which the lattice has rotated in opposite directions about an axis lying both in the plane of the boundary and in the glide plane. During the initial stages of ridge formation while only a single glide system operates, the rotation axis is crystallographically identical to that operating during simple kinking; therefore, the ridges are parallel to the kink grooves. When duplex slip conditions are attained, the rotation axis is altered and the ridge directions become irrational. There is no requirement here that ridges occur in pairs on opposite sides of a kink band, as grooves do, and this is in accord with observation. But there is the requirement that associated with a positive boundary at a ridge there be a negative boundary on each side of a rotated segment, as is, indeed, observed.

It is perhaps surprising that elasticity theory based on the assumption of isotropic medium should hold so well for the present anisotropic crystals. It appears that the chief effect of the anisotropy is to reduce the slenderness ratio at which buckling becomes the mode of failure, for kinking was found to occur even at a slenderness ratio of 1:1. This fact suggests that deformation bands in general may be the result of buckling, for a slenderness ratio of 1:1 would correspond to equiaxed grains.

Summary

1. The formation of kink bands during the compression of single crystal rods of zinc occurs by a progressive rotation of the lattice within the band as deformation proceeds, rather than by a twin-like abrupt shear to a final orientation. Rotations from a few degrees to over 80° have been measured.
2. The width of a simple kink band is fixed by the grooves that form initially on the surface; the bands do not grow wider with increasing deformation as deformation twins do in zinc.
3. These characteristics indicate that kink bands are properly considered as

deformation bands resulting from the ordinary crystal slip process, not as a new mechanism of deformation.

4. In a simple kink the angle of bend of the glide planes at a boundary changes gradually from a maximum at the concave side to a minimum on the convex side. Each boundary is initially a surface containing the direction in the glide plane that is normal to the active glide direction. After severe bending deviations can occur.

5. Complex behavior is often noted: (1) secondary boundaries may radiate out at various angles from points on the original boundaries, and (2) sharp ridges may form in areas subjected to compression. The ridges lie on the boundary between two segments that have rotated in different directions. These complexities are not incompatible with the proposal that kink

bands are special cases of deformation bands.

6. Kink band formation is accounted for by assuming that pairs of dislocations are generated between the boundaries by buckling flexures, the positive dislocations aligning themselves in a plane and the negatives in another plane (a configuration of minimum strain energy). These planes then move apart until stopped by defects or by opposing stresses in the adjoining segments of the rod. Successive planes of dislocations follow similar paths and build up continuously increasing angles of bend.

7. Ridges are accounted for by double pairs of dislocations, with positive dislocations coming together in a plane that extends out to the ridge on the surface, and the corresponding negative dislocations migrating to the

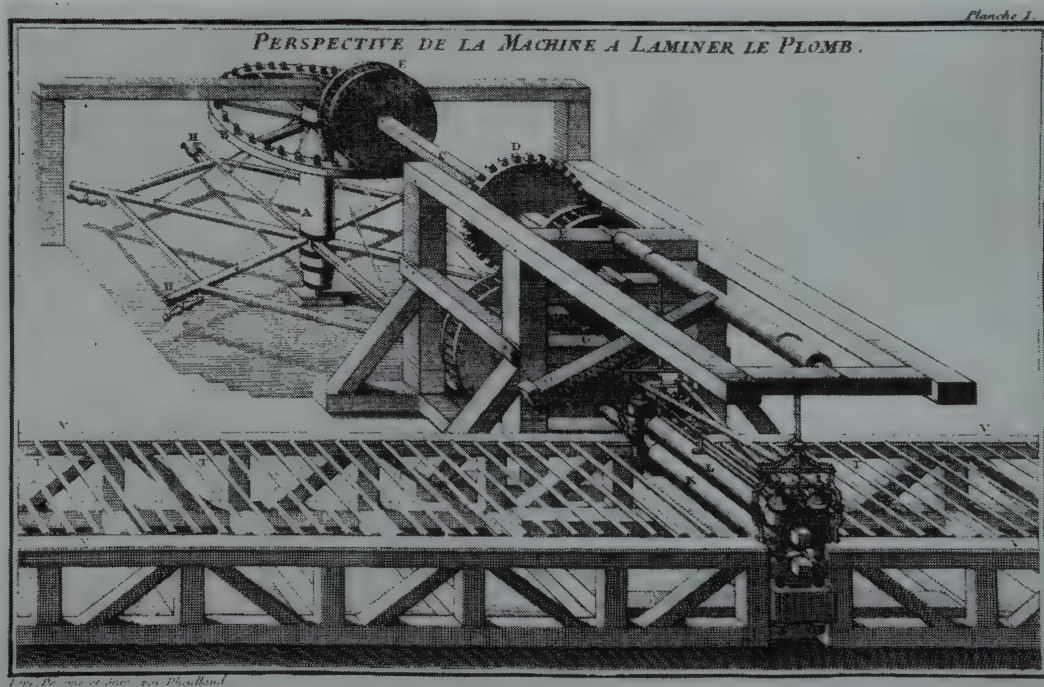
opposite boundaries of two oppositely rotated crystal segments.

Acknowledgment

The authors gratefully acknowledge the assistance of Dr. Werner Bergmann of this laboratory in preparing the long single crystals of predetermined orientation.

References

1. E. Orowan: *Nature* **149**, 643 (June 6, 1942).
2. R. F. Miller: *Trans. AIME* (1936) **122**, 176.
3. C. S. Barrett: *Trans. AIME* (1939) **135**, 296; *Structure of Metals*. McGraw-Hill, 1943, p. 305.
4. R. F. Miller: *Trans. AIME* (1934) **111**, 135.
5. J. Prescott: *Applied Elasticity*. Dover Publications, 1946.
6. W. L. Bragg: *Proc. Phys. Soc. (London)* (1940) **25**, 54.



Horse-driven reversing rolling mill for lead roofing sheets.

French, 1760. (Courtesy of C. S. Smith)

Analysis of Interstitial Diffusion Using Activity Methods

A. G. GUY

Thermodynamic activity rather than chemical composition is basic to the analysis of diffusion. This is the essential conclusion reached by Darken¹⁻³ and by Birchenall and Mehl.⁴ If so, it is reasonable to expect that diffusion calculations should be carried out using activities. This paper will illustrate a method of employing activities in analyzing interstitial diffusion.

For interstitial diffusion (of carbon in iron and probably generally) the diffusion of the solvent atoms, volume changes, and other such complexities not explicitly provided for in the usual diffusion equations cause a negligible error of the order of 1 pct. Therefore it is relatively easy to test the validity of an analysis based on activities in the instance of interstitial diffusion. The mathematical treatment of the more complex substitutional diffusion could be simplified once the adequacy of the activity method had been established for substitutional diffusion. Thus the present work has the purpose not only of providing a superior analysis of interstitial diffusion but also of indicating a possible approach to the more important question of an adequate treatment of substitutional diffusion.

Development of the Diffusion Equation

Although activities are convenient quantities to determine experimentally, they are derived from the more fundamental fugacities.⁹ Possible confusion in using activities can be avoided by basing equations involving their use on the relationship,

$$dP = -D_f \frac{\partial f}{\partial x} dt \quad [1]$$

where, dP = the number of grams of

solute crossing one cm² in the time dt sec.

D_f = the diffusion constant for use with fugacities; it is assumed to be constant at a given temperature, and has units of secs.

f = the fugacity of the solute in the solid solution; the units are those of pressure, dynes per cm².

\bar{x} = the distance in cm.

Eq 1 can be considered to be the basic form of the first Fick Law for one-dimensional diffusion.

In order to convert Eq 1 into an equation involving activities, a choice of a standard or reference fugacity, f° , must be made; then,

$$a = \frac{f}{f^\circ} \quad [2]$$

where a is the activity corresponding to the fugacity f . However, the value of a is also determined by the relation,

$$\alpha = \frac{a}{c} \quad [3]$$

where α is the activity coefficient and c is the concentration. For a given value of α (such as $\alpha = 1$) it is evident that the units used for expressing concentration will affect the numerical value of a corresponding to a given amount of carbon dissolved in γ -iron. Since weight per cent concentration is so widely used, this unit will be adopted as the standard in this paper.

When the value of f given by Eq 2 is substituted in Eq 1, the first Fick Law becomes,

$$dP = -D_f f^\circ \frac{\partial a}{\partial x} dt \quad [4]$$

Since $D_f f^\circ$ is constant (at a given temperature), the second form of Fick's Law can be obtained in the usual manner,

$$\frac{\partial c'}{\partial t} = D_f f^\circ \frac{\partial^2 a}{\partial x^2} \quad [5]$$

where c' is the concentration in g per cm³. In terms of weight per cent concentration, c , Eq 5 becomes,

$$\frac{\partial c}{\partial t} = \frac{100}{\rho} D_f f^\circ \frac{\partial^2 a}{\partial x^2} \quad [6]$$

where ρ is the density of the solid solution and will be assumed to be constant. In order to simplify Eq 6, it is necessary to consider the standard state, f° .

Standard states are chosen for convenience. There appears to be one especially convenient choice for the analysis of interstitial diffusion. If the activity coefficient, α , is set equal to unity at infinite dilution of the solute,

then $\frac{100}{\rho} D_f f_1^\circ$ is approximately equal to the usual diffusion constant in dilute solutions. This is true since the activity, a , in Eq 6 can be replaced by the concentration, c , with little error in an infinitely dilute solution.*

Here f_1° is the standard fugacity necessary to achieve this standard state. It is proposed that a diffusion constant D_A^1 be defined,

$$D_A^1 = \frac{100}{\rho} D_f f_1^\circ \quad [7]$$

where A is the metal whose diffusion is

* The second derivative of a is equal to the second derivative of c in dilute solution only if $\frac{da}{dc}$ is zero. Although theory does not require this condition, in the systems C in Fe, and Zn in Cu, $\frac{da}{dc}$ is in fact found to be essentially zero.

Cleveland Meeting, October 1949.

TP 2604 E. Discussion of this paper (2 copies) may be sent to *Transactions AIME* before December 1, 1949. Manuscript received December 31, 1948; revision received June 6, 1949.

* Associate Professor of Metallurgy, Mechanical Engineering Department, North Carolina State College, Raleigh, N. C.

† References are at the end of the paper.

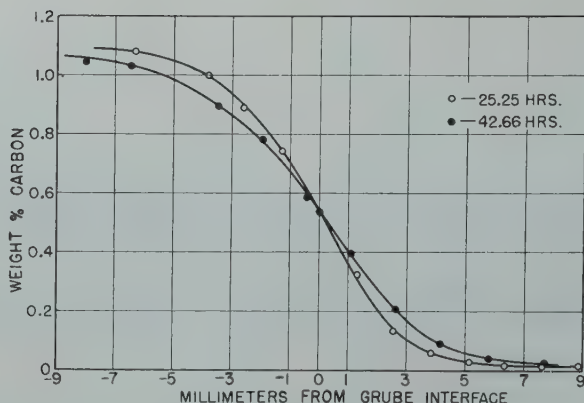


FIG 1—Concentration-penetration curves plotted from the data of Wells and Mehl for the diffusion of carbon in iron at about 1000°C.

being considered. For carbon diffusing in iron this diffusion constant is D_c^1 .

Using the definition of α given above, Eq 6 can be written,

$$\frac{\partial c}{\partial t} = D_A^1 \frac{\partial^2 a}{\partial x^2} \quad [8]$$

This equation would be in a more convenient form for calculation if it were written in terms of a alone, rather than in terms of a and c . From Eq 3,

$$\frac{\partial c}{\partial t} = \frac{\left(1 - \frac{a}{\alpha} \frac{da}{da}\right)}{\alpha} \frac{\partial a}{\partial t} \quad [9]$$

Therefore, Eq 8 becomes,

$$\frac{\partial a}{\partial t} = Z D_A^1 \frac{\partial^2 a}{\partial x^2} = D \frac{\partial^2 a}{\partial x^2} \quad [10]$$

where Z represents the quantity

$$Z = \frac{\alpha}{1 - \frac{a}{\alpha} \frac{da}{da}} \quad [11]$$

Since Z is a function of a (and therefore of concentration), D in Eq 10 is not a constant, and the exact solution of this equation involves the use of step-by-step methods.

The Error-function Solution

Fortunately there is an approximate method of applying Eq 10 to determine the value of D_c^1 corresponding to an experimental diffusion curve. The result is found to agree closely with that given by the exact solution—well within experimental error. If the variation of Z is neglected, and Z' is taken as the value corresponding to the median of the range of activities in question, then Eq 10 can be solved in a convenient manner using the error-function solution. When the boundary

conditions are those corresponding to a semi-infinite solid, Eq 10 can be shown to have the solution,⁵

$$a - a_0 = \frac{(a_1 - a_0)}{2} \left[1 \pm \operatorname{erf} \left(\frac{x}{2\sqrt{D't}} \right) \right] \quad [12]$$

where a = the activity corresponding to the carbon content at a distance x from the interface.

a_0 = the activity corresponding to the initial carbon content on one side of the interface.

a_1 = the activity corresponding to the initial carbon content on the other side of the interface.

erf = the Gauss error-function, values of which are given in numerous tables.⁶

$$D' = Z' D_c^1$$

Eq 12 can be used to analyze experimental diffusion data such as those obtained by Wells and Mehl⁷ to determine the value of D' . Since Z' is known, a value for D_c^1 can be obtained using the relation,

$$D_c^1 = \frac{D'}{Z'} \quad [13]$$

The data obtained by Wells and Mehl⁷ for the diffusion of carbon in iron were analyzed using Eq 12 to determine D' and D_c^1 at a number of temperatures. The activities of carbon in austenite (defined by Eq 3 and the choice of standard state) needed for this analysis were calculated from the activity data of R. P. Smith.⁸ Suitable interpolation and extrapolation from his data at 800° and 1000°C were required to cover the temperature range 800°–1100°C in the manner shown in Table 1.

Fig 1 is a conventional plot in terms of weight per cent carbon and distance from the Grube interface* of tests Nos. 9 and 10 of Wells and Mehl. These data can also be plotted in an analogous fashion in terms of activities. Using Eq 12, a value of D' can be calculated for each experimental point of such an activity-penetration plot. Results obtained for points near the ends of the plot are unreliable because of the effect of a small error in activity in greatly altering D' . The values of D' obtained from the five central points of the 42.66 hr data are listed in Table 2 together with the average.

To convert this average value of D' (which is that corresponding to the median activity, 0.642) to the activity diffusion constant D_c^1 , Eq 13 was used. In this instance Z' has the value,

$$Z' = \frac{\alpha}{1 - \frac{a}{\alpha} \frac{da}{da}} = \frac{1.037}{1 - (0.62)(0.262)} = 1.24 \quad [14]$$

and D_c^1 was determined to be,

* The Grube interface is defined as the plane in the specimen at which the carbon concentration is $\frac{1}{2}(c_1 + c_0)$; that is, where the carbon concentration has its median value. The activity interface is defined in terms of $\frac{1}{2}(a_1 + a_0)$.

Table 1 . . . Carbon Activities in Austenite for a Number of Temperatures

| Weight Per Cent Carbon | Temperature, °C | | | |
|------------------------|-----------------|-------------|-------|-----------|
| | 800 | 927 | 1000 | 1197 |
| 0 | | 0 | 0 | 0 |
| 0.1 | | 0.102 | 0.102 | 0.103 |
| 0.2 | | 0.200 | 0.199 | 0.200 |
| 0.3 | 0.294 | 0.298 | 0.295 | 0.297 |
| 0.4 | 0.403 | 0.404 | 0.400 | 0.402 |
| 0.5 | 0.517 | 0.510 | 0.506 | 0.513 |
| 0.6 | 0.640 | 0.620 | 0.616 | 0.624 |
| 0.7 | 0.765 | 0.747 | 0.742 | 0.748 |
| 0.8 | 0.902 | 0.875 | 0.869 | 0.877 |
| 0.9 | (0.88)1.015 | 1.015 | 1.007 | 1.015 |
| 1.0 | | 1.163 | 1.153 | 1.163 |
| 1.1 | | 1.317 | 1.310 | 1.323 |
| 1.2 | | 1.487 | 1.476 | |
| 1.3 | | (1.27)1.610 | 1.652 | |
| 1.4 | | | 1.842 | |
| 1.5 | | | 2.050 | (1.8)2.70 |

$$D_c^1 = \frac{3.31 \times 10^{-7}}{1.24} = 2.67 \times 10^{-7} \text{ cm}^2 \text{ per sec [15]}$$

at 1001°C.

Values of D' can be used to calculate approximate penetration curves by means of Eq 12. Fig 2 shows the agreement between the data of Wells and Mehl's test No. 9 (25.25 hr at 997°C) and the penetration curve calculated using the D'^* of Table 2. Somewhat poorer agreement was found in using an analogous approximate method to calculate a carburizing curve in which the concentration range exceeded 1.3 pct C.¹⁰ Exact calculations could be made using the determined value of D_c^1 and Eq 10. However, a step-by-step method of solution would then be employed.

Calculations of D_c^1 at a number of temperatures were made using suitable sets of data obtained by Wells and Mehl. The results are summarized in Table 3. Since it is to be expected that the D_c^1 values will be approximately equal to the usual diffusion constant determined at low carbon contents, the latter values reported by Wells and Mehl for 0.1 pct C are included in the table.

A plot of D_c^1 vs. $\frac{1}{T}$ is shown in Fig 3. The 1102°C point does not fall on the straight line connecting the above three points, possibly because of error in extrapolating the activity data. Assuming that the variation of the diffusion constant with temperature can be written,⁵

$$D_c^1 = A e^{-\frac{Q}{RT}} \quad [16]$$

the straight line of Fig 3 can be analyzed to give the results,

$$A = 0.17 \text{ cm}^2 \text{ per sec} \quad [17]$$

$$Q = 33,800 \text{ cal per mol} \quad [18]$$

This Q value is practically the same as that found by Wells and Mehl for 0 pct C, 33,300.

Discussion of Results

The advantage of the use of activities in diffusion analysis is that a diffusion constant independent of the concentration of the diffusing element is obtained. Not only is this fact useful mathematically, but it is also of great potential value in the fundamental understanding of metal behavior involving diffusion. However, it is neces-

sary to examine more closely the significance of the multiplicity of permissible activity diffusion constants.

At a given temperature, T , where D_f is constant, Eq 7 shows that the ratio of the activity diffusion constants referred to the two different standard fugacities f_1° and f_2° is,

$$\frac{D_{ff_1^\circ}}{D_{ff_2^\circ}} = \frac{f_1^\circ}{f_2^\circ} \quad [19]$$

But since for a given fugacity,

$$f = a_1 f_1^\circ = a_2 f_2^\circ \quad [20]$$

the ratio is also equal to a_2/a_1 . Similarly, at a different temperature, T' ,

$$\frac{D'_{ff_1^\circ}}{D'_{ff_2^\circ}} = \frac{f_1^{\circ'}}{f_2^{\circ'}} = \frac{a_2'}{a_1'} \quad [21]$$

However, since the ratio a_2/a_1 , will not in general be equal to a_2'/a_1' , it follows that the various activity diffusion constants will not vary in the same ratio with temperature; that is, the activation energies for the various activity diffusion constants will be different.

At first thought this circumstance appears to destroy the usefulness of activity diffusion constants, since the activation energy is a quantity of considerable fundamental significance. Further consideration shows the situation to be quite otherwise. Certainly the activation energy of metal A diffusing in a solid solution would be expected to depend on the concentration of A atoms in the solid solution. Specifically, different values would be expected in a dilute solution (almost pure metal B) than in a concentrated solution (almost pure metal A). It appears reasonable that the Q value determined in a

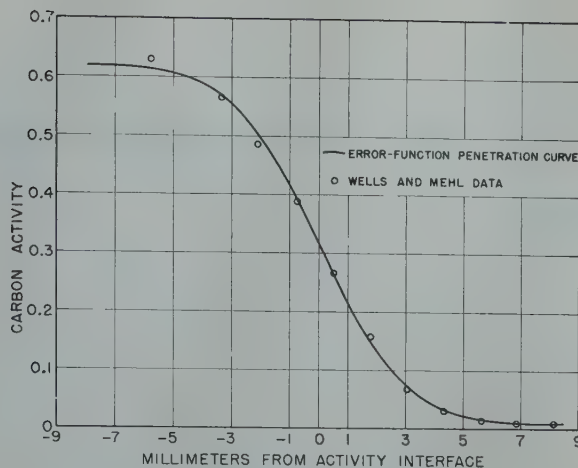


FIG 2—Comparison of the experimental data with the calculated activity-penetration curve for carbon diffusing in iron at 997°C for 25.25 hr.

Table 2 . . . Values of the Activity Diffusion Constant, D' , Determined from the 42.66 Hr Test at 1001°C

| Weight Per Cent Carbon | Carbon Activity | Distance from Interface, mm | D' cm ² per sec $\times 10^7$ |
|------------------------|-----------------|-----------------------------|--|
| 0.895 | 1.004 | -2.78 | 3.89 |
| 0.783 | 0.840 | -1.26 | 2.91 |
| 0.587 | 0.602 | +0.27 | 2.83 |
| 0.397 | 0.394 | +1.80 | 3.71 |
| 0.208 | 0.205 | +3.33 | 3.22 |
| | | Average | 3.31 |

Table 3 . . . D_c^1 Data for a Number of Temperatures

| Temp. °C | Wells and Mehl Test Number | $D' \times 10^7$ | Z' | $D_c^1 \times 10^7$ | Usual Diffusion Constant Value for 0.1 pct C ⁷ $\times 10^7$ |
|----------|----------------------------|------------------|------|---------------------|---|
| 800 | 13 | 0.274 | 1.23 | 0.222 | |
| 925 | 19 | 1.41 | 1.21 | 1.17 | 1.1 |
| 1001 | 10 | 3.31 | 1.24 | 2.67 | 2.6 |
| 1102 | 24 | 11.1 | 1.17 | 9.50 | 7.7 |

given instance is that characteristic of the standard state being used. For example, the Q obtained by plotting D_c^1 data applies to the diffusion of carbon in infinitely dilute solution in γ -iron.

Since diffusion constant values applicable for different standard states are in inverse ratio to the corresponding activities, Eq 19 and 20, it is an easy matter to determine the diffusion constant, D^i , characteristic of the standard state in which $a_i = 1$ when the concentration is c_i . Considering diffusion in a solution of concentration c_i ,

$$\frac{D^1}{D^i} = \frac{a_i c_i}{\alpha[c_i]c_i} = \frac{1}{\alpha[c_i]} \quad [22]$$

* The D' value was corrected for the 4°C difference in temperature of the two tests.

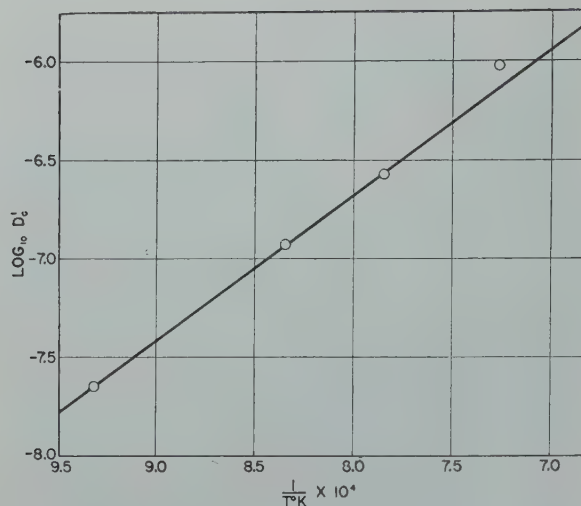


FIG 3—The variation of D_{C^1} with temperature.

where $\alpha[c_i]$ represents the value of the activity coefficient for use with dilute solutions evaluated at c_i . Using Eq 22, activation energies of 33,700 and 33,300 were calculated for 0.4 and 0.8 pct C standard states by means of the D_{C^1} values at 800° and 1001°C of Table 3 and the activity data of Table 1. These are in qualitative agreement with the results obtained by Wells and Mehl. The Q value of 42,000 given by Birchenall and Mehl⁴ is of questionable theoretical significance since it was obtained using a different standard fugacity for each temperature.

A matter that has caused some concern in previous attempts to analyze the diffusion of carbon in iron has been the "interface anomaly." This term describes the fact that the respective interfaces on which the Grube and Matano solutions are based fail generally to coincide. The question then arises as to which of these is the significant interface.

There seems little doubt that the initial interface (in the Kirkendall sense) is the significant one. The correspondence of other interfaces with this one can be summarized as follows, assuming negligible density change:

1. The Grube interface should coincide with the initial interface in perfect interstitial solid solutions. The solution of carbon in iron is not perfect, and an appreciable difference between the two interfaces is found.

2. As a consequence of its definition, the Matano interface* must coincide with the initial interface during the

* For interstitial diffusion the Matano interface definition is such that the carbon atoms gained by one side equal those lost by the other.

course of diffusion in interstitial solid solutions.

3. The interface defined by the median activity (the Grube interface marks the median concentration) will coincide with the original interface when Z (Eq 10) is constant. In the Fe-C system the variation of Z is sufficient to cause absence of perfect coincidence.

The relation between the usual diffusion constant, D^* , and the activity diffusion constant, D_{A^1} , is easily derived by equating Eq 8 and the usual form of the second Fick Law;

$$\frac{\partial c}{\partial t} = D_{A^1} \frac{\partial^2 a}{\partial x^2} = \frac{\partial}{\partial x} \left(D^* \frac{\partial c}{\partial x} \right) \quad [24]$$

Integrating the second two terms gives,

$$D_{A^1} \frac{\partial a}{\partial x} = D^* \frac{\partial c}{\partial x} \quad [25]$$

since the constant of integration must be zero. By analogy with Eq 9, Eq 25 can be written,

$$D_{A^1} Z \frac{\partial c}{\partial x} = D^* \frac{\partial c}{\partial x} \quad [26]$$

or

$$D^* = Z D_{A^1} \quad [27]$$

This equation is merely another form of the relation given by Birchenall and Mehl.⁴

Summary

1. The use of the fugacity concept has permitted a more satisfactory treatment of interstitial diffusion by activity methods.

2. Of the multiplicity of possible ac-

tivity diffusion constants, it has been proposed that D_{A^1} , corresponding approximately to the usual diffusion constant in dilute solution, be adopted as standard for analysis of interstitial diffusion.

3. An equation that permits the direct treatment of activities has been developed. A convenient approximate solution of this equation was used to analyze the data of Wells and Mehl to determine diffusion constant values. The results agreed well with those obtained by Wells and Mehl.

4. It was suggested that there is an activation energy associated with each choice of standard fugacity. That found for D_{C^1} (standard fugacity being that of an infinitely dilute solution) was 33,800, in good agreement with Wells and Mehl's extrapolated value for 0 pct C.

5. Further support for the view that the activity rather than the concentration is the basic factor in diffusion has been provided. Specifically, activity diffusion constants independent of concentration have been developed for possible application to the analysis of the more complex substitutional diffusion.

Acknowledgments

The author thanks Dr. R. F. Mehl for suggesting the problem that eventually led to this study of activity methods; Dr. K. O. Beatty, Jr., for indispensable aid with the fugacity concept; Mr. J. L. Sox for carrying out many of the calculations; and Dr. W. G. Van Note, Director of the Engineering Research Department, North Carolina State College, for his counsel and aid.

References

1. L. S. Darken: *Trans. AIME* (1942) 150, 157.
2. L. S. Darken: *Trans. AIME* (1948) 175, 184. *Met. Tech.*, Jan. 1948, TP 2311.
3. L. S. Darken: *Trans. AIME* (1949) 180, 430, *Met. Tech.*, Sept. 1948, TP 2443.
4. C. E. Birchenall and R. F. Mehl: *Trans. AIME* (1947) 171, 143. *Met. Tech.*, June, 1947.
5. R. M. Barrer: *Diffusion in and through Solids*. Cambridge Press, London, 1941.
6. B. O. Peirce: *A Short Table of Integrals*. Ginn and Co., Boston, 1929.
7. C. Wells and R. F. Mehl: *Trans. AIME* (1940) 140, 279.
8. R. P. Smith: *Jnl. Am. Chem. Soc.* (1946) 68, 1163-1175.
9. G. N. Lewis and M. Randall: *Thermodynamics*. McGraw-Hill Book Co., N. Y., 1923.
10. A. G. Guy: *Iron Age*, Jan. 27, 1949, pp. 74-76.

The Transformations in β -CuAl Alloys*

E. P. KLIER,[†] Junior Member AIME, and S. M. GRYMKO[‡]

The transformations in eutectoidal systems have been extensively studied as they occur in steels.¹ As a consequence of these studies the martensite, bainite and pearlite reactions found for most steels are widely recognized. Further, because of the work of Smith and Lindlie² and of Greninger and Troiano³ these reactions, except for the bainite reaction, are considered as typical for all eutectoidal systems.

The primary alloy studied by Smith and Lindlie² was a CuAl alloy of near eutectoid composition as was the alloy more recently studied by Mack.⁴ The transformations in these alloys were, for the most part, studied metallographically, while an X ray analysis of structures was essentially wanting. It has appeared desirable, therefore, to investigate selected CuAl alloys at and slightly away from eutectoid composition. For this purpose three alloys were prepared containing 10.5, 11.9 and 13.5 pct Al respectively. The results of a metallographic and X ray analysis of structures obtained for isothermal transformation of the β -phase are reported here for the 11.9 and 13.5 pct Al alloys.

Introduction

The phase equilibria in the CuAl alloys of immediate concern are indicated in the equilibrium diagram section presented in Fig 1. § The equilibrium and transition structures which have been reported in this system are as follows:

- α = copper rich terminal phase (f.c.c.)
- β = high temperature eutectoidal phase (b.c.c.)
- γ_2 = aluminum-rich intermediate phase (γ -brass structure)
- α' = modified α -phase postulated by Bollenrath and Bungardt.²⁶

* Taken from Metals Handbook (1948).

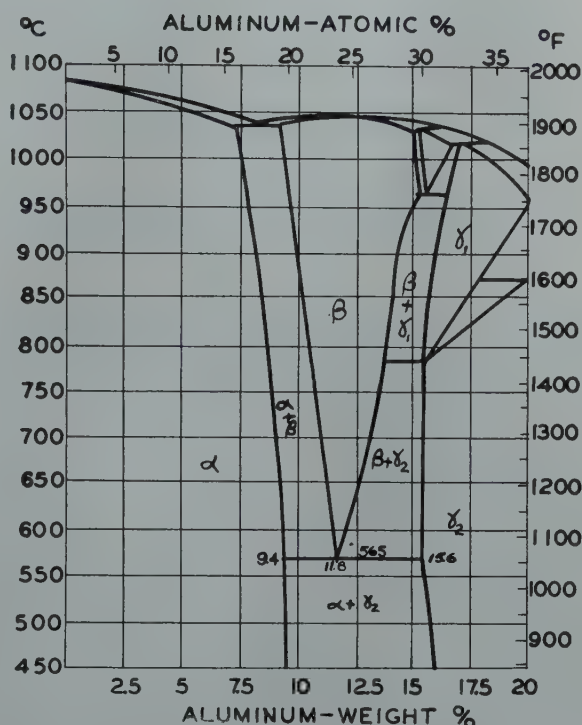


FIG 1—Phase diagram for eutectoidal Cu-Al alloys. *Metals Handbook—1948.*

- β_1 = ordered β (b.c.c.)
- β' = martensite structure: Al < 13 pct (near h.c.p.)
- β'' = β' of Smith and Lindlie²
- γ' = martensite structure: Al > 13.5 pct (h.c.p.); β_2 of Bollenrath and Bungardt.²⁶

Cleveland Meeting, October 1949.
TP 2573 E. Discussion of this paper (2 copies) may be sent to *Transactions AIME* before December 1, 1949. Manuscript received December 2, 1948; revision received May 23, 1949.

* Most of the material presented in this paper has been taken from a thesis submitted by S. M. Grymko in partial fulfillment of the requirements for the degree of Master of Science, The Pennsylvania State College, January 1949.

[†] Assistant Professor of Metallurgy, The Pennsylvania State College, State College, Pa.

[‡] Research Engineer, The Battelle Memorial Institute, Columbus, Ohio.

¹ References are at the end of the paper.

The eutectoid transformation can be suppressed at sufficiently high cooling velocities. The β -phase is then retained to about 500°C where ordering sets in. The ordering interval is not satisfactorily known but indirectly appears to be non-suppressible. Subsequent to the ordering reaction and consequently at lower temperatures, the ordered β_1 decomposes to a martensitic structure. The kinetics of these reactions and in particular those of the martensite reaction have an important bearing on the results obtained in this investigation. Since some confusion exists concerning certain reported aspects of these reactions, they will be considered in some detail.

THE MARTENSITE REACTION

The martensitic structure is formed on cooling through a critical range⁶

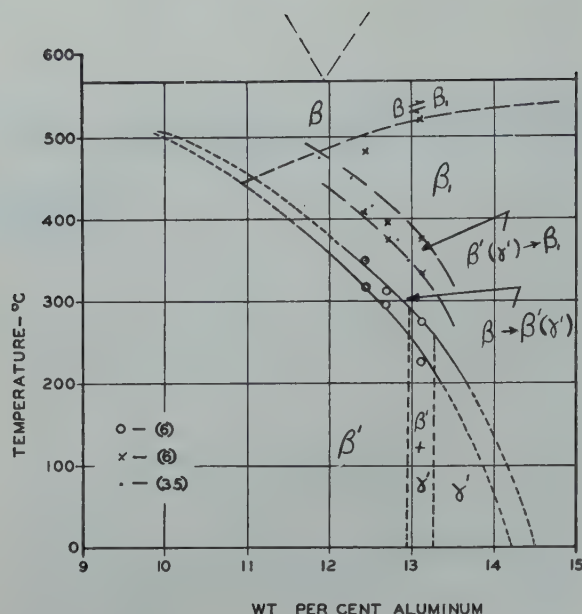


FIG 2—The effect of composition on the sub-critical transformations in eutectoidal Cu-Al alloys.

much as is martensite in steels.^{12,3} The Ar'' temperature for the CuAl alloys depends on the composition and decreases with increasing aluminum content.⁹ In certain composition ranges Ar'' is cooling velocity dependent⁸ although it is pointed out that this dependence on cooling velocity may be indirect. Thus the indicated variation in Ar'' may result from a modification of the ordering reaction with cooling velocity. At a composition of 14.5 pct Al the martensite range is entirely below room temperature but lies above -190°C .¹⁰ However, due to the reversibility of this reaction ($\beta_1 \rightleftharpoons \gamma'$) the martensitic structure is not retained at room temperature.

The inverse martensite reaction, that is, the formation of β_1 from the martensitic structure takes place on suitable heating of the martensitic structure. This reaction has been established by metallographic¹⁴ dilatometric^{7,15} and X ray^{5,6} analyses of the structures at temperature and lies above the martensite range on cooling. These data are summarized in Fig 2. The inverse martensite reaction is probably sensitive to heating velocity, but few data are available for consideration on this point.

THE STRUCTURE OF THE CuAl MARTENSITES

The microstructures of the CuAl martensites have been adequately described by Greninger.¹¹ It is sufficient to point out that two structures β' and γ' are separable on the basis of

metallographic differences. The striations in γ' arise from twin formation while those in β' seemingly do not.

The crystal structures of the martensites are close to hexagonal close packed. The departures from the close packed lattice, observed for the β' structure, are notable at low aluminum contents. Thus while the lattice for γ' containing 13.5 pct Al is described as a hexagonal close packed structure, the lattice for β' is described as differing from γ' in that the $[00.1]$ direction is at an angle of 2° to the (00.1) plane normal, and the angle between the planes (10.0) and (01.0) differs about 1° from 120° .¹³ Because of this departure from the hexagonal close packed structure the X ray pattern for the β' structure is markedly different from that for the γ' structure. This is very important as it affords an unambiguous means of determining qualitatively the compositions of the martensitic structures in partially transformed alloys without requiring the precision measurement of lattice constants.

THE REACTION $\beta \rightarrow \beta''$

The structure β'' as noted before was discovered by Smith and Lindlie² on the isothermal transformation of β for an eutectoidal alloy. Smith and Lindlie on the basis of limited X ray evidence have considered this structure as being aluminum dilute apparently tending towards the composition of the α -phase.

More recently Mack⁴ has considered this structure as being β_1 or the

ordered β structure and has defined its range of occurrence in an 11.9 pct Al alloy from about 525 to 93°C . On the basis of the discussion of the kinetics of martensite formation it is evident that the reasoning which led Mack to place the lower limit of the martensite range at 93°C is faulty.

It is emphasized that β'' is not β_1 . A specimen of 11.9 pct Al alloy quenched from 950°C is an ordered structure but does not reveal the metallographic structure β'' .

THE ISOTHERMAL TRANSFORMATION DIAGRAM FOR EUTECTOIDAL CuAl ALLOYS

Isothermal transformation diagrams in comparable eutectoidal alloys have been presented by Smith and Lindlie² and by Mack.⁴ These diagrams are in good agreement except for the martensite range which has been modified by Mack to conform with more recent knowledge about this reaction. Beyond this discrepancy both diagrams describe a pearlite range and a β'' range which stand in good agreement where comparable.

From the discussion of the inverse martensite reaction it appears that certain of Mack's tempering data may require re-evaluation.

The works of Smith and Lindlie and of Mack are the only ones in which the isothermal transformations in eutectoidal CuAl alloys have been reported in detail.

Experimental Procedure

MATERIALS

The alloys for this investigation were prepared from high purity aluminum and OFHC copper. Melting was carried out in a graphite crucible under graphite. The molten alloys were stirred several times and were then chill cast. The ingots were about $\frac{1}{4} \times 2 \times 3$ to 5 in. and were very coarse grained. These ingots were hot-rolled in part to $\frac{1}{8}$ and $\frac{1}{32}$ in. thicknesses.

The ingots were analyzed for copper by both chemical and electrolytic methods. The aluminum content was determined by difference. The results are presented in Table 1.

ISOTHERMAL STUDIES

Sliver specimens ($\frac{1}{2} \times \frac{1}{32} \times 1$ in.; $\frac{1}{8} \times \frac{1}{32} \times 1$ in.) were heated at 950°C for 10 min. in a vertical tube

furnace in an atmosphere of purified nitrogen. The specimens were quenched into a small lead furnace at the desired temperature and after holding were quenched in a 10 pct aqueous solution of sodium hydroxide. The temperature of the quenching bath was controlled to $\pm 1\frac{1}{2}^{\circ}\text{C}$. A lead-tin bath was used for the lowest transformation temperatures.

METALLOGRAPHIC EXAMINATION

The sliver specimens were polished in clamps with the final surface being obtained with magnesium oxide (Shamva) on a selvyt cloth. The specimen was etched in a fresh 1:1 solution of NH_4OH and 3 pct H_2O_2 .

X RAY EXAMINATION

The metallographic specimens were polished and etched down to slivers about $\frac{1}{64}$ in. diam. Debye-Scherrer diagrams using $\text{Cu-K}\alpha$ radiation (Ni filter) were obtained. Standard β' and γ' patterns were obtained on the 10.5, 11.9, and 13.5 pct Al alloys as quenched from 950°C into the aqueous NaOH solution. Suitable α and γ_2 reference patterns were obtained on the isothermally transformed alloys.

REPRESENTATION OF TEST RESULTS

The data have been presented in the form of isothermal transformation diagrams. Suitable micrographs and X ray diffraction patterns have been presented.

Experimental Results

Because of the emphasis with which the alloy of eutectoid composition has been studied, it appeared desirable to devote the major effort in this investigation to a study of the 13.5 pct Al alloy. The transformations in this alloy, therefore, will be considered first.

THE 13.5 PCT AL ALLOY

Metallographic Results

The isothermal transformation diagram for this alloy is presented in Fig 3. There are certain striking features to this diagram. Firstly, the temperature of maximum transformation rate for practical purposes coincides with the eutectoid temperature. Secondly, it has appeared necessary to make use of four transformation

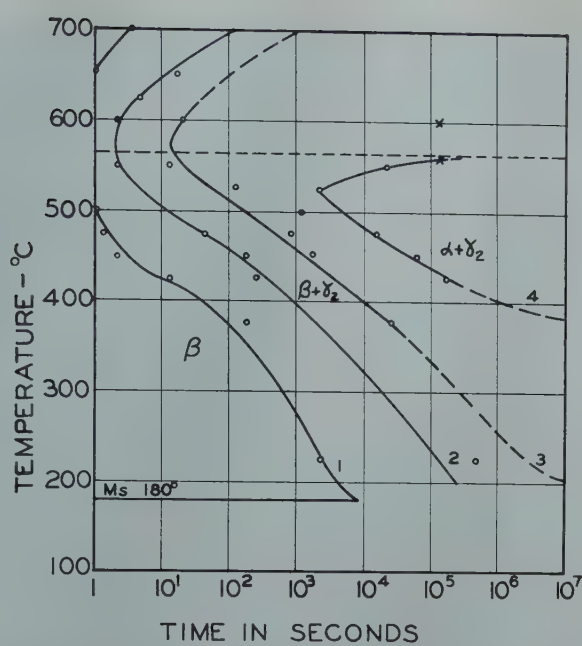


FIG 3—The isothermal transformation diagram for a 13.5 pct Al-Cu alloy.

Table 1 . . . Analyses of the Alloys

| Alloy | Pct Al by Electrodeposition | Pct Al by Chem. Analysis |
|-------|-----------------------------|--------------------------|
| 11.9 | 11.90 | 11.85 |
| | 12.00 | 11.86 |
| | 12.00 | 12.00 |
| 13.5 | 13.60 | 13.40 |
| | 13.52 | 13.43 |
| | | 13.58 |

lines to describe adequately the course of isothermal transformation, and thirdly, no pearlite reaction is indicated. These facts may best be appreciated from a consideration of the microstructures.

In Fig 4 and 5 are presented the structures corresponding to beginning and end of the first reaction at 550°C as indicated by lines 1 and 2 on the isothermal transformation diagram. The precipitate structure is truly acicular and seemingly forms on the $\langle 100 \rangle_{\beta}$ directions. The structures formed by this reaction are not stable structures and rapidly undergo alteration at this temperature. The alteration seemingly is a species of agglomeration and growth, which, as will be pointed out, is not a simple process. The third line on the diagram indicates the start of agglomeration while the fourth line indicates the time for completion of the precipitation-growth process. Further holding causes no apparent change in this final structure except for a marked coarsening. These final alterations are indicated in Fig 6 to 8. There has been no pearlite structure formed during the course of transformation. This is emphasized by a

consideration of Fig 9 which reveals the nearest approach to a pearlitic structure which has been observed in this alloy on isothermal transformation.

The transformation sequence revealed in the above micrographs is typical except for minor variations for all structures formed below the eutectoid temperature. As is implied by the fourth line on the transformation diagram, transformation above the eutectoid temperature differs in certain important respects.

The structure existing at the end of the first reaction at 650°C is presented in Fig 10. The structure existing at the end of the second reaction is presented in Fig 11. The final structure under polarized light is seen to have a matrix of an acicular nature, Fig 12. This sequence of structures emphasizes the role of the first reaction in leading to transitional structures which in turn lead to the formation of the final equilibrium structures.

The initial and final structures are modified as a function of the transformation temperature but at all temperatures the structures arising from the first reaction are closely related microstructurally.

At the highest temperatures studied the initial reaction did not lead to complete decomposition of the matrix, Fig 13. This is to be expected since presumably above the eutectoid temperature only a proeutectoid constituent should precipitate. The character of the first reaction cannot be

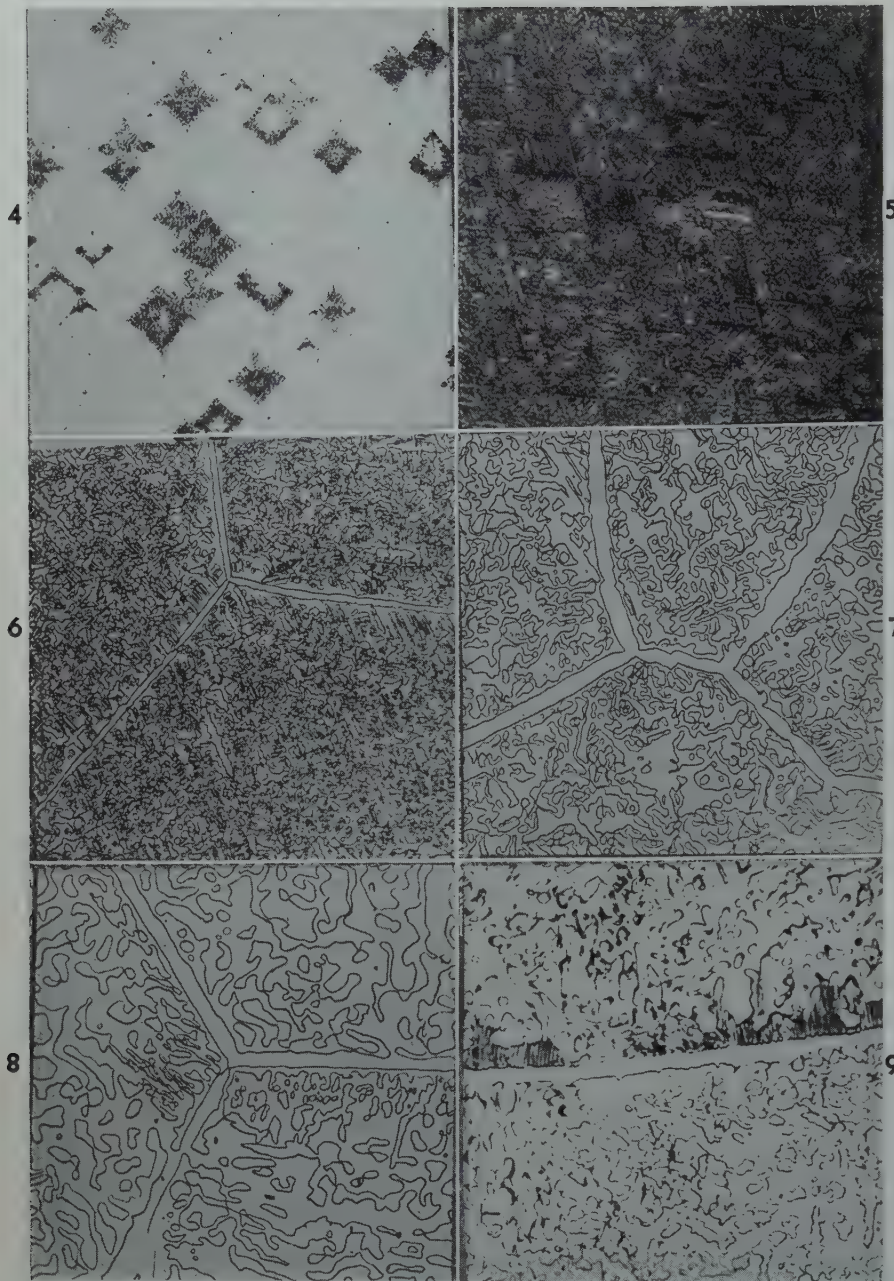


FIG 4—13.5 pct Al-Cu specimen transformed at 550°C for 1 sec. $\times 250$
 FIG 5—13.5 pct Al-Cu specimen transformed at 550°C for 3 sec. $\times 250$
 FIG 6—13.5 pct Al-Cu specimen transformed at 550°C for 32 min. $\times 250$
 FIG 7—13.5 pct Al-Cu specimen transformed at 550°C for 9 hr. $\times 250$
 FIG 8—13.5 pct Al-Cu specimen transformed at 550°C for 1 week. $\times 250$
 FIG 9—13.5 pct Al-Cu specimen transformed at 425°C for 24 hr. $\times 250$

elucidated on the basis of metallographic evidence, however.

As the transformation temperature is decreased the microstructures become finer, Fig 14 to 21. At temperatures increasingly lower than the eutectoid temperature the first reaction becomes increasingly sluggish. The times for the completion of the precipitation-growth reaction below the eutectoid temperature develop a C-shaped curve which is comparable to that developed for the pearlite reaction in steels.¹⁶ The temperature for minimum reaction time

does not coincide with the analogous temperature for the first reaction but lies below the eutectoid temperature. From this it may be concluded that stable end structures arise as a consequence of the second reaction.

These data may be summarized briefly before the X ray data are considered. The metallographic data indicate that two reactions are encountered on isothermal transformation in this alloy, one of which leads to metastable structures as indicated by its occurrence through the eutectoid tem-

perature range. After completion of this reaction a second reaction sets in and leads to the complete modification of the microstructures with the ultimate formation of stable end products. Both reactions are represented by a combination of C-shaped curves and differ in that the eutectoid temperature affects the location of the stable structures completion curve.

X Ray Results

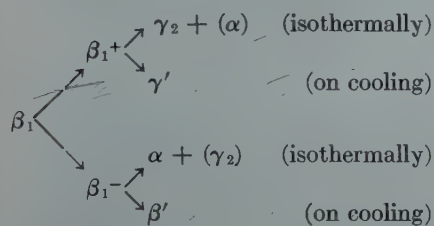
Four different crystal structures, indicated by X ray analysis may be obtained together in the transformed specimens, namely those of α , γ_2 , β' , and γ' . Positive evidence of β_1 was not obtained for the 13.5 pct Al alloy. The diffraction patterns characteristic of these four crystal structures are presented in Fig 22 to 25. The spotted lines in the pattern in Fig 23 arise from the γ_2 lattice while the continuous lines arise from α . Many of the lines in the β' and γ' patterns correspond closely to lines in the α and γ_2 patterns. Strong lines which are characteristic for the respective structures are indicated on the patterns. All diffraction patterns were checked for these strong lines. The presence or absence of the respective lines was taken as indicating the presence or absence of the respective structures.

The pattern for the β' structure was obtained from an 11.9 pct Al specimen quenched from 950°C into water + 10 pct NaOH. From the presence of the weak lines at low θ values it is evident that this structure is ordered. The γ' structure likewise is ordered.

The results of the X ray analysis are summarized in Table 2. Important diffraction patterns of the structures reported in Table 2 are presented in Fig 26 and 27. These data indicate the following sequence of composition adjustment in the transforming specimens. Prior to the start of the first reaction, the structure as quenched is γ' with possible traces of β' , Fig 25. Through the course of the first reaction the structure in the quenched specimens becomes a mixture of γ' and β' , Fig 26. This structure exists at the times corresponding to completion of the first reaction which means that the γ' revealed is not matrix γ' , or γ' which has been unaltered in composition. Rather because of the formation of large amounts of β' it is necessary that the γ' formed be very rich in aluminum. The γ' structure is next replaced by γ_2 and the structure is γ_2 and β' , Fig 27. For the fully transformed alloy the

structure is α and γ_2 , Fig 23.

The first reaction leads to the formation of structures in the as quenched specimens, which, it is known, cannot be formed at the temperature of isothermal holding. Since β' and γ' form from β_1 (or β) of characteristic composition it is concluded that the structures resulting from the first reaction prior to the quenching process consist of β_1 of two compositions, namely, β_1^+ which is aluminum rich and β_1^- which is aluminum depleted. There are thus two β_1 structures, one tending toward the composition of α , the other toward the composition of γ_2 . It is emphasized that these structures have not precipitated at temperature, rather the process throughout is a diffusion process alone. The β_1^+ becomes enriched in aluminum to the point where it can precipitate as γ_2 . The precipitation of γ_2 at the expense of the aluminum content of the β_1^- continues to the point where α can precipitate. The final structure then being α and γ_2 . This sequence of events is indicated as follows:



The reactions on isothermal holding seemingly are not interdependent. It is assumed that the same is true for the reactions on cooling.

The transformation sequence described here is in complete harmony with that for the transformation of austenite to bainite in steels.¹⁶⁻¹⁸ The composition of the structures and the manner in which the necessary composition adjustments are achieved in this CuAl alloy, however, are much more easily determined than is true for the steels.

THE 11.9 PCT Al ALLOY

Metallographic Results

The transformation data for this alloy for stock thicknesses of $\frac{1}{8}$ and $\frac{1}{32}$ in. are presented in the isothermal transformation diagram in Fig 29.

This isothermal transformation diagram, above the martensite range, is in good agreement with those diagrams presented by Smith and Lindlie² and

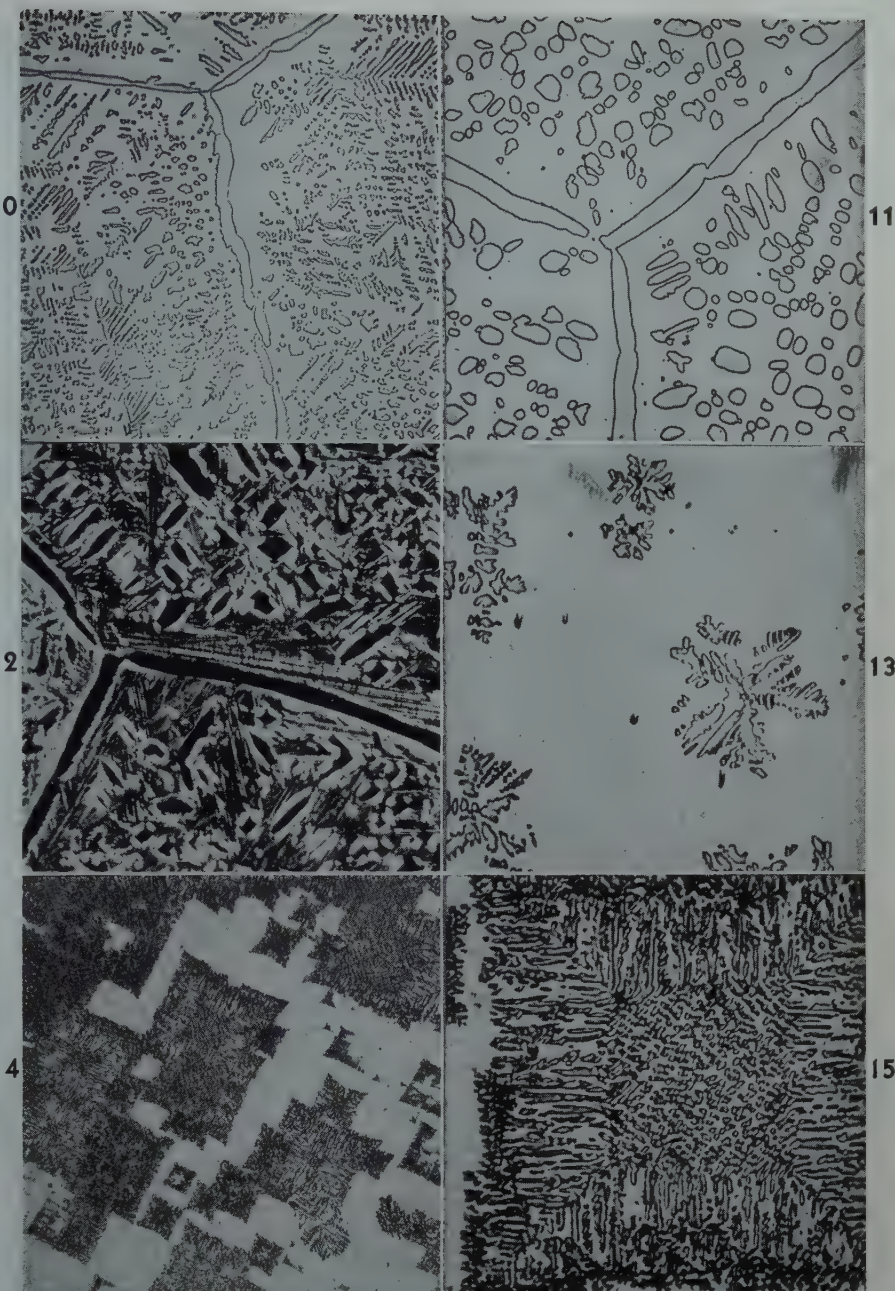


FIG 10—13.5 pct Al-Cu specimen transformed at 650°C for 5 min. $\times 250$

FIG 11—13.5 pct Al-Cu specimen transformed at 650°C for 2 hr. $\times 250$

FIG 12—13.5 pct Al-Cu specimen transformed at 650°C for 2 hr. Polarized light. $\times 250$

FIG 13—13.5 pct Al-Cu specimen transformed at 700°C for 5 sec. $\times 1000$

FIG 14—13.5 pct Al-Cu specimen transformed at 600°C for 1 sec. $\times 250$

FIG 15—13.5 pct Al-Cu specimen transformed at 600°C for 1 sec. $\times 1000$

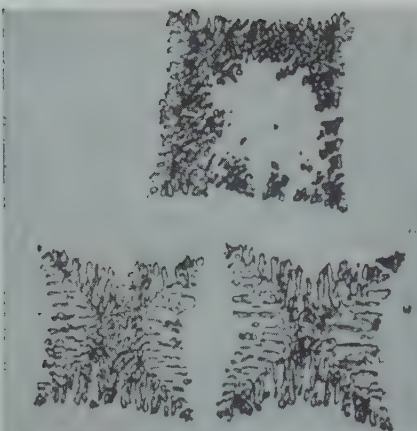
Mack.⁴ The γ_2 precipitate observed by Mack in the high temperature range of transformation is not observed for this alloy. The martensite range is presented after the data of Gawranek et al.⁹

In the intermediate range in which β'' and α are formed it is interesting to note that some disagreement in the times for the β'' and α reactions exists for the two materials. The increased working or possibly the reduced grain size of the $\frac{1}{32}$ in. thick alloy promotes

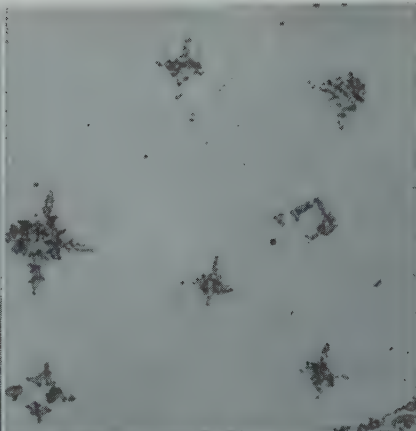
more rapid transformation in the intermediate range. The results for the $\frac{1}{32}$ in. thick stock are in satisfactory agreement with the results of Smith and Lindlie, and with those of Mack where comparable.

The metallographic data for the pearlite structures are interesting with respect to the pearlite spacing. It is generally accepted on the basis of pearlite spacings measurements on steels¹⁹⁻²³ that the pearlite structures become finer with decreasing tempera-

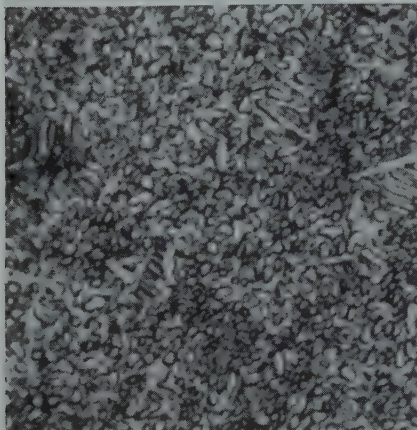
16



17



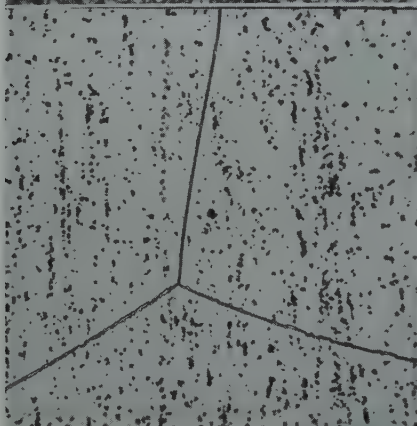
18



19



20



21

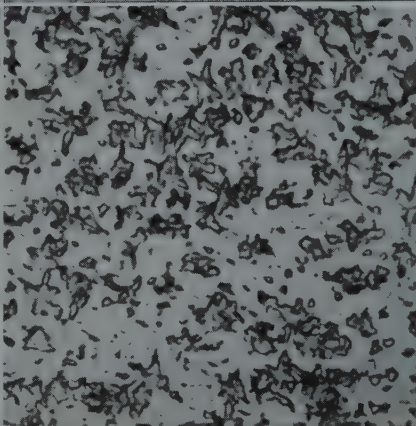


FIG 16—13.5 pct Al-Cu specimen transformed at 550°C for 1 sec. $\times 1000$
 FIG 17—13.5 pct Al-Cu specimen transformed at 475°C for 8 sec. $\times 1000$
 FIG 18—13.5 pct Al-Cu specimen transformed at 425°C for 60 sec. $\times 1000$
 FIG 19—13.5 pct Al-Cu specimen transformed at 375°C for 4 min. $\times 1000$
 FIG 20—13.5 pct Al-Cu specimen transformed at 225°C for 24 hr. $\times 250$
 FIG 21—13.5 pct Al-Cu specimen transformed at 225°C for 1 week. $\times 1000$

ture of formation. This is evidently not the case for the pearlite spacing in the CuAl alloy under investigation. For this alloy the pearlite spacing first decreases with decreasing temperature of formation. After passing through a minimum value it next increases. Thus the functional relationship between pearlite spacing and temperature cannot have the same form for this alloy as it apparently has for steels.^{20,23}

In a consideration of the relationship between pearlite spacing and temperature it is pointed out that for steels the

pearlite structures are divided into the coarse lamellar types and into the rosette (lamellar) or troostitic types. The first named occur well above the nose of the "S" curve while the second occur at about the nose of the "S" curve. (It has been pointed out that pearlitic structures as yet inadequately defined occur below the nose of the "S" curve.^{16,18}) As the temperature for pearlite formation decreases the interlamellar spacing decreases. This change in dimensions of the pearlite has been advanced as indicating a limiting car-

bide nucleus size,^{20,23} and this carbide nucleation has been used to account for the pearlite reaction. By an extension of this argument to conform to the requirements of the CuAl alloy investigated here, it would be expected that microstructural variations in the pearlitic structures would be analogous to those observed in steels. Such is not the case, however. Thus the coarse pearlites are replaced at lower temperatures by nodular pearlites—at about the "nose" of the C-curve—but these in turn give way at still lower temperatures to coarse lamellar pearlites, Fig 30 to 32. Thus the kinetics of pearlite formation in this alloy cannot be accounted for by simple comparison with the analogous reaction in steels.

X Ray Results

X ray data taken on specimens of the 11.9 pct Al alloy transformed at several temperatures are presented in Table 3. The patterns taken for transformation in the intermediate range, that is, the range in which β'' and α are formed indicate that the reaction in this range is essentially the same as that encountered in the 13.5 pct Al alloy for the first reaction. The major difference appears to be the change in the sequence in which the precipitate structures appear on isothermal transformation. Thus the structure existing in specimens quenched before α precipitates is β' . The structure after longer holding is $\alpha + \beta'$ which, on further holding, is replaced by a mixed structure of α , β' , and γ' . The amount of γ' formed is relatively small as is indicated in Fig 28. The final structure is $\alpha + \gamma_2$. The γ_2 lines are very weak.

Discussion of Experimental Results

The pearlite reaction has been considered as a reaction to be expected in general in the course of the subcritical decomposition of a high temperature eutectoidal phase. That this reaction is not generally obtained is indicated by the results presented here in the study of the 13.5 pct Al alloy. Results of a similar character have recently been reported by Hibbard et al²⁴ and by Sheehan et al.²⁵

In the CuAl alloys it appears that the pearlite reaction cannot be obtained at aluminum contents of 10.5 pct* and less or at 13.5 pct and greater. This is

*Further work on this alloy is contemplated. Results to date indicate the absence of the pearlite reaction.

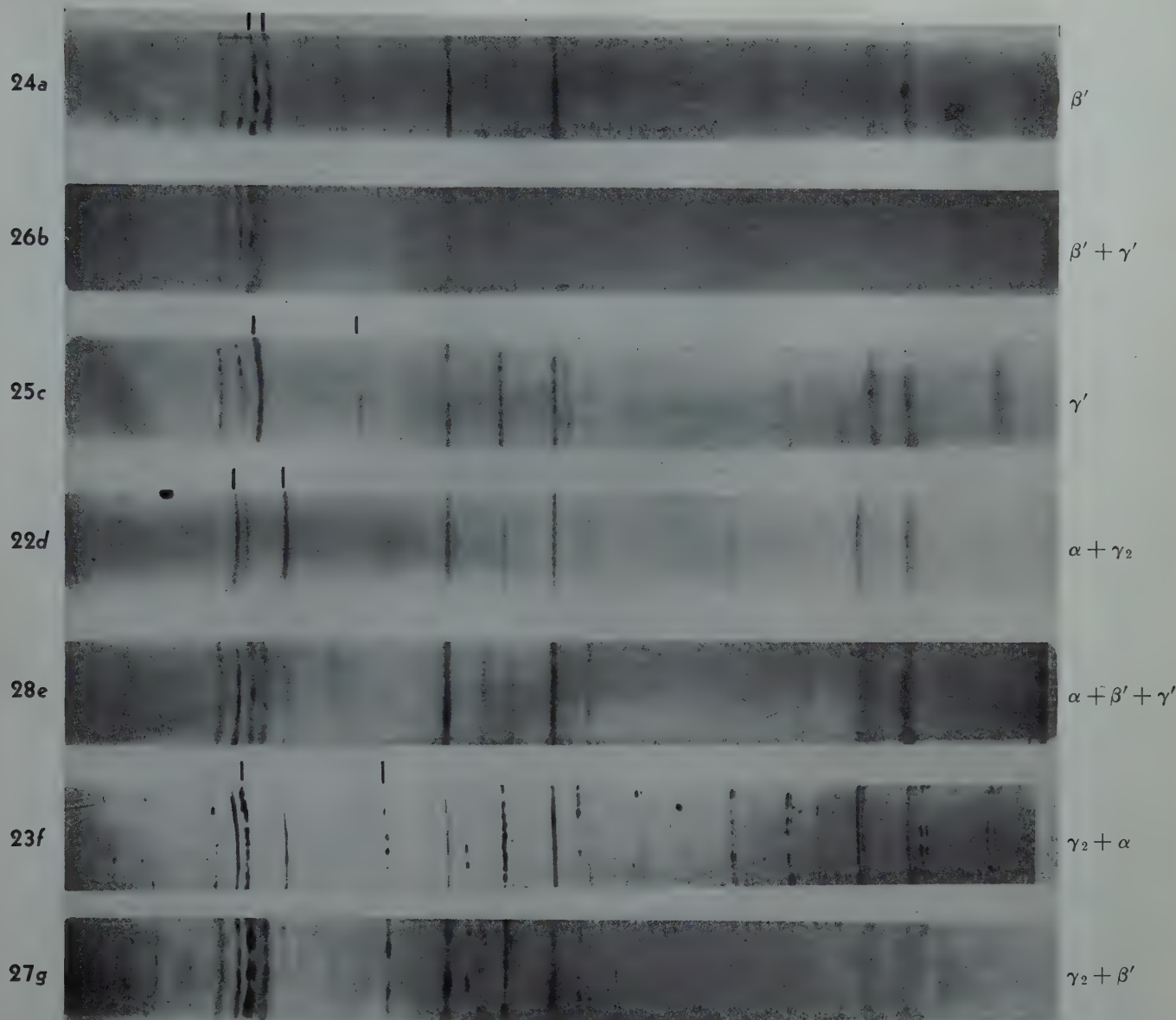


Fig 22-28—X ray Diffraction Patterns

Fig 22—(d) Alloy 11.9 pct Al held 1 hour at 500°C
 Fig 23—(f) Alloy 13.5 pct Al held 3 hours at 525°C
 Fig 24—(a) Alloy 11.9 pct Al held 60 seconds at 500°C
 Fig 25—(c) Alloy 13.5 pct Al held 1 hour at 225°C
 Fig 26—(b) Alloy 13.5 pct Al held 48 hours at 225°C
 Fig 27—(g) Alloy 13.5 pct Al held 6 seconds at 500°C
 Fig 28—(e) Alloy 11.9 pct Al held 8 minutes at 450°C

(Note: Standard patterns are indicated by underlines. Characteristic diffraction lines are indicated by vertical lines on the respective standard patterns.)

not readily explainable on the basis of the current concepts of the pearlite reaction for seemingly about 50 pct of the β -phase in both the 10.5 and 13.5 pct Al alloys should be available for pearlite formation.

The preliminary reaction which is obtained in the 13.5 pct Al alloy on isothermal holding seemingly is intimately related to the β'' reaction in the 11.9 pct Al alloy. Thus for both alloys it appears that the diffusion of aluminum takes place prior to any crystal structure change in the matrix. If the alloy is cooled before the crystal structure change in the aluminum rich or depleted zones can take place, the crystal structure change is effected during the quenching cycle. The structure at room temperature then is a martensitic structure, one made up of mar-

tensites of the various compositions of the transforming β_1 . Further since the crystallography of these zones of aluminum enriched and depleted β is fully determined, the martensitic structures formed during the quenching cycle are restricted by this crystallography. Thus neither β' nor γ' have the orientation habits determined by Greninger.¹¹ Since it is possible that the lattice relationships for the structures examined here and those examined by Greninger are the same, there arises the possibility that the martensite transformation mechanism varies with pretreatment of the matrix.

The first reaction in the 13.5 pct Al alloy and the β'' reaction in the 11.9 pct Al alloy are reactions which conform in all major details to the proposed bainite reaction¹⁷ in steels. In the 13.5

pct Al alloy the β_1 structure is modified by diffusion processes such that aluminum enriched and depleted zones are set up. These regions become evident at room temperature under metallographic examination, because of the different etching characteristics of the β' and γ' .

After the β_1^+ and β_1^- structures are formed, both decompose but evidently by more complicated processes than were observed for the bainite reaction in steels. This follows from the fact that the final structure is markedly different from the structure arising as a consequence of the first reaction. Thus if the γ_2 (in the 13.5 pct Al alloy) were formed in the matrix by a shearing mechanism such as is postulated for the bainite reaction in steels, a supersaturated γ_2 structure would be obtained and this

Table 2 . . . Structures by X ray Diffraction in Transformed Specimens of Alloy 13.5 Pct Al

| 700°C | | 600°C | | 550°C | | 525°C | | 500°C | |
|-------|---------------------|--------|---------------------|--------|---------------------|--------|---------------------------------|---------|---------------------------------|
| Time | Structure | Time | Structure | Time | Structure | Time | Structure | Time | Structure |
| 80 hr | $\beta' + \gamma_2$ | 1 sec | $\gamma_2 + \beta'$ | 1 sec | $\gamma_2 + \beta'$ | 8 sec | $\gamma_2 + \beta' + (\gamma')$ | 5 sec | $\beta' + \gamma'$ |
| | | 3 sec | $\gamma_2 + \beta'$ | 32 min | $\gamma_2 + \beta'$ | 16 sec | $\gamma_2 + \beta'$ | 15 sec | $\beta' + \gamma'$ |
| | | 10 sec | $\gamma_2 + \beta'$ | 9 hr | $\alpha + \gamma_2$ | 2 min | $\alpha + \gamma_2 + (\beta')$ | 30 sec | $\beta' + \gamma' + (\gamma_2)$ |
| Time | 650°C | 30 sec | $\gamma_2 + \beta'$ | 1 wk | $\alpha + \gamma_2$ | 30 min | $\alpha + \gamma_2$ | 60 sec | $\beta' + \gamma_2 + (\gamma')$ |
| 5 sec | $\beta' + \gamma'$ | 2 min | $\gamma_2 + \beta'$ | | | 3 hr | $\alpha + \gamma_2$ | 120 sec | $\beta' + \gamma_2$ |
| 8 min | $\beta' + \gamma_2$ | 48 hr | $\gamma_2 + \beta'$ | | | | | 5 min | $\beta' + \gamma_2$ |
| | | | | | | | | 15 min | $\beta' + \gamma_2$ |
| | | | | | | | | 1 hr | $\beta' + \gamma_2 + (\alpha)$ |
| | | | | | | | | 6 hr | $\alpha + \gamma_2$ |

| 475°C | | 450°C | | 425°C | | 375°C | | 225°C | |
|---------|---------------------|--------|---------------------------------|--------|----------------------|--------|---------------------------------|-------|---------------------------------|
| Time | Structure | Time | Structure | Time | Structure | Time | Structure | Time | Structure |
| 26.5 hr | $\alpha + \gamma_2$ | 5 sec | $\gamma' + (\beta')$ | 5 sec | $\gamma' + \gamma_2$ | 4 min | $\gamma' + (\beta')$ | 1 hr | $\gamma' + (\beta')$ |
| | | 15 sec | $\gamma_2 + \beta' + (\gamma')$ | 5 min | $\beta' + \gamma_2$ | 1 hr | $\beta' + \gamma_2 + (\gamma')$ | 24 hr | $\gamma' + (\beta')$ |
| | | 60 sec | $\gamma_2 + \beta' + (\gamma')$ | 1 hr | $\beta' + \gamma_2$ | 26 hr | $\gamma_2 + \beta'$ | 48 hr | $\beta' + \gamma' + (\gamma_2)$ |
| | | 2 min | $\gamma_2 + \beta' + (\gamma')$ | 12 hr | $\beta' + \gamma_2$ | 187 hr | $\gamma_2 + \beta'$ | 1 wk | $\beta' + \gamma' + (\gamma_2)$ |
| | | 5 min | $\beta' + \gamma_2$ | 60 hr | $\alpha + \gamma_2$ | | | | |
| | | 10 min | $\beta' + \gamma_2$ | 148 hr | $\alpha + \gamma_2$ | | | | |
| | | 16 min | $\beta' + \gamma_2$ | | | | | | |
| | | 40 min | $\beta' + \gamma_2$ | | | | | | |
| | | 1 hr | $\beta' + \gamma_2$ | | | | | | |
| | | 4.5 hr | $\beta' + \gamma_2 + (\alpha)$ | | | | | | |
| | | 17 hr | $\alpha + \gamma_2$ | | | | | | |
| | | 36 hr | $\alpha + \gamma_2$ | | | | | | |

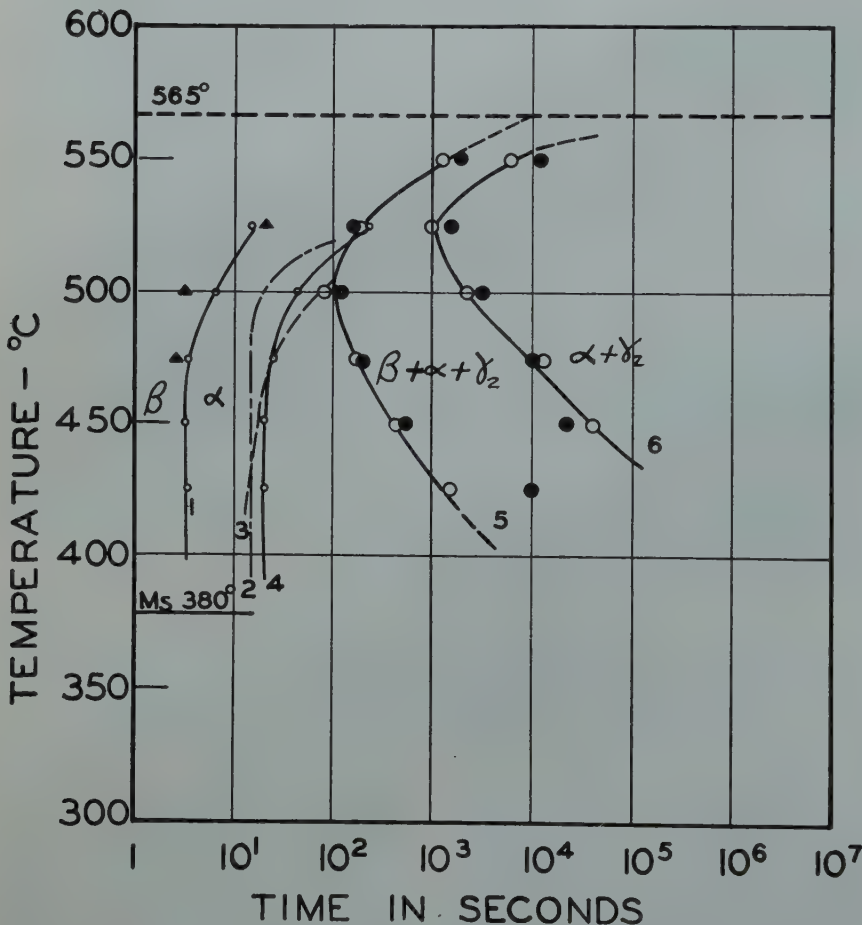


FIG 29—The isothermal transformation diagram for an 11.9 pct Al-Cu alloy.

Curve 1. α precipitation at grain boundaries. $\frac{1}{32}$ in. stock.
 Curve 2. α precipitation at grain boundaries. $\frac{1}{8}$ in. stock.
 Curve 3. α precipitation in grains. $\frac{1}{32}$ in. stock.
 Curve 4. α precipitation in grains. $\frac{1}{8}$ in. stock.
 Curve 5. Beginning of pearlite reaction.
 Curve 6. End of pearlite reaction.
 ▲ Beginning of β'' precipitation.

could be expected to decompose precipitating α . This apparently does not take place, rather the γ_2 seemingly

forms at selected sites in the lattice and grows at the expense of the aluminum content of the surrounding β_1 . On the

Table 3 . . . Structures by X ray Analysis in Transformed Specimens of Alloy 11.9 Pct Al

| 500°C | | 450°C | |
|--------|----------------------------|--------|-----------------------------|
| Time | Structure | Time | Structure |
| 60 sec | β' | 5 sec | β' |
| 30 min | α, γ_2, β' | 30 sec | $\beta', \alpha, (\gamma')$ |
| 1 hr | α, γ_2 | 4 min | β', α, γ' |
| | | 8 min | β', α, γ' |
| | | 12 min | β', α, γ' |
| | | 32 min | β', α, γ' |

| 425°C | |
|-------|--------------------|
| Time | Structure |
| 77 hr | α, γ_2 |

depletion of the β_1 to a sufficient degree α forms and in turn grows. By this mechanism the α and γ_2 lattices seemingly are not in contact, but are separated by untransformed β_1 until the final stages of transformation.

An apparent anomaly is accounted for on the basis of this mechanism. This consists in the apparent interchange of role of γ_2 from precipitate structure to matrix structure through the course of the transformations. Thus in Fig 8 it seems that the precipitate structure is γ_2 , while in Fig 9 the "precipitate" structure is α .

It seems that the β'' reaction is comparable to this reaction in the 13.5 pct Al alloy except that the β'' reaction does not go to completion. Thus the β'' formed above about 500°C is for the most part consumed by the pearlite reaction. At lower temperatures increasingly greater proportions of β'' de-

compose to form α , while, as noted before, the pearlite reaction undergoes some important alterations.

The β'' structure probably does not differ from the matrix structure in so far as ordering is concerned. Rather from the fact that α forms from β'' it appears reasonable to conclude that β'' is aluminum dilute. A quantitative evaluation of the β'' crystal structure is out of question with the X ray diffraction techniques used in this investigation, but it has appeared that β'' has essentially the same structure as β' .*

Summary

1. It has been shown that the pearlite reaction is not found at compositions appreciably away from eutectoid composition on isothermal transformation of β -CuAl alloys. This reaction cannot be considered as generally typical of eutectoidal transformations.

2. In agreement with previous work^{2,4} it has been found that the pearlite reaction exists in the alloy of eutectoid composition. It has been found, however, that the interlamellar spacing of this pearlitic structure first decreases and then increases with decreasing transformation temperature. This behavior was wholly unexpected and cannot be accounted for on the basis of current notions of the pearlite reaction.

3. A bainite type reaction or, for short, a bainite reaction has been found in the CuAl alloys studied. The first reaction in the 13.5 pct Al alloy and the β'' reaction in the 11.9 pct Al alloy are placed in this category. In both of the alloys studied the β_1 matrix forms zones enriched and depleted in aluminum. For the 13.5 pct Al alloy the enriched zones decompose to form γ_2 which grows by an accretion process. The depleted zones in turn form α which also grows by an accretion process. The formation of α occurs at a much later time than the formation of γ_2 . The β'' transformation in the 11.9 pct Al alloy differs from this mainly in that α precipitates before γ_2 .

Acknowledgment

Of the materials used in preparing the alloys studied, the OFHC copper was supplied by The American Metal Co. Ltd., New York, while the high purity aluminum was furnished by The Aluminum Company of America.

*It is evident that this discussion pertains to the structures of the quenched alloys.

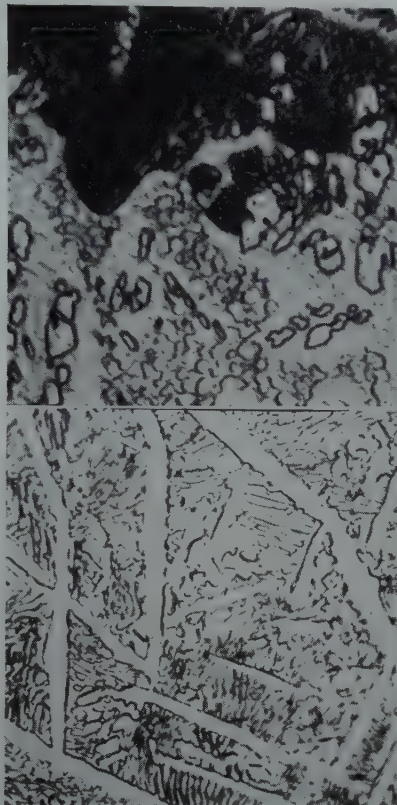
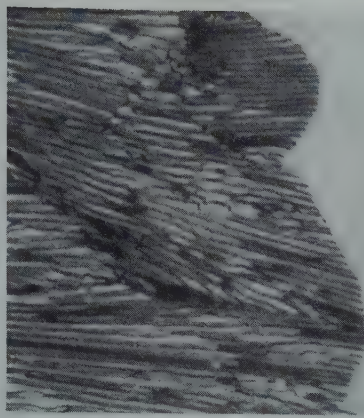


FIG 30—11.9 pct Al-Cu specimen transformed at 550°C for 30 min. $\frac{1}{32}$ in. stock. $\times 750$

FIG 31—11.9 pct Al-Cu specimen transformed at 500°C for 8 min. $\frac{1}{32}$ in. stock. $\times 1000$

FIG 32—11.9 pct Al-Cu specimen transformed at 425°C for 77 hr. $\frac{1}{32}$ in. stock. $\times 1000$

References

1. Pioneer work by E. S. Davenport and E. C. Bain: Transformation of Austenite at Constant Subcritical Temperatures. *Trans. AIME* (1930) 90, 117. Numerous articles in later volumes of *Trans. AIME* and *Trans. ASM*.
2. C. S. Smith and W. E. Lindlie: A Micrographic Study of the Decomposition of the β Phase in the Copper-aluminum System. *Trans. AIME* (1933) 104, 69.
3. A. B. Greninger and A. R. Troiano: Kinetics of the Austenite-Martensite Transformation in Steels.

- Trans. ASM* (1940) 28, 537. See also *Metals Handbook*, 1948 ed., ASM Cleveland.
4. D. J. Mack: The Isothermal Transformation of a Eutectoid Aluminum Bronze. *Trans. AIME* (1948) 175, 240. *Metals Tech.* Sept. 1947 TP 2242.
5. G. Wassermann: Über die Umwandlungsvorgänge in β Aluminumbronze. *Metallwirtschaft* (1934) 8, 133.
6. G. Kurdjumov and V. Miretski: Transformations in the Eutectoidal Alloys of Cu-Al. VII. An X-ray Study of the $\beta_1 \rightleftharpoons \beta'$ Transformation. *Jnl. Tech. Phys.* U.S.S.R. (1940) 10, 1685.
7. V. Gridnev and G. Kurdjumov: Transformation in Eutectoid Cu-Al Alloys. III Reversible Transformation of the β Solid Solution in the Metastable State. *Jnl. Tech. Phys.* U.S.S.R. (1938) 4, 1.
8. E. Söhnchen: Die Härtungserscheinungen in Aluminum Bronze. *Gieserei* (1935) 22, 289.
9. V. Gawranek, E. Kaminsky and G. Kurdjumov: Temperatur der Bildung der Metastabilen β' -Phase von Cu-Al-Legierungen und ihre Abhängigkeit von der Al-Konzentration. *Metallwirtschaft XV* (1936) No. 16, 370.
10. G. Kurdjumov and V. Miretski: Transformations in Eutectoid Cu-Al Alloys. IV. On the Reversibility on the Martensite Transformation $\beta_1 \rightarrow \gamma'$. *Jnl. Phys.* (U.S.S.R.) (1940) 2, 142.
11. A. B. Greninger: Martensite Transformation in Beta Copper-Aluminum. *Trans. AIME* (1939) 133, 204.
12. G. Tammann and E. Scheil: Die Umwandlungen des Austenits und Martensits in Gehärteten Stählen. *Ztsch. anorg. allg. Chem.* (1926) 157, 1.
13. I. Isaitschev, E. Kaminsky and G. Kurdjumov: *Trans. AIME*. (1938) 128, 361.
14. V. Gridnev: On Transformations of the Martensite Type. *Jnl. Tech. Phys.* U.S.S.R. (1938) 5, 761.
15. J. Boudloires: Etude Sur les Bronzes d'Aluminium. *Rev. d. Met.* (1927) 24, 357 and 463.
16. E. P. Klier and Taylor Lyman: The Bainite Reaction in Hypoeutectoid Steels. *Trans. AIME* (1944) 158, 394.
17. E. P. Klier: Discussion. *Trans. ASM* (1945) 35, 355.
18. E. P. Klier: Transformation of Austenite in a Steel Containing 3 Percent Chromium and 1 Percent Carbon. *Trans. AIME* (1945) 162, 186.
19. R. F. Mehl: Hardenability of Alloy Steels. *ASM Cleveland* (1939).
20. R. F. Mehl: The Structure and Rate of Formation of Pearlite. *Trans. ASM* (1942) 29, 813.
21. F. Hull and R. F. Mehl: The Structure of Pearlite. *Ibid* (1942) 30, 381.
22. G. Pellissier, M. Hawkes, W. Johnson and R. Mehl: The Interlamellar Spacing of Pearlite. *Ibid* (1942) 30, 1049.
23. C. Zener: Kinetics of the Decomposition of Austenite. *Trans. AIME* (1946) 167, 550. *Metals Tech.* (Jan. 1946) TP 1925.
24. W. R. Hibbard, Jr., G. H. Eichelmann, Jr., and W. P. Saunders: The Kappa Eutectoid Transformation in the Copper-Silicon System.

Trans. AIME (1949) 180, 92. *Metals Tech.* (Sept. 1948) TP 2441.

25. J. P. Sheehan, C. H. Julian and A. R. Troiano: The Transformation Characteristics of Ten Selected Nickel Steels. *Trans. ASM*, (1948)

Preprint No. 6.

26. F. Bollenrath and W. Bungardt: Einige Beobachtungen im System Aluminium—Kupfer an Legierungen mit 8 bis 16% Al. *Ztsch. Metallk.* (1943) 35, 153.

27. P. L. Grusin and G. Kurdjumov: Transformations in the Eutectoidal Alloys of Cu-Al. VI Specific Heat Measurements for the $\beta' \rightarrow \beta_1$ Transformation. *Jnl. Tech. Phys.* (U.S.S.R.) (1940) 10, 1680.

Compression Textures of Copper and Its Binary Alpha Solid Solution Alloys*

WALTER R. HIBBARD, JR.,† and DELMAR E. TROUT, II,‡ Junior Members AIME

Previous investigations have shown that the cold rolling textures^{1,2} and the drawn wire textures³ of copper change their secondary components after the addition of about 1 pct aluminum and 5 pct zinc, but do not change after the addition of as much as 30 pct nickel. However, few data are available on compression textures. Barrett⁴ reports from unpublished work with E. L. Layland that compression rolled copper develops a texture which is predominately {110} in the compression plane with a secondary spread to {113} and weaker spread to {100} as shown in Fig 1. However, 70-30 alpha brass similarly treated develops a texture again predominately {110} in the compression plane and with a weak secondary spread to {113} but with moderate {111} secondary intensities illustrated in Fig 2.

Experimental Procedure

Specimens of the compositions shown in Table 1 remaining from a previous investigation³ were annealed to a grain size of 0.090 mm average diam and machined to cylinders 0.20 in. diam and 0.20 in. high. Cylinders were compressed 90 pct reduction in height between lubricated steel blocks in a tensile machine. Glancing X ray photographs using copper K-alpha radiation were taken at an angle of θ degrees to the compression surface. {111}, {002} and {220} rings were analyzed to define the textures shown in Table 1.

The results are in agreement with Barrett⁴ as to types of textures and are essentially in agreement with previous work^{1,2,3} as to the effects of composition. In the wire study³ it was reported that the 4.99 pct zinc alloy had a brass-type texture, while the data in Table 1 indicate a copper-type texture for compression. The wire specimen of the 4.99 pct zinc alloy was re-examined by X rays and it was established that the {100} component still exists in the wire axis. Therefore, Table 2 of Ref. 3 is in

error and should indicate a double [111], [100] copper-type texture for this alloy. This correction results in complete consistency with regard to compositional effects, namely that copper and its alloys containing up to approximately 1 pct aluminum, 5 pct zinc and at least 30 pct nickel§ develop a copper-type texture and more concentrated copper-aluminum and copper-zinc solid solution alloys will form a brass-type texture.

Summary

Compression textures developed in copper and its alpha solid solution alloys of aluminum, nickel and zinc are essentially the same types as those re-

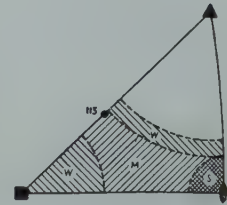


FIG 1—Orientations in copper compressed 97 pct by compression rolling (Barrett).

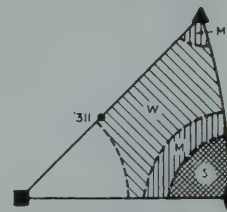


FIG 2—Orientations in 70-30 brass compressed 97 pct by compression rolling (Barrett).

Table 1 . . . Composition and Texture

| Material | Composition | | Texture of Compression Plane | | | | |
|----------|-------------|---------|------------------------------|-------|-------|-------|----------------------------|
| | Wt. Pct | At. Pct | {110} | {111} | {100} | {113} | Fig |
| Copper* | | | S | | W | M | 1 |
| Cu-Ni | 30.70 | 32.44 | S | | W | M | 1 |
| Cu-Al | 0.94 | 2.16 | S | W | W | M | Transition between 1 and 2 |
| | 3.69 | 8.28 | S | M | | W | 2 |
| | 7.76 | 16.58 | S | M | | W | 2 |
| Cu-Zn | 4.99 | 4.83 | S | | W | M | 1 |
| | 10.16 | 9.90 | S | M | | W | 2 |
| | 12.42 | 12.12 | S | M | | W | 2 |
| | 29.22 | 30.00 | S | M | | W | 2 |

* Phosphorous deoxidized electrolytic copper
Note: S = strong, M = medium and W = weak

ported by Barrett⁴ with compositional effects occurring at approximately the same percent additions as previously reported for rolled sheet^{1,2} and drawn wire.³

§ Higher nickel alloys were not investigated.

Acknowledgment

The Scovill Manufacturing Co., Waterbury, Conn., furnished the copper and brass alloys, performed certain chemical analyses and supplied laboratory facilities where needed.

References

1. Brick, Martin and Angier: *Trans. A.S.M.* (1943) 31, 675.
2. Dahl and Pawlek: *Ztsch. Metall.* (1936) 28, 266.
3. Hibbard and Yen: *Trans. AIME* 175, 126. *Metals Tech.*, Feb. 1948, TP 2334.
4. Barrett: *Structure of Metals*, McGraw-Hill (1942), 386.

Technical Note No. 18E. Manuscript received April 25, 1949.

* Some of the data included in this paper are from a report presented to the Faculty of the School of Engineering, Yale University, by Delmar E. Trout, II, in candidacy for the Degree of Master of Engineering, May 1948.

† Assistant Professor of Metallurgy, Yale University, New Haven, Conn.

‡ Scovill Manufacturing Co., Waterbury, Conn.

§ References are at the end of the note.

Surface Orientation and Rolling of Magnesium Sheet

ROBERT L. DIETRICH*

Magnesium alloy sheet has less ability to accept bending at room temperature than most of the heavier metals. In work designed to improve the bend properties, the preferred orientation of the sheet is of major importance as it is in all studies of the properties of wrought magnesium products. When rolled into sheet, all of the common magnesium alloys form an orientation texture having the basal (002) planes approaching parallel to the surface of the sheet. This texture is only slightly affected by annealing. Magnesium single crystals are highly anisotropic, and, as might be expected, so are magnesium alloy wrought products in which a strong preferred orientation is developed. It is therefore not surprising that bend properties are affected by orientation. Ansel and Betterton¹ reported that the orientation of AZ31X† sheet varies from surface to center and that bend properties are improved by etching away the sharply oriented material at the surface of the sheet to reach the more broadly oriented structure below. This paper covers a study of that orientation, either during the rolling process or by treatment of the finished sheet, in an effort to improve the bend properties and toughness of sheet.

Literature

The orientation texture of magnesium and magnesium alloy sheet has been studied extensively. Early determinations² showed that pure magnesium sheet has a preferred orientation in which the basal planes are parallel to the sheet surface within very narrow limits. J. C. McDonald³ and J. D. Hanawalt⁴ reported that sheet containing a small amount of calcium develops a "double" texture, that is, the majority of the basal planes are a few degrees from parallel to the surface and there is a noticeable vacancy at the parallel position. Bakarian⁵ made careful quantitative pole figures of both pure magnesium sheet and MI alloy

sheet which show these features. In all of these studies, however, the orientation was determined by transmission methods in which the resulting pattern is an average through the thickness of the sheet.

The tendency of wrought metal to exhibit a different orientation at the surface from that in the center has been reported by many investigators. G. von Vargha and G. Wasserman⁶ found that with copper, aluminum, iron, and brass the textures of rolled compared to drawn wires were the same at the center but differed markedly at the surface. It was also reported by investigators⁷ that the orientation of rolled aluminum varies from surface to center. Hargreaves⁸ found that the surface texture of AM503 (magnesium alloy similar to MI) sheet was different from the center texture. It is reported by Edmunds and Fuller⁹ that zinc alloy sheet sometimes had a thin layer at the surface with a strong orientation of the basal planes parallel to the surface, which, if present, impaired the bend properties of the sheet.

Part I Surface Orientation of Magnesium Alloy Sheet and the Effect on Properties

Attempts to correlate the bend properties of magnesium alloy sheet with tension ductility over short gauge lengths proved unsuccessful and the subsequent investigation showed that nonuniformity in orientation is a con-

tributing factor as the properties of the surface material have a much more important effect in bending than in tension. A program to study the relationship between surface orientation at the surface and bend properties was then undertaken.

First, the effect of etching away the surface of sheet on the bend properties and the orientations at the various depths were studied. Sheet samples of MI, AZ31X, and AZ61X were etched in dilute nitric acid to remove the surface material for various depths to 0.015 in. As may be seen in Table I, the minimum bend radius improved considerably as the surface layers were etched away but it was necessary to etch the sheet quite deeply, much more so than was found necessary by Edmunds and Fuller⁹ on zinc sheet. It is also apparent that the amount of etching required is a function of the sheet thickness. In all of this work, radii were measured as R/t , the radius divided by the sheet thickness, in order to eliminate the effect of the reduction in sheet thickness produced by the etching.

To determine the orientation texture of the sheet, X ray reflection patterns were taken using copper radiation with the beam striking the specimen at an angle of 17° to the surface, which is the Bragg angle for the (002) planes of magnesium. Two exposures were made of each specimen, one with the beam perpendicular to the rolling direction and the other with the beam parallel to the rolling direction. The symmetry of the preferred orientation in magnesium sheet is such that these two photographs gave an approximation of the pole figure sufficiently accurate for qualitative work and it was not thought worthwhile to make complete pole figures.

These X ray patterns show that the orientation has a much narrower spread at the original surface of the sheet than below the surface. The narrow spread is found in sheet having the majority of the basal planes (002) parallel to the surface, and since this is an unfavorable position for slip, it is

Cleveland Meeting, October 1949.
TP 2657 E. Discussion of this paper (2 copies) may be sent to *Transactions AIME* before December 1, 1949. Manuscript received April 27, 1949.

* The Dow Chemical Co., Midland, Michigan.

† The A.S.T.M. system of alloy designation is employed throughout this paper. AZ31X is Mg + 3%Al + 1%Zn; AZ61X is Mg + 6%Al + 1%Zn; AZ80X is Mg + 8%Al + 0.5%Zn; MI is Mg + 1.5%Mn + 0.10%Ca. X indicates high purity; h, hard rolled sheet, and a, annealed sheet. In addition, AZ31X when in sheet form contains 0.13%Ca.

‡ References are at the end of the paper.

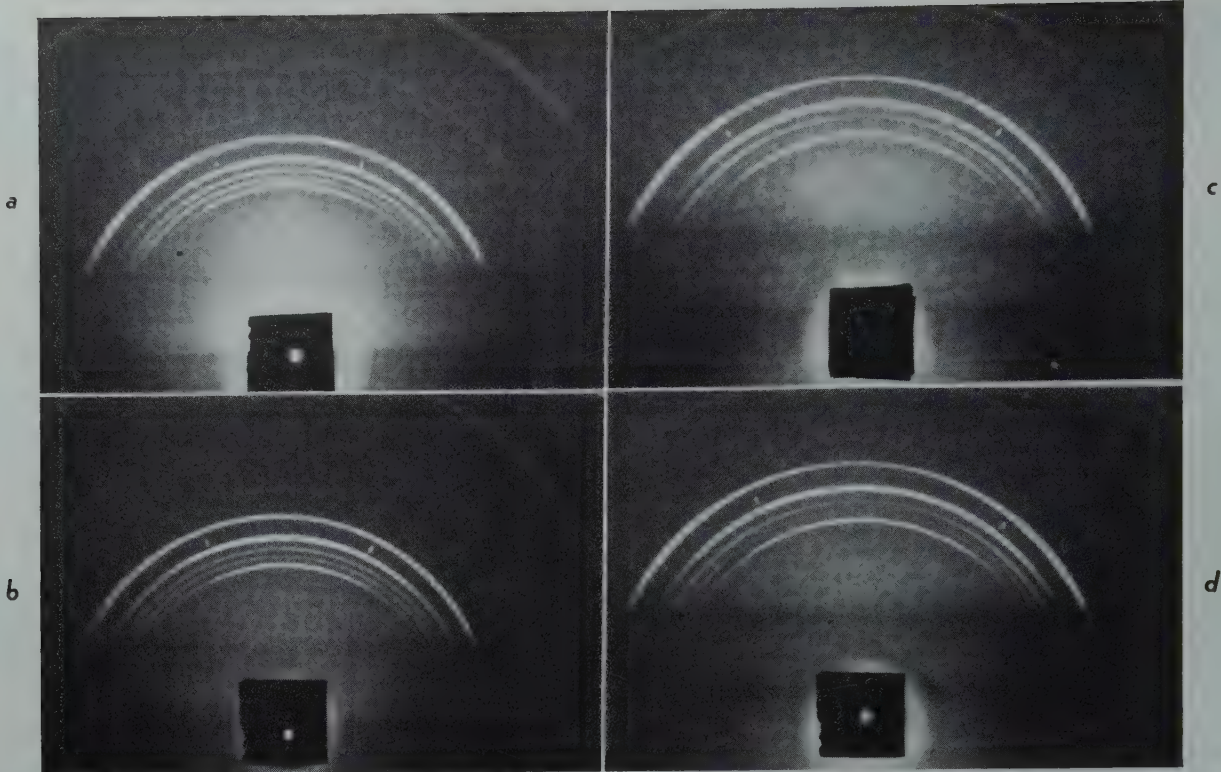


FIG 1—Effect of Etching on Surface Orientation of 0.091 in. AZ31X-h Sheet.

Original Surface (a) X ray beam perpendicular to rolling direction, (b) beam parallel; etched 0.015 in. (c) beam perpendicular and (d) beam parallel. Copper radiation. Dots are placed to show limits of maximum intensity of (002) reflections.

Table 1 . . . Effect of Etching on Bend Radius of Mg Alloy Sheet

| Alloy | Original Gauge Inches | Minimum Successful Bend Radius (r/t) Etch in In. per Side | | | | |
|---------|-----------------------|--|-------|-------|-------|-------|
| | | None | 0.001 | 0.002 | 0.005 | 0.010 |
| AZ31X-h | 0.040 | 9.7 | 7.8 | 5.7 | 5.7 | |
| AZ31X-h | 0.064 | 6.4 | 6.0 | 5.8 | 5.8 | |
| AZ31X-h | 0.091 | 6.4 | 6.3 | | 5.7 | 4.8 |
| AZ31X-a | 0.091 | 3.3 | 2.6 | | | 2.2 |
| M1-a | 0.040 | 4.4 | 4.5 | 3.9 | 2.4 | 3.5 |

not surprising that removing this layer improves the bend properties.

In the reflection patterns of 0.091 in. AZ31Xh sheet at the original surface and after etching 0.015 in. (Fig 1), the difference in spread is quite noticeable. The minimum bend radius was 6.4*t* before etching and 4.8*t* after etching. Other samples gave the same correlation, the bend properties improve as the orientation spread at the surface increases.

Tests made to determine the depth of penetration of the X ray beam in this type of reflection photograph showed that by use of copper radiation the beam penetrates to a depth of approximately 0.003 in. before its intensity is reduced to an ineffective level. The patterns must be interpreted as an integrated pattern of a layer 0.003 in. thick but heavily weighted in favor of the extreme surface. Subsequent tests showed that iron radiation, used for much of the later work, limited the depth of penetration to about 0.002 in.

EFFECT OF ETCHING ON TENSILE PROPERTIES

Although etching away the surface layers of sheet produces a marked improvement in bend properties, it was found that there is only an insignificant change in tensile properties. Tests on etched specimens showed a slight tendency for the etching to improve the elongation and lower the yield and tensile strengths; but the decrease is so slight as to be within normal tensile test variations and is only visible as a trend. This result is very reasonable, for, in a tension test, the entire cross-section of the sample is tested, whereas in bending the maximum elongation is found only in the extreme surface fibers and hence the minimum bend radius is determined by the elongation possible at the surface.

ETCHING EXTRUDED STRIP

The effect of etching on the bend properties of sheet aroused interest in

the behavior of extruded strip having a similar orientation to sheet when a transmission pattern is taken. Extruded strips, $\frac{1}{8}$ in. by $\frac{7}{8}$ in., of AZ80X, AZ61X, M1, and AZ31X were etched in the same manner as the sheet with rather startling results. Etching AZ31X strip improved the bend properties as in the sheet, but AZ80X and AZ61X strip had poorer bend properties after etching and M1 strip showed no effect. Diffraction patterns by reflection from the surface showed that the surface orientations of the various samples correlated with their bend properties. In the predominate orientation at the surface, the basal planes are not parallel to the surface, but are inclined to it at an angle of 10° to 30°.

Table 2 shows the effect of etching 0.015 in. on the bend properties of AZ80X and M1 strip and the corresponding surface diffraction patterns are shown in Fig 2. As can be seen readily, the orientation of AZ80X at a depth of 0.015 in. has a much narrower spread than at the surface, whereas in M1 strip there is little difference. Crystallites having the basal plane at an angle to the surface are in a more favorable position for basal slip than if parallel; therefore, the greater the percentage of the material at the surface in a favorable position, the better the bend properties. The results of the experiments on extruded strip confirm

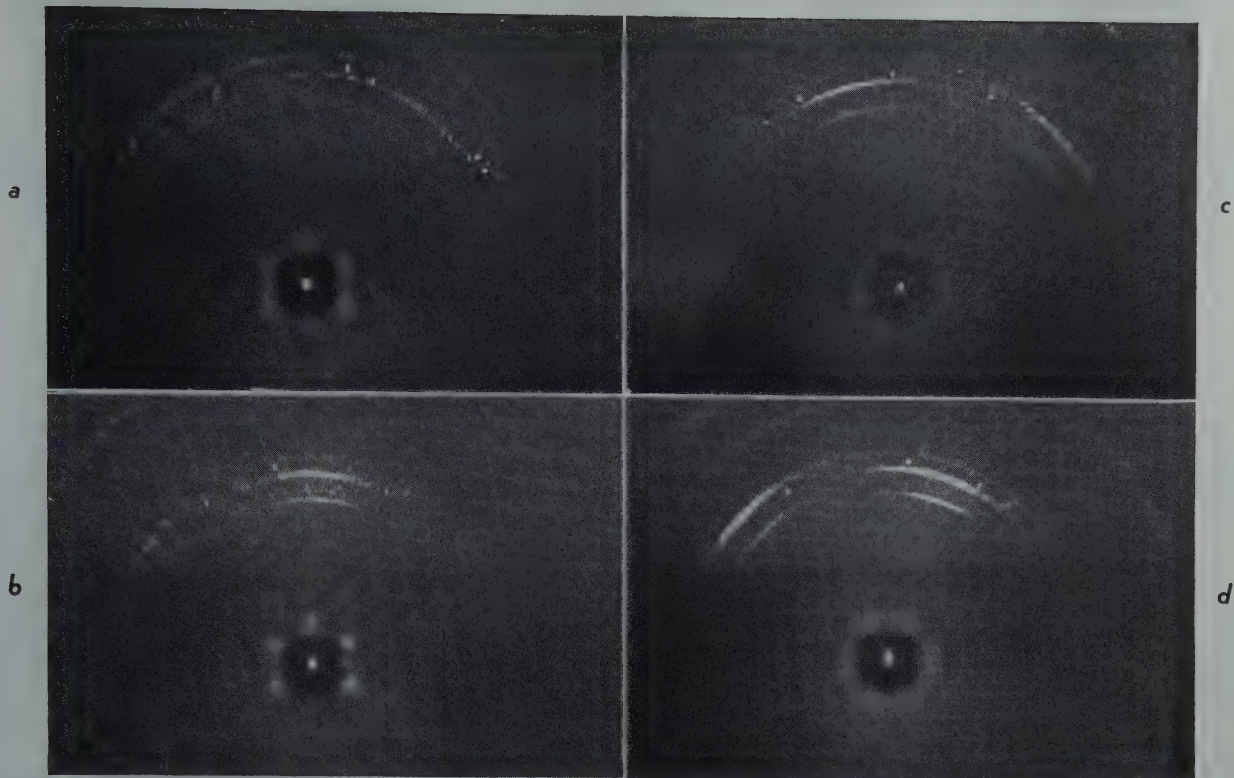


FIG 2—Effect of Etching on Surface Orientation of Extruded $\frac{1}{8}$ in. X 3 in. Strip.

(a) AZ80X as extruded and (b) Etched 0.015 in.
(c) MI as extruded and (d) Etched 0.015 in.
Copper radiation, beam perpendicular to extrusion direction.

the importance of surface orientation in determining bend properties.

SHOT PEENING

Having determined the importance of a favorable surface orientation in obtaining good bend properties in sheet, the problem of improving that orientation presents itself. There are two general ways in which this can be done; one is to alter the orientation of the rolled sheet, the other is to control the orientation during the rolling process.

One of the methods of altering the surface of the finished sheet is to etch away the unfavorably oriented material at the surface but because of the large amount of metal wasted by this process it is not commercially feasible. Shot peening offers a means of working the surface which utilizes flow characteristics entirely different from rolling. It was found that when AZ31Xa sheet was shot peened severely and then annealed at 600°F (310°C), a random orientation at the surface could be produced (Fig 3). Metallographic examination showed the affected layer to be about 0.003 in. deep. By this treatment the minimum bend radius was reduced from 3.5*t* to 2.5*t*.

REVERSE BENDING

A more effective and practical way to alter the surface orientation was

Table 2 . . . Effect of Etching on $\frac{1}{8}$ in. Extruded Strip

| Alloy | Etch | Min. Bend Radius | * Surface Orientation, Arc of Max. Intensity |
|-------|--------------------|------------------|--|
| AZ80X | None | 3.0 <i>t</i> | +10°, +54° |
| AZ80X | 0.015 in. per side | 4.0 <i>t</i> | -10°, +10° |
| MI | None | 4.0 <i>t</i> | +3°, +29° |
| | 0.015 in. per side | 3.9 <i>t</i> | +5°, +22° |

* Orientation is spread of basal planes in extrusion direction from parallel to surface.

found when it was learned that bending the sheet to about 15*t* radius through rolls, straightening, bending in the opposite direction and annealing produce a radical change in surface orientation and improve the bend properties. If the process is repeated a second time there is further broadening of orientation and further improvement in bend properties, but additional repetition is not effective. As is shown by the data in Table 3, AZ31X sheet had a 3.5*t* bend radius in the annealed condition, but if treated by reverse bending the minimum radius was reduced to 2.5*t* after the first treatment and 1.2*t* after the second. There is also an accompanying loss in yield strength, an increase in elongation, and a substantial increase in toughness.

The reverse bending process was studied in detail by X ray methods and it was found that the major orientation

change occurs during annealing, probably as a result of the twinning which takes place on the compression side of the bend. This is one of the few known cases in which annealing magnesium results in an appreciable change in orientation.

Roller leveling is somewhat similar to this reverse bending and has been cited in the literature¹¹ as a way to improve bend properties, but attempts to use this method were unsuccessful even when the two stage anneal was used. The difference is in the severity of the bends since the radii must be small enough to produce strong twinning on the compression side of the bend.

Part 2

The Control of Surface Orientation in the Rolling Process

Although the surface orientation of magnesium alloy sheet can be altered by etching, shot peening, or reverse bending, it is, of course, much more economical to roll in such a manner as to secure the desired properties without further treatment. A comprehensive program was undertaken to study the effect of hot and cold rolling variables on the surface orientation and properties of AZ31X alloy, the most widely used magnesium sheet alloy. The

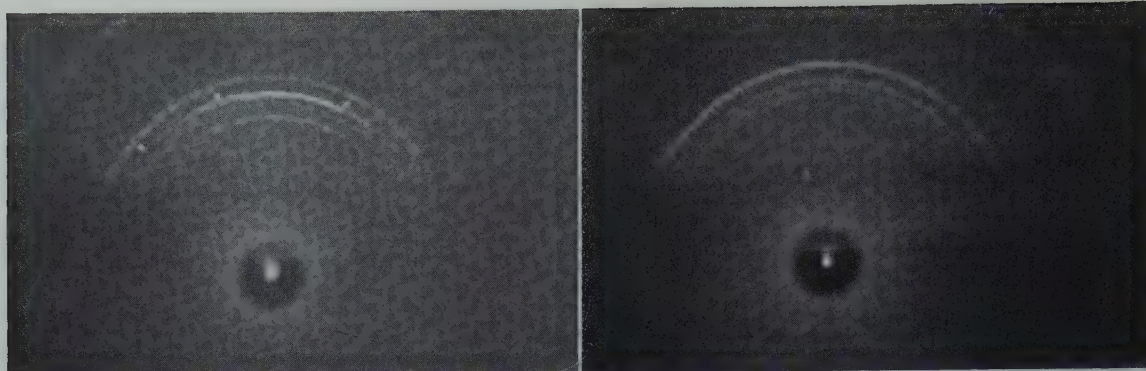


FIG 3—Effect of Shot Peening on Surface Orientation of 0.064 in. AZ31X-a Sheet.
(a) Original Surface (b) Shot peened and annealed. Copper radiation.

Table 3 . . . Effect of Reverse Bending in Both Directions on AZ31X-h

| Treatment | Tensile Properties | | | Minimum Bend Radius |
|----------------------------------|--------------------|-------------------|----------------|---------------------|
| | Ultimate psi | 0.2 Pct Yield psi | Pct E in 2 in. | |
| Original + 600°F Anneal..... | 37,800 | 23,000 | 21 | 3 5/8 |
| Reverse Bend + Anneal..... | 37,300 | 20,800 | 23 | 2 5/8 |
| (Reverse Bend + Anneal) × 2..... | 35,600 | 15,900 | 24 | 1 2/8 |

variables of temperature, reduction per pass, lubrication, and total reduction were studied as well as the effect of different combinations of them. The minimum bend radius, tension and compression strengths, and toughness gave good correlation with the resulting orientation.

EQUIPMENT

All laboratory investigations were carried out on a laboratory 2-Hi rolling mill having 8 in. diam by 12 in. rolls, and, in addition, a few pilot plant experiments were carried out on a 2-Hi mill having 32 in. by 60 in. rolls. Orientation was determined by X ray surface reflection using both copper radiation and iron radiation.

HOT ROLLING

Most of the experimental work was done on hot rolling as it was found that more could be accomplished in controlling the orientation in hot rolling even when the sheet was finished by cold rolling. The hot rolling variables of reduction per pass and temperature were studied by rolling AZ31X from 0.250 in. to 0.082 in. in four ways:

1. 800°F, (430°C), 20% reduction per pass
2. 800°F, 5% reduction per pass
3. 500°F, (260°C), 20% reduction per pass
4. 500°F, 5% reduction per pass

The resulting hot rolled material was then annealed at 700°F (370°C), cold rolled 20 pct, and final annealed at 275°F (135°C). Surface orientation and

properties were determined at each stage of the process. The higher temperatures and heavier passes produced a sheet having a much broader spread in the orientation of the basal plane at the surface. This sheet had better bend properties and, in addition, a considerably higher compression yield strength. The effect of the hot rolling conditions carried through the subsequent finishing operations of annealing and cold rolling. The properties of the sheet before and after cold rolling are given in Table 4. Surface reflection X ray pictures of the finished sheet are shown in Fig 4 with the differences in spread of the basal reflection evident.

The most probable explanation for the temperature effect is that the relative activity of the slip systems is altered by increasing temperature. There has been some indication that this may be true^{2,12,13} but no adequate proof exists. It is interesting to note Kolesnikov's¹⁴ report that three different textures were produced when zinc sheet was rolled at 20°C (70°F), 150°C (300°F), and 380°C (720°F). There are two possible reasons for the effect of reduction per pass; it may be the result of more uniform working through the thickness of the sheet or it may be the result of stress changes as discussed under lubrication. McLachlan and Davey¹⁵ found that with iron-nickel alloys, the orientation of a 0.001 in. surface layer is affected by reduction per pass but below this there is no change. Anderson and Kehl,¹⁶ on the other hand, found that with copper the reduction per pass does not influence either the surface or the overall texture.

ROLL LUBRICATION

Lubrication during hot rolling should have an effect on the stress system and possibly on the surface orientation. To study this variable, sheets were hot rolled from 0.250 in. to 0.075 in., annealed at 700°F (370°C), and cold rolled to 0.064 in. Rolling was done with palm oil on the rolls and with dry rolls. In the tests reported in Table 5, when lubricant was used for hot rolling it was also used for cold rolling; if hot rolling was dry, cold rolling was also dry. The use of lubricant causes a marked improvement in the bend properties of AZ31X but in the hard rolled condition the greatest improvement is secured if the sheet is subsequently etched to remove 0.0005 in. per side. The only explanation that can be offered for the results of etching is that even with lubrication there is a very thin layer of material with poor orientation at the surface of the sheet. The X ray method is, however, not sufficiently sensitive to prove or disprove this theory. The wider surface orientation resulting from the use of a lubricant is believed to be the result of reduction of the tensile stress on the surface due to the friction of the rolls. Experiments by the author on M1 alloy single crystals have shown that slip and fracture characteristics are different in the rolling process from those in pure compression. Single crystals having the basal plane within 5° of parallel to the rolling surface could be hot rolled successfully but fractured when subjected to compression in a testing machine operated at the same temperatures.

The use of adequate lubrication is believed to cause the stress system at the surface to approach more nearly the stresses found in the center of the sheet and, therefore, to reduce the variation in orientation from surface to center.

X ray pictures illustrating the effect of lubrication on the surface of AZ31X

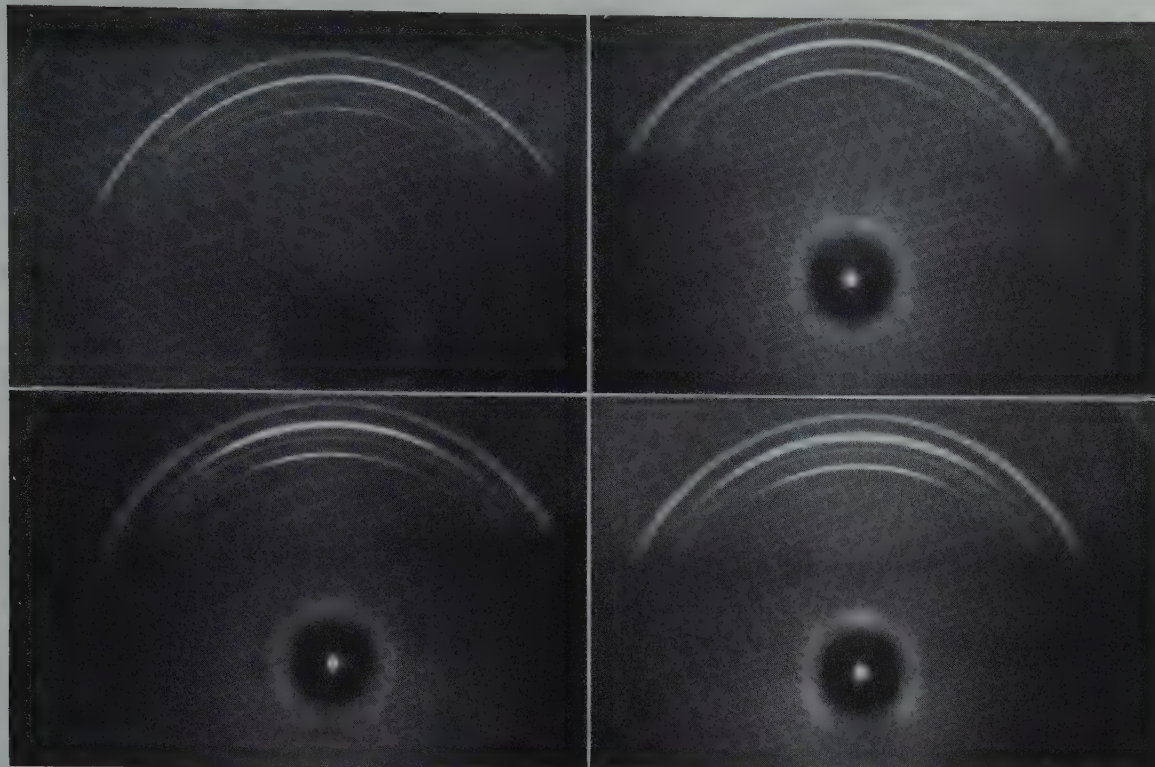


FIG 4—Effect of Hot Rolling Temperature and Reduction per Pass on Surface Orientation of Finished 0.064 in. AZ31X-h Sheet.

All sheet was annealed, cold rolled 15 pct and final annealed at 275°F (135°C)
Copper radiation, beam perpendicular to rolling direction.

(a) Hot rolled 800°F, 20 pct per pass (b) 800°F, 5 pct per pass (c) 500°F, 20 pct per pass (d) 500°F, 5 pct per pass

sheet finished by annealing and cold rolling 15 pct with dry rolls are shown in Fig 5. Further investigation shows that for best results lubrication should be confined to hot rolling, since when used for cold rolling it does not improve the resulting orientation and lubrication during cold rolling is well known to reduce the capacity of magnesium alloys to withstand cold rolling without cracking.^{1,17}

REQUIRED TOTAL REDUCTION IN HOT ROLLING

Having established that surface orientation could be altered by hot rolling conditions, tests were run to determine the minimum amount of hot rolling required under optimum conditions to secure the desired surface orientation and bend properties. These tests showed that the conditions under which the last 30 to 40 pct of the reduction in hot rolling is carried out determines the final properties.

PERSISTENCE DURING COLD ROLLING

All the data presented so far were obtained on sheet finished with 15 to 20 pct cold roll. It is surprising that the orientation produced in hot rolling persists so strongly through annealing and cold rolling operations. It would seem

Table 4 . . . Effect of Hot Rolling Temperature and Reduction per Pass AZ31X Alloy

| Hot Rolling | | Cold Roll† | Anneal °F | Min. Bend (r/t) | Tensile* | Yield* | Pct E in 2 In. | Comp. Yield* |
|-------------|------------------------|------------|-----------|-----------------|----------|--------|----------------|--------------|
| Temp. °F | Reduction per Pass Pct | | | | | | | |
| 800 | 20 | None | 700 | 3.5 | 37,100 | 21,400 | 21 | 15,700 |
| 800 | 5 | None | 700 | 5.0 | 35,400 | 21,400 | 17 | 11,900 |
| 500 | 20 | None | 700 | 6.5 | 38,200 | 25,200 | 21 | 14,900 |
| 500 | 5 | None | 700 | 6.0 | 37,200 | 23,600 | 18 | 11,600 |
| 800 | 20 | 20 % | 275 | 9 | 44,400 | 35,700 | 9 | 33,000 |
| 800 | 5 | 20 % | 275 | 9 | 41,600 | 32,800 | 7 | 28,700 |
| 500 | 20 | 20 % | 275 | 14 | 45,300 | 35,700 | 7 | 32,200 |
| 500 | 5 | 20 % | 275 | 14 | 42,400 | 34,100 | 3 | 28,200 |

* Psi.

† Annealed 1 hr 700°F before cold rolling.

probable that sufficient reduction in cold rolling would remove any influence of hot rolling conditions. Thin gauge magnesium alloy sheet is produced commercially by multiple cold rolling from a minimum hot rolled gauge of 0.075 in. Total reductions of 20 to 40 pct with intermediate anneals are used. The tests conducted in the laboratory consisted of cold rolling two batches of sheet, one of which had been hot rolled with lubricated rolls at 800°F, 20 pct per pass, and the other had been hot rolled with dry rolls at 600°F, 20 pct per pass. Two successive cold rolls of 20 pct each followed by one of 30 pct were used, annealing at 700°F (370°C) between cold rolls. The superior bend properties of the first batch persisted in the hard rolled sheet

through the entire cold rolling. It did, however, become slight after the second cold roll. In sheet final annealed at 600°F (320°C) all effect of the hot rolling conditions on bend properties was lost after the second cold roll. The sheet hot rolled at the higher temperature maintained a slightly better compression yield strength through the entire series of cold rolls.

COLD ROLLING

In addition to the work on hot rolling, the effects on surface orientation of roll lubrication, roll temperature, reversing the direction of each pass, reduction per pass, and total reduction in cold rolling were studied. The differences obtained were much less important than in the studies on hot rolling. It



FIG 5—Effect of Lubrication During Hot Rolling on Surface Orientation of Finished 0.064 in. AZ31X Sheet.

(a) Palm oil on rolls, (b) rolls dry.
All sheet hot rolled at 800°F (430°C) and 20 pct per pass.
Sheet was annealed at 700°F (370°C) and cold rolled 15 pct with dry rolls.
Iron radiation perpendicular to rolling direction.

Table 5—Effect of Lubrication during Rolling AZ31X Sheet

| Hot Rolling* | | | Anneal °F | Min. Bend Radius (r/l) | | Ulti- mate† | Yield† | Pct E in 2 In. | Comp. Yield† |
|--------------|----------------------|----------------|--------------|---------------------------|--------------------------------|----------------|--------|-------------------|-----------------|
| Temp. °F | Red. per Pass Pct | Lubri- cant | | No Etch | Etch 0.0005 in. per Side | | | | |
| 800 | 20 | Oil | 275 | 6 | 3.5 | 41,500 | 33,900 | 10 | 31,000 |
| 800 | 20 | Dry | 275 | 6.5 | 6 | 42,000 | 34,700 | 9 | 29,600 |
| 550 | 5 | Dry | 275 | 14 | 12 | 38,100 | 32,300 | 3 | 25,500 |
| 800 | 20 | Oil | 600 | 1.5 | 1.5 | 36,400 | 26,200 | 21 | 18,900 |
| 800 | 20 | Dry | 600 | 2.5 | 2.5 | 37,200 | 23,300 | 20 | 18,900 |
| 550 | 5 | Dry | 600 | 3 | 3 | 37,400 | 23,000 | 18 | 16,400 |

* All sheet annealed 700°F (378°C) and finished by cold rolling 15 pct to 0.064 in. gauge before final anneal.
† Psi.

was found that the best combination of strength and ductility in hard rolled sheet is produced by the present commercial practice of finish cold rolling 20 to 30 pct followed by a low temperature anneal at 325°F (160°C) rather than finishing with a small cold reduction without final anneal.

WARM ROLLING

As an alternative to finish cold rolling in securing the desired surface and properties, warm rolling is sometimes used. Tests on sheet finished by warm rolling at 300°F (150°C) and 400°F (200°C) showed poorer bend properties than on sheet finished by cold rolling.

OTHER MAGNESIUM ALLOYS

The work on rolling was not extended to cover magnesium alloys other than AZ31X since this alloy accounts for by far the largest quantity of production sheet, and is used almost entirely for those applications in which room temperature formability and toughness are critical factors. Some laboratory work has shown that the hot rolling temperature affects the cold rollability of AZ31X both with and without calcium and also that of AZ61X.

Summary

1. Studies of the crystallographic orientation of magnesium alloy sheet show that the spread in the orientation

of the basal plane is considerably less at the surface than in the center of the sheet.

2. A narrow orientation at the surface is detrimental to the bend properties of the sheet.

3. The layer having a narrow orientation can be removed by etching, or the orientation can be broadened by shot peening or reverse bending with a resultant improvement in bend properties.

4. The surface orientation of AZ31X sheet can be improved by higher temperature, higher reduction per pass, and adequate lubrication during hot rolling with a resultant improvement in bend properties and a slight improvement in compression yield strength.

5. The improved surface orientation resulting from hot rolling persists to a remarkable degree through subsequent annealing and cold rolling operations.

6. Variations in cold rolling have only a very slight effect on surface orientation.

Acknowledgment

The author wishes to acknowledge the assistance of J. B. Hess who did all the very considerable X ray work involved in this program.

References

1. G. Ansel and J. O. Betterton, Jr.:

- Hot and Cold Rolling of Magnesium Base Alloys. Nonferrous Rolling Practice, I.M.D. Series, 2, AIME (1948).
- A. Beck: The Technology of Magnesium and its Alloys. F. A. Hughes and Co., Ltd., London (1940).
- J. C. McDonald: Grain Orientation in Rolled Magnesium Alloys. *Physical Review* (1937) 52, 886-887.
- J. D. Hanawalt: Symposium on Radiography and X-Ray Diffraction. A.S.T.M., Phila., Pa., p. 321 (1936).
- P. W. Bakarian: Preferred Orientation in Rolled Magnesium and Magnesium Alloys. *Trans. AIME* (1942), 147, 267-271.
- G. von Vargha and G. Wasserman: On the Relation between the Crystal Orientation in Rolled Aluminum Sheet and the Thickness of the Sheet. *Metallwirtschaft* (1933) 12, 511-513.
- G. von Vargha and G. Wasserman: On the Influence of the Method of Working on the Orientation of Crystals of Wire. *Ztsch. Metallkunde* (1933) 25, 310-313.
- A. Hargreaves: The Crystal Grain Orientation in a Rolled Magnesium Alloy. *Jnl. Inst. of Met.* (1945) 71 (2), 73-86.
- G. Edmunds and M. L. Fuller: Relation of Crystals Orientation to Bending Qualities of a Rolled Zinc Alloy. *Trans. AIME* (1932) 99, 175-185.
- J. B. Hess: Unpublished work at The Dow Chemical Co.
- R. D. Lowry and F. L. Reynolds: U.S. Pat. No. 2,029,728.
- C. S. Barrett and C. T. Haller: Twinning in Polycrystalline Magnesium. *Trans. AIME* (1947) 171, 246-254. *Metals Tech.* Dec. 1946, TP 2103.
- P. W. Bakarian and C. H. Mathewson: Slip and Twinning of Magnesium Single Crystals. *Trans. AIME* (1943) 152, 226-253.
- A. T. Kolesnikov: Zhur. Eksper. i Teoret. Fiziki. (Russian) (1939) 9. *Metallurgical Abstracts* (1940) 7, 513.
- D. McLachlan, Jr., and W. P. Davey: The Preferred Orientation Produced in Pure Iron-Nickel Alloys by Cold Rolling. *Phys. Rev.* (1937) 51, (1), 60.
- H. V. Anderson and G. L. Kehl: An X-Ray Study of Preferred Orientation in Rolled Copper. *Metals and Alloys* (1937) 8, (3) 71-73.
- G. Ansel: U. S. Pat. No. 2,378,679.

Recrystallization Texture and Coarsening Texture in High Purity Aluminum

PAUL A. BECK,* Member, and HSUN HU,* Junior Member AIME

Introduction

It has been known for many years that in cold drawn polycrystalline aluminum the recrystallization texture is practically identical with the deformation texture.^{1,2,3} V. Goeler and Sachs⁴ stated that in cold rolled polycrystalline aluminum, too, the deformation texture is retained upon recrystallization. This behavior was interpreted by Dehlinger⁵ as an indication that each recrystallized grain inherits the orientation of the matrix in which it grew. However, Burgers and Basart showed⁶ that in deformed aluminum single crystals the orientation of the recrystallized grains strongly deviates from that of the matrix. Barrett demonstrated⁸ that even in deformed polycrystalline aggregates the local orientation within each deformed grain changes on recrystallization. No explanation has as yet been offered of how the aggregate texture can be retained, while the local texture is everywhere changing.

According to Burgers and Louwerse⁶ the orientation change on recrystallization in compressed and rolled aluminum single crystals corresponds to a rotation around [112] axes lying in the active slip planes and perpendicular to active slip directions. This orientation change was rationalized by them on the assumption that the orientation of the recrystallized grains is determined by the orientation of the available nuclei, and that these nuclei are small fragments of the deformed crystal, rotated in the deformation process. Barrett pointed out,⁷ however, that these assumptions were by no means proven, and that the total volume of material necessary for the nuclei is so small, that it must be available in any orien-

tation whatever. It is, therefore, unlikely that an "oriented nucleation" theory could satisfactorily explain the orientation changes in recrystallization of a deformed crystal. Furthermore, in contradiction to Burgers and Louwerse's conclusions, Barrett's results for the orientation change could be best expressed in terms of rotations around [111] axes. Thus agreement is lacking not only in the interpretations but apparently even in the experimental results contributed by the various investigators.

The orientation relationships on coarsening* in a highly oriented polycrystalline matrix were first investigated by Burgers and Basart.⁶ They produced a fine grained highly oriented matrix by the recrystallization of a compressed or rolled single crystal of

aluminum, and studied the orientation relationships in three successive generations of crystals: the "deformation texture" in the single crystal, the recrystallization texture, and the coarsening texture. Burgers^{2,4} showed that the preferred orientation of each successive generation was almost always widely different from that of the preceding one, but that the coarse grains often approximately reverted to the orientation of their grandparent, the deformed single crystal. This observation, and the idea that the orientation of the coarse grains is determined by that of the available "nuclei," led to the concept that the coarse grains are nucleated by the remnants of the deformation texture.^{12,15} On the other hand, Bowles and Boas¹⁶ found, in a carefully conducted experiment, that in recrystallized fine grained copper of cube texture coarse grains grow in orientations which can be derived from the orientation of the recrystallized matrix by rotation around a [111] direction; the coarsening texture here does not appear to be related in any simple manner to the original rolling texture from which the cube texture had been obtained by recrystallization.

It may be assumed that in a recrystallized material, even with a strong texture, there always are present some grains of practically any orientation. These may serve as "nuclei" for the coarse grains, provided that the conditions are favorable for their growth. The existence of a coarsening texture may be considered as an indication that grains with certain relative orientations with respect to the preferred orientation of their neighbors can grow much faster than others. This "oriented growth" theory was briefly suggested by van Arkel, as early as 1936,¹³ and it was mentioned by Burgers.¹⁴ Recently, C. G. Dunn produced direct

* Just as the recrystallized grains grow at the expense of the deformed matrix, and finally replace it, under suitable conditions the recrystallized grains may be in turn replaced by a new generation of grains, usually many times larger than the recrystallized grains and growing at their expense. The growth of these very large grains may be designated as discontinuous grain growth or coarsening. (The following other terms have been used by various authors: abnormal grain growth, exaggerated grain growth, germination, and secondary recrystallization. These terms are deemed to be unsuitable, as they have been used indiscriminately to describe the formation of large grains by various mechanisms.¹¹

Recent work indicates^{10,11} that an essential condition for coarsening is that in a fine grained structure continuous or gradual growth be impeded. There are at present two mechanisms known, each one of which is capable of accomplishing this, namely the inhibition by a dispersed phase and the restraint of growth resulting from a strongly developed texture. Correspondingly, one may speak of "inhibition-dependent coarsening" or "texture-dependent coarsening." In metallurgical practice intermediate cases often occur, where gradual grain growth is impeded by a combination of the two mechanisms mentioned.

Cleveland Meeting, October 1949.

TP 2675 E. Discussion of this paper (2 copies) may be sent to *Transactions AIME* before December 1, 1949. Manuscript received June 6, 1948.

* Department of Metallurgy, University of Notre Dame.

¹ References are at the end of the paper.

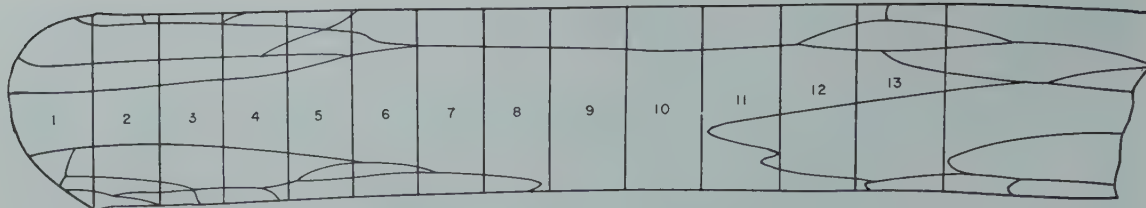


FIG 1—Outline of grain boundaries in rolled high purity aluminum bar, containing crystal I (large grain in center).

Location of saw-cuts is indicated by straight cross lines. Specimens are numbered 1 to 13.

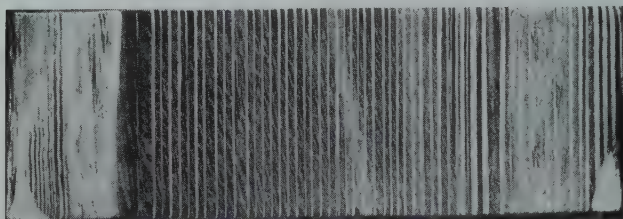


FIG 2—Spec. 7 of crystal I, as rolled, showing deformation bands in direction of rolling.

Deep etched. Magnification: $\times 3$. Reduced one half in reproduction.

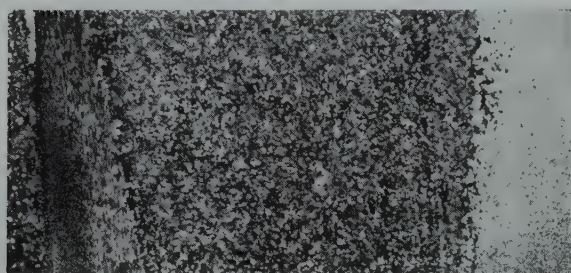


FIG 3—Spec. 4 of crystal I, rolled and annealed 25 min. at 400°C, showing fine grained recrystallized structure.

Deep etched. Magnification: $\times 4$. Reduced one half in reproduction.

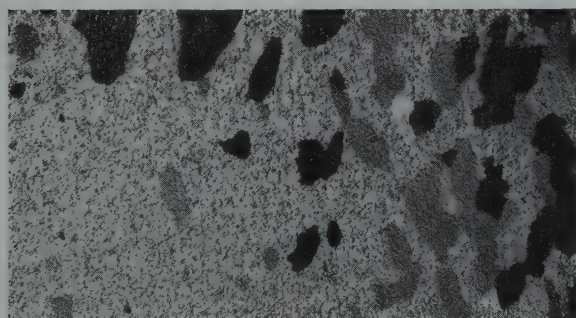


FIG 4—Spec. 8 of crystal I, rolled and annealed 745 min. at 400°C, showing several coarse grains in fine grained matrix.

Deep etched. Reduced one half in reproduction.

experimental evidence for the orientation dependence of the rate of growth in silicon ferrite.²⁵

The present investigation was undertaken in an attempt to clarify the difficulties and contradictions described above, and to rationalize both recrystallization textures and coarsening textures from the point of view of the "oriented growth" theory.

Experimental Procedure

The plan of the experiments was basically similar to that followed by Burgers and Basart.⁵ However, high purity aluminum was used in order to eliminate the possible effect of impurities on the texture relationships. Recent work indicated¹⁰ that it is possible to induce texture-dependent

coarsening in high purity aluminum. Table 1 gives the lot analysis of the aluminum.

Table 1 . . . Lot Analysis of High Purity Aluminum

| | Per Cent |
|---------|----------|
| Si..... | 0.002 |
| Fe..... | 0.002 |
| Cu..... | 0.002 |
| Mg..... | 0.003 |
| Mn..... | 0.001 |

The method of preparing the ingot was the same as previously used.¹⁶ Large crystals were grown by annealing 0.390 to 0.535 in. thick specimens for 3–4 days at 650°C. Crystals I and II were cold rolled 88 pct, and 90 pct respectively. Crystal III was compressed 75 pct between repeatedly greased ground steel plates. The deformed crystals were carefully cut into several specimens by a jeweler's saw. One specimen of each crystal was used for determining the deformation texture. The other specimens were annealed in salt baths at various temperatures and for various lengths of time.

Fig 1 gives the outlines of crystal I and its neighbors, after rolling, the location of the saw-cuts and specimen numbers. Spec. 7 was used for determining the deformation texture. As seen in Fig 2, crystal I had a large number of deformation bands extending parallel to the rolling direction. Spec. 4, (Fig 3), was annealed for 25 min. at 400°C, giving a uniformly fine recrystallized structure. Spec. 8, which had a common side with spec. 7, was annealed for 745 min. at 400°C, giving a partially coarsened structure, (Fig 4). This specimen was used to determine both the recrystallization texture and the orientation of several coarse grains. Since both structures were located in the same specimen, the relative orientation could be determined with a high degree of accuracy. For measuring the relative orientation of the deformed grain, spec. 7 was aligned by using its common edge with spec. 8. The specimens of crystals II and III were treated similarly.

The deformation texture, the re-

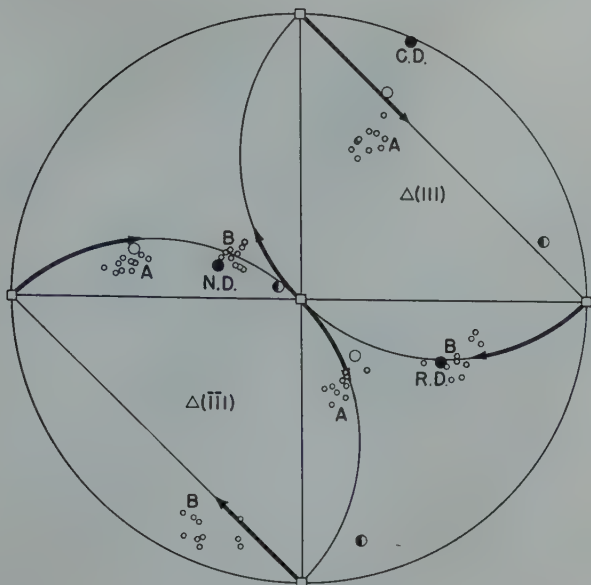


FIG 5—(100) pole figure for textures obtained in crystal I.

Recrystallization texture \square is in standard position. The main component of the deformation texture \circ , and the deformation bands \bullet , as well as groups A and B of coarse grains \circ are plotted in correct relative position, together with the rolling direction (R.D.), the cross direction (C.D.), and the normal direction (N.D.). Arrows correspond to 42° rotation around $[1\bar{1}1]$ and 35° rotation around $[111]$ respectively.

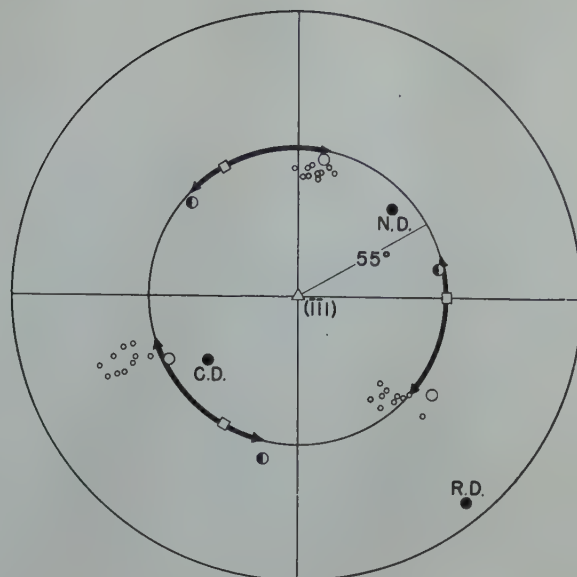


FIG 6—(100) pole figure for textures obtained in crystal I.

Recrystallization texture \square , the two components of the deformation texture \circ and \bullet , and group A coarse grains \circ are plotted in such a way that $(1\bar{1}1)$ of the recrystallization texture is the center of projection. The rolling direction (R.D.), cross direction (C.D.), and normal direction (N.D.) are indicated.

crystallization texture and the coarsening texture were determined by means of an optical goniometer similar to that described by Barrett.¹⁷ The light source used was a 2 watt concentrated arc lamp, allowing a very high degree of collimation.

The annealed specimens were polished electrolytically and etched with the reagent described by Barrett.¹⁷ It was found that about 10 to 20 min. of etching were necessary to develop the cube planes accurately. In all measurements on single grains the measured angles between the cube planes approached 90° to an accuracy of better than 1 to 2° . It was found that the crystallographic definition of the etch pit faces in deformed crystals was improved when a somewhat modified etching reagent was used as given in Table 2.

Table 2 . . . Composition of Etching Reagent Used for Developing (100) Planes in Cold Worked High Purity Aluminum

| | |
|----------------------------------|-------|
| Conc. HCl | 80 cc |
| Conc. HNO ₃ | 25 cc |
| H ₂ O | 20 cc |
| Conc. HF | 5 cc |

It was found that the texture of the fine grained recrystallized material is usually rather sharply defined, so that the mean orientation can be satisfactorily and easily determined by the optical method, if such a polycrystalline region is treated as if it was a single grain. Reproducible average orientations were obtained, and the angles

between the average cube planes so determined were close to 90° . The coarsening texture was determined by measuring the orientation of 15–20 large grains individually.

Results

Fig 5 gives the relationship between the deformation texture, the recrystallization texture and the coarsening texture obtained in crystal I. In order to show clearly the relative orientation of these textures, the pole figure is plotted for (100) poles in such a way that the recrystallization texture is in standard position. It is readily seen that the main portion of the deformed material as well as the deformation bands can be brought into fairly good alignment with the recrystallization texture by rotation around a $[111]$ direction. The coarse grains clearly fall into two groups (A and B), each with a well-developed preferred orientation. This fact is also noticeable in Fig 4, where one group of coarse grains appears black, and the other group gray. It is notable that the orientation of both groups of coarse grains deviates from that of the recrystallized matrix corresponding to a rotation around a $[111]$ direction. The angle of rotation from the deformation texture to the recrystallization texture is about 40° , that from the recrystallization texture to the group A coarse grains is of similar magnitude in the opposite direction

(or about 80° in the same direction), so that the orientation of group A coarse grains is fairly close to that of the original deformed single crystal. It is important to note that the group B coarse crystals have an entirely different orientation from either component of the deformed crystal, although they are also connected with the recrystallization texture by a $[111]$ rotation of about 35° (see Fig 1).

The extent of rotation around a $[111]$ direction can be best studied in the corresponding $[111]$ projection of the (100) poles. This is given in Fig 6 for the three successive generations of crystals: the deformation texture of crystal I (that of both the main portion and the deformation bands), the recrystallization texture and the group A coarse grains. It is apparent that with a fair degree of accuracy all these crystals have in common the $[111]$ direction which has been used as the center of projection. The group B coarse grains were omitted here, since they are connected with the recrystallization texture by rotation around a different $[111]$ direction. Similar pole figures were prepared for all cases investigated, in order to determine the angles of rotation.

Fig 7 shows the $[100]$ projection of the (100) poles for the recrystallization texture and for the coarse grains produced by the annealing of a specimen of the rolled crystal II for 25 min. at 400°C . In this instance it was found impossible to determine accurately the

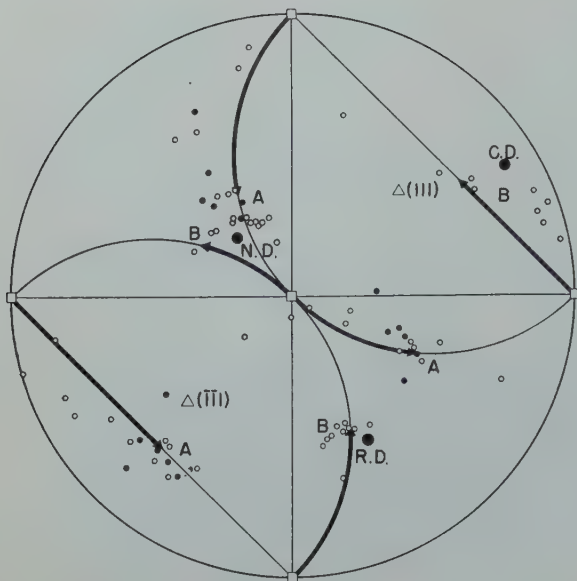


FIG 7—(100) pole figure for textures obtained in high purity aluminum crystal II.

Recrystallization texture \square is in standard position. Groups A and B of coarse grains away from sawed edges \circ , and at sawed edges \bullet are plotted together with rolling direction (R.D.), cross direction (C.D.), and normal direction (N.D.). Arrows correspond to 65° rotation around [111] and to 50° rotation around [112] respectively.

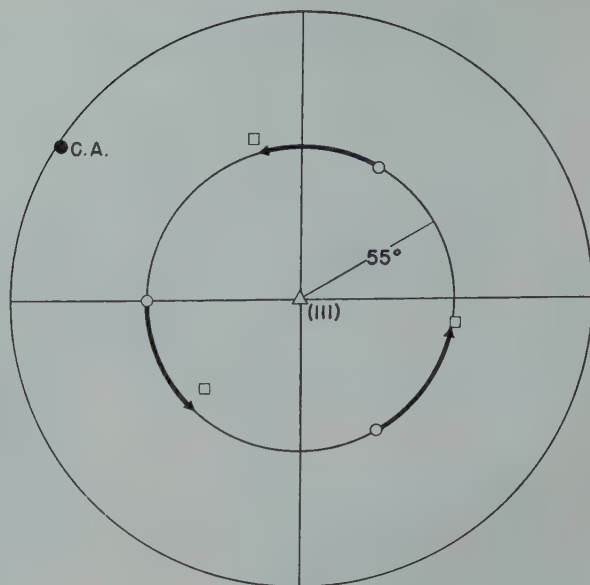


FIG 9—(100) pole figure for deformation texture \circ , and recrystallization texture \square obtained in high purity aluminum crystal III.

(111) of the deformation texture is center of projection. The compression axis (C.A.) is indicated. Arrows indicate rotation of 47° .

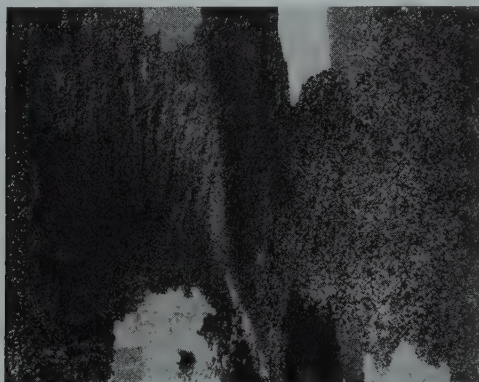


FIG 8—Specimen of high purity aluminum originally consisting of two grains, rolled and annealed 12 sec. at 400°C , showing coarse grains at sawed edges.

Reduced one half in reproduction.

deformation texture by the optical method, as the deformation bands were small, numerous and inextricably interwoven. However, the recrystallization texture was fairly sharply defined. The coarse grains showed considerable scatter, but it is apparent that even this scattered orientation range is quite clearly related to rotations around one of two [111] directions. Roughly, the scatter of one group of coarse crystals (A) may be expressed as a variation of the angle of rotation around [111] from about 17 to 65° . The orientation of the other group of coarse crystals can be derived from that of the recrystallized grains by a rotation of approximately 50° around [111].

It is of particular significance that in most specimens a tendency was noted for the coarsening to start near the two sawed edges. This is clearly shown in Fig 8. It was observed that considerable amounts of material had to be etched off the edge regions prior to annealing in order to eliminate this tendency. In Fig 7 the (100) poles for several of the grains growing from the edge are shown by solid circles. The orientation of most of these grains coincides well with the orientations of group A coarse grains, formed away from the edges.

The orientation of crystal III after compression was very similar to that shown in Fig 10, that is, the (110)

plane was close to the plane of compression. This compressed crystal had no deformation bands; its orientation was sharply defined. After annealing for 15 min. at 400°C it showed a sharply defined recrystallization texture. The relative orientation of the recrystallization texture and the deformation texture, which is shown in Fig 9 in a [111] projection, corresponds to a rotation of about 47° around [111].

Discussion of Results

The results indicate that the orientation of aluminum crystals grown in a highly oriented matrix, either by recrystallization (when the matrix is deformed) or by coarsening (when the matrix is recrystallized, fine grained), is related to the orientation of the matrix by means of a rotation around a [111] direction. The extent of the rotation is about 30 to 50° in most cases as shown in Table 3.

According to Burgers and Louwerse,⁶ the orientation relationship between a compressed single crystal of commercial purity aluminum and the recrystallization texture corresponds to a rotation around a [112] direction. Fig 10 shows a pole figure from their paper. In Fig 11 the same data are re-plotted in such a way that the [100] poles of the deformed crystal are in standard position. It is apparent that the [111] rotation expresses the orientation relationship between the compressed single

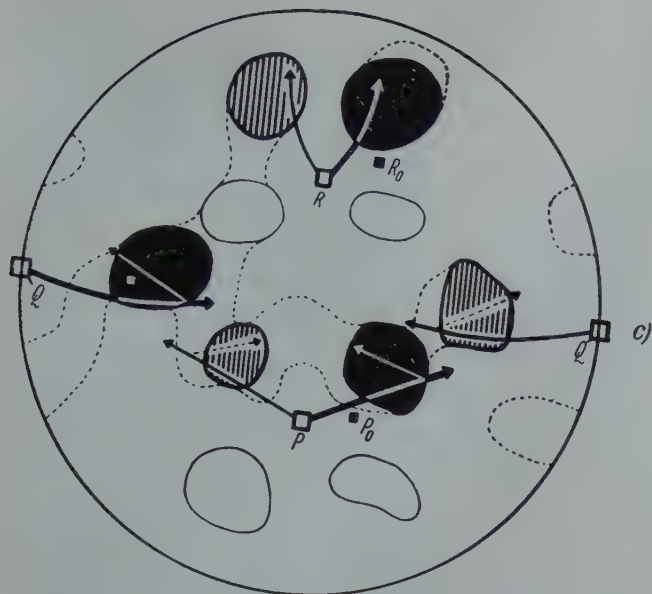


FIG 1 C—(100) pole figure for deformation texture \square and recrystallization texture obtained by Burgers⁶ in a compressed aluminum crystal of commercial purity.

Black areas represent the main component (A), and shaded areas the other important component (B) of the recrystallization texture. Arrows indicate [112] rotations.

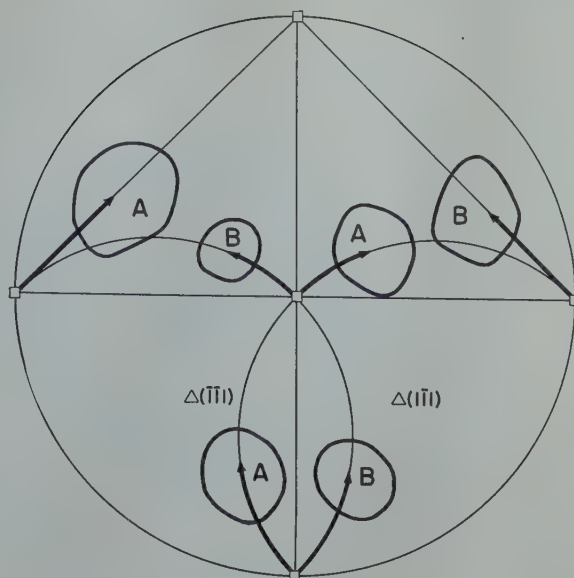


FIG 11—(100) pole figure for the data given in Fig 10, with the deformation texture in standard position.

Arrows indicate [111] rotations of 40° for A, and 37° for B.

crystal and either component of the recrystallization texture more accurately than the [112] rotations indicated by arrows in Fig 10. The orientation relationship between the deformation texture and the major component of the recrystallization texture is re-plotted in Fig 12 in a [111] projection, which again shows the excellent agreement of the data with the present interpretation. The agreement of the data reproduced in Fig 13 from ref. 6 (rolled single crystal of commercial aluminum) is again better with the [111] rotation than with the [112] rotation, as seen by comparing Fig 13 with Fig 14. It may be concluded, therefore, that the data presented by Burgers and his collaborators lend further support to the results described above. Furthermore, these data indicate that the impurities present in commercial aluminum do not affect the orientation relationship for recrystallization.

In all four instances where the relative orientation of deformation texture and recrystallization texture was determined (Fig 5, 9, 11 and 14), only one or two of the four possible [111] rotations were actually found to occur in noticeable amounts. It is to be noted that in the case of the two compressed crystals (Fig 9 and 11) the angle between the "active [111] axes and the compression axis is quite close to 90°. The [111] axes "active" in the recrystallization of the two rolled crystals (Fig 5 and 14) are those closest to the cross direction of rolling. (In the narrow deformation bands of crystal I the "active" [111]

Table 3 . . . Angle of Rotation Around [111] Direction in Degrees, Representing Orientation Change for Recrystallization and for Coarsening in a Highly Oriented Matrix

| Material | Condition before last anneal | Source of information | Recrystallization | Coarsening |
|----------------------|------------------------------|--|-------------------|------------|
| High purity aluminum | rolled single crystal | crystal I, this paper | 40 | 42, 35 |
| High purity aluminum | rolled single crystal | crystal II, this paper | 47 | 17-65, 50 |
| High purity aluminum | compressed single crystal | crystal III, this paper | 45 | |
| High purity aluminum | compressed single crystal | Barrett ⁸ | 45 | |
| Commercial aluminum | compressed single crystal | Burgers and Louwerse, ⁶ as re-interpreted above | 40, 37 | |
| Commercial aluminum | rolled single crystal | Burgers and Louwerse, ⁶ as re-interpreted above | 27, 33 | |
| Tough pitch copper | rolled polycrystal | Bowles and Boas ¹⁵ | | 30 |

direction was found to be about 2° further away from the cross direction than an inactive one. However, the accuracy of the measurements was not sufficient to make certain that this really represents an exception to the above criterion.) Since the direction of maximum compression in rolling is the normal direction, the criterion just described for rolled crystals is not unrelated to the one for compressed crystals.

The fact that the orientation of the recrystallized grains is derived from that of the deformed crystal by a [111] rotation implies, of course, that recrystallization nuclei of suitable orientation are available. It does not prove, however, that nuclei of other orientations do not exist. The occurrence of recrystallized grains of the above orientation range is favored probably because of their higher rate of growth in the deformed matrix. In the case of coarsening, this interpretation is

strongly supported by the orientation of the coarse grains nucleated at the sawed edge, as described above. Away from the edges the deformation texture is well-developed, and consequently the recrystallization texture is also quite sharply defined. Apparently, in a structure with such high degree of preferred orientation, there are but few grains with orientations deviating considerably from that of the mass, hence few "nuclei" for coarse grains. At the sawed edge the deformation is strongly heterogeneous. It may be assumed that at such locations tiny recrystallized grains of a large variety of orientations are formed upon annealing. Many of these may serve as "nuclei" in coarsening.* The fact that only those "nuclei" grow to large size which have the correct orientation with

* The described mechanism of "nucleation" of coarsening at points of inhomogeneous deformation may explain, at least in some cases, the phenomena of "forced secondary recrystallization" as reviewed by Burgers.²⁴

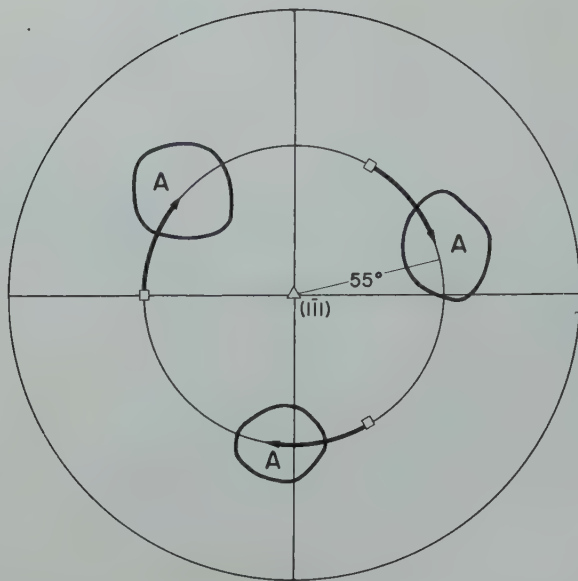


FIG 12—(100) pole figure for component *A* of the recrystallization texture, as given in Fig 10 and 11.
Center of projection is (111) of the deformation texture.

respect to the highly oriented recrystallized matrix, indicates that the selective principle involved is the orientation dependence of the rate of growth. That the coarse grains are not "nucleated" by remnants of the deformation texture is shown by the group *B* coarse grains in Fig 5, the orientation of which is quite different from that of the deformation texture. However, the orientation of both group *A* and group *B* coarse grains can be accounted for on the basis of the "oriented growth" theory.

The analogous orientation selectivity

found for recrystallization and for coarsening in high purity aluminum shows that the same orientation dependence governs the rate of growth of the grains in both cases. There is no reason to assume, however, that this analogy implies essential identity of the two processes. In fact, present evidence tends to support the view that recrystallization is connected with the elastic bending of the lamellae of deformed crystals,¹⁸ whereas coarsening is connected with the surface energy of the grain boundaries.^{16,19}

It is interesting to recall that the

fiber texture of cold drawn polycrystalline aluminum is [111] in the fiber axis, and that the recrystallization texture, developed upon annealing, is the same.^{1,2,3} In the light of the present results, the retention of the [111] fiber texture in recrystallization is easily understood, even though each deformed grain changes its orientation upon recrystallization. Fig 15 shows schematically a [111] fiber texture. If each recrystallized grain deviates from its parent matrix only by a rotation around [111], which is also the fiber axis, its (100) poles will remain within the same ring-shaped area of the pole figure, and the resulting recrystallization texture will be the same as the deformation texture. Here, as in compressed single crystals, the "active" [111] axis (around which the re-orientation takes place) is perpendicular to the directions of maximum compression (the radial directions of the rod). In copper, too, the deformation fiber texture is mainly [111], and this is retained in recrystallization.²⁰ In view of this fact, and of the observations of Bowles and Boas on coarsening, the orientation relationships for copper appear to be very similar to those for aluminum.

Fig 16 shows the rolling texture for polycrystalline aluminum, according to v. Goeler and Sachs.⁴ If this is replotted with the cross direction in the center of the projection, as in Fig 17, it becomes apparent that, in a rough approximation, the major component of this texture may be considered as an

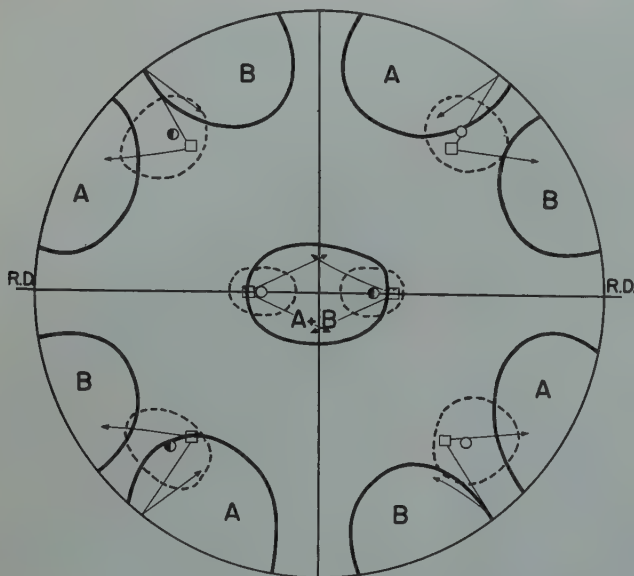


FIG 13—(100) pole figure for deformation texture (dotted lines), and for components *A* and *B* of recrystallization texture obtained by Burgers in rolled aluminum crystal of commercial purity.

Arrows indicate [112] rotations, as given by Burgers.

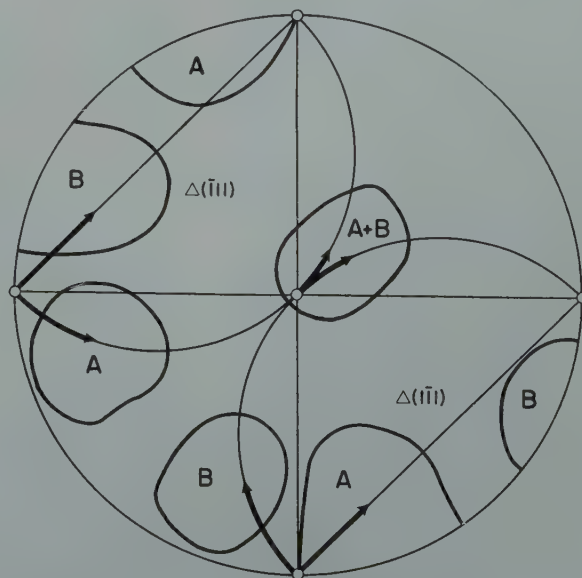


FIG 14—(100) pole figure for the data given in Fig 13, with one component of the deformation texture in standard position.

Arrows indicate [111] rotations of 27° for *A*, and 33° for *B*.

incomplete [111] fiber texture, with the cross direction as the fiber axis. Consequently, the often noted fact that the rolling texture of polycrystalline aluminum is fairly well retained upon recrystallization,⁴ may be visualized as described above for the fiber texture, even though the agreement cannot be expected to be as good as it is in the case of drawn aluminum. According to this interpretation, the "active" [111] axes in the various grains are all nearly parallel to the cross direction, in agreement with what was found above for rolled single crystals.

The behavior of rolled polycrystalline copper (with not more than about 80 pct reduction of area) is apparently very similar to that just described for aluminum. But it has been reported that the recrystallization texture of rolled silver²¹ and of certain face centered cubic copper alloys,²² such as brass, has mainly a (113) [112] position, even though the [111] fiber texture of cold drawn brass is apparently retained upon recrystallization.⁷ These conditions are not as yet clearly understood, and they are now being investigated at this laboratory.

It is known that certain body centered cubic metals have a [110] fiber texture, and that this is retained in recrystallization.²³ In analogy to the behavior of aluminum, it may be expected that in such metals the orientation relationship between a deformed grain and the recrystallized grains

growing in it may correspond to a rotation around a [110] direction. This expectation is also being tested at the present time.

Acknowledgments

The authors wish to express their appreciation to Mr. Philip R. Sperry for his conscientious and competent assistance with the experiments, and to the Aluminum Co. of America for

the grant of high purity aluminum. The continued interest and encouragement of Drs. A. R. Troiano, H. A. Dix, Jr., and A. J. Phillips is gratefully acknowledged. This work was supported by the office of Naval Research, U. S. Navy, Contract No. N6 ori-165, T.O. 1. The helpfulness of Messrs. I. R. Kramer, J. J. Harwood and James Bryson of the Materials and Mechanics Branch of the O.N.R. was of great value.

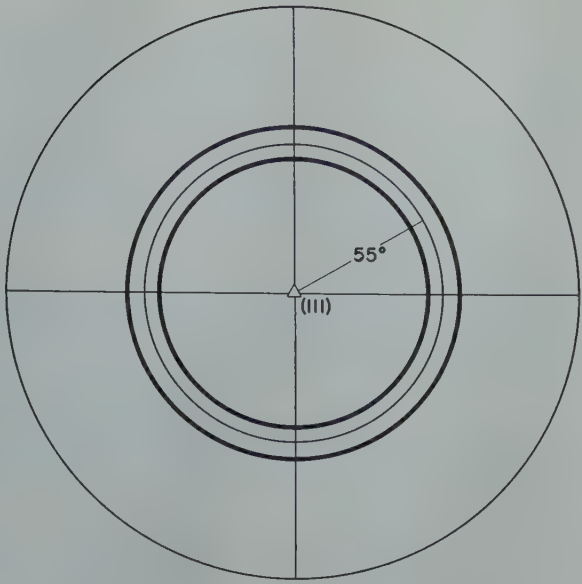


FIG 15—Schematic (100) pole figure for [111] fiber texture, with fiber axis as the center of projection.

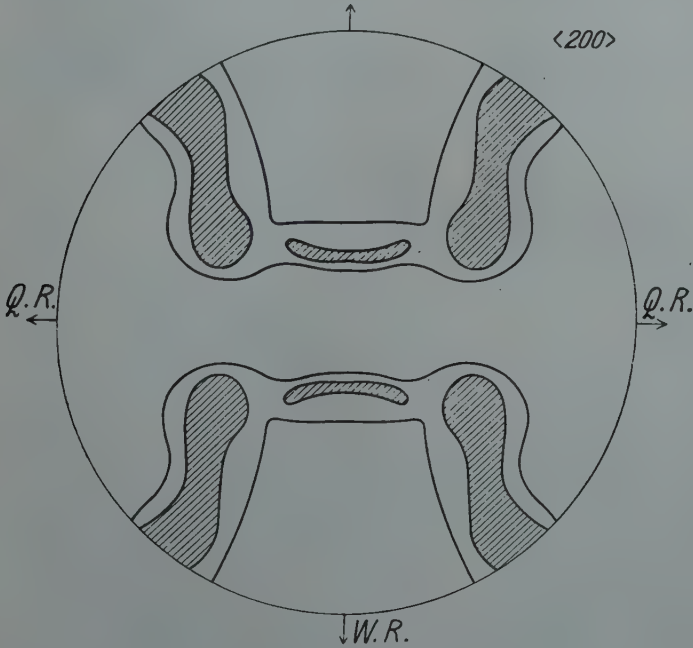


FIG 16—(100) pole figure for deformation texture of rolled polycrystalline aluminum, according to v. Goeler and Sachs.⁴ Plane of projection is the rolling plane. Rolling direction indicated by W. R.

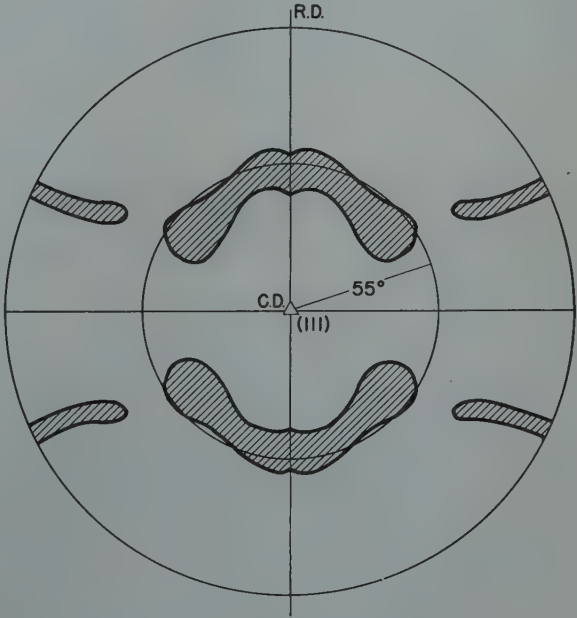


FIG 17—(100) pole figure for the data given in Fig 16, with the cross direction as the center of projection. The rolling direction is indicated.

Conclusions

1. The orientation of the recrystallized grains growing in a rolled or compressed aluminum single crystal is related to the main orientation of the deformed crystal by rotation around a [111] direction. The extent of rotation varies between about 30 and 50°. The orientation relationship for recrystallization does not appear to be affected by impurities present in commercial aluminum.

2. Since the axis of the rotation, which may be used to describe the orientation relationship between deformation texture and recrystallization texture for aluminum single crystals, is identical with the axis of the fiber texture of cold drawn polycrystalline aluminum, the retention of the [111] fiber texture in the recrystallization of this material is explained.

3. The orientation of the coarse grains growing in a matrix of fine grained recrystallized high purity aluminum with sharply defined texture is related to the main orientation of the matrix by rotation around a [111] direction. The extent of rotation may vary over wide limits, but it is usually about 30 to 50°. Important components of the coarsening texture may strongly deviate from the deformation texture. Consequently there is no reason to assume that the coarse grains are "nucleated" by remnants of the deformed material.

4. The orientation of coarse grains growing in a matrix of fine grained recrystallized high purity aluminum with sharply defined texture, from points where recrystallized grains with a large

variety of orientations are available (sawed edges) is the same as that of the coarse grains formed elsewhere. This indicates that the coarsening texture is determined by the orientation dependence of the rate of growth, rather than by "oriented nucleation."

References

1. G. Sachs and E. Schiebold: Rekristallisation und Entfestigung im Roentgenbild. *Ztsch. f. Met.* (1925) 17, 400.
2. v. Goeler and G. Sachs: Gefüge und Festigkeitseigenschaften von sehr reinem Aluminium. *Ztsch. f. Met.* (1927) 19, 90.
3. W. G. Burgers and J. Sandee: Pronounced Secondary Recrystallization of Drawn Aluminium. *Physica* (1942) 9, 996.
4. v. Goeler and G. Sachs: Walz- und Rekristallisationstextur regulärfächenzreierter Metalle I. *Ztsch. f. Phys.* (1927) 41, 873.
5. W. G. Burgers and J. C. M. Basart: Rekristallisation von Aluminium-einkristallen. *Ztsch. f. Phys.* (1929) 54, 74.
6. W. G. Burgers and P. C. Louwerse: Über den Zusammenhang zwischen Deformationsvorgang und Rekristallisationstextur bei Aluminium. *Ztsch. f. Phys.* (1931) 67, 605.
7. C. S. Barrett: Structure of Metals (1943) 420.
8. C. S. Barrett: Recrystallization Texture in Aluminum after Compression. *Trans. AIME* (1940) 137, 128.
9. U. Dehlinger: Zur theorie der Rekristallisation reiner Metalle. *Ann. d. Phys.* (1929) (5) 2, 749.
10. Paul A. Beck and P. R. Sperry: Effect of Recrystallization Texture on Grain Growth. *Trans. AIME* (1949) 185, 240. *Jnl. of Metals* March 1949.
11. P. A. Beck, M. L. Holzworth and P. R. Sperry: Effect of a Dispersed Phase on Grain Growth in Al-Mn Alloys. *Trans. AIME* 180, 163. *Metals Tech.* (Sept. 1948), TP 2475.
12. W. G. Burgers: Schematic Representation of Nuclear Growth in Deformed Metals. *Physica* (1942) 9, 987.
13. A. E. van Arkel: Quelques phenomenes de recrystallisation. *Rev. d. Met.* (1936) 33, 197.
14. W. G. Burgers: Recovery and Recrystallization viewed as processes of Dissolution and Movement of Dislocations. *Proc. K. Nederl. Akad. v. Wet.* (1947) 50, 723.
15. J. S. Bowles and W. Boas: The Effect of Crystal Arrangement on "Secondary Recrystallization" in Metals. *Jnl. Inst. Met.* (1948) 74, 501.
16. P. A. Beck, J. C. Kremer, L. J. Demer, and M. L. Holzworth: Grain Growth in High Purity Aluminium and in an Aluminium-magnesium Alloy. *Trans. AIME* (1948) 175, 372. *Metals Tech.* Sept. 1947, TP 2280.
17. C. S. Barrett and L. M. Levenson: Determination of Orientations by Etch Pits. *Trans. AIME* (1940) 137, 76.
18. P. A. Beck: Effect of Reversed Deformation on Recrystallization. *Trans. AIME* (1937) 124, 351.
19. Discussion by J. E. Burke of ref. 11. *Trans. AIME* (1949) 185, 315.
20. E. Schmid and G. Wassermann: Über die Rekristallisation von Kupferdraht. *Ztsch. f. Phys.* (1926) 40, 451.
21. R. Glocker and E. Kaupp: Beobachtungen des Rekristallisationsvorganges mittels Roentgenstrahlen. *Ztsch. f. Met.* (1924) 16, 377.
22. O. Dahl and F. Pawlek: Kornordnung und Kornwachstum bei Walzblechen. *Ztsch. f. Met.* (1936) 28, 262.
23. Z. Jeffries: The Trend in the Science of Metals. *Trans. AIME* (1924) 70, 303.
24. W. G. Burgers: Rekristallisation, Vervormter Zustand und Erholung (1941).
25. C. G. Dunn: Recrystallization Textures. Symposium on Cold Working of Metals (1948), *Trans. ASM*, 41A.

Correction June Issue

"The Statistical Nature of the Endurance Limit." By J. T. Ransom and R. F. Mehl. On page 365, June 1949 *Journal of Metals Transactions*, caption for Fig 2 should read, "Scatter Range for 210 Specimens."

Annealing Twins in Copper and 70-30 Alpha Brass*

WALTER R. HIBBARD, JR.,† Junior Member, YOU-CHAO LIU,† and STANLEY F. REITER,† Student Associates AIME

Cyril Stanley Smith in his classic 1948 Institute of Metals Lecture¹ noted in the case of annealing twins that: "It is well known that approximately the same number of twins per grain and the same general geometry are maintained in large grains as in small ones, a fact that certainly suggests a mechanism such as the above where boundaries and twins grow proportionately together. If this view is correct, a spherical grain should have no mechanism for keeping its twins." Such a constancy of twins per grain would be of particular interest as a tool for the study of the origin of annealing twins. It has been proposed by Mathewson² and later by Barrett³ that in face-centered cubic metals slip occurs in the {111} plane by $\langle 112 \rangle$ shears which combine in pairs to produce the macroscopically observed $\langle 110 \rangle$ movement. This proposal is schematically inviting since $\langle 112 \rangle$ slip permits the atoms of one plane to move along the interatomic valleys of its neighbor rather than up the hills across the atom sites. There is strong experimental evidence⁴ that annealing twins result from the growth of nuclei in the form of "twin faults" produced by single $\langle 112 \rangle$ shears.

It is possible that more twin faults would form at low deformation temperatures than at high ones, because the more rigid lattice may increase the tendency to "freeze" the twin faults

and prevent their dissipation in slip. This is suggested by (1) the greater resistance to slip at low temperatures and (2) greater tendency toward mechanical type twinning at low temperatures (a summary of these factors is presented by Seigl  and Brick⁵). These considerations would suggest the following:

- Constant twin/grain ratio for specimens deformed constant amounts at a constant temperature, but annealed at various temperatures above the recrystallization temperature.
- Larger twin/grain ratios for recrystallized specimens previously deformed constant amounts at lower temperatures.

The purpose of this investigation is to test these considerations.

Cleveland Meeting, October 1949.
TP 2677 E. Discussion of this paper (2 copies) may be sent to *Transactions AIME* before December 1, 1949. Manuscript received May 2, 1949.

* The data in this paper were taken from reports submitted by Y. C. Liu and S. F. Reiter to the School of Engineering, Yale University, in candidacy for the Degree of Master of Engineering, May 1949.

† Assistant Professor and Graduate Students, respectively, Department of Metallurgy, Yale University, New Haven, Connecticut.

¹ References are at the end of the paper.

Experimental Procedure and Results

One half in. rods of phosphorous deoxidized electrolytic copper and 70-30 alpha brass (68.36 pct Cu, 0.005 pct Pb, 0.01 pct Fe, 31.62 pct Zn remainder) were rolled to a thickness of 0.350 in., milled to specimens $0.350 \times 0.437 \times 2$ in., and annealed at 700°C to an average grain size of 0.065 and 0.090 mm, respectively. These specimens of each metal were then rolled 50 pct reduction in thickness and annealed one hour under conditions which were all combinations of the following:

| Rolling Temperatures, °C | Annealing Temperatures, °C |
|--------------------------------|----------------------------------|
| -70 | 400 |
| 25 | 500 |
| 200 | 600 |

Standard metallographic techniques⁶ were used to prepare specimens. By the method of lineal analysis⁷ using a minimum of ten samples of fifty grains each for each specimen, the ratios of twins* per total grains, twins per twinned grain, twin families* per total grains and twins per twin family were determined. Recrystallized grain size was determined by A.S.T.M. comparison methods.⁸ All observations were made on the rolling plane.

The results are tabulated in Table 1.

* Twins were counted as the number of distinguishable twins on the polished surface even though many of them were parallel. Twin families were counted as the number of different twin directions in a grain, a maximum of four.

Table 1 . . . Annealing Twins in Rolled and Recrystallized Copper and Alpha Brass

| Rolling Temperature..... | -70°C | | | 25°C | | | 200°C | | |
|-------------------------------------|-------------|-------------|-------------|-------------|-------------|-------------|-------------|-------------|-------------|
| Annealing Temperature..... | 400°C | 500°C | 600°C | 400°C | 500°C | 600°C | 400°C | 500°C | 600°C |
| Copper | | | | | | | | | |
| Twins per total grains..... | 0.95 ± 0.04 | 0.95 ± 0.04 | 1.08 ± 0.05 | 1.04 ± 0.08 | 1.14 ± 0.05 | 1.11 ± 0.05 | 1.11 ± 0.07 | 1.14 ± 0.07 | 1.06 ± 0.05 |
| Twins per twinned grains..... | 1.65 ± 0.05 | 1.67 ± 0.05 | 1.58 ± 0.05 | 1.78 ± 0.09 | 1.69 ± 0.06 | 1.68 ± 0.03 | 1.82 ± 0.08 | 1.82 ± 0.07 | 1.65 ± 0.09 |
| Twin families per total grains..... | 0.70 ± 0.01 | 0.65 ± 0.02 | 0.76 ± 0.03 | 0.68 ± 0.04 | 0.75 ± 0.02 | 0.78 ± 0.02 | 0.70 ± 0.03 | 0.71 ± 0.03 | 0.73 ± 0.02 |
| Twins per family..... | 1.35 ± 0.05 | 1.46 ± 0.04 | 1.41 ± 0.03 | 1.55 ± 0.06 | 1.52 ± 0.04 | 1.43 ± 0.03 | 1.56 ± 0.05 | 1.62 ± 0.05 | 1.46 ± 0.05 |
| Grain Size, mm..... | 0.025 | 0.035 | 0.045 | 0.035 | 0.035 | 0.045 | 0.045 | 0.045 | 0.045 |
| Brass | | | | | | | | | |
| Twins per total grains..... | 6.30 ± 0.28 | 5.85 ± 0.25 | 2.03 ± 0.08 | 6.17 ± 0.26 | 7.20 ± 0.23 | 1.87 ± 0.07 | 6.88 ± 0.23 | 7.56 ± 0.37 | 1.90 ± 0.07 |
| Twins per twinned grains..... | 6.70 ± 0.26 | 6.25 ± 0.20 | 2.23 ± 0.07 | 6.86 ± 0.25 | 7.61 ± 0.23 | 2.08 ± 0.08 | 7.58 ± 0.24 | 7.90 ± 0.40 | 2.16 ± 0.06 |
| Twin families per total grains..... | 1.83 ± 0.04 | 1.84 ± 0.05 | 1.24 ± 0.03 | 1.74 ± 0.03 | 2.01 ± 0.03 | 1.21 ± 0.03 | 1.83 ± 0.03 | 1.99 ± 0.04 | 1.26 ± 0.05 |
| Twins per family..... | 2.44 ± 0.11 | 3.16 ± 0.10 | 1.64 ± 0.03 | 3.51 ± 0.08 | 3.59 ± 0.10 | 1.52 ± 0.04 | 3.79 ± 0.11 | 3.79 ± 0.19 | 1.51 ± 0.03 |
| Grain Size, mm..... | 0.015 | 0.025 | 0.090 | 0.025 | 0.025 | 0.090 | 0.025 | 0.035 | 0.090 |

Discussion of Results

From Table 1 the following observations are apparent:

1. Under similar conditions of rolling and annealing, more annealing twins are found in 70-30 alpha brass than in copper, both from the standpoint of total number of twins and number of twin families.

2. In the case of copper, the various twin ratios are essentially independent of the annealing temperature as suggested by Smith.¹

3. In the case of 70-30 alpha brass, significantly fewer twins were formed at the highest annealing temperature under all rolling conditions. However, it was noted that a large number of nearly spherical grains survived at this temperature, again in accordance with the suggestions of Smith.¹

The tendency toward forming annealing twins is slightly but probably not significantly less for lower temperatures of deformation.

4. In the case of copper, by comparing twins per total grains with twins per twinned grains, it appears that after the 600°C anneal there were about the same number of twins per grain but significantly more twin-free grains than after the 400 and 500°C anneals. In the case of brass there were significantly fewer twins per grain but about the same number of twin-free grains at 600°C.

Observation (1) suggests that twin 70-30 alpha brass has greater tend-

faults form more readily in 70-30 alpha brass than in copper. Thus the tendency to form annealing twins is a direct function of the elastic anisotropy of the metal (that is, brass is more anisotropic than copper). This can be extrapolated to aluminum, which is nearly isotropic and in which annealing twins possibly have not been observed. It suggests that twin faults form more readily if the elastic modulus normal to the slip plane is significantly larger than that parallel to it.

Observations (2) and (4) suggest that in copper there is a tendency for twin-free grains to grow at the expense of grains containing twins, particularly those with few twins. Observations (3) and (4) suggest that in alpha brass many twins form at lower annealing temperatures (as reported by Maddigan and Blank,⁹ but that the twins coalesce within the grains at higher temperatures (600°C). This coalescence apparently starts when the grains have grown sufficiently to approach a spherical shape.

While more twin faults may have formed at lower deformation temperatures, in these experiments a proportionately larger number of them did not grow to annealing twins. Possibly the increased activity of the atoms at the annealing temperature permitted most of the twin faults to be absorbed.

Summary

encies toward annealing twin formation than copper. The twins per grain ratio is essentially constant for copper and 70-30 alpha brass over a wide range of deformation temperatures and annealing temperatures, except for the alpha brass at 600°C where an appreciable reduction in this ratio was found.

Acknowledgment

The interest, encouragement and counsel of Professor C. H. Mathewson are gratefully acknowledged. The phosphorous deoxidized electrolytic copper was furnished by the Scovill Manufacturing Co., Waterbury, Conn., and the 70-30 alpha brass rod by the American Brass Co., Torrington, Conn. Dr. Robert Maddin read and criticized the manuscript.

References

1. C. S. Smith: *Trans. AIME* (1948) 175, 15. *Metals Tech.* June 1948, TP 2387.
2. C. H. Mathewson: *Trans. A.S.M.* (1944) 32, 38.
3. C. S. Barrett: A.S.M. Symposium. Phila., Pa. Oct. 1948.
4. R. Maddin, C. H. Mathewson and W. R. Hibbard, Jr.: *Origin of Annealing Twins in Brass. Jnl. of Metals* TP 2676. (To be published.)
5. L. Siegle and R. M. Brick: *Trans. A.S.M.* (1948) 40, 813.
6. A.S.T.M. Standard E3-46T.
7. R. T. Howard and M. Cohen: *Trans. AIME* (1947) 172, 413. *Metals Tech.* Aug. 1947.
8. A.S.T.M. Standard E2-44T.
9. S. E. Maddigan and A. I. Blank: *Trans. AIME* (1940) 137, 170.



The Yielding and Strain-aging of Carburized and Nitrided Single Crystals of Iron

HARRY SCHWARTZBART,* Junior Member, and JOHN R. LOW, JR.,† Member AIME

Introduction

Annealed, polycrystalline, low carbon steel exhibits a phenomenon known as the "yield point." If such a steel is loaded in tension, the load increases steadily with elastic strain, drops suddenly, fluctuates about some constant load value for a time and then rises with further strain. The load at which the sudden drop occurs is called the "upper yield point"; the load at which deformation proceeds at constant load is known as the "lower yield point"; the amount of elongation at constant load is termed the "yield point elongation."

Deformation which occurs during the yield point elongation is heterogeneous in nature, deformed metal existing next to undeformed metal. The drop in load from the upper yield point is concurrent with the formation of a band of deformed metal which usually appears at a stress concentration such as a fillet and at an angle of approximately 45° with the direction of pull. As deformation proceeds during the yield point elongation, the deformed region grows until the entire specimen has been strained an amount equal to the strain in the first band.

A phenomenon very often associated with the yield point is that of strain aging. Aging in steels may be of two types: quench aging, or precipitation hardening, and strain-aging. Strain aging differs from precipitation hardening in that if the metal is merely strained instead of given a solution anneal and quenched, it then undergoes changes in properties similar to those

observed in quench aging.

The yield point effect and strain aging are most markedly exhibited by low carbon steel, but have been observed in other alloys. Numerous explanations for the mechanisms of both phenomena have been advanced, but the evidence for the acceptance of any of the hypotheses is incomplete. One of the explanations of the yield point phenomenon frequently proposed is that there exists a honeycomb of grain boundary material that supports the load above the yield strength of the ferrite and that when this network ruptures, the ferrite flows with no increase in load. This notion was first advanced by Dalby¹ in 1913 and has been since put forward in more concrete form by many investigators. The testing of this hypothesis was, in part, the object of the present investigation. Similarly, the mechanism by which

strain aging occurs remains to be explained. Presumably, it is a precipitation hardening phenomenon similar to quench aging, the precipitation being initiated by strain. However, it is not known whether the process is a solution and precipitation effect or a change in solubility due to strain.

One obvious method of determining whether or not the yield point is a grain boundary phenomenon is to determine if single crystals exhibit a yield point. Low and Gensamer² have shown that carbon and nitrogen are responsible for the yield point and aging in steel and that these effects can be eliminated by the removal of these elements through wet hydrogen purification. Single crystals that have been grown in wet hydrogen treated material must then be recarburized or re-nitrided in order to evaluate the effect of grain boundaries. In the present investigation, single crystals of iron which had been annealed in wet hydrogen to remove the carbon and nitrogen were cut into two specimens having the same orientation with respect to the tension axis. Of these, one specimen was pulled in tension in the wet hydrogen treated state and the other was carburized or nitrided and tested similarly. All the crystals were examined for a yield-point and strain aging.

The grain boundary hypothesis for the explanation of the yield point in steel has been tested only indirectly previously. Arrowsmith,³ Andrew and Lee,⁴ Edwards and Pfeil,⁵ Fell,⁶ Ludwik and Scheu,⁷ Winlock and Leiter⁸ and others found a decrease in proportional limit and yield point effect with an in-

Cleveland Meeting, October 1949.

TP 2603 E. Discussion of this paper (2 copies) may be sent to *Transactions AIME* before December 1, 1949. Manuscript received January 31, 1949.

This paper is based upon a thesis submitted by Harry Schwartzbart to the Pennsylvania State College in partial fulfillment of the requirements for the degree of M.S. in metallurgy.

* Formerly Research Assistant, Pennsylvania State College, State College, Pennsylvania. Presently Research Metallurgist, National Advisory Committee for Aeronautics, Cleveland, Ohio.

† Formerly Professor and Chief, Division of Metallurgy, Pennsylvania State College, State College, Pennsylvania. Presently Research Associate, General Electric Co., Schenectady, New York.

¹ References are at the end of the paper.

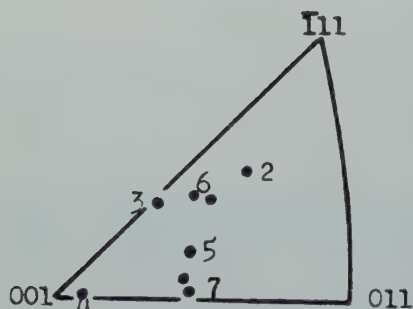


FIG 1—Orientations of the single crystals.
Checks were made on Crystals 6 and 7.

crease in grain size. Edwards and Pfeil⁵ did not find a yield point in a single crystal of hydrogen purified mild steel, but the carbon and nitrogen were probably absent in their crystals. Single crystals of iron grown in wet hydrogen purified mild steel were tested under dead weight loading by Gensamer and Mehl⁹ who found that at stresses at which yielding occurs, the rate of elongation is initially low, then increases, and finally decreases to zero. They point out that this behavior will

be observed in material whose flow curve shows a drop in load at yielding. Gensamer¹⁰ tested similar crystals in a conventional tension testing machine; these crystals showed no drop in load but the initial plastic elongation took place at substantially constant load. These crystals had not had all of the carbon and/or nitrogen removed. Holden and Hollomon¹¹ in an investigation contemporaneous with the present one found no yield point in carburized or nitrided single crystals of iron. A point-by-point comparison of the experimental procedures used in the two investigations reveals the following principal differences:

1. Holden and Hollomon's crystals were made from aluminum killed stock while those of the present investigation were made from silicon killed material. The presence of an excess of aluminum might conceivably affect the behavior of nitrided single crystals by combining with the nitrogen but would not be expected to have a similar effect in the case of carburized crystals.

2. Holden and Hollomon used $\frac{1}{8}$ -in. ga. length SR-4 strain gauges for measuring strain while the present authors used 1-in. Tuckerman gauges. The shorter gauge length used by Holden and Hollomon would tend to obscure the "drop in load" feature of the yield point, but the "strain at constant load" portion should have been observed if present.

3. Holden and Hollomon's single crystals were slowly cooled following carburizing and nitriding, whereas the present authors' were air cooled. There is no apparent reason why this difference in cooling rate should lead to the reported differences in yielding behavior.

Up to the present time, no satisfactory explanation has been found for the differing results of the two investigations.

Experimental Procedure

The single crystals used in this investigation were prepared at Carnegie Institute of Technology by the strain-anneal method and are similar to the crystals which were used in the investigation of Gensamer and Mehl⁹ discussed earlier. Details of their fabrication can be obtained from their paper. The bar stock from which the crystals were grown contained 0.36 pct Mn, 0.010 pct P, 0.025 pct S and 0.09 pct Si and it is to be expected that the single crystals contained substantially the same amounts of these elements.

Six crystals were used in the present investigation, all of which were initially in the form of $\frac{3}{8}$ in. diam round bars. No X ray examination for crystal perfection was made; however, macroscopic examination after etching to develop etch-pits did not reveal any occluded crystallites or evidence of gross crystal imperfections.

The crystals were found to contain 0.003 pct carbon when analyzed by the low pressure vacuum fusion method; hence it was not known if they had been adequately decarburized to eliminate the yield point and strain aging since this amount of carbon lies near the limit found by Low and Gensamer for these two characteristics in polycrystalline specimens. Therefore, further wet hydrogen treatment was performed on the crystals after machining into tensile specimens for this investigation.

The orientations of all the crystals were determined and the orientations

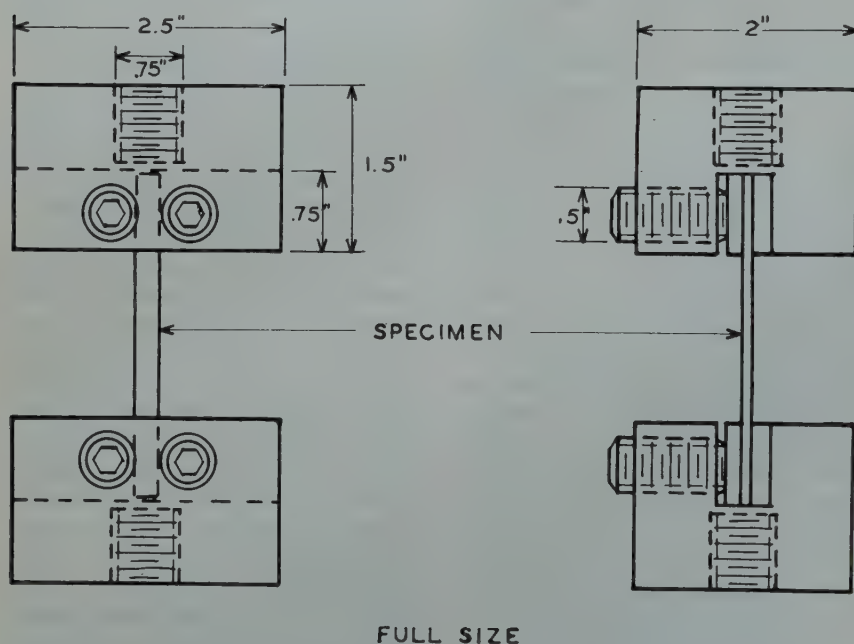


FIG 2—Grips used in single crystal tension tests.

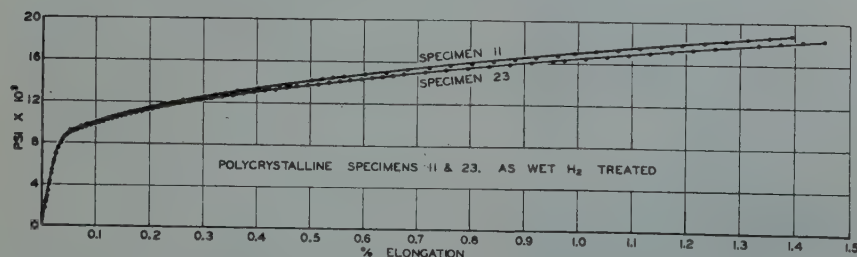


FIG 3—Stress-strain curves for polycrystalline specimens 11 and 23.
As wet hydrogen treated.

of the tension specimen axes are plotted in the stereographic triangle of Fig 1. The method used to determine orientations was similar to the etch pit technique described by Barrett and Levenson.¹² Since the success of this investigation depended on the fact that the specimens being compared were cut from the same single crystal and, therefore, had the same orientation it was not essential that the orientation be determined with a high degree of accuracy.

Each of the single crystal bars was sawed in half longitudinally and two halves ground flat to give two specimens having the same orientation with respect to the tension axis. The specimens consisted of simple rectangular prisms with no reduced section. The dimensions of the specimens before testing varied from 0.1505 in. to 0.3036 in. wide by 0.0416 in. to 0.0578 in. thick. The length of the specimens between the grips varied from 1 $\frac{5}{16}$ in. to approximately 2 $\frac{1}{2}$ in.; the distance between grips was the same for all specimens from a single crystal. All of the specimens were composed of a single crystal between the grips except the specimens of Crystal 2 which had a grain boundary about $\frac{3}{4}$ in. from one grip. In this case the knife edges of the extensometer did not contain the grain boundary between them but were placed entirely on one crystal at least $\frac{1}{4}$ in. away from the grain boundary. The results obtained on Crystal 2 are consistent with those for the other crystals.

After machining, the specimens were heated to 720°C in tank hydrogen, then held for the amounts of time shown in Table 1 in an atmosphere of hydrogen containing water vapor in the percentages noted in the same table, and air cooled. The flow rate of gas through the furnace was 2 cfhr which is equivalent to a linear flow rate of 0.037 fps. The specimens after cooling in air were coated with a thin oxide film; this was removed in 10 pct HNO₃. In some cases there was a layer of fine crystals on the specimens caused by recrystallization of the machined (cold worked) surfaces. These fine crystals were removed by alternately etching in 10 pct HNO₃ and grinding, using extremely light passes.

It can be seen in Table 1 that not all the crystals received identical wet hydrogen treatments. Since it was observed in the cases of Crystals 2, 3 and 4 that a slight yield point indication was obtained on the uncarburized

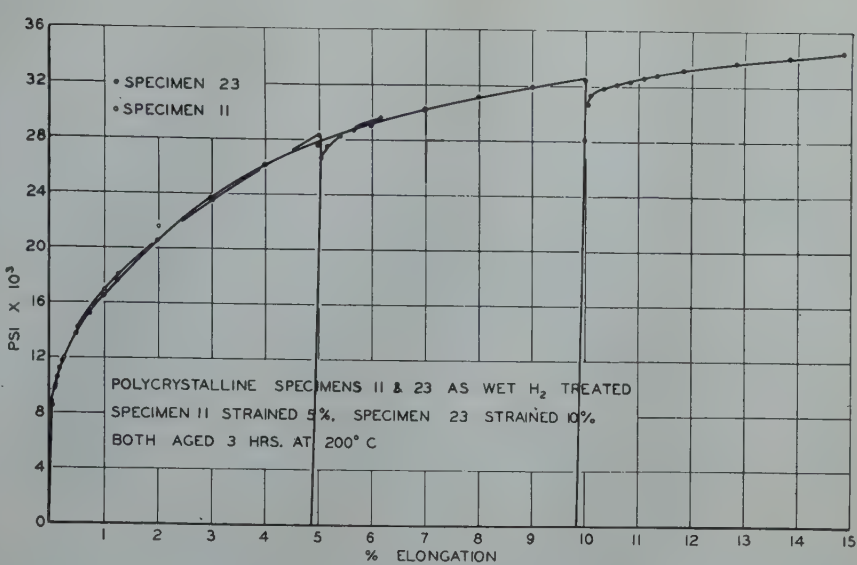


FIG 4—Composite stress-strain curves for polycrystalline specimens 11 and 23. As wet hydrogen treated.

Table 1 . . . Wet Hydrogen Treatments of Single Crystals

| Temp.—720°C; linear flow rate—0.037 fps | | |
|---|--|---|
| Crystal No. | Time of Treatment, Hr | Vol. Pct H ₂ O |
| 2, 3, and 4 | 6 $\frac{3}{4}$ 8 $\frac{1}{2}$ | 10 (saturator at 46°C) 3 (saturator at room temperature) |
| 5 and 7 | 8 $\frac{1}{2}$ + 11 $\frac{3}{4}$ | 3 (saturator at room temperature) 10 (saturator at 46°C) |

specimen in the test after aging it was desirable to learn if longer treatments would reduce the carbon and/or nitrogen to the level of complete elimination of yield point indications either before

or after aging. The treatment in which the saturator was at room temperature was a mistake. The furnaces used for all the heat treating were of the nichrome wound electric resistance type with a Sillimanite tube as the heating chamber.

One of the specimens cut from Crystals 2, 3, and 4 was heated to 700°C in tank hydrogen, then held for 10 min. in an atmosphere of hydrogen saturated with normal heptane at 22°C (this will yield a mixture containing about 5 pct heptane), and air cooled. These conditions and short carburizing time were chosen to prevent the introduction of a second phase in the crys-

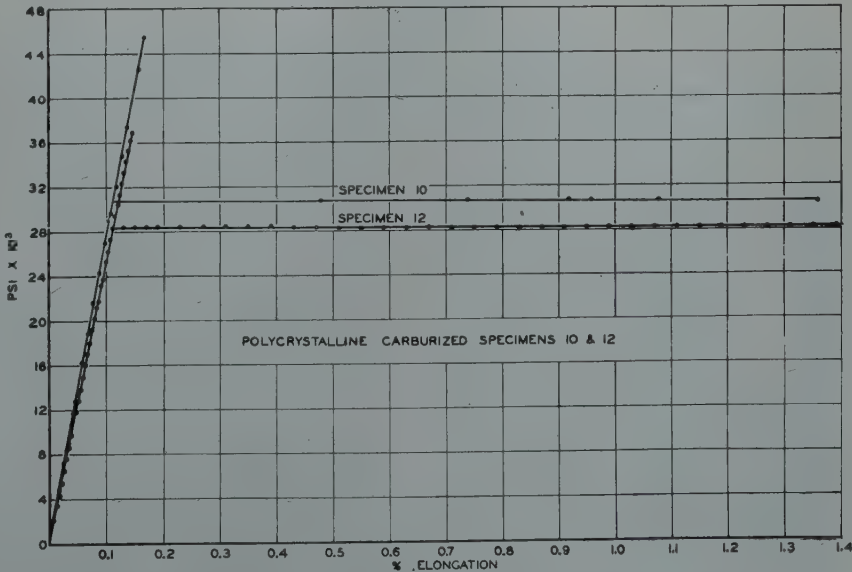


FIG 5—Stress-strain curves for polycrystalline carburized specimens 10 and 12.

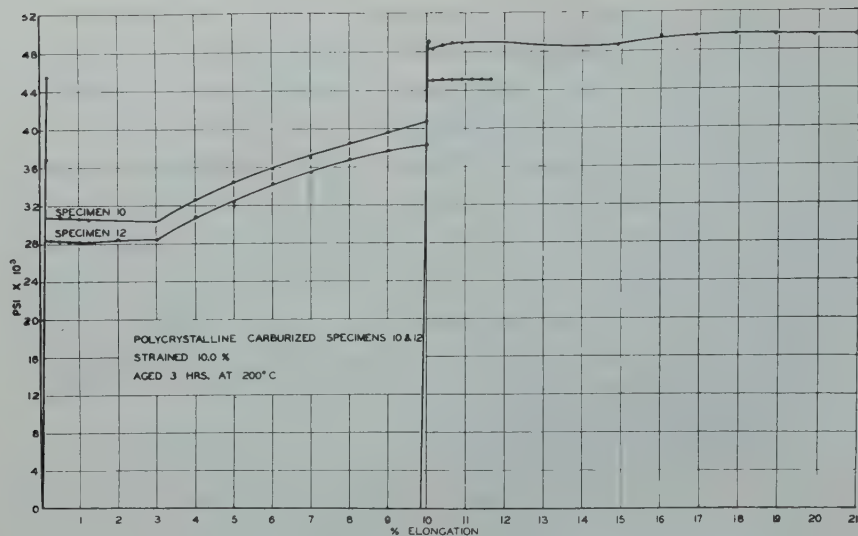


FIG 6—Composite stress-strain curves for polycrystalline carburized specimens 10 and 12.

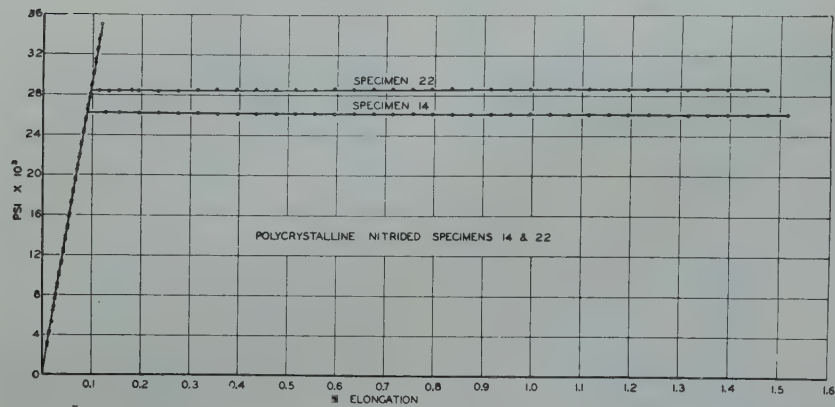


FIG 7—Stress-strain curves for polycrystalline nitrided specimens 14 and 22.

Table 2 . . . Mechanical Properties and Chemical Analyses of Carburized, Nitrided and As-hydrogen-purified Polycrystalline and Single Crystal Specimens

| Crystal or Specimen Number | Condition | Yield Strength, Psi X 10 ³ | Stress at 4 Pct Strain, Psi X 10 ³ | Pct Which Carburization or Nitriding Raised the Stress-strain Curve at 4 Pct Strain | Pct Strain Aging | Pct Carbon (Duplicate Analyses) | | Pct Nitrogen |
|-----------------------------|-------------------------------|---------------------------------------|---|---|------------------|---------------------------------|-------|--------------|
| Single Crystal 2 | Uncarburized | 10.0 | 13.0 | | 0 | 0.002 | 0.002 | |
| Single Crystal 3 | Carburized | 10.5 | 13.5 | 15 | 10 | 0.005 | 0.005 | |
| Single Crystal 4 | Carburized | 11.5 | 14.0 | 14 | 0 | 0.002 | 0.002 | |
| Single Crystal 5 | Uncarburized | 10.0 | 14.0 | 7 | 7 | 0.005 | 0.005 | |
| Single Crystal 6* | Carburized | 12.5 | 15.0 | 7 | 13 | | | |
| Single Crystal 7 | Not nitrided | 8.5 | 11.0 | | 4 | | | 0.0004 |
| Single Crystal 8 | Nitrided | 12.0 | 14.0 | 27 | 17 | | | 0.0070 |
| Single Crystal 9 | Not nitrided | 16.0 | 17.0 | | 9 | | | |
| Single Crystal 10 | Nitrided | 18.0 | 19.5 | 15 | 18 | | | |
| Single Crystal 11 | Not nitrided | 12.5 | 15.5 | | 0 | | | 0.0004 |
| Single Crystal 12 | Nitrided | 14.0 | 16.5 | 16 | 24 | | | 0.0070 |
| Polycrystalline Specimen 11 | As wet H ₂ treated | 9.0 | 26.0 | | 0 | 0.002 | 0.002 | |
| Polycrystalline Specimen 23 | As wet H ₂ treated | 9.0 | 26.0 | | 0 | | | 0.0007 |
| Polycrystalline Specimen 10 | Carburized | 29.5 | 32.5 | 25 | 17 | | | |
| Polycrystalline Specimen 12 | Carburized | 28.0 | 31.0 | 19 | 17 | 0.010 | 0.011 | |
| Polycrystalline Specimen 22 | Nitrided | 28.5 | 33.5 | 29 | 17 | | | 0.0140 |
| Polycrystalline Specimen 14 | Nitrided | 26.0 | 30.5 | 17 | 18 | | | |

* The specimens cut from this crystal were given insufficient wet hydrogen purification.

tals. The flow rate of gas through the furnace was 1.5 cfhr or 0.028 fps.

To make certain the carburization was effective, control specimens of wet hydrogen purified polycrystalline low carbon rimmed steel (ASTM grain size 8) were treated with the single crystals. The control specimens had been cut from 0.036 in. sheets previously wet hydrogen purified at 720°C for 4 hr and known to be free of either a yield point or aging. Specimens adjacent to the control specimens in the original wet hydrogen treated sheet were tested in tension and examined for yield point and strain aging. From the stress-strain curves reproduced in Fig 3, 4, and 5, it is evident that the control specimens had received sufficient purification to eliminate the yield point and strain aging and that if they exhibited these effects after carburization they were due to that carburization. The polycrystalline specimens were standard ASTM sheet specimens. Air cooling after carburization produced a scale on the specimens which was removed with 10 pct HNO₃. No recrystallization, due to carburizing, could be observed on the etched specimens.

The train used for nitriding was as follows: Tank hydrogen → CaCl₂ → empty Erlenmeyer flask at liquid air temperature → activated charcoal at liquid air temperature → liquid NH₃ saturator at -77°C → nitriding furnace. The CaCl₂ and liquid air trap were driers; the activated charcoal at -190°C was necessary for the removal of hydrocarbons present in tank hydrogen;² the ammonia saturator was maintained at -77°C to keep the concentration of ammonia in the hydrogen low enough (6 pct) to prevent the formation of iron nitrides.¹³ A venturi type flow meter between the hydrogen tank and the CaCl₂ drier indicated the flow rate which was maintained at 1.5 cfhr or 0.127 fps. The nitriding procedure was as follows: The single crystal specimens and, as in the case of carburization, the polycrystalline control specimens were placed in the cold furnace; dried ammonia vapor was introduced into the saturator where enough was condensed for one run; the specimens were heated to 500°C in hydrogen passing through the above train but by-passing the ammonia saturator; once at temperature the saturator was cut into the system by a suitable arrangement of glass T's and pinchcocks. Nitriding proceeded for 3 hr at 500°C after which the specimens were air cooled. This produced a light scale

which was removed in 10 pct HNO_3 . No recrystallization, due to nitriding, could be observed on the etched specimens.

Tensile tests were made on a Baldwin-Southwark 60,000 lb hydraulic machine with an Emery weighing system. Load readings were taken on the 1200 lb range dial of the machine to the nearest pound. The rate of head movement on all tests was approximately 0.0022 in. per min. Elongations up to about 1.6 pct were measured with a Tuckerman optical extensometer on a 1 in. ga length with a precision of 2×10^{-6} in. per in. Light punch marks were placed 1 in. apart on the single crystals and 2 in. apart on the polycrystalline specimens; elongations greater than 1.6 pct were then measured to the nearest 0.01 in., using dividers.

Axiality of loading was achieved through the use of modified Robertson shackles wherein the load is applied at the point of contact between a hardened steel plane and a steel ball. That part of the shackle which contained the threaded end of the specimen, adapter or grip could be shifted in relation to the stress axis by means of positioning screws thus correcting for any eccentricity in the system. A test for axiality is the requirement that upon a change in load in the elastic range all four sides of the specimen elongate or contract the same amount. In this investigation the specimens were aligned to the extent that, upon a change in load in the elastic range, the changes in length of any two opposite sides were within 6 pct of each other.

The polycrystalline specimens were gripped in Templin sheet grips. A special set of grips was used for the single crystals; these are illustrated in Fig 2. The specimen was fastened in the grips with the latter out of the tensile machine; the complete assembly as shown in Fig 2 was then transferred to the testing machine, with great care being exercised to avoid bending of the specimen.

The single crystals before testing had all been etched in 10 pct HNO_3 . The only difference in treatment of the two specimens cut from any single crystal was the carburization or nitriding treatment. All crystals were strained 5.0 pct, the load removed and the specimen (still in the grip assembly) was placed immediately in an oven at 200°C for 3 hr after which they were pulled again and examined for strain

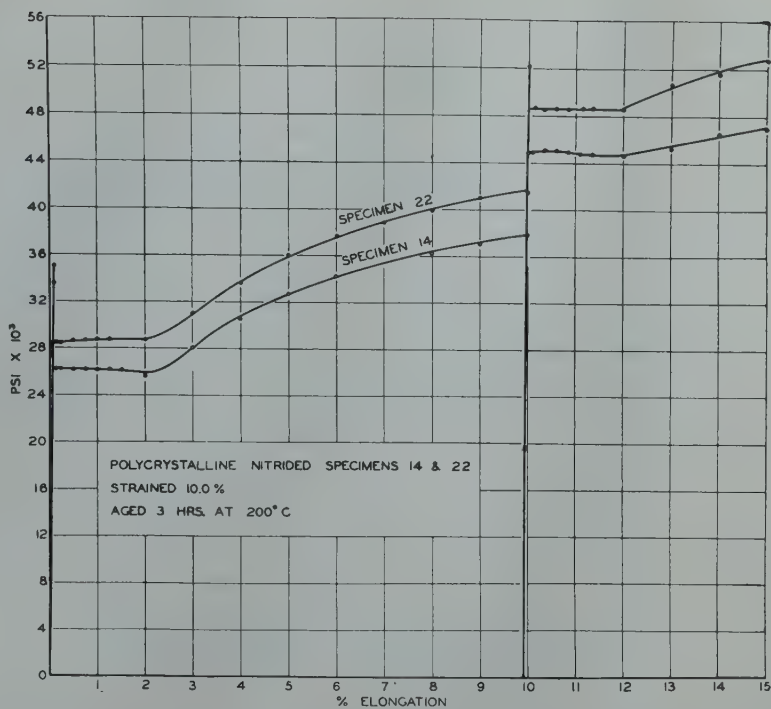


FIG 8—Composite stress-strain curves for polycrystalline nitrided specimens 14 and 22.

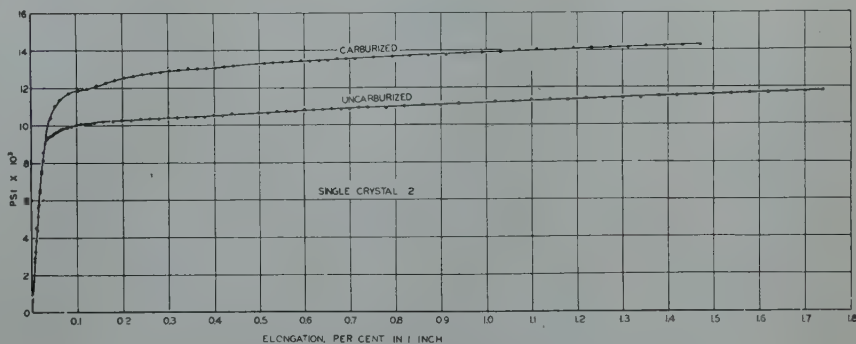


FIG 9—Stress-strain curves for single crystal 2.

aging and yield point.* The polycrystalline specimens, with one exception, were strained 10 pct before aging. In all cases, the amount of strain applied before aging was sufficient to pass through the yield point; that is, the load-elongation curve was rising steadily at the time the load was released. The amount by which the curve is raised by the aging treatment is a measure of the extent of strain aging. This was expressed as a percentage determined as follows:

$$\text{Pct strain aging} = \frac{A - B}{B} \times 100$$

where A is the yield strength in the test

* Davenport and Bain¹⁴ and Kenyon and Burns¹⁵ have shown that a marked increase in hardness occurs at this temperature in not too long an interval of time; further, that the curve of hardness vs. time has a flat maximum so that some variation in time of aging will not appreciably influence the results.

after aging and B is the stress at the time the load was released in the initial test. An exception was made in the case of the polycrystalline specimens as wet hydrogen treated. The yield strength in the test after aging was actually lower than the stress at which the load was released before aging. This was due to recovery during aging. These specimens are indicated in the results as having shown "zero" per cent strain aging. The yield strength was defined as the stress at which extensive plastic flow began; where a drop in load or constant load elongation was exhibited the stress at the lower yield point or at the level of constant load elongation was taken as the yield strength. As an arbitrary measure of the height of the flow curve after some strain, the stress at 4 pct strain was used. The ef-

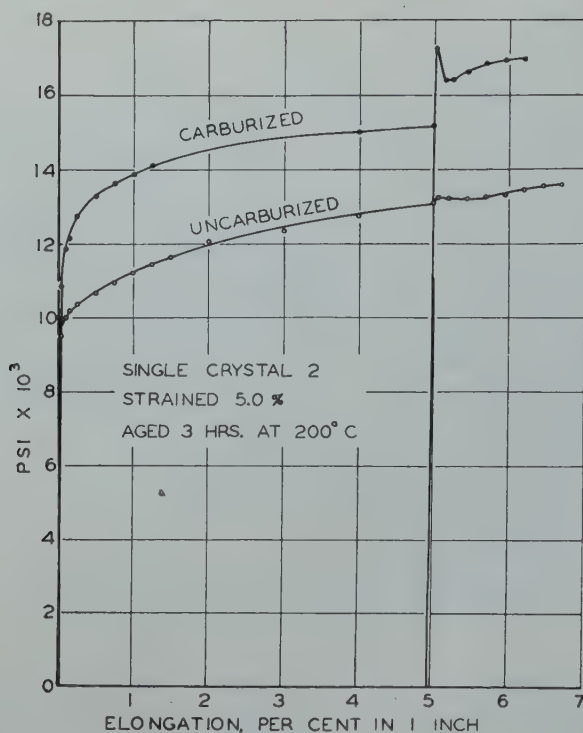


FIG 10—Composite stress-strain curves for single crystal 2.

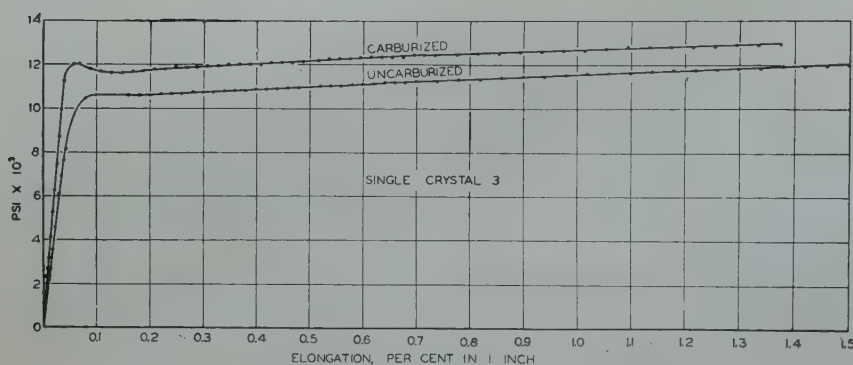


FIG 11—Stress-strain curves for single crystal 3.

fect of carburization or nitriding on the load-elongation curve is expressed as the percentage by which the treatment raised the stress at 4 pct strain. In the foregoing definition of terms the stress was computed to the nearest 500 psi based on the initial cross-sectional area. Microscopic examination of carburized and nitrided single crystals showed no evidence of a second phase.

Experimental Results

Stress-strain curves for the polycrystalline specimens are reproduced in Fig 3 to 8 and for the single crystals in Fig 9 to 20.

Some of the data derived from the stress-strain curves as well as carbon

and nitrogen analyses are tabulated in Table 2.

Discussion of Data

Examination of the stress-strain curves for the polycrystalline specimens (Fig 3 to 8) reveals results consistent with those found by Low and Gensamer.² Wet hydrogen purified material exhibited no yield point either in the initial stress-strain curve or in the test following aging. Further, no strain aging was observed. Carburizing at 700°C for 10 min. in hydrogen bearing 5 pct of normal heptane was sufficient to restore the upper yield point and some 3 pct constant load elongation at the lower yield point. The specimens

exhibited 17 pct strain aging and pronounced upper yield points in the test after aging. Nitriding at 500°C for 3 hr in hydrogen bearing 6 pct of ammonia had similar effects. These specimens exhibited upper yield points and approximately 2 pct constant load elongation. About 17 pct strain aging is observed and in the test following aging there is a constant load elongation of 2 pct; one specimen also exhibited an upper yield point in this test.

Specimens from three single crystals, 2, 3 and 4, were carburized. The uncarburized specimens from Crystals 2, 3 and 4 in every instance exhibited the following behavior: no upper yield point in the initial test nor in the test after aging; practically no constant load elongation in the initial test but 0.5 pct constant load elongation in the test after aging; no strain aging. The 0.5 pct of constant load elongation in the test after aging is consistent with the information reported by Edwards, Jones and Walters¹⁶ and Edwards, Phillips and Liu¹⁷ that low carbon steels given prolonged wet hydrogen treatment followed by slow cooling gave no yield point indication; the same samples after straining and aging gave a pronounced yield point. It was this information plus similar data for nickel, silver and copper age hardening alloys that led them to conclude that the yield point is caused by precipitation of a solute on slip planes.

Examination of the stress-strain curves of the carburized specimens of Crystals 2, 3 and 4 reveals the following information: strain aging is exhibited in every instance; Crystals 3 and 4 show a drop in load in the initial curve and Crystal 2 shows a drop in load in the test after aging; in the initial part of the curve obtained in the test after aging Crystals 3 and 4 show a low slope which rises as the test proceeds.

In summary, the uncarburized specimens of Crystals 2, 3 and 4 exhibit neither strain aging nor yield point phenomena except in the tests after aging where a slight constant load elongation was observed; the carburized specimens all show yield point indications in the initial loading as well as strain aging. Every specimen showed greater yield point indications in the test after aging than before aging.

Specimens from single Crystals 5, 6 and 7 were nitrided and the yield point and strain aging characteristics compared to non-nitrided specimens from the same crystals. It should be noted in Table 1 that the specimens cut from

Crystal 6 received insufficient wet hydrogen purification; this is evident from the yield strength and the stress level of the flow curve of the non-nitrided specimen. The non-nitrided specimens of Crystals 5 and 7 exhibited behavior similar to the non-carburized specimens of Crystals 2, 3 and 4 except for a drop in load in the initial test of Crystal 5. Examination of the stress-strain curves for the nitrided specimens reveals the following information: strain aging is exhibited in all instances, a greater amount of strain aging being observed in the nitrided specimen of Crystal 6 than in the non-nitrided specimen; a pronounced drop in load is observed in the test of Crystal 5 after aging; some constant load elongation is exhibited in most of the tests, the test of Crystal 6 after aging showing a gradually decreasing load for some 4 pct elongation after which the load rises with strain.

In summary, with the exceptions of the specimens cut from Crystal 6 which received insufficient wet hydrogen purification and a slight drop in load in the initial test of Crystal 5, the non-nitrided specimens showed no strain aging and no yield point effects while the nitrided specimens exhibit both phenomena. In the case of the exceptions noted more strain aging and yield point effect were observed in the nitrided specimens than in the non-nitrided. With one exception, greater indication of yield point behavior was exhibited in the test after aging than in the test before aging.

Addition of carbon or nitrogen had the same action, that is, to produce yield point effects and strain aging in single crystals of iron where they did not previously exist or increase these effects where they had previously existed. Aging a strained specimen, whether in the wet hydrogen purified state or carburized or nitrided, gave a greater yield point effect than in the original test.

There appeared to be no correlation between orientation and yield point behavior. A satisfactory examination of such a correlation would require a much larger number of specimens than was used in this investigation.

Microscopic evidence showed no evidence of a second phase either in the carburized or nitrided crystals. The carburized crystals contained 0.005 pct carbon and the nitrided crystals 0.007 pct nitrogen (see Table 2). The higher carbon and nitrogen contents (0.010 pct and 0.014 pct respectively) of the

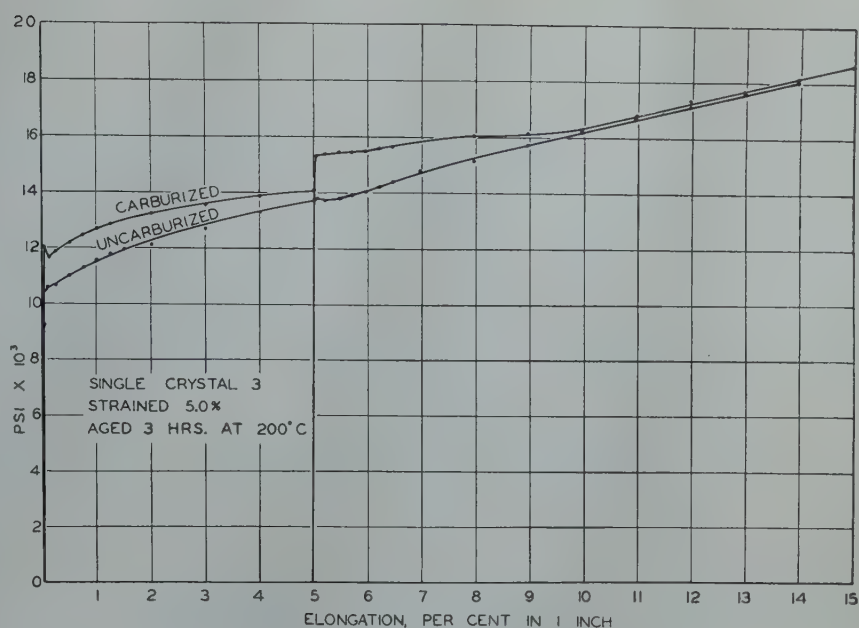


FIG 12—Composite stress-strain curves for single crystal 3.

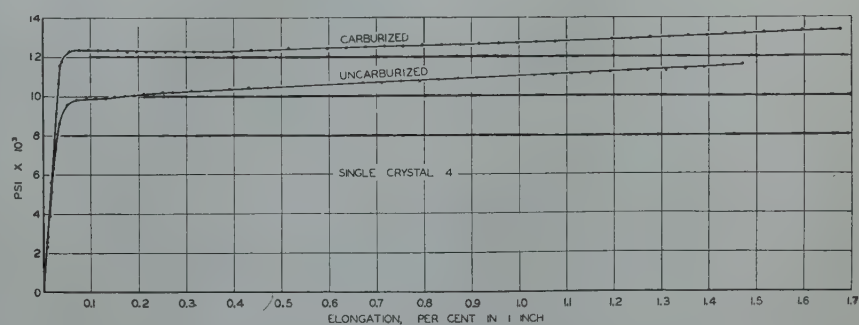


FIG 13—Stress-strain curves for single crystal 4.

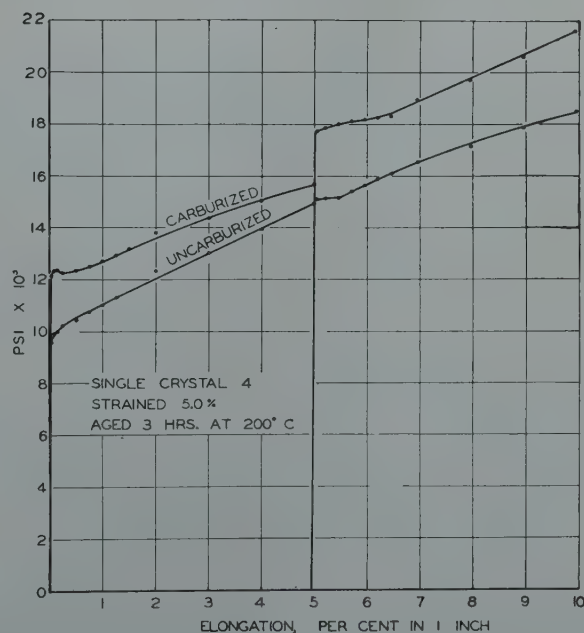


FIG 14—Composite stress-strain curves for single crystal 4.

carburized and nitrided polycrystalline specimens result from the fact that these specimens were 0.036 in. thick

while the single crystals were somewhat thicker (over 0.050 in. for the carburized crystals and about 0.043 in.

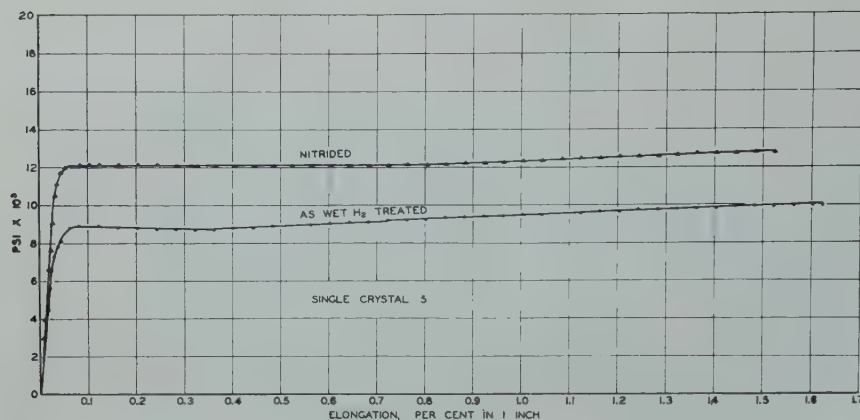


FIG 15—Stress-strain curves for single crystal 5.

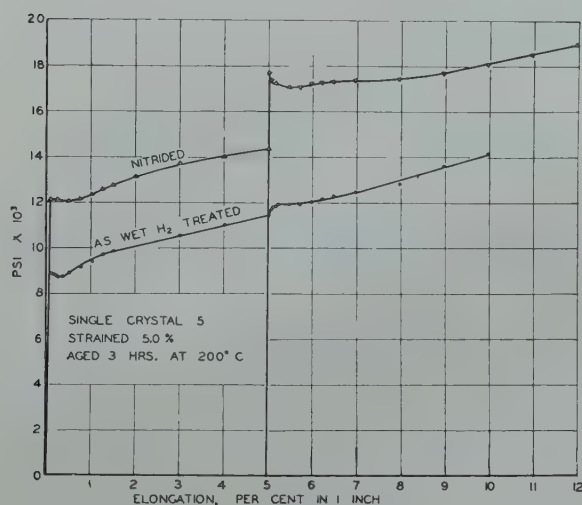


FIG 16—Composite stress-strain curves for single crystal 5.

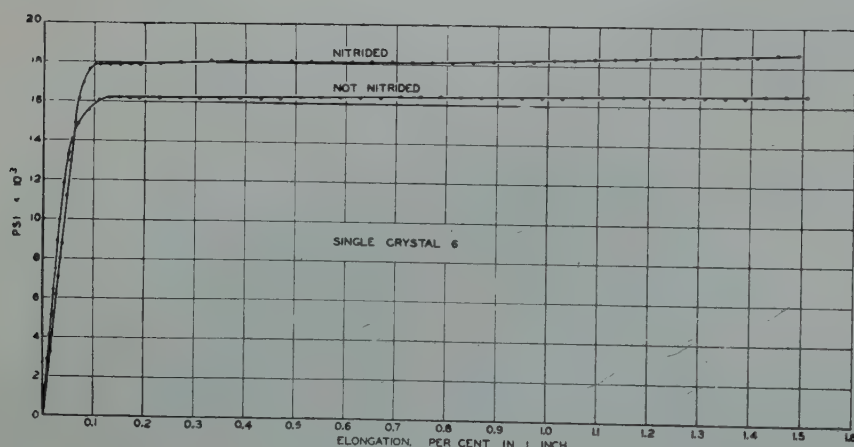


FIG 17—Stress-strain curves for single crystal 6.

for the nitrided crystals). The nitrogen analyses indicate that the polycrystalline specimens may have had higher nitrogen contents as purified than the single crystals. The presence of grain boundaries may have influenced the diffusion coefficient of carbon or nitro-

gen in alpha-iron; whether they do or to what extent is not known.¹⁸

In the light of the present data the grain boundary hypothesis as stated previously for the explanation of yield point behavior becomes untenable. Definite yield point effects have been

observed in single crystals. These effects are not as marked in the single crystals as they are in the polycrystalline specimens. Further, it has been demonstrated that single crystals which have been strained and aged show greater yield point indications after aging than before aging. This observation supports the hypothesis of Edwards, Phillips and Liu¹⁷ that the yield point is due to precipitation of solute on slip planes. Further evidence in favor of this hypothesis is the fact that mild steel as quenched exhibits no yield point but will do so if allowed to age at room temperature.^{7,19} It is suggested by the present authors that the material responsible for the yield point is in either one of two states: first, a transition state between solution and discrete second phase or, second, has just precipitated in a fine dispersion and has not had sufficient time to agglomerate. The first possibility is analogous to the transition phase which causes maximum hardness in quench aging. The second possibility was suggested by Edwards et al.

The observation is cited above that the single crystals did not exhibit yield point behavior to as great a degree as the polycrystalline specimens. It is possible that, as in quench aging, precipitation takes place preferentially at slip planes and/or grain boundaries, the latter being the more powerful in promoting yield point behavior. This would explain an increasing yield point effect with decreasing grain size as found by numerous investigators.

Conclusions

1. A yield point (drop in load and elongation at constant load) has been found in single crystals of iron containing small amounts of carbon or nitrogen. The yield point in polycrystalline iron is therefore not due to the presence of a grain boundary film as has been frequently suggested.

2. Strain aging is observed in single crystals of iron containing small amounts of carbon or nitrogen. The yield point effect is increased by strain aging in single crystals just as it is in polycrystalline irons.

Acknowledgments

The authors wish to thank Mr. F. Garofalo for his stimulating discussion and suggestions, the use of the specially

designed grips and much material assistance.

Messrs. H. F. Shannon and W. J. Frederick of the Carnegie-Illinois Steel Corporation arranged for the chemical analyses reported and their kind assistance is gratefully acknowledged.

References

1. W. E. Dalby: Load-Extension Diagrams Taken With an Optical Load-Extension Indicator. *Proc. Royal Soc.* (1913) A-88, 281.
2. J. R. Low, Jr. and M. Gensamer: Aging and the Yield Point in Steel. *Trans. AIME* (1944) 158, 207.
3. R. Arrowsmith: A Note on the Effect of Grain Size on the Extension of the Yield Point in Armco Iron. *Jnl. Iron and Steel Inst.* (1924) 11, 317.
4. J. H. Andrew and H. Lee: The Work Hardening and Aging of Steel. *Jnl. Iron and Steel Inst.* (1942) 145, 153.
5. C. A. Edwards and L. B. Pfeil: The Tensile Properties of Single Crystals of Iron. The Influence of Crystal Size on the Tensile Properties of Iron. *Jnl. Iron and Steel Inst.* (1925-II) 112, 79.
6. E. W. Fell: 'Yielding' Phenomena in Iron, Steel, Aluminum Alloys and Other Metals Under Stress. *Iron and Steel Inst., Carnegie Schol. Mem.* (1937) 26, 123.
7. P. Ludwik and R. Scheu: The Yield Point of Electrolytic Iron and Mild Steel. *Ber. Fachausschusse Ver. deut. Eisenhüttenleute* (1925) 5, 1-7.
8. J. Winlock and R. Leiter: Some Factors Affecting the Plastic Deformation of Sheet and Strip Steel and Their Relation to Deep Drawing Qualities. *Trans. ASM* (1937) 25, 163.
9. M. Gensamer and R. F. Mehl: Yield Point of Single Crystals of Iron Under Static Loads. *Trans. AIME* (1938) 131, 372.
10. M. Gensamer: Private Communication.
11. A. N. Holden and J. H. Hollomon: Homogenous Yielding of Carburized and Nitrided Single Iron Crystals. *Trans. AIME*, 185, 179: *Jnl. of Metals*, Jan. 1949.
12. C. S. Barrett and L. H. Levenson: Determinations of Orientations by Etch Pits. *Trans. AIME* (1940) 137, 76.
13. S. Brunauer, M. E. Jefferson, P. H. Emmett and S. B. Hendricks: Equilibrium in the System Iron-Nitrogen. *Jnl. Amer. Chem. Soc.* (1931).
14. E. S. Davenport and E. C. Bain: The Aging of Steel. *Trans. ASM* (1935) 23, 1047.
15. R. L. Kenyon and R. S. Burns: Aging in Iron and Steel. *ASM Symp. on Precipitation Hardening*, Chicago, (Oct. 1939).
16. C. A. Edwards, H. N. Jones and B. Walters: A Study of Strain Age Hardening of Mild Steel. *Jnl. Iron and Steel Inst.* (1939-I) 341.
17. C. A. Edwards, D. L. Phillips and Y. H. Liu: The Yield Point in Steel. *Jnl. Iron and Steel Inst.* (1943-I) 147, 145.
18. R. F. Mehl: Diffusion in Solid Metals. *Trans. AIME* (1936) 122, 11.
19. M. Kuroda: The Effect of Heat

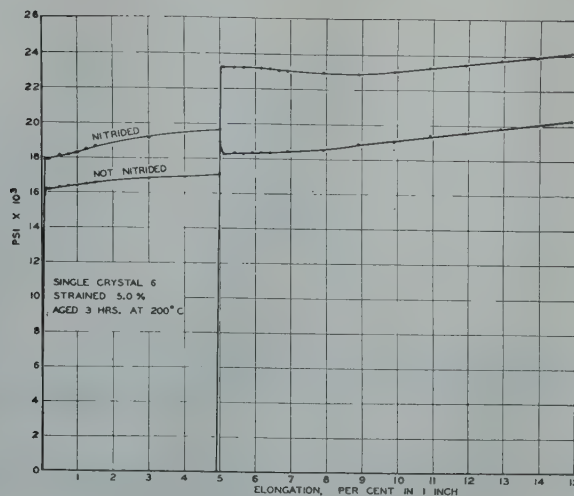


FIG 18—Composite stress-strain curves for single crystal 6.

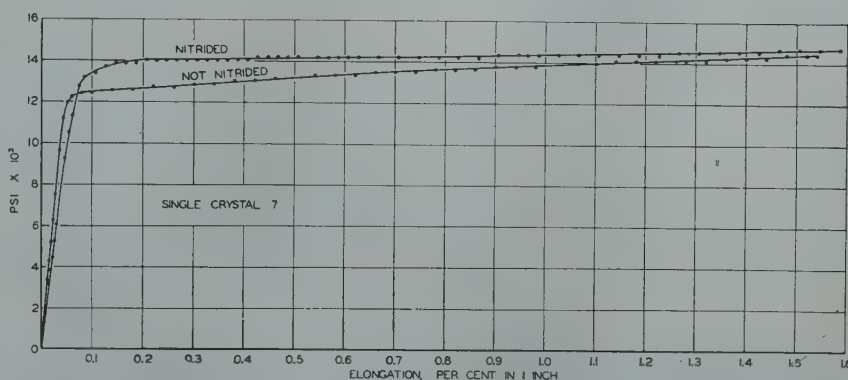


FIG 19—Stress-strain curves for single crystal 7.

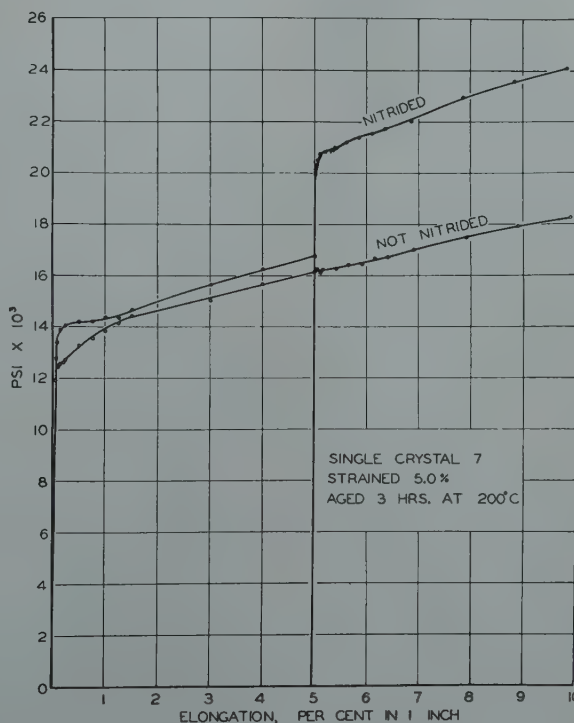


FIG 20—Composite stress-strain curves for single crystal 7.

Treatment on the Yield Point in Mild Steel. *Sci. Papers Inst. Phys. Chem. Res. (Tokyo)* (1932) 20, 29-38.

The Effect of Oxygen, Nitrogen, and Hydrogen on Iodide Refined Titanium*

ROBERT I. JAFFEE,† Member AIME, and I. E. CAMPBELL†

Oxygen, nitrogen, and hydrogen are known to be absorbed by titanium at elevated temperatures. Ehrlich¹ reports that about 30 at. pct oxygen can be dissolved in solid solution by alpha-titanium. Nitrogen also has a solid solubility in alpha-titanium, but there is no information as to its extent. The solid solubility of hydrogen in titanium also is high. Kirshfeld and Sieverts² report 50 at. pct soluble, while Hägg³ reports about 33 at. pct hydrogen to be soluble in alpha-titanium.

General statements are made in the literature that oxygen, nitrogen, and hydrogen embrittle titanium, but no quantitative measurements have been made of the effect of these gases on the mechanical properties of the metal. One reason for this is the lack of a source of titanium pure enough to be considered a suitable starting material. Iodide-refined titanium, made by thermal decomposition of titanium iodide vapor on an incandescent wire,⁴ contains small amounts of carbon, silicon, iron, and aluminum, but is very low in oxygen, nitrogen, and hydrogen content, and, therefore, was used in this work.

A further reason for the lack of quantitative information on the effect of these gases, particularly oxygen, is the difficulty of carrying out accurate analytical determinations at the low concentrations of interest in this work.

For this reason, the oxygen, nitrogen, and hydrogen were added in measured amounts as gases, and diffused into the titanium, to avoid the necessity of chemical analysis.

The purpose of the work reported here was to isolate and measure the effects of oxygen, nitrogen, and hydrogen on titanium of the highest purity available at the time. The concentrations studied were 0.25, 0.5, and 1 at. pct in each case.

Experimental Work

One-half of a 24-in. hairpin of iodide-refined titanium was available for this work. The rod was approximately

0.25-in. in diam and had a 0.003-in. tungsten core. From chemical and spectrographic analyses, the purity of the sample was estimated to be between 99.80 and 99.95 wt pct. The chief impurities (aside from the tungsten core) were iron (0.04 pct), silicon (0.01–0.1 pct), aluminum (0.05 pct), carbon (0.03 pct). The tungsten core constituted 0.05 pct by weight of the sample. Although some alloying undoubtedly took place between the tungsten and the titanium during the deposition reaction, the core remained substantially intact in the deposited metal.

The initial average hardness of the titanium as deposited was 105 Vickers (10-kg load). The maximum hardness was 116 Vickers and the minimum 91 Vickers. The metal was somewhat harder than that currently being obtained by the iodide process, that is, 75–90 Vickers.

The rod was cold swaged to 1/4-in. diam and then cold rolled in diamond shaped rolls to about 0.080-in. square, using reductions of 15 pct in area per pass. The 0.080-in.-square wire was cut into 6-in. lengths for the preparation of the alloys by the gaseous absorption and diffusion method.

ADDITION OF OXYGEN, NITROGEN, AND HYDROGEN TO TITANIUM

A modified Sieverts' absorption apparatus, shown in Fig 1, was used in

Cleveland Meeting, October 1949.
TP 2681 E. Discussion of this paper (2 copies) may be sent to *Transactions AIME* before December 1, 1949. Manuscript received May 5, 1949.

* The work covered in this paper was done at Battelle Memorial Institute for The Rand Corporation and the U. S. Air Force in an appraisal of titanium as a material for aircraft applications. Part of the data contained in this paper was summarized in a general article on the Battelle titanium alloy work by H. C. Cross, given at the Office of Naval Research Symposium on Titanium on Dec. 16, 1948, and also given in *Metal Progress*, (1949) 55, 356–358.

† Battelle Memorial Institute.

¹ References are at the end of the paper.

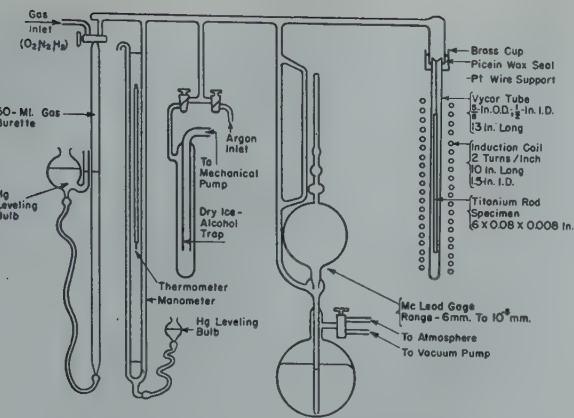


FIG 1—Gas-absorption and diffusion apparatus for producing alloys of iodide titanium with oxygen, nitrogen, and hydrogen.

adding each of the gases to the titanium samples.

Measured quantities of gas at known temperature and pressure were added to the evacuated system in each case, and the desired alloys were prepared by absorption and diffusion of the gas in the heated metal.

The samples were pickled for about 5 min. in hot, 10 pct sulphuric acid, then washed, dried, and rinsed successively in carbon tetrachloride, absolute alcohol, and acetone.

The samples were weighed to ± 0.0001 g and then suspended in an induction furnace. A No. 34 B and S ga. platinum wire was used to hold the sample.

The gas burette was flushed thoroughly with the gas to be used and then filled. Pure oxygen was obtained by slowly heating a 4:1 (by weight) mixture of C.P. potassium chlorate and manganese dioxide. The oxygen was passed through ascarite to remove traces of carbon dioxide, and then

through a dry-ice alcohol trap and magnesium perchlorate to remove water vapor. Tank nitrogen (99 pct) and tank hydrogen (99+ pct) were used as sources of those gases. Both were purified by being passed over copper turnings at 700°C and then dried in the same manner as the oxygen.

After the sample was sealed in place, the apparatus was evacuated, filled with argon, and re-evacuated. This process was repeated, but the sample tube was flamed during the final evacuation to remove occluded gas. The required volume of gas (calculated from the sample weight, barometric pressure, and temperature) was then admitted to the system from the burette and the pressure within the system redetermined. The induction-heating coil was energized, and the sample maintained at the desired temperature until the gas was completely absorbed. Additional "soaking" periods were used to obtain uniform distribution of the gas through the sample.

Data on the thermal treatment of the samples are summarized in Table 1. The oxygen was absorbed at 1000°C (observed temperature). Absorption was quite rapid and was virtually complete in 5–10 min. The samples were maintained at 1000°C for 60–80 min., however, to obtain uniform distribution of the oxygen throughout the sample.

The nitrogen was also absorbed at 1000°C but the absorption rate was much slower, 1.5–2 hr being required for complete absorption at the higher concentrations. These samples were removed as soon as absorption was complete, and given separate diffusion treatments at 1075–1100°C in vacuo.

Hydrogen, unlike nitrogen and oxygen, is absorbed reversibly, and at the higher concentrations, absorption takes place more rapidly at lower temperatures. At 650–700°C, concentrations up to one atomic per cent were completely absorbed in 2–4 min. Additional "soaking" periods were used as indi-

Table 1 . . . Identity of Specimens

| Specimen No. | Addition | Composition | | Thermal Treatment | Density, g per cc | Electrical Resistivity at 25.6°C Microhm-cm |
|--------------|----------|-------------|---------|---|-------------------|---|
| | | At. Pct | Wt Pct | | | |
| 1 | Control | Zero | Zero | 60 min. 950–1070°C in vacuum | 4.53 | 48.5† |
| 12 | | Zero | Zero | 60 min. 995–1010°C in vacuum | 4.52 | 47.7 |
| 13 | | Zero | Zero | 60 min. 1090–1125°C in vacuum | 4.515 | 47.8 |
| 2 | Oxygen | 0.27 | 0.0905 | 60 min. 1000°C in vacuum | 4.52 | 50.4 |
| 3 | | 0.51 | 0.171 | 60 min. 1000°C in vacuum | 4.51 | 51.8 |
| 4 | | 1.01 | 0.34 | 60 min. 1000°C in vacuum | 4.515 | 55.6 |
| 7 | Nitrogen | 0.245 | 0.0717 | 50 min. 1100–1110°C in vacuum* | 4.53 | 49.75 |
| 6 | | 0.496 | 0.146 | 47 min. 1075°C in vacuum* | 4.53 | 52.95 |
| 5 | | 0.996 | 0.293 | 90 min. 1080°C in vacuum* | 4.525 | 55.8 |
| 10 | Hydrogen | 0.27 | 0.00569 | 60 min. 1000°C | 4.56 | 47.2 |
| 9 | | 0.50 | 0.0106 | 15 min. 1000°C, 15 min. 775–800°C, 30 min. 650–700°C | 4.525 | 48.1 |
| 8 | | 0.99 | 0.021 | 30 min. 1000°C, 25 min. 900°C, 15 min. 750°C, 60 min. 600–700°C | 4.515 | 47.8 |

* This comprises only the diffusion treatment for the Ti-N specimens, and does not include the absorption treatment.

† Specimen No. 1 was harder than either Specimen 12 or 13, and, therefore, may not be considered as pure as those specimens. The values of 47.7 and 47.8 microhm-cm probably are better values for iodide-refined titanium.

cated in Table 1 to insure complete diffusion.

DISCUSSION OF ABSORPTION

When large amounts of oxygen or nitrogen are admitted to the absorption chamber, oxide or nitride films are formed, which act as barriers that retard the absorption process. Slow continuous addition of these gases at low pressures, therefore, gives higher overall absorption rates than step-wise additions at higher pressures. In the case of nitrogen, which is absorbed slowly, the last traces of gas may be only adsorbed, rather than absorbed, but if the sample is maintained at temperature for a few minutes, the adsorbed gas will diffuse into the metal.

Hydrogen, unlike nitrogen and oxygen, is best absorbed at higher pressures, and, for higher concentrations than those reported here, the procedure should be modified to the extent that a measured fraction of this gas should be absorbed, rather than the entire addition. At higher hydrogen concentrations, an appreciable equilibrium pressure of hydrogen is developed at temperatures where the absorption is quite rapid, and to take advantage of the rapid absorption at the higher temperatures, the hydrogen should be added at pressures up to one atmosphere and the extent of the hydrogen absorption regulated by controlling the absorption time.

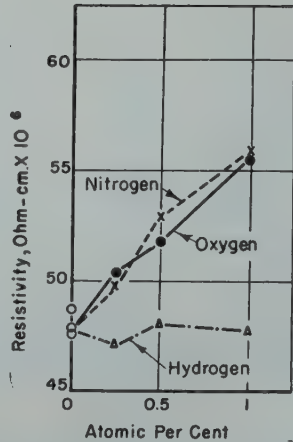


FIG 2—Effect of oxygen, nitrogen, and hydrogen on the electrical resistivity of iodide titanium.

The absorption technique used in this work provides an accurate method for adding precise quantities of hydrogen, nitrogen, and oxygen to titanium, and where the limits of solid solubility are not exceeded, homogeneous alloys can be obtained in reasonable diffusion times. Weight changes obtained upon addition of these gases to the titanium check well with the calculated weights of the gases added.

Since the amounts of gases added in this work were small, the evaporation of titanium did not introduce a significant error. The loss of titanium was insignificant in itself, and for short

absorption times the absorption of gases by titanium vapor and volatilized titanium can be neglected.

The specimens prepared were 6 in. long and approximately 0.080-in. square. Their compositions and physical condition are summarized in Table 1. For convenience, in the rest of this report the nominal compositions, 0.25, 0.5, and 1 at. pct, will be referred to, rather than the actual composition.

From each 6-in. specimen, a length 4.25 in. long was cut for determination of density, cross-section, and electrical conductivity. This was then cut into two pieces, one 3 in. long for a tensile test, and the other about 1 in. long for a cold-rolling test. The remainder of the original specimen was reserved for microscopic examination.

DENSITY, RESISTIVITY

Density at room temperature was measured by determining the displacement of the specimen, 4.25 in. long, in distilled water at a known temperature.

Results of density measurements are tabulated in Table 1. The cross-sections of the specimens were determined by calculation from the weight, length, and density of the specimens. Resistance of a 3.5-in. length of the specimen was determined at 25.6°C (78°F) by means of a Kelvin bridge. Values of the electrical resistivity were calculated from the resistance, cross-section, and length, and are given in Table 1

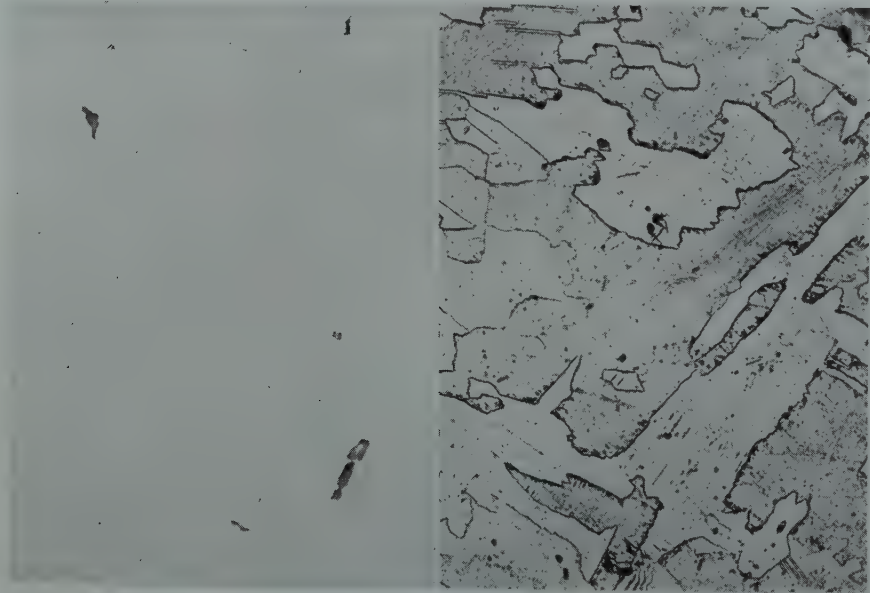


FIG 3—Unalloyed titanium. Unetched. 1000 X. FIG 4—Unalloyed titanium. Annealed at 1000°C. 250 X.

Figures reduced one-seventh in reproduction.



FIG 5—0.25 at. pct oxygen. Annealed at 1000°C. 250 \times .
 FIG 6—0.5 at. pct oxygen. Annealed at 1000°C. 250 \times .
 FIG 7—1 at. pct oxygen. Annealed at 1000°C. 250 \times .
 Figures reduced one-seventh in reproduction.

There is no significant change in the density of the alloys containing oxygen and nitrogen with alloy content. There may be a change in density with hydrogen content, as indicated by the high value for the 0.25 at. pct H alloy in Table 1, but this is rather doubtful. Most of the densities fall between 4.51 and 4.53, which are in excellent agreement with the values reported in the literature.

A plot of the electrical resistivity data is shown in Fig 2. Both oxygen and nitrogen raise the resistivity of titanium to the same extent per atomic per cent, the increase in resistivity being almost linear. This is in agreement with the reported solid solubilities of these elements in alpha-titanium. Hydrogen to one atomic per cent does not appear to affect the electrical resistivity.

The values of 47.8×10^{-6} ohm-cm and 47.7×10^{-6} ohm-cm found for the electrical resistivity at 25.6°C are in fair agreement with the value of 47.5×10^{-6} ohm-cm at 20°C reported by van Arkel.⁵ Using the value of the temperature coefficient of resistance given by van Arkel, 0.00425 per °C, the two experimental values become 46.7×10^{-6} ohm-cm and 46.6×10^{-6} ohm-cm at 20°C. Magnesium-reduced

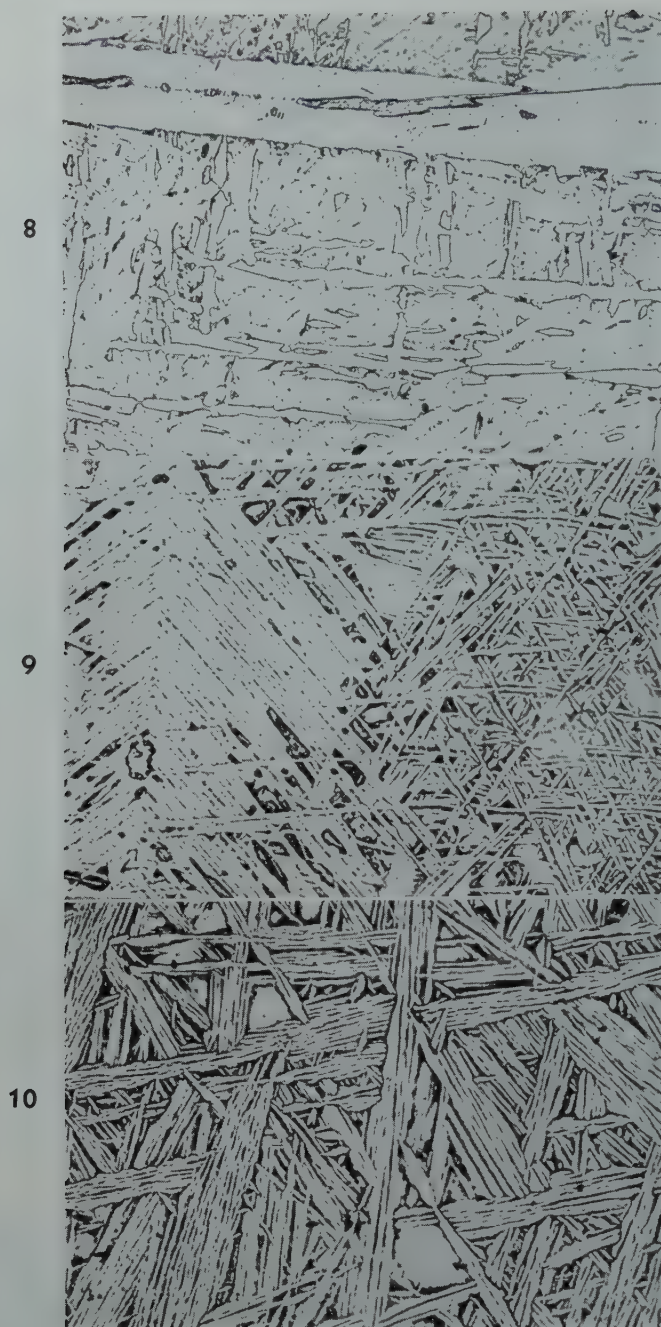


FIG 8—0.25 at. pct nitrogen. Annealed at 1100°C. 250 ×.

FIG 9—0.5 at. pct nitrogen. Annealed at 1100°C. 250 ×.

FIG 10—1 at. pct nitrogen. Annealed at 1100°C. 250 ×.

Figures reduced one-seventh in reproduction.

titanium has an electrical resistivity at 20°C of 56×10^{-6} ohm-cm, according to Dean, Long, Wartman, and Anderson,⁶ and 55.4×10^{-6} ohm-cm according to Greiner and Ellis.⁷ This higher resistivity is undoubtedly caused in part by dissolved oxygen and nitrogen, as indicated here by the potent effect of these elements on the electrical resistivity.

MICROSTRUCTURE

Cross-sections and longitudinal sections of each of the specimens were examined metallographically. No apparent lack of homogeneity was observed in the cross-sectional structure of any of the alloys, apart from the diffusion area around the tungsten core.

Polishing was done on wool laps

using 0-2-micron diamond abrasive suspended in carbon tetrachloride. In order to bring out a true structure on the titanium specimen and the softer of the alloys, it was necessary to polish and etch alternately three or four times to eliminate the worked surface. Etching was done by swabbing for 5-10 sec with an etchant containing 3 pct concentrated HNO_3 , 1.5 pct con-

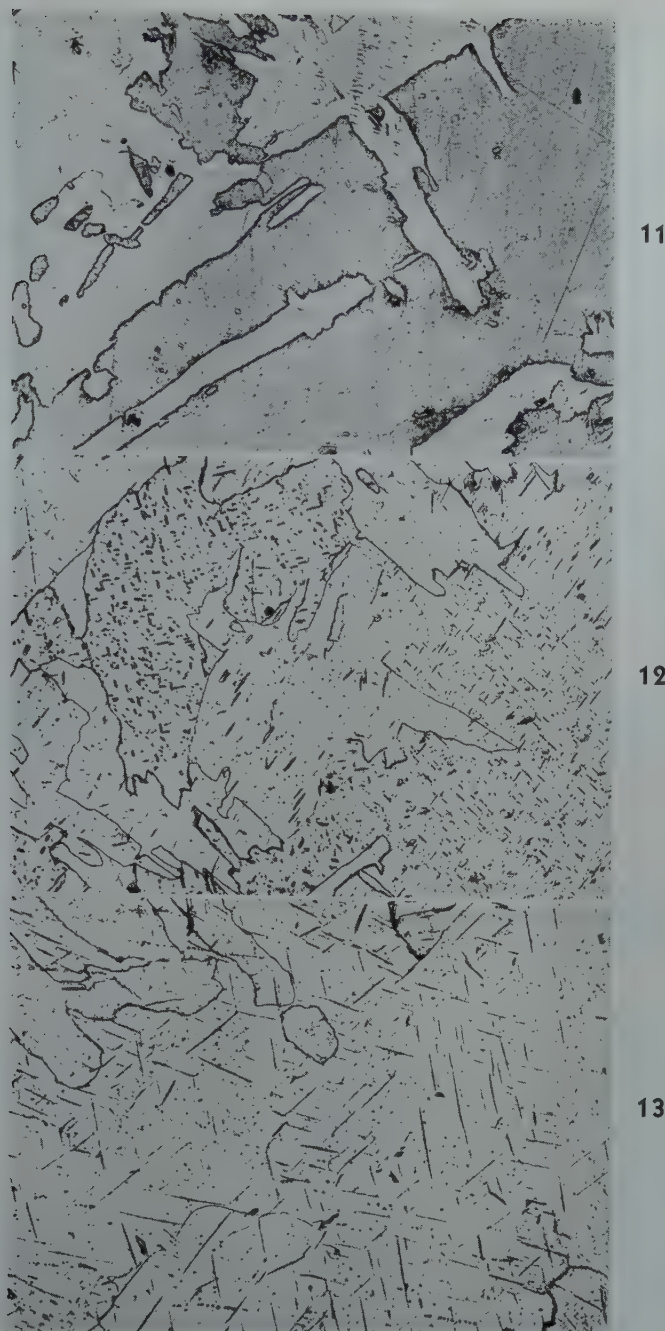


FIG 11—0.25 at. pct hydrogen. Annealed at 1000°C. 250 ×.

FIG 12—0.5 at. pct hydrogen. Annealed at 700°C. 250 ×.

FIG 13—1 at. pct hydrogen. Annealed at 700°C. 250 ×.

Figures reduced one-seventh in reproduction.

concentrated HF, balance water (volume percentages).

In the as-polished condition, all of the specimens showed a number of gray inclusions. Fig 3 shows a typical field of these inclusions at 1000 × magnification. The identity of these inclusions is not known. It is suspected that they may be titanium silicide.

Unalloyed titanium in the condition as cooled from 1000°C has the

structure shown at 250 × in Fig 4. It consists of large plates of alpha-titanium arranged in a somewhat Widmanstättenic manner; the alpha plates probably formed along the octahedral planes of the high-temperature cubic phase on cooling through the transformation temperature.

The structures of alloys with 0.25, 0.5, and 1 at. pct oxygen are shown in Fig 5, 6, and 7, respectively. The

general effect of oxygen seems to be to refine the structure, making the plates of the alpha-titanium smaller, and the Widmanstätten arrangement more regular.

The structures of the nitrogen-bearing alloys are shown in Fig 8, 9, and 10. The effect of nitrogen on the microstructure is to promote the formation of needles of alpha titanium. This is a most interesting observation, be-

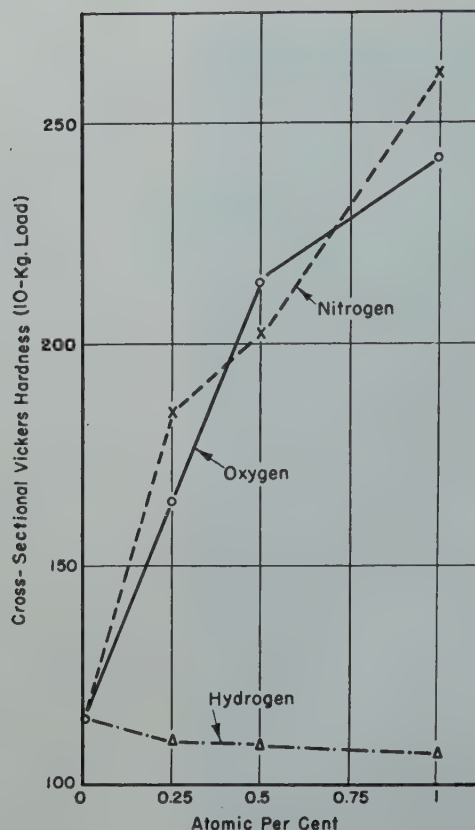


FIG 14—Average cross-sectional hardness values for alloys of iodide titanium with oxygen, nitrogen, and hydrogen.

cause this needle-like Widmanstätten structure is characteristic of most magnesium-reduced titanium that has been annealed above the alpha-beta transformation temperature. The conclusion may be drawn that the needle-like structure found in most less pure kinds of titanium is caused by nitrogen in solid solution.

The structures of the hydrogen alloys are shown in Fig 11, 12, and 13. The alloys containing 0.25 and 0.5 at. pct of hydrogen are not materially different from unalloyed titanium. They show large Widmanstätten plates of alpha-titanium. Origin of the markings shown inside the grains in Fig 12 is not known. They may be transitional structures developed by the grinding and polishing-etching operations. Fig 13, for the one atomic per cent hydrogen alloy, shows an arrangement of line markings which resembles a Widmanstätten precipitate. The origin of these marks is not known. It is doubtful that they are a second phase based on hydrogen, because one atomic per cent is very far from the accepted solid solubility of hydrogen. Another peculiar thing about them is that they cross over grain boundaries in some cases. A

possibility is that they are a kind of deformation twin, originating in the preparation of the specimen for metallographic examination.

MECHANICAL PROPERTIES

Hardnesses were taken on a cross-section of each of the specimens to see whether there was any difference in hardness between the surface and center. The only specimen for which this condition existed was No. 6, 0.5 at. pct nitrogen. Here the surface had a hardness of 245 Vickers, and the center had a hardness of 170 Vickers. This may be associated with its shorter diffusion time of 47 min. at 1075°C. Specimen No. 5, one atomic per cent nitrogen, was diffused 90 min., at 1080°C, and was uniform from center to surface.

A plot of the average cross-sectional hardness of the specimens versus their compositions is shown in Fig 14.

Tensile tests were run on 3-in. lengths of each specimen, observations being made of ultimate tensile strength and per cent elongation in one inch. Results of these tests are shown in Fig 15.

The hardness data for oxygen and nitrogen alloys are somewhat erratic, but indicate that oxygen and nitrogen

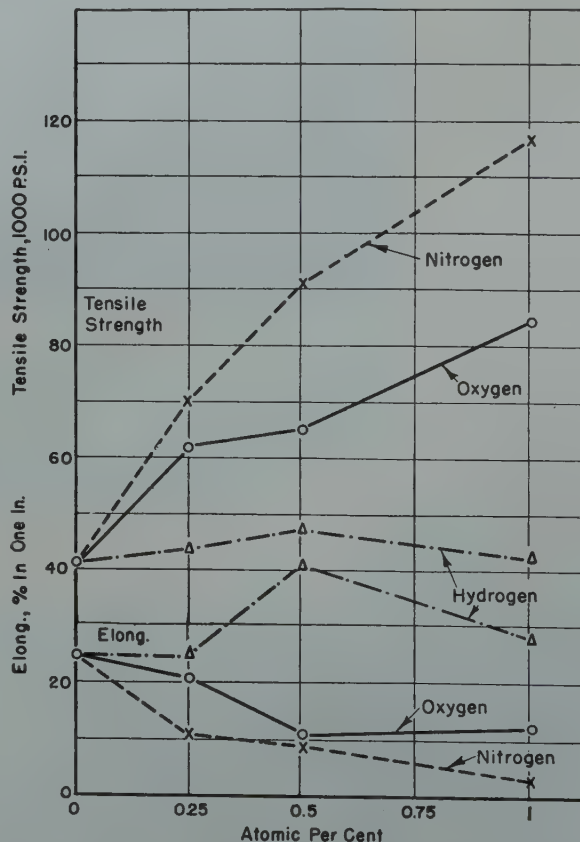


FIG 15—Tensile strength and elongation of alloys of iodide, titanium with oxygen, nitrogen, and hydrogen.

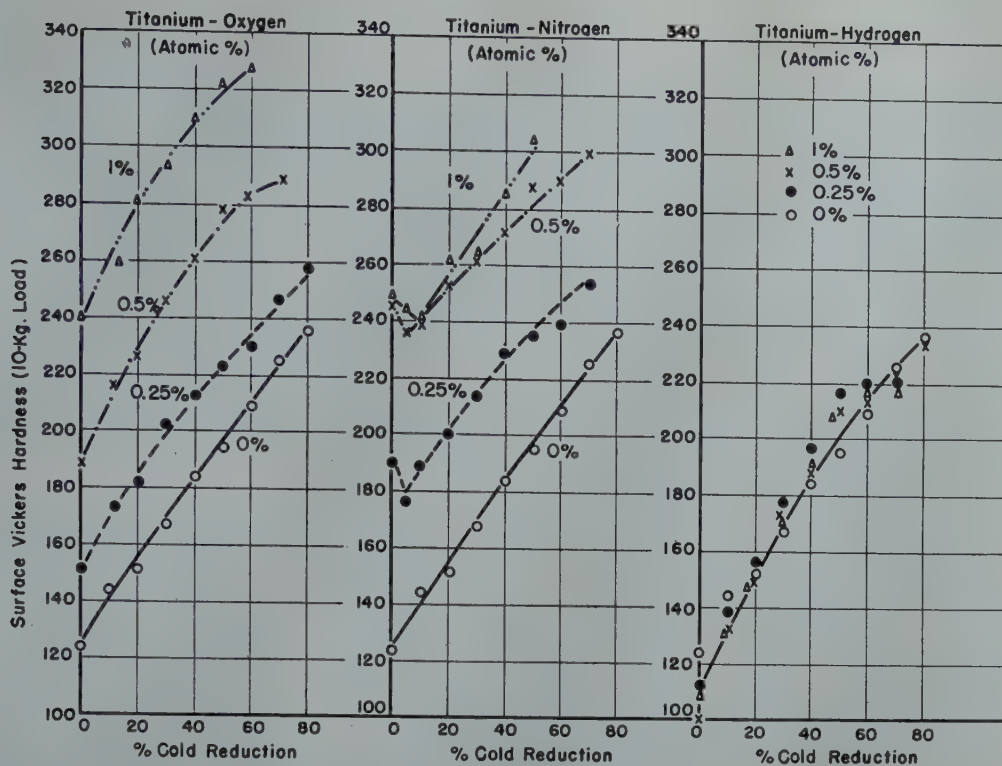


FIG 16—Work-hardening curves of iodide titanium and titanium-oxygen, titanium-nitrogen, and titanium-hydrogen alloys.

Table 2 . . . Cold Reductions Causing Edge Cracking

| Specimen No. | Composition, Atomic Per Cent | Initial Hardness, Vickers (10-kg load) | Rolled to, Inch | Per Cent Reduction | Edge Cracked |
|--------------|------------------------------|--|-----------------|--------------------|--------------|
| 12 | 100 Ti | 116 | 0.004 | 95 | No |
| 2 | 0.25 O | 164 | 0.004 | 95 | No |
| 3 | 0.5 O | 214 | 0.024 | 70 | Yes |
| 4 | 1 O | 242 | 0.032 | 60 | Yes |
| 7 | 0.25 N | 184 | 0.040 | 50 | Yes |
| 6 | 0.5 N | 202 | 0.032 | 60 | Yes |
| 5 | 1 N | 262 | 0.046-0.048 | 30-40 | Yes |
| 10 | 0.25 H | 110 | 0.004 | 95 | No |
| 9 | 0.5 H | 109 | 0.004 | 95 | No |
| 8 | 1 H | 107 | 0.004 | 95 | No |

harden titanium to about the same extent, with nitrogen possibly having a greater effect. The positions of oxygen and nitrogen are reversed at the 0.5 at. pct composition, and it is believed that this is not the actual case. As was pointed out in previous discussion, the 0.5 at. pct nitrogen alloy was incompletely diffused, and the soft center probably was given too much weight in the straight arithmetic average taken of the cross-sectional hardnesses.

Hydrogen up to one atomic per cent does not increase the hardness of iodide titanium, and actually appears to decrease it slightly, although the apparent decrease may have been caused by hardness variations in the

iodide titanium rod itself.

Nitrogen has a considerably greater strengthening effect on titanium than oxygen when added in concentrations of up to one atomic per cent, and correspondingly decreases the ductility to a greater extent. The hydrogen alloys appear to be slightly stronger and more ductile than the titanium control specimens. Since the elongation of pure titanium is generally found to be closer to 40 pct in one inch, rather than the 30 pct average found with the control specimens, the high ductilities of the hydrogen-containing specimens are more likely the result of specimen variation rather than any interaction of hydrogen with the impurities in the

titanium. Thermodynamic considerations indicate that reactions between hydrogen and the residual oxygen, nitrogen, or carbon in the titanium would not proceed to an appreciable extent under the conditions of preparation of the hydrogen-containing alloys.

COLD ROLLING CHARACTERISTICS

One-inch lengths of each of the 0.080-in.-square specimens were cold rolled at 0.001 in. per pass until edge cracking started, or to the minimum thickness the mill could roll, which was 0.004 in. Surface Vickers hardnesses (10-kg load) were taken at steps of 10

pct reduction in thickness to 70 or 80 pct reduction if the cold rolling could be carried that far.

The reductions at which edge cracking became apparent are shown in Table 2 for the various specimens.

Pure titanium and the Ti-H alloys all were very soft initially and cold rolled to 0.004 in. or 94 pct reduction without edge cracking. The 0.25 at. pct oxygen alloy, which was 164 Vickers initially, also could be rolled to 95 pct reduction without edge cracking. A completely different result was found with the 0.25 at. pct nitrogen alloy, which was 184 Vickers originally, only slightly higher than the oxygen alloy. It could be rolled only to 50 pct reduction before edge cracking. This indicates that nitrogen content is more deleterious to cold rollability than oxygen content of either the same amount or the same hardness. This adverse effect of nitrogen compared to oxygen on cold rollability shows up also in the edge-cracking limits at the 0.5- and 1-at. pct levels.

WORK-HARDENING CURVES

The work-hardening curves found for the various alloys are plotted in Fig 16.

The work-hardening curve of the unalloyed titanium (Specimen No. 1) is approximately a straight line. An 80 pct reduction about doubles the original hardness. The strip was rolled to 95 pct reduction, but determinations of hardness values were stopped at 80 pct.

Oxygen alloys had work-hardening curves very similar to the unalloyed titanium, apart from the different hardness levels from which the alloys start. This means that the relative ratios of hardness to the Ti-O alloys to titanium are unaffected by cold working.

The work-hardening data of the Ti-N alloys had some peculiarities. First, there was an initial decrease in the hardness, which was followed by

a normal increase in hardness on further cold working. This anomalous decrease in hardness may have been caused by a hard surface shell of nitrogen-rich material, which, once thinned out by a cold reduction, permitted the hardness indenter to penetrate to the softer core. The second peculiarity of the work-hardening curves of the Ti-N alloys is the closeness of the curves for the 0.5 at. pct and 1 at. pct nitrogen alloys. This does not seem to be in line with the results of the tensile tests. Actually, since the 1 at. pct nitrogen alloy only had 3 pct elongation and showed signs of edge cracking at 30 pct reduction, there probably were not enough data obtained on sound metal from which to draw conclusions. The normal part of the curve for the 0.25 at. pct nitrogen alloy shows about the same characteristics as unalloyed titanium, with the hardness level about 15 Vickers points above the curve for the 0.25 at. pct oxygen alloy.

The work-hardening data for the titanium hydrogen alloys were so similar to unalloyed titanium that no attempt was made to separate them in Fig 16.

Summary

Oxygen and nitrogen up to one atomic per cent increase the electrical resistivity at 25.6°C linearly from 48 to 56 micro-ohm-cm, while hydrogen in the same concentration has no effect.

Dissolved nitrogen changes the microstructure of annealed titanium from large Widmanstätten plates to long, narrow Widmanstätten needles. Oxygen refines and makes the Widmanstätten arrangement of the alpha-Ti plates more regular. Hydrogen does not change the microstructure of titanium at 0.25 at. pct concentration, but at higher concentrations, some markings of unknown origin appear.

Nitrogen has a more potent hardening and strengthening effect than oxygen and decreases the ductility to a greater extent. Hydrogen, when added

to one atomic per cent either does not affect the mechanical properties, or slightly improves both the strength and ductility.

Unalloyed titanium, the titanium-hydrogen alloys, and the 0.25 at. pct oxygen alloy could be cold rolled to 95 pct reduction without edge cracking. The higher oxygen alloys edge cracked at 60-70 pct reductions, while the nitrogen-containing alloys had considerably less capability for cold rolling without edge cracking. Work-hardening curves were determined for the various specimens.

Acknowledgment

Acknowledgment for support and permission to publish this paper is hereby extended to the U. S. Air Force and The Rand Corporation. The authors are grateful to Dr. B. W. Gonser for helpful discussions in planning and evaluating the work.

References

1. P. Ehrlich: Solutions of Oxygen in Metallic Titanium. *Ztsch. f. anorg. allg. Chem.* (1941) **247**, 53.
2. L. Kirschfeld and A. Sieverts: Titanium and Hydrogen. *Ztsch. f. anorg. allg. Chem.* (1929) **145A**, 227.
3. G. Hägg: X-Ray Examination of Hydrides of Titanium, Zirconium, Vanadium, and Tantalum. *Ztsch. f. Phys. Chem.* (1931), Sec. B, **II**, 433-454.
4. I. E. Campbell, R. I. Jaffee, J. M. Blocher, J. Gurland, and B. W. Gonser: Preparation and Properties of Pure Titanium. *Trans. Electrochem. Soc.* (1948) **93**, 6.
5. A. E. van Arkel: *Reine Metalle*. J. Springer, Berlin, 1939, p. 187.
6. R. S. Dean, J. R. Long, F. S. Wartman, and E. A. Anderson: Preparation and Properties of Ductile Titanium. *Trans. AIME* (1946) **166**, 379. *Metals Tech.* Feb. 1946, TP 1961.
7. E. S. Greiner and W. C. Ellis: Thermal and Electrical Properties of Ductile Titanium. *Trans. AIME* (1949) **180**, 657. *Metals Tech.* Sept. 1948 TP 2466.



The Origin of Annealing Twins in Brass

ROBERT MADDIN,* Junior Member, C. H. MATHEWSON,† Member, and WALTER R. HIBBARD, JR.† Junior Member AIME

According to conventional crystal mechanics, a face-centered cubic single crystal slips on the system $\{111\} \langle 110 \rangle$ which receives the highest shear stress in terms of the stated orientation of the stress axis of the crystal.¹ However, in brass, the slip process is never as simple as this conventional analysis indicates. There is always a second cooperating plane which contains the same slip direction as the primary plane.^{2,3} There is still another cooperating slip system commonly called the conjugate system³ previously observed to function with considerable lag only after the rotation due to the action of the first plane had produced a symmetrical condition of equal shear stress on the two systems.

In the 1943 Campbell Lecture,⁴ a slip mechanism was outlined in which the $\{111\}$ planes moved step-wise in two adjacent $\langle 112 \rangle$ directions integrating into the $\langle 110 \rangle$ slip direction. "... the slipping process would be visualized as a succession of steps 30° to the right and left of the resultant, microscopically observed, slip direction; a first step setting up the twinned configuration in the single spacing involved and an ensuing slip returning the atoms to the untwinned configuration while completing a fully integrated $\langle 110 \rangle$ movement."⁴ This process is shown diagrammatically in Fig 1 which shows two close packed layers of atoms at a slip site. A movement of the full circles through the "valleys" into the adjacent sites would produce a twin configuration with respect to the open circles. The term, "twin fault," seems most appropriate to define this faulted condition of the lattice.

Annealing twins in face-centered cubic metals may arise from preformed nuclei which could be described as twin faults produced by the first movement of this two stage slip process.

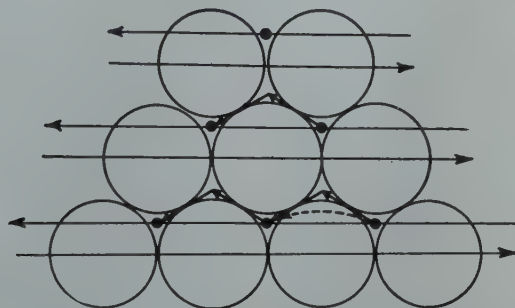


FIG 1—Hypothetical mechanical twin formation by deviation of slip from "foothills" into "valleys" of close-packed face-centered cubic structure.

(Mathewson⁴)

However, it is clear that this kind of slip does not take place so as to embrace a measurable number of adjacent planes because careful X ray examination has not conclusively shown the existence of ponderable twin lamellae (as in the case of Neumann bands in the body-centered ferrite).

In view of the imponderable character of these hypothetical twin faults, the search for evidence of their existence seems restricted to indirect methods.

The most obvious experimental technique serving this purpose is the determination by micrographic and X ray methods of the alignment of the composition planes of annealing twins with

the former slip planes in axially strained and recrystallized single crystals. In previous attempts of this sort not all of the annealing twins could be traced to slip planes known to be operative in the conventional sense and hence evidence appeared negative or inconclusive. With the discovery of additional slip systems^{2,3} operating in conjunction with the major system of highest resolved shear stress in axially strained brass it became apparent that the simple technique outlined above might be re-employed with more gratifying results.

If, on annealing single crystals of alpha brass previously strained in tension, twins are found with their composition planes parallel to all three operative slip planes and with no participation of the fourth plane there is good evidence in favor of the existence of twin faults and of the two stage slip process.

Experimental Procedure and Results

Single crystals of alpha brass of the 70-30 composition were grown by solidification from the molten state.

Cleveland Meeting, October 1949.
TP 2676 E. Discussion of this paper (2 copies) may be sent to *Transactions AIME* before December 1, 1949. Manuscript received May 2, 1949.

* Formerly Research Fellow in Metallurgy, Yale University; now Assistant Professor of Mechanical Engineering, The Johns Hopkins University, Baltimore, Md.

† Professor of Metallurgy and Assistant Professor of Metallurgy, respectively, Yale University, New Haven, Conn.

† References are at the end of the paper.

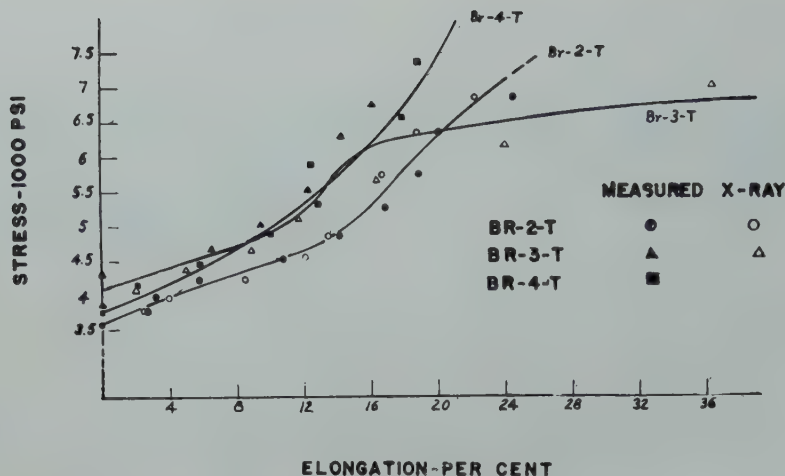


FIG 2—Stress-elongation curves for three tapered single crystals.

After a long homogenization treatment (24 hr at 800°C), central sections, about 3 in. long, were carefully tapered in a lathe to provide a linear decrease in diameter from 0.5 to 0.32 in. along the gauge length. Etching in 1:1 aqueous nitric acid solution removed the cold work, and subsequent electrolytic polishing² provided a smooth metallographic surface. Back-reflection Laue photograms were made at four different radial positions to insure that all cold work had been removed and to determine the orientation of the crystals. Fine black lines were painted on each specimen at one-quarter inch intervals; these intervals were carefully measured on a Zeiss metallograph at a magnification of X77.

The crystals were extended with a constant rate of loading until slip lines became visible within one-half inch of the large end of the gauge length. The average of repeated measurements of the gauge intervals using the same magnification gave the elongation per one-quarter inch interval. Stress values were derived from the maximum load to which the crystals were extended and the areas of the specimen after extension. A series of four back-reflection Laue photograms per gauge interval gave reorientation values in terms of λ and χ , where λ is the angle between the specimen axis and the primary slip direction and χ is the angle between the specimen axis and the primary slip plane. These values were used to calculate the elongation in the usual manner,⁵ viz.

$$\frac{l_1}{l_0} = \frac{\sin \chi_0}{\sin \chi_1} \quad [1]$$

where χ_0 and χ_1 are the original and final angles, and l_0 and l_1 are the original and final gauge lengths. The data relating stress to the measured and

calculated elongation are plotted in Fig 2. In the case of Specimen BR-4-T only measured values are shown because the reorientation was too small to yield reliable calculations.

Using the values of λ and χ determined by means of X rays, shear stress resolved in the primary $\langle 110 \rangle$ direction of slip and on the primary plane of slip was calculated by means of the usual formula.⁵

$$S = \frac{P}{A} \sin \chi \cos \lambda \quad [2]$$

where P is the load; A , the area; S , the resolved shear stress; and χ and λ , as previously designated. The shear was calculated from the two expressions;

$$t = \frac{\cos \lambda_1}{\sin \chi_1} - \frac{\cos \lambda_0}{\sin \chi_0} \quad [3]$$

and

$$t = \frac{1}{\sin \chi_0} \left(\sqrt{\left(\frac{l_1}{l_0} \right)^2 - \sin^2 \lambda_0} - \cos \lambda_0 \right) \quad [4]$$

Formulas 2 and 3 gave resolved shear stress-shear values from the X ray data and formulas 1, 2 and 4 gave resolved shear stress-shear values from the measured data. These resulting shear strengthening curves are shown in Fig 3.

The rotations of the lattice, Fig 4, are plotted from the back reflection X ray determinations of the orientations along the tapered gauge length.

These tapered specimens afforded an excellent opportunity to study the progressive formation of slip lines because of the increasing amount of deformation from zero per cent at one end to beyond 24 pct at the other. A series of representative micrographs of slip lines in Spec. Br-2-T is shown in Fig 5-16 together with the approximate extension at the respective position on the tapered specimen.

The first observable slip line, Fig 5, appeared very thin at X500. Even at this initial stage, slip on the conjugate plane is evident. Cross-slip, although not shown in Fig 5, was nevertheless present in the first group of slip lines at a different point of observation (cf Fig 17) and is shown in Fig 10 after an

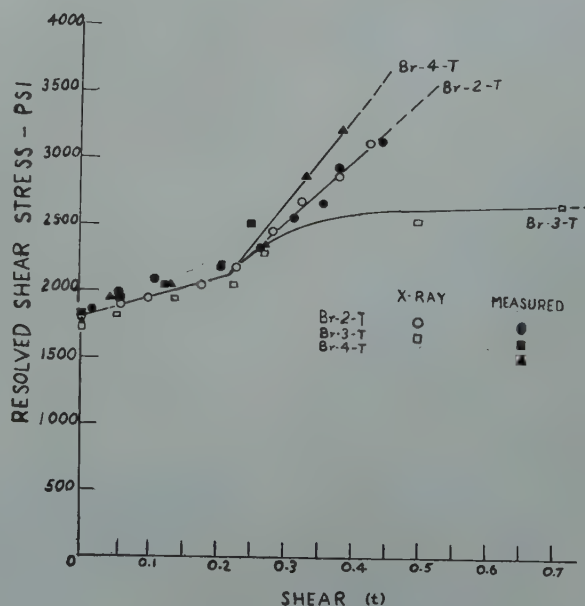


FIG 3—Resolved shear stress-shear curves for tapered single crystals.

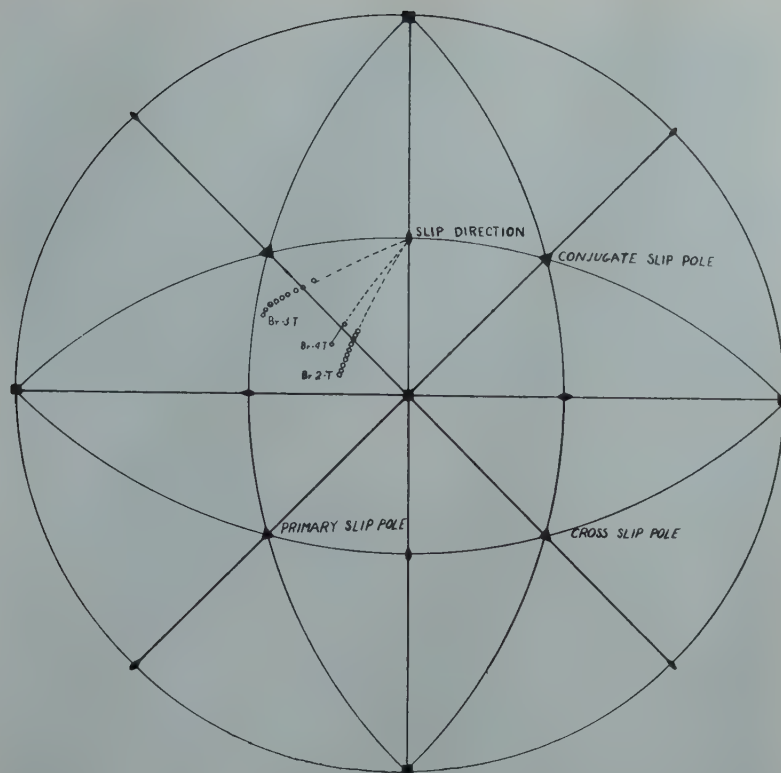


FIG 4—Stereographic projection showing the axes rotations of the tapered single crystals pulled in tension.

elongation of 4 pct. With increasing deformation, new slip lines appear adjacent to former lines, in such locations as to widen the original band, and produce the familiar clustered appearance.

At about 4 pct elongation (Fig 10) the clusters are sensibly wide and at the higher deformations, perhaps beginning with about 16 pct elongation, the clusters have overlapped to form a continuous bundle of lines which have lost their sharpness because of the proximity of many lines in and out of sharp focus.

The specimens were next wrapped loosely in thin, dead soft, brass foil of the same composition and annealed for

one hour at 800°C. After furnace cooling, they were etched in nitric acid solution followed by ferric chloride. Microscopic examination revealed that the composition planes of the many twins were nearly parallel to one of three different slip planes of the parent lattice. This structure is shown in Fig 18 and 19. The genesis of the twins was proven by X ray examination in which the X ray beam was positioned partly on the twin and partly on the adjacent material. Crystallographic analysis of the resulting double set of Laue spots gave the stereographic plot shown in Fig 20 which is typical of many such analyses made to establish the twin

relationships.

In all three specimens, recrystallization was found to extend to the location representing a minimum value of shear of about 0.22 (see Fig 3). The amount of recrystallization observed in Spec. Br-3-T was small in comparison detected in the other two specimens. Nevertheless, grains in all three specimens were large and replete with annealing twins, all of which produced boundary traces which corresponded to one of three composition planes.

From close examination of Fig 19, it may be seen that the twins seem to grow along the former slip lines.

By repolishing the specimens and

Table 1 . . . Analysis of Alignment of Twin Composition Planes with Slip Lines

| | Br-2-T Angle between Axis and Slip Line | | Br-3-T Angle between Axis and Slip Line | | Br-4-T Angle between Axis and Slip Line | |
|---------------------------|---|-----------------------------|---|-----------------------------|---|-----------------------------|
| | Measured* Degrees | Re- oriented† Degrees | Measured* Degrees | Re- oriented† Degrees | Measured* Degrees | Re- oriented† Degrees |
| Primary Slip Lines..... | 40 | 24 | 31 | 36 | 38 | 28 |
| Twin Comp. Plane..... | 32 | | 26 | | 23 | |
| Conjugate Slip Lines..... | 57 | 57 | 18 | 22 | 27 | 22 |
| Twin Comp. Planes..... | 59 | | 22 | | 30 | |
| Cross Slip Lines..... | 10 | 10 | 27 | 33 | 9 | 9 |
| Twin Comp. Planes..... | 16 | | 22 | | 10 | |

* Angles determined from stereographic analyses

† Angles measured on metallograph

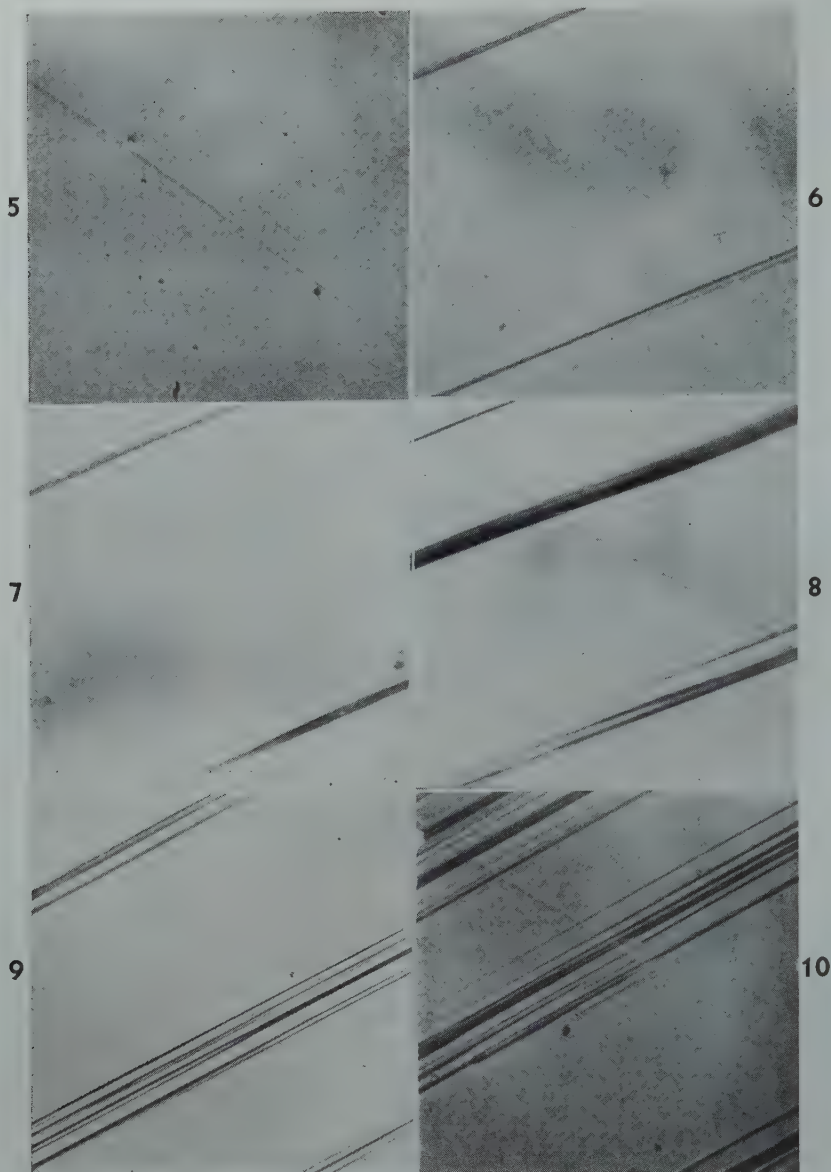


FIG 5-10—Slip lines in Specimen BR-2-T corresponding to various amounts of extension.

Except in the case of Fig 5, all micrographs were taken at a position around the conical surface of the specimen which would lie in a plane perpendicular to the plane containing the specimen axis and the primary slip direction. Stress axis vertical. Reduced one fifth in reproduction. $\times 500$

again straining in tension, slip lines were made to reappear in the unrecrystallized structure at the head of the taper and in the new grains. By aligning the composition planes of the twins with the slip lines in the parent lattice, that is, by moving the field from twin to original lattice along the axis of the specimen, these composition planes were identified as approximately parallel to former primary slip lines, cross-slip lines and conjugate slip lines. Several cases of close alignment are shown in Fig 21-26. In other cases, misalignments amounting to as much as 11° were found. Attempts were made to locate twins close to the unrecrys-

tallized structure so as to avoid misalignments due to the rotation of the lattice during the plastic extension preceding recrystallization. Since this was not always possible, stereographic analysis was used to correct the cases of misalignment by plotting the angles at the point of observation between the slip lines and the stress axis before and after straining. A typical construction is shown in Fig 27 from which the angles between the axis and the reoriented primary and cross slip planes respectively shown in column 3 of Table 1 were derived.

If observations of slip lines are made in the plane AP , then the trace of the

slip plane (primary) in the plane of observation is at the intersection of the two planes, viz., at P , and the angle AP , equal to 40° , is the measured angle between the axis and the trace of the slip plane.

If twins arising from this slip plane are observed in a part of the specimen in which the change of orientation during this extension is represented by moving the axis from A to A' , the angle $A'P$, equal to 24° will now represent the angle between the axis and their composition plane provided the latter occupies the new position of the slip plane with respect to the axis. In the case of the cross-slip plane, the

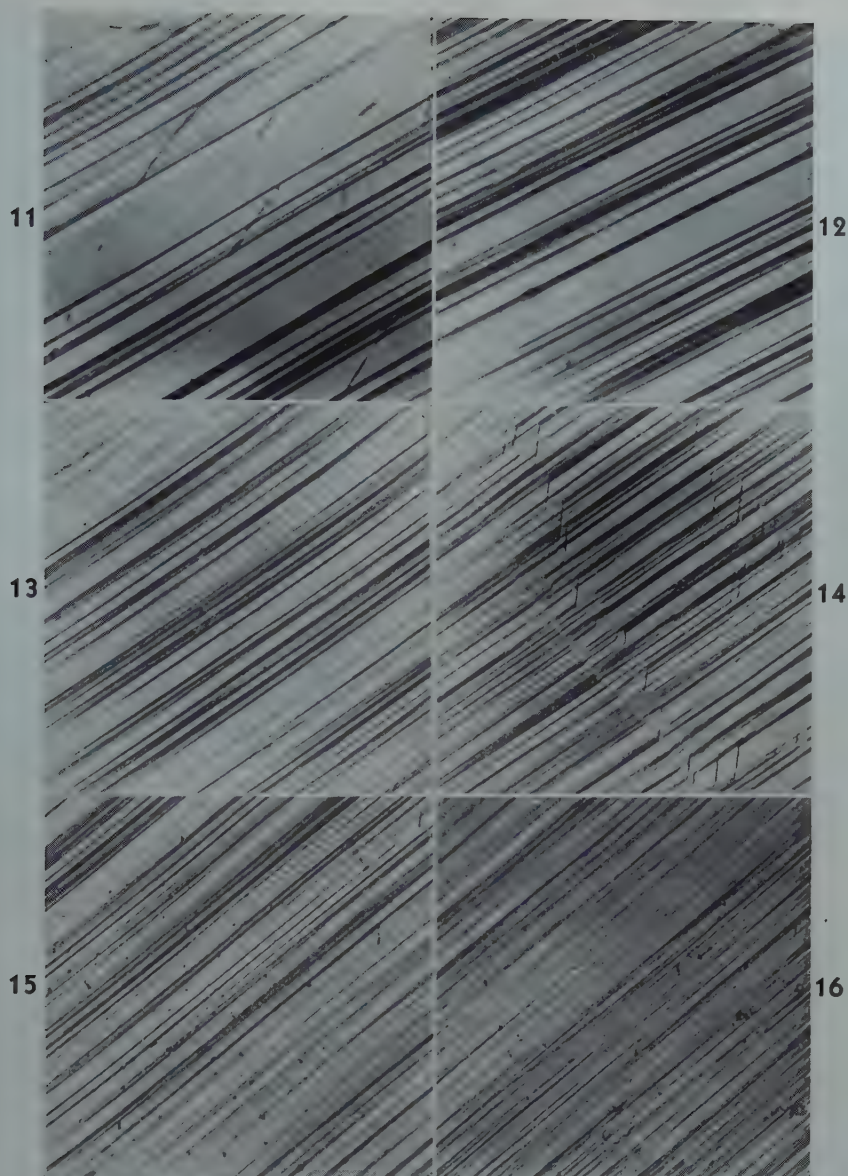


FIG 11-16—Slip lines in Specimen BR-2-T.

Positions similar to those represented in Fig 6-10. Stress axis vertical. Reduced one fifth in reproduction. $\times 500$

angle of its trace to the axis in the plane of observation AC , is equal to 10° and is practically unaltered in the new position $A'C$ after rotation. This is about 6° less than the measured angle between the axis and the twin composition plane. Similar constructions were made for the conjugate plane in this specimen and for all twinning planes in the other two specimens, BR-3-T and BR-4-T, as reported in Table 1.

The maximum error in alignment shown in Table 1 is 11° . There are four recognized sources of error in the technique used; (1) a possible 2° error in the X ray determinations from which changing positions of the stress axis were ascertained, (2) a possible 6° error introduced by the taper of the speci-

mens, (3) a possible error associated with the translation of the specimen on the microscope from the position of annealing twin to the position of the corresponding slip lines, and (4) an undetermined error in measuring the trace of the cross-slip lines because of their minute lengths. One or all of these possible errors may explain the observed deviations from perfect alignment.

Finally, the orientations of a number of grains in each specimen were determined by the Laue back-reflection technique. One group of these orientations together with the orientation of the parent lattice are shown in stereographic projection in Fig 28. These projections were drawn with the X ray beam at B , the center of the diagram,

that is, normal to the exposed grain surfaces. In the diagram, P refers to the parent lattice and the numbers refer to the specific grains outlined in Fig 29. In all of these recrystallized grains, there was an octahedral pole close to one of the octahedral poles of the parent lattice (ringed in the projection) as observed in the strained and annealed condition and in the neighborhood of the recrystallized grain, viz., at position 2 in Fig 29. It is doubtful if the term "recovered lattice" can be used in this connection since subsequent experiments have shown that the upper (least strained) part of a tapered specimen which showed no recrystallization at 800°C may recrystallize if annealed at a still higher temperature (900°C). In spite of the difference of

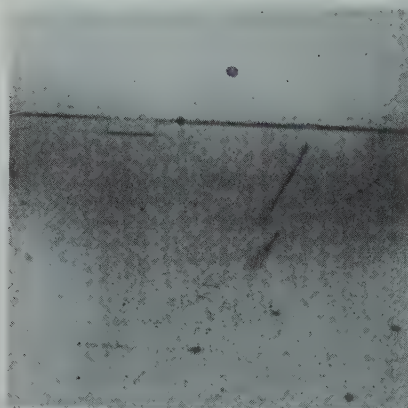


FIG 17—Appearance of first slip lines in Specimen BR-2-T.

Position perpendicular to the plane containing the specimen axis and the pole of the primary slip plane, that is, at the head of the major axis of the glide ellipse. Stress axis vertical. Note cross and conjugate slip lines. $\times 500$

orientation, which may amount to as much as 12° , between this octahedral plane as observed in the parent lattice and in the recrystallized grain, it is believed to be a common plane in the sense that it constituted the nucleus in the parent strained crystal from which the new grain grew, with a certain adjustment of orientation to the environment of strain, by a rotational process either identical with or akin to the one recently described by Kronberg and Wilson.⁶

The subsequent analytical technique was simply to perform the small rotation of the projection which was necessary to bring the so-called "common" octahedral pole in the recrystallized grain into exact coincidence with its position in the unrecrystallized structure, followed by the substantial rotation around this "common" pole which brought about complete coincidence of the two structures.

The results are shown in Table 2.

While this subject cannot be regarded as closed in view of the present meager understanding of lattice strain

in relation to recrystallization, the present experiments permit the following conclusions:

The recrystallized structure after substantial plastic deformation contains an octahedral plane obviously derived from a similar plane in the parent lattice.

The new grain does not grow out into the matrix without change of orientation or as an unreoriented twin. Its structure may be derived from the original structure by a rotation around the polar axis of the common octahedral plane.

Many of these rotations approximate the 22° and 38° rotations found by Kronberg and Wilson⁶ in their analysis of annealing twins in the secondary recrystallization of copper.

The rotation is presumably the response of the crystal to an activating strain which seems to be generally associated with twin faulting.

The Kronberg and Wilson analysis shows how a gross rotation of the lattice around an octahedral pole, for example, may be attained by small

coincidental movements of the atoms chiefly around sites which have retained their identity after the specific gross rotation. It is possible in this way to start with a twin fault and by thus moving the atoms around coincidence sites in neighboring planes on one side of the fault, to grow a new crystal whose octahedral planes are rotated 22° with respect to those of the original crystal, while growth on the other side of the fault by a similar process produces a twin structure whose poles are rotated 38° in the opposite direction around the composition plane. Other rotational possibilities are pointed out by Kronberg and Wilson. The present experiments are not wholly consistent with this crystal-geometrical pattern but offer strong evidence that the annealing twins in brass grow from twin faults parallel to the active slip planes by some rotational process of reorientation determined by the condition of strain in the plastically deformed crystal.

Inherent in the theory of two stage slip is the consideration that movement of the atoms in an octahedral slip plane determined by an active component of stress along the close packed strings of atoms $\langle 110 \rangle$ if forced to deviate into the interatomic valleys $\langle 112 \rangle$, (as shown by the arrows in Fig 1) which are assumed to be the paths of least resistance, would introduce a condition of residual stress in the hypothetical twin fault directing its alignment with the active component of shear stress. Thus the twin-faulted regions could be focal points of activation for a rotational process of atomic rearrangement and the observed annealing twins would be reoriented according to some pattern generally consistent with the reported observations.

Discussion of Results

Previous observations^{2,3,7,8,9} of lack of strain hardening in 70-30 brass single crystals during the early stages of deformation, are not in agreement with the present observations of strain hardening summarized in Fig 3. However, an explanation for these phenomena may be sought in the method of straining. In most of the experiments cited,^{2,3,7,8} the authors strained their crystals repeatedly but released the load after each individual extension. In the present investigation, the crystals attained their total extension

Table 2 . . . Rotation of Provisionally Reoriented Recrystallized Grains Around Designated Octahedral Poles Bringing Coincidence with the Original Structure

| Specimen Number | Strain (Approx.* Axis Rotation Deg.) | Direction of Rotation | Rotation Deg. | Nearest Octahedral Pole of the Parent Crystal |
|-----------------|--------------------------------------|-----------------------|---------------|---|
| BR-2-T 4 | 7 | Counter clockwise | 34 | Cross slip plane |
| 3 | 8 | Counter clockwise | 24 | Primary slip plane |
| 5 | 7 | Counter clockwise | 35 | Primary slip plane |
| 6 | 7 | Counter clockwise | 18 | Cross slip plane |
| BR-4-T 5 | 8 | Counter clockwise | 30 | Cross slip plane |
| 3 | 6 | Counter clockwise | 18 | Cross slip plane |
| 2 | 6 | Counter clockwise | 0 | Conjugate slip plane |
| 1 | 7 | Counter clockwise | 12 | Cross slip plane |
| BR-3-T 5 | 8.5 | Clockwise | 24 | Cross slip plane |

* Determined from location of grain on the tapered specimen.



FIG 18—Three views of recrystallized portion of Specimen BR-2-T. Slightly reduced in reproduction. $\times 1.5$



FIG 19—Three views of recrystallized portion of Specimen BR-4-T. Slightly reduced in reproduction. $\times 2.5$

under one application of load. This points to the possibility that a recovery process may be responsible for the lack of strain hardening previously observed and that under continuous loading, the normal process of strain hardening occurs.

A significant observation from the resolved shear stress-shear curves of Fig 3 is the constant rate of strain hardening in all three orientations investigated, up to a value of shear of about 0.22. Beyond this strain the rate of hardening appears to be a function of orientation. And this value of shear was the minimum one at which recrystallization occurred at the selected annealing temperature (800°C). The exact significance of this shear value (0.22), that is, whether or not it is constant for all orientations at all temperatures of deformation and recrystallization must be determined by further study.

The composition planes of the annealing twins formed on recrystallization of the axially strained tapered crystals of 70-30 brass were always approximately parallel to one of the active slip systems. The orientation of a new grain or part of a twin could be derived from the orientation of the parent crystal in the strained condition by rotation around their "common"

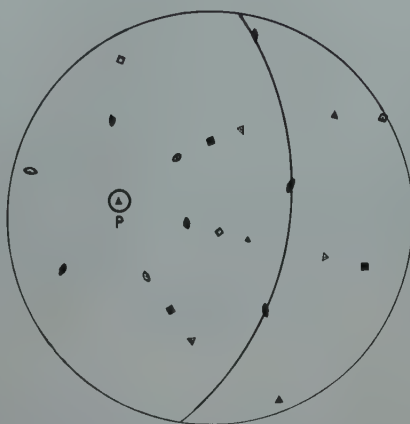


FIG 20—Stereographic plot of two sets of Laue spots showing the twin relation between the spots.

The twinning pole is labeled as *P* and its plane is shown as the arc in the plot.

octahedral pole, derived from the primary, cross or conjugate slip plane, but a certain small angular adjustment was necessary to bring the "common" pole into exact coincidence.

An attempt was made to rationalize the rotational reorientation by postulating a condition of residual stress at a twin fault due to the nature of the slip process. According to this view, the twin-fault is a preformed nucleus which activates a crystal-geometrical process of atom regrouping by rota-

tional shearing movements similar to those already reported by Kronberg and Wilson.⁶

In order to distinguish between the failure of the tapered specimens to recrystallize at 800°C in the regions which had been slightly deformed and their copious recrystallization in the severely strained regions, the following suggestions are offered on the basis of a two-stage slip process. Here a twin fault is produced in the first stage and a return to the original structure in the second stage (always accompanied by a certain configuration of residual stress).

In the early stage of slip, the atoms may be considered to move freely into their appropriate positions so as to complete the two $\langle 112 \rangle$ movements and result in an essentially unchanged lattice. However, during the later stages of the slip process, apparently beginning at about 0.22 shear, the lattice may be so strained or fragmented by the action of the three cooperating slip systems that the primary configuration can no longer be attained.

Summary

1. In the tensile straining of tapered 70-30 brass single crystals, variable de-

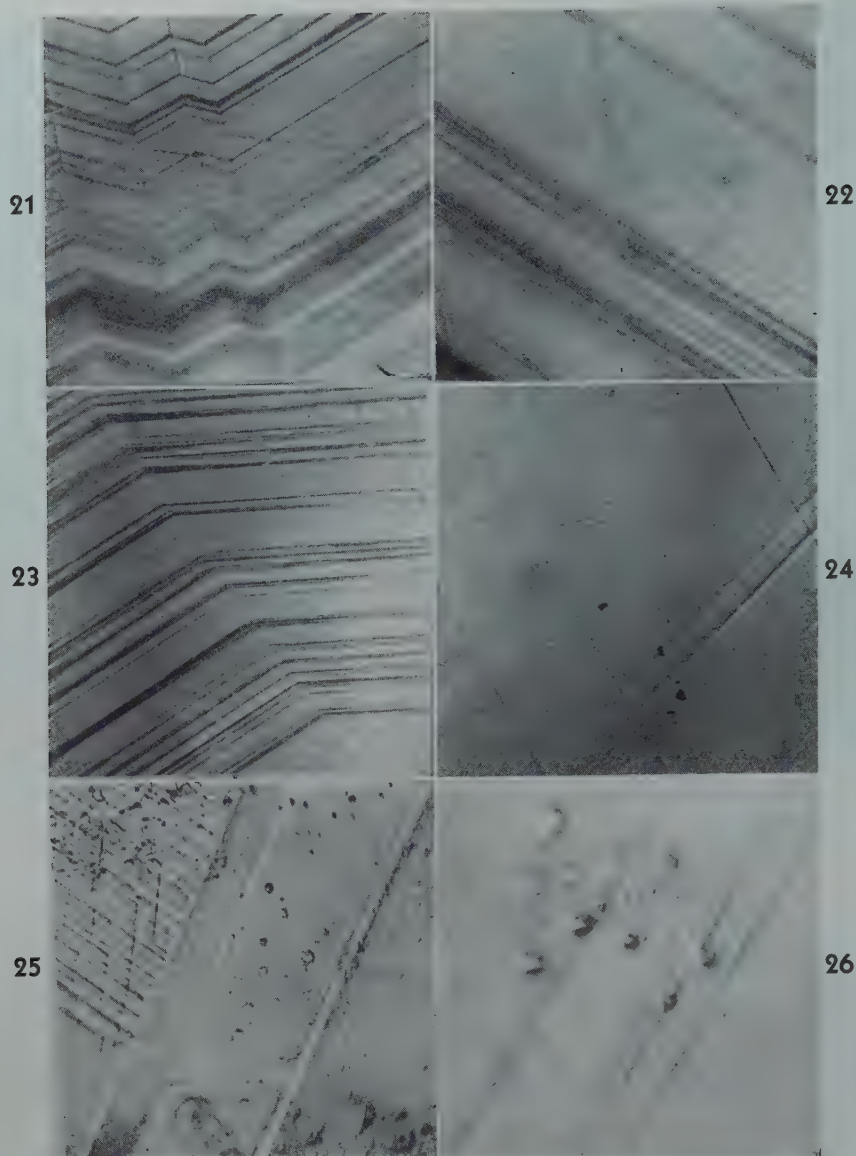


FIG 21-26—Alignment of composition planes of annealing twins with slip lines in the parent lattice.

Stress axis vertical. Reduced one fifth in reproduction. $\times 500$

formation along the specimen axis afforded the opportunity to record micrographically the progress of formation of slip lines.

2. Calculated resolved shear stress-shear curves show that there is slight strain hardening up to a value of shear amounting to about 0.22. At this point there is a marked rise in the rate of strain hardening which now appears to be a function of orientation.

3. Recrystallization on annealing at 800°C begins at a minimum value of shear of about 0.22.

4. Annealing twins are formed with composition planes parallel to the former operative primary, cross and conjugate slip planes, with no other relationships observable.

5. Recrystallized grains are found to

be related to the former parent lattice as reoriented after straining by a rotation about the pole of an operative primary, cross or conjugate slip plane. The variable amount and direction of rotation are apparently due to the difference in the strain configuration throughout the specimen.

These observations are interpreted as strong evidence in favor of coordinated $\langle 112 \rangle$ slip.

Acknowledgments

The authors' thanks are due to the New Jersey Zinc Co. of Pennsylvania for financial support which made this investigation possible and to the American Brass Co. for supplying the brass

from which the single crystals were grown.

References

1. G. I. Taylor and C. F. Elam: Distortion of an Aluminum Crystal. *Proc. Roy Soc.*, **123**, (A102) 643.
2. R. Maddin, C. H. Mathewson and W. R. Hibbard, Jr.: Unpredicted Cross Slip in Single Crystals of Alpha Brass. *Trans. AIME* **175**. *Metals Tech.* Feb. 1948, TP 2331.
3. R. Maddin, C. H. Mathewson and W. R. Hibbard, Jr.: The Active Slip Systems in the Simple Axial Extension of Single Crystalline Alpha Brass. Submitted to the *Journal of Metals* concurrently.
4. C. H. Mathewson: Structural Premises of Strain Hardening and Recrystallization, *Trans. A.S.M.* (1944) 38.
5. E. Schmid and W. Boas: *Kristallplas-*

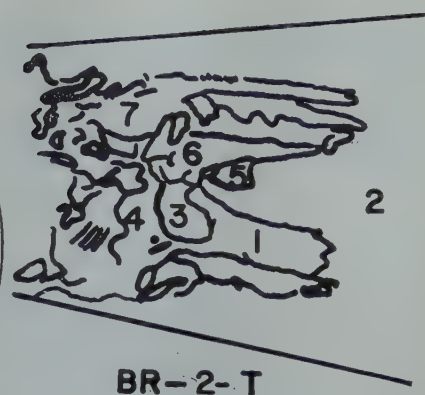
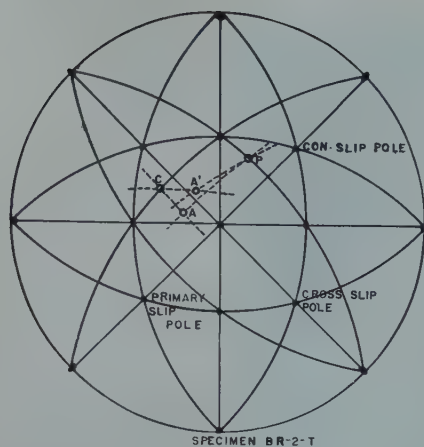


FIG 27—Stereographic analysis of the change in angle between slip lines and specimen axis at the point of observation before and after straining.

FIG 28—Stereographic plot of orientations of four grains in Specimen BR-2-T.

P refers to the parent structure and the numbers refer to the grains outlined in Fig 29.

FIG 29—Outline of grains whose orientations are shown in Fig 28.

6. M. L. Kronberg and F. H. Wilson: Secondary Recrystallization. Submitted for publication to *Jnl. of Met.*

7. D. L. Martin: Special Report (unpublished) Yale Univ. (1940).
8. R. G. Treuting and R. M. Brick: Micrographic Observations of Slip Lines in Alpha Brass. *Trans. AIME*

- (1942) 147, 128.
9. F. von Göler and G. Sachs: Zugversuche an Kristallen aus Kupfer und α Messing. *Ztsch. Phys.* (1929), 55, 581.

Some Observations on the Rate of Secondary Recrystallization in High Purity Copper

ANNA M. TURKALO* and DAVID TURNBULL †

It is well known that if copper that has been severely cold-worked by rolling (70-98 pct) is heated to high temperatures a small number of large grains are formed at the expense of the fine grained structure that appears upon primary recrystallization.

Dahl and Pawlek,¹ Cook and MacQuarie,² Ward,³ and Boas and Bowles⁴ have studied this phenomenon in copper. It has been reported as taking place with measurable velocities in the temperature range 700–1080°. Boas and Bowles have reported that the time necessary for the transformation is of the order of days at 700°C. According to Ward³ the number of secondary grains which appear in OFHC

copper decrease with increasing perfection of cubical alignment after primary recrystallization; also the perfection of cubical alignment increases with decreasing grain size prior to the final reduction.

In this investigation two heats, *A* and *B*, of especially high purity copper (99.999 pct) supplied by the American Smelting and Refining Co., were used. The behavior of samples prepared from

the two heats was qualitatively very similar providing that the grain sizes established prior to the final reduction were about the same.

We observed that in specimens prepared from bars which were relatively coarse grained prior to final reduction secondary recrystallization took place at a rapid rate at temperatures as low as 500°C. This is about 200–300°C lower than the temperature necessary to obtain fairly rapid transformation in OFHC copper. A 0.22 in. thick rectangular bar of lot *B* was cold-reduced 60 pct by straight rolling and given a penultimate annealing treatment at 250°C. Following this it was cold-reduced 90 pct and heated to various temperatures in the range 450–1040°C. The specimens were about 8 mils thick

Technical Note No. 20 E. Manuscript received April 28, 1949.

* Knolls Atomic Power Laboratory.

† General Electric Research Laboratory.

¹ References are at the end of the paper.

and $\frac{1}{2}$ sq. in. in area. They were placed in quartz specimen holders and heat treated in a hydrogen atmosphere. In general the secondary transformation was completed after about $\frac{1}{2}$ hr at 550° and in most specimens was partially complete after 6 hr at 500°C. From this it may be inferred that the linear growth rate in the transformation is at least 5×10^{-5} cm per sec at 500°C. Fig 1 shows photographs of typical specimens after heating for various times at the specified temperatures. Transformation is complete in all excepting those heated at 500°C. It is evident that the final grain size markedly increases with decreasing temperature so that at the lowest temperature only one grain appears per specimen.

Decreasing the penultimate reduction and increasing the penultimate annealing temperature tend to lower the temperature at which secondary recrystallization takes place rapidly. A sample of *B* given a penultimate reduction of 50 pct, penultimately annealed at 350°C, and cold-reduced 90 pct, exhibited complete recrystallization to several grains after 6 hr at 500°C.

In agreement with work on OFHC copper our results indicate that the tendency of secondary grains to form decreases with increasing perfection of cubical alignment. However, we have observed that the rate of appearance of secondary grains in specimens having a high degree of cubical alignment is greatly accelerated by very small strains. Specimens were prepared from heat *A* as follows: a 0.164 in. thick rectangular bar was cross-rolled to a reduction of 50 pct and annealed at 400°C for 3 hr. Because of the smaller initial grain size the grain size resulting from this treatment was much less than that obtained in lot *B* after the penultimate annealing treatments described above. The bar was cold-reduced 90 pct by straight rolling and cut into specimens having the same size as those from lot *B*. Rapid heating of these specimens to 1040°C and holding for 4 hr produced complete secondary recrystallization to 1 or 2 grains per sq. in. However, specimens recrystallized by heating at 500°C for one hour or heated slowly (200°C per hr) showed no evidence of beginning secondary recrystallization after periods of 16 to 20 hr at 1040°C provided that care was taken not to strain the specimens after primary recrystallization. If the specimens were strained by small amounts after primary recrystallization

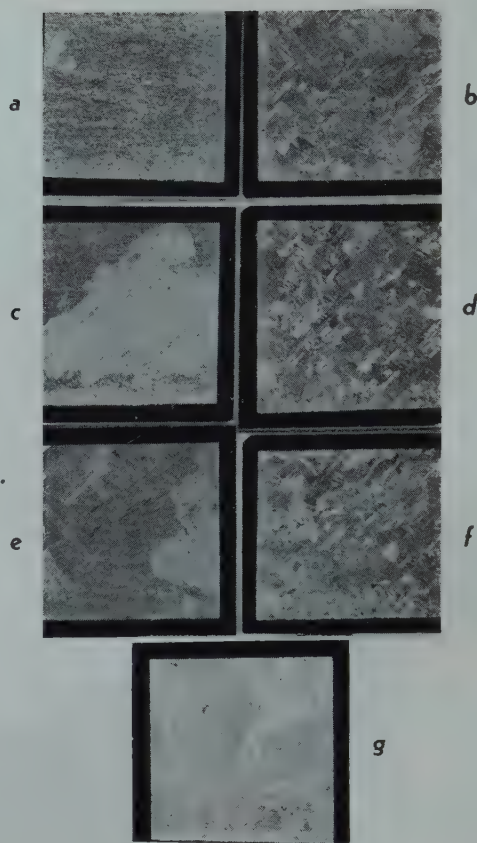


FIG 1—Copper samples annealed at various temperatures after 90 pct reduction.

a. 500°C—1 hr. b. 750°C—1 hr. c. 500°C—6 hr. d. 900°C—1 hr. e. 550°C— $\frac{1}{2}$ hr. f. 1040°C—1 hr. g. 600°C—5 min.

the secondary transformation was complete in nearly all specimens after 4–6 hr at 1040°C. Strains as small as 0.085 pct maximum, produced by bending the specimen over cylinders of a given radius of curvature, were sufficient to cause this effect. These results are in agreement with those obtained independently by Kronberg and Wilson⁵ on OFHC copper although they apparently used much larger strains to accelerate the secondary transformation.

The orientations of the secondary crystals which we observe are in fair agreement with those reported for copper by Boas and Bowles.

Our results demonstrate that the rate of the secondary transformation is much more rapid in high purity copper than in OFHC copper. At 500°C the rate of growth of secondary grains in high purity copper is at least 10^5 times greater than the value obtained for OFHC copper by extrapolation of Ward's results. Also it may be concluded that the secondary transforma-

tion takes place very slowly if at all in specimens exhibiting a high degree of perfection in cubical alignment. Secondary transformation is accelerated (or perhaps initiated) in the latter specimens by strains as small as 0.085 pct. The orientation of the grains thus obtained is very near that of the grains appearing in the secondary transformation of samples rapidly heated to the transformation temperature from the cold-rolled state. These results will be reported more completely in a subsequent paper.

References

1. O. Dahl and F. Pawlek: *Ztsch. Metallkunde* (1936) 28, (9) 266.
2. M. Cook and C. MacQuarie: *Trans. AIME* (1939) 133, 142.
3. R. Ward: Unpublished Data, General Electric Co.
4. J. S. Bowles and W. Boas: *Jnl. Inst. Metals* (1948) 74, 501.
5. M. L. Kronberg and F. H. Wilson: Seminar Hammond Laboratory, Yale Univ., Jan. 29, 1949.

Optical Temperature Scale and Emissivity of Liquid Iron

MINU N. DASTUR* and NEV. A. GOKCEN†

In metallurgical process industries a knowledge of true melting and casting temperatures is very essential for increasing the operating efficiency as well as improving the quality of the finished product. Optical pyrometers are widely used for the purpose because of their cheapness and ease of operation. It is an unfortunate fact, however, that this mode of measuring temperature entails a source of severe error inasmuch as with all non-black bodies, the temperature observed is always below the true temperature owing to deficient emissive power. Hence, the need for emissivity correction arises.

In 1913 Bidwell¹ obtained emissivity values of 0.36–0.48 for a temperature range of 1520–1800°C. He measured the true temperature of molten iron by sighting into a carbon cavity immersed in the iron under an atmosphere of hydrogen. In 1914 Burgess² determined the emissivity of a smooth surface of liquid iron free from oxide to be 0.37 under an atmosphere of hydrogen. He claimed to have attained an accuracy of within 5°C at 1500°C with an optical pyrometer using monochromatic light. He reported that no difference appeared to exist between the emissivities of pure iron and of steels containing considerable percentages of carbon, nickel or manganese; nor was there any appreciable variation of emissivity with temperature from 1530 to 1571°C. Wensel and Roeser³ found an emissivity value of 0.4 for temperatures above 1375°C for cast iron.

The average emissivity value for carbon steels reported by Leiber,⁴ Todd,⁵ Hase⁶ and Umino⁷ range from 0.4 to 0.45.

Knowles and Sarjant⁸ made an extensive study of emissivity of molten iron and steel over a wide range of workshop and laboratory conditions. Observations of true temperature were made with immersion thermocouples, and correlated with apparent temperatures indicated by optical pyrometer readings taken on the pouring stream

as it passed over the lip of the crucible. The emissivity of Armco iron was shown to be of the order of 0.4, rising slightly with increasing temperature. But for plain carbon steels containing up to 1.0 pct carbon the emissivity was shown to fall slightly with increasing temperatures. The results of their investigation are in agreement with those of Guthmann,⁹ Naeser,¹⁰ Spencer,¹¹ Todd⁵ and Hase⁶ in regard to the relation between emissivity and temperature for plain carbon steels. However,

Goller¹² has found a rise of emissivity with increasing temperature for the same steels. Results of several investigations are given in Fig 1.

Measurement of True and Apparent Temperatures

The necessity for an accurate optical temperature scale for liquid iron in studies of gas-metal equilibria led to this investigation. Experimental measurements were carried out in the induction furnace used by Dastur and Chipman¹³ in their studies of the reaction of hydrogen with oxygen in liquid iron. The furnace as modified for this work is shown in Fig 2. The atmosphere of the furnace was a mixture of purified argon with hydrogen containing a small controlled amount of water vapor. Gases were preheated by means of a platinum-10 pct rhodium resistance coil. The stream of hydrogen sweeping across the surface of molten iron vir-

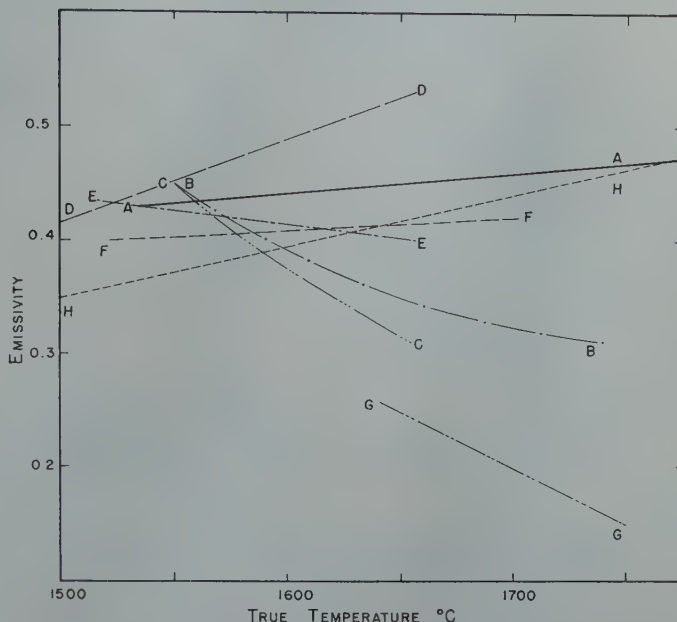


FIG 1—Results of observations of emissivity of pure iron and plain carbon steels by various investigators.

A. Present investigation, pure iron. B. Basic electric arc steel, Naeser. C. Small basic electric arc steels, Guthmann. D. Experimental basic high-frequency; steel, Goller. E. Experimental high-frequency furnace with sillimanite lining; steel, Knowles and Sarjant. F. Experimental high-frequency furnace with sillimanite lining; Armco iron, Knowles and Sarjant. G. Armco iron, Naeser. H. Iron, Bidwell.

New York Meeting, February 1950.
TP 2693 C. Discussion of this paper (2 copies) may be sent to *Transactions AIME* before April 1, 1950. Discussion is tentatively scheduled for publication in November, 1950.

Manuscript received May 12, 1949; revision received July 28, 1949.

* H. A. Brassert & Co., New York, N. Y.

† Graduate Student, Department of Metallurgy, Massachusetts Institute of Technology, Cambridge, Mass.

References are at the end of the paper.

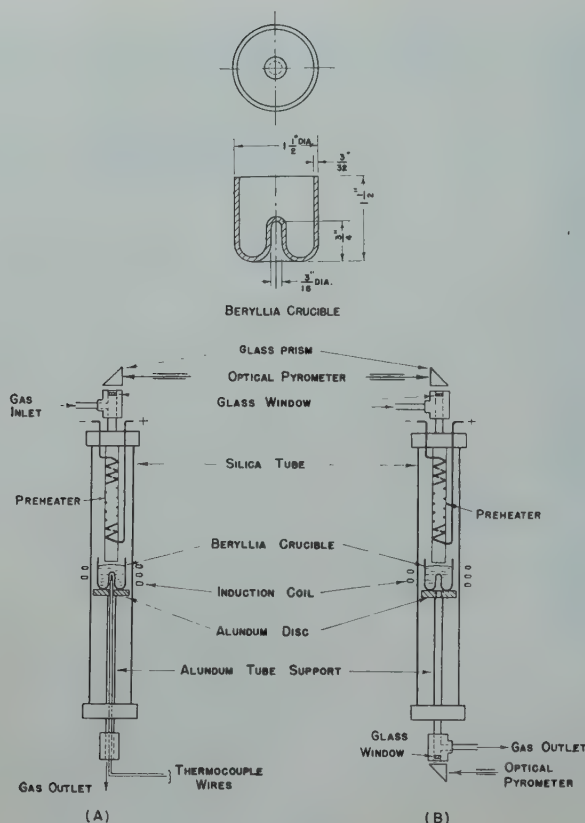


FIG 2—Furnace set-up for the determination of the true temperature scale and emissivity of liquid iron.

tually eliminates errors resulting from the presence of iron vapor except at temperatures approaching or above 1900°C. The charge consisting of about 90 g of pure iron was melted in a pure beryllia crucible especially designed for this purpose as shown in Fig 2.

Two sets of simultaneous temperature readings were obtained: (1) Optical top temperature reading by a sensitive optical pyrometer and bottom reading from a properly assembled thermocouple touching the top of the crucible cavity (see Fig 2A). (2) Top and bottom optical temperature readings by using the crucible cavity as a perfect black body for the bottom optical pyrometer (see Fig 2B).

After the charge was molten both the optical pyrometer and the thermocouple were frequently checked against the melting point of electrolytic iron in hydrogen which was taken as 1535°C. Thermocouples were also rechecked after each experimental run.

Optical temperature readings were taken when the gas preheating coil was hot and cold, and it was observed that the coil temperature has no effect upon temperature readings.

Each pair of simultaneous readings was taken when a constant and steady

temperature had been obtained by adjusting the power input from a high-frequency source. Temperature measurements obtained by stepwise heating were in agreement with those of stepwise cooling, indicating the absence of temperature gradient between the molten metal and thermocouple.

THERMOCOUPLES

Calibrated platinum-platinum rhodium and tungsten-molybdenum thermocouples were used in this investigation for establishing the true temperature of liquid iron. Platinum-platinum rhodium thermocouples were used only up to 1660°C and tungsten-molybdenum thermocouples were used from 1650 to 1900°C.

Schulze¹⁴ found that tungsten, molybdenum and tantalum were well suited for measuring high temperatures when the couples had been annealed at a higher temperature to assure constant thermal powers. The use of these thermocouples in liquid steel has been described by Taylor and Chipman.¹⁵

Schofield and Grace¹⁶ in using platinum-platinum rhodium thermocouples reported that no effect was noticed in the thermocouple output from the field

present in the induction furnace. The tungsten molybdenum thermocouples used in this investigation were from a batch calibrated and used by Potter¹⁷ and were rechecked against the melting point of pure iron.

OPTICAL MEASUREMENTS

The optical systems at the top and bottom of the furnace contained identical sight glasses and prisms and two optical pyrometers which had previously been calibrated against a standard instrument from the Bureau of Standards. No temperature difference was observed upon interchanging pyrometers or sight glasses and prisms. Since the hollow tip in the center of the crucible was more than three times longer than its diameter, it presented a perfect black body condition for the measurement of the true temperature of melt, corrected for absorption and reflection from the intervening optical system and the gas column. After checking the melting point of iron, temperatures as high as 1900°C were recorded by taking simultaneous readings with optical pyrometers from top and bottom.

Results

The results of true and apparent (optical) temperature readings are plotted in Fig 3 which gives a calibration for the given experimental conditions. Such scales may lend themselves to the evaluation of transmissivity and emissivity values, as will be shown presently.

Transmissivity correction is obtained from the optical bottom temperature reading when emissivity is unity. For this purpose the melting point of electrolytic iron (1535°C) was used as reference temperature and the transmissivity evaluated by the Wien-Planck equation:

$$\ln(E\alpha) = \frac{c_2}{\lambda} \left(\frac{1}{T_i} - \frac{1}{T_a} \right)$$

E = Emissivity

α = Transmissivity

c_2 = Fundamental constant of Planck equation, 14,330 micron-degrees

λ = Wavelength of light used (0.65 micron)

T_i = True temperature °K

T_a = Apparent temperature °K

In the special case of the melting point of iron versus bottom optical reading the apparent temperature was 1748°K and the true melting point was

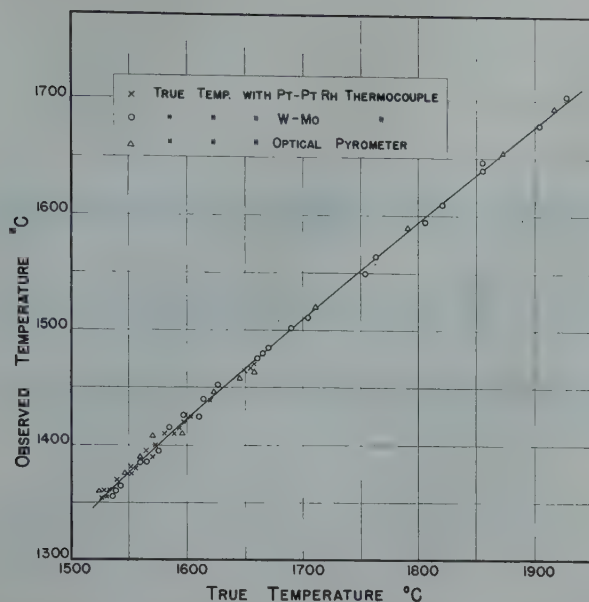


FIG 3—True temperature vs. observed (optical) temperature.

1808°K as measured by the platinum-rhodium couple. These values lead to a transmissivity of 0.65 which is considered constant within a temperature range of 1500–1900°C.

Once the transmissivity of the intervening optical system (sight glass and prism) was determined, the emissivity of liquid iron was calculated from observed top temperatures by the Wien-Planck equation using the experimental true and observed temperatures plotted in Fig 3. The scattering of the points in the emissivity plot of Fig 4 is of no great significance because even a slight error in the measurement of true or observed temperature will cause a relatively large change in the emissivity, since the logarithm of the emissivity is proportional to the difference in the reciprocal of the temperatures. An accuracy of $\pm 5^\circ\text{C}$ in observed temperature is equivalent to a change of ± 0.017 in emissivity values at 1600°C. Variation of the effective wavelength (λ) with temperature introduces a negligible error in emissivity values.

The total change in the emissivity of liquid iron over the temperature range of 1540–1900°C is from 0.42 to 0.50. The result of this investigation is presented graphically with the results of previous investigators in Fig 1 showing the inconsistency of the reported emissivity values. Variation of the emissivity of steels with temperature, investigated under plant conditions and reported by Sosman¹⁸ as 0.39 at 1425° and 0.50 at about 1650° agrees qualitatively with the present results.

Any correlation between the plant data and the emissivity is often much less accurate because of the presence of atmospheric disturbing factors as investigated by Hall¹⁹ and the surface condition of metal.²⁰

The emissivity of molten iron also varies with the addition of alloying elements. The effects of several elements have been reported rather inconsistently in the available literature. The only such element investigated here was vanadium which was found to have no effect upon the emissivity at concentrations up to 2 pct.

Acknowledgments

The authors wish to thank Professor John Chipman for suggesting the experimental method, Mrs. Virginia Mahaday for making the beryllia crucibles and Hans Elvander for assistance in the temperature measurements. This investigation forms a part of a study of the physical chemistry of steelmaking sponsored by the Office of Naval Research under contract N5 or-07816, Task Order XVI, NR-031-186.

References

1. C. C. Bidwell: *Phys. Rev.* (1913) 2, 482.
2. G. K. Burgess: Temperature Measurements in Bessemer and Open-Hearth Practice. Bur. of Standards (1917) Tech. Paper No. 91.
3. H. T. Wensel and W. F. Roeser: Temperature Measurement of Molten Cast Iron. *Trans. Amer. Foundrymen Ass'n.* (1928) 36, 191.
4. G. Leiber: Measurement of Tem-

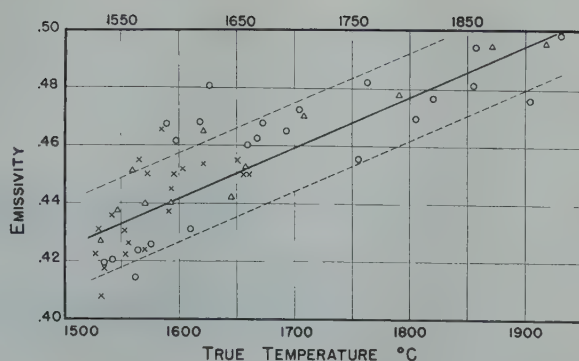


FIG 4—Emissivity of pure iron.

- perature in Steel Bath of Basic Open-hearth Furnace. *Arch. f. d. Eisenhüttenwesen* (1937) 11, 63.
5. W. J. Todd: High Temperature Measurement in a Steel Works. *Metal Treatment* (1939-40) 5, 171.
6. R. Hase: Influence of Emissivity of Liquid Iron. *Arch. f. d. Eisenhüttenwesen* (1931) 4, 261.
7. S. Umino: On the Emissivity of Substances in Steel Plants. *Tetsu-to-Hagane* (July 25, 1937) 23, 644.
8. D. Knowles and R. J. Sarjant: Emissivity of Molten Iron and Steel. *Jnl. Iron and Steel Inst.* (April 1947) 155, 577.
9. K. Guthmann: Comparative Measurements of Temperature on Molten Pig Iron, Cast Iron and Steel. *Stahl und Eisen* (1937) 57, 1245 and 1269.
10. G. Naeser: Reduction in Rejections with Radiation Measurements in Melting Practice Using Color-Intensity Pyrometer "Bioptrix." *Stahl und Eisen* (1939) 59, 592.
11. W. H. Spencer: Discussion of paper by G. R. Fitterer, *Trans. AIME* (1936), 120, 189.
12. G. N. Goller: Emissivity of Molten Stainless Steels. *Trans. Amer. Soc. for Metals* (1944) 32, 239.
13. M. N. Dastur and J. Chipman: Equilibrium in the Reaction of Hydrogen with Oxygen in Liquid Iron. *Jnl. of Metals*, Aug. 1949, 441. *AIME Trans.* (1949) 185, 441.
14. A. Schulze: Thermoelectric Properties of Tungsten, Molybdenum and Tantalum. *Ztsch. Metallkunde* (1932) 24, 206.
15. C. R. Taylor and J. Chipman: Equilibria of Liquid Iron and Simple Basic and Acid Slags in a Rotating Induction Furnace. *Trans. AIME* (1943) 154, 229.
16. F. H. Schofield and A. Grace: Quick Immersion Thermocouple for Measuring Temperature of Liquid Steel. Eighth Report on Heterogeneity of Steel Ingots, Iron and Steel Inst. Spec. Report No. 25 (1939).
17. R. D. Potter: Investigation of the Central Liquidus Surfaces and Phases of the Chromium-Molybdenum-Iron System. Sc. D. Thesis, M.I.T. (1949).
18. R. B. Sosman: Temperatures in the Open-hearth Furnace. *Trans. AIME* (1948) 176. *Metals Tech.*, Aug. 1948.
19. J. A. Hall: Influence of Smoke and Atmospheric Absorption of Optical Pyrometry. *Jnl. of Iron and Steel Inst.*
20. J. A. Hall: Photographic Investigation of the Brightness Temperature of Liquid Steel Streams. *Jnl. of Iron and Steel Inst.*, Jan. 1947, 55.

Size Effects in Quenching High-purity, Precipitation-hardenable Alloys*

WALTER L. FINLAY,† Member AIME

Introduction

Size effects in quenching steel are particularly prominent and well recognized because of the existence of a critical cooling rate separating nucleation and growth transformations, as exemplified by the formation of pearlite, from the shear type of transformation characterizing the martensite reaction. The absence of a similar, sharply demarcating cooling rate is characteristic of precipitation hardening systems and size effects in these are correspondingly less prominent. This paper is concerned with a size effect in high-purity, precipitation-hardenable alloys which appears not to have been recognized previously. This effect is believed to result from the thermal fluctuations which inevitably occur in quenching a specimen of finite size into a cooling liquid rather than from the existence of a critical cooling rate.

QUENCHING "ANOMALIES"

The precipitation hardening literature contains many references to so-called anomalous quenching and aging results. By "anomalous", investigators usually meant that their alloys did not consistently harden on aging after quenching according to some anticipated pattern; not infrequently virtually no age hardening occurred with compositions known to be precipitation-hardenable.

Perhaps the most prominent series of anomalies was reported over a 15-year

period by Gayler and coworkers on aluminum-copper.^{1,2,3,4} Working with silver-rich copper alloy, Cohen⁵ secured some very interesting Rockwell F hardness changes of from 1-5 Rockwell points between the first peak and valley. Fink and Smith borrowed one of

Cohen's specimens and, following his heat treatment and quenching practice to the letter, secured⁶ very different results in which only one peak was obtained and in which the hardness level at the aging time of Cohen's first peak was 20 Rockwell F points higher.

Fink and Van Horn⁷ encountered serious deviations in age-hardening high purity aluminum-zinc alloys. They stated that "the discrepancies were larger than might be expected from possible experimental errors in the Brinell readings."

Geisler, Barrett and Mehl⁸ likewise encountered anomalous hardening results in aluminum-silver alloys, securing quite different age-hardening curves from two identical specimens. They stated that "the treatments of these samples had been the same, so that the different behaviors could be attributed only to accidental variations in the quenching practice."

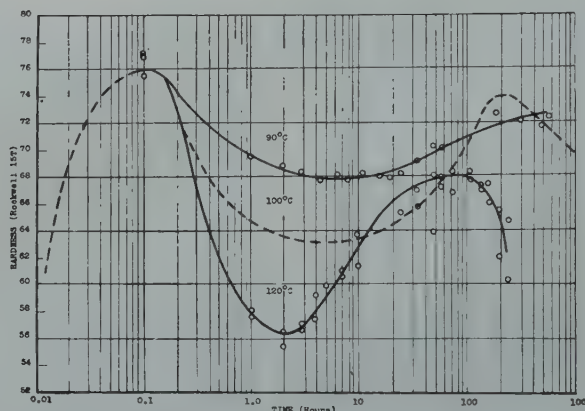


FIG 1—12 pct Al-Zn age hardening and retrogression. Longitudinal specimens with 0.1 × 0.5 in. cross-section. 2 hr at 475°C; 10°C water jet quench. Each point the average of five determinations.

Cleveland Meeting, October 1949.

TP 2694 E. Discussion of this paper (2 copies) may be sent to *Transactions AIME* before December 1, 1949. Discussion is tentatively scheduled for publication in May 1950.

Manuscript received April 29, 1949; revision received July 5, 1949.

* This paper is part of a dissertation presented by Walter L. Finlay to the Faculty of the Graduate Division of the School of Engineering of Yale University in partial fulfillment of the requirements of the degree of Doctor of Engineering, May, 1948.

† Supervisor, Metals Research, Remington Arms Co., Inc., Bridgeport, Conn.

‡ References are at the end of the paper.

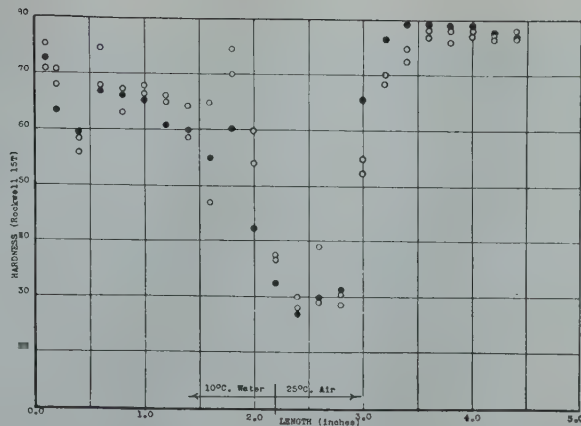
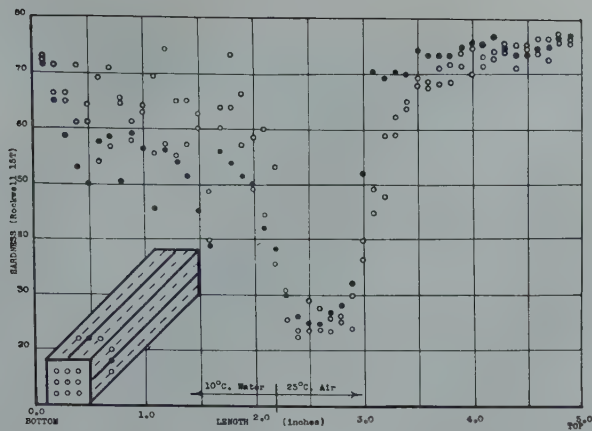


FIG 2A—12 pct Al-Zn partial immersion quenching.
Specimen with dimensions of $0.4 \times 0.4 \times 5.0$ in. solution heat treated for 2 hr at 475°C ; quickly placed vertically in quiet 10°C water with lower 2.2 in. immersed until entire specimen below 25°C . Each point a single hardness determination at locations sketched. Edge and midpoint hardnesses on one surface one hour after quenching.

FIG 2B—Same as Fig 2A except:
Edge and midpoint hardnesses on adjacent surface 24 hr after quenching.

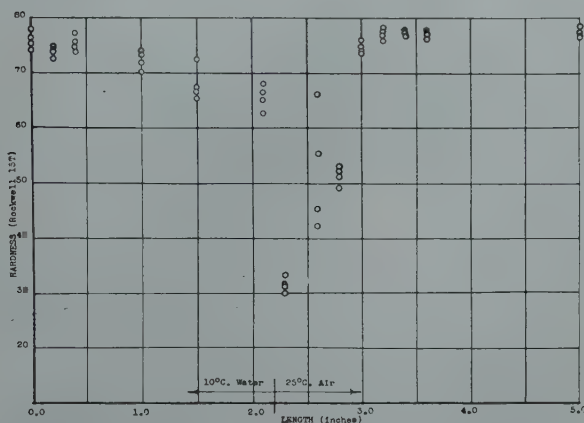


FIG 2C—Same as Fig 2A except:
Interior edge hardnesses.

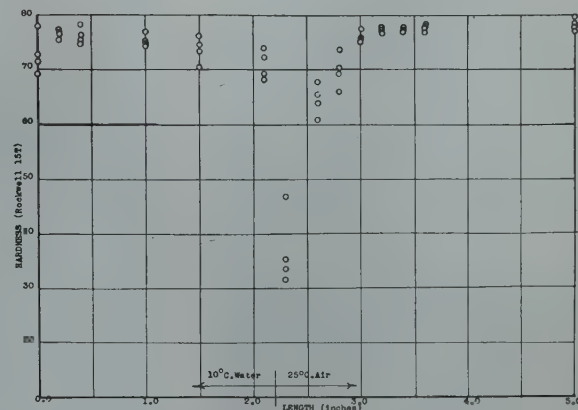


FIG 2D—Same as Fig 2A except:
Interior midpoint hardnesses.

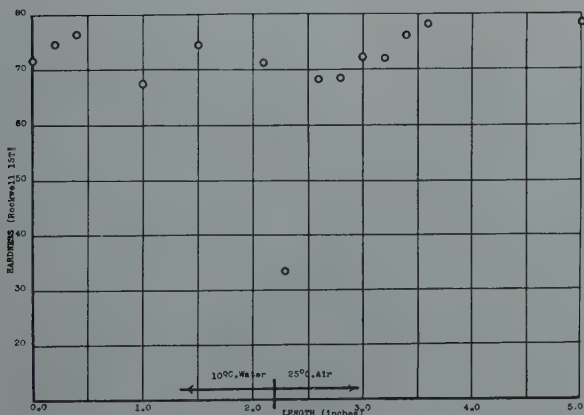


FIG 2E—Same as Fig 2A except:
Interior center hardness.

The present paper presents the view that these anomalies may be associated with retrogression effected by the thermal fluctuations accompanying quenching. Accordingly, the retrogression characteristics of the 12 pct aluminum-zinc alloy used in the investigation

being reported are outlined in the following section.

RETROGRESSION

Retrogression is a term which has been applied⁹ to the curious behavior of

certain age-hardening alloys according to which a quenched alloy partially or completely aged at a lower temperature, at first softens appreciably before slowly hardening again at a higher temperature. Masling suggested¹⁰ that the smaller of the precipitation particles which were stable at the lower temperature went back into solution at the higher temperature before additional precipitation could occur so that the observed weakening occurred. This explanation now appears to be generally accepted as valid.

A marked retrogression has been reported¹¹ for binary aluminum-rich aluminum-zinc alloys. The dashed curve in Fig 1 is a reproduction from Ref 11 for the 100°C retrogression of 12 pct aluminum-zinc; the 90 and 120°C retrogression curves also plotted in this figure present new data.

The 12 pct aluminum-zinc alloy was employed for a large part of the present investigation. Its pertinent behavior may, in terms of Rockwell 15T hardness, be summarized as follows: 1. It

quenches to a hardness of 50–55. 2. At room temperature it ages to 76–78 in 0.1–0.2 hr, and stays unchanged at that level for at least 2 yr. 3. Retrogression from its room temperature peak of 76–78 has been shown from 70°C up to at least 120°C, and doubtless this behavior is even more marked at higher temperatures. Within the temperature range investigated, the bottom of the retrogression valley is reached in 1–10 hr, and extends to depths of 56–72, the higher the temperature the shorter the time to the valley and the greater its depth. As is characteristic of the retrogression reaction, the rise from the valley is much slower than the rate of initial precipitation hardening at room temperature even though the latter is lower.

The retrogression behavior of binary aluminum-copper alloys has been studied extensively and, in principle, is not dissimilar from that of aluminum-zinc, although it differs in details, principally in that longer times or higher temperatures are required for corresponding aging effects.

Commercially pure aluminum-base alloys also retrogress and industrial use is made of this.¹⁷ In general, however, commercially pure alloys retrogress more reluctantly than their high purity counterparts.

Experimental Work

The following materials were employed in the investigation:

1. High purity 12 pct aluminum-zinc
2. High purity 4 pct aluminum-copper
3. Commercial purity 24S aluminum alloy
4. Commercial purity 75S aluminum alloy.

The preparation of the first two is described in Ref 11; the last two were purchased in the form of $\frac{1}{8}$ in. diam rod from Alcoa.

QUENCHING DIFFICULTIES

Age-hardening anomalies of the kind mentioned in the introduction were encountered in attempting to precipitation-harden high-purity, 4 pct aluminum-copper and 12 pct aluminum-zinc creep specimens having a 0.4 in. diam by 7 in. gauge length, whereas $\frac{1}{8}$ in. thick discs cut from these specimens and solution heat-treated and quenched together with the creep specimens gave consistent room temperature aging

results. With the aluminum-zinc alloy, for example, a series of 10 individual Rockwell 15T hardnesses of 77 ± 1 were common with the $\frac{1}{8}$ in. thick discs. But individual Rockwell 15T hardnesses on either the surface or cross-section of 0.4 in. round specimens were almost always low and very erratic, a typical sequence of readings being 50–38–48–22–46.

Several different quenching procedures were tried in uniformly unsuccessful attempts to secure, in the 0.4 in. round specimens of 12 pct aluminum-zinc, the 76–78 Rockwell 15T hardness level very readily attained in $\frac{1}{8}$ in. thick discs of the same material merely by dropping them into water. A special quenching unit was then built as the ultimate in quenching effectiveness. This quenching apparatus consisted of two parts: a vertical tube furnace for solution heat treating; and, axially aligned with the tube, a vertical quenching fixture into which the specimen dropped directly by gravity. A single specimen was suspended in the central portion of the vertical tube furnace by means of a wire. After a sufficient period of solution heat treating, the wire was cut and the specimen plunged directly into the jet quenching fixture. The latter consisted of a 1 in. id brass tube 10 in. long with approximately 200 holes 0.050 in. in diameter drilled into it in a uniform pattern with centers $\frac{3}{8}$ in. apart and extending from one end of the fixture to the other. Water pressure of 60 psi gave rise to 200-odd jets which symmetrically struck the specimen as it dropped through the fixture. Jets were employed both submerged and not submerged.

The result of this ultimate effort in quenching 0.4 in. diam 12 pct aluminum-zinc was a Rockwell 15T hardness averaging in the neighborhood of 50—something of an improvement over air cooling, but still far short of the hardness obtained on thin disc specimens.

Several 0.4 in. diam, 4 pct aluminum-copper rounds and $\frac{1}{8}$ in. thick discs were then jet quenched with similar results to those obtained on 12 pct aluminum-zinc, although, in the case of the 4 pct aluminum-copper, the rounds were not so markedly inferior to the discs.

The foregoing results definitely indicated a size effect. As a practical measure, therefore, all subsequent work on 12 pct aluminum-zinc and 4 pct aluminum-copper was done on specimens with a maximum thickness of 0.1

in. In order to gain some insight into the phenomena, however, a series of partial immersion quenching tests was conducted.

PARTIAL IMMERSION QUENCHING

Two rectangular bars, one with a square cross-section, 0.4 in. on a side, and another with a rectangular cross-section 0.1 in. thick and 0.4 in. wide, were employed in these tests. The specimens were solution heat treated in the standard manner and then were rapidly transferred to the quench where, in a vertical position their lower ends were immersed in the quenching medium. These experimental conditions were set up in order to secure, in one specimen, a wide range of both thermal gradients and a wide diversity of thermal fluctuations, since it was felt that the explanation for the puzzling phenomena encountered must be associated with failure, in a given region of the specimen, to maintain a uniform rate of temperature decrease during quenching.

The square cross-section bar, $0.4 \times 0.4 \times 5.0$ in., was carefully machined with its bases precisely normal to the longitudinal axis. All surfaces were flat and were polished through No. 000 paper. A hole was then drilled through one end which thereafter became the top of the vertically-quenched specimen. Three specimens were made in this manner: one from high-purity 12 pct aluminum-zinc; one from commercial 75S; and one from commercial 24S. Each was individually placed in the vertical tube furnace and solution heat treated for 2 hr. It was then quickly placed vertically in quiet 10°C water with the lower end immersed until the entire specimen had cooled to a few degrees below room temperature. One hour after quenching, pencil lines were drawn on one side of the bar as shown in Fig 2A and hardnesses were determined at 0.1 in. intervals from bottom to top of the specimen at “edge” positions (0.1 in. in from the bar edge) and at the “midpoint” position (0.2 in. in from the bar edge). The specimen was then stored for 24 hr after quenching to 25°C and hardnesses were similarly determined on an adjacent side. The hardness patterns shown in Fig 2A and 2B were thereby obtained. Because of the care with which the specimen had been machined, it was possible to determine hardnesses on the bottom of the specimen in the nine positions sketched in Fig 2A.

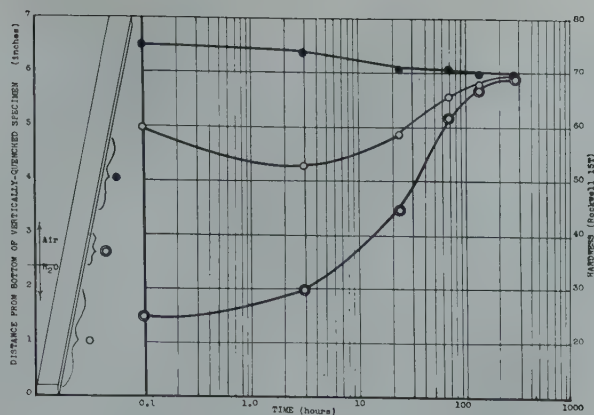


FIG 3—100°C aging of Fig 2 specimen.

After quenching as detailed on Fig 2, aged at 100°C. Each point the average of 10 determinations on the surface in the region bracketed.

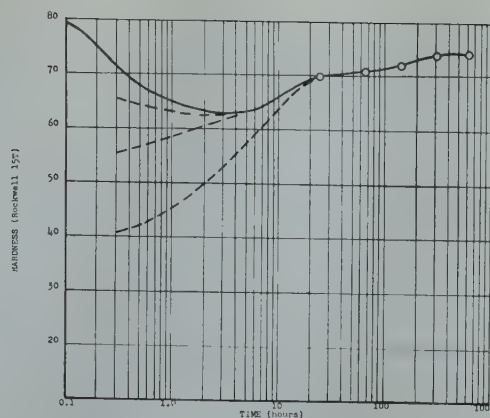


FIG 5—100°C aging of Fig 4 specimens.

After quenching as detailed on Fig 4, aged at 100°C. It was found, regardless of quenching medium and location on specimen, that after 24 hr at 100°C all hardness values were within 3 Rockwell 15T points of each other.

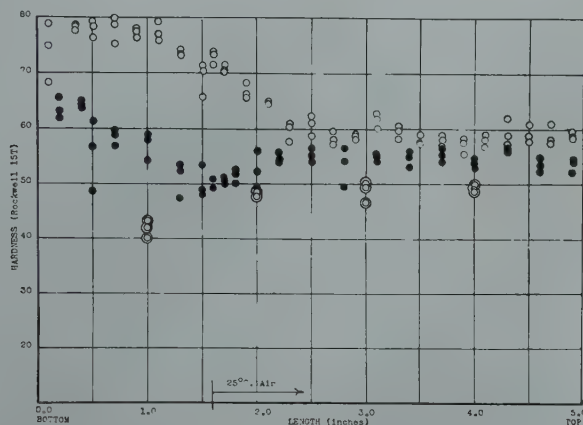


FIG 4—12 pct Al-Zn partial immersion quenching.

0.1 × 0.4 × 5 in. specimens; 2 hr at 475°C; quickly placed vertically for quenching—

○ Lower 1.6 in. in quiet 10°C water.

● Lower 1.6 in. in quiet 10°C oil.

○ Entire specimen in still 25°C air.

Each point a single hardness determination.

Hardnesses throughout the interior of the bar were then obtained by the following procedure: the specimen was clamped gently into a small vise; a line was scratched 0.1 or 0.2 in. from the end; the vise and specimen were immersed in 10°C water; by slow sawing with a fine jeweler's hack saw, a 0.1 or 0.2 in. thick specimen was cut from the end of the bar; by means of slow strokes from a clean, sharp, small-toothed file, the end of the bar specimen was squared up with the longitudinal axis; and, finally, the specimen and vise were removed from the water, the specimen was removed and hardnesses were again determined at the nine locations sketched in Fig 2A. The results of this investigation are shown in Fig 2C, 2D, and 2E. There is an excellent general correlation between the surface and interior hardnesses indicating that the necessary machining operations to secure the interior hardnesses were

carried out so that virtually no change in the actual hardnesses was effected by the machining operations. On the other hand, there are significant differences between the interior and surface hardnesses which fall into a consistent pattern when the data are analyzed from the standpoint of thermal-fluctuation-actuated retrogression and/or overaging.

The foregoing somewhat laborious procedure was carried out only on the 12 pct aluminum-zinc specimen since, as shown in Fig 6, the commercial aluminum alloys, 24S and 75S, were far less sensitive to whatever quenching variables were introduced by the test procedure and it was assumed that their interior hardnesses were the same as their surface hardnesses.

The data plotted in Fig 6 were determined one hour after quenching. Similar hardness determinations were made at intervals up to 500 hr after

quenching, resulting—in the case of both 24S and 75S—in a hardness increase of approximately 5 Rockwell 15T points uniformly along the length of the bar. Subsequent elevated temperature aging (10 hr at 190°C for 24S and 24 hr at 120°C for 75S) likewise raised the hardness uniformly along the entire length of the bar.

In order to distinguish between the effect of thick and thin specimens, the series of partial immersion quench tests graphed in Fig 4 was run on 0.1 × 0.4 × 5.0 in. specimens of 12 pct aluminum-zinc.

SUBSEQUENT AGING OF PARTIAL-IMMERSION-QUENCHED SPECIMENS

There are very few investigating means available to determine, in a polycrystalline specimen during the early stages of precipitation hardening, at just what stage is a particular region in the course of age hardening, particularly when, as in the case under discussion, the thermal history is both widely variable within the specimen and known in only a speculative way. The simplest procedure which occurred to the writer was to age the various pieces of the Fig 2 specimen, as well as the Fig 4 specimens, at 100°C, since a very large background of data had been built up on the behavior of 12 pct aluminum-zinc aged at this temperature. Results of this aging analysis are plotted in Fig 3 and 5.

Discussion of Results

The outstanding feature of the results obtained from the partial immersion quenching test is the hardness of the region just above the quenching

liquid level relative to the hardnesses of the other regions of the bar. From Fig 2, 4, and 6 the following broad details can be observed:

1. The high purity 12 pct aluminum-zinc shows a very sharp dip in hardness just above the quenching water level in the 0.4 in. square cross-section bar and the absence of any such dip in the 0.1 × 0.4 in. rectangular cross-section bar quenched in either oil or water.
2. The commercial purity 0.4 in. square cross-section bars of 24S and 75S show no dip.

The foregoing findings are the chief contribution which this paper offers to the experimental knowledge of the quenching operation. Unfortunately, time was not available to extend the investigation to other high purity systems than aluminum-zinc; but the previously-mentioned difficulties with 0.4 in. diam specimens of both high purity 4 pct aluminum-copper and 12 pct aluminum-zinc and the known lack of similar difficulties with commercial precipitation hardening aluminum alloys suggested that, in contrast to commercially pure alloys, high purity alloys may be vulnerable to unavoidable variables in even the best quenching practice. Among the possible explanations for this vulnerability and perhaps the most evident are:

1. *Critical cooling rate.* It might be assumed that a critical cooling rate exists, faster than that at which full hardening on aging subsequent to quenching is obtained and slower than that at which substantially full hardening during quenching to the temperature of the coolant is obtained. On this basis it might be argued that, after 0.1 hr at room temperature, 12 pct aluminum-zinc specimens cooled both above and below the critical cooling rate would be at approximately the same high hardness level; at about the critical cooling rate, such specimens would be soft, since very little precipitation would have occurred, yet room temperature precipitation could be very slow because the lattice defects present in volently quenched specimens would not be present to promote nucleation, despite the appreciable supersaturation.
2. *Quenching stresses.* Phillips and Brick suggested¹² that "quenching stresses are an important factor in accelerating and, perhaps, actually causing, age hardening."
3. *Thermal fluctuations.* Throughout the present paper the term "thermal fluctuations" is defined to comprise the momentary fluctuation which it is assumed would be observed if a continuous, instantaneous record could be kept of representative isotherms in a

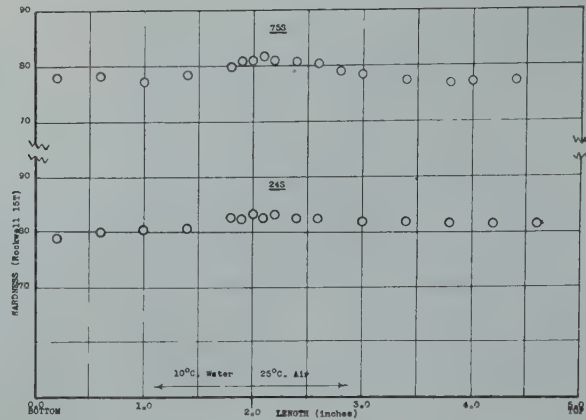


FIG 6—Commercial aluminum alloy partial immersion quenching. 24S and 75S bars with the same dimensions and heat treatment as Fig 2A. Each point the average of three determinations across the width of the specimen made one hour after quenching.

Table 1 . . . Data on Quenching Rates of 75S

| 75S Specimen and Coolant | Quenching Rate* (°F per Sec) |
|-------------------------------|------------------------------|
| 1/16 in. sheet— | |
| air..... | 4 |
| oil..... | 128–1600 |
| water..... | 2500 |
| 3/4 in. diam, water quenched— | |
| center..... | 830 |
| 4 in. diam, water quenched— | |
| 1/4 in. from surface..... | 280 |
| center..... | 42 |
| 2 in. diam, water quenched— | |
| 1/4 in. from surface..... | 430 |
| center..... | 135 |

* Average through the range 750–550°F.

specimen being quenched. Such fluctuations would mean that, in a given small region affected (that is, a volume element several hundred atoms in diameter and larger), the temperature would first fall and then, momentarily, would rise before again falling. With slow, uniform cooling presumably an isotherm would contract uniformly without appreciable fluctuations occurring. With submerged jet-quenching of thin sections, perhaps such fluctuations would be minimized. With more massive specimens, however, the combination of fluctuating vapor zone surrounding the specimen being quenched, coolant convection currents, and an appreciable quantity of heat to be removed from the interior of the specimen, is assumed to give rise to thermal fluctuations of sufficient magnitude to cause the anomalous hardening results which have been reported.

In considering the critical cooling rate possibility, the excellent experimental work of Fink and Willey¹³ is quite useful. These investigators established a "C" curve for 75ST, plotting as a function of time at isothermal quenching temperatures, the percentages of full 75ST properties attained. This work, in common with other published data by Fink and his collaborators on the precipitation hardening of high purity aluminum-copper and including the classic paper on double

aging peaks,⁶ was done with 0.064 in. thick specimens and thus, according to the findings of the present investigation, were quenched entirely satisfactorily. Fink and Willey also published¹³ extensive quenching rates for 75S, a few pertinent data being given in Table 1.

From this tabulation it can be observed that, in aluminum alloys, air cooling is negligibly slow relative to the cooling effected by conduction through the aluminum to a water quenched surface. Additional pertinent information on quenching rates in aluminum alloys has also been given by Loring, Baer, and Carlton,¹⁴ who employed a modified Jominy quench test specimen for their investigation. Extrapolating the Fink and Willey cooling rate data to the partial immersion quenching of the 0.1 and 0.4 in. thick specimens of the present investigation, one can conclude that, if a critical rate were of controlling importance, both these specimen thicknesses would have exhibited a sharp hardness dip if one did. The high purity 12 pct aluminum-zinc alloy showed a marked hardness dip in the 0.4 in. thickness but not in the 0.1 in. thickness. Hence it is concluded that the existence of a critical cooling rate does not explain the findings.

In developing their quenching stress thesis with high purity aluminum-copper alloys, Phillips and Brick used specimens from 0.0025 in. diam (filings) to 1.5 in. diam rod. Their many ingenious experiments established a very consistent trend in increasingly anomalous behavior with increasing specimen diameter. They concluded that the anomalies were related to and perhaps originated in the solution heat treatment and quench. It is perhaps

significant, in light of the data reported by the present paper, that Phillips and Brick secured quite uniform results up to a specimen thickness of 0.125 in., but that from the next greater thickness (0.25 in.) investigated, results were increasingly anomalous. In a very worthwhile discussion of the Phillips and Brick investigation, Barrett estimated the magnitude of the quenching stresses existing on a radial element near to the surface of the specimens and concluded that they reached a maximum compressive stress of about 15,000 psi. More recent work by Finlay and Hibbard¹¹ investigated the effect of 100,000 psi hydrostatic pressure on the precipitation hardening of the 12 pct aluminum-zinc alloy. This hydrostatic pressure aging is of course a different situation from that obtaining in a quenched cylinder which has tangential tensile stress and radial compressive stress present. The hydrostatic pressure aging indicated that precipitation hardening was both accelerated and intensified relative to atmospheric-pressure-aged specimens, but the differences were by no means great enough to account for those shown by the present investigation. In any case, both the region of the sharp hardness dip and the region of the high hardness plateau at the upper end of the 0.4 in. thick, 12 pct aluminum-zinc specimen were above the water level and, therefore, were in locations where quenching stresses were much less than in the region below the water level and presumably were quite low. Accordingly, it does not appear that quenching stresses can explain the results obtained.

In considering the possible action of thermal fluctuations on a precipitation hardening system, one is led to the thought that they may—under proper combinations of time, temperature, and composition—effect retrogression. From Fig 3 and 4 it is seen that the various regions of the 12 pct aluminum-zinc alloy, whether of the 0.4 in. square or 0.1×0.4 in. rectangular cross-sections, and whether water, oil, or air quenched, do indeed exhibit a 100°C aging behavior which is consistent with the hypothesis that each has been retrogressed to a different degree depending upon the kind of thermal fluctuations to which it was subjected.

The element of retrogression which appears rather definitely to be present in the hardness dip region of the 0.4 in. square aluminum-zinc specimen is the existence of a supersaturated

solid solution which is much less unstable than the same structure freshly quenched. This is evidenced by the relatively quite slow hardening rates at 100°C shown in Fig 3 compared to the much faster room temperature aging of the freshly quenched specimens shown in Fig 1. Similarly slow hardening rates are assumed in Fig 5, as shown by the dashed lines, since, unfortunately, data were not taken earlier than 22 hr on the 100°C aging of the Fig 5 specimens. Guinier's explanation¹⁵ for the reduced hardening rate of the retrogressed structure assumes that the as-quenched matrix lattice is subjected to high internal stresses and, accordingly, has many lattice defects which promote nucleation of precipitate particles. Both the initial aging at room temperature and subsequent retrogression "anneal" at 100°C given the aluminum-zinc specimen tend to diffuse these defects away, so that the nucleation rate is reduced and, with it, the rate of hardening.

Evidence for the presence of the other element of retrogression—resolution of coherent precipitate particles—is not clear from the data obtained. It seems possible that both re-solution and overaging (that is, breaking away from coherency with the matrix) of precipitate particles are involved. Thus, in the case of the air quenched specimen of Fig 4, some precipitation must have occurred during the period of relatively slow cooling and subsequent room temperature aging of one hour's duration. The low hardness can be interpreted to indicate that some of the larger precipitate particles had broken away from coherency. Upon subsequent 100°C aging, some of these noncoherent particles may have redissolved in the aluminum matrix; others may have remained noncoherent; and possibly a number of coherent precipitate particles redissolved. In any case, the typical retrogression feature of a more perfect lattice and, consequently, a lower rate of nucleation are believed to have obtained and resulted in a reduced rate of hardening to the retrogression peak. This point of view is employed in the following paragraphs to examine the details of Fig 2 and 3:

1. The Fig 2 data show generally falling hardness from the bottom of the specimen to the water line. Below the latter it is pictured that the thermal fluctuations are quickly quieted by the rapid water quenching, the more rapid and effective the quenching (as in the bottom and edges) the less the thermal

fluctuations. Thermal fluctuations, arising from heat coming from the interior, tend to begin to retrogress the outer portions so that they exhibit somewhat less than the expected room temperature hardness peak of 75–80 Rockwell 15T. Consistent with this, Fig 3 shows that on subsequent 100°C aging, retrogression continued and then recovery set in until the retrogression peak was attained. This viewpoint is consistent with the additional observations that: (a) the surface midpoint exhibits lower hardnesses than the surface edges; and (b) the surface has lower hardnesses than the interior.

2. Between the water line and 0.8 in. above the water line it is observed that (a) surface hardness is very low and does not change appreciably with distance but there is a noticeable tendency for the surface midpoints to become harder than the surface edges, and (b) like the surface, the interior hardness reaches a decided low at about the water line but, unlike the surface, the interior hardness recovers to higher values very quickly as the distance increases from the water line.

It is envisioned that because of the slower cooling just above the water line relative to that below the water line there are sufficient degree and duration of thermal fluctuations to soften the matrix to the retrogression valley. Fig 3 shows that subsequent 100°C aging raises this region out of the valley up to the retrogression peak. The interior is believed not to be subjected to as severe retrogression as the surface except at the water level and so it is generally harder but nevertheless at the retrogression valley.

3. Beyond approximately 1 in. above the water level, the hardnesses of all regions are at the highest levels attained and are matched only by the hardness at the very bottom of the specimen where presumably quenching was best. It is hypothesized that at the still slower cooling rate of this region, relative to that just above the water level, there is a longer period of severe thermal fluctuations capable of retrogressing the structure so that this region is retrogressed to the retrogression peak. Accordingly, on subsequent 100°C aging, as shown in Fig 3, the hardness falls off very slowly due to overaging.

4. From 0.8 to 1.8 in. above the water line it is observed that the surface midpoint is harder than the surface edge. This is just the opposite from the situation below the water line. Never-

theless, the thermal fluctuation retrogression theory gives a consistent explanation of the happenings. From its viewpoint it is believed that the edges both in the region under discussion and also below the water line are not retrogressed as much as the midpoints but, since in this case the hardness of the region is climbing out of the retrogression valley, the midpoints have reached the retrogression peak and are therefore harder than the edges which have not yet attained it. In the case of the region below the water the midpoints have also retrogressed more than the edges but there its advanced state meant that it had descended farther into the retrogression valley and hence was softer than the edges.

Fig 4 and 5 give the results of 0.1 in. thick bars as contrasted to the 0.4 in. thick bars of Fig 2 and 3. Similar, though less marked, results are shown in Fig 4 and 5 to those portrayed in Fig 2 and 3. The explanation for the data is also believed to be similar. No significant difference was found between the midpoints and the edges since there was not a sufficient thermal reservoir in the interior to give rise to it. For the same reason, a pronounced hardness valley was not developed just above the water line. The air-cooled specimen was discussed earlier. Subsequent aging of these specimens at 100°C resulted in the remarkably uniform hardness level characteristic of 12 pct aluminum-zinc overaging slowly from the retrogression peak.

Unlike the high-purity 12 pct aluminum-zinc, the commercial 75S and 24S bars with an 0.4 in. square cross-section did not exhibit a vulnerability to poor quenching practice. This is believed to be due to the fact that the commercial alloys have relatively very stable precipitates which resist retrogression and, indeed, this feature would appear to be a prerequisite to industrial use. As shown in Fig 6, the hardness curves, after partial immersion quenching of 75S and 24S, show no tendency whatever towards the hardness valley which is such a pronounced feature of the comparable 12 pct aluminum-zinc bar.

Summary and Conclusions

The high purity, binary, aluminum-zinc alloy containing 12 pct zinc was shown to exhibit marked retrogression at quite moderate temperatures. By means of a special testing technique, termed partial immersion quenching

and aging, it was established that this alloy was quite vulnerable to the variables encountered during quenching, and this was ascribed to its ready retrogression, possibly in concert with overaging, as effected by thermal fluctuations; further, that this vulnerability dropped to negligible proportions when the specimen thickness was not greater than 0.1 in.; and, finally, that commercial purity alloys 24S and 75S are not at all similarly vulnerable. Smaller scale tests indicated that high purity 4 pct aluminum-copper exhibited a quenching and aging behavior similar to that of the high purity 12 pct aluminum-zinc alloy.

A selection from the extensive literature on the "anomalous" quenching and aging behavior shown by high purity, binary, precipitation hardening alloys was presented. Examination of these references shows the use of specimen thicknesses considerably greater than 0.1 in. The thicknesses employed included $\frac{3}{16}$ in. for silver-aluminum;⁵ $\frac{1}{4}$ in. for aluminum-zinc;⁷ $\frac{1}{4}$ in. for aluminum-silver;⁸ $\frac{5}{32}$ in. for aluminum-copper;^{1,2,3,4} and, quite recently, $\frac{1}{2}$ in. for aluminum-copper.¹⁶ The majority, and perhaps all, of these anomalies are perhaps explicable on the basis of the size effect postulated by this paper. Additional evidence supporting this view is given in Ref. 3 wherein, when some of the anomalous-hardening $\frac{5}{32}$ in. thick specimens were forged to $\frac{1}{8}$ in. thickness, good and consistent age hardening results were obtained.

Based on the foregoing, the generalization is tentatively put forward that many precipitation hardening systems, particularly those comprising high purity binary alloys, may, because of ready retrogression and overaging, exhibit quite erratic quenching and age hardening behavior when the specimen thickness exceeds some maximum in the neighborhood of 0.1 in., since greater thicknesses inevitably give rise to excessive thermal fluctuations upon being quenched into a liquid. Commercial precipitation hardening alloys are believed not to be subject to such retrogression and overaging, since considerable tolerance to a relatively wide range of quenching conditions is presumably one of the essential prerequisites determining the suitability of an alloy for industrial use. It would appear, therefore, that the research worker dealing with noncommercial alloys should consider the possibility of a significant size effect in many precipi-

tation hardening systems and should employ some procedure such as the partial immersion quench test to insure that his quenching practice does not contain any uncontrolled variable which may invalidate his data, particularly in the early stages of aging.

Acknowledgment

Acknowledgment is made to the Remington Arms Co., Inc. for the use of equipment and facilities; and, for helpful discussions, to the writer's colleagues, M. B. Vordahl and D. R. Adessa, and to Professor W. R. Hibbard, Jr.

References

1. M. L. V. Gayler and G. D. Preston: *Jnl. Inst. Met.*, (1932) **48**, 197.
2. M. L. V. Gayler: *Jnl. Inst. Met.*, (1937) **60**, 75.
3. M. L. V. Gayler: *Jnl. Inst. Met.* (1938) **63**, 67.
4. M. L. V. Gayler and R. Parkhouse: *Jnl. Inst. Met.* (1940) **66**, 67-84.
5. M. Cohen: Aging Phenomena in a Silver-rich Copper Alloy. *Trans. AIME* (1937) **124**, 138-156.
6. W. L. Fink and D. W. Smith: Age-Hardening of Aluminum Alloys, III—Double Aging Peaks. *Trans. AIME* (1938) **128**, 223-233.
7. W. L. Fink and K. Van Horn: Equilibrium Relations in Aluminum-Zinc Alloys of High Purity. *Trans. AIME* (1932) **99**, 132-140.
8. A. H. Geisler, C. S. Barrett and R. F. Mehl: Aging in the Solid Solution of Silver in Aluminum. *Trans. AIME* (1943) **152**, 182-200.
9. R. F. Mehl and L. K. Jetter: The Mechanism of Precipitation from Solid Solution—The Theory of Age-Hardening. 1939 Symposium on Age-Hardening of Metals. *Amer. Soc. for Metals*, 342-417.
10. G. Masing: Present-Day Problems of Metallurgy. *Trans. AIME* (1933) **104**, 13-47.
11. W. L. Finlay and W. R. Hibbard, Jr.: Some Effects of Applied Stresses on Precipitation Phenomena. *Trans. AIME* **180**, 255. *Metals Tech.* Sept. 1948, TP 2470.
12. Arthur Phillips and R. M. Brick: Effect of Quenching Strains on Lattice Parameter and Hardness Values of High-purity Aluminum-Copper Alloys. *Trans. AIME* (1934) **111**, 94-112.
13. W. L. Fink and L. A. Willey: Quenching of 75S Aluminum Alloy. *Trans. AIME* (1947) **175**, *Metals Tech.*, Aug., 1947, TP 2225.
14. B. M. Loring, W. H. Baer, and G. M. Carlton: The Use of the Jominy Test in Studying Commercial Age-hardening Aluminum Alloys. *Trans. AIME* (1947), **175**, *Metals Tech.* Feb. 1948, TP 2337.
15. A. Guinier: Age-Hardening of Light Alloys. *Research* (1949) **2**, 6-11.
16. A. W. McReynolds: Plastic Deformation Waves in Aluminum. *Jnl. Inst. Met.* (1949) **1**, Sec. 3, 32-45.
17. U.S. Pat. #2,239,744 to D. W. Smith and W. L. Fink, issued on 4-29-41.

The Ternary System, Copper-manganese-zinc

T. R. GRAHAM,* J. R. LONG,† C. E. ARMANTROUT,† and A. H. ROBERSON‡

Introduction

The preparation and fabrication of copper-manganese-zinc alloys and the evaluation of their engineering properties have for some time been an integral part of a research program of the Federal Bureau of Mines. In this project, the use of electrolytic manganese, along with high purity copper and zinc, has permitted the preparation of alloys which contain a minimum of impurities which are capable of producing detectable effects in the properties studied. The initial work on the physical properties of wrought alpha solid solution alloys and a general outline of the alpha solid solution area for alloys containing up to 40 pct manganese have been presented in previous reports.^{1,2,3,4,5} The evidence accumulated in these investigations clearly showed that additions of manganese to the copper-zinc alloys improve the strength properties of the brasses without seriously reducing their characteristic ductility and that considerable quantities of manganese could be added to the copper-zinc alloys without exceeding the mutual solubilities of manganese and zinc in copper. In continuation of these studies, additional data have been obtained in a more extensive investigation of the phase relationships of the copper-manganese-zinc ternary system. The present report delineates the solid phase boundaries of the ternary system from the copper-zinc binary to the manganese-zinc binary for alloys containing up to 50 pct zinc.

Summary

The alloys used in this investigation were conditioned by working schedules designed to homogenize the structures prior to heat treatments required for

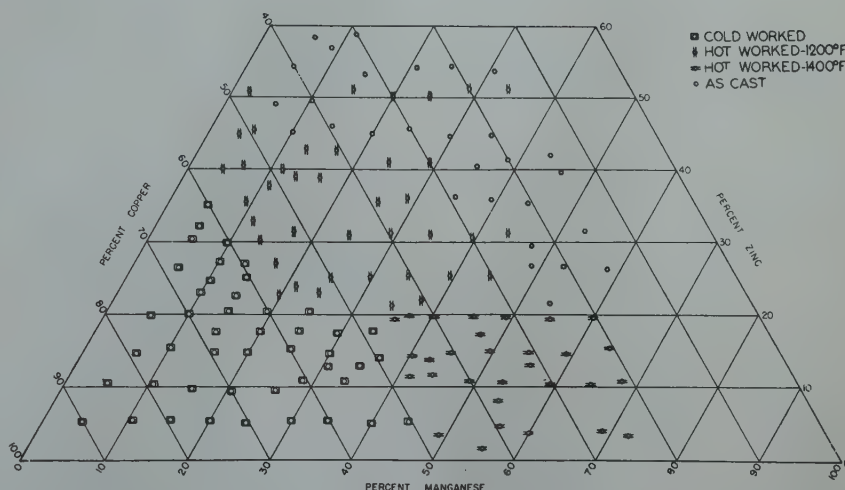


FIG 1—Condition of the alloys prior to thermal treatments used in this investigation.

the equilibrium phase study. The treated alloys were examined by metallographic methods including hardness and X ray data for confirmation.

The composite data of the investigation are summarily presented in a series of isothermal sections of the ternary system at 1100, 1200, 1300, 1400, and 1500°F. The salient features of the system as outlined by these data are: (1) the continuous alpha solid solution

which extends across the diagram to the gamma-manganese phase of the manganese-zinc system at temperatures of 1200°F and higher, (2) the beta phase of the copper-zinc system similarly forms a continuous solid solution with its counterpart the beta field of the manganese-zinc binary, (3) at 1100°F (593°C) these alpha and beta fields are greatly restricted by complications arising from the allotropic transitions of manganese and the decreasing solubility of manganese in the alpha solid solution. The alpha + beta fields intersect the alpha + alpha manganese field to produce the beta + alpha manganese field and two adjacent three phase fields consisting of alpha + beta + alpha manganese and gamma + beta + alpha manganese.

Typical microstructures representative of the various phase areas at each temperature are also presented.

Review of Previous Work

The copper-manganese-zinc alloys have periodically been the subject of numerous investigations of both prac-

Cleveland Meeting, October 1949.
TP 2699 E. Discussion of this paper (2 copies) may be sent to *Transactions AIME* before December 1, 1949. Discussion is tentatively scheduled for publication in May, 1950.

Manuscript received April 29, 1949; revision received July 13, 1949.

Papers by authors of the U. S. Bureau of Mines staff are not subject to copyright.

* Metallurgist, Rolla Branch, Metallurgical Division, Bureau of Mines, Rolla, Mo.

† Metallurgist, College Park Branch, Metallurgical Division, Bureau of Mines, College Park, Md.

‡ Metallurgist, Albany Branch, Metallurgical Division, Bureau of Mines, Albany, Ore.

References are at the end of the paper.

tical and theoretical significance.⁶ In a large measure, these studies have been concerned with the duplex, $\alpha + \beta$, alloys which constitute a commercially important group of engineering materials normally referred to as manganese bronzes. The actual manganese content of these alloys seldom exceeds 4 to 5 pct, and frequently is less than the total iron, nickel, tin and lead contents. Other investigations of the higher manganese compositions by Heusler,⁷ Bauer and Hansen,⁸ Guillet,⁹ and Hieke and Ledebur¹⁰ have been somewhat more extensive but are of limited value since their results were based on relatively impure alloys under admittedly nonequilibrium conditions. Reports by members of the Bureau's staff,^{4,5} have discussed the characteristics of a large group of the copper-manganese-zinc alloys, but did not include alloys containing more than 40 pct manganese.

The binary systems involved have been thoroughly examined in numerous studies and the principal phase boundaries are well established. The copper-zinc system has recently been reviewed by Phillips and Brick.¹¹ The copper-manganese system was thoroughly examined in the early part of the Bureau's work on alloys of electrolytic manganese.¹² Potter and Huber¹³ using powder metallurgy methods for the preparation of the alloys have determined the phase relationships of the manganese-zinc system for alloys containing up to 50 pct zinc by X ray diffraction and thermal analysis methods.

Experimental Materials and Methods

The alloys used in this investigation were prepared from electrolytic manganese, wire bar grade copper and 99.99+ zinc in substantially the same manner as described in the previous reports on these and similar alloys. It is perhaps also unnecessary to list the individual analyses for the 145 alloys examined but sufficient to point out that they were selected from some 500 heats of copper-manganese-zinc alloys which were made for a variety of experimental studies. These alloys were chosen on the basis of their suitability with due regard to their relative position in the ternary system and their low impurity content. The principal impurities present in the alloys are iron, silicon, and aluminum. Only four of the alloys contained greater than 0.020 pct iron and these contained less than 0.040 pct iron. The silicon

content of all the alloys was reported as less than 0.005 pct. The residual aluminum from the intentionally added deoxidizer did not exceed 0.04 pct and in 96 of the alloys the aluminum content was less than 0.02 pct.

Since cast alloys are not ideally suited for the determination of phase relationship because of their inherent characteristics of segregation, porosity, tendency for grain boundary constituents, persistence of agglomerated precipitates, and others, efforts were made to give the alloys a substantial amount of working before the final thermal treatments. However, this was not possible in all cases and a fixed processing schedule which would suit all the alloys could not be devised.

In this investigation one group of the copper rich alloys has been hot and then cold worked. Another group containing higher manganese and zinc was hot worked only and still other compositions were examined in the as-cast condition. The metallurgical condition and composition of the individual alloys prior to heat treatment are denoted in Fig 1. Contrary to the general tradition that high manganese alloys are normally quite brittle and unworkable, this chart shows that a substantial proportion of the alloys was hot rolled or forged. With proper adjustment of temperature in accordance with the phase boundaries subsequently developed, no doubt many of the other compositions could have been hot and cold worked. In fact, in some later work, many of the alloys containing more than 50 pct manganese with 10 to 15 pct zinc were cold rolled 60 pct reduction in thickness after quenching from 1400°F (760°C) without difficulty.

The high copper alloys which were finished by cold working, Fig 1, had, in addition to some hot reduction, three anneals with cold reductions averaging 50 to 60 pct between anneals. The hot worked alloys were reduced approximately 80 pct from the as-cast size with intermittent soaking at 1200 or 1400°F (648 or 760°C). Examination of the hot worked alloys showed the cast structures were entirely destroyed and that homogeneous or uniform structures were produced.

Several of the alloys were not worked prior to heat treatment. These alloys were primarily those highest in zinc or manganese. The castings, which were chill cast in 1¼-in. diam ingots, were quite uniform and clearly defined in structure and without serious

segregation.

Specimens of the individual alloys were heat treated for periods of 4, 8, 24, and 48 hr at 1300, 1400, and 1500°F (704, 760, and 815°C) and for 24, 48, and 200 hr at 1100 and 1200°F (593 and 648°C) in an atmosphere of helium, then quenched. In some of the highest manganese alloys slight demanganization occurred but seldom penetrated more than a few thousandths of an inch deep. All heat treated specimens were bisected so that an internal surface of one section could be used for metallographic study and the other was reserved for incidental hardness checks and X ray diffraction patterns as required for confirmation.

Approach to equilibrium conditions was determined by comparison of the structures obtained by various time periods at the same temperature. In general the structures differed but slightly and these differences were usually in amount of phases present. In a few instances, a phase was found to disappear in borderline compositions with longer heating periods. Structure of specimens held 24 and 48 hr at 1300, 1400, and 1500°F (704, 760, and 815°C) were unchanged by the longer time at temperature. Similarly structures of materials treated for 48 and 200 hr at 1100 and 1200°F (593 and 648°C) exhibit no change with the longer soaking time at temperature. The final observations from which the isothermal diagrams were drawn are based on the 48-hr treatment for 1300, 1400, and 1500°F (704, 760, and 815°C), while the 1100 and 1200°F (593 and 648°C) sections were based on 200-hr specimens.

Discussion of Results

The results of the investigation are graphically represented in Fig 2, 3, 4, 5, and 6 in which the isothermal sections for the ternary copper-manganese-zinc system at 1500, 1400, 1300, 1200, and 1100°F (815, 760, 704, 648, and 593°C) temperature levels have been drawn. In these drawings, the various phase boundaries have been extrapolated to the solubility values taken from the established copper-zinc, manganese-zinc, and copper-manganese diagrams. Where experimental observations permitted positive placement of the phase boundaries, solid lines have been drawn. Where the data are too incomplete for accurate placement of the phase boundary, but the trend of the field was known, dashed lines were used for the extension of the

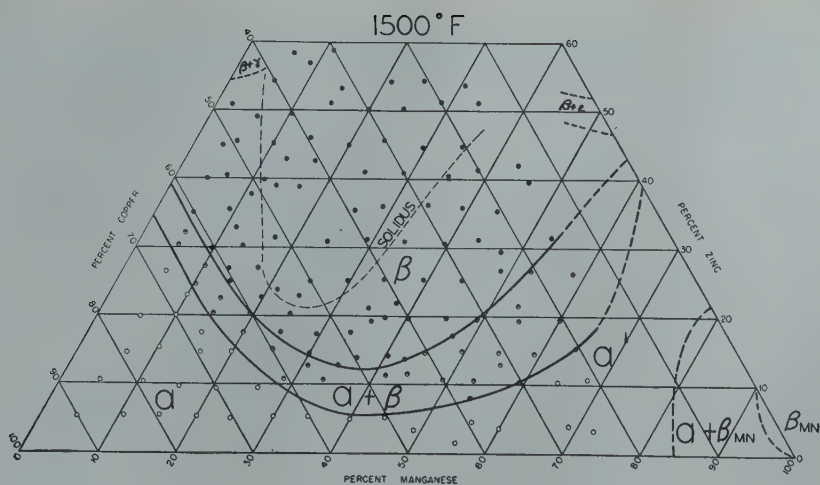


FIG 2—The isothermal section of the copper-manganese-zinc system at 1500°F (815°C).

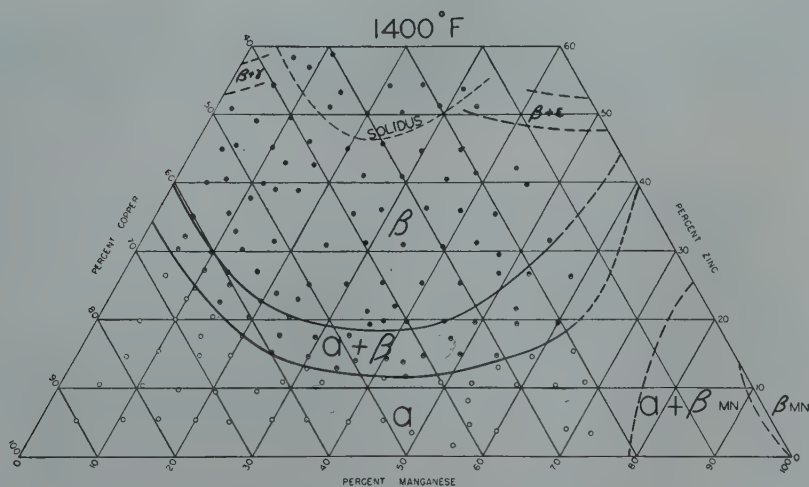


FIG 3—The isothermal section of the copper-manganese-zinc system at 1400°F (760°C).

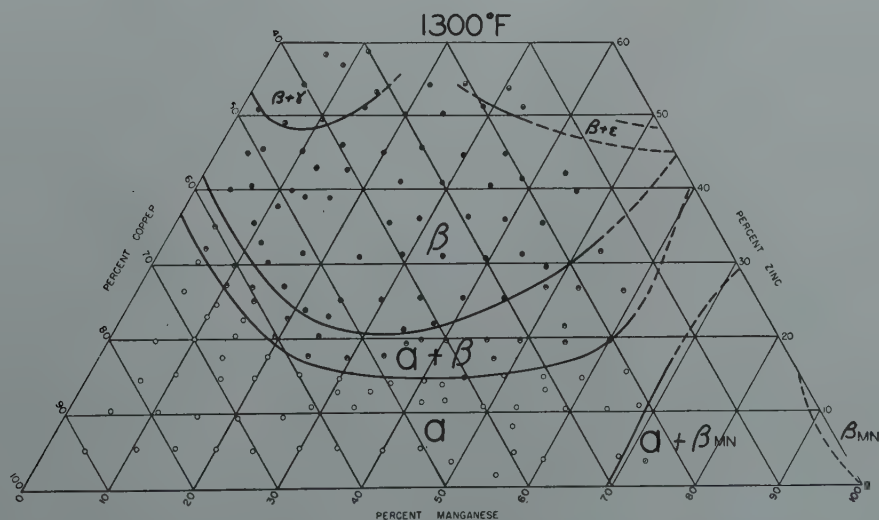


FIG 4—The isothermal section of the copper-manganese-zinc system at 1300°F (704°C).

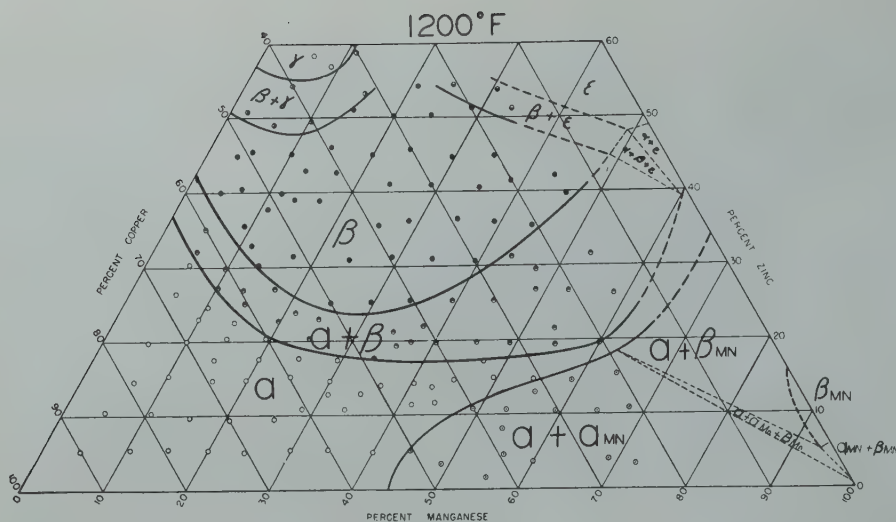


FIG 5—The isothermal section of the copper-manganese-zinc system at 1200°F (648°C).

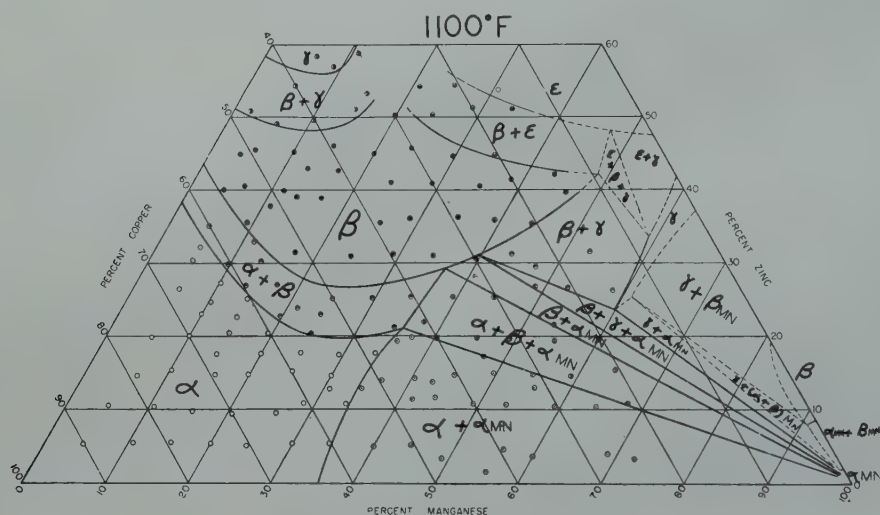


FIG 6—The isothermal section of the copper-manganese-zinc system at 1100°F (593°C).

boundary. In each of the isothermal sections, certain of the phase fields were not defined by the data but because they are necessary construction imposed by the binaries or by data in subsequent sections, dashed lines have been used to approximate their position.

At 1500°F (815°C), Fig 2, the alpha and beta solid solutions of the copper-zinc system extend uninterrupted to the manganese-zinc binary although the solubility of zinc in these phases decreases to a minimum at approximately 40 pct manganese then increases with larger amounts of manganese reaching a maximum solubility at the manganese-zinc binary. Some restriction in the alpha solid solution occurs near the manganese corner and a two phase field of alpha solid solution plus

beta manganese has been estimated on the basis of the solubility data of the manganese-copper and manganese-zinc system. The solidus line which has been incorporated in the 1500°F (815°C) isotherm is not intended as an exact solidus but has been drawn primarily to differentiate between those alloys which showed evidence of melting and those which did not exhibit melting at this temperature.

Manganese decreases the solubility of zinc in the alpha phase of the copper-zinc system. The alpha and beta solubility lines are substantially parallel to one another and parallel to the lines of constant copper up to 15 to 20 pct manganese. In general, manganese and zinc act as equivalents. The present data show slightly less solubility of

zinc in the alpha and beta phases in the range of 20 to 40 pct manganese than were previously recorded in work on the alpha solubility limits. Calculations by Hume-Rothery¹⁴ on the earlier data, showed that manganese in small amounts affected the alpha-beta equilibrium as though it were a divalent element but departed from this simple relationship at rather low manganese contents. The solubility line of the present investigation indicates the solubility curves are comparable to the theoretical curve up to 15 to 20 pct manganese if equilibrium were determined by electron concentration alone and manganese possessed a valency of 2. As the concentration of manganese increases beyond 20 pct the alpha + beta phase field tends to widen and

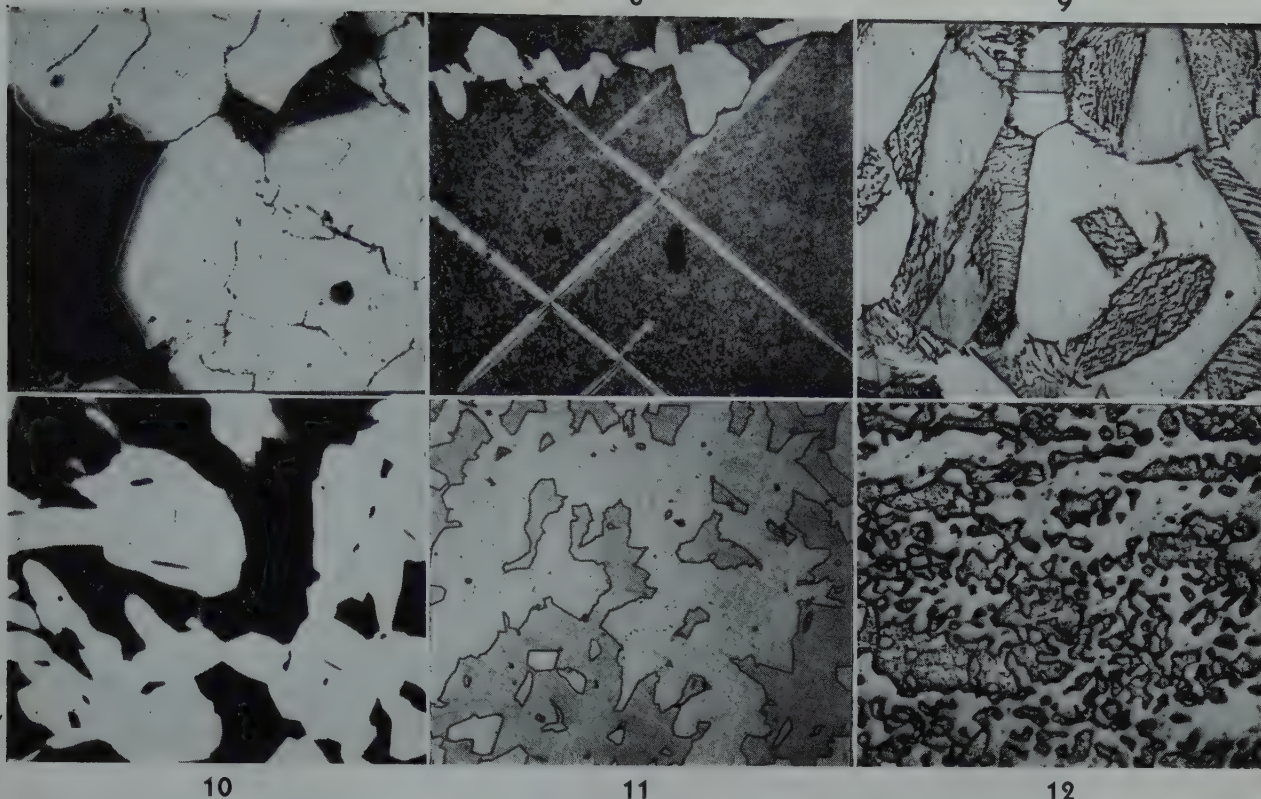


FIG 7—Alpha (light) and beta retained in the 58.0 Mn, 26.0 Zn alloy quenched from 1500°F.

× 250. ASTM copper etchant No. 11.

FIG 8—Beta (dark) and grain boundary alpha formed during cooling the 40.5 Mn, 14.2 Zn alloy from 1500°F.

× 250. ASTM copper etchant No. 11.

FIG 9—Alpha (light) and transformed beta (dark) in the 33.6 Mn 10.6 Zn alloy quenched from 1500°F.

× 250. ASTM copper etchant No. 11.

FIG 10—Alpha (light) and retained beta (dark) in the 58.0 Mn 26.0 Zn alloy quenched from 1400°F.

× 250. ASTM copper etchant No. 11.

FIG 11—Alpha (light) and beta (dark) structure of the 40.0 Mn 19.2 Zn alloy quenched from 1300°F.

× 250. ASTM zinc etchant No. 4.

FIG 12—Alpha (light) and beta manganese (dark) in the 72.1 Mn 3.2 Zn alloy quenched from 1300°F.

× 250. ASTM copper etchant No. 8 with 10 pct acetic acid added.

becomes more or less parallel to the copper-manganese binary at approximately 40 pct manganese. With larger amounts of manganese, the alpha + beta field continues to widen and the solubility of zinc in both the alpha and beta phases increases. These solubility curves are extrapolated from the 15 pct copper line to the manganese-zinc binary and decrease considerably in width with decreasing copper to correspond with the extent of this phase field in the binary system.

Similar trends of the alpha/alpha + beta and beta/alpha + beta solubility lines for the ternary system are shown in the 1400°F (760°C) isothermal section in Fig 3, although these curves are displaced to higher zinc concentrations. The solidus shifts rapidly as the temperature decreases from 1500 to 1400°F (815 to 760°C) and a rather large beta area is formed at the lower temperature. The projections of the beta + gamma field of the copper-zinc system and the beta + epsilon field of the man-

ganese-zinc system are also introduced at 1400°F (760°C).

At 1300°F (704°C), Fig 4, the general shape and contour of the alpha and beta boundaries remain substantially the same as indicated for the higher temperatures. The alpha/alpha + beta and beta/alpha + beta lines are approximately parallel giving the field a spread of 5 to 6 pct as measured on lines of constant manganese for all compositions up to about 40 pct manganese. With increasing manganese the two phase field widens to a maximum at 60 pct manganese then decreases to the manganese-zinc binary values.

The metallographic structures of specimens treated at 1300, 1400, and 1500°F (704, 760, and 815°C) are in general quite similar to the characteristic alpha and beta structures of the copper-zinc system and are readily identified. Some exceptions, however, were encountered in the beta alloys which were immediately adjacent to the beta/alpha + beta boundary.

These alloys, particularly in the low manganese range, often transform bodily to the alpha phase during the quench making it difficult to be positive of the high temperature structure. Characteristic micrographs of these structures as well as structures of the alpha and beta phases for alloys containing less than 30 pct manganese were presented in the report on the alpha solubility limits.⁴ Phillips¹⁵ has also described the mass transformation reactions for the binary copper-zinc alloys.

Representative structures for alloys containing more than 40 pct manganese and falling within the alpha + beta and beta fields are illustrated in Fig 7 to 11, inclusive. In these structures the beta phase appears as the dark or acicular constituent. In general, increasing manganese tends to stabilize the beta phase, but varying degrees of decomposition depending on composition and temperature were found to occur.

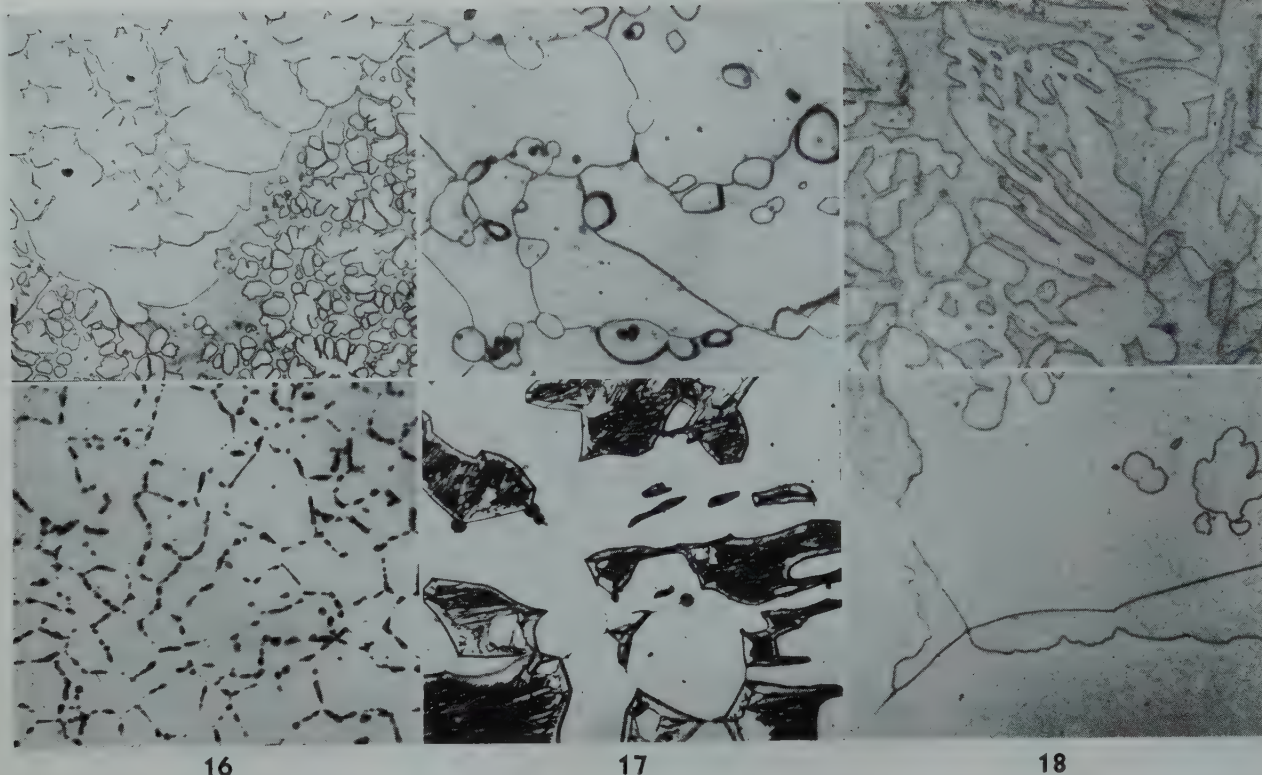


FIG 13—Beta and gamma phases in the 5.6 Mn 54.2 Zn alloy quenched from 1300°F.

× 250. ASTM copper etchant No. 11.

FIG 14—Alpha and beta structure of the 43.4 Mn 31.0 Zn alloy quenched from 1200°F.

× 250. ASTM zinc etchant No. 4.

FIG 15—Alpha and beta structure of the 37.5 Mn 22.0 Zn alloy quenched from 1200°F.

× 250. ASTM zinc etchant No. 4.

FIG 16—Alpha solid solution with alpha manganese in the 55.8 Mn 4.8 Zn alloy quenched from 1200°F.

× 250. ASTM zinc etchant No. 4.

FIG 17—Beta and epsilon structure of the 30.3 Mn 53.6 Zn alloy quenched from 1200°F.

× 250. ASTM zinc etchant No. 4.

FIG 18—Beta with a small amount of the gamma phase in the 1.75 Mn 50.8 Zn alloy quenched from 1100°F.

× 250. ASTM copper etchant No. 8 with 10 pct acetic acid added.

Fig 7 and 10 are characteristic alpha + beta structures obtained when there is little tendency for the beta phase to decompose. The formation of grain boundary and acicular alpha within the beta grain, Fig 8, occurs during the quench. Fig 9 illustrates an alpha + beta structure in which the beta phase is almost completely transformed during the cooling. In the micrograph of Fig 11, designated as an alpha + beta structure, it is quite probable that most of the alpha present was formed during the quench and that the beta/alpha + beta boundary could be lowered slightly at this point. However, evidence from the near-by compositions and the trends shown in pseudo-binary sections for higher and lower temperatures point to the position of the solubility line given.

The alpha + beta manganese structure is shown in Fig 12 for one of the alloys which falls within this field at 1300°F (704°C). The microstructure in Fig 13 is typical of the low manganese high zinc alloys in the beta + gamma

field and are similar to the structures of beta + gamma brasses.

The beta solid solution field is slightly reduced by the beta + gamma and beta + epsilon fields at 1200°F (648°C), Fig 5, and the alpha + beta boundary has shifted to higher zinc concentrations. The eutectoid decomposition of the beta phase in the manganese-zinc system requires the formation of the three phase field alpha + beta + epsilon and the alpha + epsilon field which have been tentatively positioned in the isothermal section for this temperature.

The contour of the alpha solubility line has a decided bulge at 60 pct manganese and 20 pct zinc but the field of complete miscibility remains with a narrow corridor between the manganese solubility curve and the alpha/alpha + beta line. Since the gamma manganese phase of the manganese-zinc system, which has been treated as the alpha solid solution phase of the ternary system up to this point, remains stable at this temperature and none of the beta

or alpha + beta alloys was found to contain manganese, it was assumed that these two boundaries have not joined at this temperature. It must be admitted, however, that only a limited number of alloys are positioned in this area. If a junction of the two lines did occur, it would necessarily be in the neighborhood of compositions containing less than 10 to 12 pct copper and alloys in the adjacent fields would contain precipitated manganese.

A new three phase field is introduced in the manganese rich corner of the diagram at 1200°F (648°C) based on the alpha to beta transition of manganese. Here again, the exact position of the alpha + alpha manganese + beta manganese field has been estimated, since all of the experimental compositions were found to contain only the alpha manganese phase. The beta manganese phase of the manganese-zinc system is stable at this temperature, therefore the three phase area must be placed at some intermediate position.

Microstructures representative of the

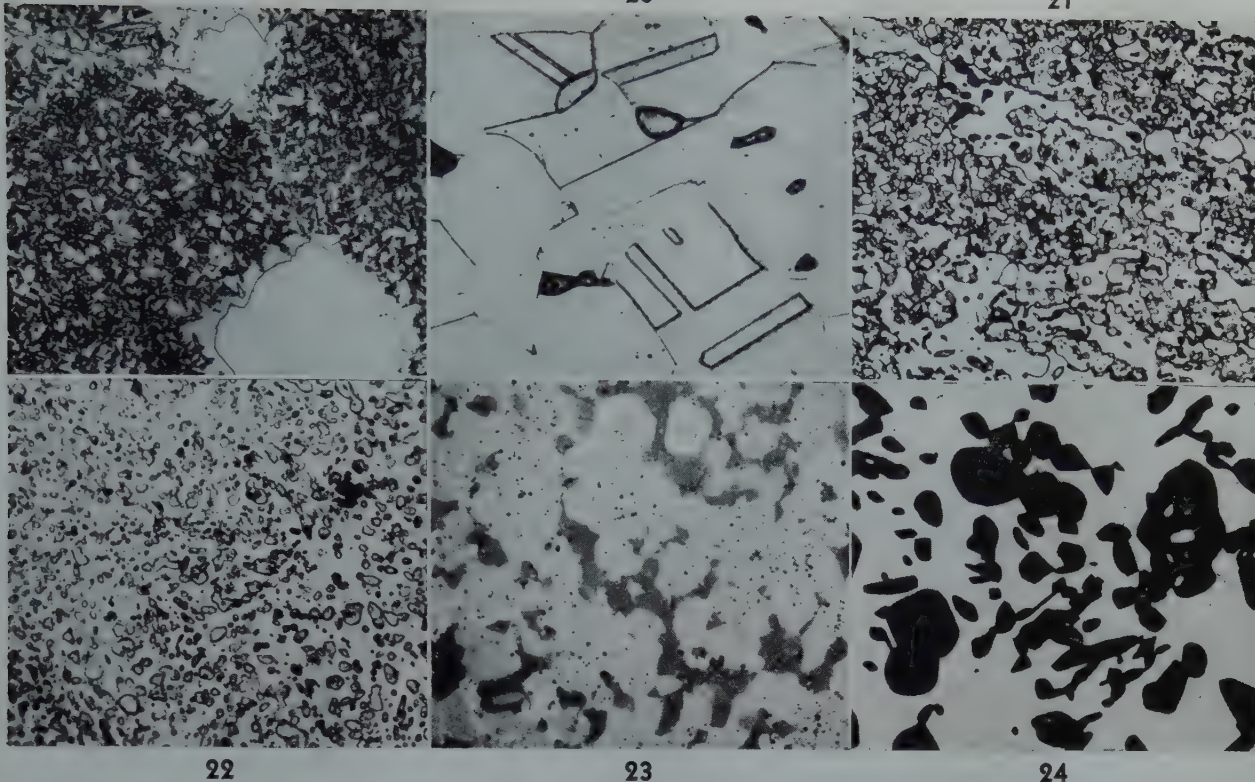


FIG 19—Transformed beta and gamma phases of the 10.2 Mn 49.6 Zn alloy quenched from 1100°F.
× 250. ASTM copper etchant No. 8 with 10 pct acetic acid added.

FIG 20—Alpha with traces of beta in the 19.7 Mn 22.2 Zn alloy quenched from 1100°F.
× 250. ASTM copper etchant No. 11.

FIG 21—Alpha + beta + alpha manganese structure in 54.5 Mn 19.2 Zn alloy quenched from 1100°F.
× 250. ASTM zinc etchant No. 4.

FIG 22—Beta solid solution with alpha manganese in the 53.2 Mn 21.2 Zn alloy quenched from 1100°F.
× 250. ASTM zinc etchant No. 4.

FIG 23—Beta (dark) + gamma of the manganese-zinc system (light) + alpha manganese (black) in the 48.4 Mn 26.4 Zn alloy quenched from 1100°F.
× 250. ASTM zinc etchant No. 4.

FIG 24—Beta (dark) and gamma of the manganese-zinc system (light) in the 47.2 Mn 29.3 Zn alloy quenched from 1100°F.
× 250. ASTM zinc etchant No. 4.

various phase fields at 1200°F (648°C) are shown in Fig 14 to 17, inclusive. Structures containing alpha and beta phases are shown in Fig 14 and 15. At this temperature, the high manganese beta phases are usually retained in the quench and do not transform or decompose. In Fig 14, the alpha phase is present in very minor amounts and the large grains of beta are restrained by the alpha. The alpha and beta structure in Fig 15 is representative of alloys which are more or less equidistant from the respective solubility limits. Fig 16 illustrates the alpha solid solution + alpha manganese alloys. Typical beta + epsilon structure is shown in Fig 17.

Sweeping changes occur in the copper-manganese-zinc ternary system as the temperature decreases to 1100°F (593°C). The construction given in Fig 6 is a complicated and radical departure from that of the isothermal section of Fig 5. The new fields are, however, dictated by positive metallographic and X ray evidence of the co-existence

of the indicated phases in these areas. The absence of beta manganese in all experimental alloys at 1100°F (593°C) and 1200°F (648°C) and the negligible solubility of copper in both alpha and beta manganese ties these fields to the manganese corner.

The zinc content of the alpha + beta field has shifted to still higher values as the temperature decreased from 1200 to 1100°F (648 to 593°C), but the respective solubility lines of this field remain essentially parallel from the copper-zinc binary to the limit of this field at approximately 36 pct manganese.

Intersection of the alpha + alpha manganese and the alpha + beta fields creates a four phase invariant plane which at 1100°F (593°C) produces the two phase field, beta + alpha manganese, and the two adjacent three phase fields, alpha + beta + alpha manganese and gamma + beta + alpha manganese. Principal evidence to support this construction is the complete absence of beta manganese in any

of the experimental alloys and the co-existence of only the beta and gamma phases without either alpha or beta manganese. The absence of beta manganese in the alloys indicates that the alpha manganese + beta manganese + alpha tentatively placed in Fig 5 must sweep toward the manganese-zinc binary before the alpha corridor is closed by the junction of the alpha + beta and alpha + alpha manganese fields. Were it otherwise, beta manganese and beta brass would be found to co-exist and this is not the case.

Representative microstructures for the two phase beta + gamma brasses are illustrated in Fig 18 and 19. Fig 18 shows the presence of a small amount of the gamma phase associated with retained beta. Transformed or decomposed beta and the gamma phase are present in Fig 19.

The microstructures observed for several of the ternary alloys containing less than 30 pct zinc annealed at 1100°F, (593°C) are reproduced in

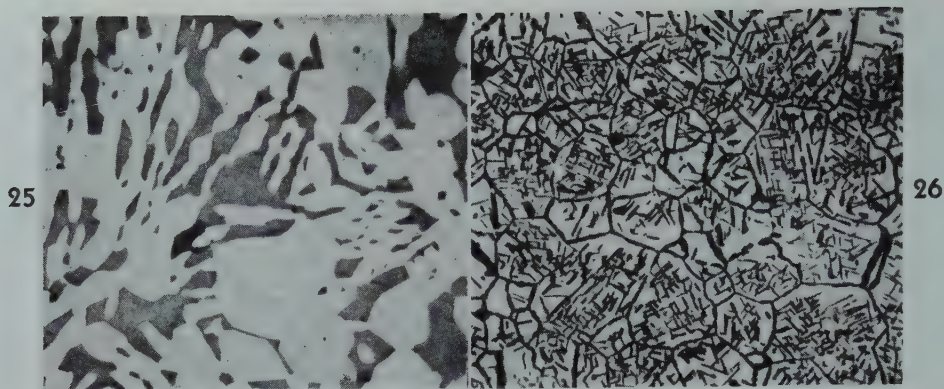


FIG 25—Beta (dark) and gamma of the manganese-zinc system (light) in the 52.6 Mn 26.3 Zn alloy quenched from 1100°F.

× 250. ASTM zinc etchant No. 4.

FIG 26—Alpha solid solution (light) and alpha manganese (dark) in the 55.4 Mn 13.0 Zn alloy quenched from 1100°F.

× 250. Unetched.

Fig 20 to 26. The copper rich alpha solid solution with traces of the beta phase is illustrated in Fig 20. The structure of Fig 21 is somewhat more complicated by the presence of alpha manganese along with the alpha and beta solid solution phases. With such structures relief polishing affords a rapid method for positive identification of the manganese constituent and subsequent etching reveals the beta and alpha phases, along with the manganese. Another characteristic of these alloys is the comparatively small grain size resulting from the presence of manganese which inhibits normal grain growth. The constituents in all specimens within this three phase area were also confirmed by X ray diffraction data. The precipitation of alpha manganese within the beta phase is shown in Fig 22. Only one specimen was found to fall within the narrow three phase field beta + gamma + alpha manganese. The microstructure of this alloy annealed at 1100°F (593°C) is given in Fig 23. Representative structures of alloys containing only the beta and gamma phases at 1100°F (593°C) are reproduced in Fig 24 and 25. These two micrographs clearly demonstrate the absence of a manganese phase. The presence of the gamma and beta constituents was confirmed by X ray diffraction. Fig 26 is characteristic of the alpha solid solution plus manganese

alloys. The formation of alpha manganese in the grain boundaries and certain crystallographic planes within the grains is quite characteristic of alloys in this area.

Acknowledgments

The authors express appreciation for the valuable assistance of the various members of the metallurgical staff of the Bureau of Mines. Particular acknowledgment is due to the group at the Salt Lake City Laboratory where the experimental work of this investigation was conducted. The X ray investigations necessary for the identification of the various phases encountered in the microstructures were conducted by E. Vernon Potter and R. W. Huber of the Physics Section.

The final manuscript was prepared at the Rolla Station Laboratory at Rolla, Missouri.

References

1. J. R. Long and T. R. Graham: Physical Properties of a 65 Cu, 10 Mn, 25 Zn Alloy. *Trans. AIME* (1944) 156, 222.
2. R. S. Dean, J. R. Long, T. R. Graham, and R. G. Feustel: Physical Properties of Cu-Mn-Zn Alloys Containing 60 Percent Cu and 5 to 25 Percent Mn. *Trans. AIME* (1946) 166, 185. *Metals Tech.* Jan. 1946, TP 1956.
3. R. S. Dean, J. R. Long, T. R. Graham, and C. W. Matthews:

A White High-Manganese Brass: *Trans. AIME* (1945) 161, 244.

4. R. S. Dean, J. R. Long, T. R. Graham, and A. H. Roberson: The Alpha Solid Solution Field of the Copper-Manganese-Zinc System. *Trans. AIME* (1945) 161, 232.
5. R. S. Dean, J. R. Long, and T. R. Graham: Copper-Manganese-Zinc Alloys—Physical Properties of Wrought Copper-Rich Alloys. *Trans. AIME* (1947) 171, 105-118. *Metals Tech.* April 1947, TP 2183.
6. O. W. Ellis: Copper and Copper Alloys. Publ. by Amer. Soc. for Metals (1948), 127.
7. O. Heusler: The Ternary System Copper-Zinc-Manganese. *Ztsch. Anorg. Chem.* (1926) 159, 37-54.
8. O. Bauer and M. Hansen: The Influence of a Third Metal on the Constitution of Brass Alloys. *Ztsch. Metallkunde* (1933) 25, 17.
9. L. Guillet: *Rev. Met.* (1905) 2, 105-111; (1906) 3, 258-262.
10. W. Heike and K. Ledebur: The Alpha Plus Gamma Eutectoid of the Brasses. *Ztsch. Metallkunde* (1924) 16, 380-381.
11. A. Phillips and R. M. Brick: Copper-Zinc Diagram. *Metals Handbook* A.S.M. 1948 Edition, 1206.
12. R. S. Dean, J. R. Long, T. R. Graham, and E. V. Potter: The Copper-Manganese Equilibrium System. *A.S.M.* (1945) 34, 443-464.
13. E. V. Potter and R. Huber: The Manganese-Zinc Diagram from 0 to 50 Percent Zinc. *A.S.M. Preprint No. 30* (Oct. 1948).
14. W. Hume-Rothery: The Effect of Manganese, Iron, and Nickel on the Alpha-Beta Brass Equilibrium. *Philosophical Mag.* (1948) Series 7, 39, 89-97.
15. A. J. Phillips: The Alpha-Beta Transformation in Brass. *Trans. AIME* (1930) 89, 194.

Discontinuous Crack Propagation—Further Studies*

L. D. JAFFE,† Junior Member AIME, E. L. REED,† and H. C. MANN†

The authors have recently published¹ evidence that brittle transgranular fracture of polycrystalline metals does *not* originate at a point and propagate continuously across the material, but rather develops at numerous related points, leading to a series of microcracks which subsequently link up. Series of related microcracks were observed in steel specimens broken in fatigue—specifically, at the central portions which broke during the final sudden fracture.

Microcracks of the type mentioned have also been reported by Baeyertz, Craig and Bumps² in steel broken under impact.‡ Some micrographs published by Irwin³ may possibly be interpreted as showing discontinuous brittle cracks. This paper presents additional observations of the authors on discontinuous crack propagation under various conditions.

Impact Test Specimens

The impact test specimens were cut longitudinally from a steel forging containing:

| C | Mn | Si | P | S | Ni | V | Mo |
|------|------|------|-------|-------|------|------|------|
| 0.24 | 0.50 | 0.15 | 0.034 | 0.027 | 1.52 | 0.03 | 0.33 |

The heat treatment consisted of oil quenching in a heavy section from 1600°F and tempering at 1260°F. The resulting yield strength was 78,000 psi, tensile strength 100,000 psi, elongation 20.0 pct in 2 in., and reduction of area 55.0 pct. Standard V-notch Charpy specimens were broken in a 217 ft-lb machine at a striking velocity of 16.8 fps. Energy absorption and fracture

‡ Since preparing this article the authors have learned that Tipper¹² observed such microcracks near the fracture of mild steel plates. As the work of Baeyertz, Craig and Bumps was carried on simultaneously and independently of that of the authors, and apparently also without knowledge of Tipper's paper,¹² the microcracks have been found independently by three separate groups.

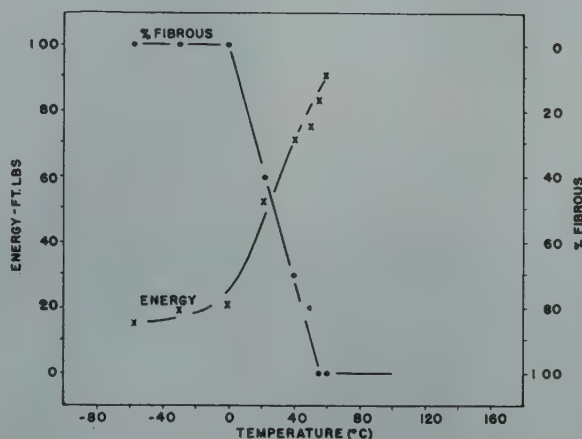


FIG 1—Impact transition curve. V-notch Charpy specimens.

appearance of this material in the V-notch Charpy test are plotted as functions of temperature in Fig 1. After test, fractured halves of specimens appearing 0, 40, 80, and 100 pct fibrous (to the unaided eye) were electroplated with nickel, sectioned longitudinally (perpendicular to the notch at its midpoint), polished and etched with Cohen-Hurlich-Jacobson (C-H-J) reagent (picric acid plus Zephiran chloride in ethyl ether)⁴ or with Vilella reagent (1 pct picric plus 5 pct hydrochloric acid in ethyl alcohol).⁵

Fig 2 and 3 show cracks near the path of final fracture in the specimen rated 0 pct fibrous. Many of the cracks terminate at the boundaries of ferrite grains, some at boundaries of pre-

existing austenite grains.* A crack often starts near the end of another. Cracks within the same ferrite grains are parallel or approximately parallel in several cases. A large percentage of the cracks are branched.†

Fig 4 illustrated a group of cracks in the 40 pct fibrous specimen. Branching and parallelism are well marked. No more than three directions of crack have been observed on the polished surface in one ferrite grain. This is consistent with the evidence⁶ that brittle fracture of ferrite takes place on the cube face crystallographic planes: the {100} planes. The appearance of some cracks suggests that they have passed around a projecting corner of a second ferrite grain by going outside the plane of polish.

In Fig 5 cracks in the 80 pct fibrous specimen may be observed. Some of

Cleveland Meeting, October 1949.
TP 2682 E. Discussion of this paper (2 copies) may be sent to *Transactions AIME* before December 1, 1949. Manuscript received May 2, 1949.

* Published by permission of the National Military Establishment.

† Watertown Arsenal Laboratory, Watertown, Mass.

‡ References are at the end of the paper.

* By "ferrite" is not meant primary ferrite, but the body-centered cubic phase, within which carbide particles may or may not be dispersed.

† One of the cracks in Fig 3 seems to contain some particles. After lightly repolishing, without re-etching, hardly any of the particles could be found, but at higher magnification the edges of the crack appeared rough. It is thought that the particles are fragments torn from the edges and lodged in the crack during polishing.

Service Fracture

A fracture was examined in a steel casting of this analysis:

| C | Mn | S | P | Si | Cr | Mo | Ni |
|------|------|-------|-------|------|------|------|------|
| 0.33 | 1.02 | 0.033 | 0.041 | 0.26 | 0.05 | 0.43 | 0.02 |

The casting had been normalized and

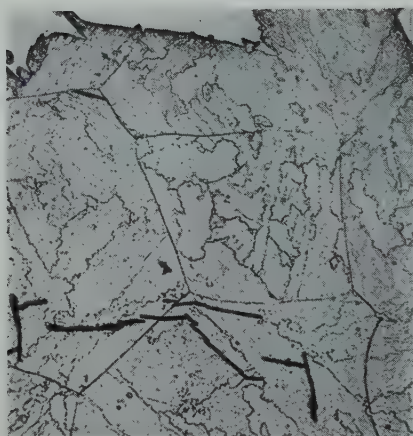


FIG 2—Microcracks near final fracture of Charpy bar rated 0 pct fibrous. Broken at -57°C , energy absorption 15 ft-lb.

$\times 500$. Etched 1 min. in C-H-J reagent, re-polished $\frac{1}{2}$ min., re-etched 10 sec. Reduced approx. one half in reproduction

the cracks have a step-like path. In the area shown the final fracture appears transgranular and brittle ("crystalline"), with little if any evidence of deformation visible. The austenite and ferrite grains are equiaxed. Fig 6 shows an area where the final fracture appeared transgranular but ductile (fibrous), with evidence of local deformation near the break. The austenite and ferrite grains are not equiaxed and it appears that the material flowed in tension perpendicularly to the eventual path of fracture. No microcracks are evident in Fig 6. None was found near fibrous portions of the final fracture in the 40 pct or 80 pct fibrous specimens, or in any portion of the 100 pct fibrous bar. All cracks observed were within 0.01 in. of a brittle transgranular portion of a final fracture.

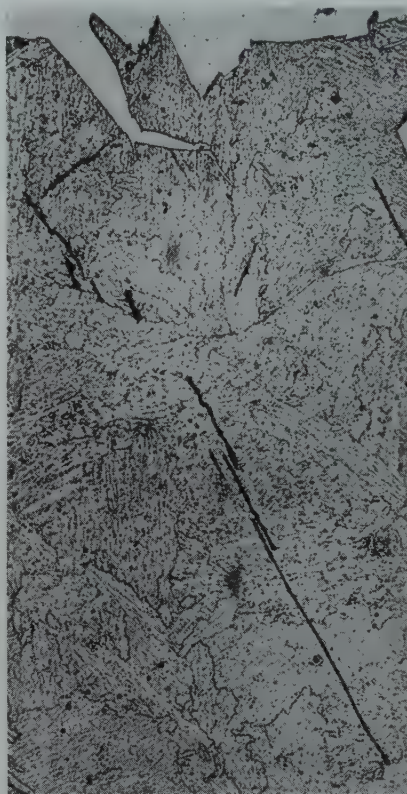


FIG 3—Microcracks very close to fracture in same Charpy bar as Fig 2.

$\times 500$. Etched 1 min. in C-H-J reagent, re-polished $\frac{1}{2}$ min., re-etched 10 sec. Reduced approx. one half in reproduction

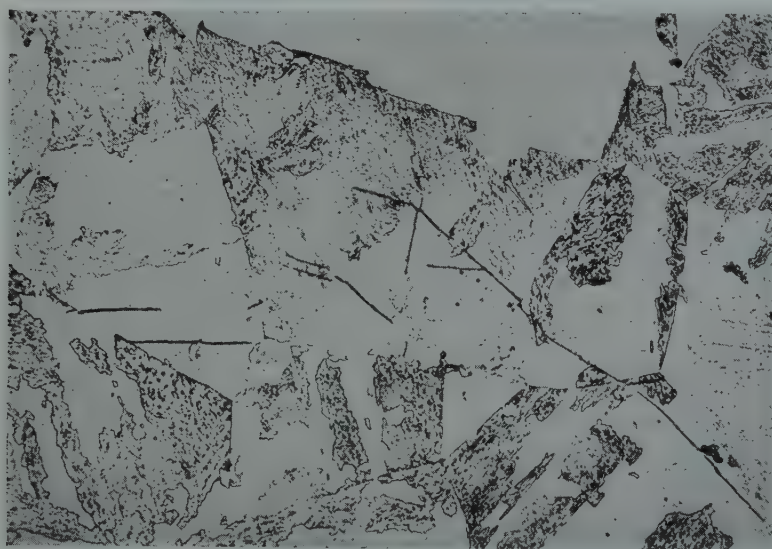


FIG 4—Group of microcracks in crystalline area near final fracture of Charpy bar rated 40 pct fibrous. Broken at $+21\frac{1}{2}^{\circ}\text{C}$, energy absorption 52 ft-lb.

$\times 500$. Etched in Vilella's reagent. Reduced approx. one half in reproduction

drawn, giving a yield strength (0.1 pct offset) of 55–58,000 psi, tensile strength of 92–95,000 psi, 12–17 pct elongation in 2 in., and 13–28 pct reduction of area, in room temperature test. Sudden fracture occurred through a machined notch under service conditions of rapid loading at a temperature of -70°F . The fracture appeared to be almost completely brittle. It was prepared for examination in the same fashion as the impact test specimens, but a 4 pct picral etch was used.

The crack in Fig 7 is "stepped" within a ferrite grain, the "treads" and "risers" appearing to lie along two sets of parallel planes. Neumann bands (deformation twins) may be seen in several ferrite grains. These twins are plainer in Fig 8. Cracks were distinguished from Neumann bands by re-polishing the specimen lightly and examining without re-etching; cracks remained visible, the twins did not. Crack segments seem to be approximately parallel to Neumann bands within the same ferrite grain; some crack segments coincide with possible extensions of the bands. This suggests that microcracks have been nucleated at the stress concentrations surrounding the ends of twins, though the converse possibility that stress concentrations at the end of stopped cracks nucleated the twins cannot definitely be ruled out. Neumann bands in iron form along $\{112\}$ crystallographic planes and not along the $\{100\}$ planes.⁷

Fig 9 is of interest because it shows that microcracks within the metal parallel the path of the final complete fracture, when both are in the same ferrite grain. There is some evidence of this in Fig 4 also.

Micrographs discussed above have been at $500\times$ magnification. Fig 10 shows at $1500\times$ some of the cracks previously noted in Fig 9. A crack that might be thought "stepped" at the lower magnification is here seen to be discontinuous, at least in the plane of polish.

Fatigue Specimens

Fatigue specimens were cut transversely from a forging of the following composition:

| C | Mn | P | S | Si | Cr | Mo | V |
|------|------|-------|-------|------|------|------|------|
| 0.28 | 0.74 | 0.014 | 0.013 | 0.20 | 1.00 | 0.49 | 0.12 |

Heat treatment consisted of annealing

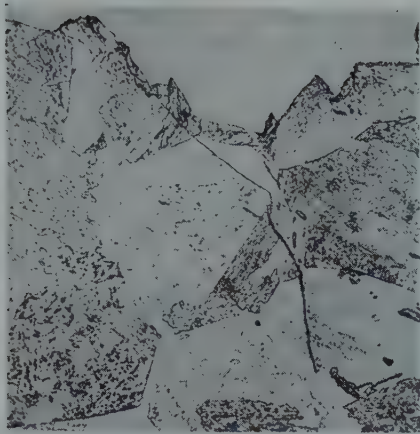


FIG 5—Some microcracks having a step-like path in crystalline area near final fracture of Charpy bar rated 80 pct fibrous. Broken at $+50^{\circ}\text{C}$, energy absorption 75 ft-lb.

$\times 500$. Etched in Vilella's reagent. Reduced approx. one half in reproduction.

from 1700°F , then holding 9 hr at 1675°F , water-quenching, holding 12 hr at 1150°F , and furnace-cooling. The material was heat-treated as a round approximately 8 in. in diam. The resulting yield strength (0.01 pct offset) was 105,000 psi, tensile strength 132,000 psi, elongation 15 pct, reduction of area 46 pct and V-notch Charpy impact energy 3-9 ft-lb at 70°F and 2 ft-lb at -40°F . The material was tested in rotating beam fatigue at 10,000 rpm as standard R. R. Moore specimens with 45° V-notch, having 0.015 in. radius at the base of the notch and a diameter across the notch of 0.220 in. All tests were at room temperature. The S-N curve is given as Fig 11.

Several specimens fractured at different stress levels were prepared for microexamination, as described for the impact bars. A micrograph of microcracks in a specimen broken under high stress has been published.¹ Fig 12 shows cracks in a specimen broken at the endurance limit: in 1,798,000 cycles at a nominal stress of 40,000 psi.* Microcracks were found in the fatigue specimens only near the path of final, complete, sudden fracture, where little or no evidence of deformation was observed, and never in the "battered" area where progressive fracture presumably took place over many cycles. No microcracks could be found below the notch in a specimen fatigued 40,880,000 cycles at 35,000 psi which did not fracture.

At the junction between the "battered" fracture and the final sudden

brittle fracture, there was always observed a projection that appeared to have been highly deformed in longitudinal tension. An example is shown in Fig 13. The significance of this projection, as well as of the microcracks, will be discussed in the next section.

Discussion of Results

Microcracks have to date been observed by the authors every time they have been looked for in areas adjacent to a brittle transgranular fracture. An explanation of the microcracks in terms of a theory of discontinuous crack propagation was given in Ref. 1. Briefly, it is suggested that a crack propagates along a crystallographic plane, in a brittle fashion, until it is stopped by a grain boundary or by a particle of a second phase. New cracks are likely to start in the zone of stress concentration at the end of the stopped crack. The

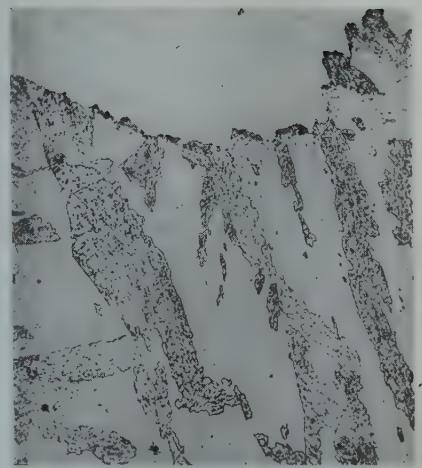
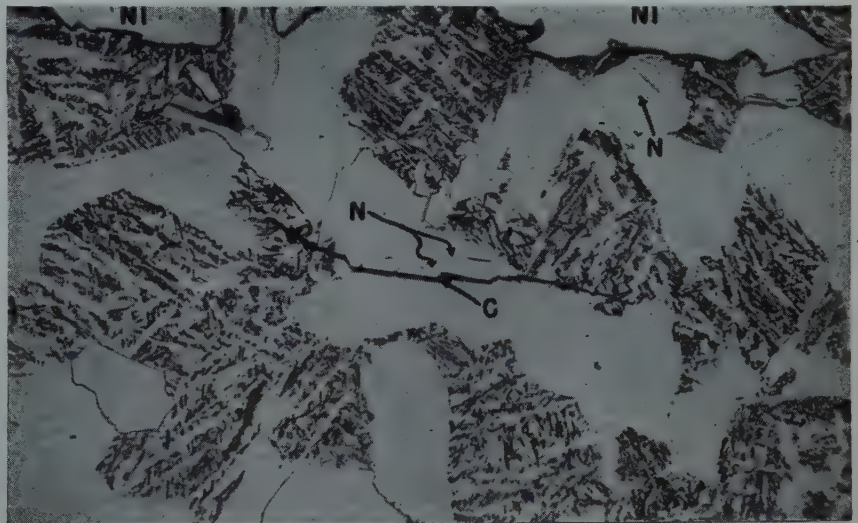


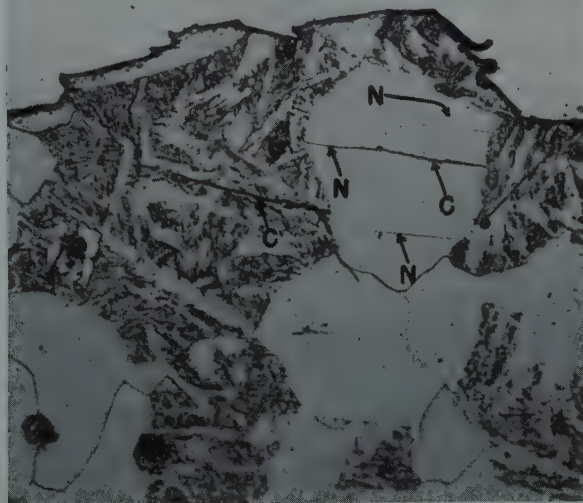
FIG 6—Local deformation in a fibrous area near final fracture of same Charpy bar as Fig 5.

$\times 500$. Etched in Vilella's reagent. Reduced approx. one half in reproduction

process then repeats, leading to discontinuous branching chains of microcracks. Cracks may also stop because



7



8

FIG 7 (above)—Step-like crack in ferrite grain near fracture of steel casting.

$\times 500$. Etched in Picral. N = Neumann bands. C = Crack. Ni = Nickel electroplate. Reduced approx. one third in reproduction

FIG 8 (below)—Neumann bands and microcracks near fracture of steel casting.

$\times 500$. Etched in Picral. N = Neumann bands. C = Cracks. Reduced approx. one third in reproduction.

* By nominal stress is meant maximum fiber stress calculated at the reduced section without considering stress concentration.

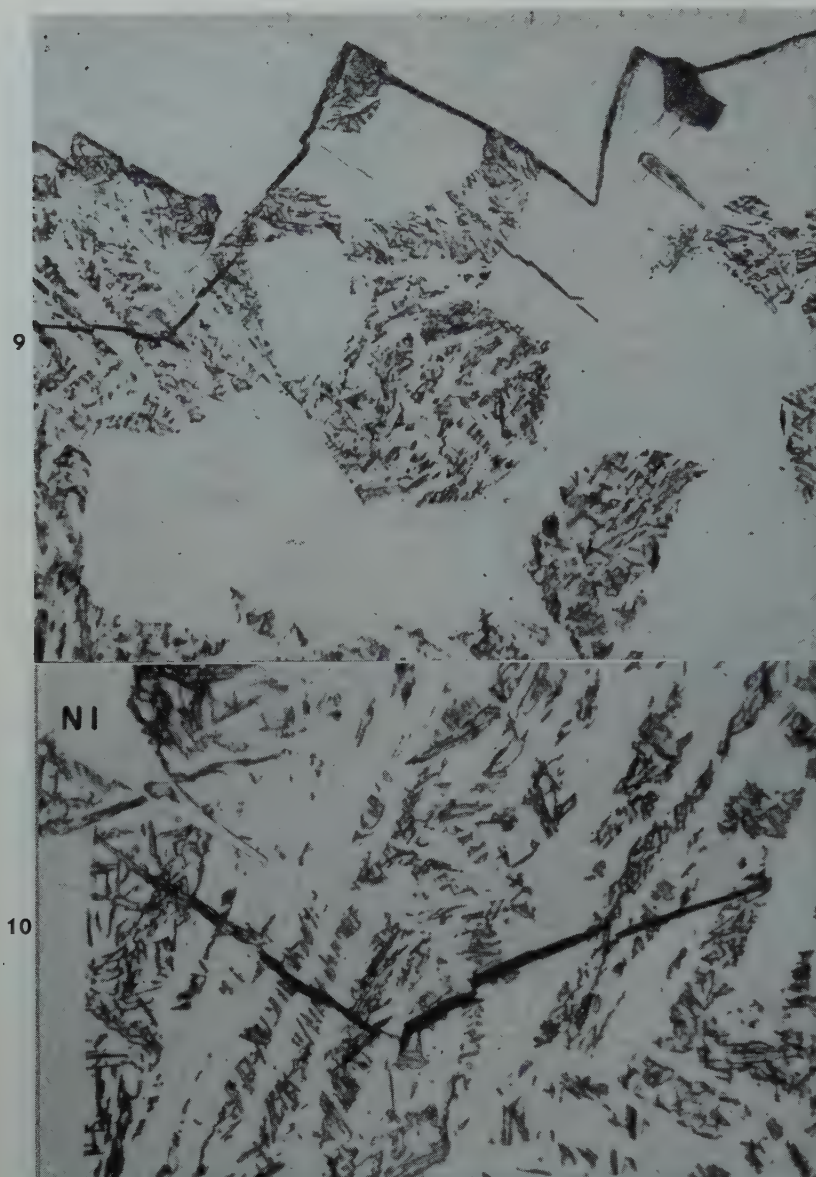


FIG 9—Microcracks near fracture of steel casting: 0.50 N.A.

× 500. Etched in Picral.

FIG 10—Same microcrack shown in Fig 9 at a higher magnification. View reversed left to right. 1.4 N.A.

× 1500. Etched in Picral. Ni = Nickel electroplate.

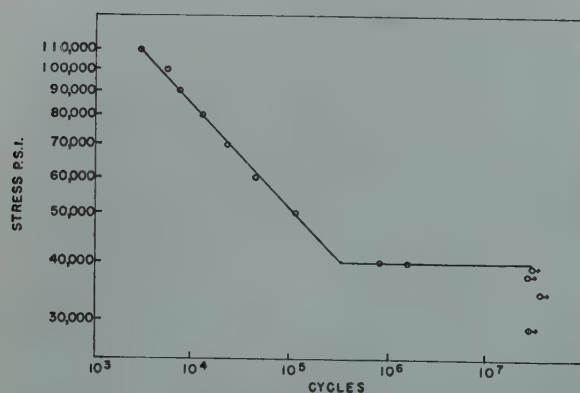


FIG 11—Fatigue test data. Notched R. R. Moore specimens.

the elastic energy released by their further spread would not be sufficient to propagate the crack (to form the new surfaces). In this last case, new

cracks would have to be at orientations which would provide greater energy release.

The probability of further cracking

near the ends of and within chains of microcracks will be much greater than elsewhere. The size of continuous crack will therefore tend to increase. This increase in size raises still further the probability of additional cracking in adjacent areas. When one continuous crack has traversed the specimen, macroscopic fracture has occurred. The brittle fractures which represent final severance of specimens or parts are series of linked microcracks.

Observation of microcracks in impact test specimens demonstrates that they are not associated with the repetitive loading which characterizes fatigue, and that series of microcracks can develop very rapidly (in the time of fracturing a brittle Charpy specimen, of the order of 10^{-5} sec).

The microcracks visible in the micrographs and discussed above are not identical with the Griffith defects,⁸ sometimes also termed "microcracks," which are supposed to exist in the material prior to stressing.

The projection observed at the junction of the battered and the brittle regions in the fatigue specimens suggests that the material represented by the projection was deforming in tension while brittle cracking was occurring nearer the axis. The final brittle fracture presumably originated (a major series of brittle microcracks first developed) either close to the axis or a small distance below the tip of the progressively advancing "fatigue crack." Fracture originating close to the axis is analogous to fracture occurring in a tensile specimen after necking.⁹ Fracture originating a small distance below the tip of the fatigue crack is analogous¹⁰ to fracture originating a small distance below the tip of a machined notch, and might be expected, because the stress there is triaxial tension, whereas at the crack or notch tip itself only biaxial stress can exist. (The stress system ahead of a fatigue crack cannot differ much from that under a sharp machined notch.¹¹) In either case final fracture does not occur by propagation inward, in a brittle fashion, of the progressive fatigue crack.

Summary

Series of apparently discontinuous microcracks have been found adjacent to the path of final brittle failure in fatigue specimens, impact specimens, and a failed part, made from steel forgings and castings. These cracks

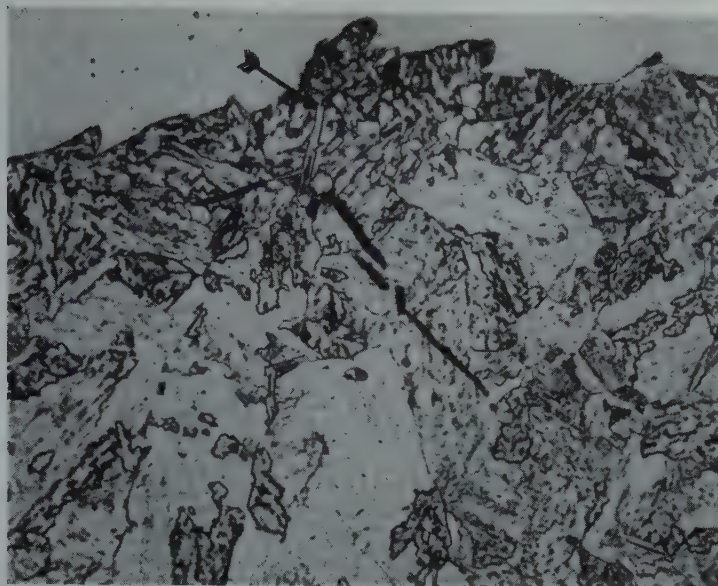


FIG 12—Microcracks near fracture of fatigue test specimen broken in 1,798,000 cycles at 40,000 psi.

White crack-like line indicated by arrow may be a crack which meets the surface outside the plane of polish and was partly filled with nickel electroplate. $\times 500$. Etched in Vilella's reagent.

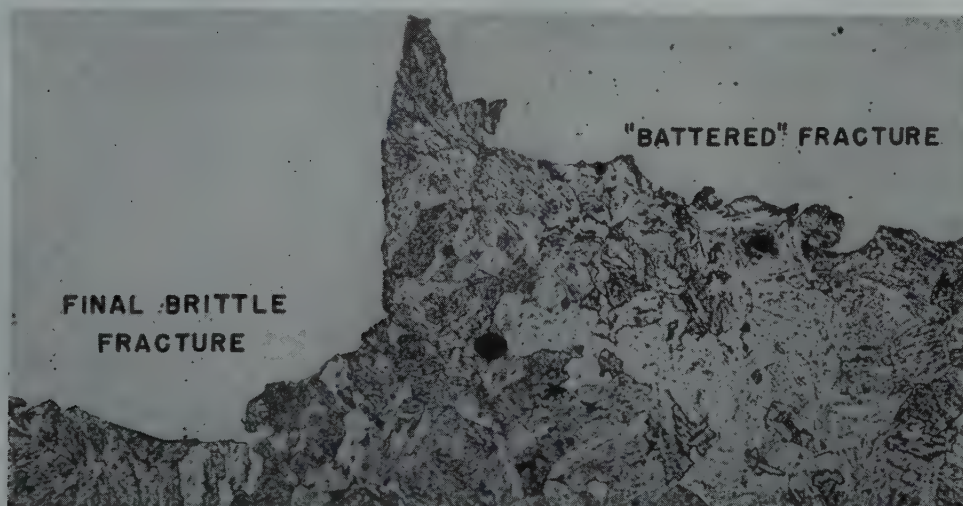


FIG 13—Projection at the junction of the "battered" (right) and final fracture (left).

Same fatigue specimen as shown in Fig 12. $\times 500$. Etched in Vilella's reagent. Reduced approx. two-sevenths in reproduction.

have been observed every time they have been sought in areas close to a brittle transgranular fracture.

It is believed that the microcracks indicate that brittle transgranular fracture of polycrystalline metals does *not* originate at one point and propagate continuously across the material, but rather nucleates at numerous related points, leading to a series of microcracks which subsequently link up.

Microscopic evidence has also been found which is interpreted to mean that final fracture in a fatigue specimen does not occur by propagation inward, in a brittle fashion, of the progressive "fatigue crack." Rather, brittle fracture originates closer to the neutral axis and links with the fatigue crack subsequently.

References

1. L. D. Jaffe, E. L. Reed, and H. C. Mann: Discontinuous Crack Propagation. *Trans. AIME* 185, 526; *Jnl. of Metals*, Aug. 1949. TN No. 16.
2. M. Baeyerly, W. Craig, and E. S. Bumps: A Metallographic Description of Fracture in Impact Specimens of a Structural Steel. *Trans. AIME*, 185, 481; *Jnl. of Met.*, Aug. 1949.
3. G. Irwin: Fracture Dynamics, *Trans. ASM* (1948) 40A, 147-166.
4. J. B. Cohen, A. Hurlich, and M. Jacobson: A Metallographic Etchant to Reveal Temper Brittleness in Steel. *Trans. ASM* (1947) 39, 109-138.
5. J. R. Vilella: Metallographic Technique for Steel. Amer. Soc. for Metals, Cleveland. (1938) 40-45.
6. F. Sauerwald, B. Schmidt, and G. Krämer: Über den Sprödigkeitsbereich von Eisen bei Teifen Temperaturen. *Ztsch. Phys.* (1931) 67, 179.
7. C. H. Mathewson and G. H. Edmunds: The Neumann Bands in Ferrite. *Trans. AIME* (1928) 80, 311-333.
8. A. A. Griffith: The Phenomena of Rupture and Flow in Solids. *Trans. Roy. Soc. (London)* (1920) A221, 163-198.
9. P. Ludwik: Bestimmung der Reißfestigkeit aus der gleichmässigen Dehnung. *Ztsch. Metallkunde* (1926) 18, 269-272.
10. E. Orowan. Private communication.
11. E. Orowan: Notch Brittleness and Ductile Fracture in Metals. *Trans. Inst. of Eng. and Shipbuilders in Scotland* (1946) 89, 165-204.
12. C. F. Tipper: Brittle Fracture in Mild-Steel Plates—II. *Engineering* (1948) 165, 594.

The Free Energy Change Accompanying the Martensite Transformation in Steels

J. C. FISHER*

Martensite transformations in steels and other alloys are characterized in part by the absence of composition changes during the growth of a new phase. Transformation occurs rapidly, and there is insufficient time for long range diffusion or partition of alloying elements to take place; martensite reactions in alloys thus are similar to phase transformations in single component systems.

A fundamental understanding of martensite transformations in steels is impossible without knowledge of the free energy change upon transforming austenite (face centered cubic iron containing alloying elements) to ferrite (body centered cubic iron containing alloying elements) of the same chemical composition. The present paper assembles the best information available concerning the influence of temperature and composition on this free energy change. Most of the material has been taken from the work of Johansson,¹ Mehl and Wells,² Zener^{3,4} and Smith;⁵ and indirectly, through these authors, from the work of Austin.⁶

In agreement with the generally accepted viewpoint, martensite is assumed to be an ordered solution of carbon in ferrite of the same composition as the parent austenite; only at high temperatures and low carbon concentrations is the carbon in ferrite distributed at random. The properties of the disordered solution are estimated by extrapolating the known properties of iron-carbon solid solutions into the range of supersaturation, and the free energy change associated with ordering is estimated from the theory developed by Zener. By incorporating Smith's recent thermodynamic measurements and Zener's theory of ordering, the present analysis modifies previous estimates of the free energy change associ-

ated with martensite transformations.

Consider a two component system consisting of a solvent *A* and a solute *B*. Let N_A and N_B represent mol fractions of *A* and *B* respectively, let $a_A = \gamma_A N_A$ and $a_B = \gamma_B N_B$ represent activities, and let superscripts 1 and 2 refer to phases 1 and 2. The partial molal free energies of *A* and *B* in phases 1 and 2 can be summarized as follows:

| | free energy | standard state |
|--------------------------------|------------------|----------------------------|
| $\bar{F}_A^1 - \bar{F}_{A0}^1$ | $= RT \ln a_A^1$ | pure <i>A</i> ¹ |
| $\bar{F}_A^2 - \bar{F}_{A0}^2$ | $= RT \ln a_A^2$ | pure <i>A</i> ² |
| $\bar{F}_B^1 - \bar{F}_{B0}^1$ | $= RT \ln a_B^1$ | pure <i>B</i> |
| $\bar{F}_B^2 - \bar{F}_{B0}^2$ | $= RT \ln a_B^2$ | pure <i>B</i> . |

The free energy of a gram atom of phase 1 is*

$$\Delta F^1 = N_A^1 \bar{F}_A^1 + N_B^1 \bar{F}_B^1$$

and that of phase 2 is

$$\Delta F^2 = N_A^2 \bar{F}_A^2 + N_B^2 \bar{F}_B^2.$$

A martensite transformation from phase 1 to phase 2 requires

$$N_A^1 = N_A^2 = N_A \text{ and } N_B^1 = N_B^2 = N_B,$$

and the free energy change per gram atom accompanying transformation is

$$\begin{aligned} \Delta F^{1 \rightarrow 2} &= N_A (\bar{F}_A^2 - \bar{F}_A^1) \\ &\quad + N_B (\bar{F}_B^2 - \bar{F}_B^1) \\ &= N_A [RT \ln (a_A^2/a_A^1) \\ &\quad + \Delta F_{A^{1 \rightarrow 2}}] + N_B RT \ln \\ &\quad (a_B^2/a_B^1) \end{aligned}$$

* A gram atom of solution contains N_A gram atoms of component *A*, N_B gram atoms of component *B*, N_C gram atoms of component *C*, and so on.

Cleveland Meeting, October 1949.
TP 2704 E. Discussion of this paper (2 copies) may be sent to *Transactions AIME* before December 1, 1949. Discussion is tentatively scheduled for publication in May 1950

Manuscript received May 2, 1949.
* General Electric Co., Schenectady, N. Y.

¹ References are at the end of the paper.

$$\begin{aligned} &= N_A [RT \ln (\gamma_A^2/\gamma_A^1) \\ &\quad + \Delta F_{A^{1 \rightarrow 2}}] + N_B RT \ln \\ &\quad (\gamma_B^2/\gamma_B^1), \quad [1] \end{aligned}$$

where γ_A^2 , γ_A^1 , γ_B^2 , γ_B^1 are activity coefficients, and where $\Delta F_{A^{1 \rightarrow 2}}$ is the free energy change upon transforming a gram atom of pure *A* from phase 1 to phase 2 at the temperature in question.

For martensite transformations in plain carbon steels, *A* = iron (Fe), *B* = carbon (C), 1 = austenite (γ), 2 = ferrite (α), and Eq 1 is

$$\begin{aligned} \Delta F^{\gamma \rightarrow \alpha} &= N_{Fe} [RT \ln (\gamma_{Fe}^\alpha/\gamma_{Fe}^\gamma) \\ &\quad + \Delta F_{Fe}^{\gamma \rightarrow \alpha}] + N_C RT \ln (\gamma_C^\alpha/\gamma_C^\gamma). \quad [2] \end{aligned}$$

Nothing is known concerning the values of γ_{Fe}^α and γ_C^α for carbon concentrations in excess of 0.025 pct. However, the approximation

$$\gamma_{Fe}^\gamma = \gamma_{Fe}^\alpha = 1$$

cannot be appreciably in error for small carbon concentrations, and Eq 2 reduces to

$$\begin{aligned} \Delta F^{\gamma \rightarrow \alpha} &= N_{Fe} \Delta F_{Fe}^{\gamma \rightarrow \alpha} \\ &\quad + N_C RT \ln (\gamma_C^\alpha/\gamma_C^\gamma). \quad [3] \end{aligned}$$

Johansson¹ and Zener³ have calculated $\Delta F_{Fe}^{\gamma \rightarrow \alpha}$ from the specific heat measurements compiled by Austin.^{6*} Their calculated values agree closely, and are summarized in Table 1.

The activity coefficients relative to graphite for carbon dissolved in iron vary with temperature according to the relationships

$$\begin{aligned} d \ln \gamma_C^\gamma / d(1/T) &= \Delta H_C^\gamma / R \\ d \ln \gamma_C^\alpha / d(1/T) &= \Delta H_C^\alpha / R \end{aligned}$$

where ΔH_C^γ and ΔH_C^α are the heats of solution of graphite in γ and α iron. Assuming the values of ΔH to be independent of carbon concentration and temperature,

$$\begin{aligned} \ln \gamma_C^\gamma &= \Delta H_C^\gamma / RT + I_1 \\ \ln \gamma_C^\alpha &= \Delta H_C^\alpha / RT + I_2 \end{aligned}$$

* Johansson employed also specific heat measurements from several other sources.

**Table 1 . . . The Free Energy Difference (calories per gram atom)
Between γ -iron and α -iron**

| Johansson ¹ | | Zener ³ | | Johansson ¹ | | Zener ³ | |
|------------------------|--|--------------------|--|------------------------|--|--------------------|--|
| °K | $-\Delta F_{Fe}^{\gamma \rightarrow \alpha}$ | °K | $-\Delta F_{Fe}^{\gamma \rightarrow \alpha}$ | °K | $-\Delta F_{Fe}^{\gamma \rightarrow \alpha}$ | °K | $-\Delta F_{Fe}^{\gamma \rightarrow \alpha}$ |
| 300 | 997 | 273 | 1045 | 1050 | 46 | 1423 | -22 |
| 350 | 938 | 373 | 924 | 1100 | 25 | 1473 | -21 |
| 400 | 873 | 473 | 784 | 1150 | +10 | 1523 | -18 |
| 450 | 805 | 573 | 622 | 1179 | 0 | 1573 | -14 |
| 500 | 735 | 673 | 487 | 1200 | -4 | 1623 | -7.5 |
| 550 | 664 | 773 | 342 | 1250 | -8 | 1673 | 0 |
| 600 | 595 | 873 | 209 | 1300 | -15 | 1773 | +32 |
| 650 | 523 | 923 | 147 | 1350 | -18 | | |
| 700 | 450 | 973 | 98 | 1400 | -18 | | |
| 750 | 379 | 1023 | 54 | 1450 | -17 | | |
| 800 | 310 | 1073 | 29 | 1500 | -16 | | |
| 850 | 247 | 1123 | +14 | 1550 | -13 | | |
| 900 | 184 | 1183 | 0 | 1600 | -8 | | |
| 950 | 121 | 1223 | -7 | 1650 | -2 | | |
| 975 | 98 | 1273 | -14 | 1674 | 0 | | |
| 1000 | 73 | 1323 | -18.5 | 1700 | +1 | | |
| 1033 | 54 | 1373 | -21 | 1750 | +6 | | |

Mean Interpolated Values

| °K | $-\Delta F_{Fe}^{\gamma \rightarrow \alpha}$ | °K | $-\Delta F_{Fe}^{\gamma \rightarrow \alpha}$ | °K | $-\Delta F_{Fe}^{\gamma \rightarrow \alpha}$ | °K | $-\Delta F_{Fe}^{\gamma \rightarrow \alpha}$ |
|-----|--|-----|--|------|--|------|--|
| 200 | 1109 | 500 | 738 | 800 | 308 | 1100 | 22 |
| 210 | 1100 | 510 | 723 | 810 | 295 | 1120 | 16 |
| 220 | 1091 | 520 | 708 | 820 | 282 | 1140 | 11 |
| 230 | 1082 | 530 | 693 | 830 | 269 | 1160 | +5 |
| 240 | 1072 | 540 | 678 | 840 | 256 | 1180 | 0 |
| 250 | 1062 | 550 | 663 | 850 | 243 | 1200 | -4 |
| 260 | 1051 | 560 | 648 | 860 | 230 | 1220 | -7 |
| 270 | 1040 | 570 | 634 | 870 | 218 | 1240 | -10 |
| 280 | 1029 | 580 | 620 | 880 | 205 | 1260 | -12 |
| 290 | 1018 | 590 | 605 | 890 | 192 | 1280 | -14 |
| 300 | 1007 | 600 | 591 | 900 | 180 | 1300 | -16 |
| 310 | 995 | 610 | 577 | 910 | 168 | 1320 | -17 |
| 320 | 983 | 620 | 563 | 920 | 156 | 1340 | -18 |
| 330 | 971 | 630 | 549 | 930 | 144 | 1360 | -19 |
| 340 | 959 | 640 | 535 | 940 | 132 | 1380 | -20 |
| 350 | 946 | 650 | 521 | 950 | 121 | 1400 | -20 |
| 360 | 933 | 660 | 507 | 960 | 111 | 1420 | -20 |
| 370 | 920 | 670 | 492 | 970 | 102 | 1440 | -20 |
| 380 | 907 | 680 | 478 | 980 | 93 | 1460 | -19 |
| 390 | 893 | 690 | 463 | 990 | 84 | 1480 | -18 |
| 400 | 880 | 700 | 449 | 1000 | 75 | 1500 | -18 |
| 410 | 866 | 710 | 435 | 1010 | 67 | 1520 | -17 |
| 420 | 853 | 720 | 420 | 1020 | 60 | 1540 | -15 |
| 430 | 839 | 730 | 405 | 1030 | 54 | 1560 | -13 |
| 440 | 825 | 740 | 391 | 1040 | 48 | 1580 | -11 |
| 450 | 811 | 750 | 377 | 1050 | 42 | 1600 | -9 |
| 460 | 797 | 760 | 363 | 1060 | 37 | 1620 | -6 |
| 470 | 782 | 770 | 349 | 1070 | 32 | 1640 | -3 |
| 480 | 767 | 780 | 335 | 1080 | 29 | 1660 | -1 |
| 490 | 753 | 790 | 321 | 1090 | 26 | 1680 | +1 |
| 500 | 738 | 800 | 308 | 1100 | 22 | 1700 | +4 |

Table 2 . . . Temperature Dependence of Zener's Order Parameter

| T/T_C | z | T/T_C | z | T/T_C | z | T/T_C | z |
|---------|-------|---------|-------|---------|-------|---------|-------|
| 1.000 | 0.377 | 0.99 | 0.502 | 0.90 | 0.742 | 0.70 | 0.924 |
| 0.999 | 0.418 | 0.98 | 0.551 | 0.88 | 0.770 | 0.65 | 0.947 |
| 0.998 | 0.434 | 0.97 | 0.588 | 0.86 | 0.795 | 0.60 | 0.964 |
| 0.997 | 0.446 | 0.96 | 0.619 | 0.84 | 0.818 | 0.55 | 0.978 |
| 0.996 | 0.457 | 0.95 | 0.645 | 0.82 | 0.838 | 0.50 | 0.987 |
| 0.995 | 0.466 | 0.94 | 0.668 | 0.80 | 0.856 | 0.45 | 0.993 |
| 0.994 | 0.474 | 0.93 | 0.689 | 0.78 | 0.873 | 0.40 | 0.997 |
| 0.993 | 0.482 | 0.92 | 0.708 | 0.76 | 0.888 | 0.35 | 0.999 |
| 0.992 | 0.489 | 0.91 | 0.726 | 0.74 | 0.901 | 0.30 | 1.000 |
| 0.991 | 0.496 | 0.90 | 0.742 | 0.72 | 0.913 | 0.25 | 1.000 |
| 0.990 | 0.502 | | | 0.70 | 0.924 | | |

Let $\phi = 2(1-z) \ln(1-z) + (1+2z) \ln(1+2z)$.

| T/T_C | ϕ | T/T_C | ϕ | T/T_C | ϕ | T/T_C | ϕ |
|---------|--------|---------|--------|---------|--------|---------|--------|
| 1.000 | 0.396 | 0.99 | 0.698 | 0.90 | 1.559 | 0.70 | 2.590 |
| 0.999 | 0.484 | 0.98 | 0.843 | 0.88 | 1.693 | 0.65 | 2.764 |
| 0.998 | 0.523 | 0.97 | 0.962 | 0.86 | 1.819 | 0.60 | 2.911 |
| 0.997 | 0.553 | 0.96 | 1.067 | 0.84 | 1.936 | 0.55 | 3.032 |
| 0.996 | 0.579 | 0.95 | 1.162 | 0.82 | 2.046 | 0.50 | 3.126 |
| 0.995 | 0.603 | 0.94 | 1.251 | 0.80 | 2.150 | 0.45 | 3.197 |
| 0.994 | 0.624 | 0.93 | 1.333 | 0.78 | 2.249 | 0.40 | 3.246 |
| 0.993 | 0.644 | 0.92 | 1.412 | 0.76 | 2.342 | 0.35 | 3.275 |
| 0.992 | 0.663 | 0.91 | 1.488 | 0.74 | 2.429 | 0.30 | 3.289 |
| 0.991 | 0.681 | 0.90 | 1.559 | 0.72 | 2.512 | 0.25 | 3.295 |
| 0.990 | 0.698 | | | 0.70 | 2.590 | 0.20 | 3.296 |

where I_1 and I_2 are integration constants. The value of $RT \ln(\gamma_C^\alpha/\gamma_C^\gamma)$ reduces to

$$RT \ln(\gamma_C^\alpha/\gamma_C^\gamma) = \Delta H_C^\alpha - \Delta H_C^\gamma + RT \Delta I. \quad [4]$$

Smith⁵ has determined quite accurately the value $\Delta H_C^\gamma = 10,000$ cal per g atom. ΔH_C^α is less accurately known, Smith having obtained a value 20,000 cal per g atom from his own experimental data, and a value 26,000 cal per g atom by making use of earlier data concerning δ -iron. The value $\Delta H_C^\alpha = 20,000$ appears to be the more reliable, particularly for use at low temperatures. Moreover, according to a recent theory of austenite decomposition,¹⁰ $\Delta H_C^\alpha = 20,500$ cal per g atom gives the best agreement between calculated M_s temperatures and those determined by Lyman and Troiano⁷ for a series of 3 pct chromium steels of varying carbon content. Therefore the value $\Delta H_C^\alpha = 20,500$ cal per g atom is assumed, and

$$RT \ln(\gamma_C^\alpha/\gamma_C^\gamma) = 10,500 + RT \Delta I. \quad [5]$$

Consider the distribution of carbon at equilibrium in the two phase $\gamma + \alpha$ region. Then

$$\Delta \bar{F}_C^\gamma = \Delta \bar{F}_C^\alpha, \\ RT \ln \gamma_C^\gamma N_C^\gamma = RT \ln \gamma_C^\alpha N_C^\alpha$$

and

$$\gamma_C^\alpha/\gamma_C^\gamma = N_C^\gamma/N_C^\alpha.$$

From the equilibrium boundaries of the iron-carbon phase diagram as determined by Mehl and Wells² and by Smith⁵ the ratio N_C^γ/N_C^α is

$$N_C^\gamma/N_C^\alpha = 0.315/0.0128 = 24.6$$

at 800°C where the carbon concentrations are relatively low and both γ_C^γ and γ_C^α are practically independent of carbon concentration.⁵ Therefore, at 800°C,

$$RT \ln(\gamma_C^\alpha/\gamma_C^\gamma) = 6825. \quad [6]$$

It is assumed that γ_C^α and γ_C^γ vary similarly with carbon concentration, so that the ratio $\gamma_C^\alpha/\gamma_C^\gamma$ is independent of N_C .

According to Eq 4, 5, 6 the value of $N_C RT \ln(\gamma_C^\alpha/\gamma_C^\gamma)$ is

$$N_C RT \ln(\gamma_C^\alpha/\gamma_C^\gamma) = N_C(10,500 - 3.425 T) \quad [7]$$

decreasing linearly from 10,500 N_C at absolute zero to 6825 N_C at 800°C. However, Eq 7 was obtained by an extrapolation that effectively assumes the solution of carbon in ferrite to remain random at low temperatures. Zener⁴ has shown that spontaneous

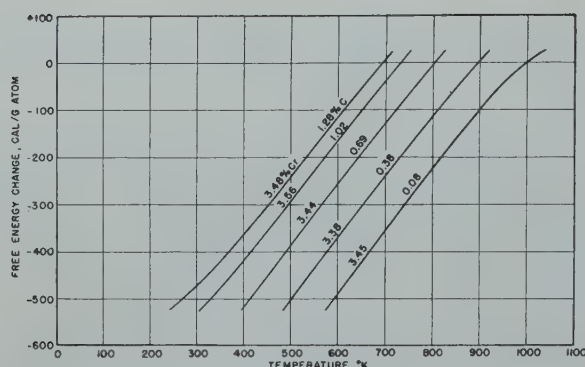


FIG 1—Variation of $\Delta F^{\gamma \rightarrow \alpha}$ with temperature for several 3.5 pct chromium steels of differing carbon content, according to Eq 12.

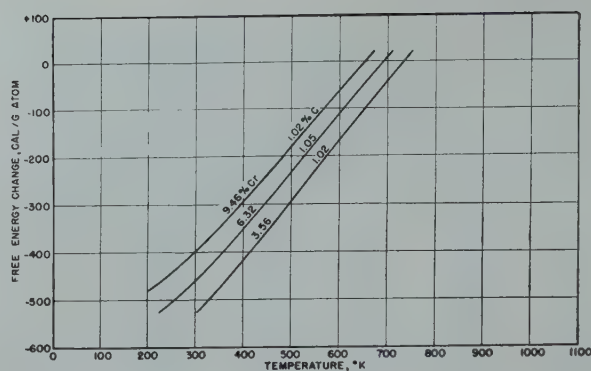


FIG 2—Variation of $\Delta F^{\gamma \rightarrow \alpha}$ with temperature for several 1.0 pct carbon steels of differing chromium content, according to Eq 12.

ordering of the carbon in ferrite takes place below the temperature

$$T_C \cong 28,000 N_C \text{ (approximately)}$$

with a decrease in free energy that is not reflected in an extrapolation based upon high temperature properties; this free energy change must be added to the value of $N_C RT \ln (\gamma_C^\alpha / \gamma_C^\gamma)$ that is given by Eq 7.

The decrease in free energy per unit volume on ordering can be derived from Zener's analysis, and is given by the expression

$$\Delta f_* = -\frac{1}{2} \left(\frac{2}{3} n_1 \lambda z \right)^2 E + \frac{1}{3} n_1 k T [2(1-z) \ln(1-z) + (1+2z) \ln(1+2z)] \quad [8]$$

ergs per cc where

$$n_1 = 6.03 (10)^{23} N_C / N_S V_0 \text{ carbon atoms per cc}$$

N_S = sum of mol fractions of all substitutional elements

V_0 = volume corresponding to a mol of lattice sites

$$\lambda = 1.68 (10)^{-24} V_0 \text{ strain per carbon atom}$$

z = Zener's order parameter

$$E = 1.30 (10)^{12} \text{ dynes per cm}^2.$$

The value of the order parameter z depends only upon the temperature ratio T/T_C , as given in Table 2, where T_C is determined by the relationship

$$T_C = 3900 V_0 N_C / N_S. \quad [9]$$

When N_C is small, $N_S \cong 1$ and $V_0 \cong 7.2$, leading to the approximate relationship $T_C \cong 28,000 N_C$. Changing to the appropriate units, the free energy change on ordering is

$$\Delta F_* = 2.39 (10)^{-8} N_S V_0 \Delta f_* \quad [10]$$

calories per gram atom.*

*Zener's numerical values have been revised, following a more accurate calculation of the value of z at the critical temperature T_C (0.3772

Combining Eq 3 and 7, and adding ΔF_* to the right hand member of Eq 7, the free energy change on transforming austenite to ferrite of the same carbon content is

$$\Delta F^{\gamma \rightarrow \alpha} = N_{Fe} \Delta F_{Fe}^{\gamma \rightarrow \alpha} + N_C (10,500 - 3.425 T) + \Delta F_* \quad [11]$$

cal per g atom for plain carbon steels.

Addition of an alloying element alters the value of $\Delta F^{\gamma \rightarrow \alpha}$ given in Eq 11 by the amount

$$N_i RT \ln (\gamma_i^\alpha / \gamma_i^\gamma)$$

where the subscript i refers to a particular alloying element. Almost nothing is known concerning the ratio $\gamma_i^\alpha / \gamma_i^\gamma$ for alloying elements other than carbon; in the absence of adequate information, perhaps the simplest assumption that can be made is that $RT \ln (\gamma_i^\alpha / \gamma_i^\gamma)$ is constant:

$$RT \ln (\gamma_i^\alpha / \gamma_i^\gamma) = K_i.$$

With this assumption, Eq 11 becomes

$$\Delta F^{\gamma \rightarrow \alpha} = N_{Fe} \Delta F_{Fe}^{\gamma \rightarrow \alpha} + N_C (10,500 - 3.425 T) + \Delta F_* + \sum N_i RT \ln (\gamma_i^\alpha / \gamma_i^\gamma)$$

vs. 0.33 as given by him), and assuming a martensite tetragonality ratio $r = 1.053$ for a completely ordered steel containing 1.28 pct carbon, as determined by Lyman and Troiano.⁷ $r = 1.053$ falls between the values $r = 1.059$ and $r = 1.051$ determined by Honda and Nishiyama⁸ and by Kurdjumov and Kaminsky⁹ respectively. The strain corresponding to a tetragonality ratio r was assumed to be $e = (r - 1) / (1 + \nu)$ where $\nu = 0.3$ is Poisson's ratio. Assuming further that the density of iron is not altered by the addition of carbon, the volume of a gram atom of alloy is $V = N_3 V_0$ cc, and the number of carbon atoms per cc is $n_1 = 6.03 (10)^{23} N_C / N_3 V_0$.

Although it was not so stated in his analysis, there must be, according to Zener's theory, a temperature region near the "critical temperature" T_C where ordered and disordered phases of differing carbon content coexist at equilibrium. Failure to consider the two phase region leads to errors in the value of Δf_* . However, the errors are small, and they are not considered further.

$$\cong N_{Fe} \Delta F_{Fe}^{\gamma \rightarrow \alpha} + N_C (10,500 - 3.425 T) + \Delta F_* + \sum N_i K_i \quad [12]$$

cal per g atom for the martensite transformation in alloy steels. The summation includes all alloying elements other than carbon.

Eq 12 is an estimate of the free energy change upon transforming austenite to martensite, obtained by extrapolating the properties of disordered iron-carbon solutions into the supersaturated range, and employing the theory of ordering developed by Zener. $\Delta F^{\gamma \rightarrow \alpha}$ values calculated from Eq 12 are used by Fisher, Hollomon, and Turnbull¹⁰ in their analysis of austenite \rightarrow martensite transformation kinetics. They suggest a value $K_{Cr} = 1200$ cal per g atom for chromium, leading to variation of $\Delta F^{\gamma \rightarrow \alpha}$ with temperature as shown in Fig 1 and 2 for a number of chromium steels.

References

1. C. H. Johansson: *Archiv f. d. Eisenhüttenwesen* (1937-38) **11**, 241.
2. R. F. Mehl and C. Wells: *Trans. AIME* (1937) **125**, 429.
3. C. Zener: *Trans. AIME* (1946) **167**, 513. *Metals Tech.* Jan. 1946. TP 1856.
4. C. Zener: *Trans. AIME* (1946) **167**, 550. *Metals Tech.* Jan. 1946. TP 1925.
5. R. P. Smith: *Jnl. Am. Chem. Soc.* (1946) **68**, 1163.
6. J. B. Austin: *Jnl. Ind. Eng. Chem.* (1932) **24**, 1225.
7. T. Lyman and A. R. Troiano: *Trans. Am. Soc. Met.* (1946) **37**, 402.
8. K. Honda and Z. Nishiyama: *Sci. Repts. Sendai* (1932) **21**, 299.
9. G. Kurdjumov and E. Kaminsky: *Ztsch. Phys.* (1929) **53**, 696.
10. J. C. Fisher, J. H. Hollomon, and D. Turnbull: *Kinetics of the Austenite-Martensite Transformation. Trans. AIME* (1949) **185**, 691. *Jnl. of Metals*, Oct. 1949.

Kinetics of the Austenite → Martensite Transformation

J. C. FISHER,* J. H. HOLLOMON,* Junior Member AIME, and D. TURNBULL*

Application of the concepts of nucleation and growth to the analysis of experimental transformation data has led to valuable descriptions of phase transformations, an outstanding example being the transformation austenite → pearlite which has been examined with particular care by Mehl and co-workers.¹⁻⁵ In addition to the pearlite transformation, the proeutectoid ferrite and proeutectoid carbide transformations are known to proceed by nucleation and growth. Martensite, on the contrary, until recently was thought to form by a mechanism involving neither nucleation nor growth; however, extension of standard nucleation theory⁶ suggests that martensite, bainite, and the other products of austenite decomposition all grow from nuclei in the parent phase. The theory that martensite forms by nucleation and growth is strongly supported by recent experimental work of Kurdjumov and Maksimova.⁷

The concepts of nucleation and growth have been fruitful also in providing a sound basis for quantitative theoretical treatments of the kinetics of phase transformations. For example, Volmer and Weber⁸ and Becker and Döring⁹ developed the theory of nucleation from fundamental considerations to a point where excellent agreement was obtained with the results of experiments on the condensation of supercooled vapors. As a result of their analysis, the kinetics of vapor-liquid transformations now can be predicted. It seems probable that application of the theories of nucleation and growth to a quantitative study of austenite decomposition similarly will clarify the nature of the individual transformations involved, and will enable the calculation of austenite transformation kinetics.

In the present paper, the theories of nucleation and growth are applied to the austenite → martensite transformation in steels. The analysis begins with a discussion of nucleation in single component systems. Martensite appears to be coherent with the parent austenite, hence the nucleation theory is modified to include the effects of elastic distortion. Nucleation in the two component iron-carbon system then is discussed, for most steels are primarily alloys of these two elements. Finally, M_s temperatures and martensite transformation curves are calculated for each of several alloy steels of varying carbon and chromium content, and are compared with those determined experimentally by Lyman and Troiano¹⁰ and Harris and Cohen.¹¹

Nucleation Theory

NUCLEATION IN SINGLE COMPONENT SYSTEMS^{6,12-14}

The work required for reversible formation of a region of phase β within the parent α phase is expressed conveniently as the sum of two terms: $W_1 = A\sigma$, the product of the area of the interface and the interfacial free energy, and $W_2 = V\Delta f$, the product of the volume of the region and the free energy increase per unit volume associated with the transformation. The total work is therefore $W = A\sigma + V\Delta f$.

When α is more stable than β , Δf is positive and W increases without limit as the volume increases. The transformation $\alpha \rightarrow \beta$ does not occur. It is nevertheless true that small regions of phase β enjoy temporary existence here and there in the α . The equilibrium number of β regions of given size is proportional to $\exp(-W/kT)$ per unit volume of α , assuring that larger β regions occur with diminishing probability.

When α is less stable than β , Δf is negative and W passes through a maximum as V increases. Assuming for simplicity that regions of β are spherical, as is true when the interfacial tension is isotropic and there are no elastic strains,

$$W = 4\pi r^2\sigma + (4/3)\pi r^3\Delta f.$$

The maximum value of W is

$$W^* = 16\pi\sigma^3/3\Delta f^2 \quad [1]$$

for regions with radius

$$r^* = -2\sigma/\Delta f. \quad [2]$$

For single component condensed systems it has been shown¹⁴ that the steady rate of nucleation of β per unit volume of untransformed α is nearly proportional to $\exp[-(W^* + Q)/kT]$ where Q is the activation energy for the unit processes of adding or removing one atom from an embryo or nucleus. If T_0 is the temperature at which α and β are in equilibrium, the rate of nucleation is a maximum at a temperature $0 < T < T_0$ where $(W^* + Q)/kT$ is a minimum.

β regions smaller than critical size are called embryos; they tend to grow smaller and disappear, only exceptionally growing larger. Regions equal to or larger than critical size are called nuclei. A critical size nucleus may grow indefinitely large or may shrink back to α , either process decreasing the free energy of the region.

Cleveland Meeting, October 1949.

TP 2674 E. Discussion of this paper (2 copies) may be sent to *Transactions AIME* before December 1, 1949. Discussion is tentatively scheduled for publication in May 1950.

Manuscript received November 1, 1948; revision received May 24, 1949.

* Research Laboratory, General Electric Co., Schenectady, N. Y.

¹ References are at the end of the paper.

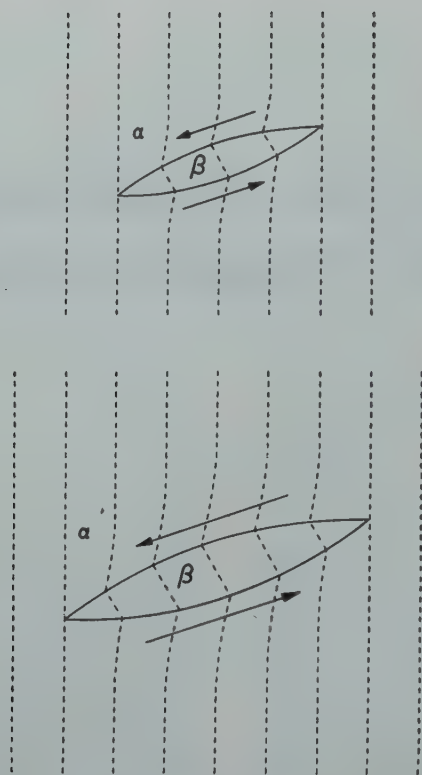
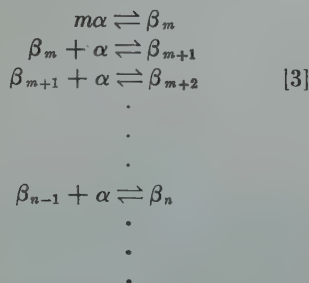


FIG 1—Growth of a martensite plate, schematic.

Arrows indicate direction of motion of parent phase.

It is important to recognize that embryos and nuclei do not suddenly appear full size in the parent phase.^{12,13} They grow larger and smaller by a series of essentially bimolecular reactions,



where α represents a single atom or molecule of phase α , and β_i represents an i -atom region of phase β . β_m , where $m \cong 10$ for metals, represents the smallest possible region having the structure of β . For β_i smaller than critical size, the specific rate of decomposition of β_i is greater than that of formation. For β_i larger than critical size the converse is true.

The unit processes of adding or removing α atoms have activation energies, and occur in finite time. If the temperature of a sample of α is changed rapidly from equilibrium at $T_1 > T_0$ where α is stable, to $T_{-1} < T_0$ where β is stable, the embryos at T_1

may be retained at the new temperature; with rapid quenching there may be insufficient time for the set of reactions $\beta_{i-1} + \alpha \rightleftharpoons \beta_i$ to lead to appreciable change toward establishment of the steady state β_i —distribution characteristic of T_{-1} .

If T_{-1} is sufficiently below T_0 , the larger embryos of β retained during quenching from T_1 will become nuclei during cooling as the critical size decreases. These nuclei then grow. The metamorphosis embryo \rightarrow nucleus that takes place during cooling is independent of thermal motion in the sense that no additional α atoms need be activated and added to the β region. For this reason nucleation resulting from the decrease in r^* with falling temperature has been termed athermal nucleation, in contrast to thermal nucleation which takes place isothermally.

It may happen that W^*/kT_{-1} is so large that the steady rate of nucleation at T_{-1} is negligible. Transformation $\alpha \rightarrow \beta$ then is initiated entirely by athermal nucleation. If the growth rate of β regions is rapid, and the size of a β grain is limited by changes in α grain boundaries, β will be observed to form only upon cooling of the α . If cooling ceases, athermal nucleation and therefore transformation also ceases. If the

cooling is continued, transformation continues.

Interrupted cooling can lead to “stabilization of the retained α ” when retained embryos of nearly critical size grow smaller and decrease in number as the steady state distribution characteristic of the holding temperature is approached. Subsequent cooling then produces fewer athermal nuclei than would have been produced by direct cooling to the final temperature.

NUCLEATION OF COHERENT PHASES

The elastic distortion accompanying transformations in solids frequently is so large that it cannot be neglected in calculating nucleation rates. Consider for example a transformation that occurs by the mechanism sketched in Fig 1. The phases are coherent in the sense that lines and planes of atoms are continuous across interfaces. The habit plane, or α plane that is parallel to the plate of β , is not necessarily rational. The transformation is evidently a “shear type” transformation; however the figure suggests that the final dimensions of a β plate are attained by growth, not by homogeneous shear or shears throughout the volume to be transformed.

The idea that “shear type” transformations are accomplished by homogeneous shears seems questionable in view of the very high activation energy associated with an entire β -plate in the partly-sheared condition. No such difficulty arises when the configuration between β -nucleus and full size β -plate is recognized to be a growing plate of intermediate size. It is suggested below that martensite is a coherent precipitate. Martensite plates are assumed therefore to form by the mechanism of Fig 1, successive layers of atoms being deposited one atom at a time as the parent phase moves relative to the plates.

Assume a coherent embryo or nucleus of radius r and of thickness δ at the center, the two surfaces of the plate being portions of spheres of large radius. The volume of the embryo is

$$V = \pi r^2 \delta / 2 \quad [4]$$

and its surface area is

$$A = 2\pi r^2 \quad [5]$$

to a good approximation when $\delta \ll r$. The formation of a coherent β embryo in α requires (1) formation of a coherent α - β interface, (2) transformation

of a volume of α to β , (3) concentration of elastic energy in the α (and to a lesser extent in the β).

Consider a sphere with center at the center of a thin coherent plate and with radius proportional to the radius of the plate. Select any point in the sphere (say on a line perpendicular to the plate at its center and at half the radius of the sphere). The elastic strain at the point is proportional to the ratio of the plate thickness to its radius,

$$e \sim \delta/r$$

as long as $\delta \ll r$. The strain energy per unit volume at the same location is proportional to the square of the strain,

$$E_v \sim (\delta/r)^2.$$

A similar proportionality holds at every point in the sphere; hence the total strain energy in the α is proportional to the product of $(\delta/r)^2$ and the volume of the sphere,

$$E = (3\theta/4) (\delta/r)^2 (4\pi r^3/3) = \theta\pi r\delta^2. \quad [6]$$

Here $3\theta/4$ is the proportionality constant.

The work associated with the reversible formation of an embryo of radius r and thickness δ is therefore

$$W = 2\pi r^2\sigma + \pi r^2\delta\Delta f/2 + \theta\pi r\delta^2. \quad [7]$$

The most probable shape for an embryo of volume V is that for which W is a minimum. Minimizing W with the condition $V = \text{constant}$ leads to the relationship

$$r = 3\theta\delta^2/4\sigma \quad [8]$$

which relates r and δ for minimum free energy embryos.

Most embryos are minimum free energy embryos. The work associated with the reversible formation of an embryo of thickness δ is therefore

$$W = 15\pi\theta^2\delta^4/8\sigma + 9\pi\theta^2\delta^5\Delta f/32\sigma^2. \quad [9]$$

W has a maximum

$$W^* = 8192\pi\theta^2\sigma^3/27\Delta f^4 \quad [10]$$

for nuclei with thickness

$$\delta^* = -16\sigma/3\Delta f \quad [11]$$

and volume

$$V^* = -32,768\pi\theta^2\sigma^3/27\Delta f^5. \quad [12]$$

Coherent nuclei grow as plates that finally are stopped at the edges by α grain boundaries, particles of a second phase, or other crystal discontinuities. Each plate thickens until the value of W associated with its formation from the α is a minimum. The plate then is

in equilibrium with the α and does not further thicken. Minimizing W at constant radius leads to the relationship

$$\delta/r = -\Delta f/4\theta \quad [13]$$

for full size coherent plates.

The ratio δ^*/r^* for coherent nuclei of critical size is also $\delta/r = -\Delta f/4\theta$ and experimental observation that $\delta \ll r$ for fully grown coherent plates justifies the assumption that $\delta \ll r$ for the corresponding nuclei and embryos.

Martensite

It is generally agreed that martensite is ferrite supersaturated with carbon of the same concentration as the parent austenite. Large amounts of dissolved carbon slightly distort the body-centered cubic structure of ordinary ferrite to a body-centered tetragonal structure. Martensite forms in thin lens-shaped plates that have definite orientation and habit relationships with the parent austenite. Transformation takes place primarily during cooling, and the growth of individual plates is very rapid.

These observations concerning martensite formation suggest the identification of martensite as supersaturated ferrite that forms by rapid coherent growth of athermal nuclei.

Martensite embryos come into being at the austenitizing temperature. Although a particular embryo has only transient existence, there is a definite equilibrium concentration of embryos of any given size. During quenching, the largest embryos find themselves supercritical for coherent growth, and they grow rapidly to full-size martensite plates.

Although both coherent and non-coherent embryos are present at the austenitizing temperature, only non-coherent embryos can be retained during quenching. Even at cooling rates as great as 10,000°C per sec, about 0.1 sec is required to reach the martensite start temperature from the austenitizing temperature. Individual martensite plates are observed to form in times of the order of 10^{-4} sec, indicating that the rate of coherent growth of martensite is very great. The life of coherent embryos therefore must be less than 10^{-4} sec, and during a time as long as 0.1 sec a given embryo will disappear; further, the largest embryos do not reform, for at lower temperatures the steady concentration of coherent embryos decreases in proportion to $\exp(-W/kT)$. Effectively,

coherent embryos always are present in the equilibrium or steady state concentration, while only noncoherent embryos, which require relatively long times to grow or shrink, can be retained during quenching.

A non-coherent α - β interface differs from a coherent interface in that non-coherent α and β structures get out of step occasionally, producing essentially a series of dislocations spaced along the interface. When β consumes α by non-coherent growth, existing dislocations move with the interface, and new dislocations appear where the interfacial area increases. However, it is possible also for β to consume α by coherent growth, leaving behind in the β the dislocations that initially were present at the α - β interface. Coherent growth of martensite from non-coherent ferrite nuclei therefore presents no contradiction.

Most martensite plates nucleate at embryos that have the minimum free energy of formation consistent with becoming nuclei at the low temperature, for these embryos are present in the greatest numbers. Let the critical size V^* for coherent growth of supersaturated ferrite (martensite) at a low temperature be as sketched in Fig 2A for a given iron-carbon alloy. Fig 2 suggests possible configurations for the embryos that are primarily responsible for martensite nucleation upon cooling to the low temperature in question.

Embryo (B) is a non-coherent ferrite region of size V^* , having the same carbon content as the austenite. Embryo (C) is a non-coherent ferrite region of the same size, but with the equilibrium amount of carbon for ferrite in contact with austenite.† The free energy of forming embryo (C) evidently is less than that of forming embryo (B), hence embryos similar to (B) do not contribute significantly to the martensite transformation.

Embryo (D) is a carbon-free austenite region of size V^* , containing a small non-coherent ferrite region just large enough to nucleate coherent growth in pure γ -iron at the low temperature. Upon quenching, the ferrite region in embryo (D) becomes a nucleus for coherent growth in carbon-free austenite; it grows to the boundary of the carbon-free region. Then, however, it is supercritical for growth in austenite of average carbon concentration, and it continues its coherent growth. The free energy of forming

† The equilibrium concentration of carbon is so low that it is assumed to be zero.

Table 1 . . . Calculated Free Energy Change in Calories per Mol of Lattice Sites for the Austenite \rightarrow Martensite Transformation in 12 Iron-Chromium-Carbon Alloys Studied by Lyman and Troiano^{10,18} and Harris and Cohen¹¹

| Pct C Pct Cr* | 0.08 3.45 | 0.15 3.39 | 0.26 3.73 | 0.38 3.38 | 0.69 3.44 | 1.02 3.56 | 1.28 3.48 | 1.13 1.18 | 1.09 2.16 | 1.04 4.36 | 1.05 6.32 | 1.02 9.46 |
|------------------|--------------|--------------|--------------|--------------|--------------|--------------|--------------|--------------|--------------|--------------|--------------|--------------|
| T°K | ΔF_m | ΔF_m | ΔF_m | ΔF_m | ΔF_m | ΔF_m | ΔF_m | ΔF_m | ΔF_m | ΔF_m | ΔF_m | ΔF_m |
| 1020 | + 12 | | | | | | | | | | | |
| 1000 | - 2 | | | | | | | | | | | |
| 980 | - 18 | + 4 | | | | | | | | | | |
| 960 | - 36 | - 13 | | | | | | | | | | |
| 940 | - 56 | - 33 | + 8 | | | | | | | | | |
| 920 | - 79 | - 55 | - 14 | | | | | | | | | |
| 900 | - 102 | - 78 | - 36 | + 2 | | | | | | | | |
| 880 | - 125 | - 102 | - 59 | - 21 | | | | | | | | |
| 860 | - 150 | - 126 | - 83 | - 44 | | | | | | | | |
| 840 | - 175 | - 150 | - 107 | - 68 | | | | | | | | |
| 820 | - 200 | - 174 | - 131 | - 92 | + 19 | | | | | | | |
| 800 | - 224 | - 199 | - 155 | - 116 | - 5 | | | | | | | |
| 780 | - 250 | - 225 | - 180 | - 140 | - 29 | | | | | | | |
| 760 | - 277 | - 252 | - 205 | - 166 | - 54 | | | | | | | |
| 740 | - 304 | - 279 | - 231 | - 192 | - 79 | + 11 | | | | | | |
| 720 | - 331 | - 306 | - 259 | - 219 | - 106 | - 16 | | | | | | |
| 700 | - 358 | - 333 | - 286 | - 246 | - 133 | - 43 | + 7 | | | | | |
| 680 | - 386 | - 361 | - 313 | - 272 | - 160 | - 69 | - 19 | - 89 | - 79 | - 49 | - 13 | |
| 660 | - 413 | - 388 | - 340 | - 299 | - 187 | - 95 | - 46 | - 116 | - 106 | - 75 | - 38 | + 11 |
| 640 | - 440 | - 415 | - 366 | - 325 | - 212 | - 121 | - 72 | - 142 | - 132 | - 101 | - 63 | - 13 |
| 620 | - 467 | - 441 | - 391 | - 351 | - 238 | - 147 | - 97 | - 168 | - 158 | - 126 | - 89 | - 37 |
| 600 | | - 467 | - 418 | - 377 | - 264 | - 172 | - 122 | - 195 | - 184 | - 152 | - 113 | - 61 |
| 580 | | - 494 | - 445 | - 402 | - 291 | - 199 | - 148 | - 222 | - 210 | - 178 | - 139 | - 86 |
| 560 | | - 521 | - 472 | - 428 | - 318 | - 225 | - 174 | - 248 | - 237 | - 204 | - 164 | - 110 |
| 540 | | | - 499 | - 456 | - 345 | - 253 | - 201 | - 276 | - 265 | - 231 | - 191 | - 135 |
| 520 | | | - 527 | - 484 | - 373 | - 280 | - 228 | - 305 | - 293 | - 259 | - 218 | - 161 |
| 500 | | | - 555 | - 511 | - 401 | - 308 | - 256 | - 333 | - 321 | - 286 | - 245 | - 187 |
| 480 | | | | - 538 | - 428 | - 335 | - 283 | - 360 | - 348 | - 313 | - 270 | - 212 |
| 460 | | | | - 566 | - 455 | - 362 | - 310 | - 387 | - 376 | - 339 | - 296 | - 237 |
| 440 | | | | - 593 | - 481 | - 388 | - 336 | - 414 | - 403 | - 365 | - 321 | - 261 |
| 420 | | | | - 618 | - 508 | - 414 | - 360 | - 441 | - 428 | - 391 | - 346 | - 285 |
| 400 | | | | - 644 | - 533 | - 439 | - 385 | - 467 | - 453 | - 415 | - 370 | - 308 |
| 380 | | | | - 669 | - 559 | - 463 | - 410 | - 492 | - 478 | - 440 | - 394 | - 331 |
| 360 | | | | - 694 | - 583 | - 487 | - 433 | - 516 | - 503 | - 464 | - 417 | - 353 |
| 340 | | | | - 718 | - 606 | - 510 | - 456 | - 540 | - 527 | - 487 | - 440 | - 375 |
| 320 | | | | - 741 | - 629 | - 532 | - 478 | - 563 | - 549 | - 509 | - 461 | - 396 |
| 300 | | | | - 762 | - 652 | - 554 | - 500 | - 585 | - 570 | - 530 | - 482 | - 416 |
| 280 | | | | | | - 574 | - 520 | - 606 | - 591 | - 549 | - 502 | - 435 |
| 260 | | | | | | - 595 | - 538 | - 626 | - 611 | - 569 | - 520 | - 454 |
| 240 | | | | | | - 614 | - 556 | - 645 | - 630 | - 588 | - 538 | - 471 |
| 220 | | | | | | | - 574 | - 662 | - 647 | - 606 | - 555 | - 487 |
| 200 | | | | | | | - 590 | - 680 | - 664 | - 622 | - 571 | - 502 |

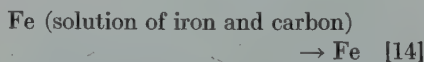
* P₁ pct manganese is counted as 2P₁ pct chromium, and P₂ pct silicon as P₂ pct iron.

embryo (D) is less than that of forming embryo (C), for embryo (C) requires a larger ferrite region with greater area of interface and greater volume of the unstable phase.

Although embryo (E), with carbon concentration increasing from zero at the boundary of the ferrite region to the average value at the boundary of the volume V^* has a free energy of formation somewhat smaller than does embryo (D), it is assumed, for ease of calculation in the following analysis, that martensite nucleates from embryos similar to embryo (D).

The free energy of formation of embryo (D) is the sum of two free energies; (1) that required to clear the carbon from a volume V^* , and (2) that associated with formation of the small ferrite region. It is assumed that the free energy required for formation of the small ferrite region is small in comparison with that required to clear the carbon from volume V^* .

The free energy change accompanying the reaction



corresponds to a transfer of all carbon from one gram atom of iron in austenite of initial carbon concentration N_C to a large reservoir of austenite of carbon concentration N_C . The activity constant for the reaction is

$$K = a_{\text{Fe}}/a_{\text{Fe}(C)} = 1/a_{\text{Fe}(C)}$$

taking the activity of pure iron as unity. The corresponding free energy change is

$$\Delta F - \Delta F_0 = RT \ln K = -RT \ln a_{\text{Fe}(C)}.$$

The standard free energy change ΔF_0 is zero, hence

$$\Delta F = -RT \ln a \quad [15]$$

cal per g atom of iron where the subscript has been dropped and $\ln a$ represents the logarithm of the activity of iron in an iron-carbon alloy.¹⁵

The activity of iron in austenite has been determined by Smith.¹⁶ He shows

that the relationship

$$-\ln a = N_C/N_s + [6.5 - 6 \exp(-1500/RT)] (N_C/N_s)^2 \quad [16]$$

gives satisfactory agreement with the experimental values over the entire temperature and composition range investigated. N_C is the mol fraction of carbon, and N_s is the mol fraction of iron. It is assumed in the following analysis that Eq 15 and 16 hold for steels of arbitrary composition when N_s is taken as the sum of the mol fractions of all substitutional elements.

The free energy change upon removing the carbon from a small region containing only n interstitial positions is

$$\Delta f_n = - (n/N) RT \ln a = -nkT \ln a. \quad [17]$$

The equilibrium number n_0 of carbon-free regions containing n lattice sites is proportional to $\exp(-\Delta f_n/kT) = \exp(n \ln a)$. Assuming ideal mixing of carbon-free regions and the remaining iron atoms the proportionality factor is N per mol of lattice sites,⁶ giving

$$n_0 = N \exp(n \ln a). \quad [18]$$

The number of regions larger than a critical size n^* is

$$n_r = \int_{n=n^*}^{\infty} n_0 dn = - (N/\ln a) \exp(n^* \ln a) \quad [19]$$

per mol of lattice sites.

CALCULATION OF M_s TEMPERATURES

Fisher¹⁷ has assembled information concerning the free energy change upon transforming austenite to martensite. The free energy change is

$$\Delta F_m' = N_{\text{Fe}} \Delta F_{\text{Fe}} + N_C (10,500 - 3.425T) + \Delta F_* + N_{\text{Cr}} RT \ln (\gamma_{\text{Cr}}^\alpha / \gamma_{\text{Cr}}^\gamma) \quad [20]$$

cal per g atom for iron-chromium-carbon alloys,[†] where the symbols have the following meanings:

$\Delta F_m'$ = free energy change upon transforming a gram atom of austenite to martensite (in the absence of elastic distortion associated with coherency).

ΔF_{Fe} = free energy change upon transforming a gram atom of γ -iron to α -iron.

ΔF_* = free energy change accom-

[†] A gram atom of iron-chromium-carbon alloy contains N_{Fe} , N_{Cr} and N_C mols of iron, chromium and carbon.

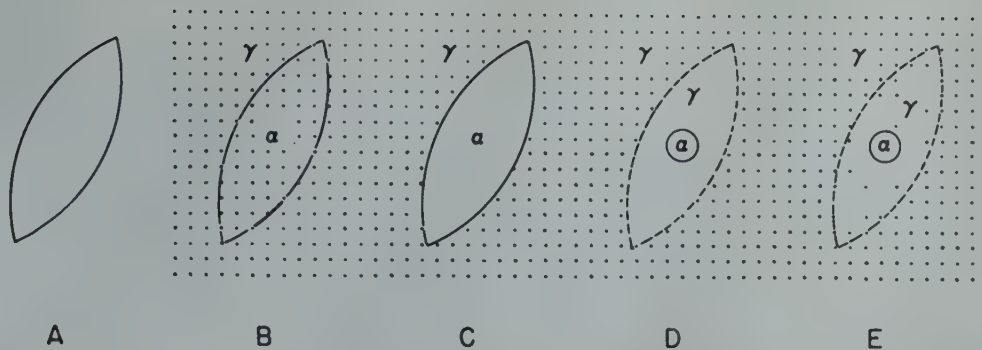


FIG 2—(A) Critical size for martensite growth. (B-E) Possible martensite embryos, schematic.

Dots represent carbon atoms.

panying the disordered-carbon \rightarrow ordered-carbon transformation in a gram atom of martensite.

N_{Fe} = mol fraction iron.

N_C = mol fraction carbon.

N_{Cr} = mol fraction chromium.

R = gas constant, 1.986 cal per mol $^{\circ}K$.

T = temperature, $^{\circ}K$.

γ_{Cr}^{α} = activity coefficient for chromium in α phase.

γ_{Cr}^{γ} = activity coefficient for chromium in γ phase.

As very little is known concerning γ_{Cr}^{α} and γ_{Cr}^{γ} , the approximation $RT \ln (\gamma_{Cr}^{\alpha}/\gamma_{Cr}^{\gamma}) = K_{Cr}$ is made, where K_{Cr} is a constant.¹⁷

Let N_s be the sum of the mol frac-

tions of all substitutional elements. The free energy change per mol of lattice sites is then

$$\Delta F_m = (N_{Fe}/N_s)\Delta F_{Fe} + (N_C/N_s)(10,500 - 3.425T) + \Delta F_{*}/N_s + (N_{Cr}/N_s)(1200). \quad [21]$$

The choice $K_{Cr} = 1200$ cal per g atom is justified in the following analysis. ΔF_m enters naturally into nucleation theory, for the free energy change per mol of lattice sites is very nearly proportional to the free energy change per unit volume. Table 1 gives values of ΔF_m vs. temperature for the 12 steels of interest in the present report.

It has been suggested that martensite nuclei form in carbon-poor austenite regions, and that the number of

martensite plates that form on cooling to a given temperature is equal to the number of carbon-free regions in the austenite that exceed the critical size for coherent growth of martensite nuclei in austenite of average carbon concentration.

According to this interpretation there is no sharply defined M_s temperature above which martensite does not form. However, there is a definite temperature, the experimental M_s temperature, at which the probability of finding a martensite plate during microscopic examination of a given specimen area is say 0.5. This temperature corresponds to a definite number of martensite plates per unit volume of iron. An equation for the experi-

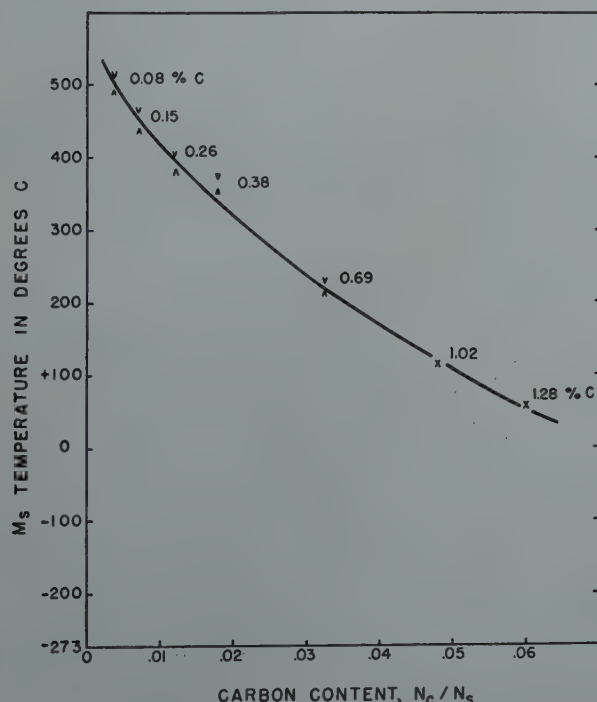


FIG 3— M_s temperature for 3 pct chromium steels as a function of carbon content.

Experimental values determined by Lyman and Troiano,¹⁰ and (0.38 pct C only) by Klier and Lyman.²⁰ Curve calculated from Eq 25.

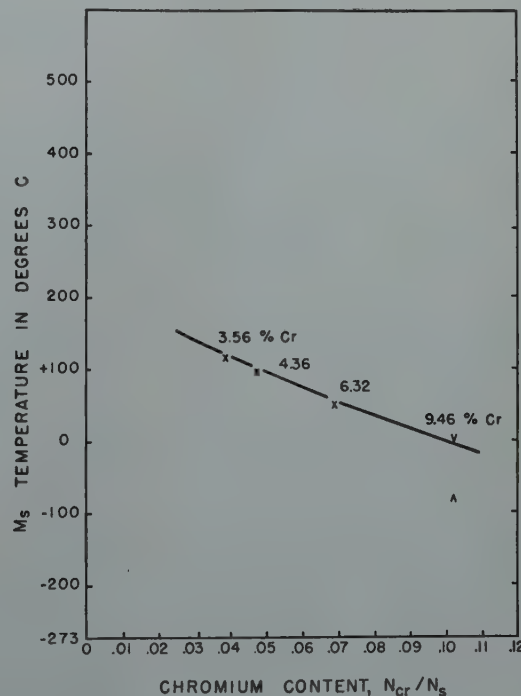


FIG 4— M_s temperature for 1 pct carbon steels as a function of chromium content.

Experimental values determined by Lyman and Troiano.¹⁰ Curve calculated from Eq 25.

mental M_s temperature can be obtained therefore by setting the expression for the number of martensite nuclei (that is, the number of carbon-free austenite regions as large or larger than the volume of a critical size martensite nucleus) per mol of lattice sites equal to a constant,

$$n_r = -(N/\ln a) \exp(n^* \ln a) = K_1. \quad [22]$$

Since the order of magnitude of $\ln a$ is the same for all steels for which M_s is determined, the above condition is practically equivalent to stating that the exponent $n^* \ln a$ is constant,

$$n^* \ln a = K_2. \quad [23]$$

The number n^* of lattice sites in a critical size martensite nucleus is proportional to its volume V^* which is in turn proportional to ΔF_m^{-5} (see Eq 12). Here $\Delta F_m \sim \Delta f$ is the free energy change in calories per mol of lattice sites for transformation to supersaturated ferrite. The equation for the M_s temperature is therefore

$$\Delta F_m = K_3(-\ln a)^{1/5} \quad [24]$$

or substituting the value $K_3 = -800$ which was found to give the best agreement with the data of Lyman and Troiano,¹⁰

$$\Delta F_m + 800(-\ln a)^{1/5} = 0. \quad [25]$$

M_s temperatures calculated from Eq 25 are compared in Fig 3 with the experimental values determined by Lyman and Troiano¹⁰ for seven 3 pct chromium steels containing from 0.08 to 1.28 pct carbon. Values of ΔF_m and $-\ln a$ required for the calculation are given in Table 1 and Eq 16.

M_s temperatures calculated for four 1 pct carbon steels of varying chromium content are compared with the experimental values of Lyman and Troiano¹⁸ in Fig 4. The value $K_{Gr} = 1200$ cal per g atom was selected to give agreement between Eq 25 and these experimental data.

MARTENSITE TRANSFORMATION CURVES

A martensite transformation curve gives the fraction of martensite, or the remaining fraction of untransformed austenite, as a function of quenching bath temperature for specimens cooled as rapidly as possible from the austenitizing temperature. The growth of individual martensite plates is stopped by austenite grain boundaries, previously formed martensite plates, and other crystal discontinuities that do

not allow coherent growth across an interface. The size of the first few martensite plates that form in a specimen of austenite containing no undissolved carbides is determined, therefore, by the austenite grain size. The size of later martensite plates is determined by the size of the pockets of untransformed austenite remaining among previously formed martensite plates. Calculation of martensite transformation curves requires an estimate of the size of these austenite pockets as a function of austenite grain size and number of martensite plates.

Let V_0 be the volume of a mol of lattice sites, let qV_0 be the volume of a single austenite grain, and let mqV_0 be the volume of an average martensite plate that forms near M_s .

After n plates have formed, the mol of lattice sites is cut up into chunks about $qV_0/(qn+1)$ cc in size. Let V_m be the volume of martensite formed. Slightly below M_s , $dV_m/dn = mqV_0/(qn+1)$ is the volume rate of transformation per martensite plate. A better approximation to dV_m/dn is

$$dV_m/dn = mq(V_0 - V_m)/(qn+1) \quad [26]$$

where V_0 has been replaced by $V_0 - V_m = V_a$, the remaining volume of untransformed austenite.

Integrating, $-\ln(V_0 - V_m) = m \ln [c(qn+1)]$ where c is the integration constant. $V_m = 0$ when $n = 0$, hence $-\ln V_0 = m \ln c$ and

$$1 - V_m/V_0 = V_a/V_0 = (qn+1)^{-m}. \quad [27]$$

Let n_0 be the number of martensite nuclei that would have appeared in the absence of nucleus growth. n , the actual number of martensite plates, is related to n_0 by the equation

$$dn/dn_0 = V_a/V_0 = (qn+1)^{-m}. \quad [28]$$

Integrating,

$$(qn+1)^{m+1}/(m+1) = qn_0 + c_2.$$

The value of c_2 is $1/(m+1)$, giving

$$(qn+1)^{m+1} = (m+1)qn_0 + 1$$

or

$$\begin{aligned} (qn+1)^{-m} &= [(m+1)qn_0 + 1]^{-m/(m+1)} \\ &\cong (qn_0 + 1)^{-m} \end{aligned} \quad [29]$$

since $m \ll 1$.

Therefore, the fraction of retained austenite is

$$V_a/V_0 = (qn_0 + 1)^{-m} \quad [30]$$

where

$$\begin{aligned} n_0 &= -(N/\ln a) \exp(n^* \ln a) \\ &= -(N/\ln a) \exp(V^* \ln a/v_0) \end{aligned} \quad [31]$$

is the number of martensite nuclei, q is the reciprocal of the number of austenite grains per mol of lattice sites, v_0 is the volume per lattice site, and $m \ll 1$ is a function of the shape of the martensite plate.

Let the ASTM grain size be g . There are then 2^{g-1} grains per sq in. visible at 100 diam, or 10^{4g-1} grains per sq in. The area of an average spherical grain cut at random is $A = 2\pi r_g^2/3$, hence the radius of a typical grain follows from the relationship

$$10^{4g-1}(2\pi r_g^2/3) = 1$$

giving

$$\begin{aligned} r_g &= 10^{-2g-2} \text{ in.} \\ &= 2.5(10)^{-2g-2} \text{ cm.} \end{aligned}$$

The volume per austenite grain is

$$V_1 = 4\pi r_g^3/3 = 65(10)^{-6g-3} \text{ cc,}$$

and the number of austenite grains per mol of lattice sites is V_0/V_1 where $V_0 = 7.2$ cc is the volume occupied by a gram atom of iron. The value of q is therefore

$$q = V_1/7.2 = 9.0(10)^{-6g-3g/2} \quad [32]$$

mol of lattice sites per austenite grain.

The volume of the average austenite grain is

$$4\pi r_g^3/3 = qV_0,$$

and the volume of the average martensite plate that forms in such a grain is

$$3(\delta/r)\pi^2 r_g^3/32 = mqV_0$$

where δ/r is the thickness to radius ratio for martensite plates. The ratio of plate volume to grain volume is

$$m = 9\pi(\delta/r)/128,$$

or

$$m = -9\pi\Delta f/512\theta = -\mu\Delta F_m \quad [33]$$

taking $\delta/r = -\Delta f/4\theta$ as given in Eq 13. μ is the constant of proportionality between m and ΔF_m .

Martensite transformation curves now can be calculated by means of Eq 30, where n_0 is given by Eq 31, q by Eq 32, and m by Eq 33. The coefficient μ in Eq 33 is the only unknown parameter. The best agreement between calculated transformation curves and those determined experimentally by Harris and Cohen¹¹ is obtained when

$$\mu = 7(10)^{-5}. \quad [34]$$

Fig 5 and 6 compare calculated and experimental curves for a 1.1 pct carbon steel and a 1.1 pct carbon, 1.5 pct

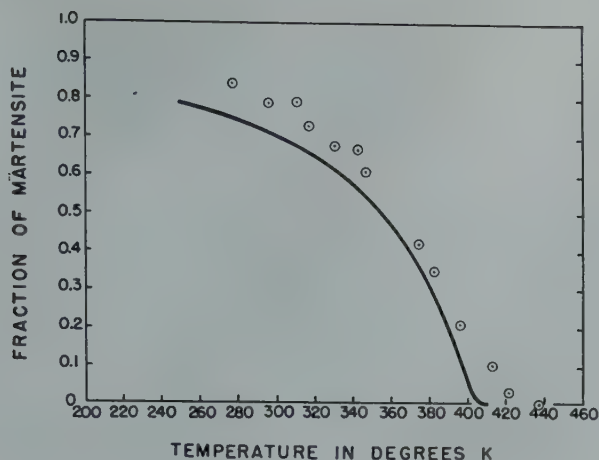


FIG 5—Martensite transformation curve for 1.1 pct carbon steel.

Experimental points determined by Harris and Cohen.¹¹ Curve calculated from Eq 30.

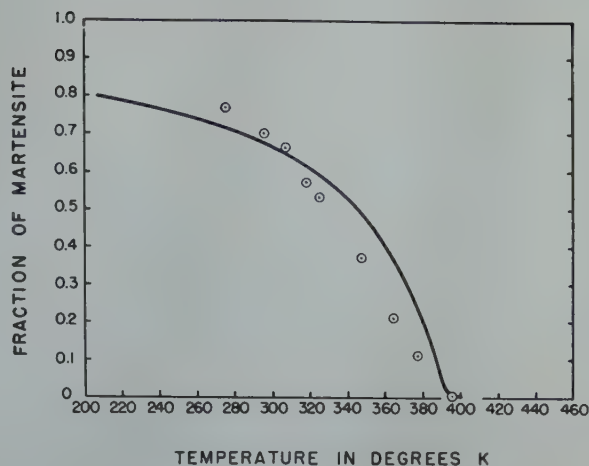


FIG 6—Martensite transformation curve for 1.1 pct carbon, 1.5 pct chromium steel.

Experimental points determined by Harris and Cohen.¹¹ Curve calculated from Eq 30.

chromium steel.

Two important effects have been neglected in calculating martensite transformation curves. It is observed frequently that the growth of one martensite nucleus immediately sets off the growth of several others in the strained austenite adjacent to the first martensite plate. Elastic strains set up by the first plate presumably have altered the critical size for growth of otherwise subcritical nuclei, so that a few of them become supercritical and grow. Further, when a significant fraction of austenite is transformed, interaction of the stress fields around neighboring martensite plates allows them to thicken considerably in comparison with the equilibrium thickness for an isolated plate. Both the multiplication effect and the thickening effect lead to increased transformation over that given by Eq 30; the discrepancy becoming large when a significant amount of martensite is present.

Significance of the Agreement between Theory and Experiment

M_s temperatures and martensite transformation curves have been calculated from the basic assumptions that martensite and austenite are coherent, and that martensite grows by the mechanism sketched in Fig 1. Agreement between theory and experiment, summarized in Fig 3-6, is satisfactory, although it can be contended that the significance of this agreement is diminished by the arbitrary choice of values for the two parameters θ (the coefficient of the strain energy term in the equation for the work of forming

a coherent embryo) and σ (the coherent interfacial free energy).

Certainly, however, the significance of the agreement will be increased if it can be shown that the value of θ required for calculation of martensite transformation curves is that given by elasticity theory, and if it can be shown that the value of σ required for calculation of M_s temperatures is reasonable in comparison with known surface and interfacial free energies.

THE SHAPE OF A MARTENSITE PLATE

The strain energy associated with a martensite plate of thickness δ and radius r is $E = \theta\pi r\delta^2$ according to Eq 6. The value of the coefficient θ can be roughly estimated by assuming that the strain in the austenite surrounding a martensite plate is uniform throughout a circumscribed sphere of radius r . The shear strain is approximately $\gamma = \phi\delta/2r$ where ϕ is the "homogeneous shear" angle of the martensite. The energy per unit volume is

$$E_v = G\gamma^2/2 = \phi^2 G(\delta/r)^2/8$$

and the total strain energy is

$$E = (4/3)\pi r^3[\phi^2 G(\delta/r)^2/8] = (\pi/6)\phi^2 Gr\delta^2,$$

whence

$$\theta = \phi^2 G/6. \quad [35]$$

Taking $\phi = 0.34$ corresponding to the Nishiyama¹⁹ orientation relationship between martensite and austenite, and $G = 8(10)^{11}$ dynes per cm² (the value for ferrite) as an approximation for austenite, the value of θ is

$$\theta_1 = 1.54(10)^{10} \text{ dynes per cm}^2. \quad [36]$$

This approximate value of θ may be

compared with the value assumed in the analysis of martensite transformation curves. Eq 33 and 34 give

$$m = -9\pi\Delta f/512\theta = -7(10)^{-5}\Delta F_m$$

whence

$$\theta = 0.46(10)^{10} \text{ dynes per cm}^2, \quad [37]$$

in satisfactory agreement with θ_1 in view of the approximations in the elastic analysis and in the assumption that austenite pockets remaining in partially transformed steel are spherical.

The thickness to radius ratio δ/r for martensite plates can be calculated from the relationship

$$\delta/r = -\Delta f/4\theta = -3.2(10)^{-4}\Delta F_m. \quad [38]$$

At the M_s temperature, the ratio δ/r calculated for 3 pct chromium steels varies from 0.084 to 0.151 as the carbon content varies from 0.08 to 1.28 pct.

THE COHERENT α - γ INTERFACIAL FREE ENERGY

The experimental martensite start temperature corresponds to the presence of a definite number of martensite plates in a quenched sample of austenite of given grain size. A reasonable estimate of the number of plates needed to provide one visible plate per microscope field suggests that there are about 10^6 martensite plates per mol of lattice sites at the M_s temperature.

Substituting the value 10^6 for the number of martensite nuclei, Eq 22 becomes

$$10^6 = n_r = -(N/\ln a) \exp(n^* \ln a) = -(N/\ln a) \exp(V^* \ln a/v_0). \quad [39]$$

For ordinary values of N_c/N_s , Eq 39 fixes the value of $V^* \ln a/v_0$ to be

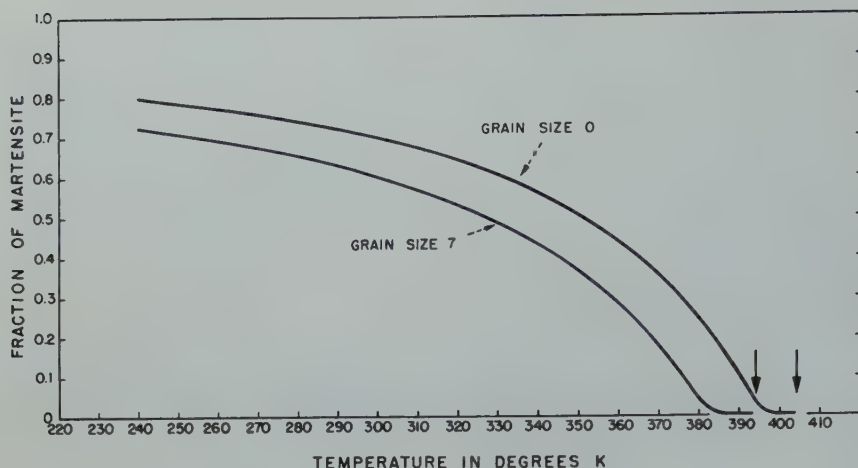


FIG 7—Calculated martensite transformation curves for 1 pct C, 3 pct Cr steel with ASTM grain sizes 0 and 7. Arrows indicate temperatures for 0.01 pct transformation.

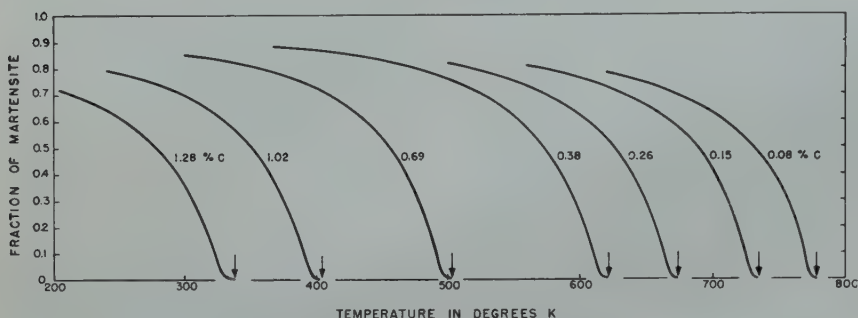


FIG 8—Calculated martensite transformation curves for 3 pct chromium steels of differing carbon content. Arrows indicate temperatures for 0.01 pct transformation.

$$V^* \ln \cong a/v_0 - 45. \quad [40]$$

Substituting the value of V^* from Eq 12,

$$32,768 \pi \theta^2 \sigma^3 \ln a/27 v_0 \Delta f^5 = 45. \quad [41]$$

Taking $[-\ln a]^{1/5}/\Delta F_m = -1/800$ and $\theta = 0.46(10)^{10}$ from Eq 25 and 37, Eq 41 can be solved for the coherent α - γ interfacial free energy σ ,

$$\sigma = 24 \text{ ergs per cm}^2. \quad [42]$$

The value $\sigma = 24$ ergs per cm^2 that must be assumed in calculating M_s temperatures can be compared with the surface and interfacial free energies of solid copper, which should not differ markedly from those of iron:

$$\sigma_1 \cong 1400 \text{ ergs per cm}^2 \quad (\text{surface tension of copper}^{20})$$

$$\sigma_2 \cong 150 \text{ ergs per cm}^2 \quad (\text{non-coherent copper-copper interface}^{21})$$

$$\sigma_3 \cong 5 \text{ ergs per cm}^2, \text{ very approximately (twin boundary}^{21}).$$

It is encouraging to note that the coherent α - γ interfacial free energy and the twin boundary free energy in cop-

per agree as to order of magnitude.

It appears that the values of the parameters θ and σ , arbitrarily chosen to give agreement between theory and experiment, are close to the values expected from independent considerations. Within the error of an approximate calculation, θ is correctly given by a purely geometrical elastic analysis. The value of σ is reasonable in the light of what is known concerning coherent interfacial free energies of solids.

Influence of Austenite Grain Size and Other Variables

The M_s temperature and the extent of martensite transformation are dependent upon the austenitic grain size. Whenever nuclei form at random in the parent phase, and rapid growth of the new phase ceases at grain boundaries of the parent phase, each transformed particle is restricted to a single parent grain. The amount of transformation is the product of the number of nuclei and the size of each transformed region. The number of nuclei is independent of

grain size, and the volume of a typical transformed region is proportional to d^3 where d is the mean grain diameter, leading to the relationship

$$(\text{pct transformation}) \sim d^3 \quad [43]$$

during the early stages of transformation. A ten-fold decrease in grain diameter decreases the volume transformed to martensite by a factor of a thousand, thereby lowering the experimental M_s temperature.

Eq 30 gives the variation in the martensite transformation curve with grain size for all stages of transformation,

$$V_a/V_0 = (qn_0 + 1)^{-m},$$

where q is the number of mols of lattice sites per austenite grain. Fig 7 compares the calculated martensite transformation curves for two specimens of 1 pct C, 3 pct Cr steel with ASTM grain sizes 0 and 7, representing approximately a ten-fold change in grain diameter. The M_s temperature is 10–13°C lower (depending upon the method of measurement) in the fine grained material, and a comparable degree of transformation is achieved in a longer temperature interval.

INFLUENCE OF COMPOSITION ON THE SHAPE OF MARTENSITE TRANSFORMATION CURVES

Consider steels of varying chromium content and fixed carbon content. For these steels the free energy change ΔF_m on transforming austenite to martensite depends to a first approximation only upon the amount of subcooling below M_s . Hence n_0 and m in the relationship $V_a/V_0 = (qn_0 + 1)^{-m}$ are the same functions of the temperature interval below M_s for all steels of a particular carbon content, and the shape of the M_s transformation curve is independent of chromium content.

Steels with different carbon contents do not have quite the same shape, however, as shown in Fig 8 where calculated curves are compared for several 3 pct chromium steels of varying carbon content. The variation in shape with carbon content is in qualitative agreement with the observations of Grange and Stewart.²²

Although grain size and carbon content influence the shape of martensite transformation curves, examination of Fig 7 and 8 indicates that for the usual grain sizes and carbon contents that are employed in commercial steels, the shape of the martensite transformation curve is relatively insensitive to these

variables. The fraction of austenite transformed depends primarily upon the temperature interval below M_s , in agreement with the observations of Harris and Cohen.¹¹

EXTRAPOLATED M_s TEMPERATURES

The extrapolated M_s temperature is that at which the nearly linear portion of the martensite transformation curve intersects the axis of zero martensite. It lies a few degrees below the M_s temperature corresponding to the first plates visible during microscopic examination, as shown in Fig 9, where the shape of a calculated martensite transformation curve is given in detail near the M_s temperature.

Averaging data from 12 martensite transformation curves determined by Harris and Cohen¹¹ the extrapolated M_s temperature was found to lie about 6°C below the highest temperature of martensite observation for steels with M_s temperatures in the range $350 < M_s < 500^\circ\text{K}$. This value compares favorably with the calculated value of about 9°C.

STABILIZATION

Consider a specimen of austenite that transforms partially to martensite upon quenching to a temperature T_{-2} . It frequently is found that holding the specimen for a time at $T_{-1} > T_{-2}$ decreases the amount of martensite formed on subsequent cooling to T_{-2} , the maximum amount of martensite corresponding to direct quenching to T_{-2} .¹¹ This process is termed stabilization.

A mechanism for stabilization in single component systems has been described in the first section on nucleation. When embryos that would have become athermal nuclei upon further cooling are present in excess of their steady state concentration at a holding temperature T_{-1} , they decrease in number with time. Subsequent cooling to $T_{-2} < T_{-1}$ then produces fewer athermal nuclei and less additional transformation. In general, stabilization requires that subcritical embryos of the new phase somehow be eliminated while the specimen is held at T_{-1} . In single component systems, only embryos that grow smaller are eliminated. In the iron-carbon system, martensite embryos perhaps may be eliminated by processes that involve the diffusion of carbon.

Harris and Cohen¹¹ have shown that

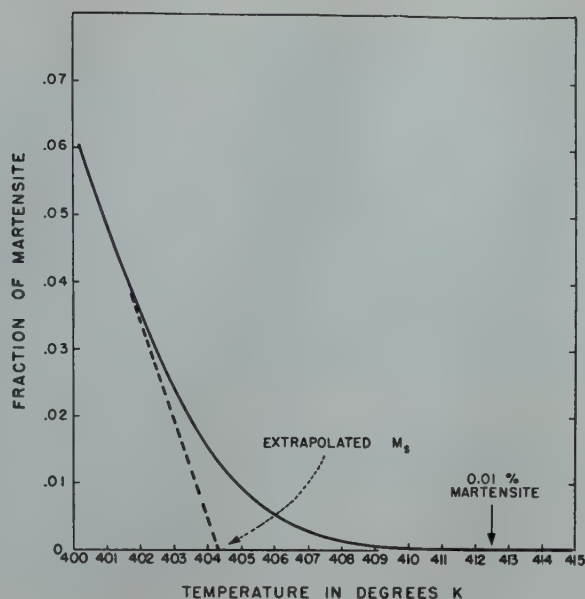


FIG 9—Shape of calculated martensite transformation curve near M_s .

stabilization does not occur at temperatures above a critical temperature σ_s , dependent upon composition, and that the amount of stabilization increases as the holding temperature decreases below σ_s . The σ_s temperature has both theoretical and practical significance, and a complete analysis of austenite decomposition should provide means for explaining and predicting its existence. However, the mechanism of stabilization appears to be more complex than that of the austenite \rightarrow martensite transformation, and lies beyond the scope of the present analysis.

RATE OF GROWTH OF MARTENSITE PLATES

Coherent growth of martensite is very rapid, for each atom need move only about 0.34 of an atomic spacing to join the new lattice. The activation energy q^* for the unit process during this sort of "diffusion" is approximately $(0.34)^2$ times that for moving an atom a full atomic spacing. The latter value is estimated by Huntington and Seitz²³ to be about 0.36 times the activation energy for self-diffusion, the remaining 0.64 of the activation energy corresponding to the formation of a lattice vacancy. Birchenall and Mehl²⁴ report the activation energy for self-diffusion in γ -iron to be 48,000 cal per g atom, hence

$$q^* \cong 0.36 (0.34)^2 (48,000) = 2000 \text{ [44]}$$

cal per g atom (very approximately) is the activation energy for coherent growth.

The value $q^* = 2000$ cal per g atom

is in excellent agreement with the experimental activation energy $q^* = 1600$ cal per g atom observed by Kurdjumov and Maksimova for isothermal transformation of austenite to martensite in the temperature range $79 \leq T \leq 173^\circ\text{K}$ where the rate of transformation is measurably slow,⁷ although these authors assumed that q^* was associated with nucleation, rather than growth, of martensite plates. The very important work of Kurdjumov and Maksimova proves that the austenite \rightarrow martensite transformation proceeds isothermally with a rate that approaches zero at the absolute zero of temperature, and is evidence strongly in favor of the nucleation and growth hypothesis of martensite formation.

Conclusions

Martensite start temperatures and martensite transformation curves have been calculated from the basic assumption that the austenite \rightarrow martensite transformation proceeds by nucleation and growth. Martensite is identified as coherent supersaturated ferrite, and martensite nuclei are identified as small carbon-free austenite regions retained from the austenitizing temperature.

Agreement between experiment and theory is satisfactory, and there is reason to believe that adequate thermodynamic data will allow accurate calculation of M_s temperatures and martensite transformation curves for steels of arbitrary composition and heat treatment.

Acknowledgment

The authors' viewpoint concerning the austenite \rightarrow martensite transformation has been influenced through study of Professor C. Zener's thought provoking article on the kinetics of austenite decomposition.²⁶ The authors are indebted to Professor M. Cohen, to Professor R. F. Mehl, and to members of the Metallurgy Division of the General Electric Research Laboratory for stimulating conversations and helpful criticism.

References

1. R. F. Mehl: *Trans. Am. Soc. Met.* (1941) **29**, 813.
2. F. C. Hull, R. A. Colton, and R. F.

- Mehl: *Trans. AIME* (1942) **150**, 185.
3. G. E. Roberts and R. F. Mehl: *Trans. AIME* (1943) **154**, 318.
4. F. C. Hull and R. F. Mehl: *Trans. Am. Soc. Met.* (1942) **30**, 381.
5. R. F. Mehl: *Jnl. Iron and Steel Inst.* (1948) **159**(2), 113.
6. J. C. Fisher, J. H. Hollomon, and D. Turnbull: *Jnl. App. Phys.* (1948) **19**, 775.
7. G. V. Kurdjumov and O. P. Maksimova: *Doklady Akad. Nauk SSSR* (1948) **61**, No. 1, 83.
8. M. Volmer and A. Weber: *Ztsch. Phys. Chem.* (1925) **119**, 277.
9. R. Becker and W. Döring: *Ann. Physik* [5] (1935) **24**, 719.
10. T. Lyman and A. R. Troiano: *Trans. Am. Soc. Met.* (1946) **37**, 402.
11. W. J. Harris, Jr. and M. Cohen: *Trans. AIME* (1949) **180**, 447, *Metals Tech.* Sept. 1948, TP 2446.
12. J. B. Zeldovich: *Acta Physicochim. URSS* (1943) **18**, 1.
13. D. Turnbull: *Trans. AIME* (1948) **175**, 774, *Metals Tech.* June 1948, TP 2365.
14. D. Turnbull and J. C. Fisher: *Jnl. Chem. Phys.* (1949) **17**, 71.
15. G. N. Lewis and M. Randall: *Thermodynamics*. McGraw-Hill, New York (1923).
16. R. P. Smith: *Jnl. Am. Chem. Soc.* (1946) **68**, 1163.
17. J. C. Fisher: *Jnl. of Metals* Oct. 1949.
18. T. Lyman and A. R. Troiano: *Trans. AIME* (1945) **162**, 196.
19. Z. Nishiyama: *Sci. Repts. Tokyo Imp. Univ.* (1934) **23**, 637.
20. H. Udin, A. J. Shaler and J. Wulff: *Jnl. of Metals* Feb. 1949, 186.
21. G. W. Sears: unpublished research.
22. R. A. Grange and H. M. Stewart: *Trans. AIME* (1946) **167**, 467, *Metals Tech.* June, 1946, TP 1996.
23. H. B. Huntington and F. Seitz: *Phys. Rev.* (1942) **61**, 315.
24. C. E. Birchenall and R. F. Mehl: *Jnl. Appl. Phys.* (1948) **19**, 217.
25. E. P. Klier and T. Lyman: *Trans. AIME* (1944) **158**, 394.
26. C. Zener: *Trans. AIME* (1946) **167**, 550, *Metals Tech.* Jan. 1946, TP 1925.

Some Observations in the Structure of Alpha Brass Single Crystals after Cutting and Polishing

ROBERT MADDIN,* Junior Member, and WALTER R. HIBBARD, JR.,† Member AIME

A series of X ray experiments conducted by G. I. Taylor¹ in 1927 and later substantiated in 1939 by J. A. Collins² both on axially strained aluminum single crystals, revealed evidence that during single slip crystallite rotation occurs in such a manner that "all parts of the material rotated about the transverse direction in the plane of slip."¹

The actual method of preparing the specimens for X ray examination is not discussed in detail by Taylor except to say that "this specimen was cut parallel to the plane of slip, as calculated from measurements of marks in the surface of the specimen. It was ground and etched till the effect of the new cuts had disappeared. This was verified by applying the same treatment to an undistorted specimen. The X ray reflections‡ in this case were perfect ones."¹

Collins, on the other hand, cut his crystals in a mechanical shaper. These

surfaces were polished on No. 1, No. 1/0, No. 2/0 and No. 3/0 papers and on a broadcloth lap using No. 600 alundum as a polishing medium. "Finally, the surface was deeply etched in Tucker's reagent. An undeformed crystal was prepared in the manner described and X rayed to determine whether or not the machining and polishing operations had produced any strain or distortion in the crystal. The Laue spots all seem to be sharp,

free from tails and streaks indicating no detectable strains had been introduced in the crystals."²

Taylor's X ray technique involved the use of "homogeneous X rays from an iron anti-cathode"; whereas Collins used K_{α} radiation of copper at 31kv and 20 milliamperes.

Glancing angle X ray photograms were taken (1) with the axis of rotation of the spectrometer table in the plane of slip and at right angles to the slip direction, and (2) with the axis of the spectrometer table lying along the slip direction.

However, eight minute exposures were used in each case and the angle setting of the spectrometer table was increased by one degree for each exposure.

With the discovery of the action of three slip systems³ in the plastic deformation of single crystalline alpha brass where, formerly, only one had

TN 23 E. Manuscript received June 24, 1949.

* Formerly Research Fellow in Metallurgy, Yale University, New Haven, Conn.; now Assistant Professor of Mechanical Engineering, The Johns Hopkins University, Baltimore, Md.

† Assistant Professor of Metallurgy, Yale University.

‡ Presumably Laue back-reflection photograms.

¹ References are at the end of the paper.

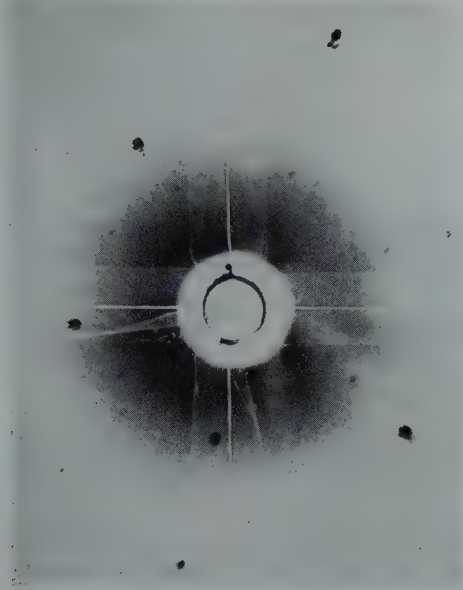


FIG 1—Laue photograph of {111} section from crystal showing absence of streaks or tails.

been considered to have operated, C. H. Mathewson suggested that the experiments of Taylor and Collins be repeated in order to examine critically the possible effects of the deformation process in terms of pole rotations introduced by the action of more than one slip system.

Consequently, the orientation of an undeformed single crystal of alpha brass was determined by the Laue back-reflection method. A disk, with its flat surfaces parallel to a convenient (111) plane, was carefully cut from the crystal with a No. 14B jeweler's saw in a goniometric miter box. The disk was polished carefully by hand on a series of fine files followed by No. 1/0, No. 2/0 and No. 3/0 metallographic papers. The disk was next etched in 1:1 HNO₃ so as to remove at least 0.125 in. from the cut surface. The (111) plane was within one degree of being parallel to the surface as determined by a Laue back-reflection photograph. The effects of cutting and polishing were seemingly removed as adjudged by the condition of the Laue spots shown in Fig 1. Although these spots are multiple indicating lineage imperfections somewhat less than 2° in magnitude, they are sharp and free from tails or streaks as they appeared in first photograph orienting the specimen.

The disk was mounted on a goniometer head set at the proper θ angle (21°30') for primary octahedral reflections. Intense monochromatic copper K radiation was obtained by reflection from the C-cleavage surface of a suitably oriented pentaerythritol crystal. The tube was operated at 31kv and 11 milliamperes. The crystal reflected beam passed through a collimator 2 in. long containing a 1 mm bore. A 1.75 in. specimen to film distance was used. Satisfactory photograms were obtained using 8-hr exposures, Fig 2.

A spread of at least 35° may be seen in Fig 2. This spread in orientation may be interpreted as indicating that mechanically cutting a single crystal affects its structure throughout a considerable thickness. Changing the θ angle to 30° (an increase of 8°30') resulted in a very weak 8° spread after 10 hr exposure.

The depth to which surface preparation disturbances can be detected in single crystals has been considered by Lacombe and Chaudron.⁴ However, their disturbed structures were measured as less than 100 microns dependent upon the material. In the present investigations a minimum of 0.125 in. was removed after mechanical cutting and polishing and yet a disturbed structure was apparent, when

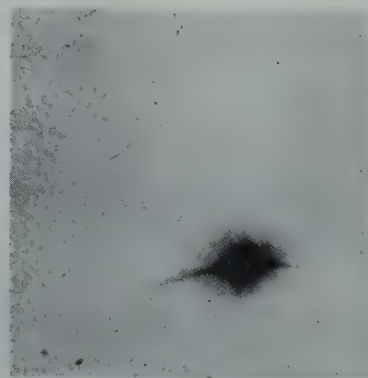


FIG 2—Glancing angle photogram of the crystal showing spread in orientation of the {111} plane.

$\theta = 21^\circ 30'$; monochromatic radiation; eight hour exposure.

investigated with directed characteristic radiation.

Since the present investigation made use of monochromatic X rays rather than white radiation to detect these disturbances and the exposures were considerably longer than those of Taylor and Collins, it would appear that they may not have removed with all certainty the mechanically disturbed surface by their treatments and the method of detection used. This suggests a reinvestigation of their findings, which is under way.

The authors would like to acknowledge the assistance of Mr. Marritt L. Kronberg of this Laboratory for setting up the monochromator.

References

1. G. I. Taylor: Resistance to Shear in Metal Crystals. Cohesion and Related Problems. The Faraday Soc., Nov. 1927, 121.
2. J. A. Collins: Yale Univ., Ph.D. Dissertation, 1939, (cf also Collins and Mathewson, *Trans. AIME* (1940) TP 1145).
3. R. Maddin, C. H. Mathewson, W. R. Hibbard, Jr.: The Active Slip Systems in the Simple Axial Extension of Single Crystalline Alpha Brass. *AIME Trans.* 185, 527 *Jnl. of Metals*, Aug. 1949. TP 2658.
4. P. Lacombe and G. Chaudron: Disc. to R. Maddin: Anomalies in the Appearance of Glide Ellipses. *Trans. AIME* (1948) 175, 355.

Simultaneous Aging and Deformation in Metals

J. D. LUBAHN*

The influence of precipitation from solid solution on the subsequent deformation resistance of alloys is well known. However, the influence of precipitation or aging that occurs simultaneously with deformation may be entirely different and of considerable importance. It is thought¹ that the presence or absence of a yield point jog in impure iron at room temperature and the presence or absence of discontinuous flow at higher temperatures may be directly related to aging phenomena, particularly since the yield point jog is absent when the carbon and nitrogen are sufficiently removed.²

As a preliminary attack on the problem of simultaneous aging and deformation, three kinds of tests—constant strain rate tensile tests, constant load creep tests, and variable strain rate tensile tests—were carried out on an age hardenable aluminum alloy.

Constant Strain Rate Tensile Tests

Stress-strain curves at a strain rate of about 0.001 min^{-1} were obtained for specimens of 61S that had been quenched into liquid nitrogen after a one-hour solution treatment at 521°C , then aged at room temperature 10 min., 20 min., 4 hr, and 26.5 hr before testing. Strain-time curves were obtained on the same chart with the stress-strain curve by means of an auxiliary pen, driven parallel to the axis of the chart drum at constant speed by a synchronous motor and gear chain. The angle of rotation of the chart drum was proportional to strain. The strain rates reported are the measured slopes of the strain time curves. Constant

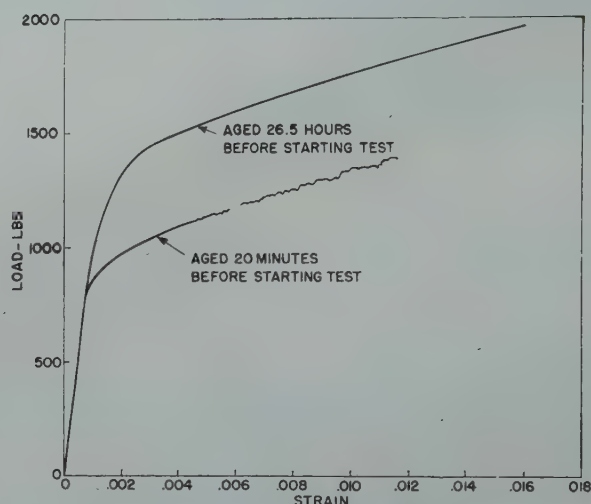


FIG 1—Effect of amount of prior room-temperature aging on the room-temperature stress-strain curve of solution treated 61S. Strain rate = 0.0013 min^{-1}

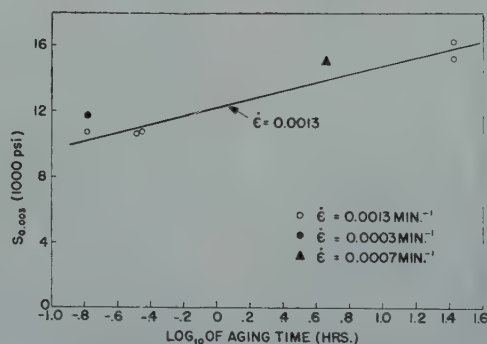


FIG 2—Effect of strain rate and prior room temperature aging on the flow stress at 0.003 plastic strain.

Cleveland Meeting, October 1949.
TP 2697 E. Discussion of this paper (2 copies) may be sent to *Transactions AIME* before Dec. 1, 1949. Discussion is tentatively scheduled for publication in May 1950.

Manuscript received May 2, 1949; revision received July 25, 1949.

*General Electric Co., Schenectady, N. Y.

¹References are at the end of the paper.

strain rate was approximated (within a factor of 2) by manual adjustment of the oil inlet valve of the hydraulic testing machine in such a way that the course of the recorder pen was parallel to pre-drawn strain-time lines of the desired slope.

The specimens were machined from $\frac{3}{16}$ in. rod. The cylindrical portion was 0.357 in. in diam by $1\frac{3}{4}$ in. long and

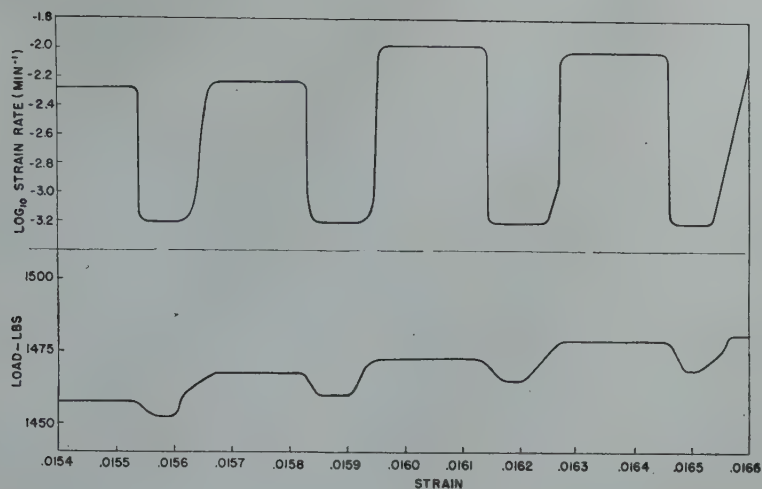


FIG 3—Discontinuous flow in 61S aged 10 min. at room temperature before room temperature testing at 0.00075 min^{-1} (or equivalent rate of head separation during discontinuous flow).

smoothed into the $\frac{1}{2}$ in. — 13 threaded ends by $\frac{1}{4}$ in. fillets. Strain was measured by an averaging Baldwin-Southwark microformer-type strain gauge with a 1.4 in. ga. length between conical points, used in conjunction with a Baldwin-Southwark stress-strain recorder and tensile testing machine.

As expected, the resulting stress-strain curves, two of which are plotted in Fig 1, show that for a given strain rate the flow stress is higher the longer the period of aging preceding the test. The entire stress-strain curve is smooth only for specimens aged for sufficiently long periods of time before testing. Although the early portions of the other curves also are smooth, the later portions exhibit discontinuous flow.*

* The term "discontinuous flow" will be used to designate any failure of the metal to follow a smooth stress-strain curve or strain-time curve.

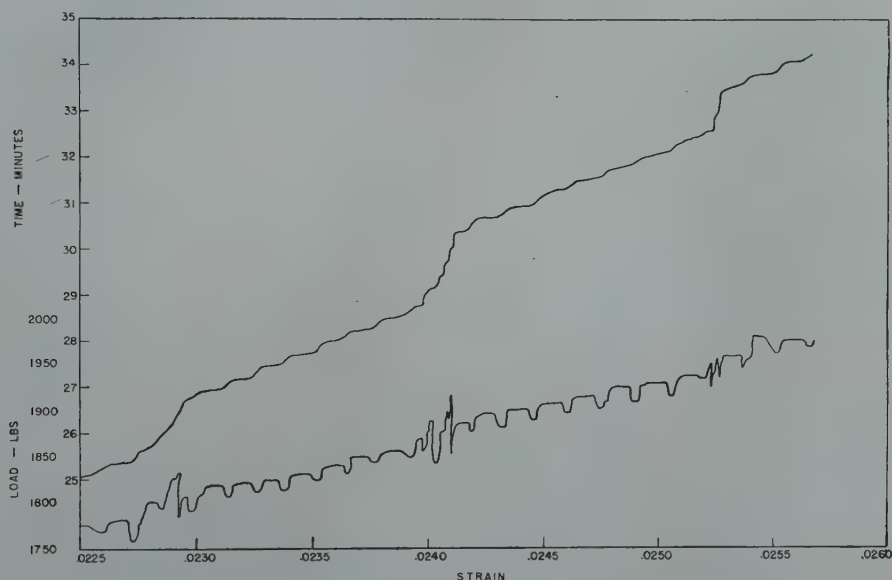


FIG 4—Discontinuous flow in 61S aged 10 min. at room temperature before room-temperature testing at 0.00075 min^{-1} (or equivalent rate of head separation during discontinuous flow).

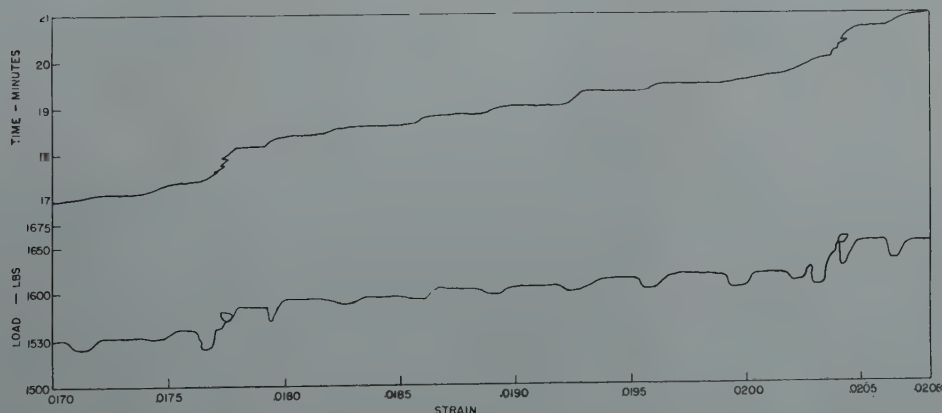


FIG 5—Discontinuous flow in 61S aged 10 min. at room temperature before room-temperature testing at 0.00075 min^{-1} (or equivalent rate of head separation during discontinuous flow).

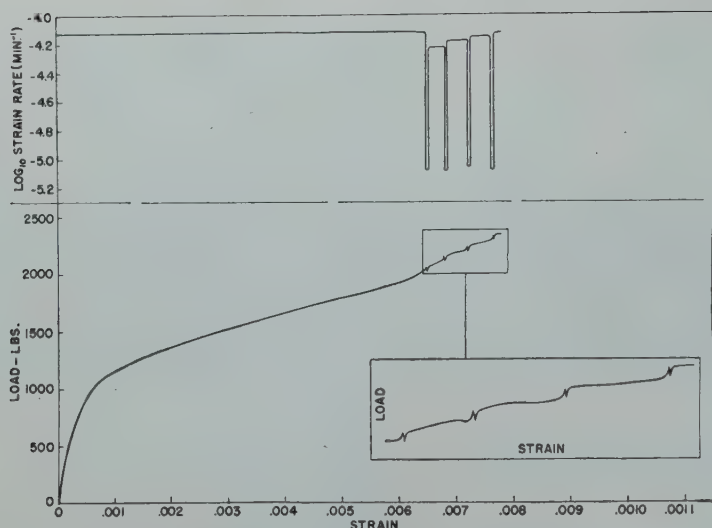


FIG 6—Discontinuous flow in 61S aged 10 min. at room temperature before testing at 0.0003 min^{-1} (or equivalent rate of head separation during discontinuous flow).

For aging times that are not too short, flow stress values can be obtained from the early, smooth portion of each stress-strain curve. Flow stress values at a plastic strain of 0.003 increase with aging time for tests at a given strain rate (Fig 2), and a few tests indicate that a slower strain rate produces a higher flow stress (for a given initial condition of aging). This reverse rate effect will be discussed in connection with another type of test to be described below.

After discontinuous flow began, a constant rate of head separation* was maintained, for it was no longer possible to keep the strain rate constant. The discontinuous flow exhibited different characteristics under different conditions of strain rate, amount of strain, and prior aging treatment. Usually there was a characteristic periodicity of rising and falling load, with slow extension prevailing during each period of falling and rising load and with sudden extension at the maximum load (Fig 3). This periodic flow sometimes was superimposed on a second kind of periodic disturbance (with a longer period) where groups of load variations occurred at regular intervals of strain (Fig 4), or where alternate lengthening and shortening combined with rising and falling load

* The Baldwin-Southwark testing machine had a pump control that provided a constant rate of oil flow for a given position of the inlet valve, regardless of the load. Thus a constant rate of head separation was obtained by keeping a constant opening of the inlet valve. Such a procedure will not produce a constant elongation rate of the gauge length if the load is changing, however, for some of the head motion is used up in fixture deflection. Variations in elongation rate as great as 20 to 1 may be expected for a constant inlet valve setting.

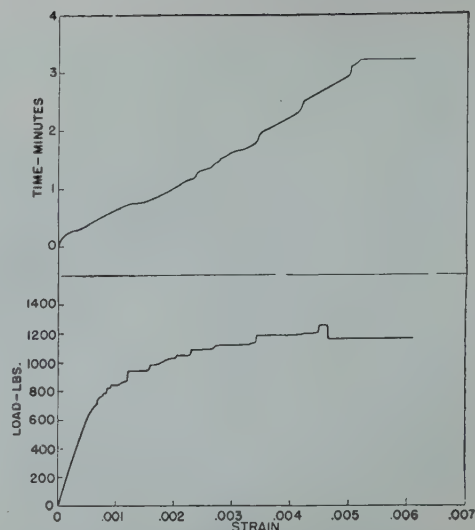


FIG 7—Discontinuous flow in 61S aged 2 min. at room temperature before room-temperature testing at 0.0008 min^{-1} (or equivalent rate of head separation during discontinuous flow).

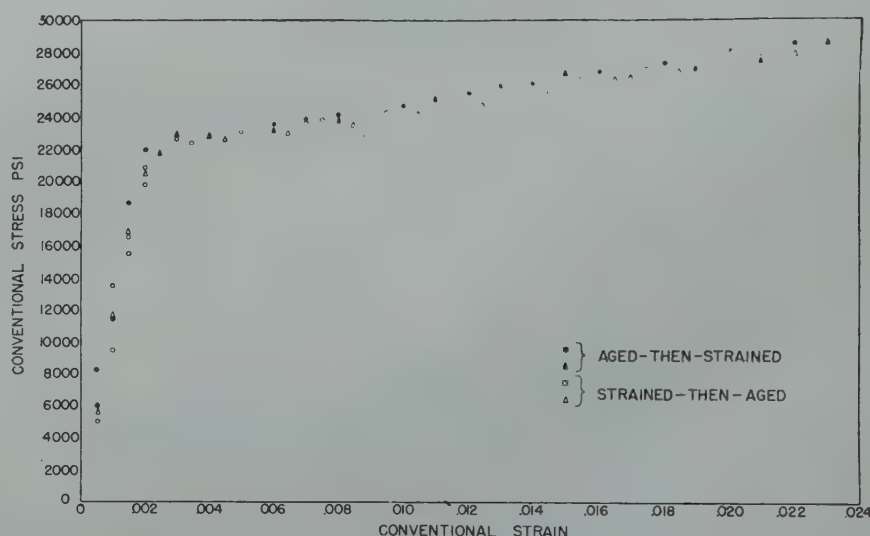


FIG 8—Creep curve for 61ST at room temperature and 41,900 psi initial stress (tested several months after aging).

actually produced loops in the stress-strain curve (Fig 5).

At a smaller rate of head separation, smooth sections of normal stress-strain curve were separated by comparatively short, uniformly-spaced, strain intervals where a very pronounced rising and falling of load accompanied unusually slow extension (Fig 6). When a specimen was tested almost immediately upon warming to room temperature from the liquid nitrogen quenching bath, discontinuous flow began immediately; and under these conditions almost square steps were observed in the stress-strain curve (Fig 7). Similar periodic flow has been observed by McReynolds³ during extension of specimens of several alumi-

num alloys. He employed a very soft tensile machine designed to produce a constant rate of increase of stress, rather than a constant strain rate.

Creep Tests

61ST was subjected to constant-load creep tests at room temperature. The load was applied through an 18:1 lever with three hardened steel knife edges. The knife edges were all in the same plane. The strain time curve was obtained with the same device employed for determining strain rates in tensile tests. The gear train for the time-drive was arranged so that quick changes in speed of 30:1 could be made as required

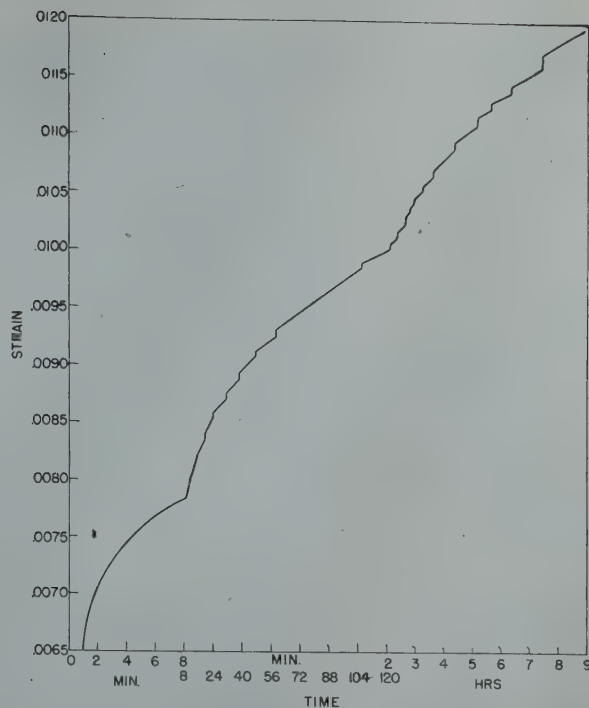


FIG 9—Creep curve for 61ST at room temperature and 42,300 psi initial stress (tested within a few hours after aging).

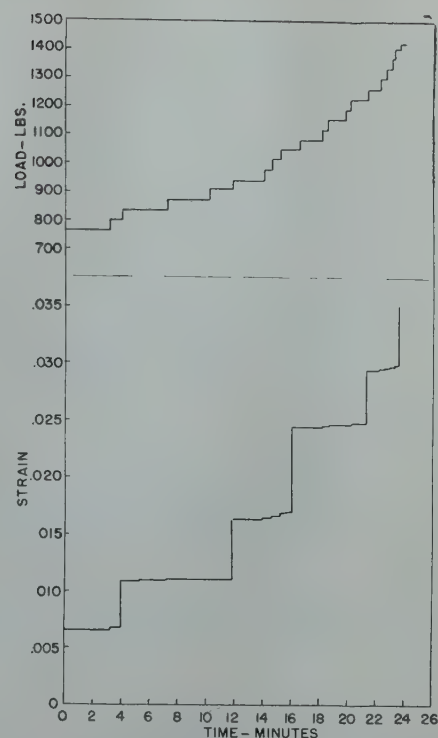


FIG 10—Room-temperature creep behavior at successively higher loads for 61S aged 10 min. at room temperature before beginning the test.

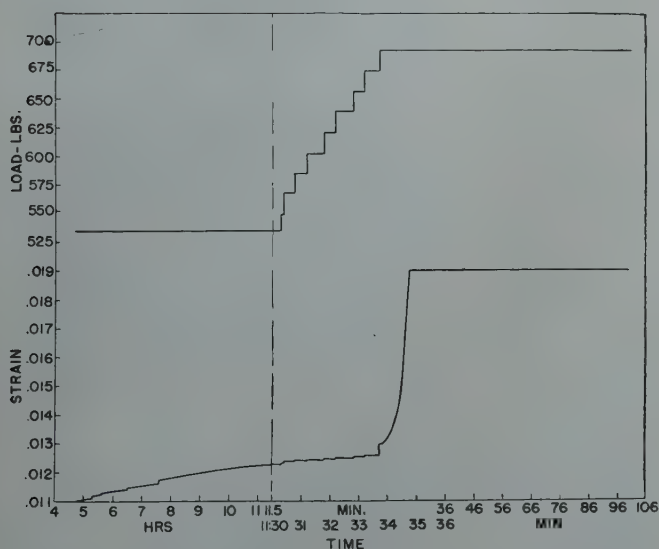


FIG 11—Creep curve for 61ST at room temperature and 42,300 psi initial stress. Tested within a few hours after aging (continuation of the test shown in Fig 9).

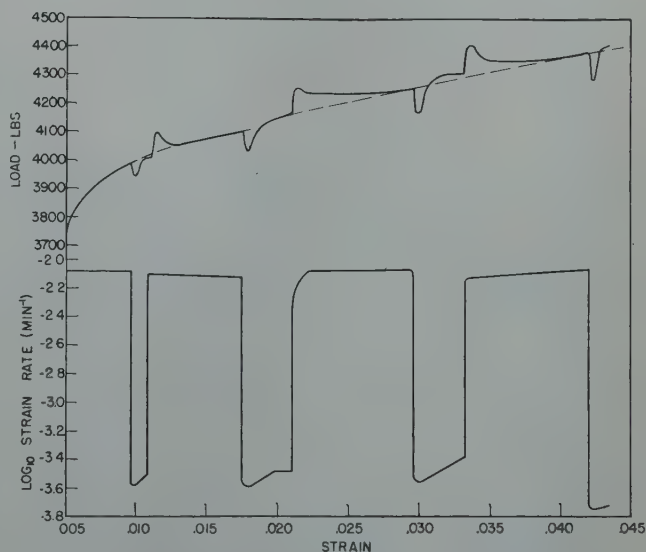


FIG 12—Transient effects in a tensile test on 61ST at room temperature.

to avoid a strain-time curve that was too nearly axial or circumferential for accurate slope measurements. 61ST tested in creep at room temperature several months after commercial aging (8 hr at 350°F) exhibited smooth strain-time curves as shown in Fig 8. On the other hand, 61ST tested within a few hours after the commercial aging treatment exhibited sudden periodic extensions superimposed on a smooth

strain-time curve, as shown in Fig 9. Similar behavior has been observed with copper.⁴ The difference in behavior between 61ST freshly aged at 350°F and that tested long after aging suggests that the freshly aged material had the greater capacity for change at room temperature.

A material that is aging rapidly during deformation ought to exhibit a very pronounced departure from the

behavior of pure metals and other non-aging materials. To check this point, a creep test was made on 61S aged 20 min. at room temperature after quenching into liquid nitrogen from 521°C. Fig 10 shows that a large plastic extension* occurred upon application of the load, after which the material did not elongate further. Furthermore, suc-

* The extension was too rapid for the recorder to follow.

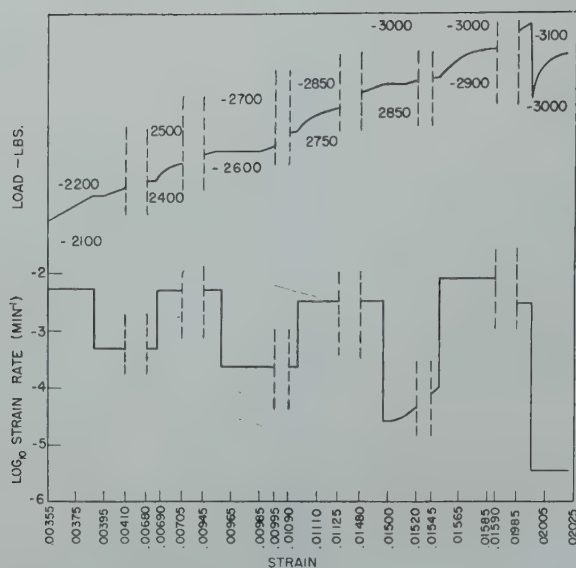


FIG 13—Tensile transients for OFHC copper at room temperature.

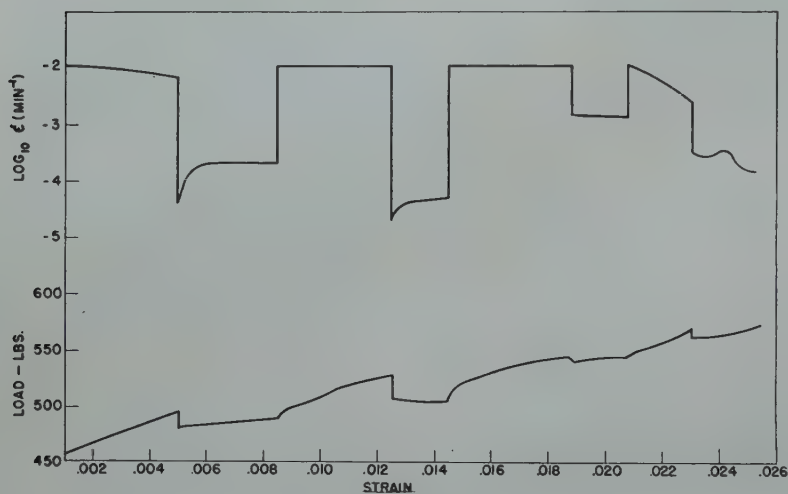


FIG 14—Tensile transients for pure (99.996 pct) aluminum at room temperature.

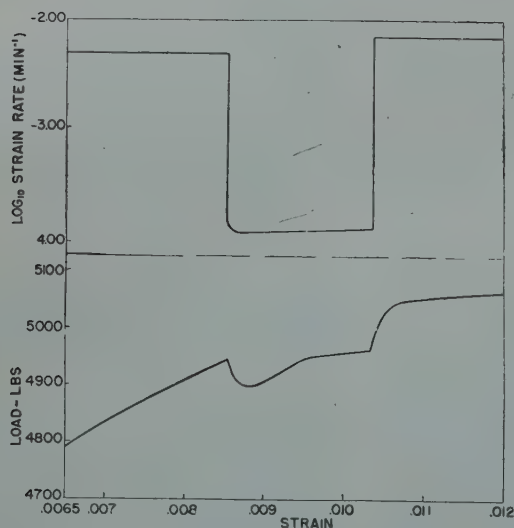


FIG 15—Transient effects in a tensile test on 61ST at the temperature of liquid nitrogen.

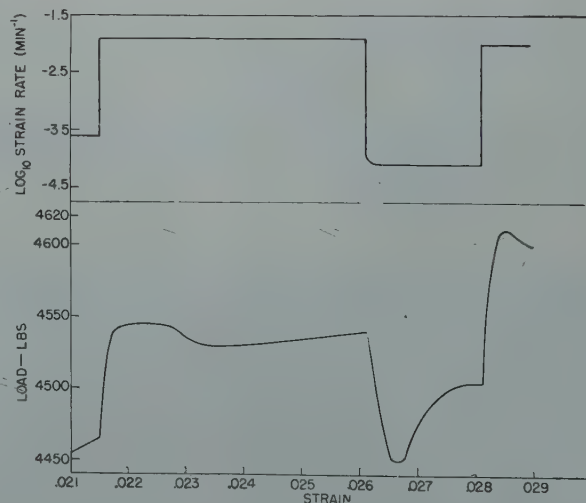


FIG 16—Transient effects in a tensile test on 61ST at the temperature of dry ice.

cessive additions of small load increments never caused gradual straining. After each load increment, either sudden plastic extension occurred or the specimen remained elastic.

The peculiar behavior observed upon successive application of small load increments to a currently aging metal was attributed to the fact that aging was proceeding during the test. If, as suggested above, the deformation behavior of recently aged 61S (61ST) can be affected by further room-temperature aging, then it might be expected that 61ST would exhibit creep behavior similar to that shown in Fig 10 for solution treated 61S. This expectation was realized (Fig 11).

Variable Strain Rate Tensile Tests

In these tensile tests the strain rate was changed suddenly from one constant value to another. When such a change is made, an immediate shift from a stress-strain curve characteristic of one rate to a second curve characteristic of the other rate might be expected. Actually, however, there is usually a period immediately following a rate change where the behavior conforms to neither curve, with rigorous conformity to the new curve being approached later. The temporary disturbance following a rate change has been called a "transient."^{5*}

A peculiar transient is observed for 61ST tested at room temperature. Fig 12 shows that after changing the

* The experimental equipment and procedure for measuring tensile transients are described in ref 5.

strain rate a new stress-strain curve appears to be approached; but then the stress changes in the opposite direction and approaches that corresponding to the curve preceding the rate change. This lack of rate effect for steady deformation (that is, after the dying-out of the transient) of 61ST at room temperature is surprising, for OFHC copper (Fig 13) and pure aluminum (Fig 14) both show a definite (though small) rate effect at room temperature.

The creep tests described above suggested that aging at room temperature could significantly affect the deformation of 61ST; it is possible that aging is responsible also for the peculiar transients and the lack of rate effect in 61ST tested at room temperature. To investigate this possibility, tensile transient tests were made at a series of temperatures. At liquid nitrogen temperature (-194°C) a definite rate effect was observed (Fig 15) and the transient consisted only of a gradual shift from one curve to another, as is observed for non-aging metals (see Fig 14). This behavior would be expected if no aging occurred at -194°C . At the temperature of dry ice (-78°C) there was still a definite rate effect, although overshooting* was observed during the transient (Fig 16). In ice water (0°C) the overshooting during the transient was more pronounced and the rate effect (though small) was in the opposite direction to that observed at lower temperatures; upon increasing the rate, a lower stress-strain curve was approached than that preceding the rate change, and conversely (Fig 17). At 93°C the rate effect was large and in the expected direction, as shown in Fig 18.

The quantity $n = (\log S_2/S_1)/(\log \dot{\epsilon}_2/\dot{\epsilon}_1)^{\dagger}$ was used as a measure of the rate effect. It was found to be roughly constant regardless of the change in rate, as illustrated in Fig 19. The influence of testing temperature on the rate effect is summarized in Fig 20, which shows n to have a pronounced minimum in the neighborhood of room temperature. It might be inferred that the rate effect in 61ST is a combination of an inherent rate effect (that observed in non-aging metals, where higher rates produce higher stresses) and a superimposed, inverse rate effect, due to aging, for which lower rates produce higher stresses. Fig 20

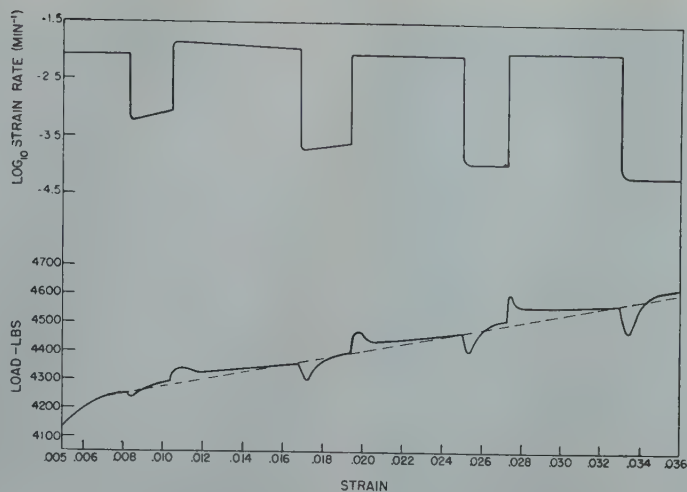


FIG 17—Transient effects in a tensile test on 61ST at 0°C .

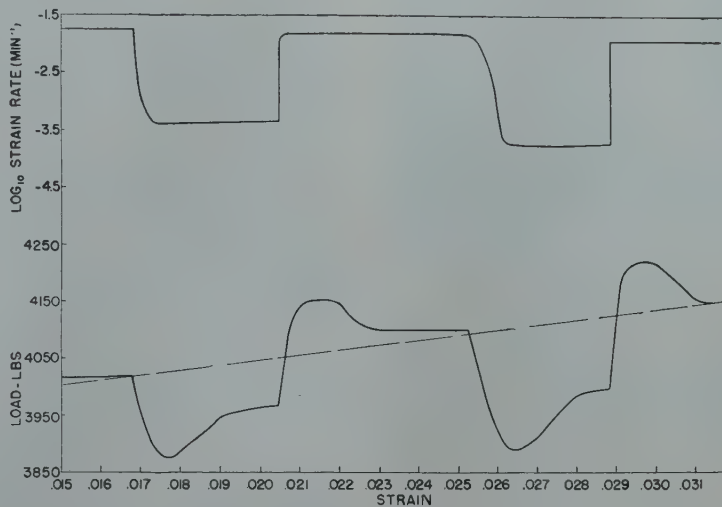


FIG 18—Transient effects in a tensile test on 61ST at 93°C .

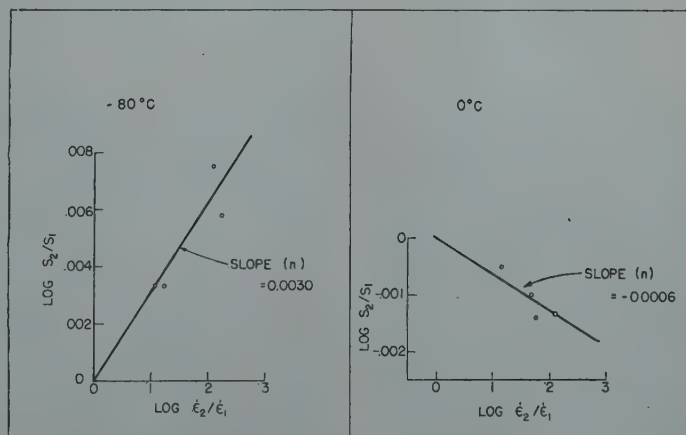


FIG 19—Determination of n values (rate effect) illustrated for two temperatures. Derived from data of Fig 16 and 17.

shows that the contribution of the aging to the overall rate effect is at a maximum near room temperature and disappears in the vicinity of -150°C .

According to the above viewpoint, transients are caused by a disturbance in the balance between two rate ef-

fects. Any disturbance of the balance between the inherent rate effect and the rate effect due to aging, such as a temporary pause in the plastic straining, might cause an unusual transient. An experiment on 61ST at room temperature in which a tensile test was

* Overshooting means that the stress changes to a value beyond that characteristic of the new strain rate, then slowly returns.
† The symbol ϵ denotes strain rate.

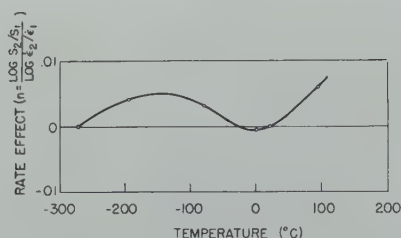


FIG 20—Effect of testing temperature on the rate effect for 61ST.

temporarily interrupted by a sojourn at a slightly lower load yielded such a transient following the interruption, even though the strain rate was the same before and after the interruption (Fig 21).

Conclusions

If a metal is aging while it is being plastically deformed, it may show unusual deformation characteristics as follows:

1. Discontinuous yielding in a tensile test.
2. Periodic sudden extensions in a constant load creep test.
3. Failure ever to undergo gradual extension at constant load.
4. Unexpected transients following a sudden rate change.
5. An inverse rate effect, where an

increase in flow stress (beyond the transient) is required to maintain a smaller strain rate.

Acknowledgment

The careful work of Miss Helen Lequear in performing the experiments is gratefully acknowledged

References

1. P. Ludwik and R. Scheu: The Yield

Point of Electrolytic Iron and Mild Steel. *Ber. Fachausschusse Ver. Deut. Eisenhüttenleute* (1925) 5, 1.

2. J. R. Low, Jr., and M. Gensamer: Aging and the Yield Point in Steel. *Trans. AIME* (1944) 158, 207.
3. A. W. McReynolds: Plastic Deformation Waves in Aluminum. *Trans. AIME* 185, 32: *Jnl. of Met.*, Jan. 1949.
4. E. N. da C. Andrade: On the Viscous Flow in Metals, and Allied Phenomena. *Proc. Roy. Soc.* (1910) 84, 1.
5. R. P. Carreker, J. G. Leschen, and J. D. Lubahn: Transient Plastic Deformation. *Trans. AIME* (1949) 180. *Metals Tech.*, Oct. 1948. TP 2477.

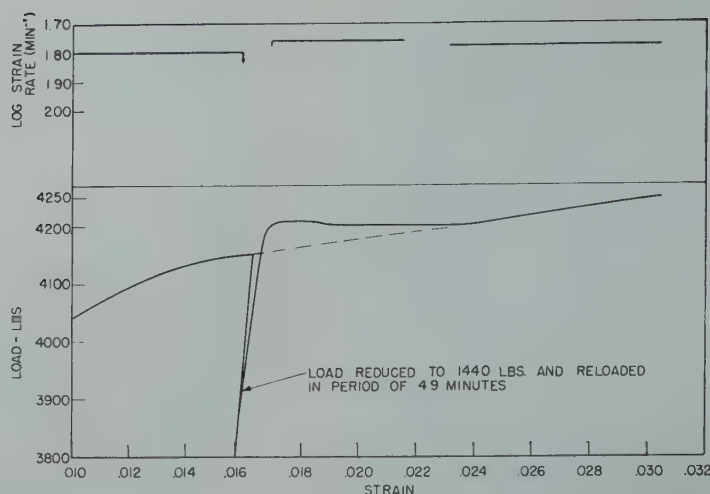


FIG 21—Transient effects at room temperature in 61ST caused by interrupting a constant strain rate tensile test.

On the Problem of Grain Boundary Movement

C. G. DUNN,* Member AIME, F. W. DANIELS,* and M. J. BOLTON*

Recent observations on grain boundary movements in silicon iron have indicated the possibility of studying grain growth phenomena in two-grain specimens in which several variables affecting growth are readily controlled. These variables are (1) the energy per unit area (γ) in the grain boundary, (2) the orientation relationship of the two grains, and (3) the radius of curvature (τ) of the moving boundary.

Ideally, one grain A should be a narrow rectangular parallelepiped adjacent to a second grain B as shown two dimensionally in Fig 1. Such a two-grain group becomes unstable when one end of grain A is shaped according to the dotted line. Since the width w of grain A remains constant during growth of grain B, τ should also remain constant. The other vari-

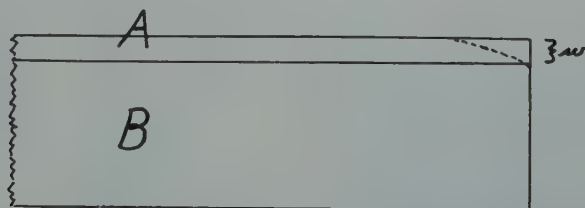


FIG 1—Schematic diagram of two grain-group for studying growth.

ables mentioned above can be controlled in the preparation of each two-grain specimen.^{1,2,3} For a particular orientation of each grain, γ is

not necessarily fixed; γ may also depend on the orientation of the grain boundary, but this may be controlled to some degree.

The energy relationships for the growth of grain B may be derived from the more simple arrangement of two grains A' and B' shown schematically in Fig 2. Here B' largely surrounds A'. Assume these grains are oriented with a common plane parallel with the flat

Technical Note No. 25 E. Manuscript received July 1, 1949.

* Research Physicist, and Metallurgists respectively, General Electric Co., Pittsfield, Mass.

¹ References are at the end of the paper.

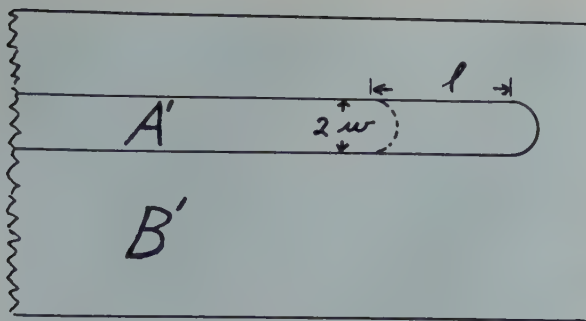


FIG 2—Schematic diagram of two grains A' and B'.

portion of the specimen. Consider equal lengths l of grains A' and A. The total grain boundary energy for A' is twice that for A. Therefore, the width of A' will be taken equal to $2w$ so that both grains have the same grain boundary energy for transferring a unit volume of metal from A to B or A' to B'. When a volume V —that is, $2wlt$, where t is the thickness of the flat specimen*—transfers to B or B', the energy E released is obviously given by the following equation:

$$\frac{E}{V} = \frac{\gamma}{w} \quad [1]$$

Thickness of the specimen does not enter this equation. Consequently, growth in such two-grain specimens should be independent of thickness. If γ is independent of grain boundary orientation, the shape of the active part of the grain boundary should reasonably approach a semicircle. When this occurs, w becomes identical with the radius of curvature τ of the advancing part of the boundary and Eq 1 then expresses the usual driving force for grain growth.⁴ If γ varies with grain boundary orientation, γ in Eq 1 applies to the straight part of the boundary.

In the application of Eq 1 to grains A and B, it is assumed that the edge of grain A does not introduce an energy term. If a surface energy is involved, Eq 1 should be modified. It is also believed that w and τ may be different merely because a groove tends to form at the open end of the curved grain boundary. The term to use in Eq 1, therefore, is w rather than τ .

The present technique permits a time-temperature investigation at constant curvature to be made. Also, the rate of grain boundary movement can be measured as a function of temperature alone and the results used to calculate activation energies.

That the above method is experi-

mentally feasible is indicated by the following example from our preliminary work. Silicon iron specimens capable of supporting exaggerated grain growth were prepared in the form of long strips 0.025 in. thick. Using a controlled grain growth technique,¹ one strip was converted into a suitable two-grain specimen with the common grain boundary lying parallel to the long dimension. The (110) planes of both grains were in the plane of the strip, and the [001] directions were 25° apart.

A 1 in. length cut from this specimen was annealed 4 hr at 1400°C in pure dry argon to eliminate boundary irregularities and to reveal the position of the boundary by thermal etching.⁵ A final small two-grain specimen was prepared from the annealed piece and given an anneal of 10 hr at 1400°C in pure dry argon.

A photograph of the specimen in the as annealed condition is shown in Fig 3. The old boundary position extends across the length of the specimen. The new boundary (one end indicated by arrow) is curved along the advancing portion and coincides with the old boundary for a short distance. Observing these thermally etched boundaries at about 300 diam magnification, the old boundary appears as a "ghost line" whereas the new boundary is well defined. Reality of the new boundary was also confirmed by an X ray Laue photograph.

The specimen was then annealed an additional 48 hr at 140°C. No movement of the grain boundary occurred. It appears that the advancement was stopped by inclusions during the first anneal.

An estimate of the available energy for growth is of interest. With γ equal to 500 ergs per cm² approximately^{6,7} and w equal to 1.3 mm, Eq 1 gives, on changing units, a driving energy of 0.00009 cal per cm³. This energy may be contrasted with the value 9 cal per cm³ reported for cold worked iron.⁸ Larger values of γ/w could be obtained using smaller values of w .



FIG 3—Photograph of a two-grain specimen showing growth of one grain. Thermal etch. $\times 10$.

More information using the present technique is anticipated from investigations now under way at this laboratory. It is hoped that results may be reported in the near future.

References

1. C. G. Dunn: Controlled Grain Growth Applied to the Problem of Grain Boundary Energy Measurements. *Trans. AIME* 185, 72; *Jnl. of Met.*, Jan. 1949, T.N. No. 9.
2. C. G. Dunn and F. Lionetti: The Effect of Orientation Difference on Grain Boundary Energies. *Trans. AIME* 185, 125; *Jnl. of Met.*, Jan. 1949.
3. T. S. Tiedema: To be published in *Cryst. Acta*. See also W. G. Burgers: Discussion TP2517E *Trans. AIME*, to be published in *Jnl. of Met.*
4. C. S. Smith: Grains, Phases and Interfaces: An Interpretation of Microstructures. (See reference to work of Zener.) *Trans. AIME* (1948) 175. *Metals Tech.* June 1948, TP2387.
5. B. Chalmers, R. King, and R. Shuttleworth: The Thermal Etching of Silver. *Proc. Roy. Soc.* (1948) A 193, 465.
6. E. Orowan: Polycrystalline Metals and the Effect of Cold Work. (Discussion), *Proc. Phys. Soc.* (1940) 52, 136.
7. W. Shockley and W. T. Read: Quantitative Predictions from Dislocation Models of Crystal Grain Boundaries. *Phys. Rev.* (1949) 75, 692.
8. H. Quinney and G. I. Taylor: The Emission of the Latent Energy Due to Previous Cold Working When a Metal is Heated. *Proc. Roy. Soc.* (1937) 163, 157.

* The value of t at the boundary is assumed to be essentially the same as the value of t everywhere else.

The Transverse Bending of Single Crystals of Aluminum*

M. K. YEN† and W. R. HIBBARD, JR.,‡ Junior Members AIME

Previous studies of plastic deformation of metals have emphasized the important role of bending and constraints during strain under relatively pure stresses.¹⁻⁵ Some new phenomena such as early conjugate slip⁶ and polygonization⁷ are intimately concerned with the relief of bending stresses, the former by slip and the latter by a process analogous to recrystallization. However, few analyses of the bending deformation of single crystals were found in the literature, and those^{8,9} are sufficiently previous to the modern interpretations of slip to invite further investigation in this area.

The transverse bending mode of testing, using the two-point loading method, was selected because the center portion of the specimen may be considered as under a theoretically pure bending stress with a uniform bending moment. Considerable attention was given to both the lattice distortion and flow characteristics of the crystals during deformation.

Experimental Procedure

A specimen under the action of equal and opposite couples at both ends is said to undergo pure bending. The shear and moment diagrams of a specimen under the two-point loading method of transverse bending are shown in Fig 1. The moment over the middle-third of the span is equal to $PL/6$, and the vertical shear is zero. Fig 2(A) illustrates the stress distribution in the elastic range on a plane across the middle of the specimen. It can be seen that the normal stress has a maximum value at the extreme surfaces on the tension and compression sides, and decreases proportionately to zero as it approaches the neutral plane.

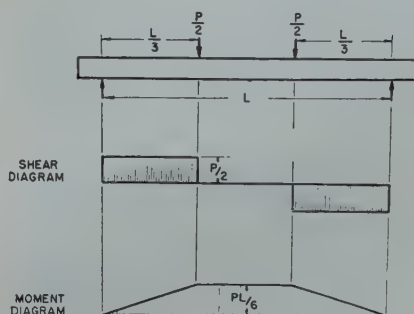


FIG 1—Shear and moment diagrams of a beam under transverse bending by the two-point loading method.

However, when the plastic range is reached, the stress distribution is no longer a straight line relation, but changes in a manner which can be best illustrated as shown in Fig 2(B). The following calculation and stress analysis are mainly in accordance with the works reported by Timoshenko¹⁰ and Kochendörfer.⁹

From the simple beam formula, the maximum normal stress will occur at the surface of the specimen. For a round specimen with a radius r and for a rectangular specimen with a height

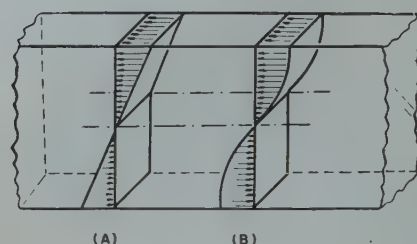


FIG 2—Stress-distribution in a beam for (A) elastic range and (B) plastic range.

$2h$ and width $2b$, the maximum normal stress, S_n , will be given by the following formulas:

For round specimen:

$$S_n = \frac{2PL}{3\pi r^3} \quad [1]$$

For rectangular specimen:

$$S_n = \frac{PL}{8bh^2} \quad [2]$$

Since it is reasonable to consider that slip takes place under the same conditions as in uniaxial loading, the resolved shear stress S_s , along the operative slip direction will be as follows:

For round specimen:

$$S_s = \frac{2PL}{3\pi r^3} \sin \chi \cos \lambda \quad [3]$$

For rectangular specimen:

$$S_s = \frac{PL}{8bh^2} \sin \chi \cos \lambda \quad [4]$$

where λ is the angle between the specimen axis and the slip direction and χ , the angle between the specimen axis and the major axis of the glide ellipse.

It was also reported by Kochendörfer⁹ that the critical bending moment, that is, the bending moment exerted on the specimen to initiate slip, should be higher than the value given by the equations stated above. Based

Cleveland Meeting, October 1949.
TP 2687 E. Discussion of this paper (2 copies) may be sent to *Transactions AIME* before December 1, 1949. Discussion is tentatively scheduled for publication in May 1950. Manuscript received May 2, 1949; revision received July 1, 1949.

* A part of a Dissertation presented by M. K. Yen to the Faculty of the School of Engineering, Yale University in Candidacy for the Degree of Doctor of Engineering, May 1949.

† Research Associate, College of Engineering, New York Univ., New York City.

‡ Assistant Professor of Metallurgy, Yale University, New Haven, Conn.

References are at the end of the paper.

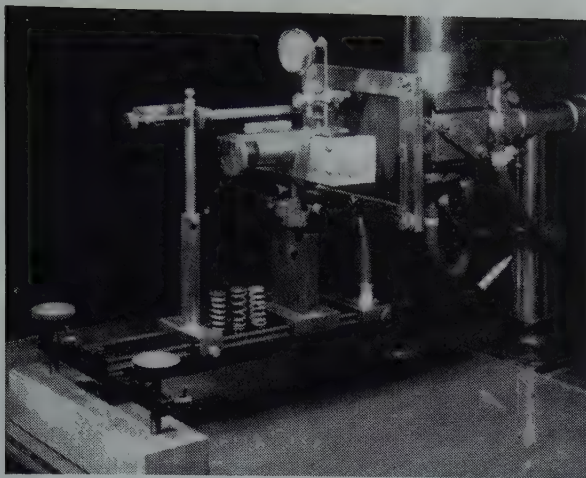


FIG 3—Bending apparatus assembly at X ray tube.

upon his analysis, the critical shear stress observed in bending may be 1.5 to 1.7 times greater than that in uni-axial loading for rectangular and round specimens respectively.

A special bending device to apply a transverse load by the two-point loading method used in this investigation consisted of three major parts: 1. Back-reflection camera with demountable pin-hole system. 2. Bending fixture with load-measuring device. 3. Deflectometer with a dial indicator.

The assembled equipment is shown in Fig 3. The back-reflection X ray camera had two interchangeable collimating pin-hole systems, 1.0 and 0.5 mm in diam.

In the bending device, the specimen was supported by two steel knife-edges with a span of exactly 3 in. The load was transmitted to the specimen through two knife-edges one inch apart which were mounted on a sliding steel plate bearing against a calibrated spring. The load was measured by reading the deflection of the compressed spring on the scale attached. The deflectometer consisted of a pivoted lever which was mounted so that the lower end contacted the center of the back side of the specimen. The upper end of the lever was attached to the stem of a dial indicator whose scale could be estimated to one ten-thousandth of an inch.

Two different types of specimens were made from high-purity aluminum rod having the following chemical compositions:

| | |
|-----------------|--|
| Pct | |
| 99.975 Aluminum | |
| 0.006 Silicon | |
| 0.015 Copper | |
| 0.006 Iron | |

Round specimens, $\frac{1}{4}$ in. in diameter and 4 in. in length were prepared by Found¹¹ using a modified Bridgman method. Flat specimens were produced by a strain-annealing method comparable to that reported by Carpenter and Elam.¹²

The round specimens, used for preliminary work, were carefully metallographically polished by hand and etched with 2 pct hydrofluoric acid. Back-reflection Laue photograms were used to insure complete removal of any distortion.

The flat specimens were cut from strain-annealed pieces mounted in a special fixture which was used as a guide for a No. 8 jeweler's saw to cut along the longitudinal axis. After the sawing was accomplished, the specimen was then alternately polished and etched using 2 pct hydrofluoric acid and emery paper down to No. 000. Subsequent wet-polishing with alumina on a slow-speed wheel provided a smooth surface ready for the final electrolytic polishing.

The electrolytic polishing process used a dilute solution of fluoboric acid with low current density. Any smudge on the surface could be removed by immersing for about one minute in a hot solution containing 35 cc of 85 pct phosphoric acid and 20 g of chromic acid per liter. A subsequent rinsing with distilled water and alcohol and a final drying operation were then necessary.

After the specimen had been prepared according to this method, a one-inch gauge length was scribed on its center portion. A scratch was also made on the end of the specimen to serve as a reference mark for aligning purposes. The specimen was then placed carefully on the bending device

and adjusted in such a manner that the two gauge marks coincided with the two knife edges for load application, and the reference mark was in a vertical position.

The back-reflection Laue method described by Greninger¹³ was used for the determination of crystal orientation.

By suitably arranging a mirror with a binocular microscope, the front and top surfaces of the specimen could be observed concurrently during loading.

The load on the specimen was applied by gradually turning the knob on the back of the compressive spring which pushed the two knife edges forward against the specimen. The compression of the spring as well as the corresponding deflection of the specimen were recorded simultaneously so that the load-deflection curve could be made. X ray photograms and micrographs were taken at successive deflections of about 50 thousandths of an inch, in addition, to analyze the various surface markings.

Discussion of Results

Ten crystals, four round specimens and six flat ones, were investigated. The round specimens, approximately $\frac{1}{4}$ in. in diam, were used for preliminary work. Flat specimens A-10, A-11, and A-12 were bent after electrolytic polishing. Flat specimens A-13, A-14, A-15 were tested after mechanical polishing and etching with a dilute solution of hydrofluoric acid. The designations, dimensions and initial orientations for all specimens are shown in Table 1. In order to simplify

Table 1 . . . Dimensions and Initial Orientations of Round and Rectangular Specimens

| Specimen | Dimension, In. | Area of Cross-section Sq In | Initial Orientation | | |
|-------------|----------------|-----------------------------|---------------------|-----------|--------------------------|
| | | | χ | λ | $\cos \chi \sin \lambda$ |
| Round | A-2 | 0.218 diam | 0.0374 | 43° | 0.431 |
| | A-3 | 0.243 diam | 0.0464 | 38° | 0.406 |
| | A-4 | 0.242 diam | 0.0461 | 52° | 0.412 |
| | A-5 | 0.241 diam | 0.0456 | 40° | 0.509 |
| Rectangular | A-10 | 0.132 × 0.221 | 0.0292 | 49° | 0.456 |
| | A-11 | 0.132 × 0.223 | 0.0294 | 49° | 0.456 |
| | A-12 | 0.129 × 0.224 | 0.0289 | 42° | 0.497 |
| | A-13 | 0.128 × 0.239 | 0.0303 | 42° | 0.497 |
| | A-14 | 0.132 × 0.227 | 0.0300 | 41° | 0.525 |
| | A-15 | 0.132 × 0.225 | 0.0297 | 41° | 0.525 |

the description of different positions on the specimen, the following designations are used: The "front" and "back" are the convex and concave sides on the bent specimen. The symbols "Top-T" and "Top-C" indicate

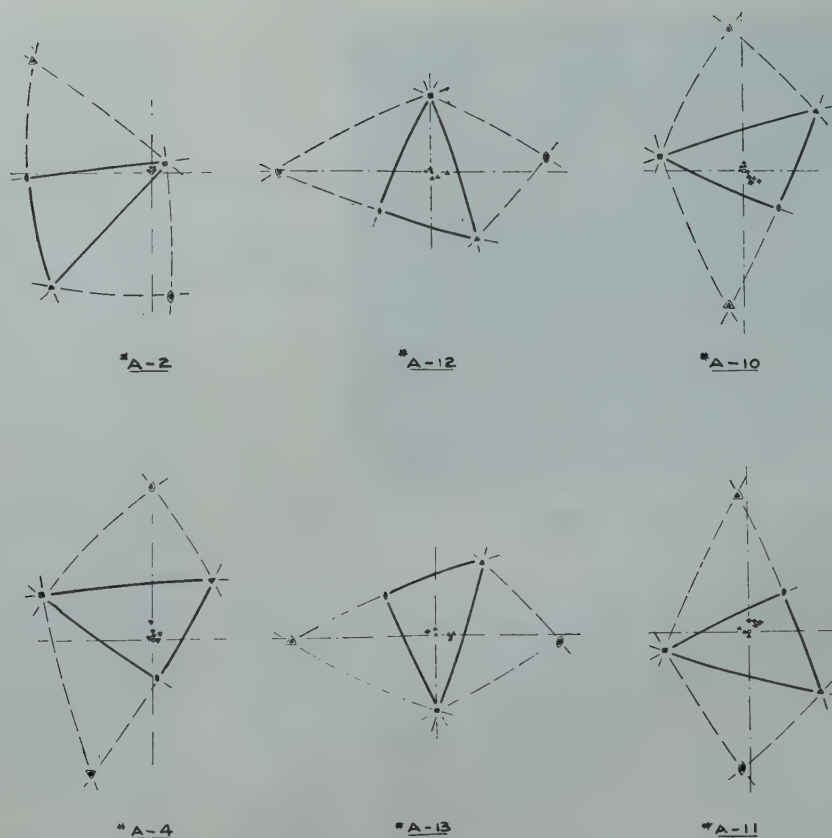


FIG 4—Axis rotations of bending specimens.
(▲) tension side and (+) compression side.

the regions on the top surface near the tension and compression edges respectively. For round specimens, only the symbols "front" and "back" are applicable. Unless otherwise noted, photograms and micrographs are taken with the stress axis horizontal and in the plane of the page.

Lattice Rotation in Bending

Axis orientations for the unstrained crystals and after various amounts of bending are shown in Fig 4. The axis of the unstrained crystal is designated by the small circle (o) at the center of the projection. The axes determined at the front and back side of the specimen after bending are represented by the triangle (▲) and cross (+) respectively. Thus the movement of the specimen axis relative to the axis of the unstrained crystal was observed.

For a single crystal subjected to tensile loading, the lattice rotation takes place in such a way that the slip direction gradually approaches the stress axis. For compression, the slip plane rotates toward a position parallel to the plane of compression. In the case of f.c.c. metals, the specimen axis dur-

ing simple slip moves toward [110] and [111] for tensile and compressive stresses, respectively, whereas in duplex slip the end positions are [112] and [110] for tension and compression respectively.^{14,15} Referring to Fig 4, it can be seen that when aluminum crystals were subjected to bending stress, the stress axis on the tension side of all specimens appeared to follow generally the Taylor and Elam rotation¹⁴ toward the active slip direction. However, in the compression side, the change of orientation deviated from the path toward the (111) pole to a certain extent. In specimens A-10 and A-11, the axis on the compression side appeared to rotate toward a (110) pole instead of the (111) pole. This deviation could be ascribed to the restriction of flow in bending and possibly the presence of a secondary slip system.

Micrographic Observations

Round specimens A-2, A-3, A-4, and A-5 were prepared by polishing and deep-etching. It was noted that both the interlineage boundaries and a slight cored structure, similar to that in copper crystals observed by Hibbard,¹⁶ were developed. However, the

interdendritic spacing of the cored structure was considerably smaller than that of copper. A considerable number of slip lines were observed on the front and back surfaces even at very low deflection. The slip lines were localized in character but were gradually propagated toward the neutral plane as the load increased. The density of the lines also increased with an increase of load, but approached a constant value of approximately 1200 per inch at higher deformation. The lines generally appeared fairly equally spaced but slightly wavy in appearance.

Flat specimens A-10, A-11, and A-12 were prepared by mechanical polishing followed by the electrolytic polishing. Fig 5 and 6 show two photographs of specimen A-10 after a total deflection of 0.554 in. It was found that the surface markings on the top surface started at the edges of the specimen and moved toward the neutral plane with an increase in deformation. The density of lines increased with the degree of deformation but decreased as they approached the neutral plane. Considerable shift of the neutral axis toward the compression side was observed at higher deformation. This can be ascribed to the difference in specimen thickness between the tension and

compression sides caused by plastic flow and the resulting change in the stress distribution.

At first glance, no marked difference in the microscopic appearance of the markings on the tension and compression sides was observable at a magnification of 100 \times . However the microstructures at high magnification exhibit a rather distinctive aspect shown in Fig 7 and 8. Parallel narrow dark lines could be resolved on the tension side, but poorly defined light-colored bands with considerable width were observed on the compression side.

The development of markings on the front surface of these specimens started with equally spaced parallel lines (see Fig 9). The density of lines increased two fold as the deflection increased from 80.5 to 250.0 thousandths of an inch. Another set of markings inclined 45° to the specimen axis then appeared during further bending. The 45° lines appeared discontinuous in nature and were displaced where they met the vertical ones (see Fig 10). It was found that the lines inclined at 45° were the expected octahedral traces, whereas the vertical ones were thought to be cubic traces at an early stage of the investigation. In Fig 11 the crystal orientation of specimen A-10 is plotted on a stereographic projection with the pole of the front surface located at the center of the primitive circle. The traces of the markings on both the front and the top surfaces are sketched in the upper-left corner of the drawing. The loci of the poles of traces Top-I and Front-I intersect at a pole of an octahedral plane which was found to be the primary operative slip-plane having the maximum value of resolved shear stress. Trace Front-III was found only with slight oblique illumination at low magnification. (See Fig 6.) It appears as a band-like structure which makes an angle of about 90° with the octahedral traces. This band-like structure could not be resolved at higher magnification and may be regarded as evidence of a type of rotation of crystallites about an axis normal to the slip plane described by previous investigators.^{17,18}

The trace Front II, which made an angle of about 90° with the specimen axis, was a somewhat confusing one. Referring back to Fig 11, the most probable plane in the zone of the axis is a cubic or a (100) plane. Since cubic slip does occur in aluminum at high temperatures, it led to the possibility that the cubic plane might slip under a

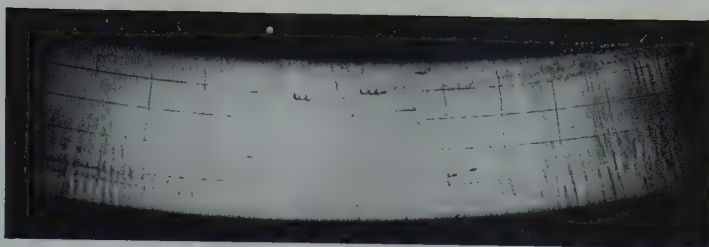


FIG 5—Specimen A-10. Top surface after 0.554 in. deflection. 4 \times .

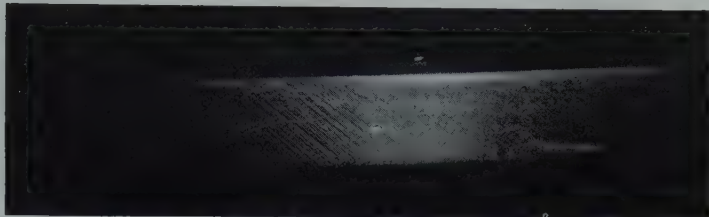


FIG 6—Specimen A-10. Front surface after 0.554 in. deflection. 4 \times .

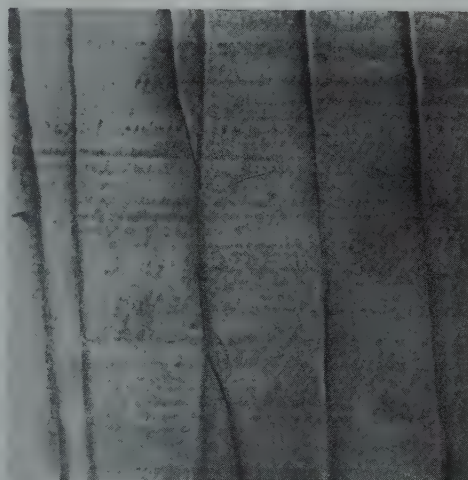


FIG 7—Specimen A-10. Surface Top-T after 0.250 in. deflection. 1000 \times .

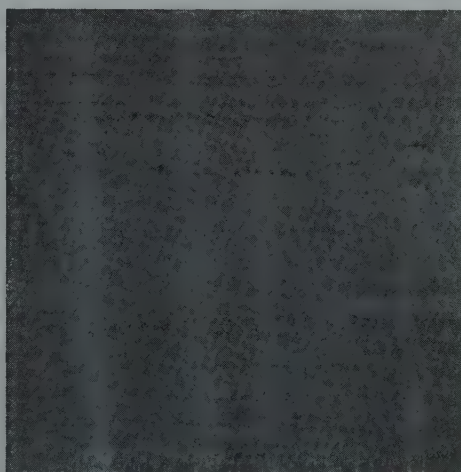


FIG 8—Specimen A-10. Surface Top-C after 0.250 in. deflection. 1000 \times .

rather complicated stress introduced by bending. Similar results were also found in specimens A-11 and A-12. The orientation of specimen A-11 is shown

in Fig 12. By further study of specimen A-11 vertical traces Front II and Top I were established as continuous traces from the same plane. Referring to Fig

12, the pole of these two vertical traces Front II and Top I must be in the neighborhood of the specimen axis, but no significant plane could be found in that region of the projection. It appears therefore, that a possible explanation is that these lines are strain markings or cracks in the anodic coating left from electrolytic polishing. Further experiments on the specimens prepared by mechanical polishing and etching substantiate this finding.

When the specimens A-10 and A-12 were subjected to bending with a deflection of a tenth of an inch, a second set of slip markings (Top Trace II) was revealed at the Top-C surface of the specimens. From the analysis of the surface markings shown by Fig 11, it can be seen that these were the traces of a secondary octahedral plane. This was found to be in the (111) plane which had the second highest resolved shear stress among the twelve (111) [110] systems. The early occurrence of the secondary slip system may be ascribed to the restriction of flow at the compression side which varies from the condition for a crystal under pure compression and thus forces the secondary system into operation. Referring back to the projections showing lattice rotation, Fig 4, it can be seen that the rotation on the compression side is different from that in uniaxial loading in that the specimen axis was rotated toward the (110) direction and not toward the pole of the slip plane as in pure compression. This appeared to collaborate the microscopic observation of double slip since it is known that the [110] direction is usually the end position of the duplex slip for face-centered

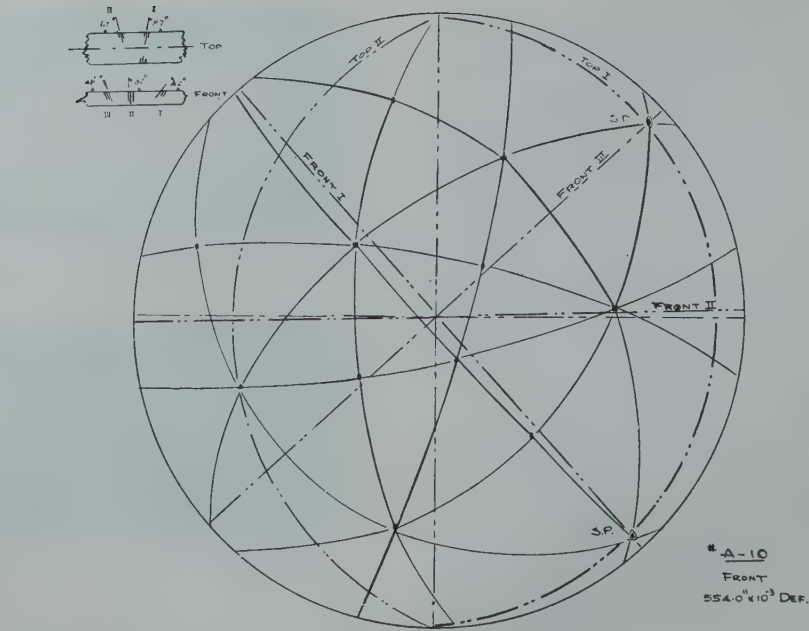


FIG 11—Stereographic profection of specimen A-10 after 0.554 in. deflection with front surface parallel to the plane of the projection.

cubic crystals under compression.

In order to eliminate the uncertainty in the surface condition introduced by electrolytic polishing, specimens A-13, A-14, and A-15 were subjected only to mechanical polishing with fine alumina followed by etching with diulte HF solution. No appreciable difference was noticed in microscopic appearance of surface markings at low magnification between specimens with or without electrolytic polishing. The band-like structure found in specimen A-15 was comparable to that in Fig 6 of specimen A-10. In addition, a similar type of band structure both parallel and per-

pendicular to the traces of the operative slip plane of specimen A-13 was found.

However, at high magnification only traces of the theoretically predicted octahedral plane were observed. Except at Top-C surface of specimen A-13, a secondary set of slip markings was found to be the traces of the octahedral plane having the second highest resolved shear stress among all twelve possible slip systems. The slip markings generally appeared to be fairly straight and equally spaced. It was found, however, in the neighborhood of the region where the slip direction intersected the specimen surface that the markings ap-

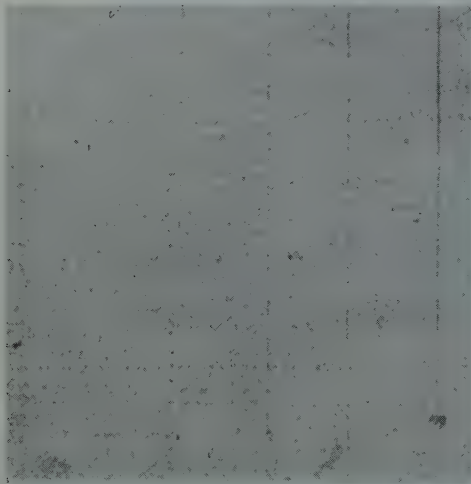


FIG 9—Specimen A-10. Front surface after 0.081 in. deflection. 500 X.

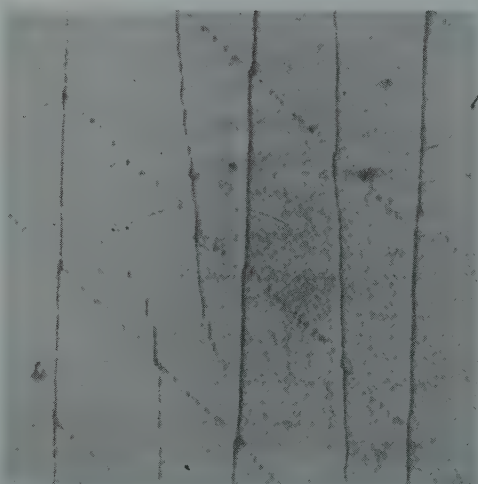


FIG 10—Specimen A-10. Front surface after 0.554 in. deflection. 1000 X.

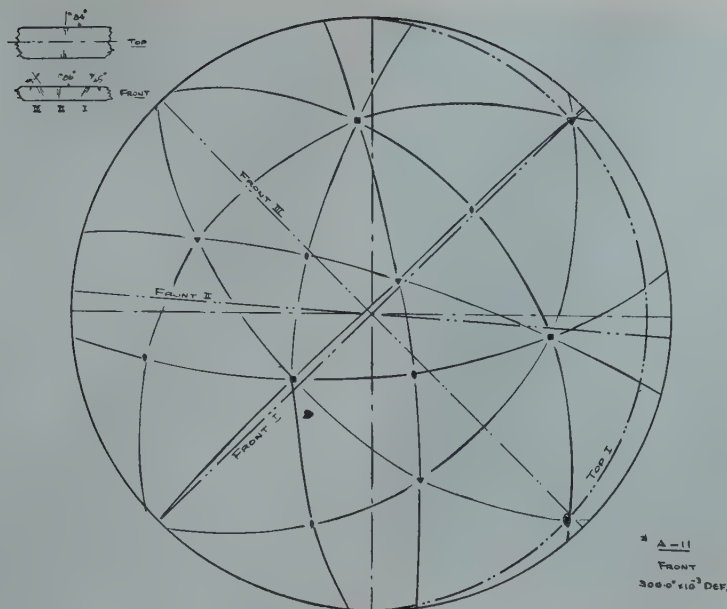


FIG 12—Stereographic projection of specimen A-11 after 0.300 in. deflection with front surface parallel to the plane of the projection.

peared to be either step-like or discontinuous in nature. Fig 13 shows slip markings on the Top-T surface and front surface of specimen A-15. The markings appeared to be straight and had an average distance between them of from 5 to 10 microns. The closest approach distance was in the order of one micron. Fig 14 shows slip markings on the front surface of specimen A-13 at $\times 1000$ magnification. The pictures were taken on the surface where it is intersected by the direction of slip. The short step-like markings appeared not to follow any definite crys-

tallographic angle as reported in alpha brass.¹⁹ This may be due to the more complicated stress condition in bending where these steps were probably too small to be identified with any particular planes. Similar results were also found in specimen A-15 on the Top-T surface where it was intersected by the direction of slip (Fig 13). Regions showing the discontinuity of markings were also observed in both specimens A-13 and A-15. These markings were similar to those reported by Crussard²⁰ in aluminum crystals as well as by Andrade²¹ in deformed lead crystals.

They generally lost their width accompanied by a great decrease in their intensities as they passed each other. It is also interesting to note that the phenomenon of bending of the glide-lamellae did take place in specimen A-15 as shown in the upper edge of Fig 13.

Slip markings of specimen A-15 under oblique illumination are shown in Fig 15, and appear to be dark and light bands on the tension and compression sides respectively. The regions free from any resolvable slip markings are close to the neutral plane, at which the stress should be theoretically zero. The density of the markings on both sides increased from the inside outward and gradually approached a constant value at the edges of the specimen.

Asterism

When a crystal is deformed by uniaxial loading, distortion generally occurs by rotation of the crystallites about an axis lying in the slip plane normal to the slip direction. This type of rotation was more or less confirmed by analysis of the Laue spots obtained from deformed crystals.²⁻⁵ Recently it was found that in addition there is also a relocation of glide-lamellae by a twisting distortion around the polar axis of the slip plane.^{17,18} However, in the present investigation, the asterism of Laue spots in the X ray photographs did not appear to follow either of these types of distortion. The change of the Laue spots always exhibited the same



FIG 13—Specimen A-15. Top-T surface after 0.389 in. deflection. 1000 X.



FIG 14—Specimen A-13. Front surface after 0.300 in. deflection. 1000 X.

pattern regardless of the initial orientation or the orientation of the operative slip plane with respect to the stress axis. In general, the Laue spots on the photograms taken from the Front surface were elongated in the direction parallel to the specimen axis, whereas those from the Back surface were distorted so as to become elongated in the direction 90° to the former ones. However, no appreciable change in the shape of Laue spots on either the Top-T or Top-C surface was noticeable.

Fig 16 shows the change in shape of Laue spots on the Front surface of specimen A-10 with an increase in deflection. It can be seen that the elongation of spots did not occur until the specimen was subjected to bending far beyond the elastic range. This may be regarded as evidence in favor of the idea that asterism does not indicate the existence of elastic strain, but rather plastic deformation resulting from bending.

Fig 17 shows the types of Laue spots obtained from the Front, Top-T and Back surfaces of two other crystals, A-11 and A-15, with different initial orientations. It is apparent that all the specimens exhibited the same type of distortion as far as the nature of the asterism is concerned. It appears that the axis of rotation causing the asterism on the tension side is in vertical direction while that on the compression side

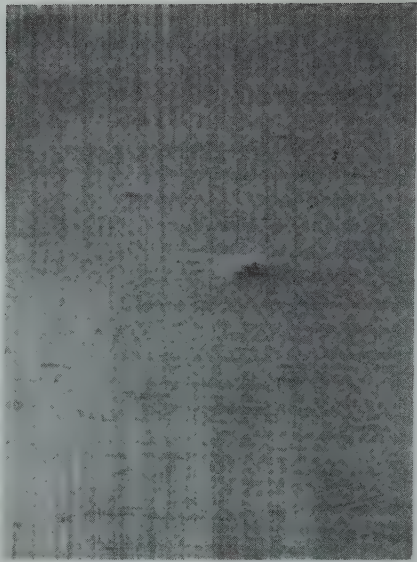


FIG 15—Slip markings on the top surface of specimen A-15 near the neutral plane. The dark markings are near the tension side and the white ones are near the compression side. 50 X.
Reduced one-half in reproduction.

is horizontal. The fact of no appreciable change of Laue spots from the top surface of the specimen further confirms these rotation axes.

Furthermore, it was also found that in specimens A-12 and A-13 the Laue spots were not only elongated but also divided into small individual areas as shown in Fig 18 and 19. The traces of the active slip plane are indicated in

the left corner of the photogram. It can be seen that the fragments of the spots appear to be aligned in a specific pattern, divided into two groups, one roughly parallel to the traces and the other normal to it. This break-up of the Laue spots in deformed crystals after annealing was observed by Collins and Mathewson¹⁷ in aluminum and by Andrade and Tsien²² in potassium and sodium. Very recently, Cahn⁷ in a study of bent zinc crystals suggested "the deformation leads to elastic bending of glide-lamellae: when the crystal is annealed, the lamellae undergo 'polygonization.' The orientation of each new grain is the same as that of the part of the original crystal from which it grew but the elastic strain has vanished." In addition, the break-up of the Laue spots was also reported even in deformed aluminum crystals by Crussard.²⁰ It appears that the discrete asterisms in specimens A-12 and A-13 may be rationalized as a process of fragmentation occurring during deformation at room temperature. In Fig 18 and 21, the fragments of the Laue spots parallel to the traces of the operative slip plane as shown at left-upper corner may be regarded as a rotation of crystallites about an axis parallel to the slip plane. The fragments oriented normal to the traces may be rationalized as a break-up of crystallites due to the torsional rota-

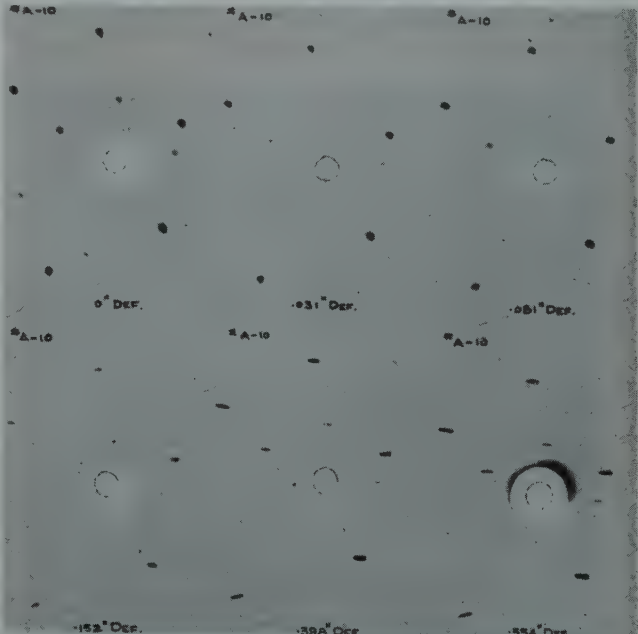


FIG 16—Laue photograms of specimen A-10 after various amounts of deflection as indicated.

FIG 17—Laue photograms of specimens A-11 and A-15 after deflections of 0.300 and 0.266 in., respectively.

Reduced approximately one-third in reproduction.

tion around the pole of the slip plane.^{17,23} The latter was reported recently by Heidenreich and Shockley¹⁸ from a study of Laue spots and Kikuchi lines produced on electron diffraction patterns of extended aluminum crystals.

Load-deflection Diagrams

The load-deflection curves for aluminum crystals under bending were found to resemble the load-elongation curves reported for the crystals under tension. A definite yield point at a total load of several pounds was usually observed. The curve then gradually flattened with an increase in deflection. The load-deflection curves for flat specimens were quite consistent with each other. The yield point was in the neighborhood of 3 lb which resulted in a normal stress on the extreme surface of the specimen of about 1150 psi with a corresponding resolved shear stress in the neighborhood of 500 psi. Fig 20 shows the data recorded for specimens A-10, A-12, and A-14 having different initial orientations. The yield point and the rate of strain-hardening indicated by the load-deflection curves did not appear to vary significantly for different orientations. This agrees with the results of shear tests in aluminum crystals reported by Burgers and Leebink.²⁴ They stated that slip in aluminum crystals deformed in shear may be found along lattice planes and directions differing from the usual slip system, (111) [110], and no appreciable variation on the shear stress required for different combinations of planes and directions was observed.

Flow-pattern in Bending

In order to understand the unique characteristics of flow in bending, two auxiliary experiments were performed. The first one was made on a study of the stress distribution pattern over the surface of a specimen by means of the commercial Stresscoat manufactured by Magnaflux Corporation, Chicago, Ill. It was found that the pattern produced by Stresscoat was practically the same as that found on specimens A-10 and A-11 prepared electrolytically and thus having an oxide coating. This may be regarded as confirmation that the anomalies in the surface markings of the electrolytically polished specimens resulted from surface cracks or strain markings in the anodic coating. It is believed that the major axis of

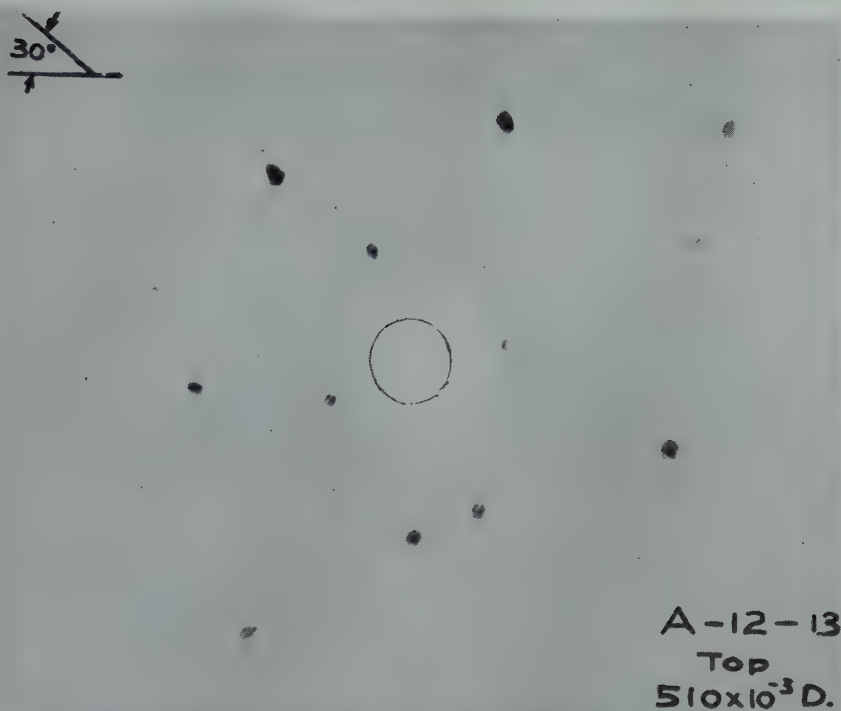


FIG 18—Laue photograph of specimen A-12, Top-T surface, after 0.510 in. deflection. 2 X.
Reduced approximately one-third in reproduction.

the strain ellipsoid on the tension side lay parallel to the specimen axis whereas that on the compression side was normal to it. A similar analysis was also reported by Yamaguchi and Tagino²⁵ who found that fissures produced in a thin oxide layer during creep

tests were oriented in the direction perpendicular to the major axis of the strain ellipsoid on the tensile specimen.

The second auxiliary experiment was the study of the flow pattern of bent specimens made of paraffin. The specimens were cast in a metallic mold hav-

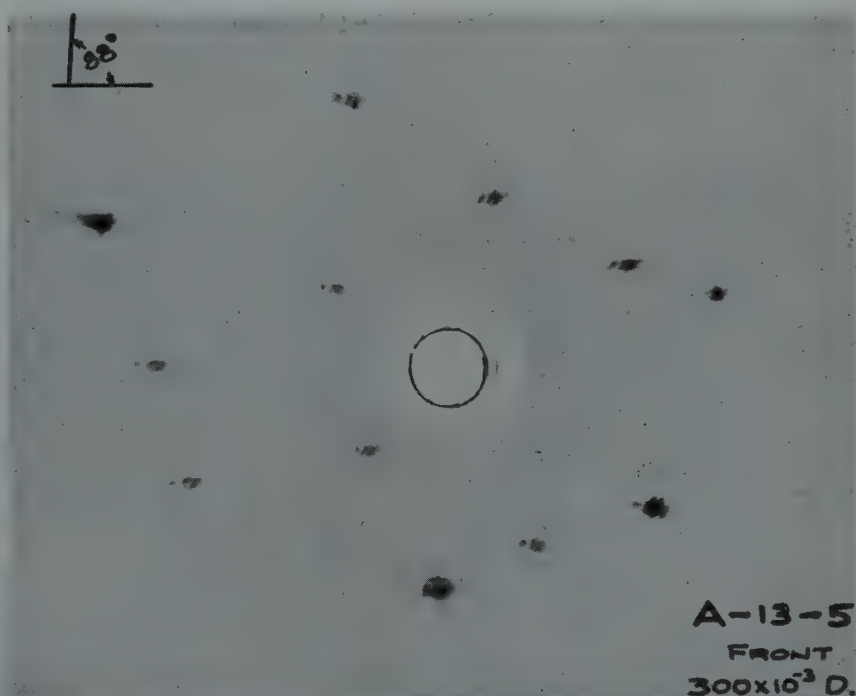


FIG 19—Laue photograph of specimen A-13, front surface, after 0.300 in. deflection. 2 X.
Reduced one-third in reproduction.

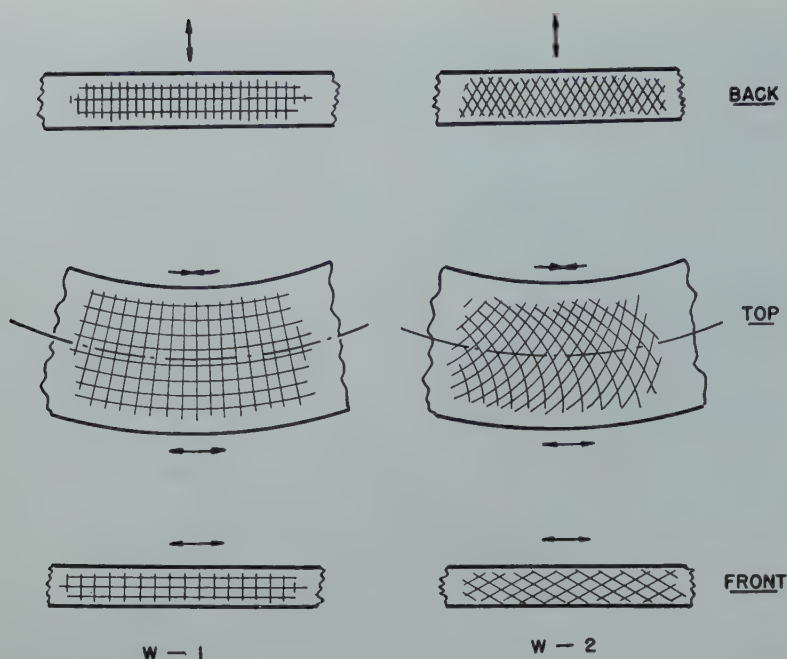


FIG 21—Schematic diagrams of flow patterns on bent wax specimens W-1 and W-2.

ing a rectangular cross-section of approximately $\frac{1}{4}$ by $\frac{1}{2}$ in. Two sets of cross-lines, one at an angle of 0° and 90° and the other at 45° with the axis of the specimen, were carefully drawn on the various surfaces of specimens W-1 and W-2. The specimens were then bent, after being warmed slightly on a gas flame, to a deflection of about $\frac{3}{4}$ in. The originally square grid was distorted to a greater or less extent at the various positions of the specimen as shown schematically in Fig 21. The arrows indicate the direction of flow derived from the flow

pattern on the paraffin specimens W-1 and W-2.

Mechanism of Deformation by Bending

A most significant characteristic of the process of plastic deformation by bending is that slip does not occur across the entire crystal but is restricted to a limited area. Slip markings appear to progress from the higher stressed to the lower stressed region, gradually losing both intensity

and width as the stress diminishes. The development of slip markings was found to consist of two different stages. At first a band-like structure was readily seen by unaided visual examination, then distinct slip markings appeared in the bands. These well-defined markings progressed toward a lower stress region with an increasing deformation. The line density was increased by the formation of new markings which appeared between the old ones under further loading. It is believed that the slip process in bending consists of an elastic bending followed by a plastic distortion, probably similar to the fragmentation processes described by Mark, Polanyi and Schmid,¹ Burgers⁴ and others.^{2,3,5} A schematic diagram of the distortion in two adjacent glide-lamellae under different stress conditions is shown in Fig 22. If the two undistorted glide-lamellae, shown in Fig 22A, were subjected to a pure shear, the lamellae would be deformed as illustrated in Fig 22B. Based upon this mechanism, the shear stress is about a thousand times larger than the observed critical shearing stress. However, it was found in this investigation that macroscopic bending of glide-lamellae did occur so that the stress distribution on the entire slip plane would be different from that produced by pure shear. This is shown schematically in Fig 22 C, D and E, that is, elastic bending, bending and plastic shear, and bending and fragmentation. It can be seen that under such conditions the slip process is composed of the successive glidings of a group of atoms at a time. The external force required to produce such a slip should be much less than the value required for an entire plane as a unit. The shear strain at the left end of the bending lamellae (Fig 22 C, D, and E) is practically equal to zero and increases gradually to a maximum value at the right end.

Furthermore, it is noteworthy that this mechanism of bending of glide-lamellae can be employed to interpret satisfactorily the asterism on Laue photograms of deformed aluminum crystals reported by Yamaguchi.² These results were criticized by Komar and Machalov⁵ who suggested that the bending of the glide-lamellae is macroscopic rather than microscopic. They found that the length of the asterism on the Laue photograms of extended magnesium crystals decreased as the surface of the crystal was etched off successively. However, referring to the

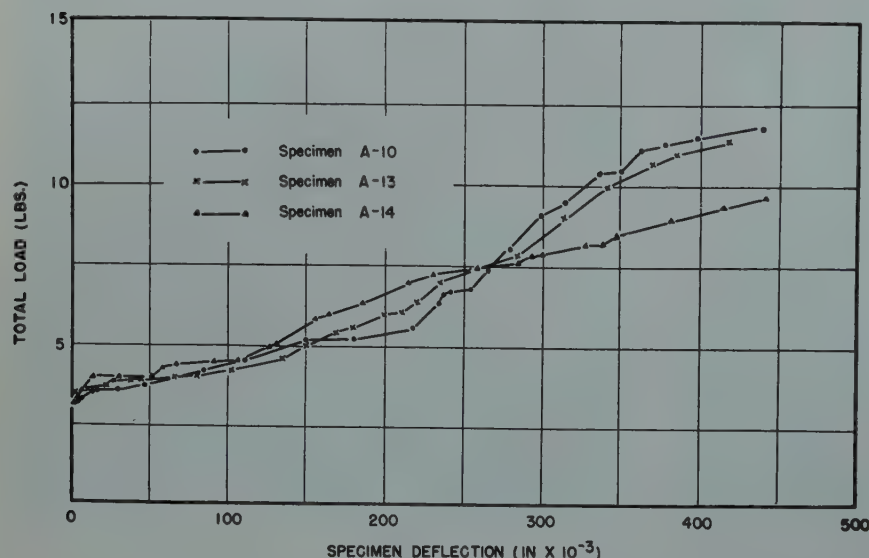


FIG 20—Load-deflection diagram of flat specimens A-10, A-13, and A-14.

mechanism of bending described in this paper, the phenomena of a decrease in the length of asterism as the outer layers of the crystal are removed by etching would be adequately explained, since the bending in the material between slip markings approaches a maximum at the outermost layer of the specimen and a greater distortion in Laue spots on X ray photograms would be expected there.

Flow Characteristics in Bending

Two different types of flow were observed on the tension and compression sides of the bent specimens. It appeared that the crystal acted as if it were divided into two parts separated by the neutral plane. The tension and compression sides experienced unusual types of axial loading where the flow of metal was restricted in a direction perpendicular to the neutral plane. There a stress-gradient existed such that the maximum stress occurred at the outermost layer of both the tension and compression sides and diminished gradually in the direction of the neutral plane. Thus the flow direction on the tension side was along the specimen axis whereas that on the compression side was in the direction roughly perpendicular to the top surface. It was found that the rectangular cross-section of all flat specimens became approximately trapezoidal during deformation, in good agreement with the characteristics of flow in a bent crystal as discussed above. The ideal flow characteristics in bending may be represented by the schematic diagram shown in Fig 23. The arrows illustrate the variation of strain introduced by the stress-gradient in a bent crystal. Sections of the undeformed crystal, shown by the dotted line, will gradually deform to those contours indicated by the solid lines during bending. Based upon this picture, the asterism on Laue photograms of a bent crystal may be interpreted as on overall bending of crystallites resulting from the process of fragmentation. Since the flow in bending is restricted in certain directions, the crystallites could not follow the type of rotation found in uniaxial loading. Instead of the usual type of rotation about an axis lying in the slip plane normal to the slip direction, the different shapes of Laue spots seem to indicate that the crystallites were bent about an axis in the slip plane and perpendicular to the direction of flow.

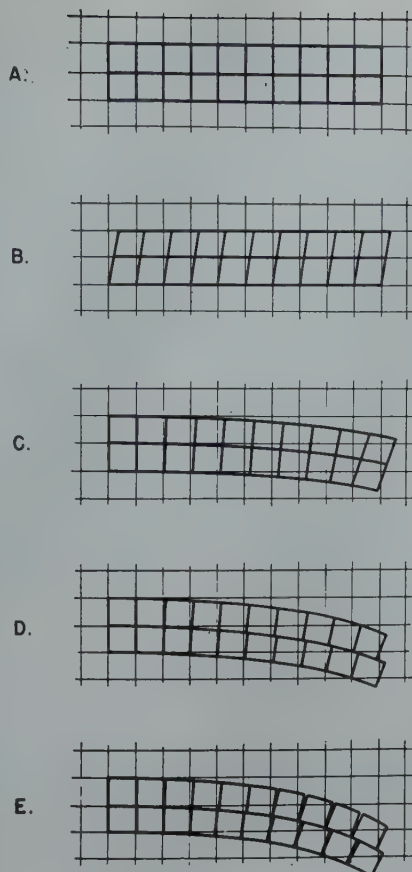


FIG 22—Schematic diagrams of slip mechanism.

(A) Undeformed, (B) Pure shear, (C) Elastic bending, (D) Bending and plastic shear and (E) Bending and fragmentation.

Summary

1. When an aluminum crystal is subjected to a bending stress, the major operative slip system is the same as for uniaxial loading. That is to say, the slip occurs on the octahedral plane which has the maximum resolved shear stress given by the equation $S_s = S_n \cos \lambda \sin \chi$, where S_n is the normal stress calculated by the simple beam formula.

2. The change of orientation on the tension and compression sides of a crystal during bending resembles closely that of two separate crystals deforming under tension and compression loading respectively. In general they appear to follow the Taylor and Elam rotation,

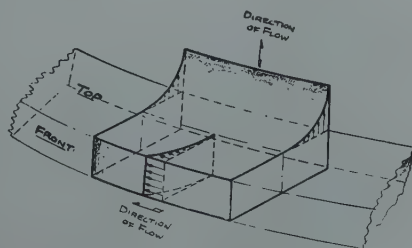


FIG 23—Schematic diagram of characteristics of flow in bending.

that is, the stress axis rotates toward a [110] slip direction on the tension side and toward (111), the pole of active slip plane, on the compression side. However, a certain amount of deviation was observed. This may be due to the complication introduced by the restriction of flow during bending and consequently requiring the early operation of a secondary slip system.

3. The anomalous surface markings on the electrolytically polished specimens may be attributed to the strain-markings or cracks on the anodic coating of the surface layer. It was found that these markings were analogous to the cracks produced on a deformed specimen treated with Stresscoat. The absence of these markings on mechanically polished and etched specimens further substantiated this interpretation.

4. "Cross-slip" or the step-like appearance of slip lines was observed on specimen surfaces intersected by the slip direction. However, no definite cross-slip plane could be identified. This may be due to the complicated stress distribution in the bending where these steps might be too small to permit the resolution of a particular plane.

5. The phenomena of slip over local regions of the specimen was noticeable in all the bending specimens. The growth of slip markings appears to undergo a process such that the slip markings occur initially at a higher stress region and move toward a lower stressed matrix, gradually losing both their intensity and width as the stress diminishes. The macroscopic bending of glide lamellae was also found.

6. From the study of the flow characteristics and the Laue spots on the X ray photograms of various bent specimens, it was found that the cause of subdividing of spots may be regarded as a result of crystallite fragmentation. The fragmentation appeared to take place by rotating the crystallites in the glide lamellae about an axis normal to the slip plane in addition to the usual type of bending about an axis lying in the slip plane perpendicular to the direction of slip. Following the rotation of crystallites, the elongation or asterism of Laue spots may be rationalized as an overall bending taking place about an axis in the slip plane and normal to the direction of flow.

Acknowledgments

The authors wish to thank Professor C. H. Mathewson for his interest and

advice concerning this work, and to acknowledge the assistance of members of Hammond Metallurgical Laboratory, Yale University, and the Research Department of Chase Brass and Copper Co. The M-B Manufacturing Co., New Haven, Conn., kindly supplied the Stresscoat equipment.

References

1. H. Mark, M. Polanyi, and E. Schmid: *Ztsch. Phys.* (1922) **12**, 58.
2. K. Yamaguchi: *Sci. Papers IPCR* (Tokyo) (1928) **8**, 289; (1929) **11**, 151, 223.
3. G. I. Taylor: *Proc. Roy. Soc. (London)* (1927) **A116**, 39.
4. W. G. Burgers and P. C. Louwerse: *Ztsch. Phys.* (1931) **67**, 605.
5. A. Komar and M. Machalov: *Phys. Z. Sowjetunion* (1936) **9**, 613.
6. R. Maddin, C. H. Mathewson, and W. R. Hibbard, Jr.: Paper submitted to AIME in March 1949.
7. R. W. Cahn: Discussion on paper by W. G. Burgers in 1947. Bristol Conference on Strength of Solids (1948) 136.
8. Y. Kidani and S. Tagino: *Bull. IPCR* (Tokyo) (1929) **8**, 118.
9. A. Kochendörfer: *Plastische Eigenschaften von Kristallen und Metallischen Werkstoffen*. J. Springer (1941) 151.
10. S. Timoshenko: *Strength of Materials*. (1940) **1**, 88, Nostrand.
11. G. Found: Yale Dissertation (1944).
12. H. C. H. Carpenter and C. F. Elam: *Proc. Roy. Soc. (London)* (1921) **A100**, 329.
13. A. B. Greninger: *Trans. AIME* (1935) **117**, 61.
14. G. I. Taylor and C. F. Elam: *Proc. Roy. Soc. (London)* (1925) **A108**, 28.
15. G. I. Taylor and W. S. Farren: *Proc. Roy. Soc. (London)* (1926) **A111**, 529.
16. W. R. Hibbard, Jr.: *Trans. AIME* (1948) **175**, 66. *Met. Tech.* Sept. 1947, TP 2244.
17. J. A. Collins and C. H. Mathewson: *Trans. AIME* (1940) **137**, 150.
18. R. D. Heidenreich and W. Shockley: *Jnl. Appl. Phys.* (1947) **18**, 1029.
19. R. Maddin, C. H. Mathewson and W. R. Hibbard, Jr.: *Trans. AIME* (1948) **175**, 86. *Met. Tech.* Feb. 1948, TP 2331.
20. M. C. Crussard: *Rev. Met.* (1944) **41**, 111, 133; (1945) **42**, 286, 321.
21. E. N. daC. Andrade: Discussion of "Deviations of Real Crystals from the Ideal Lattice Structure." Int. Conf. on Phys. II (1934) 173.
22. E. N. daC. Andrade and L. C. Tsien: *Proc. Roy. Soc. (London)* (1937) **A163**, 1.
23. C. H. Mathewson: *Trans. ASM* (1944) **32**, 28.
24. W. G. Burgers and F. J. Lebbink: *Rec. Trav. Chim. Pays. Bas.* (1945) **64**, 321.
25. K. Yamaguchi and S. Tagino: *Sci. Pap. IPCR* (Tokyo) (1929) **9**, 277.

High Temperature Sealing of Cobalt*

CHARLEY R. JOHNS† and WILLIAM MARSH BALDWIN, JR.,‡ Junior Member AIME

Introduction

Cobalt is reported^{1,2} to scale in accordance with the Pilling and Bedworth³ parabolic law:

$$w^2 = Kt \quad [1]$$

where w = weight increase per unit surface area

K = constant

t = time

The reported values of the parabolic oxidation constant, K , in the temperature range 600 to 1100°C follow an Arrhenius type of equation as inspection of Fig 1 shows. According to Valensi's theory⁵ on the scaling of metals where multiple-layered scales (for example, MeX , MeX_2 , and others) are possible, this fact could be construed as indicating that a single oxide only is formed on cobalt in this temperature range. Since the single straight line extends above 920°C where only CoO is stable in air (see Fig 2) it might be inferred that this is the only oxide formed on scaling.

Arkharov and Voroshilova¹⁰ have studied the scales formed when cobalt is heated in air in the temperature range 385 to 800°C and report that

CoO is indeed found in the scale but that Co_3O_4 is also found as an overlay and in increasing amounts in the lower temperature ranges. No quantitative data regarding the relative proportions of the two oxides were reported. Again in the light of Valensi's theory this would indicate that the straight line in Fig 1 would be expected to undergo an inflection at some point in the temperature range 385 to 800°C.

Chauvenet² has studied the oxidation rates of CoO to Co_3O_4 and has found this reaction to proceed parabolically with time but reports parabolic scaling rates which are

These authors also state that a thin exterior veneer of Co_3O_4 may have formed also but was too thin to identify with X rays. In view of the instability of Co_3O_4 in air above 400°C (see Fig 2) this is unlikely.

considerably (about ten times) larger than the scaling rates of cobalt metal itself.

This is difficult to explain in terms of Valensi's theory although a full discussion of the possible discrepancy cannot be made in view of the lack of sufficient data.

These points made an investigation of the scaling behavior of cobalt in air an attractive study.

Discussion of Results

Relatively large (approximately⁹⁵ 95 sq cm of surface area) samples of 0.020 in. thick electrolytic cobalt strip,* sanded with 2/0 paper, were heated in air in a cyclone type furnace. The samples were weighed before and after the scaling treatment. The weight increases so observed obeyed the Pilling and Bedworth parabolic law at all temperatures studied. The parabolic scaling constants when plotted on a logarithmic scale as a function of absolute temperature are reproduced

* Supplied through the kindness of Dr. O. C. Ralston, Acting Chief of the Bureau of Mines, Metallurgical Div., Washington, D. C. A qualitative spectrographic analysis showed only traces of nickel, copper, cadmium, iron, magnesium, chromium and manganese.

Technical Note No. 24 E. Manuscript received June 21, 1949.

* Abstracted from a thesis submitted by C. R. Johns to the Department of Metallurgical Engineering, Case Institute of Technology, in partial fulfillment of the degree of Master of Science in Physical Metallurgy.

† Production Metallurgist, Thompson Products, Inc.

‡ Research Professor, Case Institute of Technology.

1 References are at the end of the note.

in Fig 1. Here it may be seen that in the higher temperature ranges the present data coincide quite well with the previously reported data. There is, however, a definite inflection in the data at around 625°C, the data for the temperature range below this point showing a slope that is roughly $\frac{1}{2}$ that of the straight line drawn through the data above this point. This inflection would be expected on the basis of the reasoning presented above. If the straight line in the lower temperature range is due to the exclusive formation of Co_3O_4 , the oxidation rate of CoO to Co_3O_4 in this temperature range should follow a straight line parallel to the lower branch of the cobalt curve and lying at a value $\frac{1}{4}$ that of the aforementioned lower branch. This is, of course, at complete variance with the experimental results of Chauvenet on the oxidation of CoO and illustrates in quantitative terms how her data cannot be reconciled with the requirements of Valensi's theory. In an attempt to resolve this discrepancy, samples of cobalt were oxidized to CoO at temperatures above which none of the other oxides is stable thermodynamically (around 920°C) and then subsequently oxidized in the temperature range in which Co_3O_4 was stable. These results are entered in Fig 1. In the present case the data parallel those of Chauvenet's (and incidentally, the scaling data for straight cobalt in the temperature range above 625°C) but do not behave in accordance with Valensi's theory. It must be admitted that the present data are of the proper order of magnitude to fit Valensi's requirements, and it may be that experimental errors prevent the data from exactly duplicating the values required by his theory, but for the present we must regard the case of the scaling of cobalt in air as being still unsettled.

An internal check on the data and on Valensi's theory could have been obtained if the proportions of CoO and Co_3O_4 in the scale could have been determined quantitatively in the temperature ranges between 500 and 800°C, but the absolute thickness of the scales formed in this temperature range are extremely small compared with other metals in which such quantitative determinations have been made (for instance, copper,⁵ iron¹¹) indicating the necessity of developing special techniques for such determinations.

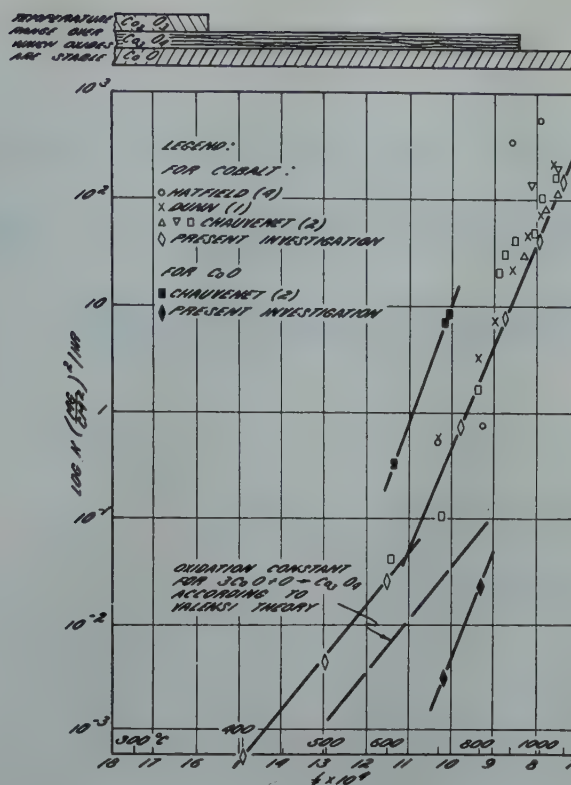


FIG 1—Relationship between the parabolic scaling constant for cobalt and CoO and temperature.

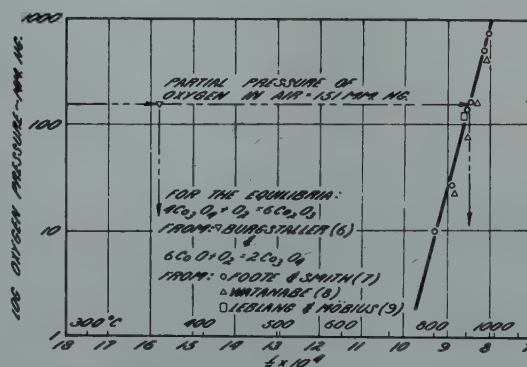


FIG 2—Dissociation pressures of various cobalt oxides as a function of reciprocal absolute temperature.

References

1. J. S. Dunn quoted by J. S. Dunn and F. J. Wilkins in "Review of Oxidation and Scaling of Heated Metals." H. M. Stationery Office (London) (1935) Sect. 4, "The Oxidation of Non-Ferrous Metals," p. 67-80.
2. G. Chauvenet: Doctor's Thesis, Univ. of Caen (1942) Order No. 34.
3. N. P. Pilling and R. E. Bedworth: The Oxidation of Metals at High Temperatures. *Jnl. Inst. Metals* (1923) 29, 529-582.
4. W. H. Hatfield: Heat Resisting Steels. *Jnl. Iron and Steel Inst.* (1927) 115, p. 483-508.
5. G. Valensi: Theoretical and Experimental Investigations about Conjugated Formation of Several Layers in Dry Corrosion. Pittsburgh International Conf. on Surface Reactions. Corrosion Publ. Co., Pittsburgh, Pa. (1948) p. 156-164.
6. S. Burgstaller: Untersuchungen über die Beständigkeit der Kobaltoxyde im Intervalle von Co_3O_4 bis CoO . *Abh. Deut. Nat. Schaft. Med. Ver. Böhmen "Lotos" in Prag.* (1912) 3, 83-143.
7. H. W. Foote and E. K. Smith: On the Dissociation Pressures of Certain Oxides of Copper, Cobalt, Nickel and Antimony. *Jnl. Amer. Chem. Soc.* (1908) 30, 1344-1350.
8. M. Watanabe: On the Equilibrium in the Reduction of Cobaltous Oxide by Carbon Monoxide. *Sci. Rep., Tohoku Imp. Univ.* (1933) 22, 892-901.
9. M. LeBlanc and E. Mobius: Untersuchungen über Kobaltoxyde und deren Systeme mit Sauerstoff. *Ztsch. Phys. Chem.* (1929) A-142, 151-176.
10. V. I. Arkharov and Z. A. Voroshilova: X-Ray Investigation on the High Temperature Oxidation of Cobalt. *Zhur. Techn. Fiziki* (1936) 6, No. 5, 781-782.
11. A. O. Tesche: *Trans. ASM* (1950) (in print).

Stages in the Deformation of Monel Metal as Shown by Polarized Light

D. H. WOODARD,* Associate Member AIME

Introduction

One of the principal uses of polarized light in metallurgy is to show the granular structure of metals by contrasting reflections. This use is confined largely to anisotropic metals, such as beryllium, tin, magnesium, and the like.¹ Recently, Hone and Pearson² have extended the use of polarized light to include the isotropic metal aluminum. This was made possible by the formation of an anodic film that was optically anisotropic and that had a fixed and reproducible structural relationship to the grains in the substrata. With their method, it was possible to indicate localized textures in annealed aluminum sheet. In the course of an investigation of plastic deformation at the National Bureau of Standards, it was found that the isotropic single phase alloy Monel could be made optically anisotropic by treatment with the usual Monel contrast etchant. Experiments soon showed that differences in orientation could be detected easily.

Previous investigations involving the use of polarized light have been restricted to annealed metals. In this paper it will be shown that inhomogeneous plastic deformation which results in lattice bending and development of deformation bands experienced by individual grains in polycrystalline Monel, is revealed in the microstructure. This interpretation of the microstructure was confirmed by a study of slip lines formed after prior plastic strain.

Materials and Procedure

The material used was Monel, the

chemical composition of which was C—0.17 pct, Mn—1.28 pct, Fe—1.61 pct, S—0.009 pct, Si—0.17 pct, Cu—30.70 pct, Ni—66.04 pct. The material was divided into 2 lots which were treated as follows: Lot A was heated at 1700°F for 3 hr to produce a fully annealed, coarse grained structure. Lot B was heated at 1400°F for 1 hr to produce a close approximation of a fully annealed structure without appreciable increase in the grain size of the original material. After each of these heat treatments the material was cooled in air.

Samples for metallographic examination were cut from tensile and compression test specimens and were prepared by grinding on lead-tin laps, followed by electrolytic polishing.[†] Etching and the development of ridges were avoided by keeping the voltage above 3.8 and by preventing contamination of the polishing solution with water.

Monel, when polished and treated with most etchants, is optically isotropic. However, when given a light etch for about 4 sec with the Monel contrast solution[‡] the surface of the metal becomes optically active. The microstructure when observed under

[†] The electrolyte was a solution of nitric acid—1 part, methyl alcohol—2 parts.

[‡] The etchant used consisted of chromic acid—3 g, nitric acid (conc.)—10 cc, ammonium chloride—5 g, water—90 cc.

Cleveland Meeting, October 1949.

TP 2696 E. Discussion of this paper (2 copies) may be sent to *Transactions AIME* before December 1, 1949. Discussion is tentatively scheduled for publication in May 1950.

Manuscript received May 2, 1949; revision received July 11, 1949.

* General Physical Scientist, National Bureau of Standards.

¹ References are at the end of the paper.



FIG 1—Appearance of the same area of plastically deformed Monel metal B under (a) (above) polarized light and (b) (below) ordinary light.

× 750. Reduced one half in reproduction.

crossed nicols* appears different from that viewed by ordinary light. This is shown by a comparison of micrographs made of the same area of a plastically deformed specimen using polarized light (Fig 1a) and white light (Fig 1b).

If Monel, which has been lightly treated with the contrast etchant, is slightly deformed by compression, rectangular figures are apparent over the specimen. However, within too short a period to be photographed, these rectangles become circular, probably because of surface tension effects within the etched film. The two observations,

* The expression "crossed nicols" employed in this paper conforms to the usages of optical crystallography. It does not mean that *Nicol prisms* are employed but merely that polarizing elements in the incident and reflected beams are crossed with respect to each other. The less explicit term "polarized light" is used in places where no ambiguity would result.

the rectangular figures becoming circular and the failure of the unetched surfaces to reflect polarized light, suggest that the Monel contrast etchant forms a film which is anisotropic.

Unless otherwise specified, all micrographs were made on a Bausch and Lomb Metallographic Research Microscope, equipped with a Foster vertical illuminator prism³ which acts also as polarizer and analyzer fixed in the crossed position. Measurements of the intensity of the reflected resolved polarized light were made at the bellows eyepiece with a specially constructed photometer, which consisted essentially of a photo-multiplier tube, RCA-931, a bank of dry cells arranged to have 90 volts across each dynode, and a microammeter. As the current coming from this photo-multiplier is proportional to the intensity of the incident light, all light intensity values are expressed in microamperes.

Differences in Orientation Shown by Polarized Light

ANNEALED MONEL

It has been shown by many investigators that the orientation of fully annealed single phase alloys is uniform

from point to point in individual grains and that the orientation varies from grain to grain in a more or less random manner. For fully annealed Monel, the intensity of the reflected polarized light is uniform over the entire area of each individual grain as illustrated by the micrographs of Fig 2. It should be noted, however, that in the case of Monel, the annealing must be complete and grain growth started before uniform reflection, that is, uniform orientation over individual grains, is obtained

The micrographs in Fig 2 show that each grain undergoes a half cycle of intensity from maximum to minimum for a 45° rotation of the plane of polarization, although the angle for maximum reflection varies from one grain to the next. It was noted that the difference in intensity between the maximum and the minimum of the reflected light may vary from one grain to another. It is, therefore, possible for two grains to be at different stages in their 90° cycle and yet reflect light with the same intensity. While the same intensity for different grains may mean different orientations, it is obvious that for any fixed direction of the planes of polarization, a difference in intensity must mean a difference in orientation. It is on this basis that

polarized light is used in this study of plastic deformation.

INDIVIDUAL GRAINS IN PLASTICALLY DEFORMED MONEL

Fig 3 shows the microstructure of Monel after extensions of 2, 14, 30, and 38 pct, when deformed at a rate of 2½ pct every 5 min. These micrographs, like others photographed under crossed nicols, are referred to as intensity patterns because the areas of extinction can be changed to areas of brightness or vice versa, although the outlines in the pattern remain the same. Obviously, plastic deformation has caused nonuniform reflections from individual grains. If differences in intensity denote differences in orientation, then it follows that plastic deformation has caused inhomogeneous distortions in the lattice structure. This is in agreement with results obtained by Barrett and Levenson⁴ who showed, by means of X rays and etch pits, that plastic deformation caused areas of nonuniform orientation over the individual grains. After a study of the intensity patterns shown in Fig 3 and other similar patterns, it was possible to classify the nonuniformities of reflection into four types shown by grains A, B, C, and D. These will be discussed under Results.



FIG 2—Variations in intensity patterns after successive rotations with respect to the plane of polarization, as indicated, of a specimen of annealed Monel metal A.
× 250. Reduced one half in reproduction.

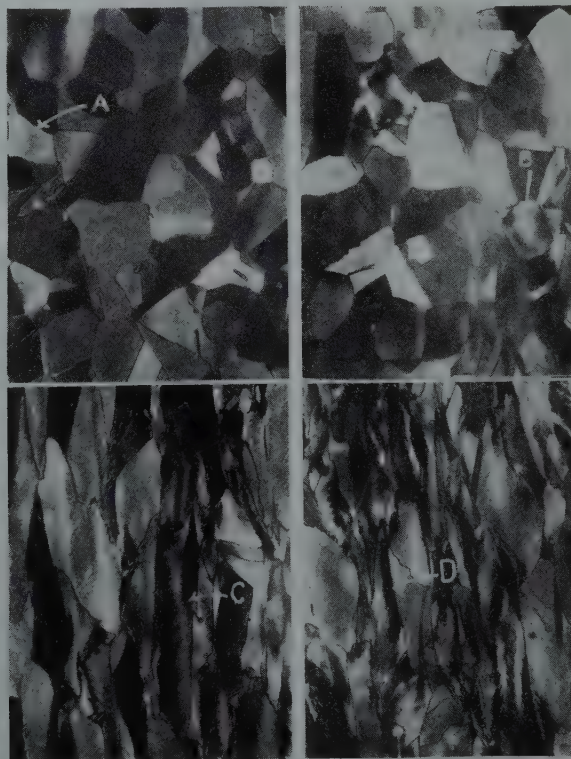


FIG 3—Variations in intensity patterns within individual grains in Monel metal B after plastic deformation in tension as indicated.
The axis of tension is in the vertical direction for all specimens.
× 750. Reduced one half in reproduction

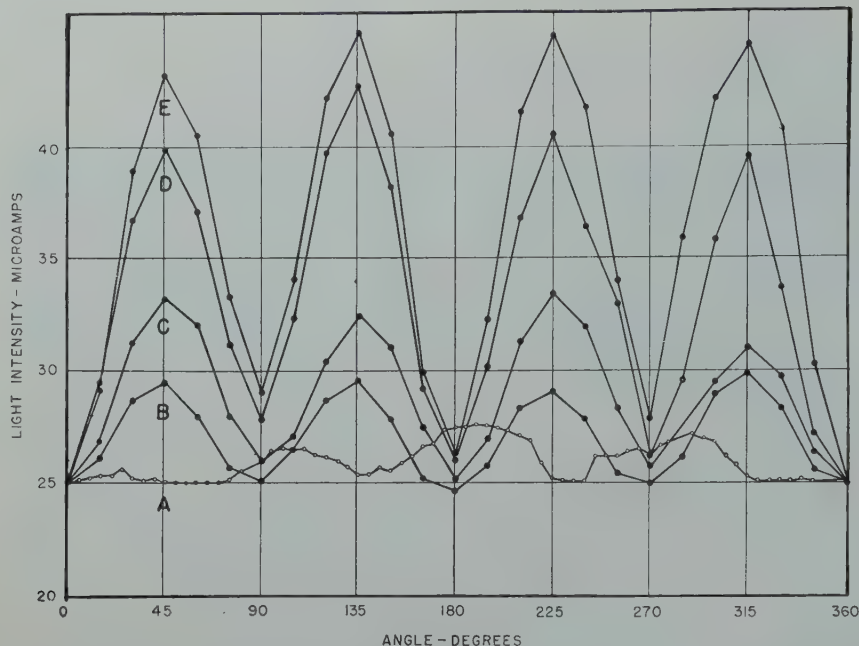


FIG 4—Effect of plastic deformation and angular rotation of crossed nicols on the overall intensity of light reflected from Monel metal B. Curves A, B, C, D, and E represent specimens extended 0, 14, 33, and 38 pct respectively.

CORRELATION OF INTEGRATED INTENSITIES WITH DEGREE OF DEFORMATION

It was observed, in examining plastically deformed specimens, that the overall intensity of the reflected polarized light with crossed nicols changed as the plane of polarization or the specimen was rotated. These changes were measured by the photometer at regular angular intervals and the results are shown in Fig 4. The data for curve A, obtained from a transverse section of a fully annealed specimen, represents a condition of random or nearly random orientation. It is evident that plastic deformation results in the formation of four peaks in each curve and that increasing plastic deformation, from 0 to 38 pct, causes the amplitude to increase.

Since any orientation of an individual grain goes through four intensity cycles, it is apparent that the integrated intensity of many grains will show four peaks as more and more grains approach a common alignment. Any such directional deviation from the original state must be considered as a development of preferred orientation. X ray studies have shown that a progressive increase in preferred orientation results when polycrystalline metals are deformed plastically in tension. There is apparently a relationship between the degree of preferred orientation and the variation in integrated intensity, where preferred orientation appears under crossed nicols before its development can be detected by X rays.

In this connection, it is interesting to note that Mebs and McAdam⁵ have interpreted variations of Poisson's ratio as showing the anisotropy of this same heat of Monel after 4 pct reduction of area. Hill⁶ has shown that the development of preferred orientation accompanies anisotropy.

If plastic deformation, accompanied by a bending of the lattice, occurred in such a manner as to permit extension in the direction of flow, a plane cutting the specimen in this direction should show more areas of certain specific planes than would be observed in the case of a purely random orientation. The development of the peaks of Fig 5 is attributed to such a phenomenon. At present, there is very little information available on the intensity of the reflection from specific planes or on the number or orientations of the planes which combine to show this preferred orientation.

EVIDENCE OF BENT LATTICE STRUCTURE

Thin straight parallel lines usually seen on polished and etched surfaces of annealed metals after slight compression are considered to be traces of crystallographic planes, that is, the intersection of these planes with the surface of the metal. Sometimes however, these lines are curved and the question has been raised as to whether a set of such curved lines represents traces of a set of crystallographic planes which are bent, or the traces of several sets of parallel crystallographic

planes which remain straight but which combine to give the effect of curved lines. The ability of polarized light to show changes in orientation along the length of a line furnishes an answer to this question and thereby yields information as to a mode of deformation.

Deformed Monel specimens were sectioned, polished, etched, and then deformed further to form traces, some of which are curved. It can be readily seen in Fig 5a and d that the slip lines bend as they go from one orientation to the other as evidenced by changes in the intensity pattern. The bends are not abrupt, as is the case at the grain boundaries, but have measurable radii of curvatures. In such cases, the intensity patterns show a gradual change in orientation which indicates a gradual change in position of the crystallographic axes. This bending of the slip lines, therefore, is interpreted as being due to a bending of the crystallographic planes of which these lines are traces. In a metal, such as Monel, which has a face-centered cubic structure, these slip lines are assumed to be traces of octahedral planes. There are four sets of these planes, each set inclined to each of the other sets at an angle of 70°.

Fig 5b, c and d show the microstructure of two specimens that had less prior strain than did the specimen whose microstructure is shown in Fig 5a. In Fig 5b, there are two sets of traces in the central grain, one set about horizontal, the other inclined about 30° to it. As the orientation changes, there is no change in direction of the horizontal set, but there is a change in the ends of the traces of the other set. The case of having two sets of traces, one straight and the other bent while going through a region of changing orientation, can be explained as follows: During the process of plastic deformation the lattice may be bent around an axis parallel to the surface in such a manner that the metal surface cuts off a longitudinal section of the cylinder. Then an octahedral plane at right angles to the axis of bending would intersect the surface of the metal in a straight line regardless of the amount of lattice bending. If the octahedral plane is at any other angle, the intersection of that plane with the specimen surface should show a change of direction with a change of orientation. The further the octahedral plane inclines toward the axis of bending, the greater is the curvature of the slip line with change in orientation. This is shown in the main grain of Fig 5c, where the traces go through the main grain with

practically no change in direction with change in orientation. However, when they go through the twin, where an octahedral plane is inclined at the twin angle, the straight lines become curved with changes in orientation. This is clearly seen in Fig 5d which is an enlargement of the twinned region.

From a study of many orientation patterns, and the slip lines formed on the surface by further plastic deformation, it appears that initial bending occurs around axes nearly perpendicular to the octahedral planes and that the slip lines run approximately perpendicular to these axes of bending. The similarity of the microstructures of Fig 3 (deformed before polishing) and of Fig 5 (deformed both before and after polishing) indicates that the curvature of the traces and the accompanying changes in intensity were not due to a rumpling of the surface.

It was found that the number of slip lines formed on a specimen initially annealed, polished, and etched increased and their spacing became more irregular as the amount of plastic deformation increased. As can be seen in Fig 5a and b, the intensity pattern of the individual grains indicates that the strain was inhomogeneous and this resulted in the irregular spacing of the slip lines. A series of annealed specimens, compressed 4, 14, 32, and 36 pct before being sectioned and polished, were etched and then given 2 pct further compression. Examination showed that the 32 pct and 36 pct specimens had fewer slip lines present than the 4 pct and 14 pct. This showed that it is more difficult to develop slip lines on specimens that had a large amount of prior compression than on those that had a lesser amount. However, the greater the deformation before sectioning, polishing, etching, and deforming further, the deeper, wider, and more irregular become the slip lines.

Discussion of Results

TYPES OF LATTICE BENDING

The concept of deformation by lattice bending has been presented by many investigators. Polanyi⁷ related the elongation of Laue spots from zinc crystals with bending of the slip plane (*Biegegleitung*). Sun and Chu⁸ interpreted Laue photographs of rock-salt crystals as showing that the first deformation occurs by a simple bending of the lattice around a fixed axis; as the crystal deforms further, bending begins around one or more new axes. Single

crystals of cadmium, when oriented so that the glide plane is nearly parallel to the axis of compression, deform by a mechanism which Orowan⁹ terms "kinking." Hess and Barrett¹⁰ have shown that the kink bands described by Orowan are a special form of deformation bands and result from a bending of the lattice.

When the intensity patterns of Fig 4 are interpreted in terms of lattice bending, four types of deformation can be seen:

1. Broad diffuse bands of brightness and extinction, as typified by grain A: These represent lattice bending around an axis which is nearly parallel to the surface. These appear on specimens that have been sectioned longitudinally after slight plastic deformation.

2. Areas of brightness surrounded by areas of extinction, as typified by grain B: These are typical of a dome type of lattice bending wherein the crystallographic planes have been bent so that they are no longer flat planes, but are wrinkled into the shape of a dome.

3. Bands of brightness and extinction with the bands ending in areas of extinction and brightness respectively, as shown in grain C: Here the change in orientation at the end of the band shows that the deformation is of the twisted or screw type.

4. Bands of brightness or extinction

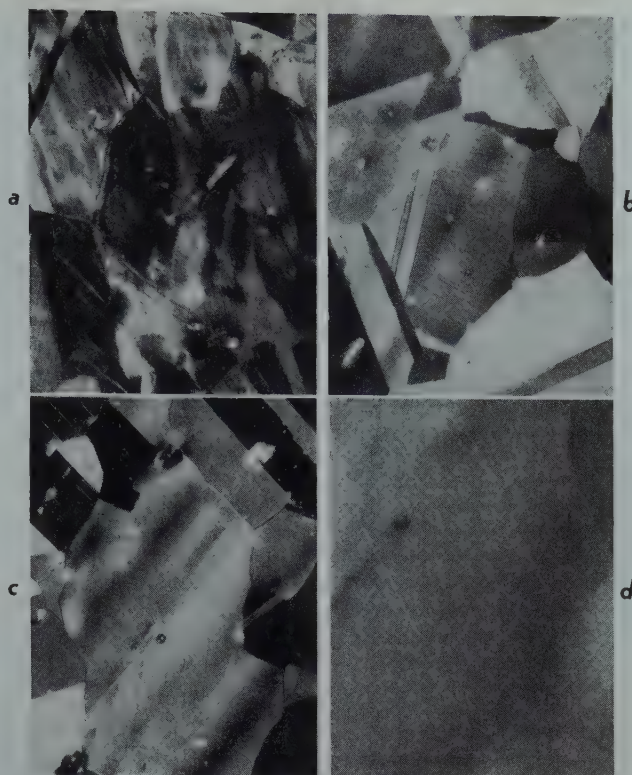


FIG 5—Effect of prior plastic deformation on the development of slip lines in Monel metal A.

(a) compressed 28 pct, (b), (c), and (d) compressed 2 pct. (a), (b), and (c) $\times 250$. (d) $\times 750$. Reduced one half in reproduction.

sharply outlined in more or less irregular shapes and mainly extending in the direction of flow as shown by grain D: Bands of this type represent fully formed deformation bends and usually appear after severe necking of the specimen.

Examination of many intensity patterns shows that initial plastic deformation occurs through the bending of the lattice around a single axis and that, as the amount of deformation increases, lattice bending takes place around several axes.

From the extreme irregularity of the intensity patterns, it is evident that directions of flow can vary within small areas and that the deformation is by no means uniform or regular as would be the case for twinning.

DEVELOPMENT OF DEFORMATION BANDS

In the early stages of plastic deformation, the changes in orientation are gradual, as seen in Fig 3a and b. As deformation increases, the changes in orientation become gradually sharper and more distinct in more or less irregular areas. After severe plastic deformation, these areas of changed orientation become elongated and sharply outlined. They are clearly seen in Fig 3d and 6a and b. As their development is a gradual process, it is quite evident that



FIG 6—Inhomogeneous deformation within individual grains in severely deformed specimens of Monel metal A.

After prior compression of 36 pct for 6(a), 28 pct for 6(b), (a) (above) $\times 500$, (b) (below) $\times 250$. Reduced one half in reproduction.

these areas are deformation bands and not deformation twins.

As these deformation bands are formed, the area bounding them becomes thinner and more distinct until, with severe plastic deformation, they become grain boundaries. Frequently, a well-defined grain boundary was seen to end in a deformation band boundary which became gradually wide and diffuse. Such a condition could exist if, due to inhomogeneous plastic flow, there is, as postulated by Mott,¹¹ a shearing action along the orientation boundary (band boundary). With severe distortion, and its accompanying shear along the newly formed orientation boundary, this oriented boundary becomes a grain boundary. Further deformation is then a unique and distinct process within each orientation. In this way, a grain can be fragmented into smaller grains by plastic deformation.

CONTINUANCE OF DEFORMATION BANDS ACROSS GRAIN BOUNDARIES

Boas and Hargreaves¹² concluded from hardness measurements that the distortion in a grain is confined largely to the areas adjacent to the grain boundaries and is transmitted to a neighboring grain along its boundaries. However, Hibbard,¹³ by means of X ray determinations of orientation, showed that deformation was not restricted to any particular area of the

grain. Examination of many intensity patterns, such as those in Fig 3, show that differences in orientation do not occur more frequently near the grain boundaries than in the center of the grain. While many areas were observed, similar to Fig 6a, in which deformation bands in one grain are adjacent to deformation bands in the next, the proportion of such areas is small. From a consideration of the intensity patterns, it is evident that the transmission of deformation across a grain boundary is dependent upon the relationship of the two adjacent orientations. The response of a grain to the deforming stress is affected not only by the orientation of the grain itself but by the restricting action of adjacent grains of different orientation.

EFFECT OF LATTICE BENDING ON THE MECHANISM OF PLASTIC DEFORMATION

If deformation of Monel is to occur through lattice bending, then the concept of deformation by slip must permit gradual changes in lattice orientation, such as are seen in Fig 3a and b, and must account for the relative proportions of deformation by lattice bending and by slip. It is quite evident that slip did not occur through the distortion of layered regions which would leave the rest of the lattice undisturbed.

It is evident that when the lattice is bent, the lattice constants on the concave side would differ from those on the convex side. In such a case, there are limitations as to the amount that the lattice can be bent elastically without deforming plastically. The plastic deformation, or atomic readjustment, could occur through the motion of dislocations, where the nonuniform stresses set up by the bending of the lattice serve as the trigger mechanism to start the dislocations into motion. It is hoped that more quantitative information will be obtained from a program now underway which will coordinate the results obtained from polarized light with those obtained from other methods.

The current widespread interest in orientation changes during plastic deformation and the inability of other methods to present these changes visually has resulted in the publication of this paper at this time.

Summary

The microstructure of Monel can be revealed, when viewed under crossed

nicols, as an intensity contrast pattern when a polished specimen has been etched with the ordinary contrast etching reagent. Differences in the intensity of the reflections were interpreted as differences in crystalline orientation. On the basis of this hypothesis, variations in crystalline orientation were shown to be present in individual grains in plastically deformed specimens. A study of these variations led to the conclusion that the individual grains were deformed in an extremely irregular flow pattern, some of the irregularity resulting from the restrictive action of neighboring grains.

A study of the microstructure of specimens that had been deformed plastically, sectioned, polished, etched, and then deformed further indicated that curved slip lines are the traces of crystallographic planes which had become bent as a result of the prior plastic deformation. Changes in lattice orientation are attributed to a bending of the lattice and are shown to become sharper and more distinct as the amount of plastic deformation is increased. These changes lead to the formation of deformation bands and to fragmentation of the grains.

It was shown that the integrated intensities of reflections from many grains varied as the specimen was rotated with respect to the plane of polarization of the incident light. The integrated intensity increased with an increase in the degree of deformation, thereby indicating that polarized light can be used to detect preferred orientation.

References

1. R. W. Drayton: *Trans. AIME* (1935) **117**, 119.
2. A. Hone and E. C. Pearson: *Metal Progress* (1948) **53**, 363.
3. L. V. Foster: *Jnl. Opt. Soc. Am.* (1938) **28**, 124.
4. C. S. Barrett and L. H. Levenson: *Trans. AIME* (1940) **137**, 112.
5. R. W. Mebs and D. J. McAdam, Jr.: Nat'l. Adv. Comm. for Aeronautics Tech. Note No. 1100.
6. R. Hill: *Proc. Roy. Soc. (London)* (1948) **A-193**, 281.
7. M. Polanyi: *F. Krist* (1925) **61**, 49.
8. Te-Yen Sun and Sheng-Lin Chu: *Acta Cryst.*, 135 (July 1948).
9. E. Orowan: *Nature* (1942) **149**, 643.
10. J. B. Hess and C. S. Barrett: Eleventh Quarterly Report, The Inst. for the Study of Metals, 70.
11. N. F. Mott: *Proc. Phys. Soc.*, 391 (April 1, 1948).
12. W. Boas and M. E. Hargreaves: *Proc. Roy. Soc. (London)* (1948) **A-193**, 89.
13. W. R. Hibbard: *Trans. AIME* (1949) **180**, *Metals Tech. Sept. 1948*. TP 2469.

Influence of Temperature on the Stress-strain-energy Relationship for Copper and Nickel-copper Alloy

D. J. McADAM, JR.,* Member AIME

Introduction

In a series of papers the author and associates have discussed the influence of temperature on the tensile properties of metals.¹¹⁻¹⁸ These papers present much information about the influence of temperature and the stress system on the conventional indices of mechanical properties, with special attention to the fracture stress. A recent study of the data, however, has revealed much additional information about the influence of temperature on the fundamental factors involved in the flow of metals. The present paper presents results of this study. Attention will be confined almost entirely to results derived from tension tests of unnotched cylindrical specimens at strain rates a little slower than those used in ordinary tension tests.

According to a concept first presented by Ludwik and elaborated in recent papers by others,^{8,9,22,23} the mechanical state of a metal depends on the total plastic strain, but not on the temperature during straining, provided that the only structural changes are those essential to plastic deformation. In the summer of 1948, however, the author made the previously mentioned study of results of a general investigation by the author and associates and reached the conclusion that the mechanical state depends not only on the total strain, but also on the temperature during the straining. A number of diagrams were then prepared. These conclusions were presented without diagrams in a discussion last October of a paper by Dorn, Goldberg and Tietz.²

The metals used in the investigation on which this paper is based were Monel and oxygen-free copper. The

Monel was supplied by the International Nickel Co. through the courtesy of Dr. W. A. Mudge. The copper was supplied by the Scomet Engineering Co. through the courtesy of Dr. Sidney Rolle. The data to be presented are based on results of tests at temperatures ranging between 165 and -188°C . Description of the apparatus and methods of test are given in previous papers.^{10,11,12}

The present paper is the first part of the general discussion of the influence to temperature on the stress-strain-energy relationship for metals. The next paper will deal with metals that are subject to structural changes other than those induced solely by plastic deformation.

Influence of Temperature and Plastic Strain on the Flow Stress of Monel and Copper

For a study of the influence of temperature on the stress-strain relationship, flow-stress curves obtained with annealed metals at various temperatures will be compared with curves obtained with the same metals after cold drawing or cold rolling at room temperature. Diagrams thus obtained with Monel and copper are shown in Fig 1 to 8. Fig 1 to 7 show the variation of the flow stress with temperature and plastic strain; Fig 8 is a diagram of a different type, derived from Fig 4 to 7. In Fig 1 to 7 strain is expressed in

terms of A_0/A , in which A_0 and A represent the initial and current areas of cross-section. Since values of A_0/A are represented on a logarithmic scale, abscissas are proportional to true strains; moreover, the true strains representing prior plastic deformation and those representing subsequent strain during a tension test are directly additive.

Fig 1 shows flow-stress curves obtained with annealed Monel. Five of the curves are based on results of tension tests. Between yield and the maximum load, the flow was under longitudinal tensile stress; between the maximum load and fracture, the local contraction induced transverse radial tensile stress. The portions of curves designated F , therefore, represent flow with increasing radial stress ratio, the ratio of the transverse stress S_3 to the longitudinal stress S_1 . Curve F_0 is based on the ultimate stresses of specimens taken from bars that had been cold drawn various amounts.¹⁷ Since the tensile stress at the maximum load is unidirectional, curve F_0 represents the course that a flow-stress curve would take if the stress during an entire tension test could be kept unidirectional.

The flow-stress curve F obtained at room temperature (Fig 1) has been established accurately by numerous measurements of the diameter of the specimen during the extension from yield to fracture.¹⁷ At the time of the experiments, however, no apparatus was available for measuring the diameter during tension tests at low temperatures. Nevertheless, curves have been established to represent with sufficient accuracy the flow at low temperatures. Each flow-stress curve must be tangent to a curve U , which starts at a point representing the ultimate stress of annealed metal. Since the ultimate stress is based on the area of

Cleveland Meeting, October 1949.
TP 2703 E. Discussion of this paper (2 copies) may be sent to *Transactions AIME* before December 1, 1949. Discussion is tentatively scheduled for publication in May 1950.

Manuscript received May 2, 1949.

* Chairman of Sect., Nat'l. Bur. of Standards.

¹¹ References are at the end of the paper.

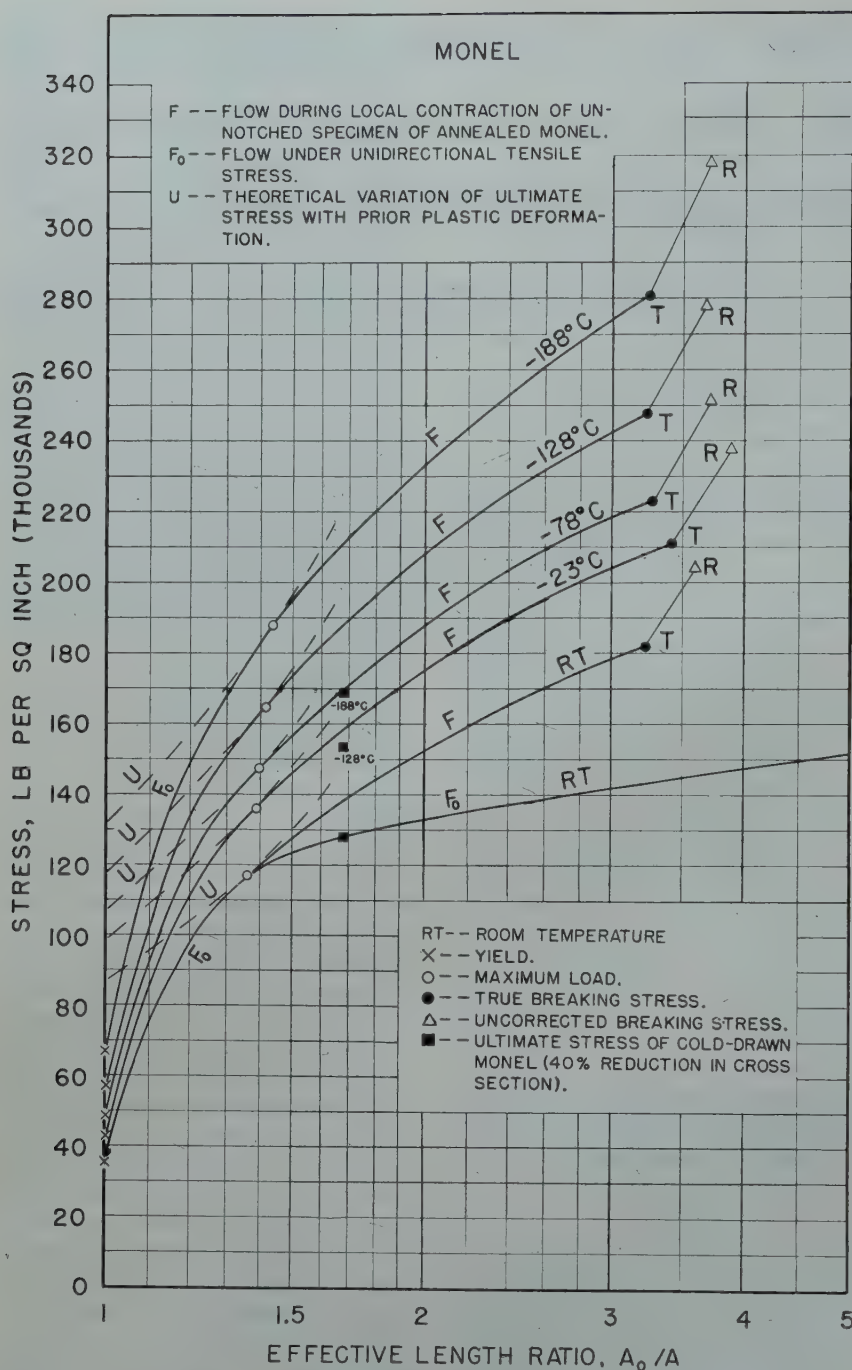


FIG 1—Flow of annealed Monel and ultimate stress of cold-worked Monel at various temperatures.

cross-section at the beginning of a tension test, this strength index varies with the amount of prior plastic deformation of the bar from which the specimen was taken. The variation is linear with L/L_0 or with A_0/A , until the load reaches a maximum and local contraction begins.* However, when A_0/A is represented on a logarithmic scale, the theoretical variation of the ultimate stress with prior plastic strain is represented by a curve U . To each curve U , the corresponding flow-stress

* L_0 and L represent the initial and current lengths.

curve must be tangent at a point representing the true stress at the maximum load. Except in some of the earliest of the tension tests by the author and associates, the extension at the maximum load was determined by means of an automatic diagram, and the point of tangency of the flow-stress curve with curve U can thus be established accurately. However, since the flow-stress curve and the tangent curve generally are close together for a considerable distance on each side of the point of tangency, the course of the flow-stress curve in this region can be

established with sufficient accuracy, even when the extension at the maximum load has not been measured. Moreover, an additional check for the point of tangency is available when the extension at the maximum load has been determined at room temperature; for Monel, the extension at the maximum load increases slightly with decrease of temperature, as illustrated in Fig 1. Between the points representing yield and maximum load, the flow-stress curves for Monel at low temperature have been constructed so as to be in proper correlation with each other and with the accurately established curve representing flow at room temperature.

In order to extend the curves beyond the points of tangency with curves U , it is necessary to establish at least approximately the points representing the beginning of fracture. Points R in Fig 1 represent breaking stresses obtained by dividing the load at beginning fracture by the cross-sectional area determined after fracture. However, because plastic deformation of a ductile metal generally continues at the rim of the cross-section while the fracture is extending from the axis to the periphery, the area of cross-section generally decreases during fracture. The breaking-stress values indicated by points R , therefore, are too high. At room temperature, the transverse measurements during flow have made it possible to determine accurately the true fracture stress, the stress when the flow-stress curve reaches a maximum and fracture begins. This stress is represented by point T . Although transverse measurements were not made during flow at low temperatures, approximate values of the true fracture stresses have been estimated on certain assumptions and are indicated by points T . These points must be on the nearly straight lines extending downward from points R at such a slope that percent decreases in stress are equal to percent decreases in A_0/A^* . Points T on these lines have been located on the assumption that the percent decrease in coordinates from R to T should be the same for low temperatures as for room temperature. The flow-stress curves between the points representing maximum load and beginning fracture have been constructed so as to be in proper correlation with each other and with the curve obtained at room temperature.

* The lines are not quite straight because the scale is semilogarithmic.

The curves thus constructed are sufficiently accurate for use in a study of the influence of temperature and plastic strain on the flow stress. The first part of this study will be a comparison of these curves with the three points representing ultimate stresses of cold-drawn Monel. Since this metal had been reduced 40 pct in cross-section by cold drawing, and since ultimate stresses of severely cold drawn metal are practically the same as flow stresses at the maximum load, the three points representing ultimate stresses in Fig 1 have been placed at an abscissa representing a value of 1.67 for A_0/A . The point representing the ultimate stress at room temperature thus coincides with curve F_0 .

If the flow stress (for a constant strain rate) were merely a function of temperature and total strain, the points representing ultimate stresses of cold-drawn Monel at -128 and -188°C would be much higher than they are in relation to the corresponding flow-stress curves. They would be below these curves, because the curves to the right of the points representing the beginning of local contraction are affected by the increasing radial stress ratio (S_3/S_1), but they would be higher than the corresponding points representing flow of annealed Monel at the maximum load. As shown in Fig 1, however, the points representing ultimate stresses of cold-drawn Monel at low temperatures are much lower in the diagram than the corresponding points representing the flow stresses of annealed Monel at the maximum load. The evidence, therefore, indicates that the flow stress at any instant depends not only on the temperature and total strain at that instant, but also on any prior changes in temperature during the flow.

For a thorough study of the influence of temperature and strain on the flow stress it is necessary to compare curves representing flow at various temperatures, but with the same stress system. Such a comparison is not made in Fig 1. The ideal stress system for this purpose is unidirectional tensile stress ($S_3/S_1 = 0$). As shown in Fig 1, a complete curve (F_0) has been derived to represent flow under this stress system at room temperature.¹⁷ In Fig 2, this curve and other curves of Fig 1 have been reproduced for comparison with curves representing flow under unidirectional tensile stress at low temperatures. Fig 2 also contains flow-stress curves for cold-drawn Monel.

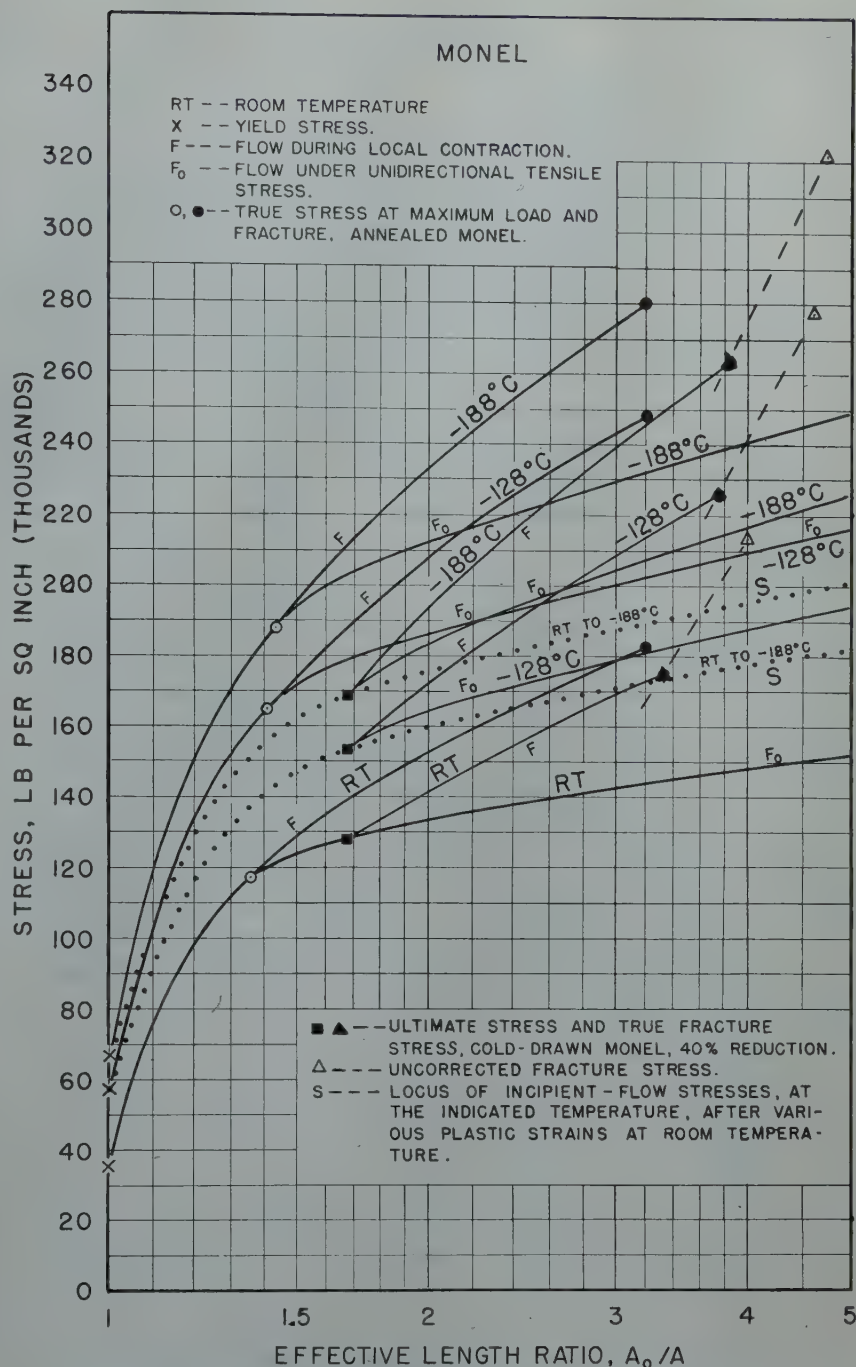


FIG 2—Influence of temperature on the flow of Monel under unidirectional tensile stress.

Curve F for cold-drawn Monel at room temperature is based on frequent transverse measurements during flow, and thus the point representing the beginning of fracture has been accurately established.¹⁷ The F curves for cold-drawn Monel at low temperatures have been established approximately by the method used in establishing the F curves of Fig 1. The F_0 curves representing flow at low temperatures are not based directly on results of experiment; experiments to extend such a curve beyond the point representing the maximum load in a tension test would involve cold drawing or cold

rolling at the low temperature. However, each of these curves in Fig 2 has been constructed with proper divergence from the corresponding F curve. Since the same amount of local contraction would cause about the same increase in the radial stress ratio (S_3/S_1) at low temperatures as at room temperature, the ratio of ordinates of corresponding F_0 and F curves at the same abscissa has been made about the same for low temperatures as for room temperature.

The junctions of the F and F_0 curves for cold-drawn Monel at low temperatures represent incipient flow at these

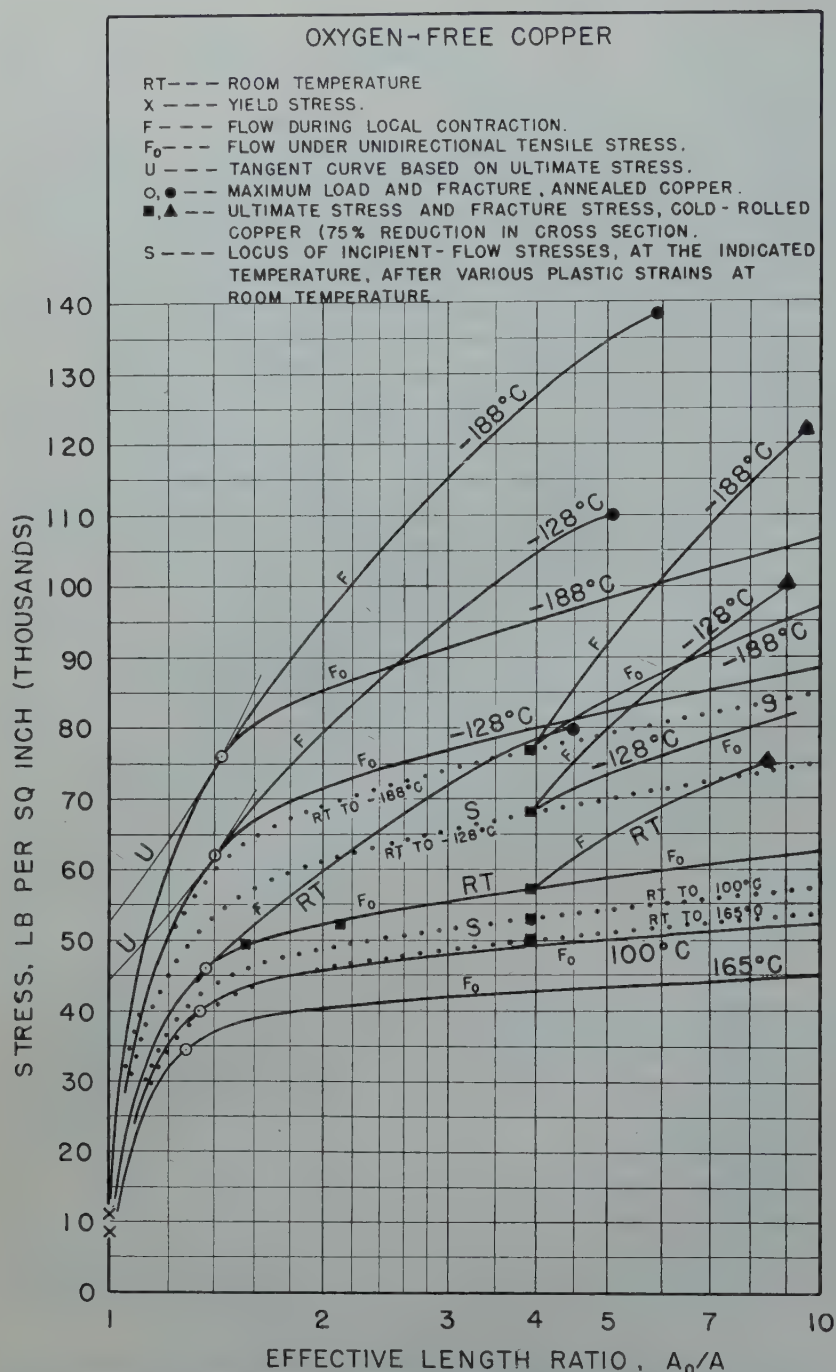


FIG 3—Influence of temperature on the flow of copper under unidirectional tensile stress.

temperatures after the indicated strain at room temperature. The dotted curve *S* passing through each of these junctions represents approximately the locus of incipient-flow stresses at the indicated temperature after various strains at room temperature. Such curves, although they do not represent continuous flow, will be termed "secondary flow-stress curves" to distinguish them from the primary curves from which they are derived. For accurate determination, such a curve should be based on results of tests of specimens that had been extended various amounts at room temperature. However, when a single point has been

established far out on a secondary flow-stress curve, the curve can be constructed in proper correlation with the primary curves, so as to be accurate enough for a study of the influence of temperature and strain on the flow stress. Each secondary curve begins at the origin of the corresponding primary curve; it diverges continuously downward from that curve and upward from the *F₀* curve for annealed Monel at room temperature. Beyond the points representing ultimate stresses of cold-drawn Monel, the ratios of corresponding ordinates of the three *F₀* curves increase very little. Comparison of the primary and secondary *F₀* curves in

Fig 2 shows that the mechanical state depends not only on the total strain, but also on the temperature during the strain.

Fig 3 shows results of tests of annealed copper rod and of rod that had been plastically deformed three different amounts before the tension tests. Two lots of the copper rod had been cold drawn to 40 and 54 pct reduction in cross-section, and one lot had been cold rolled to 75 pct reduction. The points representing ultimate stresses and the corresponding strains of the cold-worked copper coincide exactly with *F₀* curve for annealed copper at room temperature; this curve is based on numerous ultimate stress values for cold-drawn wire and cold-rolled strip.¹⁷ However, Fig 3 is based almost entirely on results obtained with the annealed rod and severely cold-rolled rod, which were tested at room temperature and at low temperatures.

Curves *F* for annealed copper and severely cold-rolled copper have been established accurately by numerous transverse measurements of the diameter of the specimen during flow.¹⁷ The true fracture stresses thus have been determined accurately. Although transverse measurements were not made during flow at low temperatures, the curves representing flow at these temperatures have been established by proper correlation with curves *U*, with the *F₀* and *F* curves for room temperature, and with the points representing fracture at room temperature. Since the points representing ultimate stresses of the severely cold-rolled copper are far out along the secondary flow-stress curves *S*, the divergence of these curves from their origins must be approximately as indicated in the figure.

Comparison of the *S* curves with the *F₀* curves from which they diverge gives additional evidence that the mechanical state of a metal depends not only on the total strain, but also on the temperature during the strain. Since "mechanical state" involves both strength and ductility, and since attention is being confined to resistance to flow, the term "strength state" will be used instead of "mechanical state," with the understanding that "strength" here means resistance to flow, not resistance to fracture. In general use, the word "strength" designates a property that varies with the temperature, as indicated by the variation of the hardness and flow stress. In the term "strength state," however, the word "strength" implies a condition

of the metal, a property independent of temperature. In future discussion, the term "intrinsic strength" will be used with the same significance as "strength state."

The lower the temperature, the more rapid is the increase of the intrinsic strength with strain. The intrinsic strength or strength state is unchanged when the temperature is changed without change in the total strain. In Fig 2 and 3 for example, points at the same abscissa on the F_0 curve for room temperature and the two secondary flow-stress curves represent the same strength state, although they represent very different flow stresses. The effect of temperature on the flow stress evidently involves two factors: (1) a direct effect; (2) an effect of temperature on the rate of increase of the intrinsic strength with strain. The direct effect is illustrated by the vertical distance between the F_0 curve for room temperature and the corresponding S curve; the effect of temperature on the rate of increase of the intrinsic strength with strain is illustrated by the divergence of the primary and secondary curves for the same temperature. For a comparison of strength states by means of flow stresses, the flow-stresses must be determined at the same temperature.

From a set of F_0 curves and secondary flow-stress curves, such as those in Fig 2 and 3, the relationship between the direct temperature factor and the intrinsic strength factor can be determined. By the use of these factors, other locus curves may be developed, each representing incipient-flow stresses at one temperature after various strains at any other temperature, higher or lower, within the range represented in the diagram. These derived curves can be established in exact correlation with the primary and secondary curves, and extended throughout the strain range of curves from which they are derived. For a systematic study of the stress-strain-temperature relationship, three groups of these derived curves should be available. In Fig 4 and 5, three groups of these curves for Monel have been assembled together with the F_0 curves and S curves, which have been reproduced from Fig 2. In Fig 6 and 7 three similar groups of curves for copper have been assembled together with the F_0 curves and S curves, which have been reproduced from Fig 3. These derived curves will be termed "tertiary flow-stress curves." Like the secondary curves,

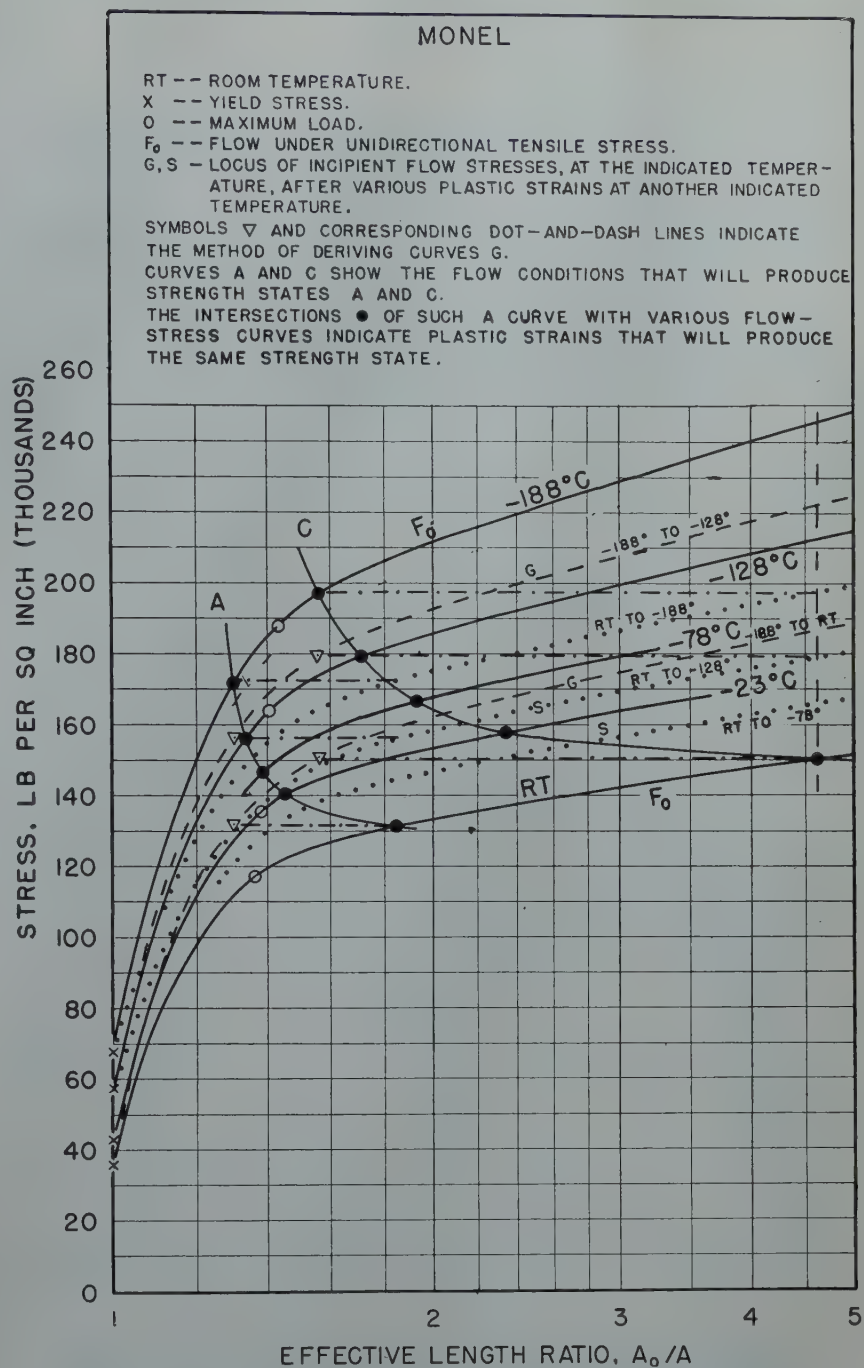


FIG 4—The flow stress of Monel as affected by temperature and total strain.

they do not represent continuous flow.

Before further consideration of the tertiary curves, attention will be given to curves of another type, the curves designated A to C in Fig 4 to 7. Each of these curves shows the influence of temperature on the strain that will produce the same strength state. These constant-state curves have been derived from the primary and secondary flow-stress curves by applying the following principles: (1) Varying the temperature without varying the plastic strain causes no change in the strength state. (2) Two specimens of the same metal, whatever their strain history, are in the same strength state if their flow

stresses are the same at the same temperature. The first principle implies that points at the same abscissa on the F_0 curve for room temperature and the S curves represent the same strength state. The second principle implies that a horizontal line drawn between a primary and a secondary curve representing flow at the same temperature will intersect these curves at points representing the same strength state.

For an example of the use of these principles in deriving a constant-state curve, reference may be made to curve C in Fig 4. A point on the F_0 curve for room temperature has been selected

MONE L

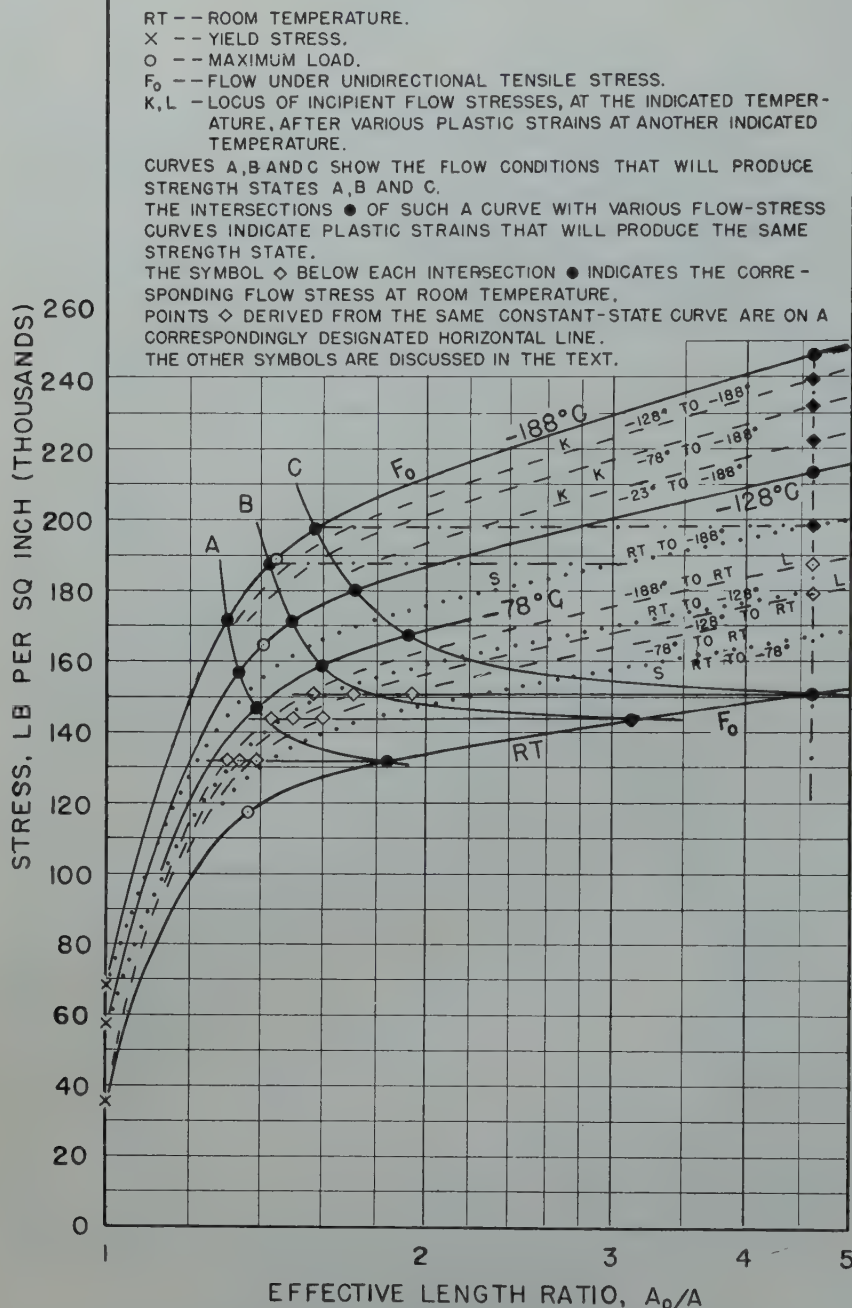


FIG 5—The flow stress of Monel as affected by temperature and total strain.

to represent state C. According to principle (1), the vertical line drawn through this point intersects the secondary flow-stress curves S at points representing the same strength state. According to principle (2), horizontal lines drawn from these intersections will intersect the corresponding F_0 curves at points representing the same strength state. The positions represented by the black circles have thus been established, and curve C drawn through these points represents a constant strength state. This method has been used in constructing all the constant-state curves in Fig 4 to 7.

Although a constant-state curve

represents constant intrinsic strength, it does not represent constant ductility. With decrease in temperature, the strain to produce constant intrinsic strength decreases, while the total ductility of Monel and copper increases. The residual ductility thus increases as the temperature is lowered. Consequently, since "constant mechanical state" implies constant strength and ductility, it is not possible to produce such a state by varying the plastic strain with the temperature. Moreover, although a constant strength state may be produced by varying the strain with the temperature, the structural state is not constant. With decrease in tempera-

ture, the strengthening effect of plastic strain of Monel and copper increases, but the damaging effect¹⁷ does not.

Attention will now be given to the three previously mentioned groups of tertiary flow-stress curves. One of the groups obtained with Monel is in Fig 4 and the other two are in Fig 5; one of the groups obtained with copper is in Fig 6 and the other two are in Fig 7. In deriving these curves, the points represented by inverted triangles have been established by a graphical method similar to the method of establishing the constant-state curves. Beyond these triangles, the tertiary curves have been extended by an arithmetical method involving the use of a direct temperature factor and an intrinsic strength factor. This method will be discussed later.

For an illustration of the graphical method, reference may be made to the inverted triangles on the G curves of Fig 4. Each of these curves represents the locus of incipient-flow stresses at the indicated temperature, after various strains at -188°C . In establishing a point on such a curve, this point should be placed at the proper distance directly below a selected point on the F_0 curve representing strain at -188°C . For convenience in establishing the two triangles on each of the G curves, the two specific strains selected are those represented by the black circles on the uppermost F_0 curve; these are the strains that will produce strength states A and C. If two specimens be strained these amounts at -188°C and then heated to room temperature, the points representing the incipient-flow stresses will be directly below the black circles on the F_0 curve. Moreover, since the two specimens will still be in states A and C, the incipient-flow stresses at room temperature should be the same as if the specimens had been strained to these states at room temperature. The two triangles on the lowest G curve, therefore, have been placed on the horizontal lines extending from the black circles on the F_0 curve for room temperature. From points directly above these two circles and on the secondary flow-stress curve S for -128°C , horizontal lines have been drawn to establish the two triangles on the G curve representing incipient-flow at -128°C . The same graphical method has been used to locate the triangles on all the tertiary flow-stress curves of Fig 5, 6 and 7.

The method of establishing these tertiary curves involves the assumption that, within the temperature range

represented, there are no structural changes other than those essential to plastic deformation. It also involves the assumption that, if the flow stresses of two specimens of the same metal with different temperature-strain histories are equal at one temperature, they will be equal at any other temperature within the range represented. This assumption implies that the direct effect of temperature on the flow stress is the same for two specimens with the same intrinsic strength, whatever may be the difference in the temperature-strain history. If this assumption were incorrect, the concept of intrinsic strength would be as untenable as the concept of absolute velocity. However, the concept of intrinsic strength is supported by scattered evidence in the literature. Moreover, it receives additional support from the results of a study of the influence of temperature on strain energy.

In Fig 4, the group of G curves is similar in one respect to the group of secondary flow-stress curves S . In each group, the curves represent incipient-flow stresses at several indicated temperatures after strains at *one temperature*. By comparison of ordinates of the curves of either group with the associated F_0 curve, information may be obtained about the direct effect of temperature on the flow stress. Similar groups of curves are shown in Fig 6. Fig 5 and 7, however, each contain two groups of a different type from those in Fig 4 and 6. The curves in each group in Fig 5 and 7 represent incipient-flow stresses at *one temperature* after strains at several indicated temperatures. Attention will be confined almost entirely to Fig 5, although the discussion would apply as well to Fig 7. The upper group, comprising the K curves, shows results of straining at several temperatures followed by determination of the incipient-flow stresses at -188°C . Since the uppermost F_0 curve represents flow at -188°C , it belongs in the same group with the K curves. The lowest curve in this group is the secondary flow-stress curve S for -188°C . All the curves of the upper group have the same origin, the point representing yield at -188°C . The lower group in Fig 5, comprising the L curves and the F_0 curve for room temperature, shows results of straining at several temperatures followed by determination of the incipient-flow stresses at room temperature. All the curves of this group have their origin at the point representing yield at room temperature.

Since the ordinates in each of these

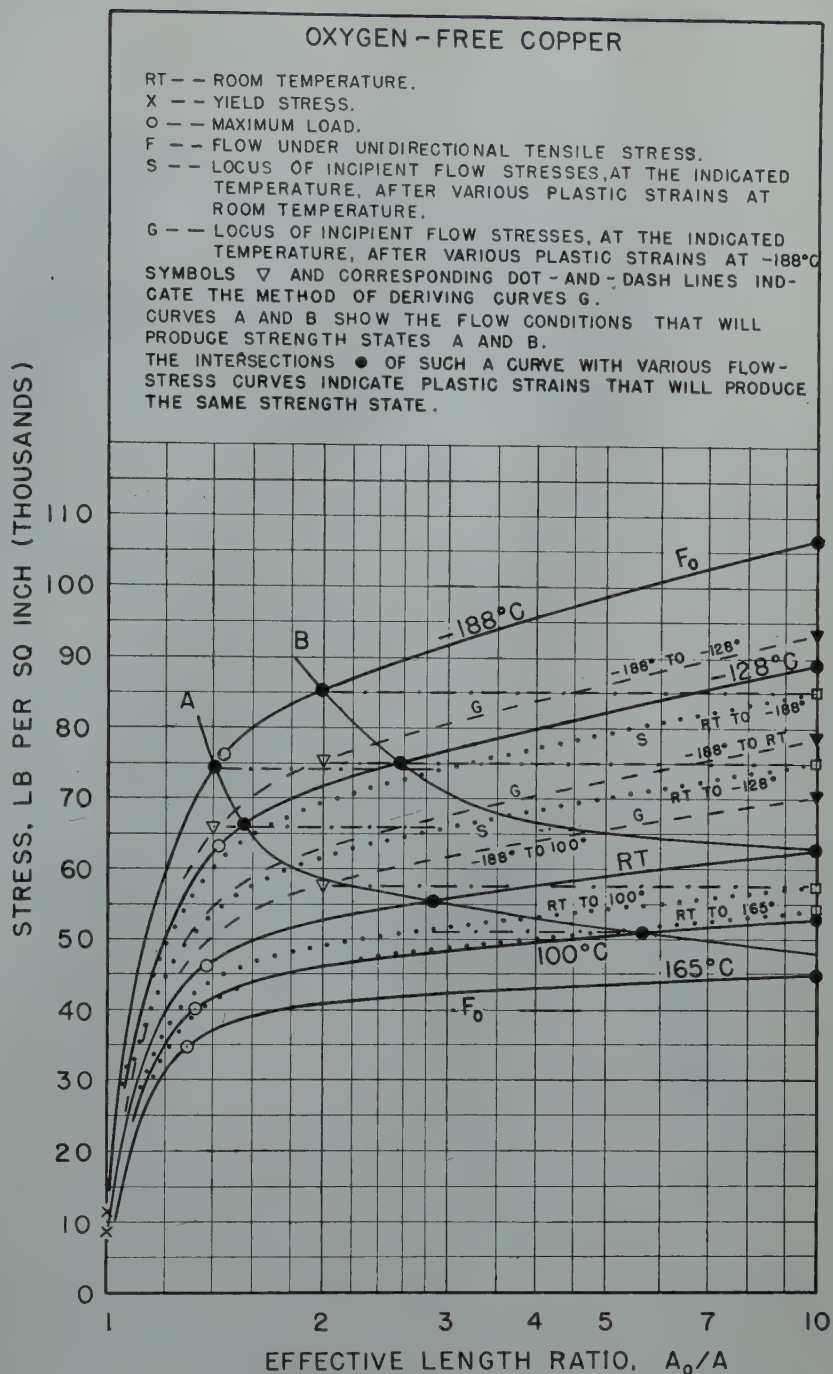


FIG 6—The flow stress of copper as affected by temperature and total strain.

groups represent incipient flow stresses at the same temperature, the ordinates at constant strain are proportional to the intrinsic strengths, and a horizontal line drawn through either of the two groups would intersect the curves at points representing the same intrinsic strength. In the lower group of curves in Fig 5, horizontal lines have been drawn to intersect the lowest F_0 curve at points representing strength states A, B and C. These horizontal lines intersect the tertiary flow-stress curves at points representing strength states A, B and C. The strength states

represented by horizontal lines A, B and C, therefore, are the same as those represented by curves A, B and C. The flow stresses represented by curves A, B and C, however, are primary flow stresses; the flow stresses represented by the horizontal lines are incipient-flow stresses after change to room temperature.

If ordinates in the curves of either the upper or lower group of Fig 5 be compared at the same abscissa, the ordinates will be proportional to the intrinsic strengths produced by the same strain at the indicated temperatures. Since the temperatures of pri-

OXYGEN-FREE COPPER

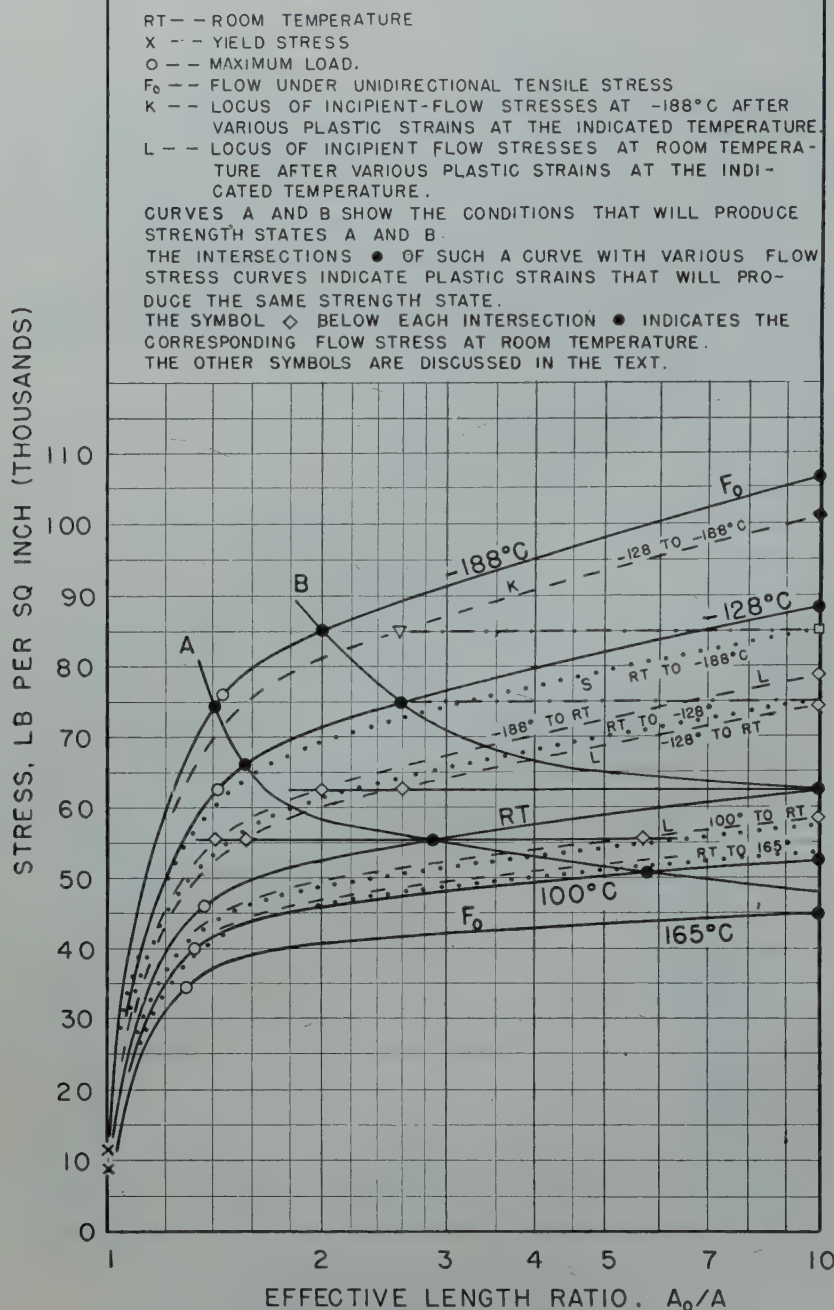


FIG 7—The flow stress of copper as affected by temperature and total strain.

mary flow were the same for both the upper and lower groups, the intrinsic strengths produced by the same strain should be in the same proportion for each group. Consequently, although the incipient-flow stresses represented by the curves of the upper and lower groups differ greatly, the ordinates at the same abscissa should be in the same proportion in each group. As will be shown in the discussion of Fig 8, the ordinates in each of the groups in Fig 5 and 7 are in correct proportion.

The effects of the difference between room temperature and -188°C are represented in Fig 5 by five ordinate

ranges. The extreme ordinate range, the range between the highest and lowest F_0 curves, represents the effect of this temperature difference on the primary flow stress. Within this ordinate range are four other significant ranges. The ordinate ranges of the upper and lower groups of curves represent the effect of the above-mentioned temperature difference on the intrinsic strength. The range below the upper group of curves and the range above the lower group of curves, each represent the *direct* effect of the same temperature difference on the flow stress. Thus there are two ordinate

ranges representing the effect of the same temperature difference on the intrinsic strength, and two ordinate ranges representing the direct effect of this temperature difference on the flow stress. However, when the effects of this temperature difference are expressed in terms of ordinate ratios instead of ordinate differences, a single ordinate ratio will represent the effect on the intrinsic strength and a single ordinate ratio will represent the *direct* effect on the flow stress. The product of these two ratios is the ordinate ratio for the highest and lowest F_0 curves in Fig 5. The effect of a temperature difference on the primary flow stress, therefore, should be expressed as the product of two flow-stress ratios, one of which will be called the intrinsic strength ratio and the other the direct temperature factor.

Plastic strain has very different effects on these two factors. Since the curves in each group from which intrinsic strength ratios are derived diverge from the corresponding point representing yield (Fig 5 and 7), the intrinsic strength ratio at yield is 1.0 and the ratio increases continuously with plastic strain. The direct temperature factor, for a change between room temperature and -188°C, is represented by the ordinate ratio for the uppermost secondary flow stress curve S and the F_0 curve for room temperature. For copper, this ratio is about 1.3 at yield, and changes little with plastic strain (Fig 7). For Monel, the ratio is about 1.9 at yield, but the ratio decreases rapidly with strain until it is about the same as for copper; thereafter the ratio changes very little.

Diagrams of a different type have been derived from Fig 4 to 7 and are shown in Fig 8. In this figure temperatures are plotted as abscissas. The temperature scale is the same that has been used in previous papers by the author and associates.^{11-16,19} Temperatures in degrees K are plotted on a logarithmic scale. Since abscissas are proportional to the logarithm of the degrees Kelvin, the scale is the same in principle as Kelvin's original thermodynamic scale. This scale has been used because, within the range from room temperature -188°C, it gives a nearly linear relationship between temperature and conventional strength indices for various metals. Ordinates in the upper division of Fig 8 represent flow stresses; in the lower division ordinates represent flow-stress ratios.

Attention will be given first to the curves in the upper division. In this

division, there are three groups of five curves, and two curves representing the influence of temperature on the yield stress. Each group of five curves represents variations of the flow stress when the plastic strain is constant at the amount indicated by the value of A_0/A . Each of these groups has been derived from corresponding groups of flow-stress curves in Fig 4 to 7 by using flow-stress values represented by the ordinates at the indicated value of A_0/A . To simplify the correlation between the curves in Fig 8 and the curves from which they are derived, the same letters have been used to designate the curves in Fig 8 and the corresponding curves in Fig 4 to 7. Moreover, the same symbols that designate established points on the curves in Fig 8 have been inserted at corresponding points on the vertical dot-and dash lines of Fig 5, 6, and 7.

In each group of five curves in Fig 8, the F_0 curve and the S curve are derived from corresponding primary and secondary flow-stress curves; the other three curves in the group are derived from tertiary flow-stress curves. The S curve and the G curve have similar meaning. The S curve represents the variation of the incipient-flow stress with temperature, after the indicated strain at room temperature; the G curve represents the variation of the incipient-flow stress with temperature after strain at -188°C . Each of these curves, therefore, represents constant intrinsic strength, and hence it represents the direct effect of temperature on the flow stress. The K curve and the L curve also have similar meaning. The K curve represents the effect of constant strain at various temperatures on the incipient-flow stress at -188°C ; the L curve represents the effect of constant strain at various temperatures on the incipient flow stress at room temperature. The flow-stress variation represented by each of these curves, therefore, is proportional to the variation of the intrinsic strength with temperature.

As indicated by the S curves in Fig 8, the direct effect of temperature on the flow stress is nearly linear between room temperature and -188°C , on this temperature scale. The linear relationship is found not only at severe strains corresponding to A_0/A values of 4.6 for Monel and 10 for copper, but also at values of 1.3 for Monel and 4 for copper, abscissas at which the secondary flow-stress curves (Fig 2 and 3) are most accurately

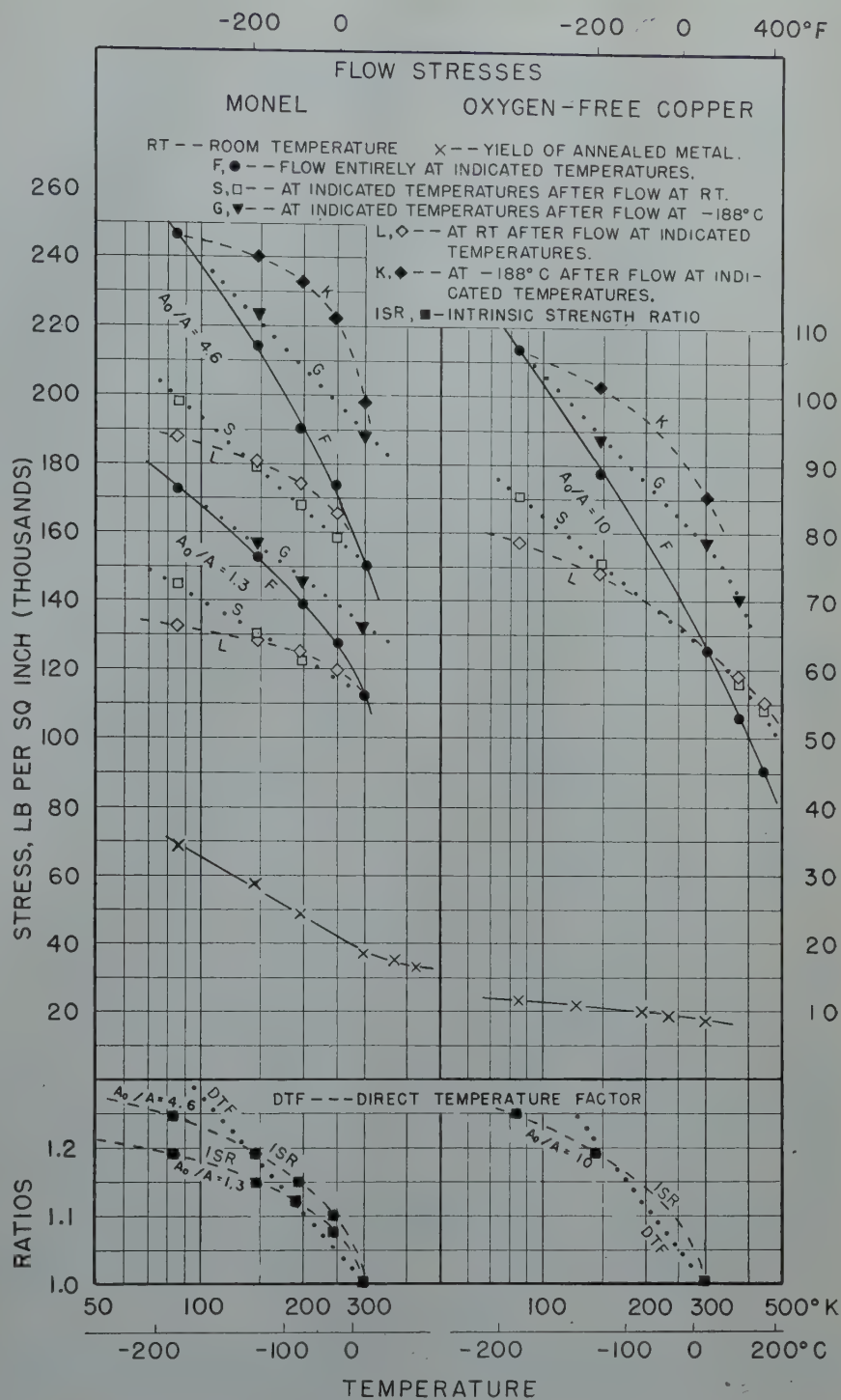


FIG 8—Influence of temperature on the flow stress of Monel and copper at constant strain.

established. The linear relationship, however, probably ends a little above room temperature. The downward bending of the S curves for copper in Fig 8 possibly is due to the softening effect of "relaxation." If the S curves for Monel were extended above room temperature, they probably would turn upward because of strain aging.¹¹ Between room temperature and -188°C neither Monel nor copper shows evidence of either strain aging or relaxation. There is some doubt that

the linear relationship persists below -188°C . Continuation of the linear relationship on this temperature scale, between -188°C and the temperature of liquid hydrogen (-252.8°C) would require about 35 pct increase in the flow stress. Results of tension tests by DeHaas and Hadfield¹ and by Kostenetz⁷ indicate that the increase in the flow stress between -188°C and -252.8°C for most of the metals tested would be not more than about 20 pct. However, results obtained by Kos-

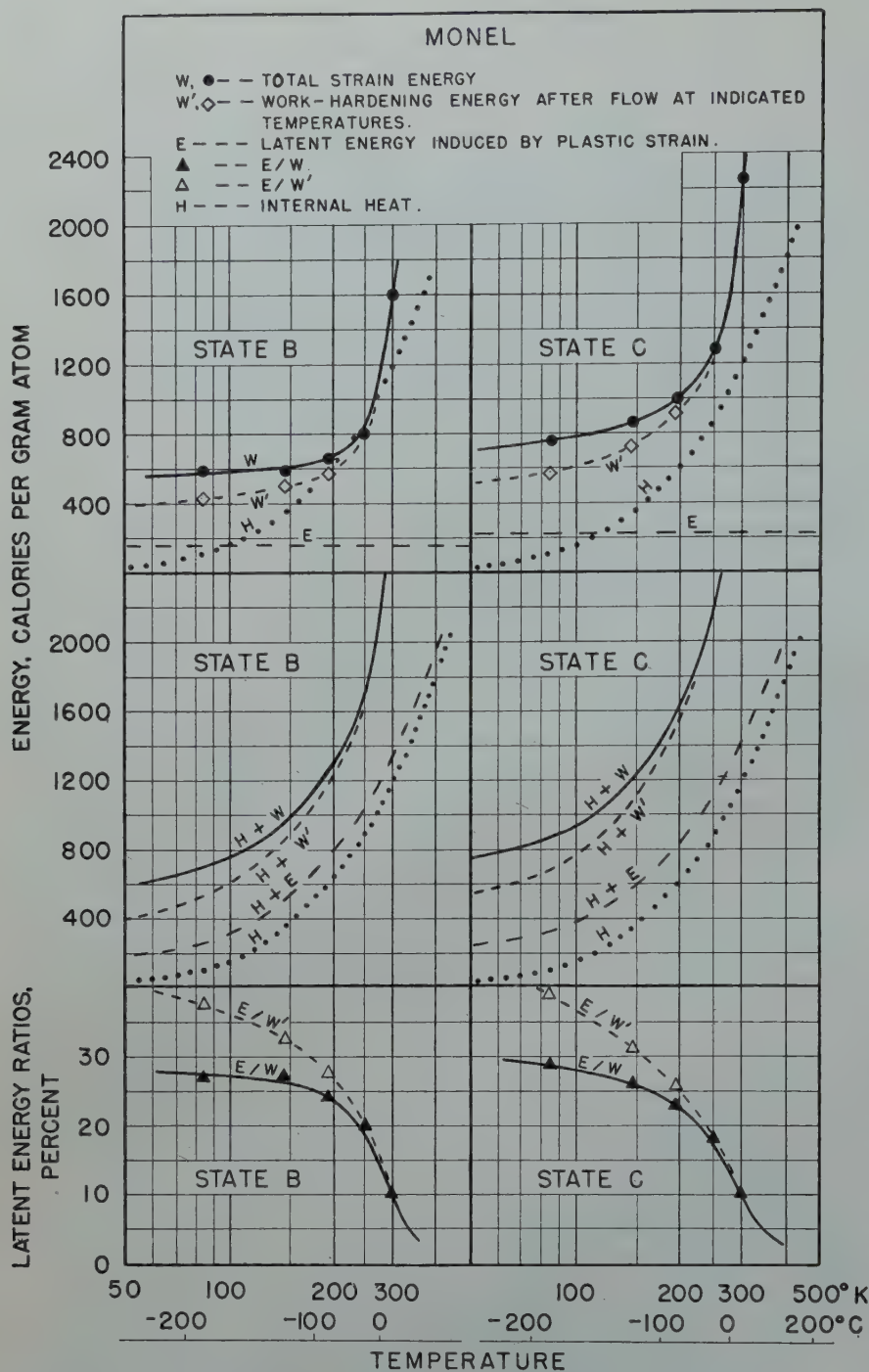


FIG 9—Influence of temperature on the strain energy of Monel for constant intrinsic strength

tenetz with some steels indicate an increase of about 35 pct, and his results for aluminum indicate an increase of 67 pct. The evidence based on these tests, therefore, is inconclusive. It appears probable, however, that the S lines for Monel and copper should be slightly curved if extended below -188°C ; the curvature would be qualitatively similar to that of the F_0 curves in Fig 8.

The F_0 curve, even in the absence of strain aging, probably would reverse its curvature if extended far enough

above room temperature. If extended over a sufficient temperature range, the curve would thus be similar in form to a curve representing the influence of temperature on the ultimate stress. Below the point of reversal the curvature is due largely to the influence of temperature on the intrinsic strength factor, as illustrated by curves K and L in Fig 8.

In each group of five curves in Fig 8, two curves represent the direct effect of the same range of temperature on the flow stress, and two curves repre-

sent the effect of the same range of temperature on the variation of the flow stress with the intrinsic strength. However, when the effect of this range of temperature on each of these four curves is expressed in terms of flow-stress ratios instead of flow-stress differences, only one curve is obtained to represent the *direct* effect of temperature, and only one curve is obtained to represent the effect of temperature on the intrinsic strength ratio. Curves so obtained are shown in the lower division of Fig 8. Lines DTF represent the variation of the direct temperature factor with temperature, and curves ISR represent the variation of the intrinsic strength ratio. Ratios are expressed in terms of the flow stress at the indicated strain at room temperature. Lines DTF are based on averages of closely agreeing ratios derived from lines S and G ; curves ISR are based on closely agreeing ratios derived from curves K and L . However, there is another way in which the ISR curves can be derived. From a pair of F_0 and S curves in Fig 8 intrinsic strength ratios can be derived by calculating ratios of corresponding ordinates. Since the S curve represents the effect of lowering the temperature without change of intrinsic strength, any point on this curve represents the intrinsic strength produced by the indicated strain at room temperature. The ratio of ordinates of the F_0 and S curves at the same abscissa, therefore, is the ratio between the intrinsic strength produced by straining at the indicated temperature and the intrinsic strength produced by the same strain at room temperature. Ratios thus obtained from the F_0 and S curves are identical with those obtained at the same abscissas from curves K and L .

The fundamental factors involved in the effect of temperature on the flow stress, therefore, can be derived directly from corresponding F_0 and S curves. These factors could then be used to establish curves G , K , L , DTF and ISR in Fig 8 without the use of the tertiary flow-stress curves in Fig 4 to 7. Moreover, the same arithmetical method can be used, in conjunction with the graphical method, to derive the tertiary flow-stress curves in Fig 4 to 7 from the F_0 and S curves.

As indicated by the ISR curves in Fig 8, the influence of temperature on the intrinsic strength factor gradually becomes less prominent as the temperature is lowered between room temperature and -188°C . However, if

the *ISR* curves were extended to some point above room temperature the steepness probably would begin to decrease, even in the absence of strain aging. The influence of prior plastic strain on the steepness of the *ISR* curve is illustrated by the relation between the two *ISR* curves for Monel. With decrease in the prior plastic strain, the steepness of the *ISR* curve decreases. At yield, the curve would become a horizontal line, and the influence of temperature on the flow stress would depend entirely on the direct temperature factor.

Influence of Temperature on the Strain Energy of Monel and Copper

The energy applied in the plastic deformation of metals is converted partly into heat and partly into latent energy. The conversion into latent energy is associated with the work-hardening, that is, the increase of intrinsic strength with strain. Since the strain energy is a function of the area beneath a flow-stress curve, the evidence in Fig 4 to 7 indicates that both the total strain energy and the latent energy vary with the temperature at which the metal is strained. The flow-stress curves in Fig 4 to 7, therefore, have been used to develop diagrams representing the influence of temperature on the strain energy of Monel and copper. The diagrams thus obtained are shown in Fig 9, 10 and 11. The energy values represented in these figures have been derived from the areas beneath flow-stress curves in Fig 4 to 7. The areas were determined by the use of original unreduced diagrams (20 in. wide) which were on coordinate paper with fine subdivisions. Since abscissas in these diagrams are proportional to true strains, the area beneath a flow-stress curve is proportional to the strain energy per unit volume of the *flowing* metal, even when this volume is decreasing because of local contraction. In calculating energy values per unit volume from the areas, a factor was used to convert abscissas to natural strains, and other factors were used so as to determine the energy equivalent of unit area in calories per gram atom.

Fig 9 and 10 show the energy relations for constant strength state; Fig 11 shows the energy relations for constant strain. Attention will be given first to the relations for constant state. States B and C represented by curves

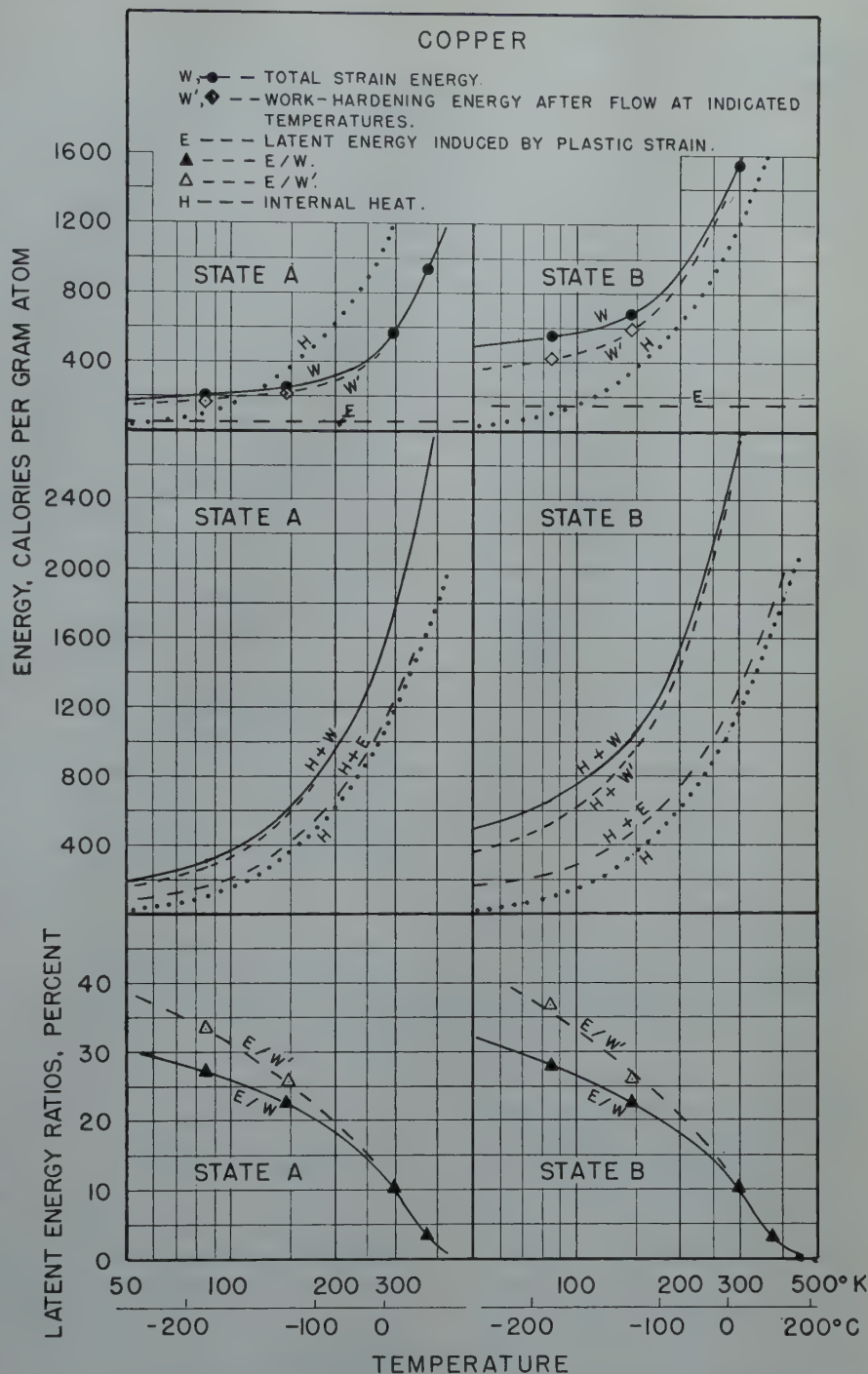


FIG 10—Influence of temperature on the strain energy of copper for constant intrinsic strength.

W in Fig 9 are the same as those represented by curves *B* and *C* in Fig 5; states *A* and *B* represented by curves *W* in Fig 10 are the same as those represented by curves *A* and *B* in Fig 7. The circles on the *W* curves in Fig 9 and 10 correspond to circles on the constant-state curves in Fig 5 and 7. Just as curve *C* in Fig 5 represents the effect of temperature on the *strain* that will produce state *C*, so curve *W* on the right side of Fig 9 represents the effect of temperature on the *strain energy* that

will produce the same strength state. The similarity in form between the *W* curves in Fig 9 and 10 and the constant state curves in Fig 5 and 7 indicates that, for constant state, the variation of the strain energy with temperature is similar to the variation of the plastic strain.

Curves *W* in Fig 9 and 10 represent the influence of temperature on the *total* strain energy. However, just as the influence of temperature on the flow stress involves a direct tempera-

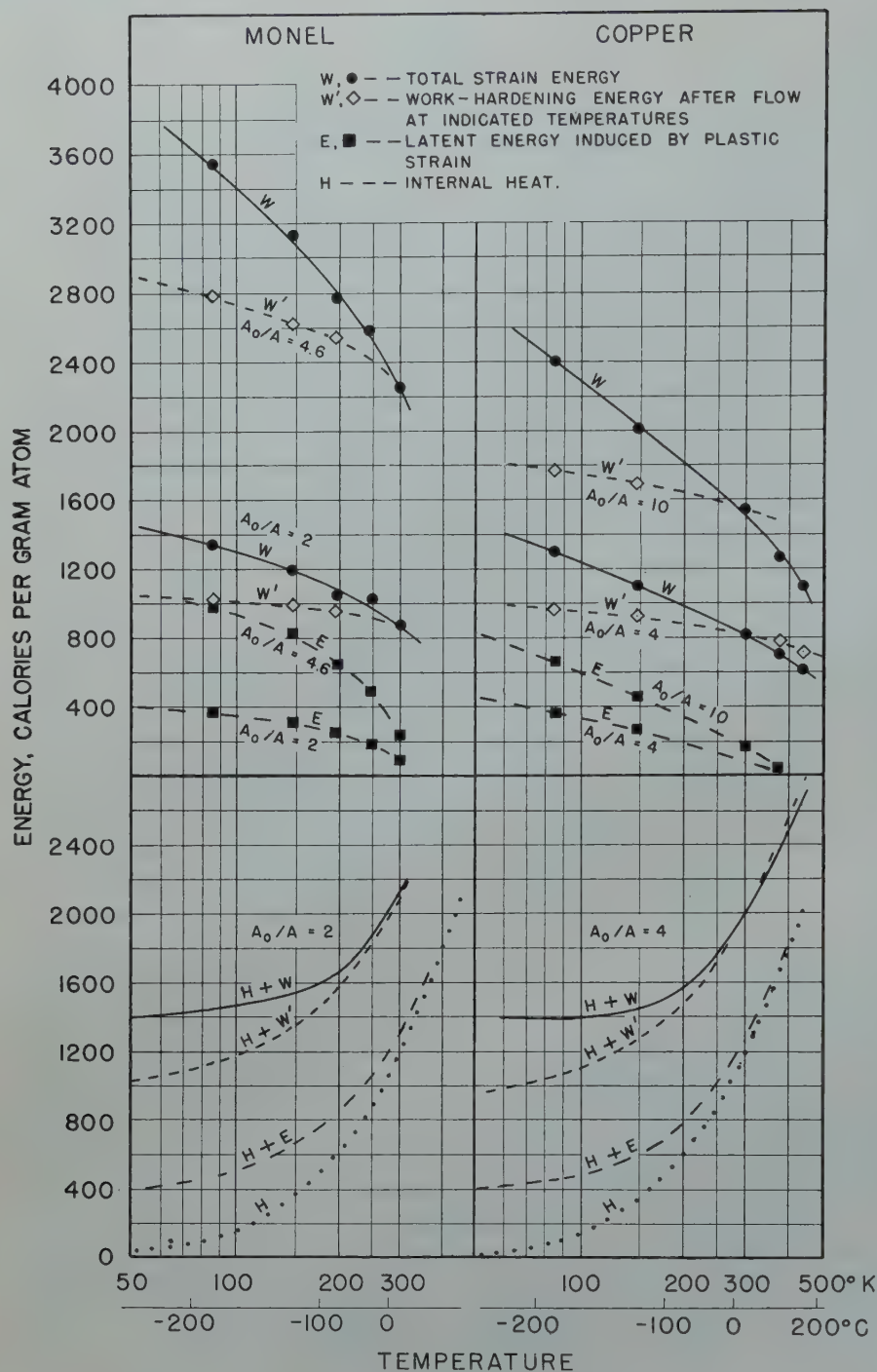


FIG 11—Influence of the temperature of Monel and copper on the strain energy for constant strain.

ture factor and an intrinsic strength factor, so the influence of temperature on the strain energy involves the same two factors. The relative influence of the two factors varies greatly with the metal. When the yield stress varies greatly with temperature, the influence of the direct temperature factor is most prominent. Curves W' have been developed to represent the influence of temperature on the work-hardening energy, the energy that remains after allowance for the influence of the direct temperature factor. Although partial

allowance for this factor may be made by utilizing only part of the area beneath a flow-stress curve, the part above the point representing the yield stress, the allowance thus made is incomplete. Complete allowance can be made by the method now to be described. Whereas curves W in Fig 9 are derived from the areas beneath F_0 curves in Fig 5, curves W' in Fig 9 are derived from areas beneath the L curves in Fig 5. The strain energy values represented by the symbols on curves W' in Fig 9 correspond to the

strain values indicated by symbols of the same kind on the horizontal lines representing strength states B and C in Fig 5. Curves W' , therefore, represent strain energy values derived from curves representing incipient flow at one temperature after strain at various temperatures. It should be emphasized that curves L in Fig 5 and 7 do not represent continuous flow. The ordinates of curves W' in Fig 9 and 10, therefore, do not represent strain energies for continuous flow at room temperature. They represent merely the energy values obtained by making allowance for the influence of the direct-temperature factor on the strain energy, and thus obtaining values for what may be called work-hardening energy. Since the values for work-hardening energy represented by a W' curve are relative to the total strain energy at room temperature, curve W'' crosses curve W at the abscissa representing room temperature (300°K). The values represented by a W' curve thus are merely relative values. They have been desired for use in the following study of the relation between applied energy and latent energy.

The relation between the total strain energy and the latent energy induced by plastic strain has been investigated by Taylor and Farren²⁰ and by Taylor and Quinney.²¹ The metals used in their experiments were copper, annealed mild steel, and annealed decarburized mild steel. For various stages during plastic deformation of these metals the increments of applied energy and latent energy were determined. With copper, the ratio of these increments (latent energy ratio) was about 9 pct throughout a wide range of plastic strain, but eventually decreased rapidly to about 4 pct. With the mild steel, the ratio decreased continuously from about 13 to about 7 pct. With the decarburized steel, the ratio decreased from about 10 to about 3 pct. With all three metals, however, the ratio of the total latent energy to the total applied energy changed very little throughout a wide range of plastic strain, a range which was much greater for copper than for the steels. For a qualitative study of the influence of temperature of the latent energy ratio, it has seemed best to assume a ratio of 10 pct for Monel and copper at room temperature. This ratio, therefore, has been used in Fig 9 and 10.

Since each of the four W curves of Fig 9 and 10 represents the strain energy relation for constant intrinsic

strength, a reasonable assumption is that each curve also represents the strain energy relation for constant latent energy. Beneath each of the W curves, therefore, a horizontal line E has been drawn to represent the influence of temperature on the latent energy E . The constant ordinate of line E is one-tenth the ordinate of curve W at room temperature. Comparison of corresponding ordinates of line E and curves W and W' shows that the latent energy ratios E/W and E/W' increase greatly with decrease in temperature. The variation of these ratios with temperature is represented directly by the curves in the lower division of Fig 9 and 10. The influence of temperature on these ratios evidently is nearly the same for both Monel and copper in each strength state. Moreover, comparison of these curves with the curves in the lower division of Fig 8 shows that the variation of the latent energy ratio with temperature is similar to the variation of the intrinsic strength ratio. The evidence indicates that the E/W ratio at -188°C is nearly three times the ratio at room temperature. If the ratio curves were extended to a point above room temperature, the steepness probably would begin to decrease. Moreover, above a certain temperature, the latent energy ratio would be affected by relaxation, and the influence of the strain rate on the ratio would become prominent.

Curves H in Fig 9 and 10 represent the total heat per gram atom, that is, the integral of the variation of the atomic heat with temperature. This will be termed "internal heat" to distinguish it from the part of the strain energy that is evolved as heat. Comparison of curves W and W' with curve H shows that the effect of temperature on the strain energy, for constant intrinsic strength, is qualitatively similar to the effect of temperature on the internal heat. The greater the internal heat, the greater is the total strain energy required to produce constant intrinsic strength, and the greater is the outflow of energy as heat. In the middle division of Fig 9 and 10, the total strain energy, work hardening energy, and latent energy are represented as superimposed on the internal heat.

Fig 11 shows the influence of temperature on the energy relations for constant strain. Curves W and W' in this figure have been derived from areas extending to the indicated abscissas beneath curves F_0 and L in Fig 5 and 7. Curves W and W' in Fig 11 are

similar in form to curves F_0 and L of Fig 8. This similarity would be expected since each curve represents results obtained with constant strain, and since the curves in both figures are derived from the F_0 and L curves of Fig 5 and 7. For constant plastic strain, therefore, the variation of the strain energy with temperature would be similar to the variation of the flow stress. Curves E in Fig 11 have been derived from the corresponding W curves by making the ordinate ratios for the two curves the same as the corresponding values of the latent energy ratio E/W , as represented by ordinates of the curves in the lower division of Fig 9 and 10. Curves E in Fig 11, therefore, are similar in form to curves E/W in Fig 9 and 10. They also are similar to the curves ISR of variation of the intrinsic strength ratio (Fig 8).

In the lower division of Fig 11, the total strain energy, work hardening energy, and latent energy for constant strain are represented as superimposed on the internal heat. The curves thus obtained should be compared with the curves representing the superimposed energies for constant intrinsic strength (Fig 8).

The diagrams in Fig 1 to 11 present various pictures of the influence of temperature on the stress-strain-energy relationship for metals that are practically free from structural changes or relaxation within the range from room temperature to -188°C .

Conclusions

1. The mechanical state of a metal depends not only on the total strain, but also on the temperature during the straining.

2. With decrease in temperature the total strain required to produce a constant strength state decreases, while the ductility of many metals increases. By "strength state" or "intrinsic strength" is meant a condition of the metal, a property independent of temperature.

3. The mechanical state which involves both strength and ductility cannot be held constant by varying the total strain with the temperature.

4. The influence of temperature on the flow stress involves two factors: (1) A direct temperature effect; (2) the influence of temperature on the rate of increase of intrinsic strength with strain. The lower the temperature, the more rapid is the increase of intrinsic strength with strain.

5. The effects of the direct temperature factor and the intrinsic strength factor on the flow stress should be expressed in terms of flow-stress ratios rather than flow-stress differences. The ratio of the flow stresses for the same total strain at two different temperatures is the product of two flow-stress ratios, one representing the direct temperature factor and the other representing the intrinsic strength ratio.

6. Both these factors can be determined from a set of primary flow-stress curves and a corresponding set of secondary curves, each representing the locus of incipient-flow stresses at a given temperature after various plastic strains at room temperature.

7. By the use of the two factors so obtained other (tertiary) locus curves can be obtained, each representing incipient-flow stresses at one temperature after various plastic strains at another temperature, either higher or lower.

8. With plastic strain the intrinsic strength ratio increases continuously, but there is not much change in the direct temperature factor.

9. The variation of the total strain energy with temperature involves the same two factors that affect the flow-stress. By making allowance for the influence of the direct temperature factor it is possible to determine the influence of temperature on the work-hardening energy.

10. The ratio of the latent energy induced by plastic strain to either the total strain energy or the work-hardening energy increases with decrease in temperature. The variation of the latent energy ratio with temperature is similar to the variation of the intrinsic strength ratio.

11. For constant intrinsic strength (constant latent energy) the variation of either the total strain energy or the work-hardening energy with temperature is qualitatively similar to the variation of the internal heat per gram atom, the integral of the variation of the atomic heat with temperature. The greater the internal heat, the greater is the total strain energy necessary to produce constant intrinsic strength, and the greater is the outflow of energy as heat.

References

1. W. J. DeHaas and R. Hadfield: The Effect of the Temperature of Liquid Hydrogen on the Tensile Properties of Forty-one Specimens of Metals. *Phil. Trans. Roy. Soc.* (1933-34) A, 232, 297-332.
2. J. E. Dorn, A. Goldberg, and T. E.

- Tietz: The Effect of Thermo-mechanical History on the Strain Hardening of Metals. *Trans. AIME* **180**, *Metals Tech.*, Sept., 1948, TP 2445. Discussion, *Trans. Jnl. of Metals* (May, 1949) 325.
3. Dushman, Dunbar and Huthsteiner: Creep of Metals. *Jnl. Appl. Phys.* (1944) **15**, 108-124.
 4. J. H. Holloman and C. Zener: Conditions of Fracture of Steel. *Metals Tech.* Dec. 1944. TP 1782.
 5. J. H. Hollomon and J. D. Lubahn: Plastic Flow of Metals. *Phys. Rev.* (1946) **70**, Nov. 1 and 15, p. 775.
 6. J. H. Holloman: The Mechanical Equation of State. *Trans. AIME* (1947) **171**, 535-543; *Metals Tech.*, Sept., 1946, TP 2034.
 7. V. J. Kostanetz: Mechanical Properties of Metals and Alloys in Tension at Low Temperatures. *Jnl. Tech. Phys.* (U.S.S.R.) (1946) **16**, No. 5, 515-554.
 8. C. W. MacGregor and J. C. Fisher: Tension Tests at Constant True Strain Rates, *Jnl. Appl. Mech.*, Dec. 1945, **12**, A217-A227.
 9. C. W. MacGregor and J. C. Fisher: A Velocity-Modified Temperature for the Plastic Flow of Metals. *Trans. ASME* 1946, **68**, A11-A16.
 10. D. J. McAdam, Jr. and R. W. Mebs: An Investigation of the Technical Cohesive Strength of Metals. *Trans. AIME* (1945) **162**, 474-536.
 11. D. J. McAdam, Jr. and R. W. Mebs: The Technical Cohesive Strength and Other Mechanical Properties of Metals at Low Temperatures. *Proc. Am. Soc. Test. Materials* (1943) **43**, 661-703.
 12. D. J. McAdam, Jr., R. W. Mebs, and G. W. Geil: The Technical Cohesive Strength of Some Steels and Light Alloys at Low Temperatures. *Proc. Am. Soc. Test. Materials* (1944) **44**, 593-644.
 13. D. J. McAdam, Jr.: The Technical Cohesive Strength of Metals in Terms of the Principal Stresses. *Trans. AIME* (1945) **162**, 542-568.
 14. D. J. McAdam, Jr., G. W. Geil, and R. W. Mebs: The Effect of Combined Stresses on the Mechanical Properties of Steels between Room Temperature and -188°C . *Proc. ASTM* (1945) **45**.
 15. D. J. McAdam, Jr., G. W. Geil and R. W. Mebs: Effects of Combined Stresses on the Mechanical Properties of Some Nonferrous Metals. *Trans. ASM* (1946) **37**, 497-536.
 16. D. J. McAdam, Jr., G. W. Geil, and R. W. Mebs: Influence of Plastic Deformation, Combined Stresses and Low Temperature on the Breaking Stress of Ferritic Steels. *Trans. AIME* (1947) **172**, *Metals Tech.* Aug. 1947, TP 2220.
 17. D. J. McAdam, Jr., G. W. Geil and Frances Jane Cromwell: Flow, Fracture and Ductility of Metals. *Trans. AIME* **175**, 306. *Metals Tech.* Jan. 1948. TP 2296.
 18. D. J. McAdam, Jr., G. W. Geil, and W. D. Jenkins: Influence of Strain Aging on the Fracture Stress of Low-carbon Steel. *Trans. AIME* (1948) **175**, *Metals Tech.* Jan. 1948. TP 2318.
 19. D. J. McAdam, Jr., G. W. Geil and F. J. Cromwell: Influence of Low Temperatures on the Mechanical Properties of 18:8 Chromium-nickel Steel. *Trans. ASM* (1949) **41**, 609-645.
 20. G. I. Taylor and W. S. Farren: Heat Developed during Plastic Extension of Metals. *Proc. Roy. Soc.* (1925) **A-107**, 425-451.
 21. G. I. Taylor and H. Quinney: The Latent Energy Remaining in a Metal after Cold Working. *Proc. Roy. Soc.* (1934) **A-143**, 307-326.
 22. C. Zener and J. H. Holloman: Plastic Flow and Rupture of Metals. *Trans. Am. Soc. Metals* (1943) **33**, 163-215.
 23. C. Zener and J. H. Holloman: Problems in Non-elastic Deformation of Metals. *Jnl. Appl. Phys.* Feb. 1946, **17**, 68-87.

The Thermodynamical Treatment of Very Small Solid Solubilities

LESTER GUTTMAN*

The question of whether classical thermodynamics alone imposes any lower limit to solid solubilities was raised during a discussion among various members† of the Institute for the Study of Metals. Although our conclusions are not new,¹ they may be worth reiterating, since confusion on this subject seems to persist.

In a binary system (A,B), the conditions for equilibrium, at constant pressure and temperature, between a solid solution and a liquid solution are

$$\mu_A^S = \mu_A^L \quad [1a]$$

$$\mu_B^S = \mu_B^L \quad [1b]$$

Here μ denotes the chemical potential either of component A or B, as shown by the subscripts, and the superscripts *s* and *l* refer to the solid and liquid solutions, respectively. These two conditions are just sufficient to determine the compositions of both phases. Suppose, however, that the solid phase is found experimentally not to contain any of component B; then we cannot evaluate μ_B^S , which is defined by

$$\mu_B^S = \left(\frac{\partial F^S}{\partial n_B^S} \right)_{n_A^S, P, T}$$

Here n_A^S and n_B^S are the number of mols of A and B, respectively, in the solid, whose free energy is F^S . Eq 1b cannot be used, but it is no longer needed: we stated at the outset that the solid has the composition "pure A," and only the liquid composition need now be determined, from Eq 1a. All the equilibrium properties of the system can be derived from Eq 1a rigorously and simply. Hence there is no purely thermodynamic reason to exclude phase diagrams which show precisely zero solid solubility. Marsh² has objected to such diagrams as implying that even the transformation of pure A begins at the eutectic temperature. In any case, the user of the diagram must have a certain minimum knowledge of how to interpret it, and

it would seem simpler to remember the general rule that eutectic temperatures have no significance for pure components, rather than to show, say, by broken lines, on a scale which will often be exaggerated, a hypothetical solid-solubility about which we know only that it is less than a certain amount.

The case of an intermetallic compound in equilibrium with a binary liquid solution does not require a separate treatment since nothing in the foregoing was dependent on the nature of the components. Therefore, thermodynamics alone does not exclude the possibility that (intermetallic) compounds may exist with compositions always precisely those given by their chemical formulas.

With the aid of *extra*-thermodynamic methods, one may conclude that the solubility of one solid in another is never exactly zero. On the other hand, one would generally expect that the solubility will be small unless the components resemble one another (as do the metals), or form weakly-bound crystals. Therefore, it is useful to know that when there is no direct evidence for solid-solubility, one may neglect it without violating thermodynamic principles.

Technical Note No. 22 E. Manuscript received June 28, 1949.

* Institute for the Study of Metals, Univ. of Chicago, Chicago, Ill.

† J. W. Stout, L. Meyer, W. Band, T. Rosenqvist, O. J. Kleppa, the writer, and others.

¹ W. Hume-Rothery: *Jnl. Inst. Metals* (1926) XXXV, 295-307.

² J. S. Marsh: *Principles of Phase Diagrams*. McGraw-Hill Book Co., N. Y., 1935. pp. 93-4.

Kinetics of the Reactions of Titanium with O_2 , N_2 and H_2

EARL A. GULBRANSEN* and KENNETH F. ANDREW*

Introduction

In a recent communication¹⁴ we have reported on the kinetics of the reactions of zirconium with O_2 , N_2 and H_2 as a function of the time, temperature and pressure variables. A systematic study was made and the results correlated with fundamental theories of gas-metal reactions. This paper will present a similar study for titanium.

Titanium and zirconium are members of the IV group of the periodic table and possess many similar physical and chemical properties as a result of their similar electronic configuration for the outer electrons. The two metals are relatively inert to both gas and liquid phase corrosion at room temperature. However, at moderate temperatures the metals become active and react readily with the common gases including O_2 , N_2 and H_2 which are of interest in this study.

A study of the kinetics of these gas-metal reactions is of interest for three reasons: (1) to understand the rate of reaction of titanium and its role in the behavior of high temperature alloys; (2) to understand the practical difficulties of the reduction, refining and working of titanium; and (3) to correlate the data with fundamental theories of gas-metal reactions and crystal structure predictions.

Literature Survey

Several review papers⁸ and books^{42,43} exist on the preparation and properties of titanium and its alloys.

THE METAL

Titanium has, at room temperature,

a hexagonal lattice of the zinc type. Hägg¹⁹ gives a value of 2.953Å for the (*a*) axis, a value of 4.729 for the (*c*) axis and a density of 4.427 at 20°C. Burgers and Jacobs⁵ have observed the transformation of the hexagonal to the body-centered cubic structure at 880°C and have established a value of 3.31 for the cube edge and a density of 4.31.

TITANIUM-OXYGEN

Carpenter and Reavell⁶ using a pressure change method have studied the reaction at temperatures of 742° and 1000°C and for a pressure of one-fifth of an atmosphere. The probabilities for reaction are calculated from kinetic theory and they report a value of 10^{-5} for O_2 at 1000°C and 10^{-6} at 740°C.

The titanium-oxygen system has been investigated by Ehrlich.^{10,11} Five phases are observed. Between (TiO_2 and $TiO_{1.90}$) an alpha-phase, consisting of a rutile lattice, is found. A beta-phase is observed between ($TiO_{1.80}$ and $TiO_{1.70}$). A gamma-phase is homogeneous between ($TiO_{1.56}$ and $TiO_{1.46}$) and has a structure of the corundum type. The delta-phase exists between $TiO_{1.25}$ and $TiO_{0.6}$ and has a sodium chloride structure. From $TiO_{0.42}$ to Ti the metal structure is observed.

The surface oxide films have been studied by Hickman and Gulbransen.²⁰

The rutile structure is observed in the temperature range studied, 300 to 700°C.

Three crystalline modifications of TiO_2 exist: rutile and anatase which are tetragonal and brookite which has an orthorhombic structure. Anatase is reported³⁶ to exist in two forms: I and II. Anatase II changes to anatase I at 642°C. Anatase I is stable up to 915°C where rutile becomes the stable modification. At 1300°C rutile transforms to brookite which melts at 1900°C. The monoxide, TiO , may be prepared from the dioxide by high temperature reduction with carbon or magnesium. Its melting point is 1750°C.

TITANIUM-NITROGEN

Carpenter and Reavell⁶ report that at 1000°C a linear rate law is observed. The probability of reaction is given as 10^{-8} at 1000°C. Fast¹² has studied the solubility of nitrogen and its effect on the mechanical properties of the metal.

The crystal structure of TiN has been shown by several workers^{2,21,44} to follow the sodium chloride structure. However, the calculated density is found to differ from the pycnometric value. This is studied by Brager^{3,4} in detail. He has suggested that the titanium sites in the lattice are only partially filled at low temperatures. As the temperature of preparation is raised the vacant sites become occupied which expands the lattice and increases the hardness and density. An (*a*) value of 4.22Å is given for room temperature.

TITANIUM-HYDROGEN

The solubility and the crystal structures observed in this system have been reviewed in a recent book by Smith.⁴⁰

Cleveland Meeting, October 1949.

TP 2684 E. Discussion of this paper (2 copies) may be sent to *Transactions AIME* before Dec. 1, 1949. Discussion is tentatively scheduled for publication in May 1950.

Manuscript received April 22, 1949; revision received July 22, 1949.

* Westinghouse Research Laboratories, East Pittsburgh, Pa.

¹⁴ References are at the end of the paper.

Table 1 . . . Equilibrium Calculations on Titanium Reactions

Table 7.7. Equilibrium Calculations on Titanium

| Reaction | | | Literature References |
|----------|---|--|--------------------------------|
| (1) | $\text{Ti(s)} + \text{O}_2(\text{g}) \rightleftharpoons \text{TiO}_2(\text{s})$ | | 24, 25, 26, 32, 35, 37 |
| (2) | $2\text{Ti(s)} + \text{CO}_2(\text{g}) \rightleftharpoons \text{TiO}_2(\text{s}) + \text{TiC(s)}$ | | CO ₂ from 35 |
| (3) | $\text{Ti(s)} + \frac{1}{2}\text{N}_2(\text{g}) \rightleftharpoons \text{TiN(s)}$ | | 24, 26, 27, 38 |
| (4) | $3\text{Ti(s)} + 2\text{CO(g)} \rightleftharpoons \text{TiO}_2(\text{s}) + 2\text{TiC(s)}$ | | CO from 35 |
| (5) | $\text{Ti(s)} + 2\text{H}_2\text{O(g)} \rightleftharpoons \text{TiO}_2(\text{s}) + 2\text{H}_2(\text{g})$ | | H ₂ O from 35 |
| (6) | $\text{Ti(s)} + 2\text{CO}_2(\text{g}) \rightleftharpoons \text{TiO}_2(\text{s}) + 2\text{CO(g)}$ | | CO ₂ and CO from 35 |
| (7) | $\text{Ti(s)} + \text{C(s)} \rightleftharpoons \text{TiC(s)}$ | | 24, 25, 26, 27, 35, 38 |

| | (1) | (2) | (3) | (4) | (5) | (6) | (7) |
|-------------|------------------------|-------------------------|------------------------|-----------------------|---|---|-----------|
| <i>t</i> °C | $-\log p_{\text{O}_2}$ | $-\log p_{\text{CO}_2}$ | $-\log p_{\text{N}_2}$ | $-\log p_{\text{CO}}$ | $-\log p \frac{\text{H}_2\text{O}}{\text{H}_2}$ | $-\log p \frac{\text{CO}_2}{\text{CO}}$ | $+\log K$ |
| 25 | 155.7 | 128.7 | 107.6 | 94.9 | 37.8 | 32.8 | 41.3 |
| 200 | 95.5 | 78.2 | 65.2 | 57.2 | 23.4 | 21.1 | 26.4 |
| 400 | 64.8 | 52.8 | 43.7 | 37.9 | 16.1 | 15.0 | 18.8 |
| 600 | 48.3 | 39.1 | 32.1 | 27.3 | 12.2 | 11.8 | 14.5 |
| 800 | 38.0 | 30.9 | 24.8 | 22.1 | 9.8 | 9.8 | 12.2 |

Systematic studies of the adsorption have been made by Huber, Kirschfeld and Sieverts²² and by Kirschfeld and Sieverts²⁹ up to temperatures of 1000°C and at various pressures. The results show the formation of two phases of variable composition, an alpha and a beta phase. Hägg¹⁹ has made an X ray crystal structure investigation of this system. The alpha phase is found to have the same structure as titanium and is homogeneous up to 33 at. pct of hydrogen. The beta phase is homogeneous from 50 at. pct to 66.7 and has a face-centered cubic structure.

Equilibria Calculations on the Reactions of Titanium with Gases

Titanium reacts with many of the common gases, with the exception of the inert gases, to form stable compounds. The chemical equilibria of these reactions may be calculated when the reaction products are TiO₂, TiN or TiC. Data on the free energy of formation of the hydride are not available.

Table I shows the reactions which are considered in this work together with the results and the literature references for each reaction.

The logarithms of the gas pressure or pressure ratios are tabulated as a function of the temperature in °C for the several reactions. For the reaction to form TiC the equilibrium constant *K* is tabulated.

The results show the following: (1) TiO₂, TiN and TiC are stable at all temperatures calculated in this study and from a thermodynamic point of view titanium will remove O₂, N₂, CO and CO₂ at the lowest pressures used in modern vacuum technology; (2) the reaction of water and carbon dioxide to form the oxide and hydrogen and carbon monoxide respectively are possible up to 800°C and perhaps higher in vacuums of the order of 10⁻⁷ mm of Hg.

Apparatus and Method

BALANCE

The vacuum microbalance and auxiliary equipment used for all of the kinetic measurements have been described.^{15,16} The sensitivity of the balance is 0.86 divisions per microgram and the weight change can be estimated to 0.3×10^{-6} g. The balance zero point is constant and the instrument is insensitive to pressure and small changes in the temperature of the surroundings.

VACUUM SYSTEM AND FURNACE TUBE

The vacuum system and furnace tube have been described.^{15,17} The system is constructed of all glass and ceramic materials. The furnace tube is double walled and is made from synthetic zircon. Vacua of McLeod gauge pressures of 10⁻⁶ mm or lower can be achieved with these tubes at temperatures of 1175°C and perhaps higher. The difficulties associated with and methods for the measurement of pressure in furnace tubes at high temperatures have been considered in another work.¹⁷

GAS PURIFICATION

The purification of the oxygen, nitrogen and hydrogen is the same as previously described.¹⁵ The source of nitrogen is specially purified nitrogen and is obtained from our Bloomfield Lamp Works. A mass spectrometer analyses of the gases used for the nitriding experiments showed oxygen to be present to about 0.01 pct (the limit of the sensitivity of the mass spectrometer for the gas sample and pressure used).

Method

The methods used have been previ-

ously described.^{14,15,16,17}

SAMPLES

Two types of titanium samples are used for the measurements: commercial titanium of approximately 99 pct purity with 0.77 pct of carbon, and iodide titanium. Both samples were obtained from the Remington Arms Co. Although no detailed analysis of the iodide titanium is available it is probably of a high degree of purity. A spectrographic analysis of the commercial titanium showed impurities of silicon and of iron. No quantitative spectrographic information is possible for these impurities since standards of known analysis are not available.

The specimens are cut from 15 mil sheets of the metal and weigh 0.6840 g. They have surface areas of 9 to 10 cm². The specimens, unless otherwise noted, were abraded starting with number one grit and finishing with 4/0 paper. The last two stages of the abrading are carried out under purified kerosene to minimize formation of oxide films.

Discussion of Results

HIGH VACUUM REACTION

The reaction of titanium in high vacua must be carefully considered if the metal is to be maintained in an essentially film free condition. This problem has been discussed in a previous paper for the case of the zirconium reaction.¹⁴ Titanium like zirconium acts as a getter for many gases at low pressures and elevated temperatures. This behavior makes the problem a difficult one.

Due to the thermodynamic stability of TiO₂ it is impossible to reduce the oxide by hydrogen. Thus, the practical solution to maintaining the titanium in a film free condition is the use of the best high vacua possible.

A number of studies show that titanium can be heated to the reaction temperature without formation of further oxide or other films. If iodide titanium is heated, for example, in a vacuum of 10⁻⁶ mm of Hg or lower no weight change of any kind is observed until a temperature of 550°C is reached. Above this temperature the specimen loses weight and at a temperature near 1000°C the rate of weight loss increases rapidly. This behavior is quite different from that observed for zirconium.¹⁴ We conclude that titanium is not as efficient a getter as zirconium and that the metal

can be heated without further film formation.

REACTION WITH OXYGEN

The reaction is studied as a function of the time, temperature and pressure and the results are presented in Fig 1, 2, 3 and 4. The weight gain in micrograms per cm² is plotted against the time in minutes. Assuming the ratio of real to measured area to be unity and the oxide to be TiO₂,²⁰ the thickness of the film in Angstroms is 58.5 times the weight gain in micrograms per cm². A scale of 1000 Å is marked on the curves.

Time

Fig 1 shows the time course of two oxidation experiments on commercial and iodide titanium at 550 and 600° respectively. A comparison is made with the oxidation reaction of iodide zirconium at 425°C. The oxygen pressure is 7.6 cm for all experiments. The iodide titanium reacts at a lower rate than commercial titanium. The comparison with zirconium shows that titanium is less reactive at these temperatures.

The shapes of the oxidation curves are similar to those observed for other metals. A rapid reaction rate is observed in the early stages of the reaction which gradually decreases as the film thickens. In this sense the oxide film has protective properties.

Time and Temperature

Fig 2 shows the effect of temperature on the reaction over the temperature range of 250 to 600°C. A comparison of the 250°C curve with the 600°C curve shows a film thickness of 210 Å after 2 hr of reaction at 250°C and a film of 7300 Å at 600°C.

The effect of temperature on the reaction rate is very marked and appears to follow an exponential law.

Time and Temperature Equations

Three equations have been used extensively to explain the time variation of the oxidation rate. These are:

- (1) the parabolic law^{33,34,39,46}
$$W^2 = Kt + C$$
- (2) the logarithmic law⁴¹
$$t = \beta(e^{W/\alpha} - 1) \text{ and}$$
- (3) the linear law
$$W = K't + C$$

In the above equation W refers to the weight gain, t the time and K' , K , C , α and β are constants.

In order to explain the temperature

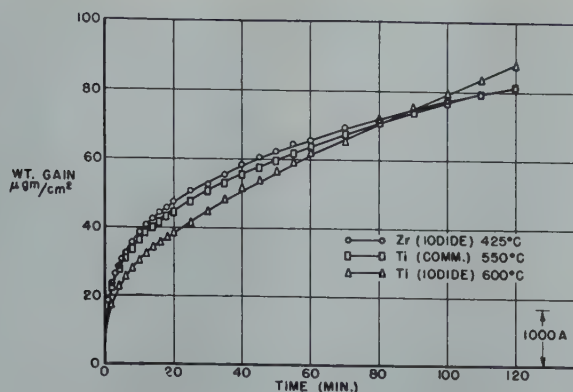


FIG 1—Reaction of Ti and Zr with O₂ 7.6 cm O₂.

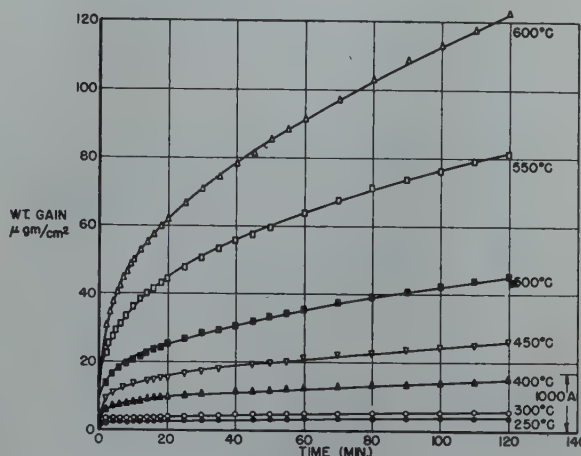


FIG 2—Reaction of Ti with O₂. Effect of temp. 250–600°C.

coefficient of the reaction rate Dunn⁹ has applied the Arrhenius equation to the parabolic rate law constant K . Mott³³ has interpreted the physical significance of the activation energy for the various types of diffusion process of ions and electrons through an oxide film. To further understand the significance of the temperature dependence one of the authors¹⁸ has applied the transition state theory¹³ of chemical reactions and diffusion processes to the oxidation reaction. The parabolic rate law constant is given by the equation:

$$K = \frac{2kT}{h} \lambda^2 e^{\Delta S^*/R} e^{-E/RT}$$

ΔS^* and E are the entropy and energy of activation, λ , the interatomic distance between diffusional states, k is Boltzman's constant and h is Planck's constant. The equation is useful since both ΔS^* and E can be calculated. ΔS^* is the probability or steric factor for a given reaction.

Time and Temperature Correlation

Plots of the weight gain vs. the

logarithm of the time show smooth curves of increasing slopes and indicate that the logarithmic law does not hold. A study of Fig 2 shows that the linear rate law is not applicable for the conditions studied.

Parabolic rate law plots are made for all of the data. In general the data deviate from the straight line during the initial stages of the reaction. However, good agreement is observed after 20 min. reaction time. This type of deviation has been predicted by Mott.³⁴

Temperature Dependence and Activation Energy

The temperature coefficient of the reaction rate is one of the most important quantities to evaluate. If the reaction can be related to a mechanism it is possible to correlate the temperature coefficient of the reaction with an energy of activation. For the oxidation of titanium it is possible to calculate diffusion constants and an energy and entropy of activation since the data can be fitted to the parabolic rate law during a large part of the reaction.

Fig 3 shows the parabolic rate law

constants K in units of cm^2 per sec plotted against $\frac{1}{T}$. These parabolic rate law constants vary from 2.8×10^{-16} cm^2 per sec at 250°C to 6.27×10^{-13} at 600°C . In terms of Angstroms of film thickness, the above rates correspond to 1.7\AA per sec at 250°C to about 80\AA per sec at 600°C . The slopes are evaluated for the time range of 60 to 120 min.

Both commercial and iodide titanium experiments are included in Fig 3. Each group appears to fit a straight line re-

lationship. The iodide titanium reacts at a slower rate. Below 350°C the data are scattered and the straight line relationship is no longer obeyed. An energy of activation of 26,000 cal per mol is calculated from the plot and the temperature independent factor $e^{\Delta S^*/R}$ evaluated from the expression derived for the parabolic rate law constant by the transition state theory.

Table 2 shows the values for the parabolic rate law constants and diffusion constants and the entropies, energies and free energies of activation of

the rate determining process. The K values are related to thickness by the use of the density of the oxide and the stoichiometric ratio of oxygen in the oxide. A surface roughness ratio of 1 is assumed.

The energy of activation of 26,000 cal per mol is higher than the value observed for the oxidation of zirconium,¹⁴ namely 18,200. The entropies of activation are less negative than those observed for the oxidation of zirconium. ΔS^* varies from -18.0 to -19.1 cal per mol per $^\circ\text{C}$ for titanium oxidation while values of -23.1 to -25.2 are obtained for the zirconium reaction.

A comparison of the reaction rate at 400°C shows a parabolic rate constant K of 0.667×10^{-14} cm^2 per sec for the titanium oxidation and a K of 13.20×10^{-14} cm^2 per sec for the zirconium reaction. Iron at the same temperature has a K value of 0.409×10^{-14} cm^2 per sec or roughly equivalent to the titanium rate.

Calculation of Diffusion Constants

Let us assume with Wagner⁴⁷ and Mott³³ that the metal ions are diffusing through the oxide lattice together with electrons by one mechanism or another. If this is done we can calculate the diffusion constant K from the parabolic rate law constants of the expression, $D = K/2$. Thus, at 400°C , the value of D is calculated to be 0.334×10^{-14} cm^2 per sec and at 600°C a value of 3.14×10^{-13} cm^2 per sec. These values represent the coefficient of self diffusion of titanium in its oxide.

The mechanisms for self diffusion of titanium are as follows: (1) formation and diffusion of interstitial titanium ions and (2) formation and diffusion of titanium defects (absence of titanium ion in lattice). Calculations by Huntington and Seitz²³ have shown that for copper the diffusion of lattice defects is the more probable process. It is at present difficult to choose between the above mechanisms for titanium oxide since calculations have not been made for systems closely analogous to this one. However, the activation energy must be associated with the formation and diffusion of either interstitial ions or lattice defects.

Pressure Effect

The effect of pressure on the reaction at 550°C is shown in Fig 4. The pressure is varied by a factor of 100 from 7.6 cm to 0.76 cm of oxygen. The effect is

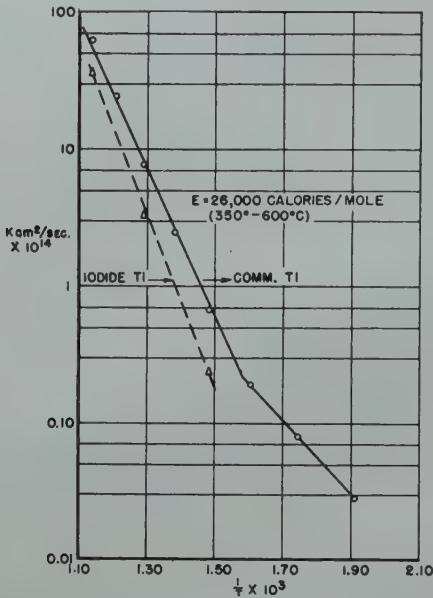


FIG 3—Reaction of Ti with O₂ log K vs 1/T 250-600°C.

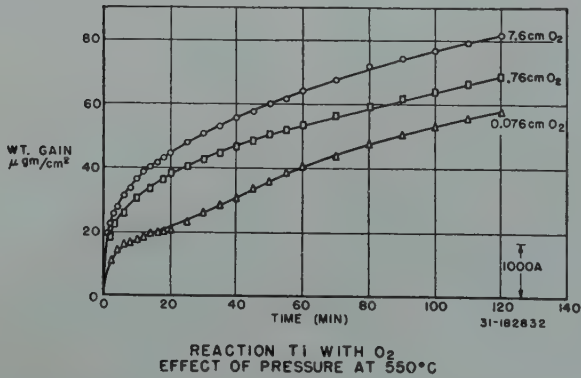


FIG 4—Reaction of Ti with O₂. Effect of pressure at 550°C.

Table 2 . . . Parabolic Rate Constants and Diffusion Constants Entropies, Energies and Free Energies of Activation for the Oxidation Process

| <i>t</i> °C | <i>K</i> , cm ² per sec | <i>D</i> ₀ , cm ² per sec | Δ <i>S</i> [*] Cal per mol °C | <i>E</i> Cal per mol | <i>T</i> Δ <i>S</i> [*] Cal per mol | Δ <i>F</i> [*] Cal per mol |
|-------------|------------------------------------|---|--|----------------------|--|-------------------------------------|
| 350 | 0.190 × 10 ⁻¹⁴ | 1.34 × 10 ⁻⁶ | -18.0 | 26,000 | -11,200 | 37,200 |
| 400 | 0.667 × 10 ⁻¹⁴ | 0.98 × 10 ⁻⁶ | -18.8 | 26,000 | -12,100 | 38,100 |
| 450 | 2.43 × 10 ⁻¹⁴ | 0.921 × 10 ⁻⁶ | -19.0 | 26,000 | -13,700 | 39,700 |
| 500 | 7.70 × 10 ⁻¹⁴ | 0.925 × 10 ⁻⁶ | -19.1 | 26,000 | -14,800 | 40,800 |
| 550 | 24.73 × 10 ⁻¹⁴ | 1.048 × 10 ⁻⁶ | -19.0 | 26,000 | -15,600 | 41,600 |
| 600 | 62.7 × 10 ⁻¹⁴ | 1.048 × 10 ⁻⁶ | -19.1 | 26,000 | -16,700 | 42,700 |

largest for the thin film range. No simple relationship with the pressure has been determined. We conclude that the effect of pressure on the reaction rate is minor for the temperature and pressure range studied. This small effect is in agreement with the mechanism of metal ion diffusion. If oxygen atoms or ions diffuse through the film one might expect the rate to follow a square root function of the pressure for some pressure and temperature conditions.

REACTION WITH NITROGEN

The difficulties associated with the study of the kinetics of the nitrogen reaction on zirconium have been discussed in a previous paper.¹⁴ These difficulties are the prevention of the high vacuum reaction with oxygen, water vapor, and others, and the prevention of secondary reactions by elimination of the impurities such as oxygen, hydrogen, and others in the nitrogen.

In this section the reactions of commercial titanium with purified lamp grade of nitrogen are studied in detail as a function of time, temperature and pressure.

The results are shown in Fig 5-8 and discussed in the following subsections. In all of the figures the weight gain in micrograms per cm² is plotted against the time and, where necessary, the temperature is given at the top of the graph.

Comparison of Nitrogen Reaction on Titanium and Zirconium

Fig 5 shows a comparison of the nitrogen reactions of the two preparations of titanium with the corresponding reaction for zirconium. The time course of the reactions for the iodide preparations of the two metals are practically identical at 600°C. The commercial preparation of titanium reacts at a greater rate. A purified lamp grade of nitrogen is used.

Time and Temperature

Fig 6 shows the time course of the reaction of commercial titanium with pure nitrogen for several temperatures. The reaction rate decreases as the reaction proceeds. The effect of temperature on the reaction rate is uniform and the rate of reaction appears to be an exponential function of the temperature. At 850°C a total reaction of 158 micrograms per cm² is found after 2 hr of reaction while at 550°C a total reaction of 6 micrograms per cm² is observed.

The shapes of the time curves are very similar to what one observes for the oxidation reaction. This leads one to apply the parabolic rate law expression to the nitride data. A plot of the square of the weight gain shows a straight line over the complete thickness range and indicates that the rate law $W^2 = Kt$ explains empirically the time course of the reaction. It is of interest to see if this rate law can be placed on a reasonable physical basis.

Van Liempt⁴⁵ in a study of the degassing of metals has solved the diffusion equation using an approximation

method. The same method may be used for the reverse adsorption process. Van Liempt's equation is $Q/Q_0 = \frac{8}{d} \sqrt{\frac{Dt}{\pi}}$ where Q is the quantity of gas evolved or taken up at any time t , Q_0 , the original quantity of gas in the metal, and D , the diffusion coefficient. This expression gives the parabolic rate law, $\frac{W}{W_0} = K \sqrt{t}$. The temperature is involved in the solubility W_0 and in K which involves the diffusion constant D . Since both W_0 and K are temperature dependent it is impossible until

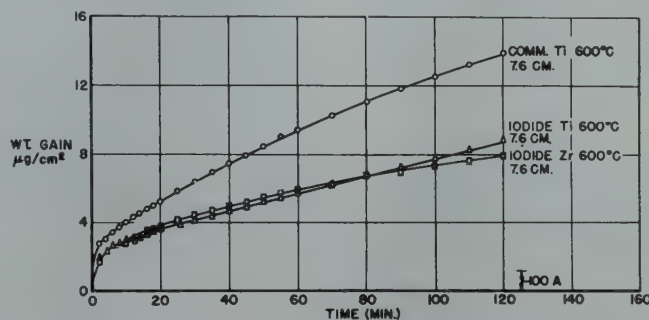


FIG 5—Reaction of Ti and Zr with pure N₂ 600°C.

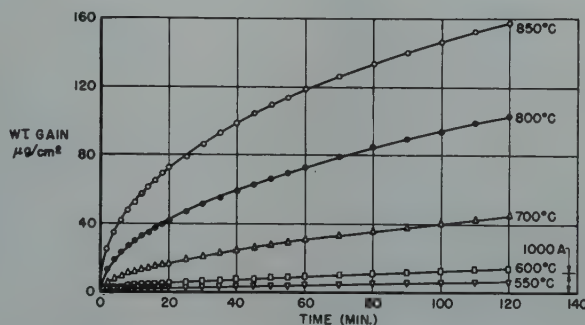


FIG 6—Reaction of Ti with pure N₂ 550-850°C.

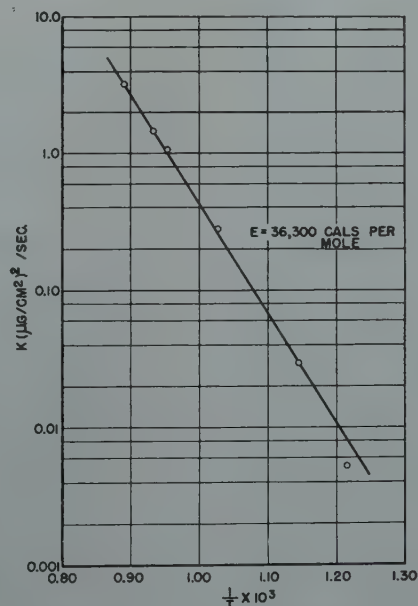


FIG 7—Reaction of Ti with pure N₂ log K vs. $\frac{1}{T}$.

data on W_0 are available to calculate D and the energy of activation E although an empirical energy of activation may be calculated.

Table 3 shows the values of the parabolic rate law constants for the temperature range of 550 to 850°C and Fig 7 shows a logarithmic plot of the parabolic rate law constant against $\frac{1}{T}$. A straight line is found for the temperature range of 550 to 850°C. An empirical energy of activation of 36,300 cal per mol is calculated. This can be compared to a value of 39,200 cal per mol obtained for the corresponding reaction with zirconium. This value is considerably higher than the energies of activation found for the oxidation process on most metals.

Table 3 . . . Parabolic Rate Law Constants Reaction Comm. Titanium with Nitrogen

| $t^{\circ}\text{C}$ | $T^{\circ}\text{K}$ | $\frac{1}{T} \times 10^3$ | k (g per cm ²) ² per sec. |
|---------------------|---------------------|---------------------------|--|
| 550 | 823 | 1.2151 | 5.28×10^{-16} |
| 600 | 873 | 1.1453 | 2.97×10^{-14} |
| 700 | 973 | 1.0276 | 2.78×10^{-13} |
| 775 | 1048 | 0.9542 | 1.08×10^{-12} |
| 800 | 1073 | 0.9329 | 1.460×10^{-12} |
| 850 | 1123 | 0.8904 | 3.2×10^{-12} |

$E = 36,300$ cal per mol

Pressure

Fig 8 shows the effect of pressure on the time course of the nitride reaction at a temperature of 800°C. The pressure is varied from 7.6 cm to 0.076 cm, or by a factor of 100. Although the rate of reaction does vary with pressure the overall effect is small when compared to the predictions of the linear or square root law.

The influence of pressure on the permeability of metals to gases has been discussed by Barrer¹ and by the authors in a previous paper.¹⁴ Two possible permeation rate-pressure equations have been used to explain the data. These are: (1) the linear rate law which is based on a mechanism of activated diffusion without dissociation and (2) the square root law which is based on a mechanism of activated diffusion with dissociation. The second type usually accounts for the permeation of gases through metals.

The pressure dependence of the reaction rate is not explained by either of the rate expressions. This indicates that the solubility term W_0 is not pressure dependent. A similar result is found for the nitrogen reaction on zirconium.¹⁴ One explanation is that a nitride film is

formed on the metal and that this film dissolves into the metal, the thickness of this film depending upon the relative rates of reaction and solution. This nitride film is not observed by visual and electron diffraction studies after removing the nitrogen and cooling at room temperature. The presence of the nitride film prevents the gas pressure from exerting its normal effect on the solubility.

REACTION WITH HYDROGEN

The reaction is studied as a function of time, temperature and pressure and a comparison is made with the hydrogen reaction on zirconium. The stability of the reaction product is studied as a function of the temperature under high vacuum conditions. Fig 9 to 14 show the results. The hydrogen is prepared by diffusion through a palladium tube after a preliminary purification.

Fig 9 shows a preliminary study of the reaction of commercial titanium with hydrogen at 2.0 cm pressure as a function of the temperature. The reaction appears to start at a temperature of about 290°C and the rate of reaction increases rapidly with temperature. Visual and electron diffraction analyses of the specimen showed no evidence of a surface film after cooling and it is assumed that the hydrogen is dissolving in the metal to form a compound or stable complex. The specimen loses weight on evacuating the hydrogen atmosphere. This indicates that the reaction product is unstable to a vacuum of 10^{-6} mm of Hg at a temperature of 400°C. This will be discussed in more detail later.

Time and Temperature

It is of interest to examine the time behavior of the reaction rate. Typical

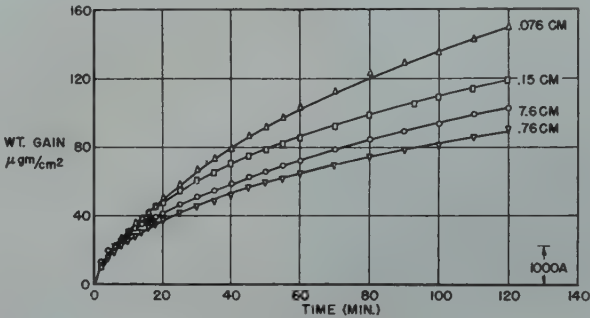


FIG 8—Reaction of Ti with pure N₂. Effect of pressure 800°C.

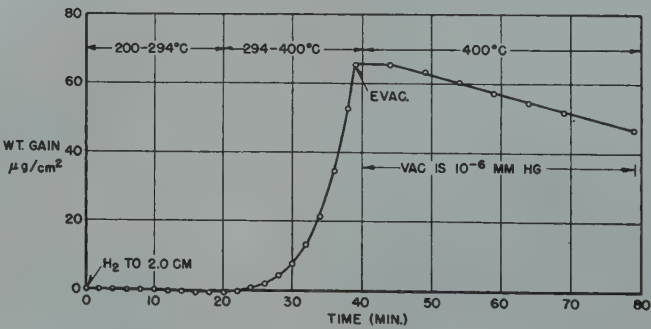


FIG 9—Reaction of Ti with H₂ and stability of hydride.

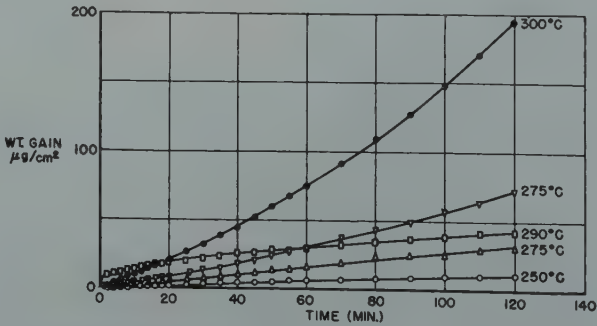


FIG 10—Reaction of Ti with H₂. Effect of temperature.

curves are shown for commercial titanium in Fig 10 for temperatures of 250 to 300°C. At temperatures of 250°C the reaction rate $\frac{dW}{dt}$ is constant with time. At a temperature of 300°C the reaction rate $\frac{dW}{dt}$ increases with the time. Some difficulty is observed in obtaining reproducible results. This may be due to the high sensitivity of the hydrogen type of reaction to impurities in the metal, to the presence of surface film, and to the lack of uniform metal specimens.

The shape of the time curves indicate that the reaction does not obey the parabolic rate law which is predicted by the equation of van Liempt⁴⁵ and discussed on p. 745. If it is considered

that cracks and blisters are forming in the metal during reaction, the time course of the reaction cannot be expected to follow the parabolic law.

The 300°C curve after 2 hr of reaction shows a hydrogen uptake corresponding to the formula $TiH_{0.13}$. Hägg¹⁹ has shown that titanium will take up hydrogen to 66.7 at. pct or to a formula TiH_2 . We have not attempted to check this value.

A comparison of the reactions of titanium and zirconium with hydrogen is shown in Fig 11. Both the iodide and commercial forms of titanium react more rapidly than the iodide form of zirconium. The shapes of the curves are different in the sense that $\frac{dW}{dt}$ decreases with time in the zirconium reaction

and increases in the titanium reaction. In regard to the hydrogen reaction titanium appears to react more rapidly on a simple weight gain basis than zirconium.

Temperature

A study of the reaction with hydrogen as a function of the temperature is necessary if the details of the reaction mechanism are to be worked out. However, the data are not of sufficient reproducibility to give a good value for the temperature coefficient. Qualitatively, very little reaction occurs at 250°C while at 300°C a very rapid reaction is observed.

Pressure

The permeation of gases through metals has been summarized by Barrer¹ and discussed briefly here, under "Reaction with Nitrogen." If the reaction is limited by a process involving activated diffusion with dissociation of the hydrogen molecules the reaction rate may be expressed by the following:

$$\frac{dW}{dt} = kp^{1/2} e^{-b/T}.$$

This formula predicts that at constant temperature the reaction rate should follow the expression:

$$\frac{dW}{dt} = Ap^{1/2}.$$

Fig 12 shows the effect of pressure on the reaction rate at 275°C for a pressure range of 6.0 cm to 0.1 cm of H_2 . The reaction is very sensitive to pressure although the 2.2 cm experiments are in disagreement with each other. The pressure effect for the hydrogen reaction is very different from the pressure effect in the nitrogen reaction.

Fig 13 shows a plot of the initial reaction rates $\frac{dW}{dt}$ as a function of the square root of the pressure. The two values of $\frac{dW}{dt}$ for the 2.2 cm pressure are averaged and included in the plot. Fair agreement with the square root law is found. This correlation shows that the diffusion of hydrogen into the metal is mainly by atoms of hydrogen rather than molecules and confirms the square root law.

Stability

Fig 14 shows the stability of the hydrogen complex with titanium as a function of temperature in a vacuum

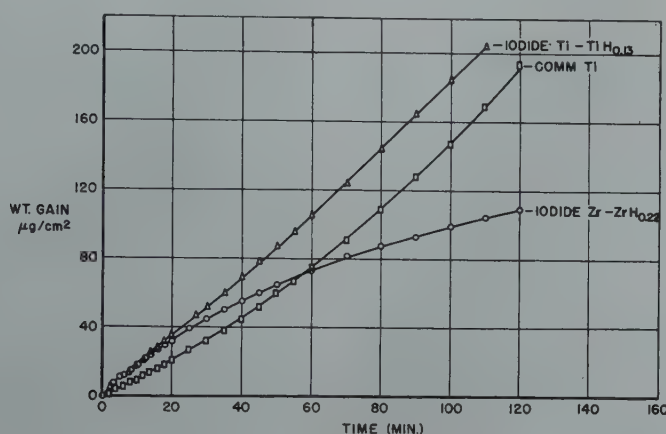


FIG 11—Reaction of Ti and Zr with H_2 300°C 2.1 cm H_2 .

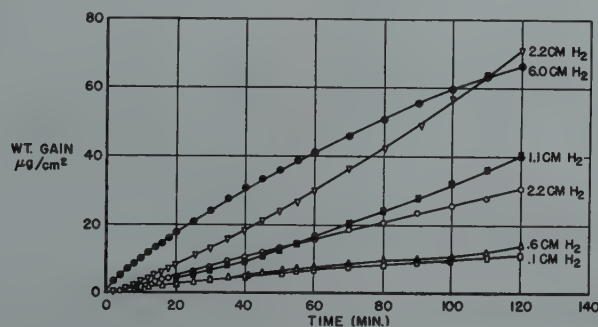


FIG 12—Reaction of Ti with H_2 . Effect of pressure.

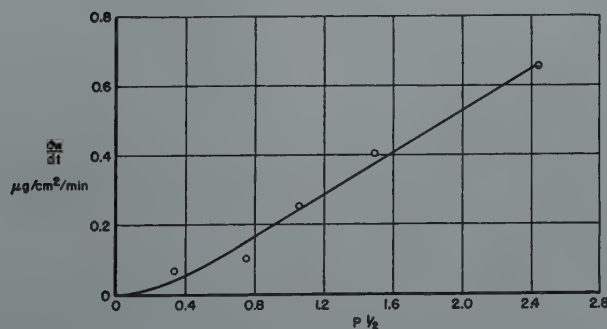


FIG 13—Reaction of Ti with H_2 . Plot of $\frac{dW}{dt}$ vs $P^{1/2}$ 275°C.

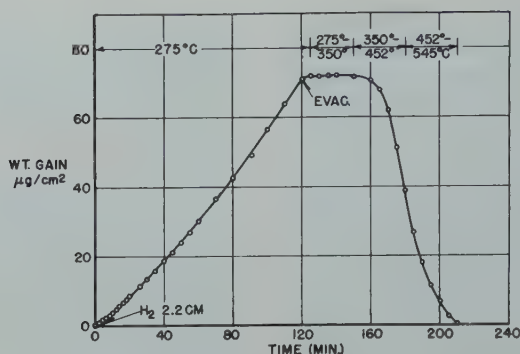


FIG 14—Reaction of Ti with H_2 275°C 2.2 cm H_2 stability curve.

of 10^{-6} mm of Hg. Hydrogen is added to titanium at a temperature of 275°C and a pressure of 2.2 cm of H_2 . The reaction product is stable at 275°C in a vacuum of 10^{-6} mm of Hg. The temperature is gradually raised. At a temperature of about 350°C the hydrogen starts to be evolved. All of the hydrogen is removed from the metal if the heating is continued. This experiment confirms the results shown in Fig 9. At 400°C in this experiment the hydrogen is evolved at an appreciable rate. A comparison may be made with the stability of the zirconium-hydrogen reaction product.¹⁴ In that case hydrogen started to be evolved at a temperature of about 435°C. This indicates that the titanium-hydrogen complex is less stable than the corresponding zirconium-hydrogen complex.

Conclusions

A study of the thermodynamic equilibria of the several gas phase reactions of titanium with oxygen, nitrogen, water vapor, carbon monoxide and carbon dioxide show the following results: (1) TiO_2 , TiN and TiC are stable at all temperatures up to the transition temperature calculated in this study; (2) from a thermodynamic point of view titanium will remove O_2 , N_2 , CO and CO_2 at the lowest pressures used in high vacuum technique; and (3) the reactions of water and carbon dioxide to form the oxide and hydrogen and carbon monoxide respectively are possible up to 800°C and perhaps higher in vacuums of the order of 10^{-7} mm of Hg.

The oxidation reaction follows a modified parabolic rate law. An energy of activation of 26,000 cal per mol is calculated from the temperature dependence of the parabolic rate law

constants. Diffusion coefficients and entropies of activation for the reaction process are calculated. The oxygen reaction is found to be insensitive to pressure.

The nitrogen reaction is of special interest. The time course of the reaction can be fitted empirically to a parabolic rate law. The temperature dependence of the parabolic rate law constants is used to calculate an empirical energy of activation of 36,300 cal per mol. The effect of pressure is small. The nature of the reaction is believed to be one involving the solution of nitride into the metal under the conditions of a nitride film present on the surface. The nitride is found to be stable to temperatures of at least 900°C.

The reaction with hydrogen obeys the square root of pressure law. In contrast to the nitrogen reaction a film is not formed during the reaction and it is shown that hydrogen is probably diffusing into the titanium lattice as atoms. The hydrogen reaction product is stable in a vacuum of 10^{-6} mm of Hg to a temperature of about 350°C.

References

1. R. M. Barrer: Diffusion In and Through Solids: University Press, Cambridge, England, 1941.
2. K. Becker and F. Ebert: *Ztsch. f. Phys.* (1925) **31**, 268-272.
3. A. Brager: *Acta physicochimica U.R.-S.S.* (1939) **10**, 593-600.
4. A. Brager: *Acta physicochimica U.R.-S.S.* (1939) **11**, 616-632.
5. W. G. Burgers, and F. M. Jacobs: *Ztsch. Kristallogr.* (1936) **A 94**, 299.
6. L. G. Carpenter and F. R. Reavell: *Metallurgia* (1948) **39**, 63-65.
7. P. Chevenard and X. Wache: *Rev. de Metall.*, May/June 1948, p. 121-128.
8. R. S. Dean and B. Silkes: Information Circular Metallic Titanium and Its Alloys. U. S. Bur. of Mines I.C. 7381 Nov. 1946.

9. J. S. Dunn: *Jnl. Chem. Soc.* (1929) 1149-1150.
10. P. Ehrlich: *Ztsch. Elektrochem.* (1939) **45**, 362.
11. P. Ehrlich: *Ztsch. anorg. allgem. Chem.* (1941) **247**, 53-64.
12. J. D. Fast: *Metallwirtschaft* (1938) **17**, 641-644.
13. Glasstone, Laidler and Eyring: The Theory of Rate Processes. McGraw Hill (1941).
14. E. A. Gulbransen and K. Andrew: *AIME Trans.* **185**, *Jnl. of Metals*, Aug. 1949, 515.
15. E. A. Gulbransen: *Trans. Electrochem. Soc.* (1942) **81**, 187-197.
16. E. A. Gulbransen: *Rev. Sci. Instr.* (1944) **15**, 201-204.
17. E. A. Gulbransen and K. Andrew: *Jnl. of Phys. and Coll. Chem.* (1949) **53**, 690-711.
18. E. A. Gulbransen: *Trans. Electrochem. Soc.* (1943) **83**, 301-313.
19. G. Hägg: *Ztsch. phys. Chem.* (1930) **B 11**, 433-454.
20. J. W. Hickman and E. A. Gulbransen: *Jnl. Anal. Chem.* (1948) **20**, 158-165.
21. W. Hofman and A. Schroeder: *Arch. Eisenhüttenwesen* (1936) **10**, 65.
22. H. Huber, L. Kirschfeld and A. Sieverts: *Ber. Deutsch. chem. Ges.* (1926) **59**, 2891-2896.
23. H. B. Huntington and F. Seitz: *Phys. Rev.* (1942) **61**, 315, 325.
24. F. M. Jaeger, E. Rosenbohm and R. Fonteyne: *Proc. Acad. Sci. Amsterdam* (1936) **39**, 442-452.
25. K. K. Kelley: *Bur. of Mines Bull.* No. 371 (1934) Washington.
26. K. K. Kelley: I and E. C. (1944) **36**, 865-866.
27. K. K. Kelley: *Bur. of Mines Bull.* No. 407 (1937) Washington.
28. K. K. Kelley: *Bur. of Mines Bull.* No. 434 (1941) Washington.
29. L. Kirschfeld and A. Sieverts: *Ztsch. phys. Chem.* (1929) **A 145**, 227-240.
30. B. Lustman: *Trans. Electrochem. Soc.* (1943) **83**, 301-313.
31. B. Lustman: Private Communication.
32. H. J. McDonald and H. Seltz: *Jnl. Am. Chem. Soc.* (1939) **61**, 2405-2407.
33. N. F. Mott: *Trans. Faraday Soc.* (1940) **36**, 472.
34. N. F. Mott: *Jnl. Inst. Metals* (1946) **72**, 367-380.
35. Nat'l Bur. of Standards Tables of Selected Values of Thermodynamic Properties, Washington.
36. Nat'l Res. Council, Bull. 107 (June 1943).
37. B. F. Naylor: *Jnl. Am. Chem. Soc.* (1946) **68**, 1077-1078.
38. B. F. Naylor: *Jnl. Am. Chem. Soc.* (1946) **68**, 370-371.
39. N. B. Pilling, and R. E. Bedworth: *Jnl. Inst. Metals* (1923) **29**, 529-582.
40. D. P. Smith: Hydrogen in Metals. Univ. of Chic. Press, Chicago, Ill. (1948).
41. G. Tammann and W. Köster: *Ztsch. anorg. Allgem. Chem.* (1922) **123**, 196.
42. W. M. Thornton: Titanium. The Chem. Catalog Co. Inc., N. Y., 1927.
43. A. E. van Arkel: *Reine Metalle*. Julius Springer, Berlin, 1939.
44. A. E. van Arkel: *Physica* (1924) **4**, 286-301.
45. J. van Liempt: Quoted by Barrer (Ref. 1).
46. C. Wagner and K. Grünwald: *Ztsch. phys. Chem.* (1938) **40 B**, 455.
47. C. Wagner: *Ztsch. f. Elektrochem.* (1941) **47**, 696-704.
48. C. Wagner: Private Communication.

Structure of Diborides of Titanium, Zirconium, Columbium, Tantalum and Vanadium*

JOHN T. NORTON,[†] Member AIME, H. BLUMENTHAL,[‡] and S. J. SINDEBAND,[‡] Member AIME

The interstitial phases formed by the transition elements with carbon, nitrogen and boron constitute a unique class of substances which are of considerable technical interest because of their well developed metallic properties and their high hardness and melting points. They are also of interest from the point of view of structure.

It was pointed out by Hägg¹ some years ago that the principal factor determining these structures was the relative sizes of metal and metalloid atoms. He predicted that if the ratio of the radii of metalloid to metal atoms was less than 0.59, the metal atoms would be arranged in a close-packed fashion of relatively simple type. This prediction has been amply confirmed. It appears, however, that this specification applies most generally to those structures in which the metalloid atoms occupy isolated positions in the lattice and there is no tendency for strong binding between the metalloid atoms themselves. The series of borides of the type MeB_2 formed from the transition elements of the fourth (Ti, Zr) and fifth (V, Cb, Ta) groups of the periodic table provide an opportunity to investigate this situation further. If one takes as a basis the radius of 0.87 Å for the boron radius and the Goldschmidt values for the metal atoms in 12 coordination, then the radius ratio varies from 0.54 for zirconium to 0.64 for vanadium, which latter is considerably greater than Hägg's limit of 0.59. It was of interest, therefore, to see if these five elements would form borides of the MeB_2 type and have simple isomorphous structures.

When this investigation was initiated, relatively little information had been published on the structure of this group of borides. McKenna² reported the preparation of ZrB_2 by a carbon reduction process. Its structure was hexagonal and the approximate lattice constants were given as $a = 3.15$ Å, $c = 3.53$ Å. Ehrlich³ reported the structure of TiB_2 as being of the C 32 type with $a = 3.02$, $c = 3.21$ and $c/a = 1.06$ Å. Recently, Kiessling⁴ published the results on ZrB_2 , showing it to be one in which the metal atoms are arranged in a simple hexagonal lattice with the boron atoms in flat sheets, midway between the layers of metal atoms. The structure is C 32 type with $a = 3.169$, $c = 3.530$ and an axial ratio = 1.11 Å. He also states that CbB_2 and TaB_2 are isomorphous with ZrB_2 .

Preparation of Borides

The borides of titanium, zirconium, columbium and tantalum were made by the electrolysis of fused salt baths after the method described by Andrieux.⁵

The bath, totalling about 6500 g in each case had the following general composition: Metal Oxide + B_2O_3 + CaO + CaF_2 . The actual proportions of the ingredients were determined for each individual case.

Although Andrieux reports the preparation of vanadium boride by the same electrolytic method, several attempts proved unsuccessful. However, it was possible to prepare VB_2 by the carbon reduction method used by McKenna to produce ZrB_2 . The mixture consisted of $V_2O_5 + 6 B_2O_3 + 11 C$ and the reduction was carried out in an induction heated graphite crucible. This method proved satisfactory for ZrB_2 and TiB_2 and undoubtedly the others could be made in the same way.

The borides, which were all in the form of fine gray metallic crystals from the electrolytic bath or gray powders from the reduction process, were carefully separated from other constituents and analyzed chemically for metal and boron content. The densities of the boride powders were measured using a standard 10 cc pycnometer at 18°C and ethyl benzene proved to be the most satisfactory liquid for this purpose.

X Ray Technique

The boride crystals, as prepared, were too small for single crystal examination so that powder techniques were employed. Patterns of the finely ground borides were prepared, using the Norelco recording X ray spectrometer. The lines on these patterns were indexed with the aid of Hull-Davy charts and the approximate dimensions

Cleveland Meeting, October 1949.
TP 2689 E. Discussion of this paper (2 copies) may be sent to *Transactions* AIME before Dec. 1, 1949. Manuscript received May 2, 1949.

* Carried out under auspices of Office of Naval Research Contract N6-ONR-256 Task Order No. 1.

[†] Professor of Metallurgy, Massachusetts Institute of Technology, Cambridge, Mass.

[‡] American Electro Metal Corporation, Yonkers, N.Y.

¹ References are at the end of the paper.

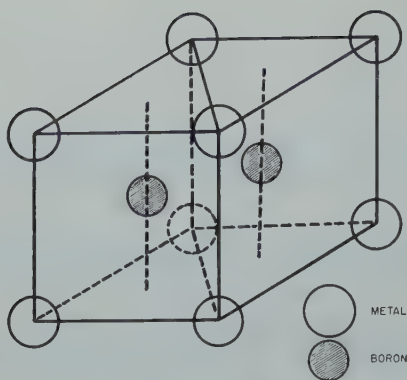


FIG 1—The unit cell of MeB_2 (C 32 type).
The open circles are metal atoms and the shaded circles are boron.

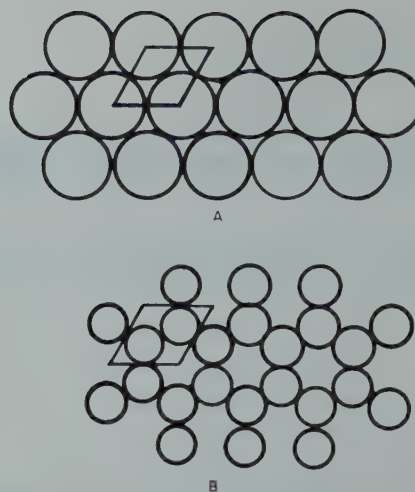


FIG 2—Sheets of metal atoms (A) and boron atoms (B) in the MeB_2 crystal.
In each case the unit cell is outlined.

of the unit cell obtained. Patterns were also made on the Phragmen focussing camera covering the angular range from 50 to 85°. It was found possible to index these lines readily and the cell constants were calculated more accurately. In order to prove the assumed structure, the density was calculated from the X ray data and compared with the measured density. Also, the diffraction line intensities were calculated and compared with those measured from the spectrometer records.

All lattice dimensions are reported in true Angstrom units and are considered correct within $\pm 0.002 \text{ \AA}$. Copper K alpha radiation was used throughout and the wavelengths used in the calculations were:

$$\alpha_1 = 1.54050 \text{ \AA}$$

$$\alpha_2 = 1.54434 \text{ \AA}$$

In calculating densities, the expression

$$\rho = 1.66020 \frac{\Sigma A}{V}$$

was used, where

ρ = density

ΣA = sum of at. wt of atoms in unit cell

V = volume of unit cell in \AA^3

Results

The borides of titanium and zirconium proved to be quite pure, possibly because there was a considerable background of experience in their preparation and they were made in considerable quantities. The other three borides were somewhat less pure as indicated by a few faint extra lines in the diffraction patterns and by the chemical analysis. These impurities consisted of graphite and constituents of the electrolytic bath and it was difficult to make a complete separation. The diffraction lines of ZrB_2 , TiB_2 and

Table 1 . . . Chemical Composition of Borides, Wt Pct

| Substance | By Analysis | | Theoretical for MeB_2 | |
|----------------|-------------|------|--------------------------------|------|
| | Me | B | Me | B |
| ZrB_2 | 80.0 | 18.9 | 80.7 | 19.4 |
| CbB_2 | 81.3 | 16.9 | 81.2 | 18.8 |
| TaB_2 | 89.2 | 10.5 | 89.4 | 10.6 |
| TiB_2 | 68.9 | 30.1 | 68.9 | 31.1 |
| VB_2 | 68.9 | 25.3 | 70.2 | 29.8 |

Table 2 . . . Lattice Constants and Density of Borides

| Substance | Lattice Constants, \AA | | | Density, G per Cm^3 | |
|----------------|---------------------------------|-------|-------|------------------------------|-------|
| | a | c | c/a | Calc. | Obs. |
| ZrB_2 | 3.170 | 3.533 | 1.114 | 6.09 | 6.17 |
| CbB_2 | 3.086 | 3.306 | 1.071 | 7.21 | 6.60 |
| TaB_2 | 3.088 | 3.241 | 1.074 | 12.60 | 11.70 |
| TiB_2 | 3.028 | 3.228 | 1.064 | 4.52 | 4.52 |
| VB_2 | 2.998 | 3.057 | 1.020 | 5.10 | 4.61 |

VB_2 were sharp but those of CbB_2 and TaB_2 were somewhat diffuse. Further work is necessary in order to decide whether or not this is an indication of a range of homogeneity.

The chemical analyses given in Table 1 show clearly, however, that the borides correspond to the formula MeB_2 . The X ray diffraction data for all five borides is in complete agreement with a structure in which the metal atoms are arranged in a simple hexagonal lattice having an axial ratio slightly greater than unity. The lattice constants decrease with decreasing atom size and the axial ratio also decreases slightly. The lattice constants and densities are given in Table 2. The structure, therefore, corresponds to space group $D_{6h}^{16} - C6/\text{mmm}$ with metal atoms at $0, 0, 0$; and boron

atoms at $\frac{1}{3}, \frac{2}{3}, \frac{1}{2}$; and $\frac{2}{3}, \frac{1}{3}, \frac{1}{2}$. This is in agreement with Kiessling's results and shows that the five borides are indeed isomorphous.

Discussion of Results

From the structure as shown in Fig 1 it will be seen that the fundamental unit is a triangular prism of metal atoms with a boron atom at the center and that the prisms are packed together so as to share faces. From another point of view, the metal atoms are arranged in layers, parallel to the basal plane with the atoms in each layer having a close-packed arrangement, each metal atom with six equidistant neighbors in the plane and two neighbors, above and below, at slightly greater distance. The boron atoms are also arranged in flat sheets midway between the metal atom layers and each boron atom has three close neighbors. This is indicated in Fig 2. It thus appears that there would be strong boron-boron binding in such a structure.

From the point of view of close-packed interstitial structures, it is of interest to observe how the lattice dimensions change with metal atom

Table 3 . . . Calculated Lattice Dimensions in \AA

| Substance | Metal to Metal in Sheet | Boron to Boron in Sheet | Metal to Boron | Separation of Sheets | Metal to Metal in Pure Metal |
|----------------|-------------------------|-------------------------|----------------|----------------------|------------------------------|
| ZrB_2 | 3.17 | 1.83 | 2.54 | 3.53 | 3.17 |
| CbB_2 | 3.09 | 1.79 | 2.43 | 3.31 | 2.85 |
| TaB_2 | 3.09 | 1.79 | 2.41 | 3.24 | 2.85 |
| TiB_2 | 3.03 | 1.75 | 2.38 | 3.23 | 2.92 |
| VB_2 | 3.00 | 1.73 | 2.31 | 3.06 | 2.63 |

size and these values, given in Table 3, afford some basis for speculation. All of these dimensions decrease with decreasing metal atom size. Perhaps it is simplest to consider the two extreme cases. In ZrB_2 , the distance of closest approach (D.C.A.) of the metal atoms in the metal atom sheet is the same as is the case in metallic zirconium. The hole in which the boron atom is placed is limited in size both by the neighboring boron atoms and by the metal atoms. This hole is larger than the normal boron radius of 0.87 Å but it appears that the boron atom must fill it, first because this is generally true in interstitial phases and secondly because the separation of the metal atom sheets is considerably greater than would be expected from the metal atoms alone. A boron radius of about 0.92 Å is consistent with this structure. The metal atoms are in contact with one another in the sheet and the boron atoms are in contact with one another and with their metal neighbors giving a close packed arrangement.

On the other hand, in VB_2 the D.C.A. of the vanadium atoms in the metal sheet is considerably greater than in vanadium metal. If the metal sheet is close packed, the boron hole is limited by the metal atoms to a radius of about 0.81 Å which probably is too small. If the vanadium atoms are not closely packed and have the same size as in the metal, then the boron hole is limited to a radius of 0.87 Å by the boron neighbors and by the metal neighbors to about 0.91 Å. Thus it seems again as if the boron atoms are essentially in contact with both metal and boron neighbors but that the packing in the metal sheets has been loosened and as a result, the separation of the metal sheets has decreased. Kiessling⁴ has reported that CrB_2 is isomorphous with the borides discussed here and it would be very interesting to know the lattice constants, for chromium is considerably smaller than vanadium and the radius ratio is 0.68.

The results show that there is no discontinuity in the series as the critical value of 0.59 for the radius ratio is

Table 4 . . . Electrical and Thermal Properties of Borides

| Substance | Electrical Resistivity Microhm-cm | Thermal Conductivity Cal per Cm per Sec °C at 200°C Avg | Wiedemann-Franz Ratio $\times 10^5$ |
|----------------|-----------------------------------|---|-------------------------------------|
| ZrB_2 | 38.8 | 0.0550 | 213 |
| TiB_2 | 28.4 | 0.0624 | 179 |

exceeded and emphasizes the fact that this limiting value should be considered specific only for phases in which the metalloid atoms are in isolated positions. That the radius ratio is not the only factor controlling structure is shown by the fact that tungsten and molybdenum, as shown by Kiessling,⁶ do not form borides which are isomorphous with the series discussed here although the radius ratio has a value of 0.62. A similar situation exists in the monocarbides.

In view of the apparent boron to boron binding, it might be expected that the borides would be less metallic than, for instance, the carbides. However, this does not appear to be the case. Electrical and thermal conductivity measurements were made on ZrB_2 and TiB_2 in the form of bars sintered without binder to about 85 pct of theoretical density. The values are given in Table 4. It will be observed that the properties are excellent and in fact compare favorably with the pure metals themselves. Also, the Wiedemann-Franz ratio is quite normal. This indicates that normal metallic linkages predominate. When sufficient quantities of the other pure borides are available, these experiments will be extended.

Another interesting aspect of the borides is the possibility of metal atom replacement to form solid solutions. On the basis of limited experiments on the series ZrB_2 - TiB_2 it appears that a continuous series of solid solutions can be formed, when the borides are mixed and heated together and that the lattice constants deviate only slightly in a negative direction from Vegard's Law. These experiments are also being extended.

Summary

1. The borides of Ti, Zr, V, Nb and Ta corresponding to the formula MeB_2 have isomorphous crystal structures with the metal atoms arranged in a simple hexagonal lattice having an axial ratio slightly greater than unity.

2. The structure is of the C 32 type, space group $D_{6h}^{16} - C6$ mmm, with metal atoms at 0, 0, 0 and boron atoms at $\frac{1}{3}$, $\frac{2}{3}$, $\frac{1}{2}$ and $\frac{2}{3}$, $\frac{1}{3}$, $\frac{1}{2}$.

3. The unit cell contains one molecule of MeB_2 .

4. This structure corresponds to alternate layers of metal and boron atoms, parallel to the basal plane of the lattice.

5. As the metal atom size increases, both a and c dimensions of the lattice increase and the axial ratio also increases slightly.

6. The borides have well developed metallic properties.

Acknowledgments

The authors wish to express their appreciation to the Office of Naval Research for the support of this investigation and permission to publish the results. They also gratefully acknowledge the important assistance of Mr. A. S. Cohan of the American Electro Metal Corporation and Mr. Albert Mahfuz of the Department of Metallurgy, Massachusetts Institute of Technology.

References

1. G. Hägg: *Ztsch. Phys. Chem.* (1929) B6, 221.
Ibid. (1931) 12, 33.
2. P. McKenna: *Ind. and Eng. Chem.* (1936) 28, 767.
3. P. Ehrlich: *Angew. Chem.* (1947) 59, 163.
4. R. Kiessling: *Acta Chem. Scand.* (1949) 3, 90.
5. L. Andrieux: *Ann. Chim.* (1929) 12, 423.
Comptes Rendus (1929) 189, 1279.
6. R. Kiessling: *Acta Chem. Scand.* (1947) 1, 893.

The Diffusion and Solubility of Carbon in Alpha Iron*

JAMES K. STANLEY,[†] Member AIME

Introduction

Knowledge of the diffusivity of carbon in the low temperature form of iron (alpha iron existing below 910°C) is at the moment of considerable interest in the study of the decomposition of austenite and martensite, the elastic after-effect,^{1,2,3} the magnetic after-effect⁴ and the decarburization of steel below 910°C. Information on the solubility of carbon in iron, and to a lesser extent its diffusion, is also important in consideration of such phenomena as blue-brittleness, temper-brittleness, "magnetic" aging, quench-aging, strain-aging, and possibly the yield point. In order to obtain more information on these subjects more fundamental knowledge is necessary. It is the purpose of this work to present data on the diffusion and solubility of carbon in the alpha iron.

The high temperature form of iron (gamma; face-centered cubic) existing above 910°C is capable of dissolving relatively large amounts of carbon, up to 1.7 pct at 1130°C, while the low temperature form (alpha, body-centered cubic) existing below 910° dissolves only a limited maximum amount of less than 0.02 pct carbon at 725°C, according to data obtained here. Since the solubility of carbon in the face-centered or gamma iron is large, relatively speaking, no great analytical difficulties have been encountered in the determination of the solubility lines⁵ or of the diffusion of carbon.⁶ The limited solubility of carbon in alpha iron offers difficulties because experimental procedures and analytical methods for low carbon contents below say 0.01 pct have to be more refined than techniques used for work with gamma iron. Because of the difficulties of applying conventional methods to the determination of the diffusion

of carbon in alpha iron, virtually no work has been done on this subject. However, by proper refinement of the analytical method for small amounts of carbon, the determination of the diffusion coefficient can be made readily using modified procedures.

The solubility of carbon in alpha iron has been determined over a temperature range by various investigators, but the agreement among them is poor. The present investigation establishes the limits quite accurately. Information of this kind is useful in establishing the correctness of equilibrium diagrams but, more significantly, such information on maximum solubilities, especially when extended to alloyed ferrites, should be extremely important in the study of aging and related phenomena.

Literature

The literature existing on the diffusion, in particular, and on the solubility of carbon in alpha iron is not extensive. The data which exist are not of a high order of accuracy, much of them being in the realm of conjecture.

THE DIFFUSION OF CARBON IN ALPHA IRON

Whiteley⁷ made the qualitative ob-

servation, using metallographic techniques, that the rate of diffusion of carbon at the A₁ (725°C) point was very rapid and that its diffusion was still rapid at 550°C.

Snoek,⁴ studying the magnetic after-effect in high purity iron, arrived at the conclusion that the after-effect could be explained by the presence of small amounts of carbon diffusing under the influence of magnetostrictive strain (lattice distortion due to magnetic interaction).

In later work, Snoek⁸ made an estimate of the ratio of carbon diffusion in alpha to its diffusion in gamma iron, and concluded that for a temperature of 910°C the ratio of D_α/D_γ was 2600. Polder,⁹ basing his calculations of D on relaxation phenomena in the elastic after-effect, estimated that D_α is about $\frac{1}{3}$ of D_γ at 910°C (1183°K) and is about $\frac{1}{12}$ of D_γ at 727°C (1000°K). Polder's equation for the diffusion of carbon in alpha iron was calculated to be

$$D = 5.2 \times 10^{-4} e^{-\frac{18000}{RT}} \text{ cm}^2 \text{ per sec}$$

Ham¹⁰ obtained data for the diffusion and solid solubility of carbon in alpha iron at two temperatures by using one technique similar to that employed in this study. He found a D of $8.0 \times 10^{-7} \text{ cm}^2 \text{ per sec}$ at 702°C and of 2.7×10^{-7} at 648°C.

THE SOLUBILITY OF CARBON IN ALPHA IRON

Although pearlite is absent in steels containing 0.06 pct,¹¹ 0.05 pct,¹² or 0.045 pct C,¹³ it appears that the carbon in these steels cannot be in solution in ferrite. The solubility of carbon at the A₁ (725°C) point was first determined by Scott¹⁴ on the basis of cooling curves, and was found to be between 0.03 and 0.04 pct C.

Tamura¹⁵ by interpolating between the solubility of carbon in delta iron at 1400°C and in alpha at room temperature (assuming zero solubility) ar-

Cleveland Meeting, October 1949.

TP 2679 E. Discussion of this paper (2 copies) may be sent to *Transactions AIME* before December 1, 1949. Discussion of Fall Meeting papers is tentatively scheduled for publication in May, 1950. Manuscript received April 4, 1949; revision received July 7, 1949.

* This paper is taken from a thesis submitted by James K. Stanley in September 1948 in partial fulfillment for the degree of Doctor of Philosophy in Metallurgical Engineering at the University of Pittsburgh.

[†] Research Metallurgist, Research Laboratories, Westinghouse Electric Corporation, East Pittsburgh, Pennsylvania.

¹ References are at the end of the paper.

rived at a solubility of carbon in alpha iron of 0.034 pct at 720°C. Whiteley⁷ using the Eggertz (colorimetric) test and metallography placed the limit of solid solubility at about 0.03 pct at 720°C. Koster¹⁶ on the basis of the Eggertz (colorimetric) test placed the maximum solubility of carbon in alpha iron at 0.04 pct at the A₁ and gave the variation of carbon solubility with temperature.

Dickie,¹⁷ using electrical resistivity measurements, made estimates of the solid solubility of carbon in Armco iron and several alloy steels by measuring the change in resistivity between the quenched and tempered states. Assuming a change of one microhm-centimeter being equivalent to 0.053 pct carbon, a calculation from his data gives the following solubility in Armco iron: 500°C, 0.008 pct; 625°C, 0.0172 pct; 710°C, 0.0194 pct; 750°C, 0.0199 pct and at 850°, 0.0204 pct.

Whiteley¹⁸ on the basis of metallographic work on Armco iron, pure iron, and electrolytic iron, concluded that the solubility of carbon was relatively constant to about 550°C, and then increased to the A₁. The line connecting the A₃ and A₁, he suggested, should be convex and gave one point (0.02 pct C at 870°C) to support this idea.

Smith,¹⁹ using a carburizing technique, arrived at the solid solubility of 0.02 pct at 750°C and 0.0128 pct at 800°C. The unpublished work of Ham¹⁰ has been mentioned; he found a solubility of 0.0185 pct at 702°C and 0.011 pct at 648°C.

In a recent work, Pennington²⁰ using a decarburizing technique, arrived at values of solid solubility of 0.025 pct C at 760°C, 0.02 pct at 790°C and 0.014 pct at 815°C.

Dijkstra,²¹ making internal friction measurements on high purity iron, arrived at the following set of solubilities at the indicated temperatures:

| | | | | | | | | | |
|----------|-------|-------|-------|-------|-------|------|-------|-------|------|
| °C..... | 250 | 400 | 450 | 500 | 550 | 600 | 650 | 700 | 710 |
| Pct..... | 0.001 | 0.002 | 0.003 | 0.004 | 0.007 | 0.01 | 0.012 | 0.016 | 0.02 |

Ziegler²² indicates that the presence of oxygen decreases the solubility of carbon.

MAGNITUDE OF THE A AND Q VALUES IN THE DIFFUSION EQUATION

A knowledge of the magnitude of the frequency factor, A, in cm² per sec and the activation energy, Q, in gram-cal per gram-atom, are of importance in the study of variation of the diffusion

coefficient with temperature.

Estimates of the Q values for the diffusion of carbon, other than those mentioned by Snoek⁸ and Polder,¹⁰ have been made. On the basis of spheroidization rates of cementite in pearlite Bailey²³ assigned a value to Q of 66,000 but this is more likely the heat of activation for spheroidization than for the diffusion of carbon. Richter^{24,25} found an activation energy Q of about 20,000 in his work on the magnetic and elastic after-effects; Snoek⁴ attributed his activation energy to the diffusion of carbon.

Ham¹⁰ by actual, though limited, experiments found A and Q values of 165 cm² per sec and 37,000 gram-cal per gram-atom, respectively.

Experimental

Two methods were used in determining the diffusion of carbon in alpha iron. The first or Van Orstrand-Dewey²⁶ method consisted of diffusing carbon from a saturated "well" into an essentially carbon-free sample. The other or Grube²⁷ method consisted of diffusing carbon from a higher carbon to a lower carbon sample with both materials being in the entirely ferritic phase. Both methods are indicated schematically in Fig 1.

THE VAN ORSTRAND-DEWEY METHOD

The Van Orstrand-Dewey method can be used successfully to determine the diffusion coefficient below 725°C in the following manner (above 725°C this method no longer applies for reasons cited):

Two cylinders, one of high carbon corresponding to a composition close to the eutectoid, and the other essentially carbon-free, were welded together into what is called a diffusion couple.

This diffusion couple is then annealed to diffuse the carbon across the weld or interface. After the diffusion anneal, the distribution of carbon with respect to the interface is determined, the concentration-penetration curve is plotted, and the curve is analyzed mathematically for the diffusion coefficient.

Below a temperature of 725°C, the high carbon side of the couple corresponds metallographically to fine pear-

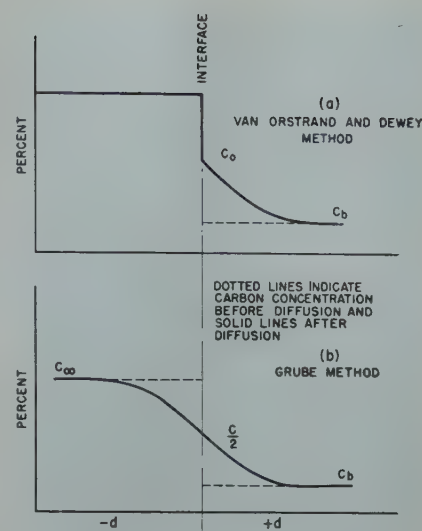


FIG 1—Schematic representation of penetration curves from which the diffusion coefficient is calculated.

ite in which the carbon is available in large concentration in carbides and which can be rapidly transmitted to the diffusion interface due to the high rate of diffusion of carbon in the ferrite lamellae. This diffusion of carbon, as shall be seen subsequently, is of the order of a hundred times faster in ferrite than it is in austenite. In this case the solution of the diffusion equation is assumed to apply because the carbon-rich side behaves as if the carbon concentration on that side of the couple were constant.

Above 725°C the Van Orstrand-Dewey solution cannot be applied because the carbon concentration on the high carbon side is not constant. Actually the diffusion of carbon in austenite is considerably slower than that in alpha iron and hence the carbon is depleted from the austenite at the interface giving rise to a gradient; also the position of the interface probably changes. For these reasons the boundary conditions which satisfy the differential equation applicable to the Van Orstrand-Dewey no longer apply.

THE GRUBE METHOD

This method, used so frequently in diffusion studies, depends on the diffusion of solute atoms in high concentration across an interface into a sample of lower concentration. In the present case one depends upon the diffusion of carbon from a high-carbon ferrite, ("high" being used advisedly since the maximum carbon is about 0.02 pct at 725°C decreasing above and below this temperature) into a carbon-free ferrite. If the carbon in the high-carbon

ferrite is purposely kept lower than the maximum solubility the diffusion can be checked above (this is an important advantage) and below 725°C.

SOLUBILITY OF CARBON IN ALPHA IRON

Information on solubility of carbon in alpha iron can be obtained by the Van Orstrand-Dewey method. As soon as the diffusion couple is annealed, there begins to be released at the interface from the high-carbon sample into the carbon-free sample a small amount of carbon which is assumed to be a measure of the carbon solubility at the diffusion temperature. This assumption appears to be valid. *Apriori*, it would seem that the carbon from a saturated "well" of carbon in iron should be released into a carbon-free ferrite at a concentration corresponding to its solubility limit, certainly at and below 725°C. Above that temperature the saturated "well" does not exist. A similar situation exists in the case of the diffusion of zinc in alpha-brass;²⁸ it has been shown that as zinc diffuses from α -brass into copper, it forms β -brass and at the α - β interface the zinc concentration is that corresponding to the limit of solid solubility given in the Cu-Zn diagram; for example, at 655°C the zinc released to the copper is 36.5 pct.

The solubility of carbon in alpha iron above 725°C can be studied by a decarburization method. In an early work Pennington²⁹ makes the statement that no carbon concentration gradient could be found in ferrite layers formed on the surface of 0.85 pct C steel decarburized between 725 and 910°C. This did not appear probable to the author who felt that a carbon gradient from zero at the immediate surface to the limit of solid solubility at the decarburization temperature must exist in the ferrite layer. If this were not the case one would have to look for another mechanism of decarburization.³⁰ The assumed lack of a gradient through the ferrite layer appeared to offer to Pennington a method of determining the solid solubility of carbon in ferrite. One could determine the solubility by analyzing the ferrite layer formed on decarburization assuming, of course, that the ferrite is saturated with carbon. Recently Pennington²⁰ used this method to determine the solubility at several temperatures.

Decarburization experiments were conducted to check Pennington's idea

| Material | C | O ₂ * | Si | Al | Cu | Mn | S | P | Others | Remarks |
|----------|-------------|------------------|-------|-------|-------|-------|-------|-------|----------|-------------------------------|
| 1 | 0.003-0.004 | 0.029 | 0.25 | 0.012 | 0.007 | 0.014 | 0.008 | 0.002 | | Deoxidized with Si and Al |
| 2 | 0.005 | 0.013 | 0.01 | 0.092 | 0.009 | 0.003 | 0.009 | 0.002 | | Deoxidized with Al |
| 3 | 0.005 | 0.055 | 0.006 | 0.005 | 0.008 | 0.005 | 0.001 | 0.002 | 0.048 Ni | Deoxidized with Al |
| 4 | 0.001 | 0.038 | 0.007 | 0.006 | 0.003 | 0.013 | 0.006 | 0.001 | 0.38 Co | Vacuum melted; no deoxidation |
| 5 | 0.006 | 0.03 | 0.21 | 0.010 | 0.007 | | 0.008 | 0.002 | | Deoxidized with Si and Al |
| 6 | 0.001 | 0.041 | 0.005 | | | | 0.005 | 0.001 | | Air melted; no deoxidation |
| 7 | 0.0044 | 0.030 | 0.007 | 0.008 | | | 0.006 | 0.002 | | Deoxidized with Si and Al |
| 8 | 0.68 | 0.011 | 0.15 | | | | 0.010 | 0.002 | | Deoxidized with Si |
| 9 | 0.0054 | | 0.004 | 0.009 | | 0.023 | 0.008 | 0.001 | | Deoxidized with Al |
| 10 | 0.001 | | 0.004 | 0.001 | | 0.011 | 0.005 | 0.002 | | Air melted; no deoxidation |
| 11 | 0.43 | | 0.06 | | | | 0.007 | 0.002 | | Deoxidized with CaSi |
| 12 | 0.0081 | | 0.004 | 0.004 | 0.007 | 0.001 | | | | Air melted; no deoxidation |

* Oxygen determined by the vacuum fusion method.

and it was found that if a high carbon alloy were decarburized and quenched from the decarburization temperature a carbon gradient in the ferrite layer existed. Even if the sample is slowly (furnace) cooled the carbon does not redistribute itself to give a uniform carbon distribution throughout the ferrite layer. The possibility exists that Pennington's analytical methods were not sensitive enough. His assumption that the carbon content of the ferrite layer should be a measure of the solid solubility cannot be considered valid. In the experiments performed by the author the limit of solid solubility by the decarburization method is the carbon concentration existing at the intersection of the decarburization curve in the ferrite with the carbon concentration in the austenitic region. Typical decarburization curves are given under *Results*.

COMPOSITION OF MATERIALS

Several materials were used for the diffusion and solubility studies. The basic material was electrolytic iron.

Ingots 12-15 lb were melted in an induction furnace and were either undeoxidized or deoxidized with silicon or aluminum or both. The high carbon materials for diffusion and decarburization were prepared by the addition of graphite to a silicon-killed melt. The materials were deoxidized for two reasons. One was that according to Ziegler²² the carbon solubility was affected by oxygen in solution and the other was that an aluminum addition was desirable to prevent grain growth. Several series of ingots were prepared, analyzed, and the desired composition was then selected for samples. Analysis was carried out on drillings taken from the

top and bottom of the ingots. When desirable compositions were found, the ingots were homogenized by heating to 950°C, holding about 15 hr and furnace cooling. The ingots were then forged at 850-900°C to one inch rounds. Sections of the rounds were analyzed at about one foot lengths and if the carbon contents of the ends of the round were in agreement, the section was used for samples. Table 1 gives the analysis of the materials used.

The possible effect of nitrogen on the diffusion of carbon was not investigated. The nitrogen content of sample 1, which was used extensively for the diffusion study, was 0.004 pct.

PREPARATION OF SPECIMENS

Cylinders of the various materials were machined, from forgings, to one-inch lengths and 0.75 in. diam and the ends were ground on a precision grinder.

Prior to the welding of the cylinders one of the faces of each was ground on several grades of metallographic paper finishing with 3/0. The cylinders were then welded on a welding machine in a hydrogen atmosphere, using 1500 lb load and 50 pulses of current (9000 amp). The welding conditions were kept as constant as possible to give identical samples. The region of the weld interface was probably heated to about 1000°C.

After the cylinders were welded they were cooled in hydrogen till black and were removed and quenched in water. The first couple welded by this procedure was tested for sufficiency of the weld. The one end of the sample was placed in a large vise and the other end was struck with a sledge hammer. The sample did not break but merely bent

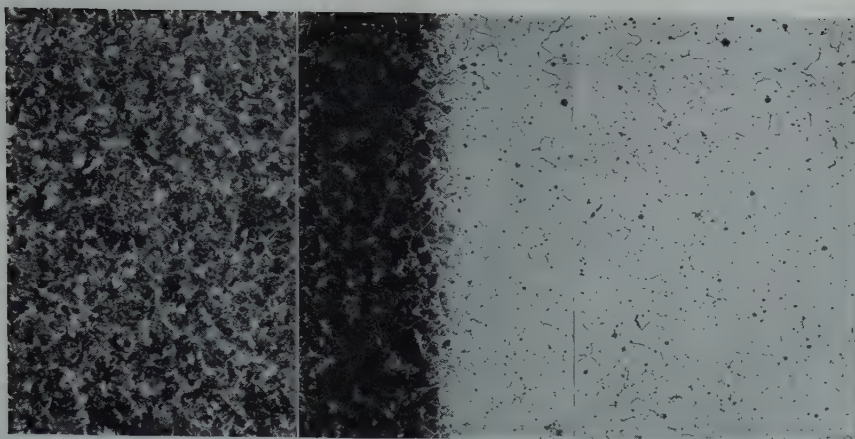


FIG 2—Diffusion weld between high-carbon and carbon-free iron.
Magnification $\times 100$. Nital etch. Reduced one-half in reproduction.

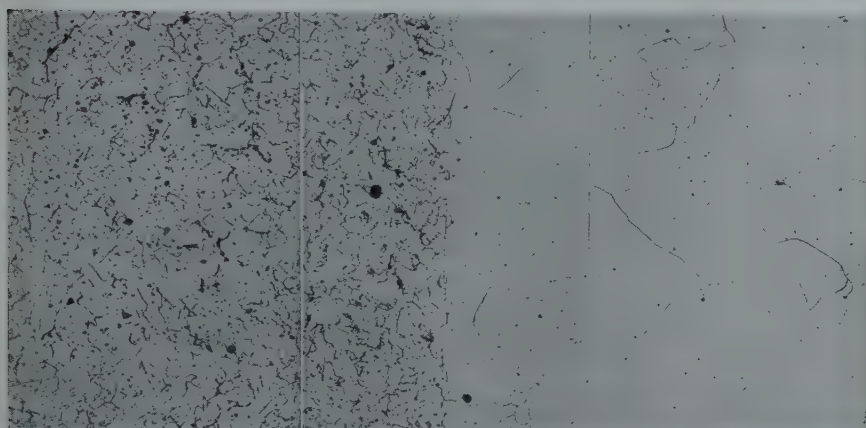


FIG 3—Diffusion weld between ferrite of different carbon contents.
(Left) 0.009 pct C and (right) 0.001 pct C. Magnification $\times 100$. Nital etch. Reduced one-half in reproduction.

under the strokes. This indicated that the fusion was satisfactory. Examination of the weld zone was also made microscopically. Fig 2 shows the zone and the region near it in a high and low carbon sample; Fig 3 shows the zone and the region near it in a sample entirely in the ferritic state.

A variation in the preparation of the diffusion sample was carried out in the following manner: A small cylinder of high carbon (0.75 in. diam by 0.25 in.) was placed between two low carbon cylinders (0.75 in. diam by 0.875 in. long) and the three pieces were welded together in sandwich fashion. Such specimens (called double couples) were used when comparisons on grain size and oxygen were desired. Fig 4 shows a macrograph of a double couple. It illustrates how the grain size of the material changes, depending on the composition, when the couples are welded. There is, in the case of undeoxidized samples (No. 4 and 6), a pronounced coarsening of the grain structure; very large elongated grains are formed. In the case of deoxidized samples (No. 2 and 3), there may be

little change in structure and sometimes even a definite refinement.

Specimens for decarburization were in the form of spools because it was desirable to have the decarburizing atmosphere (moist hydrogen) bathe the entire reduced section. The spools were $1\frac{1}{4}$ in. long; the ends of the spools were 1 in. in diam and $\frac{1}{8}$ in. wide and the central portion was 0.75 in. in diam and 1 in. long.

THE DIFFUSION ANNEAL

Since this study involves changes in carbon of low concentration, the diffusion anneals were carried out in a vacuum because it was felt that risks should not be taken with gases such as hydrogen, nitrogen, helium or argon which might be decarburizing in the presence of small amounts of oxygen or moisture.

A quartz tube vacuum furnace was used. The furnace was made so that it could slide over the quartz tube. In this way a vacuum could be obtained while the furnace was being brought to temperature. When the desired vacuum

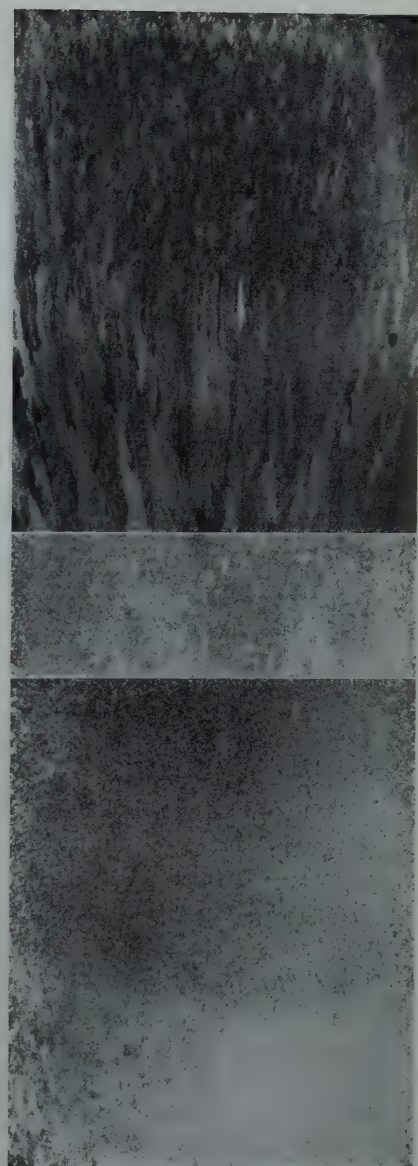


FIG 4—Grain structures in the diffusion specimens.

(Top) Deoxidized Iron, Sample No. 2.
(Middle) High carbon sample 0.68 pct C.
(Bottom) Undeoxidized iron, Sample No. 6.
(Magnification $\times 5$).
Reduced one-third in reproduction.

was obtained, the preheated furnace was pulled over the quartz tube. When the anneal was completed, the furnace was pulled away from the quartz tube.

The vacuum system consisted of a Cenco Hyper-Vac pump in series with two mercury pumps. A liquid nitrogen trap was placed between the mechanical and mercury pumps. Pressures were measured with thermocouple and ionization gauges. Even with the furnace heated to 700 or 800°C the pressures were of the order of 5×10^{-5} mm of Hg.

The furnace was wound in three sections with nichrome wire and resistors were inserted between the sections to improve the temperature distribution. An arrangement was worked out so

Table 2 . . . Details of the Diffusion and Decarburization Anneals

| Experiment | Method | Temperature °C | | | Annealing Time | | High Carbon Cylinder | | | Low Carbon Cylinder | | |
|------------|------------------|----------------|-------------------------------|-----------------------|----------------|--------------------|----------------------|--------|------------------------|---------------------|--------|------------------------|
| | | Average | Standard Deviation σ^* | Variation r^\dagger | Hours | Seconds | No | C | Grain Size ‡ | No | C | Grain Size ‡ |
| 1 | V.O.-D. | 514.3 | 2.0 | ± 1.3 | 134.8 | 4.85×10^5 | 8 | 0.68 | See Fig 3 | 7 | 0.0044 | 4 to 5 |
| 2 | V.O.-D. | 606.1 | 1.2 | ± 0.8 | 47.8 | 1.72×10^5 | 8 | 0.68 | See Fig 3 | 1 | 0.004 | 5.8 |
| 3 | V.O.-D. | 672.1 | 1.0 | ± 0.7 | 48.0 | 1.73×10^5 | 8 | 0.68 | See Fig 3 | 5 | 0.006 | 4 to 5 |
| 4 | V.O.-D. } double | 700 | 1.0 | ± 0.7 | 21.3 | 7.67×10^4 | 8 | 0.68 | See Fig 3 | 2 | 0.005 | 5.9 |
| 5 | V.O.-D. } couple | 700 | 1.0 | ± 0.7 | 21.3 | 7.67×10^4 | 8 | 0.68 | See Fig 3 | 6 | 0.001 | § |
| 6 | V.O.-D. } double | 700 | 1.0 | ± 0.7 | 21.3 | 7.67×10^4 | 8 | 0.68 | See Fig 3 | 3 | 0.005 | 5.0 |
| 7 | V.O.-D. } couple | 700 | 1.0 | ± 0.7 | 21.3 | 7.67×10^4 | 8 | 0.68 | See Fig 3 | 4 | 0.001 | §§ |
| 8 | V.O.-D. | 723.5 | 2.5 | ± 1.7 | 30.3 | 1.09×10^5 | 8 | 0.68 | See Fig 3 | 5 | 0.006 | 4 to 5 |
| 9 | Grube | 718.8 | 1.7 | ± 1.1 | 48.3 | 1.74×10^5 | 12 | 0.0081 | 5-6 | 1 | 0.003 | 5.8 |
| 10 | Grube | 761.0 | 1.1 | ± 0.7 | 40.08 | 1.44×10^5 | 9 | 0.0054 | 5-6 | 10 | 0.0008 | About 1 |
| 11 | Grube | 786.0 | 2.5 | ± 1.7 | 23.63 | 8.52×10^4 | 9 | 0.0057 | 5-6 | 10 | 0.0013 | About 1 |
| 12 | Decarburization | 750 ± 4 | | | 24.5 | 8.82×10^4 | 11 | 0.43 | | | 0.016 | (C in ferrite layer) |
| 13 | Decarburization | 775 | | | 66 | 2.38×10^5 | 11 | 0.43 | | | 0.014 | (C in ferrite layer) |
| 14 | Decarburization | 800 | | | 19.5 | 7.02×10^4 | 11 | 0.43 | | | 0.012 | (C in ferrite layer) |
| 15 | Decarburization | 825 | | | 16 | 5.76×10^4 | 11 | 0.43 | | | 0.0095 | (C in ferrite layer) |
| 16 | Decarburization | 850 | | | 24 | 8.65×10^4 | 11 | 0.43 | | | 0.0065 | (C in ferrite layer) |
| 17 | Decarburization | 875 | | | 46.5 | 1.67×10^5 | 11 | 0.43 | | | 0.004 | (C in ferrite layer) |

* Standard deviation from probability plot.

 † Error, $r_s = \sigma \times 0.6745$. ‡ Grain size; ASTM estimate; intercept method.

§ Large elongated grains in the weld zone; see figure lower portion of Fig 5.

§§ Large elongated grains in the weld zone; similar to Fig 5.

that a uniform (better than $\pm 0.25^\circ$) hot zone was maintained over a distance of 3-in.

Temperature control was obtained by using a Micromax controller-recorder in conjunction with a constant voltage transformer and an anticipator.³¹ Temperatures were measured accurately to 0.1 of a degree. The variation in temperature was from ± 0.6 to $\pm 1.70^\circ$. The temperature of the anneal was obtained by plotting readings on probability paper and determining the standard deviation from the average, which when multiplied by 0.6745 gives the \pm error.

Before the diffusion anneals were started, coils of chromel and alumel wire (24 gauge) were calibrated against a Bureau of Standards's platinum-platinum: rhodium secondary standard. This was done by placing the standard thermocouple and thermocouples prepared from each end of the coils into a 1 in. diam nickel-plated copper cylinder in which three holes had been drilled. The cylinder containing the three thermocouples was placed in the uniform temperature zone of the furnace and the readings of the thermocouples were obtained on a type K Leeds and Northrup potentiometer, using a Leeds and Northrup thermocouple selector switch. Slight differences between the ends of the chromel and alumel were noted. These were averaged and charts were prepared for the chromel-alumel thermocouples correlating millivolts and temperature. New thermocouples were used for each diffusion-anneal.

The thermocouples were placed into the low carbon end of the diffusion couple by drilling a hole sufficiently

large for the thermocouple bead and then peening over the edge of the hole to keep the thermocouple from coming out. Connection was made between the thermocouple and the potentiometer by chromel and alumel lead-in wires joined to the furnace by a kovar-glass seal.

The diffusion anneal was carried out as follows: The furnace, drawn away from the quartz tube, was heated to the required temperature. The diffusion couple was placed into the cold quartz tube and connections were made to the potentiometer. The quartz tube was closed and was pumped down to the desired vacuum. The hot furnace was then pulled over the quartz tube containing the specimen.

Table 2 gives the details of the diffusion anneals reported upon in this investigation.

DECARBURIZATION ANNEAL

Samples used for decarburization were annealed in a conventional Globar Type furnace with a quartz tube as a furnace chamber. No extraordinary effort was exercised to obtain a fine temperature control, and hence the temperature varied $\pm 4^\circ$ of the desired temperature. The gas used was hydrogen saturated with moisture at room temperature (3.1 pct moisture by volume at 25°C). When the anneal was completed the samples were quenched in water.

MACHINING OF SAMPLES

After the diffusion anneal, the couples were machined to approximately 0.7 in. diam to remove possible de-

carburized layers and to get a uniform diameter couple. The region of the interface was polished with emery cloth and metallographic papers of increasing fineness. The samples were etched in 10 pct nital to bring out the interface. With the specimen properly centered in the lathe, layers about 0.02 in. were machined off near the interface and the thickness was then progressively increased to 0.04 in. at a distance of a centimeter from the weld. The length of the specimen after each cut was measured to the thousandth of an inch and estimated to the ten thousandth.

On the spools used for decarburization, turnings were taken on layers about 0.005 in. thick. In general, machining was continued until martensitic areas were reached.

CARBON ANALYSIS

Before the carbon analyses were made, the chips were screened on a 100-mesh screen to remove very fine particles which experience has shown can be relatively high in carbon presumably because of tool wear. After screening, the chips were washed in acetone and were dried over a small flame.

The carbon analysis was carried out by the method described by Stanley and Yensen.³² The method is a modification of the conventional combustion method, employing the use of vacuum and liquid nitrogen.

The agreement between the present, also known as the Yensen, method and the conventional combustion one is reasonable. Various investigators^{33,34} using the Yensen method have

Table 3 . . . Carbon Analysis of Standard Sample

| Certified Analysis 0.014 pct C | | |
|----------------------------------|---------------------|-----|
| Investigator | | |
| Stanley and Yensen ³² | 0.0104 ± 0.0002 pct | 55a |
| Wooten and Guldner ³³ | 0.0108 ± 0.0001 pct | |
| Naughton and Uhlig ³⁴ | 0.0105 ± 0.0003* | |
| | 0.0108 ± 0.0003 | |
| | 0.0108 ± 0.0003 | |

* Naughton and Uhlig used two variations of the low pressure combustion method.

analyzed the Bureau of Standard's sample 55a and have found it somewhat lower than the certified value which was determined by conventional combustion methods. See Table 3. The differences in the two methods have been considered by Naughton and Uhlig.³⁴

ERRORS

There are certain errors in the diffusion experiment that are to be considered in obtaining the error of the diffusion coefficient. The main sources of error are those due to carbon analysis, temperature and measurement of layers. Other errors affecting D are due to: diffusion occurring during the welding of the diffusion couples, the diffusion occurring while the specimens were coming to and cooling from the diffusing temperature, and the change in dimensions due to thermal expansion.

The errors in carbon analysis and temperature can be estimated, the other errors are not readily treated. The diffusion in the welding operation is small (about 0.06 mm) as can be seen from Fig 2 but no corrections for this diffusion were made. The error due to heating up and cooling down of the diffusion couples was difficult even to approximate; however if the heating and cooling times were short compared to the time of the diffusion anneal, it was felt that no serious error was introduced. After the diffusion anneal the samples were furnace-cooled to about 500° and were then quenched. Corrections for thermal expansion can be made but were not made here because of the uncertainty of the temperature coefficient of iron in the range studied. The D values, if the expansion corrections were approximated, would be increased only by about 1 pct. It is believed that the diffusion data are good to ±10 pct.

Results

After the carbon analyses had been made they were plotted in relation to the distance from the interface on probability paper. From the best straight line obtained on the probabil-

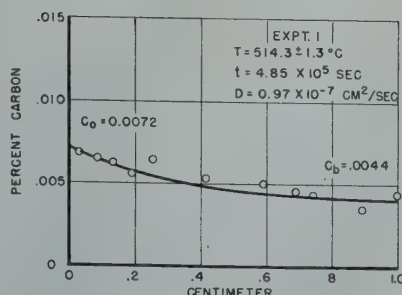


FIG 5—Carbon penetration at 514°C.

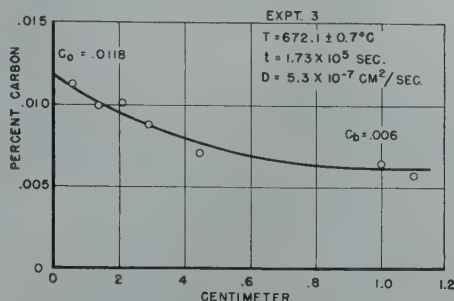


FIG 7—Carbon penetration at 672°C.

ity plot, curves were redrawn using rectangular coordinates. The types of penetration curves obtained by the Van Orstrand-Dewey method are illustrated in Fig 5 to 12 and for the Grube method in the ferritic state in Fig 13 to 15.

The D values for the curves were derived from Fick's law* of diffusion.

The differential form of Fick's equation is:

$$\frac{dC}{dt} = D \frac{d^2C}{dx^2}$$

The solution to the differential equation for the specific boundary conditions of the Van Orstrand-Dewey method is:

$$\frac{C_x - C_b}{C_o - C_b} = 1 - \phi\left(\frac{x}{2\sqrt{Dt}}\right)$$

where, using the *cgs* system,

C_x is the carbon at distance x in centimeters

C_b is the base or initial carbon content of the low carbon samples in per cent.

C_o is the carbon on the high side of the couple or the limit of solid solubility at the temperature.

D is the diffusion coefficient in centimeters squared per second.

t is the time in seconds.

ϕ is the Gauss error function.

The solution for the Grube method

* Discussions of Fick's law and the various solutions for limiting boundary conditions can be found in Jost³⁵ and Mehl.³⁶

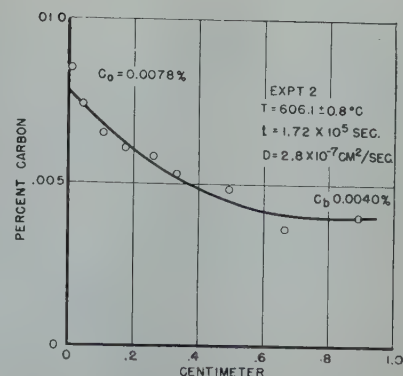


FIG 6—Carbon penetration at 606°C.

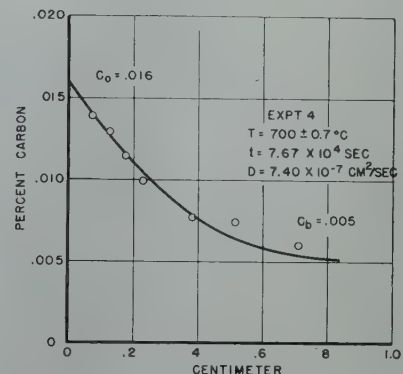


FIG 8—Carbon penetration at 700°C.

is:

$$\frac{2(C_x - C_b)}{C_\infty - C_b} = 1 - \phi\left(\frac{x}{2\sqrt{Dt}}\right)$$

where C_∞ is the carbon at infinity in the high carbon side of the couple and all other symbols remain as before.

The diffusion coefficients calculated by both methods are given in Table 4. In Fig 16, $\log D$ is plotted against the reciprocal of the absolute temperature. The agreement between points obtained by the two methods is gratifying.

The diffusion of carbon in alpha iron as a function of temperature can be represented by the equation:

$$D = 7.9 \times 10^{-3} e^{-\frac{18100}{RT}}$$

No significant difference exists in D values between deoxidized, fine-grained samples and undeoxidized, coarse-grained samples. The diffusion coefficient at 700°C calculated for deoxidized, fine-grained samples (experiments 1, 2, 3, 4, 6) using the Van Orstrand-Dewey method samples gave a value of 6.4×10^{-7} cm² per sec. The experimental D value at 700 for an undeoxidized large elongated grain sample (experiment 5) gave a value of 6.75×10^{-7} ; experiment 7 also on an undeoxidized sample should not be compared with

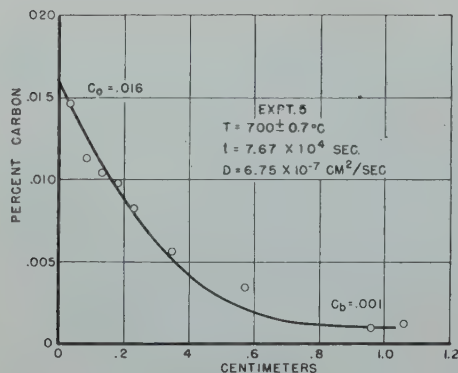


FIG 9—Carbon penetration at 700°C.

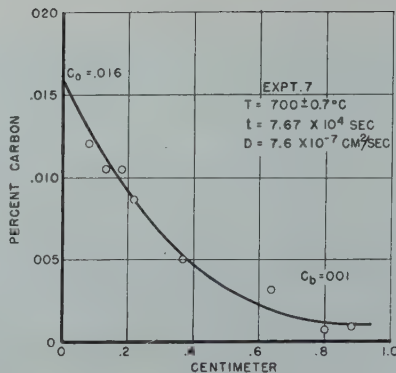


FIG 10—Carbon penetration at 700°C.

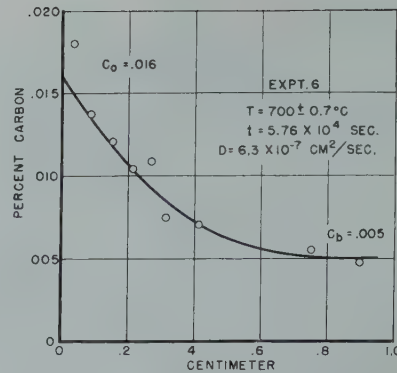


FIG 11—Carbon penetration at 700°C.

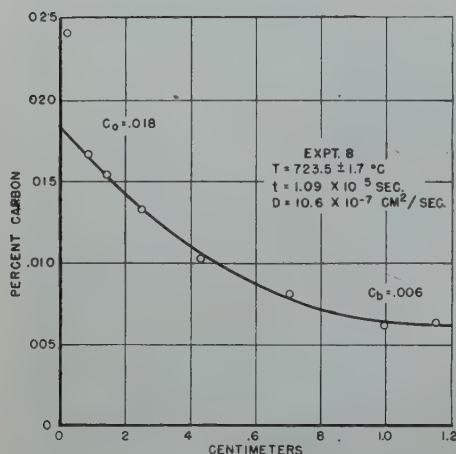


FIG 12—Carbon penetration at 723.5°C.

experiment 5 since the sample contained 0.38 pct cobalt. Reference to experiments 9, 10, 11 employing the Grube method indicates that no anomalies were observed due to differences in grain size (See Fig 3 for example).

Silicon up to 0.25 pct and cobalt up to 0.38 does not appear to affect the diffusion coefficient although it must be emphasized that the data are very meager and more work is necessary to establish the effect of these elements unequivocally. In the case of silicon (experiment 2) the calculation of D from the exponential relation derived from all the points gives a value of 2.7×10^{-7} at 606°C as against the experimental value of 2.8×10^{-7} . In the case of cobalt (experiment 7) the calculation of D from the exponential relation gives a value of 7.2×10^{-7} at 700°C as against the experimental value of 7.6×10^{-7} . These variations are both within 10 pct and no greater accuracy than this is claimed.

It has not been possible, as may be evident, to determine whether D varies with concentration as it does in the case of gamma iron.⁶

THE SOLUBILITY OF CARBON IN ALPHA IRON

The data on the solubility of carbon in alpha iron are given in Table 5. They have been obtained as the intercept carbon, C_0 , from the carbon penetration curves obtained by the Van-Orstrand-Dewey method (experiments 1-8), Fig 5 to 12, and from the concentration of carbon at the ferrite-austenite interface, C_i , as is obtained in ferrite layers by the decarburization of a medium carbon steel (experiments 12-17); typical decarburization curves are given in Fig 17 and 18 for 750°C and 875°C, respectively. The data are plotted in Fig 19 together with data obtained by other investigators. The maximum solubility of carbon in alpha iron was found to be 0.019 pct at 725°C. The lines joining the carbon solubilities obtained by the Van-Orstrand-Dewey method and the decarburization method intersect nicely at the same point indicating that both methods are complementary and that the assumptions made regarding them are justified.

Discussion

The diffusion of carbon atoms in alpha iron as well as in gamma iron is interstitial and hence one need not concern himself with the mechanism of the process as one does for the dif-

fusion of atoms in substitutional solid solutions.

The diffusion of carbon in alpha iron, however, is much more rapid than in gamma iron. Wells and Mehl⁶ report the diffusion of carbon (in the range of 0.01 pct) in gamma iron as

$$D_{\gamma} = 0.07e - \frac{32,000}{RT}$$

Using their equation and the one found here for alpha iron, comparisons in the $\frac{D_{\alpha}}{D_{\gamma}}$ ratios at various temperatures can be made. Snoek⁸ and Polder⁹ predicted that at 910°C the ratio should be 2600 and 3, respectively. Actually the ratio at 910°C is 39. At 725°C the ratio increases to 126 and at 500°C it is 835.

It should be pointed out that the activation energy of the diffusion process in alpha iron is 18,100 gram-cal per gram-mol or about half the energy for diffusion in gamma iron, that is, 32,000. This value of 18,100 is identical (18,000) with that obtained by Snoek⁸ from the theory of the magnetic after-effect and by Polder⁹ from the theory of the elastic after-effect.

THE SOLUBILITY OF CARBON IN ALPHA IRON

The solubility of carbon in alpha iron has been established between 535 and 910°C with the maximum solubility of

Table 4 . . . Summary of D Values

| Experiment | Method | Temperature °C | D cm ² per sec Observed | D cm ² per sec Calculated* | Percent Deviation from Calculated D |
|-------------------|---------|-------------------|--|---|---|
| 1 | V.O.-D. | 514.3 | 0.97×10^{-7} | 0.80×10^{-7} | +21.0 |
| 2 | V.O.-D. | 606.1 | 2.8 | 2.7 | +3.7 |
| 3 | V.O.-D. | 672.1 | 5.3 | 5.5 | -3.6 |
| 4 | V.O.-D. | 700.0 | 7.4 | 7.2 | +2.8 |
| 5 | V.O.-D. | 700.0 | 6.75 | 7.2 | -6.2 |
| 6 | V.O.-D. | 700.0 | 6.3 | 7.2 | -12.5 |
| 7 | V.O.-D. | 700.0 | 7.6 | 7.2 | +5.5 |
| 8 | V.O.-D. | 723.5 | 10.6 | 8.9 | +19.0 |
| 9 | Grube | 718.8 | 9.35 | 9.7 | -3.6 |
| 10 | Grube | 761.1 | 12.1 | 12.5 | -3.2 |
| 11 | Grube | 786.0 | 17.6 | 15.3 | +15.0 |
| Average Deviation | | | | | ±8.7 |

* Calculated from the equation of the straight line for data in Fig 16.

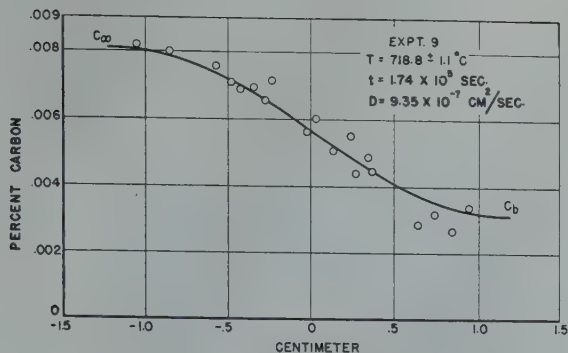


FIG 13—Carbon penetration at 719°C.

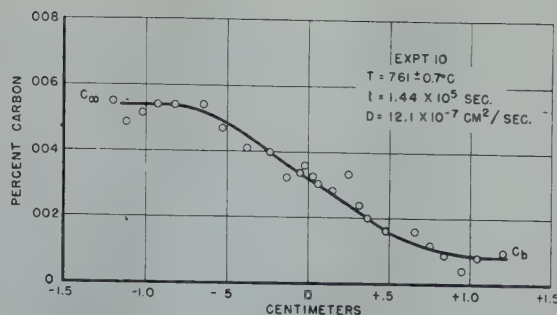


FIG 14—Carbon penetration at 761°C.

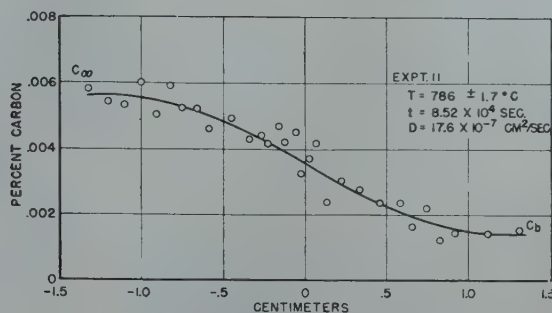


FIG 15—Carbon penetration at 786°C.

Table 5 . . . Solubility of Carbon in Alpha Iron

| Experiment | Temperature, °C | Solubility, Pct | Method |
|------------|-----------------|-----------------|-----------------|
| 1 | 514.3 | 0.0072 | V.O.-D. |
| 2 | 606.1 | 0.0078 | V.O.-D. |
| 3 | 672.1 | 0.0118 | V.O.-D. |
| 4 | 700.0 | 0.016 | V.O.-D. |
| 5 | 700.0 | 0.016 | V.O.-D. |
| 6 | 700.0 | 0.016 | V.O.-D. |
| 7 | 700.0 | 0.016 | V.O.-D. |
| 8 | 700.0 | 0.018 | V.O.-D. |
| 12 | 750 | 0.016 | Decarburization |
| 13 | 775 | 0.014 | Decarburization |
| 14 | 800 | 0.012 | Decarburization |
| 15 | 825 | 0.0095 | Decarburization |
| 16 | 850 | 0.0065 | Decarburization |
| 17 | 875 | 0.004 | Decarburization |

0.019 pct occurring at 725°C. The maximum solubility and the solubilities near it have been determined by several investigators. The present investigation is in agreement with Smith,¹⁹ Ham,¹⁰ and Dijkstra;²¹ all other determinations have tended to be high. Fig 19 gives the data of the present experiments and the data of other investigators.

The limit of solubility below 725°C is rather important because it may serve as a base line for subsequent work which is needed to determine the effect of alloying elements on solubility. Such basic information is required if progress is to be made in the study of such phenomena as quench, strain, and "magnetic" aging as well as temper and blue-brittleness.

Summary

The diffusion of carbon in alpha iron was determined by two methods. One, the Van Orstrand-Dewey method, consisted of diffusing the carbon from a high carbon iron containing 0.68 pct C—corresponding to fine pearlite—into an essentially carbon-free iron. The other or Grube method consisted of diffusing carbon from a "high" carbon ferrite into a low-carbon ferrite. The first method could be used only below 725°C (eutectoid temperature) but the second could be used above and below 725°C. Both methods gave equivalent results.

The diffusion of carbon in alpha iron can be represented by the equation:

$$D_{\alpha} = 7.9 \times 10^{-3} e^{-\frac{18,100}{RT}}$$

The diffusion of carbon does not appear to be affected by grain size, decarburization or small additions of silicon and cobalt. The present methods did not lend themselves toward determining if D varied with concentration.

At 725°C the diffusion of carbon is over 100 times as fast as it is in gamma iron.

The solubility of carbon in alpha iron below 725°C was determined by the Van Orstrand-Dewey method since the carbon leaving the pearlitic iron at

the diffusion temperature corresponds to the carbon solid solubility. The solubility above 725°C was determined by a decarburization method, the solubility being the carbon concentration where the carbon gradient in the ferrite intersects the carbon gradient of the austenite-ferrite region. Both methods of determining solubility gave lines meeting at the same point to give a maximum solubility of 0.019 pct carbon at 725°C. The solubility lines between 514 and 910°C were obtained.

Acknowledgment

The writer is most appreciative of the University of Pittsburgh-Westinghouse Electric Corporation Graduate Study Program through which this study was made possible. It was a privilege to be associated with such personalities as Dr. G. R. Fitterer, Head of the Department of Metallurgy, University of Pittsburgh, and Dr. T. D. Yensen, Westinghouse Research Laboratories; both were most helpful in the carrying out of this work.

The writer wishes to acknowledge the assistance of the following: Messrs. Julius Heuschkel (welding), R. Anderson (metallography), R. Darby (machining), and Miss Joan Von Hoene for assisting with the numerous carbon analyses.

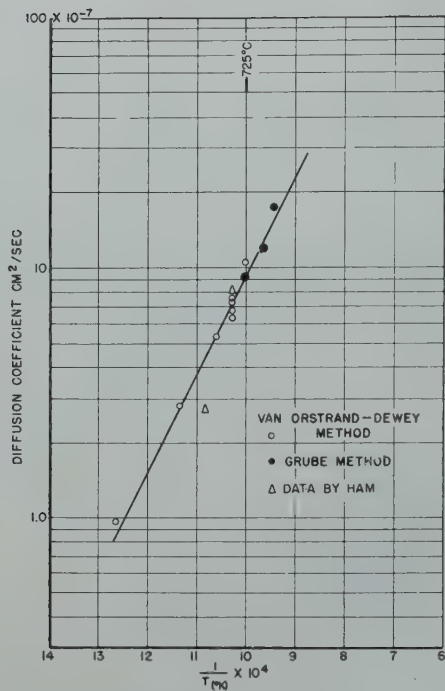


FIG 16—Plot of log D vs T.

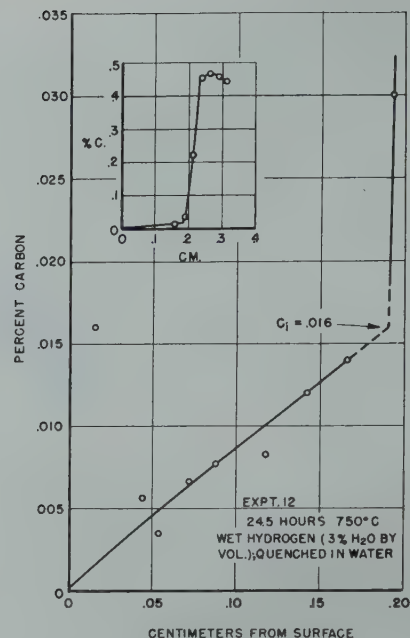


FIG 17—Decarburization curve at 750°C.

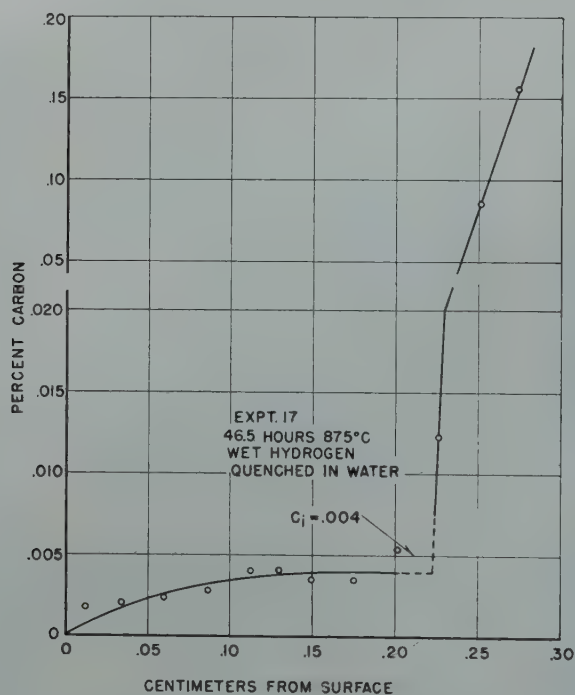


FIG 18—Decarburization curve at 875°C.

The writer also wishes to thank the following for graciously discussing the first draft of this paper: Drs. R. F. Mehl, Cyril Wells and R. Smoluchowski, Metals Research Laboratory, Carnegie Institute of Technology; Mr. F. E. Harris, Buick Motor Division, General Motors Corporation; Mr. J.

L. Ham, Climax Molybdenum Corporation of America; Dr. C. Zener, Institute of Metals, University of Chicago; and Dr. J. L. Snoek, Eindhoven, Netherlands.

References

1. J. L. Snoek: Mechanical After-effect

and Chemical Composition. *Physica* (1939) 6, 591.

2. C. Zener: Anelasticity of Metals. *Trans. AIME* (1946) 167, 155. *Metals Tech.* Aug. 1946, TP 1992.
3. J. L. Snoek: Effect of Small Quantities of Carbon and Nitrogen on the Elastic and Plastic Properties of Iron. *Physica* (1941) 8, 711.
4. J. L. Snoek: Magnetic After-Effect and Chemical Constitution. *Phys-*

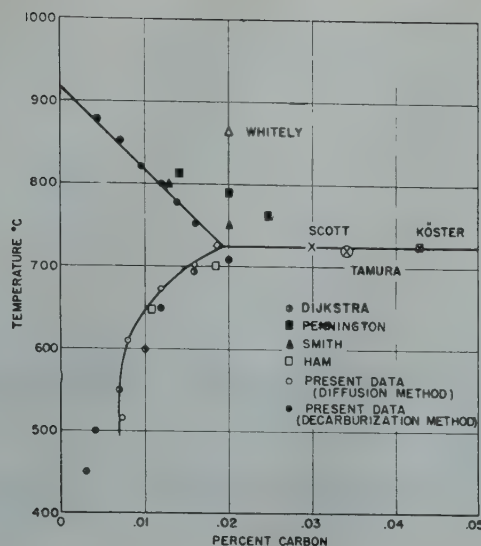


FIG 19—Solubility of carbon in alpha iron.

- ica (1939) 6, 161.
5. S. Epstein: Alloys of Iron and Carbon. McGraw-Hill Co., N.Y., 1936.
6. C. Wells and R. F. Mehl: Rate of Diffusion of Carbon in Austenite in Plain Carbon, in Nickel and in Manganese Steels. *Trans. AIME* (1941) 145, 279.
7. J. H. Whiteley: The Solution of Cementite in Alpha Iron and Its Precipitation. *Jnl. Iron and Steel Inst.* (1927) 116, 293.
8. J. L. Snoek: On the Decarburization of Steel and Related Questions. *Physica*, (1941) 8, 734.
9. D. Polder: Theory of the Elastic After-effect and Diffusion of Carbon in α -Iron. *Philips Research Reports* (1941) 1, 5.
10. Private communication from John L. Ham, Climax Molybdenum Co., dated Dec. 1, 1947 which referred to correspondence dated Oct. 21, 1946 to R. F. Mehl, Carnegie Institute of Technology.
11. A. Sauveur and V. N. Krivobok: Dendritic Segregation in Iron-Carbon Alloys. *Iron and Steel Inst.* (1925) 112, 313.
12. W. H. Hatfield: Discussion of Paper by A. L. Field on "Physical-Chemical Phenomena from Melt to Ingot." *Trans. Faraday Soc.* (1925) 21, 272.
13. A. Bramley and F. W. Haywood: Cementation of Iron and Steel. *Iron and Steel Inst.*, C.S.M. (1928) 17, 67.
14. H. Scott: What is Steel? *Chem. and Met. Eng.* (1922) 27, 1156.
15. S. Tamura: Pseudo-Twinning in Ferrite and Solubility of Carbon in α -iron at the A_1 . *Jnl. Iron and Steel Inst.* (1927) 115, 747.
16. W. Koster: Influence of Heat Treatment below the A_1 Point on the Properties of Technical Iron *Arch. f. d. Eisenhutt.* (1929) 2, 29 (503).
17. H. A. Dickie: The Solubility of Carbide in Ferrite. *Jnl. Iron and Steel Inst.* (1929) 120, 161.
18. J. H. Whiteley: A Survey of the Iron-Carbon Diagram Near Zero Carbon (Below 1000°C). *Jnl. Iron and Steel Inst.* (1936) 133, 377.
19. R. R. Smith: Equilibrium of Iron-Carbon Alloys with Mixtures of CO/CO_2 and CH_4/H_2 . *Jnl. Am. Chem. Soc.* (1946) 68, 1163-1175.
20. W. A. Pennington: Thermodynamics in the Decarburization of Steel with Mill Scales. ASM 1948 Preprint No. 38.
21. L. J. Dijkstra: Precipitation Phenomena in the Solid Solutions of Nitrogen and Carbon in α -iron below the Eutectoid Temperature. Ninth Quarterly Report to ONR on Deformation of Metals, Inst. for the Study of Metals, Univ. of Chicago, May-July 1948.
22. N. A. Ziegler: The Solubility of Oxygen in Solid Iron. A.S.M. (1932) 20, 73.
23. R. W. Bailey: Testing of Materials for Service in High Temperature Steam-Plant. *Proc. Inst. Mech. Eng.* (1932) 122, 209.
24. G. Richter: Über die Magnetische Nachwirkung um Carbonyleisen. *Ann. Phys. (Leipzig)* (1937) 29, 605.
25. G. Richter: Über die Mechanische und die magnetische Nachwirkung des Carbonyleisens. *Ann. Phys. (Leipzig)* (1938) 32, 683.
26. C. E. Van Orstrand and F. P. Dewey: Preliminary Report on the Diffusion of Solids. U.S. Geol. Survey, Prof. Paper 45-G (1915) 83-96.
27. G. Grube and A. Jedelev: Die Diffusion of Metalle in Festen Zustand. *Ztsch. f. Elektrochemie* (1932) 38, 799.
28. E. Kirkendall, L. Thomassen and C. Upthegrove: Rates of Diffusion of Copper and Zinc in Alpha Brass. *Trans. AIME* (1939) 133, 186.
29. W. A. Pennington: A Mechanism of the Surface Decarburization of Steel. A.S.M. (1946) 37, 48.
30. J. K. Stanley: Fundamentals of Carburization and Decarburization. *Steel* (1947) 120, 92.
31. M. J. Manjoine: An Anticipatory Method for Improving Automatic Temperature Control. *Instruments* (1945) 18, 454.
32. J. K. Stanley and T. D. Yensen: A Rapid Method of Determining Minute Amounts of Carbon in Metals. *Ind. Eng. Chem. (Anal. Ed.)* (1945) 17, 699.
33. L. A. Wooten and W. G. Guldner: Determination of Carbon in Low-Carbon Steel. *Ind. Eng. Chem., (Anal. Ed.)* (1944) 16, 248.
34. J. J. Naughton and H. H. Uhlig: Determination of Small Amounts of Carbon in Steel. *Anal. Chem.* (1948) 20, 477.
35. W. Jost: Diffusion Und Chemische Reaction im Festen Stoffen. Theo. Steinkopf, 1937.
36. R. F. Mehl: Diffusion in Metals. *Trans. AIME* (1936) 122, 11.



Studies of Interface Energies in Some Aluminum and Copper Alloys

K. K. IKEUYE* and CYRIL STANLEY SMITH,* Member AIME

In an earlier paper¹ one of the authors called attention to the significance of the relative free energies of grain boundaries and interphase boundaries in alloys in determining the shape and distribution of micro-constituents.

The ratio of the interphase and intercrystalline boundary energies (that is, $\frac{\gamma_{12}}{\gamma_{11}}$, where γ_{12} is the energy of the interface between a crystal of phase 1 and a crystal of phase 2, and γ_{11} is the energy of the boundary between two crystals of phase 1) will be denoted by Γ . It is this ratio that determines, by the simple triangle of forces relation,[†] the dihedral angle, θ , of phase 2 where it adjoins a boundary between two grains of phase 1. On a metallographic sample various angles are actually obtained because of the random orientation of the plane of observation, but the statistically most frequent angle is the true one. These basic principles were discussed in detail in the earlier paper.

The experiments described below show the effect of both composition and temperature on θ and Γ for some alloys containing a liquid phase, and provide data on the rate of approach to the equilibrium angles in both solid and liquid phases.

Experimental Procedure

All the alloys were melted in a graphite crucible and cast into ingots $\frac{3}{4}$ by $1\frac{1}{8}$ in. cross-section. Some of the aluminum alloys consisted of two immiscible liquids from which uniform castings could not be obtained. The amount of liquid phase varied locally to a considerable extent and the analyses were meaningless. Nevertheless, the composition of the liquid would not differ from that in an alloy of the intended gross composition, and

the synthetic composition of the alloys was therefore used in considering the surface energy results. The ingots were given initial deformation by cold-rolling to 50 pct reduction, annealed, and given a second 50 pct reduction prior to cutting into small samples for heat treatment at the times and temperatures subsequently reported. The resulting micro-samples were carefully prepared metallographically and examined at magnifications of 650, 1280, or 2500. The objectives used were 21X, 0.40 NA (dry); 41X, 0.65 NA (dry); and 80X, 1.40 NA (oil emulsion). The appropriate angles were measured by rotation of the stage of a Bausch and Lomb metallograph to align the appropriate boundaries successively with a cross-hair in a micrometer eyepiece. About 250 angles were measured on each phase. Though the angles were read to 1°, the accuracy is probably not above 3°, because of uncertainty in setting the cross-hair tangent to the sometimes curved boundary. The corners of very small particles, particularly in early stages of adjustment after cold-rolling, were difficult to measure and the results were slightly dependent on the magnification used (compare Fig 1-C and 1-D). With particles of larger size and more nearly equilibrium shape, magnification made no difference (*vide* Fig 1-F and 1-G). The measured angles were grouped in 10° intervals (5° if θ was less than 20°) and plotted in bar

Cleveland Meeting, October 1949.
TP 2691 E, Discussion of this paper (2 copies) may be sent to *Transactions AIME* before December 1, 1949. Discussion is tentatively scheduled for publication in May 1950. Manuscript received May 2, 1949; revision received July 11, 1949.

* Institute for the Study of Metals, Univ. of Chicago.

This research was done in part under contract with the Office of Naval Research.

¹ References are at the end of the paper.

$$\dagger \Gamma = \frac{\gamma_{12}}{\gamma_{11}} = \frac{1}{2 \cos \frac{\theta}{2}}. \text{ Note that } \theta$$

will be zero for $\Gamma = 0.5$ and all values below. True values for Γ can not be obtained by direct microscopic means

when $\frac{\gamma_{12}}{\gamma_{11}} < 0.5$.

graphs, of which Fig 1 is an example. The most probable angle was estimated and taken to be the true dihedral angle.

The frequency curves of even well-annealed alloys showed a greater spread of angle than that resulting from random sectioning alone, which indicates that the energies of all interphase boundaries are not identical, but vary slightly, supposedly as a result of differing orientation between the grains. Though this is of great interest and importance, it is a minor factor as far as general microscopic features are concerned and, for the present, is ignored.

Rate of Approach to Equilibrium

The distribution of dihedral angles for the liquid tin-rich phase in an aluminum-tin alloy with 5 pct tin, cold-rolled and subsequently annealed for various times at 350 and at 450°C, is shown in Fig 1 and 2. In all of these alloys, the structure consists of nearly pure aluminum grains with a tin-rich liquid dispersed as a continuous prism-like network along the edges of the three-dimensional grains. In the two-dimensional metallographic section, the tin-rich phase (solid, of course, after quenching) appears most frequently as triangles at the junction of three grains of aluminum. In the annealed samples, these triangles are essentially equilateral and equiangular, but cold-rolling distorts them considerably, resulting in a much wider spread of angles; annealing causes rapid restoration of the angles to the values determined by surface tension equilibrium. Fig 3 shows the same data as Fig 1 (that is, from the 350°C anneal) grouped according to the orientation of the apices in relation to the direction of rolling. In the rolled alloy most of the angles in the quadrants lying in the direction of rolling are smaller than the equilibrium value, while normal to this the particles have been flattened out and the angles increased. Annealing for 15 min. at 350°C gives a well-defined angle-distribution curve with a maximum at the equilibrium value, although the abnormally large spread of angles has not entirely disappeared. Annealing for 1 hr at 350°C gives liquid areas showing no anisotropy of angles, and further annealing causes no change. At 450°C (Fig 4) even the 15 min. anneal gives a structure that does not subse-

quently change, except for the size of the liquid particles.

In the solid state, restoration of distorted grain junctions to equilibrium configuration would be expected to occur at a slower rate than for a liquid phase and to be highly dependent on temperature. Tests were made on an alpha/beta bronze containing 16 pct tin at 650°C, a normal commercial annealing temperature. Annealing was done in a salt bath. Fig 5 to 8 show the microstructures obtained, while Fig 9 is a plot of the distribution of the corner angles of the beta grains after

various times of heat treatment. The grains of beta had been flattened out by rolling, and in the initial condition there is a large number of small angles in the quadrant parallel to rolling, while the normal quadrants contain larger angles than the equilibrium value. After annealing for 4 min., as can be seen from Fig 6, the alloy has completely recrystallized and the beta phase has developed apices, each one meeting a contiguous alpha boundary. The angles still show considerable spread from the equilibrium values and the strong curvature imposed on local

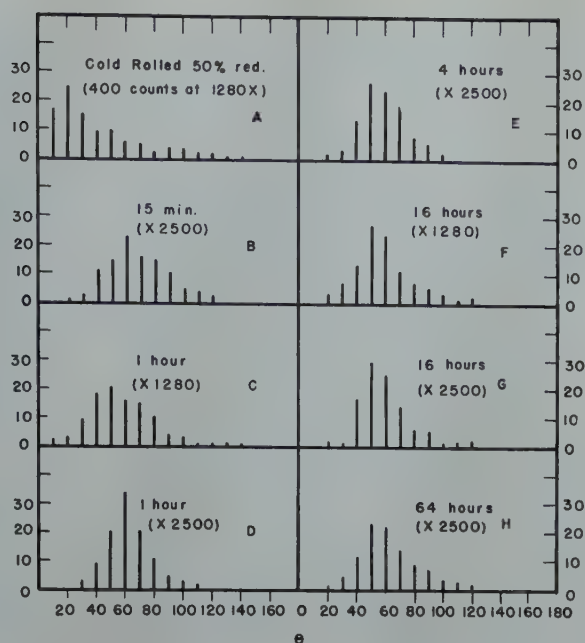


FIG 1—Distribution of measured angles in tin-rich liquid phase in longitudinal sections of 95-5 Al-Sn alloy, cold-rolled and annealed for varying times at 350°C.

250 angles measured for each sample, at 2500 X, except where otherwise noted.

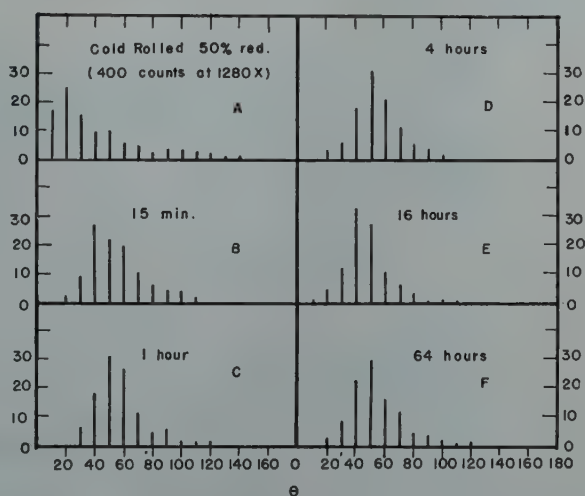


FIG 2—Distribution of measured angles of tin-rich phase in longitudinal sections of 95-5 Al-Sn alloy, cold-rolled and annealed for varying times at 450°C.

250 angles measured for each sample, at 2500 X, except where otherwise noted.

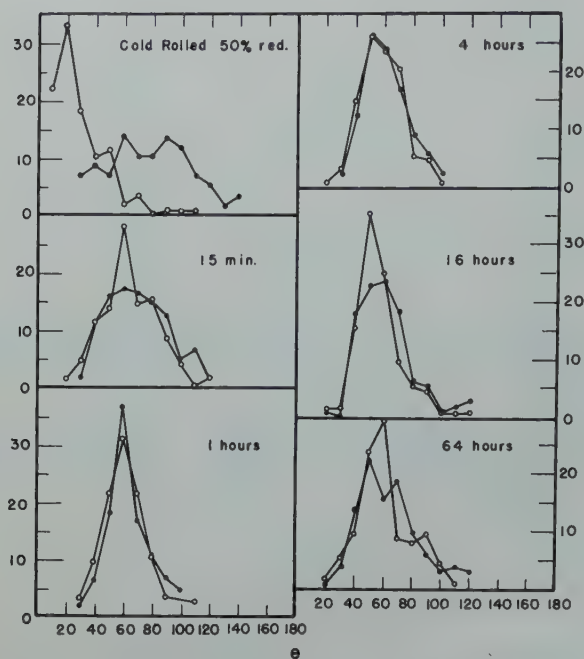


FIG 3—Same data as Fig 1, grouped in quadrants related to the rolling direction.

○ R = angles whose bisectors fall in quadrants 135–225° and 315–45° from rolling direction.
● N = angles whose bisectors fall in quadrants 45–135° and 225–315° from rolling direction.

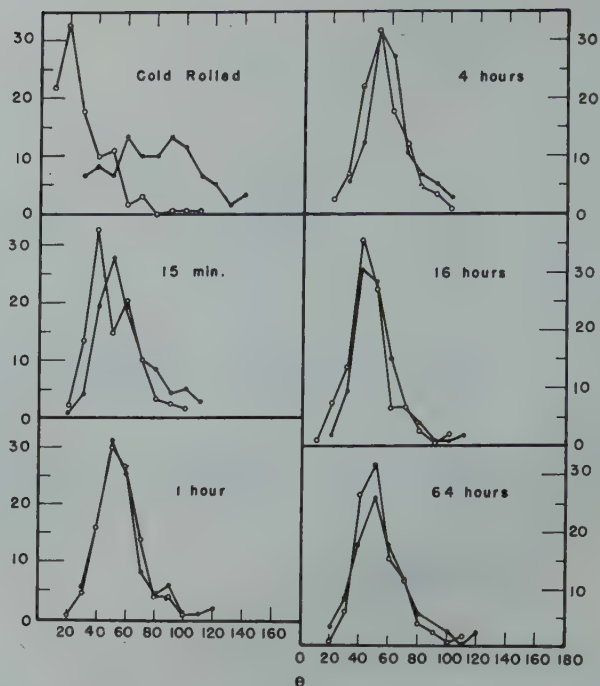


FIG 4—Same data as Fig 2, grouped in quadrants related to rolling direction.

See Fig 3 for definition of N and R quadrants.



FIG 5—Microstructure of α/β bronze (16 pct Sn) as cold-rolled 50 pct reduction following 650° anneal.

Etched with potassium dichromate, followed by ferric chloride. 250 \times .

FIG 6—Same alloy as Fig 5, annealed 4 min at 650°C.

500 \times .

FIG 7—Same alloy as Fig 5, annealed 1 hr at 650°C.

250 \times .

FIG 8—Same alloy as Fig 5, annealed 16 hr at 650°C.

250 \times . All micrographs reduced one-tenth in reproduction.

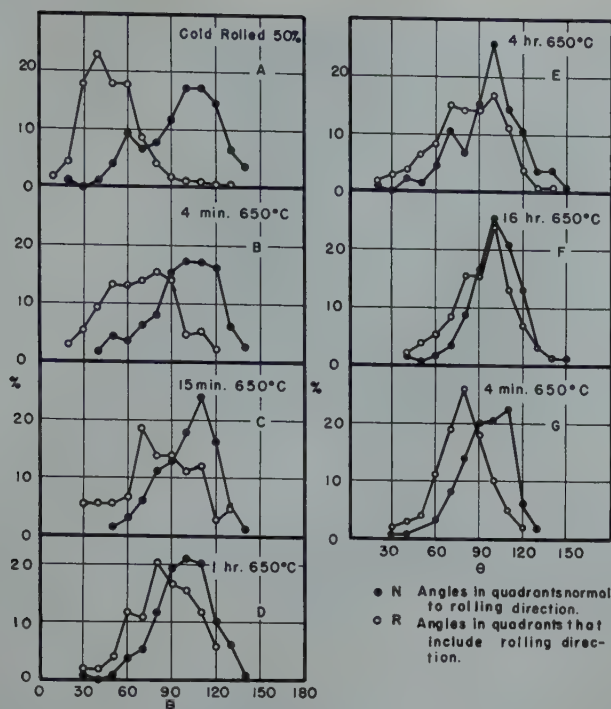


FIG 9—Distribution of angles in α/β bronze with 16 pct tin, grouped in quadrants related to the direction of rolling. 250 angles were measured in each specimen, at a magnification of 1200 \times , except Fig 9-G which was 2500 \times .

surfaces by the long-range geometry prevents equilibrium.* After 1 hr (Fig 9-D) the angles in the longitudinal and normal quadrants are nearly the same, and after 16 hr anneal at 650°C (Fig 9-F) the peaks of the two curves are almost identical, indicating that surface tension forces have entirely overcome the distortion imposed by cold-work.

*Equilibrium at a higher magnification (2500 \times) as in Fig 9-G gave a considerably sharper distribution, but still showed a definite difference between those angles near the rolling direction and normal to it. It is possible that on an atomic scale the equilibrium angle is achieved immediately after recrystallization. Samples that have been annealed for a sufficiently long time to allow the particles to acquire smooth, simply curved, outlines show no variation with magnification—provided, of course, that the metallographic preparation and optics are such as to give good resolution of the boundaries.

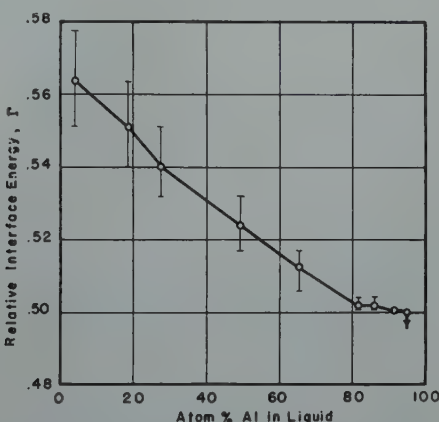


FIG 12—Relative interface energy, Γ , as a function of the composition of the liquid phase in Al-Sn alloys at various temperatures.

The answer to the question as to whether the mechanism of adjustment is by diffusion or by plastic deformation must await further study.

Effect of Temperature on the Dihedral Angle in a Binary Alloy Containing a Liquid Phase

Fig 10 shows the temperature dependence of the dihedral angle of the liquid phases in a copper-lead alloy with 1 pct lead and in an aluminum-tin alloy with 5 pct tin. Samples of these alloys were first cold-rolled and then annealed at different tempera-

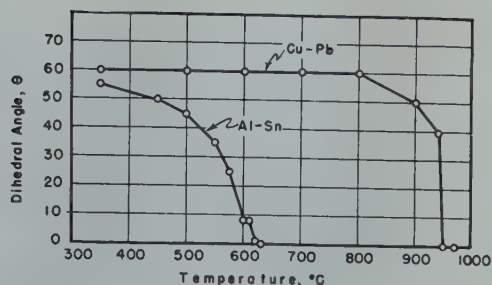


FIG 10—Temperature dependence of dihedral angles in Cu-Pb and Al-Sn alloys.

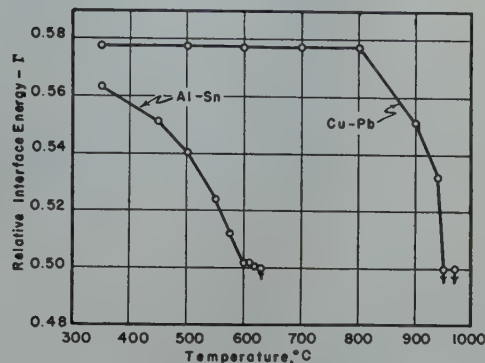
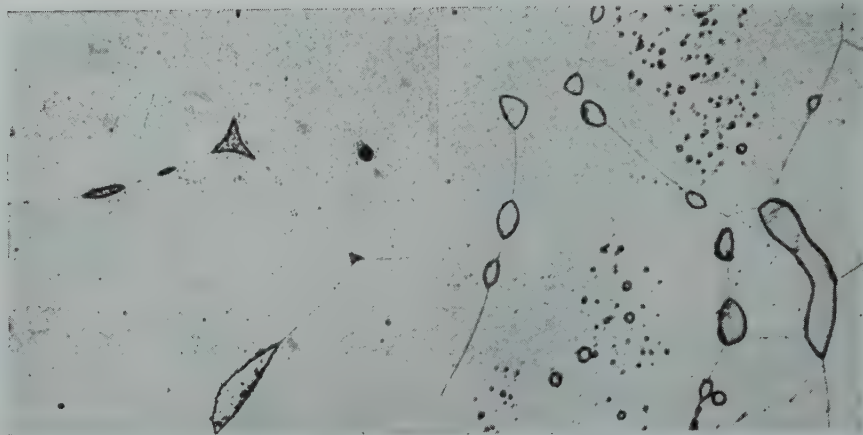


FIG 11—Effect of temperature on relative interface energy, Γ , for Cu-Pb and Al-Sn alloys.

tures for sufficient times to obtain equilibrium. Fig 11 shows values of Γ (the ratio of interphase and inter-grain boundary energies) calculated from the dihedral angles.

In the copper-lead system θ is unaffected by temperature up to 800°C, but decreases somewhat at 900 and 930°C and drops sharply to zero at 960°C. In the aluminum-tin alloy θ and Γ decrease with increasing temperature in a more uniform manner. The difference in behavior is easily explained if the constitution diagrams² are examined. In the copper-lead system, the composition of the liquid phase in equilibrium with solid copper changes

13



14

FIG 13 (left)—Microstructure of 94-3-3 Al-Cu-Sn alloy.

Cold-worked 50 pct reduction and annealed 6 hr at 550°C. Etched with 2 pct hydrofluoric acid followed by dilute Keller's etch. 250 \times . Reduced one-tenth in reproduction.

FIG 14 (right)—Microstructure of 95-5 Al-Cd alloy.

Cold-worked 50 pct reduction, annealed 6 hr at 550°C. Etched with 2 pct hydrofluoric acid, followed by dilute Keller's etch. 500 \times . Reduced one-tenth in reproduction.

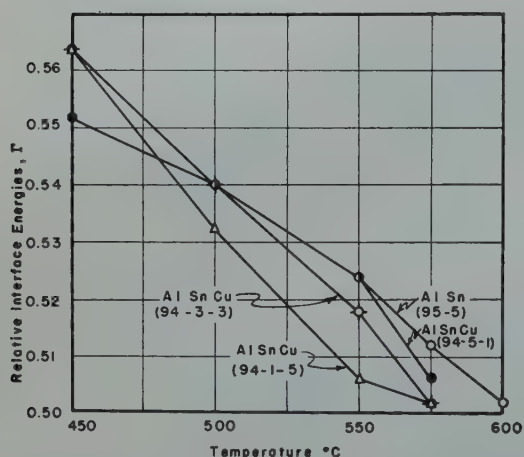


FIG 15—Relative interface energy, Γ , in Al-Sn-Cu alloys as a function of temperature.

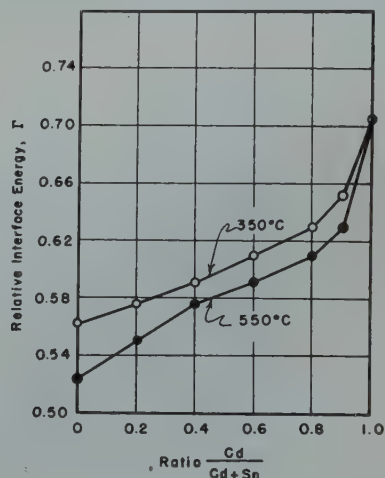


FIG 17—Relative interface energies as a function of composition in Al-Sn-Cd alloys at 350 and 550°C. (Al constant at 95 pct.)

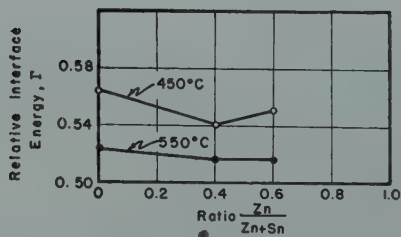


FIG 16—Relative interface energies as a function of composition in Al-Sn-Zn alloys at 450 and 550°C. (Al constant at 95 pct.)

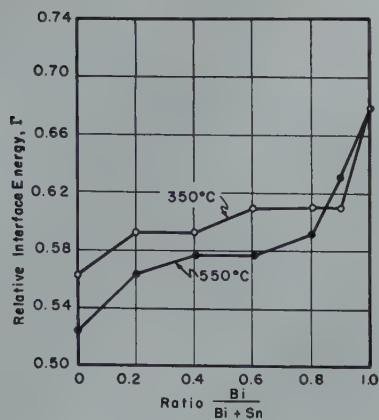


FIG 18—Relative interface energies as a function of composition in Al-Sn-Bi alloys at 350 and 550°C. (Al constant at 95 pct.)

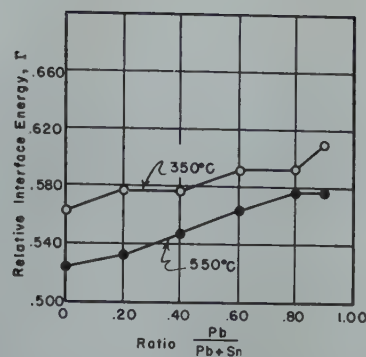


FIG 19—Relative interface energies as a function of composition in Al-Sn-Pb alloys at 350 and 550°C. (Al constant at 95 pct.)

only from 0.5 to 1.0 pct copper as the temperature rises from 500 to 800°C, and then changes with increasing rapidity to about 7.5 pct copper at the monotectic temperature, 953°C, whereupon it abruptly changes to about 60 pct copper. In the aluminum-tin system the liquid changes continuously and with increasing rapidity from 0.5 to 100 pct aluminum as the temperature is raised from that of the eutectic (229°C) to the melting point of aluminum (660°C). It seems obvious that the major effect of temperature in both alloys is to change the composition of the liquid. Although it would be expected that both γ_{allq} and $\gamma_{\alpha/\alpha}$ would decrease with temperature, though perhaps at different rates, it seems reasonable to attribute most of the change in θ and Γ to the solid/liquid interface rather than to the grain boundary.

If, as in Fig 12, the values of Γ for the aluminum-tin alloys are plotted as a function of the composition of the liquid phase, as read from the liquidus of the constitution diagram,² Γ is seen to be a smooth function of composition,* decreasing as the liquid approaches the solid in composition. This is not unexpected.

It has often been supposed that the presence of a liquid phase results in hot-shortness of an alloy. Though extreme brittleness at high temperatures is almost invariably associated with the presence of a liquid, the converse is not necessarily so, for drops of liquid with

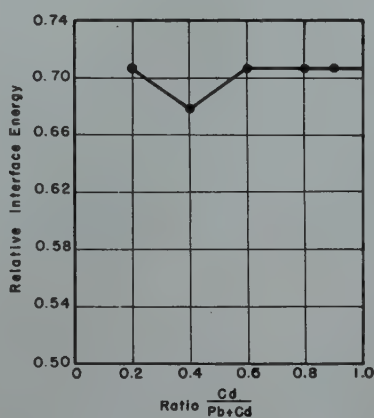


FIG 20—Relative interface energies as a function of composition in Al-Pb-Cd alloys at 350 and 550°C. (Al constant at 95 pct.)

large dihedral angles are relatively harmless. An alloy will become hot-short immediately above the solidus only if the dihedral angle is nearly zero, causing the liquid to replace a large fraction of the normal grain boundary area and to give rise to sharp notches for stress concentration. The method of determining solidus temperatures by detecting the onset of hot-shortness is an excellent one when θ is zero, but is dangerous to use on alloys where this is not known to be the case.

Interface Energies in Ternary Alloys Containing Liquid

It has been shown above that the composition change resulting from variation of solubility with temperature affects the interface energy ratio in a binary two-phase alloy. The change of

composition caused by the addition of a third element at a fixed temperature can have a similar influence. The effect of zinc and bismuth added to copper-lead alloys was discussed in an earlier paper.¹ More complete data were obtained with series of ternary alloys of aluminum containing tin and either copper, bismuth, lead, zinc, or cadmium. Except for the copper series, which contained 94 pct aluminum, the alloys investigated contained 95 pct aluminum with the remaining 5 pct divided between tin and the other element in varying proportions. Typical microstructures are shown in Fig 13 and 14.

The alloys containing copper were measured after annealing at several temperatures to show the effect both of temperature and composition (see Fig 15). The other alloys were annealed at 350 and 550°C only (for 16 and for 6 hr respectively) and gave the values of θ and Γ shown in Fig 16 to 20.

Copper and zinc (Fig 15 and 16) are soluble in both the solid and liquid phases in aluminum-tin alloys and they act slightly in the direction of decreasing the value of Γ —whether by modification of the grain boundary energy or of the liquid/solid interface cannot be said. The other elements—cadmium, lead, and bismuth—are virtually insoluble in solid aluminum, and dissolve little aluminum themselves when molten. In their ternary alloys with aluminum and tin it is therefore possible to study the equilibrium angles between an aluminum grain boundary (which, to a first approximation, may be assumed not to change in nature or

* The vertical lines drawn through the experimental points in Fig 10 represent the range of Γ corresponding to an error of 5° in measuring θ . It is obvious that the smoothness of the curve is to some extent fortuitous.

composition), and the interface between aluminum crystals and liquid that is of varying composition. The data in Fig 17 to 19 show that the energies of the interface between solid aluminum and liquid cadmium, lead,* or bismuth in the binary alloys are all higher than that of the aluminum-tin interface, but that the interface energy is decreased rapidly by the first addition of tin and more slowly as the liquid becomes richer in tin. This parallels closely the variation of surface tension with composition in binary liquid alloys and doubtless arises from a similar cause—the preferential adsorption of the element giving lower interface energy at the interface.†

Summary

Studies have been made of the angles

* The liquid phase in the pure binary alloys of aluminum and lead did not aggregate to a sufficient size to permit θ to be measured, even after annealing for 6 days at 550°C. The alloys with minor additions of cadmium or tin behaved satisfactorily.

† The behavior of the copper-bismuth-lead alloys described in Ref. 1 is not in accord with this, for the Γ curve is convex with increasing bismuth content.

‡ In the ternary Al-Pb-Cd case, there is no variation of Γ with composition (Fig 20).

existing at the corners of various microconstituents in alloys after deformation and heat treatment. Liquid phases take relatively short times to reach the angles determined by surface energy equilibrium. Solid phases are slower to adjust, but commercial annealing practice for a bronze gives dihedral angles that are not appreciably changed by longer annealing.

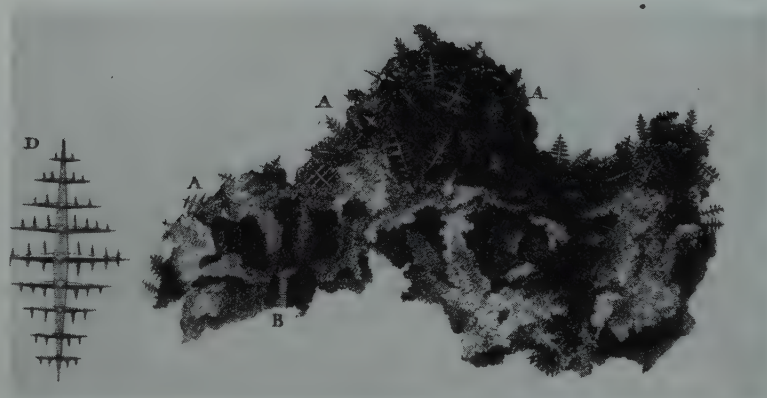
The effect of temperature on the dihedral angle and the relative energies of grain boundary and interphase boundary in copper-lead and aluminum-tin alloys is slight except when the change of temperature produces a change in the composition of the phases in equilibrium. In general, it is predicted that alloys whose constitution diagrams show a nearly vertical liquidus will be substantially unaffected by temperature change, and that alloys with a sloping liquidus will present structures that vary considerably with annealing temperature. The dihedral angle decreases as the composition of the liquid approaches that of the solid. Alloys become hot-short when heated above the solidus *only* if the liquid phase has a small dihedral angle and so replaces a large part of the

grain boundary area.

Dihedral angles were measured for a series of ternary alloys of aluminum with tin and other low melting-point elements. If the third element is soluble in both solid and liquid phases the dihedral angle may be decreased (aluminum-tin-copper, aluminum-tin-zinc) but otherwise the ternary alloys possess relative interface energies intermediate between that of aluminum-tin and that of the binary alloy of aluminum with the other component. The first addition to a binary alloy of a third element that itself has a lower interface tension against solid aluminum will cause rapid reduction of interface tension, while further additions are less potent, paralleling the behavior of surface tension in liquid binary alloys.

References

1. C. S. Smith: Grains, Phases, and Interfaces: An Interpretation of Microstructure. *Trans. AIME* (1948) 175, 15-51. *Metals Tech.* June, 1948 TP 2387.
2. M. Hansen: Der Aufbau der Zweistofflegierungen. (Berlin, Springer, 1936).



DENDRITES IN CAST BRASS.

Grignon, 1775. (Courtesy of C. S. Smith)

Preparation and Casting of Beryllium Melts*

J. G. KURA,[†] J. H. JACKSON,[‡] Member, M. C. UDY,[§] Member, and L. W. EASTWOOD,[‡] Member AIME

Introduction

The melting and casting of any commercial metal depends upon the success with which the problems attendant to the handling of the specific metal are overcome. Common difficulties encountered in the handling of commercial metals are tendencies to burn or oxidize excessively, low fluidity, entrapment of dross, hot cracking, cold embrittlement, cold shuts, and unsoundness caused by gas evolution. Beryllium is not only subject to these same difficulties but is generally more sensitive to them than are the more common metals, thus necessitating more exact founding precautions.

Characteristics of Beryllium

Certain characteristics of beryllium which make it particularly difficult to handle in the plant or laboratory are as follows:

1. The melting point of beryllium is about 2400°F and pouring temperatures vary from 2600 to 2900°F, depending upon the degree of fluidity required. The extreme chemical activity, combined with the high temperatures, makes necessary the use of inert atmospheres, slags, or vacuum for protection during melting and pouring. Furthermore, beryllium tends to react with the melting crucibles, tools, and molds, thus requiring the selection of suitable materials and proper maintenance of these items.

2. The very marked absorption of gas by molten beryllium and the subsequent evolution of gas during solidification causes a great deal of difficulty with unsoundness. Beryllium castings may also be subject to unsoundness as

a result of gas formation by chemical reaction with the mold surface during solidification.

3. The very marked chemical affinity between molten beryllium and the normal atmosphere causes the formation of dross. On relatively quiescent melts, this dross forms a very tenacious film which, if carried over to the mold, can cause defects such as the formation of skins or dross in the interior or on the surface of the casting; folds or defects similar to cold shuts may also be found.

4. During the pour and attendant turbulence, the dross may be mixed into the metal and then carried to the casting. There it may be entrapped during freezing and cause internal defects, or it may float to the surface and cause severe dross defects on the cope side of the castings.

5. Solid beryllium is very weak at a temperature near the solidus line; brittleness is also a problem at lower temperatures. Thus, hot and cold cracking must be guarded against.

Scope of the Experimental Work

All of these problems have been given consideration in the work at

Battelle. Before the work was started at Battelle, it was customary to melt beryllium in a vacuum furnace or under flux in graphite-lined induction furnaces.

Because of the difficulty of preventing gas unsoundness in beryllium castings, an investigation was undertaken primarily to study this particular problem and, secondarily, to devise methods of overcoming the other difficulties encountered in the founding of beryllium. The objectives of the laboratory work were multifold: 1. To devise a practical method of melting, other than vacuum melting, by means of which consistently sound beryllium castings could be produced. 2. To obtain fundamental data which would promote a better understanding of the causes of gas unsoundness in beryllium. 3. To develop a casting technique which would permit low melt temperatures, minimize dross defects and hot cracking, and eliminate reaction with the mold surface.

Up to the present time, a considerable amount of progress has been made on the first and third objectives, with the result that it can now be safely stated that consistently sound castings can be made by the open-pot melting method, using argon as a protective atmosphere and a proper casting technique. There has been some progress on the second objective of the project, but it cannot yet be safely stated that the problem is completely understood.

Most of the experimental work has been conducted in an enclosed melting and pouring apparatus in which very close control of melting variables has been effected. Findings based on the results of the work conducted in this small experimental apparatus have been applied to large-scale melts which have been made by techniques suitable for duplication on a commercial scale.

Cleveland Meeting, October 1949.

TP 2701 E. Discussion of this paper (2 copies) may be sent to *Transactions AIME* before Dec. 1, 1949. Discussion is tentatively scheduled for publication in May, 1950.

Manuscript received April 28, 1949; revision received July 25, 1949.

* The experimental work described in this paper was sponsored by the Atomic Energy Commission, under Contract W-7405-eng-92 and was issued as AEC D2479.

[†] Assistant Supervisor, Battelle Memorial Institute, Columbus, Ohio.

[‡] Supervisor, Battelle Memorial Institute, Columbus, Ohio.

[§] Research Engineer, Battelle Memorial Institute, Columbus, Ohio.

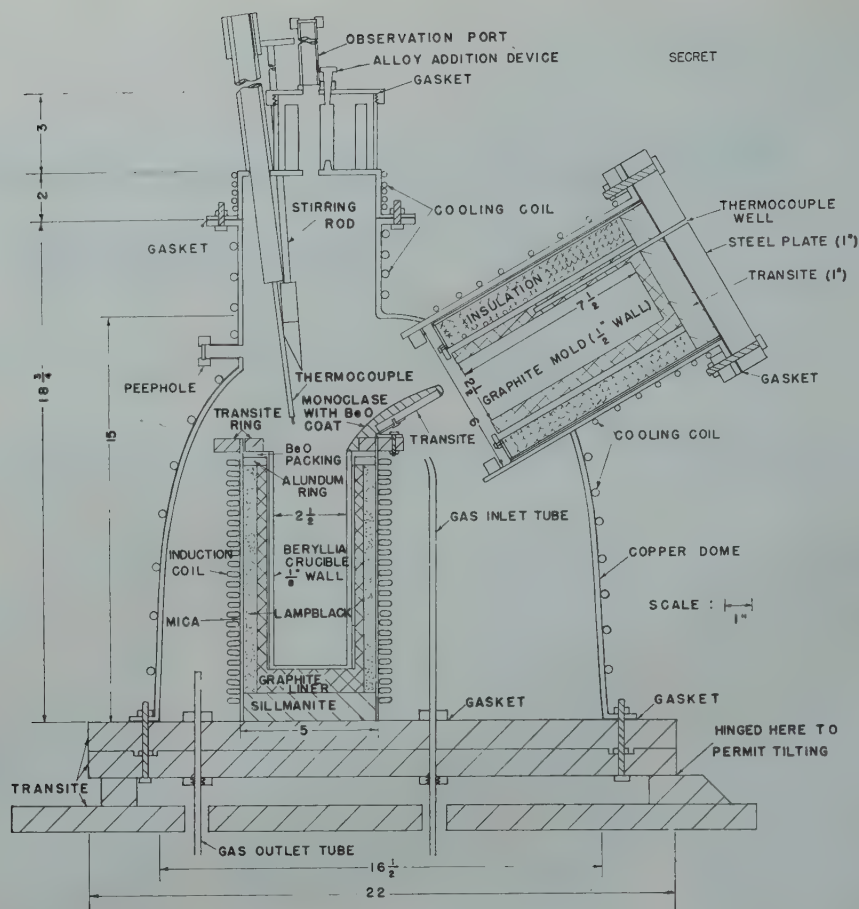


FIG 1—Sectional view of gas atmosphere induction furnace.

The Controlled-atmosphere Furnace

The experimental apparatus for melting and pouring under controlled conditions has been termed the small or controlled gas-atmosphere induction-melting furnace. A sectional view of this furnace is shown in Fig 1. The sketch shows the induction furnace lined with a beryllia crucible and equipped with a graphite mold. Other crucible and mold materials have been investigated in this apparatus, but those mentioned have been selected as the best for the work conducted to date.

As shown in Fig 1, the apparatus consists of a copper dome which fits over the induction furnace. The mold is integral with the dome. This arrangement permits the control of the composition of the ambient atmosphere used during melting and pouring. After putting the dome in place, the charge is melted in the furnace and then cast into the mold by revolving the entire assembly about the axis shown in the lower righthand corner of the drawing. Upon revolving the assembly, the

melt pours over the lip of the crucible and into the mold according to the Durville pouring method. This method of pouring is very desirable for easily oxidized or drossy metals because it permits the metal to be poured with a minimum of disturbance of the oxide film and thus prevents the inclusion of dross in the castings. The furnace assembly with the dome installed and in the melting position is shown by Fig 2.

The argon gas used as an atmosphere during melting and pouring is purified and dried, if a low humidity is desired, before it enters the dome. The rate of flow of the gas is closely controlled, its temperature inside the dome measured, and the humidity of the gas that leaves the dome determined. The temperature of the metal throughout the melting cycle is closely controlled, and the temperature of the graphite mold is also closely regulated. The dome is equipped with (1) a cooling coil through which various cooling liquids can be circulated, (2) peepholes for viewing the crucible and mold, and (3) a poking rod and an alloy addition device which permits these operations without open-

ing the dome.

Melting and Casting Large or Small Beryllium Heats

FURNACES AND FURNACE LININGS

The induction furnace is most suitable for the melting of beryllium. Graphite linings for the induction furnace have been used but are not very practical since, at a temperature of about 75° above the melting point of beryllium, the reaction $\text{Be} + \text{C} \rightarrow \text{Be}_2\text{C}$ takes place. Since the reaction is exothermic, the utility of a graphite crucible is limited by the necessity of an accurate control of the temperature of the melt.

Magnesia linings for induction furnaces, employed in melting beryllium, have been used in the past with some measure of success. The use of magnesia was abandoned when it was found that the fluxes used in melting beryllium attacked this refractory. Since fluxes are no longer necessary in the melting of beryllium, it may be possible to return to the magnesia lining. This possi-

bility should be investigated.

Large-scale melts have been made most successfully in induction furnaces lined with a graphite-bonded silicon carbide known commercially as Tercod. They are conveniently backed with lampblack for high thermal insulation. Tercod crucibles are available in a variety of sizes and shapes. In the experimental work, they have been used in the melting of heats ranging from about 3 lb up to about 85 lb.

Although Tercod crucibles have been successfully set in the large induction furnace with a silica sand backing, best results have been obtained using a lampblack (Norblack) backing. This material is rammed tightly around the crucible, the coils being protected with a layer of ramming mix next to the coil and a layer of asbestos paper between the ramming mix and the Norblack. With the 80-lb melts, melting time has been cut from $2\frac{1}{2}$ to $1\frac{1}{2}$ hr by the use of the insulating lampblack backing.

The Tercod crucible is ordinarily supplied with a borosilicate glaze. Tercod crucibles, having an aluminosilicate glaze on the outside and little or no glaze on the inside, are said to be available. Up to the present time, the glaze has been removed by melting a cryolite wash in the crucible. The cryolite is then removed by melting a wash heat of beryllium in the crucible. The wash heat may include scrap beryllium such as turnings, sawings, and others. Often, metal containing dross skimmed from previous heats is added to the wash heat which then forms a protective film of beryllium oxide on the inside of the Tercod crucible. Without this protective layer, the Tercod may be attacked by the beryllium.

The Tercod crucible does not appear to be suitable for use in the small gas-atmosphere induction furnace, because under such conditions of melting, the oxide film on the Tercod is not maintained and the melt reacts with the crucible. The use of cryolite for the removal of the glaze is undesirable from a health standpoint because, on subsequently using the crucible for melting beryllium, copious fumes of beryllium fluoride are formed as a result of the reaction between beryllium and the residual cryolite (Na_3AlF_6). It is possible that some means other than that which is used at the present time can be devised for the removal of the glaze and the attainment of a beryllia coating on the Tercod.

The development of beryllia crucibles for use in the small gas-atmosphere induction furnace (Fig 1) has been a

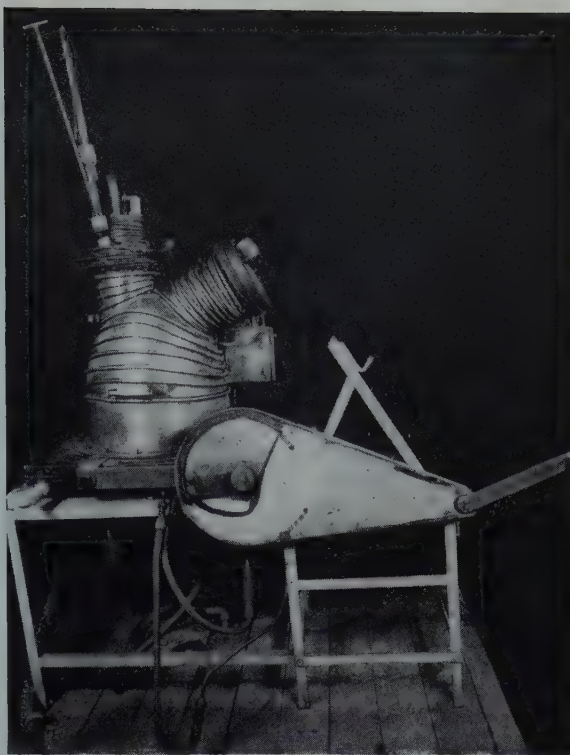


FIG 2—Photograph showing the small controlled-atmosphere induction furnace used to make melts of 1 to 2 lb each.

step of great importance in the experimental procedure. After a considerable number of trials of various materials, it was found that a beryllia crucible was satisfactory if it was fired by slow heating to 3300°F , and then held at this temperature for 4 hr before slowly cooling to room temperature. Without such treatment, the crucibles fail after each heat because they are subject to

considerable dimensional change during the heating and cooling cycle. After firing at 3300°F , the dimensional stability is very satisfactory and crucibles invariably last for 15 to 20 heats and fail through the formation of a skull of beryllium oxide on the inside of the crucible and not through cracking.

The spout of the experimental furnace is lined in such a way that during



FIG 3—Photograph of the large induction furnace with a graphite mold and tilting mechanism for making the cast 2-in.-round remelting ingots for the furnace illustrated by Fig 1 and 2.

the pour the metal contacts only the beryllia refractory.

New beryllia crucibles, even after preheating at 3300°F, are generally unsatisfactory for the melting of beryllium because the first melt made in a new crucible or in a furnace which has not been used for a considerable length of time is often very "gassy." In such instances, the use of a wash heat of beryllium for conditioning the crucible is recommended if sound castings are to be consistently obtained.

One disadvantage of the induction furnace for melting beryllium is that dross is often inductively stirred into the melt and results in dirty castings. When a Tercod crucible is used for the lining, the conductive crucible shields the melt from much of the electromagnetic field which would induce too violent agitation. A further advantage of the Tercod crucible is that it can be heated to a high temperature before the beryllium charge is added to it, thus permitting rapid melting if desired.

The stirring which occurs in the melt prepared in the controlled gas-atmosphere induction furnace (Fig 1) containing a beryllia crucible is of less importance because the use of the inert atmosphere eliminates the dross to a great extent. Furthermore, as shown in Fig 1, the beryllium melt is shielded to some extent from the inductive field by means of a graphite backer for the beryllia crucible.

Although induction heating has been used exclusively in the experimental melting of beryllium, it is conceivable that some other form of heating, such as electrical resistance heating, might be satisfactory. It is unlikely that gas-fired furnaces, unless mixtures other than city gas and compressed air were used, would be suitable because of the high-flame temperatures necessary for the melting operation and the gas absorption from the products of combustion. Arc melting probably would not be desirable because of the possible contamination of the melt by the electrodes.

SELECTION AND PREPARATION OF MELTING STOCK

Beryllium metal stock available for melting in the experimental work has ranged in purity from about 89 pct beryllium up to about 97 pct beryllium. The balance of this material has been, for the most part, fluoride flux remaining in the material from the refining operation. Very often it has also contained about 0.2 pct aluminum and up

to 1 pct magnesium. Melting this material by the open-pot method markedly reduces the content of fluoride and magnesium.

In order to prepare 1- to 2-lb charges for the experimental melts, the as-received beryllium is melted in large-scale heats weighing about 85 lb and is cast into 2-in.-diam bars. This melting is conducted in an open pot, using a Tercod-lined induction furnace with a stream of argon directed against the melt surface. The melt is poured in air into graphite molds, 4 bars per mold, using the Durville principle of pouring. Fig 3 shows the mold and apparatus used to prepare the 2-in. bars, the furnace being in a tilted position. The 2-in.-diam bars are cut to lengths weighing about 1.3 lb each. Such a bar makes an ideal material for melting stock in the experimental work because of its uniformity from piece to piece and its uniform surface area. Furthermore, during melting, the solid piece melts down uniformly with no opportunity for bridging which often occurs when lump materials are melted in the small, experimental induction furnace.

It is desirable that the beryllium melting stock, for large or small heats, be as clean as possible and dross should be removed by grinding the surface. The chances of obtaining an unsound

heat are greatly minimized by drying the stock thoroughly before melting it. This drying operation can be effectively carried out by holding the material at a temperature of 500 to 800°F for about 12 hr before melting. Naturally, the chance for gas absorption from the surface of the beryllium melting stock is minimized by using pieces as large as practicable.

MELTING TECHNIQUES

Because of the severe chemical reactivity of beryllium, it must be protected from reaction with oxygen and nitrogen during melting. Melting beryllium under a fluoride flux prevents drossing and, in a number of instances, successful castings have been poured by this method. On the other hand, the flux melting method is difficult to use because, during this type of melting, copious fumes evolve from the flux and these fluoride fumes are very toxic. A second disadvantage of this melting method is that the flux is very hygroscopic and, unless it is melted separately and added to the molten beryllium metal, a large quantity of hydrogen may be absorbed from the moisture in the flux. The flux is denser than the molten beryllium and, while it crusts over and is thus mechanically held on



FIG 4—Photograph showing a series of beryllium castings having a considerable range in unsoundness, made in the gas-controlled-atmosphere induction furnace.

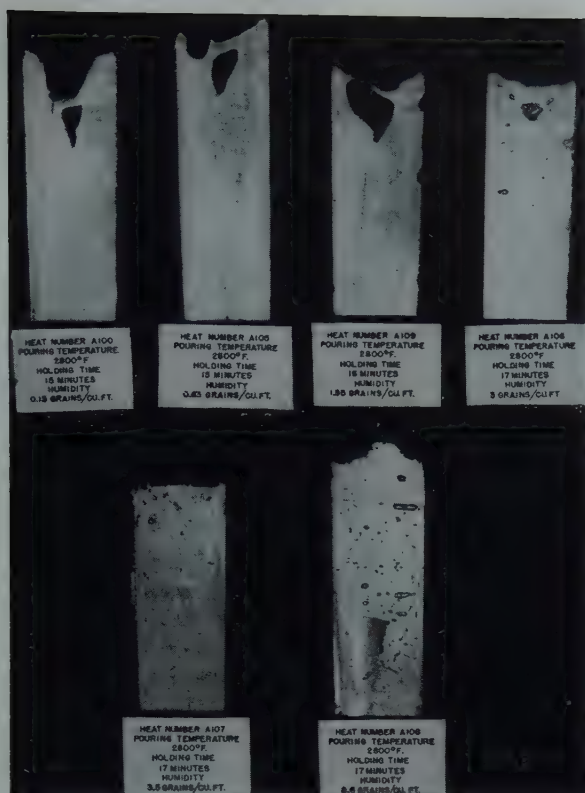


FIG 5—Series of ingots showing the relationship of gas unsoundness to the humidity of the ambient atmosphere.

top of the melt, portions of the flux invariably sink and become entrapped in the metal during the pouring operation. This entrapment of flux occasionally results in flux inclusions in the castings.

Melting under a hydrogen atmosphere has been reported in accounts on the German beryllium industry. This method has not been tried, but melting under an inert atmosphere appears to be, by far, the most practical method for melting beryllium. Inert atmospheres of the argon or helium type are satisfactory. Argon has the advantage that, being denser than air, it forms a better blanket over the surface of the melt than helium which is lighter than air and has a greater tendency to rise. Attempts have been made to use dry nitrogen, but large quantities of beryllium nitride are formed which make this gas undesirable.

Investigations of the gas unsoundness in beryllium castings poured from melts prepared in the small, experimental gas-atmosphere induction furnace have shown that a high degree of purity and of dryness of the protective gas is necessary if sound castings are to be produced. In order to produce argon of high purity for the melting unit, the gas is passed first through copper

turnings at 1200°F to remove the bulk of the oxygen present, then through a copper coil which can be refrigerated to a temperature of minus 100°F to remove most of the moisture and, finally, through titanium turnings at 1200°F to remove nitrogen and the last traces of oxygen and water vapor.

Fig 4 illustrates the range of unsoundness which can be obtained in beryllium. Microporosity, such as occurs in copper-base alloys, was not a contributing factor to the unsoundness.

The effect of the moisture content in the argon atmosphere on the soundness of beryllium castings made in the small-scale experimental furnace is shown by Fig 5. For this particular series, it is believed that the other variables were held at values which, excepting for the humidity of the ambient atmosphere, are conducive to a high degree of soundness. The transition from sound to unsound beryllium castings appears to have occurred at a moisture level of about 3 grains per cubic foot. Other series made under similar conditions have indicated that the transition level is considerably lower. In one instance, it appeared to be at about 1.0 grain per cubic foot.

In general, the longer the time that a melt of beryllium is held in the molten

state, the more unsound the resultant ingot will be. The effect of increasing the holding time of beryllium melts at the pouring temperature in the gas-atmosphere induction furnace from 4 to 30 min. before pouring is shown in Fig 6. The humidity of the ambient argon atmosphere used for the heats from which these two ingots were poured was less than 1 grain of moisture per cubic foot. The graphite mold was held at a temperature of 300°F and a pouring temperature of 2800°F was employed. This increase in gas unsoundness produced by a prolonged holding at the pouring temperature is typical of some other metals also.

The effect of the length of the holding period at pouring temperature on gas unsoundness should not be confused with the length of time required to melt the metal. The effect of the speed with which the metal is melted and then brought to the pouring temperature has not yet been investigated. Since the rapid melting of beryllium may tend to increase gas unsoundness, it should be emphasized that Fig 6 shows the effect of holding at the pouring temperature. In other words, it is known that, once the metal has reached the pouring temperature, it should be poured without further holding. It does not necessarily follow, however, that the metal should be melted as rapidly as possible. Indeed there is some evidence that slow melting is desirable.

The typical effects of the pouring temperature on the gas unsoundness of beryllium castings are shown in Fig 7. All of these ingots were poured in a graphite mold at 300°F. The heats were made in an argon atmosphere at less than 1 grain of moisture per cubic foot. The tendency to increase gas unsoundness as the casting temperature increases is typical of most metals.

Fig 8 shows a typical example of the occurrence of unsoundness in a casting made from the first melt in a beryllia crucible preheated to 3300°F before using.

MELTING POINT DETERMINATION

The melting point of beryllium, as reported in *Metals Handbook*, is 1285 $\pm 40^\circ\text{C}$ (2345 $\pm 70^\circ\text{F}$). In the course of the melting of beryllium in the controlled-atmosphere furnace, one melt was allowed to freeze in the crucible and the cooling rate determined by a calibrated platinum, platinum-rhodium thermocouple protected by a beryllium oxide tube. The resultant curve, which is shown in Fig 9, shows a



FIG 6—The effect of holding time on the occurrence of gas unsoundness in beryllium.

Pouring temperature 2800°F, mold temperature 300°F.
 A-77. Melt poured as soon as the pouring temperature was reached.
 A-78. Melt held 30 min. at the pouring temperature before pouring.

melting point of 2400°F after some supercooling. This value is near the high limit previously reported. A melt-

ing point taken as the maximum temperature after supercooling can be considered only a minimum possibility

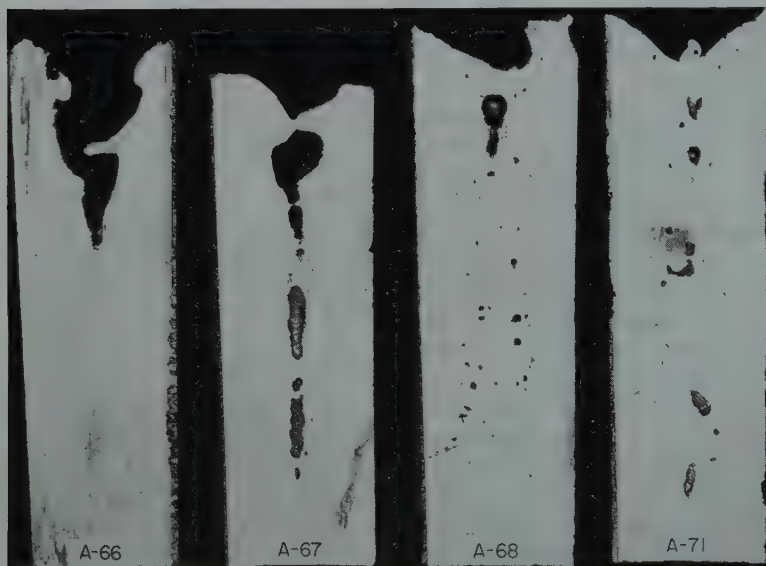


FIG 7—The effect of pouring temperature on the occurrence of gas unsoundness in beryllium.

A-66, held 16 min., poured at 2700°F, mold temp. 300°F. A-67, held 16 min., poured at 2800°F, mold temp. 300°F. A-68, held 12 min., poured at 2900°F, mold temp. 300°F. A-71, held 18 min., poured at 3000°F, mold temp. 300°F.

since it cannot be assured that the maximum temperature after supercooling is anything more than a balance between the heat released on freezing and the heat loss by natural cooling. Thus a value of 2400 + 20–10°F seems to be the melting point as determined in this test. The metal was remelted virgin beryllium. By spectrographic analysis it contained 0.10 pct Al, 0.08 pct Si, 0.10 pct Fe, < 0.05 pct Mg, and only traces of other impurities. Carbon was low, as judged by metallographic examination, but no estimate of oxygen content is available.

CASTING PRACTICE

Beryllium static castings can be produced with a minimum of difficulty from gas unsoundness and oxide and dross inclusions if they are poured directly from the furnace using the Durville method, as illustrated by Fig 1, 3, and 10. Ladling of the metal is obviously undesirable because it increases the contact of the metal with the atmosphere, makes higher melt temperatures necessary, and also increases turbulence and attendant included dross. Furthermore, ladles are often a source of gas pickup through unsatisfactory drying. In order to reduce the formation of dross, it is desirable that the molten metal be introduced into the mold with a minimum of turbulence. This can be accomplished by permitting it to run down a slight incline into the mold cavity. Although a mold can be tilted by hand to accomplish this end, the best practice is to design the mold for attachment directly to the furnace so that it tilts or can be separately tilted as the furnace is tilted. Fig 3 and 10 illustrate this technique showing the mold and method of pouring 2-in.-diam ingots and a slab about 2 in. thick and 18 in. square. The ingot mold is tilted by hand, using the special tilting mechanism, thereby permitting several to be poured from the same melt, whereas the slab mold is attached to the furnace and tilts with it, thereby permitting the pouring of one casting per melt. The metal is poured so that it runs down the slightly sloping surface of the riser and, as the furnace is tipped over, the mold is filled without causing undue turbulence. In both instances, the melt is poured direct from the furnace into the inclined mold. The end bells of the ball mill, shown by Fig 11, also illustrate castings made by this method. The end plates are sound, the dark spots being the individual coarse grain

revealed by the machining operation.

Centrifugal casting is an ideal method for producing beryllium castings when the size and shape of the casting are suitable. In order to pour a large-diameter casting, ladling metal is often necessary, though direct pouring should always be used if possible. The nature of the centrifugal casting process is such that it tends to reduce or minimize the difficulties with dross formation and gas unsoundness. A rapid pour into the mold is desirable to prevent cold shuts and to minimize the distance of travel of the metal. In the large-diameter castings, it is also desirable to pour the metal into the mold as near as possible to the periphery.

In order to cast an inside vertical wall centrifugally, it is necessary to use a rotating speed that gives a value of centrifugal force at the inside wall of the casting of at least 75 times the force of gravity. Thus the minimum speed of rotation is fixed and is dependent upon the casting diameter. Most of the centrifugal castings have been cast at this speed because it was feared that too high a speed might promote cracking. However, speeds somewhat higher than the minimum showed no harmful effects.

Some of the castings made successfully by centrifugal methods are as follows:

1. A cylinder 2¼-in. od, ¾-in. wall, 30 in. long, cast horizontally.
2. A ring 19-in. od, 1-in. wall, 5 in. high, cast vertically.
3. A ring 19-in. od, 7½-in. wall, 5 in. high, cast vertically, using a water-cooled steel mold. This casting after cutting and some machining of the inside surface is shown by Fig 12. The shrinkage on the inside periphery is to be noted.
4. A ring 52-in. od, 2-in. wall, 4 in. high, cast vertically. Fig 13 shows this casting as stripped from the mold.
5. A ball mill 9-in. od, 1½-in. wall, 8 in. long, cast vertically. This casting is illustrated by Fig 11.

A sound, fine-grained molded graphite makes an ideal mold material. It can be used successfully both in static and centrifugal casting. Although successful castings have been made in steel molds coated with acetylene soot, beryllia, or alumina, there is a tendency for beryllium metal to cut steel and, in general, the use of this material is not recommended. Baked, oil-bonded magnesite and zircon-base molds have been used, but the effects of these materials on gas unsoundness are not completely



FIG 8—The effect of the use of melting crucible on the occurrence of gas unsoundness in beryllium.

Both castings poured at 2800°F, using a mold temperature of 300°F. A-76, first heat in the crucible, namely, a wash heat. A-77, second heat in the crucible.

understood and they should be used with caution.

The extreme tendency for beryllium to hot crack must be guarded against when designing the casting. To accomplish this, the molds must be designed in such a way that the casting is not restricted during its solidification or cooling period. The development of a collapsible mold material for this metal

would be very desirable. Meanwhile, small, moderately intricate castings can be made by opening the graphite mold immediately after the casting is solidified so that the metal is subjected to a minimum of restriction as it cools.

All molds should be thoroughly dried before use. A desirable practice is to hold the graphite mold at 1000°F for about 1 hr and then cool it to not lower

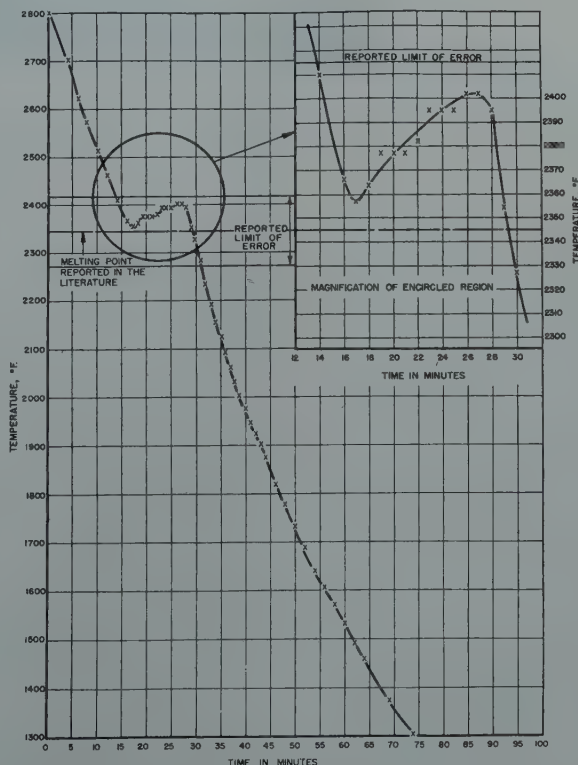


FIG 9—Cooling and solidification curve, Heat No. A-14.

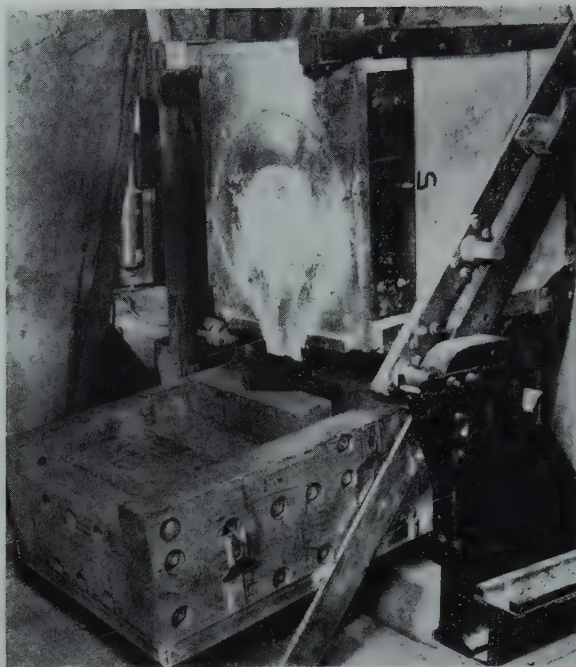


FIG 10—Photograph showing the graphite mold attached to the large induction furnace.

The mold is for a plate 18 inches \times 18 inches \times 2 inches, which is poured by the Durville method.

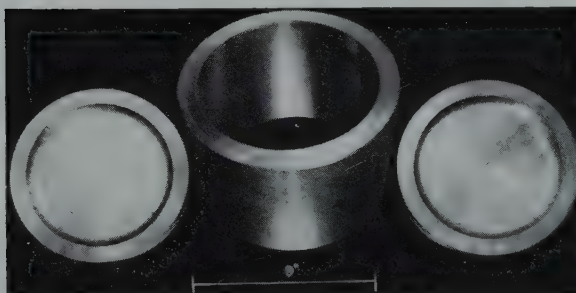


FIG 11—Photograph showing a cylindrical casting and end plates to form a small ball mill approximately 8 in. od.

than 300°F for use. In some instances, where a sufficiently large high-temperature furnace was not available, the molds were preheated to only 600°F and held for 16 hr. Graphite molds should not be allowed to cool below 300°F until all of the castings to be poured into them have been produced. If the mold is held for any length of time at room temperature, it should be reheated to 1000°F (or lower, if the higher temperature is not practicable) before subsequent use.

In the study of graphite as a mold material, it has been observed that the tendency toward gas unsoundness in the casting increases with repeated use of the mold. The reason for this behavior of the graphite is not definitely known, but to insure against the possi-

bility that the re-use of the graphite mold becomes a variable in the experimental studies, no mold is used for more than ten casting operations.

Discussion of Results

Since the experience with the founding of beryllium has not been extensive, it is difficult to evaluate the limitations of the art and science of producing high-quality castings. In this investigation, some consideration has been given to practically all of the founding characteristics of beryllium, and special attention has been given to that problem which has appeared to be the most troublesome, namely, gas unsoundness. The seriousness of the gas unsoundness problem in casting

beryllium can be appreciated by observing the range of unsoundness which may be encountered, as shown in Fig 4.

The unsoundness observed in Fig 4 is clearly caused by an evolution of gas during solidification of the metal. The precise type of gas evolution or the particular gas or gases involved is not definitely known. In general, there are two types of gas evolution, as follows: 1. Gas evolved during solidification of the metal because of the very marked decrease in solubility of the gas as the metal changes from liquid to solid. 2. The formation of a relatively insoluble gas by a reaction which occurs between two constituents dissolved in the melt. A typical example of such a phenomenon is the carbon monoxide gas evolved

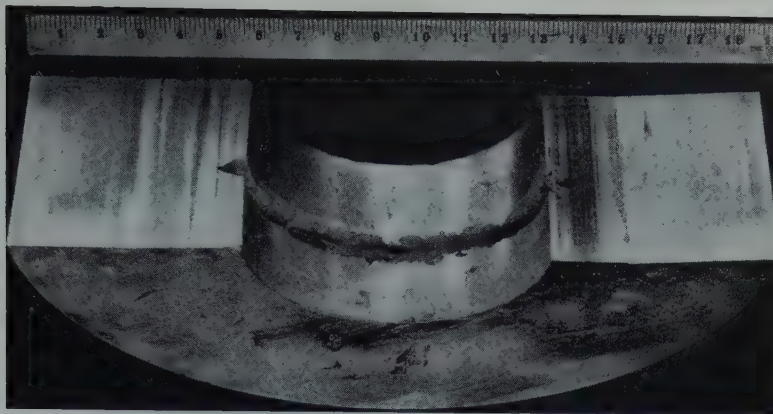


FIG 12—Photograph showing a centrifugal casting 19 in. od, a 7½-in. wall, and 5 in. high.

The casting is shown after it was sawed and some machining done on the inside surface. The shrinkage on the inside periphery is evident.

in a rimming steel ingot as a result of the reaction between dissolved carbon and oxygen. A second example is the formation of steam in copper-base alloys as the result of a reaction between hydrogen and oxygen, or an oxide dissolved in the melt. In both of these instances the gases formed, as a result of the reactions, are relatively insoluble in the solidifying metal and thus precipitate or evolve from the melt.

There are many possibilities of these two types of gas evolution which might occur in beryllium. Hydrogen, carbon monoxide, carbon dioxide, nitrogen, and possibly other gases might evolve from the melt during solidification as Type 1 gas evolution. Type 2 gas evolution could occur as a result of the reaction of hydrogen and oxygen or oxide in the melt to form steam, or the reaction of carbon or carbon monoxide with oxygen or oxide in the melt to form either carbon monoxide or carbon dioxide. If oxygen or beryllium oxide is as insoluble in molten beryllium as is oxygen or the respective oxide in the light alloys, aluminum and magnesium, Type 2 gas evolution may not occur. There have been a few instances in the experimental work where unsound ingots have shown an increased carbon monoxide content. The samples for these tests were selected to include whole gas bubbles, so that evolved as well as dissolved gases would be determined in the vacuum-fusion analyses.

Except for a few instances where carbon monoxide has been found in the unsound ingots, practically all of the gas unsoundness observed in beryllium can be explained by the supposition that hydrogen dissolved in the melt evolves during solidification as a re-

sult of decreased solubility. The principal source of hydrogen is, of course, moisture. Experimental proof of the effect of the moisture content in the argon atmosphere on the soundness of beryllium castings made in a small-scale experimental furnace is shown in Fig 5. In addition to this experimental proof of the effect of moisture, there are many indications or circumstantial evidence which place hydrogen, absorbed from moisture, at the head of the list as the main cause of gas unsoundness in beryllium. These are: 1. The necessity for melting a wash heat in a crucible before consistently sound castings can be obtained from it. 2. The necessity, when using the flux method, to melt the flux before it is added to the metal. If the flux is not melted, a considerable amount of hydrogen may be absorbed from the water in the flux. 3. The necessity for drying molds thoroughly before sound beryllium castings are made in them. 4. Melting a charge previously wet with water has produced gas unsoundness in an application where such unsoundness was desired.

In addition, there have been many other indications which have shown that moisture should not be allowed to contaminate any of the tools used in the melting process which are likely to come into contact with the molten beryllium.

Summary and Conclusions

The success with which beryllium castings can be made in the plant or laboratory depends, to a great measure, upon how well certain difficulties attendant to the handling of this metal

are overcome. These difficulties, not peculiar to beryllium alone but encountered in the handling of many commercial metals, include a high degree of reactivity with oxygen and nitrogen; this characteristic is accentuated by the high pouring temperatures of 2600–2900°F and results in the formation of dross which, if carried over to the mold, can produce serious casting defects. Another characteristic of the metal is that it is very weak and brittle at high temperatures and, therefore, tends to crack easily when hot. Its low ductility when cold can also result in cracks if the normal contraction of the casting is restrained during cooling. Finally, and perhaps the greatest difficulty encountered has been unsoundness resulting from gas evolution during solidification.

Another characteristic of the metal which must be carefully considered is the apparently extreme toxicity of the fumes evolved during melting and of the dust formed during machining, grinding, sawing, and other procedures.

The problem of gas absorption has been studied by the use of a small, controlled gas-atmosphere induction furnace. It has been found that if reasonable care is taken to prevent the exposure of beryllium to moisture during the melting and casting operations, consistently sound castings can be produced.

The reason for the occurrence of unsoundness is not completely understood but it is apparent from the experimental work that hydrogen picked up from moisture accounts for a major part of the gas which causes the unsoundness.

The results of the present investigation have added considerably to the



FIG 13—Photograph of a cylindrical casting 52 in. od, with a 2-in. wall, 4 in. high.
This casting is shown as stripped from the mold.

knowledge relating to the proper handling of beryllium in the foundry. Techniques have now been developed which will permit the production of consistently sound beryllium castings from heats weighing up to 80 lb and limited in size only by the melting equipment available for this particular operation.

The following recommendations for the melting and casting of beryllium are based upon observations made in the course of the experimental work, including the preparation of heats weighing up to 80 lb:

1. Melts may be made in thoroughly preheated beryllia or graphite-bonded, silicon carbide crucibles (Tercod). Usually, a wash heat is desirable in a new crucible to insure complete removal of moisture. High-frequency induction heating is the most convenient.

2. The beryllium melting charge should be thoroughly dried out at a temperature between 500 and 800°F. Thereafter, in the melting process, the metal should not be subjected to any atmosphere or material which might be a source of moisture, or gas, particularly hydrogen.

3. No fluxes need be employed, but the metal should be protected from the atmosphere by means of argon of the lowest possible moisture content. This can be accomplished by covering the melting crucible and introducing argon at right angles to the melt surface so that it mushrooms out over the bath. The argon can be satisfactorily dried

by passing it through a coiled copper tube held at about minus 100°F.

4. The time that the metal is kept in the molten condition, especially at the pouring temperature, should be held to a minimum, and the casting should be poured as soon as the proper melt temperature has been reached.

5. The maximum temperature should be kept low, preferably less than 2900°F, and the pouring temperature should also be kept at a minimum, consistent with the degree of fluidity necessary to fill the mold cavity completely without cold shuts or misruns.

6. Where possible, the casting should be poured directly from the furnace in order to carry out effectively these recommendations. Ladling, while not desirable, may be useful when pouring centrifugal castings.

7. The mold material should be such that the metal will not react with it. Thoroughly preheated graphite which has not been used for more than ten casting operations appears to be satisfactory, though there are considerable differences among various grades of graphite.

8. Dross entrapment should be avoided. It has been found that this can be accomplished most effectively by introducing the metal into the mold gently by permitting the molten metal to run down a low incline into the cavity, using the Durville method or a modification of it.

9. Any undue restriction to the contraction of the hot casting, such as a fin

which would result in cracking, should be prevented by proper design of the mold cavity. As far as is known to date, this means that it is feasible to cast only relatively simple shapes which do not present problems of restriction to contraction. However, the precise limitation on complexity of design has not been established. The development of collapsible molds for beryllium casting is a definite possibility.

10. Beryllium castings having fairly thin sections can be made in a graphite mold if the surface areas are relatively small. The remarkable flowability of beryllium in graphite molds and the reproduction of minute detail in the mold design should not be overlooked.

11. The size of the castings, including the gates and risers, is limited only by the size of the available melting equipment. At the present time at Battelle, the maximum is about 80 lb of beryllium.

12. Within the limitations outlined, both static and centrifugal castings can be satisfactorily made.

Acknowledgments

The authors gratefully acknowledge the contribution of Mr. E. C. Kron, who did some of the earlier work on beryllium, and the guidance of Dr. H. W. Russell and Dr. C. H. Lorig, who provided general supervision of the work.

Metallographic Examination of Beryllium Alloys*

M. C. UDY,† G. K. MANNING,† and L. W. EASTWOOD,† Members AIME

Introduction

Those who have examined beryllium and beryllium-rich alloys under the microscope have noted the results of the difficulties encountered when preparing these materials for examination. Hard constituents are readily chipped and pulled out of the matrix, and the soft ones are easily gouged out or embedded with abrasive or other material. The matrix is easily deformed, which makes it very difficult to remove the effects of scratches. Furthermore, the matrix and some of the constituents are also readily pitted during etching, which makes the structure difficult to develop.

The metallographic techniques designed to avoid these difficulties are neither radically new nor necessarily the best possible procedures. They were developed at Battelle to fill immediate requirements as part of a study of the preparation and pouring of beryllium melts as described in a separate paper.

A part of the research program on the causes of gas unsoundness in beryllium castings entailed a study of the effects of such gases or gas formers as oxygen or oxides, nitrogen or nitrides, and carbon or carbides. These gases or gas formers, if dissolved in the melt, might be an important factor in the study of unsoundness caused by gas evolution in beryllium. Because it was necessary to be able to distinguish these gases or gas formers, if present as alloy constituents, from metallic phases also present as alloy constituents, a series of alloys was prepared with additions of the various possible metallic and non-metallic constituent formers. It should be emphasized that the constituents

referred to as gases or gas formers are important in the study of gases in beryllium only if they form a part of the alloy, that is, if they dissolve in the liquid or solid metal.

During the first part of the development of metallographic techniques, the Massachusetts Institute of Technology, unpublished report (TC 3315, Nov., 1945) by Paul Gordon, describing various microconstituents in beryllium, was quite useful. Of particular interest in this report is the confirmation of one of the conclusions drawn from the present investigation, that is, that a distinct oxide phase apparently does not occur in beryllium.

The Preparation of Metallographic Specimens

GRINDING PROCEDURE

The original specimen is either sawed or cut on an abrasive wheel to a convenient size. For best results, the surface to be polished should not be more than about $\frac{1}{4}$ in. square, and it is convenient to mount the specimens in bakelite to facilitate handling. Two alternative grinding procedures have been developed. As one alternative, specimens are ground successively on

120-, 240-, and 400-grit, wet-or-dry metallographic discs. The abrasive discs are revolved at 1750 rpm on a conventional pedestal grinder. The coarsest disc (120 grit) is used either wet or dry, and in most instances, it can be eliminated from the procedure. Grinding on the two finer discs (240 and 400 grit) is accompanied by the application of kerosene. The technique consists of holding an oil can, containing kerosene, in one hand and the mounted specimen in the other hand. While the grinding is being done, several drops of kerosene are applied every few seconds close to the center of the disc. Carbon tetrachloride serves at least as well as kerosene as a lubricant; perhaps it is slightly better, but it volatilizes so readily that an additional health hazard is involved. Light oils and water are not satisfactory for the finer grinding operations.

The second procedure is perhaps slightly slower than the first and requires a more careful technique, but it eliminates the use of kerosene. The specimen is first ground wet on a 240-grit disc, followed by dry grinding on a 400-grit disc.

Finer grinding does not appear to be necessary with either of the two alternative procedures.

The pressures used throughout either grinding operation must be *extremely* light, that is, barely sufficient to hold the specimen in contact with the disc; otherwise, flow and chipping are almost certain to occur.

In both procedures, it is essential that the discs be sharp and that they be discarded as they show evidence of becoming dull or loaded. In general, not more than four or five specimens can be ground on a disc before the disc becomes dull enough to warrant discarding it.

Cleveland Meeting, October 1949.

TP 2700 E. Discussion of this paper (2 copies) may be sent to *Transactions AIME* before December 1, 1949. Discussion is tentatively scheduled for publication in May 1950. Manuscript received April 28, 1949.

* The experimental work described in this paper was sponsored by the Atomic Energy Commission, under Contract W-7405-eng-92.

† Research Engineer and Supervisors, respectively, Battelle Memorial Institute, Columbus, Ohio.

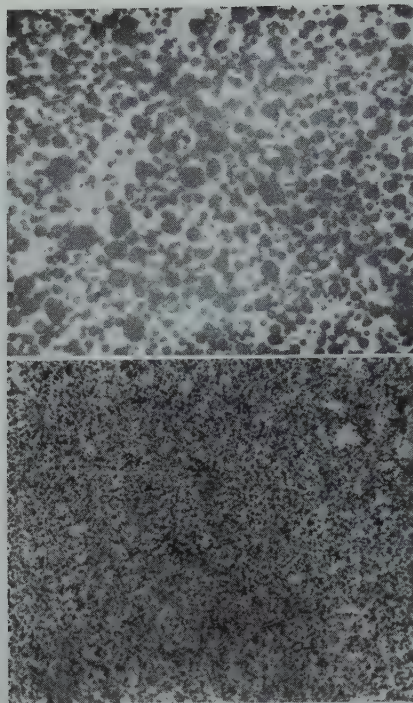


FIG 1 (above)—Heat A-9. Unetched. High carbon from mold reaction.

FIG 2 (below)—Heat A-4. Unetched. High carbon from mold reaction.

× 500. Reduced one-half in reproduction.

Hand grinding of the beryllium alloys has not been successful, even though the grinding is done under kerosene.

The preparation of the specimen may be considered more than half done when a satisfactory fine grind has been obtained. The specimen should be examined at 500 magnification in the ground condition before starting the polishing operation. After some experience, the operator will be able to judge whether or not the grinding has been accomplished without either deforming the surface of the beryllium matrix or breaking out the hard, brittle constituents. If there is evidence that some constituents have been broken out or if there is evidence of flow in the beryllium matrix, it is well to start over again because it is a waste of time to attempt to polish an improperly ground specimen.

POLISHING PROCEDURE

After a proper grind has been obtained on a specimen, the final polishing can be accomplished in a few minutes. Two successful procedures have been developed. With either method, the specimen is slowly counter-rotated on a 4-in. polishing head rotating at 1750 rpm.

The first method is more rapid but

less reproducible. The polishing head is covered with worsted serge because the use of longer nap cloths seems to promote pitting and should be avoided. A solution of 5 pct oxalic acid in water is used in conjunction with an abrasive on the polishing cloth. This is an improvement over a more complicated, glycerine-containing solution which was used earlier and which seemed, in some cases, to promote pitting of the specimen. Fine alumina is used sparingly as the abrasive. However, when soft constituents occur, such as those formed by aluminum or tin additions, levigated CP-Fe₂O₃ is better though slower than alumina. When alumina is used as the abrasive, there seems to be a greater tendency for soft constituents to be gouged out. Actual polishing of the specimens apparently requires a proper balance between chemical solution by the oxalic acid on the one hand, with the abrasive action by the alumina on the other. This procedure requires rather careful manual manipulation which can be effected only after considerable practice.

The polishing procedure consists of applying a small amount of abrasive and oxalic acid solution at the beginning of the operation and, as the polishing continues, adding only the oxalic acid solution. As the polishing operation nears completion, the addi-

tion of the oxalic acid solution is discontinued and water is added a few drops at a time to keep the wheel slightly moist.

The alternate polishing procedure, slower than the one already described is based on abrasive action alone, and requires less judgment on the part of the operator. It was developed primarily to retain magnesium-rich constituents during the polishing operation. The small-diameter, high-speed wheel is covered with ordinary green billiard cloth, the usefulness of which appears to improve with use. Merck's CP heavy MgO, suspended in 30 pct hydrogen peroxide, is used as the polishing agent. Since this suspension does not "keep" well, it is best to prepare small amounts several times daily. During the polishing operation, a considerable amount of the suspension is used on the wheel, so that, actually, the polishing is done on a layer of MgO rather than on the cloth. The peroxide has two functions. It holds the MgO on the cloth more satisfactorily than does water, and it also appears to inhibit the reaction of water with some of the microconstituents of beryllium, particularly the magnesium-rich phase. Even with this "slower" procedure, polishing can usually be completed within a few minutes.

ETCHING PROCEDURE

No systematic study of etching reagents has been made. However, a number of the common metallographic etchants were tried and, of these, only one appeared to be universally successful on the alloys. This etchant is composed of 10 cc of 48 pct hydrofluoric acid and 90 cc of 190-proof ethyl alcohol. Etching times range from 10 to 30 sec. This etchant outlines and produces many color distinctions to the different alloy phases, and not infrequently develops fine lines in the beryllium matrix which appear to be faults in the lattice structure. The etchant seems to increase in activity after standing for several hours. In general, the other etchants which have been investigated have been found to cause some pitting of the polished surface.

Identification of Constituents

A number of alloys were made especially for metallographic study. In addition, a number of specimens have been

included from heats made for other purposes.

Black and white micrographs are included in this paper, and in addition, color transparencies have been prepared of a number of the microstructures. This color photography is of great assistance in preserving and describing the colors of the various constituents. Ansco daylight film was used with a light source consisting of a 6-volt, 18-amp microilluminator, containing a 3200°K ribbon filament. Various combinations of color-correction filters were necessary because of the different reflectivities of the different constituents and, in general, it was difficult to avoid a greenish cast to the background.

No microconstituent has been found which can be identified as an oxide or as a hydride. This, however, does not preclude the possible presence of oxygen (or an oxide) or hydrogen (or a hydride) in liquid or solid solution in the metal, or even as a second phase in the solid metal.

The carbide is a distinctive phase; it is hard, angular, usually gray, and when exposed to the atmosphere, it readily stains, first to all colors of the rainbow and, eventually, to brown.

Fig 1 and 2 are specimens containing a high proportion of carbide, which is the prominent, angular gray constituent. The shadowy, lighter gray phase seen in the background, particularly of Fig 2, is unidentified, but it is probably a silicon-bearing phase. The hydrofluoric etch has no effect on the color of the carbide constituent.

Fig 3 and 4 are specimens from heats to which 1 and 2 pct carbon, respectively, were added as graphite. The angular, gray carbide constituent is easily recognizable. The lighter gray constituent (actually a light blue-gray) is a silicon-rich phase, while the bright speckled phase (actually slightly yellow) is an aluminum-rich phase. Fig 3 and 4 should be compared with

Fig 1, a high-carbon specimen, and Fig 5, a vacuum-cast material which, in this instance, contains a small amount of carbon in the form of a small quantity of angular, gray carbides. Very little of the light blue silicon-rich phase is present, but with a relatively greater amount of the yellow speckled aluminum-rich phase. It is of interest that the silicon-rich

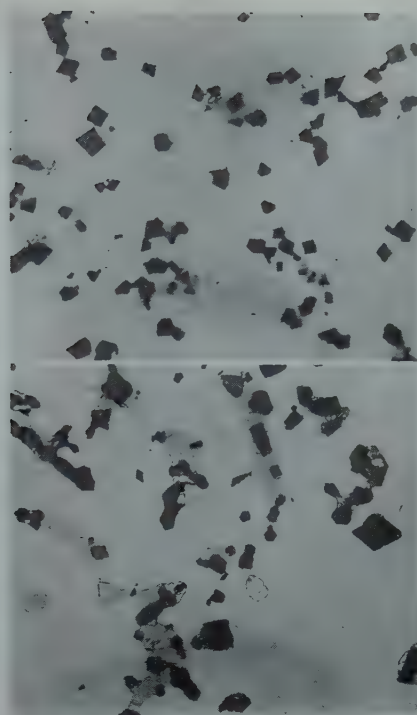


FIG 3 (above)—Heat A-6. Unetched. 1 pct C added.

FIG 4 (below)—Heat A-7. Unetched. 2 pct C added.

× 500. Reduced one-half in reproduction.



FIG 5 (left)—Vacuum-cast virgin beryllium. Light etch. × 500.

FIG 6 (right)—Heat A-11. Cold worked and deep etched to show grain boundaries. × 500.



FIG 7 (above)—Heat A-2. Made under nitrogen. Unetched.

FIG 8 (below)—Heat A-2. Isolated nitride needle.

× 500. Reduced one-half in reproduction.

and the aluminum-rich phases can exist in the same "particle" as shown just below the center of Fig 5.

Fig 6 is a photograph of a poorly prepared specimen in which the cold-worked material was not completely removed by the polishing operation. It is of interest, however, that deep etching reveals the individual grains and also delineates the grain boundaries. This treatment is unsatisfactory as a means of revealing "second" phases, however, because the aluminum-rich, silicon-rich, and carbide phases are scarcely recognizable in the figure.

The nitride phase is distinctive. It is also gray, but a darker gray than the carbide, is not affected by the HF etchant, and is usually present in needle-like form. However, in large amounts, it may also have a more massive appearance. Fig 7 is a photograph of a specimen cast from a heat melted under nitrogen and represents a badly segregated part of the ingot. An angular, gray carbide particle is also evident somewhat to the right of the center of the photograph, but other phases are not readily identifiable.

Fig 8 is a photograph of an isolated nitride needle in a portion of the same ingot represented by Fig 7. Associated with the needle are the angular carbide phase, the speckled yellow

aluminum-rich phase, and the bluish silicon-rich phase. This latter phase is barely visible in the photograph. Again, the silicon-rich phase and the aluminum-rich phase are seen to occupy the same "particle," about halfway along the top side of the needle. The aluminum-rich phase is also present as an "inclusion" in the nitride and carbide phases. The black areas are holes and a crack is also evident across the lower right-hand corner of the photograph.

One phase found in practically all samples of beryllium studied is an aluminum-rich phase. It has already been noted in the descriptions of the preceding photographs. It is soft and difficult to polish; it is bright yellow and often appears to be speckled. This speckled appearance, revealed by careful polishing, may indicate a eutectic. The HF etch does not affect the color, but does outline the phase which may be present as a grain-boundary constituent or as isolated globules, as shown by Fig 9, a photograph of a 2 pct aluminum alloy. As mentioned before, a light-blue silicon-rich phase is often associated with the bright-yellow aluminum-rich phase. This is noted again in Fig 9, where several areas in the otherwise yellow stringers are occupied by the light-blue phase. It is also possible that the speckled constituent may be the bright-blue, silicon-rich phase, or some other phase attributable to silicon. Only a few carbides are present in the specimen, represented by Fig 9, and they appear about equally abundant in the matrix and in the aluminum phase. In this instance, over-exposure has blackened their appearance considerably as well as darkened the matrix in the photograph.

Fig 10 is a photograph of a heat to which 10 pct silicon has been added. The light-blue phase attributable to silicon is seen in the grain boundaries and as isolated particles. The angular, gray carbide phase is easily recognized, as is the bright-yellow aluminum-rich phase which is associated to some extent with the silicon phase. The light-blue silicon phase is intermediate in hardness between the aluminum-rich phase and the matrix, and is outlined but not stained by the HF etch.

There are probably other phases associated with silicon; one of these is probably illustrated in Fig 11, which is a photograph of a heat that had reacted with a silicon carbide crucible. The triangular-shaped gray phase with a crack running through it is beryllium

carbide. The grain-boundary constituent is the light-blue phase previously attributed to silicon. Associated with it are small amounts of the bright-yellowish aluminum-rich phase. The dark, irregularly shaped constituent in the center of the photograph is a hard, dark blue-green constituent whose color is not affected by the HF etchant. It might be silicon carbide, although no positive identification has been made. It also occurs in heats which have had no contact with silicon carbide crucibles, but it always appears to be associated with silicon in some form.

Fig 12 shows a sample to which 10 pct titanium was added. The phase attributable to titanium is slightly pink and generally angular and its color is not affected by the HF etchant. Angular gray carbides are readily identified in the photograph. Aluminum- and silicon-rich phases, if present, have been "absorbed" in the titanium-rich phase. The fine black dots, which seem to be real, have not been identified.

Fig 13 shows a sample to which 10 pct calcium was added. Only two phases other than the matrix appear to be present. One is the angular gray phase previously identified as beryllium carbide, while the second is a light-yellow, generally angular phase present in fairly large amounts which can be

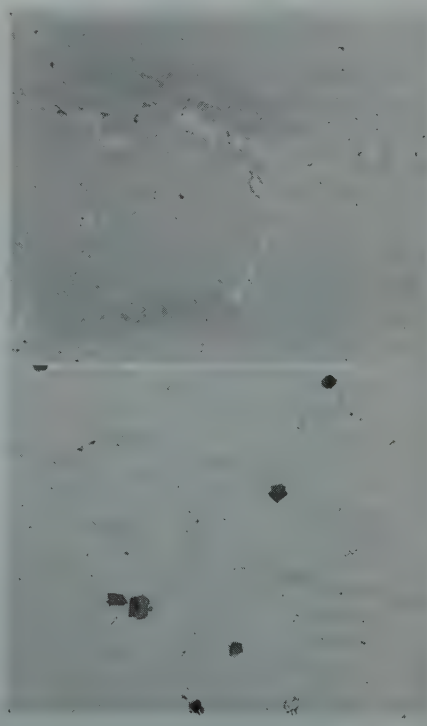


FIG 9 (above)—Heat 162. Unetched. 2 pct Al alloy.

FIG 10 (below)—Heat A-32. Lightly etched. 10 pct Si added.

× 500. Reduced one-half in reproduction.



FIG 11 (above)—Heat A-25. Unetched. Melt reacted with silicon carbide crucible.
FIG 12 (below)—Heat A-33. Lightly etched. 10 pct Ti added.
× 500. Reduced one-half in reproduction.



FIG 13 (above)—Heat A-34. Slightly etched. 10 pct Ca added.
FIG 14 (below)—Heat A-35. Unetched. 10 pct Sn added. Segregated area near 2-metal interface.
× 500. Reduced one-half in reproduction.

attributed to the calcium addition.

When tin is added to beryllium, a two-liquid system is formed which causes a two-layer ingot. The heavy tin-rich liquid settles to the bottom and mechanically carries the beryllium carbide along with it. Fig 14 shows a segregated area just above the interface between the two metals. Globules of the tin-rich phase are in evidence, and associated with them are the familiar angular gray carbides. The tin phase is yellow and similar in appearance and polishing characteristics to the aluminum rich phase previously described. It is soft and difficult to polish, as evidenced by the smeary appearance in the photograph. The beryllium layer, away from the interface, is remarkably free of inclusions. The beryllium-rich phase in the tin layer is present as a finely dispersed eutectic resolved only at × 2000 magnification.

Fig 15 and 16 are photographs of a sample to which 10 pct iron was added. Fig 15 shows the sample unetched and the phase attributed to iron appears in the grain boundaries almost entirely and is barely distinguishable from the background. The familiar gray carbides are present in the matrix and only occasionally in the iron-rich material. Other phases, if present, have been "absorbed" in the iron-rich phase. The

HF etchant (Fig 16) colors the iron phase to a reddish brown, thus affording a method of distinguishing it from other similar-appearing phases.

Ten per cent manganese was added to the specimen shown in Fig 17. The phase attributable to manganese is very similar in appearance to the iron phase. It appears in the grain boundaries and is slightly more pink than the matrix. The beryllium carbide seems to prefer the grain-boundary location in this alloy. Unlike the iron phase, the manganese phase is not stained by HF but only outlined by it.

Fig 18 shows a specimen to which 6 pct boron was added. The phase attributable to boron appears in the grain boundaries and is colored red, but is stained blue or purple by the HF etchant. The familiar carbides are present, away from the grain boundaries. The yellow aluminum-rich phase also appears as a distinct constituent which, in some locations, is closely associated with the red boron phase.

An attempt was made to produce an oxide phase in beryllium by adding silica to a melt. An increase in the light-blue silicon-rich phase was noted as well as the appearance of small amounts of the dark blue-green phase which has also sometimes been associated with silicon. Any oxide formed,

however, either went into solution and remained there, or was insoluble and separated by gravity from the melt.



FIG 15 (above)—Heat A-36. Unetched. 10 pct Fe added.
FIG 16 (below)—Heat A-36. Etched. 10 pct Fe added.
× 500. Reduced one-half in reproduction.



FIG 17 (above)—Heat A-37. Etched. 10 pct Mn added.

FIG 18 (below)—Heat A-39. Unetched. 6 pct B added.

× 500. Reduced one-half in reproduction.



FIG 19 (above)—Heat A-46. Slightly etched. 5 pct Mo added.

FIG 20 (above)—5 pct U alloy. Slightly etched.

× 500. Reduced one-half in reproduction.



FIG 21 (above)—Melting stock containing 0.75-1.00 Mg. Unetched.

FIG 22 (below)—5 pct Zr alloy. Slightly etched.

× 500. Reduced one-half in reproduction.

Five per cent molybdenum was added to the specimen, represented by Fig 19. Until it is etched, the phase attributable to molybdenum, like the iron-rich phase, appears to be about the color of the matrix. It first stains, on etching, to a chocolate color and then to a black. Carbides were substantially absent in this specimen, but the yellow aluminum-rich phase appears in small amounts.

A 6 pct copper alloy showed no phase attributable to copper. This is indicative of rather high solid solubility of copper in beryllium.

In a 5 pct uranium alloy, the uranium-rich phase was not distinguishable from the matrix in the unetched condition. However, the etchant stained the uranium-rich dendritic phase to a series of colors ranging from yellow to green. A photograph of this etched specimen is shown in Fig 20. The dendritic structure is easily seen and only a few carbides, largely in the matrix, are in evidence.

Materials containing as low as 0.35 pct magnesium have been shown to contain a phase attributable to that

material. In some of the early work, this phase was overlooked because it is soft and difficult to maintain during grinding. In addition, it is somewhat reactive to water and may disappear during polishing. Fig 21 shows this phase, believed to be a magnesium-rich constituent, in a specimen containing about 0.75 pct magnesium. It is bright "water white," very soft as compared to the matrix, and readily removed by the HF etch, leaving pits.

Fig 22 shows an alloy to which 5 pct zirconium was added. The phase attributable to zirconium is dendritic in appearance and, until etched, is barely distinguishable from the matrix, but the alcoholic HF etch outlines the phase and stains it a light blue. Further etching has no effect on the color.

Summary

Reasonably satisfactory metallographic techniques have been developed for beryllium and beryllium-rich alloys.

The following phases have been identified:

1. Carbide
2. Nitride
3. Aluminum rich
4. Silicon rich
5. Calcium rich
6. Titanium rich
7. Tin rich
8. Iron rich
9. Manganese rich
10. Boron rich
11. Molybdenum rich
12. Uranium rich
13. Magnesium rich
14. Zirconium rich

No second phase attributable to copper could be found in a 6 pct copper alloy. No phase attributable to oxygen or hydrogen has been found, but this does not preclude their presence in liquid or solid solutions.

Acknowledgments

The work of James Stevens who prepared the specimens and Clarence Barnhart who photographed them is gratefully acknowledged.

Titanium Investigations: Research and Development Work on the Preparation of Titanium Chloride and Oxide from Titanium Mattes*

R. G. KNICKERBOCKER,† C. H. GORSKI,† H. KENWORTHY,† and A. G. STARLIPER,†
Members AIME

Introduction

This report describes the progress made in the research work on the development of a new method for preparing lower-cost titanium tetrachloride and preparing titanium oxide pigment.

One of the requirements for the commercial production of ductile titanium in the process used by the Bureau of Mines is a source of lower-cost titanium tetrachloride.

The production of ductile titanium by a modification of the Kroll¹ process, recently developed by the Bureau of Mines, requires such a source of lower-cost titanium tetrachloride to make it commercially feasible. This report describes the progress of work done at the Mississippi Valley Experiment Station at Rolla, Missouri, on the development of a new method for preparing titanium tetrachloride. During the course of this research a new method for preparing pigment-grade titanium oxide was developed.

At present, the price of technical-grade titanium tetrachloride is \$0.32 a pound, which makes the price of the contained titanium \$1.28 a pound.² In addition, the titanium tetrachloride must be purified further before it is suitable for processing into metal, thus making its cost still higher.³

Columbus Meeting, September 1949.
TP 2706 D. Discussion of this paper (2 copies) may be sent to *Transactions AIME* before December 1, 1949. Manuscript received Dec. 29, 1948; revision received June 3, 1949.

Papers by Members of the staff of the Bureau of Mines are not subject to copyright.

* Laboratory work for this report was completed Sept. 1, 1948. This paper presents the results of work done by the Rolla Branch, Metallurgical Division, of the Bureau of Mines.

† Principal Metallurgical Engineer and Metallurgists, respectively, Rolla Branch, Metallurgical Div., Bureau of Mines, Rolla, Mo.

¹ References are at the end of the paper.

There were 8,562 tons of rutile produced in the United States in 1947, which was 900 tons in excess of that consumed. In addition there were 13,937 tons in various stocks, exclusive of the stocks in the Government strategic stock pile.

No estimates of the domestic production of rutile are given for any of the prewar years. However, in 1939, 442 tons of rutile were imported as compared to 14,307 tons in 1947.

One of the reasons for the large increase in the production of rutile is the working of the Florida beach sands for ilmenite, during which a considerable amount of rutile is produced as a by-product.

It would be of value to determine methods for utilizing the excess production of rutile.

The Arkansas titanium deposits in Hot Spring County produced commercial-grade rutile concentrates from 1933 to 1942. These were sold mainly to England, Germany, and Russia.

Table 1 . . . Matte Smelting of Ilmenite with Pyrite and Coke

| Product | Weight, Pct | Analysis, Pct | | | | Recovery, Pct | |
|------------------|-------------|---------------|------|-------|---------|---------------|-------|
| | | Ti | Fe | S | Total C | Ti | Fe |
| Matte..... | 64.9 | 40.7 | 14.5 | 17.9 | 1.9 | 73.3 | 20.7 |
| Metal..... | 34.3 | 1.4 | 89.5 | 1.8 | 2.7 | 1.2 | 66.2 |
| Fume..... | 0.8 | 7.4 | 9.7 | N.D.* | | 0.2 | 0.1 |
| Dust losses..... | | | | | | 25.3 | 13.0 |
| Total..... | 100.0 | | | | | 100.0 | 100.0 |

* N.D. means not determined because of lack of sample.

The ore dressing of low-grade titanium ores containing approximately 4 pct TiO_2 to a high-grade concentrate of 92 to 95 pct TiO_2 places an unusual duty upon any ore-dressing plant. A high recovery of rutile under these conditions is sacrificed to produce a high-grade product. Examination of the tailings from any rutile mill of this type operating on mine-run ore in the United States will confirm this statement. One purpose of the laboratory work on the matte smelting of titanium is to be able to utilize lower-grade titanium concentrates and thereby directly facilitate the conservation of titanium minerals. There is no present commercial use of rutile concentrates containing less than 92 pct TiO_2 . All of the laboratory work at Rolla on the matte smelting of titanium has dealt with a concentrate containing only 85 pct TiO_2 . The ilmenite concentrates treated for matte smelting were of standard grade and of the following composition: 58.4 pct TiO_2 , 25.0 pct Fe, 0.37 pct P_2O_5 , 0.11 pct V_2O_5 . It is necessary to mention that, in the production of ilmenite concentrates, the same general statement holds true in that considerable losses of ilmenite occur in the attempt to produce high-grade ilmenite mineral concentrates. The recent introduction of flotation for the recovery of fine ilmenite and rutile values has been of considerable assistance in improving these recoveries. The presence of clay minerals, however, interferes with the recovery of fine titanium minerals in flotation the same as in gravity concentration.

Preparation of Titanium Tetrachloride

GENERAL

Titanium tetrachloride is commonly prepared by one of the following processes: (1) Chlorination of titanium cyanonitride, which product is pre-

pared from pigment-grade titanium dioxide or high-grade rutile concentrate in the electric arc furnace, (2) chlorination of pigment-grade titanium dioxide at 400 to 900°C, and (3) chlorination of ilmenite or rutile concentrates at 500 to 1100°C. Methods 1 and 2 suffer from the disadvantage of requiring a relatively expensive starting material; that is, pigment-grade titanium dioxide, which has recently been quoted at \$0.19 per $\frac{1}{2}$ lb or high-grade rutile concentrates which cost approximately \$0.07 per lb.⁴ Method 3 requires a comparatively high chlorination temperature.

Chlorine is an extremely active chemical reagent at elevated temperatures. None of the common metals or alloys is resistant to its action although certain acid-resisting refractory brick and graphite are not affected by chlorine at the reaction temperatures used. In laboratory tests made on the chlorination of ilmenite-carbon mixtures several types of graphite retorts, coated with the refractory cements available, were tried. All of the tests showed that graphite was unsatisfactory because of its porosity and because of its tendency to oxidize rapidly at temperatures above red heat. None of the coating materials adhered to the graphite tubes well enough to prevent them from being oxidized.

It is believed that it would be extremely advantageous to develop a process for producing titanium tetrachloride by chlorinating a titanium compound at a temperature less than 300°C. In perusing the literature it was found that one of the most likely compounds of titanium for this purpose was the sulphide. M. Picon⁵ stated that all of the sulphides of titanium were attacked by chlorine at 175°C, titanium chloride being volatilized.

Little previous work has been done on the preparation of titanium sulphides. Some of the methods used were as follows: (1) Reaction between ti-

tanium tetrachloride vapor and hydrogen sulphide at 480 to 540°C,⁶ (2) reaction between a mixture of titanium dioxide and graphite with dry hydrogen sulphide,⁷ (3) reaction between carbon disulphide and hot titanium oxide,⁸ and (4) reaction between mixtures of iron sulphide, titanium dioxide, and carbon.⁹

Of these methods (1) is obviously unsuitable since one of the starting materials is titanium tetrachloride. However, during the course of this research some pure titanium disulphide was made by this method in order to prepare a standard X ray diffraction pattern and to determine some of its fundamental characteristics. Of the remaining three methods, a variation of (4) appeared to be the most attractive.

PREPARATION OF TITANIUM MATTES

In January 1947 a study of the reactions between rutile, pyrite, and coke, and ilmenite, pyrite, and coke was started. In the preliminary tests 200-g samples, charged in a graphite crucible, were smelted in a 3 kv-amp. high-frequency induction furnace. All of the constituents were ground to minus 200-mesh. The purpose of this work was to produce a matte containing all of the titanium in the form of the sulphide, while the reduced iron was separated from the matte in a metallic button at the bottom of the crucible. This metal should be a useful by-product as molten feed to a bessemer converter.

To determine the proper conditions for recovering the maximum amount of the charged titanium in the matte and at the same time produce a desirable titanium sulphide product, the composition of the charges, the smelting temperature, and the time were varied.

In one series of experiments the composition of the charge was varied from 20 to 60 pct ilmenite and 30 to 70 pct pyrite, and the coke was held constant at 10 pct. The results of these experiments showed that, as the pyrite in the charge was increased, the percentage of titanium in the matte decreased and the percentage of iron increased. As the percentage of titanium in the matte increased, its solubility in 10 pct and concentrated sulphuric acid decreased. It is believed that this was caused by the formation of suboxides of titanium as the amount of pyrite in the charge was decreased.

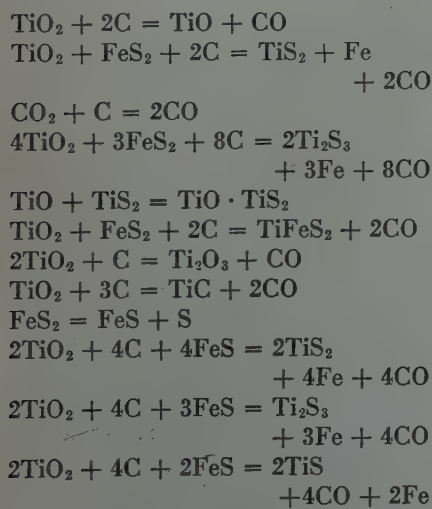
In a typical run a 200-g charge, con-

sisting of 60 pct ilmenite, 30 pct pyrite and 10 pct coke, was charged into the small induction furnace, heated to approximately 1500°C, and smelted for 45 min. at this temperature. After the smelting period the charge was allowed to cool in the crucible and the matte separated from the metal. The result of this run is shown in Table 1.

The results of these experiments were not entirely conclusive because of the large losses by "dusting" that occurred during the charging of the small induction furnace and during the reaction period. However, in larger-scale work when rutile was smelted with pyrite and coke, recoveries exceeding 90 pct of the titanium in the charge were obtained in the mattes. These initial experiments showed that it was possible to prepare titanium mattes by smelting mixtures of ilmenite, pyrite and coke at approximately 1550°C.

Several small-scale experiments were made in which mixtures of rutile, pyrite, and coke were smelted in the small induction furnace to determine whether there was any difference in the behavior of rutile in the matte smelting reaction as compared to ilmenite. No marked difference was found between the two minerals. However, rutile gave a distinctly less violent reaction than ilmenite, and the fusion temperature of the various mixes was somewhat higher. The rutile used in these and all of the following tests was an 85-pct TiO₂ mill concentrate which did not meet the specifications of commercial-grade rutile.

Little work has been done on identification of the various matte constituents and a large number of these remain to be identified. It is believed that some of the reactions which occur are as follows:



X ray studies of the mattes are being

made to determine the various constituents present in order to increase our knowledge of the reactions which occur during matte smelting.

CHLORINATION OF TITANIUM MATTES

In order to prepare a sufficiently large sample of titanium matte for chlorination experiments, several samples of matte were prepared in the 35 kv-amp. high-frequency induction furnace. This larger induction furnace was similar to the one previously described, except that the inside diameter of the graphite crucible was 3¼ in. as compared to 1¼ in. for the smaller furnace, and 1,500-g charges were smelted as compared to the 150- and 200-g charges melted in the smaller furnace.

In most of the experiments the charge was smelted for one hour at an approximate temperature of 1550°C, allowed to cool, and the matte separated from the metal. The charge compositions and chemical analyses of four typical mattes are shown in Table 2.

Table 2 . . . Matte Samples Used in Chlorination Experiments

| Sample | Analysis, pct | | | | Composition of Charge, Pct |
|--------|---------------|------|------|-----|--|
| | Ti | Fe | S | C | |
| 1 | 44.6 | 9.4 | 19.7 | 2.2 | 55 pct rutile, 35 pct pyrite, and 10 pct coke. |
| 2 | 37.2 | 14.8 | 27.2 | 2.5 | 45 pct rutile, 45 pct pyrite, and 10 pct coke. |
| 3 | 31.6 | 22.8 | 31.2 | 3.7 | 35 pct rutile, 55 pct pyrite, and 10 pct coke. |
| 4 | 37.3 | 19.3 | 28.1 | 1.5 | 45 pct rutile, 45 pct pyrite, and 10 pct coke. |

After spending considerable time in devising suitable apparatus for carrying out the chlorination experiments, it was found that a stainless-steel retort containing 25 pct chromium and 12 pct nickel was most satisfactory. A collecting system was devised that consisted of a short length of 1½-in. stainless steel pipe welded to the retort which was in turn connected by means of a length of rubber tubing to a length of 1¼-in. glass tubing that extended into a 4-liter filter flask serving as a collecting vessel. The flask was connected in series to three 500-ml Erlenmeyer flasks, the first of which contained hydrochloric acid and the other two, water. The purpose of the first Erlenmeyer was to keep the system free of water vapor, and the other two were to remove the volatile titanium com-

pounds in the exit gas. The retort was heated by a tube furnace held in a vertical position. The charge was supported on a carbon plug drilled with ⅛-in. holes, which in turn was held in position by means of the chlorine inlet tube which was flared at its end. A 1½-in. pipe cap was screwed on the bottom of the retort to make the apparatus airtight, and the cap was drilled and tapped to permit the chlorine inlet tube to pass inside the retort.

In order to keep the charge, which was ground to minus 200-mesh, from falling through the carbon plug, it had to be mixed with a binder. In several of the earlier tests fuel oil was used as binder. However, it was later found that benzol was more suitable for the laboratory work as it volatilized at a lower temperature. In some of the earlier runs activated charcoal was mixed with the titanium matte in the charge; but, as it seemed to have little effect on the chlorination reaction, its use was discontinued.

The reaction time and temperature were varied considerably during the earlier experiments. Temperatures from room temperature to as high as 400°C and reaction periods from 1 to 4 hr were used. However, in later runs, a reaction temperature of 200 to 220°C and a reaction time of 4 hr were used. After chlorination, the residues were generally leached with water to remove any of the ferric chloride formed, so as to provide an analytical sample that was not hygroscopic.

The initial experiments showed that it was possible to recover 60 pct of the titanium in the mattes by chlorination, when the charge composition of the matte contained 45 pct or more pyrite. Additional tests were made to improve the titanium recovery from mattes containing 55 pct rutile, as it was obvious that it would be more economical to prepare a matte of higher titanium content. These later runs showed that recovery could be increased and are described later.

The product obtained by the chlorination of titanium mattes was a yellow, hygroscopic, crystalline solid which fumed when exposed to the atmosphere. During the course of the reaction an amber liquid was first recovered, which was converted to the yellow solid by further reaction. The chemical composition of this solid, as determined in some 5 or 6 dozen cases was as follows: Titanium 17-21 pct, sulphur 4-6 pct, chlorine 67-75 pct. It is believed that chlorination proceeded according to the

following reactions:

1. $\text{TiS}_2 + 2\text{Cl}_2 = \text{TiCl}_4 + 2\text{S}$
2. $2\text{S} + \text{Cl}_2 = 2\text{SCl}$
3. $\text{TiCl}_4 + 4\text{SCl} = \text{TiCl}_4\text{SCl}_4 + 3\text{S}$

The product obtained from the various chlorination reactions was identified as a mixture of titanium tetrachloride and titanium sulpho-octochloride ($\text{TiCl}_4\text{SCl}_4$). It is apparent that this product must be treated further to remove the sulphur.

REMOVAL OF SULPHUR FROM CRUDE TITANIUM CHLORIDE

Several methods were tried for purifying the material obtained by the chlorination of titanium matte. Simple distillation was unsuccessful because titanium tetrachloride and sulphur monochloride have boiling points that are within 0.8°C of each other. A number of inorganic materials, that have an affinity for sulphur, were added to the crude titanium chloride, and the mixture was heated until distillation occurred. Some of the reagents used were sodium carbonate, sodium hydroxide, lime, aluminum powder, iron powder, and titanium wire and powder. None was satisfactory as the sulphur content of the product varied from 0.23 to 3.00 pct.

At the suggestion of O. C. Ralston, chief of the Metallurgical Division, Bureau of Mines, fixed oils, such as cottonseed oil, and fatty acids such as palmitic acid, coconut oil fatty acid, and oleic acid were mixed with the impure titanium tetrachloride and heated slowly for a short time until distillation occurred. The use of such an oil was to provide a material that could be chlorinated by the sulphur chloride present thus splitting the sulphur from the chlorine and forming elemental sulphur, which has a considerably higher boiling point than titanium tetrachloride.

These fatty acids and oils were more successful than the inorganic reagents which had been used previously. In several runs titanium tetrachloride with a sulphur content of as low as 0.02 pct was produced. The optimum

amount of oil used was 4 pct of the weight of the crude titanium compound charged.

In a typical run in which the charge consisted of 50 g of impure titanium compound and 2 g of soya bean oil fatty acids, three distillates were obtained. The first distillate contained 1.74 pct sulphur and consisted of 9.9 pct of the titanium charged, the second contained 0.02 pct sulphur and consisted of 52.5 pct of the titanium charged, while the third contained 0.09 pct sulphur and consisted of 24.0 pct of the titanium charged. The residue contained 13.6 pct of the titanium charged. The distillates which were high in sulphur could be returned to the still for further treatment. It should also be possible to reduce the titanium losses in the residue so that it may be safely assumed that 90 pct or more of the titanium charged should be recovered.

Further work showed that it was possible to replace the fatty acids and oils with tall oil, a cheaper material obtained as a by-product in the manufacture of paper.

At present, nothing is known of the amount of sulphur that may be tolerated in the titanium tetrachloride used in the Kroll process. It may be possible to use a product that is less pure than has been previously described, which would naturally lower the operating cost and probably increase the titanium recovery.

USE OF SILICON IN MATTE SMELTING

All of the titanium mattes prepared thus far contained a certain amount of iron, probably in the form of suspended metallics and as iron sulphide. During chlorination a considerable amount of chlorine is used in producing ferric chloride, as iron is attacked before titanium. The commercial value of this byproduct has not been investigated. Several methods were tried to lower the iron content of the mattes. Various reagents, including sodium carbonate, lime, aluminum, copper, and electrolytic manganese were added to

samples of matte in the molten condition. All of these reagents were ineffective. During a conference with Dr. William J. Kroll of the Albany, Oregon, Branch of the Bureau of Mines it was suggested by him that silicon be tried as a desulphurizer. It was believed that the silicon might react with the iron sulphide in the matte removing the sulphur in the form of volatile silicon sulphide thus forming metallic iron which would be collected in the metallic button.

Various methods of adding silicon to the charge were tried. One of the most effective ones appeared to be to smelt the batch of rutile, pyrite, and coke in the usual manner, hold it at the reaction temperature for 30 min. to one hour, then add the metallic silicon, stir the batch as thoroughly as possible and hold it for an additional shorter period, usually 15 to 30 min. at the reaction temperature, 1500 to 1550°C .

Many mattes were prepared in which silicon was added to the charge. The amount of silicon added was 2 to 4 pct of the weight of the charge. In general, the iron contents of the finished mattes were lower than those of corresponding mattes in which silicon was not used. However, all of the mattes contained some silicon, ranging from 0.11 to 8.7 pct, depending on the quantity of silicon added and the method of mixing it with the matte. In some instances, when the silicon was not thoroughly stirred into the matte it collected on the surface in the form of a slag.

Several of the silicon-containing mattes were chlorinated. In general, the titanium recoveries were somewhat higher when silicon was added to the matte. In one case, a titanium recovery in excess of 90 pct was obtained from a matte with a charge composition of 55 pct rutile, 35 pct pyrite, and 10 pct coke, to which silicon amounting to 2 pct of the original charge was added. In several other runs in which all of the experimental conditions of the previous test were duplicated, it was not possible to obtain a titanium recovery in excess of 70 pct. Apparently, this reaction of silicon with titanium matte is very sensitive and difficult to control. The function of silicon in the matte smelting reaction has not been ascertained. However, in most cases, the bulk of the silicon was not volatilized and remained in the matte, slag, and metal. Some of the metals had a silicon content of nearly 10 pct. More experimental work is necessary to determine the function

Table 3 . . . Matte Smelting in the Globar Furnace

| Product | Weight, Pct | Analysis, Pct | | | Distribution of, Pct | | |
|----------------|-------------|---------------|------|------|----------------------|-------|-------|
| | | Ti | Fe | S | Ti | Fe | S |
| Matte..... | 79.7 | 48.5 | 8.6 | 19.6 | 97.0 | 30.4 | 96.2 |
| Metal..... | 18.0 | 2.0 | 86.4 | 2.7 | 0.9 | 68.9 | 3.0 |
| Slag..... | 2.3 | 36.2 | 6.6 | 5.6 | 2.1 | 0.7 | 0.8 |
| Composite..... | 100.0 | | | | 100.0 | 100.0 | 100.0 |

of metallic silicon when introduced into molten titanium mattes.

SMELTING IN THE GLOBAL FURNACE

It was noted in the early work that an induction furnace was not entirely satisfactory for preparing titanium mattes because of its uneven heating caused by the difference in conductance of the metallics and the matte, and because of the dusting losses which occurred when the furnace was charged. The experiments made in the induction furnace, however, gave an indication of the results that might be obtained in larger-scale work.

A series of experiments was made in a global furnace to approach more nearly the hearth-type furnace and determine its suitability for titanium matte smelting. The furnace used had a hearth that was 18 in. deep and 25 in. wide. The roof was arched, and it was 17½ in. high on each side and 18½ in. in the center. There was enough room to charge four crucibles. The samples were charged into deep graphite crucibles to make a better separation between metal, matte, and slag.

In all of the experiments the charge weights were varied from 2000 to 2400 g. In the initial runs the samples were charged at 1200°C, heated to 1550°C, and held at this temperature for one hour, the total furnacing time being 7 hr. In later runs the samples were charged at 1550°C and the total furnacing time was 4½ hr. In two of the runs in which silicon was added to the samples, the charge was held at 1550°C for one hour previous to the addition. After the silicon was added the charge was stirred and held at the reaction temperature for another 30 min. The total time the samples were in the furnace was 6 hr. In some of the experiments the samples were held at the reaction temperature for 30 min.

A typical run consisted of mixing a 2000-g charge containing 55 pct rutile, 35 pct pyrite, and 10 pct coke, charging into the global furnace at 1100°C and heating for a period of 30 min. at 1550°C. The analyses of the matte, metal, and slag formed are shown in Table 3.

All of the mattes produced in the global furnace were chlorinated under various experimental conditions. The reaction temperatures were varied from 200 to 300°C, while the time was held constant at 4 hr. The results of these experiments showed that in most cases the titanium recoveries obtained from

samples made in the global furnace were approximately the same as samples made in the induction furnace. The smelts made in the global furnace, to which silicon had been added, showed that a considerable amount of the silicon was in the slag. This was probably caused by the difficulty of stirring these samples while they were being heated.

In runs in which the reaction time was reduced from one hour to ½ hr the titanium recovery was somewhat lower. In several of the samples in which the rutile was increased to more than 60 pct of the weight of the charge, the titanium recovery was markedly reduced when the sample was chlorinated. The titanium recoveries obtained by the chlorination of several mattes made in the global furnace are shown in Table 4.

SMELTING IN THE ELECTRIC ARC FURNACE

In order to prepare larger samples of titanium matte than had been made previously and also to study the smelting of these mattes in an electric arc furnace, several charges were smelted in a 100 kv-amp. single phase series arc furnace which had a carbon hearth.

In one run a charge weighing 100 lb and consisting of 55 pct rutile, 35 pct pyrite, and 10 pct coke was smelted. When the charge became molten at 1550°C, 2 pct by weight of silicon was added. After the silicon was added, the bath was thoroughly rabbled, and then poured. The total time between charging and pouring was about 2 hr, and the current and voltage were 900 amp and 70 volts, respectively. The rutile charge seemed to be ideal for smelting in an arc furnace, and the electrode consumption was considered normal. The matte from the fusion contained 42.6 pct titanium, 24.3 pct sulphur, 10.9 pct iron, and 0.11 pct silicon.

A chlorination experiment made on a sample of this matte in which the initial temperature was 150°C, the reaction time 4 hr, and the average chlorine flow 204 cc per min., gave a titanium recovery of 81.3 pct and an iron recovery of 95.0 pct. This was approximately the same titanium recovery as obtained previously in smaller-scale runs made in the induction furnace in which metallic silicon was added to the matte.

Preparation of Titanium Oxide Pigments

GENERAL

During the past 20 years the use of titanium oxide pigments has increased tremendously. Since 1939 titanium dioxide has been utilized in greater quantity than any other white pigment.¹⁰ Production and sales of titanium pigments established new high records in 1947, but the capacity production rate was inadequate by a substantial margin to fill the peak and still growing demand for the product. Because of its superior pigment properties it is reasonable to expect that the demand for titanium dioxide will continue to be strong.

During 1947, 473,154 tons of ilmenite, estimated to contain 248,231 tons of titanium dioxide, were used for making pigments in the United States.¹¹ As far as is known, no rutile was used. The reasons for this are the difficulty of extracting pigment-grade titania from rutile and the present higher cost of rutile concentrates, as compared to ilmenite. If our reserves of ilmenite should become depleted, it may become necessary to use rutile or other titanium minerals as a source of pigment-grade titanium dioxide some time in the future. The use of lower-grade rutile concentrates should lower the cost of producing titanium dioxide

Table 4 . . . Chlorination of Titanium Mattes Made in the Global Furnace

| Sample | Analysis, Pct | | | | Charge Composition, Pct and Remarks | Recovery, Pct by Chlorination | |
|--------|---------------|------|------|-----|--|-------------------------------|------|
| | Ti | Fe | S | C | | Ti | Fe |
| 5 | 33.5 | 26.0 | 31.4 | 2.8 | 35 rutile, 55 pyrite, 10 coke. Reaction time is 1 hr at 1550°C, total time in furnace is 7 hr. | 65.8 | 82.9 |
| 6 | 48.5 | 8.6 | 19.6 | 2.4 | 55 rutile, 35 pyrite, 10 coke. Reaction time is 1 hr at 1550°C, total time in furnace is 7 hr. | 63.7 | 90.4 |
| 7 | 39.5 | 17.1 | 22.8 | 3.1 | 49.4 rutile, 38.0 pyrite, 12.6 coke. Total time in furnace 4½ hr. Held at 1550°C for 1 hr. | 66.0 | 88.5 |

Table 5 . . . Leaching Titanium Matte with Sulphuric Acid

| Sample | Concentration | | Recovery | |
|-------------------|-------------------|-------------------|----------|-------|
| | Ti | Fe | Ti | Fe |
| Leach liquor..... | 21.55 g per liter | 13.94 g per liter | 60.4 | 95.4 |
| Residue..... | 36.35 pct | 1.74 pct | 39.6 | 4.6 |
| Composite..... | 43.50 pct | 17.80 pct | 100.0 | 100.0 |

from this mineral.

In the earlier work it was shown that titanium mattes made from ilmenite were soluble in 10 pct and concentrated sulphuric acid solutions. A study of the solubility of titanium mattes made from ilmenite and rutile was undertaken to determine whether the mattes would be suitable starting materials for the production of titanium oxide pigments.

LEACHING WITH AQUEOUS HYDROCHLORIC AND SULPHURIC ACID SOLUTIONS

The usual method of extracting titanium from ilmenite is by digestion with concentrated sulphuric acid solutions at 150 to 180°C. Accordingly, in the initial runs the mattes were leached with sulphuric acid solutions of various concentrations. The leaching times and temperatures were varied. In a typical run a 50-g sample of matte made by smelting a mixture of 49.4 pct rutile, 38.0 pct pyrite, and 12.6 pct coke in the 35 kv-amp. induction furnace for one hour at 1600°C and containing 43.0 pct titanium, 16.1 pct iron, 20.2 pct sulphur, and 4.8 pct carbon was leached with 143.6 g of 97 pct sulphuric acid solution for a period of 4 hr at 160 to 180°C. The mixture, which was then quite viscous, was allowed to cool and agitated for an additional ½ hr with 300 ml of water at 60 to 80°C, filtered, and washed with 200 ml of water. The results of this run are shown in Table 5.

The results of the leaching experiments with sulphuric acid solutions showed that recoveries of 25 to 75 pct of the titanium in the mattes could be obtained, dependent on the reaction conditions. Higher titanium recoveries were obtained when higher leaching temperatures and more concentrated sulphuric acid solutions were used. Increasing the amount of sulphuric acid above a 10 pct excess had no effect on titanium recovery. Increasing the leaching time to a period greater than 4 hr gave slightly higher titanium recoveries. In several cases titanium

mattes that were made from charges containing 35 pct or less rutile gave recoveries that were greater than 90 pct when leached with sulphuric acid solutions.

Several experiments were made in which hydrochloric acid solutions were used to leach some of the titanium mattes. Concentrations of 10 pct, 20.24 pct (constant boiling mixture), and 37 pct hydrochloric acid solutions were used. In no case was it possible to obtain a titanium recovery greater than 30 pct. This was considerably less than had been obtained with sulphuric acid solutions. It is believed that leaching with hydrochloric acid removed only the TiS and subsulphide contents of the mattes.

BAKING WITH SULPHURIC ACID

In the earlier experiments, it was found that, when the mattes were leached with sulphuric acid, increasing the temperature increased the titanium recovery. A series of experiments was made in which titanium mattes were baked with sulphuric acid at temperatures varying from 200 to 400°C. The amounts of sulphuric acid used, the reaction temperatures, and reaction times were varied. The general procedure was to mix the acid and matte, bake at the required temperature, allow to cool, leach with water, filter and wash the residue. The optimum experimental conditions were baking for 1 to 2 hr at a temperature of 200 to 250°C with a 100 pct stoichiometric excess of sulphuric acid. With these conditions it was possible to recover 90 to 95 pct of the titanium from

mattes of high titanium content (40–50 pct titanium). Baking these mattes with sulphuric acid increased the titanium recoveries from 15 to 25 pct as compared to similar experiments in which they were leached with aqueous sulphuric acid solutions. It is believed that the higher temperatures used in the baking experiments put the suboxides of titanium into solution.

In a typical run a 50-g sample of matte made from a batch consisting of 55 pct rutile, 35 pct pyrite and 10 pct coke, and containing 42.8 pct titanium, 9.2 pct iron, 20.2 pct sulphur, and 1.78 pct carbon was mixed with 205.5 g of concentrated sulphuric acid and heated for 2 hr at 225 to 250°C. The sample was allowed to cool, leached with 300 ml of water, filtered and the residue washed with 200 ml of water. The result of this run is shown in Table 6.

There are several advantages in treating titanium matte, as compared to ilmenite. For one, the quantity of iron in the matte is considerably lower than in ilmenite, thus reducing the amount of ferrous sulphate in the leach solution. The leach solutions obtained from high titanium mattes contained one-sixth to one-eighth the amount of iron as compared to similar solutions from ilmenite. This will simplify the purification process by reducing the amount of ferrous sulphate to be handled. Another advantage is the fact that the matte has a higher titanium content than ilmenite thus reducing the handling cost. Although considerable acid (100 pct stoichiometric excess) is necessary in most cases for a maximum titanium recovery, a large amount of this acid can be recovered in the form of sulphur trioxide and elemental sulphur.

It has been shown that titanium recoveries in excess of 95 pct can be obtained by baking titanium mattes with sulphuric acid at 200 to 250°C. Very little work has been done, however, on the precipitation of titanium dioxide or the adjustment of the concentration of the leach solution. It is believed that a countercurrent decantation system

Table 6 . . . Baking Titanium Matte with Sulphuric Acid

| Sample | Concentration | | Recovery | |
|-------------------|------------------|-----------------|----------|-------|
| | Ti | Fe | Ti | Fe |
| Leach liquor..... | 37.6 g per liter | 8.6 g per liter | 98.6 | 99.0 |
| Residue..... | 2.6 pct | 0.44 pct | 1.4 | 1.0 |
| Composite..... | 45.0 pct | 10.24 pct | 100.0 | 100.0 |

of leaching can be developed for leaching the baked matte. A sulphur balance must also be made to determine the amount that may be recovered from the system.

**BAKING CHLORINATION
RESIDUES WITH SULPHURIC
ACID**

The residues from the various chlorination tests contained 30 to 60 pct of the titanium in the original mattes and analyzed 25 to 35 pct titanium. Several runs were made on samples of these residues obtained from the chlorination of mattes prepared in the electric arc, induction, and globar furnaces. The procedure used was similar to that described in the previous section and consisted of baking the chlorination residue with sulphuric acid followed by a water leach. In all cases titanium recoveries over 90 pct were obtained. The arc-furnace product gave a recovery of 98.4 pct, the induction furnace product gave 90.6 pct, and the globar furnace gave 94.7 pct.

In Table 7 are shown the chemical analyses and over-all distribution of titanium in the various products obtained by chlorination and sulphuric acid baking of a sample of titanium matte prepared in the electric arc furnace.

A recovery of 95.2 pct of the titanium in the rutile concentrate has been obtained in usable form. It is also believed that a major part of the titanium in the slag may be recovered by sulphuric acid leaching or baking.

**Preparation of Titanium
Sulphides by Reaction of
Rutile with Carbon
Disulphide Vapor**

Several experiments were made to determine whether titanium sulphides

could be economically prepared from rutile by reaction with carbon disulphide vapor at elevated temperatures. In these tests, 85 pct rutile concentrates and a sample of low-grade rutile middling were sulphidized. Work on the low-grade material was abandoned when it was found that the gangue mineral, ankerite ($\text{CaO} \cdot (\text{MgFe})0.2\text{CO}_2$) was sulphidized before the rutile, thus causing an excessive consumption of carbon disulphide.

The procedure and apparatus used in these experiments were as follows: A weighed sample was mixed with a binder and charged into a vertical tube furnace. The charge was supported on a carbon block which was drilled with $\frac{1}{16}$ -in. holes to permit the carbon disulphide vapors to pass through the sample. The alundum or fused-silica tube was heated by an electric resistance furnace controlled by a rheostat. A weighed sample of carbon disulphide was placed in a three-necked Pyrex flask and heated by a water bath. A current of helium gas was passed over the surface of the carbon disulphide to carry it through the charge. The gases issuing from the top of the retort were passed through a water-cooled condenser to condense any unreacted carbon disulphide. The carbon disulphide was collected in a separatory funnel and returned to the distillation flask, while the tail gases were bubbled through a water trap to the atmosphere.

In a typical run a 150-g sample of 85 pct rutile was mixed with 7.9 g of sawdust and 29 g of water and heated to 800°C for 15 min. to remove the water and the volatiles in the sawdust. The charge was then heated at 1100°C for 8 hr while carbon disulphide vapor was passed through it. During the run 272 g of carbon disulphide were used. Part of this was used to sulphidize the rutile while the remainder was decomposed to form carbon and elemental sulphur. The analysis of the product obtained was 42.2 pct

titanium, 26.4 pct combined sulphur, 2.4 pct free sulphur, and 0.54 pct carbon.

A 100-g sample of this sulphidized product was chlorinated for 4½ hr at 200 to 220°C. A recovery of 59.4 pct of the titanium in the rutile was obtained. The product contained 15.3 pct titanium, 0.5 pct iron, 7.8 pct sulphur, and 78.1 pct chlorine.

It is believed that a higher recovery of titanium may be obtained, but this will be at the expense of greater carbon disulphide consumption and longer reaction times.

Conclusions

The results of the laboratory research work done thus far indicate that it is possible to produce titanium tetrachloride and titanium oxide from rutile by means of smelting the rutile with pyrite and coke and then processing the titanium matte. An impure iron is recovered as a byproduct. Ilmenite may be treated in the same way as rutile.

Recoveries of from 65 to 81 pct of the titanium in rutile may be obtained as an impure titanium tetrachloride by chlorinating titanium mattes at 150 to 250°C. When titanium matte is baked with sulphuric acid at 200 to 250°C, recoveries of 90 pct or more of the titanium in the rutile are obtained in the form of a titanium sulphate solution which is suitable for the recovery of pigment-grade titanium dioxide.

Chlorinating the mattes, followed by baking the residues with sulphuric acid gave titanium recoveries greater than 90 pct.

References

1. W. J. Kroll: The Production of Ductile Titanium. *Trans. Electrochem. Soc.* (1940) **73**, 35-47.
2. *Oil, Paint, and Drug Reporter* (April 25, 1949).
3. C. K. Stoddard and E. Pietz: Pilot Plant Distillation and Purification of Titanium Tetrachloride. *Bur. of Mines R.I.* 4153 (Dec. 1947).
4. See Ref. 2.
5. M. Picon: *Compt. Rend.* (1934) **198**, 1415-1417.
6. Biltz, Ehrlich, and Meisel: *Ztsch. anorg. allgem. Chem.* (1937) **234**, 97-116.
7. M. Picon: *Compt. Rend.* (1933) **197**, 1415-1417.
8. J. W. Mellor: A Comprehensive Treatise on Inorganic and Theoretical Chemistry, vol. 7.
9. J. Kleffner: *Metall. u. Erz.* **31**, 307-320.
10. Titanium in 1947. U. S. Dept. of the Interior, Mineral Market Reports NMS No. 1600 (Released May 22, 1948).
11. See Ref. 10.

Table 7 . . . Over-all Distribution of Titanium in Products from Titanium Matte

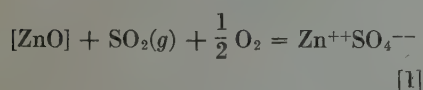
| Sample | Concentration | | | | Titanium Recovery |
|--|------------------|-----------------|--------|---------|-------------------|
| | Ti | Fe | S, Pct | Cl, Pct | |
| Chlorination product..... | 17.8 pct | 0.71 pct | 5.8 | 78.4 | 63.6 |
| Leach liquor from sulphuric acid bake | 34.5 g per liter | 1.6 g per liter | | | 31.6 |
| Leach residue..... | 4.4 pct | 0.9 pct | 4.7 | | 0.5 |
| Metallic product obtained during matte smelting..... | 0.33 pct | 85.9 pct | 1.2 | | 0.1 |
| Slag from matte smelting..... | 39.8 pct | 3.7 pct | 18.8 | | 4.2 |
| Total..... | | | | | 100.0 |

Recovery of Zinc by the Dithionate Sulphur-dioxide Leaching Process

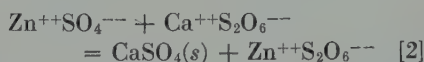
S. F. RAVITZ,* Member AIME, and A. E. BACK*

When manganese ores are leached with sulphur dioxide, a large part of any zinc in the ore usually is extracted with the manganese.¹ In the dithionate process,^{2,3} in which the manganese ore is leached with dilute sulphur dioxide gas and the manganese is subsequently precipitated by adding lime to the pregnant solution, the zinc is precipitated with the manganese. These facts suggested the possibility of applying the dithionate process to the recovery of zinc from oxidized ores or calcined sulphide concentrates. Accordingly, an investigation was begun, and preliminary tests were made on several ores and concentrates. The results were encouraging, but the need to devote available funds and personnel to other projects made it necessary to drop the work before the various factors involved in the process could be studied in detail. A brief mention of the process,⁴ however, elicited a number of inquiries, so that it appeared desirable to report the results of the preliminary work.

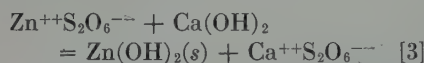
The dithionate process as applied to zinc may be summarized briefly as follows: The ore or calcined concentrate is leached with dilute SO₂ gas to dissolve the zinc, largely as zinc sulphate, in accordance with the following equation in which [ZnO] represents the "oxide zinc" in the ore or calcine:



If, in the leaching step, the ore or calcine is suspended in calcium dithionate solution, the sulphate ion, as it is formed, is precipitated immediately as calcium sulphate, which is subsequently filtered off with the insoluble ore residue:



An alternative procedure is to suspend the ore in water, filter off the insoluble ore residue after leaching, add calcium dithionate to the resulting zinc sulphate solution, and then filter off the calcium sulphate precipitate. In either event the zinc is obtained in the form of a pregnant solution of zinc dithionate, from which it can be precipitated as relatively pure zinc hydroxide by adding milk of lime:

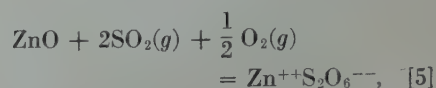


The zinc hydroxide precipitate is calcined to form the final zinc oxide product:



Theoretically the process is completely cyclic with respect to dithionate ion, the calcium dithionate required for reaction 2 being replaced by that formed in reaction 3. In practice, of course, small amounts of dithionate would be lost in the various filter cakes, depending on the economic washing limits. In the leaching step, however, some of the SO₂ is oxidized to dithionate instead of sulphate, accord-

ing to the following overall reaction:



so that the dithionate losses are made up, at least in part.

Ores and Concentrates Tested

The analyses of the ores and concentrates tested are summarized in Table 1, which also includes the analyses of the calcines produced from the concentrates. The concentrates were roasted in a laboratory muffle furnace at the temperatures indicated until evolution of SO₂ could no longer be detected; shallow clay dishes ordinarily were used; but calcines 2a and 2c were prepared in iron dishes, with the result that these two calcines were badly contaminated with iron scale.

The "complex" concentrate, sample 1, consisted essentially of sphalerite grains containing inclusions of pyrite and other sulphide minerals too minute to be liberated by grinding within economic limits. In the "marmatitic" concentrate, sample 2, the iron was present largely as marmatite (that is, as iron sulphide in solid solution in zinc sulphide) rather than as pyrite inclusions. The zinc was present largely as the carbonate in the two "oxidized" ores, samples 3 and 4, and as the silicate in the "willemite" ore, sample 5.

Leaching Tests

The leaching cell was a 3-liter glass beaker placed in an electrically heated water bath manually controlled to maintain a temperature of 35°C in the leach slurry. The slurry was agitated by means of a flat paddle-type stirrer

San Francisco Meeting, February 1949.

TP 2707 D. Discussion of this paper may be sent to *Transactions AIME* as a Technical Note. Manuscript received April 19, 1949.

* Metallurgist and former Metallurgist, respectively, Salt Lake City Branch, Metallurgical Division, U. S. Bureau of Mines, Salt Lake City, Utah.

Papers by authors of the U. S. Bureau of Mines staff are not subject to copyright.

¹ References are at the end of the paper.

Table 1 . . . Analyses of Ores, Concentrates, and Calcines

| Sample No. | Sample | Analysis, Pct or Ounces per Ton | | | | | | | | Oxide Zn, Pct of Total Zn |
|------------|--------------------------|---------------------------------|---------|------------|------|------|-----|------|-----|---------------------------|
| | | Zn | Total S | Sulphide S | Fe | Pb | Cu | Au | Ag | |
| 1 | Complex concentrate | 38.8 | 34.2 | | 13.3 | 2.5 | 1.5 | 0.08 | 6.0 | |
| 1a | Calcine, 985°C | 46.0 | 2.0 | 0.7 | 16.4 | 2.5 | 1.8 | 0.10 | 6.0 | |
| 1b | Calcine, 1035°C | 48.4 | 1.1 | 1.0 | 19.2 | 3.0 | 1.9 | 0.12 | 9.5 | |
| 1c | Calcine, 1000°C | 50.7 | 1.2 | 0.1 | 16.5 | | 2.0 | 0.12 | 8.0 | 80.0 |
| 1d | Calcine, 800°C | 43.8 | 5.8 | | 14.8 | 2.6 | 1.7 | 0.10 | 6.2 | 82.7 |
| 2 | Marmatitic concentrate | 46.1 | 30.8 | | 12.4 | 1.8 | 0.6 | 0.24 | 3.5 | |
| 2a | Calcine, 940°C | 43.2 | 0.3 | | 26.3 | | 0.6 | 0.23 | 2.9 | 71.0 |
| 2b | Calcine, 600°C | 48.9 | 4.7 | 0.3 | | | | | | 84.8 |
| 2c | Calcine, 600°C | 42.8 | 8.8 | 0.2 | | | | | | 85.8 |
| 3 | Goodsprings oxidized ore | 24.4 | 0.3 | | 4.2 | 10.3 | 0.7 | Tr | 3.2 | |
| 4 | Leadville oxidized ore | 25.4 | | | 14.2 | 0.1 | <.1 | | | |
| 5 | Willemite ore* | 47.2 | 0.1 | | 4.7 | 0.7 | 0.4 | | | |

* SiO₂, 22.2 pct.

Table 2 . . . Results of Leaching Tests

| Leach No. | Sample Leached | | SO ₂ Introduced, Gram per Gram Zn | Extraction, Pct | | | S ₂ O ₅ Formed, Lb per Ton Ore or Calcine |
|-----------|----------------|------------------------|--|-----------------|-----|----|---|
| | No. | Description | | Zn | Fe | Cu | |
| 1 | 1a | Complex concentrate | | | | | |
| | | 985° calcine | 4.3 | 83.2 | 2.8 | 44 | 61 |
| 2 | 1b | 1035° calcine | 2.1 | 60.4 | 0.3 | 1 | 30 |
| 3 | 1b | 1035° calcine | 4.3 | 82.4 | 1.2 | 34 | 46 |
| 4 | 1c | 1000° calcine | 4.1 | 80.0 | 1.0 | 33 | 77 |
| 5 | 1d | 800° calcine | 4.7 | 82.8 | 1.4 | 57 | 42 |
| 6 | 2a | Marmatitic concentrate | | | | | |
| | | 940° calcine | 4.4 | 73.9 | 1.8 | 22 | 43 |
| 7 | 2b | 600° calcine | 4.3 | 86.8 | | | 36 |
| 8 | 2c | 600° calcine | 4.3 | 86.1 | 2.8 | | 19 |
| 9 | 3 | Goodsprings ore | 4.7 | 84.8 | 3.2 | 66 | 21 |
| 10 | 4 | Leadville ore | 0.7 | 37.1 | 0.2 | | 61 |
| 11 | 4 | Leadville ore | 1.4 | 49.8 | 1.7 | | 70 |
| 12 | 4 | Leadville ore | 2.1 | 54.6 | 0.1 | | 66 |
| 13 | 4 | Leadville ore | 2.9 | 67.7 | 1.9 | | 70 |
| 14 | 4 | Leadville ore | 4.3 | 72.2 | 2.1 | | 77 |
| 15 | 5 | Willemite ore | 2.7 | 61.0 | 6.2 | | 24 |

rotating near the bottom of the cell at about 500 rpm. A mixture of SO₂ and air, containing approximately 3.5 pct SO₂ to simulate waste smelter gas, was introduced at a constant rate through two 1-mm glass orifices, the gas emerging in the direction of rotation of the stirrer at a point near the periphery of the cell about an inch above the bottom.

The material to be leached was suspended in water. In each test a quantity of minus 65-mesh ore or calcined concentrate containing approximately 50 g of zinc was placed in the cell, 1500 ml of water was added, the stirrer was turned on, and the 3.5-pct SO₂ gas was introduced at the rate of approximately 36 g per hr for the desired length of time, usually 6 hr. At the end of the leach the slurry was filtered, the residue was washed, and the products were analyzed. The results of various leaching tests are given in Table 2.

With 4.1 to 4.7 g of SO₂ per gram of zinc, 83 to 87 pct of the zinc was extracted from the calcined concentrates and from the Goodsprings ore; under similar conditions, 72 pct was extracted from the Leadville ore. Utilization of SO₂ was rather poor, since theoretically approximately 1.0 g of SO₂ would be required per gram of zinc to form zinc sulphate or sulphite and 2.0 g would be required to form zinc dithionate. The two tests on calcine 1b and the five on the Leadville ore indicate that SO₂ utilization becomes poorer as leaching progresses. The willemite ore gave an extraction of 61 pct with 2.7 g of SO₂ per gram of zinc, and it is probable that higher extraction would have been obtained with more SO₂. Extraction of silica from the willemite ore was 52 pct; the leach slurry filtered fairly well, but the filtrate sample, when examined some 46 days later, was found to have gelled. The calcine and Leadville ore slurries filtered rapidly, but the Goodsprings ore slurry filtered very slowly.

Extraction of zinc from the calcined concentrates agreed well with the percentage of zinc present as oxide, as determined by solubility in strong ammonium chloride-ammonium hydroxide solution; leaching tests with dilute sulphuric acid likewise gave approximately the same results. Microscopic, chemical, and X ray diffusion tests showed that virtually all the zinc in the leach residues was present as sulphide and ferrite, mostly the latter. Effect of ferrite formation is evident in tests 6, 7, and 8 of Table 2; when the concentrate was roasted at 940°C, zinc

extraction was 74 pct, whereas when the concentrate was roasted at only 600° to minimize ferrite formation, the extraction increased to more than 86 pct.

Extraction of iron was very low, amounting to less than 3 pct in most of the tests. Copper extraction, which was erratic, apparently depends on the extent of leaching and on the conditions of roasting. No lead and less than 3 pct of the gold or silver was extracted.

Dithionate formation ranged from 19 to 77 lb S₂O₅ per ton of ore or calcine (0.03 to 0.10 g per gram of zinc extracted). This would be ample, in most instances, to make up for washing losses in the process, which, it is estimated, would not exceed 30 lb per ton in practice. In the manganese investigation,^{2,3} however, it was found that dithionate formation depends on many factors, including size and shape of leaching tank, agitation rate, leaching rate, and method of introducing the gas, so that pilot plant tests would probably be required to determine whether dithionate formation would be adequate in leaching zinc ores or calcines under plant conditions. Dithionate formation was fairly constant in leaches 10 to 14, in which the leaching time ranged from 1 to 6 hr, indicat-

ing that most of the dithionate was formed during the first hour.

The ore and calcine samples lost a large part of their weight during leaching, so that the residues were substantially enriched in iron, lead, gold, and silver, as shown in Table 3, in which data for several typical tests are summarized. Compared with the original concentrate or ore, the increase in the iron, lead, gold, and silver assays was about threefold for the two concentrates and about twofold for the Goodsprings ore. The large losses in weight on leaching were due to the fact that the samples leached were suspended in water rather than in calcium dithionate solution; if the samples had been suspended in calcium dithionate solution, the leach residues would have contained considerable calcium sulphate formed by reaction 2, and the weight losses would have been much less.

Recovery of Zinc from Solution

Leach solutions for investigating the recovery of zinc oxide products were prepared from (A) the "complex" concentrate calcined at 600°C, (B) the "marmatitic" concentrate calcined at

Table 3 . . . Data on Leach Residues

| Leach No. | Sample Leached | Residue Weight, Pct of Ore or Calcine | Residue Assay, Pct or Oz per Ton | | | | |
|-----------|------------------------|---------------------------------------|----------------------------------|------|------|------|------|
| | | | Zn | Fe | Pb | Au | Ag |
| 1 | Complex concentrate | | | | | | |
| 3 | Calcine 1a | 40.2 | 20.0 | 38.3 | 6.0 | 0.21 | 14.2 |
| 5 | Calcine 1b | 43.4 | 19.2 | 42.0 | | | |
| 8 | Calcine 1d | 36.8 | 21.1 | 38.4 | | 0.26 | 16.1 |
| 9 | Marmatitic concentrate | | | | | | |
| 14 | Calcine 2c | 29.9 | 19.6 | 36.3 | | | |
| | Goodsprings ore | 53.6 | 7.0 | 7.5 | 19.1 | | 5.8 |
| | Leadville ore | 61.5 | 11.7 | 23.3 | | | |

Table 4 . . . Results of Precipitation Tests

| Test | pH | Analysis, Pct or Grams per Liter | | | | | | Zn Distribution, Pct | |
|-------------------------------|------|----------------------------------|-----|------|-----------------|-------------------------------|------|----------------------|---------|
| | | Zn | Fe | Ca | SO ₄ | S ₂ O ₃ | S | | L.O.I.* |
| Leach Solution | | | | | | | | | |
| A | 3.4 | 43.8 | 1.0 | 2.5 | 62.0 | 1.2 | | | 100.0 |
| B | 3.1 | 48.8 | 0.7 | | 51.2 | 1.4 | | | 100.0 |
| C | 3.7 | 27.6 | 0.3 | 0.7 | 36.4 | 1.0 | | | 100.0 |
| CaSO ₄ Precipitate | | | | | | | | | |
| A | | 0.1 | | 27.5 | 66.2 | | | | 0.2 |
| B | | 2.1 | | 26.0 | 64.5 | | | | 3.7 |
| C | | 0.05 | | 26.5 | 63.8 | | | | 0.1 |
| Pregnant Solution | | | | | | | | | |
| A | | 39.8 | | 15.0 | 5.9 | 172 | | | 99.8† |
| B | | 43.8 | | 13.6 | 11.4 | 154 | | | 96.3† |
| C | | 27.0 | | 15.7 | 1.9 | 146 | | | 99.9† |
| Zinc Precipitate | | | | | | | | | |
| A | | 54.0 | 1.3 | 2.4 | | 5.9 | 21.2 | | 99.8 |
| B-1 | | 20.5 | | 1.4 | 3.9 | 19.8 | | | 9.5 |
| B-2 | | 52.6 | 0.8 | 7.9 | | 6.8 | 14.8 | | 86.8 |
| C | | 56.4 | 0.6 | 2.8 | | 3.3 | 16.8 | | 99.9 |
| Zinc Calcine | | | | | | | | | |
| A | | 68.6 | 1.6 | 3.0 | | 1.7 | | | 99.8 |
| B-2 | | 61.6 | 0.9 | 9.3 | | 4.7 | | | 86.8 |
| C | | 67.2 | 0.7 | 3.3 | | 1.6 | | | 99.9 |
| Barren Solution | | | | | | | | | |
| A | 7.4 | <0.02 | | 27.1 | 1.1 | 121 | | | <0.1 |
| B | 10.5 | <0.02 | | 19.5 | 1.2 | 84.6 | | | <0.1 |
| C | 9.8 | <0.02 | | 22.0 | 0.8 | 97.5 | | | <0.1 |

* Loss on ignition at 1000°C.

† Includes zinc in wash solutions.

600°, and (C) the Goodsprings ore. A 200- to 300-g sample of each material was leached in 1500 ml of water with 3.5-pct SO₂ gas for about 12 hr, the residue was filtered off and the filtrate was treated as described below to precipitate calcium sulphate and zinc hydroxide successively. Each residue or precipitate was washed thoroughly, but to avoid dilution of the various solutions, the wash filtrates were discarded. The SO₂ contents of the solutions were not determined, but the odor of SO₂ was noticeable in the leach solutions and pregnant solutions, especially those from test B.

PRECIPITATION OF CALCIUM SULPHATE

To precipitate sulphate, leach solutions A and B were treated directly with finely divided crystals of CaS₂O₆·4H₂O assaying 13.3 pct Ca, 57.8 pct S₂O₆, and 0.35 pct SO₄ (theoretical

analysis: 14.7 pct Ca, 58.8 pct S₂O₆) Before adding the dithionate crystals to solution C, however, the solution was first treated with small additions of 20-pct sulphuric acid solution until the odor of SO₂ could no longer be detected and the pH remained constant at 1.9; 6.0 g of H₂SO₄ was required per liter of the solution. The quantities of calcium dithionate used per liter of leach solution were as follows:

| CaS ₂ O ₆ ·4H ₂ O Crystals Added Grams per Liter of Solution | |
|--|-----|
| A | 309 |
| B | 273 |
| C | 253 |

The analyses of the precipitates (dried at 110°C) and of the pregnant solutions are given in Table 4; the dried precipitates correspond closely to CaSO₄·½ H₂O, for which the theoretical analysis is 27.8 pct Ca and 66.1 pct SO₄.

PRECIPITATION OF ZINC

Freshly calcined lime containing 93.0

pct available CaO was used to precipitate the zinc. The lime was slaked in about 10 times its weight of water, and the milk of lime was added dropwise to the vigorously agitated pregnant solution over a period of about 45 min. Agitation was continued for several hours, after which the slurry was allowed to stand overnight, during which time the pH rose about two units. With pregnant solution B, sufficient lime was added to give a pH of 3.9, the resulting precipitate was filtered off, and the addition of lime was then continued as described. Theoretically 0.84 g of CaO is required to precipitate 1.0 g of zinc; the quantities actually used were as follows:

| | pH | Available CaO Used, Grams per Gram Zn |
|--------------|------|--|
| A | 7.4 | 0.83 |
| B—First ppt. | 3.9 | 0.10 |
| Final ppt. | 10.5 | 0.84 |
| C | 9.8 | 0.92 |

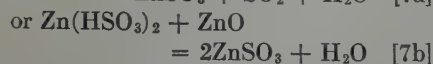
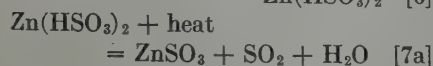
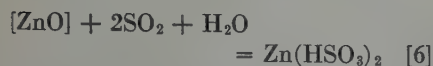
The precipitates were dried at 110°C, and portions of the final precipitates were calcined at 1000°C. The analyses of the precipitates, calcines, and barren solutions are summarized in Table 4.

The results show that virtually all the zinc in the leach solutions can be recovered as a calcine assaying nearly 70 pct Zn. No advantage appears to have been gained by acidifying the leach solution in test C. The double precipitation with lime in test B was detrimental, causing a loss of 9.5 pct of the zinc in the first precipitate. The lower grade of the product in test B compared with the other tests is due to the presence of considerable calcium sulphate as a result of the relatively high sulphate content of the corresponding pregnant solution. The reason for the differences in sulphate content of the pregnant solutions is not clear, however, since the three pregnant solutions have nearly the same calcium content. It may be that the solubility of calcium sulphate in the solutions varies with the sulphite content; pregnant solution B, which had the highest sulphate content, was known to be particularly high in sulphite, whereas pregnant solution C, which was lowest in sulphate, probably had the lowest sulphite content as a result of the acidification.

Discussion of Results

The dithionate process for zinc is similar in certain respects to two

processes investigated by Lyon and Ralston. In one of these,⁵ oxide ore or calcine is leached with sulphurous acid solution to dissolve the zinc as the hydrosulphite, the pulp is filtered, and the zinc is precipitated as the sulphite by either boiling the solution or adding zinc oxide. The precipitate is calcined to form zinc oxide and regenerate the sulphur dioxide. The reactions are as follows:



Lyon and Ralston tested several ores and calcines and obtained high extractions of zinc in solutions containing 0.2 to 4 pct SO₂. Precipitation of the zinc by boiling or by adding zinc oxide was incomplete, however, owing to the rapid air oxidation of zinc bisulphite to zinc sulphate and, in the case of calcines, to the presence of zinc sulphate formed in roasting.

In another process investigated by Lyon and Ralston,⁶ the zinc is extracted by leaching with sulphuric acid or by roasting with sulphuric acid and leaching with water. The zinc is then recovered from the zinc sulphate solution by a procedure similar to that in the dithionate process except that calcium chloride is used instead of calcium dithionate; that is, the solution is treated with calcium chloride to precipitate calcium sulphate and form zinc chloride solution, and the latter is treated with milk of lime to precipitate zinc hydroxide and regenerate the calcium chloride. Lyon and Ralston obtained precipitates assaying about 50 pct Zn, and calcination of the precipitates gave zinc oxide products assaying over 65 pct Zn. The main objection to the process, aside from the high acid consumption in leaching, was the fact that the treatment of the zinc chloride solution with lime resulted in the precipitation of basic zinc chloride

rather than zinc hydroxide, so that the precipitates contained 6 to 10 pct chlorine. This would involve a loss (in addition to normal washing losses) of 240 to 400 lb of chlorine per ton of zinc precipitated and would require 375 to 625 lb of make-up CaCl₂ per ton of zinc. Moreover, about 6 pct of the zinc was volatilized when the precipitates were calcined; this zinc would be lost unless expensive fume-collecting equipment were provided to recover it.

The present preliminary investigation of the dithionate process indicates that it may have promise for the treatment of oxidized zinc ores that cannot now be treated commercially and of off-grade complex zinc sulphide concentrates that can now be marketed with only relatively poor return for the values contained. Its advantages include (1) utilization of waste SO₂ gas for leaching; (2) possibility of forming enough dithionate during leaching to make up for losses; (3) separation of zinc from lead, gold, and silver; (4) recovery of zinc from solution by a simple precipitation with lime; and (5) production of a zinc oxide product assaying nearly 70 pct Zn. To determine the commercial feasibility of the process, however, would require a more extensive investigation. Among the factors that should be studied are effect of SO₂ concentration in the gas and of type of leaching cell on zinc extraction, SO₂ utilization, and dithionate formation; relative merits of leaching in water versus leaching in calcium dithionate solution; and effect of sulphite in the leach solution on the precipitation of calcium sulphate.

Summary

1. A new dithionate process for treating oxidized zinc ores or low-grade zinc concentrates is described. The ore or calcined concentrate is leached with dilute SO₂ gas, sulphate is precipitated by means of cyclic calcium dithionate, and the zinc is recovered from the solution by precipitation with

milk of lime.

2. In laboratory tests on several ores and calcined concentrates, 83 to 87 pct of the zinc was extracted, together with less than 3 pct of the iron, gold, or silver and none of the lead. Enough dithionate was formed during the leaching process to make up for losses. About 5 lb of sulphur dioxide was used per pound of zinc extracted.

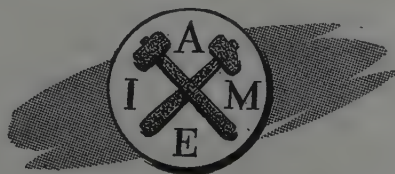
3. Virtually all the zinc in the leach solution was recovered as a precipitate which, after being calcined, assayed nearly 70 pct Zn.

Acknowledgments

The authors wish to express their appreciation to S. R. Zimmerley, Chief of the Salt Lake City Branch, Metallurgical Division, Bureau of Mines, for his helpful interest in the investigation and for arranging to obtain the samples of ores and concentrates tested; to J. D. Prater, H. E. Ohn, and the late W. F. Wyman for their invaluable assistance in the experimental work; and to the staff of the chemical laboratory of the Salt Lake City station, under the direction of H. E. Peterson, for the analytical work.

References

1. W. F. Wyman and S. F. Ravitz: Sulfur Dioxide Leaching Tests on Various Manganese Ores. U. S. Bur. Mines R.I. 4077 (1947), 12 pp.
2. S. F. Ravitz, W. F. Wyman, A. E. Back, and K. E. Tame: The Dithionate Process for Recovery of Manganese from Low-Grade Ores. *Metals Tech.* Sept. 1946, TP 2064.
3. S. F. Ravitz, A. E. Back, K. E. Tame, W. F. Wyman, and J. L. Dewey: Semi-Pilot-Plant Tests on Treatment of Manganese-Silver Ores by the Dithionate Process. U. S. Bur. Mines T.P. 723 (1949), 45 pp.
4. S. R. Zimmerley: Latest Developments in Ore Dressing. *Mining Congress Jnl.*, Feb. 1947, 39-42.
5. D. A. Lyon and O. C. Ralston: Recovery of Zinc from Low-Grade and Complex Ores. U. S. Bur. Mines Bull. 168 (1919), 81-84, 100-101, 130-131.
6. *Loc. cit.*, pp. 89-100.



Seminar on the Kinetics of Sintering

(With Discussion)

A. J. SHALER,* Member AIME

Introduction

The subject of the mechanism of sintering has received much attention in the past few years, particularly since the beginning of the series of AIME seminars in powder metallurgy of which this paper introduces the fourth. In the first of these, F. N. Rhines¹ brought together and discussed the available experimental data on the sintering of pure metallic powder, and succeeded in bringing to a sharp focus the attention of workers in this field on the established observations which a satisfactory theory must explain.

Several other authors^{3,5,6} have, in the last few years, studied the phenomena that occur when cold metallic powders, loose or in the form of compacts, are first brought to elevated temperatures. Some workers⁷ in the field of friction have recently studied the adhesion of solid metal surfaces when they are brought into close contact. These researches have indicated that several separate mechanisms operate simultaneously, at least during the first part of the sintering process. Some of them have been called *transient mechanisms*⁴ because they are in general not absolutely necessary to sintering. Powders may be so prepared and so treated that these transient phenomena do not take place during subsequent sintering. This does not mean, of course, that their industrial and scientific importance is any less than that of the *steady-state* phenomena. The latter are changes that go on during sintering no matter how the powders are made or treated; they cannot be divorced from sintering.

One way to analyze the process of sintering into its component parts is perhaps to distinguish between these

transient and steady-state phenomena. Some of the transient phenomena have been studied in the past few years. Hüttig³ has shown that, when the temperature of metallic powder is slowly raised, the following events generally occur in order: (1) physically adsorbed gases are desorbed; (2) there is an atomic rearrangement of the surface, a sort of two-dimensional "surface-recrystallization"; (3) there is a breakdown of chemically adsorbed surface compounds; (4) there is a recrystallization in the volume of the metal. All these changes are shown by Hüttig and his coworkers to be completed fairly rapidly at lower temperatures than those generally used in sintering and are therefore not a part of the mechanism whereby the density of a mass of powder continues to change after long heating at an elevated temperature. But the first and third of these changes release gases in quantities which may or may not help to control the steady-state mechanisms, depending on when the voids become isolated from the outside of the compact.

Among the phenomena studied by Steinberg and Wulff,⁸ there is the effect on sintering of residual stresses arising from the pressing operation. They found that the lateral surfaces of a green compact of iron are under a longitudinal residual tension-stress of the order of magnitude of half the yield-point for solid iron. If the outside surface is in tension, the core must be under longitudinal compression. When the compact is heated, the surface residual stress is thermally relieved

first, and the compact therefore initially expands in the direction of its axis. This is a transient phenomenon, if for no other reason than the possibility of sintering unpressed powders, as demonstrated by Delisle,⁹ Libsch, Volterra and Wulff¹⁰ and others.¹

The subject of recrystallization is dealt with further in a separate section, in view of its prominent place in sintering literature. It, too, is one of these transient phenomena.

Among the steady-state parts there may be distinguished the attraction between particles and its consequences, the spheroidization of voids in the compacts, and the densification or swelling of the compact.

There is considerable evidence^{4,7} showing that cold metallic surfaces, when brought to within a few interatomic distances of one another, are attracted to each other by forces of the order of many thousands of pounds per square inch. A calculation, discussed in greater detail in another section, shows that this force changes but slightly when the temperature of the surfaces approaches the melting point. Actual measurements of forces of adhesion of this magnitude have been made by Bradley¹² on some nonmetals, but none has yet been made on cold or hot metals. This force is of sufficient magnitude to cause some plastic deformation in powder compacts, as will be shown below.

A second force of steady-state nature is due to the surface tension, which probably has the same origin as the force of attraction between surfaces.^{16,4} A paper by Udin, Shaler, and Wulff¹³ gives the results of precise direct measurements of its value for solid copper. The demonstration of the tendency for the surface tension to shrink a pore was long ago given by Gibbs.¹⁷ He showed that its effect on a curved surface between two phases is equivalent to a pressure perpendicular to that

San Francisco Meeting, February 1949.

TP 2702 E. Manuscript received Nov. 8, 1948; revision received May 12, 1949.

* Assistant Professor of Metallurgy, Massachusetts Institute of Technology.

¹ References are at the end of the paper.

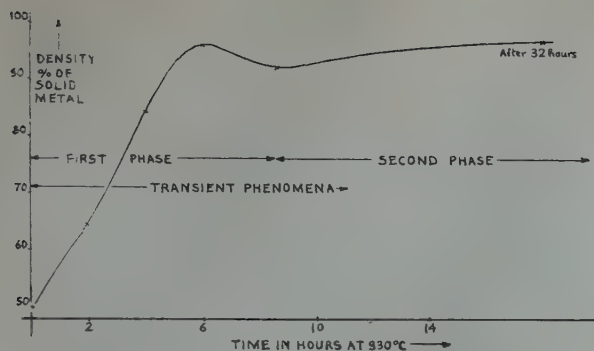


FIG 1—The progress of densification of a loose mass of copper powder (atomized #4915 MD63A, 5 pct 80 mesh, 10 pct under 150 mesh) in terms of per cent of the theoretical maximum.

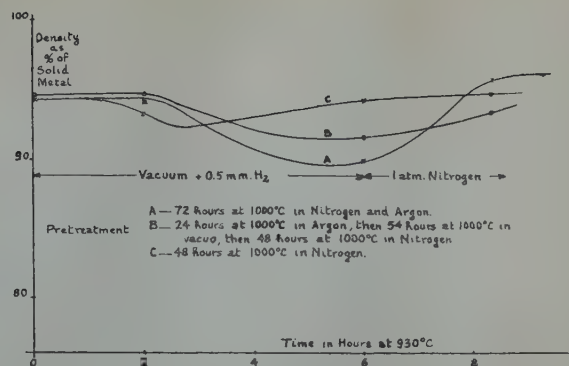


FIG 2—The progress of densification of compacts originally sintered in argon or nitrogen at one atmosphere, then subjected to heating variously in vacuo and in nitrogen.

surface and equal to twice the surface tension divided by the radius of the curvature. If the pressure of a gas within a pore is considered positive, then the pressure equivalent to the surface tension is a negative pressure directly opposed to it. Its magnitude depends on the size of the void. The interplay of this pressure and the pressure of the gases trapped within isolated voids has been described^{18,28} elsewhere.

An attempt will be made in this paper to show that the ordinary modes of plastic deformation (slip and creep) contribute appreciably only in the first-stage of sintering to the change of density of a compact, and also that surface diffusion and evaporation cannot make major contributions to the process of densification (or swelling) in most metals. Another mode of flow must be demonstrated to exist in order to account for the changes in density of a compact during later stages of sintering. The nature of this flow is at present one of the major incompletely solved problems in the theory of sintering. This meeting will probably have heard, before its close, more than one version of how surface tension and gas-pressure-differences can cause densification or expansion of compacts. After a brief discussion of recrystallization and of the contribution to sintering of surface-diffusion and evaporation, the steady-state processes will be analyzed in more detail.

Recrystallization

The term "recrystallization" has been used in two different senses. In the first, it has been applied to the reorganization of the lattice following its distortion by cold deformation; it pro-

ceeds by the diffusion of individual atoms from the distorted lattice to a nucleus; the nucleus, if it is big enough, grows into a new crystal having (despite its more perfect geometry) a lower free energy. In the second, broader, sense of the term, recrystallization means any change in crystalline shape brought about by a movement of individual atoms. If sintering takes place by a diffusion of atoms and not by slipping or twinning of blocks of atoms, then it is certainly a recrystallization in this second sense; but the term is then no more specific than "sintering" itself, and its use gives no more insight into the nature of the phenomena.

Balshin¹⁹ has advanced the hypothesis that recrystallization, presumably in the first, more restricted sense, begins at the points of contact between particles, where the greatest degree of cold deformation has been introduced during pressing, and that densification of the compact is a corollary of this recrystallization. But masses of powder need not be compressed in order to become more dense during heating. For illustration, Fig 1 shows the progress of densification of a mass of initially loose annealed copper powder (atomized, No. 4915 MD83A, Metals Disintegrating Co.) when it is heated in vacuo in a graphite container. According to this result, shrinkage does not require previous cold-working, and therefore requires no recrystallization. The converse, that recrystallization, in this sense of the word, does not result in shrinkage, can also be demonstrated. Smithells²⁰ reports that a cold-worked tungsten wire, coiled into an extremely fine coil, is recrystallized on heating in such a way that it becomes a single crystal whose orientation is independent of the direction of the axis of

the wire, as if the coil had been machined out of a single crystal in the first place. No change in shape or size occurs during this recrystallization. In the same way, it is not to be expected that a composite of particles in contact with one another should change in shape or size even if the entire mass becomes recrystallized into a single, porous, crystal.

To demonstrate further that recrystallization following cold-work cannot be responsible for changes in the density of compacts, loose masses of powder were heated in argon or nitrogen at one atmosphere (14.7 psi) until their final stable equilibrium-density was reached (this equilibrium is described below). They were then heated in vacuo, wherein a different relation existed between the driving forces of surface tension and differential gas-pressure; they were observed to expand to a new equilibrium-density, which thereafter remained relatively stable in spite of further heating in vacuo. These compacts, as detailed in Fig 2, were then reheated again in nitrogen at one atmosphere until they regained their first equilibrium-density. It is highly improbable that these changes of external stress of 14.7 psi could induce enough deformation to initiate new recrystallizations. These experiments support the conclusion of Rhines¹ that recrystallization, in this sense, proceeds no differently in powder-compacts than in more massive metals, and have nothing to do with the changes in density of these compacts during sintering.

Such simple experiments further show that the reactions between the gases within the pores and the metal surrounding them have at most an influence on sintering which is independent of the main mechanism

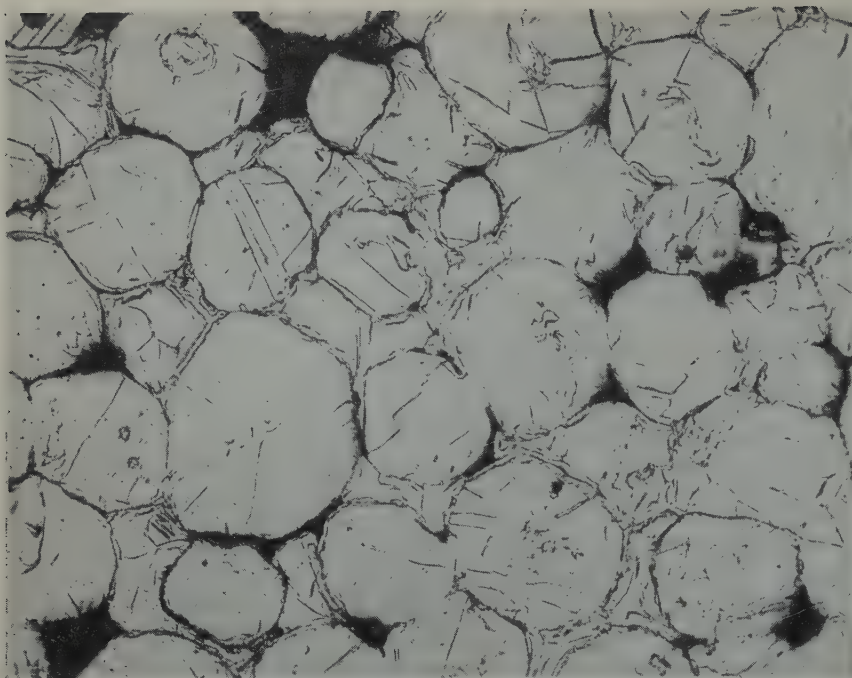


FIG 3—Micrograph at $\times 500$ of loose copper powder heated 24 hr in argon at 1 atm at 1000°C , then 54 hr in vacuo at 1025°C .

Deeply etched and repolished several times. Density 97 pct of theoretical. Note tendency of pores to become spherical. Note also recrystallized "bridges" between some particles.

whereby compacts become more or less dense. A change in the pressure of gas outside the compact can in no way influence the equilibria of reactions at the surface of pores sealed from the outside, provided the temperature is not changed. The phenomena of recrystallization and of desorption or adsorption of gases are therefore of transient influence on sintering, and their effect is not in evidence after the first heating-up period, during which they govern the amount of gas that will be trapped within the pores. After that period, the nature of the sintering process must be sought in other phenomena.

Surface Diffusion and Evaporation

Pines²¹ and more recently Ivensen²² have stated that surface diffusion and the process of evaporation from one place and condensation at another cannot change the density of a compact. This thesis has been further supported by Shaler and Wulff¹⁸ by the following argument. In a mass of powder particles, imaginary continuous lines may be drawn, passing through the centers of the particles and through the centers of the metallic "bridges" where they make contact with one another. These lines may be drawn in such a way that they never emerge from the surface of the metal

into the voids between the particles. The aggregate of these lines forms a skeleton. No process can be imagined whereby this skeleton is changed in shape or size unless there is flow within the particles themselves, or across the solid metallic "bridges." If recrystallization has permitted the lattices of the particles to be continuous through these "bridges," as countless micrographs, including that of Fig 3, have shown to be the fact in sintering, then these bridges are made of metal which is in general no different from the metal in the particles themselves. A change in size or shape of the skeleton—and hence of the compact as a whole—must involve flow in the volume of the metal. No redistribution of metal taking place at the surface of the voids between particles can cause any change in the skeleton, which never touches that surface.

If all the voids are connected by channels to the outside of the compact, of course, metal from the outside layers can proceed *via* the gas-phase or by surface-diffusion towards the interior. But this movement ceases as soon as the voids become isolated from the outside. There is other evidence to show that such a transient process can have little influence on the course of sintering—for instance, markings on the surface of compacts do not disappear during sintering.

On the other hand, surface-diffusion and vapor-phase transport do have a

function in sintering, but it is not that of changing the density. An aggregate of powder differs from a solid piece of metal chiefly in that it has a great deal more surface per unit of mass. Hüttig³ and the author⁴ show that metal powder made of micron-size particles has so much surface that its free-energy is of the order of 1000 cal per mol greater than that of solid metal. The mass of powder can reach an intermediate state of lower free-energy if the voids between the particles become spherical. Such a spheroidization of the pores has been observed, as pointed out by Rhines.¹ It can proceed by surface-diffusion or by evaporation and recondensation, for it involves only a redistribution of the metal at the surfaces of the voids. It can also proceed by a flow of the metal particles and bridges. A calculation⁴ has shown that, in nearly spherical pores (of radius 100μ) inside a copper compact at 850°C , the flow process is more rapid than the evaporation process and probably also than the surface-diffusion process. At the beginning of sintering, however, when the contact areas between the particles are small and the voids have sharper corners, the reverse may be true.

In brief, then, surface-diffusion and vapor-phase transport have a function in sintering, in that they assist the flow process in leading to a spheroidization of the pores. But these mechanisms cannot effect a change in the density of the compact, a change which requires a flow of the metal within the particles themselves.

The First Phase of Sintering

During the first phase, in the sintering of loose powder masses, the particles preserve to a great extent their original shape, and the voids are interconnected. In the second phase, which may best be studied separately, the pores are disconnected entities, and the compact may be considered a porous, but continuous, medium. Sauerwald²⁵ has shown that the mechanisms in sintering loosely pressed compacts resemble those found in sintering loose powder, whereas heavily compressed compacts already contain disconnected pores in the green state.

If the pores are all joined together and have passage to the outside, there is evidently no difference in gas pressure between the pores and the atmosphere, so that no force is to be expected

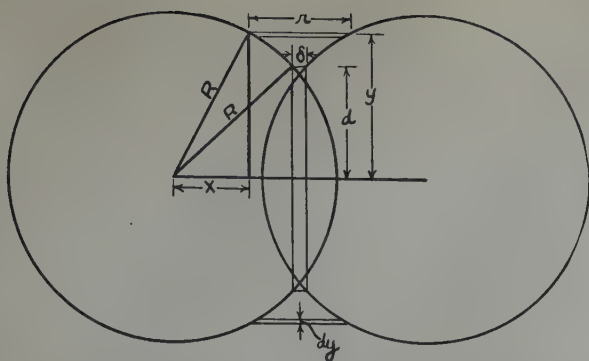


FIG 4—Two spheres, partly coalesced, separated by a minimum distance δ , and subject to attraction across cylindrical elements of length r and of thickness dy .

from this source. The surface tension exists, but it is perhaps more convenient to treat it in this phase as the force of attraction between particles. It has been shown^{4,29} that this procedure is justified, since the two forces stem from the same origin.

The force of attraction has been calculated⁴ on the following basis: according to the Sommerfeld¹¹ model of a metal, it is made up of positive ions of infinitesimal size, regularly distributed at the intersections of a geometric lattice; around the ions there is a cloud of fast-moving electrons. The electron density varies, but it is assumed to be uniform as a first approximation. The surface of the metal may be defined as the last layer of ions. The electron cloud does not stop abruptly, however, although its density falls off rapidly outside this layer. The presence of another surface nearby causes the density of the cloud to increase considerably, beyond the surface, and to fall off more gradually. If the surfaces come to within several interatomic distances of one another, there is an appreciable number of electrons moving about throughout the space between them. Each of these electrons is attracted to both the opposing surfaces, so that in effect the two surfaces are attracted to one another because they are both attracted to the electrons between them. The calculation of this force of attraction has yielded, as a first approximation, the following results: two copper surfaces, 30 Å apart, attract each other with a force of approximately 120,000 psi; this force drops to about 55,000 psi if the separation increases to 60 Å, and to about 30,000 psi when the distance is 120 Å. A rise in the temperature from 20 to 700°C decreases these values by only about 15 pct. Cleanliness of the surface is not a serious factor unless thick layers of compounds are formed. The

electronic work-function of copper, which depends on cleanliness, can vary from 1 to 5 electron volts without changing the force of attraction more than 10 pct. The calculation cannot be extrapolated to distances less than about 15 Å, because when the surfaces come that close together, the ions begin to repel one another, and the attraction falls off again. The expression is also not valid at great distances, where the presence of foreign ions and atoms interferes with electron movement. An approximate expression can be made to fit the data given above, and the unwieldy equations from which they were calculated are not necessary for practical use. If the distance r separating the surfaces, or elements of surface, is given in inches, then the force in pounds per square inch between them is given, within 10 to 15 pct, by the formula

$$f(r) = 1.4 \times 10^{-2} \frac{1}{r}$$

With this as a quantitative basis, the force of attraction between two coalescing spherical particles may be calculated. Fig 4 shows such a system. The distance δ between them is a region where, as a first approximation, the metal may be considered solid; in this disc-like region the force of attraction

becomes balanced by the ionic force of repulsion. Outside this disc, the surfaces gradually fall away from one another, and are under the influence of the force of attraction. The force pulling together the ends of the cylindrical element of thickness dy and height r at a radius y from the center-line is then

$$2\pi y f(r) dy$$

Integrating from $y = d$ to $y = R$, and remembering that δ is much smaller than R , an expression is found for the total force acting in such a way as to pull the spheres together and compress the disc between them. This expression is

$$F = 4.4 \times 10^{-2} \sqrt{R^2 - d^2} \ln \left(\frac{2}{\delta} \sqrt{R^2 - d^2} \right)$$

Since the area of the disc is πd^2 , the compressive stress acting on it is $\sigma = F/\pi d^2$. The spheres are assumed to remain spherical and to preserve their radius, a good approximation for small values of d . Fig 5 shows the values of this stress as a function of the radius d of the disc, that is, of the degree of coalescence of the two spheres, for copper spheres 0.01 cm in radius (200μ in diam). At first contact, when d is

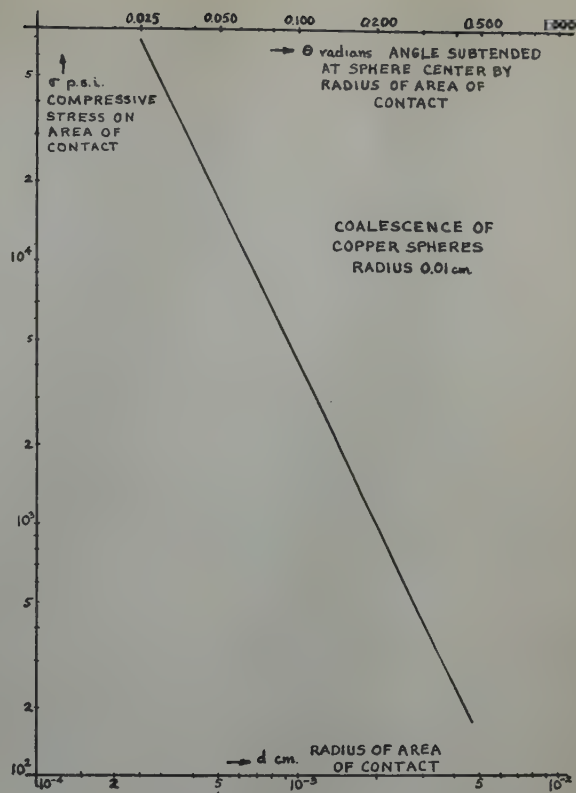


FIG 5—Plot of the compressive stress on the contact area, and of the angle subtended by the radius of that area at the sphere centers, for various degrees of coalescence of copper spheres of radius 0.01 cm.

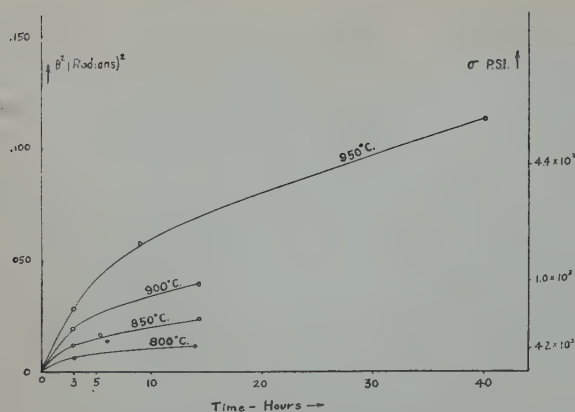


FIG 6—The growth of the area of contact of copper spheres, 0.01 cm in radius, with time at various temperatures. The ordinate is the square of the angle subtended at the sphere centers by the radius of the constant circle. Stresses corresponding to these angles, from the previous figure, are shown at the right.

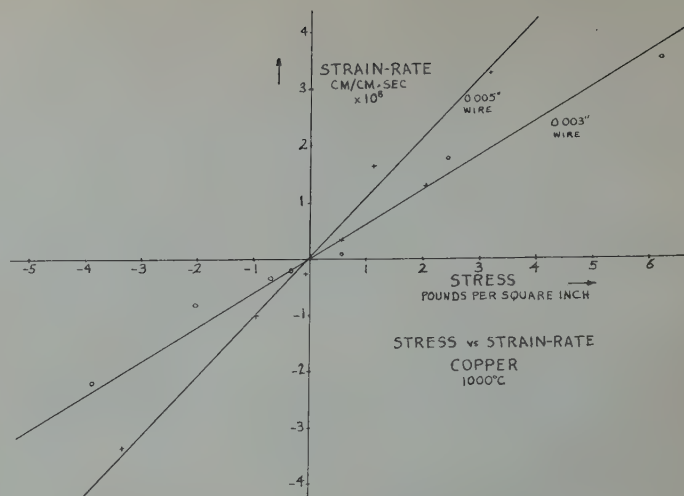


FIG 7—Plot of stress vs. strain-rate for copper wires 0.005 and 0.003 in. diam at various temperatures. Data from Udin, Shaler and Wulff.

small, the stress of compression on the contact area is very large, and unless there is interference from oxide films or layers an immediate cold-welding occurs, as it does in the friction experiments⁷ mentioned earlier, and in those of Bradley on some nonmetallic spheres.¹² Plastic deformation under this stress leads to an increase in the area of contact, and the compressive stress on that area falls off until it becomes less than the least stress necessary to cause plastic flow. But at elevated temperatures, which do not appreciably decrease the force involved, the metal is still able to creep conventionally at these lower stresses. The time factor now enters into the picture, as it does in creep. Soon the compressive stress has fallen to a value lower than the stress-limit for creep, and the first stage of sintering is at an end. By this time, the pores are disconnected, and a new type of flow becomes predominant.

Experiments on the coalescence of spheres have been carried out by the author with the assistance of H. Bernhardt. Copper spheres were selected from a commercial grade of atomized powder (described below) by first sieving for the $-70 +100$ mesh fraction, then sorting out the particles by rolling them down a narrow ground-glass plate 4 ft long, and inclined at about 4° . The few particles that rolled down the whole length of the plate were selected for the experiments. These particles were packed in carbon-black and heated for 5 hr at 750°C in an atmosphere of dry deoxidized hydrogen at 0.5 mm pressure. After slowly cooling them to room-temperature, the spheres were separated from the carbon-black in an air-classifier. Several

particles were then placed in contact with each other in a deep groove in a graphite block. After heating for various periods of time at various temperatures in an atmosphere of dry deoxidized hydrogen, the strings of spheres were observed in a microscope equipped with a micrometer eyepiece. The diameters of the areas of contact and the distances between the centers of the spheres were measured. The angle θ subtended at the center of the spheres by half the radii of the contact areas were plotted against the time at various temperatures. There was some scatter due to the fact that many of the particles were not sound throughout, and that their surfaces, after deoxidation, were not perfectly spherical. The mean deviations from the mean values of θ were of the order of 10 pct. Each point in Fig 6 is the mean of from 5 to 24 spheres, plotted on coordinates of θ^2 and time t . According to Frenkel's analysis,²⁶ if the coalescence of spheres takes place by a purely viscous flow, the points on such a plot should lie on a straight line passing through the origin, since θ^2 is then directly proportional to the time ($\theta^2 = \frac{3\gamma t}{2\eta r^3}$ where r is the sphere radius, γ is the surface tension, and η is the viscosity coefficient). In these experiments the curves are straight only at larger values of the time, and no straight line, however fitted to the points, passes through the origin. Rather, the slope of the line initially decreases rapidly with time at heat, showing that the coalescence starts with a rapid mode of flow (first stage of sintering by creep or even normal slip) and gradually becomes slower until a

viscous flow becomes dominant (the line straightens out). Experiments² reported recently by Jordan and Duwez agree with this view. Others⁵ may not.

In Fig 6, the stresses corresponding to the various values of θ^2 are given on the right-hand scale. These have been taken from Fig 5 ($\sin \theta = d/R$). Note that the linear portion of the curves, representing the second stage of flow, begins at approximately 5000 psi at 800°C , but that non-linearly continues at 950°C until the stress has fallen as low as a few hundred pounds per square inch. Flow in the first stage is thus a process which appears to begin at a critical stress-limit, decreasing as the temperature rises, as in conventional creep. The type of flow required in second-stage sintering cannot have a critical stress-limit, for flow must occur under infinitesimal stress, at a correspondingly small rate, in order to account for experimental results.

Until more is known about the creep of copper at high temperatures under stresses of the order of hundreds of pounds per square inch, it is not possible to predict the rate of this first stage of sintering, when the particles coalesce and the voids between them become disconnected. In highly compressed compacts and in the later stages of sintering of loose or lightly compressed powders, the first stage is by-passed or ended, and the mechanism of sintering involves the slower, viscous, flow described below.

The first stage of sintering is further complicated by all the transient effects described in previous sections, some of which may tend to expand the compacts, some others to shrink it.

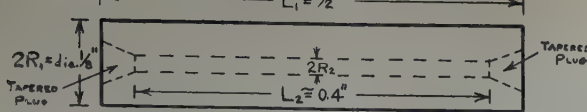


FIG 8—Artificial pore in a short length of copper wire.

Flow in the Second Phase of Sintering

In the second stage, the pores are in general disconnected, and any change in density of the compact involves a change in pore-volume and therefore in the pressure of the gas trapped within the pores. The force of shrinkage, previously manifested as the attraction between surfaces, can now be more conveniently considered as the surface tension.

Surface tensions and pressures of gas such as are encountered in powder metallurgy can form high stresses at the surface of very small pores—stresses great enough to induce plastic flow by the well-known modes of slip, twinning or creep. But it was shown that there can be no density-changes in compacts unless flow takes place inside the particles away from the surface of the pores. Here the effects of the surface tension and of the gas pressure are diluted because they act over a larger area. In the compacts described below, in which marked densification takes place, the pores have an approximate radius of 100 microns. At a distance of only 10 microns away from the surface, the stress induced by the surface tension is less than 3 psi. In the hollow tubes, whose densification is also described below, the radius of the hole is of the order of 2500 microns (0.01 in.), and the stress, even at the surface, is less than 1 psi.

• The mechanism of flow at these low stresses has not been extensively investigated. Chalmers²³ has observed the flow of tin at small stresses, and found a viscous flow at room temperature. Udin, Shaler, and Wulff¹³ measured the rate of flow of copper at elevated temperatures, under stresses of up to 6 psi on wires 0.005 and 0.003 in. in diam. Fig 7 reproduces their data in terms of stress and strain-rate. These results are consistent with a viscosity, independent of stress, expressed by the relations

$$\eta = 5.94e \frac{66490 \pm 1000}{RT}$$

for 5 mil wire, and

$$\eta = 1.32 \times 10^3 e \frac{53756 \pm 1000}{RT}$$

for 3 mil wire.

Kanter²⁷ and Frenkel²⁶ predict on theoretical grounds that the phenomenon of self-diffusion should lead to a viscous flow whose heat of activation is the same as that for self-diffusion (57,000–61,000 cal per mol for copper). The viscosities given above have a heat of activation near that range (66,000 and 54,000 cal per mol). Kê²⁴ has observed a room-temperature grain-boundary flow having the heat of activation for self-diffusion, in both iron and alpha brass. Little can be said with certainty about flow at these stresses save that it is of a viscous nature. Newtonian viscous flow is characterized by the fact that the stress vs. strain-rate curve is linear and passes through the origin. The flow is further complicated by the fact that there is evidently a dependence of viscosity on size. Possibly the self-diffusion coefficient also varies with size.

To show whether a viscous flow of this nature could be responsible for the shrinking of closed pores in sintering, a direct measurement was made. Since the artificial creation of a spherical hole of very small size in a piece of metal entails mechanical difficulties, a cylindrical hole was used. Such holes were drilled (diameters *ca.* 0.02 mm) lengthwise in three short lengths of copper wire. The drilled tubes were then heated overnight at 1000°C in dry deoxidized hydrogen at 0.5 mm pressure, and furnace-cooled. The outside diameter of the tubes was 1/8 in., and their length 1/2 in. The ends of the holes were tapered to a depth of 3/64 in., and tapered plugs were made to fit. One end of each was firmly closed by

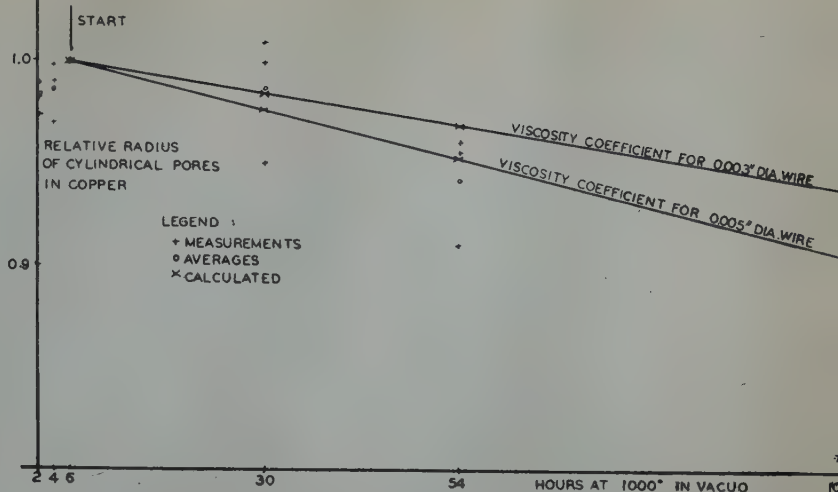


FIG 9—The relative change in radius of cylindrical "pores" in copper, compared with calculated from viscosities of copper wires.

pressing-in the plugs. In the other ends, the plugs were left loose, so that, during heating in vacuo, the holes would be evacuated before becoming sealed. A sketch of such a tube is shown in Fig 8. Being closed, as shown in a previous section, it cannot shrink by surface-diffusion or by evaporation, although by these processes the radius of the hole may expand at the expense of the length (spheroidization), but the radius and length of the hole may both decrease by flow under the action of surface tension. To heat the tubes, they were placed vertically into wells drilled in a graphite block, loosely-plugged ends uppermost. An undrilled 1/2 in. length of the same wire, similarly annealed and mounted, was used as a control. The heating chamber in which heating was carried out was a long quartz tube, sealed at one end, and fitted at the other with a waxed-in rubber stopper. Two glass tubes, fitted into the stopper, led respectively to a mechanical vacuum pump and gauge and to a source of hydrogen. The quartz tube could be evacuated and then inserted into a chromel-wound furnace. In this way, high-temperature seals were avoided, and heating and cooling-times would be cut to a minimum. The same furnace technique was used in the experiments on the coalescence of spheres and on the sintering of compacts, described elsewhere in this paper. The source of hydrogen was a commercial cylinder, from which the pressure was reduced by a conventional reducing valve to about 15 psi. The gas went to a purification train consisting of four tubes containing respectively heated copper gauze, indicating Drierite, palladium-alundum, and activated alumina. From this train, the

hydrogen passed through a constriction-flowmeter, and then through a 4 ft length of 1.2 mm capillary tubing before entering the quartz furnace-chamber. The capillary furnished a pressure differential such that atmospheric pressure could be maintained in the reducing train and flowmeter, whereas a vacuum of 0.5 mm could be easily obtained in the furnace-chamber.

The small copper tubes were first subjected to a series of three 2-hr heats at 930°C, and thereafter, since density measurements showed the metal had nearly reached stability under these conditions, to a series of 24-hr heats at 1000°C. After each heat the tubes were radiographed; their external dimensions were measured with a micrometer caliper, and their density was determined to four significant figures pycnometrically. The dimensions of the holes were found from the density determinations, and were checked by measuring the radiographs on a film-reader.

The function of the hydrogen leak at 0.5 mm pressure was to insure the reduction of any oxygen leakage and also to reduce all oxide in the metal, without introducing into the "pore" enough gas to provide appreciable pressure until the shrinkage had become considerable. Fig 9 shows the relative radius of the cylindrical "pores" plotted against time-at-heat. Also plotted are the slopes of the calculated curves to be expected if the mechanism of flow is the same as that found in wires by Udin, Shaler, and Wulff.¹³ These two curves are plotted for the viscosities observed on 0.005 and 0.003 in. wires at 1000°C. It is expected that the size-effect on the value of viscosity should disappear rapidly at larger sizes. In the tubes, the wall thickness is about 0.050 in., so that the slope should be somewhat greater than that given for 0.005 in. wires. The calculation of these curves was done as follows (see Fig 9): The incompressibility of the metal requires that the same weight enter into and flow out of a cylindrical shell of thickness dA at radius A from the pore centerline. The outermost and innermost shells yield the equations

$$\frac{dA}{dt} = \frac{R_2}{A} \frac{dR_2}{dt} = \frac{R_1}{A} \frac{dR_1}{dt}$$

The strain-rate at any radius A , in terms of the rate of decrease of R_2 , is

$$\frac{d\epsilon}{dt} = \frac{d}{dA} \left(\frac{dA}{dt} \right) = -\frac{1}{A^2} R_2 \frac{dR_2}{dt}$$

Since the stress-strain relation for viscous flow is

$$\sigma = \eta \frac{d\epsilon}{dt}$$

the heat dissipated by flow per unit volume per unit time, at radius A , is then, after Frenkel²⁶

$$dE_F = 2\sigma\epsilon = 2\eta\epsilon \frac{d\epsilon}{dt} \\ = 2\eta \left(\frac{d}{dA} \left(\frac{dA}{dt} \right) \right)^2$$

In a length l of the tube

$$E_F = 2\eta \int_{R_2}^{R_1} \left(\frac{d}{dA} \left(\frac{dA}{dt} \right) \right)^2 2\pi A l dA \\ = 2\pi\eta l R_2^2 \left(\frac{dR_2}{dt} \right)^2 \left(\frac{1}{R_2^2} - \frac{1}{R_1^2} \right)$$

The loss in surface energy per unit time, due to the reduction of both inside and outside surfaces, is, if γ is the surface tension,

$$E_s = -\frac{d}{dt} (2\pi l \gamma (R_2 + R_1)) \\ = -2\pi l \gamma \left(1 + \frac{R_2}{R_1} \right) \frac{dR_2}{dt}$$

Equating E_F to E_s , and simplifying,

$$\left(1 - \frac{R_2}{R_1} \right) dR_2 = -\frac{\gamma}{\eta} dt$$

Using the incompressibility condition, and integrating from the initial radii R_{10} and R_{20} , there results

$$(R_{20} - R_2) - (R_{10} - R_1) = \frac{\gamma}{\eta} t^*$$

from which the curves of Fig 9 are drawn, using the values of γ and η at 1000° from Udin, Shaler and Wulff.¹³

It is clear from these curves that the hollow cylinders do shrink under the influence of surface tension and it is probable that the size effect is real, and must be taken into account in sintering theory; the particle-size as well as the pore-size is a variable affecting the sintering rate of a compact.

Rate of Sintering in Second Stage

The same calculation as that made for a cylindrical pore has been made for a spherical pore by Frenkel.²⁶ In a vacuum, according to him, the energy dissipated in viscous flow becomes, if R is the pore radius at any time,

* The right-hand member should be $\frac{1}{2} \frac{\gamma}{\eta} t$ (see Discussion by Eshelby) and Fig 9 has been redrawn with the correct value.

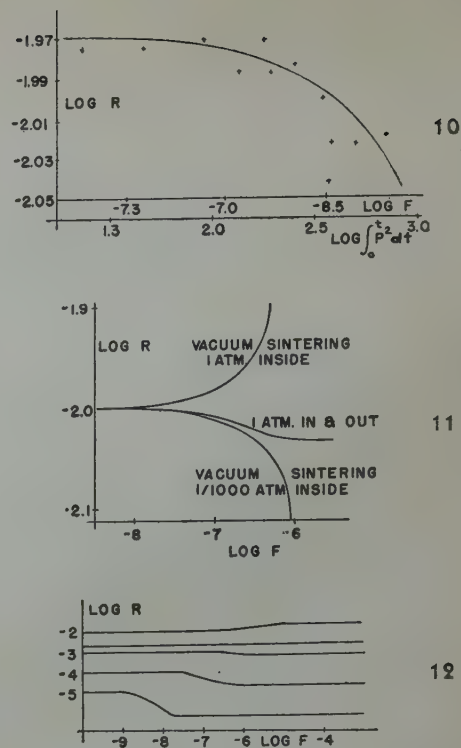


FIG 10—Change in average pore-radius during sintering of unpressed copper powder at 850°C.

After Shaler and Wulff.*

FIG 11—The change of radius of pores during various conditions of sintering in noble gas.

The top and bottom curves eventually level out also. After Shaler and Wulff.

FIG 12—The changes in the radii of pores of various initial radii, under conditions of vacuum sintering of compacts in which noble gas is trapped at an initial pressure of one atmosphere.

After Shaler and Wulff.

$$E_F = \frac{32\pi\eta R}{3\rho} \left(\frac{dR}{dt} \right)^2$$

where ρ is now the density of the porous metal surrounding the spherical void. Since the compact is usually very large compared to the void, its external radius is neglected. The density ρ varies with time during shrinkage of the compact, and therefore the rate of sintering must be measured by a parameter which combines both the time and the changing density. One such parameter, which greatly simplifies the calculations, is

$$F = \frac{3}{8\eta} \int_0^t \rho^2 dt$$

* Fig 10, 11 and 12 are reproduced from Fig 2, 3 and 4 of "Mechanism of Sintering" by A. J. Shaler and John Wulff, *Ind. and Eng. Chemistry*, May 1948. Reprinting is by permission of the copyright owner, the American Chemical Society.

Here the density ρ is introduced as a fraction of the density of solid metal. Equating E_F to the loss in surface energy E_s , as before, leads in the case of a spherical pore to

$$F = \frac{R_0}{2\gamma} - \frac{R}{2\gamma}$$

where R_0 is the initial pore radius.

Unpressed masses of powder particles, closely sized by sieving, were heated in vacuo at 850°C. The initial radius of the pores, R_0 , was calculated by assuming that the number of pores was equal to the number of particles. This assumption is valid in the case of a regular geometrical packing of the particles. Since the density of the loose mass was 0.51 of that of copper, and a simple cubic array would have a density of 0.52, this condition was judged to be fairly well obeyed. The effective radius of the pores was consequently found from the volume of voids divided by the number of particles. Since the average radius of the particles was 0.011 cm, that of the pores was 0.0103 cm. The validity of assuming that the voids are spherical is discussed in detail by Shaler⁴ and by Shaler and Wulff,¹⁸ and found to be satisfactory for voids which are not needlelike or flake-like. From Fig 6 it is observed that the end of the first phase of sintering is reached at 850°C when the contact-area radius is less than $\frac{1}{10}$ the radius of the particle. The densification corresponding to this point is very slight, so that in studying the progress of sintering of such copper compacts at this temperature, the first phase may be neglected. At higher temperatures it would have to be taken into account. After heating these compacts for various periods of time, their densities were measured, and the time and density values were combined to give values of the parameter F . When these were plotted on logarithmic paper against the changing radii of the pores, also found from the density, the points of Fig 10 resulted. The calculated curve in the figure corresponds to a coefficient of viscosity with a heat of activation near 66,000 cal per mol.^{4,18} The viscosities obtained in Udin, Shaler and Wulff¹³ have heats of activation of 66,490 cal per mol for 0.005 in. wire, and 53,756 cal per mol for 0.003 in. wire. The diameter of the particles used in the compacts was 0.008 in.

So far no account has been taken of the pressure of gas trapped within the pores. Three kinds of gas may be present: those which dissolve in the metal

or form a compound with it; those which diffuse through the metal at an appreciable rate; and those which neither diffuse, dissolve, nor react. The first kind have a pressure P_e dictated only by the temperature; when the pore shrinks, the gas is not compressed, but instead more of it goes into solution or reacts; the pressure does not change, and is constantly opposed to the stress introduced by the surface tension. Accordingly, if there is a pressure P_0 outside the compact, the pore shrinkage obeys the expression

$$\frac{dR}{dt} = \frac{3}{8\eta} [(P_0 - P_e)R - 2\gamma] \rho^2$$

Solving for F leads to⁴

$$F = \frac{2.3}{P_0} \log \frac{(P_0 - P_e)R - 2\gamma}{(P_0 - P_e)R_0 - 2\gamma}$$

If P_e is larger than P_0 , it is observed that pores initially of large size do not shrink, but expand on heating; that is, the compact swells. In copper, where γ is of the order of 1400 dynes per cm, pores larger than 5×10^{-3} cm in radius swell if $P_e - P_0$ is one atmosphere.

Gases of the second kind are more troublesome. The pressure of such gases depends on two factors: how fast the pore is shrinking; and how far inside the compact the pore is situated. No simple expression for the rate of sintering can be found except for particular cases. For instance, in the case of a very rapidly diffusing gas, the pressure stays generally low and may be neglected.

The third kind, the noble gases, are of more general interest, because all compacts pressed in air contain oxygen and nitrogen. The oxygen is generally removed during the first stage of sintering, either by the reducing atmosphere of the furnace, or in the form of compounds having a low equilibrium pressure. The nitrogen remaining behind is noble to many engineering metals. The expression for the parameter F is, in the case of a noble gas,

$$F = \int_{R_0}^R \frac{dR}{\frac{P_0 R_0^3}{R^2} - 2\gamma - P_0' R}$$

The labor of solving this equation is great, and it has been performed⁴ for one particular case only; namely, for pores 0.01 cm in radius, containing a noble gas initially at one atmosphere, the compact being sintered in a noble gas also at one atmosphere. Fig 11 compares the progress of sintering under these conditions with the prog-

ress in the case of vacuum sintering of compacts with and without any trapped gas. The limiting case where $P_0' = 0$ is easier to treat and yields:

$$F = -\sqrt{P_0 R_0^3} \left[\frac{1}{2\gamma x} + \frac{1}{2\gamma} \left(\frac{1}{2\sqrt{2\gamma}} \ln \frac{x - \sqrt{2\gamma}}{x + \sqrt{2\gamma}} \right) \right] x \sqrt{\frac{1}{R}} \sqrt{P_0 R_0}$$

where

$$x^2 = \frac{P_0 R_0^3}{R^2}$$

The curves corresponding to this expression, for P_0 equal to one atmosphere, are given in Fig 12. Pores larger than a critical size (2.4×10^{-3} cm radius) are seen to expand; finer pores shrink.

Fig 11 and 12 show another phenomenon: the change in pore-size takes place most rapidly during a relatively short time-range. The time range depends only on the pore-size, not on the conditions of gas pressure. Thus in Fig 11, the change, whether of expansion or shrinkage, is most rapid in the range of $\log F$ from -6 to -7 for pore-radii of 0.01 cm. From Fig 12 it is evident that the finer the pores are, the sooner they change. A compact pressed in air containing an assortment of pores ranging in radius from 0.0001 cm to 0.01 cm, would, upon sintering in vacuo at 850°C, first begin to shrink, in a very few minutes; and later, after an hour or more, it would expand again, and finally reach a stable density. Such a sequence is clearly shown in the work of Drapeau in cylindrical copper compacts.²⁸

In heavily pressed compacts of ductile metal powders, the voids, originally isometric, are compressed to a flake-like shape. The radius of curvature in the direction of pressing is then much larger than it is in a direction perpendicular to the pressing direction. Although the gas pressure is hydrostatic, the surface-tension force is not, and the pores may at first shrink in the lateral direction, while axially they are effectively larger and do not yet change. At a later time they may expand in the direction of pressing while remaining unchanged laterally. The final length of a cylindrical compact so compressed would be unchanged after a short sintering period, but the radius would have decreased. After a longer time of sintering the length might be greater, the diameter having suffered no further change. In such a case a short sintering time would yield a denser product than

a long sintering time, and the shrinkage of at least one dimension could be held to a minimum.

The porosity of a compact is not a direct measure of its fracture strength, as Sauerwald has often pointed out.²⁵ The shape of the voids is an important factor, because spherical pores are not as effective in concentrating stresses as are shapes containing sharper curvatures. Furthermore, long times of sintering favor conventional grain-growth, which may have a deleterious effect on strength. A more exact knowledge of the changes in shape and dimensions of pores and grains could be acquired by further study along the lines described here, and might permit powder metallurgists to select, on a more scientific basis, the proper pressures, temperatures, and times necessary to treat a compact to its best possible physical properties.

Conclusions

There remain many unsolved problems. For instance, it would be useful to know the atomistic nature of the viscous flow observed to take place at high temperatures under low stresses. In particular, the size effect observed by Udin, Shaler and Wulff¹³ and its relation to particle-size require more study. The role of oxide-films, of the thickness commonly found on metal powders, needs quantitative treatment. Such films undoubtedly affect the surface tension, the force of attraction, and govern in a large measure the pressure of gases trapped within the pores. In view of the extensive use of hydrogen-containing sintering atmospheres, the kinetics of sintering in the presence of diffusible gases is a field in which more work must be done. Finally, a great deal more experimental work must be done to test the hypotheses brought out in this paper regarding the force of attraction and the flow of metals under small stresses.

The sintering process is an extremely complicated one. In addition to the changes known to occur during the heat-treatment of massive metals—recrystallization, grain-growth, and others—the presence of a large surface-to-volume ratio increases the effects of transient phenomena such as the reactions and desorptions that occur at the surfaces of metals.

This study has given a more quantitative evaluation than any heretofore carried out of some of the mechanisms that are in operation during sintering.

Among these are the force of attraction between metal particles, the role played in the first stage of sintering by plastic flow or creep, and the nature of the last stage of the process, in which a viscous flow takes place under the combined action of surface tension and gas pressure.

Considerable attention has also been given to the part played in sintering by the transport of metal through the mechanisms of recrystallization, flow, surface-diffusion, and evaporation.

It has been shown that copper, and by inference, other metals, possess in the solid state a surface tension not widely different from that of the molten metal, and that this force alone is capable of bringing about changes in density in powder compacts. The question of why some compacts shrink, others swell, and still others do both simultaneously in different directions and at different times has been discussed. Methods of calculation have been outlined wherewith a powder metallurgist can evaluate the best conditions of time, temperature, particle-size and pressure required to meet his specifications.

In a limited range of cases it is now feasible to predict the course of sintering with some precision, and some observations, which until now have been puzzling to students in this field, can now be interpreted with less difficulty.

References

1. F. N. Rhines: Seminar on the Theory of Sintering. *Trans. AIME* (1946) 166, 474. *Metals Tech.* Aug. 1946. TP 2043.
2. C. Jordan and P. Duwez: The Densification of Copper Powder Compacts in Hydrogen and in Vacuum. *Jnl. of Metals*, 96, Feb. 1949.
3. G. F. Hüttig: Die Experimentellen Feststellungen über den Frittungsverlauf (and other papers). *Kolloid Ztsch.* (1942) 98, 6; (1941) 94, 137; (1941) 94, 258; (1942) 98, 263; *Ztsch. Anorg. Chem.* (1941) 247, 221; (1942) 249, 134; (1942) 250, 1; (1943) 257, 95.
4. A. J. Shaler: The Kinetics of the Sintering Process. ScD. Thesis, Dept. of Metallurgy, Mass. Inst. of Tech., June, 1947.
5. G. Kuczynski: Self-Diffusion in Sintering of Metallic Particles. *Jnl. of Metals*. Feb., 1949, 169.
6. R. Kamm, M. A. Steinberg and J. Wulff: Lead-grid Study of Metal Powder Compaction. *Trans. AIME* 180. *Metals Tech.* Dec., 1948 TP 2487.
7. B. W. Sakmann, J. T. Burwell, and J. W. Irvine: Measurement of the Adhesion Component in Friction by Means of Radioactive Indicators. *Jnl. App. Phys.* (1944) 15, 459.

8. M. A. Steinberg: Discussion, Density Relationships of Iron-powder Compacts. *Trans. AIME* 171, 485. *Metals Tech.* Aug. 1947, TP 2222.
9. L. Delisle: Bonding Metal Particles by Heat Alone Without Pressure. *Trans. Electrochem. Soc.* (1944) 85, 171.
10. J. Libsch, Volterra, and J. Wulff: Chap. 35 in J. Wulff: *Powder Metallurgy*. Cleveland, Am. Soc. for Metals, 1942.
11. F. Seitz: *Modern Theory of Solids*. N. Y., McGraw-Hill, 1940.
12. R. S. Bradley: The Cohesive Force Between Solid Surfaces and the Surface Energy of Solids. *Phil. Mag.* (1932) 13, 853.
13. H. Udin, A. J. Shaler and J. Wulff: The Surface Tension of Solid Copper. *Jnl. of Metals*. Feb. 1949, 186. TP 2530.
14. F. Sauerwald and Drath: Surface Tension of Molten Metals and Alloys. *Ztsch. f. Anorg. Chem.* (1927) 162, 301.
15. J. Frenkel: The Surface Electric Double Layer of Solid and Liquid Bodies. *Phil. Mag.* (1917) 35, 297.
16. A. G. Samoylovich: Electronic Theory of Surface Tension in Metals. *Comptes Rendues, Acad. of Sci., URSS* (1945) 46, 365.
17. J. W. Gibbs: *Collected Works*. N. Y., Longmans Green, 1926.
18. A. J. Shaler and J. Wulff: Mechanism of Sintering. *Ind. and Eng. Chem.* (1948) 40, 838.
19. M. Y. Balshin: A Contribution to the Theory of Metalloceramic Processes. *Vestnik Metalloprom.* (136) 16, 91.
20. C. J. Smithells: *Tungsten*. London, Chapman & Hall, Ed. 2, 1945.
21. B. Y. Pines: Mechanism of Sintering. *Jnl. Tech. Phys.* (1946) 16, 737. *Trans.* by G. Kuczynski.
22. V. A. Ivensen: Investigation of Process of Density Increase in the Sintering of Single-Phase Metal Powder Compacts. *Jnl. Tech. Phys. USSR*, (1947) 17, 1301.
23. B. Chalmers: Microplasticity in Crystals of Tin. *Proc. Roy. Soc.*, (1936) 156, 427.
24. T. S. Kê: Viscous Slip Along Grain Boundaries and Diffusion of Zinc in Alpha Brass, and other papers. *Jnl. App. Phys.* (1948) 19, 285; *Phys. Rev.* (1948) 73, 267 and *Metals Tech.*, to be published.
25. F. Sauerwald: Über die Elementarvorgänge beim Fritten und Sintern von Metallpulvern. *Kolloid Ztsch.* (1943) 104, 144.
26. J. Frenkel: USSR. *Jnl. of Phys.* (1945) 9, 385.
27. H. Kanter: The Problem of the Temperature Coefficient of Tensile Creep Rate. *Metals Tech.* (1937) 4, 8.
28. J. E. Drapeau: Sintering Characteristics of Various Copper Powders. *Powder Metallurgy*, edited by J. Wulff, Cleveland, Am. Soc. for Metals, 1942, pp. 323 ff.
29. P. Schwartzkopf: Contribution to the Theory of Sintering. *Powder Metallurgy Bull.*, 3, Sept. 1948, 74.

Discussion

(F. V. Lenel presiding)

H. H. HAUSNER*—I am surprised that Shaler in his excellent study on sintering does not apply electrical test

* Sylvania Electric Products.

methods in order to determine and distinguish the various stages of sintering. Electrical resistance or conductance measurements on sintered compacts permit a deeper insight in the process of sintering and especially in the earlier stages—or as Shaler calls it in the first phase of sintering, than any other methods.

The electrical resistance of a sintered material is composed of two different types of resistances: the particle resistances and the resistances between the particles which we call contact resistances.* In a general way (and before recrystallization) the total of the particle resistances will be the same whatever the particle size is, or whatever the respective degree of sintering of the compacts is. The contact resistances between the particles however will greatly change with the bond between the particles and will therefore be an indicator for the respective stages of sintering.

It is not only the electrical resistivity which permits conclusions on the bond between particles but also the temperature coefficient of resistance. Oxide layers, impurities or other material on the grain boundaries will greatly affect the contact resistance and especially influence its change with the temperature.

The results of a comprehensive study on the electrical properties of sintered material, especially describing the effect of the degree of sintering on the electrical resistivity of compacts will be published in the near future.

A. J. SHALER (author's reply)—I should like to thank Dr. Hausner for his excellent suggestion. I look forward with interest to the publication of his results. Owing to the complexity of the sintering process and the number of variables changing simultaneously during heating, I prefer, whenever possible, to simplify the problem by studying such models as a string of small perfect particles, or a synthetic pore. If, at some time in the future, I understand fully what is going on in these simple models, then I shall feel free to carry out experiments on the enormously more complicated problems existing in compacts made of irregular particles of various sizes and of different compositions. The state of the science concerning contact resistance and the passage of the electric current through complex surfaces in contact with one another is not yet such as to permit me to use it with much confidence as a research tool.

E. F. SWAZY† and L. S. BUSCH†—Generally, the powder metallurgist is concerned with the space between metal powder particles more than the particles

themselves. In making structural parts, he is concerned with minimizing pore space or eliminating it. In making bearings, filters, or any parts in which the pores are later filled, he is concerned with the shape, size, and degree of continuity or discontinuity of these spaces between the powder particles. Any work deserves great praise which sheds light upon the behavior of these spaces during the treatments usually afforded articles made from metal powders. Dr. Shaler's paper describes such work.

In the treatment of fine copper powder to reduce the oxides formed during storage, appreciable sintering occurs even at very low reduction temperatures. If the cake so formed is broken up, then changes which have occurred during the reduction (which can be considered a step in the elimination of the so-called transient phenomena) will affect the subsequent states through which a compact goes during sintering. We feel that any attempt to divorce completely the "steady state" and "transient phenomena" is a dangerous one and might lead to oversimplification of a difficult problem. One can consider these phenomena separately but cannot separate them finally.

We believe that the question of change in pore discontinuity during sintering deserves some discussion. It seems very dubious to us that the pores, resulting from the pressing of a compact from any metal powder particle which is not flat, ever become discontinuous.

Consider a three dimensional figure similar to Fig 4; that is, a closely packed group of spheres. It is difficult to imagine a complete discontinuity of the pores until the compact becomes completely dense, particularly if the particles retain some measure of their spherical shape on all surfaces forming a pore wall.

If the particle shape is changed before complete densification, as by repressing, it is conceivable that the pores might become discontinuous. But, as shown by the table that follows, porosity is still continuous even after severe repressing. It is conceivable then, that surface diffusion and evaporation can be considered part of the steady state phenomena. Certainly the rate at which both of these proceed would increase rapidly with increasing temperature and would also increase with time at a high temperature.

In the following table is shown the relative degree of porosity of copper compacts made from a minus 100 sieve, hydrogen reduced, copper powder sintered at 900°C for one-half hour and repressed at various pressures. The pressed density was 7.5 g per cc and the sintered density was approximately 85.5 pct of absolute in each case.

The degree of permeability was measured by noting the time required for a pressure of 90 lb of air on one side of the compact to fall to atmospheric pressure

| Final Density g per cc | Pct of Absolute Density | Relative Permeability to Air |
|---------------------------|----------------------------|------------------------------------|
| 8.00 | 89. | 5 |
| 8.25 | 92.8 | 5 |
| 8.32 | 93.5 | 1 |
| 8.40 | 94.4 | 3/4 |

on the other. The figures indicate that the pressure fell 6.6 times as fast in the 89 pct dense specimen as in the 94.4 pct dense one, but the important point is that the pores did not become discontinuous in any case. Neither do the pores in materials which develop a liquid phase become discontinuous. Porosity as low as 0.5 pct can be detected by liquid absorption methods in such materials as carbides or other high density materials and also in some materials which are pressed, sintered, and repressed to densities as high as 96 pct of absolute.

A. J. SHALER—Mr. Busch has brought up an interesting question concerning the closing of cavities. I think evidence exists that in pressing, a large proportion of the voids become isolated, and contain trapped gas at a pressure somewhere near the pressure with which the compact has been compressed. Some very thin compacts have even been observed to explode. I see no explanation unless the gas is trapped in sealed-off voids at high pressure. If Mr. Busch has made a three dimensional model of a group of spheres close-packed or otherwise, he cannot have failed to notice that in between them, on certain planes, there is a definite neck through which the passage of a gas or liquid is limited. The area of such necks must decrease in the first stage of sintering when the contact areas between spheres increase. If the sphere centers approach one another the neck is also gradually throttled down. It does not take very much increase in contact area or decrease in the distance between centers to close them completely. In later stages of sintering I cannot see any other explanation for the swelling of compacts than the presence of a force directed outward and acting on the void surface; that force to my mind can only be a gas pressure.

Other evidence in this connection is shown in the experiments reported on Fig 2, in which I was able to heat up compacts of spherical copper particles under isothermal conditions in a gas at a pressure of one atmosphere. The density of the compact increased at a gradually decreasing rate until, after a prolonged period of heating, an equilibrium density was obtained. These compacts were then heated further in vacuo. By thus forming a differential in pressure between the gas inside the voids and the gas outside the compact I was able to bring the density gradually down to a lower equilibrium value.

The reason for the residual permeability in carbides or in copper compacts

* H. H. Hausner: The Effect of Particle Size on the Electrical Properties of Sintered Materials. Powder Metallurgy Bull. (1948) 3, 4-8.
† P. B. Mallory & Co., Inc.

must be that there is a wide initial variation in the void sizes. That might in turn be due to a wide variation in the particle size or to an irregular distribution of the particles.

In that case, regions containing large pores take a considerably longer time to reach the end of the first phase of sintering than those containing only small ones. I think if regular geometrical patterns of equal spherical particles could be put together and sintered you would find the permeability reaching zero after long heating.

F. N. RHINES—If I remember correctly, Mr. Busch's sintering conditions were one hour at 900°. We have made some observations on changes in pore shapes at various temperatures and times. In the specimens that we used, the pores were definitely still connected and far from being spherical in one hour at 900°. However, as time goes on, the pores do spheroidize and by 1000 hr at 900° they are very close to being spherical and quite obviously not connected. I think that the observation under discussion is to be associated with too short a time to get into the condition of the samples to which we refer.

J. D. ESHELBY*—There are slight numerical errors in the formulas given by Dr. Shaler for the rate of closing of both cylindrical and spherical cavities. In view of the importance of these results it may be of interest to show how they may be derived by elementary, if rather tedious, methods.

In the case of the cylindrical cavity it is clear that a square of unit side with a diagonal pointing towards the center of the cavity suffers a pure shear $2\,de/dt$ per unit time. The work required to produce this shear is $\eta(2\,de/dt)^2$, twice Dr. Shaler's value.

In more complex cases this simple argument cannot be applied. We may start from the basic law of viscosity in the form: a unit surface normal to the direction of the velocity gradient has a tangential force acting on it of magnitude $\eta \times$ velocity gradient and directed parallel to the velocity. For any particular problem a volume-element can be chosen all of whose faces are subject only to shear stresses. If we choose a system of reference in which the center of the volume-element is at rest the work done on each face in unit time is then the product of η , the velocity gradient, the area of the face and the velocity of the surface in its own plane.

For the cylindrical case the appropriate volume-element is the cube, one of whose faces is the square ABCD, with BD along a radius. After unit time it has the shape A'B'C'D'. If AB = 1, then AA' = BB' = $\frac{1}{2}\sqrt{2}\,de/dt$. AB has undergone a rotation and a displacement Aa = bB'

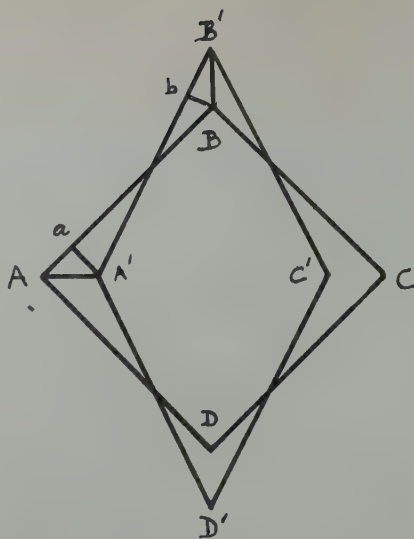


FIG 13—Sketch to illustrate calculation of rate of closing of a cylindrical cavity.

= AA'/ $\sqrt{2}$ = $\frac{1}{2}de/dt$ which is its velocity in its own direction. The shear strain is, as before, $2de/dt$: it is the velocity gradient normal to AB. The work done on the face AB per unit time is thus $\eta(de/dt)^2$. There are equal contributions from the other three faces so that the rate of dissipation of energy per unit volume is $4\eta(de/dt)^2$ as before. The corresponding value for the rate of closing of a cylindrical cavity is

$$dR/dt = -\frac{1}{2}\gamma/\eta.$$

For the spherical case the appropriate volume-element is a regular octahedron with the line joining a pair of opposite vertices pointing along the radius (Fig 13). The medium suffers an extensional strain de/dt per unit time in the radial direction. To preserve constancy of volume there must be a contractional strain $\frac{1}{2}de/dt$ in directions at right-angles to the radius. The three diagonals of the octahedron are thus parallel to the principal axes of strain: in such a case it is known* that its faces are subject only to shear stresses. The velocity gradient between opposite faces is easily shown to be $\sqrt{2}(de/dt)$. Suppose that the previous figure now represents a section of the octahedron with B,D as opposite vertices and A,C the mid-points of a pair of opposite edges. If the edge of the tetrahedron is 1 then BD = $\sqrt{2}$, AC = 1. Aa now becomes $(de/dt)/4\sqrt{3}$ and bB', $(de/dt)/\sqrt{3}$. The component along AB of the velocity of the face of the octahedron varies linearly between these limits on passing from A to B. The mean value over the face is found to be $(de/dt)/2\sqrt{3}$. The area of the face is $\sqrt{3}/4$. This leads to $\sqrt{2}\eta(de/dt)^2/8$ for the work done on this face per unit time. There are eight such faces and the volume

of the octahedron is $\sqrt{2}/3$ so that the rate of energy dissipation per unit volume is $3\eta(de/dt)^2$.

For a spherical cavity in an infinite medium $de/dt = -2(dR/dt)R^2/A^2$ so that the total rate of dissipation of energy is

$$\begin{aligned} E_F &= 12R_0^4\eta\left(\frac{dR_0}{dt}\right)\int_{R_0}^{\infty}\frac{4\pi}{A^6}A^2dA \\ &= 16\pi\eta R_0\left(\frac{dR_0}{dt}\right)^3 \end{aligned}$$

that is, $\frac{3}{2}$ times the value given by Frenkel. The error in Frenkel's paper* is the following, using his notation: with spherical polar coordinates the non-vanishing components of his v_{ik} are v_{rr} , $v_{\theta\theta}$ and $v_{\phi\phi}$, not merely v_{rr} , as he states. The condition of incompressibility gives at once $v_{\theta\theta} = v_{\phi\phi} = \frac{1}{2}v_{rr}$. In his integral v_{rr}^2 must therefore be replaced by $v_{rr}^2 + v_{\theta\theta}^2 + v_{\phi\phi}^2 = \frac{3}{2}v_{rr}^2$.

The rate of closing of the cavity is

$$dR/dt = -\frac{1}{2}\gamma/\eta$$

It is interesting to note that this is the same as for the cylindrical cavity.

These and other results can also be obtained directly from an analogy between viscous and elastic problems pointed out by Goodier.† Suppose that an incompressible elastic solid (that is, one with a Poisson's ratio $\frac{1}{2}$) is deformed by the application of surface or body forces, and that the components of elastic displacement at a point are u, v, w . If the shear modulus μ is replaced by a coefficient of viscosity η then u, v, w are the velocities of flow of a viscous liquid under the same forces. The rate of dissipation of energy is found from the elastic energy by replacing μ by η and multiplying by 2, since we require stress \times rate of strain instead of the familiar $\frac{1}{2}$ stress \times strain.

Thus, for example, the rate of contraction of the spherical cavity is equal to the displacement of the surface of a spherical cavity in a medium with shear modulus η when the same surface-tension forces are applied. The energy need not be introduced, since the solution of the elastic problem is known. As a matter of fact the elastic energy per unit volume is $\frac{1}{2}Ee^2$ where E is Young's modulus ($= 3\mu$ for an incompressible solid) and e is the radial strain. The dissipation in the viscous case is thus $3\eta(de/dt)^2$ as before.

Summary

There is an error in the formula given by Frenkel for the rate of energy-dissipation round a closing spherical pore. This has the effect of replacing the numerical factor $3\frac{2}{3}$ by 16 in Dr. Shaler's expression for E_F . For the corresponding cylindrical problem the rate of dissipation should be $4\eta(de/dt)^2$, not $2\eta(de/dt)^2$.

* H. H. Wills Physical Laboratory, Univ. of Bristol, England.

* See for example A. Nadai: *Jnl. App. Phys.* (1937), 8, 205.

* J. Frenkel: *Jnl. of Phys. USSR* (1945), 9, 385.
† *Phil. Mag.* (1936) (7), 678.

It is shown how these results may be obtained by elementary methods.

A. J. SHALER—I thank Dr. Eshelby for bringing up this point and for his elegant demonstration. He is entirely correct as I discovered some three or four weeks ago when I recalculated this entire problem by yet a third approach, namely the Rayleigh equations of hydrodynamics. The correction, as you see, alters the constant factor in the result. I have recalculated the curves of Fig 9 accordingly, and have also added some experimental points obtained since the time of writing. The results are not precise enough to show any different agreement with the corrected curves, which are shifted by a small amount. Further experiments are in progress.

R. SHUTTLEWORTH*—Goodier³⁰ has pointed out that the problem of the steady flow of a viscous fluid and the elastic displacement of an incompressible solid are mathematically identical. Suppose that two isotropic homogeneous bodies of the same shape—one purely elastic and incompressible, the other purely viscous—are loaded in the same way; the displacement of the elastic body is given by the product of μ and a function of position, while the velocity in the viscous case is given by the product of η and the same function, where μ and η are the shear modulus and the coefficient of viscosity.

It is useful to apply this correspondence to the calculation of the rate of shrinkage of a viscous fluid that contains a large number of equal spherical pores, of radius R , due to surface tension (Dr. Shaler's model of sintering). The elastic problem is the deformation of the corresponding body formed from an incompressible but shearable material, due to a hydrostatic pressure $-2\sigma/R$ inside all the pores and zero pressure outside the body, where σ is the surface tension. Because the material is incompressible the deformation depends only upon the pressure difference between the inner and outer boundaries (this immediately follows from principles of superimposition of strains and the proportionality of stress to strain); the problem thus reduces to the deformation due to a hydrostatic pressure $+2\sigma/R$ outside the body and zero pressure inside the pores.

The hydrostatic pressure produces shears in the walls separating the pores, which cause a reduction in volume of the pores (the volume of the solid, of course remains constant). It is possible to treat the body as a homogeneous continuum, and every element of volume V (supposed so large that it contains many pores) has a simple dilatation strain dV/V which is independent of the size and shape of the body, and of the position of the element. The displacement be-

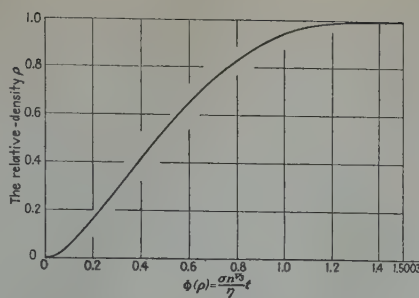


FIG 14—The increase at relative density with time at sintering.

tween any two points is proportional to their initial separation.

To make the theory quantitative it is necessary to find a relation between the dilatation and the pressure $2\sigma/R$. Here the approximation is made that the decrease in volume of a porous sphere is the same whether the pores are uniformly distributed or are all collected together at the center of the sphere. Love³¹ gives an expression for the radial displacement μ of the outer surface of a solid shell with internal and external radii a and b , due to an external pressure, from this expression

$$\frac{dV}{V} = \frac{3u}{b} = -\frac{3}{4\mu} \frac{a^3}{b^3 - a^3} \frac{2\sigma}{R}$$

A more accurate calculation could perhaps be made along the lines indicated by Bruggeman.³²

The relative-density ρ is defined by, $\rho = V_m/V$ where V_m is the volume of metal in an element of volume V , therefore

$$\frac{dV}{V} = -\frac{d\rho}{\rho}; \frac{a^3}{b^3 - a^3} = \frac{1 - \rho}{\rho}$$

If there are n pores per unit volume of metal, then

$$\frac{1}{R^3} = \frac{4\pi}{3} \frac{\rho}{1 - \rho} n$$

n can be calculated from the initial density and the initial pore radius; it does not change with time. And so

$$d\rho = \frac{3}{2} \left(\frac{4\pi}{3} \right)^{1/3} \frac{\sigma n^{1/3}}{\mu} \rho^{1/3} (1 - \rho)^{2/3}$$

In the viscous case each element of volume (together with its pores) flows towards the center of the spherical specimen with a velocity which is proportional to its distance from the center. The rate of decrease $-dV/dt$ of an element of volume V , corresponds to the decrease of volume $-dV$ in the elastic case:

$$\frac{d\rho}{dt} = \frac{3}{2} \left(\frac{4\pi}{3} \right)^{1/3} \frac{\sigma n^{1/3}}{\eta} \rho^{1/3} (1 - \rho)^{2/3}$$

The density increases uniformly throughout the whole body, at a rate which is independent of the size and shape of the body. When the last equation is integrated the relative-density is obtained as a function of time t ,

$$\frac{\sigma n^{1/3}}{\eta} t = \frac{2}{3} \left(\frac{3}{4\pi} \right)^{1/3} \int_{\rho_0}^{\rho} \frac{\rho}{\rho^{1/3} (1 - \rho)^{2/3}} d\rho = \Phi(\rho) - \Phi(\rho_0)$$

where ρ_0 is the relative-density at time $t = 0$. I am grateful to my colleague Mr. J. K. Mackenzie for evaluating the integral $\Phi(\rho)$, which is plotted in Fig 14. With the substitution $x = (1 - \rho)^{1/3} / \rho^{2/3}$, the integral can be expressed in terms of known functions. If Dr. Shaler's model is correct this equation enables the ratio σ/η to be found from the variation of the density of a powder compact with time.

Dr. Shaler, in his treatment of this problem, ignored the fact that all the pores in the body are closing simultaneously; and found that the velocity of flow decreased with the distance from a pore. This is not correct. An observer situated at the center of a pore and moving with the pore, who smooths out the change in direction of flow around the other pores, will observe that, at distances larger than the separation at pores, the velocity of flow increases in proportion to the distance.

Summary

Dr. Shaler's treatment of the rate of increase of density of a porous body is not valid, because he does not take account of the simultaneous closing of all the pores. A treatment based on the solution of the corresponding elastic problem shows that the relative-density ρ increases with time t according to the equation,

$$\frac{\sigma n^{1/3}}{\eta} t = \Phi(\rho) - \Phi(\rho_0)$$

where n is the number of pores per unit volume of metal (that is, it does not change with time) and the function $\Phi(\rho)$ is shown in Fig 14.

References

30. J. N. Goodier: *Phil. Mag.* (1936) **22**, 678.
31. A. E. H. Love: *Elasticity*. Dover: New York (1944) 142.
32. D. A. G. Bruggeman: *Annal. der Phys.* (1937) **29**, 160.

A. J. SHALER (author's reply)—I thank Dr. Shuttleworth and his colleague, Mr. Mackenzie, for the excellent discussion and for providing us with an explicit solution to the function F which I have left unintegrated. The possible skin effect, or size effect, described in the Udin, Shaler and Wulff paper¹³ may make it necessary to alter both Dr. Shuttleworth's model and my own. In the case of Dr. Shuttleworth's model, the change would lead to a more serious drawback, for it would be necessary to evaluate in a new light the validity of the approxima-

* H. H. Wills Physical Laboratory, Univ. of Bristol, England.

tion of a porous compact by a solid body with a single cavity at the center, and also the validity of extending his solution to other than spherical compacts, two unnecessary evaluations in the case of my analysis, in which the relative density is introduced into the graphical integration of F as an experimental value. A second drawback to the use of Dr. Shuttleworth's explicit solution is that the value of ρ_0 at the end of the first stage of sintering is not known, so that the value of the constant $\Phi(\rho_0)$ must in any case be deduced from experimental results.

Dr. Shuttleworth's criticism concerning the velocity of flow decreasing with distance from a pore is not in accord with the condition of continuity. For the same volume of porous material must cross each concentric spherical shell centered at any pore or at any point in the compact in the same differential time interval, during which the density is changing by the same amount throughout the compact, as he demonstrates. Hence, the velocity of any element towards the center of the shells is inversely proportional to the square of the distance. It is also inversely proportional to the density, a factor which was not left out of my equations, and appears in the function F for that reason. Dr. Shuttleworth's observer situated at the center as a pore is subject to much the same illusion as the astronomer on earth observing the recession of nebulae in an expanding universe.

G. F. HÜTTIG* (*Condensed version of translation*)—The first part of Hüttig's discussion is concerned with Shaler's distinction between "transient" and "steady state" phenomena or mechanisms in the sintering process. Hüttig considers possible different definitions of the words "mechanism" or "phenomenon," investigates whether the distinction between "steady state" and "transient" is possible on the basis of each of these definitions and comes to the conclusion that the distinction cannot be justified.

Hüttig further takes issue with Shaler's interpretation of his own theory: "I cannot agree that all the phenomena which form the basis of my theory can be considered transient for the following reasons:

"1. Even if the phenomena which I have considered are followed at higher temperature by other phenomena which complete the sintering process, this in itself would be no proof that the phenomena considered by me are transient." Hüttig argues that Shaler does not observe the final result of the sintering process, namely, a single crystal, and that it is therefore conceivable that at sintering times even longer than those employed by Shaler new phenomena are observed.

"2. It is not correct that my theory is based only on processes which are 'sub-

*Inst. f. Anorg. u. Phys. Chem. d. Tech. Hochschule, Graz, Austria.

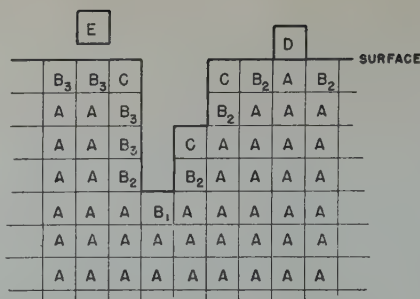


FIG 15—Representing atoms in lattice.

stantially completed in a matter of hours at temperatures considerably below those generally used in sintering.' I have taken into account all the sintering phenomena which were described in the literature up to 1941. There were 85 publications not including my own. Data on the sintering process of the metals Cu, Fe, Sn, Pb, Au, Ni, Mo, W and Al were found. Also the literature on the sintering process in oxides and other materials was collected, including data on the oxides Fe_2O_3 , ZnO , BeO , CuO , Fe_3O_4 , NaCl , organic materials and glasses. Of the properties by which the progress of sintering was measured, the following may be mentioned: electromotive forces, solubilities and chemical reactions with various liquid media, adsorption isotherms of methanol vapor and data calculated from them, densities in the vacuum pycnometer, apparent density, catalytic effects, electrical resistivities, gas evolution, strength, hardness, grain growth measured microscopically and by X rays, adsorption of dissolved dyes, and so on. All observations are presented in graphical form, in such a way that they can be compared with one another, in *Kolloidzeitschrift*, (1942) 98, 6-33. On the basis of these data a theory which takes into account all the sintering phenomena was developed in *Kolloidzeitschrift*, (1942) 98, 263-286. Other investigations based on the same methods concerned systems of two components, that is, mixtures of powders. This finally led to a theory which covers not only the sintering of single metals, but all types of chemical reactions in the solid state. These results are presented systematically in *Handbuch der Katalyse*, Vienna (1943) VI, 318-577.

"I wonder is it possible that a theory which takes into account such extended material can find its rightful place in Shaler's section on transient phenomena, which comprises only 34 typewritten lines."

Regardless of his criticism of Shaler's distinction between steady state and transient phenomena, Hüttig states: "The paper contains so much new material and new ideas, that I believe it may become a turning point in powder-metallurgical research. The ideas are not always easy to comprehend and the following is therefore meant more as com-

ment than as criticism.

"1. The paper by Sackmann, Burwell and Irvine⁷ is closely connected with the results of Thirsk and Whitmore (*Trans. Faraday Soc.* (1940) 36, 862. Other papers which concern the same phenomenon are quoted in *Handbuch der Katalyse*, VI, 474-479 and 539-544.

"2. With regard to Shaler's concept of the electron density distribution on the surface of a metal I wonder whether the method of Grimm, Brill, Hermann and Peters who determined electronic densities by means of Fourier analysis of X ray diffraction data could not be applied also to the surface layers, perhaps on the basis of electron diffraction measurements. This may result in a direct confirmation of Shaler's concept.

"3. In order to provide experimental support to the ideas about the role which a gas plays in sintering I should like to suggest the following experiment: The progress of sintering should be investigated (a) in a vacuum, (b) under a pressure of one atmosphere, (c) of 10 atm. (d) of 100 atm. of an inert gas such as argon or helium. What differences are observed, if the other experimental conditions are held constant?

"4. I am trying to develop a simple model in order to visualize Shaler's concept of the energy and force relationships in a capillary. (Regarding the use of such models see my paper together with Joos on the energy of crystal lattices (*Ztsch. Elektrochem.* (1926) 32, 294); W. Biltz and H. Grimm's calculation of the lattice energy of ammonia compounds (*Ztsch. anorg. Chem.*, 145, 63; and Pfeiffer and Goldschmidt's application of the idea of coordination number to the systematics of crystal lattices. Such a picture may possibly serve as a basis of discussion.

"Every atom tends towards a minimum free energy content. No important error is introduced when, in this statement, total energy is substituted for free energy. Fig 15, representing the atoms in a lattice, is drawn in two rather than in three dimensions and my discussion refers to this simplified two dimensional model. The heavy line represents a cross-section through the surface of a crystal.

"The atoms in the interior, A, have a minimum of energy. They therefore represent the most stable arrangement. All four positions of nearest neighbors are filled. Next in line with regard to increasing energy content are the B-atoms whose three nearest-neighbor positions are occupied (subdivided into B_1 , B_2 , B_3) then C with 2, D with one nearest-neighbor position occupied, and finally E, a freely diffusing atom with the highest energy. In a three dimensional model the coordination numbers (numbers of nearest neighbors) have to be changed accordingly.

"The surface energy is that energy which has to be expended to bring an A

atom into a B position (in general a B₃ position). The same amount of energy is given off when a surface atom becomes an atom in the interior. The surface tension in dynes per cm is identical in numerical value and dimension to the surface energy in ergs per cm². The pressure which is exerted is always directed towards the mass, that is, in the direction which tends to fill the nearest neighbor positions and never in the direction of the empty space of the capillary. The entire system reaches a minimum in free energy, that is, the most stable state, when all geometrically possible movements in the sequence E-D-C-B₃-B₂-B₁-A have taken place. This process must be connected with the filling up of the capillary. All ideas which cannot be brought into agreement with this simple picture are to me very difficult to comprehend.

5. I should like to underscore three times the sentence in the conclusion: "The sintering process is an extremely difficult one."

A. J. SHALER—I thank Dr. Hüttig for his able and kind discussion, and regret that it could not be given in full. Doubtless it is dangerous, as he and others taking part in this discussion have stated, to try to dissect the interrelated parts of the sintering process without great care; it is nevertheless a very necessary part of the scientific method, and one of which Dr. Hüttig has made full use in the papers he quotes. The separation of the process into "steady state" and "transient" "mechanisms" and "phenomena" can be debated on semantic grounds, a debate which loses as much value through the imperfection of definition in our own tongue as through the additional loss of clarity attendant upon translation. That I have dealt with Dr. Hüttig's work in but a few lines in no way reflects on my part poor judgment of its importance, but rather an acceptance of the fact that he has given as final a treatment of some of the "transient" mechanisms as I had hoped to do with some of the "steady-state" phenomena. Dr. Hüttig's suggestions concerning further refinements are welcome. Some are even now being explored. His picture of the surface energy is oversimplified. It is more useful in dealing with ionic inert-gas crystals than with metals as Dr. Shuttleworth has pointed out (The Surface Energies of Inert-Gas and Ionic Crystals. *Proc. Physical Soc.* (1949) A 62, 167) in his statement: "In metals the surface energy is best regarded as arising from the change in kinetic energy of the free electrons due to the presence of the surface."

F. N. RHINES*—One matter that I would like to mention concerns the classification of the various steps in sintering. As a process in the scientific thinking, we very properly try to break up complex

processes into small parts in order that we may look at them one at a time and thereby gain an understanding of the whole process through more simple steps. In so doing, however, I think that we should be very cautious about naming the individual steps, or about intimating that one step occurs at one time and another at another. It seems to me that the steps that Dr. Shaler has mentioned really overlap so much that all of them are going on, to some extent, most of the time. This is rather a case of one process being predominant at one moment and another being predominant later so that, perhaps, we would confuse ourselves less if we referred to the several processes without intimating so definitely that each one is associated with a specific time.

The data that I want to present are from what was to have been a paper for this meeting. Unfortunately the work was not completed in time but it is so definitely on this subject that I would like to put some of it before you.

We at Carnegie Tech have, over a period of some years, been studying the sintering process by observing the change in size and number of pores in lightly pressed compacts sintered at various temperatures and for various times in various atmospheres. I shall confine what I have to say mainly to sintering in hydrogen and at the higher temperatures, because the effects that are observed are most obvious under these conditions. Density measurements, made at intervals from 10 min. to 1000 hr at 800, 900 and 1000°C, exhibit a progressive increase, at a diminishing rate, at each temperature, the change being most rapid at 1000°C. From this observation one must conclude, as Dr. Shaler has done, that the *total volume of porosity* in the samples has been decreasing progressively. I emphasize this point to make it clear that, so far as the density measurements are concerned, there is no difference between his results and ours, because, beyond this point, our paths diverge. Our microscopic observations show very clearly that one should not further conclude that, individually, the pores are diminishing in size.

Microscope counts of the number of pores as a function of size, in single samples, show that the number rises from near zero at the smallest discernible size (of the order of 100Å in diam) to a maximum number at some intermediate size, then decreases, rapidly at first, in progressing to larger size and, then, more and more slowly, a zero number is approached just above the largest size present. With increased sintering time, the total pore count (including all sizes) diminishes and the maximum count shifts to larger pore sizes, but there is an actual increase in the number of pores of sizes greater than that at the size of the maximum count and there are a few pores of larger size than the largest observed at shorter sintering time. In other

words, the larger pores are all growing at the expense of their smaller neighbors, while the smallest pores are vanishing altogether.

This is the experimental evidence. I have given just one example out of a good many that were studied, but they all follow this same pattern. We have made an effort to devise a mechanism to describe what happens to account for these observations and I would like to outline this rather briefly.

Taking a somewhat different, but I am not at all sure that it is a fundamentally different viewpoint from that of Dr. Shaler, we have assumed that the transfer of vacant space required to bring about the changes in pore diameter is accomplished by the diffusion of vacant lattice sites. We assume that the number of vacancies present in the lattice varies from place to place in the piece of metal under the influence of the surface tension at the boundaries of the pores and at the external surface. Adjacent to a small pore the number of vacant lattice sites will be large, because the higher surface tension of the small pore will increase the probability of the birth of vacancies at its bounding surface; similarly the concentration of vacancies will be less next to a large pore and still less near the external surface of the sample. This gives rise to a complex pattern of lattice vacancy concentration gradients, such that the vacant sites will tend to diffuse away from the smallest pores and toward larger pores and the external surface.

Using the surface tension value for copper, found by Udin, Shaler and Wulff, and applying conventional assumptions with regard to the variation of the lattice vacancy concentration with surface energy and with regard to the rate of diffusion of vacancies, Dr. Birchenall has succeeded in computing the change in the number of pores of each size during a stated time interval at 1000°C. His results agree very well with the observed changes. This encourages us to believe that the mechanism that I have outlined may be reasonable.

The mathematical method that Dr. Birchenall has been forced to use is, unfortunately, very cumbersome. (It is similar to the well known analysis of the growth of water droplets in equilibrium with water vapor.) For this reason, it is taking a rather long time to test the theory on all of our observations; this work is currently in progress.

I would like to add to what I have said a few comments with regard to what all this means in connection with Dr. Shaler's paper. The main conclusion that we seem to have reached is this: all except the smallest pores grow during sintering, but the rate of the disappearance of the smallest pores is such as to produce an over-all reduction in porosity. This may be hard to understand unless it is appreciated that all outdoors is a pore too and

* Carnegie Institute of Technology.

there is diffusion of vacant space into the space surrounding the sample. That is, the increase in density must be due to the diffusion of vacant lattice sites through the external surface. This would lead us to the conclusion that the rate of density change depends upon the initial number and size distribution of the pores, the amount of external surface and the thickness of the compact. I believe that it is often observed, commercially, that the smaller compacts do reach maximum density more rapidly than large compacts. My impression is that if we had a compact of infinite size the only thing that would happen would be that there would be a tendency for all the pores to agglomerate into one great big one of the same volume as the total porosity. There would be no change in density whatever. When we have an external surface some of the vacant space goes to the external surface and is lost; that gives us our densification. The more the external surface per unit of volume, the greater the rate of densification. In a compact of small size there would be, after many hours of heating, many more pores in the interior than near the surface.

Further, it seems to me that our observations are telling us that it is risky to assume, as Dr. Shaler has done in his experiments, that the pore size obtained by piling up sorted powders is really what one would compute on the assumption that there are always the same number of pores and that the change in density results from their decrease in size. I think that is not right. Some of the pores are disappearing altogether all the time, while others are growing.

Finally, I should like to make brief mention of another interesting case: that of sintering in argon. When we observe the changes in pore diameter on sintering in argon we find that, in the early stages, the process looks just like sintering in hydrogen, as described here, but at the highest temperatures and after a long time, we found a reversal in the trend of density change. That is, there was an increase in the total porosity late in the sintering process.

We think that the explanation may be this: not only must we take account of the movement of vacant space, when we are sintering in an atmosphere rather than a vacuum, but there must be movement of the gas within the metal. This is also a diffusion process, and the rate of diffusion of the gas may be quite different from the rate of diffusion of the vacant lattice sites. If the rate of diffusion of the gas is high, we may expect that the gas will get away, (disappear through the surface of the specimen), because of the squeezing down of the pores, with a consequent building up of the pressure. But if the rate of diffusion of the gas is slow, it is much less likely that the gas will reach the external surface at a rate corresponding to the change in total pore volume. Now,

suppose that we transfer a given amount of gas from a given volume of little pores to the same volume of big pores. The little pores will have high surface tension; the big pores low surface tension. The little pores can sustain a higher pressure of the gas so that when the gas is moved on into the larger pores it will cause them to expand.

A. J. SHALER—We are all anxious to read the full account of the work of Drs. Rhines and Birchenall, and I am grateful to Dr. Rhines for presenting so much of it here. I should like to comment on some of the points he has made with a view to discovering if and where important differences exist between his views and mine.

I appreciate his very valid criticism of my attempt to separate the sintering process into steps, which in reality overlap one another to a great extent. In my model, which is only a first approximation to reality, two assumptions are made: (1) the pores are assumed to be far apart, and (2) they are assumed to be all of the same size. In my synthetic cylindrical pores I have tried to proceed according to the first. In the experiments on compacts I have tried to use spherical particles all of the same size in order to approach the second assumption.

F. N. RHINES—May I say, in connection with this, that you would have to be a micro-olive packer to get that condition experimentally; when you pile up spheres you are going to have some bridging, and it is inconceivable to me that, experimentally, you could even have, initially, all one size of pore; this situation would get progressively worse as you went on in sintering.

A. J. SHALER—That is correct. You have in that respect carried out the refinement, which I have not yet wanted to make, of dealing, not as I have with an impractical simple system, but with a practical and very complicated one, judging from the complexity of your equations.

The observations given by Dr. Rhines concerning the pore-size changes in copper sintered in hydrogen and in argon are not in disagreement with my results, although I have not carried out a quantitative analysis of the case of a diffusing gas—hydrogen—trapped in the pores. In both cases, the smallest pores first shrink to a small size, stable in the case of argon, but, with hydrogen, subsequently decreasing at a slower rate depending on the diffusion path of the hydrogen. At later times, successively larger pores shrink by lesser and lesser amounts. Later still, pores larger than a critical size swell instead of shrinking, and again, in argon, reach stable equilibrium sizes. In hydrogen, the swelling of pores of these sizes is followed by shrinkage as the gas diffuses out. Such developments should give the same qualitative change in pore counts

as those observed by Dr. Rhines, although in my analysis I have neglected the effect on each pore of the presence of neighboring pores of greater and smaller sizes. My results indicate that, in argon sintering, there should be observed a fairly large stable pore count at very small sizes. The absence of these in Dr. Rhines' observations may be due to their being too small to be seen in the microscope; alternately, the surface tension may be sufficient to drive the residual argon into solution in the metal, notwithstanding the low solubility of this gas in copper.

F. N. RHINES—I do not think there is any evidence of a large pore count at submicroscopic size. As observed with a microscope, the pore count is decreasing at an accelerating pace all the way down to the smallest visible size. The larger pores are not shrinking; they are all growing, but the smallest pore is vanishing. I am not sure that I have got my point across yet. The point that I am trying to make and the way that I see this thing is that every pore must receive vacancy from outlying space so long as there is any pore around it that is smaller, so that we observe only growth of pores, or their total disappearance.

A. J. SHALER—Not in argon.

F. N. RHINES—No, but in hydrogen.

A. J. SHALER—The mechanism whereby pores change in size and compacts change in density by the movement of lattice vacancies is not quite the same in Dr. Rhines' view as in mine. He first establishes a gradient of vacancy concentration, then states that vacancies will diffuse down the gradient. In his treatment, as in those of Pines and Kuczynski, vacancies are treated very much as if they were atoms of matter soluble in the metal, present in mass inside the pores and outside the compact, and diffusing through the metal. Shrinkage of the compacts follows if it is shown that the vacancies are more highly "concentrated" in the small pores than in the large ones; the outlying space being the largest pore of all. Such concentration differences are ascribed to the radius-sensitivity of the pressure due to surface tension.

In my view it is not necessary to have vacancy-concentration gradients. A mechanical flow takes place by motion of vacancies under the influence of mechanical stresses due to surface tensions and gas pressures. The rate of this flow was calculated by Frenkel on the approximation that no vacancy-concentration gradients exist. In criticism of Frenkel's analysis, Nabarro (private communication) has pointed out that a single vacancy cannot be persuaded to move under a unilateral stress, but a way out of this difficulty was suggested (*Physical Rev.*, 73, 8, 926, Apr. 15, 1948).

I should like to inject a note of caution in evaluating attempts to explain mechanical behavior purely on a diffusion basis. Dissolved atoms or vacancies require an activation energy before they can diffuse. It is not sufficient, as it is in the diffusion of tenuous gases, that there be a concentration gradient. If external causes, such as the presence of surfaces of various curvatures, require local readjustments of vacancy concentration in order to minimize the free energy, then the concentration gradients are not in themselves driving forces for diffusion, because a decrease in gradient would increase the free energy. It is conceivable that a region of metal near a pore has the same flow characteristics as one far from a surface, although the former may contain many more vacancies.

It appears preferable to try to solve mechanically the mechanical problem of metal flow under stresses due to surface tension and gas pressures. The growth of large pores, which standing alone would shrink, when they are surrounded by many small ones, may be simply due to the addition of a radial tension, due to the shrinkage of the small pores, on the stress field. The system is equivalent to a hollow sphere with externally applied hydrostatic tension. That Dr. Birchenall's calculations agree well with observation is evidence that in this case the distinction between a direct mechanical solution and a diffusion solution is a semantic one only, and that our explanations are not fundamentally so different as might at first appear. The approach of Drs. Rhines and Birchenall is probably on safe ground, but that of Drs. Pines and Kuczynski is not, in my opinion, as I shall try to show in answer to the latter's remarks.

Dr. Rhines' conclusion that the rate of shrinkage depends on the size of compacts is probably true, but in both his and my model the effect must be limited to a very thin skin; it should be observable only on very tiny compacts. The commercial observations to the contrary can be better explained on the basis of the size-sensitive outward diffusion of hydrogen compressed within the pores, as described above. It should not be observed on compacts in which vacuum or a noble gas only is present within the pores.

I am happy that Dr. Rhines has found experimental evidence that pore shape has little influence on kinetics of sintering, a fact deduced theoretically in my doctoral thesis (Mass. Inst. of Technology, June 1947).

E. OROWAN*—Dr. Shaler's conclusion that the attractive force between metal surfaces has a range of several hundred Angstroms is difficult to accept. During his lecture I have calculated, on the basis of his formulas, the critical diameter for which the long-range attraction between two equal copper spheres in

contact would just balance their weight; in other words, the maximum size at which we could lift up a copper sphere by means of another similar sphere in contact with it. I have repeated the calculation in another way, with the same numerical result, that is, that the critical size would be between 5 and 10 mm. If both Dr. Shaler's and my calculations were correct, therefore, metal balls of $\frac{1}{4}$ in. diam could be picked up with another similar ball as with a magnet.

A. J. SHALER—The calculation I have made for the attraction between two surfaces indicates forces greatly in excess of the technical fracture stress of copper, but not in excess of the theoretical cohesive strength calculated by the physicists for a perfect lattice. There is some experimental evidence in support of this result. Notably, Sackmann, Burwell, and Irvine (reference in paper) brought riders of copper, containing radioactive copper, gently down onto steel surfaces, and then removed them, as carefully as possible in order to prevent lateral movement. Copper could then be detected on the steel surface, indicating that the attraction between the two surfaces was greater than the fracture strength of the copper.

E. OROWAN—This can be the result of a short-range force; a short-range attraction alone, however, would not lift a copper ball by another copper ball because the force would be restricted to an extremely small circle of contact.

A. J. SHALER—I believe we are verbally performing two separate experiments. The first of these is to allow the two balls to come within a few hundred Angstroms of one another. The force of attraction will then bring the two balls into contact. The second experiment is to separate them, by allowing the weight of one to exert a tensile stress on the area of contact. As in the tensile test, the tension required to cause fracture is very low (ca. 10,000 psi for copper) compared with the strength of the bond between lattice nets. The reason for the discrepancy is still the subject of debate among fracture-theorists, but it may well reside in defects brought into being by plastic flow. A recent analysis and calculation made in our laboratory of a tensile test under pressure performed by Bridgman indicates that a stress of over 170,000 psi normal to an inactive slip plane was insufficient to cause fracture in copper, whereas fracture occurs in this metal when a stress of only 8500 psi is exerted in a direction normal to active slip planes. The two balls, one suspended from the other, are very much like a tensile specimen, and one would expect slip to take place first, followed by fracture at the consequently lowered stress value. The second experiment does not, then, invalidate the result of the hypothetical first experiment.

E. OROWAN—We can assume that the experiment with the two copper balls can be carried out so that there is no plastic deformation in either.

A. J. SHALER—Can we so assume? If the fracture problem were solved, I think it would be possible to analyze the problem of the two balls more adequately; I am not sure that it reduces the result of my calculation to absurdity. In the meanwhile, I should be embarrassed to have to lift one $\frac{1}{4}$ in. ball with another!

E. OROWAN—The assumption of forces that act over distances of several hundred Angstrom units is not only unlikely from the theoretical point of view; it also leads to immediate difficulties of which I have already mentioned one (the very large attractive forces that would act between spheres in contact). Another difficulty is this. When fracture occurs between two parts of a brittle solid, the work of the cohesive forces between the fragments must be of the order of the total surface energy of the surfaces of fracture. So long as these cohesive forces are small, they are determined by Hooke's law; in order to obtain the correct order of the surface energy, however, we have to assume that they cease to obey Hooke's law and begin to diminish when the increase of the atomic spacings between the two fragments becomes a substantial fraction of the initial interatomic spacing. If the cohesive forces continued to act over hundreds of Angstroms, the resulting work of separation would be several powers of 10 higher than the surface energy.

A. J. SHALER—The departure, which you describe, of the cohesive force from Hooke's law is shown by the well-known Morse curve, which is made up of a repulsive term, becoming negligible at a separation of several Angstroms, and an attractive term, extending to much greater distances. The resultant curve ceases to rise linearly and then reaches its maximum very nearly at the point where the repulsive term disappears; thereafter the contribution of the attractive force to the surface energy falls off. It is this part of the curve which I have calculated, making the usual simplifying assumptions. It may be that the surface energy calculated on this model is not so much greater than the observed value as Dr. Orowan believes. It is not possible to perform the calculation without a knowledge of the remainder of the curve.

E. OROWAN—That would amount to the assumption that the area below the Morse curve up to its maximum was a tiny fraction of the total area below the curve. This is only another way of postulating attractive forces of extremely long range.

G. C. KUCZYNSKI*—Dr. Shaler, what kind of an approximation did you use to calculate your forces?

* Sylvania Electric Products.

* Cavendish Laboratory, Cambridge, England.

A. J. SHALER—The electron density is calculated from the Fermi equation; the potential falls quadratically from a value at the surface equal to the work function.

G. C. KUCZYNSKI—I am afraid there is something wrong in these calculations. The electron wave functions do not extend very far. After few atomic distances they are overlapping and therefore the exchange forces are negligible.

A. J. SHALER—Dr. Kuczynski states that there is a considerable difference between the viscous flow mechanism and what he calls the volume diffusion mechanism. Since Frenkel's analysis is also based on volume diffusion, I fail to see how Dr. Kuczynski reaches this answer. I should like to see more of the calculation. For the coalescence of strings of spheres, treated as a one-step viscous flow process, I found an unreasonable value of the heat of activation for self-diffusion of some 30,000 cal per mol for copper. I do not see why Dr. Kuczynski should get 55,000 instead of 30,000.

G. C. KUCZYNSKI—I beg to differ with you, but the mechanism described in Frenkel's treatment of this problem is clearly stated as viscous flow and not diffusion flow.

The difference between the viscous flow and diffusion flow mechanisms is the following: In the case of the former mechanism no concentration gradient is required. The atoms move preferably in the direction of applied stress. In the case

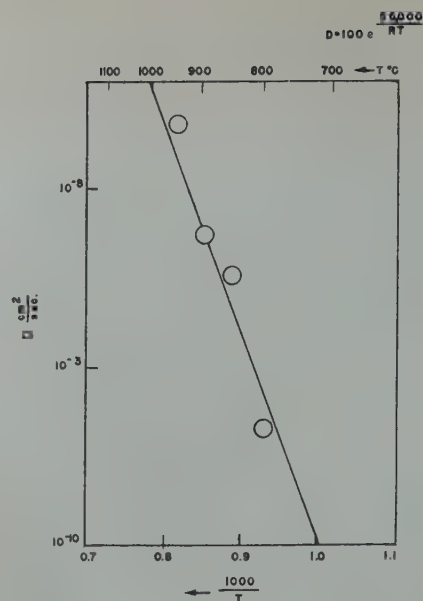


FIG 16—The variations of the coefficient of self-diffusion of copper with absolute temperature T , plotted on the semi-logarithmic scale. The points calculated from the data obtained by Dr. A. J. Shaler as represented in figure.

of diffusion flow on the other hand there has to be a gradient of vacancy concentration (or interstitial atoms). These two mechanisms represent different types of flow and their rates are different.

The relationship between the radius of the interface x and time t will be:

for viscous flow $-x^2 \sim t$ and
for diffusion flow $-x^5 \sim t$
The decrease of the radius of the spherical void r with time will be:

for viscous flow $-r = r_0 - \alpha t$ and
for diffusion flow $-r^3 = r_0^3 - \beta t$
where r_0 is the original radius of the void and α, β functions of temperature only.
On the basis of the relationship for diffusion flow the heat of activation equal to 55,000 cal per mol was obtained using your data. The plot of self-diffusion coefficient as the function of $\frac{1000}{T}$ on the semi-log scale is given in Fig 16.

A. J. SHALER—My reasons for breaking the process into two steps are given in detail in the paper. These reasons are supported by the results that Dr. Duwez presented to us this morning, in which sintering-rate curves for copper could by no stretch of the imagination be extrapolated continuously to the origin; to do so may introduce an unwarranted simplification. The fact that experimental points fall more or less on a straight line when one coordinate is a high power of one of the variables is a dangerous spring-board from which one can easily jump to arid conclusions.

G. C. KUCZYNSKI—There is no reason to separate your parabolic curves into two portions. If the correct functions were found, as I have shown in the case of the diffusion flow, these curves can be plotted as the straight lines which pass through the origin (Fig 17).

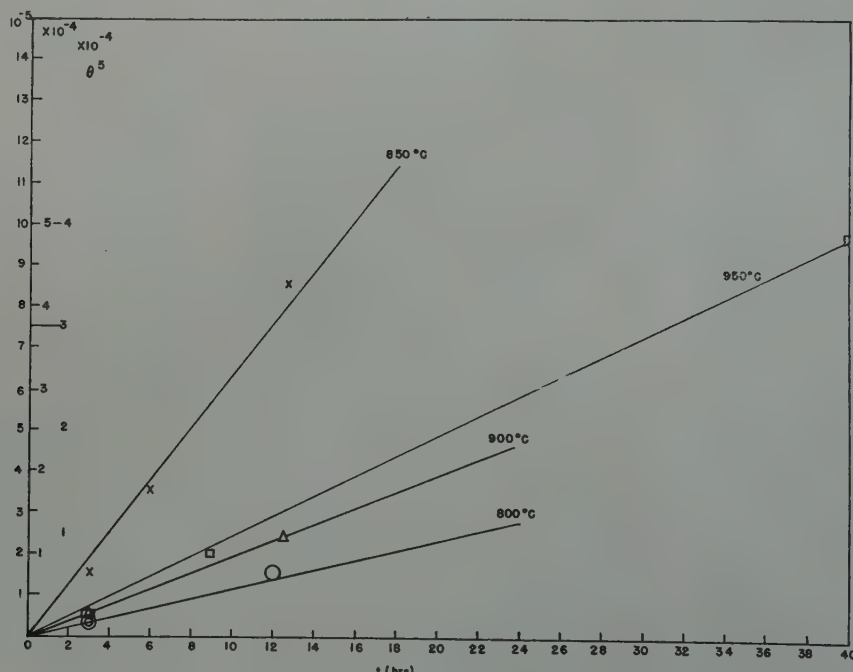


FIG 17—The plot of $\theta^5 = \left(\frac{x}{a}\right)^5$ where x is the radius of the interface and a the radius of the particles against the time of heating t in hours. The values of θ were taken from Dr. A. J. Shaler (Fig 6). It should be noted that straight lines are obtained instead of parabolic curves indicating that diffusion flow is responsible for bonding of the particles together.

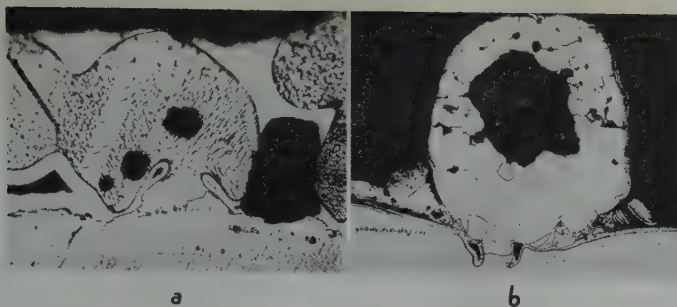


FIG 18—(a) Round copper particle sintered to nickel block at 950°C for 24 hr in hydrogen. Mag 700 X. (b) Round nickel particle sintered to copper block at 1020°C for 48 hr in hydrogen. Mag 200 X.

Both specimens were nickel plated after heating. Black spots inside the particles were blow holes caused by reduction of oxides in the hydrogen. Reduced one-half in reproduction.

A. J. SHALER—Dr. Kuczynski has shown a photograph of changes in shape during sintering of a copper sphere on a nickel plate, and also of a nickel sphere on a copper plate. I fail to see how these changes can help us to distinguish between a viscous flow based on diffusion or any other kind of flow based on diffusion.

G. C. KUCZYNSKI—I only showed this picture (Fig 18) to demonstrate clearly that the bonding of the metallic particles is not a result of viscous flow. Only diffusion phenomena can account for the peculiar shape of interfaces.

H. UDIN*—Dr. Kuczynski uses as a model for his sintering calculations a sphere on a plane, and then as sintering progresses material fills in at the fillet. I do not understand where this material comes from. I should like to ask Dr. Kuczynski if he is positive that his fifth power relationship comes from the actual mechanism of sintering, not from the geometry of the model.

G. C. KUCZYNSKI—Of course, the material comes from the particles.

F. N. RHINES—Do I understand that, in your derivation, you are saying that the copper that is filling these fillets is coming from the center of the sphere?

G. C. KUCZYNSKI—Some.

F. N. RHINES—You will develop a shell.

G. C. KUCZYNSKI—There will be

no shell. The atoms move from the body of the particle to the “neck” and the holes are diffused out to the surface.

F. N. RHINES—Eventually you must then be taking the copper from the external surface. The question in my mind is whether you would get the same mathematical expression if you wrote it on the basis of picking your copper atoms out of the surface and transferring them through the center and out to the fillet. You seem to have left the second element of the process out of the computation, the element of moving the atom from the surface into the vacated space.

G. C. KUCZYNSKI—No, it was taken care of by the diffusion coefficient.

A. J. SHALER—In Dr. Kuczynski's model the flow of material to the neck from the surface of the particle may take place by one of two paths. Either the atoms diffuse along the surface, in which case the flow of material cannot lead to densification of the compact, but only to an increase in the area of contact (spheroidization of the pores). Or the atoms diffuse through the metal in two steps; first, along a vacancy gradient, to the neck from a region inside the particle near the neck; and, second, from the surface to that region. For the second step there exists no vacancy gradient to accelerate diffusion. It is therefore the slower and the limiting step, so that the kinetics of the process should be based on a flow mechanism requiring no vacancy gradient; that is, something similar to the viscous flow we have been discussing. Furthermore it is questionable to base

the mechanism of flow even for the first step on the existence of a forced vacancy gradient; for in this case the vacancy gradient exists only in order to remove the free-energy gradient which would otherwise exist by virtue of the surface tension acting on the curved neck surfaces. A vacancy gradient alone is not sufficient for diffusion; if there is no free-energy difference between one end of the diffusion path and the other, the units of flow cannot acquire the activation energy required for motion. Therefore the first step of Dr. Kuczynski's volume diffusion process is not valid, and we must return, for a solution to the spheroidization step in sintering as well as to the densification (or swelling) stage, to a mechanical approach. In fine powders, as Dr. Kuczynski has shown, the surface-diffusion mode of spheroidization may be dominant, but densification of the compact must still occur by flow under the stresses described in my paper.

G. C. KUCZYNSKI—The process here is controlled by the slower reaction, namely self-diffusion throughout the main body of the particle. The high concentration of vacancies near the “neck” does not accelerate the rate of diffusion appreciably on the overall scale. Some variations should be noticed in the coefficient of self-diffusion (increase for the vacancy mechanism, and decrease for the interstitial atoms mechanism) during sintering of particles of only a few hundred Angstroms in diameter. But probably even in such an experiment the volume self-diffusion would be completely masked by surface diffusion.

* Massachusetts Institute of Technology.



Relative Deoxidizing Powers of Some Deoxidizers for Steel

(With Discussion)

C. E. SIMS,* Member, H. A. SALLER,* and F. W. BOULGER,* Member AIME

Introduction

Most of the data on equilibrium constant and the deoxidations potentialities of those elements, considered to be stronger deoxidizers for steel than is silicon, have been calculated from thermodynamic data. The reason for this is, primarily, the obvious difficulty of obtaining direct experimental evidence of equivalent accuracy. This is an excellent use of the principles of thermodynamics and has given valuable data not otherwise available. Such results, of course, can be no more accurate than the physical constants used in the calculations, and one can never be sure that the basic data are either complete or accurate.

In fact, as in the case with silicon,¹ there are not only discrepancies among the calculated theoretical values of the equilibrium constant for deoxidation of steel but also between the theoretical and experimental values. It is highly desirable, therefore, to obtain experimental values for checks on calculated results whenever possible. If they disagree, both cannot be right, but if there is good agreement, their value is enhanced.

The present work was done in an effort to obtain experimental evidence in regard to some of the common alloying additions but more particularly the so-called "strong" deoxidizers for steel. The method used was to determine the minimum concentration of the deoxidizer that would effect a certain definite degree of deoxidation in steel. The criterion of deoxidation was the change from the large globular Type I sulphide to the eutectic Type II as described by Sims and Dahle.² This change is sharp and definite, and inasmuch as it can be produced with equal facility by aluminum, zirconium,

and titanium, it is considered a manifestation of a certain degree of deoxidation and not an alloying effect.

Ostensibly such a procedure could give only a comparison of deoxidizing powers and no absolute values. Nevertheless, repeated observations have shown that, when increasing increments of aluminum are added to a steel, the residual aluminum content begins to increase simultaneously with the appearance of Type II inclusions. Thus it seems warranted to postulate that the Type II inclusions appear coincident with the virtual elimination of FeO as an active constituent of the steel.

Experimental Procedure

The data obtained were primarily from the microexamination of polished and unetched specimens and from chemical analysis. Experimental heats weighing 200 to 250 lb were made in a basic-lined high-frequency induction furnace. The base composition was nominally that of a medium-carbon casting steel to which the appropriate additions were made. Specimens were poured into sand-cast ingots 3 in. in diam as shown in Fig 1. Sand-cast ingots were used to prevent chilling and to allow sufficient time in freezing for normal inclusions to form of a size large enough to be studied readily. In the first few heats, the tapered wall ingot was used, but in the majority, the

extra large riser was used to prevent piping in heavily deoxidized steels. Specimens for microexamination were taken from the location shown in Fig 1, and drillings for chemical analysis were taken from a similar location.

The procedure was to melt the base composition and deoxidize with the usual manganese and silicon additions and then to pour an ingot. The furnace was then tilted back, and the first increment of strong deoxidizer or special alloy was added and allowed to disseminate through the melt, with enough power on to hold the temperature constant, for 45 sec. Then a second ingot was poured. After this, another increment was added, and after the same holding time another ingot was poured. In this way from 9 to 12 ingots were poured from each heat, each successive ingot having progressively larger total additions of alloy.

Eighteen heats were made altogether, and the range of alloys used and additions made are outlined in Table 1. The three principal types of sulphide inclusions found are illustrated in Fig 2. The globular Type I sulphides are characteristic of silicon-killed steels, the eutectic Type II are characteristic of steels deoxidized with a small amount of aluminum, while the larger, angular Type III are usually found in steels with a residual aluminum content above about 0.02 pct.

In all specimens studied, the transition from Type I to II either did not occur at all or was very abrupt and clear cut. There never was any doubt as to just which increment produced the change, although the individual additions were small, in the order of 0.01 pct. The change from Type II to Type III was considerably less sharp, and, in some cases, both types were found together. Inasmuch as the formation of Type III sulphides is apparently not a deoxidation phenomenon, they will not be discussed here.

San Francisco Meeting, February 1949.

Any further discussion of this paper may be submitted to *Transactions AIME* as a technical note.

TP 2557 C. Manuscript received November 16, 1948; revision received July 21, 1949.

* Battelle Memorial Institute.

¹ References are at the end of the paper.

INEFFECTIVE ADDITIONS

Manganese

When manganese was varied from 0.63 pct to 17.7 pct, the globular Type I inclusions remained unchanged. In the higher manganese steels, there was a greater abundance of duplex inclusions containing both silicate and sulphide, but there was no hint of a eutectic formation. This confirms common knowledge to the effect that manganese is at best a weak deoxidizer, and that it is incapable of lowering FeO to the point that Type II inclusions can form.

It was noted that, as the manganese increased, the phosphorus content also increased from 0.009 pct to 0.040 pct, while the sulphur content decreased from 0.026 pct to 0.014 pct. The phosphorus can be accounted for as an impurity in the manganese, but the loss of sulphur is from a real desulphurizing action. This was confirmed by several analytical methods. Apparently the solubility limit for manganese sulphide was reached with high manganese contents and some manganese sulphide precipitated and floated out. It is not considered a practical desulphurization method, however.

Silicon

In Heat 1467, silicon was increased in steps up to 4 pct, but no trace of Type II inclusions was observed. Silicon is apparently a stronger deoxidizer

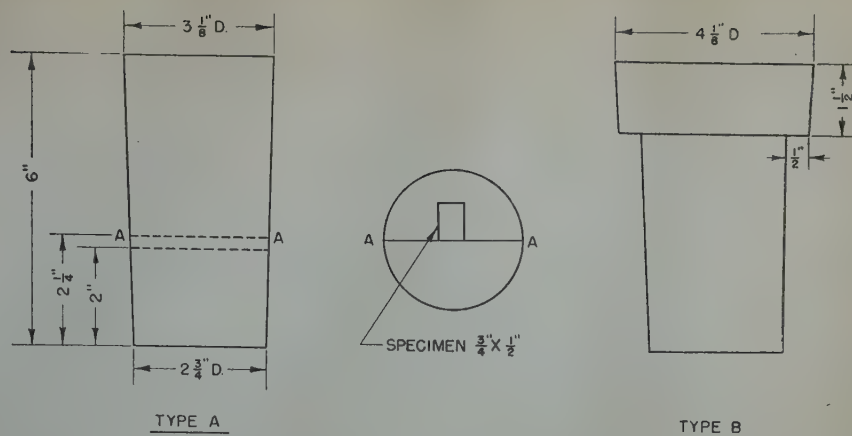


FIG 1—Sketch of experimental ingots and location of metallographic specimen.

than manganese but probably could not produce eutectic sulphides in any concentration. It was noted that the silicate inclusions increased both in size and in number as the silicon increased. They also became more transparent, indicating a higher SiO₂ content. Thus, the total silica content of the steel seemed to increase with higher silicon.

Vanadium

In Heat 1673, vanadium was added up to a content of 1 pct. The recovery of the added vanadium was practically 100 pct, indicating that it is not easily oxidized. There was no observable change in the type of sulphide inclusions. These observations plus the fact that vanadium oxide is readily

reduced by silicon warrant the conclusion that vanadium has no notable deoxidizing power in steel and does not rate a position higher than silicon.

Calcium

Although calcium has been widely regarded as a deoxidizer for steel, the present tests confirmed all previous experiments of the authors in giving completely negative results. In the tests, calcium silicide was added to the bare surface of the steel in amounts up to 0.4 pct. No change in the shape of silicates or sulphides was noted, although "birds-eye" sulphides, that is, sulphides with small, round, black spots were more prevalent after the calcium additions. Spectroscopic analysis did not show any residual calcium.

Table 1 . . . Chemical Composition of Steels Studied

| Heat Number | Special Element | Notes | Range in Chemical Analysis, Per Cent | | | | | |
|-------------|-----------------|------------------------|--------------------------------------|-----------|-------------|-------------|-----------|-------------|
| | | | C | Mn | P | S | Si | Al |
| 1466 | Mn | 0.63/17.7 manganese | 0.24/0.26 | 0.49/17.7 | 0.009/0.040 | 0.014/0.026 | 0.39/0.40 | 0.005/0.006 |
| 1467 | Si | 0.28/4.00 silicon | 0.23/0.28 | 0.61/0.65 | 0.008/0.011 | 0.032/0.043 | 0.28/4.00 | 0.004/0.008 |
| 1673 | V | 0.001/1.00 vanadium | 0.26/0.29 | 0.54/0.59 | 0.009/0.010 | 0.029/0.034 | 0.40/0.42 | |
| 1701 | Ca | 0.001/0.001 calcium | 0.24/0.27 | 0.60/0.72 | 0.010 | 0.032/0.033 | 0.22/0.76 | |
| 1503 | B | 0.0005/0.320 boron | 0.26/0.28 | 0.60/0.66 | 0.009/0.010 | 0.039 | 0.38/0.42 | |
| 1702 | Mg | 0.0005/0.01 magnesium | 0.21/0.27 | 0.60/0.70 | 0.010/0.014 | 0.034/0.035 | 0.23/2.49 | 0.004/0.012 |
| 1997 | Mg | 0.0005/0.003 magnesium | 0.30 | 0.69 | 0.006 | 0.045 | 0.66 | 0.003/0.005 |
| 1674 | Ti | 0.001/0.27 titanium | 0.24/0.26 | 0.52/0.62 | 0.010/0.018 | 0.039 | 0.36/0.41 | |
| 1741 | Zr | 0.003/0.026 zirconium | 0.32/0.33 | 0.62/0.65 | 0.010/0.011 | 0.037/0.038 | 0.25/0.34 | 0.006/0.008 |
| 1998 | Zr | 0.005/0.32 zirconium | 0.34 | 0.71 | 0.008 | 0.018 | 0.30 | 0.003/0.005 |
| 1278 | Al | Low carbon | 0.08/0.10 | 0.38/0.43 | 0.017 | 0.033/0.034 | 0.17/0.21 | 0.003/0.237 |
| 1465 | Al | Low carbon | 0.06/0.08 | 0.61/0.63 | 0.008/0.012 | 0.041/0.045 | 0.40/0.44 | 0.006/0.17* |
| 1279 | Al | Normal carbon | 0.31/0.32 | 0.57/0.59 | 0.014 | 0.034/0.036 | 0.29/0.32 | 0.007/0.287 |
| 1502 | Al | Normal carbon | 0.22/0.26 | 0.61/0.64 | 0.010 | 0.042/0.043 | 0.37/0.39 | 0.007/0.20* |
| 1742 | Al | Higher carbon | 0.48/0.52 | 0.68/0.71 | 0.010/0.012 | 0.040/0.044 | 0.34/0.39 | 0.008/0.145 |
| 1502 | Al | Normal Si, Mn | 0.22/0.26 | 0.61/0.64 | 0.010 | 0.042/0.043 | 0.37/0.39 | 0.007/0.20+ |
| 1740 | Al | Low silicon | 0.26/0.30 | 0.70/0.72 | 0.017/0.021 | 0.032/0.035 | 0.02/0.04 | 0.004/0.295 |
| 1743 | Al | Higher Mn | 0.26/0.32 | 1.42/1.44 | 0.012/0.015 | 0.040/0.044 | 0.35/0.42 | 0.003/0.105 |
| 1999 | Al | Higher Mn | 0.31 | 1.47 | 0.009 | 0.039 | 0.32 | 0.003/0.86 |

Manganese added as an 85 pct manganese, low-carbon alloy.

Silicon added to Heat 1467 as 77 pct ferrosilicon.

Vanadium added to Heat 1673 as ferrovanadium, 51 pct vanadium.

Calcium was added to Heat 1701 as a calcium-silicon alloy to the surface of the melt.

Boron added to Heat 1503 as ferrobore.

Magnesium added to Heats 1702, 1997 in the form of a powdered iron-silicon-magnesium alloy.

Titanium was added to Heat 1674 as a pure metal powder.

Zirconium added to Heat 1741 as pure metal powder and as a silicon-zirconium alloy to 1998.

Aluminum added in the form of wire to last eight heats.

* Acid-soluble aluminum—others are total aluminum values by wet or spectrographic analysis.

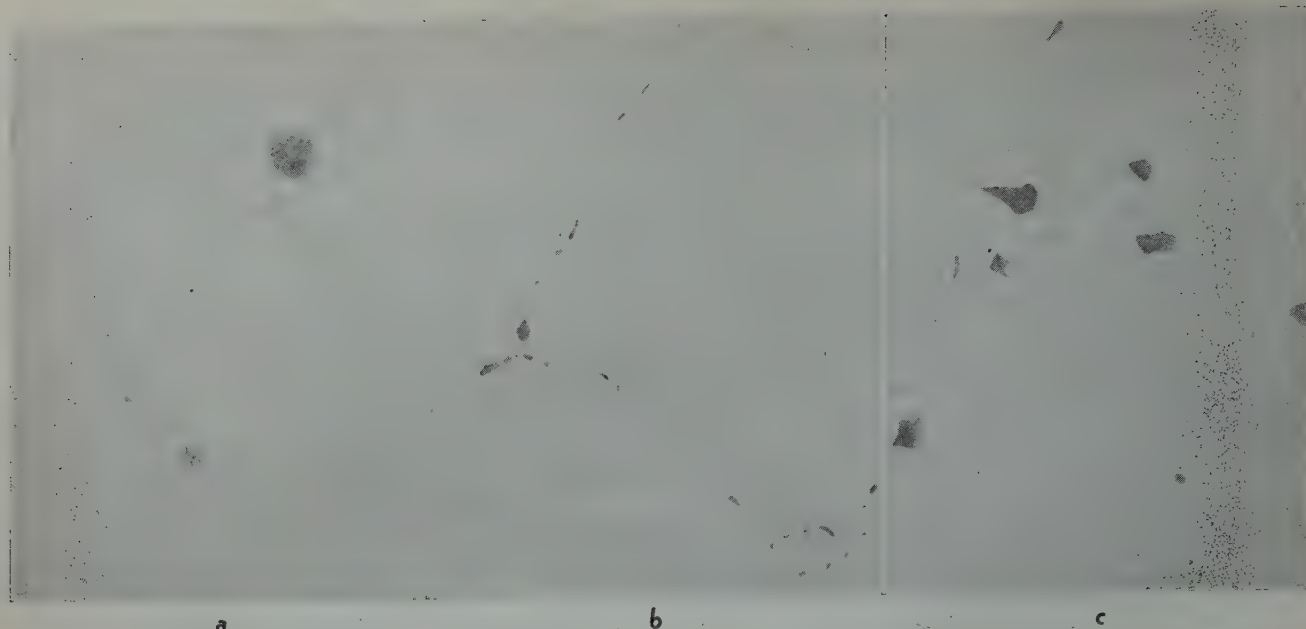


FIG 2—Typical appearance of sulphides classified on the basis of shape. 500 X.

Slightly reduced in reproduction.
a. Type I. b. Type II. c. Type III.

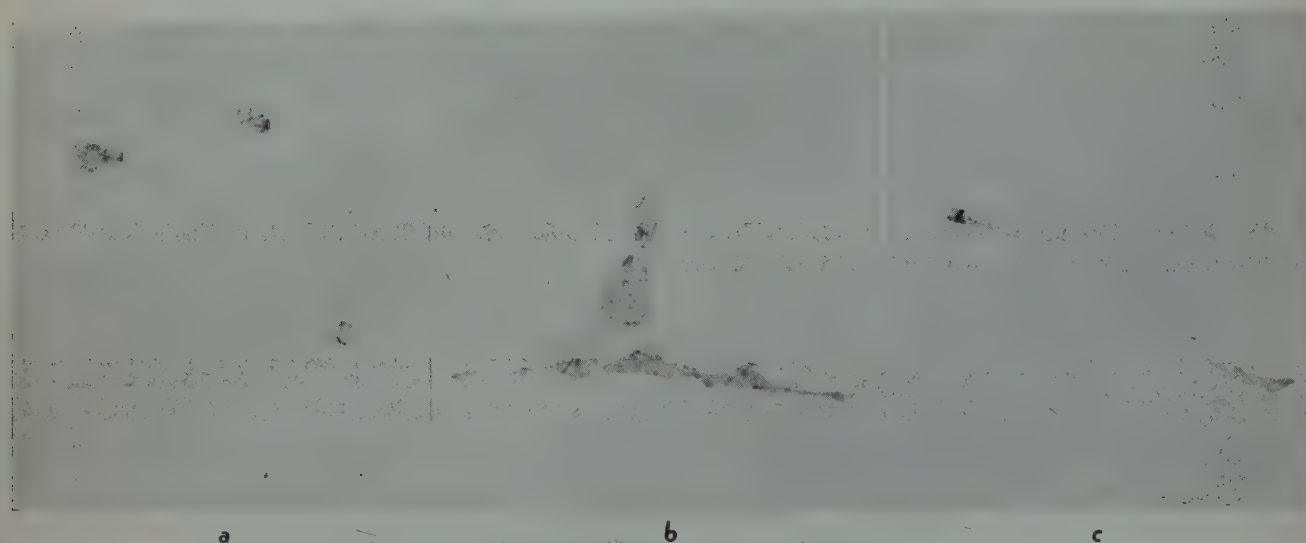


FIG 3—Typical sulphide inclusions found in Grade B steels with different boron contents. 500 X.

Slightly reduced in reproduction.
a .0.014 pct B. b. 0.034 pct B. c. 0.32 pct.

Calcium is reputedly insoluble in steel, and in molten steel, it is above its boiling point. Thus, it is under a severe handicap at best, but whether it would be a deoxidizer if it could be made to remain in contact with steel is purely hypothetical. Practically, it seems to have no deoxidizing effects.

STRONG DEOXIDIZERS

Of the elements tried, those which accomplished sufficient deoxidation to change the type of the sulphide inclusions were boron, magnesium, titanium, zirconium, and aluminum. There is some doubt regarding the deoxidation with magnesium as will be discussed later.

Boron

Boron was added to a carbon steel as 18 pct ferroboration. One effect of boron was to increase the size of the sulphides over those for similar steels containing no boron. Steels containing 0.030 pct boron, or less, were characterized by Type I sulphides and large globular silicates.

The typical sulphide inclusions in steels containing 0.034 pct or more of boron occurred as thick films in the primary grain boundaries. These inclusions have many of the characteristics of Type II sulphides in that they tend to form intergranular films, and yet they differ from those shown in Fig 2b in an important respect. Instead of being very small and forming a

fairly continuous network, they are concentrated in even larger masses than the Type I and therefore will be fewer in number and further apart. For this reason, they should not have the adverse effect on ductility that usually is associated with Type II inclusions. Typical examples are shown in the micrographs of Fig 3.

Magnesium

Magnesium is similar to calcium in being insoluble in steel and in volatility. It also has a similar position in the electromotive series. In order to add it to steel, it was made up as a master alloy by dissolving it in molten 75 pct ferrosilicon to a content of 10 pct. The first such alloy also con-

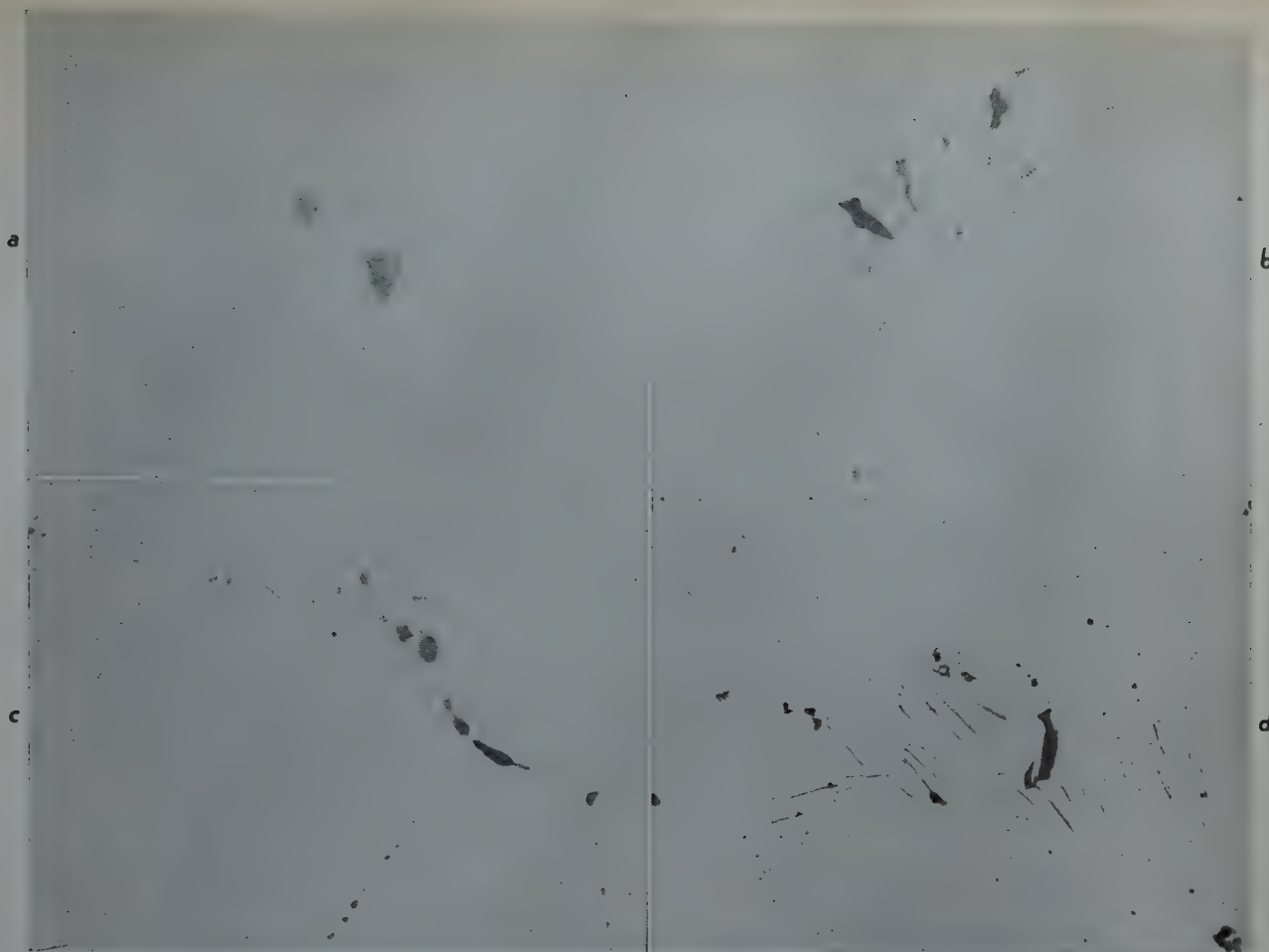


FIG 4—Typical sulphide inclusions found in Grade B steels with different titanium and magnesium additions. 500 X.
a. 0.003 pct Mg. b. 0.003 pct Mg, 0.005 pct Al. c. 0.024 pct Ti. d. 0.27 pct Ti.

tained 0.76 pct aluminum. When this alloy was added in increments to steel, the sulphides progressed from Type I to Type II and to Type III, the last being obtained with a total addition of 0.30 pct magnesium. Inasmuch as spectrographic analysis indicated less than 0.01 pct magnesium retained, but an aluminum content of 0.02 pct, it was considered that the latter element was responsible for the deoxidation.

Another series was made, using a similar alloy containing but 0.2 pct aluminum. The sulphides remained Type I up to a total addition of 0.30 pct magnesium at which point they changed to Type II; they remained Type II up to a total addition of 0.5 pct magnesium. Spectrographic analysis showed the residual magnesium never got higher than 0.003 pct, and the aluminum did not exceed 0.005 pct. This aluminum was high enough, however, to leave doubt as to whether the magnesium was effective as a deoxidizer.

Titanium

Titanium was added to Heat 1674 in

the form of pure metal pellets placed in a hollow tube fastened on a steel rod. The tube was plunged into the bath of steel where it melted off, and the titanium was dissolved. The titanium additions were made to the furnace in amounts varying from 0.01 to a total of 0.50 pct; the recoveries ranged from 50 to 60 pct. In this series of carbon steel castings, the sulphide inclusions changed from Type I to Type II at about 0.024 pct titanium. Film or eutectic sulphides were found in all samples containing more than this amount of titanium; the last ingot showed 0.27 pct titanium by analysis. Typical micrographs of titanium-bearing steels are shown in Fig 4. Data from this series suggest that titanium contents in steels should be kept below about 0.01 pct in order to avoid embrittlement by Type II distribution of sulphides.

In the steels containing comparatively large amounts of titanium, the sulphides occurred as extremely thin films, their color tending toward tan in reflected white light. These characteristics of the sulphide inclusions were noted previously in examining a medium-manganese steel with

0.16 pct titanium which had been added as low-carbon ferrotitanium. Such sulphides are presumed to contain a large proportion of titanium sulphide.

Zirconium

A silicon-zirconium alloy was used for adding zirconium to Heat 1998 after poor recoveries resulted from using pure metal powder in an earlier trial. Seventy per cent of the zirconium present was reported as being combined with oxygen when five samples were analyzed for both total zirconium and acid-soluble zirconium. This is puzzling considering that the total zirconium contents of these samples ranged from 0.01 to 0.32 pct. If the proportion of zirconium combined with oxygen was actually quite constant, it means that the oxygen content of the steel increased or that the composition of the oxide varied. In any event, the analyses agree with the metallographic examination which showed that the quantity of oxide inclusions increased with the total zirconium contents.

The micrographs in Fig 5 show the

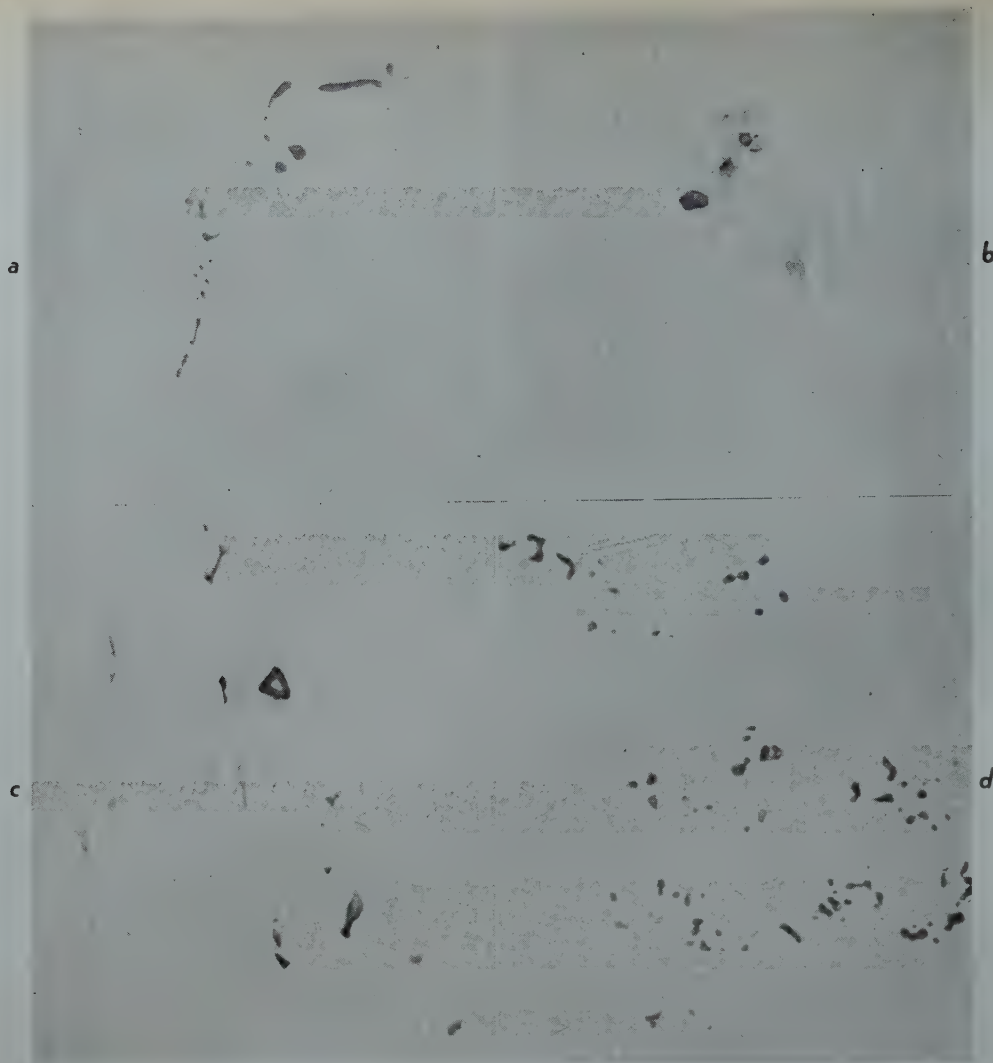


FIG 5—Typical sulphide inclusions found in Grade B steels with different zirconium contents and characteristic oxides in samples with large amounts of zirconium. 500 X.
a. 0.01 pct Zr. b. 0.03 pct Zr. c. 0.32 pct Zr. d. Oxides.

typical appearance of sulphide inclusions in three castings from the zirconium series. Eutectic film distributions existed in samples reported to contain 0.005 to 0.026 pct total zirconium. The specimen containing 0.005 pct total zirconium was found to contain 0.002 pct acid soluble zirconium and 0.003 pct was presumed to be present as oxide. Samples containing 0.03 to approximately 0.07 pct of this element were characterized by angular sulphides. As illustrated by the micrographs, the sample containing 0.32 pct zirconium indicated a reversion to film sulphides at high contents of this element. The fourth micrograph shows the inordinate number of oxide inclusions present in an ingot poured after an addition of 0.15 pct zirconium had been made to the furnace. Clouds or clusters of oxide inclusions have been found in many experimental steels treated with large quantities of zir-

conium. Such oxide inclusions have been determined, by electrolytic extraction followed by chemical analyses and petrographic examination, to be mainly zirconium silicate.

Aluminum

The last eight heats listed in Table 1 comprise the series made to study the effects of aluminum in steels of different compositions. The samples were analyzed for aluminum by three of the methods in common use. The first eighteen ingots were analyzed by wet methods to determine the acid-soluble and acid-insoluble (Al_2O_3) aluminum contents, because both fractions were considered important. This practice is cumbersome and occasionally gave erratic values. The spectrographic determination appeared to be much more reliable, and it is definitely faster and simpler. Only total alu-

minum is determined in this way, however.

Previous studies have indicated that the acid-insoluble aluminum of aluminum deoxidized steels tends to be constant, and the present data go far to verify this concept. These data for thirty samples, listed in Table 2, show that even though the total additions and the acid-soluble aluminum vary widely, the insoluble content stays close to the average value of 0.006 pct. Only three of the values varied from the average by more than 0.002 pct, and one was in a sample which contained no acid-soluble aluminum. This is within the range of precision of most wet methods of analysis. The eight heats from which these samples were taken varied in composition, but all were poured at about the same temperature of 2950°F. It appeared justifiable, therefore, to consider the insoluble aluminum a

Table 2 . . . Results of Aluminum Analyses on Test Castings

| Heat Number | Ingot Number | Aluminum, Pct | | | |
|-------------|--------------|---------------------------|-----------------------------|--------------------|-------|
| | | Acid Soluble ^b | Acid Insoluble ^a | Total ^d | Added |
| 1278 | 1 | | 0.002 | 0.002 | |
| | 2 | 0.003 | 0.006 | 0.009 | 0.01 |
| | 3 | 0.003 | 0.006 | 0.009 | 0.02 |
| | 4 | 0.002 | 0.006 | 0.008 | 0.03 |
| | 5 | 0.004 | 0.008 | 0.012 | 0.04 |
| | 6 | 0.002 | 0.006 | 0.008 | 0.05 |
| | 7 | 0.023 | 0.008 | 0.031 | 0.075 |
| | 8 | 0.025 | 0.004 | 0.029 | 0.10 |
| 1279 | 9 | 0.230 | 0.007 | 0.237 | 0.30 |
| | 1 | 0.001 | 0.004 | 0.005 | |
| | 2 | 0.001 | 0.005 | 0.006 | 0.01 |
| | 3 | 0.002 | 0.007 | 0.009 | 0.02 |
| | 4 | 0.008 | 0.005 | 0.013 | 0.03 |
| | 5 | 0.007 | 0.006 | 0.013 | 0.04 |
| | 6 | 0.015 | 0.004 | 0.019 | 0.05 |
| | 7 | 0.027 | 0.004 | 0.031 | 0.075 |
| 1465 | 8 | 0.041 | 0.005 | 0.046 | 0.10 |
| | 9 | 0.280 | 0.007 | 0.287 | 0.30 |
| 1502 | 12 | 0.17 | 0.005 | 0.175 | 0.30 |
| | 10 | 0.13 | 0.006 | 0.136 | 0.175 |

| | | Acid Soluble ^d | | Total ^c | |
|------|----|---------------------------|-------|--------------------|------|
| 1999 | 5 | 0.018 | 0.007 | 0.025 | 0.05 |
| | 10 | 0.34 | 0.005 | 0.34 | 0.40 |
| | 12 | 0.85 | 0.006 | 0.86 | 1.00 |
| 1743 | 9 | 0.049 | 0.010 | 0.059 | 0.15 |
| | 6 | 0.006 | 0.008 | 0.014 | 0.05 |
| 1742 | 12 | 0.137 | 0.008 | 0.145 | 0.30 |
| 1740 | 11 | 0.213 | 0.007 | 0.220 | 0.40 |
| | 7 | 0.067 | 0.006 | 0.073 | 0.15 |
| | 5 | 0.025 | 0.007 | 0.032 | 0.08 |
| | 3 | 0.007 | 0.012 | 0.014 | 0.04 |
| | | Avg. 0.0062 | | | |

^a Insoluble residue in wet analysis considered as Al₂O₃.

^b Acid-soluble aluminum value from wet analyses.

^c Total aluminum determined by spectrographic analysis.

^d Calculated from other two results.

constant at 0.006 pct and to simplify the determination by wet analysis for soluble aluminum only, or to use the spectrographic method and subtract 0.006 pct from the total.

In the different heats, residual aluminum contents, varying from 0.002 to 0.005 pct, were required to initiate the formation of eutectic sulphides in the various steels except for the two low-carbon Heats Al278 and Al465. In these steels, Type I sulphides persisted with an aluminum content of 0.008 pct. The Type III, angular sulphides, were readily obtained with aluminum contents of about 0.015 pct or more with all steels except those very low in silicon or carbon.

COMPARISON OF DEOXIDIZERS

Only those elements which can lower the FeO content enough to cause formation of Type II sulphides are amenable to comparison by the presently proposed method. The elements tested which fall into this category are aluminum, zirconium, titanium, and boron. None of the others apparently is a stronger deoxidizer than silicon.

Table 3 . . . The Relation Between Content of Deoxidizer and Formation of Eutectic Sulphides

| Heat No. | C | Mn | Si | S | P |
|----------|------|------|------|-------|-------|
| A 1503 | 0.26 | 0.64 | 0.42 | 0.039 | 0.010 |

| | | | | | | | | |
|--------------------------|--------|-------|-------|-------|-------|-------|-------|-------|
| Total Boron Content..... | 0.0005 | 0.006 | 0.014 | 0.023 | 0.032 | 0.041 | 0.058 | 0.062 |
| Inclusion Type..... | I | I | I | I | II | II | II | II |

| Heat No. | C | Mn | Si | S | P |
|----------|------|------|------|-------|-------|
| A 1674 | 0.26 | 0.59 | 0.36 | 0.039 | 0.018 |

| | | | | | |
|-----------------------------|-------|-------|-------|-------|------|
| Total Titanium Content..... | 0.015 | 0.020 | 0.024 | 0.037 | 0.05 |
| Inclusion Type..... | I | I | II | II | II |

| Heat No. | C | Mn | Si | S | P |
|----------|------|------|------|-------|-------|
| A 1741 | 0.33 | 0.62 | 0.32 | 0.038 | 0.011 |
| A 1998 | 0.34 | 0.71 | 0.30 | 0.018 | 0.008 |

| | | | | | | | | |
|-------------------------|---|-------|-------|-------|-------|-------|-------|-------|
| Zirconium* Content..... | 0 | 0.002 | 0.002 | 0.008 | 0.010 | 0.014 | 0.022 | 0.026 |
| Inclusion Type..... | I | II | II | II | II | II | II | II |

* First two are acid-soluble Zr, rest total Zr.

| Heat No. | C | Mn | Si | S | P |
|----------|------|------|------|-------|-------|
| A 1278 | 0.09 | 0.41 | 0.18 | 0.033 | 0.017 |
| A 1465 | 0.07 | 0.63 | 0.41 | 0.045 | 0.011 |

| | | | | | | | | | | | |
|------------------------|-------|-------|-------|-------|-------|-------|-------|-------|-------|-------|-------|
| Residual Aluminum..... | 0.002 | 0.003 | 0.004 | 0.005 | 0.006 | 0.008 | 0.011 | 0.023 | 0.024 | 0.025 | 0.037 |
| Inclusion Type..... | I | I | I | I | I | I | II | II | II | II | II |
| Res. Al..... | 0.053 | | | | | | | | | | |
| Inc. Type..... | II | | | | | | | | | | |

| Heat No. | C | Mn | Si | S | P |
|----------|------|------|------|-------|-------|
| A 1279 | 0.32 | 0.58 | 0.29 | 0.035 | 0.014 |
| A 1502 | 0.24 | 0.63 | 0.38 | 0.042 | 0.010 |

| | | | | | | |
|------------------------|-------|-------|--------|-------|-------|-------|
| Residual Aluminum..... | 0.002 | 0.002 | 0.005 | 0.007 | 0.008 | 0.014 |
| Inclusion Type..... | I | II | I & II | II | II | II |

| Heat No. | C | Mn | Si | S | P |
|----------|------|------|------|-------|-------|
| A 1742 | 0.51 | 0.69 | 0.36 | 0.043 | 0.011 |

| | | | | |
|------------------------|-------|-------|-------|-------|
| Residual Aluminum..... | 0.003 | 0.007 | 0.014 | 0.019 |
| Inclusion Type..... | I | II | II | II |

| Heat No. | C | Mn | Si | S | P |
|----------|------|------|------|-------|-------|
| A 1740 | 0.30 | 0.72 | 0.04 | 0.033 | 0.020 |

| | | | | | | |
|------------------------|-------|-------|-------|-------|-------|-------|
| Residual Aluminum..... | 0.002 | 0.009 | 0.015 | 0.027 | 0.035 | 0.066 |
| Inclusion Type..... | II | II | II | II | II | II |

| Heat No. | C | Mn | Si | S | P |
|----------|------|------|------|-------|-------|
| A 1743 | 0.30 | 1.43 | 0.36 | 0.041 | 0.012 |
| A 1999 | 0.31 | 1.47 | 0.32 | 0.039 | 0.009 |

| | | | |
|------------------------|-------|-------|-------|
| Residual Aluminum..... | 0.002 | 0.003 | 0.004 |
| Inclusion Type..... | II | II | II |

The pertinent analytical data for the stronger elements are given in Table 3; and in Fig 6 there is a graphic

representation of the quantity in the steel necessary to change the sulphides to the Type II. It will be noted that

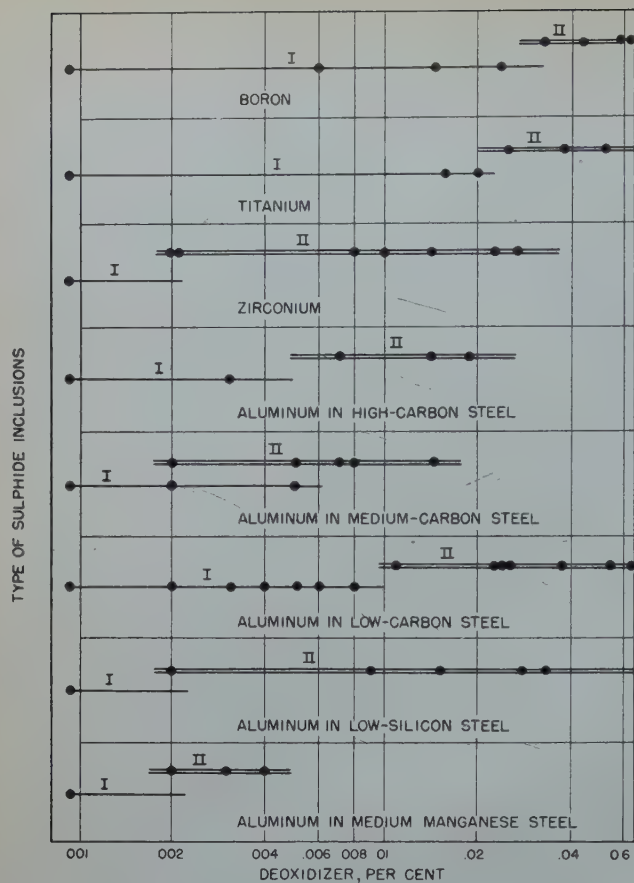


FIG 6—Showing relation between content of deoxidizing element and change to eutectic sulphide.

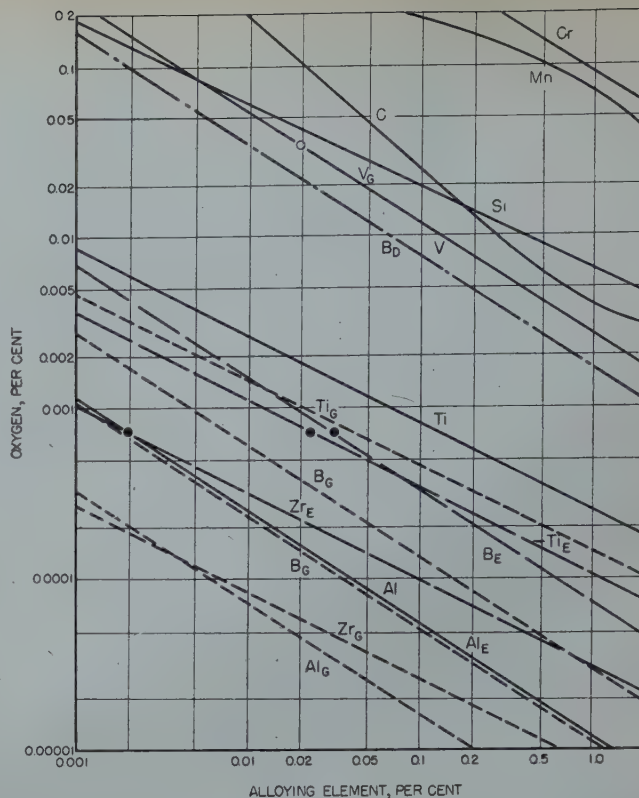


FIG 7—Comparison of deoxidizing powers at 2900°F (1600°C) for calculated and experimental values.

Solid lines Chipman's calculated values. Subscript E refers to present experimental work; subscript G refers to Gurry's calculated values; subscript D refers to Derge's experimental value.

for aluminum the change took place with a residual content of 0.002 pct for three cases, but in the steels containing 0.07 and 0.09 pct carbon, it required about 0.01 pct. In the high-carbon steel (0.51 pct C), the transition is a bit uncertain, but there was no change at 0.003 pct aluminum.

With zirconium, the transition was definite at a residual content of 0.002 pct which places it at least the equal of aluminum. In the case of titanium and boron, no distinction was made between soluble and insoluble portions, and the values given are determinations of total contents. From these it is deduced that they are considerably weaker than aluminum and zirconium.

For comparison with calculated values, the experimental values for the medium carbon steels are superimposed on Chipman's chart as it appears in "Basic Open Hearth Steel-making," 1944, p. 498, in Fig 7. No absolute values were obtained in the experimental work, and Chipman's value for aluminum was chosen as the standard, and the experimental value for aluminum made to coincide with it. Gurry's³ calculated values for aluminum, zirconium, titanium, boron,

and vanadium are also plotted as is Derge's⁴ experimental value for boron. The experimental values for titanium and boron are plotted on the basis that oxygen level is the same in all steels, regardless of deoxidizer, at the transition from Type I to Type II sulphides.

It is notable that Gurry's values for aluminum and zirconium have nearly the same relation to each other as the experimental values, but Gurry's figure for aluminum is much lower than Chipman's (stronger deoxidizer). The experimental value for titanium is lower than both Chipman's and Gurry's calculated values but is quite close to the latter. The experimental value for boron is definitely higher than either of Gurry's calculated values but also much lower than Derge's experimental value. Chipman's and Gurry's values for vanadium coincide.

SIGNIFICANCE OF THE ANALYSIS FOR ALUMINUM

One of the difficulties in obtaining data on the deoxidation with aluminum is that the limit of accuracy for analytical methods is reached for the very

low values of aluminum. The values in Table 2 were carefully checked by a skilled analyst and are believed to be accurate within the limits of the method used.* The acid-insoluble portion of the aluminum is generally believed to be present as Al_2O_3 , and in aluminum deoxidized steels, inclusions can be seen which are identifiable as Al_2O_3 and which seem to agree in quantity with the analytical results.

It has been tacitly assumed and widely believed that, when aluminum is added to steel, part of it is oxidized to Al_2O_3 (the deoxidation reaction), and that the solubility of Al_2O_3 being virtually nil, this Al_2O_3 is instantly precipitated. Much of it floats to the surface of the liquid steel, but some of it, because of its small particle size, remains suspended and is trapped when the steel freezes. Such a belief appears untenable in the face of the present data.

The constancy of the value for insoluble aluminum in steel, as shown in Table 2, has been noted before. Sims

* Insoluble aluminum separated by acid digestion, fused in potassium bisulphate, dissolved in dilute H_2SO_4 , and electrolysed on a mercury cathode. The aluminum is precipitated from this solution and determined as Al_2O_3 .

and Dahle² reported somewhat higher values. Halley⁵ analyzed some steels deoxidized with aluminum in large-sized commercial molds and obtained results as follow:

| Acid-soluble Aluminum | Al ₂ O ₃ | Insoluble Aluminum |
|-----------------------|--------------------------------|--------------------|
| 0.001 | 0.001 | 0.0005 |
| 0.009 | 0.008 | 0.004 |
| 0.038 | 0.008 | 0.004 |
| 0.073 | 0.010 | 0.005 |
| 0.169 | 0.008 | 0.004 |

Wentrup and Hieber⁶ gave analyses of 40 experimental low-carbon steels deoxidized with aluminum and with residual aluminum contents that ranged up to 0.83 pct. In 38 of these he obtained contents of acid-insoluble aluminum ranging from 0.001 to 0.012 pct with an average value of 0.005 pct. This is a significant corroboration and is considered to verify, first, that the insoluble aluminum tends to have a constant value and, second, that this value is in the neighborhood of 0.004 to 0.006 pct.

The constancy of this Al₂O₃ content cannot be accounted for on the basis that it was just the residue that failed to float out of the steel while it was still liquid. The recovery of added aluminum seldom is much higher than about 50 pct, and, in the case of a 4 lb per ton addition, the oxidized aluminum would be in the amount of 0.2 pct or thirty times the amount found in the solidified steel. If it is all precipitated, in varying amounts, why should an amount so constant remain suspended?

It cannot be accounted for as the Al₂O₃ that precipitates as a result of the shift in equilibrium constant during cooling of the steel to the freezing temperature, because the amount of oxygen involved is upwards of ten times the amount available from this source on the basis of Chipman's calculated value at 1600°C or thirty times what Gurry's value would allow, as shown in Fig 7.

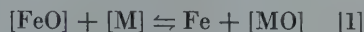
The only logical explanation seems to be that the Al₂O₃ found in the solid steel was actually in solution in some form in the liquid steel and precipitated during cooling and freezing. Moreover, it was a saturated solution in the liquid steel which accounted for the constancy. All oxide above the saturation value was precipitated instantly and floated out rapidly. The slight difference between the average value for acid-insoluble aluminum in Table 2 and Halley's value could then be due to temperature, because his heats

were probably poured at about 2800°F (1550°C); whereas, the heats of Table 2 were poured in the range of 2900 to 2950°F or a little over 1600°C. The solubility would be expected to be higher at the higher temperature.

It still remains to account for this solubility in the light of physical-chemical concepts.

A TENTATIVE THEORY ON THE DEOXIDATION REACTION AND THE FORMATION OF OXIDE INCLUSIONS

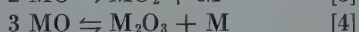
A tentative theory to account for the presence of the Al₂O₃ in solidified steel proposes that the deoxidizing reaction is first of all a homogeneous reaction in which the dissolved deoxidizing element "M" reacts with dissolved FeO in the steel to partition the oxygen and to form a monoxide of the deoxidizer. The reaction is



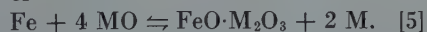
and the equilibrium constant for the reaction is

$$K_{\text{MO}} = \frac{\% \text{Fe} \times \% \text{MO}}{\% \text{FeO} \times \% \text{M}} \quad [2]$$

The MO formed has a limited solubility which varies with the concentration of M. Any excess of the MO over the solubility limit is quickly precipitated and rejected to the slag. During, or subsequent to, the precipitation, the MO disproportionates to form a higher oxide by such a reaction as



or



The disproportionation reaction may be simultaneous with the precipitation in some cases so that actually no MO exists as a separate phase, in which case it would be indistinguishable from direct precipitation of the higher oxide, or, on the other hand, it may be delayed in other systems, possibly requiring lower temperatures for completion. The presence of two oxides in the external phase, one of which is also in solution, would appear to violate the phase rule. For example, in Eq 3 to 5 above, there are two components and two phases which, at constant pressure, allow only one degree of freedom. This would mean that two solid oxides could exist at only one set of conditions (temperature, pressure, and composition). A way to avoid this objection is indicated by Willis,⁷ who postulates that oxides in

contact with molten metals cannot be regarded as classic stoichiometric compounds. For example, Wüstite, ostensibly FeO, has been found to contain too much oxygen for this composition. It cannot be regarded as a solid solution of Fe₂O₃ in FeO, because in the space lattice of the solid, there are no molecules let alone molecules of Fe₂O₃. It can be regarded only as a nonstoichiometric oxide. It seems possible, therefore, to have an oxide equivalent to MO plus M₂O₃ existing as a nonstoichiometric compound.

The importance of this to the present concept seems evident in the following quotation from Willis.⁷ "Since the composition of a nonstoichiometric compound is dependent on both temperature and the partial pressure of one of the components, any such compound must be regarded as a two-component system, where the classical compound of fixed composition represents only one component. In equilibria, involving variability of composition of a compound, an extra degree of freedom is introduced above those which would be found when the compound is counted as a single component."

Chipman⁸ has given good evidence that oxygen in liquid iron exists as a compound having one atom of oxygen, which for simplicity is assumed to be FeO. Fontana and Chipman⁹ later showed that when iron becomes saturated with FeO, as by cooling or freezing, FeO is precipitated. As the temperature falls, the FeO becomes less stable and partially disproportionates by the reaction



At any rate, some Fe₃O₄ is produced as a separate phase, and some islands of Fe can be observed in the Fe₃O₄. Although no deoxidation reaction is involved, the case is analogous and represents a condition in which the disproportionation to a higher oxide form is not complete even at room temperature.

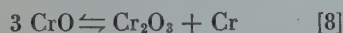
Zapffe and Sims¹ contended that SiO must play an important part in the silicon deoxidation of steel and gave some visual evidence that SiO might precipitate first and then decompose to SiO₂ plus Si. The disproportion of SiO is apparently very fast, however, and shows only in rapidly chilled specimens. Zapffe¹⁰ later elaborated this thesis with considerable additional evidence. He showed, for example, evidence of the silicon-enriched concentric envelope around the silica inclusion, which

would be the logical resultant of such a reaction.

In the carbon-oxygen reaction in steel, CO is formed and evolved (precipitated) as a gas. This gas always contains an equilibrium content of CO₂ which may be considered to have formed by the reaction



Chen and Chipman¹¹ give excellent reasons to believe that, in the Cr-O equilibrium in liquid iron, the oxygen is partitioned between FeO and CrO in a ratio that varies with Cr content. The only oxide inclusions found in the solidified Fe-Cr alloys, however, were chromite, FeO·Cr₂O₃, for those alloys containing up to 5.5 pct Cr, and chromic oxide, Cr₂O₃, in those of higher Cr content. Many of these chromite or chromic oxide inclusions contained islands of metal in a dendritic pattern. This fits very well into the picture of CrO precipitating and disproportionating as



or

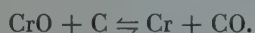


but gives no evidence that CrO ever existed as a separate phase.

Zapffe, in discussing the paper by Chen and Chipman's, argued strongly for the formation of Cr₂O₃ by the disproportionation of CrO, but he made a better case in his own paper.¹⁰

Some evidence for the existence of CrO as a separate phase in chromium alloys was obtained by Elsea, Westerman, and Manning.¹² High-chromium alloys, melted in an argon atmosphere, were found to be very high in inclusions of Cr₂O₃ when beryllia crucibles were used. When alumina crucibles were used, however, the alloys were practically free of oxide inclusions, but the crucibles had high contents of CrO·Al₂O₃ spinel. The CrO had obviously come out of the alloy as such and had combined with the alumina at the high temperature where the CrO is more stable.

Hilty¹⁵ has given very convincing evidence that in the simultaneous oxidation of carbon and chromium, from an alloy of iron, carbon and chromium, the oxides involved in the reaction are CO and CrO and that the reaction is



On the postulate that, in alloys containing up to 5.5 pct Cr, precipitated CrO disproportionates to form chromite according to Eq 9, then

Table 3 . . . Limiting Gas Compositions and Oxygen Content in Chromium-iron Alloys in Equilibrium with Chromium Refractories, Taken from Table VI of Chen and Chipman¹¹ With Calculated Values Showing Partition of Oxygen and the Constant for the Homogeneous Equilibrium

| $\frac{\text{H}_2\text{O}}{\text{H}_2}$ | Cr, pct | Total O ₂ , pct | O _{Fe} , pct | O _{Cr} , pct | FeO, pct | CrO, pct | $K_2 = \frac{\text{CrO} \times \text{Fe}}{\text{FeO} \times \text{Cr}}$ |
|---|---------|----------------------------|-----------------------|-----------------------|----------|----------|---|
| 0.162 | 1.0 | 0.045 | 0.0387 | 0.0061 | 0.174 | 0.0261 | 14.8 |
| 0.116 | 2.0 | 0.036 | 0.0272 | 0.0088 | 0.124 | 0.0374 | 14.8 |
| 0.081 | 4.0 | 0.031 | 0.0188 | 0.0123 | 0.0845 | 0.0522 | 14.8 |
| 0.070 | 5.5 | 0.030 | 0.0160 | 0.0146 | 0.0720 | 0.0620 | 14.8 |
| 0.056 | 8.0 | 0.029 | 0.0124 | 0.0170 | 0.0606 | 0.0722 | 14.8 |
| 0.046 | 10.0 | 0.028 | 0.0100 | 0.0175 | 0.0450 | 0.0742 | 14.8 |
| 0.041 | 12.0 | 0.027 | 0.0087 | 0.0187 | 0.0392 | 0.0793 | 14.8 |
| 0.034 | 16.0 | 0.027 | 0.0069 | 0.0206 | 0.0310 | 0.0878 | 14.9 |
| 0.029 | 20.0 | 0.027 | 0.0059 | 0.0220 | 0.0252 | 0.0935 | 14.8 |

$$K_1 = \frac{[\% \text{Cr}]^2}{[\text{Fe}][\text{CrO}]^4} \quad [10]$$

Since this is a heterogeneous reaction, the K₁ is really a steady state constant, but it can be treated as an equilibrium constant providing the same standard states are used for any given substance in all parts of the system. On the premise that the concentration of iron is nearly constant for such alloys, [CrO] content should be approximately proportional to the square root of [Cr]. For the higher chromium alloys, if CrO breaks down to chromic oxide according to Eq 8, then

$$K_2 = \frac{[\% \text{Cr}]}{[\text{CrO}]^3} \quad [11]$$

and the concentration of [CrO] should vary as the cube root of [Cr].

In Table 3 is listed the limiting oxygen content of alloys, containing up to 20 pct Cr, which are in equilibrium with chromite or chromic oxide at 1595°C and the gas compositions with which they would also be in equilibrium. These values were taken from Table 6 of Chen and Chipman.¹¹ In addition, values for O_{Fe}, O_{Cr}, FeO, and CrO are given which were calculated by the following formulas developed by those authors:

$$\begin{aligned} [\% \text{O}_{\text{Fe}}] &= 0.241 \left(\frac{\text{H}_2\text{O}}{\text{H}_2} \right) \frac{\% \text{Fe}}{100} \\ [\% \text{O}_{\text{Cr}}] &= 3.79 \left(\frac{\text{H}_2\text{O}}{\text{H}_2} \right) \frac{\% \text{Cr}}{100} \end{aligned}$$

The equation for [% O_{Fe}] was developed from data obtained on pure iron, whereas the formula for [% O_{Cr}] was obtained by subtracting the first equation from one for total oxygen.

In Fig 8, the values of CrO are plotted against the square root of Cr contents for alloys containing up to 5.5 pct Cr and against the cube root of Cr content for alloys containing from 5.5 to 20 pct Cr. It will be noted that acceptably straight lines, showing direct proportionality, were obtained.

This gives considerable support to the postulate regarding CrO.

Table 3 also shows that the equilibrium constant for the homogeneous equilibrium



which is

$$K_3 = \frac{[\text{CrO}] \times [\text{Fe}]}{[\text{FeO}] \times [\text{Cr}]} = 14.8 \quad [13]$$

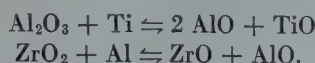
does not vary in the range 1 to 20 pct Cr. It also remains constant when [Cr] or total [O] are below the limiting values or saturation point.

This concept does not appear to violate the heterogeneous equilibrium of the chromium-iron alloys with chromite in one case and with chromic oxide in the other, as shown so well by Fig 10 of Chen and Chipman.¹¹ These higher oxides, or oxides of closely similar oxygen contents, furnish the oxygen pressure that determines the oxygen content of the alloys.

Abundant evidence has been brought forth recently to establish the knowledge that lower valence compounds of aluminum, zirconium, titanium, silicon, and chromium are stable at high temperatures under favorable (reducing) conditions. The production of ductile zirconium and titanium by the hot-wire iodide method depends, in part, on the formation of low-valence iodides which disproportionate to higher valence iodides and metal at high temperatures. Aluminum can be distilled by heating a mixture of the metal and AlF₃. The reaction 2Al + AlF₃ ⇌ 3AlF is reversible with appropriate changes in temperature and the AlF is volatile. The reaction Si + SiO₂ ⇌ SiO is used to produce volatile SiO to coat mirrors. When present in a slag, TiO₂ is an excellent flux, but under reducing conditions, it goes to a lower oxide and produces a viscous slag.

Alumina heated in vacuo at 1800°C with metallic silicon was reduced

to products identified as SiO and (probably) Al₂O.¹³ AlO has been identified definitely in the spectrum of gases at high temperature.¹⁴ When Al₂O₃ is heated in vacuo with metallic Ti or ZrO₂ with metallic Al, these refractory substances are disintegrated by the formation of suboxides



Apparently these reactions are typical and common.

THE ALUMINUM-OXYGEN EQUILIBRIUM

Evidence has been given to the effect that the alumina* found in solidified steels, which have had at least a short interval of time in the liquid state after deoxidation, represents material that was in solution while the steel was molten, and that the oxygen in this alumina far exceeds that permitted by the calculated deoxidation constants. The difference seems to be something more than experimental error.

To obtain further data, specimens having a wide variation in residual aluminum content were selected from those shown in Table 2 and were analyzed for total oxygen by the vacuum fusion analysis method, using a technique which has been shown to have a precision of ± 0.0004 pct O₂. The results are shown in Table 4.

Table 4 . . . Specimens Selected for Determination of Total Oxygen by Vacuum Fusion. The Corrected Value for Acid-insoluble Aluminum is Based on the Belief that the Average Value for this Constituent Shown in Table 2 is More Reliable than Individual Determinations. The Analyses for Oxygen are Typical of Many which Have Been Made on Aluminum Deoxidized Steels

| Sample Number | Acid-Soluble Aluminum | Insoluble Aluminum | | Total Oxygen |
|---------------|-----------------------|--------------------|-----------|--------------|
| | | Analyzed | Corrected | |
| 1279-1* | 0.001 | 0.004 | | 0.019 |
| 1279-3 | 0.002 | 0.007 | 0.006 | 0.008 |
| 1279-5 | 0.007 | 0.006 | 0.006 | 0.006 |
| 1279-6 | 0.015 | 0.004 | 0.006 | 0.005 |
| 1279-7 | 0.027 | 0.004 | 0.006 | 0.005 |
| 1279-8 | 0.041 | 0.005 | 0.006 | 0.005 |
| 1502-10 | 0.13 | 0.006 | 0.006 | 0.005 |
| 1465-12 | 0.17 | 0.005 | 0.006 | 0.005 |
| 1279-9 | 0.28 | 0.007 | 0.006 | 0.005 |

* No Al added.

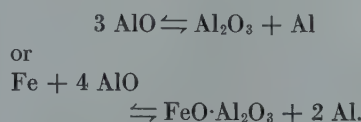
* This does not, naturally, include those streaks of aluminous inclusions found near the surface of ingots and which usually represent occluded scum.

Most outstanding is the fact that total oxygen decreases with increasing residual aluminum but only to a minimum value of 0.005 pct. For 0.006 pct Al as Al₂O₃, the stoichiometric value for oxygen would be 0.0053 pct which is well within the precision of the analytical methods. Thus, it appears that practically all of the oxygen is present as Al₂O₃ in solid steels containing as much as 0.015 pct residual Al. With contents of 0.007 pct residual Al, there is presumably some oxygen present as FeO.

According to this new concept, the deoxidation reaction is



Any AlO in excess of the solubility for the temperature is precipitated and disproportionates as



This material quickly rises out of liquid steel. The soluble portion of the AlO precipitates during cooling and freezing and forms the familiar inclusions found in aluminum deoxidized steels.

The apparent constancy of Al₂O₃ in the solid steel, which infers a similar constancy of AlO in the liquid steel, would seem to violate the theory expounded on page 821, which stipulates that AlO should vary as some function of the Al content. The typical deoxidation curve (oxygen vs. deoxidizer), however, is roughly an hyperbola and, after a certain content of deoxidizer is reached, the curve becomes nearly horizontal. With such a strong deoxidizer as aluminum, this nearly horizontal portion is quickly reached. Here the bulk of the oxygen is present as Al₂O₃, and although the content is theoretically not constant, the variation is too slight to be detected by present analytical procedures and, for purposes of calculation it may be considered constant without introducing a significant error.

The equilibrium constant can be expressed as

$$\frac{[\text{FeO}] \times [\text{Al}]}{[\text{AlO}] \times [\text{Fe}]} = K, \quad [13]$$

but since the [AlO] and Fe are nearly constant for a wide range of aluminum contents, it may be simplified to

$$[\text{FeO}] \times [\text{Al}] = K. \quad [14]$$

The constant quantity of 0.006 pct acid-insoluble aluminum can be calcu-

lated to 0.0143 pct AlO in the liquid steel. This would liberate 0.003 pct Al, most of which should be available as acid soluble, when it goes to the higher oxide form.

Using the meager data of Table 4, the values for Sample 1279-5 give $[\text{O}_{\text{FeO}}] = [\text{O}_T] - [\text{O}_{\text{AlO}}]$

$$= 0.006 - 0.0053 = 0.0007 \text{ pct} \quad [15]$$

$$[\text{FeO}] = 0.00315 \text{ pct} \quad [16]$$

$$\begin{aligned}^*[\text{Al}_R] &= \text{Al}_S - \text{Al}_L \\ &= 0.007 - 0.003 = 0.004 \text{ pct} \quad [17]\end{aligned}$$

$$\begin{aligned}K &= [\text{FeO}] \times [\text{Al}] = 0.00315 \times 0.004 \\ &= 1.26 \times 10^{-5} \quad [18]\end{aligned}$$

The best test for this constant is to see whether it can predict other conditions. In the case of Sample 1279-3, if the values 0.006 pct for insoluble Al and 0.008 pct for total O₂ are used with this value of K to calculate the residual Al, the figure of 0.004 is obtained compared with the analyzed value of 0.002 pct. For Sample 1279-6, if the values 0.006 pct for insoluble Al and 0.015 pct for soluble Al are used to calculate the oxygen present as FeO, the figure 0.00022 pct is obtained. This gives a total oxygen of 0.00552 pct as compared with the analytical value of 0.005 pct. The coincidence of the calculated and analyzed values is well within the limits of precision of the analytical methods. The quantities of FeO become unmeasurably small for still higher aluminum contents.

Because of the obvious limitations of analytical accuracy in this range, the deoxidation constant for aluminum cannot be regarded as highly accurate. The 1.26 calculated might be as low as 0.5 or as high as 2.5, but it is believed to be in the correct degree of magnitude. Total oxygen, for any given residual aluminum content, calculated from this constant, falls very close to analytical results, in contrast to previously calculated values for the deoxidation constant, as shown above.

THE ZIRCONIUM-OXYGEN EQUILIBRIUM

Data were given earlier (p. 817) to indicate that, in a steel deoxidized with silicon and zirconium, approximately 70 pct of the zirconium was present in acid-insoluble form. This was true over a range of total zirconium from 0.01 to 0.32 pct. If it be assumed that the insoluble zirconium represents oxidized zirconium (the nonmetallic inclusions seemed to be largely zirconium silicate), then it must be presumed that

* R = residual Al in liquid steel
S = acid soluble
L = liberated by disproportionation

some form of zirconium oxide, probably ZrO , has a high solubility in liquid steel and that this solubility varies with the content of residual or unoxidized zirconium. Tentatively, at least, this fits in very well with the presently postulated theory.

NOTES ON THE CHROMIUM-OXYGEN EQUILIBRIUM

When chromium is used as a deoxidizer, some chromium oxide will be precipitated, leaving some CrO in solution. The metal will, of course, be in equilibrium with the precipitated oxide and the values of dissolved CrO (when at $1595^{\circ}C$) can be taken from the curves of Fig 8. From these the following constants are obtained:

For contents up to 5.5 pct Cr

$$K_1 = \frac{(\% Cr)^{1/2}}{CrO} = 38.4$$

$$[CrO] = \frac{(\% Cr)^{1/2}}{38.4} = 0.026 (\% Cr)^{1/2}$$

For contents of 5.5 to 20 pct Cr

$$K_2 = \frac{(\% Cr)^{1/2}}{CrO} = 29.0$$

$$[CrO] = \frac{(\% Cr)^{1/2}}{29} = 0.0345 (\% Cr)^{1/2}$$

By substituting the value for $[CrO]$ in the equation

$$K_3 = \frac{[CrO] \times Fe}{[FeO] \times [Cr]} = 14.8$$

the $[FeO]$ content may be calculated. The total oxygen is then readily obtained.

It will be noted here that no activity coefficients are used and that all components are assumed to have an activity proportional to concentration. This illustrates the postulate of some physical chemists who contend that most materials at very high temperatures have activities proportional to their concentration and that, if the correct chemical species are known and used, activity coefficients, which are really correction factors, are unnecessary.

Very pertinent to the foregoing discussion is the fact that the data for $[O_{Fe}]$ also represent the activity of oxygen in the iron-chromium alloys, or $a_O = [O_{Fe}]$. The activity coefficients reported by Chen and Chipman¹¹ may be obtained as the ratio of $[O_{Fe}]$ to total $[O]$ or $\frac{[O_{Fe}]}{[O_{total}]} = f_O$.

Summary

In experimental work to test the

deoxidizing powers of commonly available elements, manganese, vanadium, and calcium were found to be no stronger than silicon. None of these is able to reduce the FeO content of steel sufficiently to form No. II type sulphides. Magnesium is somewhat doubtful but is disqualified as a deoxidizer from a practical standpoint.

Aluminum, zirconium, titanium, and boron all are capable of producing No. II type sulphides. On a comparison basis, aluminum and zirconium seem to be about equal and are the strongest deoxidizers of the elements tested. Titanium is next, though considerably weaker, while boron is not quite as good as titanium.

Alumina (acid-insoluble aluminum) was found to be quite constant in carbon steel for a wide range of residual aluminum contents. This is explained on the postulate that it was in solution in the molten steel as AlO , which precipitated and disproportionated to $Al_2O_3 + Al$ during freezing.

The theory that deoxidation is primarily a homogeneous reaction involving monoxides of Fe and the deoxidizing element is expounded. Oxides above the solubility limit precipitate and disproportionate to higher valence oxides.

By use of the proper chemical species in deoxidation, equilibrium constants may be obtained which are independent of activity coefficients.

References

1. C. A. Zapffe and C. E. Sims: Silicon-oxygen Equilibria in Liquid Iron. *Trans. AIME* (1943) 154, 192.
2. C. E. Sims and F. B. Dahle: Effect of Aluminum on the Properties of Medium-Carbon Cast Steels. *Trans. Amer. Foundrymen's Assoc.*, (1938) 46, 65-132.
3. R. W. Gurry: The Relative Deoxidizing Power of Boron in Liquid Steel and the Elimination of Boron in the Open-hearth Process. *Trans. AIME* (1944) 158, 98-106.
4. Gerhard Derge: The Boron-oxygen Equilibrium in Liquid Iron. TP 2004, *Metals Tech.* (Aug. 1946); *Trans. AIME*, (1946) 167, 93-110.
5. J. W. Halley: Grain Growth Inhibitors in Steel. TP 2030, *Metals Tech.* (June 1946); *Trans. AIME*, (1946) 167, 227.
6. H. Wentrup and G. Hieber: Unsetzungen Zwischen Aluminium und Sauerstoff in Eisenschmelzen (Reactions Between Aluminum and Oxygen in Liquid Iron). *Archiv. f. d. Eisenhüttenwesen*, (1939-40) 13, 15-20.
7. G. M. Willis: Constitution of Phases at High Temperatures in Relation to their Thermodynamic Properties. *Trans. Faraday Soc.*, Sept. 1948 (Preprint).
8. J. Chipman: Application of Thermodynamics to the Deoxidation of
9. M. G. Fontana and J. Chipman: Equilibrium in the Reaction of Hydrogen with Ferrous Oxide in Liquid Iron at $1600^{\circ}C$. *Trans. ASM*, (1936) 24, 313-332.
10. C. A. Zapffe: Dissociation Reactions within Inclusions. *Jnl. Iron and Steel Inst. London* (1946), No. II, 155-161.
11. Hsin-Min Chen and J. Chipman: The Chromium-oxygen Equilibrium in Liquid Iron. *Trans. ASM*, (1947) 38, 70.
12. A. R. Elsea, A. B. Westerman, and G. K. Manning: The Cobalt-chromium Binary System. *Trans. AIME* (1948), 175, *Metals Tech.*, TP 2393 (June 1948).
13. Metallforschung Report dated Apr. 25, 1944. B.N.F. Ser. 30,533, Ministry of Supply Translation from Kaiser Wilhelm Inst.
14. W. C. Pomeroy: *Phys. Rev.* (1927) 29, 59. Also, Selected Values of Chemical Thermodynamic Properties. Nat'l. Bur. of Standards, Washington, D. C., Dec. 31, 1947.
15. D. C. Hilty: Relation between Chromium and Carbon in the Refining of Chromium Steel. *Elec. Furn. Steel Proc.* (1948). *Jnl. of Metals Trans.* 185, 91. Feb. 1949.

DISCUSSION

J. CHIPMAN*—This paper describes the use of a new kind of indicator for studying the relative deoxidizing powers of several elements used in the deoxidation of steel. This is a very clever device and the results are interesting and possibly useful. The experimental method deserves careful scrutiny in order that there may be no uncertainty about what the indicator indicates. Molten steel, appar-

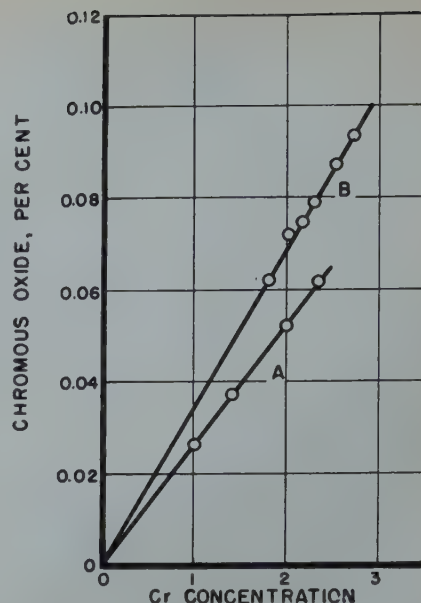


FIG 8—Values of $[CrO]$ from Table 3.

Plotted against the square root of $[Cr]$ contents up to 5.5 pct Cr (curve A) and against the cube root of $[Cr]$ contents from 5.5 to 20.0 pct (curve B).

Liquid Steel. *Trans. ASST*, (1934) 22, 385-446.

* Massachusetts Institute of Technology.

ently at 2900–2950°F in a basic-lined induction furnace, is deoxidized first with manganese and silicon and then with small increments of other deoxidizers. After each addition a 3-in. ingot is cast in a sand mold. The shape of the sulphide inclusions therein undergoes a sharp change with a critical amount of each of several deoxidizers and it is assumed that this change corresponds in each case to the same degree of deoxidation of the melt.

Two limitations on the use of this indicator must be recognized. The first is that, in order for this indicator to indicate the same degree of deoxidation with different deoxidizing elements, the composition of the indicator must be independent of the kind of deoxidizer used. Our present lack of information on the constitution of sulphide inclusions should caution us not to consider the indicator as an exact criterion of deoxidation but rather as a potentially useful approximation.

The second limitation arises from the fact that the sulphide inclusions are formed during the solidification of the metal, and the indicator can therefore be applied only to the condition of the metal during solidification. This means that its results should be compared not at 1600°C but in the freezing range, which is, of course, the condition of greater practical importance. This is a point which the authors have apparently overlooked and it deserves considerable emphasis. The degree of deoxidation indicated is not that in the furnace but rather that in the ingot during solidification. The amount of deoxidizer which must be added to the melt in the furnace must be large enough to react not only with the oxygen present but also with any additional oxygen which may be absorbed during pouring. If the solubility of the deoxidizer in the melt is very small it may be impossible to add enough of it in the furnace to maintain a high degree of deoxidation in the ingot. The solubilities of both magnesium and calcium in liquid steel are known to be very small and it seems evident that the results reported for these two elements have no bearing whatever upon their deoxidizing power. It is true that ways and means for utilizing the strong deoxidizing powers of these gaseous elements have not been developed, but the only contribution which the authors have made to this problem is another method to be avoided.

The validity of the experimental work on deoxidation with aluminum, like all previous attempts to study this reaction, is heavily dependent upon the accuracy of the analytical methods. When dealing with aluminum contents of the order of

0.006 pct, one must inquire diligently regarding the details of the method as well as possible interferences of such elements as carbon and nitrogen. Moreover, the assumed constancy of insoluble aluminum upon which so much argument is based seems hardly to be supported by the cited work of Wentrup and Hieber. Their acid-insoluble aluminum ranging from 0.001 to 0.012 pct (a twelve-fold range) can scarcely be considered a "significant corroboration" of this supposed constancy.

With regard to the theoretical sections of this paper, perhaps it will be sufficient here to record complete disagreement.

C. E. SIMS (authors' reply)—We concur with Dr. Chipman in pointing out the limitations of the deoxidation indicator used in this study. For example: at best, it is useful to indicate only one degree of deoxidation, that at which Type II sulphides first form. It is also limited to those deoxidizers substantially stronger than silicon; the others are merely lumped in the class of weak deoxidizers.

Its usefulness may be illustrated by the fact that it places vanadium very definitely among the weak deoxidizers, whereas, until recently, it has been widely regarded as a powerful deoxidizer. Statements in reference books and earlier thermodynamic calculations fostered this opinion.

The first limitation set by Chipman does not appear serious. The fact that the change from large globular to fine eutectic sulphides occurs at such low concentrations of deoxidizers, 0.002 pct for Al or Zr, makes it quite unlikely that these elements could materially alter the composition of the sulphides. It is quite obvious, on the other hand, that, at higher concentrations, sulphides of the deoxidizers do form.

In regard to Chipman's second limitation, it is emphasized again that the primary objective was a comparison of deoxidizers. The deoxidation was carried out at a nearly constant temperature of 1600°C. After that, the heats were held a standard time of 45 sec and poured directly into the mold with minimum exposure to air. Obviously, in all experimental work at high temperatures, the specimens must be solidified and cooled before they can be examined or analyzed and some conditions change during that operation. In the present case, the sulphides form during solidification, but it is postulated that the form they take is a direct result of the deoxidation that occurred at the holding temperature of 1600°C. When a different amount of deoxidizer was added, a different result

was obtained. Because of the conditions of handling, it is believed that very little change took place in the content of residual deoxidizer during pouring and solidification. This is attested by the constancy of the alumina content.

The difficulties of using such volatile and insoluble elements as calcium and magnesium as deoxidizers for steel were pointed out in the paper. Perhaps they did not have a fair chance to show their powers, although they were used in the customary manner, and perhaps they are strong deoxidizers as Chipman maintains, but what is the evidence? In another test, calcium vapor was bubbled through a rimming-type steel for a protracted period without showing any evidence of deoxidation. Although suitable under strongly oxidizing conditions, magnesia crucibles have been found unsuited to experimental work with steel under reducing conditions because the magnesia was reduced and volatilized. Alumina under the same conditions was quite satisfactory.

It is readily conceded that the present wet methods of determining Al in steel leave something to be desired. The method used is one generally approved by metallurgical laboratories. Carbon and nitrogen apparently do not interfere because the carbides and nitrides of aluminum are readily soluble in acid. The analyses reported by Wentrop and Hieber, taken by themselves, would have no significance. Although they do have considerable scatter, they lend some support to other, more consistent analyses. Because of the analytical difficulties and very low concentration, a "twelfold" variation is actually not too bad from an analytical standpoint, and, of course, most of the results were much closer to the average value. As pointed out in the paper, even the highest results of 0.012 pct represent only a small fraction of the total aluminum that was oxidized when aluminum was added.

In regard to the theoretical sections of the paper, it was fully anticipated that there would be considerable disagreement, but that alone was not a deterrent. The theory is an attempt to explain observed phenomena not covered by previous theories, but it should not be accepted without critical examination. The alternative seems to be to fall back on assertions that the oxygen content of liquid steel has a low activity because of some vague interatomic attractions and the use of a "fudge factor" called an activity coefficient, when making calculations. The present theory is immature, but, until it is disqualified, it appears to have the advantages of simplicity and workability.

Discussion*

Iron and Steel Division

San Francisco Meeting, February

1949

Contents

| | PAGE |
|---|------|
| Tracer Study of Sulphur in the Coke Oven (paper by S. F. Eaton, R. W. Hyde, and B. S. Old. <i>Met. Tech.</i> Oct. 1948, TP 2453C)..... | 826 |
| Some Correlations between Variables Affecting Sulphur in Blast Furnace Iron (paper by T. E. Brower and B. M. Larsen. <i>Met. Tech.</i> Oct. 1948, TP 2465C)..... | 830 |
| Sulphur Equilibria between Iron Blast Furnace Slags and Metal (paper by G. G. Hatch and J. Chipman. <i>Jnl. of Metals</i> Apr. 1949, TP 2556C)..... | 831 |
| Relation between Chromium and Carbon in Chromium Steel Refining (paper by D. C. Hilty. <i>Jnl. of Metals</i> Feb. 1949, TP 2507C)..... | 832 |
| The Effect of Hydrogen on the Ductility of Cast Steels (paper by C. E. Sims, G. A. Moore, and D. W. Williams. <i>Met. Tech.</i> Oct. 1948, TP 2454C)..... | 833 |
| The Origin of Silicate Inclusions in Basic Electric-arc-furnace Steel of Higher Carbon Contents (paper by A. Hultgren. <i>Met. Tech.</i> Aug. 1948, TP 2418C)..... | 834 |
| Sintering Characteristics of Minus Sixty-five and Twenty Mesh Magnetite (paper by A. Stanley and J. C. Mead. <i>Jnl. of Metals</i> , July 1949, TP 2597C)..... | 834 |
| The Influence of Temperature on the Affinity of Sulphur for Copper, Manganese, and Iron (paper by E. M. Cox, M. C. Bachelder, W. H. Nachtrieb, and A. S. Skapski. <i>Jnl. of Metals</i> , Jan. 1949, TP 2505C)..... | 837 |
| The Role of Thermochemical Factors in Basic Open Hearth Production Rate (paper by T. E. Brower and B. M. Larsen. <i>Met. Tech.</i> Oct. 1948, TP 2451C)..... | 839 |
| The Interaction of Liquid Steel with Ladle Refractories (paper by C. B. Post and G. V. Luerssen. <i>Jnl. of Metals</i> , Jan. 1949, TP 2496C)..... | 840 |
| The Ionic Nature of Metallurgical Slags. Simple Oxide Systems (paper by J. Chipman and Lo-Ching Chang. <i>Jnl. of Metals</i> , Feb. 1949, TP 2529C)..... | 841 |

* TP 2712 C.

Tracer Study of Sulphur in the Coke Oven

By S. E. EATON, R. W. HYDE, and B. S. OLD

DISCUSSION

(George McMeans presiding)

G. McMEANS*—This paper is a very good demonstration of the use of a new tool for the solution of industrial problems of a physical nature. To have solved this problem without the use of radioactive tracers would have required a far greater amount of investigation and work. The authors have described their work in such detail and in such a manner as to suggest the possibilities of the use of such tracer studies in the solution of many perplexing problems of industry.

R. E. BREWER†—The authors are to

* General Superintendent, Iron and Steel Div., Kaiser Co., Inc., Fontana, Calif.

† Chemical Engineer, Central Experiment Sta., U. S. Bureau of Mines, Pittsburgh, Pa. Papers by members of staff of U. S. Bureau of Mines are not subject to copyright.

be congratulated on this very excellent paper, which describes the results obtained by utilizing radioactive tracers in investigating the complicated reactions in the coking process. The paper has especial merit because the study was made under typical operating conditions in a commercial coke oven. Considering all the difficulties involved, the results obtained are excellent. My brief comments will relate primarily to the method used for determining the sulphur in the gas and to the value of the data obtained in stimulating further research.

In discussing their results, the authors state (p. 17) that "Of the total sulphur charged to the oven in the coal 95 pct was accounted for in the coke and gas. Most of the sulphur unaccounted for is believed to have been lost in the gas, since the gas sampling system removed all

the H₂S but probably only part of the organic sulphur compounds present in the gas. Although sulphur in the acid-insoluble tar residue in the gas scrubbing bottles was determined and added to the total sulphur determination of each sample, it is doubtful whether an aliquot portion of tar for each sample was obtained." The reviewer believes that the authors might have obtained a better sulphur balance had they used an improved procedure for determining sulphur in the gas.

The absorption train should have included a trap to remove the tar and ammoniacal liquor and a wash bottle containing 5 pct sulphuric acid to remove ammonia in the coke-oven gas before it entered the gas scrubbing bottles containing the ammoniacal cadmium chloride solution. Sulphur in the tar and

liquor could then be determined directly; and, at the same time, contamination of the precipitate by tar in the gas scrubbing bottles would be avoided. Ammonia in the gas should be removed to avoid increasing the alkalinity of the ammoniacal cadmium chloride solution, with consequent possible solution of part of the cadmium sulphide precipitate.

The authors have assumed that all of the dry, purified precipitate is cadmium sulphide from which they have calculated elemental sulphur. In addition to cadmium sulphide formed from the hydrogen sulphide, ammoniacal cadmium chloride solution also precipitates mercaptans as cadmium mercaptides and some of the carbon disulphide after partial hydrolysis as cadmium sulphide. Since the percentages of sulphur in cadmium sulphide and in cadmium mercaptide (ethyl mercaptide) are 22.2 and 27.3, respectively, calculation of the elemental sulphur from cadmium sulphide alone would be in error. Granting that the amount of elemental sulphur might thus be reported somewhat high, the higher value has not compensated for the remaining sulphur in other organic sulphur compounds that may have been present and were not precipitated either as cadmium sulphide or as cadmium mercaptide. The gas-sampling system used must therefore have removed "only part of the organic sulphur compounds present in the gas." However, since the total sulphur present in the organic sulphur compounds—such as mercaptans (ethyl and methyl), thiophene and its homologs, carbon disulphide, carbon oxysulphide, thio ethers, and alkyl disulphides—in coke-oven gas is small as compared to the sulphur in hydrogen sulphide, the total error in assuming that all of the sulphur is precipitated as cadmium sulphide would be small. A more elaborate gas-sampling system using more specific reagents in the absorption train to insure complete removal of all of the sulphur in the gas and additional laboratory analyses to determine the sulphur absorbed by each of the various reagents would, no doubt, afford a better sulphur balance. The additional labor and cost of introducing these refinements, however, to determine the 5.2 pct of unaccounted for total sulphur might not be justified in routine operations.

Fig 8 shows the percentage of sulphur content of coke-oven gas originating from the pyritic sulphur of the coal increases markedly between the 4th and 12th hours of the coking period. On the other hand, Fig 9 shows that the sulphur content of the gas originating from the organic and sulphate sulphur of the coal drops steadily after the 4th hour. These observations emphasize the need for coking coals of low pyritic sulphur content and should stimulate new developments in more effective coal-cleaning methods. Organic sulphur in coal cannot be satisfactorily

removed by present methods, but if it is not too large in amount it may be tolerated if the pyritic sulphur is small.

The authors have made a valuable contribution to the knowledge of the coking process. Their paper serves as an excellent guide for determining the principal sources of sulphur in coke. The results of this study should stimulate intensive research in the developments of methods for (1) reducing both inorganic and organic sulphur in the coal charge, (2) converting larger proportions of the coal sulphur into volatile products during coking with resulting lower sulphur in the coke, and (3) treating the coke itself to reduce its sulphur content.

(Attention is called to the following misprints in the text of the paper:

"Ind." in table on p. 4 must mean Allegheny Co., Pa.

"24,198" in line 25, p. 6, should read "24,188."

Sum of values in columns 3 and 4, Table 5, p. 12, for 2d, 5th, and 12th hr do not give the corresponding present values in column 5 of this table. After correction, the sum of all values in column 5 will be 60.5 lb or 24.6 pct of the total sulphur. This slightly higher value for sulphur in the gas, if used, will favor the sulphur balance: Table 6, p. 12; line 1, p. 13; and Table 8, p. 14.).

C. WAGGONER*—The use of a new tool is very enlightening to us who have had mixed feelings toward and recognize the need for collaboration about things like sulphur. I still ask this question. The authors talk about migration and say that it is a reasonable assumption that radioactive pyrites behave identically with the natural pyrites and then in the conclusion the results indicate that there is a migration. I would like to ask is that a migration of sulphur or is it merely a migration of radioactivity?

J. DASHER†—The radioactive sulphur. Sulphur 35 will not make any other sulphur atom radioactive. The element that is radioactive will remain so until it changes into chlorine, so the activity measured in the organic and the calcium sulphide form in the coke shows that the sulphur atoms present in that form in the coke were originally present in the pyrite, and there is no conversion of radioactivity. The atom itself is tagged.

C. WAGGONER—Before we can use a tool we must know a little bit more about it and I was interested in one other part of the paper that dealt with the background of radioactivity. If we are to tag atoms those tagged atoms may cause us trouble later in our product. We can easily calculate at what period of time it would approach the background radioactivity, is that proper?

* General Superintendent, Geneva Steel, Geneva, Utah.
† Mass. Inst. of Technology.

J. DASHER—Yes.

C. WAGGONER—And are we right in assuming that if we got reasonably close to that there would be no danger from action of radioactivity? I am not thinking about action on the person such as you described—the skin of a person would stop this activity—but I am thinking about, say, photographic plates.

J. DASHER—The activity from the sulphur in this experiment would be insufficient to affect a photographic plate.

C. WAGGONER—Will the detail of the experiment be printed?

J. DASHER—The paper was published. The analytical method in detail will be published.

C. WAGGONER—That will be excellent because I am sure it will answer a lot of questions that we who are confronted with problems of this kind will have to discuss with someone intelligently. I think the authors have made a real contribution to the methods of analyzing steel, and I only wish that we were more able to take advantage of it.

R. W. CAMPBELL*—The authors are to be congratulated on the presentation of an excellent paper and the development of a new and unique method in investigating the complicated reactions in the coking process. The results of this first large scale tracer study stress the value of the use of radioactive isotopes in the study of process metallurgy and will probably stimulate further work where similar approach would be necessary to gain the goal desired.

The rapidity of depletion of low sulphur coking coals and the advent of 100 pct mechanized coal mining in certain mining districts of the United States have given the steel industry a very perplexing problem to solve in order to obtain low sulphur metallurgical coke. The pyritic sulphur, with the exception of the very fine sizes, can be successfully removed in a modern coal washing plant, but the organic sulphur remains untouched, and it is this form of sulphur which the scientists should try to reduce in an economical way.

The Republic Steel Corporation was interested in finding out which one of the two major forms of sulphur in coal, namely, pyritic and organic, contributed the greater portion of the sulphur in the coke. Since, however, considerable quantities of sulphur are present in coke oven gas it was thought that if it could be shown definitely that the major part of the sulphur in coke originates from only one of the major forms of sulphur in the coal it would be possible to select types of coal which, although high in total sulphur, still would yield coke of fairly low sulphur content. This problem

* Superintendent Coke Div., Pittsburgh Dist., Jones & Laughlin Steel Corporation.

seemed to be suited for study using modern radioactive tracer technique while employing full-scale coking conditions, and this certainly has been accomplished by the authors.

The initial radioactive sulphur employed had an activity of only 40 micro-curies per g. Due to high dilution factor with inactive sulphur in the coal, the activity was reduced still further and it was found necessary to employ the sulphur present as the pure element in order to obtain sufficient accuracy. Since all samples contained active sulphur of the same age from the original batch, all activity measurements would be directly comparable if they were taken at the same time. As a close approximation, all sulphur samples were counted the same day with frequent checks of the background reading without sample.

The analytical data showed that 70.3 pct of the total sulphur in the coal was retained in the coke, 24.5 pct in the gas and 5.2 pct was unaccounted for. Of the total sulphur in the coal 42 pct was pyritic according to chemical analysis and from the tracer measurements it was found that 40 ± 2 pct of the total sulphur in both the resulting coke and gas evolved had pyritic origin. Thus neither of the two main forms of sulphur in coal, pyritic and organic, is removed preferentially during coking. Employing present coking methods there would be no advantage in choosing coal for its high or low pyritic or organic sulphur content.

Ferrous sulphite and carbon-sulphur complex forms represent all the sulphur in coke under high temperature and reducing conditions, as in the coke oven. After coke is pushed, some of the ferrous sulphite oxidizes to free sulphur and sulphates. However, in the top of the blast furnace, where high temperatures and reducing conditions again prevail, the free sulphur and sulphates revert to the original ferrous sulphite.

The authors conclude that in order to produce low sulphur coke, coals low in initial sulphur must be used and that in view of the large initial evolution of organic sulphur and small amounts of pyritic might be coked for a slightly shorter time to produce coke containing a given percentage of sulphur. Coals high in pyritic sulphur would have to be coked for a slightly longer period of time to obtain the same results.

Their conclusions on the possibility of helping the coke sulphur situation by controlling the coking time, depending on the types of sulphur present in the coal charge, is very interesting and should be studied further. It must be remembered, however, that the physical quality of the coke has always been the determining factor governing the coking time.

Without trying to detract in any way from the excellent work done by the au-

Table 9 . . . Distribution of Sulphur in Coal, Coke and Products of Distillation
100 Pct Raw Pittsburgh Seam Coal—Total Sulphur, 1.21 Pct

| Forms of Sulphur in Raw Coal | | | Distribution of Sulphur of Coal in Products of Distillation | | |
|------------------------------------|------|--------------|---|-------|--------------|
| | Pct | Pct of Total | | Pct | Pct of Total |
| Sulphate sulphur..... | 0.07 | 5.78 | In coke..... | 0.631 | 52.15 |
| Pyritic sulphur..... | 0.49 | 40.50 | In breeze..... | 0.104 | 8.60 |
| Organic sulphur (humus)..... | 0.52 | 42.98 | Total in gas..... | 0.387 | 31.98 |
| Organic sulphur (phenol sol.)..... | 0.13 | 10.74 | In tar..... | 0.031 | 2.56 |
| Total..... | 1.21 | 100.00 | In light oil..... | 0.016 | 1.32 |
| Inorganic sulphur..... | 0.56 | 46.28 | In final cooler water..... | 0.014 | 1.16 |
| Organic sulphur..... | 0.65 | 53.72 | In liquor as sulphide..... | 0.004 | 0.33 |
| | | | In liquor as ammonium..... | | |
| | | | Thiosulphate, sulphocyanate..... | 0.008 | 0.66 |
| | | | Total determined..... | 1.195 | 98.76 |
| | | | Undetermined and loss..... | 0.015 | 1.24 |
| | | | Total..... | 1.210 | 100.00 |

| Pct Coke Yield | Pct Sulphur in Coal | Pct Sulphur in Coke | Pct Sulphur Eliminated | Pct Sulphur Retained |
|----------------|---------------------|---------------------|------------------------|----------------------|
| 67.1 | 1.21 | 0.94 | 47.85 | 52.15 |

| | |
|---|-----------------------|
| Sulphur in furnace coke..... | 0.94 pct |
| Sulphur in coke breeze..... | 1.27 pct |
| Sulphur in gas after saturators..... | 570 grains per 100 cf |
| Sulphur in gas after final coolers..... | 550 grains per 100 cf |
| Sulphur in tar..... | 0.69 pct |
| Total sulphur in light oil..... | 1.02 pct |
| Total sulphur in liquor..... | 1.495 g per liter |
| Sulphur as sulphides in liquor..... | 0.520 g per liter |

| | Pct Retained | Accum. Pct |
|---------------------------------------|--------------|------------|
| In coke..... | 52.15 | 52.15 |
| In breeze..... | 8.60 | 60.75 |
| In gas..... | 31.98 | 92.73 |
| In tar..... | 2.56 | 95.29 |
| In light oil..... | 1.32 | 96.61 |
| In final cooler water and liquor..... | 2.15 | 98.76 |
| Undetermined and loss..... | 1.24 | 100.00 |

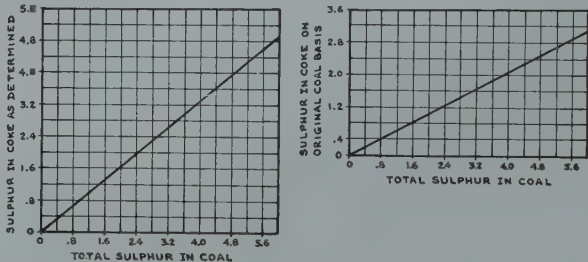


FIG 13—Coal and coke sulphur relationships.
A (left)—Relation of sulphur content of coke to sulphur content of coal.
B (right)—Sulphur content of coke, expressed on basis of original coal, as function of total sulphur content of coal.

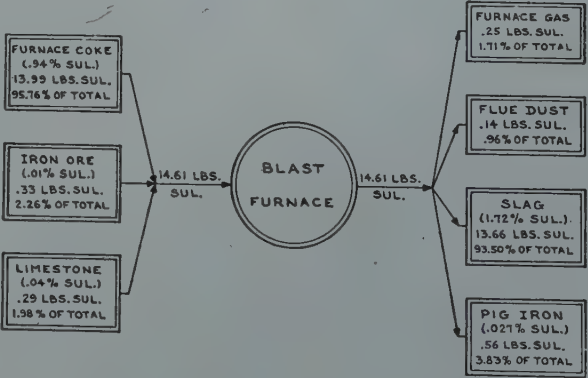


FIG 14—Sulphur distribution in the blast furnace per net ton of pig iron.

Table 10—Inland Steel Co. Coal and Coke Analyses and Yields

| | June 1941 | | | | Dec. 1948 | | | |
|------------------------|------------|---------|-----------|-----------|------------|---------|-----------|-----------|
| | Pct in Mix | Pct Ash | Pct Sulph | Pct Yield | Pct in Mix | Pct Ash | Pct Sulph | Pct Yield |
| Pocahontas..... | 35 | 5.70 | 0.60 | | 35 | 8.05 | 0.62 | |
| Wheelwright Slack..... | 40 | 4.05 | 0.74 | | 45 | 9.00 | 0.96 | |
| Wheelwright Egg..... | 25 | 2.00 | 0.66 | | 20 | 4.10 | 0.80 | |
| Mixture..... | | 4.00 | 0.67 | | | 7.40 | 0.83 | |
| Furnace Coke..... | | 5.35 | 0.58 | 68.8 | | 10.20 | 0.70 | 68.1 |
| Domestic..... | | 5.50 | 0.57 | 2.3 | | 9.75 | 0.69 | 1.9 |
| Braize..... | | 9.00 | 0.61 | 2.7 | | 15.40 | 0.76 | 4.0 |

Percent sulphur reduction during the carbonization of coal for the production of coke.

| | 1941 | 1948 |
|-------------------|---|--|
| | Pct Sulph. Yield | Sulph. Yield |
| Furnace coke..... | $0.58 \times 0.688 = 0.399$ | $0.70 \times 0.681 = 0.477$ |
| Domestic..... | $0.57 \times 0.023 = 0.013$ | $0.69 \times 0.019 = 0.013$ |
| Braize..... | $0.61 \times 0.027 = 0.016$ | $0.76 \times 0.040 = 0.030$ |
| | 0.428 | 0.520 |
| | $\frac{0.428}{0.67} \times 100 = 63.9$ pct sulphur left in coke | $\frac{0.52}{0.83} \times 100 = 62.6$ pct sulphur left in coke |

thors in their elaborate and excellent study of sulphur, it is interesting to quote the conclusions of two earlier experimenters in the same field:

Dr. A. R. Powell (1920)¹⁴—"The total sulphur of the coal is the most important factor affecting the sulphur content of the coke and the relative amount of sulphur forms does not affect it materially. Certain other factors, particularly the nature of the coal, vary the amount of sulphur in the coke to a limited extent."

Gilbert Thiessen (1935)¹⁵—"The sulphur in coke is derived from both organic and pyritic sulphur in the coal, approximately 45 pct of the organic sulphur and 60 pct of the pyritic sulphur remain in the coke.

"Because the proportions of the organic and the pyritic sulphur which remain in the coke are of the same magnitude, the sulphur content of the coke is for practical purposes directly proportional to the total sulphur content of the coal. Approximately half of the sulphur in the coal remains in the coke. Because of the loss of volatile matter, the amount of sulphur in the coke is about 80 pct of the percentage of the sulphur in the coal from which the coke was made. Iron compounds other than pyrites in the coal, arising from infiltration or from oxidation of pyrites, increase the retention of sulphur in the coke."

Fig 13 presents two curves from the experimental work of Gilbert Thiessen and shows; "A—Relation of Sulphur Content of Coke to Sulphur Content of Coal" and "B—Sulphur Content of Coke, Expressed on Basis of Original Coal, as Function of Total Sulphur Content of Coal."

Table 9 is a tabulation of some of the experimental work done at our Pittsburgh By-Product Coke Plant.

Fig 14 clearly indicates that 95.76 pct of the total sulphur in the burden is contributed by the coke containing 0.94 pct sulphur.

E. J. GARDNER*—The authors are to be commended for their careful preparation of an interesting and informative paper on the use of radioactive tracers to determine the distribution of the pyritic and organic sulphur in the carbonization of coal for the production of high temperature coke.

The gas evaluation curves, sulphur balance data on the plant scale test run, and the schematic flow of sulphur in a coke oven diagram, wherein the course of the pyritic sulphur is traced in order to determine quantitatively the amount evolved in the gas and the amount remaining in the coke, form an important contribution to our knowledge of the behavior of sulphur in the coking process.

At the Inland Steel Co., we also are concerned at the decrease in the quality of our high volatile—Elkhorn Seam—slack coal as regards ash and sulphur content. When our Wheelwright mine, because of the demand for increased production for the war emergency, went from the customary practice of careful preparation of the coal at the face, followed by hand loading of the coal into the mine cars, to the present practice of machine loading, the ash and sulphur content increased from 4.05 and 0.74 pct in June, 1941, to 9.00 and 0.96 pct respectively in Dec., 1948.

The increase in ash and sulphur in our coal blend produced furnace coke with inferior chemical and physical properties and resulted in a decrease in the quality and the iron tonnage obtained from our blast furnaces.

In order to overcome the adverse effects of mechanical loading on the ash and sulphur content of our high volatile coal, we are installing a coal cleaning plant at our Wheelwright mine. Our mining department assures us that they will deliver washed Wheelwright coal from machine loaded mining with ash and sulphur contents that are similar to the hand loaded product.

Table 10 shows comparative coal and coke analyses for our hand loaded and machine loaded coal.

Table 10 shows that in 1941 our coal mixture had 4.00 pct ash and 0.67 pct sulphur. In 1948, the coal mixture shows 7.40 pct ash and 0.83 pct sulphur. For the same periods, the analyses of our furnace coke went from 5.35 pct ash and 0.58 pct sulphur to 10.20 pct ash and 0.70 pct sulphur.

From the total sulphur analyses of the coal mixture charged and the coke produced, the amount of sulphur remaining in the coke was 63.9 pct for the 1941 and

62.7 pct for the 1948 period; in other words, the percent of the sulphur volatilized in the coking operation was practically the same for the low and high sulphur coal mixtures.

The results reported in the plant scale tracer study have given us a clearer picture than using the conventional methods of chemical analysis, of the rate of evolution and distribution of the pyritic and organic sulphur compounds during the carbonization of coal.

Although it will still be necessary to carbonize coals with low total sulphur content in order to produce low sulphur coke, the experimental data presented by the authors will form the basis for further radioactive tracer studies of the reactions that take place in the course of the transformation of coal to coke.

S. E. EATON, R. W. HYDE, and B. S. OLD (authors' reply)—The authors wish to thank R. W. Cambell and E. J. Gardner for their very interesting comments on the subject of sulphur in the coke oven and the blast furnace, and Ralph E. Brewer of U. S. Bureau of Mines for his very careful review of the paper.

In regard to the 5.2 pct of the total sulphur unaccounted for in coke and gas, Mr. Brewer is correct in saying that more of the sulphur in the coke oven gas could probably have been recovered by an improved scrubbing method. However, we wish to point out that since 95 pct of the sulphur in coke oven gas is present as hydrogen sulphide, the amount of sulphur in the gas which was not recoverable by the system used is rather small. We agree that a slight error may have been introduced by the presence of cadmium mercaptide in the cadmium sulphide precipitate but since sulphur as mercaptans is only on the order 0.3 pct of the

¹⁴ A. R. Powell: *Jnl. Ind. Eng. Chem.* (1920) 12, 1069.

¹⁵ Gilbert Thiessen: *Jnl. Ind. Eng. Chem.* (1935) 27, 473.

* Superintendent, Blast Furnace and Coke Dept., Inland Steel Co., East Chicago, Ind.

total sulphur in the gas the error should be extremely small. Undoubtedly some of the sulphur in the gas passed through the scrubbing train; to have removed all the sulphur in the gas as well as obtain an aliquot portion of tar would have involved a much more elaborate sampling system. Since we were primarily inter-

ested in the distribution of the forms of sulphur in the coke, a more elaborate system of sampling gas did not seem justified in view of the probable error involved.

Mr. Brewer also noticed a slight discrepancy in Table 5 for the 2nd, 5th, and 12 hr. The values of pyritic, organic, and

total sulphur evolved each hour were calculated to one significant figure to the right of the decimal point, that is, to the nearest tenth of a pound. We would prefer not to change any value in this table as the individual values are more accurate as they now stand.

Some Correlations between Variables Affecting Sulphur in Blast Furnace Iron

By T. E. BROWER and B. M. LARSEN

DISCUSSION

(G. MacMeans presiding)

J. SAUSSAMAN*—One thing I have to say is that when anyone mentions sulphur, we at Fontana, are ready to listen. Although we do not have too much sulphur in our coke, we run into sulphur in our ores, and that is just one more variable in the question of how to control sulphur. Inasmuch as most of the data for this paper were taken from actual operation, I thought it might be interesting to show you some places in our operation which vary from those covered in the paper. The authors talk quite a bit about magnesia in the slag, and the magnesia in the slag at Fontana runs anywhere from 15 to 18 pct, usually being closer to 18 than 15. We get very good sulphur elimination with this slag, although the calcium in the slag is very much on the low side—about 32 pct. The high magnesia content does not appear to affect seriously sulphur elimination.

At the present time the two ores we use carry quite a bit of sulphur, one of them 2 pct sulphur and the other about 0.5 pct sulphur. Of course, the 2 pct sulphur ore cannot be used in the furnace directly due to that amount of sulphur, but it is removed by sintering. That reminds me of the statement that was made in a recent paper that the best way to control sulphur is not to put it in in the first place, so that is the way we do with the ore and have very good results with the sintered product.

The other ore contains about 0.5 pct

sulphur and we control the sulphur merely by a screening operation which reduces the sulphur to about 0.2 pct in the plus $\frac{5}{8}$ in. particles with a large percentage of the sulphur following the minus $\frac{5}{8}$ in. particles to the sintering plant.

In this one ore, running about 0.5 pct sulphur, we have the problem that half of that sulphur is in the form of gypsum or calcium sulphate, and the question then comes up as to how to control sulphur when it is in the form of calcium sulphate. Does it react in the same way in the furnace as the pyritic sulphur? We do not know the answers as we have not been working with it long enough.

L. E. RIDDLE*—I do not think it right to state that some one thing is the reason sulphur in pig iron is high or low. You have to take into account a number of things—variable amounts of sulphur when using the same materials, the kinds of sulphur in the raw materials, temperature changes in the hearth of the furnace, and correlation effect.

I do not agree with Mr. Larsen that varying amounts of alumina has no effect on slag. His data show that in his study of more than 100 samples of slag the alumina did not vary 1 pct. Had he had slags with Al_2O_3 as low as 9 pct and others with 20 pct he would have found that with Al_2O_3 above 18 pct the ratio of CaO and MgO to $SiO_2 + Al_2O_3$ can be lowered greatly with sulphur removal, results equaling those when the CaO and MgO ratio to $SiO_2 + Al_2O_3$ is much higher when the Al_2O_3 is below 15 pct.

Having made pig iron with 19 and 20 pct Al_2O_3 in the slag and ferro-manganese

with 22–23 pct Al_2O_3 and the same products with half these amounts of Al_2O_3 in the slag, we learned the above fact.

B. M. LARSEN (authors' reply)—Mr. Saussaman's comments indicate approximately normal or expected S removal at 15–18 pct MgO in slag with 32 pct CaO. We have experience in one shop with 10–12 MgO and a limited run in another with 15–17 pct MgO; in both cases the ratios were lower by only a moderate amount than at what we feel to be the optimum range of 6–8 pct MgO. All such comparisons between shops must be regarded with caution because of the many factors (manganese and silicon in iron, iron and slag temperature, etc.) which appear to complicate the sulphur removal situation. As regards the division between pyritic and sulphate sulphur, we believe that essentially all the sulphur charged gets trapped in the furnace and all of it ends up in the sulphide form, so it does not matter in what form it is present in the charged materials.

As regards a member's comments on the factors of Mn and temperature, we would only say that until a lot of good temperature data are available on slag and metal casts, we probably must keep an open mind on the inter-relationships between different variables. Higher temperature may have a direct effect of speeding the rate of sulphur migration from iron to slag. On the other hand, to the extent that higher temperatures are associated with higher Mn and Si and more basic slags it is quite probable that here the temperature should be regarded as the secondary rather than the primary variable.

* Superintendent Blast Furnace, Kaiser Co., Fontana, Calif.

* Blast Furnace Consultant, Duquesne, Pa.

Sulphur Equilibria between Iron Blast Furnace Slags and Metal

By G. G. HATCH and J. CHIPMAN

DISCUSSION

(G. MacMeans presiding)

T. ROSENQVIST*—It is a pleasure to see the excellent way in which the experimental part of this work has been handled. There seems to be little doubt that the distribution data obtained corresponds most closely to thermodynamic equilibrium under the prevailing reducing conditions, namely equilibrium with graphite and one atmosphere CO pressure.

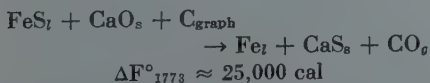
The desulphurization curves in Fig 10 show the same general feature as the curves given by Holbrook and Joseph, but the distribution ratios are from 20 to 40 times greater—undoubtedly due to a closer approach to true equilibrium.

In the theoretical discussion, the authors calculate a theoretical distribution ratio $\frac{(S)}{[S]}$ which they find to be about 50 times greater than the experimental. The deviation is so great that the basis for their calculation needs a more thorough examination.

The authors base their thermodynamic calculation on free energy expressions where diluted solutions of FeS and CaS are used as standard states. (The activity coefficient in diluted solutions is taken to equal unity.) Such a standard state will change when the nature of the solvent is changed. Taking the free energy of the reaction $[\text{FeS}] \rightarrow (\text{FeS})$, Eq 2, which is derived from the distribution of sulphur between an iron and a FeO-melt, it is very unlikely that the free energy of this reaction will be the same for a distribution between pig iron and a calcium silicate slag.

Therefore a more fundamental basis for the thermodynamic calculations seems needed, where all thermodynamic equations are referred to unambiguously defined standard states.

The most natural standard states for CaO and CaS are the pure solid substances at the same temperature. As standard state for sulphur in iron, pure liquid FeS can be used. This rules out Eq 2 $[\text{FeS}] \rightleftharpoons (\text{FeS})$ because $\Delta F^\circ = 0$. The standard equation will then be:



It would be more universal and also

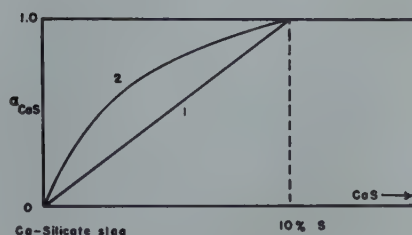
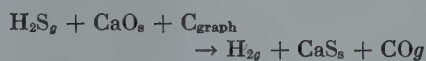


FIG 11—Chemical activity of CaS in blast furnace slag.

(Hypothetical) Curve 1. Approximately ideal solution. Curve 2. Positive deviation from ideal solution.

simpler to refer the escaping tendency of sulphur in liquid iron to the corresponding $\text{H}_2\text{S}/\text{H}_2$ ratio which can readily be determined experimentally. As standard state a gas mixture $\text{H}_2\text{S}/\text{H}_2 = 1/1$ can be used. (This corresponds at the temperature of liquid iron closely to one atmosphere S_2 vapor.) Thus the standard equation for the sulphur reaction can be formulated as follows:



The standard free energy of this reaction has been calculated from the best available data to $\Delta F^\circ_{1773} = -35,000$ cal. This gives for the equilibrium constant at 1500°C

$$K_p = \frac{A_{\text{CaS}} P_{\text{H}_2} P_{\text{CO}}}{A_{\text{CaO}} P_{\text{H}_2\text{S}} A_{\text{C}}} = 2.10^4$$

Now, the solubility of CaS in blast furnace slags has been determined by McCafferey and Oesterle* and corresponds at 1500°C to about 10 pct S (varying somewhat with the composition of the slag.)

If the activity of CaS is assumed linear between 0–10 pct as curve 1, (see Fig 11), then $a_{\text{CaO}} = 0.1 (S)$; (S) being wt. pct sulphur in the slag.

For a diluted solution of sulphur in an iron melt saturated with carbon, the ratio $\text{H}_2\text{S}/\text{H}_2$ is, according to Kitchener, Bockris and Liberman,† about 0.01 [S], [S] being wt. pct sulphur in iron. Substituting these values in the expression for K_p we find

$$\frac{(S)}{[S]} = 2.10^3 \cdot a_{\text{CaO}}$$

The value 2.10^3 is only 4 times greater than the experimental coefficient found

by Hatch and Chipman, but the value is very sensitive to a small error in ΔF° .

A better agreement with the experimental distribution coefficient can be obtained if one assumes the activity of CaS to run like curve 2 (Fig 11). This will give a lower theoretical $\frac{(S)}{[S]}$ value, a value which varies with (S) exactly as Hatch and Chipman learned. Such a shape of the activity curve, which corresponds to a positive deviation from Raoult's law, is actually to be expected from the fact that liquid silicate and sulphide phases usually show incomplete miscibility.

A closer agreement between experimental and theoretical data can not be expected before we have more complete data for the individual activities of CaS and CaO in the slag. The activities a_{CaS} and a_{CaO} referred to the solid phases as standard states, are exact defined quantities contrary to the somewhat undefined expression "free lime," and they are independent of any theory for the constitution of liquid slag.

J. CHIPMAN (authors' reply)—The authors wish to thank Mr. Rosenqvist for his very interesting and useful thermodynamic addition. Curve 2 of his figure offers the needed basis for explaining the increase in the ratio $(S)/[S]$ with increasing sulphur content. Attention is called to an error in the printed paper: Fig 2 and 3 are reversed.

M. TENENBAUM*—In the figures showing the relationship between excess base and sulphur distribution (Fig 6, 7 and 9) the slope of the curve tapers off in the negative basicity range. Somewhat the same thing is observed with open hearth slags. In that case, the fact that some sulphur distribution between slag and metal is obtained with negative basicity is interpreted as indicating some dissociation of the lime silicate compounds whose existence in oxidizing basic slags has been used to explain various observed phenomena with regard to other slag-metal reactions. In the case of the blast furnace slags, the reduced slope of the sulphur distribution curve with decreasing excess base is attributed to the amphoteric effect of alumina. Has the possibility of other explanations been investigated?

* Trans. AIME (1923) 69, 606–634.

† Discussions of The Faraday Society (1948) 4, 49.

* Inland Steel Co., East Chicago, Ind.

* Inst. for the Study of Metals, Univ. of Chicago.

B. M. LARSEN*—In view of this effect of alumina that we failed to find so far in most plant practices, if I interpret that triangular diagram correctly, it seems to me that the lines indicated very little effect of alumina and there was not any effect on sulphur at all.

I am not accustomed to using the triangular diagram, but you will notice these lines fall almost parallel to those corners (*Indicating slide*). That would indicate the alumina has a quite small effect which would agree with what our experience has been in most plant data.

There was one other thing—this departure from the distribution laws would be a very nice thing if it really worked out in practice because we are getting into higher sulphur content in the slag all the time. I am a little skeptical about

* Research Lab., U. S. Steel Corporation.

it. I feel more work should be done, probably more work with higher sulphur contents in the metal phase to minimize analytical errors. In other words, it looks as though this point is so important as to deserve more exhaustive equilibrium studies to make more sure of this effect because it would be desirable to be able to increase the sulphur in the slag.

J. CHIPMAN—We agree with you that more work needs to be done with higher precision on the sulphur analysis. These sulphur analyses were made with extreme care and the method was checked repeatedly against standards. The sulphur analysis was done by the combustion method in a manner which is perhaps better than one would normally encounter and results were always duplicable within ± 0.001 pct. Had we known that these sulphurs were going to

come so low I think we would have started out in the first place to use radio isotope methods for improving the precision of the analyses. We expected to get sulphur distribution ratios more or less in the neighborhood of what is found in the blast furnace. Even with 5 pct sulphur in the slag we were still able to get unexpectedly low sulphur contents in the metal. There is no doubt about the result that we have shown—that if you double the sulphur content of the slag you do not double the sulphur content of the metal in equilibrium. The ratio (S)/[S] is not a constant.

With regard to the effect of alumina, the results show clearly that it behaves as an acidic constituent in the basic slags. In the more acid slags this characteristic seems less pronounced. No detailed explanation of this observation is required.

Relation between Chromium and Carbon in Chromium Steel Refining

By D. C. HILTY

DISCUSSION

(B. G. Emmett presiding)

C. E. SIMS*—This is a most interesting and important paper. It is important from two standpoints. First, it has aspects of being highly accurate and therefore extremely useful to the operating man in showing how far he can go in oxidizing carbon from a steel bath while retaining chromium and the effect of temperature on this limit. Fig 5 is undoubtedly the highlight of the paper, and in checking it against available data, it seems capable of predicting actual results.

The other important aspect is the apparently significant fact that reactions within a steel bath, such as between carbon and an oxide, are homogeneous reactions which do not require equilibrium with an external phase. In this case, it seems obvious that the reaction and the equilibrium established were between dissolved carbon (or carbide) and dissolved CrO. The classic reaction which requires equilibrium with solid Cr_2O_3 did not fit the data. It was recognition of this principle that made Fig 5 possible.

G. R. FITTERER*—It might be in assuming the CrO is dissolved in the metal that you are actually approaching the correct factor for activity. If that is true and if the percentages that were used represent an equilibrium constant, this would mean, in effect, that the minimum temperature at which chromium would be reduced by an equivalent percentage of carbon would be about 2400°F from your equation. I believe that is in line with my experience particularly if you deal only with low percentages.

J. CHIPMAN†—The author in discussing the equilibrium of the reaction offers two choices of explanation. One postulates an effect of chromium on the activity coefficient of carbon; it would require perhaps more data than are available to us at the present time to test this thoroughly. The other postulate which he offers is a reaction with CrO. This explanation is consistent with physical and chemical principles provided that a solid phase CrO is present, and that is

essentially what he is postulating. If that oxide were present one would expect and, I think, almost require the kind of results that he obtained. The weakness of that postulate lies in the lack of confirmatory evidence regarding the presence of solid CrO as such. This should offer an interesting subject for further study.

It seems a pity that the theoretical arguments revolving around CrO should have obscured for a moment the very real excellence of this paper.

E. CARTER*—I think there is a problem that presents itself in practical application where the metal temperature is from 3200 to 3300 and the temperature desired in pouring is considerably less.

B. M. LARSEN†—I get the impression from some of the work that was done earlier that there is probably a localized zone of high temperature at the slag metal interface which effects the removal of the carbon. Without that I wonder if the effect is possible to have a localized superheat and an equilibrium there favorable to low carbon content and

* Univ. of Pittsburgh, Pa.

† Professor of Metallurgy, Mass. Inst. of Technology.

* Vulcan Steel Foundry.
† U. S. Steel Corporation.

still not have the whole bath heated up to that equivalent temperature.

D. REEDER*(replying for author)—I do not doubt there is a localized area there, but still the agitation of the bath, particularly at these temperatures, and the effect of applying the oxygen, (blowing the oxygen in there) will give a stirring effect; and also the temperature is so great the molten metal is very liquid and would tend to circulate more.

B. M. LARSEN—In practice you have a heavy liquid below. That heavy liquid may not get stirred very deeply.

D. REEDER—That is true. This is under very high oxidizing conditions and I believe that would have an effect on moving the metal itself.

B. G. EMMETT—I might say along those lines that our experience has been in the injection of oxygen in an arc furnace you get a violent action which would, I believe, tend to stir the metal. I would also like to comment along the lines of this paper. It has been my ex-

perience—belief at any rate—that there has been positively too much chromium steel made with no effort to boil. Consequently, when you machine the castings you find them full of holes. If you give the metal a good boil it tends to liberate hydrogen and make a good clean piece of steel rather than one that is full of gas.

D. C. HILTY (author's reply)—It is gratifying that the results presented in the paper seem to be consistent with Dr. Fitterer's experience. Mr. Larsen has brought up an interesting point for speculation. I am inclined to agree with Mr. Reeder and Mr. Emmett, however, that the rather considerable bath action that results from oxygen injection goes a long way toward equalizing temperature throughout a steel bath except, possibly, in a very localized zone immediately adjacent to the point of oxygen input.

With regard to the CrO postulate and the interpretations placed upon it by Mr. Sims and Dr. Fitterer, I believe my position has been adequately stated by Professor Chipman. As pointed out in the paper, the metallic phase was assumed to be in contact with a nonmetallic phase saturated with CrO at steelmaking tem-

peratures. In this connection it is notable that slag samples taken from chromium steel heats at the end of the oxygen blow have been observed to contain particles of metallic chromium as well as chromic oxide and chromite. One possible explanation for these observations is that at high temperatures the slags may have contained CrO which decomposed on cooling in a manner analogous to the decomposition of FeO.

The primary objective of this investigation was to establish an empirical relation that would be of practical value to the operator in establishing a practice for melting chromium steels from charges containing chromium. The chromium-carbon-temperature relation shown in Fig 5 of the paper has been checked in the field in both basic and acid arc furnaces and has been found to hold quite well under both conditions. In a number of instances practices have been deliberately devised on the basis of the curves of Fig 5, and in all cases the heats behaved in the furnace as predicted. It would appear, therefore, that regardless of the theoretical explanation of the results presented in the paper, the primary objective has been attained.

* Los Angeles Steel Casting Co.

The Effect of Hydrogen on the Ductility of Cast Steels

By CLARENCE E. SIMS, GEORGE A. MOORE, and DONALD W. WILLIAMS

DISCUSSION

(R. C. Madden presiding)

G. A. LILLIEQVIST*—I wish to compliment the authors on the excellent manner in which they have presented their data. The improvement of ductility obtained on test bars after aging at room temperature or at low temperatures of around 400°F has been a well-known fact for many years. The authors have found an explanation for this phenomenon and have presented in their paper conclusive proof that hydrogen plays an important part in controlling ductility values.

While we have never attempted to analyze for hydrogen, a great deal of our

time has been devoted to the study of aging treatments to improve the ductility of steels and we have found results similar to those presented in this paper. It was our finding that in practically 100 pct of the steels investigated there was a definite improvement when 1-in. bars were aged at 400°F for 16 hr, 550°F for 1 hr or at room temperature for 4 months. We also noted that the heavier sections were more affected than light sections and that more time was required in the aging treatment to obtain the maximum ductility.

In our investigation we also noted when an acid electric furnace heat was made as rapidly as possible, that is, to obtain a vigorous boil to reduce the carbon and then tapping as soon as possible, good results were obtained. Very little improvement was obtained in aged

bars over unaged bars. They were both very good.

I again wish to state that the authors have done an excellent job in presenting interesting information regarding the causes of low ductility values in unaged bars which should be of considerable benefit to the steel casting industry.

C. E. SIMS (authors' reply)—The authors appreciate the comments of Dr. Lillieqvist which give confirmation from practice of the data presented. The work of many investigators, including Dr. Lillieqvist, has tended to establish beyond doubt the effect of hydrogen on the ductility of steel, but this has been largely of a qualitative nature. The present work was designed to test and substantiate these observations and put them on a quantitative basis.

* Research Director, American Steel Foundries, East Chicago, Ind.

The Origin of Silicate Inclusions in Basic Electric-arc-furnace Steel of Higher Carbon

Contents

By AXEL HULTGREN

DISCUSSION

(R. C. Madden presiding)

G. R. FITTERER*—In discussing this paper I would like to state simply, that Professor Hultgren's objection to Stokes' law is interesting but not necessarily a correct interpretation. I would like to point out that Stokes' law states that the velocity of a particle, either when precipitated or rising in a fluid, is dependent chiefly upon three factors. One of these is the viscosity of the fluid which in this case is liquid steel. Another is a difference in density between the liquid steel and the nonmetallic inclusion and the third is the square of the radius of the inclusion particle itself. Now, if the particle has a radius in one case of ten times another, the one with the larger radius will be eliminated at one hundred times the velocity. This law states, in effect, that rain drops cannot become as large as watermelons and it is very fortunate that they cannot.

I would also like to point out that since it is a limiting law, it indicates that it might control either the agglomeration of the silicate particles or their dispersion. In other words, a particle may coagulate with others until the limiting size is reached. Any growth beyond this will cause the large particle to break up into smaller ones other conditions being the same. On the other hand, if in the action of pouring the heat considerable turbulence is present in pouring into the mold or even tapping in the ladle the limiting velocity as demanded by this law might be exceeded and therefore cause the break-down of the inclusions into the form that we saw here. Now, whether or not the small particles that are broken

off from the large inclusions as shown, redissolve in the steel is a point which is disputable and has not been proved by this paper.

B. M. LARSEN*—We have a few samples taken from open-hearth furnaces. I do not know whether they illuminate this question, but we took samples from the tapping stream and also out of the ladle. They came out very logically, looking at it from Hultgren's viewpoint. The tapping stream samples from open-tap heats with no block in the furnace had no inclusions except extremely tiny ones. In the ladle the inclusions jumped up to a volume percentage about the same as Hultgren found though of considerably smaller average size. The larger ones were gone in the platform samples.

A. HULTGREN (author's reply)—I wish to thank Dr. Fitterer for kindly taking the trouble to present my paper. To his comments regarding Stokes' law and its application to the present problem my reply is that I am not aware of having objected to this law, in thought or writing. If inclusions, by growth or coagulation, reach a certain size they will rise at a considerable velocity and collect at the top surface of the liquid steel. The results of experiments with steel held in the ladle for different periods, as shown in Tables 5, 10 and 13, agree well with Stokes' law.

The breaking down of large slag inclusions—or rain drops—into small ones as caused by turbulence is not demanded or governed by Stokes' law which applies to conditions of nonturbulence.

Dr. Fitterer apparently interprets Fig 10-14 as evidence of large inclusions

breaking down owing to turbulence in pouring. I think, on the other hand, that those figures support the idea of reaction products forming temporarily around inclusions which are not in equilibrium with the metal. My arguments are:

1. The inclusions had no doubt been deformed from turbulence during pouring but their round or rounded shape indicates that the turbulence had largely subsided when they were caught by the freezing steel.

2. If the satellites were formed by fragmentation of the large inclusions in connection with deformation they would not be likely to remain in a surrounding zone of uniform thickness after the latter assumed its rounded shape. Fig 15, on the other hand, shows small inclusions irregularly dispersed in relation to a large one, possibly as a result of fragmentation.

3. The lack of equilibrium at the time of formation of the inclusions is evidenced by the change in appearance of the inclusions while the steel is held in the ladle (Tables 5 and 14), the change observed indicating that the metallic oxide contents are gradually decreasing.

The absence of satellite zones around the inclusions in the samples taken from the ladle are evidence of their short-lived existence. The dissolution of small particles during the simultaneous growth of larger ones in the same matrix is a common occurrence in metallic systems. The low oxygen content of the metal would also favor dissolution. As Dr. Fitterer says, however, this is a disputable point.

The results reported by Mr. Larsen from his study of open-hearth steel supply valuable additional evidence. In conclusion, I ought, perhaps, to emphasize the limitation indicated by the title of the paper: the conclusions drawn are not necessarily all applicable to low-carbon steels.

* Head, Dept. of Metallurgy, Univ. of Pittsburgh, Pa.

* Research Lab., U. S. Steel Corporation.

Sintering Characteristics of Minus Sixty-five and Twenty Mesh Magnetite

By A. STANLEY and J. C. MEAD

DISCUSSION

(E. H. Rose presiding)

E. H. ROSE*—You have wrapped up

* Tennessee Coal, Iron and Railroad Co., Birmingham, Ala.

a great deal of new and interesting information in one quite compact package, and I wonder if it might not help the

audience a bit if you would just recapitulate your main conclusions—not all of them, but the outstanding ones about the size, the reactions, and so forth.

J. C. MEAD (authors' reply)—In our research work, the following factors were found to have a very pronounced effect on the minus sixty-five mesh magnetite.

The use of 20 to 30 pct of sized return fines in the prepared feed, when using a hearth layer over the grate area, was very beneficial. Before the sized returns were investigated, and the amount controlled, the results of the tests varied widely due to the fluctuating amount of dust in the "returns."

The control and stabilization of the moisture percentage in the magnetite and coal culm permitted more efficient mixing of these materials which raised the production rate and decreased the amount of coal culm required.

Close moisture control in the prepared feed is essential when sintering at a vacuum of 40 to 50 inches water gauge. Either too high or too low a moisture control will permit the bed to "pull holes," short-circuiting the air and decreasing the production rate.

Accurate control on the amount of sinter fuel in the prepared feed increases the quality and quantity of sinter produced. An excess amount of coal caused too high a fusion temperature which slags and makes a very brittle sinter. Too little coal resulted in too low a fusion temperature which made a weak sinter containing some unsintered material.

While the research work in the test pan showed that minus twenty mesh magnetite can be sintered without much control, in actual plant practice, very close control is needed on the magnetite, coal, and prepared feed. The plant will maintain a high production rate if the moisture in the prepared feed stays between 5.5 to 6.0 pct. Any variation above or below this range lowers the plant production rate.

A variation of $\frac{2}{10}$ pct of anthracite coal in the prepared feed will change the production rate.

Any fluctuations of "dust" from the return fines and from the dust collectors can cause wide variations in the moisture of the prepared feed. If the "dust" is used at a uniform rate, it simplifies moisture control and does not affect production.

The use of return fines having a maximum particle size of minus $\frac{3}{8}$ in. in the prepared feed and the use of a thick hearth layer over the grate area have been tried on the 250-sq ft pans and have increased the production rate. However, the use of smaller return fines requires closer moisture control than before because the bed does not hold together during the sintering quite as well as it did when using the coarse return fines in the prepared feed.

In all cases in research and in operation the closer the control maintained over the

magnetite, coal, return fines, dust, and moisture, the higher were the quality and quantity of sinter produced.

E. H. ROSE—The presentation that Mr. Mead has made here today is one of acute interest to practically all iron ore producers, particularly in view of the fact that we are going to be faced with some very finely divided material when we proceed further with low grade iron ores.

G. J. HOLT*—I missed the first part of the paper, but I heard Mr. Mead talk about pellets. I did not get the significance of the pellets.

J. C. MEAD—This pellet we found was due to fine magnetite building up around return fines, and in our test we added water into our returns in the latter part of the mixing to eliminate them. During the first part of our tests we put the water right in with the magnetite, mixing it with a concrete mixer, and we found that in going over the lifters it was rolled up into a ball. Contrary to our original idea that pellets would help us, we found that after the sintering we could take these particles and crush them with our fingers; they break up eventually; they also formed zones of weakness where in being dropped or given a tumbling test they broke down the quality of our sinter.

F. D. DE VANEY†—I just wanted to make this comment on the magnetite we are going to pelletize this year. It is about 1 pct on a hundred mesh and about 85 pct minus 200 mesh. We have recently carried on some tests using Dwight Lloyd machines and we found that for this fine material we can get a fair capacity and make a nice sinter if we roll our concentrates into balls that are from $\frac{1}{8}$ in. up to approximately $\frac{1}{2}$ in. in diam. We found with such material, contrary to pelletizing, that the added coal had to be placed on the outside of the pellets. In other words, we rolled these balls up in a drum and then we introduced this coal about a foot or two from the discharge end of the drum and put a layer of coal around the pellets; then we put them on the sintering pan and in that way we made a rather nice sintering on the Dwight Lloyd machine. Do you plan on making your pellets in a rotary drum?

MEMBER—We have not had a lot of experience, just 6 months or so on the rolling pellet, and I do not want to get into too much of a discussion on that; but we proposed using the same methods and the size of the balls is directly determined by the percentage of moisture in the balls. If you keep that moisture down the balls will get no bigger.

A. C. RICHARDSON‡—As I listened to this paper, I found it a little hard to

follow some of the conclusions reached from the data which are worthy of serious study. We have had some experience, in the laboratory, in sintering various types of ores and find that there is very little information of value in literature on this subject. I hesitate to talk about sintering in the presence of Mr. Holt, Mr. DeVaney, and Mr. Johnson who have had a lot of experience with this subject, but a lot of the sintering practice, as far as I can see, is fairly empirical; perhaps it always will be. I think, however, that the work reported by Mr. Mead, wherein he has tried to evaluate the sintering variables and then interpret them in the light of what might be encountered in practice is very valuable. I would like to suggest that more papers along this line would be helpful contributions. Mr. Mead and his company are to be complimented on publishing this information.

E. H. ROSE—Recently the American Iron and Steel Institute had a meeting on sintering in Pittsburgh which I happen to have had the pleasure of attending and there were two representatives there from, I think, practically all of the steel companies throughout the country. There were two men from Bethlehem and two from Jones and Laughlin, a couple from Carnegie, Illinois, and a couple from our place down in Birmingham. Altogether there were some thirty men there in teams of two, one a research man and the other an operating man. There was a round table discussion to see what we could formulate in the way of a program in that organization to find out what we should do to approach within shooting distance of the very thing that Mr. Mead has brought out. It is quite clear that sintering, particularly in the fine sense, is a precision operation, or should be, and yet at that meeting we paneled all of the experts and asked them a lot of questions. We all resolved to do something more about that, and a program is getting under way which I hope will result in much more information on the whole subject. Now, the astonishing thing is that none of us at that meeting could even state what is good sinter. Of course, we are all seeking a sinter that will double the production of the blast furnace and all that sort of thing. No one could define it there. Perhaps someone can define it at this meeting. If so we certainly want him to tell us about it.

F. M. HAMILTON*—This paper on sintering variables is quite interesting to us and no doubt the rest of the industry. The sintering process is being more closely scrutinized and studied since more ores require agglomeration than heretofore, and it appears as though the trend will be accelerated in the near future.

We have expended considerable time and effort on sinter research in the past

* Cleveland-Cliffs Iron Co., Ishpeming, Mich.

† Pickands, Mather and Co., Hibbing, Minn.

‡ Battelle Memorial Institute.

* Jones and Laughlin Steel Corporation, Negaunee, Mich.

few years and much of our work has been along the same line as that of National Lead. Results are in agreement with those obtained by National Lead, although the approach to the individual problems was somewhat different in some cases, and different types of material were used.

In the case of the study of moisture control of the mix, our method was to make up different types of sinter mixes at various moisture contents and then determine the amount of airflow it was possible to obtain under fixed conditions through the mix without sintering. In this manner curves were obtained which showed optimum moisture contents for maximum airflow. Then mixes were made up with moisture contents on either side of the optimum amount and subjected to sintering tests. The time, in minutes, required to sinter a test batch of 35 lb was then measured by means of a continuous strip chart record of the exhaust gas temperature. It was found that the optimum moisture content varied with the material being used. For example, New York State magnetite from Benson mines gave the best airflow values at $7\frac{1}{2}$ pct moisture while fine Minnesota hematite gave the best airflow values at 10 pct moisture. Furthermore, the best moisture content for sintering was found to be just slightly lower than the optimum indicated by airflow tests.

In connection with pellets, I note that difficulties were encountered in sintering when pellets were unintentionally formed in the mixer. Our experience has been similar in this respect but we purposely made pellets in a pelletizing drum for sintering purposes. After many trials along these lines we conclude it is quite difficult to successfully sinter pellets made from fine materials. One of the reasons for the trouble appears to be the magnitude of the difference between the optimum moisture content for sintering and the minimum moisture content at which pellets can be formed.

Our work with the surface tension properties of water in the mix agrees with that of National Lead. Wetting agents are very detrimental to sintering; however, little success has been obtained by the use of oils, lime, or limestone with our raw materials.

As a result of experiments in the plant by our New York operators, fine fractions of coal were found to be detrimental to good operation. Best results in this plant are obtained on a No. 5 Buckwheat coal.

The authors of the paper emphasize the importance of the proper use of returns in sintering fine materials. Our laboratory work indicates that large size returns are a waste of good blast furnace feed and their use as returns in the mix is of little or no value in promoting bed porosity. We expect to be in a position to carry out production runs along these lines in the near future.

The present paper is both interesting and informative on a subject of great importance to the steel industry today. It indicates recognition of the growing importance of closer metallurgical control and better plant equipment for improved sinter operations.

T. E. LLOYD*—Concerning pellets, I think that both of you are right about pellets. When you attempt to sinter a pellet that is too large, very often the coal inside of it does not burn. More often it is roasted to a coke. In such cases, obviously, it is better to have this fuel on the outside of the pellets. If the pellet is small, air gets to the coal, it burns rapidly and you have a sinter.

You have probably noted that there is a remarkable difference in pellets. A charge in which the individual small pellets have been formed by rolling until they are free of air and are solid, (a good term is "dense") will sinter faster and more uniformly than a charge of identical proportions of moisture, fuel, and others, which has not been so carefully pelletized. I believe that in many of our arguments here regarding the sintering of pellets we must first take into consideration the physical qualities of the pellets. How good is your pelletizer or mixer? To add moisture uniformly is almost an impossibility, but how close does the pelletizer approach this goal? What is the specific gravity of your individual pellet?

A few years ago, the New Jersey Zinc Co. believed that a sintering mix could be benefited if it were squeezed by running through rolls before mixing. I do not know how far they followed this up but the idea is a step in the proper direction for two reasons. First, it tends to unify the moisture content. Second, it squeezes air out of the mix which in turn serves to densify the agglomeration of particles in the individual pellets composing the mix.

H. W. JOHNSON†—It is my understanding that the commercial plant is operating on a minus twenty mesh material now.

J. C. MEAD—That is right.

H. W. JOHNSON—With a bedding about 1 in., what is the screen size of your finished product and your weight per cubic foot of the product.

J. C. MEAD—There have not been any bulk density tests taken on the plus one inch sinter. There have been bulk density tests run on the return fines and they have been the following: 101 lb per cf on minus 1 in. plus eight mesh screen size, 99.4 lb per cf on minus $\frac{1}{2}$ in. plus $\frac{3}{8}$ in. screen size. The bulk density of sinter will vary widely unless some limits on screen sizes is followed which will

exclude the "fines."

The screen size of the finished product is all plus 1 in. There have not been any screen analyses made, but by a visual check most of the sinter is plus 6 in. size with a maximum lump size of 2-ft pieces

H. W. JOHNSON—I think it would be a valuable addition to the discussion if that point were actually made—the weight per cubic foot—if there is a possibility of getting it. I think the importance of the weight of that material is of great significance. We have operated our furnaces on some test runs with high percentages of sinter with no improvement in operation. I think much of the reason for that is that we have failed to recognize the importance of the quality of the sinter used and one measure of this quality is the weight per cubic foot.

E. H. ROSE—I think that is quite true, Mr. Johnson; this also came out in Pittsburgh recently in a great many of our arguments about sintering. We can never get together because we cannot even define our subject. What defines quality? what is good sintering? In the investigation I mentioned a moment ago we are hopeful we will be able to set up some definitions. After all, just to say a sinter is hard or not hard or that it is bad or not good, very bad or very good, still does not say anything you can define and reproduce. It does not permit you to run a test with sinter as one specific definition and see what the blast furnace does and with another specific qualified quantity of sinter, what the blast furnace does on that.

Mr. Mead, did you make any porosity measurements?

J. C. MEAD—No, we did not.

T. E. LLOYD—First we know that iron ore at around 900 to 1000°C reduces two or three times faster than sinter of the same size. Secondly, it goes without saying that the structural or physical properties of iron ore fines in a furnace are impractical. Finally, it is known, but not often enough remembered, that sinter becomes increasingly more difficult to reduce as the carbon content, within practical ranges, increases. To me, the ideal sinter is a sinter coming from a charge so thoroughly and uniformly mixed that the practical range of fuel, say between 3 and 6 pct, can be held at its absolute minimum. Without the uniformity of thorough mixing, this range cannot be held. Either a trifle extra fuel is required to produce sinter or inevitably there will be portions of unsintered and channelled product.

When an ore is fine enough it can be pelletized. These pellets when roasted at around 900 to 1000°C are usually quite tough and contain about 40 pct voids. Not forgetting the difficulty of sulphur, and other elimination, if this could be

* Newark, N. J.
† Inland Steel Co.

done on a sintering machine I should think the resulting product would be even more ideal.

E. H. ROSE—Mr. Mead's mention of lime in his experiments only goes to remind me that in sinter, as in so many other affairs of this world, what is one man's meat is another's poison.

F. D. DE VANEY—I am a little bit reluctant to say anything about pelletizing. We are in the process of getting a full-size plant in operation, and one is reluctant to talk about something still to be done. The plant we have up in Aurora is a test plant in a way. In pelletizing or sintering the concentrates, we were interested in the most efficient and cheapest way. We rolled our concentrates up into balls and we learned a lot about that operation too. We rolled the material up in a drum about 8 ft in diam at a rate of 30 tons an hour, and the balls, when they came out, were hard. They would not stand shipping but they would stand movement around the plant. We fed these into what we call a tandem type furnace and then they were fired. We add our heat through a combustion chamber. The furnace is of the regenerative type, so our top gases come off at about 225°F and our pellets come out at the bottom at from 250 and 275°F. These pellets are hard when fired. I hope next year we will be able to prepare a paper and tell you just how the process works.

L. J. ERCK*—It surprised me a little to hear Mr. Mead say that the pellets which were made would not form a hard pellet on the grate inasmuch as they were a 100 pct pellet charged on a sintering grate. That point in my mind is just a little hazy now as to why the material produced in cake form would definitely sinter and yet the pellets would not. The

material we are working with at the present is a straight hematite. We have found on several occasions that the fuel has to be very thoroughly mixed, and I mean thoroughly. The pellets themselves, if not thoroughly mixed, will vary, and if that is so you will find that one pellet will burn while the next pellet will be soft. Likewise, we found that each individual pellet almost has to be a thorough and complete mixture of the ore and fuel, for if it is not you will find that one part of the pellet will be soft and the other part hard. In respect to adding lime, that problem was brought up inasmuch as the concentrate on which we are working does not present enough of the minus 325 mesh size to form favorable feed to the balling drum. There must be a certain percentage which I believe we can be safe in saying is about 50 pct—at least 50 pct. I have seen a few tests at 40 pct but 50 is certainly more satisfactory.

We thought if we could add lime of minus 325 mesh proportion in the proper percentage, we would be doing quite a trick; we would not only be making up the deficiency of the minus 325 mesh but we would also be making something equivalent to a more or less self-functioning material. The material was prepared and placed in the pelletizing furnace and we ended up with a slag mass of about 900 lb that had to be lifted with a crane, and that ended that experiment.

A. C. RICHARDSON—What was the temperature?

L. J. ERCK—That is another point I might bring up. These materials vary. We just finished running a pelletizing test down at the station under which we had no control as to the moisture content. It was a filter cake with a very high moisture and in putting it through the balling drum all the material immediately formed balls. The new material added to the returns usually built up the said

balls until they became of age. This was not the case. All the feed immediately formed balls from $\frac{1}{16}$ in. up to about $\frac{1}{4}$ in. so in placing that in the furnace we had to control the heat, not carrying it as close to the top as we usually do.

L. A. ROE—In our attempts to sinter pellets we used a batch sintering machine which was operated at a temperature of about 2475°F. Mr. Erck is speaking of firing pellets in a shaft furnace, and probably uses temperatures of 2000° or less. I wish to call attention to the fact that temperatures utilized to sinter pellets are considerably higher than temperatures used to fire pellets in a shaft furnace.

J. C. MEAD—What was the size of the feed you used in making the pellets, Mr. Erck?

L. J. ERCK—It has to be of proportion so that you do not diminish the quantity of minus 325 which is so essential for forming the pellets in the ball drum. You must be sure you have the proportionate amount of fines. Of course, the amount that you add in hematite is still relatively small.

E. H. ROSE—Is anyone familiar with the pelletizing operation at Santa Cruz on the cement?

G. J. HOLT—While trying to produce lump ore we used cement as a binder and almost everything from straw up and down. We were trying to produce lump ore. We ended up by deciding we did not know enough about it and gave up the entire project. Are you using a binder in your work?

E. H. ROSE—Yes. At the moment we are rather intrigued with the use of the paper mill waste. There are lots of paper mills in our vicinity, and we do have to heat treat it afterwards.

* Cleveland Cliffs Iron Co., Hibbing, Minn.

The Influence of Temperature on the Affinity of Sulphur for Copper, Manganese and Iron

By E. M. COX, M. C. BACHELDER, N. H. NACHTRIEB, and A. S. SKAPSKI

DISCUSSION

(D. T. Rogers presiding)

D. T. ROGERS*—The conclusions drawn in this paper have important practical significance to the steelmaker and the metallurgist if, in practice, it is demonstrated that metallic copper in the charge will pick up sulphur from the furnace atmosphere and thus increase the

sulphur content of the bath. The problem of residual copper arising out of increasing copper in the scrap available to the industry is, in itself, a matter of concern to the steel maker. If, in addition to the often detrimental effects of high residual copper upon the physical properties of some important steel grades, there is to be a complication of the sulphur problem, then we have a set of conditions that bodes no good for the open hearth melter and the open hearth metallurgist.

M. B. BEVER*—Investigations of gas-metal equilibria continue to be of interest, especially as new possibilities for improving experimental techniques emerge. Higher purity of reacting substances, better refractories, improved methods of temperature control and an increased awareness of the pitfalls of high-temperature equilibrium work are

* General Metallurgist, Jones & Laughlin Steel Corporation.

* Assoc. Prof. of Metallurgy, Mass. Inst. of Technology.

some of the factors that should contribute toward better data on gas-metal reactions.

The authors have furnished adequate and interesting information on many aspects of their experimental procedure. A more detailed discussion of several factors, however, is desirable. The loss of hydrogen from the system by diffusion, thermal diffusion within the gas phase and the thermal decomposition of hydrogen sulphide may be named. Have the authors examined the composition of the solids after each experiment, and were both the true stoichiometric sulphide and the pure metal found to be present?

It is well known that hydrogen diffuses readily through silica at high temperatures and the same is probably true of other gases and refractories, although to varying extents. The authors' procedure of checking various furnace materials against each other is to some extent a safeguard against errors of this kind but the loss of hydrogen through silica should be acknowledged as an inevitable certainty. This loss can probably be tolerated since equilibrium between the gas mixtures and the condensed phases is likely to be maintained.

The use of an impeller for keeping the gas atmosphere in motion tends to eliminate the possibility of thermal diffusion, given a sufficiently high gas velocity, but this may in turn interfere with temperature equilibrium. The thermal decomposition of hydrogen sulphide is another potential difficulty on which further comment by the authors would be desirable.

Concerning the numerical evaluation of the results of this investigation the heats of formation evidently are based on an extrapolation over a temperature interval which is altogether too wide. It also seems very doubtful whether the scattering in the plot of the logarithms of the pressure against reciprocal temperatures is any less serious than the scattering of the free energy-temperature data which the authors have rejected as a means for evaluating entropies.

The authors concede that the interpretation of their results for the steel-making process can be only tentative as far as the solid ingot is concerned. However, their interpretation of some fundamental features of the behavior of sulphur, copper and manganese in liquid steel is also open to question. They state that because of the relatively high affinity of copper for sulphur the sulphur content of the bath increases with the copper content of the scrap and that consequently the desulphurization process is hampered. This argument is equivalent to the statement that the presence of a deoxidizer in the bath raises its oxygen content and interferes with deoxidation. On the other hand it would seem to be consistent with the authors' point of view to expect that sulphur may be used to remove copper from molten steel. To

avoid such conclusions it must be recognized that this investigation deals with pure substances and its results can be applied to the physical chemistry of steel-making only by the rigorous methods of the thermodynamics of solutions.

R. E. MINTO* and H. B. EMERICK*—This discussion is aimed at the authors' principal conclusion, to wit: "... that metallic copper which is present in the scrap is to be expected to pick up sulphur from the open hearth furnace gases and thus raise the sulphur content of the bath."

An opportunity was afforded to test the validity of this conclusion in actual practice when during a recent period Jones & Laughlin Steel Corporation made 50 heats of 0.40 pct copper low alloy high tensile steel wherein the major portion of the copper requirement (all but minor final additions to adjust analysis) was obtained from high copper scrap charged with the regular scrap at the start of the heat. This scrap averaged 5 pct copper content, the copper being in the form of a heavy gild metal cladding and not as a copper-iron alloy.

A study was made to determine the effect of this added copper in the charge on melt-in sulphur and ladle sulphur chemistry. To do this, the routine sulphur and copper analyses on these heats were tabulated and compared with 50 heats made in the same period (and heat for heat chronologically as close to copper charged heats as possible) but with the practice of obtaining the copper requirement by the addition of pure copper late in the refining stage of the heat. This procedure assured reasonable constancy of lime charge and total sulphur content of the raw materials. The two practices are differentiated by calling the first group "copper charged" heats and the second group "copper addition" heats.

Preliminary copper tests are taken about 3½ hr before tap. Sulphur preliminaries are taken about 1½ hr before tap. When copper is supplied by pure copper it is added comparatively late in the heat—from ½ hr to 1¼ hr before tap. The heat at this time has been under slag cover for considerable time and subsequent absorption of sulphur from the furnace atmosphere is negligible. During the test period sulphur content of fuel oil ranged from 0.35 to 0.89 pct, averaging about 0.75 pct sulphur.

Pertinent data may be summarized as follows:

| Practice | Copper Charged | Copper Addition |
|------------------------------------|----------------|-----------------|
| No. heats..... | 50 | 50 |
| Pct preliminary copper—Range..... | 0.29/0.64 | 0.06/0.14 |
| Avg..... | 0.38 | 0.09 |
| Pct ladle copper—Avg..... | 0.41 | 0.38 |
| Pct preliminary sulphur—Range..... | 0.030/0.055 | 0.021/0.050 |
| Avg..... | 0.0373 | 0.0363 |
| Pct ladle sulphur—Range..... | 0.023/0.038 | 0.023/0.034 |
| Avg..... | 0.0271 | 0.0271 |

* Metallurgical Dept. Jones & Laughlin Steel Corporation, Pittsburgh, Pa.

These data indicate that an appreciable pickup of sulphur is not experienced when about 1000 lb of copper is charged as high copper scrap in 175 ton basic open hearth heats melting down in about 4 hr in a furnace burning 0.75 pct sulphur fuel oil. No evidence is found to support the authors' contention that metallic copper present in the scrap may be expected to pick up sulphur from the heating gases, thus increasing the sulphur content of the bath.

C. E. SIMS*—I will not discuss the experimental work, not having gone into that portion of it closely, but let us assume that the figures are correct for the sake of argument and that copper sulphide is more stable than iron sulphide or even more stable than manganese sulphide at the steelmaking temperatures. It does not seem to me, however, that such a conclusion gives the authors the right to assume that copper, when diluted down to a fraction of a per cent, as is usually the case, could still exert an important effect on the affinity of that iron copper alloy for sulphur, or its ability to pick up sulphur from the gases. Now, if metallic copper is present as pieces of copper in the scrap, during the melting of the steel it probably would pick up a larger proportion of sulphur than the steel scrap and, of course, an important contamination of sulphur does occur during the melting. Even so, when it is present in such small quantities it does not seem that it could have an important effect on the total sulphur content. However, if it is true that in the finished steel the sulphides contain a large portion of copper sulphide then I think there is a significance that has not been touched upon by the authors. We know that copper steels give considerable trouble during the hot working of plate in the form of surface checking and edge cracking. In other words, in examining steel that has been hot worked and which shows this surface cracking we find that there has been a deep penetration of oxides along grain boundaries. Now, this occurs only during the hot working, and if a copper sulphide does constitute an important portion of the sulphides it may form a liquid eutectic at these hot working temperatures that would influence the penetration of oxide along the grain boundaries and cause this phenomenon of surface and edge cracking. This probably could be checked by finding the relative trouble from a high sulphur steel and a steel very low in sulphur but with

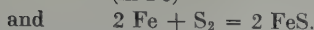
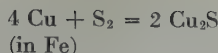
* Battelle Memorial Institute.

about the same copper content.

M. TENENBAUM*—I would like to confuse the role of copper and sulphur in the melting of plain carbon steels a little bit if I can. We make intentionally a good tonnage of steels containing over 1 pct of copper. Quite often we charge nearly all that amount of copper with the original solid charge and we have never run into any difficulty with any increased melt or final sulphur in this grade. Now, to confuse the situation, we often get complaints from our melters (and I am sure they have not read Dr. Skapski's paper) about the difficulty of removing sulphur from copper bearing heats, that is, heats containing 0.15 pct or higher copper in the liquid bath. They claim to observe this rather consistently and insist this condition actually exists. On reviewing our metallurgical reports in an attempt to get statistical evidence to support their observations, we have never been able to bring out any data that would indicate any increased difficulty in eliminating sulphur in the presence of copper.

N. H. NACHTRIEB (authors' reply)—The principal objection of Mr. Sims (supported by the evidence contributed by Messrs. Emerick and Minto) might be rephrased in this form: Is the thermodynamic activity of copper dissolved in liquid steel sufficiently high to remove sulphur from the heating gases and to fix it in the form of copper sulphide soluble in the steel? Our experiments give no answer to this question, inasmuch as they dealt with pure copper and iron with their respective sulphides, and not with copper at the level of concentration in which it prevails in actual steels. For the latter case the relevant chemical reactions may be written as:

* Inland Steel Co.



The corresponding free energy relationships are:

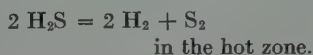
$$\Delta F^\circ_{\text{Cu}_2\text{S}} - \Delta F^\circ_{\text{Cu}_2\text{S}} = RT \ln \frac{(a_{\text{Cu}_2\text{S}})^2}{(a_{\text{Cu}})^4 (p_{\text{S}_2})}$$

$$\text{and } \Delta F^\circ_{\text{FeS}} - \Delta F^\circ_{\text{FeS}} = RT \ln \frac{(a_{\text{FeS}})^2}{(a_{\text{Fe}})^2 (p_{\text{S}_2})}$$

Whether copper is capable of competing with iron for sulphur under steelmaking conditions will depend upon whether $[\Delta F^\circ_{\text{Cu}_2\text{S}}] > [\Delta F^\circ_{\text{FeS}}]$. In turn, this depends not merely upon $\Delta F^\circ_{\text{Cu}_2\text{S}}$ and $\Delta F^\circ_{\text{FeS}}$, but also upon the activity of the copper dissolved in the steel, the activity of the copper sulphide (in the steel or in the slag), and upon the activity of the iron sulphide. We may consider the activity of the iron to be unity for all practical purposes. Since activity data are lacking, we cannot predict with any confidence that a fraction of 1 pct of copper in steel will result in an increase in the sulphur content of the steel as a result of reaction with the heating gases. The experimental evidence of Mr. Tenenbaum and that presented by Messrs. Minto and Emerick suggest that the activity of copper in steel must be *insufficient* to cause appreciable sulphur pick-up or to materially hinder the desulphurization process.

I should like to answer Mr. Bever's comments as follows:

Gas circulation, aided by the impeller, was estimated to be about 1 cm³ per sec. This, we feel, is high enough to overcome the Soret Effect of thermal diffusion. At the same time, it is probably low enough to permit the establishment of the equilibrium:



For the highest temperature run with Cu₂S (1519°K) the experimentally determined (H₂S)/(H₂) ratio has the value 5.15×10^{-3} . The pressure of sulphur vapor at this temperature is only 2.26×10^{-6} atm. (from Kelley's data for the thermal decomposition of hydrogen sulphide). This corresponds to only 0.044 pct decomposition of the hydrogen sulphide in the hot zone, and represents an error which is well within the errors in the analytical determination of hydrogen sulphide.

Mr. Bever is undoubtedly correct in stating that hydrogen diffuses through silica and other refractories at high temperatures. However, this introduces no error, since the measured ratio (H₂S)/(H₂) is maintained by the metal-hydrogen sulphide equilibrium:



Loss of hydrogen by diffusion through the furnace tube leads to a corresponding diminution in the hydrogen sulphide pressure.

Finally, Mr. Bever's comments comparing desulphurization and deoxidation may be examined. Elements serve as deoxidizers only if their oxides form a second phase whose solubility in the metal is low. Should their oxides be quite readily soluble in the metal, the oxygen content of the metal *would be increased*. Similarly, elements whose sulphides are very sparingly soluble in the metal should be effective in removing sulphur from the metal. To the extent that oxides (or sulphides) are soluble in the liquid metal the processes of deoxidation (or desulphurization) would be hindered; such elements might conceivably perform a disservice if their activities (and the solubilities of their oxides or sulphides) in the metal were sufficiently high.

The Role of Thermochemical Factors in Basic Open Hearth Production Rate

By T. E. BROWER and B. M. LARSEN

DISCUSSION

(H. C. Swett presiding)

L. REINARTZ*—In larger open hearth furnaces we have had somewhat different experience from Mr. Larsen. In the first

* Middletown, Ohio.

place, we find a very considerable increase in speed of the heat if you lower the limestone charge, and furthermore, we have found a tremendous improvement in tons per hour by using heavier scrap iron in the charge. We have recently made some experiments in different ways to charge furnaces which have shown

much greater regularity of slag run-off with about the same high percentage of pig iron being used. We have made heats containing up to as high as 70 or 75 pct of hot metal.

With this practice we have made some low carbon heats in very fast time. Some steel plants in the East have done very

good work when charging light scrap iron because they are able to charge continually. In most plants where you must use light scrap iron, charging time increases very materially, and, as a result, the length of the heat time is very much increased.

T. T. WATSON*—We have had considerable experience in all cold metal charging practice and examination of a large number of heats definitely indicated that the charging time is an extremely important factor affecting heat time. An increase in charging time will increase heat time. As the optimum charging time is approached the rate of flow of the raw materials (steel scrap and pig iron) is equally as important as the charging time.

M. TENENBAUM†—About six or seven years ago at Inland it was possible to relate our heat time with our limestone charge. About 1944 we mechanized our coal mines and we got a little poorer analysis hot metal as a result. We then found that we had to use quite a bit of our heat time in working sulphur. Accordingly, our limestone charges were increased. When we finally increased the stone charge uniformly throughout the shop, it was found that despite the in-

creased limestone charge our heat time was not affected. When our practice was standardized to the point where we did pretty well on sulphur, we then dropped the limestone charge through the shop. Again we went back to the old condition where it did not make any difference. Apparently the time saved in pulling lime was lost in working sulphur. It is just a sort of warning that where you may save a few Btu's during melting you sometimes may lose more than you have gained. The loss can appear either as poor product quality or as increased heat time used to meet quality requirements.

B. M. LARSEN (authors' reply)—The comments here on the effect of heavy scrap, charging time, etc. illustrate the need for a more rational analysis of furnace variables in general. In melting down light or heavy scrap, we have (1) the "sharpness" of the furnace, (flame intensity, direction, etc.), (2) the rate of charging and the aggregate time with doors open, and (3) the amount of oxygen absorbed by each ton of scrap during melting. These factors are all involved in furnace speed and also are somewhat interrelated. For example, the more "sharp working" the furnace is, the faster will light scrap have to be fed in to avoid delay due to periods with charge down pretty flat and fuel reduced waiting for more charge. The advantage of heavy scrap will be greater with slow charging

and also with charging conditions such that the furnace doors remain open an inordinate percentage of the charging time.

We cannot be sure even that light scrap always means more oxygen absorption, though that seems very probable in the average case. The point we tried to make in the paper was that more oxygen absorption from the gases means a lower net heat requirement by the bath; therefore, if whatever light scrap being used can be prepared and charged to the furnace about as fast as it can be melted down, with a minimum of open door periods, then we are *likely* to get faster production rate on light scrap charges. On the other hand, with the complex of factors above mentioned, it is easy to see the possibility of just the opposite effect, as mentioned by Mr. Reinartz. Also, dense piles of oily turnings or well compacted bales of sheet scrap might give a low amount of oxygen absorption, so that the detailed physical character of the scrap charge is probably involved.

Regarding Mr. Tenenbaum's comments, our experience has been that extra limestone does not always increase time of heat appreciably and this would be true especially where extra lime was needed anyhow for sulphur elimination; if it was not put in with the charge it would have to be added later so that the extra work in refining would offset any advantage from shorter melting periods.

* Lukens Steel Co.
† Inland Steel Co.

The Interaction of Liquid Steel with Ladle Refractories

By C. B. POST and G. V. LUERSSEN

DISCUSSION

(H. C. Swett presiding)

J. STEVENS*—The authors state that the contamination in the metal was due mostly to the ladle refractories. Did the contamination vary with different brands of refractories or different qualities in the ladle?

C. B. POST (authors' reply)—That would be expected. In our shop we have used a grade of firebrick which is fairly standard. We do use high refractory nozzles to combat this erosion and high refractory sleeves, but there is such a problem when you get a skull in a ladle you just cannot use these high refractory bricks; you rip out the whole ladle getting

the skull cleaned up. The acid bricks form a glass, and you can pull the skull out when you do get them. I believe you might find variations among the different refractories depending on how much silicon is in the brick. This determines how much silica is going into the interface between the steel and the brick. Our brick is about 35 pct alumina and 65 pct silica. With a brick of 35 pct alumina in the slag patches new calculations would have to be made.

R. PARDEE*—Where can you draw the line in determining the refractories as being a silica refractory?

C. B. POST—More silica than about 50 pct. I think perhaps that is generally

the criterion. The brick we use is a good high grade fire brick.

T. S. WASHBURN*—With reference to the higher silicon that is recommended as a result of this investigation, is it contemplated that the specified range would be raised to 0.40–0.60 pct silicon, or possibly 0.50–1.00 pct silicon? These higher silicon ranges would affect the physical properties of the steel and consequently there might be some complications with respect to educating the consumers to accept this revision of the conventional analysis.

C. B. POST—It will take considerable work. Take AMS 6260 as an example. Ordinarily this specification calls for 60 or 75 manganese. Silicon has some

* Murray Refractories, Murray, Utah.

* Mexico Refractories Co.

* Inland Steel Co.

hardenability in itself, and I believe if you aim for 40 to 60 for both the manganese and silicon you will have the same hardenability. At least, we have had no difficulty in meeting all the tests of the AMS 6260 specifications on that score. It might be if you had a steel too lean in hardenability for the job under the best of conditions you might get into a little trouble. I agree with you that it is going to take some work and by the people who are more qualified to talk on it than I. As far as I know, I do not think we will run into any difficulties in what work we have done.

A. A. BRADD*—The authors present very interesting and valuable information about the effect of the Mn/Si ratio on the nonmetallic inclusion content of the steels investigated. However, another factor controlling the formation of the type of nonmetallic inclusion discussed by the authors is the composition of the ladle refractories with which the steel comes in contact before entering the mold. The authors' investigations were done with 65 pct SiO_2 —30 pct Al_2O_3 —5 pct Fe_2O_3 firebrick. Rait and Pinder

* Ass't Supt. Treatment Dept., The Midvale Co.

in a paper on "The Origin and Constitution of Certain Non-Metallic Inclusions in Steel," published by the British Iron and Steel Institute in June, 1946, found that manganese aluminosilicate inclusions could be reduced to a minimum if the firebrick refractory with which the molten steel came in contact had at least 38 pct Al_2O_3 . Their work was done with steels containing about 0.30 C, 2.80 Ni and 0.65 Cr, and Mn/Si ratio ranging from 1.68 to 3.87.

The harmful effect of higher Mn/Si ratios on cleanliness ratings might not be so pronounced if more aluminous refractories were used.

The Ionic Nature of Metallurgical Slags. Simple Oxide Systems

By J. CHIPMAN and LO-CHING CHANG

DISCUSSION

(H. C. Swett presiding)

C. B. POST*—Just what are you showing that has not been shown by fixing the attention on molecular species and choosing the molecular species to give you a perfect solution?

J. CHIPMAN (authors' reply)—In general a fairly satisfactory thermodynamic treatment of slag-metal equilibria can be worked out on the basis of assumed molecular species in the slag. This has been the method used by Shenck and more recently by White, Winkler and I

also used it in studying dephosphorization. Darken and Gurry found that it did not fit satisfactorily in the case of their data on iron oxides. The ionic formulas used here conform to the data much better and probably correspond somewhat more closely with the actual structure of the slags.

C. B. POST—It does seem to be similar to you?

J. CHIPMAN—It is alternative, and may lead to a more complete understanding.

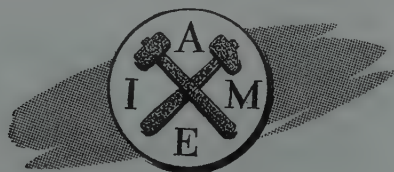
C. B. POST—Have you had a chance to talk to glass technologists on this? Have they been using this type of set-up for glass solutions?

J. CHIPMAN—Yes, and the ionic formulas have given them a little better understanding of what liquid glass is like.

C. B. POST—Nelson Taylor always said we were going about slag reactions from the wrong viewpoint when using molecular species. Evidently the glass technologists use ionic species exclusively when dealing with liquid glass reactions.

J. CHIPMAN—I agree that it seems more rational and more accurate to use ionic rather than molecular formulas. We should be cautious, however, and not suppose that we really understand the structure of a slag just because we are able to fit its reactions by ionic equations.

* The Carpenter Steel Co.



Discussion*

Extractive Metallurgy Division

San Francisco Meeting, February 1949

Contents

| | PAGE |
|--|------|
| Electrolytic Zinc at Risdon, Tasmania. Major Changes Since 1936 (paper by S. W. Ross. <i>Jnl. of Metals Trans.</i> March 1949. TP 2524D)..... | 842 |
| Cadmium Recovery Practice at the Donora Zinc Works (paper by G. T. Smith and R. C. Moyer. <i>Jnl. of Metals Trans.</i> June 1949. TP 2616D)..... | 843 |
| The Recovery of Cadmium from Cadmium-Copper Precipitate, Electrolytic Zinc Co. of Australasia, Risdon, Tasmania (paper by G. H. Anderson. <i>Jnl. of Metals Trans.</i> March 1949. TP 2525D)..... | 844 |
| Cadmium Recovery Practice in Lead Smelting (paper by P. C. Feddersen and Harold E. Lee. <i>Jnl. of Metals Trans.</i> Feb. 1949. TP 2509D)..... | 846 |
| The Effect of High Copper Content on the Operation of a Lead Blast Furnace, and Treatment of the Copper and Lead Produced (paper by A. A. Collins <i>Jnl. of Metals Trans.</i> May 1949. TP 2576D)..... | 847 |
| The Use of Oxygen Enriched Air in the Metallurgical Operations of Cominco at Trail, B. C. (paper by R. R. McNaughton, T. H. Weldon, J. H. Hargrave, and L. V. Whiton. <i>Jnl. of Metals Trans.</i> August 1949. TP 2648D)..... | 848 |
| Concentration of the SO ₂ Content of Dwight-Lloyd Sintering Machine Gas by Circulation (paper by W. S. Reid. <i>Jnl. of Metals Trans.</i> April 1949. TP 2554D)..... | 848 |
| Autogenous Roasting of Low-grade Zinc Concentrate in Multiple-hearth Furnaces at Risdon, Tasmania (paper by J. A. B. Forster. <i>Jnl. of Metals Trans.</i> Aug. 1949. TP 2624D)..... | 849 |
| Development of the Modern Zinc Retort in the United States (paper by H. R. Page and A. E. Lee, Jr. <i>Jnl. of Metals Trans.</i> Feb. 1949. TP 2523D)..... | 850 |
| Controlled Drying of Retorts (paper by R. R. Furlong and D. H. Wertz. <i>Jnl. of Metals Trans.</i> July 1949. TP 2555D)..... | 852 |
| Development of Muffle Furnaces for the Production of Zinc Oxide and Zinc at East Chicago, Indiana (paper by Gunnard E. Johnson. <i>Jnl. of Metals Trans.</i> Feb. 1949. TP 2526D)..... | 853 |
| El Paso Slag Treatment Plant (paper by T. J. Woodside. <i>Jnl. of Metals Trans.</i> August 1949)..... | 854 |
| The Morenci Smelter of Phelps Dodge Corporation at Morenci, Arizona (paper by L. L. McDaniel. <i>Jnl. of Metals Trans.</i> Jan. 1949. TP 2488D)..... | 855 |
| Distillation of Zinc from Copper Base Alloys and Galvanizers Drosses (paper by Frank F. Poland. <i>Jnl. of Metals Trans.</i> June 1949. TP 2577D)..... | 855 |

*TP 2713 D.

Electrolytic Zinc at Risdon, Tasmania. Major Changes Since 1936

By S. W. ROSS

DISCUSSION

(C. C. Long presiding)

A. A. CENTER*—This paper reminds me of the beginning of the work of the Electrolytic Zinc Company of Australasia.

Early work for this Company, as some of you may know, was done at the Bully Hill Plant in California. After working there for some time Herbert Gepp, now Sir Herbert, came to the Anaconda Co. plants in Montana where I met him. He spent some months there, in fact almost a

year if I remember rightly. That was when we were breaking in the new electrolytic zinc plant at Great Falls, Montana. From there he went back to Australia and started in on the plant there. I believe they had an original plant of about 20 tons per day of cathode zinc. We heard from them for some time, until they were able to go along on their own, and they have done very well ever since as you have heard.

Their practice, (the flow sheet, the leaching practice), has been quite different as reported in the paper and apparently they are still following that

practice to some extent.

While the earliest work on selective flotation was done down in Australia, the big companies there, strange to say, were far behind the American companies in taking it up; and it is only in comparatively recent years they have gone to the alkaline circuit and dropped out thereby more of their iron and lead. The zinc plant now is up to a capacity of 100,000 tons a year and I believe that may be notched up to about 105,000.

T. H. WELDON*—I would like to ask

* Consolidated Mining and Smelting Co.

Mr. Gordon of the Risdon staff, whether, in the handling of these high sulphide calcines, there has been a build up of manganese in the solutions and if so how is it controlled?

A. R. GORDON*—Manganese has not built up tremendously. We have manganese in solution at present to the extent of about 18 g per liter. Removal in the cells by oxidation and losses in various incompletely washed residues and precipitates maintain a state of equilibrium. However the manganese content of feed solution has varied over the years from about 6 to over 20 g per liter. We have never had to take any special steps to control the manganese build up but if the amount increased unduly we would probably institute the discard of electrolyte virtually stripped of its zinc content.

L. P. DAVIDSON†—How much depletion do you have between your purified solution and your electrolyte when your manganese is that high? It will go in about 20 or 25 g per liter. What does your cell acid run?

S. W. ROSS (author's reply)—The removal of manganese in the cells varies chiefly according to the state of the anodes. New anodes will remove several grams per liter of manganese whereas old anodes, say over 12 months old, will remove less than $\frac{1}{2}$ g per liter. On the average I would say we remove about 1 g per liter during passage through the cells.

C. C. LONG‡—Would some of the electrolytic zinc experts care to talk a bit about the removal of germanium and tin by means of soluble silica?

W. G. WOOLF§—Is the precipitation of germanium and tin by means of the soluble silica a chemical reaction or an absorption phenomenon?

S. W. ROSS—I do not think that anybody in Risdon has a very clear idea whether the removal is chemical or by absorption. I think the idea was that it might be absorption, but there is nothing definite.

* Risdon Works, Tasmania.

† American Zinc Co., Monsanto, Ill.

‡ St. Joseph Lead Co. of Pa., Monaca, Pa.

§ Bunker Hill Co., Kellogg, Idaho.

H. R. HANLEY*—I understand that the electrolytic zinc plant at Risdon, Tasmania, makes 3-day cathodes at current efficiencies above 90 pct. In this country the stripping interval is limited to one day. Do you think that superior purification is responsible for the longer cathode deposition between strippings.

S. W. ROSS—Of course in thinking about the period of stripping you must remember the difference in current density too. We use a cathode current density of upwards of 30 amp per sq ft, whereas some of your plants in this country use appreciably higher cathode densities—I think as high as about 50 amp per sq ft. At the same time we have always believed that our ability to run long stripping periods has depended mainly on three factors, (1) adequate purification, (2) a suitable combination of addition agents, and (3) maintenance of reasonably low cell temperatures.

Purification is of paramount importance, and perhaps the most vital step is that in which limestone is added. It is not difficult to drop current efficiency by many percent by improper conditions of purification in spite of the fact that the iron is completely removed. Then it took us a long time to find what was apparently the best combination of addition agents. Under our particular conditions we have never improved upon the particular combination of glue and betanaphthol referred to in the metallurgical data of the paper. Any substantial departure from these amounts adversely affects current efficiency. Finally the maintenance of reasonably low temperatures is of great importance. We have often had parts of the cell room up to over 40°C with a distinctly adverse effect on efficiency.

I would say that solution purity is probably the major factor in permitting long stripping periods but other factors are important.

H. R. HANLEY—Do you think the soluble silica in the zinc solution at Risdon has any effect on the crystal structure of the cathode?

S. W. ROSS—I am not very sure about

* Rolla School of Mines, Rolla, Mo.

this. The use of soluble silica as an addition agent in zinc electrolysis is not uncommon practice and its presence is undoubtedly beneficial under the conditions in which it is used. At Risdon about $\frac{1}{10}$ g of silica per liter survives the purification steps and enters the cells. It is quite probable that it has some influence on electrolysis and as Dr. Hanley has suggested it may affect the crystal structure. The way in which addition agents affect current efficiency and the structure of the deposit is a subject which has yet to yield many of its secrets. Much of the work done in the past has been somewhat on the hit and miss principle. We have carried out some research work on the structure of the zinc and its relationship to addition agents but I do not remember any attempt to link the effect of soluble silica with structure.

A. R. GORDON—Concerning the use of fine calcine in place of limestone for iron purification, I did not notice any reference to this in a quick look through the paper, but at Risdon we have often used fine calcine quite successfully and thereby reduced the requirements of sulphuric acid to maintain the sulphate content of the circuit.

S. W. ROSS—I note that our chairman referred to the removal of germanium and tin by means of soluble silica. I would like to draw attention to the point that no mention is made of tin in the paper in this connection. Silica appears to play an important role in the control of germanium but not of tin.

I thought that some remarks might have been provoked by the section of the paper headed "Roasting Policy." Risdon practice appears to differ widely from that employed by other plants in this regard and sometimes our roasting is looked upon as poor. However, the high sulphur oxidation per square foot of hearth area, achieved virtually in the absence of fuel addition, reduces both capital costs of the roasting plant as a whole and operating cost per unit of sulphur oxidized. On the other hand we have incurred the capital and operating costs of a flotation plant. The assessing of the debits and credits of this policy makes an interesting study.

Cadmium Recovery Practice at the Donora Zinc Works

By G. T. SMITH and R. C. MOYER

DISCUSSION

(C. C. Long presiding)

L. P. DAVIDSON*—In the analysis

* American Zinc Co., Monsanto, Ill.

of the cadmium sponge how is the sample prepared?

M. M. NEALE*—The analysis of the

* Manager, Donora Zinc Works, Donora, Pa.

cadmium sponge?

L. P. DAVIDSON—You gave a very high percentage of metallic cadmium, 2 pct zinc, 2 pct lead and say 93 pct

cadmium, or thereabouts. Just exactly how do you prepare a sample so that on a dry basis you get that analysis? Is that a dried sample?

M. M. NEALE—Yes, that is a dried sample, but I cannot answer your question as to just how it is prepared. Our chemists do that and I do not follow that through.

L. P. DAVIDSON—With the cadmium sponge from our plant we find that the chemist will give an analysis of about

70 to 75 pct, and then if you analyze it completely there is about 10 pct that you do not find; if you put it in a combustion train and actually collect the water you will find there is around 10 pct water in what is ostensibly a dry sample. We found that by washing it with alcohol one gets a sample on a dry basis so that although a part of the cadmium may be oxidized on drying, it will figure to 100 pct. Without washing by alcohol we have not been able to get it,—that is why I asked the question.

M. M. NEALE—I cannot answer your question fully on that.

A. W. SCHLECHTEN*—I merely ask for information and I fear that in doing so I may reveal my own ignorance but the question is whether the addition of zinc dust alone effectively removes germanium from the solutions.

M. M. NEALE—I cannot answer that.

* Missouri School of Mines, Rolla, Mo.

The Recovery of Cadmium from Cadmium-copper Precipitate, Electrolytic Zinc Co. of Australasia, Risdon, Tasmania

By G. H. ANDERSON

DISCUSSION

(C. C. Long presiding)

H. R. HANLEY*—I have been asked to discuss briefly the development of rotating cathodes for the electrolytic deposition of cadmium.

The earliest recorded use of rotating cathodes was by Hoepfner at Frufurt, Germany about sixty years ago. He electrolyzed zinc chloride solution using diaphragms to separate electrodes.

In the early experimental work of the Bully Hill Copper Mining and Smelting Co., Shasta County, Calif., rotating aluminum cathodes 4 ft in diam were used in the electrolysis of an acid zinc sulphate solution. Finished cathodes weighing up to 400 lb were produced. Because of mechanical difficulties, this type of cathode was abandoned for zinc, but was later used for cadmium because of the relative smoothness of deposit in comparison with stationary plates with comparable current densities. Cadmium sponge which forms on the cathode at moderate current densities (without special treatment) is entirely eliminated by a slow rotation.

The rate of rotation of the cathode has an effect on the mechanical nature of the deposit. A high rate of rotation concentrates the adhering electrolyte on the shaft; a moderate rate appears to concentrate on the cathode a short distance out from the shaft tending to corrode the deposit in the form of a ring. At a very slow rotation (2 to 3 rpm) the adhering electrolyte gravitates nearly vertically, thus avoiding the cutting ring referred to above.

The true explanation for the smoother deposits obtained on rotating cathodes

may not be given definitely as the numerous factors involved are not thoroughly understood. Smooth deposits are obtained when the orderly growth of the metal crystals in the cathode lattice are disorganized. Thus the crystals form and grow for a very short interval when they are arrested and a new crystal forms. The continued growth of the original crystals provides large crystals and a rough deposit. Also if the acidity of the electrolyte is low, hydrogen gas bubbles adhere to the deposit. As the cathode is rotated the gas surface is brought into the atmosphere where they burst; thus the deposit is made on a surface relatively gas-free.

An aluminum hub distance piece was riveted to each aluminum disk 4 ft in diam, slipped on a 4½ in. steel shaft and pressed tight to prevent acid electrolyte seeping through to the shaft.

The 9-cathode assembly was supported on insulated bearings. Electrical contact to the shaft was made through what was equivalent to a copper pulley. Sufficiently high conductivity brushes were placed on the face of the pulley to lead the current to the cathode bus bar. The assembly was driven by a link belt contacting a sprocket insulated from the shaft.

The lead anodes were semicircular and supported on porcelain insulators placed on the bottom of the cell. Two anodes were provided for each cathode to permit an 8-in. space between them without increasing the ohmic resistance. This ample spacing permitted easy stripping of deposit with the assembly in place.

Cathode cadmium was melted under 650 W cylinder oil. After casting, the primary slabs were remelted under molten caustic soda and cast into pencils 1½ in. in diam.

Rotating cathodes for deposition of

cadmium are used at Risdon, Tasmania, and at Magdeburg, Germany.

W. G. WOOLF*—This paper is very interesting to me because in our work at the Electrolytic Zinc Plant of the Sullivan Mining Co. we had an exactly similar problem—that is, a method of producing cadmium from our purification residue, the recovery of the contained copper as a copper precipitate which could be sent to a copper smelter and the production of merchantable cadmium. It is interesting to me, not knowing of the work of the Risdon people, how closely we approximate them in their main metallurgy, diverging at several interesting steps which I would like to discuss for just a moment.

For example, at Risdon they oxidize their purification residue. In our practice we take the current residue as it is produced in the purification department of the zinc plant and process it in the cadmium plant. The only oxidation that it obtains is the oxidation in the presses, the dumping of the presses and the collection and transportation of the residue to the cadmium plant.

We find that the leaching of that residue does not necessarily require the oxidation step that the Risdon people evidently find necessary.

The discussion of oxidation comes in again in the matter of the treatment of the precipitated cadmium sponge with zinc dust which again at Risdon is oxidized but which we do not attempt to oxidize except as it oxidizes itself in the storage. There is a partial oxidation which cannot be avoided, as Mr. Davidson pointed out, but we make no attempt to attain a complete oxidation and we dissolve the cadmium sponge in the sul-

* Electrolytic Zinc Plant, Sullivan Min. Co., Kellogg, Idaho.

* Missouri School of Mines and Metallurgy, Rolla, Mo.

phuric acid electrolyte of the electrolysis without any further oxidation.

Coming to the question of the rotating cathode, I have discussed this a few days ago with Mr. Gordon who visited our plant prior to this meeting and asked him why at Risdon they had the rotating cathode. He mentioned one reason perhaps was that they started with it and they continue with it because it apparently gives them satisfactory results.

The second point was that in the long-time deposition as the cathode rotates, if there are any sprouts they are easily knocked off so they obtain a smooth deposit. As a result, they are not bothered with sprouting which is one of the difficulties of cadmium electrolysis. In our procedure we have stationary cathodes. Our cathodes are stripped every 12 hr which gives us a relatively thin cathode, but the thin cathode does not bother us very much in the melting procedure.

The difference in the melting at our plant and the Risdon plant is that we melt in an iron pot with electric furnace under caustic soda. There is relatively little oxidation. The amount of dross that we obtain is comparatively small and we find no need or requirement for the thick deposits such as Risdon obtains.

A. A. CENTER*—This matter of weathering the cadmium-bearing residue is rather interesting. When we did our early work at the Anaconda Co. on cadmium about thirty years ago, we found that the cadmium copper precipitate, which we had thrown out on the ground and left there while we worked out main electrolytic zinc plant difficulties, as a weathered product leached much more easily and we got a higher leaching recovery than we got with the current production. Mr. Woolf pointed out on the other hand that they do not find it necessary. It is somewhat a matter of product at each plant, and the prior operations leading to this product in each plant.

With reference to rotating cathodes, some of you may remember, but it may be news to others, that the electrolytic zinc plant built in Park City, Utah, about thirty years ago had rotating cathodes for electro-deposition of zinc. As I recall when I was there the plant was making about 7 tons a day of zinc with rotating cathodes. The capacity of the plant, I believe, was about 20 tons of zinc per day. This plant operated a few years but shut down when the price of zinc dropped off after the first World War and was finally dismantled.

A. R. GORDON†—Regarding the question of oxidation of cadmium precipitate we have done experimental work to determine whether we could leach the precipitate directly as it comes from the zinc plant and found that it was not as

satisfactory as allowing it to oxidize first. As to why it should be so I do not know. We tried leaching it in acid with an addition of manganese mud to give oxidation in the leach, but even that was not satisfactory. Have you any explanation, Mr. Woolf, why there should be that difference in leaching?

W. G. WOOLF—The thing I neglected to point out in my discussion was the fact we return electrolyte from our cell room which carries about 270 g per liter as compared to lower acidity of your zinc electrolyte and I think perhaps that is the reason for it.

A. R. GORDON—Very likely that is the reason but we had heard about your practice before and tried out the straight leaching but in our conditions it was not satisfactory. There is another question I want to ask Mr. Woolf, what do you do with the trees that you scrape off your cathode cadmium in the cells?

W. G. WOOLF—As I pointed out we make only a 12-hr deposit and the deposit is quite free from trees and is dense and smooth.

A. R. GORDON—You have nothing to knock off to drop to the bottom of the cells?

W. G. WOOLF—No.

A. A. CENTER—I just want to say that the matter of the strong acid is not the whole answer, because, as I pointed out, our early experience at Great Falls was exactly the same as at Risdon, that the weathered material leached much more readily and yielded a higher recovery than the fresh product. Later we were able to leach fresh product with little drop in recovery using acid which was not much higher than before.

T. H. WELDON*—I do not know whether this will further confuse the issue or clarify it, but at Trail we more or less follow the same practice that Mr. Woolf mentioned was in vogue at Kellogg. We take our purification residue directly from our Shriver presses, pug it up and deliver it by pump to leach tanks with return acid. The leach pulp is circulated through the centrifugal pump and we think that a certain amount of aeration is introduced here which speeds up the leaching action. To finish the leach, we make sure that there is a slight excess of the cake. In that way, the copper is not taken into solution and yet a good recovery of cadmium is obtained. We then filter the leach to obtain a clear cadmium solution, and we use a very fine zinc dust in deficiency to precipitate high grade cadmium sponge. This particular sponge is delivered to the cadmium plant where, in the course of the operation, it is in storage for at least one week, and we think that some

oxidation there is necessary.

Someone brought up a question of thallium. We have some thallium present in our ore which reports in our purification residue and that is taken care of in our purification of the cadmium electrolyte. If the purification is properly controlled, thallium is taken out in the residue. If it is not properly controlled some thallium will get over into our cells and at the time of cleaning the anodes in the cell, we will get a sludge in those cells that might contain up to 2 pct thallium. But as I say, normally that can be taken care of in the purification step.

Also, we are making a 24-hr deposit and we think the character of the deposit is dependent on the purification. If our purification is good we get good solid deposits with very little treeing, and the small amount of trees we do get are rolled up with the cathode and melted under a caustic slag. We make about a 98½ to 99 pct melting recovery.

A. R. GORDON—Talking about thallium, in what form is the thallium removed?

T. H. WELDON—If you remove any chances of reducing power in your finished leach and you purify the solution by a permanganate purification you will oxidize that thallium and precipitate it, probably as the hydroxide.

A. R. GORDON—Do you recover that at all?

T. H. WELDON—Not at present.

A. R. GORDON—What bad effect has thallium on the electrolysis if it is not removed?

T. H. WELDON—Principally in treeing.

A. R. GORDON—I mention that because our cadmium plant electrolyte has some thallium.

T. H. WELDON—A certain amount is deposited in the cadmium as well.

A. R. GORDON—Was treeing the bad effect?

T. H. WELDON—I think so.

H. R. HANLEY—Difficulties were found in cadmium electrolysis due to the accumulation of thallium in the electrolyte. This substance causes rough deposits and increases oxidation of the cadmium during melting. It was removed by adding sodium dichromate to the neutral cadmium solution, which forms an insoluble chromate of thallium impurity.

K. MORGAN*—Our practice at Avonmouth differs somewhat from that which has been outlined in the papers we have heard this afternoon.

* Consultant, San Francisco, Calif.
† Risdon Works, Tasmania.

* Consolidated Mining and Smelting Co., Trail, B. C.

* Imperial Smelting Corporation, Avonmouth, England.

We are smelters and are consequently afraid of all electrolytic processes. We follow somewhat the practice outlined by Mr. Neale. We take our sludges and Cottrell dusts from our acid plant purification system and extract these with acid. We take the neutral solution and precipitate arsenic by controlled additions of zinc dust. During this process we volatilize about half of it, leaving 50 pct in a residue containing an equal proportion of cadmium, which is subsequently treated.

We then take our solution and slightly acidify it. Incidentally we like to leave a little arsenic in at this stage, about 0.01 g per liter. We do not use zinc dust for our main precipitating stage but use zinc rods made from high purity zinc. These are agitated in trommels, which are rotary drums, the surface of which is formed of a wire mesh screen. We place the zinc rods inside the trommels and rotate them in the solution. We find this method gives us a very dense hard sponge which settles to the bottom of the tanks. It is periodically withdrawn and filter-pressed and we find we can then melt it directly under caustic soda giving us a good yield of metallic cadmium.

The next stage depends somewhat on the purity of the metal. We use spectrographic methods and frequently find it is pure enough at that stage to cast directly into sticks or whatever is required. Sometimes the impurity content is too high and in that case we distil the metal in the furnaces somewhat similar to those outlined by Mr. Neale. If thallium is present, as it frequently is, we remove this by a melting treatment under zinc chloride. We built up a dross which contains up to 2 to 3 pct thallium. We recover this by subsequent treatment.

C. C. LONG—Mr. Morgan, what is the normal cadmium content of the solution from which the cadmium is cemented by these rotating zinc rods?

K. MORGAN—The solution runs about 100 g per liter zinc and 20 g per liter cadmium.

C. C. LONG—And the tail solution contains how much cadmium?

K. MORGAN—Our tail solution from the trommel agitators contains about 1 to 2 g per liter cadmium. We strip that cadmium by zinc dust treatment before returning the zinc liquor as a wetting down medium to our sintering plant.

L. P. DAVIDSON—What is the grade

of the zinc with your zinc rods, and have you had any trouble with the cadmium forming on the rod and giving you essentially a cadmium coated rod that did not precipitate any more cadmium? I have seen that happen.

K. MORGAN—We make our rods of high purity zinc and find that by controlling the acidity and by keeping a very little arsenic in solution we overcome the trouble.

L. P. DAVIDSON—You want the arsenic to prevent the plating of the cadmium on the rods?

K. MORGAN—Yes. At first when we developed the method we tended to form dense coats on the rods which were very difficult to deal with. We found this could be overcome by leaving a little arsenic still in the solution. Nowadays we find quite often we can strip the arsenic entirely and still get no trouble; but as a general practice, we still like to leave a little arsenic in the solution.

H. R. HANLEY—In the production of sponge cadmium from cathode or slab zinc, it is necessary that the solution move slowly around the zinc.

Turbulent solution causes the cadmium to cement on the zinc surface and prevents further precipitation.

G. H. ANDERSON (author's reply)—Regarding the necessity for the oxidation of the cadmium copper precipitate before leaching, our first work nearly 30 years ago was on an accumulation of precipitate which had weathered in a heap for a considerable time.

This material leached easily and a high cadmium extraction was obtained but rather more copper dissolved than was desired. When unoxidized precipitate was treated it was found that the cadmium extraction was poor and insufficient copper was dissolved to insure the satisfactory handling of the cadmium precipitate in the latter stage of the process.

After various tests it was found that an oxidation time of 48 hr in open bins was the most satisfactory for Risdon precipitate.

There is no doubt that the composition of the precipitate affects its rate of solution. If small amounts of arsenic and probably other elements such as cobalt, are present, the solubility is increased and this is the most likely reason for the differing behavior of the various cadmium-copper precipitates. Risdon precipitate

contains very little arsenic and cobalt.

This applies also to the high grade cadmium precipitate obtained later in the process.

At Risdon it has been considered good practice to control the oxidation of the wet high grade cadmium precipitate by applying a very low temperature to the material spread on a hearth so that a uniform product is obtained for subsequent leaching.

Our interest in the question of the oxidation of cadmium-copper precipitate was revived a few years ago when two of our staff returned from a visit to U.S.A. with the information that it was common practice to leach the precipitate without prior oxidation. Tests were conducted but it was found impracticable to obtain a high extraction of cadmium with a low finishing acidity in a reasonable time.

Referring to the revolving cathodes, it was found during the development of the process in 1922 that under the same solution conditions rotating cathodes could operate at a current density of 15 amp per sq ft whereas with stationary cathodes, a current density of only 7.5 amp per sq ft was possible over the same time of electrolysis.

Records show that in the early days of the plant, with apparently excellently pure solutions, it was possible to obtain regularly a current efficiency of 93 pct for a 96 hr stripping period with a current density of 15 amp per sq ft.

It is possible that the poorer results obtained in recent years are related to the presence of thallium.

During the early days of the plant, the whole of our raw material came from Broken Hill in New South Wales, Australia. This contained practically no thallium but now up to one third of our raw material is drawn from Rosebery, Tasmania, and this has introduced considerable quantities of thallium. As much as 20–30 mg thallium per liter is found in the cell feed solution but not more than 0.001 pct has been determined in the cadmium metal.

Also it was once the custom to purify the solution with KMnO_4 , but this was discontinued because of the very slow filtering rate of the pulp and in its place was substituted the practice of discarding cell spent solution to rid the circuit of impurities.

Apparently the KMnO_4 purification is more necessary now than prior to the use of raw material from Rosebery.

Cadmium Recovery Practice in Lead Smelting

By P. C. FEDDERSEN and HAROLD E. LEE

DISCUSSION

(C. C. Long presiding)

T. J. WOODSIDE*—In the paper it

* Amer. Smelting and Refining Co., El Paso, Texas.

was stated that many of the A. S. and R. plants probably used a process patented by Roscoe Teats in 1930. I might describe

briefly that process as used at El Paso which I believe is typical of the four or five A. S. and R. plants at which it is used. Blast furnace baghouse dust carrying anywhere from 10 to 20 pct cadmium is mixed with approximately 20 pct slack coal and 25 pct fine limerock, charged into a Godfrey roaster, roasted at a temperature of 1500°F, temperature being measured through the arch of the

roaster near the uptake, and the cadmium oxide fume running anywhere from 50 to 65 pct cadmium, the grade of the fume depending on the amount of cadmium in the feed.

A. R. GORDON*—Regarding the practice at Port Pirie mentioned in this paper, I think that cadmium is no longer recovered as carbonate. It is not treated

* Risdon Works, Tasmania.

at Risdon as it was previously. It is some years since I saw the plant at Port Pirie and then cadmium was recovered as carbonate. Also I have not seen any published material describing their present treatment, but I believe it includes precipitation of the metal from solution by means of zinc, a method similar in some respects to that described by Mr. Morgan.

The Effect of High Copper Content on the Operation of a Lead Blast Furnace, and Treatment of the Copper and Lead Produced

By A. A. COLLINS

DISCUSSION

(P. C. Feddersen presiding)

H. R. BIANCO*—I should like to ask Mr. Collins if that statement he made about the addition of drosses to the blast furnace slowing down the blast furnace is a result of his own experience or a result of the experience of some older metallurgists; and perhaps I should ask him to define the type of drosses that he means.

A. A. COLLINS (author's reply)—That has been my own personal experience with dross. On various occasions at Chihuahua we attempted to incorporate the dross in our regular blast furnace charge and to shut down the dross reverberatory to try to save some money. As expected, we had very poor results. I think that Ed Fleming will well remember on one occasion, that was back about 1933, when we attempted the first experiment along this line, and as a result of the sulphur addition to the blast furnace to matte out the copper we ended up with hanging furnaces and mushy slags and abandoned the dross experiment, once again turning to the use of the reverberatory for handling dross.

H. R. BIANCO—Is that dross you refer to from the drossing kettle?

A. A. COLLINS—Yes, the dross that I am referring to came from drossing kettles. Furthermore, to back up my previous assertion, I had occasion in 1943, while up at Leadville, to once again experience the routing of dross through the blast furnace with its sulphur addition, since they had no dross reverberatory, and to observe that once the dross was removed, the furnace was speeded up almost 100 tons a day. All of these are personal experiences and I

think that Mr. Feddersen also has had a little experience along this line—in fact, I believe all of us have had some experience.

H. R. BIANCO—I know at Trail they recirculate considerable dross through the blast furnaces and we also recirculate dross at Herculanum and I am not aware that it has done much towards slowing down the blast furnace.

A. A. COLLINS—We have always had very poor results. In the first place you have got to add a sulphur addition to pick up that copper and once you do that, that sulphur is apt to combine with some of the zinc and you are going to form a little mush; before you know it you have furnace hangs and a poor working furnace. Now of course that depends on the amount of zinc you have on charge. But in 1943, Leadville had roughly about 7 pct zinc in their slag and it worked very poorly. Previously when they had 4 or 5 pct zinc in their slag it did not matter.

B. L. SACKETT*—At Tooele we had a great deal of experience with copper. We have always been able to keep a lead well, however, in spite of the fact we have run as much as 5 pct copper and only 15 pct lead on the charge. But regarding the handling of dross, our dross reverberatory furnace is only 7 or 8 years old. Before that we recirculated the dross through the furnace and thought we were doing a pretty nice job. Of course these things are all more or less relative—in other words you establish a certain condition much better than one of a few years ago and possibly as good as any other of which you know and you think you have pretty good results.

When we first took the dross off of the blast furnace and put it through the dross

reverberatory furnace we immediately found out that we had gained something very real in furnace speed. Since that time there have been occasions when, because of the dross reverberatory being down, we have had to use dross again through the blast furnace and that has checked our original experience in slowing down the furnace very definitely.

So we feel that a dross reverberatory is a very valuable asset at the Tooele Plant.

A. A. CENTER*—Mr. Sackett's being here reminds me of trying to run with a minimum of lead concentrates the maximum of dross producing electrolytic zinc plant residue. He came up from International Smelting Co. to help us get started on that.

We took an old copper blast furnace at Great Falls, Montana, and made a lead furnace out of it by putting a lead well on the other long side which of course is a very unorthodox lead blast furnace. Our aim was to treat the residue from the electrolytic zinc plant, as I said, with a minimum of lead concentrates. That meant a maximum amount of dross. At that time selective flotation was not general practice, so our zinc concentrates ran relatively high in copper and other dross-producing elements; and of course these were largely in the zinc plant residue. I think we might call it muscle metallurgy, but we had an interesting, successful experience there and we ran for over a year thanks to Mr. Sackett's helping us get started. I have the details, but time does not permit. We did well enough so that the A. S. and R. Co. at East Helena kept boosting up the offer to us for the electrolytic zinc plant residue and there was not enough lead concentrate to supply two lead smelters there in Montana, so the matter finally finished up by the A. S. and R. Co. taking all of the residue under long term contracts.

* St. Joseph Lead Co., Herculanum, Mo.

* Tooele Smelter, Salt Lake City, Utah.

* Consultant, San Francisco, Calif.

The Use of Oxygen-enriched Air in the Metallurgical Operations of Cominco at Trail, B. C.

By R. R. McNAUGHTON, T. H. WELDON, J. H. HARGRAVE, and L. V. WHITON

DISCUSSION

(P. C. Feddersen presiding)

P. C. FEDDERSEN*—Mr. Weldon, how far do you think you can go on that? That is, how much oxygen could you use, what percentage?

T. H. WELDON (authors' reply)—That is the very interesting part of this investigation. The boys have just been theorizing a bit and it might be possible eventually to use pure oxygen in the zinc roasting in which case you could make 100 pct SO₂. Of course, you would have to redesign your furnace completely and have to supply a great amount of cooling to control temperatures. In some of the newer acid production methods where they use a cyclic process, 100 pct SO₂ would be very valuable. That would be an ultimate goal.

A. Y. BETHUNE†—What sort of zinc extraction do you get using the oxygen-enriched air in place of straight air in the roasting process? Does it change the leaching characteristics of the calcine in any way?

T. H. WELDON—No, I do not believe it does; actually with good roast using air only you will get, I think, as good a calcine as with oxygen-enriched.

A. Y. BETHUNE—Then in your opinion the application of oxygen enriched air or even straight oxygen would not have an adverse effect on the leaching properties of the calcine?

T. H. WELDON—No. We have run tests in our experimental roaster using as high as 50 pct O₂ and 50 pct air, and calcine produced is very similar to normal plant calcine.

* Bunker Hill Smelter, Kellogg, Idaho.
† Sullivan Mining Co., Electrolytic Zinc Plant Kellogg, Idaho.

C. C. LONG*—Mr. Weldon, you told us how use of oxygen in suspension roasting increases the capacity. At Joseph-town we have the opposite problem. When operating on typical low zinc, high iron concentrates we find suspension roasters quite flexible as regards capacity. When operating on high grade concentrates relatively low in iron, operations proceed smoothly at 150 tons a day. However, if the feed rate is cut down to the order of 130 or 125 tons combustion is apt to cease. It occurred to me that perhaps use of oxygen-enriched air might enhance the flexibility when oxidizing such concentrates.

T. H. WELDON—That is a very good question. Actually I think the condition there is that an iron free zinc concentrate is lower in thermal value than a high iron concentrate. Also the ignition temperature is higher. In other words Sullivan concentrate with around 12 pct iron has a fuel value of 2200 Btu's. Some of these sphalerite concentrates will have a much lower Btu value, in the order of 1800 Btu, therefore heat is not available there to maintain ignition temperature, if radiation losses are constant, or if excess air or moisture is present. I quite agree with you that a low iron concentrate is a little harder to handle and the value of oxygen-enrichment would be greater with that type of concentrate.

I did not mention that we also roast iron concentrates for the production of SO₂ for our acid plants. This iron concentrate is a pyrrhotite. In the case of the iron concentrate a larger percentage of the oxygen is tied up as metallic oxides and the theoretically possible SO₂ is only around 10 pct. Since theoretically possible SO₂ concentration is about 10 pct, if you require high gas strength, oxygen-

enrichment is of much greater value there.

W. F. JOHNSON*—I would like to mention in connection with Mr. Long's question, that I did some work 10 years ago in oxygen-enrichment and found that the ignition temperature was considerably lowered with a slight increase in oxygen content so that it probably would require a much lower temperature to get ignition, and the furnace would not go out so readily.

L. P. DAVIDSON†—In answer to Dr. Long's question about suspension roasting of low iron concentrate, we had a concentrate which we roasted successfully that had less than 2 pct iron. The only way we could roast that and get good tonnages was to updraft our furnace. We sent those data to Trail, but I think we were considered heretics.

Frankly, I like a suspension roaster that is updrafted. You can, if you want to, put some air in on the bottom hearth to finish off those last few traces of sulphide sulphur, and your updraft will permit you to do it. We were limited on the tonnage we could treat, we had no waste heat boiler and had to take our gases to a chamber acid plant. We had to keep the temperature up to get sufficient concentration in our glover tower by updrafting the furnace. Taking the gas off from the top of the combustion chamber instead of down on the seventh hearth enabled us to increase our tonnage, decrease the sulphide sulphur in the calcine and we had a much better working furnace.

Our dust loss, that is the collection in the cyclone, was no greater than when the furnace was downdrafted.

* Amer. Smelting and Refining Co., Selby Calif.
† Amer. Zinc Co., Monsanto, Ill.

Concentration of the SO₂ Content of Dwight-Lloyd Sintering Machine Gas by Circulation

By W. S. REID

DISCUSSION

(P. C. Feddersen presiding)

R. R. McNAUGHTON*—The Smelt-

* Consolidated Mining and Smelting Co. of Canada, Ltd., Trail, B. C.

ing Co. and Mr. Reid and his men at Selby are to be congratulated on the job they have done on sinter gas recircula-

tion. I think it is not going to be very long before most companies that have a sulphur dioxide emission problem will realize that they must collect and fix that sulphur some way.

T. E. LLOYD*—Between the windboxes, did you have dead plates?

W. S. REID (author's reply)—Not a dead plate as such. Ordinarily we think of a dead plate as a solid cast iron plate some 20 or 22 in. wide. Between our windboxes in the recirculation units there is a light plate, flat shaped but tapering off at either end; just an umbrella, we call it. It does prevent passage of excess air which otherwise would pass through the ribs of the pallet.

T. E. LLOYD—Just between the pallets?

W. S. REID—Wide enough to extend between two ribs of the pallet.

T. E. LLOYD—I was interested in the fact that you cool the gas there and then abandon it. The Tennessee Copper Co. at Copperhill, Tenn., are cooling a terrific amount of gas. Would you proba-

* Engineers Inc., Newark, N. J.

bly succeed better if you took the considerable amount of moisture out and recirculate the gas? What did you notice in the difference when you were running it?

W. S. REID—There are advantages in cooling and also in taking the moisture out, but our problem was entirely a practical problem. By getting the ducts cold, especially due to the periodic operation of Dwight-Lloyd Sintering Machine wherein you must close it down periodically to clean the windboxes, any moisture you get into that flue system just corrodes it greatly. It went out on us in a short time. We then tried stainless steel flues, and if the moisture is in there they go out just the same. We eventually wound up by using a lead flue from our second-over machine which is used periodically only. Lead itself stands up all right, but the expansion and contraction broke the lead flue so we were constantly welding the flue to keep it from leaking SO_2 into the building. We have eventually wound up by using wrought iron, as our tests show that wrought iron, insulated to keep the pipes warm all the time, presents no serious corrosion problem. Cooling causes

condensation of moisture and the flue goes out in a hurry.

T. E. LLOYD—You spoke of segregation, do you mean you attempted to put the charge on the pallets in such a way that you did not even have a segregation on the pallets?

W. S. REID—No, it is exactly the reverse of that. We want the segregation there, that is, a uniform segregation of the coarse material on the grates to form a grate dressing. Major segregation of coarse and fine from the feed hopper itself is bad. If the feed can be kept flowing uniformly out of the feed hopper, then by close regulation of the talus pile, there will be a uniform rolling of the coarse particles to the grate with no sluffing, and no slides; then a uniform bed throughout the machine will be obtained and that ties right in with the concentration of gas.

T. E. LLOYD—You found it necessary to have fresh air come in from around the muffle?

W. S. REID—Immediately in front of the ignition muffle until the bed is well under way on ignition and burning well.

Autogenous Roasting of Low-grade Zinc Concentrate in Multiple-hearth Furnaces at Risdon, Tasmania

By J. A. B. FORSTER

DISCUSSION

(P. C. Feddersen and T. D. Jones
presiding)

W. G. WOOLF*—The paper has a wealth of data that take careful, detailed study. As has been indicated the highlights can be only touched in the paper. The design and the arrangement of the rabble teeth as well as some of the other details of operation show a very careful study and a scientific approach to the problem which in most plants using hearth roasters are matters of trial and error with empirical conclusions and, perhaps too often, just arbitrary supervisory preferences which may be erroneous. Here the problem has been approached from a scientific angle which I think well merits careful study. The ability to treat the tonnages they get through these furnaces I think is made easier by reason of the high sulphide sulphur in the resulting calcines which the balance of the plant—the leaching and so on—can cope with.

As indicated by Mr. Weldon in his dis-

cussion earlier this morning, in most zinc plants an attempt is made to have as low a sulphide sulphur content in the roaster calcine as possible. But in the operation of the Risdon plants, they are able to cope with sulphide sulphur content up to 5 pct which is far beyond the amount of sulphide sulphur that can be handled elsewhere. I think the autogenous roasting is made easier because driving out the last percentages of sulphide sulphur brings on the necessity for extraneous heat, and that is further exemplified because even at Risdon the author shows the desirability of using some oil to better the operation, particularly for uniformity of roasting results and to obtain more regularity of furnace operation.

A. A. CENTER*—Regarding the hard crusts in the beds of the furnace and autogenous roasting, the paper speaks of the former being due, at least to a considerable extent, to lead sulphide in the crusts. I wonder if the author has considered the hard crusts as being due in large part to zinc sulphate. While I was developing large zinc operations we

ran into hard crusts which had to be dug up. I took several lumps which were so hard they showed the marks of the rabble teeth very plainly and kept them in my office for some weeks. A visitor came along one day, and as he was having similar troubles, I told him what we were doing about ours. I started to pick up one of these lumps and to my amazement the thing crumbled in my hands whereas originally it had been so hard it wore the rabbles down very rapidly in the furnace. I sent the sample to the laboratory and found that it analyzed very high in water-soluble zinc and sulphate-sulphur. The crumbling of the lumps was evidently due to the anhydrous zinc sulphate gradually taking on moisture from the air and forming crystalline zinc sulphate seven parts water. The increase in volume would, of course, result in disintegration of the lumps.

As to getting a high tonnage in the autogenous roast, that is partly because of finishing at about 5 pct sulphide sulphur. It is a real job to get down to, say, $\frac{1}{2}$ pct sulphide sulphur, which is what is usually desired, and still put through a good tonnage.

* Bunker Hill and Sullivan Co., Kellogg, Idaho.

* Consultant, San Francisco, Calif.

Autogenous, multiple-hearth roasting of zinc concentrates usually yields calcine analyzing not much under 5 pct sulphide sulphur. For example, a lithopone plant which had been used to treating only zinc wastes bought some calcine, immediately ran into troubles, and called me in. On finding where they were buying the zinc calcine, I knew they were getting calcine produced from zinc concentrates in an autogenous, multiple-hearth roaster operation, and that the calcine would probably run around $4\frac{1}{2}$ pct sulphide sulphur. This proved to be the case in spite of several disclaimers.

It is to be noted that the above discussion was sent in at the request of the AIME staff, and is based only on the abstract of the paper as heard at the San Francisco meeting.

J. A. B. FORSTER (author's reply)—Mr. Woolf is quite correct in thinking that the means used at Risdon for recovering unroasted sulphide from calcine make it easier to obtain very high roasting rates. Advantage has been taken of this at times to make up for shortage of roasting capacity by tolerating an uneconomically high sulphide sulphur in calcine.

The Risdon provision is unique in being a flotation unit which returns to the roasters a concentrate that can be roasted autogenously. It is not unusual in other roasting plants to screen the calcine, crush the oversize and re-roast it, either alone with the assistance of extraneous fuel or mixed with new concentrate. In such cases the calcine assay quoted is usually that of the screen undersize. It is not easy to compare the performance of a roaster treating low grade concentrate

and delivering unscreened calcine with one working on high grade concentrate and screening the product, but the sulphide in Risdon calcine is mainly in the coarse fraction.

By sacrificing some roasting capacity to give the material longer time in the furnace, the sulphide left in the coarse fraction can be reduced considerably, but in this case so little heat is evolved in the lower hearths that extraneous fuel is needed to maintain roasting temperature. This has been a common practice.

Additional roasting time can be given in the lower hearths by modification of rabble teeth; and since more roasting is then done in these hearths, the amount of extraneous fuel needed is less. The author hopes to demonstrate at a later date that, by carrying modification of the rabbling system to the logical conclusion, a very thorough roast can be obtained at a high hearth rate, and strictly autogenously.

Dr. Center's observations are correct, insofar as they went. There is a great difference in conditions if the space between hearths and teeth is filled with material partly roasted or with sand. In the first case, if the immobile beds are not hand-stirred every two or three days they become so hard that heavy bars and hammers are needed to chisel them. In the hottest zone where the material still contains much sulphide there is little or no sulphate formation, the binding of the bed being due to the condensation of galena vapor from the mobile bed, galena having a vapor pressure of 2 mm at 850°C and 4 mm at 920°C. Galena also condenses on the teeth which are cooler than the mobile bed, and the resulting drag on the hard hearth cake can stop a

furnace or break rabble arms. Of course a galena-free concentrate would behave quite differently in these hearths.

It is in the lower hearths, where the material is much more completely roasted and temperatures are well below that of its decomposition that zinc sulphate forms in the immobile beds. Sulphation is accompanied by expansion of volume and there develops an upward pressure against the teeth which is just as damaging as the drag in the hotter hearths.

When the immobile bed space is filled with sand the conditions are somewhat different. In the hotter hearths galena vapor still penetrates the bed causing some consolidation, and galena crusts are formed on the teeth; but provided the latter are replaced by clean ones every two or three weeks no drag develops until the bed is fully consolidated—a process which takes over three months if excessive temperatures are avoided. Owing to changes of temperature in hearths, columns and rabbles, and to growths on teeth, some sand is lost from the bed surface and is replaced by a crust similar to ordinary hearth cake, but as long as the crust is relatively thin and there is some unconsolidated sand below, no trouble occurs.

In the lower hearths the crust which forms in the same way is quickly sulphated, but as it is very thin no noticeable drag develops. The crust thickens slowly, and it is probable that under slight pressure some sand is gradually squeezed out laterally, but the beds remain in good condition for at least nine months, except around drop-holes and close to the walls where necessary cleaning results in loss of sand; consequently these beds are renewed twice a year.

Development of the Modern Zinc Retort in the United States

By H. R. PAGE and A. E. LEE, JR.

DISCUSSION

(L. P. Davidson presiding)

A. E. LEE, JR. (author)—In addition to the paper we should like to make a few remarks. First, the seriousness of bending of the clay retort cannot be overemphasized. Not only did bending limit the length of the vessel, but it permitted corrosive fluid slags to concentrate in the belly of the retort and thus increased the possibility of boring. Bending also practically prohibited the use of cleanout machines and increased the danger of excessive fume losses by allowing furnace gases to escape around the top of the retort mouth.

It will be noted that the Blackwell pottery practice places considerable emphasis on careful drying of retorts. Perhaps it is another smelter superstition, but traditionally the aging of retorts beyond a reasonable drying period has been considered important to long life. We are unable to give a good explanation of why aging should improve retorts. During the past fall in an attempt to prove a theory that the combined water in the clay decreased during aging, about 50 samples of wet retort collars were placed in a dry room when it was closed. Loss of weight, combined water and free moisture were measured each week over the 100 day drying period. The affinity

of the dried retort for moisture makes difficult the accurate measurement of free water; however, there was a clearly defined free moisture change from about 12.5 pct when freshly made to about 2 pct at the end of 18 days, then a gradual loss to about 0.25 pct at 70 days and an apparent equilibrium near this figure through the 100th day. There was no appreciable change in the combined water. The change in weight of the average sample was, however, rather unusual, there being consistently a loss of weight throughout the entire 100 days. From the 63rd day on this leveled off to about 0.03 pct per week. These were small samples and certainly should have dried

somewhat faster than the larger retort. Possibly the drying process continued although at a very low rate during the last 30 to 40 days and this caused the weight change, but our method of determining free moisture was not accurate enough to record it. In any event we have concluded that our test did not show any evidence of change in structure through loss of combined water.

An important characteristic and defect of the silica retort is its inability to withstand sudden temperature change. This is very important in starting up a furnace block. Until recently we had started a new block by filling it with green dried retorts, lighting the drops at a minimum gas setting and gradually bringing the new brickwork and green retorts up to a charging temperature over several days. This is, of course, a delicate operation and it is most difficult to hold the gas flames so low at the start as not to touch any of the retorts, especially those in the second row. We averaged a loss of at least half the original retorts during the first 3 or 4 charge cycles. A major cause of retort failure was checking about 2 ft from the mouth where the tip of the flame had touched the retort during the period of low gas firing. Recently the idea was conceived to close up the front of the furnace with butts and bring up to about the heat of a retort preheat kiln; then put in hot retorts. This method has been used on the last 3 blocks started with excellent success. The extra labor required has been more than offset by savings in retorts and by achieving normal recoveries several shifts earlier. An opportunity is afforded to measure accurately the life of the original 800 retorts and this was done on the first block started in this manner. The average life of the 800 original retorts was 34.23 cycles compared with 26.43 for all retorts in all our furnaces during the same period.

ARTHUR D. TERRELL*—That paper just given is exceedingly interesting. You only have to look at me to know that I can go back in history further than my Blackwell friends. As regards the first retort presses used in this country, they were I believe installed by the New Jersey Zinc Co., one of them at Bethlehem, Pa., and the other at Joplin, Mo., the old Empire Zinc Co. I became identified with the zinc industry in 1899 and went to Iola, Kansas in 1900 with a Mr. George E. Nicholson who sold his plant to the New Jersey Zinc Co. and I remained with it for 22 years.

These presses were installed about 1898. They were abandoned as far as those plants were concerned, and one of them was shipped to the Prime Western Spelter Co., Iola, Kansas, plant about 1903.

As regards the oval retort, they are used not only for increase in strength due

to the type of cross-section, but the heat penetration is better.

My recollection is that in a number of horizontal retort plants in the early days, a pottery consisted of two floors: one, where the retorts were made and were set on that floor for a few days until they got dry enough to be handled; then they were elevated by a one-retort-capacity hand elevator and put on the second floor, remaining there until they were taken out for use in the furnaces.

A small percentage of the zinc that goes into the walls of a fire clay retort, forms spinel.

With regard to the carborundum retort, I was with the New Jersey Zinc Co. when they made the first ones at Palmerston, Pa., and followed the results fairly closely. They were tried at some of their other plants, but never were permanently adopted as far as my knowledge goes.

The National Zinc Co., Inc., Bartlesville, Okla. made a test run on silicon carbide retorts several years ago, but did not continue their use. There have been some very unfortunate experiences and very expensive ones with the trial of carbide retorts. One of the difficulties, I believe Mr. Lee has not touched upon is the question of keeping down the blistering on the outside, particularly where you use natural gas as a firing fuel. That not only tends to weaken the retorts but makes it very difficult to get them out of the furnace after they have been in service for many months.

As far as making the retort is concerned, the indicated pressure we use for making the butt of a retort is between 2000 and 2500 psi, and the pushing out pressure is about 1200 psi. Of course, I do not think those refer to the pressure Mr. Lee has in mind. Now it is true that it seems advisable to dry clay retorts for a minimum of 30 days, unless accelerated drying is used. However, I will mention one experience we had with one of the New Jersey Zinc Co. plants at Collinsville, Okla. It had just been started the year before I became connected with it, and it grew faster than the pottery capacity did, and we got down to a 10-day life of retorts in the pottery. I confess I was very much disturbed thinking that we might have to dead fire some blocks in order to catch up on our retorts. But we ran that plant for a little while on retorts that were dried only about 10 days until we could get more rapid production of retorts which we did by putting in a new pump and a Simmons valve. Our hydraulic press capacity was then about 250 retorts in an 8-hr day instead of about 100 retorts.

As regards starting up a furnace with silica flour retorts, our experience has been just about what Mr. Lee's company's experience has been, and we had some very unfortunate results in high loss of retorts. The next time we start up a block of furnaces we are going to do about the same as Blackwell has done.

A. E. LEE—One thing I forgot to mention is a printing error in the first sentence of this paper. That is the date when commercial scale use of horizontal retorting began in the United States; that should be 1860 instead of 1890. It is interesting to note that Matthiessen and Hegeler at LaSalle, Ill. have been operating since 1860.

K. MORGAN*—It is a little difficult for me to comment on Mr. Lee's paper because our practice today at Avonmouth and also, I think, throughout Europe generally, differs in almost every respect from that outlined by Mr. Lee.

For instance it appears to be the general practice in the States to use either the silicon carbide type of retort or the silica flour type. We do not use either. We use an all clay mix. Then again on the question of de-airing, we have tried de-airing, but do not find it gives us any advantage. On our standard mix we use Belgian clays. During the war, for obvious reasons, we could not get Belgian clays and we had to use English clays. These have not the plasticity of Belgian clay and with them we do find we get some advantage from de-airing, but on Belgian clays there is no advantage at all.

There are a number of other difficulties which I am afraid would take up too much of your time, but I should like to make a few points:

The first is on this question of life. Figures for life can be very deceptive. You need to know the amount of zinc that is produced, since if you do not drive your retorts, you can get almost what life you like. It is only when you are pushed for output and have to strike a balance between output and life that life figures become significant. I should like to know from Mr. Lee how much zinc he makes per day from each retort. Our retorts are fairly big. We make about 77 lb of zinc a day from each retort. At the moment we get about a 27-day life and while we are always trying to improve it we have not been able to do so without being prepared to drop output.

The next point on which I should like to have Mr. Lee's comment and also that of the previous speaker is on the question of holing. We have to use ores containing anything up to 14 pct iron. The reason why most of our retorts fail is due to holing and when this occurs we find it is generally associated with laminations in the retort. We think that if we could stop the formation of laminations during extrusion we could greatly reduce our retort failures.

A. E. LEE—In answer to your first question about the life of the retort in terms of zinc produced, I agree this is a more accurate criterion than days. We do not figure it in terms of zinc but in terms of retorts per ton of sinter or zinc-

* Imperial Smelting Corporation, Avonmouth, England.

bearing material charged. In recent years we have gotten about 0.6 retort per ton of sinter.

I believe that the clays you have in Europe are somewhat more refractory than the ones we have available here in the States and that they withstand a higher temperature without bending. That perhaps accounts for your success with the straight clay retort.

Insofar as slagging is concerned, we have had some bad experiences with ores running as high as 12 to 15 pct iron. With ores of this character we have found retorts with the bottom half filled with a very hard iron slag after a period of several shifts.

As you point out, boring or holing occurs with furnace charges containing appreciable amounts of iron. This effect can multiply retort losses when the fluid slag drips down on retorts below. We attempt to control this by close firing so that during the latter part of the furnace cycle the charge is not so barren that the heat absorbed can be used to make the slag active.

Regarding laminations, we do not have much of that. We think perhaps this is one of the advantages of our de-airing pug mill.

L. P. DAVIDSON*—Mr. Morgan, in your slagging troubles are they all attributable to iron alone or do they become worse with a larger amount of lead?

K. MORGAN—No, I do not think we ever attributed trouble to lead. In every case we find the corrosive slag is an iron silicate.

L. P. DAVIDSON—It is not due to the formation of a very fluid lead silicate?

K. MORGAN—Not in our experience.

A. D. TERRELL—I might say we have at times gotten over 85 lb of zinc per retort. Most of the smelters are using the 48-hr cycle now and you do not reach as high top temperature to work off furnaces as you do on a 24-hr cycle, and that makes a difference in life of retorts.

C. R. KUZELL†—It has been very refreshing to hear this paper in a field of metallurgy that most of us in other fields

of metallurgy were always led to believe was rather stagnant. From what I am able to gather, having heard from some fellows of the modern-day cost of building electrolytic plants, it looks as if we are still going to be confronted with dealing with retort plants for some time.

Since we on the selling end are interested only in the question of zinc production to the point of producing zinc concentrates and selling them to these retort and other plants, of course the matter of retort life is of interest. We are often irritated by those settlement sheets showing the high penalties for iron and other fluxing impurities which cause a failure of these retorts about which we have been hearing. Consequently I have three questions which are prompted by ignorance, curiosity, and selfishness—by ignorance because I have never seen a zinc retort, by curiosity because I am naturally curious, and by selfishness because of the irritation that arises from seeing these high deducts.

I would like to ask three questions:

(1) What is the porosity of these retorts? (2) What is the relative loss of zinc through the walls of the retort? (3) Why have they never made retorts of basic refractories? As the basis for answering the question I would like to specifically recommend the hypothetical use of chemically bonded periclase subsequently burned and then used as a retort.

A. E. LEE—I do not know of any figure for retort porosity as such. However, we do have figures on the amount of zinc absorbed in the retort walls. As previously stated this was 7-9 pct of the retort weight with clay retorts. At Blackwell we recently assayed used silica retorts with a furnace life of about 26 cycles and found only 0.9 pct zinc. It has also been estimated that 2 pct of the zinc in the charge was lost through the walls of clay retorts and this is borne out by the deposits in the regenerators of some of the old producer type of furnaces. But I do not know any figure to give you on the carbide or silica retorts.

In regard to use of other refractories, I would say off hand that they might have the same failing as the early cast carbide retorts—they cannot stand the heat shocks. I would like to know what Mr. Terrell might think on that subject.

A. D. TERRELL—I feel what Mr. Lee has said would be the difficulty. They would not stand the thermal shock.

C. R. KUZELL—I would like to point out that four decades ago the copper industry in bessemerizing copper matte for the production of blister copper departed from clay and silica linings and adopted basic linings of magnesite. In some of the more recent years some of the plants have used periclase, which is a purer magnesite—purer than formerly used in magnesite brick. That has been used in the form of rammed linings and also in the production of the bricks where bricks continue to be used. The converting process is also cyclical and subject to thermal shock but nevertheless the use of the basic material has been highly successful. It would seem to me that if those who get penalized for excess iron in selling zinc concentrates would use a basic refractory like magnesite which would not be corroded by the iron and other fluxing constituents of the concentrates maybe we would be better off and get rid of some of those deducts.

A. E. LEE—There has been some experience with that type of lining. In 1900 Benjamin Sadler patented a non-corrosive retort lining. The lining consisted of magnesite, chromite or carborundum which was ground to pass a 20-mesh screen. A regular dried retort was coated on the inside with sodium silicate. Then the ground lining was added and the retort rotated until a uniform $\frac{1}{8}$ in. lining was obtained. The lining was burned into place when the retort was preheated for furnacing. This lining resisted iron slags but as in the case of the cast carbide units it cracked easily and let the slag attack the retort.

Queneau also worked out a means of making retorts consisting of layers of different materials. The inner layer was of a material resistant to attacks by the charge, the outer layer of a material resisting the action of the firing fuel, and the inner layer to form the body of the retort and give it strength. This vessel was unsuccessful because of the tendency of the layers to contract and expand at different rates, causing separation and cracking.

* American Zinc Co. of Illinois, Monsanto, Ill.
† Phelps Dodge Corporation, Douglas, Arizona.

Controlled Drying of Retorts

By R. R. FURLONG and D. H. WERTZ

DISCUSSION

(L. P. Davidson presiding)

A. E. LEE*—I would like to ask Mr. Neale if he has determined the moisture content of his dried retort. Also, has he

* Blackwell Zinc Co., Blackwell, Okla.

ever experienced difficulty with bending in the dry room where the green wet retorts contain 17 pct moisture and are placed 3 in. apart?

M. M. NEALE (replying for authors)—I cannot answer your first question as we

have had no experience with that. Setting the retorts 3 in. apart, we had no trouble with bending. We thought we would, anticipated we would, but did not.

L. P. DAVIDSON*—You mention,

* American Zinc Co. of Illinois, Monsanto, Ill.

Mr. Neale, in your opening remarks that some of your colleagues in the zinc industry were somewhat skeptical about the use of it. I can say from second-hand knowledge that about 15 years ago the Hohenlohe people in upper Silesia had

some sort of patented scheme basically such as you have done here and as the demand for zinc in 1937 came along they had a number of furnaces down—down for a long time, and did not have an adequate supply of retort to start with. They

used in principle the same process that you did and they were using the clay retort Mr. Morgan described. They had very successful drying, cut down their retort inventory tremendously, and they were very well satisfied with it.

Development of Muffle Furnaces for the Production of Zinc Oxide and Zinc at East Chicago, Indiana

By GUNNARD E. JOHNSON

DISCUSSION

(L. P. Davidson presiding)

E. D. HYMAN*—How much sorting of scrap is done?

G. E. JOHNSON (author's reply)—We do practically no sorting. We charge "run of mine" scrap to the furnace. The unmeltables, mostly iron, are in such demand today that there is no difficulty in disposing of them. It may soon be desirable to sort out from the unmeltables as much of the brass as possible.

J. J. BRUGMAN†—We have somewhat similar problems in the secondary aluminum business. What is your method of removing the unmelted material from the furnaces? Why have you such an apparently small space in which to charge your materials? Do you find that you have to seal that opening, or can you have it open and continuously charge at one end and pull out the other?

G. E. JOHNSON—Our means of melting scrap is efficient only to the extent that we use the waste heat from the vaporizing chamber to do the job. It is a batch process. We open the charge door and place the scrap on the hearth by hand shoveling. The door is then closed during the melting down period. After the melting is complete, the opposite door is opened and the unmeltables are raked out. The doors are approximately $3\frac{1}{2} \times 4\frac{1}{2}$ ft and are not sealed during the process only closed. They are nominally tight. Some metal is oxidized in the process. We have visualized a means of conveying the materials through this melting unit with the metals that are melted trickling out during its travel.

T. H. WELDON‡—Mr. Johnson, in line with the last question, is it necessary to seal the furnace between the melting down and the vaporizing unit, or have you got an inverted syphon in the bottom of the chamber?

G. E. JOHNSON—That was one of the first things we encountered. We had to have a sealed opening, and it is a

molten metal seal.

You have indirectly asked me another question, which was: "Do you have to seal up the melting unit?" I would say we should exclude as much air as possible, although we are not too efficient in doing that. We allow the melting unit doors to be open when we charge and when we remove unmeltables. You can readily see that that would lead to the idea of having a controlled atmosphere in the melting unit, and I think this would do a more efficient job of melting the scrap.

T. H. WELDON—How often do you charge the furnace?

G. E. JOHNSON—We charge the melting unit, and rake out the unmeltables, about every hour.

H. R. HANLEY*—Are any provisions made for controlling the rate of oxidation for the production of various size particles for certain characteristics of the zinc oxide product?

G. E. JOHNSON—Yes, there are many. You are getting pretty much into the fine points of zinc oxide manufacture. Some of us still think we have something to learn about that. In general, this muffle furnace as I have described it to you produces a rounded particle of zinc oxide which is generally formed by a rapid oxidation of the zinc vapor, followed by rapid cooling. We have gone to the other extreme in some of our experiments. We have changed the furnace to produce a type of zinc oxide, such as we thought was peculiar to American process zinc oxide, by controlling the temperature at the point of oxidation and maintaining that temperature for a much longer period of time than we do when we make the rounded shape.

There are other relationships that this furnace readily provides. One of the important factors is the ratio of air to zinc vapors. We can vary that by varying the air supply to the baghouse, or vary the rate at which we are vaporizing the zinc by the simple expedient of regulating the temperature over the carborundum arch. We have a number of variables that

permit us to produce all of the grades of French process zinc oxide from lead-free up through the highest grades of seal oxides. There are many controls that we can apply to the operation. What I have said is but a brief condensation.

K. MORGAN*—Can Mr. Johnson give us some idea of the fuel consumption of the furnace? How much oil does he use per ton of zinc distilled? I am also interested to know what sort of heat transmission he gets through the arch? What is the thickness of the tiles used to construct the arch? Some time ago we built a small furnace for a different purpose, using a carborundum arch, and we found that the reflectivity of the molten zinc surface was so great we had to use a very high arch temperature. We found we made an improvement by having a layer of carbon on the surface of the zinc. Has Mr. Johnson had any experience on these points? Does he make any sort of insolubles which he leaves in the furnace which he cannot tap out?

G. E. JOHNSON—I believe your first question was the fuel consumption. If I recall, somewhere in this paper there is a test that I quote. I believe we used 800 gal in a given period of time. Offhand I cannot translate that into tons of metal. I might also state that we have this understanding; that the carborundum arch, as the temperature becomes higher, becomes more efficient in heat transmission. As a matter of fact, I believe it is at about 2600°F or higher that the highest efficiency of heat transmission becomes available. We have calculations that I cannot quote from memory which indicate that the carborundum arch does a really very fine job for this type of furnace. Another point that we had considered was the fact that this furnace could be readily constructed so as to furnish an ideal source of heat for waste heat boilers. If a carborundum arch was used over the melting unit, we would have no zinc vapors in the gases at all—just clean combustion gases from which we would have removed some of the heat.

L. P. DAVIDSON†—The insolubles?

* Imperial Smelting Corporation, Avonmouth, England.

† American Zinc Co. of Illinois, Monsanto, Ill.

* San Francisco, Calif.

† Idaho Smelting, Seattle, Wash.

‡ Consolidated Mining and Smelting Co., Trail, B. C.

* Missouri School of Mines and Metallurgy, Rolla, Mo.

G. E. JOHNSON—Insolubles to me means anything that we could not tap out of the furnace. Is that correct? Let us start with the new furnace first to be technically correct. As we charge scrap into any furnace of this type there is, of course, an absorption of metal by the brickwork. That is very small in these furnaces. In fact, our recoveries of zinc over all are better than 98, probably 99 pct, accounted for. As far as I know, except for that furnace absorption and small amount of zinc we use in the molten-metal-seals, it all taps out of the furnace. You may be thinking of another thing on which I have not touched and that is the amount of dross formation in the melting of that scrap in the melting unit. There is a mush which sometimes might get into the vaporizing unit and form the insoluble you were thinking about. We have solved that. I mentioned a trough leading from the melting unit to the vaporizing unit. That trough, just before it enters the sealed opening, widens out to a large bath just outside of the vaporizing unit. If any dross forms, it collects on the surface of the metal at that point, and before it enters the

vaporizing unit. We skim it off there in an opening provided in the furnace, and thereby prevent the very large part of the dross from ever getting into the furnace.

L. P. DAVIDSON—That is, in that canal between the melting section and the vaporizing section?

G. E. JOHNSON—Yes.

E. D. HYMAN—My question concerns scrap—also scrap of the type you get from steel company's galvanizing plants. Do you treat such scrap as that commonly called sal-skims?

G. E. JOHNSON—No, we do not, since sal-skims are oxidized, and this furnace is designed primarily for distillation from metallic, zinc-bearing materials. I thought at first you were going to ask me, do we treat galvanizer's dross? We have treated much of that, as previously indicated. In treating galvanizer's dross we have had to tap out a residue metal from the vaporizing unit toward the end of the run. In fact, we have carried the distillation so far that the irony-residue had to be removed by strong arm meth-

ods, "muscular metallurgy." We finally came to the conclusion that galvanizer's dross should be treated in a furnace designed for that purpose. This is an interesting subject and I should like to know some of the answers myself.

A. D. TERRELL*—Is there any appreciable amount of blue powder formed in condensing the zinc into metallic zinc?

G. E. JOHNSON—Our figures indicate that less than one half of one percent of the zinc produced over a prolonged period of operation on zinc is formed as blue powder. That rather pleases us when you look at the figures which I have quoted on retorting where blue powder is very much more of a problem than it is on these furnaces. I think the reason is quite self-evident to us; we heat the condenser—we have facilities for heating the condenser before ever allowing the zinc vapors to enter. One detail I did not mention—we have a little outlet at the top of the condenser with a ball on it to relieve any excess pressure.

* National Zinc Co., Bartlesville, Okla.

El Paso Slag Treatment Plant

By T. J. WOODSIDE

DISCUSSION

(L. P. Davidson presiding)

A. E. LEE*—One question of the flue leading to the tube coolers. What gas velocity is maintained to prevent settling of the finely divided fume?

T. J. WOODSIDE (author's reply)—30 fps. Of course some fume settles out, but is immediately carried away by the screw conveyors.

H. R. BIANCO†—How effective are the soot blowers? Do you have to use any hand lancing?

T. J. WOODSIDE—Only one point, which is right at the top of the economizer

and which the soot blowers do not reach, we occasionally hand lance. But everywhere else the soot blowers have been very effective and no hand lancing has been done.

L. P. DAVIDSON*—Do you have considerable variation in the lead content of the fume collected if the lead is higher, and is there greater tendency for the fume to stick on the boiler tubes?

T. J. WOODSIDE—There is very little variation in the lead content. From 5 to 7 pct is the widest range variation we have had and we have noticed no difference in the behavior of the fume.

C. R. KUZELL†—Mr. Woodside has been quite generous with data pertaining

to metal and fuel economics. I think he stated that the coal consumption of the furnace was $2\frac{1}{10}$ lb for a pound of zinc recovered. I take it that that is the gross coal input to the furnace. I wonder what the net fuel consumption in terms of coal might be after crediting the fuel equivalent of the waste heat steam recovered?

T. J. WOODSIDE—The fuel value of the waste heat steam is approximately 42 pct of the heat input to the furnace. A very large part of the heat, of course, goes out in jacket water—44 pct.

A. D. TERRELL*—I would like to know how much lead is in the delead material.

T. J. WOODSIDE—It is a little less than 2 pct now.

* National Zinc Co., Bartlesville, Okla.

* Blackwell Zinc Co., Blackwell, Okla.

† St. Joseph Lead Co., Herculaneum, Mo.

* American Zinc Co. of Illinois, Monsanto, Ill.

† Phelps Dodge Corporation, Douglas, Arizona.

The Morenci Smelter of Phelps Dodge Corporation at Morenci, Arizona

By L. L. McDANIEL

DISCUSSION

(A. A. Smith, Jr. presiding)

A. A. SMITH*—This is a very complete description of one of the country's major copper producing units, and I know that it is of great interest to the copper metallurgists.

P. T. BENSON†—The matter of build-up of magnetite in a reverberatory furnace is probably of primary concern to any copper metallurgist, and I am much interested in Mr. McDaniel's remarks about using silica flux separately from the regular charge to combine with the converter slag iron rapidly and prevent deposition of magnetite.

In the description of the converter flux makeup mixing of barren quartzite with the pit run ore reduced the alumina content and the reason given for that is again to help reduce the formation of magnetite. Have you conducted experiments enough to be able to tell us just where the breaking point in the alumina content of the converter flux is with regard to the formation of magnetite?

L. L. McDANIEL (author's reply)—Probably it is not so much a matter of quantity of alumina as it is the ratio between silica and alumina, although maybe both count. We try to keep a ratio of about 5 or 6 silica to alumina. Our pit ore will run about $3\frac{1}{2}$ to ratio.

* American Smelting and Refining Co., Barber, N. J.

† American Smelting and Refining Co., Tacoma, Wash.

We change that by adding barren quartzite until we get about the ratio we want. Then we find that if we use that flux alone it is apt to be rather violent. So we add revert material to bring the silica content down to about 65. We can hold around 63 or 65 pct silica with a silica:aluminum ratio of at least 5 to 1 and get fairly good operation.

ALLAN NORRO*—I have been traveling around visiting different smelters and I also used to go to Garfield. They get about 50,000 tons of copper per converter lining and there has not been any trouble with magnetite in the bottom of the reverb. I would like to know why you do not blow magnetite linings in your converters.

L. L. McDANIEL—I think that is a matter of local practice or preference. Garfield has had very wonderful converter life which they get by magnetizing. We have not actually tried magnetizing at Morenci. But probably for the same reason that some other smelters have not, we think it might not be economical to take the time out to blow linings on a converter.

ALLAN NORRO—It just takes 5 hr once a week and this 5 hr is still production. The production will lose about 2 hr a week, and it does not take down your capacity.

L. L. McDANIEL—I repeat we have not yet done any magnetizing at Morenci.

* Boliden Mining Co., Sweden.

PAUL T. BENSON—We do practice magnetizing at Tacoma but do not get quite the life on converter lining that Garfield does. If we get 25,000 tons we consider that satisfactory. Sometimes we get 30,000 or better. We do not consider that much time is lost in magnetizing because you are blowing matte while making the magnetite lining. Our practice is, after it is completed, to go right ahead and put more matte in and begin blowing slag.

A. C. LOONAM*—I am interested in the fact that you installed multiclones instead of a cottrell. Has this been satisfactory?

L. L. McDANIEL—Our experience with multiclones on converter gases has been quite satisfactory. We have not tried the multiclones on extremely fine particle size, so I cannot give you any information on that; but on converter gases they have been satisfactory.

PAUL T. BENSON—Mr. McDaniel might add something about the multiclone performance at Douglas. I observed that a few years ago and it seemed to be very successful.

L. L. McDANIEL—We installed multiclones on converter gases at Douglas smelter of Phelps Dodge Corporation with about the same results we have had at Morenci. Very satisfactory.

* Deutsch and Loonam, New York City.

Distillation of Zinc from Copper Base Alloys

By FRANK POLAND

DISCUSSION

(A. A. Smith Jr. presiding)

S. ROLLE*—As one who has been privileged to read Mr. Poland's paper before its publication, I wish to express high praise for it and the record which it gives of the work done by the Research and Development Department of Revere Copper and Brass Inc. in developing a

satisfactory furnace for the recovery of metallic zinc from secondary metals by distillation. I have also had the opportunity of studying the operation of the furnace when running on scrap brass at the Detroit plant of Revere, and I can therefore say from knowledge gained first-hand that the unit is efficient and economical when used in conjunction with distillation. However, when I read what Mr. Poland has to say in reference to the possibility of using the furnace for

melting copper cathodes for the production of oxygen-free and tough-pitch copper shapes, I am constrained to be somewhat skeptical. No doubt the furnace can readily be modified so as to make it possible to melt cathodes, but that is only a part of what is required to produce refinery shapes.

Because of its construction the atmosphere in the furnace is highly reducing and even without protective gases such as nitrogen the copper cathodes which are

* The Scomet Engineering Co., New York City.

substantially oxygen-free will not become oxidized—that is, the copper will remain oxygen-free. If then the molten oxygen-free copper is discharged from the furnace in a closed launder and then to a pouring device which is also closed, in other words follow the Scomet process for the production of oxygen-free copper (OFHC), there is no reason why good quality oxygen-free copper cannot be made by substituting the Wilkins-Poland furnace for a Summey or Scomet furnace for the primary melting. But when we come to the production of tough-pitch copper, the matter is not quite so simple. The experience gained at the Ontario Refining Co. plant in Copper Cliff, Ont., Canada, reveals that when they allowed the copper to remain oxygen-free in the arc melting furnace and then convey it to the molds in an open launder in order to pick up the requisite amount of oxygen, it was extremely difficult, if not impossible, to control the oxygen content and to make sound tough-pitch copper castings. Even in the launder there was clear evidence that the copper was gassy by the constant discharge of copper rain; the resulting castings were of poor quality and lacked uniformity. After considerable experimentation the operators at Copper Cliff hit upon the idea of venting the arc furnace so as to permit the molten copper to pick up oxygen in the furnace. From then on there was little or no difficulty in producing tough-pitch copper of excellent quality.

It is my belief that in order to produce good quality tough-pitch copper if the Wilkins-Poland furnace is used for melting the cathodes, it will be necessary to oxidize the bath by venting the furnace so as to introduce air. What will happen to a resistor furnace of this type when operating in an oxidizing atmosphere we do not know because it has not been tried; but I should judge it would not be very satisfactory. And if the furnace is not vented and the copper emerges oxygen-free, then the same difficulties will be encountered as when Copper Cliff attempted to produce tough-pitch using the arc furnace.

Mr. L. W. Bahney, Manager of The Scomet Engineering Co., has informed me that he was unable to produce good quality tough-pitch copper wirebars at Carteret, N. J., when he attempted to introduce the proper amount of oxygen in the launder by exposing the moving stream of oxygen-free copper to the air.

In other words, he confirmed the results obtained at Copper Cliff even though the melting was done in an induction furnace instead of an arc furnace.

FRANK F. POLAND (author's reply)—I have the impression that Mr. Rolle is inferring that because air had to be vented to Copper Cliff's arc furnace it will be necessary to do the same for all other furnaces. It is my understanding that the metal as it comes from the furnace at Copper Cliff varies from about 0.005 to 0.01 pct oxygen. Can anyone present tell me if I am correct in this?

J. S. SMART*— $0.01 \pm$ is the figure that is generally used.

FRANK F. POLAND—I believe there is more than one way to obtain the same end result and Mr. Rolle does not hesitate to say that he believes the resistor furnace could, in conjunction with the proper pouring equipment, produce good sound oxygen free castings. However, he has some doubt as to the successful casting of good commercial tough pitch refinery shapes. We must not lose sight of the fact that the furnaceman has for a long time, and still is, applying his skill in the production of electrolytic copper castings and that the end result we are seeking is to get molten copper in such condition that when it solidifies in any given mold a level or slightly crown set will result. There is no doubt that fundamentally this is accomplished by the release of gas during solidification. However, there has been a lot of discussion as to how the gas got into the metal and what kind of gas it is but the fact that it is a controlled amount liberated during solidification has not been questioned.

At Copper Cliff I believe it is necessary to vent air to the furnace because it is operated with an arc and I feel quite certain they would get into a lot of difficulty with the operation of the furnace itself if this were not done.

Air is 79 pct nitrogen and in my opinion it is questionable if the amount of oxygen introduced in the arc furnace at Copper Cliff is enough in itself to assure uniform flat set. The set there I feel quite sure is controlled by their furnaceman today, as it always has been, that is between the furnace taphole and the

molds.

At Perth Amboy, N. J. some years ago we set up a gas plant where desulphurized and dehydrated producer gas was made. This gas was used to pole several 250 ton reverberatory furnace charges to an oxygen free condition. These charges after having been blown to low set by standard procedure were covered with enough charcoal to supply all the carbon needed for reduction plus an excess to cover completely the bath after completion of the deoxidation step. This furnace was equipped with two casting wheels, one casting wire bars and the other vertical cast cakes. The purpose of that experiment was to find out if copper could be made oxygen-free in large quantities. It was done successfully. The oxygen-free metal was cast into wire bars and vertical cast cakes. The set required the minimum of control by the furnaceman and the oxygen in the wire bars and cakes was approximately the same as regularly produced. This experience shows that properly prepared oxygen-free copper can absorb oxygen between the furnace and molds in an amount sufficient to produce commercial electrolytic set wire bars and cakes.

Some years ago at one of the large eastern refineries the casting equipment was such that it was necessary to pole regularly their large reverberatory furnaces down to 0.005 to 0.01 pct oxygen and during this period hundreds of thousands of good commercial set wire bars and cakes were produced. The oxygen content was 0.035 to 0.045 pct in the castings.

During the development of the continuous casting process a small resistor furnace was used to melt approximately 1000 lb of cathode copper per hour while being flushed with nitrogen. This furnace was equipped with a door so that a standard 15-lb ladle sample could be cast from the molten bath. All of these samples were sound and had a commercially good set.

The three examples that I have given and, I believe, the Copper Cliff practice prove that good commercial electrolytic copper can be cast from oxygen free metal that has been flushed with either air (nitrogen plus oxygen), commercial nitrogen or carbon monoxide plus nitrogen provided proper equipment is installed between the taphole and molds for control of the oxygen absorption from the atmosphere.

* American Smelting and Refining Co., Barber, N. J.

Discussion,*

Institute of Metals Division

San Francisco Meeting, February 1949

Contents

| | PAGE |
|--|------|
| On the Structure of Gold-silver-copper Alloys (paper by J. G. McMullin and J. T. Norton, <i>Jnl. of Metals</i> , Jan. 1949, TP 2486)..... | 857 |
| Platinum-tungsten Alloys (paper by R. I. Jaffee and H. P. Nielsen, <i>Met. Tech.</i> , Aug. 1948, TP 2420)..... | 858 |
| Use of Electrical Resistance Measurements to Determine the Solidus of the Lead-tin System (paper by Ralph Hultgren and S. A. Lever, <i>Jnl. of Metals</i> , Jan. 1949, TP 2500)..... | 859 |
| The Effect of Orientation Difference on Grain Boundary Energies (paper by C. G. Dunn and F. Lionetti, <i>Jnl. of Metals</i> , Feb. 1949, TP 2517)..... | 860 |
| Influence of Composition on the Stress-corrosion Cracking of Some Copper-base Alloys (paper by D. H. Thompson and A. W. Tracy, <i>Jnl. of Metals</i> , Feb. 1949, TP 2518)..... | 862 |
| Oxide Films Formed on Metals and Binary Alloys (paper by J. W. Hickman, <i>Met. Tech.</i> Dec. 1948, TP 2483)..... | 866 |
| Magnesium-lithium Base Alloys. Preparation, Fabrication and General Characteristics (paper by J. H. Jackson, P. D. Frost, A. C. Loonam, L. W. Eastwood and C. H. Lorig, <i>Jnl. of Metals</i> , Feb. 1949, TP 2534)..... | 867 |
| Hydrogen in Aluminum (paper by Yves Dardel, <i>Met. Tech.</i> , Dec. 1948, TP 2484)..... | 868 |
| Plastic Deformation Waves in Aluminum (paper by A. W. McReynolds, <i>Jnl. of Metals</i> , Jan. 1949, TP 2499)..... | 876 |
| Homogeneous Yielding of Carburized and Nitrided Single Iron Crystals (paper by A. N. Holden and J. H. Hollomon, <i>Jnl. of Metals</i> , Feb. 1949, TP 2521)..... | 877 |
| Temper Brittleness of Plain Carbon Steels (paper by L. D. Jaffe and D. C. Buffum, <i>Met. Tech.</i> Dec. 1948, TP 2482)..... | 880 |
| Some Factors Affecting the Rate of Grain Growth in Metals (paper by J. E. Burke, <i>Met. Tech.</i> Oct. 1948, TP 2472)..... | 881 |
| Preferred Orientation in Rolled and Recrystallized Beryllium (paper by A. Smigelskas and C. S. Barrett, <i>Jnl. of Metals</i> , Feb. 1949, TP 2522)..... | 886 |
| A Study of Textures and Earing Behavior of Cold Rolled (87-89 pct) and Annealed Copper Strips (paper by Ming-Kao Yen, <i>Jnl. of Metals</i> , Jan. 1949, TP 2506)..... | 887 |
| Pressure Distribution in Compacting Metal Powders (paper by Pol Duwez and Leo Zwell, <i>Jnl. of Metals</i> , Feb. 1949, TP 2515)..... | 888 |
| Lead-grid Study of Metal Powder Compaction (paper by R. Kamm, M. A. Steinburg and J. Wulff, <i>Met. Tech.</i> Dec. 1948, TP 2487)..... | 888 |
| Properties of Chromium Boride and Sintered Chromium Boride (paper by S. J. Sindeband, <i>Jnl. of Metals</i> , Feb. 1949, TP 2519)..... | 889 |
| Solubility Relationships of the Refractory Monocarbides (paper by J. T. Norton and A. L. Mowry, <i>Jnl. of Metals</i> , Feb. 1949, TP 2527)..... | 891 |
| The Magnetic Properties of Sintered Iron and Iron Base Alloys (paper by W. Rostoker, <i>Met. Tech.</i> Oct. 1948, TP 2437)..... | 891 |
| The Densification of Copper Powder Compacts in Hydrogen and in Vacuum (paper by C. B. Jordan and Pol Duwez, <i>Jnl. of Metals</i> , Feb. 1949, TP 2516)..... | 893 |
| The Surface Tension of Solid Copper (paper by H. Udin, A. J. Shaler and John Wulff, <i>Jnl. of Metals</i> , Feb. 1949, TP 2530)..... | 894 |
| Self-diffusion in Sintering of Metallic Particles (paper by G. C. Kuczynski, <i>Jnl. of Metals</i> , Feb. 1949, TP 2528)..... | 896 |

* TP 2690 E.

On the Structure of Gold-silver-copper Alloys

By J. G. McMULLIN and J. T. NORTON

DISCUSSION

(E. R. Jette and J. R. Long presiding)

E. R. JETTE*—The way this ternary was developed there are two directly determined points on each of the isothermals except the 700° isothermal, where I believe there is only one. How were the end points determined, and what was the basis for it? Whose work formed the basis for the silver copper line?

M. B. BEVER†—At most temperatures the authors determined three points of the isothermal line. For example it can be seen from Fig 3 and 4 how three points for the 600°C contour line

were obtained. The authors took two additional points for each temperature from the copper-silver binary diagram contained in Hansen's volume on constitution diagrams. It is correct that the 700°C contour line is based only on one point in the ternary field which was found by a slight extrapolation of Fig 4.

R. I. JAFFEE*—Are the tie lines representing phases in equilibrium parallel to the silver-copper boundary?

M. B. BEVER—Are you asking that as a matter of principle?

R. I. JAFFEE—I assumed that would follow from principle. I wonder if that is in accordance with the authors' ideas too.

M. B. BEVER—I do not believe the authors obtained any information on the tie lines in the two-phase field. Of course, in the limiting case of very low gold contents the tie-lines approach to the silver-copper boundary, but generally in the two-phase field I do not think that the tie-lines have to be parallel to the boundary.

E. R. JETTE—I am quite sure they do not have to be parallel. You cannot tell from this work in which direction they go.

E. A. GULBRANSEN*—Were any pycnometric measurements made to check the lattice parameters of the alloys?

M. B. BEVER—I did not hear any-

* Univ. of California, Los Alamos, New Mexico.
† Mass. Inst. of Technology.

* Battelle Memorial Institute.

* Westinghouse Research Laboratories, East Pittsburgh, Pa.

thing about such measurements and I think I would have if the authors had done such work.

E. R. JETTE—The cameras that were used for this work come in three ranges. Do you know whether they use the most precise range or the more convenient middle range?

M. B. BEVER—As I remember it, the authors used a Phragmen No. 3 camera.

E. R. JETTE—That covered the outer range which is the most precise, and it makes me wonder why the results are only considered good to 2/1000 Å. It is capable of doing better than that. Perhaps that is all they needed?

M. B. BEVER—I think that is so. If

you recall Fig 2, the essential quantity to be determined was the temperature above which the parameter is constant. That temperature corresponds to the intersection between the inclined and the vertical parts of the left curve in Fig 2. The precision with which this intersection could be determined was not limited by the precision of the lattice constant measurements.

J. G. McMULLIN and J. T. NORTON (authors' reply)—As Dr. Bever stated in his reply to Dr. Jaffee's question, we did not determine the tie-lines between the two phases co-existing phase in the two-phased alloys. Masing and Kloiber¹ show the lines for the 400°C isothermal section. These tie lines run roughly parallel to the Ag-Cu boundary when the compositions

are plotted in atomic percent. We know of no reason why the tie lines must lie in this direction except when they approach the Ag-Cu boundary.

In reply to Dr. Jette's question on the cameras, we used an unsymmetrical focussing type camera covering the range of θ values from 45 to 83°. We did not utilize the greatest degree of precision possible with these cameras because our specimens were relatively coarse filings instead of the very fine powders usually required for precision work. We feel that the degree of precision we did obtain was entirely adequate for this project and that the added time necessary to obtain another significant figure in the lattice constant was not justified.

Platinum-tungsten Alloys

By R. I. JAFFEE and H. P. NEILSON

DISCUSSION

(E. R. Jette and J. R. Long presiding)

C. S. SIVIL*—The authors are to be congratulated on their excellent work and on the clarity of their paper.

In our opinion the method of preparation of the platinum was perhaps not the best that could have been chosen. The precipitation of platinum by zinc results in a powder that contains not only a comparatively high percentage of zinc, but also a fairly high content of occluded gases. While the final ignition at 750°C would remove some of these gases, there may remain a considerable oxygen content, unless this ignition were carried out in hydrogen. The use of this "black" powder invariably results in swelling during sintering. A platinum powder that is freer from this objectionable swelling is that obtained by the ignition of ammonium chloro-platinate, but even such a powder will give a compact which may swell somewhat, not only when the compact is sintered but also when the compact is worked to wire. In some of our early experiments with powder metallurgy at Baker and Co. we would often make a platinum wire which, on annealing, would swell from a diameter of 0.015 in. to a diameter of 0.017–0.018 in. It is our opinion that this swelling results from (1) the cold welding of the surface of the compact due to the pressure of compacting, and (2) the sintering of this surface to a layer impervious to gas before the temperature of the inside of the compact was high enough to permit diffusion so

that the elimination of entrapped gas could not proceed. Some support is given to this view by the observation that the swelling was reduced by reducing the compacting pressure or the cross-section of the compact.

Turning our attention to the micrographs, the writer is inclined to agree with Price, Smithells and Williams that the structures of Fig 9 and 10 are due to sintering in the presence of a liquid phase, despite the argument of the authors. Is it not conceivable that the presintering of these alloys resulted in slugs that consisted mainly of a platinum-rich matrix which, when the slugs were sintered electrically, became liquid before sufficient tungsten had dissolved to raise the melting point above the sintering temperature? Prolongation of the sintering would answer this question. The writer's view would be that the high intersolubility of platinum and tungsten led to the structures observed for the alloys containing 6 pct and less platinum and 38 pct and more platinum; in the tungsten-rich, by rapid diffusion of the molten platinum into the tungsten and, in the platinum-rich, by rapid diffusion of the tungsten into the molten platinum. Perhaps Messrs. Jaffee and Nielsen kept record of the heating curves of their sintering of these alloys and such curves may give an answer to this question.

R. I. JAFFEE (authors' reply)—Mr. Sivil's comments on the swelling of high platinum content alloys are very well taken. In our work in high platinum alloys, swelling during sintering could not

be overcome. Consequently, we are glad to have his suggestion on the use of ammonium chloroplatinate ignited in hydrogen to reduce swelling. Concerning the presence of zinc in the platinum powder used, we believe that any present would have volatilized during the high temperature sintering operation. At one time we had occasion to try to make tungsten base alloys containing 10 pct Cr. By the time the bar was sintered, all of the chromium had volatilized. In view of this we believe that zinc would have volatilized also. Our point concerning the so-called "heavy metal structure" still should hold. In the theory of this structure it is assumed that the matrix present in the final product is molten at the sintering temperature, and represents the equilibrium condition. If such were the case it is highly improbable that the bar would support its own weight, which it would have to do during electrical sintering.

S. J. SINDEBAND*—Were any fusion point measurements made on bars which had been completely sintered prior to making this determination? Perhaps that would cast some light on the point just raised regarding the possible presence of liquid phases. I wonder, when the fusion point is measured in the course of the sintering operation, whether the equilibrium is always obtained prior to the initial appearance of fusion in the hole.

R. I. JAFFEE—Perhaps I did not make the point clear, but there were two steps involved. The first step was to prepare

* Baker and Co., Inc., Newark, N. J.

* American Electro Metal Corporation, Yonkers, N. Y.

the alloy, which involved taking it up to a known sintering temperature. As a second step the specimen was necked down and was taken up to the fusion point. We hoped to attain equilibrium by the first step, the sintering operation, and did not expect any further diffusion during the fusion point determination.

S. J. SINDEBAND—Perhaps the confusion comes from the text proper, because there is a statement there that the presence of the hole did not interfere with proper sintering.

R. I. JAFFEE—That is right, but the hole was put into the specimen before the sintering operation and before the fusion point determination.

H. P. NIELSEN (authors' reply)—The diffusion takes place very rapidly at the very high temperatures. While we have no complete evidence that perfect diffusion had taken place nevertheless within a matter of minutes the diffusion would have taken place so that it would be practically perfect.

E. R. JETTE*—The melting point or the solidus points seem to be very sensitive to small amounts of impurities, and perhaps the only adequate answer is to report some spectroscopic analysis of your ingots before sintering and after melting to see if there was anything that could affect the melting points.

R. I. JAFFEE—The experiments with tungstens of different nonmetallic contents indicated the extreme sensitivity of the solidus temperature impurities. It has been some time since we did this work, and I do not think the specimens are available to examine spectroscopically. It would be a good idea, however.

E. R. JETTE—We do not often get papers where the working temperatures start over 1700°C.

E. A. GULBRANSEN†—Would you

* Univ. of California, Los Alamos, New Mexico.

† Westinghouse Research Laboratories, East Pittsburgh, Pa.

elaborate on the methods used for measuring the temperature? In particular, how is the absolute temperature determined from the brightness temperature?

R. I. JAFFEE—The temperature measured was that at the bottom of a hole in the specimen, which was assumed to be radiating under black body conditions. This temperature was taken to be the true temperature. When I referred to brightness, I was referring to the relative brightness at the bottom of the hole compared to that at the surface of the bar. Perhaps I do not get the entire connotation of your question. Do you care to add anything further, Dr. Nielsen?

H. P. NIELSEN—Only that I understand that the hole should be five times as deep as the diameter or better in order to come close to black body conditions, and we made sure we had at least that depth.

E. R. JETTE—Is there any way of getting an accurate calibration of temperature under these conditions?

R. I. JAFFEE—The method used to measure temperature is admittedly not the most ideal one. A very good method employs the use of a cylindrical specimen with a small hole in it. Under such conditions a practically perfect black body is obtained. If there were no radical temperature gradients through the walls of the cylinder the conditions would be right for very reliable observations of temperature. Use of such a specimen was not feasible in the present work.

E. A. GULBRANSEN—Is it possible to interpret the etching pits as residual porosity of the material?

R. I. JAFFEE—I cannot answer that question absolutely. It is possible that they might be. However, they did not appear in the polished specimen before etching, and, also, were rather shallow.

E. A. GULBRANSEN—Did the density of the material come up to what you would normally expect of compositions of this type?

R. I. JAFFEE—We did not check density.

E. A. GULBRANSEN—How do you interpret your hardness measurements? You have a tremendous increase here, 160 to about 900. To what do you attribute this change?

R. I. JAFFEE—Straight solid solution hardening of the tungsten solid solution by platinum. A similar sort of thing, although not nearly so marked, occurs at the platinum end of the system. Tungsten is one of the most potent of the hardeners of platinum. Although I agree with you that this is a remarkable increase in hardness for a substitutional solid solution, we do not see any other mechanism for the hardening. The maximum point in the hardness curve coincided with the solubility limit.

E. A. GULBRANSEN—Are there any changes in the lattice parameters?

R. I. JAFFEE—Yes, lattice parameters were measured. Some figures are given in the paper. Thus, for pure tungsten we obtained a lattice constant of 3.1583, which checks quite well with the accepted value. A 4 pct platinum content in the tungsten causes the lattice constant to decrease to 3.1572, which amounts to a very small shift.

L. D. JAFFE*—In connection with Mr. Gulbransen's comment, is there any possibility of a precipitation on cooling from the sintering temperatures or with the specimens quenched in some fashion?

R. I. JAFFEE—Cooling from the sintering temperature was quite fast, because after the transformer is shut off, the specimen cools to below a red heat in a few seconds. Therefore the opportunity for precipitation is rather limited.

H. R. STEPHAN†—Is there a possibility that you get a high strength matrix to hold your specimen together and still have a liquid phase present.

R. I. JAFFEE—The micrographs show fairly clearly the matrix was the platinum-rich solid solution. I think that rules out that possibility.

* Watertown Arsenal Laboratory.

† Fairchild Engine and Airplane Corporation, Oak Ridge, Tenn.

Use of Electrical Resistance Measurements to Determine the Solidus of the Lead-tin System

By R. HULTGREN and S. A. LEVER

DISCUSSION

(E. R. Jette and J. R. Long presiding)

M. B. BEVER*—The method re-

* Massachusetts Institute of Technology.

ported in this interesting paper promises to be of fairly wide applicability. It may be expected that the solidus and liquidus lines in other low-melting alloy systems can also be determined by resistance measurements. As these alloys are especi-

ally slow to reach equilibrium, a static method will improve the accuracy with which these parts of their phase diagrams can be determined.

It should be noted that the sensitivity of the method for the determination of

the solidus is not the same at all compositions. The straight line representing the solid phase and the curve representing the two-phase region intersect in a decreasingly definite manner, as the temperature range of solidification increases.

A question must be raised concerning the eutectic temperature in the lead-tin system. The authors state that melting begins at 183°C, but in Fig 5 they somewhat arbitrarily place the eutectic at 185°C and in Fig 6 at 183.3°C. It may well be asked whether the resistometric method is not capable of high precision also in locating the eutectic temperature.

If the resistances of the liquid alloys reported in this paper are plotted against composition at a single temperature such as 320°C the value for the alloy containing 19 pct tin appears to be abnormally low or possibly that for the 24 pct tin alloy is unduly high. Although the authors did not intend to determine absolute values of the resistance, they perhaps have an explanation for this unexpected behavior of the resistance as a function of composition. It is of interest in this connection that Bornemann and Müller* and Matuyama† found that the resistance of liquid lead-tin alloys decreases quite regularly as their tin content

is increased.

A recently published observation may be added to the data from the literature presented in Fig 7. Borelius, Larris and Ohlsson* used resistance measurements to determine the solvus in lead-rich lead-tin alloys. They found that an alloy containing 18 pct tin on heating becomes a single phase at 182.5°C, and is still solid at 183.8°C. These data agree well with the results presented in Fig 7 by Professor Hultgren and Mr. Lever.

E. R. POTTER†—It is nice to run across papers where the authors present their data as they record them rather than making their graphs agree with their conclusions. Now in respect to this one alloy—the 19 pct tin—which happens to have a rather low value at some temperature in the liquid state, we do not know whether Dr. Hultgren used the same tube for all his alloys or whether he used various tubes during the experiment. If he had used different tubes, there would be some experimental error due to the cross-sectional area variations from tube to tube. It might be that Dr. Hultgren would have a rather simple answer to this point but I cannot answer the question.

E. R. JETTE—This is one of the oldest systems in physical metallurgy.

B. GONSER*—I might point out that the tin used is not a particularly pure tin, although it is mentioned as such. It is commercial grade. Tin of higher purity can be obtained both in commercial brands guaranteed 99.9 pct pure, and in special grades. I would recommend that similar work be done with tin of higher purity such as the 99.99 pct electrolytic tin produced by Vulcan Detinning Co. or others.

E. R. JETTE—If we are looking for the easiest possible system to try out the electrical resistance method, I would say this would be it. This is not to detract from the work but there is a certain precision attainable in handling this particular system and it would be difficult to reach in a system that melted 500° higher. Also, it is obvious that using the electric resistance method means you must be able to put the alloy in such a physical form that you can measure a resistance. This is not always easy and I suspect that the authors of the previous paper on the platinum-tungsten system might have had a great deal more difficulty in doing the job by resistance methods.

* K. Bornemann and P. Müller: *Metallurgie* (1910) 7, 396, 730, 755.

† Y. Matuyama: *Scient. Repts. Tôhoku Univ.* 1927) 16, 447.

* G. Borelius, F. Larris and E. Ohlsson: *Arkiv f. Matematik, Astronomi och Fysik.* (1944) 31A, No. 10.

† Univ. of California, Berkeley, Calif.

* Battelle Memorial Institute.

The Effect of Orientation Difference on Grain Boundary Energies

By C. G. DUNN and F. LIONETTI

(E. E. Schumacher and A. Wachter
presiding)

W. G. BURGERS*—It seems almost certain that this investigation shows the way which finally, when more analogous data have been obtained, must lead to the understanding of many features of preferential growth-directions of crystals and of the occurrence of recrystallization textures.

In this connection I should like to mention that Mr. Tiedema in my laboratory succeeded in developing an analogous method for preparing crystals in aluminum plates with a chosen crystallographic plane and direction parallel to

the surface of the plate (to be published in *Cryst. Acta*). If such crystals were grown in high purity aluminum and test-pieces containing a few crystals such as the authors describe were prepared for this metal, it might be possible that due to the absence of growth obstructing particles, even in this low-melting point metal boundary displacements approaching equilibrium positions might be realized.

With regard to the apparently marked drop in surface energy for orientation differences approaching zero degree, and orientation differences approaching those existing between twins, it seems of interest to remark that in aluminum a crystal growing at the expense of fine grained material cannot (or can only very reluctantly) absorb grains in either ap-

proximately (within 5–10°) parallel or spinel twin orientation (May, Tiedema and Burgers, *Nature* (1948) 162, 740 and *Cryst. Acta* in press). Consequently with aluminum the method of preparing a crystal with a definite orientation does not succeed when the new crystal has to absorb its own texture; for example it is not possible to grow in a polycrystalline wire with a [111]-texture a crystal with a [111]-direction parallel to the wire axis (Tiedema: *Cryst. Acta*, in press). Finally I should like to mention the well-known fact (Burgers: *Proc. Acad. Amsterdam* (1947) 50, 723) that prolonged annealing of recrystallized nickel-iron sheet with cube-texture never succeeds in transforming this into one single crystal of the same orientation; if, by "secondary recrystallization," large crystals are formed

* Laboratorium Voor Physiche Chemie, Delft, Holland.

in this process, their orientations differ considerably from the [100]-orientation. In other words, elimination of the boundaries between nearly equivalent blocks appears to be impossible. This again confirms the occurrence of a drop in surface energy for small differences in orientation.

C. G. DUNN and F. LIONETTI (authors' reply)—The authors wish to thank Dr. Burgers for his kind remarks and his very interesting discussion on the problem of recrystallization and grain growth processes. It is a pleasure to hear of the successful work done in his laboratory on growing aluminum crystals in plate specimens with each crystal having a predetermined orientation. Application of this method to the problem of grain boundary energy measurements in aluminum would be very desirable and, as Dr. Burgers indicates, the purity of the system could be controlled more completely than it can in silicon iron. Results different from our present ones might also be expected because of (1) a different type lattice and (2) a one element system.

The illustrations of lack of growth for near twins and for grains of nearly the same orientation are very welcome and we are in complete agreement with the idea expressed about low boundary energies playing an important role. For example, the presence of relatively stable island grains of near twin orientation, described by Burgers* in connection with samples supplied by P. A. Beck, is understandable on the basis of a low amount of boundary energy for twins or near twins. Further, when island grains form in a growing grain as may occur in exaggerated grain growth, a certain amount of grain boundary energy is lost for purposes of advancing the boundary and this may be important for general growth. Speculating a bit on the assumption that growth occurs, it would seem that the number of island grains would increase with sharpness of texture of the matrix provided the growing grain has about the same or a twinned orientation of the matrix texture. In such a picture not only would the total available energy drop with increasing sharpness of texture, but the amount used for general growth would also drop. From an energy standpoint, these two factors appear to explain the failure of a large grain to grow at the expense of its own texture as Dr. Burgers stated was the case.

However, Dr. Burgers is well aware that something beyond grain boundary energy appears to be involved if we consider the case when the matrix is strained. Quoting from his reference in *Nature*, "It appears from various experiments that the ease with which a crystal can grow in

a deformed matrix depends on the mutual orientation of growing and disappearing lattice domain." This idea has been stated before by van Arkel⁷ and Barrett⁸ and used recently by Dunn⁹ and Beck¹⁰ in discussing recrystallization phenomena. We believe from an energy standpoint alone, for instance, that a strained single crystal should be able to recrystallize readily to its own orientation through a nucleation and growth process. However, except for certain recovery processes,¹¹ which are very slow, recrystallization does not occur except through a change in orientation. A growing nucleus actually must build up a grain boundary energy and the amount of this increases with difference in orientation. Additional knowledge of the nature of the strain energy is needed, of course, for an understanding of this phenomenon even though such energy might be considered to reside as sub-boundary energy and be largely due to differences in orientation.^{12,13} Geometry of these sub-boundaries would be expected to be important. Geometrical relations might even provide the key to this phenomenon of orientation relations being so important to the movement of atoms from one lattice to another. On the other hand, part of the picture may be concerned merely with the rate at which atoms can leave one lattice and join another. This means that, with the same strain energy available, the nature of the boundary where atoms are moving may play a major role.

The importance of the role of orientation relationships for atomic movement also stands out for those cases where boundary energy and internal strain energy both favor the shifting of atoms. An example of this type is the strained island grain (Laue asterism), which appears to be relatively stable in a strain-free single crystal matrix of near twin orientation (see Burgers' report in *Nature* referred to by him).

A. J. SHALER*—My colleagues and I have also been doing some work on the surface energy of solid metals and we wish to assure Dr. Dunn and his collaborator that we fully appreciate the importance of their work. I should like to ask the authors if they have made any measurements of the angles formed at the intersection of the boundary with the free surface at the edges. In general, their edges were notched in the specimens shown, so that these measurements could probably not be made on them. The relation between the angles and the surface energies should be the same at these intersections as at interboundary intersections. The advantage in making such measurements would be that the boundary energy could be directly com-

pared with the surface energy of the metal (itself in the presence of hydrogen or argon). The paper by Udin, Shaler and Wulff which will be presented later shows a method of measuring directly the surface energy of the metal in the presence of its vapor or another gas. From those measurements and the measurements of the angles I am speaking of, we could then get absolute values of the grain-boundary energies.

C. G. DUNN—We observed one thing which has already made some of our next work on this problem much easier—it is the formation of grooves in the surface by thermal etching (reported also by Chalmers, King, and Shuttleworth in England for the case of silver). It seems to offer an ideal way of studying the positions of grain boundaries as well as this relationship between free surface and interboundary energies about which Dr. Shaler asked his question. I think Dr. Shaler is asking about the angle relationships of grooves at either the edge or on the large flat surface. We have measured no groove angles, but others are doing this. Our connection with this problem so far is to supply samples of silicon iron with known orientation relationships between grains. From the surface energy between the atmosphere and the metal and the groove angles, one can obtain the grain boundary energy for a particular grain boundary. If the energy of one grain boundary of our group could be determined in this way, then all our values for silicon iron could be put on an absolute basis. This we hope to do eventually. If the groove is not too near 180°, this technique may have pretty good accuracy. On the other hand if the dip is very shallow and the angle is near 180°, then I think this method would not be very accurate for determining every type of grain boundary.

Using the groove angles—if they can be measured—it should be possible to check the form of curve that we have obtained. To do this, two-grain groups suffice as specimens. You have a fixed orientation relationship for each two-grain group, and you determine γ for each configuration. If the grain boundary energy varies with orientation difference, this will cause the groove angles to vary also. Consequently, the variation of γ with orientation difference could be determined.

L. D. JAFFE—Dr. Dunn, with your techniques it seems it would be possible to control the orientation of the boundaries since they come out at about 90 and 180° angles. In any case you can adjust the orientations of the grains with respect to the boundaries. Are you planning any work in which you will simultaneously control the boundary orientations and the orientations of the grains?

C. G. DUNN—I am glad you asked

* *Nature* (1948) 162, 740.

* Massachusetts Institute of Technology.

about that. We are attempting to grow two grains from one end of the specimen in such a way that their boundary will be in a given crystallographic orientation. I think we have already succeeded in getting pretty good pseudo twins by this method. We maintain control of this direction pretty well if on subsequent annealing the motion of the boundary stays parallel to this line, otherwise control is lost. You cannot control all grain boundary orientation in three-grain groups because some have to change to establish the equilibrium angles. However, it might be possible to control one

boundary fairly well.

The other thing to do is to determine from prior data a configuration that should be fairly close to an equilibrium condition. It should be possible to grow a three-grain group near this configuration in order to obtain equilibrium conditions on a larger scale and perhaps more easily. I do not know whether you had that in mind, but it is a possibility.

References

7. A. E. van Arkel: *Rev. de Met.* (1936), 33.

8. C. S. Barrett: *Structure of Metals* (1943) 421, New York. McGraw-Hill.
9. C. G. Dunn: *Recrystallization Textures*. ASM Symp. on Cold Working of Metals (1948).
10. P. A. Beck: Private Communication.
11. C. G. Dunn: *Trans. AIME* (1946) 167, 373. *Met. Tech.*, Aug. 1946.
12. W. L. Bragg: *Proc. Phys. Soc.* (1940) 52, 105.
13. W. G. Burgers: Koninkl. Nederland. Akad. Wetenschap., *Proc.* (1947) 50, 452.

Influence of Composition on the Stress-corrosion Cracking of Some Copper-base Alloys

By D. H. THOMPSON and A. W. TRACY

DISCUSSION

(A. Wachler presiding)

E. A. ANDERSON*—At the outset, I note that you are using a humid atmosphere containing ammonia but that you make no reference to the variable of carbon dioxide content. Edmunds in his work in this laboratory found very marked effects on the rate of failure due to variations in carbon dioxide in the environment. This point is, of course, strongly related to the overall corrosion rate problem since the role of the carbon dioxide seems to be to permit the formation of hygroscopic salts which give a controlled moisture film on the specimen surface, which in turn seems to support the intergranular penetration more consistently than would otherwise occur.

(2) Your results with various copper binary systems are very striking. It is curious, however, that the time-to-failure minima all occur at percentages of the alloying element which are considerably below the solubility limits as given in the conventional equilibrium diagrams. If your theory regarding the presence of these impurities in some concentration in the grain boundaries is correct, then

either the existing diagrams are not accurate in the room temperature region, or there is a difference in solubility in the grain boundaries as compared with the grains. A study along these lines might be very revealing.

(3) The undesirable effect of silicon in copper calls to mind our own observations on the influence of silicon on the stress corrosion cracking resistance of alpha brass. In this case, silicon was found to have a very marked beneficial effect, particularly when a heat treatment capable of producing a grain boundary constituent was used. I should appreciate it if in the discussion of your paper this point should arise, you would attempt to clarify the difference between the copper-silicon binaries and the copper-zinc-silicon ternary alloys.

D. H. THOMPSON and A. W. TRACY (authors' reply)—(1) We have no data on the constancy of the carbon dioxide content of the air used for the test atmosphere but have believed that the normal carbon dioxide content of the air was as constant as could be obtained by using Edmunds' method of removing carbon dioxide from the air and then adding a measured quantity. In any event, the test atmosphere was the same for all specimens in a test run. We agree with Mr. Anderson that the carbon dioxide content is important in the formation

of a hygroscopic film on specimens.

(2) We can imagine that there could be a concentration of solute atoms at the grain boundaries which would be so small that present methods would not detect it even if it exceeded the solubility limit of the alloy. There could be somewhat greater solubility at the grain boundaries for an interstitial solute. There is a possibility that phosphorus dissolves in this way but we believe that none of the other solutes studied does. In our present studies we hope to find out something about conditions at the grain boundaries of some of the systems mentioned in the paper.

(3) Mr. Anderson points out that silicon brass, which has had a high temperature heat treatment followed by a quench, is highly resistant to stress-corrosion cracking. Although the test conditions used by Anderson* et al were different from our test conditions, it is noted that the silicon brasses which had not had the special heat treatment were less resistant to stress-corrosion cracking than copper containing approximately equal amounts of silicon.

G. R. GOHN†—Nonferrous metallurgists and particularly, materials engineers, have been accustomed to thinking

* The New Jersey Zinc Co. (of Pa.), Palmerton, Pa.

* Symposium on Stress-Corrosion Cracking of Metals. (1944), ASTM-AIME, p. 173.

† Bell Telephone Laboratories, Inc.

that copper-base alloys containing more than 85 pct copper were relatively free from spontaneous cracking under the combined effect of prolonged, high stress and corrosive attack. The data presented by the authors indicate that we must now reorient our thinking and consider that, under certain adverse conditions, copper and all copper alloys may be susceptible to stress-corrosion cracking.

For many years we have used the mercurous nitrate test as described in A.S.T.M. Designation B154 as a means of determining whether or not the residual stress in a fabricated copper-alloy part such as a rod, a tube or a manufactured piecepart was reduced to a safe level so that stress-corrosion cracking would not occur in service. Now obviously, as pointed out by Dix,* failure in this test is not caused by corrosion and hence the mercurous nitrate test leads to no understanding of stress-corrosion cracking. However, experience has indicated that fabricated parts similar to those which withstood 15 min. immersion in the mercurous nitrate test without failure, seldom failed in service; while those which did crack in the test frequently failed in service unless the residual stresses were reduced by subsequent annealing, or corrosive attack was prevented by the use of an appropriate protective finish. Tests made by Gohn and Arnold* on strip samples indicated that all of the common copper base alloys could be stressed in bending to values approximating the yield strength of the material without failure in the mercurous nitrate test and this finding correlates well with service observations. Only in the case of cylindrical and spherical parts, or screws and studs under high internal or external stresses, were stress-corrosion failures observed either in the laboratory or in service.

The findings of the authors that stress-corrosion will occur in copper and copper alloys stressed at values well below the yield strength when the corrosive agent is an atmosphere containing ammonia, water-vapor, and air is, therefore, of considerable significance and should greatly aid in the study and understanding of the mechanism of stress-corrosion cracking in copper and copper alloys. Their findings do, however, leave unanswered the relation between time-to-failure and service life. It would be interesting to know if the authors are in a position to evaluate their results in terms of expected service life.

D. H. THOMPSON and A. W. TRACY (authors' reply)—The paper describes a series of laboratory experiments designed to study fundamental causes and not intended to predict service failures. The fact that phosphorus-deoxidized copper will crack under specified

laboratory conditions does not in the least affect the probability of its cracking in service. Experience shows that the alloy does occasionally crack in service, but the event is rare indeed.

It appears that one of the necessary factors in service failures by stress-corrosion-cracking is that during cold work the alloy acquires a high internal stress, which is not relieved by subsequent creeping or relaxation. Such metal is prime for cracking. In general, phosphorus-deoxidized copper is not capable of maintaining such a residual stress and so it does not fail.

Mr. Gohn's remarks on the mercurous nitrate test cover the subject well. It is a test for the presence of internal stress in some alloys; it is not a research tool for work on stress-corrosion cracking.

H. L. BURGHOFF*—The authors have presented a large amount of data which are a most welcome addition to the available information on stress-corrosion cracking of copper alloys.

I should like to emphasize the point which they have brought out with regard to the rarity of stress-corrosion failures of phosphorus deoxidized copper. This class of material has enjoyed widespread use for many years and has a merited reputation for dependability. The only case of stress-corrosion cracking of copper in service which I definitely recall is that of a soft copper tube of small diameter. This sample was of deoxidized copper containing 0.027 pct phosphorus and had several transverse cracks which originated from the outer surface. These cracks were entirely intercrystalline in nature.

The authors mentioned the low yield point of annealed copper as making impossible the attainment of high internal stresses, thus accounting to a great degree for the scarcity of service failures of the stress-corrosion cracking type. However, such phosphorized copper is used in the cold worked condition for which the yield strength as conventionally defined is a high percentage of the tensile strength. Externally applied stresses can be high without significant deformation of the metal although residual internal stresses would be expected to be low because of the relatively low resistance of copper to stress relaxation. Stress-corrosion cracking of hard phosphorized copper is most certainly a rarity. Its extensive service record indicates great dependability in this respect.

The experiments on the effect of precipitation of iron phosphide in copper as described in the paper and summarized in Table 10 might have been more significant if the authors had used greater amounts of iron than 0.006 pct for the formation of iron phosphide with 0.024 pct phosphorus. As Fe_2P is the most likely combination of iron and phos-

phorus in copper, approximately 0.09 pct iron would be required to obtain the maximum precipitation effect with 0.024 pct phosphorus.

The test results presented for the copper-silicon series are interesting and worthy of special comment. A minimum of resistance to fracture in the ammonia atmosphere is indicated at about 1 pct silicon and work on a somewhat similar program in our laboratory is in agreement with this. The observation, however, cannot be transferred to prediction of actual service behavior of commercial silicon bronzes without consideration of other factors. For example, two important groups of silicon bronzes have nominal contents of 1.5 and 3 pct silicon respectively and their general service behavior when used as bolts does not at first glance confirm the authors' relationship. This may be due to their being used more in the cold worked state than in the annealed state, with the degree of working normally being greater in the case of the lower silicon content. The 3 pct silicon alloys, while being very serviceable, have shown a number of stress-corrosion cracking failures, whereas such failure of the 1.5 pct silicon alloys seems to be as much a rarity as in the case of copper. As far as laboratory stress-corrosion tests in ammonia atmosphere are concerned, our results on two silicon bronzes containing 1.5 and 3 pct silicon respectively and 1 pct zinc as a third element in each, indicate that the two materials will fracture in approximately the same time at a given applied stress when they are cold worked to the same level of hardness or tensile strength.

The occurrence of transcrystalline stress-corrosion cracks in alloys such as Arsenical Admiralty, as illustrated in the authors' Fig 13, is of importance in the proper diagnosis of service failures by cracking. There was a time not too long ago when transcrystalline cracks penetrating metal from a surface roughened by corrosion were considered direct evidence of corrosion fatigue. Undoubtedly the wrong conclusion has been reached in some instances on the basis of such evidence. It should not be inferred, however, that all cases of stress-corrosion cracking of such materials will be transcrystalline, for intercrystalline cracking may also be encountered in them.

Information on grain size and mechanical properties such as tensile strength and yield strength of the test material was not included in the paper. These factors may not have a great bearing on the trends which were developed, but they may be of significance in a more complete evaluation of stress-corrosion characteristics of these and other materials. It is to be hoped that the authors will tabulate them and add them to the discussion of their paper.

D. H. THOMPSON and A. W. TRACY—Dr. Burghoff points out that

* Symposium on Stress-Corrosion Cracking of Metals, ASTM-AIME (1944).

* Chase Brass and Copper Co.

the internal stress in cold-worked copper is relieved by stress relaxation and that internal stresses of the order of magnitude of the yield point therefore do not exist. Certainly it is agreed that copper rarely cracks in service. Does not the same mechanism operate in the case of silicon alloys? Our records show that service failures of cold-headed bolts containing 3 pct silicon were ended when a 1½ pct silicon alloy was substituted, paralleling the case Dr. Burghoff cites. We had ascribed this behavior to the ability of the lower silicon alloy to relax and relieve stresses both during cold heading and after installation.

The matter of iron and iron plus phosphorus requires additional work. Several heat-treatable alloys have been tested but evidence is generally lacking that precipitation or solution heat-treatments have an appreciable effect on the cracking rate of copper alloys.

The grain sizes and Rockwell hardnesses are given in Table 12. It will be observed that nearly all the grain sizes are between 0.010 and 0.040 mm.

The mechanical properties of the phosphorus alloys are given in Table 13. Samples were annealed for 1 hr at 500°C. The values are averages of two tests.

J. T. KEMP*—The paper by Messrs Thompson and Tracy is the latest in an important series on corrosion cracking. It follows in logical sequence the impressive group of reports presented at the AIME-ASTM symposium in 1944. In reading this paper it is well to look over the volume containing the earlier ones once more.

Two considerations appear to have been overlooked when one reviews these several papers with attention directed to the theory offered: 1. That the path of cracking, whether intergranular or transcrystalline, may be influenced by the structural history of the metal. 2. That the potential relationship, grain boundary to grain body, is probably inconstant, and that the intensity of anodic corrosion at the bottom of a crack may decline as the ohmic resistance of a lengthening circuit builds up.

Now the consensus of opinion regarding corrosion cracks that follow grain boundaries seems to be that such cracks are caused by localized action resulting in one way or another from precipitation or concentration of solute atoms in the grain boundary regions. It seems to be assumed that the susceptible metal was in structural equilibrium at the close of the last previous period of structural change due to the heat, that is, that the grains have been established, that the boundary precipitation or concentration has progressed to a condition approaching stability. Perhaps such conditions may be

* The American Brass Co., San Francisco, Calif.

Table 12 . . . Grain Size and Hardness of Specimens, Final Anneal 1 hour at 500°C

| Alloy No. | Alloy Addition Pct | Rockwell Hardness F | Grain Size Mm |
|-------------------|--------------------|---------------------|---------------|
| Zinc | | | |
| 8 | 0.98 | 35 | 0.035 |
| 10 | 10.03 | 51 | 0.035 |
| 11 | 20.01 | 60 | 0.035 |
| 12 | 29.82 | 64 | 0.038 |
| 14 | 39.88 | 74 | 0.025* |
| Phosphorus | | | |
| 4 | | 32 | 0.040 |
| 15 | 0.001 | 35 | 0.035 |
| 16 | 0.002 | 34 | 0.040 |
| 17 | 0.004 | 35 | 0.030 |
| 18 | 0.007 | 35 | 0.020 |
| 19 | 0.014 | 37 | 0.030 |
| 20 | 0.028 | 34 | 0.035 |
| 21 | 0.056 | 38 | 0.025 |
| 22 | 0.10 | 33 | 0.030 |
| 23 | 0.24 | 38 | 0.045 |
| 24 | 0.46 | 47 | 0.040 |
| 25 | 0.93 | 64 | 0.018 |
| Arsenic | | | |
| 4 | | 30 | 0.040 |
| 26 | 0.052 | 35 | 0.025 |
| 27 | 0.126 | 38 | 0.020 |
| 28 | 0.19 | 36 | 0.025 |
| 29 | 0.305 | 42 | 0.020 |
| 30 | 0.36 | 48 | 0.028 |
| 31 | 0.607 | 42 | 0.020 |
| 32 | 1.22 | 48 | 0.020 |
| Antimony | | | |
| 33 | 0.010 | 42 | 0.025 |
| 34 | 0.109 | 38 | 0.025 |
| 35 | 0.25 | 41 | 0.025 |
| 36 | 0.47 | 54 | 0.020 |
| 37 | 0.95 | 58 | 0.015 |
| Silicon | | | |
| 38 | 0.11 | 42 | 0.030 |
| 39 | 0.27 | 42 | 0.030 |
| 40 | 0.46 | 42 | 0.030 |
| 41 | 0.98 | 47 | 0.020 |
| 42 | 1.97 | 56 | 0.018 |
| 43 | 2.96 | 79 | 0.015 |
| 44 | 3.92 | 82 | 0.015 |
| Nickel | | | |
| 45 | 1.98 | 42 | 0.040-0.080 |
| 46 | 4.78 | 47 | 0.045-0.090 |
| 47 | 9.84 | 54 | 0.035* |
| 48 | 20.16 | 68 | 0.030† |
| 49 | 30.06 | 81 | 0.025‡ |
| Aluminum | | | |
| 50 | 0.09 | 35 | 0.028 |
| 51 | 0.24 | 40 | 0.025-0.045 |
| 52 | 0.51 | 42 | 0.025 |
| 53 | 1.03 | 56 | 0.025 |
| 54 | 1.98 | 57 | 0.022 |

* Alpha grains.

† Final anneal 700°C.

‡ Final anneal 750°C.

attained in standard laboratory operations, perhaps not. How certain can we be that more than a semblance of equilibrium has been reached in a recrystallized metal, that solute atoms have migrated from previous positions along previous grain boundaries to new positions along new grain boundaries in sufficient numbers to establish the potentials or the tensions indicated? A very considerable degree of mobility must be assumed to get the solute atoms or precipitates from place to place as new grains form in recrystallizing metal, and then to follow the boundaries as the grains grow. Is it not possible that solute atoms gathered in well established grain boundary regions, assuming that that is where these atoms do congregate, during one interval at annealing temperature may be left more or less in place during cold working and a subsequent interval at temperature, still occupying something of their original planar or zonal positions in the mass and lying across the new grains as much as along the new boundaries? If this were so, it would seem plausible to assume that the residual arrangements of solute atoms, or precipitates, would cause lattice strain within crystals and so offer favorable paths for transcrystalline cracks.

Micrographs of transcrystalline corrosion cracks, however, do not often suggest that the crack follows the polygonal alignment of former grain boundaries very faithfully. Perhaps a residual planar arrangement of residual solute in one crystal at or close to the exposed surface is enough to establish a notch in a stressed metal. The notch effect may predominate once the crack is established. It is not to be expected that the residue of any mesh work of grain boundaries would retain sharp definition through later structural changes. The traces of old boundary systems should disappear as later structures develop. Yet the persistence of coring in the wrought nickel-silvers is an evidence of the persistence of inhomogeneities in alpha copper-base alloys.

As to the electrical circuits and the progress of inter-granular cracks to considerable depth, say through and below the second layer of grains, it may be asked whether microcurrents do or do not obey the general laws governing the flow of macro-currents. Presumably they do. It must be borne in mind that there is an analogy between the flow of current in three dimensional conductors, that is, local currents in a mass of conducting metal, and the flow in restricted circuits that can be measured with precision. Specifically, it would appear that the grain boundary-grain body potential difference could operate only to promote corrosion in a crack to a depth at which the resistance of the lengthening circuit (up through the electrolytic, over the edges to whatever cathodic areas lay adjacent and back through the mass of

Table 13 . . . Mechanical Properties of Copper-phosphorus Alloys

Final Anneal 1 hour at 500°C

| Alloy No. | P Pct | Yield Point 0.50 Pct Psi | Tensile Strength Psi | Elongation Pct in 2 In. |
|-----------|-------|--------------------------|----------------------|-------------------------|
| 5 | | 8,200 | 34,000 | 48.5 |
| 17 | 0.004 | 7,100 | 33,600 | 49.0 |
| 18 | 0.007 | 6,800 | 33,300 | 50.0 |
| 19 | 0.014 | 7,200 | 34,100 | 50.0 |
| 20 | 0.028 | 6,200 | 33,600 | 48.0 |
| 21 | 0.056 | 7,800 | 35,400 | 48.0 |
| 22 | 0.10 | 6,800 | 35,000 | 50.0 |
| 23 | 0.24 | 7,300 | 36,600 | 48.0 |
| 24 | 0.46 | 8,600 | 39,000 | 48.0 |
| 25 | 0.93 | 13,300 | 43,900 | 44.0 |

metal) would reduce the active current to ineffectual values.

A simple anode to cathode circuit may exist only at the inception of a corrosion crack. As soon as appreciable depth was attained there would be modifying potential relationships between the more intensely anodic metal at the bottom of the crack and the less intensely anodic walls until the crack had widened by the removal of enough of the anodic wall metal to reveal cathodic crystal body. When this occurs, if indeed there has been no neutral point at which opposing emf's within the crack stop attack on the walls, the simple anode to cathode circuit can become re-established. Other modifying factors, chemical reactions, polarization, adsorption, and others, may all assert themselves in one or another order or intensity, perhaps inconstantly, to modify the progress of the crack.

Again, cracks that are established by potential differentials may propagate in response to other forces such as stress concentration at the sharp bottom of the notch. In any case, there should be no sharp transition from one to the other regardless of the time rate of progress in any system not subject to fluctuating external influences.

There will be many special cases—perhaps every one observed will be special in some sense—and the wide mouthed crack mentioned above is one.

No potential differences within grains have been reported in our series of corrosion-cracking papers. They would be difficult to identify and measure. Such potential differences are conceivable and have their parallels in other physics. If boundary-to-body potentials exist because of boundary precipitations or concentrations, then a similar potential should exist within a crystal if an interior concentration existed and came through to an exposed surface.

The whole subject becomes more involved the more it is studied. Perhaps the whole has become so wrapped up in words that only a clear sighted prophet can disentangle facts from fancies. May such a one emerge from the laboratories soon and reduce the laws of corrosion cracking to simple language.

D. H. THOMPSON and A. W. TRACY—In the alpha solid solutions of copper alloys, remarks about equilibrium, submicroscopical precipitation, or grain boundary concentration are all pure supposition. Perhaps the observed effects are associated with such causes; as yet proof is lacking.

In some aluminum alloys the conditions can be seen under the microscope. In his 1940 Institute of Metals Lecture,⁴ Dix shows a micrograph (Fig 2) in which

over-aging of an aluminum alloy containing 1.6 pct copper has resulted in a fine, randomly distributed precipitate that has agglomerated at the grain boundaries and left a solute-depleted zone. As Dix states in the present discussion, either the depleted zone or the precipitate may be the anode that starts stress-corrosion cracking. It is obvious, however, that the atomic movement necessary to form this precipitate and depleted zone is small, and that a solution heat-treatment would readily redissolve the precipitate. Thus, a precipitate can form and be redissolved with only small atomic movements.

In the case of copper alloys there is reason to believe that small amounts of impurities may be swept along ahead of an advancing grain boundary during grain growth. Presumably, this can occur because there is more room, more vacant lattice sites in the discontinuity of the boundary. If this mechanism takes place no precipitation heat treatment is necessary, foreign atoms are concentrated at the grain boundaries by a simple anneal. It is quite possible that the same mechanism explains why some solute atoms inhibit grain growth.

As to the lengthening current path in the deepening crack, an answer can be only conjecture, but certainly this process does not stifle the attack even in the absence of stress. In the presence of stress it has been shown (unpublished work, The American Brass Co.) that the rate of crack propagation is accelerated quite rapidly. Presumably this is the effect of the ever-increasing stress on the notch at the bottom of the crack. Mr. Kemp's idea that the walls of the crack may become cathodic and reduce the length of the current path to the corroding anodic area at the base of the crack is logical. At any rate, it is certain that if the resistance of the circuit increases, that is not the primary factor in determining the rate of crack propagation.

E. H. DIX*—The authors are to be congratulated upon a very nice piece of work which adds tremendously to our knowledge of the subject of stress corrosion cracking. I was a little bit intrigued by the introduction of the paper in which the authors refer to season-cracking of brass as being associated with internal residual stresses and stress corrosion cracking as a proper terminology when the stress is from an externally applied load. I suppose some of us who have been worrying about intergranular corrosion for a good many years do draw a distinction between ordinary intergranu-

lar penetration which occurs fairly general along the surface and not too deep in most cases, in comparison with stress corrosion cracking of a material that is susceptible to intergranular corrosion, but where the crack goes through fairly rapidly because of the applied tension stress.

There is reference here to the theory that we proposed some time back, but I think there is more emphasis put on the question of whether or not precipitation occurs than we had intended. In aluminum alloys, especially the aluminum-copper system, I think we have demonstrated pretty conclusively that the anodic condition at the grain boundaries is caused by precipitation. In that case the aluminum-copper compound is precipitated, but it leaves a depleted zone along the grain boundaries which is anodic to the remainder of the grain. In some other systems, in the aluminum alloys the precipitate is anodic. That is particularly true in the aluminum-base magnesium alloys. They are of interest because transgranular as well as intergranular cracking occurs and the transgranular cracking follows slip planes along which there is precipitated constituent. I would like to be permitted to read the conclusion from the paper since I subscribe to it 100 pct, and really it is about all that we tried to put out as a generalized theory:

"Any of these conditions makes the grain boundary region anodic to the grain bodies. Localized corrosion is accelerated and grain boundary penetration ensues. The presence of a tensile stress still further accelerates penetration by opening cracks and forming highly stressed notches."

D. H. THOMPSON and A. W. TRACY—The definitions of season cracking and stress-corrosion cracking are used by the ASTM³ and The Corrosion Handbook.²

Attack in the absence of stress cannot, of course, be called stress-corrosion cracking nor does it have the appearance of cracking. The paper refers to it only as intergranular penetration.

We agree entirely with the quoted conclusion, but we are still eager to find the cause of the shift in potential of the grain boundary in the anodic direction in copper alloys.

The authors are grateful to the several discussers for their valuable contributions to the paper and to the subject itself.

The subject can be summarized by saying that highly localized corrosion cells result from the chemical or metallurgical condition of the metal in a selected environment. Stress accelerates the failure. The paper shows how the composition of the metal may have a large effect on the formation of such cells.

* Aluminum Co. of America.

Oxide Films Formed on Metals and Binary Alloys. An Electron Diffraction Study

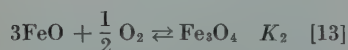
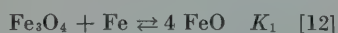
By J. W. HICKMAN

DISCUSSION

(A. Wachter presiding)

A. SQUIRE*—I am afraid I missed the explanation of the significance of Fig 3. I do not quite understand what the effect of the thickness of the film is, specifically your interpretation of the effect on the transformation of the oxide, from one type to another. In regard to tungsten copper materials, that is not a true alloy. It is just a mixture of tungsten and copper. Is there a real significance in trying to determine thermodynamic data in a mixture of that sort?

E. A. GULBRANSEN† (replying for author)—Fig 3 to which you refer, shows that the Fe_3O_4 to FeO transformation is a function of the oxide thickness. An oxide film of 4000 Å in thickness shows a transformation temperature of 500 to 550°C while an oxide film of 428 Å shows a transformation temperature of 350 to 450°C. The temperature for the thicker film is approaching the normal value of 580°C. We have noted this effect several years ago and have checked the experimental evidence several ways. I would like to interpret this phenomenon as follows: Two equations are involved in the Fe_3O_4 - FeO equilibria.



The free energy data for these reactions are well known. The logarithm of the equilibrium constants K_1 and K_2 for the two reactions are given as a function of temperature in Table 6:

Table 6 . . . Equilibrium Constants
 $\text{FeO-Fe}_3\text{O}_4$

| t°C | [12] log K_1 | [13] log K_2 |
|-----|-------------------|-------------------|
| 400 | -0.63 | 17.63 |
| 450 | -0.43 | 16.00 |
| 500 | -0.22 | 14.56 |
| 550 | -0.04 | 13.30 |
| 600 | +0.09 | 12.21 |

* Westinghouse Electric Corporation.

† Westinghouse Research Laboratories.

Eq 13 is thermodynamically possible even in oxygen pressures found in the best of high vacua at all of the temperatures shown. Eq 12, however, is thermodynamically feasible only below 570–580°C and not above. The temperature dependence of log K_1 is small and even at a temperature of 400°C log K_1 is -0.63. This is equivalent to a free energy change of 1940 calories per mol. At temperatures of 450 and 500°C the energy changes are $\frac{2}{3}$ and $\frac{1}{3}$ of the value calculated at 400°C. One may say then that the $\text{FeO-Fe}_3\text{O}_4$ equilibria is rather unique in the flatness of the free energy curve and that small energy changes associated with thin films of matter may explain the change in transformation temperature.

In regard to the question about the use of tungsten-copper materials, Dr. Hickman mentions on p. 11, of the paper the fact the metals do not form a real binary alloy and that the reactions studied may be indicative of those that obtain with a mechanical mixture of these metals.

S. E. MADDIGAN*—I will have to apologize to Mr. Gulbransen. In discussing the oxide films formed on iron he has pointed out that the transformation temperature for polymorphic transformations within these films seems to depend upon film thickness. His thermodynamic explanation for this is not quite clear to me. Although I have not had an opportunity to check the relative lattice parameters for iron and the oxides in the films, I believe that a suitable explanation can be provided by correlating crystal geometry and thermodynamic potentials. It is well known that for thin films the curves for thermodynamic potential may be displaced if suitable geometric relations exist between the substructure and the material of the deposited film, or in the present instance the chemically formed film. For instance, if one deposits a film of a polymorphic material on a suitable substructure such that the space group of the substructure has a close geometric relationship to that of one phase of the polymorphic material, and if the lattice spacings concerned

differ by only 10 to 15 pct, then one finds that the transformation temperature of the polymorphic transition is shifted quite appreciably from that normally found for gross samples of the polymorphic material. I would suggest that something of this nature is occurring in the present instance. In the first thin films mentioned by Dr. Gulbransen, from the thickness one would expect the substructure of the iron to have quite an influence on the overall thermodynamic potential. On the other hand for later thicknesses of the order of 4,000 Å, the forces operating within the volume of the oxide itself assumed the major role and the transformation temperature is then approximately the normal value, so that the film assumes the structure of the normal stable phase.

E. A. GULBRANSEN—I find myself in complete agreement with Dr. Maddigan. My previous remarks were made in order to show that small energy differences could explain the observed phenomena. The lack of matching of the two lattices may account for this difference in energy noted.

R. I. JAFFEE*—I would like to ask if these alloys, particularly those containing chromium and molybdenum and tungsten were analyzed chemically. It seems to me there is a very good possibility of losing a lot of chromium in the preparation from the powders due to the volatilization.

E. A. GULBRANSEN—Dr. Hickman does not say that the alloys have been analyzed chemically. They were prepared at our Bloomfield Lamp Division where many alloys of this type are prepared. The alloys, in both cases, were prepared by slurring in carbon tetrachloride, the molybdenum or tungsten powder together with the chromium metal powder and also the lubricant. The resulting mixture was dried and pressed into compacts which were subsequently prefired and then sintered in hydrogen atmosphere. According to the ASM Handbook 1948 Edition, both the chromium-

* British Columbia Research Council.

* Battelle Memorial Institute.

molybdenum and the chromium-tungsten systems show a solid solution equilibrium diagram.

R. I. JAFFEE—In connection with the chromium tungsten alloy, we once had occasion to try to make a 10 pct Cr-90 pct W. In an attempt to get the alloy dense it was necessary to sinter at higher and higher temperatures until finally after a dense product was obtained it was found by spectroscopic examination that there was not any chromium left as it had volatilized away. Chromium is very difficult to alloy with a high melting material such as tungsten by straight

sintering techniques.

A. SQUIRE—I might be able to shed a little light on that. Dr. Lustman of our Research Laboratories has done some rather extensive work on the preparation of molybdenum-chromium alloys. I believe one of his methods at least was actually to chromize the material, and he obtained molybdenum-chromium alloys in the entire range. On the other hand, I am almost positive that he has obtained a complete series of alloys by mixing chromium powder with molybdenum powder and sintering at a high temperature.

R. I. JAFFEE—I was referring to tungsten-chromium alloys particularly. It is necessary to get the alloy to a much higher temperature with tungsten-chromium, so that the vapor pressure of chromium is appreciably higher than it would be with molybdenum-chromium alloys.

E. A. GULBRANSEN—I have contacted our Bloomfield Works relative to Dr. Jaffee's question. They do not indicate that they had any great difficulty with the volatilization of chromium.

Magnesium-lithium Base Alloys—Preparation, Fabrication, and General Characteristics

By J. H. JACKSON, P. D. FROST, A. C. LOONAM, L. W. EASTWOOD, and C. H. LCRIG

DISCUSSION

(L. D. Jaffe presiding)

R. S. BUSK*—I wish first to congratulate the authors of this paper both for the work done and the presentation of that work. We have also been working on this type of alloy development, but any technical contribution I might have is better reserved for a separate paper which is planned in the near future.

However, I would like to insert a word of caution. The alloys described in this paper are still very much in the laboratory stage. There still remains the quite vexing problem of property stability at slightly elevated temperatures which must be solved before the properties quoted can be effectively utilized. These alloys are extremely interesting and I am confident that the problems can be solved. However, the present existence of those problems must not be overlooked.

I have one question with regard to the work-hardening test. If the work hardenability of magnesium is compared to aluminum using a more standard test such as the Meyer Analysis the magnesium is found to work harden the more rapidly. Is the test developed for this work truly a work-hardening test or a measure of something else?

J. H. JACKSON (authors' reply)—I am sure we appreciate the comments of Mr. Busk and we are pleased that the Dow Chemical Co. has also undertaken work in this field. It is a big field. We, of course, are continuing our research for the Navy Bureau of Aeronautics, since, as clearly shown in the paper, the alloys are not completely developed.

With regard to Mr. Busk's comments on the relative work-hardenability of aluminum and magnesium, the comparison we cited in the paper was intended merely to show that the results obtained by our method of testing were independent of the yield strength of the materials. We believe that this test method afforded a rough indication of the work-hardenability of the magnesium-lithium base alloys. It is not known whether this method affords greater or less accuracy than the Meyer Process, which is based upon a hardness-test impression. It is quite possible, since work-hardenability is a function of metal purity, that our results, obtained for commercial aluminum and magnesium, would be different if high-purity metals had been used.

A. C. LOONAM—Lithium has some very interesting effects on magnesium. The paper showed that even small percentages increased ductility. These small amounts changed the axial ratio of the

hexagonal magnesium from 1.624 in the pure metal to 1.606 in the saturated alpha solution, a value close to that of titanium, which has a ratio of 1.601. You will recall an article in the January, 1949, issue of the *Journal of Metals* where it was stated that titanium can be cold-rolled over 90 pct without any significant edge cracking. At 4.9 or 5 pct lithium, a change begins in crystal structure—from a hexagonal close packed to body centered cubic. There are two phases over a short range of lithium content, but at 10 pct the structure becomes completely cubic. The melting points of alloys in this range of lithium content are relatively high. Alloys even up to the six ratio have melting points above 500°C; this represents a relatively small reduction in melting point from pure magnesium itself. The magnesium-lithium system has a number of very interesting characteristics. This is only a very small part of the story.

J. H. JACKSON—I would like to remind you that Mr. Loonam is one of the authors of this paper, and the fact is that this work is based on many of his ideas. I am sure we appreciate his additional comments in this discussion.

R. LEITER*—I am interested in Fig 19 in which Mr. Jackson compares

* Dow Chemical Co., Midland, Mich.

* Philadelphia, Pa.

strength properties of various alloys after correcting for differences in weight with aluminum as the base. I have been close to the application of stainless steel in light weight structures and this chart appears to me not quite to do justice to stainless steel, particularly in the comparison with 24S-T4 and 75S-T6 aluminum alloy and SAE 1040 steel. For SAE 1040 steel to show up so well it must be in the quenched and drawn condition and the draw must be fairly low. The properties of the aluminum alloys appear to be typical rather than minimum values. The stainless steel properties as shown in the chart are fairly typical of type 301 in $\frac{1}{2}$ hard temper. However, the $\frac{3}{4}$ hard temper is about the equal of 24ST4 and full hard temper is superior to this aluminum alloy.

J. H. JACKSON—Mr. Leiter's remarks are well taken especially with regard to the comparison between stainless steel and 24S-T4. Table 11 gives the typical and minimum properties based on the most recent available data.

The typical property data for stainless steel shown in this tabulation were supplied by Mr. Leiter as being typical of

Table 11 . . . Typical and Minimum Properties

| Material | Yield Strength, psi | | | | Tensile Strength, psi | | | |
|--------------------------------------|---------------------|---------|--|---------|-----------------------|---------|--|---------|
| | Actual | | Compared to 24ST on a Strength to Weight Basis | | Actual | | Compared to 24ST on a Strength to Weight Basis | |
| | Typical | Minimum | Typical | Minimum | Typical | Minimum | Typical | Minimum |
| 24S-T4 bare | 48,000 | | 48,000 | | 68,000 | | 68,000 | |
| 24S-T4 clad | 42,000 | | 42,000 | | 64,000 | | 64,000 | |
| 75ST bare | 72,000 | | 73,000 | | 82,000 | | 83,000 | |
| 75ST clad | 67,000 | | 68,000 | | 76,000 | | 77,000 | |
| Stainless (Type 301) $\frac{1}{2}$ H | 123,000 | 110,000 | 43,000 | 39,000 | 165,000 | 150,000 | 58,000 | 53,000 |
| Stainless (Type 301) $\frac{3}{4}$ H | 145,000 | 135,000 | 51,000 | 47,000 | 185,000 | 175,000 | 65,000 | 61,000 |
| Stainless (Type 301) FH | 152,000 | 140,000 | 53,000 | 49,000 | 195,000 | 185,000 | 68,000 | 65,000 |

Budd experience. The typical data for the aluminum alloys were obtained from the publications of the Aluminum Co. of America. The data which we used originally in constructing Fig 19 were taken from the National Bureau of Standards Circular No. C147.

The relative properties shown in Fig 19 for SAE 1040 steel were for the quenched and drawn condition, the drawing temperature being about 600°F. The relative properties shown for the

stainless steel were for the $\frac{1}{2}$ -hard condition. In the $\frac{3}{4}$ -hard condition the relative properties of the stainless steel would be about equal to those of 24S-T4 but inferior to those of 75S-T6.

We wish to point out that the purpose of Fig 19 in the paper was to indicate that the magnesium-lithium alloys are comparable on a strength to weight basis with the aluminum alloy 75ST and superior on this basis to the aluminum alloy 24ST and to stainless steel Type 301

Hydrogen in Aluminum

By Y. DARDEL

DISCUSSION

(L. D. Jaffe and D. W. Smith presiding)

R. EBORALL*—The determination of the hydrogen content of aluminum alloys is of considerable technical value, particularly in the study of casting and welding processes, and any reliable method for its determination is to be welcomed, particularly if it is simple in operation and utilizes techniques which are available in any laboratory.

Modern vacuum hot extraction methods have proved very suitable for the determination of hydrogen in aluminum,^{21,22} and not only are highly reproducible results obtained by any one laboratory but there is quite good agreement between different laboratories using very different conditions of extraction.²³ Success depends upon good vacuum tech-

nique and upon extreme care in the preparation of the surface. It is standard practice to use a surface turned without lubricant—although other methods, if standardized, may be perfectly satisfactory—and to avoid touching the surface by hand at all. Under these conditions the contribution of the surface to the quantity of hydrogen obtained is constant for all practical purposes. As an illustration of this constancy, and of the reproducibility of the method generally, it may be stated that in these laboratories duplicate hydrogen determinations, even on material as thin as 0.125 in., for which the surface correction is about 0.08 cm³ per 100 g, generally agree within 0.01 cm³ per 100 g. Ordinary commercial wrought materials in this country commonly run from 0.2 to 0.5 cm³ per 100 g of hydrogen, except for high magnesium alloys which may contain rather more, so that for ordinary hydrogen determinations the method has more than adequate accuracy.

I have made this point about accuracy at some length, because Mr. Dardel emphasizes rather strongly the errors to which the work of Ransley and myself

may have been subject from variations in "surface" gas. Nevertheless, we did not claim any particular accuracy for the determinations of solid solubility, which were of a preliminary kind and a very small part of an extensive program. In fact we said: "The results do little more than indicate the order of magnitude of the solubility, since it is so small that the errors inherent in the method become serious."* Now that a series of accurate determinations has been made by Ransley and Neufeld,²⁴ there seems no reason to be dissatisfied with our earlier preliminary results.

The validity of the hydrogen contents determined by vacuum extraction receives confirmation, if any is needed, from observations obtained with a simple method for estimating hydrogen in solid wrought metal, which has been developed by my colleague A. J. Swain.²⁵

* The method referred to consisted of holding specimens in hydrogen without prior degassing, and subsequently measuring the hydrogen content. The greatest single potential source of error, in the light of later experience, was probably the formation of voids due to some of the hydrogen originally present coming out of solution at inclusions.

* Head of General Metallurgy Section, British Non-Ferrous Metals Research Association, London, England.

²¹ References not in the paper are at the end of discussion.

The principle of this method, which should be applicable to most of the aluminum engineering alloys, is to heat a thin piece of the metal for a short time in a dichromate bath at a temperature about midway between solidus and liquidus. Blisters are formed, the volume of which is a measure of the hydrogen content. It turns out that the pressure in the blisters, calculated from the known gas contents of the materials used for calibration, is about 1.1 atm. at the test temperature. The hydrogen can thus be converted into blisters which anyone can see for himself. The same sort of thing happens in castings;^{24,26} one can measure the density and find the "percentage voids" and one can measure the hydrogen content: on the average, for sand castings, a pressure between 1 and 2 atm. in the voids is obtained.

In the discussion, contained in his penultimate section, Dardel states that the values found by methods other than his own, including the vacuum hot extraction method, are greater than those which correspond to the solubility (in the solid at the melting point and at atmospheric pressure). That is commonly so. He concludes that the bulk of the hydrogen extracted therefore necessarily comes from the surface layers. That is nonsense. Some of it does of course—for our own technique we have measured the quantity and allow for it. But in a casting gas may be present in pinholes as well as in solid solution. In wrought metal it may be present in solid solution at "internal pressures" far greater than atmospheric: the metal can, and frequently does, absorb hydrogen in the solid state by the reaction with water vapor,²¹ which has ample energy,²⁷ and, moreover, the hydrogen present in pinholes in a gassy casting may be forced into solution during hot working. There are no doubt other ways in which extra hydrogen can be accommodated.

Dardel quotes Kljatschko and others to the effect that the metal is riddled by channels, increasing its surface area, and that gas is obtained from this extra surface. I thought we had disposed of this point successfully,²⁸ and do not wish to go over the same ground again. Klyachko's ideas are contrary to classical gas-metal theory and are based upon his colloidal or micellar theory of metals which is incompatible with the generally accepted one (that is, according to Klyachko's theory a metal is not truly crystalline). Tamman and Brede-meier's results, adduced in support of Klyachko, are very extraordinary; if one is to believe them, any metal is permeable throughout to large dye molecules. Since sound metals including aluminum have no detectable permeability to inert gases including helium,^{29,30,31} I suggest that the results need not be taken too seriously. Of course, if the metal contains continuous shrinkage porosity, or severe lamination owing to cold shutting, bad extrusion

practice or the like, that is a different matter.

Incidentally the author misrepresents Ransley and myself²¹ when he heads his Table 1 "Amount of Adsorbed and Dissolved Hydrogen," and continues throughout to write of "adsorbed hydrogen"²² when referring to our work. It is true that alumina formed at low temperatures is highly adsorptive, and it may be that the alumina surface film contains adsorbed hydrogen which is subsequently extracted, but we would prefer to think (and in this we agree with Klyachko) that the "surface hydrogen" is produced on heating the specimen, by the reaction of adsorbed water with the metal.

Mr. Dardel's method for determining hydrogen contents is of great ingenuity, and has the advantage that the apparatus is extremely simple. It is not however an absolute method, since it depends in the first instance upon the solubility of hydrogen in the liquid metal, which must be determined by some other method. For this, a number of published results have been averaged. In Fig 1 of the paper, representing some of the data available, the scatter is not very obvious; however, actual results at just above the melting point of aluminum are highly discordant. At 700°C they range from 0.08 cm³ per 100 g (Röntgen and Braun) to 0.95 cm³ per 100 g (Baukloh and Oesterlen); there is thus an uncertainty represented by a factor of 12, and this must be reflected in the values for hydrogen content obtained by Dardel's method. If the results of the more recent and very careful liquid solubility determinations of Ransley and Neufeld be accepted, the highest of these figures is correct and the equation used by the author yields results over three times too low.

If the results reported in the paper are multiplied by three, they accord quite well with experience. Thus in Table 4, giving the amounts of dissolved hydrogen after casting, alloys *A* and *B*, which were directionally solidified but from gassy melts, would have hydrogen contents of 0.19 and 0.16 cm³ per 100 g respectively, whereas *C*, which contains gas porosity, would have 0.38 cm³ per 100 g. These figures are entirely reasonable.

It seems rash to assume, however, that the hydrogen contents of alloys *A* and *B* are equal to the solid solubility. There may be slight supersaturation during solidification, and bubbles of gas may be trapped by the advancing crystals; only if these effects could be proved absent could the figures be accepted as representing the solid solubility. However, to return from the results to the method itself, there is a limit above which it is impossible to measure the hydrogen content of solid metal by this method; for if the hydrogen content exceeds the solubility in the liquid at the melting point, and if Mr. Dardel's assumptions are correct, the excess will boil off during melting before the pressure reading is taken. This

may not be a very serious limitation in practice, however, since such high figures (over approximately 0.69 cm³ per 100 g²⁴ are seldom encountered.

There are also further difficulties. One concerns the nucleation of a bubble. The author attempts to show that there is no nucleation difficulty; this may be true in some instances, but the experiments reported on 99.99 pct aluminum suggest that it is not always so. We do know that, in melts of commercial alloys, primary particles of one kind or another are generally present at temperatures well above the melting point; it has been possible to concentrate them with a centrifuge so that they are readily visible under the microscope.³² With high purity alloys, or even, it may be, with ordinary alloys without certain additions or impurities, these particles may not be present, and nucleation may accordingly present an obstacle to the formation of bubbles.

Another possible source of error is the possible gain or loss of hydrogen from the surface, before the pressure reading is taken. The author assumes that the metal is protected by an impermeable alumina film. That may well be true for many alloys, but no check appears to have been made on it. For some alloys, however, particularly those with high magnesium, the assumption appears of very doubtful validity, since a magnesia film may be formed and this is not likely to have a protective effect.

In short, I think this is an interesting and potentially valuable method, but that not the slightest reliance can be placed on the figures so far reported.

I should like to see the method thoroughly tried out by making a series of estimations, but using the latest liquid solubility data,³¹ and comparing the results with those obtained on the same materials by vacuum extraction. If this is not feasible, a more direct evaluation of the possible sources of error should be made.

There is great scope for a really good method of estimating rapidly the hydrogen content of molten aluminum alloys, for foundry control purposes. The ordinary Straub-Pfeiffer reduced pressure test (the author's "vacuum sample") with the 1 mm or the pressure normally used, is as the author points out, very much too sensitive for practical purposes. For a good many years we have used this test in these laboratories with a pressure of 20–60 mm of mercury, for aluminum and magnesium base alloys; actually we recommended the use of such pressures in a report issued to our member firms in 1941. At this pressure the test gives a very useful rough measure of the hydrogen content of the melt, but does not give a quantitative result (unless density measurements are subsequently made). Dardel's method on the other hand, provided it can be established on a sound basis, is ideal for this kind of purpose. It is simple,

rapid and gives a quantitative result. The apparatus, like that for the reduced pressure test, could be made robust and easily portable, so that it could be moved around a large foundry to furnaces or casting machines, to take samples at any stage in the melting and casting process and give the answer on the spot. But that answer needs to be the correct one.

M. B. BEVER*—The author finds by the method described in this paper that solid aluminum just under the melting point dissolves 0.058 cc of hydrogen in 100 g of metal. Recently Ransley and Neufeld²⁴ published solubility data for hydrogen and aluminum that were measured by a very careful equilibrium method. These authors found a hydrogen solubility of 0.036 cc in 100 g of aluminum just below its melting point.

In place of an exhaustive critical evaluation of the method described in this paper, attention will be called only to two major factors. These factors seem of such an important nature as to transcend any conclusions drawn from a statistical analysis of the experimental results. In this connection it should be emphasized that the two factors to be discussed oppose each other and under favorable conditions may partly cancel out in the resulting value of the hydrogen content.

In the first place, a marked weakness of the method is its inability to distinguish between different gases since the assumption that aluminum evolves only hydrogen is probably less well founded than the author believes. Secondly, it is inescapable that surface tension inhibits the formation of gas bubbles as Brower and Larsen³³ have shown quantitatively for the evolution of carbon monoxide from liquid steel. The presence of nuclei reduces the inhibiting effect of surface tension but does so in an unpredictable manner which cannot be reproducible under all possible conditions. In view of uncertainties such as these it seems that results obtained by the method suggested in this paper do not lend themselves to a rigorous analysis.

C. E. RANSLEY† and N. D. G. MOUNTFORD†—We have read this paper and also Dardel's previous one,¹⁹ with some care, since the subject is one with which we are closely concerned. The method he suggests for the measurement of the hydrogen content of aluminum and aluminum alloys is simple in concept, and if capable of giving reproducible and accurate results would have attractive possibilities for foundry control work. Since the publication of this paper therefore, we have constructed an apparatus similar to that described by Dardel and have carried out some experiments to determine what relation exists between

the true hydrogen content of a bath of molten metal and the value predicted by the author's bubble-pressure method. The results we have obtained are of some interest, and we would like to take this opportunity of presenting them. We may say now that we believe that the method proposed by the author is open to some criticism on fundamental grounds, and that our experiments demonstrate this. However, we have admittedly carried out only a limited number of tests, and we would welcome any comment Mr. Dardel has to make on our interpretation of them.

Before giving these results, there is one point we would like to emphasize. The method is based upon the assumption that the first bubble is formed in the liquid metal when the external pressure is reduced until it is equal to, or perhaps a little less than, the "internal pressure" of hydrogen in the melt. The value predicted for the gas-content will thus be a direct function of the value of the solubility of hydrogen in the metal at the temperature of test. The author has taken the mean value of solubility from the early published data (ignoring, however, the results of Baukloh and Oesterlen³ and Baukloh and Redjali¹³) and has derived his equations and constructed his nomograms on the assumption that these data are reliable. They are, in fact, considerably in error, particularly at the lower temperatures, which are the most important from the practical point of view. In these Laboratories we have recently²⁴ remeasured the solubility of hydrogen in liquid aluminum by an orthodox procedure and have established values which are considerably higher than those previously accepted; since the publication of our paper we have confirmed these values by an independent method, details of which we hope to publish shortly. We find that the solubility at 700°C, for example, is 0.92 cc per 100 g, whereas the value assumed by the author for this temperature is only 0.27 cc per 100 g. In other words, the values of gas-content calculated by Mr. Dardel (assuming that the deduction is otherwise valid) are wrong by a factor of more than 3. It is quite obvious, indeed, that the gas contents he quotes, that is, those given for duralumin, in his first paper, are far too low, since they are much less than the values obtained by hot-extraction measurements; the latter are now established on a firm basis and yield results in good arithmetic agreement with porosity values. We do not want to stress this point any further in the present contribution, since we have already dealt with it in the discussion of our recent paper.²⁴ We would like to make it clear, however, that we consider the values of solid solubility deduced by Mr. Dardel to be quite without significance. It is true that they are of the right order, but that is due entirely to a fortuitous combination of

circumstances.

The bubble-pressure apparatus we have constructed is very similar to that described in the paper. The vacuum chamber is exhausted by means of a rotary oil pump and the pumping line arranged so that the pressure can be reduced at a reproducible speed, that is, to 380 mm in 15 sec and to a limiting pressure of about 5 mm in 30 sec. The temperature of the metal sample is measured by means of a thermocouple inserted into a re-entrant tube in the base of the cast-iron crucible; we have kept this at about 700°C in all the tests we have so far carried out.

We used 30 lb charges of metal melted in a gas furnace for our experiments. When commencing a bubble-pressure test, a sample of the melt was taken in a small ladle and some metal poured into the crucible in the apparatus, which was preheated to the appropriate temperature; the remainder of the metal in the ladle was then cast into a chill mold to form a sample suitable for subsequent measurement of the gas-content by hot-extraction. Two commercial grades of aluminum, 99.2 and 99.8 pct, have been investigated and the results of the various measurements are summarized in Fig 9 and 10. In these figures we have plotted the true gas contents, as determined on the chill-cast samples, against the values predicted by the bubble-pressure measurements. The predicted hydrogen content m (cc per 100 g) has been calculated from the pressure observations on the assumption that it is given by the following equation derived for our own solubility results:

$$\log_{10} m = \frac{-2760}{T} + 1.356 + \frac{1}{2} \log P_{H_2} [12]$$

where P_{H_2} is the "internal pressure" of hydrogen in the melt, which is assumed to be identical with the pressure at which the first bubble is observed.

It will be seen that the results on the 99.8 pct purity metal (Fig 9) are very widely scattered and, in fact, in 4 out of 8 experiments no visible bubble had formed at the limiting pressure of the apparatus (5 mm mercury) although the hydrogen content of the samples varied from 0.16 to 0.63 cc per 100 g. The bubble formation in this alloy was obviously very irregular and the measurement worthless as a measure of gas content. This is, however, perhaps not unexpected in view of the experience of the author with 99.99 pct purity metal, and his general observation that the accuracy of the method decreases as the metal purity increases.

The results on the 99.2 pct purity metal (Fig 10) are of some interest. Unfortunately the melts used for our experiments with this metal had only a limited range of gas contents (about 0.25 to 0.45 cc per 100 g with one exception)

* Massachusetts Institute of Technology.

† Research Laboratories of the British Aluminium Co. Ltd. Gerrards Cross, Bucks, England.

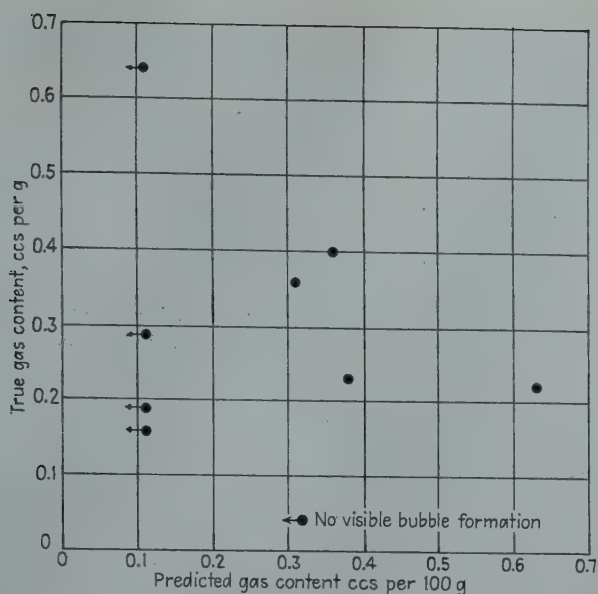


FIG 9—True gas content vs. predicted gas content. 99.8 aluminum.

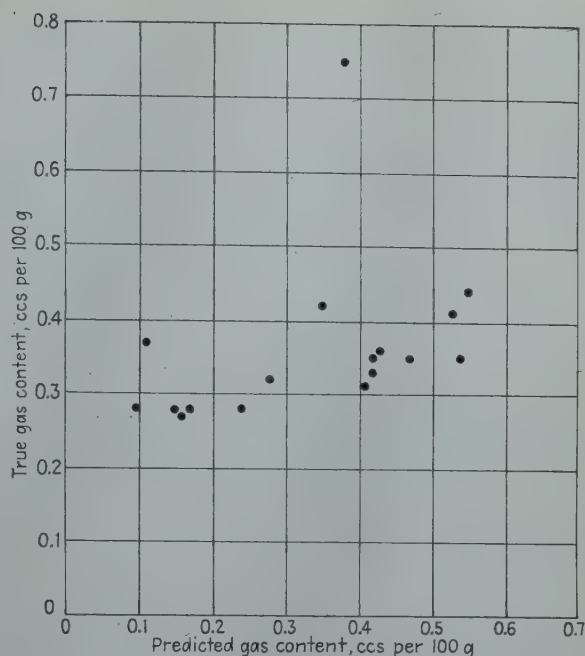


FIG 10—True gas content vs. predicted gas content. 99.2 aluminum.

and it is therefore difficult to draw any firm conclusions from the data obtained. It will be seen that in this case the bubble formation is not entirely random. If the one "rogue" point is ignored, there is statistically a significant correlation between the predicted gas content and the true gas content; in fact, knowing the relationship given by this curve, the true gas content of a melt could be predicted with a standard deviation of about ± 0.04 cc per 100 g, but this only holds over such a restricted range of true gas content that the measurement is of little value. The calibration curve is very flat, and in addition, the data plotted in Fig 10 suggest that no formation of bubbles can take place unless the gas content of the metal is greater than about 0.26 cc per 100 g. Further work would be necessary to confirm this, however, and we have not had time to carry out the necessary experiments.

It seems probable that the predicted gas—true gas relationship in the case of alloys such as duralumin will be of the same type as that shown in Fig 10. If so, it becomes possible to understand degassing curves of the type which the author has presented, such as that given, for example, in Fig 2 of his earlier paper,¹⁹ which purports to show a sevenfold decrease in the gas content of a duralumin-type alloy held in an electric furnace for 2 hr. If the values on this curve are corrected to a proper solubility basis, and then converted to true hydrogen contents with the aid of Fig 10 the decrease in gas content on standing then becomes from 0.31 to 0.27 cc per 100 g instead of from 0.07 to 0.01 cc per 100 g. Although this derivation involves several assumptions of uncertain validity, the result is very much of the order that one would predict from practical experience.

We do not propose to attempt a full explanation of the results we have given here. It seems very probable that the relationship between the gas content as predicted by bubble formation and the true value is very much influenced by the experimental conditions. For example, the loss of gas from the sample by diffusion during evacuation will obviously be a function of the rate of reduction of pressure. A fast rate of pumping is therefore desirable from this point of view. On the other hand, if the diffusion of hydrogen to a given point is a rate-determining factor in bubble-formation, a fairly slow rate of pressure reduction would be indicated. Mr. Dardel gives no information as to the rate used in his apparatus and we are unable to say how our conditions compare with his; we should be interested to have some details on this point. From the results of our tests, however, we conclude that although bubble formation is, as one would expect, influenced by the amount of hydrogen dissolved in the metal, there is another factor involved which makes it impossible to apply the simple theory proposed by the author. This factor is, we believe, primarily a question of the stability and surfacing of the gas nuclei which must pre-exist in the melt if bubble formation is to take place at all, and which a simple calculation shows must be of quite appreciable radius. The nature of these nuclei is not known with certainty, but they may well originate from particles of hydrated oxide, which enter the metal mainly from scrap additions. It is of some significance in this connection that in high-purity melts, which are likely to be entirely of virgin ingot material, bubbles are formed only with considerable difficulty. The author

has noted this effect in his paper but has not attempted any explanation as to its cause. But whatever the correct explanation may be, it seems clear that a complication exists which makes the proposed method of measuring gas contents of little value as a quantitative tool.

H. UDIN*—There is apparently a misprint in the paper on p. 5, bottom of the first column. This equation should read

$$4702 (dT/T^2) = 2.5 \text{ pct}$$

The method of determining solubility of a gas in solid metal by measuring the internal gas pressure in the remelted ingot is a very ingenious one. However, the assumption that the surface tension in the nucleating bubble can be neglected because it does not influence the scatter of the experimental results is not necessarily a valid one for several reasons. In the first place, it would be true only if there are relatively few artificial nuclei of widely different sizes present in the melt. However, experiments on undercooling indicate that this is not the case, particularly in metals which have not been especially treated to eliminate centers of nucleation.

If a batch of metal contains n artificial nuclei per unit volume (on the average), then, in measuring any phenomenon dependent on the size distribution of these nuclei, statistical theory indicates that, if the experiment is conducted on a unit volume, there will be a probable error of $1/\sqrt{n}$. If we have as few as one potential nucleus per cubic millimeter, n will equal 35,000 for a 100 g sample, and the probable error is 0.5 pct. This amount of

* Massachusetts Institute of Technology.

scatter would hardly be noticeable in the 5 pct scatter due to other factors. The surface tension term in the author's Eq 2 can thus have a real effect on the pressure without appreciably influencing the scatter of the experimental results.

We can also question the validity of the hypothesis of Eq 3 by drawing on well-known nucleation theory. The minimum size of nucleus which can grow into a bubble is determined by the balance of surface tension with the difference between external pressure and activity of the dissolved hydrogen. Relatively large nuclei may already be present as cavities on the surfaces of solid impurities. If the largest artificial nucleus is of the same order of size as the smallest stable nucleus in every experiment, little dispersion will be found in the determinations, but the error in the basic hypothesis behind Eq 3 may still be large.

Excessive pumping speed may also play a role in minimizing the dispersion of the results. Under these conditions the rate at which a bubble will grow to visible size under a favorable pressure differential would then be determined by the diffusion rate of hydrogen in aluminum as well as by the magnitude of the pressure drop. The difference in the times required for a bubble to grow to observable size from nuclei of even considerable size difference is undoubtedly small, since the volumes of the nuclei are negligible compared with the volumes of the observed bubbles. In this case the surface tension term can again effect the final answer without introducing any experimental dispersion.

Would Mr. Dardel please inform us as to whether his pumping speeds are low enough to permit an equilibrium bubble size to exist at all times?

Mr. Dardel also implies that the surface of the melt is covered by a film which is impervious to hydrogen loss by diffusion. Would he please tell us on what evidence he bases this opinion.

The author's technique may well prove to be of benefit to students of gases in metals. It is therefore of considerable importance that these theoretical questions be cleared up.

F. N. RHINES*—In connection with what has just been said, I think perhaps it is worthwhile to point out that all of the various methods that have been used for determining hydrogen in aluminum failed to take into account one imponderable which is the amount of hydrogen, perhaps combined as water, perhaps as hydrogen, which very likely exists in the oxide film. The critical experiment, it seems to me, that should be run by someone is to compare the apparent solubility by any one method for samples of varying ratios of volume to surface area, so as to find out whether there is a real effect of moisture dissolved

in the oxide film. We know, of course, that aluminum oxide is very efficient in capturing water vapor. It is my recollection that the method used by Ransley did not entirely eliminate the possibility of such contamination. Certainly in this case, it seems that some contamination of the oxide film is quite possible. Whether or not hydrogen from that source could turn up in the final analysis is still another question, but I think it needs to be proved one way or the other whether the oxide film can contribute to the apparent analysis.

E. A. GULBRANSEN*—I think one has to consider certain chemical reactions as sources of gases in aluminum. Let us consider the reaction of aluminum with water vapor from the vacuum system to form the oxide and hydrogen. This reaction is possible from thermodynamic considerations and the necessary water vapor is present if the degassing experiments are carried out in the vacuum of a rotary pump.

There are other reactions of this same type forming other gases. I feel that in discussing the liberation of hydrogen and other gases from metals one must consider the fact that certain chemical reactions may occur on the surface forming new gases.

Y. DARDEL (author's reply)—I should like to express my thanks to all contributors to the discussion on this paper for their interest and the care with which they have examined the results described.

Reply to Messrs. Ransley and Mountford:

The first point discussed by Messrs. Ransley and Mountford is of course the solubility of hydrogen in liquid aluminum. At the time of the experiments reported in the paper, the values of Röntgen and Braun, Röntgen and Möller, Bircumshaw as well as Winterhagen, were considered as the most reliable, for they gave approximately the same mean solubility, while the values of Baukloh and Oesterlen were far higher and those of Baukloh and Redjali intermediate. But the determination apparatus suggested being one of relative and not of absolute character the establishment of new and more accurate calibration curves can only be welcome. Therefore as the last measurements of Messrs. Ransley and Neufeld²⁴ confirm the values given formerly by Baukloh and Oesterlen it might be better to adopt these new values. However, before taking up this step it must be noted that the two sets of data (Röntgen and collaborators as well as Bircumshaw on one side, Baukloh and Oesterlen as well as Messrs. Ransley and Neufeld on the other) do not agree very well with the Borelius' law,³⁴ while intermediate values do (Fig 11). Of

course the Borelius' law is only an empirical one and any departure from it may be observed, but these differences should be pointed out.

The value of the solid solubility given in the paper depends of course upon the value adopted for the liquid solubility. When the solubility at melting temperature in liquid metal is equal to 0.17 cm^3 per 100 g, the solubility at the same temperature, but in solid metal, is equal to 0.058 cm^3 per 100 g. On the other hand, when the datum of 0.69 given by Messrs. Ransley and Neufeld is to be accepted the values of this paper give then 0.15–0.20 cm^3 per 100 g in solid metal. Besides, there may be a slight supersaturation as pointed out by Mr. Eborall and the values given might be a little too high. But if the liquid solubility at melting point is as high as 0.69 cm^3 per 100 g a solid solubility of only 0.036 seems rather low as can be shown from the value of the solubility ratio (Table 8 and Fig 11).

The solubility ratio $\frac{\text{liquid solubility}}{\text{solid solubility}}$ increases with the decrease in solid solubility at melting point, but it does not seem that the decrease occurs as quickly as pointed out by the datum of 19.

During the experiments reported here, the exact pumping speed has not been measured, but as all the authors who have contributed to this discussion have rightfully pointed out its importance, I shall explain at length the method used to choose the proper one.

The pressure is read at the moment given by the observer of the sample surface. The time elapsing between the observation of the bubble formation and the time of pressure reading (or dead time) must be of course so much the shorter as the speed of pressure diminution is higher. When the variation of pumping speed is rapid in the medium pressure range ($1 < p < 150 \text{ mmHg}$) where the measures are usually carried out, the values read at the higher pressure (and therefore with the higher speed of pumping) can be quite different from the actual ones corresponding to the time of bubble formation, while the measures made at lower pressure (and therefore with the lower speed of pumping) may scarcely differ from the actual one. The computation of such results can only lead to misinterpretation.

At the beginning of the experiments (preliminary experiments not reported in the paper), a one stage rotary pump without the gap G (Fig 3) was used; the variation of the speed of pumping varied rapidly with the pressure in the range of pressure measurements and the determinations were wrong.

For instance an Alpax (13 pct Si) was held at 750°C and its hydrogen content was determined at different temperatures between 750 and 580°C . In that way it was possible to vary the formation pressure of the bubble for a given amount

* Carnegie Institute of Technology.

* Westinghouse Research Laboratories.

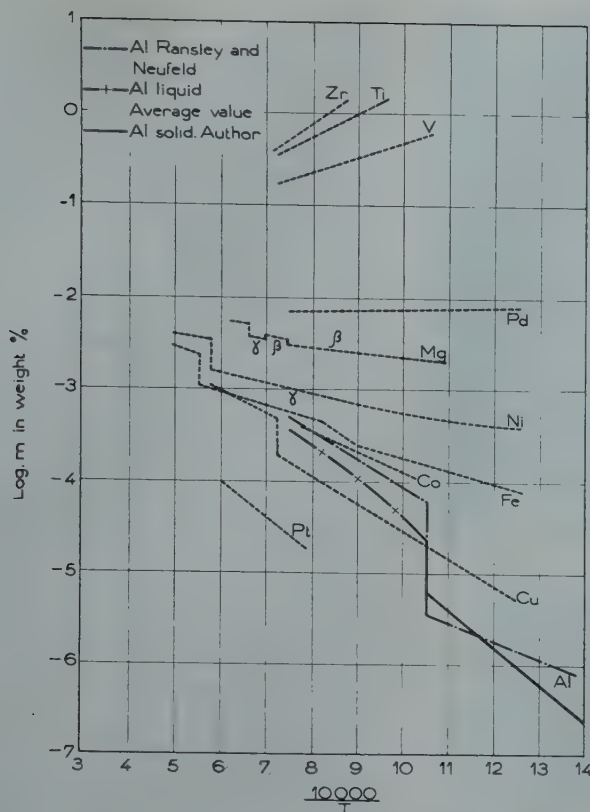


FIG 11—The solubility of hydrogen in different metals.

of hydrogen, the formation pressure being so much higher as the temperature was lower.

The results are given in Fig 12. The measured hydrogen content seemed so much lower as the pressure was higher, for at high pressure the value measured was much lower than the actual one.

On the other hand, the speed of pumping must not be too low because the diffusion of hydrogen through the surface makes the appearance of the bubble more difficult.

The speed of pumping is then limited only by the dead time of the measurement.

In a commercial apparatus it would be absolutely necessary to simplify the method of pressure reading. A push button operated by the observer would cause a hand to stop, thus giving the actual pressure.

The results of Messrs. Ransley and Mountford on hydrogen determination in high purity aluminum (99.8 pct) confirm my own results (99.99). In a similar case I have written that "any hydrogen determination with an acceptable accuracy is impossible."

Regarding the results of the determination carried out on a 99.2 pct aluminum, the departure of the correlation line from a 45° straight line can be due either to an increasing error of pressure reading when the hydrogen content rises, or to a variation in the nucleation conditions.

When the hydrogen content is higher than 0.30 cm³ per 100 g (Mr. Ransley's scale), the bubble pressure apparatus

gives, for 8 measures out of 9 with exception of the "rogue point," lower values than the hot extraction process. But I have pointed out previously that an increase in the error of reading can easily occur with an increase of pressure when the speed of pumping is too rapid. The bubble pressure determinations reported in Fig 10 have been all carried out at about 700°C, therefore the pressure bubble formation increased with the hydrogen content and likewise a possible error of reading.

For hydrogen contents lower than 0.3 cm³ per 100 g nothing can be said, for in Fig 10 all these values are distributed at random; that would mean that for hydrogen contents lower than 0.30 cm³ per 100 g according to Ransley's scale and 0.090 cm³ per 100 g according to my scale, the bubble pressure apparatus could not be used. However Fig 2 and 3 of my first paper show that almost all the values are smaller than 0.090 and are not distributed at random but follow perfectly logical laws: hydrogen content increases during heating in a gas furnace

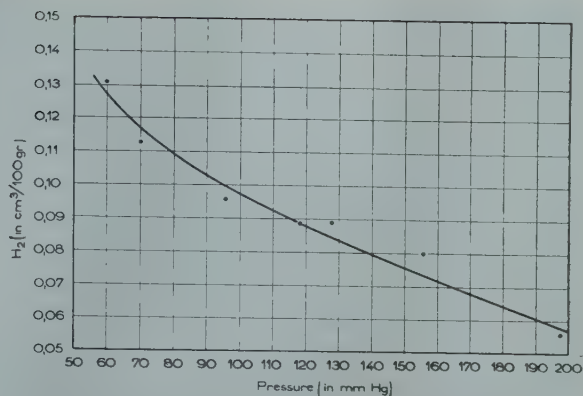


FIG 12—Variation in the determined hydrogen content, when the conditions of pumping are wrongly regulated.

and decreases during holding in a gas furnace (burners out) or in an electric furnace.

If the values of Fig 10 are not considered lower or higher than 0.3 cm³ per 100 g, but as a whole, the calculation of the correlation shows that they cannot give correct results. The application of the coefficient of correlation to the values given on Fig 2 of the paper would give a loss of only 0.04 cm³ per 100 g (Ransley's scale) or 0.012 (my own scale) by standing 2 hr in an electric furnace.

Such a small hydrogen decrease cannot be detected on the properties of an aluminum alloy (see for instance Fig 9 of the Ransley and Neufeld paper), while the effect of a 2 hr holding is well known by all aluminum foundrymen and can be very easily noted in the appearance of a vacuum sample.

Concerning the formation of a hydrogen bubble in an aluminum bath, it has been recalled in the paper that the hydrogen pressure in it was equal to

$$P_{H_2} = p_A + \frac{2n}{r}$$

and that the unobservance of the term $\frac{2n}{r}$ introduces a supplementary error which has been included in the term $\frac{df}{f}$ estimated by means of dispersion measures.

Therefore any direct comparison between bubble pressure and hot extraction measurements would be particularly welcome. Such a study would allow the analysis of the source and variation of

Table 8 . . . Value of Solubility Ratio

| Metals..... | Mn | Fe | Ni | Cu | This Paper | Al Ransley and Neufeld |
|--|--------|--------|--------|--------|------------|------------------------|
| Solubility ratio..... | 1.80 | 2.07 | 2.14 | 2.73 | 2.93 | 19 |
| Log H ₂ (H ₂ being the solubility in solid state at melting point, expressed in w pct, P _{H₂} = 1 atm.) | -2.415 | -2.922 | -2.789 | -3.753 | -5.282 | -5.49 |

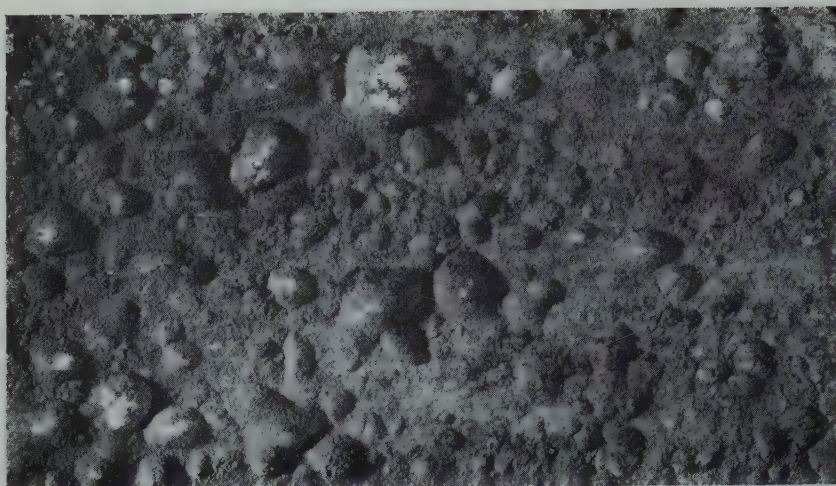


FIG 13—Aspect of surface of a wrought duralumin sample after 4 days heating at 560°C.
(Hot rolled down to 8 mm.)

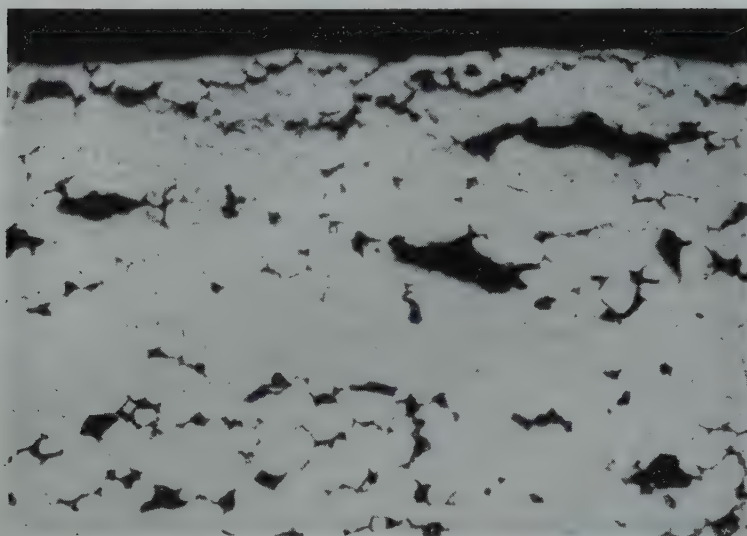


FIG 14—Formation of pores and blisters in wrought duralumin by heating at 560°C for 4 days.
(Hot rolled down to 8 mm.)

error represented by f , particularly the effect of the unobservance of $\frac{2n}{r}$ on its value.

It may be that this study would allow the estimation of the $\frac{2n}{r}$ value and through the introduction of a corrected pressure in Eq 4 more accurate results than those illustrated in Fig 5 might be obtained.

Reply to R. Eborall:

Mr. Eborall's discussion may at first seem to indicate that the determination by hot extraction of hydrogen contained in aluminum gives very accurate and indisputable results. However an examination of the papers cited by Mr. Eborall do not lead to such a conclusion. Sloman,²² whose work on hydrogen determination in steel samples is now considered a reference in all laboratories of the Continent, tried to determine the gas content of aluminum samples with an

apparatus similar to that used for steel. This author is quoted by Mr. Eborall as having given very accurate results. However, if Sloman's publication is one of the first to have cleared up the problem of gases in aluminum, the absolute values given are far from accurate in view of Ransley's work. For instance Table IV (Fig 40+) of Sloman's paper states that hydrogen in excess of that which fills voids of a porous casting is equal to 0.47–0.50–0.51. However, according to Ransley and Neufeld this value is about 0.12 cm³ per 100 g and, according to my own experiments expressed in Ransley's scale, about 0.15–0.20. The discrepancy is important. Regarding the results cited in Ref. 9, instead of discussing the difference between "adsorbed" and "surface" hydrogen—the first coming from hydrogen present in the atmosphere and adsorbed as such, while the second would come from the decomposition by heating of adsorbed water vapor—it remains that the surface correction was of the order of

the measured value and Ransley and Neufeld²⁴ could write: "Eborall and Ransley estimated the solubility in commercial aluminum at 600°C to be approximately 0.10 cm³ per 100 g, but their method involved the subtraction of a large and rather uncertain correction from their measured value"; and Ransley and Neufeld now give a value of 0.026 as solubility at 600°C.

I have recalled these values not to point out these differences, but only to make clear that a hot extraction determination remains delicate even with the most accurate apparatus and is therefore always subject to error.

The method of estimating hydrogen content by measurement of the density of an aluminum sheet after heating between liquidus and solidus is perfectly logical and is of interest to all laboratories which do not possess a hydrogen determination apparatus. It proceeds from the old qualitative method of hydrogen estimation by observation of the appearance of a sheet heated at 560°C for one hour.

The method of Mr. Swain gives the total amount of dissolved hydrogen, but can be used only with wrought material (Fig 13 and 14). Any heating of a sheet milled in as cast material leads to the formation of channels through which dissolved hydrogen escapes (Fig 15–16).

On the other hand the measurement of the density of a casting gives only the amount of gas above the limit of solubility at melting point provided that no oversaturation occurs. In fact the hydrogen content of duralumin sheet must be far lower to make sheet weldable without any defect (Fig 17).

The penultimate section on hydrogen determination by hot extraction must not be separated from the context. It has to be applied to the usual hot extraction apparatus having an accuracy of only 0.2 cm³ per 100 g.

Regarding the amount of hydrogen which can be extracted from a sample I have shown (Table 4) that hydrogen content can be higher than the solubility limit at melting point when pores are present in casting. On the other hand with commercial aluminum and duralumin I have never observed less absorption of hydrogen even by one day heating in a vapor atmosphere (and subsequent turning of the sample). Sloman's Table VII²² also could not detect any absorption of hydrogen after dipping of the samples in different solutions. Therefore if this way of gassing a sample is very common with iron, it is far from likely with aluminum.

The work of Klyachko has not been quoted to affirm that in any case aluminum is riddled by channels but only to make clear that in some cases, chiefly with castings on X ray examination, very high hydrogen content is sometimes observed. This can be explained by absorp-

tion of water vapor in microshrinkage which of course is not necessarily going throughout the metal.

The dispersion range of the liquid solubility data has already been discussed elsewhere. Therefore it will be enough to recall that the mean solubility datum given by Braun is not 0.08, but 0.24 cm³ per 100 g at 700°C, 0.08 being only one of the figures. Moreover, the dispersion range of Röntgen and Braun, Röntgen and Möller, Bircumshaw and Winterhagen is rather small. However, it may be better to adopt the new values of Ransley and Neufeld, which confirm those of Baukloh and Oesterlen. If such a step is adopted all the data reported in this paper are homogeneous to those given in Ref. 24 and can be compared to them.

The difficulties due to nucleation have already been discussed in the reply to Messrs. Ransley and Mountford and therefore will not be repeated.

I should like to point out that I agree completely with the opinion of Mr. Eborall on the respective use of an accurate hot extraction apparatus and a bubble pressure apparatus. The new hot extraction apparatus giving absolute data would be used to provide calibration curves and check the results of a bubble pressure apparatus. But while the former can be used only in a few specialized laboratories, the latter can be employed not only in any laboratory, but also on any pouring platform.

At the time the experiments were begun, this distinction could not be made since the old hot extraction apparatus had an insufficient accuracy.

Reply to M. Bever:

I think that the internal pressure of all gases except hydrogen is very small in an aluminum bath. The gases according to Sieverts' law can be dissolved only as atoms or more likely as protons and the stability of oxide and nitride shows that all dissolved oxygen and nitrogen are practically bound to metal. Only methane can also be present in the bubble, but its pressure is about 100 times smaller than that of hydrogen (Fig 4). On the other hand, the dissociation pressure of Al₂O₃, and Al N or the pressure of CO due to the reaction of oxide or carbide is extremely small and can be neglected.

The experiments of Sloman as well as those of Eborall and Ransley confirmed this point: "Hydrogen in fact, appears to be the only gaseous element which is appreciably soluble in the metal in the temperature range normally considered."

It is quite certain that surface tension inhibits the formation of the bubbles, and I have admitted that the size range of the artificial nuclei was wide open and therefore that the effect of surface tension could be reflected in the dispersion of the determinations. However, as has been very clearly pointed out by Mr. Bever, the effect of surface tension on the scatter

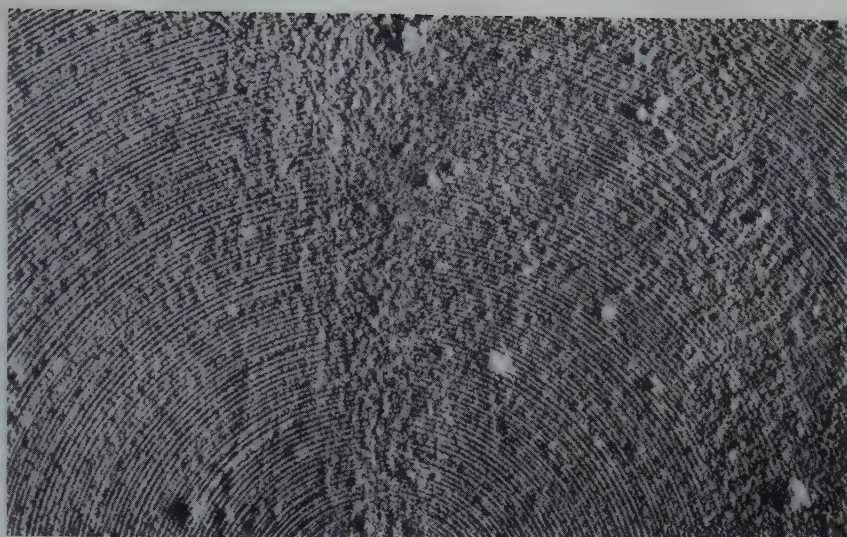


FIG 15—Aspect of surface of an as-cast duralumin sample after heating at 560°C for 4 days. (Machined down to 3 mm thickness.)

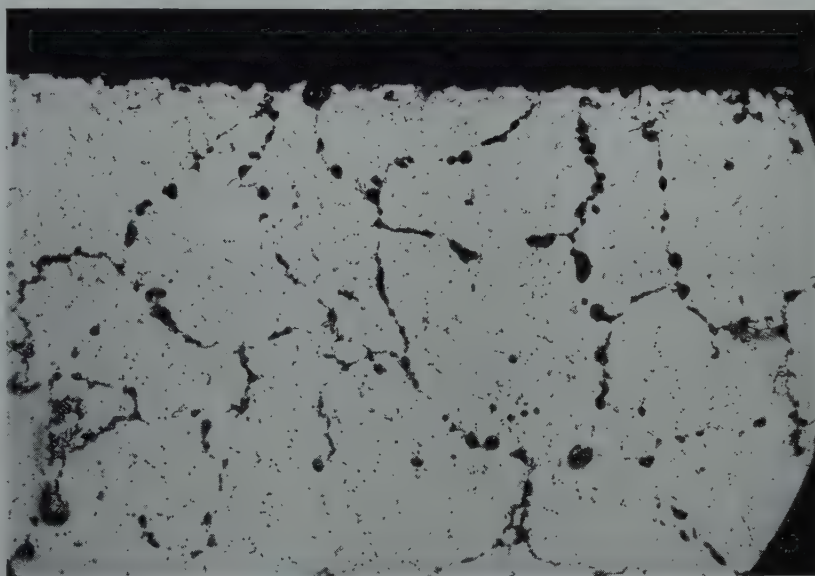


FIG 16—Formation of pores in cast duralumin after heating at 560°C for 4 days. (Machined down to 3 mm thickness.)

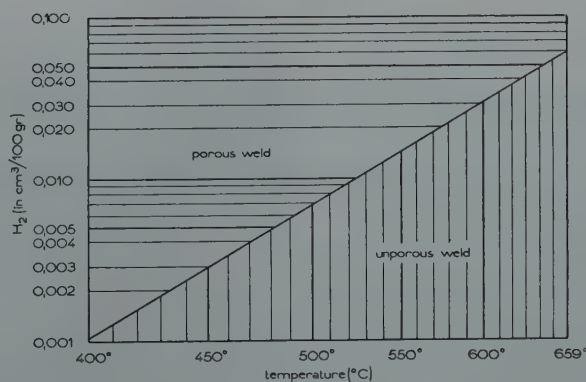


FIG 17—Relationship between the incipient melting temperature of an aluminum alloy and the maximum amount of dissolved hydrogen permissible for welding.

of the results remains small if all artificial nuclei have approximately the same size. Observations of oxides removed from an aluminum bath show that their surfaces present cavities which are not wet by the metal and which have a quite different size. However, a direct proof of the hypothesis which is the basis of Eq 3 can be made only through comparison of the results obtained by accurate hot extraction analysis and bubble pressure determination.

On the other hand I do not think that the experiments of Brower and Larsen can be opposed to the basic hypothesis as the experiments of Körber and Oelsen²⁵ show. According to these authors no formation of CO occurs when steel is melted under a silicate slag because the metal is enveloped in a hull of glassy silicate presenting no cavity acting as nuclei, while the boil starts as soon as the steel bath comes in contact with the crucible wall. An aluminum bath contains solid impurities presenting cavities and not glassy ones, therefore if the surface tension inhibits the formation of bubble, this inhibition remains small.

In fact, according to Ransley and Neufeld's determinations, the hydrogen content of an aluminum casting just free of pores varies between 0.12 and 0.18 cm³ per 100 g (Fig 9 of their paper), while the determinations of this paper (Table 4) expressed in Ransley's scale give 0.15–0.20 cm³ per 100 g. This agreement seems to offer proof that the hypothesis, which is the basis of Eq 3 can be accepted in first approximation, provided of course that the liquid solubility

given in Ref. 24 is the correct one.

No calculation of the speed of hydrogen diffusion into the bubble has been carried out, but the speed of pumping being rather low the equilibrium in the bubble size does exist at any moment.

The very low diffusion speed of hydrogen through an oxide film has been clearly shown by Ransley and Neufeld. Fig 3 of their paper confirms the old hypothesis that the gassing and degassing rate of an aluminum bath is controlled by a surface phenomenon.

Reply to F. N. Rhines:

Mr. Rhines rightfully points out the importance of the adsorbed film on the result of a gas analysis, but I think that it would be very difficult to establish whether "surface hydrogen is coming from adsorbed hydrogen or from adsorbed "water vapor." On the other hand Schmid and von Schweintz as well as Chandron and Moreau have made an extensive study of the effect due to the ratio $\frac{\text{volume}}{\text{surface}}$ of the sample. As has been shown in the paper, the sample must be turned out and as soon as the ratio $\frac{\text{volume}}{\text{surface}}$ is lower than a certain value a correction factor has to be introduced.

Reply to E. A. Gulbransen:

Mr. Gulbransen points out that certain reactions can be the source of gases in hydrogen. In fact, as I have already explained in the reply to Mr. Bever, hydrogen is the only dissolved gas able

to give bubble. On the other hand, the reaction of the water vapor of the atmosphere with the metal can occur only through the alumina film which, already impervious to hydrogen, shall be still more impervious to the diffusion of any big molecule.

References

21. R. Eborall and C. E. Ransley: *Jnl. Inst. Metals* (1945), **71**, 525.
22. H. A. Sloman: *Jnl. Inst. Metals* (1945), **71**, 391.
23. H. A. Sloman: *Jnl. Inst. Metals* (1946), **72**, 441 (discussion).
24. C. E. Ransley and H. Neufeld: *Jnl. Inst. Metals* (1948), **74**, 599.
25. A. J. Swain: *Jnl. Inst. Metals* (1949) **75**,—probably June or July 1949).
26. G. J. Metcalfe: *Jnl. Inst. Metals* (1945), **71**, 618 (discussion).
27. C. A. Zappfe: *Trans. Am. Soc. Metals* (1948), **40**, 315.
28. J. A. Klyachko, R. Eborall and C. E. Ransley: *Jnl. Inst. Metals* (1946), **72**, 712, (discussion).
29. W. D. Urry: *Jnl. Am. Chem. Soc.* (1933), **55**, 3242.
30. C. J. Smithells and C. E. Ransley: *Proc. Roy. Soc.* (1935) (A) **150**, 172.
31. A. J. Swain and R. Eborall: H. M. Stationery Office, Report No. B.D.D.A. 73, 1946. (Declassified report of work done for Dept. of Atomic Energy, Ministry of Supply.)
32. M. D. Eborall: A. Cibula: Work to be published shortly.
33. T. E. Brower and B. M. Larsen: *Trans. AIME* (1947) **172**, 137.
34. G. Borelius: *Ann. Phys.* (1927) **83**, 121.
35. F. Körber and W. Olsen: *Naturwissenschaften*. (1935) **23**, 462.

Plastic Deformation Waves in Aluminum

By A. W. McREYNOLDS

DISCUSSION

(R. S. Busk presiding)

E. OROWAN*—I observed the phenomenon of jerky yielding many years ago with zinc²⁶ and cadmium single crystals. A significant point was that the jerks occurred not only when the stress was raised but also (sometimes, after a pause of many minutes during which no trace of creep was observable) at constant stress. The phenomenon may be closely linked with the inertia of the testing machine and of the specimen, although

the inertia alone cannot account for it. If, during the test, the resistance of the material to plastic deformation suddenly diminishes while the applied force remains constant, a sudden deformation follows until the yield stress has risen, by strain hardening, to the level of the applied stress (= the value of the previous "upper yield point."). When this is reached, the rate of deformation has attained a maximum value because, up to this moment, the applied force was higher than the plastic resistance of the specimen, and the difference was used for accelerating the moving parts of machine and specimen. The kinetic energy accumulated is now transformed into

plastic work by further deformation; that is, the deformation overshoots the point at which the plastic resistance equals the applied static force. When the kinetic energy has been used up, therefore, we are left with a specimen the yield stress of which is higher than the applied stress, and no further deformation can occur (apart from a little creep) until either the applied stress has been raised to the new yield stress level, or the yield stress has fallen by thermal recovery to the level of the applied stress. While this occurs, a new upper yield point can develop, for example, by precipitation.²⁶

²⁶ A. H. Cottrell and D. F. Gibbons: *Nature* (1948) **162**, 488.

* Cavendish Laboratory, Cambridge, England.
²⁶ E. Orowan: *Zitsch. f. Phys.* (1934) **89**, 634.

There is no intrinsic contradiction in the assumption that thermal softening (by the removal of internal stresses) and precipitation hardening can occur simultaneously. The hardening effect of precipitations may be overcome by a small deformation which tears away the encircling dislocations from the precipitates,²⁷ and then the softness of the material, acquired by thermal recovery, may reveal itself. In this way, the inertia of the testing machine and of the specimen may contribute essentially to the development of upper yield points during the test, not only to the size of the jerk when an upper yield point is overcome.

Jerky extension need not be connected with the propagation of a plastic wave along the specimen. I investigated this question in 1940 for Cd crystals; the work was interrupted by the war and has not been published. I stuck nearly close-packed rows of minute shiny spheres of pure tin (about $\frac{1}{1000}$ in. diam each) to single crystal wires parallel to the wire axis; the spheres were produced by dropping filings of tin into a bath of molten stearine, the top part of which was above, and the bottom part below, the melting point of tin. The single crystal with the row of tin beads was illuminated with a distant pointolite lamp, and photographed, at about $\times 20$ to $\times 50$, with a rotating drum camera; the reflections from the beads traced extremely sharp lines on the recording paper, and the record showed directly which parts of the specimen had undergone plastic deformation: every pair of beads acted as an extensometer over a gauge length of a few thousandths of an inch. The records showed that the extension jerks were localized in a very short part of the specimen where, as a rule, many consecutive jerks occurred.

The presence of an upper yield point, if this is not re-formed during the experiment, need not cause any further jerking of the deformation. We are carrying

out experiments on the propagation of Lüders bands in mild steel wires in the Cavendish Laboratory (with Mr. W. Sylwestrowicz); in these experiments, only one Lüders band arises (usually in one of the grips, unless the ends of the wire are provided with electrodeposited heads), and this spreads over the wire in a perfectly continuous way, as slowly as is required, under a practically constant load. An essential condition of this, of course, is that the testing machine and the dynamometer must be very rigid.

E. H. DIX*—We think there is a rather clear-cut correlation between the irregular yield point elongation and the tendency to form Lüders lines. In the case of aluminum alloys containing several per cent magnesium, we get quite jagged yield point elongations and also the formation of strain lines in certain articles in which the metal is stretched in some locations during forming. In the case of annealed material, a small amount of cold work by rolling, or even by running the sheet through a series of offset rolls, that is, a roller leveler, the tendency to form Lüders lines is reduced.

Another observation is in connection with the duralumin-type alloys. Immediately after quenching, while they are in the rather unstable condition, there is a marked tendency for the Lüders lines to form, and if you watch a specimen being tested in tension you see the lines running up and down the gauge length of the specimen. It is a very interesting phenomenon to watch. After a few hours of aging that tendency disappears, and certainly after a day of aging the Lüders lines are not seen, and the yield point portion of the curve is smooth and not jagged.

R. S. BUSK†—It seems to me that one of the important points in this paper is that the phenomenon of yielding and the increase in stress necessary for subsequent yielding are so uniform. Any explanation must take into account the fact

that the steps increase in a linear fashion. I wonder if simply tensile machine inertia forces would result in such a uniform step pattern.

A. W. McREYNOLDS (author's reply)—As Dr. Orowan points out, there is considerable diversity in the manner in which irregularities in the stress-strain curve occur in different materials, as illustrated by his interesting observations on cadmium, zinc, and mild steel. It seems nevertheless profitable to view the spread of deformation through the metal as propagation of a plastic wave, even though the wave extends only through a limited region, as in Orowan's observations on cadmium and the author's observations on aluminum-copper, or spreads very slowly, as in mild steel. Whatever the mechanisms of thermal softening, precipitation hardening, and others, involved it seems clear from the continuous spreading of deformation that plastic yielding of the hardened lattice does not occur uniformly over an extended region but is initiated in the small region of inhomogeneous stress at the boundary between deformed and undeformed material. Thus a complete explanation of the phenomenon must take account of stress concentrations ahead of the plastic wave in addition to such overall properties of the material as yield stress.

As both Mr. Busk and Dr. Orowan commented, inertial effects in the tensile machine and even in the specimen itself may strongly influence the discontinuous yielding phenomena. It seems likely that most of the results to be found in the literature are complicated by this factor. The soft tensile machine used in the present experiments was specifically designed, however, such that inertial effects are eliminated insofar as possible by applying tension through a coil spring to eliminate both mass and variations of load on yielding. It is believed that, as a result of this and other special precautions, the instrumental inertia effect had no significant effect on the observed irregularities in plastic yield.

²⁷ E. Orowan: Discussion at Symposium on Internal Stresses, London 1947 (Inst. of Met. Monogr. Series No. 5, p. 451).

* Aluminum Co. of America.
† Dow Chemical Co., Midland, Mich.

Homogeneous Yielding of Carburized and Nitrided Single Iron Crystals

By A. N. HOLDEN and J. H. HOLLOMAN

DISCUSSION

(R. S. Busk presiding)

A. H. COTTRELL* and A. T.

* Dept. of Metallurgy, Birmingham Univ., England.

CHURCHMAN*—We have been making some experiments recently very similar to those reported by Messrs. Holden and Holloman. Wires of Armco iron, 0.077 in. diam. were decarburized in wet hydrogen until the yield point was

removed; they were then extended $3\frac{1}{4}$ pct and annealed at 880°C for 120 hr in dry hydrogen. This process produced large crystals which extended through the cross-section and were about $\frac{3}{4}$ in. in length. Since the length of each crystal

was thus about ten times its diameter, wires prepared in this way behaved as single crystals in tensile tests and no attempt was made to grow longer crystals. The wires were carburized by heating at 720°C for 1 hr in propane and then annealed at 680°C for 65 hr in argon. This treatment was sufficient to cause the return of a sharp yield point in polycrystalline specimens.

Before testing the crystals preliminary experiments were made to develop a method of mounting them in the testing machine; the criterion taken for a satisfactory technique was that it should permit the observation of a very sharp yield point, considerably higher than the lower yield point, on a carburized polycrystalline test-piece of the same form as the single crystal specimens. Eventually a procedure was adopted which used a 5 in. wire, the ends of which were tinned for a distance of 2 in., as a test piece. Each end was inserted to a depth of 1½ in., and soldered, in an axial hole in a ⅜ in. diam steel rod, 3 in. in length, the other end of which was attached to a shackle of the testing machine by a 5 in. piece of fine, flexible steel cable. A standard lever machine was used and the extension was measured by a screw attached to its cross-head, no extensometer or other attachment being mounted on the specimen. With this arrangement very sharp upper yield points at stresses of about 30,000 psi could be obtained consistently on polycrystalline specimens, the corresponding lower yield points occurring at about 25,000 psi.

Several single crystal specimens were tested by this method and Fig 15 shows typical results obtained. No yield point was observed on hydrogen treated specimens and extensive plastic flow began at a stress of about 4500 psi, in agreement with Holden and Holloman's results; furthermore, no yield point was developed by unloading overstrained specimens and aging them at 100°C for a few hours (curves 3, 5 and 7).

The carburized crystals, on the other hand, showed yield points. Fig 1 shows an example of this, together with the effect of overstrain in removing the yield point (curves 2, 4, 6, 8 and 10 were taken immediately after unloading) and the return of the yield point at a higher stress level on strain aging (curves 3, 5, 7 and 9 were taken after aging the unloaded specimen at 100°C for a few hours). The lower yield point is first observed at a stress of about 7500 psi, but a clearly marked upper yield point does not appear until the yield point has been raised, by strain aging, to about 15,000 psi.

While these experiments have shown the existence of inhomogeneous yielding in carburized iron crystals, they raise several questions, quite apart from the fact that they give a different result from that of Holden and Holloman's experiments. For example, why is the yield

point so small at first, compared with that of a polycrystalline specimen, and why does the upper yield point only appear after strain aging? To help answer these questions, we are at present examining the effects on the yield point of such factors as, for example, the depth of penetration of the carburized region or the condition of the surface of the specimen.

L. D. JAFFE*—It is very gratifying to be able to deduce from these new experiments that the old idea that the yield point in steels is associated with the grain boundaries, is apparently correct. It is not so gratifying, however, if we try to draw some general conclusions about the nature of the yield point phenomenon, when we remember that in brasses the yield point does appear in single crystals, and perhaps more so in single crystals than in polycrystalline material. That is unfortunate, because we would like to have similar explanations for similar phenomena. Would Mr. Holden give us any ideas he may have as to why this difference exists between behavior in brass and steel?

A. N. HOLDEN (authors' reply)—The yield point has been observed of course in single crystals of materials other than iron. For many years the yield point has been known to occur in cadmium and zinc crystals. I believe in these cases it was observed only as a consequence of strain aging. Cottrell and Gibbons¹¹ found that nitrogen was a necessary impurity in the case of cadmium.

Unfortunately I have no ready explanation for the phenomenon Mr. Jaffe described concerning yield points in brass crystals.

E. OROWAN†—The authors have performed an experiment of great importance to the theory of the yield phenomenon in steel. As far as I know, Dr. Cottrell and his collaborators in Birmingham, England, have been working on the same experimental problem for the last year or two, and it will be interesting to compare their results with the present ones.

With the experiments of Holden and Holloman, the situation in the theory of the yield phenomenon has become particularly interesting. With steel, the phenomenon occurs only in a sufficiently fine-grained polycrystalline material; with zinc and cadmium, only in single crystals.¹² It seems fairly clear why it is not observed in polycrystalline zinc or cadmium. Having only one set of easy slip planes, the grains of these metals cannot conform easily with the deformations of

the neighboring grains, so that the yield stress of the polycrystalline material is many times higher than that of a single crystal of average orientation. Since the upper yield point of Zn or Cd crystals is never more than 30 to 50 pct higher than the lower yield point, it cannot be observed in a polycrystalline metal which does not yield in any case before the average yield stress of the individual grains is exceeded by several hundred per cent.

It seems that there are (or, there had been before the experiments of the authors) three survivors among the numerous theories of the yield phenomenon. The oldest among these is the hypothesis that there is a thin film of cementite at the grain boundaries which breaks when the upper yield point is reached (Ludwik, Nádaí, and Kuroda). Edwards, Phillips and Liu¹³ abandoned this view when they observed that the yield phenomenon occurred in several nonferrous alloys only after a slight preliminary straining followed by annealing. In place of the cementite boundary layer hypothesis, Edwards, Phillips and Liu introduced the assumption that the yield phenomenon was due to a precipitation along the active slip planes.

In Cottrell's view,³ invisibly thin films of cementite could not account for the high values of the upper yield point observed in steel. He attributes the yield phenomenon to the accumulation of carbon atoms on the tensile side of dislocations where the atomic lattice is expanded; this process would reduce the energy of the dislocation, and an additional stress would be necessary to tear it away from its carbon atoms. If this is the cause of the yield phenomenon, single crystals ought to show it equally well; in fact, for the reason I have mentioned in connection with zinc and cadmium, they ought to show it rather better than polycrystalline material.

At first sight, it would seem that there is very little difference between the slip plane precipitation hypothesis of Edwards, Phillips and Liu, and the hypothesis of Cottrell; in reality, the difference is very significant. Of course, the particles precipitated in operative slip planes must have been nucleated at dislocations, for the presence of these is the only thing that makes an operative slip plane differ from plastically undistorted parts of the crystal. With this, however, the common ground of the two hypotheses ends. Cottrell assumes that a perfect crystal would be very hard; only the presence of dislocations makes it relatively soft, and it must become harder if the dislocations are made less effective by being clogged with carbon atoms. On the other hand, the slip plane precipitation hypothesis assumes that the "softest" individual slip planes in the

* Watertown Arsenal Laboratory, Watertown, Mass.

† Cavendish Laboratory, Cambridge, England.

¹¹ Nature (1948) 162, 488.

¹² E. Orowan: *Ztsch. f. Phys.* (1934) 89, 634; C. L. Smith: *Nature* (1947) 160, 466.

¹³ C. A. Edwards, D. L. Phillips, and Y. H. Liu: *Jnl. Iron and Steel Inst.* (1934) 147, 145.

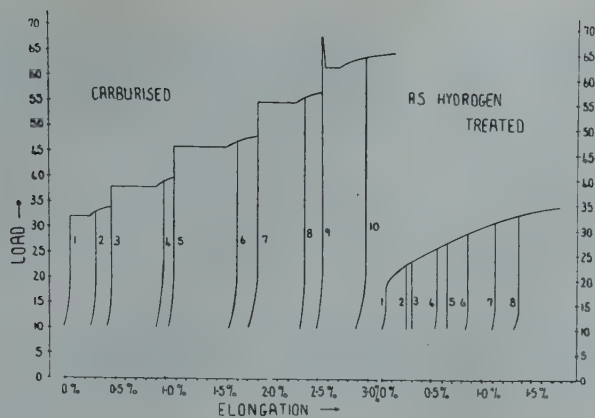


FIG 15—Load elongation curves showing the yielding behavior of carburized and decarburized iron crystals.

material, on which slip starts first, are subsequently immobilized by local precipitation hardening. The hypothesis of the clogged dislocations cannot be applied whenever prestraining is necessary for the development of the yield point; in an annealed material, there should be either no dislocations present, or only a few clogged ones, and in either case there should be an upper yield point. On the other hand, it is not easy to see how the slip plane precipitation hypothesis could explain the yield phenomenon in annealed (unstrained) materials.

Both the hypothesis of the clogged dislocations and that of slip plane precipitation might seem to face difficulties in explaining the grain size effect. It appears, however, that an explanation on this basis is not quite out of the question. In a polycrystalline metal, the interference of the neighboring grains may reduce the planes of easy slip to a small number which can be immobilized by precipitation; in a single crystal there may be numerous almost equally favorable slip planes, and even if many of these are immobilized, there are still many left on which slip may start at a not much higher stress. In this way, the slip plane precipitation hypothesis might lead to a certain grain size effect. This possibility does not exist for the hypothesis of the clogged dislocations; a grain size effect could arise here only if the important dislocations are at the grain boundaries. Since the yield phenomenon in steel needs no prestrain to arise, these dislocations must be the ones determined by the geometry of the lattice misfit between the neighboring grains, and the hypothesis is then reduced to what amounts to a re-interpretation of the boundary cementite hypothesis.

The conclusion seems to be that the cause of the yield phenomenon in steel is probably different from that in zinc, cadmium, or silver. In the latter cases, the slip plane precipitation hypothesis is very plausible; in the case of steel, the effect is probably due mainly to the resistance of the grain boundaries to slip being increased by some precipitation, in the manner expressed crudely by the

cementite film hypothesis.

A. N. HOLDEN—I wish to thank Dr. Orowan for indicating the importance of those experiments to the theory of the mechanical behavior of metals. His remarks indicate the need for a thorough experimental attack on the problem of strain aging of single crystals.

A. N. HOLDEN and J. H. HOLLOMON—The experiments of Cottrell and Churchman are very interesting, since the explanation of the yield point by Cottrell³ was somewhat embarrassed by the failure of our carburized or nitrided crystals to yield discontinuously. The unfortunate circumstance of a difference in the results of Cottrell and Churchman and the authors now exists. Furthermore, in an as yet unpublished paper,* Schwartzbart and Low have observed a horizontal portion of about 0.2 pct in extent in the stress-strain curve of single crystals of iron upon initial yielding.

This discrepancy might be explained in several ways:

1. An unlikely source of the discrepancy is the aluminum content of our crystals (an element absent or low in Armco iron). Aluminum might be expected to affect the results of nitriding, but should have no effect upon the carburized specimens. Still another material, a silicon-killed steel, was used in making the crystals tested by Schwartzbart and Low.

2. Perhaps the fine wires employed by Cottrell and Churchman were strained before testing (deformation of the wires would be difficult to prevent in handling), and even the initial yielding of their crystals arose from strain-aging.

3. The difference in the heat treat-

* Unpublished at the time of AIME San Francisco Meeting, Feb. 1949.

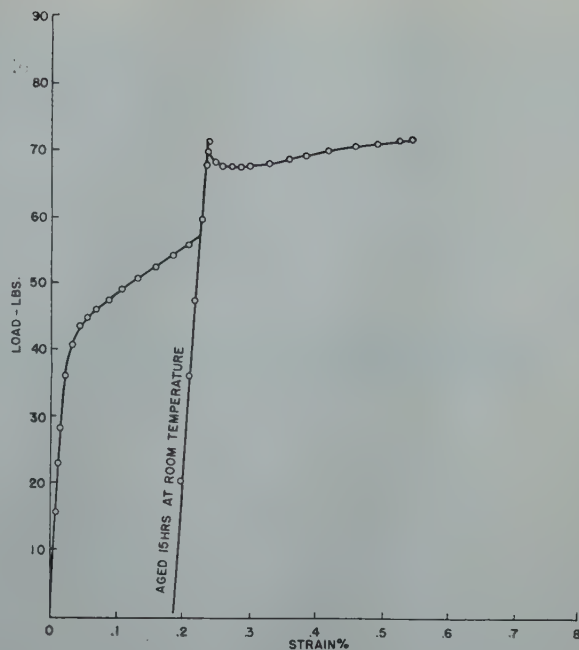


FIG 16—Strain aging of a carburized iron crystal.

ments accorded the crystals in the several experiments might lead to the different results. It is quite possible that the rate of cooling from the homogenizing temperature could affect the results. For instance, rapid cooling might introduce quenching strains allowing the crystal to strain-age prior to testing.

4. It is also a possibility that the authors (Holden and Hollomon) did not align their crystals as accurately as necessary for specimens of the shape used in the experiments. Alignment of these specimens is a serious and difficult problem, particularly if the initial yield point elongation is very small. It must be admitted, however, that with a yield point elongation of 0.2 pct such as Cottrell and Churchman observe, the misalignment would have to cause differences of this amount in strain on the two sides of a crystal to obscure the effect. The authors feel that they achieved sufficient alignment to reveal a 0.2 pct yield point elongation, but they are continuing to direct their efforts toward the development of better means of axial loading.

5. No doubt Cottrell and Churchman have considered the consequences of carburizing so close to the critical temperature. After 1 hr at 720°C in a propane atmosphere their crystals would undoubtedly be saturated with carbon. During this treatment any accidental temperature fluctuation to approximately 725°C would result in the formation of polycrystals.

Cottrell and Churchman have shown that carburized iron crystals will undoubtedly strain-age. This information will be a valuable aid in understanding the yield point phenomenon.

Since this paper was written, many experiments have been conducted by the

authors on the strain-aging of iron crystals made of carburized aluminum-killed steel. It is of interest to compare the results of one such experiment with those

of Cottrell and Churchman. Fig 16 shows the yielding of a carburized crystal. Initially there was no sign of a yield point or discontinuity. After straining

0.18 pct, unloading, aging 15 hr at room temperature, and re-straining, a definite upper yield point was observed, together with some 0.1 pct yield point elongation.

Temper Brittleness of Plain Carbon Steels

By L. D. JAFFE and D. C. BUFFUM

DISCUSSION

(R. E. Leiler presiding)

M. G. CORSON*—The low temperature brittleness of carbon steels rapidly progresses with the increase in the carbon content. The presence of nickel greatly counteracts that brittleness. For this reason a comparison of a high nickel, low chromium steel of 0.39 pct carbon content to a carbon steel of 0.47 pct C is not warranted.

Having committed this error the authors ought to present at least a table of characteristics in the static test to show that the two steels were essentially identical.

Rockwell C values of 18–19 are rather meaningless. Brinell or Rockwell B figures should have been given.

The authors succeeded only in proving that a 0.47 pct C steel of unknown characteristics tempered at 675°C for a very short period after being water-quenched (this introduces irreparable amounts of brittleness anyway) was *sharply* brittle at about -60°C ; while an alloy steel containing less carbon and quite a lot of nickel was *not so sharply* brittle in the same range.

It might have been much more to the point if the authors had examined the relative brittleness of steels of the same carbon content, one without and another with a substantial amount of chromium, but just the needed amount of Mn (0.8 pct is much too much for a plain carbon steel). Then both steels should be oil quenched and tempered at a moderate temperature (about 400°C) followed by testing at room temperature, because it is fundamentally the brittleness of troostitic steels under normal conditions that causes misgivings.

Furthermore: Half size impact test-bars should be used only in such cases where the finished piece is very small in its cross-dimensions. It is almost a foregone conclusion that full-size test bars would have shown a rather different behavior.

L. D. JAFFE and D. C. BUFFUM (authors' reply)—It is always interesting to get a discussion from Mr. Corson. We will cover a few of the points he has raised. We were not aware that the presence of nickel counteracts temper brittleness in any sense. It has always been felt that there are considerable data indicating that nickel increases temper brittleness. With respect to manganese, the manganese contents were the same in the two steels, and they were within the specified limits for those particular S.A.E. steels.

Mr. Corson would like us to have used troostitic steels and test at room temperature. We explained in the paper why martensitic steels were desirable and why it is necessary to test over a range of temperatures. We also explained that half-size test bars had to be used in order to get martensite. A comparison was made of the behavior of those small size bars with that of full-sized bars, and the results are about to be published.¹⁴

J. K. Y. HUM*—We can substantiate the results Mr. Jaffe has given on using half-size sharp bars, except our steel was an SAE 1055 steel. We achieved comparable results with his with 1040, however there is a little question about this reduced toughness of plain carbon steels. At U. C. we investigated temper brittleness by the effect of alloy elements on high purity steels. We found that with plain carbon steels of high purity (without all the usual impurities that occur in the plain carbon steels), we got a decidedly greater toughness than normally occurs with commercial plain carbon steels. Regarding the effect of alloying elements changing the transition temperature, this is quite true with one exception, which is manganese. We found small amounts have a tendency to shift to a higher shifting temperature. There might be a qualifying statement to the alloying element in regard to manganese.

That has a tendency to put a question mark on what happens to the embrittled curve.

In regard to other elements, we have done a reasonable amount of work with carbon chrome steels. We found that there is a certain amount of chrome necessary before the steel shows temper brittleness. Normally with steels up to and including 3 pct chrome temper brittleness is not evident. With over 3 pct it becomes quite temper brittle.

L. D. JAFFE and D. C. BUFFUM—We interpreted Mr. Hum's last remark to mean that in the lower chromium steels with no other alloys present there was no appreciable difference in transition temperature between the specimens slow cooled and those quenched from the draw. This, of course, may not necessarily prove that the steels are not susceptible to temper brittleness. They may have been embrittled in both conditions.

J. K. Y. HUM—That was a full-sized bar. It was not until we changed over to the half-size that we discovered the embrittlement you observed.

E. OROWAN*—In the Cavendish Laboratory, Dr. J. Nutting has studied temper brittleness by making aluminum pressings from the surfaces of fracture and examining the aluminum oxide film replicas obtained from these by the electron microscope. In all cases of true temper brittleness, the fracture was substantially intergranular, while the ordinary "notch-brittle" fracture of steel is substantially intracrystalline (cleavage fracture). If Dr. Nutting's results can be generalized, temper-brittleness is due to a lowering of intergranular cohesion, probably by some precipitation. A polycrystalline metal has, in principle, two brittle strengths: one for intergranular, and another for intracrystalline fracture. Typical temper brittleness appears when the intergranular strength drops below the intracrystalline one. A certain treatment of the material may produce brittle fracture by reducing either the inter-

¹⁴ D. C. Buffum: Investigation of Square Sub-sized Charpy Specimens. Accepted for publication, A.S.T.M. Bulletin.

* Univ. of California, Berkeley, Calif.

* Cavendish Laboratory, Cambridge, England.

granular strength, or the cleavage strength of the grains. Only in the first case are we entitled to speak of temper brittleness in the usual sense of the word. I should like to ask Mr. Jaffe, therefore, whether he and Mr. Buffum have studied the nature of the fractures microscopically or electron-microscopically in order to recognize whether the fracture was mainly intergranular or mainly intracrystalline.

L. D. JAFFE and D. C. BUFFUM—We are most interested to hear of the Cambridge electron-microscope results, which are in accord with findings of the optical-microscope.^{15,16} Miss M. R. Norton at our laboratory has also been using the optical microscope in studying the path of fracture in temper brittle steels broken at temperatures below the transition range. She has not observed as clear-cut a distinction as Dr. Orowan indicates. The embrittled specimens had primarily an intergranular fracture but there was a considerable percentage of transgranular fracture. This was often somewhat rough, suggesting that a certain amount of local deformation occurred even though the fractures appeared brittle macroscopically and absorbed little energy. In the nonembrittled specimens very little of the fracture was along grain boundaries. These transcrystalline breaks appeared to be partly by cleavage and partly with local deformation.

In response to Dr. Orowan's last question, preliminary examination of the plain carbon steel fractures has been made by Miss Norton. The fracture path appeared to be predominantly intergranular on specimens which had been embrittled either by slow cooling or isothermally. Fracture in the unembrittled specimen was chiefly transgranular. Observations of the nature of the fractures

thus support the hypothesis outlined in the paper.

J. MALTZ*—The two hypotheses described by the authors are not the only possibilities. It may simply be that the plain carbon steels are inherently less tough than alloy steels—that is, have higher transition temperatures in the absence of any embrittlement reaction.

This third hypothesis can lead to predictions (3) and (4) and reject predictions (1) and (2) just as well as the more complex one advanced by the authors. Nor is it unreasonable. Small alloy additions increase the inherent strength of ferrite, so why not the inherent toughness?

If we compare Hollomon's data⁶ for a plain carbon steel (0.39 pct C, 0.85 pct Mn), water quenched, with the data of Archer, Briggs, and Loeb¹⁷ for a chromium-molybdenum steel (0.39 pct C, 0.65 pct Mn, 0.57 pct Cr, 0.15 pct Mo) sensitized for 10 hr at 1025°F and furnace cooled, we find that the carbon steel has the higher transformation temperature. According to the authors' hypothesis, then, the plain carbon steel has more nearly completed the embrittlement reaction than has the chromium-molybdenum steel—though the time at reaction temperature was smaller by a factor of many thousand. It would be surprising if so small an alloy addition had so great a retarding effect on any reaction.

The slight differences which the authors report in an SAE 1045 steel, before and after embrittling treatments, may be caused by the relatively high manganese content, 0.81 pct. Previously published work¹⁷ indicates that carbon steels do not show such differences if the manganese content is below 0.60 pct.

L. D. JAFFE and D. C. BUFFUM—It is true that small alloy additions increase the strength of ferrite. The reason is well understood: foreign atoms in solid solu-

tion within a lattice make slip more difficult. There are no theoretical basis and no experimental data to support the belief that alloys would make ferrite tougher. On the contrary, their strengthening effect would itself be expected to make the material less tough.

The data of Hollomon⁶ cited by Mr. Maltz refer to a plain carbon steel air-cooled from the austenitizing temperature, whose microstructure would consist of tempered pearlite and primary ferrite. The data of Archer, Briggs, and Loeb¹⁷ concern a fully-hardened alloy steel, whose microstructure would consist of tempered martensite. It is well known that pearlite-ferrite mixtures have much higher transition temperatures than tempered martensites¹⁸ (other things being equal), so Mr. Maltz's comparison throws no light upon the temper brittleness of the steels. It may be noted, however, that moderate additions of molybdenum do retard one reaction—the transformation of austenite to pearlite and proeutectoid ferrite—by at least a factor of a thousand.¹⁹

We agree with Mr. Maltz that the slight differences in the SAE 1045 before and after embrittling treatments may be caused by the relatively high manganese contents.

Before closing we should like to mention a discussion that was submitted to us through private correspondence by the late Mr. Ernest Teichert of Pennsylvania State College. Mr. Teichert asked about the effects of longer embrittlement treatment. If our theory is correct, he pointed out, the carbon steel should show no additional embrittlement. As a result of this suggestion we have given the plain carbon steel a treatment of 500 hr at 455°C. The transition temperature was the same as for the 50 hr treatment.

¹⁵ J. H. Hollomon, L. D. Jaffe, D. E. McCarthy, and M. R. Norton: The Effects of Microstructure on the Mechanical Properties of Steel. *Trans. ASM* (1947) 38, 807-847.

¹⁷ J. R. Blanchard, R. M. Parke, and A. J. Herzog: The Effect of Molybdenum on the Isothermal, Subcritical Transformation of Austenite in Low and Medium Carbon Steels. *Trans. ASM* (1941) 29, 317-338.

¹⁶ D. McLean and L. Northcott: Micro-Examination and Electrode Potential Measurements of Temper Brittle Steels. *Jnl. Iron and Steel Inst.* (1948) 158, 169-177.

¹⁸ P. V. Riffin: Unpublished work, Watertown Arsenal.

* U. S. Naval Gun Factory.

¹⁷ R. S. Archer, J. Z. Briggs, and C. M. Loeb, Jr.: Molybdenum. Climax Molybdenum Co. 1948, p. 5.

Some Factors Affecting the Rate of Grain Growth in Metals

By J. E. BURKE

DISCUSSION

(S. E. Maddigan presiding)

S. E. MADDIGAN*—Dr. Orowan

* Industrial and Scientific Research Council, Univ. of British Columbia.

made the remark that in the field of cold-working of metals there was still room for a great deal of work, and he estimated it would be at least two decades before the subject became a finished article. I think in the field of recrystallization and grain growth, while it may not take two

decades, there are still a great many questions to be answered, and it is extremely fortunate that since the war there have been several groups in this country able to devote attention to a continuous study of such fundamental problems. The present paper for instance

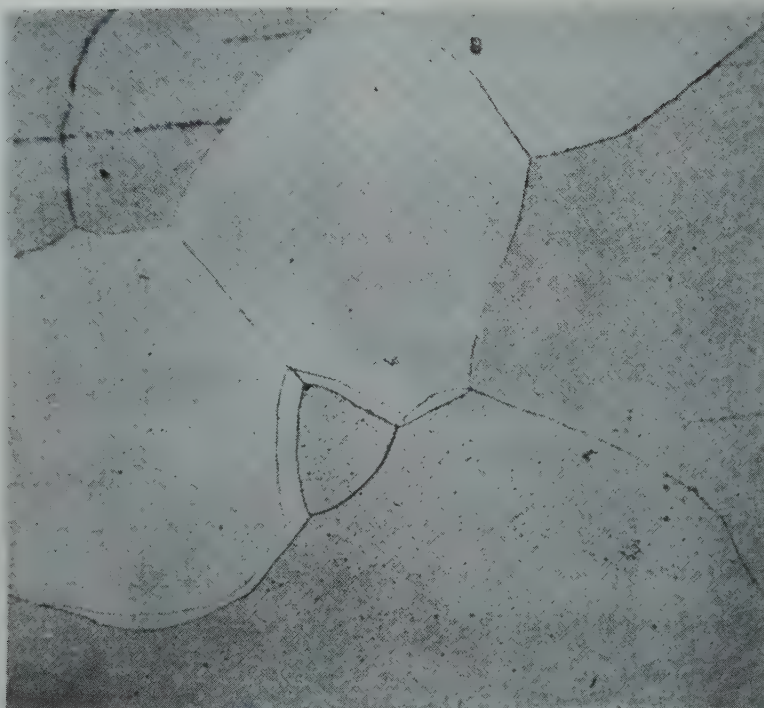


FIG 21—A time lapse micrograph illustrating a small grain in the plane of polish absorbing its larger neighbors.

The boundary migration of the small center grain is in a direction opposite that of the center of curvature of the migrating boundary.

is one of a series devoted to answering some of the questions connected with grain growth.

G. W. WENSCH*—It is readily apparent to those of us interested in the coalescence behavior of metals, that this paper is an excellent contribution to the literature. Furthermore, due to the fine control measures used in the experimental technique, the previous divergences existing between the data of Walker⁴ and Beck³ can be explained.

In observing many micrographs illustrating grain growth in metals it appeared that Harker and Parker's⁹ hypothesis was correct in that boundary migration moved in a direction toward the center of curvature of the migrating boundary. However in Carpenter and Elam's¹⁶ study on grain growth in antimony-tin alloys it was found that the migrating boundary can move in a direction opposite to that of its center of curvature as shown by Fig 21.

Since the existing theories do not satisfactorily explain the anomalous behavior cited above, could the author be induced to comment on this apparent oddity? Can the author now justify the use of Eq 3 as a basis for his derivation of Eq 7?

C. G. DUNN†—I would like to con-

gratulate the author for his beautiful piece of work on the source of energy, the driving force for grain growth. Regarding the source of energy, I might comment on the question just raised by Mr. Wensch in connection with the work of Carpenter and Elam. Their material was in a strained state, I believe. The picture is entirely different if the metal is strained for a boundary may then move away from its center of curvature. The process may still be of the nature of grain growth. Dr. Burke did some work himself showing that grain growth can occur in material slightly strained, and in cases of that type, the strain energy in the crystals adds to the driving force.

The type of grain growth considered in the present work was clearly stated in the text. Some comments on this subject, however, may be worth making. There are two types of grain growth. First there is normal grain growth, or continuous grain growth according to Professor Beck. The thickness of the sample is a limiting factor with normal grain growth. The second type is usually referred to as exaggerated grain growth, but Professor Beck calls this discontinuous grain growth. As Dr. Burke points out in the paper, the effect of sample thickness is different for exaggerated grain growth; the final grain size is entirely independent of the thickness of the material.

I would like to discuss the picture that Dr. Parker presented on the 120° angles because it is based implicitly on the assumption that the driving force or surface tension is a constant and is independent of relative orientation. Surface

tension, I believe, clearly depends on difference in orientation of adjacent grains. Data have been obtained showing that angles can depart quite far from the 120° value.¹⁷ Such variations complicate the geometrical picture a little, but I would agree with the author and Dr. Parker that the geometry is a very important factor in grain growth processes. I would question the 120° angle, however, as being particularly important. I think the 120° angle may be a sort of average value which may be seen more often than any other angle, but it is somewhat of a coincidence when only 120° angles are obtained.

E. A. GULBRANSEN*—I am concerned about the interpretation of the activation energy in Eq 2 and 8. It would be an advantage to relate the energy of activation found for the rate of grain growth to a diffusion process. If this could be done H would have a physical meaning and the value could be compared to values of H obtained from other experiments. The value obtained for H , namely, 60,000 cal per mol appears very large for a diffusion mechanism.

P. A. BECK†—The suggestion that the various structural changes occurring in cold worked metals upon annealing are the result of the surface energy associated with the internal surfaces appears to have been first clearly formulated by G. Tammann in 1912.¹⁸ As originally proposed, this theory was supposed to apply to both processes which usually take place under such circumstances, namely recrystallization and grain growth. Bengough and Hudson¹⁹ noted as early as 1910 that recrystallization may lead to grain refinement. The subsequent studies of Chappell²⁰ on iron and of Mathewson and Phillips²¹ on brass definitely proved that in the first stages of recrystallization after severe deformation, numerous small new grains are formed within each one of the deformed original grains. Mathewson and Phillips clearly realized that the "disintegration" of each deformed grain into numerous smaller ones during recrystallization is tantamount to an increase in the grain boundary surface energy, and that this energy increase must be supplied by that part of the strain energy absorbed by the metal during deformation. A detailed and lucid discussion of the energetics of recrystallization and of grain growth was given by H. Althertum in 1922,²² who carefully differentiated between these two processes, and correctly identified the driving force of grain growth (in contrast to that

* International Nickel Company Graduate Fellow, Dept. of Mining and Metallurgical Eng., Univ. of Ill.

† General Electric Co., Pittsfield, Mass.

¹⁶ H. C. H. Carpenter and C. F. Elam: Crystal Growth and Recrystallization in Metals. *Jnl. Inst. of Metals*, (1920) 24, 83.

¹⁷ C. G. Dunn and F. Lionetti: The Effect of Orientation Difference on Grain Boundary Energies. *Jnl. of Metals*, Feb. 1949, 125. *Trans. AIME* (1949) 185.

* Westinghouse Research Laboratories.

† University of Notre Dame.

of recrystallization) as the surface energy connected with the grain boundaries. His views had been accepted by most research workers for a number of years, without much further investigation of the details of the grain growth process.

It was Harker and Parker's accomplishment^{22a} to give a more detailed picture of the mechanism of grain growth in terms of movements of individual grain boundary surfaces and vertices, as described in the present paper by Burke. Recently C. S. Smith^{22b} elaborated upon Harker and Parker's proposal and contributed important refinements to the theory. Burke's experiment with partially melted brass may be considered as the first direct proof of Harker and Parker's ideas. The old and familiar concept that small crystals, surrounded by the mother liquor, are unstable in the presence of larger crystals of the same species, will have to be discarded if the basic features of the Harker-Parker theory are correct. If both the small and the large crystals are idiomorphic, according to this theory the atoms at their corresponding crystal faces should be in equally stable positions. Even though the total surface energy would decrease with an increase in the crystal size, according to the theory discussed no mechanism is available to accomplish such a change. The system may remain indefinitely in a state which is stable with respect to other immediately attainable states. Considering the critical importance of this experiment, one would like to see it repeated and confirmed by experiments involving annealing times longer than 6 min., and also with materials other than metals.

In their original paper, Harker and Parker made the additional assumption that polycrystalline metals, when annealed, will actually attain a grain boundary configuration stable in the above sense. From this assumption they derived the conclusion that, when a polycrystalline metal is annealed, grain growth eventually stops, as the stable grain boundary configuration is reached. Subsequent experimental work with high purity aluminum and with some high purity solid solutions² failed to confirm the cessation of grain growth in the postulated manner. In the present paper Burke shows that it is possible to accept the Harker-Parker mechanism of grain growth without the necessity of also accepting the assumption that a stable boundary configuration would be actually reached in the course of grain growth. As a matter of fact, experiments by C. S. Smith with soap foams, as well as the above mentioned results with high purity aluminum, indicate that the unstable boundary configuration is self-perpetuating. The stoppage of grain growth postulated by Harker and Parker may be considered very unlikely.

There are, however, other causes which may bring grain growth to a halt. The

stoppage of grain growth by a dispersed second phase was observed long ago; it was first clearly described in 1916 by Z. Jeffries.²³ A great number of investigations dealt with the subject later. In recent isothermal studies at this Laboratory,²⁴ conditions were investigated under which an initial period of grain growth is followed by stoppage of grain growth as a result of the presence of a dispersed second phase in Al-Mn alloys. The stoppage of grain growth in commercial brass, observed by Walker, was confirmed and interpreted²⁵ in the light of these results as a second-phase effect. Burke's interpretation, in the present paper, of the inhibition effect found by Walker is in complete agreement with the interpretation referred to above.^{24,25} An increase in the number of second phase particles increases the inhibiting effect which can then successfully oppose a higher level of "growth force"; consequently, grain growth stops at a smaller grain size.²⁴ The extreme sensitivity of the rate of growth, when the grain size is large, to even the smallest amounts of a second phase is clearly shown by the inhibition effects Burke found in high purity brass. Zener's interpretation as described in Burke's paper, of the inhibition by second phase particles as a surface tension effect is a notable contribution to the understanding of these phenomena.

That grain growth will cease, even in the absence of a second phase, when the grain size becomes commensurate with the specimen thickness, was shown for high purity aluminum.²² The inhibition effect discussed above is, of course, by no means in contradiction with this specimen thickness effect. The two effects may occur independently in the same material, or they may overlap, according to the conditions. This is clearly shown by the data contained in Burke's Table 4. Under the heading "Equilibrium Grain Size"* the table gives the grain size values ultimately reached at various temperatures, with specimens of commercial brass of various thicknesses. If these ultimate grain size values are plotted for each temperature as a function of the specimen thickness (Fig 22), it becomes clear that, when the specimen thickness is very small, the ultimate grain size follows the straight line corresponding to the specimen thickness effect. Thus, in commercial brass, up to a specimen thickness of approximately 0.1 mm, where the grain size is limited solely by the specimen thickness, at 700 to 850°C the ultimate grain size is independent of the annealing temperature. On the other hand, at very large specimen thicknesses, the ultimate

grain size is practically independent of the specimen thickness, but it is determined instead, by the inhibiting effect of the dispersed second phase. Under such conditions the ultimate grain size is strongly temperature-dependent. The data also indicate that between these two ranges there is considerable overlapping, so that in the intermediate range of specimen thicknesses both the specimen thickness and the inhibition by a second phase have some effect on the ultimate grain size. J. Towers Jr. at this laboratory observed similar behavior in high purity brass, except that for this material the thickness range in which the grain size is determined solely by the specimen thickness, is considerably larger. The effect of inhibition on the ultimate grain size at 800°C is not felt until a grain size of about 0.6 mm is reached.

The empirical formula Eq 7, proposed by Burke, does give a vanishing rate of growth when the grain size approaches its ultimate value, as is evident from the differential form, Eq 6. However, this formula suffers from two important disadvantages. First, it does not fit the facts and, secondly, it is not consistent within itself. As seen in Fig 23, where the dotted curves represent values computed from Eq 7, at both 700 and 800°C, there are rather large deviations between the grain sizes experimentally determined by Dr. Burke, and the calculated curves. The nature of the trouble is clear if one considers that the logarithmic expression in Eq 7 gives a gradual, asymptotic, approach to the ultimate grain size, which is only reached after an infinite time of annealing. The data obtained by Burke for 800°C are in accord with similar data obtained at this laboratory with Al-Mn alloys, in that the ultimate grain size is reached after a finite period of annealing. During a considerable part of this period the grain size increases according to the simple power law $D = K \cdot t^n$. After the period of initial grain growth, the grain size remains constant for long periods of further annealing, within the experimental accuracy of grain size determination. There appears to be in most cases only a relatively short interval of decreasing slope between the ascending and the horizontal straight line portions of the logarithmic grain growth lines (Fig 23). This rather sharp break in the curve, which is also shown by Burke's own experimental data in Fig 20, is not reproduced by his formula. The second objection to this formula is that it necessarily leads to a slope of 0.5 for grain sizes small in comparison with the ultimate grain size. (In order to make the initial slope apparent in the graph, the zero point of the time scale must be chosen to correspond with zero grain size.) As known from earlier work with high purity aluminum²² and also from the present data on high purity brass, a slope of 0.5 is approached only with very high purity

* In the physical sciences equilibrium designates states to which the system tends to return, when disturbed. In the present case the grain size will obviously not tend to return to the so-called "equilibrium grain size" if, by some means, a slightly larger grain size was reached. The term "ultimate grain size" had been proposed by Dean and Hudson,²⁶ in 1924; there does not appear to be any reason for changing this nomenclature.

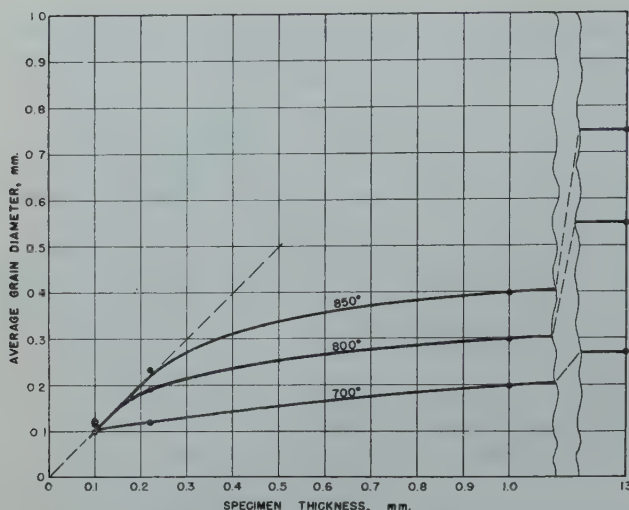


FIG 22—Ultimate grain size, D_n as a function of specimen thickness, for 70-30 brass of commercial purity, from data by J. E. Burke.

metals and solid solutions. In the presence of even small amounts of impurities forming a second phase, as in commercial brass, the initial slope becomes much smaller than 0.5. While the formula does, as intended, take into account the stoppage of grain growth after prolonged annealing periods as a result of a second phase, it represents the conditions during the period of initial grain growth as if no second phase particles were present. It is possible to devise empirical formulas, like the following one, which give considerably better approximation to the experimentally observed facts than Eq 7.

$$\log D = n \cdot \log t - C \cdot t^m + K \quad [9]$$

where n is the initial slope in accordance with the experimental data, parameters m and C are determined by the annealing time necessary to reach the ultimate grain size, and by the value of the ultimate grain size. The parameter K fixes the position of the initial ascending part of the grain growth line. This formula has the advantage of conforming to the simple power law to any extent required by the data. It has just the right number of parameters necessary to fit the data, and it reproduces the stoppage of grain growth after a finite time of annealing. Furthermore, the agreement is greatly improved by accepting the experimental fact that the ultimate grain size is temperature dependent, as discussed above. Fig 23 shows that the solid curves, calculated from Eq 9, fit Burke's experimental data for high purity brass at 700 and 800°C, considerably better than the formula proposed by him. In discussing his Eq 7, Burke introduces Eq 8 for the temperature dependence of his parameter K . However, he neglects the fact that D_f also varies with the temperature.

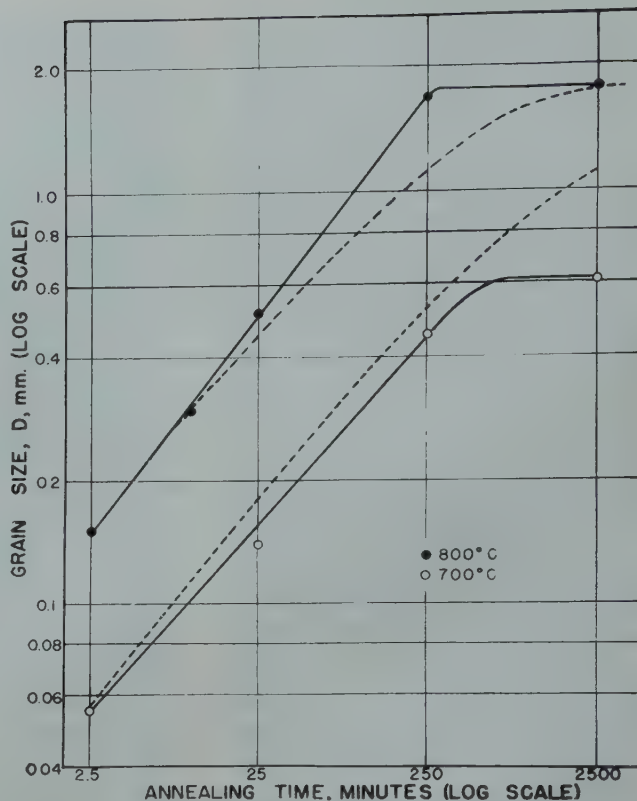


FIG 23—Comparison of grain growth data by J. E. Burke for high purity 70-30 brass with curves calculated from Burke's Eq 7 (dotted lines), and with curves calculated from Eq 9 (solid lines).

In earlier publications^{26,27} Burke proposed the following formula to take into account the initial grain size:

$$D - D_0 = K \cdot t^n$$

It has been shown⁸ that this formula does not fit the data for either high purity aluminum or for brass. It is gratifying to note that in his present paper, Dr. Burke finally abandoned this formula and that he now uses the method proposed earlier in the work on aluminum,²² to account for variations in the initial grain size.

It is a remarkable fact, discovered by Burke, that the slope of the logarithmic grain growth lines for high purity brass closely approximates the value of 0.5 over a rather wide temperature range. This value was previously derived²² for high purity metals regardless of temperature. But in experiments with high purity aluminum the slope was found to increase with the temperature, and the theoretical value of 0.5 was approached only by extrapolation to the melting point. It was observed, however, that with high purity Al-Mg solid solutions n approaches the theoretical value of 0.5 at a lower temperature and then remains almost constant near that value.²⁹ The temperature range, within which n is nearly 0.5 increases with increasing Mg content. It may be that Cu-Zn solid solutions behave similarly. If so, one might

expect that at relatively low temperatures the grain growth line for high purity brass containing lower amounts of zinc, such as 5 or 10 pct, would have a temperature dependent slope, lower than 0.5, but that, beginning with a certain temperature, the slope would approximate 0.5, and become independent of temperature. This temperature would then decrease with increasing Zn content, until it would fall below 500 or 450°C for 70-30 brass.

Burke gives a heat of activation value for grain growth in high purity brass (40 K cal per g atom), which is considerably lower than the value previously found by Burke and confirmed at this laboratory for commercial brass (60 K cal per g atom) in the range between 450 and 700°C. In the course of work with high purity brass done by John Towers, Jr. at this laboratory, using laborious and very careful grain counting techniques and a larger number of specimens, a value distinctly higher than that reported by Burke, namely 49.8 K cal per g atom, was obtained. When Dr. Burke's data were used to calculate a heat of activation from the time to reach a grain size of 0.1 mm, it was found by Mr. Towers that a value of approximately 46.5 K cal per g atom fits the data best. This is in better agreement with the above value, calculated by Towers from his own data, than the 40 K cal per g atom value given by Burke.

J. E. BURKE (author's reply)—In reply to Mr. Wensch, I believe the apparent migration of a boundary away from its center of curvature can be explained. C. S. Smith has pointed out that a surface may be curved about two axes at right angles to each other so that the net curvature at any point on the surface is zero. The surface is thus equivalent to a plane and will have no tendency to migrate. A plane will intersect such a surface in a curved line, however. Thus, on a plane polished surface of a metal specimen, it would be impossible to differentiate between it and a truly curved boundary which should migrate toward its apparent center of curvature, or even one which should migrate away from its apparent center of curvature. Any studies of grain growth on a polished surface are open to some doubt, also. A grain which intersects a surface has a different environment from a grain in the body of a specimen. Grain boundaries will intersect the surface at 90° at equilibrium, and an intersection at an angle of other than 90° may lead to grain boundary migration to readjust the angle. In reply to Mr. Wensch's second question, the quantity D which appears in Eq 3 is the same as the quantity D_i in Eq 7.

As Dr. Dunn has beautifully shown at this meeting, the surface tension of the grain boundaries does depend upon the relative orientation of the grains on opposite sides of the boundaries, and thus only rarely will the equilibrium boundary angle be precisely 120°, as called for on a simple, isotropic surface tension picture.

I agree with Dr. Gulbransen's concern about the physical significance of the activation energies presented in Eq 2 and 8. The value of 40,000 cal per mol (rather than 60,000 cal per mol for commercial purity brass) for high purity brass is very close to the reported heats of activation for diffusion of zinc in brass of that composition. One is thus tempted to suggest that grain boundary migration occurs by a diffusion mechanism. Against this is the uncertainty of the mechanism of grain boundary migration, and the fact that a change in number of inclusions with temperature may influence the temperature dependence of growth rate and the computed value of H . Later evidence which will be published shortly indicates that the temperature dependence of the rate of grain boundary migration in pure copper varies with the crystallographic direction of boundary migration. Since diffusion in cubic metals is isotropic, this indicates that grain boundary migration is not identical with bulk diffusion. However, in a two component alloy like brass, there may well be an adsorbed layer of zinc at the grain boundaries, so that this must migrate by lattice diffusion when the grain boundary migrates by any other mechanism. This could well be the rate controlling step, and thus one would

measure the activation energy for diffusion of zinc.

Mr. Beck's discussion is exhaustive, and in the interest of brevity I shall answer only those points which are pertinent to this paper and not already discussed in the body of the paper.

As was stated, a number of workers have postulated that surface energy is the driving force for grain growth, but contrary to Mr. Beck's statement, by no means all workers have accepted this explanation. In any case, it is preferable to use experiment rather than acceptance by workers in the field to test the validity of an hypothesis. The concept that the escaping tendency from a surface is a function of the curvature of the surface is not new. W. Thomson³⁰ showed that the vapor pressure of a liquid droplet is inversely proportional to its radius of curvature, and the formal proof of this may be found in most texts on Thermodynamics.³¹ Vogel and Harker and Parker applied this concept qualitatively to the migration of grain boundaries, and in the present paper it has been applied quantitatively.

It takes energy to create a new surface, therefore a small crystal, which has more surface per unit volume than a large crystal, will have more energy per atom than a large one. In solution where there is a constant interchange between surface atoms of the crystal and saturated solution, there will be a tendency for large crystals to grow at the expense of small ones. For this effect to result in an appreciable rate of growth, however, the small crystals must be very small, much smaller than the grain sizes in metals where grain growth is experimentally observed to occur at measurable rates. There is undoubtedly a slight tendency for a large grain to grow at the expense of a small one in a solid metal, across a plane interface, but the effect is so small that it is not observable, as evidenced by the fact that plane grain boundaries between grains of different length along a wire do not migrate. The greater stability of a plane surface over a curved surface is shown by the restoration of a fragment of a crystal into an ideomorphic crystal when the fragment is immersed in a saturated solution. The solubility of the curved faces and edges produced by fracturing is greater than the solubility of the perfect crystal. In polycrystalline metals the relatively rapid rate of grain boundary migration results from a convex surface (positive curvature) being in contact with a concave surface (negative curvature). The difference in escaping tendency between these two surfaces is much greater than the difference between two surfaces having similar curvatures of the same sign. As was explained in the paper, this accounts for the very low rates of grain growth in partially melted specimens. Nevertheless, if they were heated for very long periods, one would

expect small amounts of growth of the large crystals to occur at the expense of small ones.

Mr. Beck concurs with the statement in the paper that it is unlikely that grain growth will stop by the grain shapes fulfilling the Harker and Parker criterion for equilibrium, and quotes evidence from his own work that grain growth does not stop. One of the objects of this research was to reconcile the indication of his work that grain growth continues at an unabated rate until the grain size approximates the size of the specimen, with the fact mentioned by Mr. Wensch that grain growth frequently stops earlier than this. I am glad Mr. Beck now agrees that grain growth does not necessarily continue until the grain size approximates the size of the piece, and regret that his explanation of the phenomenon was not available until some time after this paper was submitted for publication. It is somewhat surprising that he agrees with the Zener formulation of the inhibiting effect of second phase particles, since it also is based on the assumption that grain boundary curvature is necessary for grain growth to occur.

As Mr. Beck mentions, the specimen thickness effect is by no means in contradiction to the inhibiting effect of inclusions, rather, as is explained in the paper, they are different manifestations of the importance of grain boundary curvature.

It is not clear what Mr. Beck intends to show by Fig 22. The data on specimen thickness were used in the paper to show that in very thin specimens the limiting grain size was a larger proportion of the specimen thickness than in thicker specimens, because in thin specimens the grain size is smaller and thus the growth force is greater. The results thus confirm the explanation given for the specimen thickness effect.

Mr. Beck objects to Eq 7 and has presented an empirical four constant equation which fits the experimental data better. It is agreed that there are numerous mathematical procedures for fitting a curve to a set of data, determining the equation for the curve, and evaluating the constants in the equation. The object in presenting Eq 7 was not to develop an empirical equation which would fit the data obtained, but to test the assumptions made as to the mechanism of grain growth. These assumptions were that the rate of growth is proportional to the effective curvature of the boundary, that is the difference between the present and the limiting curvature, and that the effect of temperature is to vary the specific reaction rate constant, K , according to the Arrhenius relationship

$$K = A \cdot e^{-H/RT}$$

The equation is semi-empirical, in that the constants K and H must be evaluated experimentally. The slopes of the curves, and the general shape are not controlled

by arbitrary constants as in the equation proposed by Mr. Beck. When the mechanism of the process is better understood, it should be possible to compute the value of H and K , and in principle, even D_f . For example, factors which will influence K are the surface energy of the boundary, and a geometric factor relating the rate of grain growth to the true rate of grain boundary migration. It is also obvious that if the temperature dependence of D_f had been taken into account a better agreement with the observed data would have been obtained. This has been stated elsewhere.³² The quite good agreement between the curves calculated from these assumptions and the observed data are taken to indicate, as stated in the paper, that these assumptions are essentially correct.

It should be pointed out that the earlier derivation of the slope of 0.5 for the log grain size versus log time curves⁵ was based upon the assumption that the rate of grain growth is proportional to the total amount of grain boundary present. The present hypothesis is that the rate of growth is proportional to the effective curvature of the grain faces. It possesses the advantage that the role of inclusions and changes in grain size distribution can be explained on this basis. Only in the absence of inclusions and only when the relative grain size distribution remains constant does the present assumption lead to a slope of 0.5 for the logarithmic curves.

The earlier heat of activation of 60,000 cal per mol (based on Walker's work, and confirmed by Beck) was shown in the present work to be influenced by solution of impurities as the temperature increases. The value of 40,000 to 43,000 cal per mol observed for the high purity brass in the present work is at least internally consistent at all temperatures. In recomputing a value from the present data, Mr. Towers has taken as his measure of rate the time

necessary to reach a grain size of 0.1 mm, and presumably measured his own value of 49.8 K cal per mol in a similar way. This method of comparing rates at different temperatures is less certain than the method of superimposing curves, since the curves must be extrapolated and there is considerable freedom in selecting the exact slope to the extrapolated. When the curves are superimposed, more of the data can be used.

It is felt that it is meaningless to give such activation energies to three significant figures, for several reasons:

1. The rate of grain growth (rate of disappearance of grains) is not the fundamental process for which an activation energy should be computed. The fundamental process is the migration of grain boundaries, and one must assume that the rate of grain boundary migration is proportional to the rate at which grains disappear.

2. There may be reasons other than a change in the number of activated atoms with temperature which cause the rate of grain growth to change with temperature. An example cited in the present paper is a change in the number of inclusions. Another possible one is a change in the mechanism of grain boundary migration.

3. Later work indicates that the activation energy for grain growth depends upon crystallographic factors, and that it may differ for different directions of migration of the same grain in a uniform matrix. Thus at best an average value will be measured in a polycrystalline material, and it might change with differences in preferred orientation.

References

18. G. Tammann: *Über die Änderung der Eigenschaften bei der Bearbeitung von Metallen. Ztsch. Elektrochemie* (1912) 18, 584.
19. G. D. Bengough and O. F. Hudson: *Heat Treatment of Brass. Jnl. Inst. Met.* (1910) 4, 92-111.
20. C. Chappell: *Recrystallization of Deformed Iron. Jnl. Iron & Steel Inst.* (1914) 89, 48.
21. C. H. Mathewson and Arthur Phillips: *Recrystallization of Cold Worked Alpha Brass on Annealing. Trans. AIME* (1916) 54, 608.
22. H. Althertum: *Zur Theorie der Rekristallisation. Ztsch. Metallk.* (1922) 14, 417.
- 22a. D. Harker and E. R. Parker: *Grain Shape and Grain Growth. Trans. ASM*, (1945) 34, 156.
- 22b. C. S. Smith: *Grains, Phases and Interfaces: An Interpretation of Microstructure. Trans. AIME* (1948) 175, 15. *Metals Tech.* June 1948. TP 2387.
- 22c. P. A. Beck, J. C. Kremer, L. J. Demer, and M. L. Holzworth: *Grain Growth in High Purity Aluminum and in Aluminum-magnesium Alloy. Trans. AIME* (1948) 175, 372; *Metals Tech.*, Sept. 1947. TP 2280.
23. Z. Jeffries: *Grain Growth Phenomena in Metals. Trans. AIME* (1916) 56, 171.
24. Paul A. Beck, M. L. Holzworth and Philip R. Sperry: *Effect of a Dispersed Phase on Grain Growth in Al-Mn Alloys. Trans. AIME* (1949) 180. *Metals Tech.* Sept. 1948. TP 2475.
25. Discussion, Institute of Metals Division. *AIME, Metals Tech.*, Aug. 1948, TP 2449, p. 60.
26. R. S. Dean and W. E. J. Hudson: *Grain Growth in Lead Containing One Per Cent of Antimony. Jnl. Amer. Chem. Soc.* (1924) 46, 1778.
27. J. E. Burke: *Grain Growth in Alpha-Brass. Jnl. Appl. Phys.* (1947) 18, 1028.
28. Paul A. Beck: *Comments on "Grain Growth in Alpha-Brass." Jnl. Appl. Phys.* (1947) 18, 1028.
29. Louis J. Demer and Paul A. Beck: *Effect of Composition on Grain Growth in Aluminum-magnesium Solid Solutions. Trans. AIME* (1949) 180. *Metals Tech.* June 1948. TP 2374.
30. W. Thomson: *Phil. Mag.* 4, 42, 448 (1881).
31. See for example Lewis and Randall "Thermodynamics" McGraw-Hill, New York (1923) p. 252.
32. *Grain Control in Industrial Metallurgy*, ASM, Cleveland (1949).

Preferred Orientation in Rolled and Recrystallized Beryllium

By A. SMIGELSKAS and C. S. BARRETT

DISCUSSION

(E. Parker presiding)

J. T. NORTON*—I think Mrs. Smigelskas Fischer has done a splendid job in working out the pole figures from

rather difficult photograms which are common to beryllium. Is there not a mistake in Fig 2 in that the pole figures B and C have been interchanged?

A. SMIGELSKAS FISCHER (authors' reply)—Yes, there is such an error in the labeling of the pole figures of Fig 2. The correct plane for Fig 2b and 2c is the

plane in parenthesis above the figure numbers and not that in the figure subtitle.

J. T. NORTON—Also, I would like to mention another method of obtaining the data for pole figures which would be particularly applicable to this problem. It is a method which has been published only

* Massachusetts Institute of Technology.

recently and some of you may not be familiar with it. In the use of thin foils, such as are involved in this problem, it again involves making up a sandwich out of several sheets cemented together with the rolling direction parallel in all sheets and then cutting out small cylindrical rods just as Mrs. Fischer did. Several rods would be cut out of the specimen with their axes making various angles with the rolling direction. These rods are then put in an X ray spectrometer fitted with a Geiger counter tube and the intensity of reflection from a particular family of planes is recorded as the rod slowly rotates. For instance, if we were to make a basal plane pole figure corresponding to Fig 2 of the paper, the cylindrical rod with its axis parallel to the rolling direction would be mounted in the direct beam of the spectrometer with the rod axis parallel to the spectrometer axis. The Geiger tube would be set at the correct angle to receive the basal plane reflection and clamped. The rod is then rotated at a constant rate and the output of the Geiger tube recorded on the chart. The resulting curve represents the intensity variation and hence the pole density variation for a diameter of the pole figure perpendicular to the rolling direction. Similarly, each of the other rods will give information about other diameters of the pole figure. Since the rods are geometrically identical, no ab-

sorption correction is necessary and all of the curves will be consistent. By drawing lines at different intensity levels above the background and measuring the angles at which these lines intersect the curves, data are available for drawing accurate pole density contours on the final pole figure. Usually six rods are sufficient to give adequate coverage of the pole figure and no part of the figure is left out. For a material as transparent as beryllium, the rods could be made fairly large and since a considerable length of the rod can be illuminated, a good integration is obtained for fairly coarse grained materials.*

A. SMIGELSKAS FISCHER—Thank you very much for describing your method. It seems to be more effective than the one we have used inasmuch as it enables one to obtain quantitatively the variation of intensity of scatter about a mean which is important in determining the exact extent of preferred orientations. We were able to estimate this extent only by eye. However, this work, which was declassified only recently, was completed several years ago. At that time, we did not have the benefit of your nice technique nor a spectrometer with which to develop any similar method.

* J. T. Norton: *Jnl. of Appl. Phys.* Dec. 1948, 19, 1176.

E. PARKER*—Everything sounds so easy the way you described it in the figures. I once tried to roll some beryllium. That was not so easy; in fact we found it very difficult. Would you care to make some comments about how the beryllium was rolled?

A. SMIGELSKAS FISCHER—I am sorry, but that is still classified information,

E. A. GULBRANSEN†—Could you use any other radiation instead of molybdenum?

A. SMIGELSKAS FISCHER—We could use other radiation but we found molybdenum best suited for our purposes.

E. A. GULBRANSEN—Though with a small figure?

A. SMIGELSKAS FISCHER—Even though the figure is small the lines are sharp and we are able to differentiate between the diffraction rings. While using longer wave lengths would spread the figure, it would also tend to broaden the lines and weaken their intensity if the same specimen to film distance and the same exposure time were used. Therefore, we felt that we would not gain any advantage from a larger figure.

* Univ. of California, Berkeley, Calif.
† Westinghouse Electric Co., East Pittsburgh, Pa.

A Study of Textures and Earing Behavior of Cold-rolled (87-89 pct) and Annealed Copper Strips

By MING-KAO YEN

DISCUSSION

(S. E. Maddigan presiding)

S. E. MADDIGAN*—I think Mr. Yen should be complimented on doing a very excellent and a very comprehensive piece of work. I was particularly pleased to note the use of X rays in a somewhat less tedious technique than pole figures. In the past I think many workers have been diverted away from the use of X rays in such investigations because of the large amount of work involved in pole figures if one is dealing with a great number of specimens. The same thing, I think, applies to the determination of orientations by counting of twins which is also a very tedious procedure; as a result several

papers which have otherwise been of excellent quality have depended upon etching techniques for determination of orientation. The present paper indicates that the results reported in those previous papers were correct, but I think the use of etching techniques alone is a rather shaky basis for setting up theories in the literature.

W. M. BALDWIN, JR.*—This discussion will be a short note of correction and apology. In my discussion of Brick, Martin and Angier's paper I incorrectly reported the orientation of phosphorus deoxidized copper annealed at temperatures. When I learned that Mr. Yen was preparing the present paper I asked that he correct this previous error, which he

most graciously consented to do. However, through my ambiguity the correction noted on p. 59 of Mr. Yen's paper is still not the proper one. For this I take full responsibility. The orientation which I observed in phosphorus deoxidized copper at high temperatures is the (112) [11 $\bar{1}$] which agrees with the pole figure given in Fig 8a, on p. 65 of Mr. Yen's paper. Our observations were made on the basis of twin counts rather than X ray determinations and therefore serve as an independent confirmation of Mr. Yen's data.

M. K. YEN (author's reply)—The author wishes to thank Dr. Maddigan for his comments in regard to the application of glancing technique to textures. As a matter of fact, considerable work has been done recently in connection with

* Univ. of British Columbia, Vancouver, B. C.

* Case Institute of Technology.

the study of rolling, wire drawing and electrolytic deposition textures for copper and its alloys by this method or some modification of it. It is to be expected

that this technique may be developed to its full practical importance. In the case of copper, it was found that the approximate position and relative height of ears

in deep drawn cups, as well as grain size and degree of recrystallization, can generally be derived from a single X ray glancing photogram.

Pressure Distribution in Compacting Metal Powders

By POL DUWEZ and LEO ZWELL

DISCUSSION

(*L. S. Busch presiding*)

L. S. BUSCH*—A very interesting use of a new engineering material, the strain gauge, is, I believe, one of the first as applied to powder metallurgy.

J. WULFF†—We have here another valuable contribution to the fundamental data on powder metallurgy from Professor Duwez's laboratory at California Institute of Technology. I am particularly pleased with the measurements which relate to the vertical pressures but not with the measurements which relate to radial pressures on the die wall. In regard to the latter, we gave up similar attempts in our own laboratory to measure radial pressures by methods

similar to those used by the authors of this paper since we believed that their very method of measurement would introduce appreciable error. For this reason, one of my coworkers, Dr. Shank, studied the pressure on the die wall by using a cylindrical thick-walled die with a goodly number of closely spaced strain gauges on the outer wall. The strain distribution in the die wall was thus obtained during pressing from both sides. This enabled the determination of both frictional and radial forces acting on the die wall. The distribution of radial forces in this work appears to be quite different from that obtained by Duwez and Zwell.

A. J. SHALER*—I am very glad that we now have some stress distribution data on the bottom plunger of a cylindrical die during pressing. These data,

along with the side-wall pressure data which the authors have given, and which have also been obtained by the method just described complete the elements required to solve the entire stress strain problem in cylindrical compacts. In previous years Kamm, Steinberg and Wulff have solved the strain distribution problem. I wonder if Professor Duwez could be induced some time when he is not too busy to put some of his strain gauges in the top plunger as well. It would not be necessary, I think, to have the top plunger stress distribution in order to solve the entire problem, but these data would certainly provide a very useful check on the result.

P. DUWEZ (authors' reply)—I think those experiments could be done very easily by using a floating die and two moving plungers instead of one.

* P. R. Mallory & Co., Inc., Indianapolis, Ind.
† Massachusetts Institute of Technology.

* Massachusetts Institute of Technology.

Lead-grid Study of Metal Powder Compaction

By R. KAMM, M. A. STEINBERG, and J. WULFF

DISCUSSION

(*L. S. Busch presiding*)

L. S. BUSCH*—We have had presented two methods of measuring these variations in powder compacts.

E. OROWAN†—In connection with the rolling mill research work carried out at the Cavendish Laboratory, Cambridge, with the help of the British Iron and Steel Research Association, Dr. E. A. W. Hoff, Mr. J. Los, and myself, have determined coefficients of friction at ex-

treme pressures for a number of liquid and solid lubricants, both by direct measurement, and by calculation from measured values of the roll force. The most efficient lubricants at these high pressures (for the small amounts of sliding that occur in rolling) were camphor and, in particular, borneol (Borneo-camphor). Perhaps such lubricants could be used with advantage in the kind of work described by Dr. Wulff.

L. S. BUSCH—I think Dr. Wulff has in the past mentioned experiments which have been performed in the extrusion and rolling of metals and which led to conclusions which can be applied to the

compacting of metal powder.

A. SQUIRE*—There have been some recent developments in the field of high pressure lubricants which indicate that boron nitride might be a very desirable material to employ as a die lubricant. At the present time its cost is prohibitive, but as the need arises for the material it will undoubtedly come down in price. The present price is \$200. a pound.

It is my understanding that one of the reasons for vacuum pressing both in ceramics and metal powders, is to prevent

* P. R. Mallory & Co., Inc.
† Cavendish Laboratory, Cambridge, England.

* Westinghouse Research Laboratories.

the formation of what we call pressure cracks on ejection. I have been assured by people who have done the work themselves in the field that it is possible to press powders at considerably higher pressures under vacuum than it is in air. Apparently the gases trapped during the pressing operation add sufficiently to the internal stress in the compact so that these pressure cracks are formed on ejection. In vacuum pressing this can be avoided.

L. S. BUSCH—I feel that Mr. Squire has a good point, but I also feel that there is another factor as far as pressure cracks are concerned and that is simple expansion as the piece comes out of the dye.

J. WULFF (author's reply)—We have not tried the borneol (Borneo-camphor) suggested by Dr. Orowan. The extremely high point pressures met with in pressing lead us to believe that it should be applicable.

In answer to Mr. Squire, we have found that boron nitride behaves as an abrasive and not as a lubricant in powder pressing. Its application to the lips of crucibles, since it is difficult to wet by molten metal, suggested its use. In an auxiliary research it was also used as a constituent of powder metallurgy bronzes which were tested for friction and wear.

No reduction in friction or wear was experienced. Indeed rolling boron-nitride torn loose from the compact accelerated the wear appreciably.

In regard to Mr. Squire's remarks on pressing, I must say that entrapped air can lead to fracture of the compact as it is ejected from the die or later during sintering. Our results indicate nevertheless that nothing is gained from a density standpoint by vacuum pressing of hard powders and little with soft powders that cannot be achieved readily by efficient lubrication.

Perhaps Professor Shaler would care to comment on Mr. Busch's remarks.

A. J. SHALER*—We have found that cracking upon ejection of the compact is not always due to the lateral elastic expansion of the compact as it comes out of the die, but must occur as soon as the pressure is released. The pattern of stresses set up in the compact when the load is removed from the die walls is such that cracks may form at the center of the compact and spread upward laterally outwards. The way to avoid cracks of this kind would not be to increase or decrease the pressure or change the lubricant, but simply to build dies of greater rigidity so that a lesser residual-stress pattern is created when the die

* Massachusetts Institute of Technology.

walls push back on the compact elastically after release of the pressure.

J. CORDIANO*—On the subject of pressure cracks in specimens on ejection from dies one of the simplest ways of preventing such cracks is to maintain a partial top pressure on the compact during ejection. One question I wanted to ask Dr. Wulff regarding pressing and sintering of these copper compacts is whether he noted bloating of the sintered specimens which were pressed at 60 tsi. Also, was there any difference in bloating tendencies when sintering in vacuum or hydrogen?

J. WULFF—The present tests on copper were sintered in a dilatometer set-up which did not permit close observation of the compact surface during sintering. I have, however, noticed the "bloating" mentioned by Mr. Cordiano on copper compacts pressed at pressure above 60 tsi and later sintered in hydrogen. Indeed, some of these specimens have even exploded in the furnace. Mr. Cordiano's remark that pressure cracks can be avoided by maintaining some pressure on the compact during ejection is well taken. S. K. Wellman has long advocated this technique in the pressing of thin specimens of large area.

* Buel Metals Co., Painesville, Ohio.

Properties of Chromium Boride and Sintered Chromium Boride

By S. J. SINDEBAND

DISCUSSION

(E. Parker presiding)

J. WULFF*—It seems to me that the author could improve the quality of his high temperature material by using less nickel as a cementing agent in hot pressing. Furthermore, to avoid the presence of undiffused nickel which would not be oxidation resistant, permit me to suggest that he use a nickel-chromium powder containing a small percentage of boron. This would give him a liquid phase at a lower temperature and accelerate both sintering and homogenization. The commercial alloy known as colmonoy contains sufficient chromium to be heat resistant

and sufficient boron to be of low melting point. Such an alloy may be applicable as a cementing agent in increasing the quality of Mr. Sindeband's alloys. Finally I believe the author unfair to himself in expecting a porous material to have properties equivalent to one of 100 pct density.

S. J. SINDEBAND—Dr. Wulff's point is well taken. Early in the program we realized the fact that we were having difficulty with these low-melting alloys, and we had hoped, since the colmonoy alloys of which you speak are at the nickel-rich end of the diagram, that by going to the other end of the diagram (chromium boride-rich) we would not have this difficulty. Thus we tried to use very small percentages of binder; but

for reasons which are not exactly apparent we found that when we did this it was necessary to raise the pressing temperature to a point which we were unable to attain. For all compositions which we tried using nickel, or for that matter any nickel iron or cobalt containing material as a binder, we found that we would get low melting boride phases, which as you point out are the commercial "strength" of the hard-facing materials. I personally believe these owe a great deal of their behavior and even hardness to the nickel boride which is considerable evidence when an alloy of chromium boride is made with nickel. Nickel boride itself is very hard. We did try pure chromium as a binder and found there was considerable difficulty in handling it, particularly since we could not just hot press under

* Massachusetts Institute of Technology.

the atmosphere conditions obtaining there. We found that when we vacuum sintered chromium boride, we developed extremely brittle materials, and had to abandon that. It looked quite fruitful at one time. We attempted to make use of materials which either did not form known borides or which formed refractory borides and used those as binders. Apparently the chromium boride itself enters into entirely too many side reactions with binders to permit us to make use of chromium boride to get the ultimate result we were seeking in this particular field.

The comparison with vitallium is a cruel one, but nevertheless it is one which I chose to make simply to indicate the goal for which we are aiming. I believe that alloys of this variety will be able to achieve high temperature strength equivalent with materials such as vitallium and better than that. What we need to do is to find if we continue with borides, a material which does not lose its boron to the binder phase but which will enter into a cementing action with the cement chosen which is similar to that observed in the case of carbides. There actual re-precipitation occurs and much of their strength comes from the matrix and not from the binder.

W. J. KROLL*—It would be of interest to know how much oxygen the powdered chromium boride contained, as well as how much oxygen was present in the chromium powder used for sintering. Wet grinding of such active metals or alloys introduces large amounts of oxide and the contaminated materials may not bind in the sintering operation.

S. J. SINDEBAND—We spent a good deal of time attempting to determine the oxygen content of the boride. Unfortunately the oxygen was largely tied up in the form of oxides of the aluminum which was used for the reduction of the original oxides in thermite reduction, and as such we met great difficulty in making any determination. It was not too clear whether it was all tied up as aluminum oxide or as some complex silicates. However, the analysis of the powders indicated that there was an unaccounted for amount, I believe, of about 3 pct. The table directly under the X ray patterns indicated, for the thermite process, that the known elements added up to 97.25. How much oxygen was in that residue we could not know. As far as the chromium is concerned, we found standard electrolytic chromium unsatisfactory as a binder with which to press the powders. The procedure that we used was to purify this chromium powder by a reduction in

extremely dry hydrogen. We found that if we got the dew point down to the temperature of liquid air we could bright anneal the chromium powder and come out with a powder considerably more ductile. We were then able to press good compacts, but still the resulting sintered cold pressed products were very brittle. The transverse rupture strength was of the order of 27,000 to 30,000 psi, or perhaps a shade higher.

MEMBER—I am particularly interested in the field of wear resistance, and I wonder whether the author has done any work or considered any work in studying these chromium boride compacts as wear resistant materials. You have shown that you had some difficulties in making the high temperature resistant material, but this might be very good wear resistant material.

S. J. SINDEBAND—We have not made any actual wear resistance tests. I believe the wear resistance of this material could be assessed on the basis of the properties that have been presented. Hardness is of major importance. The toughness of the material would be indicated by its transverse rupture strength. I believe that material of this composition has been given some use in cast form by the Wall-Colmonoy people. I would expect that this material as hot pressed would be able to do anything that that material could do, and perhaps do it better by virtue of the finer structure which is attained in this material, much the same as you would expect to get in a comparison between a cast carbide versus a cemented carbide. The wear resistance, I think, of these materials should be good. I think it would depend entirely on the actual application. If there is any acid corrosion present under the circumstances under which you want wear resistance, I think this is a very good material. We did try it as a tool material just briefly, and it cuts well. Actually I believe that if you have anything of 89 or so Rockwell hardness and a transverse rupture strength above 100,000, you can cut and cut well with it. That is good enough, I feel sure.

A. SQUIRE*—I may be mistaken but in looking at that micrograph presented in the paper it seems to me the particles are larger than 3 to 5 microns. The micrograph looks similar to those of carbide where the particle size is possibly one to two microns. Did that micrograph show that much particle size or did the grains grow?

S. J. SINDEBAND—The 3 to 5 micron particle size was the starting point.

We did observe with this material the grain growth was obtained in the hot pressing operation.

R. KIESSLING*—Binary systems, composed of a transition element and boron have been studied for four years at the Institute of Chemistry, University of Upsala. The chromium-boron system belongs to those which have been investigated. As the results in some instances are different from those published in this paper, a short note may be of interest. (The results have been received by *Acta Chemica Scandinavica* for publication.)

Five intermediary phases have been found with relatively small homogeneity ranges and boron contents of 33 (δ), 40 (ϵ), 50 (ζ), 55 (φ), and 67 (θ) at. pct. The structure of the η -phase has been mentioned in connection with a report on the system zirconium-boron (*Acta Chem. Scand.* (1949) 3, 90). The structure of the ϵ -phase is in accordance with the data given by Mr. Frueh. The position of the boron atoms has been determined using Fourier methods. The boron atoms form parallel chains through the metal lattice. The structure is closely related to the structures of the δ -phase in the systems molybdenum and tungsten-boron. (*Acta Chem. Scand.* (1947) 1, 893).

The system behaves in accordance with Hägg's rule for a content of boron up to 60 at. pct and is more complicated than the systems molybdenum-boron and tungsten-boron. The latter two systems have the radius ratio closer to the critical value. The system zirconium-boron, with a radius ratio on the other side of this value has only one simple intermediary phase.

S. J. SINDEBAND—I was very interested to note that work is continuing on a broad scale on the binary systems with boron, at the University of Upsala; particularly since so much of interest emanated from that institution in this field in the past.

I was particularly interested to find that Dr. Kiessling had made an extensive study of the chromium boron system and that his data for the structure of the phase around 50 at. pct corresponded with the data given in the paper I presented, as obtained by Mr. Frueh. In none of the X ray investigations made on chromium boride did we note lines which would correspond with the other bordering phases he has reported. It is quite possible that the method by which the material is made has something to do with this.

I shall await with interest the publication of the complete data regarding these phases.

* Northwest Electrodevelopment Laboratory, U. S. Bureau of Mines, Albany, Oregon.

* Westinghouse Electric Co., East Pittsburgh, Pa.

* Institute of Chemistry, University of Upsala, Sweden.

Solubility Relationships of the Refractory Monocarbides

By J. T. NORTON and A. L. MOWRY

DISCUSSION

(E. Parker presiding)

W. J. KROLL*—I think that since oxygen and nitrogen have a tremendous influence on the mechanical properties of these metals, it can be expected that tracers might have also considerable influence on the mechanical properties of these carbides, I wonder also how far residual oxygen and nitrogen may interfere with the determination of your lattice constants.

J. T. NORTON (authors' reply)—Thank you, Dr. Kroll, for bringing up this question about which we have thought a good deal. We have no specific analysis for oxygen on these carbides chiefly because I do not know how to do it. Maybe you have a suggestion. We do know however that in comparing careful measurements of lattice parameters of the carbides which are deficient in carbon, and where the carbon is undoubtedly

* Northwest Electrodevelopment Laboratory, U. S. Bureau of Mines, Albany, Oregon.

replaced by oxygen or nitrogen or both, there is a negligible change in the value of the lattice parameter until there is a very considerable deficiency in carbon. Titanium carbide is the one we have investigated most completely, and until about a quarter of the possible carbon atoms had been removed there was very little change in the parameter, but beyond that it drops very rapidly. It is believed titanium oxide, TiO and TiC can form a continuous series of solids. It has been investigated but the lattice parameter curve is not linear, and is almost flat at the carbon rich end. Our investigation is based on the carbides which are very nearly saturated with carbon. I am inclined to believe that these impurities which are undoubtedly present in our carbides have very little influence on the lattice parameter because both nitrogen and oxygen will replace carbon in these monocarbides atom for atom. If we had a good method for analyzing for oxygen we would feel a lot better about results of this type. Mr. Redmond of Kene-

metal Corporation has offered to provide us with some carbides made by Mr. Mackenna's process, the so-called Menstruum process you mentioned. It would be interesting to see if those carbides give any different results from the ones which we used.

J. WULFF*—Many of us peruse the literature of powder metallurgy and have been taught that double carbides of refractory metals can be made by the Menstruum method. Are we to believe from the work of the above authors that double carbides cannot be made by the Menstruum method?

J. T. NORTON—You put me on the spot. Certainly in the binary systems, which we have investigated here, there is no evidence of the formation of a double carbide. These are simple replacement solid solutions. There is no critical composition and there is only one type of structure observable over the whole range of compositions.

* Massachusetts Institute of Technology.

The Magnetic Properties of Sintered Iron and Iron Base Alloys

By W. ROSTOKER

DISCUSSION

(A. Squire presiding)

S. J. SINDEBAND*—(1) Discussing the properties of the powders used, Mr. Rostoker mentioned a silicon powder as being between 150 and 325 mesh. We always had much difficulty in measuring particle size of silicon powder by screen analysis, because of its tendency to agglomerate. I would be interested in the method used to measure these particle sizes.

(2) Mr. Rostoker maintains that the measurement of magnetic properties is more accurate in determining complete homogenization of an alloy, than is the X ray diffraction technique. I wonder whether this is really true. Even when diffusion is complete, magnetic properties

will change during continuation of the heat treatment, due to change in density and pore shapes, as has been demonstrated by Mr. Rostoker himself. Which effect is faster, the diffusion of the alloy components or the attainment of final density, will, in my opinion, depend very much on initial material and sintering conditions used. For magnetic applications, of course, the magnetic measurements are most suited for determining the point at which equilibrium conditions are reached.

(3) I was glad to see that Mr. Rostoker had used sample sizes which are similar to those I had used previously, and I believe that ring samples of about 2 in. od will become more or less standard samples for the determination of magnetic properties of powder metallurgy products. I should like to ask how the density was changed for the samples on which the effect of porosity was investi-

gated, and, further, why the sintering temperature used for this series of experiments was so low. It is somewhat surprising that a 24-hr treatment at $850^{\circ}C$ acts so much more to spheroidize the pores than a treatment for 1 hr at $1100^{\circ}C$. But the effect seems to be indisputable. I have made an investigation of the influence of sintering temperature for longer times on the maximum permeabilities of iron powder compacts which was presented at the International Powder Metallurgy Conference in Graz, in 1948, and I hope that these results will be published here within a short time. The results of this investigation are confirmed by Mr. Rostoker's findings that the change of time from 1 to 24 hr changes the permeability behavior considerably in the direction as indicated by Polder and Van Santen for spheroidization of pores. I do not quite understand Mr. Rostoker's explanation of the influ-

* American Electro Metal Corporation.

ence of "high" and "low" permeabilities on the shape of the curves for induction vs. density. Even for the large fields ($H = 100$), the permeability is still in the neighborhood of 100, that is, it is equal to the largest value Polder and Van Santen have used. I believe the fact that the permeability is not constant will make a refinement of Polder and Van Santen's theory necessary, though the general trend for flat and spherical pore shapes will probably be maintained.

(4) The densities obtained for any alloy material produced by Mr. Rostoker are rather low if compared with his excellent values for pure iron. This has to be expected, but points in the direction mentioned above, that homogenization is not necessarily connected with constant magnetic properties. An attempt to study diffusion in Fe-Si alloys by resistivity measurements was recently published by F. W. Glaser in the "Powder Metallurgy Bulletin." We are now studying the ferrosilicon materials over the full range of alloys, especially as far as resistivities and magnetic properties are concerned, and hope to publish something about these compositions within this year. Mr. Rostoker reports about a so-called anomaly in his Fe-Ni alloys with regard to the maximum permeabilities. These are inferior to data published in the literature, while, for instance, B_{100} and H_c are very close. In my opinion, the explanation for this behavior is the porosity of the alloys, as they are at the best 95 pct dense. Saturation and coercive force are much less sensitive to the influence of porosity than is maximum permeability. This might also give an explanation why there was no influence of nitrogen noticed in Fe-Co alloys, where the maximum density is still lower. The investigation by Mr. Rostoker, about the differences in properties obtainable by sintering in hydrogen or cracked ammonia, was especially interesting and might explain a number of discrepancies so far reported in the literature.

F. W. GLASER*—With regard to the preparation of the Fe-Si compacts, though not mentioned, I assume that Mr. Rostoker has mixed the Si and Fe powders by a tumbling operation. In view of the difference in density of these two powders, I myself have experienced great difficulty in obtaining the desired overall Si percentage, as it was theoretically calculated. Further, I wonder whether chemical analyses were run on the Fe-Si compacts reported. The exact overall Si content of the range of Si alloys reported in Mr. Rostoker's paper is extremely important, since as little as 0.25 pct Si in this region has quite an influence on the electrical resistivity. I should like to know to what extent Mr. Rostoker was sure that the Si percentages were really of the reported compositions.

F. N. RHINES*—I would like to say a few words in defense of the X ray method. I suppose that everyone who has thought about the problem of measuring homogenization in powdered compacts has thought of using the X ray method, and each person, in turn, seems to have become discouraged with it, but there is a basic advantage in its use, and I think we should not lose sight of it. Apparently, the thing that Mr. Rostoker has done has been simply to measure the position of maximum intensity in the reflection that he chose as his index and to watch the progress of that point of maximum intensity during heat treatment. It is fairly evident, and I think every one who has done this work has observed, that there is another phenomenon that takes place at the same time. The line first broadens so that it covers all of the parameter values from that of the pure solvent to that of the saturated solid solution. The broadened line first shows its maximum intensity somewhere near that of the pure substance; then, as time goes on, the maximum intensity shifts and, after the maximum intensity reaches somewhere near the point where it will stabilize in parameter value, the breadth of the line decreases, that is, the line becomes progressively sharper.

Now, if we could make good intensity measurements across the line we should have an index not only of the average change in composition of the material during homogenization but a detailed description of how much of each composition is present at any given time during the homogenization process. This information would be invaluable in making a complete statement of the state of homogenization at any period.

We cannot get that kind of information from any measurement which gives us only an over-all average figure, therefore it seems to me that in the long run it would be highly desirable to get the X ray method under full control and to use it for this type of research.

J. T. NORTON†—I do not believe that the X ray experiments described in this paper really indicate what the X ray method is capable of doing. A change in parameter is not a very sensitive measure of composition. As I understand this problem, it is one of determining whether or not a sample is of uniform composition; certainly the measurements of the line broadening would be much more sensitive. This is true provided the work on line broadening is carried out properly, and it is not an easy thing to do. It would require a very careful experimental technique, the use of truly monochromatic radiation and a really first-rate measurement of the line broadening as the homogenization of the compact proceeds. I believe a lot more could be

done by means of X ray than was done in this particular paper.

W. ROSTOKER (author's reply)—In reply to Mr. Steinitz, the particle size distribution of the silicon powder was determined by the use of a nest of standard screens vibrated for 15 min. No agglomeration difficulties were encountered.

Of the variables which might, in addition to inhomogeneity, affect the change of magnetic properties with time, Mr. Steinitz mentions density and pore shapes. Pore shapes at high temperatures become spheroidal early in the sintering history. The amount of porosity in the repressed and unsintered condition is 4.5 pct and after sintering for 24 hr at 1400°C is only decreased to 1.9 pct. The consolidation is therefore only slight. In accordance with the demonstrated linear effect of spheroidal porosity on permeabilities there should be little effect on the homogenization experiments.

In a similar vein, Mr. Steinitz would attribute the low maximum permeabilities of the heat treated nickel-iron alloys to porosity. Again, under the conditions of treatment the rings would be expected to, and indeed do, exhibit spheroidal porosity. The author feels that the experimental work presented definitely shows such pore shapes to exercise only slight influence on permeability at 95 pct of full density. It might also be pointed out that the maximum permeabilities of 65 and 78.5 pct nickel-iron alloys in the annealed state are quite normal. As a conjecture, the cause of this trouble might rather be in small scale inhomogeneity.

The density variations were effected by submitting samples to successively higher molding pressures. The very high densities required a double pressing operation with an intermediate short time, low temperature anneal. The final sintering times and temperatures were chosen to give conveniently the range and character of porosities.

Polder and Van Santen quantitatively calculated the effect of pore character and content on dielectric properties. They suggested that the effect on magnetic permeabilities at constant field would be analogous. There is no reason to expect that the analogy should be more than qualitative. For that reason, a permeability of 100 is referred to as "low" as compared with values of several thousands at low inductions and in accordance with usual magnetic parlance.

Mr. Steinitz implies that the large differences in maximum permeability between the sintered iron of full density and porous irons are due to differences in density. The author would rather attribute this to the extremely low carbon and oxygen contents (see Table 7) and the large grain size of the high density iron due to the prolonged heat treatment in hydrogen at 1420°C. In effect, the two

* American Electro Metal Corporation.

* Carnegie Institute of Technology.

† Massachusetts Institute of Technology.

irons are not of comparable purity. The true permeabilities of the porous irons would best be determined by extrapolation of the straight lines of Fig 7 to 100 pct of full density.

In reply to Mr. Glaser, the appropriate amounts of iron and silicon powders were weighed out and mixed for each ring individually. In this way, the required amount of silicon was introduced into each ring and it was not thought necessary to analyze the rings after heat treatment. There was no apparent segregation during the mixing operation or while pouring the powder mixture into the

molding die. The electrical resistivities do not appear to vary from other reported values by more than about 5 pct.

The author finds himself in full agreement with the comments of Professors Rhines and Norton concerning the proper study of an inhomogeneous state by X ray diffraction methods. He also feels that the experimental and interpretive difficulties involved would necessitate a separate project. Lack of proper equipment prevented the X ray studies presented here from being more detailed. But it should be remembered that this portion of the work was intended to

assist interpretation of the magnetic results. The main purpose in presenting the X ray data was to show that an apparently sharp diffraction pattern could be observed long before the structure-sensitive magnetic properties reached their ultimate values. Undoubtedly, a more careful examination of these apparently sharp lines would have indicated small scale inhomogeneity. But the pertinent conclusion to be taken was that small scale inhomogeneity affected structure-sensitive magnetic properties as severely as very small carbon and oxygen contents (T. D. Yensen, Ref. 5).

The Densification of Copper Powder Compacts in Hydrogen and in Vacuum

By C. B. JORDAN and POL DUWEZ

DISCUSSION

(A. Squire presiding)

A. J. SHALER*—I should like to congratulate the authors for having carried out such a precise set of experiments. It has been found useful, in sintering experimental compacts in vacuo, to make certain that the residual gas is not one which reacts with the metal. Since traces of oxygen can be kept away only with great difficulty, the technique is often adopted of using a "getter" of powder in the vicinity of the compacts, and, in addition, of permitting a small hydrogen leak to flow into the vacuum chamber. Did the authors use similar devices?

This paper brings up a question concerning the definition of the word 'sintering.' The authors restrict its use to the adhesion between particles. Kuczynski, in a paper presented at this meeting, applies the word to the growth of areas of contact between particles. I have used it to mean both these phenomena and also the dimensional changes which continue to take place after the first two have run their course. May I suggest that we should come to an agreement on the use of these words?

Fig 1 and 2 show an interesting feature: extrapolation of the curves to zero time does not give a densification parameter of zero. The higher the temperature, the higher is the intercept on that axis. These observations agree with the concept of a practically instantaneous densification taking place while the compact is being brought to heat. Such a change may be brought about by plastic deformation and primary creep. The

stress pattern causing this first rapid flow is, to my mind, due to the force of attraction between the surfaces of opposite particles in the regions immediately flanking their common areas of contact. The stress is not temperature-sensitive, but at room temperature plastic deformation only proceeds until the metal in the area of contact can support it elastically. As the metal is heated, the elastic limit falls, and further plastic flow occurs. At the higher temperatures, this is followed by primary creep, and finally by the steady-state rate-reaction which the authors are seeking. If they were to recalculate their densification-parameter values, using, not the initial density of the cold compact, but the density after the compacts have been brought to temperature, the systematic deviations from linearity in Fig 3 and 4 might be eliminated. Such initial densities might be obtained by extrapolating the curves of Fig 1 and 2 to zero time.

I am naturally pleased to see that such a very well done series of experiments leads to a heat of activation (for the densification process in hydrogen) that is much higher than that for self-diffusion, in confirmation of the less elaborate results reported by Wulff and myself (*Ind. and Eng. Chem.*, (1948) 40, 838).

J. T. KEMP*—I would like to comment on Dr. Shaler's remarks. There are apparently different interpretations of the word "sintering." It seems to me that an accurate definition of our word is essential in all metallurgy. May I point out, in this connection, that in practical metallurgy the word "sintering" has

been applied to a bonding process in the preparation of ores and flue dust for furnacing. It would be unfortunate if in the area of powdered metallurgy we should establish a definition that is essentially different in meaning.

F. N. RHINES*—I think that I can answer the question by saying that I see no essential difference between the use of the term "sintering" in extractive metallurgy and in powder metallurgy; physically the same things are going on. I admit sintering is used for different end purposes in the two cases. When we resort to the sintering of lead ore mixture we are doing so to obtain a chemically reactive, loose texture of some rigidity. This is only a difference in use. After all, in powder metallurgy we sometimes deliberately produce a very porous material which has just a little strength, just as in the case of sinter cake.

P. DUWEZ (authors' reply)—We agree that it would be helpful to have well-established definitions of such terms as "sintering." Since the question has now been raised, the time might be appropriate for its consideration by some suitable committee of one or more of the metallurgical societies.

In answer to Dr. Shaler's first question, no getter nor hydrogen leak was used in our vacuum experiments, except insofar as the guard disks (used to reduce friction between specimens and trays) may have acted as getters.

Dr. Shaler's statement that extrapolation of the curves of Fig 1 and 2 does not lead to zero densification at zero time apparently overlooks the logarithmic

* Massachusetts Institute of Technology.

* American Brass Co., San Francisco, California.

* Carnegie Institute of Technology.

time scale used in those figures. The intercepts he mentions are not on the line $t = 0$, but on the line $t = \frac{1}{4}$ hr. The densification parameter, as we have defined it, is necessarily equal to zero at $t = 0$, and the curves of Fig 1 and 2 would indeed intersect at $\sigma = 0$ if extended far to the left.

Since the shortest time employed in our

experiments was $\frac{1}{2}$ hr, we feel that our results should not be taken as either confirming or denying Dr. Shaler's concept of a practically instantaneous densification during the heating-up period. If the results of shorter-time experiments were such as to confirm this hypothesis, it would then be interesting to see whether the curves of Fig 3 and 4 are

more nearly straight lines if the values of σ are calculated on the basis he suggests. His idea that densification is the result of several processes which successively predominate, is in agreement with the opinion we expressed in the paper at the conclusion of the section on "Interpretation of Results."

The Surface Tension of Solid Copper

By H. UDIN, A. J. SHALER and J. WULFF

DISCUSSION

(A. Squire presiding)

G. KUCZYNSKI* and B. H. ALEXANDER*—This paper represents a most noteworthy attempt to evaluate experimentally the surface tension of a solid metal. Because of the great importance of such measurements, any proposed method should receive the closest scrutiny before the results can be considered reliable.

In regard to the experimental method, we think that the marking of the gauge length by means of tying knots in the wire may be the cause of some of the spread in the results. Such a knot may be expected to tighten slightly, and thus increase the gauge length, when placed under stress at high temperature. Although this effect would be very small, amounting at most to only a few times the wire diameter. A fairly tight knot in a wire will decrease the wire length by about ten times the wire diameter, thus only a slight tightening of the knot would cause considerable spread in the results.

Upon plotting the stress strain curves from the authors' data, the writers found that there was a fairly consistent tendency towards an S-shaped curve, instead of a straight line. Such an effect could be caused by the tightening of the knots.

The writers think, however, that the experimental results are fairly reliable, but that there may be other methods of interpreting them depending upon what mechanism is assumed to be responsible for the shrinkage of the wires. The authors have assumed that the stress due to surface tension results in viscous flow. It should be made clear that it has never been demonstrated that viscous flow can occur in metal crystals even at very high temperatures. The experiments of Chalmers¹³ on tin, which are so frequently quoted as giving evidence of viscous flow at low stresses are by no means

satisfactory. In his experiments, Chalmers found that only the initial rate of flow was approximately proportional to stress. He also found that the rate of flow varied markedly with time which, in his experiments, was less than 2 hr. Inasmuch as there is no proof of viscous flow in metals, and the authors have brought forth no conclusive evidence on this point, it may be worth while to investigate other possible mechanisms of material transport which would account for the shrinkage of the wires. The writers wish to point out that in these experiments the shrinkage of the wires can be adequately explained, according to a self diffusion mechanism. Thus, if we assume a concentration gradient for self diffusion which is a function of the radius of curvature of the wires, and assume that diffusion will occur so that the total surface area is decreased, we find the following expression for the self diffusion coefficient:

$$D = \frac{-kr_0^2 T}{\gamma \delta^3 l} \ln \epsilon \quad [19]$$

where k = Boltzmann constant

r_0 = initial radius of the wire

T = absolute temperature

γ = surface energy

δ = interatomic spacing

l = time

ϵ = strain at zero applied stress

Eq 19 may be used to evaluate the self diffusion coefficient of copper, using the strain measurements obtained by the authors for zero stress as obtained by extrapolating their curves for 5 mil wires. By inserting a reasonable value for the surface energy (1500 ergs per cm²) we find:

$$D = 5 \times 10^4 e^{\frac{-66,000}{RT}} \quad [20]$$

The activation energy is of the correct order of magnitude, but the frequency coefficient is much too high, indicating that surface diffusion may be playing an important role. This discrepancy in the action constant is much smaller than the corresponding discrepancy obtained by the authors for the viscosity coefficient.

The writers by no means propose that this proves that the shrinkage of the wires is due to self diffusion but we merely wish to point out that there are explanations other than that given by the authors. In this, as in any kinetic phenomena, it is necessary to study the rate of the process before anything can be said about the mechanism. The determination of surface tension given by the authors is based upon an interpretation of the data which embody the concept of viscous flow. The final proof of this concept will be obtained only after the time relationships confirming the authors' Eq 15 have been conclusively established. The rough linearity of the stress strain curves obtained by the authors for experiments run the same length of time should not be considered as proving that viscous flow is occurring.

H. UDIN (authors' reply)—All of the test specimens were annealed at 1000°C for an hour or more before preliminary measurements were made. During this anneal the wires recrystallize, and the greatest part of grain growth takes place. Also, the knots sinter at the cross-over points. This does not in itself eliminate the possibility of end errors, although it greatly decreases their probable magnitude. It is still possible that some extension occurs due to creep in shear at the sintered points. If so, this effect would be quite independent of and superimposed on the normal shrinkage or extension of the wire itself. Within the precision of the experimental results, straight lines satisfy the data as well as do any other simple curves. Until data of greater precision are obtained, it is futile to discuss any possible trends away from linearity.

The disagreement between Kuczynski and Alexander's Eq 19 and our Eq 18 is one of semantics and mathematics, not mechanism of flow, since Eq 18 is based on the self-diffusion concept of viscous flow. It would be interesting to learn how the mathematics leading to Eq 19 deviates from that of Eyring and of

* Sylvania Electric Products Inc.

¹³ B. Chalmers: *Jnl. Inst. of Metals* (1937) 61, 103.

Frenkel. The dependence of self-diffusion coefficient on specimen size in Eq 19 is somewhat startling.

As Dr. Orowan points out, neither the mode of flow nor its time dependence has any influence on the numerical values obtained for the surface tension of solid copper, because it is found from the interpolated value for zero strain.

A. J. SHALER (authors' reply)—Dr. Kuczynski has said, if I understand him correctly, that there may be a mechanism of material transport, no different from our atomic process, which would give him a logarithmic relationship between time and the longitudinal strain. I do not understand how he obtains an equation differing from our linear relationship. The experiments that were plotted here were carried out for various times, a random choice of times at the various temperatures. Within the limits of experimental error, these points fall on a straight line; there is no indication of a systematic deviation which would be indicative of a logarithmic relationship. I would like to ask Dr. Kuczynski if he would elaborate on why he expects this curve to be nonlinear by his method of material transport.

G. C. KUCZYNSKI—I want to say again that I do not claim that this mechanism is the true mechanism. As a matter of fact, I do not believe that it is. It is only given for the purpose of showing that something else is possible to explain the results. We have said that we are unable to distinguish which mechanism is the true mechanism because only the time relationship will give the answer to this question. The mechanism here suggested is very similar to that of closing of the cylindrical void by diffusion flow. This will take place in order to decrease the total surface area. Similarly in this case the wire by shortening its length and increasing the radius can lower the total surface. When we plot strength against stresses we may get a very similar plot to that obtained by Dr. Shaler.

L. D. JAFFE*—I first would like to congratulate the authors because this appears, if the work is correct, to be the first reliable determination of the surface energy of a solid, and I think that is going to be of tremendous importance in the years to come. I believe this paper will lay the foundation for a great deal of research both in physical metallurgy and in the more specialized field of powder metallurgy within the next few years.

I should like to raise a question with respect to one of the basic assumptions of the authors that the specimen will remain cylindrical while it is extending or contracting longitudinally. The behavior of the wires under test should be essentially analogous to the behavior of a soap film, but a soap film under the conditions

used will not remain a cylinder. A cylindrical soap film, if permitted to deform under the influence of surface tension will attempt to break down. It will develop a waist whether there is an overall extension or contraction. In fact, if the length/diameter ratio is large, as it was in the wires, the soap film will tend to break up in a series of droplets. Now, should not the wires also tend to break up into droplets? If so, then the equations used by the authors may not be applicable, and the value obtained for the surface tension may not be valid.

Dr. Kuczynski pointed out that solid crystals do not ordinarily flow in a viscous fashion. That is quite true, but it has been established by recent work of Kê that grain boundaries do behave in a viscous fashion. However, if the deformation measured by the authors is primarily due to grain boundary flow, it should not be considered as uniform on an atomic scale throughout the specimen. Also from the experimental standpoint, it would appear that the stress-strain-time relationship would then depend on the grain size of the material. Grain sizes are not mentioned in the paper. If the grain sizes were determined, would the authors give the results in their reply?

Finally, is there any possibility that the difference in the behavior of 5 mm and of 3 mm wires might be associated with differences in relative grain size?

H. UDIN—We measured the wires as carefully as we could and found no variation in diameter. That was one of the reasons why we knotted it instead of using nicks or grooves in the wire as gauge points. However, after this paper was written, we began a new series of experiments in which we nicked the wire circumferentially with a 30° angle blade. Our nicks were at least a thousandth of an inch deep in a five thousandth's diameter wire, so we were actually inviting trouble if there was any tendency for the wire to pinch off, and in every case we found the opposite tendency. The wire tended to restore its cylindricity rather than to break up at the nicks.

As to the grain size and shape, I should like to point out that after the anneal the grain boundaries are found to be perpendicular to the axis of the wire except in a few cases of twins, and I cannot quite see for this type of configuration how any grain boundary flow can occur, or at least how it can affect the length of the wire.

A. J. SHALER—If this grain boundary flow were to take place it should lead to a saturation value of strain as you proceed to longer times. Just by accident I happen to have a slide in my pocket showing the stress-strain rate relationship from these experiments. I think that this answers partly Dr. Kuczynski's question and partly Dr. Jaffe's question. There is no evidence, I think, within

experimental error of any saturation strain at long times (which are in this case coincident with high strain rates) either in compression or tension, nor of any departure from Newton's law of viscosity.

A. A. CENTER*—I wish to say that I am very interested in this attempt to measure the surface tension of solids. I am wondering about the analogy to soap filmed drops. They do have a tendency with increasing ratio of length to diameter of necking down and then of course of breaking up into droplets. The matter of the nicks in the copper specimens tending to heal under stress is certainly a very interesting observation and will require further study. We will hope to hear further on that. I have done some work in chemistry and physics of surfaces and think this is a very interesting attempt to measure the surface tension of solids. I hope there will be further work along these lines to see if they are actually measuring either surface tension or surface energy, or something else.

J. WULFF (authors' reply)—In answer to the last comment, we have been a long time trying to find quantitative measurement for the surface tension of solids. We have been worrying in our laboratory for the last five years over how we could approach this problem and we, of course, shall repeat many of these experiments, carry them on in different atmospheres, do them with silver and gold, do them with alloys. However, we are very thankful that we were able to get this far in five years.

E. OROWAN†—I should like to discuss some remarks made during the discussion, rather than the paper itself; first, however, I would say how much I enjoyed the report on this very ingenious piece of work.

The final result does not depend on the exact nature of the law of viscous flow; in principle, the method consists of observing that particular value of the applied force at which no flow occurs.

Viscous flow in a polycrystalline metal may be either sliding of the grains upon their neighbors, or crystallographic slip ("recovery flow," due to the continued removal of strain hardening by thermal agitation). Grain boundary sliding in general slows down with time, because the unevenness of the grain boundaries resists the continuation of the sliding movement; in the present case, however, the boundaries were nearly plane. On the other hand, they were also nearly perpendicular to the axis of tension, so that boundary sliding may not have played an important part; the main part of the deformation was probably by intracrystalline slip.

* Consulting Engineer, Berkeley, California.

† Cavendish Laboratory, Cambridge, England.

* Watertown Arsenal, Watertown, Mass.

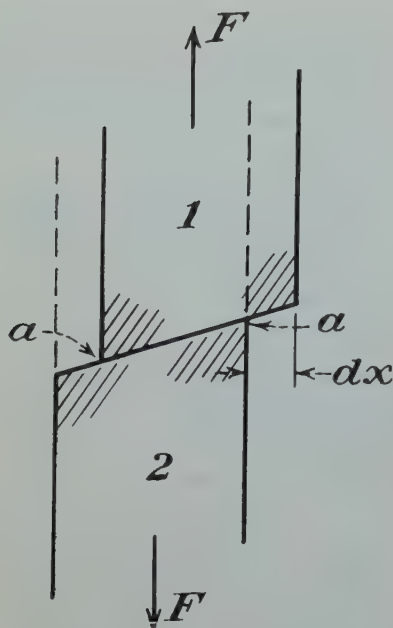


FIG 7—Energy involved in slip.

One can prove that the tendency to necking, which is typical of plastic deformation governed by a stress-strain curve of the usual type, is practically absent if the deformation obeys Newton's law of viscosity. Yet it is difficult to see why cylindrical single crystals should always retain a circular cross-section during flow. If they flatten, the value of the surface energy derived from the measurement will be different from that obtained with the assumption of a circu-

lar cross-section, although the difference will amount only to a factor of order unity.

What the authors have carried out is the counterpart of the well-known soap film experiment of Dupré. Let the forces F produce slip in a crystal with the operative slip plane indicated by the dotted line in Fig 7. If the resistance to slip is of a purely viscous nature, it vanishes for infinitesimally slow deformation, and then the forces F are opposed only by surface forces. Let ω be the (free) surface energy per unit of area of the slip plane. If the displacement between the parts 1 and 2 of the crystal increases by dx , new surfaces of area $b dx$ are laid open at the re-entrant corners a , where b is the width of the slip plane perpendicular to the plane of the figure. The increase of the total surface energy is $2\omega b dx$, and this must be equal to the work done, $F dx$; hence,

$$\omega = \frac{F}{2b}$$

This is identical with the relationship between equilibrium force and surface energy in Dupré's soap film experiment.

Clearly, the surface force that resists the applied forces F in Fig 7 must be the attraction of the opposite quadrants (shaded in the figure) resolved in the slip direction. In fact, it can be proved generally that the resolved attraction of two opposite space quadrants, per unit length of the edge, is equal to the specific surface energy of their boundary planes. This theorem, however, is valid only if the material is a continuum in the sense of the classical theory of capillarity, or at least behaves like a continuum (homopolar materials may do so; to ionic crys-

tals, the theorem cannot be applied).

A. J. SHALER—I think I speak for the other authors as well as for myself in thanking Dr. Orowan for his great interest in this work and for clearing up several points so much more beautifully than I could have done it.

Concerning the question of the cylindricity I should like to bring up once again that in the measurement of the surface tension the change from a circular cross-section to an elliptical one does not matter because at the point of measurement where zero strain occurs there is also no deformation in the cross-section. Therefore, the question of the strain pattern does not influence the measurement of the surface tension (or surface energy). If the process of flow is by slip there should be a barrier stress which would give us, in the curve of strain or strain rate against stress, a discontinuity on the zero-strain axis. It is very possible that this process is the actual one operating, and that our experimental measurement cannot detect the flat portion in the curve.

We have discussed the matter of calling our value surface tension or surface energy, and we have come to the conclusion that we ought to call it surface tension, for the reason that this measurement is a mechanical one. We are dealing with a force and surface tension is a force. An energy would only be exhibited at other than zero strain. We may be wrong. We intend to make surface tension measurements on metal single crystals and on silver chloride; we may be able then to untangle some of these problems by comparing the results between ionic crystals and metal crystals.

Self-diffusion in Sintering of Metallic Particles

By G. C. KUCZYNSKI

DISCUSSION

(F. N. Rhines presiding)

A. J. SHALER* and H. UDIN*—Bonding, and the increase in contact area, form two of the series of phenomena collectively known as 'sintering.' A third one of these is involved in changes in dimensions of the whole compact. Dr. Kuczynski's Fig 1, in which the center of the sphere does not approach the surface of the plate, shows that he is not concerned with the last of these phenomena. On the other hand, Frenkel's work is exclusively concerned with changes in dimensions. Dr. Kuczynski's rather unfortunate remarks about

Frenkel's work are therefore beside the point. The work of Wulff and myself, quoted by the author, has also been primarily concerned with what we call the 'second stage of sintering,' in which such systems as may be represented by Kuczynski's model of a sphere and a block are no longer in existence. The work of Pines also falls in this category.

Neither does Dr. Kuczynski's very masterful experimental work represent a solution to the problem of bonding. It does not seek to answer the question of why particles approach one another and form a weld in the first place. Such a study clearly reveals that the area of contact is initially rapidly deformed by direct mechanical flow caused by the same force of attraction. This initial

deformation is neglected here.

On the other hand, students of the phenomena of sintering must not underestimate the very important contribution that Dr. Kuczynski does make in this paper. It is a well-worked out study of the mechanism of 'spheroidization' of the voids, the first manifestation of which, during sintering, is the growth of the areas of contact, with no change in the dimensions of the compact. This study is very valuable as a basis for predicting the development of the strength of such compacts as filters and certain porous bearings, in which the second stage of sintering is never reached.

A few more specific points may be brought up here. If, in Table 4, the data are extrapolated to zero time, it is easily

* Massachusetts Institute of Technology.

seen that x is still considerable. I believe that this initial very rapid increase in x is due to plastic flow. If the author had used values of x/a based, not on $x = 0$ at $t = 0$, but on some value, based on later measurements, of $x = x_0$ at $t = 0$, his power relations would have been lowered. Thus, whereas he demonstrates that surface diffusion and what he calls volume diffusion are the mechanisms of spheroidization because the radius of curvature at the contact area shows a 5th or 7th power time-dependence, it is possible that, by taking into account the initial rapid plastic flow, the power relation may be considerably altered. Has Dr. Kuczynski made any calculations taking this into account? It is possible that such a treatment of the data would modify the tendency towards higher-powered relationships with finer particles.

Dr. Kuczynski has sought to demonstrate that with large particles the mechanism of vacancy diffusion is predominant in the growth of the areas of contact. Frenkel's viscous-flow theory also requires that the units of flow are diffusing vacancies. Yet Kuczynski categorically states that the viscous-flow theory is not valid. I wonder if he could clarify his position in this matter. Dr. Kuczynski states that if Frenkel's viscous-flow mechanism is responsible for sintering, the relationship between the radius of the area of contact and the time of heating should be a quadratic function. Although there is an error in the numerical constant in Eq 2, taken from Frenkel, this statement is true. Experiments which are based on this relation were published last year by Wulff and myself. They show a heat of activation for the flow process (in a hydrogen atmosphere) considerably higher than that for self-diffusion, found by the author. This (I quote the author) "by no means adequate test of theory" is strongly supported by the results of the much more adequate results found by Jordan and Duwez, which were reported at this meeting, and in which the heat of activation in hydrogen is found to be 80,000 cal per mol. These figures appear to indicate that the flow mechanism in the second stage of sintering is essentially different from the spheroidization process which Kuczynski has studied here, and for which he arrives at a heat of activation of 56,000 cal per mol for copper. I believe that our experiments, and those of Jordan and Duwez, indicate the existence, in the earliest stage of sintering, of a rapid flow rate, such as in conventional primary creep, followed by a viscous flow. These mechanisms are responsible for the densification or swelling of compacts. Superimposed on these, the spheroidization of voids proceeds by the two mechanisms adduced by Kuczynski. This spheroidization contributes to the increase in strength of the compact but

cannot explain changes in density. That these two processes are going on at the same time is shown by Kuczynski's Fig 2. His calculations are based on the relation between the radius of curvature at the edge of the contact area and the x/a ratio. Fig 2a shows a large radius of curvature and a small x/a ratio. Fig 2d shows, at a higher temperature, a much smaller radius and a larger ratio. These results are in direct conflict unless two mechanisms are at work, having different heats of activation. One is predominant at low temperature (the spheroidization), the other at high temperature (the viscous flow preceded by primary creep and perhaps by appreciable instantaneous plastic flow, in fine particles). Spheroidization produced no densification; that is, the sphere center does not approach the block in Fig 2a. Plastic or viscous flow does cause densification, and the center approaches the block, as in Fig 2d. It is not fair to base such a conclusion on two pictures which Kuczynski states to be unreliable because of lack of sphericity. But further evidence that one single mechanism may not be capable of explaining his results may be found in Fig 5, which presumably refers to copper and not to silver (the caption on Fig 4 being here applicable). In this figure the points referring to the 700° experiment at 4, 8, and 41 hr have not been plotted in accordance with the data in Tables 1 and 3. If the tables are correct, the points for 8 and 41 hr should be plotted much higher, and the average of the 5 points for 4 hr should also be higher. The line through these corrected points has a much greater slope than those shown, so that the dominant mechanism at low temperatures is not the same as at high temperatures. Plotting the widely scattering points found at 600° gives, at least initially, an even greater slope.

G. C. KUCZYNSKI (author's reply)—J. Frenkel in his paper entitled "Viscous Flow of Crystalline Bodies under the Action of Surface Tension" published in *Jnl. of Physics* (U.S.S.R.) (1945) IX, 385–391 does discuss the problem of bonding or as he calls it "welding" of the crystalline spherical particles without appreciable change of dimensions. He also states in this paper that the units of viscous flow are diffusing vacancies. The flow takes place by atoms moving to these vacancies preferably in the direction of the applied force. There is however another diffusion flow which does not require this acting force. If there is a gradient of vacancy concentration in a region of the body the atoms will move into this region. This type of mechanism was assumed in my paper. Obviously the kinetics of these two mechanisms and resulting time relationships are different. Viscous flow can produce sintering in the case of glass where the relationship

$x^2 \sim t$ predicted by Frenkel was indeed observed. In the analysis of any kinetic problem the time relationship is typical and far more important than the temperature dependence. The latter one may often be misleading.

As to the specific points stressed by Dr. Shaler I have to admit that Tables 1 and 2 contain three errors, all typographical. Some of them can easily be corrected by comparison with Table 3. In one case the diameter of the interface was introduced instead of its radius.

I have replotted the results from Table 1 and 2 on nonlogarithmic scale $\left[\left(\frac{x}{a}\right)^5 / t\right]$ and obtained straight lines which all pass through the origin, except for the curve for copper heated at 700°C. The deviations at 700°C occur for small periods of time when the diameters of the interfaces are small (few microns). Under such conditions the possible error is larger than in other cases. It is therefore quite possible that these deviations are not real.

Although the method described in the paper under discussion is not too accurate it most certainly is able to distinguish between two consecutive powers of the interface diameter.

M. BEVER*—The experimental methods described in this paper are of real interest. From the standpoint of techniques, any new quantitative use of metallographic observations is an interesting and welcome development.

A question should be raised concerning the choice of atmospheres in the sintering experiments. Hydrogen is soluble in solid copper and silver and oxygen is soluble in silver. Even if these gases are considered to have only negligible effects in solution, hydrogen can reduce oxides that may be present on the surface. It is well-known that such reduction leads to surface layers of very great activity. It is desirable to exclude even the possibility of such active surface layers from experiments in which surface phenomena may play a part.

G. C. KUCZYNSKI—I was aware of this difficulty. However I have run some silver samples in hydrogen and oxygen at 700 and 800°C for the same periods of time and no difference was observed; and recently a few copper specimens were run in an argon atmosphere at 900 and 1000°C. There was not any appreciable difference between these and those heated in hydrogen. Tentatively therefore I can state that in the case of these two metals any nonoxidizing atmosphere does not seem to have an appreciable influence upon the bonding of particles.

* Massachusetts Institute of Technology.

Evaluation of pH Measurements with Regard to the Basicity of Metallurgical Slag

CHARLES W. SHERMAN* and N. J. GRANT,* Junior Member AIME

The correlation of the high temperature chemical properties of slag-metal systems with some easily measured property of either slag or metal at room temperature has been the goal of both process metallurgists and melting operators for many years.

There are several rapid methods for estimating various constituents in steel in addition to the conventional chemical methods which are quite fast, but these do not reveal the nature of the slag as a refining agent, which is of primary interest to the steelmaker.

Furthermore, there are several methods for examining slag, the three principal ones being slag pancake, petrographic examination, and the previously mentioned chemical analysis. The main objection to the last two is the time required to make a satisfactory estimate of the mineralogical or chemical components. The objection to the first is the inadequacy of the information obtained.

A new technique has been developed by Philbrook, Jolly and Henry¹ whereby the properties of slags are evaluated from an aqueous solution leached from a finely divided sample of slag. It is known that the pH or hydrogen ion concentration (of saturated solutions that have dissolved certain basic oxides, notably calcium oxide) will indicate a pronounced basicity.

Philbrook, Jolly and Henry devised the pH measurement technique in order to supply open hearth operators with a fast, reasonably accurate method of estimating slag basicity. They offered the method as an empirical observation and made no claims as to its theoretical justification. The results were presented as an experimentally observed relationship which applied over an important range of basic open hearth slags. They found

that, in plotting the measured pH against the basicity, the best relationship existed between the pH and the log of the simple V ratio, CaO/SiO_2 .

Extensive investigation also showed that there were several variables in the experimental technique that influenced the results and necessitated following a standard procedure to obtain reproducible pH readings. These variables were: 1. Particle size of the slag powder used. 2. Weight of sample used per given volume of water. 3. Time of shaking and standing allowed before the pH was measured. 4. Exclusion of free access of atmospheric carbon dioxide to the suspension. 5. Temperature of the extract at the time the pH was measured.

In subsequent investigations of the pH method by Tenenbaum and Brown² and by Smith, Monaghan and Hay³ the general conclusions of Philbrook's work were reaffirmed. It was the object of the present investigation to extend the technique to a point where it could be used to evaluate slags of all types.

Experimental Results

PARTICLE SIZE OF SLAG POWDER

A large sample of commercial blast furnace slag of intermediate basicity (V-ratio 1.15) was selected for the

study. The slag had been put through a jaw crusher until all of it passed through a 20 mesh screen. Five fractions of this crushed material were separated, -20 to +40, -40 to +60, -60 to +100, -100 to +200, and -200 mesh.

A representative sample of 0.5 g was removed from each fraction and the pH determined using the method of Philbrook. Check pH analyses on the sample fractions varied due to the different amounts of shaking. To eliminate this variable, a mechanical shaker was employed. In order to know the exact time of contact between the slag and water, it was found necessary to filter the extract at the end of the shaking period. Using the mechanical shaker and a filtering apparatus, similar runs were made on the five fractions for contact times of 5, 10, 20, and 40 min. Random checks gave reproducible results within 0.02 pH. The data are plotted in Fig 1.

It can be seen from the plot that each slag fraction is hydrolyzed to an extent that is roughly proportional to the surface area exposed to the water. The (-100 to +200) mesh material changed very little in pH after 10 min. shaking time. The curves are symmetrical and lie in proper relation to one another. The -200 mesh curve appears to be somewhat flatter than the others, but this can be attributed to the portion of very fine material that is not present in the other fractions.

The closeness of the (-100 to +200) mesh curve to the -200 mesh curve and the fact that a -100 mesh sample would contain amounts of slag down to 1 or 2 microns in diam were considered sufficient reasons for selecting a -100 mesh sample as representative of the whole sample of slag for the purposes of this investigation.

New York Meeting, February 1950. TP 2715 C. Discussion of this paper (2 copies) may be sent to *Transactions AIME* before April 1, 1950. Discussion is tentatively scheduled for publication in November 1950. Manuscript received June 17, 1949.

* Research Assistant in Metallurgy and Associate Professor of Metallurgy, respectively, Massachusetts Institute of Technology, Cambridge, Mass.

¹ References are at the end of the paper.

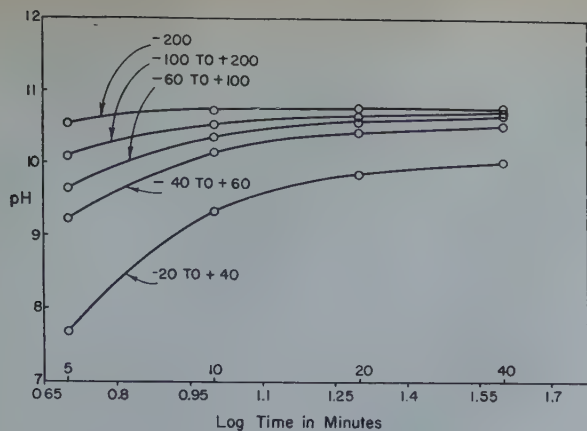


FIG 1—Effect of shaking time on pH for various particle sizes.

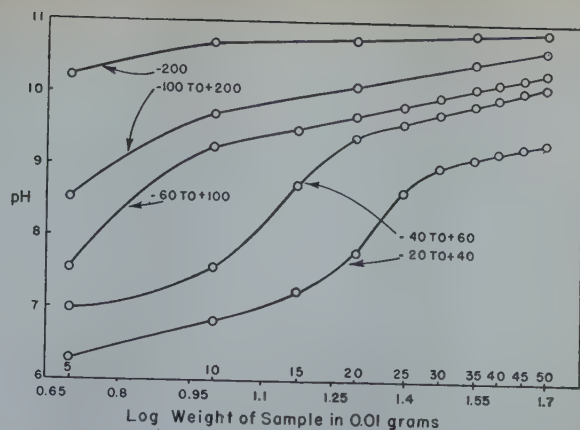


FIG 2—Effect of weight of sample on pH for various particle sizes.

EFFECT OF WEIGHT OF SAMPLE ON pH

The same commercial blast furnace slag that had been used in the study of particle size was also employed in determining the effect of weight of sample on pH. Portions of the five screen sizes were removed and weighed carefully on an analytical balance. The smallest sample taken was 50 mg and the largest sample was 500 mg. (The procedure for weighing, shaking, and filtering remained unchanged, and the time of contact between the water and the slag was held constant at 10 min.) The data are plotted in Fig 2.

It can readily be seen from the plot that the curves assume the general characteristics of potentiometric titration curves for acid-base reactions. This type of curve has a straight line portion on either side of the neutralization point. It was considered important that the sample size selected as a basis for a standard should be well within the straight line portion of the curve in order to compare different slags satisfactorily. As a consequence, the weight of sample selected as standard for the rest of the investigation was 0.5 g.

In order to shift the neutralization point further to the left, it was decided that the distilled water should be boiled to reduce the amount of acid-forming CO_2 .

Any pH value on a slag extract of less than pH 9 should be considered of doubtful value since it occurs in a region where the curve bends toward the neutralization point.

STANDARD TECHNIQUE USED FOR pH MEASUREMENT

Weigh out a representative 0.5 g

sample of slag which has been powdered so that the entire sample will pass through a 100 mesh screen. The sample should be dry and free of contamination. Weighing of each sample is recommended in order to obtain reproducible results; however, an ordinary trip balance may be used satisfactorily.

Place the sample in a clean, dry 250 ml Erlenmeyer flask. Measure with a pipette 100 ml of previously boiled, distilled water and add to the sample in the flask. As the water contacts the slag, note the time of contact. After the pipette drains, stopper the flask tightly and place in a mechanical shaker. This type of agitation prevents caking and agglomeration of the sample on the bottom of the flask.

Remove the flask from the shaker at the end of approximately $9\frac{1}{2}$ min. and pour the suspension onto a glass frit filter as the timer reaches 10 min. This sets the exact time for contact between the water and the undissolved residue remaining.

The solution should be filtered under suction in order to complete the operation as rapidly as possible. The solution is caught in a test tube suspended inside an ordinary vacuum flask. Remove the test tube and stopper it tightly. Shake well to mix the solution thoroughly. Place a 3–5 ml sample in the test cup of a precision pH meter and measure the pH of the solution with the previously calibrated meter.

The time consumed for determining the pH on each sample by this method was about 15 min. This is exclusive of the time necessary for preparation of the slag powder and the time for weighing. It was found that results could be duplicated to ± 0.03 pH as long as careful attention was paid to

the various steps in the standard technique.

CORRELATION OF pH OF BLAST FURNACE TYPE SLAGS WITH COMPOSITION

Using the standard technique, as described in the previous section, a set of slags submitted in connection with the Doctor's thesis of Gerald G. Hatch was checked.

The analyses of these slags are reported in the paper of Hatch and Chipman⁴ and will not be repeated here. In general, the slag compositions covered a much wider range of values for the four main constituents than is found in the typical commercial blast furnace bisilicate slags, but they are free of MnO . These limits of composition variation are as follows:

| | Pct |
|-------------------------------|-------|
| CaO..... | 16–52 |
| MgO..... | 0–38 |
| SiO_2 | 14–53 |
| Al_2O_3 | 0–39 |
| S..... | 0–4.5 |

Fig 3 contains a plot of the pH of each slag against its molar lime-silica ratio. In a similar manner Fig 4 relates the pH to the general molar basicity ratio, $\frac{\text{CaO} + \text{MgO}}{\text{SiO}_2 + \text{Al}_2\text{O}_3}$. These two plots are included to illustrate the diversity of the slag compositions in comparison with the slags used by Philbrook, Jolly and Henry. These authors were able to correlate their values with a plot similar to Fig 3, as were Smith, Monaghan and Hay.³ In neither instance do Fig 3 and 4 show a relationship between the chosen basicity value and the measured pH.

In Fig 5, a plot of EXCESS BASE against pH was tried. The quantity, EXCESS BASE, in this case is similar but not the same as the quantity first

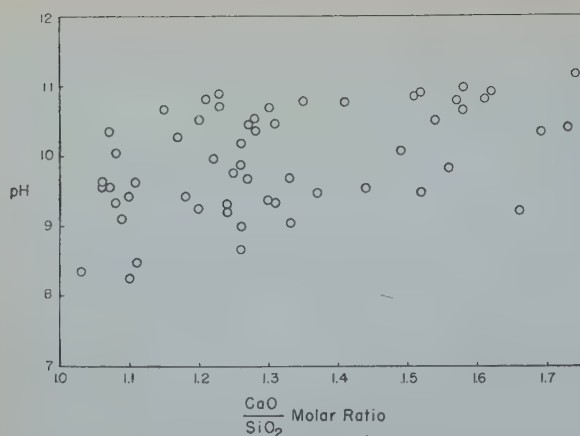


FIG 3—Effect of simple $\frac{\text{CaO}}{\text{SiO}_2}$ ratio on pH for blast furnace type slags.

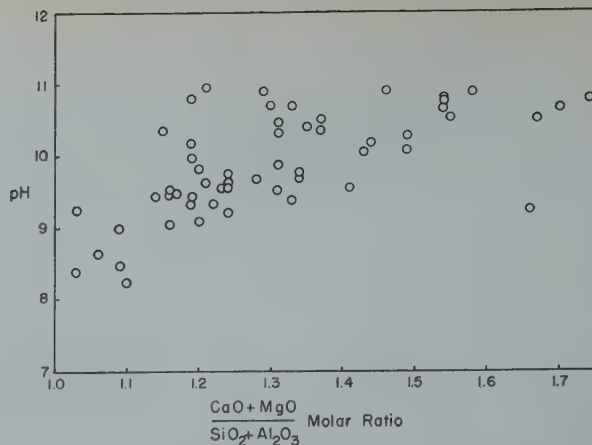


FIG 4—Effect of $\frac{\text{CaO} + \text{MgO}}{\text{SiO}_2 + \text{Al}_2\text{O}_3}$ on pH for blast furnace type slags.

calculated by Grant and Chipman.⁵ In this instance, a neutral slag is assumed to be of the bisilicate type, that is, $\text{MgO} \cdot \text{SiO}_2$, and $\text{CaO} \cdot \text{SiO}_2$. Grant and Chipman had selected a monosilicate slag as a neutral slag in their treatment of open hearth slag. Otherwise, the term EXCESS BASE is computed in the same manner for the study of blast furnace type slags. The main reason for selecting a bisilicate slag as a neutral slag is that it is known that monocalcium silicate is more stable with respect to water than is dicalcium or tricalcium silicate. This treatment of solid slags in no way contradicts the assumption that Grant and Chipman used to explain the behavior of liquid open hearth slags.

It should be pointed out that Fig 5 is the plot of millimols of EXCESS BASE per 0.5 g sample against pH. One of the practical limitations of this type of basicity measurement is the variation in the number of millimols of slag in 0.5 g. The replacement of CaO by large amounts of the lighter molecule of MgO will make the number increase, whereas the replacement of SiO_2 by substantial amounts of Al_2O_3 will cause it to decrease.

The aqueous solubilities of the various oxides found in slags formed the basis of the basicity value used in plotting Fig 6. It was noted that $\text{Mg}(\text{OH})_2$ had the largest of the solubility products after $\text{Ca}(\text{OH})_2$, but even its value was not of sufficient order of magnitude to seriously interfere as long as there was a reasonable amount of CaO present. The pH of a pure aqueous solution saturated with $\text{Mg}(\text{OH})_2$ can be computed and is found to be between pH 10 and pH 11, depending on the data used. The presence of $\text{Ca}(\text{OH})_2$ greatly suppresses the hydrolysis of MgO. Since the extracts

are not at equilibrium and are not saturated, it can be assumed that the MgO does not have an influence on pH's over 9.

The relationship between millimols EXCESS CaO and pH in Fig 6 seems quite good when it is realized that many of these slags are not fully matured and do not represent final equilibrium slags.

The calculation of EXCESS CaO involves the same procedure as the calculation of EXCESS BASE. After the value for EXCESS BASE has been found, it is multiplied by the CaO fraction of the total bases present in the slag. For example, if the slag contains 80 pct (molar) CaO and 20 pct (molar) MgO of the bases present, then the EXCESS CaO will be four-fifths of the calculated EXCESS BASE.

It should be repeated that the pH values found here are not equilibrium values but can be applied to a particular set of conditions. Qualitatively, it can be stated that longer shaking times would decrease the slope of the line shown in the various figures while shorter times would increase the slope.

CORRELATION OF pH OF OPEN HEARTH TYPE SLAGS WITH COMPOSITION

The same investigation that was carried out on blast furnace type slags was repeated for a set of open hearth type slags that had been used in the study of sulphur equilibria by Grant and Chipman.⁵

The composition range found in these slags is far larger than would be found in the ordinary commercial open hearth slags. The most complex slags contain varying amounts of nine different constituents.

In the calculation of EXCESS BASE for this investigation, the assumption was made again that a bisilicate slag is a neutral slag. The compounds SiO_2 , Al_2O_3 , and Fe_2O_3 were considered acidic and equivalent to each other on a molar basis. Also, the compounds CaO, MgO, FeO, MnO, CaS, and CaF_2 were considered basic and equivalent to each other on a molar basis. In order to compute the EXCESS BASE for a given weight of slag, subtract the acids from the bases and the remaining is the value for EXCESS BASE.

The calculation of EXCESS CaO is made by multiplying the EXCESS BASE by the CaO fraction of the total bases present in the slag. The compounds CaS and CaF_2 are included with CaO in computing the EXCESS CaO.

A plot of EXCESS BASE against pH is shown in Fig 7. The scatter of points is similar in appearance to that found for blast furnace type slags. There are more slags with higher pH's. A large portion of the open hearth type slags have pH values between 11 and 12 while the more neutral blast furnace slags seldom exceed a pH of 11. There is no significant correlation between EXCESS BASE and pH.

In Fig 8, EXCESS CaO is plotted against pH and the resulting straight line relationship is found to be quite similar to Fig 6, except that the points occur in the upper portion of the graph.

Fig 9 is a combination of Fig 6 and Fig 8 plotted together. The straight line relationship found in each case separately is the same for both types of slag. A close inspection of the plot will show that there are blast furnace slags that extend up into the more basic region of the open hearth slags, and,

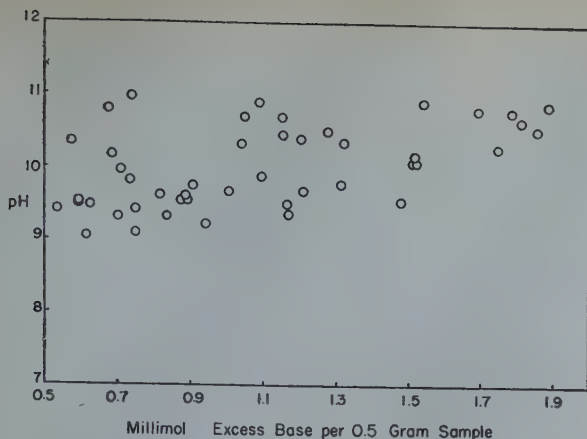


FIG 5—Effect of excess base on pH for blast furnace type slags.

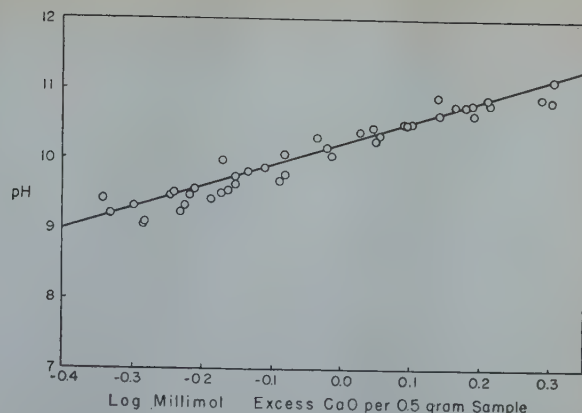


FIG 6—Effect of excess CaO on pH for blast furnace type slags.

conversely, some of the more neutral open hearth slags are found in the region of blast furnace slags.

Discussion of Results

THE pH METHOD OF ESTIMATING SLAG BASICITY

As mentioned previously, the most serious limitation in the use of the pH method as a research tool would be the variation in the number of millimols of slag in a definite weight of sample when composition varies over a wide range of molecular species of widely different molecular weights. In other words, a chemical analysis would still be necessary to check the pH results if it were expected that significant variations might occur in the low molecular weight (MgO) or high molecular weight (Al_2O_3) oxides from heat to heat.

One of the criticisms leveled against the pH method is its inability to predict V-ratios closely. This is not the fault of the pH method, but perhaps is due to the inadequacy of the V-ratio. All previous investigators of the pH method^{1,2,3} have reported some sort of correlation between the pH of the slag extracts and the V-ratio in either its ordinary or modified form. However, Smith, Monaghan and Hay³ in discussing the results of their conductance measurements infer that CaO is the controlling constituent responsible for the conductance effect. They state that it appears that the extent to which the CaO is leached out of compounds and solid solutions in the slag is in some way proportional to the V-ratio.

Since it has been found that the pH method gives a satisfactory value of EXCESS CaO, it would be expected

that EXCESS CaO and the V-ratio would not correspond in all cases. This is what was found by Philbrook. The pH method proved satisfactory for his V-ratios of 2.5 to 4.

The institution of the pH method for estimating EXCESS CaO could be accomplished with several modifications in the technique reported in this investigation.

The accurate weighing of samples would not be necessary, but since the determination would be performed by laboratory personnel, the sample could be weighed in the same manner as for the iron oxide determination which commonly uses a 0.5 g sample.

Mechanical agitation of the sample is to be preferred to intermittent shaking because it prevents caking and agglomeration of the sample on the bottom of the flask.

Boiled distilled water is a safeguard against too much CO_2 in contact with the sample. A mechanical shaker and boiled distilled water usually are employed in the steel works laboratory for the determination of phosphorus. Their use would entail the purchase of no new equipment or reagents.

The filtration of the solution after a definite time of contact between the sample and the water could probably be eliminated. This step was used to determine the exact effect of time of contact on the resulting pH. However, the desirability of a set procedure should be emphasized.

The determination of the pH of the aqueous suspensions should be performed in a section of the laboratory where there is a minimum amount of acid fume. Free H_2S , HCl , NO_2 and other acidic gases have a very deleterious effect on the pH's of the basic solutions.

ANALYSIS OF BLAST FURNACE SLAG-METAL DATA IN TERMS OF EXCESS CaO

The quantity EXCESS CaO as measured by the pH method is limited in its general usefulness unless combined with additional information to determine the EXCESS BASE value for the slag. In certain instances, this might be practical to do. Whenever other oxides such as MnO or MgO remain low or are absent altogether, the EXCESS CaO value might be combined with the chemically determined FeO content to give a reasonable estimate of overall basicity.

When the basicity of the slag has been estimated in this way, any properties that vary directly with basicity can be determined. One of the prime interests of the steelmaker is sulphur control. It is known that sulphur distribution depends on basicity of the slag. With these considerations in mind, it might be expected that the use of pH values alone to determine limiting sulphur ratios would be restricted to the case where there is no FeO present, such as the typical blast furnace slag. The slags of Hatch and Chipman⁴ used in this study were free of MnO and FeO, but contained more than residual amounts of MgO . Comparing their slags in two different ways, they found that it was necessary to make some modification in the desulphurizing effect of MgO . Both the $\frac{CaO + MgO}{Al_2O_3 + SiO_2}$ ratio and the EXCESS BASE per 100 g values showed a rather wide scatter of points when plotted against the sulphur ratio.

Realizing that Hatch and Chipman, in formulating their value for EXCESS BASE, had made many of the same assumptions that were used in this

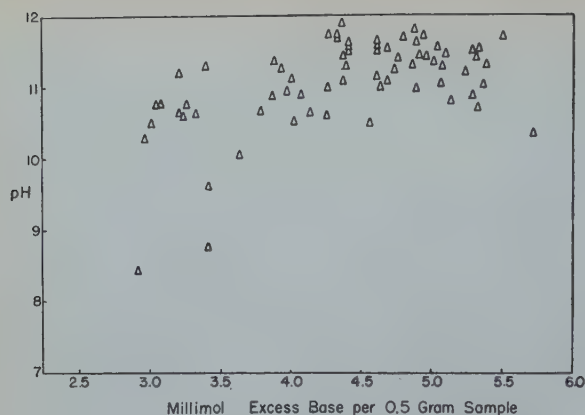


FIG 7—Effect of excess base on pH for open hearth type slags.

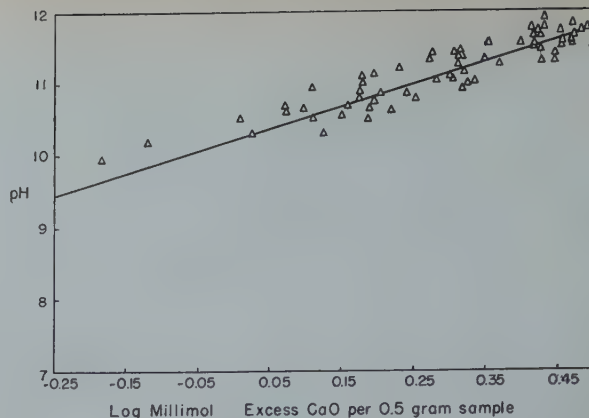


FIG 8—Effect of excess CaO on pH for open hearth type slags.

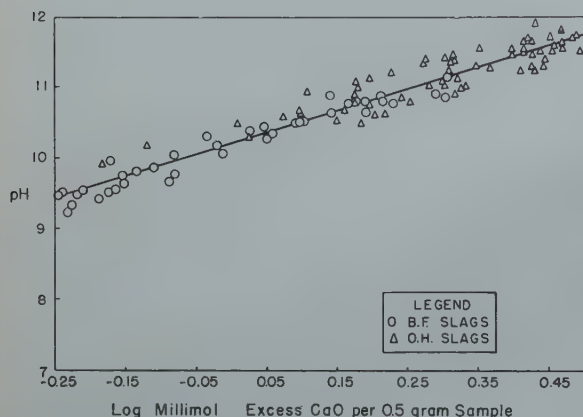


FIG 9—Effect of excess CaO on pH for blast furnace and open hearth type slags.

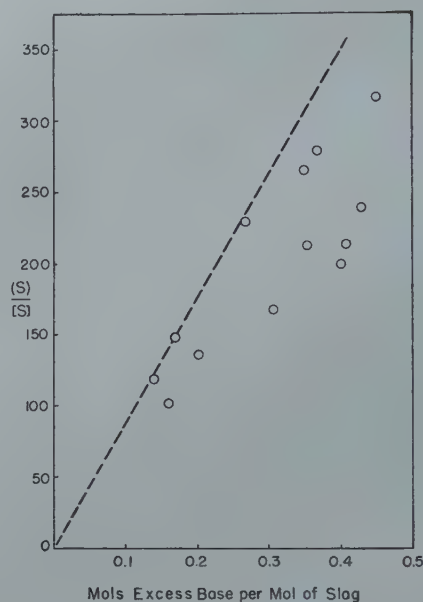


FIG 10—Effect of excess base per mol of slag on sulphur ratio for heats of Hatch and Chipman made at 1500°C.

investigation, it was thought that a better comparison might be obtained if the slags were referred to one mol of slag instead of 100 g, since there was a significant variation in the amounts of low molecular weight (MgO) and high molecular weight (Al_2O_3) oxides present. For the calculation of one mol of slag, it was assumed that the neutralized bases, CaO , SiO_2 , MgO , Al_2O_3 , and others, were one molecular species, and the "free" or EXCESS BASE was a separate molecular species.

Fig 10 shows the effect of EXCESS BASE per mol of slag on the sulphur ratio where the CaS is considered to be a base along with CaO and MgO . The point on the line drawn represents heat H-24 which has essentially no MgO . The two points that are very close to the line represent heats H-28 and H-51 which have approximately 1.5 pct MgO in the slag. Points progressively further off the dotted line show increasing MgO content.

Fig 11 is a plot of EXCESS CaO per

mol of slag against the sulphur ratio. The CaS present is considered as a part of the CaO . The relationship in Fig 11 is very good, passing through the origin and showing very little deviation from a straight line relationship.

In this particular instance (MnO free slags), the pH value will give a satisfactory estimate of the basicity of blast furnace slags. Fig 12 shows the relationship between pH and the sulphur ratio for these slags. The log of the sulphur ratio must be plotted against pH since pH is a log relationship. The scatter of points is due to the variation of the number of millimols of slag in 0.5 g sample.

A similar plot of EXCESS CaO against the sulphur ratio for the open

hearth slags was attempted, but the relationship was extremely poor, emphasizing the necessity for additional information to obtain the value for EXCESS BASE which has been correlated previously with desulphurization.⁵

Conclusions

1. The pH of the slag extracts has been studied over a very wide range of slag compositions varying from neutral bisilicate slags of the blast furnace type to the highly basic slags achieved in the open hearth process.

2. It has been found that the pH of an aqueous solution extracted from powdered slags, using a standard tech-

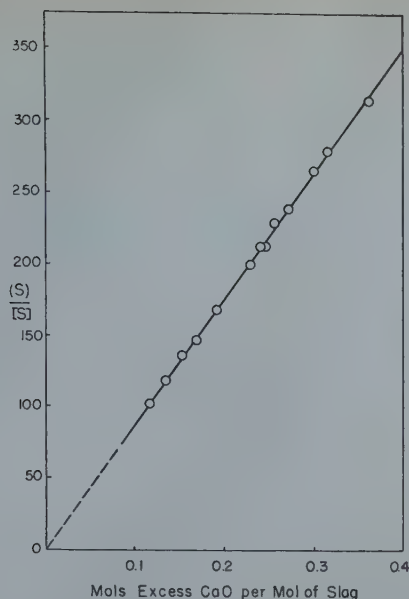


FIG 11—Effect of excess CaO per mol of slag on sulphur ratio for heats of Hatch and Chipman made at 1500°C.

nique, varies directly with the number of mols of EXCESS CaO present in the sample. EXCESS CaO is defined, in a manner similar to EXCESS BASE, as the amount of CaO remaining after subtracting the total mols of ACIDS from the total mols of BASES. The CaO is considered to be present in the EXCESS BASE in the ratio:

$\frac{\text{TOTAL MOLS CaO}}{\text{TOTAL MOLS BASES}}$ The expression, EXCESS BASE, was determined on the basis of the following set of rules.

a. One mol of base neutralized one mol of acid.

b. The compounds CaO, MgO, FeO, CaS, and CaF₂ were considered basic and equivalent to each other on a molar basis.

c. The compounds SiO₂, Al₂O₃, and Fe₂O₃ were considered acid and equivalent to each other on a molar basis.

3. In addition, it has been found that the quantity, EXCESS CaO, is useful in estimating the desulphurizing power of certain MnO-free blast furnace slags for it is shown that the sulphur ratio in these slag-metal systems is controlled by the EXCESS CaO per mol of slag. For the calculation of one mol of slag, these additional rules were followed:

d. The neutralized acids were considered one molecular species.

e. The EXCESS BASES were considered a separate molecular species.

4. For MnO-free blast furnace slags,

the pH of the slag shows a close relationship to the desulphurizing ratio; however, the pH is not closely related to the desulphurizing ratio of the basic open hearth.

Acknowledgments

The authors wish to thank the American Iron and Steel Institute that is sponsoring a steelmaking research program at the Massachusetts Institute of Technology, for its support of the above work.

References

1. Philbrook, Jolly and Henry: *Metals Tech.*, Aug. 1945. TP 1862.
2. Tenenbaum and Brown: *Metals Tech.*, Aug. 1945. TP 1863.
3. Smith, Monaghan and Hay: *Jnl. Iron and Steel Inst.*, Oct., 1948.
4. Hatch and Chipman: *AIME Trans. Jnl. of Metals*, April, 1949, 274.
5. Grant and Chipman: *Trans. AIME* (1946) 167, 134. *Metals Tech.* April 1946. TP 1988.

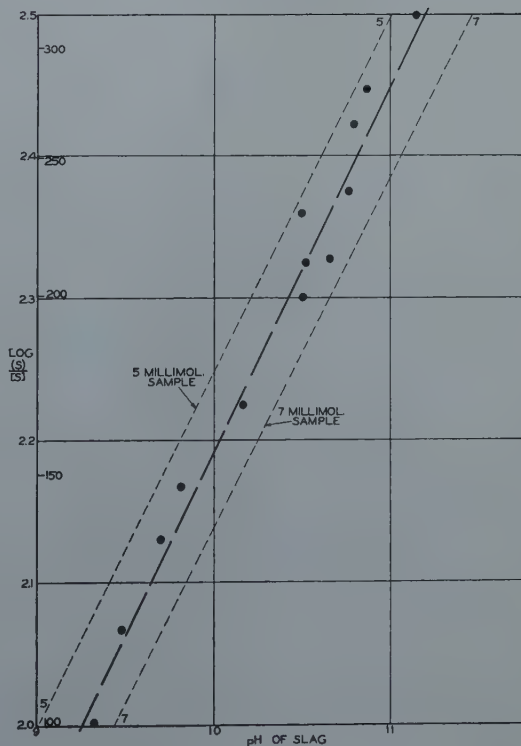


FIG 12—Effect of pH on sulphur ratio for heats of Hatch and Chipman made at 1500°C.

[illegible]

Melting Points in the System $\text{TiO}_2\text{-CaO-MgO-Al}_2\text{O}_3$

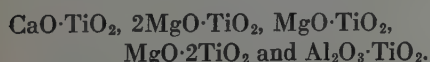
H. SIGURDSON* and S. S. COLE,* Member AIME

Introduction

The melting points of mixtures of titanium dioxide and other titanates have been reported to a limited extent as binary systems and some results have been reported in conjunction with silicon dioxide. The limited data indicated that a low melting zone might exist in a ternary or quaternary system of $\text{CaO-MgO-TiO}_2\text{-Al}_2\text{O}_3$, since the eutectics reported in the binary systems of $\text{MgO-TiO}_2\text{-TiO}_2$, $\text{Al}_2\text{O}_3\text{-TiO}_2\text{-TiO}_2$ and $\text{CaO-TiO}_2\text{-TiO}_2$ were of about equivalent composition of TiO_2 . The importance of a low melting region with a high titanium oxide value in the developing of high titanium slags is fully appreciated by metallurgists. A comprehensive study was undertaken to establish basic information on low melting titanate mixtures.

Compounds in the System $\text{CaO-MgO-TiO}_2\text{-Al}_2\text{O}_3$

Preparation of the titanates of CaO , MgO and Al_2O_3 confirmed reported data that the following compounds could be formed under oxidizing conditions in solid state reactions:



Under oxidizing conditions it was not possible to react MgO with TiO_2 in mol ratios higher than 1:2 without having unreacted TiO_2 in the product, nor was it possible to form calcium or aluminum titanates with a higher mol ratio of CaO and Al_2O_3 to TiO_2 than 1:1.

By fusing mixtures of $\text{Al}_2\text{O}_3\text{-TiO}_2$ and MgO-2TiO_2 together a series of solid solution products were obtained, which showed an MgO-2TiO_2 X ray diffraction pattern shifted to smaller interplanar spacings.

Range of Investigation

Data in the literature¹ indicated that these titanates had melting points which ranged from 1645 to 1860°C.

Since the purpose of the study was primarily to provide useful data for smelting titaniferous ores, the work was restricted to the zone of the system which would include the crystalline phases present in the slags. The explored limits were bounded by $\text{CaO-TiO}_2\text{-MgO-TiO}_2\text{-TiO}_2$ in the base plane. The system was extended to a fourth component $\text{Al}_2\text{O}_3\text{-TiO}_2$ since many titaniferous ores contain appreciable amounts of Al_2O_3 .

In the quaternary system $\text{CaO-TiO}_2\text{-MgO-TiO}_2\text{-TiO}_2\text{-Al}_2\text{O}_3\text{-TiO}_2$, a tetrahedron was used to represent graphically the components, with one component at each point of the tetrahedron.

In the base plane, mixtures were pre-

pared to represent fairly uniform changes of composition over the desired range expressed on a mol percent basis. $\text{Al}_2\text{O}_3\text{-TiO}_2$ was brought into the system in increments of 10 mol pct up to 40 pct. Mixtures were then made up for each of the $\text{Al}_2\text{O}_3\text{-TiO}_2$ planes. The ranges employed were then represented by five planes cutting the tetrahedron at 10 mol pct $\text{Al}_2\text{O}_3\text{-TiO}_2$ intervals.

Choice of Equipment

Although it was necessary for all smelting work to be done in a strongly reducing atmosphere, it was decided that all melting point determinations should be done under oxidizing conditions. This decision was prompted by the fact that TiO_2 reduced to lower oxides in a reducing atmosphere with consequent changes in melting points.

The use of a micropyrometer and a platinum strip furnace for work of this type is adequately described in the literature.² With modifications, equipment was selected which provided a fairly rapid method of determining melting points of refractory oxides.

The final assembly, which was used, consisted of a platinum strip furnace and a Leeds and Northrup disappearing filament optical pyrometer attached to a special telescope which magnified the sample about 20 diam.

The furnace assembly consisted of a platinum strip $0.005 \times 0.3 \times 2.2$ in. mounted on brass posts on a refractory base. This was enclosed in a black steel shell which had a 2-in. opening at the top for purposes of sighting the telescope.

The platinum strip was in series with two 0.04 ohm nichrome resistors connected to the secondary of a 2 kw transformer which supplied 17 volts. The current to the primary was varied

San Francisco Meeting, February 1949.

TP 2708 D. Discussion of this paper (2 copies) may be sent to *Transactions AIME* before Jan. 1, 1950.

Manuscript received March 10, 1949; revision received July 6, 1949.

* Research Chemist and Asst. Manager of Research, respectively, Research Laboratory, Titanium Division, National Lead Co., South Amboy, N. J.

¹ References are at the end of the paper.

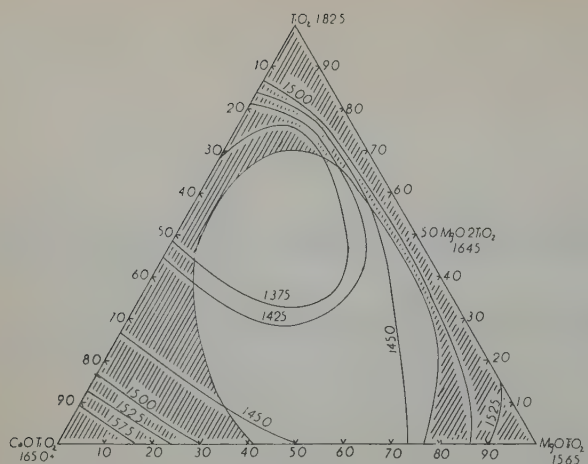


FIG 1—Melting equilibria for system $\text{CaO-TiO}_2\text{-MgO-TiO}_2$.
Clear area-fluid zone. Cross-hatched area-viscous zone.

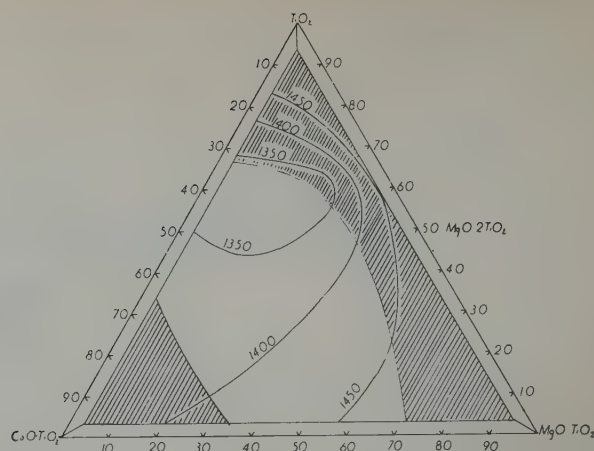


FIG 2—Melting equilibria for system $\text{CaO-TiO}_2\text{-MgO-TiO}_2\text{-Al}_2\text{O}_3\text{-TiO}_2$. (10 mol pct $\text{Al}_2\text{O}_3\text{-TiO}_2$ layer).
Clear area-fluid zone. Cross-hatched area-viscous zone.

by means of a 35 ohm variable resistor. Large increases of current in the system were made with this resistor. Very fine adjustments were made by means of the sliding contacts on the nichrome resistors.

Preparations of Mixtures

The compounds CaO-TiO_2 , MgO-TiO_2 , MgO-2TiO_2 and $\text{Al}_2\text{O}_3\text{-TiO}_2$ were prepared from spectrographically pure TiO_2 , and cp CaCO_3 , MgO and Al(OH)_3 . Stoichiometric amounts of the components were wet mixed, dried and pelletized. The pellets were then fired in platinum at 1500°C under oxidizing conditions for 3 hr to complete transformation to the compounds in each case. Chemical analyses of the compounds showed the materials to be on composition within 0.4 pct.

These compounds were then finely ground, wet-mixed in varying amounts to give the required compositions and sintered at 1200°C for at least 3 hr to give hard sintered products.

Determination of Melting Points of Mixtures

Fragments of the sintered mixtures, which had been screened through a 100 mesh screen, were placed on the platinum strip and spread evenly to insure close contact between the platinum and the sample. The temperature of the strip was then raised rapidly to about 1000°C . Time was allowed for the sample to reach temperature stability and the temperature rise was then adjusted to about 10°C per min. until the melting point was reached.

The temperatures at which melting occurred were obtained by sighting the pyrometer on the platinum strip adjacent to the sample at right angles to the length of the strip and in line with the particles under observation. These precautions were necessary since the temperature gradient across the strip was quite steep.

The emissivity of the platinum strip in the open conditions which prevailed was considerably less than in black-body conditions so temperature corrections were applied in accordance with Table 16, p. 13, of Bureau of Standards "Pyrometric Practice" No. 170. The emissivity corrections for platinum were checked against the following substances whose melting points are reported in the literature:

| Substance | Reported Melting Point $^\circ\text{C}$ | Observed* Melting Point $^\circ\text{C}$ | Deviation from Reported Value $^\circ\text{C}$ |
|------------------------------------|---|--|--|
| Gold | 1063 | 1060 | -3 |
| $\text{Na}_2\text{Ti}_2\text{O}_7$ | 1128 | 1125 | -3 |
| BaF_2 | 1280 | 1270 | -10 |
| $\text{CaMgSi}_2\text{O}_6$ | 1391 | 1385 | -6 |
| MgTi_2O_6 | 1660 | 1645 | -15 |

* Emissivity corrections for platinum applied to observed temperature reading.

The resolving power of the telescope was sufficient to permit the observance in the fluid melts of the points at which the last solid particles became molten. In these melts the particles formed spheres very sharply at the melting point. The temperature of formation of spheres and the disappearance of the solid phase coincided. As a check, the temperature of the sample was lowered through the melting point to note the temperature of appearance of the solid phase. Good agreement was obtained.

In the range of melts which were

classified as viscous, it was difficult to determine accurately the point at which the particles became spherical, since they showed a rounding of the edges at the softening point and the transition to spheres was not nearly as sharp as in the mixtures which were fluid. Chief reliance was placed on the observance of the point at which the last observable solid particles disappeared.

Quenching of the samples did not assist in determining if the mixtures were completely molten, since the crystal growth of the titanates was so rapid that isotropic phases could not be obtained. Hence the actual determination of the points at which samples were completely molten rested very much with the judgment of the operator.

Definition of Melting and Softening Points

The following definition of the melting point of a refractory material was used,² "The melting point of an irregularly shaped refractory particle is that temperature at which the viscosity (or crystalline rigidity) is overcome by the random motion of the molecules and at which the surface tension is sufficient to draw the particle into a globular shape."

In contrast to this, the "softening" point was considered to be "the temperature at which the corners of an angular piece of the refractory substance first became rounded." At this point there would be considerable unfused material present in the particle whereas at the melting point there would be only a trace of solid material in equilibrium with the fused portion.

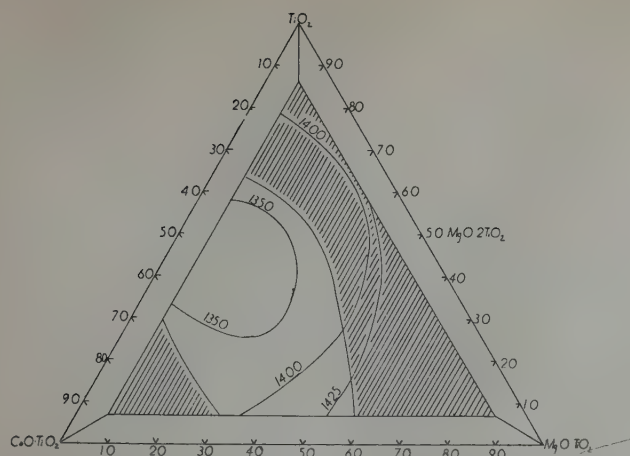


FIG 3—Melting equilibria for system $\text{CaO} \cdot \text{TiO}_2$ - $\text{MgO} \cdot \text{TiO}_2$ - TiO_2 - $\text{Al}_2\text{O}_3 \cdot \text{TiO}_2$. (20 mol pct $\text{Al}_2\text{O}_3 \cdot \text{TiO}_2$ layer.)
Clear area-fluid zone. Cross-hatched area-viscous zone.

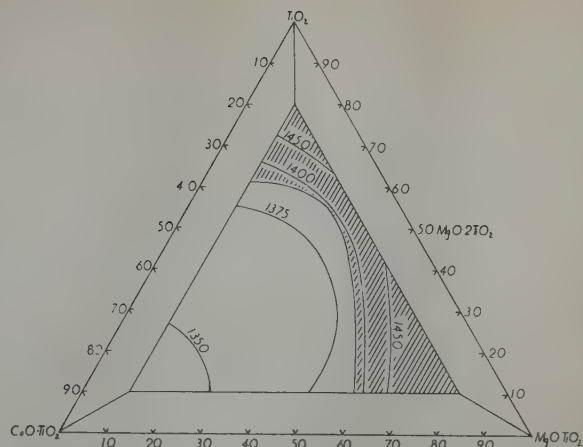


FIG 4—Melting equilibria for system $\text{CaO} \cdot \text{TiO}_2$ - $\text{MgO} \cdot \text{TiO}_2$ - TiO_2 - $\text{Al}_2\text{O}_3 \cdot \text{TiO}_2$. (30 mol pct $\text{Al}_2\text{O}_3 \cdot \text{TiO}_2$ layer.)
Clear area-fluid zone. Cross-hatched area-viscous zone.

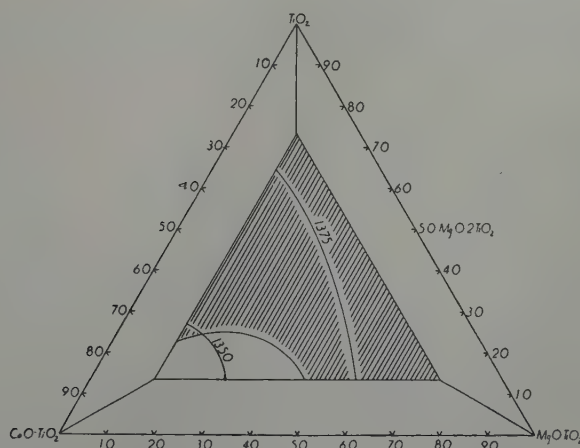


FIG 5—Melting equilibria for system $\text{CaO} \cdot \text{TiO}_2$ - $\text{MgO} \cdot \text{TiO}_2$ - TiO_2 - $\text{Al}_2\text{O}_3 \cdot \text{TiO}_2$. (40 mol pct $\text{Al}_2\text{O}_3 \cdot \text{TiO}_2$ layer.)
Clear area-fluid zone. Cross-hatched area-viscous zone.

Table 1 . . . Patterns of $\text{MgO} \cdot 2\text{TiO}_2$, $\text{Al}_2\text{O}_3 \cdot \text{TiO}_2$ and Intermediate Series of Mixed Crystals Spectrometer, $\text{Cu } K_{\alpha, \lambda} = 1.5374 \text{ \AA}$, 2 rpm scan. No Corrections Applied

| $\text{MgO} \cdot 2\text{TiO}_2$ | | 80Mol % $\text{MgO} \cdot 2\text{TiO}_2$ 20Mol % $\text{Al}_2\text{O}_3 \cdot \text{TiO}_2$ | | 60Mol % $\text{MgO} \cdot 2\text{TiO}_2$ 40Mol % $\text{Al}_2\text{O}_3 \cdot \text{TiO}_2$ | | 40Mol % $\text{MgO} \cdot 2\text{TiO}_2$ 60Mol % $\text{Al}_2\text{O}_3 \cdot \text{TiO}_2$ | | 20Mol % $\text{MgO} \cdot 2\text{TiO}_2$ * 80Mol % $\text{Al}_2\text{O}_3 \cdot \text{TiO}_2$ | | $\text{Al}_2\text{O}_3 \cdot \text{TiO}_2$ | |
|----------------------------------|------|--|------|--|------|--|------|--|-----|--|------|
| d/n Å | I/I | d/n Å | I/I | d/n Å | I/I | d/n Å | I/I | d/n Å | I/I | d/n Å | I/I |
| 5.0 | 0.12 | 4.9 | 0.2 | 4.8 | 0.3 | 4.8 | 0.4 | 4.8 | 0.7 | 4.71 | 0.47 |
| 4.9 | 0.12 | 4.8 | 0.4 | 4.7 | 0.7 | 4.6 | 1.00 | 4.6 | 1.0 | 3.35 | 1.00 |
| 3.51 | 1.00 | 3.44 | 1.00 | 3.43 | 0.05 | 3.40 | 0.7 | 3.39 | 0.5 | 2.65 | 0.7 |
| 2.86 | 0.09 | 2.83 | 0.08 | 2.82 | 1.00 | 2.70 | 0.09 | | | | |
| 2.75 | 0.6 | 2.72 | 1.00 | 2.71 | 0.1 | 2.44 | 0.12 | | | 2.36 | 0.20 |
| 2.45 | 0.2 | 2.42 | 0.2 | 2.41 | 0.05 | 2.41 | 0.15 | | | 2.14 | 0.31 |
| 2.42 | 0.15 | 2.39 | 0.2 | 2.37 | 0.1 | 2.16 | 0.2 | 1.91 | 0.2 | 2.11 | 0.30 |
| 2.22 | 0.15 | 2.21 | 0.2 | 2.19 | 0.25 | 1.931 | 0.4 | 1.81 | 0.4 | 1.897 | 0.52 |
| 2.19 | 0.2 | 2.17 | 0.25 | 2.16 | 0.25 | 1.822 | 0.3 | | | 1.792 | 0.44 |
| 1.967 | 0.3 | 1.951 | 0.3 | 1.943 | 0.1 | 1.713 | 0.15 | | | 1.687 | 0.28 |
| 1.876 | 0.6 | 1.850 | 0.6 | 1.836 | 0.1 | 1.629 | 0.09 | | | 1.606 | 0.27 |
| 1.846 | 0.15 | 1.836 | 0.1 | 1.725 | 0.1 | 1.601 | 0.1 | | | 1.578 | 0.28 |
| 1.754 | 0.15 | 1.738 | 0.1 | 1.613 | 0.1 | | | | | 1.519 | 0.06 |
| 1.665 | 0.15 | 1.653 | 0.2 | 1.524 | 0.15 | | | | | 1.484 | 0.36 |
| 1.634 | 0.2 | 1.621 | 0.2 | 1.514 | 0.1 | | | | | 1.449 | 0.08 |
| 1.551 | 0.3 | 1.532 | 0.2 | | | | | | | 1.371 | 0.14 |
| 1.535 | 0.2 | 1.528 | 0.2 | | | | | | | 1.305 | 0.16 |
| 1.424 | 0.09 | 1.409 | 0.1 | | | | | | | 1.266 | 0.11 |
| 1.378 | 0.08 | | | | | | | | | 1.253 | 0.11 |
| 1.358 | 0.15 | 1.343 | 0.1 | | | | | | | 1.219 | 0.09 |
| 1.318 | 0.08 | 1.283 | 0.09 | | | | | | | | |
| 1.265 | 0.10 | 1.256 | 0.1 | | | | | | | | |
| 1.245 | 0.10 | 1.235 | 0.07 | | | | | | | | |

—After relative intensity means wide line or lines.

*—Very weak pattern.

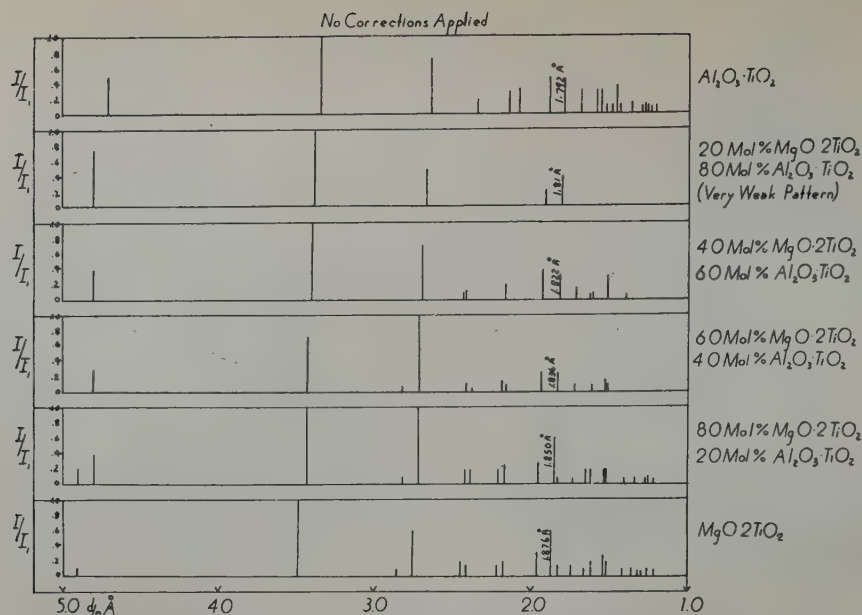


FIG 6—Patterns of $\text{MgO} \cdot 2\text{TiO}_2$ - $\text{Al}_2\text{O}_3 \cdot \text{TiO}_2$ and intermediate series of mixed crystals. Spectrometer, $\text{Cu K}\alpha, \lambda = 1.5374 \text{ \AA}$, 2 rpm scan.

Differentiation between Fluid and Viscous Melts

Preliminary investigation of the melting points of mixtures of the titanates disclosed, in many cases, that if a sample were heated above the melting point, the surface tension was sufficient for several neighboring spheres to migrate into one mass.

If this occurred within 100°C of the observed melting point, the mixture was classified as "fluid." If this migration did not occur within this range the mixture was classified as "viscous."

Phase Relationships

Equilibrium conditions prevailing at high temperatures were not obtained, since any possible transitions could not be prevented by the quenching method. No attempts were made to determine these equilibria by a method such as X ray diffraction studies of compounds at high temperatures.

In mixtures which had been fused and subsequently cooled to room temperature, the following compounds were observed:

1. In the base-plane $\text{CaO} \cdot \text{TiO}_2$ - $\text{MgO} \cdot \text{TiO}_2$ - TiO_2 (See Fig 1).

(a) Below the $\text{CaO} \cdot \text{TiO}_2$ - $\text{MgO} \cdot 2\text{TiO}_2$ tie-line, $\text{CaO} \cdot \text{TiO}_2$, $\text{MgO} \cdot \text{TiO}_2$ and $\text{MgO} \cdot 2\text{TiO}_2$ were present in the proportions expected from the position of the mixture on the phase diagram.

(b) Above the $\text{CaO} \cdot \text{TiO}_2$ - $\text{MgO} \cdot 2\text{TiO}_2$

tie-line, $\text{CaO} \cdot \text{TiO}_2$, $\text{MgO} \cdot 2\text{TiO}_2$ and TiO_2 were present in expected proportions.

2. In the 10, 20, 30 and 40 mol pct $\text{Al}_2\text{O}_3 \cdot \text{TiO}_2$ layers of the System (See Fig 2, 3, 4 and 5).

Melts of the mixtures falling within these four planes crystallized to give $\text{CaO} \cdot \text{TiO}_2$, $\text{MgO} \cdot \text{TiO}_2$ and mixed crystals of $\text{MgO} \cdot 2\text{TiO}_2$ and $\text{Al}_2\text{O}_3 \cdot \text{TiO}_2$. X ray diffraction studies of mixtures of the series $\text{MgO} \cdot 2\text{TiO}_2$ - $\text{Al}_2\text{O}_3 \cdot \text{TiO}_2$, which had been fused and crystallized, showed that the two compounds form a continuous series of mixed crystals. The interplanar spacings derived from X ray powder diffraction patterns of representative members of the series are shown in Table 1 and Fig 6. Similar studies of mixtures falling within the above four planes, showed shifted patterns for $\text{MgO} \cdot 2\text{TiO}_2$ or $\text{Al}_2\text{O}_3 \cdot \text{TiO}_2$ depending upon the composition of the mixture. Uncombined Al_2O_3 was never present in a melt of these mixtures.

Conclusions

(1) The melting points of the various mixtures investigated are presented in Fig 1, 2, 3, 4 and 5. Mixtures which were classified as "fluid" in the molten state are within the clear areas of each figure. Shaded areas show the compositions which were classified as "viscous" in the molten state.

(2) In the base plane $\text{CaO} \cdot \text{TiO}_2$ - $\text{MgO} \cdot \text{TiO}_2$ - TiO_2 a eutectic at 1360°C was established between $\text{CaO} \cdot \text{TiO}_2$ and

$\text{MgO} \cdot 2\text{TiO}_2$ at 40 mol pct $\text{CaO} \cdot \text{TiO}_2$ and 60 mol pct $\text{MgO} \cdot 2\text{TiO}_2$.

It was found, however, that melting points at about 1375°C were obtained with mixtures much higher in TiO_2 than this combination (for example, a mixture of 13.5 mol pct $\text{MgO} \cdot \text{TiO}_2$, 20 mol pct $\text{CaO} \cdot \text{TiO}_2$ and 65 mol pct TiO_2 had a melting point of 1375°C). This gave promise of the feasibility of working with fluid combinations much higher in TiO_2 than would be encountered with CaO and MgO additions sufficient to place the resultant mixture on the tie-line between $\text{CaO} \cdot \text{TiO}_2$ and $\text{MgO} \cdot 2\text{TiO}_2$.

3. $\text{Al}_2\text{O}_3 \cdot \text{TiO}_2$ additions up to 30 mol pct did not adversely affect the melting temperatures of the mixtures, but a shift in the zone of fluidity toward the $\text{CaO} \cdot \text{TiO}_2$ part of the system was evident.

40 mol pct $\text{Al}_2\text{O}_3 \cdot \text{TiO}_2$ additions to the system caused a sharp decrease in the zone of fluid melts and a 50 mol pct $\text{Al}_2\text{O}_3 \cdot \text{TiO}_2$ addition gave only viscous melts.

References

- (a) H. V. Wartenburg and E. Prophet: System $\text{MgO} \cdot \text{TiO}_2$. *Ztsch. anorg. u. allgem. Chem.* (1932) **208**, 373.
(b) E. N. Bunting: System $\text{Al}_2\text{O}_3 \cdot \text{TiO}_2$. *Bur. Standards Jnl. Research.* (1933) **11**, 725.
(c) H. V. Wartenburg, H. J. Reusch and E. Saran: System $\text{CaO} \cdot \text{TiO}_2$. *Ztsch. anorg. u. allgem. Chem.* (1936-37) **230**, 257.
- G. R. Fitterer and M. B. Royer: Rept. of Invest. Use of Micropyrometer for High Temperature Melting Point Investigations. R. I. 3151, March 1932.

Laboratory Smelting of Titaniferous Ores

D. L. ARMANT* and S. S. COLE,* Member AIME

Introduction

The smelting of titaniferous ores for the past hundred years has not been successful because of thickening of the slags in the furnaces. The interest in the utilization of these iron bearing materials has been due to the extensive deposits which have been found in various parts of the world.¹ The literature contains references² to the use of titaniferous ores in blast furnaces. None of these attempts has met with success due to the lack of sufficient information as to the cause of failures and to economic considerations. Evaluation of the published information, as to the probable cause of failure in various attempts, has indicated that the presence of lower valence titanium oxide and formation of titanium carbide contributed to the failure. It was apparent that severe reducing conditions which are present in a blast furnace had been one of the factors for such failures. The previous smelting operations had as a primary objective the recovery of iron from these ores. Under these conditions the highest recovery of iron could only occur with severe reducing conditions.

Application of Melting Point Data

The application of the melting point data, from the system $\text{CaO-MgO-Al}_2\text{O}_3\text{-TiO}_2$ reported in another paper,³ to the smelting of titaniferous ores required an extrapolation of these melting points due to the presence of other impurities from the ores. Likewise, a study of the effect of varying FeO and reduced titanium content of the slag was necessary before the data could be fully applied. The melting point data under oxidizing conditions had clearly indicated that a fluid slag with a melting point in the temperature range of 1370°C could be obtained. The smelting of a titaniferous ore had as a

primary objective the production of a high titanium slag which was fluid and substantially free of iron and low in trivalent titanium. Since production of a high titanium slag was of primary importance, rather than the recovery of iron from these ores, the smelting concept could be altered to a marked degree. The ferrous oxide could be maintained at higher levels than is the normal practice in iron ores slags without being detrimental to the slags, although a loss in iron recovery resulted.

During the reduction of the molten mixtures of ferrous iron and titanium, carbon acts as the reductant for changing the valence of the titanium and iron. The reaction can go further than in the case of the reduction which occurs in iron-titanium solutions. The formation of metallic iron removes iron from the system, so that the titanium oxide can be reduced to trivalent and divalent titanium oxides and also form titanium carbide which removes the titanium from the slags as a soluble constituent. The problem, therefore, resolves itself into maintaining the proper amount of ferrous iron in the slag thereby avoiding the formation of appreciable amounts of trivalent titanium and no divalent titanium oxide or titanium carbide. The latter two have been found in the viscous

San Francisco Meeting, February 1949.

TP 2662 D. Discussion of this paper (2 copies) may be sent to *Transactions AIME* before Jan. 1, 1950. Manuscript received March 10, 1949.

* Research Chemist and Assistant Manager of Research, respectively, Research Laboratory, Titanium Division, National Lead Co., South Amboy, N. J.

¹ References are at the end of the paper.

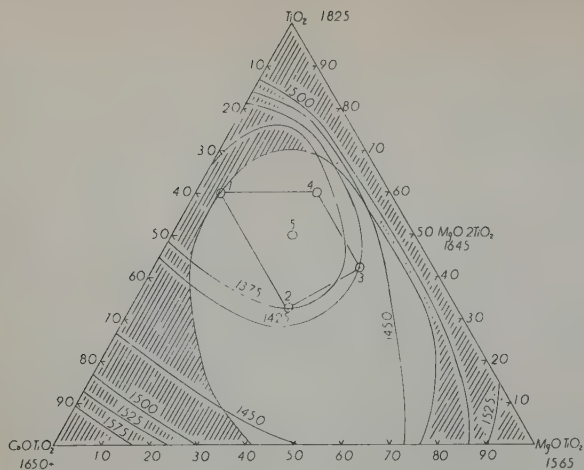


FIG 1—Melting equilibria for system $\text{CaO-TiO}_2\text{-MgO-TiO}_2\text{-TiO}_2$.

Clear area—Fluid zone
Cross hatched area—Viscous zone
Areas 1, 2, 3, 4—Normal slag zone

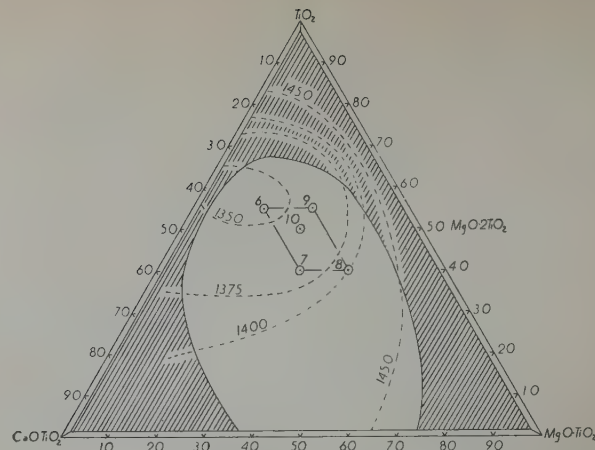


FIG 2—Melting equilibria for system $\text{CaO-TiO}_2\text{-MgO-TiO}_2\text{-TiO}_2\text{-Al}_2\text{O}_3\text{-TiO}_2$ (5 mol pct $\text{Al}_2\text{O}_3\text{-TiO}_2$ layer) interpolated from Fig 1 and 3.

Clear area—Fluid zone
Cross hatched area—Viscous zone
Areas 6, 7, 8, 9—Normal slag zone

slags which have been made from the titaniferous ores in blast furnace operation. The avoidance of the formation of Ti_2O_3 was also an important consideration since it is known that this oxide is homologous with Al_2O_3 . It would be expected that the formation of Ti_2O_3 would cause a viscous condition in a slag since this would be equivalent to addition of Al_2O_3 . Likewise, the presence of reduced titanium in the slag was to be avoided since this was not desirable in the final solutions obtained from the digestion of the slag.

Most titaniferous ores contain as normal impurities small amounts of Al_2O_3 , MgO , CaO and SiO_2 . Since the four component system which had been studied did not include SiO_2 , it was necessary in any preliminary calculations to assume that the SiO_2 would function the same as TiO_2 . This assumption was in slight error, but the characteristics of the slag produced were not appreciably affected. The titaniferous ores which were considered of primary importance in this study were the large ore bodies which are proven deposits in New York, Canada and Norway. Typical analyses of the ores used for the smelting are given in Table 1. The amount of Al_2O_3 in these ores with reference to the TiO_2 content varies slightly. The analyses have been calculated to show the TiO_2/CaO , TiO_2/MgO , and $\text{TiO}_2/\text{Al}_2\text{O}_3$ ratios. These ratios are the basic minima that would be obtained in a slag if no flux were to be used. The same information is utilized in considering the general composition that

Table 1. . . Analysis of Titaniferous Ores

| | MacIntyre Ilmenite Tahawus, N. Y. Pct | Baie St. Paul Ore Baie St. Paul, Quebec, Pct |
|--------------------------------------|--|---|
| TiO_2 | 44.6 | 38.8 |
| FeO | 36.7 | 28.3 |
| Fe_2O_3 | 8.2 | 19.7 |
| CaO | 0.8 | 0.9 |
| MgO | 2.6 | 3.8 |
| SiO_2 | 4.0 | 3.5 |
| Al_2O_3 | 3.2 | 2.8 |
| V_2O_5 | 0.04 | 0.29 |
| Cr_2O_3 | 0.02 | 0.09 |
| S | 0.24 | 0.67 |
| P_2O_5 | 0.045 | 0.04 |
| TiO_2/CaO | 55.7 | 43.0 |
| TiO_2/MgO | 17.2 | 10.2 |
| $\text{TiO}_2/\text{Al}_2\text{O}_3$ | 13.9 | 13.8 |

should be adopted from melting point data. The ratio of $\text{TiO}_2/\text{Al}_2\text{O}_3$ is the most critical in considering different ores with respect to general smelting and production of a fluid slag. This is particularly the case in ores which cannot be dressed to produce a low Al_2O_3 content.

With this basic amount of $\text{TiO}_2/\text{Al}_2\text{O}_3$ in the final slags established it is necessary only to select the area in the four component system which will yield a low melting zone and in which the aluminum oxide in the final composition would fit into this range of composition. This necessitated considering the compositions that were in the 0, 5, 10 and 20 mol pct $\text{Al}_2\text{O}_3\text{-TiO}_2$ plane. The compositions which fitted in this region are given in Table 2 and Fig 1-4 and are for the region of the highest fluidity and lowest melting points. The data in Table 2 have the greatest bearing on the titaniferous ores which have been investigated.

The weight percent is calculated so that all TiO_2 in excess is considered to be in solid solution with MgO-2TiO_2 . The areas on the 5 and 10 mol pct $\text{Al}_2\text{O}_3\text{-TiO}_2$ plane are typical for most slags produced from ores. The areas were selected for varying the CaO and MgO additions because this was the lowest melting and most fluid zone. The slags from the ores would approach the 5 mol pct $\text{Al}_2\text{O}_3\text{-TiO}_2$ with respect to minimum $\text{TiO}_2/\text{Al}_2\text{O}_3$ and TiO_2/MgO . The flux additions were calculated so that the final slag would have a general composition within these areas, after correcting for SiO_2 and FeO in the slag. The usual practice was to add the minimum amounts of flux. This practice was followed since it was desirable to have as high a TiO_2 content in the slag as possible.

Smelting Practice

The investigation was primarily divided into two sections: first, the induction furnace work and second, the single phase arc furnace. Based upon the composition diagram which appeared to give the most fluid slags, a series of mixtures were prepared in which varying amounts of CaO and MgO were incorporated using petroleum coke as a reducing agent. The use of petroleum coke was practiced in order to avoid any introduction of ash from other types of coke.

The induction furnace utilized for this work was a standard Ajax 6KW high frequency induction furnace,

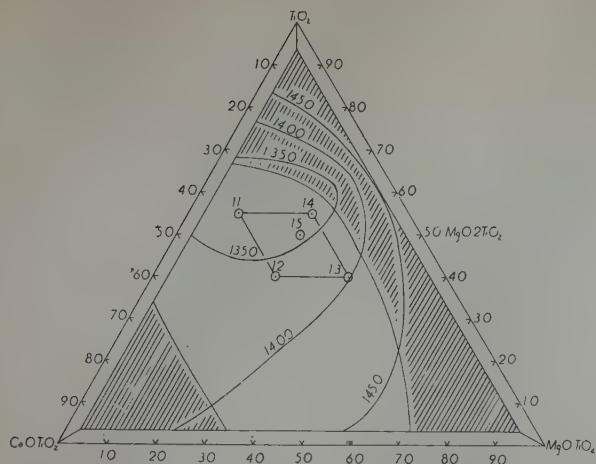


FIG 3—Melting equilibria for system CaO·TiO₂-MgO·TiO₂-TiO₂-Al₂O₃·TiO₂ (10 mol pct Al₂O₃·TiO₂ layer).
Clear area—Fluid zone
Cross hatched area—Viscous zone
Areas 11, 12, 13, 14—Normal slag zone

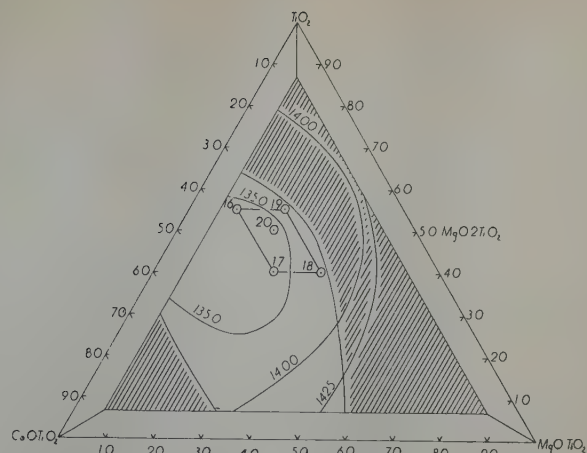


FIG 4—Melting equilibria for system CaO·TiO₂-MgO·TiO₂-TiO₂-Al₂O₃·TiO₂ (20 mol pct Al₂O₃·TiO₂ layer).
Clear area—Fluid zone
Cross hatched area—Viscous zone
Areas 16, 17, 18, 19—Normal slag zone

using a standard 2 lb graphite crucible (3 in. od \times 2½ in. id \times 3½ in. inside height \times 4 in. outside height). The period of time for a smelting test was varied in order to establish the change in ferrous oxide content of the slag and to observe the change in fluidity as the reduced titanium content increased. Normally the one pound batch required about 30–35 min. to form a molten mixture and this was held in a fluid state for 10–20 min. before removing from the furnace. A holding time of 15 min. was found to be the time required to obtain the necessary reduction of the iron to the metal. The molten slag and metal were poured into a small metal mold and allowed to cool. The metal formed a solid button which was readily separated from the slag above it. The various heats were analysed for TiO₂ and the total ferrous iron as well as carrying out

metallographic, X ray and digestion tests.

Results Obtained

The results from a series of mixtures which were smelted in order to study the influence of composition upon fluidity of the slag are given in Table 3. The shift in mineral composition is directly related to the amount of trivalent titanium in the slag.⁴ The formation of Ti(OC) also occurs when the slag is over-reduced. The fluidity of these slags was not noticeably affected by the high Ti³⁺ content. Longer holding in the furnace, however, did cause the slags to become viscous and even formed a sintered mass, which was predominantly Ti(OC).

The change in viscosity in the slag is shown in the results given in Table 4 in which the calcium content of the

burden was varied over the range of composition which would give viscous and fluid slags based upon the melting point data observations. The observed fluidity was obtained in accordance with predictions. The calculated slag composition agrees quite well with the observed values.

The maximum and minimum amounts of CaO and MgO required to give suitable slags from various ores was then established. Since the melting point data and fluidity observations appeared to be valid, it was necessary only to delineate the general results for a given ore. These data are given in Table 5 for slags made from the three ores. The maximum amount of MgO that could be used with minimum CaO addition was not established since it was desirable to keep the MgO addition at a minimum. The slags were fluid and furnace behavior was entirely

Table 2 . . . Mineral and Chemical Composition of Low Melting and Fluid Zones

| | Mol Pct | | | | Wt Pct | | | Composition-Wt Pct | | | | TiO ₂ /MgO | TiO ₂ /Al ₂ O ₃ |
|----|--|----------------------|----------------------|------------------|--|-----------------------|----------------------|--------------------|------|------|--------------------------------|-----------------------|--|
| | Al ₂ O ₃ ·TiO ₂ | MgO·TiO ₂ | CaO·TiO ₂ | TiO ₂ | Al ₂ O ₃ ·TiO ₂ | MgO·XTiO ₂ | CaO·TiO ₂ | TiO ₂ | CaO | MgO | Al ₂ O ₃ | | |
| 1 | 0 | 5 | 35 | 60 | 0 | 53 | 47 | 78.8 | 19.2 | 2.0 | 0 | 39.4 | |
| 2 | 0 | 33 | 35 | 32 | 0 | 58 | 42 | 70.9 | 17.4 | 11.7 | 0 | 6.1 | |
| 3 | 0 | 43 | 15 | 42 | 0 | 81 | 19 | 75.8 | 7.9 | 16.3 | 0 | 4.7 | |
| 4 | 0 | 25 | 15 | 60 | 0 | 79 | 21 | 81.3 | 8.5 | 10.2 | 0 | 8.0 | |
| 5 | 0 | 25 | 25 | 50 | 0 | 67 | 33 | 77.0 | 13.4 | 9.6 | 0 | 8.0 | |
| 6 | 5 | 14 | 29 | 52 | 8 | 45 | 37 | 75.0 | 15.2 | 5.2 | 4.8 | 14.4 | 15.6 |
| 7 | 5 | 28 | 29 | 38 | 8 | 57 | 35 | 71.1 | 14.4 | 10.0 | 4.5 | 7.1 | 15.8 |
| 8 | 5 | 38 | 19 | 38 | 8 | 69 | 23 | 72.1 | 9.6 | 13.7 | 4.6 | 5.2 | 15.7 |
| 9 | 5 | 24 | 19 | 52 | 9 | 66 | 25 | 76.1 | 10.0 | 9.1 | 4.8 | 8.4 | 15.9 |
| 10 | 5 | 24 | 24 | 47 | 8 | 52 | 30 | 74.0 | 12.4 | 8.9 | 4.7 | 8.3 | 15.7 |
| 11 | 10 | 9 | 31.5 | 49.5 | 16 | 46 | 38 | 71.8 | 15.8 | 3.2 | 9.2 | 22.4 | 7.8 |
| 12 | 10 | 22.5 | 31.5 | 36 | 16 | 46 | 38 | 68.5 | 15.1 | 7.7 | 8.7 | 8.9 | 7.9 |
| 13 | 10 | 36 | 18 | 36 | 16 | 63 | 21 | 69.7 | 8.8 | 12.6 | 8.9 | 5.5 | 7.8 |
| 14 | 10 | 22.5 | 18 | 49.5 | 17 | 61 | 22 | 73.3 | 9.2 | 8.2 | 9.3 | 8.9 | 7.9 |
| 15 | 10 | 22.5 | 22.5 | 45 | 16 | 57 | 27 | 71.5 | 11.3 | 8.1 | 9.1 | 8.7 | 7.9 |
| 16 | 20 | 8 | 28 | 44 | 30 | 38 | 32 | 67.1 | 13.1 | 2.7 | 17.1 | 24.9 | 3.9 |
| 17 | 20 | 20 | 28 | 32 | 30 | 39 | 31 | 64.6 | 12.6 | 6.4 | 16.4 | 10.1 | 3.9 |
| 18 | 20 | 28 | 20 | 32 | 30 | 48 | 22 | 65.0 | 9.2 | 9.2 | 16.6 | 7.1 | 3.9 |
| 19 | 20 | 16 | 20 | 44 | 31 | 46 | 23 | 67.8 | 9.5 | 5.4 | 17.3 | 12.6 | 3.9 |
| 20 | 20 | 16 | 24 | 40 | 30 | 43 | 27 | 66.6 | 11.1 | 5.3 | 17.0 | 12.6 | 3.9 |

Table 3 . . . Influence of Fe²⁺ and Ti³⁺ on Slag Properties

| | | | | | | |
|--|--------------------|-------|-------|-------|-------|-----|
| Burden..... | Baie St. Paul..... | | | | | 100 |
| | CaO..... | | | | | 5 |
| | MgO..... | | | | | 1 |
| | C..... | | | | | 15 |
| | | | | | | |
| Heat No. | 206-4 | 212-4 | 208-3 | 210-3 | 211-3 | |
| TiO ₂ Pct..... | 58.7 | 63.2 | 65.8 | 67.5 | 66.4 | |
| Fe ²⁺ Pct..... | 9.2 | 8.3 | 4.5 | 2.5 | 0.7 | |
| Ti ³⁺ Pct..... | 0 | 0.4 | 3.3 | 7.8 | 8.9 | |
| Mineral Composition—Pct | | | | | | |
| CaO·TiO ₂ | 25 | 25 | 30 | 20 | 10 | |
| (Fe,Mg)O·2TiO ₂ | 45 | 65 | 60 | 40 | 30 | |
| FeO·TiO ₂ | 20 | 0 | 0 | 0 | 0 | |
| Ti(O,C)..... | 0 | 0 | 0 | 5 | 5 | |
| Glass..... | 10 | 10 | 10 | 10 | 10 | |
| MgO·Ti ₂ O ₃ | 0 | 0 | 0 | 25 | 45 | |

Table 4 . . . Furnace Characteristics of Slag with Variation in CaO Addition

| | | | | | | |
|--------------------------------------|--------------------|---------|----------|----------|----------|-----|
| Burden..... | Baie St. Paul..... | | | | | 100 |
| | CaO..... | | | | | 3-7 |
| | MgO..... | | | | | 1 |
| | C..... | | | | | 15 |
| | | | | | | |
| CaO..... | 3 | 4 | 5 | 6 | 7 | |
| Slag Analysis | | | | | | |
| TiO ₂ | 70.5 | 68.9 | 67.5 | 62.0 | 61.0 | |
| Fe ²⁺ | 2.5 | 2.0 | 2.5 | 5.0 | 4.6 | |
| Observed Fluidity..... | Cinder | Viscous | V. Fluid | V. Fluid | V. Fluid | |
| Fluidity Expected..... | Sinter | Viscous | Fluid | Fluid | Fluid | |
| Mineral Composition—Pct | | | | | | |
| CaO·TiO ₂ | 10 | 20 | 30 | 40 | 45 | |
| (FeMg)O·2TiO ₂ | 80 | 70 | 60 | 50 | 45 | |
| Glass..... | 10 | 10 | 10 | 10 | 10 | |
| Calculated Chemical Composition—Pct | | | | | | |
| TiO ₂ | 70.3 | 69.0 | 67.8 | 65.0 | 63.9 | |
| Fe ²⁺ | 2.5 | 2.5 | 2.4 | 4.9 | 4.8 | |
| CaO..... | 7.1 | 8.7 | 10.3 | 11.6 | 12.7 | |
| MgO..... | 8.7 | 8.5 | 8.4 | 8.0 | 7.9 | |
| Al ₂ O ₃ | 5.1 | 5.0 | 4.9 | 4.7 | 4.6 | |

satisfactory. This series indicated that within limits a slag could be prepared of desired composition with proper fluidity if within the area of fluidity as indicated by the melting point diagrams. The absolute maximum amount of fluxes was not determined since the objective was to produce a high titanium slag.

Arc Furnace Smelting

The induction furnace tests had shown that the formation of a fluid slag which had the necessary chemical, mineralogical and digestible characteristics could be accomplished. The application of the observations of the induction furnace to arc furnace practice was the next step. A small arc furnace was utilized which was a modi-

fied Pittsburgh Lectromelt size "X" single phase unit. The power supply was a 440 volt primary transformer with variable secondary taps. The taps used for this smelting work was 78 volts with 60 pct reactance. The usual operation of the furnace was about 40 KVA utilizing a 1¼ in. electrode. The input to the furnace was controlled by manually raising and lowering the electrode.

The furnace was lined with graphite blocks forming a hearth approximately 80 sq in. and had a depth of about 9 in. The furnace was covered and an opening for charging the furnace was allowed through the top. The slag and metal were removed from the furnace through a tap hole in the bottom.

Since the ores of primary interest were the Canadian ore from Baie St. Paul and the MacIntyre ilmenite con-

Table 5 . . . Fluid Slags from Various Ores—Maximum and Minimum Flux Addition

| Ore | MacIntyre | | Baie St. Paul | |
|--------------------------------------|-----------|------|---------------|------|
| Burden | 100 | 100 | 100 | 100 |
| Ore..... | 6 | 8 | 4 | 7 |
| CaO..... | 1 | 5 | 0 | 3 |
| MgO..... | 15 | 15 | 15 | 15 |
| C..... | | | | |
| Slag Analysis | | | | |
| TiO ₂ | 70.8 | 63.5 | 67.4 | 59.2 |
| Fe ²⁺ | 4.9 | 4.0 | 4.2 | 5.5 |
| Mineral Composition—Pct | | | | |
| CaO·TiO ₂ | 20 | 50 | 25 | 40 |
| (Fe,Mg)O·2TiO ₂ | 70 | 40 | 65 | 50 |
| Glass..... | 10 | 10 | 10 | 10 |
| Calculated Chemical Composition—Pct | | | | |
| TiO ₂ | 68.6 | 62.8 | 69.0 | 61.8 |
| Fe ²⁺ | 4.6 | 3.9 | 4.3 | 4.6 |
| CaO..... | 10.2 | 12.4 | 8.7 | 12.3 |
| MgO..... | 5.5 | 10.7 | 6.8 | 10.8 |
| Al ₂ O ₃ | 4.8 | 4.5 | 5.0 | 4.5 |
| SiO ₂ | 6.1 | 5.6 | 6.2 | 5.6 |

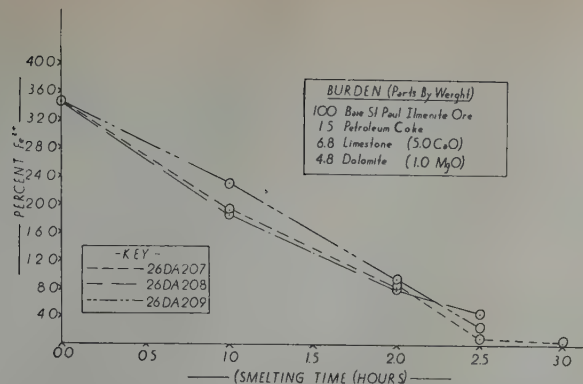


FIG 5—Progressive reduction of Baie St. Paul ore during smelting in arc furnace.

centrate the arc smelting was limited to these two materials. The burdens selected for the tests were those which had shown the best properties from induction furnace tests and were as follows:

| | Baie St. Paul, Pounds | MacIntyre, Pounds |
|---------------------|-----------------------|-------------------|
| Ore..... | 50 | 50 |
| Petroleum coke..... | 7.5 | 7.5 |
| Limestone..... | 3.4 | 4.3 |
| Dolomite..... | 2.4 | 2.4 |

The flux addition is equivalent to 5.0 parts of CaO and 1 part of MgO added to the burden for Baie St. Paul and 6.0 parts CaO and 1 part MgO for MacIntyre.

It was a regular practice to heat the furnace first by arcing the electrodes on a carbon block for about $\frac{1}{2}$ hr prior to adding the charge. Approximately $\frac{1}{3}$ of the charge was dumped into the furnace after removing the carbon block and melted down. The balance of the charge was added gradually as the melting proceeded. The total time required for charging varied from 20–30 min. In order to establish the time required to obtain the necessary reduction, samples of slags were taken at various intervals for analyses. The total smelting time varied from 2–3 hr, depending upon the general operating procedure. The temperature of the slag as it flowed from the furnace, observed with an optical pyrometer, was normally about 1500°C. The slag was tapped into a ladle in which iron settled out in the bottom and the slag formed as a separate layer on top. The slags

which had proven most satisfactory in the induction furnace could be duplicated on a larger scale in the arc furnace.

The progressive reduction of the charge in several tests made from Baie St. Paul ilmenite is given in Fig 5. The reproducibility of the smelting was fairly consistent when the power input was maintained very carefully.

Observation of the mechanics of the reduction definitely indicated that the slag and carbon were reacting. The reduction was found to be affected by type of carbon used. Coke, because of its high surface area, was better suited for a reductant than anthracite. As a result of the high secondary voltage delivered by the transformer, the electrodes could not be maintained in the slag during the final period of reduction. The change in resistivity of the slag was quite apparent and appeared to be a function of the ferrous iron content.

Summary

1. The adaptation of melting point data to slag formation is shown.
2. Ilmenites having 38–44 pct TiO_2 were smelted in laboratory to produce fluid slags with 65–69 pct TiO_2 .
3. A high titanium slag can be produced in which the formation of appreciable amounts of Ti^{3+} may be avoided.
4. The final slag with 62–69 pct TiO_2 requires 5–11 pct MgO and 9–13 pct CaO in order to have desired fluidity from MacIntyre and Baie St.

Paul ilmenites.

5. High titanium slags can be produced in an arc furnace with slag temperatures of 1450–1550°C which were identical in behavior and properties to the induction furnace slags.

References

1. J. R. Linney: Adirondack Iron Mining. *Mining and Metallurgy* (1943) 24, 480–487.
2. a. F. E. Bachman: The Use of Titaniferous Ore in the Blast Furnace. Yearbook, Amer. Iron and Steel Inst. (1914), 370–419.
 b. D. Forbes: Composition and Metallurgy of Some Norwegian Titaniferous Iron Ores. *Chem. News* (1868) 18, 275–276.
 c. W. M. Goodwin: Smelting of Titaniferous Iron Ores. *Trans. Roy. Can. Inst.* (1921) 13, 35–49.
 d. A. H. A. Robinson: Titanium Department of Mines, Mines Branch, Ottawa, Canada (1922) No. 579, 7–38.
 e. A. J. Rossi: Titanium in Blast Furnaces. *Jnl. Am. Chem. Soc.* (1890) 12, 19–117 Titaniferous Ores in the Blast Furnace. *Trans. AIME* (1892–93) 21, 832–867. The Smelting of Titaniferous Ores, I and II. *Iron Age* (1896) 57, 354–356; 464–469.
 f. A. Stansfield and W. A. Wissler: The Smelting of Titaniferous Ores of Iron. *Trans. Roy. Soc. Canada* (1916) 10, No. 111, 33–42.
 g. W. Tillmann: Smelting of Titanium Containing Iron Ores in the Blast Furnace. *Stahl u. Eisen* (1940) 60, 469–474.
 h. C. E. Wood, T. L. Joseph, and S. S. Cole: Smelting of Vanadium Bearing Titaniferous Sinter in an Experimental Blast Furnace. U.S. Bur. of Mines, Rep't of Invest. 3679 (1943) 1–24.
3. H. Sigurdson and S. S. Cole: Melting Points in the System TiO_2 –CaO– MgO – Al_2O_3 .
4. C. H. Moore and H. Sigurdson: Petrology of High Titanium Slags.

Petrology of High Titanium Slags

CHARLES H. MOORE, JR.,* Member AIME and H. SIGURDSON*

Introduction

Extensive studies have been carried out on electric furnace and blast furnace slags obtained in the winning of iron from its ores. These slags normally consist of elements of the gangue minerals present in the ores, as well as the added flux materials. In consequence, melts of CaO , MgO , Al_2O_3 and SiO_2 can be considered as representing typical slag compositions. When a slag of this composition cools, it usually crystallizes according to predictions possible from an equilibrium diagram of these constituents, providing the melt is not undercooled to form glass. The melt is either viscous or fluid, depending upon the ratio of binary cations to silica, and crystallizes easily or forms a glass for the same reasons. If the melt is not overheated so that carbides of the metal components of the slag are formed and if the composition of the slag is so adjusted that it has a high fluidity, liquid equilibrium is attained and the slag can be held in a liquid state for extended periods of time. Upon tapping, the slag crystallizes into minerals, the type and proportion of which are determined by the melt composition. Since equilibrium is attained, the holding period is not critical.

In melts containing a large increment of titanium, however, the normal slag procedures are not applicable. Titanium, as one of the atomic transition elements, is, at elevated temperatures, capable of being reduced to form metalloid compounds much more readily than the refractory oxides present in normal slags. In consequence, an oxide melt containing titanium never reaches equilibrium in a reducing environment, but continues to shift its composition until cooled. If melts of this nature are cooled and samples submitted to metallographic and X ray analysis the course

of reaction and crystallization in this type of slag can be determined.

Preparation of Slag

The slags investigated fell into the system $\text{CaO-MgO-TiO}_2\text{-Al}_2\text{O}_3\text{-SiO}_2$ and were produced from ilmenite ores reduced by carbon in an electric furnace. Since the equilibrium series¹ and the laboratory smelting of ilmenite² are described in two of the accompanying papers, detailed description of the smelting procedure is not required here. However, certain essentials must be mentioned.

Two types of melts were used to produce slags studied in this investigation. The first series of smelts made to determine proper flux addition were produced in a 4 lb Ajax induction furnace. The charge, consisting of ore with the proper flux addition, was heated in a graphite crucible until fluid, held fluid for a sufficient time period to obtain 1-5 pct FeO content, and poured. Because of the small size of the charge only the final sample of these melts could be examined. In the melts made in the 50 lb arc furnace, however, grab samples taken at 10 min. intervals between time of initial melting and final pouring were available for examination. These samples allowed a much clearer picture of the course of reaction and crystallization.

Sample Preparation

Any material containing appreciable

San Francisco Meeting, Feb. 1949.
TP 2714 DH. Manuscript received
March 10, 1949.

* Department Supervisor and Research Chemist, respectively, Research Laboratory, Titanium Div., National Lead Co., South Amboy, N. J.

¹ References are at the end of the paper.

amounts of ferrous oxide and reduced titanium compounds is opaque to transmitted light. Therefore, all petrographic studies had to be made on polished slag sections. A representative sample of slag was cut or broken, mounted in a thermosetting plastic, ground flat using 400 grit silicon carbide, the coarse scratches removed with 600 grit silicon carbide and polished on billiard cloth using levigated alumina. Rouge was avoided because of the entrainment of the red particles in pores in the slag, causing a possible confusion with some of the mineral phases. In order to prevent sample projection above the plastic surface red bakelite was used to hold the sample, and backed up with clear lucite. In this manner sample labels could be permanently retained in the mounting. The polished samples were examined on a Bausch and Lomb metallograph at magnifications of 250 \times , 500 \times , 1000 \times and 1800 \times . The instrument was equipped for examination of specimens under bright field illumination and with crossed nicols. A magenta tint plate to aid in color tone differentiation was also used.

Petrology of Slags

In order to determine the composition and mineral relations of a previously unreported system petrologically, it is essential that the starting composition, reaction temperature and final composition be known. The chemical composition of the ilmenite ore used in these smelts is given in Table 1, and the complete analysis of a typical high titanium, low iron slag is given in Table 2.

In the winning of TiO_2 from ilmenite by a smelting process it is necessary to produce a slag which will melt at an economically feasible temperature, remain molten as the iron is removed by reduction, be fluid enough to be readily removed from the furnace, contain a high percentage of TiO_2 and a low percentage of reduced titanium com-

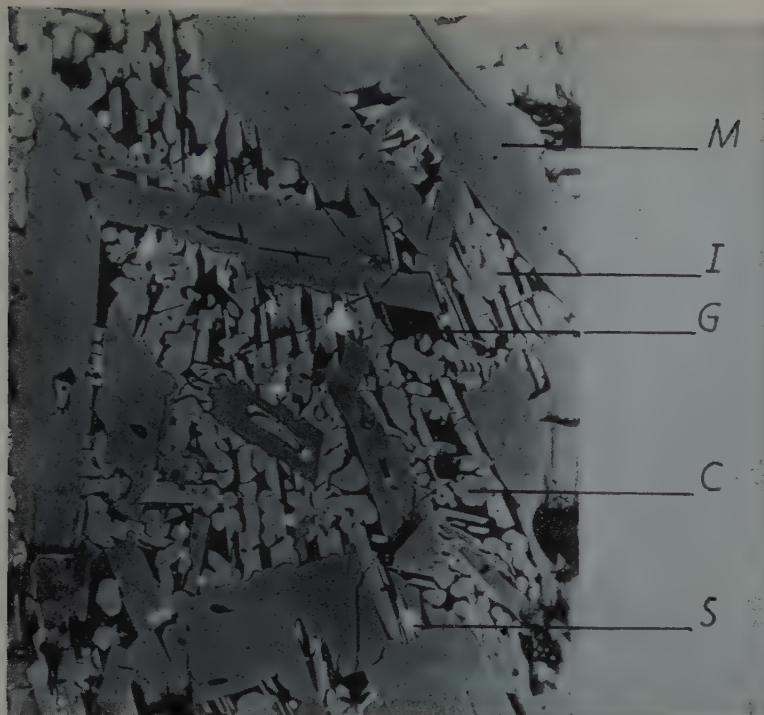


FIG 1—Micrograph of slag sample No. 1. X 500.

Slightly reduced in reproduction. The slag at this early stage of reduction contains 16.2 pct FeO and 58.8 pct TiO₂. The presence of this amount of ilmenite indicates that reduction of the slag has not progressed to the desired final composition. Mineralogical composition is as follows:

I—20 pct ilmenite
C—10–20 pct CaO·TiO₂
M—50–60 pct (Fe, Mg)O·2 TiO₂
G—10 pct silicate glass
S—Small amount Fe, FeS, etc.

Table 1 . . . Chemical Composition of Baie St. Paul Ilmenite (Weight, Pct)

| | |
|--------------------------------------|-------|
| TiO ₂ | 39.7 |
| FeO..... | 28.6 |
| Fe ₂ O ₃ | 20.6 |
| CaO..... | 0.7 |
| MgO..... | 3.6 |
| Al ₂ O ₃ | 2.4 |
| SiO ₂ | 3.4 |
| V ₂ O ₅ | 0.32 |
| Cr ₂ O ₃ | 0.11 |
| P ₂ O ₅ | 0.045 |

Table 2 . . . Chemical Composition of Typical High TiO₂—Low FeO Slag (Weight, Pct)

| | |
|--------------------------------------|------|
| TiO ₂ | 68.5 |
| Ti ³⁺ | 5.1 |
| FeO..... | 3.1 |
| CaO..... | 9.5 |
| MgO..... | 7.2 |
| Al ₂ O ₃ | 5.4 |
| SiO ₂ | 5.1 |
| S..... | 0.91 |
| V ₂ O ₅ | 0.32 |
| C..... | 0.06 |

pounds, and be amenable to digestion in sulphuric acid. In light of the melting data obtained in the accompanying paper on slag equilibria it is apparent that at least part of these requirements was fulfilled by the additions of lime and magnesia fluxes to ilmenite.

Course of Reduction

As ilmenite is heated with carbon, the iron begins to reduce to metal at

1000°C, by a solid state reaction, leaving a composition that appears to be FeO·2TiO₂. At 1150°C, and when the amount of FeO·2TiO₂ reaches 70 pct an apparent eutectic occurs in the system FeO·TiO₂–FeO·2TiO₂ and the charge becomes pasty.*

If reduction continues, the charge remains pasty until the temperature reaches 1450°C. Here a probable equilibrium between FeO·TiO₂, (Fe,Mg)O·2TiO₂ and calcium magnesium silicate makes the melt fluid. If frozen at this point, the slag consists of ilmenite, FeO·2TiO₂ (probably with some magnesium replacing the iron), minor amounts of CaTiO₃ and a glass. The FeO content of such a slag is 11–14 pct. If reduced further the last skeletal crystals of ilmenite disappear at 7–8 pct FeO and the slag consists of a (Fe,Mg)O·2TiO₂ structure and CaTiO₃ (near the 60–40 eutectic proportion)

* Grieve and White² indicate two eutectics and only pseudobrookite and ilmenite in the thermal equilibrium diagram FeO–TiO₂. However, they mention an undetermined amount of Fe₂O₃ in their system. We have found that if conditions are sufficiently oxidizing to transform FeO to Fe₂O₃, the compound FeO·2TiO₂ does not form, being replaced by ilmenite or pseudobrookite and rutile. If the compound FeO·2TiO₂ (with minor amounts of magnesium in solid solution) is heated to 500°C in air it dissociates to pseudobrookite and anatase. This indicates that the (Fe, Mg)O·2TiO₂ structure is stable only when deficient in oxygen.

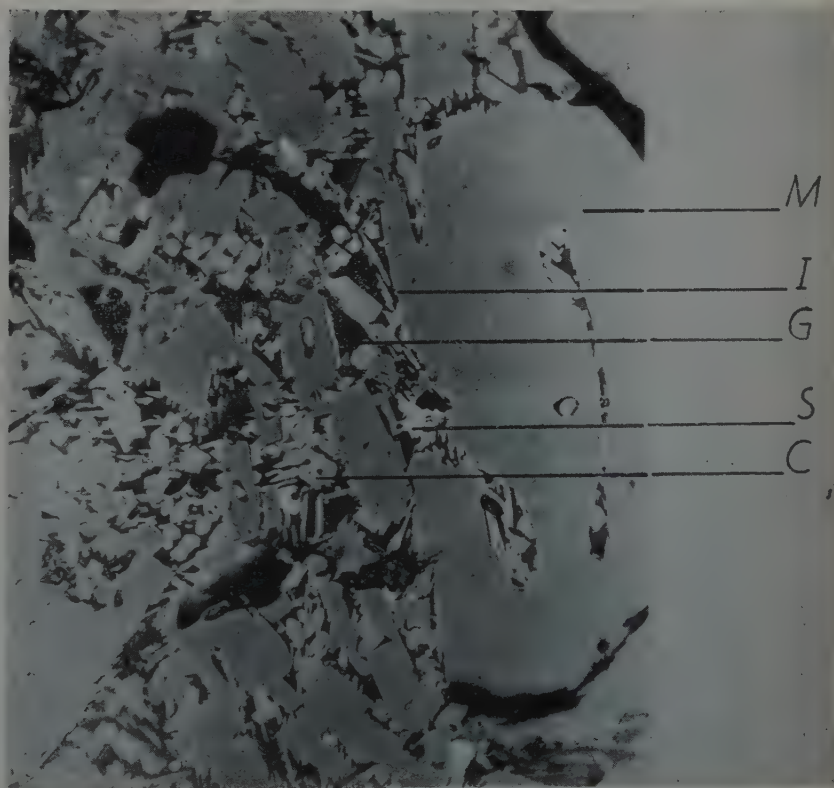


FIG 2—Micrograph of slag sample No. 2. X 500.

Slightly reduced in reproduction. The slag at this stage of reduction contains 13.3 pct FeO and 60.3 pct TiO₂. Ilmenite still remains in sufficient quantity as acicular particles to indicate the reduction has not progressed to the optimum composition. The mineralogical composition is as follows:

I—10–15 pct ilmenite
C—10–20 pct CaO·TiO₂
M—50–60 pct (Fe, Mg)O·2TiO₂
G—10 pct silicate glass
S—Small amount of Fe, FeS, etc.

and glass. $(\text{Fe,Mg})\text{O}\cdot 2\text{TiO}_2$ is the primary phase, CaTiO_3 the secondary phase and finally, an interstitial glass, which may on slow cooling partially devitrify to poorly crystallized silicates. As reduction proceeds, the mineralogical relationship of the constituents remains essentially the same except that iron is isomorphously replaced by magnesium in the compound $(\text{Fe,Mg})\text{O}\cdot 2\text{TiO}_2$. However, as the iron content of the slag system falls below 3 pct the titanium begins to reduce. If frozen here the slag is still amenable to processing, but the compound is designated as MgTi_3O_8 . As the loss of oxygen from the system continues the $\text{MgO}\cdot 2\text{TiO}_2$ type structure is no longer stable and shifts to a structure designated as MgTi_2O_4 . When this occurs, the melt becomes more refractory and hence less fluid and is no longer amenable to standard sulphuric acid digestion procedure. The slag is then called "over-reduced." If reduction is allowed to continue $\text{Ti}(\text{O,C})$ and finally TiC , are formed and the melt freezes. As far as can be determined, the amount and composition of the CaTiO_3 remains constant, from its first crystallization in eutectic proportions, throughout the course of reduc-

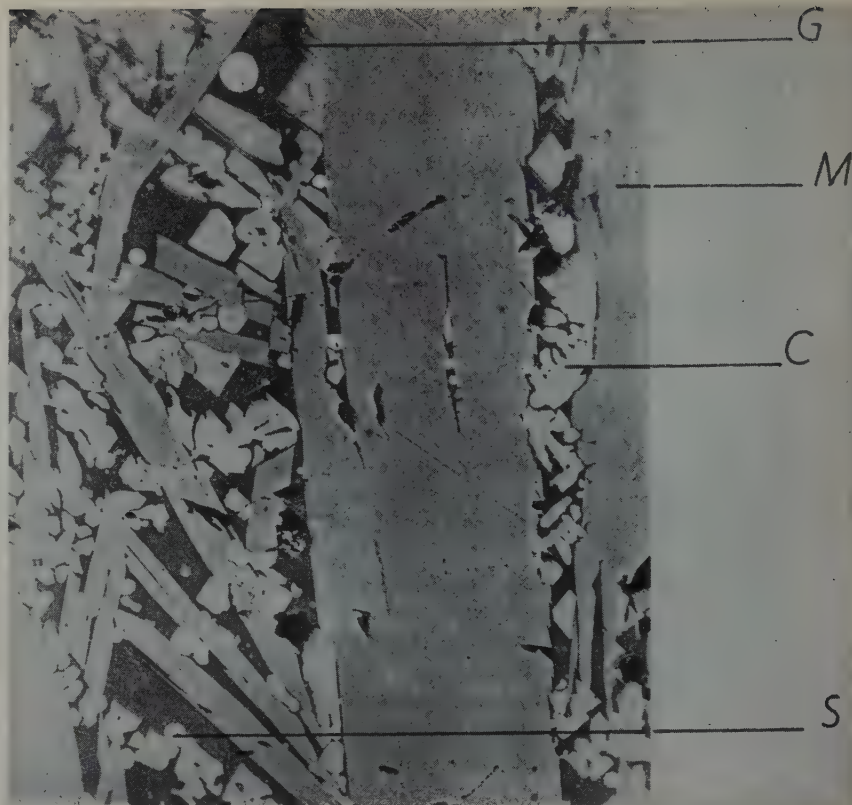


FIG 4—Micrograph of slag sample No. 4. $\times 500$.

At this stage of reduction the slag contains 4.9 pct FeO and 67.8 pct TiO_2 . The presence of the MgTi_3O_8 phase indicates slight over-reduction of the $(\text{Fe,Mg})\text{O}\cdot 2\text{TiO}_2$ phase which apparently is not detrimental to optimum digestion of the slag. Mineralogical composition is as follows:

C—20–30 pct $\text{CaO}\cdot\text{TiO}_2$
M—60 pct $(\text{Fe,Mg})\text{O}\cdot 2\text{TiO}_2$
5 pct MgTi_3O_8 (not evident at $\times 500$)
G—10 pct silicate glass
S—Small amount Fe, FeS, etc.

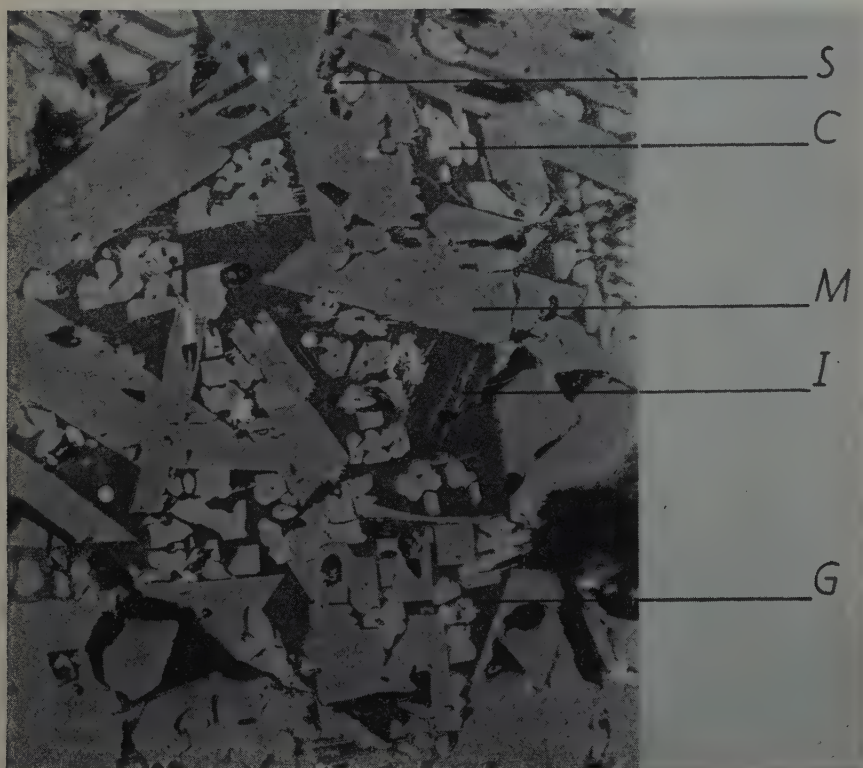


FIG 3—Micrograph of slag sample No. 3. $\times 500$.

The slag now contains 8.7 pct FeO and 63.8 pct TiO_2 . It has now been reduced almost to the optimum composition since ilmenite remains only as small crystals surrounding the $(\text{Fe,Mg})\text{O}\cdot 2\text{TiO}_2$ phase and no over-reduction of the dititanate phase is evident. The mineralogical composition is as follows:

I—5 pct ilmenite
C—20–30 pct $\text{CaO}\cdot\text{TiO}_2$
M—50–60 pct $(\text{Fe,Mg})\text{O}\cdot 2\text{TiO}_2$
G—10 pct silicate glass
S—Small amount Fe, FeS, etc.

tion. The series of micrographs shown in Fig 1 through 5 illustrates the course of reduction but does not in all cases indicate the proportions of phases present in the melts. The representative phase proportions were determined from a large number of samples.

Mineral Phases

The isomorphous series $\text{FeO}\cdot 2\text{TiO}_2$ – $\text{MgO}\cdot 2\text{TiO}_2$ is by far the most interesting mineral phase in this type of slag. It not only is the primary crystallization phase in the slags, but incorporates the greatest amount of titanium in the system. The shift from $\text{FeO}\cdot 2\text{TiO}_2$ to $(\text{Fe,Mg})\text{O}\cdot 2\text{TiO}_2$ is continuous and occurs as iron is removed from the system. This composition shift is difficult to detect. It is distinguished microscopically only by a change in color of the laths from dark gray to light gray as the amount of iron is decreased. X ray powder patterns of $\text{FeO}\cdot 2\text{TiO}_2$ and $(\text{Fe,Mg})\text{O}\cdot 2\text{TiO}_2$ are apparently identical.

Under reducing conditions $\text{MgO}\cdot 2\text{TiO}_2$ is not stable and always contains vacant titanium equipoints. As

mentioned above, the formula MgTi_3O_6 is assumed and is used to indicate this. The structure and habits of this compound are identical with $\text{MgO} \cdot 2\text{TiO}_2$ and are not distinguishable by X ray powder patterns. Under reflected light the color is a very light gray with a pink tone.

The next reduction stage, however, is readily distinguished under the microscope. It is a dark red to purple in reflected light and assumes a quadratic habit. Although the structure has not been completely delineated it is apparently cubic and has been assigned the probable formula MgTi_2O_4 .

The flexibility of the structure which is called " $\text{MgO} \cdot 2\text{TiO}_2$ type" is indicated by its ability to lose iron, gain magnesium and lose oxygen, and still preserve its identity.

There are indications that it is capable of far more flexibility. It was shown early in the investigation that the amount of TiO_2 determined chemically to exist in these slags was not accounted for by the $(\text{Fe}, \text{Mg})\text{O} \cdot 2\text{TiO}_2$ and CaTiO_3 present. In consequence a series of synthetic slags was prepared under both reducing and oxidizing conditions in which the proportions MgO to TiO_2 were varied.

Under oxidizing conditions, no success has been obtained in attempts to form magnesium titanates higher in TiO_2 than $\text{MgO} \cdot 2\text{TiO}_2$. All attempts to form $\text{MgO} \cdot 3\text{TiO}_2$ have given $\text{MgO} \cdot 2\text{TiO}_2$ and rutile.

Under strongly reducing conditions, however, it has been found that the $(\text{Fe}, \text{Mg})\text{O} \cdot 2\text{TiO}_2$ structure will take TiO_2 into solid solution up to explored limits of the order of 12 mol of TiO_2 per mol of $(\text{Fe}, \text{Mg})\text{O}$, without a breakdown in structure. The solid solution compound with TiO_2 values of this order has been produced readily during smelting of low gangue ilmenite ores and also from mixtures of Fe_2O_3 , MgO and TiO_2 . X ray examination of the compound shows a shift in the structure to larger interplanar spacings (for example, $(\text{Fe}, \text{Mg})\text{O} \cdot 12\text{TiO}_2$ showed a strong line at 1.894\AA in contrast to the typical line at 1.876\AA in $\text{MgO} \cdot 2\text{TiO}_2$ and $(\text{Fe}, \text{Mg})\text{O} \cdot 2\text{TiO}_2$).

Oxidation of the $(\text{Fe}, \text{Mg})\text{O} \cdot 2\text{TiO}_2$ ($\text{Fe}, \text{Mg})\text{O} \cdot 12\text{TiO}_2$ series in air at 500°C for several hours causes a breakdown in the structure to the compounds which are stable under oxidizing conditions. These compounds are Fe_2O_3 , TiO_2 , $\text{MgO} \cdot 2\text{TiO}_2$, $\text{MgO} \cdot \text{TiO}_2$ and TiO_2 . At 500 – 800°C the TiO_2 is present as anatase. At temperatures higher than 800°C , the TiO_2 which is crys-

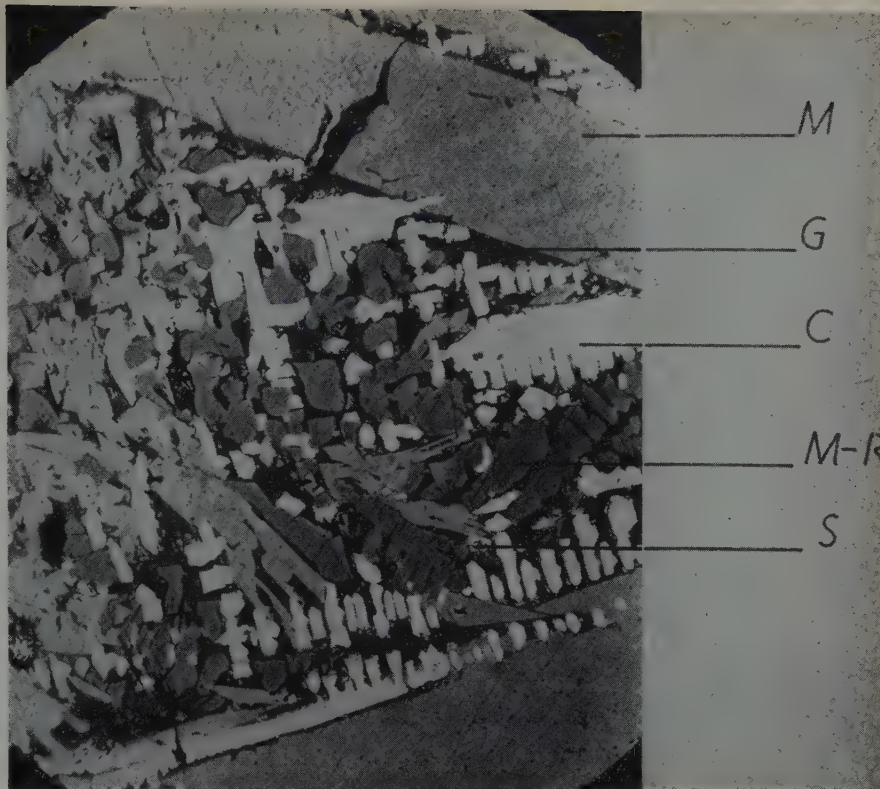


FIG 5—Micrograph of slag sample No. 5. $\times 500$.

At this stage of reduction the slag contains 1.0 pct FeO and 70.7 pct TiO_2 . The presence of the MgTi_2O_4 stage indicates serious over-reduction of the $(\text{Fe}, \text{Mg})\text{O} \cdot 2\text{TiO}_2$ phase and this phase is detrimental to optimum digestion. Mineralogical composition is as follows:

C—20 pct $\text{CaO} \cdot \text{TiO}_2$
M—20–30 pct $(\text{Fe}, \text{Mg})\text{O} \cdot 2\text{TiO}_2$
M-R—30–40 pct MgTi_2O_4
G—15 pct silicate glass
S—Small amount Fe, FeS, etc.

tallized from the $(\text{Fe}, \text{Mg})\text{O} \cdot 2\text{TiO}_2$ structure exists as rutile.

The fact that TiO_2 cannot be retained in the structure under oxidizing conditions indicates that the solid solution of TiO_2 in the dititanate struc-

ture is possible under reducing conditions because of an oxygen deficient lattice in the dititanate. Data on the degree of oxygen deficiencies in the lattice have not been completely determined.

Table 3 . . . Patterns of Titanates. Spectrometer, Cu, $K\alpha$, $\lambda = 1.5374\text{\AA}$, 2 Rpm Scan. No Corrections Applied

| $\text{MgO} \cdot 2\text{TiO}_2$ or $(\text{Fe}, \text{Mg})\text{O} \cdot 2\text{TiO}_2$ | | 50 Mol Pct $\text{MgO} \cdot 2\text{TiO}_2$ 50 Mol Pct $\text{Al}_2\text{O}_3 \cdot \text{TiO}_2$ (oxidizing conditions) | | $\text{Al}_2\text{O}_3 \cdot \text{TiO}_2$ (oxidizing conditions) | | $(\text{Fe}, \text{Mg})\text{O} \cdot 2\text{TiO}_2$ + 20 Pct Al_2O_3 (by wt.) with TiO_2 in Solid Soln. (reducing conditions) | | $(\text{Fe}, \text{Mg})\text{O} \cdot 2\text{TiO}_2$ structure (Empirical Formula $(\text{Fe}, \text{Mg})\text{O} \cdot 12\text{TiO}_2$) (reducing conditions) | |
|---|---------|---|---------|---|---------|--|---------|---|---------|
| $d/n, \text{\AA}$ | I/I_1 | $d/n, \text{\AA}$ | I/I_1 | $d/n, \text{\AA}$ | I/I_1 | $d/n, \text{\AA}$ | I/I_1 | $d/n, \text{\AA}$ | I/I_1 |
| 5.0 | 0.12 | 4.83 | 0.38w | 4.71 | 0.47 | 4.86 | 0.4 | 4.97 | 0.23w |
| 4.9 | 0.12 | | | | | | | | |
| 3.51 | 1.00 | 3.43 | 1.00 | 3.35 | 1.00 | 3.44 | 1.00 | 3.54 | 1.00 |
| 2.86 | 0.09 | | | | | | | | |
| 2.75 | 0.6 | 2.71 | 0.8 | 2.65 | 0.7 | 2.71 | 0.9 | 2.76 | 0.6 |
| 2.45 | 0.2 | | | | | 2.43 | 0.2 | 2.47 | 0.23 |
| 2.42 | 0.15 | 2.40 | 0.20w | 2.36 | 0.20 | 2.37 | 0.15 | 2.43 | 0.19 |
| 2.22 | 0.15 | 2.18 | 0.22 | 2.14 | 0.31 | 2.20 | 0.2 | 2.24 | 0.22 |
| 2.19 | 0.2 | 2.16 | 0.20 | 2.11 | 0.30 | 2.17 | 0.2 | 2.21 | 0.15 |
| 1.967 | 0.3 | 1.939 | 0.34w | 1.897 | 0.52 | 1.951 | 0.24 | 1.98 | 0.25 |
| 1.876 | 0.6 | 1.829 | 0.43w | 1.792 | 0.44 | 1.854 | 0.35 | 1.894 | 0.75 |
| 1.846 | 0.15 | | | | | 1.839 | 0.1 | 1.857 | 0.15 |
| 1.754 | 0.15 | 1.723 | 0.14w | 1.687 | 0.28 | 1.73 | 0.1w | 1.763 | 0.15 |
| 1.665 | 0.15 | 1.645 | 0.11 | 1.606 | 0.27 | 1.648 | 0.1 | 1.67 | 0.10w |
| 1.634 | 0.2 | 1.632 | 0.11 | 1.578 | 0.28 | 1.621 | 0.2 | 1.65 | 0.15w |
| | | 1.606 | 0.16 | 1.55 | 0.08w | 1.598 | 0.1 | | |
| 1.551 | 0.3 | | | 1.519 | 0.06 | | | 1.559 | 0.32 |
| 1.535 | 0.2 | 1.515 | 0.29w | 1.484 | 0.36 | 1.530 | 0.3 | 1.542 | 0.10 |
| 1.424 | 0.09 | 1.400 | 0.09w | 1.449 | 0.08 | 1.413 | 0.1 | 1.43 | 0.10w |
| 1.378 | 0.08 | 1.352 | 0.11w | 1.371 | 0.14 | 1.364 | 0.1 | 1.37 | 0.10w |
| 1.358 | 0.15 | | | 1.32 | 0.09w | 1.350 | 0.2 | | |
| 1.318 | 0.08 | | | 1.305 | 0.16 | | | | |
| 1.265 | 0.10 | | | 1.266 | 0.11 | 1.251 | 0.1 | 1.268 | 0.08 |
| 1.245 | 0.10 | | | 1.253 | 0.11 | | | 1.251 | 0.07 |
| | | | | 1.219 | 0.09 | | | | |

w — after relative intensity means wide line or lines.

Spectrometer, $Cu K\alpha, \lambda = 1.5374 \text{ \AA}$, 2 rpm scan

No Corrections Applied

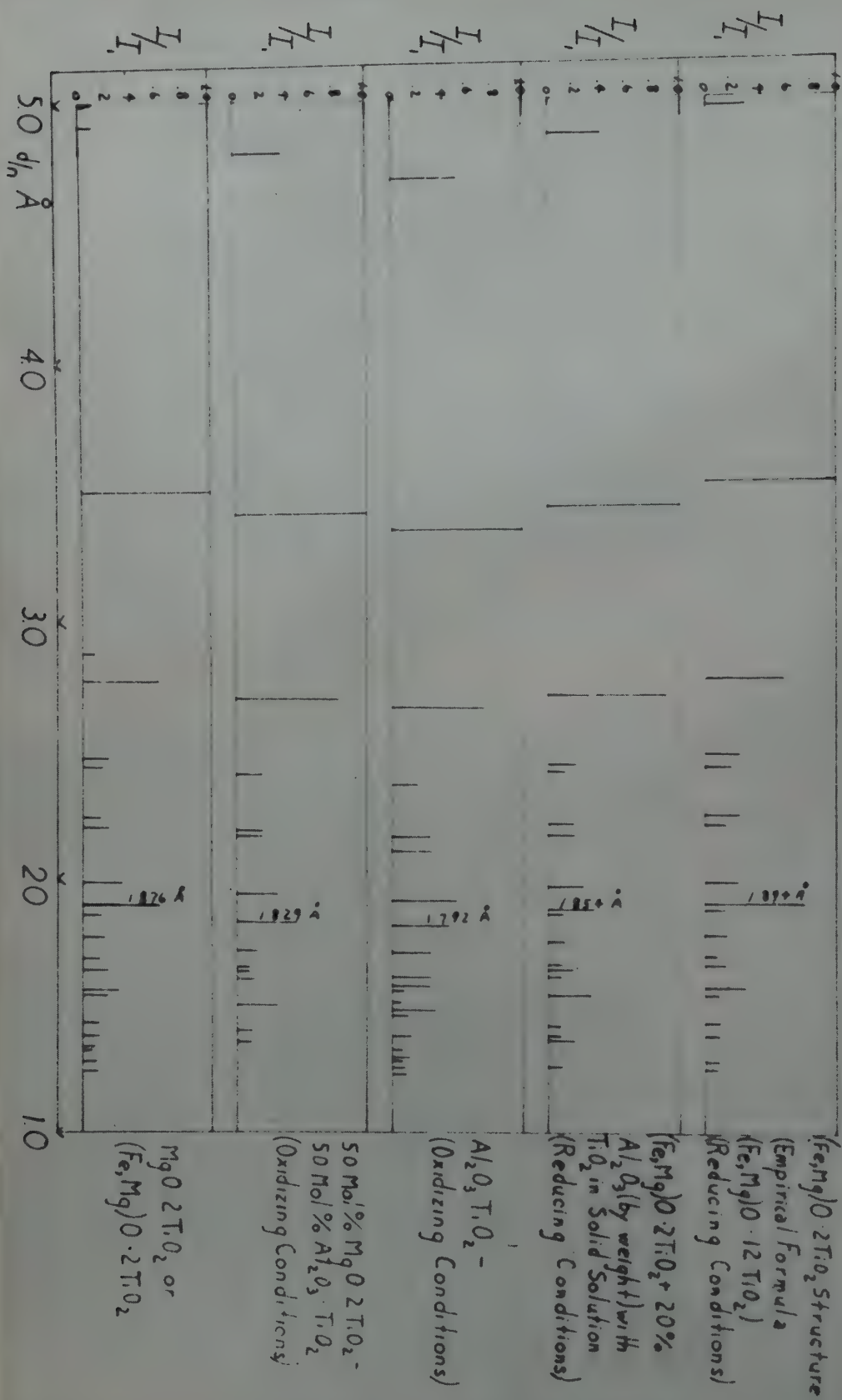


FIG 6—Patterns of Titanates.

Table 4 . . . Properties in Reflected Light of Phases Present in High Titanium Slags Made by Fluxing Ilmenite with CaO and MgO

| Phase | Bright Light with Blue Filter Screen | | Crossed Nicols | | Sensitive Tint Plate | |
|--------------------------------------|--------------------------------------|---|----------------------------|---|------------------------|---|
| | Color | Habit | Color | Habit | Color | Habit |
| CaO-TiO ₂ | Light gray to white | Dendritic aggregates or individual blocky crystals. | Very bright white to brown | Birefringent in all positions of stage. | Highly reflecting blue | Blue in all positions of stage. |
| FeO-TiO ₂ (Ilmenite)..... | Light gray to pale brown | Occurs as laths in glass or as rims around (Fe,Mg)O-2TiO ₂ | Black to dark gray | Extinct parallel to horizontal cross hair. Gray parallel to vertical cross hair. | Pink to blue | Pink parallel to horizontal cross hair. Blue parallel to vertical cross hair. |
| (Fe,Mg)O-2TiO ₂ | Light to dark gray | Well defined laths | Dark gray to black | Extinct parallel to vertical cross hair. Gray parallel to horizontal cross hair. | Pink to blue | Pink parallel to vertical cross hair. Blue parallel to horizontal cross hair. |
| MgTiO ₃ | Gray black to light brown | Well defined laths | Black to light brown | Extinct parallel to vertical cross hair. Light brown parallel to horizontal cross hair. | Pink to blue | Pink parallel to vertical cross hair. Blue parallel to horizontal cross hair. |
| MgTiO ₄ | Brownish red | Quadratic crystals | Black to brown | Extinct in 90° positions. Brown in 45° positions. | | |
| Glass..... | Dark gray | Fills interstices of crystals. | Black | Black in all positions of stage. | | |

Under oxidizing conditions there is a continuous solid solution series Al₂O₃-TiO₂-MgO.2TiO₂ as discussed in the accompanying melting equilibria paper. Under reducing conditions Al₂O₃ is taken into solid solution in the (Fe,Mg)O-2TiO₂ structure up to approximately 20 pct by weight, without the formation of Al₂O₃-TiO₂. This solid solution compound shows a considerable shift in the structure to smaller interplanar spacing (for example, the shift is from 1.876Å for normal MgO-2TiO₂ or (Fe,Mg)O-2TiO₂ to 1.854Å for (Fe,Mg)O-2TiO₂ with 20 pct Al₂O₃ (by weight) present in solid solution. Fig 6 shows X ray powder pattern comparisons of the effects of solid solution of TiO₂ and Al₂O₃ on the (Fe,Mg)O-2TiO₂ structure. Additions of over 20 pct Al₂O₃ gave the above solid solution compound and Al₂O₃-TiO₂. The line position for Al₂O₃-TiO₂ in this region of the X ray pattern is 1.792Å. Table 3 shows the d/n values for these compounds.

No change in the structure of the compound from the normal (Fe,Mg)O-2TiO₂ is discernible under the metallographic microscope when TiO₂ or

Al₂O₃ are present in solid solution even at the higher values of these oxides.

CaTiO₃ apparently always crystallizes as the secondary phase in the range of composition used in slag formation. These crystals are cubic in crystallization, quadratic in habit and usually the only colorless constituent of the slag. In slag samples which were quickly frozen the CaTiO₃ occurs as skeletal outlines in the glass. In slowly cooled slags the large cubic crystals are fully developed. No evidence of structural shift or solid solution in CaTiO₃ was observed at any reduction stage by either X ray diffraction patterns or petrographic character.

The role of the silicate glass in these melts is rather ambiguous. It apparently helps fluidization of the melt by incorporating at least part of the alumina to form a probable FeO-CaO-Al₂O₃-SiO₂ melt. The index of refraction of the glass preserved in the quickly frozen slags is ±1.55. The silicates which are observed in the slowly cooled slags are so poorly crystallized that their identity could not be determined.

Table 4 is a compilation of the opti-

cal properties in reflected light of the phases which occur in titanium bearing slags when fluxed with lime and magnesia.

Acknowledgment

The writers wish to express thanks to Dr. S. S. Cole, Assistant Research Manager, Titanium Division, National Lead Co., for technical suggestions and aid in preparation of the paper and to Mr. C. H. North of the Research Laboratory for the X ray data which have been of great value in this investigation.

References

1. H. Sigurdson and S. S. Cole: Melting Equilibria for System CaO-MgO-TiO₂-Al₂O₃. AIME Trans. AIME (1949) 185, 905. *Jnl. of Metals*, Dec. 1949.
2. D. L. Armant and S. S. Cole: Laboratory Smelting of Titaniferous Ores. AIME Trans. AIME (1949) 185, 909. *Jnl. of Metals*, Dec. 1949.
3. J. Grieve and J. White: *Jnl. Roy. Techn. Coll. (Glasgow)*, (1939) 4, 441-448.

Notes on the Electrolytic Isolation of Carbides in Steel

GUSTAF WRANGLÉN*

On account of the possibility of isolating carbides in steel it is generally assumed that the electrode potential of iron carbide is more noble than that of ferrite.^{1,2,3,4,5} Differences from 0.032 V¹ to 0.4 V⁴ have been recorded. However, it is important to realize that the more noble behavior of

cementite in relation to ferrite is not

Technical Note No. 28 E.
Manuscript received July 18, 1949.
* Chemical Engineer, Div. of Appl. Electrochemistry, Royal Inst. of Technology, Stockholm, Sweden.
¹ References are at the end of the paper.

an issue of thermodynamics but of reaction kinetics. Theoretically, cementite is less noble than ferrite, which is a direct consequence of its thermodynamic instability. With the value ΔF^o₂₉₈ = +4700 cal per mol for the free energy of formation of cementite⁶ it is easily calculated that the electrode

potential of the reaction $\text{Fe}_3\text{C} = 3\text{Fe}^{2+} + \text{C} + 6\text{e}^-$, found to be the relevant one, particularly in neutral solution,⁵ is -0.47 V (cf. $e^\circ_{\text{Fe}} = 0.44\text{ V}$). There are great hindrances to this reaction, however, implying a slow reactivity, which has to be termed high chemical polarization in this case. Hence, the electrolytic isolation of iron carbide is *not* a parallel to the retention of noble metals as an anode slime in electrolytic refining.

It is evident, furthermore, that the reaction referred to cannot be even chemically reversible, the less so thermodynamically. An equilibrium corresponding to the computed figure will never be reached. On measurement more noble and varying values will be obtained. These static potentials are of minor interest. It would be more valuable to determine the actual dissolution potentials during electrolysis and then select those conditions for separation, under which the difference between the dissolution potentials of cementite and ferrite is the greatest.

Structure is the most important factor influencing the isolation. If the carbide is present as large spheroid particles it is fairly insensible to varying conditions of electrolysis. If the structure is unfavorable (lamellar pearlite, cementite network) the operating conditions become important. Current density has to be kept fairly high in order to bring down the time of electrolysis. Elevation of temperature greatly diminishes the chemical polarization of iron but the same applies to cementite. Chemical attack by the electrolyte also increases strongly with rising temperature. The latter has to be kept low, therefore, and the anodic polarization of iron has to be reduced by other means, such as presence of chloride ions stirring, frequent removal of carbide and possibly superimposed alternating current.^{7,8}

The most effective stirring is rotation of the anode, preferably cylindrical, but this is usually not enough to remove the carbide particles. The specimen has to be scraped or at least knocked now and then. A brush in contact with the rotating specimen often gives poorer results, presumably

due to disaggregation of carbide, increasing its reactivity. If hydrochloric acid is employed as electrolyte, evolution of hydrogen occurs even at the anode and aids in loosening the carbide. In this case the carbide ought to be better protected on the anode than out in the solution to begin with. In no case, however, must the carbide remain on the anode to form a thick layer since that causes the current density and anodic polarization to be greatly increased and then the carbide also will begin to dissolve.

Regarding the electrolyte there is a wide-spread erroneous theory for the choice of anion. Treje and Benedicks^{9,10} used sodium citrate as an electrolyte for isolation of both slag inclusions and carbide. With this electrolyte alone they expected to get oxygen evolution at the anode. They therefore wanted to add another anion that might be discharged instead of oxygen. They considered the electrode potentials SO_4 1.90, Cl 1.34, O 1.33, Br 0.99 and I 0.52 V and concluded from them that sulphates and chlorides could not be used as they would not exclude oxygen evolution. The only rational anions would be Br and I which are discharged more easily than oxygen.

As far as the author has been able to find there have been no objections to this theory but it has been widely spread in the literature^{3,11,12,13,14} and has exerted a great influence. Electrolytes containing bromides and iodides have been employed in a great many investigations, particularly by German workers.

In reality, however, the quoted anion potentials have nothing to do with the dissolution of iron. The electrode potential of significance is that of iron itself, -0.44 V . Discharge of hydroxyl ions or other anions will occur only at very high current densities if the iron salts formed at the anode are not removed quickly enough or if the anode becomes passivated. Chloride ions are a very good means for counteracting passivity and a chloride, such as hydrochloric acid or ammonium chloride, is therefore a very suitable electrolyte. There are no valid reasons for using

bromides or iodides. Furthermore, iodide solutions are easily decomposed under the formation of iodine which attacks the carbide.

To support their theory, Treje and Benedicks⁹ carried out some potential measurements. In a FeBr_2 -solution at $2\text{--}4\text{ A/dm}^2$ they normally found anode potentials as high as $0.70\text{--}0.79\text{ V}$, that is, somewhere between the electrode potentials of iodine and bromine. However, these values are erroneously calculated, since the authors failed to see that the anode potential was negative in relation to the calomel electrode and hence added 0.286 to the positive value of the bridge reading instead of to its negative value. Recalculated, the true values are -0.22 to -0.13 V . Similar results were obtained in a control measurement by the author. In German literature^{15,16} there is a precept that the anode potential should be kept below $+0.50\text{ V}$ in order to exclude oxygen evolution. Presumably, this high limit originates from the erroneous figures referred to. As shown above, the anode potential need not and should not be higher than -0.3 to -0.2 V .

References

1. G. Tammann and K. Ewig: *Ztsch. anorg. Chem.* (1927) **167**, 391.
2. Gmelins Handbuch der Anorg. Chemie, Eisen A:2, 1207, 1220.
3. E. Houdremont *et al*: *Archiv Eisenhüttenw.* (1941-1942) **15**, 257.
4. A. Trawers and R. Diebold: *Compt. rend.* (1937) **205**, 797.
5. W. Koch: *Stahl Eisen* (1949) **69**, 1.
6. H. Seltz *et al*: *Trans. AIME* (1940) **140**, 263.
7. A. G. Arend: *British Steelmaker* (1943) **9**, 32.
8. P. Klinger and W. Koch: *Stahl Eisen* (1948) **68**, 321.
9. R. Treje and C. Benedicks: *Jernkontorets Ann.* (1932) **106**, 165.
10. R. Treje and C. Benedicks: *Jnl. Iron and Steel Inst.* (1933) **128**, 205.
11. C. Benedicks: *Trans. AIME* (1933) **105**, 195.
12. K. Kippe and O. Meyer: *Archiv Eisenhüttenw.* (1936-1937) **10**, 93.
13. P. Klinger *et al*: *Trans. AIME* (1939) **125**, 308.
14. F. W. Scott *et al*: *Metals Handbook*, 1939 Ed., p. 717.
15. P. Klinger and W. Koch: *Archiv Eisenhüttenw.* (1936-1937) **11**, 571.
16. *Handbuch für das Eisenhüttenlaboratorium* (Düsseldorf, 1941), **2**, 447.



Effect of Prestraining Temperatures on the Recovery of Cold Worked Aluminum

T. E. TIETZ,* R. A. ANDERSON* and J. E. DORN,* Member AIME

Introduction

Recent investigations^{1,2,3,4} have conclusively shown that the strain hardened state of metals depends upon the temperature and strain rate of prestraining as well as on the total plastic strain. A typical example of the effect of temperature of prestraining on the work hardening of metals is reproduced in Fig 1. When pure aluminum is strained at liquid nitrogen temperature the upper solid stress-strain curve (OFGH) is obtained. But when pure aluminum is prestrained to $\epsilon_2 = 0.153$ at atmospheric temperature and the test is then completed at liquid nitrogen temperature, the curve OBCD results. Thus a prestrain $\epsilon_2 = 0.153$ at atmospheric temperature gives a flow stress *C* when continued at liquid nitrogen temperature, whereas a higher flow stress *G* results when the specimen is strained exclusively at liquid nitrogen temperature to the same strain ϵ_2 . Consequently the metal strain hardens more rapidly at the lower temperature. Obviously the strain alone is not a measure of the strain hardened state in metals.

Inspection of Fig 1 reveals that the flow stress at *C* is identical with that at *F*. This fact suggests that a strain $\epsilon_2 = 0.153$ at atmospheric temperature induces the same work hardened state as a strain $\epsilon_1 = 0.058$ at liquid nitrogen temperature. But this concept of equivalent strains is also in error. If curve *CD* is shifted to the left so that point *C* falls on *F*, point *D* becomes *D'*. Inspection of the curves reveals that the rate of increase of stress with strain at *C* is greater than the rate of increase of stress with strain at *F* even though the flow stresses are identical. Consequently *C* and *F* do not represent

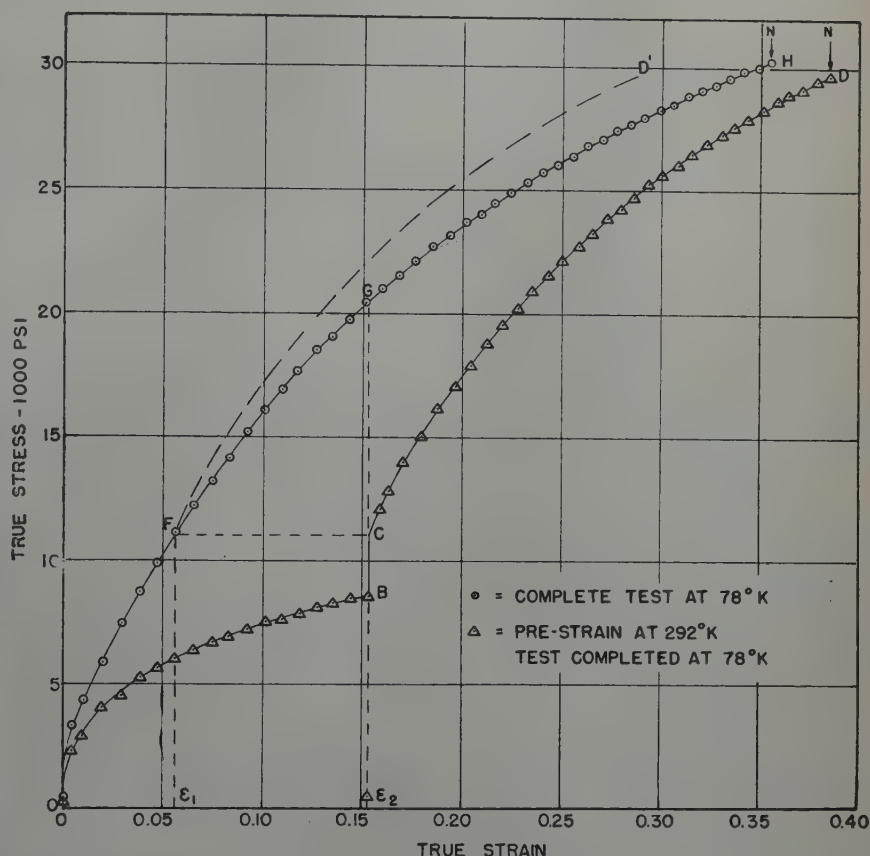


FIG 1—Effect of temperature of straining on the strain hardening of pure aluminum (99.987 pct).

identical work hardened states. It therefore becomes important to ascer-

tain how the strain hardened states at *C* and *F* might differ from each other.

In a more recent report⁴ it was shown that straining at higher rates of strain increases the amount of strain hardening in a manner quite analogous to straining at lower temperatures. These observations suggested that the flow stress is not only a function of the strain but also a function of the strain rate-temperature history of straining, perhaps in accord with the Zener-Hollomon parameter $p = \dot{\epsilon} e^{\frac{\Delta H}{RT}}$ (where

New York Meeting, February 1950. TP 2716 E. Discussion of this paper (2 copies) may be sent to *Transactions AIME* before April 1, 1950. Discussion is tentatively scheduled for publication in November 1950.

Manuscript received May 27, 1949; revision received Aug. 1, 1949.

* Research Engineer, Engineer, and Professor of Metallurgy, respectively, University of California, Berkeley, California.

¹ References are at the end of the paper.

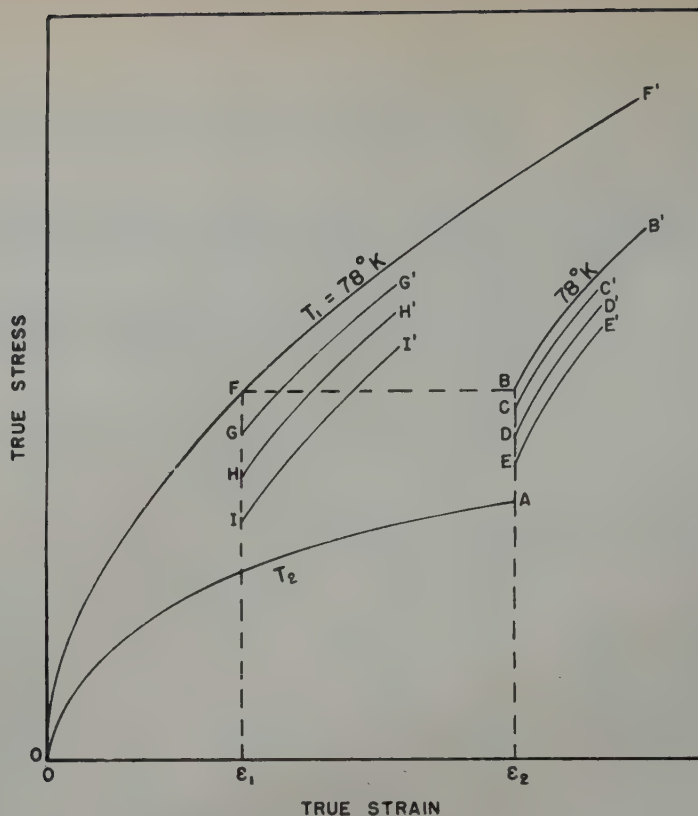


FIG 2—Method of evaluating the recovery.

e = base, natural logarithm, and $\frac{\Delta H}{RT}$ is an exponent of e). If then a specimen is strained ϵ_1 at ρ_1 and ϵ_2 at ρ_2 etc., the flow stress might be given by

$$\sigma = \sigma(\epsilon_1, \rho_1; \epsilon_2, \rho_2; \dots)$$

Such concepts have practical utility for correlation and analyses of data but they fail to identify the fundamental causes for the effect of strain rate and temperature histories on the strain hardening of metals.

The well known effect of the strain hardened states of metals on their recovery rates suggested that a more complete identification of the effect of strain rate and temperature histories on the strain hardening of metals might be obtained from recovery tests. Preliminary data from two recovery tests¹ appeared to confirm this thought. The tests described in the following pages of this report were made in order to obtain more conclusive evidence on the effect of temperature of prestraining on the recovery of the flow stress.

Materials and Testing Techniques

Pure aluminum (99.987 pct Al) was selected for these studies in order to minimize the effect of such factors as strain aging on the interpretation of

the data.

All of the tests were performed with equipment previously described in the literature.^{2,4} Strains were measured to 0.001 and stresses were determined to about ± 25 psi. All recorded data are given in terms of true stresses and true plastic strains.

Method of Evaluating the Recovery

The procedure used to determine the amount of recovery in this investigation is shown schematically in Fig 2. A specimen strained exclusively at liquid nitrogen temperature has the true stress-true plastic strain curve OFF' whereas a specimen strained to ϵ_2 at some higher temperature T_2 and then immediately tested at liquid nitrogen temperature gives the curve $OABB'$. Thus a prestrain ϵ_2 at T_2 gives the same flow stress (B) at liquid nitrogen temperature as is obtained by straining exclusively at liquid nitrogen temperature to ϵ_1 . If the strain hardened states at B and F are identical the recovery rates of the two specimens should also be identical. But if the recovery rates are dissimilar the strain hardened states must be different even though the flow stresses are approximately the same at liquid nitrogen temperature.

The recovery of specimens prestrained to ϵ_1 at liquid nitrogen temperature was obtained by aging the specimens at some appropriate temperature for various times and then testing again at liquid nitrogen temperature. In this way a series of curves GG' , HH' , etc. were obtained for the partially recovered material. For the data reported here these curves exhibited a sharp knee at the yield stress so that rather accurate determinations of the stresses G , H , I , etc. were obtainable by extrapolation to zero additional plastic strain upon restraining after recovery.

One complication arose in the analyses of the recovery data. Due to minor variations in properties from specimen to specimen, the flow stress F after prestraining to ϵ_1 at liquid nitrogen temperature was not quite the same for all specimens. The F value, however, was obtained for each specimen as well as the recovered stress, for example, G . The amount of recovery was then calculated as $F-G$ for each specimen. In this way the effect of minor variations from specimen to specimen on the calculated amount of recovery was reduced to a negligibly small value.

A somewhat similar procedure was used to determine the recovery after prestraining an amount ϵ_2 at a temperature T_2 . In order to evaluate the

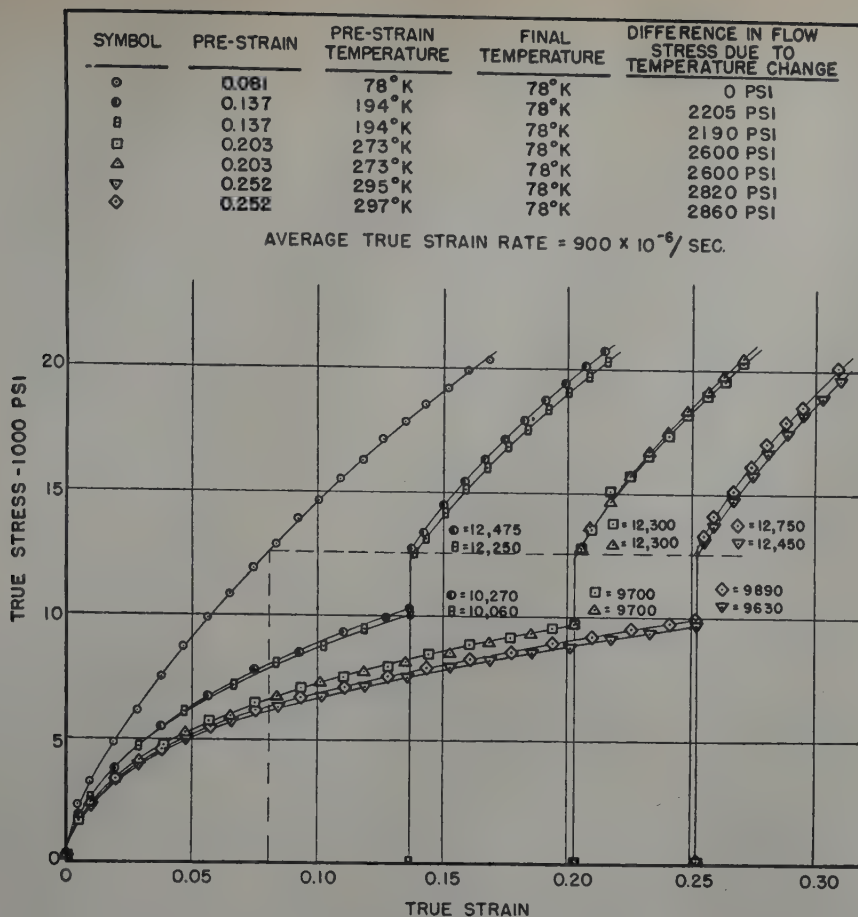


FIG 3—Effect of prestraining at various temperatures on the flow stress at liquid nitrogen temperature.

amount of recovery on a comparable basis, all tests after a recovery treatment were conducted at liquid nitrogen temperature, providing in this way curves CC' , DD' , etc. The stress A differed slightly for each specimen strained to the same value ϵ_2 but stress B was found to vary in an analogous way so that $B-A$ was substantially constant. This value was then used as a basis for calculating the amount of recovery. A specimen to be treated for recovery was strained to ϵ_2 and the stress A for the specimen was measured. After recovery the stress-strain curve CC' was obtained at liquid nitrogen temperature. In this way $C-A$ was determined for the recovered specimen. The amount of recovery was then calculated as $(B-A) - (C-A)$.

Experimental Data

The question of prime interest in the present study concerns possible differences in the work hardened state as revealed by recovery experiments after the metal has been subjected to various prestraining histories of such extent that the instantaneous flow stress is

constant. If different recovery rates are obtained for specimens that have been so prestrained that their flow stress at liquid nitrogen temperature is about 12,500 psi, it follows that the instantaneous flow stress under constant conditions of temperature and strain rate is not a measure of the work hardened state. Under such conditions the relative rates of recovery for the various prestraining treatments will serve to qualify the existing differences in the work hardened states that were generated. In order to permit this evaluation the metal must be prestrained just that amount at various temperatures to give a constant flow stress (12,500 psi in the following tests) when the test is continued at liquid nitrogen temperature. The conditions of prestraining used to accomplish this are shown in Fig 3. Prestraining to 0.252 at 296°K, 0.203 at 273°K, 0.137 at 194°K and 0.081 at 78°K gave approximately the same flow stress of 12,500 psi when the temperature was changed rapidly from that for prestraining to liquid nitrogen. In all cases the transfer to liquid nitrogen temperature was accomplished in less than 15 sec in order to reduce the

amount of recovery that might have occurred during the transfer interval.

It is significant to note that the two specimens prestrained at atmospheric temperature (296°K) gave slightly different stress-strain curves, but that the differences between the flow stress at liquid nitrogen and room temperatures were $12,750 - 9,890 = 2,860$ psi, and $12,450 - 9,630 = 2,820$ psi respectively, which are identical within the limits of experimental error. Similarly the difference in flow stress at liquid nitrogen (78°K) and CO_2 -acetone (194°K) for the two specimens prestrained at CO_2 -acetone temperature $12,475 - 10,270 = 2,205$ psi and $12,250 - 10,060 = 2,190$ psi which is again within the limits of experimental error. These data suggest that the effects of sampling can be largely eliminated by the procedure previously described for calculating the amount of recovery.

The recovery data are recorded in Fig 4 and 5. The amount of recovery was determined by the decrease in the flow stress at liquid nitrogen temperature upon recovery as described previously. Although there is some scatter in the data, the results are nevertheless

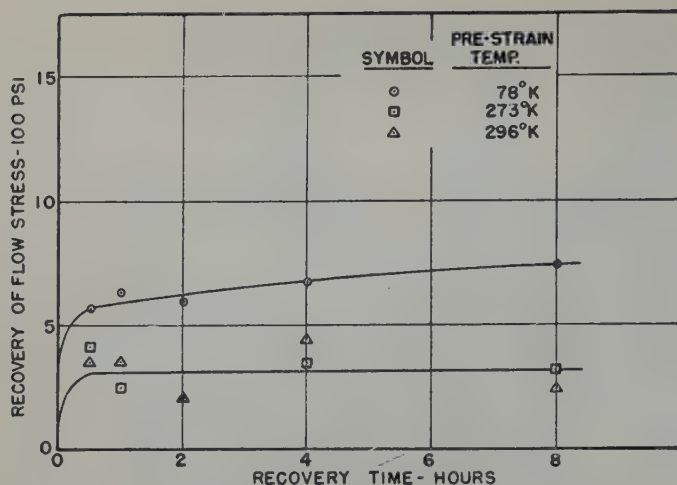


FIG 4—Effect of prestrain temperature on recovery at 273°K.

less conclusive. At 273°K the rates of recovery were relatively slow whereas satisfactorily higher recovery rates were obtained at 305°K. At both of these temperatures the specimens prestrained at 273 and 296°K presented approximately identical recovery rates indicating thereby almost identical work hardened states. But for both of the recovery temperatures used here the specimens that were prestrained at liquid nitrogen temperature (78°K) recovered most rapidly. Fig 6 shows the recovery data at 305°K on a log-log plot. As shown in Fig 4 and 5 the specimens prestrained at CO₂-acetone temperature (194°K) recovered at an intermediate rate.

The data recorded in Fig 4 and 5 reveal that the high purity aluminum used in these tests recovers somewhat at atmospheric temperature after prestraining at atmospheric temperature. Such recovery must, therefore, also occur during the straining. It might, therefore, appear that the observed differences in the recovery rates after various prestrain histories is attributable to the possibility that recovery occurring during prestrain reduces the subsequent recovery for those specimens prestrained at the higher temperatures. In Fig 7 are shown recovery tests at the testing temperature for 273, 194, and 78°K. Although recovery does occur at 273°K in 1 hr, no recovery was detected in 4 hr at 194°K or in 1 hr at 78°K. Evidently the data obtained by prestraining at 78 and 194°K are not clouded by possible recovery during prestraining. Therefore, evidence is substantial that metal prestrained at the lower temperature recovers more rapidly than metal prestrained at a higher temperature even when the two conditions of prestrain-

ing result in the same instantaneous values of the flow stress at the lower temperature.

It is possible of course that greater rates of recovery are induced by the applied stresses during prestraining. In order to test this thought six recovery tests were made under stresses approximating the yield stress at the recovery temperature. No indication of a significant effect of stress on the rate of recovery was detected, thereby disqualifying this suggestion.

Discussion of Results

The preceding experimental data reveal that high purity (99.987 pct Al) aluminum work hardens more rapidly for lower temperatures of prestraining. By appropriate selection of the amount of prestraining for each prestrain temperature it is possible to induce a work

hardened state that gives the same flow stress when straining is continued at liquid nitrogen temperature. In order to accomplish this, the specimens must be prestrained a greater amount for the higher prestraining temperatures. Although the instantaneous flow stresses at liquid nitrogen temperature are adjusted to the same value by this procedure, the rates of strain hardening differ systematically for the various prestraining temperatures. Specimens prestrained at the higher temperatures have higher rates of strain hardening for identical flow stress when they are subsequently tested at liquid nitrogen temperature. This fact suggests that although the flow stresses are the same, the work hardened states nevertheless differ in some yet obscure way as a result of the previous prestrain temperature history.

Specimens prestrained at the higher temperatures to a strain that induces a fixed flow stress at liquid nitrogen temperatures exhibit much slower rates of recovery of the flow stress upon storage at the same recovery temperature than specimens prestrained at lower temperatures. This not only occurs under conditions where the prestraining temperature is high enough to cause some recovery during prestraining, but it also occurs for prestraining temperatures at which the amount of recovery during prestraining is so small that it cannot be detected. The evidence is thus unmistakable that lower temperatures of prestraining to a fixed flow stress yield a more rapidly recoverable work hardened state. Consequently specimens of a metal so treated by various histories that they have the same in-

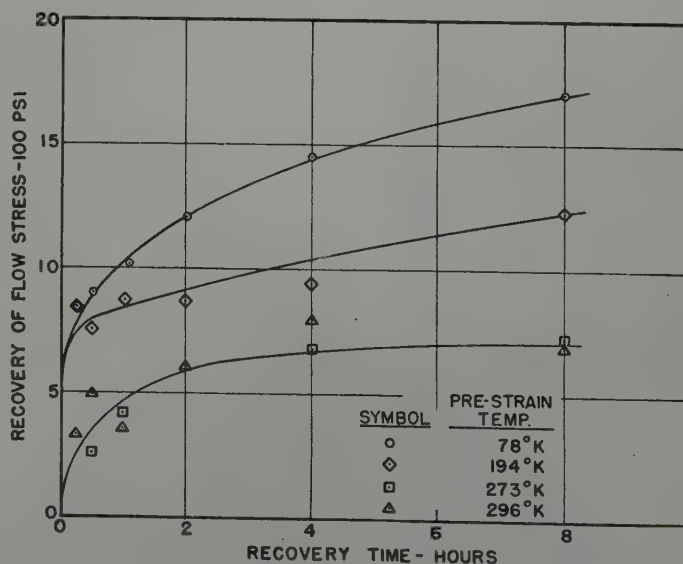


FIG 5—Effect of prestrain temperature on recovery at 305°K.

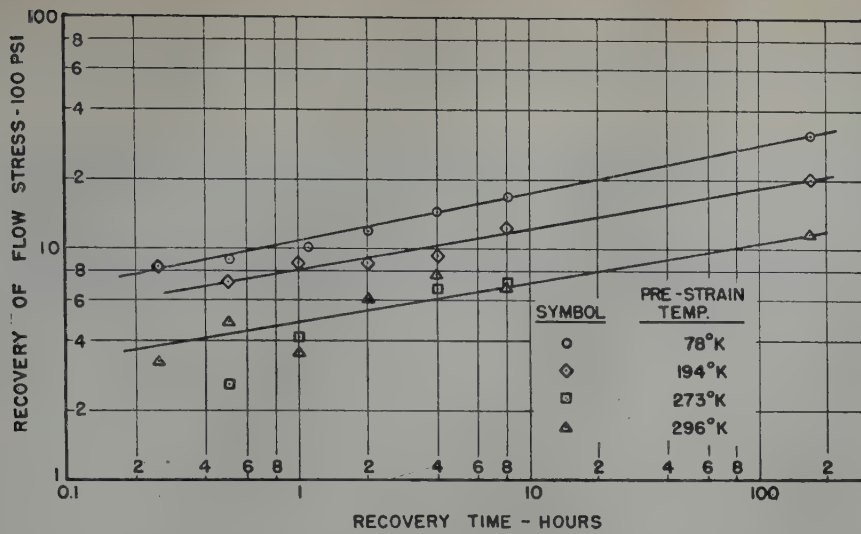


FIG 6—Effect of prestrain temperature on recovery at 305°K.

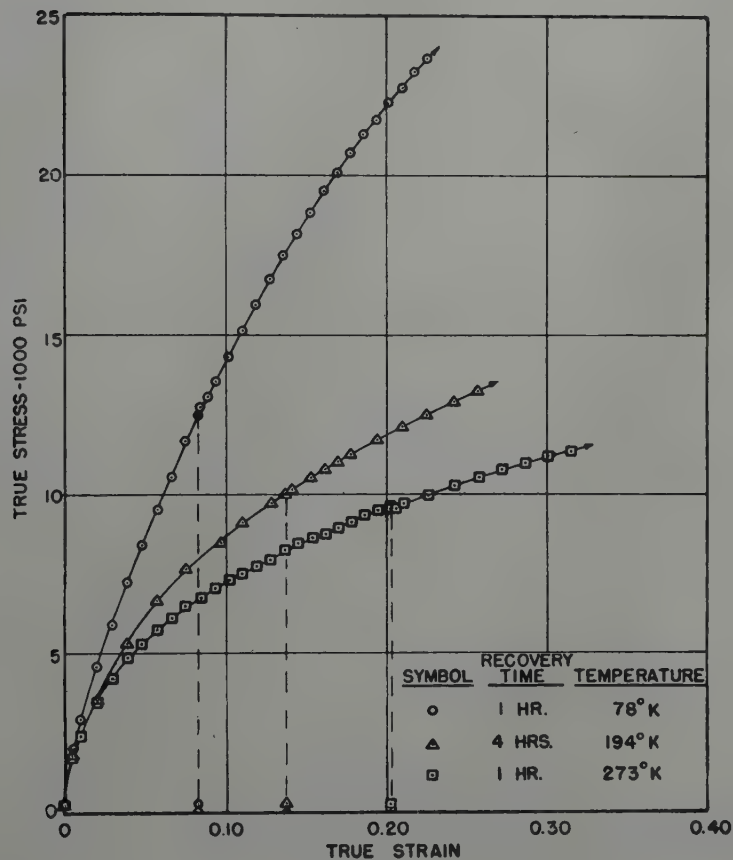


FIG 7—Recovery at testing temperature.

stantaneous flow stress under specified conditions of testing do not necessarily exhibit the same work hardened state.

The differences in these work hardened states is somewhat elucidated by their relative rates of recovery. It appears justifiable to assume that the work hardened state induced in cold worked metals is essentially attributa-

ble to imperfections of a type that are perhaps analogous to dislocations. The work hardened state is then determined by the size, distribution and density of the dislocations. Prestraining under different conditions of temperature, strain-rate and strain induced unique sizes, distributions and densities of the dislocations. Thus it is pos-

sible to acquire the same flow stress in a metal by various strain histories and yet have differences in the size, distribution and density of the dislocations. Upon recovery the more mobile dislocations will be activated and might migrate out of the mosaic blocks or be otherwise annihilated. The rate with which such a recovery process

would occur at a stated recovery temperature would depend upon the relative activation energies for the various sizes, distributions and densities of dislocations. The new work hardened state and the new flow stress following recovery would depend on the resulting dislocation statistics. Inasmuch as those specimens which were prestrained to a stated flow stress at the lower temperatures recovered most rapidly it appears logical to conclude that they also contain a larger number of more easily activated dislocations. Perhaps they contain a greater number of more readily activated dislocations more propitiously distributed as a result of the lower prestrain temperature to give nevertheless the same flow stress as is obtained by an appropriately larger prestrain at a higher temperature. Perhaps the dislocations generated at the lower prestrain temperatures are smaller, (as has been suggested on the basis of other evidence by Taylor⁶ and Kauzmann⁶ and Dushman⁷) but more numerous so that the same flow stress is achieved as is obtained by more extensive prestraining at the higher temperatures. The latter suggestion is of interest and will constitute the subject for further investigations.

Conclusions

1. The mechanical properties of cold-worked metals depend not only on the instantaneous values of the

strain, strain rate and temperature but on the entire past history of temperature and strain rate during prestraining.

2. Neither the instantaneous value of the total strain nor the instantaneous value of the flow stress under stated conditions of strain rate and temperature are adequate for characterizing the strain hardened state.

3. Specimens of a metal can be so prestrained at various temperatures that the same flow stress is obtained when they are subsequently tested at the same instantaneous temperature and strain-rate. Those prestrained at the higher temperatures require greater amounts of prestrain.

4. Although such specimens have the same instantaneous flow stress, those prestrained at the higher temperatures have greater instantaneous rates of strain hardening.

5. The recovery rate of pure aluminum depends upon the temperature of prestrain; specimens prestrained at the lower temperatures exhibit much higher rates of recovery.

6. These observations appear to suggest that lower temperatures of prestraining induce the formation of smaller or otherwise more readily activated dislocations.

Acknowledgments

This investigation was sponsored by the Office of Naval Research as part of

a more extensive program of investigation on the plastic properties of aluminum alloys. The authors express their sincere gratitude to the O.N.R. for their sponsorship of these studies and their substantial contributions to the planning and execution of this program of study. In addition they wish to thank Messrs. C. Peters and E. Berliner for their aid in conducting the tests and Mrs. G. Pelatowski for the preparation of the figures in this report.

References

1. E. Orowan: The Creep of Metals. West Scotland Iron and Steel Inst., Feb. 14, 1947.
2. J. E. Dorn, A. Goldberg and T. E. Tietz: The Effect of Thermal-mechanical History on the Strain Hardening of Metals. AIME, *Trans.* 180 (1949) *Metals Tech.* Sept. 1948. TP 2445.
3. E. J. Ripling and G. Sachs: The Effect of Strain-temperature History on the Flow and Fracture Characteristics of an Annealed Steel. AIME *Trans.* (1949) 185, 78. *Jnl. of Metals*, Feb. 1949. TP 2514.
4. T. E. Tietz and J. E. Dorn: The Effect of Strain Histories on the Work Hardening of Metals. *Trans. ASM* 41A (1949).
5. G. I. Taylor: The Mechanism of Plastic Deformation of Crystals. *Proc. Roy. Soc. (London)* A145 (1934) 362.
6. W. Kauzmann: Flow of Metals from the Standpoint of the Chemical-Rate Theory. *Trans. AIME* (1941) 143, 57.
7. S. Dushman, L. W. Dunbar and H. Hothsteiner: Creep of Metals. *Jnl. Appl. Phys.* (1944) 15, 108.

CORRECTION

M. K. Yen and W. R. Hibbard, Jr.: The Transverse Bending of Single Crystals of Aluminum. *Journal of Metals*, Oct. 1949, p. 716. Fig 16 and 17 are transposed.



Flow and Fracture Characteristics of a Die Steel at High Hardness Levels*

L. J. KLINGLER,† C. C. CHOW,‡ and G. SACHS,§ Member AIME

Introduction

Most structural parts which are heat treated are designed using strength properties which have been determined in the principal direction of the wrought material. For example, for rolled or drawn materials, properties are given for the rolling or drawing direction. The structures, however, may be loaded so that the critical stress is in some direction other than that for which the properties of the material are known.

Investigations of forged products,^{1,2,3} have shown that while the yield strength and tensile strength of carbon steel billets and bars vary little with the direction of the test specimen in relation to the fiber, the contraction in area in tension tests and the impact strength in notched bar impact tests decrease in the transverse direction. The contraction in area and, consequently, the fracture stress of hard aluminum and magnesium alloy forgings have also been found to be lower in the transverse direction.

An investigation on aluminum alloy plate⁴ likewise has shown the dependence of the fracturing characteristics upon the direction* of the test specimens, the longitudinal direction being considerably stronger than the transverse direction and the normal direction, with the normal direction being the least strong.

The variation of properties with direction has been explained by a type of anisotropy called mechanical anisotropy. This anisotropy results from the elongation, in the direction of the principal strain, of certain phases, inclusions, and/or cavities in the metal

during working. A mechanical fibering is thus produced which seems to persist through annealing and heat treatment.

This investigation was initiated to determine the flow stress and fracture stress, at high hardness levels, at 90° to the rolling direction in a round steel bar. It is this direction which receives the critical stress in drawing dies machined from round bars. Preliminary tests showed a large difference in properties between the 0° and 90° directions. Consequently, it was felt that a more complete investigation, utilizing several types of tests, was warranted to determine the flow and fracture characteristics of a steel at various orientations, for a number of hardness levels. This investigation was conducted on an air hardening nondeforming die steel.

Material and Procedure

The distribution of properties was

made on a 3-in. round bar of annealed high-carbon, high chromium steel of the following analysis:

| | Pct |
|-----------------|-------|
| Carbon..... | 1.53 |
| Manganese..... | 0.39 |
| Silicon..... | 0.27 |
| Chromium..... | 11.76 |
| Vanadium..... | 0.25 |
| Molybdenum..... | 0.81 |

The 3-in. bar was produced from an 8-in. ingot, which was annealed and forged to a 4-in. square billet. The billet was annealed and rolled to a 3-in. round which was then annealed and straightened.

This steel is an air hardening die steel which has very good dimensional stability on hardening; therefore, the residual stresses resulting from hardening would be expected to be low. A hardness survey across the diameter of the annealed bar showed no difference in hardness from the center to the outside. However, the test sections of all the specimens were taken approximately half way between the center of the bar and the surface to avoid any surface effect or possible porosity at the center.

Tension, compression and bend tests were made on specimens hardened and tempered at six different temperatures.

The tension test specimens, Fig 1, were machined from the bar at orientations of 0, 22.5, 45, 67.5 and 90° from the axis of the steel bar. The specimens were rough machined, heat treated and then ground to size. The test section on each specimen was lapped in a direction parallel to the axis of the specimen to remove any transverse scratches which might act as stress raisers. The specimens were tested in fixtures which insured concentricity of loading of less than 0.001 in.⁵ The transverse strains were measured with a radial strain gauge,⁵ the least count of which was 0.0001 in. change in diam.

The compression specimens, Fig 1, were machined from the bar at ori-

New York Meeting, February 1950.

TP 2724 E. Discussion of this paper (2 copies) may be sent to *Transactions AIME* before April 1, 1950. Discussion is tentatively scheduled for publication in November 1950.

Manuscript received May 23, 1949; revision received Aug. 31, 1949.

* This paper is one of a series of reports in a research program conducted at the Metals Research Laboratory, Case Institute of Technology, Cleveland, Ohio, under the direction of W. M. Baldwin, Jr., and in cooperation with the Office of Naval Research, U. S. Navy.

† Research Associate, Metals Research Laboratory, Case Institute of Technology.

‡ Academia Sinica, Shanghai, China; formerly Research Assistant, Metals Research Laboratory, Case Institute of Technology.

§ Formerly Director Metals Research Laboratory, Case Institute of Technology.

¹ References are at the end of the paper.

* The direction of a test specimen can be defined as the relation of the axis of the specimen to a set of axes made up of the longitudinal, transverse, and normal directions in the material.

entations of 0° and 90° from the axis of the steel bar. The specimens were rough machined, heat-treated, and then ground to size. The specimens were tested between hardened ground steel blocks in a specially built ball-bearing die set, which assured pure compression. The ends of the specimen were lubricated with a drawing compound to minimize the friction. The transverse strain was measured with the same radial strain gauge which was used for the tension specimens. All the specimens were strained in excess of 4 pct (increase-in-area). No perceptible bending or barreling of the specimens was noted at these strains.

The bend test specimens, Fig 1, were machined from the bar at orientations of 0° and 90° from the axis of the bar. The specimens were rough machined, heat treated, and then ground to size. A photogrid, 100 lines per in.⁶ was applied on the tension surface of the bend bar. Readings were made from this grid after fracture to give the strain at the middle of the tension surface. The strains were measured with a Filar eyepiece, using a gauge length of 0.01 in. Five gauge-lengths were meas-

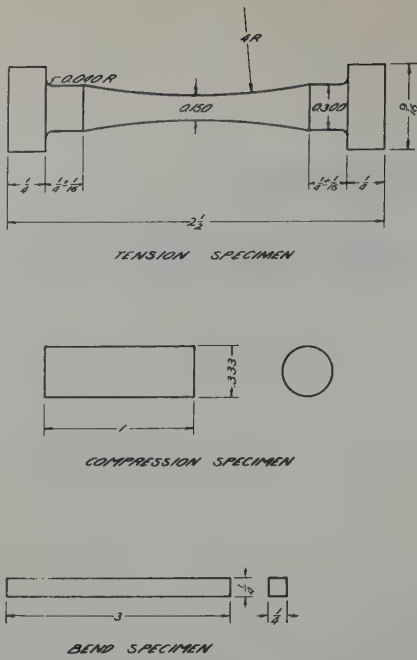


FIG 1—Test specimens.
a. Tension specimen. b. Compression specimen.
c. Bend specimen.

ured on each side of the fracture and the strain at the fracture was extra-

polated from these measurements. The specimens were bent in a "Wrap Former" around a 1.25 in. radius die.⁶ All of the specimens fractured during testing at relatively small angles of bend. The bend angle was measured after fracture on a microprojector.

All of the test specimens for each tempering temperature were heat treated together, the specimens being held 40 min. at 1820°F, in a Vapo Carb Atmosphere furnace and cooled in still air. The specimens were tempered in a forced air convection furnace at 1000, 1025, 1050, 1100, 1150 and 1200°F for one hour.

The corresponding hardness values for the various tempering temperatures were as follows:

| Tempering Temperature °F | Hardness Rockwell C |
|--------------------------|---------------------|
| 1000 | 62.5 |
| 1025 | 62.5 |
| 1050 | 59. |
| 1100 | 54.5 |
| 1150 | 50. |
| 1200 | 45. |

Results

STRUCTURE

In order to show the disposition of

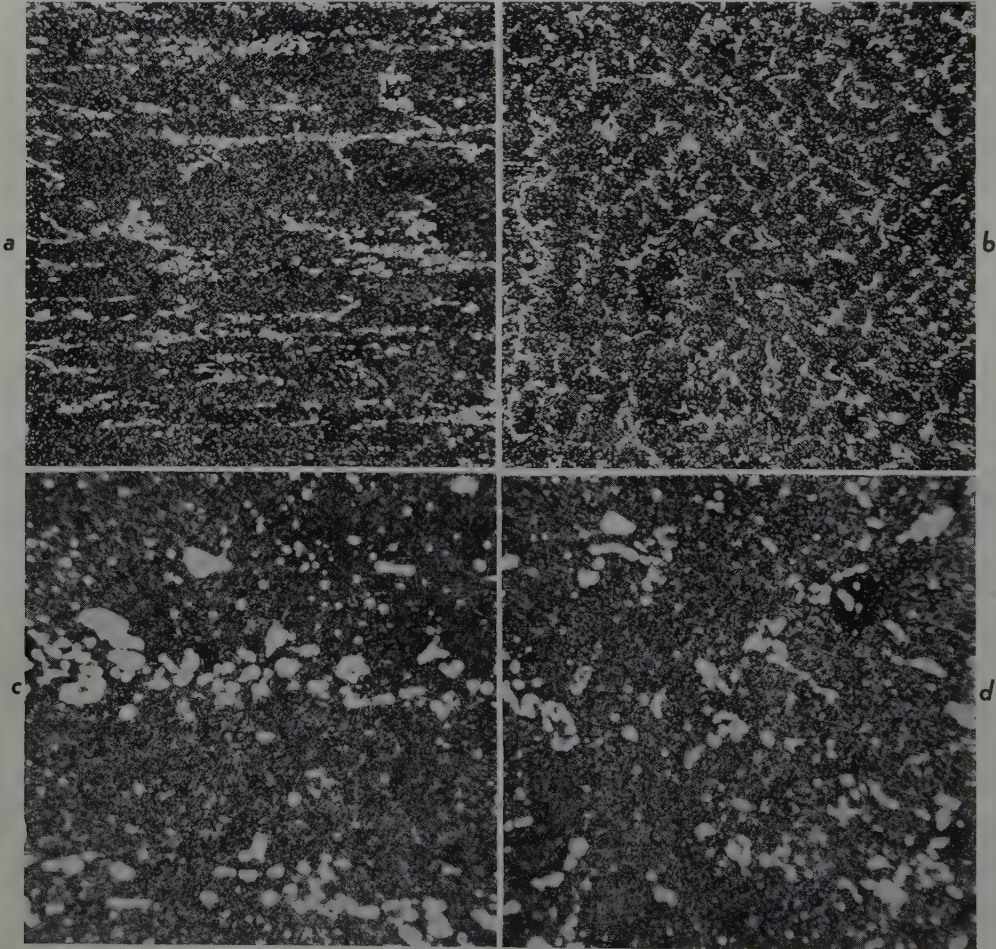


FIG 2—Structure of a 3-in. diam bar of die steel, quenched and tempered at 1200°F. Nital etch. a. Longitudinal direction, X 100. b. Transverse direction X 100. c. Longitudinal direction, X 500. d. Transverse direction, X 500.

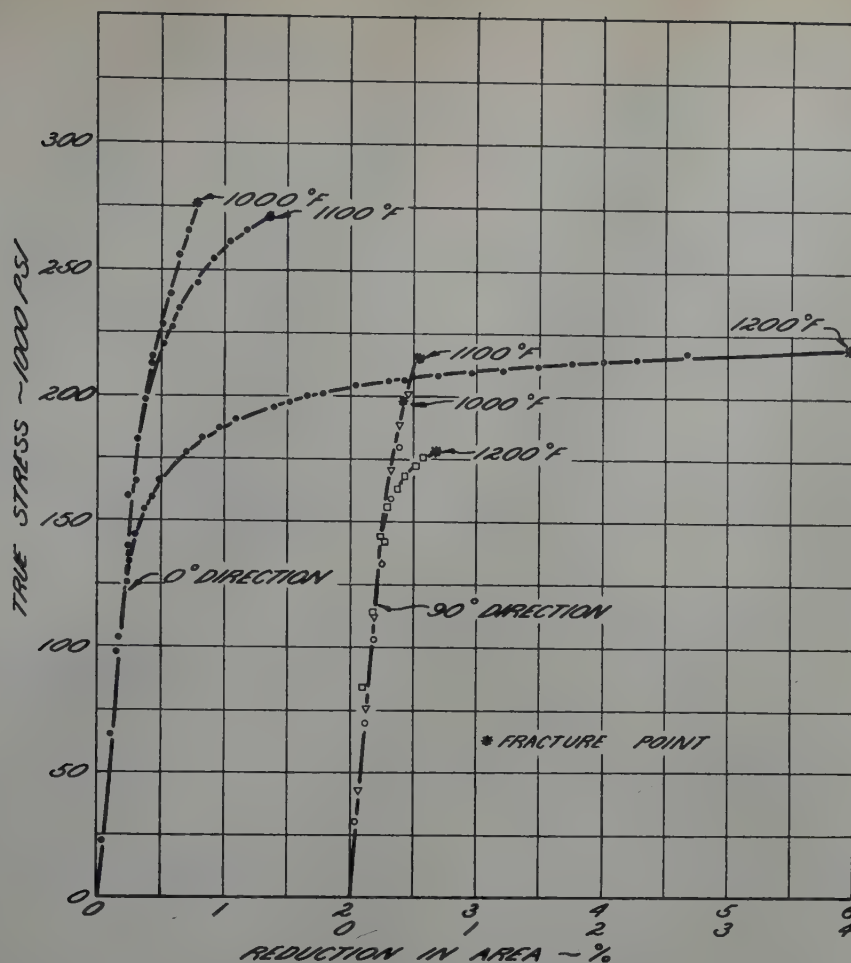


FIG 3—Typical stress-strain curves in tension for a die steel tempered at various temperatures and tested at several directions to the rolling direction.

the carbides, micrographs were made in the longitudinal and transverse directions of the bar in specimens which had been quenched and tempered at 1200°F. These micrographs are shown in Fig 2 at both 100 and 500 magnifications. It can be seen that the undissolved carbides have been strung out in the longitudinal direction of the bar by the fabricating operations.

TENSION TESTS

The results of the tension tests are shown in Fig 3, 4, 5, and 6. In Fig 3 a few typical tension curves are shown for the longitudinal and transverse directions at three different tempering temperatures. The fracture stress, ductility, and yield stress are shown in Fig 4, 5, and 6 as functions of tempering temperature and of specimen direction for three selected temperatures.

The fracture stress, Fig 4, for every orientation reached a maximum at a tempering temperature between 1025 and 1050°F. At 1000°F the fracture stress fell off for all of the orientations. The fracture stress at each tempering temperature decreased from a maxi-

mum at the 0° direction to a minimum at the 90° direction.

The reduction in area, Fig 5, was small for all of the tests but showed an increase with tempering temperature for all orientations. The increase in ductility was greater at each tempering temperature as the orientation changed from 90 to 0°. The yield stress, 0.2 pct offset, Fig 6, was the same for all orientations at each tempering temperature. The yield stress increased as the tempering temperature was lowered until a maximum was reached at 1025°F and then the yield fell off at 1000°F in a manner similar to the fracture stress.

COMPRESSION TESTS

Typical stress strain curves in compression are shown in Fig 7 for the longitudinal direction at three different tempering temperatures. The stresses in compression for 0.1, 0.2, 0.5, 1.0 and 2.0 pct plastic flow are shown in Fig 8. A small but consistent difference was noted between the orientations of 0° and 90°, the values for 0° always being higher. The values of yield stress in-

creased with decreasing tempering temperature and unlike the yield stress in tension, did not have a maximum at 1025°F.

BEND TESTS

The strains measured at the center of the tension surfaces and the angles of bend after fracture are given in Fig 9 and 10. Considerable difference is shown between the 0° and 90° orientations for both the bend strain and bend angle, this difference becoming larger with increasing tempering temperature. Both the strain and the angle increased with increasing tempering temperature for both 0° and 90° orientations.

Discussion of Results

A high degree of directionality was shown in the fracture stress and ductility for this material. At 1200°F tempering temperature the strength in the transverse direction was 18 pct less than the longitudinal direction and this difference increased at lower tempering temperatures. An even greater

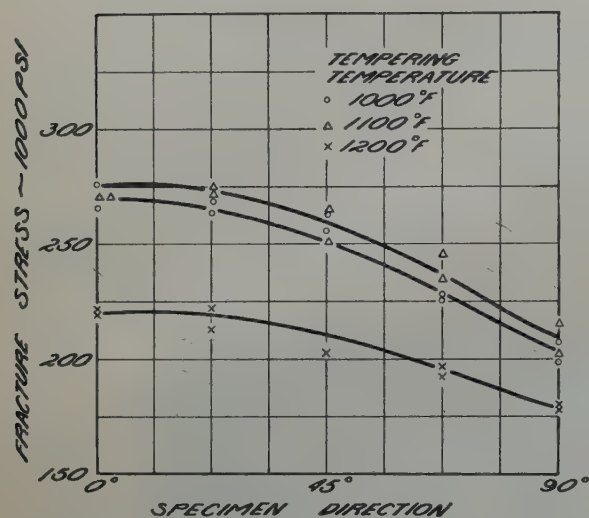
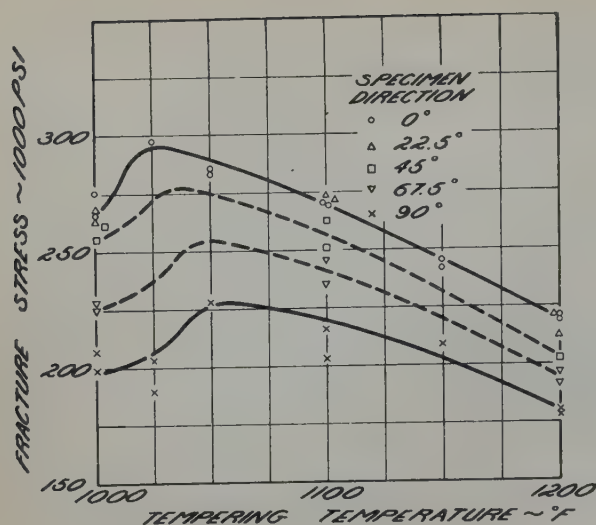


FIG 4—Dependence of fracture stress on tempering temperature and orientation.

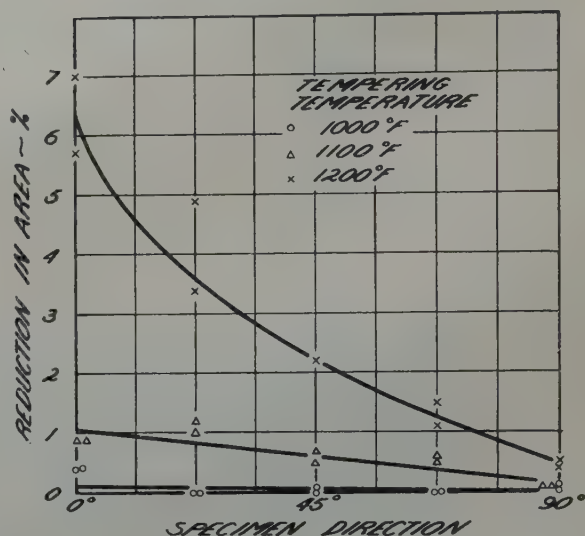
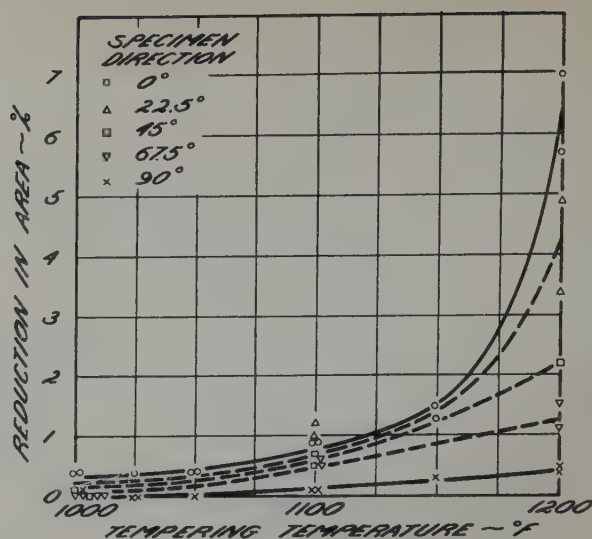


FIG 5—Dependence of ductility in tension on tempering temperature and orientation.

difference was shown by the ductility over the whole range of tempering temperatures used.

The decrease in fracture stress expressed as a percentage of the fracture stress at 0°, is shown in Fig 11 for the different orientations at three tempering temperatures. This decrement appears to be a function of the specimen direction and is also dependent upon the structure, particularly at 90°. This behavior is of the type which would be expected if discontinuities or cavities existed parallel to the axis of the bar. The yield stress in tension, however, showed no such directionality (the yield stress in compression showed a slight degree of directionality). This further supports the belief that mechanical anisotropy is the cause of the differences in fracture stress and ductility since a crystallographic preferred orientation normally causes differences in yield strength in various directions. Cubically aligned copper is

one exception, in that it shows little dependence of yield stress upon the direction of testing.⁷

The decrease in yield stress in the vicinity of 1000° tempering temperature may be due to the retention of residual stresses which lower the apparent yield strength. The sharp drop in yield stress was not observed in compression. A comparison of the yield stress in tension with the yield stress in compression (0.2 pct), Fig 12, shows that between 1200 and 1100°F the yield stress in compression was slightly higher than that in tension. This is the usual case. However, below 1100°F, the tension yield stress decreased, whereas the compressive yield stress continued to increase.

The ductility of this steel is extremely low in the range of tempering temperatures used. On hardening, the steel retains a high percentage of

austenite (30 to 40 pct) which transforms on tempering.⁸ A secondary hardening range is observed at tempering temperatures about 1000°F, Fig 2, where additional chromium carbides are formed. Consequently a mixed structure is obtained which is composed of variously tempered marten-sites, carbides, retained austenite, and possibly other transformation products. Small amounts of carbides, retained austenite or other transformation products would all cause a lowering of the ductility.

In the range of tempering temperature from 1000 to 1050°F the ductility is reduced to less than one per cent. Consequently, the fracture stress is lowered in this range.

The bend tests showed considerable difference between the 0° and 90° orientations when measured either by the strain or the bend angle. A comparison

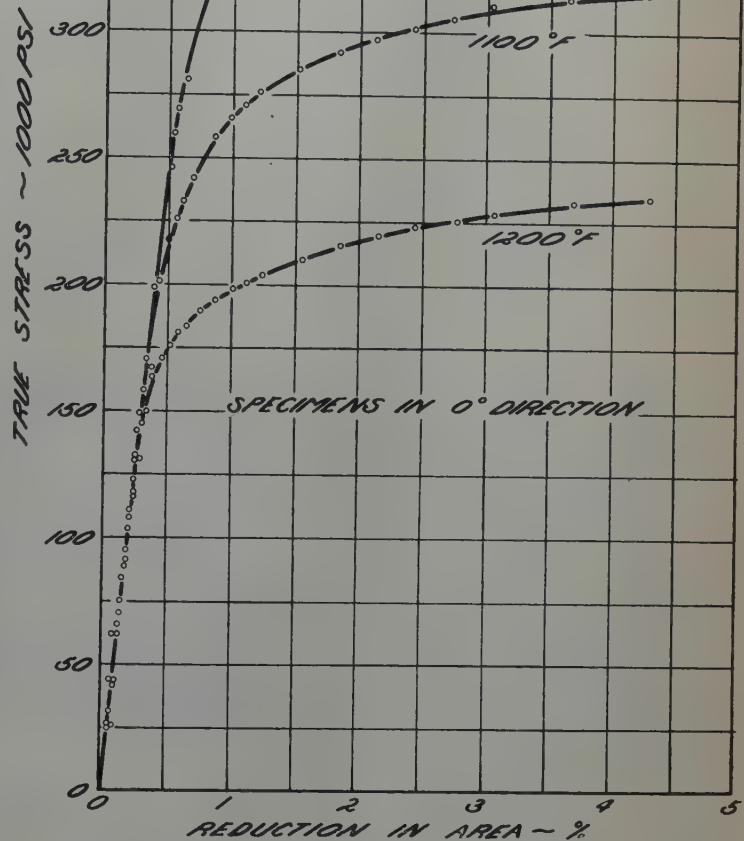
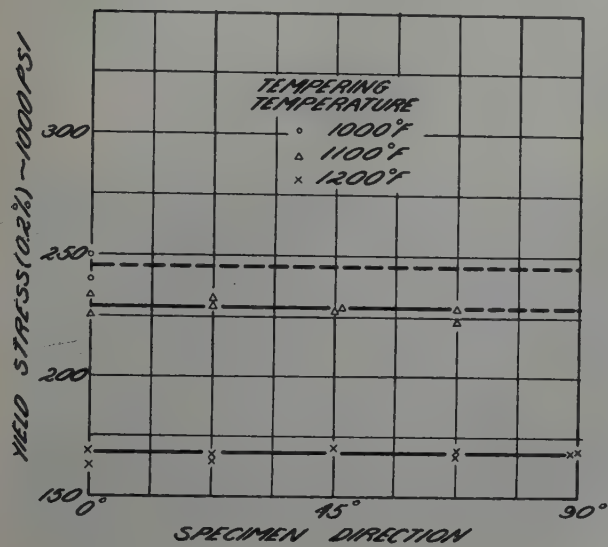
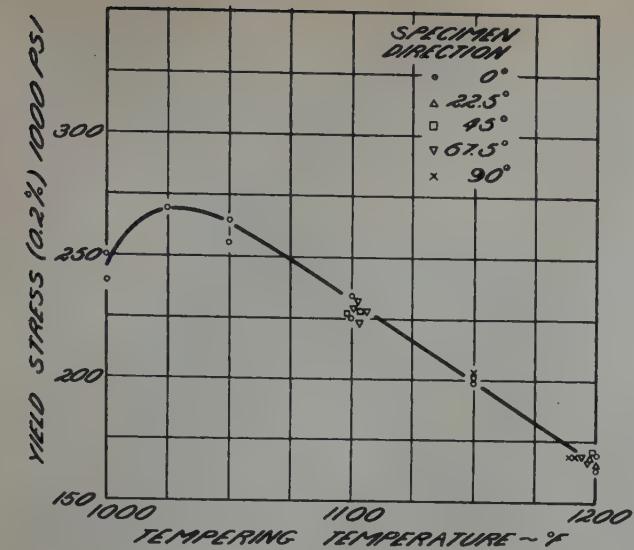


FIG 6 (Upper left)—Dependence of yield stress in tension on tempering temperature and orientation.

FIG 7 (Above)—Typical stress strain curves in compression for a die steel tempered at various temperatures and tested in the rolling direction.

FIG 8 (Lower left)—Dependence of yield stress in compression on tempering temperature and orientation for various amounts of strain.

of the strains measured in the bend tests with those in tension shows that the strains were greater for the bend tests although a slight degree of biaxiality* exists at the center of the tension surface of a square bar.

Conclusion

As a result of this investigation, the

* On bending a square bar, a small transverse stress results at the center of the tension surface due to lateral restraint.⁶

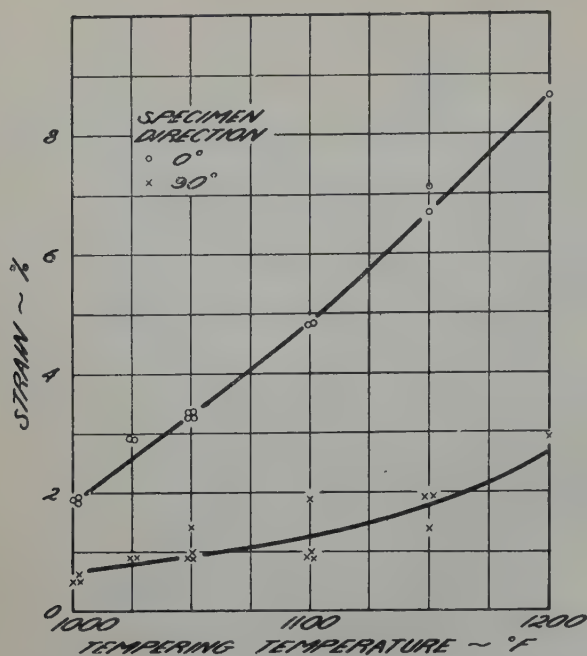


FIG 9—Dependence of bending strain on tempering temperature and orientation.

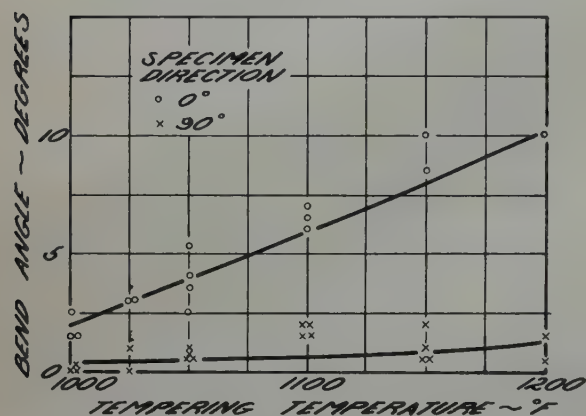


FIG 10—Dependence of bend angle on tempering temperature and orientation.

following conclusions can be drawn:

1. The fracture stress and ductility in tension and the ductility in the bend test exhibited pronounced directionality, properties always being higher in the longitudinal direction for every tempering temperature chosen.

2. The yield stress in tension did not vary with direction. The yield stress in compression varied only slightly with direction.

3. The directionality can be attributed to mechanical anisotropy caused by the carbide stringers developed in the fabrication of the material.

Acknowledgment

The authors are indebted to the Office of Naval Research, U. S. Navy, for permission to publish this

information.

References

1. G. Sachs: Properties of Heavy Forgings. *Steel*, Apr. 6, 1942, 110, 76-77, 101-109.
2. G. Sachs and K. R. Van Horn: Practical Metallurgy. A.S.M. Cleveland (1940).
3. G. Sachs: Some Observations on the Forgings of Strong Aluminum Alloys. *Jnl. Inst. Metals* (1939) 64, 261-283.
4. L. J. Klingler and G. Sachs: Fracturing Characteristics of Aluminum Alloy Plate. *Jnl. Aero. Sci.* (1948) 15,

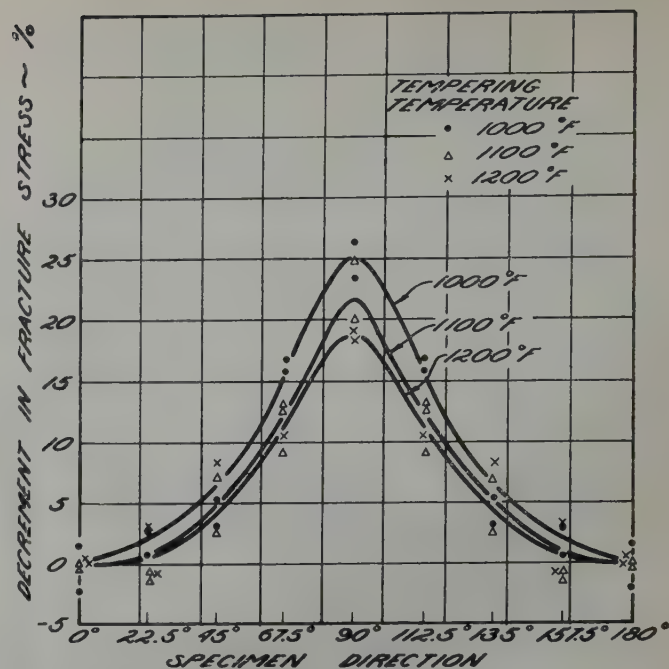


FIG 11—Decrement in fracture stress as a function of orientation.

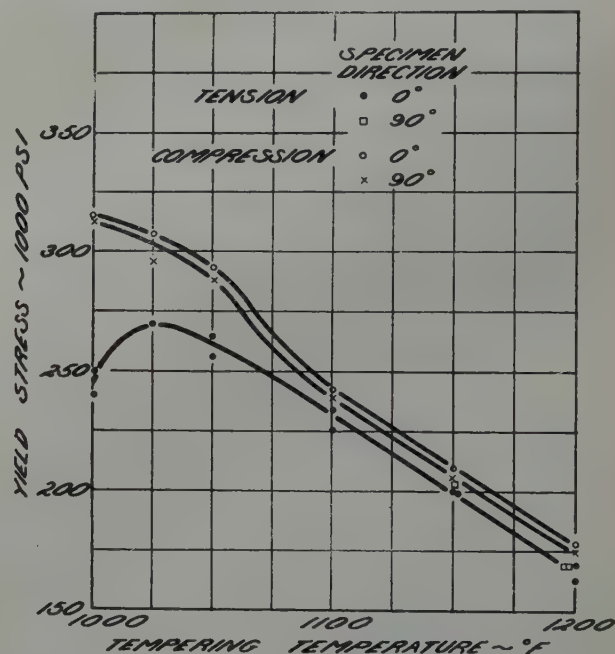


FIG 12—Comparison of yield stresses in tension and compression for 0.2 pct plastic strain.

731-734.

5. G. Sachs, J. D. Lubahn, and L. J. Ebert: Notched Bar Tensile Test Characteristics of Heat Treated Low Alloy Steels. *Trans. A.S.M.* (1944) 33, 340-391.
6. G. S. Sangdahl, Jr., E. L. Aul, and G. Sachs: An Investigation of the Stress and Strain States Occurring in Bending. *Experimental Stress Analysis* (1948) 6, No. 1, 1-18.
7. F. H. Wilson and R. M. Brick: Textures, Anisotropy and Earing Behavior of Brass. *Trans. AIME* (1945) 161, 173-200.
8. W. H. Wills: Further Study of a High Carbon-High Chromium Tool Steel. *Trans. A.S.M.* (1937) 25, 1013-1029.

The Effect of Working and Heating Eutectic Structures

J. S. BROWN* and A. G. GUY*

With the exception of the work of Tammann and Hartmann,¹ no published information has been found on the structural changes produced in eutectic structures as the result of heating following plastic deformation. In part this lack of information may be due to the fact that many eutectic structures contain an intermetallic compound as a prominent phase, and as a consequence have been considered to be unworkable. For example, Tammann and Hartmann were able to obtain useful data only on those alloys that they could greatly reduce in thickness

cooling in the mold from about the eutectic temperature. The fairly coarse eutectic structure thus obtained was too brittle to work at room temperature without cracking. Fig 1b shows the worked structure obtained by compressing a $\frac{1}{2}$ -in. cube 70 pct in about 15 sec at 550°F and then water quenching. The pronounced changes in the distribution of the two phases produced by heating the worked alloy at 850°F for 1 hr are shown in Fig 1c. Recrystallization of both phases appears to have taken place, and the mechanical properties of the cast alloy

tion, to have a granular structure after heat treatment: Sn-9 pct Zn (98 pct); Cd-82.5 pct Pb (60 pct); and Bi-43.5 pct Pb (90 pct). On the other hand the alloy Al-11.7 pct Si (60 pct) showed no change after heating. Tammann and Hartmann observed a distinct shrinking of the needles in unworked eutectics subjected to heat-treatment. In the present work inappreciable change in the eutectic structure was found on heating undeformed alloys.

In summary, it appears that eutectic structures can be recrystallized into a "spheroidized" condition by heating

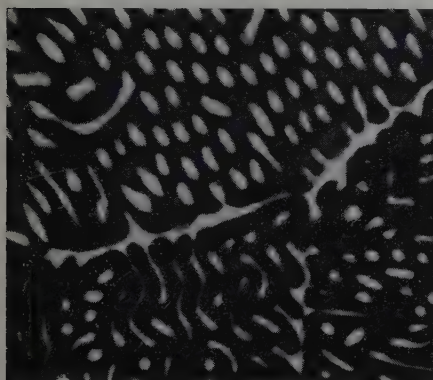


FIG 1a—The cast structure of the Pb-33.2 pct Mg alloy; the Mg_2Pb intermetallic compound appears dark and the Mg solid solution light.

Unetched. 1000 \times .

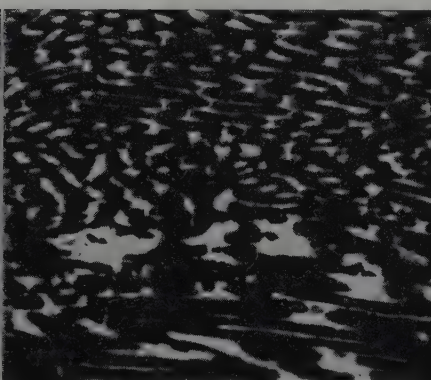


FIG 1b—The Pb-33.2 pct Mg alloy reduced pct by pressing at 550°F.

Unetched. 1000 \times .



FIG 1c—The 70 pct reduced Pb-33.2 pct Mg alloy after heating for one hour at 850°F.

Unetched. 1500 \times .

by cold rolling. This restriction placed on the investigation of alloys containing intermetallic compounds has been largely removed by the work of Savitskii² which showed that large deformations of such alloys can be produced by relatively slow compression at temperatures near the melting range. It was possible, therefore, to carry out the present work on a range of binary eutectics including one composed of two intermetallic compounds.

The essential results obtained on the alloy systems studied are illustrated by the Pb-Mg eutectic containing 33.2 pct Mg, Fig 1. The cast structure, Fig 1a, was obtained by melting together magnesium of 99.8 pct purity and chemically pure test lead, casting into a heated, small steel mold, and furnace

must have been significantly changed by the working and heat treatment.

Similar results were obtained with the Mg-59.5 pct Bi, Mg-36.4 pct Sn, Mg-65.4 pct Cu, and Bi-40 pct Cd eutectics, only the last of which could be worked at room temperature. Tammann and Hartmann reported a thickening and shortening of the needles of the eutectics which they heated about 10°C below the melting range for 1 hr after drastic cold rolling. They found the following eutectics, given the indicated amounts of reduc-

near the eutectic temperature after severe deformation. If the eutectic contains one or more brittle phases the necessary deformation can be accomplished by pressing at high temperatures. It is reasonable to expect that this tendency towards equiaxed grains from the plate- or needle-like eutectic structure should be general since the energy relations and mode of growth in recrystallization are so different from those that hold for eutectic crystallization.

References

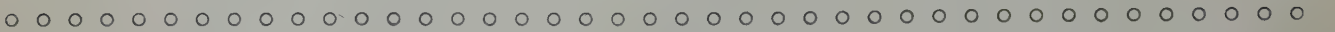
1. G. Tammann and H. Hartmann: *Ztsch. Metallkunde* (1937) **29**, 141-144.
2. E. M. Savitskii: *Doklady Akad. Nauk S.S.S.R.* (1948) **62**, 349-351. Abstr. in *Metal Prog.* (July, 1949) **56**, 126, 128.

Technical Note No. 27 E. Manuscript received July 27, 1949.

* Graduate Student and Associate Professor of Metallurgy, respectively, Mechanical Engineering Dept., North Carolina State College, Raleigh, N. C.

¹ References are at the end of the note.

The Fume and Dust Problem in Industry



HARRY V. WELCH,* Member AIME

Introduction

In this paper, as prepared for delivery at the Southern California regional meeting on Oct. 14, 1948, it was thought best to interpret the term "economics" in a rather broad manner and to include, in addition to the material losses and recoveries and associated monetary values (Part I), a limited discussion of the increased difficulties or the particular problem and the special requirements, as the particle sizes of the suspended particles range down from the relatively coarse to 100, to 10, to 1 micron or even to a fraction of one micron (Part II). Further, it is not quite in order to overlook entirely the community and individual health problems, although space requires the economics of this to be considered only very incompletely. Therefore, Part III, covering this phase of the subject, is very limited.

This paper, then, is divided into 5 parts or headings as follows: I Losses and/or values in suspended solids. II Particle size. III Dust and fumes in community and individual living. IV Means and Procedures for dust and fume collection. V Description or examples of specific equipment in service and of the several types used for dust and fume collection. Because of the wide extent and wealth of subject material available and the space and time limitation imposed, presentation and discussion are less than originally planned.

I—Losses and/or Values in Suspended Solids

The weight involved in moving streams of industrial plant gases is commonly not appreciated, neither is their carrying power in the weight of solids maintained in suspension and

moved with the gas stream from a point of origin or pick-up to a point of dissipation or settlement. These, however, are major weight figures; for example, in a modern iron blast furnace there may be five tons of gas for every ton of iron produced and by the time this blast furnace gas has been burned in stoves or under boilers the weight of gas discharged to atmosphere is on the order of eight times the weight of iron produced. Similarly for nonferrous metallurgy there may readily be from 10 to 20 times the weight of gases discharged to atmosphere as there is metal produced.

A cement kiln in operation or a kiln in service to produce metallurgical lime may have on the order of 5 to 6 times the weight of stack gases as of clinker or lime produced, and at least the cement kiln, because of the very fine nature of its feed, is a very heavy dust producer.

It may be noted that there have been two developments in progress for nearly three decades. Both are extraordinary in the industrial economics effected and in their ready availability to ever larger units of operation and their ever widening importance in industry, and both are productive of great quantities of finely divided material in furnacing. The first of these is the flotation process for ores, especially the metallics such as copper, lead, and zinc; and the second, powdered fuel combustion for power plant, industrial plants and metallurgical operations. Today, new developments, for

example, flotation for the nonmetallics such as higher grade limestone for cement manufacture which requires still finer grinding and the powdered-coal-fired boilers with production ratings of over 1,000,000 lb of steam per hr, bring still more concentrated and hugely increased quantities of stack emission.

Perhaps the honors for the greatest interest in the quantities and values escaping in waste furnace and equipment gases belong to the nonferrous metallurgical operations. Their record of achievement in the installation of dust and fume collection equipment, largely baghouses or Cottrell electrical precipitators, is exceeded by no other industry.

Something of the magnitude and variety of equipment utilized in such recovery systems was covered by the writer in two papers presented to the Institute some 10 years ago.^{1,2} It is not intended to repeat the material of those articles, but it is thought that they complement this offering and should be noted.

COPPER ROASTERS

As the copper roasters are the first of the series of furnaces handling the copper-bearing concentrates in the usual copper smelter of today, it is in order to make them the first consideration.

Multiple hearth sulphide roasters, not hard driven, often maintain their dust loss through exit gases at 3 pct or below of feed to furnace; in hard-driven or maximum-driven furnaces, exit gas losses often approximate 7 pct of charge with a ± 2 pct variation for special conditions prevailing at some plants. A 5 pct loss of feed in a roaster gas exit, unless reclaimed, often makes the difference between a profit and loss operation, and in many cases substantial recovery is the very basis of dividend payments. As there is available very practical and successful equipment for the collection of the

California Fall Meeting, Los Angeles, Oct. 1948, and New York Meeting, February 1950.
To be presented at the Fume and Dust Collection Symposium, Feb. 1950.
TP 2727 D. Discussion of this paper (2 copies) may be sent to *Transactions AIME* before Feb. 1, 1949.
Manuscript received Dec. 8, 1948; revision received Sept. 17, 1949.
* Chief Chemist, Western Precipitation Corporation, Los Angeles, Calif.
¹ References are at the end of the paper.

suspended solids in the acid-bearing copper roaster gases, all plants handling good tonnages of through-put material are equipped with some form of collection equipment; the most common and quite the most successful collection equipment makes use of high potential electrical discharge—the process of *Electrical Precipitation*, more commonly referred to as the Cottrell process. In general, the values in copper roaster feed are not confined to the copper only but include both gold and silver. Copper and gold show no appreciable fume production and their recovery in a normal roaster precipitator may be on the order of 10 pct higher than that of total solids (commonly there are present in the precipitate minor amounts of fumes and dust—as oxides and/or sulphates of lead, zinc, arsenic, antimony and the like) and 5 pct better than the silver recovery efficiency. Silver has a greater volatility than copper and gold, and particularly so in the presence of volatilized lead compounds.

No two copper smelters are alike as to losses with their flue gases, the variation being surprisingly large and usually excessive in hard-driven plants or older plants, or with poor maintenance as indicated by leaky flues and general large air infiltration conditions. It is, however, worthwhile to go through a sample set of figures of furnace losses and collections for a copper smelter and while the figures are not those of any one smelter they are more or less representative of all. Consider a custom smelter, as an example, with a charge of 1000 tons per day of crushed ore averaging 7 pct copper, and 1000 tons per day of concentrates averaging, say, 35 pct copper. The crushed ore which may be considered coarse in comparison with concentrates, is fine when considering only run-of-mine ore. However, even on their crushed ore, say, $\frac{1}{8}$ to $\frac{1}{4}$ in. dimensions, there is much decrepitation and production of fines in the actual furnacing operation, so that it will be productive of finely divided particles readily carried off by the furnace-exit gas stream. Nevertheless, the major dust will be derived from the concentrate fraction of furnace feed, and the collection in a precipitator will approximate 15 to 20 pct copper, say, $17\frac{1}{2}$ pct as an average. On flotation concentrates alone the dust loss may reach 10 pct of feed. On crushed ore with appreciable decrepitation taking place, dust loss is often 5 pct and if we say $7\frac{1}{2}$ pct as an average dust loss and a precipitator

recovery of 98 pct on the copper, the distribution of copper may be placed as follows: In new feed to roaster 420 tons copper, in Cottrell collection 73.5 tons, in stack gases 1.5 tons. The latter, the stack loss, is 0.36 pct of the copper in furnace feed and it is very evident that there is the desirability of high efficiency of recovery. With copper at a market of 23¢ per lb (1948) even the recovery of 98 pct and the accompanying loss of $1\frac{1}{2}$ tons of metallic copper, or roughly $\frac{1}{8}$ of 1 pct, is an item of some interest and will bear further consideration.

REVERBERATORY FURNACES

In the past, the operation of reverberatory furnaces has varied so widely from plant to plant and from time to time in the same plant, that the majority of operators have considered their waste-heat boiler installation as a good enough collector and have disregarded further dust and fume-collecting equipment.

Reverberatory practice, however, is divided into two types, first with all feed passing through the multiple-hearth roaster, and second, that type in which the wet concentrate is directly fed to the reverberatory furnace. As is to be expected, the latter type of operation uses more fuel and has a greatly increased gas volume. Both these conditions are normally productive of a higher dust loss from furnace. In addition, however, the wet feed, although preventing dusting at charge time, is often after an interval of time productive of disruptive surface conditions due to the very rapid change of water particles to steam vapor, and this effect is productive of dusting.

A reverberatory, with roasters pre-treating its feed and working on a mixture of crushed ore and fine concentrates, is considered operating as well as may be reasonably expected if its stack loss is on the order of $\frac{1}{2}$ to $\frac{1}{4}$ of 1 pct of furnace feed in copper—about the same fraction of a percent loss in gold, and 1 to 1+ pct in silver—the latter increasing with the presence of lead fume in the gases. On the basis of a smelter operation with new copper-bearing feed of 1000 tons per day, 20 pct copper, 0.3 oz gold and 2 oz silver and present-day market (1948) of 23¢ per lb for copper, such reverberatory loss is considerable, amounting to approximately \$250.00 per day. However, 85 pct of the total value is in the copper and since the present price is nearly twice that of war-time fixed

price, it does not follow that such losses would warrant the immediate construction of high efficiency and relatively expensive recovery equipment. Perhaps it is in order to consider means for a relatively lower-efficiency mechanical recovery.

Where the reverberatories are directly fed with undried and unroasted concentrates the losses in the exit gases after boilers are appreciably greater (commonly double or even more) than stated above for calcine-fed reverberatories, and the dust collection is justified. Commonly such investment where the copper content in the feed is high, is returned within a very few years of service of collecting equipment by the value of recovery.

COPPER CONVERTERS

Generally, modern and large converters will lose from the furnace, with their exit gases, on the order of 1 to 2 tons copper per day and this may be 1 to 3 pct of the copper produced. It varies widely from plant to plant due to grade of matte, type of flux and procedure of operation.

The actual solids lost, both dust and fume, may be several times the copper loss and in lead and zinc-bearing mattes the elimination of these two constituents as oxides or sulphate compounds is almost 100 pct with the gases.

Because of the necessities of operation there is always a tremendous infiltration of outside air at the converter hoods, and thus a volume in the flue just back of the converter stands may be on the order of 100,000 to 150,000 cfm for a present-day large converter. Such excessively large gas volume, in proportion to air supplied to converter at tuyeres or to tonnage of material treated, or to weight and nature of suspended solids in the exit flue gases, makes the economic handling of converter losses a rather uncertain problem. A portion, approximately one half the total suspended solids, is relatively coarse particles, being essentially the material expelled mechanically by the effects of converter blast, and this is substantially collected in a flue or settling chamber. The remaining fraction, however, is normally very fine and it may justify only a mechanical collector, say, with 80 to 90 pct (on copper) efficiency or it may justify an electrical precipitator of about 98 pct efficiency and perhaps, with the latter, at least twice as expensive to build.

Roughly, one can say the North

American capacity for production of copper (in copper reduction works) and in some 30 plants, approximates 1,000,000 tons per year, or at \$400.00 per ton copper, \$400,000,000.00. Certainly this is a primary sizable, and for the security and good of the country, a most important industry! On the basis of a furnace loss of 7 pct of the copper content and a recovery from the furnace gases of 96½ pct of the furnace loss there is a copper recovery in flue dust of around 67,550 tons copper, or expressed in dollars at \$400.00 per ton a total of approximately \$27,000,000.00 with a final loss from stack of about ¼ of 1 pct of original plant input of new copper-bearing material. These are, of course, quite generalized figures but show the magnitude and ability of our copper smelter metallurgists to confine their stack losses to an exceedingly small minimum through the installation and skilled use of a large variety of dust collecting equipment. The main dependence, however, is on electrical precipitation for the collection in acid-carrying gases and of the exceedingly large amount of fines which the modern flotation milling plant provides.

DIFFERENTIATION OF DUSTS, FUMES, AGGLOMERATES, ETC.

As a distinction between recoveries of copper values and those of lead and zinc in exit furnace gases, it is to be noted the copper is recovered almost entirely as a "dust," while in the lead and zinc suspensions both dust and fume are present, with the fume often the largest fraction. We define a dust particle as substantially a fragmental particle derived by percussion or crushing as the ore and fuel and flux are processed and handled through mines, mills and furnaces. It commonly has a chemical and mineralogical composition approaching that of the furnace feed. In practice the major fraction of the dust is said to average 5 to 50 microns, but blasting and crushing operations always produce a minor fraction below the 3 or 5 micron range and a minute portion may be not over or even less than 1 micron.

A very special suspension product results from solid carbonaceous fuel combustion. This runs in composition from the raw coal and partly burned particles of fuel to tar fogs, soot, soot agglomerates, fragmented ash particles and the fused, rounded and commonly hollow particles, the so-called "fly ash" of powdered-fuel suspension combustion. The fly ash particles cover a fair

range in size but a goodly portion are on the order of 1 micron, and broken sphere fragments less than a micron. Other than the tar fogs they are all solids and do not represent a volatilized product but no doubt some of the finer carbon or soot particles, before agglomeration has taken place, are products of decomposition, probably carrying with them traces of actual tar, and may be looked upon for size and function, too, as "fume"-like or "fog" particles.

Fumes, as compared to dust, are constituents or compounds as of or from the charge, vaporized in the hottest areas of the furnaces and chilled to a solid form out of contact with walls. These fumes bear no physical resemblance to the new materials of furnace feed, often existing in the flue gas suspensions as an "igneous concentration" product. They are generally assumed to be of rounded form and of exceedingly small diameter, from a few hundredths of a micron to one micron in diameter or occasionally somewhat larger. There is always an appreciable agglomeration present, probably due to the effects of electrical charges on the solid particles occurring in fume-laden gases. Similar agglomeration effects are to be noted in liquid suspended particles, that is, in mists and fogs. Examples of the latter are tar and acid fog. The effect of agglomeration or of agglomeration and coalescence is to produce fewer and larger particles and thus increase the settlement rate.

LEAD AND ZINC FURNACING UNITS

Lead and zinc reduction works, in the roasting and reduction departments, produce both dust and fume, perhaps to the gross amount of 5 to 10 pct of the new metal-bearing material to reduction works, but thanks to modern development in dust and fume-collecting equipment, including both baghouses and electrical precipitators, actual stack losses in modern lead smelters and zinc works of the electrolytic type, including the roasting or sintering operations essential thereto, may be on the order of a small fraction of 1 pct of new metal input. In fact these enterprises today rarely are in trouble from dust-fall, but doubtless some who do not convert their SO₂ production into acid, or liquid SO₂ or elemental sulphur, do have what is termed an SO₂ problem.

IRON AND STEEL WORKS

Our main mineral wealth producers here in the West have, in the past,

been our lead, zinc and copper enterprises and therefore we have been particularly interested in their dust problems. However, we have, within recent years, developed several plants in ferrous or iron metallurgy and these plants have dust problems, quite as great in volume and weight as copper and lead smelter enterprises, but with values in the collected products for which most iron smelter men are entirely unwilling to set any worthwhile figure. Nevertheless, modern iron and steel plants are eager to clean their combustible gases from blast furnaces and coke ovens and public officials look with concern at open hearth stacks and sintering machine stacks with large and objectionable "plumes."

There are three main sources of dust-bearing furnace gases passing to atmosphere in an iron and steel works, first the iron blast furnace, second the sintering machine and third, the open hearth reverberatories. In plants of a generation ago, there were only the crudest, if any, dust and fume-collecting devices on blast furnace equipment. From the stack discharge gases from the blast furnaces, the stoves and adjacent boiler plants burning the blast furnace gas, there was almost a rain of reddish colored dust, giving the blast furnace a most undesirable reputation. Today, however, all modern plants realize the savings and benefits of clean gas in stoves and boilers, and even greater economic advantages are secured in plant operation by burning the low Btu blast furnace gas under coke ovens, and the high Btu gas from coke ovens in domestic or steel plant operation. For by-product coke oven service the blast furnace gas must be practically as clean as outside air, the usual specification calling for not over 0.002 grains of solids per cf of gas calculated at N.T.P. Almost equally important is clean gas for modern closely spaced checkerwork of the blast furnace stoves, but here a specification not quite as rigid as considered necessary for use in coke oven combustion, is permissible and the usual figure is stated as not over 0.007 grain per cf as calculated to N.T.P. conditions. To accomplish the degree of cleaning, the usual current design calls for (1) a dry dust settler adjacent to the blast furnace providing a 180° turn for the gases, in other words, an impingement type dry cleaner; (2) such dry dust collector to be followed by an efficient wet scrubber, usually counter-current type in baffle or tile packed chamber; (3) the scrubber to be followed by a

wet or film-type electrical precipitator. The dry dust collector may have an inlet concentration of 10 to 15 grains per cf, an outlet of 3 to 5 grains per cf, the scrubber with an inlet which is the outlet of the dry dust catcher and an outlet of 0.25 to 0.3 grains per cf and lastly an electrical precipitator with an inlet concentration of the scrubber outlet and precipitator outlet concentration of 0.007 grains per cf. These correspond to average efficiency for each piece of series-operating equipment and as developed only on its own average inlet and outlet concentration, of approximately 70 pct for the dry dust collector, 94 pct for the scrubber and 97 pct for the precipitator. The precipitator collection is substantially all fumes, largely those of the alkali or alkali-earth compounds but occasionally fumes of zinc are present.

The economic results of this train of dust and fume collection equipment are very considerable indeed. Clean gases to stoves mean nearly theoretical combustion, with high heat; no suspended solids in gases permits close packing of brick work and greatly increases the storage and release of heat, and the absence of any fine deposits upon the checker work permits rapid accumulation of heat and its equally ready release. Thus the furnace is better served and responds by greatly increased uniformity of operation, by increased daily production or greater capacity and by simplicity and ease of handling. These are not readily-figured benefits over one day's operation, but over several years provide noteworthy economics of operation and the maximum of production.

The numerous reheating and soaking pits of a steel works do not commonly discharge visible or appreciable quantities of suspended solids but the sintering plants and open hearth furnaces are at times producers of considerable clouds of dust with some fume. These pieces of plant equipment, in their stack discharge, reflect the nature of the dry feed to the furnace; where there is much fines there is corresponding furnace loss, where there is fume-making material (for instance, galvanized iron scrap) a fume discharge will be evident.

The open hearth reverberatories, in particular the newer and larger units, say 100 to 150 tons of steel production per charge and above, are now very generally being equipped with waste heat boilers. Such boiler installations in themselves are fair dust collectors and provide the very decided additional

advantage of cooling the furnace exit gas volume and thereby correspondingly decreasing the gas volume to be handled, so that additional collection means after the boilers are relatively easily supplied and installed. In reverberatory furnaces where blast furnace pig iron is a major constituent of the feed it is also common practice to add iron ore as a means of effecting the combustion of the carbon of the pig iron. At the time of feeding that charge to the reverberatory and perhaps for an hour or more thereafter, there will be heavy reddish stack discharge. This is not a serious loss as regards weight of materials or of values at the furnace but it is certainly one of the items that give the steel works an evil name as a maker of community dust. Reverberatory furnaces, depending upon their size, condition of feed or of fineness and fuming characteristics, and degree of "hard driving," range in dust loss from around 2 tons per day in a small hearth to around 10 tons of furnace dust loss per day in a very large furnace. As in a great many cement plants, it has been the practice to provide one chimney for each furnace, and this practice adds to the cost and inconvenience of any form of dust collecting devices. Once the procedure is adopted of installing waste heat boilers on each reverberatory and bringing all the boiler exit gases to a central point for treatment, the cost and feasibility of dust and fume collection installation will be greatly simplified, which makes for the minimum of expense. It is evident that one central recovery plant will cost less and be easier to handle than several individual dust recovery units.

The sintering machines in use at iron works are of comparatively recent introduction. The usual type is commonly provided with a large diameter, horizontal type of cyclone which serves to collect a coarse constituent of suspended material passing the grates; but in general, when fine ore or flue dust constitutes a major element of the sinter feed, there is a nuisance stack loss if not an important material loss. This equipment will receive due attention for dust collection along with the reverberatory department if and when the collection question is not one of plant economy but one of community betterment as regards appearance, cleanliness, saving in wear and tear, and the like. The installation of collecting equipment is neither more nor less pressing than in many other industrial operations or plants, such as cement plants, modern powdered-fuel-

fired power plants, railroad yards, handling equipment and the like.

CEMENT PLANTS

Cement plants are large producers of dusts and fumes in their furnace gases, as would readily be expected from the nature of their operation. This operation includes preparation of a furnace feed of exceedingly finely ground limestone and clay or shale, 86 to 90 pct or above of minus 200 mesh (a 74 micron particle size just passes a 200 mesh screen), and the furnacing of this mixture to a point and temperature sufficient to produce a sinter. Commonly the prevailing temperature in the clinkering zone of the kiln is in the range of 2500 to 2700°F. On the basis of 600 lb of raw mix to 1 bbl finished cement, dust losses in stack discharges have been reported all the way from 10 to 120 lb per bbl. Needless to say the latter is abnormal, and good plant operation will not long permit such a loss. However, 30 to 40 lb per bbl kiln loss is quite ordinary and at 40 lb per bbl and 5,000 bbl per day the kiln dust loss (not stack loss) per day is 100 tons.

In former days of cement plant operation, before government regulations became the dominating and costly practice they are today for all of us, manufacturers were disposed to figure the value of their clinker so low that they were reluctant to give worthwhile values to the recovered kiln discharge dust. Today, however, with high labor and operation costs and still higher prices for cement, the dust becomes of considerable value to the producer—such figures of \$1.00 to \$2.00 per ton, occasionally more, being the practical basis of consideration. Since the U. S. production of Portland cement for 1947 is given as 185 million bbls it is evident we are talking of a kiln dust loss of over 3 million tons per year. It is to be understood that not all this dust reaches the atmosphere and is distributed around the surrounding community as a rain of dust, for the great majority of cement plants have some provision for collection. Their dust-collecting equipment runs all the way from an enlarged kiln-end housing or a boiler setting to an electrical precipitator, and includes baghouses or settling chambers, scrubbing systems, or one large or several small cyclones. On the whole, good collection service is provided by the industry. Possibly over half the total dust produced is collected—between one and two million tons per year.

POWER PLANTS

A field somewhat similar to that of cement manufacture as far as large gas volumes and dust loadings are concerned, is that of the new powdered fuel-fired-boiler power plants. Units in this field are ever growing larger and boilers producing 1,000,000 lb of steam per hr, are being built with corresponding gas volumes of around one half million cfm at the average prevailing temperature of about 300°F. In the earlier powdered-fuel power plants and even in some modern ones upwards of 90 pct of the ash in the coal is discharged with the stack gases. The practice of burning coal in suspension has permitted the use of coal, without combustion difficulties, much higher in ash content than formerly was permissible. This, no doubt, along with the tremendous size of the modern power plant, has led to the very general complaint of the discharge of chimney solids (fly ash). As an example, take a power plant of a million kw capacity burning 12,000 tons of coal per day of possibly 12 pct ash, and assume 75 pct of ash in chimney discharge and not the 90 pct which has been occasionally reported. There results a stack loss of fly ash, so named, of approximately 1000 tons per day. Part of such stack loss is excessively fine, with many 1 micron particles, and usually 1/3 of the total dust particles are less than 10 microns in diameter. While American practice has favored the dry collection and predominantly that by the Cottrell process of electrical precipitation, the English have leaned toward the scrubber types with neutralization of the acidity resulting from sulphur dioxide collection.

In a British power plant³ which has been reported in successful operation with better than 95 pct removal of dust and sulphurous acid from plant gases, the neutralization has been effected by use of a mixture of lime and limestone so that the active neutralization agent is reported as the bicarbonate of lime. This operation of neutralization, they state, is accomplished without the building of caked material, or scale (which we assume is a bisulphite salt) of the usual and very serious insoluble and voluminous calcium deposits so commonly encountered in non-precisely controlled scrubbing of waste gases containing SO₂ with suspended lime or limestone in the scrubbing liquor. Past experience in attempts to scrub the dust and sulphur-bearing compounds from cement plant gases does, indeed, make one most hesitant to accept with-

out thorough proof any scrubbing scheme for sulphur-bearing dust-carrying gases in which the neutralization is to be accomplished with a lime compound, and where the assumption or the assurance is given that no serious build-up of lime-carrying deposits will occur.

All indications point to more severe restrictions as to stack emanations from power plants and city factories for the future, and it is well if it is so understood by technical staff and plant management and plans and equipment are provided to accomplish the desired end. A statement was made some years ago by an English investigator that the damage resulting to structures, furnishings, clothing and health of the people was not less than 3/4 shillings for every ton of raw coal burned. Since at that time 3/4 shillings probably equalled about 55¢ of our money, it is easy to figure raw coal combustion without treatment of discharge combustion gases as running to hundreds of millions of dollars. The damage and nuisance and unpleasant results of raw untreated coal combustion are, of course, open to a wide range of interpretation, evaluation and even argument and one whose interests are normally technical is well advised to be cautious and conservative in his figures and remarks.

GENERAL

In the preceding account there has been covered in a brief and general discussion the losses of wastes from stacks and chimneys of metallurgical operation of industrial and power plants. Stack losses for the entire United States, without the incorporation of present-day quality and recovery equipment of industry, smelting and power plants, would easily reach a billion dollars or more per year in values. With suitable equipment installed to collect suspended solids from furnace and industry exit gases, community savings of the above amount may be effected. Nevertheless, for health, for community, for good house-keeping and for the acceptance of the responsibility to be a credit to the community, which every industrial plant really plans to provide, there are required still further effort, expansion and investment for suppression or collection of vent or stack emission.

II—Particle Size

If one would understand the problem of handling, controlling and collecting suspended particles in gases,—aerosols

as they have been termed—it is necessary to have a mental picture of the relative sizes and the special characteristics that go with such range of particle sizes. Over the years various relationships have been developed by one observer after another and these scattered data have been gathered into a very useful chart (Fig 1) by C. E. Miller and published in *Chemical and Metallurgical Engineering* in March, 1938 (p. 113). Due to the large amount of convenient and related information, this is reproduced here for convenience and by the courtesy of the publisher, McGraw-Hill Co.

It is of interest to point out several of the interesting features of this chart compilation. Reference to the lower left hand corner shows the relationship of standard screen size as compared to micron sizes. The particles just passing a 325 mesh screen are approximately 44 microns in diameter and while this is about as fine as one cares to go with screen sizes it is to be noted that 44 micron is still in the first third of size range given and such 325 screen, passing a 44 micron particle, is just about midway point or the sizes of many industrial operations, for example, sulphide ore, flotation pulps, pulverized coal, combustion ash (flyash) cement, and others. It will be noted few dusts go as low as 1 micron but many fumes and mists (including fogs) go down to about 0.02 micron, for instance, zinc oxide fume, tobacco smoke, and oil smoke. A half micron particle is nearing the edge of visibility with the most powerful optical microscopes and at 0.1 micron diameter particles show Browning movement and thereby display no tendency to settle.

To place the respective diameters and rates of fall in figures more common to our experience, Table 1 taken from Gibbs⁴ and here somewhat extended to express the rate of fall both in foot per second and miles per hour is presented.

Table 1 . . . Particle Diameter vs. Rate of Fall (Spherical and Still Air)

| Diameter of Particles | | Mi-crons | Rate of Settling | | |
|-----------------------|------------------|----------|------------------|---------|--------------|
| | | | Cm per Sec | Fpm | Miles per hr |
| Screen Size* | Cm | | | | |
| | 10 ⁻² | 100 | 30 | 59.0 | 6.711 |
| | 10 ⁻³ | 10 | 0.3 | 0.6 | 0.06711 |
| | 10 ⁻⁴ | 1 | 0.003 | 0.006 | 0.00067 |
| | 10 ⁻⁵ | 0.1 | 0.00003 | 0.00006 | 0.0000007 |

* Tyler Standard screen size, 200 mesh = 74 micron; 325 mesh = 44 micron.
† Approximate, size of opening in mesh to pass 100 micron (spherical) particle.

It is obvious from Table 1 that a mild breeze, of about 5 miles per hr, would permit settlement of only 100 micron particles or those rounded particles passing a 150 mesh screen; and for 10 microns diam and below, no settlement should be expected in the ordinary always-moving air currents about us. It is therefore a welcome and well-known phenomenon that atmospheric particles below settlement size are continually agglomerating into larger particles and in due course of time do settle. Observing the ordinary Tyndall beam and the huge mass of floating particles observable therein it is a satisfaction to realize that there is not a continuously increasing density of particles and that normally the Tyndall beam reflects an equilibrium condition wherein about as many old particles are agglomerated and removed by settlement as there are new particles entering the beam. The dust particles usually seen in a Tyndall beam are from 1 micron downward and that fraction from about 1/2 micron downward is invisible individually. However, when sufficiently concentrated into masses, the appearance is that of a cloud.

Two types of suspended particles are of particular interest to those whose activities in mining and smelting operations are in the West, and in the non-ferrous field. The first of these is silica dust, which in a certain size range has a health hazard. On the Miller chart the range is given as from 10 microns with a lower limit somewhat indefinite, as there is a question mark showing at 0.25 micron; others give the danger size range as from 5 micron to 1/2 micron. More particular mention will be made of this under a later division of this paper. The second type of suspended particle is white SO₃, (or SO₃ · xH₂O) a so-called "fumé," but in actuality a fog or mist that escapes in such tremendous volumes particularly from our copper plant stacks. On Miller's chart the diameters of these SO₃ particles are given for the range of approximately 3 microns down to 1/2 micron. One series of interesting investigations of size of fumes for a number of products such as ammonium chloride, sulphur trioxide, phosphorus pentoxide, sodium peroxide and the like, were carried out about 25 years ago by H. Remy⁵ in Germany. He followed the size change from formation until it was "aged," that is, agglomeration took place. He found these fume products aged very slowly after formation about 1/2 micron in size and that on "aging," that is agglomerating and

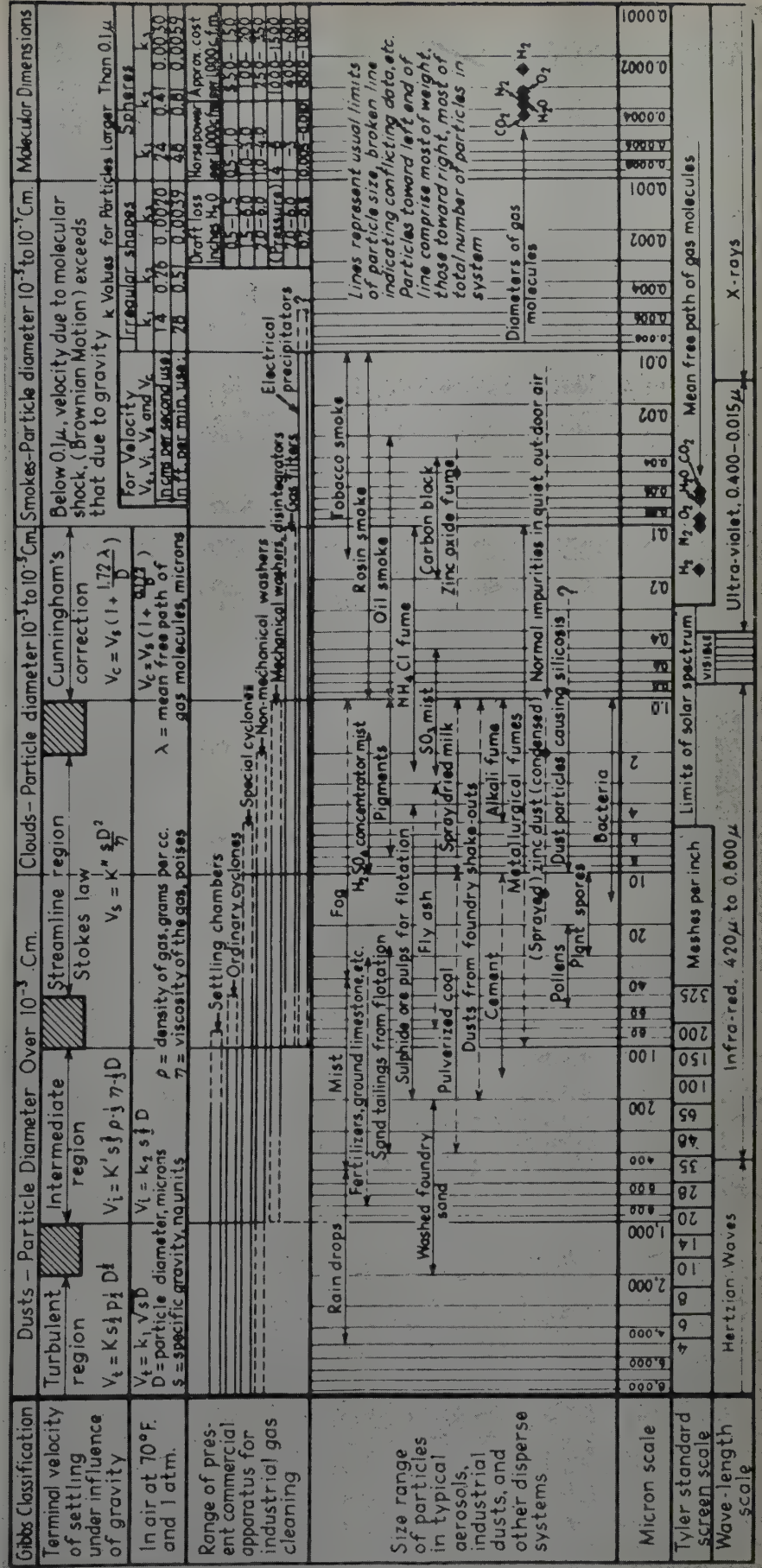


FIG 1—Summary of properties of some typical aerols. Size relationship to physical characteristics.
Compiled by C. E. Miller, *Chem. and Met. Eng.* (1938) 45, 133. (Courtesy Chemical and Metallurgical Engineering.)

settling, they were somewhat over 1 micron in size. It is to be interpreted that if the settling distance had been that of many feet instead of the inches of his glass vessel, the agglomerates would have still further increased in size to the upper limits we often detect on a slide of settled fume, that is, to 3 microns or more.

III—Dust and Fumes in Community and Individual Living

One who worked around our Western mines and lead smelters about 40 years ago noted a general indifference to possible health dangers. There were cases of silicosis on the one hand and lead poisoning on the other, occasionally both in one individual. Similar plant visits today make one realize the great advances that have been made in today's practice. Nevertheless, we still have a long way to go to reach desirable working conditions that are free of health hazards. Much of the betterment has come from understanding the necessity of proper ventilation and the installation and operation of proper equipment plus the equally vital understanding that cleanliness is an important consideration. Particularly around lead mines and smelting enterprises it is essential that simple health measures be enforced; such as the washing of hands before eating, the shower bath at the end of a shift, and changing and washing of underwear and work clothing. The reduction of incidence of lead poisoning by such measures is striking, and one has only to remember the poorly-kept plant of earlier years and compare it with an intelligently operated mine or plant of today to realize the change.

The average productivity per man hour in a well-run lead smelter or lead mine or in the handling and treatment of relatively high silica carrying ores, is more than sufficient to cover the costs of good working conditions, and in not a few places makes the difference between a profitable and nonprofitable operation.

Where it is a matter of health hazard there is the greatest anxiety to be certain and precise on the atmospheric content and character and state of subdivision of the suspended solids. In spite of a vast amount of endeavor, the development of many types of equipment and practices and procedures for particle counting and particle-collection weighing, there has resulted no one

method of procedure or equipment which may be called standard. Dust and fumes differ enormously in their collection characteristics, and while one type of equipment may give the most consistent and most accurate analysis of dust content in a given gas, it by no means follows that it will serve with equal fidelity on another type of suspended solid, or in a greatly changed set of conditions even with the original suspended solids. Therefore it may be said that there are some uncertainties still existing in reporting suspended solid concentration by any of the half dozen or more widely used types of apparatus.

Added to the problem of equipment is that of whether the basis should be expressed as the number of particles in a given gas volume or the weight of the suspended solids. The problem may be visualized by considering 1 cm cube of quartz and subdividing it into cubes of 1 micron edge length. The original 1 cm cube has 6 sq cm of total area while the equivalent mass in 1 micron cube has 6 sq meters and the number of micron particles becomes 10^{12} or a million million. On the basis of 100 million particles per cf of air the 1 cc of the original quartz would be dispersed in an air volume of 10,000 cf.

Health authorities in investigating the hazards of occupation have leaned to the consideration of a count of number of particles rather than weight on the basis that the relatively coarse particles and that portion of the fines below about $\frac{1}{2}$ micron are not relatively reactive to lung tissue; the coarse, because the moist and hair-like lining of the air passages collects and removes them, and the very fine ($\frac{1}{2}$ micron and below) because they substantially conform to the characteristics of gases and move in and out of the lungs without chemical action with the tissues.

In a practical sort of understanding the particle counters and the weight followers have agreed that 1 mg of crushed quartz material contains about 300 million particles.⁸

The count-the-particle investigators are largely responsible for our laws on permissible concentrations of dust particles per cubic foot of air and such specifications are for particles which are less than 10 microns in diam as counted on microscopic fields. For example, the State of Illinois⁶ through its health department specified permissible limits of dust by count as follows:

Total dust—50 million particles per

cf of air.

Free silica—5 million particles per cf of air.

Asbestos—5 million particles per cf of air.

Silicates—5 million particles per cf of air.

Alundum—15 million particles per cf of air.

Carborundum—15 million particles per cf of air.

Particles counted in microscopic field are limited to the all minus 10 micron sizes. Immediately after firing a blast to break rock in almost any hard rock mine a dust count will show about 50 million particles per 1 cf and it is usually necessary to reduce this to around 10 million particles in order to keep to 5 million or under of silica. Such a specification as this involves extended studies in mine ventilation. Allowable settling periods, use of sprays, bags, filters and the like all help to reduce the particle concentration to an acceptable figure. It seems the old days of one shift a day at a mine, blasting at end of shift and allowing 8 to 16 hr for workings to clear of dust particles resulting from the use of high explosives, are passing, and in our large low grade underground operations it is customary to work around the clock. Whereas in the old days a full shift was required to move the broken rock, substantially all by hand power, nowadays with a modern mucking machine the broken rock is removed in a couple of hours. Equally reduced is the drilling cycle and thus the opportunity for natural settling of rock particles is greatly lessened in comparison with the old days, and an acute problem in maintenance of limited dust concentration confronts the modern operator of larger tonnage in the lower grade ore mines.

IV—Means or Procedures for Dust and Fume Collection. Both Test or Laboratory Equipment and Commercial Installation in Mine, Smelter, Power-house and Factories

The type of equipment effective for collection in commercial operations varies with the fineness of the suspended particles as will be noted by reference again to the Miller chart. That chart indicates 5 fundamental types of equipment, *viz*, (1) settling chambers (including wire-hung dust chambers), (2) Inertial or cyclonic

equipment (including baffled chambers and many types and kinds of cyclone collectors), (3) Spray chambers and/or scrubbers, (4) Filters (baghouses), (5) Electrical precipitators. A 6th, however, is on its way, industrially, and that is supersonic precipitation. For test work, little use is made of cyclone equipment if very high or complete collection is the end object, but the other four procedures mentioned are all used in test and laboratory work and in a large number of modifications. Two additional procedures have had considerable study: (1) thermal precipitation, and (2) impingement on a prepared surface with the particular object of counting the particles as they appear on a glass slide under suitable magnification. Impingement on liquid wet wall surfaces in a bath is also used for weight samples by health authorities.

Due to the protracted discussion required for any worthwhile review of the test methods proposed and used, which would unduly lengthen this paper, it is felt those particularly interested in this field should consult the extensive literature available.^{7,8,9,10}

However, it is worth our while to consider some cost figures in commercial operations and respective efficiencies of the several types of collection equipment. You will note on the Miller chart several small tables on the right giving draft loss, power requirements and cost per 1000 cf of gas treated and, except for the cost item which needs to be doubled or more for today's installation, the data are quite in line.

It is cheapest to collect only the coarsest dust and here, if we can afford to pass everything on the order of 100 micrograms and finer, a settling chamber is the most economic type of equipment. However, you will note from the Miller chart that 100 microns or 150 mesh is less than halfway along the range of usually suspended dusts in the majority of industries. Note, for example, sulphide ore pulps from flotation, foundry dusts, cement, fly ash and the like. Of course such settling chambers have low draft losses and corresponding requirements for power are small (commonly a stack is sufficient) but, if a fan is required, it may be for ½ in. or less of draft loss and require ½ hp or less per 1000 cf of gas treated. As far as the writer knows, no enterprise having a modern dust problem has attempted to solve it by settling chambers during the last 25 years or thereabouts. Such settling chambers as are used today are inci-

dental—for example, a particularly large flue originally constructed and in anticipation of greatly increased plant size. One device, making use of the fact that decreasing the distance of fall increases collection, proposes a chamber with large number of superimposed shelves spaced a few inches apart—the Howard collector. At one time it was of particular interest to acid manufacturers using pyrites to prevent pyrites cinder from reaching the Glover tower. However, the restricted spacing between plates resulted in much trouble from choking of passageways so that gradually their use was abandoned.

Quite the contrary development has taken place with regard to inertial or cyclonic type of equipment. Special designs and modifications, almost without limit, have appeared during the last 15 to 20 years and many of these have added to the efficiency and range of fineness susceptible to collection by centrifugal equipment. Probably the most notable advance has been the recognition of the importance of decreasing the diameter for increasing efficiency and offsetting the capacity loss per item of equipment by using a multiplicity of cyclone units instead of one on a given gas volume. A number of investigators have reported such studies in various technical society proceedings or in the technical press, to which those desiring more details should refer.^{11,12,13} Some of these special cyclones do good work on particle sizes appreciably below 10 microns, although there is also an escape of 10 microns and minus 10 micron particles. The basis of these newer studies on effect on recovery are well illustrated by a table prepared by Evald Anderson¹⁴ which sets up the increased gravitational pull as the radius of collector is decreased from a 10 ft radius to a 1.5 in. radius while maintaining, through all changes in radius, a 60 fps tangential velocity (Table 2).

Table 2 . . . The Centrifugal Separating Force in a Circular Gas Stream with a 60 fps Tangential Velocity for Different Radii, Expressed in Terms of Gravity, that is, Gravity = 1 in.

| Radius of Curvature of Gas Path | Separation Force |
|---------------------------------|------------------|
| Gravity..... | 1 |
| 10 ft..... | 11 × gravity |
| 5 ft..... | 22 × gravity |
| 2.5 ft..... | 45 × gravity |
| 1.0 ft..... | 112 × gravity |
| 6 in..... | 224 × gravity |
| 4 in..... | 336 × gravity |
| 2.5 in..... | 548 × gravity |
| 1.5 in..... | 896 × gravity |

The above appears almost too good, but as a practical consideration there

must be taken into consideration the turbulence existing at the interface of the stationary cylindrical wall and the high-velocity centrifugally-moving gas stream. This is of considerable magnitude and lowers the collection or separating efficiency. Pressure drop is an important consideration on all centrifugal equipment and in general, at least up to 6 or 8 in., efficiency is improved by increasing pressure drop. Commonly such equipment runs at pressure drops of 1½ to 6 in., and doubling the cost figure given by Miller for 1000 cf of capacity is in order, viz., \$200.00 to \$400.00 per M. of gas treated.

SCRUBBERS

Of extraordinary extent of field of application, varying from simple to complex design, and from small to extraordinary large power requirements are *spray chambers* and *scrubbers*.

Their service is, of course, limited to materials or products which it is permissible to wet and collect as a sludge, and if ordinary steel is to be the structural material, then only to that type of gases with their suspended solids which are not acid, or if acid then with a continuous addition of neutralization agent as a protection against corrosion. The simplest of these starts with a spray in a flue or a stream of water running over grid or lattice work and ends at the combined cyclone-scrubber construction of Theisen,¹⁵ the Pease-Anthony¹⁶ and the very recent Venturi scrubber.¹⁷ Both the Theisen and the Venturi scrubber perform excellent service on very fine materials such as the fines present with the dusts and fumes from black liquor furnace combustion of kraft paper mills, the fumes and fine dusts of open hearth steel manufacture, iron blast furnace gas and the like. Their handicap is the large power requirement to drive the special-bladed Theisen scrubber runner, or the power required to provide the pressure drop and high gas velocity in the throat of the Venturi scrubber.

It will be noted in the Miller chart that the "Mechanical Washer, Disintegrators" cover the Theisen, and the latter is often known as a "disintegrator." The Theisen has an efficiency of recovery practically to the 1 micron size and it will also be noted the power requirements are on the order of 4-6 hp hr per 1000 cf. Many of the old Theisen washer-disintegrators handling iron blast furnace gas required power on the order of 500 to 1000 hp

and the gas leaving the Theisen disintegrator was clean enough for use in gas engine operation.

This Theisen scrubber was developed about a generation ago and, disregarding its heavy power requirement, has not been equalled by a scrubber of any other type up to very recently. However, within the last few years the Venturi scrubber followed by a Pease-Anthony scrubber has shown a capacity equal to the Theisen to collect fine particles, for example, soda fume from paper mill recovery furnaces, and fumes from reverberatory steel furnaces, with an overall efficiency of around 98 pct. The equipment, however, is about on a par with the Theisen as to power requirements and pressure drops—for example, on a paper mill, the combined Venturi-Pease-Anthony scrubber gas collecting sodium compounds, largely as fumes, and for a gas volume of some 45,000 cfm, required an induced-fan motor unit of between 225 and 250 hp.¹⁸ The velocity of gases in the narrow section of the Venturi was about 300 fps and the pressure drop across the Venturi section something over 12 in. of water gauge. Its good efficiency is proportional to the power consumed, since the latter expresses the energy necessary to break up the water into independent small particles and it has been stated that, for good collection, the water particles should be reduced in size so that the diameter ratio between water particles and suspended dust or fume particle is not greater than 10 diam for the water to 1 diam of solid particle. It is evident if one is trying to collect particles of 1 micron and less a very fine subdivision of the wash waters is required and both the Theisen and the Venturi do that very thing but at a corresponding expense for power.

Packed towers (with coke or tile) have always given a good account of themselves but their efficiency is quite largely dependent on the pressure drop which again represents a power consumption to subdivide the water or increase its total surface, and the weakness of these packed towers is their tendency to choke with deposited solids.

The simplest design of scrubber, a coarse spray in a tower, is a good gas cooler but, except for the coarser particles of dust, is a poor collector. It uses relatively little power.

FILTERS OR FILTRATION

Filters or filtration, as a means of dust and fume recovery, are very widely

used throughout industry, largely as baghouses. The temperature limit is quite low—for cotton bags it should not exceed 200°F and for woolen bags 250°F. Acid gases or corrosive compounds, of course, greatly shorten the life of bags but in very low concentrations or after partial neutralization, are encountered in many gases going to bag houses, for example, lead smelter gases.

A newer material for bag manufacture has become available during the last 10 years and gives promise, indeed, of great future service. This is glass fiber cloth, and while the earlier material tended to plug, new methods of weaving and new physical types of thread appear to offer fabrics having the filtering characteristics of wool, that is, filtering on the surface rather than through the pores of the medium. Present price and delivery are perhaps drawbacks but undoubtedly the future use of material such as woven glass fibers for baghouse service will become much more general, both for large and small units.

Bag house operation is generally on a basis of about 2 in. of draft loss but some are made to operate on 6 to 8 in. One difficulty is the passing of fume-like material through the bag weave at high pressure loss, while the same material may be satisfactorily collected at lower pressure drops, say 1 to 2 in. Cost of good baghouses or filter chambers are commonly less than electrical precipitators but still on the order of two to three times that of the best designs in centrifugal equipment. Filtration with a nearly new bag properly coated with a filter layer of particles removed from the gas stream and at a reasonable pressure drop is nearly perfect, that is, nearly 100 pct. The efficiency varies downward from this as the bags get old and worn, or as pressure drop is increased and as rapping or shaking of bags must be done to prevent buildup of flow resistance across the bag wall. In bag house operation, where the bags are being shaken or rapped at regular intervals of time, there is usually to be noted a good "puff" to atmosphere as the rapping period starts. Some test work would indicate as very good practice a 95 pct collection efficiency, considered over a period of baghouse operation.

ELECTRICAL PRECIPITATION

The last of the commercial types of equipment to be discussed is the *Electrical Precipitation* of suspended

particles in gases, perhaps as well known by the name of its inventor, the Cottrell process, after Dr. Frederick G. Cottrell, former professor of physical chemistry of the University of California, Berkeley.

You will observe from Miller's chart that its limit in degree of fineness of the material which it can collect far exceeds any other device or method of collection considered. Tobacco smoke, which is a tar fog, plus some carbon particles, is given a particle size of from 0.15 down to 0.01 micron, individually far too small to be seen under the highest magnification of a microscope. It has been stated that in the visible cloud exhaled from a cigarette there are some 5 million particles of tar fog per cc. In a laboratory apparatus the instantaneous precipitation of such tobacco smoke is quite a striking demonstration of electrical precipitation.

Strange as it may seem, the electrical phenomenon of precipitation as the result of a high potential direct current discharge and field, was a very early discovery. Hohlfield, in 1824, noted that a bottle filled with smoke and with a wire led into the bottle through the cork, could be almost instantly cleared when the knob of a charged Leyden jar was made to contact the wire into the bottle. That was at a date in history in which electricity was truly still a mystery and the only known way to generate it was the rubbing of a glass or wax rod with a silk or wool cloth.

As an industrial process it did not become of interest or successful until Cottrell, in the early years of this century,¹⁹ applied our modern electromagnetic means of producing abundant high potential electricity. It is true a first effort was made at industrial application by Sir Oliver Lodge and associates in 1884-5, in attempting the precipitation of lead fumes in a lead smelter flue in Wales. His source of electrical power was a Wimshurst machine (developed in 1881) of two 5-ft glass plates driven by a 1 hp steam engine. We know now that such a Wimshurst machine could energize only a few inches of a pipe electrode and that to handle successfully the gases from an average lead smelter requires thousands of feet of electrode pipe and perhaps 50 to 100 kw of installed high potential electrical equipment for service therewith. The conversion of high potential alternating current readily obtained from modern power plant equipment into direct current (true, of an intermittent or pulsating type) by

means of a synchronous rotating make-and-break switch, was a major contribution by Cottrell and by this means he was enabled to pass to his electrically insulated high potential discharge electrode the necessary power to provide the electron or corona glow essential for dust charging and static precipitation.

While electrical precipitators for dust, fumes, mists and fogs have been built in a great variety of size, shape and outline designs, in essence they conform closely and are commonly either of plate or pipe design. The spacing between plates or the diameter of electrode pipes varies generally from 6 to 12 in., is tied directly to the available or desirable high voltage, and the latter, for general working conditions, is specified in the range of 50,000 to 100,000 volts. Always the high potential or discharging electrode possesses elements of small diameter, that is, from a No. 16 wire up to $\frac{1}{4}$ in. rod from which there is obtained an electron discharge, commonly visible as a corona glow. Such electron emission produces a rupture stress upon the electrical neutral gas molecules immediately adjacent to the discharge electrode, and while the positive charge must fall into the negative discharge electrode, the negative charge, i.e., the electron charge attaches itself to a gas molecule and such charged gas particle under the strong electrical field between the discharge and collecting electrodes starts to migrate to the collecting electrode. As it encounters dust or fume particles it either gives up its charge thereto or the charged gas particle is adsorbed or attached to the dust particle and thereby the suspended dust or fume particle is moved toward the positive or collecting electrode. Upon reaching the collecting electrode such charged dust particle should give up its charge and become grounded and form one particle of a cake which may later be rapped or shaken down into a hopper beneath the plate electrode. The readiness of suspended particles to receive a charge, to release such charge upon reaching the electrode of opposite polarity and the mechanical adherence of deposited particles, all are modified and are increased or decreased by conditions within the gas stream. Therefore for "poorly conducting dusts" it is common to "condition" the gases and particles, that is, improve their collectability by adding to the gas stream such agents as moisture, acids, bases, salts, oils, and others. In general

each installation and the operations to which it is attached provide a special problem and require specific handling.

With the provisions as outlined above, the field of collection of industrial dusts and fumes is broad indeed and the actual application and plant installation are ever widening and the units in service always increasing in numbers.

Since its cost of installation is several times that of cyclonic equipment or a settling chamber, its use is justified only where the amount and value of recovered products are large or where the degree of gas cleaning is of the highest importance. Good examples of the latter are to be found in the gas cleaning necessary for contact acid manufacture from gas produced in the roasting of mineral sulphides, and the cleaning of iron blast furnace gas for use as a dust and fume-free fuel in stoves and coke oven retorts.

One phase of electrical precipitation not covered in the preceding discussion, is its use in the purification of air for human habitations. Here the recovery in the precipitator may be bacteria, pollen and the like, as well as minute floating particles of solids and mists. Its construction and operation vary from those of the usual commercial plant by the use of very much reduced spacing and corresponding voltage reduction and the use of very fine wires for ionization and of a double plate field for the static collection of the charged particles. It is essential in this field that ozone and oxides of nitrogen be reduced below detectable amounts, which is accomplished by the relative low voltage and the use of a static field following upon a gas and dust-charging field.

V—Description of Equipment of the Several Types Discussed Previously for Dust and Fume Collection

SETTLING CHAMBERS

In 1902 the Anaconda Copper Mining Co. completed a new copper smelter which, at that time, was the largest and the best equipped of any such type of plant in the world. In design and provision for the possibilities of the future, no plant built had had better engineering or more skill of design. Each unit of operation such as roaster, blast furnace, and converter department had its own stack and its own dust collection settling chamber. These

chambers, approximately 40 ft wide, 40 ft high and 260 ft long had a net height for dust settling of 30 ft, since about 10 ft from ground level a chamber floor was installed and below this was a system of tracks and means of dust removal and transport. Since the furnace feed, as compared with today's, was relatively coarse, comprising crude ore and the output of the best of gravity mills of the day, the settling chambers gave a very good account of themselves on the basis of copper recovery, but still there was a stack discharge which reached the valley areas well below the smelter level and several miles away, which brought on complaints of harm to livestock and growing crops. To secure still more provision for settlement, for cooling and condensing of certain constituents and to discharge the smelter gases at a greatly increased height above the valley, a combined settling chamber and flue for the combined smelter gases was carried up a hillside, the lower section being 60 ft wide, 20 ft on its side walls, both sides sloping to the middle with an underground cleanout tunnel on the middle line with 36 ft from top of flue to top of tunnel. This lower section was built approximately 1000 ft long and with a brick jack arch roof. The upper 1000 ft was made just twice as wide and twice the cross-section and with a steel top to promote condensation, particularly of the arsenic trioxide, the constituent of the stack gases to which most objection had been raised. This entire system of settling chambers and extended flues comprised about 6,000,000 cf of settling space and represented a heavy investment even for those days. Due to the acid character of the gases, the only other competing equipment of that date, the baghouse, was entirely out of consideration, and the system installed did represent the best of engineering and scientific application.

Nevertheless the complaints continued and the evidence of operation indicated the inability of a settling chamber to collect satisfactorily the "fumes" or volatilized and condensed metallic compounds such as the oxides of arsenic, lead and antimony. Years later, to bring the collection of all products up to a high degree of recovery, an extended Cottrell or electrical precipitation installation was built to operate in series with and after the settling chamber system. Its collection, largely fumes, brought the overall recovery of both dust and fume from

furnace to stack to the present highly efficient operation.

An interesting modification or improvement of the simple settling chamber is the wire-hung dust chamber of which the largest was that installed at the Boston and Montana Company's Smelter plant at Great Falls, Montana, in 1908 or 1909.²⁰ As a matter of fact a wire-hung dust chamber is really a combination of a settling and an inertial type of recovery equipment, since the gas stream in striking the wire must sharply turn while the dust particles move forward and strike the wire surface, yielding their energy thereto and falling. This wire-hung dust chamber was 177 ft wide, 367 ft long, 21 ft high. It had a completely hoppers bottom (over 1000 hoppers) with wires attached to and guided by heavy screens of about 2 in. mesh. Over one million wires in two banks were hung in this chamber. A mechanical rapping device was provided for the suspended system of vertical wires. Its collection efficiency, on total solids, was about $3\frac{1}{2}$ times that of the simple open dust chamber and it undoubtedly collected more efficiently on the finer fractions; but in course of time, due partly to shutdown periods and consequent corrosion, it was found too expensive to maintain the wire hung feature of construction and the wires were removed. This settling chamber, without its wires, operated for a number of years but eventually was replaced by a Cottrell, the latter making use of hoppers and supporting steel work of a portion of the old chamber.

INERTIAL OR CENTRIFUGAL

For the inertial or centrifugal type of collectors it is proposed to discuss briefly three installations, two on boiler plant gases and one on converter dust recovery.

Modern combustion of coal in a power house required the coal to be finely ground and then burned in suspension. This results in most of the ash appearing in suspension in the gases as finely divided small spheres, some hollow, and of which a fair proportion—say a third—may be in the size range of 1 to 10 microns. The percentage of the ash leaving the boiler as so-called "fly ash" is usually better than 80 pct of the total ash and occasionally some plants get into the 90 pct class of ash to stack gases. While the huge central station plants with their requirement of overload for limited periods have generally, in the past, used electrical precipitators, some of

the new plants today are choosing a combination of cyclonic tubes followed by an electrical precipitator. This mechanical collector between the boiler and the precipitator, for a 1,000,000 lb per hr boiler with over 400,000 cfm of flue gas, comprises a series of Multiclone units all operating in parallel from a common flue of boiler width, there being 5 units of Multiclones, each unit with 156 tubes in parallel position, the tubes being of a uniform inside diameter of 9 in. and each tube provided with a stationary cyclonic vane at its top and inlet heading.

Plants of an industrial nature are not usually so severely restricted as to amount of emission and an example without the auxiliary electrical precipitator, in series, is a sugar mill at Vancouver, B.C. It is an excellent example of a reasonable efficiency utilizing a small-diameter type of cyclonic collector with a multiplicity of tubes. The gases derived from three boilers at this Vancouver plant and totaling approximately 70,000 to 80,000 cfm, pass to a battery of Multiclone units, each unit of 30 tubes and each tube 9 in. in diam. A system of dampers is provided for the Multiclone units so that as a boiler is taken off or put on the line the number of Multiclone units in service can be proportionately varied. Normally the pressure drop across the Multiclone is maintained at 2 to 3 in. of water column. The pulverized coal is of local supply of relatively high ash and usual efficiency is on the order of 85 pct.

Multiclones with a larger diameter of tube, that is, 16 in. diam tubes have found service at several copper smelter converter installations in the West. As an example, there may be taken the installations at the McGill, Nevada, Smelter of the Kennecott Copper Corp. Here 4 units of Multiclones, each of 45 tubes 16 in. in diam are installed to serve three converters. The gas volume approximates 273,000 cfm at 600°F. For movement of the gases through the flue system and to supply the approximately 3 in. pressure drop across the Multiclones, a large induced draft fan is located on the exit flue from the Multiclone units and is driven by a 150 hp motor. Due to the corrosive nature of converter gases at lowered temperature, ample heat insulation has been provided, mainly in the form of a rock wool blanket 4 in. in thickness. On the copper content only of the converter dust and fine discharge, the Multiclone collects 90 pct or better but on the overall of dust and fume the

collection is considerably below the copper collection.

FILTRATION

The third method of dust collection to be illustrated by plant example is that of baghouse and we have selected two baghouse installations; one at a copper smelter and one at a lead plant.

While present-day practice does not favor a baghouse on copper plant gases but does favor its use at lead reduction works, it is of interest to note an example of a baghouse installation on a copper plant works which for its day and time was a signal success. Early in this century the Mammoth Smelting Co. at Kennett, California, operated a copper smelter of 4 blast furnaces and 2 converters. The copper ore, a sulfide, also carried enough zinc so that the gases were approximately free of SO_3 or H_2SO_4 and, by lowering the temperature by radiation-cooler pipes, plus further cooling by dilution with outside air, successful operation on the baghouse was obtained. The installation of the baghouse was not necessitated by plant requirements as the collected product was not returned to furnaces, and unless it has been washed away or dissolved by the rains since the plant was shut down about 30 years ago, it is still on hand at the smelter site. Its construction was due to a desire of the smelter company to meet the objections to smelter dust fall from communities in the upper end of the Sacramento Valley.

The gases from the furnaces averaged about 600°F and were passed to a radiation cooler consisting of a number of 2-ft pipes operating in parallel, which discharged to the inlet flue of the baghouse. Into this same header flue a fan forced outside air and the resulting air-smelter gas mixture was maintained at about 200°F. The baghouse discharged to atmosphere through the 5 large square stacks. Approximately 3000 woolen bags, 18 in. diam by 35 ft high were installed in the baghouse and the gas volume, as cooled and diluted to approximately 200°F, amounted to 350,000 cfm. The tonnage of ore smelted amounted to approximately 1000 tons per day, and the baghouse collection to 18 to 20 tons per day.

Typical baghouses for lead smelter service have been described by several authors and the one in service at Murray Smelter²¹ in the Salt Lake area is representative of good design and good construction. The housing for the bag sections is of heavy brick construc-

tion and has outside dimensions of 216.5 ft long, 90.5 ft wide and a height to roof trusses of 51.5 ft. The lower 16 ft of wall is 21 in. thick, the next 18 ft 17 in. thick and the remaining height 13 in. wall. Forty-eight brick buttresses are spaced along the walls and add stiffness and rigidity to construction. There are four bag compartments separated by brick partition walls from floor line to roof trusses. Each compartment below the chamber floor is separated into 4 divisions by brick walls, each with its own cleanout door. Installed in the four compartments is a total of 4032 bags, each bag 18 in. diam and 30 ft long and these bags are made of wool to very careful specifications. As originally built there was provided 570,012 sq ft of filtering area to handle 165,000 cfm of gas or at the rate of 3.45 sq ft of bag surface to 1 cf of gas per min. Mechanical rapping or shaking of the bags was provided at their top ends.

Some later and smaller baghouses at lead smelters have been able to increase greatly the ratio of cfm per square foot of area by means of fully automatic operation of damper and bag shaking, some reporting a ratio of 1 to 1. In the case of a true fume such as arsenic or lead, however, increasing velocity through the filter cloth openings tends to cause increased escape of unagglomerated particles, and so increased economy of investment is offset by somewhat lower efficiencies. However, it is to be recollected that baghouses at lead smelters are as much a consideration for employee and community health as they are an investment in equipment to provide an economic return, and therefore are always planned for relatively ample capacity and high efficiency.

SCRUBBERS

The fourth means of collection, that is, scrubbers, "disintegrators," and the like, making use of water as a medium to collect fume and dusts, have rarely found practical use at lead and copper works except for the small volumes encountered in silver and gold refining, and this, no doubt, has been largely due to the corrosion hazard. More than half a century ago, around iron blast furnaces, they received much attention and many units were installed. The combined inertial and wetting procedures used, for example, the Theisen disintegrator gas washer, were the most efficient collectors on the market and

collected not only the dust, but also the zinc and alkali fumes which often appear in the iron blast furnace gases. In principle, this Theisen scrubber is a fan with the usually solid blades replaced by perforated plates or a heavy screen mesh. Water is introduced with the inlet gases near the center of the fan runner and is broken up into fine particles in passing through or from center to periphery of runner. To collect particles of dust and fume, the water particles must be on the order of not over 10 times the diameter of the dust or fume particles and where particles of around 1 micron or less are to be collected, an enormous subdivision of water particles is required and this subdivision requires extraordinary high power consumption. In the older steel works of continental Europe, often the largest power unit of the works was attached to the Theisen washer and from 2 to 10 hp per 1000 cf of gas treated was the rule. The Theisen disintegrator, however, did prepare iron blast furnace gas for combustion in gas engines with a content in solid suspended particles not far from that of outside air. Today their use has greatly decreased, the same degree of cleaning being secured by a film type of electrical precipitator with a power consumption only a few percent of that of the Theisen. Nevertheless, it should be noted that at the time of its first introduction, 50 years or more ago, it was an outstanding success and for the service it rendered over a generation or more, no other equipment of that period was in its class.

However, within the last few years a new scrubber has been brought on the market, known as the Venturi¹⁷ which, combined with the Pease-Anthony scrubber¹⁶ shows reported efficiencies on the order of 98 pct on paper mill fume. On reverberatory open hearth waste gases containing fumes and the like, equally good efficiencies have been reported. In the Venturi scrubber a high velocity of gas stream is maintained at the throat, about 250 to 300 fps with a corresponding pressure drop across the throat section approximating 12 in. of water column. A series of water connections surround the throat of the Venturi, and in the throat conditions are such that an extraordinarily violent turbulence is set up, sufficient to provide for the wetting and collection into the moving water gas mixture, of the dust and fume particles suspended in the gas stream. From the Venturi the gases

either pass to a simple cyclone for separation of water particles and gas, or to a Pease-Anthony scrubber, which is a cyclone with tangential gas entrance near the bottom and a central column with an array of spray heads discharging in such a manner that the longest possible path in the cylindrical shell is obtained for spray discharge and passing the gas stream. On paper mill (soda) fume, the Venturi alone has been reported as collecting approximately 90 pct and the combined Venturi and Pease-Anthony 98 pct of the suspended fumes in the gases. The latter figure and also that for the combined Venturi-Pease Anthony have been reported on an open hearth reverberatory with oxygen in the bath, the latter to speed the refining operation at top temperatures. The drawback of the Venturi scrubber, like that of the Theisen, is the high power consumption required for induced fan and to provide the throat velocity or the pressure drop across the Venturi and the Pease-Anthony. About 220 hp was used on the reverberatory tests handling approximately 45,000 cfm. Should it prove practical to reduce the power consumption without decreasing the efficiency appreciably, this type of scrubber should have most excellent industrial possibilities.

Excepting these two types of Theisen and Venturi which do collect fume, the general run of scrubbers is used on dust particles (say, 100 to 1000 times the weight of a fume particle) and there they do acceptable work with relative low power consumption. Probably best in practice are the countercurrent tile-packed towers, although commonly these require periods of special flushing or cleaning to prevent choking and buildup. They are generally planned for a 1 to 3 in. pressure drop across the tile sections but with only a small buildup of mud or caked material will promptly double or triple their pressure drop.

On hot gases and series operation of two or more spray chambers, the first at a higher temperature, the second cooling the gases below dew point, it is practical to vaporize more moisture into the first chamber than the gases can retain in the cooler conditions of the second spray chamber with the result of the condensing out of a proportion of the water vapor produced in the first chamber. Such condensed precipitates make use of fine particles of dust and fume as nuclei for their condensation and thus permit of high effi-

ciencies. On a calcining kiln, where only a fine dust escaped, a reported 97 pct removal of suspended solids in gases was reported in this manner of operation.

The great objection to scrubbing in general is the need to care for large volumes of water containing a relatively small amount of solids. Thickeners, filters, storage tanks and extensive pumping and piping are commonly required to complete a properly operating plant.

ELECTRICAL PRECIPITATION

We now come to the fifth and last method under discussion for dust and fume collection, *viz.* *Electrical Precipitation*. So many plants have been described in the literature that it seems questionable if anything new may be offered here. However, we propose to describe briefly two types of precipitators: (1) that aimed at collection of large quantities of dust or dust and fume, and (2) that aimed at the final cleanup of a gas so that such cleaned gas may be advantageously used in further processes or equipment.

For the first classification above, it is proposed to describe an electrical precipitator recently installed at a cement plant in the South, and a power plant precipitator going into service in the near future. For the second classification above or purification of gases it is proposed to describe a plant installed to "fine"-clean iron blast furnace gas and a plant to clean roaster gas for contact acid manufacture.

The cement plant of the Universal Atlas Cement Co. at Leeds,²² Alabama, is not far from the center of the town and while producing only at a minimum or average capacity did not discharge from its stack an objectionable quantity of dust. Along with the war and the aftermath of war, with its huge demand for cement, came the necessity to increase to the limit the plant's capacity to produce and, with this increase, came immediate evidence of greatly increased dust discharge from the stacks. To meet the desired reduction in stack emission of solids a three-unit precipitator was installed, each unit to handle 100,000 cfm at the prevailing temperature of approximately 700°F. The actual efficiency for slightly less than the rated gas volume was 94 pct or better. Each of the three units of precipitator are provided with three sections or electrode banks in series, the first two sections being of 15 gas passageways or ducts on 8 in.

centers and the last section of a V or pocket type with 12 gas passageways or ducts on 10 in. centers. Each collecting electrode approximates a dimension of 8 by 18 ft, the discharge electrodes being square twisted rods $\frac{1}{8}$ in. in diam in a supporting frame. Six special electrical units each with a 75,000 volt transformer and mechanical rectifier serve the installation. Automatic or push button controls are provided for all operating equipment including rapping both discharge and collecting electrodes, dampers, screw conveying equipment and the like. The return of the dry dust to a wet process plant is always a difficult problem and here 55 pct of the collected dust is returned as a dry feed to the center of a vortex of slurry just as it enters the feed pipe to kiln.

Power plants and boiler sizes are ever growing larger and in some of the newer power plants gas volumes exceed anything but those of our very largest copper smelters. The boilers of huge size now being installed are possible because of powdered fuel combustion developments and since, in powdered fuel plants, the major portion of the ash is suspended in the spent gases from boiler and normally passing to stack, collection equipment for ash particles has become an essential requirement. Electrical precipitation is generally favored because of the degree of fineness, (20 to 50 pct minus 10 microns) of the ash and the fact that its collection is dry, thus avoiding a corrosion problem.

At the present time there is under construction a power plant involving three boilers each of one million lb steam evaporation per hour and each producing somewhat under $\frac{1}{2}$ million cf of gas as measured at exit of air heater at approximately 300°F. Each boiler gas discharge has its own collection installation and a brief description follows: The collector is a combined inertial and electrical precipitator in which the electrical precipitator for each boiler is preceded by a Multiclone installation as described under the heading of inertial or centrifugal equipment. The precipitator for each boiler is divided into five units, each with an outlet damper and each precipitator unit consists of 15 gas passageways or ducts, and while only one section long, each duct carries three collecting plates, each plate 3 ft wide by 16 ft high with 2 ft of settling and agglomerating space between each two plates in the direction of gas flow. The duct width,

or from center to center of two collecting plates, is 9 in. Discharge electrodes consist of the usual square twisted $\frac{1}{8}$ in. bars. The gas volume per boiler is 400,000 cfm at prevailing temperature of 325°F and the total for three boilers is 1,200,000 cfm at 325°F. For the three-boiler plant there is a total of 2340 Multiclone tubes preceding the precipitator and a total of 225 gas passageways or ducts in the electrical precipitator. This gas volume is larger than the usual nonferrous metallurgical plant except for several of the very largest copper smelters. Eventually the power plant will have a fourth and a fifth boiler, each of one million lb per hour production of steam or perhaps even larger—a million and a quarter is even under discussion.

From collection of the major portion of a nuisance waste at a power plant with a huge gas volume, we turn now to a plant handling a much more limited gas volume, a mere 100,000 cfm, but which is required to clean the gas almost to the equal of outside air, that is, to 0.007 grain per cf or better. This is entirely an operation of purification of the gases and the recovered material, mostly fume, is of no value or use.

Modern steel works find it profitable to have the cleanest obtainable fuel gas from iron blast furnace operation in order (1) to prevent slagging of the checker work in the stoves, (2) to permit closer packing of refractory brick in stoves, (3) to permit satisfactory operation of automatic air and gas regulators on blast furnace stoves and of fuel at coke oven plants without danger of slagging the brick work. All this they obtain with a train of collection equipment on the gases coming from the iron blast furnace top. The train consists of (1) a dry dust catcher or chamber where the very coarse dust is caught and where dust concentration is reduced from around 12 grains per cf to around 3 or 4 grains per cf. (2) The gases then enter a scrubber provided either with a checker work of wooden strips or a series of sections of tile packing with heavy coarse sprays at top and commonly at two or three intermediate points with gases passing upward and water downward, that is, countercurrent operation. The gas entering the scrubber has a concentration of 3 to 4 grains and the gas leaving the scrubber has a concentration in solid suspension of 0.25 to 0.3 grain. From the scrubber the gases enter the precipitator and are cleaned in the

precipitator down to a concentration of approximately 0.007 grain per cf. This reduction in suspended solids of 0.3 to 0.007 corresponds to an efficiency of 97.7 pct. From the precipitator the clean gases go to the receiver and to special services where extreme cleanliness is desired. The gas volume at precipitator approximates 100,000 cfm and 4 units of precipitator are placed in two circular shells, each with a division wall down its center. Each unit has 126 pipe electrodes 8 in. in diam by 15 ft long or a total for the 4 units of 504 tubes. Three electrical sets, each 25 kva, with 75,000 volt transformers supply the special direct current required for precipitator operation.

A second field where electrical precipitators are used in the purification of gases is in the manufacture of sulphuric acid by the contact process with the SO_2 derived by combustion of the usual run of sulphide ores or sulphide concentrates—commonly zinc, iron, or copper sulphides or mixtures usually with minor amounts of arsenic, antimony, lead and the like.

Arsenic oxide, and some of the other constituents, poison the platinum catalyst and others merely coat over the active mass, so it is necessary to have the gas, before going to the SO_2 to SO_3 converters, cleaned down to a few parts in 100,000 of arsenic figured as As_2O_3 and as grains per cf. This is accomplished by a thorough wetting and cooling of the roaster gas in towers and scrubbers of various design, occasionally a packed tower is required, and the passage of the gas at 80 to 100°F to a lead type precipitator. The gases reaching the precipitator are fully saturated with water vapor and contain in addition mist particles of very weak acid. These latter usually contain the minute particles of arsenic probably as the nuclei of mist particle formation. In one acid plant with a gas volume of about 7500 cfm at the prevailing temperature of 80 to 100°F, a precipitator was used consisting of 72 pipes, 70 of these 10 in. in diam by 12 ft long and two pipes carrying stiff rods to lower grid, 13 in. diam by 12½ ft high.

The actual precipitate was a very light liquid sludge which drips from pipes and eventually finds its way to a waste sump. One electrical set with a 75,000 volt transformer and two mechanical rectifiers (one a spare) serves the pipe section. The discharge electrodes are lead-covered iron wires in a star cross-sectional design and held straight and true by lead weights. Many lead pipe units of the same general design are used at acid-concentrating plants such as are to be found at munitions works and occasionally at chemical and oil works. Both material savings and improvement in health conditions are derived benefits from the precipitator operation on waste acid gases.

Conclusion

It may be true we have tried to cover too much, too sketchily in this paper. However, it is thought the object in view, *viz*, to acquaint our member engineers both with a birds-eye view of the problems of collection of suspended dusts and fumes as a whole and also to offer enough of the practical in description of types of equipment and specific installation as will permit of fair engineering visualization, has been reasonably well accomplished. It is recognized that books have been written and more are in prospect on particular phases of the subject matter here handled and that is as it should be, for truly to meet the modern requirements in dust and fume control in mines and mills, in industrial plants and smelters, will require some technical knowledge of the problem by nearly all engineers and a great deal on the part of those directly involved in collection. Also this latter class in industry will constitute a staff many times that of today and the expenditure for equipment will approximate hundreds of millions and this is limited to the near continental area of our United States.

References

1. H. V. Welch: Recovery of Suspended

Solids from Furnace Gases in Copper Smelters; with Special Reference to the Cottrell Process. *Trans. AIME* (1934) 106, 296.

2. H. V. Welch: Collection of Lead and Zinc Dusts and Fumes by the Cottrell Process. *Trans. AIME* (1936) 121, 304.
3. G. Nonhebel: Commercial Plant for Removal of Smoke and Oxides of Sulphur from Flue Gases. Disperse Systems in Gases. Faraday Soc. (1936), p. 1291.
4. W. E. Gibbs: Clouds and Smokes (1924) p. 129.
5. H. Remy: *Ztsch. anorg. allgem. Chemie* (1924) 138, 167.
6. Industrial Health Code, III. State Dept. of Public Health.
7. J. J. Bloomfield and J. M. Dallavale: Determination and Control of Industrial Dust. Public Health Bull. 217 (1935).
8. P. Drinker, T. Hatch: Industrial Dust. (1936).
9. Disperse Systems in Gases, Dust, Smoke and Fog. *Trans. Faraday Soc.* (1936).
10. W. E. Gibbs: Clouds and Smokes. (1924).
11. Marcel A. Lissman: Dust Collection on Analysis of Mechanical Methods. *Chem. and Met. Eng.* Oct. 1930, 37.
12. Evald Anderson: Effect of Tube Diameter in Cyclonic Dust Collectors. *Chem. and Met. Eng.* Oct. 1933, 40.
13. F. Miller and M. Lissman: Calculation of Cyclone Pressure Drop. *Trans. ASME*, Dec. 1941.
14. Evald Anderson: Chem. Eng. Handbook. Perry 1st Ed. (1934) 1539.
15. F. G. Breyer: Efficiency of Theisen Washers. *Bull. AIME*, Apr. 1917, p. 554.
16. R. V. Kleinschmidt and A. W. Anthony, Jr.: Recent Developments of the Pease-Anthony Gas Scrubber. *Trans. ASME* (1941) 63, 349.
17. Editorial Article. The Venturi Scrubber, Power Generation. May, 1948. 52.
18. T. T. Collins, Jr.: Scrubbing of Sulphate Recovery Furnace Stack Gases. *Paper Industry and Paper World*. Aug., Sept., Oct. 1948.
19. Cottrell, F. G.: Problems in Smoke, Fume and Dust Abatement. Smithsonian Inst. Rep. for 1913. Pub. 2307, (1914) pp. 653-685.
20. C. W. Goodale and J. H. Klepinger: Great Falls Flue System and Chimney. *Bull. AIME* Aug. 1913 P. 1934; also *Eng. and Min. Jnl.* (1910) 89, 368.
21. A. Eilers: Notes on Bag Filtration Plants. *Trans. AIME* (1912) 44, 708.
22. Nordberg, Bror: High Efficiency in Stack Dust Recovery. *Rock Products*, Aug. 1947.



Some Observations on the Recovery of Cold Worked Aluminum

T. V. CHERIAN,* P. PIETROKOWSKY* and J. E. DORN,* Member AIME

Introduction

The phenomenon of recovery of cold-worked metals is interesting not only because of its practical importance but also because of its fundamental significance in solid state reactions. Although extensive investigations^{1,2} have already been made in an attempt to discover the mechanics of the recovery process, many of the observations have not yet been satisfactorily correlated to provide a completely consistent model for the process. The wide differences in the recovery rates of various properties can be cited as a typical example of one of the difficulties that are encountered. Frequently, for example, the electrical resistance will have almost completely recovered before any recovery in tensile strength can be detected. Of course, such differences in the recovery rates of different properties might be explained by assuming that each property is a unique function of the work-hardened state, and consequently each property exhibits its own unique recovery rate. The assumption that different properties are uniquely related to the work-hardened state cannot be denied. On the other hand, the properties that recover at different rates often exhibit more or less parallel changes upon work-hardening. This suggests that the microstructural changes attending recovery are not exactly the reverse of the changes attending work-hardening. Several types of imperfections must be postulated in order to account for this apparent anomaly. The different recovery rates for various properties, then, are due to the different recovery rates of the type of imperfection to which each property is most sensitive as well as the unique dependence of each property on the cold-

worked state. This concept assumes that a simple model of the work-hardened state consisting only of one type of imperfection, such as Taylor's type of dislocation patterns, is inadequate to cope with the diversified phenomena attending work-hardening and recovery.

Although current models for the work-hardened state are not useful for describing all aspects of the recovery process, the general trends of the recovery of each postulated type of imperfection as a function of time and temperature should be at least qualitatively deducible from the rather well developed laws of kinetics of reactions in the solid state. Consequently, recovery data might prove useful for elucidating some aspects of the complexities of the work-hardened state of metals. A preliminary attempt to study work-hardening by investigating recovery rates of cold-worked metals is outlined in the following pages of this report.

Experimental Procedure

Many properties recover when cold-worked metals are annealed below their recrystallization temperature. Therefore, electrical resistivity, thermal electromotive force, X ray diffraction line

widths, X ray diffraction line intensities, elastic spring back, density and other physical and chemical properties have been used to study the recovery process. Major interest, however, has generally been directed toward the recovery of the mechanical properties such as hardness, yield strength, and tensile strength. But a search of the literature suggests that the effect of recovery on the true stress-true strain curve has been neglected, in spite of the current recognition of the fundamental importance of such an investigation. An investigation on the effect of recovery treatment on the true stress-true strain curves in tension, therefore, was undertaken in the present study.

Commercially pure aluminum (99. + pct Al) in the form of 0.100 in. thick rolled sheet of 2S-O aluminum alloy was selected as the material for this investigation because rather extensive correlatable data are already available on the recovery of some of its properties. Tensile specimens having a 6 in. long gauge section and a uniform reduced section width of 0.500 in. were machined from the sheet in accordance with a design that has previously been reported.³ All specimens were selected with their axes aligned in the rolling direction. In order to eliminate the effects of previous work-hardening and the effects of machining, the specimens were annealed for 15 min. at 750°F before testing.

During tensile testing the loads were measured by means of a proving ring (sensitive to $\frac{1}{2}$ lb) in series with the specimen.⁴ Strains were determined from the extension of a rack and pinion strain gauge sensitive to a strain of ± 0.0001 . The stress was recorded as the true stress, namely

New York Meeting, February 1950.
TP 2721 E. Discussion of this paper (2 copies) may be sent to *Transactions AIME* before April 1, 1950. Discussion is tentatively scheduled for publication in November 1950.

Manuscript received August 8, 1949.

* Graduate Student, Research Engineer, and Professor of Metallurgy, respectively, University of California, Berkeley, California.

¹ References are at the end of the paper.

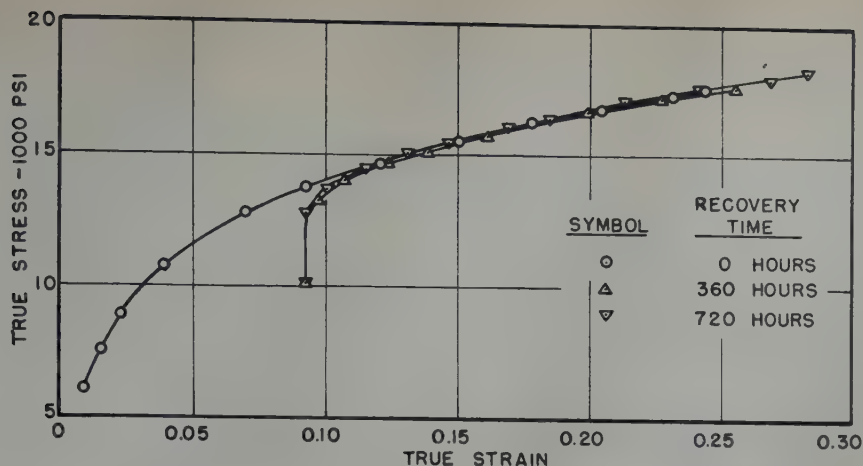


FIG 1—Recovery of 2S-O alloy at 90°F after a prestrain of 0.092.

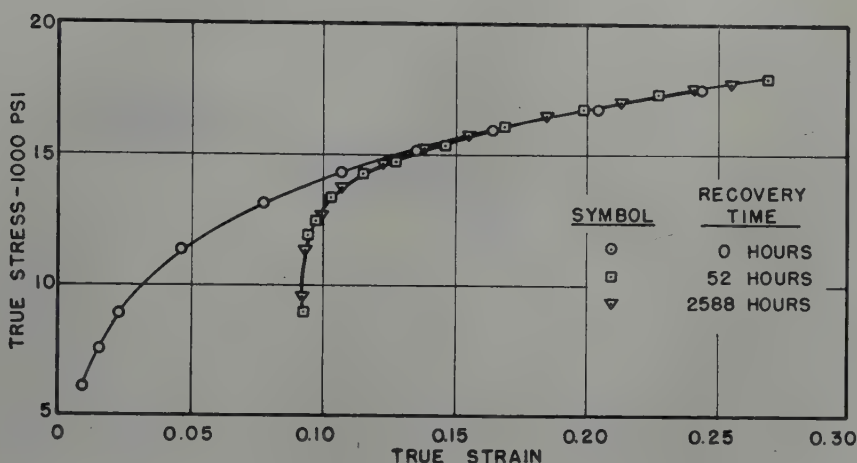


FIG 2—Recovery of 2S-O alloy at 212°F after a prestrain of 0.092.

$$\text{Stress} = \frac{\text{Load}}{\text{Instantaneous Area}}$$

and the total true strain was evaluated by

$$\text{Strain} = \log_e \frac{\text{Instantaneous Length}}{\text{Initial Length}}$$

The true plastic strain was then calculated by subtracting the known elastic component from the total true strain.

Experimental Results

Several typical experimental results are given in Fig 1 to 4 in the form of true stress-true plastic strain curves. The upper curve of each figure is the work-hardening curve for the annealed specimens. The remaining curves were obtained from specimens that had been strained to $\epsilon = 0.092$ at atmospheric temperature, recovered for the recorded time and temperature, and then re-tested at atmospheric temperature. Only a few representative data are shown in Fig 1 to 4. Other prestrains

(0.048 and 0.125) and intermediate times of annealing yielded analogous results.

Discussion of Results

The data recorded in Fig 1 reveal that cold-worked aluminum recovers upon annealing at 90°F. The recovery rate is quite rapid initially, but it ceases before complete recovery of the initial flow stress is achieved. It is significant to note, however, that upon restraining only the initial flow stress appears to have recovered, and after an additional strain of about 0.04 the stress-strain curve of the recovered material coincides with that of the virgin annealed specimen at the same total strain. Consequently those imperfections that are readily activated at this low recovery temperature are readily reintroduced upon restraining. The exact coincidence of the latter portion of the stress-strain curve of recovered specimens with the curve for the virgin

annealed material at the same total strain suggests that the work-hardened states in the two cases are substantially identical.

As shown in Fig 2 the phenomenon of recovery at 212°F is qualitatively analogous to that which occurs at 90°F. The only significant difference is that a greater amount of recovery of the initial flow stress results at the higher annealing temperature. Nevertheless the constant value of the initial flow stress is yet above that for complete recovery.

The term metarecovery will be used to describe the type of recovery experienced by cold-worked aluminum 2S-O alloy upon annealing at 90 and 212°F. Metarecovery, then, consists of the removal of readily activated imperfections at low recovery temperatures. The removal of these imperfections causes an appreciable decrease in the initial flow stress; they are again readily restored upon restraining. After small additional strains (about 0.04) have been imposed on the recovered

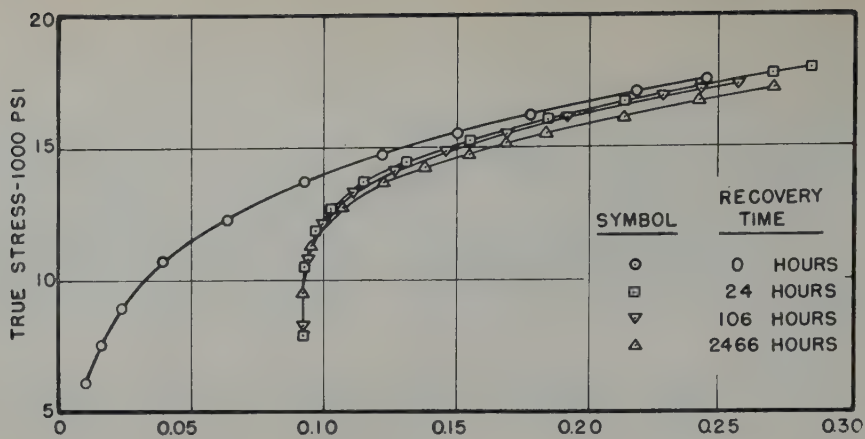


FIG 3—Recovery of 2S-O alloy at 300°F after a prestrain of 0.092.

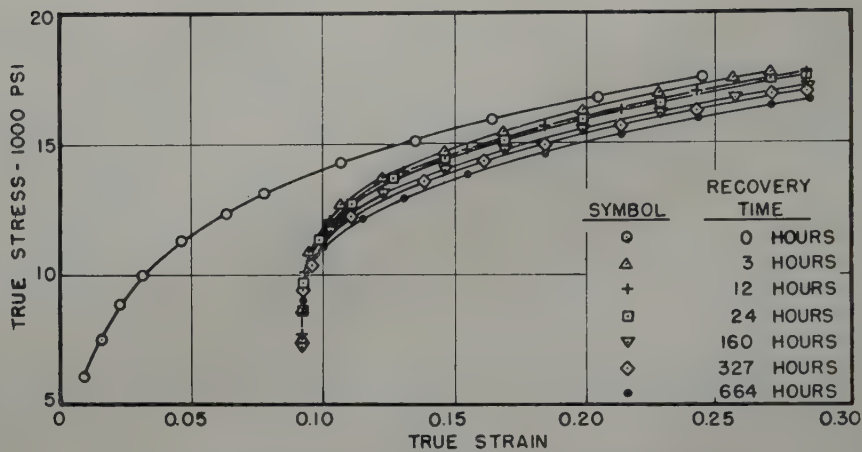


FIG 4—Recovery of 2S-O alloy at 400°F after a prestrain of 0.092.

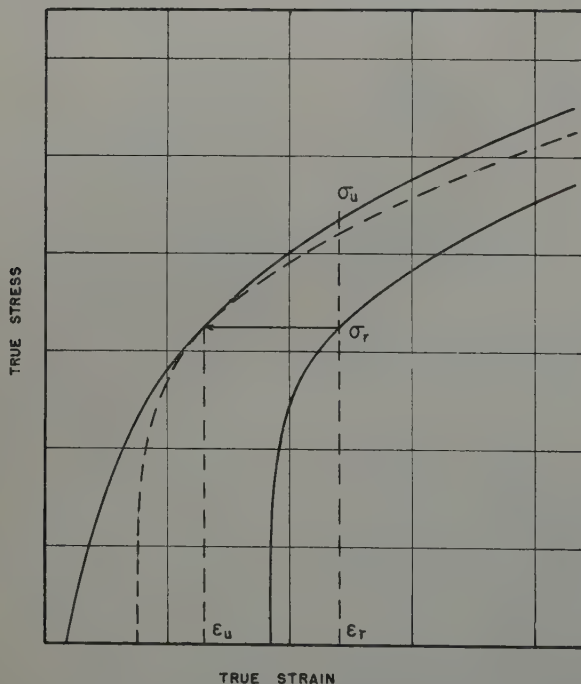


FIG 5—A method of evaluating the amount of orthorecovery.

specimen it responds plastically in a manner identical with that of a virgin specimen which has been deformed to the same total strain. Metarecovery takes place at a high initial rate but the specimen soon acquires constant plastic properties before complete recovery occurs. The amount of metarecovery, as dictated by the reduction in the initial flow stress below the value in the work-hardened specimen, is greater the higher the annealing temperature. Two possible interpretations can be ascribed to this observation. If the type of imperfections that are removed upon metarecovery do not interact with each other, they must individually have activation energies for recovery over a broad band of values. The imperfections having the lower values of activation energies are then removed at the lower annealing temperatures, whereas higher annealing temperatures are required to remove those imperfections that have higher activation energies. In this way it is

possible to account for the early termination of metarecovery before complete recovery is achieved. On the other hand, the imperfections might exhibit interactions such that the activation energy for metarecovery is a function of the density of the imperfections. In order to account for the observations it must be assumed that the activation energy for recovery increases rapidly with a decrease in the density of imperfections. The present evidence does not permit identification of which of the two alternate mechanisms of metarecovery is correct; it is interesting to note, however, that only the second mechanism is compatible with recovery of Taylor's stable patterns of edge type dislocations.⁵⁻¹⁰

The stress-strain curves given in Fig 3 and 4, for specimens annealed at 300 and 400°F, appear to be slightly different from those shown in Fig 1 and 2. They not only exhibit the previously described metarecovery, as indicated by the decrease in the initial flow stress after annealing, but they also show permanent effects of the annealing treatment. The flow stress after recovery at these higher temperatures never acquires the same value as the flow stress of the virgin material at the same total strain. Beyond an additional strain of about 0.05 after recovery treatment at these higher temperatures, the stress-strain curves for the recovered specimens fall below but parallel to that for a virgin annealed specimen at the same total strain. It will be convenient to describe this type of recovery as orthorecovery. Two important characteristics serve to distinguish orthorecovery from metarecovery. First the true stress-true strain curve of a material which has been subject to orthorecovery is below that for the virgin material at the same total plastic strain for all strains. And secondly, whereas orthorecovery appears to continue until complete restoration of the annealed properties is achieved, metarecovery practically ceases far short of complete recovery. This conclusion is immediately apparent when it is noted that even after annealing 2466 hr at 300°F or after 664 hr at 400°F additional orthorecovery is yet occurring.

It is not immediately apparent as to how a quantitative measure of orthorecovery might be obtained. It might be thought that shifting the stress-strain curve of a partially recovered specimen to the left would bring the latter portion of the stress-strain curve

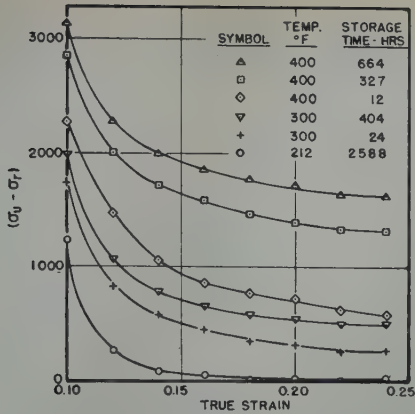


FIG 6—The reduction in flow stress upon recovery as a function of total strain.

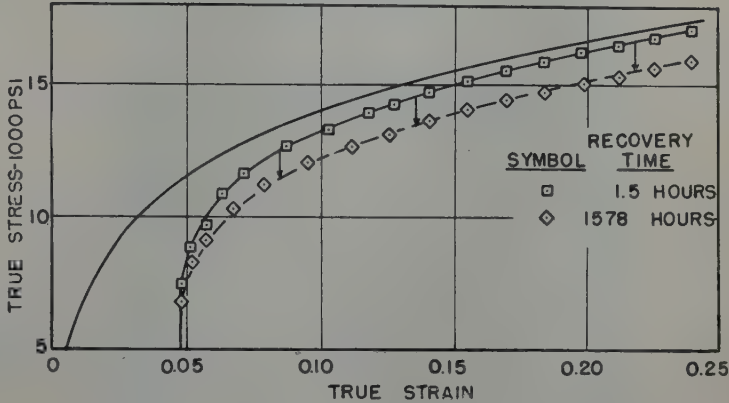


FIG 7—The effect of recovery at 400°F on the stress-strain curve for 2S-O alloy prestrained 0.048.

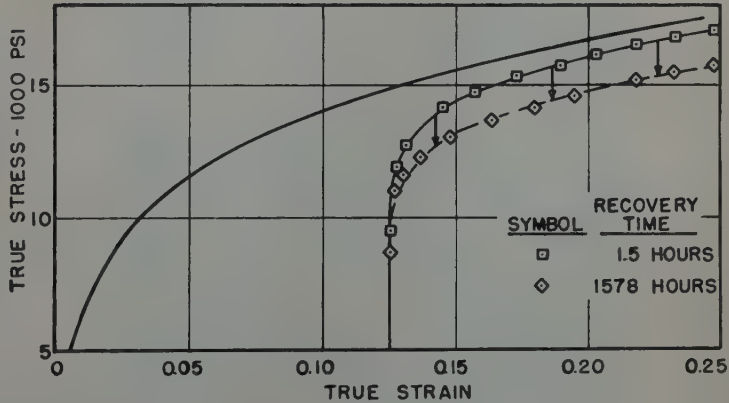


FIG 8—The effect of recovery at 400°F on the stress-strain curve for 2S-O alloy prestrained 0.125.

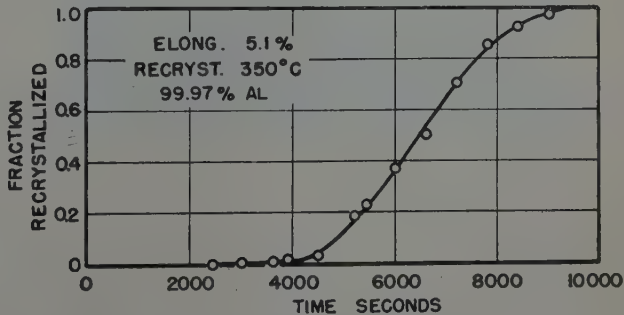


FIG 9—Typical curve for fraction recrystallized vs. time relationship. (After W. A. Anderson and R. F. Mehl.)

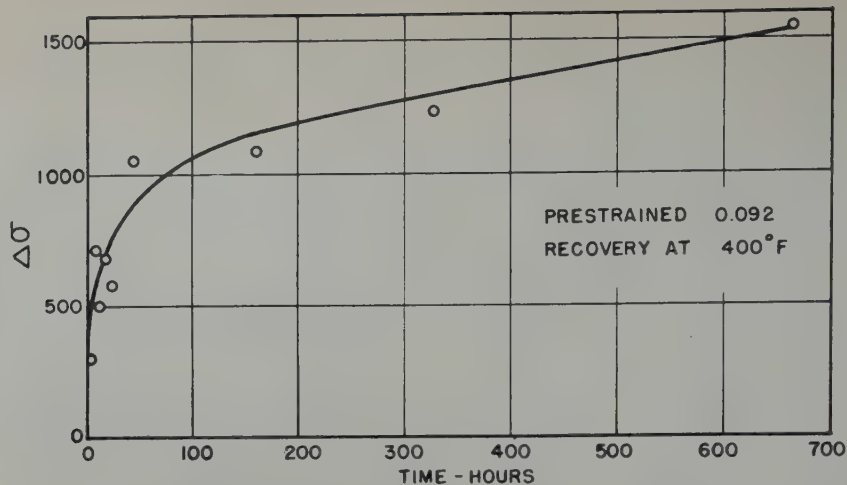


FIG 10—The effect of annealing time on orthorecovery.

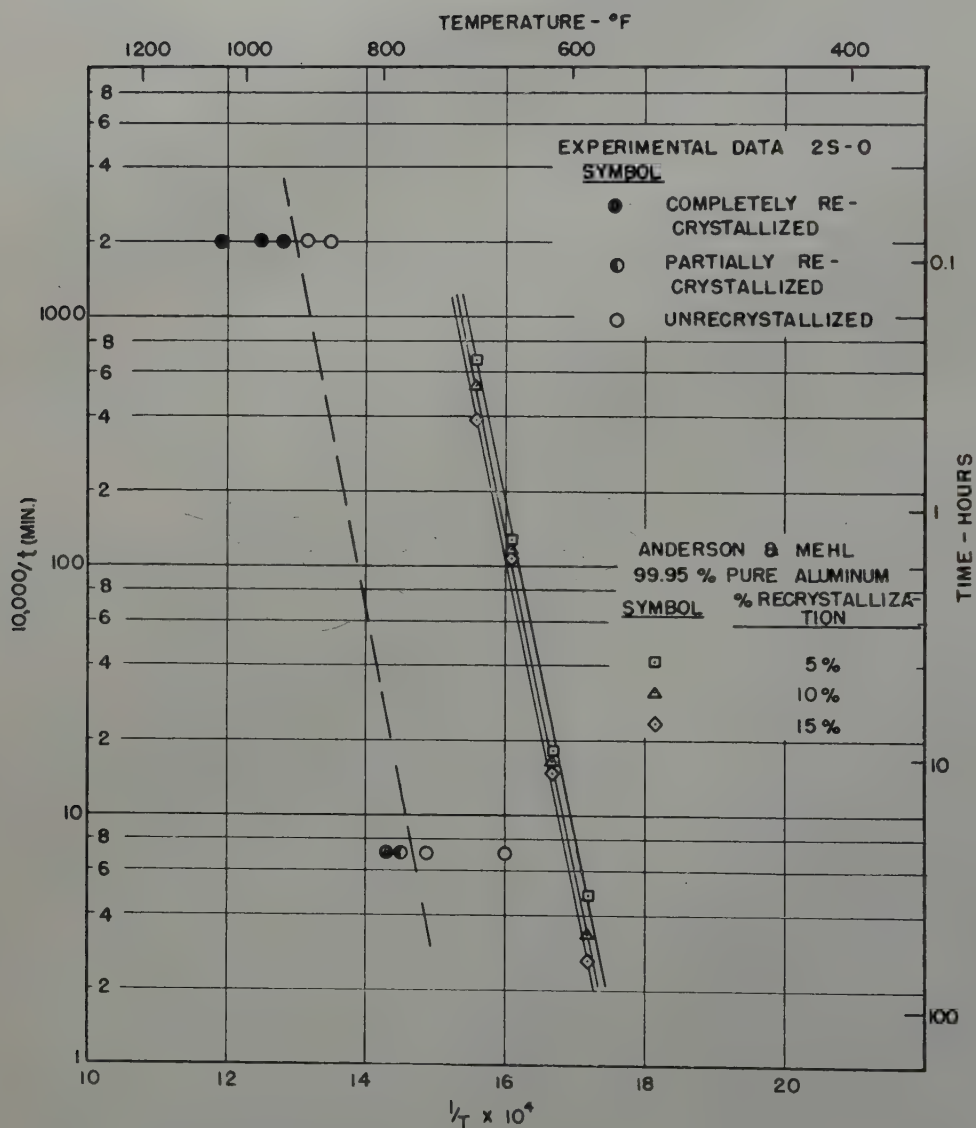


FIG 11—Recrystallization of 2S-O alloy.

of the recovered specimen into coincidence with that for a virgin specimen. Then $\epsilon_r - \epsilon_u$ shown in Fig 5, would serve as a measure of the strain-recovery. This method should work if only one kind of an imperfection is present. But, as shown in Fig 5, coincidence of the stress-strain curves for the virgin and annealed materials is obtained at only one point, a fact that not only disqualifies the proposed procedure, but also implies that several types of imperfections responsible for work-hardening are induced by cold-work.

In order to obtain a method of measuring the amount of orthorecovery, consider evaluation $\sigma_u - \sigma_r$ (illustrated in Fig 5) as a function of the total strain. Several typical curves for various recovery treatments are shown in Fig 6. It is immediately apparent that the various curves are substantially parallel. After annealing for 2588 hr at 212°F the lowest curve representing the effect of almost complete metarecovery is obtained. The remaining curves represent the effect of both meta- and orthorecovery for various recovered states. The parallel trends of these curves suggest that metarecovery is almost complete after annealing at 212°F for 2588 hr and that orthorecovery results in a uniform decrease in the flow stress below that for the virgin unrecovered specimen independent of the subsequent strain.

In order to test this concept consider now the data of Fig 7 obtained by prestraining about 0.048 and annealing at 400°F for recovery. If after annealing for 1.5 hr at 400°F all of the metarecovery has taken place as well as some orthorecovery, the difference between the stress-strain curve after 1.5 hr of annealing and that following 1578 hr of annealing is attributable to orthorecovery. Furthermore, if orthorecovery causes a uniform decrease in the flow stress for all strains a vertical shift of the stress-strain curve after annealing 1.5 hr should yield a curve that coincides exactly with that obtained after annealing 1578 hr. Upon shifting the stress-strain curve after 1.5 hr of annealing to lower stress values, the broken curve of Fig 7 is obtained. The excellent agreement between the experimental data and the broken curve support the concept that orthorecovery consists of a uniform lowering of the flow stress for all strains, whereas metarecovery consists in decreasing only the initial flow stress. Consequently, $\sigma_u - \sigma_r$ at high total strains might be taken as a measure of

orthorecovery.

This concept was also checked and found to give equally good agreement for values of prestrain equal to 0.092 and 0.125. The results of this correla-

tion after a prestrain of 0.125 are shown in Fig 8.

No justification has been presented in the previous discussion in favor of the use of the term orthorecovery. It is

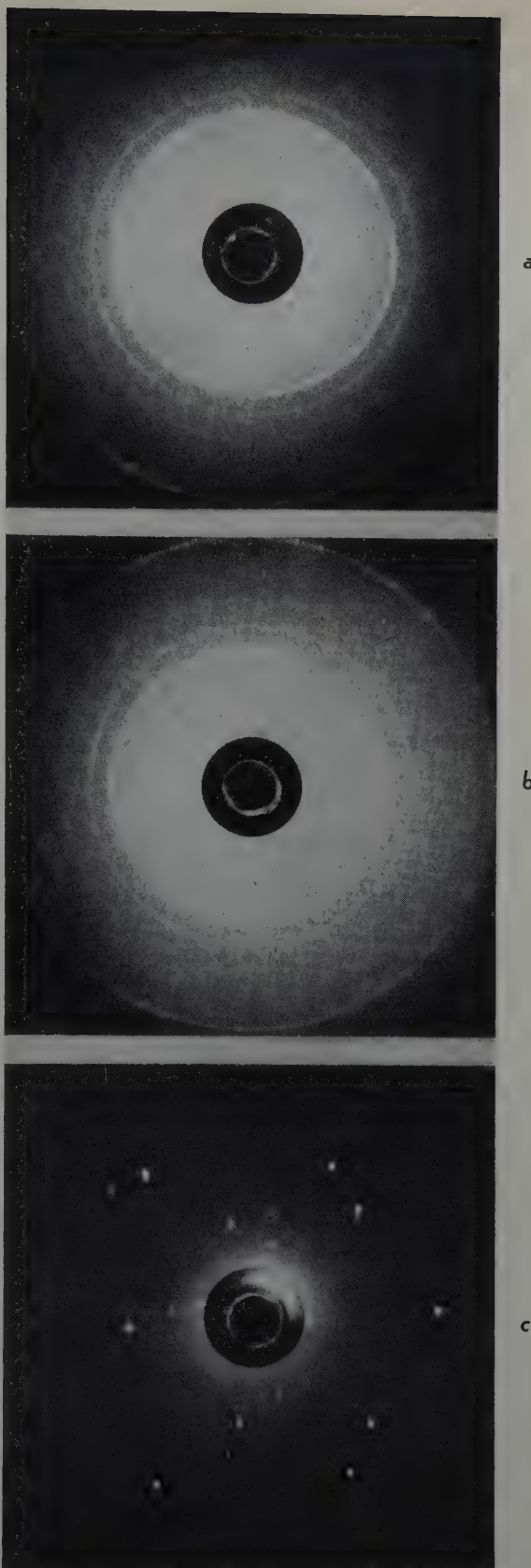


FIG 12—Back reflection X ray patterns. W radiation.

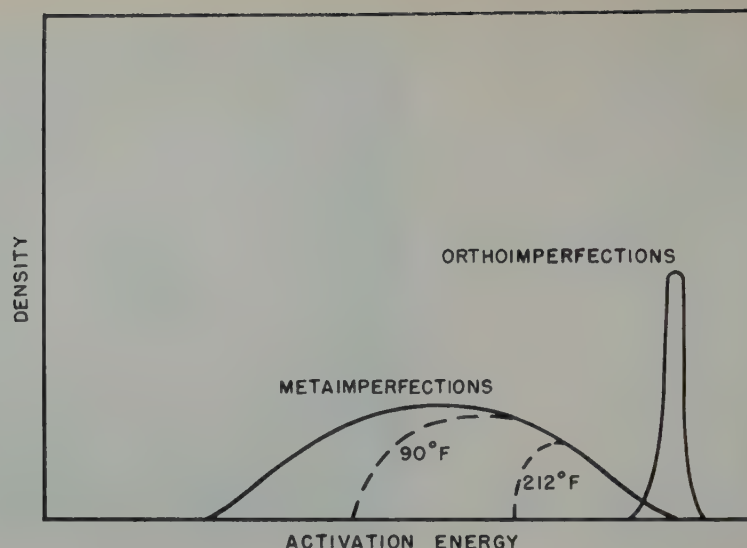


FIG 13—Schematic representation of distribution of imperfections induced by cold work as a function of activation energy for recovery.

quite possible, of course, that the specific phenomena peculiar to what has been called orthorecovery is actually due to recrystallization. Therefore, this possibility was explored.

Mehl et al.¹¹⁻¹⁴ have demonstrated that the fraction recrystallized-time curve is sigmoidal as illustrated in Fig 9. Although the mechanical properties need not vary linearly with the fraction recrystallized, nevertheless, some sigmoidal relationship would again be expected between the change in flow stress and time of annealing at temperatures of annealing if recrystallization takes place. In order to check this concept, the data for orthorecovery were plotted as a function of time as shown in Fig 9. The value $\Delta\sigma$ was obtained by taking $\sigma_u - \sigma_r$ (see Fig 5) at a large total strain ($\epsilon = 0.24$) where metarecovery no longer affects the flow stress. The $\Delta\sigma$ -time curve of Fig 10 illustrates that the process termed orthorecovery has its greatest rate at $t = 0$ in sharp contrast to phenomena that depend upon nucleation and growth. This evidence, then, suggests that what has been called orthorecovery is not a true recrystallization process. Furthermore, no detectable difference in microstructure was discernable upon careful comparison of the structures of a specimen strained 0.13 and another strained the same amount and then annealed at 400°F for 1577 hr.

The most conclusive evidence that recrystallization was absent in the annealing treatments leading to ortho-

recovery, however, is shown in Fig 11. It is well known that when the logarithm of the reciprocal of the time to achieve a certain percentage of recrystallization is plotted as a function of the reciprocal of the absolute temperature, a linear relationship, dictated by the laws of kinetics of reaction rates, is obtained. The data recorded by the solid lines of Fig 11 were taken from the excellent investigation of Anderson and Mehl¹⁴ on the recrystallization of high purity aluminum (99.95 pct Al). Thus the linear relationship that is obtained when recrystallization data are plotted in this manner is well established. Now 2S-O alloy is less pure than the material investigated by Anderson and Mehl and, therefore, longer times or higher temperatures of annealing would be required to cause equivalent recrystallization of 2S-O alloy.

A complete investigation of the recrystallization of 2S-O was not attempted, but only an estimate of its recrystallization temperatures and times was made in this study. Specimens of 2S-O alloy were strained 0.09 at atmospheric temperature and annealed for 15 min. and 24 hr respectively at a series of temperatures. Back reflection Laue patterns, using W radiation, were then taken to establish whether or not recrystallization was obtained. Three typical radiographs are shown in Fig 12a, 12b and 12c after annealing for 24 hr at a series of temperatures. Fig 12a exhibits the continuous rings (due to the L radiation)

of the fine grained cold-worked 2S-O. Fig 12c illustrates a coarse grained structure after complete recrystallization, whereas Fig 12b shows some rings attributable to the initial fine grain size as well as some spots resulting from the larger recrystallized grains. These data and analogous results for the recrystallization in 15 min. are recorded in Fig 11. Of course, the location of the line representing a given small amount of recrystallization cannot be ascertained accurately from these data. But the approximate curve shown by the broken line is not seriously in error. It is interesting to note that this line is practically parallel to that obtained in the more thorough microscopic investigation on the recrystallization of higher purity aluminum by Anderson and Mehl.

Assuming that the linear relationship of this plot is admissible, the calculated time for incidence of recrystallization of 2S-O alloy prestrained 0.09 and annealed at 400°F is of the order of magnitude of 10^{10} hr. Since the phenomenon described as orthorecovery is already clearly discernable in less than 18 hr after annealing the cold-worked 2S-O alloy, orthorecovery is distinctly separate from a recrystallization process. Orthorecovery appears to be a true recovery process.

Burgers¹⁵ has already discussed the mechanics of the recovery process in terms of dislocations but it will nevertheless be interesting to deduce what kinds of models of work-hardening are consistent with the preceding observa-

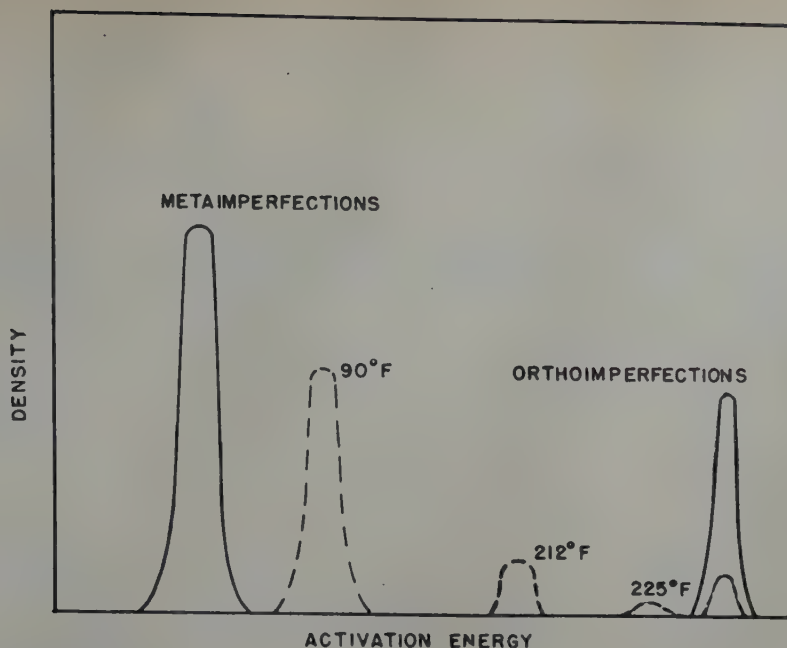


FIG 14—Schematic representation of distribution of imperfections induced by cold work as a function of activation energy for recovery.

tions on the recovery of the flow stress of cold-worked aluminum. It will be convenient to designate those imperfections that are removed by meta-recovery as metaimperfections and those that are removed by pure orthorecovery as orthoimperfections.

The activation energies for the removal of orthoimperfections by recovery must be higher but may overlap the activation energies for annihilation of metaimperfections. The rather uniformly continuing process of orthorecovery suggests that orthoimperfections do not have strong interaction energies and consequently the activation energy for orthorecovery appears to be independent of the density of orthoimperfections.

The process of metarecovery is more complex than that for orthorecovery. First two alternate models appear to be possible. One is shown in Fig 13 based on the assumption that the activation energies for recovery of the metaimperfections consist of a broad band of values and that there is no interaction between the metaimperfections so that their activation energies are independent of their densities. The broken curves marked 90 and 212°F give a schematic representation of the distribution of metaimperfections following several hours recovery at these temperatures. After annealing at 300 and 400°F for a few hours all of the

metaimperfections will have been removed and some of the orthoimperfections will have been eliminated. Since the orthoimperfections exist over a narrow band of activation energies, the process of orthorecovery will continue (but at an ever decreasing rate because of the decrease in the density of orthoimperfections) until complete recovery is achieved.

An alternate model is shown in Fig 14. Here it is assumed that the metaimperfections have an activation energy for recovery that is a function of their density. As they are removed by metarecovery their activation energy increases as shown by the broken curves which represent the metastable states achieved after annealing a few hours at 90 and 212°F respectively. At temperatures of 300 and 400°F recovery of all of the metaimperfections occurs in a very short period of time and thereafter pure orthorecovery continues, the orthoimperfections being eliminated without major changes in the activation energies of those that remain.

It is helpful now to define more precisely the kinetics of the recovery process. To a first approximation the process might be considered analogous to a unimolecular reaction wherein the rate of recovery is proportional to the number of imperfections per unit volume, namely

$$-\frac{dN}{dt} = kN$$

where N is the density of dislocation, t is the time and k is the rate constant. For metarecovery the rate constant k is probably given by

$$k = k_0 e^{-\{E-f(N)\}/RT}$$

where $f(N)$ is some function of the density of imperfections, E is the activation energy, R the gas constant and T the absolute temperature.

Thus, as recovery takes place $E - f(N)$ increases and the process substantially ceases before complete recovery is achieved. Unfortunately the present evidence on metarecovery rates is too incomplete to evaluate $f(N)$.

For orthorecovery, however, no interaction energy is assumed and k is simply given by

$$k = k_0 e^{-E/RT}$$

Consequently

$$\ln \left(\frac{Ni}{N} \right) = kt = tk_0 e^{-E/RT}$$

where Ni is the number of orthoimperfections at $t = 0$. Then

$$\ln \ln \left(\frac{Ni}{N} \right) = \ln k_0 - \frac{E}{RT} + \ln t$$

Assuming that when $\sigma_u - \sigma_r$ reaches some value upon orthorecovery, Ni/N is constant, the activation energy E is obtainable by plotting $\ln t$ vs. $1/T$ for constant values of $\sigma_u - \sigma_r$. The data for orthorecovery reported here for 2S-O alloy reveal that E is a constant

independent of the time of recovery. Furthermore, E is about 33,000 cal per mol. It is scarcely accidental that this value agrees well with the activation energies in Table 1 quoted by Zener.¹⁶

According to either of the postulated mechanisms, orthorecovery is not compatible with the recovery of Taylor's patterns of dislocations, whereas meta-recovery of the kind illustrated in Fig 13 is not inconsistent with Taylor's concept of the work-hardened state.

The assumption that work-hardening introduced two distinctly different types of imperfections, namely the meta- and the orthoimperfections, not only facilitates the analysis of the recovery data reported here, but it also clarifies several issues of long standing regarding the recovery process. First, the models for recovery based on the presence of meta- and orthoimperfections demand that the work-hardened state, after partial recovery, be dissimilar from any state achieved by work-hardening alone. This conclusion is necessary for at the lower annealing temperatures only the metaimperfections are eliminated whereas both imperfections are introduced simultaneously upon strain-hardening. Consequently, recovery is not exactly the reverse of strain-hardening. Secondly, it now becomes clearer why properties exhibit unique recovery rates upon annealing. Some properties, such as the yield strength, (and perhaps the electrical resistivity) are sensitive to recovery of metaimperfection whereas other properties, such as tensile strength, are rather insensitive to the metaimperfections and respond most effectively to the recovery of the orthoimperfections. Consequently, some properties may exhibit almost complete recovery before any appreciable recovery is detectable in other properties.

Conclusions

1. After recovery at low tempera-

Table 1 . . . Activation Energies for

| Aluminum | |
|---|--------|
| Process | |
| Volume Diffusion ¹⁶ | 37,500 |
| Grain Boundary Slip ¹⁶ | 34,500 |
| Creep ¹⁶ | 37,000 |
| Orthorecovery..... | 33,000 |

tures (90 and 212°F) cold-worked aluminum exhibits a low initial flow stress upon restraining. But after an additional strain of about 0.04 the flow stress is restored to essentially that value which would have been obtained if the specimen had not been recovered. This is called metarecovery.

2. At higher temperatures (300 and 400°F) not only is metarecovery observed, but a permanent decrease in the flow stress is obtained such that the stress-strain curve for the recovered metal is below that for the virgin metal at the same total strain for all strains. This is called orthorecovery.

3. The kinetics of meta- and orthorecovery appear to be distinctly different. This suggests that during work-hardening at least two kinds of imperfections are introduced, one which is rapidly recoverable, and a second which is more slowly recoverable. This assumption rationalizes the observed differences in recovery rates of different properties.

4. These observations strongly suggest that the work-hardened state is characterized by at least two essentially distinct types of imperfections.

Acknowledgment

This investigation was partly supported by the Office of Naval Research as part of a more extensive project on the plastic properties of aluminum alloys. The authors express their sincere appreciation to the O.N.R. and its personnel for support of this investigation. In addition they wish to thank Messrs. T. Tietz, R. Anderson and E. Berliner for their aid in conducting some of the tests, and Mrs. G. Pel-

towski for the preparation of the figures.

References

1. W. G. Burgers: Rekristallization Verformter Zustand und Erholung. *Handbuch der Metallphysik*, BdIII TeilIII, Leipsig (1941).
2. R. F. Mehl: Recrystallization. *Metals Handbook* (1948) p. 259-263.
3. A. E. Flanigan, L. F. Tedsen, and J. E. Dorn: Stress Rupture and Creep Tests on Aluminum-Alloy Sheet at Elevated Temperatures. *Trans. AIME* (1948) 175. *Metals Tech. Sept. 1947*. TP 2033.
4. J. E. Dorn, A. Goldberg and T. E. Tietz: The Effect of Thermal-mechanical History on the Strain Hardening of Metals. *Trans. AIME* (1949) 185, 20. *Jnl. of Metals*. Jan. 1949. TP 2445.
5. R. Becker: *Physik* 2. (1925) 26, 919.
6. E. Orowan: *Ztsch. Physik* (1934) 89, 605, 614, 634; (1935) 97, 573; (1936) 98, 382. *Proc. Phys. Soc.* (1940) 52, 8.
7. G. I. Taylor: *Proc. Roy. Soc.* (1934) A145, 362, 388, 405; *Proc. Fourth Intern. Congr. Appl. Mech.* Cambridge (1934) p. 113; *Ztsch. Kristallog* (1934) 89, 375.
8. M. Polanyi: *Ztsch. Phys.* (1934) 89, 660; *Ztsch. Metallk.* (1925) 17, 94.
9. J. M. Burgers: *Trans. Roy. Acad. Sci. Amsterdam* (1938) 16, 200; (1939) 42, 293; *Proc. Phys. Soc.* (1940) 52, 23.
10. W. G. Burgers and J. M. Burgers: *Nature* (1935) 135, 960; *Trans. Roy. Acad. Sci. Amsterdam* (1935) 15, 173.
11. W. A. Johnson and R. F. Mehl: *Trans. AIME* (1939) 135, 416.
12. J. K. Stanley and R. F. Mehl: *Trans. AIME* (1942) 150, 260.
13. F. C. Hull, R. A. Colton and R. F. Mehl: *Trans. AIME* (1942) 150, 185.
14. W. A. Anderson and R. F. Mehl: *Metals Tech.* Feb. 1945, TP 1805.
15. W. G. Burgers: Recovery and Recrystallization Viewed as Processes of Dissolution and Movement of Dislocations. *Proc. Udelandische Akademie van Wetenschappen L.*
16. C. M. Zener: Elasticity and Anelasticity of Metals. Univ. of Chicago Press (1948).



Carbides in Isothermally Transformed Chromium Steels

WALTER CRAFTS,* Member AIME, and JOHN L. LAMONT*

Electrolytic extraction of carbides from quenched and tempered steel and their examination under the electron microscope were found to be helpful in understanding the mechanism of secondary hardening in alloy steels¹ and the same technique has been applied to isothermally transformed steels. A preliminary survey of the utility of the method has indicated that it has promising possibilities for investigating the characteristics of pearlite and bainite. The examination of a few carbon and chromium steels has suggested that pearlite is formed with carbides of two varieties representing the lamellar and nonlamellar forms and that bainite appears to form with a structure analogous to, but significantly different from, martensite.

Procedure

The method used for examining the carbides was similar to that described previously.¹ The chromium steels used in the investigation were made from an Armco iron base in an induction furnace and were not treated with grain-refining deoxidizers. The composition of the steels is given in Table 1.

Three-inch square ingots were forged and rolled to $\frac{1}{8}$ -in. thick sheet for use in the isothermal studies. After rolling, the sheets were sandblasted to remove the rolling scale.

Specimens approximately $\frac{3}{4}$ -in. wide and $1\frac{1}{2}$ -in. long were prepared from the $\frac{1}{8}$ -in. sheet. They were heated in a salt bath at 2100°F (1150°C) for $\frac{1}{2}$ hour, transferred to other salt baths at 1300°F (704°C), 1000°F (538°C), 800°F (426°C), or 600°F (315°C), held

Table 1 . . . Composition of Steels

| Steel | Pct C | Pct Mn | Pct Si | Pct Cr |
|-------|-------|--------|--------|--------|
| A | 0.20 | 0.55 | 0.20 | 5.06 |
| B | 0.43 | 0.52 | 0.23 | 5.41 |
| C | 1.17 | 0.43 | 0.33 | 5.95 |

for various periods up to 100 hr and finally quenched in water. After quenching, the specimens were cut in half, one half being submitted to microscopic examination and the other half being used for the electrolytic extraction. The isothermally transformed specimens were submitted to examination under the light microscope to determine the degree of transformation and type of structure and were photographed at 2000 \times .

Carbide residues were obtained by electrolyzing in 10 pct hydrochloric acid and collecting the residue in glycerine to minimize attack by the acid. As pointed out in the earlier paper, the carbides are attacked to some degree during electrolysis. This attack is relatively minor on the coarser carbides but may be quite severe on the fine bainitic carbides. The residues were washed free of the

glycerine with water and alcohol. The alcohol was removed by repeated washings of amyl acetate, and the amyl acetate suspensions were transferred to stoppered vials. Debye-Sherrer X ray diffraction patterns of the residues were prepared using a chromium target. A selection based on the microstructure and X ray data was then made of samples considered most illustrative of the progress of transformation. Electrolytically extracted residues from these samples were submitted to examination by W. D. Forgeng and A. C. Jenkins on the electron microscope at the Research Laboratories of The Linde Air Products Co. and electron micrographs were made at $\times 5000$ and enlarged to 25,000 \times . The micrographs obtained with both the light and the electron microscopes are mounted side by side in the accompanying figures.

Although no effort was made to establish the T-T-T diagram for the chromium steels, the times for holding in the salt bath were adjusted with the intention of making the samples represent different stages in the transformation at temperatures of 600, 800, 1000, and 1300°F. The degrees of transformation and results of X ray examination are shown in Tables 2-4. The carbide designations refer to orthorhombic or trigonal carbide types and are not meant to imply that the compositions are exactly as indicated.

X ray Diffraction Data

The occurrence of Fe_3C and Cr_7C_3 in these steels was found to be consistent with published data on comparable chromium steels. Steels A and B with relatively low ratios of carbon to chromium contained Cr_7C_3 in the pearlitic structures and Fe_3C in the

New York Meeting, February 1950.

TP 2709 E. Discussion of this paper (2 copies) may be sent to *Transactions AIME* before May 1, 1950. Discussion is tentatively scheduled for publication in November 1950.

Manuscript received June 2, 1949.

* Chief Metallurgist and Research Metallurgist, respectively, Union Carbide and Carbon Research Laboratories, Inc., Niagara Falls, N. Y.

¹ References are at the end of the paper.

Table 2 . . . Constituents in X Ray Patterns of Extracted Residues of Steel A—0.20 Pct C—5.06 Pct Cr After Indicated Degree of Transformation

| 1300°F | | | | | | |
|-------------------------|--------|-------|--|--|---|---|
| Time at Temp. | 36 Sec | 6 Min | 20 Min | 1 Hr | 10 Hr | 100 Hr |
| Pct transformation..... | 0 | 1-2* | 15 | 99* | 99 | 100* |
| X ray pattern..... | (a) | Blank | Cr ₇ C ₃ (3) Cr ₂ N (2) p (b) (1) | Cr ₇ C ₃ (3) Cr ₂ N (1) p (b) (4) | Cr ₇ C ₃ (4) Cr ₂ N (4) | Cr ₇ C ₃ (4) Cr ₂ N (4) |
| 1000°F | | | | | | |
| Pct transformation..... | 0 | 0 | | 0 | 0 | 1* |
| X ray pattern..... | (a) | (a) | | (a) | (a) | Blank |
| 800°F | | | | | | |
| Pct transformation..... | 1-2 | 85* | | 90 | 95 | 98* |
| X ray pattern..... | Blank | Blank | | Fe ₃ C (2) | Fe ₃ C (2) | Fe ₃ C (2) |

* Residues submitted to electron microscope studies.
(a) No extractions made.
(b) Unidentified constituent—For d-values see Table 5.
(1) Very faint pattern.
(2) Poor pattern.
(3) Fair pattern.
(4) Good pattern.

Table 3 . . . Constituents in X Ray Patterns of Extracted Residues of Steel B—0.43 Pct C—5.41 Pct Cr After Indicated Degree of Transformation

| 1300°F | | | | | | |
|-------------------------|-------|---|---|--|---|---|
| Time at Temp. | 6 Min | ½ Min | 12 Hr | 1 Hr | 10 Hr | 100 Hr |
| Pct transformation..... | 5 | 20* | 95 | 98* | 99 | 100* |
| X ray pattern..... | Blank | Cr ₇ C ₃ (2) p (b) (1) | Cr ₇ C ₃ (3) p (b) (2) | Cr ₇ C ₃ (3) p (b) (4) Cr ₂ N (1) | Cr ₇ C ₃ (4) Cr ₂ N (4) | Cr ₇ C ₃ (4) Cr ₂ N (4) |
| 1000°F | | | | | | |
| Pct transformation..... | 0 | | | 0 | 1 | 35* |
| X ray pattern..... | (a) | | | (a) | Blank | Cr ₇ C ₃ (4) p (b) (4) |
| 600°F | | | | | | |
| Pct transformation..... | 1 | | 20* | 75 | 80* | 95 |
| X ray pattern..... | Blank | | Fe ₃ C (1) | Fe ₃ C (3) | Fe ₃ C (4) | Fe ₃ C (4) |

* Residues submitted to electron microscope studies.
(a) No extractions made.
(b) Unidentified constituent—For d-values see Table 5.
(1) Very faint pattern.
(2) Poor pattern.
(3) Fair pattern.
(4) Good pattern.

Table 4 . . . Constituents in X Ray Patterns of Extracted Residues of Steel C—1.17 Pct C—5.95 Pct Cr After Indicated Degree of Transformation†

| 1300°F | | | | | | |
|-------------------------|---|---|--|--|--|---|
| Time at Temp | 3.25 Min | 6 Min | 1 Hr | 3 Hr | 10 Hr | 100 Hr |
| Pct transformation..... | 65* | 95 | 99* | | 99 | 100* |
| X ray pattern..... | Cr ₇ C ₃ (2) Fe ₃ C (3) | Cr ₇ C ₃ (3) Fe ₃ C (3) | Cr ₇ C ₃ (4) Fe ₃ C (3) p (b) (4) | | Cr ₇ C ₃ (4) Fe ₃ C (3) p (b) (1) | Cr ₇ C ₃ (4) |
| 1000°F | | | | | | |
| Pct transformation..... | | Trace | 5* | 50* | 95 | 98* |
| X ray pattern..... | | Cr ₇ C ₃ (2) | Cr ₇ C ₃ (2) Fe ₃ C (2) | Cr ₇ C ₃ (3) Fe ₃ C (3) p (b) (4) | Cr ₇ C ₃ (3) p (b) (4) | Cr ₇ C ₃ (4) p (b) (4) |
| 600°F | | | | | | |
| Pct transformation..... | | 0 | 0 | | 1 | 5* |
| X ray pattern..... | | (a) | (a) | | Cr ₇ C ₃ (3) | Cr ₇ C ₃ (2) Fe ₃ C (2) |

* Residues submitted to electron microscope studies.
† Cr₇C₃ noted in X ray pattern of direct quenched sample.
(a) No extractions made
(b) Unidentified constituent—For d-values see Table 5.
(1) Very faint pattern.
(2) Poor pattern.
(3) Fair pattern.
(4) Good pattern.

bainitic range. A pattern of the Cr₂N type was also found in steels A and B transformed at 1300°F. In general, the patterns of Fe C, Cr₇C₃, and Cr₂N increased in definition and intensity with the length of time the specimens were held at temperature.

Undissolved carbide was present after austenitizing steel C and X ray diffraction revealed a corresponding Cr₇C₃ pattern in all specimens. The carbide formed as the initial product of transformation at all temperatures appeared to be Fe₃C, but this pattern tended to disappear from pearlitic structures, leaving only Cr₇C₃ after long holding at temperature. As shown in Table 5, the dimensions of the

Table 5 . . . d-Values of Cr₇C₃ Type Carbides and Unidentified Constituent in 5 Pct Chromium Steel Residues

| Cr ₇ C ₃ Type from Steels A and B | | Cr ₇ C ₃ Type from Steel C | | Unidentified Constituent | |
|---|--------------------|--|--------------------|--------------------------|--------------------|
| d-Å | Relative Intensity | d-Å | Relative Intensity | d-Å | Relative Intensity |
| 2.28 | 5 | 2.27 | 5 | 2.43* | 2 |
| 2.11 | 5 | 2.10 | 6 | 2.08 | 3 |
| 2.03 | 10 | 2.02 | 10 | 2.06 | 2.5 |
| 2.01 | 2 | 1.99 | 2 | 1.93 | 1.5 |
| 1.89 | 1 | 1.90 | 1 | 1.59 | 2 |
| 1.84 | 2 | 1.82 | 3 | 1.23 | 1.5 |
| 1.80 | 4 | 1.79 | 5 | | |
| 1.74 | 3 | 1.73 | 3 | | |
| 1.60 | 0 | 1.59 | 1 | | |
| 1.43 | 2 | 1.42 | 3 | | |
| 1.34 | 2 | 1.34 | 3 | | |
| 1.32 | 1 | 1.315 | 2 | | |
| 1.25 | 1 | 1.245 | 1 | | |
| 1.199 | 4 | 1.195 | 5 | | |
| 1.175 | 4 | 1.172 | 5 | | |
| 1.163 | 3 | 1.159 | 3 | | |
| 1.159 | 3 | 1.154 | 3 | | |

* Not known if this value is a result of this constituent.

Cr₇C₃ pattern found in the 1.17 pct carbon steel C were different from those in the Cr₇C₃ pattern found in the lower carbon steels A and B. The Cr₇C₃ pattern of a steel containing 0.70 pct carbon and 5 pct chromium was also of the same dimensions as that found in the lower carbon steels, so that the change would seem to be discontinuous and probably represents a decided difference in composition.

In addition to the normally expected phases, the residues of specimens held for intermediate periods at temperatures producing pearlitic structures also contained a phase that gave a pattern with "d" values as given in Table 5. The pattern of this phase tended to appear only after the transformation was well advanced and to disappear on holding after completion of transformation. The nature of the phase has not been identified.

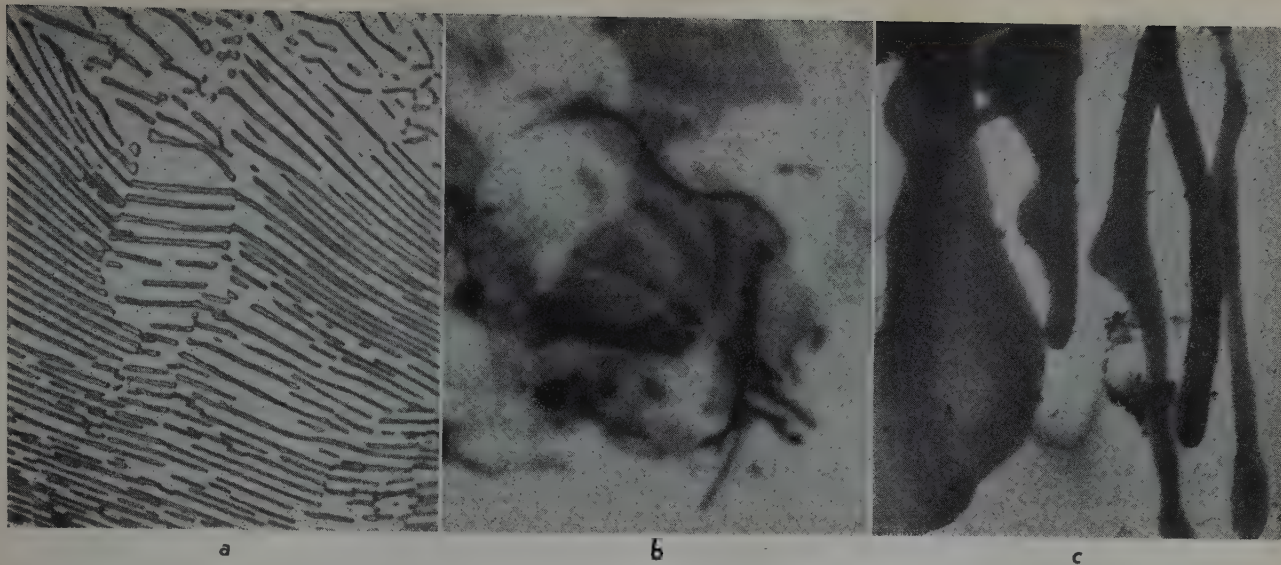


FIG 1—Eutectoid carbon steel, cooled very slowly from 1850°F.

A—Micrograph of steel. $\times 2000$. B—Micrograph of extracted residue. $\times 2000$. C—Electron micrograph of extracted residue. $\times 20,000$.

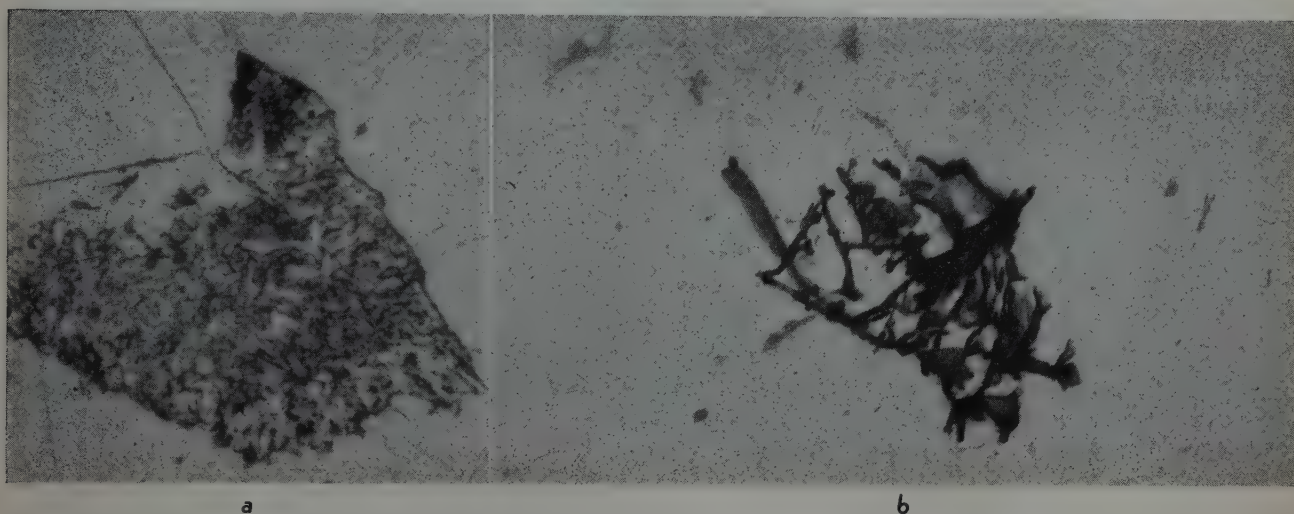


FIG 2—Steel A—0.20 pct C, 5.06 pct Cr. Transformed 1–2 pct after 6 min at 1300°F.

A—Steel structure. $\times 2000$. B—Extracted residue. Electron micrograph. $\times 25,000$.

Microscopic Examination of Carbides in Pearlite

A limited number of carbon steels, transformed isothermally and by continuous cooling, as well as the chromium steels, have been studied by electrolytic extraction and examination of the carbide residue on both the light and electron microscopes. Only the coarser structures permit a direct comparison at comparable magnification between the structure found in the metal and the appearance of extracted carbides as revealed by transmitted light and the electron beam. However, the structures are sufficiently similar to make the higher magnification electron micrographs of finer structures quite convincing.

The pearlitic structures found in the 5 pct chromium steels were quite fine,

only partly lamellar, and generally of a confused and granular appearance rather than the well defined lamellar structure of slowly cooled carbon steel. The carbides extracted from well developed lamellar pearlite in a slowly cooled eutectoid carbon steel are illustrated by light and electron micrographs in Fig 1. The typical carbide is a thin, very irregularly shaped, and often curled plate. It may contain holes and usually has deeply indented bays. There are thickened knobs and fingers at the edges and sometimes within the body of the plate. The thickened edges appear to correspond with the clubby ends of pearlite lamellae seen in polished cross-sections of steel. This type of carbide was illustrated by Koch² using a similar procedure.

The predominant carbides extracted

from the fine pearlite of carbon steels transformed at relatively low temperatures are thicker skeletal or rod-like shapes of very irregular appearance. This type of carbide is illustrated in many of the micrographs of chromium steel residues where it will be seen that it is too thick to be penetrated by the electron beam. Because the thin plate type is predominant in specimens with well developed lamellar pearlite and the more massive skeletal type occurs mainly in specimens with little of the lamellar structure, it would appear that confused pearlite structures are actually not lamellar, but are composed mainly of carbides of the massive skeletal type. Both types of carbide are specific to pearlitic structures and may be readily distinguished from the residues of bainitic or tempered martensitic structures.

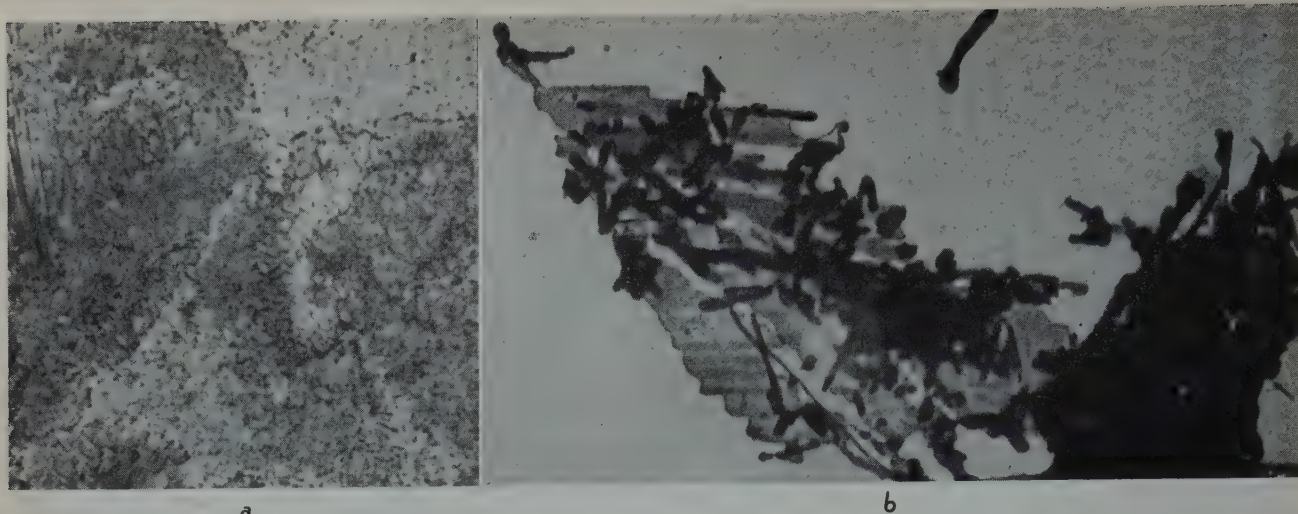


FIG 3—Steel A—0.20 pct C, 5.06 pct Cr. Transformed 99 pct after 1 hr at 1300°F.
A—Steel structure. $\times 2000$. B—Extracted residue. Electron micrograph. $\times 25,000$.

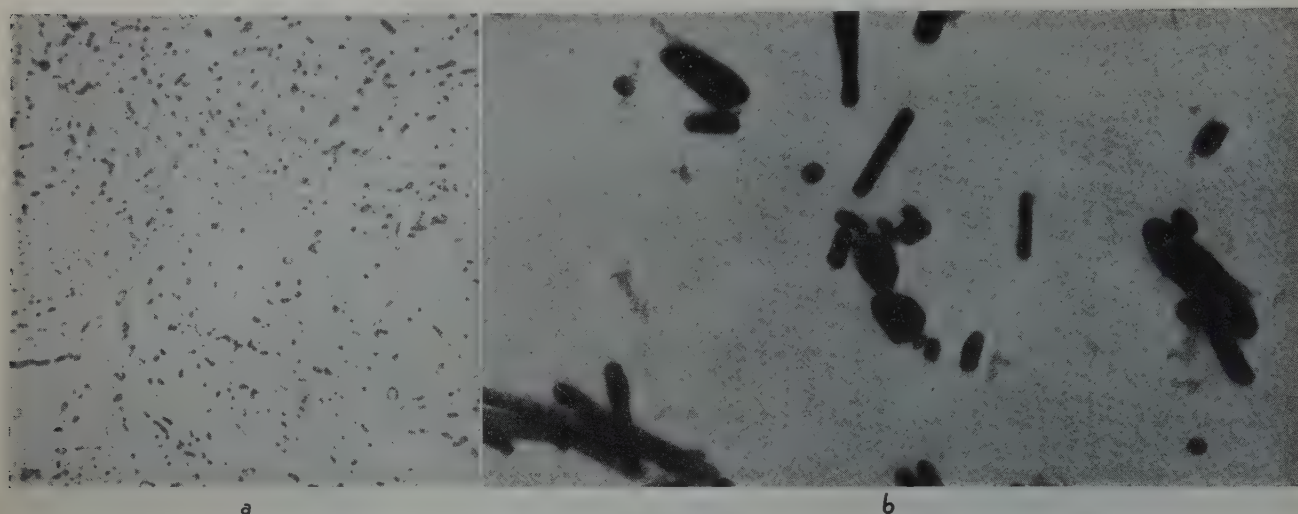


FIG 4—Steel A—0.20 pct C, 5.06 pct Cr. Transformed 100 pct after 100 hr at 1300°F.
A—Steel structure. $\times 2000$. B—Extracted residue. Electron micrograph. $\times 25,000$.

The carbides extracted from the pearlitic chromium steels, as well as micrographs of the corresponding steel structures are shown in Fig 2-5, 8-12, 14-19, and 21-22.

The carbides found in steel A transformed at 1300°F, as shown in Fig 2, show an initially fine structure composed mainly of the massive type of carbide in a complex irregular pattern. After 1 hr at 1300°F, as shown in Fig 3, the transformation was virtually complete, and the carbide particles are much coarser than in Fig 2. Both thin and thick carbides are present in a much more well developed form. The thin plate is seen to be corrugated or ribbed to a degree that was not observed in carbon steels, and the massive types are more crystalline in shape than at earlier stages in the transformation. After 100 hr at 1300°F, as shown in Fig 4, the light microscope revealed a spheroidized structure with virtually no lamellae, and the extracted residue

contained only massive, more or less idiomorphic, crystals. The thin plates were absent and had either been absorbed or had coalesced into the idiomorphic carbides. Similar carbide particles were shown by Koch and Wiester³ after an extended tempering of pearlite.

Both thin and massive carbides in steel B transformed at 1300°F, as shown in Fig 8-10, tend to be very long and relatively narrow, but are qualitatively similar to those found in steel A. The tendency toward thickening at the edges of the thin plates is particularly well illustrated in Fig 8. Some of the thin carbides are still present after 100 hr, although the predominant type is the well developed crystals. The appearance of the thin carbide shown in Fig 10 is somewhat more dense than is typical of specimens held for a shorter time at temperature, and there is a tendency toward local thickening. It is presumed that this represents a

typical mechanism by which the thin particles are converted to a more massive form, although the time involved is so great that a good deal of absorption and reprecipitation could occur. It is probable that the growth of the massive particles also progresses by a diffusion reaction.

The carbides found in steels A and B after 100 hr at 1000°F, Fig 5 and 11, are appreciably smaller than the carbides found after a comparable degree of transformation at 1300°F. However, they are quite similar in character even though the structure as seen in the light microscope is too fine to be resolved satisfactorily.

The carbides produced at 1300°F in steel C, as shown in Fig 14-16, are quite similar to those found in steel A. Although some undissolved carbide was present in these samples, it was not observed in the extracted residues. Ordinarily large carbide particles are too heavy to be supported by the suspend-

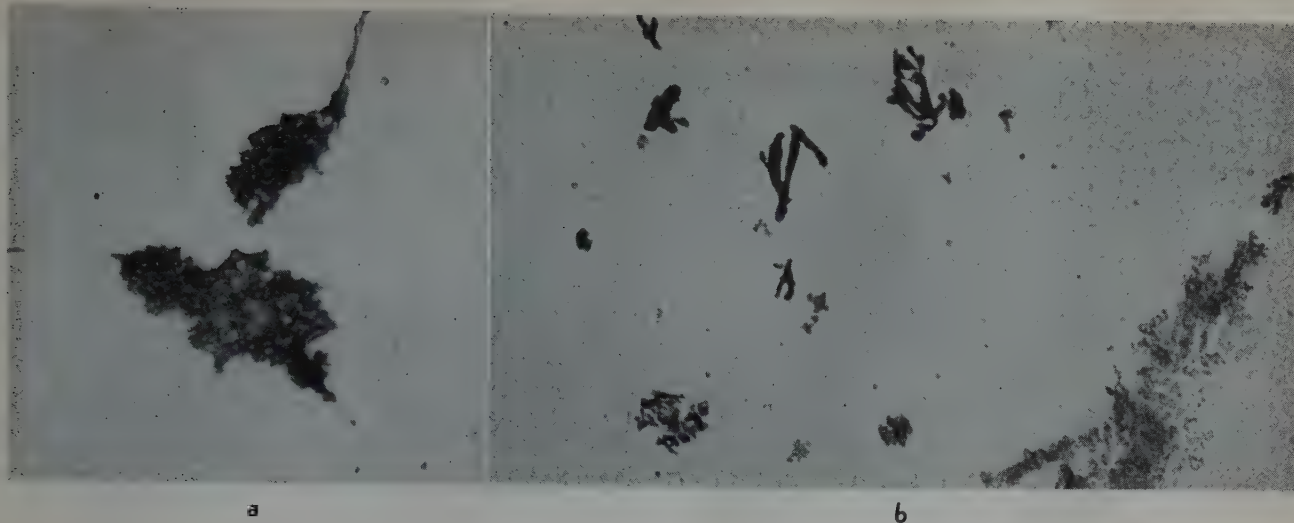


FIG 5—Steel A—0.20 pct C, 5.06 pct Cr. Transformed 1 pct after 100 hr at 1000°F.
A—Steel structure. $\times 2000$. B—Extracted residue. Electron micrograph. $\times 25,000$.

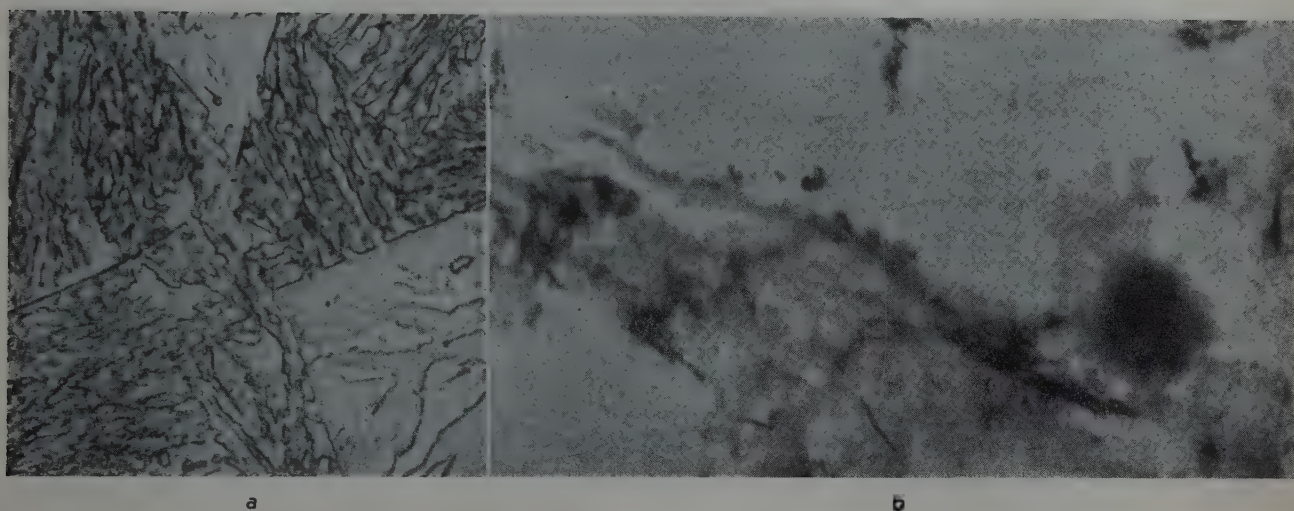


FIG 6—Steel A—0.20 pct C, 5.06 pct Cr. Transformed 85 pct after 6 min at 800°F.
A—Steel structure. $\times 2000$. B—Extracted residue. Electron micrograph. $\times 25,000$.

ing film used for electron microscope examination, so that they may not be observed in the examination of extracted residues. Transformation of steel C at 1000°F produced “arborescent” pearlite structures as shown in the light micrographs of Fig 17–18. Although the extracted carbides are quite small in the initial stages of transformation, they do not appear to be significantly different from those formed at 1300°F. In the same manner as at higher temperatures, the carbides become progressively larger as the specimens are held longer at temperature.

In general, it would appear that the carbide particles in pearlite are of a similar character regardless of the specific composition of the steel or temperature of transformation. There are two well defined types of carbide shape. The difference in character between the thin plates and the more massive carbide particles is shown in Fig 21. The extracted residue was

shadowed with gold before examination on the electron microscope, and the resulting electron micrographs clearly show the relative thickness of the carbide particles. One is a thin plate of very irregular shape tending toward heavier knobs and fingers at the edges. The other is a more massive type that occurs in an irregular skeletal or rod-like form. Both types eventually grow into the idiomorphic form illustrated in Fig 22. The thin type occurs more commonly in well organized lamellar structures and the more massive skeletal type tends to be formed in the more confused sublamellar structures. It would seem reasonable to believe that the plates represent the carbides of strictly lamellar pearlite. Pearlite in which it is difficult to see lamellae is presumably composed principally of the more massive skeletal type of carbides. It would appear that those nonlamellar areas of pearlite that are sometimes considered to be oriented

unfavorably to visualize lamellae are actually nonlamellar.

A tempering process with growth of the carbide particles seems to start immediately after transformation and to progress continuously before and after transformation is completed. It was not possible to isolate small carbide particles in the later stages of transformation and identify them as having been formed more recently than the larger carbides. Because of the time involved in the later stages of transformation, it is considered probable that even the freshly formed carbides would be tempered appreciably before examination. It is doubted, therefore, whether it would be reasonable to expect that this method of examination will readily reveal whether the size of carbides transformed late are affected by the growth of previously formed carbides. The progress of tempering of both the thin plates and the skeletal carbides to larger massive and ultimately

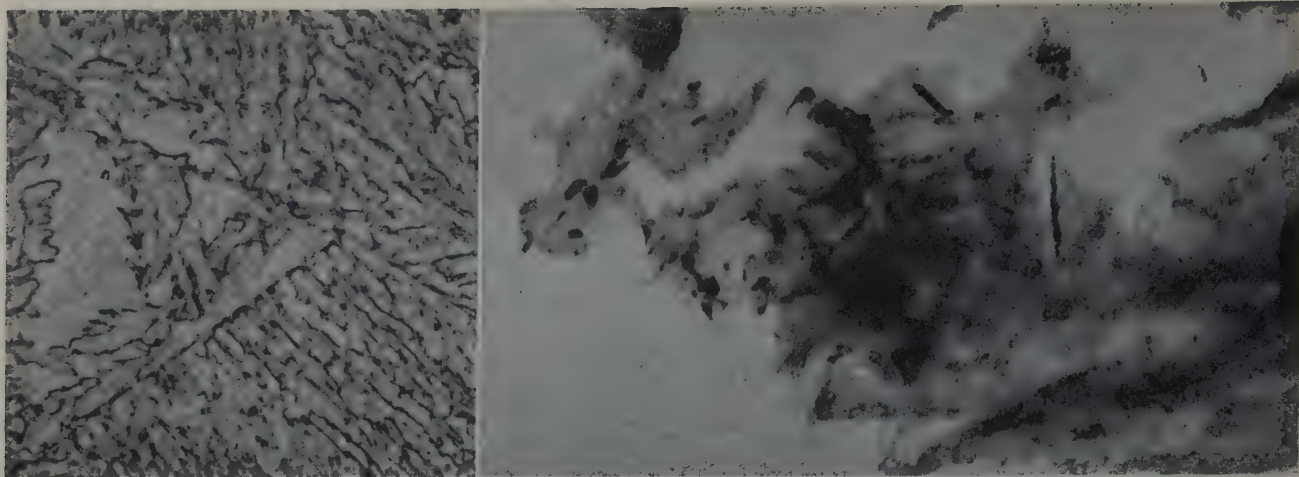


FIG 7—Steel A—0.20 pct C, 5.06 pct Cr. Transformed 98 pct after 100 hr at 800°F.
A—Steel structure. $\times 2000$. B—Extracted residue. Electron micrograph. $\times 25,000$.

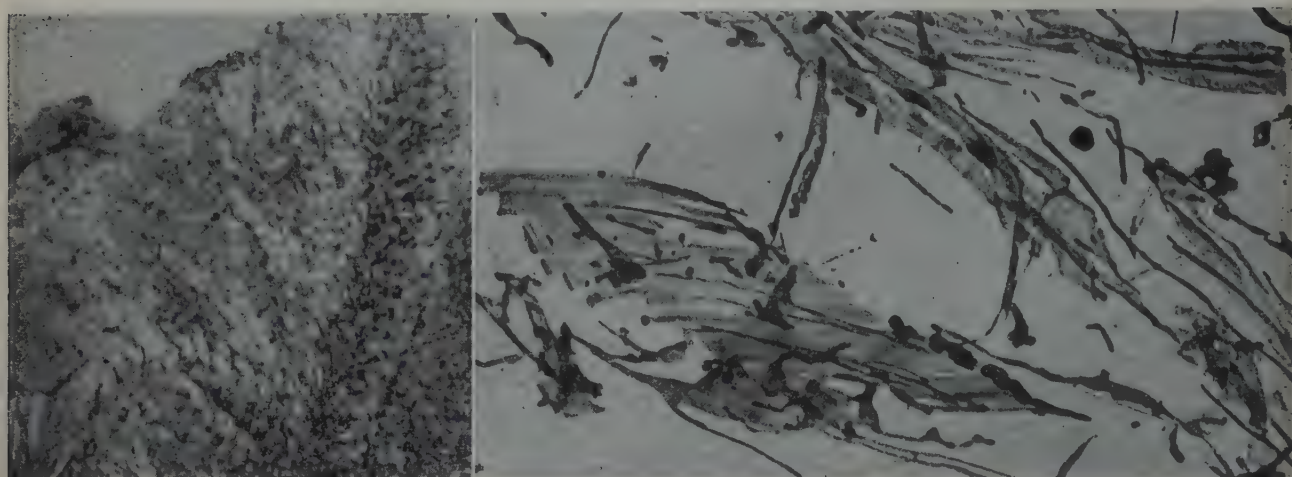


FIG 8—Steel B—0.43 pct C, 5.41 pct Cr. Transformed 20 pct after 12 min at 1300°F.
A—Steel structure. $\times 2000$. B—Extracted residue. Electron micrograph. $\times 25,000$.



FIG 9—Steel B—0.43 pct C, 5.41 pct Cr. Transformed 98 pct after 1 hr at 1300°F.
A—Steel structure. $\times 2000$. B—Extracted residue. Electron micrograph. $\times 25,000$.

idiomorphic particles seems to be accomplished in part by coagulation of the more extended shapes as well as by normal diffusion and growth.

Microscopic Examination

of Residues from Bainitic Structures

The structures formed in chromium steel specimens treated to produce bainite are illustrated in Fig 6-7, 12-13,

20 and 23. The structures of the extracted residues appear to consist of a nebulous cloud of very fine particles in which there is a concentration of many or larger particles on certain planes as well as a number of well defined par-



FIG 10—Steel B—0.43 pct C, 5.41 pct Cr. Transformed 100 pct after 100 hr at 1300°F.
A—Steel structure. $\times 2000$. B—Extracted residue. Electron micrograph. $\times 25,000$.

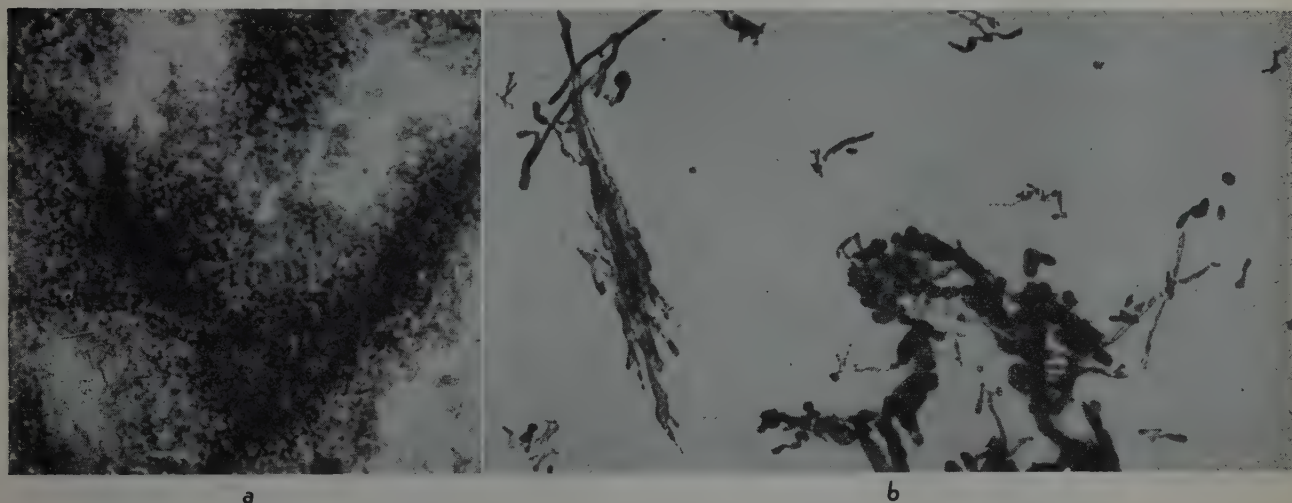


FIG 11—Steel B—0.43 pct C, 5.41 pct Cr. Transformed 35 pct after 100 hr at 1000°F.
A—Steel Structure. $\times 2000$. B—Extracted residue. Electron micrograph. $\times 25,000$.

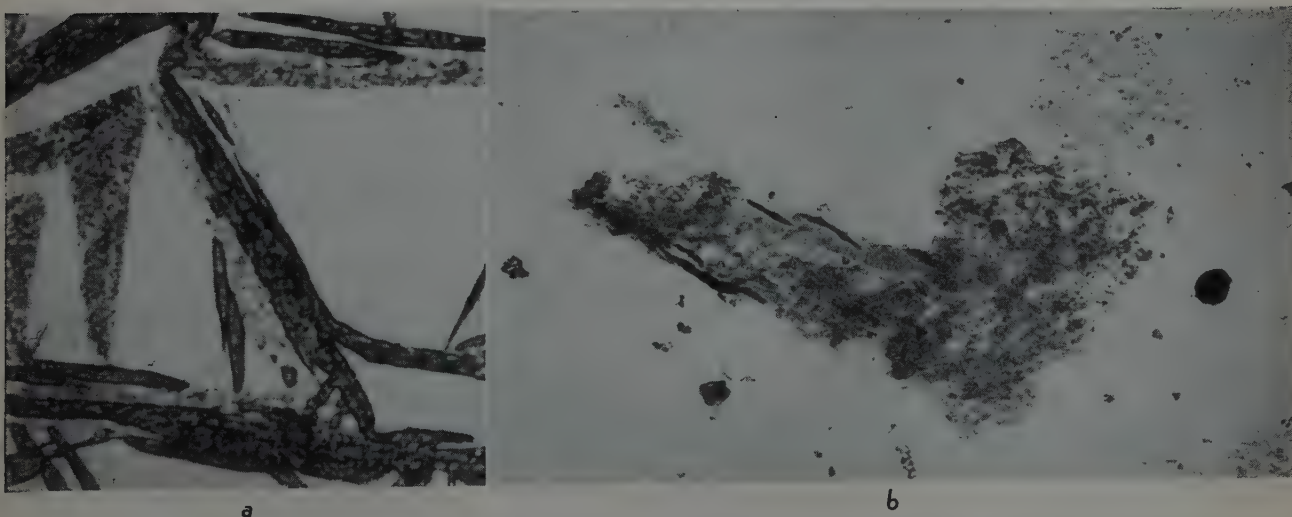


FIG 12—Steel B—0.43 pct C, 5.41 pct Cr. Transformed 20 pct after 30 min at 600°F.
A—Steel structure. $\times 2000$. B—Extracted residue. Electron micrograph. $\times 25,000$.

ticles of a larger order of size. The "graininess" or size of the particles seems to increase as time at temperature and degree of transformation increase, but the structure never becomes sufficiently well defined to give

much assurance that the structures are adequately resolved.

Each group or cloud that appears to be a cluster of a myriad of particles has been shown by gold shadowing in Fig 23 to have a considerable thickness,

so that the electron beam has partially penetrated a great volume of fairly low density. The velvety black zones in Fig 6 and 20 are typical of residues extracted from martensite in which it is probable that the residue itself is only

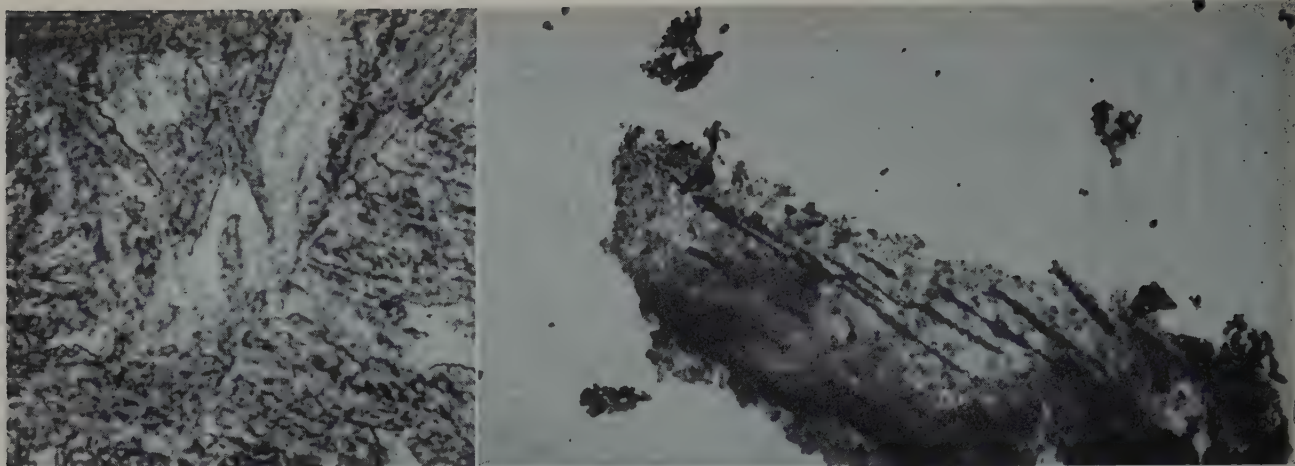


FIG 13—Steel B—0.43 pct C, 5.41 pct Cr. Transformed 80 pct after 10 hr at 600°F.
A—Steel structure. $\times 2000$. B—Extracted residue. Electron micrograph. $\times 25,000$.

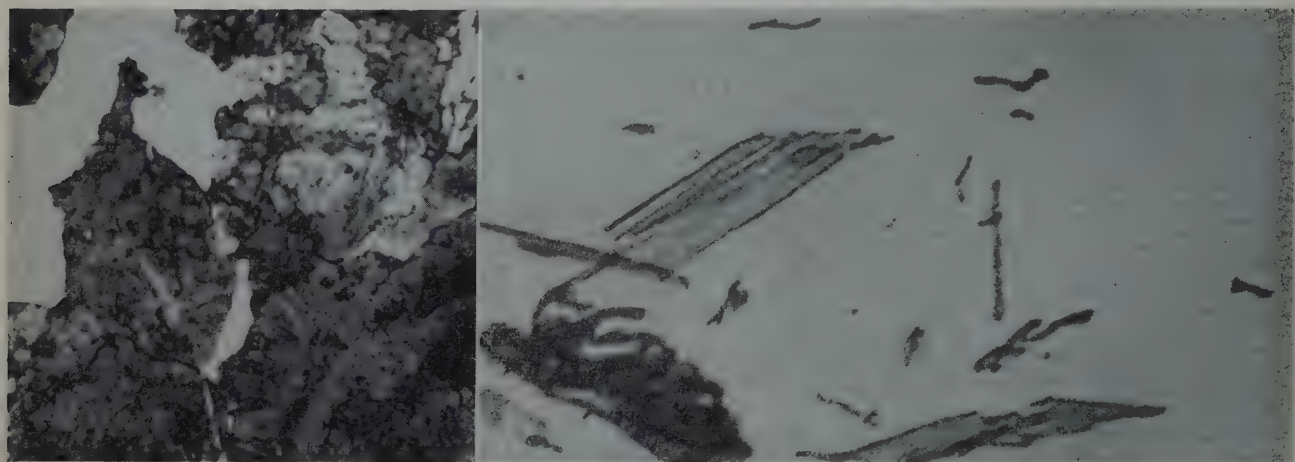


FIG 14—Steel C—1.17 pct C, 5.95 pct Cr. Transformed 65 pct after 3.25 min at 1300°F.
A—Steel structure. $\times 2000$. B—Extracted residue. Electron micrograph. $\times 25,000$.

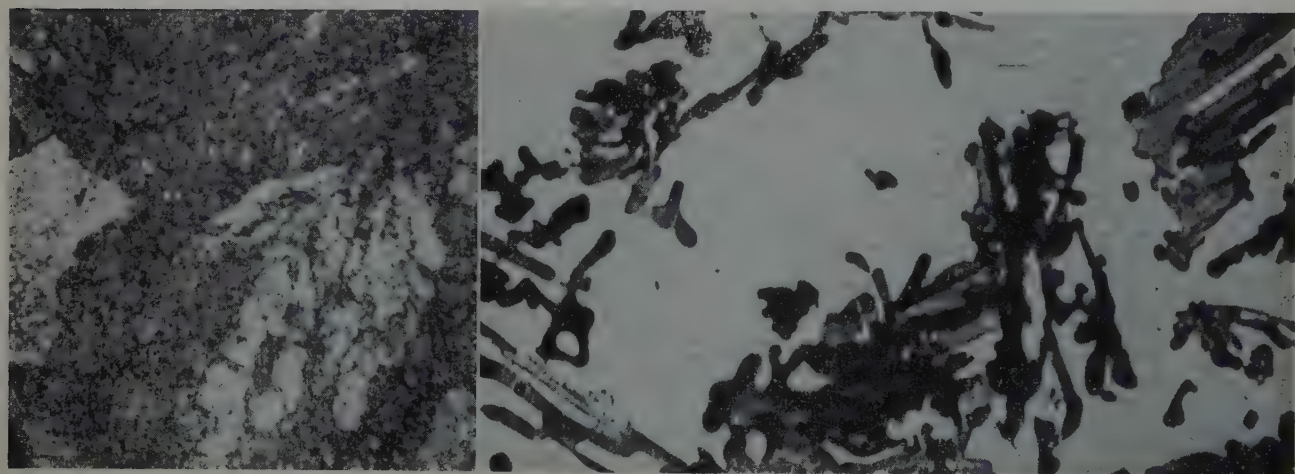


FIG 15—Steel C—1.17 pct C, 5.95 pct Cr. Transformed 99 pct after 1 hr at 1300°F.
A—Steel structure. $\times 2000$. B—Extracted residue. Electron micrograph. $\times 25,000$.

amorphous carbon. No analytical work has been done on these bainite residues, so that it is possible that the residue is not carbide but a metamorphosed representation. The granular structure of the "clouds" is quite different from

that previously found¹ in tempered martensite residues in which indications of individual particles were not observed. As time at temperature and degree of transformation increase, the structure becomes even more granular,

probably reflecting an increase in the size of the individual particles. It has also been observed that residues of bainitic carbon steels transformed in shorter periods are intermediate in appearance between the bainitic chro-

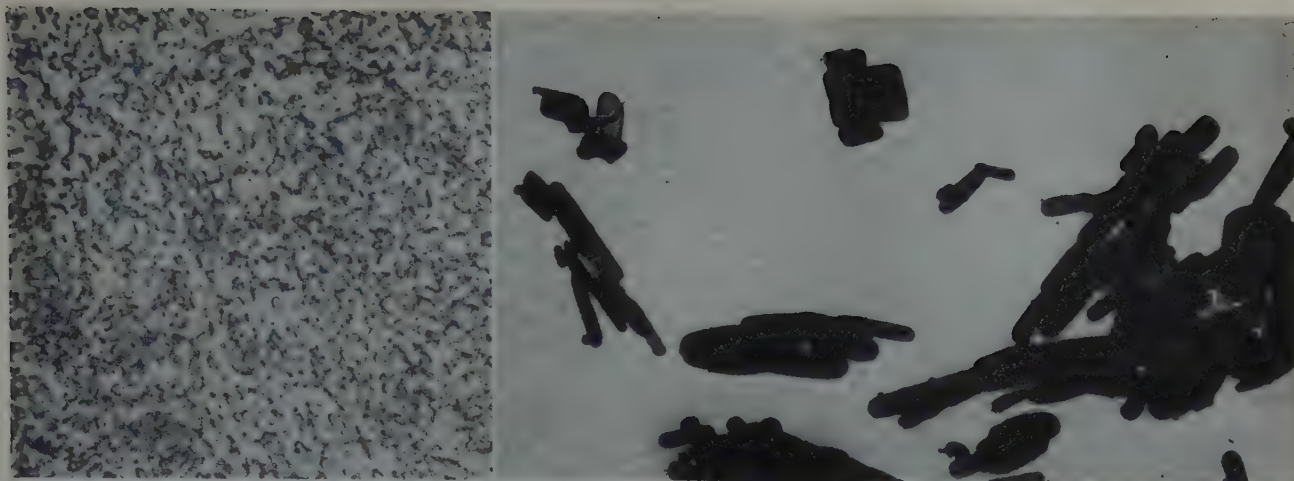


FIG 16—Steel C—1.17 pct C, 5.95 pct Cr. Transformed 100 pct after 100 hr at 1300°F.
A—Steel structure. × 2000. B—Extracted residue. Electron micrograph. × 25,000.

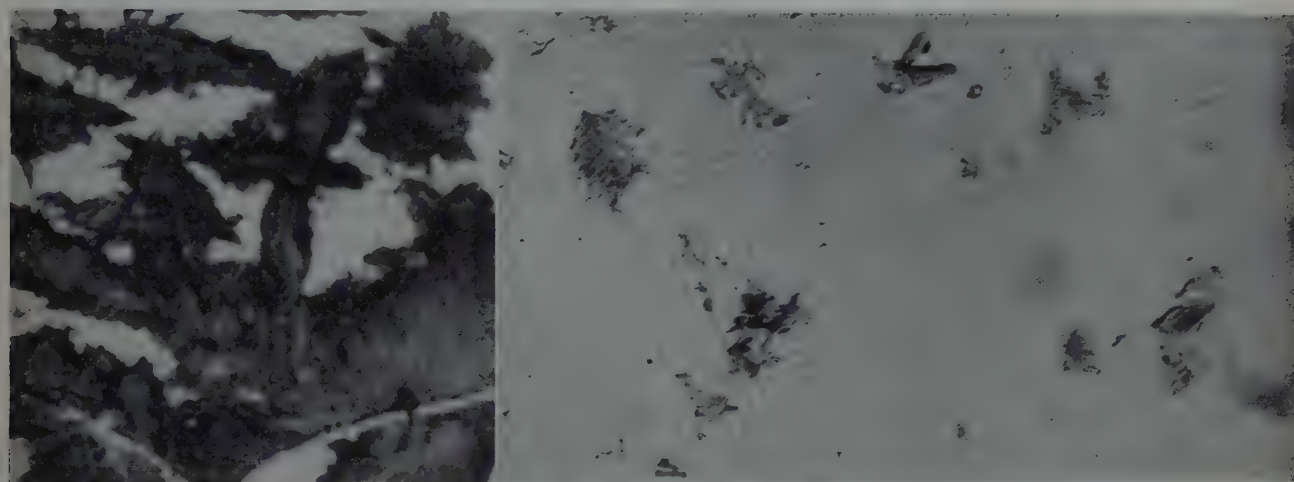


FIG 17—Steel C—1.17 pct C, 5.95 pct Cr. Transformed 5 pct after 1 hr at 1000°F.
A—Steel structure. × 2000. B—Extracted residue. Electron micrograph. × 25,000.

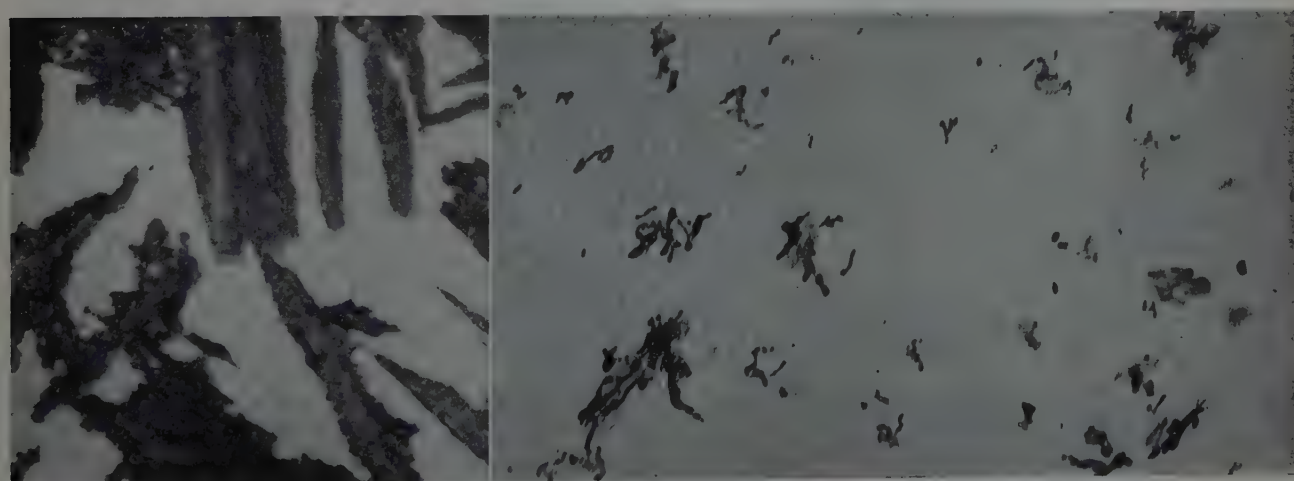


FIG 18—Steel C—1.17 pct C, 5.95 pct Cr. Transformed 50 pct after 3 hr at 1000°F.
A—Steel structure. × 2000. B—Extracted residue. Electron micrograph. × 25,000.

mium steel residues and martensitic residues, and it is inferred that the growth of the fine particles to dimensions visible at this magnification results from a tempering process.

In a similar manner the thickened

planes that are seen in the cloudy matrix are significantly different from similar planes in martensite residues. The character of these planes is best shown in Fig 13 where three small zones are separated from the main

cluster. These are believed to be the fragments of the thickened planes that appear to contain larger particles than the matrix. The size of the particles and possibly their number increase with time at temperature. Such structures

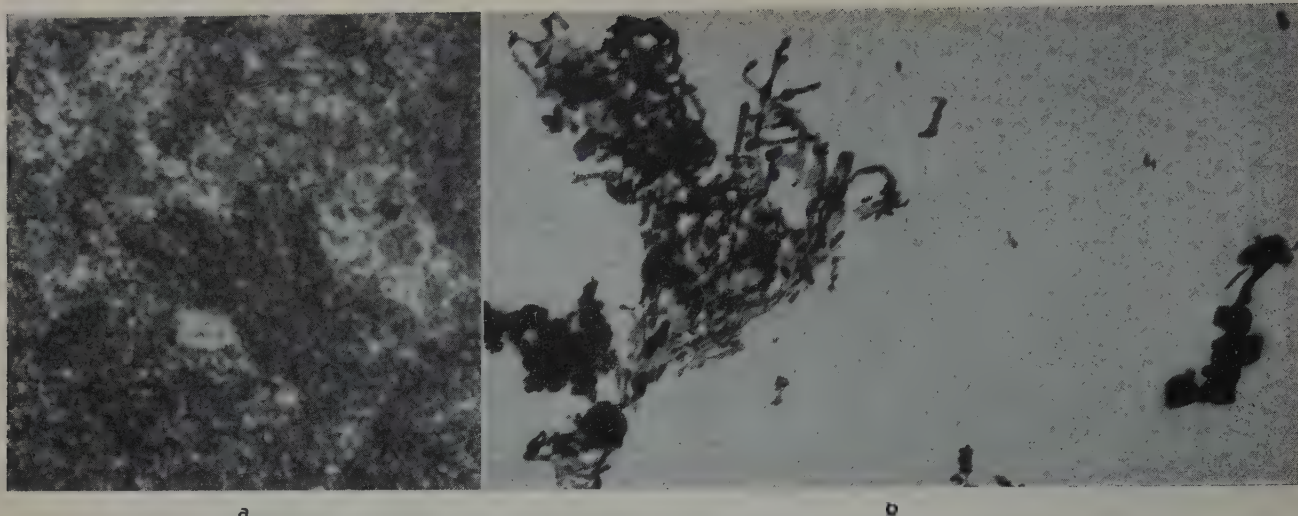


FIG 19—Steel C—1.17 pct C, 5.95 pct Cr. Transformed 98 pct after 100 hr at 1000°F.
A—Steel structure. $\times 2000$. B—Extracted residue. Electron micrograph. $\times 25,000$.

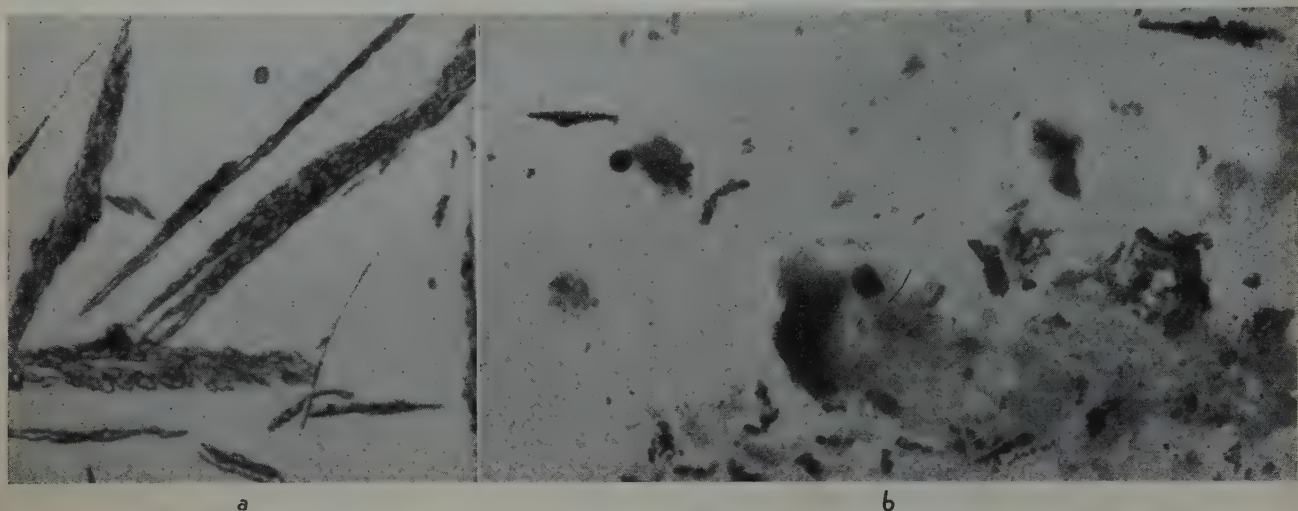


FIG 20—Steel C—1.17 pct C, 5.95 pct Cr. Transformed 5 pct after 100 hr at 600°F.
A—Steel structure. $\times 2000$. B—Extracted residue. Electron micrograph. $\times 25,000$.

have not been observed in tempered martensite where the density of the matrix is lessened by precipitation along many planes in the form of continuous two-dimensional plates rather than a number of fine particles. The well defined larger particles, shown best in Fig 7 and 20, seem to be of a different character and may have been formed by a different mechanism than that by which the main structure was formed.

Although it is not presumed that these structures are adequate to answer the question of whether bainite forms initially as a single phase or as an aggregate, the structures are quite suggestive. With respect to these steels it is evident that, if it be assumed that the bainite formed initially by a martensite-like reaction and that it was tempered immediately, the resulting structure is significantly different from that formed when a truly martensitic structure is tempered by reheating.

Thus, if bainite in these steels were formed by the decomposition of a martensite-like constituent, either the transitional structure or the manner of its tempering is significantly different from martensite. However, the structure is so closely related to that of martensite that it is not possible to infer, as an obvious corollary, that bainite forms as an aggregate. An examination of bainite residues at much higher magnification would be desirable to obtain a better understanding of the structure.

Summary

Examination of carbide residues extracted electrolytically from chromium steels has been shown by X ray diffraction to be consistent with the normally expected constituents of these steels, except for observation of two forms, differing in lattice dimensions, of Cr_7C_3 and of an unidentified transi-

tional constituent in pearlitic specimens. Electron micrographs of the residues have shown characteristic forms of carbide for pearlite and bainite.

The carbides associated with pearlite are of two shapes. One is a thin irregularly shaped plate with thickened edges that is considered to be the lamellar carbide of regular pearlite and the other is a skeletal, rod-like or massive type that is considered to be the nonlamellar carbide in confused pearlite. The more extended forms of both types tend to coagulate locally, and the resulting massive particles, as well as the initially formed massive type carbides, grow by diffusion until they assume idiomorphic shapes in spheroidized pearlite structures. The tendency toward either type is controlled by the conditions of transformation rather than by specific effects of composition, and similar appearing carbides may be produced regardless of whether the carbide is of

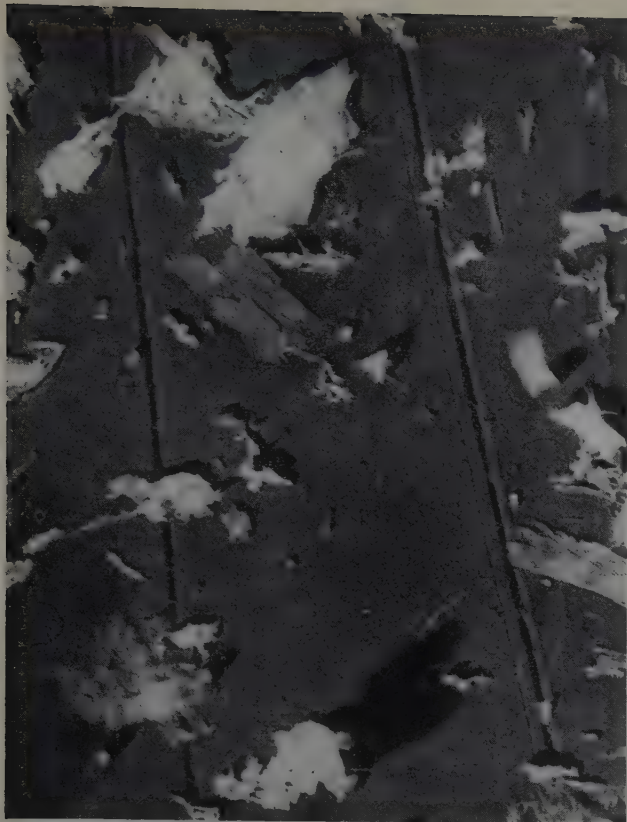


FIG 21—Electron micrograph of shadow-cast residues of Steel C.
× 10,000.

Transformed 65 pct after 3.25 min. at 1300°F.



FIG 22—Electron micrograph of shadow-cast residues of Steel C.
× 10,000.

Transformed 100 pct after 100 hr at 1300°F.

the Fe_3C or Cr_7C_3 type.

Residues from bainitic structures are closely analogous to those of martensite, but are significantly different. In bainite the residues have a nebulous, but granular, matrix, and discrete particles are found in the planes on which carbide tends to concentrate, rather than the unresolvable matrix and the continuous plates of tempered martensite residues. The bainite residues also contain fairly large particles not found in martensite residues. These characteristics suggest that although bainite may be formed in a manner analogous to martensite, the differences in structure are sufficiently great to indicate a significant difference in the mechanism. Further examination at much higher magnification should be helpful in understanding bainite formation.

Although this study of extracted carbides has been limited to the cursory examination of a few steels, it would appear that this use of the electron microscope is capable of adding considerably to our understanding of the structures of steel.

Acknowledgments

The authors wish to acknowledge the generous cooperation of the staff of the Union Carbide and Carbon Research

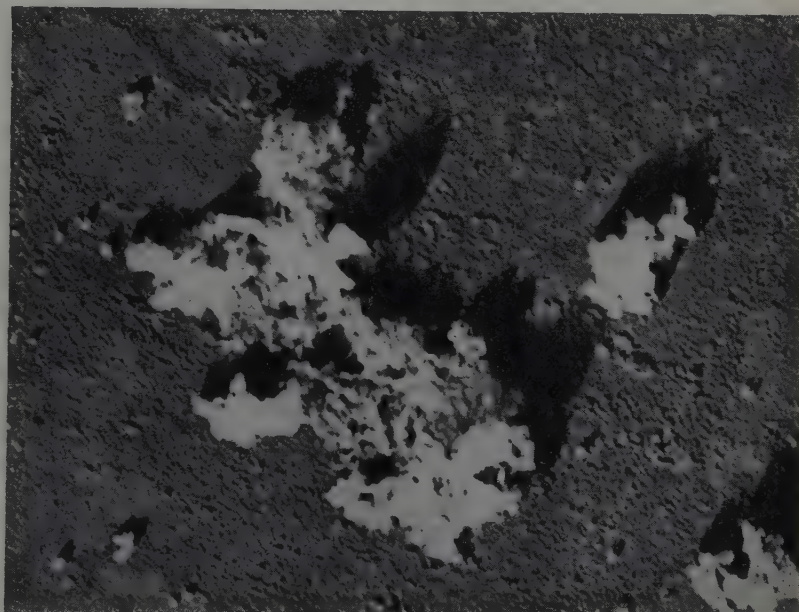


FIG 23—Electron micrograph of shadow-cast residue of Steel B. × 25,000
Transformed 95 pct after 100 hr at 600°F.

Laboratories, Inc. Special acknowledgment is due to W. D. Forgeng for the metallographic and X ray studies and to A. C. Jenkins of the Research Laboratories of The Linde Air Products Co. for preparing the electron micrographs.

References

1. W. Crafts and J. L. Lamont: Second-

ary Hardening of Tempered Martensitic Alloy Steels. *Trans. AIME* (1949) 180. *Metals Tech.*, Sept. 1948, TP 2439.

2. W. Koch: Electrolytic Separation of Carbides in Alloyed and Unalloyed Steels. *Stahl und Eisen*, 69, 1-8. Jan. 6, 1949.
3. W. Koch and H-J. Wiester: New Contributions to the Knowledge of Carbides in Alloy Steels. *Stahl und Eisen* 69, 73-79. Feb. 3, 1949.

The Properties of Sand Cast Magnesium-Rare Earth Alloys

THOMAS E. LEONTIS,* Junior Member AIME

Introduction

Several publications¹⁻⁷ during the past few years have demonstrated the markedly greater effect of cerium, as compared to all other alloying elements, in enhancing the strength and creep resistance of magnesium at elevated temperature either with or without the presence of other elements. In the work reported in Ref. 1-6, the cerium was added in the form of Mischmetal, which contains all the rare earth elements in essentially the same proportions as they occur in monazite sand, the principal ore of these metals. Mellor and Ridley⁷ have presented the creep characteristics at 200°C of magnesium alloys prepared both with pure cerium and with Mischmetal. Up to the present time, however, no comprehensive study of the effect of the various component elements of Mischmetal on the properties of sand-cast magnesium has been made. This hiatus in magnesium technology undoubtedly is associated with the difficulty in obtaining the rare earth metals separately.

This investigation provides such a survey, the object of which was to determine which of the elements present in Mischmetal contributes the greatest effect in developing high strength and high resistance to creep at elevated temperatures. Toward this end the compositional variation of these properties has been determined as a function of temperature in the following alloy systems:

- 1. Magnesium-Mischmetal
- 2. Magnesium-cerium-free Mischmetal
- 3. Magnesium-didymium
- 4. Magnesium-praseodymium-lanthanum
- 5. Magnesium-cerium

Table 1 . . . Chemical Analyses of Rare Earth Metals

| Producer's Designation of Material | Pct Total Rare Earths | Pct Ce | Pct Nd | Pct Pr | Pct Th† | Pct La* | Pct Fe | Pct Si | Pct Cr | Pct Other Impurities† |
|------------------------------------|-----------------------|--------|--------|--------|---------|---------|--------|--------|--------|-----------------------|
| Mischmetal..... | 97.8 | 50.6 | 18.2 | 6.4 | nil | 22.6 | 0.59 | 0.16 | 0.03 | 1.42 |
| Ce-free Mischmetal.... | 94.5 | 0.2 | 35.2 | 12.2 | 0.9 | 46.0 | 3.24 | 0.20 | 0.31 | 1.79 |
| Didymium..... | 89.8 | 0.8 | 72.3 | 7.9 | nil | 8.8 | 7.05 | 0.56 | 0.75 | 2.84 |
| Cerium..... | 94.8 | 92.2 | 0.9 | 0.3 | nil | 1.4 | 2.37 | 0.02 | 0.50 | 2.21 |
| Lanthanum..... | 96.5 | 0.5 | 0.7 | 0.2 | nil | 95.1 | 1.77 | 0.08 | 0.25 | 1.40 |
| Praseodymium..... | 95.2 | 0.8 | 2.9 | 65.6 | nil | 25.9 | 2.61 | 0.60 | 0.19 | 1.40 |

* Lanthanum obtained by difference from total rare earth content and therefore includes all the lesser elements such as Sa, Tb, Y, etc.
† Thorium included in Total Rare Earth Content.
‡ Other impurities obtained by difference from 100 pct. These impurities consist of oxygen and probably Al, Mn, Mg, and Cu in varying amounts. Some carbides and nitrides are also present.

Table 2 . . . Typical Analysis of Electrolytic Magnesium by Spectrographic Method

| Al | Ca | Cu | Fe | Mn | Ni | Pb | Si | Sn | Zn |
|-------|-------|-------|------|-----------|--------|--------|-------|--------|-------|
| <0.01 | <0.01 | <0.01 | 0.03 | 0.05-0.10 | <0.001 | <0.001 | <0.01 | <0.001 | <0.01 |

6. Magnesium-lanthanum
This designation, based on the names of the metals as furnished by the producer, is used throughout the paper in order to avoid the complicated system of listing all the elements present in the more complex alloys. The composition of the metals and the alloys is discussed in detail below.

Preparation of Alloys

ALLOYING INGREDIENTS

The chemical composition of each of

the six alloying ingredients used to prepare the alloys reported in this paper is given in Table 1. In each case, the percent total rare earths, percent cerium, percent neodymium, percent praseodymium, and percent thorium were determined in addition to the listed impurities. The percent lanthanum was determined by difference from the total rare earth content and consequently includes the other elements (samarium, terbium, yttrium, etc.) present in Mischmetal. These additional elements, however, seldom amount to more than 1 to 2 pct of the total rare earth content of Mischmetal. The iron content of the Mischmetal is considerably lower than that of the other metals. This grade of Mischmetal is now readily available.

The metals are listed in the order of decreasing complexity. Elimination of the cerium from Mischmetal results in what the trade calls "Cerium-free Mischmetal." Carrying the separation a step further by eliminating the lantha-

New York Meeting, February 1950.
TP 2726 E. Discussion of this paper (2 copies) may be sent to *Transactions AIME* before April 1, 1950. Discussion is tentatively scheduled for publication in November, 1950.
Manuscript received April 22, 1949; revision received Aug. 18, 1949.
* Metallurgist, Magnesium Laboratories, The Dow Chemical Co., Midland, Michigan.
† References are at the end of the paper.

num yields what is commonly called "didymium" and should consist essentially of neodymium and praseodymium. Unfortunately, the material obtained for this work also contains 8 pct lanthanum (10 pct of the total rare earths) and the praseodymium content is rather low compared to that of Ce-free Mischmetal. The cerium and the lanthanum metals are both practically free of other rare earth metals. The praseodymium, however, contains a large proportion of lanthanum; consequently, the alloys made with it are called magnesium-praseodymium-lanthanum alloys.

MELTING AND CASTING OF ALLOYS

All the alloys used in this study were prepared in small laboratory melts according to the melting practice described by Nelson⁸ as the "Crucible Method." The special precautions necessary in the alloying of Mischmetal with magnesium have been described in detail by Marande.⁹ The same procedure was followed in introducing the other rare earth metals into magnesium.

A 50- to 100-lb melt of each alloy was prepared except for the didymium alloys and the praseodymium-lanthanum alloys, in which case smaller melts were necessitated by the smaller amounts of alloying ingredients available. Test bars of 6½ in. length with a 2½ in. long reduced section of ½ in. diam were cast in sand molds using a four-bar pattern. Electrolytic magnesium was used as the starting material; a typical analysis of this grade of magnesium is shown in Table 2.

In order to conserve the rare-earth metals, the alloy containing the highest percentage of the added element in each group was made first. Alloys of lower content were then prepared by remelting the scrap from the preceding melt and adding magnesium to obtain the desired composition of the next alloy in the series. All the melts were poured at 1300-1325°F in an attempt to obtain as fine a grain size as possible.

ANALYSIS

Chemical analysis to determine the rare earth content of each alloy was made on a sample taken from a test bar, whereas the spectrographic analysis of impurities was performed on separately cast specimens poured immediately before filling the test bar molds. The results of both analyses are given in Table 3; only the impurities which are present in major proportions

or those which differ markedly from the amounts present in electrolytic magnesium (Table 2) are tabulated.

As indicated in Table 3, two alloys from each series were analyzed for cerium, neodymium, praseodymium, and total rare earths; in all the other alloys, only the total rare earth content was determined. The lanthanum values represent the difference between cerium + neodymium + praseodymium and the total rare earths as mentioned

above. The method of analysis of cerium and of total rare earths is given in another publication.¹⁰ These analyses are accurate to ±0.10 pct rare earth. The neodymium and the praseodymium were determined by the spectrophotometric method described by Rodden.¹¹ The accuracy of the analyses by this method is believed to be ±5 pct for neodymium and ±10 pct for praseodymium. The same analytical methods were used in determining the composi-

Table 3 . . . Composition and Grain Size of Alloys

| Alloy Number | By Chemical Analysis | | | | | By Spectrographic Analysis | | | | | Grain Size 0.001 in. |
|---|-----------------------|--------|--------|--------|---------|----------------------------|--------|--------|--------|--------|--|
| | Pct Total Rare Earths | Pct Ce | Pct Nd | Pct Pr | Pct La* | Pct Al | Pct Fe | Pct Mn | Pct Pb | Pct Si | |
| Magnesium-Mischmetal Alloys | | | | | | | | | | | |
| 1 | 0.18 | 0.09 | 0.03 | 0 | 0.06 | < .01 | 0.041 | 0.17 | 0.005 | < .01 | 14-28 14-16 60-90 (10-80 pct Columnar) |
| 2 | 0.40 | 0.21 | 0.06 | 0.02 | 0.11 | < .01 | 0.06 | 0.18 | 0.008 | < .01 | |
| 3 | 1.15 | 0.59 | 0.19 | 0.06 | 0.31 | 0.014 | 0.030 | 0.14 | 0.023 | 0.018 | |
| 4 | 1.43 | 0.67 | 0.22 | 0.07 | 0.35 | 0.015 | 0.019 | 0.14 | 0.022 | 0.05 | 45-60 35-60 (10-30 pct Columnar) |
| 5 | 1.62 | 0.83 | 0.27 | 0.09 | 0.43 | 0.026 | 0.042 | 0.16 | 0.014 | < .01 | |
| 6 | 2.50 | 1.28 | 0.42 | 0.14 | 0.66 | < .01 | 0.009 | 0.17 | 0.007 | 0.02 | |
| 7 | 2.85 | 1.47 | 0.47 | 0.16 | 0.75 | 0.023 | 0.042 | 0.15 | 0.006 | < .01 | 14-22 |
| 8† | 3.23 | 1.69 | 0.51 | 0.17 | 0.86 | < .01 | 0.048 | 0.09 | 0.005 | < .01 | 20-28 |
| 9† | 6.33 | 3.21 | 1.10 | 0.36 | 1.66 | < .01 | > .05 | 0.06 | 0.005 | < .01 | 12-16 |
| 10 | 10.11 | 5.20 | 1.68 | 0.56 | 2.67 | < .01 | > .05 | 0.04 | 0.007 | | 10-14 |
| Magnesium-Ce-free Mischmetal Alloys | | | | | | | | | | | |
| 11 | 0.14 | 0 | 0.05 | 0.01 | 0.08 | < .01 | 0.035 | 0.11 | 0.031 | 0.02 | 70-100 pct Columnar |
| 12 | 0.26 | 0 | 0.08 | 0.02 | 0.16 | 0.015 | 0.022 | 0.12 | 0.028 | 0.04 | 80-100 pct Columnar |
| 13 | 0.51 | 0 | 0.17 | 0.04 | 0.30 | 0.015 | 0.021 | 0.10 | 0.025 | 0.04 | 50-70 (30-70 pct Columnar) |
| 14 | 0.93 | 0.01 | 0.31 | 0.08 | 0.53 | 0.019 | 0.024 | 0.12 | 0.042 | 0.05 | 40-70 (10-60 pct Columnar) |
| 15 | 1.87 | 0.03 | 0.62 | 0.17 | 1.05 | 0.034 | 0.057 | 0.08 | 0.013 | < .01 | 40-50 (20-40 pct Columnar) |
| 16 | 1.89 | 0.03 | 0.62 | 0.17 | 1.07 | < .01 | 0.064 | 0.11 | 0.035 | < .01 | 30-40 |
| 17 | 2.11 | 0.03 | 0.70 | 0.19 | 1.19 | < .01 | 0.030 | 0.12 | 0.039 | < .01 | 30-45 |
| 18 | 2.59 | 0.04 | 0.85 | 0.23 | 1.47 | < .01 | 0.020 | 0.17 | 0.030 | < .01 | 18-30 |
| 19† | 3.00 | 0.07 | 0.86 | 0.21 | 1.86 | < .01 | 0.044 | 0.12 | 0.015 | < .01 | 12-16 |
| 20 | 5.05 | 0.07 | 1.67 | 0.45 | 2.86 | < .01 | 0.052 | 0.16 | 0.047 | < .01 | 8-15 |
| 21 | 5.74 | 0.03 | 2.14 | 0.62 | 2.94 | 0.039 | 0.051 | 0.10 | 0.020 | < .01 | 12-14 |
| Magnesium-didymium Alloys | | | | | | | | | | | |
| 22 | 0.65 | 0.01 | 0.51 | 0.06 | 0.07 | 0.019 | 0.032 | 0.04 | 0.008 | < .1 | 30-50 (30-80 pct Columnar) |
| 23 | 1.63 | 0.02 | 1.29 | 0.14 | 0.18 | < .01 | 0.040 | 0.07 | 0.010 | < .01 | 40-80 (10-70 pct Columnar) |
| 24 | 2.60 | 0.03 | 2.05 | 0.22 | 0.30 | 0.043 | 0.044 | 0.09 | 0.017 | 0.02 | 16-28 |
| 25† | 3.85 | 0.06 | 3.00 | 0.31 | 0.48 | < .01 | 0.045 | 0.09 | 0.020 | < .01 | 12-20 |
| 26† | 6.03 | 0.07 | 4.82 | 0.56 | 0.58 | < .01 | 0.062 | 0.09 | 0.027 | < .01 | 16-24 |
| Magnesium-praseodymium-lanthanum Alloys | | | | | | | | | | | |
| 27 | 0.69 | 0.0 | 0.02 | 0.47 | 0.20 | < .01 | 0.030 | 0.07 | 0.004 | < .01 | 40-50 (30-70 pct Columnar) |
| 28 | 1.59 | 0.01 | 0.05 | 1.08 | 0.45 | < .01 | 0.040 | 0.07 | 0.008 | < .01 | 30-40 |
| 29† | 3.00 | 0.02 | 0.11 | 2.03 | 0.84 | < .01 | 0.033 | 0.08 | 0.011 | < .01 | 14-20 |
| 30† | 6.19 | 0.05 | 0.17 | 4.20 | 1.77 | < .01 | 0.030 | 0.07 | 0.023 | < .01 | 8-14 |
| Magnesium-cerium Alloys | | | | | | | | | | | |
| 31 | 0.15 | 0.15 | 0 | 0 | 0 | < .01 | 0.030 | 0.14 | 0.013 | 0.02 | 80-100 pct Columnar |
| 32 | 0.45 | 0.44 | 0 | 0 | 0.01 | < .01 | 0.013 | 0.12 | 0.033 | 0.03 | 80-90 pct Columnar |
| 33 | 1.09 | 1.05 | 0.01 | 0 | 0.03 | < .01 | 0.038 | 0.14 | 0.030 | 0.02 | 30-60 (10-30 pct Columnar) |
| 34 | 1.54 | 1.49 | 0.02 | 0.01 | 0.03 | < .01 | 0.024 | 0.14 | 0.030 | 0.04 | 30-50 (20-40 pct Columnar) |
| 35 | 2.01 | 1.95 | 0.02 | 0.01 | 0.03 | < .01 | 0.019 | 0.18 | 0.030 | < .01 | 60-80 (40-80 pct Columnar) |
| 36 | 2.39 | 2.31 | 0.03 | 0.01 | 0.04 | < .01 | 0.038 | 0.17 | 0.025 | < .01 | 30-50 |
| 37† | 2.60 | 2.48 | 0.04 | 0.02 | 0.06 | < .01 | 0.037 | 0.14 | 0.018 | < .01 | 30-40 |
| 38 | 3.57 | 3.45 | 0.04 | 0.02 | 0.06 | < .01 | 0.040 | 0.12 | 0.031 | < .01 | 10-20 |
| 39† | 5.70 | 5.56 | 0.05 | 0.02 | 0.07 | 0.028 | 0.062 | 0.10 | 0.014 | < .01 | 50-80 |
| 40 | 6.73 | 6.50 | 0.08 | 0.04 | 0.11 | < .01 | > .05 | 0.06 | < .001 | < .01 | 14-16 |
| Magnesium-lanthanum Alloys | | | | | | | | | | | |
| 41 | 0.20 | 0 | 0 | 0 | 0.20 | < .01 | 0.014 | 0.11 | 0.028 | 0.04 | 28-38 |
| 42 | 0.32 | 0 | 0 | 0 | 0.32 | < .01 | 0.028 | 0.10 | 0.030 | 0.04 | 40-60 |
| 43 | 0.54 | 0 | 0 | 0 | 0.54 | < .01 | 0.004 | 0.14 | 0.028 | 0.03 | 40-60 (10-20 pct Columnar) |
| 44 | 0.89 | 0.01 | 0 | 0 | 0.88 | 0.011 | 0.022 | 0.04 | 0.022 | 0.04 | 40-50 (10 pct Columnar) |
| 45 | 1.39 | 0.01 | 0.01 | 0 | 1.37 | < .01 | 0.003 | 0.10 | < .01 | < .01 | 35-100 (10-30 pct Columnar) |
| 46 | 1.60 | 0.02 | 0.01 | 0 | 1.57 | 0.012 | 0.048 | 0.12 | 0.020 | 0.04 | 60-80 (20-70 pct Columnar) |
| 47 | 2.47 | 0.02 | 0.01 | 0 | 2.44 | < .01 | 0.044 | 0.11 | 0.011 | < .01 | 40-50 (10 pct Columnar) |
| 48 | 2.74 | 0.03 | 0.02 | 0 | 2.69 | 0.02 | 0.016 | 0.10 | 0.022 | < .01 | 20-30 |
| 49 | 2.80 | 0.03 | 0.02 | 0 | 2.75 | < .01 | 0.030 | 0.12 | 0.006 | 0.02 | 60-70 |
| 50 | 3.59 | 0.04 | 0.02 | 0.01 | 3.52 | < .01 | 0.045 | 0.14 | 0.008 | 0.04 | 60-100 (10-50 pct Columnar) |
| 51† | 3.85 | 0.04 | 0.02 | 0.01 | 3.78 | 0.014 | 0.032 | 0.08 | 0.022 | 0.02 | 30-35 |
| 52 | 6.51 | 0.06 | 0.04 | 0.02 | 6.39 | < .01 | 0.045 | 0.09 | 0.006 | < .01 | 30-80 |
| 53† | 6.70 | 0.06 | 0.04 | 0.02 | 6.58 | 0.03 | 0.041 | 0.12 | 0.047 | 0.02 | 10-18 |

* By difference from Total Rare Earth Content.
† Alloys analyzed separately for Ce, Nd, Pr, and Total Rare Earths.

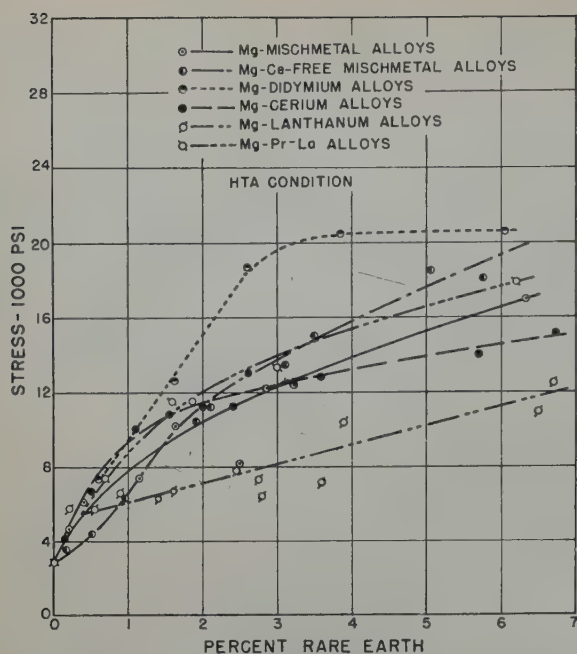


FIG 1—Tensile yield strength at room temperature.

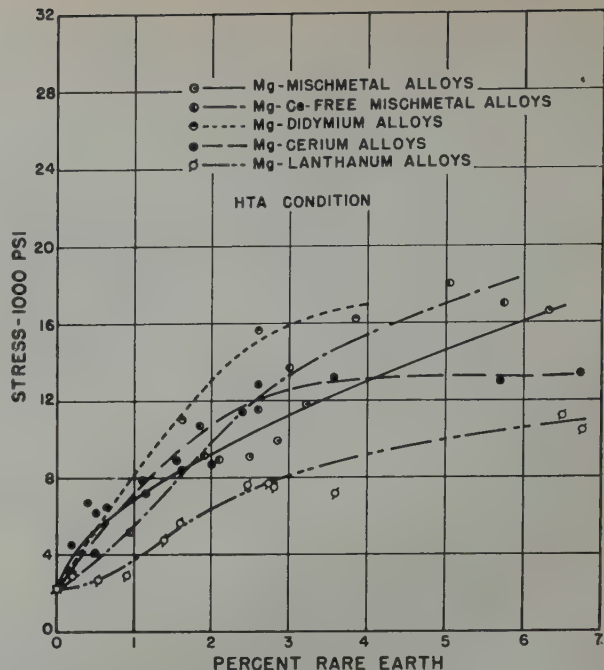


FIG 2—Tensile yield strength at 200°F.

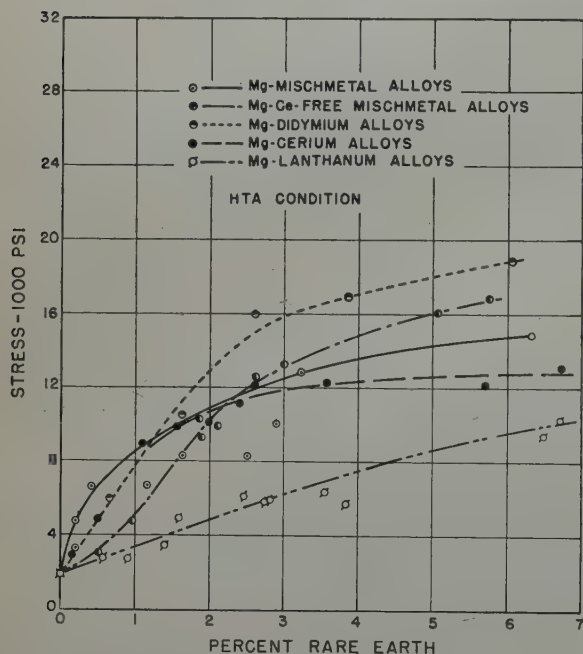


FIG 3—Tensile yield strength at 300°F.

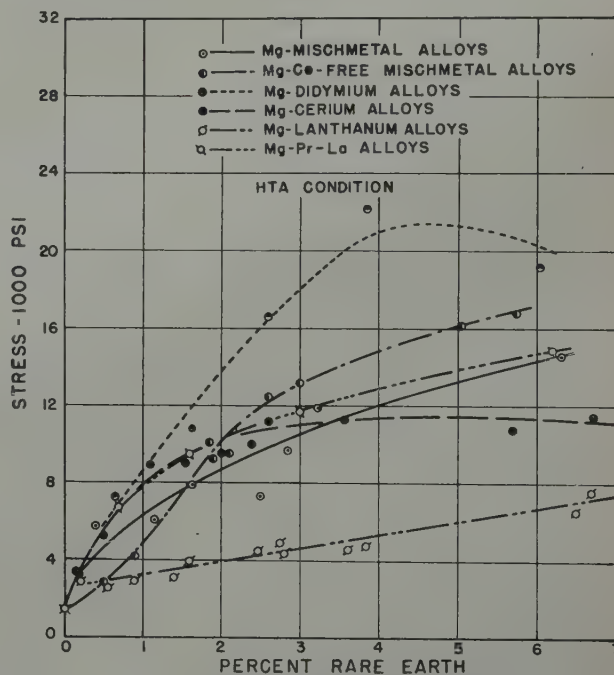


FIG 4—Tensile yield strength at 400°F.

tion of the rare earth metals given in Table I.

In the alloys analyzed for the separate rare earth metals, the proportion of each of the four elements agrees reasonably well with that of the same element in the corresponding alloying ingredient. This observation, together with the good agreement between the two alloys analyzed in each group, indicates that there is no preferential loss of any of these elements either in alloying with magnesium or in remelting. With these findings on hand,

it was deemed justifiable to apportion the total rare earth content of all the other alloys among the four elements. For each series of alloys, the proportioning factors used were based on the average of the two complete analytical determinations in the series.

HEAT TREATMENT

A preliminary study was conducted to determine the maximum possible solution heat treating temperature for each type of alloy. This was done by

heat treating small specimens of alloys containing 6 pct and 3 pct rare earths in the as-cast condition at a series of temperatures followed by quenching in cold water. Metallographic examination of these specimens has established the following minimum temperatures of liquation:

| | °F |
|--|----------|
| Magnesium-Mischmetal alloys..... | 1095 ± 5 |
| Magnesium-Ce-free Mischmetal alloys..... | 1100 ± 5 |
| Magnesium didymium..... | 1000 ± 5 |
| Magnesium-praseodymium-lanthanum alloys..... | 1100 ± 5 |
| Magnesium-cerium alloys..... | 1095 ± 5 |
| Magnesium-lanthanum alloys..... | 1125 ± 5 |

These temperatures are in good agree-

Table 4 . . . Tensile Properties of Alloys in the As-cast, Heat Treated, and Heat Treated + Aged Conditions at Room Temperature

| Alloy Number | Pct Total Rare Earths | As-Cast | | | Heat Treated | | | Heat Treated + Aged | | |
|-------------------------------------|-----------------------|---------|------|------|--------------|------|------|---------------------|------|------|
| | | Pct E | TYS | TS | Pct E | TYS | TS | Pct E | TYS | TS |
| Magnesium | | 6.0 | 2.9 | 12.6 | | | | | | |
| Magnesium-Mischmetal Alloys | | | | | | | | | | |
| 1 | 0.18 | 9.5 | 4.4 | 20.4 | 10.2 | 4.2 | 20.9 | 10.0 | 4.7 | 21.4 |
| 2 | 0.40 | 9.1 | 5.1 | 20.7 | 7.8 | 4.0 | 13.8 | 8.2 | 6.1 | 16.6 |
| 3 | 1.15 | 4.6 | 5.3 | 14.3 | 6.0 | 5.3 | 16.0 | 6.0 | 7.4 | 18.0 |
| 5 | 1.62 | 2.9 | 7.0 | 14.4 | 5.5 | 7.8 | 20.0 | 3.5 | 10.2 | 19.3 |
| 6 | 2.50 | 1.9 | 8.7 | 15.5 | 3.0 | 6.8 | 15.4 | 2.2 | 8.2 | 17.0 |
| 7 | 2.85 | 1.7 | 9.0 | 15.4 | 5.0 | 10.5 | 18.6 | 1.7 | 12.2 | 19.4 |
| 8 | 3.23 | 1.1 | 9.1 | 14.9 | 3.4 | 8.9 | 18.7 | 1.5 | 12.4 | 20.5 |
| 9 | 6.33 | 0.5 | 13.1 | 16.6 | 2.0 | 13.8 | 16.8 | 1.0 | 17.0 | 20.4 |
| Magnesium-Ce-free Mischmetal Alloys | | | | | | | | | | |
| 11 | 0.14 | 6.6 | 3.0 | 14.3 | 6.5 | 3.2 | 15.3 | 6.2 | 3.6 | 14.1 |
| 12 | 0.26 | 5.3 | 3.5 | 12.2 | 5.2 | 3.9 | 12.4 | 5.5 | 4.2 | 13.5 |
| 13 | 0.51 | 5.7 | 4.0 | 14.1 | 6.5 | 4.0 | 15.3 | 6.0 | 4.4 | 15.0 |
| 14 | 0.93 | 4.8 | 5.0 | 14.0 | 5.7 | 6.3 | 15.5 | 5.7 | 6.4 | 16.0 |
| 15 | 1.87 | 3.5 | 6.9 | 15.9 | 5.2 | 6.7 | 16.1 | 3.5 | 11.5 | 19.4 |
| 16 | 1.89 | 4.3 | 6.9 | 16.3 | 7.5 | 7.7 | 20.1 | 3.2 | 10.4 | 21.5 |
| 17 | 2.11 | 4.1 | 7.5 | 16.4 | 5.8 | 8.5 | 19.5 | 2.3 | 11.2 | 21.3 |
| 18 | 2.59 | 3.5 | 8.6 | 16.6 | 6.0 | 8.8 | 20.5 | 2.2 | 13.5 | 23.0 |
| 19 | 3.00 | 3.1 | 9.4 | 17.3 | 7.0 | 10.1 | 20.2 | 2.2 | 15.0 | 23.4 |
| 20 | 5.05 | 0.5 | 12.7 | 16.0 | 2.7 | 12.0 | 19.3 | 0.7 | 18.5 | 24.5 |
| 21 | 5.74 | 1.3 | 13.1 | 17.3 | 4.0 | 13.1 | 20.6 | 1.5 | 18.1 | 25.4 |
| Magnesium-didymium Alloys | | | | | | | | | | |
| 22 | 0.65 | 7.2 | 5.1 | 19.1 | 8.2 | 4.5 | 19.4 | 5.7 | 7.3 | 22.3 |
| 23 | 1.63 | 6.7 | 7.2 | 19.5 | 7.2 | 7.2 | 16.8 | 5.0 | 12.6 | 23.4 |
| | | | | | | | 21.6 | | | 29.0 |
| 24 | 2.60 | 5.0 | 11.3 | 21.0 | 9.0 | 11.8 | 25.2 | 3.7 | 18.7 | 31.9 |
| 25 | 3.85 | 3.0 | 13.8 | 21.9 | 4.2 | 14.1 | 23.7 | 2.2 | 20.5 | 28.9 |
| 26 | 6.03 | 0.5 | 18.5 | 20.7 | 1.5 | 14.7 | 20.2 | 0.5 | 20.6 | 25.7 |
| Magnesium-cerium Alloys | | | | | | | | | | |
| 31 | 0.15 | 5.2 | 3.3 | 12.6 | 6.0 | 4.0 | 11.9 | 4.5 | 4.2 | 14.2 |
| 32 | 0.45 | 5.0 | 4.2 | 13.7 | 5.0 | 5.0 | 16.4 | 5.0 | 6.7 | 20.2 |
| 33 | 1.09 | 5.5 | 5.6 | 16.1 | 3.5 | 6.9 | 18.9 | 2.5 | 10.0 | 22.3 |
| 34 | 1.54 | 4.1 | 6.3 | 15.2 | 6.0 | 8.8 | 21.5 | 3.7 | 10.8 | 21.6 |
| 35 | 2.01 | 2.5 | 6.6 | 12.8 | 6.3 | 8.9 | 18.0 | 2.3 | 11.2 | 18.4 |
| 36 | 2.39 | 1.9 | 8.3 | 14.5 | 3.7 | 7.4 | 16.7 | 1.7 | 11.2 | 18.2 |
| 37 | 2.60 | 1.9 | 8.9 | 15.3 | 3.7 | 9.8 | 18.4 | 1.5 | 13.0 | 19.9 |
| 38 | 3.57 | 1.0 | 9.9 | 14.9 | 4.2 | 10.6 | 17.4 | 1.7 | 12.8 | 19.1 |
| 39 | 5.70 | 0.5 | 12.5 | 14.0 | 1.0 | 12.2 | 14.4 | 1.5 | 14.0 | 15.6 |
| 40 | 6.73 | 0.7 | 17.1 | 19.5 | 1.2 | 12.1 | 16.6 | 0.5 | 15.2 | 18.0 |
| Magnesium-lanthanum Alloys | | | | | | | | | | |
| 41 | 0.20 | 6.6 | 4.5 | 17.1 | 6.7 | 5.7 | 18.0 | 7.0 | 5.8 | 18.3 |
| 43 | 0.54 | 5.3 | 4.8 | 15.6 | 5.7 | 5.2 | 17.0 | 6.0 | 5.8 | 16.9 |
| 44 | 0.89 | 4.5 | 5.5 | 15.1 | 5.2 | 6.0 | 17.0 | 4.5 | 6.6 | 17.1 |
| 45 | 1.39 | 2.6 | 5.4 | 10.2 | 4.0 | 6.5 | 11.6 | 3.5 | 6.3 | 12.0 |
| 46 | 1.60 | 3.2 | 5.9 | 13.0 | 3.5 | 6.5 | 15.0 | 4.0 | 6.7 | 15.0 |
| 47 | 2.47 | 2.0 | 8.1 | 14.2 | 3.2 | 7.8 | 15.4 | 3.2 | 8.1 | 15.3 |
| 48 | 2.74 | 1.5 | 8.4 | 14.8 | 2.5 | 7.1 | 14.5 | 3.0 | 7.4 | 15.2 |
| 49 | 2.80 | 1.1 | 7.8 | 11.2 | 2.7 | 6.3 | 12.3 | 2.7 | 6.4 | 12.1 |
| 50 | 3.59 | 0.6 | 8.7 | 11.2 | 1.7 | 6.9 | 11.0 | 1.7 | 7.2 | 11.8 |
| 51 | 3.85 | 1.0 | 9.9 | 15.1 | 2.0 | 10.0 | 15.0 | 1.7 | 10.4 | 14.9 |
| 52 | 6.51 | 0.0 | 14.1 | 15.0 | 0.5 | 10.7 | 14.4 | 1.0 | 11.0 | 14.8 |
| 53 | 6.70 | 0.0 | 14.1 | 17.7 | 0.5 | 12.0 | 15.6 | 1.0 | 12.5 | 16.1 |

Pct E—Percent elongation in 2 in.
TYS—Tensile yield strength in 1000 psi
TS—Tensile strength in 1000 psi

ment with the eutectic temperatures of the published magnesium-rare earth diagrams;^{12,13,14,15} no information is available on the principal constituent of didymium, that is, the magnesium-neodymium system.

With these determinations as a guide, the following heat treating temperatures were selected and used throughout this investigation:

Magnesium-didymium alloys.....

All other alloys.....

°F9751070

The higher temperature possible with magnesium-lanthanum alloys was not used in order to avoid the dangers of oxidation and sagging of the test bars. All heat treatments were of 24-hr duration followed by cooling on a thick iron

plate under a fan blast. The aging treatment consisted of heating for 16 hr at 400°F.

All the heat treatments were conducted in circulating air furnaces, electrically heated and controlled to $\pm 5^\circ\text{F}$. The atmosphere of the furnace was rendered protective by the maintenance of a concentration of 0.5 to 1.0 pct sulphur dioxide.

GRAIN SIZE

The grain size of each alloy (Table 3) was determined on a sample from the reduced section of every test bar after being tested either in tension or in creep. The measurements were made

by the comparison method described by P. F. George.¹⁶ A range of grain size is given for each alloy. This represents the variation from bar to bar. The figures given for columnar structure represent the percent of the area covered by columnar grains. It may be stated that, in general, the grain size decreases with increasing alloy content. The suppression of a columnar structure in the lower alloy contents is very erratic. No evidence of grain coarsening upon heat treatment was observed.

Testing Methods

Detailed descriptions of the methods of tension and creep testing have been given in earlier publications.^{4,17} All the properties were determined on cast test bars without machining the surface. Tensile properties are the average of two tests. All creep data are from tests of 100 to 160 hr duration. Space does not permit the presentation of detailed creep data. The creep characteristics of each alloy are defined in this paper by three parameters:

1. Limiting stress to give 0.1 pct creep extension in 100 hr

2. Limiting stress to give 0.2 pct total extension in 100 hr

3. Limiting stress to give 0.5 pct total extension in 100 hr.

These values were determined by interpolation of log-log plots of stress vs. extension as described previously.^{4,17} A minimum of 3 and as many as 8 stress levels were used to establish the log stress vs. log extension relationship for each alloy at each temperature. The total extension figures include the elongation obtained during loading as well as the creep extension. No significance has been attached to creep rates in this investigation because during the 100-hr test the secondary stage of creep, which gives the minimum creep rate, is not established in many tests.

The method of determining electrical conductivity has been described earlier.¹⁸

The density of each alloy in the heat treated plus aged condition was determined on a $\frac{5}{8}$ in. diam by 1 in. long specimen machined from the shoulder of a test bar. Each sample was weighed on an analytical balance under two conditions: (1) in air, and (2) in kerosene of known density. The density of the alloy was calculated from these two weighings.

Discussion of Results

TENSILE PROPERTIES

The room temperature tensile properties of all the alloys in the as-cast, solution heat treated (HT), and heat treated and aged (HTA) conditions are presented in Table 4. The yield and tensile strengths in the HTA condition are plotted as a function of composition for all temperatures investigated in Fig 1 through 13. The total rare earth content of all the alloys is used to represent the composition in these as well as all subsequent plots. Graphs of elongation vs. composition have been omitted in order to conserve space; furthermore, the scatter in these data renders them rather inconvenient for graphical representation. Elongation values at all temperatures are given in Table 5.

Marked differences exist in the degree to which the strength of magnesium is enhanced by the various rare earth elements. The highest properties at all temperatures over the entire composition range investigated are developed by the addition of didymium, whereas the lowest properties are found in magnesium-lanthanum alloys. Intermediate to these lie the alloys containing cerium-free Mischmetal, praseodymium + lanthanum, Mischmetal, and cerium in that order of decreasing properties for alloys containing 3 to 6 pct total rare earths. Among these four types of alloys there is little difference in strength in compositions of less than 2 to 2.5 pct alloying elements. In general, the elongation decreases with increasing amounts of rare earth elements; the slight increase in this property in alloys containing 0.18 and 0.40 pct Mischmetal is undoubtedly associated with the unusually fine grain size of these alloys as compared to that of electrolytic magnesium which is 100 pct columnar.

It can readily be seen from the data in Table 4 that all the alloys, with the exception of the magnesium-lanthanum alloys, exhibit a certain degree of age hardening. The alloys may be rated in the following order of decreasing age hardening: magnesium-didymium, magnesium-cerium-free Mischmetal, magnesium-Mischmetal, magnesium-cerium, magnesium-lanthanum. From these observations it may be concluded that of the four principal elements in Mischmetal, neodymium contributes the most to age hardening. Quenching from the heat treating temperature into water at 180°F instead of air cooling effects no increase in the properties or in the degree of age hardening of any of these alloys. The

Table 5 . . . Elongation of Alloys in the Heat Treated + Aged Condition at Room and Elevated Temperatures

| Alloy Number | Percent Total Rare Earths | Percent Elongation in 2 In. | | | | | | |
|---|---------------------------|-----------------------------|-------|-------|-------|-------|-------|-------|
| | | Room Temp. | 200°F | 300°F | 400°F | 500°F | 600°F | 700°F |
| Magnesium | | 6.0 | 16.1 | 23.2 | 38.0 | 59.0 | 81.0 | 101.0 |
| Magnesium-Mischmetal Alloys | | | | | | | | |
| 1 | 0.18 | 10.0 | 13.2 | 24.7 | 25.2 | 28.0 | 59.0 | |
| 2 | 0.40 | 8.2 | 20.5 | 24.0 | 23.7 | 28.5 | 52.0 | 107.6 |
| 3 | 1.15 | 6.0 | 10.7 | 13.2 | 18.2 | 18.7 | 29.5 | 65.0 |
| 5 | 1.62 | 3.5 | 11.0 | 15.0 | 15.0 | 19.0 | 32.5 | 76.6 |
| 6 | 2.50 | 2.2 | 3.0 | 5.8 | 8.5 | 16.5 | 32.7 | 56.6 |
| 7 | 2.85 | 1.7 | 5.0 | 10.0 | 9.7 | 11.2 | 28.2 | |
| 8 | 3.23 | 1.5 | 2.7 | 7.0 | 4.7 | 11.7 | 24.2 | 113.6 |
| 9 | 6.33 | 1.0 | 2.2 | 2.0 | 2.0 | 4.2 | 12.5 | 77.9 |
| Magnesium-Ce-free Mischmetal Alloys | | | | | | | | |
| 13 | 0.51 | 6.0 | 12.0 | 17.5 | 20.0 | 20.7 | 25.5 | 70.7 |
| 14 | 0.93 | 5.7 | 12.2 | 15.5 | 19.0 | 16.3 | 25.5 | 58.3 |
| 15 | 1.87 | 3.5 | 5.2 | 8.5 | 11.0 | 14.5 | 22.2 | |
| 16 | 1.89 | 3.2 | 8.5 | 15.5 | 17.0 | 21.2 | 34.2 | 121.0 |
| 17 | 2.11 | 2.3 | 5.5 | 14.5 | 14.5 | 17.7 | 26.0 | 133.0 |
| 18 | 2.59 | 2.2 | 3.5 | 12.5 | 15.0 | 18.0 | 35.0 | 133.9 |
| 19 | 3.00 | 2.2 | 2.5 | 9.2 | 14.0 | 15.2 | 40.7 | 153.3 |
| 20 | 5.05 | 3.5 | 5.2 | 8.5 | 11.0 | 14.5 | 22.2 | |
| 21 | 5.74 | 1.5 | 2.5 | | 4.5 | 9.2 | 34.0 | 146.0 |
| Magnesium-didymium Alloys | | | | | | | | |
| 22 | 0.65 | 5.7 | 13.7 | 16.7 | 19.0 | 23.5 | 34.0 | 70.2 |
| 23 | 1.63 | 5.0 | 10.2 | 15.5 | 15.0 | 13.5 | 33.5 | 41.7 |
| 24 | 2.60 | 3.7 | 9.0 | 13.0 | 12.7 | 12.7 | 31.5 | 77.0 |
| 25 | 3.85 | 2.2 | 5.0 | 6.5 | 9.0 | 11.7 | 37.5 | 78.0 |
| 26 | 6.03 | 0.5 | | 2.5 | 3.2 | 6.5 | 26.6 | 51.0 |
| Magnesium-praseodymium-lanthanum Alloys | | | | | | | | |
| 27 | 0.69 | 4.5 | | | 18.0 | | 39.0 | |
| 28 | 1.59 | 5.2 | | | 20.0 | | 31.0 | |
| 29 | 3.00 | 2.7 | | | 14.5 | | 38.0 | |
| 30 | 6.19 | 0.7 | | | 3.0 | | 27.0 | |
| Magnesium-cerium Alloys | | | | | | | | |
| 31 | 0.15 | 4.5 | 8.2 | 15.7 | 15.7 | 19.2 | 27.5 | 49.9 |
| 32 | 0.45 | 5.0 | 9.2 | 12.2 | 17.0 | 16.2 | 32.0 | 55.6 |
| 33 | 1.09 | 2.5 | 15.0 | 18.5 | 15.5 | 17.2 | 32.2 | 52.7 |
| 34 | 1.54 | 3.7 | 7.7 | 10.2 | 16.7 | 14.0 | 29.7 | |
| 35 | 2.01 | 2.3 | 4.2 | 9.7 | 13.0 | 16.5 | 27.2 | 55.7 |
| 36 | 2.39 | 1.7 | 3.2 | 9.0 | 14.5 | 18.7 | 38.5 | 78.3 |
| 37 | 2.60 | 1.5 | 4.7 | | 11.2 | 17.2 | 31.5 | 83.6 |
| 38 | 3.57 | 1.7 | 3.7 | 7.0 | 13.5 | 12.0 | 40.0 | 109.3 |
| 39 | 5.70 | 1.5 | 2.0 | 2.0 | 3.2 | 6.5 | 32.5 | 90.6 |
| 40 | 6.73 | 0.5 | 1.2 | 1.7 | 3.0 | 3.2 | 33.0 | 62.3 |
| Magnesium-lanthanum Alloys | | | | | | | | |
| 41 | 0.20 | 7.0 | 14.0 | 19.5 | 26.0 | 26.2 | 43.0 | |
| 43 | 0.54 | 6.0 | 13.0 | 19.2 | 24.0 | 22.5 | 36.5 | |
| 44 | 0.89 | 4.5 | 12.2 | 16.7 | 20.7 | 23.0 | 34.5 | |
| 45 | 1.39 | 3.5 | 7.0 | 10.5 | 24.0 | 23.0 | 24.2 | |
| 46 | 1.60 | 4.0 | 9.0 | 14.7 | 22.0 | 23.5 | 40.7 | |
| 47 | 2.47 | 3.2 | 7.5 | 13.7 | 23.0 | 21.0 | 45.0 | |
| 48 | 2.74 | 3.0 | 4.5 | 12.2 | 21.0 | 26.7 | 48.7 | |
| 49 | 2.80 | 2.7 | 4.2 | 9.5 | 19.2 | 22.0 | 28.2 | |
| 50 | 3.59 | 1.7 | 2.7 | 5.0 | 14.7 | 15.8 | 38.5 | |
| 51 | 3.85 | 1.7 | | 9.0 | 18.5 | 23.5 | 48.7 | |
| 52 | 6.51 | 1.0 | 2.2 | 3.0 | 8.7 | 11.5 | 34.7 | |
| 53 | 6.70 | 1.0 | 1.5 | 2.5 | 7.5 | 10.5 | 40.0 | |

properties of magnesium-lanthanum alloys after heat treating at 1100°F are the same as those reported here after the 1070°F heat treatment.

The specific effect of each rare earth metal is more clearly illustrated by the property vs. temperature plots shown in Fig 14, 15, 16 and 17. These graphs have been derived from the property-composition curves for two levels of alloy content, 3 and 6 pct total rare earths; below 3 pct alloy content the properties decrease quite rapidly to the values for electrolytic magnesium. The curves in these figures do not necessarily pass through all the points read

from the property-composition plots, but deviations from them are no greater than 1000 psi.

EFFECT OF EXPOSURE AT 600°F

Table 6 shows the tensile properties of two compositions of magnesium-Mischmetal, magnesium-cerium-free Mischmetal, magnesium-didymium, magnesium-cerium, and magnesium-lanthanum alloys at room temperature and 600°F after holding the test bars at 600°F for 5000 hr. This long-time exposure treatment was conducted in an atmosphere containing ½ to 1 pct sulphur dioxide in order to prevent any

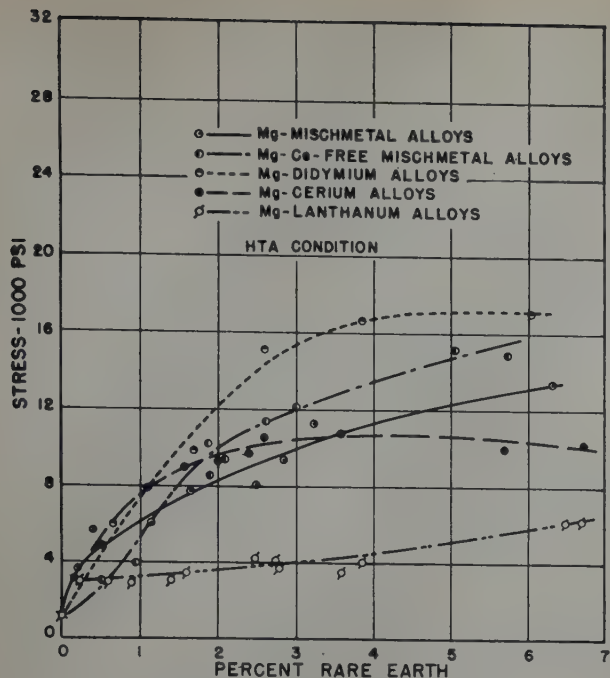


FIG 5—Tensile yield strength at 500°F.

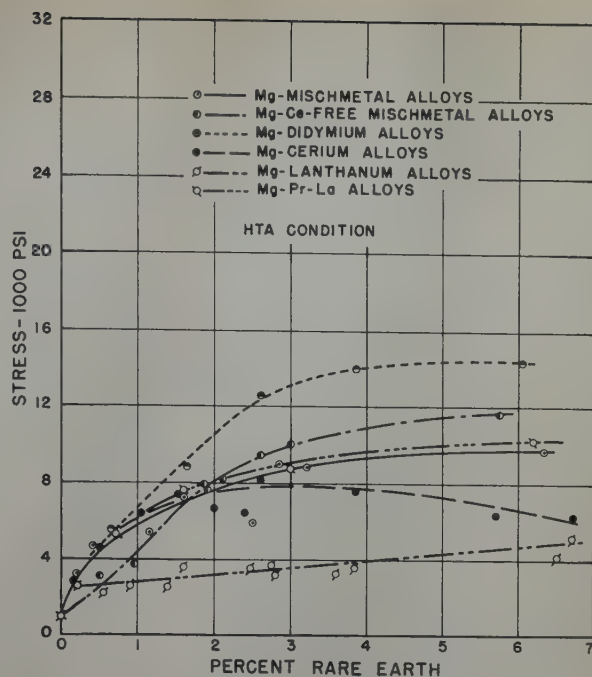


FIG 6—Tensile yield strength at 600°F.

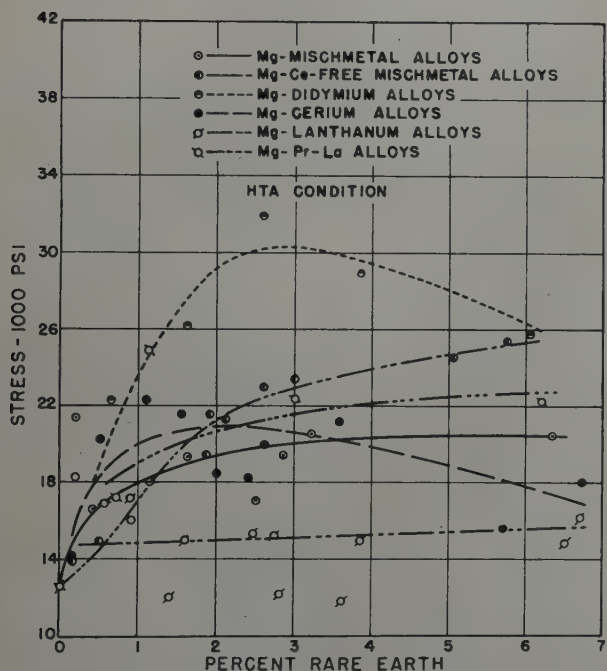


FIG 7—Tensile strength at room temperature.

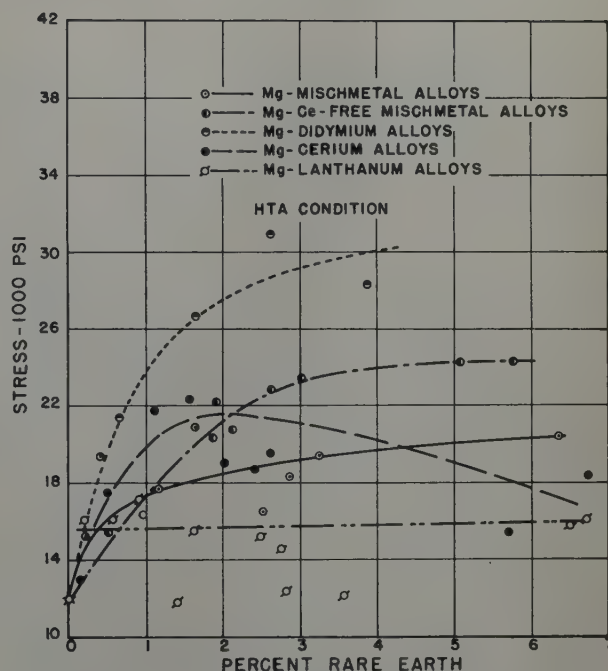


FIG 8—Tensile strength at 200°F.

preferential oxidation of the rare earth intermetallic compounds.

Compared to their properties in the HTA condition, the alloys containing Mischmetal, cerium-free Mischmetal, didymium, and cerium suffer a much greater loss in strength at room temperature and 600°F from this exposure than do the magnesium-lanthanum alloys. In fact, there is no change in the room temperature properties of magnesium-lanthanum alloys. However, the best combination of strength

at room temperature and 600°F after the prolonged exposure is exhibited by the magnesium + 5.74 pct cerium-free Mischmetal alloy.

Similar data have been reported by McDonald⁶ for an alloy containing 6 pct Mischmetal plus 1.5–2.0 pct manganese. His results showed that the strength of this alloy decreases within 16 to 24 hr exposure at 600°F to a value that is maintained out to 1000 hr exposure. Subsequent experiments on the same material have been extended

to 5000 hr without any further change in the properties.

CREEP RESISTANCE

The creep characteristics of all six alloy systems at 400 and 600°F are depicted as a function of composition in Fig 18 through 21. Only a limited number of alloys, other than magnesium-Mischmetal alloys, have been investigated at 500°F; the results of these tests together with the data at

300°F for magnesium-Mischmetal alloys are summarized in Table 7.

The pronounced differences among the various rare earth metals in their respective effect on the creep resistance of magnesium at 400°F is demonstrated clearly by all three indices of creep resistance used to represent the data. All the rare earth elements, with the exception of lanthanum, effect a marked increase in this property in the composition range between 0 and 2 pct. In general, the alloys may be listed in the same order with respect to creep resistance as was found in their relative tensile properties. This listing applies specifically in the range of 3 to 6 pct rare earth content; in lower compositions some of the curves cross one another. The decrease in creep strength in magnesium-cerium alloys between 3 and 7 pct cerium content is difficult to explain. The reason does not lie in grain size variation inasmuch as of the two alloys containing 5.70 and 6.73 pct cerium, the former has a grain size of 0.050-0.080 in. and the latter 0.014-0.16 in. Furthermore, alloys of lower cerium content having higher creep resistance than either of the two high cerium compositions have grain size values which fall at both ends of the range covered by the high cerium alloys.

The results of tests at 500°F show much the same trends as indicated at 400°F. It will be noted that again there is a drop in creep resistance between 3 and 6 pct cerium. Alloys containing 1.15, 1.62, 2.50 and 2.85 pct Mischmetal exhibit anomalously low creep resistance at 300°F and high creep resistance at 500°F. These effects appear to correlate with the abnormally large grain size of these alloys.

The situation at 600°F is a little more confused; many anomalies exist in the data rendering them difficult to evaluate on a comparative basis. To illustrate these effects, Table 7a has been prepared from Fig 21 for three levels of alloy content:

These results may be summarized by saying that the relative merits of the various magnesium-rare earth alloys depend upon the temperature. Furthermore, there definitely appears to be a grain size effect, but it is not the same for all alloy systems. This effect is most pronounced in magnesium-cerium-free Mischmetal and magnesium-didymium alloys at 600°F, and in magnesium-Mischmetal alloys at 300 and 500°F. The selection of an alloy for applications demanding high creep resistance at elevated temperatures must, there-

Table 6 . . . Effect of 5000 Hr Exposure at 600°F on the Tensile Properties of Magnesium-rare Earth Alloys

| Alloy Number | Pct. Total Rare Earths | Tested at Room Temperature | | | | | | Tested at 600°F | | | | | |
|-------------------------------------|------------------------|----------------------------|------|------|----------------|------|------|-----------------|------|------|----------------|-----|------|
| | | HTA | | | HTA + Exposure | | | HTA | | | HTA + Exposure | | |
| | | Pct E | TYS | TS | Pct E | TYS | TS | Pct E | TYS | TS | Pct E | TYS | TS |
| Magnesium-Mischmetal Alloys | | | | | | | | | | | | | |
| 7 | 2.85 | 1.7 | 12.2 | 19.4 | 3.0 | 8.2 | 16.4 | 28.2 | 9.0 | 14.2 | 48.0 | 3.5 | 8.2 |
| 9 | 6.33 | 1.0 | 17.0 | 20.4 | 1.0 | 10.3 | 14.1 | 12.5 | 9.8 | 14.3 | 34.2 | 4.4 | 9.8 |
| Magnesium-Ce-free Mischmetal Alloys | | | | | | | | | | | | | |
| 18 | 2.59 | 2.2 | 13.5 | 23.0 | 3.0 | 8.5 | 16.7 | 35.0 | 9.5 | 14.7 | 63.5 | 4.1 | 9.6 |
| 21 | 5.74 | 1.5 | 18.1 | 25.4 | 1.5 | 11.5 | 17.7 | 34.0 | 11.7 | 17.0 | 58.5 | 5.9 | 12.4 |
| Magnesium-didymium Alloys | | | | | | | | | | | | | |
| 24 | 2.60 | 3.7 | 18.7 | 31.9 | 7.0 | 3.8 | 21.4 | 31.5 | 12.6 | 15.9 | 63.5 | 4.4 | 10.4 |
| 26 | 6.03 | 0.5 | 20.6 | 25.7 | 3.0 | 9.5 | 15.7 | 26.2 | 14.4 | 19.3 | 46.0 | 5.2 | 13.2 |
| Magnesium-cerium Alloys | | | | | | | | | | | | | |
| 37 | 2.60 | 1.5 | 13.0 | 19.9 | 2.2 | 6.9 | 14.8 | 31.5 | 8.1 | 11.3 | 49.7 | 2.5 | 7.0 |
| 39 | 5.70 | 1.5 | 14.0 | 15.6 | 1.5 | 9.9 | 14.4 | 32.5 | 6.4 | 10.6 | 25.7 | 3.6 | 8.8 |
| Magnesium-lanthanum Alloys | | | | | | | | | | | | | |
| 48 | 2.74 | 3.0 | 7.4 | 15.2 | 4.0 | 7.4 | 15.4 | 48.7 | 3.7 | 7.4 | 75.5 | 2.4 | 5.2 |
| 53 | 6.70 | 1.0 | 12.5 | 16.1 | 1.0 | 12.8 | 15.5 | 40.0 | 5.2 | 10.8 | 44.5 | 3.6 | 8.2 |

Pct E—Percent elongation in 2 in.
TYS—Tensile yield strength in 1000 psi
TS—Tensile strength in 1000 psi

fore, take into consideration the temperature range as well as the stress level. In order to illustrate the range in properties that exists in magnesium alloys, the tensile properties and creep limits of three rare earth alloys are compared with those of two commercial casting alloys and magnesium-6 pct zinc-zirconium alloy¹⁸ in Table 8. The superiority of the alloys containing rare earth metals over the other alloys at 400°F is clearly demonstrated. In addition, this table illustrates in a concise form the quantitative differences among the rare earth alloys.

ELECTRICAL CONDUCTIVITY

The results of electrical conductivity measurements are given in Fig 22 for various conditions of heat treatment. The experimental points have been omitted from these plots in order to render the curves more clearly discernible. It can be said that the curves

Table 7 . . . Creep Limits at 500°F

| Alloy No. | Composition | Creep Limits— 1000 psi | | |
|-----------|----------------------------|-------------------------------|-------------------------------|-------------------------------|
| | | 0.1 pct Creep Extension | 0.2 pct Total Extension | 0.5 pct Total Extension |
| 300°F | | | | |
| 2 | Pct 0.40 Mischmetal | 5.5 | 5.2 | 5.7 |
| 3 | 1.15 Mischmetal | 7.9 | 6.1 | 7.2 |
| 5 | 1.62 Mischmetal | 9.0 | 6.8 | 8.7 |
| 6 | 2.50 Mischmetal | 9.7 | 7.3 | 9.2 |
| 7 | 2.85 Mischmetal | 10.1 | 7.3 | 9.0 |
| 8 | 3.23 Mischmetal | 10.0 | 8.4 | 10.2 |
| 9 | 6.33 Mischmetal | 10.6 | 9.6 | 11.8 |
| 500°F | | | | |
| 2 | 0.40 Mischmetal | 3.1 | 3.2 | 4.2 |
| 3 | 1.15 Mischmetal | 5.6 | 5.0 | 6.1 |
| 5 | 1.62 Mischmetal | 6.1 | 5.8 | 6.3 |
| 6 | 2.50 Mischmetal | 6.5 | 5.5 | 7.4 |
| 7 | 2.85 Mischmetal | 7.4 | 6.8 | 8.3 |
| 8 | 3.23 Mischmetal | 4.7 | 4.7 | 6.2 |
| 9 | 6.33 Mischmetal | 5.3 | 5.5 | 6.7 |
| 19 | 3.00 Ce-free Mischmetal | 5.5 | 5.5 | 7.0 |
| 21 | 5.74 Ce-free Mischmetal | 5.2 | 5.6 | 7.4 |
| 25 | 3.85 Didymium | 6.0 | 5.9 | 7.8 |
| 38 | 3.57 Cerium | 4.8 | 4.8 | 5.6 |
| 39 | 5.70 Cerium | 3.7 | 3.8 | 4.5 |

Table 7a . . . Comparison of Creep Limits at 600°F

| Rare Earth Metal | Creep Limit—1000 psi | | | | | | | | |
|--------------------------|---------------------------|---------------|---------------|-------------------------|---------------|---------------|-------------------------|---------------|---------------|
| | 1.5 pct Total Rare Earths | | | 3 pct Total Rare Earths | | | 6 pct Total Rare Earths | | |
| | 0.1 pct Creep | 0.2 pct Total | 0.5 pct Total | 0.1 pct Creep | 0.2 pct Total | 0.5 pct Total | 0.1 pct Creep | 0.2 pct Total | 0.5 pct Total |
| Mischmetal | 1.9 | 2.1 | 2.7 | 2.3 | 2.5 | 2.9 | 2.5 | 2.7 | 3.1 |
| Cerium-free Mischmetal | 1.8 | 1.9 | 2.5 | 1.5 | 1.9 | 2.2 | 1.5 | 1.9 | 2.2 |
| Didymium | 1.7 | 2.1 | 3.2 | 1.0 | 1.4 | 1.7 | 1.0 | 1.4 | 2.6 |
| Praseodymium + lanthanum | 2.0 | 2.1 | 2.5 | 1.7 | 2.1 | 2.2 | 1.7 | 2.0 | 2.2 |
| Cerium | 2.3 | 2.5 | 2.7 | 2.4 | 2.5 | 2.9 | 1.8 | 2.1 | 2.4 |
| Lanthanum | 1.1 | 1.2 | 1.4 | 1.2 | 1.3 | 1.5 | 1.4 | 1.6 | 2.1 |

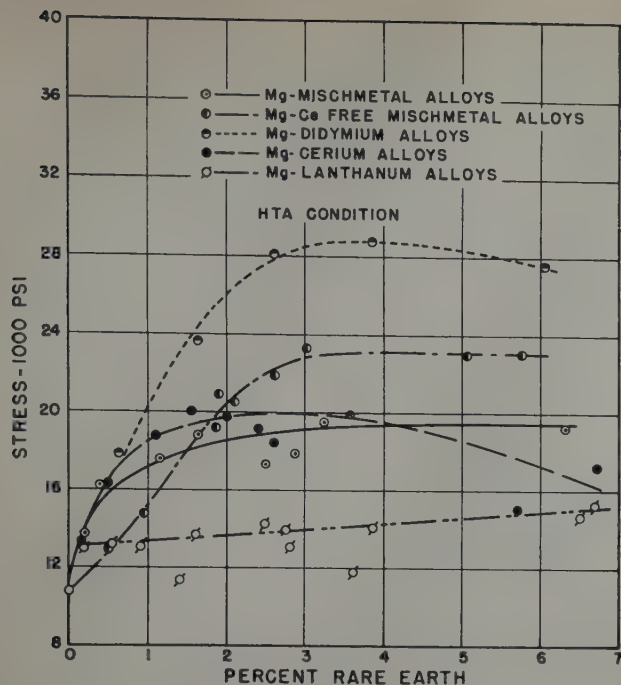


FIG 9—Tensile strength at 300°F.

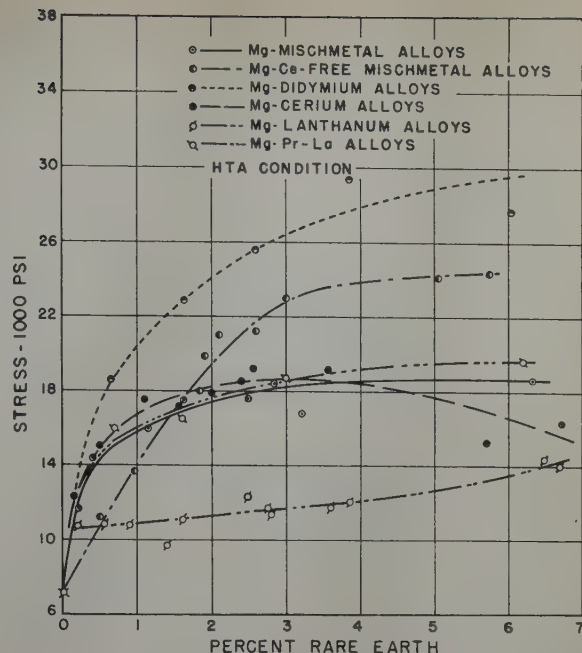


FIG 10—Tensile strength at 400°F.

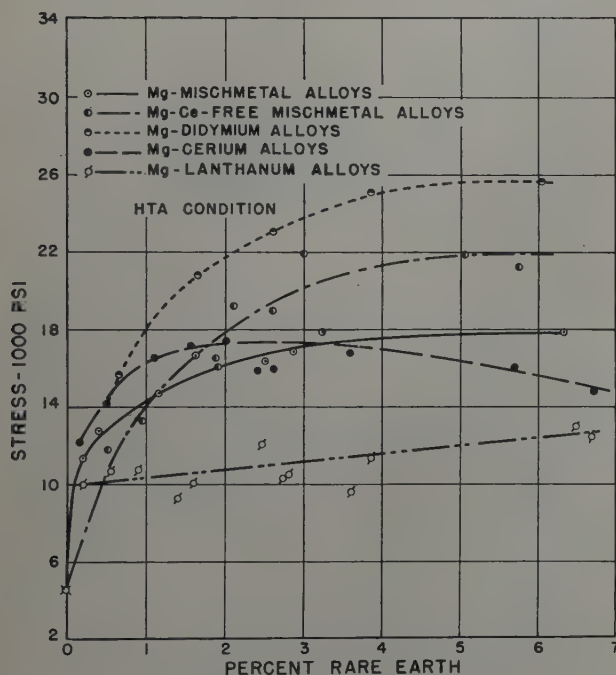


FIG 11—Tensile strength at 500°F.

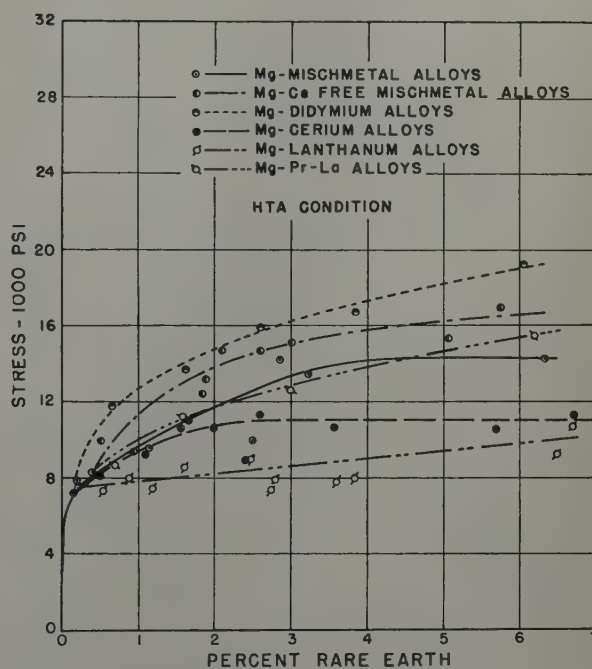


FIG 12—Tensile strength at 600°F.

as drawn follow faithfully the experimental data. The zero point of each series of curves is the conductivity of cast electrolytic magnesium in the same condition of heat treatment as the alloys in the series. The conductivity of this grade of magnesium is naturally a little lower than the value of 0.23 reciprocal microhm-cm reported for pure magnesium.

The decrease in conductivity with composition in each of the alloy sys-

tems is well illustrated by the curves. Considering the conductivity changes that take place upon aging, it may be predicted that the solid solubility of neodymium in magnesium is greater than that of any of the other rare earth elements. On the other hand, the relative insensitivity of the conductivity of magnesium-lanthanum alloys to heat treatment and to aging leads one to the conclusion that the solubility of lanthanum in magnesium is very low, cer-

tainly lower than that of cerium. This is in contradiction of the findings of Weibke and Schmidt¹³ and of Haughton and Schofield¹² both of whom have reported essentially equivalent solid solubilities of cerium and of lanthanum in magnesium. The measurements on magnesium-lanthanum alloys were repeated after heat treating the alloys at 1100°F; no change was recorded in the conductivity after this heat treatment nor did any change occur upon

Table 8 . . . Comparison of Properties of Magnesium-Rare Earth Alloys with Other Magnesium Alloys

| Alloy and Condition | Pct E | TYS* | TS* | Creep Limits* (100 hr) | | |
|---|-------|------|------|-------------------------------|-------------------------------|--------------------------------|
| | | | | 0.1 pct Creep Extension | 0.2 pct Total Extension | 0.5 pct. Total Extension |
| Room Temperature | | | | | | |
| Mg + 6.33 pct Mischmetal (HTA)..... | 1.0 | 17.0 | 20.4 | | | |
| Mg + 5.74 pct Ce-free Mischmetal (HTA)..... | 1.5 | 18.1 | 25.4 | | | |
| Mg + 6.03 pct didymium (HTA)..... | 0.5 | 20.6 | 25.7 | | | |
| Mg + 6Zn + 1Zr (HTA)†..... | 4.9 | 23.9 | 39.5 | | | |
| AZ92-HTA‡..... | 2 | 23 | 40 | | | |
| AZ63-HTS§..... | 7 | 17 | 40 | | | |
| 400°F | | | | | | |
| Mg + 6.33 pct Mischmetal (HTA)..... | 2.0 | 14.7 | 18.6 | 10.7 | 9.6 | 11.8 |
| Mg + 5.74 pct Ce-free Mischmetal (HTA)..... | 4.5 | 16.8 | 24.3 | 13.5 | 10.3 | 15.5 |
| Mg + 6.03 pct Didymium..... | 3.2 | 19.2 | 27.7 | 14.7 | 11.2 | 17.0 |
| Mg + 6Zn + 1Zr..... | 21.5 | 15.1 | 18.1 | 4.1 | 4.3 | 6.0 |
| AZ92-HTA..... | 36.0 | 10.9 | 16.9 | 0.9 | | |
| AZ63-HTS..... | | 12.0 | 17.5 | 1.3 | 1.7 | 2.5 |

* 1000 psi
† Heat treated and aged at 400°F (16 hr)
‡ Mg-9Al-2Zn-0.2Mn:—Heat treated and aged at 425°F (10 hr)
§ Mg-6Al-3Zn-0.2Mn:—Heat treated and aged at 500°F (4 hr)

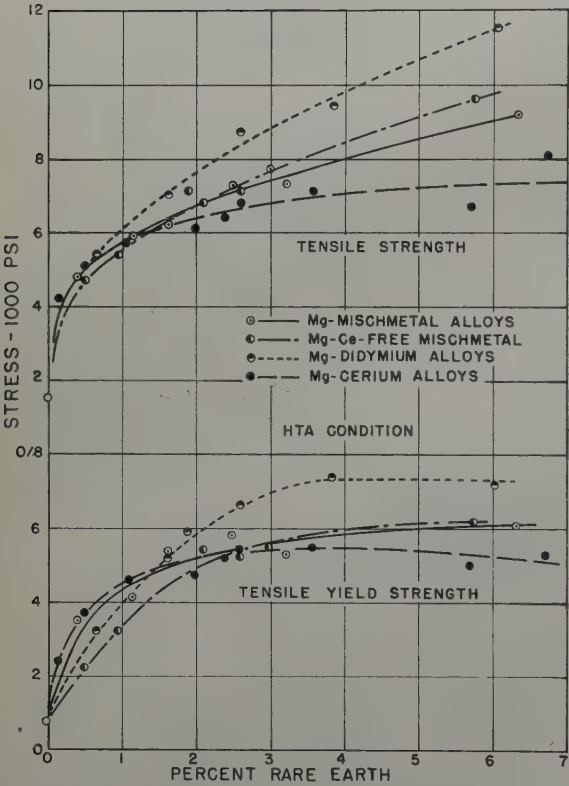


FIG 13—Tensile yield strength and tensile strength at 700°F.

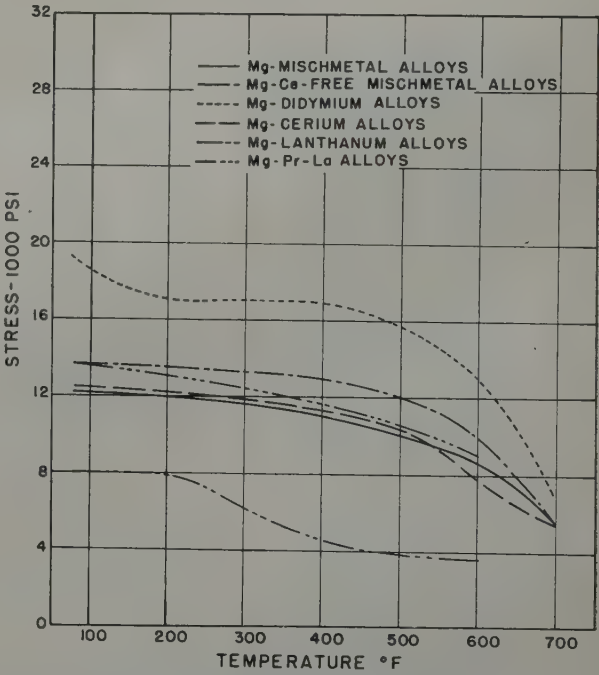


FIG 14—Tensile yield strength of magnesium—3 pct rare earth alloys as a function of temperature. HTA condition.

aging at 400°F for 16 hr subsequent to the same heat treatment.

DENSITY

The density of magnesium-Mischmetal, magnesium-didymium, magnesium-cerium and magnesium-lanthanum alloys, all in the HTA condition, is shown as a function of composition in Fig 23. There is no significant difference in the density of these four types

of alloys. With this information on hand, it can be predicted that the density of magnesium-cerium-free Mischmetal alloys and that of magnesium-praseodymium-lanthanum will fall in the same range.

METALLOGRAPHY

Considerable attention was given to the microstructure of the alloys throughout this investigation; a few

micrographs (Fig 24 through 30) are presented to illustrate some of the most important features of the structures. The etchants used have been described by P. F. George.¹⁶

The as-cast structure of the 6 pct composition of each of the six alloy systems is shown in Fig 24 at a magnification of 100 × and in Fig 25 at 250 ×. The general distribution of second phase is clearly illustrated in Fig 24.

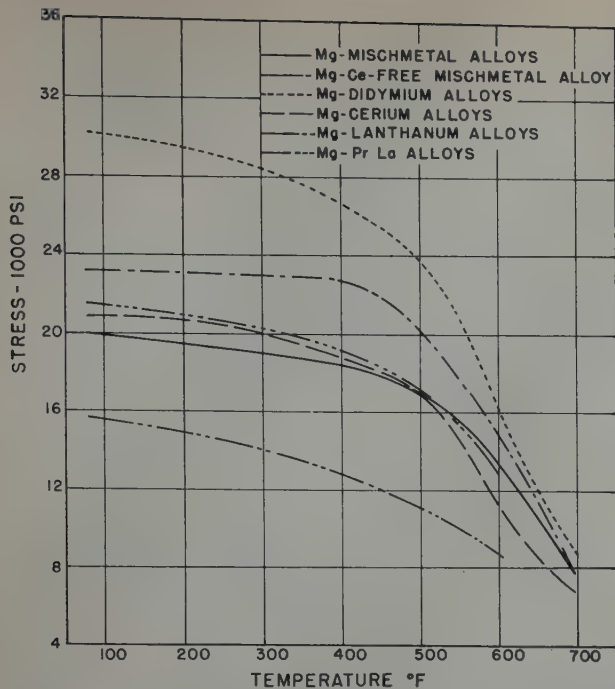


FIG 15—Tensile strength of magnesium—3 pct rare earth alloys as a function of temperature. HTA condition.

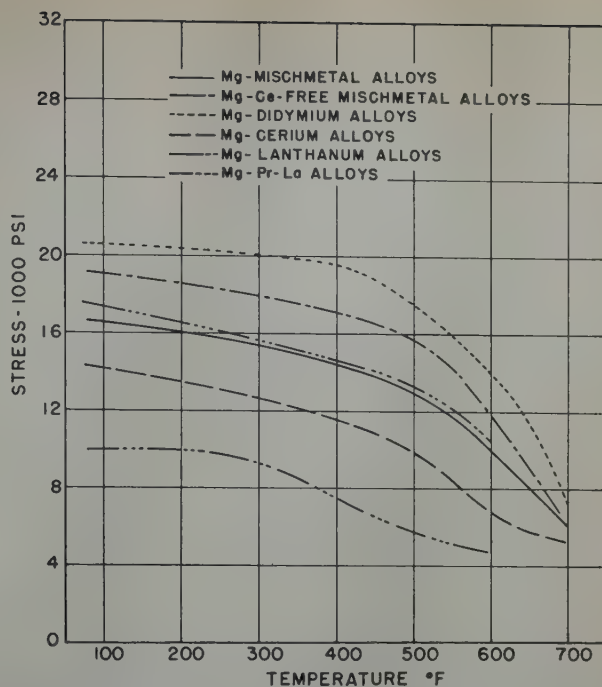


FIG 16—Tensile yield strength magnesium—6 pct rare earth alloys as a function of temperature. HTA condition.

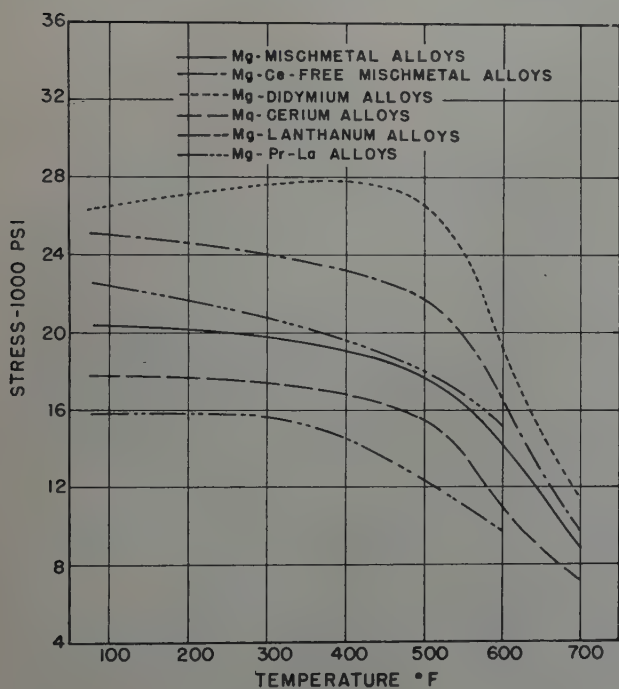


FIG 17—Tensile strength of magnesium—6 pct rare earth alloys as a function of temperature. HTA condition.

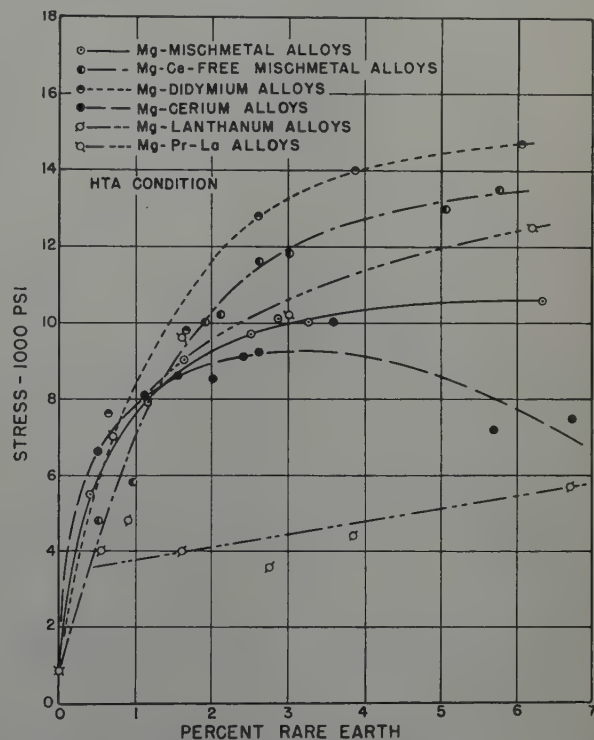


FIG 18—Limiting stress for 0.1 pct creep extension in 100 hr at 400°F.

All the alloys have a dendritic structure. There is a distinct difference in the nature of the eutectic in alloys containing more than one rare earth element from that in the magnesium-cerium alloy and in the magnesium-lanthanum alloy. Both the magnesium-cerium and the magnesium-lanthanum alloys have a very fine eutectic which can be resolved only with difficulty at

250 \times . However, in all the other alloys, there is a very strong tendency for the eutectic to become divorced, in fact in magnesium-didymium alloys it is completely divorced, and what eutectic is present is in the form of massive compound areas with particles of magnesium solid solution imbedded in them. The magnesium-cerium and the magnesium-lanthanum eutectics are

shown more clearly at higher magnification in Fig 26 and 27 and for still better resolution of their structure the electron microscope was used with the results shown in Fig 28 and 29. That these two eutectics differ in the distribution of their respective components is apparent.

The structure of alloys containing lower amounts of rare earths are not

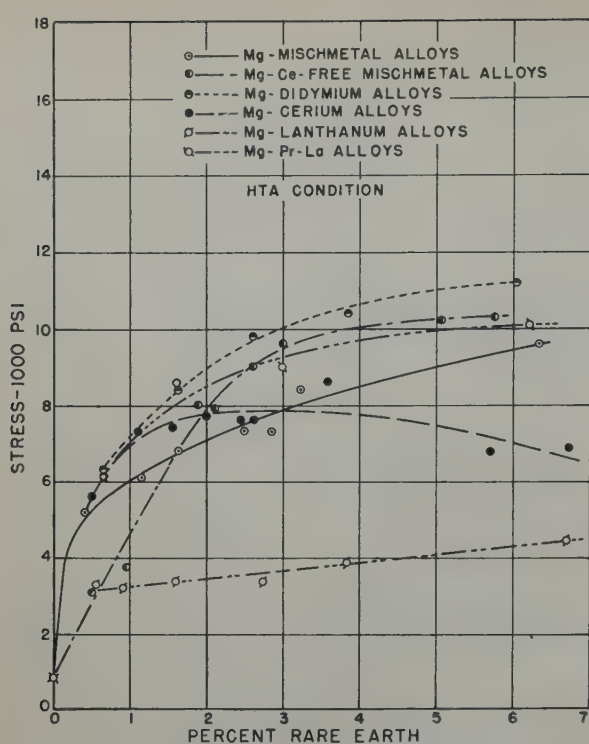


FIG 19—Limiting stress for 0.2 pct total extension in 100 hr at 400°F.

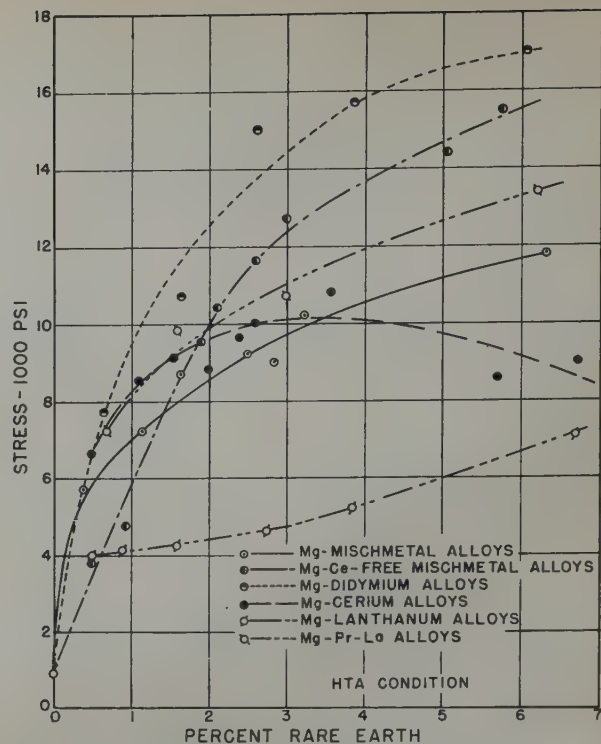


FIG 20—Limiting stress for 0.5 pct total extension in 100 hr at 400°F.

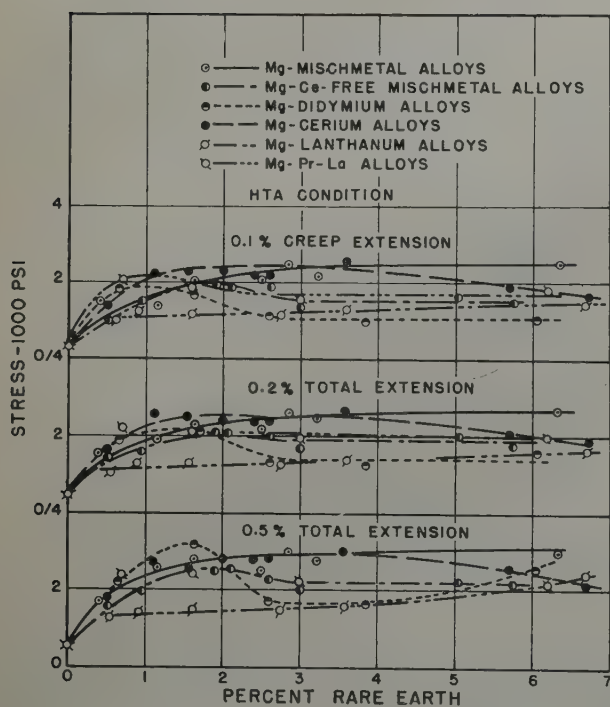


FIG 21—Limiting stresses for 100 hr creep at 600°F.

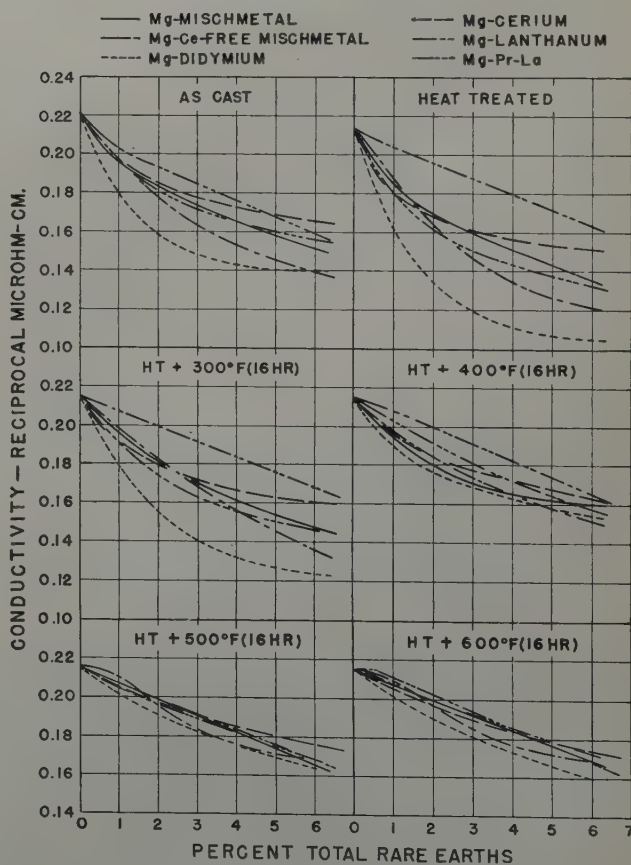


FIG 22—Electrical conductivity of magnesium—rare earth alloys at 95°F.

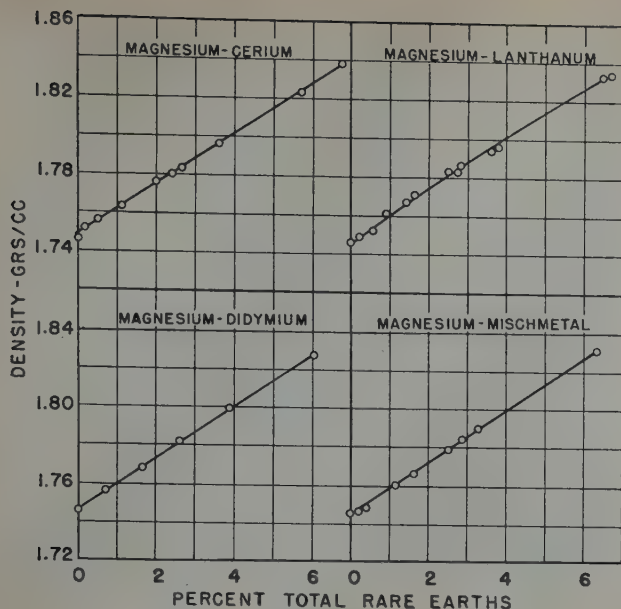


FIG 23—Density of magnesium—rare earth alloys at 25°C (77°F). HTA condition.

shown. The amount of eutectic decreases with decreasing alloy content and the eutectic network ceases to be the continuous phase in alloys containing less than 2 to 3 pct rare earth elements. The eutectic in the complex alloys is completely divorced and the magnesium-lanthanum eutectics show increasing tendency to divorce in lower alloy contents. There is compound or eutectic present in alloys containing as little as 0.10 pct total rare earths.

The microstructures of the 6 pct alloys after heat treating and aging are shown in Fig 30. In all the alloys the compound of the eutectic has been

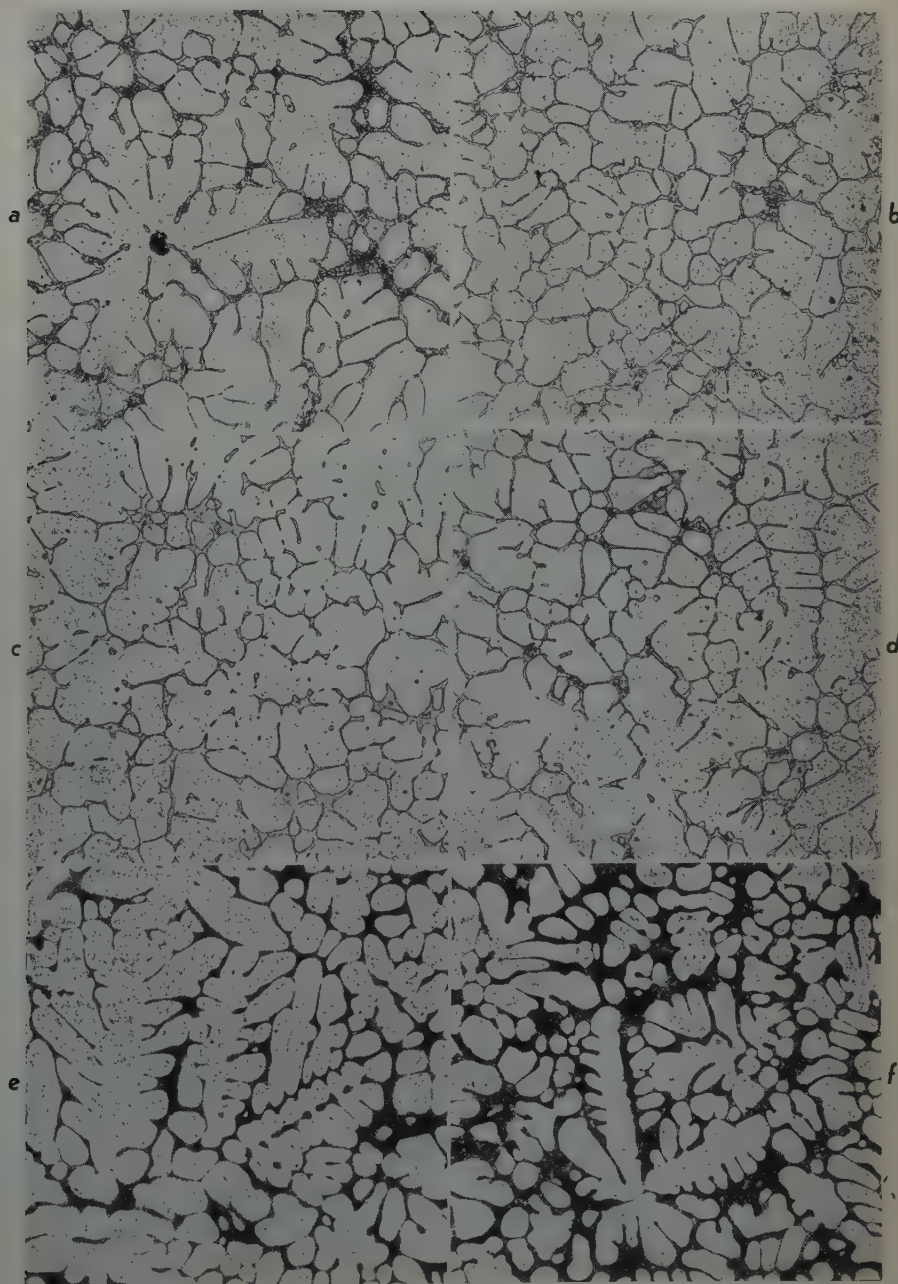


FIG 24—Structure of as-cast magnesium—rare earth alloys.

Glycol etchant. 100 X. Slightly reduced in reproduction. *a.* Mg + 6.33 pct Mischmetal. *b.* Mg + 5.74 pct Ce-free Mischmetal. *c.* Mg + 6.03 pct didymium. *d.* Mg + 6.19 pct (Pr + La). *e.* Mg + 6.73 pct cerium. *f.* Mg + 6.70 pct lanthanum.

coalesced and the continuity of the network has been broken so that the matrix is the continuous phase. For any given alloy content, the magnesium-didymium alloy has the least compound, and the magnesium-lanthanum alloy the most. The compositions of each alloy system which consists only of magnesium solid solution with no rare earth intermetallic compound after heat treatment are listed below:

| | |
|----------------------------------|---|
| Magnesium-Mischmetal | 0.18 pct total rare earth |
| Magnesium-cerium-free Mischmetal | 0.20 pct total rare earth |
| Magnesium-didymium | 0.65 pct total rare earth |
| Magnesium-praseodymium-lanthanum | None, lowest composition available was 0.69 pct |
| Magnesium-cerium | 0.15 pct total rare earth |
| Magnesium-lanthanum | None, lowest composition examined was 0.16 pct |

Increasing the heat treating time to 96 hr does not change these results.

Increasing the heat treating temperature for magnesium-lanthanum alloys does not decrease the amount of Mg₂La nor does it result in a completely homogeneous structure even in the lowest composition available. These findings confirm the conclusions formed from conductivity; neodymium has the greatest solid solubility in magnesium and lanthanum, the least.

Aging at 400°F for 16 hr produces a visible precipitate in the magnesium-cerium-free Mischmetal alloy but even here the amount of precipitate is small and the particles are very fine (Fig 30b). In a previous publication,⁴ it has been shown that in the magnesium + 6 pct Mischmetal alloy in the HTA condition precipitate can be revealed only by the electron microscope.

Aging at 600°F produces a large amount of coarse precipitate in all the magnesium-rare earth alloys except magnesium-lanthanum, as shown previously for magnesium-Mischmetal alloys.⁴ The time required to produce this precipitate is considerably longer in alloys containing 3 and 6 pct didymium than in all other alloys. Extending the aging time at 600°F to 5000 hr fails to produce any precipitate in magnesium-lanthanum alloys, whereas this treatment leads to the coalescence of the precipitate into fairly large particles in the case of magnesium-didymium and to the coalescence of the precipitate with the undissolved compound already present in magnesium-Mischmetal and magnesium-cerium alloys. Only magnesium-

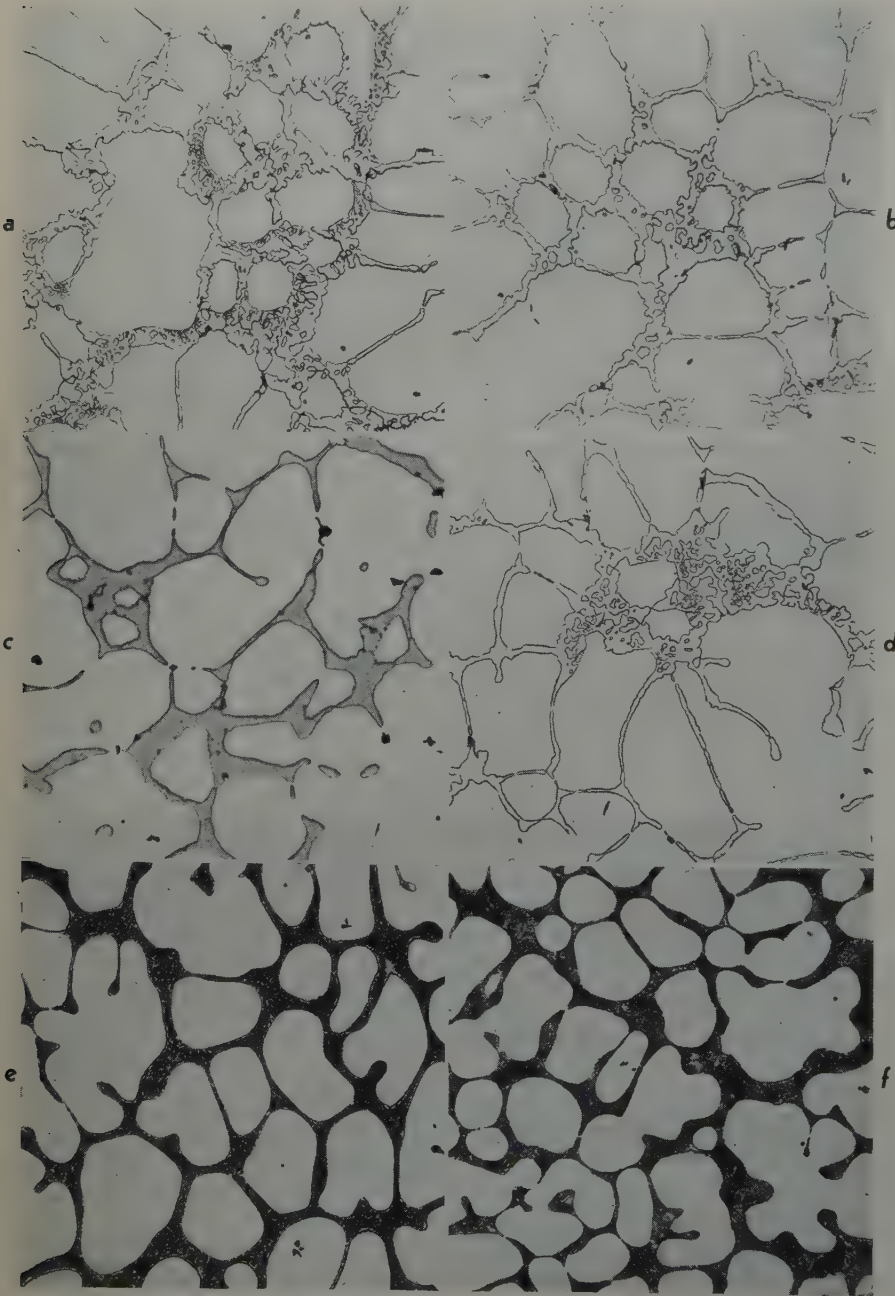


FIG 25—Structure of as-cast magnesium—rare earth alloys.

Glycol etchant. 250 X. Slightly reduced in reproduction. a. Mg + 6.33 pct Mischmetal. b. Mg + 5.74 pct Ce-free Mischmetal. c. Mg + 6.03 pct didymium. d. Mg + 6.19 pct (Pr + La). e. Mg + 6.73 pct cerium. f. Mg + 6.70 pct lanthanum.

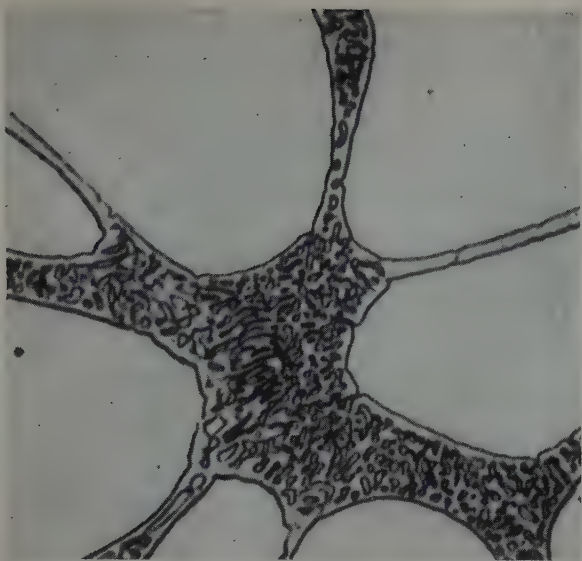


FIG 26 (left)—Eutectic in Mg + 6.73 pct Ce alloy. As-cast condition.
Glycol etchant. 1000 \times .

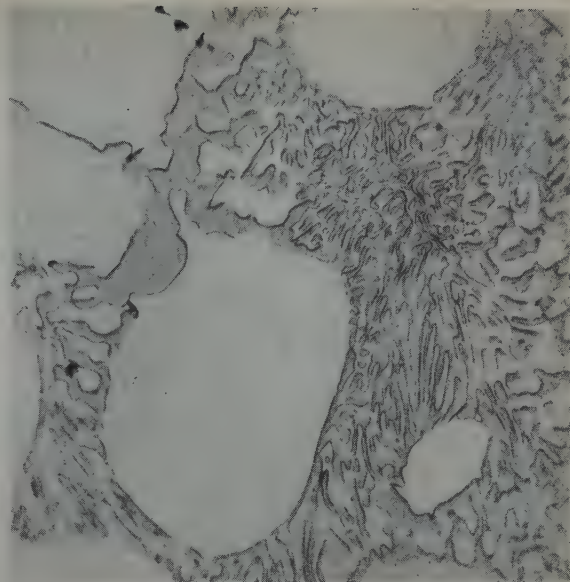


FIG 27 (right)—Eutectic in Mg + 6.70 pct La alloy. As-cast condition.
Glycol etchant. 1000 \times .

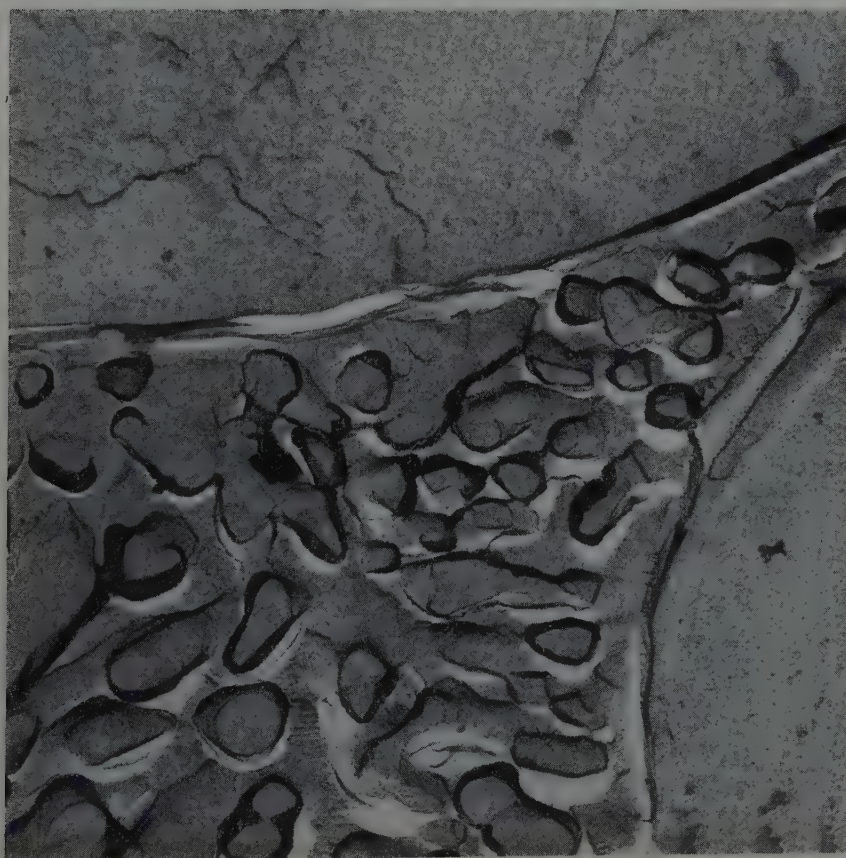


FIG 28—Electron micrograph of eutectic in Mg + 6.73 pct Ce alloy. As-cast condition.
Methyl iodide etchant. 10,000 \times .

cerium-free Mischmetal alloys retain a uniform distribution of precipitate after this prolonged aging treatment. This may explain the somewhat higher strength of these alloys after this treatment.

Summary

All the rare earth metals investigated enhance the strength, hardness, and creep resistance of magnesium at room and elevated temperatures. There are, however, marked differences among the metals in the degree to which they improve these properties.

The various magnesium-rare earth alloys may be rated in the following order of decreasing tensile properties at room and elevated temperatures and creep resistance at 400 and 500°F:

- 1. Magnesium-didymium. 2. Magnesium-cerium-free Mischmetal. 3. Magnesium-praseodymium-lanthanum. 4. Magnesium-Mischmetal. 5. Magnesium-cerium. 6. Magnesium-lanthanum.

The relative effect of each rare earth metal on the creep resistance of magnesium at 600°F depends upon the composition level and, to a certain extent, upon the grain size.

Of the rare earth metals investigated, neodymium exhibits the greatest solid solubility in magnesium and lanthanum, the least. The solid solubility of lanthanum is much less than that reported in the literature. Cerium also appears to have a somewhat lower solid solubility in magnesium than that reported in the literature.

The results of this investigation have shown that considerably higher elevated temperature properties can be developed in magnesium-didymium and magnesium-cerium-free Mischmetal alloys than those exhibited by magnesium-Mischmetal alloys. At 400°F, for example, the properties of magnesium-didymium alloys are 20 to 50 pct higher than those of magnesium-Mischmetal alloys. Although the superiority of these alloys may not hold over the

entire temperature range, their advantage at certain temperatures may warrant their serious consideration for commercial applications. Further development of these alloys will depend upon the availability of the rare earths and a possible reduction in their cost.

References

- 1. J. L. Haughton and W. E. Prytherch: Magnesium and Its Alloys. London, 1937. H. M. Stationery Office.
- 2. A. Beck: The Technology of Magnesium and Its Alloys. London, 1940. F. A. Hughes and Co., Ltd.
- 3. K. Wellinger and E. Keil: *Ztsch. Metallkunde* (1943) 35, 169.
- 4. T. E. Leontis and J. P. Murphy: *Trans. AIME* (1946) 166, 295. *Metals Tech.* Apr. 1946.
- 5. A. J. Murphy and R. J. M. Payne: *Jnl. Inst. Metals* (1946), 73, 105.
- 6. J. C. McDonald: *Proc. ASTM* (1948) 48.
- 7. G. A. Mellor and R. W. Ridley: *Jnl. Inst. Metals* (1949) 75, 679.
- 8. C. E. Nelson: *Trans. AIME* (1944) 159, 392.
- 9. R. F. Marande: *Materials and Methods* (1946) 23, 418.

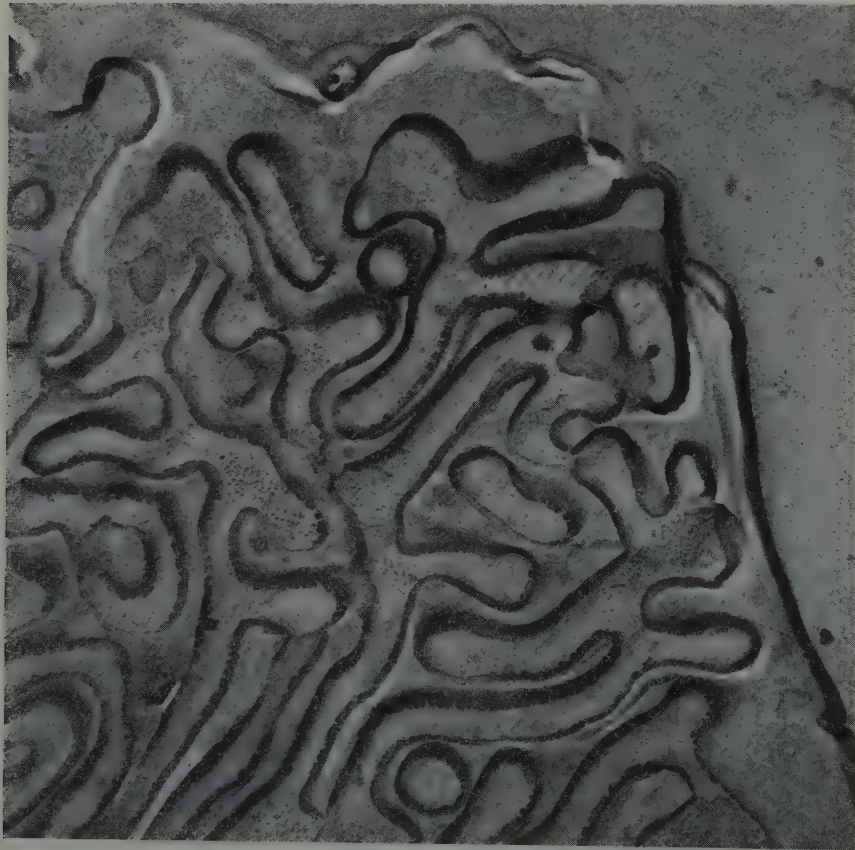


FIG 29—Electron micrograph of eutectic in Mg + 6.70 pct La alloy. As-cast condition. Methyl iodide etchant. 10,000 X.

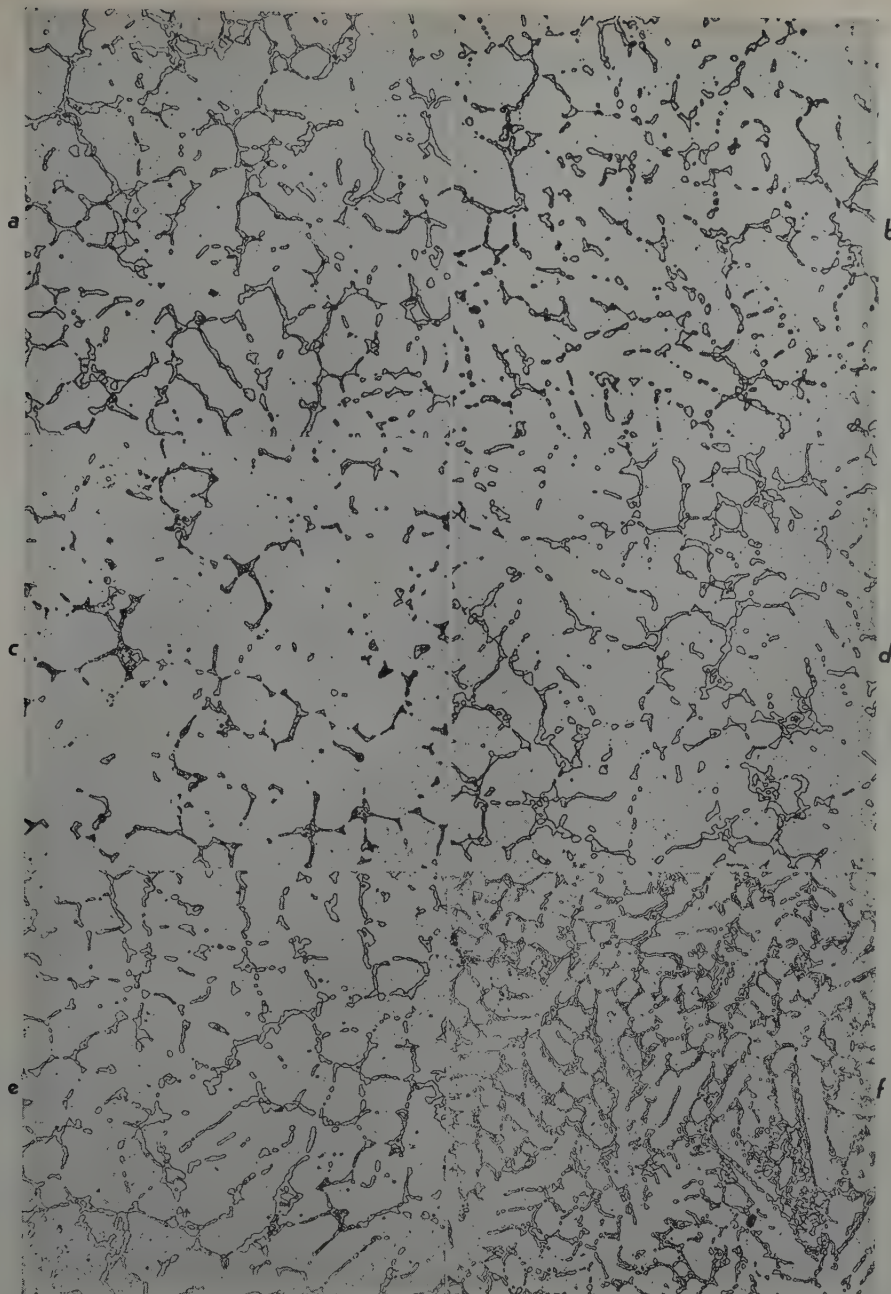


FIG 30—Structure of magnesium—rare earth alloys in the heat treated + aged condition.
Glycol etchant, 100 X. Slightly reduced in reproduction. *a.* Mg + 6.33 pct Mischmetal. *b.* Mg + 5.74 pct Co-free Mischmetal. *c.* Mg + 6.03 pct didymium. *d.* Mg + 6.19 pct (Pr + La). *e.* Mg + 6.73 pct cerium. *f.* Mg + 6.70 pct lanthanum.

- | | | |
|--|---|---|
| 10. Magnesium Laboratory Methods. The Dow Chemical Co., Midland, Mich. | 13. F. Weibke and W. Schmidt: <i>Ztsch. Elek.</i> (1940) 46, 357. | (Aug. 1944), 35. |
| 11. C. J. Rodden: <i>Jnl. Res. Nat. Bur. Stds.</i> (1941) 26, 557. | 14. G. Canneri: <i>Met. Italiana</i> (1931) 23, 803. | 17. A. A. Moore and J. C. McDonald: <i>Proc. ASTM</i> (1946) 46, 970. |
| 12. J. L. Haughton and J. H. Schofield: <i>Jnl. Inst. Metals</i> (1937) 60, 339. | 15. G. Canneri: <i>Met. Italiana</i> (1933) 25, 250. | 18. T. E. Leontis: <i>Trans. AIME</i> (1948) 175. <i>Metals Tech.</i> , June 1948, TP 2371. |
| | 16. P. F. George: <i>ASTM Bull.</i> No. 129 | |

The Relationship Between Electrical Conductivity and Composition of Molten Lead Silicate Slags

A. KENNETH SCHELLINGER,* Junior Member AIME and ROBERT P. OLSEN†

Molten silicate salts, the important industrial byproducts termed "slags," are known to be electrolytic conductors at furnace temperatures. This property is due to their partial dissociation into ions with the ion kind and size being closely related to the slag composition. Ionic conductance, in liquids, is a function of the viscosity, which in turn is a function of the temperature. It could be anticipated, therefore, that a semi-log plot of conductivity vs. reciprocal absolute temperature might yield a straight line, in the case of molten silicates and salts. As liquids, the viscosity of these slags should follow the Shepard¹ relationship:

$$\log \text{ viscosity} = \frac{A}{T} + B$$

Then, if the resistance of the molten slag is directly proportional to the viscosity:

$$\log R_s = \frac{A}{T} + B$$

Resistance measurements of molten halide salts,² and silicate salts^{3,4} by various investigators have, indeed, shown this straight line relationship between resistance and temperature.

A further relationship between the

conductivity versus the degree of ionization, the size of the ions, and the slag composition is, also, to be expected. Large ions, and fewer ions, would move more slowly in a potential field and could not carry as much current as smaller, more numerous, and mobile, ions. Conductivity, therefore, would be smaller in the presence of such large ions and higher slag viscosities.

The conductivity-composition relationship is of considerable interest in the case of the industrial slags produced in iron blast furnaces, and non-ferrous smelting furnaces. These slags usually approximate three component systems with several minor components as impurities. At least one of the major

components is commonly purchased for the sole purpose of rendering the slag less viscous at a reasonable furnace temperature. Should the conductivity be related rather directly to the concentration of such a purchased slag component (that is, CaO) instrumental measurement and control at the furnace might be possible. Modern telemetric control methods in aqueous chemical process industries are often based on the property of conductivity of solutions, and its variation with composition.

Investigators³ of the phenomenon of electrical conductivity in molten blast furnace slags have established that these systems show lines of equal conductivity on their ternary diagrams at one temperature level. These isoconductivity lines form closed contours on the diagrams, and at times, minimum areas occur at which these contours are essentially closed down to a point. The conductivity reading at such a point, at one temperature, would, of course, locate one on the diagram, and give the slag composition.

Research in this field is understandably scanty. The reactive nature of

New York Meeting, February 1950. TP 2728 D. Discussion of this paper (2 copies) may be sent to *Transactions AIME* before April 1, 1950. Discussion is tentatively scheduled for publication in November 1950.

Manuscript received Aug. 1, 1949.
* Instructor of Metallurgy, Stanford University, Stanford, California.

† Metallurgist, Selby Plant, American Smelting and Refining Co., Selby, Calif.

¹ References are at the end of the paper.

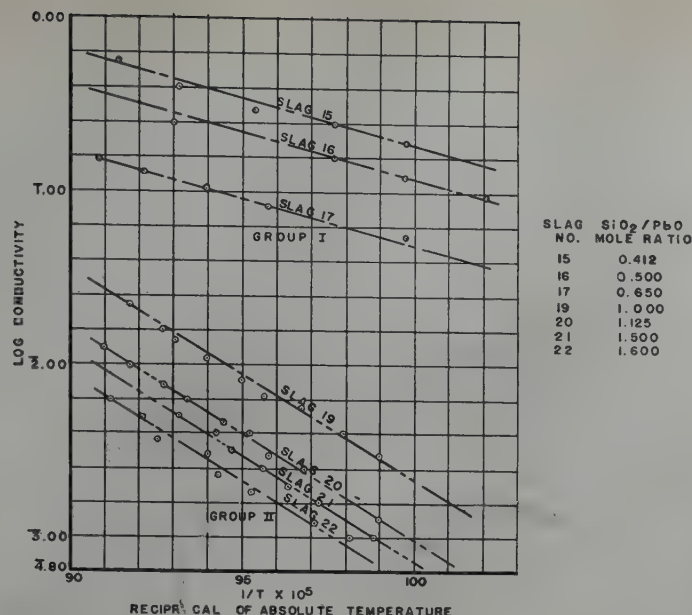


FIG 1—Log conductivity vs. reciprocal of absolute temperature for PbO-SiO₂ slags in liquid state.

these slag systems at their liquid temperatures renders the construction of a measuring apparatus extremely difficult. Temperature control is, also, not easy to achieve. Complex ternary systems often obscure experimental data by the introduction of uncontrollable variables.

Experimental Procedure and Apparatus

The present research was started with the hope of obtaining some further data on industrial systems. However, preliminary work on low-melting lead silicate systems seemed like a logical starting point in establishing the validity of the conductivity-composition control method. Accordingly, several artificial slags were made up from cp litharge and silica. These ranged in content from 10 pct SiO₂ to 30 pct SiO₂, by weight. These slags were melted in 10-g silica assay crucibles held in an electrically-heated pot furnace. An assembly, consisting of two platinum electrodes, plus a chromel-alumel thermocouple, was fitted on the top of the crucible. This allowed the electrodes and thermocouple to dip into the molten slag to a predetermined depth.

Temperature and conductivity were read simultaneously at each point; first with the temperature increasing, and then with it decreasing. Temperature was read on a Leeds and Northrup

portable potentiometer. Conductivity readings required 1000-cycle current, supplied by an audio-oscillator, and a resistance bridge circuit, calibrated in ohms. The null-point method was then used for both resistance and temperature. The conductivity apparatus was calibrated to yield specific conductivities, according to the formula:

$$L_s = \frac{K}{R} \quad \text{where } K \text{ is the cell constant and } R \text{ is the resistance reading in ohms.}$$

K was determined by a calibration using standard KCl solutions.

Results

A number of temperature-conductivity points were read for each slag composition, above its melting point. Fig 1 shows these points plotted to a log conductivity-reciprocal absolute temperature scale. It will be seen that the points for slag composition can be averaged as a straight line of formula:

$$\log L_s = \frac{-A}{T} - B$$

Where A is a constant for each line—the slope of the line—and B is a second constant.

This formula can be derived from the Shepard¹ formula for viscosity:

$$\log \mu = \frac{A}{T} + B$$

by assuming molten slag specific resistance as directly proportional to viscosity, whence:

$$\log R_s = \frac{A}{T} + B$$

and as, $R_s = \frac{1}{L_s}$ then,

$$\log \frac{1}{L_s} = \log 1 - \log L_s = \frac{A}{T} + B,$$

$$\text{or, } \log L_s = \frac{-A}{T} - B.$$

The correspondence between this formula and the one for the plotted points in the lead silicate system is considered good evidence of the direct relationship between viscosity and conductivity in these slags.

It will be noted, also, that the four slags with SiO₂/PbO ratios of 1.00, or greater, all have almost equal slopes. That is, for these compositions, A is a constant. Further, the three slags of SiO₂/PbO ratios less than 1.00 yield lines with approximately equal slopes, or Constant A .

A_2 has an average value of 11,200, which makes the equation of the lines in group II:

$$\log L_s = \frac{-11,200}{T} - B$$

Similarly, the equation for group I is:

$$\log L_s = \frac{-5000}{T} - B$$

If we take unit conductivity ($L_s = 1$) as a reference point, then for group II:

$$B = \frac{-11,200}{Tu} \quad \text{and} \quad Tu = \frac{-11,200}{B}$$

and for the group I:

$$Tu = \frac{-5000}{B}$$

where Tu is the absolute temperature of unit conductivity for each slag composition, corresponding to its constant B .

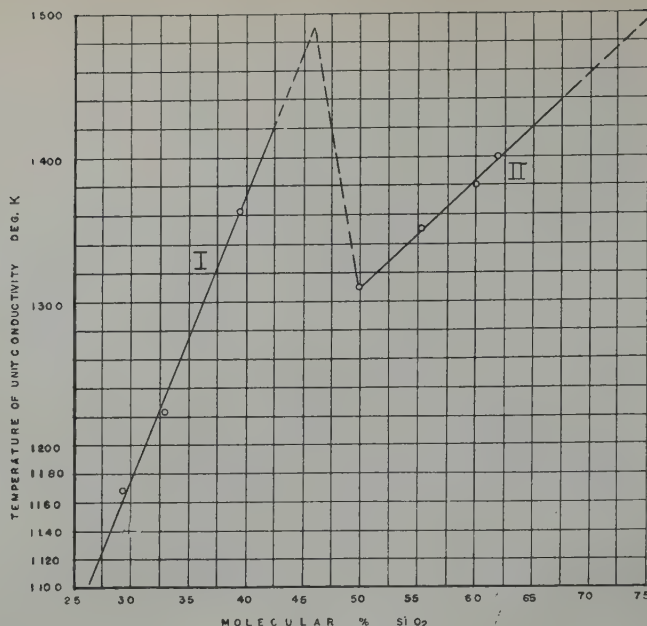


FIG 2—Temperature of unit conductivity vs. mol pct SiO₂.

When these Tu values are plotted against molecular percentage of SiO₂, the points can be averaged by two straight lines of different slopes, one for each group. This will be seen by a glance at Fig 2. The break between these two curves is seen to occur at about 50 mol pct SiO₂, or about 21 pct by weight of SiO₂. This break is such that the temperature of unit conductivity drops sharply at this composition. The slag suddenly conducts the same amount of electricity at a much lower temperature. This seems to indicate an increase in the number of ions and a decrease in the size of the ions, or both. Such an event could occur by the ionization, and disappearance, of a large molecular association such as PbO.SiO₂. It is interesting to note that the constitutional diagram⁵ of PbSiO₃ vs. temperature shows a temperature maximum in its liquidus line at 21 pct, by weight, SiO₂. This maximum is at 1137 degrees absolute and corresponds to the compound PbO.SiO₂.

The equation for line I, in Fig 2, is:

$$Tu = 20N + 570, \text{ or}$$

$$N = \frac{Tu - 570}{20} = 0.05Tu - 28.5$$

and as, $Tu = \frac{-5000}{B}$ for group I

(when $Ls = 1$) then $N = \frac{-250}{B} - 28.5$
 $= \text{mol pct SiO}_2$ where B , for group I, is given by:

$$-B = \log Ls + \frac{5000}{T}$$

Similarly, for line II, in Fig 2:

$$N = \frac{Tu - 917}{7.8} = 0.128Tu - 117.6$$

and, substituting, $Tu = \frac{-11,200}{B}$ for

group II, whence $N = \frac{-1432}{B} - 117.6$

and, B for group II is given by:

$$-B = \log Ls + \frac{11,200}{T}$$

These equations can be used to predict the mol pct SiO₂ of lead silicate slags, in the absence of Fig 1 and 2, as follows:

Suppose that a slag of unknown silica content gave a specific conductivity reading of $Ls = 0.00725$ mho at a temperature of 800°C or 1073°K. Here $\log Ls = 3.860$. Assume that any reading with a log value less than 2.00 will be in group II. Then,

$$-B = \log Ls + \frac{11,200}{T} \\ = 3.860 + 10.42 = 8.28$$

$$\text{and } N = \frac{-1432}{B} - 117.6 = 173.2 -$$

117.6 = 55.6 mol pct SiO₂. This is seen to be one of the points of slag 20, in group II. This slag therefore, has a composition of 25 pct SiO₂, by weight.

For this simple binary system, these equations, or corresponding nomographs will convert specific conductivity, plus temperature readings to composition. Small amounts of impurities probably will not affect this relationship; however, this fact has not been definitely established. Extension of this method to other binary, and, perhaps, ternary systems would place a useful tool in the hands of the furnace metallurgist.

References

1. Prutton and Maron: Fundamental Principles of Physical Chemistry. 1st Ed., 1944, MacMillan, p. 106.
2. C. L. Mantell: Industrial Electrochemistry, Second Ed., 1940, Chap. XIX, McGraw-Hill.
3. A. E. Martin and G. Derge: The Electrical Conductivity of Molten Blast Furnace Slags. *Trans. AIME* (1943) 154, 104.
4. A. Wegnarth: Current Conducting Properties of Slags. *Trans. Electrochem. Soc.* (1934) 65, 177.
5. O. C. Shepard and W. F. Dietrich: Fire Assaying. 1st Ed., 1940, McGraw-Hill.

Cemented Titanium Carbide

JOHN C. REDMOND,* Member AIME, and E. N. SMITH*

Introduction

The increasing need for materials capable of withstanding higher operating temperatures for various applications such as gas turbine blading and other parts, rocket nozzles, and many industrial applications, has brought consideration of cemented carbide compositions. The well known usefulness of cemented carbides as tool materials is attributable to their ability to retain their strength and hardness at much higher temperatures than even complex alloys. However, it has been found that the temperatures encountered in cutting operations do not approach by several hundred degrees¹ those involved in the applications mentioned above where the interest is in materials possessing strength and resistance to oxidation at temperatures of 1800°F and above. At these latter temperatures, the tool type compositions which are made up essentially of tungsten carbide are found to oxidize very rapidly and to produce oxidation products of a character which offer no protection to the remaining body. As a further consideration, the density of the tungsten carbide type compositions is high, from about 8.0 to 15.0.

The refractory metal carbides as a class are the highest melting materials known as shown by Table 1 which summarizes the available data from the literature for the carbides of the elements which are sufficiently available for consideration for these uses. The density is also included in the table, since as mentioned above, it is an important consideration in many of the applications for which the materials would be considered. It has been established that in the tool compositions the mechanism of sintering with cobalt is such as to result in a continuous carbide skeleton and that the properties of the sintered composition are thus essen-

Table 1 . . . Melting Points and Density

| Carbide | Melting Point °C | Density g per cc |
|--------------------------------|---------------------|---------------------|
| TaC | 3880 | 14.49 |
| CbC | 3500 | 7.82 |
| TiC | 3140 | 4.90 |
| WC | 2870 | 15.50 |
| VC | 2810 | 5.36 |
| Mo ₂ C | 2380 | 8.9 |
| Cr ₃ C ₂ | 1890 | 6.68 |

tially those of the carbide.² On the hypothesis that this mechanism holds to a greater or less degree in cementing most of the refractory metal carbides with an auxiliary metal, it appears from Table 1 that titanium carbide compositions would offer possibilities for a high temperature material.

Titanium carbide has extensive use for supplementing the properties of tungsten carbide in tool compositions. Although the literature contains several references to compositions containing only titanium carbide with an auxiliary metal,^{3,4,5,6} it may be inferred from the meager data that such compositions were deficient in strength and were considered to have poor oxidation resistance.⁷ Kieffer, for instance, reports the transverse rupture strength of a hot pressed TiC composition at 100,000 psi as compared to up to 350,000 psi for WC compositions.

The work described herein was undertaken to determine the properties of compositions consisting of titanium carbide and an auxiliary metal and to improve the oxidation resistance of

such compositions. It appeared possible that the inclusion of one or more other carbides with titanium carbide might improve the oxidation resistance and also that this might be more desirable than other means from the point of view of maintaining the highest possible softening point. Consideration of the available carbides in Table 1 suggests tantalum and columbium carbides because of their high melting points and general refractoriness. The work on improving oxidation resistance was concentrated on the addition of tantalum carbide or mixtures of tantalum and columbium carbide. The auxiliary metals used included cobalt, nickel and iron. It was also desired to learn the general physical properties of these compositions.

Experimental Procedure

The compositions used in this study were made by the usual powder metallurgy procedure applicable to cemented tungsten carbide compositions. The powdered carbide or carbides and auxiliary metal were milled together out of contact with air. In some cases cemented tungsten carbide balls and in other instances steel balls were used to eliminate any effect of tungsten carbide contamination. A temporary binder, paraffin, was then included in the mix and slugs or ingots were pressed with care to obtain as uniform pressing as possible. The ingots were presintered and the various shapes of test specimens were formed by machining, making the proper allowance for shrinkage during sintering. Thereafter the shapes were sintered in vacuum at temperatures of from 2800 to 3500°F. Final grinding to size was carried out by diamond wheels under coolant.

The titanium carbide used contained a minimum of 19.50 pct total carbon and a total of 0.50 pct metallic impurities as indicated by chemical and spectrographic analysis. It was found by X ray diffraction examination with

New York Meeting, February 1950.
TP 2725 E. Discussion of this paper
(2 copies) may be sent to *Transactions*
AIME before April 1, 1950. Discussion
is tentatively scheduled for publica-
tion in November 1950.

Manuscript received May 23, 1949.

* Research Director and Research
Engineer, respectively, Kennametal,
Inc., Latrobe, Pa.

¹ References are at the end of the
paper.

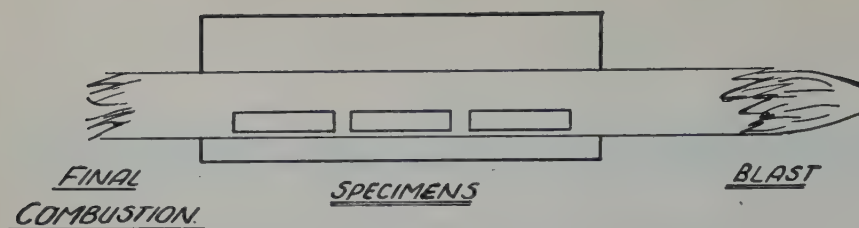


FIG 1—Arrangement of apparatus used for gas oxidation tests.

a Norelco Recording Spectrometer to have the usual NaCl type of cubic lattice with a parameter of 4.32 Å. The auxiliary metals were in the form of pure hydrogen reduced powders. The carbides used to modify the TiC for increasing its oxidation resistance were made by the McKenna "menstruum" process.⁸ These were TaC and a three-carbide solid solution of the following approximate composition: Cb, 50.0 pct, Ta, 32.5 pct, Ti, 7.0 pct and carbon 10.5 pct. The latter is of interest because it offers a more available source of columbium and tantalum being made directly from suitable columbite ore without the need for separations.

Two tests were used to determine oxidation resistance. In the first test used in the earlier phases of the work a tube furnace arrangement combining electric and gas heating as shown in Fig 1 was used. The blast burner fuel gas ratio was so adjusted that combustion was not complete until the gases had passed over the specimens and through the tube and some flame was maintained at the exit end of the tube. An analysis of the gas at the specimens showed the following:

| | Pct |
|--|---------|
| CO..... | 5.1 |
| CO ₂ | 4.0 |
| O ₂ | 6.1 |
| N ₂ and H ₂ O..... | Balance |

The temperature of the specimens was maintained at 2100°F. This condition was found to be insufficiently severe.

The second procedure consisted of heating the ground specimens on ceramic or carbon supports in an unsealed muffle furnace without atmosphere control. Various conditions with respect to time and temperature were used as noted later.

The problem of measuring deterioration is difficult. The scales or coatings formed are highly adherent and cannot be removed mechanically; and they cannot be removed chemically without the danger of attacking the sound body. Methods based on weight increase appear to be satisfactory although somewhat difficult of interpretation because of the varying stoichiometric increases associated with the oxidation

of the various constituents. Measurement of the increase in thickness was found to agree well with weight increase values and was used as a measure for most of the work. In a few instances, strength measurements made after exposure demonstrated the decrease in strength to be proportional to the thickness increase. In a few instances microscopic examination was also made on polished cross-sections.

The strengths were determined at room temperature and at 1800°F by the transverse bending method. The particular arrangement used is shown in Fig 2 and has been widely used for testing the strength of the tool compositions. It is satisfactory as long as the materials being tested are of high compressive strength so that the failure is by tension rather than by shear. It was found by a compressive-strength test using the method of Bridgeman⁹ that the compressive strength of the composition of 80 pct TiC and 20 pct Co was 550,000 psi at room temperature and it was therefore considered that the short span specimen would yield satisfactory values for comparison purposes. This has since been confirmed qualitatively by work done on longer span specimens $\frac{1}{4}$ by $\frac{1}{2}$ by 4 in.¹⁰ For the high temperature tests the specimen was heated by induction with a coil surrounding the supports and the specimen and with the thermocouple placed directly in contact with the bottom surface of the specimen. Additional tests were carried out at other temperatures up to 2000°F in the case of two of the compositions. The room temperature tests were made on a calibrated hydraulic testing machine or on a Brinell testing machine. The high temperature tests were made on a hand operated hydraulic press calibrated with a proving ring.

The density of the sintered compositions was measured in all cases to determine completeness of sintering. This was carried out on ground specimens using the water immersion method and with a commercial wetting agent in the water. The theoretical density was calculated on the assumption that

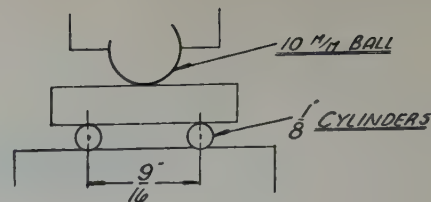


FIG 2—Arrangement for transverse rupture testing. Specimen cross section is 0.200 in. thick X 0.375 in. wide.

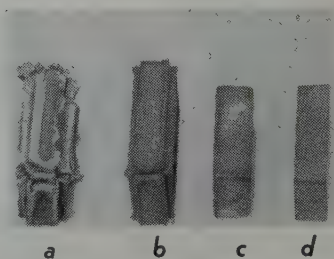


FIG 3—Comparison of oxidation of tungsten carbide and titanium carbide compositions.

a. 94 pct WC—6 pct cobalt. b. 73 pct WC—11 pct cobalt—16 pct titanium, columbium and tantalum as carbides. c. 80 pct TiC—20 pct cobalt. d. 60 pct TiC—20 pct cobalt—20 pct titanium, columbium and tantalum as carbides.

there was no retention of any of the carbides in solution in the auxiliary metal phase or change of any of the constituents in compositions. This was deemed a satisfactory criterion for determining completeness of sintering.

Other properties, including hardness, thermal and electrical conductivity and thermal expansion, were measured on two of the compositions to determine their general character.

Experimental Results

Early oxidation tests with the apparatus shown in Fig 1 indicated the oxidation rate of TiC compositions to be as little as 0.0002 in. thickness increase per face per hr at temperatures up to 2100°F with an adherent coating formed. The transverse rupture strength at room temperature for the 80 pct TiC—20 pct Co composition was found to be from 160 to 190,000 psi and at 1800°F it was found to be of the order of 100,000 psi. Further oxidation tests made in the muffle furnace for 18 hr periods showed that while these TiC compositions oxidized somewhat rapidly at 1800°F (up to 0.0011 in. thickness increase per face per hr), they were considerably superior to the tungsten carbide base materials which showed rates as high as 0.050 in. and oxidation products of inferior character as shown by Fig 3. The first composition is 94 pct WC and 6 pct Co, the

second 73 pct WC and 11 pct Co and the balance titanium, tantalum and columbium as carbides. In both instances the oxides are fluffy and non-adherent. The third specimen is 80 pct TiC and 20 pct Co. The fourth composition is the same as the third except that 20 pct of the solid solution of columbium and tantalum and titanium carbides was included as will be discussed later.

The oxidation rates of compositions containing varying quantities of cobalt, nickel and iron with TiC only and of compositions including TaC and the three carbide solid solution were determined in an 18 hr muffle test as shown in Table 2. The rates for the various auxiliary metals are observed to be of the same order of magnitude. In these preliminary tests it was found that from 25 to 35 pct of TaC substituted for an equal weight of TiC reduced the oxidation by tenfold as is shown in Table 2. This same result could be accomplished equally well by smaller percentages of the columbium, tantalum, titanium carbide solid solution. A series of compositions was therefore prepared using cobalt as the auxiliary metal maintained at 12.3 pct by volume of the composition. The three carbide solid solution content was varied as shown in Fig 4. The sintered test pieces were subjected to a 64 hr test in the muffle with the results shown. The marked effect of the columbium and tantalum in even small percentages in reducing the oxidation is to be noted as well as the fact that compositions which are very high in columbium and tantalum carbide oxidize more rapidly than the high TiC

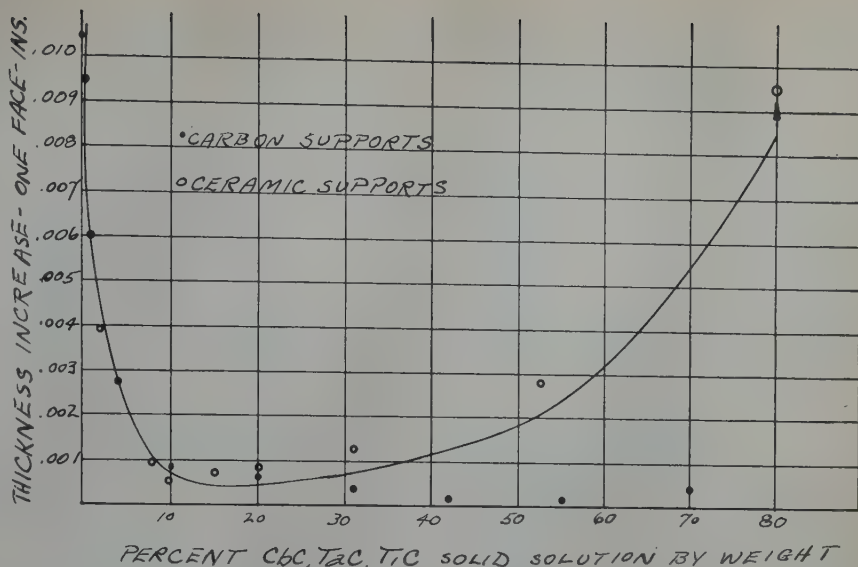


FIG 4—Effect of CbC, TaC, TiC solid solution on oxidation of TiC compositions. 64 hr at 1800°F in open muffle furnace.

compositions. Two tests were made in one of which the specimens were supported on ceramic boats and in the other on carbon supports. The difference in the results should be noted.

A 210 hr oxidation test at 1800°F in the open muffle on a few selected compositions showed substantially the same results as the 64 hr test as shown in Table 3. Fig 5 shows the character of coating formed on the composition containing 18.7 pct Co, 15 pct three carbide solid solution and 66.3 pct TiC after heating for 210 hr at 1800°F in the open muffle. The overall coating thickness is approximately 0.003 in. A short test of 18 hr at 2200°F showed relative oxidation rates to be unchanged with the composition contain-

ing 20 pct of the three carbide solid solution being highly resistant. The thickness increase was 0.0182 in. for the 80 TiC-20 Co composition and 0.0014 in. for the equivalent composition containing 15 pct solid solution.

A study was made to determine whether any change in the rate of oxidation occurred with time with the results shown in Fig 6. The two compositions used were the 80 pct TiC-20 pct Co composition and the similar composition containing 15 pct of the columbium, tantalum, titanium solid solution. It is observed that within the accuracy of the measurements both compositions show straight line though widely varying rates of oxidation.

The effect of the addition of the three

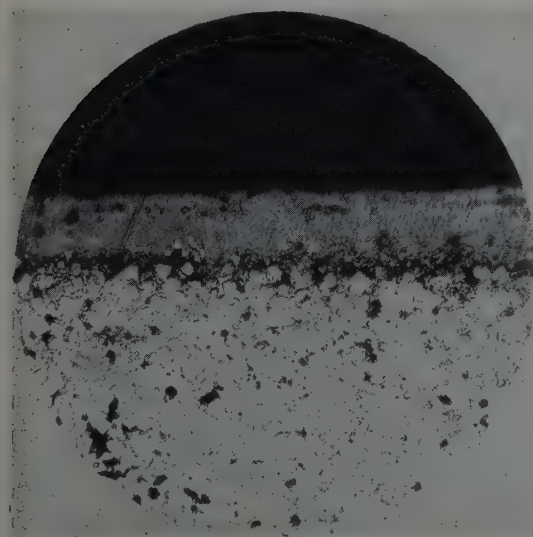


FIG 5—Coating on TiC composition heated 210 hr in muffle at 1800°F. 66.3 pct TiC, 15 pct solid solution of CbC, TaC, and TiC, 18.7 pct Co. 100 X.

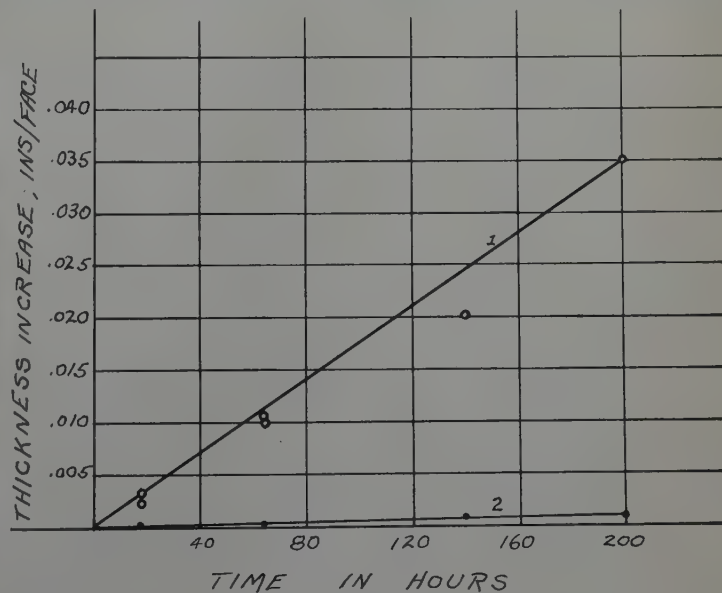


FIG 6—Variation of rate of oxidation of TiC composition with time. (1) 80 pct TiC—20 pct cobalt. (2) 66.3 pct TiC—15 pct solid solution of CbC, TaC and TiC.

Table 2 . . . Oxidation of Various TiC Compositions
18 hr at 1800°F—Muffle Test

| Composition Ingredients and Pct | Increase in Thickness In. Per Face |
|------------------------------------|--|
| 95 TiC, 5 Co..... | 0.0021 |
| 90 TiC, 10 Co..... | 0.0025 |
| 80 TiC, 20 Co..... | 0.0022 |
| 70 TiC, 30 Co..... | 0.0038 |
| 90 TiC, 10 Ni..... | 0.0015 |
| 85 TiC, 15 Ni..... | 0.0031 |
| 80 TiC, 20 Ni..... | 0.0028 |
| 80 TiC, 20 Fe..... | 0.0040 |
| 60 TiC, 25 TaC, 15 Ni..... | 0.0003 |
| 50 TiC, 35 TaC, 15 Ni..... | 0.0001 |
| 71 TiC, 10 S.S.* 19 Co..... | 0.0006 |
| 62 TiC, 20 S.S., 18 Co..... | 0.0003 |

* S.S. refers to the solid solution of columbium, tantalum and titanium carbides.

Table 3 . . . Oxidation Test of TiC Compositions
210 hr at 1800°F—Muffle Test

| Composition Ingredients and Pct | Increase in Thickness In. Per Face |
|------------------------------------|--|
| 80 TiC, 20 Co..... | 0.0359 |
| 66.3 TiC, 15 S.S.* 18.7 Co..... | 0.0009 |
| 51.7 TiC, 31 S.S., 17.3 Co..... | 0.0009 |
| 41.8 TiC, 41.8 S.S., 16.4 Co..... | 0.0019 |
| 66.3 TiC, 15 S.S., 18.7 Ni..... | 0.0020 |

* S.S. refers to the solid solution of columbium, tantalum and titanium carbides.

carbide solid solution upon the room temperature strength was determined upon the same series of compositions as used to obtain the oxidation data of Fig 4. The results are shown in Fig 7. The consistent effect of the columbium and tantalum in reducing strength is to be noted. The strengths at room temperature and 1800°F of various other compositions are given in Table 4. It is to be noted that although the strengths of various TiC-Ni compositions are greater at room temperature than those of the TiC-Co compositions, the strength decreases more rapidly with temperature so that at 1800°F, they are somewhat weaker. The compositions using iron show promise. It has been suggested that, since TiC

Table 4 . . . Strength and Density of Various TiC Compositions

| Composition No. | TiC Pct | Other Carbide Pct | Auxiliary Metal Pct | Transverse Rupture psi × 1000 | | Density | |
|--------------------|------------|-------------------------|---------------------------|----------------------------------|--------|------------------|--------|
| | | | | Room Temp. | 1800°F | Theo- retical | Actual |
| 1 | 95 | | Co 5 | 126 | | 5.12 | 5.26 |
| 2 | 90 | | Co 10 | 122 | | 5.23 | 5.23 |
| 3 | 80 | | Co 20 | 160 | 111 | 5.47 | 5.42 |
| 4 | 65 | | Co 35 | 152 | | 5.91 | 5.84 |
| 5 | 90 | | Ni 10 | 123 | | 5.23 | 5.26 |
| 6 | 85 | | Ni 15 | 151 | 90 | 5.35 | 5.40 |
| 7 | 80 | | Ni 20 | 173 | 91 | 5.47 | 5.45 |
| 8 | 70 | | Ni 30 | 154 | | 5.61 | 5.60 |
| 9 | 90 | | Fe 10 | 124 | | 5.19 | 5.11 |
| 10 | 80 | | Fe 20 | 136 | | 5.42 | 5.32 |
| 11 | 60 | TaC 25 | Ni 15 | 85 | 71 | 6.51 | 6.52 |
| 12 | 50 | TaC 35 | Ni 15 | 93 | 42 | 7.08 | 7.02 |
| 13 | 66.3 | S.S* 15 | Ni 18.7 | 147 | 82 | 5.85 | 5.78 |

* S.S. refers to the solid solution of columbium, tantalum and titanium carbides.

compositions were known to have inferior strengths, the strengths obtained in this work were the result of approximately 3 pct of tungsten resulting from the milling of these compositions with cemented tungsten carbide balls. Accordingly, a composition was prepared containing 80 pct TiC and 20 pct Co wherein steel balls were used for the milling. Analysis showed this composition to contain only spectrographic traces of tungsten. The room temperature transverse rupture strength of this composition averaged 153,000 psi as compared with 160,000 with the same composition milled with tungsten carbide balls. The elevated temperature strengths of two of the compositions, that containing 80 pct TiC and 20 pct Co and the equivalent containing 15 pct three carbide solid solution are shown in Fig 8 for temperatures up to 2000°F. The slow rate of falling off of strength is to be noted. The lower rate of decrease

of the composition containing the columbium and tantalum carbide is of note. Table 4 also includes some high temperature modulus of rupture values for some of the other compositions. The theoretical and actual densities have been shown in Table 4 and it will be noted that the actual densities correspond very closely. Discussion of Results The most notable result is the marked decrease in oxidation of TiC compositions effected by the minor addition of TaC or of CbC and TaC in the form of the three carbide solid solution. This reduction in the amount of oxidation ranged up to 40 times in some instances. The effect cannot be accounted for on the basis of the oxidation characteristics of the additive carbides since, of themselves, the other carbides do not possess the oxidation resistance of

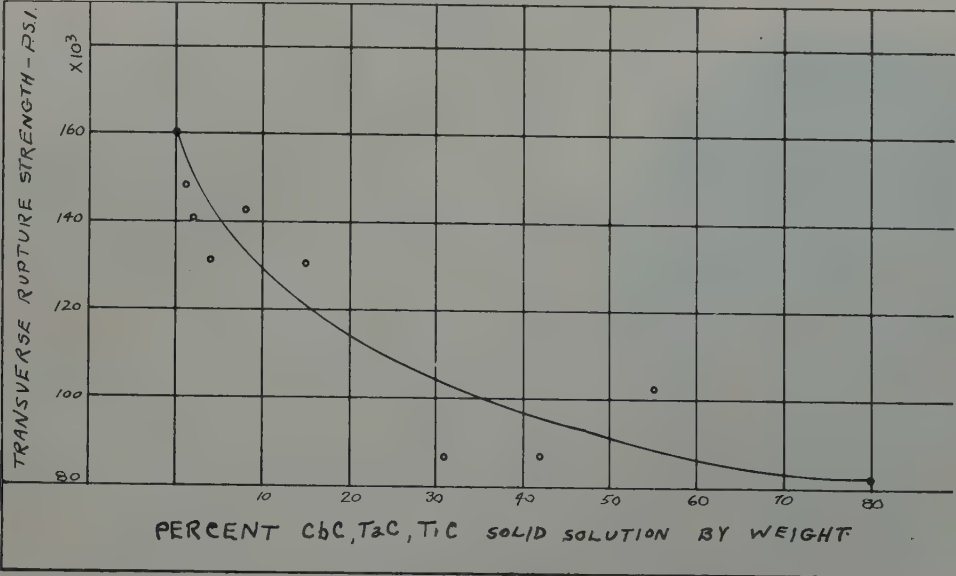


FIG 7—Effect of increasing percentages of CbC, TaC, TiC solid solution upon strength of TiC compositions, 12.3 pct Co by volume throughout.

TiC. The explanation which would appear to hold is that the ratio of the oxides in the oxidation product and their character must be such as to form an adherent continuous film and thus prevent further access to the carbide structure. Although no tests were conducted on the effect of CbC alone as an additive to TiC compositions, the combined effect of the columbium and tantalum carbides contained in the three carbide solid solution indicates that the columbium contributes considerably to the protection obtained.

The use of various auxiliary metals has little effect on the oxidation rate and as a secondary observation the percentage of auxiliary metal has small influence on the oxidation rate. It thus appears that the rate of oxidation is largely determined by the carbide constituents.

The data on modulus of rupture show in general that titanium carbide compositions may have strengths as much as 75 pct higher than those previously reported. Although these strengths are considerably below the general level of those of the cemented tungsten carbide compositions, the cemented titanium carbide compositions are strong materials. A better basis upon which to compare these materials with other materials, at least with alloys, is tensile strength and work upon this phase is now being carried out. However, based on the work of a number of laboratories the short time tensile strength of brittle materials may be expected to be from 0.4 to 0.6 the modulus of rupture value.¹⁰ This would make the high temperature tensile

strengths of cemented titanium carbide comparable with the best alloys and ceramics.

The marked difference in the rate of oxidation observed between the gas fired tube furnace and the muffle furnace, which was the equivalent of the differences found with and without columbium and tantalum carbides, emphasizes the effect of variations in the atmosphere upon oxidation results. The importance of even small variations in atmosphere upon oxidation results is shown by the results in the muffle furnace when ceramic vs. carbon supports are used for the specimens. Such differences in the effect of furnace atmosphere are insignificant in the case of compositions which have high oxidation resistance as shown by Fig 4.

Other Properties

It is of interest to know other properties of these TiC compositions, some of which are summarized in Table 5 for two of the compositions.

Table 5 . . . Additional Properties of TiC Compositions

| | Pct 80 TiC 20 Co | Pct 66.3 TiC 15.0 S.S.* 18.7 Co |
|---|------------------------|--|
| Young's Modulus of Elasticity | | |
| Room Temperature..... | 55.0×10^6 psi | 57.3×10^6 psi |
| Hardness, RA, Room Temperature..... | 90.5 | 89.5 |
| Thermal Expansion per °F 100 to 1800°F..... | 5.0×10^{-6} | 4.5×10^{-6} |
| Thermal Conductivity cal per sec per °C per cm..... | 0.085 | 0.075 |
| Electrical Conductivity Per Cent of Copper Standard..... | 5.0 | 4.0 |

* S.S refers to the solid solution of columbium, tantalum and titanium carbides.

YOUNG'S MODULUS OF ELASTICITY

These values were determined by the sonic vibration method¹¹ using ground bars $\frac{1}{4} \times \frac{1}{2} \times 3$ in. Comparisons were made with cemented tungsten carbide bars. These high moduli are indicative of the formation of a continuous carbide skeleton as in the case of the tungsten carbide compositions.

HARDNESS

These values were determined using a special Rockwell A Brale which was calibrated upon a cemented tungsten block calibrated by the Wilson Mechanical Instrument Co.

THERMAL EXPANSION

These values were determined by the use of a Bureau of Standards type dilatometer. Virtually straight line expansion curves were obtained. While these values are somewhat higher than the general level of those for cemented tungsten carbide compositions, they

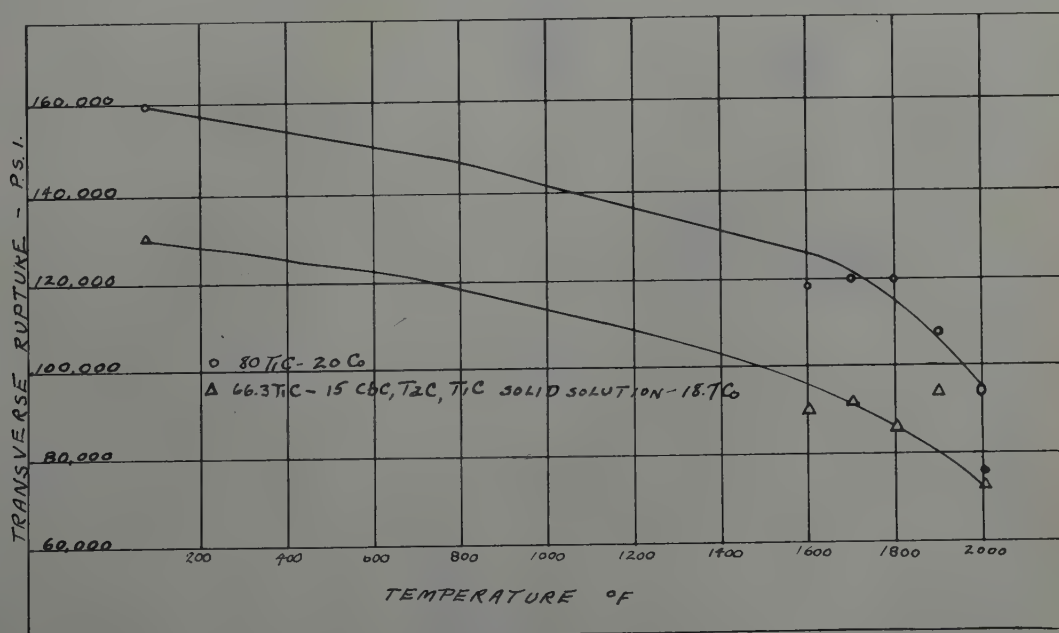
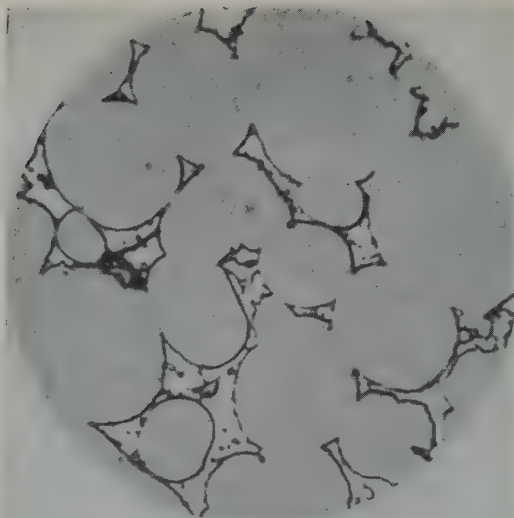


FIG 8—Effect of temperature upon the strength of TiC compositions.

9



10



11

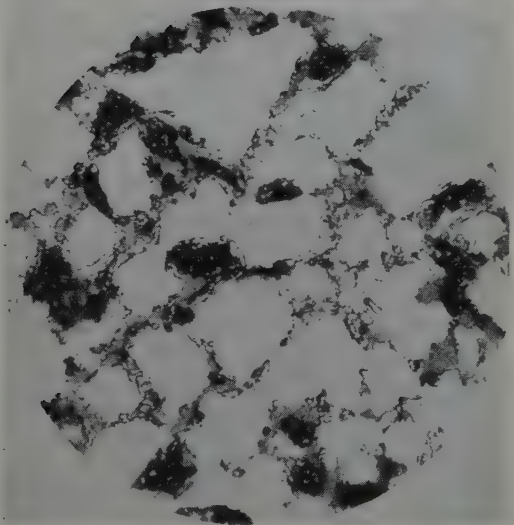


FIG 9—Structure of cemented TiC—80 pct TiC, 20 pct Co. $\times 1500$, nital etch.

FIG 10—Structure of cemented TiC—66.3 pct TiC, 15 pct CbC, TaC, TiC solid solution, 18.7 pct Co. $\times 1500$, nital etch.

FIG 11—Composition of Fig 10 after 210 hr at 1800°F. $\times 1500$, nital etch.

are one half or less those for ferrous base alloys and of the order of those for ceramics. The thermal expansion is an important consideration in the resistance of materials to thermal shock.

THERMAL CONDUCTIVITY

These values were obtained by the method described by McKenna.¹² The apparatus was standardized on pure

iron and lead. The conductivity of the cemented titanium carbide compositions is somewhat below that of the tungsten carbide compositions although above the level of highly alloyed ferrous base materials and many times higher than ceramics. The thermal conductivity of a material has a large bearing on its ability to resist thermal shock resulting from rapid temperature changes.

ELECTRICAL CONDUCTIVITY

These values were obtained by the Kelvin Bridge method using ground bars $\frac{1}{4}$ in. diam by 12 in. long and calibrating against a 0.1 ohm standard accurate to ± 0.02 pct.

Structure

Fig 9 and 10 show the etched structures of two of the compositions at 1500 magnifications which is largely used for examining cemented tungsten carbide tool compositions. The polishing is done with diamond dust using lead-tin laps as in the case of tungsten carbide compositions but greater care is needed to avoid scratches because of the lower abrasion resistance of these compositions. The 2 pct nital etch has been found to produce preferred etching to the conventional alkali ferricyanide etch used on tool compositions.

The structures are comparable to those of the tungsten carbide compositions in that they show two phases, the carbide phase and the phase which is predominately auxiliary metal. The grains are much more rounded than is the case with tungsten carbide compositions. The effect of CbC and TaC in causing larger grain size is to be noted. A specimen prepared for the composition of Fig 10 after 210 hr exposure at 1800°F is shown in Fig 11. There appears to be no significant change in structure.

X ray diffraction examination of the compositions of Fig 9 and 10 with the Norelco Recording Spectrometer shows that in both cases only a single carbide phase is present. In the case of the TiC-Co composition the TiC phase has a lattice parameter of 4.32 Å as for the TiC used in making the composition. This indicates that no more than a small quantity of Co could be held in solution in the TiC. The lattice parameter of the composition containing titanium, columbium and tantalum carbides was found to be 4.34 Å indicating a complete solid solution, as would be expected from the work of Norton and Mowry.¹³ The amount of

TiC retained in the Co phase in the sintered compositions has not yet been determined.

Summary

This work has shown that cemented titanium carbide compositions prepared by powder metallurgy methods have transverse rupture strengths up to 175,000 psi or 75 pct greater than previously reported in the literature. Either cobalt, nickel or iron may be used as an auxiliary metal. The two former appear very nearly equivalent in titanium carbide compositions. Iron is somewhat inferior.

Compositions containing only titanium carbide and an auxiliary metal are considerably superior to the tungsten carbide compositions with respect to the character of the oxidation products. It has also been found that the addition of minor percentages of tantalum carbide or of columbium and

tantalum carbide reduces the oxidation rate of the titanium carbide compositions to very small values at temperatures up to 2200°F.

The general properties of cemented titanium carbide compositions are comparable with those of the cemented tungsten carbide compositions. When the strength, oxidation resistance, thermal expansion and conductivity are considered, these compositions offer excellent possibilities as high temperature materials.

Acknowledgment

The authors acknowledge the work of J. R. Bridge in obtaining the data upon the general properties of these materials and of others in this laboratory for their assistance in this work.

References

1. W. Dawihl: *Ztsch. Metallkunde* (1940) 32, 320-325.

2. W. Dawihl and J. Hinnueber: *Kolloid Ztsch.* (1943) 104, 233-236.
3. F. Skaupy: *Kolloid Ztsch.* (1943) 102, 269-271.
4. R. Kieffer and F. Kolbl: *Powder Metallurgy Bull.*, 4, 4-16.
5. Kieffer and Hotop: *Pulvermetallurgie und Sinterwerkstoffe* (1943) p. 298, Springer, Verlag—Berlin.
6. U. S. Pat. No. 2,193,143. P. Wright: *Process for Producing Hard Metal Carbide Alloys.*
7. S. J. Sindeband: *Trans. AIME* (1949) 185, 198. *Jnl. of Metals*, Feb. 1949.
8. U. S. Pat. No. 2,124,509. P. M. McKenna: *Carbides of Tantalum and Like Metals and Method of Producing the Same.*
9. P. N. Bridgeman: *Harvard Univ.*, Private Communication.
10. A. R. Bobrowsky: *The Applicability of Ceramics and Ceramals as Turbine Blade Materials for the Newer Aircraft Power Plants*, ASME-ASTM Symp. on Effect of Temperature on Properties of Metals. New York, Dec. 1948.
11. S. V. Fogue and G. A. Loomis: *Bull. American Ceramic Society* (1941) 20, 425-430.
12. Philip M. McKenna: *Trans. AIME* (1938) 128, 90.
13. John T. Norton and A. L. Mowry: *Trans. AIME* (1949) 185, 133. *Jnl. of Metals*, Feb. 1949.

Binary Chart for Interconversions of Mol, Weight, and Volume Percent

JOHN B. SEABROOK,* Student Associate AIME

The accompanying Fig 1 is a graphical scheme of intermediate accuracy for expediting interconversions of mol, weight, and volume percents. This chart consists of a family of curves of mol or atomic or volume percent plotted against weight percent, each curve in the family providing for a certain ratio of molecular or atomic weights or densities. Thus, the whole range of variations is presented in a very familiar format, and the conversion is effected simply by choosing the proper curve and reading off the required values. An entire series of conversions for a given binary system can be found by following the appropriate curve.

It is interesting to examine the analytical geometry of the plots. The curves, which must fit into a square

and all join at the 0 and 100 pct points, may be shown to be hyperbolas with their centers on the extension of the diagonal of the square which they intersect. Multiplying out the expression

$$\text{atomic fraction of } A = y = \frac{\frac{x}{A}}{\frac{x}{A} + \frac{1-x}{B}}$$

where x is the weight fraction of A , and A and B are atomic weights, we get

$$xy + \frac{A}{B}y - \frac{A}{B}xy = x$$

Upon rotating and translating axes and

avoiding imaginaries, it is found that the angle of rotation is -45° , the origin

$$\text{moves up } \frac{\sqrt{2}}{2} \text{ units and } \frac{\sqrt{2}}{2} \left(\frac{\frac{A}{B} + 1}{\frac{A}{B} - 1} \right)$$

units to the right, and the standard form is

$$\frac{1}{2} \left[\left(\frac{\frac{A}{B} + 1}{\frac{A}{B} - 1} \right)^2 - 1 \right] = 1$$

Thus the curves are equilateral hyperbolas, their centers are

$$\sqrt{\frac{1}{2} \left[\left(\frac{\frac{A}{B} + 1}{\frac{A}{B} - 1} \right)^2 - 1 \right]}$$

units away from their intersection with

Technical Note 30 E. Manuscript received April 28, 1949.

* Metallurgical Engineer, General Electric Co., West Lynn, Mass.

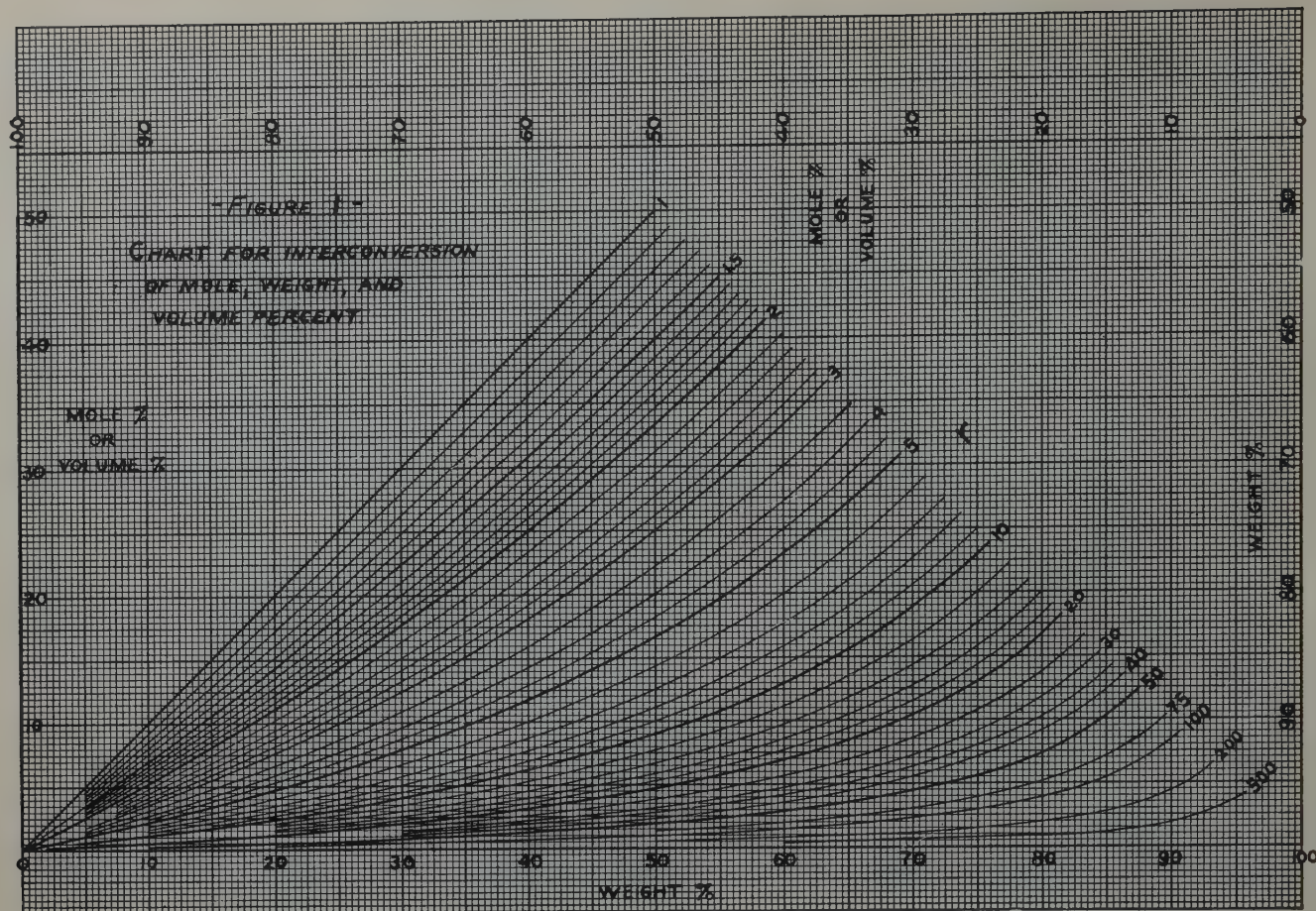


FIG 1—Chart for interconversion of mol, weight, and volume percent.

the diagonal and are on that diagonal, and the curves are symmetrical with respect to that diagonal. As the ratio of $A:B$ increases, both the center of the curve and the intersection of the curve with the diagonal approach the lower right hand corner of the square plot from opposite sides.

In the actual chart only one triangular quarter of the entire square is shown. Elimination of half of the square is accomplished by setting up the rule that the larger ratio always be taken, in other words, by making A the component with the larger atomic or molecular weight. Then, since the curves are symmetrical, only half of the remaining plot need be drawn, and the diagram may be turned as required. The scales are labeled so as to prevent error.

A few examples of the use of the chart may be useful. As may be seen on the chart, the atomic or molecular weight ratio, or density ratio is called r . Suppose it is desired to convert 20 wt

pct of Ag in the Ag-Cu system to atomic percent Ag. Choosing the larger

$$\text{ratio, } r = \frac{108}{63.6} = 1.70. \text{ This may be}$$

obtained from a slide rule or a prepared table of atomic weight ratios. Selecting the curve for a ratio of 1.7, the at. pct of 12.8 pct Ag is readily obtained. As a second example, suppose the wt pct of Ag were 70 pct in the same system. This combination requires the interchanged scales, and therefore the chart must be turned 90° clockwise. Atomic percent of A is again found by the single reading of the graph, using the same $r = 1.7$ curve. A final example is provided by the problem of determining what weight of Fe will be contained in a given weight of Fe_3C . This is an atomic percent to weight percent conversion. Fe being the heavier component, the atomic percent to be considered is obviously 75 pct, and $r = \frac{55.9}{12.0} = 4.65$. Using the chart in the sideways position, the value of 93.3 wt

pct of Fe is obtained, estimating the last digit. Thus, every 6.7 g of C in the carbide are combined with 93.3 g of Fe.

It is at once recognized that the chart becomes quite inaccurate for the low and high percents and also for the high ratios. This can be overcome, if the need so warrants, by making enlarged plots of limited areas of the original whole plot. Another variation in accuracy occurs in that simple interpolation between curves becomes inaccurate as the ratio becomes large.

To summarize the conditions for which the chart is set up: (1) the percents indicated on the scales of the chart refer to the component which has the larger atomic or molecular weight or density, (2) the ratio, r , which selects the appropriate curve, is the larger ratio of weights or densities, (3) whenever a combination of percent and r falls outside the triangular area covered by the curves, the chart must be turned 90°.

Intergranular Parting of Brass during Anneals

F. H. WILSON,* and E. W. PALMER,* Members AIME

Brass mills are familiar with a recurring problem which reveals itself during deformation of annealed metal as an opening up of cracks which are suggestive of a grain boundary pattern. A typical example is seen in Fig 1, which shows part of the convex surface of a cartridge brass disc which was slightly dished by the punching operation. Another illustration of the same type of defect was found in the surface of a finished cartridge case which split open on firing. These cracks, shown in Fig 2, were away from the split but indicate the presence of the type of weakness which permitted the splitting. Usually the weakness consists of separate cracks, the lengths of which are of the same order of magnitude as the grain size prior to the final anneal. Their typical appearance in a polished section is shown in Fig 3. This structure was found below the surface of a fractured tensile-specimen that had been cut from a large cartridge blank showing the defects on its convex surface.

While the pattern formed by these cracks suggests a grain boundary origin, the cracks bear no relation to the currently existing grain structure. Thus Fig 3 shows that the grains have grown up to cracks already present. Since it is doubtful that the cracks were present in the metal before the anneal, they must have formed during the anneal but prior to recrystallization. The term "fire-cracking" has been generally applied to cracking that occurs during an anneal under the influence of internal stress, but refers more specifically to obvious macroscopic cracking attributable to the presence of a low melting phase, usually lead. Since the type of cracking described above may occur when the lead content is very low, we have considered it a somewhat different phenomenon, and have called it "intergranular parting." While most examples involve cartridge brass, intergranular parting has also been observed in the fabrication of large seamless tubes from discs of both 85/15 red brass and 70/30 cupro-nickel. Similar cracking in

nickel silver was investigated by Jones and Whitehead,¹ who showed that it could occur during heating or cooling. That which occurred on heating they called "fire cracking," and they suggested that a transformation at about 320°C might account for its occurrence.

It was felt in this laboratory that the observed parting was probably one aspect of the general observation, first made by Rosenhain and Archbutt,² that a tendency toward intergranular fracture under tensile stress increases with increasing temperature and decreasing rate of strain. In this case the stress involved would be internal. The rate of strain would be exceedingly slow, a localized internal creep. Reference to the literature uncovered no efforts to extend the observations of Rosenhain to conditions involving only internal stress.

Accordingly, an exploratory research, sufficient in detail to satisfy us as to the probable truth of this explanation of the observed intergranular parting, was undertaken. The internal stresses present during the early stages of an anneal (prior to recrystallization) would be from two sources: residual stresses developed during deformation, and thermal stresses caused by uneven heating and expansion. Thermal stresses would vary widely according to shape, size and manner of heating, and can be considered as supplementary to residual stresses. It seemed necessary to determine the stress and temperature conditions under which parting would occur in a relatively short time, and then to establish whether or not in-

ternal stresses may persist to an extent adequate to cause parting at such temperatures. (Jones and Whitehead¹ and Moore and Beckinsale³ made tests which indicated that stress relief required an appreciable time.) During the course of the research the desirability of studying the effect of grain size became apparent, and this factor is one of the major variables of our investigation.

Intergranular Parting under Tension at Elevated Temperatures

In early experiments, hard 70/30 brass tensile specimens, with unknown residual stresses, held for 10 min. at applied stresses from 30,000 to 40,000 psi at temperatures from 300 to 350°C, showed no macroscopically visible cracks when unloaded and cooled, but cracks very similar in appearance to those observed in commercial practice were revealed in these specimens by pulling them to fracture. Annealed specimens, on the other hand, showed no cracks in such experiments, apparently because they deformed plastically at stresses below those necessary to cause parting in a reasonable time. Hence, the specimens used for this study were first strengthened by cold tensile elongation, giving them an unavoidable residual stress pattern (determined largely by grain size and orientation) which would, however, correspond in direction, at least, to the stress pattern obtained under stress at temperature. A variation in these residual stresses might be expected with variations in grain size, but following any given anneal the reproducibility of stress pattern should be as good as that of the grain size measurement.

With no information as to the effect of the amount of prior deformation, tests were conducted on specimens given the same cold elongation, using a stress applied at temperature which was a constant proportion of the stress required to produce this elongation. In

New York Meeting, February 1950.

TP 2717 E. Discussion of this paper (2 copies) may be sent to *Transactions AIME* before April 1, 1950. Discussion is tentatively scheduled for publication in November 1950.

* Assistant Research Metallurgist and Research Metallurgist, respectively, The American Brass Co., Waterbury, Conn.

¹ References are at the end of the paper.

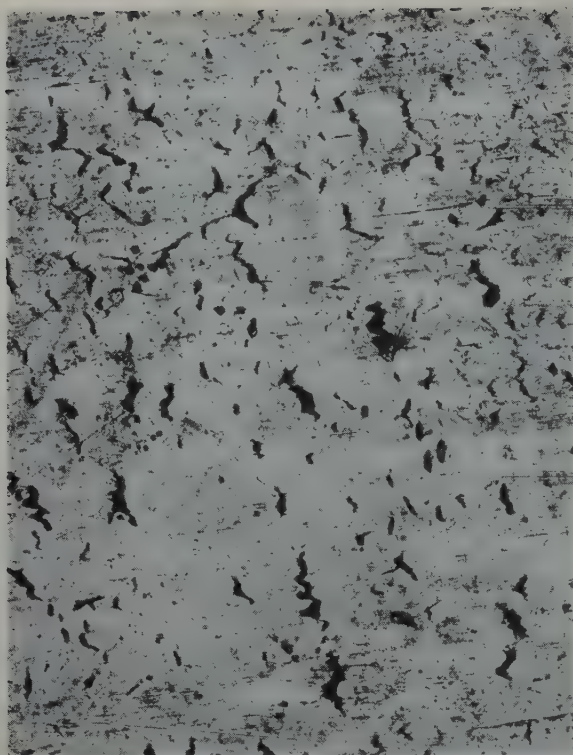


FIG 1—The convex surface of a 70/30 brass cartridge disc (6.29 in. diam \times 0.525 in.). Slightly dished during punching. $\times 10$



FIG 2—Cracks near head of 70/30 brass 0.270 cal. cartridge which split on firing. $\times 30$

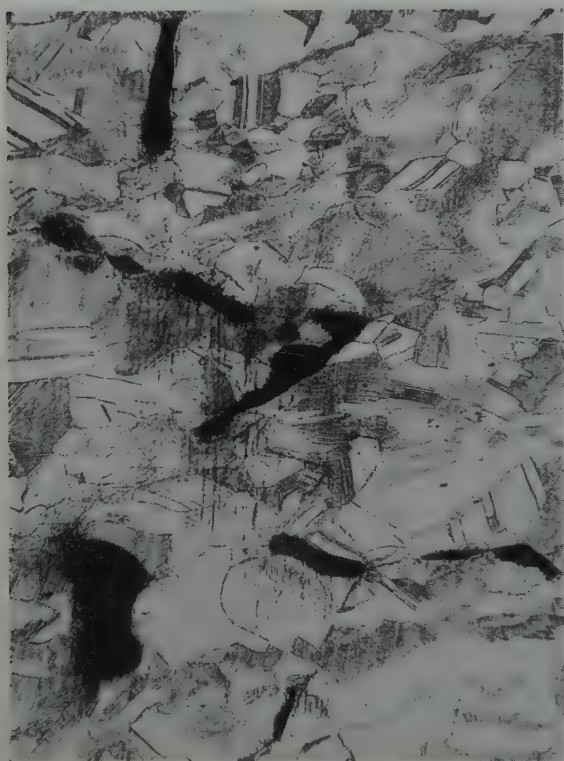


FIG 3—Cracks in a broken tensile specimen cut from a 70/30 brass cartridge disc ($16\frac{1}{16}$ in. diam \times $1\frac{1}{16}$ in.) which showed surface cracks as punched. $\times 75$

this way the stress applied at temperature was approximately related to the yield strength of the material tested. As a result, large grained specimens were held under lower stresses at tem-

perature than the fine grained ones. Later tests determined the relative behavior of specimens having different grain sizes which were given the same stress at the same temperature.

Tests at Elevated Temperatures under Sustained Loads

Tensile specimens were machined to a $\frac{3}{8}$ in. diam over a 2 in. ga length from $\frac{9}{16}$ in. diam 70/30 brass rod, which had been given a final reduction of about 30 pct. The ready-to-finish grain size was 0.065 mm. Analysis showed the following composition:

| | Pct |
|-------------|---------------------|
| Copper..... | 69.64 |
| Zinc..... | 30.33 by difference |
| Lead..... | 0.02 |
| Iron..... | 0.01 |

Specimens were annealed for 1 hr at 400, 500, 600, 700 and 800°C and developed grain sizes of 0.020, 0.035, 0.1, 0.2 and 1 mm respectively. For each test, a specimen was stretched 25 pct, noting the maximum load and final diameter. It was then set in the tensile machine and brought to within $\pm 3^\circ$ of the desired temperature by means of an electric furnace. After soaking 15–20 min. it was loaded quickly to 80 pct of its prior maximum load. This load was automatically maintained for 10 min., save in a few cases where a maximum crosshead travel of 0.01 ipm failed to compensate for creep. The extent of damage by cracking was revealed by subsequently pulling the specimen to fracture at room temperature, the maximum load and the diameter at fracture being observed. Tensile

Table 1 . . . Intergranular Parting of 70/30 Brass Under Stress at Elevated Temperatures

| Specimens Stretched 25 Pct before Stressing | | | | | |
|---|------------------------------------|-----------------------|-------------------|-----------------------------------|-----------------------|
| | | Stress at Temperature | | Room Temperature Test to Fracture | |
| Temperature during Stressing | Pre-stress psi $\times 10^{-3}$ | Stress psi | Pct of Pre-stress | Tensile Strength | Reduction of Area Pct |
| | | | | Based on Area after Pre-Stressing | |
| 400° Anneal—0.020 mm grain diam | | | | | |
| °C | | | | | |
| 225 | 56.7 | 45,300 | 80 | 63,300 | 71.2 |
| 250 | 55.7 | 44,500 | 80 | 62,900 | 64.6 |
| 275 | 56.7 | 45,400 | 80 | 63,500 | 54.8 |
| 300 | 56.5 | 45,400 | 80 | 62,300 | 54.0 |
| 325 | 56.3 | 31,500 | 56 | 61,200 | 53.6 |
| 450° Anneal | | | | | |
| 323 | 53.6 | 31,000 | 58 | 55,600 | 39.6 |
| 500° Anneal—0.035 mm grain diam | | | | | |
| 225 | 52.3 | 41,800 | 80 | 60,600 | 68.8 |
| 250 | 49.3 | 40,200 | 80 | 58,400 | 61.8 |
| 275 | 50.0 | 39,900 | 80 | 56,900 | 47.2 |
| 287½ | 52.1 | 40,400 | 77.5 | 54,800 | 28.2 |
| 300 | 50.3 | 34,500 | 68.5 | 54,600 | 38.3 |
| 323½ | 50.7 | 31,400 | 62 | 52,400 | 32.2 |
| 600° Anneal—0.1 mm grain diam | | | | | |
| 225 | 44.9 | 36,000 | 80 | 55,800 | 70.6 |
| 250 | 42.0 | 33,500 | 80 | 53,200 | 64.8 |
| 275 | 41.9 | 33,400 | 78.5 | 49,300 | 35.8 |
| 286* | 44.8 | 35,850 | 80 | | 5.4 |
| 300* | 44.8 | 35,800 | 80 | | 2.0 |
| 700° Anneal—0.2 mm grain diam | | | | | |
| 225 | 38.8 | 31,100 | 80 | 51,100 | 61.6 |
| 250 | 36.9 | 29,500 | 80 | 50,600 | 69.4 |
| 275 | 37.5 | 29,900 | 80 | 48,800 | 49.8 |
| 277 | 38.8 | 31,100 | 80 | 47,100 | 36.3 |
| 280½ | 38.9 | 31,100 | 80 | 46,700 | 40.5 |
| 300* | 40.9 | 32,600 | 80 | | 5.7 |
| 800° Anneal—1 mm grain diam | | | | | |
| 225 | 36.8 | 29,500 | 80 | 50,100 | 56.3 |
| 250 | 30.7 | 24,500 | 80 | 45,300 | 63.1 |
| 275 | 32.0 | 25,500 | 80 | 43,100 | 42.9 |
| 279* | 37.2 | 29,700 | 80 | | 8.3 |
| 300* | 36.8 | 29,400 | 80 | | 5.4 |

* Broke at temperature in furnace.

strength and reduction of area values, based on the diameter of the specimen just before the final tests, were recorded.

With this procedure, tests were made on specimens representing all the grain sizes listed above at temperatures of 225, 250, 275 and 300°C. In addition, tests were made at 325°C for specimens annealed at 400, 450 and 500°C, and a few other tests were made at intermediate temperatures.

The results of these tests, as recorded in Table 1, are grouped according to the temperature of anneal, and within each group are in the order of increasing temperature of stressing. The value in the "pre-stress" column (the maximum true-stress reached with cold elongation) is an indication of the strength of the specimen under load.



FIG 4—The variation of intergranular parting with grain size and temperature.
Longitudinal sections showing cracks opened up by room temperature fracturing of 70/30 brass tensile specimens annealed 1 hr at the indicated temperatures, stretched 25 pct, and stressed at 80 pct of the prior maximum stress for 10 min. at the indicated temperatures. $\times 2\frac{1}{2}$.

It will be noted that for anneals of 500°C, and below, it was not possible to reach 80 pct of the pre-stress at some of the temperatures. In such cases, the specimen stretched continuously at the maximum permitted loading rate of 0.01 ipm for the full 10 min. under load. As indicated, several specimens broke in the furnace before the 10 min. had elapsed. In these cases the fracture was completely intergranular and there was no evidence of local necking before fracture.

Damage from cracking is indicated by a lowering of tensile strength and of ductility as measured by reduction of area. Inspection of the data shows that for any one grain size the amount of damage increases with the temperature of stressing. There is an apparent downward trend of tensile strength and ductility with increasing grain size, and the reality of this effect will be shown in tests at constant stress which will be discussed later. Photographs of polished longitudinal sections through the fractures of most of the specimens (Fig 4)

demonstrate a correlation between ductility and cracking. Cracks, present even in the fine grained specimen tested at 225°C, increase in number with the temperature of test and with the grain size up to the 600°C anneal. The greater magnitude of each crack in the larger grained specimens overcompensates for the decreased number of cracks, and represents greater damage as measured by reduction of area.

Cracks on the surface near the fracture of specimens annealed at 600, 700 and 800°C are illustrated in Fig 5. These bear a strong resemblance to those found when intergranular parting is encountered in commercial fabrication, as illustrated in Fig 1 and 2.

The data from this series of tests are also presented graphically in Fig 6. Three variables are plotted. (A fourth, stress at temperature, is not included, but can be found by reference to Table 1.) The vertical axis indicates the reduction of area, the variation of which with the temperatures of anneal (grain size) and the temperatures of

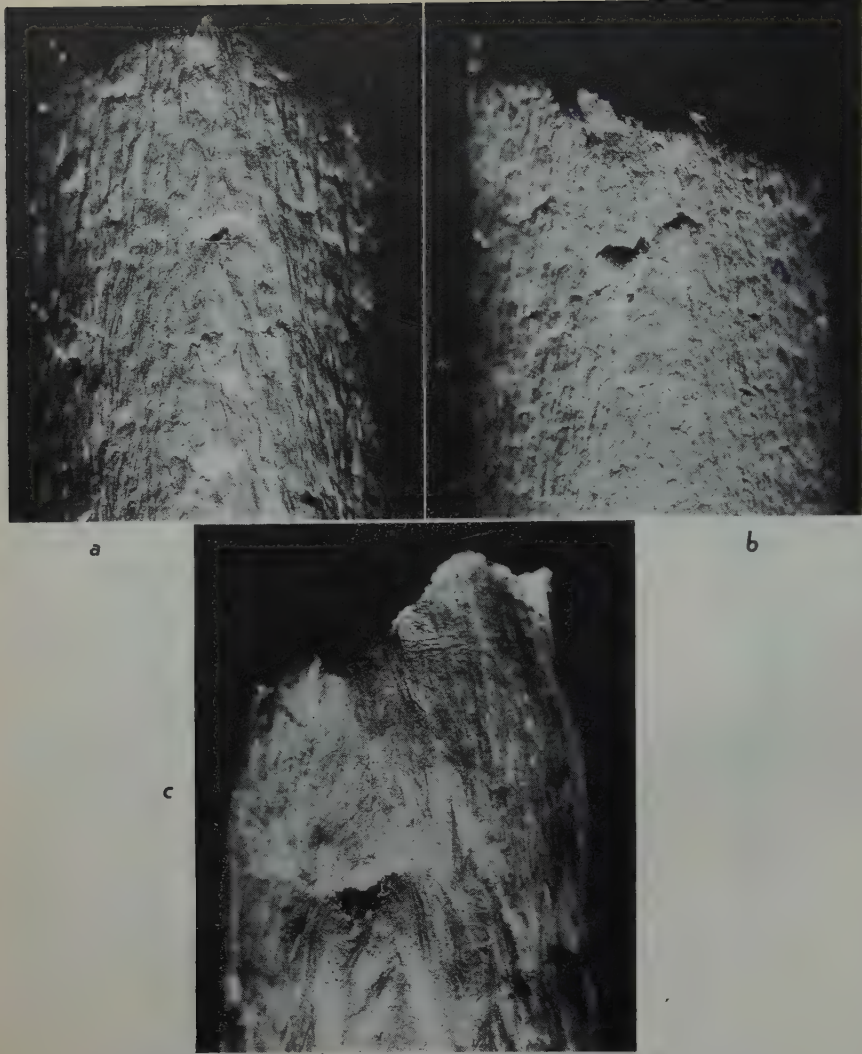


FIG 5—Intergranular parting revealed by room temperature fracturing.

Tensile specimens annealed 1 hr at indicated temperature, elongated 25 pct, and loaded for 10 min. at indicated stresses and temperatures. $\times 10$.

| | Anneal, °C | Stress, psi | Temperature, °C |
|-----|------------|-------------|-----------------|
| (a) | 600 | 33,400 | 275 |
| (b) | 700 | 31,100 | 280 |
| (c) | 800 | 25,500 | 275 |

stressing constitutes a surface. Contour lines of constant temperature of stressing and constant grain size are drawn to indicate this surface. Points on the surface indicate single tests. The reduction

of area figures for specimens which broke in the furnace are included and are responsible for a sharp break in the slope of the surface. In the region of low grain size and high temperature of

Table 2 . . . Effect of Magnitude of Pre-stressing on Intergranular Parting

| Grain Size Anneal | Pre-stress psi $\times 10^{-3}$ | Pre-stretch Pct | Stress at Temperature, 275°C | | Test to Fracture | |
|-------------------|------------------------------------|--------------------|---------------------------------|----------------------|---|------------------------------|
| | | | psi $\times 10^{-3}$ | Pct of Pre-stress | Tensile Strength psi $\times 10^{-3}$ | Reduction of Area, Pct |
| 700°C | 36.3 | 22.5 | 18.2 | 50 | 50.4 | 71.7 |
| | 21.4 | 10.0 | 18.2 | 85 | 45.6 | 72.1 |
| | 35.7 | 20.5 | 21.4 | 60 | 50.8 | 67.8 |
| | 25.2 | 11.0 | 21.4 | 85.5 | 47.0 | 60.6 |
| | 35.7 | 20.0 | 25.0 | 70 | 48.7 | 47.0 |
| | 29.1 | 16.5 | 25.0 | 86 | 47.1 | 48.8 |
| 800°C | 83.6 | 29.0 | 19.3 | 50 | 49.1 | 57.5 |
| | 22.2 | 12.5 | 18.8 | 85 | 43.4 | 57.2 |
| | 44.3 | 33.5 | 22.1 | 50 | 50.8 | 53.3 |
| | 26.0 | 16.5 | 22.1 | 85 | 43.1 | 49.6 |
| | 50.1 | 40.0 | 25.0 | 50 | 53.2 | 41.9 |
| | 29.6 | 20.0 | 25.2 | 85 | 38.9 | 39.1 |

stressing, dotted contour lines are drawn through points representing tests in which 80 pct of the prior load could not be attained.

A few tests were made which compared pairs of specimens given the same stress at temperature following different prior deformations. These were made only on specimens annealed at 700 and 800°C; specimens were stressed at about 18,500, 21,500 and 25,000 psi for 10 min. at 275°C. The results of these tests are listed in Table 2. Referring to the reduction of area figures, it will be seen that the damage is almost independent of the amount of prior deformation.* The results confirm the expectation that the parting increases with stress. Moreover, comparison can be made between specimens of differing grain size which are given the same stress at the same temperature, and it is seen that loss of ductility from parting does increase with increasing grain size. For each pair, differing only in the amount of prior reduction, the tensile strengths are less consistent measures of damage than the reduction of area values. In each case a higher tensile strength is indicated for the higher prior deformation and, since the strength value is based on the area after deformation, this is due to work hardening in uncracked portions of the specimen. All of these specimens showed visual evidence of parting except the 700°C annealed specimen stressed at 18,200 psi.

Discussion of Results

Since these test results involve only single specimens under each condition, there is no claim that any absolute values can be read from the table; nor does it seem necessary to try to establish absolute values, since in the practical application of this information actual stress, temperature, and grain size values are rarely known. The important points are the approximate determination of the conditions which will cause intergranular parting and the directions of the effects of the variable factors studied.

It is shown that 70/30 brass will part in less than 10 min., at grain boundaries, at temperatures below those which cause recrystallization in a reasonably short time, under the influence of

* That this is not universally true was learned in a few comparable tests on silicon bronze. Specimens of equivalent grain size, given identical true-stresses at the same temperature, were profoundly affected by the amount of prior deformation, or the concomitant variable, specimen diameter. The greater parting occurred on specimens where the true stresses were a higher percentage of the previously applied true stress.

stresses of approximately the same order as those which may be found internally. The extent of parting will increase with both increasing temperature and stress. The loss of ductility resulting from the parting increases with increasing grain size even when the number of cracks per unit volume decreases. At least for 70/30 brass, susceptibility to parting is independent of prior cold work, provided the metal has been strengthened sufficiently to support the required level of stress.

The type of test performed here differs from tensile tests at low rates of strain at elevated temperatures in that, by holding the load constant at a stress below the yield strength, the strain rate is exceedingly low. The test differs from stress-rupture and creep tests in the time allowed for stress application at temperature. However, as in these other types of test, failure occurs by parting at the grain boundaries and it is believed that the present data add to an accumulation of results^{2,4-12} which indicate that the only conditions necessary to cause parting at grain boundaries under stress are a sufficiently high temperature and a sufficiently low rate of strain. Theoretical interpretation of this behavior is ably discussed by Zener¹³ in terms of the viscous behavior of grain boundaries.

Experimental Study of Some Factors Influencing Relief of Stresses by Annealing

Having demonstrated that intergranular parting can occur under the influence of externally applied stress at elevated temperatures, there remained an investigation of the probability that adequate stresses, thermal and residual, can be present internally when metal is heating up in commercial anneals. The many unpredictable factors involved in the development of thermal stresses makes an investigation of these quite difficult. However, relaxation tests on bent strips, while limited for quantitative studies by the fact that stress formulas assume a linear stress distribution, can give at least a qualitative estimate of the rate of relief of internal residual stress and can determine the factors which influence it.

STRESS RELIEF TESTS

Relaxation tests, involving measurements of residual curvature of initially

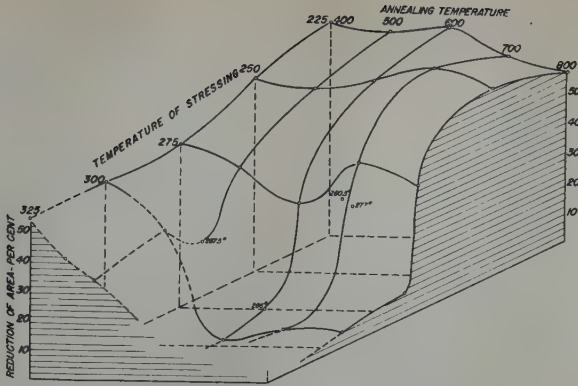


FIG 6—The effect of grain size and temperature of stressing on ductility. Same specimens as in Fig 4. Reduction of area values based on dimensions after stressing. Temperature in °C.

flat specimens annealed while constrained against a cylindrical block, were made at four different stresses (by varying the strip thickness), for five different grain sizes, and at three temperatures in the relief annealing range. The specimens were cut from four strips of 70/30 brass fabricated from hot rolled stock having the following composition:

| | Pct |
|-------------|---------------------|
| Copper..... | 69.81 |
| Zinc..... | 30.16 by difference |
| Lead..... | 0.02 |
| Iron..... | 0.01 |

Table 3 outlines the course of fabrication for the four gauges. The ready-to-finish anneals resulted in the following grain sizes, substantially the same for all four gauges:

| | |
|----------------|----------------|
| 400°C—0.012 mm | 600°C—0.115 mm |
| 500°C—0.038 mm | 700°C—0.325 mm |
| 800°C—0.450 mm | |

It will be noted that the strip was in all cases finished with a 25 pct reduction, since, as in the case of the tensile specimens stressed at elevated temperatures, a hard material was necessary to permit development of stresses of the desired magnitude. Half inch wide specimens 6 in. long were cut from the finished strip, straightened somewhat by stretching, and milled to 0.45 in. width.

A few additional tests were made at one temperature on even thinner material, in two grain sizes, which was prepared by taking some of the 0.049

in. material rolled 25 pct and processing as follows:

| | Anneal 1 hr at 650°C | |
|---------------------|----------------------|----------------|
| | 5E, 6E, 7E, 8E | 5A, 6A, 7A, 8A |
| Cold roll to..... | 0.022 in. | 0.022 in. |
| Anneal 1 hr at..... | 400°C | 800°C |
| Cold roll 15 pct to | 0.0185 in. | 0.0185 in. |

Samples 5A–8A had uniform grain sizes of about 0.375 mm while samples 5E–8E had an uneven grain size averaging 0.020 mm. Note that this material was finished with a reduction of only 15 pct, rather than the 25 pct used for the more extensive series above.

The stress measurements were based on calculations of outer fiber stresses in bent strips, assuming a linear distribution of stress. The amount of bend was determined from the height of the segment intercepted by a 5 in. chord. The stress required to change the curvature from that determined by a segment height d_a to that determined by d_b is

$$S_a - S_b = Et/6.25 (d_a - d_b)$$

where $E = 16,400,000$ psi and t is the thickness. With d_1 the height after holding a specimen against a 20 in. radius surface for 5 min. at room temperature, d_2 the height after a subsequent 60 min. anneal of the bent specimen, and d_0 the segment height for a 20 in. radius of curvature,

Table 3 . . . Preparation of Strips for Stress Relief Tests

| Final Gauge..... | 0.037 in. | 0.049 in. | 0.0615 in. | 0.0735 in. |
|---------------------|---|-----------|------------|------------|
| | Hot rolled stock milled to 0.500 in. | | | |
| | Annealed 2 hr at 750°C—pickled | | | |
| Cold rolled to..... | 0.200 in. | 0.260 in. | 0.300 in. | |
| | Annealed 1 hr at 650°C—pickled | | | |
| Cold rolled to..... | 0.100 in. | 0.130 in. | 0.160 in. | 0.200 in. |
| | Annealed 1 hr at 550°C—pickled | | | |
| Cold rolled to..... | 0.049 in. | 0.065 in. | 0.0815 in. | 0.098 in. |
| | 1 piece of each annealed at 400, 500, 600, 700, 800°C | | | |
| Cold rolled to..... | 0.037 in. | 0.049 in. | 0.0615 in. | 0.0735 in. |
| | (25 Pct Reduction on Finished Strip) | | | |

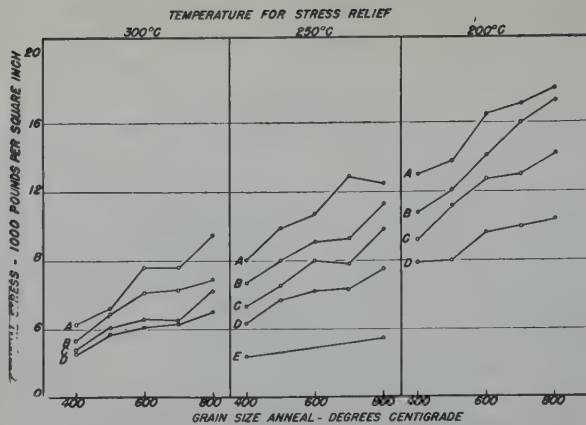


FIG 7—The effect of grain size and temperature on stress relief.

Residual stresses in bent 70/30 brass strips after 1 hr at indicated temperatures when initially stressed to about: A. 26,000 psi B. 22,000 psi C. 19,000 psi D. 15,000 psi E. 7,000 psi

$S_0 - S_1$ is the applied stress before relief annealing.

$S_2 - S_1$ is the stress relieved by the anneal

$S_0 - S_2$ is the residual stress which returns the specimen to its final position after the anneal.

The assumption of linearity of stress distribution is known to be inaccurate in two ways: 1. Any plastic flow occurring during the 5 min. bending at room temperature leaves a residual stress which decreases the applied stress below that calculated by an undetermined amount.¹⁴ 2. The stress relief, occurring disproportionately in the outer fibers, destroys any linearity of stress distribution and calculations based on the final curvature give an outer fiber stress higher than that

actually present.

Nevertheless, since the actual stresses must be related to the measured ones, the technique is useful for determining the relative effect of variable factors affecting stress relief, such as temperature, time, grain size and the magnitude of applied stress.

The 20 in. radius bend was obtained by the use of a steel block with a surface having this curvature against which the specimens were free to slide in expanding. Due to the fact that the heavier gauges took on a permanent set at room temperature the calculated applied stresses were 15,000, 19,000, 22,000 and 26,000 psi rather than the intended (assuming flat specimens) 15,000, 20,000 25,000 and 30,000 psi. In the anneals, 60 min. was allowed for the assembly to reach temperature.

Table 4 . . . Stress Relief in 70/30 Brass

| Gauge Inch Av. | Grain Size mm | Applied Stress | | | Stress Relieved Thermally | | | | | | | | | Residual Stress | | |
|----------------------|---------------------|-------------------------------------|-------|-------|-------------------------------------|-------|-------|--|-------|-------|-------------------------------------|-------|-------|-----------------|-------|-------|
| | | $S_0 - S_1$ psi $\times 10^{-3}$ | | | $S_2 - S_1$ psi $\times 10^{-3}$ | | | $\frac{S_2 - S_1}{S_0 - S_1} \times 100$ per cent | | | $S_0 - S_2$ psi $\times 10^{-3}$ | | | | | |
| | | 200°C | 250°C | 300°C | 200°C | 250°C | 300°C | 200°C | 250°C | 300°C | 200°C | 250°C | 300°C | 200°C | 250°C | 300°C |
| 0.0735 | 0.450 | 26.3 | 25.6* | 26.7 | 8.4 | 13.0* | 17.3 | 31.9 | 50.8* | 64.8 | 18.0 | 12.5* | 9.5 | | | |
| | 0.325 | 26.4 | 28.4 | 25.8 | 9.3 | 15.5 | 18.2 | 35.2 | 54.6 | 70.5 | 17.1 | 12.9 | 7.6 | | | |
| | 0.115 | 26.8 | 24.3 | 26.2 | 10.3 | 13.7 | 18.5 | 38.4 | 56.4 | 70.6 | 16.5 | 10.7 | 7.6 | | | |
| | 0.038 | 25.7 | 27.4 | 23.9 | 11.9 | 17.5 | 18.7 | 46.3 | 63.9 | 78.2 | 13.8 | 9.9 | 5.2 | | | |
| | 0.012 | 27.5 | 26.4* | 26.8 | 14.4 | 18.3* | 22.4 | 52.4 | 69.3* | 83.6 | 13.0 | 8.0* | 4.3 | | | |
| 0.0615 | 0.450 | 24.9 | 23.6 | 21.6 | 7.6 | 12.2 | 14.8 | 30.5 | 51.7 | 68.5 | 17.3 | 11.3 | 6.9 | | | |
| | 0.325 | 24.6 | 21.6 | 21.6 | 8.6 | 12.3 | 15.3 | 35.0 | 56.9 | 70.8 | 16.0 | 9.3 | 6.3 | | | |
| | 0.115 | 23.1 | 23.2 | 21.3 | 8.9 | 14.1 | 15.2 | 38.5 | 60.8 | 71.4 | 14.1 | 9.1 | 6.1 | | | |
| | 0.038 | 22.1 | 21.6 | 20.3 | 10.0 | 13.6 | 15.5 | 45.2 | 63.0 | 76.4 | 12.1 | 8.0 | 4.9 | | | |
| | 0.012 | 22.2 | 22.9 | 20.2 | 11.4 | 16.2 | 16.9 | 51.4 | 70.7 | 83.7 | 10.8 | 6.7 | 3.3 | | | |
| 0.0495 | 0.450 | 19.8 | 19.5 | 18.7 | 5.7 | 9.7 | 12.5 | 28.8 | 49.7 | 66.8 | 14.2 | 9.8 | 6.2 | | | |
| | 0.325 | 19.2 | 18.7 | 17.6 | 6.1 | 10.9 | 13.1 | 31.8 | 58.3 | 74.4 | 13.0 | 7.8 | 4.5 | | | |
| | 0.115 | 20.1 | 20.0 | 19.1 | 7.4 | 12.1 | 14.5 | 36.8 | 60.5 | 75.9 | 12.7 | 8.0 | 4.6 | | | |
| | 0.038 | 19.2 | 18.6 | 18.8 | 8.0 | 12.1 | 14.8 | 41.7 | 65.1 | 78.7 | 11.2 | 6.5 | 4.1 | | | |
| | 0.012 | 18.5 | 17.4 | 17.7 | 9.3 | 12.2 | 14.9 | 50.3 | 70.1 | 84.2 | 9.2 | 5.3 | 2.8 | | | |
| 0.0375 | 0.450 | 14.7 | 15.0 | 14.7 | 4.3 | 7.5 | 9.6 | 29.2 | 50.0 | 65.3 | 10.4 | 7.5 | 5.0 | | | |
| | 0.325 | 14.9 | 14.2 | 14.6 | 4.9 | 7.9 | 10.3 | 32.9 | 55.6 | 70.5 | 10.0 | 6.3 | 4.3 | | | |
| | 0.115 | 15.3 | 14.6 | 14.5 | 5.7 | 8.3 | 10.4 | 37.2 | 56.8 | 71.7 | 9.6 | 6.2 | 4.1 | | | |
| | 0.038 | 14.9 | 15.2 | 15.3 | 7.0 | 9.6 | 11.6 | 47.0 | 63.2 | 75.8 | 8.0 | 5.7 | 3.7 | | | |
| | 0.012 | 15.4 | 14.7 | 14.8 | 7.5 | 10.4 | 12.2 | 48.7 | 70.7 | 82.4 | 7.9 | 4.3 | 2.5 | | | |
| 0.0185 | 0.375 | | | | | 3.9 | | | 52.7 | | | 3.5 | | | | |
| | 0.020 | | 7.4 | | | 4.3 | | | 64.2 | | | 2.4 | | | | |

* Tests used for comparison with tests on specimens having smaller gauge. See p. 1001.

EFFECT OF TEMPERATURE, GRAIN SIZE AND THE MAGNITUDE OF APPLIED STRESS ON STRESS RELIEF

Specimens for each grain size in the four heavier gauges were relief annealed for 1 hr at 200, 250 and 300°C. The 0.0185 in. strips were relief annealed only at 250°C. Data as determined from measurements before and after the anneal are given in Table 4 and plotted in Fig 7 and 8. The per cent stress relieved thermally based on the applied stress is also included. These data illustrate the expected lower residual stresses resulting from higher relief annealing temperatures. It is clear from the consistency of behavior for all gauges and temperatures that specimens with finer grain sizes have less residual stress than those with coarse grains. Moreover, the amount of residual stress increases with applied stress, the curves in Fig 8 demonstrating about the same level of per cent stress relief at any one temperature, regardless of the magnitude of the applied stress.

With reference to the 0.0185 in. specimens stressed to only 7,000 psi (Table 4 and Fig 7), it will be seen that, at least at 250°C, if there is any minimum stress below which there is no relief annealing it must be very low. It is interesting to note that even at low stresses the per cent stress relief is not affected by applied stress. The fine grained (0.020 mm) thin specimen shows a per cent stress relief between the averages for 0.012 mm (400°C) and 0.038 mm (500°C) thicker specimens, and the coarse grained (0.375 mm) thin specimen a value between those for 0.325 mm (700°C) and 0.450 mm (800°C) thicker specimens.

Even under conditions of least stress relief (that is, with large grained specimens), the magnitudes of residual stresses at temperature, after 1 hour of relief annealing, are well below those required for intergranular parting at any of the temperatures employed. Since it seemed probable that the stresses remaining after shorter times at temperature would be higher, the change of residual stress with time was tested for one applied stress on both fine and coarse grained specimens.

EFFECT OF TIME ON STRESS RELIEF

For studying the effect of time on relief annealing, the steel block was unsatisfactory since it required an hour to reach temperature. A thin walled

tube, 10.1 in. od \times 0.063 in. wall, which required only 6 min. to reach temperature, was employed. The smaller radius called for thinner specimens for equivalent stresses, and the 0.0185 in. thick material designated by 5A-8A and 5E-8E was sheared to size for these tests. Strip having this gauge should develop outer fiber stresses of 30,000 psi when bent to the 5.05 in. radius of the tube support. However, as a result of initial curvature and permanent set at room temperature, the applied stresses were of the order of magnitude of 25,000-29,000 psi.

One specimen for each grain size was held to the tube with wire. Again d_1 after 5 min. at room temperature, and d_2 after the anneal, were measured. Allowing 6 min. to reach temperature, the specimens were annealed for 0, 3 and 6 min. at 200, 250 and 300°C. An additional test was made for 60 min. at 250°C.

Data corresponding to those assembled for specimens bent to the 20 in. radius are recorded for these specimens in Table 5. The effects of grain size and temperature of relief annealing are again evident.

The effect of time is presented graphically in Fig 9. Since tests for 60 min. were made only at 250°C, the data for the points at 60 min. for the 200 and 300°C curves are taken from Table 4 and are indicated by filled circles. These results were obtained with thicker and harder specimens bent to a larger radius of curvature, and justification for their inclusion can be made by comparing the stress relief in thick and thin specimens under equivalent stresses at 250°C for 60 min. For instance, data for specimens 6A60 and 6E60 may be compared with the two starred specimens in Table 4. By bending to different radii, these 4 specimens were given about the same applied stress and all were relief annealed for 1 hr at 250°C.

| Specimen | Gauge Inch | Grain Size mm | Radius Inch | Applied Stress psi | Per Cent Stress Relief | Retained Stress psi |
|----------|------------|---------------|-------------|--------------------|------------------------|---------------------|
| 1 | 0.0735 | 0.450 | 20 | 25,600 | 50.8 | 12,500 |
| 2 | | 0.012 | 20 | 26,400 | 69.3 | 8,000 |
| 3(6A60) | 0.0185 | 0.375 | 5 | 24,800 | 50.0 | 12,400 |
| 4(6E60) | | 0.020 | 5 | 28,300 | 66.8 | 9,300 |

Specimens 1 and 3 show almost identical stress relief and the difference between 2 and 4 may be due to the effect of their difference in grain size. It is evident that with a constant applied stress specimen thickness may vary widely without greatly influencing the extent of stress relief as tested by bend-

| Specimen | Grain size mm | Applied Stress $S_0 - S_1$ psi | Relief Annealing Temperature °C | Time at Temperature min. | Stress Relieved Thermally | | Residual Stress $S_0 - S_2$ psi |
|----------|---------------|--------------------------------|---------------------------------|--------------------------|---------------------------|--|---------------------------------|
| | | | | | $S_2 - S_1$ psi | $\frac{S_2 - S_1}{S_0 - S_1} \times 100$ Pct | |
| 7A0 | 0.375 | 26,000 | 200 | 0 | 5,300 | 20.4 | 20,700 |
| 7A3 | 0.375 | 26,800 | 200 | 3 | 6,600 | 24.6 | 20,200 |
| 7A5 | 0.375 | 26,900 | 200 | 6 | 6,700 | 24.9 | 20,200 |
| 7E0 | 0.020 | 28,400 | 200 | 0 | 8,600 | 30.3 | 19,800 |
| 7E3 | 0.020 | 28,400 | 200 | 3 | 9,900 | 34.9 | 18,500 |
| 7E5 | 0.020 | 26,600 | 200 | 6 | 9,700 | 36.5 | 16,900 |
| 6A0 | 0.375 | 26,800 | 250 | 0 | 7,900 | 29.5 | 19,000 |
| 6A3 | 0.375 | 28,000 | 250 | 3 | 10,200 | 36.4 | 17,800 |
| 6A5 | 0.375 | 26,600 | 250 | 6 | 10,300 | 38.7 | 16,300 |
| 6A60 | 0.375 | 24,800 | 250 | 60 | 12,400 | 50.0 | 12,400 |
| 6E0 | 0.020 | 27,200 | 250 | 0 | 12,500 | 46.0 | 14,700 |
| 6E3 | 0.020 | 29,200 | 250 | 3 | 15,600 | 53.4 | 13,500 |
| 6E5 | 0.020 | 27,600 | 250 | 6 | 15,600 | 56.5 | 12,000 |
| 6E60 | 0.020 | 28,300 | 250 | 60 | 18,900 | 66.8 | 9,300 |
| 5A0 | 0.375 | 26,800 | 300 | 0 | 13,300 | 49.6 | 13,400 |
| 5A3 | 0.375 | 27,000 | 300 | 3 | 16,100 | 59.6 | 10,900 |
| 5A5 | 0.375 | 27,200 | 300 | 6 | 16,000 | 58.8 | 11,200 |
| 5E0 | 0.020 | 28,200 | 300 | 0 | 18,600 | 66.0 | 9,600 |
| 5E3 | 0.020 | 29,600 | 300 | 3 | 21,500 | 72.6 | 8,200 |
| 5E5 | 0.020 | 29,700 | 300 | 6 | 21,900 | 73.7 | 7,800 |

ing strips.

As seen in Table 5 and Fig 9, the values at "zero" time show that there has been a rapid initial decrease in residual stress (from an applied stress of 25,000-29,000 psi) during the 6 min. heating up period to each of the temperatures, and this is greater as the temperature increases and the grain size decreases. However, this rapid decrease does not constitute the whole of the stress relief and residual stresses remain after 10 min. in the furnace (4 additional min.) which are appreciably higher than the stresses remaining in the earlier tests after 60 min.

The curves suggest that, after the initial rapid stress relief, the rate of stress relief is independent of grain size and temperature.

DISCUSSION OF RESULTS

The data show that the amount of stress relief increases with time and temperature. This behavior would be expected of reactions involving atomic motions which require an activation

energy and are thus functions of the probability that a given atom will be given sufficient energy to move into a more stable position.

The present research also shows that the amount of stress relief decreases with increasing grain size. Perhaps the grain size effect is not surprising in view

of the fact that stress relaxation and creep are fundamentally alike¹⁵ and the creep rate of brass varies inversely with grain size.¹⁶

The experiments were not complete enough to establish whether, given sufficient time, specimens would reach the same residual stress for a given temperature regardless of initial stress; but the results suggest that this would not be true. Thus, if there were a residual stress determined only by temperature after a very long time, it could be inferred from the curves that for some of the more highly stressed samples (for example, 28,000 psi-250°C), the final residual stress could not be much below 10,000 psi. However, a sample stressed initially at 7,000 psi drops in 60 min. to 3,500 psi. More extensive studies of Moore and Beckinsale³ on the effect of time show that, except for much harder strip in which stress was entirely relieved (presumably by recrystallization) at 250-300°C, a dependence of residual stress on initial stress is maintained after the time curves become horizontal.

Thermodynamic considerations would suggest that, if the metal were homogeneous, uniform stress in an elastically strained specimen would tend to approach, with time, a residual stress characteristic of the temperature and independent of the magnitude of the initial stress. The experimental evidence that the residual stress is a definite function of the applied stress can be understood by analysis of the inhomogeneities present and of the stress distribution. Considering, first, the lack of homogeneity of stress in a polycrystalline metal, the total stress can be considered as a composite of

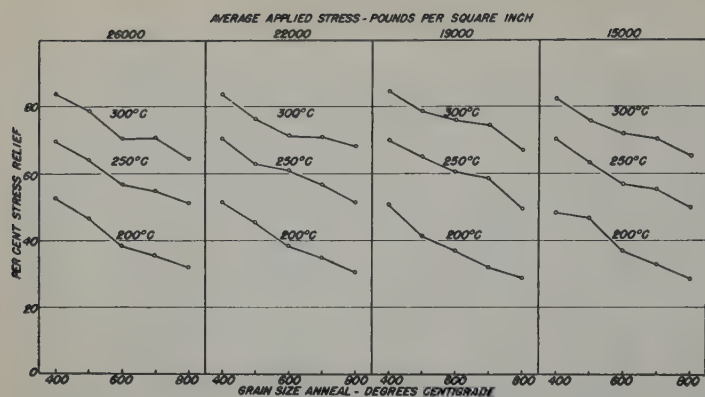


FIG 8—The constancy of per cent stress relief with varying initial applied stress. The same data as in Fig 7.

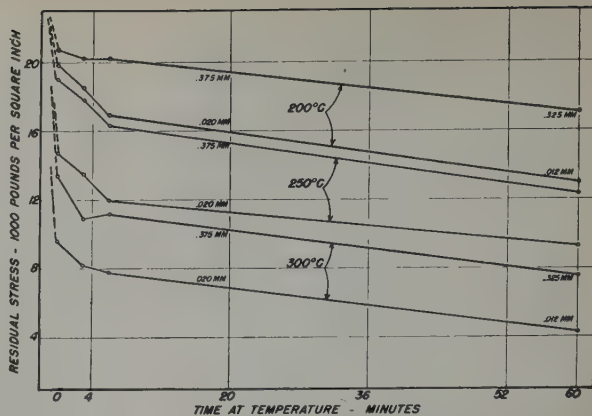


FIG 9—Rate of stress relief as affected by grain size and temperature.

Initial applied stress: 25–29,000 psi.
Datum points are residual stresses after 0, 3, 6, and 60 min. at temperature.

microstresses which vary in magnitude because of the anisotropy of elastic modulus. If each local site of microstress were considered homogeneous, overall stress relief at a given temperature would consist of a reduction of all higher stresses to a level characteristic of the temperature, and residual stress would be a composite of all the unchanged lower stresses and an increased number of stresses at the maximum level characteristic of the temperature.

Increasing the applied stress increases each microstress proportionally causing the total stress to consist increasingly of microstresses higher than the stress to which a given temperature will relax them. Thus there is more stress relief in specimens having a greater initial stress. However, the residual stress will also be greater because the extent to which the total residual stress consists of the highest stresses possible at the temperature of annealing will increase with initial stress.

With respect to the stress distribution in an elastically bent specimen, there is again a range of stress, in this case increasing linearly from the neutral axis to the surface. The same argument applies and stress relief results in a reduction of all higher stresses to a level characteristic of the time and temperature. A nonlinear stress distribution results, but the total stress will be higher the higher the initially applied stress.

Because of the uncertainty introduced by the fact that the calculated residual stresses indicate values which are higher than the actual residual stresses in the outer fibers by an undeterminable amount, it is not safe to estimate from the experimental results the magnitude of residual stress which might be found within a metal

after any particular time in an annealing furnace. The results do show, however, that whatever the magnitude of stress remaining after a given treatment of brass in a given condition it will be greater after shorter times, at lower temperatures, with larger grain sizes and with higher initial internal stresses.

Intergranular Parting During Anneals

It has been shown that “intergranular parting,” a type of failure occasionally observed in commercial fabrication of 70/30 brass, has a structural appearance which can be duplicated by holding tensile specimens at a constant stress at elevated temperatures. The most probable time in commercial fabrication that the metal is under appreciable stress at an elevated temperature is during the heating up period of an anneal. That parting occurs at this time is shown by tests which indicate that annealed brass will not support stresses adequate to cause parting in a short time (at least when they are only uniaxial), and by the observation in commercial failures that recrystallization occurs after cracking. (Some examples are known in which thermal stresses during rapid spray cooling of annealed metal appear to have caused intergranular parting).

In investigations as to whether internal stresses can be responsible for cracking, qualitative measurements of the residual stresses still present after a few minutes at the temperatures favorable to parting, at least with initial stresses up to 28,000 psi, have shown that such residual stresses may be fairly high but probably not high enough to cause the parting. Higher

residual stresses may be present when the initial internal stresses are greater. Total stresses adequate to cause parting can be accounted for, by assuming that, when this type of failure does occur, the residual stresses are supplemented by thermal stresses from uneven expansion.

The tests have shown the importance of grain size, since both the tendency toward intergranular parting and the tendency toward slow relief of stress are increased with increasing grain size.

The comparative rarity of occurrence of intergranular parting suggests that extreme variations of some of the factors contributing to it, or a fortuitous combination of several of them, must be necessary. Very high internal stresses can be sustained by heavily worked brass; the extent and persistence of thermal stresses can vary according to the type of heating and furnace construction; the rate of heating can be very rapid, minimizing stress relief and increasing thermal stresses; grain sizes may be particularly large especially in heavy gauge material, which is more susceptible to uneven thermal expansion and in which, as a matter of fact, most examples of intergranular parting are found.

Corroboration of the conclusions drawn from this work can be found in practical solutions to commercial fabrication problems, based on this explanation for the cause of intergranular parting. For example, in the early stages of fabrication of large seamless 85/15 brass tubing, intergranular parting at the shoulders of large cups can be caused, or eliminated, depending upon the position of the cups during annealing. With the open face up, the inside surface of the cup is heated most rapidly and

transfers tensile stresses to the outside. These add to the internal stresses already present at the shoulder, and frequently cause cracking. If the cup is placed bottom up on the pan, the outside surface is heated first, and the residual tensile stress at the shoulder tends to be relieved by the thermal expansion of the metal so that no cracking occurs. This evidence suggests that parting can be caused solely by the effect of stress at an elevated temperature. The possibility that compositional or precipitation effects may be contributory is not denied, but they alone are not adequate to cause parting.

The tendency toward intergranular parting can be minimized by: 1. Minimizing internal stress left by cold working. 2. Keeping the grain size down. 3. Providing for uniform heating. 4. Heating slowly enough to permit some stress relief before cracking temperatures are reached. 5. Placing the work in the furnace in such fashion that surfaces known to be internally stressed in tension reach temperature first.

The finding of cracks in the heads of 3 in., 50 caliber cartridge cases made from hot-rolled 70/30 brass has recently been reported by Arnold.¹⁷ The report lacks sufficient detail to indicate whether or not the factors discussed in this paper are responsible, but it is suggested that the results of this research should be considered in that connection.

Acknowledgment

The authors wish to express their thanks to Mr. J. R. Freeman, Jr., Technical Manager of The American Brass Co., for his interest in and encouragement of this research, and to the Company itself for permission to publish. The assistance of Mr. J. J. Breen, who carried out many of the tests, is also gratefully acknowledged.

References

1. E. O. Jones and E. Whitehead: *Trans. AIME* (1926) 73, 334.
2. W. Rosenhain and S. L. Archbutt: *Proc. Roy. Soc.* (1919-20) 95, 55.

3. H. Moore and S. Beckinsale: *Symp. on Failure of Metals under Internal and Prolonged Stresses*. Faraday Soc., London. 1921, p. 162.
4. Z. Jeffries: *Trans. AIME* (1919) 60, 474.
5. D. Hanson and M. A. Wheeler: *Jnl. Inst. Metals* (1931) 45, 229.
6. A. E. White, C. L. Clark and R. L. Wilson: *Trans. A.S.M.* (1938) 26, 52.
7. R. H. Thielemann and E. R. Parker: *Trans. AIME* (1939) 135, 559.
8. R. H. Thielemann: *Proc. A.S.T.M.* (1940) 40, 788.
9. C. H. M. Jenkins, G. A. Mellor, and E. A. Jenkinson: *Jnl. Iron and Steel Inst.* (1942) 145, 51.
10. R. F. Miller, G. V. Smith, and G. L. Kehl: *Trans. A.S.M.* (1943) 31, 817.
11. E. R. Parker and C. F. Riisness: *Trans. AIME* (1944) 156, 117.
12. D. L. Martin and E. R. Parker: *Trans. AIME* (1944) 156, 158.
13. C. Zener: *Elasticity and Anelasticity of Metals* p. 158. The Univ. of Chicago Press, (1948).
14. G. Forrest: *Symp. on Internal Stresses in Metals and Alloys*. Inst. of Metals Monograph and Report Series #5 (1948), p. 153.
15. T. S. Kê: *Phys. Rev.* (1947) 71, 533.
16. H. L. Burghoff, A. I. Blank and S. E. Maddigan: *Proc. A.S.T.M.* (1942) 42, 668.
17. F. M. Arnold: *Metal Progress* (1949) 55, 158.

A Proposed Microbending Mechanism of Plastic Deformation*

M. K. YEN,[†] Junior Member AIME

The distortion of crystal structures referred to as "biege gleitung",¹ "local curvature"²⁻⁴ and "deformation bands"^{5,6} is believed to be an unavoidable characteristic of deformed single crystals. The presence of asterism on Laue photograms of Al single crystals either deformed by pure shear⁷ or extended in a condition relatively free from the grip effect² indicates strong evidence substantiating this point of view. The type of localized bending described in connection with the bending test of Al single crystals by Yen and Hibbard⁸ could conceivably exist either microscopically or submicroscopically in all types of deformation. The purpose of this note is to extend this idea to the postulate of a hypothetical "microbending site," as applied to the mechanism of slip in a general sense.

The mosaic structure, as postulated by Darwin,⁹ is that crystals were actually composed of small blocks which have a linear dimension 10^{-4} to 10^{-6} cm on the edge and deviate from each other by an angle of about one-tenth of a degree. The following discussion is based on the assumption

that when slip is propagated from one mosaic block to the adjacent one, bending of the lattice at the region of their boundary is produced in order to maintain the continuity of the gliding process along a certain slip plane.

Consider a two-dimensional diagram of two ideal mosaic blocks on the cross-section perpendicular to the slip plane and containing the active direction of slip. When an external force is applied, the localized bending or "microbending site," would be generated at the region as illustrated in Fig 1A at point B.

A schematic diagram of a "microbending site," generated at a mosaic boundary, is illustrated in Fig 1B. It may be seen that once the curvature

of the bending site reaches sufficient magnitude, the interaction force encountered by pairs of atoms symmetrical with respect to the center of the bending is equal but opposite in sign. Consequently, the overall energy required to displace the atoms near the center is approximately zero.¹⁰⁻¹²

Based upon the finding that the misalignment between two mosaics is 0.1 degree,⁹ the assumption is made that "microbending sites" may possibly exist in the region where one plane will have one more row of atoms than an adjacent plane. It is probable that the origin of the bending site will be where the distance between two mosaic boundaries is " $2d$ " as shown in Fig 1A at point B, where " d " is the interatomic distance. Thus, the distance between two "microbending sites" is in the range of about 600 interplanar spacings. In the case of aluminum, the spacing between two octahedral planes is about 2.33 Å. The distance between two bending sites will be approximately 2.5×10^{-5} cm. It is interesting to note that according to Woods¹³ these values approach closely the size of the domains of a cold-worked metal whose minimum

Technical Note No. 29 E. Manuscript received August 29, 1949.

* A part of dissertation presented by M. K. Yen to the Faculty of the School of Engineering, Yale University in partial fulfillment of the requirements for the degree of Doctor of Engineering, May, 1949.

[†] Research Associate, Research Division, College of Eng., New York Univ., N.Y.C.

¹ References are at the end of the paper.

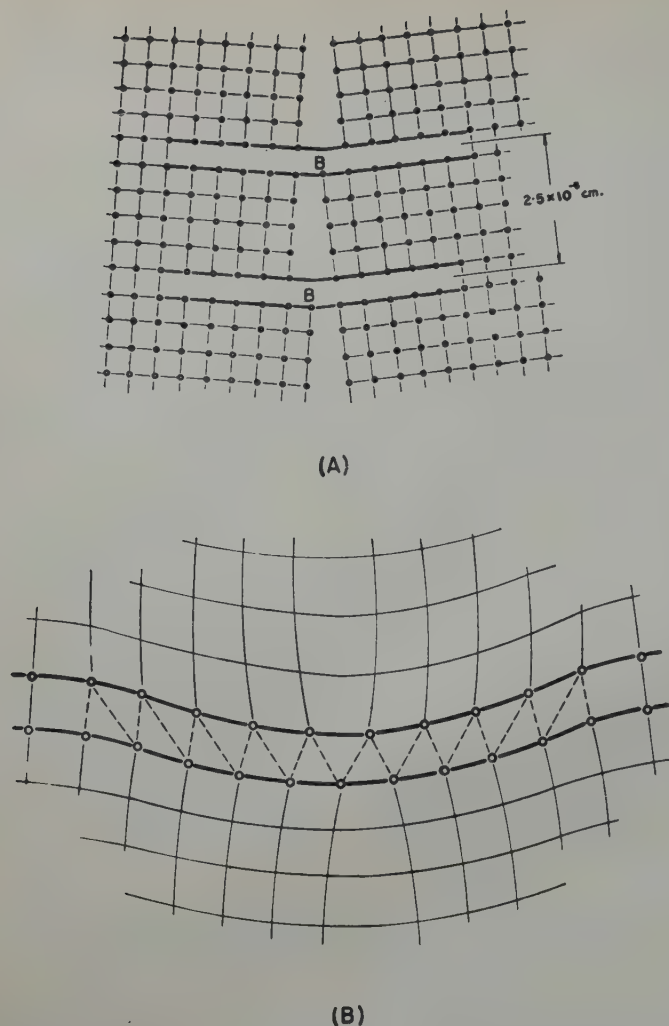


FIG 1—Schematic diagrams showing "microbending sites."

dimension should be about 10^{-6} cm.

Since different mosaic blocks in a crystal may bear various angular relationships with neighboring ones, the "microbending sites" could be classified into two types. The one with the concave side upward as shown in Fig 1B is designated as the concave type and the other with the convex side upward as the convex type. A greater interference would be exerted between a concave and a convex bending site, one immediately above the other, than two similar ones, because of the distortion produced in the adjacent lattice. The interaction force between two "microbending sites" of opposite curvature may be either attractive or repulsive, depending upon their relative position to each other. For instance, if two "microbending sites" have both concave sides opposite to each other, the tensile strain in the lattice between them would have a tendency to pull them together. If two bending sites have both convex sides opposite to each other, the interaction force becomes a repulsive one.

However, both of these two arrangements can be considered to be responsible for the strain-hardening effect in plastically deformed crystals.

One of the essential features of the mechanism proposed here is that the slip process is based upon the idea that slip starts at those planes where the location of "microbending sites" happens to be close enough to form a sub-microscopically wavy layer which is composed of a number of curved surfaces each having a low resistance to shear. As soon as the external force reaches this magnitude, slip takes place along the slip direction in the manner of a sequence of local processes. The time required from the generation of the "microbending site" to the commencement of slip appears to be the same as the incubation period in the nucleation theory recently proposed.^{14,15} It may be seen that once slip commences, the distortion produced in the adjacent lattice may destroy the regular pattern of the "microbending sites." This results in the phenomenon of strain-hardening

which tends to prevent further gliding along the same plane. If, however, the external stress increases sufficiently to overcome the barriers between "microbending sites" which have relatively large misalignment at the ends, new slip markings between the old ones are produced.

In Fig. 1B only a two-dimensional "microbending site" is illustrated. Since this may be out of registry along the direction perpendicular to the paper, a type of distortion by bending about an axis parallel to the paper would be required to provide the continuity of the slip process. If, however, a second set of slip planes becomes active, it is conceivable that strain-hardening of latent slip plane would always exceed that of the operative ones in order to pass through the highly distorted lattice and to initiate slip.

In summary, "microbending sites" may be described as atomistically dislocated local curvatures which act as nuclei for the slip process. Thus, the mechanism for plastic deformation in crystals could be interpreted in accordance with the theory of local curvature,¹⁻⁴ the theory of dislocation¹⁰⁻¹² and the theory of nucleation.^{14,15}

Acknowledgment

The author wishes to thank Professor W. R. Hibbard, Jr., of Yale University and Professor John P. Nielsen of New York University for their helpful discussion and criticism.

References

1. Mark, Polanyi and Schmid: *Ztsch. Phys.* (1922) **12**, 58.
2. Yamaguchi: *Sci. Pap. IPCR (Tokyo)* (1928) **8**, 289.
3. Taylor: *Proc. Roy. Soc. (London)* (1927) **A116**, 39.
4. Burgers and Lauwerse: *Ztsch. Phys.* (1931) **67**, 605.
5. Barrett: *Trans. AIME* (1939) **135**, 296.
6. Barrett and Levenson: *Trans. AIME* (1940) **137**, 112.
7. Burgers and Lebbink: *Rec. Trav. Chim. Pays-Bas* (1945) **64**, 321.
8. Yen and Hibbard: *Trans. AIME* **185**, 710. *Jnl. of Metals* Oct. 1949. TP 2687.
9. Darwin: *Phil. Mag.* (1914) **27**, 315, 675; (1922) **43**, 800.
10. Orowan: *Ztsch. Phys.* (1934) **89**, 634.
11. Polanyi: *Ztsch. Phys.* (1934) **89**, 660.
12. Taylor: *Proc. Roy. Soc. (London)* (1934) **A145**, 362.
13. Woods: *Proc. Roy. Soc. (London)* (1939) **A172**, 231.
14. Turnbull: *Trans. AIME* (1948) **175**, 774. *Metals Tech.* June 1948. TP 2365.
15. Leschen, Carreker and Holloman: *Trans. AIME* (1949) **180**. *Met. Tech.* Sept. 1949. TP 2476.

The Low Temperature Properties of Tin-antimony and Tin-cadmium Alloys*

F. J. DUNKERLEY,[†] Junior Member, H. B. HUNTER[‡] and F. G. STONE,[§] Junior Member AIME

Introduction and Literature Survey

This is the second in a series of papers coming from this laboratory on the correlation of the low temperature tensile properties of tin-binary alloys with microstructure. These engineering data and those of the previous paper¹ were obtained as the initial part of a long-range program to determine the changes in the fundamental mechanical properties accompanying the beta to alpha phase change in tin and its binary alloys below 13.2°C. Since it appears now that the more fundamental studies will be delayed,* and since no summary of the low temperature properties of these tin-base white bearing alloys was found in the literature, it was decided to publish all the engineering data thus far obtained. Accordingly, the tensile properties of thirteen binary alloys containing from 0.1 to 60 pct cadmium and 0.1 to 10.43 pct antimony measured at six temperatures from -196 to +23°C are presented here and their variations rationalized in terms of microstructure.

A literature search showed that these systems had not been investigated at low temperatures, although both the tin-cadmium and tin-antimony^{2,3,4,5}

and the tin-rich corner of the ternary system^{6,7} have been studied at room temperature. Hanson and Pell-Walpole⁵ and Homer and Plummer⁴ determined the tensile properties of alloys containing from 0 to 10 pct cadmium. The same authors³ determined the

tensile strength and elongation in the tin-antimony system from 2 to 18 pct antimony at room temperature while Pell-Walpole et al.^{6,7} studied the properties of high tin and tin-antimony-cadmium alloys. Since there were many variables besides composition in these tests, it was difficult to make a valid comparison with the room temperature data of the present study, but in general the tensile strength and ductility values are in reasonable agreement.

Pell-Walpole² also determined the effect of grain size on the tensile strength of pure tin and 1 pct alloys of both antimony and cadmium. The true maximum stress was found to decrease exponentially as the number of grains in the cross-section increased. This effect of grain size was strikingly revealed in the present work, as indicated in a later section.

Hanson and Pell-Walpole⁸ placed the solid solubility limit of antimony in tin at 3.5 pct at 20°C, increasing to 4 pct at 190°C, and then sharply increasing to 10.3 pct at 246°C (the latter being a peritectic point). Their results are in disagreement with those of previous investigators,⁹ and the discrepancy seems to lie in the microscopic observation of the second phase

New York Meeting, February 1950. TP 2723 E. Discussion of this paper (2 copies) may be sent to *Transactions AIME* before April 1, 1949. Discussion is tentatively scheduled for publication in November 1950. Manuscript received June 1, 1949.

* A contribution from the University of Pennsylvania Thermodynamics Research Laboratory, operated originally under Contract NObs 2477 with the U.S. Navy Department, Bureau of Ships. The contract terminated July 1, 1948 and subsequently the research on tin and its alloys has been curtailed.

[†] Assistant Professor of Metallurgy and Member of the Staff of the Thermodynamics Research Laboratory, University of Pennsylvania.

[‡] Formerly Assistant Instructor and Graduate Student in the Department of Metallurgical Engineering, University of Pennsylvania.

[§] Formerly Graduate Student in the Department of Metallurgical Engineering and Research Assistant, Thermodynamics Research Laboratory, University of Pennsylvania; now Research Metallurgist, General Electric Co., Pittsfield, Mass.

¹ References are at the end of the paper.

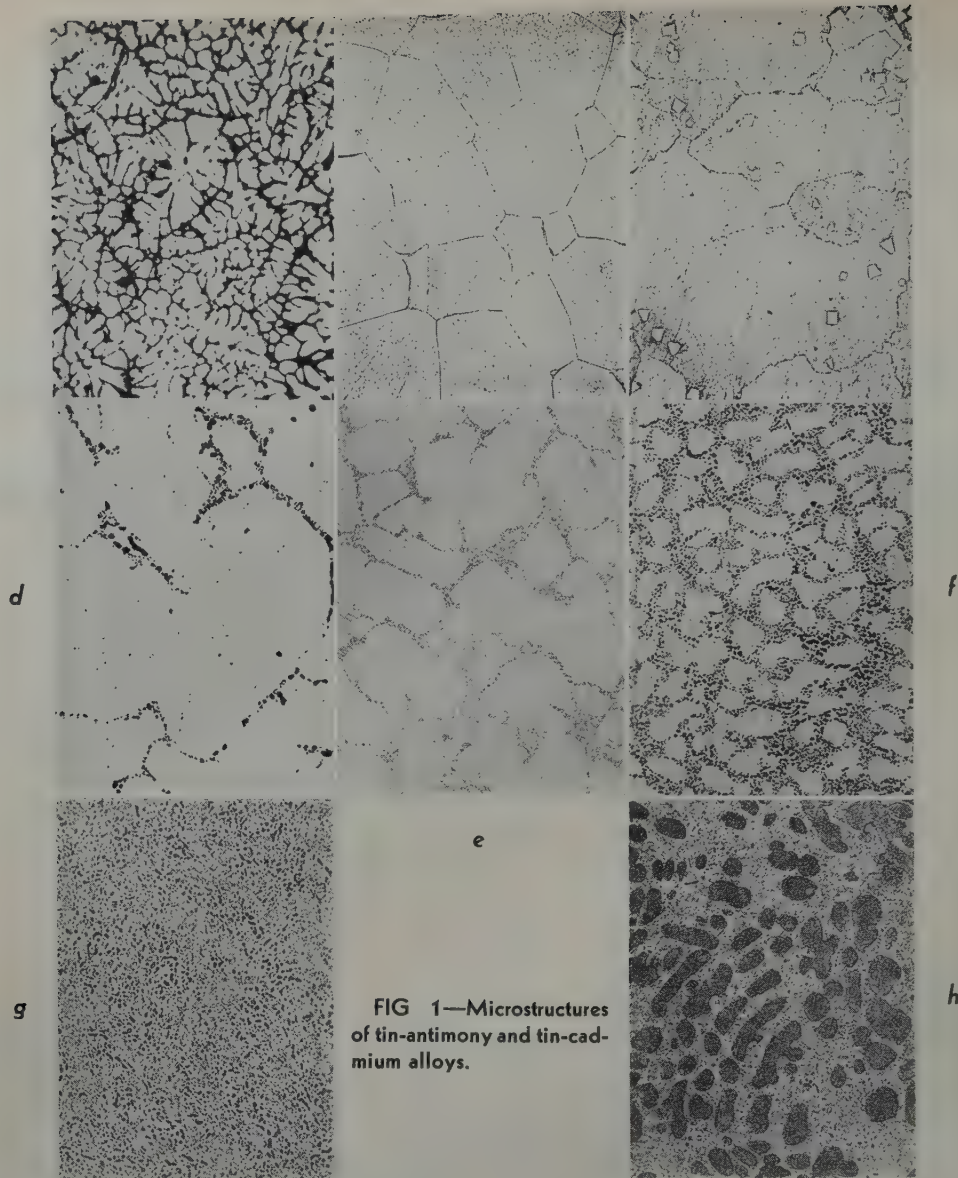


FIG 1—Microstructures of tin-antimony and tin-cadmium alloys.

a 3.38 pct Sb, as cast; b 3.38 pct Sb, homogenized 150 hr at 190°C; c 10.43 pct Sb, homogenized; d 2.65 pct Cd, homogenized; e 10 pct Cd, homogenized; f 20 pct Cd, homogenized; g 33 pct Cd, homogenized; h 60 pct Cd, homogenized. Etched in 8 parts glycerine, 1 part acetic acid, 1 part nitric. 100 X. Reduced one third in reproduction.

SbSn. This is ordinarily seen as large cuboids first appearing at about 9 pct antimony, but Hanson and Pell-Walpole showed that it also appears as a fine precipitate, preferentially along the grain boundaries, in compositions as low as 3.5 pct. They employed thermal analysis, resistance measurements and micrographic methods, and the results seem quite conclusive.

The same authors,^{5,9,10} investigating the tin-cadmium system, found the room temperature solid solubility limit at 1.0 pct and this limit remained essentially constant to 133°C, the temperature of the eutectoid transformation.

In the present investigation, the equilibrium diagrams of Hanson and Pell-Walpole for both systems have been accepted as conclusive, since they are the most recent and the most

comprehensive. Moreover, the limited metallographic study carried out here for purposes of correlating microstructure and tensile properties, confirmed their findings.

Materials and Methods

PURITY AND PREPARATION OF ALLOYS

The tin was the same grade (99.9965 pct pure) used in the early investigation.¹ The antimony metal was Mallinckrodt reagent quality in crushed granular form and was 99.84 pct pure. Cadmium metal of 99.97 pct purity was obtained in the form of $\frac{3}{8}$ in. rods from the American Smelting and Refining Co.

Using the melting procedure previ-

ously described,¹ tin-cadmium alloys containing 0.092, 0.26, 0.90, 2.65, 10.0, 20.0, 33.0, 60.0 pct cadmium, and antimony alloys containing 0.0, 0.31, 1.11, 3.38 and 10.43 pct antimony were melted and cast tensile bars, 0.25 in. in diam and 1 in. in gauge length, were prepared. Chemical analyses were made on all compositions, antimony and cadmium contents being determined spectrographically, while wet analytical methods were used for the higher values. Spot checks on the finished test specimens showed that iron, in amounts of 0.005 pct, was the greatest impurity.

HEAT TREATMENT AND MICROSTRUCTURE

Heat treatments to provide a variety of microstructures were possible with

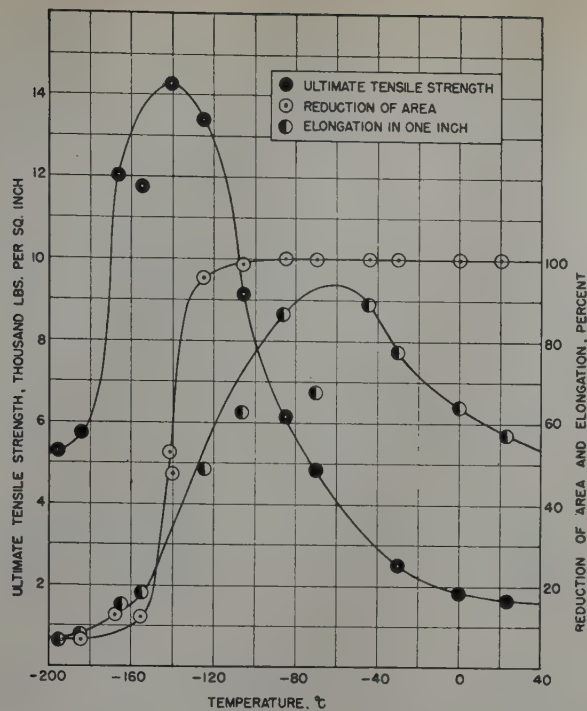


FIG 2—The effect of temperature on the tensile properties of pure tin.

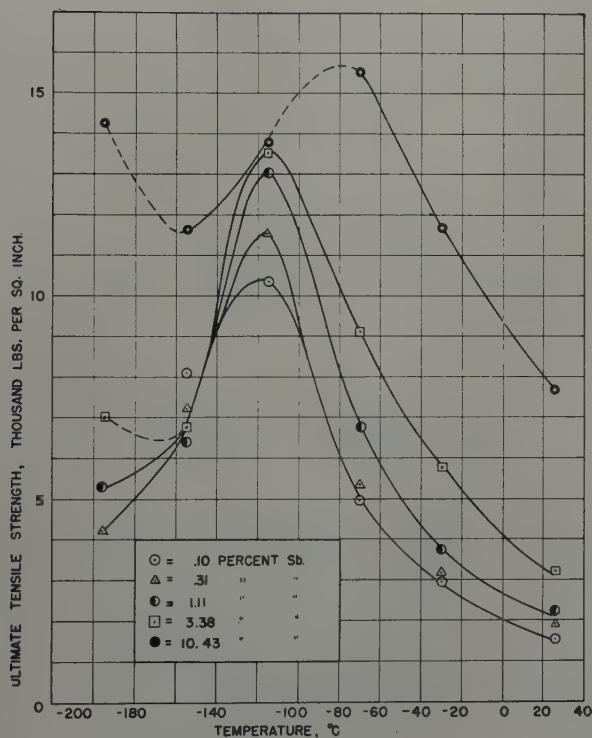


FIG 3—The tensile strength from -195°C to 23°C of tin-antimony alloys containing 0.1 to 10.43 pct antimony.

these alloys, but a structure stable at room temperature was selected as most desirable for these studies. Consequently, the bars were annealed at a temperature such that, in cooling down to room temperature, no phase change

and only slight changes in solubility would occur. Homogenizing anneals of 150 hr at 190°C for the antimony alloys and 350 hr at 120°C for the cadmium alloys, while immersed in silicone oil, fulfilled these conditions. For con-

venience, all compositions of the respective systems were heat treated at the same temperature, since this did not violate the above imposed conditions. After the homogenization, the bars were slowly cooled in the furnace

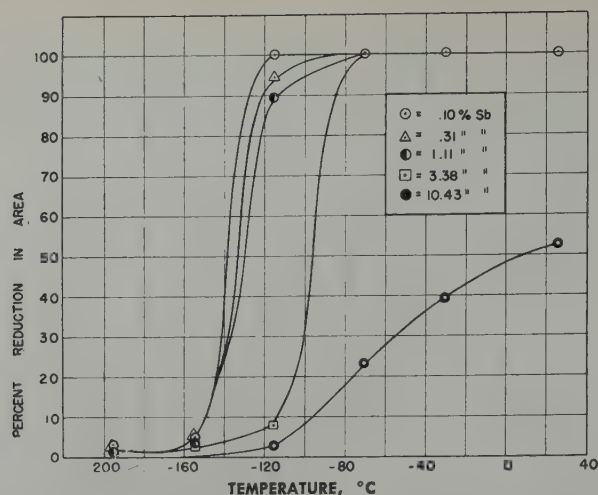


FIG 4—The effect of various temperatures on the reduction in area for tin-antimony alloys containing from 0.1 to 10.43 pct antimony.

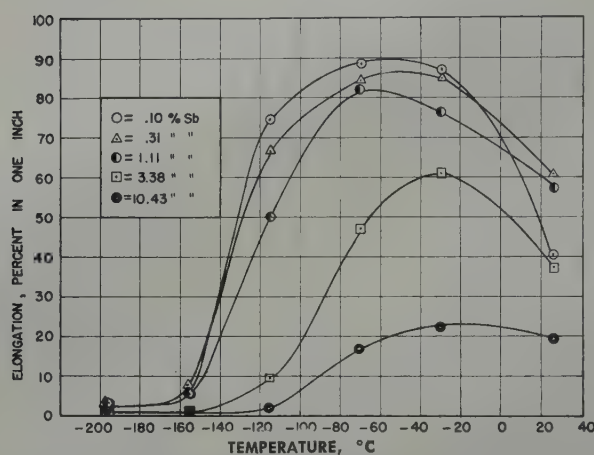


FIG 5—The percent elongation in one inch from -195°C to 23°C for tin-antimony alloys containing from 0.1 to 10.43 pct antimony.

to room temperature.

Fig 1a shows the typical cast structure with pronounced coring obtained in the 3.38 pct antimony alloy. The structure after homogenization at 150 hr at 190°C is shown in Fig 1b. Attention is called to the definite grain boundary constituent appearing in Fig 1b. This evidence substantiates the findings of Hanson and Pell-Walpole who placed the solubility limit at 3.5 pct. These authors noted a definite tendency for the second phase to appear at grain boundaries, and Fig 1c, representing an alloy of 10.43 pct antimony, clearly shows the presence of the compound SbSn in the form of cubic crystals in the grain boundaries.

It should be noted here that a more complete metallographic investigation would have been desirable to supplement existing knowledge concerning solid-solubility limits, distribution of

second phases, and others, but the limited studies reported here were considered sufficient for purposes of this research. Fig 1d shows the microstructure of the 2.65 pct cadmium alloy in the homogenized condition. The eutectic structure is evident in Fig 1d, and it is clear that the solubility limit (1 pct) has been exceeded. This alloy undergoes a peritectic reaction at 223°C , and the resulting beta structure is stable down to 133°C . However, this reaction is easily suppressed by rapid cooling,¹⁰ so that the eutectic of Fig 1d is believed to be present in nearly the equilibrium amount. Special attention is called to the dispersion of fine material throughout the grains in this 2.65 pct cadmium alloy. Whether this represents a small amount of the now metastable β phase, or whether the particles are γ which has transformed *in situ* from the β and perhaps slightly

agglomerated, is an interesting question and one which could not be further investigated here. The authors are inclined to the latter opinion, since the long homogenizing treatment (350 hr) is believed to represent a close approach to structural equilibrium.

Fig 1e, f, g and h show typical microstructures of the 10, 20, 33 and 60 pct cadmium alloys. Before discussing the individual structures, it will be noted that in all four compositions, the α or continuous phase is much finer grained than in the lower cadmium alloys. As will be explained in the discussion of results, and mentioned later in this section, this is an important factor to be considered in the interpretation of the tensile data.

The structure of the 10 pct cadmium alloy (Fig 1e) is seen to be two phase with the γ phase forming an almost continuous grain boundary envelope

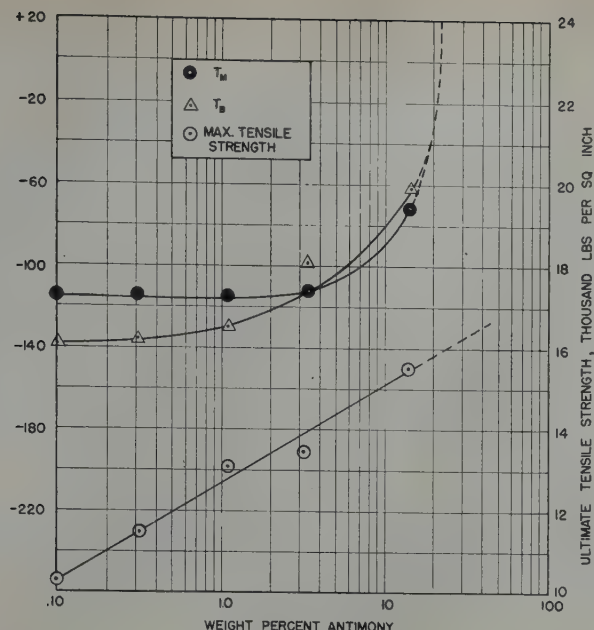


FIG 6—Variation of T_B , T_M , and the maximum tensile strength at T_M , with composition.

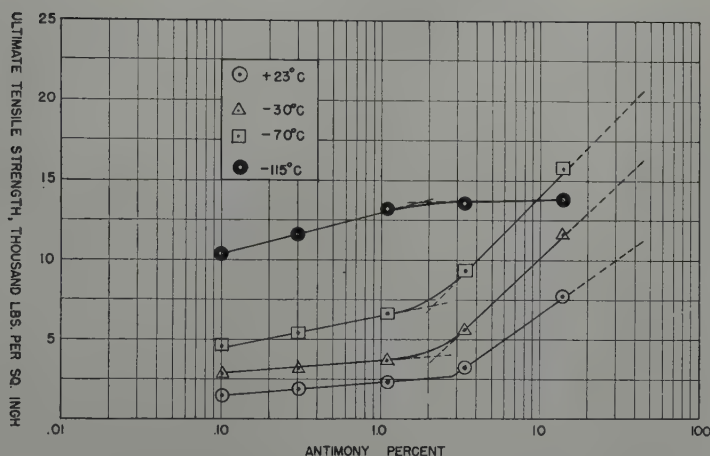


FIG 7—The effect at various temperatures of composition on the ultimate tensile strength of tin-antimony alloys containing from 0.1 to 10 pct antimony.

about the predominant α matrix. The α phase of the 20 pct alloy (Fig 1f), on the other hand, is even finer grained than that in the 10 pct alloy, and is composed of a network of both fine and agglomerated γ phase enclosing the white α phase. In both these alloys, homogenization has caused extensive agglomeration, as indicated by the presence of large intergranular black particles along with the finer spheroidized grain-boundary precipitate also present. The eutectic alloy containing 33 pct cadmium, Fig 1g, is seen to contain even more of the black γ phase uniformly dispersed along with the finer γ spheroids in the α matrix. Fig 1g shows the very interesting microstructure of the 60 pct cadmium

alloy. Here the large massive particles are primary γ , which appeared as massive dendrites in the cast structure. Homogenization has broken up these dendrites into very large particles of γ , although the distribution of the phase has been altered little from that in the cast structure. Also the lamellar structure lying between the γ dendrites in the cast alloy has been completely spheroidized and appears as a fine precipitate in the white α matrix.

The influence of grain size on tensile properties has been investigated by other workers who used the total number of grains in the specimen cross-section as a variable.² For normal fine grain sizes, the effect is not significant, but tensile properties are considerably

influenced when the cross-section of the bar represents only a few grains. Since the base metal tin has a recrystallization temperature below room temperature for ordinary amounts of plastic strain, grain growth during the homogenizing anneal is possible. In the present case, however, both alloying elements raised the recrystallization temperature sufficiently so that no troublesome grain growth was encountered except in the 0.1 and 0.3 pct antimony alloys. Here the cross-section of the bar may frequently have contained only two or three grains, but in no case was a monocrystalline, chisel-type fracture obtained. The pronounced grain refining effect of cadmium on the cast structure resulted in extremely fine

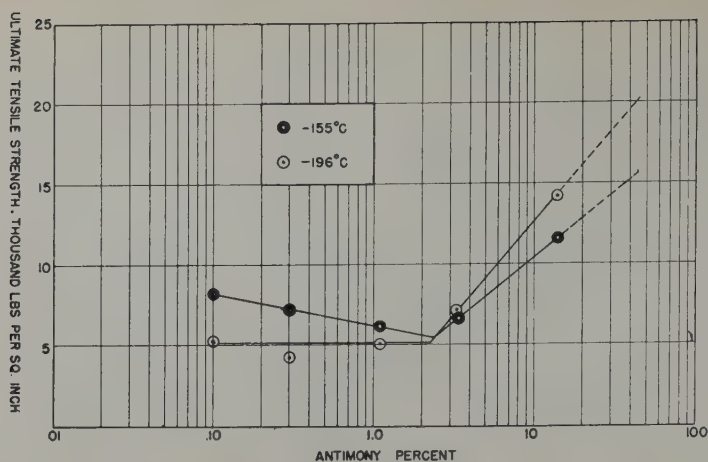


FIG 8—The effect at various temperatures of composition on the ultimate tensile strength of tin-antimony alloys containing from 0.1 to 10 pct antimony.

grain sizes in most of the cadmium alloys, especially those containing more than 3 pct cadmium.

TESTING METHODS

Complete details of test specimen and testing procedure were those described in Ref. 1, except that isopentane was used for the immersion liquid for temperatures near -155°C . The strain rate was maintained at 0.2 iipm for all tests, and testing temperatures were held to $\pm 0.4^{\circ}\text{C}$. The deviation of the measured load, using the weigh bar, was ± 1.0 lb or ± 0.05 pct at the highest load in all cases when the ductility was sufficient to allow ample time to balance the strain indicator. The elongation and reduction of area data represent the usual degree of accuracy attained in tensile testing, except that with coarse-grained fractures, the reduction of area is somewhat less accurate because of the difficulty in accurately measuring the final diameter.

As in the tin-lead studies¹ tensile specimens, 0.25 diam with 1-in. ga length, were tested either in duplicate or triplicate at each temperature and the results are summarized below in graphical form. In the event of considerable discrepancy between the duplicates, or if the fractured surface showed casting defects, a third test was made in nearly all cases.

Discussion of Results

The data obtained in this investigation are presented graphically in Fig 3, 4, 5, 9, 10, and 11, the tensile strength

being plotted in various ways as functions of both temperature and composition. The pertinent data reported here include ultimate tensile strength, per cent elongation in a one inch gauge length, and per cent reduction in area. The values of true maximum stress were calculated for a few bars, but because of the experimental errors in the measurement of the true area and the doubtful accuracy of the breaking load values, no coherent data were obtained. Also, yield data are not reported because neither the "weigh bar," "drop-of-the-beam" or offset methods gave reproducible values.

In previous studies,¹ the low temperature tensile properties of pure tin were rationalized in terms of the effect of decreasing temperature on (1) the critical flow stress, (2) the extent or amount of cold work, and (3) the technical cohesive strength (true fracture stress at nil cold work). It is believed that a similar analysis can be made in the case of these data, with the stipulation, as given earlier, that when two or more phases are present in alloys, the measured tensile properties will be the net result of these three factors operating simultaneously on the separate phases. Thus the relative amount, form and distribution of the phases present will influence the magnitude of the net temperature effects. Also, since pure white tin is metastable below 13.2°C , all the tests except those at room temperature are subject to possible effects of the α (white) to β (grey) transformation. It is known that rolling, bending or drawing enormously increases the velocity of transformation at -50°C , the velocity being proportional to the intensity of deformation.¹¹

In general, alloying elements are known to retard the transformation velocity but their effect on the equilibrium has never been determined. Both the kinetics and phase equilibria are being studied in this laboratory as major research problems; but until these data are available, it cannot be stated whether or not the present series of alloys were in a metastable condition when tested. However, in over 125 tests at sub-zero temperatures some of which lasted 15 min. or more, no visual evidence of the transformation from white to grey tin was observed, and it will therefore be eliminated as a variable.

As in the earlier work,¹ certain terms used in this discussion will be defined so that their use in this discussion will be clearly understood. Reduction in area, rather than elongation, will be used exclusively as the measure of ductility; temperature of embrittlement, T_B , is defined as the temperature at which 50 pct of maximum ductility, that is, 50 pct of maximum reduction in area, occurs in the given alloy. Temperature of maximum ultimate tensile strength, T_M , is self-defining. Technical cohesive strength is used here as the fracture stress at nil cold work. The critical flow stress is defined as the applied stress required to start flow.

To make this an integral report, a summary of the previous explanation of the pure tin properties will be given. For this purpose, Fig 2 containing the tensile properties of pure tin as a function of temperature from -195 to $+23^{\circ}\text{C}$ has been reproduced here. It has been postulated that for pure tin fracture at temperatures down to -125°C occurred principally by flow, since 100 pct of the ductility remained

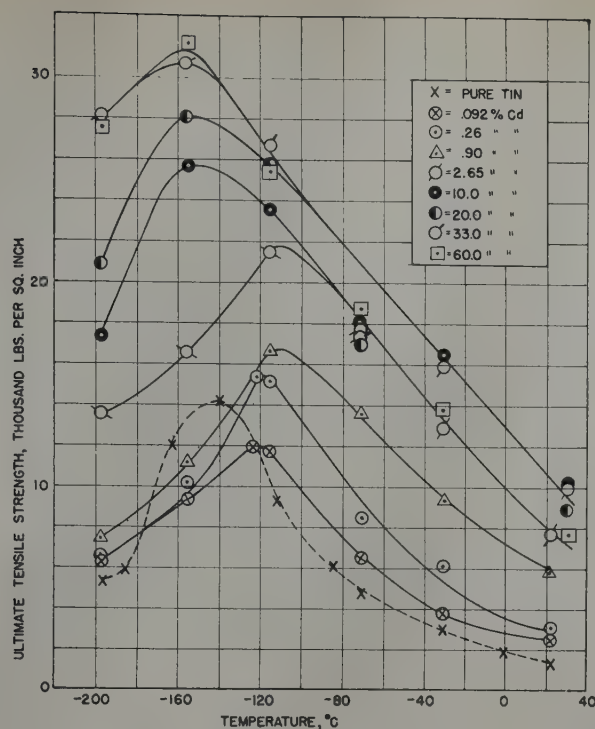


FIG 9—The effect of temperatures on the ultimate tensile strength of tin cadmium alloys containing from 0 to 60 pct cadmium.

at that temperature. Down to -60°C , the rapid increase in tensile strength was caused partially from the increase of the flow stress with decreasing temperature, but principally from the increasing contribution of the work hardening, as evidenced by the increase in elongation to a maximum at this temperature. Below -60°C the amount of work hardening decreased and the critical flow stress, increasing as the temperature decreased, became the main component of the tensile strength. At -130°C as the ductility (R.A.) began falling off and approached 50 pct R.A., failure in tension occurred half by cleavage and half by flow, and the metal could then be considered brittle. At this point, work hardening was still contributing to the cleavage stress because considerable ductility still remained. However, as the ductility fell off, the contribution of the flow stress correspondingly decreased until failure occurred principally by cleavage. Finally, as the ductility decreased the cleavage stress simultaneously decreased and approached the true fracture stress at nil cold work.

An examination of the tensile data at the various subatmospheric temperatures for both the tin-antimony and tin-cadmium alloys indicates that the same three fundamental factors operating in the case of pure tin may also be responsible for the various alloy

properties. Of course, certain differences between the alloys and pure tin do exist, and these will be pointed out as the specific data for each system are considered. However, as in the case of the tin-lead alloys,¹ it will be assumed that because of the graphical analogies, the measured temperature effects on the properties of the alloys differ from those of pure tin only in degree. Hence the main emphasis in the following discussion will be placed on the correlation of the tensile data with composition and the explanation of these relations on the basis of microstructure.

The data for both binary systems have been presented graphically in various ways, as were the tin-lead data, in order to reveal pertinent relationships. These include (1) plots of tensile, elongation, and reduction in area or ductility values versus temperature, (2) T_B , T_M vs. composition and maximum tensile strength vs. composition, the latter on a logarithmic scale, (3) tensile strength at each of the six test temperatures vs. log composition, and (4) for the tin-cadmium series only, log of tensile strength at each temperature level vs. composition on a linear scale.

For ease of reading, the same sequence as was followed in the earlier discussion will be adhered to here. That is, relationships between composition and tensile strength will be brought out by appropriate crossplots of the

data, and with the aid of these, the influence of composition on (1) the temperature of maximum tensile strength T_M , (2) the temperature of embrittlement T_B , (3) the maximum tensile strength at T_M , and (4) the tensile strength at the six testing temperatures will be described. A rationalization of these four specific composition-property relations in terms of the microstructures of the alloys will then be discussed in the indicated order.

TIN-ANTIMONY ALLOYS

It will be noted in Fig 3 that, for the tin-antimony alloys, increasing amounts of the second phase, that is, brittle β (SbSn) phase, has caused definite differences in the magnitude of the changes in tensile properties with decreasing temperature. On the other hand, the only significant difference between the shape of these curves and that for pure tin is that below -160°C , where nil ductility is possessed by both pure tin or the tin-antimony alloys, the fracture stress increased with decreasing temperature for the 3 and 10 pct antimony alloys. This was also observed in the case of the 50-50 tin-lead alloys¹ as well as other metals, and further confirms the postulate that the fracture stress of metals in general increases with decreasing temperature.

Examination of the tensile data presented in Fig 3 shows that additions of 2.5 pct antimony and less had no measurable effect on the temperature of maximum tensile strength, T_M , or on the temperature of embrittlement, T_B . The higher antimony additions, however, definitely affected T_M and T_B , and these effects are obvious in Fig 6. Here it is seen that T_M and T_B are not synonymous in these alloys, the maximum difference being as much as 25°C for some alloys. As in the earlier work,¹ it is believed this difference is a result of the interaction of the three fundamental factors acting simultaneously either on the solid solutions of varying composition, or on the two phases present in some of the alloys.

In Fig 6 it can be seen that T_M remains essentially constant up through

3.38 pct antimony while T_B is consistently 25°C lower through 1 pct antimony. Then above 3.38 pct antimony for T_M and 1 pct for T_B , a rapid rise occurs, with T_B rising above T_M by from 10 to 15°C until at about 10 pct antimony they become synonymous. The maximum ultimate tensile strength (at T_M) increases exponentially with increased antimony, as shown by the straight line relationship of the tensile strength at T_M vs. the logarithm of the composition (wt pct antimony). Variations of the tensile strength with composition at the six test temperatures is also of interest and is shown in Fig 7 and 8. Above T_B , additions of antimony up to about 2 pct had only a slight strengthening effect, but 3 pct antimony and higher caused an abrupt rise in the strength. These data for each

temperature seem to be represented satisfactorily by two straight lines intersecting between 2.2 and 2.8 pct antimony. At -115°C, additions of antimony up to about 1.8 pct have a strengthening effect but further additions had no apparent effect on the tensile strength. Below T_B , antimony contents up to 2 pct either decreased the strength slightly, as at -155°C, Fig 8, or have little or no effect, as at -196°C. Between 2.3 and 2.5 pct antimony, a sharp break in the curve is seen, with further additions of antimony causing a pronounced increase in strength.

These data and the various relationships between composition and tensile strength can be rationalized quite satisfactorily in terms of the heterogeneous microstructures developed in these alloys. Antimony additions up to about 2.5 pct did not affect T_M or T_B appreciably because the antimony remained in solid solution in tin. As mentioned earlier, the solid solubility of antimony in tin at room temperature has been reported recently as 3.5 pct by Hanson and Pell-Walpole.¹² However, the sharp break in the tensile strength vs. composition curves shown in Fig 7 and 8 may be interpreted as evidence that the solid solubility at 20°C lies between 2.2 and 2.8 pct antimony. The following explanation is thus offered: Antimony up to 2.2 pct had no effect on T_M or T_B because the alloys in this composition range were single phase. In this solid solution range, however, solution of antimony in the parent tin lattice formed a substitutional solid solution and strengthened the alloy in direct proportion to the percent antimony added at temperatures above T_B . Thus the maximum tensile strength and the ultimate tensile strength at and above -115°C increase with increased antimony. On the other hand, at -155°C and -196°C antimony in the solid solution range either decreases the tensile strength or has only a slight effect. Since both these temperatures are below T_B , the alloys in this composition range possess no measurable ductility and the observed tensile strength plotted in Fig 8 is really the true fracture stress of the alloys. These data thus indicate that antimony atoms, corresponding to 2 pct antimony or less, dissolved substitutionally in tin either slightly decrease or have little or no effect on their true fracture stress at temperatures below T_B .

Between 2.2 and 2.8 pct antimony, particles of β phase (SbSn) precipitated preferentially at the grain boundaries

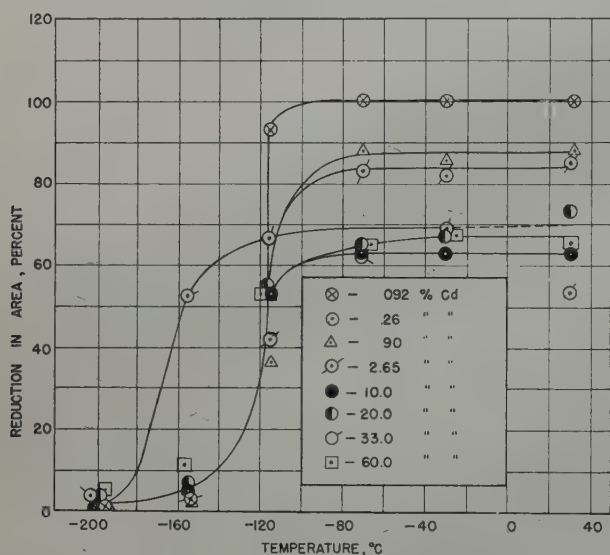


FIG 10—The effect of temperature on the reduction in area for tin-cadmium alloys.

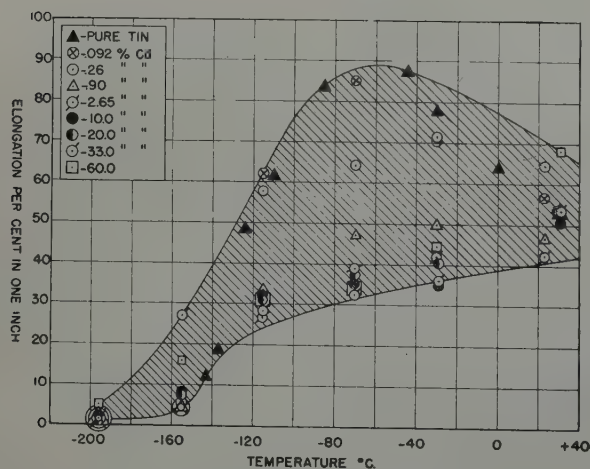


FIG 11—The percent elongation in one inch as a function of temperature for the cadmium alloys containing from 0 to 60 pct cadmium.

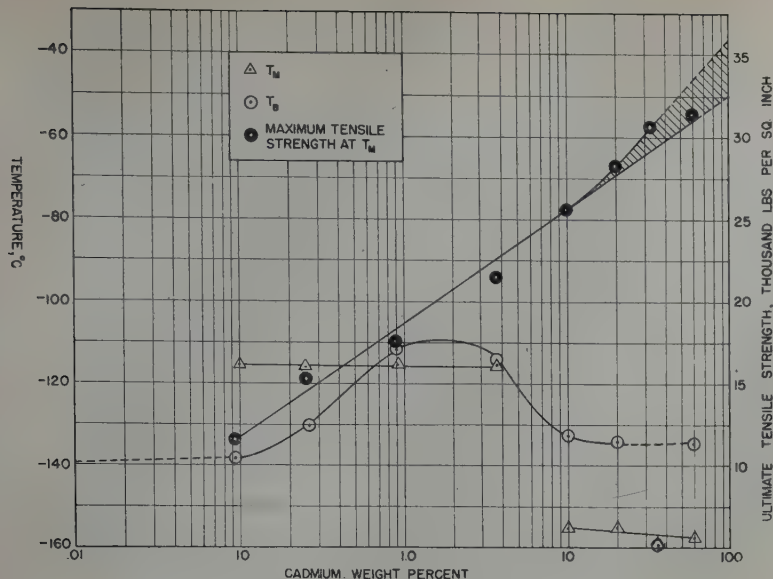


FIG 12—Variation of temperature of maximum tensile strength, T_M , temperature of embrittlement, T_B , and tensile strength at T_M with composition.

and this would be expected to cause precipitation hardening. The closest composition to this range included in this survey was a 3.38 pct alloy, and as seen in Fig 1b, this alloy was found to contain a grain boundary constituent, which was presumed to be particles of β phase. Property-wise, this was reflected by a slight rise in T_M and T_B , for here the β particles were either large or numerous enough to facilitate slip. However, the particles had not exceeded the critical particle size for hardening because the maximum tensile strength and the tensile strength above T_B , for this alloy, were higher than for the lower alloys. At the same time, at -115°C the fact that the 3.38 pct alloy had no higher tensile strength than the 1.1 pct alloy at first appears anomalous. This is to be expected, however, since -115°C is between T_B and T_M . The continuous α (tin-rich) phase is of course predominant and is believed to determine the properties of this alloy. These results mean, then, that the true fracture stress of the α tin-rich phase is the major remaining component of the tensile strength and in this case it is no higher than the combined critical flow stress, fracture stress and work hardening contribution making up the tensile strength of the lower solid solution alloys. Similarly the same explanation is offered to account for the ultimate tensile strength values obtained at -155 and -196°C .

In the 10.38 pct alloy, the β particles were considerably larger and more numerous, appearing intragranularly as

well as in the grain boundaries. These large brittle particles of β in the grain boundaries acted as discontinuities and consequently T_M and T_B increased abruptly. At the same time, sufficient intragranular precipitation occurred to cause the maximum tensile strength to increase. Above T_B the ultimate tensile strength also increased rapidly, presumably because as seen in Fig 4 and 5, considerable ductility remained so that critical flow stress and work hardening of both the continuous α tin phase and discontinuous β phase was appreciably higher than that for the lower alloys. That the true fracture stress at this temperature remains small is indicated by the fact that at the lower tempera-

ture of -115°C , that is, 50°C below T_B for this alloy, the net tensile strength, being essentially the true fracture stress (only 2 pct ductility remaining), is still equal only to the strength of the 3.38 pct alloy. Continuing this line of reasoning, at -155 and -196°C , the tensile strength increased appreciably because the fracture stress markedly increased with decreasing temperature. It is significant to note that the 10.38 pct antimony alloy was about 2500 psi stronger at -196°C than at -155°C , in further confirmation of the negative temperature coefficient of the true fracture stress.

Thus the variations with composition of T_M , T_B , the maximum tensile strength at T_M , and the ultimate tensile strength at subatmospheric temperatures as low as -196°C can be rationalized in a straightforward and logical manner in terms of the microstructure developed in the alloys. It is hoped that more fundamental data, such as true-stress strain measurements, yield data, tensile properties of variously strained alloys, creep data, and other information may soon be available to test the basic reasoning and perhaps separate the several variables used here necessarily in a qualitative way. Extension of this work to higher antimony alloys would be very desirable, especially from the fundamental standpoint. Extrapolation of the curves of Fig 6 indicates that T_M and T_B for the single phase β alloy (45 pct antimony) should be approximately $+20^\circ\text{C}$, and its maximum tensile strength should be about 16,500 psi. These predictions were confirmed in

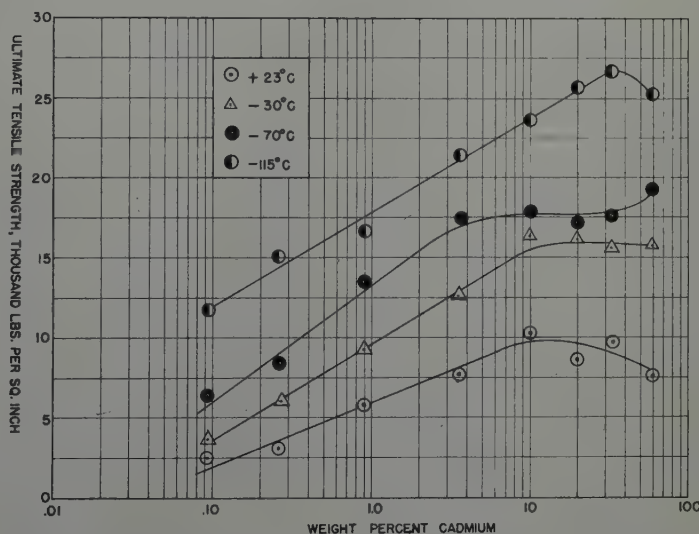


FIG 13—The effect at various temperatures of composition on the ultimate tensile strength of tin-cadmium alloys.

part when a 30 pct alloy was found to be brittle at about 0°C. However, since sound castings of this and higher compositions proved difficult to prepare, sufficient specimens were not available for these initial studies.

TIN-CADMIUM ALLOYS

The tensile data for the tin-cadmium alloys containing from 0.01 to 60 pct cadmium are summarized graphically in Fig 9 to 11. Also, the curves for pure tin are superimposed on these for the tin-cadmium alloys for comparison purposes. As indicated above, a comparison of the tin-cadmium alloy curves with pure tin shows they are all similar in shape, except, of course, the magnitude of the effect of decreasing temperature on the tensile properties varies with the composition.

It will be noted first that the maximum in the tensile strength vs. temperature curve of Fig 9 for the alloys containing from 0.1 to 2.65 pct cadmium occurs at -115°C , which is about 25°C higher than that for pure tin. Alloys containing from 10 to 60 pct cadmium appear to form another family of curves with the maximum at -155°C . This apparent demarcation of the curves into two families with maxima from 35 to 40°C apart first appears to be anomalous, but it is believed to be caused by grain size differences rather than an effect of composition changes. The first four cadmium alloys were cast into slightly hotter molds than were the pure tin and the four higher cadmium alloys. Consequently, the grain size of the latter four alloys and tin was much finer and this not only shifted the maxima in tensile strength to a lower temperature, but raised the entire level of each tensile strength vs. temperature curve. Cursory microscopic examination confirmed this reasoning, but considerably more experimental work than was possible to include in this investigation would be required to establish more specifically the effect of grain size on low temperature tensile properties.

This effect must be considered to explain the data plotted in Fig 12 which shows the relation between T_M , T_B , maximum tensile strength and composition. Two separate curves have been drawn for the T_M vs. composition data in line with the reasoning that the grain size of the four lower alloys was considerably larger than that of the four with higher cadmium contents. The effect of grain size, however, on the ductility and T_B of the eight alloys was

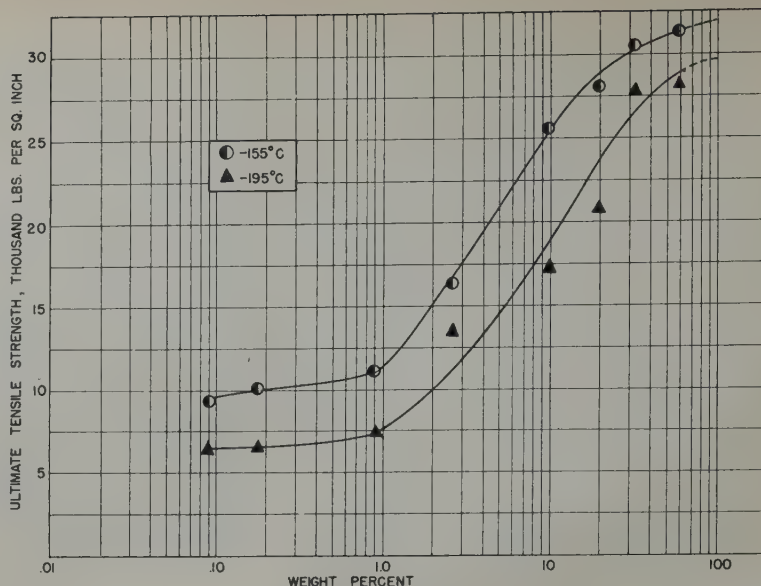


FIG 14—The effect of composition on the ultimate tensile strength of tin cadmium alloys at -155°C and -195°C .

not as pronounced as that on T_M . Composition had no apparent effect on T_M through 2.65 pct cadmium. Variation of the cadmium content from 10 to 60 pct, on the other hand, decreased T_M slightly. T_B follows a similar trend to that of the tin-lead¹ and tin-antimony alloys. Although the T_B vs. log of cadmium composition curve theoretically could only approach -140°C , that is, T_B for pure tin at $-\infty$ (since $\log 0$ is $-\infty$), an approximate extrapolation is pertinent to show that the first additions of cadmium up to 0.1 pct had little or no effect on T_B . T_B then increased steadily for the 0.26 and 0.90 pct alloys to a maximum between 1.0 and 2.65 pct cadmium followed by an abrupt decrease for the 10 to 60 pct alloys. A value for T_B constant within $\pm 5^{\circ}\text{C}$ for pure tin was then approached. Finally an extremely low value for the eutectic 33 pct alloy was obtained. The maximum tensile strength at T_M increased uniformly over the entire composition range from 0.1 to 60 pct cadmium, the data following a straight line relationship quite well. The isothermal tensile strength-composition data plotted in Fig 13 and 14 show that above T_B , the tensile strength increases as the cadmium content increases, the curve approaching maxima at about 10 pct cadmium and either decreasing slightly or remaining constant for the 20, 33 and 60 pct cadmium compositions. At -115°C , pronounced strengthening from cadmium additions continues and obeys a straight line relationship until a maximum is reached at 33 pct fol-

lowed by a decrease in strength for the 60 pct alloy. Below T_B , that is, at -155 and -196°C , however, additions of cadmium up to 1 pct have only a slight strengthening effect. Then a sharp break occurs at the 1 pct composition level, with further additions causing very marked increases in tensile strength to either approach or attain maxima at from 33 to 60 pct cadmium. As in the case of the tin-lead¹ and tin-antimony systems, this break in the tensile strength vs. log composition below T_B corresponds with the terminal solid solution limit of cadmium in tin, and is taken as confirmation of this 10 pct solid solubility of cadmium in tin reported by Hanson and Pell-Walpole.⁵ Further, if the tensile data for temperatures above T_B are replotted with the tensile strength on a logarithmic scale, a very definite break in the curves occurs at about 1 pct cadmium, Fig 15. These data are also considered to confirm the 1 pct cadmium solid solubility in tin. It is undoubtedly significant that two distinctly different relationships between tensile strength and composition are obeyed for above and below T_B respectively, but without additional fundamental data it can only be speculated that this difference is related to the fact that the fundamental process operating above T_B is cleavage by flow, whereas below T_B , failure occurs principally by fracture. At any rate, having confirmed the most recent tin-cadmium phase diagram reported in the literature,⁵ the following correlation of low temperature tensile properties and

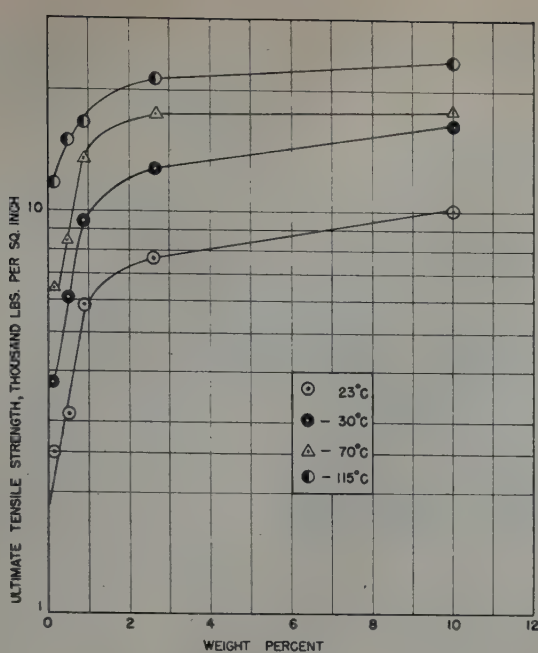


FIG 15—The ultimate tensile strength for various temperatures as a function of composition in the range from 0 to 10 pct cadmium.

microstructure is offered. All the data and relationship revealed by various graphical treatments will be considered except T_M vs. composition curve since, because of grain size effects, it is somewhat anomalous.

The first additions of cadmium (up to 0.1 pct) had no effect on T_B , however, because the substitutional cadmium atoms were too few to change the flow-fracture properties of the resulting solid solution from those of the pure tin. Increasing numbers of cadmium atoms, however, corresponding to 0.26 and 0.9 pct cadmium distorted the parent tin lattice increasingly, so that cleavage by flow was facilitated and T_B increased. The tensile strength at T_M also increased continuously in this composition range, presumably because increased numbers of cadmium atoms dissolved substitutionally increased the critical flow stress and work-hardening contribution of these homogeneous solid solutions. The tensile strengths of these alloys above T_B also increased progressively for the same reason. Below T_B , however, increasing cadmium up to 0.9 pct had only a slight strengthening effect, indicating that dilution of the tin-rich matrix with substitutional cadmium atoms did not appreciably influence the true fracture stress values of the various alloys.

At 1.0 pct cadmium, however, a fine precipitate of γ phase began appearing preferentially at the grain boundaries, slip was thus facilitated and T_B in-

creased to a maximum between 1 and 3 pct cadmium. The maximum tensile strength continued to increase, however, probably because of precipitation hardening and because the fracture stress of the γ phase, occurring both inter- and intragranularly in the 2.65 pct alloy, was sufficient to supplement the composite flow, work hardening, and fracture stress of the continuous tin phase. The tensile strength above T_B continued to increase in the range from 0.1 to 3 pct cadmium, probably because of precipitation hardening. At -155 and -196°C , however, or below T_B , the increase in tensile strength must be attributed to the higher combined fracture strengths of the precipitated γ and the continuous α phases. It is significant to note that as T_B is more nearly approached or exceeded, the slopes of the curves of Fig 13 increase in the 0.1 to 3 pct cadmium range. This can be interpreted as indicating that the technical cohesive strength component of the net tensile strength is increasing and becoming more predominant with decreasing temperature. Ultimately, the tensile strengths at -155 and -196°C are the true fracture strengths, since no ductility remains at these low temperatures.

As the composition reached and exceeded 2.65 pct cadmium, the intergranular γ precipitate increased in amount so that flow was facilitated in this phase as well as the α phase and thence T_B decreased to a constant

value of about -134°C at the 10 pct cadmium level. The maximum tensile strength increased in the 2.65 to 10 pct cadmium range probably because the γ phase was uniformly distributed and the critical flow stress and work-hardening of the two-phase alloy increased with increasing amounts of γ phase. The tensile strengths at $+23$ and -30 were also improved because both the α and β phases had higher critical flow stresses and were strengthened by work hardening to give higher tensile strengths with increasing cadmium contents. At -70°C , however, the γ phase, appearing in increasing amounts in the 2.65 to 10 pct range to form a grain boundary envelope, was probably brittle and the tensile strength of the alloy was thus determined by the strength of the continuous tin phase. Since the composition of this α tin phase remains essentially constant, its strength remained constant as shown by the fact that the tensile strength of the nominal 2.65 and 10 pct cadmium alloys is essentially constant. At -115°C , the fracture stress of the intergranular γ phase increased, so that the net tensile strength of the 10 pct alloys is higher, and this strengthening, caused by the increase of the fracture stress of both the α and γ phases, increased in degree as the temperature decreased. This accounts for the increasing slopes of the tensile strength vs. log composition curves as the temperature decreased.

In the 20 and 33 pct alloys, the γ phase was agglomerated into quite massive particles which probably became brittle before the continuous α phase, as suggested above. Thus since the composition of the α phase remained constant in the 10–20 and 33 pct alloys T_B also remained constant. The maximum tensile strength, however, did continue to increase, presumably because the fracture stress of the increasing γ phase contributed appreciably, that is, corresponding to the amount of γ present. The tensile strength at $+23$, -30 and -70 remains essentially constant in the 10 to 33 pct composition range, either (1) because the massive γ phase is brittle and its fracture stress at all these temperatures is low so that the tensile strength of the alloy was determined by the constant composition α phase, or (2) at $+23$ and -30 , the critical flow stress, work hardening contribution and the fracture stress of the γ phase is less than those of the α phase, and the latter still determined the tensile strength of the alloy. At

-115°C, the fracture stress of the γ phase increased and the net tensile strength thus increased. At -155 and -196°C, that is, below the embrittlement temperature for both the α and γ phases, the increase of fracture stress with decreasing temperature accounts satisfactorily for the increase in tensile strength in the 10 to 33 pct cadmium range.

Again, in the case of the 60 pct cadmium alloy, the continuous α phase determined T_B , and thus, since the tin matrix is of constant composition, as in the 10 pct higher alloy, T_B remained constant. The maximum tensile strength continued to increase, however, for the same reasons as given for those in the 10 to 33 pct range. The tensile strengths at +23 and -30°C decrease slightly for the 60 pct alloy, probably because the critical flow stress, work-hardening contribution and fracture stress of the massive γ phase is considerably less than the corresponding factors for the α phase. At -70°C, the 60 pct alloy is slightly stronger as a result of the increase of the fracture stress of the γ phase with decreasing temperature. On the other hand, at -115°C the tensile strength decreased for this 60 pct alloy, possibly because the decrease of the work hardening component with decreasing temperature was greater than the increase of fracture strength accompanying this fall in temperature. The decrease of strength for this alloy at -155°C cannot be explained according to this reasoning, and thence must be considered anomalous until more information is available. At -196°C, the abrupt improvement in strength for this alloy is undoubtedly a result of the increase of the fracture strength of both phases with decreased temperature.

This correlation of microstructure and low temperature tensile properties has necessarily been qualitative, but it is hoped that these rationalizations may be helpful to design engineers who need to know the properties of similar white bearing alloys for low temperature service. Certain anomalies have been pointed out throughout the discussion, and as might be expected in such survey investigations, many other undelineated questions must go unanswered at this time. A rather extensive long range fundamental research program on low temperature phenomena is underway in this laboratory, however, and it is hoped that a rigorous analysis of these and other related low

temperature behaviors will soon be forthcoming.

Conclusions

1. The tin-antimony alloys containing up to 3 pct antimony remain ductile down to -100°C, whereas the 10 pct antimony alloy becomes brittle at -60°C. Extrapolation would indicate that pure β (SbSn) is brittle at room temperature, a fact confirmed by other workers.³ Tin-cadmium alloys containing from 0.01 to 2.65 pct cadmium become brittle below -120°C, while the 10 to 60 pct cadmium alloys as tested did not become brittle until about -155°C was reached. Since these higher cadmium alloys were finer grained than the lower alloys, this behavior was interpreted as a grain size effect superimposed on a composition effect.

2. All the tin-binary alloys tested increased in strength as the temperature decreased prior to embrittlement. This increase in tensile strength with decreasing temperature has been explained on the basis of (1) the increase of the critical flow stress with decreasing temperature, (2) the effects of work hardening accompanying plastic deformation below the recrystallization temperature, and (3) the increase of technical cohesive strength (fracture stress at nil cold work) with decreasing temperature. The properties measured, of course, were the net or composite strengths arising from the operation of these three factors on the two or more phases present in most of the alloys.

3. Antimony in solid solution has little effect on the tensile strength at any temperature above and below the embrittlement temperature, but as a second phase, it greatly strengthens the alloys. Cadmium, on the other hand, has an appreciable strengthening effect above the embrittlement temperature, whether in solid solution or as a second phase. Below the embrittlement temperature, however, solid-solution strengthening is only slight, whereas cadmium-rich second phase (γ) increases the strength markedly.

4. Antimony raises the embrittlement temperature as soon as an antimony-rich phase appears. Cadmium, either in solid solution or as a second phase, has little effect on the temperature of embrittlement.

5. The use of low temperature tensile tests to verify the solvus lines of

binary phase diagrams near room temperature has been demonstrated both in the tin-antimony and tin-cadmium systems.

Acknowledgment

The authors wish to thank the U.S. Navy, Bureau of Ships, for supporting this work. We are also grateful to Dr. R. M. Brick who initiated the long range research program on tin binary alloys and, by discussion of these data, contributed to its interpretation. It is also a pleasure to acknowledge the aid of our laboratory assistant, David Goldstein, who did the difficult metallographic work on these tin alloys.

References

1. H. S. Kalish and F. J. Dunkerley: The Low Temperature Properties of Tin and Tin-lead Alloys. *Trans. AIME* (1949) 182. *Met. Tech.*, Sept. 1948, TP 2442.
2. W. T. Pell-Walpole: The Effect of Grain Size on the Tensile Strength of Tin and Tin Alloys. *Jnl. Inst. Metals* (1943) 69, 131.
3. D. Hanson and W. T. Pell-Walpole: A Study of the Mechanical Properties of Tin-Rich Antimony-Tin Alloys. *Jnl. Inst. Metals* (1938) 63, 87.
4. C. E. Homer and H. Plummer: Mechanical Properties of Some White Bearing Metals and Other Tin-Base Alloys at Various Temperatures. T.P. International.
5. D. Hanson and W. T. Pell-Walpole: The Constitution and Properties of Cadmium-Tin Alloys. *Jnl. Inst. Metals* (1935) 56, 165.
6. W. T. Pell-Walpole: Non-Equilibrium Structures in Chill Cast Tin-Antimony-Cadmium Alloys and Their Effects on Mechanical Properties. *Jnl. Inst. Metals* (1945) 71, 441.
7. D. Hanson and W. T. Pell-Walpole: A Study of the Mechanical Properties of Tin-Rich Antimony-Cadmium-Tin Alloys. *Jnl. Inst. Metals* (1937) 61, 123.
8. D. Hanson and W. T. Pell-Walpole: The Constitution of the Tin-Rich Antimony-Tin Alloys. *Jnl. Inst. Metals* (1936) 58, 299.
9. E. S. Hedges and C. E. Homer: Equilibrium Diagrams of Binary Alloys of Tin. T.P. International Tin Res. Dev. Council, Ser. B, 1935, No. 2.
10. D. Hanson and W. T. Pell-Walpole: A Further Study of the Constitution of the Cadmium Tin Alloys. *Jnl. Inst. Metals* (1936) 59, 281.
11. E. Cohen, W. A. T. Cohen,—De Meester and A. K. W. A. van Lieshout: The Velocity of Polymorphic Change III. Effect of Mechanical Deformation on the Velocity of Change. *Ztsch. Physik. Chem.* (1935) (A) 173, 169.
12. D. Hanson and W. T. Pell-Walpole: *Jnl. Inst. Metals* (1936) 58, adv. copy.

Metals Transactions

January-December 1949

Index to Volume 185

PAGES IN EACH ISSUE

| | | | |
|----------|---------|-----------|----------|
| January | 1-72 | July | 393-440 |
| February | 73-204 | August | 441-552 |
| March | 205-260 | September | 553-664 |
| April | 261-296 | October | 665-784 |
| May | 297-348 | November | 785-904 |
| June | 349-392 | December | 905-1016 |

| | Page | | Page | | Page |
|---|------|---|------|---|------|
| Academia Sinica, Shanghai, China: flow and fracture characteristics of a die steel at high hardness levels..... | 927 | and composition of molten lead silicate slags..... | 984 | Avery, H. S.: Discussion: Cobalt-chromium Binary System..... | 299 |
| Aerotex M-3: use as a mounting material.. | 229 | American Steel and Wire Co.: Controlled Drying of Retorts..... | 393 | Avery, H. S.: Discussion: Fractographic Study of Cast Molybdenum..... | 308 |
| Alexander, B. H., and Kuczynski, G.: Discussion on The Surface Tension of Solid Copper..... | 894 | Anaconda Copper Co.: slag fuming plant.... | 473 | | |
| Alloys, precipitation-hardenable; size effects in quenching high-purity..... | 668 | Anderson, E. A.: Discussion on Influence of Composition on the Stress-corrosion Cracking of Some Copper-base Alloys..... | 862 | | |
| Alnico magnet..... | 418 | Anderson, G. H.: The Recovery of Cadmium from Cadmium-copper Precipitate, Electrolytic-Zinc Co. of Australasia, Risdon, Tasmania..... | 205 | | |
| Alpha brass: annealing twins in..... | 635 | discussion..... | 846 | | |
| some observations in structure of single crystals after cutting and polishing | 701 | Anderson, R. A., et al.: Effect of Pretraining Temperatures on the Recovery of Cold Worked Aluminum..... | 921 | | |
| Alpha iron: diffusion and solubility of carbon in..... | 752 | Andrew, Kenneth F. and Gulbransen, Earl A.: Kinetics of the Reactions of Titanium with Os, Ni and H..... | 741 | | |
| Aluminum, alloys, studies of interface energies..... | 762 | Kinetics of the Reactions of Zirconium with Os, Ni and H..... | 515 | | |
| bending single crystals of..... | 710 | Ansoco film..... | 781 | | |
| flow-pattern in..... | 717 | Argonne National Laboratory: preferred orientation in rolled and recrystallized beryllium..... | 145 | | |
| flow characteristics in..... | 719 | Armant, D. L., and Cole, S. S.: laboratory smelting of titaniferous ores..... | 909 | | |
| load-deflection diagrams..... | 717 | Armantrout, C. E., et al.: The Ternary System, Copper-manganese-zinc..... | 675 | | |
| transverse..... | 710 | Armco Iron: emissivity..... | 665 | | |
| effect of pretraining temperatures on recovery of cold worked..... | 921 | Armour Research Foundation of Illinois Institute of Technology: a metallographic description of fracture in impact specimens of a structural steel..... | 481 | | |
| recovery from residue metal..... | 124 | effects of molybdenum and commercial ranges of phosphorus upon the toughness of 0.40 pct carbon chromium steels..... | 535 | | |
| recrystallization and coarsening texture in | 627 | Arrhenius equation..... | 518 | | |
| Aluminum Co. of America: liquid solubility of manganese in a magnesium-aluminum-tin alloy..... | 405 | Asterism..... | 715 | | |
| American Brass Co.: influence of composition on the stress-corrosion cracking of some copper-base alloys..... | 100 | Atomic Energy Commission: metallographic examination of beryllium alloys..... | 779 | | |
| intergranular parting of brass during anneals..... | 995 | preparation and casting of beryllium melts | 769 | | |
| secondary recrystallization in copper..... | 501 | Auger machine: use in forming retorts..... | 74 | | |
| American Electro Metal Corporation: electrical resistivity measurements on iron-silicon compacts prepared by the powder metallurgy procedure..... | 475 | Aust, K. T., and Pidgeon, L. M.: Solubility of Titanium in Liquid Magnesium.. | 585 | | |
| properties of chromium boride and sintered chromium boride..... | 198 | Austenite-martensite transformation, kinetics of..... | 691 | | |
| structure of diborides of titanium, zirconium, columbium, tantalum and vanadium..... | 749 | Averbach, B. L.: Recovery and Recrystallization in Brass..... | 491 | | |
| American Iron and Steel Institute..... | 903 | | | | |
| American Metal Co..... | 416 | | | | |
| American Smelting and Refining Co.: concentration of the SO ₂ content of Dwight-Lloyd sintering machine gas by recirculation..... | 261 | | | | |
| relationship between electrical conductivity | | | | | |

| | Page | | Page | | Page |
|---|----------|---|----------|---|------|
| Barrett, C. S., and Smigelskas, A.: <i>Preferred Orientation in Rolled and Recrystallized Beryllium</i> | 145 | Boss, G. H.: <i>Discussion: on Nucleation of Slip Bands and Transient Plastic Deformation</i> | 320 | Carwile, N. L., and Geil, G. W.: <i>Discussion on The Effect of Thermal-mechanical History on the Strain Hardening of Metals</i> | 325 |
| Bash, F. E.: <i>Discussion on An Electron Diffraction Study of Oxide Films Formed on Nickel-chromium Alloys</i> | 305 | Boulger, F. W., et al.: <i>Relative Deoxidizing Powers of Some Deoxidizers for Steel</i> | 814 | Case Institute of Technology: high temperature scaling of cobalt | 720 |
| Battelle Memorial Institute: comparative creep properties of several types of commercial coppers | 409 | Bradd, A. A.: <i>Discussion on The Interaction of Liquid Steel with Ladle Refractories</i> | 841 | stress and strain states in elliptical bulges | 49 |
| effect of oxygen, nitrogen, and hydrogen on iodide refined titanium | 646 | Brass: annealing twins in | 655 | Cenco Hyvac fore pump | 516 |
| investigation of temper brittleness in low-alloy steels | 366 | dendrites in cast | 768 | Center, A. A.: <i>Discussion on Autogenous Roasting of Low-grade Zinc Concentrate in Multiple-hearth Furnaces at Risdon, Tasmania</i> | 849 |
| magnesium-lithium base alloys—preparation, fabrication, and general characteristics | 149 | Brassett & Co.: equilibrium in the reaction of hydrogen with oxygen in liquid iron | 441 | Center, A. A.: <i>Discussion on The Effect of High Copper Content on the Operation of a Lead Blast Furnace, and Treatment of the Copper and Lead Produced</i> | 847 |
| metallographic examination of beryllium alloys | 779 | optical temperature scale and emissivity of liquid iron | 665 | Center, A. A.: <i>Discussion on Electrolytic Zinc at Risdon, Tasmania. Major Changes Since 1936</i> | 842 |
| preparation and casting of beryllium melts relative deoxidizing powers of some deoxidizers for steel | 769 | Brewer, R. E.: <i>Discussion on Tracer Study of Sulphur in the Coke Oven</i> | 826 | Center, A. A.: <i>Discussion on The Surface Tension of Solid Copper</i> | 895 |
| transformations in β -CuAl alloys | 611 | Brick, R. M.: discussion on Mechanism of Precipitation in a Permanent Magnet Alloy | 301 | Center, A. A.: <i>Discussion on The Recovery of Cadmium from Cadmium-copper Precipitate, Electrolytic Zinc Co. of Australasia, Risdon, Tasmania</i> | 845 |
| Bausch and Lomb, metallograph | 914 | on Some Effects of Applied Stresses on Precipitation Phenomena | 302 | Chalcocite | 348 |
| metallographic research microscope | 723 | Bristol meter | 436 | Chalcocyprite | 348 |
| Beck, P. A.: <i>The Sigma Phase in Ternary Cr-Co-Fe and Cr-Co-Ni Alloys</i> | 354 | Brookhaven National Laboratories: the beryllium-iron system | 285 | Chang, L., and Chipman, J.: <i>The Ionic Nature of Metallurgical Slags. Simple Oxide Systems</i> | 191 |
| Beck, P. A.: <i>Discussion on Some Factors Affecting the Rate of Grain Growth in Metals</i> | 882 | Brugman, J. J.: <i>Discussion on Development of Muffle Furnaces for the Production of Zinc Oxide and Zinc at East Chicago, Ind.</i> | 853 | Charpy test | 683 |
| Beck, P. A., and Hu, Hsun: <i>Recrystallization Texture and Coarsening Texture in High Purity Aluminum</i> | 627 | Buffum, D. C., and Jaffe, L. D.: <i>Reply to discussion on Temper Brittleness of Plain Carbon Steels</i> | 880 | Chase Brass and Copper Co.: a study of textures and earing behavior of cold-rolled (87-89 pct) and annealed copper strips | 59 |
| Beck, P. A., and Manly, W. D.: <i>The Sigma Phase in Ternary Cr-Co-Fe and Cr-Co-Ni Alloys</i> | 354 | Buffum, D. C., et al.: <i>Effect of Carbon and Nitrogen on Temper Brittleness</i> | 499 | Chaudron, G., et al.: <i>Discussion on Some Effects of Applied Stresses on Precipitation Phenomena</i> | 302 |
| Beck, P. A., and Sperry, P. E.: <i>Effect of Recrystallization Texture on Grain Growth</i> | 240 | Bumps, E. S., et al.: <i>A Metallographic Description of Fracture in Impact Specimens of a Structural Steel</i> | 481 | Chazy Lime and Stone Co. | 436 |
| Beck, P. A., et al.: <i>Grain Coarsening in Copper</i> | 203 | Bunker Hill Smelter: cadmium recovery practice in lead smelting | 110 | Cheggwidden, R. A.: <i>Rectangular Hysteresis Loops of Co-Ni-Fe Alloys</i> | 570 |
| Bell Telephone Labs: microstructures of silicon ingots | 389 | Burgers, W. G.: <i>Discussion on The Effect of Orientation Difference on Grain Boundary Energies</i> | 860 | Cheng, C. H., and Birchenall, C. E.: <i>The Vapor Pressures of Zinc and Cadmium over Some of Their Silver Alloys</i> | 428 |
| rectangular hysteresis loops of Co-Ni-Fe alloys | 570 | Burghoff, H. L.: <i>Discussion on Influence of Composition on the Stress-corrosion Cracking of Some Copper-base Alloys</i> | 863 | Cherian, T. V., et al.: <i>Some Observations on the Recovery of Cold Worked Aluminum</i> | 948 |
| p-type and n-type silicon and the formation of the photovoltaic barrier in silicon ingots | 383 | Burke, J. E.: <i>Discussion on Effect of Composition on Grain Growth in Aluminum-magnesium Solid Solutions</i> | 309 | Chihuahua Smelter: effect of high copper content on the operation of a lead blast furnace, and the treatment of the copper and lead produced | 347 |
| Benson, P. T.: <i>Discussion on The Morenci Smelter of Phelps Dodge Corporation at Morenci, Arizona</i> | 855 | Burke, J. E.: <i>Discussion on Effect of a Dispersed Phase on Grain Growth in Al-Mn Alloys</i> | 315 | Chipman, J.: <i>Discussion on Relation between Chromium and Carbon in Chromium Steel Refining</i> | 832 |
| Beryllium, casting practice | 774 | Burke, J. E.: <i>Reply to discussion on Some Factors Affecting the Rate of Grain Growth in Metals</i> | 885 | Chipman, J.: <i>Discussion on Relative Deoxidizing Powers of Some Deoxidizers for Steel</i> | 824 |
| characteristics of | 769 | Burns, J. R.: <i>Discussion on The Room and Elevated Temperature Properties of Some Sand Cast Magnesium-base Alloys Containing Zinc</i> | 327 | Chipman, J.: <i>What Is Metallurgy?</i> | 349 |
| melting of | 770 | Busch, L. S.: <i>Discussion on Lead-grid Study of Metal Powder Compaction</i> | 888, 889 | Chipman, J., and Chang, L.: <i>The Ionic Nature of Metallurgical Slags. Simple Oxide Systems</i> | 191 |
| metallographic examination of alloys | 779 | Busch, L. S.: <i>Discussion on Pressure Distribution in Compacting Metal Powders</i> | 888 | discussion | 841 |
| preparation and casting | 769 | Busch, L. S., and Swazy, E. F.: <i>Discussion on Seminar on the Kinetics of Sintering</i> | 805 | Chipman, J., and Dastur, M. N.: <i>Equilibrium in the Reaction of Hydrogen with Oxygen in Liquid Iron</i> | 441 |
| rolled and recrystallized, preferred orientation in | 145 | Busk, R. S.: <i>Discussion on Magnesium-lithium Base Alloys—Preparation, Fabrication, and General Characteristics</i> | 867 | Chipman, J., and Hatch, G. G.: <i>Sulphur Equilibria between Iron Blast Furnace Slags and Metal</i> | 274 |
| Beryllium-iron system: as developed by Gordon | 286 | Busk, R. S.: <i>Discussion on Plastic Deformation Waves in Aluminum</i> | 877 | discussion | 831 |
| Berzelius: first producer of ferrosilicon | 475 | | | Chisholm, O. P.: development of dross reverberatory | 348 |
| Bethune, A. Y.: <i>Discussion on The Use of Oxygen-enriched Air in the Metallurgical Operations of Cominco at Trail, B. C.</i> | 848 | | | Chow, C. C., et al.: <i>Stress and Strain States in Elliptical Bulges</i> | 49 |
| Bever, M. B.: <i>Discussion on Hydrogen in Aluminum</i> | 870 | | | Chow, C. C., et al.: <i>Flow and Fracture Characteristics of a Die Steel at High Hardness Levels</i> | 927 |
| Bever, M. B.: <i>Discussion on The Influence of Temperature on the Affinity of Sulphur for Copper, Manganese and Iron</i> | 837 | | | Chromium,—oxygen equilibrium | 824 |
| Bever, M. B.: <i>Discussion on Self-diffusion in Sintering of Metallic Particles</i> | 897 | | | use in steel refining | 91 |
| Bever, M. B.: <i>Discussion on the Structure of Gold-silver-copper Alloys</i> | 857, 858 | | | substituting molybdenum for, for hardenability | 537 |
| Bever, M. B.: <i>Discussion on Use of Electrical Resistance Measurements to Determine the Solids of Lead-tin System</i> | 859 | | | Chromium boride: air corrosion tests | 202 |
| Bever, M. B., and Barer, R. D.: <i>The Effect of Quenching on the Age Hardening of Two Aluminum Alloys</i> | 544 | | | current investigation of crystal structure | 199 |
| Bianco, H. R.: <i>Discussion on The Effect of High Copper Content on the Operation of a Lead Blast Furnace, and Treatment of the Copper and Lead Produced</i> | 847 | | | effect of pressing and sintering | 200 |
| Bianco, H. R.: <i>Discussion on El Paso Slag Treatment Plant</i> | 854 | | | high temperature testing | 201 |
| Biegegleitung (bending of slip plane) | 725 | | | Chromium steel refining, chromium-carbon-temperature relations | 91 |
| Binary Chart | 993 | | | Citrate cell: for electrolytic isolation of carbides | 579 |
| Birchenall, C. E., and Cheng, C. H.: <i>The Vapor Pressures of Zinc and Cadmium over Some of Their Silver Alloys</i> | 428 | | | Clancy, W. P., et al.: <i>Effect of Carbon and Nitrogen on Temper Brittleness</i> | 499 |
| Blackwell Zinc Co.: development of the modern zinc retort in the United States | 73 | | | Clapeyron-Clausius equation | 431 |
| Blank, A. I.: <i>Discussion on Effect of Grain Size on Tensile Strength, Elongation, and Endurance Limit of Deep Drawing Brass</i> | 339 | | | Clark, Howard T., Jr.: <i>The Lattice Parameters of High Purity Alpha Titanium; and the Effects of Oxygen and Nitrogen on Them</i> | 588 |
| Blickwede, D. J.: <i>Discussion on Secondary Hardening of Tempered Martensitic Alloy Steel</i> | 345 | | | Cobalt: disposal of precipitate | 214 |
| Blickwede, D. J., and Cohen, M.: <i>The Isolation of Carbides from High Speed Steel</i> | 578 | | | high temperature sealing of | 720 |
| Blumenthal, H., et al.: <i>Structure of Diborides of Titanium, Zirconium, Columbium, Tantalum and Vanadium</i> | 749 | | | thermal expansion curves | 575 |
| Bolton, M. J., et al.: <i>On the Problem of Grain Boundary Movement</i> | 708 | | | Cohen, M., and Balluffi, R.: <i>Discussion on Secondary Hardening of Tempered Martensitic Alloy Steel</i> | 345 |
| Boss, J. H.: <i>Discussion: on Fractographic Study of Cast Molybdenum</i> | 308 | | | Cohen, M., and Blickwede, D. J.: <i>The Isolation of Carbides from High Speed Steel</i> | 578 |
| | | | | Cohen, M., and Teltel, R. J.: <i>The Beryllium-Iron System</i> | 285 |
| | | | | Cole, S. S., and Armand, D. L.: <i>Laboratory Smelting of Titaniferous Ores</i> | 909 |
| | | | | Cole, S. S., and Sigurdson, H.: <i>Melting Points in the System TiO₂-CaO-MgO-Al₂O₃</i> | 905 |
| | | | | | |
| | | | | | |
| | | | | | |
| | | | | | |
| | | | | | |
| | | | | | |
| | | | | | |
| | | | | | |
| | | | | | |
| | | | | | |
| | | | | | |
| | | | | | |
| | | | | | |
| | | | | | |
| | | | | | |
| | | | | | |
| | | | | | |
| | | | | | |
| | | | | | |
| | | | | | |
| | | | | | |
| | | | | | |
| | | | | | |
| | | | | | |
| | | | | | |
| | | | | | |
| | | | | | |
| | | | | | |
| | | | | | |
| | | | | | |
| | | | | | |
| | | | | | |
| | | | | | |
| | | | | | |
| | | | | | |
| | | | | | |
| | | | | | |
| | | | | | |
| | | | | | |
| | | | | | |
| | | | | | |
| | | | | | |
| | | | | | |
| | | | | | |
| | | | | | |
| | | | | | |
| | | | | | |
| | | | | | |
| | | | | | |
| | | | | | |
| | | | | | |
| | | | | | |
| | | | | | |
| | | | | | |
| | | | | | |
| | | | | | |
| | | | | | |
| | | | | | |
| | | | | | |
| | | | | | |
| | | | | | |
| | | | | | |
| | | | | | |
| | | | | | |
| | | | | | |
| | | | | | |
| | | | | | |
| | | | | | |
| | | | | | |
| | | | | | |
| | | | | | |
| | | | | | |
| | | | | | |
| | | | | | |
| | | | | | |
| | | | | | |
| | | | | | |
| | | | | | |
| | | | | | |
| | | | | | |
| | | | | | |
| | | | | | |
| | | | | | |
| | | | | | |
| | | | | | |
| | | | | | |
| | | | | | |
| | | | | | |
| | | | | | |
| | | | | | |
| | | | | | |
| | | | | | |
| | | | | | |
| | | | | | |
| | | | | | |
| | | | | | |
| | | | | | |
| | | | | | |
| | | | | | |
| | | | | | |
| | | | | | |
| | | | | | |
| | | | | | |
| | | | | | |
| | | | | | |
| | | | | | |

| Page | Page | Page |
|--|------|---|
| Collins, A. A.: <i>The Effect of High Copper Content on the Operation of a Lead Blast Furnace, and the Treatment of the Copper and Lead Produced</i> | 347 | recovery of cadmium from cadmium-copper precipitate, Electrolytic Zinc Co. of Australasia, Risdon, Tasmania.... |
| discussion | 847 | 205 |
| Columbium: structure of diborides..... | 749 | electrolytic zinc at Risdon, Tasmania. Major changes since 1936..... |
| Compacts: copper-nickel | 574 | 211 |
| copper-zinc | 575 | Electropolishing |
| iron powder | 575 | 395 |
| swelling caused by gas pockets..... | 573 | Elliott turbine driven blower..... |
| thermal expansion curves, of chromium-molybdenum | 577 | 474 |
| of copper-nickel | 576 | Ellis, W. C.: <i>Discussion on Nucleation of Slip Bands and Transient Plastic Deformation</i> |
| of copper-zinc | 576 | 319 |
| Consolidated Mining and Smelting Co. of Canada, Ltd.: use of oxygen enriched air in the metallurgical operations of Cominco at Trail, B. C..... | 447 | <i>Discussion on Statistical Rate Theory of Metals—I. Mechanism of Flow and Application to Tensile Properties</i> .. |
| Converters | 8 | 316 |
| Copper, annealing twins in..... | 635 | El Paso Smelting Works: El Paso slag treatment plant |
| compression textures of..... | 620 | 472 |
| densification of | 96 | Elsa, A. R., and Herres, S. A.: <i>Investigation of Temper Brittleness in Low-alloy Steels</i> |
| influence of temperature on tensile properties of | 727 | 366 |
| on strain energy..... | 737 | Emerick, H. B., and Minto, R. E.: <i>Discussion on the Influence of Temperature on the Affinity of Sulphur for Copper, Manganese and Iron</i> |
| recovery from residue metal..... | 124 | 838 |
| Copper alloys: stress-corrosion of | 100 | Emmett, B. G.: <i>Discussion on Relation between Chromium and Carbon in Chromium Steel Refining</i> |
| studies of interface energies..... | 762 | 833 |
| CuAl alloys, transformations in..... | 611 | Eppelsheimer, D. S., and Hancock, F. A.: <i>Ferromagnetic Alloys in the Systems Cu-Mn-In and Cu-Mn-Ga</i> |
| Copper-indium system, diagram..... | 496 | 495 |
| Copper-gallium system, diagram..... | 496 | Eprelian, E., and Harker, D.: <i>The Crystal Structure of NiW</i> |
| Copper-manganese-gallium system | 498 | 267 |
| Copper-manganese-indium system | 497 | Erck, L. J.: <i>Discussion on Sintering Characteristics of Minus Sixty-five and Twenty Mesh Magnetite</i> |
| Copper sulphide, as aid in sintering..... | 348 | 837 |
| Copper test: cadmium-copper precipitate leach | 210 | Eshelby, J. D.: <i>Discussion on Seminar on the Kinetics of Sintering</i> |
| cadmium precipitate leach..... | 210 | 806 |
| Cordiano, J.: <i>Discussion on Lead-grid Study of Metal Powder Compaction</i> | 889 | |
| Corson, M. G.: <i>Discussion on A High Strength-High Conductivity Copper-silver Alloy Wire</i> | 340 | F |
| Corson, M. G.: <i>Discussion on Temper Brittleness of Plain Carbon Steels</i> | 880 | FeO: distribution between molten iron and oxide slags |
| Cottrell, A. H.: <i>Discussion on Nucleation of Slip Bands and Transient Plastic Deformation</i> | 320 | 195 |
| Cottrell, A. H., and Churchman, A. T.: <i>Discussion on Homogeneous Yielding of Carburized and Nitrided Single Iron Crystals</i> | 877 | slags containing lime or magnesia..... |
| Cox, E. M., et al.: <i>Influence of Temperature on the Affinity of Sulphur for Copper, Manganese, and Iron</i> | 27 | 195 |
| Crack propagation, discontinuous—further studies | 683 | Feddersen, P. C.: <i>The Use of Oxygen-enriched Air in the Metallurgical Operations of Cominco at Trail, B. C.</i> |
| Craig, W. E., Jr., et al.: <i>A Metallographic Description of Fracture in Impact Specimens of a Structural Steel</i> | 481 | 848 |
| Craig, W. E., Jr., et al.: <i>Effects of Molybdenum and Commercial Ranges of Phosphorus upon the Toughness of 0.40 Per Cent Carbon Chromium Steels</i> | 535 | Feddersen, P. C., and Lee, H. E.: <i>Cadmium Recovery Practice in Lead Smelting</i> |
| Crafts, W., et al.: <i>Carbides in Isothermally Transformed Chromium Steels</i> | 957 | 110 |
| Creep tests, constant load..... | 704 | Fink, W. L.: <i>Discussion on Mechanism of Precipitation in a Permanent Magnet Alloy</i> |
| Churchman, A. T., and Cottrell, A. H.: <i>Discussion on Homogeneous Yielding of Carburized and Nitrided Single Iron Crystals</i> | 877 | 300 |
| Crucible: silicon carbide..... | 771 | Finlay, W. L.: <i>Size Effects in Quenching High-purity, Precipitation-hardenable Alloys</i> |
| Crucible Steel Co. of America: ionic nature of metallurgical slags, simple oxide systems | 191 | 668 |
| Cupping tests | 59 | Fisher, J. C.: <i>The Free Energy Change Accompanying the Martensite Transformation in Steels</i> |
| | | 688 |
| D | | Fisher, J. C., et al.: <i>Kinetics of the Austenite-Martensite Transformation</i> .. |
| Dana, A. W., et al.: <i>Stress and Strain States in Elliptical Bulges</i> | 49 | 691 |
| Daniels, F. W., et al.: <i>On the Problem of Grain Boundary Movement</i> | 708 | Fitterer, G. R.: <i>Discussion on Relation between Chromium and Carbon in Chromium Steel Refining</i> |
| Dardel, Y.: <i>Reply to discussion on Hydrogen in Aluminum</i> | 872 | 832 |
| Darwin formula | 492 | <i>Discussion on The Origin of Silicate Inclusions in Basic Electric-arc Furnace Steel of Higher Carbon Contents</i> ... |
| Dasher, J.: <i>Discussion on Tracer Study of Sulphur in the Coke Oven</i> | 827 | 834 |
| Dastur, M. N., and Chipman, J.: <i>Equilibrium in the Reaction of Hydrogen with Oxygen in Liquid Iron</i> | 441 | Flanigan, A. E.: <i>Discussion on Mechanism of Precipitation in a Permanent Magnet Alloy</i> |
| Dastur, M. N., and Goken, N. A.: <i>Optical Temperature Scale and Emissivity of Liquid Iron</i> | 665 | 301 |
| Davidson, L. P.: <i>Discussion on Cadmium Recovery Practice at the Donora Zinc Works</i> | 843 | 517 |
| on Controlled Drying of Retorts..... | 852 | Forster, J. A. B.: <i>Autogenous Roasting of Low Grade Zinc Concentrate in Multiple Hearth Furnaces at Risdon, Tasmania</i> |
| on Development of the Modern Zinc Retort in the United States..... | 852 | 461 |
| on Development of Muffle Furnaces for the Production of Zinc Oxide and Zinc at East Chicago, Indiana..... | 853 | 850 |
| on Electrolytic Zinc at Risdon, Tasmania. Major Changes Since 1936..... | 843 | discussion |
| on El Paso Slag Treatment Plant..... | 854 | Frost, P. D., et al.: <i>Magnesium-lithium Base Alloys—Preparation, Fabrication, and General Characteristics</i> .. |
| on The Recovery of Cadmium from Cadmium-copper Precipitate, Electrolytic Zinc Co. of Australasia, Risdon, Tasmania..... | 846 | 149 |
| on The Use of Oxygen-enriched Air in the Metallurgical Operations of Cominco at Trail, B. C. | 848 | Fume and Dust Problem..... |
| | | 934 |
| | | Furlong, R. R., and Wertz, D. H.: <i>Controlled Drying of Retorts</i> |
| | | 393 |
| | | Furnace: Ajax 6 KW..... |
| | | 910, 914 |
| | | electric arc..... |
| | | 789, 912 |
| | | fuming |
| | | 472 |
| | | gas atmosphere induction..... |
| | | 770 |
| | | Global type |
| | | 766, 789 |
| | | Herreshoff type |
| | | 461 |
| | | muffle |
| | | 118 |
| | | Skinner type |
| | | 461 |
| | | G |
| | | Gallium |
| | | 363 |
| | | Gardner, E. J.: <i>Discussion on Tracer Study of Sulphur in the Coke Oven</i> |
| | | 829 |
| | | Gas tenor, relation to heat balance..... |
| | | 471 |
| | | Geiger-counter spectrometer |
| | | 491 |
| | | Gell, G. W., and Carville, N. L.: <i>Discussion on The Effect of Thermal-mechanical History on the Strain Hardening of Metals</i> |
| | | 325 |
| | | General Aniline and Film Co.: carbonyl iron |
| | | 565 |
| | | General Electric Co.: controlled grain growth applied to the problem of grain boundary energy measurements.... |
| | | 72 |
| | | crystal structure of NiW..... |
| | | 267 |
| | | effect of orientation difference on grain boundary energies |
| | | 125 |
| | | free energy change accompanying the martensite transformation in steels.... |
| | | 688 |
| | | homogeneous yielding of carburized and nitrided single iron crystals..... |
| | | 179 |
| | | kinetics of the austenite-Martensite transformation |
| | | 591 |

| | Page | | Page | | Page |
|---|----------|--|----------|---|----------|
| low temperature properties of tin-antimony and tin-cadmium alloys | 1005 | on Electrolytic Zinc at Risdon, Tasmania. Major Changes Since 1936 | 843 | Ikeuye, K. K., and Smith, C. S.: <i>Studies of Interface Energies in Some Aluminum and Copper Alloys</i> | 762 |
| mechanism of martensite formation | 590 | on The Recovery of Cadmium from Cadmium-copper Precipitate, Electrolytic Zinc Co. of Australasia, Risdon, Tasmania | 844, 846 | Ilmenite, Baie St. Paul, reduction of charge | 913 |
| observations on the rate of secondary recrystallization in high purity copper | 663 | Hargrave, J. H., et al.: <i>Oxygen Enriched Air in the Metallurgical Operations of Cominco at Trail, B. C.</i> | 446 | MacIntyre | 913 |
| problem of grain boundary movement | 708 | Harker, D., and Epreman, E.: <i>The Crystal Structure of NiW</i> | 267 | Winning TiO ₂ from, by Smelting process | 914 |
| rapid determination of orientations of cubic crystals | 417 | Hatch, G. G., and Chipman, J.: <i>Sulphur Equilibria between Iron Blast Furnace Slags and Metal</i> | 274 | Indium | 363 |
| yielding and strain-aging of carburized and nitrided single crystals of iron | 637 | Hausner, H. H.: <i>Discussion on Seminar on the Kinetics of Sintering</i> | 804 | Indium Corp. of America | 499 |
| Germanium | 363 | Herenguel, J., et al.: <i>Discussion on Some Effects of Applied Stresses on Precipitation Phenomena</i> | 302 | Inland Steel Co. | 829 |
| Gibbs-Duhem equation | 456 | Herrres, S. A., and Elsea, A. R.: <i>Investigation of Temper Brittleness in Low-alloy Steels</i> | 366 | Intergranular Parting of Brass during Anneals | 995 |
| Giove, J. L., et al.: <i>Hardenability Effect of Molybdenum</i> | 218 | Hess, J. B.: <i>Discussion on Property Changes during Aging</i> | 337 | International Nickel Co. | 727 |
| Glaser, F. W.: <i>Discussion on The Magnetic Properties of Sintered Iron and Iron Base Alloys</i> | 892 | Hess, J. B., and Barrett, C. S.: <i>Structure and Nature of Kink Bands in Zinc</i> | 599 | Ionic solutions | 193 |
| Glaser, Frank W.: <i>Electrical Resistivity Measurements on Iron-silicon Compacts Prepared by the Powder Metallurgy Procedure</i> | 475 | Hibbard, W. R., Jr.: <i>Effect of Composition on the Wire Features of Copper and Its Solid Solution Alloys</i> | 598 | Iron, alpha: diffusion and solubility of carbon in | 752 |
| Gleekman, L. W.: <i>Discussion on Effects of Grain Size on Tensile Strength, Elongation, and Endurance Limit of Deep Drawing Brass</i> | 339 | Hibbard, W. R., Jr., et al.: <i>Annealing Twins in Copper and 70-30 Alpha Brass</i> | 635 | Iron Crystals: heat-treating and testing | 180 |
| Gohn, G. R.: <i>Discussion on Influence of Composition on the Stress-corrosion Cracking of Some Copper-base Alloys</i> | 862 | Hibbard, W. R., Jr., and Maddin, R.: <i>Some Observations in the Structure of Alpha Brass Single Crystals after Cutting and Polishing</i> | 700 | Iron, liquid: temperature scale and emissivity of | 665 |
| Gokcen, N. A., and Dastur, M. N.: <i>Optical Temperature Scale and Emissivity of Liquid Iron</i> | 665 | Hibbard, W. R., Jr., and Maddin, R.: <i>Discussion on Transient Plastic Deformation</i> | 318 | Thermocouples for establishing true temperature of | 666 |
| Gonser, B.: <i>Discussion on Use of Electrical Resistance Measurements to Determine the Solidus of the Lead-tin System</i> | 860 | Hibbard, W. R., Jr., et al.: <i>Active Slip Systems in the Simple Axial Extension of Single Crystalline Alpha Brass</i> | 527 | Isothermal recrystallization of rimmed and aluminum killed steel | 242 |
| Gonser, B. W.: <i>Discussion on Thermal and Electrical Properties of Ductile Titanium</i> | 336 | Hibbard, W. R., Jr., and Trout, D. E., II: <i>Compression Textures of Copper and Its Binary Alpha Solid Solution Alloys</i> | 620 | effect of temperature of | 243 |
| Gordon, A. R.: <i>Discussion on Cadmium Recovery Practice in Lead Smelting</i> | 847 | Hibbard, W. B., Jr., and Yen, M. K.: <i>The Transverse Bending of Single Crystals of Aluminum</i> | 710 | effect of treatment prior to cold reduction | 244 |
| <i>Discussion on Electrolytic Zinc at Risdon, Tasmania. Major Changes Since 1936</i> | 843 | Correction | 926 | on continuous heating | 245 |
| <i>Discussion on The Recovery of Cadmium from Cadmium-copper Precipitate, Electrolytic Zinc Co. of Australasia, Risdon, Tasmania</i> | 845 | Hill, R.: <i>Discussion on Plastic Flow in Anisotropic Sheet Steel</i> | 323 | | |
| Gorski, C. H., et al.: <i>Titanium Investigations: Research and Development Work on the Preparation of Titanium Chloride and Oxide from Titanium Mattes</i> | 785 | Hilty, D. C.: <i>Relation between Chromium and Carbon in Chromium Steel Refining</i> | 91 | Jackson, J. H., et al.: <i>Magnesium-lithium Base Alloys—Preparation, Fabrication, and General Characteristics</i> | 149 |
| Graham, T. R., et al.: <i>The Ternary System, Copper-manganese-zinc</i> | 675 | discussion | 833 | discussion | 867, 868 |
| Grain boundary, energies, effect of orientation difference on | 125 | Hodge, J. M., et al.: <i>The Hardenability Effect of Molybdenum</i> | 218 | Jackson, J. H., et al.: <i>Preparation and Casting of Beryllium Melts</i> | 769 |
| movement, on problem of | 708 | Hodge, J. M., et al.: <i>The Effect of Ferrite Grain Size on Notch Toughness</i> | 233 | Jackson, L. R., et al.: <i>Comparative Creep Properties of Several Types of Commercial Coppers</i> | 409 |
| Grant, N. J., and Kates, L. W.: <i>Discussion on The Cobalt-chromium Binary System</i> | 298 | Holden, A. N., and Hollomon, J. H.: <i>Homogeneous Yielding of Carburized and Nitrided Single Iron Crystals</i> | 179 | Jaffe, L. D.: <i>Discussion on the Effect of Orientation Difference on Grain Boundary Energies</i> | 861 |
| Grant, N. J., and Sherman, C. W.: <i>Evaluation of pH Measurements with Regard to the Basicity of Metallurgical Slag</i> | 898 | discussion | 879 | on Homogeneous Yielding of Carburized and Nitrided Single Crystals | 878 |
| Greenawalt sintering plant | 434 | Hollomon, J. H.: <i>Discussion on The Effect of Thermal-mechanical History on the Strain Hardening of Metals</i> | 325 | on Nucleation of Slip Bands and Transient Plastic Deformation | 319 |
| Greninger, A. B., and Trolano, A. R.: <i>The Mechanism of Martensite Formation</i> | 590 | Hollomon, J. H., et al.: <i>Kinetics of the Austenite-Martensite Transformation</i> | 691 | on Platinum-tungsten Alloys | 859 |
| Grube method, for determination of diffusion of carbon in alpha iron | 753 | Hollomon, J. H., and Holden, A. N.: <i>Homogeneous Yielding of Carburized and Nitrided Single Iron Crystals</i> | 179 | on Stabilization of the Austenite-martensite Transformation | 344 |
| Grymko, S. M., and Klier, E. P.: <i>The Transformation in 8-CuAl Alloys</i> | 611 | discussion | 879 | on the Surface Tension of Solid Copper | 895 |
| Gulbransen, E. A., and Andrew, K. F.: <i>Kinetics of the Reactions of Titanium with O₂, N₂ and H₂</i> | 741 | Holt, G. J.: <i>Discussion on Sintering Characteristics of Minus Sixty-five and Twenty Mesh Magnetite</i> | 835, 837 | Jaffe, L. D., et al.: <i>Discontinuous Crack Propagation—Further Studies</i> | 526 |
| Guettel, C. L.: <i>Discussion on An Electron Diffraction Study of Oxide Films Formed on Nickel-chromium Alloys</i> | 306 | Horsting, C. W.: <i>Discussion on Fractographic Study of Cast Molybdenum</i> | 308 | Jaffe, L. D., et al.: <i>Effect of Carbon and Nitrogen on Temper Brittleness</i> | 499 |
| Gulbransen, E. A.: <i>Discussion on Hydrogen in Aluminum</i> | 872 | Howe Memorial Lecture | 349 | Jaffe, L. D., and Buffum, D. C.: <i>Reply to discussion on Temper Brittleness of Plain Carbon Steels</i> | 880 |
| on Oxide Films Formed on Metals and Binary Alloys. An Electron Diffraction Study | 866, 867 | Hu, Hsun and Beck, P. A.: <i>Recrystallization Texture and Coarsening Texture in High Purity Aluminum</i> | 627 | Jaffee, R. I.: <i>Discussion on The Low Temperature Properties of Tin and Tin-lead Alloys</i> | 335 |
| on Platinum-tungsten Alloys | 859 | Huber, R. W., et al.: <i>Transformation of Gamma to Alpha Manganese</i> | 399 | on Oxide Films Formed on Metals and Binary Alloys, An Electron Diffraction Study | 866, 867 |
| on Preferred Orientation in Rolled and Recrystallized Beryllium | 887 | Hull, F. C.: <i>Discussion on Property Changes During Aging</i> | 337 | on the Structure of Gold-silver-copper alloys | 857, 858 |
| on Some Factors Affecting the Rate of Grain Growth in Metals | 882 | Hultgren, A.: <i>Reply to discussion on The Origin of Silicate Inclusion in Basic Electric-arc Furnace Steel of Higher Carbon Contents</i> | 834 | Reply to discussion on Platinum-tungsten Alloys | 858, 859 |
| on the Structure of Gold-silver-copper Alloys | 857 | Hultgren, R., and Lever, S. A.: <i>Use of Electrical Resistance Measurements to Determine the Solidus of the Lead-tin System</i> | 67 | Jaffee, R. I., and Campbell, I. E.: <i>Effect of Oxygen, Nitrogen, and Hydrogen on Iodide Refined Titanium</i> | 646 |
| Gulbransen, E. A., and Andrew, K. F.: <i>Kinetics of the Reactions of Zirconium with O₂, N₂ and H₂</i> | 515 | Hum, J. K. Y.: <i>Discussion of Temper Brittleness of Plain Carbon Steels</i> | 880 | Jessup, A. C., and Wilson, J. B.: <i>Discussion on The Room and Elevated Temperature Properties of Some Sand Cast Magnesium-base Alloys Containing Zinc</i> | 330 |
| Guinier, A.: <i>Discussion on Property Changes During Aging</i> | 338 | Hunter, H. B., et al.: <i>The Low Temperature Properties of Tin-antimony and Tin-cadmium Alloys</i> | 1005 | Jette, E. R.: <i>Discussion on Platinum-tungsten Alloys</i> | 859 |
| Guttman, L.: <i>Thermodynamical Treatment of Very Small Solid Solubilities</i> | 740 | Hüttig, G. F.: <i>Discussion on Seminar on the Kinetics of Sintering</i> | 808 | on the Structure of Gold-silver-copper alloys | 857, 858 |
| Gutzeit's test | 208 | Hyde, R. W., et al.: <i>Reply to discussion of Tracer Study of Sulphur in the Coke Oven</i> | 829 | on Use of Electrical Resistance Measurements to Determine the Solidus of the Lead-tin System | 860 |
| Guy, A. G.: <i>Analysis of Interstitial Diffusion Using Activity Methods</i> | 607 | Hydraulic press: use in forming retorts | 74 | Jillson, D. C.: <i>Discussion: on Effect of Composition on Grain Growth in Aluminum-magnesium Solid Solutions</i> | 309 |
| | | Hydrochloric acid cell: drawing | 583 | Johns, C. R., and Baldwin, W. M., Jr.: <i>High Temperature Sealing of Cobalt</i> | 720 |
| | | Hyman, E. D.: <i>Discussion on Development of Muffle Furnaces for the Production of Zinc Oxide and Zinc at East Chicago, Ind.</i> | 853 | Johns Hopkins University: the active slip systems in the simple axial extension of single crystalline alpha brass | 527 |
| | | | | some observations in the structure of alpha brass single crystals after cutting and polishing | 700 |
| | | | | origin of annealing twins in brass | 655 |
| | | | | Johnson, G. E.: <i>Development of Muffle Furnaces for the Production of Zinc Oxide and Zinc at East Chicago, Ind.</i> | 118 |
| | | | | discussion | 853 |
| | | | | Johnson, H. W.: <i>Discussion on Sintering Characteristics of Minus Sixty-five and Twenty Mesh Magnetite</i> | 836 |
| | | | | Johnson, W. A.: <i>Discussion on Thermal and Electrical Properties of Ductile Titanium</i> | 336 |
| | | | | Johnson, W. F.: <i>Discussion on The Use of Oxygen-enriched Air in the Metallurgical Operations of Cominco at Trail, B. C.</i> | 848 |

| Page | Page | Page |
|--|---------------|------|
| Jordan, C. B., and Duwez, P.: <i>Densification of Copper Powder Compacts in Hydrogen and in Vacuum</i> | 96 | |
| K | | |
| Kalin, S. H., et al.: <i>Recrystallization and Microstructure of Aluminum Killed Deep Drawing Steel</i> | 242 | |
| Kates, L. W., and Grant, N. J.: <i>Discussion on The Cobalt-chromium Binary System</i> | 298 | |
| Ké, T. S., and Zener, C.: <i>Discussion on Statistical Rate Theory of Metals—1. Mechanism of Flow and Application to Tensile Properties</i> | 316 | |
| Kemp, J. T.: <i>Discussion on The Densification of Copper Powder Compacts in Hydrogen and in Vacuum</i> | 893 | |
| on Influence of Composition on the Stress-corrosion Cracking of Some Copper-base Alloys..... | 864 | |
| Kennametal, Inc.: <i>cemented titanium carbide</i> | 987 | |
| Kennecott Copper Corp..... | 543 | |
| Kenworthy, H., et al.: <i>Titanium Investigations: Research and Development Work on the Preparation of Titanium Chloride and Oxide from Titanium Mattes</i> | 785 | |
| Kiessling, R.: <i>Discussion on Properties of Chromium Boride and Sintered Chromium Boride</i> | 890 | |
| Kinetics: of Austenite-Martensite Transformation..... | 691 | |
| of reactions of titanium with O ₂ , N ₂ and H ₂ | 741 | |
| of sintering..... | 796 | |
| Kink bands, in zinc..... | 589 | |
| conditions for kink formation..... | 600 | |
| boundaries..... | 601 | |
| dislocation theory of..... | 603 | |
| reorientation..... | 600 | |
| Klier, E. P., and Grymko, S. M.: <i>Transformations in β-CuAl Alloys</i> | 611 | |
| Klingler, L. J., et al.: <i>Flow and Fracture Characteristics of a Die Steel at High Hardness Levels</i> | 927 | |
| Knickerbocker, R. G., et al.: <i>Titanium Investigations: Research and Development Work on the Preparation of Titanium Chloride and Oxide from Titanium Mattes</i> | 785 | |
| Knolls Atomic Power Lab.: <i>some observations on the rate of secondary recrystallization in high purity copper</i> | 663 | |
| Kodak type K X-ray film: <i>use in Lane photographs</i> | 422 | |
| Kronberg, M. L., and Wilson, F. H.: <i>Secondary Recrystallization in Copper</i> | 501 | |
| Kroog filter press..... | 208 | |
| Kroll, W. J.: <i>Discussion on Properties of Chromium Boride and Sintered Chromium Boride</i> | 890 | |
| on Solubility Relationships of the Refractory Monocarbides..... | 891 | |
| Kuczynski, G. O.: <i>Discussion on the Kinetics of Sintering</i> | 811, 812, 813 | |
| on The Surface Tension of Solid Copper..... | 895 | |
| Self-diffusion in Sintering of Metallic Particles..... | 169 | |
| discussion..... | 897 | |
| Kuczynski, G., and Alexander, B. H.: <i>Discussion on The Surface Tension of Copper</i> | 804 | |
| Kura, J. G., et al.: <i>Preparation and Casting of Beryllium Melts</i> | 769 | |
| Kutzell, C. R.: <i>Discussion on Development of the Modern Zinc Retort in the United States</i> | 852 | |
| on El Paso Slag Treatment Plant..... | 854 | |
| L | | |
| Labbe, A. L.: <i>patent entitled "Method and Apparatus for Sintering"</i> | 263 | |
| Lachance, M.: <i>Discussion on Decarburization of Chrome Nickel Alloys by Their Surface Oxides in High Vacua and at Elevated Temperatures</i> | 308 | |
| Lacombe, P., et al.: <i>Discussion: on Some Effects of Applied Stresses on Precipitation Phenomena</i> | 302 | |
| Lamont, J. L., et al.: <i>Carbides in Isothermally Transformed Chromium Steels</i> | 957 | |
| Larsen, B. M.: <i>Discussion on The Origin of Silicate Inclusions in Basic Electric Furnace Steel of Higher Carbon Contents</i> | 834 | |
| Discussion on Relation between Chromium and Carbon in Chromium Steel Refining..... | 832, 833 | |
| on Sulphur Equilibria between Iron Blast Furnace Slags and Metal..... | 832 | |
| Reply to Discussion on The Role of Thermochemical Factors in Basic Open Hearth Production Rate..... | 840 | |
| Reply to discussion on Some Correlations between Variables Affecting Sulphur in Blast Furnace Iron..... | 830 | |
| Lead smelting: <i>cadmium recovery practice in Lead-tin system: solidus and liquidus</i> | 71 | |
| Lee, A. E.: <i>Discussion on Controlled Drying of Retorts</i> | 852 | |
| on El Paso Slag Treatment Plant..... | 854 | |
| Lee, A. E., Jr., and Page, H. R.: <i>Development of the Modern Zinc Retort in the United States</i> | 738 | |
| correction..... | 296 | |
| discussion..... | 850, 851, 852 | |
| Lee, H. E., and Feddersen, P. C.: <i>Cadmium Recovery Practice in Lead Smelting</i> | 110 | |
| Leeds and Northrup: <i>potentiometer</i> | 756 | |
| pyrometer..... | 905 | |
| recording microphotometer..... | 374 | |
| thermocouple selector switch..... | 756 | |
| Leiter, R.: <i>Discussion on Magnesium-lithium Base Alloys—Preparation, Fabrication, and General Characteristics</i> | 867 | |
| Lement, B. S.: <i>Discussion on Stabilization of the Austenite-Martensite Transformation</i> | 844 | |
| Leontis, T. E.: <i>The Properties of Sand Cast Magnesium-Rare Earth Alloys</i> | 968 | |
| Lever, S. A., and Hultgren, R.: <i>Use of Electrical Resistance Measurements to Determine the Solidus of the Lead-tin System</i> | 67 | |
| Lillieqvist, G. A.: <i>Discussion on The Effect of Hydrogen on the Ductility of Cast Steels</i> | 833 | |
| Linde Air Products Co..... | 91 | |
| Lionetti, F., and Dunn, D. G.: <i>Effect of Orientation Difference on Grain Boundary Energies</i> | 125 | |
| discussion..... | 861 | |
| Liquid iron oxide slags..... | 193 | |
| Liu, You-chao, et al.: <i>Annealing Twins in Copper and 70-30 Brass</i> | 635 | |
| Lloyd, T. E.: <i>Discussion on Concentration of the SO₂ Content of Dwight-Lloyd Sintering Machine Gas by Recirculation</i> | 849 | |
| on Sintering Characteristics of Minus Statfive and Twenty Mesh Magnetite..... | 836 | |
| Long, C. C.: <i>Discussion on Electrolytic Zinc at Risdon, Tasmania. Major Changes Since 1936</i> | 843 | |
| on Recovery of Cadmium from Cadmium-copper Precipitate, Electrolytic Zinc Co. of Australasia, Risdon, Tasmania | 846 | |
| on Use of Oxygen-enriched Air in the Metallurgical Operations of Cominco at Trail, B. C..... | 848 | |
| Long, J. R., et al.: <i>The Ternary System, Copper-manganese-zinc</i> | 615 | |
| Loonam, A. C.: <i>Discussion on The Morenci Smelter of Phelps Dodge Corp. at Morenci, Ariz.</i> | 855 | |
| Loonam, A. C., et al.: <i>Magnesium-lithium Base Alloys—Preparation, Fabrication, and General Characteristics</i> | 149 | |
| discussion..... | 867 | |
| Lorig, C. H., et al.: <i>Magnesium-lithium Base Alloys—Preparation, Fabrication, and General Characteristics</i> | 149 | |
| Low, J. R., Jr.: <i>Discussion on Low Temperature Properties of Tin and Tin-lead Alloys</i> | 335 | |
| Low, J. R., Jr., and Schwartzbart, H.: <i>Yielding and Strain-aging of Carbureted and Nitrided Single Crystals of Iron</i> | 637 | |
| Lubahn, J. D.: <i>Simultaneous Aging and Deformation in Metals</i> | 702 | |
| Luerssen, G. V., and Post, C. B.: <i>Interaction of Liquid Steel with Ladle Refractories</i> | 15 | |
| Lukens, H. C., et al.: <i>Transformation of Gamma to Alpha Manganese</i> | 399 | |
| M | | |
| MacIntyre Development, National Lead Co..... | 435 | |
| MacIntyre ilmenite..... | 913 | |
| Mackenzie, J. T., Jr., et al.: <i>Recrystallization and Microstructure of Aluminum Killed Deep Drawing Steel</i> | 242 | |
| Maddigan, S. E.: <i>Discussion on Oxide Films Formed on Metals and Binary Alloys. An Electron Diffraction Study</i> | 866 | |
| on Some Factors Affecting the Rate of Grain Growth in Metals..... | 881 | |
| on A Study of Textures and Baring Behavior of Cold-rolled (87-89 pct) and Annealed Copper Strips..... | 887 | |
| Maddin, R., and Hibbard, W. R., Jr.: <i>Some Observations in the Structure of Alpha Brass Single Crystals after Cutting and Polishing</i> | 700 | |
| Maddin, R., et al.: <i>Origin of Annealing Twins in Brass</i> | 655 | |
| The Active Slip Systems in the Simple Axial Extension of Simple Crystalline Alpha Brass..... | 527 | |
| Magnafux Corp..... | 717 | |
| Magnesium-lithium base alloys: <i>corrosion resistance</i> | 163 | |
| melting techniques..... | 150 | |
| metallography..... | 164 | |
| preparation, fabrication, characteristics..... | 149 | |
| work-hardening capacity..... | 158 | |
| Maltz, J.: <i>Discussion on Temper Brittleness of Plain Carbon Steels</i> | 881 | |
| Mann, H. C., et al.: <i>Discontinuous Crack Propagation</i> | 526 | |
| Discontinuous Crack Propagation—Further Studies..... | 683 | |
| Martensite, formation of..... | 590 | |
| lattice relationships and habits..... | 590 | |
| shear..... | 592, 594 | |
| stereographic analysis of..... | 596 | |
| Maddin, R., and Hibbard, W. R., Jr.: <i>Some Observations in the Structure of Alpha Brass Single Crystals after Cutting and Polishing</i> | 700 | |
| Discussion on Nucleation of Slip Bands and Transient Plastic Deformation..... | 318 | |
| Magnus, P.: <i>Discussion: on A Copper-base Alloy Containing Iron as a High-strength High-conductivity Wire Material</i> | 840 | |
| on A High Strength-High Conductivity Copper-silver Alloy Wire..... | 840 | |
| Magnesium alloys: <i>manganese segregation in AM65S</i> | 405 | |
| solubility of manganese..... | 406 | |
| effects of manganese on tensile properties and resistance to corrosion..... | 407 | |
| Manganese, gamma: <i>transition</i> | 400 | |
| Manganese silicon: <i>effect of balance on cleanliness of steel</i> | 17 | |
| effect of ratio on silica content of slag patches on ingot surfaces..... | 21 | |
| Manly, W. D., and Beck, P. A.: <i>Sigma Phase in Ternary Cr-Co-Fe and Cr-Co-Ni Alloys</i> | 354 | |
| Manning, R. D., et al.: <i>Effect of Ferrite Grain Size on Notch Toughness</i> | 233 | |
| Metallographic Examination of Beryllium Alloys..... | 779 | |
| Martens, H., and Duwez, P.: <i>A Dilatometric Study of the Sintering of Metal Powder Compacts</i> | 571 | |
| Martensite, embryos..... | 893 | |
| free energy change accompanying transformation in steels..... | 688 | |
| transformation curves..... | 696 | |
| influence of austenite upon..... | 698 | |
| Martin, W. W., and Dunn, C. G.: <i>Rapid Determination of Orientations of Cubic Crystals</i> | 417 | |
| Martinson, M. W.: <i>Discussion on The Room and Elevated Temperature Properties of Some Sand Cast Magnesium-base Alloys Containing Zinc</i> | 329 | |
| Massachusetts Inst. of Technology: <i>beryllium-iron system</i> | 285 | |
| determination of boundary stresses during the compression of cylindrical powder compacts..... | 561 | |
| effect of quenching on the age hardening of two aluminum alloys..... | 544 | |
| equilibrium in the reaction of hydrogen with oxygen in liquid iron..... | 441 | |
| evaluation of pH measurements with regard to the basicity of metallurgical slag..... | 898 | |
| isolation of carbides from high speed steel..... | 578 | |
| on the structure of gold-silver-copper alloys..... | 46 | |
| optical temperature scale and emissivity of liquid iron..... | 885 | |
| recovery and recrystallization in brass..... | 491 | |
| seminar on the kinetics of sintering..... | 796 | |
| solubility relationships of the refractory monocarbides..... | 133 | |
| structure of diborides of titanium, zirconium, columbium, tantalum and vanadium..... | 749 | |
| sulphur equilibria between iron blast furnace slags and metal..... | 274 | |
| surface tension of solid copper..... | 186 | |
| what is metallurgy?..... | 349 | |
| Mathewson, C. H., et al.: <i>Origin of Annealing Twins in Brass</i> | 655 | |
| Active Slip Systems in the Simple Axial Extension of Single Crystalline Alpha Brass..... | 527 | |
| McAdam, D. J., Jr.: <i>Influence of Temperature on the Stress-strain-energy Relationship for Copper and Nickel-copper Alloy</i> | 727 | |
| Discussion on Effect of Thermal-mechanical History on the Strain Hardening of Metals..... | 326 | |
| McDaniel, L. L.: <i>The Morenci Smelter of Phelps Dodge Corp. at Morenci, Ariz.</i> | 1 | |
| discussion..... | 855 | |
| McDonald, J. C.: <i>Discussion on Factors Affecting the Tensile Notch Sensitivity of Magnesium Alloy Extrusions</i> | 338 | |
| McLeod gauge..... | 554, 742 | |
| McMeans, G.: <i>Discussion on Tracer Study of Sulphur in the Coke Oven</i> | 825 | |
| McMullin, J. G., and Norton, S. T.: <i>On the Structure of Gold-silver-copper Alloys</i> | 46 | |
| discussion..... | 858 | |
| McNaughton, R. R.: <i>Discussion on Concentration of the SO₂ Content of Dwight-Lloyd Sintering Machine Gas by Recirculation</i> | 848 | |
| McNaughton, R. R., et al.: <i>Use of Oxygen Enriched Air in the Metallurgical Operations of Cominco at Trail, B. C.</i> | 446 | |
| discussion..... | 848 | |
| McReynolds, A. W.: <i>Plastic Deformation Waves in Aluminum</i> | 82 | |
| discussion..... | 277 | |

| | Page | | Page | | Page |
|---|---------------|--|----------|---|--------------------|
| Mead, J. C., and Stanley, A.: Sintering Characteristics of Minus Slats-five and Twenty Mesh Magnetite..... | 435 | National Research Corporation..... | 499, 500 | Phelps Dodge Corp.: the Morenci smelter of Phelps Dodge Corp. at Morenci, Ariz. | 1 |
| discussion..... | 835, 836, 837 | Neale, M. M.: Discussion on Cadmium Recovery Practice at the Donora Zinc Works | 843, 844 | Phosphorus, effect on electrical conductivity and softening temperature of copper on temper embrittlement..... | 370, 535, 539 |
| Mehl, R. F.: Discussion on Plastic Deformation of Large Grained Copper Specimens | 323 | on Controlled Drying of Retorts..... | 852 | in 5140 steel..... | 541 |
| on Plastic Flow in Anisotropic Sheet Steel | 324 | Nehrenberg, A. B.: Discussion on the Effect of Chromium on the Ms Point..... | 341 | in molybdenum-chromium steels with hardenability similar to 5140 steel..... | 541 |
| Mehl, R. F., and Ransom, J. T.: Statistical Nature of the Endurance Limit..... | 364 | New York University: the transverse bending of single crystals of aluminum.... | 710 | Photovoltaic cells, preparation from silicon ingots | 385 |
| Meier, J. W.: Discussion on The Room and Elevated Temperature Properties of Some Sand Cast Magnesium-base Alloys Containing Zinc..... | 328 | a proposed microbending mechanism of plastic deformation | 1003 | Pickens-Waiter diffraction unit..... | 874 |
| Melara, P.: Discussion on Property Changes During Aging | 337 | Nielson, H. P.: Reply to discussion on Platinum-tungsten Alloys | 859 | Pidgeon, L. M., and Aust, K. T.: Solubility of Titanium in Liquid Magnesium... | 585 |
| Metallurgical slag, evaluation of pH measurements with regard to basicity..... | 898 | Nielsen, J. P.: Discussion on Effect of a Dispersed Phase on Grain Growth in Al-Mn Alloys | 314 | Pietrowsky, P., et al.: Some Observations on the Recovery of Cold Worked Aluminum | 948 |
| analysis in terms of excess CaO..... | 901 | Nelson, B. J., and Sager, G. F.: Liquid Solubility of Manganese in a Magnesium-aluminum-iron Alloy | 405 | Pilling and Bedworth parabolic law..... | 720 |
| Metal powders: pressure distribution in compacting of | 137 | Norblack (lampblack) | 771 | Pirani gauge | 58 |
| Metals, aging and deformation in..... | 702 | Norro, A.: Discussion on the Morenci Smelter of Phelps Dodge Corp. at Morenci, Ariz. | 855 | Plastic Deformation, Proposed Microbending Mechanism | 1003 |
| Metals Disintegrating Co..... | 797 | North Carolina State College: analysis of interstitial diffusion using activity methods | 607 | Poisson's ratio | 724 |
| Micomax controller-recorder | 756 | Norton, J. T.: Discussion on The Magnetic Properties of Sintered Iron and Iron Base Alloys..... | 892 | Poland, F. F.: Distillation of Zinc from Copper Base Alloys and Galvanizers Drosses | 355 |
| Milek, J. T.: Discussion on Diffusion of Carbon in Austenite with a Discontinuity in Composition..... | 304 | on Preferred Orientation in Rolled and Recrystallized Beryllium | 886 | discussion | 856 |
| on An Electron Diffraction Study of Oxide Films Formed on Nickel-chromium Alloys | 306 | Norton, J. T., and Mowry, A. L.: Solubility Relationships of the Refractory Monocarbides | 133 | Porter, G. V.: Discussion on An Electron Diffraction Study of Oxide Films Formed on Copper-nickel Alloys at Elevated Temperatures | 307 |
| on An Electron Diffraction Study of Oxide Films Formed on Copper-nickel Alloys at Elevated Temperatures..... | 307 | discuss ion | 891 | Post, C. B., and Luerssen, G. V.: Interaction of Liquid Steel with Ladle Refractories | 15 |
| on Thermal and Electrical Properties of Ductile Titanium | 336 | Norton, J. T., et al.: Structure of Diborides of Titanium, Zirconium, Columbium, Tantalum and Vanadium | 749 | Post, C. B.: Discussion on The Ionic Nature of Metallurgical Slags, Simple Oxide Systems | 841 |
| Minto, R. E., and Emerick, H. B.: Discussion on The Influence of Temperature on the Affinity of Sulphur for Copper, Manganese and Iron..... | 838 | Norton, J. T., and McMullin, J. G.: On the Structure of Gold-silver-copper Alloys | 46 | Potter, E. R.: Discussion on Use of Electrical Resistance Measurements to Determine the Solidus of the Lead-tin System | 860 |
| Missouri School of Mines and Metallurgy: ferromagnetic alloys in the systems Cu-Mn-In and Cu-Mn-Ga..... | 495 | discuss ion | 858 | Potter, E. V., et al.: Transformation of Gamma to Alpha Manganese..... | 399 |
| Merrick Feedweight | 473 | Norton Co.: Pure-oxide..... | 452 | Promethues | 350 |
| Molybdenum, influence on temper brittleness | 369, 536, 574 | Nucleation theory | 691 | Purdue University: the study of grain boundaries with the electron microscope | 395 |
| thermal expansion curves..... | 574 | of coherent phases..... | 692 | Pyrometer, for optical top temperature reading | 606 |
| Monel metal, influence of temperature and plastic strain on flow stress of..... | 727 | O | | Q | |
| influence of temperature on stress-strain energy relationship for copper and nickel-copper alloy | 727 | Oak Ridge National Lab.: sigma phase in ternary Cr-Co-Fe and Cr-Co-Ni alloys | 354 | Quenching, of high-purity, precipitation-hardenable alloys | 668 |
| stages in deformation of, shown by polarized light | 722 | Old, B. S., et al.: Reply to discussion of Tracer Study of Sulphur in the Coke Oven | 829 | R | |
| differences in orientation..... | 723 | Olsen, R. P.: The Relationship Between Electrical Conductivity and Composition of Molten Lead Silicate Slags..... | 981 | Rabble teeth, improvement in design and arrangement | 46 |
| Monocarbides, solubility of..... | 133 | Optical temperature scale and emissivity of liquid iron | 665 | Radavich, J. F.: Study of Grain Boundaries with the Electron Microscope..... | 395 |
| Morgan, K.: Discussion on Development of the Modern Zinc Retort in the United States | 851, 852 | Orowan, E.: Discussion on Homogeneous Yielding of Carbureted and Nitrided Single Iron Crystals..... | 878 | Radabaugh, R. A.: Discussion on Property Changes During Aging | 338 |
| on Development of Muffle Furnaces for the Production of Zinc Oxide and Zinc at East Chicago, Ind..... | 853 | on Lead-grid Study of Metal Powder Compaction | 888 | Ransley, C. E., and Mountford, N. D. G.: Discussion on Hydrogen in Aluminum | 870 |
| on the Recovery of Cadmium from Cadmium-copper Precipitate, Electrolytic Zinc Co. of Australasia, Risdon, Tasmania | 845, 846 | on Plastic Deformation Waves in Aluminum | 876 | Ransom, J. T., and Mehl, R. F.: Statistical Nature of the Endurance Limit..... | 364 |
| Moore, C. H., and Sigurdson, H.: Petrology of High Titanium Slags..... | 914 | on Seminar on the Kinetics of Sintering | 811 | Ravitz, S. F., and Back, A. E.: Recovery of Zinc by the Dilithionate Sulphur-dioxide Leaching Process..... | 792 |
| Morrill, F. R.: Discussion on An Electron Diffraction Study of Oxide Films Formed on Nickel-chromium Alloys | 305 | on The Surface Tension of Solid Copper | 895 | Ray-O-Tube | 91 |
| on Fractographic Study of Cast Molybdenum | 308 | Temper Brittleness of Plain Carbon Steels | 880 | Rectifier, point contact, modern version of "crystal detector" | 383 |
| Mountford, N. D. G., and Ransley, C. E.: Discussion on Hydrogen in Aluminum | 870 | Orthoink | 570 | Redler elevator | 473 |
| Moyer, R. C., and Smith, G. T.: Cadmium Recovery Practice at the Donora Zinc Works | 360 | Orthomol | 570 | Redmond, J. O., et al.: Cemented Titanium Carbide | 987 |
| Mowry, A. L.: Solubility Relationships of the Refractory Monocarbides..... | 133 | P | | Reed, E. L., et al.: Discontinuous Crack Propagation | 526 |
| Mudge, W. A.: Discussion: on Property Changes during Aging..... | 337 | Pachuca discharge, classification and thickening | 213 | Discontinuous Crack Properties—Further Studies | 683 |
| N | | Page, H. R., and Lee, E. Jr.: Development of the Modern Zinc Retort in the United States..... | 73 | Reeder, D.: Discussion on Relation between Chromium and Carbon in Chromium Steel Refining | 833 |
| Nachtrieb, N. H., et al.: Influence of Temperature on the Affinity of Sulphur for Copper, Manganese and Iron..... | 27 | correction | 296 | Reichhold, H. M., et al.: Effect of Ferrite Grain Size on Notch Toughness..... | 233 |
| discussion..... | 839 | Palmer, E. W.: Discussion: on Effect of Grain Size on Tensile Strength, Elongation, and Endurance Limit of Deep Drawing Brass..... | 339 | Reid, W. S.: Concentration of the SO ₂ Content of Dwight-Lloyd Sintering Machine Gas by Rectriculation..... | 261 |
| National Aeronautical Research Institute, Amsterdam, Holland: the relation between indentation hardness and strain for metals..... | 904 | on A High Strength-High Conductivity Copper-silver Alloy Wire | 341 | discussion | 849 |
| National Bureau of Standards: influence of temperature on the stress-strain-energy relationship for copper and nickel-copper alloy | 727 | Palmer, E. W., and Wilson, F. H.: Intergranular Parting of Brass during Anneals | 995 | Reinartz, L.: Discussion on The Role of Thermochemical Factors in Basic Open Hearth Production Rate..... | 839 |
| stages in the deformation of Monel metal as shown by polarized light..... | 722 | Palm, J. H.: Relation Between Indentation Hardness and Strain for Metals..... | 904 | Reiter, S. F., et al.: Annealing Twins in Copper and 70-30 Alpha Brass..... | 635 |
| National Advisory Committee for Aeronautics: the yielding and strain-aging of carburized and nitrided single crystals of iron..... | 637 | Paranjpe, V. G.: Discussion on Diffusion of Carbon in Austenite with a Discontinuity in Composition..... | 304 | Remington Arms Co.: lattice parameters of high purity alpha titanium; and the effects of oxygen and nitrogen on them | 588 |
| National Lead Co.: sintering characteristics of minus sixty-five and twenty mesh magnetite | 435 | on Some Effects of Applied Stresses on Precipitation Phenomena | 301 | size effects in quenching high-purity, precipitation-hardenable alloys | 668 |
| laboratory smelting of titaniferous ore.. | 909 | Pardee, R.: Discussion on The Interaction of Liquid Steel with Ladle Refractories | 840 | Republic Steel Corp..... | 445, 827 |
| melting points in the system TiO ₂ -CaO-MgO-Al ₂ O ₃ | 905 | Parker, E.: Discussion on Preferred Orientation in Rolled and Recrystallized Beryllium | 887 | Retorts | 73 |
| petrology of high titanium slags..... | 914 | Pearlite, possibility of arresting cleavage. "Peeling," experiments to avoid, in high speed steel | 489 | silica | 75 |
| National Military Establishment: effect of carbon and nitrogen on temper brittleness | 499 | Pennington, decarburization experiments..... | 580 | performance | 76 |
| discontinuous crack propagation..... | 526 | Pennsylvania State College: transformations in 9-CuAl alloys..... | 754 | silicon carbide | 74 |
| | | yielding and strain-aging of carburized and nitrided single crystals of iron..... | 611 | Reverberatory furnace | 4 |
| | | Pessel, L.: Discussion on A Copper-base Alloy Containing Iron as a High-strength High-conductivity Wire Material | 637 | Revere Copper and Brass Inc.: distillation of zinc from copper base alloys and galvanizers drosses | 355 |
| | | Pfann, W. G., and Scaff, J. H.: Microstructures of Silicon Ingots..... | 340, 389 | Rhines, F. N.: Discussion on Densification of Copper Powder Compacts in Hydrogen and in Vacuum..... | 893 |
| | | | | on hydrogen in aluminum..... | 872 |
| | | | | on Magnetic Properties of Sintered Iron and Iron Base Alloys..... | 892 |
| | | | | on Seminars on the Kinetics of Sintering | 806, 809, 810, 811 |

| | Page | | Page | | Page |
|--|--------------------|---|----------|---|----------|
| Rhodin, T. N., Jr.: Oriented Arrangements of Thin Aluminum Films on Ionic Substrates..... | 371 | Seabrook, J. B.: Binary Chart for Interconversions of Mol. Weight, and Volume Percent..... | 993 | Smith, E. N., et al.: Cemented Titanium Carbide..... | 987 |
| Richardson, A. C.: Discussion on Sintering Characteristics of Minus Sixty-five and Twenty Mesh Magnetite..... | 835, 837 | Shaler, A. J.: Seminar on the Kinetics of Sintering..... | 796, 813 | Smith, G. T., and Moyer, R. C.: Cadmium Recovery Practice at the Donora Zinc Works..... | 360 |
| Rickett, R. L., et al.: Recrystallization and Microstructure of Aluminum Killed Deep Drawing Steel..... | 242 | On Effect of Orientation Difference on Grain Boundary Energies..... | 861 | Smith, K. F., et al.: Comparative Creep Properties of Several Types of Commercial Coppers..... | 409 |
| Riddell, G. C.: development of double roasting..... | 347 | on Lead-grid Study of Metal Powder Compaction..... | 889 | Smoluchowski, R.: Discussion on Diffusion of Carbon in Austenite with Discontinuity in Composition..... | 304 |
| Riddle, L. E.: Discussion on Some Correlations between Variables Affecting Sulphur in Blast Furnace Iron..... | 830 | on Pressure Distribution in Compacting Metal Powders..... | 888 | Spence, N. S.: Discussion on The Room and Elevated Temperature Properties of Some Sand Cast Magnesium-base Alloys Containing Zinc..... | 329 |
| Ripling, E. J.: Discussion on The Effect of Thermal-mechanical History on the Strain Hardening of Metals..... | 326 | Shaler, A. J., and Udin, H.: Discussion on Self-diffusion in Sintering of Metallic Particles..... | 896 | Spendlove, M. J., and St. Clair, H. W.: Low Pressure Distillation of Zinc from Al-Zn Alloy..... | 553 |
| Ripling, E. J., and Sachs, G.: Effect of Strain-temperature History on the Flow and Fracture Characteristics of an Annealed Steel..... | 78 | Shaler, A. J., et al.: Surface Tension of Solid Copper..... | 186, 896 | Sperry, P. R., and Beck, P. A.: Effect of Recrystallization Texture on Grain Growth..... | 240 |
| Risdon Works of Electrolytic Zinc Co. of Australasia, Ltd.: electrolytic zinc at Risdon, Tasmania, major changes since 1936..... | 211 | Shank, M. E., and Wulff, J.: Determination of Boundary Stresses during the Compression of Cylindrical Powder Compacts..... | 561 | Sperry, P. R., et al.: Grain Coarsening in Copper..... | 203 |
| Roberson, A. H., et al.: Ternary System, Copper-manganese-zinc..... | 675 | Sheehan, J. P., et al.: Effects of Molybdenum and Commercial Ranges of Phosphorus upon the Toughness of 0.40 Pct Carbon Chromium Steels..... | 535 | Squire, A.: Discussion on Lead-grid Study of Metal Powder Compaction..... | 888 |
| Roe, L. A.: Discussion on Sintering Characteristics of Minus Sixty-five and Twenty Mesh Magnetite..... | 837 | Sherman, C. W., and Grant, N. J.: Evaluation of pH Measurements with Regard to the Basicity of Metallurgical Slag Shriver press..... | 115 | on Oxide Films Formed on Metals and Binary Alloys. An Electron Diffraction Study..... | 866, 867 |
| Rogers, D. T.: Discussion on The Influence of Temperature on the Affinity of Sulphur for Copper, Manganese and Iron..... | 837 | Shuttleworth, R. L.: Discussion on Seminar on the Kinetics of Sintering..... | 807 | on Properties of Chromium Boride and Sintered Chromium Boride..... | 890 |
| Rolle, S.: Discussion on Distillation of Zinc from Copper Base Alloys and Galvanizers Drosses..... | 855 | Sigurdson, H., and Cole, S. S.: Melting Points in the System TiO ₂ -CaO-MgO-Al ₂ O ₃ | 905 | Stanford Univ.: the relationship between electrical conductivity and composition of molten lead silicate slags..... | 984 |
| Rose, E. H.: Discussion on Sintering Characteristics of Minus Sixty-five and Twenty Mesh Magnetite..... | 834, 835, 836, 837 | Sigurdson, H., and Moore, Charles H.: Petrology of High Titanium Slags..... | 914 | Stanley, A., and Mead, J. C.: Sintering Characteristics of Minus Sixty-five and Twenty Mesh Magnetite..... | 435 |
| Rosenqvist, T. A.: A Thermodynamic Investigation of the System Silver-sulphide..... | 451 | Silicon, effect of boron on resistivity and rectification characteristics..... | 385, 386 | Stanley, J. K.: Diffusion and Solubility of Carbon in Alpha Iron..... | 752 |
| Discussion on Sulphur Equilibria between Iron Blast Furnace Slags and Metals..... | 831 | effect of boron and phosphorus..... | 386 | Starlipper, A. G., et al.: Titanium Investigations: Research and Development Work on the Preparation of Titanium Chloride and Oxide from Titanium Mattes..... | 785 |
| Ross, S. W.: Electrolytic Zinc at Risdon, Tasmania. Major Changes Since 1936..... | 211 | dependence of uniformity of resistivity on boron-phosphorus ratio..... | 387, 391 | Steel, temperature history on flow and fracture characteristics..... | 78 |
| discussion..... | 843 | Silicon iron, grain boundary movements in..... | 708 | electrolytic isolation of carbides in..... | 919 |
| Rostoker, W.: Reply to discussion on The Magnetic Properties of Sintered Iron and Iron Base Alloys..... | 892 | Silver, effect on creep properties of copper..... | 411 | relative deoxidizing powers of some deoxidizers..... | 814 |
| Royal Institute of Technology, Stockholm, Sweden: notes on the electrolytic isolation of carbides in steel..... | 919 | Silver-zinc, diagram according to Andrews, Davies, Hume-Rothery and Oswin..... | 431 | martensite transformation in..... | 688 |
| S | | Sims, C. E.: Discussion on The Influence of Temperature on the Affinity of Sulphur for Copper, Manganese and Iron on Relation between Chromium and Carbon in Chromium Steel Refining..... | 838 | Stephan, H. R.: Discussion on Platinum-tungsten Alloys..... | 859 |
| Sachs, G., et al.: Stress and Strain States in Elliptical Bulges..... | 49 | Reply to discussion on The Effect of Hydrogen on the Ductility of Cast Steels..... | 833 | Stevens, J.: Discussion on the Interaction of Liquid Steel with Ladle Refractories..... | 840 |
| Sachs, G., et al.: Flow and Fracture Characteristics of a Die Steel at High Hardness Levels..... | 927 | Sims, C. E., et al.: Relative Deoxidizing Powers of Some Deoxidizers for Steel..... | 814, 825 | Stokes briquetting machine..... | 116 |
| Sachs, G., and Ripling, E. J.: Effect of Strain-temperature History on the Flow and Fracture Characteristics of an Annealed Steel..... | 78 | discussion..... | 814, 825 | Strain gauges, measurement of pressure distribution on wall of a die..... | 137 |
| Sackett, B. L.: Discussion on The Effect of High Copper Content on the Operation of a Lead Blast Furnace, and Treatment of the Copper and Lead Produced..... | 847 | Sindecand, S. J.: Properties of Chromium Boride and Sintered Chromium Boride..... | 198, 890 | Stone, F. G., et al.: The Low Temperature Properties of Tin-antimony and Tin-cadmium Alloys..... | 1005 |
| Sager, G. F., and Nelson, E. J.: Liquid Solubility of Manganese in a Magnesium-aluminum-Hin Alloy..... | 405 | discussion..... | 198, 890 | Storm, R. G., et al.: Hardenability Effect of Molybdenum..... | 218 |
| St. Clair, H. W., and Spendlove, M. J.: Low Pressure Distillation of Zinc from Al-Zn Alloy..... | 553 | on The Magnetic Properties of Sintered Iron and Iron Base Alloys..... | 858, 859 | Stresscoat..... | 717 |
| St. Venant's relation..... | 54, 58 | Sindecand, S. J., et al.: Structure of Dihydrides of Titanium, Zirconium, Tantalum and Vanadium..... | 891 | Sully, A. H.: Discussion on Nucleation of Slip Bands and Transient Plastic Deformation..... | 321 |
| Saller, H. A., et al.: Relative Deoxidizing Powers of Some Deoxidizers for Steel..... | 814 | Sinter machine, down-draft, development by Dwight and Lloyd..... | 749 | Sully, A. H.: Discussion on The Cobalt-chromium Binary System..... | 298 |
| Saunders, J.: Discussion on Some Correlations between Variables Affecting Sulphur in Blast Furnace Iron..... | 830 | Sintering, seminar on kinetics..... | 796 | Suspension roasting..... | 446 |
| Sayre, M. F.: Discussion on Plastic Flow in Anisotropic Sheet Steel..... | 324 | recrystallization..... | 797 | Sway, E. F., and Busch, L. S.: Discussion on Seminar on the Kinetics of Sintering..... | 805 |
| Scaff, J. H.: Discussion on An Electron Diffraction Study of Oxide Films Formed on Nickel-chromium Alloys..... | 306 | surface diffusion and evaporation..... | 797, 798 | Sweeny, W. O.: Discussion on The Cobalt-chromium Binary System..... | 299 |
| Scaff, J. H., and Pfann, W. G.: Microstructures of Silicon Ingots..... | 389 | first phase..... | 798 | Sylvania Electric Products Inc.: self-diffusion in sintering of metallic particles..... | 169 |
| Scaff, J. H., et al.: P-type and N-type Silicon and the Formation of the Photovoltaic Barrier in Silicon Ingots..... | 383 | second phase..... | 798, 801 | a method of examination of sections of fine metal powder particles with the electron microscope..... | 228 |
| Schellinger, A. K., et al.: The Relationship Between Electrical Conductivity and Composition of Molten Lead Silicate Slags..... | 984 | Sivil, C. S.: Discussion on Platinum-tungsten Alloys..... | 858 | T | |
| Schlechtern, A. W.: Discussion on Cadmium Recovery Practice at the Donora Zinc Works..... | 844 | Skapski, D. S., et al.: Influence of Temperature on the Affinity of Sulphur for Copper, Manganese, and Iron..... | 27 | Tantalum, structure of diborides..... | 749 |
| Schumacher, E. E., et al.: P-type and N-type Silicon and the Formation of the Photovoltaic Barrier in Silicon Ingots..... | 383 | Skinner, E. N.: Discussion on Decarburization of Chrome Nickel Alloys by Their Surface Oxides in High Vacua and at Elevated Temperatures..... | 307 | Teitel, R. J., and Cohen, Morris: The Beryllium-iron System..... | 284 |
| Schwartzbart, H., and Low, J. R., Jr.: Yielding and Strain-aging of Carbureted and Nitrided Single Crystals of Iron..... | 697 | Slag-metal (see Metallurgical slag)..... | 898 | Temper brittleness, definition..... | 366 |
| Schwöpe, A. D., et al.: Comparative Creep Properties of Several Types of Commercial Coppers..... | 409 | Slags, evaluation of pH of..... | 898 | Tenenbaum, M.: Discussion on the Influence of Temperature on the Affinity of Sulphur for Copper, Manganese and Iron..... | 839 |
| Scmet Engineering Co..... | 727 | powder, particle size of..... | 898 | The Role of Thermochemical Factors in Basic Open Hearth Production Rate..... | 840 |
| Scrap brass, melting of refinery..... | 355 | pH method of estimating basicity..... | 901 | on Sulphur Equilibria between Iron Blast Furnace Slags and Metal..... | 831 |
| converting residual metals..... | 357 | Smart, J. S.: Discussion on Distillation of Zinc from Copper Base Alloys and Galvanizers Drosses..... | 856 | Tensile tests, constant strain rate..... | 702 |
| metallurgical results..... | 357 | on Effect of a Dispersed Phase on Grain Growth in Al-Mn Alloys..... | 310 | variable strain rate..... | 706 |
| | | Smelter oxygen system..... | 448 | Tercod crucible..... | 406, 671 |
| | | Smelting, metallurgy..... | 1 | Ternary system, copper-manganese-zinc..... | 775 |
| | | Smigelskas, A., and Barrett, C. S.: Preferred Orientation in Rolled and Recrystallized Beryllium..... | 145, 887 | Terrell, A. D.: Discussion on Development of the Modern Zinc Retort in the United States..... | 851, 852 |
| | | discussion..... | 886, 887 | on Development of Muffle Furnaces for the Production of Zinc Oxide and Zinc at East Chicago, Indiana..... | 854, 854 |
| | | Smith, A. A.: Discussion on the Morenci Smelter of Phelps Dodge Corp. at Morenci, Ariz..... | 855 | on El Paso Slag Treatment Plant..... | 854 |
| | | Smith, C. S.: Discussion on Effect of a Dispersed Phase on a Grain Growth in Al-Mn Alloys..... | 312, 204 | Thermodynamic relations in the molten state, silver-silver sulphide..... | 457 |
| | | Solid Nuclei in Liquid Metals..... | 204 | Theuerer, H. O., et al.: P-type and N-type Silicon and the Formation of the Photovoltaic Barrier in Silicon Ingots..... | 383 |
| | | on The Kappa Eutectoid Transformation in the Copper-silicon System..... | 343 | Thompson, D. H., and Tracy, A. W.: Influence of Composition on the Stress-corrosion Cracking of Some Copper-base Alloys..... | 100 |
| | | Smith, C. S., and Ikeuye, K. K.: Studies of | | | |

